META 2023 Paris - France

The 13th International Conference on Metamaterials, Photonic Crystals and Plasmonics



July 18 – 21, 2023
Paris - France

Proceedings

ISSN 2429-1390

metaconferences.org

META 2023 Paris - France

The 13th International Conference on Metamaterials, Photonic Crystals and Plasmonics

Edited by

Philippe Lalanne | Institut d'Optique d'Aquitaine - CNRS, France
Said Zouhdi | Paris-Saclay University, France

TABLE OF CONTENT

ORGANIZATION I COMMITTEES 3

SPONSORS I EXHIBITORS 5

PLENARY SPEAKERS 7

KEYNOTE SPEAKERS 13

TUTORIALS 25

INDUSTRIAL WORKSHOPS 26

GUIDELINES FOR PRESENTERS I IN-PERSON 27

GUIDELINES FOR POSTER PRESENTERS I ONLINE 28

USEFUL INFORMATION 29

TABLE OF CONTENTS 31

ORGANIZATION I COMMITTEES

Conference Chairs



Philippe Lalanne
Institut d'Optique d'Aquitaine - CNRS, France



Said Zouhdi
Paris–Saclay University, France

International Advisory Committee

Federico Capasso (USA)
Nader Engheta (USA)
Teruya Ishihara (Japan)
Yuri Kivshar (Australia)
Graeme W. Milton (USA)
Manuel N.-Vesperinas (Spain)
Susumu Noda (Japan)
Franco Nori (Japan & USA)
Masaya Notomi (Japan)
Vladimir Shalaev (USA)
David R. Smith (USA)
Martin Wegener (Germany)
Xiang Zhang (Hong Kong)
Nikolay Zheludev (UK)

Technical Program Committee

Pierre-Michel Adam (France)
Ishwar Aggarwal (USA)
Antonio Ambrosio (Italy)
Benfeng Bai (China)
Mohamed Bakr (Canada)
Xavier Begaud (France)
Henri Benisty (France)
Jamal Berakdar (Germany)
Svetlana V. Boriskina (USA)
Shah Nawaz Burokur (France)
Che Ting Chan (Hong Kong)
Debashis Chanda (USA)
Johan Christensen (Spain)
Alfredo De Rossi (France)
Alexander Dmitriev (Sweden)
Monika Fleischer (Germany)
Denis Garoli (Italy)
Alexander Govorov (USA)
Tatjana Gric (Lithuania)
Jean-Philippe Groby (France)
Ortwin Hess (UK)
Eugene Kamenetskii (Israel)
Howard (Ho Wai) Lee (USA)
Jensen Li (Hong Kong)
Qiang Li (China)
Yang Li (China)
Anatole Lupu (France)
Nicolò Maccaferri (Sweden)
Martin McCall (UK)
Marco Miniaci (France)
Taiichi Otsuji (Japan)
Willie Padilla (USA)
Dorota Pawlak (Poland)
Lucia Petti (Italy)
Virginie Ponsinet (France)
Min Qiu (China)
Giorgio Quaranta (Switzerland)
Jun Suk Rho (Korea)
Junichi Takahara (Japan)
Takuo Tanaka (Japan)
Hong Wei (China)

Special Sessions Organizers

Guillermo Acuna (Switzerland)
Angela Barreda (Germany)
Xavier Begaud (France)
Alessandro Belardini (Italy)
Maha Ben Rhouma (France)
Henri Benisty (France)
Jamal Berakdar (Germany)
Sven Burger (Germany)
Shah Nawaz Burokur (France)
Giulio N. F. Cerullo (Itlay)
Debashis Chanda (USA)
Hyuck Choo (Korea)
Kaveh Delfanazari (UK)
Giuseppe Della Valle (Itlay)
Marc Dubois (France)
Kofi Edee (France)
Braulio García-Cámara (Spain)
Denis Garoli (Itlay)
Li Ge (USA)
Jonathan Gratus (UK)
Tatjana Gric (Lithuania)
Thierry Grosjean (France)
Simon Horsley (UK)
Han Htoon (USA)
Xiao Hu (Japan)
Kotaro Kajikawa (Japan)
Alina Karabchevsky (Israel)
Mercedeh Khajavikhan (USA)
Paul Kinsler (UK)
Panagiotis Kosmas (Greece)
Philippe Lalanne (France)
Anatole Lupu (France)
Nicolò Maccaferri (Sweden)
Konstantinos Makris (Greece)
Martin McCall (UK)
Khaled Mnaymneh (Canada)
Galan Moody (USA)
Ziad Musslimani (USA)
Willie Padilla (USA)
Dorota Pawlak (Poland)
Lucia Petti (Italy)
Francesco Pineider (Italy)
Virginie Ponsinet (France)
Edik Rafailov (UK)
Massimo Rippa (Italy)
Sergey Saveliev (UK)
Rebecca Seviour (UK)
Radwanul H. Siddique (USA)
Junichi Takahara (Japan)
Ventsislav K. Valev (UK)
Frank Vollmer (UK)
Simone Zanotto (Italy)

Special Symposia Organizers



Jerome Plain
France



Alexander Govorov
USA



Davy Gérard
France



Pedro H. Martinez
Singapore



Junsuk Rho
Korea



Hakjoo Lee
Korea



Namkyoo Park
Korea



Seong Ok Han
Korea



Howard Lee
USA



Pin-Chieh Wu
Taiwan



Eugene
Kamenetskii
Israel



Jensen Li
Hong Kong



Jean-Philippe Groby
France



Marco Miniaci
France



Vicente R. García
Spain



Vincent Pagneux
France



Noé Jiménez
Spain

SPONSORS I EXHIBITORS

Gold Sponsor

Raith develops leading edge lithography systems enabling compound semiconductor customers to drive innovation and production. Our maskless electron beam, laser beam and focused ion beam patterning solutions cover the full range, from µm structures to sub 10 nm critical device fabrication. The Raith product portfolio is being complemented by automated SEM based chip analysis and process control systems. Our worldwide service and customer support structures are backed by experienced experts in our international applications and development centers. We are fully committed to further push the limits of nanofabrication in close collaboration with our outstanding customer base.

Silver Sponsor

The Synopsys Optical Solutions Group provides design tools that model all aspects of light propagation. Our innovative software packages include CODE V® imaging design software, LightTools® illumination design software, the LucidShape® products for automotive lighting, and the RSoft™ Photonic Device Tools for passive and active photonic devices. And our optical measurement solutions give customers access to precision light scattering data for materials and media used in optical systems.

At META 2023, Synopsys will demonstrate MetaOptic Designer, an unprecedented inverse design tool that takes user-specified criteria and generates metalenses/metasurfaces for optimal design performance. Metalens design traditionally requires extensive physics knowledge and many hours of development. MetaOptic Designer removes these barriers with exclusive AI that automatically yields the best metalens designs as fast as possible.

PHASICS, founded in 2003, offers state-of-the-art optics metrology and imaging solutions, from standalone SID4 wavefront sensors to fully automated test benches, Kaleo MTF, Kaleo MultiWAVE, and a fully modular metrology solution, Kaleo Kit. This range of wavefront measurement systems and quantitative phase imaging solutions is based on innovative, high-resolution wavefront-sensing technology. PHASICS' unique, patented wavefront sensing technology is called QuadriWave Lateral Shearing Interferometry (QWLSI). This technology was developed to overcome the Shack- Hartmann limitations: it offers ultra-high resolution, high sensitivity (sub-nanometric), and a wide dynamic range (hundreds of microns).

PHASICS has a strong customer focus and cares about satisfying all its customers' needs. Its robust R&D team develops innovative features, explores new applications, and customizes standard configurations to customers' requests. Thanks to these large innovative projects, PHASICS covers a wide range of applications, including laser testing, adaptive optics, lens alignment and quality control, refractive index mapping in materials, quantitative phase imaging for biology, and plasma and gas density measurements.

ENSEMBLE3 is a newly established Centre of Excellence in nanophotonics, advanced materials and technologies based on crystal growth. The Centre was established under the "Teaming for Excellence" program funded by the European Commission and the "International Research Agendas" program funded by the Foundation for Polish Science and works in collaboration with renowned national and international scientific institutions.

The Centre works on the development of new material technologies and advanced materials with exceptional electromagnetic properties that can be applied in areas such as photonics, optoelectronics, telecommunications, solar energy conversion, medicine, aeronautics, security and defense.

Other Partners

Université Paris-Saclay is a research university based in Paris, France. Université Paris-Saclay offers a comprehensive and varied range of Undergraduate, Master's and PhD degrees, renowned internationally thanks to the University's reputation for research excellence and the commitment of its academic staff. The University's constituent faculties, institutes and component institutions all contribute to the curricula with cutting-edge specialised courses in Science and Engineering, Life Sciences and Health, and Social Sciences and Humanities.
Université Paris-Saclayis ranked 1st in France and 13th in the world according to the Academic Ranking of World Universities (ARWU).

AEM - Advanced Electromagnetics is a peer-reviewed, Gold Open Access journal. It covers recent international research results in the general field of Electromagnetic Waves, Antennas and Propagation. Authors of articles published in Advanced Electromagnetics retain the copyright of their articles and are free to reproduce and disseminate their work (under a Creative Commons Attribution License). AEM is widely indexed and has a Scopus CiteScore of 2.2 (2021).

ACS Photonics is an interdisciplinary forum to communicate on the latest advances in the field of photonics, all the way from basic research to applied research and technology. Embracing the transversality of photonics, it connects scientists and technologists from a broad scientific spectrum, at the interface between physics, chemistry, biology, and engineering. It also aims at bridging the gap between the academic and industrial worlds.

Nanophotonics (De Gruyter) covers recent international research results, specific developments in the field and novel applications. It publishes all article in a Gold Open Access model and belongs to the top journals in the field. Nanophotonics focuses on the interaction of photons with nano-structures, such as carbon nano-tubes, nano metal particles, nano crystals, semiconductor nano dots, photonic crystals, tissue and DNA.

PLENARY SPEAKERS



Andrea Alù

City University of New York, USA

Extreme Control of Light and Sound with Metamaterials

Andrea Alù is a Distinguished Professor at the City University of New York (CUNY), the Founding Director of the Photonics Initiative at the CUNY Advanced Science Research Center, and the Einstein Professor of Physics at the CUNY Graduate Center. He received his Laurea (2001) and PhD (2007) from the University of Roma Tre, Italy, and, after a postdoc at the University of Pennsylvania, he joined the faculty of the University of Texas at Austin in 2009, where he was the Temple Foundation Endowed Professor until Jan. 2018. Dr. Alù is a Fellow of the National Academy of Inventors (NAI), the American Association for the Advancement of Science (AAAS), the Institute of Electrical and Electronic Engineers (IEEE), the Materials Research Society (MRS), Optica, the International Society for Optics and Photonics (SPIE) and the American Physical Society (APS). He is the President of Metamorphose, a Highly Cited Researcher since 2017, a Simons Investigator in Physics, the director of the Simons Collaboration on Extreme Wave Phenomena Based on Symmetries, and the Editor in Chief of Optical Materials Express. He has received several scientific awards, including the NSF Alan T. Waterman award, the Blavatnik National Award for Physical Sciences and Engineering, the IEEE Kiyo Tomiyasu Award, the ICO Prize in Optics, the OSA Adolph Lomb Medal, and the URSI Issac Koga Gold Medal.

Extreme Control of Light and Sound with Metamaterials
In this talk, I discuss recent developments in this field of research, with an emphasis on the role of symmetries in establishing emerging optical responses for metamaterials based on otherwise simple constituents. Geometrical rotations, suitably tailored perturbations, and broken time reversal symmetry can be carefully engaged to tailor waves in robust and efficient ways, control their propagation, break Lorentz reciprocity and enable topological order and phase transitions.



Nader Engheta

University of Pennsylvania, USA

Structuring light with media with higher dimensions: space, time, and more

Nader Engheta is the H. Nedwill Ramsey Professor at the University of Pennsylvaniain Philadelphia with affiliations in the Departments of Electrical and Systems Engineering, Physics and Astronomy, Bioengineering, and Materials Science and Engineering. He received his BS degree from the University of Tehran, and his MS and Ph.D. degrees from Caltech. His current research activities span a broad range of areas including optics, metamaterials, electrodynamics, microwaves, photonics, nano-optics, graphene photonics, imaging and sensing inspired by eyes of animal species, microwave and optical antennas, and physics and engineering of fields and waves. He has received several awards for his research including the 2023 Benjamin Franklin Medal in Electrical Engineering, Election to the American Academy of Arts and Sciences (2023), Caltech Distinguished Alumni Award (2023), the 2020 Isaac Newton Medal and Prize from the Institute of Physics (UK), the 2020 Max Born Award from the OPTICA (formerly Optical Society), the 2019 Ellis Island Medal of Honor, the 2018 IEEE Pioneer Award in Nanotechnology, the 2022 Hermann Anton Haus Lecture at MIT, the 2015 SPIE Gold Medal, the 2014 Balthasar van der Pol Gold Medal from the International Union of Radio Science (URSI), the 2017 William Streifer Scientific Achievement Award, the Canadian Academy of Engineeringas an International Fellow the Fellow of US National Academy of Inventors (NAI), the IEEE Electromagnetics Award, the Vannevar Bush Faculty Fellowship Awardfrom DoD, the Wheatstone Lecture in King's College London, 2006 Scientific American Magazine 50 Leaders in Science and Technology, and the Guggenheim Fellowship. He is a Fellow of nine international scientificand technical organizations, i.e., IEEE, OPTICA, APS, MRS, SPIE, URSI, AAAS, IOP and NAI. He has received the honorary doctoral degrees from the Aalto University in Finland in 2016, the University of Stuttgart, Germany in 2016, and Ukraine's National Technical University Kharkov Polytechnic Institute in 2017.

Structuring light with media with higher dimensions: space, time, and more

In this talk, I will present some of our most recent results on exploring light-matter interaction in material media with high degrees of freedom and dimensions including spatial and/or temporal inhomogeneities, and other degrees of freedom such as anisotropy, ellipticity, and hyperbolicity. We show how light manipulation with such metastructures with high degrees of freedom can lead to exciting novel wave phenomena with potential applications in wave-based reconfigurable analog computing, 4D optics, and other optical devices and components.



Sylvain Gigan

Sorbonne Université, France

Imaging and Computing with disorder

Sylvain Gigan is professor of physics at Sorbonne Université in Paris and group leader in Laboratoire Kastler-Brossel at Ecole Normale Supérieure. His research interests range from fundamental investigations of light propagation in complex media, biomedical imaging, computational imaging, and signal processing, to quantum optics and quantum information in complex media. After graduating from Ecole Polytechnique (Palaiseau France) in 2000 and a Master specialization in optics from University Paris XI (Orsay, France), he obtained a PhD in physics in 2004 from University Pierre and Marie Curie (Paris, France) in quantum and non-linear Optics. From 2004 to 2007, he was a postdoctoral researcher in Vienna University (Austria). from 2007 to 2014, he was at ESPCI ParisTech as Associate Professor, and started working on optical imaging in complex media and wavefront shaping techniques, at the Langevin Institute. Dr. Gigan is also the cofounder of a spin-off called LightOn (www.lighton.ai), aiming at performing optical computing for machine learning and big data. He was awarded the Fabry de Gramont Prize of the French Optical Society in 2016, The Joseph Fourier ATOS prize in 2018, the Jean Jerphagnon Prize in 2019.

Imaging and Computing with disorder

Light propagation in complex media, such as paint, clouds, or biological tissues, is a very challenging phenomenon, encompassing fundamental aspects in mesoscopic and statistical physics. It is also of utmost applied interest, in particular for imaging. Although this scattering process seems to mix and completely destroy all information, thus preventing imaging or communication, a different approach has emerged. I will discuss how this powerful concept has recently triggered a wealth of advances in imaging and computing.



Marin Soljačić

Massachusetts Institute of Technology (MIT), USA

Nanophotonics for tailoring radiation from fast electrons

Marin Soljačić is a Professor of Physics at MIT. He is a founder of WiTricity Corporation (2007), LuxLabs (2017), as well as Lightelligence (2017). His main research interests are in artificial intelligence as well as electromagnetic phenomena, focusing on nanophotonics, non-linear optics, and wireless power transfer. He is a recipient of the Adolph Lomb medal from the Optical Society of America (2005), and the TR35 award of the Technology Review magazine (2006). In 2008, he was awarded a MacArthur fellowship “genius” grant. He is an international member of the Croatian Academy of Engineering since 2009. In 2011 he became a Young Global Leader (YGL) of the World Economic Forum. In 2014, he was awarded Blavatnik National Award, as well as Invented Here! (Boston Patent Law Association). In 2017, he was awarded "The Order of the Croatian Daystar, with the image of Ruđer Bošković", the Croatian President’s top medal for Science. In 2017, the Croatian President also awarded him with "The Order of the Croatian Interlace" medal. He was also Highly Cited Researcher according to WoS for 2019, 2020 and 2021.

Nanophotonics for tailoring radiation from fast electrons

Nanophotonic methods provide intriguing options for manipulating scintillation phenomena. We will outline recent developments in this domain, along with our theoretical framework for modeling these occurrences, supported by our experimental findings. Additionally, Smith-Purcell radiation, characterized by fast electrons interacting with nano-structured materials to produce light, offers a broad spectrum of possibilities for creation of novel light sources. We will discuss our new theoretical framework designed to comprehend and tailor such phenomena, as well as our techniques for boosting Smith-Purcell radiation.



Isabelle Staude

Friedrich Schiller University Jena, Germany

Active photonic metasurfaces empowered by 2D semiconductors

Isabelle Staude is professor at the Institute of Solid State Physics at the Friedrich Schiller University Jena, Germany. She studied physics at the University of Konstanz, Germany, received her Ph.D. degree from the Karlsruhe Institute of Technology, Germany, in 2011, and spent several years as a postdoc at the Australian National University, Canberra, Australia. She received an Emmy-Noether Grant from the German Research Foundation and the Hertha Sponer Prize 2017 from the German Physical Society. She is a member of the German Young Academy (Junge Akademie) and a Fellow of the Max Planck School of Photonics..

Active photonic metasurfaces empowered by 2D semiconductors

This talk reviews our recent and ongoing activities in hybridizing optical metasurfaces composed of resonant metallic or dielectric building blocks with 2D-TMDCs. We demonstrate that the ability of the nanoresonators to concentrate light into nanoscale volumes can be utilized to carefully control the properties, such as pattern and polarization, of light emitted by 2D-TMDCs via photoluminescence or nonlinear optical processes. Furthermore, we investigate the ability of tailored nanostructures to interact selectively with exciton populations located at inequivalent conduction band minima at the corners of the 2D-TMDC's Brillouin zone.



Jelena Vuckovic

Stanford University, USA

Scalable classical and quantum photonics

Jelena Vuckovic (PhD Caltech 2002) is the Jensen Huang Professor in Global Leadership in the School of Engineering, and Professor of Electrical Engineering and by courtesy of Applied Physics at Stanford, where she leads the Nanoscale and Quantum Photonics Lab. She is also the Fortinet Founders Chair of the Electrical Engineering Department at Stanford, and was the inaugural director of Q-FARM, the Stanford-SLAC Quantum Science and Engineering Initiative. Vuckovic has received many awards and honors including recently the Vannevar Bush Faculty Fellowship (2022), the Mildred Dresselhaus Lectureship from MIT (2021), the James Gordon Memorial Speakership from the OSA (2020), the IET A. F. Harvey Engineering Research Prize (2019), Distinguished Scholarship of the Max Planck Institute for Quantum Optics (2019), the Hans Fischer Senior Fellowship from the Institute for Advanced Studies in Munich (2013), and Humboldt Prize (2010). She is a Fellow of the APS, of the Optica (OSA), and of the IEEE, and an associate editor of the ACS Photonics.

Scalable classical and quantum photonics

Novel computational techniques such as photonics inverse design, along with new nanofabrication approaches, play a crucial role in building scalable integrated classical and quantum photonics. Inverse design, a departure from the traditional photonics design approach, can lead to photonics much better than state of the art in many metrics (smaller, more efficient, more robust, a much higher density of integration). This is enabled by development of a computer software which efficiently searches through the space of all possible and fabricable photonic geometries, in any material of interest. On the other hand, future photonic systems also require integration and fabrication of traditional and non-traditional photonic materials, including silicon, silicon-carbide, diamond, sapphire, and strong electro-optic materials such as lithium niobate, strontium and barium titanate.

KEYNOTE SPEAKERS



Harry Atwater

California Institute of Technology, USA

Active Metasurfaces in Space and Time

Harry Atwater is the Otis Booth Leadership Chair of the Division of Engineering and Applied Science, and the Howard Hughes Professor of Applied Physics and Materials Science at the California Institute of Technology. Atwater's scientific effort focuses on nanophotonic light-matter interactions. His work spans fundamental nanophotonic phenomena and applications, including active wavefront shaping of light using metasurfaces, optical propulsion of lightsails, quantum and 2D nanophotonics as well as solar energy conversion.

Atwater was an early pioneer in nanophotonics and plasmonics and gave a name to the field of plasmonics in 2001. He is Chair of the LightSail Committee for the Breakthrough Starshot program. Currently Atwater is also the Director for the Liquid Sunlight Alliance (LiSA), a Department of Energy Hub program for solar fuels, and was also the founding Editor in Chief of the journal ACS Photonics. Atwater is a Member of the US National Academy of Engineering, a Web of Science Highly Cited Researcher, and the recipient of the 2021 von Hippel Award of the Materials Research Society.

Active Metasurfaces in Space and Time
Active dielectric and plasmonic metasurfaces enable new modalities for spatiotemporal beam control for beam steering and wavefront shaping at multiple frequencies. In this talk, I will discuss metasurfaces with high quality factor, local, resonant elements capable of two-dimensional phase gradient generation, in both passive and active metasurface designs. I will also describe active metasurfaces with both spatial and temporal phase gradients, and an active metasurface as a lens-less imaging system, and compare the characteristics to conventional lens-coupled image sensors.



Alexandra Boltasseva

Purdue University, USA

Crossroads of Nanophotonics and Machine Learning

Alexandra Boltasseva is a Professor at the School of Electrical & Computer Engineering at Purdue University. She received her PhD in electrical engineering at Technical University of Denmark, DTU in 2004. Boltasseva specializes in nanophotonics, nanofabrication, optical materials, plasmonics and metamaterials. She is 2018 Blavatnik National Award for Young Scientists Finalist and received the 2013 IEEE Photonics Society Young Investigator Award, 2013 Materials Research Society (MRS) Outstanding Young Investigator Award, the MIT Technology Review Top Young Innovator (TR35), the Young Researcher Award in Advanced Optical Technologies from the University of Erlangen-Nuremberg, Germany, and the Young Elite-Researcher Award from the Danish Council for Independent Research. She is a Fellow of the Optical Society of America (OSA) and Fellow of SPIE. She served on MRS Board of Directors and is Editor-in-Chief for OSA's Optical Materials Express.

Crossroads of Nanophotonics and Machine Learning
We report on advancing machine-learning-assisted optical inverse design optimization for metasurfaces with applications in thermophotovoltaics, reflective optics, and lightsail technology as well as for on-chip quantum photonic components and super-resolution imaging.



Mark Brongersma

Stanford University, USA

Flat Optics for Dynamic Wavefront Manipulation

Mark Brongersma is the Stephen Harris Professor in the Departments of Materials Science and Applied Physics at Stanford University. He leads a research team of ten students and five postdocs. Their research is directed towards the development and physical analysis of new materials and structures that find use in nanoscale electronic and photonic devices. He is on the list of Global Highly Cited Researchers (Clarivate Analytics). He received a National Science Foundation Career Award, the Walter J. Gores Award for Excellence in Teaching, the International Raymond and Beverly Sackler Prize in the Physical Sciences (Physics) for his work on plasmonics, and is a Fellow of the OSA, the SPIE, and the APS. Dr. Brongersma received his PhD from the FOM Institute AMOLF in Amsterdam, The Netherlands, in 1998. From 1998-2001 he was a postdoctoral research fellow at the California Institute of Technology.

Flat Optics for Dynamic Wavefront Manipulation
In this presentation, I will highlight our recent efforts to realize electrically-tunable metasurfaces employing nanomechanics, microfluidics, phase change materials, and atomically-thin semiconductors. Such elements are capable of dynamic wavefront manipulation for optical beam steering and holography. I will also discuss how the nanostructured, planar optical elements can be fabricated by scalable fabrication technologies, opening the door to a wide range of commercial applications.



Demetrios Christodoulides

University of Southern California, USA

Optical thermodynamics of highly multimode nonlinear photonic systems

Demetrios Christodoulides is an Endowed Chair Professor in the Department of Electrical and Computer Engineering at the University of Southern California. He received his Ph.D. from Johns Hopkins University in 1986. After earning his doctorate degree, he joined Bellcore as a postdoctoral research fellow, and was a faculty member in the Department of Electrical Engineering at Lehigh University from 1988 to 2002. Between 2002 and 2022 he was a Pegasus Professor and the Cobb Family Endowed Chair at CREOL–The College of Optics and Photonics at the University of Central Florida. Christodoulides' contributions have been in the general field of optics and photonics. Among them is the first prediction of discrete self-trapped states in optical lattices, Bragg solitons in nonlinear gratings, vector solitons, and the development of the theory describing nonlinear optical interactions in soft matter and biological colloidal systems. His group proposed and demonstrated optical accelerating beams, which today find applications in microscopy and nonlinear optics. In the last ten years or so, his work has focused on the ramifications and applications of some special symmetries in optics, such as those of parity-time symmetry and supersymmetry. Most recently he has been exploring new theoretical avenues in describing the complex dynamics of highly multimode nonlinear photonic systems by means of optical thermodynamics. He has served as an associate editor for the IEEE Journal of Quantum Electronics and JOSA B. He is a Fellow of APS and Optica. He is the recipient of the Optica's 2011 R.W. Wood Prize and 2018 Max Born Award, and of the 2023 Arthur L. Schawlow Prize in Laser Science of APS.

Optical thermodynamics of highly multimode nonlinear photonic systems
In this talk, a thermodynamic theory capable of describing complex, highly multimoded, nonlinear optical systems is presented. It is shown that the mode occupancies in such nonlinear multimode arrangements follow a universal behavior that always tends to maximize the system's entropy at steady-state. This thermodynamic response takes place irrespective of the type of nonlinearities involved and can be utilized to either heat or cool an optical multimode system. Aspects associated with adiabatic compressions and expansions will be discussed along with the possibility for all-optical Carnot cycles.



Javier García de Abajo

ICFO-Institut de Ciencies Fotoniques, Spain

Quantum optical phenomena in two-dimensional materials

Javier García de Abajo received his PhD from the University of the Basque Country in 1993 and then visited Berkeley National Lab for three years. He was a Research Professor at the Spanish CSIC and in 2013 moved to ICFO-Institut de Ciencies Fotoniques (Barcelona) as an ICREA Research Professor and Group Leader. He is Fellow of both the American Physical Society and the Optical Society of America, and he has co-authored 300+ articles on different aspects of nanophotonics, atomic physics, surface science, and electron microscope spectroscopies. See http://www.nanophotonics.es for more details.

Quantum optical phenomena in two-dimensional materials
We discuss new approaches to the synthesis, design, and exploitation of two-dimensional materials for nanophotonics, including plasmonics in ultrathin crystalline metals, a disruptive class of quantum-phase materials, recent advances in the solution to the problem of coupling between free-space light and ultraconfined optical excitations, and the application of these developments to the study of ultrafast nonlinear phenomena and quantum optics at the atomic scale.



Wolfgang Fritzsche

Leibniz Institute for Photonic Technology, Germany

Bioanalytics using plasmonic nanostructures

Wolfgang Fritzsche is heading the Nanobiophotonics Department at the Leibniz Institute for Photonic Technology (IPHT) in Jena, Germany. His scientific interest is in localized surface plasmon resonance, focused on novel effects in the interaction of molecular components with plasmonic nanostructures, with a special emphasis on biosensing. Here, multiplexed assays based on imaging spectrometry readout are targeted, in order to allow for the paralleled monitoring of molecular binding reactions for potential bioanalytical applications.

Bioanalytics using plasmonic nanostructures
The effect of localized surface plasmon resonance (LSPR) on chemically synthesized gold nanoparticles is utilized to setup a biosensing platform with the potential for sensitive and specific detection of biomolecules of interest such as biomarkers. This principle is demonstrated both on a single particle level for DNA detection, then extended also to proteins, and to arrays of particles. In order to readout the arrays, imaging spectrometer were developed.



Sven Höfling

University of Würzburg, Germany

Semiconductor quantum dot based quantum technologies

Sven Höfling received his Ph.D. degree from Würzburg University. He was with the Fraunhofer Institute of Applied Solid-State Physics, Freiburg, Germany from 2001 to 2002 working on blue and white light emitting diodes. From 2006 to 2013, he was head of the Optoelectronic Materials and Devices Group at Technische Physik, Würzburg University. Sven Höfling was a full professor at the University of St Andrews, Scotland from 2013 to 2021. In 2015 he rejoint the University of Würzburg, Germany as a professor of physics and as the Head of the Chair of Applied Physics and the Gottfried-Landwehr-Laboratory for Nanotechnologies. He is running a 550 sqm clean room with a full chain of semiconductor growth, processing and characterization tools. Dr. Höfling is a member of German Physical Society (DPG), a Senior member of IEEE and SPIE, and a fellow of the Institute of Physics (IOP) and Optica.

Semiconductor quantum dot based quantum technologies
We will summarize recent progress made within our group on self-assembled quantum dot device,development for quantum repeater and quantum computer applications. A particular emphasis will be on,semiconductor quantum dots embedded in circular Bragg grating cavities. For scalability, spatially deterministic, placement of quantum dots in bullseye cavities is pursued and tuning by electric and strain fields are,implemented. To apply electric fields, a new device design for electrically contactable circular Bragg grating,cavities in labyrinth geometry is employed.



Jiří Homola

Institute of Photonics and Electronics of the Czech Academy of Sciences, Czech Republic

Plasmonic biosensors for biomedical applications

Jiří Homola is Deputy Director and the Head of Optical Biosensors research group at the Institute of Photonics and Electronics of the Czech Academy of Sciences. He received his PhD (1993) from the Czech Academy of Sciences. From 1993 to 1997 he worked at the Institute of Photonics and Electronics, Prague as a Research Scientist. From 1997 to 2002 he was with the Department of Electrical Engineering, University of Washington, Seattle (USA), since 2001 as a Research Associate Professor. From 2003, he has been with the Institute of Photonics and Electronics in Prague and has been responsible for the optical biosensors research program. In 2009, he received his DSc. degree in technical sciences from the Czech Academy of Sciences and in 2014 he became Professor of physics at Charles University in Prague. From 2009 to 2019, he was Affiliate Professor at the University of Washington, Seattle. He has received the Roche Diagnostics Prize for Sensor Technology, Award for Outstanding Research of the Ministry of Education of the Czech Republic, among other awards. He has been elected Fellow of the Learned Society of the Czech Republic and Fellow of the International Society for Optical Engineering (SPIE). He serves as associate editor of Biosensors and Bioelectronics (Elsevier).

Plasmonic biosensors for biomedical applications
Optical biosensors hold potential for applications in numerous important areas. Herein, we discuss the main challenges in developing plasmonic biosensors for applications in biomedicine and present selected advances in biosensor research that aim to address these challenges. We cover advances in plasmonic nanostructures, sensor instrumentation, transport of target molecules in microfluidic systems, functional coatings, and detection assays. We also highlight applications of plasmonic biosensors related to the investigation of biomolecular interactions related to Alzheimer's disease and diagnosis of Myelodysplastic syndromes.



Mercedeh Khajavikhan

University of Southern California, USA

Micro- and Nano-lasers: From One to Many, Unleashing Endless Possibilities

Mercedeh Khajavikhan is a Professor of Electrical and Computer Engineering at the University of Southern California. She has also a joint appointment at the Department of Physics & Astronomy at USC. She received her Ph.D. in Electrical Engineering from the University of Minnesota in 2009. Subsequently, she joined the University of California in San Diego as a postdoctoral researcher, where she worked on the design and development of nanolasers, plasmonic devices, and silicon photonics components. Prior to joining USC, she was a faculty at the College of Optics and Photonics (CREOL) at the University of Central Florida (UCF), working primarily on unraveling novel phenomena in active photonic platforms. She is the recipient of the NSF Early CAREER Award in 2015, the ONR Young Investigator Award in 2016, the DARPA Young Faculty Award in 2018, the University of Central Florida Reach for the Stars Award in 2017, UCF Luminary Award in 2018, and DARPA Director's Fellowship in 2020. She is a fellow of Optica (formerly known as Optical Society of America OSA).

Micro- and Nano-lasers: From One to Many, Unleashing Endless Possibilities

Micro- and nano-lasers form a crucial category of optical components with significant scientific and technological implications. In this presentation, I will discuss the utilization of non-Hermiticity, supersymmetry, and topology principles to design arrays of these devices, resulting in intriguing and unexpected lasing phenomena. By considering the interaction between cavity modes, array geometry, and both short- and long-range coupling among the array elements, we can achieve novel laser phase locking regimes, high radiance emission, rapid beam steering, photonic spin machines, and unidirectional lasing.



Tobias J. Kippenberg

EPFL, Switzerland

Ultra low loss nonlinear integrated photonic circuits: from soliton microcombs, traveling wave parametric amplifiers, chip based Erbium amplifiers to cryogenic quantum interconnects

Tobias J. Kippenberg is Full Professor in the Institute of Physics and Electrical Engineering at EPFL in Switzerland since 2013 and joined EPFL in 2008 as Tenure Track Assistant Professor. Prior to EPFL, he was Independent Max Planck Junior Research group leader at the Max Planck Institute of Quantum Optics in Garching, Germany. While at the MPQ he demonstrated radiation pressure cooling of optical micro-resonators, and developed techniques with which mechanical oscillators can be cooled, measured and manipulated in the quantum regime that are now part of the research field of Cavity Quantum Optomechanics. Moreover, his group discovered the generation of optical frequency combs using high Q micro-resonators, a principle known now as micro-combs or Kerr combs. For his early contributions in these two research fields, he has been recipient of the EFTF Award for Young Scientists (2011), The Helmholtz Prize in Metrology (2009), the EPS Fresnel Prize (2009), ICO Award (2014), Swiss Latsis Prize (2015), as well as the Wilhelmy Klung Research Prize in Physics (2015), the 2018 ZEISS Research Award and 2020 OSA R. Wood Award. Moreover, he is 1st prize recipient of the "8th European Union Contest for Young Scientists" in 1996 and is listed in the Highly Cited Researchers List of 1% most cited Physicists in 2014-2019. He is founder of the startup LIGENTEC SA, an integrated photonics foundry.

Ultra low loss nonlinear integrated photonic circuits: from soliton microcombs, traveling wave parametric amplifiers, chip based Erbium amplifiers to cryogenic quantum interconnects
Recent advances in attaining ultra low loss highly confining silicon nitride waveguides with loss in the dB-meter range, and their heterogeneous integration with MEMS and Lithium Niobate have opened up novel applications that exhibit both low cost, and scalable manufacturing but also performance that is on par or exceeding that of legacy optical systems. I will describe a range of novel advances, including photonic integrated circuit based frequency agile lasers, wave amplifiers, as well as soliton frequency combs.



Naoto Nagaosa

RIKEN Center for Emergent Matter Science (CEMS), Japan

Chirality and nonreciprocal responses in quantum materials

Naoto Nagaosa was born in Hyogo Prefecture in 1958, and graduated from Department of Applied physics, The University of Tokyo in 1980. From 1983 to 1986, he was a research associate in Institute for Solid State Physics, Univ. Tokyo, and received a D.Sci from Univ. Tokyo in 1986. From 1988 to 1990, he worked as a visiting scientist at Department of Physics, Massachusetts Institute of Technology, before joining the Department of Applied Physics in Univ. Tokyo, where he is now a professor. From 2013 he has joint appointment with the Deputy Director of the RIKEN Center for Emergent Matter Science (CEMS). He is now serving as Senior Advisory Group (SAG) Scientist of APCTP, and also the chairman of c5 commission (Low Temperature Physics) of IUPAP. His research field is theoretical condensed-matter physics, especially involving the strong electron correlation, optical responses of solids, topological aspects of condensed matter, and superconductivity. For his accomplishments, he has received the Yukawa Prize, Japan IBM Prize, Nissan Science Prize, Nishina Memorial Prize, Fujihara Prize, Purple Ribbon, Benjamin Lee Professorship, and is now a Foreign member of National Academy of Science.

Chirality and nonreciprocal responses in quantum materials
We study the chiral dynamics and consequent nonreciprocal responses in quantum materials, where the most fundamental principles in physics manifest themselves, i.e., the symmetries especially the time-reversal and spatial inversion, dissipation, quantum-classical crossover/transition, quantal Berry phase and topology, and many-body correlation effects. They include (1) magnetochiral anisotropy of semiconductors, Weyl semimetals, and superconductors, and (2) the photovoltaic effect, e.g., the shift currents under photo-excitations.



Dragomir Neshev

Australian National University, Australia

Dielectric metasurfaces with fast and ultra-fast tunability

Dragomir Neshev is the Director of the Australian Research Council Centre of Excellence for Transformative Meta-Optical Systems (TMOS) and a Professor in Physics at the Australian National University (ANU). He received a PhD degree from Sofia University, Bulgaria in 1999. Since then, he has worked in the field of optics at several research centres around the world and joined ANU in 2002. He is the recipient of several awards and honours, including a Highly Cited Researcher (Web of Science, 2022 and 2021), a Queen Elizabeth II Fellowship (ARC, 2010), and a Marie-Curie Individual Fellowship (European Commission, 2001). His activities span over several branches of optics, including periodic photonic structures, singular optics, plasmonics, and optical metasurfaces.

Dielectric metasurfaces with fast and ultra-fast tunability
This talk will overview the recent advances and challenges in tunable metasurfaces. I will discuss metasurface tunability through several mechanisms, including electrical and all-optical drives. Such drives allow for fast and ultrafast responses with high modulation strength. We demonstrate how all-optical control can lead to and high ultrafast transmission modulation of 80%. The presented developments hold promise for real-world applications of active meta-optics.



Sir John Pendry

Imperial College London, UK

Extreme time modulation of material properties and Hawking radiation

John Pendry is a condensed matter theorist working at Imperial College London. His early work addressed electronic and structural properties of surfaces developing the theory of low energy diffraction, EXAFS, and of electronic surface states later moving on to studies of transport in disordered systems. In the mid 1990's he turned his attention to metamaterials and proposed several structures which radically influenced the development of the field leading to the experimental discovery of negative refraction by the Smith group and later, also in collaboration with David Smith, the design of a cloak of invisibility. His investigation of negative refraction led to the discovery that it is theoretically possible to design a lens whose resolution is limited only by the perfection of manufacture, not by the well known Abbé law which limits resolution to the order of the wavelength. The technique of transformation optics which he pioneered has led to many applications in the field of plasmonics, particularly building on the perfect lens concept and showing how to concentrate light into sub nanoscale volumes. His most recent work moves the study of metamaterials on to structures that vary in time as well as in space, invoking quantum aspects of metamaterials.

Extreme time modulation of material properties and Hawking radiation
Experiments demonstrating extremely rapid modulation of the permittivity have been performed by exploitingthe enhanced non-linear effects possible in the presence of plasmonic resonances. These experiments measure anextreme rise time by exploiting the analogy between Young's slits which produce diffraction in momentum space,and closely spaced time windows which produce diffraction in frequency space.



Luca Razzari

Centre Energie, Matériaux et Télécommunications (INRS-EMT), Canada

Structured surfaces for enhanced radiation-matter interaction and nonlinear optics

Luca Razzari is a Full Professor at Institut National de la Recherche Scientifique – Centre Energie, Matériaux et Télécommunications (INRS-EMT) in Montreal, Canada, since 2020. He received his Laurea (2001) and PhD (2004) degrees from the University of Pavia, Italy. He completed part of his PhD research at Institut d'Optique in Orsay, France (2004). He then had three postdoctoral experiences: from 2005 to 2006, he worked at the Institute for Complex Systems (CNR-ISC) in Rome, Italy. From 2006 to 2010, he made his first move to Canada as a Marie Curie Fellow at INRS-EMT. From 2010 to 2012, he was with the Italian Institute of Technology (IIT) in Genoa, Italy. In November 2012, he finally joined the INRS-EMT as a junior faculty member. Dr. Razzari's research interests include nanoscale light-matter interactions, metasurfaces, nonlinear optics, as well as terahertz science and technology. He has been recently elected a Fellow of Optica (2023).

Structured surfaces for enhanced radiation-matter interaction and nonlinear optics
In this talk, I will review our main results regarding the exploitation of nanoresonators and,metasurfaces for: (i) enhanced terahertz spectroscopy of low-dimensional materials; (ii) nanoscale phonon strong coupling; and (iii) nonlinear wavelength conversion.



Mikael Rechtsman

Pennsylvania State University, USA

Quantized Fractional Thouless Pumping of Solitons

Mikael Rechtsman is an Associate Professor of Physics at the Pennsylvania State University in the US. His research group studies different aspects of nonlinear optics and photonics, with a focus on topological structures and devices. He is the recipient of the Packard and Sloan Fellowships, the Office of Naval Research Young Investigator Award, and the ICO prize of the International Commission of Optics.

Quantized Fractional Thouless Pumping of Solitons
I will present my group's recent work on the fractional pumping of solitons in photonic Thouless pumps. Specifically, I will show that the displacement (in unit cells) of solitons in Thouless pumps is strictly quantized to the Chern number of the band from which the soliton bifurcates in the low power regime, whereas in the intermediate power regime, nonlinear bifurcations lead to fractional quantization of soliton motion. This fractional quantization can be predicted from multi-band Wannier functions.



Moti Segev

Technion, Israel

Photonic Time-Crystals

Moti Segev is the Robert J. Shillman Distinguished Professor of Physics and Electrical Engineering, at the Technion, Israel. His interests are mainly in photonics, solitons, lasers, and quantum optics. He won numerous international awards, among them the 2007 Quantum Electronics Prize of the EPS, the 2009 Max Born Award of the OSA, and the 2014 Arthur Schawlow Prize of the APS. In 2011, he was elected to the Israel Academy of Sciences, in 2015 to the National Academy of Science of the USA. In 2014 he won the Israel Prize (highest honor in Israel). Above all his achievements, Moti takes pride in the success of his graduate students and postdocs, among them are currently 23 professors in the USA, Germany, Taiwan, Croatia, Italy, India, China and Israel, and many holding senior R&D positions in the industry.

Photonic Time-Crystals
Time-Crystals (PTCs) are materials in which the refractive index varies periodically and abruptly in,time. They conserve momentum but not energy, and display momentum bands separated by gaps. The,fundamentals of PTCs will be presented, with an emphasis on light-matter interactions ranging from light,emission by atoms and free electrons to superluminal k-gap solitons and recent experiments.



Vladimir M. Shalaev

Purdue University, USA

Near-Zero-Index Materials for Nonlinear Optics and Beyond

Vladimir M. Shalaev, Scientific Director for Nanophotonics at Birck Nanotechnology Center and Distinguished Professor of Electrical and Computer Engineering at Purdue University, specializes in nanophotonics, plasmonics, and optical metamaterials. Vladimir M. Shalaev has received several awards for his research in the field of nanophotonics and metamaterials, including the Max Born Award of the Optical Society of America for his pioneering contributions to the field of optical metamaterials, the Willis E. Lamb Award for Laser Science and Quantum Optics, IEEE Photonics Society William Streifer Scientific Achievement Award, Rolf Landauer medal of the ETOPIM (Electrical, Transport and Optical Properties of Inhomogeneous Media) International Association, the UNESCO Medal for the development of nanosciences and nanotechnologies, OSA and SPIE Goodman Book Writing Award. He is a Fellow of the IEEE, APS, SPIE, MRS and OSA. Prof. Shalaev has authored three books, thirty invited book chapters and over 500 research publications.

Near-Zero-Index Materials for Nonlinear Optics and Beyond
We discuss Near-Zero-Index (NZI) materials based on transparent conducting oxides (TCOs) that open new avenues in nonlinear optics including exotic time-varying media phenomena, such as negative refraction, time refraction/reflection, and photonic time crystals.



Kerry Vahala

California Institute of Technology, USA

High-Q photonics

Kerry Vahala is Professor of Applied Physics at Caltech and holds the Jenkins Chair in Information Science and Technology. His research on chip-based high-Q optical resonators and related low-power nonlinear optical devices has advanced miniature frequency and time systems, microwave sources, parametric oscillators, astrocombs and gyroscopes. Vahala also made early contributions to the subject of cavity optomechanics and demonstrations of chip-based devices to cavity QED phenomena. A member of the National Academy of Engineering and Fellow of the IEEE and Optica, he received the IEEE Sarnoff Medal for research on quantum-well laser dynamics, the Alexander von Humboldt award and MPQ Distinguished Scholar Award for work on ultra-high-Q optical microcavities, a NASA achievement award for application of microcombs to exoplanet detection, and the Optica Forman Team Engineering Excellence Award for a 2-photon optical clock. Vahala is the Executive Officer of the Department of Applied Physics and Materials Science at Caltech.

High-Q photonics

After a brief overview of their history, I will review recent applications. These include Sagnac gyroscopes, microwave signal sources, clocks, and high-coherent sources. The current and possible future limits of microresonator performance, and untapped application areas, will also be discussed.



Xiangrong Wang

The Hong Kong University of Science and Technology, Hong Kong

Recent progress in magnetic skyrmion physics

Xiangrong Wang is a full professor in the physics department of The Hong Kong University of Science and Technology (HKUST). He obtained his PhD in 1990 from University of Rochester and joined the Physics Department of HKUST in 1992. Professor Wang is a condensed matter theorist and is interested in revealing the physics principles behind the novel physics phenomena. Currently, he is working on the interplay of charges, spins, and phonons in nano-systems and devices. His current research focus on topological states of matter, magnetization dynamics, and spin/charge transport. The research topics include skyrmion physics, magnonics, magnetic domain wall motion, spin current generation and detection, and magneto-effects.

Recent progress in magnetic skyrmion physics

In this talk, I will discuss several progresses made in our group about fundamental properties of skyrmions in chiral magnetic films. These include 1) skyrmion sizes in isolated, in crystal, or in stripy forms, 2) skyrmion nucleation, formation, and potential barrier energies, 3) the roles of magnetic field in skyrmion crystal formation, 4) the stability and existing conditions of composite skyrmions such as target skyrmions and skyrmion bags/cluster, 5) topological equivalence of stripy phases and skyrmion crystals.



Martin Wegener

KIT, Germany

Roton-like dispersion relations in metamaterials

Martin Wegener is Professor at the Institute of Applied Physics at KIT and one of the Directors of the Institute of Nanotechnology at KIT. He is also spokesperson of the Excellence Cluster "3D Matter Made to Order". He initiated (2006) and co-founded (2007) the company Nanoscribe GmbH. His current research interests are in 3D additive manufacturing driven towards the nanometer scale and applications thereof, for example in 3D metamaterials.

Roton-like dispersion relations in metamaterials
We review our work on mimicking the dispersion relation of rotons in liquid helium in different systems (acoustic, elastic, and electromagnetic waves) and using three different strategies (nonlocal metamaterials, chiral metamaterials, and monomode metamaterials).



Gary Wiederrecht

Argonne National Laboratory, USA

Ultrafast Optical Studies of Hybrid Nanomaterials of Interest for Optoelectronic and Energy Conversion Applications

Gary Wiederrecht is currently the Deputy Division Director and Senior Scientist in the Nanoscience & Technology (NST) Division at Argonne National Laboratory. He received a B.S. degree in chemistry from UC Berkeley in 1987 and a Ph.D. in physical chemistry from MIT in 1992. He moved to Argonne National Laboratory as a postdoctoral fellow in 1992, working with Michael Wasielewski on molecular photonics, and became a scientific staff member in 1995. His research interests center on the photochemistry and photophysics of hybrid nanostructures, photochemical energy conversion, quantum science, biomimetic materials, and the ultrafast optical responses of nanoparticles and nanoparticle assemblies. He is also working to develop novel approaches to time-resolved optical microscopy and imaging applications. He has received an R&D100 award, the DOE Young Scientist Award, the Presidential Early Career Award for Scientists and Engineers (PECASE), and the Argonne National Laboratory Distinguished Service Award. He has authored or co-authored approximately 165 peer-reviewed research articles and has several patents. He is a Fellow of the American Physical Society.

Ultrafast Optical Studies of Hybrid Nanomaterials of Interest for Optoelectronic and Energy Conversion Applications
Ultrafast optical spectroscopy is used to monitor energy flow in nanostructures of interest for optoelectronic and energy conversion applications. The impact of hybrid nanostructures on aiding in the efficiency of desired energy flow outcomes following the absorption of photons is further described. Using ultrafast spectroscopy to probe hybrid structures designed to increase light-matter interactions, such as through optical cavities, is also discussed.



Eli Yablonovitch

UC Berkeley, USA

The Challenge of Photonic Crystals (and Meta-Materials) is Inverse Electromagnetic Design (Aperiodic)

Eli Yablonovitch is a Professor of Electrical Engineering and Computer Sciences at UC Berkeley, where he holds the James & Katherine Lau Chair in Engineering. He is the Director of the NSF Center for Energy Efficient Electronics Science (E3S), a multi-University Center headquartered at Berkeley.

Prof. Yablonovitch introduced the idea that strained semiconductor lasers could have superior performance due to reduced valence band (hole) effective mass. With almost every human interaction with the internet, optical telecommunication occurs by strained semiconductor lasers. He is regarded as a Father of the Photonic BandGap concept, and he coined the term "Photonic Crystal". The geometrical structure of the first experimentally realized Photonic bandgap, is sometimes called “Yablonovite”. In his photovoltaic research, Yablonovitch introduced the 4(n squared) (“Yablonovitch Limit”) light-trapping factor that is in worldwide use, for almost all commercial solar panels. His mantra that "a great solar cell also needs to be a great LED”, is the basis of the world record solar cells: single-junction 28.8% efficiency; dual-junction 31.5%; quadruple-junction 38.8% efficiency; all at 1 sun. His startup company Ethertronics Inc., has shipped over one billion cellphone antennas.

Prof. Yablonovitch is elected as a Member of the National Academy of Engineering, the National Academy of Sciences, the American Academy of Arts & Sciences, and is a Foreign Member of the Royal Society of London. He has been awarded the Buckley Prize of the American Physical Society, the Isaac Newton Medal of the UK Institute of Physics, the Rank Prize (UK), the Harvey Prize (Israel), the IEEE Photonics Award, the IET Mountbatten Medal (UK), the Julius Springer Prize (Germany), the R.W. Wood Prize, the W. Streifer Scientific Achievement Award, and the Adolf Lomb Medal. He also has an honorary Ph.D. from the Royal Institute of Technology, Stockholm, & the Hong Kong Univ. of Science & Technology, and is honorary Professor at Nanjing University.

The Challenge of Photonic Crystals (and Meta-Materials) is Inverse Electromagnetic Design (Aperiodic)
Inevitably, in electromagnetics, there is a goal, and it may be that the goal is best achieved by an,aperiodic rather than a periodic design. Then there is a universal question: What is the best design to achieve,a specific goal?



Nikolay Zheludev

University of Southampton, UK and NTU, Singapore

Continuous Time Crystals on Opto-Mechanical Platform

Nikolay Zheludev’s research interest are in nanophotonics and metamaterials. He is the Deputy Director of the Optoelectronics Research Centre in Southampton University, UK and co-Director of The Photonics Institute at Nanyang Technological University, Singapore.

Prof. Zheludev is elected as a Fellow of the Royal Society (UK) and Member of the USA National Academy of Engineering. He is a Fellow of the European Physical Society (EPS), the Optical Society (OSA) and the Institute of Physics (London). He has been awarded the Michael Faraday Gold Medal, Thomas Young Medal and President of Singapore Science and Technology Award.

Continuous Time Crystals on Opto-Mechanical Platform
We overview recent developments in the field of photonic time crystals, a state of matter with broken time-translation symmetry.

TUTORIALS



Prof. Philippe Lalanne

Institut d'Optique d'Aquitaine - CNRS, France

Wednesday 19st July
14:00 - 15:00 — Amphi Fournel

Disordered optical metasurfaces

Philippe Lalanne is a CNRS Research scientist. Optician by adoption, he is an expert in nanoscale electrodynamics. His first works with Pierre Chavel at Orsay focused on optoelectronic machines for implementing neural networks operating by simulated annealing at video rate. After a sabbatical year at the Institute of Optics (Rochester), he undertook work in the field of diffractive optics. At the Laboratoire Charles Fabry in Palaiseau, he then designed the first high-efficiency metasurfaces, gave general rules for designing microcavities with high quality factor and explained the role of plasmons in the extraordinary optical transmissions. At the Laboratoire Photonique, Numérique et Nanosciences in Bordeaux, he is currently studying the non-Hermitian dissipative coupling of light with nanoresonators and the properties of disordered optical metasurfaces. From 2018 to 2022, he was director of the GDR Ondes. He received several distinctions, including a 2022 ERC Advanced grant. He is associate editor of the journal Optica and is a fellow of IOP, SPIE and OPTICA.

Disordered optical metasurfaces
Shaping the far-field radiation diagrams of surfaces engraved with high-index subwavelength structures belongs to a longstanding and fundamental ambition of wave science. The problem comes in different forms, but generally consists of angularly and spectrally controlling polychromatic light scattering with nanostructures smartly arrayed on a surface. We discuss important challenges in the emerging field of disordered metasurfaces to address applications such as light focusing, light extraction and detection, color and appearance creation.



Dr. Anja Wecker

Editor in Chief of Advanced Optical Materials (WILEY), Germany

Thursday 20th July
14:00 - 15:00 — Amphi Bezier

Publishing Research with Impact in the Optics and Photonics Field

Anja Wecker studied chemistry at Saarland University in Saarbrücken where she completed her diploma as well as well as her PhD thesis in the field of physical chemistry. She joined Wiley in 2012.

Publishing Research with Impact in the Optics and Photonics Field
For researchers, it's a long road from the idea to the published article. Producing great research results does not necessarily mean they will automatically be appreciated by the community. Choosing the right journal, convincing editors and reviewers, and making work visible to others are essential steps on the way to success. In this tutorial talk, I will give an insight into publishing opportunities in relevant journals and the related peer review process. From an editorial perspective, I will provide some guidance on how to best pass peer review and maximize success in scientific publishing.

INDUSTRIAL WORKSHOPS

SYNOPSYS®

18th & 19th July, 16:40 - 17:40 — Salle des Conseils

Automated Inverse Design Solution for Metalenses

Chenglin Xu, Maryvonne Chalony, Yijun Ding

To help researchers design metalenses easily and quickly, Synopsys has developed MetaOptic Designer, a fully automated design tool for metalenses. Based on a few inputs from designers, such as a pre-built metaatom library and basic lens configuration, MetaOptic Designer generates an optimized design to meet all design targets. Synopsys will introduce and demonstrate MetaOptic Designer in two workshop sessions at META 2023.

On July 18, we will provide a general overview of the MetaOptic Designer optimization algorithm, followed by quick demonstrations of the tool's capability.

On July 19, we will demonstrate advanced metalens applications with tips and tricks; applications will include:

- Achromatic metalens
- Wide-angle metalens
- Chiral hologram
- Reflective metalens
- Hybrid optical system with both metasurfaces and traditional refractive lenses

The workshop is free and open to all META conference attendees.

GUIDELINES FOR PRESENTERS I **IN-PERSON**

In-person Oral Presentations

Each session room is equipped with a stationary computer connected to a LCD projector. Presenters must load their presentation files in advance onto the session computer. Technician personnel will be available to assist you.

Scheduled time slots for oral presentations are 15 mn for regular, 20 mn for invited presentations, 30 mn for keynote talks and 35 mn for plenary talks, including questions and discussions. Presenters are required to report to their session room and to their session Chair at least 15 minutes prior to the start of their session.

The session chair must be present in the session room at least 15 minutes before the start of the session and must strictly observe the starting time and time limit of each paper.

In-person Poster Presentations

Presenters are requested to stand by their posters during their session. One poster board, A0 size (118.9 x 84.1 cm), in portrait orientation, will be available for each poster. Pins or thumbtacks are provided to mount your posters on the board. All presenters are required to mount their papers 30mn before the session and remove them at the end of their sessions. Posters must prepared using the standard AES poster template (available on the conference website).

GUIDELINES FOR PRESENTERS I **ONLINE**

All Oral presentations will be in person with option for remote viewing via Zoom.

Poster sessions will be hybrid, consisting of both in person and virtual presentations. Instructions for **virtual poster presenters** can be found here: guidelines).

USEFUL INFORMATION

Venue

META 2023 will be held at
Ecole Nationale Supérieure d'Arts et Métiers (ENSAM) - Paris Campus
155 boulevard de l'Hôpital, 75013, Paris

https://artsetmetiers.fr



A leading science & technology Grande École in France with an international reputation in education and research, Arts et Métiers is one of France's oldest and best engineering schools specializing in mechanical, industrial and energy engineering. Arts et Métiers has more than 250 years of tradition in technical innovation and industrial engagement.

Getting to Venue

Getting to ENSAM

By Metro
Lines 5, 6, 7; Metro station: Place d'Italie
Line 5; Metro station: Campo-Formio

By Bus
Lines 57 & 67; Bus station: Rubens – Ecole des Arts et Métiers

Planing the fastest itinerary between two locations in Paris : https://www.ratp.fr/en

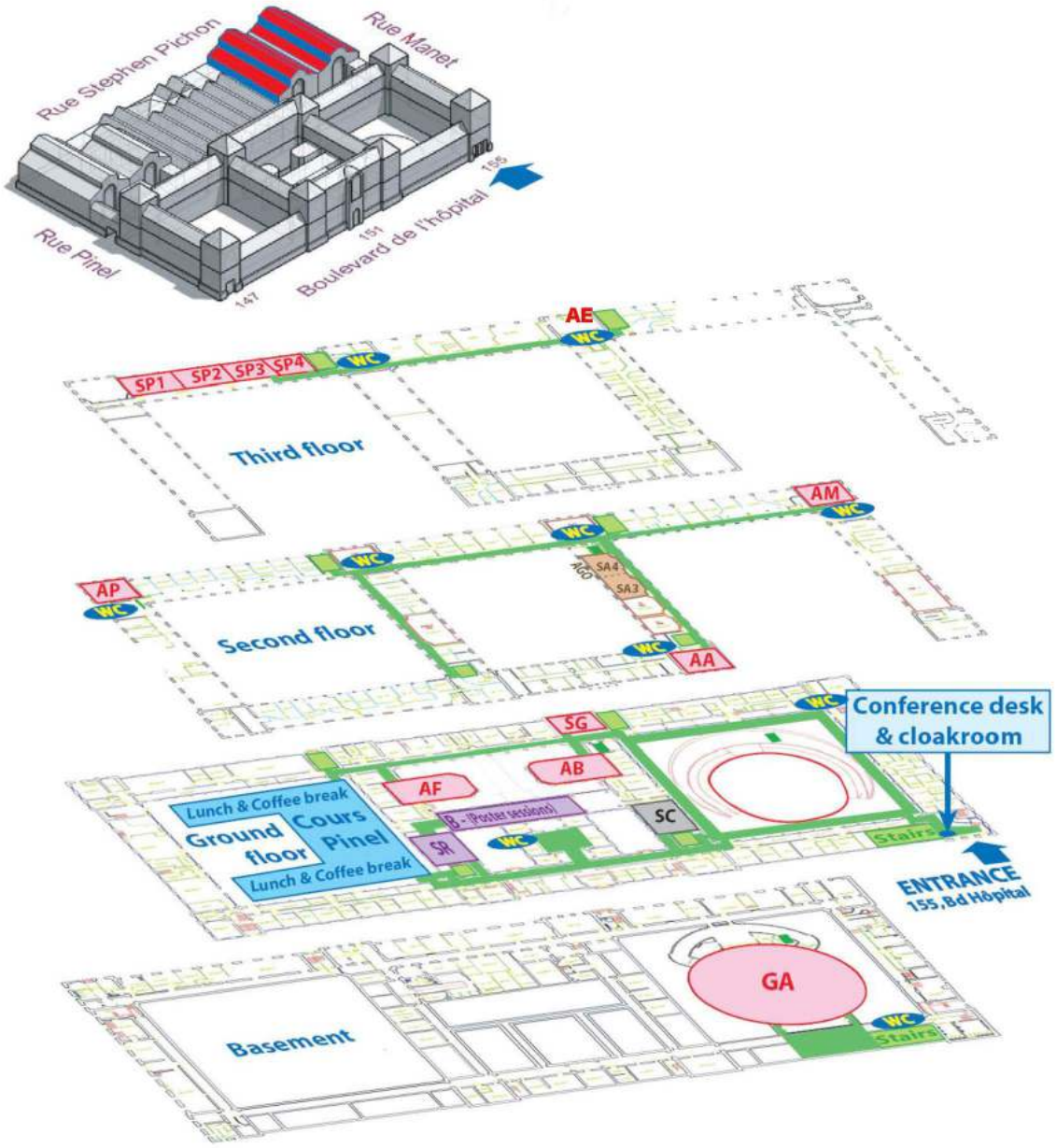

Rue Stephen Pichon
Rue Manet
Rue Pinel
Boulevard de l'hôpital
147
151
155
AE
WC
SP1
SP2
SP3
SP4
Third floor
AM
AP
SA4
SA3
AGO
Second floor
AA
SG
AB
AF
Conference desk
& cloakroom
Lunch & Coffee break
Ground floor
Cours Pinel
Lunch & Coffee break
SC
SR
Stairs
ENTRANCE
155, Bd Hôpital
GA
Basement
Toilets
Lunches/Breaks
Walkways
GA Grand Amphi
AF Amphi Fournel
AB Amphi Bezier
AA Amphi A
AM Amphi Manet
AP Amphi Pinel
Sγ Salle Gamma
SP1 Salle P1
SG Salle Gautherin
SC Salle des Conseils
AE Amphi Esquillan

TABLE OF CONTENTS

Plenary presentation

Nanophotonics for tailoring radiation from fast electrons (pp. 94)
Marin Soljacic,

Structuring light with media with higher dimensions: space, time, and more (pp. 95)
Nader Engheta,

Scalable classical and quantum photonics (pp. 96)
Jelena Vuckovic,

Active photonic metasurfaces empowered by 2D semiconductors (pp. 97)
Isabelle Staude,

Imaging and Computing with disorder (pp. 98)
Sylvain Gigan,

Extreme Control of Light and Sound with Metamaterials (pp. 99)
Andrea Alu,

Keynote presentation

Ultra low loss nonlinear integrated photonic circuits: from soliton microcombs, traveling wave parametric amplifiers, chip based Erbium amplifiers to cryogenic quantum interconnects (pp. 101)
Tobias Kippenberg,

Quantized Fractional Thouless Pumping of Solitons (pp. 102)
Marius Juergensen, Sebabrata Mukherjee, Christina Joerg, Mikael Rechtsman,

Photonic Time-Crystals (pp. 103)
Moti Segev,

Optical thermodynamics of highly multimode nonlinear photonic systems (pp. 104)
Demetrios N. Christodoulides,

Dielectric metasurfaces with fast and ultra-fast tunability (pp. 105)
Dragomir Neshev,

Semiconductor quantum dot based quantum technologies (pp. 106)
Q. Buchinger, G. Peniakov, J. Michl, I. Gamov, J. Kaupp, P. Gschwandtner, S. Kruger, A. Pfenning, T. Huber-Loyola, Sven Hofling,

Recent progress in magnetic skyrmion physics (pp. 108)
Xiangrong Wang,

Chirality and nonreciprocal responses in quantum materials (pp. 110)
Naoto Nagaosa,

Near-Zero-Index Materials for Nonlinear Optics and Beyond (pp. 112)
Vladimir M. Shalaev,

Crossroads of Nanophotonics and Machine Learning (pp. 113)
Alexandra Boltasseva,

Active Metasurfaces in Space and Time (pp. 114)
Harry Atwater,

Continuous Time Crystals on Opto-Mechanical Platform (pp. 116)
Nikolay Zheludev,

Conference Tutorials

Publishing Research with Impact in the Optics and Photonics Field (pp. 118)
Anja Wecker,

Disordered optical metasurfaces (pp. 119)
Philippe Lalanne,

Hybrid Nanomaterials and Metastructures for Photonics, Sensing and Energy

Ultrathin Suspended Chiral Metasurfaces for Enantiodiscrimination and Circularly Polarized Luminescence (pp. 121)
Mengjia Cen, Huilin He, Jiawei Wang, Jianxun Liu, Tun Cao, Yanjun Liu,

Locally controlling quantum yields in 2D semiconductors via electron tunneling (pp. 122)
Ricardo Javier Pena Roman, Remi Bretel, Delphine Pommier, Luis Enrique Parra Lopez, Etienne Lorchat, Elizabeth Boer-Duchemin, Gerald Dujardin, Andrei G. Borisov, Luiz F. Zagonel, Guillaume Schull, Stephane Berciaud, Eric Le Moal,

Photoluminescence Engineering with Surface Lattice Resonances (pp. 124)
Shunsuke Murai,

DNA Origami as a Versatile Method for Bottom-Up Fabrication of Plasmonic Metamaterials (pp. 125)
Christoph Sikeler, Susanne Kempter, Franziska Haslinger, Tim Liedl,

Oriented Colloidal Quantum Wells: Pushing the Limits, Breaking Records (pp. 127)
Hilmi Volkan Demir,

Guided mode resonance enhanced upconversion luminescence of upconversion nanoparticles for immunoassay with ultralow limit of detection (pp. 128)
Yu-Chung Chiu, Yen-Ta Tseng, Van Dai Pham, Wen-Hsuan Wu, Thanh Thu Le Vu, Chao-An Chang, Lai-Kwan Chau, Shiao-Wei Kuo, Michael WY Chan, Hung-Chih Kan, Jiunn-Yuan Lin, Chia Chen Hsu,

Chiro-optical gradient forces in chiral nanomaterials (pp. 130)
Hiromi Okamoto, Junsuke Yamanishi, Hyo-Yong Ahn,

Local photochemical nanoscopy of plasmonic photocatalysts at work (pp. 132)
Alberto Naldoni,

Tailoring the emission and the photodynamics of quantum emitters with high index dielectric nanostructures (pp. 133)
Melodie Humbert, Romain Hernandez, Peter Wiecha, Nicolas Mallet, Frank Fournel, Vincent Larrey, Aurelie Lecestre, Guilhem Larrieu, Christian Girard, Vincent Paillard, Laurence Ressier, Aurelien Cuche,

Novel Second Harmonic Rayleigh and Mie scattering chiroptical effects (pp. 135)
Ventsislav K. Valev,

Chiral Generation of Hot Carriers Towards Enantioselective Plasmonic Photocatalysis (pp. 137)
Miguel Comesana-Hermo,

Near-Infrared plasmon-induced hot electron extraction in an Indium Tin Oxide/Monolayer Molybdenum Disulfide Heterostructure (pp. 138)
Michele Guizzardi, Michele Ghini, Andrea Villa, Luca Rebecchi, Qiuyang Li, Giorgio Mancini, Xiaoyang Zhu, Ilka Kriegel, Francesco Scotognella,

Measuring the Ultrafast Dynamic of Nanoparticle Temperature on the fs-to-ps Time Scale (pp. 140)
Francesco Bisio, Marzia Ferrera, Maria Sygletou, Michele Magnozzi, Daniele Catone, Patrick O'Keeffe, Alessandra Paladini, Francesco Toschi, Stefania Benedetti, Gian Marco Pierantozzi, Riccardo Cucini, Alessandro di Bona, Piero Torelli, Giuseppe Della valle, Giancarlo Panaccione, Maurizio Canepa,

Merging bound states in the continuum and van der Waals materials for enhanced light-matter coupling (pp. 142)
Andreas Tittl,

Characterization and bio-applicability of inexpensive plasmonic nanoparticles and complex-shaped nanocrystals (pp. 143)
Veronica Bahamondes Lorca, Oscar Avalos-Ovando, Christoph Sikeler, Liedl Tim, Dongling Ma, Andrei Kabashin, Shiyong Wu, Martin Kordesch, Alexander Govorov,

Theoretical models for chiral photogrowth in plasmonic nanocrystals (pp. 144)
Lucas Vazquez Besteiro, Miguel Correa-Duarte, Zhiming M. Wang, Alexander O. Govorov,

Chirality without mirrors (pp. 145)
Rahul Kumar, Ben Trodden, Anastasiia Klimash, Affar Karimullah, Nikolaj Gadegaard, Peter J. Skabara, Shun Hashiyada, Gordon J. Hedley, Malcolm Kadodwala,

Enhancing Light-Matter Interaction in MoS2 Monolayer deposited on Metalic Nanostructures (pp. 146)
Matheus Fernandes Sousa Lemes, Guilherme Migliato Marega, Riccardo Chiesa, Andras Kis, Euclydes Marega Junior,

Toward the Control of Excitonic flux in 2D materials (pp. 148)
Jean-Marie Poumirol, Hassan Lamsaadi, Dorain Beret, Ioannis Paradisanos, Ziyang Gan, Emad Najafidehaghani, Antony George, Tibor Lehnert, Ute Kaiser, Shivangi Shree, Ana Estrada-real, Delphine Lagarde, Xavier Marie, Pierre Renucci, Vincent Paillard, Laurent Lombez, Andrey Turchanin, Bernhard Urbaszek,

Metamaterial Thermal Management (pp. 150)
Wakana Kubo,

Hyperbolic meta-antennas: magnetic and electric modes (pp. 151)
Sema Ebrahimi, Alina Muravitskaya, Ali Adawi, Anne-Laure Baudrion, Pierre-Michel Adam, Jean-Sebastien Bouillard,

Ultrafast hot-carrier spatial transients in photonic metasurfaces: experiments, modeling, design (pp. 153)
Andrea Schirato, Giulia Crotti, Andrea Toma, Remo Proietti Zaccaria, Paolo Laporta, Costantino De Angelis, Alessandro Alabastri, Giulio Cerullo, Margherita Maiuri, Giuseppe Della Valle,

Ultrafast phenomena at the interface of plasmonic/semiconductor hybrid systems (pp. 155)
Margherita Zavelani-Rossi,

Nanophotonic Tools for Lipid Membrane Sensing and Manipulation (pp. 157)
Theo Lohmuller,

Photodoping of plasmonic doped metal oxide nanocrystals for the direct storage of solar energy (pp. 159)
Ilka Kriegel,

Opto-thermal effects in plasmonic nanocrystals with complex shapes (pp. 160)
Oscar Avalos-Ovando, Lucas Besteiro, Artur Movsesyan, Alexander Govorov,

Chiral sensing with semiconductor nanophotonics (pp. 161)
Alberto G. Curto,

Top-down and bottom-up fabrication of electro-optic flat photonic devices (pp. 162)
Rachel Grange,

Multiresonant and Nonlinear Metasurface-Waveguide Hybrid Structures (pp. 163)
Mikko Huttunen, Jussi Kelavuori, Ali Panah Pour, Timo Stolt, Anna Vesala,

Chiral plasmonic metasurfaces self-assembled from non-chiral metallic nanowires and nanorods (pp. 164)
W. Wu, V. Lemaire, Matthias Pauly,

Active photonics using nanocrystal and application for infrared sensing (pp. 166)
Emmanuel Lhuillier, Yoann Prado, Tung Huu Dang, Audrey Chu, Gregory Vincent, Angela Vasanelli,

Ultra-sensitive Plasmonic Biosensors based on Two-Dimensional NanoMaterials (pp. 167)
Shuwen Zeng,

Active control of the nanoparticle self-assembly for photonic applications (pp. 168)
Talha Erdem,

Single photon nanophotonics using hybrid plasmonics (pp. 170)
Aurelie Broussier, Regis Deturche, Safi Jradi, Sylvain Blaize, Renaud Bachelot, Christophe Couteau,

Twisted waveguides as arbitrary unitary gates in polarization-encoded quantum information processing circuits (pp. 172)
F. Morozko, A. Novitsky, A. Mikhalychev, Alina Karabchevsky,

Controlling Heat Anisotropy at the nanoscale inside cross arrays (pp. 174)
Jean-Francois Bryche, Marlo Vega, Julien Moreau, Paul-Ludovic Karsenti, Mondher Besbes, Philippe Gogol, Denis Morris, Paul G Charette, Michael Canva,

Perspectives and Challenges for the Fabrication of Plasmonic Nitride Nanostructures (pp. 176)
Panos Patsalas, Nikolaos Pliatsikas, Spyridon Kassavetis, David Babonneau, Sophie Camelio, Gregory Abadias,

Photochemical imaging of near-field and dissymmetry factor of chiral nanostructures (pp. 177)
Thinhinane Aoudjit, A. Horrer, S. Koscheev, R. Bachelot, J. Plain, D. Gerard,

Unidirectional ultracompact self-assembled optical antennas (pp. 178)
Maria Sanz-Paz, Fangjia Zhu, Mauricio Pilo-Pais, Guillermo Acuna,

In situ and real-time studies of ultrathin silver films grown by physical vapor deposition: The role of nitrogen additive (pp. 180)
David Babonneau, Gregory Abadias, Karan Solanki, Anny Michel, Julien Ramade, Sophie Camelio, Andrea Resta, Alina Vlad, Alessandro Coati, Yves Garreau, Kostas Sarakinos, Michal Kaminski, Barbel Krause,

Foerster-Type Nonradiative Energy Transfer in Media with Complex Permittivity (pp. 182)
Pedro Ludwig Hernandez Martinez, Abdulkadir C. Yucel, Hilmi Volkan Demir,

Vacuum Ultraviolet Light Generation and Circular Polarization Control Using Dielectric Nanomembranes (pp. 183)
Kuniaki Konishi,

Laser direct writing of crystallized metal oxide from sol-gel using thermoplasmonic effect (pp. 184)
Laurent Noel, Amine Khitous, Celine Molinaro, Olivier Soppera,

Chiral Nanostructures (pp. 185)
Yurii Gun'ko,

Metal-Induced Polymerization of Diazonium Salts for Controlled Spatial Deposition of QDs in Hot Spots (pp. 187)
Liudmila Trotsiuk, Aurelie Broussier, Sylvie Marguet, Anne-Laure Baudrion, Yun Luo, Claire Mangeney, Nordin Felidj, Pierre-Michel Adam, Renaud Bachelot,

Publishing in Nature journals (pp. 189)
Rachel Won,

The kinetics of plasmon-induced chemical reactions studied by surface-enhanced Raman scattering (SERS) and X-ray photoelectron spectroscopy (XPS) (pp. 190)
Ilko Bald, S. Kogikoski Jr., A. Dutta, R. Schurmann,

Non-Thermal Activation of Reactants in Plasmon-Assisted Chemical Reactions: Roles of Molecular Structure and Metal-Molecule Contact (pp. 192)
Zee Hwan Kim,

Ultrafast Optical Studies of Hybrid Nanomaterials of Interest for Optoelectronic and Energy Conversion Applications (pp. 193)
Gary Wiederrecht,

Bioanalytics using plasmonic nanostructures (pp. 194)
S. Kastner, E. Podlesnaia, F. Seier, Y. Luximun, A. Dietel, M. Urban, A. Csaki, Wolfgang Fritzsche,

Structured surfaces for enhanced radiation-matter interaction and nonlinear optics (pp. 196)
Luca Razzari,

Photoluminescence from Ultrathin Monocrystalline Gold Flakes (pp. 197)
Alan Bowman, Fatemeh Kiani, Alvaro RodriÌ•guez Echarri, Ted Tsoulos, Joel Cox, Javier GarciÌ•a de Abajo, Giulia Tagliabue,

An approach to fabricating plasmonic Titanium Nitride nanoparticles by pulsed laser ablation for biological applications (pp. 199)
Nikolaos Pliatsikas, Spyros Kassavetis, Afroditi Koutsogianni, Stavros Panos, Tamara Odutola, Ilias Fekas, Evi Rampota, Christos Kapnopoulos, Maria Gioti, Panos Patsalas,

Liquid crystal templated chiral films: chiral plasmonics and circularly polarized luminescence (pp. 201)
Wiktor Lewandowski,

Dual-Band and High-Speed Plasmonic Metafiber Electrooptic Modulators (pp. 203)
Jiyong Wang, Lei Zhang, Min Qiu,

Conducting polymers as optical actuators for addressable structural colors (pp. 204)
Stefano Rossi, Magnus P. Jonsson,

Au@Pd supercrystals as plasmonic photocatalysts for Suzuki C-C coupling (pp. 206)
Charlene Brissaud, Wajdi Chaabani, Lucas Vazquez Besteiro, Miguel Comesana-Hermo, Jean-Yves Piquemal,

Experimental and theoretical study of the plasmonic properties of Cobalt nanoparticles (pp. 208)
Wajdi Chaabani, Miguel Comesana-Hermo, Jaysen Nelayah, Nordin Felidj, Jean-Yves Piquemal,

Strong coupling in aluminum optical antennas (pp. 209)
Thomas Simon, Gabriel Arditi, Xiaoyan Li, Florian Lamaze, Julien Proust, Jerome Martin, Mathieu Kociak, Odile Stephan, Davy

Gerard,

Light-matter-coupling effects in pentacene thin films on nanorod antenna arrays (pp. 210)
Christoph Theurer, Florian Laible, Jia Tang, Katharina Broch, Frank Schreiber, Monika Fleischer,

Optoelectronic properties of FeSe nanomaterials with diverse dimension (pp. 212)
Hyojin Kang, Jaebeom Lee,

Chiral photothermal effect induced by plasmonic metasurface for fluid motion (pp. 214)
Peng Yu, Alexander Govorov, Zhiming Wang,

Metasurface design by capillarity-assisted nanoparticles assembly in a microfluidic channel and their applications (pp. 216)
Juan Xin, Julien Proust, Jeremie Beal, Anne-Laure Baudrion, Abdelhamid Hmima, Jerome Plain,

Nanolasing in Self-Assembled Metasurfaces (pp. 218)
Tomas Tamulevicius, Mindaugas Juodenas, Nadzeya Khinevich, Domantas Peckus, Asta Tamuleviciene, Joel Henzie, Sigitas Tamulevicius,

Biocompatible fluorescent carbon dots nanoparticles used for anti-counterfeiting of cultural artefacts (pp. 219)
Theo Duarte, Aurelie Broussier, Sabine Fourrier, Alexandre Rabot, Anne-Laure Baudrion, Jerome Plain, Julien Proust,

Optical Mie resonances of DNA-assembled three-dimensional gold superlattice crystals (pp. 221)
Doxi Misatziou, H. J. Singh, Angela de Fazio, Martinus Werts, Alvaro Buendia, Vincenzo Giannini, Jose Sanchez-Gil, Afaf El-Sagheer, Tom Brown, Antonios Kanaras, Otto Muskens,

Spectrally-Resolved Polarized Cathodoluminescence in STEM (pp. 223)
Malo Bezard, Yves Auad, Davy Gerard, Jeremie Beal, Jerome Martin, Mathieu Kociak,

New trends in nanophotonics and advanced materials

Active aerosols to control the propagation of light (pp. 225)
Jake Fontana, Chuck A. Rohde, Kristin M. Charipar, Paul Johns, Ashlin G. Porter, Nicholas J. Greybush,

Integrated 2D GaGeTe Electro-Optic Phase Shifter in Silicon Photonics (pp. 227)
S. R. Tamalampudi, G. Dushaq, J. E. Villegas, Mahmoud Rasras,

Two-dimensional photonic crystal: an ideal nanophotonics platform for both fundamentals and applications (pp. 229)
Heonsu Jeon,

Plasmon and Graphene-based Nano-tweezers for Raman Imaging (pp. 230)
Changjun Min,

Topological polaritonics with organic materials (pp. 232)
Dmitry Solnyshkov, J. Ren, Y. Li, O. Bleu, J. Yao, C. Leblanc, T. Long, X. Ma, S. Schumacher, J. De, F. Yin, F. Li, H. Fu, G. Malpuech, Q. Liao,

A multi-modal nonlinear optical technique to study in-situ polymer nanostructure formation (pp. 234)
Thierry Verbiest, K. Aerts, Y. de Coene,

Lithium niobate metasurfaces-A bright nonlinear light source (pp. 236)
Mengxin Ren, Lun Qu, Lu Bai, Wei Wu, Jingjun Xu,

Semi-solid Beam Steering System Based on Micro-Meta-Lens Arrays (pp. 237)

Rui Chen, Yifan Shao, Yungui Ma,

Hierarchical Micro/Nanostructures for Light Harvesting and Photovoltaic Device Applications (pp. 238)
Jae Su Yu,

PT-symmetric non-Hermitian plasmonic systems for switchable radiation control (pp. 240)
Yuto Moritake,

Electromagnetic Signal Propagation Through Lossy Media (pp. 242)
Igor Smolyaninov,

Microscopic Study of Effective 2+1 Dimensional Gravity in Ferrofluid-Based Hyperbolic Metamaterials (pp. 244)
Vera Smolyaninova, J. Cartelli, N. Christopher, B. Kist, J. Perry, S. Spickard, M. S. Devadas, I. I. Smolyaninov,

Plasmonic h igh entropy alloy materials for midinfrared metasurfaces towards efficient photo thermal energy conversion (pp. 246)
Yoshiaki Nishijima,

Color Selective 3D Polarization Profiles (pp. 248)
Xianzhong Chen,

Switch from mono- to multi-mode polariton laser in a GaN ridge waveguide (pp. 250)
Christelle Brimont, H. Souissi, M. Gromovyi, T. Gueye, L. Doyennette, D. D Solnyshkov, G. Malpuech, E. Cambril, S. Bouchoule, B. Alloing, S. Rennesson, F. Semond, J. Zuniga-Perez, T. Guillet,

Image processing with metaoptics: phase imaging and asymmetric optical transfer functions (pp. 252)
Niken Priscilla, Shaban Sulejman, Wendy Lee, Lukas Wesemann, Timothy Davis, Ann Roberts,

Flat Band Induced Metal-Insulator Transitions With Weak Disorder and Many Body Interactions (pp. 254)
Sergej Flach,

Deep ultraviolet to visible absorbing and sensing applications by stacking film with highly lossy ultra-thin film (pp. 255)
Yuusuke Takashima, Shunsuke Furuta, Kentaro Nagamatsu, Masanobu Haraguchi, Yoshiki Naoi,

Research on Intelligent Photonic Computing Chips (pp. 257)
Xiaoyong Hu, Kun Liao,

Plasmon Resonance Mode Evolution in a Semiconductor Nanodimer in the Overlapping Regime (pp. 259)
Zi Wang, Thomas Wong,

Strong coupling between two-dimensional excitons and plasmonic nanocavities with a low exciton number (pp. 261)
Xiulai Xu,

High performance silicon photonic devices with subwavelength metamaterials (pp. 263)
Pavel Cheben, Jens H. Schmid, Winnie N. Ye, Daniel Benedikovic, Pablo Ginel-Moreno, Shahrzad Khajavi, Jose-Manuel Luque-Gonzalez, Alejandro F. Hinestrosa, Daniel Pereira-Martin, Abdel Hadij-ElHouati, Radovan Korcek, William Fraser, Alejandro Sanchez-Postigo, Alejandro Ortega-Monux, Juan-Gonzalo Wanguemert-Perez, Inigo Molina-Fernandez, Robert Halir, Daniele Melati, Carlos Alonso-Ramos, David Gonzalez-Andrade,

Color centers in ZnO nanowires (pp. 265)
Carsten Ronning,

Extremely Localized Optical Modes and Direct Electro-optical Modulation (pp. 266)

Xuewen Chen,

External Laser Mirror for Oscillation Wavelength Stabilization and Waveguide Input Coupling (pp. 268)
Junichi Inoue, Akari Watanabe, Keisuke Ozawa, Kenji Kintaka, Shogo Ura,

Discovering new high-refractive-index dielectric materials (pp. 270)
Soren Raza,

Heavily doped semiconductors: a platform for integrated nonlinear plasmonics (pp. 272)
Federico De Luca, Michele Ortolani, Huatian Hu, Cristian Ciraci,

Symmetry, connectivity, and topology in photonic crystals (pp. 274)
Thomas Christensen,

Chemical interface damping by electrochemical oxidation of gold (pp. 275)
Maurice Pfeiffer, Manfred Eich, Alexander Petrov,

Reconfiguring electric and magnetic resonances of individual meta-atoms using phase-change materials (pp. 276)
Lukas Conrads, Andreas HeÃŸler, Thomas Taubner,

3D nanoprinting using light (pp. 278)
Maria Farsari,

Plasmon-enhanced nano-spectroscopies for highly sensitive biomolecular detection (pp. 279)
Taka-Aki Yano, Ryo Kato, Takuo Tanaka,

Hybrid bullseye-nanotip antennas for bright directional single photon sources (pp. 280)
Hamza Abudayyeh, Annika Mildner, Julia Fulmes, Regina Jager, Dror Liran, Boaz Lubotzky, Lars Luder, Florian Laible, Alfred Meixner, Dieter Kern, Ronen Rapaport, Monika Fleischer,

Proximity Induced Chiral Quantum Light Generation in Strain Engineered WSe2/MPX3 Heterostructures (pp. 282)
Han Htoon,

Three-dimensional metasurface absorber for gas sensing devices (pp. 284)
Takuo Tanaka,

Highly conformable terahertz metasurfaces via two-photon polymerization on polymeric ultra-thin films (pp. 285)
Andrea Ottomaniello, Paolo Vezio, Omar Trincici, Frank Marco Den Hoed, Paul Dean, Alessandro Tredicucci, Virgilio Mattoli,

Ellipsometric probing of hot electrons in plasmonic media (pp. 287)
Judit Budai, Zsuzsanna Papa, Peter Petrik, Peter Dombi,

Bound States in the Continuum with High Q-factors in Deep Ultraviolet Light Source (pp. 289)
Omar A. M. Abdelraouf, Aravind P. Anthur, Xiao Renshaw Wang, Qijie Wang, Hong Liu,

A small spectrometer with extremely high resolution (0.07 nm) realized with an improved reconstruction algorithm (pp. 291)
Takasumi Tanabe, Junnosuke Kokubu, Ryo Sugano,

Epsilon-near-zero materials enhance infrared vibrational spectroscopy (pp. 293)
Rafik Smaali, Antoine Moreau, Emmanuel Centeno,

Advances in multiphysics modeling of phase change materials based metasurfaces (pp. 294)

Dmitry Chigrin,

Photo-Induced Sources within Multilayer Optics: from Light Scattering to Micro-cavities and Thermal Radiation (pp. 295)
Claude Amra, Paul Rouquette, Myriam Zerrad, Gabriel Soriano, Michel Lequime,

Purcell factor for plasmon-enhanced metal photoluminescence (pp. 297)
Tigran Shahbazyan,

Graphene-based 2D Plasmonic Metamaterials for Terahertz Laser Transistors (pp. 299)
Taiichi Otsuji, S. Boubanga-Tombet, C. Tang, A. Satou, V. Ryzhii, K. Wojciech, D. Yadav, K. Narahara, M. Ryzhii, V. Mitin, M. S. Shur,

All-optical Control of Nonlinear Light Interaction with Topological Photonic (pp. 301)
Yupei Wang, Jitong Wang, Nicolae-Coriolan Panoiu,

Fluid-coupled Lamb waves for self-assembling three-dimensional photonic crystals (pp. 302)
Y.-H. Chen, Y.-M. Huang, P.-K. Tsai, M.-H. Li, J.-S. Chen, Yu-Bin Chen,

Topological Tamm states based on flat band symmetry inversion (pp. 303)
Soufyane Khattou, Amina Rezzouk, Madiha Amrani, Mohamed El Ghafiani, El Houssaine El Boudouti, Abdelkrim Talbi, Bahram Djafari Rouhani,

Ultrafast nanophotonics: from all-optical control of exciton dynamics towards plasmon-tailored nano-chemistry and information processing based on cavity-electrodynamics (pp. 305)
NicolÃ² Maccaferri,

Dielectric nanostructures for novel photonics devices: from Solar Cells to NanoLEDs. (pp. 307)
Braulio Garcia-Camara, Lorena Escandell, Angela Barreda, Eduardo Lopez-Fraguas, Ricardo Vergaz, Jose Manuel SÃ¡nchez-Pena,

Enhanced electric field and emission directionality of gap mode (pp. 308)
Dai Zhang, Peng Miao, Felix Schneider, Yang Zhao, Tim Parker, Alfred Meixner,

Chiral Phase Change Nanomaterials: A nanoscale path to microscopic optics (pp. 310)
Imad Agha,

Strong light matter interaction in plexcitonic crystals (pp. 312)
Marzia Ferrera, Jacopo Stefano Pelli Cresi, Vincenzo Aglieri, Elena Ghidorsi, Andrea Toma,

Characterization of Nano-grating Profiles using Standard Ellipsometry and Deep Neural Networks (pp. 314)
Zijie Jiang, Wen-Di Li,

Colloidal Metal Nanoparticles under Ultrafast Laser Pulses (pp. 316)
Andres Guerrero Martinez,

Self-powered Flexible Devices: Piezo-sensor and microLED (pp. 317)
Keon Jae Lee,

Controllable generation of frequency-encoded qubits and qudits using silicon photonics nano-engineered devices (pp. 318)
Massimo Borghi, Noemi Tagliavacche, Federico Andrea Sabattoli, Houssein El Dirani, Laurene Youssef, Camille Petit-Etienne, Erwine Pargon, Corrado Sciancalepore, J. E. Sipe, Marco Liscidini, Matteo Galli, Daniele Bajoni,

PT Symmetric Non-Hermitian Polaritonic System with Single Hexagonal Microcavity on Loss-modulated Substrate (pp. 320)
Yong-Hoon Cho,

Hybrid-Integrated Quantum Optics on a Silicon Nitride Platform (pp. 321)
Khaled Mnaymneh, Edith Yeung, David B. Northeast, Jeongwan Jin, Patrick Laferriere, Sofiane Haffouz, Robin L. Williams, Philip J. Poole, Dan Dalacu,

Independent electrical control of phase and magnitude of second harmonic generation using intersubband polaritonic metasurfaces (pp. 322)
Jaeyeon Yu, Gerhard Boehm, Mikhail Belkin, Jongwon Lee,

Functionalization of gold nanoparticles by localized surface plasmon resonance photopolymerization of molecularly imprinted polymers - An easy route for selective and specific sensors (pp. 324)
Amine Khitous, Celine Mollinaro, Simon Gree, Karsten Haupt, Olivier Soppera,

Microscopic theory of cavity-enhanced interactions of dipolaritons (pp. 325)
Esben Rohan Christensen, A. Camacho-Guardian, O. Cotlet, A. Imamoglu, M. Wouters, G. M. Bruun, I. Carusotto,

Meta-Optical Fibers (pp. 326)
Andrew Palmer, Stuart Love, Leon Zhang, Howard Lee,

Direct and Inverse design forNon-Hermitian light management (pp. 328)
Muriel Botey, R. Herrero, K. Staliunas,

Roton-Like Dispersion Relations in Metamaterials (pp. 330)
Martin Wegener,

Quantum optical phenomena in two-dimensional materials (pp. 331)
Javier Garcia de Abajo,

High-Q Photonics (pp. 332)
Kerry Vahala,

The Challenge of Photonic Crystals (and Meta-Materials) is Inverse Electromagnetic Design (Aperiodic) (pp. 333)
Eli Yablonovitch,

Micro- and Nano-lasers: From One to Many, Unleashing Endless Possibilities (pp. 335)
Mercedeh Khajavikhan,

Retrieving optical parameters of emerging van der Waals microcrystals (pp. 336)
Mitradeep Sarkar, Mehrdad Shokooh-Saremi, Michael Enders, Georgia Papadakis,

Atypical light extraction technologies for organic light emitting diodes with spontaneously formed buckling patterns of soft materials (pp. 338)
Byung Doo Chin, J. Y. Yoo, S.-H. Hwang, Ohyoung Kim, S. M. Cho, W. H. Koo,

Towards Predictable 2D/3D Plasmonics via FEBID (pp. 340)
Verena Reisecker, David Kuhness, Harald Plank,

Alternative Plasmonic Metamaterials based on Titanium Nitrides and Oxynitrides with Tunable Properties (pp. 341)
Cristina Mancarella, Ludovica Tovaglieri, Gianluigi Baiardi, Alessio Lamperti, Vincenzo Caligiuri, Antonio De Luca, Andrea Li Bassi,

Tailoring coupling conditions between silicon metasurfaces and molecular vibrations (pp. 343)
Keisuke Watanabe, Hemam Rachna Devi, Iwanaga Masanobu, Tadaaki Nagao,

Optical Metafluids Composed of Colloidal Mie-Resonant Silicon Nanospheres (pp. 345)
Hiroshi Sugimoto, Minoru Fujii,

Some 2D Magnetic Topological Photonic Crystals (pp. 347)
Baile Zhang,

Charge Transfer Process on Plasmonic Cathode Electrode (pp. 349)
Hiro Minamimoto, Yuto Tajiri, Minoru Mizuhata,

Advanced passive and active metasurfaces and zero-index materials

Harnessing the properties of emerging low-dimensional and phase-change materials for mid-IR photonics (pp. 351)
Mitradeep Sarkar, Maxime Giteau, Michael Enders, Aleksandra Deeva, Georgia Theano Papadakis,

Plasmonic metasurfaces and waveguide devices based on epsilon-near-zero materials (pp. 353)
Pierre Berini,

Magnetic Nearfield Reshaping Metasurfaces (pp. 355)
Hanwei Wang, Xiaodong Ye, Joshua Yu, Yun-Sheng Chen, Yang Zhao,

Leveraging Thermo-optical Effects in Nanoantennas and Metasurfaces (pp. 357)
Giulia Tagliabue,

Metasurface Image Sensors for Optical Spatial Filtering and Quantitative Phase Imaging (pp. 358)
Jianing Liu, Yuyu Li, Hao Wang, Lei Tian, Roberto Paiella,

Optical pulse-shaping with plasmonic metasurfaces (pp. 360)
Rene Geromel, Philip Georgi, Maximilian Protte, Shiwei Lei, Tim Bartley, Lingling Huang, Thomas Zentgraf,

Building Uncooled Infrared Camera based on One Atom Thick Graphene (pp. 362)
Debashis Chanda,

Conductive Nitrides for Plasmonics in the Visible Region: Properties and Applications (pp. 363)
Yu-Jung Lu,

Integrated optofluidic devices for medium-switchable metasurfaces and metasurface-based biosensors (pp. 365)
Hao Wang, Nanzhong Deng, Yue Xiao, Haogang Cai,

Exciton resonances in two-dimensional materials for dynamic wavefront manipulation (pp. 367)
Melissa Li, Claudio Hail, Souvik Biswas, Harry Atwater,

Quasi-Bound State in the Continuum in Intra-Coupled Si Dielectric Metasurface (pp. 368)
Wen-Hui (Sophia) Cheng,

Physics-informed reinforcement learning for nanophotonic device design (pp. 369)
Min Seok Jang,

Active metamaterials and devices: from rapidly-tunable lenses to emergent polaritonic materials (pp. 370)
Gennady Shvets,

Dielectric and Transient Optical Properties of Ultrathin TiN and Ti1-xAlxN (pp. 371)
I Hung Ho, Hyeyoung Ahn,

Metallic quantum well based extreme nonlinear materials and metasurfaces (pp. 373)
Zhaowei Liu,

Generation and Control of Ultrafast Directional Photocurrents at Nanoscale Using Symmetry-Broken Hybrid Graphene Nanoplasmonic Metasurfaces (pp. 374)
Jacob Pettine, Hou-Tong Chen,

Piezoelectric Shifter for Wideband Tunability in Chalcogenide Metamaterials (pp. 376)
Jesse Frantz, Jason Myers, Anthony Clabeau, Robel Bekele, Austin Moore, Vinh Nguyen, Jasbinder Sanghera,

Ultrathin Titanium Nitride Epitaxial Structures for Tunable Infrared Plasmonics (pp. 378)
Shangjr Gwo,

Nanophotonics-based chiroptical sensing of drug solutions (pp. 379)
R. Adhikary, A. Sahoo, M. Aschi, I. Daidone, M. Silvestri, M. Venturi, C. Ferrante, A. Mecozzi, Andrea Marini,

Merging Nanophotonics with Optical Fibers through 3D Nanoprinting: a novel platform for flexible beam manipulation (pp. 381)
Markus Schmidt, Henrik Schneidewind, Uwe Huebner, Matthias Zeisberger, Malte Plidschun, Jisoo Kim, Oleh Yermakov, Yuri Kivshar, Andrey Bogdanov, Haoran Ren, Stefan A. Maier,

Modulating and Spinning thermal radiation with incandescent metasurfaces (pp. 383)
Anne Nguyen, Leo Wojszvzyk, Jean-Paul Hugonin, Anne-Lise Coutrot, Enrique Garcia-Caurel, Benjamin Vest, Jean-Jacques Greffet,

Full color Imaging with Large-Aperture Meta-Optics (pp. 385)
Arka Majumdar,

Flat Optics for Dynamic Wavefront Manipulation (pp. 387)
Mark Brongersma,

Tailoring the visual appearance with disordered arrays of resonant metaatoms (pp. 388)
A. Agreda, T. Wu, A. Hereu, M. Treguer-Delapierre, G. Drisko, K. Vynck, Philippe Lalanne,

Lithography-free control of thermal emission. (pp. 390)
Mitradeep Sarkar, Maxime Giteau, Michael Enders, Georgia Papadakis,

Reconfigurable and polarization-dependent grating absorber for large-area emissivity control based on the plasmonic phase-change material In3SbTe2 (pp. 392)
Lukas Conrads, Natalie Honne, Andreas Ulm, Andreas HeÃŸler, Matthias Wuttig, Robert Schmitt, Thomas Taubner,

Shape-multiplexed conformable holographic metasurfaces (pp. 394)
Sebastian Schulz, Jianling Xiao, Robert Hunter, Duncan Robertson, Graham Smith, Simon Horsley, Andrea Di Falco,

Rotary metaswimmers powered by linearly polarized light (pp. 396)
Mahdi Shanei, Einstom Engay, Vasilii Mylnikov, Mikael Kall,

Active Huygens' metasurface based on in-situ grown conductive polymer (pp. 398)
Wenzheng Lu, L. de S. Menezes, A. Tittl, H. Ren, S. A. Maier,

Gap-plasmon Resonance based Energy-efficient Electro-tunable Metasurface for Polarization-independent Optical Intensity Modulation (pp. 400)
Tanmay Bhowmik, Jegyasu Gupta, Debabrata Sikdar,

Chirality, magnetism, and magnetoelectricity: Separate phenomena and joint effects in metamaterial structures

Magnetoelectric coupling of topological magnets for spintronic and quantum information applications (pp. 403)
Tomoki Hirosawa,

Observation of bulk chiral anomaly in photonic crystal systems (pp. 405)
Hongwei Jia, Mudi Wang, Che Ting Chan,

Non-reciprocal spin wave beams in thin magnetic films (pp. 406)
Vincent Vlaminck, Loic Temdie, Vincent Castel, Dinesh Wagle, M. Benjamin Jungfleisch, Carsten Dubs, Gyandeep Pradhan, Jose Solano, Hicham Majjad, Romain Bernard, Yves Henry, Daniel Stoeffler, Matthieu Bailleul,

Giant Magnetoimpedance Effect in amorphous magnetic materials (pp. 408)
Arcady Zhukov, Paula Corte-Leon, Mihail Ipatov, Juan Maria Blanco, Jesus Olivera, Valentina Zhukova,

Extreme time modulation of material properties and Hawking radiation (pp. 410)
John B. Pendry,

Electric-field Control of Magnetism and Topological Spin Textures (pp. 411)
Masahiro Sato, Shunsuke C. Furuya,

Hyperbolic Anisotropic and Bianisotropic Media (pp. 413)
Maxim Durach,

Mimicking TMDs by Plasmonic Topological Metasurface with a broken time-reversal symmetry (pp. 415)
E. D. Epstein, D. Cheskis, Yuri Gorodetski,

Creation, Manipulation and Switching of Topological Magnetisms in Spin-Charge Coupled Magnets (pp. 417)
Masahito Mochizuki,

Flat optical devices for 4D light manipulation through orbital angular momentum (pp. 419)
Antonio Ambrosio,

Identifying topology directly from Maxwell's equations: Band structures and Bloch eigenstates not required (pp. 420)
Alexander Cerjan, Terry Loring,

Photocurrent induced by the momentum-space Berry phase in magnetic materials at a microwave frequency (pp. 421)
Hiro Ishizuka, Akira Harada,

Circular Polarization in absorption and emission of light by molecules and molecular assemblies (pp. 423)
Stefan Meskers,

Nonreciprocal Magneto-optical Metasurfaces (pp. 425)
Weihao Yang, Shuang Xia, Jun Qin, Longjiang Deng, Lei Bi,

Rational Design and Fabrication of UV-Resonant Plasmonic Nanoantennas for Enhanced CD Spectroscopy (pp. 427)
Bjoern Reinhard,

Nonlocal response of magnons in photonic structures (pp. 428)
Hajime Ishihara, Kenta Kato, Tomohiro Yokoyama,

Spin Relaxation, Diffusion and Edelstein Effect in Chiral Metal Surface (pp. 430)
Yuta Suzuki, Yusuke Kato,

Emergent inductance by dynamical ferromagnetic nanostructures (pp. 432)
Jun'ichi Ieda,

Topological textures and CP2 Skyrmion crystals in quantum spin-nematics (pp. 434)
Yutaka Akagi,

Nonreciprocal charge transport and phase transitions in noncentrosymmetric superconductors (pp. 436)
Akito Daido, Youichi Yanase,

Ultrathin magneto-optical devices based on all-dielectric metasurfaces (pp. 438)
Yasutomo Ota, Siyuan Gao, Satoshi Iwamoto,

Bose-Einstein condensation of freely evolving overpopulated magnon gas to the uniform precession state (pp. 440)
Oleksandr (Alexander) Serha (Serga),

Non-linear ferrite dynamics for microwave thin film technologies (pp. 442)
Feodor Ogrin,

Wavelength-Independent Bragg-Like Effect (pp. 443)
Martin McCall, Stefanos Koufidis,

Symmetry control of strong chiral light-matter interactions in photonic nanocavities for efficient circularly polarised emission (pp. 445)
Rahul Kumar, Ben Trodden, Anastasiia Klimash, Affar Karimullah, Nikolaj Gadegaard, Peter J. Skabara, Shun Hashiyada, Gordon J. Hedley, Malcolm Kadodwala,

Optical response of magnetic metals from first principles (pp. 447)
Mariia Pogodaeva, Sergey Levchenko, Vladimir Drachev,

Quantum theory of magnetic quadrupole moment and its relation to orbital magnetoelectric effect (pp. 449)
Nobuhiro Arai, Yang Gao, Di Xiao, Shuichi Murakami,

Novel materials with magnetic skyrmions and their three-dimensional dynamics (pp. 450)
Shinichiro Seki,

Magnetoelectric fields for chirality discrimination (pp. 451)
Eugene Kamenetskii,

Angular-Momentum Dynamics in Ferromagnets on Ultrashort Timescales: Electron-Magnon Interactions vs. Spin-Orbit Coupling (pp. 452)
Felix Dusabirane, Kai Leckron, Barbel Rethfeld, Hans Christian Schneider,

Magneto-Optical Chirality in a Coherently Coupled Exciton-Plasmon System (pp. 454)
Samarth Vadia, Johannes Scherzer, Kenji Watanabe, Takashi Taniguchi, Alexander Hoegele,

Chiral quantum phase shifters (pp. 455)
Nir Rotenberg,

Gain-enhanced chiral sensing with achiral metasurfaces (pp. 456)
Sotiris Droulias,

The optical Dirac equation and confined modes at chiral, magnetoelectric, and non-Hermitian interfaces (pp. 458)
Simon Horsley,

Spin-Orbit-Coupling Mediated by an Epsilon-Near-Zero Interface (pp. 460)
Peter Banzer, J. S. Eismann, L. Ackermann, B. Kantor, S. Nechayev, M. Z. Alam, R. Fickler, R. W. Boyd,

Spin-orbit Coupling and Topology of Optical Fields in Metamaterials (pp. 461)
Vittorio Aita, Diane Roth, Alexey Krasavin, Anatoly Zayats,

Chiro-optical characterization of self-assembled plasmonic nanostructures (pp. 463)
Emilija Petronijevic, Hari Prasat Ram Kumar, Grigore Leahu, Roberto Li Voti, Concita Sibilia, Alessandro Belardini,

Chirality sensing employing parity-time symmetric and general gain-loss media (pp. 465)
Ioannis Katsantonis, Maria Kafesaki,

Noncollinear chiral orbitronics (pp. 467)
Tom G. Saunderson, Fabian R. Lux, Dongwook Go, Wanxiang Feng, Mathias Klaui, Yuriy Mokrousov,

Mixed Quantum/Classical Approach to Surface-Enhanced Spectroscopies (pp. 469)
Tommaso Giovannini, Chiara Cappelli,

Creating, Reading, and Switching Skyrmions in a Magnetic Tunnel Junction (pp. 471)
Shaohai Chen,

Parity-broken vacuum as a chiral catalyst (pp. 472)
Yanzhe Ke, Zhigang Song, Qingdong Jiang,

Chiral photonic cavity based on multiferroic layers (pp. 473)
Vakhtang Jandieri, Ramaz Khomeriki, Koki Watanabe, Daniel Erni, Douglas H. Werner, Jamal Berakdar,

Chirality of the electromagnetic fields of resonant nanostructures (pp. 475)
Mathieu Nicolas, Jayeeta Amboli, Lingfei Cui, Per Magnus Whalmsness, Xingyu Yang, Catherine Schwob, Guillaume Demesy, Mathieu Mivelle, Morten Kildemo, Souhir Boujday, Nicolas Bonod, Bruno Gallas,

Microwave-to-Optical Quantum Transduction Utilizing the Topological Magnetoelectric Effect (pp. 477)
Akihiko Sekine, Mari Ohfuchi, Yoshiyasu Doi,

Dynamic magnetoelectric effects at dielectric/ferromagnetic metal interface: generation of spin currents and modulation of spin wave amplitude (pp. 478)
Piotr Graczyk, Maciej Krawczyk,

Optical interface for a hybrid magnon-photon resonator (pp. 480)
Eyal Buks,

Pushing the limits of magnetoplasmonics by (meta)material design (pp. 481)
Francesco Pineider,

Interfaces of B20 compounds with exotic spin currents (pp. 483)
Gina Pantano, Cole Gibson, Samuel Tkacik, Jacob Gayles,

Hot-electron generation in chiral plasmonic nanocrystals as a mechanism for chiral photo-growth and photochemistry (pp. 485)
Alexander Govorov,

Orbital angular momentum of light creates exotic chiral structures (pp. 486)
Takashige Omatsu,

Driving and imaging achiral-to-chiral transitions in an all-optical setup (pp. 488)
E. Binns, J. Terentjevas, L. Rego, David Ayuso,

Microbundle array of Magnetoplasmonic Nanorods for reconfigurable chiral Metasurface (pp. 490)
Juyong Gwak, Hyojin Kang, Jaebeom Lee,

Giant Magnetoimpedance effect at GHz frequencies in amorphous microwires (pp. 492)
Valentina Zhukova, Mihail Ipatov, Paula Corte-Leon, Juan Maria Blanco, Arcady Zhukov,

Casimir Force Between Pasteur Materials (pp. 494)
Zixuan Dai, Qingdong Jiang,

Phononics and acoustic metamaterials

Tailoring MIMO transfer of sound using reflective reconfigurable intelligent surfaces (pp. 497)
Hongkuan Zhang, Qiyuan Wang, Guancong Ma,

Subwavelength broadband perfect absorption for unidimensional open-duct problems (pp. 499)
Yang Meng, Vicente Romero-Garcia, Gwenael Gabard, Jean-Philippe Groby, Charlie Bricault, Sebastien Goude,

Strain-gradient-driven and magnetoelectric operation with order parameters in Cr2O3 (pp. 501)
Oleksandr Pylypovskyi,

Backscattering reduction in a twisted water wave channel (pp. 503)
Samantha Kucher, Adrian Kozluk, Philippe Petitjeans, Agnes Maurel, Vincent Pagneux,

How to steer acoustic waves in a random medium in a programmable way? (pp. 505)
Anastasiia Krushynska, Martin van Hecke,

Control of wave propagation in networks of gyro-elastic discrete strips (pp. 507)
Giorgio Carta, Michael Nieves, Michele Brun,

A nonlinear acoustic topological system through active control (pp. 509)
Xinxin Guo, Lucien Jezequel, Mathieu Padlewski, Herve Lissek, Pierre Delplace, Romain Fleury,

Deep learning models for acoustic wave scatterings (pp. 510)
Waqas Ahmed, Mohamed Farhat, Pai-Yen Chen, Xiangliang Zhang, Ying Wu,

Wave reflection, transmission and antireflection layers at a temporal boundary using a Shive wave machine (pp. 512)
Motonobu Tomoda, Tetsu Omiya, Hayato Takeda, Osamu Matsuda, Oliver B. Wright,

Quasi-Bound States in the Continuum for Acoustic and Elastic Waves (pp. 514)
Marc Marti-Sabate, Junfei Li, Bahram Djafari-Rouhani, Steven Cummer, Daniel Torrent Marti,

Latent symmetry in acoustic wave systems (pp. 515)
Malte Rontgen, Christian V. Morfonios, Peter Schmelcher, Vincent Pagneux,

Meso-scale analysis of non-periodic and periodic discrete flexural waveguides (pp. 516)
Michael Nieves, Alexander Movchan,

A pathway to lossless non-reciprocal scattering based on synchronization (pp. 517)
Nicolas Noiray,

Topologically invisible defects in chiral mirror lattices (pp. 518)
Antonin Coutant, Li-Yang Zheng, Vassos Achilleos, Olivier Richoux, Georgios Theocharis, Vincent Pagneux,

A solution to cloaking with Willis materials (pp. 520)
Phillip Brucks, Hussein Nassar,

Novel photonic materials enabled by crystal growth (pp. 521)
Dorota Pawlak, Piotr Paszke, Piotr Piotrowski, Monika Tomczyk, Katarzyna Sadecka, Kingshuk Bandopadhyay, Krzysztof Markus, Barbara Surma, Andrzej Materna, Johann Toudert, Alessandro Belardini, Concita Sibilia,

State of the art on the recovery of mechanical energy in the city. The role of seismic metamaterials (pp. 523)
Stephane Brule, Sebastien Guenneau, Stefan Enoch,

Tunable topological protection from auxeticity and nonlinearity (pp. 525)
Maryam Morvaridi, Federico Bosia, Michele Brun, Vinicius Dal Poggetto, Antonio Gliozzi, Marco Miniaci, Nicola Pugno, Giorgio Carta,

Design, fabrication and performance assessment of an acoustic focusing metamaterial lens (pp. 527)
Feng Qin, Jie Zhang, Bruce W. Drinkwater,

Acoustic metagratings: From principle to applications (pp. 529)
Jun Mei,

Exceptional points and skin modes in non-Hermitian elastic phononic beams (pp. 530)
Yabin Jin, Runcheng Cai, Wenxin Zhong, Timon Rabczuk, Xiaoying Zhuang, Yan Pennec, Bahram Djafari Rouhani,

Long-time dynamics of one-dimensional topological lattice models (pp. 532)
Bertin Many Manda, Georgios Theocharis,

Airborne Transverse Sound: from Spin-Orbit Interactions to Circular Dichroism (pp. 533)
Shubo Wang, Qing Tong, Guancong Ma,

Study on acoustic metasurface controlling phase of transmitted waves (pp. 534)
Jia-Hong Sun, Ching-Yun Chang,

Aiming of water waves in a time-varying metabathymetry (pp. 536)
Magdalini Koukouraki, A. Maurel, P. Petitjeans, V. Pagneux,

Invariance of the transmitted field in a periodic waveguide (pp. 538)
Elie Salemeh, S. Felix, Vincent Pagneux,

Bottom-up approaches, new fabrication routes and ENSEMBLE3

Alignment of quantum rods for single- and multi-layered luminescence-based circular polarization convertors (pp. 541)
Yutaka Okazaki, Hayaki Shimizu, Kaito Nakamura, Shusaku Kubota, Kan Hachiya, Takashi Sagawa,

DNA identification using surface-enhanced Raman spectroscopy (pp. 543)

A. Kowalczyk, A. M. Nowicka, J. Krajczewski, A. Michalowska, E. Pyrak, A. Kowalik, J. L. Weyher, I. Dziecielewski, M. Chlopek, S. Gozdz, Andrzej Kudelski,

Review of Remote Epitaxy and Blue Spectral Intensity Enhancement Using Surface Plasmon Resonance (pp. 545)
Jun Hee Choi, Kiho Kong, Eunsung Lee, Joo Hun Han, Jung Hun Park, Nakhyun Kim, Jinjoo Park, Joosung Kim, Dong Chul Shin, Sunil Kim,

In situ growth: Bottom-up wet-chemical preparation of plasmonic gold nanostructures on substrates (pp. 547)
Gail Vinnacombe-Willson,

Self-organization of eutectic two-phase composites: insights from phase-field simulations (pp. 549)
Mathis Plapp,

Non-resonant enhancement of photoluminescence based on metallic nanocubes (pp. 551)
Mohammad Khaywah, Audrey Potdevin, Francois Reveret, Rachid Mahiou, Youcef Ouerdane, Anthony Desert, Stephane Parola, Genevieve Chadeyron, Emmanuel Centeno, Rafik Smaali, Antoine Moreau,

Fabrication and properties of GaAs Tamm plasmon confined light emitting diodes (pp. 553)
Joel Bellessa, Vincent Toanen, Clementine Symonds, Jean-Michel Benoit, Alban Gassenq, Aristide Lemaitre,

Bioinspired Colorimetric Metasurfaces for Next Generation, On-Chip Imaging of Tissue Microstructure (pp. 555)
Paula Kirya, Zaid Haddadin, Dev Shah, Loren Phillips, Omonigho Aisagbonhi, Lisa Poulikakos,

Tailoring Anisotropies in NIR-plasmonic Semiconductor Nanocrystals (pp. 556)
Jisoo Oh, Yannis Cheref, Capucine Cleret de Langavant, Louise Daugas, Florian Lochon, Alexandre Baron, Thierry Gacoin, Jongwook Kim,

Scalable self-assembled plasmonic metamaterials: fabrication and application (pp. 557)
Anastasiia Zaleska, F. Lotti, A. Krasavin, W. Dickson, A. V. Zayats,

Escaping the flatland: fabrication and application of volume metamaterials (pp. 559)
Thomas Pertsch,

Novel surface interactions of 2D TMDs with different bacteria and virus models (pp. 561)
Manjo Singh,

Tailoring Surface Reflectance Using Self-Assembled Block Copolymer Nanopatterns (pp. 562)
Gregory Doerk, Charles Black,

Self-assembled hexagonal array or correlated disorder plasmonic metasurfaces: optical properties comparison (pp. 564)
Gil Cardoso, Frederic Hamouda, Vy Yam, Beatrice Dagens,

Designing Mode Coupling in Two-Phase Metamaterials made by Sequential Self-Assembly (pp. 566)
Jelena Wohlwend, Georg Haberfehlner, Ralph Spolenak, Henning Galinski,

Direct Fabrication of Plasmonic Nanoantennas onto Tapered Optical Nanofibers with Electron Beam Induced Deposition for Enhanced Single Photon Emission (pp. 568)
Antonio Balena, Chengjie Ding, Marianna D'Amato, Muhammad Fayyaz Kashif, Filippo Pisano, Marco Pisanello, Gaia De Marzo, Massimo De Vittorio, Alberto Bramati, Ferruccio Pisanello,

3D Topological Insulators and Eutectics at a crossroad (pp. 570)
Kingshuk Bandopadhyay, Andrzej Materna, Krzysztof Markus, Marta Buza, Cheng Chen, Piotr Piotrowski, Alexei Barinov, Fumikazu Murakami, Masayoshi Tonouchi, Yulin Chen, Dorota Pawlak,

Dynamic plasmonics based on conducting polymers (pp. 571)
Shangzhi Chen, M. P. Jonsson,

Bottom-up fabrication of 2D MoS2: from thermochromic sensing to hyperbolic metamaterials. (pp. 572)
Jose Luis Ocana Pujol, Ramon Camilo Rodriguez Ordonez, Christof Vockenhuber, Ralph Spolenak, Henning Galinski,

Plasmonic Metasurfaces of Self-assembled Gold Nanoparticle Superlattices with Tunable Sub-nanometer Gaps (pp. 574)
Bin Lu, Karol Vegso, Simon Micky, Christian Ritz, Michal Bodik, Yuriy Fedoryshyn, Peter Siffalovic, Andreas Stemmer,

Light-matter interaction on a chip

Efficient grating coupling strategies for silicon photonics (pp. 577)
Periklis Petropoulos, V. Vitali, T. Dominguez Bucio, F. Y. Gardes, C. Lacava,

Generation of spatial rogue waves in a Q-switched Nd:YAG laser (pp. 579)
Roza Navitskaya, Ihar Stashkevich, Stanislav Derevyanko, Alina Karabchevsky,

Integrated Photonics for Machine Learning Assisted Signal Processing (pp. 581)
Imtiaz Alamgir, Luigi Di Lauro, Celine Mazoukh, Stefania Sciara, Bennet Fischer, Abdul Rahim Aadhi, Armaghan Eshaghi, Brent E. Little, Sai T. Chu, David. J Moss, Roberto Morandotti,

Wafer-scale fabrication of metasurfaces for infrared and energy applications (pp. 582)
Otto Muskens, K. Sun, C. Wheeler, J. J. Ou, C. H. de Groot,

Anapole metallic nanostructures for metarsurface applications (pp. 583)
Emadeldeen Hassan, Andrey Evlyukhin, Antonio Cala Lesina Cala Lesina,

Emission enhancement of erbium in a reverse nanofocusing waveguide (pp. 584)
Nicholas Gusken, Ming Fu, Max Zapf, Michael Nielsen, Paul Dichtl, Robert Roder, Alex Clark, Stefan Maier, Carsten Ronning, Rupert Oulton,

Simulation of Plasmonic Absorption Interplays in Hybridized Semiconductor/Metal Nanostructures (pp. 586)
Atefeh Habibpourmoghad, Wenyong Xie, Antonio Cala Lesina,

Green-Extraction of Graphene from Natural Mineral Shungite (pp. 588)
Anastasia Novikova, A. Karabchevsky,

Plasmonic Nanomaterials for Bio-diagnostics, Environmental Monitoring and Food Safety

Plasmonic Metasurface for Enhanced Infrared Spectroscopy: a method to monitor protein denaturation (pp. 591)
Valentina Di Meo, Gennaro Sanita, Massimo Moccia, Alessio Crescitelli, Annalisa Lamberti, Vincenzo Galdi, Ivo Rendina, Emanuela Esposito,

Development of a hybrid plasmonic/photonic nanoscale strategy for multi-level anti-counterfeit labels in the framework of food safety (pp. 593)
Vincenzo Caligiuri, Aniket Patra, Maria Penelope De Santo, Agostino Forestiero, Giuseppe Papuzzo, Dante M. Aceti, Giuseppe E. Lio, Riccardo C. Barberi, Antonio De Luca,

Plasmonic Metasurfaces for Enhanced Spectrochemical Tissue Diagnostics (pp. 595)
S. Rosas, K. A. Schoeller, E. Chang, H. Mei, M. A. Kats, K. W. Eliceiri, X. Zhao, Filiz Yesilkoy,

Plasmon Resonances in Ga Nanoparticles and Plasmonic Antennas for Biosensing (pp. 597)

Michal Horak, Vojtech Calkovsky, Vlastimil Krapek, Joseph Riley, Victor Pacheco-Pena, Jindrich Mach, Tomas Sikola,

Plasmonic metamolecular units for biological analytes investigation (pp. 599)
Massimo Rippa, Valentina Marchesano, Ambra Vestri, Domenico Sagnelli, Lu Zhou, Giovanna Fusco, Joseph Zyss, Jun Zhou, Lucia Petti,

Development of plasmonic platforms for sensitive and selective detection of macromolecules for food-quality assessment and environmental monitoring (pp. 601)
Giulia Rusciano,

Optical metasurfaces with hybrid TE-TM collective resonances for spectroscopic applications (pp. 603)
Radoslaw Kolkowski, Andriy Shevchenko,

Plasmonic sensing for application in food science and eco/nanotoxicology (pp. 605)
Duncan Sutherland,

Nanoplasmonic sensing of food product and neurochemistry (pp. 607)
Jean-Francois Masson,

Optomechanical disk resonators for real-time environmental monitoring and single-nanoparticle detection (pp. 608)
Elena Sentre-Arribas, Eduardo Gil-Santos, Oscar Malvar, Jose Jaime Ruz, Samantha Sbarra, Louis Waquier, Aristide Lemaitre, Maurits van der Heiden, Robert Altmann, Dimitris Papanastasiou, Diamantis Kounadis, Ilias Panagiotopoulos, Ivan Favero, Montserrat Calleja, Javier Tamayo,

Optical pushing of plasmonic nanoparticles for high-sensitivity spectroscopy of molecules and nanoplastics (pp. 610)
Maria Grazia Donato, S. Bernatova, M. Kizovsky, A. Foti, J. Jezek, O. Samek, O. M. Marago, P. Zemanek, P. G. Gucciardi,

Portable Microfluidic Plasmonic Chip for Fast Real-Time Cardiac Troponin I Biomarker Detection (pp. 611)
Andreea Campu, Ilinca Muresan, Monica Potara, Diana Lazar, Florin Lazar, Simona Cainap, Dana Maniu, Simion Astilean, Monica Focsan,

Numerical optimization of the optical scattering response of plasmonic nanostructures (pp. 612)
Sven Burger, Fridtjof Betz, Felix Binkowski, Martin Hammerschmidt, Lilli Kuen, Phillip Manley, Matthias Plock, Philipp-Immanuel Schneider, Ivan Sekulic, Lin Zschiedrich,

Mass customized optical metasurfaces (pp. 614)
Anders Kristensen,

Bright-field imaging of nanoscale bioparticles with Gires-Tournois photonic platform (pp. 616)
Young Min Song,

Plasmonics on neural implants (pp. 618)
Filippo Pisano, Liam Collard, Di Zheng, Antonio Balena, Barbara Spagnolo, Marco Bianco, Linda Piscopo, Maria Samuela Andriani, Cinzia Montinaro, Francesco Tantussi, Antonella D'Orazio, Francesco De Angelis, Manuel Valiente, Liset M. de la Prida, Marco Grande, Massimo De Vittorio, Ferruccio Pisanello,

Nanophotonics for biosensing: development of optical platforms for high sensitivity and specificity (pp. 620)
Giovanna Palermo,

Plasmonic nanomaterials for detection and degradation of pesticedes (pp. 622)
Alexa Guglielmelli, R. Mazzei, G. Palermo, P. Strangi, L. Giorno, T. Poerio,

Nanophotonic biosensors based on bound state in continuum (pp. 624)

Vito Mocella, Silvia Romano, Gianluigi Zito, Ivo Rendina,

Plasmonic biosensors for biomedical applications (pp. 626)
T. Springer, M. BockovÃ¡, J. Slaby, E. HemmerovÃ¡, Jiri Homola,

Au/Ag SERS active substrate for broader wavelength excitation (pp. 627)
Sebin Augustine, Mahesh Saini, Sooraj KP, Mukesh Ranjan,

Nanophotonic chiral sensing: How does it actually work? (pp. 629)
Shaikhah Almousa, Harald Giessen, Steffen Both, Egor Muljarov, Diana Shakirova, Thomas Weiss,

Coherent control of absorption in structured materials

High-Fidelity Reprogrammable Signal Processors Built Off the Anti-Laser (pp. 632)
Philipp del Hougne,

Quantum and thermal aspects of coherent perfect absorption (pp. 634)
Inigo Liberal,

A Massively Degenerate Coherent Perfect Absorber (pp. 636)
Yevgeny Slobodkin, Gil Weinberg, Helmut Hoerner, Kevin Pichler, Stefan Rotter, Ori Katz,

Coherent Retroreflector, Coherent Asymmetric Absorber, and Bianisotropy Emulation using Coherent Illumination (pp. 638)
Francisco Cuesta, M. S. Mirmoosa, Sergei Tretyakov,

Nontrivial application of coherent quantum absorption (pp. 640)
Anton Vetlugin, Ruixiang Guo, Shuyu Dong, Filippo Martinelli, Cesare Soci, Nikolay Zheludev,

Non-Hermitian Wavefront shaping and Optical Limiting (pp. 642)
Tsampikos Kottos,

Quantum Coherent Absorption of Squeezed Light (pp. 644)
Umit Hardal, Devashish Pandey, Sanshui Xiao, Martijn Wubs,

Many-body Quantum Metasurfaces with Coherent Perfect Absorption with PT Symmetry Breaking (pp. 645)
Kyle Ballantine, Janne Ruostekoski,

Multipolar Coherent Amplification of Chiroptical Scattering and Absorption from a Magnetoelectric Core-shell Nanoparticle (pp. 647)
Hsin-Yu Wu, Frank Vollmer,

Beyond CPA: A General Theory of Reflectionless Scattering (pp. 649)
A. Douglas Stone, W. R. Sweeney, C.-W. Hsu, A. Alhulaymi, P. Del Hougne,

Controlling wave phases and absorption in curved space for light (pp. 651)
Yangjie Liu, Z. K. Xiong, Z. Mao, B. Zhou,

Optical control of collective states in 1D ordered atomic chains beyond the linear regime (pp. 653)
Nikos Fayard, Igor Ferrier-Barbut, Antoine Browaeys, Jean-Jacques Greffet,

Chiroptical phenomena

Computational implementation of the hyper-Rayleigh scattering optical activity: theory, symmetry considerations and quantum chemistry applications (pp. 655)
Andrea Bonvicini, Benoit Champagne,

Maximum Chirality Achieved with Resonant Dielectric Metastructures (pp. 656)
Maxim Gorkunov, Alexander Antonov, Denis Baranov, Yuri Kivshar,

Signature of the Chiral Tensor Elements of the First Hyperpolarizability in Metallic Nanoparticles in Hyper Rayleigh Scattering Experiments (pp. 658)
Zacharie Behel, Michalina Slemp, Katarzyna Matczyszyn, Stephane Parola, Pierre-Francois Brevet,

Transition Metal Nitride and Oxide Thin Films for Chiral Structures: Spectral and Environmental Applicability (pp. 660)
Ryan Bower, Peter Petrov,

Photogalvanics of chiral topological insulator metamaterials (pp. 662)
Alexander M. Dubrovkin, Giorgio Adamo, Nikolay I. Zheludev, Cesare Soci,

Multifunctional Chiral Meta-Platform for Dynamic Spin-Encoded Phase Multiplexing (pp. 663)
Hafiz Saad Khaliq, Junhwa Seong, Asad Nauman, Jae-Won Lee, Jung-Yeop Shin, Junsuk Rho, Hak Rin Kim,

Strong broadband circular dichroism in chiral plasmonic woodpiles (pp. 665)
B. Abdennadher, R. Iseli, U. Steiner, Matthias Saba,

BSW-based transducer for surface mode polarization control (pp. 667)
Erika Mogni, Giovanni Pellegrini, Jorge Gil-Rostra, Francisco Yubero, Giuseppina Simone, Stefan Fossati, Jakub Dostalek, Rebeca Martinez Vasquez, Roberto Osellame, Michele Celebrano, Marco Finazzi, Paolo Biagioni,

Circular dichroism in plasmonic array of elliptical nanoholes with square lattice (pp. 669)
Hanan Ali, Emilija Petronijevic, Giovanni Pellegrini, Concita Sibilia, Lucio Andreani,

A characterization method for an achiral magnetic photonic antenna with arbitrary excitation (pp. 671)
Lingfei Cui, Xingyu Yang, Catherine Schwob, Mathieu Mivelle, Bruno Gallas,

Resonant Optics - Fundamentals and Applications

Microstar cavities: Ray-wave correspondence in the semiclassical regime (pp. 674)
Julius Kullig, Jan Wiersig,

Resonant Photonic Galleries of Dielectric Particles (pp. 676)
N. S. Solodovchenko, M. E. Bochkarev, K. B. Samusev, Mikhail Limonov,

Plasmonic nanocavities: From resonant modes to semi-persistent sub-radiant states (pp. 678)
Angela Demetriadou,

Predicting nonlinear optical scattering with physics-driven neural networks (pp. 680)
Carlo Gigli, Amirhossein Saba, Ahmed Bassam Ayoub, Demetri Psaltis,

Polarization Singularities in Optical Near Fields: Topology and Chirality (pp. 683)
Shubo Wang, Jie Peng, Shiqi Jia, Ruo-Yang Zhang,

Computing partial derivatives of quasinormal modes (pp. 685)
Felix Binkowski, Fridtjof Betz, Martin Hammerschmidt, Philipp-Immanuel Schneider, Lin Zschiedrich, Sven Burger,

Quasi-normal mode expansions of resonant scattering responses (pp. 686)
Jorn Zimmerling, Rob Remis,

Optomechanics of Quasi-Bound States in the Continuum of Dielectric Metasurfaces (pp. 688)
Simone Zanotto,

Photon-Pair Generation in Resonant Dielectric Nanostructures (pp. 690)
Maximilian Weissflog,

Light scattering and dipole emission in resonant periodic structures (pp. 692)
Lin Zschiedrich, Felix Binkowski, Phillip Manley, Martin Hammerschmidt, Philipp Schneider, Sven Burger,

Towards a highly directional hybrid Mie-Tamm optical cavity for high-performance single-photon sources (pp. 693)
Jose Manuel Llorens Montolio, Anna Nowak, Jose Maria Ulloa, Benito Alen,

Calculating resonant states in optical systems: Exact theory and approximations (pp. 695)
Egor Muljarov,

Bound-State-in-the-Continuum Resonances in Monolithic Cavities on a Substrate (pp. 696)
Cindy Peralle, Sushanth Kini Manjeshwar, Anastasiia Ciers, Witlef Wieczorek, Philippe Tassin,

Quantum confinement effects in atomic-scale polaritons (pp. 698)
Javier Garcia de Abajo,

Nanolasers: Dynamics and Phase Locking (pp. 699)
Yeshaiahu Fainman, Sizhu Jiang, Suruj Deka, Athena Pan,

Resonantly confining light in air: The dielectric Mie voids (pp. 701)
Masoud Hamidi, Kirill Koshelev, Mario Hentschel, Adria CanÃ³s-Valero, Yuri Kivshar, Harald Giessen, Thomas Weiss,

Design and Simulation of Large-Scale Metalenses (pp. 702)
Jens Niegemann, Dan-Nha Huynh, Federico Gomez, Dylan McGuire, James Pond,

Engineered Solid-State Quantum-Light Sources for Quantum Networking (pp. 703)
Tobias Heindel,

MAN: A freeware to compute and analysis modes of resonators (pp. 704)
Tong Wu, D. Arrivault, W. Yan, Philippe Lalanne,

Complex chi(3) of polyaniline and silver nanoparticle metafluids (pp. 705)
Giuseppe Leo, Giorgio Guercio, Maeva Laffitte, Virginie Ponsinet, Olivier Mondain-Monval, Alexandre Baron,

Quasi-Normal Mode Expansion in Unbounded Photonic structures: Perfectly Matched Layers (PML) vs. Bayliss-Turkel (BT) Absorbing Boundary Condition (pp. 706)
Guillaume Demesy, Andre Nicolet, Frederic Zolla,

Exploiting and Engineering non-Hermiticity in Photonics (pp. 707)
Massimo Gurioli, Nicoletta Granchi, Francesca Intonti,

Double helical plasmonic antennas for enhanced chiroptical interactions (pp. 709)
A. Tsarapkin, S. Jurgensen, Th. Feichtner, K. Mackosz, V. Deinhart, I. Utke, S. Reich, Katja Hoflich,

Tailored local fields for nonlinear optics, strong coupling and chiral recoil forces (pp. 710)

Bert Hecht, Jessica Meier, Luka Zurak, Rene Kullock, Andrea Locatelli, Daniel Friedrich, Jin Qin, Tommaso Tufarelli, Benedikt Schurr, Thorsten Feichtner,

Self-assembled DNA-origami inverse diamond lattice with a photonic band gap in the UV (pp. 712)
Gregor Posnjak, Xin Yin, Paul Butler, Oliver Bienek, Mihir Dass, Ian Sharp, Tim Liedl,

Photonic resonances in next-level metrology and precision experiments (pp. 714)
Stefanie Kroker, Bernd Bodermann, Johannes Dickmann, Tim Kaseberg, Mika Gaedtke, Steffen Sauer, Thomas Siefke,

Measuring Feibelman's d parameters in the optical domain (pp. 715)
Yi Yang,

Auto-differentiable Computational Photonics and its application to optimization (pp. 716)
Benjamin Vial, Yang Hao,

Tailoring resonant interactions in suspensions of disordered particles to achieve near zero reflection (pp. 718)
Cedric Blanchard, Timothee Guerra, Jean-Paul Hugonin, Olivier Rozenbaum,

Quasinormal Mode Theory for Nanoscale Electromagnetism informed with the Feibelman's d-Parameter Treatment (pp. 720)
Qiang Zhou, Pu Zhang, Xue-Wen Chen,

Quasi normal mode perturbation theory to achieve Q factor optimization of resonances in disordered photonic systems (pp. 722)
Nicoletta Granchi, Francesca Intonti, Massimo Gurioli, Guillermo Arregui,

Anisotropic Light Scattering from Tunable Self-Assembled Submicron Resonators (pp. 724)
Maeva Lafitte, Ranjeet Dwivedi, Rajam Elancheliyan, Philippe Barois, Alexandre Baron, Olivier Mondain-Monval, Virginie Ponsinet,

Purcell Enhanced Intrinsic Linear and Nonlinear Optical Responses in Colloidal Dielectric Resonators (pp. 726)
Jeanne Heintz, Gauthier Roubaud, Samuel Gresillon, Sebastien Bidault,

Generalized Lorentz Model and Quasinormal Mode theory for Nonlocal Media (pp. 728)
Xuewen Chen,

Resonances in doubly anisotropic, high-index nanoplatelets (pp. 730)
Bingying You, Tom Sistermans, Alberto Curto,

Analog optical differentiation using metal-dielectric layered structures (pp. 732)
Artem Kashapov, Leonid Doskolovich, Evgeni Bezus, Nikita Golovastikov, Dmitry Bykov,

Optical properties of resonant gratings with spatially varying period (pp. 734)
Dmitry Bykov, Evgeni Bezus, Artem Kashapov, Andrey Morozov, Vladimir Podlipnov, Leonid Doskolovich,

Bound states in the continuum in the waveguide structure covered by the 2D-rectangular plasmonic lattice (pp. 736)
Sergey Pavlov, S. A. Dyakov, D. P. Markov, S. A. Grudinkin, N. A. Feoktistov, A. B. Pevtsov,

Metamaterials and Metasurfaces for Medical and Healthcare Applications

Super-Resolution Ultrasonic Cellular Imaging by Localization of Meta-Nanodroplets (pp. 739)
Chengzhi Shi,

Metamaterial Antenna for High Field MRI (pp. 740)
Anton Nikulin, Benoit Larrat, Djamel Berrahou, Alexandre Vignaud, Redha Abdeddaim, Abdelwhabed Ourir, Julien de Rosny,

Enhancing the performance of antennas for biomedical applications with inverse-designed nonlocal-inspired metamaterials (pp. 742)
Dimitrios Tzarouchis, Maria Koutsoupidou, Dionisios Rompolas, Ioannis Sotiriou, Efthymios Kallos, Panagiotis Kosmas,

The benefit of reconfigurable metamaterials in Magnetic Resonance Imaging (pp. 744)
Matthias Guenther, Endri Stoja, Simon Konstandin, Thomas Bertuch, Johannes Mueller, Dennis Philipp,

Comparison between a highly sensitive H-shape Terahertz metasurface absorber and an EIT-like terahertz Metasurface for refractive index biosensing (pp. 746)
Tomas Pereira Pires, Ruobin Han, Shoreh Nourinovin, Akram Alomainy, Hasan Abbas, Muhammad Imran, Qammer Abbasi,

Metasurface Pads for body imaging at 3T (pp. 749)
Marc Dubois, Stefan Enoch, David Bendahan, Abdeddaim Redha,

Metamaterials for 7T Ultra High Field MRI (pp. 750)
Redha Abdeddaim, Marc Dubois, Stefan Enoch,

Segmentation of individual muscles in MR images from patients with neuromuscular diseases (pp. 751)
David Ben Dahan,

On the design, control, and AI-driven optimization of reconfigurable metamaterials for Magnetic Resonance Imaging (pp. 752)
Dennis Philipp, Endri Stoja, Simon Konstandin, Thomas Bertuch, Johannes Mueller, Marina Schmidt, Matthias Guenther,

Boosting received magnetic field (B1-) strength using wearable metasurface-based add-ons for 1.5T MRIs (pp. 754)
Jegyasu Gupta, Tanmay Bhowmik, Ratnajit Bhattacharjee, Debabrata Sikdar,

New Trends in Topological Matematerials

Topological singular points and skin modes in asymmetric dielectric structures (pp. 757)
Masaya Notomi, Taiki Yoda, Yuto Moritake,

3D Magnetic Topological Photonic Crystals (pp. 759)
Baile Zhang,

Topological Transport in a Nanoscale Optomechanical Array (pp. 761)
Florian Marquardt,

Topological Thouless Pumping in Photonic Time Crystals (pp. 762)
Xiang Ni, Shixiong Yin, Huanan Li, Andrea AlÃ¹,

Hyperbolic topological states with first-order and higher-order Chern numbers (pp. 764)
Weixuan Zhang, Xiangdong Zhang,

Optical holography and coding based on topological light field in real space (pp. 766)
Lingjun Kong, Xiangdong Zhang,

Experimental observation of the bulk-edge correspondence in anomalous-Chern topological insulators in a synthetic photonic lattice (pp. 768)
Rabih El Sokhen, Albert F. Adiyatullin, Alvaro GÃ³mez de Leon, Stephane Randoux, Pierre Delplace, Alberto Amo,

Topological transport of GHz surface acoustic wave (pp. 769)
Yoichi Nii, Yoshinori Onose,

Non-Hermitian topological light manipulations in integrated waveguide lattices (pp. 771)
Wange Song, Luqi Yuan, Shining Zhu, Tao Li,

Beam Trajectory Steering by Distorted Photonic Crystals (pp. 772)
Kyoko Kitamura, J. Hashizume, Y. Kawamoto, A. Onishi, H. Kitagawa,

Filling anomalies and chiral winding numbers in higher-order topological metamaterials (pp. 774)
Wladimir Benalcazar,

Adiabatic topological photonics (pp. 775)
Anton Vakulenko, Svetlana Kiriushechkina, Daria Smirnova, Sriram Guddala, Filipp Komissarenko, Andrea Alu, Monica Allen, Jeffery Allen, Alexander Khanikaev,

Nanophotonic structures to control propagation, emission and topological behavior of light (pp. 777)
Ganapathi Subramania,

Harness Light with Spinor Wavefunction (pp. 778)
Xiao Hu,

Topological photonic integrated circuits for controlling optical vortex signal (pp. 779)
Tomohiro Amemiya, Hibiki Kagami, Sho Okada, Itsuki Sakamoto, Nobuhiko Nishiyama, Xiao Hu,

High-throughput generation of topological metamaterials (pp. 781)
Sebastian Huber,

Probing bulk topology of one dimensional synthetic frequency lattice (pp. 782)
Greta Villa, Iacopo Carusotto, Tomoki Ozawa,

Photonic Bimorphic Floquet Topological Insulators (pp. 783)
Julius Beck, Georgios G. Pyrialakos, Matthias Heinrich, Lukas J. Maczewsky, Mercedeh Khajavikhan, Nikolaos V. Kantartzis, Alexander Szameit, Demetrios N. Christodoulides,

Surface states in double diamond nodal line photonic crystals (pp. 785)
Haedong Park, Sang Soon Oh,

Laser based on Bound States in the Continuum in the Ultraviolet Region (pp. 787)
Mu-Hsin Chen, Di Xing, Vin-Cent Su, Yang-Chun Lee, Ya-Lun Ho, Jean-Jacques Delaunay,

Topological corner states in photonic bilayer square lattice with Ï€flux (pp. 789)
Natsuko Ishida, Motohiko Ezawa, Guangtai Lu, Wenbo Lin, Yasutomo Ota, Yasuhiko Arakawa, Satoshi Iwamoto,

Photonic topological phases in pseudochiral metamaterials (pp. 791)
Ruey-Lin Chern, Ti-Jung Hsu,

Generation and applications of textured photonics fields

Nanofemto vectorial texturing of electromagnetic fields by spin-orbit interaction of light (pp. 793)
Hrvoje Petek, Atreyie Ghosh, Sena Yang, Yanan Dai,

Tailoring vortex light sources with planar optical devices (pp. 795)

Michael Almeida de Oliveira, Marco Piccardo, Antonio Ambrosio,

Photonic N00N-sates with spatially structured photons (pp. 797)
Markus Hiekkamaki, Rafael F. Barros, Marco Ornigotti, Robert Fickler,

Novel Effects in Propagation and Absorption of Optical Vortices (pp. 799)
Andrei Afanasev,

Generation of Extreme-Ultraviolet structured fields with the seeded Free Electron Laser FERMI, and applications in atomic and molecular physics. (pp. 801)
Carlo Callegari,

High efficiency interface between multi-mode and single-mode fibers (pp. 803)
Oussama Korichi, Markus Hiekkamaki, Robert Fickler,

Thermal plasmonics and metamaterials for sustainable society

Quasi-resonance of surface plasmons for near-infrared sensitivity improvement of silicon image sensor (pp. 806)
Atsushi Ono, Takahito Yoshinaga, Kazuma Hashimoto, Nobukazu Teranishi,

Optical magnetic field distribution imaging using a single-gap, crescent-shaped metal split-ring resonator (pp. 808)
Toshihiro Okamoto, K. Takabatake, K. Yamaguchi, M. Haraguchi,

Fabrication of metasurfaces for heat-shielding windows and 6G communications and investigation of the possibility of near-infrared reflection control by movable thin films (pp. 810)
Yoshiaki Kanamori,

Si Plasmonic MEMS device for infrared sensing (pp. 812)
Masaaki Oshita, Elyas Ashenafi Abadi, Tetsuo Kan,

Material systems for metamaterial based selective thermal emitters (pp. 814)
Eich Manfred, G. V. Krishnamurthy, M. Stormer, A. Yu. Petrov,

Spectrally selective infrared emitters enabled by 1D metamaterials (pp. 815)
Yongkang Gong, Sang Soon Oh,

Dynamic emissivity modulating thermoregulating fabric using metallic particles (pp. 817)
Muluneh Geremew Abebe, Gilles Rosolen, Bjorn Maes,

Zero-dimensional thermal light emitters in the infrared based on silicon microspheres (pp. 819)
Roberto Fenollosa, Fernando Ramiro-Manzano, Moises Garin, Francisco Meseguer,

Refractory metamaterials for tuning thermal emission at high temperature (pp. 821)
Alima Nzie, Syreina Sayegh, Olivier Rozenbaum, Mikhael Bechelany, Quentin Flamant,

Perfect Absorbers and Photothermal Control of Light by Single Crystalline Silicon Metasurface (pp. 823)
Junichi Takahara,

Transition Metal Nitride Metasurface Broadband Absorbers for Plasmon-Enhanced Solar-Driven Hydrogen Evolution (pp. 825)
Yu-Jung Lu,

A Sustainable Power Scavenger Using Zebra-Inspired In-Plane Radiative Cooler/Heater (pp. 827)

Se-Yeon Heo, Young Min Song,

Realization of true perfect absorber metasurfaces (pp. 829)
Yoshiaki Nishijima,

Non-radiative cooling materials with high transparency (pp. 831)
H. TT. Tam, M. Toma, Kotaro Kajikawa,

New trends in opto-magnetism and magneto-optics

Twisted light affects ultrafast demagnetization (pp. 833)
Eva Prinz, Jonas Hoefer, Benjamin Stadtmuller, Martin Aeschlimann,

Magnetoplasmonics beyond metals: the case of plasmonic Transparent Conductive Oxide Nanocrystals (pp. 835)
Alessio Gabbani,

Nanoscale and ultrafast magnetophotonics (pp. 837)
Alexandre Dmitriev,

Magneto-Optical Light-Matter interactions in Weyl Semimetals (pp. 838)
Dima Cheskis,

Ultrafast Driving of Orbital Magnetism in Metallic Nanoparticles using Circularly Polarized Light (pp. 839)
Paul-Antoine Hervieux, Rajarshi Sinha-Roy, Jerome Hurst, Giovanni Manfredi,

Optics and THz for ultrafast magnetization manipulation in ferro and ferrimagnetic systems (pp. 841)
Jon Gorchon,

Amplification of magneto-optical activity via plasmonic modes hybridization (pp. 843)
Paolo Vavassori, Terunori Kaihara, Pablo Rodriguez-Suarez,

Magnetic Helicoidal Dichroism with XUV Light Carrying Orbital Angular Momentum (pp. 845)
Mauro Fanciulli, Matteo Pancaldi, Emanuele Pedersoli, Mekha Vimal, David Bresteau, Martin Luttmann, Dario De Angelis, Primoz Rebernic-Ribic, Benedikt Rosner, Christian David, Carlo Spezzani, Michele Manfredda, Ricardo Sousa, Ioan-Lucian Prejbeanu, Laurent Vila, Bernard Dieny, Giovanni De Ninno, Flavio Capotondi, Maurizio Sacchi, Thierry Ruchon,

Ultrafast control of spins using resonant light excitation (pp. 847)
Dmytro Afanasiev,

Structured ultrafast electric and magnetic fields by design (pp. 848)
Hrvoje Petek, Atreyie Ghosh, Sena Yang, Yanan Dai,

Microwaves and millimeter waves applications of metamaterials and metasurfaces for the real world

Deep learning-driven all-optical operations utilizing metasurfaces (pp. 851)
Zihan Zhao, Yue Wang, Xumin Ding,

Emulating Fast-Fading Rician Wireless Environments with Electronically Adjustable K-Factors in a Programmable-Metasurface-Stirred Reverberation Chamber (pp. 853)
Ismail Ahmed, Matthieu Davy, Philippe Besnier, Philipp Del Hougne,

Intelligent Surfaces for Wireless Communications: Living at the Interface of Electromagnetic and Communication Theories

(pp. 855)
Marco Di Renzo,

Metagratings for wavefronts manipulation: Theory and design (pp. 856)
Zhen Tan, Jianjia Yi, Badreddine Ratni, Shah Nawaz Burokur,

Modulated metasurface antennas and arrays for millimeter wave and sub-terahertz applications (pp. 858)
David Gonzalez Ovejero, Jerome Taillieu, Christos Bilitos, Ronan Sauleau, Olivier De Sagazan,

Perfect Control of Diffraction Patterns with Phase Gradient Metasurfaces (pp. 860)
Yuxiang Wang, Kuang Zhang, Guohui Yang, Shah Nawaz Burokur, Qun Wu,

Holographic Metasurfaces for Wireless Communications and Extended Reality (pp. 861)
Alexandros Pitilakis, Odysseas Tsilipakos, Anna Tasolamprou, Ageliki Tsioliaridou, Traianos Yioultsis, Nikolaos Kantartzis, Dionysios Manessis, George Kenanakis, Sotiris Ioannidis, Maria Kafesaki, Christos Liaskos,

A Dual Polarized Metagrating to Manipulate Wavefronts (pp. 863)
Wei Zhou, Lina Zhu, Jianjia Yi,

Composite based metasurface for surface wave excitation in HF band (pp. 865)
Gildas Briand, Andre Barka, Shah Nawaz Burokur,

A Compact, Quad-Band, and Wideband Antenna Using Triple-Band AMC (pp. 867)
Rafael Goncalves Licursi de Mello, Anne Claire Lepage, Xavier Begaud,

Design and measurement of an oblique wide-angle metamaterial absorber for RF space applications (pp. 871)
Anne Claire Lepage, Xavier Begaud, O. Rance, K. Elis, N. Capet,

Transparent Passive Reflector for Coverage Enhancement in 5G Millimeter Wave (pp. 873)
Konstantinos Dovelos, Panagiotis Kosmas, Efthymios Kallos, Ragip Pala,

GRIN Lens Design by Defining Phase Function and Using Optical Path Rescaling (pp. 875)
Hossein Eskandari, Mehrdad Shokooh-Saremi, William Whittow, Tomas Tyc,

Time-varying OAM beams generation by a metasurface (pp. 877)
Jingxin Zhang, Peixing Li, Ray C. C. Cheung, Alex M. H. Wong, Jensen Li,

A Non-Interleaved Bidirectional Janus Metasurface with Full-Space Scattering Channels (pp. 879)
Guanyu Shang, Zihan Zhao, Xumin Ding,

Reconfigurable Intelligent Surface as MIMO (pp. 881)
Sotiris Droulias, Angeliki Alexiou,

Cross-wavelength Metasurface Based on Carbon Nanotubes (pp. 883)
Jin Zhang, Peng Liu, Zhipei Sun,

Classical and Quantum Phononics

Single electron spin dynamics in a two-electron double quantum dot under a nonequilibrium phonon environment (pp. 886)
Kazuyuki Kuroyama, Sadashige Mastuo, Shunsuke Yabunaka, Sascha R. Valentin, Arne Ludwig, Andreas D. Wieck, Yasuhiro Tokura, Seigo Tarucha,

Quantum interference of electron-phonon coupled states in semiconductors using phase-locked femtosecond pulses (pp. 888)
Kazutaka Nakamura, Itsuki Takagi, Yosuke Kayanuma,

Generation of entangled electron-photon-phonon states in nanocavity-QED systems (pp. 890)
Mikhail Tokman, Maria Erukhimova, Qianfan Chen, Alexey Belyanin,

Engineering optomechanical and nonlinear effects in nanostructured silicon photonics (pp. 892)
Paula Nuno Ruano, Jianhao Zhang, Thi-Thuy-Duong Dinh, David Gonzalez-Andrade, Xavier Le Roux, Miguel Montesinos Ballester, Christian Lafforgue, David Medina Quiroz, Daniel Benedikovic, Pavel Cheben, Samson Edmond, Etienne Herth, David Bouville, Norberto Daniel Lanzillotti-Kimura, Delphine Marris-Morini, Eric Cassan, Laurent Vivien, Carlos Alonso Ramos,

Nano-optomechanical systems for ultrasensitive mass measurement (pp. 894)
Wayne Hiebert, C. Thrideep, M. Belov, J. Westwood-Bachman, S. K. Roy, M. P. Maksymowych, V. T. K. Sauer, T. S. Lee, T. Firdous, A. Venkatasubramanian, A. Kobryn,

Diamond X-band Optomechanical Crystals (pp. 896)
Elham Zohari, Waleed El-Sayed, Joseph Losby, Gustavo de Oliveira Luiz, Paul Barclay,

Optomechanics in the microwave regime: leveraging strong non-linearities for cooling (pp. 898)
David Zoepfl, Lukas Eng, Olivier-Michel Tardif, etienne Pilon, Mercier-Coderre Laurence, David Tran, Gerhard Kirchmair, Mathieu Juan,

Applications of phonon-electron devices for microwave frequency signal processing (pp. 899)
Matt Eichenfield,

Photonic Implementation of Non-Adiabatic Holonomies for Quantum Computing (pp. 900)
Vera Neef, Julien Pinske, Matthias Heinrich, Stefan Scheel, Alexander Szameit,

Quantum explorations and applications of phonon-electron interactions (pp. 902)
Matt Eichenfield,

Thermalization and condensation of light waves: Wave turbulence theory and experiments in multimode optical fibers (pp. 903)
Kilian Baudin, Josselin Garnier, Nicolas Berti, Adrien Fusaro, Katarzyna Krupa, Lucas Zanaglia, Claire Michel, Valerie Doya, Guy Millot, Antonio Picozzi,

Thermalization of weakly non-integrable Josephson junction networks (pp. 905)
Gabriel Lando,

Diffusion without Spreading of Wavepackets in Nonlinear Lattices with linear Anderson Localization (pp. 906)
Serge Aubry,

Thermodynamics and pressure of composite multimoded optical systems (pp. 907)
Nikolaos Efremidis, D. N. Christodoulides,

Controlling optical thermalization via spectral engineering: A Kinetic Equation Approach (pp. 909)
Tsampikos Kottos,

Recent Advances in Non-Hermitian Photonics: Topological, Disordered and Quantum systems

The bosonic skin effect: boundary condensation in asymmetric transport (pp. 912)

Louis Garbe, Yuri Minoguchi, Julian Huber, Peter Rabl,

Non-unitary boson sampling dynamics - distinguishability, complexity, and noise (pp. 913)
Ken Mochizuki, Ryusuke Hamazaki,

Extended Nielsen-Ninomiya theorem and non-Hermitian topological phenomena (pp. 914)
Masatoshi Sato,

Continuum of Bound States in a Non-Hermitian Model (pp. 915)
Qiang Wang, Changyan Zhu, Xu Zheng, Haoran Xue, Baile Zhang, Y. D. Chong,

Non-orthogonality of Bogoliubov modes and the laser linewidth (pp. 917)
Ivan Amelio, Iacopo Carusotto,

Non-Hermitian quantum optics in cold atomic ensembles (pp. 919)
Georgios Siviloglou, J. F. Chen,

Observation of tailored non-Hermiticity induced transparency and photonic constant-intensity waves in optical mesh lattices (pp. 920)
Andrea Steinfurth, Ivor Kresic, Sebastian Weidemann, Mark Kremer, Konstantinos Makris, Matthias Heinrich, Stefan Rotter, Alexander Szameit,

Observation-dependent enhancement and suppression of two-photon coincidences by tailored losses (pp. 922)
Max Ehrhardt, Matthias Heinrich, Alexander Szameit,

Compressibility and fluctuations of an optical quantum gas (pp. 924)
Julian Schmitt,

Stability of Non-Hermitian Hamiltonians with Different Periodicities Using Floquet Theory (pp. 925)
Avadh Saxena, Julia Cen, Yogesh N. Joglekar,

Classifying topological solitons using local markers (pp. 926)
Stephan Wong, Terry Loring, Alexander Cerjan,

Experimentally realizable PT phase transitions in reflectionless quantum scattering (pp. 928)
Micheline Soley, Carl Bender, A. Douglas Stone,

Restoration of the non-Hermitian bulk-boundary correspondence via topological amplification (pp. 930)
Matteo Brunelli, C. C. Wanjura, A. Nunnenkamp,

Non-Hermitian dispersive hydrodynamics and Riemann problems (pp. 932)
Sathyanarayanan Chandramouli, Nicholas Ossi, Ziad Musslimani, Konstantinos Makris,

Models and other phenomena in photonic Chern insulator systems (pp. 934)
Mark Ablowitz, Justin Cole, Sean Nixon,

Exceptional robustness of anomalous topological scattering network (pp. 935)
Zhe Zhang, Pierre Delplace, Romain Fleury,

Topological framework for directional amplification in driven-dissipative cavity arrays (pp. 936)
Clara Wanjura, Matteo Brunelli, Andreas Nunnenkamp,

Non-Hermitian optical design by coordinate transformations and mapping (pp. 938)

Ivor Kresic, Konstantinos Makris, Andre Brandstotter, Ulf Leonhardt, Stefan Rotter,

Graph parity-time symmetry for bipartite graphs and system stability analysis (pp. 940)
Henri Benisty, L.A. Moreno-Rodriguez, Claudia T. Martinez-Martinez, Jose Antonio Mendez-Bermudez,

Electrically injected first-order gratings broken Parity-Time symmetry DFB lasers: insight on device design rules and experimental results (pp. 942)
Yaoyao Liang, Quentin Gaimard, Jean-Rene Coudevylle, Alexandre Garreau, Arnaud Wilk, Olivier Delorme, Henry Benisty, Abderrahim Ramdane, Anatole Lupu,

Experimental observation of lasing over Anderson-localized modes at exceptional points using quantum echoes (pp. 944)
Sushil Mujumdar, Krishna Joshi,

Level statistics and Anderson localization transitions of non-Hermitian systems with exceptional points (pp. 946)
Chen Wang,

Enhanced avionic sensing based on Wigner's cusp anomalies (pp. 948)
Rodion Kononchuk, Joshua Feinberg, Joseph Knee, Tsampikos Kottos,

Emergence of non-Hermitian dynamics in a quantum gas leading to a self-driven topological pump (pp. 949)
Alexander Baumgartner,

Non-Hermitian microresonators at an Exceptional Point (pp. 950)
Riccardo Franchi, Stefano Biasi, Lorenzo Pavesi,

Non-Hermitian topological disclination defect in a valley-Hall sonic lattice (pp. 951)
Julio Iglesias Martinez, Rene Pernas SalomÃ³n, Penglin Gao, Muamer Kadic, Johan Christensen,

Non-Hermitian resonant energy transfer (pp. 952)
Andrey Novitsky, Fyodor Morozko, Denis Novitsky, Alina Karabchevsky,

A Hermitian Bypass to the non-Hermitian Quantum Theory (pp. 954)
Tanmoy Das,

Non-Hermitian modulations for stabilization of VCSEL, EEL and EEL arrays (pp. 955)
Ramon Herrero, S. B. Ivars, M. Botey, K. Staliunas,

Time-Refraction Optics at Single Cycle Modulation (pp. 957)
Ohad Segal, Eran Lustig, Soham Saha, Eliyahu Bordo, Sarah N. Chowdhury, Yonatan Sharabi, Avner Fleischer, Mustafa Ozlu, Alexandra Boltasseva, Oren Cohen, Vladimir M. Shalaev, Mordechai Segev,

Statics and Dynamics of non-Hermitian Many-body Localization (pp. 959)
Arijeet Pal,

Reflectionless Scattering in Disordered Media: exceptional points and anti-reflection structures (pp. 960)
Matthieu Davy, Clement Ferise, Michael Horodynski, Matthias Kuhmayer, Stefan Rotter, Simon Felix, Vincent Pagneux,

Sensitivity and robustness in non-Hermitian topological lattices (pp. 962)
Ioannis Komis, Dimitrios Kaltsas, Shiqi Xia, Hrvoje Buljan, Zhigang Chen, Konstantinos Makris,

Physical limitations on the observability of non-Hermitian effects in passive systems (pp. 964)
Henning Schomerus,

Pseudomagnetic suppression of non-Hermitian skin effect (pp. 966)
Hau Tian Teo, Subhaskar Mandal, Yang Long, Haoran Xue, Baile Zhang,

Probing the spatial and temporal decay of quasimodes in non-Hermitian Vogel spirals via localization maps (pp. 968)
Marcus Prado, Fabrizio Sgrignuoli, Yuyao Chen, Luca Dal Negro, Felipe Pinheiro,

Engineering localised modes via drive and dissipation in photonic lattices (pp. 970)
O. Jamadi, B. Real, K. Sawicki, C. Hainaut, A. Gonzalez-Tudela, N. Pernet, I. Sagnes, M. Morassi, A. Lemaitre, L. Le Gratiet, A. Harouri, S. Ravets, J. Bloch, Alberto Amo,

Non-Hermitian Spin-Hall Effect in Topological Metasurfaces (pp. 971)
Svetlana Kiriushechkina, Anton Vakulenko, Daria Smirnova, Sriram Guddala, Filipp Komissarenko, Monica Allen, Jeffery Allen, Alexander Khanikaev,

Higher order exceptional points in photonic lattices (pp. 973)
Dimitrios Kaltsas, Ioannis Komis, Konstantinos Makris,

Metasurfaces for Nonlinear and Ultrafast Nanophotonics

Broadband control of topological-spectral correlations in space-time beams (pp. 976)
Marco Piccardo, Michael De Oliveira, Veronica Policht, Mattia Russo, Benedetto Ardini, Matteo Corti, Gianluca Valentini, Jorge Vieira, Cristian Manzoni, Giulio Cerullo, Antonio Ambrosio,

Third-order Infrared Upconversion Imaging with Silicon Metasurfaces (pp. 978)
Ze Zheng, Lei Xu, Lujun Huang, Daria Smirnova, Khosro Zangeneh Kamali, Arman Yousefi, Fu Deng, Rocio Camacho-Morales, Cuifeng Ying, Andrey E. Miroshnichenko, Dragomir N. Neshev, Mohsen Rahmani,

Generation of quantum entanglement from a nonlinear metasurface and its application in quantum imaging (pp. 980)
Jinyong Ma, Jihua Zhang, Marcus Cai, Rocio Camacho Morales, Xu Lei, Jinliang Ren, Yuxin Jiang, Tongmiao Fan, Matthew Parry, Dragomir Neshev, Andrey Sukhorukov,

Piezoelectric MEMS-empowered dynamic optical metasurfaces (pp. 982)
Fei Ding,

Ultrafast nanophotonics of subwavelength semiconductor resonators beyond the perturbative regime (pp. 983)
Anton Rudenko, Anastasiia Zalogina, Jerome Moloney, Yuri Kivshar, Sergey Kruk,

Reconfigurable nonlinear dielectric metasurfaces (pp. 985)
Davide Rocco, Luca Carletti, Marco Gandolfi, Attilio Zilli, Michele Celebrano, Marco Finazzi, Unai Arregui Leon, Antonio Ferraro, Roberto Caputo, Giuseppe Leo, Giuseppe Della Valle, Costantino De Angelis,

Photon-pair generation in thin-film materials (pp. 987)
Frank Setzpfandt,

K-space engineering in nonlinear metasurfaces (pp. 989)
Domenico de Ceglia, Costantino De Angelis,

From light to heat: electronic dynamics and photothermal effects in engineered metasurfaces (pp. 990)
Andrea Schirato, Yage Zhao, Pratiksha Dongare, Joao Cunha, Luca Mascaretti, Margherita Maiuri, Giulio Cerullo, Remo Proietti Zaccaria, Alberto Naldoni, Giuseppe Della Valle, Naomi Halas, Peter Nordlander, Alessandro Alabastri,

Quantum optical metasurfaces: new avenues for generating and engineering entangled photons (pp. 992)
Tomas Santiago-Cruz,

Stimulated Emission Tomography of Spontaneous Four Wave Mixing from a Metasurface (pp. 994)
John Yang, Paul Dichtl, Jefferson Florez, Nathan Gemmel, Sylvain Gennaro, Xiaofei Xiao, Chris Phillips, Alex Clark, Rupert Oulton,

Combining plasmonic nanostructures and diamond for emission of electrons using visible light. (pp. 996)
Patrick O'Keeffe, Giuseppe Ammirati, Alessandro Bellucci, Valerio Campanari, Daniele Catone, Faustino Martelli, Matteo Mastellone, Silvia Orlanducci, Riccardo Polini, Francesco Toschi, Daniele Trucchi, Stefano Turchini, Veronica Valentini,

Ultrafast optical switching in Si-metasurfaces for wireless and space optical communication (pp. 998)
Kaloyan Georgiev, Anton Trifonov, Khosro Kamali, Dragomir Neshev, Giulia Crotti, Giuseppe Della Valle, Lyuben Petrov, Ivan Buchvarov,

Two-Dimensional Electronic Spectroscopy of Strong Exciton-Surface Plasmon Polariton Coupling (pp. 1000)
Christoph Lienau,

Modelling and Inverse Design of Complex Nanophotonic Systems (pp. 1002)
Lora Ramunno,

All-optical routing of upconverted light by dielectric metasurfaces through coherent control (pp. 1003)
Agostino Di Francescantonio, Attilio Zilli, Davide Rocco, Fabrizio Conti, Vincent Vinel, Adrien Borne, Martina Morassi, Aristide Lemaitre, Paolo Biagioni, Lamberto Duo, Costantino De Angelis, Giuseppe Leo, Marco Finazzi, Michele Celebrano,

Ultrafast optical control of nonlinear dielectric nanoantennas (pp. 1005)
Eva A. A. Pogna, Michele Celebrano, Andrea Mazzanti, Lavinia Ghirardini, Luca Carletti, Giuseppe Marino, Andrea Schirato, Daniele Viola, Paolo Laporta, Costantino De Angelis, Giuseppe Leo, Giulio Nicola Cerullo, Marco Finazzi, Giuseppe Della Valle,

Disentangling the ultrafast optical response of Titanium Nitride (pp. 1007)
Silvia Rotta Loria, B. R. Bricchi, A. Schirato, L. Mascaretti, C. Mancarella, A. Naldoni, A. Li Bassi, G. Della Valle, M. Zavelani-Rossi,

Ultrafast Polarization Control via All-Optical Modulation in Anisotropic Metasurfaces (pp. 1009)
Giulia Crotti, Mert Akturk, Andrea Schirato, Vincent Vinel, Remo Proietti Zaccaria, Margherita Maiuri, Anton Trifonov, Ivan Buchvarov, Dragomir Neshev, Giuseppe Leo, Giulio Cerullo, Giuseppe Della Valle,

All-Optical Modulation of Birefringence in Nonlinear All-Dielectric Metasurfaces (pp. 1011)
Mert Akturk, Giulia Crotti, Andrea Schirato, Vincent Vinel, Remo Proietti Zaccaria, Anton A. Trifonov, Ivan C. Buchvarov, Dragomir N. Neshev, Giuseppe Leo, Margherita Maiuri, Giuseppe Della Valle, Giulio Cerullo,

Tensorial artifical optical nonlinearity in dielectric metasurfaces (pp. 1013)
Fuyong Yue, Nicola Montaut, Fabrizio Riminucci, Giacomo Balistreri, Andrea Toma, Riccardo Piccoli, Stefano Cabrini, Roberto Morandotti, Luca Razzari,

Metasurface Design with Robust Resonances for Nonlinear Photonics (pp. 1015)
Gianni Quimey Moretti, Benjamin Tilmann, Andreas Tittl, Emiliano Cortes, Stefan Maier, Andrea Veronica Bragas, Gustavo Grinblat,

Ultrafast modulation of surface plasmon dispersion in metallic bilayers by hot non-equilibrium electrons (pp. 1017)
Artur Avdizhiyan, Andrzej Stupakiewicz, Ilya Razdolski,

Advanced Computational Electromagnetics for the Analysis and Design of Nanophotonic Devices

Modeling the Acousto-Plasmonic Coupling: Raman Energy Density Framework (pp. 1020)

Nicolas Large, Jose Luis Montano-Priedeâ€¬, A. Mlayah,

Heat transfer modelling in the crossover regime between conduction and radiation (pp. 1022)
Mauricio Gomez Viloria, Philippe Ben-Abdallah, Riccardo Messina,

Strategies to Tailor Thermal Properties of Metamaterials: Perforation and Amorphisation (pp. 1024)
Konstantinos Termentzidis,

Nanostructures for Photocatalysis - From regular to dendritic Architectures (pp. 1026)
Christin David,

Smart Sensing and Spectroscopy using Thermal Emission (pp. 1028)
Yuzhe Xiao,

Nanophotonic scintillators for enhanced x-ray detection and imaging (pp. 1029)
Charles Roques-Carmes,

A multimode quasi-normal mode framework for nonlinear harmonic generation with 2D materials (pp. 1030)
Thomas Christopoulos, Emmanouil Kriezis, Odysseas Tsilipakos,

Green's tensor inverse design of light-matter interactions (pp. 1032)
Robert Bennett,

Efficient computation of EM scattering from a dielectric cylinder partially covered with a graphene strip (pp. 1033)
Youssef Jeyar, Brahim Guizal, Mauro Antezza,

Improving Photonic Crystal Waveguide Simulation Efficiency: A Journey from 3D approaches to Deep Neural Networks (pp. 1035)
Caspar Schwahn, Sebastian Schulz,

Modeling and Applications of Nonlocal Asymmetric Metasurfaces (pp. 1037)
Karim Achouri, Sergejs boroviks, Olivier Martin,

An overview of spatial spectral methods with complex-plane deformations for the representation of waves in homogeneous and layered media without absorbing boundary conditions (pp. 1039)
Roeland J. Dilz, Martijn C. van Beurden,

Effect of top metallic contacts on radiation transfer and conversion efficiency for near-field thermophotovoltaics (pp. 1041)
Kevin Austry, Youssef Jeyar, Minggang Luo, Brahim Guizal, Riccardo Messina, Rodolphe Vaillon, Mauro Antezza,

Inverse design of dispersive optical nanostructures and tunable metasurfaces (pp. 1043)
Antonio Cala' Lesina,

Energy Efficient Back-to-Back Neural Networks to Design Photonic Devices (pp. 1045)
Ergun Simsek,

The Fourier Modal Method simplified for crossed subwavelength gratings (pp. 1047)
Brahim Guizal,

Enhanced and Tunable Kerr effect on InSb/graphene hybrid magnetoplasmonic structure at Terahertz waves (pp. 1048)
Maha Ben Rhouma, K. Edee, B. Guizal,

Ray Tracing Model for Non-Rotationally Symmetric Geodesic Lens Antennas with Full Beam Scanning Range in the

Azimuthal Plane (pp. 1050)
Sarah Clendinning, Oskar Zetterstrom, Francisco Mesa, Oscar Quevedo-Teruel,

Numerical methods for topological polaritonics (pp. 1052)
Ismael Septembre, Charly Leblanc, Dmitry Solnyshkov, Guillaume Malpuech,

Analyzing Invisibility using a Nonlinear Eigenvalue Formulation (pp. 1054)
Zitao Mai, Ya Yan Lu,

Local-rational models for the adaptive frequency sampling of nanophotonic simulations (pp. 1056)
Francesco Ferranti, Dries Peumans,

Enhanced photoluminescence of ZnO nanowire coatings and gratings (pp. 1057)
Emmanuel Centeno, Aubry Martin, Michel Langlet, Audrey Potdevin, Francois Reveret, Rafik Smaali, Elena Kachan, Yves Jourlin, Genevieve Chadeyron,

Time-Varying Photonics (pp. 1058)
Matias Koivurova, Charles Robson, Marco Ornigotti,

Deep Learning and Optimization for Efficient and Robust Nanophotonic Design (pp. 1059)
Sawyer Campbell, Ronald Jenkins, Pingjuan Werner, Douglas Werner,

Chiral nanophotonic waveguides for spin-based quantum optical devices (pp. 1061)
Hamidreza Siampour, Christopher O'Rourke, Alistair J. Brash, Maxim N. Makhonin, Rene Dost, Dominic J. Hallett, Edmund Clarke, Pallavi K. Patil, Maurice S. Skolnick, A. Mark Fox,

Multifunctional metasurface optics for imaging and sensing (pp. 1063)
Fan Yang, Hung-I Lin, Juejun Hu, Tian Gu,

Towards cm-scale full-wave metasurface simulation and design (pp. 1064)
Owen Miller,

Fabrication-Conscious Inverse Design of Single-Material Variable-Index Multilayer Films (Invited) (pp. 1065)
Omer Yesilyurt, Samuel Peana, Vahagn Mkhitaryan, Karthik Pagadala, Vladimir Shalaev, Alexandra Boltasseva, Alexander Kildishev,

Efficient Design of 2D Slanted Gratings using Polynomial Modal Method (pp. 1067)
Kofi Edee, Gerard Granet, Pierre Bonnet,

Photonic crystal design targeting room temperature operation of GaN-based ridge polariton laser (pp. 1069)
Valentin Develay, Laetitia Doyenette, Christelle Brimont, Guillaume Malpuech, Jesus Zuniga-Perez, Sophie Bouchoule, Thierry Guillet,

Quantum Hydrodynamic Theory for Plasmonics: a Computational Perspective (pp. 1071)
Cristian Ciraci, Michele Castriotta, Henrikh Baghramyan, Muhammad Khalid, Fabio Della Sala,

Radiative heat exchange driven by acoustic modes between two solids at the atomic scale (pp. 1073)
Mauricio Gomez Viloria, Riccardo Messina, Philippe Ben-Abdallah,

Nonlinear generation of vortex beams on optical metasurfaces (pp. 1074)
Laure Coudrat, Kimon Moratis, Pascal Filloux, Rana Tanos, Julien Claudon, Jean-Michel Gerard, Aloyse Degiron, Giuseppe Leo,

DNA nanotechnologies for photonics and sensing

Interfacing quantum emitters and plasmonic resonators with DNA (pp. 1076)
Jeanne Heintz, Claudia Corti, Sylvie Marguet, Gaetan Bellot, Sebastien Bidault,

DNA origami assembled nanoantennas for manipulating single-molecule spectral emission (pp. 1078)
Maria Sanz-Paz, Fangjia Zhu, Nicolas Bruder, Karol Kolataj, Mauricio Pilo-Pais, Antonio Fernandez-Dominguez, Guillermo Acuna,

DNA Precision Placement Allows for Studying and Exploiting Energy Transfer beyond the Classical FRET Limit (pp. 1080)
Matthew Chiriboga, Christopher Green, Divita Mathur, Youngchan Kim, Joseph Melinger, Igor Medintz, Sebastian Diaz,

DNA-origami-based plasmonic assemblies with tailored stimuli and optical responses (pp. 1082)
Anton Kuzyk, M-K. Nguyen, J. Ryssy, J. Loo, R. Klajn, P. Albella, Y. Huang,

Colloidal Silicon Nanospheres as Building Blocks for Photonic Applications (pp. 1083)
Hiroshi Sugimoto,

Neurotransmitter Sensing via Ionic Flux Modulation Through Aptamer Conformational Rearrangement (pp. 1085)
Annina Stuber, Ali Douaki, Julian Hengsteler, Denis Buckingham, Dmitry Momotenko, Denis Garoli, Nako Nakatsuka,

Probing fast dynamics of single DNA molecules in real-time using plasmon-enhanced fluorescence (pp. 1087)
S. Nooteboom, K. Okholm, V. Lamberti, B. Oomen, S. Dey, D. Sutherland, Peter Zijlstra,

Colorimetric sensing with hybrid gold-DNA origami nanostructure (pp. 1088)
Claudia Corti, Elise Gayet, Nesrine Aissaoui, Sylvie Marguet, Gaetan Bellot, Sebastien Bidault,

Superconducting Josephson classical and quantum metamaterials

Slowing down microwave photons in a superconducting quantum metamaterial (pp. 1091)
Alexey Ustinov,

Quantum Analogues of Dissipative Circuit Elements (pp. 1092)
Alexandre Zagoskin,

Improved Method for Characterizing Resonance Quality Factor in Superconducting Resonators (pp. 1094)
Martin Weides,

Development of high temperature superconducting terahertz emitters (pp. 1095)
Takanari Kashiwagi,

Ultrastrongly coupled THz metasurfaces: from large arrays to single meta-atom spectroscopy (pp. 1097)
Giacomo Giacomo Scalari, Elsa Jochl, Shima Rajabali, Sergey Markmann, Erika Cortese, Simone DeLiberato, Mattias Beck, Jerome Faist,

Josephson terahertz plasmonics with layered superconductor microcavity arrays (pp. 1099)
Samane Kalhor, Sergey Savel'ev, Kaveh Delfanazari,

Creation and annihilation of Josephson vortex loops in a Junction with nanopillar (pp. 1101)
G. R. Berdiyorov, M. V. Milosevic, F. Kusmartsev, F. M. Peeters, Sergey Savel'ev,

Quantum electrodynamics of non-demolition detection of single microwave photon by superconducting qubit array (pp. 1103)
Patrick Navez,

Metamaterials Meeting Industry

Modelling hot carrier generation in large metallic nanoparticles (pp. 1106)
Johannes Lischner,

Dynamic plasmonics and optics with organic conducting polymers (pp. 1107)
Magnus Jonsson,

Surface Susceptibility Synthesis of Spatially Dispersive Metasurfaces (pp. 1108)
Jordan Dugan, Tom Smy, Francesco Monticone, Suhlabh Gupta,

Time-resolved NIR to Visible Upconversion Luminescence from Single NaYF4:Yb3+,Tm3+ Nanoparticles on Plasmonic Nanowire Composites (pp. 1110)
K. Y. Chiok, A. Haghizadeh, A. Ahmed, A. Baride, R. B. Anderson, S. May, Steve Smith,

Topological Trapped-Rainbow and Nonreciprocal Guides Beyond the Time-Bandwidth Limit (pp. 1111)
Konstantinos Baskourelos, Kosmas Tsakmakidis,

From synthesis to assembly: a Silicon based metasurface fabrication (pp. 1113)
Juan Xin, Wajdi Chaabani, Julien Proust, Jerome Plain,

The effect of periodically corrugated substrate on SERS anisotropy of organic molecules (pp. 1115)
Ephraim Thomas Mathew, Jacek Jenczyk, Zygmunt Milosz, Weronika Andrzejewska, Mikolaj Lewandowski, Maciej Wiesner,

Bio-Inspired Nanophotonics

Bioinspired coating for bird-safe glazing optimised for avian and human vision (pp. 1118)
Sebastien Mouchet, Remy Wauters, Emile Haye, Stephane Lucas, Olivier Deparis,

Cross-reactive plasmonic arrays as optical tastebuds (pp. 1119)
Justin R. Sperling, William J. Peveler, Alasdair Clark,

Effective refractive index determination and light propagation mechanisms in natural scattering media (pp. 1120)
Dominic T. Meiers, Georg von Freymann,

Transparent and Durable Dust-Repellent Coatings for Photonics Application (pp. 1122)
Pritha Sarkar, Kausik Mukhopadhyay,

Bio-inspired surface nanopatterning using Femtosecond Lasers and its Applications (pp. 1123)
Chunlei Guo,

Cuttlefish-eye inspired vision systems with high-quality imaging capabilities (pp. 1124)
Young Min Song,

Quasi-ordered photonic structures colour the bluespotted ribbontail ray (pp. 1126)
Julien Bouchat, Fabio Cortesi, Karen Cheney, Pete Vukusic, N. Justin Marshall, Olivier Deparis, Sebastien Mouchet,

SERS Detection of Neurotransmitters through Gold Nanoislands-Decorated Tapered Optical Fibers (pp. 1128)
Di Zheng, Filippo Pisano, Liam Collard, Antonio Balena, Marco Pisanello, Barbara Spagnolo, Linda Piscopo, Cristian Ciraci, Massimo De Vittorio, Ferruccio Pisanello,

Ultralight, Energy Saving Plasmonic Structural Color Paint (pp. 1130)
Pablo Cencillo, Debashis Chanda,

Plasmonic Colors - Valuable Members of the Structured Colors Family (pp. 1132)
Samuel Peana, Sarah Chowdhury, Ludmila Prokopeva, Alexander Kildishev,

Parity-Time and quasi-normal modes in Photonics, Plasmonics, Acoustics

Acoustic nonreciprocity in a linear viscous medium with broken P symmetry (pp. 1135)
Arkadii Krokhin, Hyeonu Heo, Arup Neogi, Yuri Zubov, Ezekiel Walker,

Spectral response at hierarchically-constructed exceptional points (pp. 1137)
Jan Wiersig,

Efficient analysis and design of edge states (pp. 1139)
Henning Schomerus,

Shaping the Topological States (pp. 1141)
Hamidreza Ramezani, Elnaz Hamdarsi, Cem Yuce, Prineha Narang,

Parity-time symmetric waveguides with tailored dipoles and chiral features (pp. 1143)
Alice De Corte, Mondher Besbes, Henri Benisty, Bjorn Maes,

Stabilizing topological transport in a non-Hermitian optomechanical system (pp. 1145)
Justin Lane, Chitres Guria, Vishnuteja Chavva, Toni Montalvo, Hugo Ribeiro, Jack Harris,

Maximally transmitted states in non-Hermitian photonics (pp. 1146)
Konstantinos Makris,

Switching between topological edge states in nanophotonic structures using phase-change materials (pp. 1148)
Georgios Veronis, Yin Huang, Yuecheng Shen,

Exceptional-point sensing with a quantum interferometer (pp. 1149)
Wai Chun Wong, Jensen Li,

Landau-Zener transitions through a pair of higher order exceptional points (pp. 1151)
Eva-Maria Graefe, S. Malzard, R. Melanathuru,

Dispersion curves of guided modes in a PT symmetric waveguide (pp. 1152)
Nan Zhang, Y. Y. Lu,

Scanning Quantum Interference across PT-symmetry Breaking (pp. 1154)
Friederike Klauck, Tom A.W. Wolterink, Matthias Heinrich, Alexander Szameit,

Symmetry-protected topological exceptional chain (pp. 1156)
Xiaohan Cui, Ruoyang Zhang, Guancong Ma, C. T. Chan,

Quantum exceptional points of metasurfaces (pp. 1157)
Wai Chun Wong, Hong Liang, Kai Ming Lau, Tsz Kit Yung, Bei Zeng, Jensen Li,

A Coherent Perfect Absorber for Arbitrary Wavefronts (pp. 1159)
Yevgeny Slobodkin, Gil Weinberg, Helmut Hoerner, Kevin Pichler, Stefan Rotter, Ori Katz,

Photon production in cavity: Quasinormal modes as a tool for quantum dynamics (pp. 1161)
Maxime Federico, Hans-Rudolf Jauslin,

Machine learning for metamaterials and metasurfaces

Deep learning based inverse design: Neural adjoint for free-form geometries (pp. 1164)
Peter Wiecha, Abdourahman Khaireh-Walieh, Tom Radford, Alberto Politi, Otto Muskens,

Digital Twins for Generic Radio Environments Parametrized by Reconfigurable Intelligent Surfaces: Physics-Based vs. Physics-Agnostic Surrogate Models (pp. 1166)
Hugo Prodhomme, Philipp del Hougne,

Exploring Multiple Network Architectures to Solve Selected Challenges in Computational Nanophotonics (pp. 1167)
Yannick Augenstein, Lina Kuhn, Taavi Repan, Carsten Rockstuhl,

Deep-Neural-Network for Meta-Lens Image Reconstruction (pp. 1168)
Yunxi Dong, Bowen Zheng, Sensong An, Hang Li, Hong Tang, Yi Huang, Mohammad Haerinia, Hualiang Zhang,

Normalization flows for designing metasurfaces (pp. 1170)
Kebin Fan, Jia-Qi Yang, Yu-Cheng Xu, Jingbo Wu, Caihong Zhang, De-Chuan Zhan, Biaobing Jin, Willie J. Padilla,

Adaptive physics-driven neural networks for electromagnetic inverse problems and design of ultracompact diffractive devices (pp. 1172)
Luca Dal Negro, Y. Zhu, R. Riganti,

Importance of Metric Learning and Manifold Learning in Knowledge Discovery and Inverse Design of Nanophotonic Structures (pp. 1174)
Mohammadreza Zandehshahvar, Muliang Zhu, Mohammad Hadighehjavani, Ali Adibi,

Multipolar Resonance Engineering Using Machine Learning (pp. 1175)
Wenhao Li, Hooman Barati Sedeh, Willie J. Padilla, Jordan Malof, Natalia Litchinitser,

Meta-Atom Design for a Highly-Sensitive Liquid Sensor (pp. 1176)
Kazunori Serita, Luwei Zheng, Kazuki Hara, Masayoshi Tonouchi,

Broadband invisibility cloaking design of concentric multilayered cylindrical metamaterials based on genetic algorithm (pp. 1177)
Tomoya Momose, Mana Toma, Kotaro Kajikawa,

Enabling the inverse design of metasurfaces at the unit cell and the supercell level using neural network approaches for industrial applications (pp. 1179)
Konstantinos Dovelos, Evangelos Galaris, Vasiliki Vardakastani, Panagiotis Kosmas, Dimitrios Tzarouchis,

Metasurfaces for light control emission

Universal light encoders: artificial intelligent hardware for nanoscale light control (pp. 1182)
Andrea Fratalocchi,

All-dielectric metasurfaces for enhancing and tuning the emission of quantum emitters (pp. 1183)
Angela Barreda, Chengjun Zou, Artem Sinelnik, Evgenii Menshikov, Ivan Sinev, Thomas Pertsch, Isabelle Staude,

Electroluminescent Metasurface Light Emitting Diodes (pp. 1185)
Jon Schuller,

Amplifying nanophotonics lattices (pp. 1186)
Femius Koenderink,

Topological exciton-polaritons in metasurfaces integrated with transition metal dichalcogenides (pp. 1187)
Ivan Sinev, Mengyao Li, Fedor Benimetskiy, Tatiana Ivanova, Svetlana Kiriushechkina, Anton Vakulenko, Sriram Guddala, Dmitry Krizhanovskii, A. Alu, Anton Samusev, Alexander Khanikaev,

Nonlinear generation and detection of valleys in atomically thin semiconductors (pp. 1189)
Paul Herrmann, Sebastian Klimmer, Thomas Lettau, Mohammad Monfared, Isabelle Staude, Ioannis Paradisanos, Ulf Peschel, Giancarlo Soavi,

Approaching the thin-film absorption limit with monolayer semiconductor superlattices (pp. 1190)
Sara Elrafey, Lennart M. Heijnen, Rasmus H. Godiksen, Alberto Curto,

Capturing near-field circular dichroism enhancements from far-field measurements (pp. 1192)
Jorge Olmos-Trigo, Jon Lasa-Alonso, Iker Viloria-Gcomez, Gabriel Molina-Terriza, Aitzol Garcia-Etxarri,

Optical nanostructures for boosting fluorescence from magnetic dipolar transitions (pp. 1194)
Ayesheh Bashiri, Marijn Rikers, Aleksandr Vaskin, Katsuya Tanaka, Angela Barreda, Michael Steinert, Duk-Yong Choi, Thomas Pertsch, Isabelle Staude,

Engineering spatial dispersion in metasurfaces through materials dispersion (pp. 1196)
Sergejs Boroviks, Adrei Kiselev, Christian Santschi, Karim Achouri, Olivier Martin,

Exploiting light-matter interactions to realize selective artificial photosynthesis (pp. 1198)
Zelio Fusco, Christin David, Fiona Beck,

Multifunctional Optical Surfaces with Ultrathin Materials and Nano-structuring (pp. 1200)
Javier Arres Chillon, D. Martinez-Cercos, C. Graham, A. Mezzadrelli, I. Karadzhov, W. Senaratne, R. Bellman, D. Thelen, P. Mazumder, Valerio Pruneri,

Enhanced light-matter interaction in a hollow nanocuboid metasurface supporting delocalised quasi-BIC modes (pp. 1201)
Jose Francisco Algorri, Pablo Roldan-Varona, Luis Rodriguez-Cobo, Jose Miguel Lopez-Higuera, Dimitris Zografopoulos,

Structure dependent photoluminescence of colloidal PbS quantum dots in low refractive index dielectric 3D infrared metamaterials (pp. 1203)
Angelos Xomalis, Lorenzo J. A. Ferraresi, Oriol P. de G. Busquests, Krzysztof Mackosz, Dmitry N. Dirin, Ivo Utke, Johann Michler, Maksym V. Kovalenko, Jakob Schwiedrzik, Ivan Shorubalko,

Nonlinear dielectric metasurfaces for infrared imaging and light sources (pp. 1206)
Dragomir Neshev,

Light source engineering of directive photoluminescent metasurfaces with the local Kirchhoff's law (pp. 1207)
Elise Bailly, J.-P. Hugonin, B. Vest, J.-J. Greffet,

Stick-and-play nanoantenna stickers to control photoluminescence (pp. 1209)
Shunsuke Murai, TienYang Lo, Katsuhisa Tanaka,

Reciprocity Violation in Time-Modulated Structures for Enhanced Optical Heating (pp. 1210)
Valeriya Levkovskaya, A. V. Kharitonov, S. S. Kharintsev,

Quantum Light Emitters and Photonic Heterogeneous Integration

Heterogeneous III-V on Diamond Nanophotonics for Quantum Nodes based on Defects in Diamond (pp. 1213)
Alexander Abulnaga, S. Karg, D. Huang, A. Pakpour-Tabrizi, Z. Zhang, N. P. de Leon,

Plug & play quantum light sources with fiber-integrated quantum emitters (pp. 1215)
W. B. Jeon, Jehyung Kim,

Spin and level structure of positioned sulfur vacancies in MoS2 acting as quantum emitters (pp. 1217)
Alex Holleitner,

Modeling exciton dynamics behind single-phonon emission by interacting solid-state defects (pp. 1218)
Andrei Piryatinski,

Efficient outcoupling of light from single-photon emitters in 2D materials (pp. 1220)
Rudolf Bratschitsch,

Nanometric axial localization of color centers in hexagonal boron nitride flakes (pp. 1222)
Pankaj Jha,

Carbon nanotubes and atomically thin materials integrated with silicon photonic crystal nanocavities (pp. 1223)
Yuichiro K. Kato,

Stimulated Emission from a Three-Level Quantum Ladder System (pp. 1225)
Eva Scholl, Bjorm Jonas, Friedrich Sbresny, Lukas Hanschke, Dirk Heinze, Patricia Kallert, Timo Langer, William Rauhaus, Bianca Scaparra, Katarina Boos, Eduardo Zubizarreta Casalengua, Hubert Riedl, Elena del Valle, Dirk Reuter, Stefan Schumacher, Jonathan J. Finley, Artur Zrenner, Kai Muller, Klaus D. Jons,

Room-temperature ultrabright single photon sources based on colloidal quantum dots on directional resonator-antennas: towards high dimensional encoding of photonic qudits (pp. 1226)
Ronen Rapaport,

Generating Quantum Emitters in 2D Semiconductors Using UV Light (pp. 1228)
Xuedan Ma,

Low Energy Focused Ion Beam Implantation (pp. 1229)
Michael Titze, Jonathan Poplawsky, Barney Doyle, Edward Bielejec, Alex Belianinov,

Integrated Quantum Dot Optomechanics (pp. 1231)
M. Weiss, D. Wigger, D. D. Buhler, E. D. S. Nysten, M. Choquer, M. Lienhart, B. Mayer, A. Vogele, A. Crespo-Povedo, K. Muller, J. J. Finley, A. Rastelli, T. Kuhn, P. Machnikowski, M. M. de Lima Jr., P. V. Santos, G. Moody, Hubert Krenner,

Indistinguishable telecom-band single photons from a coupled cavity-nanotube system at room temperature (pp. 1233)
L. Husel, J. Trapp, M. Nutz, M. Forg, J. Noe, T. Hummer, P. Wang, J. Wu, Y.-H. Wang, Alexander D. Hunger, Alexander Hogele,

Hybrid high-Q nanocavities for 2D materials and their heterostructures (pp. 1234)
C. Qian, V. VillafaÃ±e, P. Soubelet, A. Hotger, T. Taniguchi, K. Watanabe, N. P. Wilson, A. V. Stier, A. W. Holleitner, Jonathan Finley,

Exciton photophysics in MoSe2-WSe2 Moire hetero-bilayers (pp. 1235)
Arnab Barman Ray, Arunabh Mukherjee, Liangyu Qiu, Sefaattin Tongay, Nick Vamivakas,

From flask to devices: Exceptionally functional colloidal quantum emitters and deterministic integration (pp. 1237)
E. Dolgopolova, E. G. Bowes, R. Rapaport, A. Piryatinski, H. Htoon, Jennifer Hollingsworth,

Localized Dipolar Excitons in 2D Semiconductors for Quantum Sensing of Correlated Electrons (pp. 1239)
Ajit Srivastava,

Site Controlled Integration of SiN/SiO2 Single Photon Emitters with a Topologically-Optimized Coupler (pp. 1240)
Samuel Peana, Omer Yesilyurt, Zachariah Martin, Alexander Senichev, Vahagn Mkhitaryan, Alexei Lagutchev, Alexandra Boltasseva, Alexander Kildishev, Vladimir Shalaev,

Two-photon interference from a position-controlled quantum emitter in hexagonal boron nitride (pp. 1242)
Clarisse Fournier, Sebastien Roux Roux, Aurelie Pierret, Michael Rosticher, Stephanie Buil, Julien Barjon, Jean-Pierre Hermier, Aymeric Delteil,

Activation of a quantum emitter in a hBN waveguide for integrated quantum photonics (pp. 1244)
Domitille Gerard, Michael Rosticher, Stephanie Buil, Jean-Pierre Hermier, Julien Barjon, Aymeric Delteil,

Dynamic control of emission from quantum emitters embedded in ultra thin ENZ media (pp. 1246)
Arun Mambra, Joy Mitra,

Exotic Meta-media â€“ Time-dependent, Nonlocal and Other Novel Responses

Manifestations of thermal hysteresis in theoretical studies of scattering, columnar thin films, and surface-plasmon-polariton wave propagation (pp. 1249)
Tom Mackay, Tran Son, Alain Hache, Waleed Waseer, Akhlesh Lakhtakia,

Temporal boundaries in electromagnetic materials (pp. 1251)
Jonathan Gratus, Rebecca Seviour, Paul Kinsler, Dino Jaroszynski, Shankaranandh Balakrishnan,

Solution generation in electrodynamics (pp. 1253)
Robert Thompson, Martin McCall,

Spatial dispersion with Mathieu's equation for EM generation and particle acceleration (pp. 1255)
Jonathan Gratus, Taylor Boyd, Sergey Siaber, Steven Jamison, Rebecca Seviour,

Twisting an optomechanical cavity (pp. 1257)
Daigo Oue, Mamoru Matsuo,

Time-varying fundamental acoustic equations (pp. 1259)
Ruben PicÃ³, Javier Redondo, Victor Jose SÃ¡nchez-Morcillo,

Time-varying metasurfaces for parametric amplification of electromagnetic waves (pp. 1261)
Fedor Kovalev, I. V. Shadrivov,

The operator theory of dispersive time varying media (pp. 1263)
Simon Horsley,

Surface plasmon polaritons are not polaritons, and not plasmons either (pp. 1265)
Antoine Moreau,

Metamaterials with Temporal Inhomogeneity for Analog Optical Computing (pp. 1267)
Anton Kharitonov, Aidar Minibaev, S. S. Kharintsev,

Nanophotonics in Biomedical Applications

Holographic control of plasmonic structures on the distal facet of multimode optical fibers (pp. 1270)
Liam Collard, Filippo Pisano, Di Zheng, Antonio Balena, Linda Piscopo, Muahmmad Fayyaz Kashif, Marco Pisanello, Liset M. de la Prida, Cristian Ciraci, Marco Grande, Massimo De Vittorio, Ferruccio Pisanello,

Inversely design a phase mask for an extended depth of focus through adjoint optimization (pp. 1272)
Huade Mao, Jiqiang Kang, Kenneth K. Y. Wong,

Plasmonic infrared sensor aided with artificial intelligence and immunoassay for structural protein biomarker-based neurodegenerative disease detection (pp. 1274)
Deepthy Kavungal, Pedro MagalhÃ£es, Senthil Kumar, Rajasekhar Kolla, Hilal Lashuel, Hatice Altug,

LSPR sensors with antiadhesive layer made of DNA: nanostructure pitch study (pp. 1276)
Remigiusz Trojanowicz, A. Vestri, M. Rippa, J. Zyss, K. Matczyszyn, Lucia Petti,

New materials for photonics (Graphene, MoS2, WS2, etc)

Chirality nonlinear optics enabled modulator and logic gates (pp. 1279)
Yi Zhang, Juan Arias Munoz, Zhipei Sun,

Layer-Dependent Optical Properties of 2D CrI3 from Monolayer to Mesoscale Mapped by Hyperspectral Imaging (pp. 1281)
Fernando Ramiro-Manzano, Marta Galbiati, Jose Joaquin Perez Grau, Fernando Cantos-Prieto, Jaume Meseguer-Sanchez, Ivona Kosic, Filippo Mione, Andres Cantarero, David Soriano, Efren Navarro-Moratalla,

Radiative suppression of exciton-exciton annihilation in a two-dimensional semiconductor (pp. 1283)
Luca Sortino, Merve Gulmus, Benjamin Tilmann, Leonardo de S. Menezes, Stefan A. Maier,

Atomically thin waveguides for photonics with 2D light waves (pp. 1284)
Myungjae Lee, Hanyu Hong, Jaehyung Yu, Fauzia Mujid, Andrew Ye, Ce Liang, Jiwoong Park,

S Vacancies-Triggered High SERS Activity of MoS2 for Ultrasensitive Detection of Trace Diclofenac (pp. 1285)
Yingnan Quan, X. J. Huang, W. Q. Liu,

Mesoporous g-C3N4/TiO2 photonic film with a chiral nematic structure: slow photonic effect inducing improved H2 generation (pp. 1287)
Masa Johar, C. Wang, M. N. Ghazzal,

Non-Unity Magnetic Permeability in 2D Hybrid Organic/Inorganic Perovskites (pp. 1289)
Jon Schuller, Ryan DeCrescent, Rhiannon Kennard, Michael Chabinyc,

Flexible Interdigitated Pd/ZnO-SWCNT/Pd Ultraviolet Photodetectors (pp. 1291)
M. R. Sabity, Ghusoon M. Ali,

Metal-insulator transition in vanadium dioxide studied by analytical transmission electron microscopy (pp. 1293)
Michal Horak, Jan Krpensky, Jakub Planer, Peter Kepic, Jiri Kabat, Tomas Sikola, Andrea Konecna, Vlastimil Krapek,

Fabrication of Mie-resonant nanostructures using laser annealing for highly sensitive fluorescence spectroscopy (pp. 1295)
Tatsuya Fukuta, Ryo Kato, Takuo Tanaka, Taka-Aki Yano,

Graphene-based plasmonic nanostructures for efficient SERS detection of odor molecules (pp. 1296)
Shinnosuke Ozeki, Ryo Kato, Takuo Tanaka, Taka-Aki Yano,

Twist-tunable polaritonic nanoresonators in a van der Waals crystal (pp. 1297)
Olga Matveeva, A. I. F. Tresguerres-Mata, R. V. Kirtaev, K. V. Voronin, J. Taboada-Gutierrez, C. Lanza-Garcia, J. Duan, J. Martin-Sanchez, V. S. Volkov, Pablo Alonso-Gonzalez, A. Y. Nikitin,

Fluctuation imaging of nanoscale disorder in monolayer semiconductors (pp. 1299)

Tom Sistermans, Rasmus Godiksen, Alberto Curto,

Towards Graphene-comprising Waveguide Resonators for Kerr Comb Generation in the Non-Perturbative Electrodynamic Nonlinearity Regime (pp. 1301)
Alexandros Pitilakis, Emmanouil Kriezis,

Non-linear Optical Properties Investigation on the Colloidal WS2 nanosheets (pp. 1303)
Yang Zhao, Marcus Frohlich, Onno Strolka, Tim Parker, Jannika Lauth, Alfred Meixner, Dai Zhang,

Enhanced As(III) detection under near-neutral conditions: Synergistic effect of boosted adsorption by oxygen vacancies and valence cycle over activated Au NPs loaded on FeCoOx nanosheets (pp. 1305)
Cong-Cong Huang, Xing-Jiu Huang, Meng Yang,

Optical antennas and plasmonics-based devices

Improved Control over Multipole Excitations in Multi-Shelled Particles Leads to Higher Directivity Scattering (pp. 1308)
Seokhwan Min, Jonghwa Shin,

Plasmonic addressing structure (pp. 1310)
Marius Crouzier, Vy Yam, Giovanni Magno, Thomas Lopez, Beatrice Dagens,

Room-temperature waveguide-coupled plasmonic crystal lasers on GaAs substrate (pp. 1312)
Yue-Ting Tsai, Yu-Hsun Wu, Chu-Chun Wu, Sheng-Di Lin,

Electrical excitation of surface plasmon polaritons with a nanoantenna tunneling junction (pp. 1314)
Delphine Pommier, Cheng Zhang, Yunhe Lai, Eric Le Moal, Christophe Sauvan, Jean-Jacques Greffet, Jianfang Wang, Elizabeth Boer-Duchemin,

Visible range active metasurface device fabrication and characterization (pp. 1316)
Yong-Hae Kim, Kyunghee Choi, Chi-Sun Hwang, Jong-Heon Yang, Jooyeon Kim, Jaehyun Moon, Ji-Hoon Choi,

Plasmonically-enhanced phase-change integrated photonic memory device (pp. 1318)
Junchao Song, I. Bente, W. H. P. Pernice, H. Bhaskaran, C. D. Wright,

Plasmon-mediated wavelength-selective photoactuation for multi-directional soft robots (pp. 1320)
Dong-Jin Lee, Dae Yu Kim,

Controlling Forster Resonance Energy Transfer in Plasmonic Nanopatch Antennas (pp. 1322)
Abdullah O. Hamza, Francesco N. Viscomi, Jean-Sebastien G. Bouillard, Ali Adawi,

Hybrid Dielectric-Plasmonic Nanoantenna with Multiresonances for Subwavelength Photon Sources (pp. 1323)
Emmanuel Lassalle, Pavel A. Dmitriev, Lu Ding, Darren C. J. Neo, Vytautas Valuckas, Ramon Paniagua-Dominguez, Joel K. W. Yang, Hilmi V. Demir, Arseniy I. Kuznetsov,

Tailoring Nanowire Lasing Modes via Coupling to Metal Gratings (pp. 1325)
Francesco Vitale, Daniel Repp, Thomas Siefke, Uwe Zeitner, Ulf Peschel, Thomas Pertsch, Carsten Ronning,

Near unity Raman beta-factor of surface enhanced Raman scattering in a waveguide (pp. 1327)
Ming Fu, Monica Mota, Xiaofei Xiao, Andrea Jacassi, Nicholas Gusken, Huaifeng Xiao, Yi Li, Ahad Riaz, Stefan Maier, Rupert Oulton,

A Terahertz Lens Antenna Array Design for Beam Steering in Time-Domain (pp. 1329)
Ahmet Canberk Songur, Ahmet Oguz Sakin, Hasan Alper Gunes, Beyza Akcay, Mehmet Unlu,

A Terahertz Time-Domain Antenna Array based on a Parametric Study (pp. 1331)
Ahmet Canberk Songur, Ahmet Oguz Sakin, Beyza Akcay, Hasan Alper Gunes, Mehmet Unlu,

Realization of electromagnetically-induced transparency in the mid-infrared with symmetry-broken metamaterials (pp. 1333)
The Linh Pham, Fei Han, Kacper Pilarczyk, Joris Van de Vondel, Niels Verellen, Thanh Tung Nguyen, Ewald Janssens,

Actively Real-time Controllable Metal-Graphene Hybrid Metasurfaces (pp. 1335)
Fei Han, Bart Raes, The Linh Pham, Nguyen Thanh Tung, Xuezhi Zheng, Guy A. E. Vandenbosch, Joris van de Vondel, Niels Verellen, Ewald Janssens,

Optical characterization of polymer-based Fresnel zone plate probe structures combined with hyperbolic metamaterial by means of SNOM (pp. 1337)
Patrik Micek, Alexandr Belosludtsev, Dusan Pudis, Dorota Pawlak, P. Gaso, M. Goraus,

Enhancement of a single molecule triplet depopulation rate by a dielectric nanoantenna (pp. 1339)
Remigiusz Trojanowicz, Simon Vassant, F. Charra,

Multiresonant nano-optical trap of Rayleigh particles with coaxial plasmonic apertures (pp. 1341)
HipÃ³lito Alan Arredondo Champi, Rina Huamanrayme Bustamante, Daniel Reinaldo Cornejo, Walter Jaimes Salcedo, Jose Roberto Castilho Piqueira,

Photothermal and photoelectric nanophotonics

Overcoming color limitation of sub-ambient radiative cooler for full color expression (pp. 1344)
Suwan Jeon, Soomin Son, Seokhwan Min, Hyeonjin Park, Heon Lee, Jonghwa Shin,

Surface absorbers for thermomechanical bolometers (pp. 1346)
Benedetta Bertoni, Leonardo Vicarelli, Simone Zanotto, Stefano Roddaro, Alessandro Tredicucci, Alessandro Pitanti,

Designing tunable, broadband absorber/emitter using epsilon near zero media (pp. 1348)
Sraboni Dey, Joy Mitra,

Plasmon-enhanced photovoltaics, photocatalysis, and solar fuels

Pd nanoparticles as Visible and near-IR plasmonic catalysts (pp. 1351)
Yukie Yokota, A. Fujita, M. Abe,

Cathodoluminescence spectroscopy of Au dendritic structures for photocatalysis applications (pp. 1353)
Zelio Fusco, Asim Riaz, Christin David, Fiona Beck,

Synergistic Photonic and Morphology Design of Solar Powered Redox Cells (pp. 1355)
Jiaming Ma, Kiseok Oh, Giulia Tagliabue,

Layer transfer of multispectral plasmonic absorbers onto graphene for enhanced selective photo-absorption (pp. 1357)
Hyo-Seung Park, Gyu Won Hwang, Jongkil Park, Joon Young Kwak, Doo-Seok Jeong, Kyeong Seok Lee,

Plasmonics and nano-optics

Artificial intelligence-based refractive index sensing achieving atto-mol detection limit (pp. 1360)
Ning Li, Qizhou Wang, Zhao He, Arturo Burguete-Lopez, Fei Xiang, Andrea Fratalocchi,

Effect of Mirror Quality on the Optical Properties of Nanoparticle-on-Mirror Plasmonic Nanocavities (pp. 1362)

Zhenxin Wang, Alexey V. Krasavin, Pan Wang,

Stark Effect Control of the Scattering Properties of Plasmonic Nanogaps (pp. 1364)
Donatello Pagnotto, Alina Muravitskaya, David M. Benoit, Jean-Sebastien G. Bouillard, Ali Adawi,

Microscopic Theory of Tip-Enhanced Nonlinear Raman Scattering with Self-Consistent Nonlocal Response (pp. 1365)
Hiroyuki Ikagawa, Mamoru Tamura, Tomohiro Yokoyama, Hajime Ishihara,

CdZnO nanoparticles for SEIRA sensing in the mid-infrared (pp. 1367)
Pablo Ibanez Romero, Eduardo Martinez Castellano, Javier Yeste, Vicente Munoz Sanjose, Miguel Montes Bajo, Adrian Hierro Cano,

Synergetic hot carrier generation due to coherent couplings of plasmon-carrier excitations and plasmon hybridization in a metallic nano-chain array (pp. 1369)
Soshun Inoue, Tomohiro Yokoyama, Hajime Ishihara,

Hybrid gold-(CdSe/CdS/CdZnS) nanocrystal supraparticles emission: from FRET inhibition to collective emission of a mesoscopic ensemble of NCs (pp. 1371)
V. Blondot, Domitille Gerard, Guillaume Quibeuf, Christophe Arnold, Aymeric Delteil, Alexandra Bogicevic, Thomas Pons, Nicolas Lequeux, Jean-Paul Hugonin, Jean-Jacques Greffet, Stephanie Buil, Jean-Pierre Hermier,

Investigation of Terahertz SSPP Waveguides Using TRL Calibration (pp. 1373)
Yusuf Colak, Mesut Demircioglu, Mehmet Unlu,

Design of Subwavelength Confinement Waveguides at 1 THz Band (pp. 1375)
Mesut Demircioglu, Muhammed Abdullah Unutmaz, Mehmet Unlu,

Metasurface-driven surface-enhanced infrared absorption spectroscopy for superior characterization of electrocatalytic reactions (pp. 1377)
Luca Maria Berger, Malo Duportal, Leonardo de Souza Menezes, Emiliano Cortes, Stefan Maier, Andreas Tittl, Katharina Krischer,

A TD-DFT Approach for Polariton Chemistry: Polaritonic and Charge Transfer Excitations in Azobenzene Photoisomerization (pp. 1379)
Lucia Cascino, Stefano Corni, Stefano Corni, Stefania D'Agostino,

Coherent coupling between the individual and collective excitations by radiative fields in nanoscale materials (pp. 1381)
Tomohiro Yokoyama, Masayuki Iio, Takeshi Inaoka, Hajime Ishihara,

Reconfigurable Non-Volatile Silicon Photonics Using Ultralow-Loss Phase-Change Chalcogenide Sb2Se3 (pp. 1383)
Sophie Blundell, Daniel Lawson, David Thomson, Ioannis Zeimpekis, Otto Muskens,

High resolution plasmonic-based impedance microspectroscopy (pp. 1385)
Sidahmed Abayzeed,

Enhancing Optical Chirality Detection through Collective CD Resonance (pp. 1386)
Ji-Hyeok Huh, Ryeong Myeong Kim, SeokJae Yoo, Tae Gyun Kim, Changwon Kim, Hyeohn Kim, Jeong Hyun Han, Nam Heon Cho, Yae-Chan Lim, Sang Won Im, EunJi Im, Jae Ryeol Jeong, Min Hyung Lee, Tae-Young Yoon, Ho-Young Lee, Q-Han Park, Ki Tae Nam, Seungwoo Lee,

Experimental Realization of Quantum Walks near Synthetic Horizons on Photonic Lattices (pp. 1388)
Chong Sheng, R. Q. He, Y. L. Zhao, J. C Duan, Y. Wei, C. W. Sun, L. L. Lu, Y. X. Gong, S. N. Zhu, H. Zhu,

Ultrasmall and tunable TeraHertz surface plasmon cavities in the deep plasmonic regime (pp. 1390)
Ian Aupiais, Romain Grasset, Tingwen Guo, Dmitri Daineka, Javier Briatico, Sarah Houver, Luca Perfetti, Jean-Paul Hugonin, Jean-Jacques Greffet, Yannis Laplace,

Surface material dependance in tip enhanced Raman spectroscopy (pp. 1392)
Tim Parker, Felix Schneider, Yang Zhao, Alfred J. Meixner, Dai Zhang,

Plasmonic single-nanoantennas enabling fast and nanoscale-controllable insulator-to-metal transition of VO2 (pp. 1394)
Luca Bergamini, Bigeng Chen, Daniel Traviss, Yudong Wang, Cornelis H. de Groot, Jeffrey M. Gaskell, David W. Sheel, Nerea Zabala, Javier Aizpurua, Otto L. Muskens,

Orbit-Orbit Interaction of Light: Harnessing Vortex-Trajectory Interplay for Light Manipulation (pp. 1396)
Raghvendra P. Chaudhary, Avraham Reiner, Nir Shitrit,

Low Loss All-Oxide Plasmon-Assisted Electro-Optic Modulator (pp. 1398)
Dhruv Fomra, Mohammad Sojib, Vitaliy Avrutin, umit ozgur, Amit Agrawal, Henri J. Lezec, Nathaniel Kinsey,

Automated Inverse Design Solution for Metalenses (pp. 1400)
Chenglin Xu,

Photonic Band Structure Calculations of 3D Finite Nanostructured Supercrystals (pp. 1401)
Nicolas Large, Jose Luis Montano-Priedeâ€¬,

Directional scattering by composite SiO2/Au nanoparticles (pp. 1403)
Thomas Kotte, A. J. L. Adam, H. P. Urbach,

Displacement trajectory of nanoparticles illuminated by pulsed photonic jet and photonic hook (pp. 1405)
Maya Hen Shor Peled, Paolo Maioli, Alina Karabchevsky,

Integrated Polarization Control for Trapped-Ion Quantum Computers (pp. 1407)
Guochun Du, Carl-Frederik Grimpe, Anastasiia Sorokina, Pascal Gehrmann, Elena Jordan, Steffen Sauer, Stefanie Kroker, Tanja Mehlstaubler,

Vertical Injection and Wideband Grating Coupler Based on Asymmetric Grating Trenches for Higher Coupling Efficiency (pp. 1409)
Md Asaduzzaman,

Nonlinear optical generation of photon pairs using hybrid plasmonic nanostructures (pp. 1411)
Sandy Mathew, Guillaume Laurent, Nicolas Chauvet, Gilles Nogues, Aurelien Drezet, Guillaume Bachelier,

Strain sensors based on Fano resonance in plasmomechanical system (pp. 1413)
Najat Ahmidayi, W. d'Orsonens, Th. Maurer, G. Leveque,

Propagating surface plasmons for plasmonic nanocavities (pp. 1415)
Arsenios Gisdakis, K. Bedingfield, J. J. Baumberg, A. Demetriadou,

Manipulating the Modes of Radially Symmetric Resonators (pp. 1417)
James Capers, Dean Patient, Stephen Boyes, Alastair Hibbins, Simon Horsley,

Near-field seeing the colorful nano-world (pp. 1419)
Xuezhi Ma, Qian Wang, Ming Liu,

Supersymmetric Reshaping and Higher-Dimensional Rearrangement of Photonic Lattices (pp. 1421)

Tom Wolterink, Matthias Heinrich, Alexander Szameit,

Quasi-Dark States: A New Frontier in Light Enhancement and Control based on metasurface structures (pp. 1423)
Hicham Mangach, Abdenbi Bouzid, Younes Achaoui, Shuwen Zeng,

Imaging of Anti-ferroelectric Dark Modes in an Inverted Plasmonic Lattice (pp. 1425)
Javier Rodriguez Alvarez, Amilcar Labarta, Juan Carlos Idrobo, Rossana Dell'Anna, Alessandro Cian, Damiano Giubertoni, Xavier Borrise, Albert Guerrero, Francesc Perez-Murano, Arantxa Fraile Rodriguez, Xavier Batlle,

A Planar, NEMS-Based Terahertz Phase Shifter Using Subwavelength Confinement Waveguides (pp. 1427)
Mesut Demircioglu, Muhammed Abdullah Unutmaz, Mehmet Unlu,

Coupling of semiconductor nanowire lasers to dielectric cylinders (pp. 1429)
Daniel Repp, Francesco Vitale, Carsten Ronning, Thomas Pertsch,

Tests for large-scale fabrication of plasmonic metasurfaces with fluorescence enhancement applications (pp. 1431)
Roxana Tomescu, Veronica Anastasoaie, Catalin Parvulescu, Iuliana Mihalache, Dana Cristea,

Single-shot mapping of the second harmonic 3D radiation pattern by harmonic holography (pp. 1433)
Serena Goldmann, Samuel Gresillon, Ignacio Izeddin, Gilles Tessier, Yannick De Wilde,

Spectral Control of Plasmonic response and Spontaneous Emission Reinforcement from Quantum Dot near Nanoplasmonic Structures (pp. 1435)
Riya Choudhary, Sachin Kumar Srivastava,

Improvement of photoluminescence quality of MoS2 monolayers by an atomic hydrogen beam (pp. 1437)
Mahan Bakhshikhah, Jiri Liska, Sayed Hossein Mirdamadi Khouzani, Ondrej Cervinka, Jindrich Mach, Miroslav Kolibal, Tomas Sikola,

Spin-coating Based Nanosphere Lithography (pp. 1439)
Alejandro Descalzo Ruiz, Lu He, Teresa Isabel Picoto Pena Madeira, Dietrich R. T. Zahn,

Size-dependent Localized Surface Plasmon Resonance of Structures Prepared by Nanosphere Lithography (pp. 1441)
Milad Karami, Lu He, Teresa Isabel Picoto Pena Madeira, Dietrich R. T. Zahn,

Highly directional plasmomechanic stretchable strain sensor (pp. 1443)
Asad Nauman, Jae-Won Lee, Jun-Chan Choi, Hafiz Saad Khaliq, Junkai Wang, Hak-Rin Kim,

Development of a novel optical label-free voltage sensing technique (pp. 1445)
Oscar Barajas Gonzalez, Joseph Sollini, Michael Somekh, Sidahmed Abayzeed,

Investigation of the optical properties and the emission behavior of nanoscale Yagi-Uda antennas using nonlinear optics and back focal plane imaging (pp. 1447)
Felix Schneider, Felix Nagele, Alfred Meixner, Monika Fleischer, Dai Zhang,

High resolution impedance imaging with plasmonic nanostructures (pp. 1449)
Finlay Nelson, Rafael Fuentes-Dominguez, Fei He, Richard Smith, Matt Clark, George Gordon, Sidahmed Abayzeed,

Quasi minimum-scattering-superabsorbed nanowires (pp. 1451)
Jeng Yi Lee,

Plasmonic surface lattice resonances in 2D hexagonal arrays of Au nanoparticles (pp. 1453)
Rina Huamanrayme Bustamante, HipÃ³lito Alan Arredondo Champi, Daniel Reinaldo Cornejo, Walter Jaimes Salcedo,

Metal-insulator-metal metamaterial as optoplasmonic biosensor for refractive index sensing (pp. 1455)
Zohreh Ayareh, D. Sutherland, M. Moradi,

LSPR enhanced In-situ Ellipsometry as a Label-free Optical Sensing Platform (pp. 1461)
Natasha Mandal, Rakesh Singh Moirangthem,

Exploring Propagation Characteristics of Ga:ZnO Thin Films in the Epsilon-near-zero Region (pp. 1463)
Ranjeet Dwivedi, Dorota A. Pawlak,

Photonic nanojet enhanced Raman scattering: A new platform for Raman nanoscopy (pp. 1465)
Gour Mohan Das, Piotr Paszke, Katarzyna Sadecka, Dorota A. Pawlak,

Quantum and topological photonics

Optical control of topological and correlated electronic states (pp. 1468)
Mohammad Hafezi,

Luminescence of molecular polaritons in a microcavity: non-Markovian Fano â€Žresonances, motional narrowing, and nonlinearity associated with vibronic â€Žcoupling (pp. 1469)
Boris Fainberg, Vladimir Osipov,

Order-Invariant Quantum Correlations in non-Hermitian Interferometers (pp. 1471)
Tom Wolterink, Matthias Heinrich, Stefan Scheel, Alexander Szameit,

Space-time Quantum Metasurfaces (pp. 1473)
Wilton Kort-Kamp, Abul Azad, Diego Dalvit,

Photonic circuit simulation of topological arrays compared with experimental results in tantalum pentoxide (pp. 1475)
Bradley Thompson, Ricky Gibson, Stefan Badescu,

Fabrication of GaN Topological Photonic Crystals and Observation of Edge Modes in Visible Region (pp. 1477)
Yamato Takano, Umito Kurabe, Koji Yoneta, Taiju Kudo, Mirai Akimoto, Takuto Honda, Xiao Hu, Kikuchi Akihiko,

Polarization singularities and far-field optical properties in dielectric metasurfaces (pp. 1479)
Luca Zagaglia, Simone Zanotti, Momchil Minkov, Marco Liscidini, Dario Gerace, Lucio Andreani,

Controlling Spontaneous Emission with Nanomaterials at the Single-Emitter Level (pp. 1481)
R. Margoth Cordova-Castro, Clement Cabriel, Dirk Jonker, Mario Zapata-Herrera, Alexey Krasavin, Arturo Susarrey-Arce, Riccardo Sapienza, Yannick De Wilde, Valentina Krachmalnicoff, Anatoly Zayats, Ignacio Izeddin, Robert W. Boyd,

Quantum remote control of vortex beams using a metasurface (pp. 1483)
Hong Liang, Hammad Ahmed, Wing Yim Tam, Xianzhong Chen, Jensen Li,

Quantum dynamics and dissipation-driven formation of entangled dark states in strongly coupled many-qubit systems in solid-state nanocavities (pp. 1485)
Mikhail Tokman, Alexandra Behne, Brandon Torres, Maria Erukhimova, Yongrui Wang, Alexey Belyanin,

Prime comb lasing in a fiber ring at low temperatures (pp. 1487)
Eyal Buks,

Super-resolution imaging

Analysis of tip-enhanced photoluminescence image of single molecule based on nonlocal response theory (pp. 1490)

Yoshitsugu Tomoshige, Mamoru Tamura, Tomohiro Yokoyama, Hajime Ishihara,

Terahertz virtual superlens via evanescent amplification in the radiating near-field (pp. 1492)
Alessandro Tuniz, Boris Kuhlmey,

Acoustic and seismic metamaterials

Sound insulation performance of ventilated labyrinthine metamaterial described by enriched homogenized continuum (pp. 1495)
Renan Liupekevicius Carnielli, Hans van Dommelen, Marc Geers, Varvara Kouznetsova,

Reflection of ultrasound by underwater phase-gradient acoustic metasurfaces (pp. 1496)
Jin-Chen Hsu, H. Alwi, K.-L. Liao, J.-T. Huang,

Acoustic anechoic coatings based on flexible honeycomb corrugated composite sandwich panel (pp. 1498)
Janghao Wu, Debao Ji, Yu Xie, Junyi Wang, Jiaming Hu, Yun Chen,

Metamaterial Based Miniaturized Broad Band Acoustic Absorber (pp. 1500)
Santosh Dasila, Venkatachalam Subramanian, C. V. Krishnamurthy,

Scattering of acoustic valley Hall modes through different turns (pp. 1502)
Theo Torres, Antonin Coutant, C. Bellis, R. Cottereau,

Superradiant Scattering from Nonlinear Wave-Mode Coupling (pp. 1504)
Tiemo Pedergnana, Nicolas Noiray,

Introduction to Functionally Graded Unit Cell of Nonlinear Metamaterial that Controls Harmonic Responses of Elastic Waves (pp. 1506)
Pravinkumar Ghodake,

Fundamental Study of Elastic Wave Damping by Metamaterials with Local Resonant Structures in Electrical Systems (pp. 1508)
Kyogo Sato, Keisuke Nishida, Toshihiko Sugiura,

High-resolution medical ultrasound focusing and temperature rise with acoustic metamaterial (pp. 1510)
Jiajie He, Xue Jiang, Dean Ta,

Chiral and hyperbolic metamaterials

Spin-momentum locking breakdown on plasmonic metasurfaces (pp. 1513)
Fernando Loren, L. Martin-Moreno,

Engineering of a THz time-reversal symmetry breaking chiral metamaterial (pp. 1515)
Lorenzo Graziotto, Johan Andberger, Luca Sacchi, Mattias Beck, Giacomo Scalari, Jerome Faist,

Machine learning for metamaterial design

Polarization holograms assisted with deep-learning (pp. 1518)
Jiawei Xi, Jian Shen, Man To Chow, Tan Li, Jack Ng, Jensen Li,

Machine Learning Techniques and Practical Advice for the Free-Form Inverse Design of Nanophotonic Devices (pp. 1520)
Timo Gahlmann, Philippe Tassin,

Beyond Periodic pillar-wise library for metasurface: a stochastic approach (pp. 1522)
Loumi Tremas, Mathys Le Grand, Denis Rideau, Louis Henri Fernandez-Mouron, Jeremy Grebot, Bruce Rae, James Downing, Pascal Urard, Valerie Serradeil, Lucie Dilhan, Habib Mohamad, Gonzague De Carpentier, Enrico Giuseppe Carnemolla, Matteo Fissore, Christophe Sauvan,

Metamaterial-based devices

Design of a beam-modulable vertical cavity using a dielectric metasurface with a full phase change encircling an exceptional point (pp. 1525)
Jaewon Jang, Yeonsang Park,

Converged wireless infrastructure with acoustic holography (pp. 1527)
Chuanxin Zhang, Xue Jiang, Dean Ta,

Atomic-level engineered transition-metal alloy photoanodes with record efficiency for solar water splitting (pp. 1529)
Fei Xiang, Ning Li, Arturo Burguete-Lopez, Zhao He, Maxim Elizarov, Andrea Fratalocchi,

Breathalyzer-based Prompt Coronavirus Screening Test using Terahertz Spectroscopy of Viruses in LC-Resonant Metamaterial Nano-Antenna Array (pp. 1531)
Rudrarup Sengupta, Heena Khand, Gabby Sarusi,

Electronic beam steering using a reconfigurable metasurface (pp. 1533)
Nawel Meftah, Badreddine Ratni, Mohammed Nabil El Korso, Shah Nawaz Burokur,

Modifying the integer quantum Hall effect with cavity vacuum fields (pp. 1535)
Josefine Enkner, F. Appugliese, G. L. Paravicini-Bagliani, M. Beck, C. Reichl, W. Wegscheider, G. Scalari, C. Ciuti, Jerome Faist,

Conductive coupling induced Dark multipole plasmon modes in hybrid cavities (pp. 1538)
Sukhvinder Kaur, Ravendra Kumar Varshney, Dibakar Roy Chowdhury,

Highly Sensitive Flexible Terahertz Metasensor for Thin Film Sensing (pp. 1540)
Parveen Joon, Sukhvinder Kaur, Ravendra Kumar Varshney,

Engineering a multifunctional TiO2 BIC metasurface (pp. 1542)
Haiyang Hu, Ludwig Huttenhofer, Oliver Bienek, Alwin Wester, Thomas Weber, Ian D. Sharp, Stefan A. Maier, Emiliano Cortes, Andreas Tittl,

Demonstration of an ultra-sharp bend in 1D grating waveguides based on inverse design (pp. 1544)
Ahmet Oguz Sakin, Ahmet Canberk Songur, Hasan Alper Gunes, Beyza Akcay, Mehmet Unlu,

Metamaterial-Assisted Power Division: An Inverse Design Study in 1D Grating Waveguides (pp. 1546)
Ahmet Oguz Sakin, Beyza Akcay, Hasan Alper Gunes, Ahmet Canberk Songur, Mehmet Unlu,

Ultracompact Tapers & Splitter for Fishbone-Like Grating Waveguides (pp. 1548)
Ahmet Oguz Sakin, Hasan Alper Gunes, Beyza Akcay, Ahmet Canberk Songur, Mehmet Unlu,

Flexible metamaterial microwave absorbers with polymer nanocomposite as substrates (pp. 1550)
Murugan Anjali, Kumaran Rengaswamy, Abhishek Ukey, Lincy Stephen, Chitti Venkata Krishnamurthy, Venkatachalam Subramanian,

Active metasurface using Ag/ITO nano antenna for visible wavelength (pp. 1551)
Chi-Sun Hwang, Yong Hae Kim, Jong-Heon Yang, Joo Yeon Kim, Kyunghee Choi, Jaehyun Moon, Ji Hun Choi,

Label-Free Protein Detection based on Surface-Enhanced Infrared Absorption Spectroscopy with vertical Nanogap (pp. 1553)
Mingyun Kim, Dohyun Kang, Jongwon Lee, Joo-Yun Jung,

Metasurface Augmented Camera for General Optical Metrology Applications (pp. 1555)
Arturo Burguete Lopez, Maksim Makarenko, Qizhou Wang, Fedor Getman, Andrea Fratalocchi,

Attribute of attenuation band in smart negative indexed mechanical metamaterials (pp. 1557)
Ankur Dwivedi, S. A. R. Horsley,

Scanning Reflectance Anisotropy Microscopy (SRAM): strain mapping of metasurfaces and beyond (pp. 1559)
Fabian Haake, Joan Sendra, Henning Galinski, Ralph Spolenak,

Line modes in elastic mechanical metamaterials (pp. 1561)
Ankur Dwivedi, S. A. R. Horsley,

Fabrication of two-dimensional magnonic crystal using yttrium iron garnets and non-magnetic metals (pp. 1563)
Kanta Mori, Takumi Koguchi, Toshiaki Watanabe, Mitsuteru Inoue, Kazushi Ishiyama, Taichi Goto,

Temporal modulation of Bound States in the Continuum at Mid-IR wavelengths (pp. 1565)
Saurabh Kishen, Poludasu Sahaan, Jinal Tapar, Naresh Kumar Emani,

Morphing design of Network of Beams to Maximize Absolute Bandgaps using Spectral Element Method (pp. 1567)
Theo Bonneval, Maxime Lanoy, Leonardo Sanches, Caroline Lyszyk, R. Tanays, Adrien Pelat, Guilhem Michon,

Numerical method for the inverse design of three-component metamaterial multilayers (pp. 1569)
Takamichi Terao,

Twisted Polaritonic Crystals in Thin Anisotropic Van der Waals Slabs (pp. 1571)
Nathaniel Capote-Robayna, O. Matveeva, V. S. Volkov, P. Alonso-Gonzalez, A. Y. Nikitin,

Arbitrarily-broadband dispersion compensation with ultrathin multiresonant metasurfaces (pp. 1573)
Odysseas Tsilipakos, Thomas Koschny,

ZrO2 Holographic Metasurfaces for Biophotonics Applications (pp. 1575)
Mohammad Biabanifard, Tomasz Plaskocinski, Jianling Xiao, Andrea Di Falco,

Ray-based design of hybrid metalens refractive imaging systems (pp. 1577)
Yijun Ding, Bryan Stone,

Metasurface-based optical concentrators monolithically integrated with Barrier infrared detectors (pp. 1579)
Tobias Wenger, Richard Muller, Cory J. Hill, Anita M. Fisher, David Z. Ting, Dan Wilson, Sarath D. Gunapala, Alexander Soibel,

Phase sensing with meta-optical devices for wavefront recovery and biological imaging (pp. 1581)
Lukas Wesemann, Shaban Barney Sulejman, Timothy J. Davis, Ann Roberts,

Metasurface enabled multifunctional microscopy (pp. 1583)
Muhammad Afnan Ansari, Yuttana Intaravanne, Hammad Ahmed, Narina Bileckaja, Huabing Yin, Xianzhong Chen,

Dielectric polarization-insensitive metasurfaces for Bessel beam generation in light sheet microscopy (pp. 1585)
Anna Archetti, Matteo Bruzzone, Giulia Tagliabue, Marco dal Maschio,

Large Field-of-View and Multi-Color Imaging with Quadratic Metalenses (pp. 1587)

Emmanuel Lassalle, Anton V. Baranikov, Egor Khaidarov, Damien Eschimese, Joel Yeo, N. Duane Loh, Ramon Paniagua-Dominguez, Arseniy I. Kuznetsov,

Photonic bound states in the continuum in asymmetric bi-slot metasurfaces (pp. 1588)
Ti-Jung Hsu, Ruey-Lin Chern,

Highly angle-sensitive and efficient optical metasurfaces (pp. 1589)
Nayoung Kim, Myungjoon Kim, Joonkyo Jung, Taeyong Chang, Suwan Jeon, Jonghwa Shin,

Morphogenetic engineering of radiating metasurfaces (pp. 1591)
Thomas Fromenteze, Okan Yurduseven, Eric Arnaud, David R. Smith, Cyril Decroze,

Enabling and perfectioning advanced large Area Metalens Nanofabrication by Electron Beam Lithography (EBL) (pp. 1593)
Frank Nouvertne, C. Aulbach, G. Piaszenski, J. Munchenberger, V. Boegli,

Transmittance analysis of dielectric optical metasurfaces (pp. 1595)
Ivan Moreno, Carlos Basilio-Ortiz,

Pancake metalens for compact imaging systems (pp. 1597)
Chen Chen, Shining Zhu, Tao Li,

Investigating the Bound States in the Continuum Phenomenon in hBN Nano-antenna Arrays (pp. 1598)
Harsh Gupta, James Edgar, Francesco De Angelis, Andrea Toma, Michele Tamagnone,

Polarization Dichroic Fabry-Perot Cavities Enabled By Metasurface Structures (pp. 1600)
Behrooz Semnani, Mohammad Soltani, Sema Kuru, Michal Bajcsy,

Three-dimensional varifocal device by mechanical tuning of metalens doublet and auxiliary visual alignment guiding hologram (pp. 1602)
Hyeonhee Kim, Joonkyo Jung, Jonghwa Shin,

Fully Beam Scanning Transmissive Mechanical Metasurface with Polarization Conversion (pp. 1604)
Chhungheng Lor, Sungjoon Lim,

Angle sensitivity of extraordinary optical transmission and resonant spatial frequency filtering (pp. 1606)
Sun-Je Kim, Hanbyul Chang,

Electrical tunning of metasurfaces via transparent conducting oxide micro heaters (pp. 1607)
Khosro Zangeneh Kamali, Lei Xu, Nikita Gagrani, Hark Hoe Tan, Chennupati Jagadish, Andrey E. Miroshnichenko, Dragomir N. Neshev, Mohsen Rahmani,

Investigation of Field Effect Tuning of Refractive Index in Transparent Conducting Oxide Thin Film Fabry-Perot Cavity Structures (pp. 1609)
Evan Roy, Nishtha Shelly, Chris Murray, David McCloskey,

Optical Metasurfaces for Grafted Vortex Beams Generation (pp. 1611)
Hammad Ahmed, Muhammad Afnan Ansari, Xianzhong Chen,

Performance Analysis of Patch-HIS Arrays for Visually Impaired Aid System (pp. 1613)
Alicia Florez Berdasco, Jaime Laviada Martinez, Maria Elena de Cos Gomez, Fernando Las-Heras Andres,

Silicon metalens using Fresnel zone plate with subwavelength gratings (pp. 1615)

William Fraser, Winnie Ye,

Optical matrix computation using programmable metalens array (pp. 1617)
Randy Stefan Tanuwijaya, Hong Liang, Jiawei Xi, Tsz Kit Yung, Wing Yim Tam, Jensen Li,

Switching of Phase-Change Optical Metasurfaces via Remote Thermal Sources (pp. 1619)
George Braid, Carlota Ruiz de Galarreta, Andrew Comley, Jacopo Bertolotti, C. David Wright,

Metasurface-enabled molecular spectroscopy and machine learning resolve lipid membrane photoswitching (pp. 1621)
Martin Barkey, Rebecca Buchner, Alwin Wester, Stefanie Pritzl, Maksim Makarenko, Qizhou Wang, Thomas Weber, Stefan A. Maier, Andrea Fratalocchi, Theobald Lohmuller, Andreas Tittl,

Tuning optical properties of individual Sb2S3 nanostructures (pp. 1623)
Peter Kepic, Petr Liska, Beata Idesova, Filip Ligmajer, Tomas Sikola,

Efficient broadband mid-infrared linear-to-circular polarization conversion using a nanorod-based metasurface (pp. 1625)
Huanling Zou, Geoff Nash,

Complete linear control based on universal metasurfaces and their applications (pp. 1627)
Joonkyo Jung, Taeyong Chang, Sang-Hyeon Nam, Hyeonhee Kim, Jong Uk Kim, Nayoung Kim, Suwan Jeon, Minsung Heo, Jonghwa Shin,

Miniaturized Metamaterial Absorber Using Lossy Effective Dielectric-Medium and Resistive Metasurface (pp. 1629)
Jyoti Yadav, Mondeep Saikia, Kumar Vaibhav Srivastava, J. Ramkumar,

Metasurface-Based Radome for Wearable Antenna at 24GHz (pp. 1631)
Maria Elena de Cos Gomez, Alicia Florez Berdasco, Fernando Las-Heras Andres,

Active phase control with metasurfaces in the visible by electrochemistry (pp. 1633)
Junhyung Park, Min Gwan Jo, Jonghwa Shin,

All metal 1D plasmonic metasurface broadband absorber for refractive index sensing in Mid-IR regime (pp. 1635)
Sagar Kumar Verma, Sachin Kumar Srivastava,

Metasurfaces for illumination and light concentration (pp. 1637)
Ivan Moreno, C. P. CastaÃ±eda-Almanza, Thaire V. Galvan,

Analysis of Reliability of Flexible Microwave Absorbing Meta-Surface under Bending Stress (pp. 1638)
Doo-Sun Choi, Ji-Youn Kwak, Jun Sae Han, Eun-Ji Gwak, Eun-Chae Jeon,

Reconfigurable On-Chip Waveguide-fed cELC-based Metasurface Antenna (pp. 1640)
Khaled Boubekeur, Nicolas Zerounian, Badr Eddine Ratni,

Dielectric metalens and polarization beam splitter for UV wavelengths (pp. 1642)
BeÃ¡ta IdesovÃ¡, Katarina Rovenska, Ondrej Cervinka, Martin Hrton, Filip Ligmajer, Tomas Sikola,

Epsilon near zero metasurfaces (ENZ) at visible wavelengths (pp. 1644)
Iman Alhamdan, S. A. Schulz,

Supercell Metasurfaces: Hierarchical Designs and Experimental Validation (pp. 1646)
Tatiana Contino, Michele Tamagnone,

Non-Uniform Array of Polarizable Particles as a Locally Linear Space Invariant (LSI) Metasurface (pp. 1648)

Jordan Dugan, Tom Smy, Joao G. Nizer Rahmeier, Suhlabh Gupta,

Adjoint Optimized Mid-Wave Infrared Metalenses (pp. 1650)
Joshua Rollag, Raymond Wambold, Ricky Gibson,

Self-assembly of magnetoplasmonic nanowires for structural colors and chiral metasurfaces (pp. 1652)
My-Chi Nguyen, Huu-Quang Nguyen, Jaebeom Lee,

Dynamic phase-modulated metasurface for beam scanning antenna (pp. 1654)
Zakaria Zouhdi, Badr Eddine Ratni, Shah Nawaz Burokur,

Tuning of Fano resonance in mirrored array of split ring resonators (pp. 1657)
Dalius Seliuta, Andrius Kamarauskas, Gediminas Slekas, Zilvinas Kancleris,

Nonlinear metamaterials

Broadband Terahertz Emitter with All-Dielectric Metasurface Based on the Quasi-Bound States in the Continuum (pp. 1660)
Yang Guo, L. Y. Hu, B. Wang, S. Du, C. Z. Gu,

Nonlinear Effects of Linear Time-Dependent Metamaterials (pp. 1662)
Pravinkumar Ghodake,

Nonlinear optics of quasistatic origin from a deep-subwavelength metallic meta-atomical system (pp. 1664)
Avi Niv,

Controlling High-Q Lattice Resonances in Bipartite Plasmonic Arrays through Nanoparticle Geometry and Orientation (pp. 1666)
Timo Stolt, Jussi Kelavuori, Ali Panahpour, Mikko J. Huttunen,

Enhanced Generation of Higher Harmonic from Halide Perovskite Metasurfaces (pp. 1668)
Pavel Tonkaev, Kirill Koshelev, Mikhail Masharin, Sergey Makarov, Sergey Kruk, Yuri Kivshar,

Optical bistability in Su-Schrieffer-Heeger lattice with Kerr nonlinearity (pp. 1670)
Ghada Alharbi, Sang Soon Oh,

Large Enhancement in Visible to UV Nonlinear Frequency Conversion by a Plasmonic Gold Nanograting (pp. 1672)
Shroddha Mukhopadhyay, Laura Rodriguez-SuÃ±e, Crina Maria Cojocaru, â€¦Maria Antonietta Vincenti, Kent A. Hallman, Giuseppe Leo, Metodi Belchovski, Domenico de Ceglia, Michael Scalora, Jose Francisco Trull Silvestre,

Epsilon-Near-Zero coupled Surface Lattice Resonances as a Nonlinear Activation Function (pp. 1674)
Dhruv Fomra, Adam Ball, Amit Agrawal, Henri J. Lezec, Nathaniel Kinsey,

Suppression of filamentation in Kerr media by photonic crystals (pp. 1676)
Edvinas Aleksandravicius, Darius Gailevicius, Audrius Dubietis, Kestutis Staliunas,

Stable periodic solutions in fractional dissipative systems with non-Hermitian modulation (pp. 1678)
Salim Benadouda Ivars, Muriel Botey, Ramon Herrero, Kestutis Staliunas,

Laser and cavities

Hybrid External Cavity Laser based on a novel Si3N4 1D Photonic Crystal cavity for label-free on-chip sensing applications (pp. 1681)

Taynara De Oliveira, Simone Iadanza, Jesus Hernan Mendoza-Castro, Gautham Paikkath, Bernhard Lendl, Marco Grande, Liam O'Faolain,

Integrated polariton condensate in SOI high contrast grating microcavities (pp. 1683)
Pietro Tassan, Darius Urbonas, Bartos Chmielak, Thorsten Wahlbrink, Rainer Mahrt, Thilo Stoferle,

Integrated Q-switched lasing element in the NIR with transition metal dichalcogenide gain and graphene saturable absorption (pp. 1685)
Georgios Nousios, Thomas Christopoulos, Odysseas Tsilipakos, Emmanouil Kriezis,

Tunable band structures coupled by spin-orbit interaction in self-organized photonic potential inside a liquid crystal optical microcavity (pp. 1687)
Marcin Muszynski, Przemyslaw Oliwa, Eva Oton, Rafal Mazur, Przemyslaw Morawiak, Wiktor Piecek, Przemyslaw Kula, Barbara Pietka, Jacek Szczytko,

Silicon Nitride Ring Resonators Operating at 450nm (pp. 1689)
Samira Jastan, S. Iadanza, L. O'Faolain,

Interlayer Exciton Lasing in Atomically Thin Heterostructures (pp. 1691)
Qiaoling Lin, Hanlin Fang, Yuanda Liu, Yi Zhang, Moritz Fischer, Juntao Li, Nicolas Stenger, Zhipei Sun, Martijn Wubs, Sanshui Xiao,

Photonic bandgap structures

Fabrication of All-Garnet Bragg Mirror using Cerium Substituted Yttrium Iron Garnet (pp. 1693)
Yuki Yoshihara, Pang Boey Lim, Mitsuteru Inoue, Kazushi Ishiyama, Taichi Goto,

Morphogenetic Design of Self-Organized Correlated Disordered Media (pp. 1695)
Fadhila Chehami, Cyril Decroze, Thomas Fromenteze,

Directional emission enhancement measurements in terahertz photonic crystals (pp. 1697)
Kseniia Lezhennikova, Sahand Mahmoodian, Boris Kuhlmey, Redha Abdeddaim, Stefan Enoch, Martijn de Sterke, Alessandro Tuniz,

Nonlinear 2D Photonic Crystal Tunable Switch (pp. 1699)
Amel Bounouioua, Ahlem Benmerkhi, M. Bouchemat,

Nanophotonics with stratified architecture for bright phosphor-based nano LEDs (pp. 1701)
Debapriya Pal, Femius Koenderink,

Emerging applications

Theoretical study of optomechanical effects by luminescence-induced optical force on micromechanical membranes (pp. 1704)
Hideki Arahari, Sota Konishi, Seiji Akita, Hajime Ishihara,

Inverse design of fabrication-compatible monolithic metasurfaces for optically interfacing deeply embedded solid-state qubits (pp. 1706)
Amelia Klein, Nader Engheta, Lee Bassett,

Applications of Eutectic Materials for 5G Technology (pp. 1708)
Hamid Reza Darabian, Jerzy Krupka, BartÅ‚omiej Salski, Dorota Anna Pawlak,

Micro/Nano fabrication and characterization techniques

Sub-wavelength silicon nano-structuring with direct laser writing (pp. 1711)
Rana Asgari Sabet, Onur Tokel,

MBE substrate deoxidation surveillance via RHEED image analysis with Deep-Learning (pp. 1713)
Abdourahman Khaireh-Walieh, Alexandre Arnoult, Sebastien Plissard, Peter Wiecha,

Laser Anneal for Selective Crystallization of Magnetooptical Film (pp. 1715)
Hibiki Miyashita, Yuki Yoshihara, Takumi Koguchi, Pang Boey Lim, Mitsuteru Inoue, Kazushi Ishiyama, Taichi Goto,

Dyes emission mediated by plasmonic nanostructures revealed by SNOM (pp. 1717)
Anna Mercedi, Lucio Litti,

Characterization of Optical Fourier Volumes made by Holographic Recording on Photo-reactive Polymers (pp. 1718)
Kwangjin Kim, Yongjun Lim, Heeju Son, Seung Jae Hong, Chang-Won Shin, Dongjae Baek, Hyeon Ho Kim, Joona Bang, Seungwoo Lee,

Rewritable Optical Fourier Volumes using Photoaddressable Polymers containing Azobenzene and Liquid Crystals (pp. 1720)
Heeju Son, Kwangjin Kim, Yongjun Lim, Seungjae Hong, Changwon Shin, Dongjae Baek, Hyeonho Kim, Nam Kim, Joona Bang, Seungwoo Lee,

Design and Fabrication for Optical Fourier Surfaces Reaching the Theoretical Upper Limit of Diffraction Efficiency (pp. 1722)
Yongjun Lim, Seung Jae Hong, Heeju Son, Joona Bang, Seungwoo Lee,

Characterizing Far-Field Plasmonic Resonances of Au and AuAl2 Structures using Dark Field Spectroscopy (pp. 1724)
Tiernan McCaughery, Achyut Maity, R. Bowman,

3D Micro-imprinted Flexible Plasmonic PDMS-based Platform for SPR-SERS Detection of the Formalin Contaminant (pp. 1725)
Andreea Campu, Monica Potara, Simion Astilean, Monica Focsan,

Ion beam doping of phase-change materials: a platform for active metasurfaces (pp. 1726)
Martin Hafermann, Robin Schock, Annkathrin Kohler, Jacob Grandmontagne, Carsten Ronning,

Large area high-resolution nanostructure fabrication with focused ion beam for surface-enhanced Raman spectroscopy (pp. 1728)
Liga Bikse, Reinis Ignatans, Juris Prikulis, Annamarija Trausa, Krisjanis Smits,

Periodically modulated photonic structures for light manipulation (pp. 1729)
Julianija Nikitina, Ceren Babayigit, Kestutis Staliunas, Lina Grineviciute,

Laser-Induced Nanostructuring of Material Phase and Shape for 3D Light Control (pp. 1731)
Maxim Elizarov, Ning Li, Andrea Fratalocchi,

Modeling and computational techniques

Micromagnetic Simulation of Sub-micron Scaled Magnetic Domains in Magnetic Garnet Films (pp. 1734)
Takumi Koguchi, Yuki Yoshihara, Pang Boey Lim, Mitsuteru Inoue, Kazushi Ishiyama, Taichi Goto,

Explaining an Anomalous Thermally Activated Delayed Fluorescence (TADF) Response for a Phenothiazine Derivative

through a TD-DFT Approach (pp. 1736)
Lucia Cascino, Antonio Maggiore, Ivan Rivalta, Gian Paolo Suranna, Roberto Grisorio, Daniele Conelli, Vincenzo Maiorano, Stefania D'Agostino,

Inverse Design of Metalens Systems Including Refractive Lenses (pp. 1738)
Jan Bos, Evan Heller, Rob Scarmozzino, Mayank Bahl, Li-Ce Hu, Chenglin Xu,

Level-set optimization of non-reciprocal media (pp. 1740)
Claire Cisowski, Robert Bennett,

Ray-Optical Analysis for Optimization of Light Absorption in the Double-Junction III-V Solar Cells with Luminescent Solar Concentrators (pp. 1741)
Dongjae Baek, Shin Hyung Lee, Kwangjin Kim, Sung-Min Lee, Seungwoo Lee,

Band gap tuning based on adjustable stiffness of local resonators (pp. 1743)
Hossein Alimohammadi, K. Vassilyeva, H. Hosseinnia, E. Petlenkov,

Plenary presentation

META 2023, PARIS - FRANCE, JULY 18 – 21, 2023

Nanophotonics for tailoring radiation from fast electrons

Marin Soljačić

Physics Department, Massachusetts Institute of Technology, Cambridge, MA, USA
soljacic@mit.edu

Abstract: Nanophotonic methods provide intriguing options for manipulating scintillation phenomena. We will outline recent developments in this domain, along with our theoretical framework for modeling these occurrences, supported by our experimental findings. Additionally, Smith-Purcell radiation, characterized by fast electrons interacting with nano-structured materials to produce light, offers a broad spectrum of possibilities for creation of novel light sources. We will discuss our new theoretical framework designed to comprehend and tailor such phenomena, as well as our techniques for boosting Smith-Purcell radiation.

Structuring light with media with higher dimensions: space, time, and more

Nader Engheta[1]

[1]Department of Electrical and Systems Engineering, University of Pennsylvania, Philadelphia, PA 19104, USA
*corresponding author, E-mail: engheta@seas.upenn.edu

Abstract

In this talk, I will present some of our most recent results on exploring light-matter interaction in material media with high degrees of freedom and dimensions including spatial and/or temporal inhomogeneities, and other degrees of freedom such as anisotropy, ellipticity, and hyperbolicity. We show how light manipulation with such metastructures with high degrees of freedom can lead to exciting novel wave phenomena with potential applications in wave-based reconfigurable analog computing, 4D optics, and other optical devices and components.

META 2023, PARIS - FRANCE, JULY 18 – 21, 2023

Scalable classical and quantum photonics

Jelena Vuckovic

Stanford University, CA, USA
*corresponding author: jela@stanford.edu

Abstract: Novel computational techniques such as photonics inverse design, along with new nanofabrication approaches, play a crucial role in building scalable integrated classical and quantum photonics. Inverse design, a departure from the traditional photonics design approach, can lead to photonics much better than state of the art in many metrics (smaller, more efficient, more robust, a much higher density of integration). This is enabled by development of a computer software which efficiently searches through the space of all possible and fabricable photonic geometries, in any material of interest. On the other hand, future photonic systems also require integration and fabrication of traditional and non-traditional photonic materials, including silicon, silicon-carbide, diamond, sapphire, and strong electro-optic materials such as lithium niobate, strontium and barium titanate.

META 2023, PARIS - FRANCE, JULY 18 – 21, 2023

Active photonic metasurfaces empowered by 2D semiconductors

Isabelle Staude

Friedrich Schiller University Jena, Institute of Solid State Physics, Max-Wien-Platz 1, 07743 Jena, Germany
*corresponding author: Isabelle.staude@uni-jena.de

Abstract: Optical metasurfaces, namely two-dimensional arrangements of designed nanoresonators, have been in the limelight of nanophotonics research during the last decade. Such metasurfaces can impose a spatially variant phase shift onto an incident light field, thereby providing control over its wave front. As such, metasurfaces have been suggested for numerous wavefront-shaping applications, including lensing, beam shaping, and holographic imaging [1]. However, most metasurfaces realized so far were passive and linear, and their optical response was permanently encoded into the structure during fabrication. Recently, a growing amount of research is concentrating on the integration of active materials, in particular emitters, optical nonlinearities, and responsive materials into the metasurface architectures. The resulting active, i.e. light-emitting, nonlinear, and tunable, metasurface systems can provide many functionalities beyond pure wavefront shaping, and are of huge interest for a large range of potential applications.

While many different active materials have been explored in the context of creating active metasurfaces, the semiconducting representatives of the family of two-dimensional transition metal dichalcogenides (2D-TMDCs) stand out by their unique optoelectronic properties, including a strong direct bandgap photoluminescence in the monolayer phase, excitonic-dominated properties at room temperature, strong second-order nonlinear susceptibility, strong spin-valley coupling and associated chiral photoluminescence emission, as well as tunability of their optical response by electronic gating. Furthermore, due to their flat nature, their integration with likewise flat optical metasurfaces is particularly intuitive [2].

This talk reviews our recent and ongoing activities in hybridizing optical metasurfaces composed of resonant metallic or dielectric building blocks with 2D-TMDCs. We demonstrate that the ability of the nanoresonators to concentrate light into nanoscale volumes can be utilized to carefully control the properties, such as pattern and polarization, of light emitted by 2D-TMDCs via photoluminescence or nonlinear optical processes [3,4]. Furthermore, we investigate the ability of tailored nanostructures to interact selectively with exciton populations located at inequivalent conduction band minima at the corners of the 2D-TMDC's Brillouin zone. Finally, we suggest that resonant nanoantennas can be used to probe the nature of chiral emission from 2D-TMDCs. Altogether, our results contribute to a better fundamental understanding of coupling of photonic nanostructures to excitons in 2D-TMDCs and are an important step towards the realization of future miniaturized active metasurface and valleytronic devices.

[1] N. Yu and F. Capasso, "Flat optics with designer metasurfaces", Nat. Mater. 13, 139–150 (2014).

[2] R. Mupparapu et al., "Integration of two-dimensional transition metal dichalcogenides with Mie-resonant dielectric nanostructures", Advances in Physics: X 5, 1734083 (2020).

[3] T. Bucher et al., "Tailoring photoluminescence from MoS_2 monolayers by Mie-resonant metasurfaces", ACS Photonics 6, 1002–1009 (2019).

[4] F. J. F. Löchner et al., „Hybridization of dielectric metasurfaces with chemical vapor deposition grown MoS_2 monolayers for enhanced second-harmonic generation", ACS Photonics 8, 218–227 (2021).

META 2023, PARIS - FRANCE, JULY 18 – 21, 2023

Imaging and Computing with disorder

Sylvain Gigan
Laboratoire Kastler Brossel, Sorbonne Université, Ecole Normale Supérieure-Paris Sciences et Lettres (PSL) Research University, Centre Nationale de la Recherche Scientifique (CNRS) UMR 8552,Collège de France, 24 rue Lhomond, 75005 Paris, France
sylvain.gigan@lkb.ens.fr

Abstract: Light propagation in complex media, such as paint, clouds, or biological tissues, is a very challenging phenomenon, encompassing fundamental aspects in mesoscopic and statistical physics. It is also of utmost applied interest, in particular for imaging. Although this scattering process seems to mix and completely destroy all information, thus preventing imaging or communication, a different approach has emerged — exploiting this apparently detrimental effect to one's advantage by processing information carried by waves. I will discuss how this powerful concept has recently triggered a wealth of advances in imaging and computing.

META 2023, PARIS - FRANCE, JULY 18 – 21, 2023

Extreme Control of Light and Sound with Metamaterials

Andrea Alù
Photonics Initiative, Advanced Science Research Center, City University of New York
Physics Program, Graduate Center, City University of New York
Department of Electrical and Computer Engineering, City College of New York
85 St. Nicholas Terrace, New York, NY 10031, U.S.A.
aalu@gc.cuny.edu, http://alulab.org

Abstract: The field of metamaterials, artificial materials engineered at the nanoscale, has been rapidly evolving in the past two decades, demonstrating extreme optical and acoustic phenomena and unprecedented control over wave propagation. In this talk, I discuss recent developments in this field of research, with an emphasis on the role of symmetries in establishing emerging optical responses for metamaterials based on otherwise simple constituents. Geometrical rotations, suitably tailored perturbations, and broken time reversal symmetry can be carefully engaged to tailor waves in robust and efficient ways, control their propagation, break Lorentz reciprocity and enable topological order and phase transitions. In particular, the use of strongly coupled wave and matter interactions in polaritonic systems enables extreme responses at the nanoscale, well suited for classical-wave and quantum applications. In my talk, I will discuss the underlying physical principles that span over a wide range of frequencies, and their impact on practical technologies, from imaging, energy and sensing to computing and communications..

Keynote presentation

META 2023, PARIS - FRANCE, JULY 18 – 21, 2023

Ultra low loss nonlinear integrated photonic circuits: from soliton microcombs, traveling wave parametric amplifiers, chip based Erbium amplifiers to cryogenic quantum interconnects

Tobias Kippenberg

EPFL, Switzerland
*corresponding author: tobias.kippenberg@epfl.ch

Abstract: Recent advances in attaining ultra low loss highly confining silicon nitride waveguides with loss in the dB-meter range, and their heterogeneous integration with MEMS and Lithium Niobate have opened up novel applications that exhibit both low cost, and scalable manufacturing but also performance that is on par or exceeding that of legacy optical systems. I will describe a range of novel advances, including photonic integrated circuit based frequency agile lasers with fiber laser phase noise, parametric traveling wave amplifiers, Erbium amplifiers on chip, as well as soliton frequency combs.

META 2023, PARIS - FRANCE, JULY 18 – 21, 2023

Quantized Fractional Thouless Pumping of Solitons

Marius Juergensen[1], Sebabrata Mukherjee[1,2], Christina Joerg[1,3], and Mikael C. Rechtsman[1]

[1]The Pennsylvania State University, University Park, PA, USA 16802
[2]Indian Institute of Science, Bangalore, India
[3]Technical University of Kaiserslautern, German

[*]corresponding author: mcrworld@psu.edu

Abstract: I will present my group's recent work on the fractional pumping of solitons in photonic Thouless pumps. Specifically, I will show that the displacement (in unit cells) of solitons in Thouless pumps is strictly quantized to the Chern number of the band from which the soliton bifurcates in the low power regime; whereas in the intermediate power regime, nonlinear bifurcations lead to fractional quantization of soliton motion. This fractional quantization can be predicted from multi-band Wannier functions associated with the states of the pump.

META 2023, PARIS - FRANCE, JULY 18 – 21, 2023

Photonic Time-Crystals

Mordechai (Moti) Segev

Technion, Israel

Abstract: Time-Crystals (PTCs) are materials in which the refractive index varies periodically and abruptly in time. They conserve momentum but not energy, and display momentum bands separated by gaps. The fundamentals of PTCs will be presented, with an emphasis on light-matter interactions ranging from light emission by atoms and free electrons to superluminal k-gap solitons and recent experiments.

Optical thermodynamics of highly multimode nonlinear photonic systems

Demetrios Christodoulides

University of Southern California, USA
*corresponding author: demetri@usc.edu

Abstract: The past few years have witnessed a resurgence of interest in multimode structures, predominantly driven by the ever-increasing demand for higher information capacities. This renaissance, in turn, incited a flurry of activities in the general area of nonlinear multimode optics. The sheer complexity associated with the presence of hundreds or thousands of nonlinearly interacting modes that collectively act as a many-body system, has led to new opportunities in observing a multitude of novel optical effects that would have been otherwise impossible in single-mode settings. In this talk, a thermodynamic theory capable of describing complex, highly multimoded, nonlinear optical systems is presented. It is shown that the mode occupancies in such nonlinear multimode arrangements follow a universal behavior that always tends to maximize the system's entropy at steady-state. This thermodynamic response takes place irrespective of the type of nonlinearities involved and can be utilized to either heat or cool an optical multimode system. Aspects associated with adiabatic compressions and expansions will be discussed along with the possibility for all-optical Carnot cycles.

META 2023, PARIS - FRANCE, JULY 18 – 21, 2023

Dielectric metasurfaces with fast and ultra-fast tunability

Dragomir Neshev
ARC Centre of Excellence for Transformative Meta-Optical Systems (TMOS), Department of Electronic Material Engineering, Research School of Physics, Australian National University, Canberra, Australia
*corresponding author: Dragomir.Neshev@anu.edu.au

Abstract: This talk will overview the recent advances and challenges in tunable metasurfaces. I will discuss metasurface tunability through several mechanisms, including electrical and all-optical drive. Such drives allows for fast and ultrafast response with high modulation strength. We demonstrate the how all-optical control can lead to and high ultrafast transmission modulation of 80%. The presented developments hold promises for real-world applications of active meta-optics.

Optical metasurfaces are sub-wavelength patterned surfaces that interact strongly with light. The field has been driven by the key advantages of this technology, including the ultimate miniaturization of optical elements, empowering novel functionalities that process hidden modalities of light, and the opportunity to tune their properties on demand. Several exciting applications have been demonstrated over the past years, including high-efficiency metalenses and holograms. However, many exciting new applications require metasurfaces with dynamically reconfigurable and programable functionalities. Such applications include 3D imaging, holographic displays, and light detection and ranging (LIDAR). This talk will overview the recent advances and challenges in reconfiguring optical metasurfaces. I will discuss metasurface tunability by utilizing different control mechanisms to tune the properties of the constituent elements. In particular, I will present the development of optically and electrically driven metasurfaces to perform fast amplitude modulation. We demonstrate the highest ultrafast modulation of over 80% and multi-pixel operation with over 70% transmission modulation. The presented developments aim to advance the field of tunable optical metasurface for real-world applications of active meta-optics.

Semiconductor quantum dot based quantum technologies

Q. Buchinger[1], G. Peniakov[1], J. Michl[1], I. Gamov[1], J. Kaupp[1], P. Gschwandtner[1], S. Krüger[1], A. Pfenning[1], T. Huber-Loyola[1], and S. Höfling [1*]

[1]Julius-Maximilians-Universität Würzburg, Physikalisches Institut, Lehrstuhl für Technische Physik, Am Hubland, 97074 Würzburg, Deutschland
[*]corresponding author: sven.hoefling@physik.uni-wuerzburg.de

Abstract: We will summarize recent progress made within our group on self-assembled quantum dot device development for quantum repeater and quantum computer applications. A particular emphasis will be on semiconductor quantum dots embedded in circular Bragg grating cavities. For scalability, spatially deterministic placement of quantum dots in bullseye cavities is pursued and tuning by electric and strain fields are implemented. To apply electric fields, a new device design for electrically contactable circular Bragg grating cavities in labyrinth geometry is employed.

In this presentation, we will summarize recent progress made within our group and plans on device development with self-assembled quantum dots intended for quantum repeater and quantum computer applications [1]. A particular emphasis will be on semiconductor quantum dots embedded in circular Bragg grating cavities [2,3]. For scalability, spatially deterministic placement of quantum dots in bullseye cavities is pursued and techniques for tuning by electric and strain fields are implemented. To apply electric fields, a new device design for electrically contactable circular Bragg grating cavities in labyrinth geometry is employed [4]. We report on the challenges experienced in obtaining high performance devices based on circular Bragg grating cavities and figures of merits achieved, outlining the prospects for these devices in quantum technology applications.

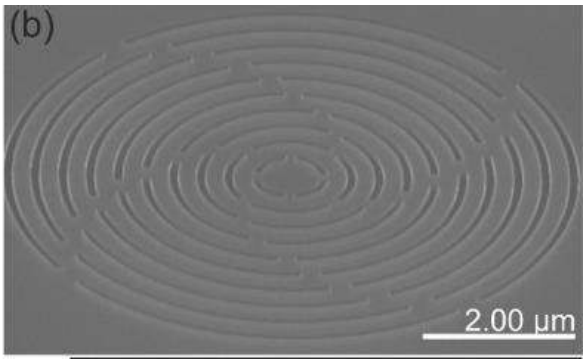


Figure 1 Circular Bragg grating cavity in labyrinth geometry for electrical contacting.

We are grateful for financial support of this work by the German Federal Ministry of Education and Research (BMBF) within the projects Q.Link.X, QR.X, MHLASQU, PhotonQ and QD-E-QKD. Expert technical assistance by Silke Kuhn, Adriana Wolf and Margit Wagenbrenner is gratefully acknowledged.

References

1. C.-Y. Lu and J.-W. Pan, “Quantum-dot single-photon sources for the quantum internet.” Nature Nanotechnology, Vol.

16, 1294-1296, 2021.
2. J. Scheuer and A. Yariv, “Coupled-Waves Approach to the Design and Analysis of Bragg and Photonic Crystal Annular Resonators”, IEEE J. Quantum Electron. Vol. 39, 1555-1562, 2003.
3. M. Davanco, M. T. Rakher, D. Schuh, A. Badolato, and K. Srinivasan, “A circular dielectric grating for vertical extraction of single quantum dot emission,” Appl. Phys. Lett., Vol. 99, 041102, 2011.
4. Q. Buchinger, S. Betzold, S. Höfling and T. Huber-Loyola, “Optical properties of circular Bragg gratings with labyrinth geometry to enable electrical contacts,” Appl. Phys. Lett., Vol. 122, 111110, 2023.

META 2023, PARIS - FRANCE, JULY 18 – 21, 2023

Recent progress in magnetic skyrmion physics

Xiangrong Wang[1,2 *]

[1]Physics Department, The Hong Kong University of Science and Technology, Clear Water Bay, Kowloon, Hong Kong

[2]HKUST Shenzhen Research Institute, Shenzhen 518057, China

[*]corresponding author: phxwan@ust.hk

Abstract: In this talk, I will discuss several progresses made in our group about fundamental properties of skyrmions in chiral magnetic films. These include 1) skyrmion sizes in isolated, in crystal, or in stripy forms; 2) skyrmion nucleation, formation, and potential barrier energies; 3) the roles of magnetic field in skyrmion crystal formation; 4) the stability and existing conditions of composite skyrmions such as target skyrmions and skyrmion bags/cluster; 5) topological equivalence of stripy phases and skyrmion crystals.

The summary Magnetic skyrmions have attracted much attention in recent years for their academic interest and potential applications in information technology [1]. They are two-dimensional magnetic solitons with localized topological spin textures which can move and be manipulated by external forces. Various aspects of magnetic skyrmions have been extensively and intensively studied, including characterizations, generations, control, etc. With all advances in skyrmion physics, many fundamental properties of skyrmions were not adequately known, such as the role of magnetic field in skyrmion crystal (SkX) formation, relationship between SkXs and stripy spin structures that often appear together with SkXs, parameter dependences of skyrmion size in isolated circular skyrmions, in SkXs, and in stripe skyrmions, skyrmion nucleation energy, skyrmion energy barrier and skyrmion energy. Other than different elementary skyrmions, many localized magnetic structures, topologically different from the elementary skyrmions and with arbitrary integer skyrmion numbers, were found in

the past eight years. The increasing number of newly discovered topologically non-trivial localized spin structures in chiral magnetic films reminisces the discovery of a huge number of elementary particles in the first half of last century that resulted in the quark model of elementary particles. It calls for a “quark model” to properly organize these newly discovered topological magnetic structures. This talk shall address above mentioned fundamental issues related to magnetic skyrmion physics.

We use a perpendicularly magnetized chiral magnetic film as a model to demonstrate these progresses. The films are characterised by a Dzyaloshinskii–Moriya interaction (DMI) and normal ferromagnetic exchange interaction characterized by parameter D and A, respectively, as well as magnetic anisotropy measured by K and magnetic field H.

We show that only skyrmions with positive formation energy are intrinsically circular [2-5]. Allowed spin structures are fully determined by parameters defined as $\kappa \equiv (\pi D)2/(16AK)$ and $\kappa' \equiv (\pi D)2/(16A\mu_0 M_s H)$. Critical κ and κ' separates isolated circular skyrmions from condensed stripe skyrmions [3]. The natural morphology of skyrmions of negative formation energy are stripes of well-defined width. Condensed stripy skyrmions, ranging from irregular maze to periodically arranged helical states, is the preferred thermodynamic equilibrium state [5] when skyrmion-skyrmion separation is much larger than the stripe width. It is generally believed that helical states and SkXs are topologically unconnected \cite{roadmap}, and transformations from stripy states to SkXs are phase transitions, even though stripy states are the precursors of SkXs. However, these beliefs are inconsistent with recent findings that skyrmions at lower density have stripe morphology in their condensed phase [4,5]. The irregular stripy phases transform smoothly into SkXs as stripe width increases via material parameter engineering or as the skyrmion density increases through thermal agitations and/or the assistances of external forces [4,5]. Thus, SkXs and helical states are topologically connected.

We show that the stability and properties of various types of composite skyrmions are very sensitive to κ and κ'. Magnetic skyrmions show strong particle-continuum-medium duality. As particles, one or many circular and stripe skyrmions can be embedded inside another larger skyrmion, which act as a glue or a bag, to form a skyrmionium or skyrmion bag/cluster. The embedding can continue layer by layer to form all kinds of target skyrmions and cascade skyrmion bags. In the absence of the external magnetic field and for $\kappa \leq 1$ where isolated circular skyrmions are metastable and $\kappa > 1$ where condensed stripe skyrmions are stable. 1) Topologies of stable static magnetic textures are fully determined by κ, and A/D defines their length scale. 2) The maximal number of cascade layers in target skyrmions for $\kappa \leq 1$ increases monotonically from 1 at $\kappa=0.7$ to 2 at $\kappa=0.8$, and to 4 at $\kappa=0.94$, and eventually diverges at $\kappa=1$ for an infinite large system. 3) An

unstable target skyrmion or skyrmion bag for $\kappa < 1$ can be stabilized by inserting enough skyrmions inside the innermost bag and/or the next innermost bag. The maximal number of skyrmions needed to stabilize a skyrmion bag decreases from a larger value at small κ, say 4 at $\kappa=0.7$, to the lowest possible 1 when κ approaches 1. This number increases also as the number of cascade layers increases. Furthermore, skyrmion size inside the innermost bag increases with the number of skyrmions inside the bag, and approaches the size of isolated elementary skyrmions. 4) For $\kappa>1$, the number of target stripe skyrmions and cascade stripe skyrmion bags can be any number as long as the average space-size occupied by each skyrmion is larger than twice of elementary stripe width. Furthermore, stripe width and stripe spin profile of any target stripe skyrmions and cascade stripe skyrmion bags are the same as those of elementary stripe skyrmions. 5) When the average skyrmion-skyrmion distance inside a stripe skyrmion bag is comparable to the elementary stripe width for $\kappa>1$, stripe skyrmions in the innermost layer become disk-like objects and form an SkX.

In conclusion, I will present several progress made in our group about some fundamental properties of skyrmions in chiral magnetic films. Depending on skyrmion formation energy, a magnetic skyrmion is a circular object for a positive formation energy, and irregular stripe for a negative formation energy, in contrast to the common belief that stripy spin textures are topological trivial objects. In fact, many spiral/helical/cycloid orders are skyrmions, siblings of circular skyrmions in skyrmion crystals (SkXs) and cousins of isolated circular skyrmions. At the extreme of one or a few skyrmions in the whole sample, the skyrmion is a ramified stripe. As the skyrmion number density increases, skyrmion shapes gradually change from ramified stripes to circular objects, forming SkXs. Skyrmion size in a SkX has a different parameter dependence as those for isolated skyrmions and stripes, and size formulas in three different cases are obtained. A generic theory about SkX formation in chiral magnetic thin films and its fascinating thermodynamic behaviours will be presented. The lowest energy state in the presence of an external magnetic field has a finite skyrmion density. This explains why a chiral magnetic film is often in a stripy state at a low field and a SkX only around an optimal field when an important parameter, called κ, is above a critical value. Both stripy states and SkXs are skyrmion condensates and they are topologically equivalent. By gradually tuning the stripe width, the morphology of a skyrmion condensate transforms smoothly and continuously from various stripy phases to crystals. A huge number of all kinds of topologically protected localized magnetic solitons observed in experiments and simulations can be understood from the duality of particle and elastic continuum-medium nature of skyrmions. Skyrmions can be building blocks for cascade skyrmion bags and target skyrmions. They can also act as bags and glues to hold many other skyrmions together. The principles and rules for stable composite skyrmions are explained and presented, revealing their rich and interesting physics. In summary, recent progress shows that magnetic skyrmions have very rich and interesting physics.

This work is supported by the National Key Research and Development Program(No. 2020YFA0309600), the NSFC Grant (No. 11974296), and HK RGC Grants (No. 16301619, 16300522, and 16302321).

References

1. C. Back, et. al., “The 2020 skyrmionics roadmap”, Phys. D: Appl. Phys., 2020, **53**, 363001.
2. X. R. Wang, X. C. Hu, and H. T. Wu, “Stripe skyrmions and skyrmion crystals”, Commun. Phys. 4, 142, 2021.
3. H. T. Wu, X. C. Hu, K. Y. Jing, and X. R. Wang, “Size and profile of skyrmions in skyrmion crystals”, Commun. Phys. 4, 210, 2021.
4. H. T.Wu, X. C. Hu, and X. R. Wang, “Nematic and smectic stripe phases and transformations”, Science China 65, 247512, 2022.
5. X. C. Hu, H. T. Wu, and X. R. Wang, “A theory of skyrmion crystal formation”, Nanoscale 14, 7516, 2022.

META 2023, PARIS - FRANCE, JULY 18 – 21, 2023

Chirality and nonreciprocal responses in quantum materials

N. Nagaosa*
RIKEN Center for Emergent Matter Science (CEMS), Japan
*corresponding author: nagaosa@riken.jp

Abstract: We study the chiral dynamics and consequent nonreciprocal responses in quantum materials, where the most fundamental principles in physics manifest themselves, i.e., the symmetries especially the time-reversal and spatial inversion, dissipation, quantum-classical crossover/transition, quantal Berry phase and topology, and many-body correlation effects. They include (1) magnetochiral anisotropy of semiconductors, Weyl semimetals, and superconductors, and (2) the photovoltaic effect, e.g., the shift currents under photo-excitations.

When the system lacks both parity and mirror symmetries, it is called “chiral” and can be classified into right-handed and left-handed materials. Chirality is one of the most fundamental issues in many branches of sciences [1]. This is on the structure of the system, while we are interested in the dynamics particularly the flow of the particles in solids here. In that case, the time-reversal symmetry is also important, and the nonreciprocal responses are classified into 4 categories according to the
(a) linear or nonlinear, and (b) with and without the time-reversal symmetry breaking [2].

(1) The magnetochiral anisotropy of quantum materials:
Under the external magnetic field which breaks the time-reversal symmetry, the band dispersion becomes asymmetric between k and -k in noncentrosymmetric materials, which results in the nonreciprocal response of the resistivity called “magnetochiral anisotropy”, where the resistivity contains the term expressed by the product of the magnetic field B and the current I. We employed the Boltzmann transport theory to analyze the magnetochiral anisotropy in BiTiBr, which shows the giant bulk Rashba splitting [3]. This effect is found to be enhanced by the chiral anomaly in Weyl semimetals [4]. Even larger magnetochiral anisotropy is observed experimentally in superconductor MoS2. We have constructed the Ginzburg-Landau free energy functional which contains the third order terms in the momentum of the order parameter, and calculated the nonlinear paraconductivity due to the fluctuating order parameter. This theory explains the huge enhancement of the nonreciprocal resistivity [5].

(2) Photovoltaic effect in noncentrosymmetric materials:
The spontaneous creation of the bulk photocurrent induced by the irradiation of light without the external bias is called photovoltaic effect. We have formulated this effect in terms of the Floquet theory combined with the Keldysh Green’s function to reveal the role of relaxation [6]. Furthermore, we have extended this formalism to the electron-phonon coupled system, and predict the direct current production in ferroelectric insulator by exciting phonon, which is observed experimentally in BiTiO3 [7].

The collaborators of these works are T. Morimoto, K.W. Kim, R. Wakatsuki, K. Hamamoto, M. Ezawa, H. Ishizuka, S. Hoshino, S. Koshikawa, S. Shimizu, Y. Kaneko Y. Saito, T. Ideue, Y. Iwasa, and Y. Tokura. This work was supported by JST CREST Grant Number JPMJCR1874 and JPMJCR16F1, Japan, and JSPS KAKENHI Grant number 18H03676.

References

1. Gardner, M. “The Ambidextrous Universe. Left, Right and the Fall of Parity,” *Basic Books Inc.*, 1964.
2. Tokura, Y. and N. Nagaosa, “Nonreciprocal responses from non-centrosymmetric quantum materials”, Nature Commun., **9**, 3740, 2018.
3. Ideue. T. et al., “Bulk rectification effect in a polar semiconductor”, Nature Phys. **13**, 578-583, 2017.
4. Morimoto, T. and N. Nagaosa, “Chiral Anomaly and Giant Magnetochiral Anisotropy in Noncentrosymmetric Weyl Semimetals”, Phys. Rev. Lett. **117**, 146603, 2016.
5. Wakatsuki, R. et al., “Nonreciprocal charge transport in noncentrosymmetric superconductors”, Science Advances **3**, e1602390, 2017.
6. Morimoto, T. and N. Nagaosa, “Topological nature of nonlinear optical effects in solids”, Science Advances **2**, e1501524, 2016.
7. Okamura, Y. et al., “Photovoltaic effect by soft phonon excitation”, Proc. Natl. Acad. Sci. U.S.A., **119(14)**, e2122313119, 2022.

META 2023, PARIS - FRANCE, JULY 18 – 21, 2023

Near-Zero-Index Materials for Nonlinear Optics and Beyond

Vladimir M. Shalaev
Purdue University, U.S.A.
shalaev@purdue.edu

Abstract: We discuss Near-Zero-Index (NZI) materials based on transparent conducting oxides (TCOs) that open new avenues in nonlinear optics including exotic time-varying media phenomena, such as negative refraction, time refraction/reflection, and photonic time crystals.

META 2023, PARIS - FRANCE, JULY 18 – 21, 2023

Crossroads of Nanophotonics and Machine Learning

Alexandra Boltasseva[1,2]

[1]School of Electrical and Computer Engineering, Birck Nanotechnology Center and Purdue Quantum Science and Engineering Institute, Purdue University, West Lafayette, IN 47907, USA
[2]The Quantum Science Center (QSC), a National Quantum Information Science Research Center of the U.S. Department of Energy (DOE), Oak Ridge, TN 37931, USA

aeb@purdue.edu

Abstract: Advancing optical inverse design via machine learning promises to enable the next generation of efficient on-chip circuitry, high-resolution imaging and sensing, sustainable energy concepts, and quantum information technology. In this talk, we discuss photonic design approaches and emerging material platforms for showcasing machine-learning-assisted topology optimization for metasurface designs with applications in thermosphotovoltaics, reflective optics, and lightsail technology. We demonstrate the effectiveness of autoencoders for compressing the vast design space of metasurfaces into a smaller search space. By employing global optimization via adjoint methods or quantum annealing, one can find the optimal metasurface designs within the smaller space constructed by the autoencoder. The quantum-assisted machine learning framework, named bVAE-QUBO, presented in this work is the first demonstration of a generic machine learning framework that compresses an arbitrary continuous optimization problem into an Ising-model formalism for quantum sampling. When compared to other global optimization techniques, bVAE-QUBO has the potential for quantum speedups and achieving higher quality designs than traditional adjoint optimization methods. The techniques employed in this work extend well beyond the metasurface optimization space and into many inverse design problems for engineering and physics.

Acknowledgements: This work is supported by the U.S. Department of Energy (DOE), Office of Science through the Quantum Science Center (QSC), a National Quantum Information Science Research Center, and Purdue's Elmore ECE Emerging Frontiers Center 'The Crossroads of Quantum and AI'. The authors also acknowledge support from the National Science Foundation award 2029553-ECCS.

Active Metasurfaces in Space and Time

Harry A. Atwater[1]

[1]California Institute of Technology, USA
*corresponding author: haa@caltech.edu

Abstract: Active dielectric and plasmonic metasurfaces enable new modalities for spatiotemporal beam control for beam steering and wavefront shaping at multiple frequencies.

Electro-optically tunable active metasurfaces that enable dynamic modulation of reflection and transmission amplitude, phase, and polarization using resonantly excited materials and phenomena are powerful design elements for meta-imaging and computation. As flat, low-profile optical elements, active metasurfaces have potential serve as cascadable, programmable components in optical meta-imaging systems, such as lens-less cameras and single-photon imaging systems.

Active metasurfaces that enable dynamic complex index modulation to vary the amplitude, phase and polarization have been recently explored using several active materials and modulation phenomena, including carrier index in plasmonic ENZ structures, reorientation of liquid crystal molecules, electrooptic effects in quantum well heterostructures and polar perovskite materials, as well as index changes in phase change materials. Recently also, metasurfaces that employ dielectric phase-gradient elements with high quality factor non-local as well as local resonances have expanded the design space for active metasurfaces by enabling silicon and other more conventional dielectric materials with modest values of index change to be utilized.

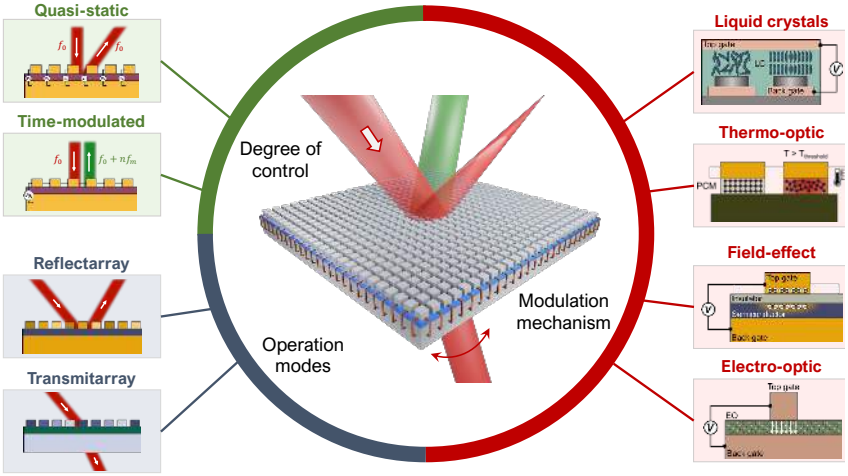


Figure 1. Active metasurface configurations (left) and physical mechanisms for modulation(right). (image credit: P. Thureja)

We can develop a taxonomy for active metasurfaces based on the attainable degree of spatial and temporal control. The spatial phase gradient arising from phase-reconfigurable array elements can enable continuous phase gradient tuning for beam steering or varifocal lensing. The degree of temporal control is connected to the reconfiguration timescale: In *quasistatic* metasurfaces, temporal gradients are slow compared to the period of electromagnetic waves, while *time-modulated* structures feature temporal gradients modulated fast enough to alter the frequency of the scattered beam. This opens the possibility to frequency multiplex scattered beams from active metasurfaces to facilitate harmonic beam steering in which a single active aperture steers scattered beams for different frequencies at independent angles.

In this talk, I will discuss metasurfaces with high quality factor, local, resonant elements capable of two-dimensional phase gradient generation, in both passive and active metasurface designs. I will also describe active metasurfaces with both spatial and temporal phase gradients, and an active metasurface as a lens-less imaging system, and compare the characteristics to conventional lens-coupled image sensors.

This work is supported by the Air Force Office of Scientific Research Meta-Imaging MURI under grant #FA9550-21-1-0312 as well as grant #FA9550-18-1-0354.

References

1. Lastname, F. M. “Title of the journal paper,” Journal Title Abbreviation, Vol. 34, No. 10, 1064–1076, 1986.
2. Lastname, F. M. and F. M. Lastname, “Title of the journal paper,” Journal Title Abbreviation, Vol. 34, No. 10, 1064–1076, 1986.
3. Lastname, F. M., F. M. Lastname and F. M. Lastname, “Title of the journal paper,” Journal Title Abbreviation, Vol. 34, No. 10, 1064–1076, 1986.

META 2023, PARIS - FRANCE, JULY 18 – 21, 2023

Continuous Time Crystals on Opto-Mechanical Platform

Nikolay I. Zheludev[1,2]

[1]University of Southampton, UK; [2]Nanayan Technological University, Singapore
zheludev@soton.ac.uk

Abstract: We overview recent development in the field of photonic time crystals, a state of matter with broken time-translation symmetry.

Recent advances in picometer scale visualization and localization techniques with electron beams [1] and topologically structured light [2] allow the detection of atomic level displacements in opto-mechanical systems and the study of dynamics and statistics of their picometre scale thermal and driven movements. This opens opportunity to develop pico/nano-opto-mechanical systems, in particular flexible plasmonic metamaterial arrays as a powerful platform to investigate classical many-body effects in the strongly correlated regime induced by light that complements the cold atom and spin platforms where many-body quantum states of bosonic or fermionic matter can be studied.

Among these many-body strongly correlated systems is the time crystal that is an eagerly sought phase of matter with broken time-translation symmetry. Quantum time crystals with discretely broken time-translation symmetry have been demonstrated in trapped ions, atoms and spins while continuously broken time-translation symmetry has only been observed in an atomic condensate inside an optical cavity.

We have demonstrated [3] that a classical metamaterial nanostructure, a two-dimensional array of plasmonic metamolecules supported on nanowires, exhibit complex picometer scale dynamics in presence of light. It can be driven to a state possessing all the key features of a continuous time crystal: continuous coherent illumination by light resonant with the metamolecules' plasmonic mode triggers a spontaneous first order phase transition to a superradiant-like state of transmissivity oscillations, resulting from many-body interactions among the metamolecules, characterized by long-range order in space and time. The continuous time crystal state results from synchronization of picometer scale stochastic thermal movements of the nanowires that is driven by light-induced interactions of plasmonic metamolecules. In interpretation of these experiments, we discuss different routes to synchronization including the Kuramoto-like mechanism that rely on nonlinearity of the mechanical sub-system of the array and the mechanism involving non-reciprocal non-Hamiltonian forces of light pressure.

We argue that the continuous time crystal state is of interest to applications in all-optical modulation, frequency conversion, timing and all-optical computing.

References

1. . T. Liu, J. Y. Ou, N. Papasimakis, K. F. MacDonald, V. E. Gusev, N. I. Zheludev. Ballistic dynamics of flexural thermal movements in a nanomembrane revealed with subatomic resolution. **Science Adv.** 8, eabn8007 (2022) doi: 10.1126/sciadv.abn8007
2. T. Liu, J. Y. Ou, K. F. MacDonald, N. I. Zheludev. Photonic metamaterial analogue of a continuous time crystal. **Nature Phys.** (in press) doi: 10.48550/arXiv.2209.00324
3. T. Liu, C. H. Chi, J. Y.Ou, J. Xu, E. A. Chan, K. F. MacDonald, N. I. Zheludev. Picophotonics - subatomic optical localization beyond thermal fluctuations. **Nature Mat.** (in press) doi: 10.48550/arXiv.2205.01475

Conference Tutorials

META 2023, PARIS - FRANCE, JULY 18 – 21, 2023

Publishing Research with Impact in the Optics and Photonics Field

Anja Wecker
Wiley, Germany
anwecker@wiley.com

Abstract: For researchers, it's a long road from the idea to the published article. Choosing the right journal, convincing editors and reviewers, and making work visible to others are essential steps on the way to success. In this tutorial talk, I will give an insight into publishing opportunities in relevant journals and the related peer review process. From an editorial perspective, I will provide some guidance on how to best pass peer review and maximize success in scientific publishing.

META 2023, PARIS - FRANCE, JULY 18 – 21, 2023

Disordered optical metasurfaces

Philippe Lalanne
Institut d'Optique d'Aquitaine - LP2N, France
philippe.lalanne@institutoptique.fr

Abstract: Shaping the far-field radiation diagrams of surfaces engraved with high-index subwavelength structures belongs to a longstanding and fundamental ambition of wave science. The problem comes in different forms, but generally consists of angularly and spectrally controlling polychromatic light scattering with nanostructures smartly arrayed on a surface. We discuss important challenges in the emerging field of disordered metasurfaces to address applications such as light focusing, light extraction and detection, color and appearance creation.

Hybrid Nanomaterials and Metastructures for Photonics, Sensing and Energy

Ultrathin Suspended Chiral Metasurfaces for Enantiodiscrimination and Circularly Polarized Luminescence

Mengjia Cen,[1,2] Huilin He,[1] Jiawei Wang,[1] Jianxun Liu,[1] Tun Cao,[2,3] and Yan Jun Liu,[1,*]

[1]*Department of Electrical and Electronic Engineering, Southern University of Science and Technology, Shenzhen 518055, China*

[2]*Department of Biomedical Engineering, Dalian University of Technology Dalian, Dalian 116024, China*

[3]*School of Optoelectronic Engineering and Instrumentation Science, Dalian University of Technology, Dalian 116024, China*

*Corresponding author: yjliu@sustech.edu.cn

Artificially designed chiroptical metasurfaces can exhibit a strong circular dichroism, but they are usually limited by the complicated fabrication procedure and alignment errors. Here, we demonstrate a new type of self-aligned suspended bilayer metasurface with only one-step electron beam lithography exposure [1,2]. A significant optical chirality of 221° μm^{-1} can be realized using suspended metasurfaces with a thickness of 100 nm. Furthermore, we demonstrate that 1) such suspended chiral metasurfaces can be utilized for label-free discrimination of the chiral molecules at zeptomole level, exhibiting a much higher sensitivity (orders of magnitude) compared to the conventional circular dichroism spectroscopy [1]; 2) such suspended chiral metasurfaces can be utilized to induce strong circularly polarized luminescence from achiral nanocrystals including both upconversion nanoparticles (UCNPs) and quantum dots (QDs) [2,3]. Due to the giant chiroptical response, the proposed metadevice may offer promising applications for ultrathin circular polarizers, chiral molecular discrimination, imaging and sensing, etc.

References:

1. M. J. Cen, J. W. Wang, J. X. Liu, H. L. He, K. Li, W. F. Cai, T. Cao, and Y. J. Liu, Ultrathin Suspended Chiral Metasurfaces for Enantiodiscrimination, *Adv. Mater.* 34, 2203956 (2022).
2. M. J. Cen, J. W. Wang, J. X. Liu, Y. Li, W. F. Cai, D. L. Kong, D. Luo, T. Cao, and Y. J. Liu, Plasmonic Surface Lattice Resonances in Suspended Symmetric Double-Layer Gratings, *Photonics* 9, 890 (2022).
3. H. L. He, M. J. Cen, J. W. Wang, Y. W. Xu, J. X. Liu, W. F. Cai, D. L. Kong, K. Li, D. Luo, T. Cao, and Y. J. Liu, Plasmonic Chiral Metasurface-Induced Upconverted Circularly Polarized Luminescence from Achiral Upconversion Nanoparticles, *ACS Appl. Mater. Interfaces* 14, 53981–53989 (2022).

META 2023, PARIS - FRANCE, JULY 18 – 21, 2023

Locally controlling quantum yields in 2D semiconductors via electron tunneling

R. J. Peña Román[1], R. Bretel[2], D. Pommier[2], L. E. Parra López[3], E. Lorchat[4], E. Boer-Duchemin[2], G. Dujardin[2], A. G. Borisov[2], L. F. Zagonel[1], G. Schull[3], S. Berciaud[3], and E. Le Moal[2,*]

[1]Institute of Physics "Gleb Wataghin", Department of Applied Physics, State University of Campinas-UNICAMP, 13083-859 Campinas, Brazil
[2]Institut des Sciences Moléculaires d'Orsay, Université Paris-Saclay, CNRS, 91405 Orsay, France
[3]Institut de Physique et de Chimie des Matériaux de Strasbourg, Université de Strasbourg, CNRS, IPCMS, UMR 7504, F-67000 Strasbourg, France
[4]Physics & Informatics (PHI) Laboratories, NTT Research, Inc., Sunnyvale, California 94085, United States
[*]corresponding author: eric.le-moal@universite-paris-saclay.fr

Abstract: Using a scanning tunneling microscope, the radiative recombination yield of excitons in a laser-excited two-dimensional semiconductor is locally and electrically controlled.

Monolayer transition-metal dichalcogenides (TMDs)[1,2] are direct-bandgap two-dimensional (2D) semiconductors that have potentially groundbreaking applications in nanodevice technologies thanks to their unique optical and electronic properties. Even at room temperature, the photophysics of monolayer TMDs is governed by the exciton dynamics, i.e., the dynamics of bound electron-hole pairs that can diffuse in the 2D lattice and interact with each other or with charge carriers. Manipulating the elementary excitonic processes (i.e., exciton creation, diffusion and recombination) is key for the performance of TMD-based devices. In particular, the control of the luminescence quantum yield is a long sought-after goal in 2D optoelectronics and nanophotonics.[3] Attempts to control trion formation in monolayer TMDs on the nanoscale have been reported, e.g., using the plasmonic tip-substrate nanocavity of an atomic force microscope.[4] Nevertheless, distinguishing charge injection and electromagnetic effects in such plasmon-based experiments is challenging. Moreover, most of the techniques to locally control or excite excitons in 2D materials that are based on a scanning probe (or a focused electron beam) provide virtually no direct information about the diffusion and local recombination processes of these excitons,[5,6] a key aspect for the integration of these materials in realistic devices.

In this communication, we introduce a new method to locally and electrically control the radiative quantum yield of monolayer TMDs on transparent electrodes (i.e., indium tin oxide-coated glass) using the tip and the tunneling current of a scanning tunneling microscope (STM).[7] Via a combination of STM and wide-field photoluminescence microscopy, we uncover the effects of the biased tip-sample junction on the excitonic properties a WS_2 monolayer. The radiative quantum yield is modified in two ways, both of which are shown to be reversible. First, the near-field electromagnetic non-radiative transfer of energy from excitons to the non-plasmonic tungsten tip of the STM quenches the photoluminescence in an almost diffraction-limited area just below the tip. Secondly, bias and current-dependent photoluminescence quenching and enhancement occur within micrometer-scale areas around the tip position. We ascribe such "long-range" effects to lateral spatial gradients in the charge carrier density in the monolayer, which presumably modify the relative contributions of neutral and charged excitons to the photoluminescence and the radiative quantum yield of the excitons. Such doping gradients result from electron tunneling between the tip and the semiconductor and a partial electronic decoupling of the monolayer from the underlying conducting substrate.[7]

This work was supported by public grants from the French National Research Agency (H2DH ANR-15-CE24-0016, Intelplan ANR-15-CE24-0020, M-Exc-ICO ANR-16-CE24-0003, and ATOEMS ANR-20-CE24-0010) and overseen by the ANR as part of the "Investissements d'Avenir" program (Labex NIE ANR-11-LABX-0058-NIE and Labex NanoSaclay ANR-10-LABX-0035). This project has received funding from the European Research Council (ERC) under the European Union's Horizon 2020 research and innovation program (grant agreement no. 771850). This work has received financial support from the Fundação de Amparo à Pesquisa do Estado de São Paulo (FAPESP), through projects 18/08543-7, 20/12480-0, and 14/23399-9.

References

1. Mak, K. F. and J. Shan, "Photonics and optoelectronics of 2D semiconductor transition metal dichalcogenides," Nat. Photonics, Vol. 10, 216, 2016.
2. Wang, G., A. Chernikov, M. M. Glazov, T. F. Heinz, X. Marie, T. Amand, and B. Urbaszek, "Colloquium: Excitons in atomically thin transition metal dichalcogenides," Rev. Mod. Phys., Vol. 90, 021001, 2018.
3. Lien, D.-H., S. Z. Uddin, M. Yeh, M. Amani, H. Kim, J. W. Ager, E. Yablonovitch, and A. Javey, "Electrical suppression of all nonradiative recombination pathways in monolayer semiconductors," Science, Vol. 364, 468−471, 2019.
4. He, Z., Z. Han, J. Yuan, A. M. Sinyukov, H. Eleuch, C. Niu, Z. Zhang, J. Lou, J. Hu, D. V. Voronine, and M. O. Scully, "Quantum plasmonic control of trions in a picocavity with monolayer WS_2," Sci. Adv., Vol. 5, eaau8763, 2019.
5. Park, K.-D., O. Khatib, V. Kravtsov, G. Clark, X. Xu, and M. B. Raschke, "Hybrid Tip-Enhanced Nanospectroscopy and Nanoimaging of Monolayer WSe_2 with Local Strain Control," Nano Lett., Vol. 16, 2621−2627, 2016.
6. Bonnet, N., H. Y. Lee, F. Shao, S. Y. Woo, J.-D. Blazit, K. Watanabe, T. Taniguchi, A. Zobelli, O. Stéphan, M. Kociak, S. Gradečak, and L. H. G. Tizei, "Nanoscale Modification of WS_2 Trion Emission by Its Local Electromagnetic Environment," Nano Lett., Vol. 21, 10178−10185, 2021.
7. Peña Román, R. J., R. Bretel, D. Pommier, L. E. Parra López, E. Lorchat, E. Boer-Duchemin, G. Dujardin, A. G. Borisov, L. F. Zagonel, G. Schull, S. Berciaud, and E. Le Moal, "Tip-induced and electrical control of the photoluminescence yield of monolayer WS_2," Nano Lett., Vol. 22, No. 23, 9244–9251, 2022.

Photoluminescence Engineering with Surface Lattice Resonances

S. Murai*

Department of Material Chemistry, Graduate School of Engineering, Kyoto University, Japan
*Corresponding author: murai@dipole7.kuic.kyoto-u.ac.jp

Abstract: We combined a luminescent layer or substrate with metallic or dielectric nanoantennae to harness the photoluminescence into a specific direction predefined by the antenna design. A notable (> 10 times) enhancement in in radiation intensity into a designated direction is demonstrated. We describe the mechanism using a simple analytical model. We also fabricated "nanoantenna sticker" where the nanoantenna is embedded in a flexible polymer. The sticker can be stacked on any clean surfaces and act as nanoantenna.

Nanoantenna is a periodic array of scattering elements that can harness light into a specific direction. Combination of nanoantenna with phosphors enables spatial and spectral control over the luminescence (Fig. 1) [1-3]. In this presentation, we use several sets of nanoantennae (metallic or dielectric) and phosphors (organic or inorganic) to demonstrate the luminescence control. Typical nanoantenna consists of aluminum [1], silicon [2], and titanium dioxide [3]. We will discuss the difference of conversion efficiency from blue excitation to yellow-red luminescence for the metallic and dielectric nanoantenna.

We also introduce the nanoantenna stickers, which are the nanoantenna embedded in the flexible polymer [4]. We place this sticker on top of the luminescent layers to modulate their emission directionality. Because of its flexibility, the sticker gives control over luminescent directionality via stretching/compressing it.

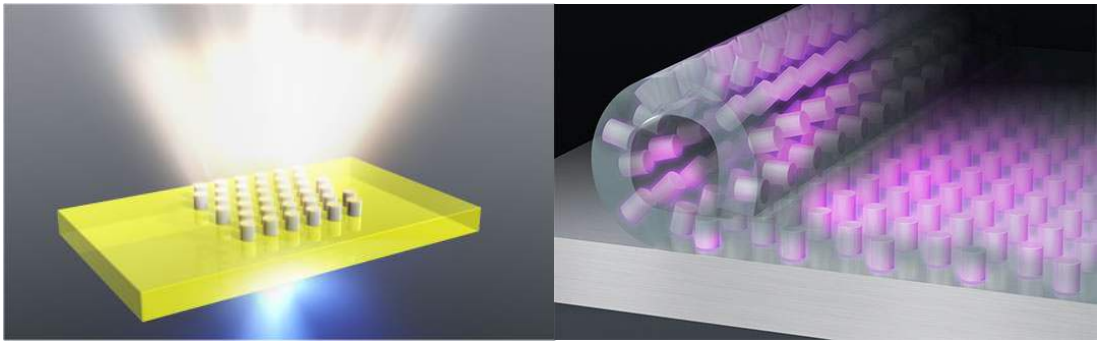


Fig. 1: (left) Sketch of the nanoantenna phosphor, converting a blue light into yellow photoluminescence with a directionality. (right) Sketch if the nanoantenna sticker, which is flexible and can be attached to any clean surfaces.

We acknowledge financial support from MEXT (Kekanhi 22K18884, 22H01776), Izumi Science and Technology Foundation, Casio Science Promotion Foundation and The Futaba Foundation.

References

1. Kamakura, R. et al., "Enhanced photoluminescence and directional white-light generation by plasmonic array," *J. Appl. Phys.* **124**, (2018) 213105
2. Liu, L. et al., "Loss Control with Annealing and Lattice Kerker Effect in Silicon Metasurfaces," *Adv. Photon. Res*., (2021) 2100235
3. Murai, S. et al., "Photoluminescence engineering with nanoantenna phosphors," *J. Mater. Chem. C* **129**, (2023) 163101 11, 472-479
4. Agata, K. et al., "Stick-and-play metasurfaces for directional light outcoupling," *Appl. Phys. Lett*. **118**, (2021) 021110

DNA Origami as a Versatile Method for Bottom-Up Fabrication of Plasmonic Metamaterials

Christoph Sikeler[1*], Susanne Kempter[1], Franziska Haslinger[1] and Tim Liedl[1]

[1]Ludwig-Maximilians-Universität, Germany
[*]corresponding author: C.Sikeler@physik.uni-muenchen.de

Abstract: In this work, we exploit the flexibility of DNA origami to create different kinds of metamaterials. DNA origami structures are created in a bottom-up, self-assembly process and plasmonic nanoparticles can be attached at predesigned locations. This can be used to create periodic lattices in solution as well as on a surface.

DNA origami is a very versatile technique to fabricate arbitrary nanostructures in a bottom-up, highly paralyzed manner. It utilizes the specificity of Watson-Crick base pairing to assemble designed structures from a long single-stranded DNA strand (scaffold) and multiple short oligonucleotides (staples). The desired geometry is built from multiple DNA double helices, which can be approximated by a cylindrical shape and are tightly connected by repeating DNA crossover motives[1].

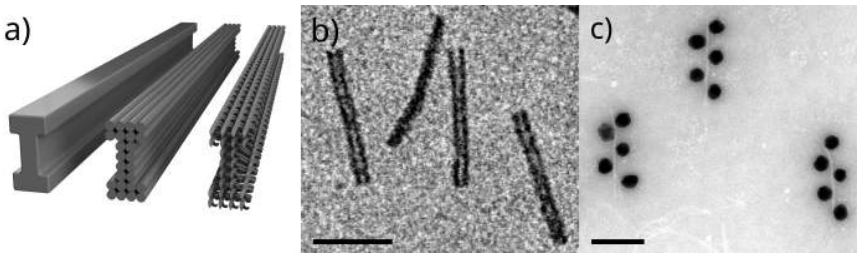


Figure 1: *Left: Illustration of an H-beam. Middle: Illustration of an H-beam structure filled with cylinders. Right: Illustration of an H-beam build from DNA double helices. (b) TEM image of an H-beam DNA origami structure. (c) TEM image of an H-beam DNA origami structure to form a zigzag pattern with five attached gold nanospheres.*

There are many ways to chemically modify DNA strands. Therefore, a large variety of molecules and particles can be functionalized with DNA. By extending staple strands in the DNA origami structure with a sequence that is complementary to the sequences of strands that are conjugated to the molecules of interest, it is possible to introduce these guest molecules at specific locations on the DNA origami structure (Figure 1). Guest molecules can for example be metallic nanoparticles, quantum dots, fluorophores or proteins. Consequently, DNA origami structures decorated with metallic nanoparticles can be used to build plasmonic systems with high accuracy and without the need for lithography.

On the other hand, one can use e-beam lithography to arrange DNA origami structures on a surface[2]. Once attached to the surface, the origami structures can be used to capture metallic nanoparticles like gold nanospheres, see Fig. 2 a and b. The specific interaction between the DNA origami structure and the nanoparticles allows for a very precise positioning. Therefore, e-beam lithography combined with DNA origami enables us to build functional surfaces with metallic nanoparticles whose geometry would be difficult to produce with lithography.

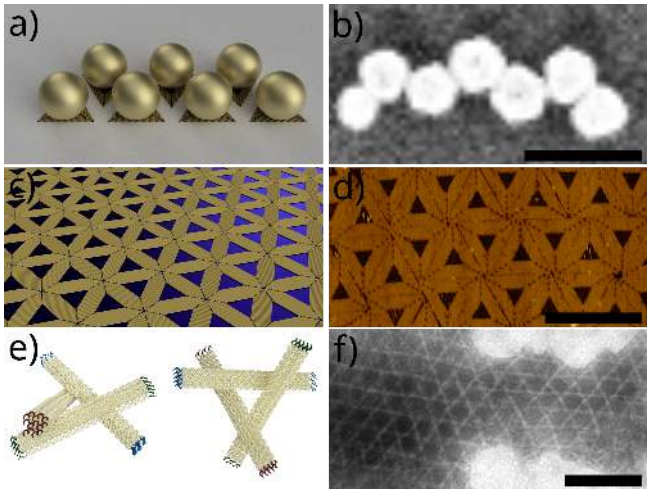


Figure 2: *Illustration and experimental implementation of DNA origami structures. (a) Illustration of gold nanospheres arranged in a zigzag pattern using DNA origami and e-beam lithography. (b) SEM image of gold nanospheres arranged on DNA origami structures in a zigzag pattern. (c) Illustration of a periodic DNA origami surface. (d) AFM image of triangular origami structures forming a closed packed pattern on a mica surface. (e) Illustration of a DNA origami structure which can be multimerized to build a rhombohedral crystal. (f) TEM image of a rhombohedral crystal formed by DNA origami.*

Furthermore, periodic surfaces can be created even without any lithography. Under certain conditions the DNA origami structures accumulate at the surface. In order to fit as many DNA origami structures to the surface as possible, the structures will arrange in a closed packed pattern[3]. For example, incubating a triangular DNA origami structure at a surface will result in a hexagonal pattern, see Fig. 2 c and d. Each of the origamis can subsequently capture guest molecules. Hence, a periodic pattern of plasmonic particles can be created completely by a bottom-up, self-assembly process.

DNA origami can also be used to build periodic crystals in liquid. By employing the specificity of DNA base pairing, DNA origamis can be programmed to attach to each other. Therefore, a single DNA origami structure forms a unit cell which multimerizes into a large periodic lattice[4], see Fig. 2 e and f. Again, this lattice can bind guest particles at predesigned locations in each unit cell. As a result, one ends up with a periodic one-, two- or three-dimensional array of plasmonic particles.

References

1. Rothemund, P. W. K. “Folding DNA to create nanoscale shapes and patterns”, Nature, Vol. 440, 297-302, 2006
2. Kershner, R. J., Bozano, L. D., Micheel, C. M., Hung, A. M., Fornof, A. R., Cha, J. N. Rettner, C. T., Bersani, M., Frommer, J. Rothemund, P. W. K., Wallraff, G. M., “Placement and orientation of individual DNA shapes on lithographically patterned surfaces”, Nature Nanotechnology, Vol. 4, 557-561, 2009
3. Xin, Y., Shen, B., Kostiainen, M. A., Grundmeier, G., Castro, M., Linko, V., Keller, A., “Scaling Up DNA Origami Lattice Assembly”, Chem. Eur. J., Vol. 27, 8564, 2021
4. Zhang, T., Hartl, C., Frank, K., Heuer-Jungmann, A., Fischer, S., Nickels, P. C., Nickel, B., Liedl, T., “3D DNA Origami Crystals”, Adv. Mater., Vol. 30, 1800273, 2018

Oriented Colloidal Quantum Wells:
Pushing the Limits, Breaking Records

Hilmi Volkan Demir
NTU Singapore – Nanyang Technological University, School of Electrical and Electronic Engineering, School of Physical and Mathematical Sciences, School of Materials Science and Engineering, Singapore

Bilkent University UNAM, Department of Electrical and Electronics Engineering, Department of Physics, Institute of Materials Science and Nanotechnology, National Nanotechnology Research Center, Ankara, Turkey
hvdemir@ntu.edu.sg, volkan@bilkent.edu.tr

We introduce a powerful, large-area self-assembly technique for orienting colloidal quantum wells in all face-down configuration. We demonstrate three-dimensional constructs of such oriented self-assemblies with monolayer precision. We present the most recent examples of LEDs and lasers using these oriented assemblies for lighting and displays. Here we also show record high efficiency from their LEDs and record thin gain medium from their laser structures. These solution-processed quantum wells hold great promise to challenge their epitaxial thin-film counterparts in semiconductor optoelectronics.

Guided mode resonance enhanced upconversion luminescence of upconversion nanoparticles for immunoassay with ultralow limit of detection

Yu-Chung Chiu[1], Yen-Ta Tseng[1,2], Van Dai Pham[1], Wen-Hsuan Wu[1], Thanh Thu Le Vu[1], Chao-An Chang[1], Lai-Kwan Chau[2], Shiao-Wei Kuo[3], Michael WY Chan[4], Hung-Chih Kan[1], Jiunn-Yuan Lin[1], Chia-Chen Hsu[1,*]

[1] Department of Physics, National Chung Cheng University, Ming-Hsiung, Chia-Yi, 621, Taiwan
[2] Department of Chemistry and Biochemistry National Chung Cheng University, Chia-Yi, 621, Taiwan
[3] Department of Materials and Optoelectronic Science, National Sun Yat Sen University, Kaohsiung, 804, Taiwan
[4] Department of Biomedical Science, National Chung Cheng University, Chia-Yi, 621, Taiwan
[*]corresponding author: phycch@ccu.edu.tw

Abstract: A low refractive index resonant waveguide grating (RWG) is integrated with up-conversion nanoparticles (UCNPs) to from a sandwich type immunoassay. Guided mode resonance enhanced evanescent field is formed atop of the RWG to enhance upconversion luminescence of UCNPs in aqueous and the detection sensitivity of the bioassay is greatly increased. The limit of detection of the bioassay is 0.42 fg/mL for the detection of cardiac troponin I, which is 6 orders lower than acute myocardial infarction threshold value (~28 pg/mL).

In this work, a novel sandwich type immuneassay, based on the integration of a low refractive index resonant waveguide grating (low-n RWG) and upconversion nanoparticles (UCNPs), hereafter called as low-n RWG + UCNPs sandwich bioassay, is presented for the detection of the concentration cardiac troponin I, (cTnI). Figure 1 displays the structure of a 3x3 sandwich type low-n RWG + UCNPs bioassay. In each pixel, capture antibodies (anti-cardiac troponin I) are immobilized on the low-n RWG surface to seize cTnI. UCNP-conjugated detection antibodies are bound to cTnI to form a sandwich structure. The use of UCNPs in the assay provides the following advantages: (1) no background luminescence is generated from the carrier fluid or the assay biochemistry because UCNPs are excited with near-infrared (NIR) light. It can significantly reduce the limit of detection (LOD) to a value much lower than those of conventional assays. (2) The upconversion luminescent (UCL) properties of UCNPs are inert to the environment. The detection process is not influenced by the sampled fluid and the variation of environmental sampling conditions. In our previous investigation, we found that as the low-n RWG is illuminated by NIR light with resonant excitation configuration, i.e. incident light matching with guided mode resonance (GMR) condition, strong local field can be formed atop of the low-n RWG. As a result, UCL of UCNPs can be greatly enhanced [1-3], and thus significantly improves the detection sensitivity of the low-n RWG + UCNPs bioassay.

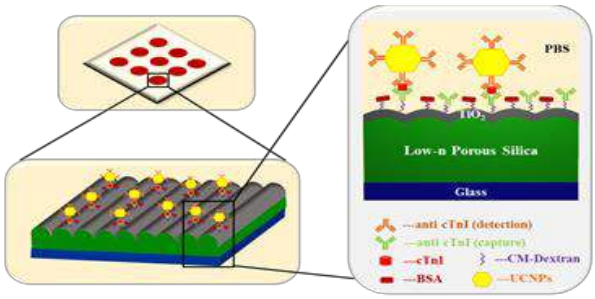


Figure 1 Schematic diagram of a 3x3 sandwich type low-n RWG + UCNPs bioassay

Figure 2 (a) shows UCL spectra of the low-n RWG + UCNPs bioassay with cTnI concentration of 1 pg/ml obtained with two different excitation angles $\theta=22^0$ (resonant excitation) and $\theta=0^0$ (non-resonant excitation). The result confirms that the resonant excitation indeed can greatly enhance UCL intensity of UCNPs. The inset shows UCL images of the low-n RWG + UCNPs bioassay taken with the aforementioned excitation angles. Figure 2 (b) shows UCL spectra at 450 nm of low-n RWG + UCNPs bioassays varying with concentrations of cTnI in PBS obtained under resonant excitation condition ($\theta=22^0$). As displayed, the UCL intensity increases as the concentration of cTnI increases. Figure 2 (c) plots UCL peak intensity at 450 nm versus the concentration of cTnI obtained by three different chips. From the plot, the LOD of the bioassay for the detection of cTnI was found to be 0.42 fg/mL. The bioassay offers the detection range over 7 orders of magnitude of cTnI concentration from 1 fg/mL to 1 ng/mL. To address the challenges of matrix effects and interference, two human sera were diluted 100 times with PBS and spiked with known cTnI concentrations as internal controls. Their recoveries are 113.2% and 96.3%. Our results confirm that the low-n RWG+UCNPs sandwich bioassay indeed can improve LOD to fg/ml level, about three to five orders lower than those of obtained by other techniques. Therefore, the low-n RWG + UCNPs sandwich bioassay should be useful for detecting very low concentration of biomarkers in blood.

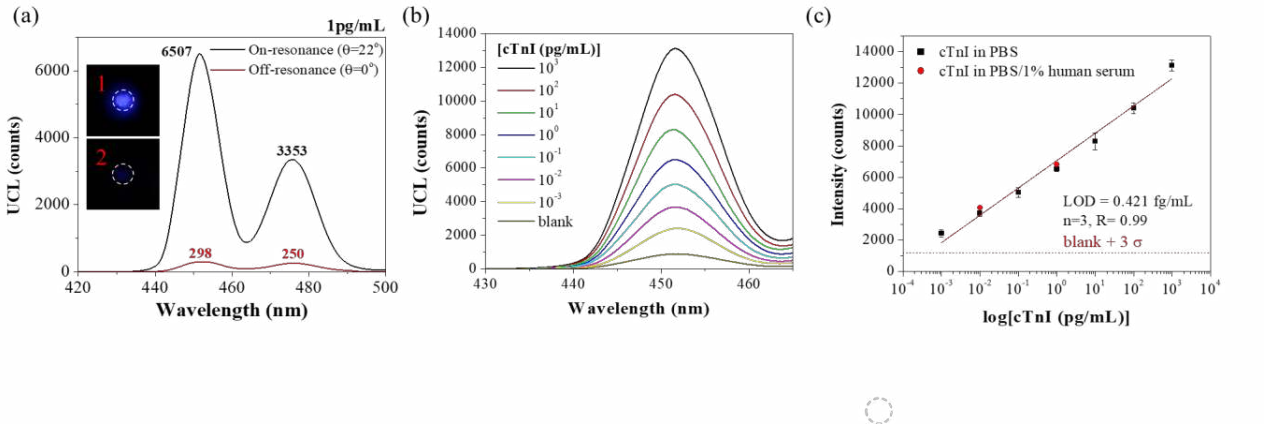


Figure 2 (a) UCL spectra of the low-n RWG + UCNPs bioassay with cTnI concentration of 1 pg/ml obtained with $\theta=22^0$ and $\theta=0^0$. (b) UCL spectra at 450 nm of the low-n RWG + UCNPs bioassays varying with concentrations of cTnI in PBS obtained with $\theta=22^0$. (c) UCL peak intensity at 450 nm versus the concentration of cTnI obtained by three different chips.

References

1. Lin, J. H. Liou, H. Y. Wang, C. D. Tseng, C. Y. Lee, C. T. Ting, C. C. Kan, H. C. and Hsu, C. C. " Giant enhancement of upconversion fluorescence NaYF4:Yb^{3+},Tm^{3+} nanocrystals with resonant waveguide grating substrate", ACS Photonics, 2, 4, 530-536, 2015.
2. Vu, D. T. Chiu, H. W. Nababan, R. Le, Q. M. Kuo, S. W. Chau, L. K. Ting, C. C. Kan, H. C. and Hsu, C. C. "Enhancing upconversion luminescence emission of rare earth nanophosphors in aqueous solution with thousands fold enhancement factor by low refractive index resonant waveguide grating" ACS Photonics, 5, 8, 3263-3271, 2018.
3. Vu, D. T. Tsai, Y. C. Le, Q. M. Kuo, S. W. Lai, N. D. Benisty, H. Lin, J. Y. Kan, H. C. and Hsu, C. C. "A synergy approach to enhance upconversion luminescence emission of rare earth nanophosphors with million-fold enhancement factor" Crystals, 11, 10, 1187, 2021.

Chiro-optical gradient forces in chiral nanomaterials

Hiromi Okamoto[1*], Junsuke Yamanishi[1], and Hyo-Yong Ahn[1,2]

[1]Institute for Molecular Science, National Institutes of Natural Sciences, Japan
[2]Center for Novel Science Initiatives, National Institutes of Natural Sciences, Japan
[*]corresponding author: aho@ims.ac.jp

Abstract: When a chiral nanomaterial is irradiated by circularly polarized light, the material in general exhibits chiro-optical effects. The chiro-optical effects appear as various forms. Here we report chiral optical gradient force observation on chiral nanoparticles and nanoscale imaging of chiro-optical force fields.

When a chiral nanomaterial is irradiated by circularly polarized light, the material in general exhibits chiro-optical effects. The chiro-optical effects appear as various forms, typified by circular dichroism (CD) and optical rotation (OR). When a small particle is illuminated with strong focused laser beam, the particle is trapped at the focal point due to the optical gradient force, which is known as optical trapping. Chiral nanoparticles are expected to exhibit chiro-optical trapping effects. That is, the optical gradient force exerted on the chiral particle depends, when trapped by circularly polarized light, on the handedness of the circular polarization. In this paper, we report studies related to chiro-optical effects on the optical gradient forces on chiral nanostructures.

Chiral optical gradient force on chiral nanoparticles. We investigated the chiral characteristics of gradient force for chiral nanoparticles, which has not previously been studied experimentally. Three-dimensional helicoid-shaped chiral gold nanoparticles[1] (Fig. 1) were trapped by circularly polarized light and the characteristics depending on the handedness of the trapping light and on the handedness of the particle were examined.[2] The colloidal solutions of the chiral nanoparticles showed strong CD (and OR) bands in visible to near-infrared region, in resonance with the surface plasmon modes. We trapped the particles in water with loosely focused circularly polarized laser beam in the wavelength region near the plasmon resonance (680-720 nm).

The experimental results showed that the gradient force depended on the handedness of the CP of the trapping light and the particle chirality. The wavelength dependence of the gradient force tends to follow the CD spectrum of the colloidal solution rather than the OR, and this result indicates that the spectral features of the chiral gradient

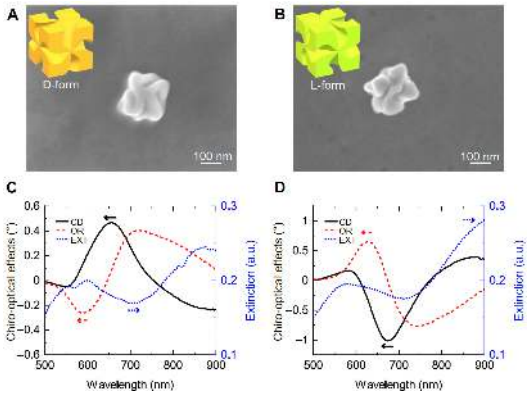


Fig. 1 SEM images (A,B) and CD, OR, and extinction spectra (C,D) of D-form (A,C) and L-form (B,D) helicoid gold nanoparticles.[2]

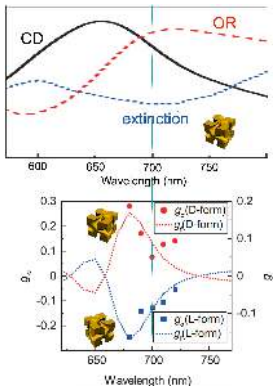


Fig. 2 Optical spectra of the colloidal solution of D-form particles (top) and experimental (dots) and simulated (curves) wavelength dependences of gradient force dissymmetries (bottom).[2]

force are influenced not only by the real part of the refractive index but also by the electromagnetic field perturbed by the chiral particle. This is in sharp contrast to the well-known behavior of the gradient force, which is governed by the real part of the refractive index. The extended aspect of the chiral optical force obtained here can provide novel methodologies on chirality sensing, manipulation, separation, enantioselective biological reactions, and so forth.

Nanoscale imaging of chiro-optical force. Atomic force microscopy is based on detection of forces between the probe tip and the matter to be observed. This principle can be applicable to optical forces due to interaction between dipoles on the probe and on the sample, induced by irradiation of light. This method of microscopic imaging has been known as photoinduced force microscopy. By detecting difference between the force under left- and right-handed circularly polarized illumination with the photoinduced force microscopy, we can expect to visualize chiral optical fields on the sample under irradiation of light.

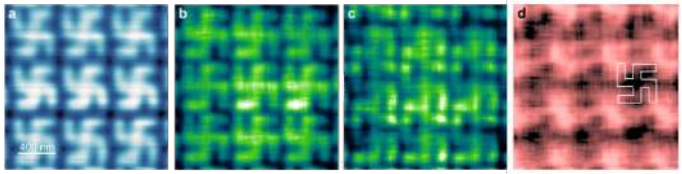


Fig. 3 (From left to right) AFM image, photoinduced force images under right- and left-circularly polarized light at 785 nm, and the differential image between the two photoinduced force images, for right-handed gold gammadion array structure. The unit cell size is 540 nm.

We thus developed an experimental system for nanoscopic observation of chiro-optical force and imaging of chiral optical fields on the samples, based on photoinduced force microscope. We adopted gold coated AFM tip as the probe to detect interaction with the sample induced by irradiation of the system by circularly polarized light. Heterodyne frequency modulation technique[3] was utilized to eliminate the thermal effects by the light. The photoinduced force images under illumination of left- and right-circularly polarized light were recorded, and the chiro-optical image was obtained as the difference between the two. As the test sample, we fabricated left- and right-handed gold gammadion structure arrays by electron-beam lithography method. The result of chiro-optical image of the sample is demonstrated in Fig. 3. We succeeded in visualizing nanoscale chiral optical fields in the vicinity of the nanostructures. It is seen that the local chiro-optical effect is prominent at the corners of each gammadion. The technique provides a new method to investigate chiral optical near-fields and paves the way for revealing the physical phenomena of nanoscale chiro-optical effects and technological development based on that.

The authors thank Drs. S. Hashiyada, H. Yamane, and Profs. K. T. Nam and H. Ishihara for their contributions. This work was supported by Grants-in-Aid for Scientific Research (KAKENHI Nos. JP22225002, JP15H02161, JP15K13683, JP15J01261, JP16H06505, JP17H07330, JP21H04641, JP21K18884, and JP22H05135).

References

1. H.-E. Lee, H.-Y. Ahn, J. Mun, Y. Y. Lee, M. Kim, N. H. Cho, K. Chang, W. S. Kim, J. Rho, K. T. Nam, "Amino-acid- and peptide-directed synthesis of chiral plasmonic gold nanoparticles," *Nature*, **556**, 360-365, 2018.
2. J. Yamanishi, H.-Y. Ahn, H. Yamane, S. Hashiyada, H Ishihara, K. T. Nam, H. Okamoto, "Optical gradient force on chiral particles," *Sci. Adv.*, **8**, eabq2604, 2022.
3. J. Yamanishi, Y. Naitoh, Y. J. Li, Y. Sugawara, "Heterodyne Frequency Modulation in Photoinduced Force Microscopy," *Phys. Rev. Appl.*, **9**, 024031, 2018.

META 2023, PARIS - FRANCE, JULY 18 – 21, 2023

Local photochemical nanoscopy of plasmonic photocatalysts at work

A. Naldoni[1]

[1]Department of Chemistry and NIS Centre, University of Turin, 10125 Turin, Italy
[*]corresponding author: alberto.naldoni@unito.it

Abstract: Recent investigations have demonstrated the strength of investigating the interactions occurring between plasmonic materials and molecules at the nanoscale to elucidate the richness of reactivity offered by plasmon−driven photocatalysis. In this talk, I will present a photochemical nanoscopy technique that enables the 2D mapping of plasmonic reaction products, and thus of the hot carriers driving photocatalysis, with subwavelength resolution. This approach opens the way to a deeper understanding of how photonic low-dimensional materials drive chemical transformations.

META 2023, PARIS - FRANCE, JULY 18 – 21, 2023

Tailoring the emission and the photodynamics of quantum emitters with high index dielectric nanostructures

Mélodie Humbert[1,2], R. Hernandez[1,2], Peter R. Wiecha[3], Nicolas Mallet[3], Frank Fournel[4], Vincent Larrey[4], Aurélie Lecestre[3], Guilhem Larrieu[3], Christian Girard[1], Vincent Paillard[1], Laurence Ressier[2], and Aurélien Cuche[1,*]

[1]CEMES-CNRS, Université de Toulouse, CNRS, UPS, Toulouse, France
[2]LPCNO, Université de Toulouse, CNRS, INSA, UPS, 135 Avenue de Rangueil, 31077 Toulouse, France
[3]LAAS-CNRS, Université de Toulouse, CNRS, INP, Toulouse, France
[4]Université Grenoble Alpes, CNRS, CEA-Leti Minatec, Grenoble, France
*corresponding author, E-mail: aurelien.cuche@cemes.fr

Abstract: We show both experimentally and theoretically that the photodynamics of quantum emitters (NV colored centers in nanodiamonds), accurately positioned by AFM nanoxerography in the near field of silicon dimer nanoantennas, can be controlled by these simple high-index dielectric nanostructures. Then, in order to go a step further and control the directive emission of such quantum sources, we explore numerically and optimize with an evolutionary optimization algorithm, the geometry of silicon nanoantennas, made of a limited number of building blocks.

Introduction

Improving the brightness and efficiency of single photon sources by the mean of optically resonant nanostructures is a major stake for the development of efficient nanodevices for quantum communications.

For a couple of decades, these resonant nanostructures have mainly been made of noble metal that sustain strong localized resonances (LSPR) that can be used to manipulate, concentrate or redirect visible light. Such properties have led to numerous actual or potential applications in integrated optics, sensors, nonlinear optics, field-enhanced spectroscopies, or photovoltaics. Recently, an alternative emerged with high refractive index dielectric nanostructures, which offer the same range of applications as plasmonics by manipulating Mie optical resonances instead of LSPR [1].

These resonances can be efficiently tuned by modifying the size, shape, and material of those nanostructures (e.g. silicon, n ~ 4) [2]. Furthermore, high index dielectric nanostructures offer several key advantages when compared to their metallic counterparts: absorption losses are far weaker for wavelengths longer than the direct band gap, access to semiconductor (CMOS) technology for nanostructure fabrication, and presence of intrinsic strong magnetic and electric resonances, providing an unique opportunity to spatially separate and redistribute the energy of the magnetic and electric parts of the electromagnetic field in the near field, otherwise inextricably connected in the far field [3].

Discussion

We discuss here the effect of simple high index dielectric nanoantennas on the spontaneous emission of model quantum emitters. First, we accurately positioned arrays of nanodiamonds hosting NV colored centers in the gap of silicon dimer nanoantennas, using atomic force microscopy (AFM – [4]) nanoxerography [5]. The NV center is an ideal model system exhibiting single photon emission properties at room temperature, which is well adapted for proof of concept experiments in quantum nano-optics. Since the emission rate of the emitters, and therefore the local density of photonic states (LDOS), are modified by the nanostructure, we show by the mean of time-resolved photoluminescence acquisitions that the photodynamics of these electric dipoles can be enhanced by the coupling to the nanoantenna down to the single photon emission regime [5]. Our experimental results are in good agreement with multipolar analysis and numerical simulations based on the Green Dyadic Method - GDM.

Second, in order to go a step further, we explore numerically the control of the directive emission from quantum dipolar sources by the mean of complex Si antennas. The latter, made of a given number of building (nano)blocks, are optimized by an Evolutionary Algorithm (EA). The geometries obtained allow to tailor the emission direction of a single dipolar source, maximizing the intensity of the emitted light within a given solid angle. Our numerical experiments demonstrate the efficiency of such EA-optimized antennas.

Acknowledgements

This work was supported by Programme Investissements d'Avenir under the program ANR-11-IDEX-0002-02, reference ANR-10-LABX-0037-NEXT, by the HiLight ANR project ANR-19-CE24-0026, by LAAS-CNRS micro and nanotechnologies platform member of the French Renatech network, by the CNRS and INSA (M.H. PhD grant), by the Région Midi-Pyrénées via the Institute for Quantum technologies in Occitanie (IQO), and by the computing facility center CALMIP of the University of Toulouse under grants P12167 and P1107.

References

[1] H. Kallel, A. Arbouet, G. Benassayag, A. Chehaidar, A. Poti, B. Salem, T. Baron, V. Paillard, Tunable enhancement of light absorption and scattering in Si1xGex nanowires, *Phys. Rev. B* 12: 085318, 2012.

[2] P.R. Wiecha, A. Cuche, A. Arbouet, C. Girard, G. Colas des Francs, A. Lecestre, G. Larrieu, F. Fournel, V. Larrey, T. Baron, V. Paillard, Strongly directional scattering from dielectric nanowires, *ACS Photonics* 4: pp 2036–2046, 2017.

[3] P.R. Wiecha, C. Majorel, C. Girard, A. Arbouet, B. Masenelli, O. Boisron, A. Lecestre, G. Larrieu, V. Paillard, A. Cuche, Enhancement of electric and magnetic dipole transition of rare-earth-doped thin films tailored by high-index dielectric nanostructures, *Appl. Opt.* 58, 1682, 2019.

[4] M. Humbert, Y. Hallez, V. Larrey, F. Fournel, E. Palleau, V. Paillard, A. Cuche, L. Ressier, Versatile, rapid and robust nanopositioning of single-photon emitters by AFM-nanoxerography, *Nanotechnology* 33, 215301, 2022.

[5] M. Humbert, R. Hernandez, N. Mallet, G. Larrieu, V. Larrey, F. Fournel, F. Guérin, E. Palleau, V. Paillard, A. Cuche, L. Ressier, Large-scale controlled coupling of single-photon emitters to high index dielectric nanoantennas using AFM nanoxerography, *Nanoscale* 15, 599-608, 2023.

META 2023, PARIS - FRANCE, JULY 18 – 21, 2023

Novel Second Harmonic Rayleigh and Mie scattering chiroptical effects

Ventsislav K. Valev[1,2,3]
1 Centre for Photonics and Photonic Materials, University of Bath, Bath, BA2 7AY, United Kingdom
2 Centre for Nanoscience and Nanotechnology, University of Bath, Bath, BA2 7AY, United Kingdom
3 Department of Physics, University of Bath, Bath, BA2 7AY, United Kingdom
*corresponding author, E-mail: v.k.valev@bath.ac.uk

Abstract: Following our recent discovery of the Hyper Rayleigh Scattering Optical Activity (HRS OA) [1,2], we report both novel forms of harmonic chiroptical scattering and novel materials in which these effects can be observed. The new effects are enable chiroptical characterization in tiny volumes of illumination. They are also highly sensitive and capable of characterizing the chirality of a single metal nanoparticles, floating freely in an isotropic liquid environment.

Chirality – the geometric property of breaking mirror-symmetry – is omnipresent in nature. It is exhibited in the spiral shapes of galaxies in motion, in the storm systems of planetary atmospheres, in the shape of human hand, the shells of many snails, in the twist of seeds and bacteria, as well as in molecules, such as DNA, proteins, sugars and amino acids. In molecules, the handedness (i.e. their direction of twist) is extremely important as it can determine the nature of chemical reactions or the expression of genes. Circular dichroism and optical rotation are among the main chiral optical (chiroptical) techniques that serve to routinely characterize the handedness of chiral molecules and inorganic particles. However, these optical effects are considered intrinsically weak, and, in order to accumulate a large measurable signal, they rely on large illumination volumes and large amounts of chiral analytes.

By contrast, in the case of nonlinear chiral optical method, the effects are orders of magnitude more pronounced. These effects are usually limited in space to the only the focal point of illumination. The caveat is that such nonlinear chiral optical methods have been considered technologically complex and their applications beyond the laboratory environment have been limited.

To cite a few examples, second harmonic generation circular dichroism[3] and second harmonic generation optical rotation [4] were the first nonlinear chiroptical effects reported but they are based on symmetry breaking interfaces and are therefore not suited for investigating chirality in liquids, such as water – the medium of life. For such isotropic liquids, chirality can be characterized by sum frequency generation.[5,6] This technique is a good example of the technological complexity often associated with nonlinear chiroptical methods – it requires it requires two light pulses on two non-collinear beam paths, with different polarization to be superimposed at the same point, both in space and in time. Going to higher nonlinear chiroptical effects (those that engage the third susceptibility, or second hyper-polarizability), good examples are nonlinear circular dichroism or optical rotatory dispersion [7]. These methods are measured against the background of linear effects, which is also the case for Polarimetric z-scan [8], where the linear optical effect serves to calibrate the nonlinear method.

In 2019, our team reported the first experimental observation of the effect – Chiroptical Harmonic Scattering – at the second harmonic, from Ag nanohelices[1]. This paper settled the 40-year old scientific question. We later reported the effect from chiral Au nanocubes [9], from semiconductor (CdTe) nanoparticles [10] and at the third harmonic wavelength (together with Andrews) [11]. In [9], we also set a sensitivity record, reporting the first chiroptical characterisation of a single nanoparticle floating freely in a liquid environment, a sensitivity that was further confirmed in [12].

Here, we report chiroptical Mie scattering at the Second Harmonic and chiroptical second harmonic Rayleigh scattering in a class of materials where the effects had not been seen before.

Acknowledgements

V.K.V. acknowledges support for this work from the Royal Society through the University Research Fellowships and the Royal Society grants PEF1\170015 and RGF\EA\180228, as well as the STFC grant ST/R005842/1. Acknowledged also is funding and support from the Engineering and Physical Sciences Research Council (EPSRC) Centre for Doctoral Training in Condensed Matter Physics (CDT-CMP), Grant No. EP/L015544/1 and EP/T001046/1.

References

1. J. T. Collins, K. R. Rusimova, D. C. Hooper, H.-H. Jeong, L. Ohnoutek, F. Pradaux-Caggiano, T. Verbiest, D. R. Carbery, P. Fischer, V. K. Valev, First Observation of Optical Activity in Hyper-Rayleigh Scattering, Phys Rev. X 9, 011024 (2019).
2. L. D. Andrews, T. Thirunamachandran, Hyper−Raman scattering by chiral molecules. J. Chem. Phys. 70, 1027 (1979).
3. T. Petralli-Mallow, T. M. Wong, J. D. Byers, H. I. Yee, and J. M. Hicks, Circular dichroism spectroscopy at interfaces: a surface second harmonic generation study J. Phys. Chem. 97, 1383 (1993).
4. J. D. Byers, H. I. Yee, and J. M. Hicks, A second harmonic generation analog of optical rotatory dispersion for the study of chiral monolayers, J. Chem. Phys. 101, 6233 (1994).
5. M. A. Belkin, S. H. Han, X. Wei, and Y. R. Shen, Sum-Frequency Generation in Chiral Liquids near Electronic Resonance, Phys. Rev. Lett. 87, 113001 (2001).
6. R. Boyd, “Nonlinear Optics”, 3rd edition, Elsevier, 2008, p. 270.
7. H. Mesnil, F. Hache, Experimental Evidence of Third-Order Nonlinear Dichroism in a Liquid of Chiral Molecules, Phys. Rev. Lett. 85, 4257 (2000).
8. P. P. Markowicz, M. Samoc, J. Cerne, P. N. Prasad, A. Pucci, G. Ruggeri, Modified Z-scan techniques for investigations of nonlinear chiroptical effects, Opt. Express, 12, 5209 (2004).
9. L. Ohnoutek, N. H. Cho, A. W. A. Murphy, H. Kim, D. M. Răsădean, G. D. Pantoș, K. T. Nam, V. K. Valev, Single Nanoparticle Chiroptics in a Liquid: Optical Activity in Hyper-Rayleigh Scattering from Au Helicoids, Nano Lett. 20, 5792–5798 (2020).
10. L. Ohnoutek, J.-Y. Kim, J. Lu, B. J. Olohan, D. M. Răsădean, G. Dan Pantoș, N. A. Kotov, V. K. Valev, Third harmonic Mie scattering from semiconductor nanohelices, .Nat. Photonics 16, 126-133 (2022).
11. L. Ohnoutek, H.-H. Jeong, R. R. Jones, J. Sachs, B. J. Olohan, D. M. Răsădean, G. Dan Pantoș, D. L. Andrews, P. Fischer, V. K. Valev, Optical activity in third-harmonic Rayleigh scattering: a new route for measuring chirality, Laser. Photonics. Rev. 12, 2100235 (2021).
12. L. Ohnoutek, R. R. Jones, X. Zheng, H.-H. Jeong, V. K. Valev, Second harmonic Rayleigh scattering optical activity of single Ag nanohelices in liquids, Nanoscale 14, 3888-3898 (2022).

Chiral Generation of Hot Carriers Towards Enantioselective Plasmonic Photocatalysis

Miguel Comesaña-Hermo

Université Paris Cité, CNRS, ITODYS, F-75013 Paris, France
*corresponding author: miguel.comesana-hermo@u-paris.fr

Abstract: We present the synthesis of inorganic assemblies composed by the adsorption of Au nanoparticles onto chiral silica nanostructures in order to study the features of non-thermalized charge carriers obtained under circularly polarized radiation. We demonstrate that such materials can be implemented as photocatalytic platforms in polarization-dependent chemical reactions.

It has been recently predicted that the formation of plasmonic assemblies with chiroptical activities can induce an asymmetric response on the hot charges generated via electromagnetic excitation of the plasmonic component.[1,2] In this manner, hot electrons and holes could be used for the development of polarization-sensitive photochemistry. In the present work we use silica-Au nanoribbons as chiral templates for the controlled assembly of plasmon-based photocatalysts, leading to the formation of hybrid materials with asymmetric catalytic features. More precisely, we demonstrate that an improved reaction yield can be obtained when the helicity of the circularly polarized light used for the activation of the plasmonic component matches the handedness of the chiral substrate.[3] Subsequently, we take advantage of this feature to investigate the photo-induced growth of a metal onto the chiral substrate. The photo-reduction of metal ions induced by the photo-generated charge carriers can lead to the formation of a chiral plasmonic system with novel morphological and optical features.[4]

References

1. Liu, T. “Chiral Plasmonic Nanocrystals for Generation of Hot Electrons: Toward Polarization-Sensitive Photochemistry” Nano Lett., 19, 1395-1407, 2019.
2. Khorashad, L. K., “Hot Electrons Generated in Chiral Plasmonic Nanocrystals as a Mechanism for Surface Photochemistry and Chiral Growth” J. Am. Chem. Soc., 142, 4193-4205, 2020.
3. Negrín-Montecelo, Y. “Chiral Generation of Hot Carriers for Polarization-Sensitive Plasmonic Photocatalysis” J. Am. Chem. Soc., 144, 1663-1671, 2022.
4. Besteiro, L. V. “Local Growth Mediated by Plasmonic Hot Carriers: Chirality from Achiral Nanocrystals Using Circularly Polarized Light” Nano Lett., 21, 10315-10324, 2021.

META 2023, PARIS - FRANCE, JULY 18 – 21, 2023

Near-Infrared plasmon-induced hot electron extraction in an Indium Tin Oxide/Monolayer Molybdenum Disulfide Heterostructure

Michele Guizzardi*[1], Michele Ghini[2], Andrea Villa[1], Luca Rebecchi[2,3], Qiuyang Li[4,5], Giorgio Mancini[6], Xiaoyang Zhu[4], Ilka Kriegel[2], Francesco Scotognella[1]

1 Dipartimento di Fisica, Politecnico di Milano, piazza Leonardo da Vinci 32, 20133 Milano, Italy

2 Functional Nanosystems, Istituto Italiano di Tecnologia, via Morego 30, 16163, Genova, Italy

3 Dipartimento di Chimica , Università degli Studi di Genova, Via Dodecaneso 31, 16146 Genova, Italy

4 Department of Chemistry, Columbia University, 3000 Broadway , Havemeyer Hall · New York, NY 10027, USA

5 Department of Physics, University of Michigan, 450 Church Street, Ann Arbor, MI 48109-1040, USA

6 Smart Materials, Fondazione Istituto Italiano Di Tecnologia, Via Morego 30, 16163, Genova, Italy

*corresponding author: michele.guizzardi@gmail.com

Abstract:

In this work, we observe near-infrared plasmon induced hot electron extraction in a heterostructure between indium tin oxide nanocrystals and monolayer molybdenum disulphide. We excite the sample at 1750 nm, resonant with the indium tin oxide plasmon and we observe the excitonic features of molybdenum disulphide in the visible range, close to the exciton of molybdenum disulphide. Such phenomenon can be ascribed to a charge transfer between indium tin oxide nanocrystals and monolayer molybdenum disulphide upon plasmon excitation.

Alternative ways to produce energy from the Sun also include plasmon induced hot electron extraction based solar cells [1,2]. In 2016, Reineck[3] et al. have demonstrated photon-to-electron conversion efficiency by employing a solar cell with an interface between gold nanoparticles and titanium dioxide. Visible light excites the gold nanoparticles generating hot electrons. Such hot electrons are higher in energy with respect to the bottom of the conduction band of titanium dioxide.

With materials that show the plasmonic resonance in the visible it is possible to observe plasmon-induced hot electron extraction[4]. In recent years the attention on plasmons in heavily doped semiconductor nanocrystals has increased. Doping levels around 10^20-21 cm^-3 place their plasmon resonances in the near infrared. Of particular interest are transparent conducting oxide nanocrystals

Herein, we show plasmon-induced hot electron extraction in an indium tin oxide nanocrystal / monolayer molybdenum disulphide structure (Figure 1a). By exciting the heterostructure at 1750 nm, where molybdenum disulphide is not absorbing light and indium tin oxide shows a strong absorption, we observe the excitonic feature of molybdenum disulphide. We ascribe this phenomenon to plasmon-induced hot electron transfer between indium tin oxide nanocrystals and monolayer molybdenum disulphide.

In figure 2a, we show the MoS2 transient signal excited below the bandgap at 1750 nm (0.7
eV), which is much lower with respect to the optical bandgap. We have chosen 1750 nm to ensure that even by two-photon absorption we could not reach the excitonic energy that is around 660 nm (1.87 eV). In this case, we can only see an artifact at zero-time delay between the pump and probe. Finally, in Figure 3d, we show the results of the heterojunction of ITO and MoS2 excited at 1750 nm. After the coherent artifact, we observe the fingerprint of the exciton around 630 and 660 nm. We assign this to an ultrafast plasmon induced hot electron transfer from ITO to MoS2. The high energy tail of the hot FD distribution has enough energy to overcome the Schottky barrier and jump to the MoS2. When now the probe arrives, we have created a different dielectric environment for the MoS2 having those charges in the valence band.

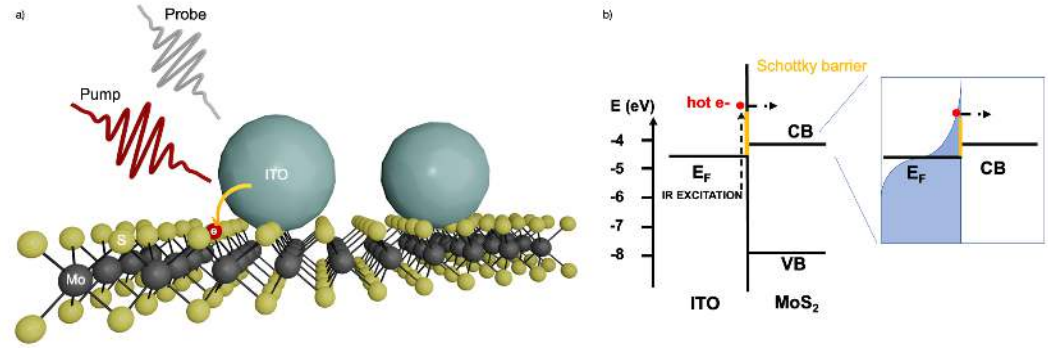


Figure 1 a) ITO/MoS2 heterojunction sketch; b) Band alignment between ITO and MoS2, on the right-hand side we have the sketch of the hot Fermi Dirac Distribution and Schottky barrier.

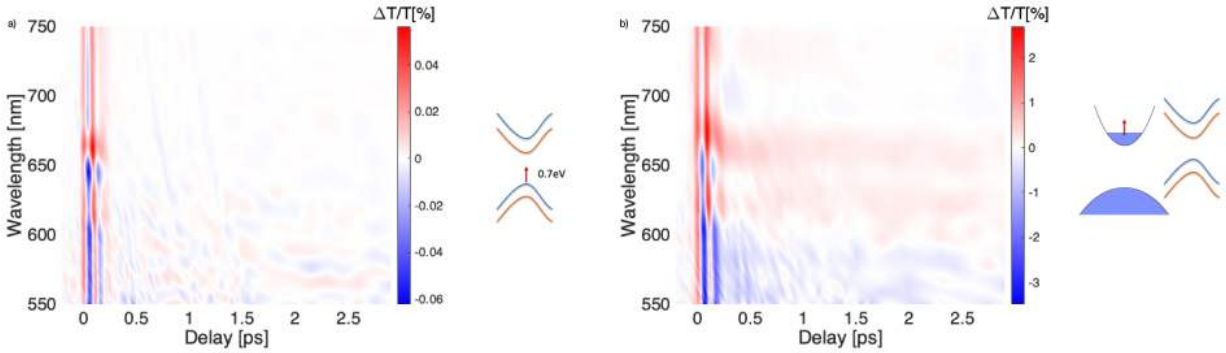


Figure 2 a) Pump probe map of bare MoS2 excited in the NIR at 1750nm b) Pump probe map of the heterostructure ITO/MoS2 excited in the infrared at 1750nm

In conclusion, we have used ultrafast spectroscopy to see charge transfer processes from indium tin oxide to a single layer MoS2 heterojunction excited resonant to the plasmon at 1750 nm.

References

1. Leenheer, A. J.; Narang, P.; Lewis, N. S.; Atwater, H. A. Solar Energy Conversion via Hot Electron Internal Photoemission in Metallic Nanostructures: Efficiency Estimates. J. Appl. Phys. 2014, 115 (13),
2. Wu, K.; Chen, J.; McBride, J. R.; Lian, T. Efficient Hot-Electron Transfer by a Plasmon-Induced Interfacial Charge-Transfer Transition. Science 2015, 349 (6248), 632−635
3. Reineck, P.; Brick, D.; Mulvaney, P.; Bach, U. Plasmonic Hot Electron Solar Cells: The Effect of Nanoparticle Size on Quantum Efficiency. J. Phys. Chem. Lett. 2016, 7 (20), 4137−4141.
4. Clavero, C. Plasmon-Induced Hot-Electron Generation at Nanoparticle/Metal-Oxide Interfaces for Photovoltaic and Photocatalytic Devices. Nature Photon 2014, 8 (2), 95−103

META 2023, PARIS - FRANCE, JULY 18 – 21, 2023

Measuring the Ultrafast Dynamic of Nanoparticle Temperature on the fs-to-ps Time Scale

F. Bisio[1*], M. Ferrera[2], M. Sygletou[2], M. Magnozzi[2], D. Catone[3], P. O'Keeffe[3], A. Paladini[3], F. Toschi[3], S. Benedetti[4], G. M. Pierantozzi[5], R. Cucini[5], A. di Bona[4], P. Torelli[5], G. Della Valle[6], G. Panaccione[5], M. Canepa[2]

[1]CNR-SPIN, 16152 Genova, Italy
[2]Optmatlab, Dipartimento di Fisica, Università di Genova, Italy
[3]CNR-ISM, 00133 Rome, Italy
[4]CNR-NANO, 41125 Modena, Italy
[5]CNR-IOM, 34149 Trieste, Italy
[6]Dipartimento di Fisica, Politecnico di Milano, 20133 Milano, Italy
[*]corresponding author: francesco.bisio@spin.cnr.it

Abstract: The impulsive photoexcitation of nanoparticles kicks off the time-dependent re-equilibration of the electron gas, ion lattice, and environment. For better understanding and harnessing these processes, for thermoplasmonics or photocatalysis applications, it is paramount to know the dynamic, time-dependent evolution of the temperature of each system subcomponents. We report two different methods to directly deduce the temporal evolution of the electronic and lattice temperature of plasmonic Au nanoparticles excited by ultrashort laser pulses on the fs-ps time scale.

Following the impulsive photoexcitation of bulk materials and nanoparticles (NPs), a non-thermal electron population is generated. The nonthermal gas internally thermalizes on a sub-picosecond time scale via electron–electron (e-e) collisions, giving rise to a hot electron gas that subsequently releases its energy to the lattice by means of electron–phonon (e-p) collisions, on the few-ps time scale. Once electron gas and ionic lattice are in mutual thermal equilibrium, heat is dissipated to the environment via phonon–phonon (ph-ph) interactions within few hundred ps.

These dynamic processes and the energy redistribution among the system's degrees of freedom following the photoexcitation lie at the very heart of several highly-intriguing light-induced physical phenomena, such as photocatalysis, thermoplasmonics and solar energy conversion. Highly energetic non-thermal electrons (available in the first few hundreds of fs following the excitation), in particular, play a pivotal role in determining the final outcome of photocatalytic reactions, whereas the lattice-temperature evolution is instrumental for thermoplasmonics heating. In any case, knowing the electron and lattice temperature throughout the relaxation process paves the way to a better understanding of the physical processes occurring during the energy relaxation. We report the direct, model-independent measurement of the electronic and lattice temperature of impulsively excited Au plasmonic nanoparticles, on a time scale ranging from the hundred-fs to the hundred-ps regime.

The ultrafst-electron temperature (T_e) measurements were performedby means of ultrafast, high-resolution photoemission spectroscopy, on ensembles of plasmonic gold NPs, laid onto a transparent conductive oxide substrate [1]. Experiments were performed in pump-probe configuration by photo-exciting the NPs close to the LSP resonance and collecting ultrafast time-resolved photoemission spectra (tr-PES) by means of ultrashort energetic light pulses obtained by high-harmonic generation from the pump beam (Fig.1, left).

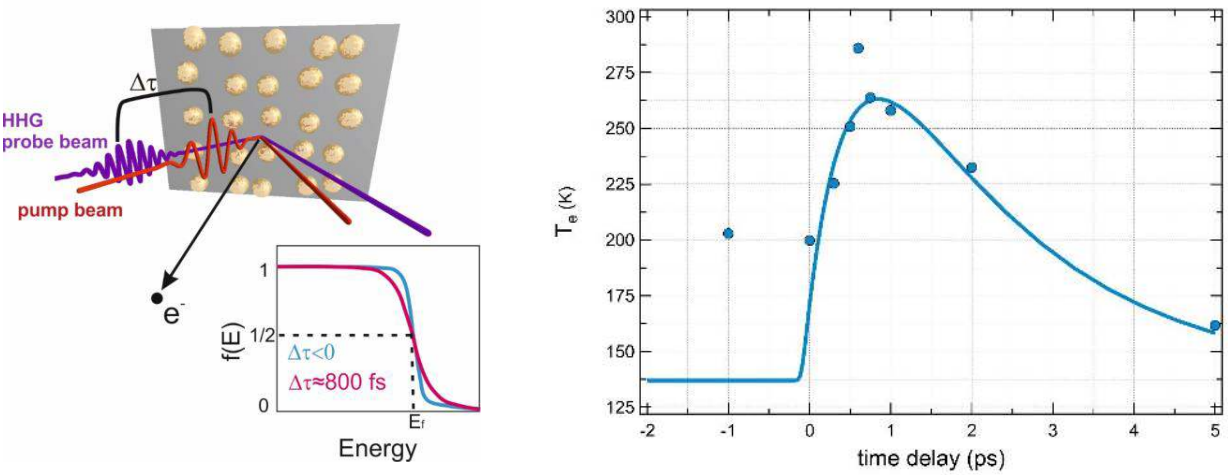


Figure 1: Left: experimental configuration for the ultrafast pump-probe photoemission experiment. Right: evolution of the electronic temperature as a function of the time elapsed since the photoexcitation.

T_e was evaluated exploiting its own definition expressed by the Fermi distribution function, without resorting to any kind of model. Its temporal evolution showed a marked increase up to 800 fs, followed by a gradual relaxation toward environment temperature (Fig. 1, right). The deviations of the electronic distribution function with respect to the Fermi-Dirac were below experimental sensitivity.

At longer delays time, where electron gas and ion lattice are in thermal equilibrium, the nanoparticle temperature was deduced by means of a direct comparison between the differential absorbance of the excited system recorded in a femtosecond- transient absorption spectroscopy measurement, and the differential absorbance recorded in a static thermo-optical experiment [2]. The overlap between time-dependent spectra and temperature-dependent spectra allows to reconstruct the temperature evolution of the nanoparticles in the 20 ps-300 ps time interval, whereupon the relaxation towards ambient temperature is almost complete.

References

1. Sygletou, M.; Benedetti, S.; Ferrera, M.; Pierantozzi, G. M.; Cucini, R.; Della Valle, G.; Carrara, P.; De Vita, A.; di Bona, A.; Torelli, P.; Catone, D.; Panaccione, G.; Canepa, M.; Bisio, F. Quantitative Ultrafast Electron‐Temperature Dynamics in Photo‐Excited Au Nanoparticles. Small 2021, 17 (26), 2100050.
2. Ferrera, M.; Della Valle, G.; Sygletou, M.; Magnozzi, M.; Catone, D.; O'Keeffe, P.; Paladini, A.; Toschi, F.; Mattera, L.; Canepa, M.; Bisio, F. Thermometric Calibration of the Ultrafast Relaxation Dynamics in Plasmonic Au Nanoparticles. ACS Photonics 2020, 7 (4), 959–966.

Merging bound states in the continuum and van der Waals materials for enhanced light-matter coupling

Andreas Tittl[1]

[1]Chair in Hybrid Nanosystems, Nanoinstitute Munich, Faculty of Physics,
Ludwig-Maximilians-Universität München, Königinstraße 10, 80539 München, Germany

[*]corresponding author: Andreas.Tittl@physik.uni-muenchen.de

Abstract: Metasurfaces supporting bound states in the continuum (BICs) have emerged as a powerful nanophotonic platform because of their exceptional resonance control and large field enhancements ideal for light-matter coupling. Van der Waals (vdW) materials are particularly interesting for nanophotonics because of their unique optical and electronic properties. This talk will introduce BIC-driven metasurface concepts based on the prominent vdW materials hexagonal boron nitride and the transition metal dichalcogenide WS_2, demonstrating broad spectral tunability, ultrasharp resonances, and strong light-matter coupling.

The introduction of the physical concept of bound states in the continuum has sparked a revolution in nanophotonics, enabling breakthrough applications ranging from ultrasensitive biospectroscopy to efficient higher harmonic generation and beyond. Because of their exceptional control over high-Q resonances accompanied by large field enhancements, symmetry-protected BIC-driven metasurfaces have seen particular interest for enhancing and probing light-matter interactions. Many realizations of such metasurfaces have so far relied on established nanophotonic materials such as silicon, germanium, or titanium dioxide. Layered materials composed of individual atomic planes bonded together by weak van der Waals (vdW) interactions can open exciting new perspectives for nanophotonic light-matter coupling because of their unique optical and electronic properties, especially for on-chip quantum optics and optoelectronics.

In my talk, I will introduce several recent examples of BIC-driven metasurface concepts based on vdW materials such as hexagonal boron nitride (hBN) and the transition metal dichalcogenide (TMDC) WS_2, demonstrating broad spectral tunability throughout the visible wavelength range, high resonance quality factors, and strong light matter coupling [1,2]. Uniquely, these concepts leverage material-intrinsic BICs, where the vdW structures themselves act as the optically active materials. We harness WS_2-intrinsic BIC modes with sharp and tailored linewidths to tune the resonances over the WS_2 exciton, resolving the distinct anti-crossing signature of strong coupling with large values of the Rabi splitting of 116 meV that can be precisely controlled by modifying the metasurface geometry. Material-intrinsic BIC platforms are broadly applicable for a multitude of vdW materials, where they can deliver both basic insights and practical polaritonic device applications.

References

1. L. Kühner, L. Sortino, B. Tilmann, T. Weber, K. Watanabe, T. Taniguchi, S. A. Maier, and A. Tittl, “High-Q Nanophotonics Over the Full Visible Spectrum Enabled by Hexagonal Boron Nitride Metasurfaces”, Advanced Materials, DOI: 10.1002/adma.202209688 (2022).
2. T. Weber, L. Kühner, L. Sortino, A. B. Mhenni, N. P. Wilson, J. Kühne, J. J. Finley, S. A Maier, and A. Tittl, “Strong light-matter interaction with self-hybridized bound states in the continuum in monolithic van der Waals metasurfaces”, arXiv: 2209.01944 (2022).

META 2023, PARIS - FRANCE, JULY 18 – 21, 2023

Characterization and bio-applicability of inexpensive plasmonic nanoparticles and complex-shaped nanocrystals

V. A. Bahamondes Lorca[1,2*], O. Avalos-Ovando[1], Christoph Sikeler[3], Tim Liedl[3], Dongling Ma[4], Andrei Kabashin[5], S. Wu[1], M. E. Kordesch[1], and A. Govorov[1*]

[1] Ohio University, USA

[2] Universidad de Chile, Chile

[3] Ludwig-Maximilians-Universität, Germany

[4] Center Energy, Mater. & Telecommun, Institut national de la recherche scientifique (INRS), Canada

[5] Aix-Marseille University, France

[*]corresponding authors: bahamondeslorca@ohio.edu, Govorov@ohio.edu

Abstract: With the recent developments in biomedical sciences, we have witnessed the impact and application of nanoparticles (NPs) in bio-diagnostics. Since gold-NPs play an important role, our concern about the availability of gold natural resources and prices, made us analyze options to replace gold-NPs usage. Here, we will show the characterization and applicability of novel, affordable, and abundant plasmonic NPs that could be used in this field as an alternative to gold-NPs. Our results concern technologies for preparing NPs and bio-conjugation.

The authors acknowledge the generous financial support from the OURC/Baker Fund from Ohio University.

META 2023, PARIS – FRANCE, JULY 18 – 21, 2023

Theoretical models for chiral photogrowth in plasmonic nanocrystals

Lucas V. Besteiro[1], Miguel A. Correa-Duarte,[1] Zhiming M. Wang[2], Alexander O. Govorov[3]

[1]CINBIO, Universidade de Vigo, 36310 Vigo, Spain
[2]Institute of Fundamental and Frontier Sciences, University of Electronic Science and Technology of China, Chengdu 610054, China
[3]Department of Physics and Astronomy, Ohio University, Athens, Ohio 45701, United States

Abstract

Plasmonic systems can act as photocatalysts, with energy deposited in their resonant modes driving local chemical reactions. Furthermore, the spatial inhomogeneity of the local response of a plasmonic nanostructure can be used to tailor its properties as a nanoantenna, perhaps most notably through the creation of electromagnetic hot spots. Such locally differentiated response can be combined with circularly polarized light to create and amplify local chiral symmetry of the particle-light system. We present computational results suggesting the potential for developing chiral plasmonic nanostructures from achiral templates by exploiting this phenomenon.

Chirality without mirrors

Rahul Kumar*[1], Ben Trodden[1], Anastasiia Klimash[1], Affar Karimullah[1], Nikolaj Gadegaard[2], Peter J. Skabara[1], Shun Hashiyada,[3, 4] Gordon J. Hedley[1*] and Malcolm Kadodwala[1]*

[1] School of Chemistry, Joseph Black Building, University of Glasgow, Glasgow, G12 8QQ, UK

[2] School of Engineering, Rankine Building, University of Glasgow, Glasgow G12 8LT, U.K

[3] Innovative Photon Manipulation Research Team, RIKEN Center for Advanced Photonics, 2-1 Hirosawa, Wako, Saitama 351-0198, Japan

[4] Department of Electrical, Electronic, and Communication Engineering, Chuo University, 1-13-27 Kasuga, Bunkyo-Ku, Tokyo 112-8551, Japan.

Abstract

Chiral excited electronic states of molecules have an intrinsic sense of handedness, or twist, and are the active component in energy efficient display technologies and in new photosynthetic routes to produce pharmaceuticals. Creating chiral states is achieved by manipulating the "twistiness" of the geometric molecular structure. This is a demanding problem adding complexity due to the need to precisely control molecular geometry. Here we demonstrate a novel concept for creating chiral excited states which does not rely on molecular structure. Instead, it depends on hybridising a non-chiral molecule with a chiral electromagnetic field, producing a hybrid light-matter chiral polariton state. This is achieved by a symmetry-controlled strong chiral-light–matter interaction between an electromagnetic mode of a chiral nanocavity and an achiral molecule, a concept referred to as the electromagnetic-enantiomer. This electromagnetic mechanism simplifies the creation of chiral electronic states since it is far less demanding in terms of materials design. We have illustrated the concept using an exemplar system relevant to organic optoelectronic technology, producing efficient circularly polarised emission from a non-chiral emitter molecule.

Enhancing Light-Matter Interaction in MoS_2 Monolayer deposited on Metalic Nanostructures

M. F. Sousa Lemes [1], G. M. Marega[2], R. Chiesa[2], A. Kis[2] and E. Marega Jr.*[1]

[1]Instituto de Física de São Carlos, Universidade de São Paulo, São Carlos. Brazil
[2]Institute of Electrical and Microengineering, École Polytechnique Fédérale de Lausanne (EPFL) Lausanne, Switzerland
*corresponding author: euclydes@ifsc.usp.br

Abstract: Monolayer transition metal dichalcogenides (TMDs) with a direct bandgap hold enormous potential for designing novel electronic and optoelectronic devices. However, their atomic-thin thickness leads to inefficient light-matter interactions and hinders more versatile applications. One promising solution to overcome this problem is hybridizing the 2D-TMDs with plasmonic structures to increase the optical absorption of the monolayer materials.

Since the discovery of graphene in 2004, an impressive development of other 2D materials has followed. Some examples are transition metal dichalcogenides (TMDs), e.g. molybdenum disulfide (MoS_2), molybdenum diselenide ($MoSe_2$), tungsten disulfide (WS_2), hexagonal boron nitride (h-BN), and many others. However, monolayer TMDs have a low optical cross-section due to their atomic thickness, which results in low light absorption and hinders their systematic use in light harvesting and conversion applications. Various designed systems have been studied to improve the light-matter interaction in 2D materials, such as chemical treatment (1) and quantum doping (2), but they suffer from a high degree of complexity for practical implementation. One effective way to enhance the optical response of monolayer TMDs relies on using plasmonic metal nanomaterials that localize and enhance the electromagnetic field within their proximity (3-4). Here, we report on the fabrication of MoS_2-coated metallic nanostructures and their characterization by Confocal photoluminescence microscopy and lifetime image measurements (Figure 1). Confocal photoluminescence microscopy analysis at room temperature was employed to understand the influence on the emission properties of the MoS_2 (figure 2) when deposited on top of a metallic nanostructure. When the microscopy incident photon energy is above the bandgap of the MoS_2 (excitation at 405 nm), the PL radiative emission is greatly enhanced, ~400-fold, at the Au grating region (red square) and quenched outside (blue square). However, when the excitation is below the bandgap (excitation at 800 nm), the emission at the Au grating is also enhanced 120-fold, and it shows different behavior that can attribute to the absorption of light by the plasmonic metal nanostructure, its conversion into hot electron-hole pairs, and subsequent excitation transfer into MoS_2 layer. In the blue square region in figure 2c again, a quenching in the photoluminescence is observed. It is important to note that the quantum yield of the two-photon

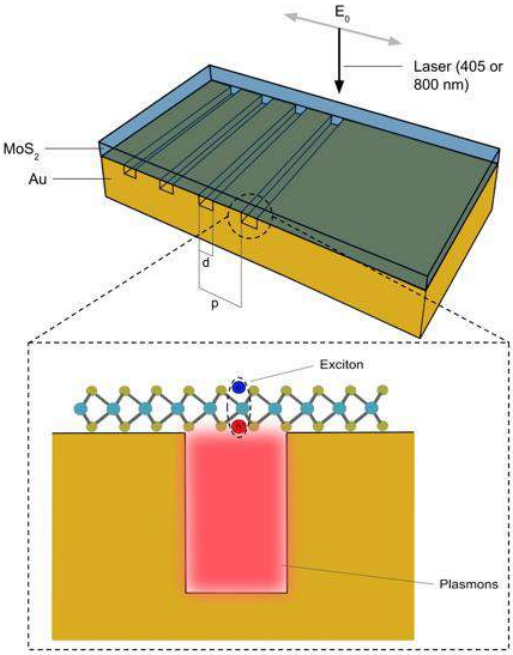


Figure 1 - Schematic diagram of MoS_2 deposit on metallic nanostructures.

absorption of the MoS_2 is extremely low.

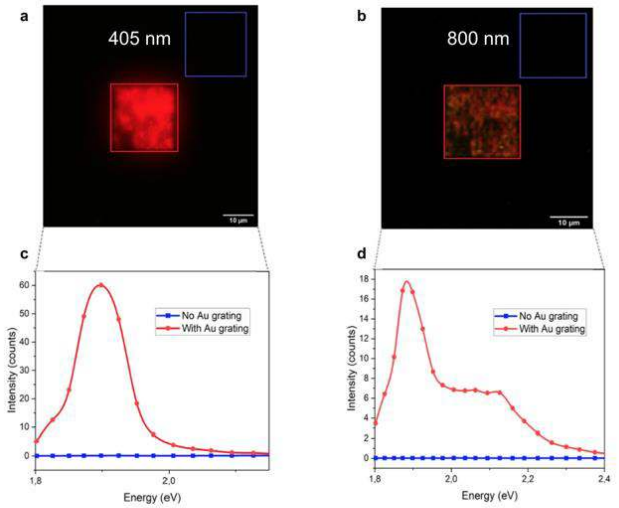


Figure 2 – a) and b) confocal spectral images of 20x20μm square metallic grating with slits separated by 400nm and a width of 50nm. c) and d) spectral deconvolution of the red and blue square regions.

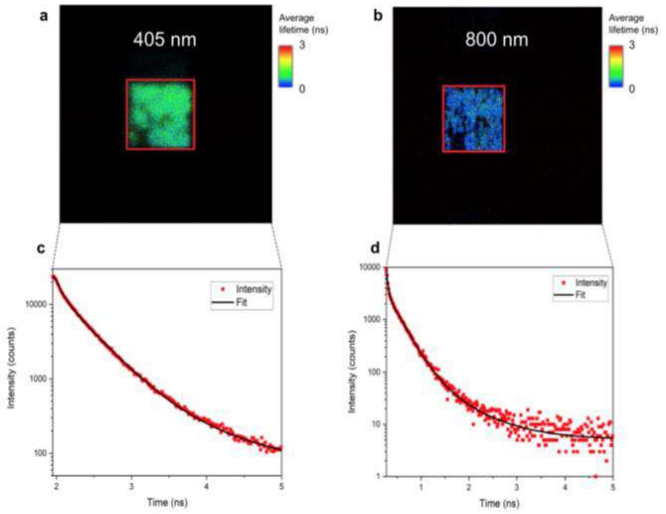


Figure 3 – a) and b) Fluorescence lifetime confocal images of the same structures as in figure 2. c) and d) the average time decay of the red square region.

Fluorescence lifetime images were performed to investigate the mechanisms between the emission properties at the two incident photon energies (see figure 3). The average lifetimes on the Au grating structure are significantly larger when the excitation is at 405 nm compared with the 800nm excitation. This shows that the recombination mechanisms happen faster for plasmon-mediated processes and must be considered when designing optoelectronic devices operating in this energy range.

This study can provide a new understanding of the plasmonic-excitonic interaction in these hybrid metal/semiconductor devices and paves the way toward implementing plasmon-enhanced transition metal dichalcogenide photodetectors, sensors, and emitters.

Acknowledgments: This work was supported by a cooperation between the Brazilian agency FAPESP grant 2021/03311-3 and Swiss National Science Foundation grant 200021L_205114.

References

1. AMANI, M. et al. Near-unity photoluminescence quantum yield in mos2. Science, American Association for the Advancement of Science, v. 350, n. 6264, p. 1065–1068, 2015.
2. KONSTANTATOS, G. et al. Hybrid graphene–quantum dot phototransistors with ultrahigh gain. Nature Nanotechnology, Nature Publishing Group, v. 7, n. 6, p. 363–368, 2012.
3. FERNÁNDEZ-GARCÍA, R. et al. Design considerations for near-field enhancement in optical antennas. Contemporary Physics, Taylor & Francis, v. 55, n. 1, p. 1–11, 2014.
4. SRIRAM, P. et al. Hybridizing strong quadrupole gap plasmons using optimized nanoantennas with bilayer mos2 for excellent photo-electrochemical hydrogen evolution. Advanced Energy Materials, Wiley Online Library, v. 8, n. 29, p. 1801184, 2018.

META 2023, PARIS - FRANCE, JULY 18 – 21, 2023

Toward the Control of Excitonic flux in 2D materials

J-M Poumirol[1], H. Lamsaadi[1], D. Beret[2], I. Paradisanos[2], Z. Gan[3], E. Najafidehaghani[3], A. George[3], T. Lehnert[4], J. Biskupek[4], U. Kaiser[4], S. Shree[5], A. Estrada-real[2,6], D. Lagarde[2], X. Marie[2], P. Renucci[2], S. J. Weber[1], V. Paillard[1], L. Lombez[2], A.Turchanin[3] and B. Urbaszek [1,6]

[1]CEMES-CNRS, Université de Toulouse, Toulouse, France
[2]Université de Toulouse, LPCNO, 135 Avenue Rangueil, 31077 Toulouse, France
[3]Friedrich Schiller University Jena, Institute of Physical Chemistry, 07743 Jena, Germany.
[4]Ulm University, Central Facility of Electron Microscopy, D-89081 Ulm, Germany.
[5]Department of Physics, University of Washington, Seattle, WA, USA.
[6]Institute of Condensed Matter Physics, Technische Universität Darmstadt, Germany.
[*]Corresponding author: jean-marie.poumirol@cemes.fr

Abstract: Being able to control the excitonic flux is a mandatory step for the development of future room-temperature excitonic quantum devices. Transition metal dichalcogenides (ML-TMD) with stable and mobile excitons are highly attractive in this prospect. However, generating an efficient and controlled exciton diffusion over long distances has proven quite complex. Here we demonstrate that ML-TMD based lateral heterostructure (MoSe2/WSe2) acts as an efficient excitonic diode[1], with an excitonic flux that can be controlled through near-field engineering.

In our work, we investigate experimentally and theoretically the effect of atomically sharp $MoSe_2/WSe_2$ lateral heterostructure (LH) over the exciton diffusion. Using Tip Enhanced Photoluminescence measurements (TEPL), in combination with a modified diffusion theory[2], we show that at the steady state, due to the presence of the excitonic asymmetric potential at the interface, an area is formed in which the diffusion properties are modified becoming strongly asymmetric. This partition zone is extending hundreds of nanometers away from the LH forcing excitons to move, toward the junction, up to five time their diffusion length (LD) before recombining without affecting neither the potential, recombination rate, or mobility of the propagating quasi-particles. Furthermore, we performed time dependent PL imaging experiments that show that in WSe_2, LD is strongly dependent on the excitonic density (n). By comparing the diffusion properties of fully h-BN encapsulated LH and h-BN supported LH, without top h-BN layer, we demonstrate that the diffusion properties of the LH can be tuned by increasing the excitation laser power or by modifying the optical near field configuration[3] (at constant laser power).

References

1. D. Beret, I. Paradisanos, H. Lamsaad, "Exciton spectroscopy and unidirectional transport in MoSe2-WSe2 lateral heterostructures encapsulated in hexagonal boron nitride ", npj 2D Materials and Applications, (2022)
2. W. K. Lewis and W. G. Whitman. Principles of Gas Absorption. Industrial & Engineering Chemistry, 16(12), 1215–1220, (1924)
3. Jean-Marie Poumirol, Ioannis Paradisanos, Shivangi Shree, et. al. Unveiling the Optical Emission Channels of Monolayer Semiconductors Coupled to Silicon Nanoantennas. ACS Photonics, 7(11), 3106–3115, (2020)

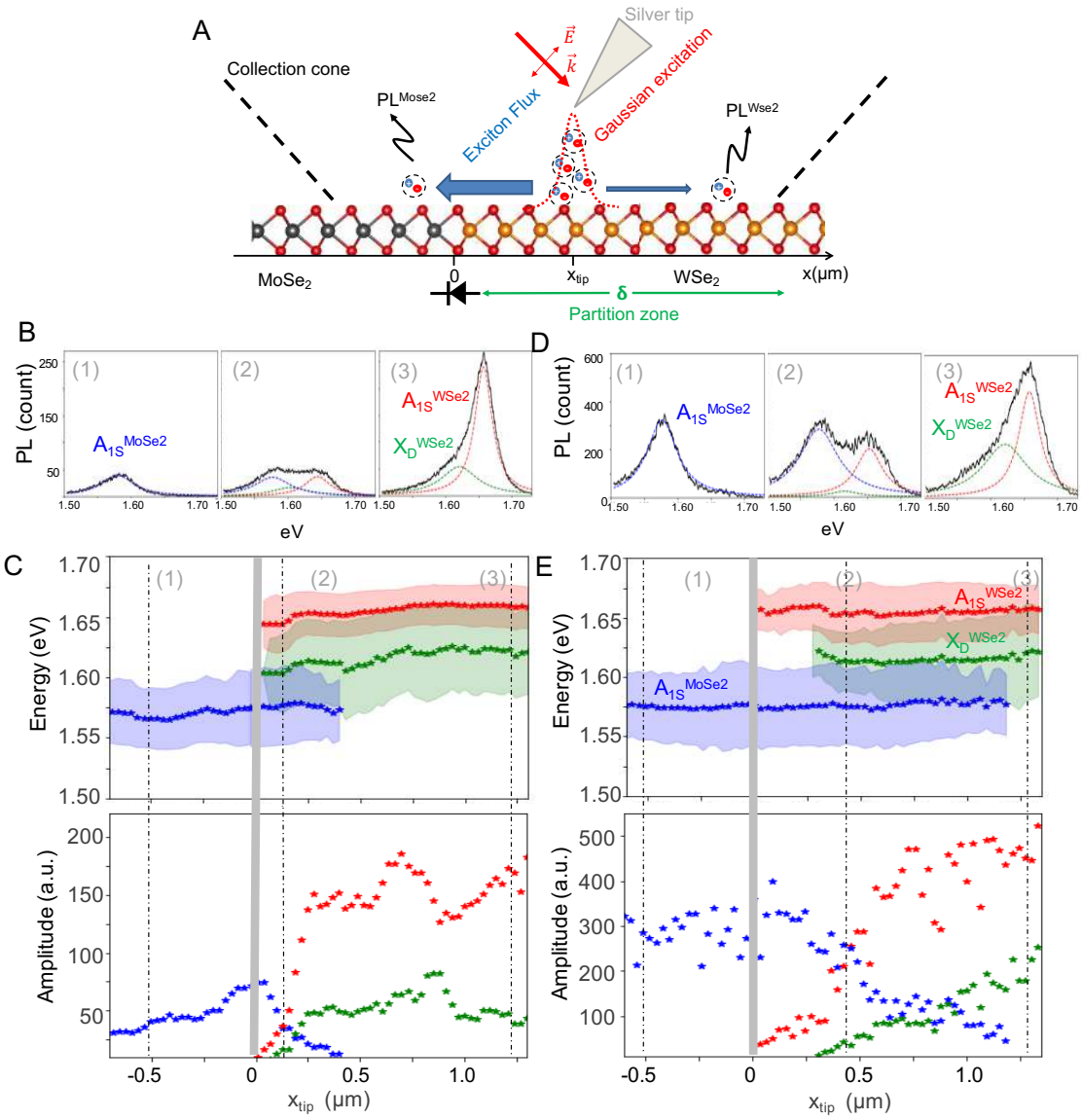


FIG. **A.** Schematic of the lateral heterojunction, TEPL measurement and the resulting excitonic diffusion properties. **B. (D.)** Typical TEPL spectra taken across the interface in e-LH (respectively un-LH) (1) 500 nm to the left of the interface, (2) 100 nm (300 nm) and (3) 1,25μm to the right of the interface. The excitonic contributions are fitted using individual Lorentzian function, neutral WSe_2 exciton in red ($A_{1s}{}^{WSe2}$), neutral $MoSe_2$ exciton in blue ($A_{1s}{}^{MoSe2}$) and the dark exciton (out-of-plan) in WSe_2 green ($X_D{}^{WSe2}$). **C. (E.)** Top: Energy and FWHM of each Lorentzian peak obtained from the fitting procedure as shown in B (D). Bottom: Amplitude of each Lorentzian peak obtained from the fitting procedure as shown in B. (D.) The red, blue and green stars indicate $A_{1s}{}^{WSe2}$, $A_{1s}{}^{MoSe2}$, $X_D{}^{WSe2}$ respectively.

Acknowledges funding from ANR HiLight, ANR Ti-P and NanoX project 2DLight

Metamaterial Thermal Management

Wakana Kubo

Division of Advanced Electrical and Electronics Engineering, Tokyo University of Agriculture and Technology,

2-24-16 Naka-cho, Koganei-shi, Tokyo 184-8588, Japan
*corresponding author: w-kubo@cc.tuat.ac.jp

Abstract: To increase the efficiency of energy harvesting, technologies that can utilize weak thermal energies existing in environments are in demand; however, conventional technologies fail to realize this objective because energy accumulation does not occur in them. Herein we propose a metamaterial thermal engineering technique by which thermal energy can be accumulated from the surrounding environment and can be converted into electricity.

Thermal energies existing in the environment are one of the reliable energy resources. Technologies that can utilise weak such thermal energies are needed to satisfy the demands for increased energy utilisation. However, thermal energies are emitted from objects into the atmosphere, e.g. cars, machines, and buildings, and are present in extremely diluted form in the atmosphere, making it difficult to accumulate and utilise the energies.

Herein we propose metamaterial thermal management that can be used to accumulate diluted thermal energies existing in ambient air. Using the metamaterial thermal engineering, we realised a thermoelectric device that can produce electricity even in a uniform-temperature environment. We attached a metamaterial absorber (MA) on the surface of one of the thermoelectric device edges (Fig. 1(a,b)) and kept the device in a uniform-temperature environment. Using the large difference in absorptivity of the device edges produced by the MA, a temperature gradient is produced even when the device is subjected to uniform and isotropic thermal radiations, leading to thermoelectric generation (Fig. 1(c)).

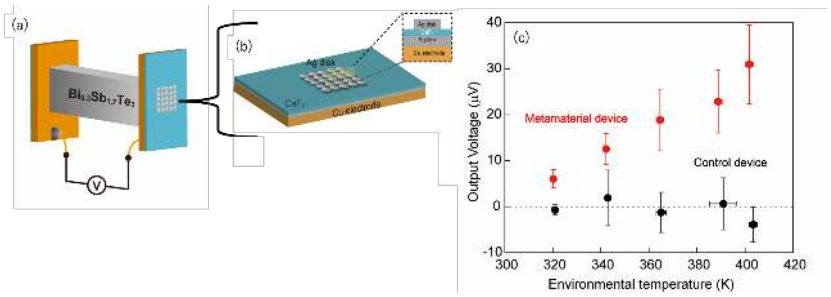


Fig. 1 Schematics of (a) a thermoelectric device loaded with the metamaterial electrode and (b) metamaterial array. (c) Dependence of the output voltages generated on the metamaterial device (red) and a control device (black) on the measured environment temperatures.

References

1. T. Asakura, T. Odaka, R. Nakayama, S. Saito, S. Katsumata, T. Tanaka & W. Kubo*, "*Metamaterial Thermoelectric Conversion*", arXiv:2204.13235 (2022).
2. S. Katsumata, T. Tanaka, W. Kubo*, "*Metamaterial perfect absorber simulations for intensifying the thermal gradient across a thermoelectric device*", *Opt. Express*, **29**, 16396-16405 (2021).

META 2023, PARIS - FRANCE, JULY 18 – 21, 2023

Hyperbolic meta-antennas: magnetic and electric modes

Sema Ebrahimi,[1,2,3,*] Alina Muravitskaya,[2,3] Ali M. Adawi,[2,3] Anne-Laure Baudrion,[1] Pierre-Michel Adam,[1,*] Jean-Sebastien G. Bouillard[2,3,*]

[1]University of Technology of Troyes, Light, Nanomaterials, Nanotechnologies Laboratory, CNRS EMR 7004, F-10004 Troyes Cedex, France

[2]University of Hull, Department of Physics and Mathematics, Cottingham Road, HU6 7RX, Hull, UK

[3]University of Hull, G.W. Gray Centre for Advanced Materials, Cottingham Road, HU6 7RX, Hull, UK

[*]corresponding authors: semaebrahimi@gmail.com, pierre_michel.adam@utt.fr, j.bouillard@hull.ac.uk

Abstract: Coupling hyperbolic metaparticles is the next step in metamaterial applications, providing tunable electromagnetic properties on demand. Here we present the magnetic and electric modes in hyperbolic meta-antennas arising from the coupling of metaparticles. We show the existence of two coupling regimes for the magnetic modes, and demonstrate a fine control over the electrical field spatial distribution, opening the route towards a wide range of applications from magnetic nanolight sources and magnetic forces engineering, to single photon sources, and subwavelength lasers.

Metamaterials, by providing custom engineered optical properties, offer new ways of manipulating electromagnetic waves. Hyperbolic metamaterials specifically can support high-k modes, large increases in photonic density of states, and high refractive index structures beyond what is available in nature, therefore enabling new ways to engineer light-matter interactions.[1,2] It is therefore not surprising that HMM have found a vast range of applications encompassing single-antenna biosensing, plasmonic-based lasing, photovoltaics, and hot-electron generation technologies.[3-5]

Hyperbolic metaparticles, created by nanostructuring hyperbolic metamaterials, represent additional possibilities to bulk metamaterials, and have therefore been at the center of recent research with the promise of many exotic applications. Hyperbolic metaparticles built from alternating metal-dielectric multilayers support two well-separated electric and magnetic resonances. However, the study of hyperbolic nanostructures has so far focused on isolated metaparticles, despite the fact that mode coupling in metamaterial nanostructures will pave the way for novel optical phenomena unavailable in isolated metaparticles and allow to fully capitalize on their many opportunities.

Here we introduce a new class of hyperbolic bowtie meta-antenna based on a type II hyperbolic bulk metamaterial. The meta-antenna is constructed from a gold-titanium dioxide multilayer system, in which both the geometrical and material parameters are kept within the possibilities of current experimental nanofabrication techniques. Using finite difference time domain (FDTD) simulations, we explore the mode structure supported by such a hyperbolic system and evidence the existence of both electric and magnetic coupling in those meta-antennas.

After identifying the modes supported by this type of meta-antenna, we compare the optical behaviour of full multilayer geometry to the corresponding effective medium system for a range of filling factors. We then study the mode coupling inside such a meta-antenna by fully exploring the parameter space, including the gap size, filling factor, and incident polarisation. Whereas the coupled electric mode results in a field enhancement along the height of the meta-antenna nanogap, the magnetic coupling, on the other hand, follows two regimes depending on the interplay of the individual magnetic dipole moments. With both coupling controllable through the effective permittivity, gap size, and incident polarization, such novel hyperbolic meta-antennas open the

route for applications in optical sensors, single photon sources, sub-wavelength meta-cavity lasers, as well as magnetic nanolight sources, chiral quantum optics, magnetic forces engineering, active control of metamaterial nanostructures, and quantum interfaces for non-reciprocal processing of light.

Acknowledgments

The authors acknowledge the Ministère and FEDER (fonds européens) and the University of Hull for financial support through a PhD scholarship. This work has been made within the framework of the Graduate School NANO-PHOT (École Universitaire de Recherche, contract ANR-18-EURE-0013). A. Muravitskaya, A. M. Adawi, J.-S. G. Bouillard acknowledge the support of the EU Horizon 2020 research and innovation programme under grant number 861950, project POSEIDON. The authors also acknowledge the Viper High Performance Computing facility of the University of Hull and its support team.

References

1. Poddubny, A. *et al.*, "Hyperbolic metamaterials," Nature Photonics **7**(12), 958–967 (2013)
2. Lu, L., Simpson, R. E., and Valiyaveedu, S. K., "Active hyperbolic metamaterials: Progress, materials and design," Journal of Optics (United Kingdom) **20**(10), 103001 (2018)
3. Shekhar,P., Atkinson, J. and Jacob, Z., "Hyperbolic metamaterials: fundamentals and applications," Nano Convergence **1**(1), 14 (2014)
4. Wang , P. *et al.*, "Metaparticles: Dressing Nano-Objects with a Hyperbolic Coating," Laser & Photonics Reviews **1800179** (2018)
5. Morgan, S. O. *et al.*, "Using adsorption kinetics to assemble vertically aligned nanorods at liquid interfaces for metamaterial applications," Phys. Chem. Chem. Phys. **24**(18), 11000–11013 (2022)

META 2023, PARIS - FRANCE, JULY 18 – 21, 2023

Ultrafast hot-carrier spatial transients in photonic metasurfaces: experiments, modeling, design

A. Schirato[1,2], G. Crotti[1,2], A. Toma[2], R. Proietti Zaccaria[2,3], P. Laporta[1,5], C. De Angelis[6], A. Alabastri[4], G. Cerullo[1,5], M. Maiuri[1,5], and G. Della Valle[1*,5,7]

[1]Dipartimento di Fisica, Politecnico di Milano, Italy
[2]Istituto Italiano di Tecnologia, Genova, Italy
[3]Cixi Institute of Biomedical Engineering, Cina
[4]Department of Electrical and Computer Engineering, Rice University, Texas USA
[5]Istituto di Fotonica e Nanotecnologie, CNR, Italy
[6]Department of Information Engineering, University of Brescia, Italy
[7]Istituto Nazionale di Fisica Nucleare, Milano, Italy
[*]corresponding author: giuseppe.dellavalle@polimi.it

Abstract: Hot carriers photoinduced by fs-laser pulses in photonic nanostructures have been widely investigated. In most of the works a spatially homogeneous excitation pattern is assumed. Here we show how ultrafast hot carrier spatial inhomogeneities at the nanoscale can manifest and even dominate the transient transmission of photonic metasurfaces. An inhomogeneous version of the three-temperature model has been validated on pump-probe spectroscopy measurements in plasmonic metasurfaces. Our results pave the way for the design of novel ultrafast nanophotonic devices.

Hot carriers photoinduced by intense laser pulses in nanomaterials have been the subject of intensive research, both for fundamental aspects and novel applications. Among the latter, ultrafast all-optical modulation of light has recently attracted a strong interest (see, e.g., Refs. 1, 2 for an overview). However, despite the many papers published so far in the field, it is only until very recently that spatial inhomogeneities of the photogenerated hot electrons have come into play [2-10].

Here we report on an agile modeling approach based on an extended, inhomogeneous, version of the more classic three temperature model (I3TM) [1,2], capable of grasping the key phenomena involved in the spatio-temporal dynamics of hot carriers photogenerated at the nanoscale. The theoretical predictions of the I3TM have been validated on ultrafast broadband pump-probe measurements of gold metaatoms.

We then show how it is possible to engineer the metaatom configuration so to exploit these spatial transients for novel functionalities. In particular, we demonstrate unprecedented ultrafast reconfiguration of giant dichroism by simply acting on the polarization of the fs-laser control pulse in plasmonic metasurfaces with Au nanocross metaatoms [8]. Moreover, we highlight the key role of spatial inhomogeneities on the temporal dynamics of the ultrafast reconfiguration for plasmonic metaatoms with high aspect ratio. Pronounced discrepancies between homogeneous and inhomogeneous models are indeed retrieved, possibly resulting in opposite signs for the predicted transient signal even for relatively low fluences (~mJ/cm^2 level) [9].

Finally, we show how a similar modeling approach can be applied to all-dielectric nanomaterials, and provides the capability to explain the origin of the picosecond time delay with which the peak of the transient optical response is observed in AlGaAs nanopillars excited with ~100 fs laser pulses [10].

This work is part of the METAFAST project that received funding from the European Union Horizon 2020 Research and Innovation program under grant agreement no. 899673.

References

1. Brongersma, M., N. J. Halas, and P. Nordlander, “Plasmon-induced hot carrier science and technology,” Nat. Nanotechnol. Vol. 10, 25-34, 2015.
2. Schirato, A., M. Maiuri, G. Cerullo, and G. Della Valle, “Ultrafast hot electron dynamics in plasmonic nanostructures: experiments, modelling, design,” Nanophotonics Vol. 12, No. 1, 1-28, 2023.
3. Rudenko, A., K. Ladutenko, K., S. Makarov, and T. E. Itina, T., “Photogenerated free carrier-induced symmetry breaking in spherical silicon nanoparticle,” Adv. Opt. Mater. Vol. 6, 1701153, 2018.
4. Kong, X.-T., L. K. Khorashad, Z. Wang, and A. O. Govorov, “Photothermal Circular Dichroism Induced by Plasmon Resonances in Chiral Metamaterial Absorbers and Bolometers,”, Nano Lett. Vol. 18, 2001-2008, 2018.
5. Nicholls, L.H., et al., “Designer photonic dynamics by using non-uniform electron temperature distribution for on-demand all-optical switching times,” Nat. Commun. 10, 2967, 2019.
6. Schirato A., et al., “Transient optical symmetry breaking for ultrafast broadband dichroism in plasmonic metasurfaces,” Nat. Photon. Vol. 14, 723-727, 2020.
7. Sivan, Y., and M. Spector, “Ultrafast dynamics of optically-induced heat gratings in metals,” ACS Photon. Vol. 7, No. 5, 1271-1279, 2020.
8. Schirato, A., et al., “All-Optical Reconfiguration of Ultrafast Dichroism in Gold Metasurfaces,” Adv. Optical Mater. 10, 2102549, 2022.
9. Schirato, A., G. Crotti, R. Proietti Zaccaria, A. Alabastri, and G. Della Valle, “Hot carrier spatio-temporal inhomogeneities in ultrafast nanophotonics,” New J. Phys. 24, 045001, 2022.
10. Mazzanti, A., et al., “All-Optical Modulation with Dielectric Nanoantennas: Multiresonant Control and Ultrafast Spatial Inhomogeneities,” Small Sci. Vol. 1, 2000079, 2021.

Ultrafast phenomena at the interface of plasmonic/semiconductor hybrid systems

M. Zavelani-Rossi[1,2]

[1] Dipartimento di Energia, Politecnico di Milano, Via Ponzio 34/3, 20133 Milano, Italy
[2] IFN-CNR, piazza Leonardo da Vinci 32, 20133 Milano, Italy
*corresponding author: margherita.zavelani@polimi.it

Abstract: Hybrid plasmonic/semiconductor junction allow providing and controlling interesting physical functionalities, such hot-electron charge transfer or plasmon induced resonance energy transfer. Ultrafast transient absorption spectroscopy is an effective tool to study the junction behavior. Here, gold plasmon nanostripes coupled to a 2D transition metal dichalcogenide (MoS_2) and silver nanoparticles decorating ZnO nanorods are considered. Experimental data together with an analytical model and crossed results, allow disclosing the physics of the systems, providing important information for fundamental knowledge and future applications.

Targeted design of plasmonic/semiconductor hybrid assemblies can promote new physics and new high-performance functionalities in optoelectronic devices. In particular, the interaction of the electromagnetic optical field with a structure composed by a low dimensional plasmonic noble metal coupled to a semiconductor can give rise to various physical phenomena, that can be exploited for energy harvesting, photocatalysis and biological sensing, to mention a few examples.[1–2] The strong light interaction, induced by plasmonic effects, fosters several unique phenomena such as electric field enhancement, tunable light absorption (from visible to infrared region) and generation of hot-electrons. The study of the carrier redistribution after photo-excitation in a plasmonic/semiconductor junction is crucial to determine the physical process, to assess the relaxation routes and to characterize the time-scale of the phenomena involved. This knowledge is beneficial both for fundamental physics of hybrid systems and for practical applications.

Among various interesting systems, the junction between a noble metal plasmonic object and a semiconductor is particularly interesting because hot-electrons generated in the metal can possibly overcome the barrier offset and travel into the conduction band of the neighboring semiconductor. The physics is very intriguing and highly debated because different routes mechanisms can take place, like direct electron transfer, or plasmon induced resonance energy transfer.[3,4] These processes occur on an ultrashort time scale, ranging from a few tens of femtoseconds to a few picoseconds.

Here, I will discuss two notable examples. The first one consisting of a 2D transition metal dichalcogenide (TMDs), a few-layer MoS_2, coupled to gold plasmonic nanostripes (NSs);[5,6] the second consisting of ZnO nanorods (NRs) decorated with silver plasmonic nanoparticles (NPs).[7] I will show the ultrafast transient absorption dynamics, obtained on a wide spectral range (350-700 nm), with high temporal resolution (<100 fs), and tunable pump excitation (in the near UV-visible spectral region). Experimental results are compared with an analytical model and with other data. A comprehensive scenario of the charge/energy transfer is thus provided.

For the Au NSs/MoS_2 architecture, multiple transient absorption measurements are presented (Figure 1a), enabling quantitative comparison between the ultrafast behavior of metal nanostructures, TMDs, and their assembly. This allows providing the evidence of plasmon-enhanced charge injection from Au NSs to the 2D semiconductor, which occurs in less than 200 fs. Numerical modeling corroborates the charge transfer mechanism.

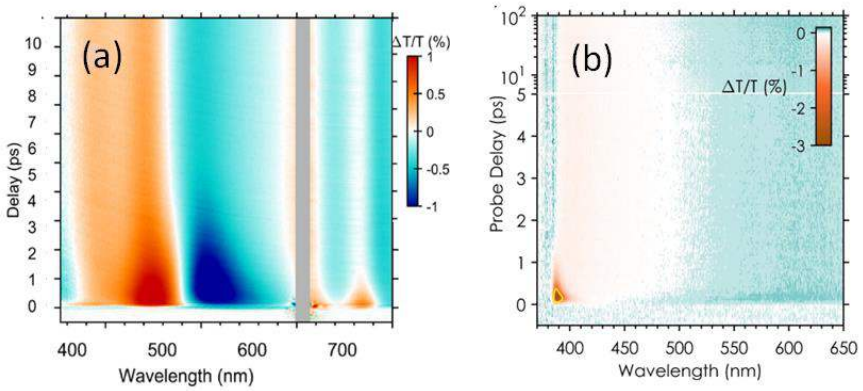


Figure 1: Transient absorption maps, (a) Au NSs/MoS_2, (b) Ag NPs/ ZnO NRs.

For the Ag NPs/ ZnO NRs system, a comparison is made between decorated and non-decorated NRs. Photoluminescence, transient absorption (Figure 1b) and photoresponse are studied. Following photo-excitation of the system, a fast electron redistribution is evidenced, favored by the tiny energy difference between the conduction band of ZnO and the Fermi level of Ag. Moreover, a fast and effective population of ZnO NRs trap states, mediated by Ag NPs plasmonic response, appears. All together, the whole set of data indicate a non-radiative optical field coupling mechanism of Ag NPs with ZnO, with hot-electron injection, that takes place in less than 500 fs.

Overall, it appears that ultrafast transient spectroscopy is an effective tool to shed light on the physical processes in metal plasmonic/semiconductor systems. It is noteworthy to mention that these results can be applied to different hybrid architectures.

MIUR financial support, through the project MIUR-PRIN 2015 Grant No. 2015WTW7J3, is acknowledged.

References

[1] Brongersma M. L., Halas N. J., Nordlander P., "Plasmon-induced hot carrier science and technology", Nat. Nanotechnol., 10, 25, 2015

[2] Nbelayim P, Kawamura G., Kian Tan W., Muto H. and Matsuda A., "Systematic characterization of the effect of Ag@TiO2 nanoparticles on the performance of plasmonic dye-sensitized solar cells, Sci. Rep., 7, 1–12, 2017.

[3] Clavero C., "Plasmon-induced hot-electron generation at nanoparticle/metal-oxide interfaces for photovoltaic and photocatalytic devices", Nat. Photonics, 8, 95, 2014.

[4] Cushing S. K., Li J., Meng F., Senty T. R., Suri S., Zhi M., Li M., Bristow A. D. and Wu N., "Photocatalytic Activity Enhanced by Plasmonic Resonant Energy Transfer from Metal to Semiconductor" J. Am. Chem. Soc., 134, 15033–15041, 2012.

[5] Camellini A., Mennucci C., Cinquanta E., Martella C., Mazzanti A., Lamperti A., Molle A., Buatier de Mongeot F., Della Valle G. and Zavelani-Rossi M., "Ultrafast Anisotropic Exciton Dynamics in Nanopatterned MoS2 Sheets", ACS Photonics 5, 3363-3371, 2018

[6] Camellini A., Mazzanti A., Mennucci C., Martella C., Lamperti A., Molle A., Buatier de Mongeot F., Della Valle G. and Zavelani-Rossi M., "Evidence of Plasmon Enhanced Charge Transfer in Large-Area Hybrid Au–MoS2 Metasurface" Adv. Opt. Mater., 8, 2000653, 2020.

[7] Gilzad Kohan M., You S., Camellini A., Concina I., Zavelani-Rossi M. and Vomiero A., "Optical Field Coupling in ZnO Nanorods Decorated with Silver Plasmonic Nanoparticles" J. Mater. Chem. C 9, 15452-15462, 2021.

META 2023, PARIS - FRANCE, JULY 18 – 21, 2023

Nanophotonic Tools for Lipid Membrane Sensing and Manipulation

T. Lohmüller[1]

[1] Photonics and Optoelectronics Group, Nano-Institute Munich, Department of Physics, Ludwig-Maximilians-Universität (LMU), Königinstraße 10, 80539 Munich, Germany
*corresponding author: t.lohmueller@lmu.de

Abstract: A new approach is presented for monitoring the photoisomerization dynamics of photolipid bilayer membranes on the nanoscale using plasmonic sensing. The azobenzene group in photolipids enables optical control over various membrane parameters, such as lipid mobility and thickness, but measuring the switching dynamics in a bilayer is challenging. We demonstrate that plasmonic sensing with single gold nanorods allows for analyzing membrane photoisomerization and corresponding changes in bilayer thickness with high spatio-temporal accuracy.

Synthetic lipid bilayer membranes are a key model system to study and emulate the physical properties of native plasma membranes. However, controlling membrane dynamics and reorganization with high spatio-temporal resolution is challenging and often involves drastic changes in experimental conditions. At the same time, lipid bilayer properties are mostly characterized by fluorescence techniques, which provide high sensitivity but require a fluorescent label that itself might interfere with bilayer properties. To overcome these limitations, we developed nanophotonic tools that enable precise control and monitoring of membrane properties at fast time-scales.

We used photolipids containing an azobenzene group in their lipid tails, which undergoes a conformational change upon illumination with UV and visible light, as a model system[1]. Introducing this lipid photoswitch into a bilayer membrane provides optical control over a variety of membrane parameters, including fluidity[2], mechanical properties[1], and thickness, among others[3,4]. However, analyzing the fast switching dynamics in the bilayer, which is only ~4 nm thin, is challenging due to a lack of sensitive tools. X-ray scattering (e.g. SAXS) is widely used, but it does not provide sufficient time resolution to monitor fast switching dynamics.

To address this challenge, we conducted an experiment using plasmonic gold nanorods deposited on a glass substrate and coated with a supported photolipid bilayer. We demonstrate that analyzing the scattering spectra obtained from single nanorods makes it possible to resolve the dynamics of the azobenzene switch between *cis* and *trans* isomer. We found that membrane photoisomerization leads to a reversible shift of the plasmon resonance over many switching cycles, which highlights the potential of plasmonic nanoparticles as sensitive probes to study the dynamics and photostationary states of lipid bilayer membranes with high accuracy and within nanoscale environments.

Our results demonstrate the potential of using hybrid nanosystems of photolipid molecules and plasmonic nanoparticles as light-sensitive nanoagents for controlling biological systems in space and time. By enabling precise control and monitoring of membrane properties, these nanophotonic tools can offer new insights into the behavior of biological membranes and pave the way for the development of new therapeutic and diagnostic applications.

References

1. Pernpeintner, C. *et al.*, “Light-Controlled Membrane Mechanics and Shape Transitions of Photoswitchable Lipid Vesicles” Langmuir, 33 (16), 4083–4089, 2017.
2. Urban, P., *et al.*, “A Lipid Photoswitch Controls Fluidity in Supported Bilayer Membranes” Langmuir, 36 (10), 2629–2634, 2020.
3. Urban, P., *et al.*, “Light-Controlled Lipid Interaction and Membrane Organization in Photolipid Bilayer Vesicles” Langmuir, 34 (44), 13368–13374, 2018.
4. Pritzl, S., *et al.*, “Photolipid Bilayer Permeability is Controlled by Transient Pore Formation” Langmuir, 36 (45), 13509–13515, 2020.

META 2023, PARIS - FRANCE, JULY 18 – 21, 2023

Photodoping of plasmonic doped metal oxide nanocrystals for the direct storage of solar energy

Ilka Kriegel

[1]Functional Nanosystems, Italian Institute of Technology, via Morego 30, Genova, Italy

[*]corresponding author: ilka.kriegel@iit.it

Abstract: We are currently investigating novel processes that work towards the direct storage of solar energy by investigating nanomaterials that act as light-charged (nano-)capacitors. In this talk, I will present our work towards the understanding of the fundamental processes underlying this novel concept. I will present our endeavors in the production of novel nanomaterials, their photophysical and theoretical characterization. Finally, I will give insights into the challenges of device fabrication for this novel system.

Energy from sunlight is a promising alternative solution for the global sustainable energy crisis. However, there is a significant drawback related to the intermittency of the Sun. Potential solutions relate to the use of solar energy to produce useful chemicals, i.e. photocatalysis. Alternatively, novel technologies are developed that permit the direct storage of solar energy. A promising approach towards the latter is the photodoping of plasmonic, doped metal oxide nanocrystals, such as indium tin oxide or doped zinc oxides. The fundamental physical process initiates with the absorption of photons with light beyond the bandgap. An electron hole pair is created. When the hole reacts with sacrificial hole scavengers, such as ethanol, the extra electrons remain stored within the nanocrystal. This process can be repeated multiple times accumulating up to hundreds of electrons per nanocrystal,[1, 2] thus, photodoping displays the potential to combine light absorption, charge separation, and accumulation in the same set of materials.[3] Capacitance values, comparable to commercially available supercapacitor materials have been reported for this light-driven charging process.[4] Within this talk I will give fundamental insight into the mechanism of charge storage within metal oxide nanocrystals. I will further discuss open questions with regards to their implementation as novel light-driven multi-charge accumulation components in the next generation of solar energy devices.

For this work, the authors acknowledge the support of both European Union's Horizon 2020 European Research Council, under grant agreement no. 850875 (Light-DYNAMO) and European Union's Horizon 2020 Research and Innovation program under grant agreement no. 101017821 (LIGHT-CAP).

References

1. M. Ghini, N. Curreli, M. B. Lodi, N. Petrini, M. Wang, M. Prato, A. Fanti, L. Manna, I. Kriegel, Nat Commun 2022, 13, 537.
2. M. Ghini, A. Rubino, A. Camellini, I. Kriegel, Nanoscale Adv. 2021, 3, 6628–6634.
3. M. Ghini, N. Curreli, A. Camellini, M. Wang, A. Asaithambi, I. Kriegel, Nanoscale 2021, 13, 8773–8783.
4. I. Kriegel, M. Ghini, S. Bellani, K. Zhang, A. W. Jansons, B. M. Crockett, K. M. Koskela, E. S. Barnard, E. Penzo, J. E. Hutchison, J. A. Robinson, L. Manna, N. J. Borys, P. J. Schuck, J. Phys. Chem. C 2020, 124, 8000–8007.

META 2023, PARIS - FRANCE, JULY 18 – 21, 2023

Opto-thermal effects in plasmonic nanocrystals with complex shapes

O. Avalos-Ovando[1*], L. V. Besteiro[2], A. Movsesyan[1], and A. O. Govorov[1]

[1]Ohio University, USA
[2]CINBIO, Universidade de Vigo, Spain
[*]corresponding author: oa322219@ohio.edu

Abstract: The careful geometrical design of plasmonic nanocrystals (NCs) allows not only to manipulate their optical response, but also to generate heat efficiently. Here we present a opto-thermal study of plasmonics NCs but with complex shapes. We use a two-temperature model to study the ultrafast photothermal responses, and we solve for the lattice and the electronic temperatures. We observe the creation of local modifications of the dielectric function via the temperature, which leads to the thermal imprint of plasmonic hotspots.

Acknowledgements: O.A.-O. and A.O.G. acknowledge the generous support from the United States−Israel Binational Science Foundation (BSF), and the Nanoscale & Quantum Phenomena Institute at Ohio University. L.V.B. acknowledges support from the Spanish Ministerio de Ciencia e Innovacción under Project PID2020-118282RA-I00.

META 2023, PARIS - FRANCE, JULY 18 – 21, 2023

Chiral sensing with semiconductor nanophotonics

Alberto G. Curto[1,2,3]

[1] Photonics Research Group, Ghent University-imec, Ghent, Belgium

[2] Center for Nano- and Biophotonics, Ghent University, Ghent, Belgium

[3] Department of Applied Physics and Eindhoven Hendrik Casimir Institute, Eindhoven University of Technology, Eindhoven, The Netherlands

[*]Corresponding Author: Alberto.Curto@UGent.be

Abstract: Detecting molecular chirality is crucial in biochemistry. It is, however, limited by low sensitivity at low concentrations. I will discuss our progress to push the limits of chiral sensing by exploiting semiconductor nanophotonics.

Chirality plays a pivotal role in the functionality of biomolecules such as proteins, amino acids, and carbohydrates. Circular dichroism can distinguish enantiomers thanks to a small difference in the absorption of circularly polarized light. However, chiral sensing faces significant limitations due to inherently weak chiroptical signals. It is thus severely limited by low sensitivity and low spatial resolution. As a result, it is challenging to resolve the chirality of individual nanoscale objects using light for critical applications such as detecting protein aggregates linked to various diseases. In this presentation, I will discuss our progress in pushing the sensitivity limits of optically resolvable chirality by exploiting semiconductor nanophotonics. I will show several strategies to optimize chiral molecular sensors based on silicon metasurfaces to detect low molecular concentrations. Specifically, I will present our recent results on tailoring silicon nanostructures to enhance polarized fluorescence [1, 2] and Raman spectroscopies, increase optical chirality and maximize chirality transfer [3, 4]. Our results promise an increase in sensitivity towards the detection of single chiral molecules compatible with high-resolution imaging.

Acknowledgements. This work was financially supported by The Netherlands Organisation for Scientific Research (NWO) through an NWO START-UP Grant (740.018.009) and the European Research Council (ERC) under the European Union's Horizon 2020 research and innovation program (grant agreement 948804, CHANSON).

References

1. A.F. Cihan, A.G. Curto, S. Raza, P. G. Kik, M. L. Brongersma “Silicon Mie resonators for highly directional light emission from monolayer MoS_2” *Nature Photonics* 12, 284–290, 2018.
2. S. Murai, G. W. Castellanos, T. V. Raziman, A. G. Curto, J. G. Rivas, “Enhanced light emission by magnetic and electric resonances in dielectric metasurfaces”, *Adv. Opt. Mat.* 8 (16), 1902024, 2020.
3. E. Mohammadi, A. Tittl, K. L. Tsakmakidis, T. V. Raziman, A. G. Curto, “Dual Nanoresonators for Ultrasensitive Chiral Detection,” *ACS Photonics*, 8, 6, 1754, 2021.
4. T. V. Raziman, R. H. Godiksen, M. A. Müller, A. G. Curto, “Conditions for Enhancing Chiral Nanophotonics near Achiral Nanoparticles,” *ACS Photonics* 6, 10, 2583, 2019.

META 2023, PARIS - FRANCE, JULY 18 – 21, 2023

Top-down and bottom-up fabrication of electro-optic flat photonic devices

R. Grange*[1]

[1]ETH Zurich, Optical Nanomaterial Group, Institute for Quantum Electronics, Department of Physics, 8093 Zurich, Switzerland
*corresponding author: grange@phys.ethz.ch

Abstract: We will demonstrate the fabrication of devices with lithium niobate and barium titanate material for applications in telecommunication and quantum optics.

Nonlinear and electro-optic devices are present in our daily life with many applications: light sources for microsurgery, green laser pointers, or modulators for telecommunication. Most of them use bulk materials such as glass fibres or high-quality crystals, hardly integrable or scalable. Even the fast developments of thin film lithium niobate face the challenging etching of metal-oxides. Therefore, the quest for a non-centrosymmetric material system, easy to fabricate and to scale up while maintaining its functionality is still ongoing. Here we will present our recent advances in top-down fabrication of lithium niobate devices[1], and bottom-up assemblies of randomly oriented nanocrystals to produce electro-optic, nonlinear and parametric down conversion signals[2]. First, barium titanate metalenses synthesized by a sol-gel technique will be demonstrated. Then, we will show how the electro-optic response in assembled nanostructures can be as strong as certain other perfect crystalline structure. Finally, we will generate photon pairs from free-standing lithium niobate microcubes through the spontaneous parametric down-conversion process[3].

References

1. Maeder, A., Weigand, H. and Grange, R., “Lithium niobate on insulator from classical to quantum photonic devices,” 116, Photoniques(116), 48–53, 2022.
2. Vogler-Neuling, V. V., Karvounis, A., Morandi, A., Weigand, H., Dénervaud, E. and Grange, R., “Photonic Assemblies of Randomly Oriented Nanocrystals for Engineered Nonlinear and Electro-Optic Effects,” ACS Photonics 9(7), 2193–2203, 2022.
3. Duong, N. M. H., Duong, N. M. H., Duong, N. M. H., Saerens, G., Saerens, G., Timpu, F., Buscaglia, M. T., Buscaglia, V., Morandi, A., Müller, J. S., Maeder, A., Kaufmann, F., Solntsev, A. S., Grange, R. and Grange, R., “Spontaneous parametric down-conversion in bottom-up grown lithium niobate microcubes,” Opt. Mater. Express 12(9), 3696–3704, 2022.

Multiresonant and Nonlinear Metasurface–Waveguide Hybrid Structures

M. J. Huttunen, J. Kelavuori, Ali Panah Pour, T. Stolt, and A. Vesala

Photonics Laboratory, Physics Unit, Tampere University, FI-33014 Tampere, Finland
*corresponding author: mikko.huttunen@tuni.fi

Abstract: Collective lattice excitations known as surface lattice resonances (SLRs) enable to realize high-Q factor metasurface resonators. Here, we show how multiple high-Q SLRs can be utilized to realize flat resonators with a potential of increasing the nonlinear optical responses of metasurfaces. We will also theoretically demonstrate an approach towards ultra-high-Q SLRs (Q>10 000) by studying hybrid metasurface–waveguide structures.

Nonlinear optical processes provide the basis for many photonic applications, such as all-optical switches and frequency comb-based spectroscopy. Current trend in improving energy-efficiency of such nonlinear devices is to move towards small-scale and integrated devices. But it is challenging to realize strongly nonlinear integrated components by using conventional nonlinear materials, which motivates the search for alternative material platforms. Nonlinear metasurfaces have recently emerged as an interesting candidate to enable nanoscale/flat nonlinear optics [1–3]. Despite steady progress, the so far achieved conversion efficiencies have not yet rivalled conventional material platforms [4], motivating to increase the achievable conversion efficiencies of metasurfaces by increasing their associated Q-factors.

We will present our recent works to develop more efficient nonlinear metamaterials exhibiting high-Q-factor SLRs [1–3]. These resonances are associated with very narrow spectral features, showing potential to dramatically boost nonlinear processes via resonant light–matter interactions [2]. We will first discuss of our recent experimental demonstrations of multiply-resonant metasurfaces [3], and demonstrate that the lattice-sum approach (LSA) is a simple yet powerful method to understand the optical responses of SLR-supporting metasurfaces. Then, we will discuss of our recent theoretical work where we extend the LSA formalism to multipartite arrays, arbitrary incidence angles, and hybrid metasurface–waveguide structures. In particular, we show how placing metasurfaces inside waveguiding structures, the coupling between nanoparticles can be dramatically increased providing a clear route towards higher Q-factors. Even more interestingly, the associated waveguide modes become strongly dispersive near their cut-off frequencies, which provides a new mechanism to further increase the attainable Q-factors. This is particularly interesting, since it may enable to experimentally realize ultrahigh-Q-factor metasurfaces (Q>10 000) with smaller number of nanoparticles.

References

1. Bin-Alam, M. S. *et al.* "Ultra-high-Q resonances in plasmonic metasurfaces," Nat. Commun., Vol. 12, 974, 2021.
2. Stolt, T. *et al.*, "Multiply-resonant second-harmonic generation using surface lattice resonances in aluminum metasurfaces," Opt. Express, Vol. 30, No. 3, 3620–3631, 2022.
3. Stolt, T. and Huttunen, M. J., "Broadband frequency conversion of ultrashort pulses using high-Q metasurface resonators," New J. Phys., Vol. 24, 025004, 2022.
4. Vermeulen, N. *et al.* "Post-2000 nonlinear optical materials and measurements: Data tables and best practices" J. Phys. Photonics, accepted, 2022.

Chiral plasmonic metasurfaces self-assembled from non-chiral metallic nanowires and nanorods

W. Wu, V. Lemaire and M. Pauly*
Université de Strasbourg, CNRS, Institut Charles Sadron, Strasbourg, France
*corresponding author: matthias.pauly@unistra.fr

Abstract: Large-area chiral multilayer thin films are prepared by combining Grazing Incidence Spraying and Layer-by-Layer assembly from anisotropic plasmonic nanoparticles. The resulting giant chiroptical properties can be finely tuned over a broad wavelength range using simple design principles, reaching ellipticity values higher than 13° and g-factor values up to 1.6 in the visible and near-IR range. The chiroptical properties of helicity-preserving chiral mirrors will also be discussed.

Chiral assemblies of plasmonic nanoparticles have attracted increasing attention over the last years due to promising applications in fields such as molecular sensing or as optical circular polarizing elements.[1] Metamaterials that can control the flow of electromagnetic waves in unprecedented ways need to have subwavelength dimensions, i.e. in the range of tens of nm for optical applications, and their properties are not only governed by the constitutive materials but also often depend on the nanoscale structure and hierarchical organization of the individual building blocks. Such metamaterials have mostly been manufactured by top-down technologies that have the disadvantage of being expensive and slow. Obtaining large areas and regular (3D) ordering is difficult, and nanoparticle self-assembly is a promising alternative. A big challenge resides in the hierarchical organization of the nanoscale building blocks into two- or three-dimensional structures with well-controlled location and orientation across multiple length scales.

In this talk, I will present how Grazing Incidence Spraying can be used to assemble anisotropic nanoparticles as mono- and multilayer thin films[2-3] on large areas with tuneable particle density and orientation (Fig. 1a). Furthermore, the combination with the Layer-by-Layer assembly technique[4] allows building helical (and thus chiral) multilayer large-area thin films in which the composition and orientation can be controlled independently in each layer (Fig. 2b, c).[5]

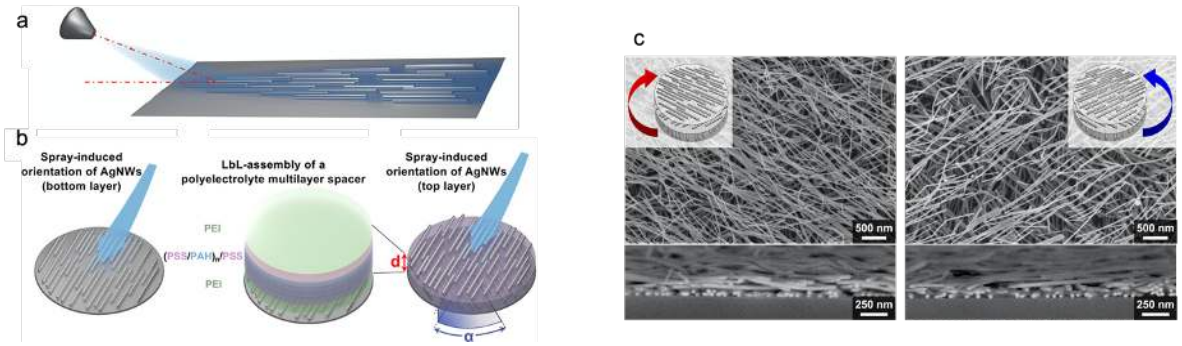


Figure 1: a) Schematic of the spray-induced orientation of nanowires. b) Schematic of the Layer-by-Layer assembly of oriented nanowire layers to prepare chiral Bouligand metasurfaces. c) SEM images (top-view and cross-section) of left-handed and right-handed 3-layer silver nanowire metasurfaces.

These films display very high chiroptical activity over a broad wavelength range (Fig. 2a) with g-factor values up to 1.8 in the near IR range (Fig. 2b).[6] The optical properties (polarized transmittance, CD spectroscopy and Mueller Matrix Polarimetry) as function of the thin film geometry will be detailed, with a special emphasis on how the chiroptical properties depend on the architecture of the assembly. The properties of chiral mirrors built from these assemblies will also be discussed.

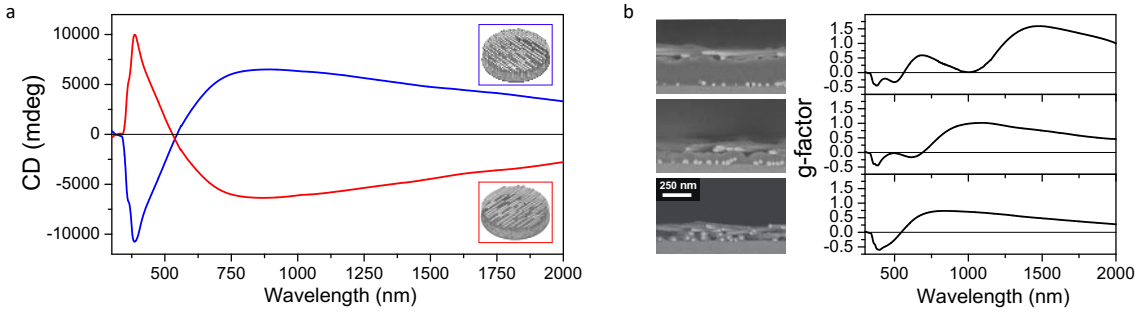


Figure 2: a) CD spectra of left-handed and right-handed chiral plasmonic nanostructures. b) Cross-section SEM images and g-factor spectra of chiral plasmonic thin films of increasing interlayer spacing.

References

1. W. Wu and M. Pauly "Chiral plasmonic nanostructures: recent advances in their synthesis and applications" Mater. Adv. Vol. 3, 186-215, 2022.
2. S. Sekar, V. Lemaire, H. Hu, G. Decher and M. Pauly "Anisotropic optical and conductive properties of oriented 1D-nanoparticle thin films made by spray-assisted self-assembly." Faraday Discuss. Vol. 191, 373-389, 2016.
3. H. Hu, M. Pauly, O. Felix and G. Decher "Spray-assisted alignment of Layer-by-Layer assembled silver nanowires: a general approach for the preparation of highly anisotropic nano-composite films." Nanoscale Vol. 9, 1307-1314, 2017.
4. G. Decher "Fuzzy Nanoassemblies: Toward Layered Polymeric Multicomposites." Science Vol. 277, 1232-1237, 1997.
5. H. Hu, S. Sekar, W. Wu, Y. Battie, V. Lemaire, O. Arteaga, L. V. Poulikakos, D. J. Norris, H. Giessen, G. Decher and M. Pauly, "Nanoscale Bouligand Multilayers: Giant Circular Dichroism of Helical Assemblies of Plasmonic 1D Nano-Objects" ACS Nano Vol. 15, 13653-13661, 2021.
6. W. Wu, Y. Battie, V. Lemaire, G. Decher and M. Pauly, "Structure-Dependent Chiroptical Properties of Twisted Multilayered Silver Nanowire Assemblies" Nano Lett. Vol. 21, 8298-8303, 2021.

META 2023, PARIS - FRANCE, JULY 18 – 21, 2023

Active photonics using nanocrystal and application for infrared sensing

Emmanuel Lhuillier[1], Yoann Prado[1], Tung Huu Dang[2], Audrey Chu[1], Gregory Vincent[3], Angela Vasanelli[2]

[1]Sorbonne Université, CNRS, Institut des NanoSciences de Paris, INSP, F-75005 Paris, France

[2]Laboratoire de physique de l'Ecole Normale Supérieure, ENS, Université PSL, CNRS, Sorbonne Université, Université Paris Cité, 75005 Paris, France

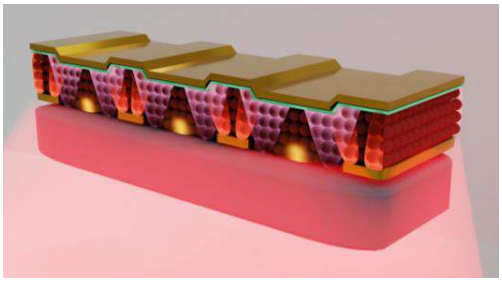
[3]ONERA - The French Aerospace Lab, 6, chemin de la Vauve aux Granges, BP 80100, F-91123 Palaiseau, France.

[*]corresponding author: el@insp.upmc.fr

Abstract: talk discusses how photonic cavities can be coupled to an infrared nanocrystal film not only to reshape the absorption but also to achieve new properties such as bias reconfigurable response.

To motivate this work, I will start by a few words regarding the integration of infrared nanocrystal as active material for infrared sensing and imaging [1]. In particular I will discuss how nanocrystal ink have dramatically simplify the coupling between the active layer and the at circuit making pixel pitch reduction possible.

In spite of this success, current devices still present a poor coupling to the incident light and most of it is generally not absorbed, limiting the overall device performance. This raises the need for a control of the light matter coupling though the coupling of the film to photonics cavity. I will review some of the development made in the group [2] relying on grating used both as cavity and contact electrodes. Though the initial goal was to boost the absorption and photoresponse of device we also have realized that it enables the design of bias reconfigurable photoresponse [3]. Two key ingredients are required which are (i) an inhomogeneous absorption generated by the cavity and (ii) a bias dependence diffusion length which comes for free thanks to hopping conduction. I will discuss some development that we have made in this direction starting from observation of small bias induced shift up to the development of structure where broad spectral window can be turned on and off



Figures schematic of a nanocrystal-based infrared sensor presenting optical resonance to reshape the absorption spectra

References

1. Photoconductive focal plane array based on HgTe quantum dots for fast and cost-effective short-wave infrared imaging, C Gréboval *et al*, Nanoscale 14, 9359 (2022)
2. Helmholtz Resonator Applied to Nanocrystal-Based Infrared Sensing, C Abadie *et al*, Nano Letters 22, 8779 (2022)
3. Bias Tunable Spectral Response of Nanocrystal Array in a Plasmonic Cavity, TH Dang *et al*, Nano Letters 21, 6671 (2021)

META 2023, PARIS - FRANCE, JULY 18 – 21, 2023

Ultra-sensitive Plasmonic Biosensors based on Two-Dimensional NanoMaterials

Shuwen ZENG[1]

[1] Light, Nanomaterials & Nanotechnologies (L2n), CNRS-EMR 7004, Université de Technologie de Troyes, France

E-mail : shuwen.zeng@utt.fr

Abstract: Surface plasmon resonance sensors are commonly used an effective tool for real-time monitoring biomolecular interactions. The sensing mechanism is based on the evanescent field perturbation at the metallic sensing substrate induced by the binding of chemical and biological molecules. Molecular binding interactions could be measured from the signal of reflected light, under the condition that the surface plasmon resonance is excited by the incident light. In this talk, I will present the use of hybrid 2D nanomaterials-based metasurface nanostructure as an enhanced sensing substrate. The thickness of the plasmonic sensing substrate is tuned in an atomic scale and optimized to improve the sensing capability. Here, both a sharp phase signal change and phase-related Goos-Hänchen signal shift were achieved due to the strong resonance at the surface of the sensing film. The enhanced plasmonic sensitivities of 2D nanostructures were systematically investigated. It is worth noting that the tunability of atomic layer led to the sensing substrate optimized with a narrow scale < 1 nm. Through a precise engineering of the metasurface substrates, 3 orders of magnitude improvement of the sensitivity were demonstrated compared to the one with pure gold sensing substrate. This hybrid 2D nanomaterial-based metasurfaces would provide a good opportunity for developing portable theranostic devices in clinical applications.

META 2023, PARIS - FRANCE, JULY 18 – 21, 2023

Active control of the nanoparticle self-assembly for photonic applications

T. Erdem[1*]

[1]Department of Electrical-Electronics Engineering, Abdullah Gül University, Erkilet Bul. Sumer Campus, Kayseri Turkey
[*]corresponding author: erdem.talha@agu.edu.tr

Abstract: Colloidal nanoparticles enable collective utilization of the inherent properties of the nanoparticles. Furthermore, their collective optical response can be fine-tuned employing DNA-driven self-assembly. Here, we present that the optical transmission of self-assembled DNA-functionalized gold nanoparticle network can be actively manipulated using an external optical excitation. We also show control of optical polarization of emitted light from semiconducting supraparticle networks hybridized with magnetic supraparticles. These results prove the potential of programmed nanoparticle self-assembly in tailoring optical features of colloidal systems.

Conventional technologies of fabricating optical materials are usually complex, costly, and energy consuming. Chemical syntheses and functionalization of colloidal nanoparticles, which may possess semiconducting, metallic, or dielectric characteristics, offer solutions to some of these problems. Especially, programmed self-assembly of the nanomaterials using DNA-DNA interactions allows for obtaining optical features that cannot be easily obtained using conventional micro- and nanofabrication methodologies. We now add another functionality to the optical systems made of colloidal nanoparticles. Our idea relies on tailoring the structure of the colloidal nanomaterial network using external means leading to controlling the optical features of these systems.

In our first study, the temperature dependence of DNA-DNA interaction was utilized. A double-stranded DNA molecule consists of two different single-stranded DNA molecules with complementary base chains linked by hydrogen bonds. When the temperature of the environment increases, the hydrogen bonds break and the double-stranded DNA molecule splits into two single-stranded DNA molecules. When the temperature decreases, recombination occurs. In our study, we focused on controlling the binding-unbinding process of the nanoparticles with the help of an external light source and tailoring the light transmittance, not by changing the temperature on a macroscopic scale [1]. For this purpose, gold nanoparticles with a diameter of 20 nm were synthesized, and then single-stranded DNA molecules functionalized with thiol groups were attached to these particles. The nanoparticle sample was split into two groups such that complementary DNA strands were attached to the nanoparticles in each group. Next, a nanoparticle network was successfully produced from these materials by mixing DNA-functionalized gold nanoparticles. Then, using a green handheld laser, the nanoparticle network was successfully heated locally, enabling the separation of the gold nanoparticles that had formed a nanoparticle network. As a result, the optical transmittance of the structure was increased by 30%. Furthermore, clear openings were detected using an optical microscope in the regions illuminated by the laser beam.

In another study [2], which aims to actively control optical properties, supraparticles were formed from semiconductor quantum dots and magnetic nanoparticles. Complementary single-stranded DNA molecules were attached to these particles via copper-free click chemistry. By mixing the two types of supraparticles, magnetic supraparticles were connected to supraparticles containing semiconductor quantum dots. Thus, a hybrid particle

network was formed. By applying an external magnetic field to this particle network, the magnetic particles were forced to line up in the direction of the magnetic field. In this way, the linear polarization of the light emanating from the semiconductor quantum dots was successfully changed and the polarization ratio was increased to 1.9. In this study, it has been successfully demonstrated that radiation can be actively controlled by an external effect.

We expect our work, briefly summarized above, to open the door to innovative fabrication methods and innovative applications of nanophotonic structures.

We are grateful to Tübitak for 2247-A Program Grant No. 120C124.

References

1. Şenel, Z., İçöz, K. and T. Erdem, "Tuning optical properties of self-assembled nanoparticle network with external optical excitation", J. Appl. Phys. Vol. 129, 153106 (2021).
2. Erdem, T., Zupkauskas, M., O'Neill, T., Caciagli, A., Xu, P., Altintas, Y., Mutlugün, E. and E. Eiser, "Magnetically controlled anisotropic light emission of DNA-functionalized supraparticles," MRS Bulletin Vol. 47, 1-7 (2022) https://doi.org/10.1557/s43577-022-00352-z

Single photon nanophotonics using hybrid plasmonics.

Aurélie Broussier[1*], Régis Deturche[1], Safi Jradi[1], Sylvain Blaize[1], Renaud Bachelot[1,2,3], Christophe Couteau[1*]

[1] Light, nanomaterials, nanotechnologies (L2n) Laboratory. CNRS EMR 7004. Université de Technologie de Troyes, 12 rue Marie Curie, 10004 Troyes Cedex, France
[2] Sino-European School of Technology, Shanghai University, 200444 Shanghai, China
[*]corresponding author: aurelie.broussier@utt.fr, christophe.couteau@utt.fr

Abstract: The need for photon and electron transport is necessary for quantum information, although very difficult in practice due to the different scales involved. In this work, we propose two different approaches to tackle this problem. The first consists of a hybrid plasmonic nanosystem comprising two types of nanosources placed strategically on a nanowire electromagnetic waveguide. The second is based on the integration of a single photon source, with a photonic structure consisting of optical waveguide used in photonics integrated circuits.

For nanophotonics and quantum photonics, it is of paramount importance to be able to efficiently couple nanoemitters and quantum emitters with photonic structures such as photonic waveguides[1], in order to be able to scale-up for any practical purposes. As a proof of concept, we use colloid semiconductor nanocrystals[2] (NCs) as nanosources of light which are also capable of single photon emission. At first, we couple different NCs on the same plasmonic structure based on a silver nanowire (Ag-NW) waveguide[3]. We then move on to another photonic platform which compatible on a larger scale with standard photonics (such as optical fibers) using ion exchanged waveguides (IEW).

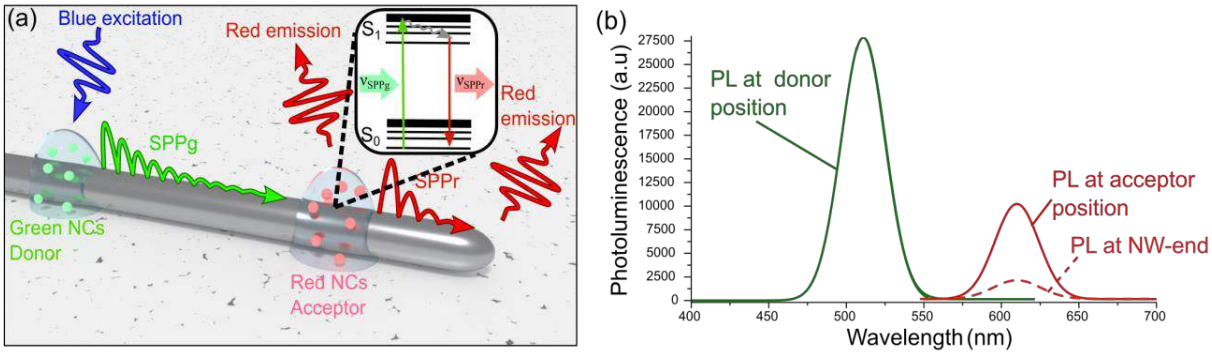


Figure 1-a Artistic view of a hybrid plasmonic nanosystem, -b PL spectra of emission on different zones. 405 laser focused on the intersection of the lines containing green QDs and the NW – donor position.

In the first case, using silver nanowires, we realize efficient acceptor-donor hybrid nano-systems where different nano-nodes can interact with each other as depicted in Fig.1-a, where 'green' surface plasmon polaritons are transformed into red plasmon polaritons at controlled sites of the silver plasmonic nanowaveguide, as a result of a plasmon-polariton conversion. Fig.1-b shows the photoluminescence (PL) obtained at different locations of the nanowire for excitation of donor NCs via a 405 nm laser. We demonstrate that Ag-NW nanowaveguides can support multi-mode propagating surface plasmon polaritons and thus defining a fundamental building block for plasmonic/nanophotonic integrated circuits.

To go even further, a single photon emitter NC was coupled to a glass waveguide connected to an optical fiber. Fig. 2-a provides a schematic of our system where we have the photonics structure made of a semi-buried IEW and a single NC as a quantum emitter on top of it. In between, a secondary waveguide has been fabricated in order to have a smooth adiabatic coupling of the NC with the micro-size waveguide. The NC emitter was then tested to demonstrate single photon emission as depicted in Fig. 2-b by the second order correlation function $g^{(2)}$ where the lowered central peak is a clear evidence that we have a single photon source from a single NC emission and this was obtained after connecting the glass waveguide to an optical fiber.

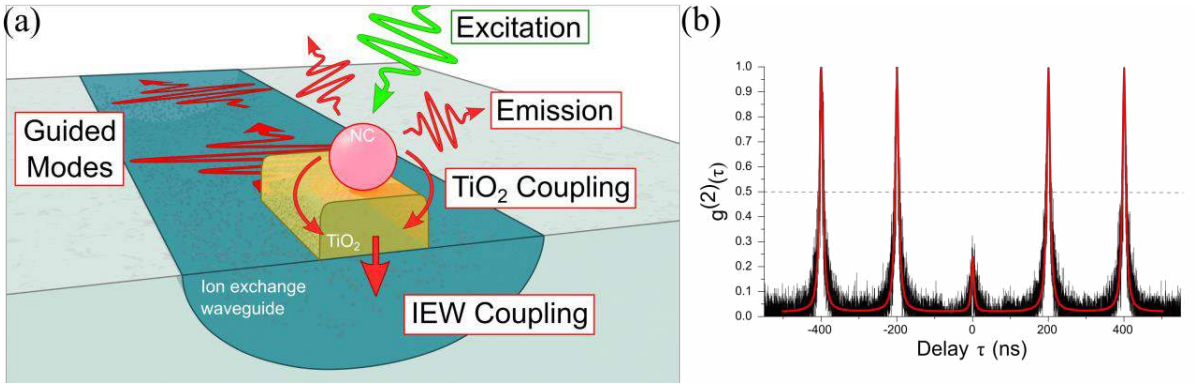


Figure 2 (a) Artistic view a single photon source integrated on Ion Exchange Waveguide. (b) Second order correlation function for the single NDs on the IEW/TiO_2 with a pulsed excitation laser at 532 nm.

We demonstrate in this that it is possible to effectively couple and control the position of nanoemitters to different photonic structures. Perspectives of this work are to optimise the coupling of nanoemitters to photonic structures as well as the use of color centres in nanodiamonds[4] as nanoemitters which are more compatible with more complex quantum photonic networks[5].

Acknowledgments

French Research Agency (ANR) ACTIVE NANO-PHOT/MULHYN and STRONG-NANO projects, CNRS-Innovation project InteQ, SATT SAYENS project InteQ2, the facility and the French RENATECH+ network, the Graduate School NANO-PHOT (École Universitaire de Recherche, contract ANR-18-EURE-0013).

References

[1] J. Beltran Madrigal *et al.*, "Hybrid integrated optical waveguides in glass for enhanced visible photoluminescence of nanoemitters," *Applied Optics*, vol. 55, no. 36, p. 10263, Dec. 2016, doi: 10.1364/AO.55.010263.

[2] P. Benalloul *et al.*, "Manipulating emission of CdSe/ZnS nanocrystals embedded in synthetic opals," *J. Phys.: Conf. Ser.*, vol. 187, p. 012004, Sep. 2009, doi: 10.1088/1742-6596/187/1/012004.

[3] A. Broussier *et al.*, "Hybrid plasmonic nanosystem with controlled position of nanoemitters," *Applied Physics Letters*, vol. 114, no. 16, p. 163106, Apr. 2019, doi: 10.1063/1.5093360.

[4] M. Nahra *et al.*, "Single germanium vacancy centers in nanodiamonds with bulk-like spectral stability," *AVS Quantum Science*, vol. 3, no. 1, p. 012001, Jan. 2021, doi: 10.1116/5.0035937.

[5] H. Wei, Z. Wang, X. Tian, M. Käll, and H. Xu, "Cascaded logic gates in nanophotonic plasmon networks," *Nature Communications*, vol. 2, no. 1, Sep. 2011, doi: 10.1038/ncomms1388.

META 2023, PARIS - FRANCE, JULY 18 – 21, 2023

Twisted waveguides as arbitrary unitary gates in polarization-encoded quantum information processing circuits

F. Morozko[1,2], A. Novitsky[2], A. Mikhalychev[3], and A. Karabchevsky[1*]
[1]School of Electrical and Computer Engineering, Ben-Gurion University of the Negev, Beer-Sheva, Israel
[2]Belarusian State University, Minsk, Belarus
[3]B. I. Stepanov Institute of Physics, NAS of Belarus, Minsk, Belarus.
[*]corresponding author: alinak@bgu.ac.il

Abstract: Integrated photonics is a remarkable platform for the realization of quantum computations due to its flexibility and scalability. Here we propose a novel paradigm exploiting twisted waveguides as a building block for polarization-encoded quantum photonic computations on a chip. We unveil a transformation (gate) matrix in the closed form and demonstrate that twisted waveguides can implement arbitrary Bloch sphere rotations. The outcomes of this research may open a new direction in the development of quantum computing architectures on a chip.

To encode information in a single photon one must use its physical degrees of freedom such as path, momentum, angular momentum, and polarization. For reaching a higher information processing capability per chip footprint it is desirable to make use of the maximum possible number of them. Photon polarization is an always-available natural degree of freedom and is thus among the most widely used encoding mechanisms. To benefit from using an integrated platform it is crucial to perform most or ideally all light manipulations on a chip as most losses occur at a stage of coupling light into a chip or from a chip. However, despite the recognized strength of integrated photonics in controlling light, manipulation of polarization on a chip yet remains elusive.

Although integrated photonic polarization-encoded CNOT gate has been demonstrated in laser-written chips, the polarization manipulation in the reported works [1]–[3] was performed using either bulk or fiber optics. On-chip polarization manipulation schemes based on tilted basis waveguides are typically used serving as waveplates [4], [5] where the waveguide symmetry axis is the optical axis. Such schemes, however, suffer from a number of drawbacks: they are extremely sensitive to fabrication intolerances and due to the cross-section mismatch with normal waveguides exhibit significant coupling losses [6].

Here we report general polarization transformation with twisted waveguides. We note that twisted waveguides are capable not only to rotate the linear polarization but also to cause the polarization transformation due to their structural elliptical birefringence. Therefore, twisted waveguides can be suggested as arbitrary unitary gates in polarization-encoded quantum information processing circuits.

Results

Using modal expansion in helical reference frame and perturbation theory we have obtained an analytical expression for the transmission matrix of a twisted waveguide which is a general Bloch sphere rotation [7]. The main conclusion is that twisted waveguides can approximate arbitrary unitary operations with arbitrary precision and reasonable design constraints. Our results pave the way to robust yet simple building block for integrated photonic polarization-encoded quantum information processing with twisted waveguide architectures. Figure 1 summarizes the results of the investigation.

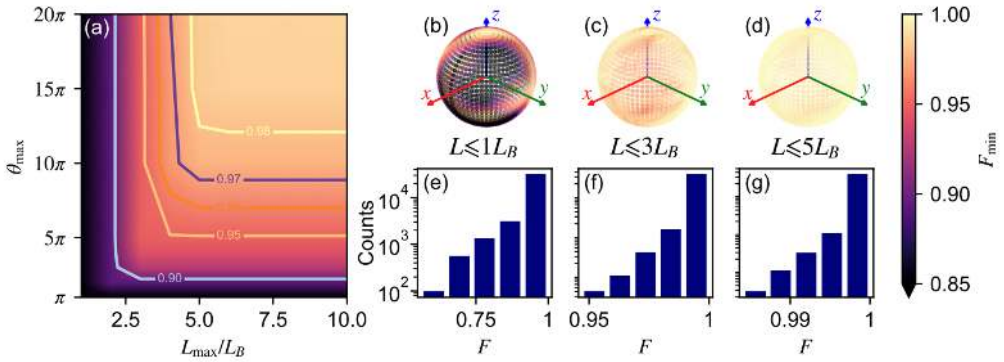


Figure 1. Twisted waveguide approximation of arbitrary single-qubit gates. (a) shows worst fidelity $F_{\min}$ over all single qubit gates as a function of twisted waveguide design constraints, where $\theta_{\max}$ is the maximum twist angle, $L_{\max}$ is the maximum twist length measured in terms of linear beat lengths L_B. (b-d) show the worst fidelity over rotations around a given axis with $\theta_{\max} = 20\pi$ and three different $L_{\max}$ constraints, histograms (e-g) below the spheres visualize the distribution of approximation fidelities. *Cited from* [7].

Acknowledgements

A.K. acknowledges the support of the Israel Science Foundation (ISF no. 2598/20).

References

[1] L. Sansoni *et al.*, "Polarization Entangled State Measurement on a Chip," *Phys. Rev. Lett.*, vol. 105, no. 20, p. 200503, Nov. 2010, doi: 10.1103/PhysRevLett.105.200503.

[2] A. Crespi *et al.*, "Integrated photonic quantum gates for polarization qubits," *Nat Commun*, vol. 2, no. 1, p. 566, Sep. 2011, doi: 10.1038/ncomms1570.

[3] J. Zeuner *et al.*, "Integrated-optics heralded controlled-NOT gate for polarization-encoded qubits," *npj Quantum Inf*, vol. 4, no. 1, p. 13, Dec. 2018, doi: 10.1038/s41534-018-0068-0.

[4] G. Corrielli *et al.*, "Rotated waveplates in integrated waveguide optics," *Nat Commun*, vol. 5, no. 1, p. 4249, Sep. 2014, doi: 10.1038/ncomms5249.

[5] R. Heilmann, M. Gräfe, S. Nolte, and A. Szameit, "Arbitrary photonic wave plate operations on chip: Realizing Hadamard, Pauli-X and rotation gates for polarisation qubits," *Sci Rep*, vol. 4, no. 1, p. 4118, May 2015, doi: 10.1038/srep04118.

[6] M. F. Baier, "Polarization multiplexed photonic integrated circuits for 100 Gbit/s and beyond," Technische Universität Berlin, 2018. Accessed: Dec. 28, 2020. [Online]. Available: https://depositonce.tu-berlin.de//handle/11303/8125

[7] F. Morozko, A. Novitsky, A. Mikhalychev, and A. Karabchevsky, "Arbitrary single-qubit rotations on chip with twisted waveguides." arXiv, Dec. 27, 2022. Accessed: Feb. 15, 2023. [Online]. Available: http://arxiv.org/abs/2212.13530

[8] A. Nicolet, F. Zolla, and S. Guenneau, "Modelling of twisted optical waveguides with edge elements," *Eur. Phys. J. Appl. Phys.*, vol. 28, no. 2, pp. 153–157, Nov. 2004, doi: 10.1051/epjap:2004189.

[9] D. M. Shyroki, "Exact Equivalent Straight Waveguide Model for Bent and Twisted Waveguides," *IEEE Trans. Microwave Theory Techn.*, vol. 56, no. 2, pp. 414–419, 2008, doi: 10.1109/TMTT.2007.914637.

META 2023, PARIS - FRANCE, JULY 18 – 21, 2023

Controlling Heat Anisotropy at the nanoscale inside cross arrays

Jean-François Bryche[1,2,3,*†], Marlo Vega[1,2,4†], Julien Moreau[4], Paul-Ludovic Karsenti[3], Mondher Besbes[4], Philippe Gogol[1,2,5], Denis Morris[1,2,3], Paul G. Charette[1,2] and Michael Canva[1,2]

[1] Laboratoire Nanotechnologies Nanosystèmes (LN2), CNRS, Université de Sherbrooke - Sherbrooke, QC, Canada.

[2] Institut Interdisciplinaire d'Innovation Technologique (3IT), Université de Sherbrooke - Sherbrooke, QC, Canada

[3] Faculté des Sciences, Université de Sherbrooke - Sherbrooke, QC, Canada.

[4] Université Paris-Saclay, Institut d'Optique Graduate School, CNRS, Laboratoire Charles Fabry - Palaiseau, France.

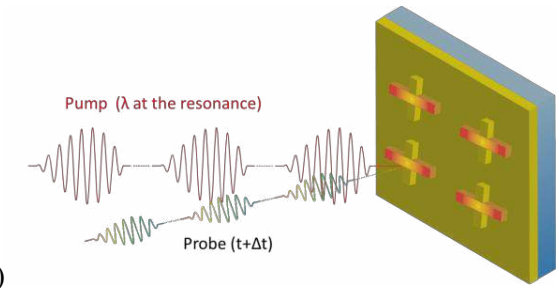
[5] Centre de Nanosciences et de Nanotechnologies, Université Paris-Saclay, CNRS - Palaiseau, France.

[*]corresponding author: jean-francois.bryche@cnrs.fr
[†]*first shared co-authorship.*

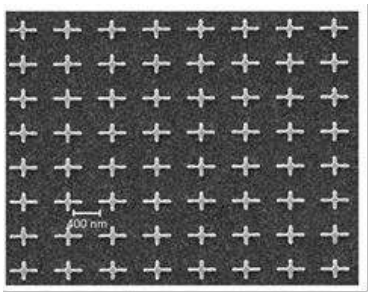
Abstract: In this work, we investigate the photothermal heating of asymmetric nano-crosses by ultrashort light pulses. We show experimentally and numerically that non-thermal energy density and temperature inside the two arms of the crosses can be controlled with the polarization of the pump pulse. We also demonstrate the importance of considering non-thermal electron ballistic displacement to reproduce the measured experimental data.

Nanoparticles (NPs) can absorb and convert light into heat, making them useful as localized sources of heat [1]. However, the dynamics of heat distribution inside NPs must be better understood and modeled. This is a challenging task due to the time and space scale involved in the photothermal process (femtosecond and nanometer scale). Firstly, we have developed a two-temperature model for uniform gold film [2]. In this work, we go further and realize pump-probe spectroscopy on cross-shaped gold nanoparticles on gold film (see figure 1 a-b). We predict with our numerical model heat transfer inside the nanoparticles and confirm it with experiments [3]. This NP geometry is known to support polarization-dependent localized plasmonic resonance (LSPR) along each of its branches (see figure 1-c). Here we obtain two resonances around 600 nm for the TM polarization and 680 nm for TE polarization. By selectively exciting one LSPR, we can heat only one branch, then, the heat will propagate along the other branch.

a)



b)



c)

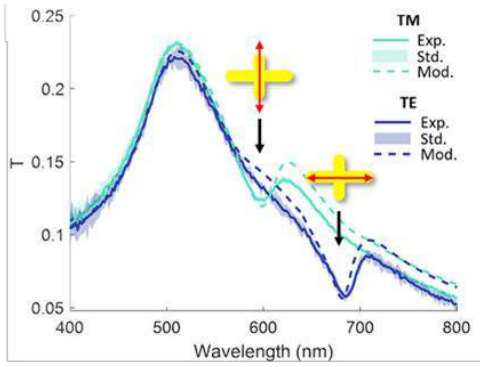


Figure 1. a) schema of the pump-probe experiment on gold cross-shaped nanoparticles b) SEM pictures of an array of nanocross of 300-410nm size, 60nm of height, and a period of 530 and 640 nm respectively in horizontal and vertical axes. c) Experimental (solid lines) and modeled (dashed lines) steady-state transmission spectra through the array at normal incidence for both polarizations. The arrows indicate the transmission minima at resonance for each arm in the cross. The standard deviation with a 95% confidence interval over six spectra is represented in a lighter color for each curve. ***Figures b) and c) Reproduced from [2] copyright ACS Photonics.***

By measuring the temporal delay between the modulation of LSPR intensity of each branch with pump-probe setup, we put in evidence the thermal transport inside the cross-shaped NP. The measured optical response delay between the longitudinal and transverse LSPR of the nanocross was around 140 ± 50 fs, in agreement with the simulated one (100 fs). More details on the numerical model as the experiments are provided in [3]. We also demonstrate the importance of considering a non-thermal ballistic electron displacement inside the improved two-temperatures model to match the experiment.

Acknowledgements. This work was supported by the Natural Sciences and Engineering Research Council of Canada (NSERC) with Discovery Grants for M.C. and P.G.C. A doctoral scholarship from IDEX Paris-Saclay supports M.V. This work is supported by the "ADI" project funded by the IDEX Paris-Saclay, ANR-11-IDEX-0003-02 Grant from CMC Microsystems and the MNT Financial Assistance Voucher (8774 & 10451). J-F B. was supported by the Fonds de recherche du Québec−Nature et Technologies (FRQNT) and his Merit scholarship program for international students (no. 273433). LN2 is an International Research Laboratory (IRL) funded and co-operated by Université de Sherbrooke (UdeS), Centre National de la Recherche Scientifique (CNRS), École Centrale Lyon (ECL), Institut National des Sciences Appliquées de Lyon (INSA Lyon), and Université Grenoble Alpes (UGA). We thank also CMC Microsystems.

References

1. Baffou, G., & Rigneault, H. (2011). Femtosecond-pulsed optical heating of gold nanoparticles. In Physical Review B (Vol. 84, Issue 3). https://doi.org/10.1103/physrevb.84.035415
2. Bresson, P., Bryche, J.-F., Besbes, M., Moreau, J., Karsenti, P.-L., Charette, P. G., Morris, D., & Canva, M. (2020). Improved two-temperature modeling of ultrafast thermal and optical phenomena in continuous and nanostructured metal films. In Physical Review B (Vol. 102, Issue 15). https://doi.org/10.1103/physrevb.102.155127
3. Bryche, J.-F.†,, Vega, M.†,, Moreau, J., Karsenti, P.-L., Bresson, P., Besbes, M., Gogol, P., Morris, D., Charette, P. G., & Canva, M. (2023). Ultrafast Heat Transfer at the Nanoscale: Controlling Heat Anisotropy. ACS Photonics. https://doi.org/10.1021/acsphotonics.2c01968.

Perspectives and Challenges for the Fabrication of Plasmonic Nitride Nanostructures

P. Patsalas[1,*], N. Pliatsikas[1], S. Kassavetis[1], D. Babonneau[2], S. Camelio[2], G. Abadias[2]

[1] Physics Department, Aristotle University of Thessaloniki, Thessaloniki, Greece
[2] Institut Pprime, UPR 3346 CNRS-Université de Poitiers-ENSMA, Département Physique et Mécanique des Matériaux, 86073 Poitiers, France
[*]Corresponding author: ppats@physics.auth.gr

Abstract: The refractory character of plasmonic transition metal nitrides[1] and their growth predominantly by reactive sputtering are simultaneously blessings and curses[2], as they limit the fabrication of nitride plasmonic nanostructures to top-down processes, which is time consuming, costly, and of limited scalability. In this work, alternative routes of fabrication of TMN nanostructures are critically reviewed and presented. We focus on the fabrication of nano-islands by nanosphere lithography[3], dichroic nanowires by glancing angle deposition[4], and colloidal nanoparticles laser ablation in liquids.

Με σχόλια [NP1]: Max. 80 words

The research project was supported by the Hellenic Foundation for Research and Innovation (H.F.R.I.) under the "2nd Call for H.F.R.I. Research Projects to support Post-Doctoral Researchers" (Project Number: 1099).



References

1. P. Patsalas, N. Kalfagiannis, S. Kassavetis, G. Abadias, D.V. Bellas, Ch. Lekka, E. Lidorikis, "Conductive nitrides: Growth principles, optical and electronic properties, and their perspectives in photonics and plasmonics" Mater. Sci. Eng. R, Vol. 123, 1–55, 2018.
2. M. Gioti, J. Arvanitidis, D. Christofilos, K. Chaudhuri, T. Zorba, G. Abadias, D. Gall, V.M. Shalaev, A. Boltasseva, P. Patsalas, Plasmonic and phononic properties of epitaxial conductive transition metal nitrides, J. Opt. Vol. 22, art. no. 084001, 2020.
3. S. Panos, D. Tselekidou, S. Kassavetis, I. Fekas, J. Arvanitidis, D. Christofilos, D. Karfaridis, S. Dellis, S. Logothetidis, P. Patsalas, "Etchless Fabrication of High-Quality Refractory Titanium Nitride Nanostructures" Physica Status Solidi B, Vol. 258, No. 7, art. no 2170033, 2021.
4. D. Babonneau, S. Camelio, G. Abadias, D. Christofilos, I. Arvanitidis, S. Psilodimitrakopoulos, G.M. Maragkakis, E. Stratakis, N. Kalfagiannis, P. Patsalas, "Self-Assembled Dichroic Plasmonic Nitride Nanostructures with Broken Centrosymmetry for Second-Harmonic Generation" ACS Applied Nanomaterials Vol. 4, No. 9, 8789–8800, 2021.

Photochemical imaging of near-field and dissymmetry factor of chiral nanostructures

T. Aoudjit[1*], A. Horrer[1], S. Koscheev[1], R. Bachelot[1], J. Plain[1] and D. Gerard[1]

[1] Lumière, nanomatériaux, nanotechnologies (L2n), Université de Technologie de Troyes & CNRS ERL 7004, Troyes 10004, France.

[*]corresponding author: thinhinane.aoudjit@utt.fr

Abstract: We present here a subwavelength imaging approach that is based on the interaction between the highly exalted near-field of chiral nanostructures and an azobenzene molecule (DR1, disperse red 1) grafted to a polymeric chain (i.e., PMMA). The aim of the study is to experimentally demonstrate the visibility factor.

Under illumination, the azobenzene molecules (DR1) undergo photo-isomerization cycles, which induce a displacement of matter inducing measurable topographical modifications that can be tracked using atomic force microscopy [1]. Therefore, we obtain in the polymer a map of the near-field of the chiral nanostructures . We recently demonstrated that chiral effects in plasmonic nanostructures can be imaged with this technique [2]. Here, we apply photochemical imaging to chiral metallic nanostructures composed of two coupled gold nanorods. Each rod has a length of 140 nm, a width of 70 nm and a height of 50 nm. They are separated by a 40 nm wide gap and are shifted with respect to each other by a distance '**s**' along their long axis. We show that the near-field chiral response can be imprinted in the photopolymer (figure 1.a-b). It is shown that it is possible to experimentally map the near-field dissymmetry factor, which is the contrast in the local near-field response of the object under RCP and LCP excitation (figure 1.c) [3].

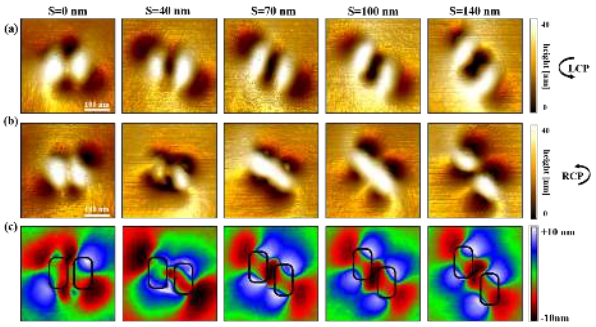


Figure 1 : (a,b) AFM images after irradiation by the left (LCP) and right (RCP) polarization. (c) V-factor maps.

References

1. Plain, J., G. P. Wiederrecht,S. K. Gray,P. Royer, R. Bachelot, "Multiscale optical imaging of complex fields based on the use of azobenzene nanomotors," *J. Phys. Chem. Lett*, 4, 2124-2132, 2013.
2. Horrer, A., Y. Zhang, D. Gérard, J. Beal, M. Kociak, J. Plain, R. Bachelot,"Local optical chirality induced by near-field mode interference in achiral plasmonic metamolecules," *Nano Lett*. 20, 509–516, 2019.
3. Aoudjit, T., A. Horrer, S. Kostcheev, R. Bachelot, J. Plain and D. Gerard, "Photochemical imaging of near-field and dissymmetry factor in chiral nanostructures," Adv. Optical Mater, 2203015, 2023.

Unidirectional ultracompact self-assembled optical antennas

Maria Sanz-Paz[1], Fangjia Zhu[1], Mauricio Pilo-Pais[1], Guillermo Acuna[1]*

[1] Department of Physics, University of Fribourg, Chemin du Musée 3, Fribourg CH-1700, Switzerland
*corresponding author: guillermo.acuna@unifr.ch

Abstract: We report unidirectional emission of a single fluorophore using an ultracompact optical antenna. The design consists of two side-by-side gold nanorods self-assembled via DNA origami, which also controls the positioning of the single-fluorophore. Our results show that when a single fluorescent molecule is positioned at the tip of one nanorod and emits at a frequency capable of driving the antenna in the anti-phase mode, unidirectional emission with a forward to backward ratio of up to 9.9 dB can be achieved.

Optical antennas have been widely used for manipulating light-matter interactions at the nanoscale in order control the emission intensity, lifetime and directivity of single molecules [1], [2]. In particular, increasing the directionality of single emitters takes on crucial significance, for example in the context of future integrated optical circuits or quantum communication and computing schemes, which hold potential for lower energy consumption and higher efficiency using states that can be controlled up to the fundamental quantum limit [3], [4]. To date most efforts were focused on designs adapted from the Yagi-Uda antenna that can reach high directionality with a significant number of elements spanned over approximately a wavelength [5]. Despite this tremendous proof of concept, further development of these antennas is hindered by the challenges involved in the fabrication and positioning of the single emitters and metallic elements that limits the coupling control and performance that can be achieved.

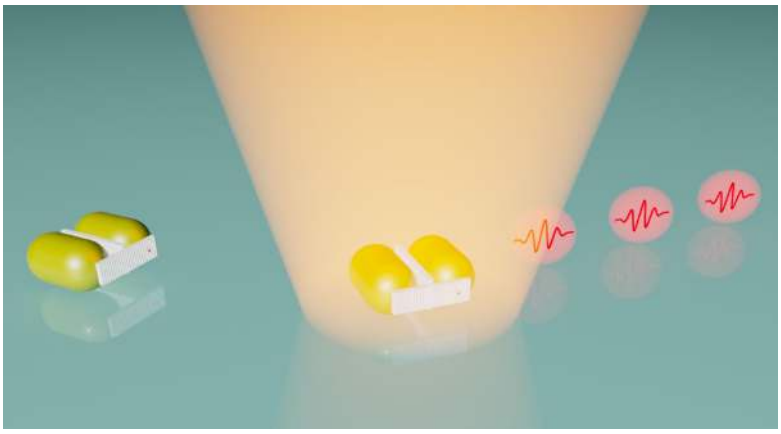


Fig. 1: sketch of an ultracompact antenna showing unidirectional emission

In this contribution, we report on the realization of ultra-compact directional antennas for single photon emitters by means of DNA self-assembly. Adapting the design proposed by Pakizeh et al. [6], we used the DNA origami technique [7] to place two gold nanorods in a side-to-side (or end-fire) arrangement with an overall footprint an order of magnitude smaller than the optical Yagi-Uda antenna. By coupling a single fluorescent molecule to one of the nanorods, unidirectional emission is registered red-shifted from the bonding mode [8], when the nanorods are driven close to the antiphase mode

References

[1] P. Biagioni, J.-S. Huang, and B. Hecht, “Nanoantennas for visible and infrared radiation,” Reports Prog. Phys., vol. 75, no. 2, p. 024402, 2012.

[2] A. F. Koenderink, “Single-Photon Nanoantennas,” ACS Photonics, vol. 4, no. 4. pp. 710–722, 2017.

[3] O. Benson, “Assembly of hybrid photonic architectures from nanophotonic constituents,” Nature, vol. 480, no. 7376. pp. 193–199, 2011.

[4] A. Alù and N. Engheta, “Wireless at the nanoscale: Optical interconnects using matched nanoantennas,” Phys. Rev. Lett., vol. 104, no. 21, 2010.

[5] A. G. Curto, G. Volpe, T. H. Taminiau, M. P. Kreuzer, R. Quidant, and N. F. Van Hulst, “Unidirectional emission of a quantum dot coupled to a nanoantenna,” Science (80-.)., vol. 329, no. 5994, pp. 930–933, 2010.

[6] T. Pakizeh, M. Käll, M. Ka, and M. Käll, “Unidirectional Ultracompact Optical Nanoantennas,” Nano Lett., vol. 9, pp. 2343–2349, 2009.

[7] P. W. K. Rothemund, “Folding DNA to create nanoscale shapes and patterns,” Nature, vol. 440, no. 7082. pp. 297–302, 2006.

[8] E. Prodan, C. Radloff, N. J. Halas, and P. Nordlander, “A Hybridization Model for the Plasmon Response of Complex Nanostructures,” Science (80-.)., vol. 302, no. 5644, pp. 419–422, 2003.

META 2023, PARIS - FRANCE, JULY 18 – 21, 2023

In situ and real-time studies of ultrathin silver films grown by physical vapor deposition: The role of nitrogen additive

D. Babonneau[1*], G. Abadias[1], K. Solanki[1], A. Michel[1], J. Ramade[1], S. Camelio[1], A. Resta[2], A. Vlad[2], A. Coati[2], Y. Garreau[2,3], K. Sarakinos[4], M. Kamiński[5], and B. Krause[5]

[1]Université de Poitiers, CNRS, Institut Pprime, Poitiers, France
[2]Synchrotron SOLEIL, Saint-Aubin, France
[3]Université Paris Cité, CNRS, Laboratoire Matériaux et Phénomènes Quantiques, Paris, France
[4]University of Helsinki, Department of Physics, Helsinki, Finland
[5]Institut für Photonenforschung und Synchrotronstrahlung, Karlsruher Institut für Technologie, Karlsruhe, Germany
[*]corresponding author: david.babonneau@univ-poitiers.fr

Abstract: In this talk, we discuss growth strategies to produce transparent and conductive silver layers by physical vapor deposition in the presence of nitrogen additive. We use a combination of *in situ* and real-time diagnostics (substrate curvature measurements, surface differential reflectance spectroscopy, grazing incidence x-ray diffraction, and grazing incidence small-angle x-ray scattering) during deposition, which provides valuable insights into the effects of nitrogen additive on the early-film-formation stages and related optical properties.

Ultrathin silver films with thickness below a few nanometers are interesting candidates for use as transparent conductive electrodes in flexible optoelectronic devices [1]. However, early growth stages of Ag films deposited by 'conventional' physical vapor deposition on weakly interacting substrates are dominated by a natural tendency to form disconnected 3D islands, which manifests itself in high electrical resistivities and broad absorption bands in the visible range due to the excitation of localized surface plasmons. Growth strategies to produce continuous, ultrathin and ultrasmooth Ag films without compromising their electrical conductivity and optical transparency have lately been deployed. Among them, the use of gaseous additives, such as nitrogen or oxygen, appears to be an effective means of promoting wetting of Ag on the substrate surface, resulting in the formation of a continuous layer at a lower nominal Ag thickness [2-4]. However, understanding the impact of additives on the early-growth stages of ultrathin Ag films, in terms of both structural and optical/electrical properties, requires the implementation of *in situ* and real-time diagnostics.

In the present work, we study nitrogen-mediated growth of Ag on weakly-interacting amorphous carbon and SiO_x substrates. We explore the influence of nitrogen addition on the evolution of the film morphology, crystal structure, stress development, and optical response by coupling complementary *in situ* and real-time observations during the deposition by magnetron sputtering or electron-beam evaporation. Laboratory-scale real-time studies include substrate curvature measurements together with surface differential reflectance spectroscopy to determine the morphological transition thicknesses (percolation and continuous formation thickness) [5] as a function of nitrogen partial pressure. These investigations are augmented by real-time synchrotron experiments at SOLEIL (SIXS beamline) combining simultaneous grazing incidence small-angle x-ray scattering (GISAXS), grazing incidence diffraction (GID), and substrate curvature measurements. This enables us to monitor the evolution of the island morphology (size and shape), texture and stress, from the initial growth stages until the formation of a continuous layer, as well as during growth interruptions.

Acknowledgements: This work is part of the IRMA project funded by the ANR and DFG (reference ANR-21-CE09-0041-01). It also pertains to the French Government programs "Invertissements d'Avenir" (EUR

INTREE, reference ANR-18-EURE-0010) and LABEX INTERACTIFS (reference ANR-11-LABX-0017-01

References

1. Yun, J. “Ultrathin metal films for transparent electrodes of flexible optoelectronic devices”, Adv. Func. Mater., Vol. 27, 1606641, 2017.
2. Yun, J. *et al.*, “An unexpected surfactant role of immiscible nitrogen in the structural development of silver nanoparticles: an experimental and numerical investigation”, Nanoscale, Vol. 12, 1749–1758, 2020.
3. Jamnig, A. *et al.*, “3D-to-2D morphology manipulation of sputter-deposited nanoscale silver films on weakly interacting substrates via selective nitrogen deployment for multifunctional metal contacts”, ACS Appl. Nano Mater., Vol. 3, 4728–4738, 2020.
4. Pliatsikas, N. *et al.*, “Manipulation of thin silver film growth on weakly interacting silicon dioxide substrates using oxygen as a surfactant”, J. Vac. Sci. Technol. A, Vol. 38, 043046, 2020.
5. Abadias, G. *et al.*, “Volmer-Weber growth stages of polycrystalline metal films probed by *in situ* and real-time optical diagnostics”, Appl. Phys. Lett., Vol. 107, 183105, 2015.

META 2023, PARIS - FRANCE, JULY 18 – 21, 2023

Foerster-Type Nonradiative Energy Transfer in Media with Complex Permittivity

Pedro Ludwig Hernandez-Martinez [1], Abdulkadir C. Yucel [1], and Hilmi Volkan Demir [1,2]

[1]*LUMINOUS!* Centre of Excellence for Semiconductor Lighting and Display, School of Electrical and Electronic Engineering, Nanyang Technological University, Singapore, 639798, Singapore
[2]Department of Electrical and Electronics Engineering, Department of Physics, UNAM−National Nanotechnology Research Center, and Institute of Materials Science and Nanotechnology, Bilkent University, Ankara 06800, Turkey
[*]corresponding author: pedro@ntu.edu.sg

Abstract: We present the effects of the complex permittivity of a background medium on Foerster-type nonradiative energy transfer (FRET) and the changes in FRET as a function of the relative permittivity of the medium. We discuss examples of enhanced FRET via tuning the complex permittivity of the medium and illustrate that FRET can significantly increase when the denominator of the FRET screening factor approaches zero.

The Foerster-type nonradiative energy transfer (FRET) is a crucial proximity effect that strongly modifies the emission kinetics of nano-emitters serving as donors and acceptors and has numerous applications such as color tuning, biosensing, light-harvesting, and light-generation. FRET strongly depends on the distance between the donor and acceptor pair, limiting its applications. Two main approaches have been used to boost FRET: the dimensionality effect from the change in the exciton confinement due to the difference in the nanostructure geometry [1] and the local electric field enhancement from a localized surface plasmon (LSP). However, these approaches have their limitations, and in the case of LSP, the lossy properties of the plasmonic nanostructure can decrease FRET if it is not appropriately designed. FRET can be significantly enhanced by using artificially engineered materials of complex dielectric medium with carefully tuned permittivity [2]. In such a medium, the FRET pair can effectively confine and guide the electromagnetic energy within them, owing to their low wavenumber and very large wavelength in the medium, introducing the proximity effect in the long-range interactions, leading to a dramatic increase in FRET. To illustrate the effects of the background medium's permittivity, we discuss examples where the background medium is tuned to enhance FRET.

The authors acknowledge support from Singapore Agency for Science, Technology, and Research (A*STAR) MTC program, Grant No. M21J9b0085. This research is supported by the Ministry of Education, Singapore, under its Academic Research Fund Tier 1 (MOE-RG62/20). The authors also gratefully acknowledge the financial support in part from TUBITAK 119N343, 120N076, 121N395, and 20AG001. H.V.D. also acknowledges the support from TUBA.

References

1. P.-L. Hernández-Martínez, A.-O. Govorov, and H.-V. Demir, Generalized Theory of Förster-type Nonradiative Energy Transfer in Nanostructures with Mixed Dimensionality, *J. Phys. Chem. C*, Vol 117, No 19, 10203−10212, 2013.
2. P. L. Hernández-Martínez, A. C. Yucel, and H. V. Demir, "Ultraefficient Förster-Type Nonradiative Energy Transfer Enabled by the Complex Dielectric Medium with Tuned Permittivity" J. Phys. Chem. C 125, 12405, 2021.

Vacuum Ultraviolet Light Generation and Circular Polarization Control Using Dielectric Nanomembranes

Kuniaki Konishi

Institute for Photon Science and Technology, The University of Tokyo, Japan
kkonishi@ipst.s.u-tokyo.ac.jp

Abstract: We have demonstrated that dielectric free-standing thin film (Nanomembranes) with a thickness of several-hundred nanometers can generate coherent vacuum ultraviolet (VUV) light efficiently and tunably based on third harmonic generation (THG). We have also demonstrated the generation of circularly-polarized VUV THG in a dielectric nanomembrane with a square periodic lattice of circular hole. The presented results show that nanomembranes and their nanostructures are an effective new way to generate and control vacuum ultraviolet coherent light.

Vacuum ultraviolet (VUV) coherent light sources have been used for many applications for probing the electronic states of excited atoms and molecules and for controlling chemical reactions, time-resolved angle-resolved photoemission spectroscopy, and circular dichroism measurement of biomolecules. For such applications, it is important to develop a method for simple light generation for VUV spectroscopy. Though third or higher harmonic generation from gases has been used to generate vacuum and extreme-ultraviolet light, it is still more practical and convenient to use solids for wavelength conversion. Recently, new types of solid nonlinear materials for VUV generation, such as dielectric metasurfaces [1], which are artificial nanostructures with sizes comparable with or smaller than the light wavelength, have been proposed and demonstrated, but it is required to increase the intensity and control the polarization state of generated VUV coherent light for practical spectroscopic application.

We have developed that dielectric free-standing thin film (Nanomembranes) with a thickness of several-hundred nanometers or less can generate coherent VUV light efficiently and tunably based on third harmonic generation (THG) [2]. We evaluate that THG in SiO_2 nanomembranes excited at 470 nm enables VUV radiation at 157 nm with photon flux (10^{10} photon per second), which is sufficient to be used for spectroscopic application. We also demonstrate the generation of circularly-polarized VUV THG in a photonic crystal nanomembrane with a square periodic lattice of circular hole (Fig. 1) [3]. It is known that the rotational symmetry of the structure allows for a nonlinear optical response of circularly polarized light, [4], and we demonstrate that it is also applicable to rotational symmetry of periodic all-dielectric nanostructures, i.e., photonic crystals.

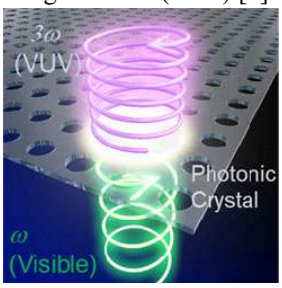


Fig. 1 Schematic of vacuum ultraviolet circular polarization wavelength conversion using a photonic crystal nanomembrane.

The presented results show that nanomembranes and their nanostructures are an effective new way to generate and control vacuum ultraviolet coherent light.

References

1. M. Semmlinger et al., “Vacuum Ultraviolet Light-Generating Metasurface,” Nano Lett., Vol. 18, No. 9, 5738–5743, 2018.
2. K. Konishi et al., “Tunable third harmonic generation in the vacuum ultraviolet region using dielectric nanomembranes,” APL Photon., Vol. 5, 066103, 2020.
3. K. Konishi et al., “Circularly polarized vacuum ultraviolet coherent light generation using a square lattice photonic crystal nanomembrane,” Optica, Vol. 7, No. 8, 855–863, 2020.
4. K. Konishi et al., “Tunable and nonlinear metamaterials for controlling circular polarization,” J. Appl. Phys. Vol. 127, 230902, 2020.

Laser direct writing of crystallized metal oxide from sol-gel using thermoplasmonic effect

L. Noel[1,2], A. Khitous[1,2], C. Molinaro[1,2], and O. Soppera*[1,2]

[1]Université de Haute-Alsace, CNRS, IS2M UMR 7361, F-68100 Mulhouse, France
[2] Université de Strasbourg, France
*corresponding author: olivier.soppera@uha.fr

Abstract: The development of semiconducting thin films represents a large and important area of research, due to their interesting optical and electrical properties. Metal oxide (MO) films are indeed used in a wide range of applications, including photodetectors, gas sensors, biosensors or photocatalysis.
Near infrared (NIR) laser annealing was successfully used to crystallize TiO_2 thin films from a sol-gel solution deposited on gold nanoparticle arrays (AuNPs). The AuNPs were used as nano-heaters allowing a local temperature increase up to 500°C in the film. The temperature reached under laser is deduced from the presence of the anatase phase in the samples obtained by laser exposure, showing that crystallized TiO_2 can be obtained by thermoplasmonic effect. Different analytical techniques supported this study, such as grazing X-ray diffraction (GIXRD), UV-visible and Raman spectroscopy. The temperature increased was confirmed by a numerical model that emphasized the role of NPs coupling in the thermoplasmonic effect. Direct laser patterning by NIR laser and in combination with Deep-UV photolithography (DUV) has also been demonstrated. This fabrication method opens new perspectives in applications such as photonics, photocatalysis or biosensing.

Acknowledgements: The authors would like to acknowledge the support of Agence Nationale pour la Recherche (Project ANR-18-CE24-0028) for funding.

References

1. F. Kameche, W. Heni, S. Telitel, D. Ge, L. Vidal, F. Dumur, D. Gigmes, J. Lalevée, S. Marguet, L. Douillard, C. Fiorini-Debuisschert, R. Bachelot, O. Soppera, Materials Today 2020, 40, 38.
2. A. Khitous, C.-F. Lin, F. Kameche, H.-W. Zan, J.-P. Malval, D. Berling, O. Soppera, ACS Applied Nano Materials 2021, 4, 8770.
3. F. Kameche, W. Heni, S. Telitel, L. Vidal, S. Marguet, L. Douillard, C. Fiorini-Debuisschert, R. Bachelot, O. Soppera, The Journal of Physical Chemistry C 2021, 125, 8719.
4. C.-F. Lin, A. Khitous, H.-W. Zan, O. Soppera, Advanced Optical Materials 2021, 2100045.
5. C. C. Yeh, H. W. Zan, O. Soppera, Advanced Materials 2018, 30, 24.

META 2023, PARIS - FRANCE, JULY 18 – 21, 2023

Chiral Nanostructures

Y. K. Gun'ko*

School of Chemistry and CRANN, Trinity College Dublin, Dublin 2, Ireland
*corresponding author: igounko@tcd.ie

Abstract: Our primary aim is to create novel chiral nanostructured materials that exhibit optical activity and chirality, and to investigate their properties, nature, and potential applications. The chiroptically active nanostructures have unique physical and chemical properties that have attracted significant attention in recent years. Here we present the progress in various approaches for the synthesis of these nanostructures. The study of chiral nanostructures is an exciting and rapidly growing field with promising future prospects for various technological advancements.

Our primary aim is to create novel chiral nanostructured materials that exhibit optical activity and chirality, and to investigate their properties, nature, and potential applications. As part of our efforts, we have successfully synthesized new types of chiral nanomaterials, such as chiral II-VI semiconducting quantum dots and chiral nanoparticles of metal oxides that are of significant technological importance. Furthermore, we have shown that chiral quantum dots have promising applications in chiral recognition and luminescent chemo- and bio-sensing. Chiral nanostructures have unique physical and chemical properties that have attracted significant attention in recent years. They have potential applications in various fields such as optics, electronics, catalysis, and biomedicine. Chiral nanostructures can be synthesized using various techniques, and researchers are continually exploring new ways to create and control their chirality to optimize their properties [1-4]. The main goal of our work is to develop new types of technologically important inorganic nanosteuctured materials possessing optical activity and chirality, study their properties, investigate their nature and explore their potential applications (Figure 1).

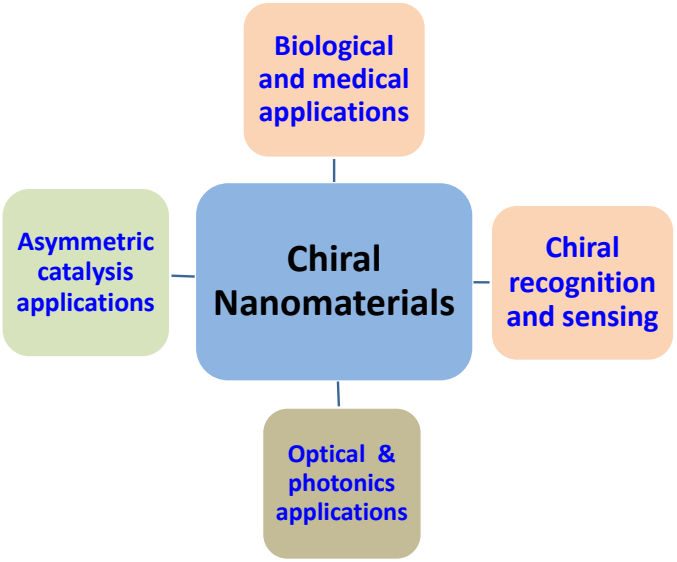


Figure 1. Potential applications of chiral nanomaterials.

We have developed new chiral nanomaterials including a range of chiral semiconducting nanoparticles (quantum dots) and chiral nanoparticles of technologically important metal carbonates, transition metal dichalcogenides and oxides. In addition, we explored the properties of new anisotropic chiral nanomaterials [5-7]. The new nanomaterials have shown a very interesting optical activity and unusual chiral morphologies which were confirmed by various instrumental techniques. The use of chiral ligands enabled us to transfer these nanostructures into aqueous phases and enhance their chiroptical activity. We have also demonstrated potential applications of chiral quantum dots for chiral recognition and luminescent chemo- and bio- sensing. We have also found that live cells demonstrate an enantioselective uptake of chiral quantum nanostructures. It is expected that chiral nanomaterials will find applications in sensing, nanomedicine, asymmetric synthesis, catalysis and other areas.

Acknowledgements

The authors gratefully acknowledge financial support from the Science Foundation of Ireland (Grant SFI 20/FFP-A/8904) and BiOrbic, Bioeconomy Research Centre (grant number SFI 16/RC/3889).

References

1. Govorov, A.O., Gun'ko, Y.K., Slocik, J.M. Gerard, V.A., Fan, Z., Naik, R.R. "Chiral nanoparticle assemblies: circular dichroism, plasmonic interactions, and exciton effects", Journal of Materials Chemistry, Vol. 21, 16806-16818, 2011.
2. Ben-Moshe, A., Maoz, B.M., Govorov, A.O., Markovich, G., "Chirality and chiroptical effects in inorganic nanocrystal systems with plasmon and exciton resonances", Chemical Society Reviews, Vol. 42, 7028-7041, 2013.
3. Milton, F.P., J. Govan, M.V. Mukhina, Y.K. Gun'ko, "The chiral nano-world: chiroptically active quantum nanostructures", Nanoscale Horizons, Vol 1, 14-26, 2016.
4. Kuznetsova, V., Gromova, Y., Martinez-Carmona, M., Purcell-Milton, F., Ushakova, E., Cherevkov, S., Maslov, V., Gun'ko, Y. K. "Ligand-induced chirality and optical activity in semiconductor nanocrystals: theory and applications", Nanophotonics, Vol. 10, 797-824, 2021.
5. Kuznetsova, V.A., Mates-Torres, E., Prochukhan, N., Marcaste, M., Purcell-Milton, F., O'Brien, J., Visheratina, A.K., Martinez-Carmona, M., Grornova, Y., Garcia-Melchor, M., Gun'ko, Y.K., "Effect of Chiral Ligand Concentration and Binding Mode on Chiroptical Activity of CdSe/CdS Quantum Dots" ASC Nano, Vol. 13, 13560-13572, 2019.
6. Baimuratov, A.S., Pereziabova, T.P., Leonov, M.Y., Zhu, W., Baranov, A.V., Fedorov, A.V., Gun'ko, Y.K., Rukhlenko, I.D., "Optically Active Semiconductor Nanosprings for Tunable Chiral Nanophotonics", ACS Nano, Vol12, 6203-6209, 2018.
7. Purcell-Milton, F., McKenna, R., Brennan, L.J., Cullen, C.P., Guillemeney, L., Tepliakov, N.V., Baimuratov, A.S., Rukhlenko, I.D., Perova, T.S., Duesberg, G.S., Gun'ko, Y.K., "Induction of Chirality in Two-Dimensional Nanomaterials: Chiral 2D MoS_2 Nanostructures", ACS Nano, Vol.12, 954-964, 2018.

Metal-Induced Polymerization of Diazonium Salts for Controlled Spatial Deposition of QDs in Hot Spots

L. Trotsiuk[1*], A. Broussier[1], S. Marguet[2], A.-L. Baudrion[1], Y. Luo[3], C. Mangeney[3], N. Felidj[4], P.-M. Adam[1] and R. Bachelot[1]

[1] Light, nanomaterials, nanotechnologies (L2n), CNRS EMR 7004, Université de Technologie de Troyes, France
[2] Université Paris Saclay, France
[3] LCBPT, CNRS UMR 8601, Université Paris Cité, France
[4] ITODYS, CNRS UMR 7086, Université Paris Cité, France

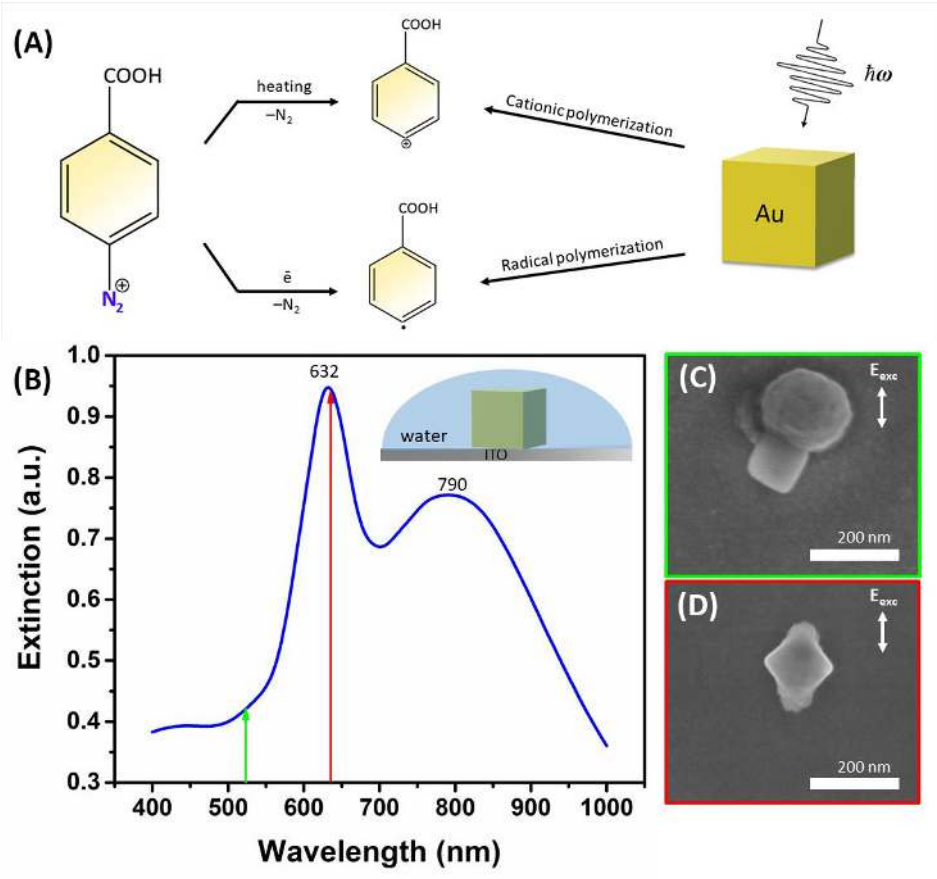
[*]corresponding author: liudmila.trotsiuk@gmail.com

Abstract: In this work, we demonstrate the possibility of the local functionalization of gold nanoparticle surface using metal-induced diazonium salt polymerization for spatial control of quantum dot deposition. Varying the wavelength of excitation of gold nanoparticles, we can choose the polymerization mechanism, which leads to different polymerization pattern.

Hybrid metal-semiconductor nanostructures are of a great importance as promising elements of integrated photonics.[1] Successful implementation of hybrid structures into real applications depends on the efficiency of plasmon-exciton coupling in them. Plasmonic nanoparticles can significantly alter the optical and electronic properties of semiconductor nanocrystals (e.g. quantum dots, QDs).[2] However, the main problem during the fabrication of hybrid systems remains a poor control over semiconductor nanocrystals deposition in the vicinity of plasmonic structures. Since the enhanced field is not eventually distributed around a metal nanoparticle, for the efficient plasmon-exciton coupling an attachment of QDs in hot spots is required. Chaotic deposition of QDs reduces “beneficial” effect of plasmonic nanoparticles leading to a loss in the efficiency of the hybrid system.

In this work, we demonstrate the advantage of using metal-induced polymerization of diazonium salts to create anchoring sites for QDs in plasmonic hot spot. Diazonium salts, molecules containing easily removed N_2-group, have been widely used for electrochemical grafting of electrodes.[3] The large choice of substitution groups in these molecules allows binding varied molecules or particles to the grafted layer via electrostatic interaction or covalent bonding.[3] There are two possible pathways of dediazonation and therefore polymerization of diazonium salts (Fig. 1a). The first mechanism goes through the formation of a cation, which then interact with negatively charged surface, and is initiated by heating. Another mechanism requires electron transfer and goes through the radical formation step, which can further easily attach to any surface.

The ability of gold nanoparticles to generate under irradiation both local heat and hot electrons allow us to induce the both mechanisms of polymerization of diazonium salts resulting in different spatial image. Under the excitation that matched interband transition, we observe polarization-independent thermal growth of polymer on the gold nanoparticle surface (Fig. 1c). At the same time, the excitation of the plasmon resonance of the gold nanocube (Fig. 1b) leads to the polymerization pattern corresponding to hot spots (Fig. 1d). Further electrostatic interaction of negatively charged diazonium structures with positively charged QDs leads to controlled QD attachment in plasmonic hot spots.



Figures 1: (a) Schematic representation of possible polymerization pathways of diazonium salts in the presence of a metal nanoparticle; (b) FDTD simulated extinction spectrum of a gold nanocube; (c) and (d) SEM-images of gold nanocubes after polymerization of diazonium salts at the 514 nm and 633 nm excitation correspondingly.

Acknowledgements

This study was financially supported by the French Research Agency (ANR) in the frame of ADVANSPEC project. Fabrication and characterization were made by the facilities of Nano'mat platform and the French RENATECH+ network.

References

1. Pelucchi, E.; Fagas, G.; Aharonovich, I.; Englund, D.; Figueroa, E.; Gong, Q.; Hannes, H.; Liu, J.; Lu, C.-Y.; Matsuda, N.; et al. "The Potential and Global Outlook of Integrated Photonics for Quantum Technologies", Nat. Rev. Phys., Vol. 4, No. 3, 194–208, 2021.

2. Bitton, O.; Gupta, S. N.; Haran, G. "Quantum Dot Plasmonics: From Weak to Strong Coupling", Nanophotonics, Vol. 8, No. 4, 559–575, 2019.

3. Mahouche-Chergui, S.; Gam-Derouich, S.; Mangeney, C.; Chehimi, M. M. "Aryl Diazonium Salts: A New Class of Coupling Agents for Bonding Polymers, Biomacromolecules and Nanoparticles to Surfaces", Chem. Soc. Rev., Vol. 40, No. 7, 4143, 2011.

META 2023, PARIS - FRANCE, JULY 18 – 21, 2023

Publishing in Nature journals

Rachel Won
Nature Photonics
r.won@nature.com

Abstract: In this talk, I will tell you all you need to know about publishing your work in Nature journals, right from preparing your manuscript and options you have during your submission, through to the editorial and review processes.

.

META 2023, PARIS - FRANCE, JULY 18 – 21, 2023

The kinetics of plasmon-induced chemical reactions studied by surface-enhanced Raman scattering (SERS) and X-ray photoelectron spectroscopy (XPS)

I. Bald[1*], S. Kogikoski Jr.[1], A. Dutta[1] and R. Schürmann[2]

[1]Institute of Chemistry, University of Potsdam, Germany

[2]Physikalisch Technische Bundesanstalt (PTB), Berlin, Germany
[*]corresponding author: bald@uni-potsdam.de

Abstract: The rate constants of plasmon-induced transformation of brominated adenine and thiophenol derivatives is studied by SERS and XPS. We identified relevant parameters determining the reactivity of molecules on plasmonic nanostructures, among them the material and size of nanoparticles, as well as the local density of states. Furthermore we attempt to exploit these systems for site-selective functionalization of nanoparticles and radical induced polymerization reactions.

Plasmonic nanoparticles such as gold and silver nanoparticles absorb visible light very efficiently through excitation of their surface-plasmon resonance (SPR). The SPR can decay into ("hot") electron-hole pairs that are able to induce chemical reactions in adsorbed molecules by a charge transfer. In the case of the transfer of an electron the chemical processes occurring in the adsorbed molecules can be described by dissociative electron attachment (DEA). This opens the new field of plasmonic chemistry, which promises new chemical pathways and selectivities in bond breaking/activation through low-energy electrons.[1] We have investigated this process in brominated Adenine and Guanine on Au and AgNPs using surface-enhanced Raman scattering (SERS), which allows to determine the kinetics of the electron-induced debromination reaction by monitoring the vibrational fingerprint of reactants and products.[2,3] The same technique has been applied to a range of thiophenol molecules, and along with synchrotron XPS measurements we were able to identify important parameters determining the reactivity of molecules towards electrons released from the nanoparticle surface.[4-6] Currently, we are exploring possibilities to apply the gained mechanistical knowledge to modify nanoparticles site-selectively using plasmon-induced reactions, and to create light-controlled polymers using controlled radical polymerization.

Support by the European Research Council (ERC) is gratefully acknowledged (Consolidator Grant 772752).

References

1. C. Zhan et al., "From plasmon-enhanced molecular spectroscopy to plasmon-mediated chemical reactions", Nat. Rev. Chem., 2, 216, 2018.
2. A. Dutta, R. Schürmann, S. Kogikoski Jr., N. S. Mueller, S. Reich and I. Bald, "Kinetics and Mechanism of Plasmon-Driven Dehalogenation Reaction of Brominated Purine Nucleobases on Ag and Au" ACS Catal., 11, 8370, 2021.
3. S. Kogikoski Jr., A. Dutta and I. Bald, "Spatial Separation of Plasmonic Hot-Electron Generation and a Hydrodehalogenation Reaction Center Using a DNA Wire", ACS Nano, 15, 20562, 2021.
4. R. Schürmann, K. Ebel, C. Nicolas, A. R. Milosavljevic, I. Bald, „Role of Valence Band States and Plasmonic Enhancement in Electron-Transfer-Induced Transformation of Nitrothiophenol", J. Phys. Chem. Lett., 10, 3153, 2019.
5. R. Schürmann, A. Dutta, K. Ebel, K. Tapio, A. R. Milosavljević and I. Bald, "Plasmonic reactivity of halogen thiophenols on gold nanoparticles studied by SERS and XPS", J. Chem. Phys., 157, 084708, 2022.

6. R. Schürmann, E. Titov, K. Ebel, S. Kogikoski Jr., A. Mostafa, P. Saalfrank, A. R. Milosavljević and I. Bald, “The electronic structure of the metal–organic interface of isolated ligand coated gold nanoparticles”, Nanoscale Adv., 4, 1599, 2022.

Non-Thermal Activation of Reactants in Plasmon-Assisted Chemical Reactions: Roles of Molecular Structure and Metal-Molecule Contact

Zee Hwan Kim*
Department of Chemistry, Seoul National University, Seoul 08826, Korea
E-mail: zhkim@snu.ac.kr

Recent studies on plasmon-assisted chemical reactions postulate that the hot carriers of plasmon-excited nanostructures may induce a non-thermal vibrational activation of metal-bound reactants. However, a quantitative validation at the level of molecular quantum states is currently missing. In this talk, I will present our recent spectroscopic studies on metal-bound reactants, which proves the non-thermal vibrational molecular excitations caused by plasmons: We find that such a plasmon-induced vibrational excitation causes hyper-thermal vibrational population distribution of a specific molecular vibrational mode, and bring significant population in overtone-excited states. Such excitation is found to be critically dependent on the metal-molecule chemical contact. The inelastic molecule-electron scattering model could fully explain what are observed. The result provides the physical basis for the plasmon-assisted chemical reactions and paves the way for controlling chemical reactions on metal surfaces.

META 2023, PARIS - FRANCE, JULY 18 – 21, 2023

Ultrafast Optical Studies of Hybrid Nanomaterials of Interest for Optoelectronic and Energy Conversion Applications

G. P. Wiederrecht[1*]

[1]Center for Nanoscale Materials, Argonne National Laboratory, Lemont, IL, 60439, USA
[*]corresponding author: wiederrecht@anl.gov

Abstract: Ultrafast optical spectroscopy is used to monitor energy flow in nanostructures of interest for optoelectronic and energy conversion applications. The impact of hybrid nanostructures on aiding in the efficiency of desired energy flow outcomes following the absorption of photons is further described. Using ultrafast spectroscopy to probe hybrid structures designed to increase light-matter interactions, such as through optical cavities, is also discussed.

Ultrafast spectroscopy is useful for monitoring various pathways for energy flow following the photoexcitation of a nanomaterial. The ability of modern ultrafast laser systems to excite and probe over a broad spectral range, from ultraviolet through terahertz energies, allows for monitoring energy and charge flow within and between nanostructures, as well as to their local environments. Such capabilities enable the study and optimization of optically-induced processes that impact the efficiency of optoelectronic and light harvesting/energy conversion materials. With that said, ultrafast spectroscopy remains challenging and frequently very time-consuming for a number of reasons, such as phototoxicity of many materials (particularly under ambient conditions) and high optical scattering that can limit signal to noise in a pump-probe or time-resolved emission experiment.

Hybrid nanomaterials represent an additional handle with which to impact pathways of photoinduced energy flow and dissipation, through coupling that can modify both radiative and nonradiative processes. In this talk I describe our recent efforts to time-resolve energy flow in hybrid plasmonic and excitonic nanomaterials. I also describe our recent efforts to improve the rate of data acquisition of time-resolved optical studies in these and similar nanostructures, which can potentially have the added benefit of enabling a larger range of materials to be studied since less exposure time to illumination enables more photosensitive materials to be studied. Time-resolved studies of collective nanostructures designed for light harvesting and energy conversion are also described. Finally, the dynamics of excitonic-plasmonic hybrid nanostructures in which the plasmonic material functions as an optical cavity to alter radiative rates are discussed. For example, the dynamics of nanomaterial photoprocesses as a function of photon energy relative to the cavity resonance is explored in detail and impact on applications is described.

Work performed at the Center for Nanoscale Materials, a U.S. Department of Energy Office of Science User Facility, was supported by the U.S. *DOE*, Office of Basic Energy Sciences, under Contract No. DE-AC02-06CH11357.

META 2023, PARIS - FRANCE, JULY 18 – 21, 2023

Bioanalytics using plasmonic nanostructures

S. Kastner, E. Podlesnaia, F. Seier, Y. Luximun, A. Dietel, M. Urban, A. Csaki, W. Fritzsche*

Leibniz Institute of Photonic Technology (IPHT) Jena, Germany
*corresponding author: wolfgang.fritzsche@ipht-jena.de

Abstract: The effect of localized surface plasmon resonance (LSPR) on chemically synthesized gold nanoparticles is utilized to setup a biosensing platform with the potential for sensitive and specific detection of biomolecules of interest such as biomarkers. This principle is demonstrated both on a single particle level for DNA detection, then extended also to proteins, and to arrays of particles. In order to readout the arrays, imaging spectrometer were developed.

Today, innovative tools for diagnostics and bioanalytics are needed. They should be able to detect molecules of interest with sufficient sensitivity, preferably label-free and multiplexed, to be usable outside of dedicated laboratories and with less qualified personnel, at minimal costs.

Plasmonic nanostructures promise to provide sensing capabilities with the potential for ultrasensitive and robust assays in a high parallelization and miniaturization, and without the need for markers. When functionalized with certain biomolecules (such as single-stranded DNA or antibodies) which bind the target molecule of interest (e.g., a biomarker like DNA or a protein), they should capture this target molecule with high specificity. Upon binding of target molecules, the localized surface plasmon resonance (LSPR) of these structures is changed, and can be used as sensoric readout [1]. This is possible even on a single nanostructure level, using optical darkfield detection introduced more than 100 years ago [2], as demonstrated for DNA detection [3]. In contrast to SPR, LSPR senses only in a very thin layer (on the scale of the particle diameter), resulting in an efficient background suppression [4,5]. Only molecules bound directly at the surface contribute significantly to the signal, but much less molecules farer away.

In order to multiplex this approach, imaging spectrometer setups, e.g. based on a Michelson interferometer or multiple LEDs have been developed, able to readout a whole array of sensors in one step [6,7]. On the sensor side, microarrays of gold nanoparticle spots were fabricated using spotting of pre-synthesized gold nanoparticles [8]. Such chemically synthesized particles allow for a cost-efficient generation of highly crystalline particles as nanosensors; by using microfluidic approaches, a higher quality and reproducibility can be achieved [9]. Using this microarray approach, a multiplex DNA-targeting detection of fungal pathogens involved in sepsis could be demonstrated [10]. DNA-based signal amplification, e.g. by hybridization chain reaction, improves the sensitivity [11. Beyond DNA detection, LSPR sensing is also applicable for the detection of protein targets, such as CRP [5].

In conclusion, the results demonstrate the potential of this LSPR-based array platform for molecular detection of biomolecules of interest, with possible applications in bioanalytics and diagnostics.

Acknowledgements:
Funding by BMBF (02WIL1521, 01DR20010A and 13N15717) and TAB (2018 VF 0015; 2018 FE 9039).

References

1. A. Csaki, T. Schneider, J. Wirth, Jahr N, Steinbrück A, Stranik O, Garwe F, Müller R and Fritzsche W: Molecular Plasmonics – light meets molecules at the nanoscale. Phil Trans A 369, 3483-3496 (2011).
2. T. Mappes, N. Jahr, A. Csaki, N. Vogler, J. Popp, W. Fritzsche: The Invention of Immersion Ultramicroscopy in 1912 – The Birth of Nanotechnology? Angew Chem Int Ed 51, 11208-11212 (2012)
3. T. Schneider, N. Jahr, J. Jatschka, A. Csaki, O. Stranik, W. Fritzsche: Localized surface plasmon resonance (LSPR) study of DNA hybridization at single nanoparticle transducers, J Nanopart Res 15, 1531 (2013)
4. J. Jatschka, A. Dathe, A. Csaki, W. Fritzsche, O. Stranik: Propagating and localized surface plasmon resonance sensing - a critical comparison based on measurements and theory. Sensing and BioSensing Research 7, 62-70 (2016)
5. S. Kastner, P. Pritzke, A. Csaki, W. Fritzsche: The effect of layer thickness and immobilization chemistry on the detection of CRP in LSPR assays. Scientific Reports 12, 836 (2022)
6. D. Zopf, J. Jatschka, A. Dathe, N. Jahr, W. Fritzsche, O. Stranik: Hyperspectral imaging of plasmon resonances in metallic nanoparticles. Biosensors and Bioelectronics 81, 287-293 (2016); S. Kastner, M. Urban, A.-K. Dietel, A. Csaki, W. Fritzsche: Cost-Effective and Robust Multispectral Light-Emitting Diode Device for the Readout of Plasmonic Microarray Sensors. Adv Photon Res 2200252 (2022)
7. S. Kastner, M. Urban, A.-K. Dietel, A. Csaki, W. Fritzsche: Cost-Effective and Robust Multispectral Light-Emitting Diode Device for the Readout of Plasmonic Microarray Sensors. Adv Photon Res 2200252 (2022)
8. A. Pittner, S. Wendt, D. Zopf, A. Dathe, N. Grosse, A. Csaki, W. Fritzsche, O. Stranik: Fabrication of micro-patterned substrates for plasmonic sensing by piezo-dispensing of colloidal nanoparticles. Analytical and Bioanalytical Chemistry 411, 1537-1547 (2019)
9. M. Thiele, J.Z.E. Soh, A. Knauer, D. Malsch, O. Stranik, R. Mueller, A. Csaki, T. Henkel, J.M. Koehler, W. Fritzsche: Gold nanocubes - Direct comparison of synthesis approaches reveals the need for a microfluidic synthesis setup for a high reproducibility. Chemical Engineering Journal 288, 432-440 (2016)
10. D. Zopf, A. Pittner, A. Dathe, N. Grosse, A. Csaki, K. Arstila, J. Toppari, W. Schott, D. Dontsov, G. Uhlrich, W. Fritzsche, O. Stranik: Plasmonic Nanosensor Array for Multiplexed DNA-based Pathogen Detection. ACS Sensors 4, 335-343 (2019) Biosensors and Bioelectronics 167, 112465 (2020)
11. A. Miti, S. Thamm, P. Müller, A. Csaki, W. Fritzsche, G. Zuccheri: A miRNA biosensor based on localized surface plasmon resonance enhanced by surface-bound hybridization chain reaction. Biosensors and Bioelectronics 167, 112465 (2020)

META 2023, PARIS - FRANCE, JULY 18 – 21, 2023

Structured surfaces for enhanced radiation-matter interaction and nonlinear optics

Luca Razzari

Institut National de la Recherche Scientifique, Centre Énergie Matériaux Télécommunications (INRS-EMT), Canada
*corresponding author: luca.razzari@inrs.ca

Abstract: In this talk, I will review our main results regarding the exploitation of nanoresonators and metasurfaces for: (i) enhanced terahertz spectroscopy of low-dimensional materials; (ii) nanoscale phonon strong coupling; and (iii) nonlinear wavelength conversion.

META 2023, PARIS - FRANCE, JULY 18 – 21, 2023

Photoluminescence from Ultrathin Monocrystalline Gold Flakes

A. R. Bowman[1], F. Kiani[1], A. Rodríguez Echarri[2], T. V. Tsoulos[1], Joel D. Cox[3,4,5], F. Javier García de Abajo[2,6] and G. Tagliabue[1*]

[1]Laboratory of Nanoscience for Energy Technologies (LNET), STI, École Polytechnique Fédérale de Lausanne (EPFL), Lausanne 1015, Switzerland
[2]ICFO–Institut de Ciencies Fotoniques, The Barcelona Institute of Science and Technology, 08860 Castelldefels (Barcelona), Spain
[3]Center for Nano Optics, University of Southern Denmark, Campusvej 55, DK-5230 Odense M, Denmark
[4]POLIMA–Center for Polariton-driven Light–Matter Interactions, University of Southern Denmark, Campusvej 55, DK-5230 Odense M, Denmark
[5]Danish Institute for Advanced Study, University of Southern Denmark, Campusvej 55, DK-5230 Odense M, Denmark
[6]ICREA–Institució Catalana de Recerca i Estudis Avançats, Passeig Lluís Companys 23, 08010 Barcelona, Spain
[*]corresponding author: giulia.tagliabue@epfl.ch

Abstract: Photon emission from gold has recently received increased attention, particularly in the context of nanoplasmonics. However, this signal's origin remains unclear. Here we study photoluminescence from ultrathin monocrystalline gold flakes, allowing us to decouple nanoscale from plasmonic effects. We explain our measurements through first-principles theory accounting for electronic and optical properties of the gold films. Our results resolve a fundamental scientific debate and provide insight for the exploitation of photoluminescence as a probe of light-matter interactions in metals.

Photon emission from gold was first observed in 1969 [1], and has since received increased interest from a number of fields that employ gold nanostructures, including fundamental nanoscale studies [2,3], monitoring surface and electronic temperature [4–6], and probing gold-molecule interactions in plasmonic picocavities [7]. Despite its usefulness, significant uncertainty surrounds the origin of emitted light in different structures, especially whether it is due to inelastic Raman scattering or recombination of hot electrons and holes [3,8–11]. This is further complicated by enhancement of emission at specific wavelengths due to plasmonic resonances and spatial confinement effects in nanostructures.

Here we present photon emission measurements from monocrystalline gold flakes with 14 nm to 110 nm thicknesses. Uniquely, our flakes have atomically flat, clean surfaces and, at the time of writing, they have the world's best aspect ratio [12]. This enables us to probe the relationship between photon emission and spatial confinement directly as a function of sample thickness and temperature at varying excitation wavelength and power. We reveal that long-wavelength photon emission is independent of excitation wavelength: conclusive evidence that this signal is due to photoluminescence (PL) rather than Raman scattering. We also demonstrate that photon re-absorption plays an extremely significant role in gold PL, which has previously not been fully understood. We use photon re-absorption to spatially resolve the origin of PL from within the flakes, revealing that there is minimal charge transport prior to PL. We reproduce experimental signals with first-principles calculations based on density functional theory. Finally, we show that PL can be used to probe local temperature without the need to measure the anti-Stokes components [5], enhancing the possibilities of gold thermometry. Our study provides crucial insight into the nature of light emitted from gold, decoupling spatial confinement from plasmonic enhancement, and paves the way to probing hot carriers in a wide variety of devices.

References

[1] A. Mooradian, *Photoluminescence of Metals*, Phys. Rev. Lett. **22**, 185 (1969).

[2] M. R. Beversluis, A. Bouhelier, and L. Novotny, *Continuum Generation from Single Gold Nanostructures through Near-Field Mediated Intraband Transitions*, Phys. Rev. B **68**, 115433 (2003).

[3] Y.-Y. Cai, J. G. Liu, L. J. Tauzin, D. Huang, E. Sung, H. Zhang, A. Joplin, W.-S. Chang, P. Nordlander, and S. Link, *Photoluminescence of Gold Nanorods: Purcell Effect Enhanced Emission from Hot Carriers*, ACS Nano **12**, 976 (2018).

[4] E. Pensa, J. Gargiulo, A. Lauri, S. Schlücker, E. Cortés, and S. A. Maier, *Spectral Screening of the Energy of Hot Holes over a Particle Plasmon Resonance*, Nano Lett. **19**, 1867 (2019).

[5] Y.-Y. Cai, E. Sung, R. Zhang, L. J. Tauzin, J. G. Liu, B. Ostovar, Y. Zhang, W.-S. Chang, P. Nordlander, and S. Link, *Anti-Stokes Emission from Hot Carriers in Gold Nanorods*, Nano Lett. **19**, 1067 (2019).

[6] T. Jollans, M. Caldarola, Y. Sivan, and M. Orrit, *Effective Electron Temperature Measurement Using Time-Resolved Anti-Stokes Photoluminescence*, J. Phys. Chem. A **124**, 6968 (2020).

[7] W. Chen, P. Roelli, A. Ahmed, S. Verlekar, H. Hu, K. Banjac, M. Lingenfelder, T. J. Kippenberg, G. Tagliabue, and C. Galland, *Intrinsic Luminescence Blinking from Plasmonic Nanojunctions*, Nat Commun **12**, 2731 (2021).

[8] P. Y. Yu, Y. R. Shen, Y. Petroff, and L. M. Falicov, *Resonance Raman Scattering at the Forbidden Yellow Exciton in Cu 2 O*, Phys. Rev. Lett. **30**, 283 (1973).

[9] J. R. Solin and H. Merkelo, *Resonant Scattering or Absorption Followed by Emission*, Phys. Rev. B **12**, 624 (1975).

[10] J. T. Hugall and J. J. Baumberg, *Demonstrating Photoluminescence from Au Is Electronic Inelastic Light Scattering of a Plasmonic Metal: The Origin of SERS Backgrounds*, Nano Lett. **15**, 2600 (2015).

[11] S. Wu, O. H.-C. Cheng, B. Zhao, N. Hogan, A. Lee, D. H. Son, and M. Sheldon, *The Connection between Plasmon Decay Dynamics and the Surface Enhanced Raman Spectroscopy Background: Inelastic Scattering from Non-Thermal and Hot Carriers*, Journal of Applied Physics **129**, 173103 (2021).

[12] F. Kiani and G. Tagliabue, *High Aspect Ratio Au Microflakes via Gap-Assisted Synthesis*, Chem. Mater. **34**, 1278 (2022).

An approach to fabricating plasmonic Titanium Nitride nanoparticles by pulsed laser ablation for biological applications

N. Pliatsikas[1,*], S. Kassavetis[1], A. Koutsogianni[1], S. Panos[1], T. Odutola[1], I. Fekas[1], E. Rampota[1], C. Kapnopoulos[1], M. Gioti[1], P. A. Patsalas[1]

[1] Physics Department, Aristotle University of Thessaloniki, Thessaloniki, Greece
[*]Corresponding author: nipliats@physics.auth.gr

Abstract: The need to manufacture plasmonic materials with absorption in the Near-Infrared window is imperative even today for biomedical applications due to the efficient absorption and heating when at the same time the use of Traditional plasmonic metal nanoparticles have failed. We could pave the way by the controlled fabrication of refractory transition metal nitrides nanoparticles, such as Titanium Nitride, by pulsed laser ablation process in solvents.

Plasmonics is one of the most dynamic and fast-developing scientific and technological fields nowadays. Metal nanoparticles (NPs) with plasmonic response in the Near-Infrared (NIR) spectral range can be applied for biological applications due to the efficient absorption and heating at extremely confined volume in the vicinity of the NPs. “Traditional” plasmonic metal NPs, such as Au and Ag, fail to endure high temperatures and/or the high electric fields of NIR concentrated light, required for biological applications [1]. We could pave the way to emerging plasmonic bio-applications by the fabrication of refractory transition metal nitrides NPs, such as Titanium Nitride (TiN), whose plasmonic performance can extent into the NIR spectral range by varying their stoichiometry or via alloying to form ternary systems [2]. The most promising route to fabricate plasmonic TiN NPs, in terms of reproducibility and ease process upscaling, is by pulsed laser ablation in solvents (LA). As the NIR plasmonics are extremely sensitive to the stoichiometry and/or doping of TiN, LA emerges as the undisputed method of choice, because the ablated NPs retain in the elemental composition of the solid target.

In this work, we present the controlled fabrication of functional refractory and stable plasmonic TiN NPs with absorption in the NIR biological window by LA. The initial targets have been developed by reactive Magnetron Sputtering at room temperature while the final shaping of the colloidal NPs was performed through a laser ablation process by the 532 nm beam of a picosecond laser system and/or by 1064 and 532 nm beam of a nanosecond Nd:YAG pulsed laser system. TiN NPs structure and morphology as well as the quality of the materials have been analyzed by XRD, SEM, EDX, AFM and XPS. The optical properties of the TiN target materials have been evaluated by NIR-Vis-UV Spectroscopic Ellipsometry, while an optical absorbance characterization was performed on the colloidal TiN NPs. The photothermal properties of these colloidal NPs have also been investigated, and preliminary biocompatibility tests have been carried out using proteins such as albumin and fibrinogen in PBS solvent.

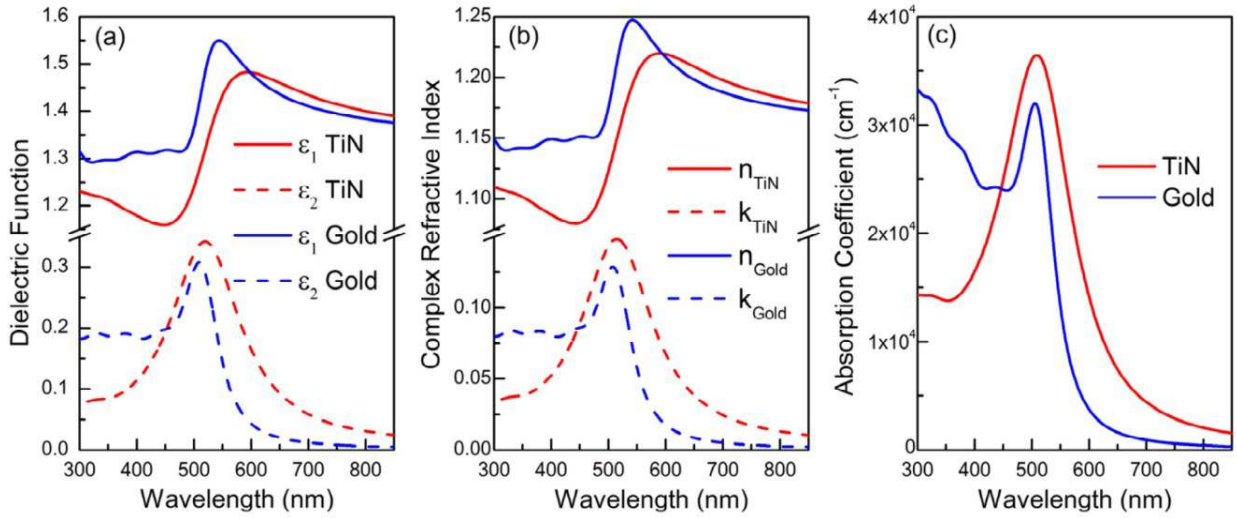


Figure 1. The predicted plasmonic performance of TiN NPs and 40 nm gold NPs [1].

The research project was supported by the Hellenic Foundation for Research and Innovation (H.F.R.I.) under the "2nd Call for H.F.R.I. Research Projects to support Post-Doctoral Researchers" (Project Number: 1099).

References

1. Patsalas, P. A., N. Kalfagiannis, and S. Kassavetis, "Optical properties and plasmonic performance of titanium nitride," Materials, Vol. 8, No. 6, 3128–3154, 2015.
2. Patsalas, P. A., N. Kalfagiannis, S. Kassavetis, G. Abadias, D.V. Bellas, Ch. Lekka, and E. Lidorikis "Conductive nitrides: Growth principles, optical and electronic properties, and their perspectives in photonics and plasmonics," Materials Science and Engineering: R: Reports, Vol. 123, 1–55, 2018.

Liquid crystal templated chiral films: chiral plasmonics and circularly polarized luminescence

W. Lewandowski[1]

[1]Faculty of Chemistry, University of Warsaw, Warsaw, Poland
[*]corresponding author: wlewandowski@chem.uw.edu.pl

Abstract: Nanostructures with chiroptical properties highly desired for photonic technologies. Here, we present endeavors towards achieving nanostructured chiral thin films, which show tunable, highly dissymmetric optical properties. Namely, chiroptical properties of gold or semiconductor nanocrystals are induced by mixing them with (chiral) liquid crystals. Owing to the soft character of liquid crystals, these nanocomposites exhibit durability, tunability and strong dissymmetry (g-factor up to 0.1) attractive for real world applications.

Thin films exhibiting plasmonic chirality or circularly polarized luminescence hold a great potential for photonic technologies relying on the emission or detection of circularly polarized light. However, most approaches of chiroptical thin films fabrication focus on top-down methods yielding static structures. To fully capitalize on the potential of chiral photonic materials the bottom-up fabrication of switchable films, showing high optical dissymmetry desired for applications, is required.

Recently, we proposed an efficient method for the preparation of chiral assemblies of nanoparticles which combats switchability and dissymmetry issues in thin films. The proposed method relies on melting and freezing a mixture of liquid crystal (LC) and either gold or semiconductor nanoparticles (NPs). Particularly, we proposed using LC that forms helically twisted fibers, that serves as a chiral matrix for guiding the assembly of NPs.[1,2] This way, we induce chiroptical properties of NPs.

From the perspective of the organic LC matrix, it's worth noting that upon cooling in the film state, the molecular architecture of the achiral LC supports the formation of layered assemblies that twist into helical nanofibers. These fibers grow dendritically from crystallization points, preserving their. This mechanism results in local symmetry breaking, that is mm-scale domains of both handedness are formed. It is possible to achieve macroscopic symmetry breaking by adding small amounts of a chiral, molecular dopant. To induce helical assembly of NPs within such LC films NPs need to mix well with LC in the melted state (at an elevated temperature), while on freezing they should be selectively pushed to the boundaries of the helical nanofibers. It is thus crucial to endow NPs with chemical compatibility to the matrix. For this purpose we cover gold and semiconductor NPs with organic ligands that are structurally similar to the LC compound.

The major contributions achieved using our methodology revolve around structure and optical properties of LC/NP composites, probed with e.g. TEM, AFM, XRD, CD, CPL methods and explained with modelling. Our films show a highly hierarchical structure of double helical assembly of NPs. This results in uniform composites, translating to strong optical dissymmetry of the films. Namely, for assemblies of spherical and rod-like gold NPs with sizes up to 50 nm, we recorded circular dichroism featured with dimensionless g-factor values of absorption on the state-of-the-art level of 0.1.[3] Similarly, when using InP/ZnS semiconductor NPs circularly polarized luminescence with strong dissymmetry was detected.[4] Importantly, the proposed method enables tuning of the chiroptical response into different parts of the visible spectrum by the choice on NPs and LC design.[5,6] A unique feature of the films is their thermal responsiveness driven by the soft character of LC matrix. It enables dynamic

switchability of the structure endowing the formed films with actively controlled chrioptical properties.[4,5] It is also worth to note that the described method for chiroptical film formation is highly scalable and energy efficient, increasing it's applicative potential.

In summary, the developed methodology of co-crystallization of liquid crystals and nanoparticles allows to realize chiral plasmonic and circularly polarized luminescent thin films with strong optical dissymmetry, precisely controlled structure, and (actively) tunable optical properties. These properties are achieved for thin films exhibiting high durability and scalable fabrication, which makes us believe that the described method may unlock the full potential of chiral photonics in the aspects of e.g. increasing the speed of data transfer.

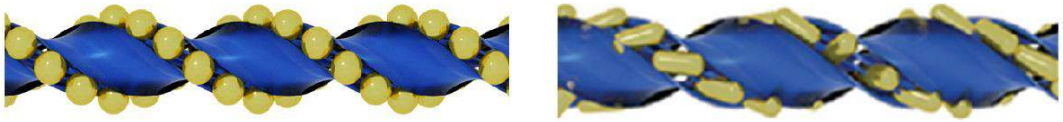


Figure 1. 3D models of a single helical nanofiber decorated with either spherical or rod-like nanoparticles.

I acknowledge support from the National Science Center Poland under the OPUS Grant UMO-2019/ 35/B/ST5/04488.

References

1. Lewandowski, W., N. Vaupotič, D. Pociecha, E. Górecka, E. and L. M. Liz-Marzán, "Chirality of Liquid Crystals Formed from Achiral Molecules Revealed by Resonant X‐Ray Scattering," Adv. Mater. Vol. 32, 1905591, 2020.
2. Baginski, M., M. Tupikowska,, G. Gonzaez-Rubio, M. Wojcik and W. Lewandowski, „Shaping Liquid Crystals with Gold Nanoparticles: Helical Assemblies with Tunable and Hierarchical Structures Via Thin‐Film Cooperative Interactions," Adv. Mater. Vol. 32, 1904581, 2020.
3. Szustakiewicz, P. N. Kowalska, D. Grzelak, T. Narushima, M. Góra, M. Bagiński, D. Pociecha, H. Okamoto, L. M. Liz-Marzán, W. Lewandowski, "Supramolecular Chirality Synchronization in Thin Films of Plasmonic Nanocomposites," ACS Nano, Vol. 14, 12918–12928, 2020.
4. Parzyszek, S., J. Tessarolo, A. Pedrazo-Tardajos, A. M. Ortuño, M. Bagiński, S. Bals, G. H. Clever, W. Lewandowski, "Tunable Circularly Polarized Luminescence via Chirality Induction and Energy Transfer from Organic Films to Semiconductor Nanocrystals," ACS Nano, Vol. 16, 18472–18482, 2022.
5. Grzelak, D. M. Tupikowska, D. Vila‐Liarte, D. Beutel, M. Baginski, S. Parzyszek, M. Gora, C. Rockstuhl, L. M. Liz-Marzan, W. Lewandowski, "Liquid Crystal Templated Chiral Plasmonic Films with Dynamic Tunability and Moldability," Adv. Funct. Mater. Vol. 32, 2111280, 2022.
6. Pawlak M., M. Bagiński, P. Llombart, D. Beutel, G. González-Rubio, E. Górecka, C. Rockstuhl, J. Mieczkowski, D. Pociecha, W. Lewandowski, "Tuneable Helices of Plasmonic Nanoparticles Using Liquid Crystal Templates: Molecular Dynamics Investigation of an Unusual Odd–Even Effect in Liquid Crystalline Dimers," Chem. Commun. Vol. 58, 7364–7367, 2022.

Dual-Band and High-Speed Plasmonic Metafiber Electrooptic Modulators

Jiyong Wang[1*], Lei Zhang[2,3], and Min Qiu[2,3]

[1] School of Electronics and Information, Hangzhou Dianzi University, Hangzhou, 310018, China.
[2] Key Laboratory of 3D Micro/Nano Fabrication and Characterization of Zhejiang Province, School of Engineering, Westlake University, 18 Shilongshan Road, Hangzhou 310024, Zhejiang Province, China.
[3] Institute of Advanced Technology, Westlake Institute for Advanced Study, 18 Shilongshan Road, Hangzhou 310024, Zhejiang Province, China.
[*]corresponding author: jiyongwang@hdu.edu.cn

Abstract:

Electro-optic modulators (EOMs) are one of the vital elements in optical communications for digitalizing optical signals through electric driving signals. Most of current EOM devices are targeting on-chip integrations, which routinely suffer from high coupling losses, complex optical alignments and single-band operations. Here, we report that a lumped EOM device is fully integrated on the single-mode optical fiber tips for fast amplitude modulations. Profiting from ultrathin and high quality-factor plasmonic metasurfaces, nanofabrication-friendly and highly efficient EO polymers and coupling-free connections with fiber networks, our EOM is demonstrated to allow dual-band operations (telecom O band and S band) and high-speed modulations (~ 1 GHz at a bias voltage of ± 9 V). This work offers an avenue to 'plug-and-play' implementations of EO devices and ultracompact "all-in-fibers" optical systems for communications, imaging, sensing and many others.

Conducting polymers as optical actuators for addressable structural colors

S. Rossi[1], **M. P. Jonsson**[1*]

[1]Laboratory of Organics Electronics, Department of Science and Technology, Linköping University, Sweden

[*]corresponding author: magnus.jonsson@liu.se

Abstract: Conducting polymers change their electronic and optical properties when doped with counter-ions. The doping process can be dynamically and reversibly done electrochemically, exposing the polymer to an electrolyte. The permittivity and thickness change upon redox cycling changes the effective refractive index. We demonstrate an application to tune the color of reflective optical nanocavities in all the visible spectrum, using a low-bandgap conducting polymer. The outcome is promising for reflective displays but can be extended to other active nanophotonic systems.

Summary

Many modern optical and optoelectronic devices require to be actively addressable, changing dynamically their response to an electric stimulus. Nanophotonics has been revolutionizing the optical field, with many new applications and opportunities given by the light-matter interaction at the subwavelength scale. However, the active tunability of those systems is still a technological challenge and new strategies and materials for optical actuation are needed. In our recent works, we focused on addressable structural colors for application in color reflective displays with ultralow power consumption. **The aim was to integrate metal-insulator-metal reflective optical nanocavities** that we developed in our previous work [1] **with conducting polymers for active electrochemical color tuning** [2]. Those materials are conjugated polymers that can be doped with counter ions to induce charge carriers in the polymeric chains. The doping process can be done by exposing the polymeric film to a suitable electrolyte in an electrochemical cell and is reversible by redox cycling. Conducting polymers have been having a fundamental role in the development of organic electronics and have shown great potential for photonics. They have been applied for solar cells, organic light-emitting diodes (OLED), electrochromic windows and displays, but only recently have found applications in optics. When charges (holes or electrons, depending on if p- or n-type) are injected in the polymeric chains applying a potential difference between the polymer and a counter electrode, counter-ions need to diffuse in the polymeric matrix to maintain charge neutrality. This causes swelling and thickness change, coupled with permittivity variation due to the modulation of the electronic properties of the

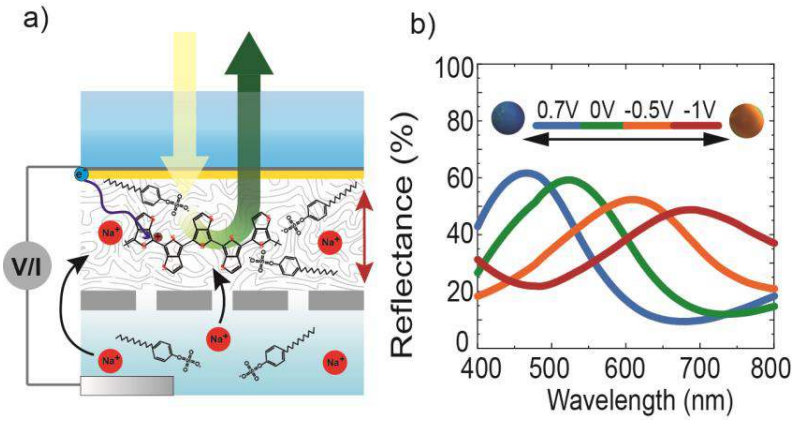


Figure 1. Electrochemically tunable reflective optical nanocavities. **a)** Schematic of the nanocavities integrated in the electrochemical cell. **b)** Experimental reflectance spectra at different potentials.

conjugated chains, leading to an effective refractive index variation that can be exploited for optical actuation. **We focus here on our recent efforts in studying and exploiting conducting polymers for electrochemically addressable structural colors**. We showed that a low-bandgap polymer, thienothiophene, exhibits a relatively low absorption in the visible for all the redox states, which makes it a good candidate for actuating reflective structural colors. We integrated thienothiophene as the spacer of optical nanocavities and placed the sample in an electrochemical cell with a water-based electrolyte (Fig. 1a). We achieved complete coverage of the visible spectrum, maintaining a high reflectance for all the colors while using a low voltage range (Fig. 1b). This was made possible by a synergistic combination of the variation of the optical properties and thickness change of the polymeric spacer. We attributed the actuation of the optical nanocavity mainly to the thickness variation of the polymeric spacer due to electrolyte swelling. The low-bandgap of the material ensured to obtain similar reflectance values for all the colors, in contrast with most conducting polymers, because the absorption peak is in the near-infrared for both the reduced (undoped) and oxidized (p-doped) states. The addition of nanoholes to the fully reflective mirror, further improved the ion diffusion, extending the wavelength tunability up to 400nm. Those cavities can be considered as the proof of concept of a "monopixel" that can cover the entire visible spectrum. The samples suffered from low color uniformity and limited cycling stability, but we expect that those issues can be solved by the lateral microstructuration of the nanocavities to lower the ionic diffusion path. **Therefore, conducting polymers have the potential to be used in hybrid nano-optical systems to actively address structural colors.** Besides optical nanocavities**,** they can also be applied to plasmonic nanopixels [3] and photonic crystals, Moreover, we demonstrated UV-patterning possibilities by using a different thin film deposition method based on vapor phase polymerization [4], which is promising for display applications. Those materials have also recently found application in actively addressable metasurfaces for beam steering [5] and holography [6] when coated over optical nanoantenna, extending their optical actuation capabilities beyond structural coloration.

References

[1] S. Rossi and M. P. Jonsson, "Highly reflective optical nanocavities for structural coloration by combining broadband absorber and Fabry-Pérot effects," J. Opt., vol. 23, no. 1, 2021.

[2] S. Rossi et al., "Dynamically Tuneable Reflective Structural Coloration with Electroactive Conducting Polymer Nanocavities," Adv. Mater., vol. 33, no. 49, 2021.

[3] J. Peng et al., "Scalable electrochromic nanopixels using plasmonics," Sci. Adv., vol. 5, pp. 1–9, 2019.

[4] S. Chen et al., "Tunable Structural Color Images by UV-Patterned Conducting Polymer Nanofilms on Metal Surfaces," Adv. Mater., vol. 33, no. 33, 2021.

[5] J. Karst et al., "Electrically Switchable Metasurface for Beam Steering Using PEDOT Polymers," J. Opt., vol. 22, p. 124001, 2020.

[6] R. Kaissner et al., "Electrochemically controlled metasurfaces with high-contrast switching at visible frequencies," Sci. Adv., vol. 7, no. 19, 2021.

Au@Pd supercrystals as plasmonic photocatalysts for Suzuki C-C coupling

C. Brissaud[1*], W. Chaâbani[1], L. V. Besteiro[2], M. Comesaña-Hermo[1], and J.-Y. Piquemal[1]

[1]Université Paris Cité, CNRS, ITODYS, F-75013 Paris, France
[2]CINBIO, Universidade de Vigo, Departamento de Química Física, Vigo 36310, Spain
*charlene.brissaud@u-paris.fr

Abstract: We use Au@Pd core-shell nanorods self-assembled into supercrystals as plasmonic photocatalysts for the Suzuki C-C coupling reaction between bromobenzene and m-tolylboronic acid under simulated sunlight. Such plasmonic device is an interesting model system to understand the relative importance that the electromagnetic field enhancement generated via plasmonic coupling between nanorods, the photogenerated hot charge carriers and the temperature rise may have on this particular reaction.

With the aim of benefiting from the synergistic effect between the optical properties of plasmonic nanoparticles and the well-known catalytic features of palladium, we synthesize Au@Pd core-shell nanorods (NRs) as efficient plasmonic photocatalysts.[1] The use of an evaporation-induced self-assembly method allows us to obtain the well-organized packing of Au@Pd NRs into supercrystals (SCs) by drop-casting a concentrated solution of the resonators on a silicon substrate.[2] Such nanoarchitectures enable us to induce plasmonic hot spots thanks to the coupling between the tips of the particles, generating, at the scale of the SC, a homogeneous enhancement of the electric field over a large area.

In order to investigate the photocatalytic features of our plasmonic device, we perform the Suzuki-Miyaura C-C coupling, a well-established method for carbon-carbon cross-coupling between an organoboron species and an aryl halide in the presence of a base, as model reaction.[1] This reaction usually requires an energy input in order to overcome the activation barrier, being usually performed at elevated temperatures (>50 °C) and using a palladium species as catalyst.[3] In this work we demonstrate that our Au@Pd SCs are efficient photocatalysts to drive this organic transformation, modulating chemical reactivity under irradiation thanks to the unique characteristics of the plasmonic objects and their collective features.[4],[5]

In this context, the relative importance of the different processes behind plasmonic photocatalysis (electromagnetic field enhancement, photogenerated charge carriers and photothermal effects) is also discussed.[6] Our experimental data is complemented by thermal simulations of the thermal contribution of the system under study.

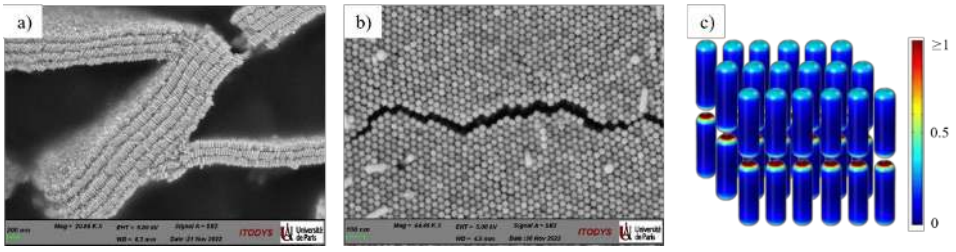


Figure 1. SEM images of Au@Pd SCs a) horizontally and b) vertically self-assembled and c) calculated field enhancement bteween the tips of the nanorods.

References

1. Rodal-Cedeira, S. *et al.* "Plasmonic Au@Pd Nanorods with Boosted Refractive Index Susceptibility and SERS Efficiency:

A Multifunctional Platform for Hydrogen Sensing and Monitoring of Catalytic Reactions." Chem. Mater. 28, 9169–9180, 2016.

2. Scarabelli, L. *et al.* "Design and Fabrication of Plasmonic Nanomaterials Based on Gold Nanorod Supercrystals." Chem. Mater. 29, 15–25, 2017.
3. Miyaura, N. and Suzuki, A. "Palladium-Catalyzed Cross-Coupling Reactions of Organoboron Compounds." Chem. Rev. 95, 2457–2483, 1995.
4. Shin, H. H. *et al.*"Recent Progress in Plasmonic Hybrid Photocatalysis for CO_2 Photoreduction and C–C Coupling Reactions." Catalysts 11, 155, 2021.
5. Beletskaya, I. P. *et al.* "The Suzuki-Miyaura reaction after the Nobel prize." Coordination Chemistry Reviews 385, 137–173, 2019.
6. Negrín-Montecelo, Y. *et al.* "Plasmonic photocatalysis in aqueous solution: assessing the contribution of thermal effects and evaluating the role of photogenerated ROS." Nanoscale 14, 11612–11618, 2022.

Experimental and theoretical study of the plasmonic properties of Cobalt nanoparticles

W. Chaâbani[1*], M. Comesana-Hermo[1], J. Nelayah[2], N. Flédij[1], and J.-Y. Piquemal[2]
[1]Université de Paris-Cité, Laboratoire ITODYS, CNRS, F-75006 Paris, France

[2] Université de Paris, MPQ, CNRS, F-75006 Paris, France

[*]corresponding author: wajdi.fss@yahoo.com

Abstract: The control of optical properties at the nanoscale is a current topic of intense research. It has been shown recently in our group that the regular arrays of Co nanoparticles obtained by electron-beam lithography present intense plasmon resonances in the visible range of electromagnetic spectrum. In this work, we purpose to focus our attention on the study of the optical properties of colloidal Co nanoparticles synthesized by the polyol process. The nanoparticles obtained present an anisotropic shape in the form of nanorods and are relatively polydisperse in length while their thickness remains very homogenous (Figure 1a). FDTD simulations show that Co nanorods of thes dimensions have a plasmon resonance in the visible range, as shown in Figure 1b. Subsequently, the plasmonic properties of Co nanoparticles are characterized experimentally by electron energy loss spectroscopy (EELS) at the single-nanoparticle level, allowing us to take into consideration the polydispersity at the sample. Our finding highlights the potential of such objects as a new platform for studying light-matter interactions at the nanoscale.

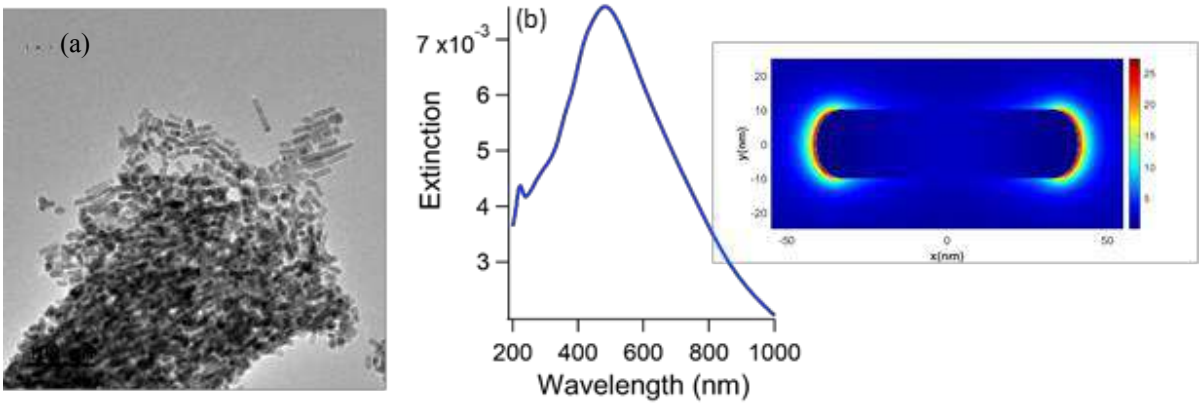


Figure 1: (a) TEM image of Co nanoparticles, (b) FDTD simulation of optical spectrum and electric field

References

1. Braik, M., Sow, I., Nelayah, J., Belkhir, A., Faustini, M., Mercone, S., Nowak, S., Decorse, P., Piquemal, J.-Y., and Félidj, N., "Introducing cobalt as a potential plasmonic candidate combining optical and magnetic functionalities within the same nanostructure" Nanoscale, Vol. 13, 2639–2647, 2021.
2. Fiévet, F., Ammar-Merah, S., Brayner, R., Chau, F., Giraud, M., Mammeri, F., Peron, J., Piquemal, J.-Y., Sicard, L. and Viau, G., "The polyol process: a unique method for easy access to metal nanoparticles with tailored sizes, shapes and compositions", Chem. Soc. Rev., Vol. 47, 5187-5233, 2018.

META 2023, PARIS - FRANCE, JULY 18 – 21, 2023

Strong coupling in aluminum optical antennas

Thomas Simon[1], Gabriel Arditi[2], Xiaoyan Li[2], Florian Lamaze[1], Julien Proust[1], Jérôme Martin[1], Mathieu Kociak[2], Odile Stéphan[2], and Davy Gérard[1,*]

[1]Light, nanomaterials, nanotechnologies, CNRS EMR 7004, Université de Technologie de Troyes, Troyes, France
[2]Laboratoire de Physique des Solides, Bâtiment 510, UMR CNRS 8502, Université Paris-Saclay, Orsay, France
[*]corresponding author: davy.gerard@utt.fr

Abstract: We analyze the plasmonic response of aluminum nanorods using both optical and electronic spectroscopies. We experimentally evidence a strong coupling phenomenom between the multiple orders of the nanorod's plasmonic resonance and the interband transition of aluminum. The resulting hybrid modes are analyzed using a model for strong coupling to extract the Rabi energies.

Aluminum is an appealing plasmonic material, combining a broadband metallic behavior, a wide availability and CMOS compatibility [1]. Here, we study the optical properties of aluminum nanostructures using electron energy-loss spectroscopy (EELS), a powerful technique allowing direct imaging and spectroscopy with nanoscale spatial resolution [2]. We focus on the coupling between the plasmonic modes of an Al nanorod and the interband transition of aluminum. Using both EELS and optical spectroscopy, we experimentally evidence a strong coupling between the antenna's plasmonic resonances and the interband transition (Fig. 1). This interesting phenomenon (as the antenna couples *with itself* to create hybrid modes) is analyzed using a model for strong coupling.

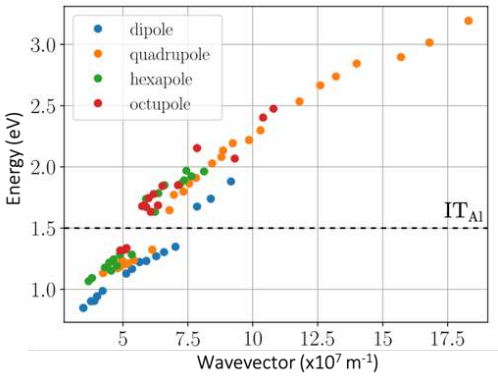


Figure 1: Dispersion curves of the plasmonic resonances of an Al nanorod, as obtained from EELS measurements. The horizontal dotted line denotes the position of the interband transition at 1.5 eV. A clear energy gap is observed around the interband, associated with strong coupling (Rabi splitting).

Acknowledgements: We acknowledge financial support from CNRS-CEA "METSA" French Network Grant FR CNRS 3507 on the platform LPS-STEM.

References

1. D. Gérard and S. K. Gray, "Aluminium plasmonics", J. Phys. D : Appl. Phys. 48, 184001, 2015.
2. T. Simon, X. Li, J. Martin, D. Khlopin, O. Stephan, M. Kociak, D. Gérard, "Aluminum Cayley trees as scalable, broadband, multiresonant optical antennas", PNAS **119** e2116833119, 2022.

Light-matter-coupling effects in pentacene thin films on nanorod antenna arrays

C. P. Theurer[1], F. Laible[1], J. Tang[1], K. A. Broch[1], F. Schreiber[1], and M. Fleischer[1*]

[1]Institute for Applied Physics and Center for Light-Matter-Interaction, Sensors and Analytics LISA+, Eberhard Karls University Tübingen, Tübingen, Germany
[*]corresponding author: monika.fleischer@uni-tuebingen.de

Abstract: By harnessing light-matter coupling in optical cavities, the chemical and photophysical properties of organic semiconductor films can be tailored without the need for chemical modification. Here, strong coupling is demonstrated in polycrystalline pentacene thin films on top of silver nanorod antenna arrays. Such an open configuration offers advantages in view of device applications. Simultaneous coupling of the two Davydov transitions to surface lattice resonances is observed.

Under the influence of strong light-matter coupling within cavities exciton-polariton quasi-particles can form in organic semiconductors [1.]. While most studies so far consider either single crystals or diluted molecules in closed cavities between two mirrors for maximum effect, open cavities and polycrystalline thin films can have practical advantages in terms of applications. Strong coupling has been demonstrated e.g. in organic crystals on plasmonic nanorod arrays [2., 3.]. Such arrays offer the possibility to excite surface lattice resonances that present excellent spectral tunability and narrow bandwidths [4.-7.].
In the present work, pentacene thin films are prepared on silver nanorod arrays by organic molecular beam deposition. Pentacene is chosen as a common organic semiconductor with the added feature that it presents a singlet fission material [8.]. Singlet fission, i.e. the spontaneous splitting of an excited singlet state into two triplet states, is of considerable interest since it leads to a duplication of the excitons in a material. The singlet fission dynamics can be accelerated by strong light-matter coupling [9.]. The present work shows that the two Davydov transitions couple to surface lattice resonances excited in the nanorod array with different coupling strengths. The resulting energy splitting is evident when the system is compared to an inert polystyrene reference film with a comparable refractive index on the same arrays (see Figure 1). The strong coupling regime is reached for the lower transition in pentacene, leading to a reduction of the energy gap to the triplet pair state [10.].

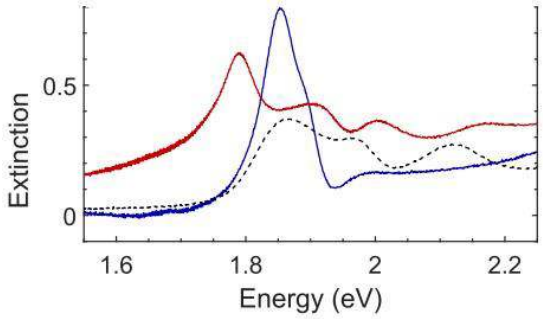


Figure 1: Extinction spectrum of a plasmonic silver nanorod array covered with a pentacene thin film (red) in comparison to the same array covered by a polystyrene reference film (blue). The black line shows the extinction of the bare pentacene film.

Support by the German Research Foundation (DFG) and the Vector-Stiftung is gratefully acknowledged.

References

1. Lidzey, D. G., Bradley, D. D. C., Skolnick, M. S., Virgili, T., Walker, S., Whittaker, D. M., "Strong exciton–photon coupling in an organic semiconductor microcavity," Nature, 395, 53–55, 1998.
2. Berghuis, A. M., Serpenti, V., Ramezani, M., Wang, S., Gómez Rivas, J., "Light–matter coupling strength controlled by the orientation of organic crystals in plasmonic cavities," J. Phys. Chem. C, 124, 12030–12038, 2020.
3. Bai, P., ter Huurne, S., van Heijst, E., Murai, S., Gómez Rivas, J., "Evolutionary optimization of light-matter coupling in open plasmonic cavities," J. Chem. Phys., 154, 134110, 2021.
4. Kravets, V. G., Kabashin, A. V., Barnes,W. L., Grigorenko, A. N., "Plasmonic surface lattice resonances: A review of properties and applications," Chem. Rev., 118, 5912–5951, 2018.
5. Utyushev, A. D., Zakomirnyi, V. I., Rasskazov, I. L., "Collective lattice resonances: Plasmonics and beyond," Rev. Phys., 6, 100051, 2021.
6. Gollmer, D. A., Lorch, C., Schreiber, F., Kern, D. P., Fleischer, M., „Enhancing light absorption in organic semiconductor thin films by one-dimensional gold nanowire gratings," Phys. Rev. Mater., 1, 054602, 2017.
7. Gollmer, D. A., Lorch, C., Schreiber, F., Kern, D. P., Fleischer, M., „Shaping and polarizing fluorescence emission of a polycrystalline organic semiconductor film by plasmonic nanogratings," J. Opt. Soc. Am. B, 36, E9–E14, 2019.
8. Hinderhofer, A., Heinemeyer, U., Gerlach, A., Kowarik, S., Jacobs, R. M. J., Sakamoto, Y., Suzuki, T., Schreiber, F., "Optical properties of pentacene and perfluoropentacene thin films," J. Chem. Phys., 127, 194705, 2007.
9. Climent, C., Casanova, D., Feist, J., Garcia-Vidal, F. J., "Not dark yet for strong light-matter coupling to accelerate singlet fission dynamics," Cell Rep. Phys. Sci., 3, 100841, 2022.
10. Theurer, C. P., Laible, F., Tang, J., Broch, K. A., Fleischer, M., Schreiber, F., „Strong light-matter coupling in pentacene thin films on plasmonic arrays," submitted (2023).

Optoelectronic properties of FeSe nanomaterials with diverse dimension

Hyojin Kang[1] and Jaebeom Lee[1,2*]

[1]Department of Chemical Engineering and Applied Chemistry, Chungnam National University, Republic of Korea[2] Department of Chemistry, Chungnam National University, Republic of Korea
[*]corresponding author: nanoleelab@gmail.com

Abstract: Metal chalcogenides, such as molybdenum sulfide (MoS_2), nickel sulfide (Ni_3S_2), and copper-based chalcogenides, are mainly a two-dimensional structure and have been studied in various fields for the past 10 years. Herein, we report dimension-controlled FeSe nanomaterials (0D, 1D and 2D) to have unprecedented electron structure using absorption coefficient driven by investigating transmittance spectra via Fourier-transform infrared spectroscopy, breaking conventional charge-phase transition. This approach could be applied as a next-generation electronic device due to its specific band gap and photo-reactivity.

The discovery of two-dimensional atomic crystals with rich photonic and optoelectronic properties has sparked renewed interest in next-generation optoelectronic devices. Among them, FeSe superconductors and related systems corresponding to transition metal chalcogenides have received particular attention due to their simple crystal structures and unique electronic and physical properties[1]. However, recently, studies on FeSe quantum dots as semiconductor light emitting materials have been actively conducted.[2] These quantum dots showed multi-colored excitation dependent emission (MEDE) characteristics that only appear in organic quantum dots, and this was reported to be caused by unusual electronic states that appear in semiconductors and Mott physics. In this study, various sizes and morphologies of FeSe nanocrystals were utilized to investigate and compare their anomalous band gaps and optical properties. 0D FeSe QDs were synthesized with chiral ligands of L-, D-cysteine (Cys), resulting in MEDE characteristics controlled by ligand-induced interlayer distance change. In addition, the inorganic MEDE is predicted to originate from the strong correlation effect in the local impurity state of the band edge occurring in the Fe-3d-orbital, where the interlayer extension by the Cys ligand promotes the MEDE degree of the FeSe NPs.

In the size/shape-dependent properties of FeSe, a new type of room temperature phase transition is clearly observed, including band gap instability seen in strongly correlated d-p orbital interaction effects. In particular, an unusual situation was found in the synthesis of FeSe nanospheres (d. 3.6 nm) and 2D nanoplates (l. 20, 500 nm). The optical coefficient spectra show significant bandgap differences in both, which are predicted to be attributed to the reduced bandgap by possible quantum confinement and electrical continuity in the first and second dimensions, respectively. This approach can be applied to analyze the electronic band structure of other relevant systems, disrupting the existing charge phase transition and achieving a feasible approach for electronic devices.

Acknowledgements

This work was supported by the National Research Foundation (NRF) of Korea and grants funded by the Ministry of Science, ICT, and Future Planning (MSIP) of Korea (NRF-2019R1A2C2007825), and Regional Innovation Strategy (RIS) through the National Research Foundation of Korea (NRF) funded by the Ministry of Education (MOE) (2021RIS-004).

References

1. Kwon, J.; Jun, S.; Choi, S.; Mao, X.; Kim, J.; Koh, E.; Kim, Y.-H.; Kim, S.-K.; Hwang, D.; Kim, C.-S. FeSe quantum dots for in vivo multiphoton biomedical imaging. *Science advances* **2019**, *5* (12), eaay0044.
2. Kwon, J.; Jun, S. W.; Kim, J.; Lee, M.; Choi, Y.; Kim, D.; Kim, M.; Lee, S. G.; Lee, S.; Kang, S. H. Excitation-dependent emissive FeSe nanoparticles induced by chiral interlayer expansion and their multi-color bio-imaging. *Nano Today* **2022**, *43*, 101424.

Chiral photothermal effect induced by plasmonic metasurface for fluid motion

Peng Yu[1*], Alexander Govorov[2], and Zhiming Wang[1]

[1]Institute of Fundamental and Frontier Science, University of Electronic Science and Technology of China, Chengdu 610054, China
[2]Department of Physics & Astronomy, Ohio University, Athens, Ohio 45701, United States
[*]corresponding author: peng.yu@uestc.edu.cn

Abstract: The plasmonic photothermal effect can be used as an efficient heat source due to enhanced light-matter interaction. This talk will introduce recent advances in plasmonic photothermal effect-driven motion. Also, we will discuss the chiral photothermal effect and chiral optofluidics induced by chiral plasmonics.

The plasmonics photothermal effect is an emerging field in photonics that aims at harnessing the kinetic energy of light to generate heat at the nanoscale.[1] Meanwhile, along with the expanding application of circularly polarized light, a growing number of investigations on chiral plasmonic metasurfaces have been conducted.[2] This talk aims to introduce recent advances in chiral photothermal effect and their applications.

First, we will introduce the concept of the chiral photothermal effect. The chiral photothermal effect is a phenomenon that the process of different heat generation, conduction, and dissipation after circularly polarized light is absorbed by chiral materials.[3]

Second, we will introduce a theoretical conception of chiral optofluidics induced by the chiral photothermal effect.[4] As shown in figure 1a and figure 1b, the proposed metasurface exhibits giant circular dichroism in absorption and thus leads to a strong photothermal effect. Based on the multiphysical analysis, including optics, thermodynamics, and hydrodynamics, we propose a concept of chiral spectroscopy termed optofluidic circular dichroism. Our results show that different fluid velocities of thermally induced convection appear around a chiral plasmonic metasurface under different circularly polarized excitation. The chiral fluid convection is induced by an asymmetric heat distribution generated by absorbed photons in the plasmonic heater. This concept can be potentially used to induce chiral fluid convection utilizing the chiral photothermal effect. Our proposed structure can potentially be used in various optofluidics applications related to biochemistry, clinical biology, and so on.

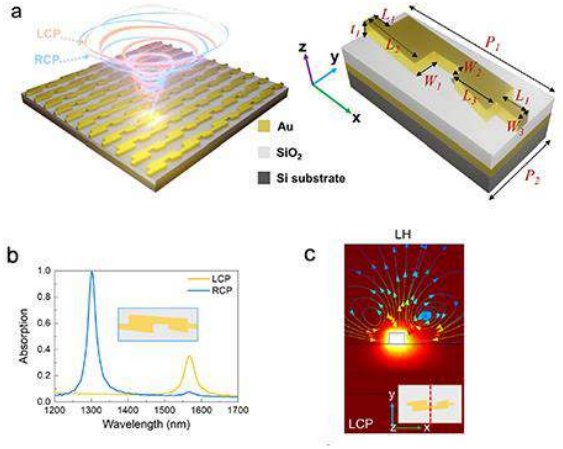


Figure 1. (a) Schematic of the chiral metasurface consisting of Au nanoantenna arrays and a bottom Au film separated by a SiO_2 layer; the geometry of a unit cell in the chiral metasurface. The thicknesses of the top Au chiral structure and bottom Au layer are 55 and 100 nm, respectively; the thickness of the SiO_2 spacer is 150 nm. For the top

resonator: L1 = 100 nm, L2 = 350 nm, L3 = 200 nm, W1 = 100 nm, W2 = 50 nm, W3 = 61 nm, P1 = 800 nm, P2 = 350 nm. (b) Simulated optical response of RH metasurface under RCP illumination. (c) Thermal-induced chiral fluid convection of the RH metasurface.

In the end, we summarize chiral photothermal phenomena and discuss their potential applications.

References

1. Baffou, G.; Cichos, F.; Quidant, R., Applications and challenges of thermoplasmonics. *Nature Materials* **2020,** *19* (9), 946-958.
2. Hentschel, M.; Schäferling, M.; Duan, X.; Giessen, H.; Liu, N., Chiral plasmonics. *Science Advances* **2017,** *3* (5), e1602735.
3. Kong, X.-T.; Khosravi Khorashad, L.; Wang, Z.; Govorov, A. O., Photothermal Circular Dichroism Induced by Plasmon Resonances in Chiral Metamaterial Absorbers and Bolometers. *Nano Letters* **2018,** *18* (3), 2001-2008.
4. Ma, C.; Yu, P.; Wang, W.; Zhu, Y.; Lin, F.; Wang, J.; Jing, Z.; Kong, X.-T.; Li, P.; Govorov, A. O.; Liu, D.; Xu, H.; Wang, Z., Chiral Optofluidics with a Plasmonic Metasurface Using the Photothermal Effect. *ACS Nano* **2021,** *15* (10), 16357-16367.

Metasurface design by capillarity-assisted nanoparticles assembly in a microfluidic channel and their applications

Juan Xin[1,*], Julien Proust[1], Jérémie Béal[1], Anne-Laure Baudrion[1], Abdelhamid Hmima[1], and Jérôme Plain[1,*]

[1]Light, nanomaterials, nanotechnologies (L2n), Universite de Technologie de Troyes & CNRS EMR 7004, 10004 Troyes, France

[*]corresponding authors: juan.xin@utt.fr or jerome.plain@utt.fr

Abstract: The metasurfaces consist of arrays of sub-wavelength nanostructures, called meta-atoms. The periodic arrangement of these meta-atoms plays a key role in determining the functionality of the metasurface device.[1] In this project, Si nanoparticles are synthesized in solution[2] and assembled by a capillary force-based technique,[3] overcoming some of the drawbacks of the top-down approach. Furthermore, the metasurface structure assembled by Si NPs with high refractive index can realize strong magnetic field response with low loss.[4]

We have demonstrated the development of an aggregation-free colloidal dispersion of Si NPs with spheroidal shape using a kitchen blender,[2] based on exfoliation processes without addition of any surfactant. We obtained crystalline Si NPs with diameters controlled in the range of 45−250 nm. Nanoholes with different sizes were obtained by e-beam lithography (EBL). After a silanization reaction, Si NPs were filled into the hole with the help of capillary force using SmartForce. Finally, PMMA is removed by acetone and a certain size of nanoparticle metasurface can be obtained.

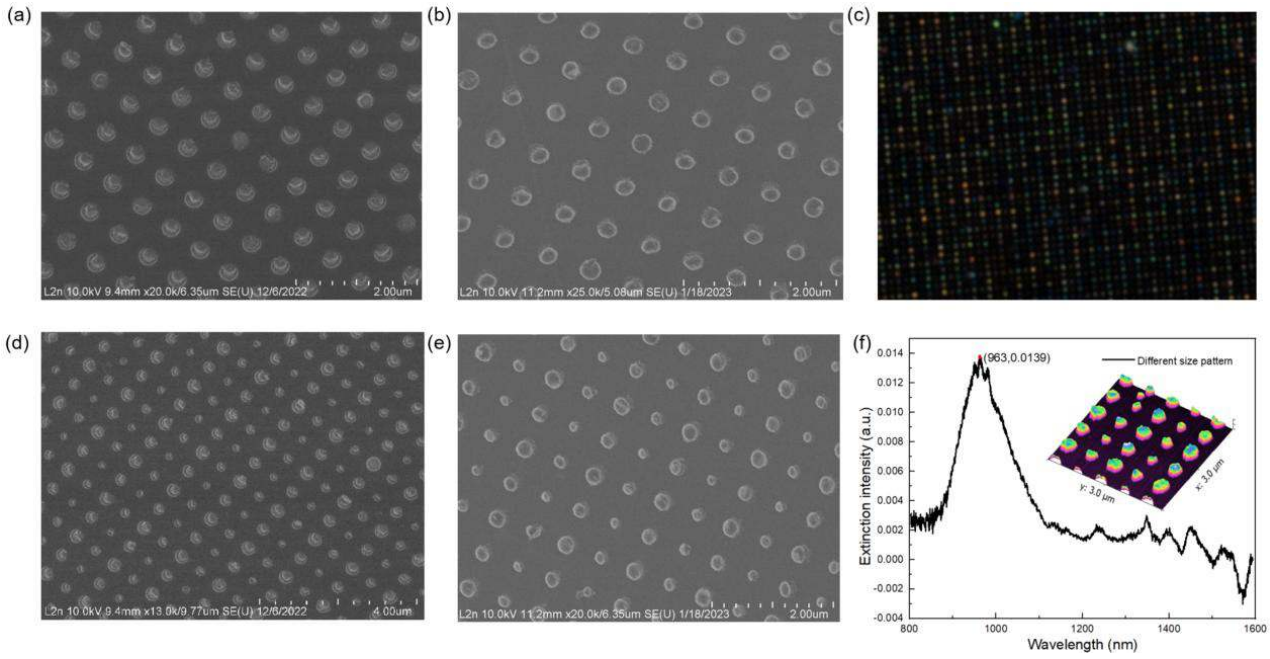


Fig. 1 NP assembly. SEM micrograph of a randomly selected assembly area 1 showing the deposition of single NPs (a) with PMMA matrix and (b) after removing the mask. (c) Dark field optical image of a randomly selected assembly area after removing PMMA mask. SEM micrograph of a randomly selected assembly area 2 showing the deposition of single NPs (d)

with PMMA matrix and (e) after removing PMMA. (f) Extinction spectrum of area 2 assembled by SmartForce after removing PMMA. The inset picture is the corresponding AFM image for this area.

We present a microfluidic platform to produce a pattern with particular size design within a microchannel, based on sequential capillarity-assisted Si nanoparticles assembly. The NPs assembly result is shown in Fig.1, the SEM micrograph of a randomly selected assembly area 1 and area 2 showing the deposition of single NPs is presented. The filling rate is almost 100%, and the Si NPs arrays stays well organized on the substrate after removing PMMA. This is also confirmed by AFM image shown in Fig.1 (f inset). First transmission optical measurement has been obtained and presented in Fig.1 (f) and shows an optical resonance in NIR. Other optical measurements on a larger range are in progress and will be presented.

The polarization, phase and amplitude of incident light can be controlled by the metal metasurface composed of metal structural elements. With the research of metasurface entering the near-infrared and visible wavelengths, the intrinsic loss of metals becomes increasingly prominent and cannot be ignored. The proposed dielectric metasurface avoids the loss problem of metal metasurface and the structural and functional design of dielectric metasurface is based on Mie scattering. Using a dielectric material in place of the plasmonic one, it will be possible to explore new optical and thermal properties. With the plethora efforts of researchers, we believe optical metasurfaces would spread through in our life sooner or later.

Acknowledgment:
Financial support of Nano'Mat (www.nanomat.eu) by the Ministère de l'enseignement supérieur et de la recherche, the "Fonds Européens de Développement Régional (FEDER) fund", the "région Grand-Est", and the "Conseil départemental de l'Aube", are acknowledged. Parts of this project were supported by the SUSTECH and the Agence nationale de la recherche (ANR), contract NOSE (contract ANR 21-CE39-0014). The support provided by China Scholarship Council (CSC), contract 202208070142. This work has been made within the frame of the Graduate School (Ecole Universitaire de Recherche) "NANO-PHOT", contract ANR-18-EURE-0013.

References

1. Jung, C., et al., Metasurface-driven optically variable devices. Chemical Reviews, 2021. 121(21): p. 13013-13050.
2. Chaabani, W., et al., Large-scale and low-cost fabrication of silicon mie resonators. ACS nano, 2019. 13(4): p. 4199-4208.
3. Pioli, R., et al., Sequential capillarity-assisted particle assembly in a microfluidic channel. Lab on a Chip, 2021. 21(5): p. 888-895.
4. Miroshnichenko A E., et al., Magnetic light: optical magnetism of dielectric nanoparticles. Optics and Photonics News, 2012. 23(12): p. 35-35.

META 2023, PARIS - FRANCE, JULY 18 – 21, 2023

Nanolasing in Self-Assembled Metasurfaces

T. Tamulevicius[1,2,3*], M. Juodenas[1,4], N. Khinevich[1], D. Peckus[1], A. Tamuleviciene[1,2], J. Henzie[5], and S. Tamulevicius[1,2]

[1]Institute of Materials Science, Kaunas University of Technology, Kaunas 51423, Lithuania
[2]Physics Department, Kaunas University of Technology, Kaunas 51368, Lithuania
[3]UAB Nanoversa, Kaunas 51423, Lithuania
[4]Physics Department, Chalmers University of Technology, Gothenburg 41296, Sweden
[5]International Center for Materials Nanoarchitectonics, National Institute for Materials Science, Tsukuba 305-0044, Japan
[*]corresponding author: tomas.tamulevicius@ktu.lt

Abstract: Plasmonic surface lattice resonance-based (SLR) nanolasers are attractive because of their small mode volumes and footprint, ultrafast dynamics, and good beam directionality.[1] Underlying plasmonic nanocavities are usually produced by conventional lithography processes. We have developed a deposition method to arrange monodisperse, colloidal nanoparticles onto macroscopic, patterned substrates, otherwise metasurfaces, with a high assembly yield.[2,3] Furthermore, we have shown that the SLR can drive the lasing modes from the fluorescence spectra of the organic dye when pumped with ultra-short laser pulses.
This research was performed within a project LaSensA under the M-ERA.NET scheme.

References

1. Zhou, W., et al, “Lasing action in strongly coupled plasmonic nanocavity arrays,” Nature Nanotech, Vol. 8, 506–511, 2013.
2. Juodenas, M., et al, “Surface Lattice Resonances in Self-Assembled Arrays of Monodisperse Ag Cuboctahedra,” ACS Nano, Vol. 13, No. 8, 9038–9047, 2019.
3. Juodenas, M., et al, “Effect of Ag Nanocube Optomechanical Modes on Plasmonic Surface Lattice Resonances,” ACS Photonics, Vol. 7, No. 11, 3130–3140, 2020.

META 2023, PARIS - FRANCE, JULY 18 – 21, 2023

Biocompatible fluorescent carbon dots nanoparticles used for anti-counterfeiting of cultural artefacts

Theo Duarte[1]*, Aurélie Broussier[1], Sabine Fourrier[2], Alexandre Rabot[2], Anne-Laure Baudrion[1], Jérôme Plain[1], Julien Proust[1]

[1] Lumière, nanomatériaux et nanotechnologie (L2n), CNRS EMR 7004 & Université de Technologie de Troyes, 12 rue Marie Curie, 10004 Troyes Cedex, France
[2] Histoire et sources des mondes antiques - CNRS UMR 5189 – Lyon, France
*corresponding author: theo.duarte@utt.fr

Abstract: In this work, fluorescent biocompatible carbon nanoparticles were synthesized using high-pressure bottom-up synthesis. The influence of the different synthesis parameters was studied to investigate the formation mechanism of this method and their influence on the photophysical properties of the nanoparticles.
The carbon dots formed by this method were then integrated into various mediums to produce safe anti-counterfeiting markings used to protect cultural artefacts discovered in archaeological sites with a high risk of looting.

For many years, cultural property in general and archaeological artefacts especially have been liable to be stolen during and after the excavation process to be introduced to the black market. Globally, it is commonly estimated that the illicit trafficking of cultural heritage ranks among the biggest illicit trade in the world, grossing several billion dollars[1].

To tackle this problem a safe technical solution is needed to trace stolen archaeological artefacts. Biocompatible fluorescent nanoparticles can be used to produce original anti-counterfeiting markings that are safe for use without training and hard to reproduce by looters.

In 2004 Xu et al[2] discovered nanoparticles composed of carbon that produced blue photoluminescence. Carbon dots are a 0D nanomaterial made of a hybrid structure with graphene-like clusters of sp2 carbon linked within a shell of amorphous sp3 carbon comprised of organic functional groups on its surface. They present properties ideal for anticounterfeiting applications such as biocompatibility[3], stability and narrow fluorescence that can also be dependent on the excitation wavelength.
Since they are mainly composed of carbon, they constitute a safer alternative to heavy metal quantum dots and allow us to avoid trace contamination before analysis. As of today, carbon black is the basis of the black inks currently used for marking and it is chemically identical to Carbon Dots.
Various structures of carbon dots can be synthesized by bottom-up high-pressure synthesis from organic precursors. Conditions of pressure and temperature as well as the precursors used in the synthesis are chosen by investigating the emission properties and the quantum yield of the carbon dots. Structural characterizations such as FTIR and Raman spectroscopy are also investigated to bring new information on the origin of the fluorescence in their structure.

As a proof of concept, carbon dots synthesized from 1,6-dihydroxynaphtalene using a protocol developed by Yan et al.[4] were synthesized. After purification by silica column chromatography, we obtained a colloidal solution with a fluorescent emission at 590nm under UV or green excitation. This solution showed an absolute quantum yield of 22.6% under 530nm excitation. Integration of these nanoparticles inside commercial clear nail

polish used by archaeologists for protection of artefacts was performed by drying and redispersion in ethyl acetate. The coatings produced were unrecognizable from usual protection coatings with the naked eye but fluoresce under the correct excitation allowing for identification of the cultural artefact.



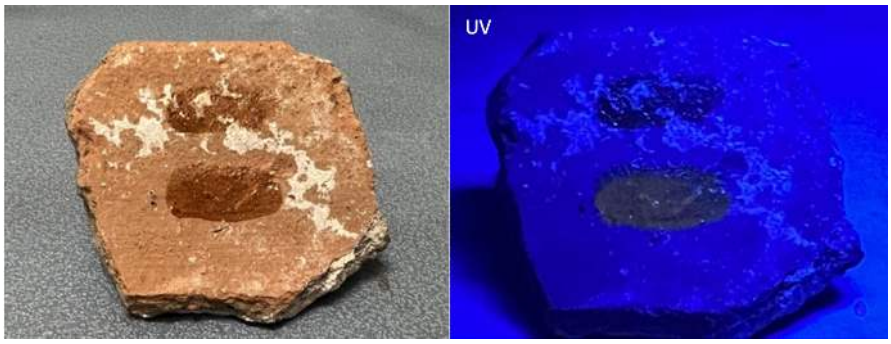


Figure 1. Carbon dots in solution under green laser excitation;

Figure 2. Clear nail polish for classic marking (left) and carbon dots incorporated to clear nail polish for marking (right) under visible and UV light.

References

(1) Barker, A. W. Looting, the Antiquities Trade, and Competing Valuations of the Past. *Annu. Rev. Anthropol.* **2018**, *47* (1), 455–474.

(2) Xu, X.; Ray, R.; Gu, Y.; Ploehn, H. J.; Gearheart, L.; Raker, K.; Scrivens, W. A. Electrophoretic Analysis and Purification of Fluorescent Single-Walled Carbon Nanotube Fragments. *J. Am. Chem. Soc.* **2004**, *126* (40), 12736–12737.

(3) Emam, A. N.; Loutfy, S. A.; Mostafa, A. A.; Awad, H.; Mohamed, M. B. Cyto-Toxicity, Biocompatibility and Cellular Response of Carbon Dots–Plasmonic Based Nano-Hybrids for Bioimaging. *RSC Adv.* **2017**, *7* (38), 23502–23514.

(4) Yan, F.; Zhang, H.; Yu, N.; Sun, Z.; Chen, L. Conjugate Area-Controlled Synthesis of Multiple-Color Carbon Dots and Application in Sensors and Optoelectronic Devices. *Sens. Actuators B Chem.* **2021**, *329*, 129263.

Acknowledgements: We thank the Laboratory Histoire et sources des mondes antiques (HISOMA) for providing cultural artefacts for testing, the Centre de recherche de l'École National Supérieur de Police (CRENSP) for their collaboration on security subjects and the Agence National de Recherche (ANR) for financing our project ANR-21-CE39-0014.

META 2023, PARIS - FRANCE, JULY 18 – 21, 2023

Optical Mie resonances of DNA-assembled three-dimensional gold superlattice crystals

D.Misatziou[1], H.J. Singh[1], A. De Fazio[1], M. Werts[2], Á. Buendía[3], V. Giannini[3,4,5], J. A. Sánchez-Gil[3], A. El Sagheer[6,7], T. Brown[6], A. G. Kanaras[1], and O.L. Muskens[1*]

[1]Physics & Astronomy, Faculty of Engineering and Physical Sciences, University of Southampton, UK
[2] Univ. Rennes, CNRS, SATIE–UMR, Rennes, France
[3]Instituto de Estructura de la Materia (IEM), Consejo Superior de Investigaciones Científicas (CSIC), Madrid, Spain
[4]Technology Innovation Institute, Building B04C, Abu Dhabi, United Arab Emirates
[5]Centre of Excellence ENSEMBLE3 sp. z o.o., Warsaw, Poland
[6]Department of Chemistry, University of Oxford, Chemistry Research Laboratory, Oxford, UK.
[7]Chemistry Branch, Department of Science and Mathematics, Faculty of Petroleum and Mining Engineering, Suez University, Suez, Egypt.

[*]corresponding author: O.Muskens@soton.ac.uk

Abstract: We report the DNA-mediated assembly of gold nanoparticles into 3D superlattice crystals and their subsequent stabilization using carbazol-mediated DNA cross-linking. The visible-near infrared optical properties of the gold-DNA superlattice crystals is shown to be mediated by a broad spectrum of higher order Mie resonances.

Bottom-up approaches for developing new types of hybrid nanomaterials using DNA-mediated assembly are of great interest for their ability to encode the hierarchical structuring through the microscopic building blocks. In recent work our team has established methods for stabilization of the resulting superlattice structures using reversible DNA cross-linking via carbazole groups incorporated into the oligonucleotide structure.[1]

In this work we explore the optical response of three-dimensional Au superlattices mediated by DNA-assembly and carbazole cross-linking, down to the level of single isolated crystals using hyperspectral imaging and micro-spectroscopy. A broadband optical microscopy setup was constructed equipped with a supercontinuum laser as the main light source, a Si and InGaAs photodetectors for signal detection enabling a broad range from 400 nm to 1700 nm. As for the measurement we use a NA, 0.5, 100x objective to focus the light source on to the sample plane, resulting a diffracted limited spot with a diameter equal to the optical wavelength. An identical 100x objective was used to collect the transmitted or scattered light from the sample.

The originally prepared superlattice crystals are kept in a colloidal solution. A small amount (~ 10-20 µl) of the solution was drop casted on a freshly cleaned microscope glass slide and then let to dry overnight. Figure 2a shows the bright field image and the corresponding darkfield image under white lamp (focused laser spot is seen as a bright spot). As seen from the images the crystals on the film tend to form mostly aggregates but there are regions also where they are dispersed and isolated.

A hyperspectral imaging map is generated by scanning the laser focus over the dotted area in Figure 1a. The result under bright field illumination is shown in Figure 1b. The map looks like the exact replica of the digital image shown in Figure 1a expect that now each pixel in such a map contains detailed spectral information as shown in Figure 1c. The transmittance spectra show features around 650-700 nm due to plasmon resonance

effects. Also, the supercrystals exhibit features at higher wavelength >1000 nm which we attribute to the Mie-type resonances of the supercrystals.

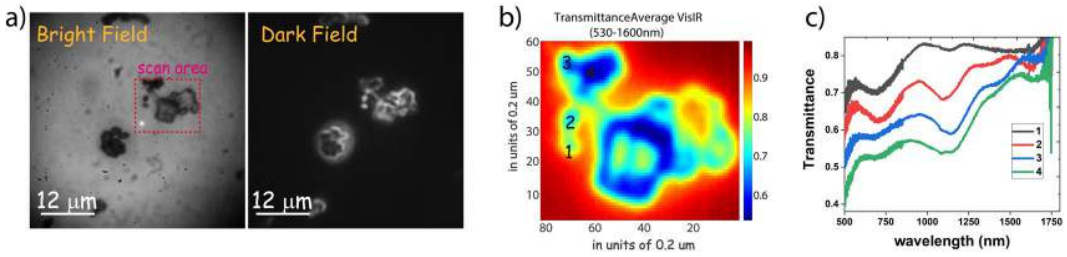


Figure 1. (a) Bright field and dark field images of Au superlattice crystals drop casted on a glass slide. (b) Hyperspectral map (scanned area in (a)) for average transmittance measured under bright field configuration. (c) Transmittance spectra corresponding to points marked in (b).

The setup allowed us to reveal a polarization-insensitive optical response with distinct scattering features in the visible and near-infrared range. The experimental observations were supported by detailed numerical simulations of the microcrystals under a resonant effective medium approximation in the regime of capacitively coupled nanoparticles. The study identifies a universal characteristic optical response which is defined by a band of multipolar Mie resonances, which only weakly depend on the crystal size and light polarization.

The authors acknowledge support from Dstl through a PhD studentship of ADF and The Leverhulme Trust through research grant RPG-2018-251.

References

1. De Fazio, A.F., A. H. El-Sagheer, J. S Kahn, I. Nandhakumar, M. R. Burton, T. Brown, O. L. Muskens, O. Gang, A. G. Kanaras, "Light-Induced Reversible DNA Ligation of Gold Nanoparticle Superlattices," ACS Nano, Article 5, 5771-5777, 2019.
2. Singh, H. J., D. Misatziou, C. Wheeler, A. Buendía, V. Giannini, J. A. Sánchez-Gil, M. H. V. Werts, T. Brown, A. H. El-Sagheer, A. G. Kanaras, O. L. Muskens, "Optical Mie Scattering by DNA-Assembled Three-Dimensional Gold Nanoparticle Superlattice Crystals," ACS Appl. Opt. Mater., 1, 1, 69–77, 2022.

Spectrally-Resolved Polarized Cathodoluminescence in STEM

M. Bézard [1)*], Y. Auad [1)], D. Gérard [2)], J. Beal [2)], J. Martin [2)], M. Kociak [1)]

[1)] Univ. Paris-Saclay, CNRS, Laboratoire de Physique des Solides, 91400 Orsay, France
[2)] Univ. Technologique de Troyes, CNRS, Light nanomaterials nanotechnologies (L2n), 10000 Troyes, France

[*]Corresponding author: malo.bezard@universite-paris-saclay.fr

Far-field optical methods are hindered by the optical diffraction limit. This is probably one of the reason of the success of electron-based optical spectroscopies available in a Scanning Transmission Electron Microscopy (STEM) such as Electron Energy Loss Spectroscopy (EELS) and Cathodoluminescence (CL), among others. One objective of the last decades is to unveil information about the electric field polarization of various excitations (plasmons, excitons, phonons, etc.) using Electron Microscopy, and measure the linear and the circular dichroism as it can be achieved in Optics. A first method to access this information is to measure, in EELS, the Orbital Angular Momentum transfers between the electron beam and the excitations to probe the near-field polarization. A second way to access the polarization measurement in the far-field, is to study the polarization of photons emitted by the sample after having been exited by the electron beam using CL. Some experiments have already combined the use of energy-filtered and polarized light and Scanning Electron Microscope to study achiral and chiral objects [1-3]. One object of interest is a well-known system called a Born-Kuhn System (BKS). This complex nanoparticle exhibits two plasmonic modes which have opposite chirality. This property already has been studied in optics on BKS networks [4] but has never been observed on a single nanoparticle. In this seminar, we discuss the way to perform such an experiment on BKS using a STEM, what are the limitations we can face of and what are the considered solutions to overcome them.

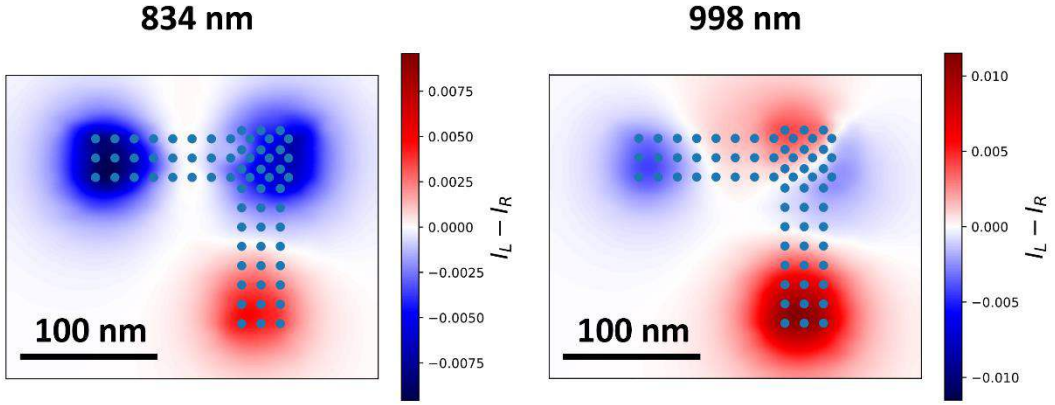


Figure : Simulated Right (R) and Left (L)-handed polarized cathodoluminescence on a gold BKS structure. Each arm has a length of 150 nm and a width of 50 nm. (pyGDM2)

References

[1] N. Yamamoto, K. Araya and F. J. Garcia de Abajo, Physical Review B, 64 205419 (2001)
[2] C. I. Osorio, et. al., ACS Photonics, 3 147-154 (2016)
[3] S. Zu, et. al., Nano Letter, 19, 775-780 (2019)
[4] L. Gui, et. al., ACS Photonics, 6, 3306-3314 (2019)

New trends in nanophotonics and advanced materials

Active aerosols to control the propagation of light

Jake Fontana[1*], Chuck A. Rohde[1], Kristin M. Charipar[1], Paul Johns[1], Ashlin G. Porter[1] and Nicholas J. Greybush[1]

[1]U.S. Naval Research Laboratory, 4555 Overlook Ave. SW, Washington, DC 20375, USA
[*]corresponding author: jake.fontana@nrl.navy.mil

Abstract: This work connects the fields of active plasmonics and aerosols to establish an active aerosol. We report the experimental dynamics and control of ensembles of gold nanorods suspended in air by varying the magnitude and frequency of externally applied electric fields, thereby demonstrating an active aerosol. We further show light filter, valve and gradient-index responses, demonstrating active aerosols as a novel type of optical element we define as component-less optics.

Aerosols commonly impede the propagation of light and the ability to make observations in a variety of research fields, from cosmic dust in astronomy, to clouds in climate science and fog in navigation. Traditionally, aerosols have been regarded as passive, disordered media. If aerosols can be actively ordered, then spatial, spectral and temporal windows of opportunity may open to govern the propagation of light in air. External fields are regularly used to order individual aerosol particles. Though, control of an ordered aerosol ensemble of particles and resultant macroscale optics has yet to be realized, generally due to the need for significant coupling of the external field to a large number of particles in low pressure environments to overcome the disordering forces of Brownian motion.

Experiments were carried out to guide the optical response of an aerosol ensemble and understand the dynamic anisotropic properties of these materials in air when placed in external fields. Plasmonic nanorods were aerosolized into the gas state [1] and coupled to external electric fields [2], as conceptually illustrated in Figure 1.

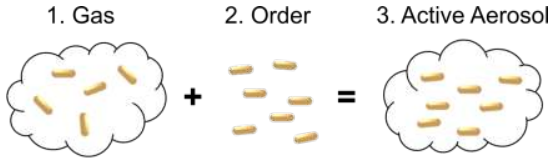


Figure 1. Active aerosol: Electric field induced order in plasmonic aerosols. Reprinted with permission from [3] © The Optical Society.

Active aerosols are shown as three illustrative optical elements, we term component-less optics [3]: (i) The absorption spectrum of gold nanorods in air is shown in Figure 2(a), with longitudinal and transverse absorption peaks at 1020 nm and 520 nm respectively, showing a stop-band light filter element at the absorption peak wavelengths. (ii) The orientational order of the ensemble of gold nanorods suspended in air is controlled by placing an AC electric field across the aerosol, aligning the longitudinal axis of the nanorods in the applied field direction, resulting in a light valve response, Figure 2(b). (iii) The positional order of the aerosol is modulated by introducing a DC electric field, pushing/pulling the nanorods in the field direction, and demonstrating a mechanism to create a gradient index behavior from the aerosol, Figure 2(c).

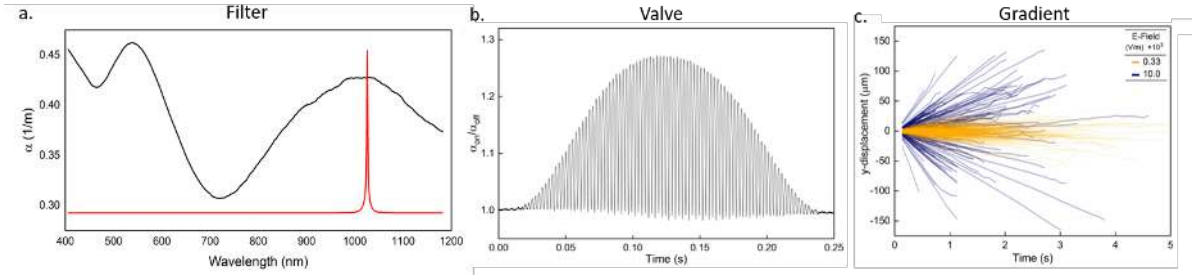


Figure 2. Component-less optics: light filter (a) valve (b) and gradient-index (c) responses. Adapted with permission from [3] © The Optical Society.

We thank the Office of Naval Research (N0001421WX00025, N0001422WX00600) and the Defense Advanced Research Projects Agency (HR0011256798) for support.

References

1. Geldmeier, J., Johns, P., Greybush, N. J., Naciri, J., and Fontana, J., "Plasmonic aerosols," Phys. Rev. B, Vol. 99, 081112 2019.
2. Fontana, J., da Costa, G. K. B., Pereira, J. M., Naciri, J., Ratna, B. R., Palffy-Muhoray, P., Carvalho, I. C. S., "Electric field induced orientational order of gold nanorods in dilute organic suspensions" Appl. Phys. Lett., Vol. 108, No. 8, 081904-4, 2016
3. Rohde, C.A., Charipar, k. M., Johns, P., Porter, A.G., Greybush, N. J., and Fontana, J., "Active aerosols," Opt. Express, Vol. 30, 42276-42282, 2022.

Integrated 2D GaGeTe Electro-Optic Phase Shifter in Silicon Photonics

S. R. Tamalampudi[1], G. Dushaq[1], J. E. Villegas[2], and M. S. Rasras[1*]

[1] Department of Electrical Engineering, New York University Abu Dhabi, UAE

[2] Department of Electrical and Computer Engineering, New York University Tandon School of Engineering, NY, 11201, Brooklyn, USA

[*]Corresponding author: mrasras@nyu.edu

Abstract: We present a high-speed and compact optical phase-shifter using multi-layered GaGeTe hybrid integrated on silicon micro-ring resonator (Si-MRR) structure. Under static DC bias, a blue-shift of wavelength is observed for both the Transverse Electric (TE) and Transverse Magnetic (TM) polarizations corresponding to -1.78 pm/V and - 6.65 pm/V, respectively. The device showed a remarkable tuning speed of 2.1 MHz with low optical insertion losses <0.25 dB. The Pockels effect is expected to dominate the observed phase shift.

The two-dimensional (2D) multi-layered GaGeTe crystals are a non-centrosymmetric structure Recently, those crystals have gained a lot of attention due to their superior electrical and optical properties. They also exhibit high chemical stability under ambient conditions[1-5]. The GaGeTe crystals are part of the MXTe 2D layered group made up of stacks of monolayers connected by weak van der Waals interactions [5].

In this work, we present an electro-optic device based on the hybrid integration of GaGeTe into a silicon micro-ring resonator (Si-MRR). Figure 1 (a) inset shows a schematic of the device, and optical image of the device. A compact phase shifter is used with a total length of 28µm. The device operates in the O-band centered at the telecom wavelength of 1310 nm. As shown in Fig. 1(a and b), for the TE polarization, a blue shifted phase of -1.78pm/V is observed which is attributed to changes in the real part of the index of refraction. A higher blue shift of -6.65 pm/V is observed for devices operating in the TM mode. We expect this blue shift with the positive applied bias to be due to the Pockels effect.

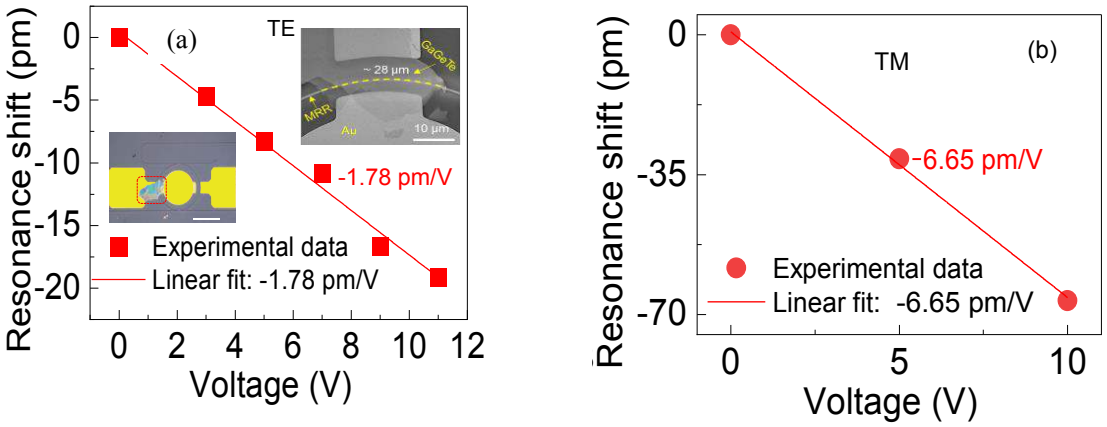


Fig. 1. The electro-static response of the hybrid Si-MRR/GaGeTe flake for TM mode with coverage lengths of 28 µm for different DC voltages. The measured resonance shift versus applied voltage (a) TE mode (b) TE mode.

In summary, the hybrid integration of GaGeTe on Si waveguides expands the silicon photonics device library by introducing a new class of highly tunable and linear electro-optical materials. The proposed structure can be used to construct optical phase shifters, high-speed modulators, small-footprint switches, and a variety of other active integrated photonic devices.

Acknowledgements, this work was supported by NYUAD Research Enhancement Fund. The experimental characterization was conducted in the NYUAD Photonics Lab and simulations were performed on the NYU IT High-Performance Computing resources given its services and staff expertise.

References

1. M. Lipson, "Compact Electro-Optic Modulators on a Silicon Chip," IEEE Journal of Selected Topics in Quantum Electronics, vol. 12, no. 6, pp. 1520-1526, 2006.
2. V. Kucek, C. Drasar, J. Navratil, L. Benes, and P. Lostak, "Optical and transport properties of GaGeTe single crystals," Journal of Crystal Growth, vol. 380, pp. 72-77, 10/01 2013.
3. S. R. Tamalampudi et al., "Short-wavelength infrared (SWIR) photodetector based on multi-layer 2D GaGeTe," Opt. Express, vol. 29, no. 24, pp. 39395-39405, 2021/11/22 2021, doi: 10.1364/OE.442845.
4. J. Zhang et al., "Two-dimensional GaGeTe film: a promising graphene-like material with tunable band structure and high carrier mobility," Journal of Materials Chemistry C, 10.1039/C7TC03001K vol. 5, no. 34, pp. 8847-8853, 2017
5. S. R. Tamalampudi, G. Dushaq, J. Villegas, B. Paredes, and M. S. Rasras, “A Multi-layered GaGeTe Electro-Optic Device Integrated in Silicon Photonics,” IEEE J. Lightwave Technol., Jan. 2023. doi: 10.1109/JLT.2023.3237818

Two-dimensional photonic crystal: an ideal nanophotonics platform for both fundamentals and applications

Heonsu Jeon[1,2,3*]

[1]Department of Physics and Astronomy, Seoul National University, Seoul 08826, Korea
[2]Inter-university Semiconductor Research Center, Seoul National University, Seoul 08826, Korea
[3]Institute of Applied Physics, Seoul National University, Seoul 08826, Korea
[*]corresponding author: hsjeon@snu.ac.kr

Abstract: Two-dimensional photonic crystal (PhC) in a planar geometry has enabled many sophisticated photonic functions and devices, such as PhC phosphors, photonic Anderson localizations, random lasers, and topological lasers, all demonstrated by the author's group. It is expected to continue to play pivotal roles in photonics. In this talk, some of the salient features and properties of those devices will be presented.

Two-dimensional (2D) photonic crystals (PhCs) have been exploited to demonstrate various important concepts and devices in nanophotonics, which include nanocavities with extreme Q factors, nanowaveguides with negligible bending-loss or cross-talk, zero or negative dispersions, nanolasers, etc. The author's group also has been working on both pure and applied physics based on the 2D PhCs with the emphasis on photonic band-edge modes. As for pure physics, photonic band-tail states manifested in composition-disordered PhCs and their relationship to photonic Anderson localizations were clarified [1]. For applications, a number of technologically important milestones in nanophotonic devices have been achieved, including PhC-based random lasers prepared by a top-down approach (Fig. 1) and the active controls on their modal properties [2], PhC phosphors with unprecedentedly high color-conversion efficiency [3], and topological PhC lasers that are immune to structural imperfections and irregularities [4]. This talk will summarize the concepts and characteristics of those devices, along with the future perspectives.

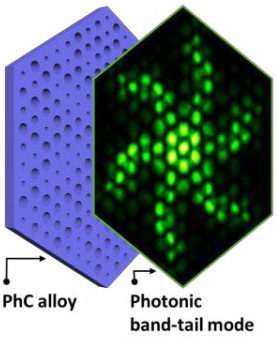


Figure 1. 2D PhC with compositional disorder in the air-hole sizes. A six-fold rotational symmetry is assumed for clarity.

This work was supported by Samsung Research Funding and Incubation Center, Samsung Electronics Co., and the National Research Foundation of Korea.

References

1. Lee, M., et al., "Anderson localizations and photonic band-tail states observed in compositionally disordered platform", Sci. Adv. 4, e1602796, 2018.
2. Lee, M., et al., "Taming of random lasers", Nat. Photon. 13, 445-448, 2019.
3. Lee, H., et al., "Structurally engineered colloidal quantum dot phosphor using TiO2 photonic crystal backbone", Light Sci. Appl. 11, 318, 2022.
4. Han, C., et al., "Laing at topological edge states in a photonic crystal L3 nanocavity dimer array", Light Sci. Appl. 8, 40, 2019.

Plasmon and Graphene-based Nano-tweezers for Raman Imaging

Changjun Min[1*]

[1]Nanophotonics Research Centre, Institute of Microscale Optoelectronics, Shenzhen University, Shenzhen, China
[*]corresponding author: cjmin@szu.edu.cn

Abstract: To enhance the optical trapping precision and functions, we propose two new nano-tweezers technologies, including the plasmonic-thermoelectric tweezers and the graphene-based opto-thermoelectric tweezers. The plasmonic-thermoelectric tweezers offer both high trapping stability and high electric-field enhancement, and achieves Raman imaging with resolution of ~λ/4.5 by dynamically scanning a single metallic nanoparticle. The graphene-based opto-thermoelectric tweezers significantly reduces the required incident power and extends the working bandwidth, and shows great application potential in intracellular Raman spectroscopic detection.

Optical tweezers and associated manipulation tools have had a major impact on scientific and engineering research by offering precise manipulation of small objects. More recently, the use of surface plasmon techniques enables excitation of hotspots much smaller than the free-space wavelength; with this confinement, the plasmonic tweezers could achieve trapping of various nanostructures and materials with higher precision, and thus have contributed to various applications such as nanoparticle (NP) transport and sorting, biomanipulation, and spectrographic sensing and imaging [1].

Surface-enhanced Raman spectroscopy (SERS) technology usually uses metallic nanoparticles to enhance Raman scattering signals, thereby adding significantly to molecule-level recognition and detection. However, realization of nanometre-scaled SERS imaging in liquid environments is extremely difficult due to the requirements of both precise scanning of single metallic nanoparticle and high enhancement field, and thus has never been achieved before. To overcome this obstacle, we propose and demonstrate an immersive nanometre-scaled SERS mapping technology, based on dynamic scanning of a single metallic nanoparticle with a plasmonic-thermoelectric tweezers (PTT) system [2], as shown in Figure 1. The PTT is based on the combination of plasmonic focus and thermoelectric effect, and is demonstrated to possess both high trap stability and Raman enhancement. The results indicate that, for a trapped gold NP of radius 100 nm, its range in fluctuation shrinks sharply to 1/10 of the size observed within traditional focused plasmonic tweezers. By scanning the trapped NP over a molybdenum disulfide (MoS2) sample, two-dimensional Raman imaging with a deep-subwavelength resolution of 118.5 nm is achieved, thereby breaking the diffraction limitation significantly. This enables exciting new functionalities for optical tweezer systems, for example, imaging and detection of biological samples, plasmon-mediated photocatalysis, molecular detections, and many others.

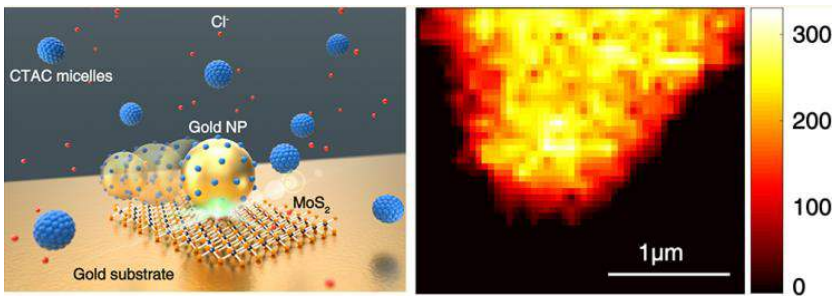


Figure 1. Schematics of SERS imaging based on the PTT system, and the resultant Raman imaging of the MoS_2.

Besides the plasmonic-thermoelectric tweezers based on the metallic nano-film, we also introduce graphene to the field of optical-tweezer technology and demonstrate the graphene-based opto-thermoelectric tweezers (GOTT) [3]. The GOTT technology not only reduces the incident light energy required by two orders of magnitude (compared with traditional optical tweezers), it also brings new advantages such as a much broader working bandwidth and a larger working area compared to those of widely researched gold-film-based opto-thermoelectric tweezers. Compared with gold film, graphene exhibits higher thermal conductivity and higher uniformity and is easier to process. Thus, we have found that even monolayer graphene provides stable trapping for particles in a broad bandwidth and that performance is enhanced as the number of graphene layers increases. Furthermore, parallel trap multiple particles as desired shapes can be easily generated with structured graphene patterns. This work demonstrates the enormous application potential of graphene in optical-tweezer technology and will promote their application to the trapping or concentration of cells and biomolecules as well as to microfluidics and biosensors.

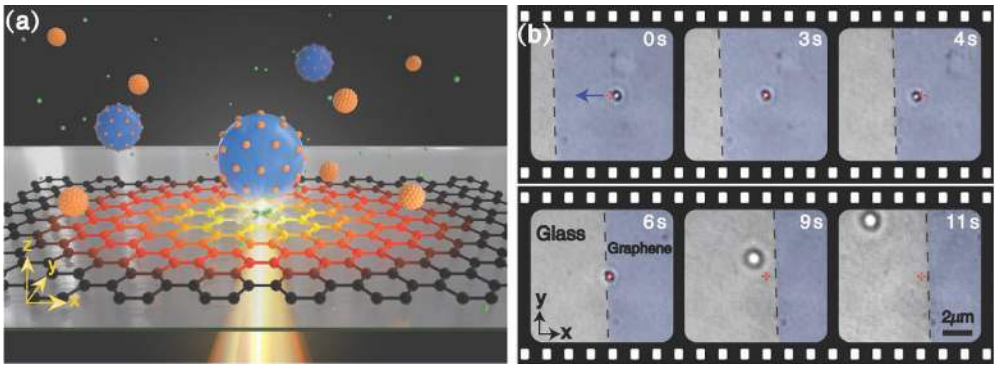


Figure 2. (a) A schematic of the GOTT featuring a graphene substrate. (b) Successive images showing a 500-nm-diameter PS particle stably trapped and dragged to the left.

Moreover, we demonstrate that the GOTT system can be used for in situ intracellular Raman spectral detection [4]. Because of the excellent photothermal conversion effect of the graphene substrate, a potent thermoelectric effect is generated to not only strengthen the trap for biological cells, but also accelerate metallic nanoparticles to permeate into these cells for intracellular Raman enhancement. An in situ intracellular Raman spectrum is thus acquired that offers the opportunity to distinguish the intracellular elements. This work provides a promising approach for use in cytobiology research and is expected to enable exciting new applications in the detection of complex intracellular life processes.

References

1. Y. Q. Zhang, C. J. Min, X. J. Dou, X. Y. Wang, H. P. Urbach, M. G. Somekh, and X. C. Yuan, “Plasmonic tweezers: for nanoscale optical trapping and beyond,” Light: Science & Applications, Vol.10, 59, 2021.
2. X. Y. Wang, Y. Q. Zhang, J. H. Yu, X. Xie, R. P. Deng, C. J. Min, and X. C. Yuan, “Plasmonic-Thermoelectric Nanotweezers for Immersive SERS Mapping,” ACS Nano, Vol. 16, No. 11, 18621–18629, 2022.
3. X. Y. Wang, Y. Q. Yuan, X. Xie, Y. Q. Zhang, C. J. Min, and X. C. Yuan, “Graphene-based Opto-thermoelectric Tweezers,” Advanced Materials, Vol. 34, No. 8, 2107691, 2022.
4. R. P. Deng, Y. Q. Zhang, X. Y. Wang, X. Xie, Y. Song, J. Bu, C. J. Min, and X. C. Yuan, “In situ intracellular Raman spectroscopic detection with graphene-based thermoelectric optical tweezers,” Sensors and Actuators B: Chemical, Vol. 361, No. 15, 131722, 2022.

Topological polaritonics with organic materials

D. D. Solnyshkov[1], J. Ren[2,3], Y. Li[4], O. Bleu[1], J. Yao[3], C. Leblanc[1], T. Long[2], X. Ma[5], S. Schumacher[5,6], J. De[2], F. Yin[3], F. Li[4], H. Fu[2,3], G. Malpuech[1], and Q. Liao[2]

[1]Institut Pascal, Université Clermont Auvergne, CNRS, INP, France
[2]Capital Normal University, Beijing, China
[3]Tianjin University, Tianjin, China
[4]Xi'an Jiaotong University, Xi'an, China
[5]University of Paderborn, Paderborn, Germany
[6]University of Arizona, Tucson, USA
[*]corresponding author: dmitry.solnyshkov@uca.fr

Abstract: Organic materials exhibit excitonic resonances capable of showing strong light-matter coupling at room temperature. We present a review of our recent results on organic microcavities with 3 different materials (perylene, DPAVBi, and TTPSB polymers). We demonstrate emergent optical activity (equivalent to Rashba-Dresselhaus spin-orbit coupling) leading to the formation of topological valleys capable of helical lasing, and selective strong coupling creating exceptional points. We also demonstrate ultrafast switching between bands, enhancing the polariton interactions by an applied electric field.

Topological photonics is a very active research field [1]. It exploits various types of spin-orbit coupling and symmetry-breaking terms giving rise to topological bands or valleys, often responsible for the formation of protected interface states which can have one-way propagation properties.

Combining topology with interactions is crucial for the fabrication of future devices. Strong interactions even allow reaching the quantum regime. Optical non-linearities can be obtained by different means, including the so-called strong light-matter coupling, generating optical eigenstates with a significant "material" fraction, for example, due to the coupling of the light modes with excitonic resonances. This coupling is characterized by the Rabi splitting between the mixed eigenstates. Room-temperature operation requires excitons with large binding energies and high oscillator strengths giving rise to Rabi splittings $\hbar\Omega_R > k_B T$. This is why organic semiconductors are particularly interesting for the studies of non-linear topological photonics with applied purposes. Apart from the strong light-matter coupling, organic semiconductors possess other interesting optical properties, including strong anisotropy of the excitonic resonances. One can even achieve polarization-dependent strong light-matter coupling. This can be interpreted as a strong linear birefringence.

In a recent paper [2], we have demonstrated experimentally and theoretically that a microcavity with an active region exhibiting a sufficiently strong birefringence capable of putting in resonance the cavity modes of opposite parity gives rise to an emergent optical activity. This phenomenon was originally discovered in liquid crystal microcavity [3], where it has been interpreted as a Rashba-Dresselhaus spin-orbit coupling with equal strength. This emergent optical activity is a key ingredient allowing to achieve topological valleys in cavity modes, with other ingredients universally present in many cavity systems: the TE-TM splitting (ubiquitous in all inhomogeneous systems) and the residual linear birefringence. The two latter ingredients provide valleys with tilted Dirac cones, whereas the optical activity opens topological gaps at these Dirac points. This first work, where the topology of these valleys was measured directly from the optical eigenstates, was based on the use of

an organic crystal polymer called perylene, which is often used as a dye.

In the following work, we have demonstrated the possibility to achieve helical lasing from such valleys formed in microcavities with another organic polymer, TTPSB [4]. Polariton relaxation is assisted by the vibron resonance. The circular polarization degree at the band extrema of the valleys is protected by their topological invariants, the valley Chern numbers. The device can be used as a source of directional circular-polarized laser beams.

In parallel, we have studied a different organic polymer, DPAVBi, which manifests selective strong coupling. With one polarization coupled to excitons and another uncoupled, the mass of the cavity modes is very different. This allows a single weakly coupled photonic mode to cross several strongly coupled polaritonic modes of the opposite polarization, with half of them of opposite parity, allowing the observation of emergent optical activity. Moreover, selective strong coupling gives rise to a very different linewidth of strongly and weakly coupled modes (x2 difference), thus creating conditions for the formation and observation of exceptional points [5]. Thanks to these unique properties, we have managed to demonstrate experimentally the hyperbolic divergence of the quantum metric in the vicinity of exceptional points, which is important for the beam dynamics.

Finally, using the same organic polymer DPAVBi embedded in a cavity, we have demonstrated polariton lasing assisted by an electric field [6], which improves the polariton-polariton interactions by inducing an excitonic dipolar moment and changing their radius, while at the same time increasing the exciton lifetime. The electric field thus strongly changes the properties of polaritons and controls their relaxation, allowing us to fabricate an ultrafast electric switch.

This work was supported by the National Key R&D Program of China (Grant No. 2018YFA0704805, 2018YFA0704802 and 2017YFA0204503), the National Natural Science Foundation of China (22150005, 22090022, 21833005 and 21873065), the Natural Science Foundation of Beijing, China (KZ202110028043), Beijing Talents Project (2019A23), Capacity Building for Sci-Tech Innovation-Fundamental Scientific Research Funds, Beijing Advanced Innovation Center for Imaging Theory and Technology. The Paderborn group acknowledges support by the Deutsche Forschungsgemein-schaft (DFG) through the collaborative research center TRR142 (project A04, No. 231447078). We also acknowledge the support of the European Union's Horizon 2020 program, through a FET Open research and innovation action under the grant agreement No. 964770 (TopoLight), the ANR Labex Ganex (ANR-11-LABX-0014), and of the ANR program "Investissements d'Avenir" through the IDEX-ISITE initiative 16-IDEX-0001 (CAP 20-25).

References

1. Ozawa, T. et al “Topological photonics,” Rev. Mod. Phys., Vol. 91, 015006, 2019.
2. Ren, J. et al “Nontrivial band geometry in an optically active system,” Nat. Comm., Vol. 12, 689, 2021.
3. Rechcinska, K. et al “Engineering spin-orbit synthetic Hamiltonians in liquid-crystal cavities,” Science, Vol. 366, 727 (2019).
4. Long, T. et al “Helical Polariton Lasing from Topological Valleys in an Organic Crystalline Microcavity,” Advanced Science, Vol. 2022, 2203588, 2022.
5. Liao, Q. et al “Experimental Measurement of the Divergent Quantum Metric of an Exceptional Point,” Phys. Rev. Lett., Vol. 127, 107402, 2021.
6. De, J. et al “Room-Temperature Electrical Field-Enhanced Ultrafast Switch in Organic Microcavity Polariton Condensates,” J. Am. Chem. Soc., Vol. 145, 3, 1557-1563, 2023.

A multi-modal nonlinear optical technique to study *in-situ* polymer nanostructure formation

T. Verbiest[1,*], K. Aerts[1], and Y. de Coene[1]

[1]KU Leuven, department of chemistry, Belgium
[*]Corresponding author: Thierry.verbiest@kuleuven.be

Abstract: We describe a new multi-modal optical technique to study the formation of (polymer) nanostructures in solution. The technique is based on linear and nonlinear light scattering combined with multi-photon fluorescence and optical transmission.

Conjugated polymers in solution are extremely attractive materials for various optical and opto-electronic applications, because of their semiconducting and fluorescent properties. They have been investigated for their applications in spintronics, metamaterials and photovoltaic applications.[1,2,3] Unfortunately, predicting and reproducing their (optical) properties has proven to be extremely difficult.[4] One possible explanation is polymorphism that is commonly found in their nanostructures.[5,6] Indeed, different nanostructures can be formed depending on the processing or preparation conditions, but little is known about steering the formation process of the nanostructures towards one particular polymorph. The key in understanding lies in the mechanism of nanostructure formation, but this requires powerful *in-situ* techniques that are sensitive to aggregation and self-organization.

We have recently developed a new analytical technique to study such processes based on the simultaneous measurement of second-and third-harmonic scattering (harmonic scattering), and multi-photon fluorescence.[7] Here we describe an in-situ multi-modal optical detection scheme that combines static linear light scattering, harmonic light scattering, multi-photon fluorescence and optical transmission. We will show that it can serve as a powerful benchtop technique for studying nanostructure formation in conjugated polymers. A schematic of the technique is shown in Figure 1.

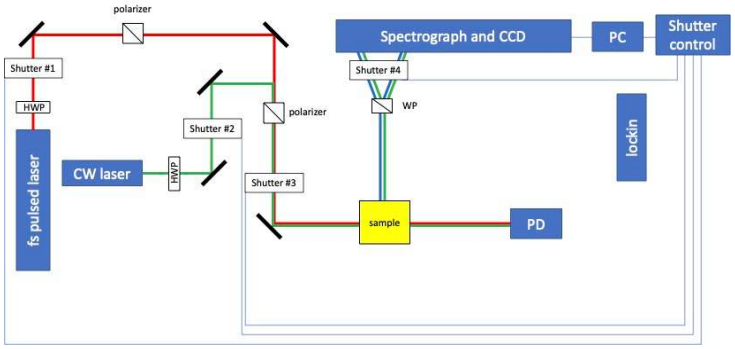


Figure 1: schematic representation of the multi-modal set-up. HWP = half-waveplate, WP = Wollaston prism, PD= photodiode. When shutter#1 and #4 are open, light from the fs laser is focused into the sample cuvette. Harmonic light scattering and multi-photon fluorescence are detected by a lens system, send through a Wollaston prism and detected by a spectrograph coupled to a CCD camera. When shutters#2 and #3 are open, light from the CW laser (532 nm) is focused on the sample and the (linearly) scattered light is collected in the same way as the harmonic scattering signals. The transmitted light through the sample is detected by a photodiode.

A typical measurement is performed as follows: a conjugated polymer is dissolved in a good solvent, and slowly a non-solvent is added to induce nanostructure formation while simultaneously recording 5 different observables (three light scattering signals, multi-photon fluorescence and optical transmission). The three light scattering signals give complementary information: linear light scattering reveals size while second- and third-harmonic scattering are sensitive to size, symmetry, and molecular conjugation. Multi-photon fluorescence and optical transmission give molecular information. Combining all these signals yields a complete view of the dynamics of the nanostructure formation. While demonstrated for conjugated polymers, the technique is suitable to apply to any type of material, either metallic, inorganic, or organic.

References

1. Gong, Z. L.; Zhu, X.; Zhou, Z.; Zhang, S. W.; Yang, D.; Zhao, B.; Zhang, Y. P.; Deng, J.; Cheng, Y.; Zheng, Y. X.; et al. Frontiers in Circularly Polarized Luminescence: Molecular Design, Self-Assembly, Nanomaterials, and Applications. *Sci. China Chem.* **2021**, *64* (12), 2060–2104.
2. Nowacki, B.; Oh, H.; Zanlorenzi, C.; Jee, H.; Baev, A.; Prasad, P. N.; Akcelrud, L. Design and Synthesis of Polymers for Chiral Photonics. *Macromolecules* **2013**, *46* (18), 7158–7165.
3. Lu, H.; Li, X.; Lei, Q.; Conjugated conductive polymer materials and its applications: a mini-review. *Frontiers in chemistry* **2021**, *9:*732132
4. Timmermans, B.; de Coene, Y.; Van Oosten, A.; Clays, K.; Verbiest, T.; Koeckelberghs, G. Influence of the Irregularity of the Molecular Structure on the Chiral Expression of Poly(Fluorene)S. *Macromolecules* **2022**, *55*, 8303–8310.
5. Schulz, G. L.; Ludwigs, S. Controlled Crystallization of Conjugated Polymer Films from Solution and Solvent Vapor for Polymer Electronics. *Adv. Funct. Mater.* **2017**, *27* (1).
6. Poelking, C.; Andrienko, D. Effect of Polymorphism, Regioregularity and Paracrystallinity on Charge Transport in Poly(3-Hexylthiophene) [P3HT] Nanofibers. *Macromolecules* **2013**, *46* (22), 8941–8956.
7. Moris, M.; Van Den Eede, M. P.; Koeckelberghs, G.; Deschaume, O.; Bartic, C.; Van Cleuvenbergen, S.; Clays, K.; Verbiest, T. Harmonic Light Scattering Study Reveals Structured Clusters upon the Supramolecular Aggregation of Regioregular Poly(3-Alkylthiophene). *Commun. Chem.* **2019**, *2* (1), 1–9.

Lithium niobate metasurfaces—A bright nonlinear light source

Mengxin Ren[*], Lun Qu, Lu Bai, Wei Wu, and Jingjun Xu[†]
The Key Laboratory of Weak-Light Nonlinear Photonics, Ministry of Education, School of Physics and TEDA Applied Physics Institute, Nankai University, Tianjin, China
[*]corresponding author: ren_mengxin@nankai.edu.cn
[†]corresponding author: jjxu@nankai.edu.cn

Abstract: Metasurfaces have demonstrated themselves as a promising platform for enhanced second harmonic generation (SHG) to achieve ultracompact nonlinear light sources. Lithium niobate (LN), particularly the crystalline LN thin film on insulators (LNOI) has emerged recently as a promising platform to manufacture metasurfaces. In this talk, we will present our recent work about nonlinear LN metasurfaces with high SHG conversion efficiencies.

Second harmonic generation (SHG), which converts the frequency of a laser ω to twice its frequency 2ω, plays a key role in extending spectral coverage of laser sources to wavelengths that are difficult to access by standard laser gain media. As we enter the Nano-era, the SHG at nanoscales with controllable performance is highly desired. Nonlinear metasurfaces have provided us with a revolutionary concept to engineer nonlinear responses from nanoscale. In addition, it also acts as a new platform to realize novel nanoscale SHG light sources. However, the current nonlinear metasurfaces made of noble metals or semiconductors suffer problems of either high loss or narrow transparent band, which imposes strict constraints on their applications. Recently, crystalline lithium niobate thin film on insulators (LNOI) has emerged as an excellent solution for the novel SHG metasurfaces and nonlinear light sources. However, their SHG conversion efficiencies are still limited, which seriously limits their applications. How to further enhance the SHG efficiency has become an urgent problem to address. In this talk, we will present our recent results on the topic of nonlinear LN metasurfaces [1,2,3], which show a strong nonlinear conversion efficiency larger than 10^{-4}. Our work paves an effective way for enhancing nonlinear optical processes within the framework of metasurfaces, which can be used to develop ultracompact nonlinear light sources for photonics and optoelectronics.

References

1. Lun Qu, Lu Bai, Chunyan Jin, Qiang Liu, Wei Wu, Bofeng Gao, Juntao Li, Wei Cai, Mengxin Ren, Jingjun Xu. “Giant Second Harmonic Generation from Membrane Metasurfaces,” Nano Lett. 22, 9652, 2022.
2. Junjun Ma, Fei Xie, Weijin Chen, Jiaxin Chen, Wei Wu, Wei Liu, Yuntian Chen, Wei Cai, Mengxin Ren, Jingjun Xu. “Nonlinear lithium niobate metasurfaces for second harmonic generation,” Laser Photonics Rev., 15, 2000521, 2021.
3. Junjun Ma, Jiaxin Chen, Mengxin Ren, Wei Wu, Wei Cai, Jingjun Xu. “Second harmonic generation and its nonlinear depolarization from lithium niobate thin films,” Opt. Lett., 45, 145, 2020.
4. Bofeng Gao, Mengxin Ren, Wei Wu, Hui Hu, Wei Cai, Jingjun Xu. “Lithium niobate metasurfaces,” Laser Photonics Rev., 13, 1800312, 2019.

Semi-solid Beam Steering System Based on Micro-Meta-Lens Arrays

Rui Chen, Yifan Shao, and Yungui Ma*

State Key Lab of Modern Optical Instrumentation, Centre for Optical and Electromagnetic Research, College of Optical Science and Engineering; International Research Center for Advanced Photonics, Zhejiang University, Hangzhou, 310058, China.

Corresponding author. Email: yungui@zju.edu.cn

ABSTRACT

Optical beam steerers have been widely employed for information acquisitions. Numerous beam steering schemes have been developed and each of them can satisfy practical requirements for certain scenarios. However, there is still a lack of a comprehensive approach able to balance all the critical technical parameters for wide range of applications. In this talk, we will present a semi-solid micro-mechanical beam steering system based on micro-meta-lens arrays (MMLAs). It is operated by manipulating the probe beam over two sets of decentered MMLAs potentially driven by high-speed piezo-electric motors. Small *f*-numbers, well-corrected aberration and easy lateral reproduction of micro-meta-lenses in optimizing the overall technical parameters. As a proof-of-concept, we implement such a device exhibiting diffraction-limited resolution within a large field of view of 30°×30°. A three-dimensional depth sensing is also performed to demonstrate its potential in light detection and ranging (LiDAR) applications. In this talk, we will exhibit that this MMLAs could be employed to design a two-dimensional optical ruler with nanometric resolution.

References

1. Rui Chen, Yifan Shao, Yi Zhou, Yongdi Dang, Hongguang Dong, Sen Zhang, Yubo Wang, Jian Chen, Jian, Bing-feng Ju, and Yungui Ma*, A Semisolid Micromechanical Beam Steering System Based on Micrometa-Lens Arrays, Nano Letters 22, 1595-1603 (2022).

Hierarchical Micro/Nanostructures for Light Harvesting and Photovoltaic Device Applications

Jae Su Yu[1*]

[1]Department of Electronic Engineering, Institute for Wearable Convergence Electronics, Kyung Hee University, 1732 Deogyeong-daero, Gihung-gu, Yongin-si, Gyeonggi-do 17104, Republic of Korea
[*]corresponding author: jsyu@khu.ac.kr

Abstract: Hierarchical micro and nanostructures based on inorganic and organic materials for the manipulation of light behaviors such as reflection, transmission, scattering, etc. are demonstrated. The fabrication of the micro and nanostructures on material surfaces is performed via various manufacturing techniques, together with the design by numerical modelling and simulations. Optical properties of the fabricated micro and nanostructures are theoretically and experimentally evaluated. Eventually, the hierarchical micro and nanostructures are applied to light harvesting and photovoltaic devices to enhance their performances.

Over the past years, antireflective structures including subwavelength grating structures instead of conventional antireflection multilayers and high hazed structures have been developed, based on micro and nanoarchitectured structures. For fabrication, electron-beam/photo lithography, laser interference, nanoimprint, thermal-wetted particles, and nano/microspheres for patterning, followed by dry etching processes, were traditionally employed. Bioinspired micro or nanoarchitectures which can enable efficient antireflection in the wide ranges of incident wavelengths and angles have been widely studied. These structures have been fabricated on the silicon, III-V semiconductors, metal oxides, glass, etc. In case of polymers, antireflective micro/nanostructures could be easily fabricated by a soft imprint lithography method which takes advantage of simple, cost-effective, and fast manufacturing.

On the other hand, in photovoltaic devices, both subwavelength structures and micrograting architectures can efficiently increase the light absorption by reducing the surface reflection owing to the linearly gradient refractive-index profile. Furthermore, micrograting extend light path lengths as well as promote diffuse lights and induce strong electromagnetic fields, which leads to a high haze factor. Additionally, micro/nanostructured polymer films can be used as the antireflection and protection layer of coverglasses to enhance the conversion efficiency of photovoltaic systems. In this presentation, I would like to report hierarchical micro and nanostructures for light harvesting and photovoltaic device applications, together with finite-difference time-domain and rigorous coupled-wave analysis simulations. For various photovoltaic devices based on hierarchical micro and nanostructures, light incident angle-dependent characteristics are also investigated in a broad angle range.

This work was supported by the National Research Foundation of Korea (NRF) grant funded by the Korean government (MSIP) (No. 2018R1A6A1A03025708).

References

1. M Choi, J. W. Leem, and J. S. Yu, “Antireflective gradient-refractive-index material distributed microstructures with high haze and superhydrophilicity for silicon-based optoelectronic applications,” RSC Adv., Vol. 5, No. 32, 25616–25624, 2015.

2. J. W. Leem, S. Kim, S. H. Lee, J. A. Rogers, E. Kim, and J. S. Yu, “Efficiency Enhancement of Organic Solar Cells Using Hydrophobic Antireflective Inverted Moth-Eye Nanopatterned PDMS Films,” Adv. Energy Mater., Vol. 4, No. 8, 1301315, 2014.
3. B. Dudem, J. W. Leem, J. H. Lim, S. H. Lee, and J. S. Yu, “Multifunctional polymers with biomimetic compound architectures via nanoporous AAO films for efficient solar energy harvesting in dye sensitized solar cells,” RSC Adv., Vol. 5, No. 109, 90103–90110, 2015.
4. J. W. Leem and J. S. Yu, “Artificial inverted compound eye structured polymer films with light-harvesting and self-cleaning functions for encapsulated III–V solar cell applications,” RSC Adv., Vol. 5, No. 75, 60804–60813, 2015.
5. B, Dudem, J. W. Jung, and J. S. Yu, “Improved light harvesting efficiency of semitransparent organic solar cells enabled by broadband/omnidirectional subwavelength antireflective architectures,” J. Mater. Chem. A, Vol. 6, No. 30, 14769–14779, 2018.
6. B. Dudem, I. S. Jin, A. R. Mule, J. W. Jung, and J. S. Yu, “High-Efficiency and Thermally Sustainable Perovskite Solar Cells with Sandpaper-Aided Flexible Haze/Antireflective Films,” ACS Sustain. Chem. Eng., Vol. 7, No. 15, 12981–12989, 2019.

PT-symmetric non-Hermitian plasmonic systems for switchable radiation control

Yuto Moritake[1,2,*]

[1]Department of Physics, Tokyo Institute of Technology, Japan
[2]PRESTO, Japan Science and Technology Agency, Japan
[*]corresponding author: moritake@phys.titech.ac.jp

Abstract: Non-Hermitian photonics is research fields utilizing phenomena induced by non-Hermiticity. Especially, systems with *PT* symmetry is important due to *PT*-phase transition across an exceptional point (EP) where the eigenvalues and eigenmodes coalesce. In this presentation, we introduce our recent results on switchable radiation control with *PT*-symmetric non-Hermitian plasmonic systems. Coupled split ring resonators and coupled plasmonic wires were proposed for switching of unidirectional radiation and polarization states, respectively. The studies provide exotic photonic functionalities based on non-Hermiticity in the systems.

Recently, non-Hermitian (NH) physics has attracted a great deal of attention from researchers. Especially, the NH systems with *PT* symmetry exhibit *PT* phase transition across an exceptional point (EP). The eigenvalues and eigenmodes coalesce at the EP, which is very unique property of NH systems with *PT* symmetry and cannot be found in Hermitian systems. Since photonic systems naturally have non-Hermiticity due to radiation and material gain and loss, many photonic systems involving NH photonics have been reported and shown variety of intriguing phenomena [1].

In this paper, we introduce our recent studies on switchable radiation control with NH plasmonic systems. In the studies, we take advantage of the singular eigenstates at EPs, in which the resonators oscillate in $\pm\pi/2$ phase difference. First, we explain switchable unidirectional radiation from artificial Huygens dipoles in coupled split ring resonators (SRRs) [2]. And the second, switching of circular polarization eigenstates in coupled plasmonic dipoles at EPs is presented [3]. The studies would provide new root to realize novel photonic functionalities based on the singular eigenstates at EPs in NH systems.

Figure 1(a) shows a unit structure of coupled SRRs to realize artificial Huygens dipoles. Huygens dipole is formed by orthogonal arrangement of electric and magnetic dipoles which oscillate in- or anti-phase [4]. A Huygens dipole radiates unidirectionally due to interference between electric and magnetic dipoles. Here, LC resonance in SRRs are used for mimicking the electric and magnetic dipoles. *PT* symmetry was achieved by difference in radiation losses between the SRR1 and SRR2, which manifests the existence of EPs in a parameter space. Here, we sweep the geometrical parameters α (arc angle of SRR1) and d_x (displacement between SRRs along x-axis). Importantly, induced electric and magnetic dipoles in SRRs has initial phase difference of $\pi/2$ so that the Huygens dipole conditions, in- or anti-phase, are satisfied by the singular EP eigen states. Therefore, unidirectional radiation originating from Huygens dipole formation is observed (Fig. 1(b)). Moreover, by appropriate control of coupling between SRRs, we can realize the other EP, which has different sign of phase difference, giving rise to radiation to he opposite direction. We can switch the direction by choosing these EPs through the geometric parameters.

Figure 1(c) shows a unit structure of coupled plasmonic dipole resonators to realize single circular eigen states for normal incidence. The structures are composed of x- and y-dipole resonators in which GST (lossy materials) is added only y-resonator to realize a *PT*-symmetric system. At an EP, two resonators oscillate in $\pi/2$

phase difference which means polarization eigen state becomes a single circular polarization [5]. This strong chirality for normal incidence is originate from non-Hermiticity while generally optical chirality requires three dimensional structures. When the GST film is in crystal phase, the loss of GST induces non-Hermiticity and *PT*-phase transition in a polarization space as shown in Fig. 1(d). Here, polarization eigen states approach the circular polarization, which is EP eigen states, in the way of *PT* phase transition. On the other hand, once the GST is changed into an amorphous phase, its material loss becomes negligible, giving rise to disappearance of non-Hermiticity and only linear polarizations are allowed (Fig. 1(e)). These results demonstrated switching of polarization state, non-Hermitian to Hermitian transition, by material phase transition.

In summary, we introduced two studies on switching of photonic states based on non-Hermiticity using coupled plasmonic systems. Taking advantage of the singular eigenstates at EPs, unique photonic functionality can be achieved, which would be applicable to realize reconfigurable NH photonic devices.

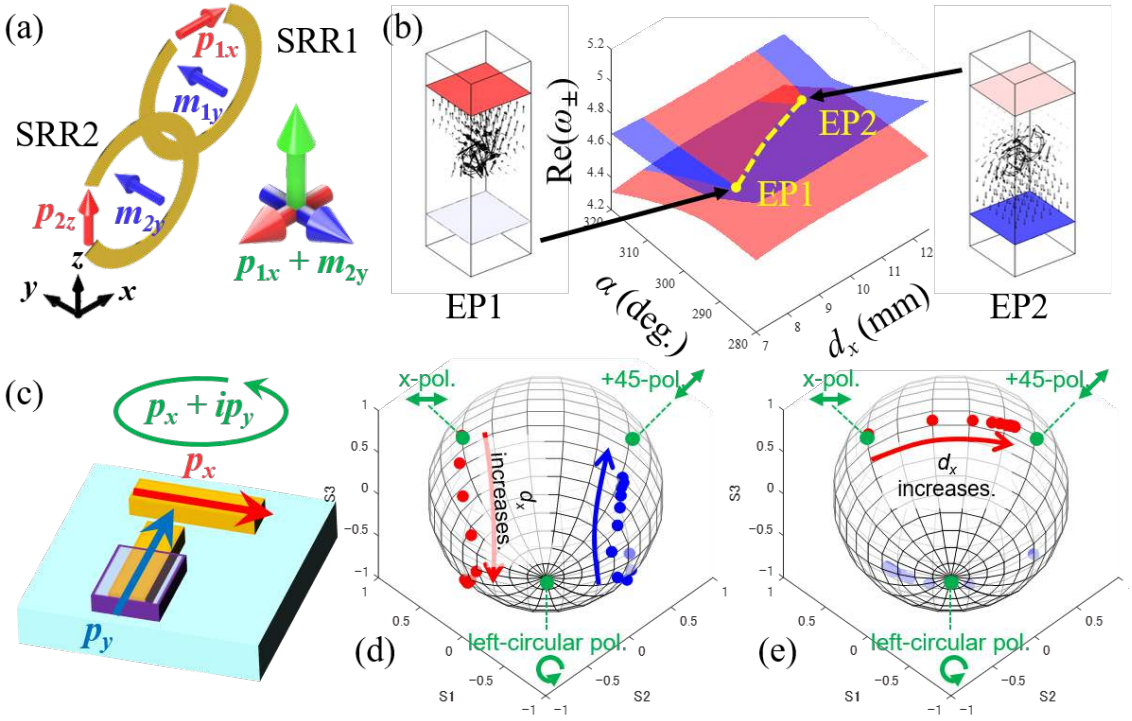


Fig. 1 (a) Coupled SRRs exhibiting artificial Huygens dipole at EPs. (b) Riemann surface structure in a parameter space and switchable unidirectional radiation from Huygens dipoles at EPs. (c) Coupled plasmonic dipole resonators for single circular eigen polarization. Change in polarization eigen states on Poincare sphire when the GST film is in (d) crystal and (e) amorphous phases.

Acknowledgements

This work has been supported by JST, PRESTO Grant Number JPMJPR18L9, Japan, by JSPS, Grant-in-Aid for Scientific Research (S), 20H05641, Japan, and by Grant-in-Aid for Early-Career Scientists, 21K14551.

References

[1] L. Feng *et al.* Nat. Photon. **11**, 752 (2017). [2] Y. Moritake and M. Notomi, arXiv:2110.01884.

[3] Y. Moritake and M. Notomi, CLEO 2021. [4] M. F. Picardi *et al.* Phys. Rev. Lett. **120**, 117402 (2018).

[5] M. Lawrence *et al.* Phys. Rev. Lett. **113**, 093901 (2014).

META 2023, PARIS - FRANCE, JULY 18 – 21, 2023

Electromagnetic Signal Propagation Through Lossy Media

I. I. Smolyaninov[1*]

[1]Saltenna LLC, 1751 Pinnacle Drive, Suite 600 McLean VA 22102, USA
[*]corresponding author: igor.smolyaninov@saltenna.com

Abstract: It is commonly believed that electromagnetic waves cannot propagate in lossy conductive media and that they quickly decay inside such media over short length scales of the order of skin depth. I will demonstrate that contrary to this belief, surface electromagnetic waves in stratified lossy conductive media may have propagating character, and their propagation length may be considerably larger than the skin depth. This result has important consequences across the electromagnetic spectrum from radio signals propagation underwater to UV nanophotonics.

It was recently demonstrated that surface electromagnetic waves in stratified lossy conductive media may have propagating character, and the propagation length of such waves may be considerably larger than the skin depth [1,2]. The comparison of these novel surface wave solutions with the properties of the more well-known surface waves, such as surface plasmons [3] and Zenneck waves [4], is summarized in Table 1. Similar to surface plasmons, the wavelength of this wave may be considerably shorter than the light wavelength in free space, which may enable its applications in super-resolution microscopy and nanolithography techniques. However, unlike plasmonics-based nanophotonic devices, which are typically built using a very limited number of low loss optical materials, the newly found class of surface waves may be supported by a much broader range of lossy media.

Utilization of the newly discovered class of surface electromagnetic waves, which propagate along gradual interfaces of lossy optical media, should bring about quite a few developments in linear and nonlinear nanophotonics. These novel surface waves may bring the spatial resolution of 2D microscopes down to 10 nm scale and beyond [2]. Unlike plasmonics-based nanophotonic devices, which are typically built using a very limited number of low loss optical materials, the newly found class of surface waves may be supported by a much broader range of lossy media. Such materials as graphite and silicon seems to be ideal in UV nanophotonics applications where the classical plasmonic materials are not operational [2].

Indeed, such a classic CMOS material as silicon appears to be highly suitable for gradient-index nanophotonics applications. Similar to graphite, silicon exhibits very large and purely imaginary dielectric permittivity in the UV range, which strongly depends on the doping level. Therefore, silicon-based gradient index nano waveguides may potentially be fabricated using CMOS technology, which would greatly extend various silicon photonics applications. Deeply subwavelength UV nanoresonators may become possible, leading to numerous applications in sensing and UV nanolasers. In addition, such applications as deep UV high harmonic generation in these nanostructures may also become possible. Such developments have a potential to completely revolutionize UV nanophotonics.

Based on the same ideas, we also demonstrated several underwater portable radio communication systems operating in the 30-50 MHz band and capable of transmitting voice and high-definition live video images underwater. The system operation is based on launching surface electromagnetic waves propagating along the water-air and water-seafloor interfaces using specially designed surface wave antennas. Since the propagation

surface wave type	interface type	bounding media	wavelength range
Surface plasmon	abrupt	low loss metal-dielectric	from free space to deep subwavelength
Zenneck wave	abrupt	lossy conductor-dielectric	similar to free space
Interfacial wave	continuous	lossy conductor-lossy conductor	deep subwavelength

Table 1. Comparison of the basic properties of different kinds of surface electromagnetic waves.

length of the surface electromagnetic waves far exceeds the classical skin depth of conventional radio waves at the same frequency, this technique is useful for radio and video communication and object detection underwater. For example, in the experiments performed in a freshwater lake (Lake Phoenix, VA), a 50 MHz underwater radio operated at 5 W transmit power in combination with SEW antennas achieved clear voice communication underwater over distances up to 85 m and depth up to 8 m. The described system also appears to be efficient at communicating through the water-air interface, which is traditionally believed to be a very difficult problem.

References

1. Smolyaninov, I. I., "Surface electromagnetic waves in lossy conductive media: tutorial", JOSA B Vol. 39, 1894-1901, 2022.
2. Smolyaninov, I. I., "Gradient-index nanophotonics", Journal of Optics Vol. 23, 095002, 2021.
3. Zayats, A. V., Smolyaninov, I. I. and Maradudin, A. "Nano-optics of surface plasmon-polaritons", Physics Reports Vol. 408, 131-314, 2005.
4. Michalski, K. A. and Mosig, J. R. "The Sommerfeld half-space problem revisited: from radio frequencies and Zenneck waves to visible light and Fano modes", Journal of Electromagnetic Waves and Applications Vol. 30, 1-42, 2016.

META 2023, PARIS - FRANCE, JULY 18 – 21, 2023

Microscopic Study of Effective 2+1 Dimensional Gravity in Ferrofluid-Based Hyperbolic Metamaterials

V. N. Smolyaninova[1*], J. Cartelli[1], N. Christopher[1], B. Kist[1], J. Perry[1], S. Spickard[1], M. S. Devadas[1] and I. I. Smolyaninov[2]

[1]Towson University, 8000 York Rd., Towson, MD 21252, USA
[2]Saltenna LLC, 1751 Pinnacle Drive, Suite 600 McLean VA 22102, USA
[*]corresponding author: vsmolyaninova@towson.edu

Abstract: Recent theoretical and experimental work demonstrated that nonlinear optics of ferrofluid-based hyperbolic metamaterials exhibits very unusual 2+2-dimensional spatiotemporal dynamics. Here we report a detailed microscopic study of mutual interactions of individual self-focused optical filaments inside this metamaterial. In agreement with theoretical expectations, the observed mutual interactions of individual filaments exhibit strong similarities with general relativity in 2+1 dimensions.

Optical space is the central concept of the transformation optics paradigm. A metric of optical space inside an electromagnetic metamaterial differs from the metric of physical space, and in such unusual cases as hyperbolic metamaterials, the optical space may behave like an "optical spacetime" [1]. It was reported that the nonlinear optical dynamics of this system should have very unusual character [2], and it may have strong resemblance with gravitational physics. In particular, in several experimental situations the nonlinear optics of hyperbolic metamaterials may be reduced to effective general relativity (GR) in 2+1 dimensions, which is very interesting since such a theory may be solved exactly, even in the quantum mechanical limit.

One of such situations involves using a monochromatic CW laser light illuminating a hyperbolic metamaterial, so that at high enough power laser light passing through the metamaterial develops filamentation. The nonlinear dynamics of such light filaments looks similar to gravity in 2+1 dimensions. Initial experimental evidence of such a filamentation inside a ferrofluid-based hyperbolic metamaterial has been communicated in [2]. Here we report a detailed microscopic study of this effect. We substantially improved the spatial resolution of our experimental setup, so that the properties of individual filaments and details of their mutual interaction have been revealed in fine detail. The schematic diagram of our experimental setup is shown in Fig. 1. Compared to the original setup described in detail in [2], we have implemented a high-resolution telescopic objective mounted on the LWIR camera. An example of high-resolution image of the extraordinary laser beam propagated through the metamaterial sample is shown in Fig. 2. This 6.48 mm x 6.48 mm image frame was taken from a recorded video of the extraordinary beam evolution as a function of time. This image was recorded at 960 mW CO_2 laser power. The average (approximately Gaussian) laser beam profile was subtracted from the image. This background subtraction allowed to reveal the optical filaments formed within the beam and study the temporal dynamics of their mutual interactions. The filaments appeared to be quite stable, having an average lifetime of about 10 s. At higher laser powers, when the filaments appeared to be well-defined, their width to intensity ratio was approximately constant (Fig.2b). The increase of laser power passing through the metamaterial led to increase of the number of filaments (Fig.2c), while their relative sizes remained mostly similar. This initial increase was followed by eventual near saturation of the number of filaments at higher powers.

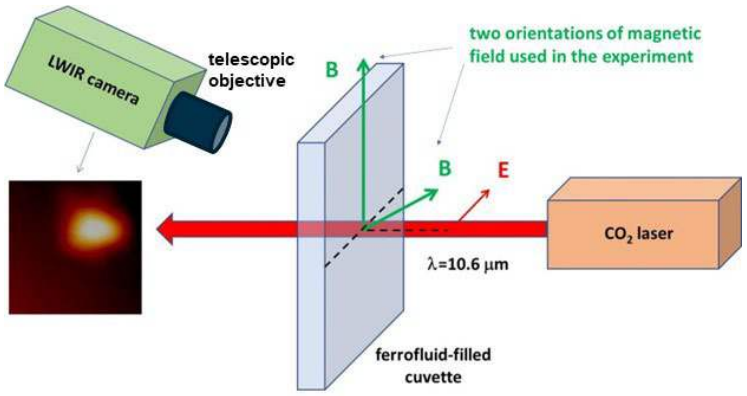
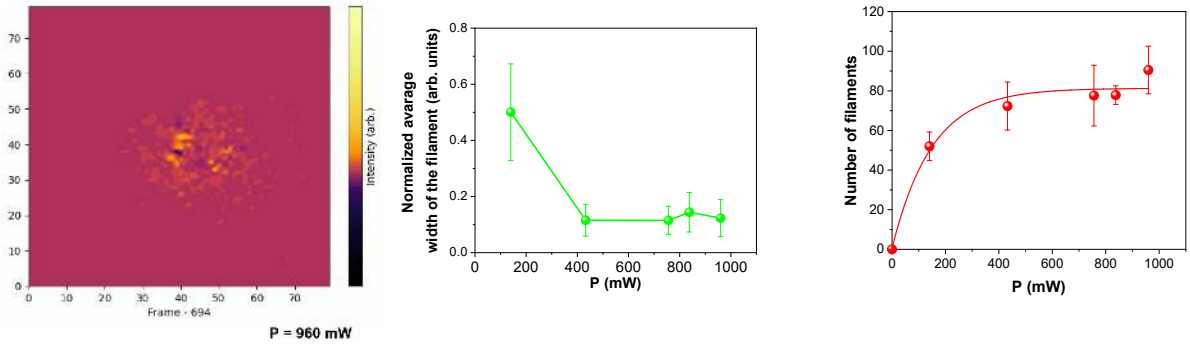


Fig. 1. Schematic diagram of the experimental setup. A LWIR camera with an attached telescopic objective is used to study propagation of CO_2 laser beam through the ferrofluid-based hyperbolic metamaterial, which is subjected to external DC magnetic field. The inset shows the measured beam shape of the CO_2 laser in the absence of the metamaterial sample. Two orientations of the external magnetic field B used in our experiments are shown by green arrows. The red arrow shows polarization of laser light.



(a) (b) (c)

Fig. 2. (a) A 6.48 mm x 6.48 mm image of the extraordinary CO_2 beam. This image was recorded at 960 mW laser power. The average (approximately Gaussian) laser beam profile was subtracted from the image to reveal optical filaments within the beam. (b) At higher laser powers, when the filaments appeared to be well-defined, their width to intensity ratio is approximately constant. (c) The increase of laser power passing through the metamaterial leads to increase of the number of filaments. The line is a guide to the eye.

In agreement with theoretical expectations, the analysis of mutual interactions of individual filaments exhibit strong similarities with general relativity in 2+1 dimensions.

This work was supported in part by FDRC, SET and Fisher Endowment grants at Towson University.

References

1. Smolyaninov, I. I. and Narimanov, E. E. “Metric signature transitions in optical metamaterials”, Phys. Rev. Letters Vol. 105, 067402, 2010.
2. Smolyaninova, V. N., Cartelli, J., Augstein, B., Devadas, M. S. and Smolyaninov, I. I. “Experimental observation of effective gravity and two times physics in ferrofluid-based hyperbolic metamaterials”, Advanced Photonics Vol. 2, 056001, 2020.

META 2023, PARIS - FRANCE, JULY 18 – 21, 2023

Plasmonic high entropy alloy materials for midinfrared metasurfaces towards efficient photo-thermal energy conversion

Yoshiaki Nishijima[1*]

[1] Department of Electrical and Computer Engineering, Graduate School of Engineering, Yokohama National University, 79-5 Tokiwadai, Hodogaya-ku, Yokohama, 240-8501, Japan

[*]corresponding author: nishijima-yoshiaki-sp@ynu.ac.jp

Abstract: We have realized High entropy alloy, (HEA) materials for plasmon applications, especially midinfrared absorption metasurfaces. Optical obtained permittivity realized FDTD simulations that can well reproduce the experimental data. Also FDTD results indicate that HEA metasurface became true perfect absorption condition.

Conventional plasmon resonance materials have been studied using simple metals such as gold (Au), silver (Ag), copper (Cu), and aluminum (Al). And some rare earth, alkaline metals were not used for plasmonic research, but they show plasmon resonance from considering the permittivity. The limitation of materials comes from the richness of free electrons (free carrier density) and relaxation time or dumping of oscillation during resonances. These properties has appeared in the permittivity that can be described using Drude-Lorenz model. To overcome this limitation, alloying metals is one of the promising ways. We have studied the alloying metals such as Au-Ag-Cu, and Au-Pd for plasmon resonance and hydrogen sensing applications, beyond the material limitation. We have primarily focusing experimentally determined optical permittivity of such alloy materials for quantitative evaluation of plasmon resonances [1].

In recent years, high-entropy alloys (HEA) composed of more than five metals have attracted attention. This is because they can realize the highest configuration entropy in their crystal. In particular, HEA forms homogeneous phases without phase separation, exhibiting stronger physical properties than components. In addition, HEA also focused on new catalytic materials. For example, when HEA was composed with Au, Ag, Cu, Pt, Pd, HEA can improve catalytic activity [2].

The aim of this study is to apply such HEAs for plasmonic metasurfaces, which consists of metal-insulator-metal nanostructures. Especially in mid infrared wavelength region, metasurfaces have important roles of efficient photo-thermal energy conversion materials [3-6]. To evaluate the optical properties of metasurfaces quantitatively, it is essential to obtain the complex optical permittivity ($\varepsilon = \varepsilon_1 + \imath\varepsilon_2$). We have experimentally determined the optical permittivity of HEA materials from visible to mid-infrared wavelength and evaluated their plasmon resonances.

An alloy system consisting of gold, silver, copper, platinum, and palladium was selected as a HEA. HEA film on a glass substrate was prepared by a sputtering method. Their optical permittivity was measured using spectrometric ellipsometer UV-VIS (250 to 1000 nm) and MIR (1700 nm to 20000 nm), respectively. Also, Metal-insulator metal (MIM) metasurfaces were fabricated using electron beam lithography. Their optical responses were analyzed with FTIR and FDTD simulations.

Figure 1 shows the experimentally obtained optical permittivity of Au, Ag, Cu, Pd, Pt, and HEA. The optical permittivity of HEA located between Pd and Pt. When we apply them to mid-infrared metasurfaces, the absorption band of the MIM metasurface can be obtained only in a limited range concerning the film thickness of SiO_2. In contrast, the HEA has good absorption properties over the range of 2-7 μm in the mid-infrared wavelength region. This suggests that HEA is the better material for MIM metasurfaces for optical light absorbers and thermal radiators.

In the presentation, we will discuss the detail experiments, numerical simulation results, and future application of HEA for efficient midinfrared photonic materials.

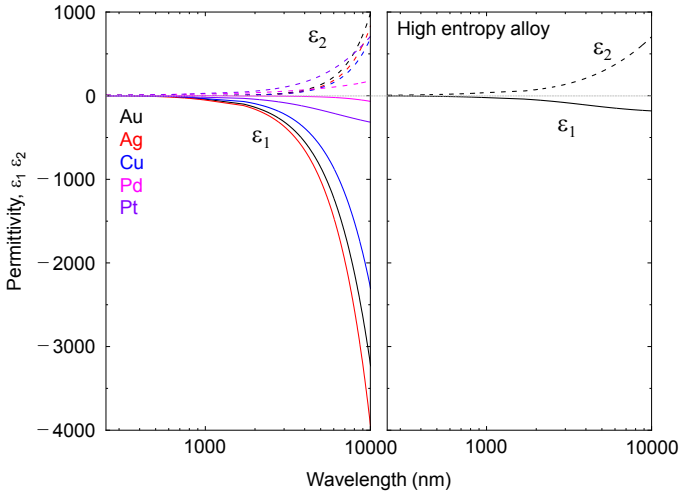


Fig. 1 Optical permittivity of Au, Ag, Cu, Pd, Pt (left panel) and their HEA materials (right panel).

References

1. Y. Hashimoto, G. Seniutinas, A. Balčytis, S. Juodkazis and Y. Nishijima, "Au-Ag-Cu nano-alloys: tailoring of permittivity," Sci. Repo., 6, 25010, 2016.
2. D. Wu, K. Kusada, Y. Nanba, M. Koyama, T. Yamamoto, T. Toriyama, S. Matsumura, O. Seo, I. Gueye, J. Kim, L. S. R. Kumara, O. Sakata, S. Kawaguchi, Y. Kubota, and H. Kitagawa, "Noble-Metal High-Entropy-Alloy Nanoparticles: Atomic-Level Insight into the Electronic Structure," J. Am. Chem. Soc., 144, 3365–3369, 2022
3. Y. Nishijima, S. Morimoto, A. Balčytis, T. Hashizume, R. Matsubara, A. Kubono, N. To, M. Ryu, J. Morikawa, and S. Juodkazis, "Coupling of molecular vibration and metasurface modes for efficient mid-infrared emission," J. Mater. Chem. C, 10, 451-462, (2022).
4. Y. Nishijima, S. Juodkazis, "Control of Vibration-Metasurface Coupling at the Mid-Infrared Spectral Window for Inorganic Thermal Emitters," Bull. Chem. Soc. Jpn, 95, 1411-1418, (2022).
5. Y. Nishijima, S. Juodkazis, "The Tunable Coupling between Metasurface and Molecular Vibration towards the Platform of Spectral Analysis," Bull. Chem. Soc. Jpn, 95, 1318-1324, (2022).
6. Y. Nishijima, N. To, A. Balčytis, and S. Juodkazis, "Absorption and scattering in perfect thermal radiation absorber-emitter metasurfaces," 30, 4058-4070 (2022).

Color Selective 3D Polarization Profiles

Xianzhong Chen*

School of Engineering and Physical Sciences, Heriot-Watt University, Edinburgh, UK
*corresponding author: x.chen@hw.ac.uk

Abstract: We propose and experimentally demonstrated a single metasurface device that can realize color selective 3D polarization structures. The device design includes multi-foci design, polarization rotation, and color multiplexing in 3D space. The efficacy of this approach was exemplified through the demonstration of multiple 3D knots with controlled local polarization states. The unprecedented design degree of freedom of optical metasurfaces has provided a compact platform to develop ultrathin optical devices with engineered 3D polarization profiles and color selective functionality.

Vector beams have been recognized as a promising future technology in quantum memories, particle trapping, and high-resolution lithography. However, the real-life applications remain limited, mainly because of complexity of the experimental system and the inability to arbitrarily manipulate polarization state of light at subwavelength scale. It has found many applications ranging from quantum to classical optics (e.g., polarized sunglasses and 3D cinema). Polarization control has been used to record, process and store information. Light beams with spatially inhomogeneous polarization distributions have received great attention owing to their peculiar optical features and practical applications such as higher resolution lithography and patterning of lyotropic chromonic liquid crystals by photoalignment.

Driven by device miniaturization and system integration, there is huge interest in developing ultrathin (light wavelength scale) and lightweight planar optical devices with novel functionalities that cannot be obtained with conventional optical elements. Optical metasurfaces are planar nanostructured interfaces and have recently attracted tremendous interests due to their unprecedented capability in the manipulation of the amplitude, phase and polarization at subwavelength scale. The emergent optical metasurface based flat optics has revolutionized design concepts in photonics, providing a new platform to develop unusual ultrathin optical devices (e.g., dual-polarity lenses, polarization sensitive holograms). Optical metasurfaces have shown much promise for polarization manipulation [1]. We have experimentally demonstrated 2D polarization profiles with uniform intensity to hide high-resolution images in a light beam based on optical metasufaces [3, 4]. The target images are encoded in the spatially variant polarization states in 2D space. We designed and demonstrated metalenses that can achieve arbitrary 3D focal curves with customized polarization profiles without the aid of additional optical elements [5]. A number of focal curves ranging from a simple ring to a more complicated 3D knot are observed in the focal region of metalenses. The proposed approach is very flexible and robust to generate various polarization profiles of the focal curves, including linear and nonlinear relations between polarization rotation angles and positions along the curves.

Multispectral polarization manipulation will add more degrees of freedom. Furthermore, multifunctional optical devices have profound implications for the research fields where light weight and integrated optical systems are highly desirable. There is an urgent need to develop multifunctional ultrathin devices that can simultaneously encode color and intensity information into 3D polarization profiles. However, how to realize color selective 3D polarization structures has not been reported. Here we propose and experimentally demonstrate color selective

three-dimensional (3D) polarization structures with a single metasurface. The geometric metasurfaces are designed based on color and phase multiplexing and polarization rotation, creating various 3D polarization knots. Remarkably, different 3D polarization knots in the same observation region can be achieved by controlling the incident wavelengths, providing unprecedented polarization control with color information in 3D space. Our research findings may be of interest to many practical applications such as vector beam generation, virtual reality, volumetric displays, security and anti-counterfeiting.

Metasurface enabled arbitrary polarization manipulation is a new research field. The precise control over the polarization state of light in 3D space can be faithfully mapped onto the intensity profile for each color. By combining multiple 3D polarization structures and dispersion effect of a metalens, this work provides a compact platform to realize different 3D polarization structures. Multispectral polarization manipulation will add more degrees of freedom. The small volume, light weight, and color selective functionality bring 3D polarization engineering capabilities closer to being feasible on integrated polarization optics system and wearable devices with smaller footprints. The flexible and controllable generation of 3D polarization distributions with customized intensity profiles of different colors (wavelengths) may be of interest to many practical applications such as vector beam generation, virtual reality, color displays, information security, anti-counterfeiting, and high-density information storage.

Acknowledgements

This work is supported by Engineering and Physical Sciences Research Council of the United Kingdom (Grant Ref: EP/P029892/1), the Leverhulme Trust (RPG-2021-145), and the Royal Society International Exchanges (IES\R3\193046).

References

1. Y. Intaravanne, X. Chen, Recent advances in optical metasurfaces for polarization detection and engineered polarization profiles, Nanophotonics, 9, 1003-1014, 2021.
2. F. Yue, C. Zhang, X.-F. Zang, D. Wen, B. D. Gerardot, S. Zhang, X. Chen, High-resolution grayscale image hidden in a laser beam, Light Sci. Appl. 7, 17129, 2018.
3. C. Zhang, D. Wen, F. Yue, Y. Intaravanne, W. Wang, X. Chen, Optical metasurface generated vector beam for anticounterfeiting, Phys. Rev. Applied 10: 034028, 2018.
4. X. Zang, F. Dong, F. Yue, C. Zhang, L. Xu, Z. Song, M. Chen, P. Chen, G. S. Buller, Y. Zhu, S. Zhuang, W. Chu, S. Zhang, X. Chen, Polarization encoded color image embedded in a dielectric metasurface, Adv. Mater. 30: 1707499, 2018.
5. R. Wang, Y. Intaravanne, S. Li, J. Han, S. Chen, J. Liu, S. Zhang, L. Li, and X. Chen, “Metalens for Generating a Customized Vectorial Focal Curve.,” Nano Lett., 21, 2081-2087, 2021.
6. Y. Intaravanne, R. Wang, H. Ahmed, Y. Ming, Y. Zheng, Z.-K. Zhou, Z. Li, S. Chen, S. Zhang, and X. Chen. Color-selective three-dimensional polarization structures, Light Sci. Appl. 11, 302, 2022.

META 2023, PARIS - FRANCE, JULY 18 – 21, 2023

Switch from mono- to multi-mode polariton laser in a GaN ridge waveguide

C. Brimont[1]*, H. Souissi[1], M. Gromovyi[2] T. Gueye[1], L. Doyennette[1], D.D Solnyshkov [3], G. Malpuech [3], E. Cambril [2], S. Bouchoule [2] B. Alloing[4], S. Rennesson[4], F. Semond[4], J. Zúñiga-Pérez[4], T. Guillet [1]

[1]Laboratoire Charles Coulomb (L2C), UMR 5221 CNRS-Université de Montpellier, France
[2]Centre de Nanosciences et de Nanotechnologies, CNRS, Université Paris-Saclay, France
[3]Université Clermont Auvergne, CNRS, SIGMA Clermont, Institut Pascal, Clermont-Ferrand, France
[4]UCA, CRHEA-CNRS, Rue Bernard Gregory, Valbonne, France
*corresponding author, E-mail: christelle.brimont@umontpellier.fr

Abstract: We report a polariton laser in a GaN ridge waveguide, switching from mono to multi-mode laser operation as temperature is increased. The free spectral range's study between the modes first leads to the unambiguous proof that the polaritons are in strong coupling regime; and above 150K, during the transition to multi-mode lasing, a flattening of the FSR demonstrates a synchronization of the modes. These results therefore pave the way to the investigation of harmonic mode-locking in polariton waveguide lasers.

Polaritons in microcavities are a rich playground that has led to numerous researches for more than thirty years. The polariton laser has a specificity compared to a more conventional ridge laser: the absence of reciprocity between the processes leading to gains and losses. A new trend in polaritonics is developing, based on the waveguide geometry. By studying the operation of a CW polariton laser in a GaN waveguide geometry with distributed Bragg reflectors (DBR) forming the cavity, we have shown that the lasing effect is achieved even for a pump length of only 15% of the cavity length with only a threefold increase in overall threshold in stark contrast to conventional ridge lasers [1]. Waveguide polaritons form a new platform of choice for integrated photonics relying on both laser pumping specificity, potential nonlinearities, low losses and long propagation distances. The small footprint of the cavities studied, the choice of base materials, namely gallium nitrides, outline this promising future in terms of a device operating at room temperature [5].

Half-light and half-matter, polaritons exhibit a large nonlinearity which eclipses the values of the photonic nonlinearities in semiconductors by several orders of magnitude. Thus, an experimental observation of nonlinear self-modulation of UV pulses in an AlInGaN-based waveguide has been reported [2]. Other waveguide geometries are investigated such as polaritonic micro-rings, where mode-locking and soliton formation was predicted [3] and cw lasing was experimentally demonstrated [4].

For this presentation we will focus on the extension of the study we conducted previously. We perform spatially- and spectrally-resolved power-dependent microphotoluminescence experiments on GaN/(AL,Ga)N planar waveguide with DBR. We evidence at 70K, the laser operation which above

threshold happens to be CW and mono-mode. The increase in the temperature of the structure above 150K makes a switch towards a laser which is, at threshold, directly multi-mode.

Below the threshold, for all investigated temperatures, our photoluminescence spectra exhibit, over a large part of the measured energy range, so-called Fabry-Perot modes. A detailed study of the experimental free spectral range (FSR) of these modes compared to that calculated from the dispersion of the LPB will, assesses the strong coupling regime in our polaritonic device. We will see that the change in laser regime with temperature causes two phenomena. Just before the threshold, the FSR decreases near the exciton resonance and just above the threshold, a flattening of the FSR. This last point is important, because it happens to be the signature of mode synchronization arising from the nonlinearity recently evidenced under resonant excitation [2]. These results therefore opens interesting prospects regarding harmonic mode-locking in polariton waveguide lasers.

The authors acknowledge funding from the French National Research Agency (ANR-16-CE24-0021-03, ANR-11 LABX-0014, ANR-21-CE24-0019-01), the French Renatech network and the Region Occitanie (ALDOCT-001065).

References

1. H. Souissi et al. Phys. Rev. Appl., Vol. 18, 044029, 2022.
2. D. M. Di Paola et al. Nat. Commun., Vol 12, 3504, 2021.
3. O. A. Egorov et al. Optics Express, Vol. 26, 18, 2018.
4. A. Delphan et al. APL Photonics, Vol. 8, 021302, 2023.
5. C. Brimont et al. Phys. Rev. Appl. Vol 14, 054060, 2020.

META 2023, PARIS - FRANCE, JULY 18 – 21, 2023

Image processing with metaoptics: phase imaging and asymmetric optical transfer functions

N. Priscilla[1], S. B. Sulejman[1], W. S. Lee[1], L. Wesemann[1], T. J. Davis[1], and A. Roberts[1*]

[1] ARC Centre of Excellence for Transformative Meta-Optical Systems, School of Physics, University of Melbourne, Victoria 3010, Australia

[*]Corresponding author: ann.roberts@unimelb.edu.au

Abstract: The capacity to modify images in the Fourier domain using all-optical methods in real-time is well-known but there is an emerging interest in manipulating images using metasurfaces in the object or image plane leading to an orders-of-magnitude reduction in size and weight. Many applications, however, require the introduction of a transverse asymmetry in the optical transfer function. Here approaches to introducing the required asymmetry will be discussed and their application to phase contrast imaging of transparent objects will be highlighted.

Although the use of optical systems to perform image processing in the Fourier plane has been well-known since the 1940s, most commonly used modifications (such as edge enhancement) are more widely performed digitally. Furthermore, information carried in an optical wavefield introduced by, for example, propagation through transparent objects or turbulence, is lost on acquisition with a camera. Although sophisticated computational strategies for extracting phase from intensity images exist, these can be relatively slow. Conventional all-optical approaches for image processing and phase contrast imaging, however, typically require relatively bulky, and sometimes expensive, optics. The increasing amount of data being generated, the drive for miniaturization of optical components, and advances in nanoscience have underpinned a renewed interest in all-optical image processing.

When considering the propagation of an optical wavefield carrying an image we typically consider the decomposition of the field into a superposition of plane waves each with a characteristic amplitude and phase. Conventional spatial filtering involves introducing an amplitude and/or phase mask into the focal plane of a lens taking advantage of the Fourier transforming property. This places constraints on the positioning of the filter as well as requiring bulky lenses and the inclusion of propagation distances from the object to Fourier plane. Another approach that we are currently investigating involves directly manipulating the spatial frequencies via a device that has a reflection or transmission that depends on the angle of incidence of a plane wave. In 1979 it was shown that the introduction of a suitably tailored phase grating into the object plane of an optical system generated an edge-enhanced output [1]. It was highlighted that there was considerable flexibility in the positioning of the device since spatial filtering was no longer required a the angular spectrum was manipulated directly. The emergence of metaoptics has reignited interest in this approach since concepts from nanophotonics can produce compact devices with a tailored angular dispersion and, hence, expanded capacity to manipulate images and, more generally, perform analogue computing [2,3].

We have considered both reflective and transmissive geometries. One system with a well-known angular sensitivity is a simple, commercially available notch filter that can be used to perform edge detection in

transmission at the design wavelength [4]. A planar metal-insulator-metal also can be used to enhance edges in reflection at the resonant wavelength [5] as can a resonant waveguide grating in transmission [6]. Many mathematical operations, however, require an inherent asymmetry in the optical transfer function that is used to describe the way that spatial frequencies propagate through the metasurface. Although some devices have been demonstrated that can generate the derivative of the device after interaction with the metaoptic, detection with a camera results in a loss of phase information that precludes determining the sign of the gradient which is particularly important when imaging phase objects. The introduction of a simple tilt of the device introduces a phase ramp that shifts the effective transfer function so that is no longer symmetric about normal incidence [4,6,7]. This generates a pseudo-3D phase contrast images of transparent objects similar to those seen in Differential Interference Contrast microscopy but with a simple thin device. Furthermore, through appropriate device design and choice of polarization, it is possible to create an asymmetric transfer function about normal incidence removing the requirement to tilt the device. In this talk two metasurfaces [8,9] that have this capacity will be discussed and recent experimental results presented.

This research was funded by the Australian Government through the Australian Research Council Centre of Excellence grant (CE200100010). S.B.S also gratefully acknowledges the support of the Ernst & Grace Matthaei Scholarship and the Australian Government Research Training Program Scholarship.

References

1. Case, S.K. “Fourier processing in the object plane”, Opt. Lett. Vol. 4, No. 9, 286-288, 1979.
2. Zangeneh-Nejad, Sounas, D.L., Alù, A. Fleury, R, “Analogue computing with metamaterials,”, Nature Reviews Materials, Vol. 6, 207-225, 2021
3. Wesemann, L., Davis, T. J., & Roberts, A. “Meta-optical and thin film devices for all-optical information processing,” Applied Physics Reviews, Vol. 8 No. 3, 031309, 2021.
4. S.B. Sulejman, N. Priscilla, L. Wesemann, W. S. L. Lee, J. Lou, E. Hinde, T. J. Davis, A. Roberts, “Thin film notch filters as platforms for biological image processing,” arXiv:2209.09539, 2022.
5. Wesemann, L., Panchenko, E., Singh, K. Della Gaspera, E., Gómez, D.E., Davis, T.J., Roberts, A. “Selective near-perfect absorbing mirror as a spatial frequency filter for optical image processing,” APL Photonics, Vol. 4, 100801, 2019.
6. Wesemann, L., Rickett, J., Song, J., Lou, J., Hinde, E., Davis, T.J., Roberts, A. "Nanophotonics enhanced coverslip for phase imaging in biology" Light Sci. Appl., Vol. 10, No. 1, 98, 2021.
7. Roberts, A., Gómez, D.E., Davis, T.J., “Optical image processing with metasurface dark modes,” J. Opt. Soc. Am. A, Vol. 35, No. 9, 1575-1584, 2018.
8. Davis, T.J., Eftekhari, F., Gómez, D.E., Roberts, A. “Metasurfaces with asymmetric optical transfer functions for optical signal processing,” Phys. Rev. Lett. Vol. 123, 013901, 2019.
9. Wesemann, L., Rickett, J., Davis, T.J., Roberts, A. "Real-time phase imaging with an asymmetric transfer function metasurface,”ACS Photonics, Vol. 9, No. 5, 1803-1807, 2022.

Flat Band Induced Metal-Insulator Transitions With Weak Disorder and Many Body Interactions

Certain lattice wave systems in translationally invariant settings have one or more spectral bands that are strictly *flat* or independent of momentum in the tight binding approximation, arising from either internal symmetries or fine-tuned coupling [1]. Originally considered as a theoretical convenience useful for obtaining exact analytical solutions of ferromagnetism, flat bands have now been observed in a variety of settings, ranging from electronic systems to ultracold atomic gases and photonic devices [1],[2]. I will review the design and implementation of flat bands, classification schemes, discuss recent results on adding many-body interactions [3] and disorder[4], and chart future directions of this exciting field.

[1] *Artificial flat band systems: from lattice models to experiments*. Daniel Leykam, Alexei Andreanov, Sergej Flach. Adv. Phys.: X **3**, 1473052 (2018)
[2] *Photonic Flat Bands*. Daniel Leykam, Sergej Flach. APL PHOTONICS **3**, 070901 (2018)
[3] *Many body flatband localization*. Carlo Danieli, Alexei Andreanov, Sergej Flach. Phys. Rev. B **102**, 04116(R) (2020); *Heat percolation in many-body flatband localizing systems*. Ihor Vakulchyk, Carlo Danieli, Alexei Andreanov, Sergej Flach. Phys. Rev. B **104**, 144207 (2021); *Many-body localization transition from flatband finetuning*. Carlo Danieli, Alexei Andreanov, Sergej Flach. Phys. Rev. B **105**, L041113 (2022).
[4] *Metal-insulator transition in infinitesimally weakly disordered flatbands*. Tilen Cadez, Yeongjun Kim, Alexei Andreanov, Sergej Flach. Phys. Rev. B **104**, L180201 (2021); *Flatband-induced metal-insulator transitions for weak magnetic flux and spin-orbit disorder*. Yeongjun Kim, Tilen Cadez, Alexei Andreanov, Sergej Flach. arXiv:2211.09410; *Critical-to-insulator transitions and fractality edges in perturbed flatbands*. Sanghoon Lee, Alexei Andreanov, Sergej Flach. Phys. Rev. B **107**, 0142024 (2023).

META 2023, PARIS - FRANCE, JULY 18 – 21, 2023

Deep ultraviolet to visible absorbing and sensing applications by stacking film with highly lossy ultra-thin film

Y. Takashima[1,2*], S. Furuta[1], K. Nagamatsu[1,2], M. Haraguchi[1,2] and Y. Naoi[1,2]

[1]Faculty of Science and Technology, Tokushima University, Tokushima, Japan
[2]Institute of Post-LED Photonics, Tokushima University, Tokushima, Japan
[*]corresponding author: takashima@tokushima-u.ac.jp

Abstract: Stacking films with ultra-thin highly lossy material provides unique destructive interference condition in complex phase space far from the real axis. Utilizing the interference, we demonstrated the broadband deep ultraviolet and visible perfect light absorbers with large angle tolerance and the highly sensitive refractive index sensing technique in planer structure.

Broadband perfect light absorbers with insensitive for the incident angle and the polarization states are extremely suitable for photodetectors and solar cells. Especially, perfect absorption into the ultra-thin film is highly desirable for efficient light-photocurrent conversion.

Perfect absorption can be obtained by the simultaneously vanishing reflection (R) and transmission (T). The enhancement of the absorption has been reported using quarter wavelength thin films [1, 2] and meta-materials [3] and -surfaces [4]. However, the suppression of both R and T for broad wavelength, wide angle, and both polarizations (p- and s-polarizations), is challenging.

We utilized the unique interference in the highly lossy ultra-thin film to overcome the above issue and demonstrated the attractive deep ultraviolet (DUV) to visible (VIS) applications, such as ultra-broadband perfect absorbers. The highly lossy film (namely, the real and the imaginary parts of its complex refractive index with sane order) causes a non-zero or $-\pi$ phase shift of Fresnel coefficients. The large complex valued Fresnel coefficients can provide unique destructive interference condition in the complex phase space and enhances the light-matter interaction inside deep subwavelength region [5-9]. The destructive interference of our optimized multi-stacking system with highly lossy film realized almost perfect DUV and VIS absorptions into the much thinner film than the incident wavelength. The properly designed structures also show polarization-insensitive flat-top absorption spectra with large angle tolerance. The features are very advantageous for several applications of the high-efficiency conversion between light and photocurrent.

Moreover, we applied the destructive interference of the highly lossy films to the refractive index sensing applications. The destructive interference of the optimized highly lossy film shows very high sensitivity for the refractive index of the incident medium.

Acknowledgements

This work is supported in part by JSPS KAKENHI (Grant Number: JP21K14515), Adaptable and Seamless Technology Transfer Program through Target-driven R&D (A-STEP) (Grant number: JPMJTM20GK), Iketani Science and Technology Foundation (Grant number: 0331109-A).

References

1. Dallenbach, W. and W. Kleinsteuber, “Reflection and absorption of decimeter-waves by plane dielectric layers,” Hochfrequenztech. Elektroakustik, Vol. 51, 152–156, 1938.
2. Fante, R. L. and M. T. McCormack, “Reflection properties of the Salisbury screen,” IEEE Trans. Antennas Propag., Vol. 36, No. 10, 1443–1454, 1988.
3. Yu, P., L. V. Besteiro, Y. Huang, J. Wu, L. Fu, H. H. Tan, C. Jagadish, G. P. Wiederrecht, A. O. Govorov and Z. Wang, “Broadband metamaterial absorbers,” Adv. Opt. Mater., Vol. 7, Iss. 3, 1800995, 2019.
4. Glybovski, S. B., S. A. Tretyakov, P. A. Belov, Y. S. Kivshar and C. R. Simovski, “Metasurfaces: from microwaves to visible,” Phys. Rep., Vol. 634, 1-72, 2016.
5. Kats, M. A. and F. Capasso, “Optical absorbers based on strong interference in ultra-thin films,” Laser Photonics Rev., Vol. 10, No. 5, 735–749, 2016.
6. Kats, M. A., D. Sharma, J. Lin, P. Genevet, R. Blanchard, Z. Yang, M. M. Qazilbash, D. N. Basov, S. Ramanathan and F. Capasso, “Ultra-thin perfect absorber employing a tunable phase change material,” Appl. Phys. Lett., Vol. 101, Iss. 22, 221101, 2012.
7. Park, J., J.-H. Kang, A. P. Vasudev, D. T. Schoen, H. Kim, E. Hasman and M. L. Brongersma, “Omnidirectional near-unity absorption in an ultrathin planar semiconductor layer on a metal substrate,” ACS Photonics, Vol. 1, Iss. 9, 812-821, 2014.
8. Lee, K.-T., C. Ji and L. J. Guo, “Wide-angle, polarization-independent ultrathin broadband visible absorbers,” Appl. Phys. Lett., Vol. 108, Iss. 3, 031107, 2016.
9. Takashima, Y., K. Nagamatsu, M. Haraguchi and Y. Naoi, “Ultra-thin deep ultraviolet perfect absorber using an Al/TiO_2/AlN system,” Opt. Express, Vol. 30, No. 24, 44229-44239, 2022.

META 2023, PARIS - FRANCE, JULY 18 – 21, 2023

Research on Intelligent Photonic Computing Chips

Xiaoyong Hu*, Kun Liao

Department of Physics, Peking University, Beijing 100871, China

*corresponding author: xiaoyonghu@pku.edu.cn

Abstract:

With the rapid development of advanced engineering computing, economic data analysis, and cloud computing, the demand for ultra-high speed and energy-efficiency computing is growing exponentially. However, for electronic processors, the scaling of computing time and power consumption is limited by data transfer between memory and processing units, RC delay associated with integrated circuits and excessive heating due to Ohmic losses. Integrated photonics adopting photons as information carriers with multiple degrees of freedom benefiting from the CMOS-compatible manufacturing with modularity and scalable fabrication technology of integrated circuits, could reach a high computational efficiency with minimal power consumption and low-latency at the speed of light.

One of the most important applications of combining machine learning and integrated photonics is Photonic Hardware for AI. As one of the artificial intelligent algorithms, neural network has strong judgment in solving inference tasks because of its superior learning ability. In addition, neural networks implemented on photonic platforms can take advantages of photonic computing, including ultralow energy consumption, ultra-fast time response, low integration crosstalk, and multidimensional degrees of freedom. In recent years, photonic neural networks have achieved superior performance in artificial intelligence tasks such as pattern recognition and image classification. So far, there are still some challenges in the field of photonic neural networks that need to be further studied, including expanding the functions of neural networks by taking full advantage of using photons for computing; improving computing efficiency by designing new configurations of neural networks adapted to photonic hardware platforms; increasing complexity of neural networks by realizing reliable all-optical nonlinear activation layers; and saving the computing power by realizing hardware on-chip training [1].

Here, we have done some corresponding research from several aspects of the challenges mentioned above. Firstly, we proposed an all-optical computing chip based on the convolutional neural network from the perspective of extending the functions of neural networks [2]. We extended the function of the optical neural network to realize logical operations and solve complex mathematical operations for the first time, providing a potential direction for a new generation of intelligent all-optical computing chips. In addition, we also proposed a matrix eigenvalue solver based on reconfigurable photonic neural network [3]. The designed principle of the network is simple and reconfigurable with the efficient and scalable implementation scheme. Secondly, starting from improving network efficiency, we proposed the concept of "photonic diffraction neuron", and designed a silicon-based optical neural network based on the proposed photonic diffraction neurons [4]. The inverse-designed photonic neurons provide higher-density optical connection, achieving efficient signal processing from low to high dimensional datasets. Afterwards, from the perspective of increasing the complexity of the network, we proposed the graphene/silicon heterojunction-based reconfigurable optical activation functions [5]. Here we used complex amplitude activations, demonstrating that the proposed activations in complex networks outperform the classical computer activations. This work realized rich and effective nonlinear activation layers, which provides a feasible way for the effective implementation of all-optical neural networks on integrated photonic platforms.

References

1. K Liao, X Hu*, et al, "Integrated Photonic Neural Networks: Opportunities and Challenges", ACS Photonics, Accepted, 2023.
2. K Liao, X Hu*, et al, "All-optical computing based on convolutional neural networks", Opto-Electron. Adv., 4 (11), 200060, 2021.
3. K Liao, X Hu*, et al, "Matrix eigenvalue solver based on reconfigurable photonic neural network", Nanophotonics, 11 (17), 4089-4099, 2022.
4. K Liao, X Hu*, et al, "Optical Neural Network Based on Integrated Photonic Diffraction Neurons", In preparation.
5. C Zhong, K Liao, X Hu*, et al, "Graphene/silicon heterojunction for reconfigurable phase-relevant activation function in coherent optical neural networks", Nat. Commun., Under Review.

META 2023, PARIS - FRANCE, JULY 18 – 21, 2023

Plasmon Resonance Mode Evolution in a Semiconductor Nanodimer in the Overlapping Regime

Z. Wang and T. Wong*
Illinois Institute of Technology, USA

*corresponding author: twong@ece.iit.edu

Abstract: Field intensification and polarization enhancement are exhibited by semiconductor nanodimers (SND) in the non-overlapping regime. On the other hand, an SND in the overlapping regime exhibits unique characteristics of geometrical influence on space charge interactions, leading to secondary resonance that is strongly dependent on the amount of overlap between the constituent particles. The charge distribution, interior and exterior field, and dipole moment induced on a model SND by a terahertz electric field is studied by a charge transport formulation for carrier dynamics with a quasi-static framework for the polarizing field. Spectral components observed are interpreted by considering the evolution of charge distribution within the semiconductor material.

Being the simplest form of nanoparticle clusters, the nanodimer is of particular interest in the study of polarization coupling between particles in multiple particle systems. Nanodimers can be categorized into non-overlapping and overlapping types. The former exhibits field intensification in the gap region between the particles when they are placed in a linearly polarized electric field parallel to the axis of the dimer (1). When a semiconductor nanodimer (SND) is made up of particles with different doping levels, the enhanced field in the gap sways from one side to the other as the frequency of the applied field is varied from the surface plasmon resonance (SPR) of one particle to that of the other (2). The absence of the gap in the overlapping case implies the dimer is actually a single-body nanostructure whose shape varies from that resembling a dumbbell to that of an elongated sphere as shown in Fig. 1.

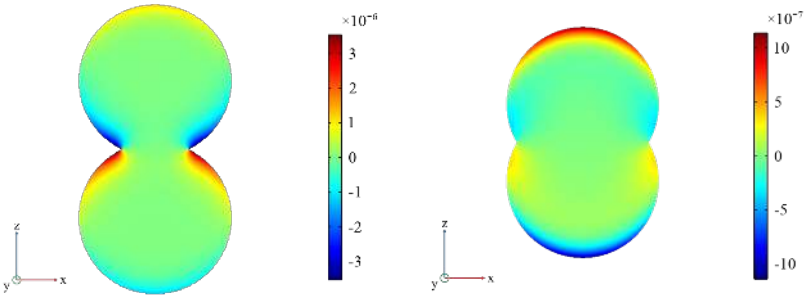


Figure 1. Charge distribution in SND with different amount of overlap at frequency of applied field close to the SPR frequency of the isolated particles making up the dimer. The SNP has radius of 50 nm and doping of 10^{18} cm^{-3}.

In this paper, an account of investigation on the polarization in an overlapping SND immersed in a terahertz electric field is presented. Numerical solution for the space-charge dynamics in an SND is obtained by a finite-element simulation tool applied on a system of equations derived from the moments of the Boltzmann

transport equation for the charge carriers coupled with the field equations (3). A general observation from the results of computation is that the SND in the overlapping regime exhibits SPR with resemblance to that of the standalone SNP with a slight red shift in the resonance frequency. When the amount of overlap between the constituent SNPs is small, an additional resonance with a smaller amplitude appears at a frequency slightly above the intrinsic SPR of the SNP. This secondary SPR can be attributed to the space charge accumulated at the waist of the SND as shown on the left of Fig. 1. This observation is in qualitative agreement with prior results obtained for metallic nanodimers (4). As the overlap increases, both resonant modes blue shift while the weaker resonant mode at higher frequency diminishes in amplitude and eventually vanishes. Results of computation for the charge density, interior field and exterior field, and the total induced dipole moment are presented.

References

1. T. Shen, Z. Hu, X. Fu, Y. Li, and T. Wong, "Intensification of Terahertz Electric Field in a Semiconductor Nanodimer," *Proc. 39th IRMMW-THz Conf.*, Tucson, September 2014.
2. Z. Wang and T. Wong, "Field Dynamics in the Gap of a Semiconductor Nanodimer", Z. Wang and T. Wong, *Proc. IEEE NANO 2021*, Montreal, July, 2021.
3. T. Shen, M. Yan, and T. Wong, "Charge Polarization and Current Distribution in a Conductive Particle in the Rayleigh Region", *IEEE Trans. Antennas and Propagation*, v. 61, pp. 4229-4238, Aug. 2013.
4. I Romero, J Aizpurua, G.W. Bryant, F.J.G. De Abajo, "Plasmons in nearly touching metallic nanoparticles: singular response in the limit of touching dimers", *Optics Express*, v. 14, pp. 9988-9999, Oct. 2006.

Strong coupling between two-dimensional excitons and plasmonic nanocavities with a low exciton number

Xiulai Xu[1*]

[1]School of Physics, Peking University, Beijing, China
[*]corresponding author: xlxu@pku.edu.cn

Abstract: The interaction between two-dimensional excitons and plasmon nano-cavities has a potential to realize exciton-polaritons in quantum regime. Here, we report on a robust strong exciton-plasmon coupling with MoS_2 layers and bowtie nanocavities. With a proper exciton transition dipole moment, we estimated that the exciton number contributing to the coupling is reduced to 40, which is the lowest for this type of work so far. The interacting between 2D excitons and chiral nanocavities will be also discussed.

Atomically thin transition-metal dichalcogenides (TMDs) have been exploited widely for numerous photonic applications. One of the intriguing properties is the large exciton binding energy, providing the opportunity to realize exciton-polariton at room temperature when embedded in a microcavity. Plasmonic nanocavities with mode volumes beyond the diffraction limit make it possible to demonstrate strong coupling with a small number of excitons, which has rich applications in the research of quantum many-body phenomena, photon blockade with many emitters, cavity cooling and so on. However, achieving a robust plasmon−exciton coupling with nanocavities is still very challenging, such as the layer area is usually small in the conventional approaches and the two-dimensional excitons are hard to couple with the cavity modes effectively.

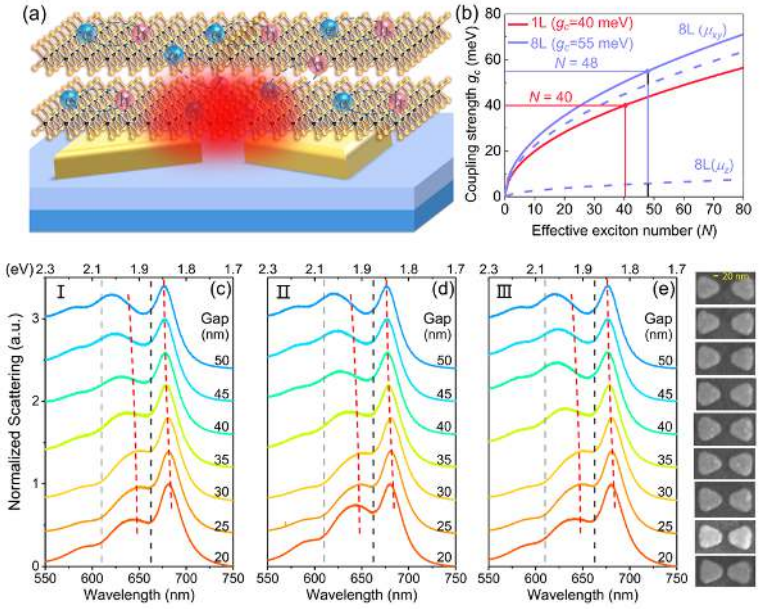


Figure 1. Strong coupling of individual bowtie resonators with layered MoS_2. (a) Schematic of the system with layered MoS_2 on a single gold bowtie resonator. (b) Coupling strength g_c as a function of the effective exciton number (N) for single-layer and eight-layer systems. (c)-(e) The dark-field scattering spectra of coupled hybrid systems of three groups with the same parameters. The image on the right shows the bowties with different gaps.

In our work, we obtained a robust strong exciton−plasmon coupling between the gap mode of a bowtie and the excitons in MoS_2 layers utilizing gold-assisted mechanical exfoliation and nondestructive wet transfer techniques. Due to the ultrasmall mode volume and strong in-plane field, the estimated effective exciton number contributing to the coupling is largely reduced. For estimating the exciton number contributing to the coupling, we corrected the value of exciton transition dipole moment in two-dimensional layer by quantum well method and absorbance measurements. With a corrected exciton transition dipole moment, the exciton numbers are extracted as being 40 for the case of a single layer and 48 for eight layers, which is the lowest for this type of work so far. Our work paves the way to realize strong exciton-plasmon coupling in quantum regime at room temperature.

References

1. Longlong Yang, Xin Xie, Jingnan Yang, Mengfei Xue, Shiyao Wu, Shan Xiao, Feilong Song, Jianchen Dang, Sibai Sun, Zhanchun Zuo, Jianing Chen, Yuan Huang, Xingjiang Zhou, Kuijuan Jin, Can Wang, and Xiulai Xu. Strong Light–Matter Interactions between Gap Plasmons and Two-Dimensional Excitons under Ambient Conditions in a Deterministic Way. Nano Letter, 22, 2177 (2022)

META 2023, PARIS - FRANCE, JULY 18 – 21, 2023

High performance silicon photonic devices with subwavelength metamaterials

P. Cheben[1], J.H. Schmid[1], W. N. Ye[2], D. Benedikovič[3], P. Ginel-Moreno[4], S. Khajavi[2], J.M. Luque-González[4], A. F. Hinestrosa[4], D. Pereira-Martín[4], A. Hadij-ElHouati[4], R. Korček[3], W. Fraser[2], A. Sánchez-Postigo[4], A. Ortega-Moñux[4], J. G. Wangüemert-Pérez[4], I. Molina-Fernández[4], R. Halir[4], D. Melati[5], C. Alonso-Ramos[5], D. González-Andrade[5], L. Vivien[5], J. Zhang[1], M. Milanizadeh[1], D.-X. Xu[1], Y. Grinberg[1], S. Janz[1], R. Cheriton[1], S. Wang[1], M. Vachon[1], M. Dado[3], R. Fernández de Cabo[6], and A. V. Velasco[6]

[1]National Research Council Canada, Ottawa, Canada
[2]Carleton University, Ottawa, Canada,
[3]Dept. Multimedia and Information-Communication Technologies, University of Zilina, Zilina, Slovakia
[4]University of Malaga, Malaga, Spain
[5]Centre de Nanosciences et de Nanotechnologies, CNRS, Universite Paris-Saclay, Palaiseau, France
[6]Instituto de Óptica Daza de Valdés, Consejo Superior de Investigaciones Científicas (CSIC), Madrid, Spain
[*]corresponding authors: Pavel.Cheben@nrc-cnrc.gc.ca and Winnie.Ye@carleton.ca

Abstract: Incorporating subwavelength grating metamaterials in nanophotonic waveguides has opened new degrees of freedom to control light propagation on a photonic chip. In this invited contribution, we will present our recent advances in development of subwavelength-engineered metamaterial devices for silicon photonics.

Subwavelength grating (SWG) waveguides and components comprising nanophotonic structures with dimensions on a scale below the wavelength of light, have enabled development of integrated photonic devices with unprecedented performance. Since their first demonstration in the early 2000's by NRC Canada [1,2], SWG metamaterial waveguides have attracted a strong research interest and are being extensively used as a powerful engineering tool for overcoming performance limitations of conventional integrated photonic devices [3,4,5]. Here we present an overview of our recent advances in this surging field and discuss how on-chip optical metamaterials improve the performance of state-of-the-art silicon photonics devices, including fiber-chip couplers, nanophotonic waveguides with controlled anisotropy, complex spectral filers and nanoantennas for Optical Phased Arrays (OPAs).

References

1. P. Cheben, D-X. Xu, S. Janz, and A. Densmore, "Subwavelength waveguide grating for mode conversion and light coupling in integrated optics," Opt. Express 14(11), pp. 4695-4702 (2006).
2. P. Cheben, P. J. Bock, J. H. Schmid, J. Lapointe, S. Janz, D.-X. Xu, A. Densmore, A. Delâge, B. Lamontagne, and T. J. Hall, "Refractive index engineering with subwavelength gratings for efficient microphotonic couplers and planar waveguide multiplexers," Opt. Lett. 35(15), pp. 2526-2528 (2010).
3. P. Cheben, R. Halir, J. H. Schmid, H. A. Atwater, and D. R. Smith, "Subwavelength integrated photonics," Nature 560(7720), 565–572 (2018).
4. R. Halir, A. Ortega-Moñux, D. Benedikovic, G. Z. Mashanovich, J. G. Wangüemert-Pérez, J. H. Schmid, Í. Molina-Fernández, and P. Cheben, "Subwavelength-Grating Metamaterial Structures for Silicon Photonic Devices," Proc. IEEE 106(12), 2144–2157 (2018).
5. J. M. Luque-González, A. Sánchez-Postigo, A. Hadij-ElHouati, A. Ortega-Moñux, J. G. Wangüemert-Pérez, J. H.

Schmid, P. Cheben, Í. Molina-Fernández, and R. Halir, "A review of silicon subwavelength gratings: building break-through devices with anisotropic metamaterials," Nanophotonics 10(11), pp. 2765–2797 (2021).

Color centers in ZnO nanowires

Carsten Ronning*

Institute of Solid State Physics, Friedrich Schiller University Jena, Helmholtzweg 3, 07743 Jena, Germany

*corresponding author: carsten.ronning@uni-jena.de

Abstract: Even though intrinsic semiconductor nanowires have already extraordinary optical properties, doping them with optically active impurities significantly expands the potpourri of photonic applications. This talk therefore supplies a snapshot of the most recent progress on the structural and optical properties of transition metal and rare earth element doped ZnO nanowires using ion beam implantation. Here, ion implantation is advantageous, as concurrent defect generation and diffusion upon subsequent annealing allows the formation of defect complexes. This scenario is in many cases even inevitable for the optical activation of the intra-shell luminescence of the implanted impurities, as density functional theory calculations demonstrate. Analysis of the prepared systems was partly performed by a new experimental setup installed at the synchrotron ESRF in Grenoble, which will be presented in detail and allows the detection of the carrier dynamics and the luminescence in respect to the elemental composition and the local environment of the color centers in single zinc oxide nanowires.

The author acknowledges the ESRF for the beamtime allocated on the beamline ID16B (experiment: MA-4444), and the financially supported by the German Federal Ministry of Education and Research under the streakXEOL project (Contact No. 05K19SJ2).

References

1. C.T. Plass, V. Bonino, M. Ritzer, L.R. Jäger, V.R. Bakaikoa, M. Hafermann, J. Segura-Ruiz, G. Martínez-Criado, C. Ronning “Spatially Resolved Dynamics of Cobalt Color Centers in ZnO Nanowires,” Advanced Science, 10, 2205304, 2023.

Extremely Localized Optical Modes and Direct Electro-optical Modulation

Xue-Wen Chen[*1,2]

[1]School of Physics and Wuhan National Laboratory for Optoelectronics, Huazhong University of Science and Technology, Wuhan, China.
[2]Wuhan Institute of Quantum Technology, Wuhan, China.
[*]corresponding author: xuewen_chen@hust.edu.cn

Abstract: Recent developments of nanoscience and nanofabrication techniques have enabled optical confinement into deep nanoscale or even atomic scale in space, offering exciting new opportunities. Here we discuss the physics to devise extremely localized optical modes that feature quantum-optical mode volumes down to one cubic nanometer. In particular, we present the approaches to overcome Landau damping to make the modes far-field accessible. Moreover, we introduce the concept of nanoscopic electron reservoir for direct electro-optical coupling that potentially allows energy-efficient ultrafast modulation.

In the past decade, the dramatic advents of nanomaterial science and precision nanofabrication techniques have been pushing the optical confinement from micro/nano scale down to deep nanoscale or even sub-nanoscale. These developments lead to a new frontier of nanophotonics, *i.e.*, extreme nanophotonics, that lies at the nexus of photonics, electronics, and nanoscience. It provides opportunities to simultaneously have extreme optical confinement and nanoscopic electronics as well as their interaction.

Firstly, we report the discovery and the rationale to devise bright single optical eigenmodes with mode volumes about 1 nm^3 and the lowest down to 0.5 nm^3[1]. Our discovery originates from a fundamentally new understanding of electromagnetic modes associated with extreme field localization. The discovery is possible because we develop an advanced theoretical platform capable of describing microscopic details of a macroscopic system. Moreover, we provide a strategy to resolve the longtime difficulty of huge loss occurring with extreme localization. The finding will enable to venture into a new regime of optical physics as the optical modes could now approach the scale of electron wave functions in an atom or a molecule.

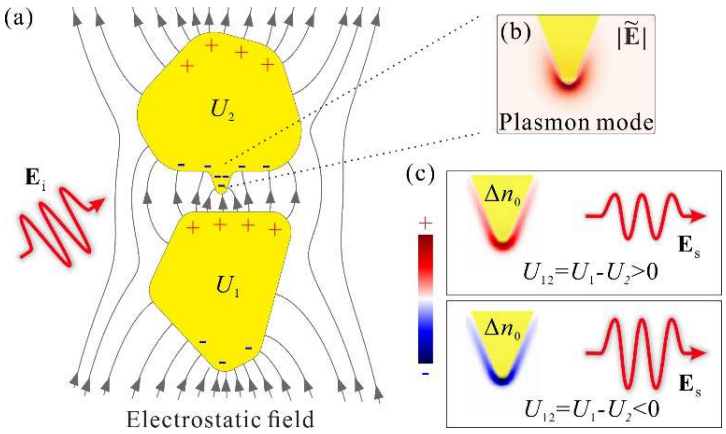


Fig. 1 Schematic illustration of an electro-optic modulation via a nanoscopic electron reservoir (NER) situated on a metal host. The details can be found in Ref. [2].

Secondly, we discuss the interaction of the extremely localized optical modes with the static electric field, which, as shown in Fig. 1, will lead to the direct electrical tuning of the localized modes and its far-field response [2]. Direct electrical tuning of localized plasmons at optical frequencies boasts the fascinating prospects of being ultrafast and energy efficient and having an ultrasmall footprint. However, the prospects are obscured by the grand challenge of effectively modulating the very large number of conduction electrons in three dimensional metallic structures. Here we propose the concept of nanoscopic electron reservoir (NER) for direct electro plasmonic and electro-optic modulation. A NER is a few-to-ten-nanometer size metal feature on a metal host and supports a localized plasmon mode. We provide a general guideline to construct highly electrically susceptible NERs and theoretically demonstrate pronounced direct electrical tuning of the plasmon mode by exploiting the nonclassical effects of conduction electrons with the help of quasinormal mode analysis [3]. Moreover, we show the electro-plasmonic tuning can be efficiently translated into modulation of optical scattering by utilizing the antenna effect of the metal host for the NER. Our calculations show it is possible to have electro-optic modulation at a speed of 20 fs/bit and with an energy consumption rate of 100 atto-joule/bit. Our work extends the landscape of electro plasmonic modulation and opens appealing new opportunities for quantum plasmonics.

We acknowledge partial financial support from the National Natural Science Foundation of China (Grants No. 9215011 and No. 11874166).

References

1. W. Li, Q. Zhou, P. Zhang, X.-W. Chen, “Bright optical eigenmode of 1 nm^3 mode volume”, *Phys. Rev. Lett.* 126, 257401 (2021).
2. W. Li, Q. Zhou, P. Zhang, X.-W. Chen, “Direct Electro Plasmonic and Optic Modulation via a Nanoscopic Electron Reservoir”, *Phys. Rev. Lett.* 128, 217401 (2022).
3. Q. Zhou, P. Zhang, X.-W. Chen, “General framework of canonical quasinormal mode analysis for extreme nano-optics”, *Phys. Rev. Lett.* 127, 267401 (2021).

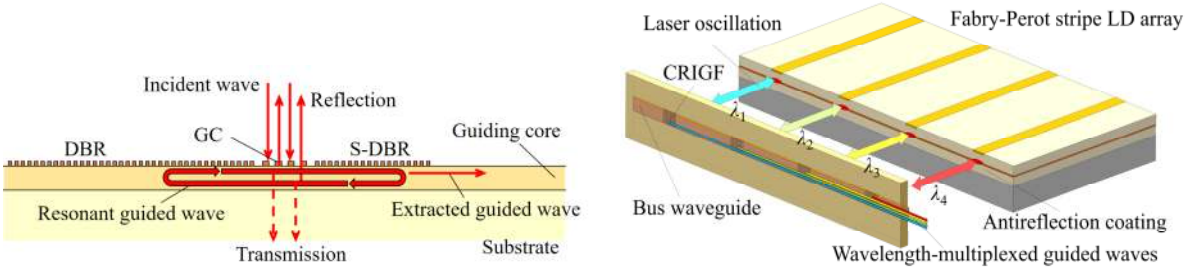
External Laser Mirror for Oscillation Wavelength Stabilization and Waveguide Input Coupling

J. Inoue[1*], A. Watanabe[1], K. Ozawa[1], K. Kintaka[2], and S. Ura[1]

[1]Kyoto Institute of Technology, Japan
[2]National Institute of Advanced Industrial Science and Technology, Japan
[*]corresponding author: inoue@kit.ac.jp

Abstract: The potential application of guided-mode resonance devices as an external laser mirror with oscillation wavelength stabilization and waveguide input coupling functions that is a key component for constructing a future ultra-compact multi-wavelength light source is discussed.

A guided-mode resonance (GMR) filter consists of a subwavelength surface grating integrated in a thin-film optical waveguide on a transparent substrate, and shows a narrowband reflection spectrum for an incident free-space wave [1]. GMR filters have much attention for use as external mirrors of fiber or waveguide lasers due to their advantages of fabrication convenience, design flexibility, polarization selectivity, and so on. However, a normal GMR filter needs a sub-millimeter-size aperture for nanometer-order reflection bandwidth. We proposed a cavity-resonator-integrated GMR filter (CRIGF) for aperture miniaturization [2]. Figure 1(a) shows the basic configuration of the CRIGF. It has a micro-aperture grating coupler (GC) in a waveguide cavity resonator composed of two distributed Bragg reflectors (DBRs). Only at the resonance wavelength of the waveguide resonator, a vertically incident wave is coupled by the GC to the resonant guided wave, and the substrate radiation from the guided wave cancels out the transmission, resulting in a strong reflection. In addition, by shortening the coupling length of one of the DBRs and thereby reducing its reflectance, the excited guided wave can be extracted from the CRIGF through the shortened DBR (S-DBR).



(a) (b)

Figure 1. (a) Schematic cross-sectional view of CRIGF. (b) Concept image of ultra-compact multi-wavelength light source based on CRIGFs and stripe LD array.

Because of this multifunctionality of narrowband reflection and guided wave extraction, CRIGF is expected to serve as an external laser mirror which stabilizes oscillation wavelength to the reflection wavelength and couples the laser light to the waveguide. In addition, since the resonance wavelength of CRIGF is determined by the cavity length, integration of CRIGFs of different wavelengths will enable wavelength multiplexing. The authors have proposed and investigated an ultra-compact multi-wavelength light source without separate multiplexers, such as an arrayed waveguide grating or a multimode interference coupler by combining a stripe laser diodes (LDs) array and different CRIGFs integrated on a bus waveguide as shown in Figure 1(b). The

lasing wavelength is determined by a reflection peak of the CRIGF because antireflection coating is made on the facing end of the LD. However, there are several issues to the practical application of this multi-wavelength light source. In this presentation, our results on fundamental study to solve them are introduced.

One of key issues is the optimization of CRIGF reflectance for giving the highest electrical-optical power conversion efficiency. Lower reflectance of S-DBR for higher efficiency of a guided-wave extraction gives lower vertical reflection of the CRIGF, resulting in higher threshold current and lower differential efficiency of the stripe LD. The S-DBR reflectance needs to be optimized to maximize the conversion efficiency from the input electrical power to the multiplexed optical power. Another issue is DBR bandwidth limiting the wavelength spacing. The guided wave should pass through other CRIGFs to reach an output waveguide. The bandwidth of the DBR reflection is set to be narrower than the wavelength spacing in order to avoid undesirable reflection of other multiplexed signals. Four CRIGFs with a wavelength spacing of 15 nm on the same waveguide were designed and fabricated. Simultaneous guided wave extraction with vertical reflection and the possibility of four-wavelength multiplexing were experimentally confirmed [3].

The diameter of an incident beam to the CRIGF must coincide with the aperture size to obtain high reflectance. The aperture size will be several microns at least even though it is much smaller than normal GMR filters. Meanwhile, a field diameter of the guided mode of an LD waveguide is submicron. We cannot expect high-efficiency direct butt coupling of the LD to the CRIGF and need some beam-size conversion. We proposed a focusing CRIGF (F-CRIGF) for reflecting and focusing a diverging wave back to the divergence point. [4]. A focusing GC (FGC) and a high-reflection substrate are used in an F-CRIGF instead of the GC and a transparent substrate, respectively. An F-CRIGF can retroreflect the emitted light from the LD. As a result, we can avoid the unpreferable integration of additional lens. An F-CRIGF was designed and fabricated not only for narrowband retroreflection but also for guided wave extraction. An external cavity laser was constructed by combining this F-CRIGF and a gain chip, and the simultaneous realization of wavelength stabilized laser oscillation and input coupling was demonstrated [5].

This work was supported in part by JSPS KAKENHI Grant Number JP19K04522. A part of this work was supported by Kyoto University Nano Technology Hub in “Nanotechnology Platform Project” sponsored by the Ministry of Education, Culture, Sports, Science and Technology (MEXT), Japan. The authors would like to express sincere thanks to Dr. T. Sugawara, Mr. T. Matsudaira, and Mr. K. Sato in Shincron Co., Ltd. who deposited the multilayer on a substrate.

References

1. Magnusson, R. and S. S. Wang, “New principle for optical filters,” Appl. Phys. Lett., Vol. 61, No. 9, 1022–1024, 1992.
2. Kintaka, K., T. Majima, J. Inoue, K. Hatanaka, J. Nishii, and S. Ura, “Cavity-resonator-integrated guided-mode resonance filter for aperture miniaturization,” Opt. Express, Vol. 20, No. 2, 1444–1449, 2012.
3. Inoue, J., A. Tsuji, K. Kintaka, K. Nishio, and S. Ura, “Wavelength division multiplexer based on cavity-resonator-integrated guided-mode resonance filters for a compact multiwavelength light source,” Opt. Express, Vol. 26, No. 3, 2212–2219, 2018.
4. Inoue, J., T. Kusuura, R. Ueda, K. Kintaka, and S. Ura, “Narrowband focusing retroreflector with a thin-film structure,” Appl. Phys. Express, Vol. 14, No. 8, 082003, 2021.
5. Ozawa, K., A. Taniguchi, R. Ueda, S. Teranishi, A. Watanabe, J. Inoue, K. Kintaka, and S. Ura, “Integrated Photonic Device for Wavelength-Stable Laser Oscillation and Simultaneous Input Coupling,” IEEE Photonics J., Vol. 15, No. 1, 6600506, 2023.

META 2023, PARIS - FRANCE, JULY 18 – 21, 2023

Discovering new high-refractive-index dielectric materials

Søren Raza
Department of Physics, Technical University of Denmark, Fysikvej, DK-2800 Kongens Lyngby, Denmark

E-mail: sraz@dtu.dk

Abstract: Dielectric materials with a high refractive index are key in the design of optical nanoantennas and metasurfaces. Here, we use a high-throughput screening method combined with optical Mie theory to evaluate the performance of more than 2000 materials and discover a new promising material, boron phosphide, which has so far been elusive. We prepare boron phosphide nanoparticles and experimentally demonstrate that they support Mie resonances across the visible and the near ultraviolet using both optical measurements and electron energy-loss spectroscopy.

Optical metasurfaces and nanoantennas based on high-refractive-index materials offer efficient manipulation of light on the nanoscale due to low optical losses and their ability to support both magnetic- and electric-type Mie resonances.[1] The development of all-dielectric nanophotonics has been largely driven by the availability of just a few high-index materials, such as silicon, gallium phosphide, and titanium dioxide, which offer low-loss operation in most of the visible spectral range and where lithographic processing has been well established.[2] For applications in the important ultraviolet spectral range, the availability of high-index materials is even more scarce. Identifying new optical materials that may outperform the ones currently available, offer new functionalities or give access to other spectral regions is critical for many applications.

In this work,[3] we discover new high-index materials using high-throughput screening based on density functional theory (DFT). Starting from a library of more than 2000 thermodynamically stable binary materials, we develop a workflow to identify isotropic high-index dielectric materials across a spectral range spanning from mid infrared to the deep ultraviolet. The wavelength-dependent complex refractive indices of these materials are calculated within the random phase approximation and used as input for Mie scattering calculations to evaluate their optical performance. Our methodology identifies all of the known high-index materials as well as other materials, which have been less investigated. In particular, we identify boron phosphide (BP), which offers a refractive index above 3 with very low absorption losses in a spectral range spanning from the infrared to the near ultraviolet.

To support our computational discovery, we prepare BP nanoparticles and experimentally demonstrate that they support Mie resonances across the visible and ultraviolet spectral ranges using dark-field optical measurements and electron energy-loss spectroscopy. The Mie resonance energies can be tuned with particle size. We also demonstrate a laser reshaping method to realize spherical BP nanoparticles, which host multiple Mie resonances in quantitative agreement with full-field optical simulations. Our experimental measurements of Mie resonances in BP nanoparticles demonstrate the potential of high-index BP across a broad spectral range as well as validate the refractive index obtained from DFT calculations. Besides the discovery of BP, we believe that our high-throughput screening results provide an overview of existing materials as well as a pathway for realizing new high-index materials.

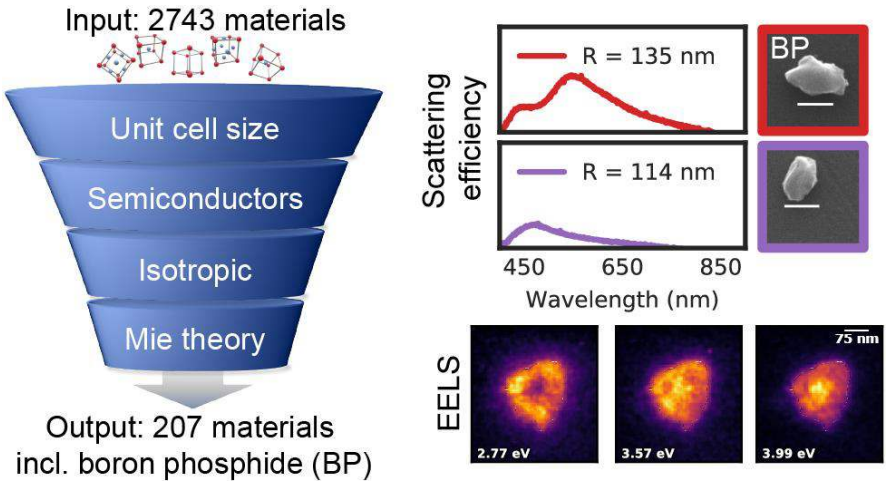


Fig. 1. High-throughput screening of a large library of materials identifies many high-refractive-index materials across a broad spectral range. Boron phosphide (BP) appears particularly promising due to its refractive index above 3 in a spectral range covering the visible and reaching the near ultraviolet. BP nanoparticles are prepared and their scattering properties are measured using far-field dark-field spectroscopy and near-field electron energy-loss spectroscopy (EELS). Combined with full-field optical simulations, these measurements demonstrate that BP nanoparticles support Mie resonances at visible and ultraviolet energies.

References

1. Kuznetsov, A. I., Miroshnichenko, A. E., Brongersma, M. L., Kivshar, Y. S. & Luk'yanchuk, B. Optically resonant dielectric nanostructures. *Science* **354**, aag2472 (2016).
2. Baranov, D. G. *et al.* All-dielectric nanophotonics: the quest for better materials and fabrication techniques. *Optica* **4**, 814 (2017).
3. Svendsen, M. K. *et al.* Computational Discovery and Experimental Demonstration of Boron Phosphide Ultraviolet Nanoresonators. *Adv. Opt. Mater.* **2200422**, 2200422 (2022).

META 2023, PARIS - FRANCE, JULY 18 – 21, 2023

Heavily doped semiconductors: a platform for integrated nonlinear plasmonics

Federico De Luca[1,2,3], Michele Ortolani[4], Huatian Hu[1], Cristian Ciracì[1,*]

[1]Center for Biomolecular Nanotechnologies, Istituto Italiano di Tecnologia, IT-730101 Arnesano, Italy
[2]Dipartimento di Matematica e Fisica "E. De Giorgi," Università del Salento, IT-73100 Lecce, Italy
[3]Photonics Initiative, Advanced Science Research Center, City University of New York, New York, NY 10031, USA.
[4]Department of Physics, Sapienza University of Rome, IT-00185 Rome, Italy
[*]corresponding author: cristian.ciraci@iit.it

Abstract: In this talk we numerically investigate heavily doped semiconductors as a platform for integrated nonlinear plasmonics at mid-infrared frequencies. We study free-electron nonlinearities and use surface charge density modulation to control and enhance the nonlinear response.

The control and the concentration of light at subwavelength scales are of extreme importance for the realization of integrated optical technologies, especially to reach operational efficiencies in devices based on nonlinear optical effects. In this context, the study of light interaction with free electrons (FEs), i.e. plasmonics, in materials characterized by a high carriers density has a central role. Notoriously, noble metals have been the main material choice for plasmonic devices in the visible spectrum for many years. Heavily doped semiconductors (i.e. with charge densities $n_0 \sim 10^{19}$ - 10^{20} cm^{-3}), on the other hand, have recently emerged as alternative materials for plasmonics in the near-infrared (NIR), i.e. $0.8 < \lambda < 2$ μm, and in the mid-infrared (MIR), i.e. $2 < \lambda < 20$ μm [1]. Being low-loss high-quality materials that can be compatible with standard microelectronics fabrication processes, and being their optical response tunable through electrical or optical doping, heavily doped semiconductors offer a unique perspective for integrated optical devices in the NIR and in the MIR. [2].

In this talk we show that FE nonlinearities could be up to two orders of magnitude larger than conventional semiconductor lattice nonlinearities [3,4]. We use a hydrodynamic description that includes terms up to the third order, usually negligible for noble metals. Within the hydrodynamic formalism, the third-order response, expressed through the third-order polarization vector is inversely proportional to the squared equilibrium charge density, i.e. $\mathbf{P}_{\mathrm{NL}}^{(3)} \propto \frac{1}{n_0^2}$. Indeed, doped semiconductors with a plasma wavelength in the MIR have a charge density ($n_0 \sim 10^{19}$ cm^{-3}) much lower than noble metals, such as gold ($n_0 \sim 10^{22}$ cm^{-3}). Hence, FE nonlinearites may grow as much as six orders of magnitude, overcoming by far the contributions originating in the crystal lattice nonlinear susceptibility $\chi^{(3)}$, which instead represents the dominant third-order nonlinear source in gold due to the high concentration of charge carriers. Moreover, the nonlinear active volumes are expected to increase in semiconductors due to their smaller effective masses [3].

Finally, we consider modifications of the charge density at the semiconductor surface obtained through the application of an external bias, i.e. by means of field-effect modulation (Fig. 1). We present a model for describing the influence of surface charge depletion on FE nonlinearities and make quantitative predictions about the role of field-effect modulation for the control of the optical nonlinear response of heavily doped semiconductors [5]. This technique may provide the unique ability to externally and dynamically modulate the nonlinear coefficients of heavily doped semiconductors by a simple setting of DC electric potential levels.

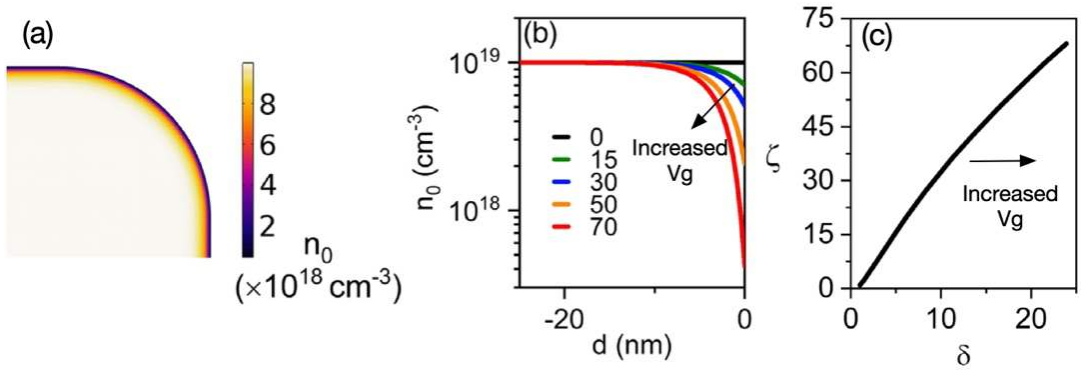


Fig. 1 Effects of surface charge depletion on the FE THG efficiency η of a doped InP semi-infinite grating: (a) charge density distribution along the contour of the grooves. (b) equilibrium charge density as a function of the distance *d* from the surface of the slab for different levels of modulation (in V/μm); (c) enhancement factors ζ as a function of the depletion factor δ in correspondence of the peak efficiencies λ_{FF} = 12.2 μm.

M.O., H.H., and C.C. acknowledge funding from the European Innovation Council through its Horizon Europe program with Grant Agreement No. 101046329.

References

1. M. P. Fischer, *et al*., *"Plasmonic mid-infrared third harmonic generation in germanium nanoantennas,"* Light: Science & Applications, vol. 7, 106, 2018.
2. T. Taliercio, P. Biagioni, *"Semiconductor infrared plasmonics,"* Nanophotonics, vol. 8, 949, 2019.
3. F. De Luca, M. Ortolani, C. Ciracì, *"Free electron nonlinearities in heavily doped semiconductors plasmonics,"* Phys. Rev. B, vol. 103, 115305, 2021.
4. F. De Luca, M. Ortolani, C. Ciracì, *"Free electron harmonic generation in heavily doped semiconductors: the role of the materials properties,"* EPJ Applied Metamaterials, vol. 9, 13, 2022.
5. F. De Luca, C. Ciracì, *"Impact of Surface Charge Depletion on the Free Electron Nonlinear Response of Heavily Doped Semiconductors,"* Phys. Rev. Lett., vol. 129, 123902, 2022.

META 2023, PARIS - FRANCE, JULY 18 – 21, 2023

Symmetry, connectivity, and topology in photonic crystals

Thomas Christensen[1]

[1] Department of Electrical and Photonics Engineering, Technical University of Denmark, Denmark
[*] thomas@dtu.dk

Abstract: Symmetry imposes strong constraints on the frequency dispersion and topology of photonic crystal bands. I will describe several interesting consequences of these constraints, highlighting implications for the connectivity of photonic bands, the prevalence of photonic topology, and the outlook for having frequency-isolated topological degeneracies at high-symmetry points in the Brillouin zone.

The transverse nature of photons produces a polarization singularity at zero frequency which distinguishes the lowest bands of photonic crystals from those of other quasiparticles. I will discuss our recent work [1] on how symmetry, topology, and this polarization singularity lead to constraints on where the first photonic band gap can be opened. These constraints can be solved by a symmetry-based framework that allows determining the minimum connectivity of bands below the first photonic gap as well as the any associated symmetry-identifiable topology. By systematically examining the topology of all possible minimal configurations, we find a new, uniquely photonic topological effect which obstructs symmetry-allowed gap-openings by requiring the presence of topological nodal lines.

The framework developed to answer these questions allows the whole-sale application of recent methods from electronic topology – known as symmetry indicators or topological quantum chemistry – to the photonic context; I will highlight a few interesting examples of the opportunities that this brings, including an assessment of the prevalence of topology in two-dimensional photonic crystals and whether frequency-isolated Weyl points can exist at high-symmetry points of the Brillouin zone.

References

1. T. Christensen, H.C. Po, J.D. Joannopoulos, & M. Soljačić, “Location and Topology of the Fundamental Gap in Photonic Crystals”, Phys. Rev. X **12**, 021066 (2022).

Chemical interface damping by electrochemical oxidation of gold

M. Pfeiffer[1], **M. Eich**[1,2], **A. Yu. Petrov**[1,2*]

[1]Institute of Optical and Electronic Materials, Hamburg University of Technology, Germany
[2]Institute of Photoelectrochemistry, Helmholtz-Zentrum Hereon, Geesthacht, Germany
[*]corresponding author: a.petrov@tuhh.de

Abstract: Chemical interface damping (CID) is a change of the effective collision frequency of electrons in metal due to chemical change of the metal interface. We show that electrochemical oxidation of gold leads to CID effect. The increase in collision frequency is determined by in-situ ellipsometric measurements during oxidation of flat single crystal and polycrystalline gold films.

Chemistry at the surface of metals can change the effective collision frequency of electrons in a free electron model determining the dielectric properties of metals. This effect is widely discussed. The increase in effective collision frequency was observed in plasmonic nanostructures due to thiol [1] and metal-oxide [2] coatings. Different explanations for the underlining physical effect exist, such as additional roughness seen by electrons at the surface or temporal electron transfer into states at the surface [3].

Here we investigate the CID effect on flat single crystal gold films due to electrochemical surface oxidation. We conduct in-situ measurement of ellipsometric data of the sample inside an electrochemical cell. The Ψ and Δ measured by ellipsometric method correspond to the ratio of s and p polarized light reflection and the phase shift between them and are used to fit a layer stack of gold and gold oxide with varying collision frequency as well as oxide thickness. Previously similar investigations were done disregarding the increase in collision frequency of gold; the change of reflection was attributed solely to oxide coating [4]. Including the change in collision frequency in the consideration we can clearly demonstrate both increase in the oxide thickness and increase in collision frequency. Important is also the fact, that at some point further oxide growth does not lead to further increase of collision frequency as the structure of the interface between gold and oxide does not change any more. This is an additional confirmation for the ellipsometric model that we use.

The collision frequency increase in the order of 10 meV observed for bulk gold can be recalculated in terms of electron mean free path, which allows the comparison to the results obtained with thiols and other oxides on gold nanoparticles. We show that electrochemical gold oxidation provides a stronger effect on collision frequency than coatings. The results of these ellipsometric study can be used to design electrochemically tunable gold nanostructures.

References

1. B. Foerster, V. A. Spata, E. A. Carter, C. Sönnichsen, and S. Link, “Plasmon damping depends on the chemical nature of the nanoparticle interface,” Sci. Adv., Vol. 5, No. 3, p. eaav0704, 2019
2. B. Foerster, M. Hartelt, S. S. E. Collins, M. Aeschlimann, S. Link, and C. Sönnichsen, “Interfacial states cause equal decay of plasmons and hot electrons at gold-metal oxide interfaces,” Nano Lett., Vol. 20, No. 5, pp. 3338–3343, 2020
3. J. B. Khurgin, A. Petrov, M. Eich, and A. V. Uskov, “Direct Plasmonic Excitation of the Hybridized Surface States in Metal Nanoparticles,” ACS Photonics, Vol. 8, No. 7, pp. 2041–2049, 2021
4. Y.-T. Kim, R. W. Collins, and K. Vedam, “Fast scanning spectroelectrochemical ellipsometry: In-situ characterization of gold oxide,” Surf. Sci., vol. 233, no. 3, pp. 341–350, 1990

META 2023, PARIS - FRANCE, JULY 18 – 21, 2023

Reconfiguring electric and magnetic resonances of individual meta-atoms using phase-change materials

Lukas Conrads[1], Andreas Heßler[1]

and Thomas Taubner[1,*]

[1] I. Institute of Physics (IA), RWTH Aachen University, Germany
[*]corresponding author: taubner@physik.rwth-aachen.de

Abstract: We employ Phase-Change Materials (PCMs) for local addressing of individual meta-atoms in both metallic and low-loss dielectric metasurfaces, with special emphasis on tuning electric dipole (ED) and magnetic dipole (MD) resonances simultaneously or individually. Individual control of the electric and magnetic dipole resonances of split-ring resonators (SRRs) is demonstrated by locally changing the refractive index of aluminum SRRs in the corresponding hotspots of the antenna resonances and by direct writing and reconfiguration of SRRs in the new plasmonic PCM In_3SbTe_2.

For miniaturized active nanophotonic components, resonance tuning of nanoantennas is a key ingredient. Phase-change materials (PCMs) provide a switchable dielectric environment for resonant nanostructures, altering their resonance wavelengths in a non-volatile, reversible way. While PCMs usually exhibit a high optical contrast between their amorphous and crystalline phases [1], the "plasmonic" PCM In_3SbTe_2 (IST) has optical properties which change from dielectric to metallic upon crystallization in the whole infrared spectral range [2]. Resonant metallic and dielectric nanostructures (meta-atoms) can host a variety of different modes, ranging from electric dipole (ED) over electric quadrupole to even magnetic dipole (MD) modes etc. The full control over each resonance mode individually was not yet been obtained, although this could dramatically improve the design freedom of individually addressable meta-atoms and allow for post-fabrication fine-tuning.

Here, I will present our recent progress on the local optical addressing of individual meta-atoms in metallic [3] and low-loss dielectric [4] metasurfaces, with special emphasis on tuning ED and MD resonances either simultaneously or individually. While a homogeneous change of the refractive index around a meta-atom shifts both ED and MD in a similar way [4], the controlled optical addressing or modification within each meta-atom unit cell allows to specifically tune ED and MD separately.
For example, PCM-covered aluminum split-ring resonators (SRRs) are switched locally to tune both the electric dipole resonances as well as the magnetic dipole resonances. By selectively switching the PCM at different hotspots of the SRRs, both resonances can be tuned individually. The field enhancement in the magnetic resonance allows continuous tuning of surface-enhanced infrared absorption (SEIRA) of native SiO_2 [5]. Exploiting the "plasmonic" PCM IST, split-ring resonators (SRRs) are directly optically written and reconfigured in their arm size to continuously tune their magnetic dipole resonances over a range of 2.4 µm without changing their electric dipole resonances [6].

Our concepts are well-suited for rapid prototyping of ultrathin, tunable, plasmonic devices for infrared nanophotonics, telecommunications or (bio)sensing, and fine-tuning functionalities of metasurfaces on a meta-atom level by locally changing the refractive index at the hotspots of the selected antennas.

Acknowledgements

The authors acknowledge support by the Deutsche Forschungsgemeinschaft (DFG No. TA848/7-1 & SFB 917 “Nanoswitches”).

References

1. Wuttig, M. et al., “Phase-change materials for non-volatile photonic applications” *Nat. Photon*., **11**, 465–476 (2017)
2. Heßler, A. et al., “In_3SbTe_2 as a programmable nanophotonics material platform for the infrared” *Nat. Commun.* **12**, 924 (2021)
3. Michel, A.-K. U. et al., “Advanced optical programming of individual meta-atoms beyond the effective medium approach”, *Adv. Mat.* **31**, 1901033 (2019)
4. Leitis, A. et al., “All-dielectric programmable Huygens’ metasurfaces”, *Adv. Func. Mat.* **30**, 1910259 (2020).
5. Conrads, L. et al., “Infrared resonance tailoring of individual split-ring resonators with phase-change materials by locally changing the dielectric surrounding of the antenna hotspots” (submitted) (2023)
6. Heßler, A., Conrads, L. et al., “Reconfiguring Magnetic Infrared Resonances with the Plasmonic Phase-Change Material In_3SbTe_2” *ACS Photonics* **9**, 5 (2022)

META 2023, PARIS - FRANCE, JULY 18 – 21, 2023

3D nanoprinting using light

Maria Farsari[1, *]

[1]FORTH/IESL, N. Plastira 100, Heraklion, 70013, Greece
[*]mfarsari@iesl.forth.gr

Abstract:

Multiphoton Lithography is a laser-based additive manufacturing technique which allows fabrication with resolution down to a few tens of nanometres. Based on nonlinear absorption, Multiphoton Lithography has unique capabilities that no-other technique can provide. It has been implemented with a variety of materials and several components and devices have been fabricated such as metamaterials, biomedical devices, photocatalytic systems and mechanical models

The unique capability of Multiphoton Lithography lies in that it allows the fabrication of computer-designed, fully functional 3D devices. In this talk, I summarize the principles of microfabrication, and present recent research in materials processing and functionalization of 3D structures. Finally, I discuss future applications and prospects for the technology.

Plasmon-enhanced nano-spectroscopies for highly sensitive biomolecular detection

T. Yano[1, 2*], R. Kato[1, 2], and T. Tanaka[1, 2]

[1]Institute of Post-LED Photonics, Tokushima University, Tokushima, Japan
[2]Innovative Photon Manipulation Research Team & Metamaterials Laboratory, RIKEN, Saitama, Japan
[*]corresponding author: yano.takaaki@tokushima-u.ac.jp

Optical biosensing has attracted considerable attention due to its capability of highly sensitive molecular detection and analysis. We have been developing a variety of nanostructure-enhanced biomolecular spectroscopies in combination with plasmonics and metamaterials where optical nanostructures play a crucial role in enhancing various optical signals (visible absorption/reflection, Raman scattering, fluorescence, and infrared absorption) from targeting biomolecules. Here in this talk, we focus on our recent works on high-sensitivity and super-resolution optical sensing and imaging for biomedical analysis [1-7].

The first topic is plasmonic detection of single biomolecules. A nanometric gap between a silver tip and gold substrate enabled us to enhance and detect Raman scattering from a single gold-binding peptides (GBP) which exhibited specific binding affinity to gold surface, resulting in spectroscopic elucidation of the binding sites and mechanisms. The second topic is nanoparticle-enhanced surface plasmon resonance (SPR) sensing of coronavirus (SARS-CoV-2). A crucial plasmonic role in significantly enhancing the limit of detection (LOD) is revealed for exceptionally large gold nanoparticles with diameters of hundreds of nm. SPR enhanced by these large nanoparticles lowered the LOD of SARS-CoV-2 N protein to 85 fM, resulting in the highest SPR detection sensitivity ever obtained for SARS-CoV-2 N protein. We also developed a digital SPR biosensing technique based on plasmon hybridization, which improved the SPR sensitivity down to sub-fM level. The last topic is plasmon-enhanced fluorescence spectroscopy using polymer-coated silver nanoparticles. The polymer layer coated was adequately thin to efficiently achieve plasmonic enhancement of fluorescence and also thick enough to effectively suppress quenching of fluorescence, achieving a huge net enhancement of fluorescence. The polymer-coated plasmonic nanoparticles are a promising platform for demonstrating highly sensitive biosensing for medical diagnostics.

References [our recent publications on plasmon-enhanced nanospectroscopies]:

[1] *Sci. Rep.* **12**, 1060 (2022). [2] *Sci. Adv.* **8**, eabo4021 (2022). [3] *ACS Omega*, **5**, 4286 (2022). [4] *Vib. Spectro.* **118**, 103333 (2022). [5] *Nanophotonics*, **11**, 2541 (2022). [6] *Opt. Continuum*, **1**, 565 (2022). [7] *Anal. Sci.* **38**, 1497 (2022).

META 2023, PARIS - FRANCE, JULY 18 – 21, 2023

Hybrid bullseye-nanotip antennas for bright directional single photon sources

H. Abudayyeh[1], A. Mildner[2,3], J. Fulmes[2,3], R. Jäger[3,4], D. Liran[1], B. Lubotzky[1], L. Lüder[2,3], F. Laible[2,3], A. J. Meixner[3,4], D. P. Kern[2,3], R. Rapaport[1], M. Fleischer[2,3*]

[1]Racah Institute of Physics, Center for Nanoscience and Nanotechnology, and Applied Physics Department, The Hebrew University of Jerusalem, Jerusalem 9190401, Israel
[2]Institute for Applied Physics, Eberhard Karls University Tübingen, Tübingen Germany
[3]Center for Light-Matter-Interaction, Sensors and Analytics LISA+, Eberhard Karls University Tübingen, Germany
[4]Institute of Physical and Theoretical Chemistry, Eberhard Karls University Tübingen, Tübingen Germany
[*]corresponding author: monika.fleischer@uni-tuebingen.de

Abstract: Single-photon sources that form the basis for various quantum applications have seen fast development. The deterministic generation of single photons can amongst others be realized by semiconductor quantum dots. To achieve efficient sources, parameters such as the brightness, photon rates, directionality, room-temperature stability, etc. need to be optimized. To modify the emission properties of individual quantum dots, they can be coupled to nano-antennas. Here a design that enables bright room-temperature quantum light sources is demonstrated.

The authors independently developed techniques for enhancing the directionality of quantum dot-based single photon sources by positioning single nanocrystals at the center of concentric Bragg antennas [1.-3.] and for enhancing emission rates via coupling to a nanocone antenna [4., 5.]. In the presented configuration, both approaches are combined, see Figure 1 [6.]. The Bragg antennas are numerically optimized for their collimation effect and narrow emission angles, which allow for high collection efficiencies even in systems with low numerical apertures. The attachment to the apex of a nanotip leads to a reduction of the lifetime and consequently to a brightness enhancement.

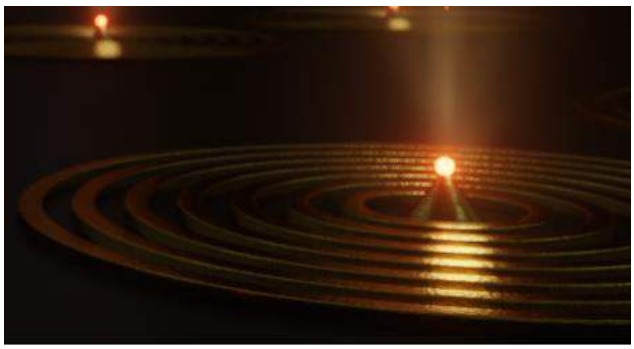


Figure 1: Schematic illustration of a bullseye antenna with a central nanocone to which a single quantum dot is attached, resulting in directional emission [courtesy of L. Lüder].

In the presentation, the design considerations for the overall hybrid bullseye-nanocone-nanoemitter device will be outlined. The geometry is illustrated by scanning electron microscopy images, and the optical performance is evaluated in terms of the projected photon rates.

Support by COST (European Cooperation in Science and Technology) Action MP1302, the German Excellence Initiative, the Israeli Innovation Authority: Quantum Communication Consortium, and the Center for Nanoscience and Nanotechnology at the Hebrew University of Jerusalem is gratefully acknowledged.

References

1. Harats, M. G., Livneh, N., Zaiats, G., Yochelis, S., Paltiel, Y., Lifshitz, E., Rapaport, R., "Full spectral and angular characterization of highly directional emission from nanocrystal quantum dots positioned on circular plasmonic lenses," Nano Lett., 14, 5766–5771, 2014.
2. Harats, M. G., Livneh, N., Rapaport, R., "Design, fabrication and characterization of a hybrid metal-dielectric nanoantenna with a single nanocrystal for directional single photon emission," Opt. Mater. Express, 7, 834, 2017.
3. Abudayyeh, H., Lubotzky, B., Blake, A., Wang, J., Majumder, S., Hu, Z., Kim, Y., Htoon, H., Bose, R., Malko, A. V., Hollingsworth, J. A., Rapaport, R., "Single photon sources with near unity collection efficiencies by deterministic placement of quantum dots in nanoantennas," APL Photonics, 6, 036109, 2021.
4. Fulmes, J., Jäger, R., Bräuer, A., Schäfer, C., Jäger, S., Gollmer, D. A., Horrer, A., Nadler, E., Chassé, T., Zhang, D., Meixner, A. J., Kern, D. P., Fleischer, M., „Self-aligned placement and detection of quantum dots on the tips of individual conical plasmonic nanostructures," Nanoscale, 7, 14691-14696, 2015.
5. Meixner, A.J., Jäger, R., Jäger, S., Bräuer, A., Scherzinger, K., Fulmes, J., zur Oven Krockhaus, S., Gollmer, D. A., Kern, D. P., Fleischer, M., „Coupling single quantum dots to plasmonic nanocones: optical properties," Faraday Discuss., 184, 321-337, 2015.
6. Abudayyeh, H., Mildner, A., Liran, D., Lubotzky, B., Lüder, L., Fleischer, M., Rapaport, R., „Overcoming the rate-directionality tradeoff: A room-temperature ultrabright quantum light source", ACS Nano, 15, 17384-1791, 2021.

META 2023, PARIS - FRANCE, JULY 18 – 21, 2023

Proximity Induced Chiral Quantum Light Generation in Strain Engineered WSe_2/MPX_3 Heterostructures

Han Htoon
Center for Integrated Nanotechnologies, Materials Physics and Applications Division, Los Alamos National Laboratory, Los Alamos, NM 87545
*htoon@lanl.gov

Abstract: We report free-space generation of highly chiral single photons from QEs created via nanoindentation of monolayer WSe2 - NiPS3 heterostructures at zero external magnetic field. These QEs emit with a degree of circular polarization and single photon purity as high as 0.89 and 80% respectively, independent of pump laser polarization. The chiral quantum light emission arises from magnetic proximity interactions between localized excitons in the WSe_2 monolayer and the out-of-plane magnetization of defects in antiferromagnetic (AFM) order of NiPS.

Generation of chiral quantum light is critically needed for realization of non-reciprocal single photon devices, deterministic spin-photon interfaces, and complex quantum networks.[1] To date however, emission of such chiral quantum light has only been achieved through the application of intense external magnetic fields,[2] by electrical/optical injection of spin-polarized carriers/excitons,[3] or by coupling with complex photonic/meta-structures.[1] We exploit *magnetic proximity interactions* for the first time to realize free-space, zero-field generation of chiral quantum light.

"Proximity effects" – the class of phenomena by which an atomically-thin material borrows properties of an adjacent material (such as magnetism) via quantum mechanical interactions – has recently been explored by coupling transition metal dichalcogenides (TMD) with various bulk and 2D magnetic materials.[4] However, chiral light emission without spin polarized carrier/exciton injection at zero magnetic field remains elusive to date. A van der Waals antiferromagnetic (AFM) material, $NiPS_3$, has recently been identified as fertile ground for exploring emergent phenomena of 2D magnetism.[5] Because this material displays in-plane AFM order, it is not conventionally expected to induce ferromagnetic proximity interactions necessary for chiral light emission. Surprisingly, however, our work shows that chiral quantum light sources with a high degree of circular polarization and 80% single-photon purity *can* be realized by strain-engineering the $WSe_2/NiPS_3$ heterostructure with nanoscale indentations. Through state of art scanning diamond NV microscopy experiment and temperature dependent magneto-photoluminescence studies, we show that the chiral quantum light emission arises from magnetic proximity interactions between localized excitons in the WSe_2 monolayer and out-of-plane magnetization of AFM defects in $NiPS_3$, both of which are co-localized by the strain field arising from the nanoscale indentations. Interestingly, a similar chiral localized excitonic emission is also observed in our more recent experiment performed on $WSe_2/MnPS_3$ and $WSe_2/FePS_3$ heterostructure with nano-indents (See Extended Data Fig. 10).

Our work establishes TMD/$TMPX_3$ (TM = Mn, Ni, Fe, Co; X = S, Se) heterostructures as a novel material platform for not only exploring proximity-induced emergent phenomena but also for the development of spin-photon interfaces, magnon based quantum transduction, and sensing schemes. Our observations also reveal that local strain

engineering can be utilized not only to create QEs, but also to localize ferromagnetic proximity effects required for creation of chiral single photon emitters in $WSe_2/NiPS_3$ heterostructures.

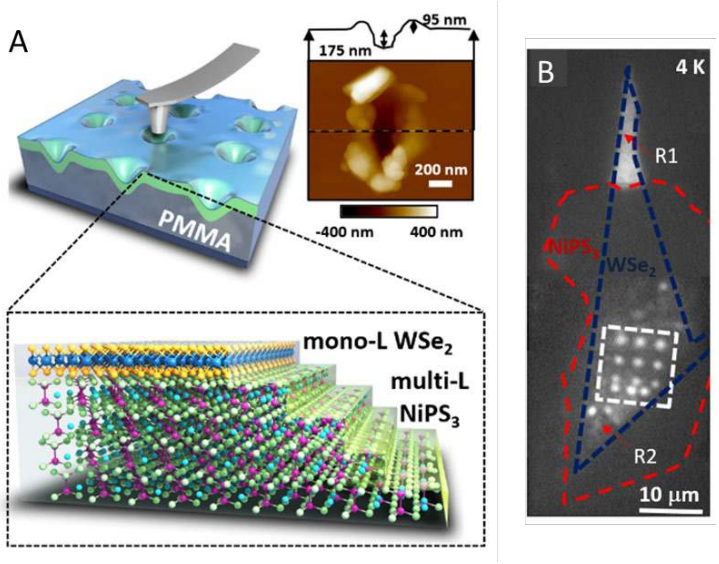


Figure 1. (A) Schematic of sample structure and an atomic force microscopy topography image and cross section of a representative indentation. (B) photoluminescence images of a $WSe_2/NiPS_3$ heterostructure.

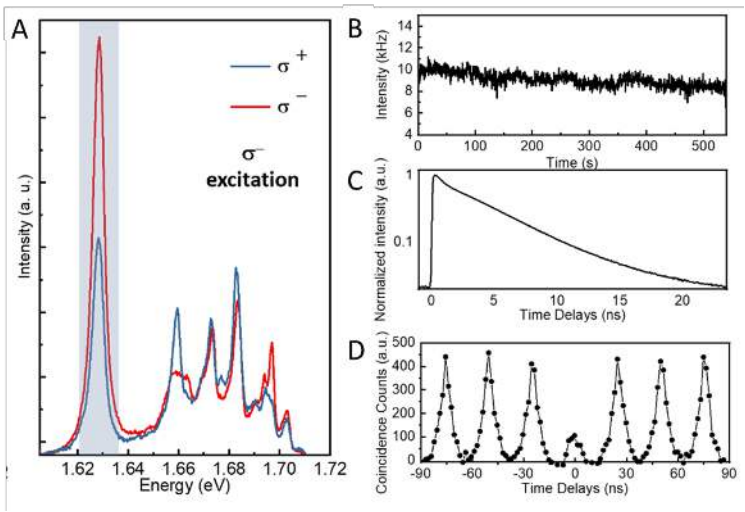


Figure 2. A.σ^+ (blue) and σ^- (red) polarized PL spectra of an indented $WSe_2/NiPS_3$ heterostructure showing circularly polarized PL emission spectra of a QE. B-D**.** PL intensity time trace (B), PL decay curve (C), 2nd order photon correlation trace (D) showing evidence of quantum light emission.

References

1. Lodahl, P. Nature 541, 473, 2017; **2**. Mak, K. F Nat. Photon. 12, 451 2018; Aivazian, G. Nat. Phys. 11, 148, 2015; **3**. Huang, Y. Nat. Photon. 15, 475, 2021; Seyler, K. L. Nature 567, 66 2019; Tran, K. Nature, 567, 71, 2019; **4**. Zhao, C. Nat. Nanotech. 12, 757, 2017; Zhong, D. Nat. Nanotech. 15, 187 2020; Huang, B. Nat. Mater. 19, 1276, 2020; **5**. Kang S. Nature 583, 785, 2020; Hwangbo, K. Nat. Nanotech. 16, 655, 2021; Wang, X. Nature Mater. 20, 964, 2021

Three-dimensional metasurface absorber for gas sensing devices

Takuo Tanaka[1, 2, 3]

[1]RIKEN Cluster for Pioneering Research, Japan
[2]RIKEN Center for Advanced Photonics, Japan
[3] Institute of Post-LED Photonics, Tokushima University, Japan
*corresponding author: t-tanaka@riken.jp

Abstract: We discuss about ultra-sensitive infrared spectroscopic techniques enhanced by 3D metasurfaces. To suppress unwanted background and noises in IR spectroscopy, metasurface absorber with three-dimensional vertical-oriented metal-insulator-metal (v-MIM) structure was introduced. Owing to small footprint of v-MIM, the density of hot spots was dramatically increased resulting in strong signal enhancement and efficient suppression of background light. Using this device, 20 ppm concentration of carbon dioxide and butane molecule detection was demonstrated.

Metasurfaces have attracted considerable attention due to their capabilities to manipulate light. Recently we applied metasurface light absorber for improving the sensitivity of IR spectroscopy. Owing to its plasmonic interaction with incident light wave, and molecules, unwanted background and noises in IR spectroscopy were suppressed and molecular signals are enhanced. This technique has already been applied for self-assembled monolayer of 16-mercaptohexadecanoic acid molecules on the device surface and atto-molar (10^{-18} mol) level molecular sensitivity was realized [1]. For liquid samples, to introduce target molecules into the hot spot region of the metamaterial, we proposed a metamaterial absorptive device that incorporates with nanofluidics, and demonstrated an ultra-high sensitivity of IR absorption detection [2]. In this paper, we introduced metasurface absorber with three-dimensional vertical-oriented metal-insulator-metal (v-MIM) structure for ultra-sensitive infrared spectroscopic techniques for gas sensing [3]. We designed and fabricated the v-MIM structure with a nano-gap of 25 nm channel which enabled the delivery of small molecules into hot-spot region. Figure 1 shows the electron micrographs of the fabricated v-MIM array structure. Owing to small footprint of v-MIM comparing conventional lateral MIM structure, the density of hot spots was dramatically increased resulting in strong signal enhancement and efficient suppression of background light.

This metamaterial was applied to carbon dioxide and butane detection designing to exhibit a resonance at 4033 cm^{-1} and 2945cm^{-1} which spectral overlap with the C=O and $–CH_2$ vibration mode, respectively. The mutual coupling of these two resonant modes creates a Fano resonance, and their distinct peaks are clearly observed in the corresponding transmission dips. In addition, owing to its small footprint, v-MIM structure allows the detection of a 20 ppm concentration with suppressed background and high selectivity in the mid-infrared region.

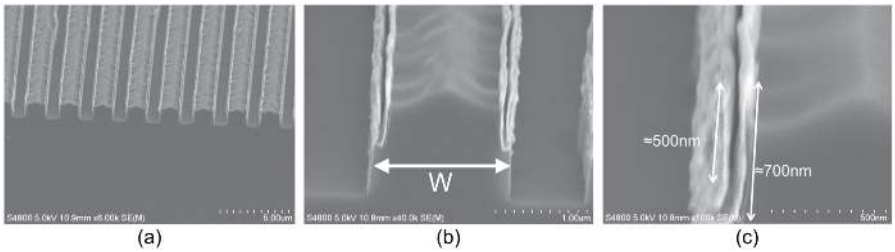


Figure 1 Fabricated vertically-oriented metal-insulator-metal (v-MIM) metasurface absorber.

[1] A. Ishikawa and T. Tanaka, Scientific Reports **5**, 12570 (2015).
[2] T. H. H Le and T. Tanaka, ACS Nano **11**, 9780-9788 (2017).
[3] D.-S. Su, D. P. Tsai, T.-J. Yen, and T. Tanaka, ACS Sensors **4**, 2900-2907 (2019).

Highly conformable terahertz metasurfaces via two-photon polymerization on polymeric ultra-thin films

A. Ottomaniello[1], P. Vezio[2], O. Tricinci[1], F. M. Den Hoed[1,3], P. Dean[4], A. Tredicucci[2,*], and V. Mattoli[1]

[1]Center for Materials Interfaces, Istituto Italiano di Tecnologia, Via R. Piaggio, 34, 56025 Pontedera, PI, Italy
[2]Dipartimento di Fisica E. Fermi, Università di Pisa, Largo Pontecorvo 3, 56127 Pisa, Italy
[3]Engineering and Technology Institute Groningen (ENTEG), University of Groningen, Nijenborgh 4, Groningen, 4747 AG, The Netherlands
[4]School of Electronic and Electrical Engineering, University of Leeds, Leeds LS29JT, UK
[*]corresponding author: alessandro.tredicucci@unipi.it

Abstract: The interest in flexible and integrated photonics requires new strategies for device manufacturing on arbitrary complex surfaces. THz technology can particularly benefit from this approach to implement compact systems for generation, detection, and manipulation of THz radiation. Here we present a novel fabrication method to realize conformable metasurfaces. The flexible and versatile character of polymeric nanomembranes is combined with direct laser writing and metal deposition to develop freestanding ultra-thin THz devices with an unprecedentedly high level of conformability.

Optical metasurfaces are a very promising platform to go beyond traditional metamaterials in terms of both compactness and functionality. Here, we propose a novel fabrication method for ultra-sub-wavelength free-standing plasmonic THz metasurfaces with high degree of conformability. The developed technique merges direct laser writing via two-photon polymerization (2PP) and transfer printing using ultra-thin polymeric membranes. As proof of concept, we focused on developing a highly absorbing structure using a suspended membrane consisting of a dielectric thin film encapsulated by two metallic layers. By inscribing in the top metallization a terahertz metasurface, an absorption resonance is introduced, whose depth is strongly enhanced by the presence of a homogeneous bottom metallization. Regulating the thickness of the dielectric material, high levels of absorption are demonstrated in an ultra-subwavelength thickness (even < λ/100).

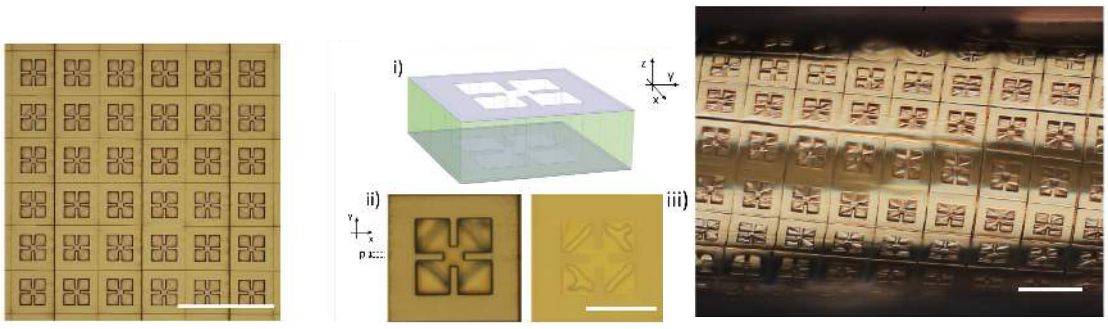


Figure 1: Optical images of a representative 2 μm-thick conformable THz metasurface absorber showing the square array of split ring resonators. (i): 3D sketch highligthing the two metal surfaces displaced by the resist thickness. Front (ii) and back (iii) view of the metasurface unit-cell of 45 μm size. Scale bars are 100 and 30 μm, respectively. Image showing the all-round conformability of the metasurface around a 100 μm-radius wire. Scale bar is 50 μm.

A fabricated sample 2 µm-thick is shown in the optical image of Figure 1. It shows the metasurface pattern where it is possible to observe the square array arrangement and geometry of the unit-cell with size a = 43 µm. The realized resonator shape belongs to the most widely used class of sub-wavelength optical resonators at microwave, THz and FIR frequencies known as split-ring resonators (SRRs), which can present electric and/or magnetic response by design.

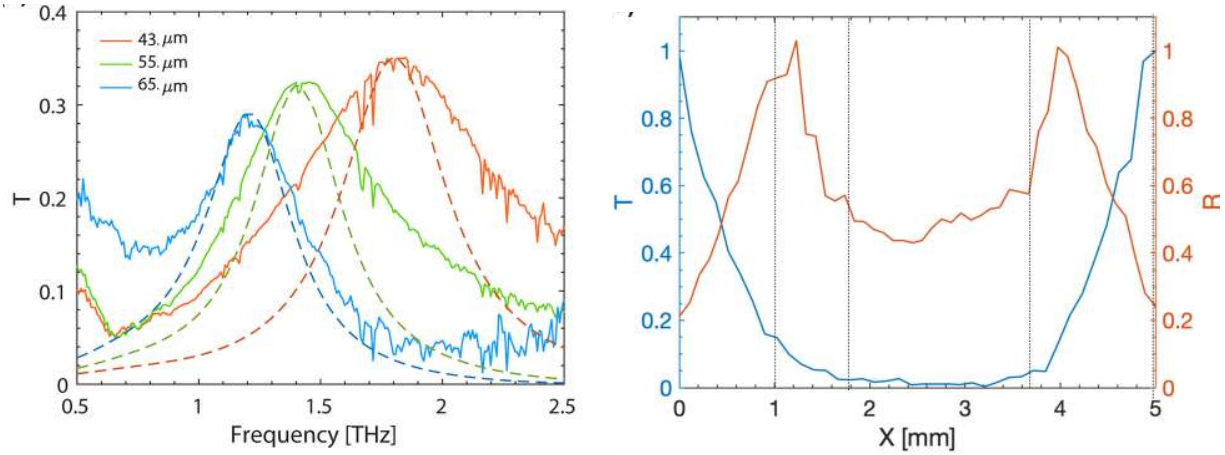


Figure 2: Left: transmission spectra for three metasurfaces having only the top metallization with 43, 55 and 65 µm unit-cell represented by the orange, green and blue solid curves, respectively. Dashed lines with same darker colors report the corresponding calculated results obtained via full-wave finite-element simulations. Right: transmission and reflection profiles for the double-metal metasurface.

THz transmission measurements were first performed on single-metal membranes using time-domain spectroscopy (TDS) in the frequency range from 0.5 to 3.5 THz to check the SRR resonances. The measured transmittance of three devices with a = 43 µm, 55 µm and 65 µm is shown in Figure 2 (left). A clear resonance is observed for each sample, with a linear blueshift of the frequency peak according to the downscaling of the metasurface unit-cell.

In order to investigate the absorption of the dual-metal devices fabricated with one continuous metal ground plane, a single-mode quantum cascade laser, nominally emitting at the 3.5 THz of the chosen metasurface resonance peak, is used. Figure 2 (right) shows the acquired transmission and reflection profiles. They highlight the absorbing character of the metasurface placed in the middle of the scan. Even if a considerable (>40 %) absorption is observed, the deviation from a quasi-perfect absorption can be ascribed to a possible frequency resonance detuning of the laser emission frequency due to a discrepancy between nominal and real geometrical parameters of the structure.

The authors acknowledge support from the EC Horizon 2020 research and innovation program under the FET Open grant agreement 5DNanoPrinting – no. 899349.

References

1. Ottomaniello, A., P. Vezio, O. Tricinci, F. M. Den Hoed, P. Dean, A. Tredicucci and V. Mattoli “Highly conformable terahertz metasurface absorbers via two-photon polymerization on polymeric ultra-thin films,” Nanophotonics, https://doi.org/10.1515/nanoph-2022-0667, 2023.

Ellipsometric probing of hot electrons in plasmonic media

J. Budai[1], Z. Pápa[1,2], P. Petrik[3], and P. Dombi[1,2]

1. ELI-ALPS Research Institute, Szeged, Hungary

2. Wigner Research Centre for Physics, Budapest, Hungary

3. Institute of Technical Physics and Materials Science, Centre for Energy Research, Budapest, Hungary

*E-mail: dombi.peter@wigner.hu

Abstract: We show that ellipsometry is an ultrasensitive tool for spatiotemporal probing of surface plasmon-generated hot electrons.

The strong localization of plasmon-assisted photon absorption facilitates the emergence of so-called hot electrons with energy levels deviating from Fermi-Dirac distribution. We demonstrated that spectroscopic ellipsometry is capable of grabbing the in-depth distribution and the temporal evolution of surface plasmon polariton (SPP) mediated hot electron populations [1].

For the excitation of SPPs, a Kretschmann-geometry involving a glass right angle prism coated with 50 nm gold was applied. SPPs were excited from the backside of the film using either an 808 nm cw diode laser or the 35 fs pump pulses of an amplified Ti:sapphire laser under resonance angle. Spectroscopic ellipsometry was applied at the top side of the films (Fig. 1. left panel), illuminating the samples with a broadband cw light source or white light continuum probe.

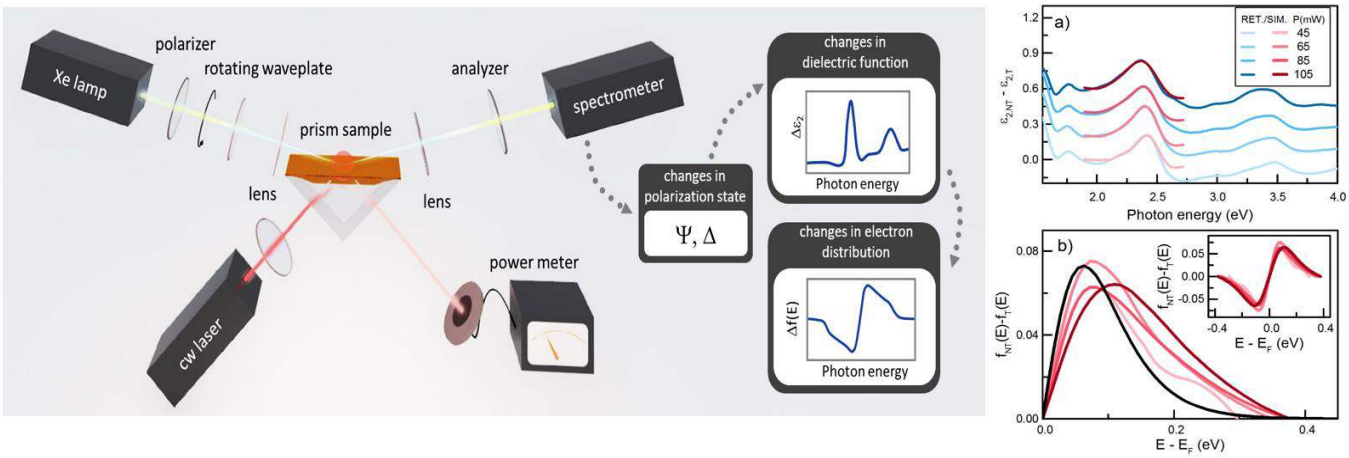


Fig. 1 Left) Experimental setup for ultrasensitive probing of plasmonic hot electrons with spectroscopic ellipsometry. SPPs are excited by a cw laser at the resonant angle of incidence from the backside, while ellipsometric data is recorded on the gold-air interface with white-light probing from the top. These measurements are capable of accessing the dielectric function of the investigated system, the changes of which are in close correlation with the electron distribution function. Right a) retrieved and simulated differences between the dielectric function of the non-thermalized top layer (NT) and the thermalized part (T) of the gold film and b) the corresponding electron occupancies for cw excitation.

In the case of cw excitation of SPPs, ellipsometry revealed - besides the temperature raise of the gold layer -

the presence of a surface layer accounting for the appearance of SPPs and the associated hot electron generation. The spatial extent of this non-thermalized layer (1.5-4 nm) and its dielectric function became also visible. We retrieved the changes in the electron occupancies based on the proportionality of ε_2 with the electron distribution and the band structure. The observed changes provide a clear indication of the existence of a hot-electron population with moderately increased energies close to the film surface where plasmon excitation takes place (Fig. 1 right panel a) and b)).

For the pump-probe experiments, the pseudo dielectric function of the gold layer was deduced. These dielectric functions were modelled by assuming different electron distributions describing the different mechanisms following the SPP excitation. The very good accordance between the measured and calculated curves supports the applicability of our method.

The authors received funding from the National Research, Development and Innovation Office of Hungary (TKP2021-NVA-04, KKP-137373). This work was also supported by a FET Open grant of the EU ("PetaCOM").

References

1. J. Budai, Z.Pápa, P. Petrik, P. Dombi "Ultrasensitive Probing of Plasmonic Hot Electron Occupancies in Gold", Nature Comm. 13, 6695 (2022) .
2. T. Heilpern et al., "Determination of hot carrier energy distributions from inversion of ultrafast pump-probe reflectivity measurements", Nature Comm. 9, 1853 (2018).
3. Y. Dubi et al., "Hot" electrons in metallic nanostructures—non-thermal carriers or heating?", Light: Science & Applications 8, 89 (2019).

Bound States in the Continuum with High Q-factors in Deep Ultraviolet Light Source

Omar A. M. Abdelraouf[1, 2], Aravind P. Anthur[2], Xiao Renshaw Wang[1, 3*], Qi Jie Wang[1, 3*], Hong Liu[2*]

[1] School of Physical and Mathematical Sciences, Nanyang Technological University, Singapore 637371, Singapore
[2] Institute of Materials Research and Engineering, Agency for Science, Technology and Research (A*STAR), 2 Fusionopolis Way, #08-03, Innovis, Singapore 138634, Singapore
[3] School of Electrical and Electronic Engineering, 50 Nanyang Avenue, Nanyang Technological University, Singapore 639798, Singapore
[*] corresponding authors: renshaw@ntu.edu.sg, qjwang@ntu.edu.sg, h-liu@imre.a-star.edu.sg

Abstract: Traditional deep ultraviolet (DUV) light sources using nonlinear optical crystals exhibit limitations such as bulky size, inadequate efficiency, and requirement of phase-matching conditions. We proposed a crystalline silicon metasurface with symmetry breaking, which can excite bound states in the continuum (BIC) resonance to enhance third harmonic generation (THG) at the DUV regime. We experimentally realized a high Q-factor of ~ 180 and the measured THG power is around 200 pW at a pump power of 200 mW.

1. Introduction

Traditional coherent light sources in the DUV regime (200 nm – 300 nm) have been widely adopted in applications such as optical lithography,[1] bioimaging,[2] and medical inspection.[3] Although conventional nonlinear crystals exhibit high conversion efficiency, the optical loss in the DUV regime limits their operating ranges to visible and longer wavelength only. In addition, nonlinear optical crystals suffer from their bulky size, low efficiency and stringent requirement of phase-matching conditions, which hinders their applications where miniaturized and compact light sources are needed. In recent years, optical bound states in the continuum (BIC) have emerged as a new paradigm for trapping and confining resonant modes for numerous applications.[4] BIC metasurfaces have been manifested to be able to confine the incident light efficiently with very high Q-factors. Metasurfaces consisting of high-quality nonlinear materials, such as silicon (Si) would enhance the nonlinear conversion efficiency.[5] In this work, we have theoretically proposed a BIC resonant structure inside c-Si metasurface and experimentally obtained a high Q-factor BIC. Our finding shows that c-Si is a good candidate for THG in the DUV regime due to its high nonlinearity. In addition, exciting the BIC resonance via the c-Si metasurface can significantly boosted the THG efficiency.

2. Results and discussion

The concept of the proposed BIC resonance inside the c-Si metasurface and its unit cell consisting of two resonators are sketched in Fig. 1a. The key design parameters include the width of top and bottom sides denoted by L_1 and L_2, respectively. The shape of the two resonators is a right-angle trapezoid. In the case of L_1=L_2, the BIC resonance is confined so that it cannot be coupled to the radiation spectrum. The BIC resonance is observed only after inducing a lattice symmetry breaking, i.e., creating a difference of ΔL between L_1 and L_2, as shown in Fig 1b. A maximal theoretical Q-factor of up to 900 is calculated upon for ΔL =20 nm.

The BIC metasurfaces was fabricated via electron beam lithography followed by dry etching to transfer the nanopattern from the hydrogen silsesquioxane (HSQ) to the c-Si and the SEM image of the unit cell of the fabricates BIC metasurfaces is shown in the inset of Fig. 2a. We pumped the fabricated c-Si metasurface using a linearly polarized fs-laser with the polarization in the horizontal direction. The measured THG power as a function of the pump power is plotted in Fig. 2a, showing a third order dependence between the pump and the THG signals.

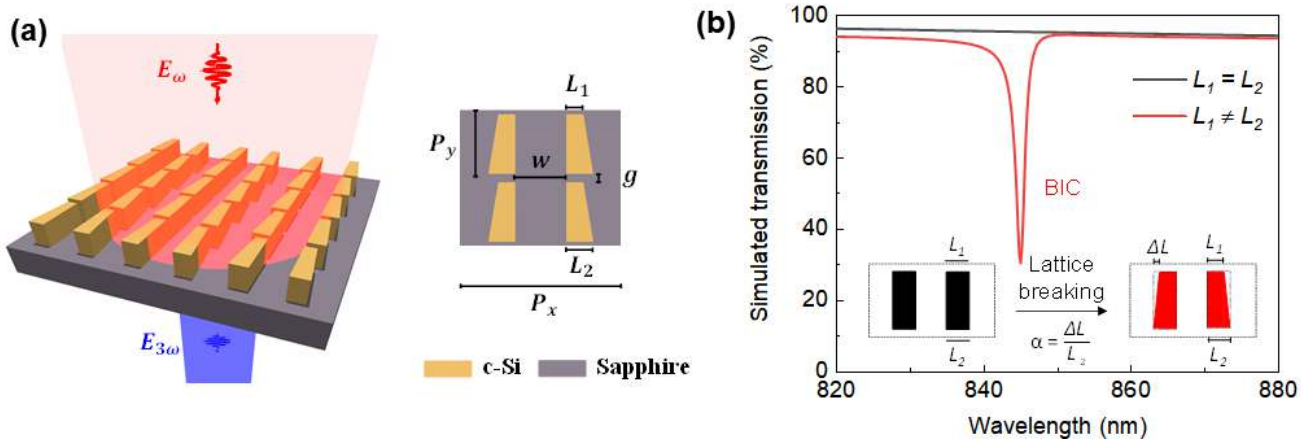


Figure 1. Metasurface design and parameters of c-Si metasurface supporting BIC resonance. (a) The schematic of c-Si metasurface on sapphire under an incidence of a pump fs-laser at the wavelength of 840 nm denoted by E_ω, and the collected THG at the wavelength of 280 nm denoted by $E_{3\omega}$. (inset): the dimensions of unit cell of c-Si metasurface: periods P_x = 550 nm, P_y = 320 nm, horizontal gap g_x = 155 nm. The width of pillars L_1 varies while L_2 is fixed to break lattice symmetry. (b) Simulated transmission before and after the lattice symmetry breaking showing the BIC near 840 nm.

The maximum THG power was up to 200 pW at a pump power of 200 mW. In addition, we measured the THG spectrum, and the results are plotted in Fig. 2b. The experimental Q-factor was more than 120. Our results indicate that c-Si metasurfaces have great potential to develop highly efficient ultracompact DUV light sources.

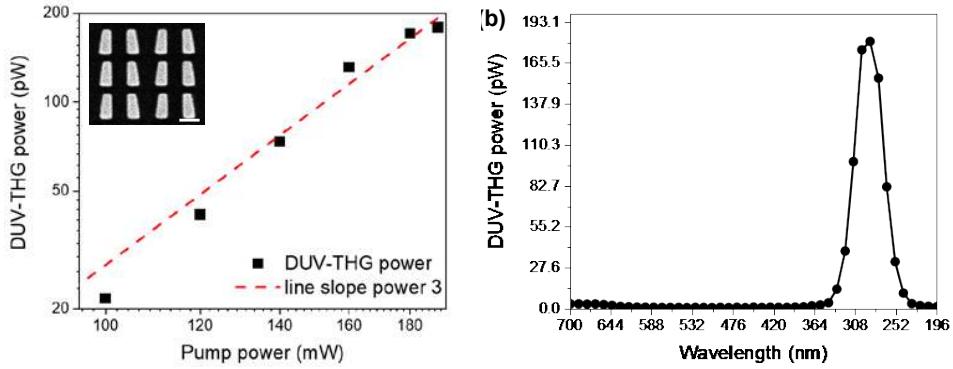


Figure. 2 THG measurement of c-Si BIC metasurface. (a) The measured THG versus pump power at a wavelength around 280 nm. (inset) the SEM image of the fabricated c-Si metasurface, with a scale bar of 200 nm. (b) The measured THG spectrum versus wavelength.

Acknowledgement

This work is supported by A*STAR AME programmatic grant (grant no. A18A7b0058), Academic Research Fund (AcRF) Tier 2 (Grant No. MOE-T2EP50220-0005) from Singapore Ministry of Education and the Agency for Science, Technology and Research (A*STAR) under its AME IRG grant (Project No. A20E5c0094).

References

[1] Wu, B.; Kumar, A., Extreme ultraviolet lithography: A review. *J Vac Sci Technol B Microelectron Nanometer Struct Process Meas Phenom*. 25, 1743-1761 (2007).

[2] Weigelin, B.; Bakker, G.-J.; Friedl, P., Third harmonic generation microscopy of cells and tissue organization. *Journal of Cell Science* 129, 245-255 (2016).

[3] Ager III, J. W.; Nalla, R. K.; Breeden, K. L.; Ritchie, R. O., Deep-ultraviolet Raman spectroscopy study of the effect of aging on human cortical bone. *Journal of biomedical optics* 10, 034012 (2005).

[4] Hsu, C. W.; Zhen, B.; Stone, A. D.; Joannopoulos, J. D.; Soljačić, M., Bound states in the continuum. *Nat. Reviews Materials*. 1, 1-13 (2016).

[5] Abdelraouf, Omar AM, *et al*. Multistate Tuning of Third Harmonic Generation in Fano-Resonant Hybrid Dielectric Metasurfaces. *Adv. Func. Mater*. 31, 2104627 (2021).

A small spectrometer with extremely high resolution (0.07 nm) realized with an improved reconstruction algorithm

Takasumi Tanabe, Junnosuke Kokubu, and Ryo Sugano

[1]Departament of Electronics and Electrical Engineering, Faculty of Science and Technology, Keio University Japan

*corresponding author: takasumi@elec.keio.ac.jp

Abstract: We successfully reconstruct the spectrum of a multi-wavelength input by using the inverse matrix method for data obtained with a random chirped photonic crystal waveguide.

With conventional spectrometers, there is a tradeoff between device compactness and high spectral resolution. Although integrated photonic devices are expected to overcome this issue, they suffer from fabrication errors that degrade the resolution. We have already reported spectrometer operation based on photonic crystal waveguides with randomness [1, 2] that can overcome this problem. The process is based on capturing the wavelength-dependent light localization pattern of a photonic crystal waveguide with a camera and reconstructing the spectrum. Since the localizations usually exhibit a Q of 10^5 or higher, corresponding to a ~ 0.01 nm spectrum width, we expect a wavelength resolution of the same order. We used simulated annealing [1] and deep learning [2] to reconstruct the spectra, but these approaches were slow and could not provide a high resolution.

Here, we report our significant process as regards wavelength resolution, where we show that a value of 0.07 nm is possible by improving the reconstruction method, employing low-rank approximation, and regularizing least squares for the algorithm while realizing real-time operation, which was not possible with the previous method [1]. We should note that a device that has such a high resolution (0.07 nm) and a footprint as small as mm^2 outperforms other spectrometer devices.

The chirped waveguide structure is shown in Fig. 1(a), where the cut-off frequency is shifted up in each section by reducing the waveguide width by 2 nm. Since Anderson localization occurs close to the mode gap, usually exhibiting Qs of 10^5, we can use them to reconstruct the spectrum information. Localization patterns were captured from the top of the chip while scanning the wavelength of the incident laser (Fig. 1(b)).

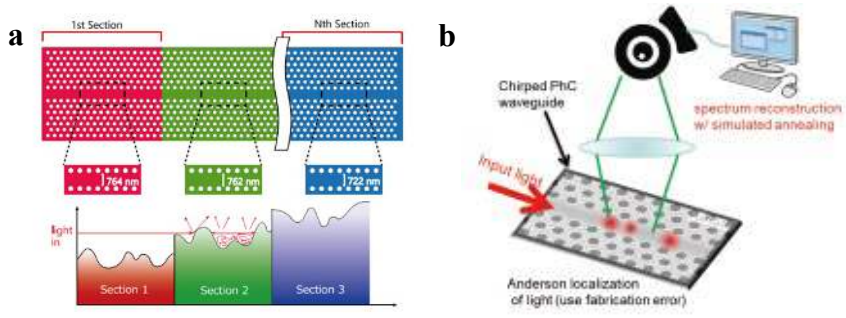


Fig. 1: (a) PhC waveguide and conceptual diagram of the waveguide mode gaps. (b) Schematic diagram of the experimental system.

The captured images are processed by cropping, deforming, and averaging, and then converted to one-dimensional data. By arranging them in wavelength order, a matrix T is obtained. Therefore, the localization

pattern $\vec{I}$ when an unknown spectrum $\vec{S}$ is injected satisfies the following,

$$\vec{I} = T\vec{S}. \tag{1}$$

Therefore, ideally, the spectrum is reconstructed using the inverse matrix of *T*. We must also take account of the noise during processing. Hence, we consider a singular value decomposition of *T* given as [3],

$$T = USV^T. \tag{2}$$

Since lower singular values are more strongly affected by noise, a threshold value is set, and singular values below the threshold are truncated. This is called low-rank approximation. Using S_{tr} consisting only of singular values above a threshold, we correct the *T* matrix to

$$T_{tr} = US_{tr}V^T. \tag{3}$$

Furthermore, a regularized inverse matrix is obtained by introducing a constant λ that compensates for the sensitivity to noise. The reconstructed spectrum is then given as,

$$S = [(\lambda I - T_{tr}^T T_{tr})^{-1} T_{tr}]I. \tag{4}$$

We obtained the *T* matrix based on this algorithm, as shown in Fig. 2(a). The wavelength step is 0.1 nm, which will give the resolution. Figure 2(b) shows the localized pattern for two different wavelength inputs simultaneously. We assume that the localization pattern is the superposition of the two patterns at different wavelengths. Indeed, the blue line of the numerically multiplied pattern agrees well with the red line, which is the experimentally obtained localized pattern. Figure 2(c) is the spectrum reconstructed using our algorithm. It demonstrates that our approach can reconstruct a multi-wavelength input at a wavelength separation of 0.8 nm, which is beyond the designed wavelength resolution of the chirped photonic crystal waveguide. The calculation time was only 0.097 sec.

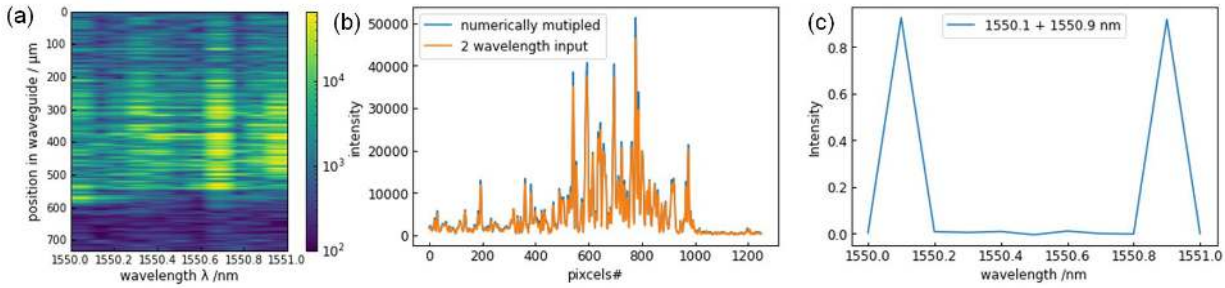


Fig. 2 (a) Obtained *T* matrix. (b) Localization patterns at two wavelength inputs. The blue line is the numerically calculated (as the superposition of two different inputs) pattern. The red line is the obtained pattern. (c) A reconstructed spectrum of a multi-wavelength input from the obtained localization pattern.

In conclusion, we show that we can distinguish the peak of an input light of the order of sub-seconds with a resolution of 0.07 nm by using a chirped photonic crystal waveguide where randomness is inherent.

References

1. T. Kodama, *et al.*, in CLEO:2022, paper SM3K.6.
2. J. Hofs, *et al.*, in CLEO:2020, paper SF1J.4.
3. B. Redding, *et. al.*, Opt. Express **21**, 6584 (2013)

Epsilon-near-zero materials enhance infrared vibrational spectroscopy

R. Smaali[1*], A. Moreau[1], and E. Centeno[1]

[1]Université Clermont Auvergne, CNRS, SIGMA Clermont, Institut Pascal, F-63000 Clermont-Ferrand, France
[*]corresponding author: rafik.smaali@uca.fr

Abstract:
Surface-enhanced infrared absorption (SEIRA) spectroscopy is a powerful technique for a label-free identification of molecular species. The low infrared absorption cross sections of molecules are made up for the electromagnetic field enhancement provided by the excitation of surface and/or localized plasmons of metallic structures [1]. The design of actual plasmonics detectors is a trade-off between the detection of very small volumes of molecules and the signal to noise ratio level. We demonstrate that an epsilon-near-zero (ENZ) material combined with nano-slits lifts this constraint and provides both extreme enhancement factor up to 10^7 and highly contrasted SEIRA signal for an extremely low amount of material of interest [2]. These results are explained by the modification of the electromagnetic field of the gap plasmon mode sustained by the slits in the presence of the ENZ material, Fig. 1. We propose to implement this concept with a semiconductor whose doping level engineering provides a versatile way to scan the whole molecules' fingerprint frequency range.

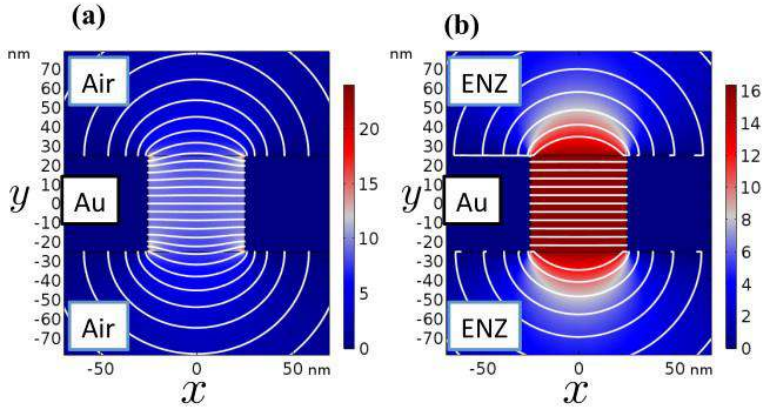


Figure 1: Modulus of the x-component of the normalized electric field for 50 nm silts filled with air, when the slit is, respectively, surrounded by air (a) and by an ENZ medium (b). The permittivity of the ENZ medium is equal to -0.01. The electric field lines are represented in white.

We wish to acknowledge the support received from the Agence Nationale de la Recherche of the French government through the program investissements d'avenir (No. 16-IDEX-0001 CAP 20-25) and the IMobS3 Laboratory of Excellence (No. ANR10-LABX-0016). Antoine Moreau is an Academy CAP 20-25 chair holder.

References

1. T. Tanaka, T-A. Yano and R. Kato, "Nanostructure-enhanced infrared spectroscopy", *Nanophotonics* **11**, 2541-2561 (2021).
2. R. Smaali, T. Taliercio, A. Moreau and E. Centeno, "Reshaping plasmonic resonances using epsilon-near-zero materials for enhanced infrared vibrational spectroscopy", *Applied Physics Letters* **119**, 183701 (2021).

META 2023, PARIS - FRANCE, JULY 18 – 21, 2023

Advances in multiphysics modeling of phase change materials based metasurfaces

Dmitry N. Chigrin[1,2]

[1]I. Physikalisches Institut (1A), RWTH Aachen University, Aachen, Germany
[2] DWI Leibniz Institute for Interactive Materials, Aachen, Germany
*corresponding author: chigrin@physik.rwth-aachen.de

Abstract: Phase change materials are substances that can undergo rapid and reversible phase transitions, leading to significant changes in their physical properties. By incorporating these materials into metasurface design, it is possible to create programmable photonics components that can be reconfigured. This is particularly important in the fields of artificial materials, neuromorphic computing, and integrated photonics, where there is a growing demand for adaptivity and reconfigurability. In this presentation, we report on recent developments of the multiphysics description of complex composite active metasurfaces that incorporate phase change materials as building blocks. We provide a detailed discussion of the method and examples of its application.

META 2023, PARIS - FRANCE, JULY 18 – 21, 2023

Photo-Induced Sources within Multilayer Optics: from Light Scattering to Micro-cavities and Thermal Radiation

C. Amra, P. Rouquette, M. Zerrad, G. Soriano, M. Lequime

Aix Marseille Univ, CNRS, Centrale Marseille, Institut Fresnel, Marseille, France
*corresponding author: claude.amra@fresnel.fr

Abstract: We use the same formalism to analyze light scattering, luminescence, and photo-induced thermal radiation in optical interference filters. The 4D spatio-temporal regime is considered. Analytical techniques are presented to design strong inhibition (case of scattering) or huge enhancement (luminescence, thermal radiation) of the pattern emitted from these multi-dielectric coatings.

Optical interferential filters [1,2] are currently used to modify the spectral properties of substrates. This has led to numerous multilayer designs of varying complexity, such as broadband antireflection coatings and beam splitters, dichroic filters with steep edges, multi-cavity narrowband filters, notch filters, chirped mirrors and others. In the field of manufacturing (dual ion beam sputtering, magnetron sputtering, ion assisted deposition...), the know-how is very advanced so that these amorphous coatings can be produced up to 1000 thin films with sub-micron thicknesses.

In addition to the mechanical properties of these components, their energy balance remains a key issue in high precision optics (space optics, gyro-laser mirrors, gravitational wave detection). This balance requires that the total losses due to absorption and scattering be less than 10^{-6} of the incident flux (1ppm), a barrier to be overcome in the coming years. For this reason, light scattering is still the subject of extensive research [3], including the role of interface roughness, bulk inhomogeneities, and local defects. We first show how to analyze these phenomena using electromagnetic theory and high-end laboratory equipment. Scattering sources are described with fictitious currents at all interfaces and bulks, which interfere to produce the scattering pattern of multilayers in free space. Thanks to a mutual coherence factor close to unity, these interferences can be destructive, opening the door to anti-scattering effects with great advantages.

Multilayer optics can also be used in the form of microcavities [4,5], where the illumination beam is replaced by one or more luminescent layers in the stack. The deposition techniques are different (epitaxial growth on crystalline substrates), but the formalism is similar, since physical bulk sources take account of the luminescence processes. A key difference with light scattering is the lack of coherence between these currents. In this context, we present an analytical technique to design huge pattern enhancements of these micro-cavities, which finds applications in the field of sensors and micro-sources. Huge enhancements can be designed for arbitrary polarizations, wavelengths, or angles, which can also occur simultaneously [6].

Photo-induced thermal radiation [7,8,9] is also predicted and designed with the same formalism [10]. In fact, thermal radiation originates from stochastic bulk currents, both magnetic and electric, with no mutual coherence. The main difference is that these currents are temperature dependent, which requires first calculating the absorption heat source in the multilayer and then solving the 4D spatio-temporal heat equation in the stack [11]. The results allow to predict the photo-induced thermal radiation in the most general case, versus time, direction and wavelength, and versus illumination parameters (incident energy, pulse duration and repetition rate,

polarization and incidence). Finally, we show how multi-dielectrics allow to design narrow-band huge emissivity [10] of controlled amplitude at predetermined frequencies and polarizations.

To be complete, for all processes (scattering, luminescence and thermal radiation) we quantify both the amount of light that merges outside the coating in free space, and the amount of trapped light that is transferred to the guided modes of the multilayer. Depending on the coating design, one (free space) or the other (guided modes) process may dominate the energy balance [12].

We acknowledge the French Space Agency (CNES), the French Research Agency (ANR) and Cilas ArianeGroup for their support.

References

1. H. A. Macleod, Thin-Film Optical Filters, 4th ed, Series in Optics and Optoelectronics, CRC Press/Taylor & Francis (2010).
2. Claude Amra, Michel Lequime, Myriam Zerrad. Electromagnetic Optics of Thin-Film Coatings: Light Scattering, Giant Field Enhancement, and Planar Microcavities. Cambridge University Press, 2020, 9781108772372.
3. Imran Khan, Michel Lequime, Myriam Zerrad, Claude Amra. Detection of Ultralow Light Power Back-Reflected or Back-Scattered by Optical Components Using Balanced Low-Coherence Interferometry. Phys.Rev.Applied, 2021, 16 (4), pp.044055. <10.1103/PhysRevApplied.16.044055>
4. Claude Amra and Sophie Maure, "Electromagnetic power provided by sources within multilayer optics: free-space and modal patterns," J. Opt. Soc. Am. A 14, 3102-3113 (1997).
5. H. Benisty, H. De Neve and C. Weisbuch, "Impact of planar microcavity effects on light extraction-Part I: basic concepts and analytical trends," *IEEE Journal of Quantum Electronics*, 34, 9, 1612-1631, (1998).
6. Paul Rouquette, Claude Amra, Myriam Zerrad, and Michel Lequime, "Micro-cavity optimization for ultra-sensitive all-dielectric optical sensors," Opt. Express 30, 15344-15364 (2022)
7. S. M. Rytov, Yu. A. Kravtsov, and V. I. Tatarskii, Principles of Statistical Radiophysics 3: Elements of Random Fields (Springer-Verlag, 1989).
8. Z. M. Zhang, Nano/Microscale Heat Transfer, 2nd ed., Mechanical Engineering Series (Springer International Publishing, 2020).
9. J.-J. Greffet, R. Carminati, K. Joulain, J.-P. Mulet, S. Mainguy, and Y. Chen, "Coherent emission of light by thermal sources," Nature 416, 61–64 (2002).
10. P. Rouquette, C. Amra, M. Zerrad, C. Grèzes-Besset, H. Krol, “Thermal Radiation Photo-Induced in Optical Interference Coatings”, submitted to Optics Express
11. P. Rouquette, C. Amra, M. Zerrad, C. Grèzes-Besset, and H. Krol, "Photo-induced temperature in optical interference coatings," Opt. Express 30, 46575-46601 (2022)
12. Claude Amra, Myriam Zerrad, and Michel Lequime, "Trapped light scattering within optical coatings: a multilayer roughness-coupling process," Opt. Express 29, 25570-25592 (2021)

Purcell factor for plasmon-enhanced metal photoluminescence

Tigran V. Shahbazyan

Department of Physics, Jackson State University, Jackson, MS 39217 USA
shahbazyan@jsums.edu

Abstract: We present an analytical model for plasmonic enhancement of metal photoluminescence (MPL) in metal nanostructures. We obtain a universal expression for MPL Purcell factor in terms of metal dielectric function, plasmon frequency, and the system volume. We find that the lineshape of MPL spectrum is affected by the interference between direct carrier recombination processes and those mediated by plasmonic antenna which leads to a blueshift of MPL spectral band relative to scattering spectra observed in the experiment.

The origin of bright MPL from plasmonic nanostructures was suggested [1] to be due to excitation of the localized surface plasmon (LSP) by a recombining electron-hole pair [2] followed by the LSP radiative decay. This plasmonic antenna scenario has been confirmed by MPL measurements from single gold nanorods which revealed strong similarities between the MPL spectra and scattering spectra measured from the same structures [3-5]. At the same time, a persistent blueshift of MPL peak positions relative to LSP resonance in scattering spectra has been reported, which has not so far been explained.

We present an analytical model for MPL from plasmonic structures of arbitrary geometry with characteristic size is below the diffraction limit. For such systems, we derive an explicit expression for the MPL Purcell factor, which describes the plasmonic antenna effect, and trace the observed blueshift of MPL spectral band to destructive interference between the direct and antenna-assisted recombination processes. For frequencies w close to the LSP frequency w_n, we obtain the MPL Purcell:

$$\mathrm{F}(\omega) = \frac{2\pi \mathrm{c}^3}{\omega^3 V_\mathrm{m}} \frac{\varepsilon''(\omega)}{|\varepsilon(\omega) - \varepsilon'(\omega_n)|^2} \tag{1}$$

where $\varepsilon(\omega) = \varepsilon'(\omega) + i\varepsilon''(\omega)$ is metal dielectric function, c is speed of light, and V_m is metal volume. With such Purcell factor, we obtain the MPL enhancement factor relative to bulk MPL background as

$$M(\omega) = A_n \left| \frac{\varepsilon'(\omega_n) - 1}{\varepsilon(\omega) - \varepsilon'(\omega_n) - (2i\omega^3/3c^3)[\varepsilon(\omega) - 1]V_n} \right|^2 \tag{2}$$

where V_n is the effective system volume and the coefficient A_n depends on system geometry. The enhancement factor (2) can be used to describe the MPL spectra for systems of various shapes and sizes.

To illustrate our results, we present the MPL spectra for several gold nanostructures immersed in water by plotting Eq. (2) for a single LSP mode. In all calculations, we use the experimental gold dielectric function and, accordingly, the LSP wavelength range extends above 530 nm, which corresponds to the interband transitions onset in gold. Specifically, we choose the LSP peak positions at the wavelengths 620 nm, 670 nm, 710 nm and 750 nm, which are close to those measured in the MPL experiments [3-5]. We assume no particular shape but specify the overall nanostructure volume as $V_\mathrm{m} = L^3$, where L is the characteristic linear size. For gold structures, the optimal L lies in the interval between 20 nm and 60 nm, in which the MPL quenching is relatively weak while the LSP radiative damping is not too strong.

In Fig. 1, we plot the MPL enhancement factor (2) for general-shape gold nanostructures with L = 20 nm, in which the LSP resonance position can be tuned by varying the structure shape (e.g., by varying the aspect ratio of nanorods). The MPL enhancement factor exhibits nearly-Lorenzian resonances, whose amplitude increases with the wavelength, consistent with MPL quantum yield measurements [3-5].

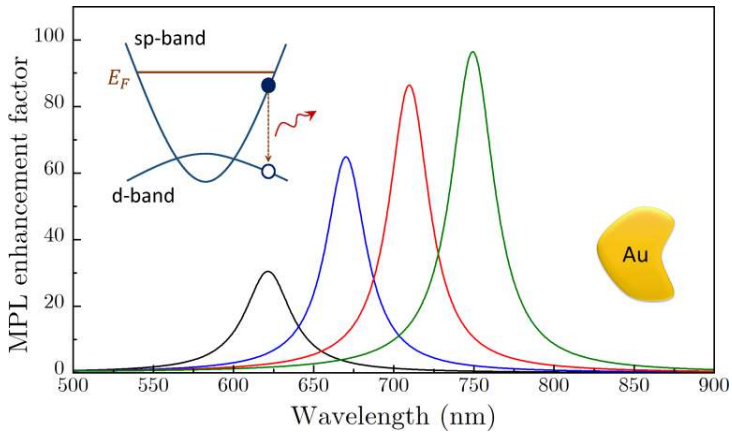


Figure 1. MPL enhancement factor for gold nanostructures with characteristic size 20 nm at various LSP wavelengths 620 nm, 670 nm, 710 nm and 750 nm. Inset: Schematics of interband transitions in gold.

In Fig. 2, we compare the MPL spectra for L = 40 nm gold nanostructures at same LSP wavelength values and the scattering spectra, which are both normalized to their maxima. A clear blueshift of the MPL spectral band relative to the LSP resonance in scattering spectra persists for all structures but is more pronounced for shorter wavelengths, consistent with the experiment [3-5]. This blueshift and the change in the resonance lineshape originate from the interference between the direct and LSP-mediated recombination processes, which is incorporated in the MPL enhancement factor (2).

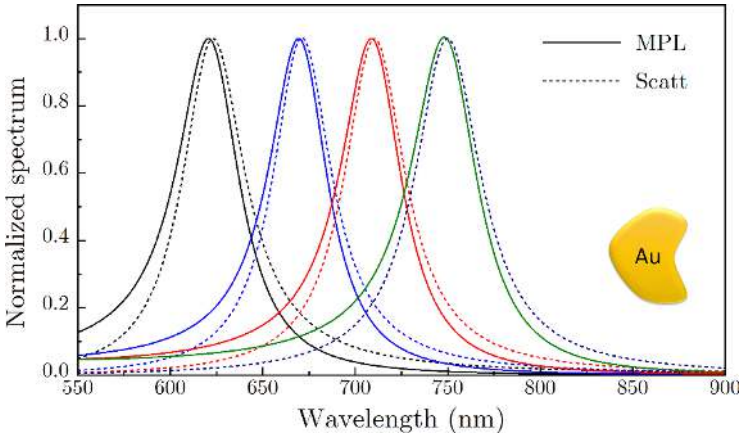


Figure 2. Normalized MPL and scattering spectra for gold nanostructures with characteristic size 40 nm at the same LSP wavelengths as in Fig. 1.

References

1. Dulkeith, E. *et al*., "Plasmon emission in photoexcited gold nanoparticles," Phys. Rev. B, Vol. 70, 205424 (2004).
2. Shahbazyan, T. V., I. E. Perakis, and J.-Y. Bigot, "Size-dependent surface plasmon dynamics in metal nanoparticles," Phys. Rev. Lett. Vol. 81, 3120, 1998.
3. Yorulmaz, M. *et al*., "Luminescence Quantum Yield of Single Gold Nanorods," Nano Lett. Vol. 12, 4385 (2012).
4. Fang, Y. *et al*., "Plasmon Emission Quantum Yield of Single Gold Nanorods as a Function of Aspect Ratio," ACS Nano Vol. 6, 7177, 2012.
5. Rao, W., Q. Li, Y. Wang, T. Li, and L. Wu, "Comparison of Photoluminescence Quantum Yield of Single Gold Nanobipyramids and Gold Nanorods," ACS Nano Vol. 9, 2783, 2015.

META 2023, PARIS - FRANCE, JULY 18 – 21, 2023

Graphene-based 2D Plasmonic Metamaterials for Terahertz Laser Transistors

T. Otsuji[1], S. Boubanga-Tombet[1], C. Tang[1], A. Satou[1], V. Ryzhii[1], K. Wojciech[2], D. Yadav[3], K. Narahara[4], M. Ryzhii[5], V. Mitin[6], and M.S. Shur[7]

[1]Research Institute of Electrical Communication, Tohoku University, Japan
[2]CENTERA, Institute of High Pressure Physics, Polish Academy of Sciences, Poland
[3]Center for Advanced Photonics, RIKEN, Japan
[4]Kanagawa Institute of Technology, Japan
[5]University of Aizu, Japan
[6]University at Buffalo, SUNY, USA
[7]Rensselaer Polytechnic Institute, USA
[*]corresponding author: otsuji@riec.tohoku.ac.jp

Abstract: This paper reviews recent advances in the research and development of graphene-based 2D plasmonic metamaterials for terahertz (THz) laser transistors.

The authors' theoretical discovery of THz laser transistors in 2007 [1-4] was realized in 2018 [5] as a distributed-feedback dual-gate graphene-channel field-effect transistor (DFB-DG-GFET). However it had small output power (single-mode emission at 5.2 THz with ~0.1 μW output intensity) and operated at a low lasing threshold temperature (100K). Various approaches have been introduced and discussed to realize room temperature, dry-cell battery operating, and intense THz lasing with fast direct modulation, based on graphene plasmonic metamaterials The proposed designs include (i) replacement of the laser photonic cavity with a plasmonic cavity enormously improving the THz photon field confinement with larger gain overlapping [6], (ii) introduction of THz amplification of stimulated emission via current-driven instability of graphene Dirac plasmons (GDPs) [7-12], and (iii) controlling the parity and time-reversal symmetry of GDPs enabling ultrafast direct gain-switch modulation [13-15]. Possible device structures and design constraints were discussed as a promising pathway towards coherent light sources for future 6G- and 7G-class THz wireless communication systems. The graphene plasmonic metamaterial solutions offer new ways for designing efficient devices for future robust far-infrared and THz plasmonic device technology. New physical models should meet new important challenges for theoretical physics and provide a full quantitative description of current-driven plasma phenomena in graphene and other 2D systems with Dirac-like energy band structure.

This work was supported by JSPS KAKENHI # 21H04546 and 20K20349, and RIEC Nation-Wide Collaborative Research Project #R04/A10, Japan. The work at RPI was supported by the Office of Naval Research (contract # N00014-23-1-2289, USA. The device process responsible for T. Otsuji was carried out at the Laboratory for Nanoelectronics and Spintronics of RIEC, Tohoku University, Japan.

References

1. Ryzhii, V., Ryzhii, M., Otsuji, T. "Negative dynamic conductivity in optically pumped graphene," J. Appl. Phys., Vol. 101, 083114, 2007.
2. Ryzhii M, Ryzhii V. "Injection and population inversion in electrically induced p-n junction in graphene with split gates," Jpn. J. Appl. Phys., Vol. 46, L151-L153, 2007.

3. Otsuji T, Boubanga-Tombet S, Satou A, Ryzhii M, Ryzhii V. “Terahertz-wave generation using graphene-toward new types of terahertz lasers,” IEEE J. Selected Topics in Quantum Electron., Vol. 19, 8400209, 2013.
4. Ryzhii V, Ryzhii M, Mitin V, Otsuji T. “Toward the creation of terahertz graphene injection laser,” J. Appl. Phys., Vol. 110, 094503, 2011.
5. Yadav D, Tamamushi G, Watanabe T, Mitsushio J, Tobah Y, Sugawara K, Dubinov AA, Satou A, Ryzhii M, Ryzhii V, Otsuji T. “Terahertz light-emitting graphene-channel transistor toward single-mode lasing,” Nanophotonics, Vol. 7, 741–752, 2018.
6. Dubinov A A, Sleshkin V Ya, Morozov SV, Ryzhii V, Otsuji T. “Terahertz plasmon-emitting graphene-channel transistor,” Opto-Electron. Rev., Vol. 27, 345-347, 2019.
7. Boubanga-Tombet S, Knap W, Yadav Y, Satou A, But DB, Popov VV, Gorbenko IV, Kachorovskii V, Otsuji T. “Room temperature amplification of terahertz radiation by grating-gate graphene structures,” Phys. Rev. X, Vol. 10, 031004, 2020.
8. Boubanga-Tombet S, Satou A, Yadav Y, But DB, Knap W, Popov VV, Gorbenko IV, Kachorovskii V, Otsuji T. “Paving the way for tunable graphene plasmonic THz amplifiers,” Frontiers in Phys., Vol. 7, 726806, 2021.
9. Ryzhii V, Ryzhii M, Mitin V, Shur MS, and Otsuji T. “S-shaped current-voltage characteristics of n+-i-n-n+ graphene field-effect transistors due to the Coulomb drag of quasi-equilibrium electrons by ballistic electrons,” Phys. Rev. Appl., Vol. 16, 014001, 2021.
10. Ryzhii V, Ryzhii M, Mitin V, Shur MS, and Otsuji T. “Coulomb drag mechanism of terahertz plasma instability in n+-i-n-n+ graphene FETs with ballistic injection,” Appl. Phys. Lett., Vol. 119, 093501, 2021.
11. Ryzhii V, Ryzhii M, Satou A, Mitin V, Shur MS, and Otsuji T, “Ballistic injection terahertz plasma instability in graphene n+-i-n-n+ field-effect transistors and lateral diodes,” Phys. Status Solidi A, Vol. 219, 2100694, 2022.
12. Ryzhii V, Ryzhii M, Satou A, Otsuji T, Mitin V, and Shur MS. “Effect of Coulomb carrier drag and terahertz plasma instability in p+-p-i-n-n+ graphene tunneling transistor structures,” Phys. Rev. Appl., Vol. 16, 064054, 2021.
13. Bender CM, Boettcher S. “Real spectra in non-Hermitian Hamiltonians having PT symmetry,” Phys. Rev. Lett., Vol. 80, 5243-5246, 1998.
14. Ramezani H, and Kottos T. “Unidirectional nonlinear PT-symmetric optical structures,” Phys. Rev. A, Vol. 82, 04383, 2010.
15. Miri M-A, Alu A. “Exceptional points in optics and photonics,” Science, Vol. 363, 42, 2019; Krasnok A, Alu A. “Active nanophononics,” Proc. IEEE, Vol. 108, 628-564, 2020.
16. Otsuji T, Boubanga-Tombet SA, Satou A, Yadav D, Fukidome H, Watanabe T, Suemitsu T, Dubinov AA, Popov VV, Knap W, Kachorovskii V, Narahara K, Ryzhii M, Mitin V, Shur MS, and Ryzhii V. "Graphene-based plasmonic metamaterial for terahertz laser transistors," Nanophotonics, Vol. 11, 1677-1696, 2022.

META 2023, PARIS - FRANCE, JULY 18 – 21, 2023

All-optical Control of Nonlinear Light Interaction with Topological Photonic Structures

Yupei Wang[1], Jitong Wang[1], and Nicolae C. Panoiu[1*]

[1]Department of Electronic and Electrical Engineering, University College London, Torrington Place, London WC1E 7JE, UK

[*]corresponding author: n.panoiu@ucl.ac.uk

Abstract: In this talk I will review some recent results regarding nonlinear interactions and all-optical control of one-way edge-modes of topological photonic crystals (PhCs) and graphene metasurfaces. Thus, I will show that the Kerr effect in graphene can be used to effectively control the valley-Hall topological transport in certain waveguides implemented in graphene metasurfaces. I will also demonstrate that pairs of bound states in the continuum of certain PhC slabs can be employed to achieve a remarkable enhancement of second-harmonic generation.

Topological photonics aims to utilize topological photonic bands and corresponding edge modes to implement robust light manipulation, which can be readily achieved in the linear regime of light-matter interaction. In this talk, I will review some recent results regarding nonlinear optical interactions and all-optical control of one-way edge-modes in frequency mixing processes in topological photonic crystals (PhCs) and graphene metasurfaces. Thus, I demonstrate that the influence of Kerr effect on valley-Hall topological transport in graphene metasurfaces can be used to implement an all-optical switch. To this end, by taking advantage of the large Kerr coefficient of graphene, the index of refraction of a topologically protected graphene metasurface can be tuned *via* a pump beam, which results in an optically controllable frequency shift of the photonic bands of the metasurface. This spectral shift can in turn be employed to control the propagation of an optical signal in certain domain-interface waveguide modes of the graphene metasurface. Our theoretical and computational analysis reveals that the threshold pump power needed to optically switch ON/OFF the signal is strongly dependent on the group velocity of the pump, especially when the device is operated in the slow-light regime. Certain methods for coupling light into the domain-interface waveguide modes of the graphene metasurface are also discussed.

In the second part of my talk, I will illustrate how bound states in the continuum (BICs) of certain silicon nitride (SiN) PhC slabs, engineered to possess sharp resonances with high quality factors at both the fundamental frequency (FF) and second-harmonic (SH) can be used to achieve an orders-of-magnitude enhancement of the SHG. By investigating the angle-resolved reflection spectra and corresponding modal analysis, we demonstrate that two PhC slabs with different configurations but same lattice constant, operating at telecommunication wavelengths, support a pair of at-Γ and a pair of off-Γ resonances. In both cases, BIC-type resonances are observed at the FF while BIC-like resonances are found at the SH. This double-resonance phenomenon is subsequently used to significantly enhance the SH generation (SHG) from the PhC slabs. The electric field patterns corresponding to the optical resonances reveal that there is a strong spatial overlap between the optical field of the modes for both at-Γ and off-Γ resonances. To quantify the efficiency of the nonlinear optical processes, we explore the dependence of SHG intensity on the angle of incidence. The existence of peaks in SHG spectra reveals the strong light-matter interaction facilitated by the double-resonance effect. The corresponding peak values of the SHG signal are several orders of magnitude larger than those corresponding to homogeneous SiN slabs with the same thickness.

META 2023, PARIS - FRANCE, JULY 18 – 21, 2023

Fluid-coupled Lamb waves for self-assembling three-dimensional photonic crystals

Y.-H. Chen[1], Y.-M. Huang[1], P.-K. Tsai[1], M.-H. Li[1], J.-S. Chen[2], and Y.-B. Chen[1*]

[1]Department of Power Mechanical Engineering, National Tsing Hua University, Hsinchu City, Taiwan 30013
[2] Department of Engineering Science, National Cheng Kung University, Tainan City, Taiwan 70101
[*]corresponding author: ybchen@pme.nthu.edu.tw

Abstract:

Fluid-coupled Lamb waves (LWs) were proposed to facilitate the self-assembling of three-dimensional (3D) photonic crystals (PCs) in this work. Numerical models were constructed for proof-of-concept, and a fabrication set-up was developed for experimental demonstration. LWs were initially generated by a piezoelectric substrate. A couplant altered the propagating direction of these LWs to form the fluid-coupled LWs at a superstrate. The coffee-ring effect (CRE) of a suspension droplet on the superstrate was thus suppressed. The suspended nanospheres formed 3D PCs after the droplet dried out. Diversified PCs were fabricated using the developed set-up. Their transmittance spectra demonstrated the corresponding bandgap clearly. Advantages of utilizing fluid-coupled LWs for self-assembling 3D PCs include flexibility in excitation frequency, fabrication cost-effectiveness, acceptance for a passively oscillating substrate, and enlargement of sample area.

References

1. Ni, Z. Xu, G. Huang, J. Yao, G. Tu, J. Guo, X. and Zhang, D. “Lamb wave coupled resonance for SAW acoustofluidics,” Appl. Phys. Lett. Vol. 118, 051103, 2021.
2. Hsu, J. C. and Chao, C. L. “Acoustophoretic patterning of microparticles in a microfluidic chamber driven by standing Lamb waves,” Appl. Phys. Lett. 119, 103504, 2021.
3. Chen, Y.-H. Huang, Y.-M. Tsai, P.-K. Li, M.-H. Chen, J.-S. and Chen, Y.-B. “Fluid-coupled Lamb waves for self-assembling three-dimensional photonic crystals,” J. Appl. Phys. Vol. 132, 065301, 2022.

META 2023, PARIS - FRANCE, JULY 18 – 21, 2023

Topological Tamm states based on flat band symmetry inversion

S. Khattou[1], Y. Rezzouk[1], M. Amrani[1], M. El Ghafiani[1], E. H. El Boudouti[1], A. Talbi[2], and B. Djafari-Rouhani[2*]

[1]LPMR, Département de Physique, Faculté des Sciences, Université Mohammed I, Oujda, Morocco

[2]CNRS – Univ. Lille - UPHF - Ecole Centrale – JUNIA, UMR 8520 -IEMN - F-59000 Lille, France

[*]corresponding author: bahram.djafari-rouhani@univ-lille.fr

Abstract: We study topological Tamm states at the interface between two comb-like photonic or phononic crystals based on a new mechanism of band inversion symmetry due to the existence of flat bands. Several arguments such as the Zak phase or the phase of the reflection coefficients support the topological nature of the interface states. The analytical results are well reproduced by experiments using coaxial cables.

1. Introduction and methodology

The interface between two photonic or phononic crystals (PCs) can support localized states called optical or acoustic Tamm states[1]. In this work, we are interested by topological Tamm states at the interface between two one-dimensional PCs, each consisting of a periodic array of stubs attached along a waveguide (Fig. 1 (a)). Several works have addressed such Tamm states in comb-like PCs[2] in the framework of the well-known Su-Schrieffer-Heeger (SSH) model[3], a dimerized chain based on two resonators per unit cell. This PC exhibits a Dirac cone at the boundaries of the Brillouin zone. By changing the parameters of the PC, a gap opens at the Dirac cone and a common gap between two topologically different PCs (characterized by a symmetry inversion of their bulk edge modes) supports an interface state of topological nature. In this work[4-5], we propose a new concept for the existence of topological interface states which results from band edge symmetry inversion around a flat band, namely the mechanism is based on the vanishing of the width of a passband instead of the closing of a bandgap. The flat bands originate from the local resonances of the stubs constituting the PC.

We start from the geometrical parameters and a frequency where the flat band occurs. Then, by changing the periods of the PCs from the initial value, we realize two crystals with different topological properties around the initial flat band and demonstrate the existence of Tamm states in the common gaps of the two PCs. Different arguments and approaches are used to discuss the Tamm states and their topological character, namely the topology of the passband from the determination of their Zak phases and the symmetry of their edge modes, or a condition on the phases of the reflection coefficients when each PC is attached to a waveguide at its extremity. These interface states manifest themselves as peaks in the local density of states. They also appear as peaks or dips in the transmission and reflection spectra when a finite structure constituted by two combined PCs is inserted in a waveguide or is vertically attached to a waveguide. For some specific geometrical parameters, the interface state becomes a bound state in the continuum (BIC) which is characterized by an infinite lifetime. All the theoretical demonstrations are based on semi-analytical calculations using a Green's function method. They are supported by simple experiments using coaxial cables in the radiofrequency range.

2. Theoretical and experimental illustrations

The comb-like PC (Fig. 1(a)) is defined by the length of the stubs $\mathbf{d'_1}$, chosen as the unit of length, and the period $\mathbf{d_1}$. Figure 1(b) shows the successive passbands of an infinite PC as a function of the period $\mathbf{d_1}$. The points labeled 1 to 4 represent the position of the flat bands where the bands close and reopen. The edge modes of two

bands in the vicinity of a flat band are characterized by the same symmetry. The lines with pink and cyan colors indicate the symmetric and antisymmetric band edge states and the Zak phase of each band is respectively zero or π depending on whether the symmetry of its edge states is the same or different (area respectively colored in gray and dark cyan). From the band diagram of Fig. 1(b), one can easily select two PCs with different periods exhibiting a common band gap such that the edges of their lower passbands have two different symmetries. Such a gap necessarily supports a topological interface state. As an example, for the pair of PCs called PC1 and PC4 (with d_1=0.5 and 1.7 respectively), there is an interface mode in their common gap around the dimensionless frequency Ω = 0.6 and not in their other common bandgaps around Ω = 0.5 and Ω = 1.5. This result is confirmed by a dip indicated T (Fig. 1(c)) in the reflection spectrum of a finite structure constituted by an association of PC1 and PC4 and embedded inside a waveguide (Fig. 1(a)). The theoretical results in presence of loss (blue lines) are confirmed by an experimental validation (open circles). Another example with an association PC2-PC3 is shown in Fig. 1(d), where two interface states appear in two consecutive gaps separated by a flat band in their middle around Ω = 1.5. Finally, let us mention that the above results can be easily transposed to acoustic waves in slender tubes[5] and plasmonic metal-insulator-metal waveguides operating in the telecommunication domain[6].

Acknowledgments: The work of BDR is supported by HORIZON-CL4-2022-RESILIENCE-01-10 project No. 101091968 MAGNIFIC and by the CHIST-ERA ERA-NET project MUSICIAN.

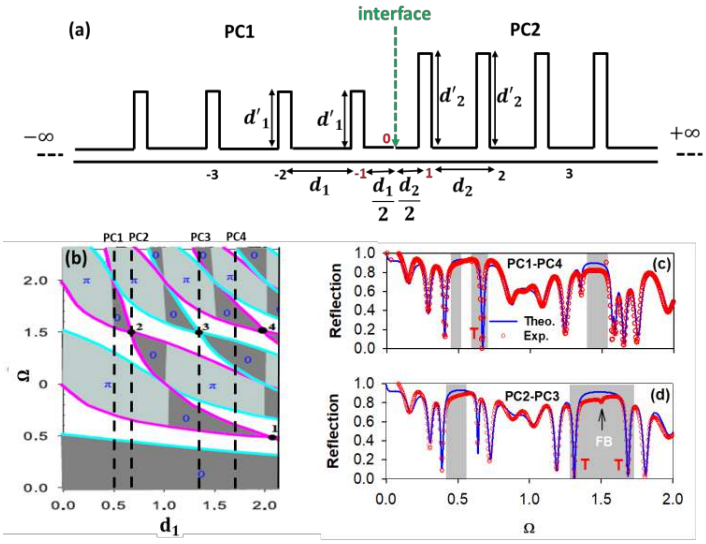


Figure 1: (a) Interface between two PCs (PC1 and PC2), each composed of a unit cell made of a stub of length $\mathbf{d'}_i$ and period $\mathbf{d}_i$ (i =1, 2). (b) Band structure (in dimensionless units) of an infinite PC. The black dots 1 to 4 indicate the band crossing points where the bands close and reopen. The lines in pink and cyan colors indicate symmetric and antisymmetric band edge states, respectively. Gray and dark cyan colors indicate that the Zak phase of the band is 0 and π, respectively. (c), (d) Reflection amplitude for a finite PC made of PC1-PC4 and PC2-PC3, respectively. Solid lines represent the theoretical results in presence of loss, while open circles give the experimental measurements. Gray areas indicate the common gaps between each combination. The symbol T refers to Tamm states.

References

1. M. Kaliteevski, I. Iorsh, S. Brand, R. Abram, J. Chamberlain, A. Kavokin, I. Shelykh, Phys. Rev. B 76, 165415 (2007).
2. W. Zhu, Ya-Q Ding, J. Ren, Y. Sun, Y. Li, H. Jiang, and H. Chen, Phys. Rev. B 97, 195307 (2018).
3. W. Su, J.R. Schrieffer, and A.J. Heeger, Phys. Rev. Lett. 42, 1698, 1979.
4. S. Khattou, Y. Rezzouk, M. El Ghafiani, M. Amrani, M. Elaouni, E. H. El Boudouti, A. Talbi, A. Akjouj, B. Djafari-Rouhani, Phys. Rev. B (2023) (in press)
5. S. Khattou, Y. Rezzouk, M. Amrani, M. El Ghafiani, E. H. El Boudouti, A. Talbi, B. Djafari-Rouhani, Crystals 12, 1685 (2022).
6. Y. Rezzouk, M. Amrani, S. Khattou, E. H. El Boudouti, B. Djafari-Rouhani, J. Opt. Soc. Am. B 39, 600-610 (2022).

Ultrafast nanophotonics: from all-optical control of exciton dynamics towards plasmon-tailored nano-chemistry and information processing based on cavity-electrodynamics

N. Maccaferri[1,2*]

[1]Department of Physics, Umeå University, 901 87 Umeå, Sweden
[2]Department of Physics and Materials Science, University of Luxembourg, 1511 Luxembourg City, Luxembourg
[*]corresponding author: nicolo.maccaferri@umu.se

Abstract: Light as information career can revolutionize how we store and process information. At the same time, nanoscale confinement of electromagnetic fields can change the way we approach photo-chemical reactions and electronic energy landscapes. This rich potential can pave the way to develop new hardware enabling faster and more energy-efficient computing schemes, thus contributing to the raise of photonic quantum nanotechnologies.

Ultrafast control of light-matter interactions is fundamental in view of new technological frontiers, for instance in light-driven information processing and nanoscale photochemistry [1]. In this framework, we explore metal-dielectric nanocavities to achieve all-optical modulation of the light reflectance at a specific wavelength. Without the need of driving higher order effects, our system is based on linear absorption, provides large relative modulation exceeding 100% and switching bandwidths of few hundred GHz at moderate excitation fluence [2]. This archetypical system becomes even more interesting if the "gain medium" is an inorganic van der Waals bonded semiconductor, like a transition metal dichalcogenide (TMD). TMDs are subject of intense research due to their electronic and optical properties which are promising for next-generation optoelectronic devices. In this context, understanding the ultrafast carrier dynamics, as well as charge and energy transfer at the interface between metals and semiconductors is crucial and yet quite unexplored. By employing a pump-push-probe scheme, we experimentally study how thermally induced ultrafast charge carrier injection affects the exciton formation dynamics in bulk WS2 [3], opening up excellent opportunities also in nano-chemistry. In fact, if an electronic transition strongly interacts with the light modes of a resonator, we can tailor the energetics and the morphology of a molecular state. By combining quantum mechanical modelling and pump-probe spectroscopy, we shed light on the ultrafast dynamics of a hybrid system composed of photo-switchable dye molecules coupled with optically anisotropic plasmonic nanoantennas, which allow us to selectively switch between two regimes where the light-matter interaction is either weak or strong [4]. Our synergistic approach is instrumental to devise new strategies for tailoring electronic states by using plasmons for applications in polaritonic chemistry on femtosecond timescales.

We acknowledge support from the Swedish Research Council (grant n. 2021-05784), Kempestiftelserna (grant n. JCK-3122), the European Innovation Council (grant n. 101046920 'iSenseDNA'), and the Luxembourg National Research Fund (grant n. C19/MS/13624497 'ULTRON') and the European Commission (grant n. 964363 'ProID').

References

1. Koya, A. N. et al., "Advances in ultrafast plasmonics," arXiv:2211.08241.
2. Kuttruff, J. et al., "Ultrafast all-optical switching enabled by epsilon-near-zero-tailored absorption in metal-insulator

nanocavities," Commun. Phys., Vol. 33, No. 114, 2020.
3. Keller, K. R. et al., "Ultrafast Thermionic Electron Injection Effects on Exciton Formation Dynamics at a van der Waals Semiconductor/Metal Interface," ACS Photonics, Vol. 9, No. 8, 2683–2690, 2022.
4. Kuttruff, J. et al., "Ultrafast dynamics of a hybrid plasmon polariton-molecular system at the weak and strong coupling regimes," arXiv:2205.06358.

Dielectric nanostructures for novel photonics devices: from Solar Cells to NanoLEDs.

B. García-Cámara, L. Escandell, A.I. Barreda, E. López-Fraguas, R. Vergaz and J.M. Sánchez-Pena

[1]Groups of Displays and Photonic Applications, Carlos III University of Madrid, Spain
[*]corresponding author: braulio.garcia@uc3m.es

Abstract: This work shows a review of our last works in the design of dielectric nanostructures and dielectric metamaterials to improve the performance of photonics devices and/or development new ones.

It is well known that dielectric nanostructures with a refractive index such that there is a high contrast respect to the surrounding medium are able to support Mie resonances with a myriad of interesting properties. In this sense, this kind of nanostructures are able to present an effective magnetic behavior, produce light scattering directionality or enhance non-linear effects [1-4]. In the last years, the main efforts are focused on the exploration of using these nanostructures and their unique properties in the improvement and/or development of new photonic devices. In this sense, several research groups are currently working on the integration of all-dielectric nanostructures to improve the performance of optical biosensors or functional communications devices, among others.

In this work, we review our last works in the numerical design of dielectric nanostructures and dielectric metamaterials for different applications. In particular, we are mainly focused on the development of novel designs for optical emitters, such as LEDs, and detectors, such as solar cells.

This work was funded by the Spanish Research Agency (AEI) through the grants PID2019-109072RB-C31/AEI/10.13039/501100011033 and PDC2021-121370-C22 and Comunidad de Madrid by SINFOTON2-CM (grant number S2018/NMT-4326). These grants are also co-founded by the European Fund for Regional Development.

References

1. Kuznetsov, A., A.E. Miroshnichenko, M.L. Brongersma, Y.Kivshar , and B. Luk'yanchuk "Optically resonant dielectric nanosctructures" Science, Vol- 354, No. 6314, aag2472, 2016.
2. Xu, J., Y. Wu, P. Zhang, Y.Wu, R.A.L. Vallée, S. Wu and X. Liu, "Resonant Scattering Manipulation of Dielectric Nanoparticles" Adv. Opt. Mater., Vol. 9, No. 15, 2100112, 2019.
3. Ullah, K. B. García-Cámara, M. Habib, X. Liu, A. Krasnok, S. Lepeshov, J. Hao, J. Liu and N.P. Yadav. "Chiral all-dielectric trimmer nanoantenna" J. Quant. Spect. Rad. Trans., Vol. 208, 71-77, 2018.
4. Liu, T., S. Xiao, B. Li, M. Gu, H. Luan, X. Fang. "Third- and second-harmonic generation in all-dielectric nanoastructures: A mini review" Front. Nanotechnol., Vol. 4, 891892, 2022.

Enhanced electric field and emission directionality of gap mode

D. Zhang,* P. Miao, F. Schneider, Y. Zhao, T. Parker, A. Meixner

Institute of Physical and Theoretical Chemistry,

Eberhard Karls Universität Tübingen, Tübingen, Germany

*e-mail of corresponding author: dai.zhang@uni-tuebingen.de

Abstract: The localized plasmonic resonance and electric field in small gaps will be discussed. To evaluate the enhanced excitation electric field, the intensities and energies of the photoluminescence, and Raman signals are compared by varying the gap sizes systematically. Further insights into the gap-mode emission properties in the k-space are obtained by combining the back focal plane technique with parabolic mirror assisted optical microscopy.

High-resolution optical technique combining scanning probe microscopy and optical microscopy has shown its distinct capability in characterizing materials with high chemical and spatial resolution. In the past years this technique has witnessed an extremely active development, which has shown to be operated at low temperature, ultra-high vacuum or electrochemical environment [1].

In this talk, our work about applying tip-enhanced Raman and fluorescence microscopy to study the nanometer scale structural properties of optoelectronic materials will be reported. [2] Further, back focal plane imaging of gap mode that is formed either by single nanoparticle-on-ultrasmooth gold film or gold tip/gold crystal, will be presented. The influences of nanoparticles and tips of different geometries on the directionalities of the emission signals from the narrow gap will be discussed. [3]

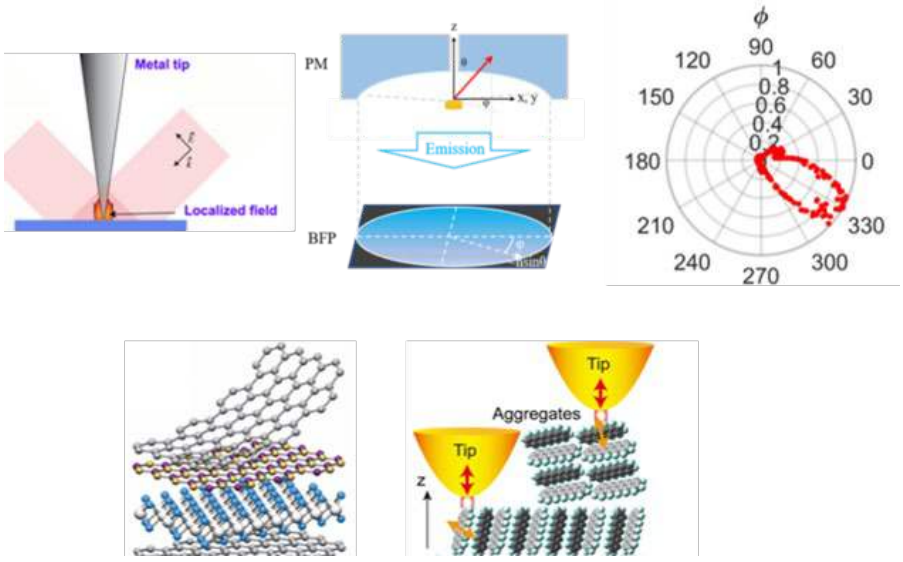


Figure 1. Plasmonic enhanced optical microscopy and k-space imaging visualize the local structural properties of semiconductive molecules at the nanometer scale.

Acknowledgements: This work was financially supported by the German Research Foundation (Nos. ZH 279/13-1 and ME 1600/21-1), and the Chinese Scholarship Council.

References

1. S.-C. Huang, et al., Annu. Rev. Phys. Chem., 2021, 72, 213-234. DOI: 10.1146/annurev-physchem-061020-053442; Y. Zhang, et al., National Science Review 2019, 6, 1169-1175. https://doi.org/10.1093/nsr/nwz180; T. Touzalin, et al. 2019, 108, 106557. https://doi.org/10.1016/j.elecom.2019.106557
2. P. Miao, Y.-T. Chen, L. Pan, A. Horneber, K. Greulich, T. Chassé, H. Peisert, P.-M. Adam, P. Xu, A. Meixner, D. Zhang, The Journal of Chemical Physics, 2022, 156, 034702. https://doi.org/10.1063/5.0078113. M. van den Berg, A. J. Meixner, D. Zhang et al., Beilstein J. Nanotechnol., 2020, 11, 1147. https://doi.org/10.3762/bjnano.11.99. Y. C. Zhao, D. Zhang, C. Brabec et al, Nature Comm., 2020, 11, 6328. 10.1038/s41467-020-20066-7.
3. Yu-Ting Chen, PhD thesis, 2021, Tip-Enhanced Optical Spectroscopy: Resonance, Hotspot, Imaging, and Radiation, Eberhard Karls University of Tübingen.

Chiral Phase Change Nanomaterials: A nanoscale path to microscopic optics

Imad Agha[1,2,*]

[1]Department of Physics, University of Dayton, Dayton, OH, USA
[2]Department of Electro-Optics and Photonics, University of Dayton, Dayton, OH, USA
[*]corresponding author: iagha1@udayton.edu

Abstract: In this talk, we present our most recent results on phase change nanomaterials, based on bottom-up self-assembly fabrication techniques, as well as their use in phase, amplitude, and polarization control.

Due to their optical and electrical tunability aspect, there has been a renewed and strong interest in Phase change materials (PCMs) in1many fields beyond traditional memories. Given their unique characteristic of changing phase on-demand from amorphous to crystalline1 and vice versa, they can be applied in many applications ranging from optical filters to rewritable metasurfaces. The ultimate limitation, however, has been the thickness at which these materials can be switched. Due to the thermal distribution in the thin film, PCMs have been limited to switching at sub-100nm thicknesses. In our work[1], we found that through a self-assembly technique, commonly referred to as Glancing Angle Deposition (GLAD) (Fig. 1), it is possible to beat the limit of thickness on Chiral Phase Change Nanomaterials (PCNMs), and produce devices for phase, amplitude, and polarization control.

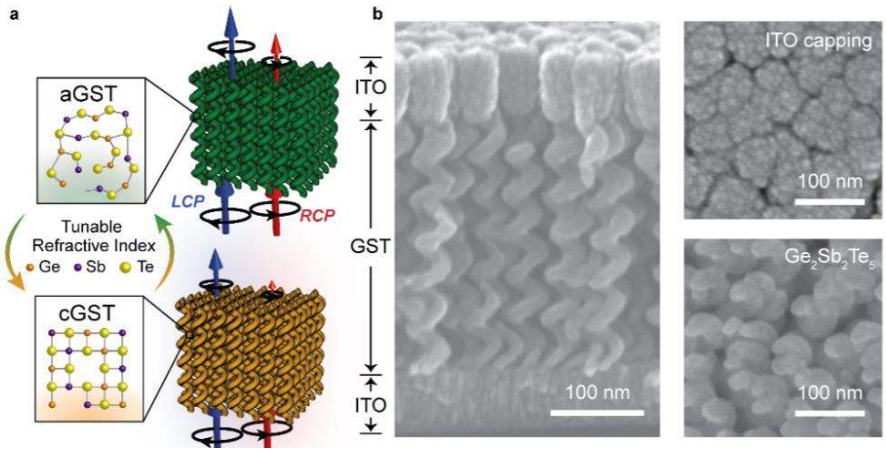


Fig 1: Growth of Chiral PCNMs (a) and SEM of structures (b)

The PCNMs are grown using glancing angle deposition, whereby a substrate is placed at a sharp angle and rotated during electron beam evaporation. Two targets were used here: Germanium Antimony Telluride (GST) and Antimoney Selenide (SbSe). While GST is highly opaque in the visible regime, it produces sharp resonances due to absorption, that can be exploited in highly resonant processes, such as optical chirality, in which selective absorption between left and right handed polarizations can be amplified through the left or right-handed geometry. In the case of SbSe nanorods, the effect is less pronounced, however these structures are useful as

they allow for the growth of very thick films well beyond the growth methods for bulk thin films. Additionally, due to the low packing density, it is possible to optically (and potentially electrically) cycle much thicker films than the earlier reported limit of ~ 100 nm between the amorphous and crystalline phases. This method will open the door to a variety of future devices that hitherto have been impossible to implement due to fundamental limitations of PCMs in their bulk thin film structure.

References

1. Burrow, J. A., Shah Alam, MD, Smith, E. M., Yahiaoui, R., Laing, R., Shah, P. J., Searles, T. A., Vanagala, S., Hendrickson, J., Sarangan, A., and Agha, I., Chiral Phase Change Nanomaterials, arXiv:2111.09940v1 (2021)

Strong light matter interaction in plexcitonic crystals

M. Ferrera[1], J. S. Pelli Cresi[1], V. Aglieri[1], E. Ghidorsi[1] and A. Toma[1*]

[1]Istituto Italiano di Tecnologia, via Morego 30, 16163 Genova, Italy
[*]corresponding author: andrea.toma@iit.it

Abstract: Nanohybrid platforms featuring strong light-matter interactions were fabricated and spectroscopically investigated. Both steady-state and ultrafast pump-probe spectroscopies were exploited to investigate the radiative properties of the hybrid systems and to assess the strong-coupling regime achievement.

The interaction of electromagnetic radiation with matter plays an instrumental role in our everyday life and typically involves an energy exchange between an external electromagnetic field and a photon emitter (dye molecules, low-dimensional semiconductors, etc.). The possibility of controlling/engineering the interplay between the electromagnetic field and quantum states of matter -through *ad-hoc* designed optical resonators- provides a key to reshape the energy landscapes of the nanomaterial elementary excitations [1]. In particular, if the exchange rate of energy is faster than any other competing relaxation process, the system can enter the so-called "strong coupling" regime. New hybrid light/matter states, called polaritons, are formed [2], which in turn offer huge potential for a wider class of technological applications, including quantum computing [3], non-linear photonics and polariton chemistry [4].

Here, the focus is on hybrid platforms, where quantum emitters are combined with nanopatterned metallic surfaces in order to obtain strongly coupled states. The radiative properties of the plasmonic-excitonic heterostructures has been characterized by both steady-state and ultrafast pump-probe spectroscopies. The presence of the anti-crossing behavior has been assessed, and results in terms of Rabi splitting energy and polariton relaxation dynamics reported. Experiments of time-resolved spectroscopies can indeed shed light on the intrinsic photophysics of such heterostructures by revealing the dynamics of the hybrid states. Among the various architectures, the attention has been addressed to long-range ordered plasmonic crystals. The present systems, with their open architecture, offers an appropriate platform where the excitonic material can be easily placed, thus concurrently allowing for the proper excitation and investigation of the newly formed plexcitonic states [5,6]. This work sets the base for further studies on the design, fabrication and investigation of novel nanohybrid architectures featuring strong light-matters interactions, and their exploitation towards functional devices.

Acknowledgement

The authors acknowledge support by the European Research Council (ERC) under the European Union's Horizon 2020 research and innovation program "REPLY ERC-2020-COG Grant agreement No. 101002422".

References

1. Rivera, N. and I. Kaminer "Light-matter interaction with photonic quasiparticles," Nat. Rev. Phys., Vol. 2, 538–561, 2020.
2. Törmä, P. and W. L. Barnes, "Strong coupling between surface plasmon polaritons and emitters: a review," Rep. Prog. Phys., Vol. 78, No. 1, 013901, 2014.
3. Kavokin, A., T. C. H. Liew, C. Schneider, P. G. Lagoudakis, S. Klembt and S. Hoefling, "Polariton condensates for

classical and quantum computing", Nat. Rev. Phys., Vol. 4, 435-451, 2022.

4. Yuen-Zhou, J. and V. M. Menon, "Polariton chemistry: thinking outside the (photon) box", Proc. Natl. Acad. Sci., Vol. 116, No. 12, 5214-5216, 2019.
5. Wang, H., H.-Y. Wang, H.-B. Sun, A. Cerea, A. Toma, F. De Angelis, X. Jin, L. Razzari, D. Cojoc, D. Catone, F. Huang and R. Proietti Zaccaria, "Dynamics of strongly coupled hybrid states by transient absorption spectroscopy", Adv. Funct. Mater., Vol. 28, 1801761, 2018.
6. Salomon, A., S. Wang, J. A. Hutchison, C. Genet and T.W. Ebbesen, "Strong light-molecule coupling on plasmonic arrays of different symmetries", ChemPhysChem, Vol. 14, 1882-1886, 2013.

META 2023, PARIS - FRANCE, JULY 18 – 21, 2023

Characterization of Nano-grating Profiles using Standard Ellipsometry and Deep Neural Networks

Zijie Jiang[1] and Wen-Di Li[1*]

[1]Department of Mechanical Engineering, Univ. of Hong Kong, Hong Kong, China
[*]corresponding author: liwd@hku.hk

Abstract: In-situ measurement of nano-grating profiles is of great importance in the semiconductor industry. We propose a new method based on deep neural networks and gradient descent method to fully reconstruct the profile of nano-gratings using standard ellipsometry data (i.e., ψ and Δ) rather than commonly used Muller matrix ellipsometry. A wide range of samples of fabricated by wafer-scale interference lithography were used to train and test our model with promising performance for fast, non-destructive, and in-situ characterization of nanostructure profiles.

In-situ measurement of nano-grating profiles is of great importance in the semiconductor industry. Recently, as a popular and powerful tool, deep learning is applied to infer key parameters of gratings from measured spectral and ellipsometry information. Compared with conventional characterization techniques, such as scanning electron microscopy (SEM) and atomic force microscopy, deep-learning-based methods possess the advantages of high efficiency and high throughput. However, most reported methods of this type rely on Muller matrix ellipsometry [1] or some special optical measurement systems [2], which is typically expensive and not commonly available. Moreover, geometric models used in these methods are over-simplified and usually limited to a single patterning method or material, hindering their adoption in practical applications.

In this research, we propose a new method based on deep neural networks and gradient descent method to fully reconstruct the profile of nano-gratings using standard ellipsometry data (i.e., ψ and Δ). As shown in Figure 1(a), twelve parameters are adopted to describe the grating. The application of round corners, waist width, and refractive index makes the model compatible with various kinds of patterning techniques and different resists. Figure 1(b) illustrates the architecture of the algorithm. To relieve the problem of multiple solutions, seven sets of spectra from different azimuthal angles are fitted simultaneously as an additional constraint, which can improve the accuracy and stability of our method. Notably, these azimuthal angles can be arbitrarily selected within a predefined range. The candidate solution is updated by the gradient descent algorithm to minimize the mean square error (MSE) between predicted and measured spectra. As a demonstration, samples made by interference lithography are tested. To emulate measurement data, simulated ellipsometry spectra are added with Gaussian noise. Yellow dashed lines shown in Figure 2 display the inferred profile, which is consistent with SEM images. The mean absolute errors (MAE) of profiles for three gratings are 7, 9, and 9 nm respectively. MSEs of fitted and target spectra are only 15.4, 1.8, and 0.5.

References

1. 1. K. Meng, B. Jiang, and K. Youcef-Toumi, Appl. Surf. Sci. 570, 151219 (2021).
2. 2. T. Li, A. Chen, L. Fan, M. Zheng, J. Wang, G. Lu, M. Zhao, X. Cheng, W. Li, X. Liu, H. Yin, L. Shi, and J. Zi, Light: Sci. Appl. 10, 154 (2021).

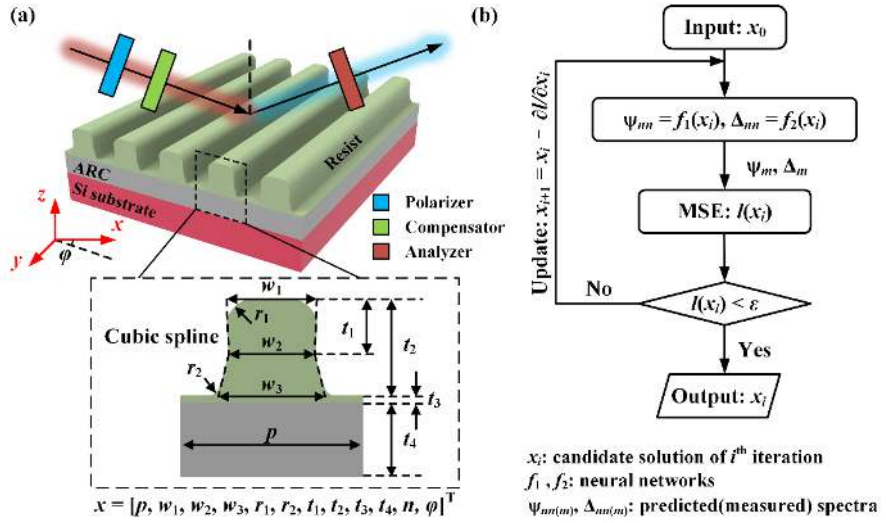


Figure 1. (a) Schematic of a standard ellipsometer (top inset) and model of the grating profile (bottom inset). Twelve parameters are used to describe both geometric and optical properties (refractive index *n* of resist) of measured gratings. (b) Flow chart to iteratively infer satisfactory parameters from measured ellipsometry data.

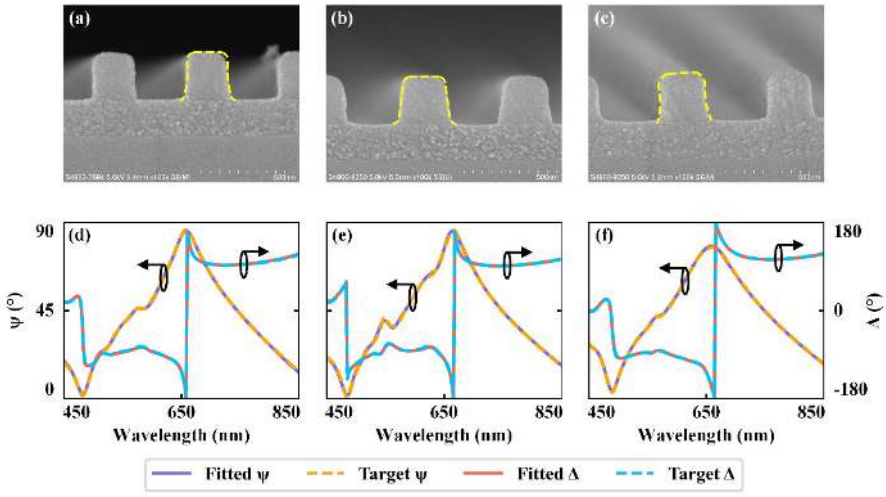


Figure 2. (a) – (c) Comparisons between SEM images and profiles (yellow dashed lines) inferred by the proposed method. (d) – (f) Ellipsometry data of fitted (solid lines) and measured (dashed lines) results under azimuthal angles near 0°.

Colloidal Metal Nanoparticles under Ultrafast Laser Pulses

A. Guerrero-Martínez

Departamento de Química Física, Universidad Complutense de Madrid, Avda. Complutense s/n, 28040 Madrid, Spain
aguerrero@quim.ucm.es

Abstract: The control of the excitation of the localized surface plasmon resonances of colloidal metal nanoparticles with ultrafast laser pulses, from the nanosecond to the femtosecond timescales, can be used to prepare highly monodisperse metal nanoparticles, hollow metal nanoparticle morphologies, alloyed metal nanoparticles, or assembled and welded nanostructures.

The vast majority of the applications of metal nanoparticles developed during the last two decades have arisen from their unique optical properties. Within this context, rational synthesis and assembly of metal nanoparticles have been the main research focus, aiming at the design of nanoplasmonic devices with tailored optical functionalities. The progress made in this field is thus to be ascribed to the understanding of the origin of the interaction between light and such nanostructures, the dynamics of which have been thoroughly investigated with significant contributions from short and ultrashort pulse laser technologies.[1] This presentation focuses on the potential of pulse lasers to provide new fundamental insights into the electron dynamics involved in the interaction of light with the free conduction electrons of metal nanoparticles, that is, localized surface plasmon resonances (LSPRs). The excitation of LSPRs with a femtosecond pulse laser is followed by thermalization of the metal nanoparticle electrons and the subsequent relaxation of the nanocrystal lattice and the surrounding environment, which generally results in surface melting.[2] By contrast, nanosecond irradiation usually induces metal nanoparticle fragmentation and uncontrolled melting due to overlapping excitation and relaxation phenomena. These concepts have been exploited toward the preparation of highly monodisperse metal nanoparticles via femtosecond pulse laser irradiation of polydisperse colloids, or in the fabrication of hollow metal nanoparticles.[3] In addition, pulse laser irradiation has been proven a unique tool for the controlled assembly and welding of colloidal metal nanoparticles by electromagnetic field enhancement at the hot spots of assembled metal nanoparticles. The combination of different nanometals with pulse lasers promises significant chemical advances, including the preparation of alloyed nanostructures with potential applications in sensing and catalysis.

References

1. González-Rubio, G., Guerrero-Martínez, A. and Liz-Marzán, L. M., “Reshaping, Fragmentation, and Assembly of Gold Nanoparticles Assisted by Pulse Lasers”, Acc. Chem. Res., 49, 678–686, 2016.
2. González-Rubio, G., Díaz-Núñez, P., Rivera, A., Prada, A., Tardajos, G., González-Izquierdo, J., Bañares, L., Llombart, P., Macdowell, L. G., Palafox, M. A., Liz-Marzán, L. M., Peña-Rodríguez O. and Guerrero-Martínez, A., “Femtosecond laser reshaping yields gold nanorods with ultranarrow surface plasmon resonances”, Science, 358, 640–644, 2017.
3. González-Rubio, G., Díaz-Núñez, P., Albrecht, W., Manzaneda-González, V., Bañares, L., Rivera, A., Liz-Marzán, L. M., Peña-Rodríguez, O., Bals, S. and Guerrero-Martínez, A., “Controlled Alloying of Au@Ag Core-Shell Nanorods Induced by Femtosecond Laser Irradiation” Adv. Opt. Mater., 9, 2002134, 2021.

META 2023, PARIS - FRANCE, JULY 18 – 21, 2023

Self-powered Flexible Devices: Piezo-sensor and microLED

Keon Jae Lee[1*]

[1]Department of Materials Science and Engineering, KAIST, South Korea

[*]corresponding author: keonlee@kaist.ac.kr

Abstract: This seminar introduces recent progresses of self-powered flexible devices; piezo-sensors and microLED. The first part, we reported a machine learning-based acoustic sensor by mimicking the basilar membrane of human cochlear. Highly sensitive self-powered flexible piezoelectric acoustic sensor (f-PAS) with a multi-resonant frequency band was employed for voice recognition. The second part will discuss the highly efficient flexible vertical micro LED (f-VLED) for full color displays and biomedical applications. We introduces the flexible vertical GaAs/GaN microLED on plastic substrates using micro-vacuum transfer and anisotropic conductive film. The superb properties of the flexible inorganic LED enable the dramatic extension of flexible displays toward not only full color displays and wearable phototherapy patches for skin research like hair growth and melanogenesis inhibition.

References

1. "Machine Learning-based Self-powered Acoustic Sensor for Speaker Recognition", Nano Energy, 53, 658, 2018
2. "Flexible Piezoelectric Acoustic Sensor and Machine Learning for Speech Processing", Adv. Mater., 32, 1904020, 2020
3. "Biomimetic and Flexible Piezoelectric Mobile Acoustic Sensors with Multi-Resonant Ultrathin Structures for Machine Learning Biometrics", Sci. Adv., 7, eabe5683, 2021
4. "Optogenetic Control of Body Movements via Flexible Vertical Light-Emitting Diodes on Brain Surface", Nano Energy, 44, 447, 2018.
5. "Monolithic Flexible Vertical GaN Light-Emitting Diodes for Transparent Wireless Brain Optical Stimulator", Adv. Mater. 30, 1800649, 2018

META 2023, PARIS - FRANCE, JULY 18 – 21, 2023

Controllable generation of frequency-encoded qubits and qudits using silicon photonics nano-engineered devices.

Massimo Borghi[1,*], Noemi Tagliavacche[1], Federico Andrea Sabattoli[2], Houssein El Dirani[3], Laurene Youssef[4], Camille Petit-Etienne[5], Erwine Pargon[5], Corrado Sciancalepore[6], J.E. Sipe[7], Marco Liscidini[1], Matteo Galli[1], and Daniele Bajoni[8]

[1]Dipartimento di Fisica, Università di Pavia, Via Agostino Bassi 6, 27100 Pavia, Italy

[2]Advanced Fiber Resources Milan S.r.L, via Fellini 4, 20097 San Donato Milanese (MI), Italy

[3]LIGENTEC SA, 224 Bd John Kennedy, 91100 Corbeil-Essonnes, France

[4]IRCER, Centre Européen de la Céramique, 12 rue Atlantis, 87068 Limoges, France

[5]Univ. Grenoble Alpes, CNRS, LTM, 38000 Grenoble, France

[6]SOITEC SA, Parc technologique des Fontaines, Chemin des Franques, 38190 Bernin, France

[7]Department of Physics, University of Toronto, 60 St. George Street, Toronto, ON, M5S 1A7, Canada

[8]Dipartimento di Ingegneria Industriale e dell'Informazione, Università di Pavia, Via Adolfo Ferrata 5, 27100 Pavia, Italy

[*]Corresponding author: massimo.borghi@unipv.it

Abstract: We present silicon photonic devices designed for the generation of frequency bin entangled qubits and qudits. We show through quantum tomography experiments that bin spacing, qudit dimension, and bipartite quantum state can be directly controlled using on-chip devices. We discuss further developments and the possible applications in several key quantum technologies.

Encoding quantum information in systems with dimensionality of the Hilbert space larger than 2 (qudits) is important in the development of large scale architectures for many quantum technologies. This strategy is particularly suitable when using photons as carriers of quantum information, due to the variety of degrees of freedom they possess. For example, frequency bin encoding, i.e., the use of different frequency bands to encode logical states, has been shown to be very effective in creating qudits by means of integrated quantum optical microcombs [1]. In these experiments spontaneous four wave mixing (SFWM) in a microresonator with a comb spacing (FSR) of the order of few tens of GHz is used to generate photon pairs, while coherent manipulation is achieved through off-the-shelf fiber optic components such as electro-optic modulators (EOM) and waveshapers [2].

The use of single rings and commercial EOMs generally compromises the source brightness, which scales with the inverse square of the FSR. Recently, it has been shown that this trade-off can be removed by the use of multiple resonators, each associated with the generation of a pair of non-degenerate frequency bins [3], and this paradigm has been experimentally demonstrated for a two qubit system [4,5]. In this work we exploit this concept to demonstrate the generation of entangled frequency bin qudits up to a dimension of four fully controllable via the use of photonic devices integrated on the same chip.

Our source is realized on a silicon photonic chip and is shown in Fig. 1 a). Three Mach-Zehnder interferometers are used to divide the pump power into four paths with adjustable amplitudes, to excite four identical ring resonators (R0-R3) of radius 22 microns. The comb lines of each pair of rings are offset by an amount tunable using thermal phase shifters. We use four mutually coherent pumps at different frequencies to trigger pair generation by SFWM, each pump associated with a resonance of a different ring, and we operate at a pump

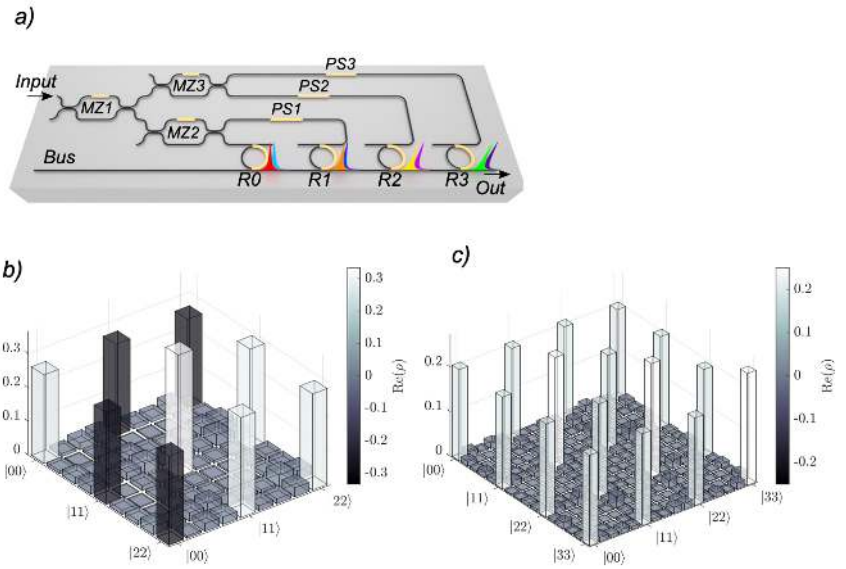


Figure 1: a) Scheme of the device. b) and c) Reconstructed density matrices of the target states as described in the text for b) a pair of qutrits and c) a pair of ququarts. The bar height indicates the modulus of the matrix element, while the color indicates the real part.

power level such that multiple-pair events are negligible.

The average brightness of the four rings is about 0.15 MHz per square mW. To show the capability to generate qudit states, we set the bin spacing to 15 GHz, and reconfigure the device to generate the target states $|\Phi_3\rangle = \frac{1}{\sqrt{3}}(|00\rangle - |11\rangle - |22\rangle)$ and $|\Phi_4\rangle = \frac{1}{\sqrt{4}}(|00\rangle + |11\rangle + |22\rangle + |33\rangle)$, for a three level qudit (qutrit) and four level qudit (ququart) respectively. Note that the former state can not be directly generated from a single resonator without external manipulation of the state, for example by using a waveshaper. The target states are confirmed through quantum state tomography, and their reconstructed density matrices are shown in Fig. 1 b) and c) respectively. In the case of the qutrit state, we obtained a fidelity of 86.2 ± 0.3 % with the target state, and a purity of 78.3 ± 0.5 %. In the case of the ququart state, we get 84.5 ± 0.2 % for the fidelity and 74.4 ± 0.4 % for purity.

To certify entanglement, we also computed the high-dimensional CGLMP inequalities [6] from the reconstructed density matrices, proving their violations by tens of standard deviations in both cases.

In summary, we experimentally demonstrated a bright and reconfigurable source of entangled frequency bin qudits. Our approach allows to simultaneously achieve high brightness and small bin spacing, which are key requirements for the efficient generation and manipulation of high dimensional, frequency-bin-encoded multipartite states.

References

1. M. Kues, et al., Nat. Phot., 13.3 pp. 170-179 (2019).
2. H. H. Lu, et al. Phys. Rev. Lett., 125 120503 (2020).
3. M. Liscidini and J. E. Sipe, Opt. Lett., 44.11, pp. 2625-2628 (2019).
4. F. A. Sabattoli, et al. Opt. Lett. 47, 6201 (2022)
5. M. Clementi, et al. arXiv:2212.13191 (2022).
6. D. Collins, et al. Phys. Rev. Lett. 88, (2002) 040404.

PT Symmetric Non-Hermitian Polaritonic System with Single Hexagonal Microcavity on Loss-modulated Substrate

Yong-Hoon Cho
Department of Physics and KI for the NanoCentury,
Korea Advanced Institute of Science and Technology (KAIST), Daejeon, Republic of Korea
*corresponding author: yhc@kaist.ac.kr

Abstract: Photonic systems with complementary gain and loss profiles have recently been studied using non-Hermitian system with parity-time reversal symmetry. Indirect coupling via near-fields between two or more identical photonic components has been used in these systems because photons are non-interactive. In this talk, we present direct coupling via exciton nature of polaritons within a single hexagonal microcavity on a loss-modulated substrate. This polariton-based PT symmetric system provides opportunities for the investigation of non-Hermitian physics and the development of practical applications.

Exciton-polaritons are quasi-particles that have a combination of excitonic and photonic properties. They can be created and condensed into a coherent ground state within a strongly coupled microcavity and have the ability to directly interact with each other. Microcavities based on group III-nitride semiconductors are an ideal platform for studying polaritonics even at room temperature, due to their high oscillator strength and large exciton binding energy. Recently, there has been a lot of interest in non-Hermitian systems with parity-time symmetry (PT symmetry), which involves photonic systems with complementary gain and loss profiles. In most non-Hermitian photonic systems, indirect coupling via near-fields has been used to mediate interaction between two or more identical photonic components. In this talk, we present direct coupling via the excitonic nature of polaritons within a single hexagonal microcavity on a loss-modulated substrate. By using a high-quality GaN hexagonal microrod, we were able to observe the whispering gallery polariton condensate at room temperature and ballistic transport phenomenon depending on the excitation size-related potential gradient.[1] The naturally formed sixfold symmetry of the hexagonal GaN microrod provides degenerate modes between two quasi-whispering gallery polariton modes, each with upwards (equilateral) and downwards (inverted) triangular paths. By combining the coupled polariton pair with a loss-controlled substrate having gradual loss variation, we were able to realize a phase transition from an unbroken to a broken phase, creating a polariton-based PT symmetric system with only a single microcavity at room temperature.[2] This polaritonic PT-symmetric platform can be utilized to study non-Hermitian physics and to develop versatile practical applications.

References

1. H. G. Song, S. Choi, C. H. Park, S. H. Gong, C. Lee, M. S. Kwon, D. G. Choi, K. Y. Woo, and Y. H. Cho*, “Tailoring the potential landscape of room-temperature single-mode whispering gallery polariton condensate,” Optica Vol. 6, 1313, 2019.
2. H. G. Song, M. Choi, K. Y. Woo, C. H. Park, and Y. H. Cho*, “Room-temperature polaritonic non-Hermitian system with single microcavity,” Nature Photonics Vol. 15, 582, 2021.

META 2023, PARIS – FRANCE, JULY 18 – 21, 2023

Hybrid-Integrated Quantum Optics on a Silicon Nitride Platform

Khaled Mnaymneh[1]*, Edith Yeung[1,2], David B. Northeast[1], Jeongwan Jin[1], Patrick Laferrière[1,2], Sofiane Haffouz[1], Robin L. Williams[1], Philip J. Poole[1] and Dan Dalacu[1,2]

[1]National Research Council Canada, 1200 Montreal Road, Ottawa, Canada K1A 0R6
[2]Dept. of Physics, University of Ottawa, 150 Louis-Pasteur Private , Ottawa, Canada K1N 6N5
*corresponding author: khaled.mnaymneh@nrc.ca

Abstract: We present our progress towards scalable quantum-technology solutions on a silicon nitride platform. Using a pick-and-place technique, we demonstrate hybrid integration of single InAs quantum dots on a Si_3N_4 optical waveguide and show that the hybrid-integrated process does not ruin the single emitter properties, and may even enhance them.

Independent electrical control of phase and magnitude of second harmonic generation using intersubband polaritonic metasurfaces

Jaeyeon Yu[1], Gerhard Boehm[2], Mikhail A. Belkin[2], and Jongwon Lee[1*]

[1]Department of Electrical Engineering, Ulsan National Institute of Science and Technology, Republic of Korea
[2]Walter Schottky Institute, Technical University of Munich, Germany
[*]corresponding author: jongwonlee@unist.ac.kr

Abstract: We present electrically tunable intersubband nonlinear polaritonic metasurfaces for second harmonic generation. The phase and magnitude of effective nonlinear susceptibility of these metasurfaces can be controlled independently, with a range of 0 to 160 nm/V in magnitude and 0 to 2π in phase.

Metasurfaces made up of two-dimensional arrays of subwavelength unit structures have demonstrated new methods for producing efficient frequency mixings with relaxed phase matching constraints, opening up new avenues for innovative applications such as nonlinear holography, optical encryption, and quantum optics [1]. However, most of these metasurfaces have been passive devices with fixed nonlinear optical responses. Recently, nonlinear intersubband polaritonic metasurfaces have been developed, which leverage the giant nonlinear response of intersubband transitions (IST) in multiple quantum well (MQW) structures, coupled with electromagnetic modes of plasmonic resonators [2]. To address the static limitation in nonlinear response, an electrically reconfigurable nonlinear polaritonic metasurface has been reported by integrating electrically tunable giant nonlinear response from Stark tunable ISTs in a semiconductor heterostructure with plamonic nanocavity structures, demonstraing unprecedentedly high intensity modulation and local phase tuning of the second harmonic generation (SHG) response, reaching up to 135° [3].

To maximize the utility of electrically tunable nonlinear metasurfaces, the phase and magnitude of the second harmonic signal need to be independently controllable from 0 to its maximum value. To enable ultimate electrical control of the nonlinear response, we propose the use of electrically tunable intersubband polaritonic metasurfaces with new unit cell design. These metasurfaces can cover a full phase tuning range from 0 to 2π while maintaining a constant magnitude or cover a large range of magnitude of the nonlinear response while maintaining a constant phase.

For the experimental demonstration of these novel features, we first optimized the MQW structure by analyzing the main factors that affect the perturbation of IST energies, dipole elements, and spectral tunability. The MQW structure used in this study was made up of a three-quantum-well system in which the centers of the first three electron subbands were spatially separated [3], as shown in Fig. 1(a). The ISTs provide a giant second order nonlinear response, $\chi_{zzz}^{(2)}$, and a broadband spectral tuning of $\chi_{zzz}^{(2)}$ can be induced through the quantum confined Stark effect (QCSE). The magnitude and phase spectra of $\chi_{zzz}^{(2)}$ for different bias voltages are plotted in Fig. 1(b) and 1(c), respectively. While the theoretical coverage of $\chi_{zzz}^{(2)}$ is almost 2π phase, its magnitude rapidly decreases as the phase difference from 0V increases. To overcome this limitation, a unit cell structure with two meta-atoms was designed, as illustrated in Fig. 1(d). The two meta-atoms, which are geometrically inverted, generate effective second order nonlinear responses that are π phase shifted from each other, as depicted in Fig.

1(e). By selecting the appropriate bias voltages for the two meta-atoms, it is possible to attain complete phase control of the SHG signal from 0 to 2π with a constant amplitude in this configuration.

To achieve 2π tuning of SHG with nearly constant conversion efficiency (represented by a circle in a complex plane), we combined the two effective second-order susceptibilities of the two meta-atoms with the same phase by applying external bias voltages V_a and V_b to the two meta-atoms, as depicted in Fig. 1(d). We were able to find two bias voltages that generate an SHG signal at any location within the circle on the complex plane. Similarly, we also obtained to bias voltages that produces a particular SHG intensity with any phase within the circle, as demonstrated in points A-F in Fig. 1(f). Our calculations showed a maximum SH power conversion efficiency of 0.01% for an input pump power of 200 mW at a wavelength of 10 μm. Additionally, the proposed device can operate in a broadband range. For the input pump wavelength range from 9 to 10.6 μm, the device can cover most of the complex plane for various combinations of the two bias voltages, and the calculation results at the pump wavelength of 9 and 10.6 μm are plotted in Fig. 1(g) and 1(h), respectively.

This work was supported by a Basic Science Research Program through the National Research Foundation of Korea (NRF) grant funded by the Korea government (MSIT) (No. 2020R1A4A3079834 and 2022R1A2C301189811)

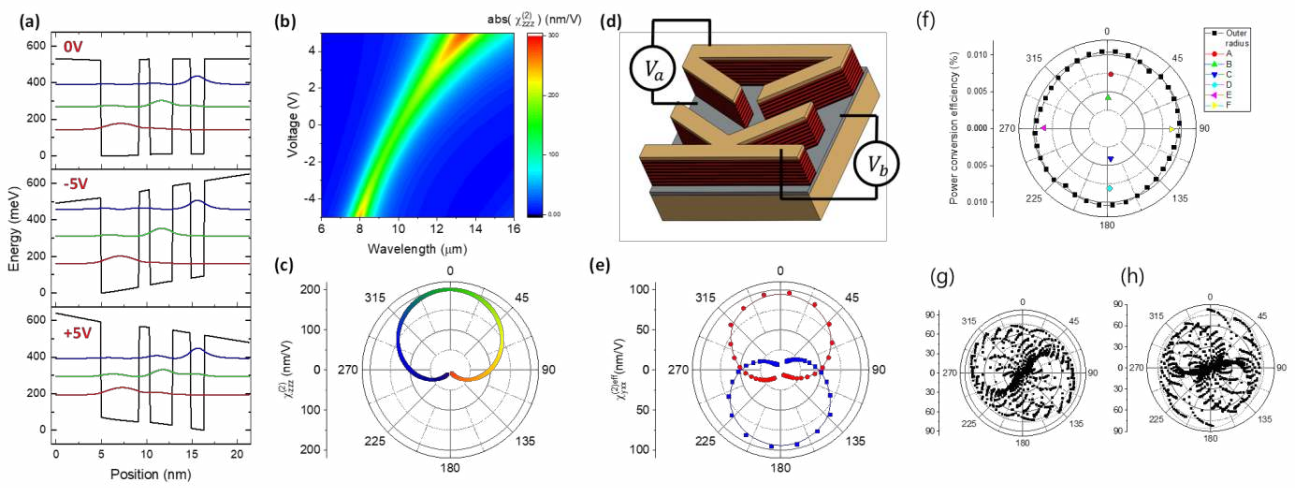


Fig. 1. (a) One period of conduction band of MQW with external bias voltages (top : 0V, middle : -5V, bottom : 5V). (b) Magnitude of second order susceptibility spectra with external bias voltage. (c) Second order susceptibility in the complex plane according to different bias voltages (blue -5V, green 0V, red +5V). (d) Unit cell structure of the metasurface (yellow : Au, red : MQWs, gray : Cr), (e) The effective second order nonlinear susceptibilities of the upper meta-atom (red, it changes clockwise as bias voltage increases) and the lower meta-atom (blue, it changes counterclockwise as bias voltage increases). (f) Calculated SHG conversion efficiency at input pump wavelength of 10μm (maximum intensity combinations : black dots). Points A to F are calculated SHG conversion efficiencies for different V_a and V_b values. (g,h) Calculated effective second order nonlinear susceptibilities at pump wavelength of (g) 9 μm and (h) 10.6 μm for all combinations of V_a and V_b from -5V to 5V with 0.25V step.

References

1. Li, G., Zhang, S., and Zentgraf, T. “Nonlinear photonic metasurfaces,” Nat. Rev. Mater., Vol. 2, 17010, 2017.
2. Lee, J. et al., “Giant nonlinear response from plasmonic metasurfaces coupled to intersubband transitions,” Nature, Vol. 511, 65–69, 2014.
3. Yu, J. et al., “Electrically tunable nonlinear polaritonic metasurface,” Nat. Photon., Vol. 16, 72–78, 2022.

META 2023, PARIS - FRANCE, JULY 18 – 21, 2023

Functionalization of gold nanoparticles by localized surface plasmon resonance photopolymerization of molecularly imprinted polymers – An easy route for selective and specific sensors

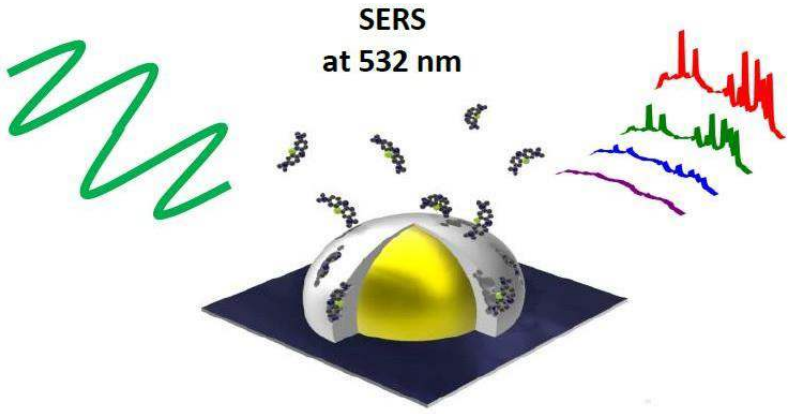
A. Khitous[1,2], C. Molinaro[1,2], K. Haupt[1,2], S. Gree[1,2] and O. Soppera[1,2*]

[1]Université de Haute-Alsace, CNRS, IS2M UMR 7361, F-68100 Mulhouse, France

[2]Université de Strasbourg, France
[3]Université de Technologie de Compiègne, France
[*]Corresponding author: olivier.soppera@uha.fr

Abstract:

Using the localized surface plasmon resonance (LSPR) to enhance the electromagnetic field in optical near field, a new simple, fast and versatile method for the functionalization of gold nanoparticles (AuNPs) by a nanoscale layer of molecularly imprinted polymers (MIPs) was developed[1,2]. The key step is based on near-field radical photopolymerization of a MIP pre-polymerization mixture. This allows the preparation of hybrid AuNPs@MIPs nanoparticles which are used as substrates for LSPR and surface enhanced Raman spectrometry (SERS) analyses with excellent sensitivity and specificity. To demonstrate the performance of AuNPs@MIPs, MIPs specific to methylene blue (MB) were prepared. The sensitivity of spectroscopic detection is in the range of 10 nM3. Specificity is demonstrated by comparing the response with a control non-imprinted polymer (NIP) and by interference tests with two analogues (Rhodamine 6G and Rhodamine 110)[3]. This fabrication method allowed us to obtain robust and recyclable sensing surfaces with high sensitivity and selectivity. The nanometric thickness of MIP allows a short analysis time (10 min), which improves the performance of MIP-based sensors and opens new perspectives to detect molecules at very low concentrations.



References

1. Khitous, A.; Molinaro, C.; Thomas, C.; Haupt, K.; Soppera, O. "Synthesis and Integration of Hybrid Metal Nanoparticles Covered with a Molecularly Imprinted Polymer Nanolayer by Photopolymerization". *Sensors*, *23* (8), 3995, 2023.
2. Fuchs, Y.; Soppera, O.; Haupt, K. "Photopolymerization and Photostructuring of Molecularly Imprinted Polymers for Sensor Applications"—A Review. *Analytica chimica acta*, *717*, 7–20, 2012.
3. Khitous, A.; Molinaro, C.; Gree, S.; Haupt, K.; Soppera, O. "Plasmon-Induced Photopolymerization of Molecularly Imprinted Polymers for Nanosensor Applications". *Advanced Materials Interfaces*, 2201651, 2023.

Microscopic theory of cavity-enhanced interactions of dipolaritons

E. R. Christensen[1*], A. Camacho-Guardian[2], O. Cotlet[3], A. Imamoglu[3], M. Wouters[4], G. M. Bruun[1,5], and I. Carusotto[6]

[1]*Center for Complex Quantum Systems, Department of Physics & Astronomy, Aarhus University, Denmark*
[2]*Departamento de Física Química, Instituto de Física, Universidad Nacional Autónoma de México, Mexico*
[3]*Institue for Quantum Electronics, ETH Zurich, Switzerland*
[4]*TQC, Universiteit Antwerpen, Belgium*
[5]*Shenzhen Institute for Quantum Science and Engineering and Department of Physics, Southern University of Science and Technology, China*
[6]*INO-CNR BEC and Dipartimento di Fisica Center, Università di Trento, Italy*
[*]corresponding author: esbenrohan@phys.au.dk

Abstract: We develop a microscopic theory of interacting dipolar polaritons. Numerical results in a wire geometry together with a Born-Oppenheimer type approach showcase three emerging regimes, including a polariton blockade regime that should be reachable in realistic systems. We extend our theory to higher dimensions and compare dipolar polaritons to non-dipolar ones, highlighting the roles of light-matter coupling and interaction range. Dipolar polaritons in TMDs and/or with multiple quantum wells are promising candidates for realizing strongly correlated fluids of light.

Recent advances in experiments with quantum particles formed by a superposition of light and matter excitations promise an era of realizing entirely new hybrid light-matter quantum systems with far reaching perspectives both for fundamental science and for future opto-electronic technologies [1]. To reach these goals, an outstanding challenge is to make these hybrid light-matter particles, called polaritons, interact strongly with each other.

We address this by developing a theory for the collisional properties of polaritons whose matter component carries a static electric dipole moment [2]. The repulsion between these dipolar light-matter particles is shown to make them promising candidates for realizing strong photon-photon interactions. The theoretical model is based on microscopic numerical calculations for one-dimensional geometries and on a Born-Oppenheimer type approach. We identify three different interaction regimes from impenetrable polaritons in long wires to a polariton blockade regime for smaller but still realistic wire lengths. The results are then analytically continued to two-dimensional polariton systems and highlight the light-matter coupling as a crucial ingredient to realize strong polariton interactions. In contrast to expectations, such dipolar polaritons turn out to be even more favorable in materials with tightly bound excitons and multiple quantum wells.

Our predictions suggest dipolar polaritons as a most promising solid-state platform for realizing strongly correlated fluids of light and harness them as a quantum light source for quantum technology applications.

References

1. Christensen, E. R., et al., "Microscopic theory of cavity-enhanced interactions of dipolaritons," arXiv preprint arXiv:2212.02597, 2022
2. Carusotto, I. and Ciuti. C, "Quantum fluids of light," Rev. Mod. Phys. **85**, 299-366, 2013

“Meta”-Optical Fibers:

Andrew Palmer, [1,2] Stuart Love, [1,2] Leon Zhang, [1,2] **Ho Wai Howard Lee**[1,2,*]

[1] *Department of Physics & Astronomy, University of California, Irvine, United States*
[2] *Beckman Laser Institute and Medical Clinic, University of California, Irvine, United States*
Howardhw.lee@uci.edu

Optical fiber is a well-established and efficient light-guiding medium. Although optical fiber is efficient for transmitting light, its functionality is limited by the dielectric material of the core, which has poor optoelectronic, magneto-optical, and nonlinear-optical responses and has a dielectric diffraction limit. Therefore, the optical properties of the optical fiber such as phase, amplitude, polarization, and mode profile, cannot be altered after the fiber drawing fabrication, thus limiting the development of novel in-fiber devices. Integration of new materials and nanostructures into fiber will enhance processing/transmission capabilities and novel functionalities.

In this talk, I will present our recent development of “Meta”-optical fiber, an advanced optical fiber integrated with emerging nanophotonic concepts such as optical metasurfaces, plasmonic nanowires, and zero-index photonics. I will present the development of ultrathin optical metalens which is cascaded on the facet of a photonic crystal fiber that enables light focusing. I will also discuss the first experimental demonstration of zero-index resonance excitation in an optical fiber coated with AZO nanolayer and excitation of plasmonic resonances on holey optical fiber for advanced optical sensing and tip-enhanced Raman spectroscopy. These advanced “meta”-optical fibers open a pathway to revolutionary in-fiber lasers/spectroscopies, optical imaging/sensing, and optical communication devices.

This work was supported in part by the AFOSR (FA9550-21-1-02204)

META 2023, PARIS - FRANCE, JULY 18 – 21, 2023

Direct and Inverse design forNon-Hermitian light management

M. Botey[1*], R. Herrero[1*], K. Staliunas[1,2]

[1] Universitat Politecnica Catalunya, Dep. de Fisica, Rambla Sant Nebridi 22, 08222, Terrassa (Barcelona) Spain

[2]ICREA, Passeig Lluís Companys 23, 08010, Barcelona, Spain

[*]corresponding author: Muriel.botey@upc.edu

Abstract: We present direct and inverse-design strategies to achieve 'on demand' management of light by scattering cancellation in non-Hermitian media. The direct approach is based on our recently proposed generalized Hilbert Transform as a recipe to design complex potentials to tailor the flow of light following any arbitrary direction. Beyond this fundamental approach, we present supervised and unsupervised learning techniques for knowledge acquisition in non-Hermitian systems which accelerate the inverse the "on demand" design process. The different proposals may have direct applications to control the wave dynamics in semiconductor lasers or other linear and nonlinear physical systems including cloaking sensors and arbitrary shaped objects.

Non-Hermitian Physics has emerged as a fertile ground for a smart control of waves [1]. In turn, the pursuit of artificial materials to control and shape light is possibly one of the most attracting research areas in photonics in the last decades. In this context, we recently proposed a strategy to achieve 'on demand' dynamical manipulation of light by non-Hermitian potentials that mimics the time symmetry breaking at the basis of causality. In fact, the cancellation of the response before the arrival of the signal is warranted by a Hilbert Transform relating the spectral dependence of the real and imaginary components of the response function of the system, see Fig. 1a. Therefore, a Hilbert Transform (HT) relating the real and imaginary distributions of the complex permittivity allows to control the flow of light by scattering cancellation, Fig. 1b. A recipe that can be extended to 2D, widening the concept Kramers Kronig relations in space [2], to design complex potentials to tailor the propagation of light following any vector field [3], or to generate invisible potentials where light propagates as in free space [4], Fig. 1c. The approach allows restricting the dimensionality of the complex susceptibility within practical limits for a feasible realization or even avoiding the use of gain [5].

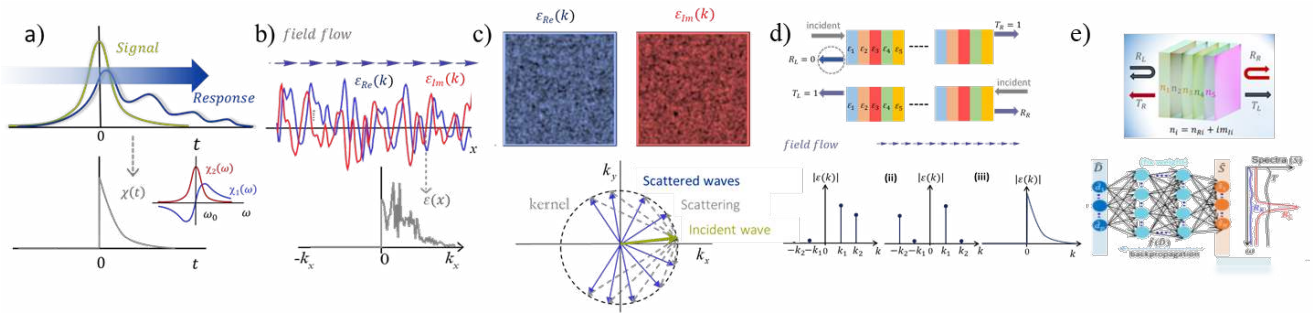


Figure 1. a) Causality imposes the cancellation of the response before the arrival of the signal; the spectral dependence of the real and imaginary components of the response function are related by a HT. b) Backward scattering cancellation in a 1D system is warranted by any complex random potential which real and imaginary parts are rated by a HT, ensuring $\varepsilon(k_x)=0$ for $k_x<0$. c) Generalization to a random potential in 2D, where the kernel of the HT uncouples incident radiation from particular backward scattering

directions. d) Algorithm assisted inverse design for a 1D structure for frequency-selective operation or broadband unidirectionality. e) Machine learning approach from ref. [7].

Beyond this fundamental approach, we also we also present supervised and unsupervised learning techniques for knowledge acquisition in non-Hermitian systems which accelerate the inverse the “on demand” design process. As a first step, proposed a general inverse-design strategy based on genetic algorithm optimization to achieve ‘on demand’ manipulation of light in 1D and 2D non-Hermitian systems [6], see Fig. 1d. Moreover, just recently, supervised and unsupervised learning techniques for knowledge acquisition in non-Hermitian systems have shown to accelerate the inverse design process while may trigger a trigger a route for intelligent inverse design and contribute to the understanding of physical mechanism in general non-Hermitian systems [7], see Fig. 1e.

These different proposals may have direct applications to control the wave dynamics in semiconductor lasers or other linear and nonlinear physical systems, including cloaking sensors and arbitrary shaped objects. Both the direct and inverse design approaches are not restricted to optical systems, and it can be applied directly to find accurate solutions to other kind of waves.

References

[1] El-Ganainy, R., Makris, K., Khajavikhan, M., et al. "Non-Hermitian physics and PT symmetry," Nat. Phys. 14, 11–19 (2018)

[2] Horsley, S., Artoni, M. and La Rocca, G., "Spatial Kramers–Kronig relations and the reflection of waves," Nat. Photon. 9, 436–439 (2015).

[3] Ahmed, W. W., Herrero, R., Botey, M., Hayran, Z., Kurt, H. and Staliunas, K., "Directionality fields generated by a local Hilbert transform," Phys. Rev. A 97, 033824 (2018)

[4] Hayran, Z., Herrero, R., Botey, M., Kurt, H., Staliunas, K. "Invisibility on demand based on a generalized Hilbert transform," Phys. Rev. A, 98(1), 013822 (2018)

[5] Ahmed, W. W., Herrero, R., Botey, M., Wu, Y., and Staliunas, K., "Restricted Hilbert transform for non-Hermitian management of fields,” Physical Review Applied, 14, 044010 (2020).

[6] Ahmed, W. W., Herrero, R., Botey, M., Wu, Y., and Staliunas, K. "Inverse-design of non-Hermitian potentials for on-demand asymmetric reflectivity," Optics express, 29(11), 17001-17010 (2021).

[7] Ahmed, W. W., Farhat, M., Staliunas, K., Zhang, X., & Wu, Y. Machine learning for knowledge acquisition and accelerated inverse-design for non-Hermitian systems. Communications Physics, 6(1), 2 (2023)

META 2023, PARIS - FRANCE, JULY 18 – 21, 2023

Roton-Like Dispersion Relations in Metamaterials

M. Wegener[1,2,*]

[1]Institute of Applied Physics, Karlsruhe Institute of Technology (KIT), 76128 Karlsruhe, Germany
[2]Institute of Nanotechnology, Karlsruhe Institute of Technology (KIT), 76128 Karlsruhe, Germany

[*]corresponding author: martin.wegener@kit.edu

Abstract: We review our work on mimicking the dispersion relation of rotons in liquid helium in different systems (acoustic, elastic, and electromagnetic waves) and using three different strategies (nonlocal metamaterials, chiral metamaterials, and monomode metamaterials).

The roton dispersion relation in liquid helium starts with frequency being proportional to wavenumber, followed by a maximum, a region of backward waves, a minimum, and a further increase of frequency versus wavenumber. We start by briefly reviewing our work towards mimicking this dispersion relation in elastic and acoustic metamaterials [1,2] by using nonlocal interactions.

We emphasize more recent work on electromagnetic waves and nonlocal interactions [3], elastic waves and chirality in 3D cubic-symmetry metamaterials [4], and elastic waves in monomode metamaterial beams [5].

I thank all of the authors on the below references for their corresponding contributions. This research has been funded by the Deutsche Forschungsgemeinschaft (DFG, German Research Foundation) under Germany's Excellence Strategy via the Excellence Cluster “3D Matter Made to Order” (EXC-2082/1-390761711), which has also been supported by the Carl Zeiss Foundation through the “Carl-Zeiss-Foundation-Focus@HEiKA”, by the State of Baden-Württemberg, and by the Karlsruhe Institute of Technology (KIT). We further acknowledge support by the Helmholtz program “Materials Systems Engineering” (MSE) and by the Karlsruhe School of Optics & Photonics.

References

1. “Roton-like acoustical dispersion relations in 3D metamaterials”,
   Y. Chen, M. Kadic, and M. Wegener,
   Nature Commun. **12**, 3278 (2021).
2. “Experimental Observation of Roton-Like Dispersion Relations in Metamaterials,
   J. A. Iglesias Martinez, M.F. Groß, Y. Chen, T. Frenzel, V. Laude, M. Kadic, and M. Wegener,
   Science Adv. **7**, eabm2189 (2021).
3. “Nonlocal cable-network metamaterials”,
   Y. Chen, M.A.A. Abouelatta, K. Wang, M. Kadic, and M. Wegener,
   in review (2023).
4. “Observation of Chirality-Induced Roton-Like Dispersion in a 3D Micropolar Elastic Metamaterial”,
   Y. Chen, J.L.G. Schneider, M. Groß, K. Wang, C. Wang, M. Kadic, and M. Wegener,
   in preparation (2023).
5. “Observation of roton-like dispersion relations in an elastic monomode metamaterial beam”,
   M. Groß, Y. Chen, J.L.G. Schneider, M. Kadic, and M. Wegener,
   in preparation (2023).

META 2023, PARIS - FRANCE, JULY 18 – 21, 2023

Quantum optical phenomena in two-dimensional materials

F. Javier García de Abajo[1,2*]

[1] ICFO-Institut de Ciencies Fotoniques, The Barcelona Institute of Science and Technology, Barcelona, Spain
[2] ICREA-Institució Catalana de Recerca i Estudis Avançats, Barcelona, Spain
[*] javier.garciadeabajo@nanophotonics.es

Abstract: We discuss new approaches to the synthesis, design, and exploitation of two-dimensional materials for nanophotonics, including plasmonics in ultrathin crystalline metals, a disruptive class of quantum-phase materials, recent advances in the solution to the problem of coupling between free-space light and ultra-confined optical excitations, and the application of these developments to the study of ultrafast nonlinear phenomena and quantum optics at the atomic scale.

Atomically thin materials have emerged as a robust platform for manipulating and exploiting light at the nanoscale thanks to a wide variety of polaritonic modes, ranging from plasmons in thin metals and doped graphene to excitons in transition metal dichalcogenides and phonons in ionic insulators. The electromagnetic behavior of these modes can be well understood in terms of effective surface conductivities, which capture their strong dependence on temperature and external static electric and magnetic fields. Recent advances have also been produced in the synthesis of thin noble-metal films,[1,2] which open a new regime in plasmonics. In this talk, we overview the general characteristics of the optical response of these materials, which can be understood in terms of simple theoretical models. We also discuss more sophisticated models, aiming at the exploration of genuinely quantum-mechanical effects. We further review recent advances in the control of ultrafast and nonlinear optical processes,[3,4] as well as potential applications in light modulation[5,6] and quantum optics.[7] The in/out coupling problem between external light and strongly confined polaritons remains a major challenge, for which we propose innovative solutions.[8,9] We conclude with emerging directions in the design of polaritonic materials relying on quantum phase effects.[10]

References

1. Z. M. Abd El-Fattah et al., “Plasmonics in atomically thin crystalline silver films,” ACS Nano 13, 7771, 2019.
2. V. Mkhitaryan et al. (in preparation).
3. F. Iyikanat et al., “Nonlinear tunable vibrational response in hexagonal boron nitride,” ACS Nano 15, 13415, 2021.
4. Y. Wang, et al., “Probing electronic states in monolayer semiconductors through static and transient third-harmonic spectroscopies,” Adv. Mater. 34, 2107104, 2022.
5. A. J. Sternbach et al., “Negative refraction in hyperbolic hetero-bicrystals,” Science 379, 555, 2023.
6. H. Hu et al., “Gate-tunable negative refraction of mid-infrared polaritons,” Science 379, 558, 2023.
7. A. Rodríguez Echarri et al., “Direct generation of entangled photon pairs in nonlinear optical waveguides,” Nanophotonics 11, 1021, 2022.
8. E. J. C. Dias and F. J. García de Abajo, “Fundamental limits to the coupling between light and 2D polaritons by small scatterers,” ACS Nano 13, 5184, 2019.
9. E. J. C. Dias and F. J. García de Abajo, “Complete coupling of focused light to surface polaritons,” Optica 8, 520, 2021.
10. V. Di Giulio et al., Nat. Commun. “An image interaction approach to quantum-phase engineering of two-dimensional materials,” 13, 5175, 2022.

META 2023, PARIS - FRANCE, JULY 18 – 21, 2023

High-Q Photonics

Kerry Vahala

California Institute of Technology
*corresponding author: vahala@caltech.edu

Abstract: High-Q microresonators in the form of rings or disks provide access to nonlinear optical phenomena at milli-Watt power levels. Their resulting functionality is paving the way to integrated optical systems for sensing, metrology, spectroscopy, microwave generation, time keeping, and data transmission. Once discrete and reliant upon specialized processing techniques for optical loss reduction, high-Q microresonators are today planar, capable of integration, and in some cases fabricated on CMOS foundry lines. After a brief overview of their history, I will review recent applications. These include Sagnac gyroscopes, microwave signal sources, clocks, and high-coherent sources. The current and possible future limits of microresonator performance, and untapped application areas, will also be discussed.

META 2023, PARIS - FRANCE, JULY 19, 2023

The Challenge of Photonic Crystals (and Meta-Materials) is Inverse Electromagnetic Design (Aperiodic)

Eli Yablonovitch

Electrical Engineering and Computer Sciences Dept.,
UCLA/University of California, Berkeley, USA
eliy@eecs.berkeley.edu

Abstract: Inevitably, in electromagnetics, there is a goal, and it may be that the goal is best achieved by an aperiodic rather than a periodic design. Then there is a universal question: What is the best design to achieve a specific goal?

The problem is exacerbated by the reality that any geometrical design could have millions of design parameters that define a desirable shape. With a particular goal in mind, the adjustment of any one design parameter, requires a revision of all the other parameters, making it hard, or impossible to converge on a good design. Essentially this is a problem in multi-variable calculus: How to co-optimize the millions of parameters that are implicit in any geometrical shape? It might be called "Shape Calculus".

Fortunately there are elegant mathematical methods that have emerged in recent years that permit the co-optimization of millions of variables, but requiring only two solutions of Maxwell's Equations [1]. The mathematical approach is called the "Adjoint Method", and it is a merger the chain rule of calculus, with linear algebra [2]. Indeed this method has been rediscovered numerous times in the past 70 years, within numerous fields, wherever some optimization over many variables is needed. This has many names. For example, in neural networks this is called "Back-Propagation", in photolithography it's called Inverse Lithography Technology, (ILT), but it is also used in Control Theory, mechanical design, etc.

One of the first electromagnetic applications of the "Adjoint Method" was toward the design of lithographic masks for the photographic process by which electronic chips are manufactured. These masks consist of thin-film Chromium on glass, intricately patterned, to photographically project out the sub-wavelength shapes of transistors, wires, and other components on an integrated circuit. These metal film masks, so heavily used in electronics manufacturing, can be regarded as the original "meta-surface" [3].

Sub-wavelength transistor images were desired, but it was not at all clear what the mask pattern should be, that would produce those desired sub-wavelength images. The first company founded to employ the "Adjoint Method" for photo-lithography was Luminescent Inc., (2002). Luminescent introduced the slogan ILT "Inverse Lithography Technology" to be understood as a sub-category of Inverse Electromagnetic Design. Today, almost all memory chips and micro-processors use thin-film chromium masks and ILT software in their design and manufacture, meta-surfaces indeed [4].

Whether it's a meta-lens or any other type of electromagnetic function, there is no need to slavishly follow a

periodicity constraint. Mathematical methods have been developed, to efficiently optimize any type of electromagnetic function. I will provide some examples: “Silicon Photonics” couplers, optical antennas, solar cell surface textures, etc

References

1. Burger, M., Osher, S., Yablonovitch, E., “Inverse Problem Techniques for the Design of Photonic Crystals,” IEICE Transactions on Electronics, vol E87-C, no. 3, pp. 258-265, March 2004.
2. Kao C.Y., Osher S., Yablonovitch E., “Maximizing band gaps in two-dimensional photonic crystals by using level set methods,” Applied Physics B-Lasers & Optics, vol. B81, no.2-3, July 2005, pp.235-44.
3. Daniel S. Abrams, Linyong Pang, "Fast inverse lithography technology," Proc. SPIE 6154, Optical Microlithography XIX, 61541J (15 March 2006); doi: 10.1117/12.658876
4. T. Cecil, D.P, Peng, D. Abrams, S. Osher, & E. Yablonovitch, “Advances in Inverse Lithography” ACS Photonics, (2022). https://doi.org10.1021/acsphotonics.2c01026

Micro- and Nano-lasers: From One to Many, Unleashing Endless Possibilities

Mercedeh Khajavikhan

University of Southern California, USA

Abstract: Micro- and nano-lasers form a crucial category of optical components with significant scientific and technological implications. In this presentation, I will discuss the utilization of non-Hermiticity, supersymmetry, and topology principles to design arrays of these devices, resulting in intriguing and unexpected lasing phenomena. By considering the interaction between cavity modes, array geometry, and both short- and long-range coupling among the array elements, we can achieve novel laser phase locking regimes, high radiance emission, rapid beam steering, photonic spin machines, and unidirectional lasing.

Retrieving optical parameters of emerging van der Waals microcrystals

M. Sarkar, M.S. Saremi, M.T. Enders and G. T. Papadakis*

ICFO-Institut de Ciencies Fotoniques, The Barcelona Institute of Science and Technology, Spain
*corresponding author: georgia.papadakis@icfo.eu

Abstract: To achieve high-quality in low-dimensional layered van der Waals materials, microcrystals are typically exfoliated. The small size of exfoliated flakes makes their optical characterization with conventional far-field optics challenging. Thus, flake-characterization has typically required delicate spatial scanning via a near-field tip. We present a simple method for determining the optical properties of optically small flakes. Our method is based on far-field spectroscopy and requires minimal numerical fitting. We demonstrate the robustness of our method using hexagonal boron nitride and α-MoO_3.

The mid-long infrared (MLIR) spectral range is highly relevant for energy applications, thermal radiation control, molecular sensing and IR spectroscopy[1]. In recent years, emerging discovered low-dimensional layered and van der Waals materials (LDM) have become relevant to LMIR photonics; in particular, they often support phonon polariton resonances arising from lattice vibrations, with strong dielectric permittivity resonances within the Reststrahlen band. As exemplary LDMs, we mention classes of metal oxides (like α-MoO_3)[2] as well as dielectrics, such as hexagonal Boron Nitride (hBN), which are being explored in the MLIR range[3].

Despite significant interest in such low-dimensional composites, standard approaches for the experimental retrieval of their dielectric properties cannot be easily applied. In particular, standard Fourier Transform Infrared Spectroscopy (FTIR) and Spectroscopic Ellipsometry (SE) have characteristic beam sizes on the order of millimeters, whereas sample sizes of exfoliated flakes are typically on the order of tens to hundreds of micrometers, yielding a beam-sample size mismatch. Furthermore, a highly relevant property of LDMs is their strong optical anisotropy, often in-plane (such as in α-MoO_3)[2] . For this anisotropy to be experimentally detectable, sample sizes on the order of hundreds of micrometers to millimeters are necessary to eliminate the effect of random orientation of sub-crystals. Hence, experimental determination of the complex refractive index for LDM and van der Waals microcrystals is not trivial[4]. In this work, we present a method to retrieve the in-plane complex dielectric permittivity of microcrystals of hBN (isotropic) and α-MoO_3 (in-plane anisotropic), based on reflectivity measurements on exfoliated flakes on a gold substrate. The method applies to *any* other material.

Fig.1a shows a 1μm-thick microcrystal of α-MoO_3 on a gold substrate of cross-sectional area close to ~100μm×50μm. In Fig. 1b, the corresponding FTIR reflectivity spectra are shown, taken on two different locations of the flake. By comparing the two measurements, there exists a strong mismatch in the amplitude of the reflectance (ΔR), owing to the non-uniformity of the flake, and such a discrepancy is typical in such flakes. On the other hand, the spectral position of the dips in reflectivity ($\Delta\omega_d$) shows statistically much less variation with sample location, as also seen in Fig. 1b. The frequencies (ω_d) are related to the real part of the material refractive index (Re{n}) as[5]:

$$\omega_d = \frac{1}{2d}\left[\frac{2m+1}{2Re\{n(\omega_d)\}} - \frac{1}{2\pi Re\{n(\omega_d)\}} tan^{-1}\left\{\frac{-2Re\{n(\omega_d)\}k_s}{Re\{n(\omega_d)\}^2 - n_s^2 - k_s^2}\right\}\right] \quad (1)$$

where *d* is the flake's thickness and n_s and k_s are the real and imaginary parts of the refractive index of the metal substrate respectively.

The flake thicknesses (*d*) were measured with Atomic Force Microscopy (AFM). From Eq.1, Re{n} of the microcrystal was deterministically evaluated at each ω_d. This is shown with the black points in Figs. 1c,d for multiple microcrystals with different thicknesses, along the two optical crystal axes of a-MoO3. For values of Re{n} within the Reststrahlen band, the reflectivity spectra were measured with incident light polarized at 45° with respect to the crystal axes. Hence, from predetermined values of n_x we can derive the values of n_y. To obtain the complex refractive index of the material, the obtained Re{n} was fitted to the Lorentz oscillator model:

$$Re\{n(\omega)\} = Re\left\{\sqrt{\epsilon_{inf}\left(1+\frac{\omega_{LO}^2-\omega_{TO}^2}{\omega_{TO}^2-i\gamma\omega-\omega^2}\right)}\right\} \quad (2)$$

The fit (Fig. 1c,d) is used to retrieve the parameters of the complex permittivity namely ω_{TO}, ω_{LO}, γ and ε_{inf}.

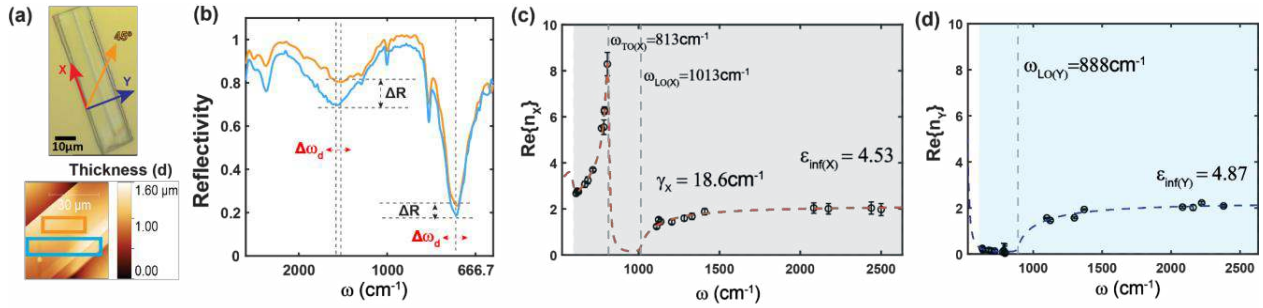


Figure 1 a) Microscope image of a MoO_3 microcrystal (d=1μm) on gold. The thickness measured by AFM is shown below. b) The reflectivity spectrum obtained by FTIR microscope on two different locations of the microcrystal. (c) Retrieval of complex refractive index along the crystal axis X. (d) The same along Y.

This work presents a method to retrieve accurately the in-plane complex refractive index of optically small flakes, without needing elaborate fitting algorithms or near-field tip-based measurements. The method was applied to retrieve complex refractive indices of two van der Waals materials in exfoliated flakes, namely hBN and α-MoO_3:

The project that gave rise to these results received the support of a fellowship from "la Caixa" Foundation (ID 100010434) and from the European Union's Horizon 2020 research and innovation programme under the Marie Skłodowska-Curie grant agreement No 847648.

References

1. Caldwell, J. D. & Novoselov, K. S. Mid-infrared nanophotonics. *Nat Mater* **14**, 364–366 (2015).
2. Álvarez-Pérez, G. *et al.* Infrared Permittivity of the Biaxial van der Waals Semiconductor α-MoO3 from Near- and Far-Field Correlative Studies. *Advanced Materials* **32**, 1908176 (2020).
3. Lu, G. *et al.* Engineering the Spectral and Spatial Dispersion of Thermal Emission via Polariton–Phonon Strong Coupling. *Nano Lett* **21**, 1831–1838 (2021).
4. Yoo, S. J. & Park, Q. H. Spectroscopic ellipsometry for low-dimensional materials and heterostructures. *Nanophotonics* **11**, 2811–2825 (2022).
5. Park, K. C. The Extreme Values of Reflectivity and the Conditions for Zero Reflection from Thin Dielectric Films on Metal. *Appl Opt* **3**, 877–881 (1964).

Atypical light extraction technologies for organic light emitting diodes with spontaneously formed buckling patterns of soft materials

B. D. Chin[1*], J. Y. Yoo[1], S.-H. Hwang[1], O. Kim,[1], S. M. Cho[2], and W. H. Koo[2]

[1]Department of Polymer Science and Engineering, Dankook University, Korea
[2]LG. Display Co, Ltd, Korea
[*]corresponding author: bdchin@dankook.ac.kr

Abstract: There exist a lot of technologies for a light extraction of organic light emitting diodes (OLEDs). However, for the successful commercial application, the restriction on the cost of manufacturing, directionality of color, and the requirement to maintain a high-quality image are severe. In this work, some of the simple fabrication process for the microscale light-extraction pattern formation are introduced. However, for a top-emitting OLED (TOLED), a useful platform of display for high-resolution mobile and non-transparent substrates, colors and spectra are significantly sensitive to those light extraction structures and intrinsic micro-cavity effects [1]. Here, a quasi-periodic, controllable buckling patterns [1] with broad size distribution for outcoupling-enhancing structures of top-emitting OLED are described in detail [2-3]. The formation of buckling patterns is spontaneously driven by the mismatch of thermal expansion coefficient of the organic and polymeric layers, which are easily deposited by simple deposition process. Further experimental studies on the effect of molecular weight, segmental softness/rigidity, and phase separation behavior of material combination will be investigated.

As for OLED performance, luminous efficiency of device with buckling patterns was increased without change of the spectral characteristics and color stability. Such a result, observed in case of optimum buckling structure on the transparent electrode of device, can be explained by the suppression of light loss by the surface plasmon polariton (SPP) mode at metal/air interface. Experimental data for different scale of buckling patterns at top emitting OLED were analyzed with the wavelength-dependent grating pitch and scattering order, indicating that efficiency is increased with larger periodic patterns.

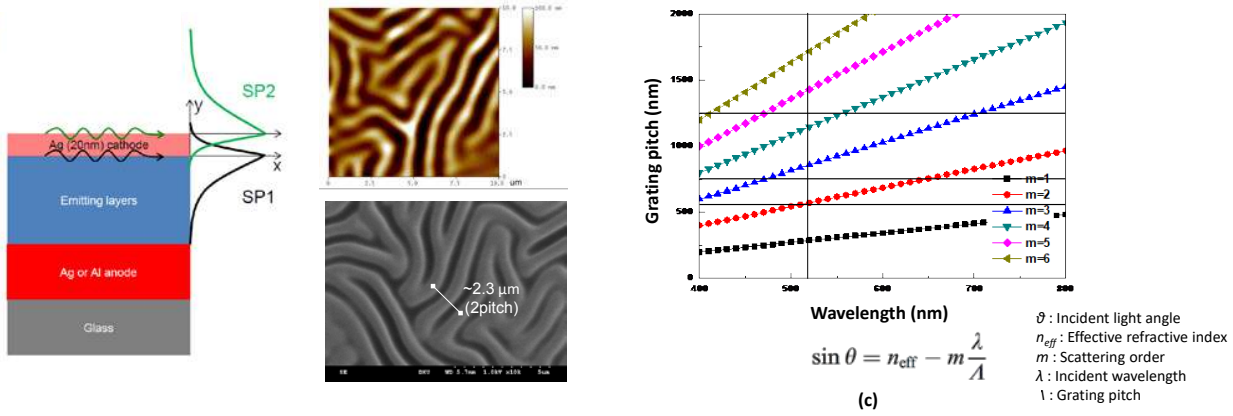


Figure (a) Effect of surface plasmon (SP) resonance at top-emission OLED. (b) Spontaneously-formed buckling/corrugated pattern of soft organic materials by the thermal expansion/contracting process on top of the (semi) transparent electrode of top-emission OLED. (c) Estimation of scaling for grating pitch vs. wavelength for enhanced scattering order, with the theory explained [4]

Acknowledgements; Industrial strategic technology development program (20011059 funded by MOTIE, Korea), and the Soft Chemical Materials Research Center by Gyeonggi Regional Research Center program (GRRC Dankook 2016-B01).

References

1. E. Kim, J. Chung, J. Lee, H. Cho, N. S. Cho, S. Yoo "A systematic approach to reducing angular color shift in cavity-based organic light-emitting diodes" Organic Electronics Vol 48, 348-356, 2017.
2. W. H. Koo, S. M. Jeong, F. Araoka, K. Ishikawa, S. Nishimura, T. Toyooka, and H. Takezoe Lastname, F. M. and F. M. Lastname, "Light extraction from organic light-emitting diodes enhanced by spontaneously formed buckles," Nature Photonics Vol 4, 222-226, 2010.
3. W. H. Koo, B.D. Chin, S. M. Jo, Korea Patent 10-2293473 "Organic Light Emitting Display Device and Method of Manufacturing the Same" 2021.
4. T. Fuhrmann, K. Samse, J. Salbeck, A. Perschke, H. Franke, "Guided electromagnetic waves in organic light emitting diode structures", Organic Electronics 4, 219–226, 2003.

META 2023, PARIS - FRANCE, JULY 18 – 21, 2023

Towards Predictable 2D/3D Plasmonics via FEBID

V. Reisecker[1], D. Kuhness[2] and H. Plank[1,2,3*]

[1]Institute of Electron Microscopy and Nanoanalysis (FELMI), Graz University of Technology, Austria
[2]Christian Doppler Laboratory DEFINE, FELMI, Graz University of Technology, Austria
[3]Graz Centre for Electron Microscopy (ZFE), Austria
[*]corresponding author: harald.plank@tugraz.at

Abstract:
Focused Electron Beam Induced Deposition (FEBID) is a mask-less nano-printing technique that allows for the reliable fabrication of planar and even complex, free-standing 3D nanostructures. Herein, we demonstrate its suitability for creating flexible plasmonic nanostructures, which are not producible with standard lithography techniques. We start with printing simple 2-3D Au nanostructures and evaluate their plasmonic activity via STEM-EELS further corroborated by simulations with the aim to generate an upfront design tool.

Alternative Plasmonic Metamaterials based on Titanium Nitrides and Oxynitrides with Tunable Properties

C. Mancarella[1*], L. Tovaglieri[1], G. Baiardi[1], A. Lamperti[2], V. Caligiuri[3,4], A. De Luca[3,4] and A. Li Bassi[1,5]

[1]Nanolab, Department of Energy, Politecnico di Milano, Milano, Italy
[2]CNR-IMM, Agrate Brianza (MB), Italy
[3]Department of Physics, Università della Calabria, Rende (CS), Italy
[4]CNR-Nanotec, Rende (CS), Italy
[5]CNST-IIT – Italian Institute of Technology, Milano, Italy

[*]Corresponding author: cristina.mancarella@polimi.it

Abstract: the established potentialities of plasmonic effects in boosting light-matter interactions are at the basis for next-generation metamaterials merging multifunctionality, tunability of properties and broader spectral responses. The archetypal plasmonic materials, i.e. noble metals, show limited modulation outside the visible spectrum. Here, original meta-structures (e.g. hyperbolic metamaterials) based on non-metal plasmonic materials (titanium nitrides, oxynitrides) has been experimentally developed to finally pursue tailorable plasmonic features from VIS to IR towards extreme light manipulation in energy or nanophotonic applications.

At present, plasmonic excitations (e.g. Localised Surface Plasmon Resonances LSPRs) are at the forefront of research because they allow an ultra-fine tailoring and intensification of light-matter interactions at the nanoscale, to be exploited for example in solar-driven energy conversion devices [1]. Noble metals are the most widespread plasmonic materials (e.g. Au) due to high-quality LSPR in the visible (VIS) range. However, the impossibility to modulate plasmons outside the VIS (fixed carrier density) justifies the spreading interest for alternatives [2].

Conducting transition metal nitrides (e.g. TiN) are nowadays appointed as ideal substitutes to traditional plasmonic materials because of low-cost, CMOS compatibility and the tailored plasmonic responses in the VIS-near IR through stoichiometry [3]. Besides, thermal, chemical and mechanical stability are added advantages for operation in extreme environments. Oxynitrides (e.g. TiO_xN_y) are rising interest as well, due to the unique capability to cross twice the zero value of the real permittivity ε_1 in a wide spectral range (double epsilon-near-zero property, D-ENZ) at which new exotic phenomena arise, such as enhanced non-linear optical responses, super-intensification of light or improved photocatalysis [4]. Conversely, transparent conductors possess tunable carrier density, thus are promising for shifting the plasmonic features in the infrared (IR) [2].

In this framework, the interest is now focusing on meta-structures based on alternative materials, possessing intrinsic multifunctionalities and vast tunability of properties to fulfill at once multiple needs, spanning different applications (energy, optoelectronics, biosensing, nano-photonics). Specifically, peculiar multilayer structures, namely Hyperbolic Metamaterials (HMMs) show an anisotropic permittivity ε (parallel $\varepsilon_{//}$ and perpendicular $\varepsilon_{\perp}$ to the multilayer surface) resulting from the periodic alternation of conductors ($\varepsilon_1<0$) and dielectrics ($\varepsilon_1>0$) [5]. At the hyperbolic regime, unconventional electromagnetic phenomena are enabled (e.g. high-k modes) resulting, for instance, in unprecedented light confinement and manipulation. However, by investigating and merging alternative materials (transition metal nitrides or oxynitrides) with innovative design routes, metamaterial research can be further advanced by exploiting potentialities coming from unusual combinations of materials and properties (material stability, conductivity, broadband VIS-IR plasmonics, tunability).

In this work, single films and multilayers based on titanium nitrides TiN and oxynitrides TiO_xN_y (**Fig. 1a**),

have been developed at room temperature, on cheap substrates (Si, glass). Pulsed Laser Deposition (PLD) has been consciously selected for the one-step and manageable deposition procedure of 1-dimensional layered nanostructures. Besides, stoichiometry, composition and morphology in the growing films can be modified directly at the synthesis stage, by acting on deposition parameters (e.g. background gas pressure, laser fluence etc.) or through post-processing (e.g. thermal annealing). Great efforts have been devoted to materials characterization, understanding the physics behind while keeping a material science outlook.

First, TiN have been implemented as metal element in conducting TiN/TiO_2 multilayers, where this material couple for HMMs is a novelty and intriguing due to the good knowledge and versatility of TiO_2 as a wide-band gap semiconductor, high thermal stability of TiN and easiness in production. Material properties of the metasystem can be tailored with geometry (structural, electrical, optical/plasmonic properties). The existence of the hyperbolic character has been found by first evaluating the permittivities of single constituents through ellipsometry, then performing simulations of the anisotropic components ($\varepsilon_{\parallel}$ and $\varepsilon_{\perp}$) and final assessing the wavelength window at which $\varepsilon_{\parallel} \cdot \varepsilon_{\perp} < 0$ (HMM behaviour). Notably, a very wide HMM character in VIS-near IR (600-2100 nm) is present (**Fig. 1b**), although open to improvements by increasing the quality of the single layer materials (avoiding oxidation and internal stresses). Then, single films of oxynitrides have been synthetized from TiN by finely engineering the level of oxygen through deposition parameters (base vacuum, H_2-N_2 pressure). The not-trivial challenge is increasing the oxygen incorporation while maintaining the structure of TiN, i.e. preventing transition to TiO_2. Relationship between synthesis and structural/optical characteristics is complex and not straightforward to investigate. However, the approach is successful in obtaining D-ENZ character, since ε_1 has two zero-crossing points strongly tunable with deposition conditions at 400– 1700 nm (**Fig. 1c**). The next obligatory step is the integration in designed multilayers for broadband and multi-resonant D-ENZ HMMs.

Concluding, nitride-based alternative plasmonic nanomaterials merging multifunctional, tunable and broader plasmonic responses are starting guidelines to design real devices where the enhancement of light-matter interactions is at the core for technologically-relevant applications (thermal management in photovoltaics, plasmon-mediated broadband solar absorption/manipulation and photocatalysis).

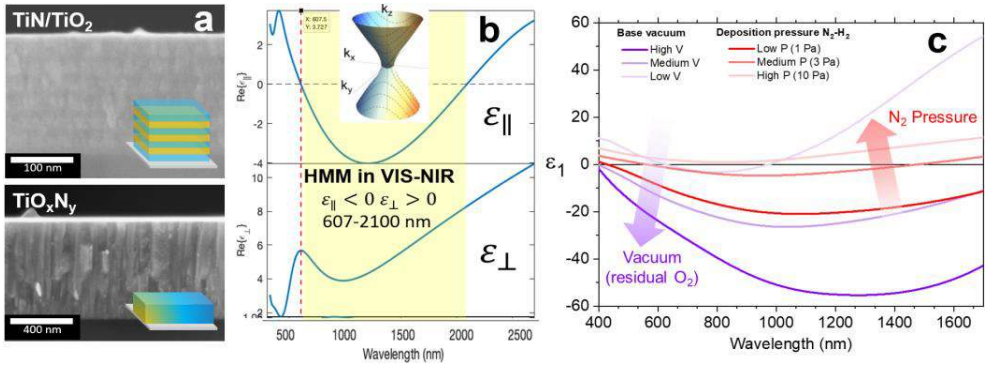


Figure 1: (a) SEM images of TiN/TiO_2 multilayers and TiO_xN_y films. **(b)** $\varepsilon_{//}$ and $\varepsilon_{\perp}$ of TiN/TiO_2. **(c)** ε_1 of TiO_xN_y showing D-ENZ.

References

1. Naldoni, A. et al., "Solar-Powered Plasmon-Enhanced Heterogeneous Catalysis", *Nanophotonics* 5, 112–133, 2016
2. Naik, G. V. et al., "Alterantive Plasmonic Materials: Beyond Gold and Silver", *Adv. Mater.* 25, 3264–3294, 2013
3. Patsalas, P. et al., "Conductive nitrides: Growth principles, optical and electronic properties, and their perspectives in photonics and plasmonics", *Mater. Science and Engineering R* 123 1-55, 2018
4. Braic, L., et al., "Titanium Oxynitride Thin Films with Tunable Double Epsilon-Near-Zero Behavior for Nanophotonic Applications", *ACS Appl. Mater. Interfaces*, 9, 29857−29862, 2017
5. Shekhar, P. et al., "Hyperbolic metamaterials: fundamentals and applications", *Nano Convergence*, 1, 14, 2014.

Tailoring coupling conditions between silicon metasurfaces and molecular vibrations

K. Watanabe[1*], H. R. Devi[2], M. Iwanaga[3], and T. Nagao[2,4]

[1]International Center for Young Scientists (ICYS), National Institute for Materials Science (NIMS), Japan
[2]International Center for Materials Nanoarchitectonics (MANA), National Institute for Materials Science (NIMS), Japan
[3]Research Center for Functional Materials, National Institute for Materials Science (NIMS), Japan
[4]Department of Condensed Matter Physics, Graduate School of Science, Hokkaido University, Japan
[*]corresponding author: watanabe.keisuke@nims.go.jp

Abstract: Vibrational coupling to quasi-bound states in the continuum (qBICs) in silicon-based dielectric metasurfaces is experimentally demonstrated. The judicious selection of the asymmetry parameter of qBICs offers tailored coupling between the resonance mode and polymethyl methacrylate (PMMA) molecules from weak to strong coupling regimes. We also show the existence of the asymmetry parameter at which the enhanced molecular signal is maximized. We believe that these findings serve as a bases for highly sensitive surface-enhanced infrared spectroscopy based on all-dielectric materials.

Identifying a small number of molecules based on surface-enhanced infrared spectroscopy is conventionally realized by utilizing the interactions between the molecular vibrations and the strongly localized electric fields in plasmonic platforms [1]. Recently, loss engineering strategies for maximizing the molecular absorptions at the vibrational modes have been reported as another strategy [2]. The ratio of the radiative to the nonradiative intrinsic loss rates originating from the metallic nanostructures can be controlled by changing the structural parameters, giving a large vibrational signal at an optimum condition [3]. This method provides significant enhancement effects without a precise nanofabrication such as a few nanometer gaps [4]. Nevertheless, it still requires elaborate structural design, and the loss tunability is limited by metal absorptions. In this respect, dielectric nanostructures have advantages in terms of their low material losses and tunability of radiative quality (Q) factors [5]. Especially, dielectric metasurfaces at quasi-BICs have great potential for the significant surface enhancement effects in vibrational coupling to the resonance modes as the radiative losses can be controlled simply by changing their asymmetry parameters.

In this work, we report on the tunability of the coupling conditions between silicon metasurfaces and molecular vibrations. Figure 1(a) shows the proposed metasurface structure on a silicon-on-insulator (SOI) wafer with a 400-nm silicon layer and a 2000-nm buried oxide layer. The period of the array P is 3900 nm, the primitive silicon rod length L is 2625 nm, the rod height w is 985 nm, and the distance between the centers of the upper and lower rods is 1825 nm. Here, the asymmetry parameter is defined as $\alpha = 2\Delta L/L$. The electric field intensity in the xy-plane ($\alpha = 0.2$) is strongly localized at the sidewalls of the silicon rods (Fig. 1(b)), which induces a strong interaction with the coupled molecules. For the field intensity in the yz-plane, the field strengths in the upper and lower rods are asymmetric (Fig. 1(c)), giving rise to the net electric component in the x-direction. Figure 1(d) shows experimental transmission spectra obtained using Fourier transform infrared spectroscopy. Both the resonance peak amplitudes and the linewidths increased with the parameter α. Notably, only the linewidths could be tuned while the resonance peak wavelengths remained nearly constant when changing α. Next, a 111-nm PMMA layer was spin-coated onto the bare metasurfaces. As can be seen in Fig. 1(e), the two split peaks appeared at the shorter and longer wavelengths of the PMMA absorption peak (C=O stretching mode) when α is large. The amplitudes of the split modes increased with increasing α. The Rabi splitting Ω was evaluated by observing the anti-crossing behavior in structures with varied detuning, indicating that strong coupling conditions were satisfied when α was smaller or equal to

0.27, where the Ω exceeded the linewidths of both the C=O absorption and qBIC modes. When α was larger than 0.27, the coupled systems were in weak coupling conditions. The enhanced molecular signal, which was calculated by subtracting transmission amplitude of the coupled qBIC-PMMA modes from the qBIC modes, was maximized at a specific α. The molecular signal can be explained by the temporal coupled mode theory [6], indicating that the surface enhancement effect originated from the radiative loss engineering based on the qBIC modes. The wide tunability of the loss in dielectric metasurfaces favors the optimization of the coupling conditions of the vibrational mode, opening potential applications for highly sensitive surface-enhanced infrared spectroscopy without using metals.

This work was financially supported by JSPS KAKENHI Grant Number JP22K20496.

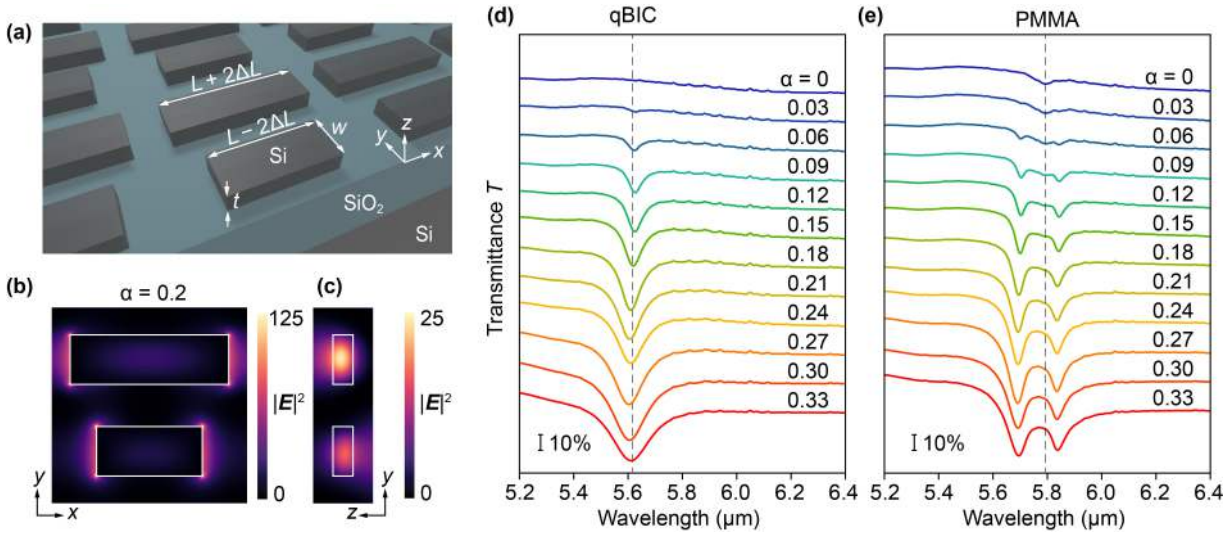


Figure. 1 Silicon metasurfaces at quasi-BICs. (a) Schematic of a silicon metasurface fabricated on a SOI wafer composed of two parallel asymmetric rods. (b)(c) $|\boldsymbol{E}|^2$ profiles at the resonance peak wavelengths in the *xy*-plane at half height of the silicon nanostructures and *zy*-plane at the center of the unit cell, respectively. (d)(e) Experimental transmission spectra of the bare and PMMA coated metasurfaces, respectively, with different α.

References

1. F. Neubrech, C. Huck, K. Weber, A. Pucci, and H. Giessen, "Surface-enhanced infrared spectroscopy using resonant nanoantennas," *Chemical Reviews*, vol. 117, no. 7. American Chemical Society, pp. 5110–5145, 2017.
2. R. Adato and H. Altug, "In-situ ultra-sensitive infrared absorption spectroscopy of biomolecule interactions in real time with plasmonic nanoantennas," *Nat. Commun.*, vol. 4, no. 1, p. 2154, 2013.
3. R. Adato, A. Artar, S. Erramilli, and H. Altug, "Engineered absorption enhancement and induced transparency in coupled molecular and plasmonic resonator systems," *Nano Lett.*, vol. 13, no. 6, pp. 2584–2591, 2013.
4. H. Zhou, Z. Ren, C. Xu, L. Xu, and C. Lee, "MOF/Polymer-integrated multi-hotspot mid-infrared nanoantennas for sensitive detection of CO2 gas," *Nano-Micro Lett.*, vol. 14, no. 1, p. 207, 2022.
5. K. Watanabe and M. Iwanaga, "Nanogap enhancement of the refractometric sensitivity at quasi-bound states in the continuum in all-dielectric metasurfaces," *Nanophotonics*, vol. 12, no. 1, pp. 99–109, 2023.
6. W. Suh, J. D. Joannopoulos, and S. Fan, "Temporal coupled-mode theory for the Fano resonance in optical resonators," *J. Opt. Soc. Am. A*, vol. 20, no. 3, pp. 569–572, 2003.

Optical Metafluids Composed of Colloidal Mie-Resonant Silicon Nanospheres

H. Sugimoto[1*], and M. Fujii[1]

[1]Department of Electrical and Electronic Engineering, Graduate School of Engineering at Kobe University, Japan
[*]corresponding author: sugimoto@eedept.kobe-u.ac.jp

Abstract: Colloidal suspension of resonant nanostructures exhibiting optical magnetism may have very high and low effective index un-achievable in natural liquids, which can be exploited for the applications different from solid-state optical metamaterials. Here, dual nanoparticles with electric and magnetic resonances dispersed in solution dubbed as "dual metafluids" were developed based on Mie-resonant silicon nanospheres. In addition to the strong magnetic response in optical regime, the helicity preserved light scattering from size-purified silicon nanoparticles dispersed in solution were demonstrated.

Dielectric nanoparticles that exhibit both electric and magnetic responses provide rich functionalities for manipulating light waves in the field of metasurfaces, by enabling 2π phase control, Kerker-type directionality, enhanced chirality, negative refractive index, etc. The dielectric nanoantennas have been mostly lithographically fabricated on the substrate and used as building blocks of solid photonics devices. When the dielectric nanoantennas are synthesized in solution, they can also be a constituent of a liquid-phase metamaterial or a "metafluid". Such metafluid may be promising for applications in chemical and biology. The nanoantennas with electric and magnetic responses satisfy duality symmetry condition and they preserve the helicity of the incident light (*i.e.*, "dual"). In the helicity-preserving nanoantennas, the chirality of the local fields around the constituent nanospheres are strongly enhanced, which improves the sensitivity of enantiomer-selective chiral molecular sensing. However, experimental demonstration of the "dual" behaviors of nanoantennas in solution is not successful yet.



Figure 1. Dual nanoantennas. Helicity of incident light is preserved at Kerker condition of dielectric nanoantennas.

Over the past decades, plasmonic nanoparticles and nanoclusters have been explored as constituents of a metafluid. However, magnetic response of plasmonic nanoparticles is usually much weaker than the electric responses, i.e., the optical response is "non-dual". Here, we propose an all-dielectric metafluid composed of crystalline silicon nanospheres having the electric dipole (ED) and magnetic dipole (MD) Mie resonances at the optical frequencies At the Kerker condition, where the ED and MD resonances have the same amplitude and are in-phase, a silicon nanoparticle is "dual". We first experimentally demonstrate that a silicon nanosphere metafluid exhibits strong electric and magnetic dipolar Mie responses across the visible to near-infrared spectral range. The intensity ratio of the magnetic-to-electric responses reaches unity. We show that a solution of size-purified silicon nanospheres can be "dual" and "anti-dual" metafluids. This is the first experimental demonstration of a

liquid that can control the helicity of scattered light. The helicity-preserving metafluids with large enhancement of chiral near-fields may have applications in the fields of chiral molecular sensing.

References

1. Sugimoto, H, *et al.*, "Mie Resonator Color Inks of Monodispersed and Perfectly Spherical Crystalline Silicon Nanoparticles", Advanced Optical Materials, Vol. 8, Issue 12, 2000033, 2020.
2. Hinamoto, T *et al.*, "Colloidal Solutions of Silicon Nanospheres toward All-Dielectric Optical Metafluids", Nano Letters, Vol. 20, Issue 10, 7737-7743, 2020.
3. Sugimoto, H, Fujii, M, "Colloidal Mie Resonant Silicon Nanoparticles", Nanotechnology, Topical Review, Vol. 32, Number 45, 452001, 2021.
4. Negoro, H. *et al.*, "Helicity Preserving Metafluids", *under review*

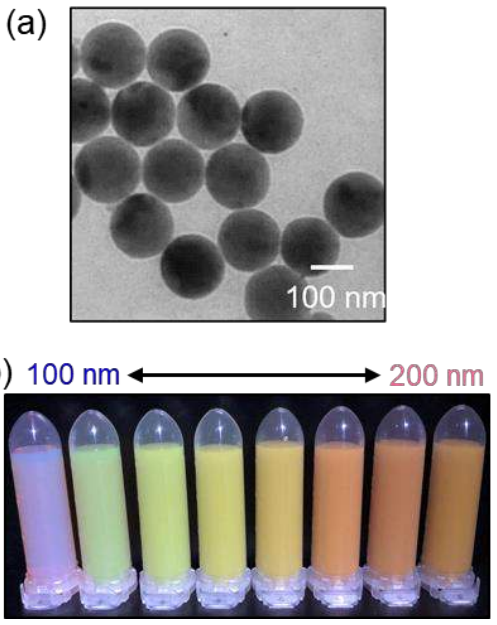


Figure 2. (a) TEM image of crystalline Si nanospheres. (b) Photograph of colloidal dispersion of Si nanospheres with different average diameters under white LED illumination.

Some 2D Magnetic Topological Photonic Crystals

Baile Zhang[1, 2‡]

[1]Division of Physics and Applied Physics, School of Physical and Mathematical Sciences,
Nanyang Technological University, Singapore 637371, Singapore
[2]Centre for Disruptive Photonic Technologies, Nanyang Technological University, Singapore 637371, Singapore
corresponding authors: ‡blzhang@ntu.edu.sg

Abstract: Over a decade ago, topological photonics came into existence with the discovery of the first photonic topological insulator, which comprised a two-dimensional (2D) periodic lattice of gyromagnetic rods or a magnetic photonic crystal. Despite the significant progress made in the field of topological photonics in recent years, the potential of 2D magnetic photonic crystals remains largely unexplored. In this talk, we present some of our recent research on 2D magnetic topological photonic crystals.

The field of topological photonics [1] emerged a decade ago with the discovery of the first photonic topological insulator, a periodic lattice of gyromagnetic rods or a magnetic photonic crystal [2] that supports chiral edge states propagating in a unidirectional way. This groundbreaking achievement marked the first demonstration of the Chern insulator phase, known as the quantum Hall effect without Landau levels [3], characterized by the topological invariant of Chern number.

In this talk, I will present some of our recent studies on two-dimensional (2D) magnetic topological photonic crystals. The first study is focused on the localization of chiral edge states. According to the topological bulk-boundary correspondence, the chiral edge states should be "topologically protected" against any disorder or defect, without the possibility of being localized as long as the Chern number is valid in a non-closed band gap. However, we will discuss the possibility of localizing chiral edge states even when the Chern number is intact.

We will start by considering the non-Hermitian skin effect [4], which is the result of a non-Hermitian band topology that applies to the chiral edge states. By introducing non-Hermiticity (loss/gain) into a magnetic topological photonic crystal, we can construct the coexistence of a point band gap (for the non-Hermitian skin effect) and a line band gap (for the Chern number-protected chiral edge states), leading to skin effect of chiral edge states and causes their localization.

The second study focuses on the topological phase transition to a quadrupole topological insulator phase [5]. The quadrupole topological insulator is the first higher-order topological phase that has sparked the rise of higher-order topological physics in recent years. The typical construction of a quadrupole topological insulator requires the negative coupling and time-reversal symmetry, as required in the Benalcazar-Bernevig-Hughes (BBH) model [6]. We will show that a magnetic topological photonic crystal can exhibit a phase transition from the Chern insulator phase to a quadrupole topological insulator phase.

References

1. Ozawa, T., H. M. Price, A. Amo, N. Goldman, M. Hafezi, L. Lu, M. C. Rechtsman, D. Schuster, J. Simon, O. Zilberberg and I. Carusotto, "Topological Photonics," Rev. Mod. Phys., Vol. 91, 015006, 2019.
2. Wang, Z., Y. D. Chong, J. D. Joannopoulos and M. Soljacic, "Observation of Unidirectional Backscattering-Immune Topological Electromagnetic States," Nature, Vol. 461, 772, 2009.

3. F. D. Haldane, “Model for a quantum Hall effect without Landau levels: condensed-matter realization of the ‘parity anomaly’,” Phys. Rev. Lett., Vol. 61, 2015, 1988.
4. E. J. Bergholtz, J. C. Budich and F. K. Kunst, “Exceptional topology of non-Hermitian systems,” Rev. Mod. Phys., Vol. 93, 015005, 2021.
5. P. Zhou, G.-G. Liu, Z. Wang, Y.-H. Hu, S. Li, Q. Xie, Y. Zhang, X. Xi, Z. Gao, L. Deng, and B. Zhang, “Realization of a quadrupole topological insulator phase in a gyromagnetic photonic crystal,” arXiv:2302.03184.
6. W. A. Benalcazar, B. A. Bernevig, and T. L. Hughes, “Quantized electric multipole insulators”, Science, Vol. 357, 61, 2017.

Charge Transfer Process on Plasmonic Cathode Electrode

Hiro Minamimoto*, Yuto Tajiri, and Minoru Mizuhata

Department of Chemical Science and Engineering, Graduate School of Engineering, Kobe University

1-1 Rokkodai-cho, Nada, Kobe, 657-8501, Japan.
*corresponding author: minamimoto@godzilla.kobe-u.ac.jp

Abstract: The visible-light energy conversion is one of the important challenges for the sustainable society. Recently, various photocatalytic systems, such as molecular catalysts, semiconductors, or plasmonic systems, have been established. In this study, we have focused on the plasmonic photoenergy conversion system and established the new plasmonic cathode electrode system. Through the examination of photoelectrochemical measurements, we have successfully clarified the detail information about charge transfer processes on plasmonic cathode electrodes.

The establishment of high efficient visible light energy conversion system is an attractive challenge in the field of photoelectrochemical region. In order to achieve it, the wide-band gap semiconductor electrodes are often recognized as the promising candidates. However, the available wavelength region is often limited to the ultraviolet region because of their wide band gap energy. Recently, as the breakthrough for it, the introduction of the plasmonic metal nanostructures into the semiconductor electrode surfaces has been received much attention. In that system, the excited electrons or holes are injected into the semiconductor while remained holes or electrons trigger the chemical reactions at metal-semiconductor interfaces. Until now, various anodic systems which are the combination of plasmonic metal nanostructures with n-type semiconductor electrodes have been proposed. And also, the detail information and absolute electrochemical potential of excited holes were also investigated [1]. Recent study also proposes the plasmonic cathode by using the p-type semiconductor to control the reduction reactions at electrode surfaces. In our previous study, we have also proposed the plasmonic cathodic system which consists of p-type GaP and Ag nanostructures to control the visible light driven hydrogen evolution reactions [2]. In that report, the unique pH dependence of the reaction characteristic was observed, indicating unique molecular selectivity of plasmon-driven reactions. Although we have clarified unique reaction characteristics, the detail information about the charge transfer process on it was still under discussion. In this study, we have investigated its information through various photoelectrochemical measurements. At the present system, the chemically synthesized Au nanorod structures were supported on various types of p-type semiconductors to achieve the multi-color response ability. Through the photoelectrochemical measurements, we have found that the absolute electrochemical potential of excited electrons was dependent on not only the incident wavelength but also the flat band potential of substrates. As the results, we have confirmed the unique isotope effects which cannot be observed the conventional cathode system. Our current research would provide the novel insight for the accurate design of the high efficient light conversion device.

References

1. H. Minamimoto et al., J. Phys. Chem. C, Vol. 120, 16051–16058, 2018.
2. H. Minamimoto et al., Chem. Lett., Vol. 49, 806–808, 2020.

Advanced passive and active metasurfaces and zero-index materials

Harnessing the properties of emerging low-dimensional and phase-change materials for mid-IR photonics

Mitradeep Sarkar[1], Maxime Giteau[1], Michael Enders[1], Aleksandra Deeva[1], and Georgia T. Papadakis[1*]

[1]ICFO-Institut de Ciencies Fotoniques, The Barcelona Institute of Science and Technology, Spain

[*] georgia.papadakis@icfo.eu

Abstract: In this talk I will discuss the properties of several emerging low-dimensional materials that are typically exfoliated in the laboratory, rather than grown in large scale. First, I will introduce a method for retrieving the mid-IR dielectric properties of exfoliated flakes, which are typically too small to be characterized via the standard spectroscopic ellipsometry. Second, several low-dimensional materials exhibit significant anisotropy in the mid-IR range. I will discuss approaches to leverage this property for deep-subwavelength control of optical chirality and polarization control of a mid-IR beam. Finally, I will present simple design rules that can be applied in lithography-free mid-IR absorbers and emitters for active tunability via temperature-controlled phase-change materials.

The mid-infrared (IR) spectral range is of particular importance for applications in thermal energy harvesting, spectroscopy, molecular sensing and detection, and thermal camouflage. There has recently been significant interest in harvesting relevant properties of emerging materials for mid-IR photonics. Of particular interest are materials that support strong dielectric resonant features in the mid-IR range, with most prominent the case of surface phonon polaritons (SPhPs) that span the whole range from mid-IR to THz. These excitations can be found in various low-dimensional materials, such as hexagonal boron nitride (hBN) and molybdenum trioxide (MoO_3). Other than their strong dielectric resonances due to SPhPs, these materials also exhibit strong optical anisotropies, often behaving like a metal in one coordinate direction and like a dielectric in another coordinate direction. These properties have been considered by the mid-IR photonics community in the last decade as ways to control thermal radiation.

Nonetheless, these materials are not yet widely reproducible in the large-scale. Most experimental demonstrations, to ensure high material quality, utilize exfoliation to isolate thin flakes. Exfoliated flakes are typically very small as compared to a mid-IR beam, yielding a beam-sample mismatch for standard far-field mid-IR spectroscopy. This challenge also pertains to spectroscopic ellipsometry: the approach used traditionally to experimentally retrieve the optical properties of materials. Thus, exfoliated flakes with interesting mid-IR excitations are typically characterized insufficiently with near-field methods such as near-field optical microscopy (NSOM) and others. These methods are typically too delicate and sensitive to mechanical vibrations, and the reported dielectric properties deriving from them are the result of significant numerical fitting. In contrast, in this talk I will present a method to characterize small flakes of low-dimensional materials with a standard Fourier Transform Infrared Spectroscopy (FTIR) with minimal a priori knowledge of the dielectric properties of the samples. This method extends to strongly anisotropic materials, and I will present results for hBN and a-MoO_3 flakes that are close to literature values.

The SPhP resonances of several low-dimensional materials are highly relevant for directional control of mid-IR light. I will present a numerical study of how the interplay between real and imaginary part of their

dielectric permittivity dictate the degree of directional control that one may achieve. Furthermore, the strong anisotropies of low-dimensional materials can be a useful property for controlling different features of light propagation. I will present experimental results for a deep-subwavelength a-MoO_3 half waveplate operating both in transmission and reflection, and being at least two orders of magnitude thinner than standard mid-IR materials that serve as quarter waveplates. I will also discuss ways to control the chirality of mid-IR beams by leveraging this in-plane anisotropy of several low-dimensional materials.

In the final part of my talk, I will introduce design rules, compatible with any planar heterostructure, for achieving maximal dynamic tunability via temperature-control. In particular, I will discuss an approach to yield arbitrarily large shifts in mid-IR absorptivity or emissivity, as well as an approach to obtain maximal ON/OFF contrast ratio on-resonance.

Funding

We acknowledge funding from “la Caixa” Foundation (ID 100010434), from the PID2021-125441OA-I00 project funded by MCIN /AEI /10.13039/501100011033/ FEDER, UE, and from the European Union’s Horizon 2020 research and innovation program under the Marie Sklodowska-Curie grant agreement No 847648. The fellowship code is LCF/BQ/PI21/11830019. This work is part of the R&D project CEX2019-000910-S, funded by MCIN/ AEI/10.13039/501100011033/ , from Fundacio Cellex, Fundacio Mir-Puig, and from Generalitat de Catalunya through the CERCA program.

META 2023, PARIS - FRANCE, JULY 18 – 21, 2023

Plasmonic metasurfaces and waveguide devices based on epsilon-near-zero materials

Pierre Berini

School of Electrical Engineering and Computer Science, University of Ottawa, Ottawa, Canada
Department of Physics, University of Ottawa, Ottawa, Canada
*corresponding author: berini@eecs.uottawa.ca

Abstract: We report work on tunable plasmonic metasurfaces and on polarization-independent broadband plasmonic modulators (>200 GHz), exploiting epsilon-near-zero effects in metal-oxide-semiconductor structures fabricated using conductive oxides. The tunable metasurfaces comprise subwavelength pixels that produce no grating diffraction and are used in reflection to control the magnitude and phase of the reflected beam. The broadband modulators share the same material set but are fabricated on embedded Si waveguides and designed to operate with TE or TM light.

Results

Resonant nanometallic structures, such as plasmonic nanoantennas, are essential to the conversion of light to surface plasmon-polaritons (SPPs) localized to ultra-small volumes. Such structures can provide highly enhanced fields, strong confinement, high surface sensitivity, and can double as a device electrode for applying voltages or passing currents to active regions in optoelectronic devices. In optoelectronics, plasmon enhancement can be exploited for high-performance electro-optic modulators and beam-steering devices [1-6].

Fig. 1 shows an electrically-tunable plasmonic metasurface on fused silica. The metasurface consists of an array of Au dipole nanoantennas contacted perpendicularly by electrical contact lines (Fig. 1(b)). The contact lines are centred on the nanoantennas (dipoles), which ensures that they are minimally invasive optically, due to their orthogonal alignment relative to the incident polarisation (along the nanoantenna axes). The nanoantennas are connected to an electrical fan-out structure (Fig. 1(a)) and coated with a HfO_2 layer then an ITO layer (Fig. 1c)), and finally by a metal mirror structure (Fig. 1(d)). Electrically the structure operates as a MOS capacitor (Au-HfO_2-ITO) with the top Au mirror structure also acting as the Ohmic contact to the ITO. When driven into strong accumulation, the ITO enters the epsilon-near-zero regime [6] resulting in large changes in the resonant behaviour of the nanoantennas. The structure produces a reflection coefficient at telecom wavelengths ($\lambda_0 \sim$ 1550 nm) that varies significantly (magnitude and phase) with applied voltage. The individual pixels (meta-atoms) in this structure are subwavelength such that grating diffraction upon reflection is completely avoided. The structure forms the basis of a solid-state optical phased array or a spatial light modulator.

Using the same material set (Au-HfO_2-ITO) a broadband plasmonic electro-optic modulator operating at telecom wavelengths and based on free carrier dispersion in ITO is enabled [5]. MOS structures are integrated into a pair of coupled metal-insulator-metal (MIM) waveguides aligned on a planarized silicon waveguide. The coupled MIM waveguides support symmetric and asymmetric plasmonic supermodes, excited adiabatically using mode transformation sections, by the fundamental TM and TE modes of the underlying silicon waveguide, respectively, such that the modulator can operate in either mode. The modulators are 1.5 to 2 μm long, due to the strong interaction of the plasmonic modes with the perturbed ITO layer, and an electrical bandwidth exceeding 200 GHz. The modulators produce an extinction ratio in the range of up to 6 dB and an insertion loss in the range of 4 to 7.5 dB including input/output mode conversion losses. The AC drive voltage is ±1.75 V.

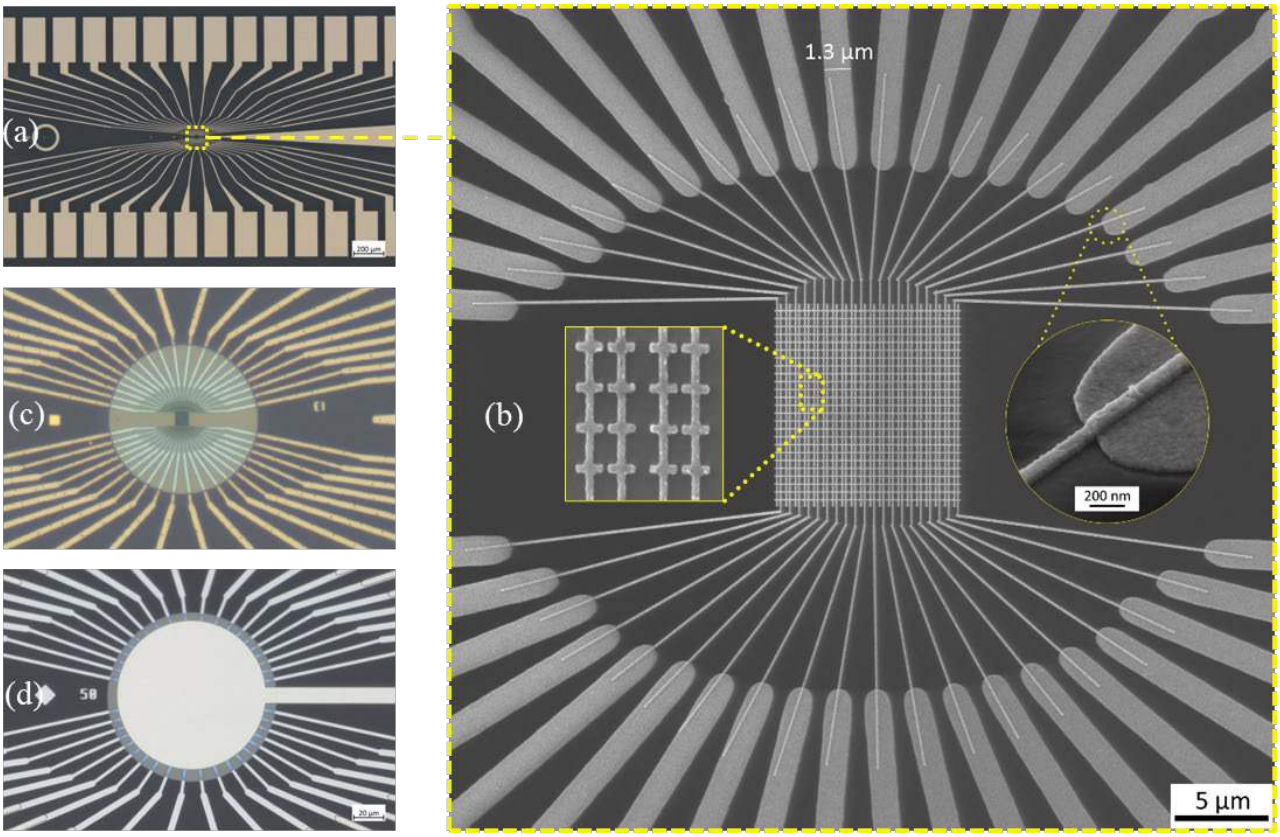


Fig. 1. Electrically-tunable plasmonic metasurface on fused silica: (a) First layer metal (Au contacts, alignment marks), (b) Au nanoantennas (He+ litho), (c) HfO_2 and ITO deposition followed by etching, (d) backside metal (Ohmic contacts, mirror).

References

1. Berini, P., "Optical Beam Steering Using Tunable Metasurfaces," ACS Photonics, Vol. 9, 2204-2218, 2022
2. Calà Lesina, A., Goodwill, D., Bernier, E., Ramunno, L., Berini, P., "Tunable Plasmonic Metasurfaces for Optical Phased Arrays," IEEE J Sel. Top. Quant. Electr., Vol. 27, 4700116, 2021
3. Calà Lesina, A., Goodwill, D., Bernier, E., Ramunno, L., Berini, P., "On the performance of optical phased array technology for beam steering: effect of pixel limitations," Opt. Express, Vol. 28, 31637-31657, 2020
4. Rashid, S., Walia, J., Northfield, H., Hahn, C., Olivieri, A., Calà Lesina, A., Variola, F., Weck, A., Ramunno, L., Berini, P., "Helium ion beam lithography and liftoff," Nano Futures, Vol. 5, 025003, 2021
5. Dhingra, N., Mehrvar, H., Berini, P., "Broadband plasmonic modulator operating with the fundamental TM or TE modes of a planarized silicon waveguide," submitted
6. Shabaninezhad, M., Ramunno, L., Berini, P., "Tunable plasmonics on epsilon-near-zero materials: the case for a quantum carrier model," Optics Express, Vol. 30, pp. 46501- 46519, 2022

META 2023, PARIS - FRANCE, JULY 18 – 21, 2023

Magnetic Nearfield Reshaping Metasurfaces

Hanwei Wang[1], Xiaodong Ye[1], Joshua Yu[1], Yun-Sheng Chen[1], Yang Zhao[1*]

[1]Department of Electrical and Computer Engineering, University of Illinois Urbana Champaign, USA
[*]corresponding author: yzhaoui@illinois.edu

Abstract In this talk, I will discuss a wearable metasurface that can actively reshape the magnetic nearfield to form a desired mode. The active tuning of the metasurface enables an on-demand magnetic field distribution that can be used for efficiently wirelessly charging embedded medical devices. We show that our metasurface can be worn on hands and enhances the delivered power by 10 fold.

Summary

Over 2 million patients in the United States benefit from electrically powered, implanted medical devices, such as cardiac pacemakers, implanted insulin pumps, and cochlear implants. The implants significantly prolong the patients' lifetime and improve their living quality. For example, cardiac pacemakers yield an average life increase of 9.5 to 20 years. In 1988, among the 1152 elderly patients over 65 years old who took surgical implantations of cardiac pacemakers due to chronic heart failure, 73% survived over five years after the surgery.4 Most medical implants use batteries as their power supply. The battery level needs to be checked frequently and replaced through a surgical procedure when they are out of charge. To enable an easier replacement, the batteries are usually placed in a pocket site underneath the skin and connected through a wire to the executing device inside the body. The leading wire can cause infection, blood vessel damage, and allergic reactions. Most patients report discomfort caused by the wire and the battery pocket. To overcome these problems, researchers have developed integrated devices without wires, i.e., leadless micro-implants. In 2009, Medtronic developed the first leadless pacemaker that can be implanted into the ventricle through minimally invasive surgery. The power consumption is optimized so that the battery can last 12 years, longer than the average lifetime of its patients. However, in the cases that the battery is running low, the devices have to be replaced with open-heart surgery.

Self-powering implants have been a research hotspot for decades. Researchers have utilized power from percutaneous light, blood flow, and body motion. However, these approaches require a complicated energy harvesting device that either needs to be installed invasively or has relatively low efficiency or reliability. To date, none of these approaches have been clinically approved. Radiofrequency (RF) electromagnetic waves, on the other hand, have high penetration depth in tissues and can be easily received by a resonant antenna.[1] Ubiquitous RF power from radio and television stations has proved to be capable of powering battery-free sensors and cameras, where milliwatt-level power can be harvested from a 6-inch antenna at the frequency of 915 MHz.[2, 3] However, medical devices, especially those deeply implanted, such as in the ventricle or cochlea, do not have the space for a 6-inch antenna. Therefore, techniques, such as adaptive phase-tuning have been developed to efficiently capture the energy for charging deeply implanted medical devices. Regardless of the energy harvesting efficiency, the maximum power is limited by the RF field intensity; therefore, power transducers are still required.

Metasurfaces, as a promising man-made material that can manipulate electromagnetic fields and waves, open a new path to overcome the challenges of self-powering the implants with ubiquitous RF fields. Metasurface uses an array of phase-tunable resonators to reshape the wavefront of the radiative wave and,

theoretically, can focus the electromagnetic field into any desired beam form. Different from the applications of the conventional metasurfaces,[4] the physical scale of the medical devices is much smaller compared to the wavelength (~30 cm for 915 MHz RF wave). In our recent work, we pioneered the theory and a design of a highly subwavelength metasurface that is capable of manipulating electromagnetic field in the nearfield range with an arbitrary target field distribution and orientation.[5] We have demonstrated its ability to enhance the signal-to-noise ratio for magnetic resonance imaging.[6]

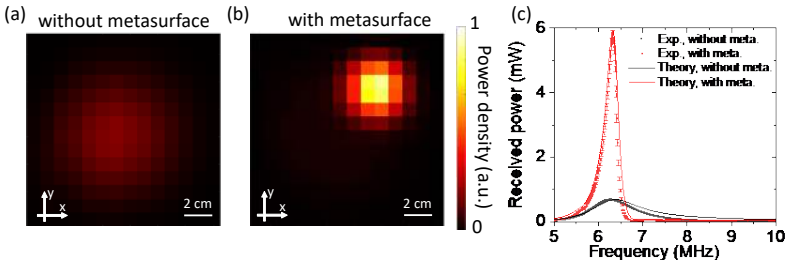


Figure 1. Experimental demonstration of the magnetic nearfield reshaping capability using metasurface. (a) Magnetic field from a coil without metasurfaces. (b) The reshaped magnetic field using the metasurface that 'refocus' the magnetic beam and re-directs the beam to an off-center location. (c) Experimentally demonstration of the enhanced power delivery using the metasurface by more than 10 fold compared to that without the metasurface. The experimental demonstration matches well with our theory.

In this talk, I will discuss recent advances in wearable metasurfaces for enhancing efficiency and delivered power by actively reshaping the magnetic nearfield distribution.[7] We inversely design the metasurface impedance based on the targeted mode distribution using coupled mode theory; we then configure the reactance distribution of the metasurface so that the resulting mode of the metasurface resembles the targeted mode due to strong coupling among the metasurface unit cells and with the transmitting and receiving coils. We have demonstrated two sets of metasurfaces. One operates at 6.8 MHz, compatible with AirFuel Alliance standard, and another one operates at 190 KHz, compatible with the Qi standard. In both devices, we show enhanced power delivery by more than 10 times.

References

1. Kurs, A. et al. Wireless Power Transfer via Strongly Coupled Magnetic Resonances. *Science* **317**, 83-86 (2007).
2. Ho, J.S. et al. Wireless power transfer to deep-tissue microimplants. *Proceedings of the National Academy of Sciences* **111**, 7974-7979 (2014).
3. Philipose, M. et al. Battery-free Wireless Identification and Sensing. *IEEE Pervasive Computing* **4**, 37–45 (2005).
4. Yu, N. et al. Light Propagation with Phase Discontinuities: Generalized Laws of Reflection and Refraction. *Science* **334**, 333-337 (2011).
5. Wang, H., Chen, Y.-S. & Zhao, Y. A wearable metasurface for high efficiency, free-positioning omnidirectional wireless power transfer. *New Journal of Physics* **23**, 125003 (2021).
6. Wang, H., Huang, H.-K., Chen, Y.-S. & Zhao, Y. On-demand field shaping for enhanced magnetic resonance imaging using an ultrathin reconfigurable metasurface. *VIEW* **2**, 20200099 (2021).
7. Hanwei Wang, Joshua Yu, Xiaodong Ye, Yun-Sheng Chen & Zhao, Y. Qi standard metasurface for free-positioning and multi-device supportive wireless power transfer. (2023).

META 2023, PARIS - FRANCE, JULY 18 – 21, 2023

Leveraging Thermo-optical Effects in Nanoantennas and Metasurfaces

G. Tagliabue[1]

[1]Laboratory of Nanoscience for Energy Technologies (LNET), Ecole Polytechnique Federale de Lausanne (EPFL), CH

corresponding author: giulia.tagliabue@epfl.ch

Abstract: Thermo-optical effects in dielectric nanoresonators open new opportunities for contactless manipulation of metasurfaces.

In the last decade, optical nanoantennas have revolutionized light manipulation and control at the nanoscale. Light absorption was initially considered a purely detrimental process, reducing the efficiency of optoelectronic devices. Recently, however, it has attracted growing interest, enabling novel light-energy conversion pathways and offering intriguing opportunities for reconfigurable systems.

In this talk, I will discuss self-induced optical heating effects in highly absorbing Silicon (Si) and Germanium (Ge) nanoresonators. In particular, I will show recent calculations demonstrating that, due to thermo-optical effects, self-heating can give rise to a complex, non-linear relationship between illumination intensity and temperature, even for moderate illumination intensities relevant for applications such as Raman scattering [1]. Subsequently, I will discuss how self-induced optical heating could be employed for thermally reconfigurable optical devices and metasurfaces [2]. Finally, I will discuss our recent effort in controlling the temperature field in multi-dimensional arrays of nanoantennas, highlighting the importance and opportunities offered by thermo-optical effects [3].

References

1. T. V. Tsoulos, G. Tagliabue, Self-induced thermo-optical effects in silicon and germanium dielectric nanoresonators, Nanophotonics 9 (12), 3849-3861
2. A. Archetti, RJ Lin, N. Restori, F. Kiani, T. V. Tsoulos, G. Tagliabue, Thermally Reconfigurable Metalens, Nanophotonics 2022.
3. A. Naef, T. V. Tsoulos, G. Tagliabue, Photothermal and Thermo-optical Effects in 3D Arrays of Dielectric and Plasmonic Nanoantennas, ArXiV: 2211.11832.

Metasurface Image Sensors for Optical Spatial Filtering and Quantitative Phase Imaging

Jianing Liu, Yuyu Li, Hao Wang, Lei Tian, and R. Paiella*

Department of Electrical and Computer Engineering and Photonics Center,
Boston University, 8 St. Mary's St., Boston, MA 02215, USA
*corresponding author: rpaiella@bu.edu

Abstract: We report the development of angle-sensitive photodetectors based on specially designed metasurfaces that can map the phase distribution of the incident light and visualize transparent phase objects without any external spatial-filtering elements. Pixel arrays of these devices can provide quantitative phase reconstruction in a single shot with state-of-the-art sensitivity.

Traditional image sensors detect light incident from all directions with equal responsivity, and as a result can only measure the intensity distribution of a visual scene. At the same time, all information associated with the phase profile and local directions of light propagation is lost in the image acquisition process. The ability to capture such information, however, would allow for more advanced image sensing and processing functionalities, such as image differentiation by optical spatial filtering and the visualization of transparent phase objects, which normally require rather bulky and complex setups. In turn, these functionalities have important applications ranging from computer vision to biomedical microscopy.

Here we report the development of angle-sensitive image sensors that can measure the phase profile of the incident optical field directly, without the need for any external optical elements other than standard imaging lenses. These devices consist of photodetectors stacked with a composite plasmonic metasurface that introduces a strong dependence of responsivity on illumination angle. Specifically, the metasurface is designed to couple light incident at the desired detection angles into surface plasmon polaritons supported by an underlying metal film, which are then scattered into the photodetector active layer by a set of subwavelength slits perforated through the metal film [Figs. 1(a) and 1(b)]. Light incident along all other directions is instead simply reflected back or diffracted away from the device.

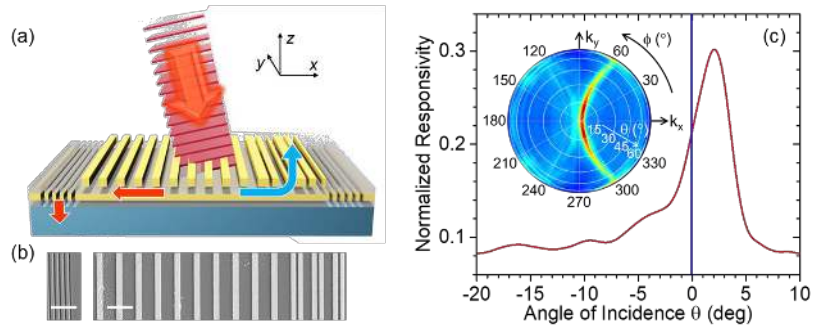


Fig. 1. Angle-sensitive metasurface photodetectors. (a) Schematic device structure. (b) Top-view SEM images of an experimental sample, showing the slits (left image) and nanostripes (right). The scale bars are 2 μm. (c) Inset: measured responsivity of this device at $\lambda = 1550$ nm versus polar θ and azimuthal ϕ illumination angles, normalized to the responsivity of an identical photodetector without any metasurface. Main plot: horizontal line cut of the color map. The vertical blue line indicates normal incidence.

In prior work, similar devices have been developed to demonstrate a planar lensless camera with ultrawide field of view, based on the compound-eye vision modality [1]. The same devices can also be used as optical

spatial filters, based on the notion that different spatial-frequency components of an illuminated object correspond to optical plane waves propagating from the object along different directions [2]. Here we focus on the ability of angle-sensitive photodetectors to visualized transparent phase objects, where light transmission generally involves a deflection in the direction of light propagation proportional to the local phase gradient. To maximize the device sensitivity to small deflection angles, the metasurface is designed to produce an asymmetric dependence of responsivity on angle of incidence around the surface normal. The measured angular response of this device (i.e., responsivity versus polar and azimuthal angles of incidence) is shown in Fig. 1(c).

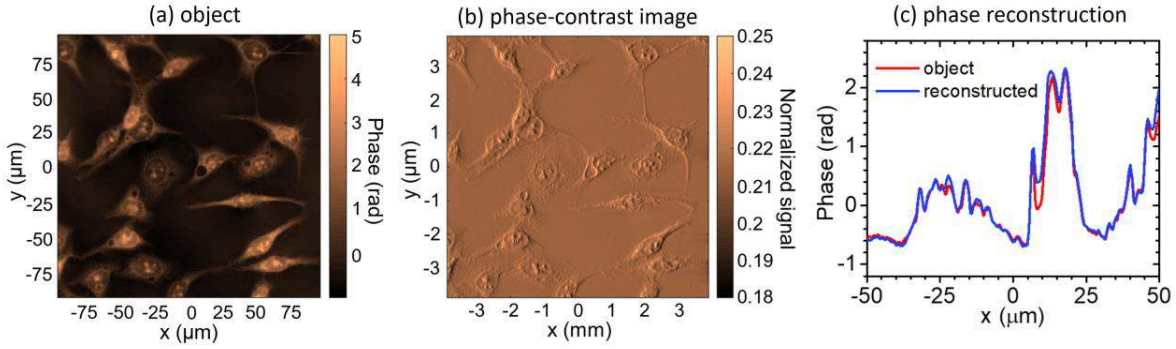


Fig. 2. Phase imaging results. (a) Representative phase object. (b) Corresponding image detected by an array of identical angle-sensitive pixels. (c) Red trace: phase distribution along the horizontal line at y = 0 in the object of (a). Blue trace: reconstructed phase profile from an array partitioned into blocks of four adjacent pixels, each coated with the metasurface of Fig. 1 oriented along one of four orthogonal directions.

These measurement results, combined with computational imaging simulations, indicate that a standard camera or microscope based on such devices can directly map the phase gradient of the incident light and therefore visualize any phase object in its field of view. As an illustration, Figs. 2(a) and 2(b) show, respectively, a phase object of practical interest (HeLa cancer cells) and its phase-contrast image recorded with this approach. A detailed analysis based on the noise properties of high-performance image sensors also show that the minimum detectable phase contrast is smaller than 10 mrad, which is comparable with state-of-the-art phase imaging systems involving significantly more complex and bulky setups [3].

Furthermore, the combination of sensors with equal and opposite angular response on the same pixel array can be used to perform quantitative phase reconstruction in a single shot with a straightforward computational protocol [Fig. 2(c)]. At the same time, with this approach the overall imaging system can be significantly simplified and miniaturized compared to traditional setups for quantitative phase imaging, e.g., based on optical spatial filtering, interferometry, or structured illumination. As a result, this approach is particularly promising for applications where space is highly constrained, such as point-of-care and in vivo microscopy and measurements involving freely moving objects.

This work was supported by NSF under Grant ECCS 2139451.

References

1. Kogos, L. C., Y. Li, J. Liu, Y. Li, L. Tian, and R. Paiella, “Plasmonic ommatidia for lensless compound-eye vision,” Nat. Commun., vol. 11, 1637, 2020.
2. Liu, J., H. Wang, L. C. Kogos, Y. Li, Y. Li, L. Tian, and R. Paiella, “Optical spatial filtering with plasmonic directional image sensors,” Opt. Express, vol. 30, 29074–29087, 2022.
3. Bonati, C., T. Laforest, M. Kunzi, and C. Moser, “Phase sensitivity in differential phase contrast microscopy: limits and strategies to improve it,” Opt. Express, vol. 28, 33767-33783, 2020.

META 2023, PARIS - FRANCE, JULY 18 – 21, 2023

Optical pulse-shaping with plasmonic metasurfaces

René Geromel[1,2,*], Philip Georgi[1,2], Maximilian Protte[1,2], Shiwei Lei[3,4]
Tim Bartley[1,2], Lingling Huang[3] and Thomas Zentgraf[1,2]

[1] Department of Physics, Paderborn University, 33098 Paderborn, Germany
[2] Institute for Photonic Quantum Systems (PhoQS), Paderborn University, 33098 Paderborn, Germany
[3] School of Optics and Photonics, Beijing Institute of Technology, 100081, Beijing, China
[4] Kunming Institute of Physics Key Laboratory of Low-light Night Vision Technology, Xi'an 710065, China

[*]corresponding author: thomas.zentgraf@uni-paderborn.de

Abstract: We present a miniaturized pulse shaping device that creates an arbitrary dispersion through the interaction of multiple metasurfaces on less than 2 mm^3 volume. For this, a metalens and a grating-metasurface between two silver mirrors are fabricated. The grating contains further phase information to achieve the device's pulse shaping functionality.

Ultrashort laser pulses are an important part for nonlinear applications; however, inherent dispersion in optical components tends to distort these pulses. To compensate the dispersion, pulse shaping devices usually utilize bulky prisms or gratings. Furthermore, prism-based pulse shapers are limited to correcting second order dispersion only, whereas newer applications involving metasurfaces promise a more compact design and allow for an arbitrary phase control [1]. Still, these metasurface based devices often rely on free space propagation to generate angular dispersion which leads to extended setups [2,3]. In this work, we report a compact pulse shaping device on a single glass substrate. We demonstrate the application of arbitrary dispersion to an input laser pulse, and analyze the experimental data by second-harmonic generation frequency-resolved optical gating (SHG-FROG) measurements.

The fabricated sample consists of an off-axis focusing metalens (MS1) and a grating metasurface (MS2) embedded in a spacer layer, on one side of a single 2 mm thick BK7 glass-substrate (Fig. 1). Both sides of the substrate are covered with a silver mirror. MS1 focuses the laser beam on MS2 while also introducing angular dispersion, which spreads the laser pulse's bandwidth over the second metasurface. MS2 acts as a grating with half the grating period of MS1 in order to redirect the beam back to MS1. Furthermore, additional wavelength dependent phase information is encoded onto MS2, which is used to alter the laser pulse dispersion.

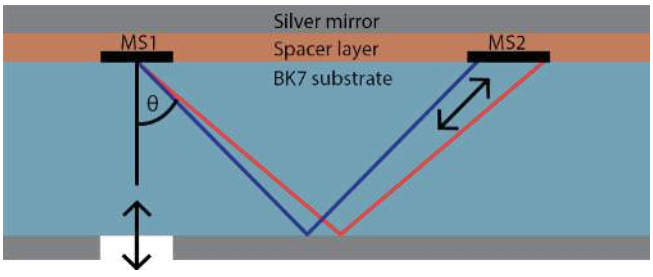


Fig. 1: Schematic image of the pulse-shaping device. A laser beam can pass the aperture in the silver mirror and hit the off-axis metalens (MS1) which redirects the beam under the angle θ towards MS2 while also causing angular dispersion. MS2 contains further phase information which can introduce wavelength dependent arbitrary dispersion.

Multiple MS1 and MS2 pairs with different functionality are fabricated, such as the compensation of the device's inherent dispersion caused by the material and angular dispersion, third order dispersion and phase information which leads to the generation of two laser pulses. The signal from the pulse shaping device is evaluated in an SHG-FROG measurement, consisting of an autocorrelator and a spectrometer, from which the existing pulse dispersion can be retrieved. To illustrate the device's ability of creating a complex pulse shape, Figure 2 compares the reference measurement with an SHG-FROG trace for an MS1-MS2 configuration that is designed to generate a double pulse. In order to achieve this double pulse, a periodic π phase shift encoded on MS2 is applied to the spectrum with a modulation that corresponds to the desired temporal separation of 200 fs between the two laser pulses.

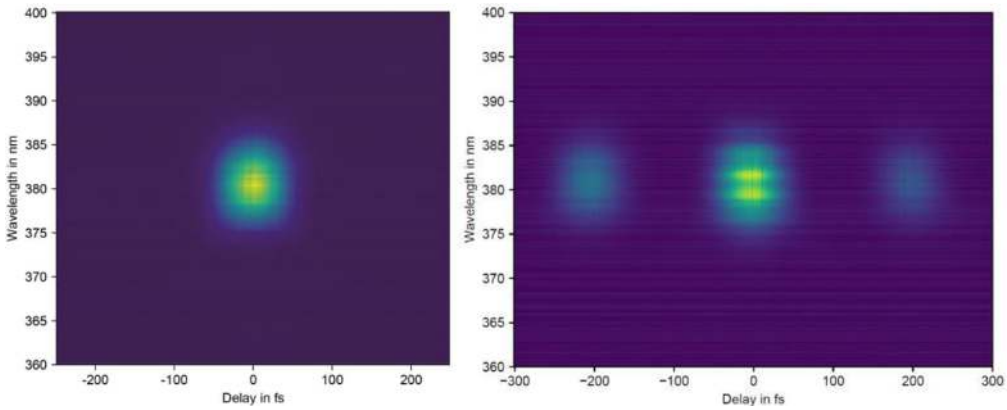


Fig. 2: Left) Measured SHG-FROG trace for a 45 fs laser pulse as second harmonic wavelength over the delay time τ (reference measurement). Right) Measured SHG-FROG trace for a generated double pulse with 200 fs temporal separation.

Our work presents a pulse shaping meta device that can apply arbitrary dispersion which is verified by our measurements. We show that by adding a well-defined phase information, a double pulse with a desired temporal separation can be generated as expected. Further pulse shaping such as the control of second- and third-order dispersion are also demonstrated. The device manages such functionality on a volume of less than 2 mm^3 and on a single substrate, making it compact and easy to use in space limited applications.

Acknowledgment: This project received funding from the Deutsche Forschungsgemeinschaft (DFG, German Research Foundation) – Collaborative Research Center TRR142 (project no. 231447078, project B09).

References

[1] Faraji-Dana, M., et al. (2019). "Hyperspectral Imager with Folded Metasurface Optics." ACS Photonics 6(8): 2161–2167.

[2] Zhu, A. Y., et al. (2017). "Ultra-compact visible chiral spectrometer with meta-lenses." APL Photonics 2(3): 036103.

[3] Divitt, S., et al. (2019). "Metasurface-Enabled Fourier-Transform Optical Pulse Shaper." CLEO/Europe-EQEC 2019, paper cf_12_3.



Dr. Debashis Chanda
Professor
NanoScience Technology Center,
Dept. of Physics,
CREOL, College of Optics and Photonics,
University of Central Florida, Florida, USA
Debashis.Chanda@ucf.edu
http://www.nanoscience.ucf.edu/chanda

Title: Building Uncooled Infrared Camera based on One Atom Thick Graphene

Abstract: The talk will outline a novel strategy for uncooled, tunable, multispectral infrared detection. Due to the low photon energy, detection of infrared photons is challenging at room temperature. One atom thick graphene offers an alternative mechanism bypassing material bandgap restriction. Further, the ability of carrier concentration modulation on graphene via external voltage offers dynamic spectral selectivity for "color" night vision/sensing. The performance of preliminary demonstration compares favorably even with present cryogenically cooled detection schemes paving the path for commercial development of many applications from space exploration to healthcare.

Prof. Debashis Chanda is a Professor, jointly appointed with NanoScience Technology Center, Dept. of Physics and College of Optics and Photonics (CREOL), University of Central Florida (UCF). Dr. Chanda received his PhD from University of Toronto. His PhD work was recognized in the form of several awards, including prestigious National Sciences and Engineering Research Council (NSERC) fellowship. Dr. Chanda completed his post-doctoral research with Prof. John A. Rogers at Beckman Institute, University of Illinois at Urbana-Champaign. Quite a few of this research works were extensively covered by National Science Foundation news, BBC, Daily Mail, NBC, Fox, Science Radio and other national/international media outlets. His research has appeared on American Scientist magazine as focused article where it was outlined how companies like Intel, Toshiba etc are trying to adopt some of the printing techniques which were developed in his group. Dr. Chanda is a recipient of the 2012 DOE Energy Frontier Research Center (EFRC) Solar Energy Future Direction Innovation Proposal Award, 2013 NSF Summer Institute Fellowship and International Displaying Future Award-2016 by Merck Germany, UCF Reach of the Stars Award (2018), Samsung Global Research Outreach (GRO) Award (2022), Sony Research Award 2022. Dr. Chanda's research has been supported by NSF, DoD, DARPA, Florida Space Institute/NASA, Northrop Grumman, Lockheed Martin etc. Apart from that Dr. Chanda is the founder of start-up, E-Skin Displays Inc., out of his research in California.

META 2023, PARIS - FRANCE, JULY 18 – 21, 2023

Conductive Nitrides for Plasmonics in the Visible Region: Properties and Applications

Yu-Jung Lu*[1,2]

[1]*Research Center for Applied Sciences, Academia Sinica, Taipei 11529, Taiwan*

[2]*Department of Physics, National Taiwan University, Taipei 10617, Taiwan*

*corresponding author: yujunglu@gate.sinica.edu.tw

Abstract: In this presentation, I will discuss emerging plasmonic platforms based on transition metal nitrides. We demonstrated that the refractory hafnium nitride (HfN) plasmonic crystals could generate full-visible color with a high image resolution of ~63,500 dpi while withstanding a high temperature (900 °C). In addition, I will present an overview of my research works over the past five years on the plasmon-enhanced light-matter interactions in visible regions and their applications.

Plasmonic nanostructure based on silver and gold that produces LSPR to withstand ultrahigh temperatures without damage remains a great challenge for future ultra-compact integrated circuits, and high-power enabled photonic devices. In principle, the shapes of plasmonic nanostructures containing noble metals would change after the heat treatment that altered the plasmonic resonance. Thus, discovering refractory plasmonic materials that can exhibit plasmonic resonance in the visible range is essential. A challenge in refractory plasmonic materials is the bulk plasmon frequency is usually in the near-infrared range, making it difficult to generate plasmonic colors in the visible. We first reported a new refractory plasmonic material HfN, one of the conductive nitrides, that has a relatively high bulk plasmon frequency ($\lambda = 400$ nm) with a high melting point ($T \sim 3583$ K) and a relatively large magnitude of the real part of the permittivity, which enables intense local electromagnetic field confinement to form LSPR in the visible region. We use this unique property to develop full-color plasmonic pixels with sub-diffraction resolution through tailoring HfN plasmonic crystals and demonstrate that HfN refractory plasmonic crystals can withstand high-temperature annealing (900 °C) without damage. The novel HfN refractory plasmonic materials unlock new opportunities for ultra-compact integrated functional plasmonic devices. Especially the unique property of HfN, implying a bright future for emerging plasmonic materials at visible wavelengths [1]. In addition, I will present an overview of my research works over the past five years on the plasmon-enhanced light-matter interactions in the visible regions and their applications [1-6], including the plasmonic nanolasers [2-3], tunable plasmonic modulators [4], plasmonic phototransistors [5], plasmon-enhanced solar energy harvesting [6], and the refractory plasmonic colors for back-light free displays [1]. My group discovered several unique working mechanisms that utilize plasmonic nanocavities to improve optoelectronic device performance. By engineering the local electromagnetic field confinement, the light-matter interaction strength can be enhanced, which results in efficient energy conversion in the designed nanosystem. Moreover, I will discuss the detailed mechanisms and possible applications. These results have broad implications for the use of alternative plasmonic nanocavities in high-performance optoelectronic devices.

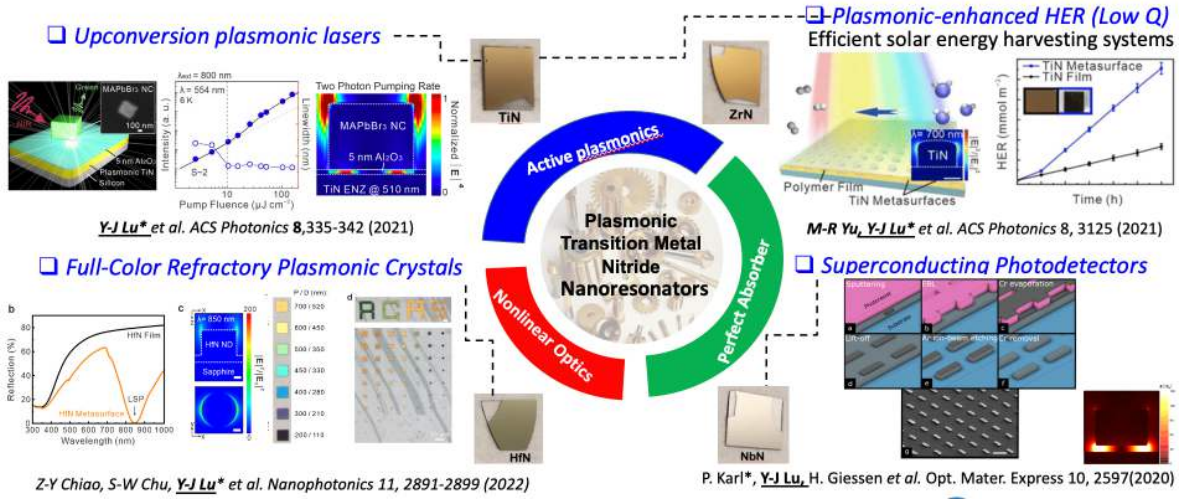


Figure 1. Research works based on plasmonic transition metal nitrides (TiN, HfN, NbN) as plasmonic platforms that reported by our Lab. By engineering the local electromagnetic field confinement, the light-matter interaction strength can be enhanced, which results in efficient energy conversion in the designed nanosystem for various applications.

References

[1] Z-Y Chiao, Y-C Chen, J-W Chen, Y-C Chu, J-W Yang, T-Y Peng, W-R Syong, H W H. Lee, S- W Chu, and Y-J Lu*, Full-Color Generation Enabled by Refractory Plasmonic Crystals. Nanophotonics 11, 2891-2899 (2022)

[2]. Y-H Hsieh, B-W Hsu, K-N Peng, K-W Lee, C W Chu, S-W Chang, H-W Lin*, T-J Yen*, and Y-J Lu*, Perovskite Quantum Dot Lasing in a Gap-Plasmon Nanocavity with Ultralow Threshold, ACS Nano 14, 11670 (2020). (Issue cover)

[3]. Y-J Lu*, T L Shen, K-N Peng, P-J Cheng, S-W Chang, M-Y Lu, C W Chu, T-F Guo, H. Atwater*, Upconversion Plasmonic Lasing from an Organolead Trihalide Perovskite Nanocrystal with Low Threshold. ACS Photonics 8,335-342 (2021).

[4]. Y-J Lu, R. Sokhoyan, W-H Cheng, G. Kafaie Shirmanesh, A. Davoyan, R. A. Pala, K. Thyagaraja n, and H. A. Atwater*, Dynamically Controlled Purcell Enhancement of Visible Spontaneous Emissi on in a Gated Plasmonic Heterostructure, Nature Communications 8, 1631 (2017).

[5]. H-Y Lan, Y-H Hsieh, Z-Y Chiao, D. Jariwala, M-H Shih, T-J Yen, O. Hess, and Y-J Lu*, Gate- Tunable Plasmon-Enhanced Photodetection in a Monolayer MoS2 Phototransistor with Ultrahigh Phot oresponsivity. Nano Lett. 21, 3083 (2021).

[6]. M-J Yu, C-L Chang, H-Y Lan, Z-Y Chiao, Y-C Chen, H W H. Lee, Y-C Chang, S-W Chang, T. Tanaka, V. Tung, H-H Chou*, and Y-J Lu*, Plasmon-Enhanced Solar-Driven Hydrogen Evolution Using Titanium Nitride Metasurface Broadband Absorbers. ACS Photonics 8, 3125-3132 (2021).

Integrated optofluidic devices for medium-switchable metasurfaces and metasurface-based biosensors

Hao Wang[1], Nanzhong Deng[2], Yue Xiao[3] and Haogang Cai[1,2*]

[1]Tech4Health Institute and Department of Radiology, NYU Langone Health, New York, USA
[2]Department of Biomedical Engineering, New York University, Brooklyn, USA
[3]College of Art and Science, New York University, New York, USA
[*]corresponding author: haogang.cai@nyu.edu

Abstract: Active tunable metasurfaces have been demonstrated by various methods including mechanical actuation and phase change materials. Metasurfaces can be easily infiltrated with liquids through microfluidics. The change in refractive index will tune the resonance of meta-atoms and therefore can be used to modulate the optical properties and functions of the given metasurface. Here we demonstrate a series of integrated optofluidic metasurface devices, with wide applications including transparent displays, tunable color filters based on structural color, switchable meta-holograms and biosensors.

Comprised of a planar thin layer of nanostructures, optical metasurfaces enable the engineering of optical resonance and wavefront within sub-wavelength thickness, which will promote a new generation of ultra-compact optical systems [1]. Conventional metasurfaces have static optical functions, because the sub-wavelength meta-atoms are static and fixed after fabrication. Active tunable metasurfaces have been drawing increasing attention, and demonstrated by various methods including mechanical actuation and phase change materials. Among all the different approaches, we are particularly interested in the interactions between metasurfaces and their surrounding media. Metasurfaces can be easily infiltrated with liquid crystals [2-4], or liquids [5] by adding superstrates or microfluidic chambers, respectively. The change in refractive index (RI) of the infiltration medium will tune the resonance of meta-atoms and therefore can be used to modulate the optical properties and functions of the given metasurface.

The integrated optofluidic metasurface device is schematically shown in Fig. 1a. Titanium oxide (TiO_2) was selected due to the excellent optical properties in the visible spectrum. TiO_2 nanostructures of different geometries (i.e., nanodisk radius and disk-to-disk gap) were fabricated on glass substrates using electron beam lithography, as shown in the scanning electron microscope images (Fig. 1b). A polydimethylsiloxane (PDMS) chamber was formed in a mold, and then bonded on top of the metasurface after Oxygen plasma treatment. Microfluidic tubes were inserted to the PDMS chamber, forming inlet and outlet channels. Liquids with different RI can be injected and exchanged. For example, the metasurface surrounding medium can be switched between water (n = 1.33), and a medium with a higher n = 1.40 (e.g., 40% glucose or 50% glycerine solutions by weight).

Huygens metasurfaces based on Mie resonance are used in this work. From the finite-difference time-domain (FDTD) simulation, the metasurface resonance spectrum shifts in response to the medium RI change (Fig. 1c). Based on the resonance tuning, the integrated optofluidic devices provide a simple implementation of active tunable metasurfaces. The change in transmission amplitude could switch on/off a single-wavelength light, with potential applications in tunable transparent displays [6]. Furthermore, TiO_2 metasurfaces form structural colors in the visible region [7], so the device can be used as a tunable color filter, which changes the transmitted color under white light (Fig. 1d). More importantly, in addition to amplitude modulation, the phase modulation enables wavefront engineering. For example, tunable holographic

metasurfaces can be achieved by the microfluidic medium change (Fig. 1e) [5]. The dynamic tunable meta-holograms are useful in holographic display, optical information processing and encryption. Finally, medium-induced resonance change can be used not only for medium-switchable metasurfaces, but also for refractometric sensing (Fig. 1c). Using the same optofluidic devices, we demonstrated a sensitive detection of RI change down to 0.001 RIU. The devices can be further bio-functionalized for biosensing applications.

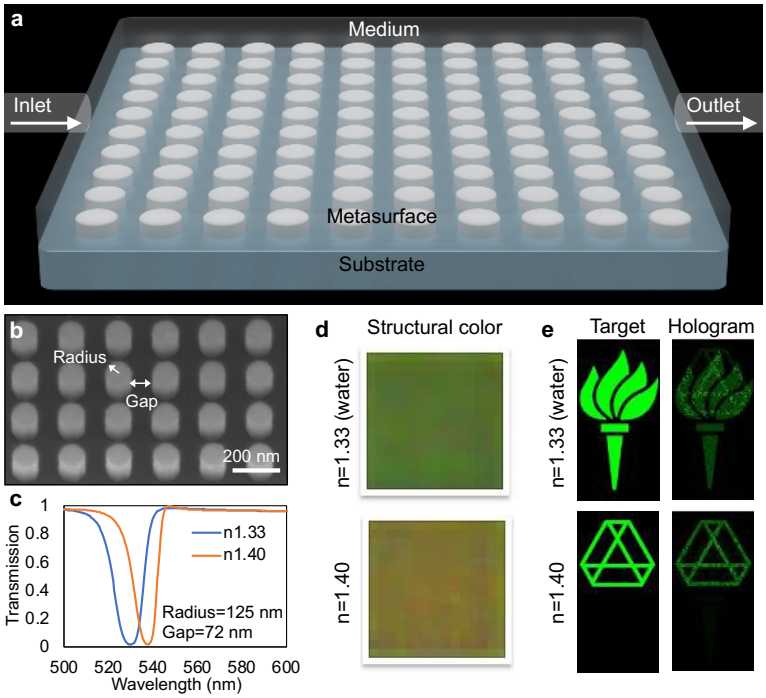


Figure 1. (a) Schematic diagram of the integrated optofluidic metasurface device. (b) SEM images of the fabricated TiO_2 metasurfaces. (c) Spectral shift of resonance, (d) structural color change, and (e) meta-hologram switching in response to the medium refractive index change between water (n = 1.33) and n = 1.40.

References

1. Khorasaninejad, M. and F. Capasso, Metalenses: Versatile multifunctional photonic components. Science, Vol. 358, No. 6367, 1146-1154, 2017.
2. Li, S.Q., et al., Phase-only transmissive spatial light modulator based on tunable dielectric metasurface. Science, Vol. 364, No. 6445, 1087-1090, 2019.
3. Lininger, A., et al., Optical properties of metasurfaces infiltrated with liquid crystals. Proceedings of the National Academy of Sciences, Vol. 117, No. 34, 20390-20396, 2020.
4. Dolan, J. A., Cai, H., Delalande, L., Li, X., Martinson, A. B. F., de Pablo, J. J., Lopez, D., Nealey, P. F.. Broadband liquid crystal tunable metasurfaces in the visible: liquid crystal inhomogeneities across the metasurface parameter space. ACS Photonics, Vol. 8, No. 2, 567-575, 2021.
5. Cai, H., Dolan, J. A., Gordon, G. S. D., Chung, T., Lopez, D. Polarization-Insensitive Medium-Switchable Holographic Metasurfaces. ACS Photonics, Vol. 8, No. 9, 2581-2589, 2021.
6. Zou, C., et al., Electrically Tunable Transparent Displays for Visible Light Based on Dielectric Metasurfaces. ACS Photonics, 2019. 6(6): p. 1533-1540.
7. Sun, S., et al., All-Dielectric Full-Color Printing with TiO_2 Metasurfaces. ACS Nano, Vol. 11, No. 5, 4445-4452, 2017.

Exciton resonances in two-dimensional materials for dynamic wavefront manipulation

Melissa Li, Claudio Hail, Souvik Biswas, Harry Atwater

Thomas J. Watson Laboratory of Applied Physics, California Institute of Technology,
Pasadena, California 91125, United States

Dynamic control of the scattering properties of resonant nanophotonic structures is central to the realization of active metasurfaces. However, concepts thus far primarily employ geometrical resonances, e.g. plasmonic or Mie resonances, in three-dimensional nanostructures and show very weak electro-optic effects. As structures for light manipulation become increasingly complex and compact, the demand for novel materials that exhibit strong tunable light-matter interactions in the ultra-thin regime is rapidly growing.

Exciton resonances in two-dimensional (2D) van der Waals materials have gained widespread attention for opto-electronics based multifunctional devices due to their large binding energies, strong oscillator strengths, and high tunability through electrostatic gating. In this talk, we discuss how excitons in these layered materials can be engineered to achieve a wide range of optical wavefront manipulation. We demonstrate how in a field-effect heterostructure, the radiative and nonradiative rates of excitons in monolayer molybdenum diselenide ($MoSe_2$) can be actively tuned, thereby strongly modulating the light-scattering properties. By applying spatially-varying amplitude and phase gradients across the monolayer $MoSe_2$ with electrostatic gates, we observe large tuning of the complex refractive index at various excitonic frequencies and demonstrate dynamic beam steering. We show how optical cavities, otherwise needed to enhance light-matter interactions, can be eliminated by using a high quantum yield 2D semiconductor that serves both as the resonant scatterer and the tunable material. Our results uncover conceptually new metasurface design principles by engineering material resonances and have broad implications for the use of low-dimensional excitonic materials for atomically-thin, active nanophotonic devices.

References

1. Li, M., Biswas, S., Hail, C. U. & Atwater, H. A. Refractive Index Modulation in Monolayer Molybdenum Diselenide. *Nano Lett*. **21**, 7602–7608 (2021)
2. Li, M., Hail, C. U., Biswas, S. & Atwater, H. A. Excitonic Beam Steering in an Active van der Waals Metasurface. *Nano Lett*. **23**, 2771–2777 (2023)

Quasi-Bound State in the Continuum in Intra-Coupled Si Dielectric Metasurface

Wen-Hui (Sophia) Cheng*
National Cheng Kung University, Taiwan
*corresponding author: wcheng@gs.ncku.edu.tw

Abstract: A structure of all-dielectric metasurface with the concept of q-BIC is introduced and studied. Magnetic quadrupole being induced by asymmetry and near field coupling contribute to the high Q resonance. The effect of pitch, size, and scaling factor will be discussed for better understanding of the system.

Metasurfaces present a viable prospect for the alteration of electromagnetic wave properties, including amplitude, phase, and polarization, through the customization of meta-atom geometry. Notably, dielectric metasurfaces have garnered significant interest in recent times owing to their minimal radiative loss. In this work, we incorporate the concept of quasi-bound state in the continuum (q-BIC) with the dielectric metasurface. By introducing the asymmetry factor and parameter optimization in our metasurface, we theoretically obtain a resonance with a quality factor (Q-factor) of 650 with a bi-radius four-unit structure. We performed a multipole decomposition analysis of the resonance, revealing that the resonance is resulted from addition of the magnetic quadrupole to the electric dipole. In addition, we explore the pitch effect and find that the resonances are influenced not only by pitch in x-direction but also y-direction. We attribute this result to magnetic quadrupole being induced by asymmetry and near field coupling. Therefore, the pitch size should not be too large for the maintain of the q-BIC resonance. For practical application, we also examine the tunability of the q-BIC resonance with scaling factor. A broadband tunability from 600nm to 1200nm without sacrificing much the Q-factor can be realized. Our studies with fundamental understanding of the q-BIC in the proposed structure support the potential application of the all-dielectric metasurface including sensing, emission control, and nonlinear optics.

The work is supported by National Science and Technology Council, Taiwan (2030 Cross-Generation Young Scholars Program, 111-2628-E-006-007), and Ministry of Education (Yushan Fellow Program), Taiwan, and in part from the Higher Education Sprout Project of the Ministry of Education to the Headquarters of University Advancement at National Cheng Kung University (NCKU).

META 2023, PARIS - FRANCE, JULY 18 – 21, 2023

Physics-informed reinforcement learning for nanophotonic device design

M. S. Jang[1 *]

[1]School of Electrical Engineering, Korea Advanced Institute of Science and Technology (KAIST), Korea
[*]corresponding author: jang.minseok@kaist.ac.kr

Abstract: The increasing demand on a high-performance metasurface requires a freeform design method that can handle a huge design space. Accordingly, various nanophotonic device design schemes have been investigated including the ones based on machine learning. In this presentation, I discuss design approaches based on deep reinforcement learning, which have achieved great success in many different fields spanning video games, the game of Go, protein folding problems, to matrix multiplication algorithms. Reinforcement learning has not yet been actively explored in the field of nanophotonics compared to other machine learning methods such as generative or discriminative models. I will introduce how to apply deep reinforcement learning to design a metasurface beam deflector with large degrees of freedom, and discuss how to increase the sample efficiency by informing the agent of the reinforcement learning using physical constraints that govern the electromagnetic system.

Active metamaterials and devices: from rapidly-tunable lenses to emergent polaritonic materials

Gennady Shvets

Cornell University, USA

Abstract: One of the attractions of resonant metamaterials is the possibility of tuning their resonant frequencies in real time by integrating them with actively-controlled materials. In this talk, I will describe how metasurfaces can be combined with liquid crystals to develop a new class of electrically-controlled varifocal metalenses operating at multiple wavelengths. Experimental demonstrations of imaging using actively controlled varifocal and bifocal metalenses will be presented, and new approaches to making widefield electrically-tunable metalenses will be described. I will also describe how electrically-biased plasmonic metasurfaces – also known as metagates – can be integrated with 2D materials to simultaneously modify the band structure of free carriers and plasmons. The resulting active material possesses emergent polaritonic properties that are absent without the metagate.

Dielectric and Transient Optical Properties of Ultrathin TiN and $Ti_{1-x}Al_xN$

I-H. Ho and H. Ahn*

Department of Photonics, College of Electrical and Computer Engineering, National Yang Ming Chiao Tung University, Hsinchu 30010, Taiwan.
*corresponding author: hyahn@nycu.edu.tw

Abstract: Titanium nitride (TiN) with excellent optical and thermal properties has recently attracted attention in the fields of plasmonics and photothermal applications. We report the dielectric as well as the transient optical responses of ultrathin TiN and $Ti_{1-x}Al_xN$ ($0 \leq x \leq 0.67$) films grown by molecular-beam-epitaxy method. With increasing Al compositions, drastic increase of VIS-NIR absorption and the redshift of the epsilon-near-zero wavelength is observed for $Ti_{1-x}Al_xN$. Strong sub-picosecond electron-phonon coupling and nanosecond-long heat-preservation is observed for $Ti_{1-x}Al_xN$ in the whole visible spectral range.

Along with hafnium nitride (HfN) and zirconium nitride (ZrN), titanium nitride (TiN) is a refractory transition metal nitride with high melting temperature (~3000 °C) and many excellent optical and plasmonic properties comparable or superior to gold (Au), making it a good candidate for robust and low cost metallic material with compatibility to complementary metal–oxide–semiconductor (CMOS) fabrication technologies. TiN possesses the epsilon-near-zero wavelength (λ_{ENZ}) at ~2.47 eV, emerging as an alternative plasmonic and ENZ material to gold operating in the visible range. Typically, wide tunability in λ_{ENZ} has been realized by using metamaterials requiring complicated structural engineering. In our work, we prepared the high crystalline quality ultrathin TiN and $Ti_{1-x}Al_xN$ epitaxial layers by using the molecular-beam epitaxy (MBE) method. We have achieved the tunable λ_{ENZ} from 470 nm to 530 nm in the ultrathin TiN films by reducing the thickness from 30 to 2.4 nm. Moreover, even wider tunability from visible to near-infrared range could be achieved by alloying with Al in $Ti_{1-x}Al_xN$. This talk would be divided into two topics; Dielectric, optical, and electrical properties of ultrathin TiN and the Al composition dependence of transient behavior for TiN and $Ti_{1-x}Al_xN$.

Ultrathin metal film is a promising transparent and conductive electrode (TCE) material, but noble metal films grown by evaporation or sputtering methods exhibit poor morphology at the initial stage and its percolation thickness is in the range of 6 – 10 nm. While TiN films grown via sputtering, PLD, or ALD techniques show relatively low quality films, the influence of oxygen-related defects is greatly reduced for MBE-grown TiN films owing to ultrahigh vacuum growth. Our ultrathin (<6 nm) TiN epilayers have high optical transparency (≥75%) over the whole visible spectra regime and λ_{ENZ} could tuned with different film thickness, as shown in Figure 1a.[1]

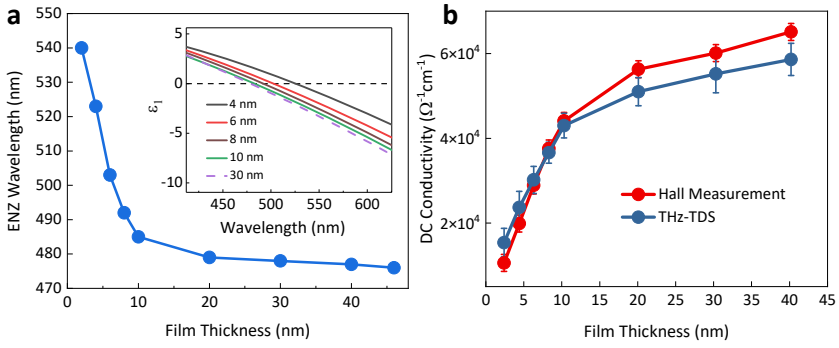


Figure1. (a) Film thickness dependence of ENZ wavelength. Inset; Real dielectric functions (ε_1) measured by spectroscopic ellipsometry. (b) Thickness dependence of DC conductivity measured by THz spectroscopy and Hall-effect techniques.

The electrical properties of ultrathin films are explored by the terahertz time-domain spectroscopy (THz-TDS) and the Hall effect techniques which are the optical and direct contact measurement method, respectively. In Figure 1b, we found an excellent agreement between optically and electrically measured results.

Recently, several contradictory results have been reported in electron-phonon (*e-ph*) coupling time of TiN, namely, either strong and ultrafast (sub-ps)[2] or weak and slow (a few tens of ps). From the comprehensive study of broadband transient reflectivity spectroscopy, we found that these two distinct *e-ph* coupling processes are concurrently occurring in TiN, but critically depending on the probe wavelength. In particular, the one with sub-picosecond coupling time occurs only within a narrow ENZ region. As shown in Figure 2a, the visible light absorption for Ti-rich (x<0.5) $Ti_{1-x}Al_xN$ is enhanced by doping with Al and more importantly, the ultrafast *e-ph* coupling is observed in the whole visible spectral range, demonstrating that $Ti_{1-x}Al_xN$ can play an important role in development of a new family of plasmonic and ENZ-based opto-electronic devices. Figure 2b also shows that following the e-ph coupling process, the magnitude of transient reflectivity is high and decay to equilibrium in a nanosecond, indicating the great potentials of TiN and TiAlN films as highly efficient materials in photothermal and photochemical applications.

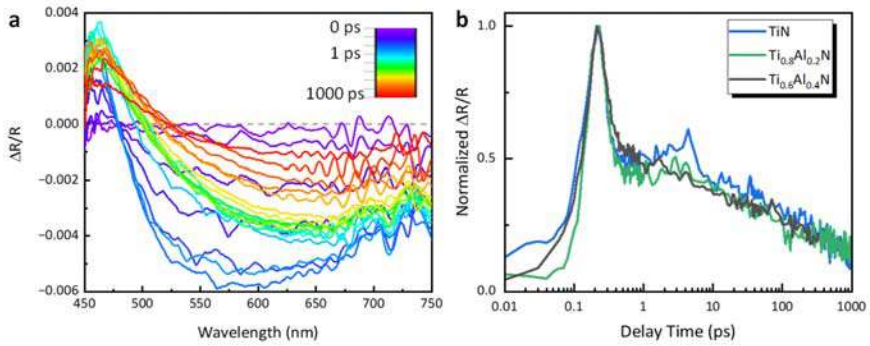


Figure2. (a) Spectral cuts of transient reflectivity of $Ti_{0.6}Al_{0.4}N$ at different delay times from 0 ps to 1000 ps, indicated by the color bar. (b) Temporal evolution of transient reflectivity for TiN, $Ti_{0.8}Al_{0.2}N$, and $Ti_{0.6}Al_{0.4}N$.

We acknowledge C.-W. Chang and S. Gwo in National Tsing Hua University, Taiwan for providing TiN and TiAlN films and physical property data used in this work. This work is financially supported by the National Science and Technology Council of Taiwan (NSTC 110-2124-M-A49-009-MY3 and NSTC 111-2112-M-A49-044).

References

1. Ho, I H., C.-W. Chang, Y.-L. Chen, W.-Y. Chang, T.-J. Kuo, Y.-J. Lu, S. Gwo, and H. Ahn, "Ultrathin TiN epitaxial films as transparent conductive electrodes," ACS Appl. Mater. Interfaces. Vol. 14, 16839–16845, 2022.
2. Diroll, B. T., S. Saha, V. M. Shalaev, A. Boltasseva, and R. D. Schaller, "Broadband ultrafast dynamics of refractory metals: TiN and ZrN," Adv. Optical Mater. Vol. 8, 2000652, 2020.

Metallic quantum well based extreme nonlinear materials and metasurfaces

Zhaowei Liu*
Department of Electrical and Computer Engineering, University of California, San Diego
9500 Gilman Drive, La Jolla, California, USA
*Corresponding author: zhaowei@ucsd.edu

Abstract: Optical power dependent nonlinear metasurface has attracted much attention recently due to its great potential in ultrafast meta-optics, optical image and signal processing. Here, we review our recent studies about the development of various metallic quantum well systems with extremely high Kerr nonlinear coefficients and a few examples of applying those materials to nonlinear metasurfaces. We think nonlinear metasurface with exceptionally high nonlinear effect is becoming a promising candidate in real time image processing and parallel analog computing.

Exceptionally large Kerr nonlinearity has been demonstrated in various quantum well heterostructures due to the inter-sub-band (ISB) transitions. In order to achieve the operational frequency to visible and near infrared range, we developed metallic quantum well with film thickness around 3nm or less. Specifically, TiN/Al_2O_3 multiple layers show not only high nonlinearity ($\chi^{(2)}$ ~1500 pm/V, and $\chi^{(3)}$ ~2×10^{-15} m^2/V^2 in the VIS/NIR), but also ultra-high damage threshold, rendering them compatible for nonlinear optical studies. However, TiN is a lossy metal with relatively high linear optical loss. There is a desire to further improve performance through different material platforms that offer additional resonant characteristics with lower linear material losses.

Materials that can be characterized as possessing free charge carrier, such as metallic films and highly doped semiconductor films have a special regime where the real permittivity of the material approaches zero, denoted as the Epsilon-Near-Zero (ENZ) regime. There is significant interest in this class of material, as they display a variety of exotic nonlinear effects, such as near-unity refractive index change, and harmonic generation enhancement. Stemming from the continuity of the normal E-field through a medium, when the permittivity for a medium approach zero, the normal E-field component within the ENZ film is greatly enhanced. In addition, ultrathin ENZ films support leaky modes that further enhance the E-field enhancement by an order of magnitude than its bulk counterparts.

We will discuss our new strategy to combine the extreme nonlinearity in metallic quantum wells and the ENZ to achieve much stronger nonlinear effects and the applications in nonlinear metasurfaces.

References

1. Zhou, J., Zhao, J., Wu, Q., Chen, C., Lei, M., Cheng, G., Tian, F., and Liu, Z., “Nonlinear computational edge detection metalens,” Adv. Funct. Mater, Vol. 32, No. 34, 2204734, 2022.
2. Zhou, J., Qian, H., Chen, C., Chen, L., and Liu, Z., “Kerr metasurface enabled by metallic quantum wells,” Nano Lett. Vol. 21, No. 1, 330-336, 2020.
3. Qian, H., Li, S., Li, Y., Chen, C., Chen, W., Bopp, S.E., Lee, Y.U., Xiong, W., and Liu, Z., “Nanoscale optical pulse limiter enabled by refractory metallic quantum wells,” Sci. Adv., Vol. 6, No. 20, eaay3456, 2020.

Generation and Control of Ultrafast Directional Photocurrents at Nanoscale Using Symmetry-Broken Hybrid Graphene Nanoplasmonic Metasurfaces

Jacob Pettine[1] and H.-T. Chen[1*]

[1]Center for Integrated Nanotechnologies, Los Alamos National Laboratory, Los Alamos, NM 87545, USA
[*]Corresponding author: chenht@lanl.gov

Abstract: The generation of directional photocurrents via a variety of mechanisms is essentially linked to the breaking of spatial inverse and/or time-reversal symmetries. Here we introduce a class of optoelectronic metasurfaces, more specifically hybrid graphene nanoplasmonic metasurfaces with broken inversion symmetry, for the generation of arbitrarily and spatially varying ultrafast directional photocurrents at nanoscales. We further apply this concept for efficient emission of pulsed THz radiation and direct generation of THz vector beams.

The generation of directional electrical currents is ubiquitous, with obvious examples including applying a voltage bias using a battery and illuminating a photodiode with light. The directionality is essentially linked to symmetry breaking associated with applying extrinsic stimuli (voltage bias), device structural designs (p-n junction), and/or intrinsic material properties (noncentrosymmetric crystal structures). This enables a variety of device applications for microelectronics, energy harvesting, and sensing, to name a few. The generation of directional currents can be also exploited to investigate material and structural properties due to the broken spatial inversion and/or time-reversal symmetries, e.g., circular photogalvanic effects in topological insulators, two-dimensional van der Waals heterostructures, Weyl semimetals, and other emerging quantum materials [1]. However, the generation of directional photocurrents so far are mostly at the macroscopic and mesoscopic scales; the ability to generate arbitrarily and spatially varying directional currents at nanoscale remains a considerable challenge, although it may find important applications in microelectronics and signal transductions.

Here, we introduce a class of optoelectronic metasurfaces for light-driven vectorial charge flow at ultrafast timescales and nanometer spatial scales. The hybrid graphene nanoplasmonic metasurfaces (Fig. 1(a)) consist of an array of teardrop-shaped gold nanoantennas on top of a CVD-grown graphene monolayer. The inversion symmetry breaking of gold teardrop nanoantennas makes them act as lightning rods; strong plasmonic hot spots at the sharp (< 15 nm radius) tips occur under resonant photoexcitation. Directional photocurrents will emerge

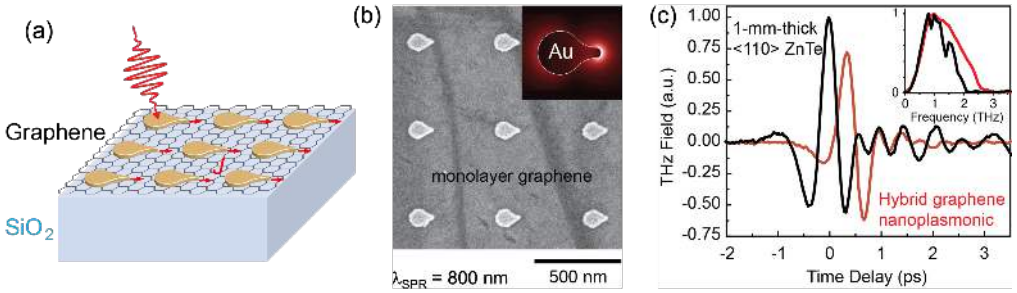


Figure 1. (a) Schematic of the hybrid graphene nanoplasmonic metasurface. (b) SEM image of a fabricated sample, with inset showing the plasmonic resonance. (c) Radiated THz pulses from the metasurface and from a 1-mm-thick ZnTe crystal.

within the underlying graphene monolayer due to the strong asymmetry in the plasmonic field mode and the corresponding hot carrier excitation, acceleration, and/or injection. The direction of the generated photocurrents is locally determined by the orientation of the gold teardrop nanoantennas, and the ultrafast timescales are enabled by the femtosecond laser excitation as well as the picosecond hot carrier relaxation within the graphene. Such hybrid graphene nanoplasmonic optoelectronic metasurfaces can be scaled to operate at arbitrary excitation wavelengths ranging from near-infrared to terahertz (THz) regimes. This provides a versatile and adaptive light-based control over ultrafast, nanoscale vectorial currents with designer spatially varying magnitude and direction.

We validate the optoelectronic metasurfaces by fabricating millimeter-scale devices through a wet transfer process of graphene and electron-beam lithography process for the gold teardrop nanoantenna array (Fig. 1(b)), along with a suite of electrical and optical measurements. We first investigated the metasurfaces with gold teardrop nanoantennas all aligned to form a uniform square array. The resonant properties of the fabricated metasurfaces were first verified via white light transmission spectroscopy, revealing excellent agreement with the designs. Under optical excitation using wavelength-tunable femtosecond lasers with linear polarization along the principal axis of the gold teardrop nanoantennas, we observed directional photocurrents by directly reading out the time-averaged photocurrents, the magnitude of which also revealed strong dependence on the excitation wavelength, with highest photocurrents right at the resonance wavelength. The ultrafast characteristic of the generated photocurrents was verified by successful probing of emission of picosecond pulses (i.e., broadband THz radiation) to free space, measured in the time domain (Fig. 1(c)). The radiated THz pulses provide indications of the light-matter interactions and hot carrier dynamics, limited here only by the bandwidth of the THz detector. Our experiments showed that this THz emission is highly efficient, approaching that of a widely used THz emitter (1-mm-thick ZnTe nonlinear crystal) under the same experimental conditions. With this result, we continued to investigate optoelectronic metasurfaces with designer spatial profiles of gold teardrop nanoantenna orientation, and successfully generated high-quality radial and azimuthal THz vector beams when the nanoantenna orientation is aligned at the radial and azimuthal directions, respectively.

By judicious considerations of symmetry-breaking in structural designs and integration of materials with desirable properties, hybrid nanoplasmonic metasurfaces can provide a pathway for the generation and control of nanoscale ultrafast directional currents. Such optoelectronic metasurfaces can also inspire the discovery of new efficient THz sources [2] and the direct generation of arbitrary THz (vector) beams, thus manifesting the importance of metasurfaces for advancing THz science and technology [3].

This work was partially supported by the LANL/LDRD program, and performed, in part, at the Center for Integrated Nanotechnologies, an Office of Science User Facility operated for the U.S. Department of Energy (DOE) Office of Science. Los Alamos National Laboratory, an affirmative action equal opportunity employer, is managed by Triad National Security, LLC for the U.S. Department of Energy's NNSA, under contract 89233218CNA000001.

References

1. Orenstein, J., J. E. Moore, T. Morimoto, D. H. Torchinsky, J. W. Harter, and D. Hsieh, "Topology and symmetry of quantum materials via nonlinear optical responses," Annu. Rev. Condens. Matter Phys., Vol. 12, 247–272 (2021).
2. Pettine, J., P. Padmanabhan, N. Sirica, R. P. Prasankumar, A. J. Taylor, and H.-T. Chen, "Ultrafast terahertz emission from emerging symmetry-broken materials," Light Sci. Appl. (2023).
3. Chen, H.-T., A. J. Taylor, and N. F. Yu, "A review of metasurfaces: physics and applications," Rep. Prog. Phys., Vol. 79, No. 7, 076401 (2016).

Piezoelectric Shifter for Wideband Tunability in Chalcogenide Metamaterials

J. A. Frantz[1*], J. D. Myers[1], A. Clabeau[2], R. Y. Bekele[1], A. F. Moore[3], V. Q. Nguyen[1] and J. S. Sanghera[1]

[1]U.S. Naval Research Laboratory, USA
[2]University Research Foundation, USA
[3]Jacobs, USA
[*]corresponding author: jesse.frantz@nrl.navy.mil

Abstract: A large-area thin film, with position carefully controlled by a piezoelectric transducer, can be used as a "shifter," a mechanism that provides a large shift in the resonance of a metasurface. Designs for such devices, based on chalcogenide glasses (ChGs) and operating in the midwave infrared (MWIR) are presented, demonstrating resonance shifts of >400 nm for a shifter translation of only several hundred nanometers.

Tunability has been long sought after in photonic metamaterial devices. A variety of approaches to achieving tuning have been explored including mechanical tuning, i.e. physically changing the geometry of a device; incorporating a material with tunable optical properties such as a phase change material or liquid crystal; applying electromagnetic fields; or by incorporating a material with optical nonlinearity [1,2]. Each of these methods has distinct advantages for different types of devices, yet it remains challenging to provide optical tuning over large bandwidths, on the order of hundreds of nanometers.

One promising approach is to provide tuning with a piezoelectric transducer. Some recent work has taken advantage of piezoelectric transducers to alter the near-field environment of a metamaterial and thus produce tuning [3,4]. To date, most work has shown small changes in optical properties and provided tuning over a small physical area. For many applications, tuning over large bandwidths and large areas is required. To do so, a piezoelectric shifter configuration is evaluated. In the proposed configuration, illustrated in Fig. 1 where (a) shows the top view of a metasurface (MS) and (b) shows the device in cross section, a piezoelectric actuator is used to operate a shifter—an optically transparent thin film that changes the near-field environment of the MS. The shifter is displaced above the waveguide by *d,* the shifter spacing, and a piezoelectric actuator is employed to vary *d*. When the shifter assembly is sufficiently close to the waveguide, it alters the position optical response of the MS. Fig. 1(c) shows simulation results for these devices indicating that, for the design illustrated, varying *d* from 0-600 nm changes the position of a resonance of the structure from approximately 4.1 to 3.65 μm, a change of >400 nm.

To experimentally demonstrate this effect, we designed and fabricated several devices based on arsenic sulfide (As_2S_3) glass, a ChG with high MWIR transparency. Bulk As_2S_3 samples were batched from purified precursors in an N_2 purged glovebox, melted, and quenched to obtain a glass boule. Small pieces of the boule were used as deposition sources. Films of As_2S_3 were deposited via thermal evaporation while maintaining the substrate at approximately 25 °C.

Prior to testing the shifting approach with a MS, experiments were first carried out with a waveguide device, where the shifter is applied to tune the effective index, n_e, of the waveguide, in order to ensure that the mechanism works over a large area. For these experiments, we used a MWIR nonmechanical beam steering (NMBS) chip [5] that consists of a silicon substrate and a planar waveguide with an As_2S_3 subcladding, and an

As_2Se_3 core. A shifter, consisting of 500 nm of As_2S_3 on a CaF_2 substrate is brought into near-contact with the waveguide. A quantum cascade laser with a wavelength of 4.7 μm is coupled into the waveguide. A piezoelectric transducer is used to control *d* by moving the shifter position. Steering is achieved by varying n_e in the output coupling region. In this experiment, steering angles of up to ~8 mrad were observed, showing that modulation of n_e has been achieved. Experiments to apply this same approach to a MS in order to shift its resonance are ongoing.

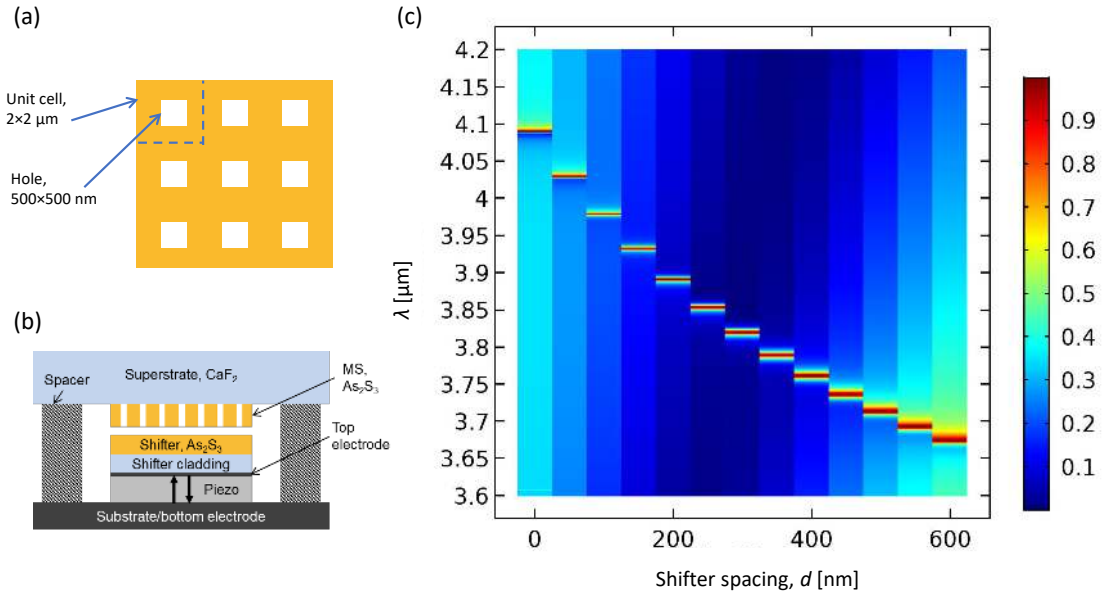


Figure 1. A shifter-tunable MS: (a) top view of the ChG MS showing a unit cell; (b) cross section of a device including the MS, a shifter, and the piezoelectric transducer; and (c) a heat map of reflectance from the device as a function of wavelength and shifter spacing.

Acknowledgement: The authors would like to acknowledge funding from the U.S. Naval Research Laboratory 6.1 Base Program.

References

1. A. Q. Liu, W. M. Zhu, D. P. Tsai, and N. I. Zheludev, "Micromachined tunable metamaterials: a review," J. Opt. **14**, 114009 (2012).
2. S. Bang, J. Kim, G. Yoon, T. Tanaka, and J. Rho, "Recent Advances in Tunable and Reconfigurable Metamaterials," Micromachines **9**, 560 (2018).
3. V. Annamdas and C. Soh, "A Perspective of Non-Fiber-Optical Metamaterial and Piezoelectric Material Sensing in Automated Structural Health Monitoring," Sensors **19**, 1490 (2019).
4. R.-J. Xu and Y.-S. Lin, "Actively MEMS-Based Tunable Metamaterials for Advanced and Emerging Applications," Electronics **11**, 243 (2022).
5. J. A. Frantz, J. D. Myers, R. Y. Bekele, C. M. Spillmann, J. Naciri, J. Kolacz, H. G. Gotjen, V. Q. Nguyen, C. C. McClain, L. Brandon Shaw, and J. S. Sanghera, "Chip-based nonmechanical beam steerer in the midwave infrared," J. Opt. Soc. Am. B **35**, C29 (2018).

META 2023, PARIS - FRANCE, JULY 18 – 21, 2023

Ultrathin Titanium Nitride Epitaxial Structures for Tunable Infrared Plasmonics

Shangjr Gwo

National Tsing-Hua University, Taiwan
shangjr@hotmail.com

Abstract: Titanium nitride (TiN) is an excellent material for infrared plasmonics due to unique optical properties (comparable to gold), refractory material nature, mechanical and chemical stabilities, as well as bio- and CMOS compatibilities. In this work, we demonstrate that ultrathin and scalable TiN epitaxial structures can be applied for tunable infrared plasmonics, extending from near- (NIR) to mid-infrared (MIR) spectral region.

META 2023, PARIS - FRANCE, JULY 18 – 21, 2023

Nanophotonics-based chiroptical sensing of drug solutions

R. Adhikary[1], A. Sahoo[1], M. Aschi[1], I. Daidone[1], M. Silvestri[1], M. Venturi[1], C. Ferrante[2], A. Mecozzi[1] and A. Marini[1*]

[1] Department of Physical and Chemical Sciences, University of L'Aquila, Via Vetoio, 67100 L'Aquila, Italy
[2] Consiglio Nazionale delle Ricerche, CNR-SPIN, Via Vetoio 10, 67100 L'Aquila, Italy
[*]corresponding author: andrea.marini@univaq.it

Abstract: We theoretically model the bi-anisotropic linear response of reparixin, ladarixin and levodropropizine solutions, discussing the potential of photonic crystal fibers, metasurfaces and photonic nanostructures for chiroptical sensing of drug solutions.

Chirality plays a central role in fundamental and applied physics, chemistry, biology and pharmaceutics, where the specific enantiomeric form of drugs affects their functionality, as in particular pharmacodynamics, pharmacokinetics and toxicity [1]. In turn, chiral sensing plays a central role in pharmaceutics, drug discovery and particularly in nanomedicine to optimise biological tissue penetration and to gain enhanced control of contrast agents, detection markers and biosensors. Currently, the enantiomeric excess of chiral molecular mixtures is assessed by nuclear magnetic resonance, X-ray crystallography, gas chromatography, capillary electrophoresis and high performance liquid chromatography. However, such techniques are not suitable for real-time analysis, lab-on-a-chip integration and wider nanomedicine applications.

Here we discuss the potential of nanophotonics-based devices for chiroptical sensing of drug solutions. Specifically, we focus on isotropic assemblies of reparixin (an inhibitor of the CXCR2 function attenuating inflammatory responses [2,3] that has been adopted in clinical trials for the treatment of hospitalized patients with COVID-19 pneumonia [4]) dissolved in water with dilute number molecular density of the order $n_{mol}=n^{(R)}_{mol}+n^{(S)}_{mol} \approx 10^{-2}$ nm^{-3} (corresponding to a concentration of 5 mg/ml), where $n^{(R,S)}_{mol}$ indicate the number densities of R and S enantiomers, respectively. We further focus on ladarixin dissolved in water and levodropropizine dissolved in a mixture of ethanol and hexane (40:60 volume ratio). Our results are based on molecular dynamics (MD), time-dependent density functional theory (TD-DFT) and Perturbed Matrix Method (PMM) simulations for the calculation of the drugs electronic structure and of their static and transition electric/magnetic dipole moments. All macroscopic optical parameters (including the dielectric permittivity ε_r, the magnetic permeability μ_r and the chiral parameter κ of the isotropic chiral mixtures, see Fig. 1) are calculated from first principles by perturbatively solving the density matrix equations accounting for the leading electronic absorption peaks and by averaging the obtained first/second-order hyper-polarizability tensors over the random molecular orientation through the Euler rotation matrix approach.

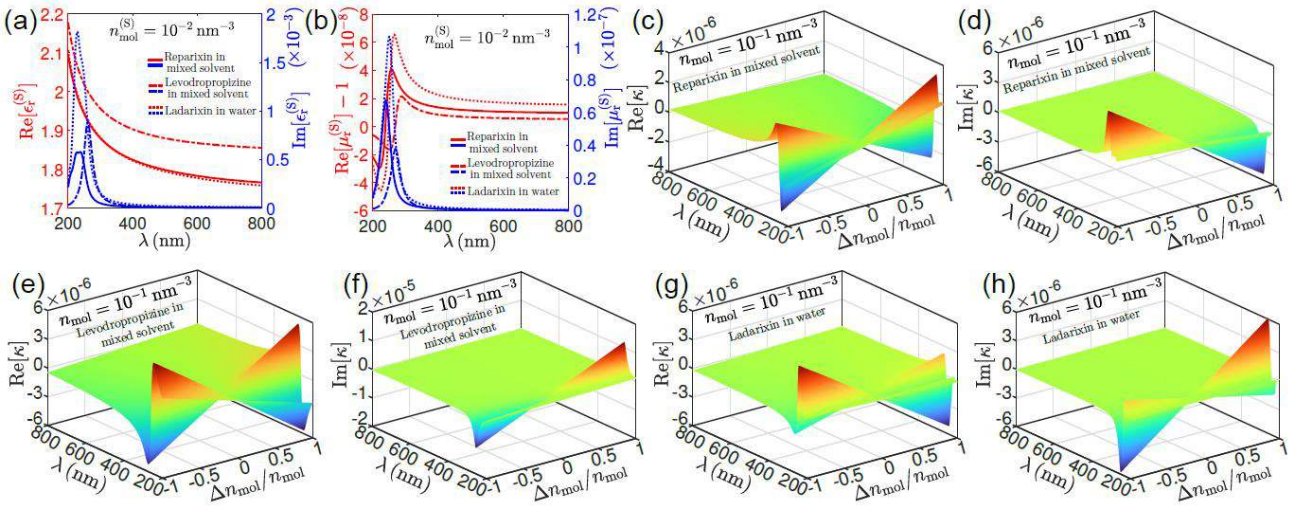


Fig. 1 Real (red curves) and imaginary (blue curves) parts of the **(a)** relative permittivity ϵ_r and **(b)** permeability μ_r of the S-type chiral enantiomer of the three pharmaceutical molecules (with concentration $n_{mol} = 10^{-2}$ nm^{-3}) in different solvents. Here, the left (red) and right (blue) axes represent the real and imaginary parts of ϵ_r and μ_r. The solid curves correspond to reparixin dissolved in $CH_3CN + H_2O$ (50:50 volume ratio), the dashed curves indicate levodropropizine dissolved in $C_6H_{14} + C_2H_5OH$ (40:60 volume ratio), and the dotted curves correspond to ladarixin dissolved in water. **(c,e,g)** Real and **(d,f,h)** imaginary parts of κ as a function of wavelength (λ) for relative concentration ($\Delta n_{mol}/n_{mol} = [n^{(S)}_{mol} - n^{(R)}_{mol}]/n_{mol}$) of an enantiomeric mixture of R and S enantiomers.

References

1. Nguyen, L. A., He, H. and Pham-Huy, C. “Chiral drugs: an overview,” Int J Biomed Sci. Vol. 2, 85 – 100, 2006.
2. Bertini R. et al. “Noncompetitive allosteric inhibitors of the inflammatory chemokine receptors CXCR1 and CXCR2: Prevention of reperfusion injury,” PNAS Vol. 101, 11791 - 11796, 2004.
3. Bertini R. et al. “Receptor binding mode and pharmacological characterization of a potent and selective dual CXCR1/CXCR2 non-competitive allosteric inhibitor,” British Journal of Pharmacology Vol. 165, 436 – 454, 2012.
4. Landoni, G., Piemonti, L., d’Arminio Monforte, A., Grossi, P., Zangrillo, A., Bucci, E., Allegretti, M., Goisis, G., Gavioli, E. M., Patel, N., De Pizzol, M., Pasedis, G. & Mantelli, F. “A multicenter phase 2 randomized controlled study on the efficacy and safety of reparixin in the treatment of hospitalized patients with COVID-19 pneumonia,” Infect Dis Ther. Vol. 11,1559 – 1574, 2022.

Merging Nanophotonics with Optical Fibers through 3D Nanoprinting: a novel platform for flexible beam manipulation

Markus A. Schmidt[1,2,3], Henrik Schneidewind[1], Uwe Hübner[1], Matthias Zeisberger[1], Malte Plidschun[1], Jisoo Kim[1], Oleh Yermakov[4], Yuri Kivshar[5,6], Andrey Bogdanov[6], Haoran Ren[7], Stefan A. Maier[7,8,9]

[1]Leibniz Institute of Photonic Technology, Jena, Germany
[2]Otto Schott Institute of Materials Research (OSIM), Friedrich Schiller University of Jena, Germany
[3]Abbe Center of Photonics and Faculty of Physics, Friedrich-Schiller-University Jena, Germany
[4]V. N. Karazin Kharkiv National University, Kharkiv, Ukraine
[5]Nonlinear Physics Centre, Australian National University, Canberra, Australia
[6]Harbin Engineering University, Harbin, China
[7]School of Physics and Astronomy, Monash University, Melbourne, Australia
[8]Chair in Hybrid Nanosystems, Nanoinstitute Munich, Faculty of Physics, Ludwig-Maximilian University of Munich, 80539 Munich, Germany
[9]Department of Physics, Imperial College London, London SW7 2AZ, UK
[*]corresponding author: userid@institution.edu

Abstract: Here, we will demonstrate how the fusion of optical fibers with nanostructures creates a new category of fiber-integrated devices – hybrid optical fibers - that unlocks novel applications. We achieve this by leveraging 3D nanoprinting, which is highly compatible with the fiber geometry, to integrate high-NA holographic meta-lenses, achromatic metasurface-based lenses, and dielectric ring-like gratings onto the end faces of single-mode fibers, allowing to trap biological relevant objects, to focus light across the telecommunication range, and to boost incoupling efficiencies.

The development of nanostructures on the end faces of commercially available optical fibers offers a promising approach for unlocking new functionalities across various fields, such as biophotonics, quantum technologies, and optical sensing. However, conventional top-down fabrication methods are challenging to apply to optical fibers due to their unique geometry that differs from commonly used wafers [1,2]. In this presentation, we show our recent findings on 3D nanoprinting using direct laser writing, which circumvents this bottleneck. With this approach, we can implement intricate nanostructures on the end face of optical fibers, resulting in significant performance enhancements compared to fibers with unstructured end faces, as demonstrated in the following examples.

Optical trapping with single fiber (Figs. 1(a) and (b)): Effective focussing of light is crucial for various applications, such as optical imaging and microscopy, biophotonics, quantum technology, and materials processing. However, optical fibers have limitations in that respect due to the divergence of light emitted from the fiber facet. Note that to achieve single-focus optical trapping, a numerical aperture of greater than 0.8 is necessary. In this study, we used 3D nanoprinting to integrate ultra-high numerical aperture holographic meta-lenses onto functionalized single-mode fibers [3]. By considering the fiber environment, we achieved a record-high numerical aperture of up to 0.9 with diffraction-limited spots. This breakthrough allowed us to optically trap microspheres and biologically relevant bacteria, such as E. coli, with individual single-mode fibers, overcoming a significant limitation in fiber optic research.

Achromatic light focusing (Figs. 1(c) and (d)): The efficient and tailored focusing of light is crucial for future applications of optical fibers. An open issue in the field of telecommunications is achromatic light focusing, for which no satisfactory solution exists so far. By integrating a nano-printed metasurface-based lens onto a fiber, we have been able to achromatically and efficiently focus the output light of a SMF-28 over the entire telecommunications range [4]. Crucial here is the possibility of realizing nanopillars of different heights within one single metasurface, which is a unique feature provided by the nanoprinting process and has actually enabled the wavelength independent focussing of the light. With the conducted study we could thus show that metasurfaces can be very relevant for fiber optic applications with respect to telecommunication.

Boosting in-coupling efficiency (Figs. 1(e) and (f)): Conventional commercial fibers suffer from the limitation of low numerical aperture, which restricts light coupling to small angles. To address this problem, we have integrated axial-symmetric nanogratings consisting of nanoprinted concentric rings onto the core of single-mode fibers (SMF-28) [5]. This integration has already resulted in an impressive improvement of coupling efficiency at near-grazing incidence by more than four orders of magnitude compared to fibers with unstructured end faces. This improvement is based on an additional wave vector provided by the grating, which suppresses the electric field oscillation on the fiber surface at a certain angle, thereby allowing for exciting specific fiber modes. Additionally, we were able to achieve incoupling at preselected angles and across large angular intervals by employing an optimization procedure and 3D nanoprinting. This approach has helped to overcome the low numerical aperture limitation of commercial fibers and can lead to advancements in the field of fiber optics.

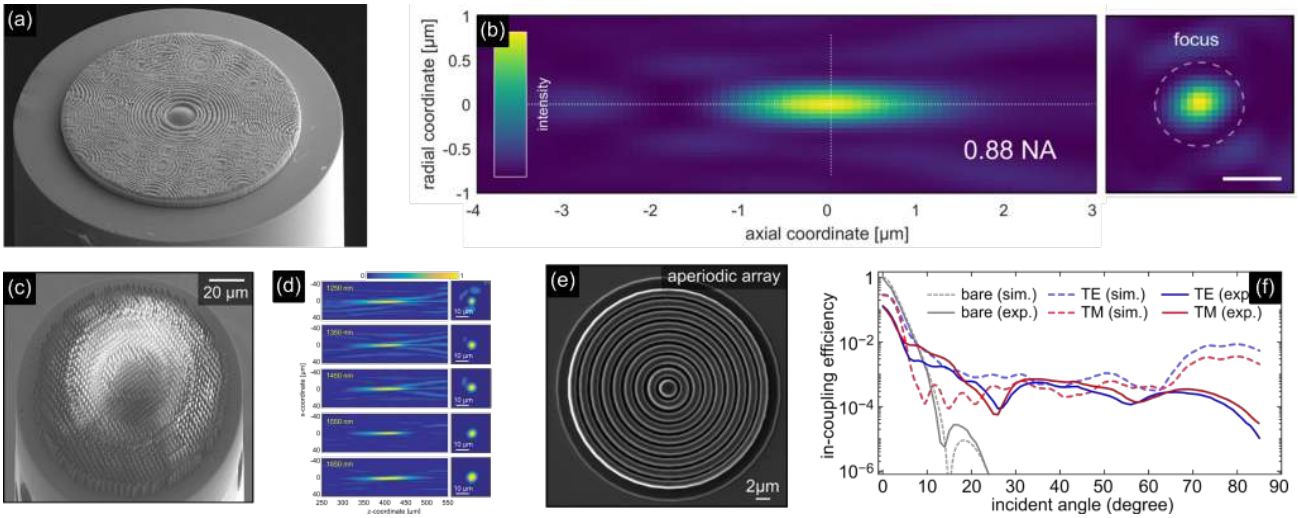


Fig. 1: Examples of printed nanostructures on optical fibers. (a) High-NA holographic metalens located on the end face of an optical fiber [3]. (b) Corresponding measured beam profile in water (632 nm). (c) Nanopillar-based metasurface located on an optical fiber and used for achromatic light focusing [4]. (d) Measured profile of the focus at different telecommunication wavelengths. (e) An aperiodic nano-grating on SMF-28 [5]. (f) Measured coupling efficiency vs. angle of incidence for a bare fiber (gray) and a nanostructured-interfaced fiber (1.55 µm).

We have demonstrated that the integration of optical fibers with nanostructures results in a new category of fiber-integrated devices that offer unprecedented applications in fiber optics. With the implementation of versatile application strategies, we anticipate broader use of nanostructured fibers in various fields, including quantum technology, bioanalytics, and nanophotonics.

References

1 Wang, N., Zeisberger, M., Hübner, U. & Schmidt, M. A. Boosting Light Collection Efficiency of Optical Fibers Using Metallic Nanostructures. *Acs Photonics* **6**, 691-698, doi:10.1021/acsphotonics.8b01560 (2019).

2 Wang, N., Zeisberger, M., Hübner, U. & Schmidt, M. A. Nanotrimer enhanced optical fiber tips implemented by electron beam lithography. *Opt Mater Express* **8**, 2246-2255, doi:10.1364/OME.8.002246 (2018).

3 Plidschun, M. *et al.* Ultrahigh numerical aperture meta-fibre for flexible optical trapping. *Light: Science & Applications* **10**, 57, doi:10.1038/s41377-021-00491-z (2021).

4 Ren, H. *et al.* An achromatic metafiber for focusing and imaging across the entire telecommunication range. *Nat Commun* **13**, 4183, doi:10.1038/s41467-022-31902-3 (2022).

5 Yermakov, O. *et al.* Advanced fiber in-coupling through nanoprinted axially symmetric structures. *Applied Physics Reviews* **10**, doi:10.1063/5.0127370 (2023).

Modulating and Spinning thermal radiation with incandescent metasurfaces

B. Vest[1]

[1]Université Paris-Saclay, Institut d'Optique Graduate School, CNRS, Laboratoire Charles Fabry, 91127, Palaiseau, France.

[*]email: benjamin.vest@institutoptique.fr

Abstract: Blackbody radiation is intrinsically isotropic, broadband and unpolarized. However, these properties can be strongly modified using appropriate nanostructures. Here we report about the design, fabrication and characterization of incandescent metasurfaces based on subwavelength metallic gratings. When heated by Joule effect, the grating acts as a thermal emitter that can be modulated at frequencies higher than the MHz. The system geometry can also be engineered to provide circularly polarized light with a polarization degree around 35%.

Thermal emission is an intrinsically incoherent process, delivering broadband, isotropic and unpolarized radiation. Therefore, generation of a circularly polarized beam from an incandescent source generally requires the use of several components, such as filters and waveplates, in order to provide the adequate retardance at chosen frequencies. This limits the compactness of the whole device. In this presentation, we report about the design, fabrication and characterization of thermal metasurfaces, designed to provide light at fast modulation regimes, and that can be designed to provide either linearly or circularly polarized light in the mid-wave infrared domain. We follow a design method based on a generalized Kirchhoff's law approach : we engineer the absorptivity features of the metasurfaces in order to shape the properties of light emitted by the structure by reciprocity [1].

In the first part of the presentation, we report the performances of a device designed to achieve fast modulation of IR emission (see Fig. 1). In our work, the emission modulation relies on fast temperature modulation of thin emitters placed on a cold substrate [2]. Thanks to heat conduction, the emitters can cool down within a characteristic time which varies as the square of its thickness. In the proposed structure, we use a sub-wavelength metallic grating as the emitting source, thus demonstrating a MWIR source linearly polarized with the emission modulation up to 10 MHz.

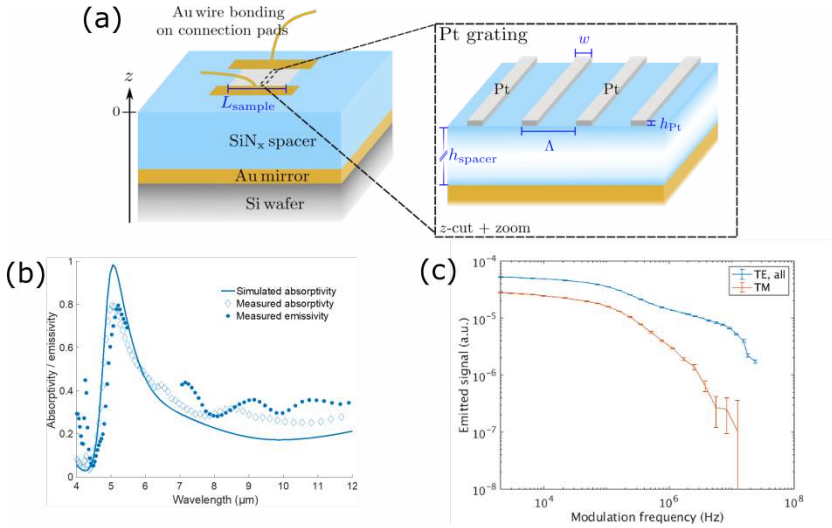


Fig. 1 Experiments on fast modulation of incandescence. (a) Design of the structure. The platinum grating lays the role of the emitting source (b) Simulated and experimentally measured absorptivities and emissivities showing peak emission at 5.5 µm. (c) Evolution of the average emitted power as a function of modulation frequency in both polarizations.

In the second part, we present a similar where the top surface is paved with a subwavelength metallic grating following a chiral pattern [3] (See Fig 2.). The dimensions of the system are chosen in order to make the grating a good chiral absorber : we maximize the contrast in absorption of the system when illuminated respectively by right-handed circularly polarized light (RCP) and left-handed circularly polarized light (LCP). The top metallic grating is then heated by Joule effect. It acts a thermal emitter with a contrast in emissivity between LCP and RCP.

We designed a specific protocol to accurately measure the different Stokes vector components of the highly polychromatic emission over a broad range of wavelengths between 3 and 5 microns, thus evaluating with precision the polarization state of the infrared light as a function of the emission wavelength. Our devices emits light with a degree of circular polarization (DCP) up to 35% at 4.7 microns, to be compared to simulations predicting a maximum of 50% for our design.

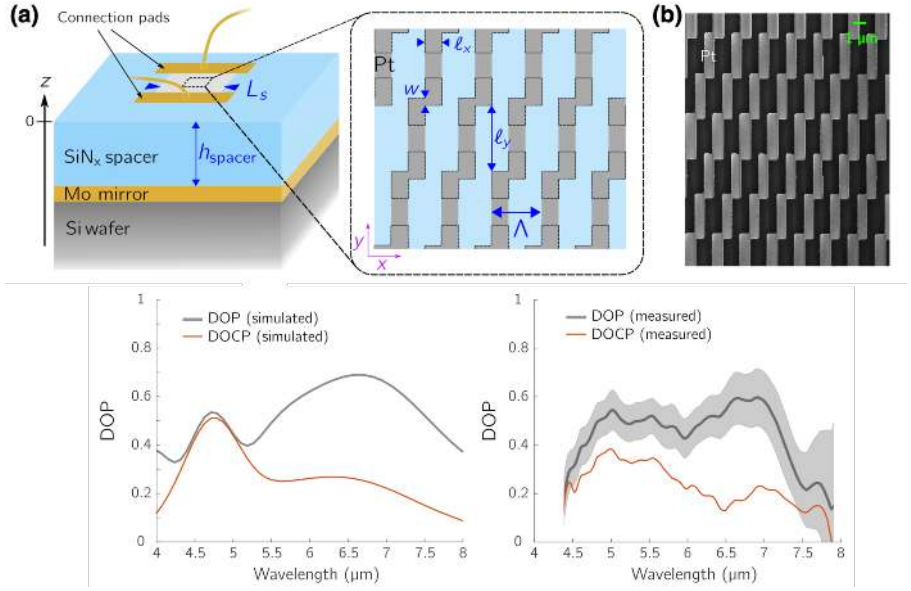


Fig. 2 Experiments on circularly polarized light emission of incandescence. (a) Design of the structure. The platinum grating follows a chiral pattern (b) SEM picture of the fabricated device. (c) Simulated and measured degree of polarization (DOP) and degree of circular polarization (DOCP). Shaded areas represent one-sigma error bars.

Our system paves the way towards cheap and compact devices to generate infrared light with a decent DCP using only one single component, for applications in communication, sensing, security and counterfeiting.

Funding. This project ackowledges funding from Agence Nationale de la Recherche (ANR-17-CE24-016).

References

1. Greffet, J.J., Bouchon, P., Brucoli, G., Marquier F. “Light emission by nonequilibrium bodies: local Kirchhoff law” Phys.Rev.X 8, 021008, 2018.
2. Wojszvzyk, L., Nguyen, A., Coutrot, A.-L.,, Zhang, C. Vest, B. and Greffet, J.-J. “An incandescent metasurface for quasimonochromatic polarized mid-wave infrared emission modulated beyond 10 MHz,” Nat. Commun. 12, 1492, 2021.
3. Nguyen, A., Hugonin, J. P., Coutrot, A. L., Garcia-Caurel, E., Vest, B., & Greffet, J. J “Large circular dichroism in the emission from an incandescent metasurface”. Optica, 10(2), 232-238, 2023

META 2023, PARIS - FRANCE, JULY 18 – 21, 2023

Full color Imaging with Large-Aperture Meta-Optics

Arka Majumdar[1,2,*]
[1] *Department of Electrical and Computer Engineering, University of Washington, Seattle, WA 98195, USA*
[2] *Department of Physics, University of Washington, Seattle, WA 98195, USA*
[*] *arka@uw.edu*

Abstract: By exploiting computational backend, coupled with a designer meta-optics we demonstrate high-quality imaging using a single meta-optics with an aperture of 1cm.

The miniaturization of image sensors in recent decades has made today's cameras ubiquitous across many application domains, including medical imaging, smartphones, security, robotics, and autonomous transportation. However, only imagers that are an order of magnitude smaller could enable novel applications in nano-robotics, in vivo imaging, mixed reality, and health monitoring. While sensors with sub-micron pixels exist now, further miniaturization has been primarily prohibited by fundamental limitations of conventional optics. Traditional imaging systems consist of a cascade of refractive elements that correct for aberrations, and these bulky lenses impose a lower limit on camera footprint. A further fundamental barrier is the difficulty of reducing focal length, as this induces greater chromatic aberrations.

We employ computationally designed meta-optics to close this gap and enable ultra-compact cameras that could allow for unprecedented capabilities in bio-imaging or mixed reality systems. Ultrathin meta-optics utilize subwavelength scatterers to modulate incident light with greater design freedom and space-bandwidth product over conventional diffractive optics. Existing meta-optics, however, achieve an order of magnitude higher reconstruction error than achievable with refractive compound lenses due to severe, wavelength-dependent aberrations that arise from discontinuities in their imparted phase. Dispersion-engineered meta-optics aim to mitigate this by exploiting group delay and group delay dispersion to focus broadband light, but this technique is fundamentally limited, constraining designs to apertures of only ~10's of micron with low f-number (high numerical aperture). As such, existing approaches have not been able to increase the achievable aperture sizes without significantly reducing the numerical aperture or supported wavelength range. Other attempted solutions only suffice for discrete wavelengths or narrowband illumination, which cannot be used for broadband imaging under ambient light.



Figure 1: 1cm meta-optics integrated camera.

Our solution is to design the meta-optics such that the modulation transfer function (MTF) of all the wavelength across the desired optical bandwidth are same at the sensor plane. Additionally, the area under the MTF curve needs to be large, such that enough information is captured and the orginal image can be reconstructed. Same intuition can be employed for different angles to mitigate the geometric aberrations as well. However, designing such meta-optics is not trivial.

We have developed essentially three different methods to solve this problem. In the first approach we used well-known designs of extended depth of focus (EDOF) meta-lenses, such as cubic [1] or log-asphere lenses [2]. Such EDOF property allows light at different wavelengths to reach the sensor in identical way. The computational backend involves either Wiener filtering or Total-Variation (TV) regularization. In the second approach, we employ inverse design to create the meta-optics, but the computational post-processing remains same [3,4]. Finally, we can co-design the meta-optics and computational algorithm. Such an "end-to-end" designed optics and computational algorithm [5] can provide high quality imaging. Specifically we obtained photographic-quality imaging with a single meta-optics,

rendering the total volume of the sensor at least four orders of magnitude smaller. The image quality improves from the first to last approach, while the design becomes more complex. By exploiting rotational symmetry and different field propagators, we recently extend the designs to upto 1cm diameter, which for the first time allows comparing imaging between a refractive and a meta-optics. Figure 1 shows the fabricated metalens and direct integration with a camera. We then compare the imaging between different versions of the 1cm meta-optics and refractive for an OLED screen in lab (Figure 2). Finally, we performed imaging under ambient light (Figure 3).

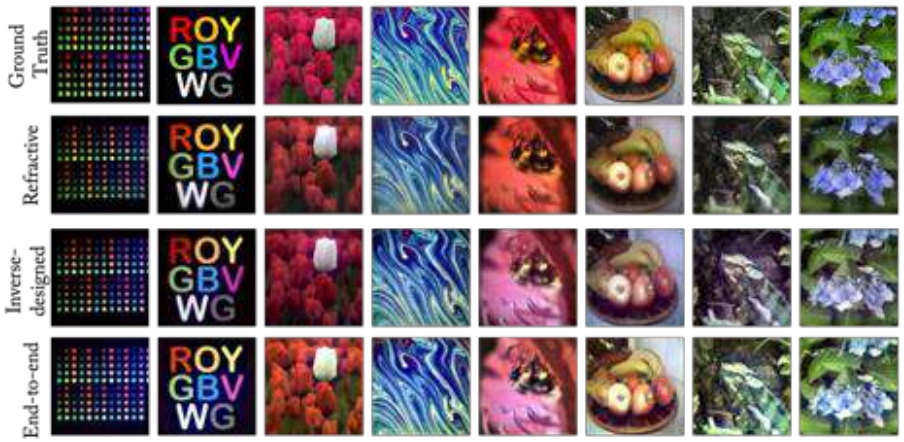


Figure 2: Full-color imaging with meta-optics against refractive (ground thruth)



Figure 3: Ambient imaging with simple Wiener deconvoution and diffusion network deconvolution.

Acknowledgements: This research was supported by DARPA (Contract no. W31P4Q21C0043).

References

[1] S. Colburn, A. Zhan, and A. Majumdar, "Metasurface optics for full-color computational imaging," *Science Advances,* vol. 4, 2018.

[2] L. Huang, J. Whitehead, S. Colburn, and A. Majumdar, "Design and analysis of extended depth of focus metalenses for achromatic computational imaging," *Photonics Research,* vol. 8, pp. 1613-1623, 2020/10/01 2020.

[3] E. Bayati, R. Pestourie, S. Colburn, Z. Lin, S. G. Johnson, and A. Majumdar, "Inverse Designed Metalenses with Extended Depth of Focus," *ACS Photonics,* vol. 7, pp. 873-878, 2020/04/15 2020.

[4] E. Bayati, R. Pestourie, S. Colburn, Z. Lin, S. G. Johnson, and A. Majumdar, "Inverse designed extended depth of focus meta-optics for broadband imaging in the visible," *Nanophotonics,* vol. 11, pp. 2531-2540, 2022.

[5] E. Tseng, S. Colburn, J. Whitehead, L. Huang, S.-H. Baek, A. Majumdar, and F. Heide, "Neural nano-optics for high-quality thin lens imaging," *Nature Communications,* vol. 12, p. 6493, 2021/11/29 2021.

META 2023, PARIS - FRANCE, JULY 18 – 21, 2023

Flat Optics for Dynamic Wavefront Manipulation

Mark Brongersma

Stanford University, United States
*corresponding author: brongersma@stanford.edu

Abstract: Since the development of diffractive optical elements in the 1970s, major research efforts have focused on replacing bulky optical components by thinner, planar counterparts. The more recent advent of metasurfaces, i.e. nanostructured optical coatings, has further accelerated the development of flat optics through the realization that nanoscale antenna elements can be utilized to facilitate local and nonlocal control over the light scattering amplitude and phase.

In this presentation, I will highlight our recent efforts to realize electrically-tunable metasurfaces employing nanomechanics, microfluidics, phase change materials, and atomically-thin semiconductors. Such elements are capable of dynamic wavefront manipulation for optical beam steering and holography. I will also discuss how the nanostructured, planar optical elements can be fabricated by scalable fabrication technologies, opening the door to a wide range of commercial applications.

Tailoring the visual appearance with disordered arrays of resonant metaatoms

A. Agreda[1*], T. Wu[1], A. Hereu[2], M. Tréguer-Delapierre[2], G. Drisko[2], K. Vynck[3], and P. Lalanne[1]

[1]LP2N, CNRS, Institut d'Optique Graduate School, Univ. Bordeaux, F-33400 Talence, France

[2]Institut de Chimie de la Matière Condensée de Bordeaux, CNRS, Pessac, France

[3]Institut Lumière Matière, CNRS, Université Claude Bernard Lyon 1, Villeurbanne, France
[*]corresponding author: philippe.lalanne@institutoptique.fr

Abstract: Metasurfaces have flourished in the last few years thanks to their extraordinary capabilities in the manipulation of light. In this work, we propose a theoretical tool that can effectively and intuitively predict the visual appearance of disordered resonant metasurfaces.

In a recent work, some of the authors succeeded in designing the very first simulation tool to predict the appearance of disordered metasurfaces made of array of resonant meta-atoms [1]. The modelling platform may find use in several branches of visual arts, to predict the appearance of augmented reality devices using metasurfaces, design unusual effects for counterfeiting applications or luxury goods …

Importantly, the tool predicts the possibility to create fancy appearances, unseen so far with the nanostructures available in nature,



see also the Supplementary Videos 1 & 2 in [1] for a rapid glance.

The tool in [1] relies on an approximate model that predicts the Bidirectional Reflection Distribution Function (BRDF) of disordered metasurfaces. Because the BRDF is a huge multidimensional function, the tool relies on repeating many full-wave electromagnetic simulations for all wavelengths, incidence angles and polarizations of the incident light. However, such a brute force approach is inefficient and, more importantly, completely hides the physics. It clearly lacks from intuition and does not provide any feedback on how the nanoscale morphology affects the BRDF first, and subsequently the visual appearance.

We need a tool not only for calculating but also for understanding the processes and for conceptualizing the problem before we even begin to calculate. In this work, such a tool is proposed, implemented and tested for disordered metasurfaces made by silver nanoparticles deposited on a reflective substrate coated with a submicrometric SiO_2 spacer [2]. The tool is

based on recent advances [3] on the analysis of electromagnetic nanoresonators in the basis of their natural resonance modes, also known as quasinormal modes (QNMs). We stress that the modal tool not only result in a considerable reduction of the computational loads, but also provides an advanced conceptualization of the form factor which unveils the physics and the control knobs at play to harness the appearance. The tool quantitatively predicts and intuitively explains a remarkable iridescence phenomenon, in which the diffuse light exhibits only two **very distinct** colors, irrespective of the viewing and illumination directions [2]. The modal tool also explains why, despite the renowned strong sensitivities of the resonance wavelength of nanoresonators to shape and size variations that are present in our samples, the observed colors remain vivid and accurately predicted with simulations assuming monodispersity. This resilience to fabrication imperfections is crucial for genuine applications because it considerably lowers fabrication costs and enables large-scale fabrication.

Acknowledgements

This work has received financial support from the GPR Light of the University of Bordeaux and the ANR contract "NANO-APPEARANCE" (ANR-19-CE09-0014).

References

1. Vynck, K., Pacanowski, R., Agreda, A., Dufay, A., Granier, X. & Lalanne, P. The visual appearances of disordered optical metasurfaces. Nat. Mater. 21, 1035–1041 (2022).
2. Agreda A. et al., "Diffuse iridescence of disordered metasurfaces coated on reflective substrates," Arxiv 2022.
3. Sauvan, C., Wu, T., Zarouf, R., Muljarov, E. A. & Lalanne, P. Normalization, orthogonality, and completeness of quasinormal modes of open systems: the case of electromagnetism. Opt. Express 30, 6846-6885 (2022).

Lithography-free control of thermal emission.

M. Sarkar, M. Giteau, M.T. Enders and G. T. Papadakis*

ICFO-Institut de Ciencies Fotoniques, The Barcelona Institute of Science and Technology, Spain
*corresponding author: georgia.papadakis@icfo.eu

Abstract: Blackbody thermal emission is spatially diffuse. Achieving highly directional thermal emission typically requires nanostructuring the surface of the thermally emissive medium. Here, we revisit the simple motif of a planar Salisbury screen and show that hexagonal Boron Nitride thin films can enable grating-like thermal emission lobes in a lithography-free platform.

Gaining control over the spatial and spectral characteristics of mid-infrared (IR) thermal emission is central to various applications like thermophotovoltaic systems, radiative cooling, IR sources, thermal camouflage and molecular sensing[1]. Blackbody thermal emission is spectrally broad and spatially diffuse, however with photonic design, one can narrow the spectral range and control the directionality of thermal emission[2]. Previously, this was achieved by coupling light into the phonon polaritons in polar materials[3]. To couple into these modes and to achieve strong directionality, typically, one requires a grating structure [4]. Other than being lithographically complex, this approach is also limited to p-polarization.

In contrast, here we introduce an approach that allows omni-polarization directional control of thermal emission without *any* lithography. To achieve this, we leverage the strong dielectric permittivity resonances of polar materials. We introduce design rules for achieving both narrowband diffuse and narrowband directional thermal emission in a three-layer heterostructure.

Our meta-structure is shown in Fig 1a. It is based on the Salisbury screen configuration[5]: a dielectric spacer layer is sandwiched between a thin lossy emitter and a perfect electric conductor (PEC). For maximum emissivity at a given incidence angle θ, it is necessary for light to experience constructive interference in the spacer. Considering an acquired phase of π and Ψ for reflections at the PEC and lossy material respectively, we derive the condition for constructive interference:

$$2k_0 h_m \aleph_m + \pi + \Psi = 2l\pi \quad (1)$$

where l is an integer denoting the interference order and $k_0 = 2\pi/\lambda$, with λ the wavelength of light. The emitter (with subscript e) and the spacer (with subscript m) can be considered anisotropic, having a diagonal permittivity tensor with elements ϵ, ϵ/α_Y^2 and ϵ/α_Z^2 along x, y and z axes respectively. The terms $\aleph_Z^2 = \epsilon - \alpha_Z^2 sin^2\theta$ and $\aleph_Y^2 = (\epsilon - \alpha_Y^2 sin^2\theta)/\alpha_Y^2$ are the effective index of the anisotropic medium. It can be shown that for maximum directional control, we need $\Psi = \pi$ while, for minimum angular dependence, (diffuse thermal emission), we need $\Psi = 0, 2\pi$. We have derived the acquired phase on reflection from the lossy material as

$$\Psi_P = \pi - 2tan^{-1}\frac{\aleph_{Ze}\,\epsilon_m}{\epsilon_e \aleph_m}\frac{\epsilon_e cos\theta + i\aleph_{Ze}T_e}{\epsilon_e cos\theta\, T_e - i\aleph_{Ze}} \quad (2)$$

for P polarization with $T_e = tan(h_e k_0 \aleph_{Ze/Ye})$. A similar equation can be derived for the S polarization.

By optimizing the geometrical parameters of the metastructure and using Eq.1 and Eq.2, complete directional control can be achieved. We demonstrate this concept with hexagonal Boron Nitride (hBN) as the emitter[6]. The

high permittivity near the phonon resonances (Reststrahlen band) of hBN allows for strong directional control while the narrow bandwidth of these resonances also yields spectral control. This is shown in Fig 1c and d for the metastructure and the directional control achieved is comparable to lithographically complex nanostructures (grating) shown in Fig.1b.

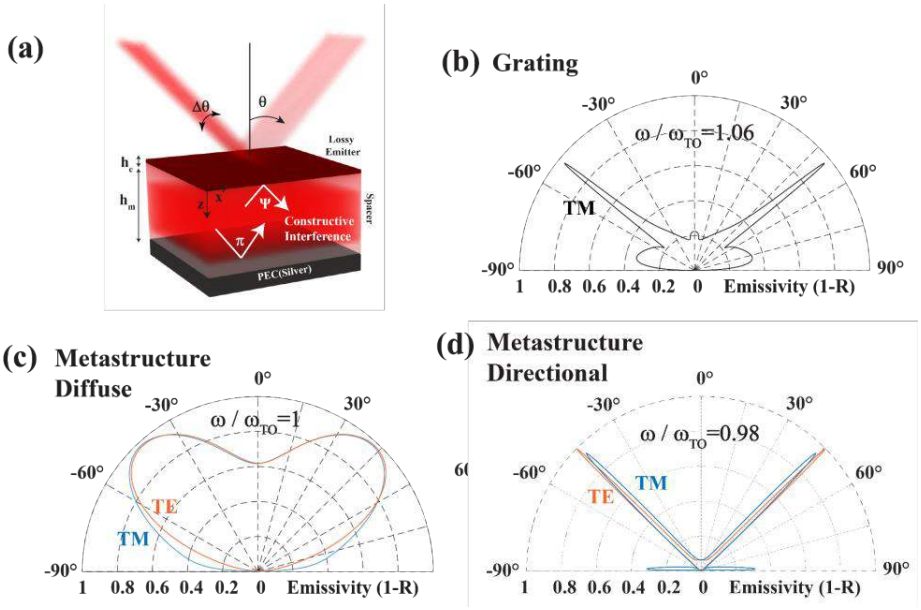


Figure 1 a) The schematic of the meta-structure in the Salisbury screen configuration. b) The polar plot for P polarized emission from a grating structure[2] for a frequency in the center of the Reststrahlen band of hBN. (c) The polar plot for the meta-structure for diffuse emission for both P and S polarizations. (c) The same for a frequency where the emission is directional for both polarizations.

In this work, we present a method to bypass the inherent difficulty in achieving strong spatial and spectral control of thermal emission. We present a standard geometry involving a Salisbury screen and, via optimizing the emitter and spacer thicknesses, we have shown that one can strongly confine light emitted due to the volume polaritons of polar materials in the lossless spacer.

The project that gave rise to these results received the support of a fellowship from “la Caixa” Foundation (ID 100010434) and from the European Union’s Horizon 2020 research and innovation programme under the Marie Skłodowska-Curie grant agreement No 847648.

References

1. Baranov, D. G. *et al.* Nanophotonic engineering of far-field thermal emitters. *Nat Mater* **18**, 920–930 (2019).
2. Greffet, J. J. *et al.* Coherent emission of light by thermal sources. *Nature* **416**, 61–64 (2002).
3. Caldwell, J. D. *et al.* Low-loss, infrared and terahertz nanophotonics using surface phonon polaritons. *Nanophotonics* **4**, 44–68 (2015).
4. Li, W. & Fan, S. Nanophotonic control of thermal radiation for energy applications [Invited]. *Opt Express* **26**, 15995–16021 (2018).
5. Salisbury, W. W. Absorbent body for electromagnetic waves. (1952).
6. Sarkar, M., Giteau, M., Enders, M. & Papadakis, G. T. Lithography-free directional control of thermal emission. *ArXiv* (2022) doi:https://doi.org/10.48550/arxiv.2210.01026.

META 2023, PARIS - FRANCE, JULY 18 – 21, 2023

Reconfigurable and polarization-dependent grating absorber for large-area emissivity control based on the plasmonic phase-change material In_3SbTe_2

Lukas Conrads[1,*], Natalie Honné[1], Andreas Ulm[2], Andreas Heßler[1], Matthias Wuttig[1], Robert Schmitt[2], and Thomas Taubner[1]

[1] I. Institute of Physics (IA), RWTH Aachen University, Germany

[2] Fraunhofer Institute of Production Technology (IPT), Germany

[*]corresponding author: conrads@physik.rwth-aachen.de

Abstract: The plasmonic phase-change material In_3SbTe_2 can be reversibly switched from an amorphous dielectric to a crystalline metallic state. Infrared emissivity control by patterning a grating absorber metasurface for different polarizations, which can be only seen in the long-wave infrared regime, is demonstrated. Additionally, a 1x1 cm² metasurface is fabricated with enhanced emissivity to display an apparent local temperature pattern.

Metasurfaces with perfect infrared absorption promise integrated filters and compact detector elements with narrowband thermal emission. Phase-change materials (PCMs) are prime candidates for active, non-volatile absorption tuning [1]. Commonly, the response of the entire metasurface is tuned, while local adaptions remain elusive. Currently, a novel material class of switchable infrared plasmonic PCMs, like In3SbTe2 (IST), is emerging. Since IST can be locally optically switched between dielectric (amorphous phase) and metallic (crystalline phase) states in the whole infrared range, it becomes possible to directly change the geometry and size of nanoantennas to tune their infrared resonances [2,3]. In this work, we show flexible encoding of different absorption/emission properties within a metasurface. We employ the plasmonic PCM IST to obtain control over the emissivity by patterning an adaptable grating absorber metasurface. Using a commercial direct laser writing setup, we locally switch the IST from an amorphous dielectric into a crystalline metallic state and write cm-sized stripe gratings above a reflecting mirror. We demonstrate modification of already written patterns by changing the laser power and thus the IST stripe width to encode different polarization-sensitive patterns with nearly perfect absorption into the same metasurface. Finally, we measure an apparent local temperature pattern due to our large-area emissivity shaping metasurface with a conventional thermal camera [4]. Our results pave the way towards low-cost, large-area and adaptable patterning of metasurfaces with wavelength and polarization-selective perfect absorption, enabling applications like enhanced thermal detection, infrared camouflage or encoding anti-counterfeiting symbols.

Acknowledgements

L.C., N.H., M.W. and T.T. acknowledge support by the Deutsche Forschungsgemeinschaft (SFB 917 “Nanoswitches”).

References

1. Wuttig, M. et al., “Phase-change materials for non-volatile photonic applications” *Nat. Photon*., **11**, 465–476 (2017)
2. Heßler, A. et al., “In3SbTe2 as a programmable nanophotonics material platform for the infrared” *Nat. Commun.* **12**, 924 (2021)
3. Heßler, A., Conrads, L. et al., “Reconfiguring Magnetic Infrared Resonances with the Plasmonic Phase-Change Material In3SbTe2” *ACS Photonics* **9**, 5 (2022)
4. Conrads, L. et al., “Reconfigurable and polarization-dependent perfect absorber for large-area emissivity control based on the plasmonic phase-change material In3SbTe2” *Adv. Opt. Mat.* (2023)

Shape-multiplexed conformable holographic metasurfaces

Sebastian A. Schulz[1], Jianling Xiao[1], Robert. I. Hunter[1], Duncan A. Robertson[1], Graham M. Smith[1], Simon Horsley[2], Andrea Di Falco[1]

[1]SUPA, School of Physics and Astronomy, University of St Andrews, St Andrews, UK
[2]Department of Physics and Astronomy, University of Exeter, Exeter, UK
*corresponding author: sas35@st-andrews.ac.uk

Abstract: Conformal metasurfaces hold great potential for retro-fitting optical functionality and decoupling the complexity of the final shape from the constraints of nanofabrication. Here we demonstrate a reflective conformable metasurface that shows one of two independent holographic images, where we can switch between two independent holographic images, by changing from a concave to a convex shape and vice versa.

Metasurfaces - two-dimensional distributions of meta-atoms – allow control over the phase, polarization and amplitude of scattered light [1]. Within metasurfaces two developments are of particular interest, flexible and conformable metasurfaces, and multiplexed metasurfaces. In multiplexed metasurfaces different, independent information is encoded into different states (e.g. polarization or wavelength) of light [2], enabling applications such as encryption, sensing or displays [3-5]. Flexible and conformable metasurfaces on the other hand can be used to encode and retrieve information [6] or decouple the optical response from an object's shape [7] when applied to non-flat surfaces. Here we combine these two fields and present a conformal metasurface that displays two independent holographic images, dependent on the curvature of the object that it is applied to [8].

Fig. 1(a) and (b) show a schematic of the metasurface and its operation. When in a convex shape the displayed hologram features two focal spots, in the top left and bottom right corner of the image plane respectively. However, when in a concave shape the metasurface displays a holographic image featuring three focal spots

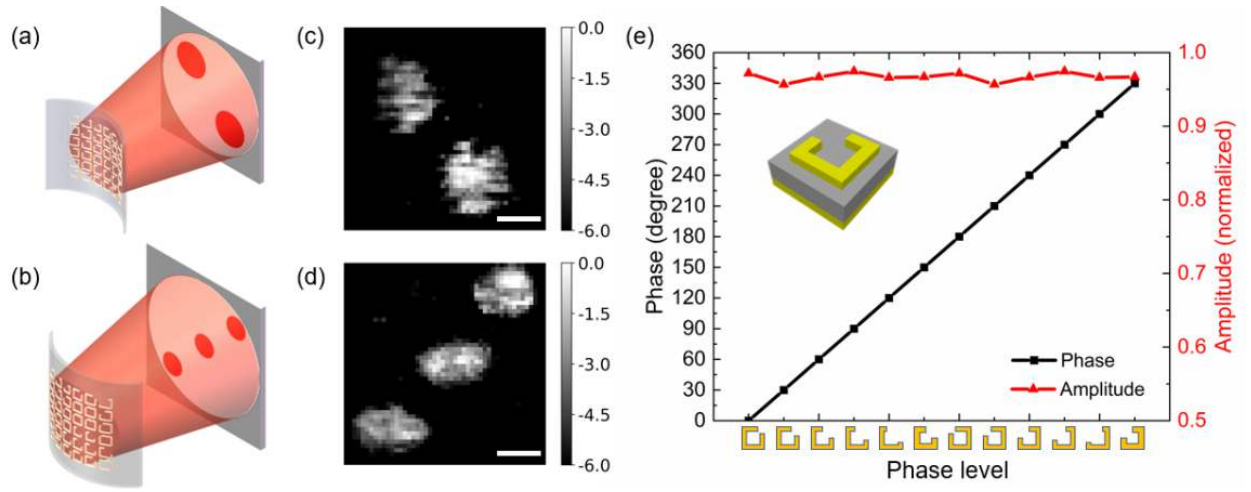


Figure 1: Schematic of the (a) convex and (b) concave operation of the metasurface. (c) and (d) experimental observation of the expected holographic image, obtained at 94 GHz. The scalebar corresponds to 20 mm. (e) Phase and amplitude response of the underlying c-ring resonators that form the meta-atoms.

along the opposite diagonal, i.e. from the bottom left to the top right corner of the image plane.
For our experimental realization of these images (see fig. 1(c) and (d)), we implement a radius of curvature of 35 mm and -100 mm for the convex and concave shape respectively. These images are obtained using a reflective metasurface operated in the mm-wave regime (illuminated with 94 GHz mm-waves). The metasurface consists of an array of copper c-ring resonators with varying gap positions and sizes, giving us a uniform amplitude response and 12-level full 2π-phase coverage, as shown in Fig.1(e). The c-ring resonators have a thickness of 200 nm and are on a 380 μm PMMA layer, followed by a 200 nm copper back reflector. This is a mm-wave band implementation of the popular, high-reflectance metal-dielectric-metal metasurface geometry [7].
To achieve the shape multiplexing we interleave two independent holograms, each designed for the relevant radius of curvature of the metasurface, using the Gerchberg-Saxton algorithm, with the Rayleigh-Sommerfeld integral as a propagator.
We believe that the demonstration of shape-multiplexed metasurfaces paves the way towards novel applications in reconfigurable antennas, optomechanical sensors, and actuators across a wide range of wavelengths and operating bands.

Aknowedgments
S. A. Schulz acknowledges funding from EPSRC through grant [EP/V029975/1].

References

1. H.-T. Chen and A. J. Taylor and N. Yu, "A review of metasurfaces: physics and applications," *Reports on progress in physics* **79**, 076401 (2016).
2. R. Zhao and L. Huang and Y. Wang, "Recent advances in multi-dimensional metasurfaces holographic technologies," *PhotoniX* **1**, 1-24 (2020).
3. J. Li and S. Kamin and G. Zheng and F. Neubrech and S. Zhang and N. Liu, "Addressable metasurfaces for dynamic holography and optical information encryption," *Science advances* **4**, eaar6768 (2018).
4. X. Fang and H. Ren and M. Gu, "Orbital angular momentum holography for high-security encryption," *Nature Photonics* **14**, 102-108 (2020).
5. L. Yan and J. Xiao and T. Plaskocinski and M. Biabanifard and S. Persheyev and M. Askari and A. D. Falco, "Two-tier manipulation of holographic information," *Optics Express* **30**, 19145-19151 (2022).
6. J. Burch and A. Di Falco, "Surface topology specific metasurface holograms," Acs Photonics **5**, 1762-1766 (2018).
7. J. Burch and J. Ma and R. I. Hunter and, S. A. Schulz and D. A. Robertson and G. M. Smith and J. Wang and A. Di Falco “Flexible patches for mm-wave holography” *Applied Physics Letters* **115**, 021104 (2019).
8. J. Xiao and R. I. Hunter and D. A. Robertson and G. M. Smith and S. Horley and S. A. Schulz and A. D. Falco, "Shape dependent conformable holographic metasurfaces," *Advanced Materials Technologies* (2023) (accepted for publication).

META 2023, PARIS - FRANCE, JULY 18 – 21, 2023

Rotary metaswimmers powered by linearly polarized light

M. Shanei[1*], E. Engay[1], V. Mylnikov[1], and M. Käll[1]

[1] Department of Physics, Chalmers University of Technology, Gothenburg, Sweden

[*]corresponding author: mahdi.shanei@chalmers.se

Abstract: Metasurfaces offer great possibilities to manipulate the momentum of light. Changes in linear optical momentum can result in forces and torques acting on a movable metaswimmer. Here, we demonstrate that by spatially distributing the changes in the linear momentum of light across the metasurface, these optomechanical effects can be utilized to generate optical torques able to rotate metaswimmers that are tens of micrometers wide in aqueous environments. We delineate the counterintuitive dynamics resulting from physical and hydrodynamic interactions between metaswimmers.

Metasurfaces are flat structures with engineered subwavelength building blocks that provide various possibilities for tailoring optical forces and momentum exchange. In the process of shaping a light beam, a metasurface is itself subject to momentum exchange and optical forces. This effect can be observed if a metasurface is incorporated into a micro-scale object allowed to move freely across a surface [1,2]. In this work, metaparticles are designed based on defining silicon-based deflectors that mimics conventional blazed gratings. The deflection of light from the propagation axis by the grating adds an in-plane linear momentum onto the outgoing beam. Conservation of the system's total momentum generates a reaction force that results in the translation of the particle as shown in Fig 1.

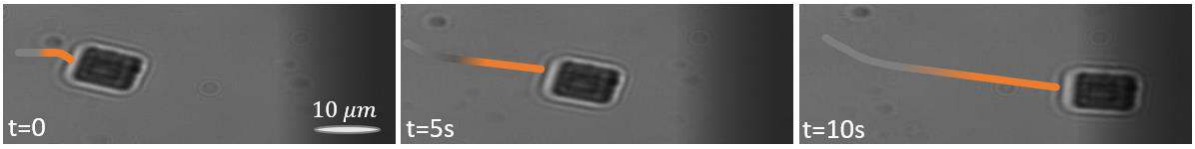


Figure 1. Translation of a metaswimmer due to the reaction force resulting from high-angle deflection of an incident plane wave.

The exchange of linear momentum between light and matter can also be exploited to rotate particles and micro-swimmers. Different approaches have been used to rotate an object with a linearly polarized plane wave [3], such as using chiral or birefringent structures, breaking the symmetry of objects, or utilizing unbalanced light-matter interactions in different sections of a particle. Figure 2 illustrates that when a spatial dependency is added by placing different grating orientations on the body of a metaswimmer, the interaction of the incident light and the meta-swimmer can generate an optical torque. In this presentation, we will discuss the fabrication, optical properties, dynamics and mutual interactions of rotary metaswimmers that range in lateral size from a few microns to several tens of microns, while still being essentially flat. We envisage that these kinds of structures could find use in microfluidics and bionanotechnology, and may serve as testbeds for probing the dynamics of physically diverse systems, such as microorganisms or other biological entities.

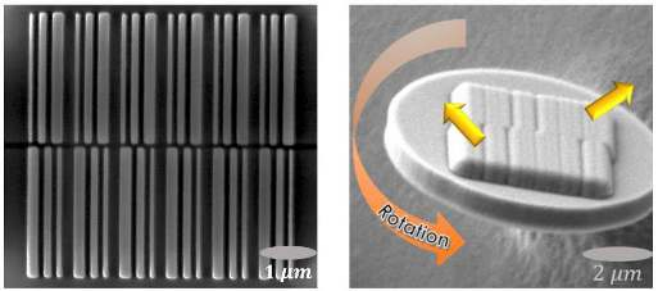


Figure 2. SEM images of a rotary metaswimmer propelled by the deflection of incident light in opposite directions.

Acknowledgments. This work was performed in part at Myfab Chalmers and funded by Knut and Alice Wallenbergs Foundation.
and

References

1. Andrén, Daniel, et al. "Microscopic metavehicles powered and steered by embedded optical metasurfaces." Nature Nanotechnology Vol. 16, No.9, 970-974, 2021.
2. Wu, Xiaofei, et al. "Light-driven microdrones." Nature Nanotechnology Vol. 17, No. 5, 477-484, 2022.
3. Mitra, Shirsendu, and Mitali Basak. "Recent trends in non-reactive light driven Micro/-nano propellers and rotors." Applied Materials Today Vol. 31, 101748, 2023.

META 2023, PARIS - FRANCE, JULY 18 – 21, 2023

Active Huygens' metasurface based on in-situ grown conductive polymer

W. Lu[1,*], L. de S. Menezes[1,2,3], A. Tittl[1], H. Ren[4] and S. A. Maier[4,5,*]

[1]Chair in Hybrid Nanosystems, Nano-Institute Munich, Faculty of Physics, Ludwig-Maximilians-Universität München, Munich, 80539, Germany.
[2]Departamento de Física, Universidade Federal de Pernambuco, 50670-901 Recife-PE, Brazil.
[3]Center for Nanoscience, Faculty of Physics, Ludwig-Maximilians-Universität München, Munich, 80539, Germany.
[4]School of Physics and Astronomy, Monash University, Clayton, Victoria 3800, Australia.
[5]Department of Physics, Imperial College London, London SW72AZ, UK.
[*]corresponding author: Wenzheng.Lu@physik.uni-muenchen.de; Stefan.Maier@monash.edu

Abstract: Active metasurfaces provide unique advantages for on-demand light manipulation at a subwavelength scale for emerging applications of 3D displays, augmented/virtual reality (AR/VR) and light detection and ranging (LiDAR). Here, we introduce an electrically active Huygens' metasurface based on in-situ grown conductive polymer with holistic switching performance. Our active metasurface design can be readily incorporated into other metasurface concepts to deliver high-reliability electrical control over optical response, paving the way for compact and robust electro-optic metadevices.

Active metasurfaces, often alternatively termed as tunable or reconfigurable metasurfaces, are rapidly emerging as a major frontier in photonic research and have launched tremendous breakthroughs in modern optics[1]. Compared with their passive counterparts, active metasurfaces consist of ultrathin planar arrays of subwavelength active nanoantennas, whose optical responses can be dynamically modulated on-demand. The active tuning schemes mainly rely on varying optical properties of the nanoantennas or their surrounding materials through chemical reactions[2], mechanical displacements[3], electrical switching[4], thermal modulation[5] and all-optical switching[6]. Among these modulation schemes, electrical switching is of particular interest because it promises compact integration of meta-optics with miniaturized on-chip electro-optic systems, which can be readily incorporated into electronic smart devices for practical applications[1], such as 3D displays, augmented/virtual reality (AR/VR) glasses, dynamic holograms, beam steering and light detection and ranging (LiDAR).

To this end, a number of active metasurfaces have been implemented by using different electro-active materials. Previous active metasurfaces exhibit only distinct subsets of key performance metrics[1], including switching speed, cycling duration, controllability over intermediate states, modulation contrast, optical efficiency and operation voltages. However, these performance attributes are hardly met simultaneously, making them almost impossible for any practical use. For instance, even though phase-change-materials metasurfaces can provide a switching speed of up to 2 MHz[7], they require high operation voltage and large cell manipulation. Recently, conductive polymers have shown many desired properties for electrically active metasurfaces, such as large variation of refractive index, fast switching speed, superior cycling stability and low operation voltages[8]. However, previous active metasurfaces purely based on conductive polymers are disadvantaged by low diffractive efficiency, due to the geometric phase design and the weak resonant nature of the nanostructured polymer[4]. Moreover, the fabrication of the conductive polymer relying on spin-coating prevents long-term switching durability since the contact issue between the polymer and the substrate.

In this work, we introduce an electrically active Huygens' metasurface based on the in-situ grown conductive polymer, polyaniline (PANI), and experimentally demonstrate its holistic active switching performance. We combine the superior electro-optical response of PANI with the accurate and continuous phase modulation of the Huygens' nanoantennas, and achieve an unprecedented switching performance covering all key requirements for display applications. Our active Huygens' metasurface exhibits a high modulation contrast of 1400% and a diffraction efficiency up to 28%, which is 25 times higher than the previous polymer-based metasurface6,14 and comparable to liquid crystal-based metadevices[9]. The manufacture of the active PANI layer is realized by in-situ polymer growth on the pre-fabricated metasurface. The solid contact between the nanoantennas and the grown PANI facilitates mechanical and electrical durability, enabling a superior cycling duration of over 2000 switching cycles without noticeable degradations. The intrinsic dynamic properties of PANI endow the active metasurface with fast switching speed of 60 fps and virtually hysteresis-free controllability over continuous intermediate states within a low operation voltage range from -0.2 V to +0.6 V. Unlike previous active metasurfaces performing well only in subsets of performance metrics, our electrically active metasurface with holistic switching performance holds great promise towards practical display applications.

References

1. Gu, T., Kim, H. J., Rivero-Baleine, C. & Hu, J. Reconfigurable metasurfaces towards commercial success. *Nat. Photon.* **17**, 48–58 (2023).
2. Li, J. et al. Addressable metasurfaces for dynamic holography and optical information encryption. *Sci. Adv.* **4**, eaar6768 (2018).
3. Ee, H.-S. & Agarwal, R. Tunable metasurface and flat optical zoom lens on a stretchable substrate. *Nano Lett.* **16**, 2818–2823 (2016).
4. Karst, J. et al. Electrically switchable metallic polymer nanoantennas. *Science* **374**, 612–616 (2021).
5. Komar, A. et al. Dynamic beam switching by liquid crystal tunable dielectric metasurfaces. *ACS Photonics* **5**, 1742–1748 (2018).
6. Shcherbakov, M. R. et al. Ultrafast all-optical tuning of direct-gap semiconductor metasurfaces. *Nat. Commun.* **8**, 17 (2017).
7. Wang, Y. et al. Electrical tuning of phase-change antennas and metasurfaces. *Nat Nanotechnol.* **16**, 667–672 (2021).
8. Chen, S. & Jonsson, M. P. Dynamic conducting polymer plasmonics and metasurfaces. *ACS Photonics* **10**, 571–581 (2023).
9. Li, S.-Q. et al. Phase-only transmissive spatial light modulator based on tunable dielectric metasurface. *Science* **364**, 1087–1090 (2019).

Gap-plasmon Resonance based Energy-efficient Electro-tunable Metasurface for Polarization-independent Optical Intensity Modulation

Tanmay Bhowmik, Jegyasu Gupta, and Debabrata Sikdar
Department of Electronics and Electrical Engineering, Indian Institute of Technology Guwahati, Assam 781039, India.
*corresponding author: tanmay18@iitg.ac.in, deb.sikdar@iitg.ac.in

Abstract: Ultra-thin artificially engineered nanoscale scatterers, known as metasurfaces, have gained immense attention in recent years to realize dynamic nanophotonic components by engineering meta-atoms. In this study, we propose an electrically tunable metasurface for optical intensity modulation by leveraging gap-plasmon resonance effect. The presented metasurface exhibits ~15 dB modulation depth at 1550 nm for both TE- and TM-polarized incident wave with an energy-consumption as low as 213 fJ/bit.

Introduction: The metasurfaces can provide enormous degrees-of-freedom to dynamically control the light–matter interactions at the nanoscale [1]. Recently, metasurface-assisted optical modulators find potential candidature to realize active nanophotonic components [2]. Various design strategies have been demonstrated to achieve large modulation depth by incorporating numerous active materials *viz.* ITO (indium-tin-oxide), VO_2 (vanadium dioxide) and graphene [3]. Among these, ITO has gained huge attention due to its astonishing electro-optical properties by external applied bias induced free-carrier accumulation [4]. By leveraging this technique, numerous metasurface based modulators have been proposed *via* exploiting gap-plasmon resonance (GPR) and guided-mode resonance [5]–[7]. However, realization of a polarization-independent modulator that can exhibit a low energy consumption remains a great challenge. In this regard, our design of energy-efficient electro-tunable polarization-insensitive metasurface is crucial to find prospective applications in future nanophotonic systems.

Structural Overview: Our presented metasurface comprises a 2D Ag-nanodisk array (with radius, r = 300 nm and height, h = 100 nm) on cascaded layers of ITO, HfO_2 (Hafnium oxide), and Ag-ground layer, as presented in Fig. 1(a). We leverage GPR-effect combined with free-electron accumulation in ITO under applied bias-voltage, to realize the modulation of light reflected from the metasurface. A side-view of the meta-atom is shown in Fig. 1(b). To study the optical response, a 3D finite-difference-time-domain simulation model has been considered.

Results and Discussion: The permittivity of ITO can be defined by the Drude model, given as [8]:

$$\varepsilon_{\mathrm{ITO}} = \varepsilon'_{\mathrm{ITO}} + j\varepsilon''_{\mathrm{ITO}} = \varepsilon_\infty - \frac{\omega_\mathrm{p}^2}{\omega^2 + \mathrm{j}\Gamma\omega}, \qquad \omega_\mathrm{p} = \sqrt{N\mathrm{e}^2/\varepsilon_0 m_\mathrm{e}^*} \qquad (1)$$

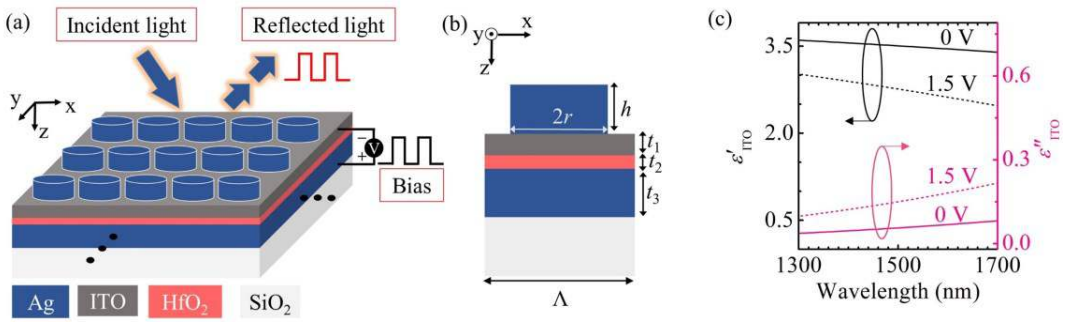


Fig. 1. Schematics of the metasurface presenting (a) perspective view and (b) a unit-cell side view with 700 nm periodicity (Λ) along x- and y axis. Note: t_1 =10 nm, t_2 = 5 nm, and t_3 = 100 nm. Here, the direction of propagation light is along z-axis. (c) The deviation of complex permittivity of ITO inside the accumulation layer for two different biasing conditions.

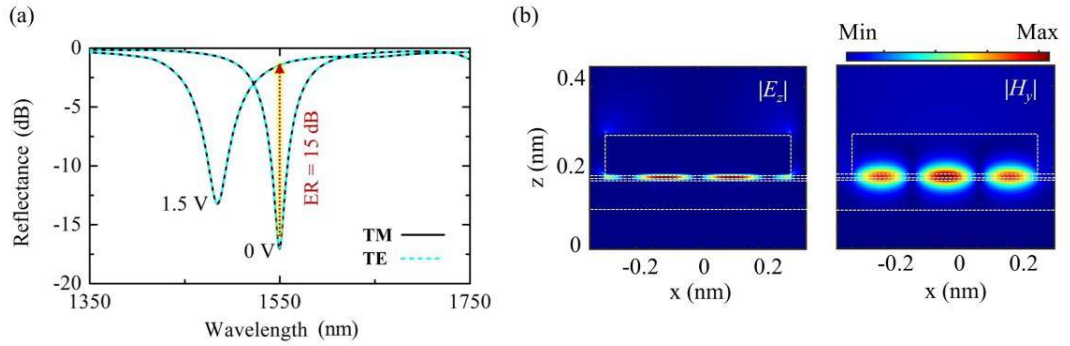


Fig.2. (a) Variation of the resonance dip in reflectance spectrum as a function of bias-voltage for both TM- and TE-polarized light. The arrowed-dotted line denotes the achieved ER = 15 dB at 1550 nm. (b) electric- (E_z) and magnetic-field (H_y) distributions for 0 V bias at 1550 nm.

where high-frequency permittivity, plasma frequency, oscillation frequency, and damping constant are represented by ε_∞, ω_p, ω, and Γ, respectively [1]. Note that ω_p varies with carrier concentration (N) and effective electron mass m_e*. We have considered $N = 6 \times 10^{19}$ cm^{-3} for 0 V bias. With an increase in bias-voltage, the free-electrons of ITO start accumulating at the ITO–HfO_2 interface, leading to a formation of ultra-thin (~3 nm) accumulation region. This leads to a modulation of the complex ITO permittivity, as shown in Fig. 1(c).

With 0 V bias, we observe excitation of third-order GPR-mode at 1550 nm, as shown in Fig. 2, which leads to a dip in the reflectance (R) spectrum. On the contrary, with 1.5 V biasing, the resonance dip gets blue-shifted due to the deviation in the permittivity of the accumulation layer. Thus, we realize an amplitude modulation of reflected beam with an extinction ratio (ER [dB]= $R_{1.5\,V} - R_{0\,V}$) as high as 15 dB while operating between 0 V and 1.5 V biasing states, as presented by the vertical dotted-arrow in Fig.2(a) for both TM and TE polarized plane wave. The electric (E_z) and magnetic (H_y) field distributions at resonance wavelength for 0 V bias are shown in Fig. 2 (b) and 2(c), respectively, where we can clearly observe the excitation of third-order GPR-mode [9].

The per bit energy-consumption of the device can be calculated as, E_b (= $CV^2/4$), where C denotes the total capacitance of the device. Based on electrostatic simulations, we can estimate the unit-cell capacitance (C_{unit}) as ~15 fF/μm^2. Hence, with a total device footprint around 5 × 5 μm^2 (containing 50 meta-atoms), the estimated $C \approx$ 376 fF. Therefore, the estimated energy requirement per bit is $E_b \approx$ 213 fJ/bit for 1.5 V applied bias.

Conclusion: In summary, we have presented an electro-tunable polarization-insensitive metasurface for optical intensity modulation by utilizing the astonishing electro-optic behavior of ITO. For both TM- and TE-modes, the device exhibits an ER of ~15 dB at 1550 nm while marinating a low energy-consumption of 213 fJ/bit.

References

[1] G. Kafaie Shirmanesh, R. Sokhoyan, R. A. Pala, and H. A. Atwater, "Dual-Gated Active Metasurface at 1550 nm with Wide (>300°) Phase Tunability," *Nano Lett.*, vol. 18, no. 5, pp. 2957–2963, May 2018, doi: 10.1021/acs.nanolett.8b00351.

[2] T. Bhowmik and D. Sikdar, "Electrically tunable metasurface for dual-band spatial light modulation using the epsilon-near-zero effect," *Opt. Lett.*, vol. 47, no. 19, 2022, doi: 10.1364/OL.471974.

[3] O. Reshef, I. De Leon, M. Z. Alam, and R. W. Boyd, "Nonlinear optical effects in epsilon-near-zero media," *Nat. Rev. Mater.*, vol. 4, no. 8, pp. 535–551, Aug. 2019, doi: 10.1038/s41578-019-0120-5.

[4] H. W. Lee *et al.*, "Nanoscale Conducting Oxide PlasMOStor," *Nano Lett.*, vol. 14, no. 11, pp. 6463–6468, Nov. 2014, doi: 10.1021/nl502998z.

[5] A. Forouzmand and H. Mosallaei, "Electro-optical Amplitude and Phase Modulators Based on Tunable Guided-Mode Resonance Effect," *ACS Photonics*, vol. 6, no. 11, Nov. 2019, doi: 10.1021/acsphotonics.9b00950.

[6] Q. Chen, S. Song, H. Wang, L. Liang, Y. Dong, and L. Wen, "Ultra-broadband spatial light modulation with dual-resonance coupled epsilon-near-zero materials," *Nano Res. 2020 148*, vol. 14, no. 8, pp. 2673–2680, Dec. 2020, doi: 10.1007/S12274-020-3271-1.

[7] T. Bhowmik, A. K. Chowdhary, and D. Sikdar, "Grating-Assisted Polarization-Insensitive Dual-Mode Spatial Light Modulator Design Using Epsilon-Near-Zero Material," *IEEE J. Quantum Electron.*, vol. 58, no. 4, pp. 1–8, Aug. 2022, doi: 10.1109/JQE.2022.3166653.

[8] T. Bhowmik and D. Sikdar, "Parallel directional coupler based dual-polarization electro-absorption modulator using epsilon near-zero material," *J. Phys. D. Appl. Phys.*, vol. 55, no. 13, p. 135107, Mar. 2022, doi: 10.1088/1361-6463/ac4455.

[9] A. K. Osgouei, A. Ghobadi, B. Khalichi, and E. Ozbay, "A spectrally selective gap surface-plasmon-based nanoantenna emitter compatible with multiple thermal infrared applications," *J. Opt.*, vol. 23, no. 8, p. 085001, Aug. 2021, doi: 10.1088/2040-8986/AC16B7.

Chirality, magnetism, and magnetoelectricity: Separate phenomena and joint effects in metamaterial structures

META 2023, PARIS - FRANCE, JULY 18 – 21, 2023

Magnetoelectric coupling of topological magnets for spintronic and quantum information applications

T. Hirosawa

Aoyama Gakuin University, Japan
*corresponding author: hirosawa@phys.aoyama.ac.jp

Abstract: In multiferroic materials, the magnetic and electric dipole moments are strongly coupled with each other. Here, we propose a novel method to control multiferroic skyrmions via magnetoelectric coupling, which have swirling spin textures characterized by an integer topological charge. Firstly, we consider skyrmions under high-frequency laser irradiation. We find the laser-driven skyrmion motion and laser-controlled magnon band topology. Secondly, we introduce the magnetoelectric magnon-photon coupling by placing skyrmion crystals inside a microwave cavity and discuss potential applications in quantum information.

Magnetic skyrmions are microscopic magnetic vortices with an integer topological charge. They attract much attention as future information carriers in the field of spintronics [1]. Furthermore, they are recently proposed as a qubit, a fundamental building block of quantum computers [2]. In this work, we show that the magnetoelectric effect of multiferroic materials could broaden and enhance the functionality of magnetic skyrmions in spintronics and quantum information science [3,4].

Firstly, we consider the classical spin dynamics of skyrmions under circularly polarized lasers at terahertz frequencies [3]. In multiferroic systems, the coupling between electromagnetic fields and magnets is written as

$$H_{EM}(t) = -\sum_{i}^{N} [\boldsymbol{p}_i(t) \cdot \boldsymbol{E}(\boldsymbol{r}_i, t) + \boldsymbol{m}_i(t) \cdot \boldsymbol{B}(\boldsymbol{r}_i, t)] , \quad (1)$$

where $\boldsymbol{p}_i(t)$ are $\boldsymbol{m}_i(t)$ denote electric and magnetic dipole moments at *i*th site, respectively. The spin-driven electric moment is assumed to arise from the d-p hybridization mechanism as observed in a skyrmion-hosting insulator Cu_2OSeO_3 [5]. Our method combines the numerical simulation of Landau–Lifshitz–Gilbert equation and Floquet-magnus expansion for classical spin systems. We demonstrate that via a delicate balance between the energy injection from a high-frequency laser and dissipation processes, single skyrmions can be driven with a velocity and propagation direction that can be tuned by the laser field amplitude and polarization, respectively. Moreover, we uncover an ultrafast Floquet magnonic topological phase transition in a laser-driven skyrmion crystal.

Secondly, we introduce a theory of magnetoelectric magnon-photon coupling in cavities hosting noncentrosymmetric magnets [4]. Analogously to nonreciprocal phenomena in multiferroics, the magnetoelectric coupling is time-reversal and inversion asymmetric. This asymmetry establishes a means for exceptional tunability of magnon-photon coupling, which can be switched on and off by reversing the magnetization direction. We reveal the electrical activity of skyrmion eigenmodes and propose it for magnon-photon splitting of ``magnetically dark'' elliptic modes. Furthermore, we predict a cavity-induced magnon-magnon coupling between magnetoelectrically active skyrmion excitations. We discuss applications in quantum information processing by proposing protocols for all-electrical magnon-mediated photon quantum gates, and a photon-mediated SPLIT operation of magnons.

References

1. Nagaosa, N. and Y. Tokura, “Topological properties and dynamics of magnetic skyrmions”, Nat. Nanotech., Vol. 8, 899, 2013.
2. Psaroudaki, C. and C. Panagopoulos, “Skyrmion Qubits: A New Class of Quantum Logic Elements Based on Nanoscale Magnetization”, Phys. Rev. Lett., Vol. 127, 067201, 2021.
3. Hirosawa, T., J, Klinovaja, D. Loss, and S. A. Díaz, "Laser-Controlled Real- and Reciprocal-Space Topology in Multiferroic Insulators", Phys. Rev. Lett., Vol. 128, 037201, 2022.
4. Hirosawa, T., A. Mook, J, Klinovaja, and D. Loss, “Magnetoelectric Cavity Magnonics in Skyrmion Crystals", PRX Quantum, Vol. 3, 040321, 2022.
5. Seki, S., X. Z. Yu, S. Ishiwata, and Y. Tokura, “Observation of Skyrmions in a Multiferroic Material”, Science, Vol 336, 198, 2012.

META 2023, PARIS - FRANCE, JULY 18 – 21, 2023

Observation of bulk chiral anomaly in photonic crystal systems

H.W. Jia[1], M.D. Wang[1], and C.T. Chan [1*]

[1]Physics Department, Hong Kong University of Science and Technology, Hong Kong, China
[*]corresponding author: phchan@ust.hk

Abstract: We show that chiral anomaly can be induced in the bulk of 2D photonic crystal systems using the inhomogeneous effective mass or by imposing special boundary conditions. We experimentally characterized the associated transport properties.

We observed chiral Landau levels in 2D Dirac cone systems which carries inhomogeneous effective mass. Chiral zeroth Landau levels are topologically protected bulk states that give rise to chiral anomaly. It is known that 3D Weyl degeneracies can give rise to such chiral Landau levels. We show that such chiral anomaly can be realized using 2D photonic crystal systems that have Dirac point. We introduce an inhomogeneous effective mass in the photonic crystal through breaking local parity inversion symmetries. Zeroth-order chiral Landau levels with one-way propagation characteristics emerged and they are experimentally observed. In addition, the chiral zeroth mode are shown to demonstrate robust transport of the against defects in the system.

We also observed boundary condition induced chiral anomaly bulk states. The most useful property of topological materials is perhaps the robust transport of topological edge modes, whose existence depends on bulk topological invariants. We suggest here that instead of designing the bulk to create topological transport on the edges, we can create topological transport in some bulk modes by imposing certain boundary conditions on the edge. The idea is demonstrated by showing that a topologically trivial 2D hexagonal phononic crystal waveguide bounded by some specific boundaries guarantees the existence of bulk modes with chiral anomaly inside a pseudogap due to finite size effect. We experimentally observed robust valley-selected transport, complete valley state conversion, and valley focusing of the chiral anomaly bulk states. The same concept applies to phononics and electromagnetics.

If time permits, we will discuss some topological transport properties of disordered magnetic photonic crystals.

Acknowledgements: We acknowledge support from Research Grants Council (RGC) Hong Kong and the Croucher Foundation.

META 2023, PARIS - FRANCE, JULY 18 – 21, 2023

Non-reciprocal spin wave beams in thin magnetic films

V. Vlaminck[1,2], L. Temdie1[1,2], V. Castel[1,2], D. Wagle[3], B. Jungfleisch[3], C. Dubs[4], G. Pradan[5], J. Solano[5], H. Majjad[5], R. Bernard[5], Y. Henry[5], D. Stoeffler[5], M. Bailleul[5]

[1] IMT Atlantique, Institut Mines Telecom Atlantique, Microwave Dpt., CS 83818, 29238 Brest, France

[2] Lab-STICC (UMR 6285), CNRS, Technopole Brest-Iroise, CS 83818, 29238 Brest Cedex 3, France

[3] University of Delaware, Dept. of Physics and Astronomy, Newark, Delaware, USA

[4] INNOVENT e.V. Technologieentwicklung, Prussingstrasse 27B, 07745 Jena, Germany

[5] IPCMS – Institut de Physique et Chimie des matériaux de Strasbourg, France

*corresponding author: vincent.vlaminck@imt-atlantique.fr

Abstract: We present several approaches that allows exciting non-reciprocal spin wave beams in thin magnetic films. Using primarily the spin wave spectroscopy techniques performed in both in- and out-of-plane geometries, we show that the spin wave beamforming can be tailored using concepts inspired from optics. We also developed a near-field diffraction model that benchmarks spin wave diffraction in thin films for any geometry, and is readily applicable for future designs of magnon interferometric devices.

Magnonic devices, which take advantage of the versatility of spin waves, are anticipated to be a propitious alternative for efficient signal processing. Spin waves constitute the building blocks of novel wave computing methods such as spectral analysis [1], and neuromorphic computing [2], which are all interference based techniques. Recently, basics concepts of optics applied to spin waves demonstrated the possibility to shape and stir spin wave beams, suggesting prominent performance in particular tasks such as image processing and speech recognition [3]. Along these ideas, we demonstrated that the beamforming in ferromagnetic thin films follows directly the near-field interference pattern of the excitation geometry [4-6].

In this communication, we focus on the beam shaping of spin wave using different methods such as curvilinear antennas, grating of nanomagnets, and sharp constrictions. Firstly, we will introduce our near-field diffraction model, which is applicable for all spin wave modes in thin magnetic films, and serves as a decisive tool to identify proper designs of spin wave beam antennas. Secondly, we will present measurements done via spin wave spectroscopy on various pairs of antenna whose designs allows characterizing the propagation properties in the 2D plane as shown in Fig. 1. Thirdly, using spatially resolved micro-focused Brillouin light spectroscopy, we will show how a sharp constriction in an antenna can directly excite caustic beams in an extended film when the suitable conditions of field and frequency meets an inflection point in the dispersion relation. These findings have important implications for the development of switchable spin wave splitters, passive spin-wave frequency-division demultiplexers, and magnonic interferometry.

This work was supported by the French ANR project MagFunc, the Département du Finistère through the project “SOSMAG”, the U.S. Department of Energy, Office of Basic Energy Sciences, Division of Materials Sciences and Engineering under Award DE-SC0020308, and the Transatlantic Research Partnership, a program

of FACE Foundation and the French Embassy.

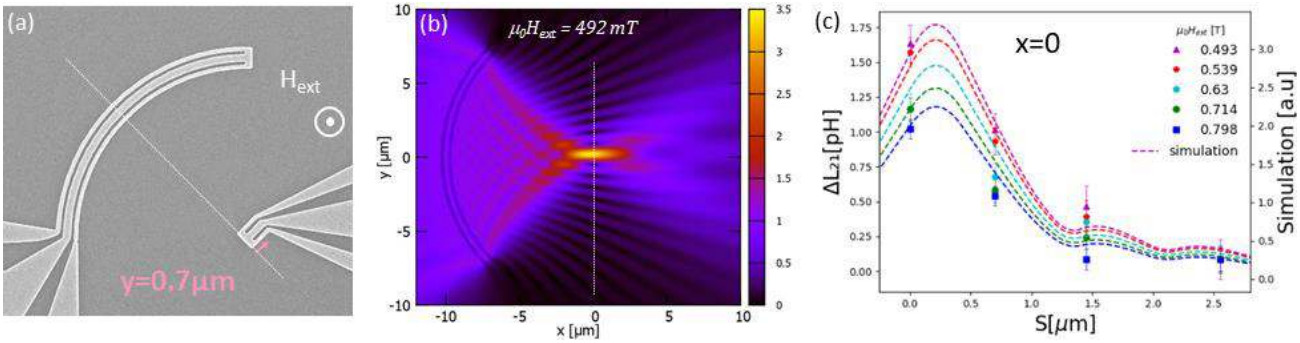


Figure 1: (a) SEM image of a spin wave concentrator. (b) Near-field diffraction simulation for an out-of plane field of 492mT, and a frequency of 8.5 GHz. (c) Discrete mapping of the spin wave intensity in the vicinity of the focal point.

References

1. Papp, A. and Porod, W. and Csurgay, A. I. and Csaba, G. “Nanoscale spectrum analyzer based on spin-wave interference”, Scientific Reports 7, 9245, 2017.
2. Papp, A. and Porod, W. and Csaba, G. “Nanoscale neural network using non-linear spin-wave interference”, Nature Communications 12, 6422, 2021.
3. Albisetti, E and Tacchi, S. and Silvani, R. and Scaramuzzi, G. and Finizio, S.and Wintz, S. and Rinaldi, C. and Cantoni, M. and Raabe, J. and Carlotti, G. and Bertacco, R. and Riedo, E. and Petti, D., “Optically inspired nanomagnonics with nonreciprocal spin waves in synthetic antiferromagnets”, Advanced Materials 32, 1906439, 2020.
4. Loayza, N. and Jungfleisch, M. B. and Hoffmann, A. and Bailleul, M. and Vlaminck, V., “Fresnel diffraction of spin waves”, Physical Review B 98, 144430, 2018.
5. Vlaminck, V. and Temdie, L. and Castel, V. and Jungfleisch, M. B. and Stoeffler, D. and Henry, Y. and Bailleul, M., “Spin wave diffractionmodel for perpendicularly magnetized films”, Journal of Applied Physics 133, 053903, 2023.
6. Temdie, L. and Castel, V. and Dubs, C. and Pradhan, G. and Solano, J. and Majjad, H. and Bernard, R. and Henry, Y. and Bailleul, M. and Vlaminck, V., “High wave vector non-reciprocal spin wave beams”, AIP Advances, 13, 2, 025207, 2023.

Giant Magnetoimpedance Effect in amorphous magnetic materials

A. Zhukov[1,2,3,4*], P. Corte-Leon[1,2,4], M. Ipatov[1,2], J.M. Blanco[2,4] J. Olivera[5] and V. Zhukova[1,2,4]

[1] Dpto. de Polímeros y Materiales Avanzados, University of Basque Country, UPV/EHU, San Sebastian, Spain

[2] Dpto. de Fisica Aplicada, EIG, University of Basque Country, UPV/EHU, San Sebastian, Spain

[3]IKERBASQUE, San Sebastian and Bilbao, Spain

[4] EHU Quantum Center, University of the Basque Country, UPV/EHU, Spain.

[5] Instituto de Física, Facultad de Ciencias, Universidad Autónoma de Santo Domingo, Dominican Republic

[*]corresponding author: arkadi.joukov@ehu.es

Abstract: We studied the factors affecting the giant magnetoimpedance, GMI, effect value and magnetic field dependence in magnetic microwires. Generally, excellent magnetic softness and high GMI effect have been observed in as-prepared Co-rich microwires. Specially designed postprocessing allows also to improve substantially the GMI effect in less expensive Fe-rich microwires. There is a relationship between the optimal frequency for the GMI performance and the wire diameter: to achieve the maximum GMI effect a trade-off between wire dimensions and frequency is required. Considerable GMI effect in thin microwires is observed up to GHz frequency range. A new sensing method involving free space microwave spectroscopy using inclusions of ferromagnetic microwires presenting the GMI effect at GHz frequencies is proposed for the stress, temperature and magnetic field monitoring in carbon fiber containing composites.

Studies of Giant magnetoimpedance, GMI, effect have attracted considerable attention in the last few years owing to it suitability for sensor applications [1,2]. The GMI effect was interpreted in terms of the classical skin effect in a magnetic conductor assuming the dependence of the penetration depth of the AC current flowing through the magnetically soft conductor on the DC applied magnetic field [1-3].

Commonly, the GMI effect is described as the magnetoimpedance ratio, ΔZ/Z, defined as:

$$\Delta Z/Z = [Z(H) - Z(H_{max})] / Z(H_{max}), \quad (1)$$

where H_{max} is the axial DC-field with maximum value up to few kA/m.

Extremely high sensitivity of the GMI effect to applied magnetic field attracted great interest for magnetic sensors applications. Cylindrical shape and high circumferential permeability observed in amorphous wires are quite favorable for achievement of high GMI effect [1-3]. At low frequency range (roughly up to 10 MHz depending on sample diameter/thickness) the GMI effect originates basically from variations of the magnetic penetration depth due to strong changes of the effective magnetic permeability caused by a DC magnetic field [3,4]. However, for GHz frequencies, the magnetization rotation is strongly influenced by the gyromagnetic effect. With increasing the frequency, the GMI peaks are shifted to larger fields where sample is magnetically saturated. At this frequency range strong changes of the sample's impedance have been attributed to the ferromagnetic resonance (FMR)[4,5].

Recently major attention is focused on high frequencies (GHz range) GMI applications owing to the development of thinner magnetically soft materials and recent tendency in miniaturization of magnetic field sensors [4]. Another promising application of GMI effect at GHZ frequencies is use of soft magnetic wire inclusions presenting the GMI effect at GHZ frequency in composites, enabling wireless stresses, temperature and magnetic field monitoring [1,5].

The purpose of this paper is present last results on the GMI effect in soft magnetic wires at high frequencies and explore the application of such microwires in carbon containing tunable composites with thin microwires inclusions.

We measured magnetic field dependences of impedance, Z, and GMI ratio, ΔZ/Z, of

magnetic microwires prepared by the Taylor-Ulitovsky method using specially designed micro-strip sample holder. The sample holder was placed inside a sufficiently long solenoid that creates a homogeneous magnetic field, H. The sample impedance Z was measured using vector network analyzer from reflection coefficient S11, using the expression:

$$Z=Z_0(1+S_{11})/(1-S_{11}), \qquad (2)$$

where Z_0=50 Ohm is the characteristic impedance of the coaxial line [1]. Described technique allows measuring of the GMI effect in extended frequency, *f*, ranges up to GHz frequencies.

As discussed elsewhere [1], for amorphous materials characterized by the absence of magneto-crystalline anisotropy the main sources of magnetic anisotropy are the shape and magnetoelastic anisotropy, K_{me}. The latter is determined by the magnetostriction coefficient, λ_s, and the internal stresses, σ_i, by the relation [1]:

$$K_{me} = 3/2\ \lambda_s\sigma_i, \qquad (3)$$

Nearly-zero λ_s – values can be achieved in the Co_xFe_{1-x} ($0 \leqslant x \leqslant 1$) or Co_xMn_{1-x} ($0 \leqslant x \leqslant 1$) systems at x about 0,03 – 0,08 [1]. Such compositions present better magnetic softness [1]. From ΔZ/Z(H) dependencies measured in Co-rich microwires with vanishing λ_s – values with but with different diameters, d (d=25.6 μm and d=10.8μm) was observed that thicker microwires present higher ΔZ/Z ratio at f=100 MHz. However, at 700 MHz the opposite tendency is observed: higher ΔZ/Z ratio is observed for thinner microwire. Accordingly, the diameter of ferromagnetic metallic nucleus must be mentioned among the other factors relevant for the GMI ratio optimization at a given frequency. The observed behaviour confirms the relationship between the optimal frequency for the GMI performance and the wire diameter: to achieve the maximum GMI effect a trade-off between wire dimensions and frequency is required [1,4]. The diameter reduction must be associated with the increasing of the optimal GMI frequency range [1].

Magnetic softness and GMI of Fe-rich microwires with high and positive λ_s – values can be substantially improved, when Fe-rich microwires were subjected to stress-annealing allowing induction of transverse magnetic anisotropy [1].

The integration of such ferromagnetic microwires into composite materials significantly modify the effective microwave response, making it possible to obtain a new tunable and self-sensing composite material [5]. In the case of the composites containing carbon fibers, the surrounding conductive carbon fibers interfere in the microwave signal generated by ferromagnetic microwires, making it difficult to be measured. However, low frequency magnetic field modulation allows to extract the microwave signal from ferromagnetic microwires inclusions. These results demonstrate the capability for the integration of ferromagnetic microwire inclusions into structural carbon composite parts for wireless monitoring of external stimuli, such as applied stress, temperature or magnetic field.

References

[1] Zhukov, A., Corte-Leon, P., Gonzalez-Legarreta, L., Ipatov, M., Blanco, J.M., Gonzalez, A., Zhukova, V. “Advanced functional magnetic microwires for technological applications”, J. Phys. D: Appl. Phys., vol. 55, 253003, 2002.

[2] Phan, M.-H., Peng, H.-X. “Giant magnetoimpedance materials: Fundamentals and applications”, Prog.Mater. Science vol. 53, 323–420, 2008

[3] Panina L.V. and Mohri, K. “Magneto-impedance effect in amorphous wires”” Appl. Phys. Lett. vol. 65, 1189-1191, 1994.

[4] Ménard, D., Britel, M., Ciureanu, P. and Yelon,A. “Giant magnetoimpedance in a cylindrical conductor,” J. Appl. Phys., vol. 84, 2805–2814, 1998.

[5] Makhnovskiy, D., Zhukov, A., Zhukova, V. and Gonzalez, J. “Tunable and self-sensing microwire composite materials incorporating ferromagnetic microwires,” Advances in Science and Technology, Vol. 54, 201–210, 2008.

META 2023, PARIS - FRANCE, JULY 18 – 21, 2023

Extreme time modulation of material properties and Hawking radiation

J. B. Pendry

The Blackett Laboratory, Department of Physics, Imperial College London, London SW7 2AZ, UK

Abstract:

Experiments demonstrating extremely rapid modulation of the permittivity have been performed by exploiting the enhanced non-linear effects possible in the presence of plasmonic resonances. These experiments measure an extreme rise time by exploiting the analogy between Young's slits which produce diffraction in momentum space, and closely spaced time windows which produce diffraction in frequency space.

I go on to discuss some theoretical consequences of space-time modulated structures. Diffraction gratings moving at trans-luminal velocities contain points where wave and grating velocity are equal. We show these points can be understood as a series of optical event horizons where wave energy can be trapped and amplified, leading to radiation from the quantum vacuum state. We calculate the spectrum of this emitted radiation, finding a quasi-thermal spectrum with features that depend on the grating profile, and an effective temperature that scales exponentially with the length of the grating, emitting a measurable flux even for very small grating contrast. Stimulated emission also takes place under the influence of incident photons, but in contrast to emission from excited atoms, transluminal systems radiate correlated photon pairs.

References

1. Romain Tirole et al, "Double-slit time diffraction at optical frequencies" arXiv:2206.04362, 2023
2. Simon A. R. Horsley and J. B. Pendry, "Time varying gratings model Hawking radiation", ArXiv.2302.04066 2023

Electric-field Control of Magnetism and Topological Spin Textures

Masahiro Sato[1*] and Shunsuke C. Furuya[2]

[1]Department of Physics Chiba University, Chiba, Japan
[2]Department of Basic Science, University of Tokyo, Tokyo, Japan
[*]corresponding author: sato.phys@chiba-u.jp

Abstract: Effects of dc electric fields on nano materials have been investigated, especially, in the fields of multiferroics and spintronics. However, their microscopic theories have not been developed enough. We have theoretically tackled this issue, focusing on Mott insulators in Hubbard-like models under a strong electric field. As a result, we predict that a strong enough electric field can generate spin textures (magnetic skyrmion, soliton, hedgehog, etc.) and phase transitions in thin films of chiral magnets and other magnetic systems.

A dc electric field (or an electric voltage) is one of the few things that human beings can quantitatively apply to materials in order to control their properties. In the last decades, effects of this external field have been actively studied from the viewpoints of both pure and applied physics. Particularly, studies of such effects in spintronics [1] and multiferroics [2] have been largely developed. However, even now it is not easy to quantitatively explain experimental results driven by an electric field in quantum, microscopic level. It means that solid theories for electric-field effects have not been established enough and there are several open issues there.

In recent years, we have developed theories for several effects of dc electric fields applied to nano systems (thin films, one-dimensional systems, etc.) of magnetic Mott insulators, by analyzing Hubbard like models [3,4,5]. Using the second- and fourth-order strong coupling expansion (large-U expansion), we have computed direct- and super-exchange couplings and some magnetic anisotropies like Dzyaloshinskii-Moriya (DM) interaction as a function of the electric field and microscopic parameters (strengths of electron hopping, on-site Coulomb repulsion, Hund coupling, spin-orbit coupling, etc.). From these results, we can predict several magnetic phenomena driven by an electric field in magnets in a quantitative manner.

If our result is used in nano-scale systems with a magnetic order, we conclude that a sufficiently strong electric field can generate several spin textures such as magnetic skyrmions, magnetic soliton lattices, and magnetic hedgehogs (see Fig.1) when we add the field to nano materials in a proper setup. For instance, if we apply both electric and magnetic fields to a thin film of a chiral ferromagnet in a proper way, we can create or annihilate the skyrmion lattice phase as shown in Fig. 2. For quantum spin systems, we predict electric-field induced quantum phase transitions and field-induced spin gaps in several models. Particularly, we show that when we apply a strong electric field to Kitaev honeycomb model [6] (see Fig. 3), the field-induced DM interaction or Gamma anisotropy can create new quantum spin liquid states such as a sort of Chern insulators.

In the conference, we will report these theoretical results of the electric-field effects.

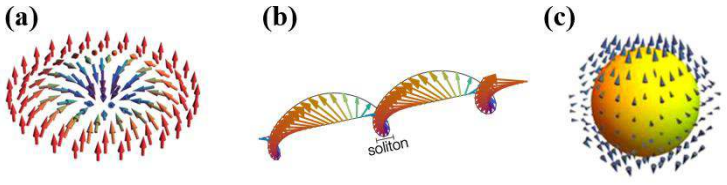


Fig.1: (a) Magnetic skyrmion, (b) magnetic soliton lattice, and (c) magnetic hedgehog. If we apply a strong electric field in proper magnetic systems, we can create these topological spin textures.

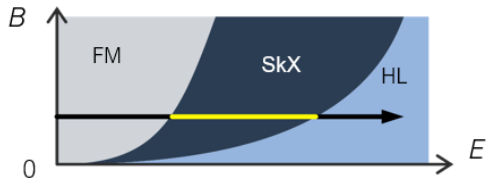


Fig.2: Phase diagram of a film of chiral ferromagnet in the space of an electric field (E) and a magnetic field (B). FM, SkX and HL are respectively forced ferromagnetic, skyrmion lattice, and helical ordered phases.

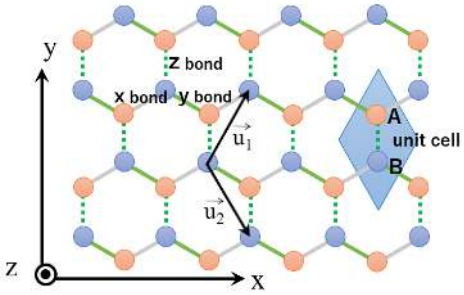


Fig.3: Kitaev honeycomb model [6] whose ground state is a quantum spin liquid state with fermion excitations. This model is exactly solved and regarded as an effective low-energy model for a class of spin-orbit coupled Mott insulators.

References

1. F. Matsukura, Y. Tokura, and H. Ohno, Nat. Nanotech. 10, 209 (2015).
2. H. Katsura, N. Nagaosa, and A. V. Balatsky, Phys. Rev. Lett. 95, 057205 (2005); Y. Tokura, S. Seki, and N. Nagaosa, Rep. Prog. Phys. 77, 076501 (2014).
3. K. Takasan and M. Sato, Phys. Rev. B 100, 060408(R) (2019).
4. S. C. Furuya, K. Takasan, and M. Sato, Phys. Rev. Research 3, 033066 (2021).
5. S. C. Furuya, and M. Sato, arXiv:2110.06503.
6. A. Kitaev, Ann. Phys. 321, 2 (2006); G. Jackeli and G. Khaliullin, Phys. Rev. Lett. 102, 017205 (2009).

META 2023, PARIS - FRANCE, JULY 18 – 21, 2023

Hyperbolic Anisotropic and Bianisotropic Media

M. Durach[1*]

[1]Georgia Southern University, USA
[*]corresponding author: mdurach@georgiasouthern.edu

Abstract: We report on the work of Durach et al. at Georgia Southern University demonstrating that anisotropic and bianisotropic media can be classified as belonging to one of the five classes: non-hyperbolic, hyperbolic, bi-hyperbolic, tri-hyperbolic, and tetra-hyperbolic according to the high-k plane waves in the media. This determines the topology of the Fresnel iso-frequency surfaces, the reflection and transmission properties, resonances, and surface electromagnetic waves in both anisotropic and bianisotropic media.

Bianisotropics, as the electromagnetic research of bianisotropic media is known [1-4], was started in 1888 by investigations of magnetoelectric effects in moving media first observed by Roentgen and Wilson [4,5]. Magnetoelectric crystals were first studied by Landau, Lifshitz, and Dzyaloshinskii [7,8]. To unify the research on moving media and on magnetoelectric crystals, the concept of a bianisotropic medium was coined in 1968 by Cheng and Kong [9] describing the most general case of linear local media. Today, the metamaterial research is central to electromagnetics in all frequency bands [10-13]. Metamaterials feature many properties important for applications, such as superresolution imaging and sensing, optical cloaking, subwavelength optical confinement, guiding, emission rate and directivity control, optical magnetism etc. These properties are mostly due to metamaterials being anisotropic and bianisotropic.

Metamaterials with extreme anisotropy can exhibit both plasmonic and dielectric properties depending on the excitation direction and polarization. Such metamaterials are known as hyperbolic due to formation of high-k states in momentum space where transition between metal and dielectric properties occur, which leads to open Fresnel iso-frequency k-surfaces [14]. Hyperbolic metamaterials find numerous applications [15,16]. In 2016 Kruk et al. [17] experimentally observed magnetic hyperbolic metamaterials, with hyperbolicity due to the extreme anisotropy in the magnetic permeability tensor. In 2017 Tuz, Fedorin and Fesenko [18] predicted that simultaneous extreme anisotropy in dielectric permittivity and magnetic permeability tensors can be observed in non-reciprocal gyrooptic magnetic-semiconductor superlattice resulting in bi-hyperbolic optical phase.

Here we report on the work conducted by Durach et al. at Georgia Southern University [19-24] in relation to the taxonomy of bianisotropic media. In a bianisotropic medium with effective medium parameters tensors $\hat{\epsilon},\hat{\mu},\hat{X},\hat{Y}$ for the dielectric permittivity, magnetic permeability, and magnetoelectric couplings the equation describing the direction of propagation of the high-k modes is given by the *high-k characteristic function*:

$$(\boldsymbol{k}^T\hat{\epsilon}\boldsymbol{k})(\boldsymbol{k}^T\hat{\mu}\boldsymbol{k}) - \left(\boldsymbol{k}^T\hat{X}\boldsymbol{k}\right)\left(\boldsymbol{k}^T\hat{Y}\boldsymbol{k}\right) = 0 \qquad (1)$$

The complete Fresnel wave surface of bianisotropic media can be characterized using the *index of refraction operator method* [22,23,24], follows a quartic dispersion equation, and, therefore, should follow a topological classification into the 5 hyperbolic classes, which include the following topological classes: non-, mono-, bi-, tri-, and tetra-hyperbolic materials. The prefix in the name of each topological class indicates the number of the double cones that the iso-frequency k-surface has in the high-k limit.

In principle, the tri- and tetra-hyperbolic phases require magnetoelectric coupling and in the purely anisotropic regime (i.e. without magnetoelectric coupling) only non-, mono-, and bi-hyperbolic phases can be achieved [22]. However, the formation of tri- and tetra-hyperbolic-like topological phases in media without

magnetoelectric coupling by hybridization of plasmonic and magnetic high-k waves is possible when the double cones due to plasmonic and magnetic anisotropies intersect [23]. This leads to the separation of the 2 double cones of the bi-hyperbolic dispersion into 3 or 4 double cones via anti-crossing whose width is inversely proportional to the magnitude of the k-vector as k tends to infinity.

The properties of the high-k waves topologically determine the parameters of the Fabry-Perot resonances and surface electromagnetic waves (SEWs) in bianisotropic objects [24]. For example, thin subwavelength bianisotropic layers support high-k Fabry-Perot resonances if the bianisotropic material is oriented such that the high-k directions, given by the zeros of high-k characteristic function [Eq. (1)], are close to perpendicular to the interfaces of the layer. As the thickness of the layer increases, the resonance spectrum becomes more populated with lower-k modes of the bulk bianisotropic media. The SEWs appear as arcs in the regions where evanescent waves are supported between the regions with propagating waves [20,21,24], which are topologically separated by the high-k characteristic function [Eq. (1)]. This is in line with the statement that the high-k states separate the parameter space into regions where metal-like and dielectric-like properties of bianisotropic media occur.

Acknowledgements: this work was supported by Georgia Southern University through Faculty Research Council Scholarly Pursuit Awards, COUR Scholars Program, and McNair Scholars Program.

References

1. Kamenetskii, E. O. “Bianisotropics and electromagnetics,” arXiv preprint cond-mat/0601467, 2006.
2. Sihvola, A., I. Semchenko, and S. Khakhomov, Photonics and Nanostructures, Vol. 12, No. 4, 279–283, 2014.
3. Tretyakov, S. A., F. Bilotti, and A. Schuchinsky, METAMATERIALS, 361–363, IEEE, 2016.
4. Mackay, T. G. and A. Lakhtakia, “Electromagnetic Anisotropy and Bianisotropy”, World Scientific, 2010.
5. Roentgen, W. C., Annalen der Physik, Vol. 271, No. 10, 264–270, 1888.
6. Wilson, H. A., Phil. Transactions of the Royal Society of London. Series A, Vol. 204, Nos. 372–386, 121–137, 1905.
7. Landau, L. D. and E. M. Lifshitz, Electrodynamics of Continuous Media. Theoretical Physics, Vol. 8, Fizmatlit, 2005.
8. Dzyaloshinskii, I. E., J. Exp. Theoret. Phys., Vol. 37, 881, 1959 [Soviet Phys. — JETP, Vol. 10, 628, 1960].
9. Cheng, D. K. and J. A. Kong, “Covariant descriptions of bianisotropic media,” Proc. IEEE, 56, 3, 248–251, 1968.
10. Noginov, M. A. and V. A. Podolskiy (eds.), Tutorials in Metamaterials, CRC Press, 2011.
11. Engheta, N. and R. W. Ziolkowski (eds.), Metamaterials: Physics and Engineering Explorations, Wiley & Sons, 2006.
12. Noginov, M. A., G. Dewar, M. W. McCall, and N. I. Zheludev, Tutorials in Complex Photonic Media, SPIE, 2009.
13. Tretyakov, S. A., “A personal view on the origins and developments of metamaterials,” J. Opt., 19, 1, 013002, 2016.
14. D. R. Smith, D. Schurig, Phys. Rev. Lett. 90, 077405 (2003).
15. A. Poddubny, I. Iorsh, P. Belov, Y. Kivshar, “Hyperbolic metamaterials,” Nature Photonics 7, 948-957, 2013.
16. P. Shekhar, J. Atkinson, and Z. Jacob, Nano Convergence 1, 14, 2014.
17. S. S. Kruk et al., Nat. Com. 7(1), 1-7, 2016.
18. V. R. Tuz, I. V. Fedorin, V. I. Fesenko, Optics Letters 42, 4561, 2017.
19. Mulkey, T., J. Dillies, and M. Durach, Optics Letters, Vol. 43, No. 6, 1226–1229, 2018.
20. Durach, M., OSA Continuum, Vol. 1, No. 1, 162–169, 2018.
21. LaBalle, M. and M. Durach, OSA Continuum, Vol. 2, No. 1, 17–24, 2019.
22. Durach, M., R. F. Williamson, M. Laballe, and T. Mulkey, Applied Sciences, Vol. 10, No. 3, 763, 2020.
23. Durach, M., Optics Communications, Vol. 476, 126349, 2020.
24. Durach M., R. Williamson, J. Adams, T. Holtz, P. Bhatt, R. Moreno, F. Smith, PIER, Vol. 173, 53-69, 2022.

Mimicking TMDs by Plasmonic Topological Metasurface with a broken time-reversal symmetry

E. D. Epstein[1,4], **D. Cheskis**[2,4], **Y. Gorodetski**[1,3,4,*]

[1]Electrical and Electronics Engineering Department, Ariel University, 407000, Ariel, Israel
[2]Physics Department, Ariel University, 407000, Ariel, Israel
[3]Mechatronics and Mechanical Engineering Department, Ariel University, 407000, Ariel, Israel
[4]Ariel Photonics Center
[*]Corresponding author: yurig@ariel.ac.il

Abstract

In this paper we present a topological plasmonic metasurface exhibiting spin-dependent distribution in the k-space analogical to the behaviour of the K and K' valleys in 2D materials. We intentionally break the lattice inversion-symmetry by local rotation of the lattice features and analyze the helicity dependence in the isofrequency plane. We attribute the characterisic valleytronic behavior to the local geometric Berry phase induced between the structure sublattices.

Two dimensional (2D) materials have been a subject of great interest for many years, since the discovery of graphene. In recent years the field has developed rapidly with the discovery of many more types of 2D materials such as transition metal dichalcogenide (TMD) monolayers [1]. Due to their unique physical properties and potential applications in a wide range of technologies, much research has been devoted to fabrication methods, together with theoretical and experimental studies of their underlying physics. TMDs are semiconductors of the form MX_2 where M is a transition metal atom such as Mo or W and X is a chalcogen atom such as S, Se or Te. It has been shown that these materials, when cleaved to a monolayer, have a direct band-gap and strong spin-orbit coupling, together with favourable electrical and mechanical properties. With these properties, TMDs such as MoS_2 have a valley degree of freedom, enabling the development of valleytronic devices [2]. They also posses topological phases due to their symmetry giving rise to a non-trivial Berry phase and many TMDs behave as topological insulators (TIs) hosting topologically protected conducting edge states [3]. Because of the great promise of these materials, further understanding of the physical processes is needed. The Berry phase [4] is a phase which is being added

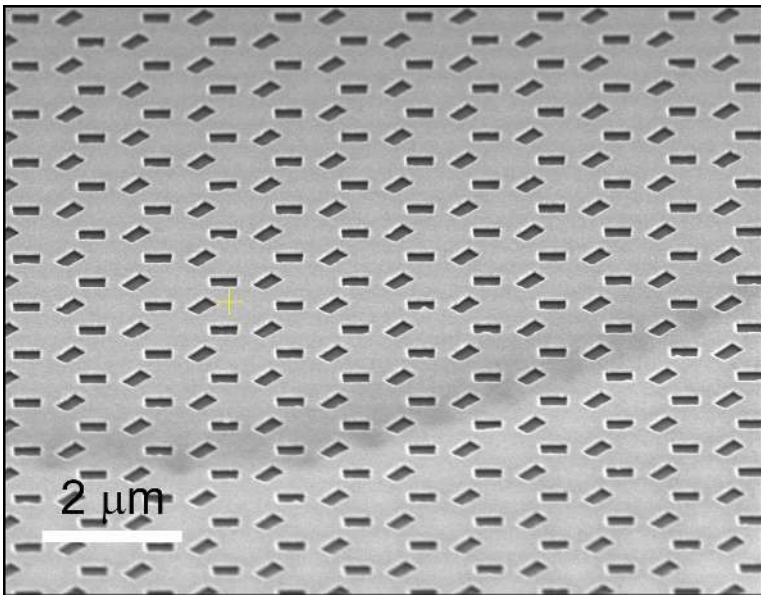


Fig. 1. Scanning electron micrograph of the graphene-like topological structure with broken inversion symmetry.

to an eigenstate after completing a closed loop in the parametric state defining it. It is caused by non trivial topology of the state-space, therefore it is often called a "geometric phase". In points of level degeneracy in the parameter space, topological monopoles appear giving rise to the Berry curvature resulting in parallel transport of the particle's state [5]. In crystals with

Corresponding author: Y. Gorodetski (email: yurig@ariel.ac.il).

broken time-reversal or inversion symmetry the level degeneracy of the chiral eigenstates (quasi-spins) is lifted giving rise to so called Berry curvature which can be compared to appearance of magnetic monopoles. Apparently, a strong magnetic field can be used to break a time-reversal symmetry in originally symmetric structures such as graphene. TMDs such as MoS_2 and WSe_2 also have a hexagonal graphene-like structure, but unlike the latter, the different atoms in the honeycomb unit cell, break inversion symmetry. Therefore, the Berry phase accumulated by Bloch electrons at their Dirac points, which are degenerate in graphene, are of opposite sign making the K and K' valleys distinguishable. The parameter space that defines a state of a polarized light is the Poincaré sphere. A gradual cyclic change of the polarization state induces a measurable and helicity-dependent Pancharatnam-Berry (PB) phase [6]. This phase is equal to the half of the solid angle enclosed by the loop. The PB phase is responsible for the spin-Hall effect of light [5] and has played an important role in numerous applications in optics [7] and plasmonics [8], [9].

Here we consider plasmonic PB phase metasurfaces with a graphene-like structures but with broken inversion symmetry. Plasmonic metasurfaces with subwavelength space-variant anisotropic scatterers have previously been shown to produce the PB phase [10]. By measuring the plasmonic response upon illumination with different spin states in momentum space, we show that the excited plasmonic modes strongly depend on the helicity of the incident light. Explicitly we observe a spin-degeneracy lifting analogical to the behavior of TMD lattices in K and K' valleys while the inversion symmetry is broken here by varying the angle between adjacent apertures in the metasurface. This angle leads to opposite PB phases in K and K' directions resulting in different contrast between the two circular polarizations in both the near and far field. These results are consistent with numerical calculations that we performed.

It seems that an analogy can be drawn between our structures and 2D materials and we believe that this could open many doors to further understanding of TMDs and other topological materials.

REFERENCES

[1] N. Mounet, M. Gibertini, P. Schwaller, D. Campi, A. Merkys, A. Marrazzo, T. Sohier, I. E. Castelli, A. Cepellotti, G. Pizzi, *et al.*, "Two-dimensional materials from high-throughput computational exfoliation of experimentally known compounds," *Nature nanotechnology*, vol. 13, no. 3, pp. 246–252, 2018.

[2] J. R. Schaibley, H. Yu, G. Clark, P. Rivera, J. S. Ross, K. L. Seyler, W. Yao, and X. Xu, "Valleytronics in 2d materials," *Nature Reviews Materials*, vol. 1, no. 11, pp. 1–15, 2016.

[3] F. Wu, T. Lovorn, E. Tutuc, I. Martin, and A. MacDonald, "Topological insulators in twisted transition metal dichalcogenide homobilayers," *Physical review letters*, vol. 122, no. 8, p. 086402, 2019.

[4] M. V. Berry, "Quantal phase factors accompanying adiabatic changes," *Proceedings of the Royal Society of London. A. Mathematical and Physical Sciences*, vol. 392, no. 1802, pp. 45–57, 1984.

[5] K. Y. Bliokh, A. Niv, V. Kleiner, and E. Hasman, "Geometrodynamics of spinning light," *Nature Photonics*, vol. 2, no. 12, pp. 748–753, 2008.

[6] S. Pancharatnam, "Generalized theory of interference and its applications," in *Proceedings of the Indian Academy of Sciences-Section A*, vol. 44, pp. 398–417, Springer, 1956.

[7] C. McDonnell, J. Deng, S. Sideris, T. Ellenbogen, and G. Li, "Functional thz emitters based on pancharatnam-berry phase nonlinear metasurfaces," *Nature communications*, vol. 12, no. 1, pp. 1–8, 2021.

[8] K. Y. Bliokh, Y. Gorodetski, V. Kleiner, and E. Hasman, "Coriolis effect in optics: unified geometric phase and spin-hall effect," *Physical review letters*, vol. 101, no. 3, p. 030404, 2008.

[9] K. Y. Bliokh, "Geometrical optics of beams with vortices: Berry phase and orbital angular momentum hall effect," *Physical Review Letters*, vol. 97, no. 4, p. 043901, 2006.

[10] M. Fox and Y. Gorodetski, "Generalized approach to plasmonic phase modulation in topological bi-gratings," *Applied Physics Letters*, vol. 120, no. 3, p. 031105, 2022.

META 2023, PARIS - FRANCE, JULY 18 – 21, 2023

Creation, Manipulation and Switching of Topological Magnetisms in Spin-Charge Coupled Magnets

Masahito Mochizuki

Department of Applied Physics, Waseda University, Japan
email: masa_mochizuki@waseda.jp

Abstract: We discuss our recent theoretical studies on the dynamical creation, manipulation and switching phenomena of topological magnetisms in a spin-charge coupled magnet described by the Kondo-lattice model.

Dynamical switching, creation, and manipulation of topological magneism, e.g., skyrmions, merons, hedgehogs and Z2 vortices, by application of electromagneic waves (i.e., light and microwave) are subject of intensive study in recent research of condensed-matter physics. In this talk, we discuss our recent theoretical studies on dynamical phenomena and dynamical manipulation of such topological magnetic textures in spin-charge coupled magnets via light or microwave irradiation.

We start with the Kondo-lattice model which describes metallic magnets with localized spins coupled to itinerant electrons via exchange interactions called Kondo coupling. The localized spins are mutually coupled through effective interactions mediated by the conduction electrons. These effective interactions result in emergence of rich magnetically ordered phases including various types of skyrmion crystals as superpositions of multiple magnetic helices. Taking this model, we theoretically demonstrate the microwave-induced skyrmion creations [1], the microwave-induced switching of magnetic topology [2], and the photoinduced 120-degree spin order with topological Z2 vortices [3].

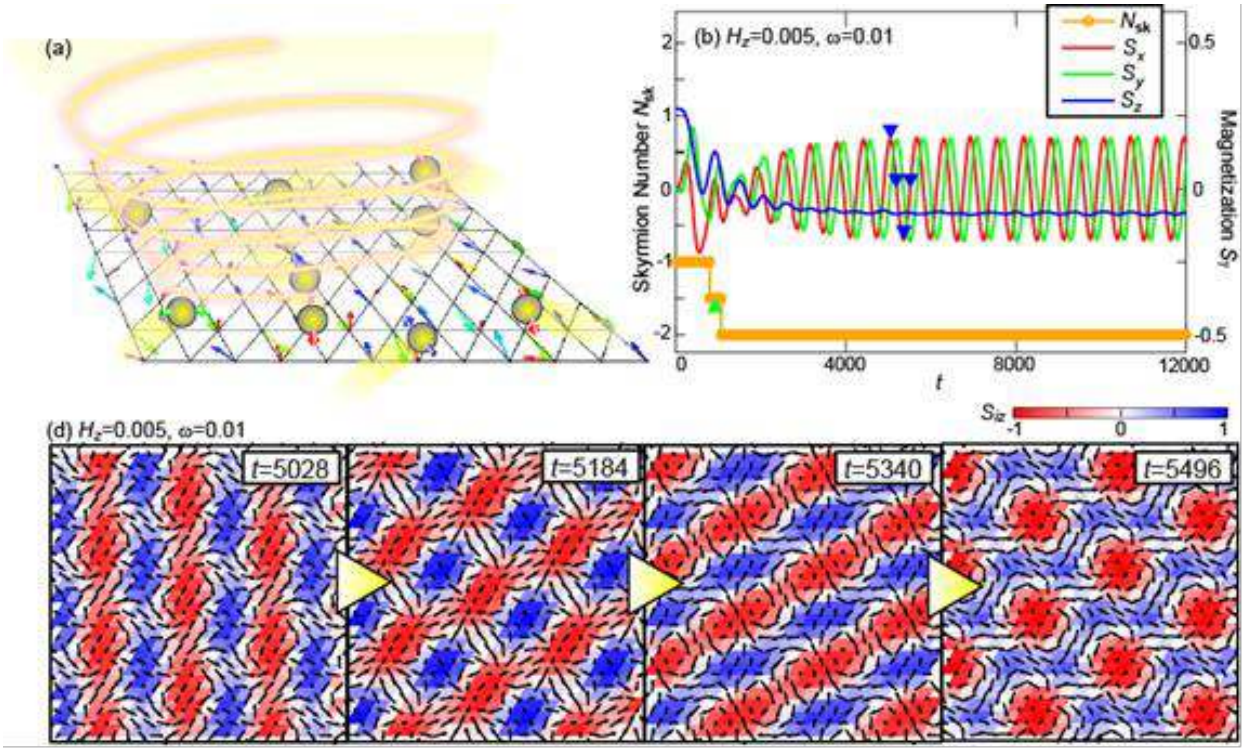


Figure *(a) Schematics of the Kondo-lattice magnet irradiated with electromagnetic waves. (b), (c) Simulated results of the microwave-induced magnetic topology switching.*

Acknowledgements: This work was supported by JSPS KAKENHI (No. 20H00337), JST CREST (No. JPMJCR20T1), and the Waseda University Grant for Special Research Projects (No. 2022C-139).

References

1. T. Inoue, and M. Mochizuki, Phys. Rev. B 105, 144422/1-15 (2022).
2. R. Eto, and M. Mochizuki, Phys. Rev. B, 104, 10442/1-13 (2021).
3. M. Miyake, and M. Mochizuki, Phys. Rev. B 101, 094419/1-9 (2020).

META 2023, PARIS - FRANCE, JULY 18 – 21, 2023

Flat optical devices for 4D light manipulation through orbital angular momentum

A. Ambrosio[1]

[1]Istituto Italiano di Tecnologia, Via Raffaele Rubattino 81, 20134 -Milano Italy
*corresponding author: antonio.ambrosio@iit.it

Abstract: By controlling amplitude, phase and polarization of light, optical metasurfaces have recently allowed spin-to-orbital angular momentum transformations with a single device that are not possible with standard optical components. We will present our most recent results in developing flat optical components for orbital angular momentum manipulation.

In our research activity, we developed a structured light laser capable of producing vortex laser arrays with actively tunable topologies and non-local coupling dictated by the array's topology. The gain medium of our laser has a large transverse cross-section supporting many transverse modes that we forced to organize and form a lattice of a hundred laser beams by inserting a metasurface mask that modulates the phase and amplitude of the field. More specifically, the phase profile was designed to produce vortex beams with an annular intensity profile, useful for communication, microscopy and lithography applications. In our scheme, the optical cavity resulted to be effectively partitioned into two sections—one on either side of the mask— each emitting a laser array imbued with a different topological charge (Orbital Angular Momentum). We achieved spatial coupling of the lasers in the array exploiting dissipative losses in the cavity, making the system stable and coherent. Importantly, in our new laser arrays, the coupling network is not limited to the nearest neighbours as for arrays of Gaussian lasers with no topological charge, but instead can be tailored to mix vortices that are widely separated in the lattice. Although different schemes for generating a single vortex inside a resonator have been demonstrated, we demonstrated the conditions for generating vortex laser arrays in a single cavity, realizing a platform to explore complex topological transformations and collective vortex effects at the source. Furthermore, we demonstrated the robustness of the designed complex light distribution to defects in the metasurface mask. This opens up the possibility of iteratively manipulating structured light parameters and could be used to develop photonic simulators.

References

1. Piccardo, M., de Oliveira M., Toma, Aglieri, V., A. Forbes, A., Ambrosio, A. "Vortex laser arrays with topological charge control and self-healing of defects," Nature Photonics, Vol. 16, 359–365, 2022.

META 2023, PARIS - FRANCE, JULY 18 – 21, 2023

Identifying topology directly from Maxwell's equations: Band structures and Bloch eigenstates not required

A. Cerjan[1*], and T. A. Loring[2]

[1]Center for Integrated Nanotechnologies, Sandia National Laboratories, Albuquerque, New Mexico 87185, USA
[2]Department of Mathematics and Statistics, University of New Mexico, Albuquerque, New Mexico 87131, USA
[*]corresponding author: awcerja@sandia.gov

Abstract: We develop the mathematical framework for determining a photonic structure's topology directly from its real-space description (i.e., Maxwell's equations), without the need to calculate its band structure or Bloch eigenstates. We illustrate the generality of this approach in three different systems, a standard 2D photonic crystal topological insulator, a novel class of gapless topological photonic crystals, and photonic topological crystalline insulators.

Recently, the study of topological structures in photonics has generated significant excitement, due to these systems' ability to realize robust, non-reciprocal chiral edge states and cavity-like confined states that may have applications in both linear and non-linear devices. However, traditional band theoretic approaches can present some challenges for identifying the topology of photonic crystals and metasurfaces due to both fundamental and numerical difficulties. In this talk, I will develop a mathematical framework for determining a photonic structure's topology directly from its real-space description (i.e., Maxwell's equations), without the need to calculate its band structure or Bloch eigenstates [1]. Instead, this framework is based on the photonic system's spectral localizer, which yields a set of local invariants, protected by local gaps, for every symmetry class [2,3]. Using this framework, I will show that non-trivial topology, and associated boundary-localized resonances, can appear in photonic crystals that lack complete band gaps. Finally, I will show how to develop local invariants for topology stemming from a system's crystalline symmetries, which allows for the prediction of spatially localized topological states without the construction of Wannier centers or the calculation symmetry indicator invariants.

Acknowledgements: This work is part-funded by Sandia National Laboratories (SNL). SNL is managed and operated by NTESS under DOE NNSA contract DE-NA0003525.

References

1. A. Cerjan and T. A. Loring, "An operator-based approach to topological photonics," Nanophotonics, Vol. 11, No. 21, 4765–4780, 2022.
2. T. A. Loring, "K-theory and pseudospectra for topological insulators," Ann. Physics, Vol. 356, 383–416, 2015.
3. A. Cerjan and T. A. Loring, "Local invariants identify topology in metals and gapless systems," Phys. Rev. B, Vol. 106, 064109, 2022.

Photocurrent induced by the momentum-space Berry phase in magnetic materials at a microwave frequency

Hiroaki Ishizuka and Akira Harada

[1]Department of Physics, Tokyo Institute of Technology, Japan

*corresponding author: ishizuka@phys.titech.ac.jp

Abstract: The low symmetry of chiral materials realizes electromagnetic phenomena prohibited by symmetry in most materials. For instance, recent studies on Weyl semimetals discovered the photovoltaic effect and magnetoresistance reflecting the Berry phase. Drawing inspiration from the adiabatic charge pump, we discuss that another kind of Berry phase, the Berry phase arising from the magnetic dynamics, induces a photocurrent through a mechanism similar to the adiabatic pump, a topological effect known in driven systems.

Materials with low crystal symmetries, such as a chiral crystal structure, host rich electronic states such as chiral topological semimetal. The optical properties of such topological electrons have attracted attention in recent years as they give rise to unique features reflecting the topological properties, such as unique properties in the circular photogalvanic effect and Fermi arcs. These phenomena are related to the unique distribution of the Berry phase in the momentum space, which characterizes the topological state. The recent discovery of magnetic topological semimetals further enlarged the possibility of realizing novel phenomena arising from the interplay of magnetism and topological electronic state.

To explore the novel photovoltaic response in magnetic semiconductors, we focus on a Weyl semimetal, a topologically nontrivial electronic state often realized in chiral materials. The effective Hamiltonian reads

$$H(t) = \sum_{\boldsymbol{k},\alpha,\beta} c^{\dagger}_{\boldsymbol{k}\alpha} \left[v\boldsymbol{k}\cdot\boldsymbol{\sigma} - \{v_0 k_z + \mu(t)\}\delta_{\alpha\beta} - J_K \boldsymbol{m}(t)\cdot\boldsymbol{\sigma} \right]_{\alpha\beta} c_{\boldsymbol{k}\beta} \qquad (1)$$

where $\sigma = (\sigma_x, \sigma_y, \sigma_z)$ ($\sigma_{x,y,z}$ are the Pauli matrices), $\mu(t)$ is the chemical potential, v is the velocity of the Weyl electron, v_0 ($|v_0| < |v|$) is the velocity of the tilting term, J_K is the Kondo coupling, $c_{k\alpha}$ ($c^{\dagger}_{k\alpha}$) is the annihilation (creation) operator of an electron with momentum $k = (k_x, k_y, k_z)$, and $m(t) = [m_x(t), m_y(t), m_z(t)]$ ($|m(t)| = 1$) is a unit vector parallel to the ferromagnetic moment. The response of magnetic moment to the microwave is calculated using the Landau-Lifshitz-Gilbert equation, and the electronic response to the magnetic dynamics is calculated using a Boltzmann theory taking account of the Berry phase effect [1].

As a demonstration of how magnetic dynamics affects electron transport, we particularly focus on a setup similar to the ferromagnetic resonance, namely, illuminating a ferromagnet using an electromagnetic wave in the microwave to the terahertz regime [Fig. 1(a)]. We show that the precession of the ferromagnetic moment modifies the electronic band, moving the Weyl cone in a circular motion in the momentum space. A similar effect was previously proposed in non-magnetic Weyl semimetals [2,3]. However, the radius of the circular motion is orders of magnitude larger than the non-magnetic semimetals. As a consequence, the circular motion of the Weyl nodes by magnetic precession induces a larger Berry curvature. The Berry phase effect results in a macroscopic current, resulting in a photocurrent by a microwave or the terahertz wave.

From the viewpoint of the Berry phase, this phenomenon is similar to the adiabatic pump proposed by D. J. Thouless [4]. The induction of Berry phase by the circular motion of Weyl cone resembles Faraday's law of electromagnetism, in which the circular electric current induces a magnetic field. Similarly, the circular motion of the Weyl node, a magnetic charge in the momentum space, induces a momentum-space electric field that appears in the adiabatic pump [3].

In a different view, this phenomenon is a spin motive force, an electric current induced by magnetic dynamics. Unlike the conventional spin motive force, however, this phenomenon produces a finite current without a magnetic gradient. The result shed light on a novel material property arising from the Berry phase effect and its potential for spintronics application.

This work is supported by JSPS KAKENHI (Grant Numbers JP18H03676 and JP19K14649).

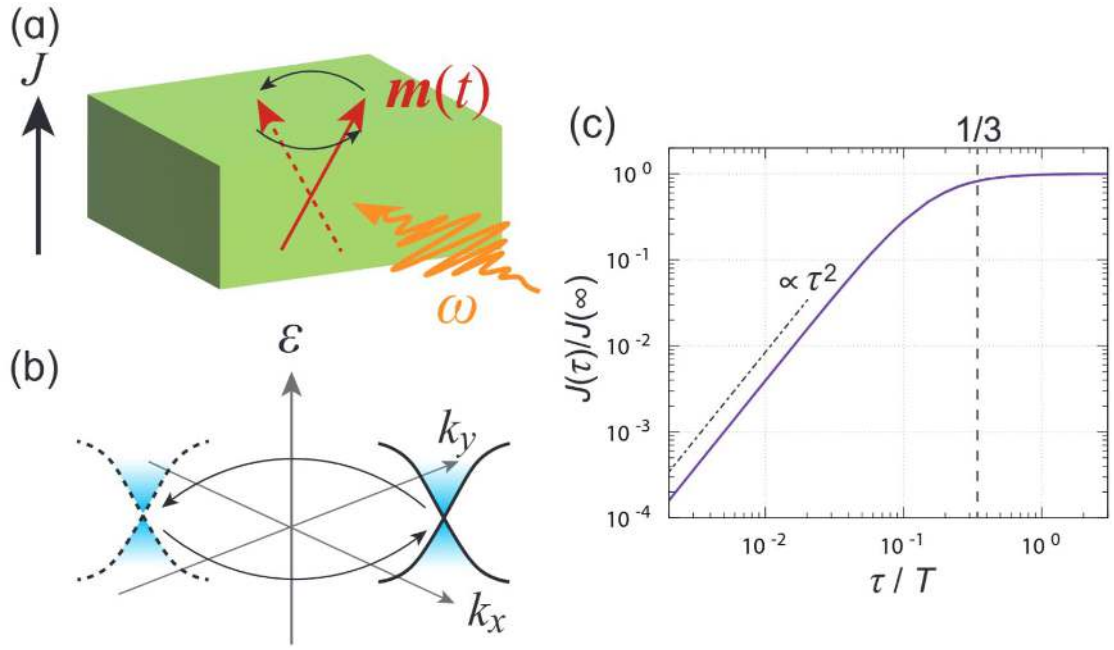


Figure: Photocurrent in Weyl semimetals induced by the microwave. (a) A schematic of the experimental setup. A setup similar to ferromagnetic resonance experiment induces an electric current along the net magnetization direction (noted by J). (b) The deformation of electron bands and the shift of Weyl node. (c) The relaxation time dependence of the induced photocurrent for $\mu/v = 1$, $v_0 / v = 0.1$, and $J_K m / v = 0.1$.

References

1. Harada, A. and H. Ishizuka, "Spin motive force by the momentum-space Berry phase in magnetic Weyl semimetals," arXiv:2201.10180, 2022.
2. Ishizuka, H. *et al.*, "Emergent Electromagnetic Induction and Adiabatic Charge Pumping in Noncentrosymmetric Weyl Semimetals," Phys. Rev. Lett., Vol. 117, 216601, 2016.
3. Ishizuka, H. *et al.*, "Momentum-space electromagnetic induction in Weyl semimetals," Phys. Rev. B, Vol. 95, 245211, 2017.
4. Thouless, D. J. "Quantization of particle transport," Phys. Rev. B. Vol. 27, 6083, 1983.

Circular Polarization in absorption and emission of light by molecules and molecular assemblies

S.C.J. Meskers[1*]

[1]Molecular Material and Nanosystems, Technische Universiteit Eindhoven, The Netherlands
[*]corresponding author: s.c.j.meskers@tue.nl

Abstract: Chiral molecules and materials preferentially absorb and emit one of the circular polarizations of light. Yet the reverse statement is not necessarily true. Recent developments in circular polarization in topologically chiral molecules, supramolecular assemblies and materials with strong light-matter coupling are discussed.

Chiral molecules preferentially absorb and emit one of the two circular polarizations of light. The degree of circular polarization, or dissymmetry factor, g for isotropically oriented molecules

$$g = \frac{4\,\mathrm{Im}(\vec{\mu}\cdot\vec{m})}{|\vec{\mu}|^2 + |\vec{m}|^2} \qquad (1)$$

is determined by the relative magnitude and orientation of the electric (μ) and magnetic (m) transition dipole moments of the transition. The electric dipole represents the translational motion of the electron during the spectroscopic transition while the magnetic dipole cover the rotational, circular aspect of the electron oscillation.[1] An electron oscillating along a helical polymer chain, executes linear and circular oscillatory motion resulting in selective absorption/emission of light.[2] As a recent example we mention helical ladder polymers, where g can be used to gauge the delocalization of the excited state responsible for light emission. The circular differential absorption of light by chiral molecules can be used to make compact detectors for the circular polarization of light.[3]

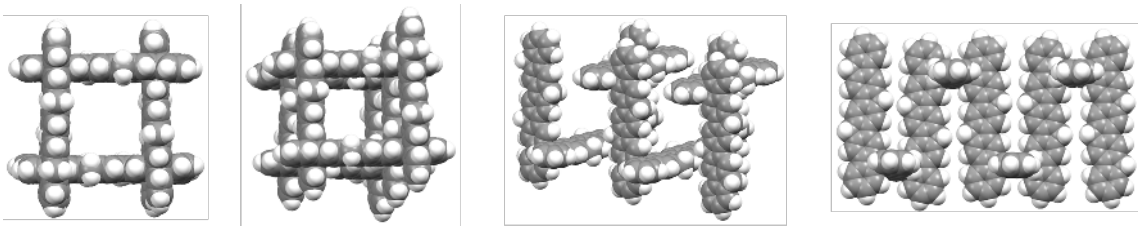


Figure 1. A helical ladder polymer seen from different angles

Interestingly, g reaches its extremal values (±2) for molecules whose electric and magnetic dipoles are equally large and parallel, thus extending the electric-magnetic duality symmetry of the free field to the transition dipoles describing the molecule-light interaction. In general, g is a tensorial property, i.e. it varies with the direction in which the photon is absorbed/emitted. Recent experiments on individual polymer nanoparticles indeed confirmed this anisotropy.[4]

Selective absorption and emission of circular polarized light is not an exclusive property of chiral molecules. Also achiral molecules may show a difference in the interaction with left and right polarized light for a particular

orientation of the molecules with respect to the light beam. In the isotropic limit i.e., when averaging over all orientations this circular selectivity should vanish for achiral systems. Also, molecules that have been magnetized via excitation with circularly polarized light can show circular polarization of their photoluminescence in one direction. For these magnetized systems, the circular polarization should average out when measuring over photon emission directions. A distinguishing feature of these magneto-optical systems is that the time inversion symmetry operation, the sign of the circular polarization should change whereas for truly chiral molecules the circular preference is invariant.

The spectroscopic properties of supramolecular assemblies and materials are obviously more complex than those for isolated small molecules because of the many possible intermolecular interactions. Interestingly, for some systems it is now possible to program the circular polarization in absorption and emission by irradiation with circularly polarized light.[5,6] Understanding the complex electrodynamic couplings within the aggregates can be guided by the notion that the interaction between distant molecules may be described in terms of optics. As an example, the circular polarization of light emitted by an achiral dye in a chiral nematic host material does not originate directly at the site of photon emission but arises gradually as the photon travels out through the chiral matrix. A key challenge are systems with strong coupling the light and matter, where electromagnetic waves acquire mass and molecular electronic excited states wave character.

References

1. Meskers, S.C.J. “Circular Polarization of Luminescence as a Tool To Study Molecular Dynamical Processes,” ChemPhotoChem, Vol. 6, No. 1, e202100154, 2022.
2. Ammenhäuser, R., Klein, P., Schmid, E., Streicher, S., Vogelsang, J., Lehmann, C., Lupton, J. M., Meskers, S. C. J. and Scherf, U. “Circularly Polarized Light Probes Excited-State Delocalization in Rectangular Ladder-type Pentaphenyl Helices”, Angew. Chem. Int. Ed., Vol. 62, No. 29, e202211946, 2023.
3. Liu, L., Wei, Z. and Meskers, S.C.J., “Semi-Transparent, Chiral Organic Photodiodes with Incident Direction-Dependent Selectivity for Circularly Polarized Light,” Adv. Mater., Early view, 10.1002/adma.202209730.
4. Oki, O., Kulkarni, C., Yamagishi, H., Meskers, S.C.J., Lin, Z.-H., Huang, J.-S., Meijer, E.W. and Yamamoto, Y., ”Robust Angular Anisotropy of Circularly Polarized Luminescence from a Single Twisted-Bipolar Polymeric Microsphere,” J. Am. Chem. Soc., Vol. 143, No. 23, 8772 – 8779, 2021.
5. Hou, J., Toyoda, R., Meskers, S.C.J. and Feringa, B. L. “Programming and Dynamic Control of the Circular Polarization of Luminescence from an Achiral Fluorescent Dye in a Liquid Crystal Host by Molecular Motors,” Angew. Chem.Int. Ed.Vol. 61, No. 41, e202206310, 2020
6. Sakaino, H., Broer, D. J., Meskers, S.C.J., Meijer, E.W. and Vantomme, G., “Photo-Imprinting of the Helical Organization in Liquid-Crystal Networks Using Achiral Monomers and Circularly Polarized Light,” Angew. Chem. Int. Ed. Vol. 61, No.15, e202200839, 2022.
7. Kulkarni, C., Curvers, R.H.N., Vantomme, G., Broer, D. J., Palmans, A. R. A., Meskers, S. C. J. and Meijer, E.W., “Consequences of Chirality in Directing the Pathway of Cholesteric Helix Inversion of π-Conjugated Polymers by Light,” Adv. Mater., Vol. 33, No. 2, 2005720, 2021.
8. Liu, L., Wei, Z. and Meskers, S. C. J., “Polaritons in a Polycrystalline Layer of Non-fullerene Acceptor,” J. Am. Chem. Soc. Vol. 145, No. 4, 2040 – 2044, 2023.

Nonreciprocal Magneto-optical Metasurfaces

W. Yang[1], S. Xia[1], J. Qin[1], L. Deng[1] and L. Bi[1*]

[1]University of Electronic Science and Technology of China, China
[*]corresponding author: bilei@uestc.edu.cn

Abstract: Unconstrained by Lorentz reciprocity, nonreciprocal metasurfaces may provide unique functionalities with distinctive characteristics for forward and backward electromagnetic wave propagation. In this work, we report our recent progress on nonreciprocal metasurfaces based on magnetic meta-atoms, demonstrating nonreciprocal phase gradient, magnetic bias free properties and anomalous magneto-optical effects.

Metasurfaces have attracted great research interest recently. Most metasurfaces reported to date follow the Lorentz reciprocity theorem, where the wave propagation characteristics is the same between forward and backward directions. Nonreciprocal metasurfaces unconstrained by Lorentz reciprocity may provide distinctive characteristics between forward and backward propagating waves, which is important for applications in antennas, radomes and full-duplex communications. Magnetic materials are naturally nonreciprocal. However, limited by the weak magneto-optical effect and large biasing magnet, nonreciprocal metasurfaces have rarely been demonstrated using magnetic nanostructures. In addition, the biasing magnetic field make all materials magnetized along the same orientation, causing significant challenge to achieve nonreciprocal phase gradient.

In this work, we report our recent progress on nonreciprocal magneto-optical metasurfaces. We first report Mie resonance enhanced magneto-optical effect in magnetic meta-atoms, showing several new magneto-optical effects such as optical gyromagnetic properties. Then we report a magnetic bias-free, phase-gradient nonreciprocal magneto-optical metasurface in the Ku band. Finally, we discuss the possibility to achieve strong nonreciprocal light propagation in optical frequencies based on high quality factor metasurface designs

First, we report the observation of optical gyromagnetic properties, where the effective permeability, rather than permittivity tensor of the metamaterial is gyrotropic in a Si/Ce:YIG/YIG/SiO_2 all-dielectric magneto-optical metasurface. As shown in Fig. 1, we observe giant transverse TMOKE up to 7 % under s-polarized incidence in the infrared. The effective gyrotropic permeability and permittivity were both retrieved using 4 x 4 transfer matrix methods, demonstrating the bi-gyrotropic nature of the device.

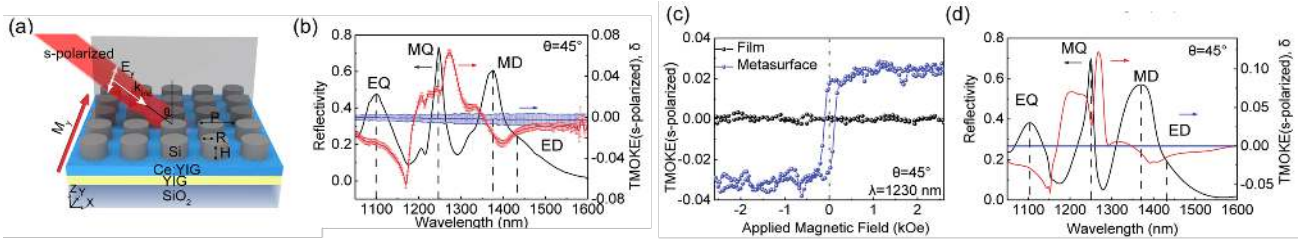


Fig. 1. Reflection spectrum and giant TMOKE for s-polarized incident light. (a) Schematic diagram of the s-polarized TMOKE characterization set-up. (b) Measured s-polarized TMOKE and reflection spectra of the metasurface compared with bare Ce:YIG/YIG thin films. (c) Measured TMOKE hysteresis for the metasurface and the bare MO films at 1230 nm wavelength. (d) Simulated reflection spectra and TMOKE responses of the metasurface for s-polarized light and θ=45° incidence angle.

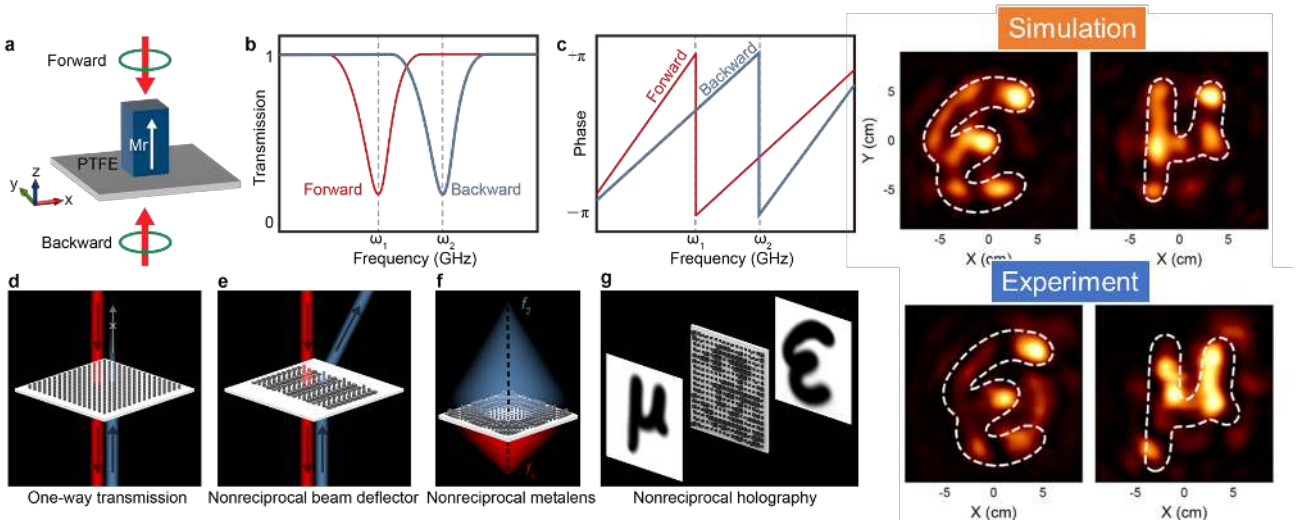


Fig. 2. Self-biased nonreciprocal MO metasurfaces. (a) Operation mechanism of the a self-biased magnetic metaatom. (b) Illustration of nonreciprocal transmission near Mie resonance modes, leading to nonreciprocity in transmission amplitude. (c) Illustration of nonreciprocal transmission and phase near Mie resonance modes. Metasurfaces functions: (d) one-way transmission (e) nonreciprocal beam deflector (f) nonreciprocal metalens and (g) nonreciprocal holography metasurfaces. Also shown are the simulation and experiment results of the nonreciprocal metasurface.

Second, we report a self-biased MO metasurface with nonreciprocal phase gradients, as shown in Fig. 2. Thanks to the large remanent magnetization and coercivity of hexaferrite materials, the biasing magnetic field is not required. Moreover, the magnetization of each meta-atom can be directed along independent directions, facilitation the realization of phase gradient metasurfaces. At ~15 GHz frequency, we experimentally demonstrated unidirectional transmission with an isolation of 9.18 dB and insertion loss of 1.35 dB. We demonstrate a non-reciprocal deflector reaching 0°/29° forward/backward deflection angles. We also demonstrate a nonreciprocal lens with forward focal length of 110 mm and backward focal length of 54 mm. Finally, we showed nonreciprocal holograms with ε and μ patterns in the far-field for forward and backward propagations, respectively.

The authors are grateful for support by National Natural Science Foundation of China (NSFC) (Grant No. U22A2014, No. 51972044, No. 52021001, No. 52102357.), the Ministry of Science and Technology of the People's Republic of China (MOST) (Grant No. 2021YFB2801600.), Sichuan Provincial Science and Technology Department (Grant Nos. 2019YFH0154, 2021YFSY0016 and 99203070) and the Fundamental Research Funds for the Central Universities (Grant No. ZYGX2020J005).

References

1. Tsakmakidis, K. et al. "Breaking Lorentz reciprocity to overcome the time-bandwidth limit in physics and engineering" , Science, Vol. 356, 1260–1264, 2017.
2. Rosenthal, E. I., Chapman, B. J., Higginbotham, A. P., Kerckhoff, J. & Lehnert, K. "Breaking Lorentz reciprocity with frequency conversion and delay" , Phys. Rev. Lett., Vol. 119, 147703, 2017.
3. A. I. Kuznetsov, A. E. Miroshnichenko, M. L. Brongersma, Y. S. Kivshar, B. Luk'yanchuk, "Optically Resonant Dielectric Nanostructures", Science, Vol. 354, 2016.
4. Y. Yang, Kravchenko, II, D. P. Briggs, J. Valentine, "All-Dielectric Metasurface Analogue of Electromagnetically Induced Transparency", Nat. Commun., Vol. 5, 5753, 2014.

Rational Design and Fabrication of UV-Resonant Plasmonic Nanoantennas for Enhanced CD Spectroscopy

B. M. Reinhard[1]

[1]Department of Chemistry and The Photonics Center, Boston University, United States
*corresponding author: bmr@bu.edu

Abstract: Rational electromagnetic optimization strategies for plasmonic aluminum antennas in the ultraviolet range of the electromagnetic spectrum are presented, evaluated, and discussed. Scalable fabrication strategies for UV resonant plasmonic antennas for applications in CD spectroscopy are experimentally evaluated.

Circular dichroism (CD) spectroscopy provides important structural information about biomolecules in solution, but the method suffers from low sensitivity, which makes high sample concentrations necessary. Especially for valuable biomolecules, the need for high concentrations is a significant impediment. One potential strategy to overcome this challenge is in the development of adequate antenna structures that can enhance the CD signal. Electronic CD arises from differential absorption of left and right circularly polarized light. Since molecular electronic transitions lie in the ultraviolet (UV), there is an urgent need for antennas that can enhance electromagnetic fields in this wavelength range. Aluminum supports localized plasmon resonances in the UV which make it an interesting material for UV-resonant plasmon resonances. In this presentation, we will review our recent work in the design, fabrication, and characterization of UV-resonant aluminum nanoantennas.

Although electromagnetic simulations can provide reliable predictions of the performance of a nanoantenna with defined geometry, by themselves they cannot predict the best antenna design. In order to optimize the structure of an antenna design they need to integrated in a rational optimization algorithm. Genetic optimization strategies have shown promise for the rational design of plasmonic nanoantennas.[1–3] Inspired by these studies, we have investigated genetic optimization algorithms to achieve a rational design of aluminum nanoclusters that optimize the performance at a desired wavelength in the UV. The implemented algorithm, the resulting structural predictions, and some general implications for designing UV-resonant nanoclusters will be discussed.

In addition to the optimization of the antenna design through electromagnetic simulations, scalable fabrication strategies for aluminum nanoantennas are necessary for CD application. In this presentation, we will review our strategy for large scale fabrication of defined aluminum nanostructures. At the end of the presentation, we will provide an outlook about how the performance of the current generation of aluminum antennas can be further enhanced.

(1) Forestiere, C.; Pasquale, A. J.; Capretti, A.; Miano, G.; Tamburrino, A.; Lee, S. Y.; Reinhard, B. M.; Dal Negro, L. Genetically Engineered Plasmonic Nanoarrays. *Nano Lett.* **2012**, *12* (4), 2037–2044. https://doi.org/10.1021/nl300140g.

(2) Feichtner, T.; Selig, O.; Kiunke, M.; Hecht, B. Evolutionary Optimization of Optical Antennas. *Phys. Rev. Lett.* **2012**, *109* (12), 127701. https://doi.org/10.1103/PhysRevLett.109.127701.

(3) Feichtner, T.; Selig, O.; Hecht, B. Plasmonic Nanoantenna Design and Fabrication Based on Evolutionary Optimization. *Opt. Express* **2017**, *25* (10), 10828. https://doi.org/10.1364/OE.25.010828.

META 2023, PARIS - FRANCE, JULY 18 – 21, 2023

Nonlocal response of magnons in photonic structures

H. Ishihara*, K. Kato, and T. Yokoyama

Department of Materials Engineering Science, Osaka University, Japan
*corresponding author: ishi@mp.es.osaka-u.ac.jp

Abstract: We develop a nonlocal response theory of magnons and discuss the spatial correlation between microwaves and magnon waves that leads to unconventional effects of magnon-polaritons (MPs). Based on this framework, we theoretically demonstrate anomalous selective coupling of MPs in layered magnetic thin films in the absence and presence of one-dimensional photonic structures. Further, we show the magnonic antenna effect that transcribes the functionality of the thick-layer MPs to the nanoscale thin-layer MPs.

The design of the interaction between fields and matter elementary excitations is crucial for probing quantum properties of materials and field control. The important degree of freedom for controlling the interaction is their spatial structures. However, although both of them have wave characters, the correlation of each spatial structure has not been fully exploited. In the presence of the spatial correlation between both waves, the nonlocal response occurs, namely, the response appears at sites remote from the excited sites through the spatial extension of matter wavefunctions. For example, the excitonic nonlocal response has been extensively studied and unconventional optical effects have been revealed [1][2].

The present study develops the nonlocal theory of magnons, which is an elementary excitation of magnetic materials and demonstrates functional microwave responses of magnetic thin films. A coupled system of magnons and microwaves is known as magnon-polariton (MP) which is drawing attention recently because of its potential applications. In particular, the coupling between microwave cavities and magnons is one of the representative targets of study these days [3]. However, no study has been conducted for designing the coupling of magnons and fields as waves. In our theory, we solve the constitutive equations and Maxwell equations of the magnetic field H and the magnetization M self-consistently. We should note that the induced polarization P appears for photonic structures in the coupled equations of H and M. Since P affects H in the magnetic optical response, we should treat all of E, P, H, and M self-consistently.

One of the theoretical demonstrations is the microwave response of Yttrium-Iron-Garnet (YIG) film with mm thickness (see, Fig. 1(a)). In this case, the single-mode magnon exhibits both level repulsion and level attraction-like effects. The interference between the incident field and radiative field plays an important role, and these spectral behaviors are the intrinsic response of the magnon. On the other hand, all the magnon modes (along the film axis) with different numbers of nodes energetically degenerate. However, the degeneracy is lifted by the coupling between the magnon mode and the same parity Fabry-Perot mode, which enables a selective excitation of MPs. It can be applied to control the spin texture by the spatial structure of the microwave. For the micrometer-scale YIG layer in the one-dimensional photonic crystals (see, Fig. 1(b)), where a single cavity mode couples to the separated magnon modes, the spatial correlation between the magnon and microwave appears even in a μm thin magnetic film by controlling the parity of field mode in the cavity. When the cavity mode has a node at the thin YIG layer, the coupling component to the "traveling" wave can be larger than that of the "standing" wave. By selecting the parameters of dielectric layers and the number of layers, such a situation is achieved, and the level attraction-like behavior is obtained although the MPs do not show the level attraction. Note that the level attraction-like and repulsion-like spectra are controllable by the external magnetic field.

Another demonstration is an antenna effect of magnon [4]. We have proposed a multilayered magnetic structure to demonstrate a large and switchable magnon current in the integrable thin magnetic layer (see, Fig. 2). We consider the nanoscale YIG film and macroscopic YIG substrate separated by a μm dielectric layer. Although nm films are favorable for the fabrication of MP circuit, magnons in such a thin film cannot couple with the field. On the other hand, the process of the circuit with nanoscale depth fabricated only on the surface of the thick film does not work because of MP motion is dominated by the whole thick film. Our proposed structure overcome such difficulties by the mechanisms: "waveguide modes" and a "magnonic antenna effect". The formation of the waveguide mode is attributed to the spatial structure of the dielectric constant, which considerably enhances the light–magnon coupling caused by the spatial interplay between the magnons and microwaves. The magnonic antenna effect, originating from the thickness of YIG and the magnon–magnon interaction (longitudinal field), increases the excited magnon densities in the thin layer and transcribes the functionality of the thick layer MPs to the nanoscale thin layer MPs. By analyzing the dispersion relations of the MPs in this system based on nonlocal response theory, we exhibited an enlarged and switchable magnon current in the nanometer-scale thin film. Moreover, from the radiative damping of MPs, we evaluated the coherence length for the MP transport and the figure of merit for the magnonic antenna effect. The evaluations indicate high efficiency of our proposed structure as magnonic devices.

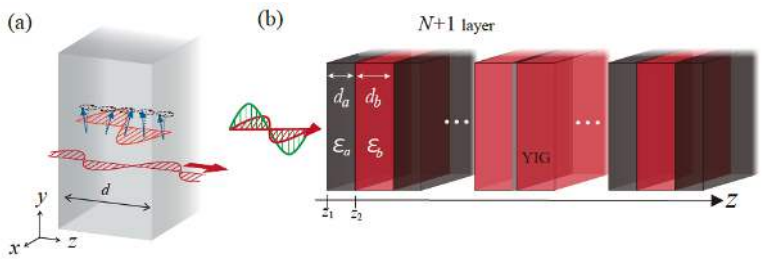


Fig. 1: Schematic figures of our system. (a)The YIG film confines the microwave and becomes the microwave cavity when the incident energy has the Fabry-Perot resonance. The microwave has standing and traveling mode and both of these modes couple with the spin waves. (b) Photonic crystal consisted of periodic N-layer.

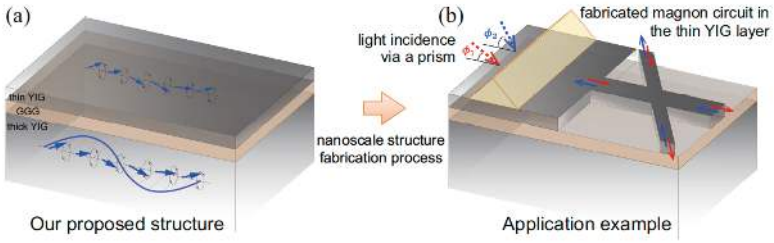


Fig. 2: Schematic of the proposed multi-layer structure for magnonic devices. (a) Proposed structure comprising thin YIG, thin gadolinium gallium garnet (GGG), and thick YIG layers. (b) Imaginary processed structure. [4]

As seen above, the nonlocal description of magnon has revealed novel coupling schemes of magnon-polaritons and their potential applications. We hope this study will stimulate future experimental studies to demonstrate our proposed effects of MPs.

References

1. H. Ishihara, Comprehensive Nanoscience and Nanotechnology 2nd Edition Vol. 4, p323-346 “Nanoscale Optical Response” (Academic Press) 2019.
2. T. Kinoshita, et al., “Synergetic Enhancement of Light-Matter Interaction by Nonlocality and Band Degeneracy in ZnO Thin Films, Phys. Rev. Lett. **122**, 157401 (2019).
3. X. Zhang, C.-L. Zou, L. Jiang, and H. X. Tang, “Strongly Coupled Magnons and Cavity Microwave Photons”, Phys. Rev. Lett. **113**, 156401 (2014).
4. K. Kato, T. Yokoyama, and H. Ishihara, “Functionalized high-speed magnon-polaritons resulting from magnonic antenna effect”, Phys. Rev. Appl. to be published (2023).

Spin Relaxation, Diffusion and Edelstein Effect in Chiral Metal Surface

Y. Suzuki[1*] and Y. Kato[1, 2]

[1]Department of Physics, The University of Tokyo, Japan
[2]Department of Basic Science, The University of Tokyo, Japan
[*]corresponding author: suzuki@vortex.c.u-tokyo.ac.jp

Abstract: Motivated by recent experiments on spin polarization in chiral-crystalline metals, we investigate spin transport at the surface/interface of the chiral metals. Through eigenmode analysis of the Boltzmann equation, we first define spin relaxation time and diffusion length for the spin-splitting surface. We then describe charge–spin interconversion via the Edelstein effect at the interface between the chiral metal and a nonmagnetic metal with finite thickness. We finally show the Onsager's reciprocal relationship at that composite system.

There has been much interest in electron spin generation, detection and transport in surfaces, interfaces, and non-centrosymmetric crystals over the last three decades. Recent observations of current-induced magnetization in chiral-crystalline metals $CrNb_3S_6$, $TaSi_2$ and $NbSi_2$ [1–4] bring a new perspective to these fields of spin transport. The chiral metals display parallel coupling of current and spin, in contrast to the Rashba system where spin and momentum are coupled perpendicularly. Furthermore, two remarkable features of spin transport have been found in the chiral metals: nonlocal spin polarization in the absence of net charge current [3,4], which is recently of theoretical interest [5,6], and highly efficient charge–spin interconversion at the interface [1,3,4]. To describe these two features, it is a fundamental issue to examine spin diffusion length in the chiral metals, as well as to formulate the conversion process between charge current and spin current across the interface.

In this study [7], we describe spin relaxation and diffusion in a two-dimensional metal with anisotropic spin–orbit coupling, as a prototypical model of the chiral metals (Fig. 1 (a)). We also discuss the Edelstein effect and associated charge–spin interconversion at the interface between the two-dimensional system and a nonmagnetic metal with finite thickness (Fig. 1 (b), (c)). Our calculation is based on the Boltzmann transport equation beyond the relaxation time approximation, with which we take account of impurity scattering at the two-dimensional metal.

Our contributions are three-fold: (i) We have defined spin diffusion length for each spin component and for each diffusion direction in the chiral metal surface. Our definition does not rely on spin-dependent chemical

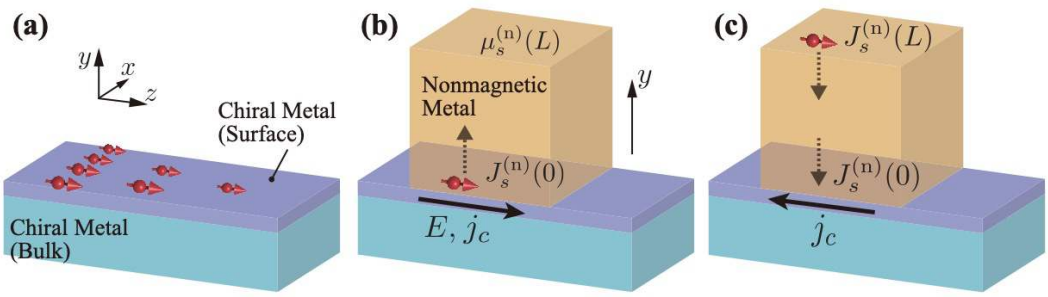


Figure 1. (a) Spin relaxation and diffusion, (b) direct Edelstein effect, (c) inverse Edelstein effect

potential, which is conventionally employed but is ill-defined under strong spin–orbit coupling of the chiral metals. (ii) We have obtained analytical expressions for the conversion efficiencies at the chiral metal interface, from charge current to spin current, and vice versa. Here in accordance with the spin-current-injection experiment, we take account of a finite thickness of the nonmagnetic metal attached on the chiral metal. Such a realistic description has been done for the first time by this study, in contrast to previous theoretical studies on the Edelstein effect [8–11]. (iii) We have developed the Onsager's reciprocity for the Edelstein effect, originally given by Ref. [8] at a surface, to the interface system. Our findings (i)–(iii) will pave the way for the future analysis of the spin transport properties in the bulk chiral metals.

Acknowledgements

We are grateful to Y. Togawa, H. Shishido, J. Ohe, Y. Fuseya, T. Kato, J. Kishine, H. M. Yamamoto, H. Kusunose, E. Saitoh and S. Sumita for fruitful discussions. This work was supported by JSPS KAKENHI Grant Numbers 22J12348, 20K03855, and 21H01032. This work was also supported by Special Project by Institute for Molecular Science (IMS program 21-402). Y.S. is supported by World-leading Innovative Graduate Study Program for Materials Research, Industry, and Technology (MERIT-WINGS) of the University of Tokyo.

References

1. Inui, A., R. Aoki, Y. Nishiue, K. Shiota, Y. Kousaka, H. Shishido, D. Hirobe, M. Suda, J.-i. Ohe, J.-i. Kishine, H. M. Yamamoto and Y. Togawa, "Chirality-induced spin-polarized state of a chiral crystal $CrNb_3S_6$," Phys. Rev. Lett. Vol. 124, 166602, 2020.
2. Nabei, Y., D. Hirobe, Y. Shimamoto, K. Shiota, A. Inui, Y. Kousaka, Y. Togawa and H. M. Yamamoto, "Current-induced bulk magnetization of a chiral crystal $CrNb_3S_6$," Appl. Phys. Lett. Vol. 117, 052408, 2021.
3. Shiota, K., A. Inui, Y. Hosaka, R. Amano, Y. Ōnuki, M. Hedo, T. Nakama, D. Hirobe, J.-i. Ohe, J.-i. Kishine, H. M. Yamamoto, H. Shishido and Y. Togawa, "Chirality-induced spin polarization over macroscopic distances in chiral disilicide crystals," Phys. Rev. Lett. Vol. 127, 126602, 2021.
4. Shishido, H., R. Sakai, Y. Hosaka and Y. Togawa, "Detection of chirality-induced spin polarization over millimeters in polycrystalline bulk samples of chiral disilicides $NbSi_2$ and $TaSi_2$," Appl. Phys. Lett. Vol. 119, 182403, 2021.
5. Tatara, G., "Nonlocality of electrically-induced spin accumulation in chiral metals," J. Phys. Soc. Jpn. Vol. 91, 073701, 2022.
6. Roy, A., F. T. Cerasoli, A. Jayaraj, K. Tenzin, M. B. Nardelli and J. Sławińska, "Long-range current-induced spin accumulation in chiral crystals," npj Comput. Mater. Vol. 8, 243, 2022.
7. Suzuki, Y. and Y. Kato, "Spin Relaxation, Diffusion and Edelstein Effect in Chiral Metal Surface," (submitted). Preprint: arXiv:2212.04202.
8. Shen, K., G. Vignale and R. Raimondi, "Microscopic theory of the inverse Edelstein effect," Phys. Rev. Lett. Vol. 112, 096601, 2014.
9. Zhang, S. and A. Fert, "Conversion between spin and charge currents with topological insulators," Phys. Rev. B Vol. 94, 184423, 2016.
10. Dey, R., N. Prasad, L. F. Register and S. K. Banerjee, "Conversion of spin current into charge current in a topological insulator: Role of the interface," Phys. Rev. B Vol. 97, 174406, 2018.
11. Isshiki, H., P. Muduli, J. Kim, K. Kondou and Y. C. Otani, "Phenomenological model for the direct and inverse Edelstein effects," Phys. Rev. B Vol. 102, 184411, 2020.

META 2023, PARIS - FRANCE, JULY 18 – 21, 2023

Emergent inductance by dynamical ferromagnetic nanostructures

J. Ieda[1*]

[1] Advanced Science Research Center, Japan Atomic Energy Agency, Japan
[*]corresponding author: ieda.junichi@jaea.go.jp

Abstract: Emergent inductance appears universally when magnetization dynamics is coupled with conduction electrons based on a sequential action of spin torque and spinmotive force effects under ac currents. An original version of the emergent inductor using a spiral magnet can be extended to include the spin-orbit coupling effects. A striking common feature among emergent inductors is their size dependence of the effect; the inductance is inversely proportional to the sample cross-sectional area, opening a way for integrating an inductor element.

The interaction of spin current and magnetization dynamics has been a central interest in spintronics for a long time, and it is continuously being developed for better and lower power consumption device applications in the nano-scale size. S-d exchange coupling is a key factor that controls spin-dependent transport and magnetization dynamics in ferromagnetic conductors and ferromagnetic/nonmagnetic interfaces. This is due to the transfer of angular momentum and energy between conduction spin and magnetization texture. These characteristic properties are the basis for spin-transfer torque (STT), and spinmotive force (SMF) [1].

Because the SMF is the spin version of Faraday's law of induction, one can envisage the spin-extension of inductor operation in magnetic nanostructures. This was actually invented by a theoretical proposal of the so-called "emergent inductor" using a spiral magnet [2]. When an electric current flows in a spiral magnet, it stores the energy in the spiral structure formed by the local magnetization via its exchange coupling with conduction electrons. In terms of the Berry phase formalism, where the spin Berry phase is given by the solid angle sustained by magnetization dynamics, the emergent inductance can be thought of as an extension of the dynamical Aharonov–Bohm effect to a spiral magnet where the electromagnetic potential is replaced by a spin-dependent Berry connection generated by the spatial variation of the magnetization. In this presentation, we discuss the basic notion of the emergent inductance based on the well-studied theories of spin torques and spinmotive forces in ferromagnetic nanostructures.

Focusing on the adiabatic processes of STT and SMF, the inductance originating from spiral dynamics can be expressed as the following simple formula [2]:

$$L = \left(\frac{p\hbar q}{2e\sqrt{K}} \right) \frac{l}{A} \tag{1}$$

where p is the spin polarization, $\hbar$ is the Dirac constant, q is the spiral wave number, e is the elementary charge, K is the magnetic hard axis anisotropy constant, l is the spiral magnet length, and A is the spiral magnet cross-sectional area. A prominent feature of emergent inductors is their inductance magnitude dependence on physical size. Contrary to the coil inductance that is proportional to the coil cross sectional area, A ($L \propto A$), the emergent inductance is inversely proportional to the area that the current passes through ($L \propto A^{-1}$). This property opens an innovative avenue for downsizing inductor elements. Soon after the theoretical proposal, the concept was experimentally demonstrated in a centrosymmetric helical magnet, $Gd_3Ru_4Al_{12}$ in low temperatures

(T < 20 K) [3] where the inductance was reported comparable to that of a commercial one (~ 400 nH), but in a volume about a million times smaller. Theoretical studies have shown that two excitation modes of a spiral magnetic texture, namely, its translational displacement and rotation of the spiral plane, contribute to emergent inductance with opposite signs [4,5]. This may explain the negative inductance observed in the experiment [3]. Another observation of emergent inductance has been achieved in YMn_6Sn_6 at room temperature [6]. The discovery of emergent inductance has arisen a revision of electronics theories, and we are at the beginning of a new chapter exploring inductance by quantum mechanical mechanisms.

The concept of the emergent inductor is not limited to original spiral magnetization dynamics. In fact, a novel inductance of a spin-orbit coupling (SOC) origin was proposed [7] where an SOC stores the energy in itself and mediates the energy conversion with the electric energy. The spin–orbit inductance results from the time derivative of the Aharonov–Casher phase in magnetic materials, where the Berry connection originating from SOCs depends on the electron's momentum and spin. The spin–orbit inductance can be formulated based on a dynamical spin Berry phase acquired by an electron moving in arbitrary magnetic textures in the presence of SOCs. Exploring spin–orbit inductance with spatially uniform magnetization is of particular interest, where the other inductance mechanisms are ruled out, and it provides nearly frequency independent inductance, except in the vicinity of the ferromagnetic resonance frequency ~1–10 GHz. This can resolve the issue related to a limitation in the operating frequency in the previous experiments [3,6] reflecting the dynamics of spiral magnets.

A next issue to be addressed is the quality (Q-) factor of emergent inductors, defined as $Q = |\omega L/R|$, where R denotes the sample resistance leading to the energy dissipation. Because both L and R scale with the sample size in the same way, miniaturization does not improve the Q-factor. To tackle this problem, new material combinations including topological and ferromagnetic insulators are currently under investigation [8].

This work is done in collaboration with Y. Yamane and Y. Araki and is financially supported by JSPS KAKENHI (No. 19H05622).

References

1. Maekawa, S. *et al.* Eds, *Spin Current*, 2nd ed., Oxford University Press, Oxford, 2017.
2. Nagaosa, N. "Emergent inductor by spiral magnets," Jpn. J. Appl. Phys., Vol. 58, 120909, 2019.
3. Yokouchi, T. *et al.*, "Emergent electromagnetic induction in a helical-spin magnet," Nature, Vol. 586, 232-236, 2020.
4. Ieda, J. and Y. Yamane, "Intrinsic and extrinsic tunability of Rashba spin-orbit coupled emergent inductors," Phys. Rev. B, Vol. 103,. L100402, 2021.
5. Kurebayashi, D. and N. Nagaosa, "Electromagnetic response in spiral magnets and emergent inductance," Commun. Phys., Vol. 4, 260, 2021.
6. Kitaori, A. *et al.*, "Emergent electromagnetic induction beyond room temperature," Proc. Natl. Acad. Sci. U.S.A., Vol. 118, e2105422118, 2021.
7. Yamane, Y., S. Fukami, and J. Ieda, "Theory of emergent inductance with spin-orbit coupling effects," Phys. Rev. Lett., Vol. 128, 147201, 2022.
8. Araki, Y. and J. Ieda, "Emergence of inductance and capacitance from topological electromagnetism," arXiv:2211.14007v1, 2022.

META 2023, PARIS - FRANCE, JULY 18 – 21, 2023

Topological textures and CP^2 Skyrmion crystals in quantum spin-nematics

Yutaka Akagi*

The University of Tokyo, Japan
*corresponding author: yutaka-akagi@g.ecc.u-tokyo.ac.jp

Abstract: Recently, topological spin textures such as Skyrmions have attracted scientific and technological interest. However, in most studies on topological spin textures, magnetic moments are approximated as O(3) vectors. This simplification neglects key features of quantum magnets. Thus, we develop the theoretical methods in models with spin–1 moments for quantum spin-nematics. Using the methods, we have found that CP^2 Skyrmion crystals and their relatives are realized in a new type of model for quantum spin-nematics, having a generalized Dzyaloshinskii-Moriya interaction.

Topological excitations (textures) play an important role in both conventional liquid crystals, i.e., nematic phase, and in spin systems. However, little is known about their role in quantum spin nematic phases (quadrupolar phases) [1,2] which are invisible to conventional probing techniques due to the absence of dipole long-range order. Thus, we consider the topological excitations in these nontrivial phases. The model is the spin-1 bilinear biquadratic (BBQ) model on the triangular lattice [3,4]. Using homotopy analysis and a numerical optimization technique, we identify a new family of Skyrmions with dipole moment at a particular point in parameter space, in which the system has global SU(3) symmetry. The Skyrmion with higher topological charges spontaneously decays into “elementary” Skyrmions with emergent interactions [5]. We have also found nontrivial fine structures of point-like defects in spin-nematics, which induce dipole moments as well [6]. In addition, we have examined the thermodynamic properties and dynamics of $\mathbf{Z}_2$ point-like defects in ferro-nematic order by using a molecular dynamics technique based on the framework of a u(3) algebra which we have developed [7].

Recently, through interdisciplinary collaboration (see Collaborators below), we have numerically found that CP^2 Skyrmion crystals (spin nematic Skyrmion crystals) possessing both dipole and quadrupole moments are stabilized as the ground state in SU(3) chiral magnets [8], which are SU(3) magnets endowed with a generalized Dzyaloshinskii-Moriya interaction [9]. The new type of model for quantum spin-nematics could be implemented using spin-1 spinor Bose-Einstein condensates (BECs) with an artificial spin-orbit coupling [10] in an optical lattice. We have investigated the ground state structure of SU(3) chiral magnets for wide parameter regions and found various exotic phases, for example, CP^2 Skyrmion crystal, CP^2 Skyrmionium crystal, and CP^2 Helical phase [11]. We have clarified the properties of these nontrivial phases using several physical quantities like energy, topological charge, and structure factors, mapping out the phase diagram.

Collaborators

The works on the dynamics of topological excitations have been done in collaboration with Rico Pohle (UTokyo), Kimberly Remund (OIST), Judit Romhányi (UC-Irvine), and Nic Shannon (OIST). The interdisciplinary studies have been done in collaboration with high-energy physicists, Yuki Amari (UTokyo, JINR, Tokyo Univ. of Sci., Toyama Prefectural Univ., Keio Univ.), Nobuyuki Sawado (Tokyo Univ. of Sci.), Sven Bjarke Gudnason (Henan Univ.), Muneto Nitta (Keio Univ., International Institute for $SKCM^2$, Hiroshima Univ.), and Yakov Shnir (JINR, Univ. of Oldenburg).

Acknowledgements

The works were supported by JSPS KAKENHI Grants No. JP17K14352, No. JP18H01217, No. JP20K14411, No. 22H01221, and JSPS Grant-in-Aid for Scientific Research on Innovative Areas “Quantum Liquid Crystals” (KAKENHI Grant No. JP19H05825, No. JP20H05154 and No. JP22H04469). Y. Akagi is supported by JST PRESTO Grant No. JPMJPR2251. The works were also support by the WPI program “Sustainability with Knotted Chiral Meta Matter ($SKCM^2$)” at Hiroshima University, the National Natural Science Foundation of China (Grants No. 11675223 and No. 12071111), and the Ministry of Education of Russian Federation, project FEWF-2020-0003. Numerical calculations were carried out using HPC facilities provided by OIST, the Supercomputer Center of the Institute of Solid State Physics, The University of Tokyo, and the “GOVORUN” cluster supported by the LIT, JINR.

References

1. B. A. Ivanov, R. S. Khymyn, and A. K. Kolezhuk,
   “Pairing of Solitons in Two-Dimensional S=1 Magnets,”
   Phys. Rev. Lett. **100**, 047203 (2008).
2. J. Takano and H. Tsunetsugu,
   “Theory of Impurity Effects on the Spin Nematic State,”
   J. Phys. Soc. Jpn. **80**, 094707 (2011).
3. A. Lauchil, F. Mila, and K. Penc,
   “Quadrupolar Phases of the S=1 Bilinear-Biquadratic Heisenberg Model on the Triangular Lattice,”
   Phys. Rev. Lett. **97**, 087205 (2006).
4. H. Tsunetsugu and M. Arikawa,
   “Spin Nematic Phase in S=1 Triangular Antiferromagnets,”
   J. Phys. Soc. Jpn. **75**, 083701 (2006).
5. H. T. Ueda, Y. Akagi, and N. Shannon,
   “Quantum solitons with emergent interactions in a model of cold atoms on the triangular lattice,”
   Phys. Rev. A. **93**, 021606(R) (2016).
6. Y. Akagi, H. T. Ueda, Y. Amari, and N. Shannon, in preparation.
7. K. Remund, R. Pohle, Y. Akagi, J. Romhányi and N. Shannon,
   “Semi-classical simulation of spin-1 magnets,”
   Phys. Rev. Research **4**, 033106 (2022).
8. Y. Amari, Y. Akagi, S. Gudnason, M. Nitta, Y. Shnir,
   “CP^2 skyrmion crystals in an SU(3) magnet with a generalized Dzyaloshinskii-Moriya interaction,”
   Phys. Rev. B **106**, L100406 (2022).
9. Y. Akagi, Y. Amari, N. Sawado, and Y. Shnir,
   “Isolated skyrmions in the CP^2 nonlinear sigma model with a Dzyaloshinskii-Moriya type interaction,”
   Phys. Rev. D **103**, 065008 (2021).
10. G. Juzeliūnas, J. Ruseckas, J. Dalibard,
    “Generalized Rashba-Dresselhaus spin-orbit coupling for cold atoms,”
    Phys. Rev. A **81**, 053403 (2010).
11. Y. Amari, Y. Akagi, S. Gudnason, M. Nitta, Y. Shnir, in preparation.

META 2023, PARIS - FRANCE, JULY 18 – 21, 2023

Nonreciprocal charge transport and phase transitions in noncentrosymmetric superconductors

A. Daido[1] * and Y. Yanase[1]

[1]Departrment of Physics, Kyoto University, Japan
*corresponding author: daido@scphys.kyoto-u.ac.jp

Abstract: Nonreciprocal phenomena are attracting attention as the novel functionality and probes of noncentrosymmetric materials. In this talk, we discuss nonreciprocal charge transport and phase transitions in noncentrosymmetric superconductors under magnetic fields. We reveal the close connection of nonreciprocal phenomena and finite-momentum superconductivity. The obtained results show that nonreciprocal charge transport offers a versatile probe of the finite-momentum superconductivity.

Recent studies have revealed that noncentrosymmetric materials show various nonreciprocal phenomena such as the directional resistance (magnetochiral anisotropy), nonlinear Hall effect, and superconducting diode effect. They are appealing not only for engineering purposes but also as novel probes of noncentrosymmetric systems and are among the hallmarks of modern condensed matter physics. Further study of nonreciprocal phenomena would shed light on unprecedented phenomena in noncentrosymmetric materials. In particular, noncentrosymmetric superconductors offer a fertile ground to explore exotic physical phenomena arising from the interplay of nonreciprocity and macroscopic quantum coherence of Cooper pairs.

In this talk, we theoretically study the intrinsic nonreciprocity in the charge transport and phase diagrams of noncentrosymmetric superconductors under magnetic fields. In such systems, it is known that Cooper pairs spontaneously acquire a finite center-of-mass momentum in equilibrium because of the magnetoelectric coupling of electrons due to the Rashba spin-orbit coupling. We discuss the fingerprint of finite-momentum Cooper pairs in nonreciprocal charge transport such as the directional resistance, nonlinear Hall effect, and superconducting diode effect as well as the phase diagrams under the supercurrent injection [1,2,3]. The obtained results uncover the novel aspect of finite-momentum superconductors and show that nonreciprocal charge transport offers a versatile probe of the finite-momentum superconductivity.

This work was supported by JSPS KAKENHI (Grant Nos. JP18H01178, JP18H05227, JP20H05159, JP21K13880, JP21K18145, JP22H01181, JP22H04476, JP22H04933) and SPIRITS 2020 of Kyoto University.

References

1. Akito Daido and Youichi Yanase, Phys. Rev. B **106**, 205206 (2022).
2. Akito Daido and Youichi Yanase, to be submitted.

While SDE is a powerful probe of the finite-momentum superconductivity, it works only in small-width samples to capture the intrinsic contribution. Unfortunately, this condition is not satisfied in general thin-film samples, including the candidate finite-momentum superconductors known so far.

Considering the great interest of the research community in finite-momentum superconductivity, versatile smoking-gun probes is highly desired. To resolve this issue, we pay renewed attention to the nonreciprocal paraconductivity, the nonreciprocal transport of Cooper pairs thermally excited above the superconducting transition temperature. The focus of the pioneering works has been on the magnetochiral anisotropy at low magnetic fields, to explain the experiment in MoS_2 [R. Wakatsuki, *et al*., Sci. Adv. **3**, e1602390 (2017)]. Therefore, the previous formulation is not applicable to moderate and high magnetic fields, and finite-momentum superconductors are out of its scope.

the connection of nonreciprocal phenomena and intrinsic properties of superconducting states has not been fully uncovered, offering

Indeed, it has been pointed out that SDE can detect finite-momentum superconductivity[1] , which has been sought after for a long time.

predict the colossal nonreciprocal charge transport of finite-momentum superconductors, by developing a generalized formulation of the nonreciprocal paraconductivity. The formulation is applicable to general finite-momentum superconductors, while we mainly study the finite-momentum superconductivity in noncentrosymmetric superconductors (called the helical superconductivity). By studying the Rashba-Zeeman superconductors in two dimensions, we elucidate that both the longitudinal and Hall nonlinear conductivity are enhanced by several orders of magnitude under the moderate- and high-magnetic fields compared to the low-magnetic-field region which has been studied in previous works. The enhancement of nonreciprocal charge transport is attributed to the development of the finite-momentum Cooper pairs. It naturally follows from the obtained results that finite-momentum superconductors in centrosymmetric materials also show huge nonreciprocal transport once the symmetry-protected degeneracy of Cooper-pair momenta is lifted by external fields. We also study the case of quasi-two-dimensional superconductors by deriving a Kubo-type formula of the nonreciprocal paraconductivity. The formula can describe general situations including the system under orbital magnetic fields as well as with multiple pairing channels. It turns out that the huge nonreciprocal charge transport is also obtained in the presence of the cyclotron motion of Cooper pairs. Thus, nonreciprocal charge transport is established as powerful probes of finite-momentum superconductivity regardless of the sample dimensionality.

The enhanced nonreciprocity is accompanied by the development of finite-momentum Cooper pairs and gives strong evidence of finite-momentum superconductivity when observed in experiments. Thus, we believe that this work meets the criteria for publication in Physical Review Letters based on the promising impacts on a broad readership.

META 2023, PARIS - FRANCE, JULY 18 – 21, 2023

Ultrathin magneto-optical devices based on all-dielectric metasurfaces

Y. Ota[1*], S. Gao[2] and S. Iwamoto[2]

[1]Department of Applied Physics and Physico-Informatics, Keio University, Japan
[2]Research Center for Advanced Science and Technology, The University of Tokyo, Japan
[*]corresponding author: ota@appi.keio.ac.jp

Abstract: Magneto-optical (MO) devices play a key role in introducing nonreciprocity in optical systems, but tend to be bulky due to weak MO effects available in the optical regime. In this talk, we discuss our recent efforts to design of all-dielectric MO metasurfaces toward ultrathin MO devices. We found that large Faraday rotations and high light transmittance can be realized in MO metasurfaces that are much thinner than the operating wavelength.

Free-space magneto-optical (MO) devices, such as polarization-based Faraday isolators, are indispensable for regulating the flow of light beams in optical systems. They tend to be bulky to gain long-enough interaction lengths to compensate for the weak MO effects in transparent MO materials in the optical domain. For example, Faraday rotators based on yttrium iron garnets (YIG) or their derivatives, which are the materials of the first choice at the telecommunication wavelengths, typically require a few hundred micrometers or longer to attain the required 45° non-reciprocal polarization rotation.

Downsizing MO devices has been of great interest for the last few decades. Early trials employed optical resonances in one-dimensional photonic crystals[1] and plasmonic structures[2]. However, the measured Faraday rotation angles (θ_f) and transmittance (T) were insufficient for practical use. Recently, all-dielectric metasurfaces have emerged as an alternative route to realize ultrathin Faraday rotators[3-5]. The numerical simulation in the report[3] demonstrated a large θ_f of 7° at a telecom wavelength with a 260-nm-thick metasurface based on bismuth iron garnet (BIG). However, this study did not consider the influence of fabrication imperfections, which could be inevitable in this material system considering the notorious difficulty of nanopatterning of iron garnets[6]. More recently, a novel design of an ultrathin Faraday rotator based on a silicon metasurface place on a plane cerium-substituted YIG film has been proposed and experimentally demonstrated[7]. This approach allows for avoiding the direct nanopatterning of the iron garnet layer. However, the reported value of θ_f was less than 1° even in the design, which will limit the application of the device.

In this talk, we will discuss our recent efforts to design ultrathin Faraday rotators based on all-dielectric MO metasurfaces. First, we examined the influence of fabrication imperfections on the MO metasurface design reported previously[3] (see Fig. 1(a)). We found rapid degradation of θ_f and light transmittance when introducing tilted sidewalls in the constituent BIG microresonators (Figs. 1(b) and (c)). As a result, a figure of merit of the device, defined as $\theta_f T^{1/2}$, also exhibits significant reduction by reclining the sidewall just by 10°. Interestingly, we found that asymmetric cladding of the metasurface can significantly recover the performance of the Faraday rotator[8] (not shown). As another approach, we also investigated a Faraday rotator structure based on a Si photonic crystal slab on a plane YIG thin film[9] (not shown). By employing guided mode resonance in the 500-nm-thick YIG layer, we achieved high Q factor resonances, which largely enhance Faraday rotation available in the thin-film device. We numerically observed a θ_f of 45° with a transmittance of ~ 70% in an optimized design.

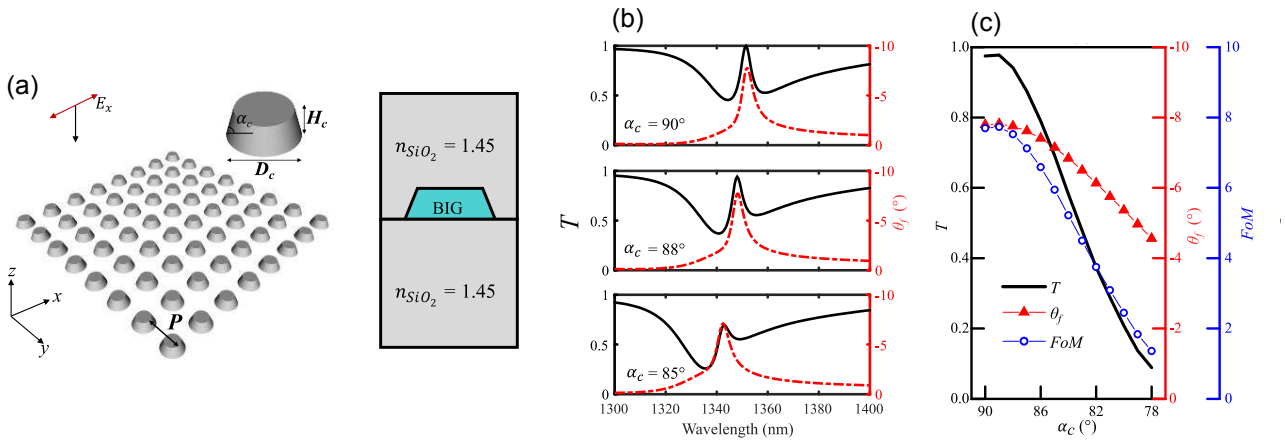


Figure 1 (a) Investigated metasurface composed of BIG microdisks with tilted side walls. (b) Faraday rotation (red dash lines) and transmission (black solid) spectra when varying the sidewall angle (α_c). (c) Faraday rotation angles, light transmittance and figures of merit as a function of sidewall angle.

Acknowledgements: We thank T. Liu, F. Tian, T. Kitai, S. Ishida, H. Matsukiyo, H. Otsuki, Y. Narazaki, Y. Tanimura and K. Taniguchi for their technical support and fruitful discussions. This work was supported by KAKENHI (17H06138, 19K05300, 22H00298, 22H01994, 22K18989), JST CREST(JPMJCR19T1), JST FOREST Program (JPMJFR213F), Nippon Sheet Glass Foundation.

References

1. M. Inoue, K. Arai, T. Fujii and M. Abe, “One-dimensional magnetophotonic crystals”, J. Appl. Phys. 85, 5768 (1999).
2. V. I. Belotelov, *et al*.,” Enhanced magneto-optical effects in magnetoplasmonic crystals”, Nat. Nanotechnol. 6, 370 (2011)
3. A. Christofi, Y. Kawaguchi, A. Alù and A. B. Khanikaev, “Giant enhancement of Faraday rotation due to electromagnetically induced transparency in all-dielectric magneto-optical metasurfaces”, Opt. Lett. 43, 1838 (2018).
4. T. Kiel, P. Varytis, B. Beverungen, P. T. Kristensen and K. Busch,” Enhanced Faraday rotation by dielectric metasurfaces with Bayesian shape-optimized scatterers”, Opt. Lett. 46, 1720 (2021).
5. D. O. Ignatyeva, D. M. Krichevsky, V. I. Belotelov, F. Royer, S. Dash and M. Levy, “All-dielectric magneto-photonic metasurfaces”, J. Appl. Phys. 132, 100902 (2022).
6. D. O. Ignatyeva, *et al*., “All-dielectric magnetic metasurface for advanced light control in dual polarizations combined with high-Q resonances”, Nat. Commun. 11, 5487 (2020)
7. S. Xia, *et al*., ” Enhancement of the Faraday Effect and Magneto-optical Figure of Merit in All-Dielectric Metasurfaces” ACS Photon. 9, 1240 (2022).
8. S. Gao, Y. Ota, T. Liu, F. Tian and S. Iwamoto, “Faraday rotation in a conical frustum metasurface made of a magneto-optical material”, OPIC-ICNN, ICNN7-02 (2022).
9. S. Gao, Y. Ota, T. Liu, F. Tian and S. Iwamoto, submitted.

META 2023, PARIS - FRANCE, JULY 18 – 21, 2023

Bose–Einstein condensation of freely evolving overpopulated magnon gas to the uniform precession state

A. A. Serga[1*]

[1]Fachbereich Physik and Landesforschungszentrum OPTIMAS,
Rheinland-Pfälzische Technische Universität Kaiserslautern-Landau, 67663 Kaiserslautern, Germany
[*]corresponding author: serha@rptu.de

Abstract: Bose–Einstein condensate (BEC), which magnons can form even at room temperature, is now a promising object for developing new computational concepts. Most studies employ Brillouin light scattering spectroscopy to observe a short-wavelength BEC in planarly magnetized ferrimagnetic films. However, electrical detection is essential for the implementation of magnon BEC devices. Using parametric electromagnetic pumping of magnons in perpendicularly magnetized films, we achieved a new long-wavelength type of BEC and investigated its behavior by inductive detection.

Coherent spin-wave states, such as Bose–Einstein condensates (BECs), which spontaneously form in an overpopulated magnon gas even at room temperature [1], have considerable potential for wave-based computing and information processing at microwave frequencies [2, 3].

The magnon condensate is usually created in the low-damping yttrium iron garnet (YIG) films by the parametric pumping of magnons by a microwave electromagnetic field. In this process, external microwave photons split into magnon pairs with half of the pumping frequency and opposite wavevectors. They populate a gaseous magnon distribution with internal interactions provided by the four-magnon scattering processes. Eventually, the magnon gas thermalizes to the bottom of the frequency spectrum, and if the applied pumping power exceeds a certain threshold, a BEC forms there. In in-plane magnetized YIG films, magnons condense at two frequency-degenerated minima with opposite wavevectors along the magnetization direction. Since the wavelength of such magnon condensate is only a few microns, its observation is quite challenging and is usually performed using Brillouin light scattering spectroscopy. Only recently, by exploiting the magnon wavelength transformation in a bulk YIG sample's inhomogeneous internal magnetic field, we have observed such a condensate using an inductive antenna [4].

Here, I present the formation of a new long-wavelength type of magnon BEC in perpendicularly magnetized YIG films. Under such magnetization conditions, the magnon spectrum has only one energy minimum at zero wavenumber. This state corresponds to the so-called magnon Kittel mode and represents a homogeneous precession of the magnetic moment of the sample at the ferromagnetic resonance frequency. The signal of such a precession is easily detected by a conventional inductive microstrip antenna, and its temporal evolution and spectral characteristics can be measured with high accuracy.

In our experiment, parametric magnons are generated 800 MHz above the spectral minimum at 3090 MHz and are broadly distributed around half of the pumping frequency. The intense pumping leads to a significant perturbation of the magnon distribution and often prevents BEC formation during its action [4, 5]. The same behavior of the spin system is observed in our case; only after the parametric pumping is terminated the spectrally-narrow BEC state with a linewidth of about 1 MHz is formed in the freely evolving magnon gas.

This research was funded by the European Research Council within the Advanced Grant No. 694709 “SuperMagnonics” and by the Deutsche Forschungsgemeinschaft (DFG, German Research Foundation) within the Transregional Collaborative Research Center – TRR 173/2 – 268565370 “Spin+X” (project B04).

References

1. Demokritov, S. O., V. E. Demidov, O. Dzyapko, G. A. Melkov, A. A. Serga, B. Hillebrands and A.N. Slavin, “Bose–Einstein condensation of quasi-equilibrium magnons at room temperature under pumping,” Nature, Vol. 443, 430–433 (2006).
2. P. Pirro, P., V. I. Vasyuchka, A. A. Serga and B. Hillebrands, “Advances in coherent magnonics,“ Nat. Rev. Mater., Vol. 6, 1114–1135, 2021.
3. Mohseni, M., V.I. Vasyuchka, V.S. L’vov, A.A. Serga and B. Hillebrands, “Classical analog of qubit logic based on a magnon Bose–Einstein condensate,” Commun. Phys., Vol. 5, 196, 2022.
4. Noack, T. B., V. I. Vasyuchka, A. Pomyalov, V. S. L’vov, A. A. Serga and B. Hillebrands, “Evolution of room-temperature magnon gas: Toward a coherent Bose–Einstein condensate,” Phys. Rev. B, Vol. 104, No. 10, L100410, 2021.
5. Serga, A. A., V. S. Tiberkevich, C. W. Sandweg, V. I. Vasyuchka, D. A. Bozhko, A. V. Chumak, T. Neumann, B. Obry, G. A. Melkov, A. N. Slavin and B. Hillebrands, “Bose–Einstein condensation in an ultra-hot gas of pumped magnons,” Nat. Commun., Vol. 5, 3452, 2014.

Non-linear ferrite dynamics for microwave thin film technologies

Feodor Y. Ogrin

School of Physics and Astronomy, University of Exeter, Exeter, UK

Electromagnetic (EM) shock waves are normally associated with nuclear explosions, and as such a rare phenomenon. Analogous to a sonic boom, it is an interference effect, resulting in a surge of EM power, propagating with a speed of light. Since early 60s there was an interest to harness the effect to make it more technologically practical. One possible way to do that is within the configuration of a magnetically loaded transmission line (e.g. coaxial line). While the coaxial design has been proven to be viable for generating high power microwaves [1], its practicality in consumer technology is less so obvious due to high voltages (typically 10-100th kV) needed in order to obtain the effect. Theoretically, this problem can be resolved by scaling down the dimensions of the transmission line. Reducing down to microscopic dimensions, it is possible to obtain the effect at voltages as low as 1-10 Volts. At this level the effect can be usefully utilised in a range of electronic devices, and particularly the high frequency communications, which are of great demand in the development of modern IC technologies. Modelling extremely non-linear EM dynamics is however a challenging problem, that can not be done by the available conventional solvers. Here we approach the problem by using a unique modelling technique allowing to solve Maxwell equations in parallel to Landau-Lifshits-Gilbert's (LLG) [2]. The unique nature of our 3D FDTD-LLG code, is in the fact that LLG equation is solved exactly, accounting for the given geometry with the presence of any type of conducting or non-conducting materials [3]. This means that all non-linear effects can be calculated precisely without any linearization or imposed constraints.

In this contribution I will demonstrate the main characteristics and parameters of the shock wave propagation in microstrip transmission line. In particular, I will show the dispersion characteristics of the wave, its dependence on the geometric and material parameters of the device and those of the source of actuation. As well as the typical effects, such as applied field dependence and anisotropy, I will demonstrate some unique features, such as tuneability with the electric field pulse, allowing to manipulate the response in a broad GHz frequency range. I will also demonstrate the possibility of guiding the waves in microstripes with non-linear geometric designs, and discuss the potential for application in communication technologies.

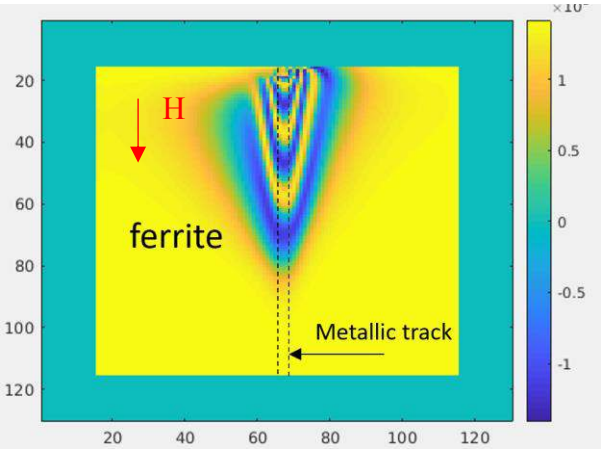


Figure 1. **Electromagnetic shock-wave propagation in a thin-film microstrip transmission line**. The wave is actuated with a short electric pulse between the microstrip (shown with dashed lines) and the base plane. Ferrite thin film (10micron) extended over the base line. Shock wave propagates below the strip, but deviates also into the whole slab. Intensity map: out-of-plane magnetisation. Initial orientation of the magnetisation is parallel to the field.

[1] Ulmasculov et al. (2017), J. Phys.: Conf. Ser. 830 012027.

[2] M. M. Aziz, Progress In Electromagnetics Research B 15, (2009) 1–29.

[3] .https://www.maxllg.com/

Wavelength-Independent Bragg-Like Effect

M. W. McCall* **and S. F. Koufidis**

Blackett Laboratory, Department of Physics, Imperial College London, London, United Kingdom
*corresponding author: m.mccall@imperial.ac.uk

Abstract: We have recently established that a uniform birefringent medium can exhibit an arbitrarily broadband Bragg-like response, based solely on matching the chirality parameter to the medium's average refractive index rather than on the usual Bragg condition. Here, we demonstrate that such a response can also be achieved in a broader family of optically active media, which relaxes the previously identified hard-to-achieve resonance condition while offering control over the resonance bandwidth via an externally applied static magnetic field.

The Drude-Born-Fedorov model for circular birefringence may be phenomenologically generalised, as in **[1]**, to include the effect of gyrotropy induced by an externally applied magnetic field. The constitutive relations read

$$\mathbf{D} = \epsilon_0[\boldsymbol{\epsilon} \cdot \mathbf{E} + (\chi - i\alpha)\eta_0\mathbf{H}] \quad \text{and} \quad \mathbf{B} = \mu_0[(\chi + i\alpha)\eta_0^{-1}\mathbf{E} + \mu\mathbf{H}], \tag{1}$$

where all the symbols have their usual meaning, α, χ are the chirality parameter and Tellegen coefficient, respectively, and for the static magnetic field $\mathbf{B}_0$ being aligned along the positive z-axis, the permittivity tensor is

$$\boldsymbol{\epsilon} = \begin{pmatrix} \epsilon & -ig & 0 \\ ig & \epsilon & 0 \\ 0 & 0 & \epsilon_z \end{pmatrix}. \tag{2}$$

Although the constitutive relations in Eq. (1) are oversimplified, since gyrotropy will in principle affect both the chirality and the permeability (see **[2]**), such an approximation is indeed widely-adopted as it leads to more insightful dispersion relations. Aligning the direction of propagation in a suitable z'-axis, so that the angle between the wavevector $\mathbf{k}$ and $\mathbf{B}_0$ is θ, the supported refractive indices will then satisfy the equation

$$n^4 + \beta n^2 + \gamma n + \delta = 0, \tag{3}$$

where β, γ, δ are generally functions of the medium's parameters and, crucially, of the declination angle.

In the absence of the Faraday effect ($g = 0$), the tensor in Eq. (2) describes a uniaxial medium which combined with Eq. (1) yields that of **[3]**. Then, plane-waves propagating at an angle θ off the optical axis z, along z', experience a linear birefringence $\boldsymbol{\epsilon}_\perp = \mathrm{diag}(\epsilon_1(\theta), \epsilon_2(\theta))$. Then, the solutions to Eq. (3) are given by

$$\pm n^{(\pm)} = \pm\sqrt{\alpha^2 + \bar{\epsilon}\mu - \chi^2 \pm \sqrt{4\alpha^2(\bar{\epsilon}\mu - \chi^2) + \Delta\epsilon^2\mu^2}}, \tag{4}$$

where $\bar{\epsilon}(\theta)$ is the average dielectric constant and $\Delta\epsilon(\theta)$ measures the birefringence. In the absence of absorption, it turns out that Eq. (4) becomes purely imaginary whenever the chirality parameter α lies in the regime

$$(\bar{\epsilon} - |\Delta\epsilon|)\mu - \chi^2 < \alpha^2 < (\bar{\epsilon} + |\Delta\epsilon|)\mu - \chi^2, \tag{5}$$

which signifies that a bulk medium will then support evanescent modes. For a fixed θ, calculation of the eigenmodes demonstrates that there, the upper branch of Eq. (4) refers to circular polarisation, whereas the lower to linear polarisation, which is a combination of forward and backward propagating circular polarisations. From the chirality-domain dispersion of Fig. 1, and the chirality-domain intensity transmittances for a slab of the considered medium in Fig. 2, it is evident that we have a Bragg-like response, similar to that of structurally chiral media (SCM), without however matching the wavelength of light to a spatial period but by resonant tuning of the chirality parameter to $\alpha^2 = \bar{\epsilon}\mu - \chi^2$. Such a resonant condition signifies extreme values of chirality, leading to the negative refraction regime, that has recently been achieved in meta-media at THz frequencies **[4]**.

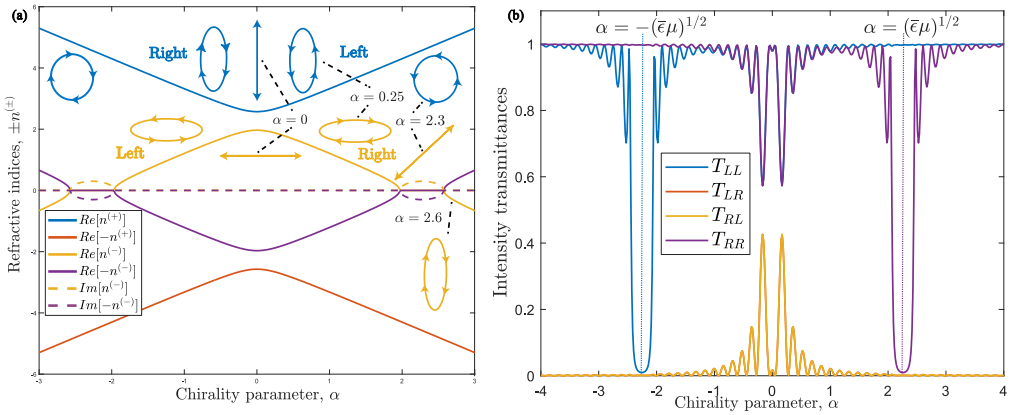


Figure 1 Bragg-like response of a linearly and circularly birefringent medium: **(a)** chirality-domain dispersion and **(b)** intensity transmittances for a slab of the considered medium. The non-reciprocity parameter $\chi = 0$, and the angle is fixed so that the slab is impedance-matched with the surrounding dielectric **[3, arXiv preprint]**.

Comparison of Fig. 1b with the well-studied case of SCM, characterised by a pitch $h\Lambda$ with $h = \pm 1$ for right/left handedness, provides a clear analogy: the chirality parameter can be mapped to the pitch $h\Lambda$, whereby $\alpha > 0$ corresponds to a right-handed SCM that back-scatters right circular polarisations, whereas $\alpha < 0$ corresponds to a left-handed SCM that reflects left circular polarisations. For $\alpha = 0$ (correspondingly, $\Lambda = 0$), the medium becomes purely linearly birefringent and an exchange between circular states ensues (cf. Fig. 1b at $\alpha \approx 0$). Unlike the case of **[3]**, here, the key-parameters $\bar{\epsilon}(\theta)$ and $\Delta\epsilon(\theta)$, which determine the centre of resonance and bandwidth, are θ-dependent offering the possibility of relaxing the hard-to-achieve tuning condition $\alpha^2 \approx \bar{\epsilon}\mu$ by manipulating the angle between the direction of wave propagation and the medium's optical axis. We note that considering material dispersion and realistic losses will not significantly alter the medium's response (see **[3]**).

In a chiroplasma medium ($g \neq 0, \chi = 0$) **[1]**, or in a so-called G-chiral medium ($g \neq 0, \chi \neq 0$) with the permeability being a scalar, the aforementioned electromagnetic response can be achieved. Indeed, for the direction of propagation being perpendicular to the static magnetic field, Eq. (3) is once again rendered bi-quadratic, like Eq. (4), but with the centre of resonance and the chirality-domain bandwidth now depending, necessarily, on the gyrotropic parameter g. Remarkably, this dependence significantly eases the resonance condition of **[3]** to $\alpha^2 = (\bar{\epsilon} - g^2/\epsilon_1)\mu$, offering at the same time a convenient platform for manipulating the reflection/transmission bandwidth $\Delta\epsilon = |\epsilon_1 - \epsilon_2| + g^2/\epsilon_1$. As the required parameters are within reach of current meta-media technology, applications in optoelectronics, waveguiding, or fibre Bragg grating sensors are expected.

References

1. Engheta, N., D. L. Jaggard, and M. W. Kowarz. "Electromagnetic waves in Faraday chiral media," IEEE Trans. Antennas Propag., Vol. 40, No. 4, 1064–1076, 1992.
2. Weiglhofer, W. and S. Hansen, "Faraday chiral media revisited. I. Fields and sources," IEEE Trans. Antennas Propag., Vol. 47, No. 5, 807–814, 1999.
3. McCall, M. W. and S. F. Koufidis, "Broadband Bragg phenomenon in a uniform birefringent medium," Opt. Lett., Vol. 48, No. 5, 1096–1099, 2023.
4. Liu, M. et al., "Temperature-controlled optical activity and negative refractive index," Adv. Funct. Mater., Vol. 31, No. 14, 2020149, 2021.

META 2023, PARIS - FRANCE, JULY 18 – 21, 2023

Symmetry control of strong chiral light–matter interactions in photonic nanocavities for efficient circularly polarised emission

Rahul Kumar[*1], Ben Trodden[1], Anastasiia Klimash[1], Affar Karimullah[1], Nikolaj Gadegaard[2], Peter J. Skabara[1], Shun Hashiyada[3,4], Gordon J. Hedley[1] and Malcolm Kadodwala[1*]

[1]School of Chemistry, Joseph Black Building, University of Glasgow, Glasgow, G12 8QQ, UK
[2] School of Engineering, Rankine Building, University of Glasgow, Glasgow G12 8LT, U.K
[3] Innovative Photon Manipulation Research Team, RIKEN Center for Advanced Photonics, 2-1 Hirosawa, Wako, Saitama 351-0198, Japan
[4] Department of Electrical, Electronic, and Communication Engineering, Chuo University, 1-13-27 Kasuga, Bunkyo-Ku, Tokyo 112-8551, Japan.
[*]Corresponding author: Rahul.kumar.2@glasgow.ac.uk, Malcolm.kadodwala@glasgow.ac.uk

Abstract: We demonstrate a novel concept for creating chiral excited states which does not rely on molecular structure. Instead, it depends on hybridising a non-chiral molecule with a chiral electromagnetic field, producing a hybrid light-matter chiral polariton state. This is achieved by a symmetry-controlled strong chiral-light–matter interaction between an electromagnetic mode of a chiral nanocavity and an achiral molecule. This electromagnetic mechanism simplifies the creation of chiral electronic states since it is far less demanding in terms of materials design.

Chirality, the property of asymmetry, is generally perceived as a geometric concept, with chiral materials existing in otherwise identical mirror forms known as enantiomers. Thus, creating chiral molecules, which have applications spanning pharmaceuticals to next generation photonic technologies[1-3], requires precise control of 3-D structure, is a challenging chemical problem. In contrast, if chirality could be conveyed on to an achiral molecule without the need for specific stereostructural control, then it would simplify the synthesis and broaden potential applications. Therefore, in this work, we show such an effect, where chirality is induced in achiral molecules by virtue of the chiral electromagnetic (EM) environment they occupies, a concept referred to as the electromagnetic-enantiomer, shown in Figure 1(a). We have synthesised and spin coated fluorescence achiral molecules -in various concentration with respect to PMMA- on Chiral Metamaterial (CM) of two periodicity i.e., 1000 nm and 1500 nm to realise ≈200 nm thick film. The molecular structure of the synthesized achiral molecules and schematic & SEM image of CM used is shown in figure 1(b) and 1(c) respectively. The chiral photoluminescence (CP) emissions from for Left-handed (LH) CM structure for both periodicity is shown in Figure 1(d). It can be seen from the figure that, in the case of 1000 nm metafilms, the luminescence showed two distinct regions of structure centered at λ≈ 560 nm and 620 nm. The structure observed around λ≈ 560 nm for mis-matched combinations of metafilm handedness and emitted light helicity (LH/RCP and RH/LCP) is a single peak, which appear to split into two less intense components for matched combinations, with the splitting being equivalent to ~ 107 meV (Δλ~ 28 nm). This splitting in PL peak is a definitive fingerprint of strong coupling[4]. Relatively weaker structure occurs in the region around λ≈ 620 nm, with a single peak observed for the mis-matched combinations and weaker, less defined features observed for the matched combinations. For the 1500 nm metafilms, the structure is less pronounced and the most noticeable feature, a single peak, occurs close to λ≈ 594 nm. The absence of strong coupling in the 1500 nm cavity indicates relatively weak electric fields compared to those for the 1000 nm. The EM simulations do show this effect where the maximum enhancement in the Electric field was observed for 1000 nm matched combinations of metafilm handedness and light helicity. The molecule displays distinctly different luminescence behaviour i.e., peak splitting under strong coupling, and

enhanced emission under weak coupling. This provides a simple route to create efficient (≈30%) circularly polarised emission. Such a level of efficiency has previously required structurally complex and multicomponent chemical systems. A potential application of the phenomenon is in making the manufacture of OLED sources of CP light a less challenging chemical problem, since current strategies rely on the challenging synthesis and isolation of chiral geometric molecular structures in high enantiomeric excess.

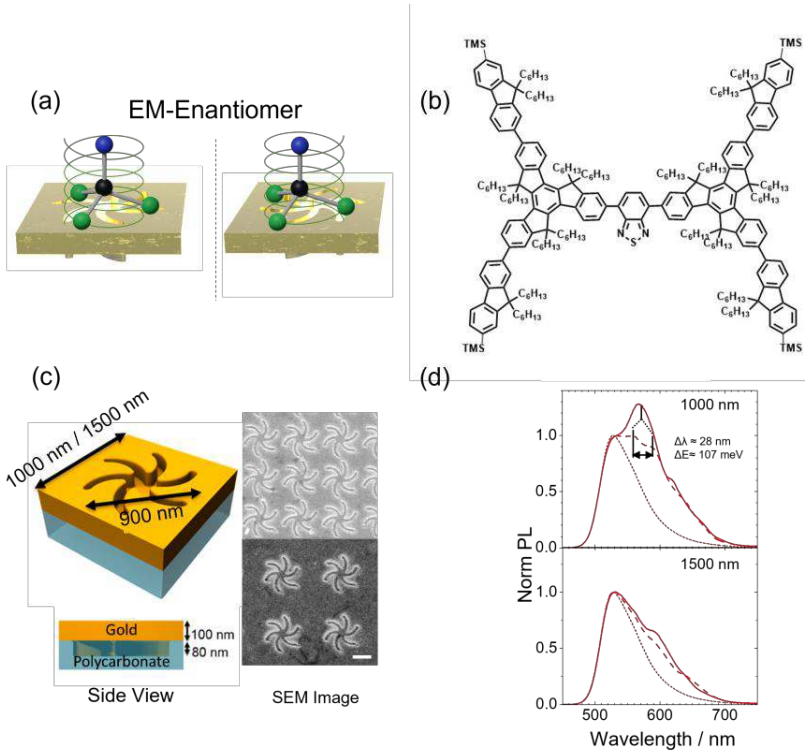


Figure 1 *(a) The interaction of chiral nearfields with achiral molecules results in EM-enantiomers, through the symmetry dependent creation of polariton states. (b) Molecular structure of MHeB14 dye. (c) SEM images and schematic showing orthographic (top) and side view (bottom) of LH nanocavity. (d) Normalised PL for both structures. The black vertical lines are guidance for eyes, highlighting the presence or absence of peak splitting. The dashed line and solid line respectively show the RCP and LCP PL emission from the structures. The overlapping dotted lines show LCP and RCP PL emission of dye when present on the flat gold. All spectra have been self-normalised to value at λ=533 nm*

References

1. Balavoine, G., Moradpour, A., & Kagan, H. B. J. "Preparation of chiral compounds with high optical purity by irradiation with circularly polarized light, a model reaction for the prebiotic generation of optical activity." J. Am. Chem. Soc., 96(16), 5152-5158, 1974.
2. Sallembien, Q., Bouteiller, L., Crassous, J., & Raynal, M. "Possible chemical and physical scenarios towards biological homochirality" Chem. Soc. Rev., 2022.
3. Noorduin, W. L., Bode, A. A., Van Der Meijden, M., Meekes, H., Van Etteger, A. F., Van Enckevort, W. J., ... & Vlieg, E. "Complete chiral symmetry breaking of an amino acid derivative directed by circularly polarized light". Nat. Chem, 1(9), 729-732, 2009.
4. Leng, H., Szychowski, B., Daniel, M. C., & Pelton, M." Strong coupling and induced transparency at room temperature with single quantum dots and gap plasmons". Nat. Commun., 9(1), 4012, 2018.

Optical response of magnetic metals from first principles

M.K. Pogodaeva[1*], S.V. Levchenko[1], V.P.Drachev[1]

[1]Skolkovo Institute of Science and Technology, Russia
[*]corresponding author: mariia.pogodaeva@skoltech.ru

Abstract: We present a first-principle methodology to calculate spin-resolved dielectric function of magnetic metals applying Drude model. Interband and intraband contributions to the dielectric function are calculated using density functional theory in an all-electron full-potential framework. The results are compared to the experiments. We find a significant difference between the contribution of the spin-up and spin-down electrons. Our results allow to explain the existence of unexpected plasmon resonance in cobalt nanoparticles.

There is no clear understanding of the effects of magnetization on plasma frequency so far. Our recent research in plasmonics has shown an inconsistency between theoretical predictions and experimental measurements of optical properties of cobalt nanoparticles [1]. Specifically, a plasmon resonance was observed at 280 nm for cobalt nanoparticles that could not be reproduced by permittivity measurements for large-area films (see fig. 1).

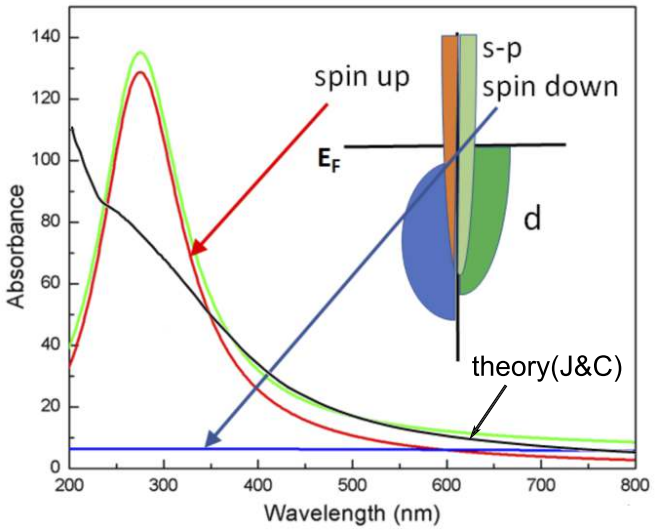


Fig. 1. Two-plasmon model for absorbance in cobalt nanoparticles. Red line shows the contribution from spin-majority electrons, while blue line shows the contribution from spin-minority electron. Green line shows experimentally observed spectrum from [1]. Black line shows theoretical prediction for spectrum of cobalt nanoparticles using data from [2].

The Mott model suggests that in magnetic metals there are two largely independent spin channels of conductivity. The probability of spin-flip scattering is low, and scattering rates for spin-up and spin-down channels are sufficiently different. The position of the absorption peak in the nanoparticles depends of the plasmon frequency, which is proportional to bulk plasma frequency where is the dielectric permittivity of the host medium, and is the interband contribution to the metal permittivity. Thus, separate consideration of spin channels for bulk optical properties will allow us to understand the unexpected plasmon resonances in magnetic nanoparticles, which the plasmonics currently fails to predict.

In our work [3] we have presented a methodolody to calculate spin-resolved plasma frequency of magnetic metals. We have applied the methodolody to calculate spin-up and spin-down plasma frequencies for cobalt and have shown that they are sufficiently different. We have shown, that the inclusion of spin-orbit coupling mixes spin channels and does not allow to fully resolve between spin-up and spin-down electrons, however, approximate resolution is still possible. The plasmon frequency in nanoparticles depends on the above described plasma frequency as follows:

$$\omega_p^2 = \frac{\omega_{pl}^2}{\varepsilon_{ib} + 2\varepsilon_h} \tag{1}$$

Here ε_{ib} is the interband contribution of bulk metal and ε_h is host permittivity. Calculated plasma frequency tensors for spin-up and spin-down channels in hexagonal cobalt have the following values: 5.03 eV and 3.44 eV for *xx* and *yy* components of the tensor and 4.89 eV and 4.63 eV for *zz* component of the tensor. Generally, the interband contribution is a frequency-dependent dielectric function, but for transition metals it is frequently considered as approximately constant small value ~1.

The dielectric function tensor of bulk metals can be separated to the vacuum, interband and intraband contributions:

$$\varepsilon_{i,j}(\omega) = \delta_{i,j} + \varepsilon_{i,j}^{inter}(\omega) + \varepsilon_{i,j}^{intra}(\omega) \tag{2}$$

In this work we are focusing on interband contribution to the dielectric function:

$$\varepsilon_{i,j}^{inter}(\omega) = \lim_{\mathbf{q}\to 0}\left\{\frac{4\pi e^2}{|\mathbf{G}+\mathbf{q}||\mathbf{G}'+\mathbf{q}|}\chi_{\mathbf{G},\mathbf{G}'}^{KS}(\mathbf{q},\omega)\right\}_{\mathbf{G},\mathbf{G}'=0} \tag{3}$$

Within the random-phase approximation (RPA), the Kohn-Sham dielectric permittivity χ^{KS} at **G**,**G**′=0 depends on wavevector **q**, difference between Fermi functions Δf_{mn} at states m and n, and difference between Kohn-Sham eigenenergies $\Delta\varepsilon_{mn}$ a of the given system:

$$\chi_{\mathbf{G},\mathbf{G}'=\mathbf{0}}^{KS}(\mathbf{q},\omega) = \sum_{m\neq n\mathbf{k}} \langle n|\mathbf{qr}|m\rangle\langle m|\mathbf{qr}|n\rangle \frac{\Delta f_{mn}}{\Delta\varepsilon_{mn}-\omega} \tag{4}$$

References

1. Bhatta, H. L., A. E. Aliev, and V. P. Drachev, “New mechanism of plasmons specific for spin-polarized nanoparticles”, Sc. Rep., Vol 9, No. 1, 1-8, 2019.
2. Johnson, P.B., and R.W. Christy, “Optical constants of transition metals: Ti, V, Cr, Mn, Fe, Co, Ni and Pd”, Phys. Rev. B, Vol. 9, No 12, 5056, 1974.
3. Pogodaeva, M. K., S. V. Levchenko, and V. P. Drachev, “Spin-dependent plasma frequency from all-electron ab initio calculations including spin-orbit coupling”, Phys. Rev. B, Vol.107, No. 4, 045113, 2023.

META 2023, PARIS - FRANCE, JULY 18 – 21, 2023

Quantum theory of magnetic quadrupole moment and its relation to orbital magnetoelectric effect

Nobuhiro Arai[1], Yang Gao[2], Di Xiao[3,4], Shuichi Murakami[1*]

[1] Department of Physics, Tokyo Institute of Technology, Ookayama, Meguro-ku, Tokyo 152-8551, Japan
[2] University of Science and Technology of China, Hefei, Anhui 230026, China
[3] Department of Materials Science & Engineering, University of Washington, Seattle WA 98915, USA
[4] Department of Physics, University of Washington, Seattle WA 98915, USA
[*] corresponding author: murakami@stat.phys.titech.ac.jp

Abstract: We find that the known formula for the orbital magnetic moment misses a term in its diagonal elements. In this work, by considering a response to the magnetic fields including a monopole, we derive a modified formula for the magnetic quadrupole moment. We show that the trace of the magnetic quadrupole moment now has the Chern-Simons axion term, as expected from the relationship between the orbital magnetic quadrupole moment and the orbital magnetoelectric tensor.

Recently, the quantum formula of orbital magnetic quadrupole moment Q_{ij} was derived, which is defined as a response to the spatial modulation of magnetic fields[1,2]. Nonetheless, this result needs to amendments, because it does not satisfy the thermodynamic property that the derivative of the magnetic quadrupole moment Q_{ij} with respect to the chemical potential is equal to the orbital magnetoelectric tensor α_{ij}. In this work, by considering a response to the spatial modulation of magnetic fields including a monopole field, we derive a modified formula for the magnetic quadrupole moment, whose derivative correctly reproduces the orbital magnetoelectric tensor α_{ij} including the Chern-Simons term in its diagonal elements[3]. We show that the trace of the magnetic quadrupole moment comes from the correction of density of states due to the monopole field. We note that the magnetic quadrupole moment derived as such is not equal to the classically defined quadrupole moment, but it has additional terms[3]. We also discuss axion insulators, which have a quantized orbital magnetoeletric tensor. This class of systems is equivalent to higher-order topological insulators with chiral hinge states, and we explain that these hinge states are not primarily related with magnetoelectric response or orbital magnetic quadrupole moment.

Y.G. acknowledges the support of the 363 Fundamental Research Funds for the Central Universities, 364 China (Grant No. WK2340000102). D.X. is supported by DOE Award No. DE-SC0012509. S. M is supported by JSPS KAKENHI Grant Numbers JP22K18687 and JP22H00108.

References

1. Shitade, A. H. Watanabe, and Y. Yanase, Phys. Rev. B 98, 020407(R) (2018).
2. Gao, Y. and D. Xiao, Phys. Rev. B 98, 060402(R) (2018).
3. Arai, N., Y. Gao, D. Xiao, and S. Murakami, in preparation (2023).

META 2023, PARIS - FRANCE, JULY 18 – 21, 2023

Novel materials with magnetic skyrmions and their three-dimensional dynamics

S. Seki[1*]

[1]Department of Applied Physics & Institute of Engineering Innovation, University of Tokyo, Japan
[*]corresponding author: seki@ap.t.u-tokyo.ac.jp

Abstract: Topological swirling spin textures, such as skyrmions and merons, have attracted much attention as a unique building block for high-density magnetic information devices. In this talk, I overview recent discovery of novel materials and mechanisms to realize a rich variety of nanometric magnetic quasi-particles with nontrivial symmetry and topology.

Magnetic skyrmion, i.e., a topologically stable swirling spin configuration, has recently attracted attention as a particle-like object potentially suitable for the design of high-density information bits. Previous observations of skyrmions have mostly focused on noncentrosymmetric systems, where Dzyaloshinskii-Moriya interaction plays an important role[1,2]. On the other hand, recent theoretical studies suggest that skyrmions can be stabilized even in centrosymmetric systems by considering different microscopic mechanisms. For example, geometrical frustration of short-range exchange interactions on triangular lattice is predicted to stabilize a hexagonal lattice of skyrmions[3]. Another potential mechanism is the RKKY and four-spin interactions mediated by itinerant electrons, which is expected to favor a skyrmion lattice state for highly-symmetric (such as hexagonal or tetragonal) crystal lattice systems[4].

In this talk, I overview the recent experimental discovery of skyrmions in centrosymmetric systems[5-9]. In particular, we focus on the case of centrosymmetric tetragonal magnets, where the square lattice of skyrmions with extremely small diameter (1.9 nm for $GdRu_2Si_2$, i.e. the smallest value ever reported for single-component bulk materials) has been observed[7-9]. These compounds also host various non-trivial topological spin textures, and the present findings demonstrate that even a simple centrosymmetric magnet with competing interactions can be a promising material platform to realize a rich variety of nanometric magnetic quasi-particles with distinctive symmetry and topology.

If time allows, I will also discuss the recent experimental observation of skyrmion strings in three-dimensional systems and their excitation dynamics[10,11].

References

1. S. Muhlbauer *et al.*, Science **323**, 915 (2009).
2. S. Seki *et al*., Science **336**, 198 (2012).
3. A. O. Leonov *et al*., Nature Commun. **6**, 8275 (2015).
4. S. Hayami *et al.*, Phys. Rev. B **95**, 224424 (2017).
5. T. Kurumaji *et al*., Science **365**, 6456 (2019).
6. M. Hirschberger *et al*., Nature Commun. **10**, 5831 (2019).
7. N. D. Khanh, S. Seki *et al*., Nature Nanotechnology **15**, 444 (2020).
8. Y. Yasui, S. Seki *et al*., Nature Commun. **11**, 5925 (2020).
9. R. Takagi, S. Seki *et al.*, Nature Commun. **13**, 1472 (2022).
10. S. Seki *et al*., Nature Commun. **11**, 256 (2020).
11. S. Seki *et al*., Nature Materials **21**, 181 (2022).

META 2023, PARIS - FRANCE, JULY 18 – 21, 2023

Magnetoelectric fields for chirality discrimination

E. O. Kamenetskii

School of Electrical and Computer Engineering, Ben Gurion University of the Negev, Israel

corresponding author: kmntsk@bgu.ac.il

Chirality is fundamentally related to a magnetoelectric response. But the magnetoelectric response is characterized by the violation of both spatial and temporal symmetry. It is claimed that time-even pseudoscalar optical chirality gives enantioselective fields. Are only time-even pseudoscalars required to describe local properties of chiral light-matter interactions? We argue that near fields with both spatial and temporal symmetry breaking, called magnetoelectric near fields, are true enantioselective fields for describing local properties of chiral light-matter interactions.

META 2023, PARIS - FRANCE, JULY 18 – 21, 2023

Angular-Momentum Dynamics in Ferromagnets on Ultrashort Timescales: Electron-Magnon Interactions vs. Spin-Orbit Coupling

F. Dusabirane, K. Leckron, B. Rethfeld, and H. C. Schneider*

Physics Department and Research Center OPTIMAS, University of Kaiserslautern-Landau, Germany
*corresponding author: hc.schneider@rptu.de

Abstract: We analyze the contributions of electron-magnon scattering and Elliott-Yafet spin-flip scattering to ultrafast magnetization dynamics in a model metallic ferromagnet. We find that far-from-equilibrium magnon distributions are created after ultrashort-pulse excitation and play an important role in the demagnetization process. We compare these findings to earlier calculations using the Elliott-Yafet mechanism alone.

Ever since its experimental discovery mor than 20 years ago, the demagnetization dynamics in ferromagnets has mostly been described in terms of effective temperature models for electrons, spins and lattice. Also, the spin-lattice coupling was mostly envisaged as being due to electron-phonon spin-flip scattering, similar to the Elliott-Yafet spin-relaxation mechanism in semiconductors and normal metals. Recently, there have also been suggestions that the angular momentum of phonons may be of importance. In order to compare the different contributions to the demagnetization process and how they affect the conservation/flow of angular momentum, one needs to understand them in microscopic detail.

In the past, we have used a microscopic description of electron-phonon scattering to study the spin-dependent electron dynamics of ferromagnetic metals [1] and ferromagnetic model systems [3] after ultrashort-pulse excitation. In this way, the electron-lattice coupling and its effect on the electronic spin polarization can be studied directly on ultrashort, i.e., sub picosecond, time scales, where the system is far from equilibrium and also far from any quasi-equilibrium as assumed in the 3-temperature mode..

More recently, we have investigated the coupling of electrons to magnons on the same ultrashort timescales. We introduce magnons as separate degrees of freedom by adapting the approach of Ref. [3]. We then compute the dynamics of momentum resolved electron and magnon distributions due to electron-magnon and statically screened Coulomb electron-electron scattering, which are treated at the level of Boltzmann scattering integrals, and electron-phonon scattering. The coupled equations for the spin and momentum dependent distribution function thus have the general form

$$\frac{\partial}{\partial t} n_{\boldsymbol{k},\sigma} = \frac{\partial}{\partial t} n_{\boldsymbol{k},\sigma}\Big|_{e-m} + \frac{\partial}{\partial t} n_{\boldsymbol{k},\sigma}\Big|_{e-e} \frac{\partial}{\partial t} n_{\boldsymbol{k},\sigma}\Big|_{e-pn}$$

We find that the electron-magnon scattering leads to a pronounced non-equilibrium for magnon modes that couple directly to spin-flip transitions in the spin-split ferromagnetic band structure. For reasonable parameters for iron, the electronic spin-flip scattering with magnons results in a transient electron spin polarization on a timescale of a few ten femtoseconds. We find that the transient electronic spin polarization and magnon distributions are similar for excitations either within the minority or the majority band. The connection of the calculated results to experimental findings and other models will be discussed.

We acknowledge funding by the Deutsche Forschungsgemeinschaft (DFG, German Research Foundation) through No. TRR 173–268565370 (project B03).

References

1. Essert, S, and H. C. Schneider, “Electron-phonon scattering dynamics in ferromagnetic metals and their influence on ultrafast demagnetization processes,” Phys. Rev. B, Vol. 84, 224405, 2011.
2. Leckron, K, S. Vollmar and H. C. Schneider, “Ultrafast spin-lattice relaxation in ferromagnets including spin-orbit fields,” Phys. Rev. B, Vol. 96, 140408, 2017.
3. Woolsey, B and R. M. White, “Electron-magnon interaction in ferromagnetic semiconductors”, Phys. Rev. B, Vol. 1, 4474, 1970.

Magneto-Optical Chirality in a Coherently Coupled Exciton–Plasmon System

Samarth Vadia[1,2,3,†,*], Johannes Scherzer[1,†], Kenji Watanabe[4], Takashi Taniguchi[5], and Alexander Högele[1,2]

[1] Fakultat für Physik, Munich Quantum Center, and Center for NanoScience (CeNS), Ludwig-Maximilians-Universität München, Geschwister-Scholl-Platz 1, 80539 Munich, Germany

[2] Munich Center for Quantum Science and Technology (MCQST), Schellingtr. 4, 80799 Munich, Germany

[3] attocube Systems AG, Eglfinger Weg 2, 85540 Haar, Germany

[4] Research Center for Functional Materials, National Institute for Materials Science, 1-1 Namiki, Tsukuba 305-0044, Japan

[5] International Center for Materials Nanoarchitectonics, National Institute for Materials Science, 1-1 Namiki, Tsukuba 305-0044, Japan

[†] These authors contributed equally to this work

[*] corresponding author: samarth.vadia@physik.lmu.de

Chirality is a fundamental asymmetry phenomenon, with chiral optical elements exhibiting asymmetric response in reflection or absorption of circularly polarized light. Recent realizations of such elements include nanoplasmonic systems with broken mirror symmetry and polarization-contrasting optical absorption known as circular dichroism. An alternative route to circular dichroism is provided by spin-valley polarized excitons in atomically thin semiconductors. In the presence of magnetic fields, they exhibit an imbalanced coupling to circularly polarized photons and thus circular dichroism. Here, we demonstrate that polarization-contrasting optical transitions associated with excitons in monolayer WSe_2 can be transferred to proximal plasmonic nanodisks by coherent coupling. The coupled exciton-plasmon system exhibits magneto-induced circular dichroism in a spectrally narrow window of Fano interference, which we model in a master equation framework. Our work motivates exciton-plasmon interfaces as building blocks of chiral metasurfaces for applications in information processing, non-linear optics and sensing.

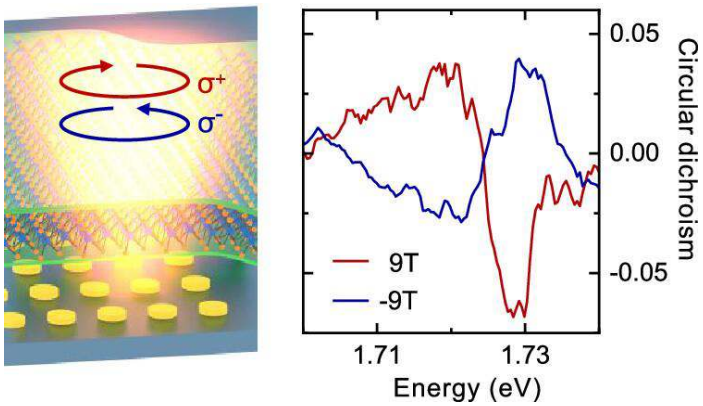


Figure 1: Left: Schematic of the chiral metasurface combining monolayer semiconductor and metallic nanodisk array. Right: Circular dichroism response of the metasurface in the presence of magnetic field.

References

1. Vadia, S., Scherzer, J., Watanabe, K., Taniguchi, T., and Högele, A., *Magneto-Optical Chirality in a Coherently Coupled Exciton–Plasmon System.* Nano Lett., 23, 614–618, 2023.

Chiral quantum phase shifters

N. Rotenberg[1*]

[1] Centre for Nanophotonics, Department of Physics, Engineering Physics & Astronomy, Queen's University, Kingston, Canada

[*]corresponding author: nir.rotenberg@queensu.ca

Abstract: Phase-shifters are a key component of photonic circuits, including those that process quantum information. This talk introduces such a phase-shifter based on a single, solid-state quantum emitter chirally coupled to a nanophotonic waveguide, covering both the basics of such a device and its performance in the presence of realistic imperfections. Finally, the fidelity of simple quantum photonic circuits based on these phase-shifters is considered.

The basic element of a reconfigurable quantum photonic circuit are phase shifters integrated within a Mach-Zehnder-Interferometer (MZI), with meshes of these devices enabling universal quantum information processing [1]. The phase-shifters must provide a phase shift spanning 2π in a controllable and accurate manner, and to date this is overwhelmingly accomplished by thermal shifters where a change of temperature by an applied current changes the optical properties of a section of the waveguide through which photons travel. Although highly accurate, such thermo-optical phase-shifters are slow, bulky and in general incompatible with cryogenic temperatures at which single-photon detectors (another critical component of integrated circuits) operate.

Here, we suggest a different type of phase-shifter, one based on a single quantum-emitter chirally-coupled to a nanophotonic waveguide [2]. We show how such an emitter-waveguide system can be used to shift the phase of passing photons by the requisite 2π range, and how this performance is altered by the presence of imperfections. Specifically, we consider imperfect emitter-waveguide coupling (leading to losses), directionality (i.e. sub-optimal chiral coupling, leading to reflections), pure-dephasing (a fast, scrambling of the quantum coherence) and spectral diffusion (a slow drift of the system response). We identify regions within this rich phase-space where high fidelity operation is possible, and show that it is compatible with current experimental chiral quantum systems, providing an additional route towards phase-shifters that meet the stringent requirements of quantum photonic technologies.

References

1. Carolan, J., *et al.,* "Universal linear optics," Science, 349, 711–716, 2015.
2. P. Lodahl, *et al.*, "Chiral quantum optics," *Nature* 541: 473−480, 2017.

META 2023, PARIS - FRANCE, JULY 18 – 21, 2023

Gain-enhanced chiral sensing with achiral metasurfaces

S. Droulias[1*]

[1]Department of Digital Systems, University of Piraeus, Piraeus 18534, Greece

[*]corresponding author: sdroulias@unipi.gr

Abstract: Metasurfaces are ideal platforms for enhancing the inherently weak chiroptical signals of natural optically active molecules. Intuitively, the introduction of gain could provide the desired enhancement, however requires gain media that can couple directly to the chiral medium. In this work, it is shown that metasurfaces can mediate the coupling between the gain and chiral medium, enabling enhanced chiral sensing. The coupling mechanisms are analyzed and, through numerical simulations, the regimes and conditions for enhanced chiral sensing are demonstrated.

Among the most widely used techniques for chiral sensing are the polarimetric techniques of optical rotatory dispersion (ORD) and circular dichroism (CD), both routinely applied in industrial applications [1]. However, for measurements of dilute samples, and, particularly, of nanometer-scale thin films (e.g., protein monolayers), these signals become extremely weak, close to or even below the detection limits of modern instrumentation, practically rendering the chiral medium undetectable. To overcome this limitation, modern nanophotonic-based schemes rely on the utilization of resonant near fields, rather than propagating waves [2-5]. Alternatively, one could attempt to achieve the desired enhancement in the chiroptical signals, simply by introducing gain in the vicinity of a thin chiral film, for example, thus circumventing the need for the fabrication of sophisticated nanophotonic platforms. However, this would require gain media that can couple directly to the chiral medium.

In this work it is shown that metasurfaces that generate collinear electric and magnetic dipole moments can mediate the coupling between the chiral medium and gain, leading to signals stronger than those achieved from the chiral medium alone or when combined with the same metasurface without gain [6]. It is found that the indirect coupling between the chiral medium and the gain medium depends on how strongly gain couples with the metamaterial. For weak coupling, incident waves can be amplified without the metamaterial resonance being undamped (regime of background amplification), however for strong coupling the resonance becomes undamped (sharpened), i.e. loss compensated (regime of loss compensation) [7]. In this context, it is shown that the chiroptical signal enhancement occurs within the regime of loss compensation, as background amplification may as well result in amplified transmitted fields, but does not guarantee the enhancement of their chiral far-field signatures.

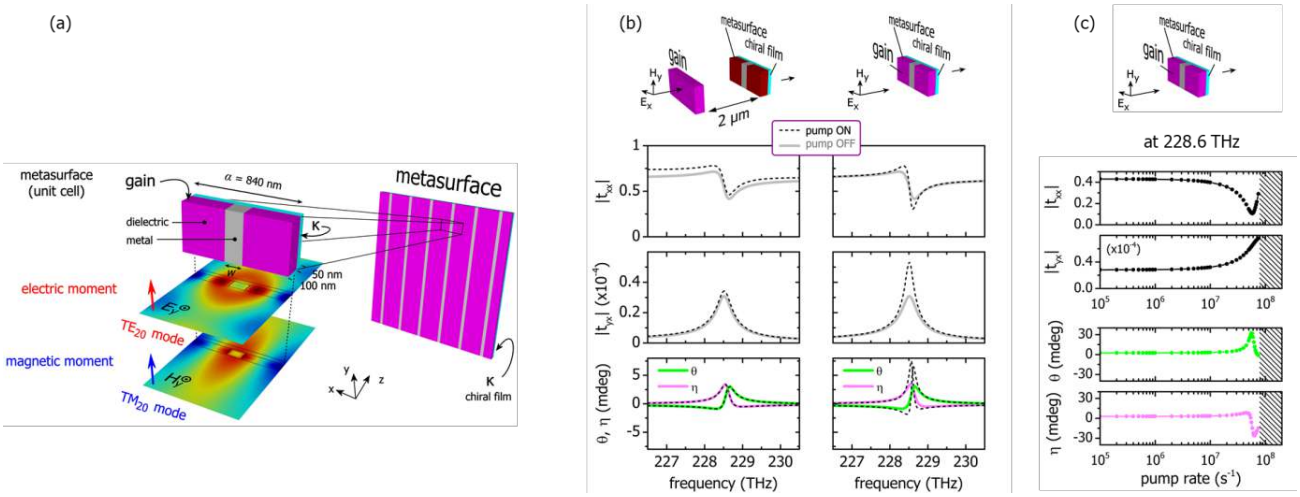


Figure 1. Achiral metasurface for gain-enhanced chiral sensing. (a) Implementation of gain-enhanced chiral sensing in the infrared, illustrating a single unit cell and a schematic of the metasurface containing 6 unit cells. The spatial field distribution of TE_{20}, the electric-type mode (that provides the electric dipole moment), and TM_{20}, the magnetic-type mode (that provides the magnetic dipole moment) are also shown. (b) Chiroptical signal enhancement for constant pump rate $R_p = 3\times10^7$ s^{-1}. *Left panel*: Gain coupled weakly to the metasurface leads to background amplification (enhanced t_{xx}, t_{yx} signals), however no chiroptical signal enhancement (optical rotation θ, ellipticity η). *Right panel*: Gain coupled strongly to the metasurface leads to loss compensation and enhanced chiroptical signals. (c) Pump-dependent study of the gain-assisted metasurface with chiral inclusions. Measurements of co-polarization (t_{xx}), cross-polarization (t_{yx}) transmission amplitudes and chiroptical signals θ, η as a function of the pump rate R_p at 228.6 THz, the resonant frequency of the metasurface's electric and magnetic modes, TE_{20} and TM_{20}, respectively.

Acknowledgements

This work was supported by the European Commission Horizon 2020, project ULTRACHIRAL (Grant No. FETOPEN-737071).

References

1. Busch, K. W., and Busch, M. A., "Chiral Analysis", Elsevier, Amsterdam, 2006.
2. Zhao, Y., Askarpour, A. N, Sun, L., Shi, J., Li, X., and Alù, A., "Chirality detection of enantiomers using twisted optical metamaterials", Nat. Commun. 8, 14180, 2017.
3. García-Guirado, J., Svedendahl, M., Puigdollers, J., and Quidant, R., "Enhanced Chiral Sensing with Dielectric Nanoresonators", Nano Lett. 20, 585-591, 2020.
4. Droulias, S., "Chiral sensing with achiral isotropic metasurfaces", Phys. Rev. B 102, 075119, 2020.
5. Droulias, S. and Bougas, L, "Chiral sensing with achiral anisotropic metasurfaces", Phys. Rev. B 104, 075412, 2020.
6. Droulias, S., "Enhanced chiral sensing using achiral metasurfaces with gain", J. Opt. Soc. Am. B 38(9), C210, 2021.
7. Droulias S., Koschny T., Kafesaki M., Soukoulis C.M., "On loss compensation, amplification and lasing in metallic metamaterials", Nanomaterials and Nanotechnology, 9, 2019.

META 2023, PARIS - FRANCE, JULY 18 – 21, 2023

The optical Dirac equation and confined modes at chiral, magnetoelectric, and non-Hermitian interfaces

S. A. R. Horsley[1*]

[1]School of Physics and Astronomy, University of Exeter, Stocker Road, Exeter, EX4 4QL UK
[*]corresponding author: s.horsley@exeter.ac.uk

Abstract: Despite describing particles of different spin, the structure of the classical Maxwell equations and the Dirac equation is almost identical. I will show this is useful for navigating the space materials, where in differing cases we can understand magneto-electric materials as an effective mass, or gauge field for light. I shall show how this analogy enables us to find new interface modes without ever solving Maxwell's equations, in addition to finding one-way propagating optical edge modes, and perfect absorbers.

The Dirac equation was developed to describe high energy electrons, but describes any spin ½ particle. For massless particles it reduces to simply the differential equation $c\,\boldsymbol{\alpha}.\nabla\,\psi+\partial_t\,\psi=0$,where $\boldsymbol{\alpha}$ is a 4x4 matrix. Interestingly, Maxwell's equations take exactly the same form as the Dirac equation when the curl equations are grouped together

$$c\begin{pmatrix}0 & -\nabla\times\\ \nabla\times & 0\end{pmatrix}\begin{pmatrix}\boldsymbol{E}\\ \eta_0\boldsymbol{H}\end{pmatrix}+\frac{\partial}{\partial t}\begin{pmatrix}\boldsymbol{E}\\ \eta_0\boldsymbol{H}\end{pmatrix}=0 \qquad (1)$$

The only modification is that the matrix $\boldsymbol{\alpha}$ is now a 6x6 matrix, consistent with the EM field being spin 1. In this form ("the optical Dirac equation") Barnett [1], and more recently Dennis et al. [2] have explored the connection between free space optics and spin half fields.

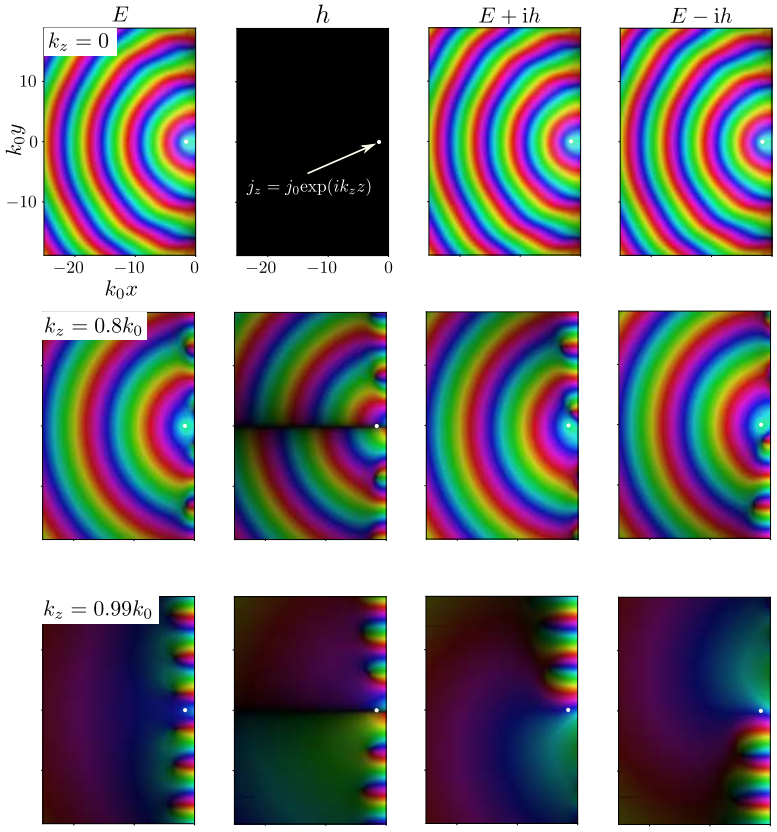
Here we use the same connection to design materials. Working at a single frequency, and introducing a set of linear material parameters (permittivity $\boldsymbol{\epsilon}$, permeability $\boldsymbol{\mu}$, and bi-anisotropy $\boldsymbol{\xi}$) , Maxwell's equations becomes

$$c\begin{pmatrix}0 & \nabla\times\\ -\nabla\times & 0\end{pmatrix}\begin{pmatrix}\boldsymbol{E}\\ \eta_0\boldsymbol{H}\end{pmatrix}=-i\,\omega\begin{pmatrix}\boldsymbol{\epsilon} & \boldsymbol{\xi}\\ \boldsymbol{\xi}^{\dagger} & \boldsymbol{\mu}\end{pmatrix}\begin{pmatrix}\boldsymbol{E}\\ \eta_0\boldsymbol{H}\end{pmatrix} \qquad (2)$$

Comparing Eq. (2) with the Dirac equation, the bianisotropy can play the role of a gauge field $\boldsymbol{\xi}$ for the EM field, a "mass" can be associated with $\boldsymbol{\epsilon}-\boldsymbol{\mu}$, and an "energy" with $\boldsymbol{\epsilon}+\boldsymbol{\mu}$ (for details see [3-4]). Using known analytical results for the Dirac equation in one and two dimensions we can use this equivalence between electromagnetic material parameters and gauge fields, mass, and energy to design materials with a given effect on the EM field.

In this talk I will review three applications of this analogy. Firstly I shall demonstrate cases of interface states between electromagnetic materials, showing that analogues of the Jackiw-Rebbi mode of the two dimensional Dirac equation occur in many chiral and non-chiral electromagnetic materials. These modes are unusual in that they are insensitive to the details of the interface, depending only on the asymptotic material

parameters. Secondly I shall explore an unusual aspect of the Dirac equation, where at zero energy the wave becomes an analytic function of position $\psi = \psi(x + i\,y)$. This analyticity indicates that the wave is only able to circulate in one sense, and is thus forced to propagate in only one direction at a boundary. Through using our Dirac-Maxwell equivalence and imposing this same condition on the material parameters in Maxwell's equations, we thus find a general condition for materials supporting unidirectional propagation, without every using topological arguments [5]. An interesting special case of this is free space, when one component of the wave-vector is fixed equal to ω/c (see Fig. 1).



Finally I will discuss the application of the Dirac-Maxwell analogy to design non-Hermitian media with controlled reflection and transmission properties, using known properties of the Dirac equation to design perfectly reflectionless index profiles [6].

Figure 1: *The Dirac equation, free space propagation, and chiral modes:* Taken from [7]. Shows the electric and magnetic fields from a line source (out of the page) along which the current is modulated with propagation constant k_z. When $k_z = k_0$ the Dirac-Maxwell analogy tells us that the wave is forced to circulate in one sense, and thus interface modes can propagate in only one direction (bottom right).

SARH acknowledges the Royal Society and TATA (URF\R\21103)

References

[1] S. M. Barnett, "*The Optical Dirac Equation*", *New J. Phys.* **16**, 093008 (2014).

[2] M. R. Dennis, T. Tijssen, and M. A. Morgan, "*On the Majorana representation of the Optical Dirac equation*" *J. Phys. A: Math. Theor.* **56**, 024004 (2023).

[3] S. A. R. Horsley, "*Topology and the Optical Dirac Equation*", *Phys. Rev.* A **98,** 043837 (2018).

[4] S. A. R. Horsley, "*Indifferent electromagnetic modes: bound states and topology*" *Phys. Rev.* A **100**, 053819 (2019).

[5] S. A. R. Horsley and M. Woolley, "*Zero-refractive-index materials and topological photonics*", *Nat. Phys.* **17** (2021).

[6] D. A. Patient and S. A. R. Horsley, "*Supersymmetry, half bound states, and grazing incidence reflection*", *J. Opt.* 075602 (2021).

[7] S. A. R. Horsley "*Tutorial: topology, waves, and the refractive index*" *arxiv:2202.08643* (2022).

META 2023, PARIS - FRANCE, JULY 18 – 21, 2023

Spin-Orbit-Coupling Mediated by an Epsilon-Near-Zero Interface

P. Banzer[1,2,3,4*], J. S. Eismann[1,2,3], L. Ackermann[3], B. Kantor[1], S. Nechayev[2], M. Z. Alam[4], R. Fickler[5], R. W. Boyd[4]

[1]Institute of Physics, University of Graz, NAWI Graz, Austria

[2]Max Planck Institute for the Science of Light, Erlangen, Germany

[3]Institute of Optics, Information, and Photonics, University Erlangen-Nuremberg, Germany

[4]Max Planck-University of Ottawa Centre for Extreme and Quantum Photonics, 25 Templeton St., Ottawa, Ontario K1N 6N5, Canada

[5]Photonics Laboratory, Physics Unit, Tampere University, Tampere, FI-33720, Finland

*corresponding author, E-mail: peter.banzer@uni-graz.at

Abstract: Taking advantage of a fundamental laws of geometrical optics, i.e., Fresnel equations, allows for coupling polarization and spatial phase degrees of freedom. We show that this conversion of spin to orbital angular momentum can be accomplished by a simple planar, homogeneous, and isotropic layer of an epsilon-near-zero material.

Epsilon-near-zero (ENZ) materials give rise to extraordinary linear and nonlinear optical effects [1]. Here we show that an unstructured circularly polarized beam incident on a planar and isotropic ENZ layer is converted into a beam carrying orbital angular momentum and, hence, a structured phase front [2,3]. While this effect can be realized for almost any interface, the vanishing permittivity of an epsilon-near-zero material environment leads to a special set of Fresnel coefficients, which greatly enhance the spin-orbit-coupling between the incident field and the converted light mode.

References

1. O. Reshef, I. De Leon, M. Z. Alam et al., “Nonlinear optical effects in epsilon-near-zero media”. Nat Rev Mater 4, 535–551, 2019.
2. H. Rubinsztein-Dunlop et al., “Roadmap on structured light,” Journal of Optics 19.1, 013001, 2016.
3. J. S. Eismann, L. Ackermann, B. Kantor, S. Nechayev, M. Z. Alam, R. Fickler, R. W. Boyd, P. Banzer, "Enhanced spin–orbit coupling in an epsilon-near-zero material," Optica 9, 1094-1099, 2022.

META 2023, PARIS - FRANCE, JULY 18 – 21, 2023

Spin-orbit Coupling and Topology of Optical Fields in Metamaterials

Vittorio Aita[1], Diane J. Roth[1], Alexey V. Krasavin[1], Anatoly V. Zayats[1*]

[1]Department of Physics and London Centre for Nanotechnology, King's College London, Strand, London WC2R 2LS, United Kingdom

[*]corresponding author: anatoly.zayats@kcl.ac.uk

Abstract: We will discuss spin-orbit coupling manifestations in interaction of complex vector beams with plasmonic metamaterials. Spin-orbit coupling and topology of evanescent waves and vector beams propagating in epsilon near-zero metamaterials will be considered.

The ability to engineer and manipulate the properties of optical wavefronts and pulses, such as phase, polarisation and amplitude, and dispersion is very important in various applications including imaging, metrology, optical communications as well as biomedical and quantum technologies [1]. As light waves carry both spin and angular optical momenta, their interactions are important in controlling the flow of light, especially on the nanoscale. Optical spin-orbit coupling describes how spin angular momentum of light (associated with circular polarisation of an electromagnetic wave) influences its extrinsic and intrinsic orbital angular momenta, associated with the propagation direction and energy flow. This effect provides interesting applications in polarisation-enabled control of optical signals, or in reverse, controlling light polarisation, sensing applications, optical forces and quantum optical processes [2–14].

In this talk, we will discuss spin-orbit coupling in guided waves and complex vector beams, both carrying longitudinal fields, their topological manifestations, interaction with anisotropic and epsilon-near-zero metamaterials, and applications. Topologically protected states in guided and propagating beams, and polarisation structure stability and transformations will be considered. Strongly anisotropic metamaterials provide a flexible platform for tailoring complex vector beams and pulses for harvesting functionalities and applications of complex light beams with complex polarisation and phase distributions in numerous photonic and quantum technologies, imaging and metrology.

This work was supported by the ERC iCOMM project (789340).

References

1. K. Y. Bloch et al, Roadmap on structural waves, arXiv 2301.05349 (2023).
2. M. F. Picardi, C. P. T. McPolin, J. J. Kingsley-Smith, X. Zhang, Sh. Xiao, F. J. Rodríguez-Fortuño, and A. V. Zayats, "Integrated Janus dipole source for selective coupling to silicon waveguide networks," Appl. Phys. Rev. 9, 021410 (2022).
3. M. F. Picardi, M. Neugebauer, J. Eismann, G. Leuchs, P. Banzer, F. J. Rodriguez-Fortuno, and A. V. Zayats, "Experimental demonstration of linear and spinning Janus dipoles for polarisation and wavelength selective near-field coupling," Light: Sci. Appl. 8, 52, (2019).
4. A. V. Krasavin, P. Segovia, R. Dubrovka, N. Olivier, G. A. Wurtz, P. Ginzburg, and A. V. Zayats, "Generalization of optical theorem: experimental proof for radially polarized beams," Light: Sci. Appl. 7, 36 (2018).
5. J. S. Eismann, L. H. Nicholls, D. J. Roth, M. A. Alonso, P. Banzer, F. J. Rodríguez-Fortuño, A. V. Zayats, F. Nori, and K. Y. Bliokh, "Transverse spinning of unpolarized light," Nature Photonics 15, 156 (2021).

6. A. Ciattoni, C. Conti, A. V. Zayats, and A. Marini, "Electric control of spin orbit coupling in graphene-based nanostructures with broken rotational symmetry," Laser Phot. Rev. 14, 2000214 (2020).
7. L. Du, A. Yang, X.-C. Yuan, and A. V. Zayats, "Deep-subwavelength features of photonic skyrmions in a confined electromagnetic field with orbital angular momentum," Nature Physics 15, 650 (2019).
8. X. Lei, A. Yang, P. Shi, Z. Xie, L. Du, A. V. Zayats, and X.-C. Yuan, "Photonic spin lattices: symmetry constraints for skyrmion and meron topologies," Phys. Rev. Lett. 127, 237403 (2021).
9. P. Shi, L. Du, C. Li, A. V. Zayats, and X.-C. Yuan, "Transverse spin dynamics in structured electromagnetic guided waves," Proc. Nat. Acad. Sci. 118, e2018816118 (2021).
10. X. Lei, L. Du, X. Yuan, and A. V. Zayats, "Optical spin–orbit coupling in the presence of magnetization: photonic skyrmion interaction with magnetic domains," Nanophotonics 10, 3667 (2021).
11. A. Afanasev, J. J. Kingsley-Smith, F. J. Rodriguez-Fortuno, and A. V. Zayats, "Non-diffractive 3D polarisation features of optical vortex beams," Adv. Photon. Nexus 2, 026001 (2023).
12. Y. Shen, B. Yu, H. Wu, C. Li, Z. Zhu, and A. V. Zayats, "Topological transformation and free-space transport of photonic hopfions, "Adv. Photon. 5, 015001 (2023).
13. V. Aita, A. V. Zayats, "Enhancement of optical spin-orbit coupling in anisotropic ENZ metamaterials," IEEE Phot. Journ. 15, 0600108 (2023).
14. Y. Shi, T. Zhu, J. Liu, D. P. Tsai, H. Zhang, S. Wang, C. T. Chan, P. C. Wu, A. V. Zayats, F. Nori, A. Q. Liu, "Stable optical lateral forces from inhomogeneities of the spin angular momentum," Sci. Adv. 8, eabn2291 (2022).

Chiro-optical characterization of self-assembled plasmonic nanostructures

E. Petronijevic[1], H. P. Ram Kumar[1], G. Leahu[1], R. Li Voti[1], C. Sibilia[1], and A. Belardini[1]*

[1]Sapienza Università di Roma, SBAI Department, Italy
*corresponding author: Alessandro.belardini@uniroma1.it

Abstract: In order to control the circular polarization of light at nanoscale, complex structures can be realized. Among different fabrication techniques, self-assembled approach can produce high reproducible, low cost, large area asymmetric metasurfaces that present different optical functionalities, and in particular can exhibit chiral optical response both in the near field and in the far field. Here we show the optical chiral properties of different self-assembled metasurfaces measured by different characterization techniques, both in linear and nonlinear regime.

.

Symmetry breaking in plasmonic nanostructures can lead to strong manipulation of the circular polarization at the nanoscale. Among different complicated fabrication techniques, self-assembled procedure can be a suitable way for low-cost, time-reduced, large area, chiral-effective metasurfaces production. In this talk, after summarizing the relationship between chirality and symmetry breaking that leads to the concept of pseudo-chirality or extrinsic chirality [1], we show that this concept, together with real chirality gives rise to effective chiro-optical signal in different self-assembled plasmonic nanostructures. We apply different measurement techniques, based on transmission/reflection of light, absorption measured by photoacoustic technique (PA), second harmonic generation (SHG) on nanostructures, showing that managing the symmetry of the investigated system can lead to a tuning of the spatial localization of the circular polarized components of the electromagnetic radiation in proximity of the plasmonic nanoantennas. This fact open the possibility to fine tune the chiro-optic properties of the different nanostructures under study.

We start showing results on very simple geometries like nanowires and nanopillars. First example is a metasurface formed by tilted gold nanowires: by depositing gold at grazing incidence on a silicon substrate maintained at a temperature of ~300 K (Glancing Angle Deposition-GLAD) were realized a self-ordered forest of tilt Au 300nm long nanowires (NWs). The asymmetric orientation of the gold wires with respect to the pumping light orientation (Fig.2a) leads to the excitation of extrinsic chiral response in reflection, PA and SHG response that can be evaluated by using circular polarized pump light [2]. Second example is a sample formed by Au partially covered GaAs nanowires 5 microns long fabricated on Si substrate by a by a self-catalyzed approach. Also in this case we present reflection, PA and SHG measurements [3]. Comparison with the same sample without asymmetric gold covering gives rise to a dramatic circular dichroism enhancement.

The last set of samples that we show present a planar arrangement of polystyrene nanospheres (PNS) covered by asymmetric metallic shell. From that sample, by removing the polystyrene spheres is obtained a elliptical nanohole array (NHA) that exhibit chiral properties in a broad near-infrared range [4].

Here, we demonstrate the broadband chiral properties of such nanostructures exhibit interesting resonant features which are widely tunable by means of the incident angle.

Chiral optical properties namely the circular dichroism (CD) of the NHA are governed by the incident angle-dependent coupling of the light with Rayleigh anomalies and surface plasmon polaritons (see figure 1). On

this samples we performed chiral transmission measurements, photoacoustic absorption (PA) and photothermal deflection (PD) experiments [5-8].

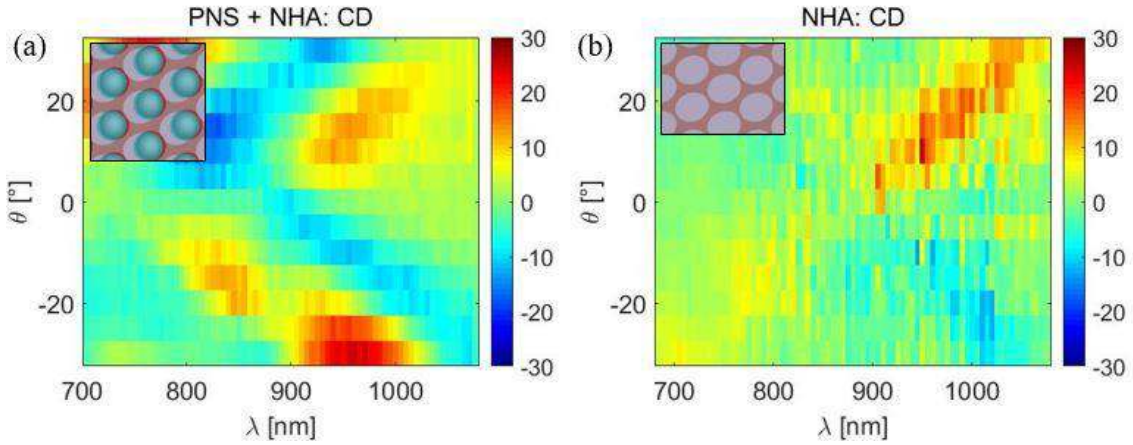


Figure 1. Map of circular dichroism as a function of the wavelength and the incident angle θ, for the sample with (a) PNS and NHA, and (b) with NHA only (after PSN removal).

A.B. acknowledges LASAFEM Sapienza Università di Roma Infrastructure Project prot. n. MA31715C8215A268 and the Sapienza Research Grant prot. n. RG1221816B6FA2E9.

References

1. A. Belardini, M. C. Larciprete, M. Centini, E. Fazio, C. Sibilia, D. Chiappe, C. Martella, A. Toma, M. Giordano, and F. Buatier de Mongeot, Phys. Rev. Lett. 107, 257401 (2011).
2. A. Belardini, M. Centini, G. Leahu, D.C. Hooper, R. Li Voti, E. Fazio, J. W. Haus, A. Sarangan, V. K. Valev, C. Sibilia, Scientific Reports 6, 31796 (2016).
3. G. Leahu, E. Petronijevic, A. Belardini, M. Centini, C. Sibilia, T. Hakkarainen, E. Koivusalo, M. Rizzo Piton, S. Suomalainen, and M. Guina, Adv. Optical Mater. 2017, 1601063 (2017).
4. E. Petronijevic, G. Leahu, R. Li Voti, A. Belardini, C. Scian, N. Michieli, T.Cesca, G.Mattei, and C. Sibilia, "Photo-acoustic detection of chirality in metal-polystyrene metasurfaces", Appl. Phys. Lett. 114, 053101 (2019).
5. E. Petronijevic, H. Ali, N. Zaric, A. Belardini, G. Leahu, T. Cesca, G. Mattei, L. C. Andreani, and C. Sibilia, "Chiral effects in low-cost plasmonic arrays of elliptic nanoholes," Opt Quant Electron 52, 176 (2020).
6. E. Petronijevic et al., Sci. Rep. 11, 4316 (2021).
7. E. Petronijevic et al., Phys. Rev. Appl. 16(1), 014003 (2021).
8. R. Li Voti et al., Appl. Sci. 12, 1109 (2022).

META 2023, PARIS - FRANCE, JULY 18 – 21, 2023

Chirality sensing employing parity-time symmetric and general gain-loss media

I. Katsantonis[1,2], M. Kafesaki[1,2]

[1] Institute of Electronic Structure and Laser, Foundation for Research and Technology Hellas (FORTH), N. Plastira 100, 70013 Heraklion, Crete, Greece

[2] Dept. of Materials Science and Technology, University of Crete, 70013 Heraklion, Crete, Greece

*corresponding author: kafesaki@iesl.forth.gr

Abstract: We demonstrate the potential of gain materials and parity-time symmetric systems to enhance the circular dichroism response and the dissymmetry factor of molecular chiral systems, highly facilitating thus the sensing of such systems and the discrimination of the different enantiomers, issue critical in biology and pharmaceutics.

Molecular chirality sensing and enantiomer discrimination is an issue of particularly high importance for biology, medicine and pharmaceutical industry. This is due to the fact that the two different enantiomers of a chiral substance (e.g. a medicine), although they share the same physical properties, they can have completely different biological activity. To detect chirality, a common approach to date is based on the exploitation of another difference of the two enantiomers: their different interaction with circularly polarized light, and in particular the different absorption of left- and right-handed circularly polarized waves, known as circular dichroism (CD=A_+-A_-; $A_{+/-}$ is the absorption of right/left-handed circularly polarized waves; denoted by +/- respectively). Circular dichroism (CD) response signal though of chiral molecules is usually extremely weak, making difficult the detection of small quantities of a chiral substance. Recently it was shown that a very promising way to enhance the CD signal is through the interaction of a chiral substance with super-chiral local fields, i.e. fields with optical chirality, C, larger than that of circularly polarized light ($C \propto \mathrm{Im}(\boldsymbol{E}\cdot\boldsymbol{H}^*)$, with $\boldsymbol{E}$, $\boldsymbol{H}$, electric and magnetic field, respectively; Im denotes the imaginary part and * complex conjugation). Such local fields can be produced in the vicinity of properly designed nanophotonic or metamaterial structures. The realization of the C-mediated CD enhancement stimulated an intense research effort to devise design rules for super-chiral field generation and to design appropriate structures and strategies.

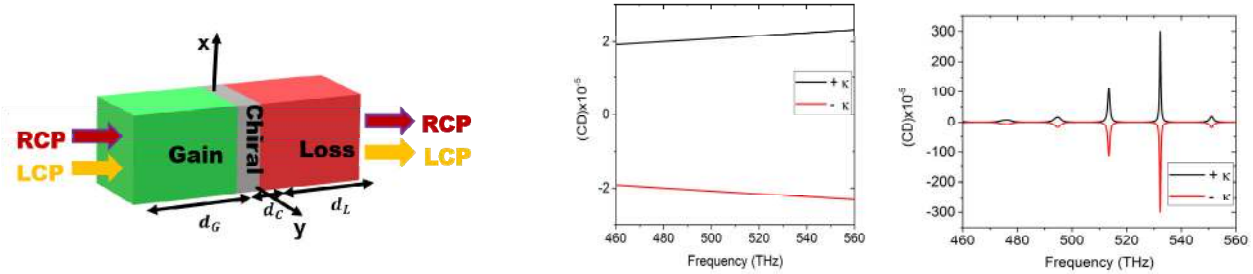


Fig. 1: Left panel: A PT-symmetric bilayer with a thin (10 nm) chiral layer in between the gain and loss layers (of μm thickness); RCP and LCP denote the right and left-handed circular polarization respectively. The gain and loss here are considered constant (frequency independent). For details see [1]. Middle panel: Circular dichroism of the chiral layer alone. Black and red lines show the CD for layers made of the two different enantiomers of the chiral substance.

Right panel: Circular dichroism for the chiral layer in the middle of the gain-loss bilayer. An up to x1500 CD enhancement compared to the chiral layer alone can be observed. The maximum enhancement is achieved at the lasing threshold of the PT-symmetric system.

Here we propose an approach that is able to be combined with nanophotonics-based structures and strategies and enhance not only the CD response of a chiral substance but also the dissymmetry factor, *g*. (*g* is crucial not only for chirality sensing but also for enantio-specific synthesis; it is defined as the ratio of the circular dichroism to the average absorption, $(A_+ + A_-)/2$). This is by employing gain media. Gain media, by providing "negative" absorption, can highly extend the absorption-related properties and capabilities of any structure and device that they are involved. To test the potential of gain materials in chirality sensing we examined the simplest possible gain-loss system, i.e. a gain-loss bilayer (see Fig. 1), empowering it though with Parity-Time-symmetry, which gives the possibility of zero total absorption and advanced tailoring of the optical modes of a system. The chiral medium was placed initially in the middle of the PT-bilayer, as shown in Fig. 1 [1]. Even in this simple geometry we achieved an enormous circular dichroism enhancement (see Fig. 1), with the CD reaching values up to 1500 times larger than the ones achieved for chiral layer alone. The largest CD enhancement was achieved at the lasing threshold of the PT-bilayer, close to the exceptional point of the system. Besides, we overserved in the system an up to 15 times dissymmetry factor enhancement compared to the chiral layer alone, with the *g*-peaks to coincide with the anisotropic transmission resonances of the PT-bilayer.

Similar to the above results were obtained also when the chiral layer was placed next to the gain layer of the bi-layer (at the left side of the structure of Fig. 1), while placing it next to the loss layer led to significant deterioration of the observed response. Moreover, in all cases we examined the CD enhancement was always associated with enhancement of the field chirality in the position of the chiral structure.

To test the impact of gain and PT-symmetry in structures more favorable for super-chiral near fields than the PT-bilayer (which is actually a Fabry-Perot resonator), we examined also metasurfaces based on dielectric cylindrical pillars with incorporated gain material. In all the cases the gain-involving structure led to significant enhancement of both circular dichroism and dissymmetry factor response, verifying that the employment of gain media can lead to a novel path in the molecular chirality sensing research and applications.

References

1. Katsantonis I., Droulias S., Soukoulis C. M., Economou E. N., Rakitzis P. T., Kafesaki M., "Chirality sensing employing parity-time-symmetric and other resonant gain-loss optical systems", Phys. Rev. B, Vol. 105, 174112, 2022.

META 2023, PARIS - FRANCE, JULY 18 – 21, 2023

Noncollinear chiral orbitronics

T. G. Saunderson[1,2*], F. R. Lux[1,3], D. Go[1,2], W. Feng[4], M. Kläui[1,5] and Y. Mokrousov[1,2]

[1]Institute of Physics, Johannes Gutenberg-University, Staudingerweg 7, 55128 Mainz, Germany
[2]Peter Grünberg Institut and Institute for Advanced Simulation, Forschungszentrum Jülich, 52425 Jülich, Germany
[3]Department of Physics, Yeshiva University, New York, NY, USA
[4]Beijing Institute of Technology, Beijing 100081, China
[5]Centre for Quantum Spintronics, Norwegian University of Science and Technology, 7491 Trondheim, Norway
[*]corresponding author: tsaunder@uni-mainz.de

Abstract: Non-collinear antiferromagnets (NC-AFM) have attracted much attention recently due to the observation of the anomalous Hall effect (AHE) in these materials despite the small magnetic moments present in their unconventional spin structures, in addition to the giant piezomagnetism and a strain-induced anomalous Nernst effect. These fascinating qualities have hints of multiple competing orders that could be harnessed to enable chirality switching and bring these materials ever closer to realistic antiferromagnetic spintronic devices.

Modern spintronics must adapt to meet the challenges of the new era. Computer processors can no longer follow Moore's law yet the demand for greater computational power is ever increasing. Inventive solutions are therefore required to achieve the desired processing power whilst also being more energy efficient to combat the increasing effects of climate change. Chiral magnetic textures have emerged as a promising avenue for addressing these challenges, as they have already shown to exhibit a wide range of exotic phenomena such as skyrmionic textures [1], large anomalous [2], spin [3] and chiral hall [4] effects and even long-range triplet supercurrents have been generated when interfaced with superconductors [5,6].

Furthermore, the new and upcoming field of orbitronics [7] has established itself as a possible successor to spintronics due its prolific orbital current generation and efficient orbital-to-spin conversion [8,9]. The materials which exhibit large orbital currents do not correlate with the spin-orbit interaction and some are very light such as 3d elements [7], paving the way for extremely efficient devices which do not require expensive materials to manufacture. Whilst recently the potential for a 'chiral' spin current and subsequent chirality switching has been addressed [4], the addition of the orbital degree of freedom presents a new channel which, when coupled to the chiral degree of freedom, could allow for more flexibility when designing realistic antiferromagnetic spintronic devices.

In this talk, I will discuss our recent work unpacking the competing orders present in chiral magnetic textures in noncollinear antiferromagnets using a combination of first principles and model techniques to introduce the orbital degree of freedom. We construct an efficient basis set of maximally localized Wannier functions to describe the orbital textures complete with spin orbit coupling, and introduce the noncollinear magnetic textures with a combination of fully noncollinear first principles spin relaxation calculations and exchange fields in the Wannier functions. Such a technique represents the first ever attempt to combine both noncollinear magnetism with orbital currents in a first principles-based approach. This work aims to shed light on the complex interplay of competing magnetic orders present in the latest experiments on noncollinear antiferromagnets, whose response to current, strain and temperature go beyond the current understanding of the state-of-the-art.

We gratefully acknowledge the Jülich Supercomputing Centre for providing computational resources under project jiff40. This work was funded by the Deutsche Forschungsgemeinschaft (DFG, German Research

Foundation) - Grants No. TRR 173/2 - 268565370 Spin+X (projects A01, BO2 and A11), No. TRR 288 - 422213477 (project B06) and CRC 1238 -- 277146847 (project C01).

References

1. Shibata, K., Yu, X. Z., Hara, T., Morikawa, D., Kanazawa, N., Kimoto, K., Ishiwata, S., Matsui, Y. and Tokura, Y., "Towards Control of the Size and Helicity of Skyrmions in Helimagnetic Alloys by Spin–Orbit Coupling", Nat. Nanotech., Vol. 8, No. 10, 723, 2013.
2. Nayak, A. K., Fischer, J. E., Sun, Y., Yan, B., Karel, J., Komarek, A. C., Shekhar, C., Kumar, N., Schnelle, W., Kübler, J., Felser, C. and Parkin, S. S. P., "Large Anomalous Hall Effect Driven by a Nonvanishing Berry Curvature in the Noncolinear Antiferromagnet Mn3Ge", Sci. Adv., Vol. 2, No. 4, e1501870, 2016.
3. Kimata, M., Chen, H., Kondou, K., Sugimoto, S., Muduli, P. K., Ikhlas, M., Omori, Y., Tomita, T., MacDonald, A. H., Nakatsuji, S. and Otani, Y., "Magnetic and Magnetic Inverse Spin Hall Effects in a Non-Collinear Antiferromagnet", Nature, Vol. 565, No. 7741, 627-630, 2019.
4. Go, D., Sallermann, M., Lux, F. R., Blügel, S., Gomonay, O. and Mokrousov, Y., "Noncollinear Spin Current for Switching of Chiral Magnetic Textures", Phys. Rev. Lett., Vol. 129, No. 9, 097204, 2022.
5. Jeon, K. R., Hazra, B. K., Cho, K., Chakraborty, A., Jeon, J. C., Han, H., Meyerheim, H. L., Kontos, T. and Parkin, S. S. P., "Long-Range Supercurrents through a Chiral Non-Collinear Antiferromagnet in Lateral Josephson Junctions", Nat. Mater., Vol. 20, No. 10, 1358-1363, 2021.
6. Chan, A. K., Cubukcu, M., Montiel, X., Komori, S., Vanstone, A., Thompson, J. E., Perkins, G. K., Blamire, M., Robinson, J. W. A., Eschrig, M., Kurebayashi, H. and Cohen, L. F., "Controlling Spin Pumping into Superconducting Nb by Proximity-Induced Spin-Triplet Cooper Pairs", arXiv:2202.01520, 2022.
7. Go, D., Jo, D., Lee, H. W., Kläui, M. and Mokrousov, Y., "Orbitronics: Orbital Currents in Solids", Europhys. Lett., Vol. 135, No. 3, 37001, 2021.
8. Ding, S., Ross, A., Go, D., Baldrati, L., Ren, Z., Freimuth, F., Becker, S., Kammerbauer, F., Yang, J., Jakob, G., Mokrousov, Y. and Kläui, M., "Harnessing Orbital-to-Spin Conversion of Interfacial Orbital Currents for Efficient Spin-Orbit Torques", Phys. Rev. Lett. Vol. 125, No. 17, 177201, 2020.
9. Ding, S., Liang, Z., Go, D., Yun, C., Xue, M., Liu, Z., Becker, S., Yang, W., Du, H., Wang, C., Yang, Y., Jakob, G., Kläui, M., Mokrousov, Y. and Yang, J., "Observation of the Orbital Rashba-Edelstein Magnetoresistance", Phys. Rev. Lett., Vol. 128, No. 6, 067201, 2022.

META 2023, PARIS - FRANCE, JULY 18 – 21, 2023

Mixed Quantum/Classical Approach to Surface-Enhanced Spectroscopies

T. Giovannini[1*], and C. Cappelli[1]

[1]Scuola Normale Superiore, Piazza dei Cavalieri 7, 56126, Pisa, Italy

[*]corresponding author: tommaso.giovannini@sns.it

Abstract: We present a novel theoretical approach to calculate the optical response of molecular systems interacting with plasmonic substrates, either metallic or graphene-based.

Peculiar electromagnetic responses arise when a molecular system is adsorbed on plasmonic substrates under the effect of an external radiation. As an example, surface enhanced Raman scattering (SERS) has become a widely used analytical technique, taking advantage of the huge enhancement of the Raman signal when a target molecule is adsorbed on metal nanoaggregates [1]. This phenomenon can allow single molecule detection, thanks to enhancement factors as much as 10^{10} [1]. In this contribution, we present a novel theoretical approach to treat surface-enhanced spectroscopies, including SERS. The plasmonic structure is described by means of fully atomistic classical electromagnetic models, which have recently been developed by the present authors [2-5]. The adsorbed molecular system is treated at the quantum mechanical (QM) level. The approach can treat nanostructures of complex shape, and are general enough to describe both metal nanoparticles [2,3,5] and graphene-based materials [4,6] at the same level of accuracy. The approach has huge potential for large scale nanoplasmonic simulations (more than 1 million atoms), also for systems dominated by quantum effects, such as subnanometer junctions [2,5], or geometrical defects [6,7].

The robustness and reliability of the developed method is demonstrated for selected test cases and by the comparison with experimental spectra [8].

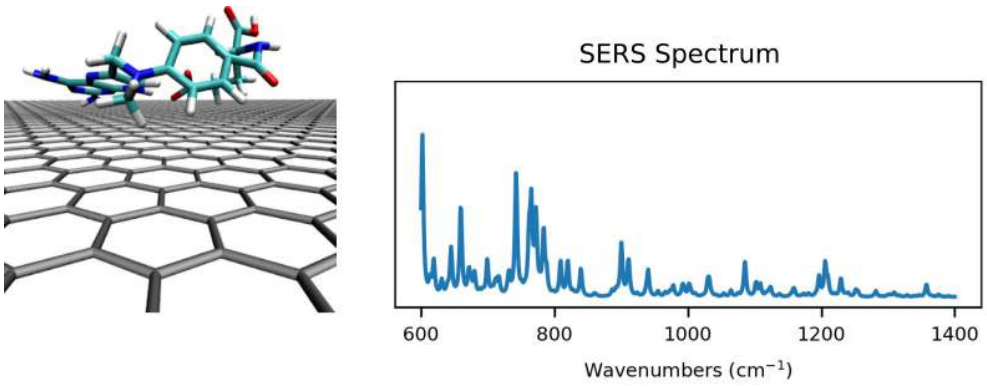


Fig. 1 Graphical depiction of methotrexate adsorbed on a graphene disk (left) and the corresponding calculated SERS spectrum (right).

This work has received funding from the European Research Council (ERC) under the European Union's Horizon 2020 research and innovation programme (grant agreement No. 818064).

References

1. Langer, J. et al. "Present and future of surface-enhanced Raman scattering", ACS Nano, Vol. 14, 28–117, 2019.
2. Giovannini, T., M. Rosa, S. Corni and C. Cappelli, "A classical picture of subnanometer junctions: an atomistic Drude approach to nanoplasmonics", Nanoscale, Vol. 11, 6004–6015, 2019.
3. Bonatti, L., G. Gil, T. Giovannini, S. Corni and C. Cappelli, "Plasmonic resonances of metal nanoparticles: Atomistic vs. continuum approaches", Front. Chem., Vol. 8, 340, 2020.
4. Giovannini, T., L. Bonatti, M. Polini and C. Cappelli, "Graphene plasmonics: Fully atomistic approach for realistic structures", J. Phys. Chem. Lett., Vol. 11, 7595–7602, 2020.
5. Giovannini, T., L. Bonatti, P. Lafiosca, L. Nicoli, M. Castagnola, P. Grobas Illobre, S. Corni and C. Cappelli, "Do we really need quantum mechanics to describe plasmonic properties of metal nanostructures?", ACS Photonics, Vol. 9, 3025–3034, 2022.
6. Bonatti, L., L. Nicoli, T. Giovannini and C. Cappelli, "In silico design of graphene plasmonic hot-spots", Nanoscale Adv., Vol. 4, 2294–2302, 2022.
7. Zanotto, S., L. Bonatti, M. F. Pantano, V. Miseikis, G. Speranza, T. Giovannini, C. Coletti, C. Cappelli, A. Tredicucci and A. Toncelli, "Strain-Induced Plasmon Confinement in Polycrystalline Graphene", ACS Photonics, (2023), Vol. 10, 394–400, 2023.
8. Lafiosca, P., L. Nicoli, L. Bonatti, T. Giovannini, S. Corni and C. Cappelli, "QM/Classical Modeling of Surface Enhanced Raman Scattering Based on Atomistic Electromagnetic Models", submitted.

META 2023, PARIS - FRANCE, JULY 18 – 21, 2023

Creating, Reading, and Switching Skyrmions in a Magnetic Tunnel Junction

Shaohai Chen[1]

[1] Institute of Materials Research & Engineering, Agency for Science, Technology &

Research (A*STAR), 138634 Singapore

Abstract: Magnetic skyrmions – nanometre-scale topological spin textures – are promising active elements for scalable, energy-efficient bio-inspired and unconventional computing electronic devices. A key technological roadblock to unleashing their potential is achieving deterministic electrical readout and manipulation. Here we present wafer-scale realization of a nanoscale skyrmionic magnetic tunnel junction (SK-MTJ) shown to host a single skyrmion in addition to uniform states, and systemically investigate its electrical and magnetic properties.

Besides the parallel and antiparallel MR states possessed by conventional MTJ, the SK-MTJ exhibits an additional skyrmion state with sizeable MR (20-70%), whose magnitude scales proportionally with skyrmion size. A suite of electrical and imaging techniques demonstrates that the nanoscale SK-MTJ consistently nucleates skyrmion with a fixed polarity, albeit via two distinct, asymmetric mechanisms. The distinguishing feature in turn facilitates the zero-field stability of distinctly sized skyrmions, with established promise towards multi-state functionality. Crucially, it is found that such SK-MTJs can be electrically switched by using a low current density of about ~10^7 A/m^2, ~1000 times lower than achievable via conventional spin torques. The possible originations are attributed to the voltage control of magnetic anisotropy (VCMA) and spin transfer torque (STT) effects, which collaboratively drive skyrmion nucleation and deletion in our SK-MTJs. Together, our findings provide a platform to incorporate electrical readout, writing and erasing within skyrmionic devices, and provide a springboard for their use in unconventional computing applications.

META 2023, PARIS, JULY 19 – 22, 2022

Parity-broken vacuum as a chiral catalyst

Yanzhe Ke[1], Zhigang Song[2], and Qing-Dong Jiang[1*]

[1]Shanghai Jiao Tong University, China
[2]Harvard University, America
[*]corresponding author: qingdong.jiang@sjtu.edu.cn

Abstract: A material with symmetry breaking inside can transmit the symmetry breaking to its vicinity by vacuum fluctuations. The vacuum in proximate to a symmetry-broken material is referred as its quantum atmosphere[1]. Here, we show that a parity-symmetry-broken quantum atmosphere can induce a chirality-dependent shift of the ground-state energy of a chiral molecule, resulting in a chemical reaction process that favors producing one chirality over the other[2]. We evaluate the chirality production rate for concrete examples, showing the promise of quantum atmospheric selectivity.

Summary: Chemical and physical systems can occur in two forms distinguished solely by being images of each other. This phenomenon, known as chirality, interlocks the physical and biochemical sciences and attracts continuous interest. Two related research directions are of great importance: i) What is the origin of molecular handedness? ii) How to find a universal and efficient way to select chirality?

In this paper[4], we propose an entirely new route to select chirality by using quantum fluctuations near parity-symmetry-broken materials. The vacuum in proximate to a symmetry-broken material is referred as its quantum atmosphere[1,2,3]. Using quantum atmosphere to select chirality is efficient yet dramatically different from previous proposals where real fields are needed. We show that parity-symmetry breaking and quantum fluctuations can induce a chirality-dependent shift of the molecular ground-state energy, leading to a chemical reaction process that favors producing one chirality over the other. Besides analytical analysis, we further perform the first-principle calculation to find specific examples, showing that our proposal gives significant chirality selectivity.

Acknowledgements: The authors are sponsored by Pu- jiang Talent Program 21PJ1405400 and TDLI starting up grant and Jiaoda 2030.

References

1. Qing-Dong Jiang, and Frank Wilczek, Quantum atmospherics for materials diagnosis, Phys. Rev. B 99, 201104(R).
2. Qing-Dong Jiang and Frank Wilczek, Axial Casimir force, Phys. Rev. B 99, 165402 (2019).
3. Qing-Dong Jiang and Frank Wilczek, Chiral Casimir forces: Repulsive, enhanced, tunable, Phys. Rev. B 99, 125403 (2019).
4. Yanzhe Ke, Zhigang Song, and Qing-Dong Jiang, Can vacuum select chirality in chemical reactions? arXiv: 2211.11132
5. Yanzhe Ke, and Qing-Dong Jiang, in preparation.

META 2023, PARIS - FRANCE, JULY 18 – 21, 2023

Chiral photonic cavity based on multiferroic layers

Vakhtang Jandieri[1,2], Ramaz Khomeriki[3], Koki Watanabe[4], Daniel Erni[2], Douglas H. Werner[5], and Jamal Berakdar[1,*]

[1]Martin-Luther University, Halle-Wittenberg, 06099 Halle, Germany
[2]Faculty of Engineering, Center for Nanointegration Duisburg-Essen, 47048 Duisburg, Germany
[3]Physics Department, Tbilisi State University, 3 Chavchavadze, 0128 Tbilisi, Georgia
[4]Department of Information and Communication Engineering, Fukuoka Institute of Technology, Fukuoka 811-0295, Japan
[5]Department of Electrical Engineering, The Pennsylvania State University, University Park, PA 16802, USA
[*]corresponding author: jamal.berakdar@physik.uni-halle.de

Abstract: An electrically controllable multilayer structure for discerning and confining chiral electromagnetic fields is demonstrated. Upon scattering, the chiral nature of the noncollinear spin texture in multiferroic layers is imprinted on the electromagnetic fields resulting in well-defined and electrically controlled chirality density of the standing waves within the resonator. Analytical and full-numerical, material-specific simulations endorse the feasibility and flexibility of the proposed scheme.

Schemes for generating externally tunable chiral photonic fields and resonators are of key importance to studying and functionalizing chiral matter (1). Considering dielectric stacks of oxide helical multiferroic (2) layers, we propose a setup for electrically-controllable resonator that efficiently traps purely chiral photonic fields (Fig.1).

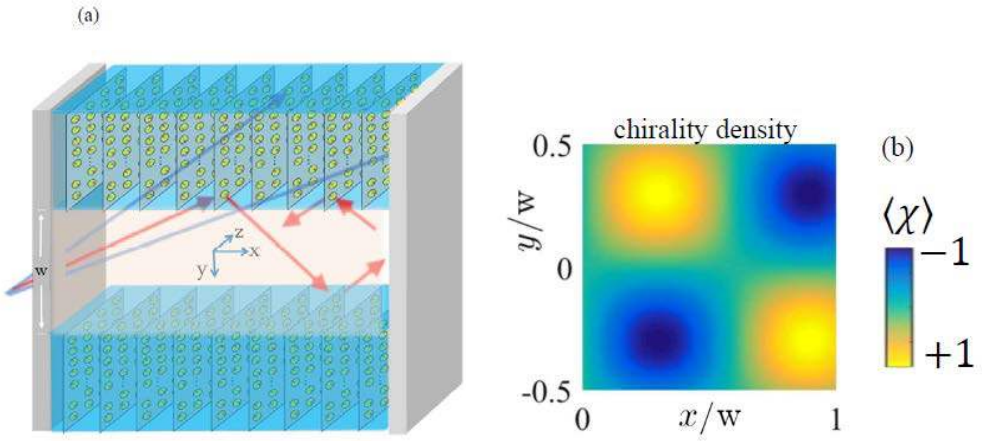


Figure 1: (a) Proposal for an electrically controlled generation of purely chiral light between chiral multiferroic multilayers. The modes are bounded by perfect mirrors attached to the left and right sides of the resonator. *w* is the thickness of the confining region. Radiative modes (blue arrows) leak out from the guiding region. Standing wave modes (red arrows) are purely chiral due to the spin-dependent scattering of electromagnetic waves from the non-collinear spin texture (small red arrows in the yellow circles) in the multiferroic layers. (b) The calculated, time-averaged chiral density of the standing waves within the resonator. The spin texture is tunable by a DC voltage.

Using analytical and the rigorous coupled wave methods (3) we performed simulations and analysis that expose the dispersion and scattering properties of electromagnetic waves in multiferroic (2) multilayers. The results evidence that due to scattering from the non-collinear spin texture in the multiferroic layers, only modes with a particular transverse wavenumber leads to the formation of standing chiral waves in the resonator. All other modes leak out from the cavity. An external static electric field leads to a change in the spin texture in the multiferroic layers. Therefore, also the enclosed modes in the cavity and their chirality are affected and can be tuned to a certain extent.

Acknowledgements: This work is funded by the DFG.

References

1. Mun, J. et al. "Electromagnetic chirality: from fundamentals to nontraditional chiroptical phenomena," Light: Science & Applications 2020, 9, 139.

2. Fiebig, M., Lottermoser, Th., Meier, D., and Trassin, M., "The evolution of multiferroics," Nature Reviews Materials 2016, 1, 16046. 3.

3. Jandieri, V., Khomeriki, R., Chotorlishvili, L., Watanabe, K., Erni, D., Werner, D. H., and Berakdar, J., "Photonic signatures of spin-driven ferroelectricity in multiferroic dielectric oxides," Phys. Rev. Lett. 2021, 127, 127601.

Chirality of the electromagnetic fields of resonant nanostructures

M Nicolas[1,2], J. Amboli[3], L. Cui[1], P.M. Whalmsness[4], X. Yang[1], C. Schwob[1], G. Demesy[3], M. Mivelle[1], M. Kildemo[4], S. Boujday,[2] N. Bonod[3], B. Gallas[1,*]

[1]Sorbonne Université-CNRS, Institut des NanoSciences de Paris, UMR 7588, 75005 Paris, France
[2]Sorbonne Université – CNRS, Laboratoire de Réactivité de Surface, UMR 7197, 75005 Paris, France
[3]Institut Fresnel-CNRS, UMR 7249, 13013 Marseille, France
[4]Department of Physics, NTNU, Trondheim, Norway
[*]corresponding author: Bruno.gallas@insp.jussieu.fr

Abstract: Metallic nanostructures support localized surface plasmon resonances (LSPR) resulting from the collective motion of the electrons excited by electromagnetic fields. At the LSPR, the intensity of the electromagnetic near-field is also strongly enhanced, which find applications in many domains of Physics, Chemistry, Biology… Lately, there has also been a strong interest in the vectorial properties of the electromagnetic nearfield, in particular for generating strong chiral fields which may be used for biodetection applications.

The chirality of the interaction of light with resonant nanostructures is generally characterized through the measurement of Circular Dichroism (CD) which measures the difference in the absorption rates of the nanostructures for light of opposite helicities. However, in the case of supported and/or oriented nanostructures, the measured CD does not necessarily mean chirality. Secondly, the farfield measured CD does not give all the information about the nearfield polarimetric properties of the electromagnetic field.

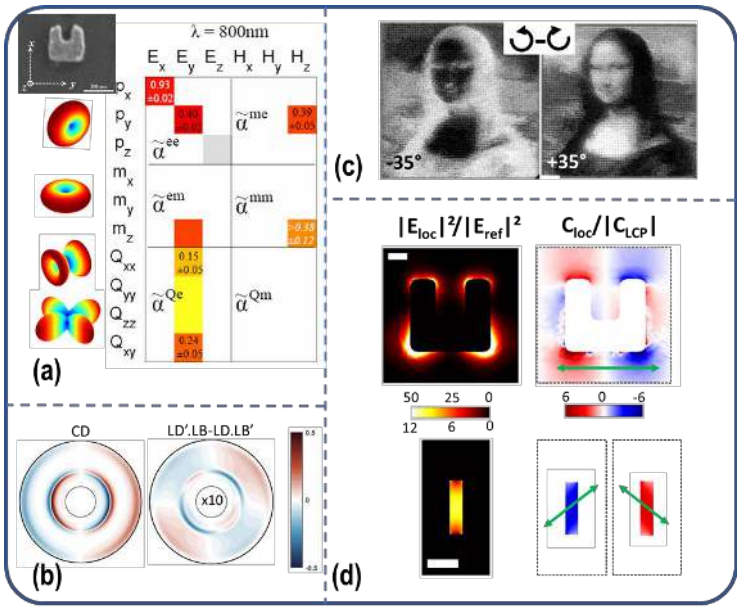


Figure 1: (a) polarizability tensor of achiral resonators exhibiting chiral optical response. (b) True CD and contribution of linear retardance and diattenuation to the CD of U-shaped resonators as a function of wavelength and azimuthal angle. (c) Image showing contrast reversal in CD based on achiral resonators. (d) Calculated chiral near field intensity and chirality density for incident linear polarization for U-shaped resonators and nanoslits in gold. The white scale bar is 50 nm.

Nanostructures obtained through top-down techniques (lithography, ion etching…) are very useful for the precise control of the shape and the organization they offer. Even achiral nanostructures supporting multipolar modes can exhibit chiral electromagnetic fields which chirality can be reversed upon changes in the illumination conditions (Figure 1(a) and (b)). [1] Farfield polarimetric properties can then been used to generate contrast in CD that is controllable spatially [2]. The link with the nearfield is more difficult to establish and relies on extensive numerical simulations. Numerical simulations show the generation of unexpected effects like asymmetric or uniform and reversible chiral fields (Figure 1(d)) for illumination conditions that do not yield any farfield CD. [3] These effects are very promising effects for the detection of chiral biomolecules because they offer additional degrees of freedom and increased sensitivity.

This work was realized partly thanks to the support of the ANR (n◦ ANR-18-CE09-0010). LC and XY acknowledge support from the Chinese Science Council.

References

1. Proust, J., Grand, J., Bonod, N., Gallas, B., “Optical monitoring of the magneto-electric coupling in individual plasmonic scatterers”, ACS Photonics, Vol. 3 1581-1588, 2016
2. Sang Hyuk Yoo, T., Berthelot, J., Guida, G., Demaille, D., Garcia-Caurel, E., Bonod, N., B. Gallas, “Circularly polarized images with contrast reversal using pseudochiral metasurfaces”, ACS Photonics 4068-4073, 2018
3. Cui, L., Yang, X., Reynier, B., Schwob, C., Bidault, S., and Gallas, B., & Mivelle, M. “An achiral magnetic photonic antenna as a tunable nanosource of superchiral light.,” https://doi.org/10.48550/arXiv.2301.11044

Microwave-to-Optical Quantum Transduction Utilizing the Topological Magnetoelectric Effect

Akihiko Sekine[1*], Mari Ohfuchi[1], and Yoshiyasu Doi[1]

[1]Fujitsu Research, Fujitsu Limited, Japan
[*]corresponding author: akihiko.sekine@fujitsu.com

Abstract: The quantum transduction between microwave and optical photons is essential for realizing scalable quantum computers with superconducting qubits. Due to the large frequency difference between microwave and optical ranges, the transduction needs to be done via intermediate bosonic modes or nonlinear processes. In this study, we focus on the transduction via the magneto-optic Faraday effect (i.e., the magnon-photon interaction) and propose that the transduction efficiency can be greatly improved by utilizing magnetically doped topological insulator thin films.

The quantum transduction, or equivalently quantum frequency conversion, is an important quantum technology which enables the interconnects between quantum devices. Especially, the quantum transduction between microwave and optical photons has so far gathered attention in pursuit of large-scale quantum computers with superconducting qubits [1]. Due to the large frequency difference between microwave and optical ranges, the transduction needs to be done via the interaction between photons and intermediate bosonic modes or via the nonlinear interaction between photons, such as optomechanical effect, electro-optic effect, and magneto-optic effect. To date, the transduction efficiency, whose maximum value is 1 by definition, has recorded the highest value $\sim 10^{-1}$ with optomechanical effect.

In this study, we focus on the microwave-to-optical quantum transduction via the magneto-optic Faraday effect (i.e., the magnon-photon interaction). A previous experimental study has observed the transduction efficiency $\sim 10^{-10}$ by using a ferromagnet YIG [2]. We take advantage of the fact that three-dimensional topological insulators exhibit a universal Faraday rotation angle from the topological magnetoelectric effect, leading to a large value of the Verdet constant in the thin-film geometry. We show theoretically that the transduction efficiency can be greatly improved to $\sim 10^{-4}$ by utilizing magnetically doped topological insulator thin films [3]. The transduction efficiency can be further improved to $\sim 10^{-3}$ in a heterostructure of a few dozen of layers consisting of magnetically doped topological insulator thin films and nonmagnetic substrates. We also expect that the transduction efficiency can be further improved by incorporating an optical cavity. Our study paves the way for a possible application of topological materials in achieving an efficient quantum transduction.

We would like to thank Shintaro Sato for his advice, encouragement, and support on this project.

References

1. Han, X. *et al*., “Microwave-Optical Quantum Frequency Conversion”, Optica **8**, 1050 (2021).
2. Hisatomi, R. *et al*., “Bidirectional Conversion between Microwave and Light via Ferromagnetic Magnons”, Phys. Rev. B **93**, 174427 (2016).
3. Sekine, A., Ohfuchi, M., and Doi, Y., in preparation.

Dynamic magnetoelectric effects at dielectric/ferromagnetic metal interface: generation of spin currents and modulation of spin wave amplitude

Piotr Graczyk[1*] and Maciej Krawczyk[2]

[1]Institute of Molecular Physics, Polish Academy of Sciences, Poznań, Poland
[2]Institute of Spintronics and Quantum Information, Adam Mickiewicz University, Poznań, Poland
[*]corresponding author: graczyk@ifmpan.poznan.pl

Abstract: We present the operation of the device which non-resonantly modulates the spin-wave amplitude by the ac electric field. The spin accumulation is generated by the charge-mediated magnetoelectric effect at the dielectric/ferromagnetic metal interface and interacts with magnetization through the spin transfer torque.
We show the criteria for the effective amplification and dependences of the obtained gain on the applied voltage amplitude and spin-wave frequency.

Spin waves are potential candidates to replace electrons in logical systems to operate faster, with ultralow energy consumption and operating at sub-micrometer scale. Much effort has been devoted to develop methods of spin-wave generation, steering and conversion which led to the first laboratory realization of the spin-wave-based logic units [1]. However, the main challenge for the magnon computing, which is relatively high attenuation, remains unresolved. In our proposition [2], the modulation of spin-wave attenuation/amplitude takes place in the magnetoelectric cell (MEC, Fig. 1) which consists of two high-permittivity dielectric (D)

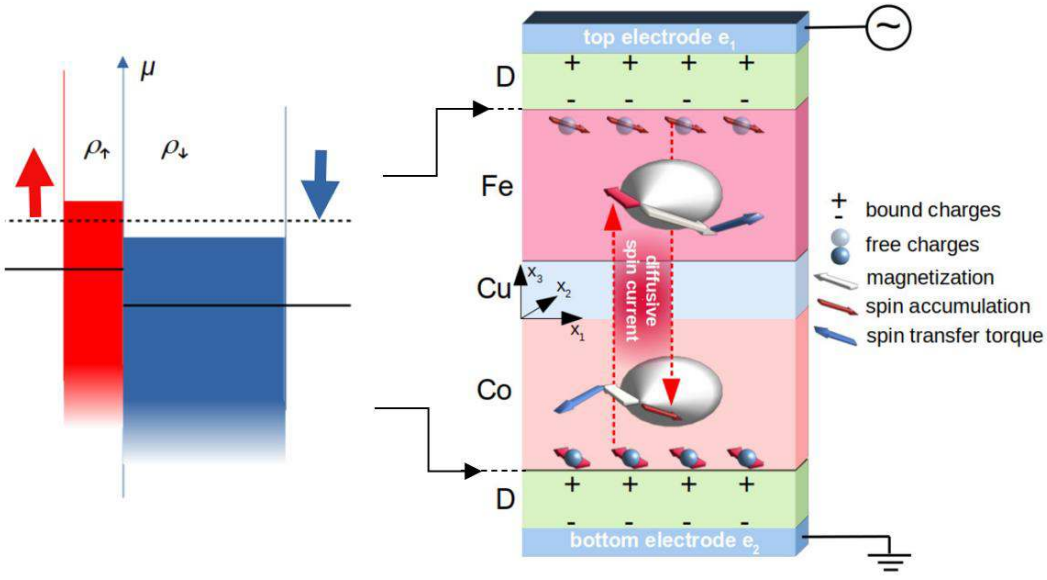


Fig. 1. The principle of operation of magnetoelectric cell subjected to the ac voltage. The dynamic splitting of the spin-up and spin-down subbands (i.e. spin-dependent surface screening, left part of the figure) at the Fe/dielectric and Co/dielectric interfaces generates the spin accumulation which diffuses through the Fe/Cu/Co layers and exerts the spin-transfer torque on the local magnetization.

nanocapacitors in series connected through a conductive ferromagnetic bilayer. The thin ferromagnetic layers, made from Fe and Co are separated by a nonmagnetic metal (Cu).

The principle of operation is as follows (see, Fig. 1). The ac voltage applied to the MEC generates time-varying screening charges at the ferromagnetic interfaces with dielectrics. Because the density of the screening charge is spin-dependent [3]–[5], the dynamic spin-dependent potential produces nonequilibrium spin density at the interfaces, as we have demonstrated in Ref. [6]. Importantly, the strength of the effect depends on the magnetoelectric constant. The spin accumulation is polarized along the local, precessing magnetic moment at the interface with the dielectric, and it diffuses between the layers. If the magnetization of the second layer is non-collinear to that spin accumulation (i.e., to the magnetic moment at the surface of the first layer), it exerts a spin-transfer torque.

To describe the coupled charge-spin-magnetization dynamics of the system and demonstrate usefulness of the MEC we solve numerically the set of coupled differential equations for magnetization dynamics and charge/spin transport. We show that the spin accumulation driven by the spin-dependent surface screening in ultrathin magnetoelectric cell effectively modulates coherent spin wave modes of specific symmetry and group velocity. The signal is periodically modulated: amplified and suppressed with the frequency of the ac voltage applied to MEC. We discuss in detail the spin-wave amplitude gain in dependence on the ac voltage amplitude, spin-wave mode and frequency.

The presented mechanism is non-resonant and may be useful e.g., for the modulation of the spin-wave amplitude, amplification of short impulses or when the effect is used for two parallel spin-wave conduits operating on the split signal with respective microwave fields delayed by π.

The study has received financial support from the National Science Centre of Poland under grant 2018/28/C/ST3/00052.

References

[1] A. V. Chumak, V. I. Vasyuchka, A. A. Serga, and B. Hillebrands, ‘Magnon spintronics’, *Nature Physics*, vol. 11, p. 453, 2015.

[2] P. Graczyk and M. Krawczyk, ‘Nonresonant amplification of spin waves through interface magnetoelectric effect and spin - transfer torque’, *Scientific Reports*, vol. 11, no. 15692, Art. no. 15692, 2021, doi: 10.1038/s41598-021-95267-1.

[3] S. Zhang, ‘Spin-Dependent Surface Screening in Ferromagnets and Magnetic Tunnel Junctions’, *Physical Review Letters*, vol. 83, no. 3, Art. no. 3, 1999, doi: 10.1103/PhysRevLett.83.640.

[4] M. Y. Zhuravlev, S. Maekawa, and E. Y. Tsymbal, ‘Effect of spin-dependent screening on tunneling electroresistance and tunneling magnetoresistance in multiferroic tunnel junctions’, *Physical Review B*, vol. 81, no. 10, Art. no. 10, 2010, doi: 10.1103/PhysRevB.81.104419.

[5] M. K. Niranjan, J. D. Burton, J. P. Velev, S. S. Jaswal, and E. Y. Tsymbal, ‘Magnetoelectric effect at the SrRuO3/BaTiO3 (001) interface: An ab initio study’, *Applied Physics Letters*, vol. 95, p. 52501, 2009, doi: 10.1063/1.3193679.

[6] P. Graczyk and M. Krawczyk, ‘Spin-polarized currents driven by spin-dependent surface screening’, *Physical Review B*, vol. 100, no. 19, Art. no. 19, Nov. 2019, doi: 10.1103/PhysRevB.100.195415.

META 2023, PARIS - FRANCE, JULY 18 – 21, 2023

Optical interface for a hybrid magnon-photon resonator

E. Buks[1*]

[1]Andrew and Erna Viterbi Department of Electrical Engineering, Technion, Haifa 32000 Israel
[*]Corresponding author: eyal@ee.technion.ac.il

Abstract: We study magneto-optical coupling in a ferrimagnetic sphere resonator made of Yttrium iron garnet. Methods to manipulate quantum entanglement induced by light-matter interaction are explored.

We study optical detection of magnetic resonance of a ferrimagnetic sphere resonator (FSR), which is strongly coupled to a microwave loop gap resonator [1, 2]. Optical fibers are employed for coupling the FSR with light in the telecom band. We find that magnetic resonance can be optically detected in the region of anti-crossing between the loop gap and the ferrimagnetic resonances. By measuring the response time of the optical detection, we rule out the possibility that microwave induced heating is responsible for the optical detectability.

We study a device composed of an FSR integrated with an optical interferometer. Magneto-optic coupling can be employed in such a device to manipulate entanglement between optical pulses that are injected into the interferometer and the FSR [3]. The device is designed to allow measuring the lifetime of such macroscopic entangled states in the region where environmental decoherence is negligibly small. This is achieved by recycling the photons interacting with the FSR in order to eliminate the entanglement before a pulse exits the interferometer. The proposed experiment may provide some insight on the quantum to classical transition associated with a measurement process.

References

1. Banoj Kumar Nayak, Cijy Mathai, Dekel Meirom, Oleg Shtempluck and Eyal Buks, "Optical interface for a hybrid magnon-photon resonator", Appl. Phys. Lett. 120, 062404 (2022).
2. Banoj Kumar Nayak and Eyal Buks, "Polarization-selective magneto-optical modulation", Journal of Applied Physics 132, 193905 2022.
3. Eyal Buks and Banoj Kumar Nayak, "Quantum measurement with recycled photons", Phys. Rev. B 105, 014421, 2022.

Pushing the limits of magnetoplasmonics by (meta)material design

F. Pineider[1,2]

[1]Department of Chemistry and Industrial Chemistry, University of Pisa, Italy

[2] Department of Physics and Astronomy, University of Florence, Italy
*francesco.pineider@unipi.it

Abstract: The field of magnetoplasmonics has reached a relatively mature state and is currently striving to take the step toward technological application. In this talk, I will show some interesting approaches to increase the magnetoplasmonic modulation, based on rational material design and structuration into metasurfaces. Finally, I will discuss a (failed) attempt to observe magnetochiral behaviour in a nickel-silver metasurface.

In its simplest form, the interaction between charge carriers of a plasmonic unit with a static magnetic field can be rationalized as a Lorentz force component that alters carriers' trajectories in the conductor. [1,2,3] In recent years, several approaches have been proposed to capitalize on this interaction and boost it up to a usable magnitude. [4,5]

In this contribution, I will give a general description of the factors that must be balanced to improve magnetoplasmonic performance and describe the critical rules to design efficient materials. As an application of these rules, I will present the case of plasmonic degenerately doped semiconductors, [6] which have recently shown outstanding magnetic field response, even if completely non-magnetic (Figure 1). [7,8] Further discussion on the possibilities offered by magnetic co-doping of the semiconductor matrices will follow.

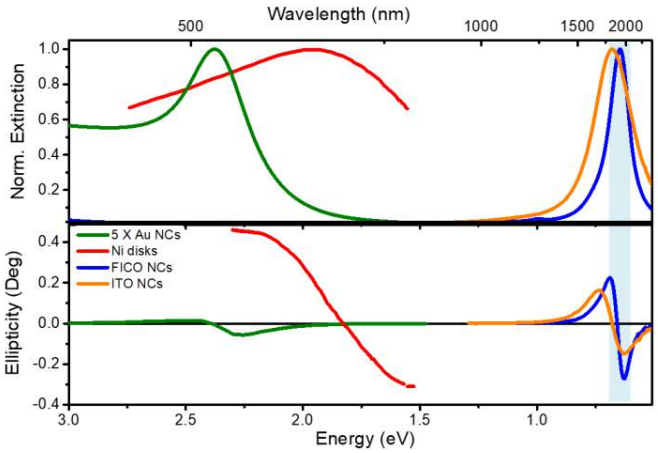


Figure 1. Optical and magneto-optical response of doped semiconductors compared to noble metal and ferromagnetic metal plasmonic structures.

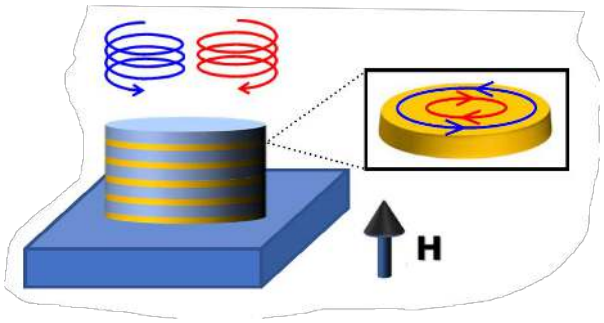


Figure 2. Sketch of a hyperbolic metamaterial unit and of its interaction with circularly polarized light in the presence of a static magnetic field.

Besides the features of the plasmonic material, which should maximise the effect of magnetic field on their optical properties, I will also give a preliminary account on ways in which the organization of plasmonic resonators in metasurfaces can give rise to novel types of magneto-optical response (Figure 2) [9] and increase the general magnetoplasmonic performance. [10]

Finally, I will describe a brief venture in the fascinating yet still partly elusive field of magnetochirality, i.e. one of the manifestations of simultaneous spatial and temporal non-reciprocity. [11] In our attempt, we prepared a plasmonic chiral and magnetic metasurface, and looked for signs of magnetochiral effects. [12] Although no effects were observed, we were able to derive important design guidelines for plasmonic magnetochiral candidates.

References

1. F. Pineider et al. “Circular Magnetoplasmonic Modes in Gold Nanoparticles”, Nano Lett., 13 (2013) 4785
2. B. Sepúlveda et al. “Plasmon-Induced Magneto-Optical Activity in Nanosized Gold Disks.”, Phys. Rev. Lett. 104, 147401 (2010)
3. Gabbani, A. et al. “Magneto-Optical Methods for Magnetoplasmonics in Noble Metal Nanostructures”, J. Appl. Phys. 129, 211101 (2021)
4. G. Armelles et al.” Magnetoplasmonics: Combining Magnetic and Plasmonic Functionalities”, Adv. Opt. Mater. 1, 10 (2013)
5. N. Maccaferri et al. “Magnetoplasmonics: Current challenges and Future Opportunities”, Appl. Phys. Lett. 122, 120502 (2023)
6. J.M. Luther et al. “Localized Surface Plasmon Resonances Arising from Free Carriers in Doped Quantum Dots”, Nature Mater., 10, 361 (2011)
7. A. Gabbani et al. “Magnetoplasmonics beyond Metals: Ultrahigh Sensing Performance in Transparent Conductive Oxide Nanocrystals”, Nano Lett., 22, 9036 (2022)
8. K.H. Hartstein et al. “Cyclotron Splittings in the Plasmon Resonances of Electronically Doped Semiconductor Nanocrystals Probed by Magnetic Circular Dichroism Spectroscopy”, J. Phys. Chem. Lett. 8, 1831 (2017)
9. Kutruff, J. et al. “Magneto-Optical Activity in Nonmagnetic Hyperbolic Nanoparticles”, Phys. Rev. Lett., 127, 217402 (2021)
10. Pourjamal, S. et al. “Hybrid Ni/SiO2/Au Dimer Arrays for High-Resolution Refractive Index Sensing.” Nanophotonics, 7, 905 (2018)
11. Rikken, G. and Raupach, E. “Enantioselective magnetochiral photochemistry”, Nature 405, 932 (2000)
12. Petrucci et al. “Macroscopic Magneto-Chiroptical Metasurfaces”, Appl. Phys. Lett. 118, 251108 (2021)

META 2023, PARIS - FRANCE, JULY 18 – 21, 2023

Interfaces of B20 compounds with exotic spin currents

G. Pantano[1], C. Gibson[1], S. Tkacik[1] and J. Gayles[1*]

[1]Department of Physics, University of South Florida, Tampa, FL 33620, USA
[*]corresponding author: gayles@usf.edu

Abstract: We use first principal calculations to investigate 2D planar twinning interfaces in B20 compounds. We employ supercell calculations where the area of the interface is restricted to the primitive cell interface. The calculations are carried out for the Weyl semimetal CoGe. Our results show that the spin and anomalous Hall effect can be significantly increased due to the increase in spin-orbit coupling with the change in atomic potential at the interface.

Modern electronics have reached their full maturity due to the unprecedented increase in the demand for computation and data management. However, the inability to miniaturize electronic components to the atomic scale and eliminate crystal imperfections severely limits the performance and efficiency of devices. Crystal imperfections are near unavoidable during the growth of materials and often reduce their physical properties, such as the ability to conduct electricity. Furthermore, removing crystal imperfections is costly and detrimental to the environment. The challenge is overcoming these technological constraints; we must classify and understand the symmetries of crystal imperfections, discover new materials whose electronic properties are enhanced by crystal imperfections, and develop new mechanisms to carry and manipulate information [1-7]. The research will contribute to substantial breakthroughs in the design of energy-efficient low-power devices and help mitigate the toxic purification process of materials. Materials in modern devices are nominally restricted by various impurities and defects, reducing desired transport phenomena and increasing waste heat. This leads to a substantial investment in creating high-quality single crystals. However, 2D planar defects can potentially increase select transport phenomena such as the spin and anomalous Hall effect in systems that break inversion symmetry [7-9]. Intuitive tight-binding Hamiltonians are used to understand the role of symmetry and to reduce the complexity of the interface band structure.

Here we use first principle calculations on crystal domain boundaries of CoGe [10] with distinct symmetries on either side of the boundary interface. Figure a), b), and c) show the effect of spin-orbit coupling (SOC) strength on bulk CoGe on the bandstructure and Fermi arcs. Figure d) shows a schematic of the opposite chirality interfaces with a sharp interface highlighted in green. We compare the total energies to find stable interface boundaries that are predictable to form under finite temperatures in experimental conditions. In figure e), we show the total energy comparisons for a few boundary interfaces compared to the vacuum state in orange and the bulk in black. A strain analysis of the systems is also considered, based on symmetries, which allows for selecting distinct interface boundaries with topological electronic structure. Depending on the interface, the SOC strength can be varied by two orders of magnitude compared to that of the bulk CoGe [10].

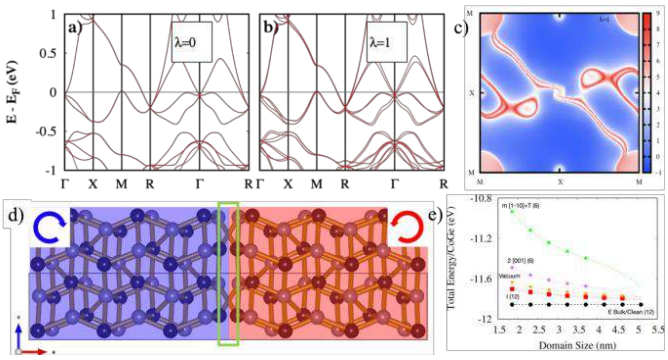


Figure showing band structure calculations, schematic of an interface boundary with opposite chiralities and the total energy comparison of interfaces.

Additionally, a finite magnetic moment is stabilized close to the boundary interface, which allows for Dzyaloshinkii-Moryia interaction. We calculate the spin and anomalous Hall effect, which show a

considerable variation for the boundaries distinct from the bulk and related to the topological surface states that survive on specific boundary systems. We develop tight-binding models, motivated by first principle calculations, to intuitively understand the effect of symmetry and the interface on transport. Unique combinations of boundaries suggest novel topological states not present in bulk can be stabilized due to the interface [5,7,10].

References

1. Lanzillo, N. A., Bajpai, U., Garate, I., & Chen, C.-T. "Size-Dependent Grain-Boundary Scattering in Topological Semimetals," Physical Review Applied, Vol. 18, No. 3, 2022. URL: https://doi.org/10.1103/physrevapplied.18.034053
2. Lien, S.-W., Garate, I., Bajpai, U., Huang, C.-Y., Hsu, C.-H., Tu, Y.-H., Lanzillo, N. A., Bansil, A., Chang, T.-R., Liang, G., Lin, H., & Chen, C.-T. "Unconventional Resistivity Scaling in Topological Semimetal CoSi," npj Quantum Materials, Vol. 8, No. 1, 2023. URL: https://doi.org/10.1038/s41535-022-00535-6
3. D A Pshenay-Severin, D. A., Ivanov, Y. V., Burkov, A. A., and Burkov, A. T. "Band Structure and Unconventional Electronic Topology of CoSi," J. Phys.: Condensed Matter, Vol. 30, No. 13, 2018. DOI: 10.1088/1361-648X/aab0ba
4. Chen, C. -T., Bajpai, U., Lanzillo, N. A., Hsu, C. -H., Lin, H. & Liang, G. "Topological Semimetals for Scaled Back-End-Of-Line Interconnect Beyond Cu," 2020 IEEE International Electron Devices Meeting (IEDM), San Francisco, CA, USA, 2020, pp. 32.4.1-32.4.4, DOI: 10.1109/IEDM13553.2020.9371996.
5. Chang, G., Xu, S.-Y., Wieder, B. J., Sanchez, D. S., Huang, S.-M., Belopolski, I., Chang, T.-R., Zhang, S., Bansil, A., Lin, H., & Hasan, M. Z. "Unconventional Chiral Fermions and Large Topological Fermi Arcs in RhSi," Physical Review Letters, Vol. 119, No. 20, 2017. URL: https://doi.org/10.1103/physrevlett.119.206401.
6. Jeong, T., & Pickett, W. E. "Implications of the B20 Crystal Structure for the Magnetoelectronic Structure of MnSi," *Physical Review B*, Vol. *70, No. 7, 2004*. URL: https://doi.org/10.1103/physrevb.70.075114
7. Hu, L. -H., Guo, C., Sun, Y., Felser, C., Elcoro, L., Moll, P. J. W., Liu, C. -X., & Bernevig, B. A. "Hierarchy of Quasi-Symmetries and Degeneracies in Chiral Crystal Materials CoSi," arXiv, 2022. DOI: 10.48550/ARXIV.2209.02745.
8. Takane, D., Wang, Z., Souma, S., Nakayama, K., Nakamura, T., Oinuma, H., Nakata, Y., Iwasawa, H., Cacho, C., Kim, T., Horiba, K., Kumigashira, H., Takahashi, T., Ando, Y., & Sato, T. "Observation of Chiral Fermions with a Large Topological Charge and Associated Fermi-arc Surface States in CoSi," Physical Review Letters, Vol. 122, No. 7, 2019. URL: https://doi.org/10.1103/physrevlett.122.076402
9. Ishii, F., Kotaka, H., & Onishi, T. "Spin-Orbit Interaction Effects in the Electronic Structure of B20-Type CoSi: First-Principles Density Functional Study," Proceedings of the International Conference on Strongly Correlated Electron Systems (SCES2013), 2014. DOI: 10.7566/JPSCP.3.016019
10. C. S. Spencer, J. Gayles, N. A. Porter, S. Sugimoto, Z. Aslam, C. J. Kinane, T. R. Charlton, F. Freimuth, S. Chadov, S. Langridge, J. Sinova, C. Felser, S. Blügel, Y. Mokrousov, and C. H. Marrows, Phys. Rev. B 97, 214406 (2018), e-print arXiv:1803.03281. https://doi.org/10.1103/PhysRevB.97.214406,

META 2023, PARIS - FRANCE, JULY 18 – 21, 2023

Hot-electron generation in chiral plasmonic nanocrystals as a mechanism for chiral photo-growth and photochemistry

Alexander O. Govorov[1]

[1]**Department of Physics and Astronomy, Ohio University, Athens, USA**
govorov@ohio.edu

The generation of energetic (hot) electrons and the photoheating are intrinsic properties of any optically excited plasmonic nanocrystal [1,2]. In addition, high-energy hot electrons and phototemperature contribute to the kinetic processes observed in colloidal nanocrystals, metal-semiconductor hybrids, plasmonic Schottky photodetectors, and metastructures [1,2]. In this talk, we will focus on the theory of hot electron injection and present related applications for chiral photo-growth, plasmonic photochemistry and plasmonic photocatalysis [3,4,5,6].

References:

[1] L. Chang, L. V. Besteiro, J. Sun, E. Y. Santiago, S. K. Gray, Z. Wang, A. O. Govorov, *ACS Energy Lett*., 4, 10, 2552-2568 (2019).
[2] L. V. Besteiro, P. Yu, Z. Wang, A. W. Holleitner, G. V. Hartland, A. O. Govorov, *Nano Today*, 27, 120-145 (2019).
[3] T. Liu, L.V. Besteiro, T. Liedl, M.A. Correa-Duarte, Z. Wang, A. Govorov, *Nano Letters*, 19, 1395–1407 (2019).
[4] L. Khosravi Khorashad, L. V. Besteiro, M. A. Correa-Duarte, S. Burger, Z. M. Wang, A.O. Govorov, *J. Am. Chem. Soc.*, 142, 9, 4193–4205 (2020).
[5] O. Ávalos-Ovando, L.V. Besteiro, A. Movsesyan, G. Markovich, T. Liedl, K. Martens, Zh. Wang, M.A.Correa-Duarte, and A.O. Govorov, *Nano Letters* (2021); DOI: 10.1021/acs.nanolett.1c02479.
[6] A. Movsesyan, E. Y. Santiago, S. Burger, M. A. Correa-Duarte, L. V. Besteiro, Zh. Wang, and A.O.Govorov, *Advanced Optical Materials* (2022); https://doi.org/10.1002/adom.202102663.

META 2023, PARIS - FRANCE, JULY 18 – 21, 2023

Orbital angular momentum of light creates exotic chiral structures

T. Omatsu[1,2]

[1]Graudate School of Engineering, Chiba University, Japan
[2]Molecular Chirality Research Center, Chiba University, Japan
[*]corresponding author: omatsu@faculty.chiba-u.jp

Abstract: We herein report on the demonstration of chiral engineered optical materials, including chiral crystallization of $NaClO_3$, galaxy-shaped reliefs of azopolymers with spiral arms, and self-written helical fibers, by the illumination of light fields possessing orbital angular momentum.

Light field possessing an orbital angular momentum (OAM), that is optical vortex, exhibits an annular spatial form originated from its helical wavefront with an on-axis phase singularity [1,2]. In recent years, optical chirality and optical activity of optical vortex have been widely studied [3]. In fact, it has been discovered that the optical vortex with OAM twists the irradiated materials, including metals, semiconductors, polymers, and even crystals, towards clockwise (right-handed) or counter-clockwise (left-handed) direction to form nano/microscale helical structures [4,5]. This phenomenon never happens with only the spin angular momentum (SAM) associated with a circular polarized light field with a planar wavefront.

Such chiral structures under optical vortex illumination will offer new avenues to develop chiral engineered optical materials with exotic physical properties beyond natural materials.

In this work, we review the formation of chiral structures under optical vortex illumination, including chiral crystallization of $NaClO_3$ [6], galaxy-shaped reliefs of azopolymers with spiral arms, and self-written helical fibers [7] by employing optical vortex and its hybrid mode. Surprisingly, we discover that the chirality of $NaClO_3$ crystals is selectively controlled (crystal enantiomeric excess (CEE)>55%) by altering the helicity of an irradiating optical vortex. This demonstration will provide us new fundamental insights into the origin of homochirality.

Also, galaxy-shaped reliefs of azopolymers reflect full physical parameters (not only handedness and but also topological charge) of the irradiated optical vortices, and they allow the development of advanced photo-induced chiral engineered optical materials with the freedom of chirality and topological charge.

References

1. L. Allen, M. W. Beijersbergen, R. J. C. Spreeuw, and J. P. Woerdman, "Orbital angular momentum of light and the transformation of Laguerre-Gaussian laser modes," Phys. Rev. A 45, 8185–8189 (1992).
2. J. Leach, M. J. Padgett, S. M. Barnett, S. Franke-Arnold, and J. Courtial, "Measuring the Orbital Angular Momentum of a Single Photon," Phys. Rev. Lett. 88, 257901 (2002).
3. K. A. Forbes, D. L. Andrews, “Orbital angular momentum of twisted light: chirality and optical activity”, J. Phys. Photonics, 3, 022007 (2021).
4. T. Omatsu, K. Miyamoto, K. Toyoda, R. Morita, Y. Arita, and K. Dholakia, "A New Twist for Materials Science: The Formation of Chiral Structures Using the Angular Momentum of Light," Adv. Opt. Mater. 7, 1801672 (2019).
5. T. Omatsu, K. Masuda, K. Miyamoto, K. Toyoda, N. M. Litchinitser, Y. Arita, and K. Dholakia, "Twisted mass transport enabled by the angular momentum of light," J. Nanophotonics 14, 1 (2020).
6. K. Toyoda, H.-T. Su, K. Miyamoto, T. Sugiyama, T. Omatsu, “Chiral crystallization manipulated by orbital angular

momentum of light," Optica 10, 332-338 (2023).
7. Y. Arita, J. H. Lee, H. Kawaguchi, R. Matsuo, K. Miyamoto, K. Dholakia, T. Omatsu, "Photopolymerization with high-order Bessel light beams," Opt. Lett. 45, 4080-4083 (2020).

META 2023, PARIS - FRANCE, JULY 18 – 21, 2023

Driving and imaging achiral-to-chiral transitions in an all-optical setup

E. Binns[1], J. Terentjevas[1], L. Rego[1,2,3] and D. Ayuso[1,4,*]

[1]Department of Physics, Imperial College London, SW7 2AZ London, United Kingdom
[2]Universidad de Salamanca, 37008 Salamanca, Spain
[3]Departamento de Química, Universidad Autónoma de Madrid, 28049 Madrid, Spain
[4]Max-Born-Institut, Max-Born-Str. 2A, 12489 Berlin, Germany
[*]d.ayuso@imperial.ac.uk

Abstract: We show how to imprint chirality into achiral matter using tailored light, and how to monitor such achiral-to-chiral phase transitions in an all-optical setup. Our proof-of-principle simulations reveal that the hydrogen atom undergoes ultrafast and nonlinear chiral electron dynamics when exposed to a locally chiral laser pulse, giving rise to chiral high harmonic generation. Furthermore, the atom remains in a chiral superposition of stationary states after the pulse is gone, emitting chiral free-induction decay radiation which reveals the imprinted handedness.

Chiral molecules owe their handedness to the spatial arrangements of their *nuclei*, which form chemical structures which are not superimposable with their mirror images. However, chirality can also be related to *electronic* degrees of freedom. Indeed, as shown by Ordoñez and Smirnova, even the hydrogen atom can have chiral superpositions of electronic excited states [1].

Synthetic chiral light [2] enables ultrafast and highly efficient imaging of molecular chirality. Such light is locally chiral: the tip of the electric-field vector draws a chiral (3D) Lissajous figure in time, at each point in space. Interestingly, such tailored light can also be used to create chiral electronic states in atoms [3,4], which emit chiral photoelectron currents and exhibit photoelectron circular dichroism [3].

Here we show how to apply synthetic chiral light which is both locally and globally chiral [2] to drive ultrafast chiral electron motion in systems which are initially achiral, such as atoms, thus driving ultrafast achiral-to-chiral phase transitions. This tailored light can be created with the two-colour noncollinear setup introduced in [2].

We solved the time-dependent Schrödinger equation for the hydrogen atom exposed to an ultrashort, intense, locally chiral field. The induced polarization, proportional to $\langle\Psi(t)|\mathbf{r}|\Psi(t)\rangle$, is depicted in Fig. 1. As shown in Fig. 1a, the laser drives ultrafast chiral electron motion at its fundamental frequencies (800 and 400nm), although nonlinear effects are also evident. Indeed, the high-frequency components, shown in Fig. 1b, also create a chiral structure in time, and give rise to chiral high harmonic generation (HHG).

Chiral HHG is suppressed after the pulse is gone, but chiral electron motion does not stop. Indeed, the atom remains in a chiral coherent superposition of stationary states, and thus the electron continues to undergo ultrafast chiral dynamics, see Fig. 1c. This chiral electron motion results from having populated excited stationary states of the atom with different energy and angular momentum. The ultrafast chiral current shown in Fig. 1c gives rise to chiral free-induction decay radiation with elliptical polarization. As we will show in this conference, the imprinted handedness is recorded in the polarization of the emitted light.

We believe that this work creates exciting opportunities for driving and monitoring achiral-to-chiral phase transitions in all-optical setups, also in complex systems, as well as for driving chiral photo-chemical reactions using achiral reagents.

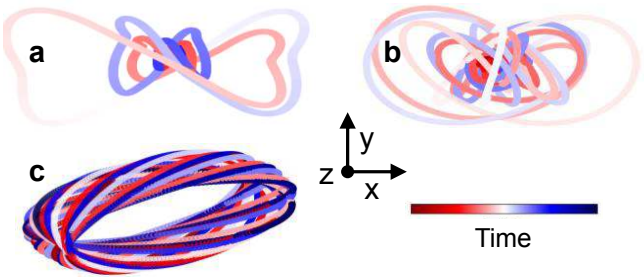


Fig. 1. Ultrafast polarization induced in the hydrogen atom by our locally chiral field [2]. **a**, total polarization the presence of the field. **b**, high-order components, resulting from filtering out the linear response in **a**. **c**, induced polarization after the pulse is gone. Laser parameters: wavelengths 800 and 400nm, intensity 10^{14} Wcm^{-2}, pulse duration 7fs (FWHM).

References

1. A. Ordonez and O. Smirnova, "Propensity rules in photoelectron circular dichroism in chiral molecules. I. Chiral hydrogen", *Phys. Rev. A* **99**, 043416 (2019)
2. D. Ayuso et al, "Synthetic chiral light for efficient control of chiral light-matter interaction", *Nat. Photonics* **13**, 866-871 (2019)
3. N. Mayer et al, "Imprinting chirality on atoms using synthetic chiral light fields", *Phys. Rev. Lett.* **129**, 243201 (2022)
4. G. P. Katsoulis et al, "Momentum scalar triple product as a measure of chirality in electron ionization dynamics of strongly driven atoms", *Phys. Rev. A* **106**, 043109 (2021)

Microbundle array of Magnetoplasmonic Nanorods for reconfigurable chiral Metasurface

Juyong Gwak[1], Hyojin Kang[1] and Jaebeom Lee[1,2*]

[1]Department of Chemical Engineering and Applied Chemistry, Chungnam National University, Republic of Korea[2] Department of Chemistry, Chungnam National University, Republic of Korea
[*]corresponding author: nanoleelab@gmail.com

Abstract: Flexible devices are a fascinating application for wearable electronics, life & healthcare, and stealth technology. In this study, a metasurface film was fabricated by arranging core-shell magnetoplasmonic nanowires in microbundles on a flexible polymer substrate. Its chirality is manipulated by the tilt angle (θ), i.e. the angle between the applied magnetic field vector (B) and the tangent vector (T) of the curved metasurface. These flexible chiral metasurface platform could be useful for fabricating integrated enantiomeric sensing and AR devices.

Chirality is a property that appears everywhere from simple molecular structures to galaxies in the universe.[1] To study the chirality of nanomaterials and amplify their signals, inducing chirality in three-dimensional nanostructures has been well researched and developed over the past decade.[2] In particular, 2D planar metasurface has obtained a novel field of research.[3] They reported the smart metasurface, which has a uniform nanopattern, can control the chirality by inducing external curvature at the microscale. Active planar chiral metamaterials and reconfigurable metasurfaces have drawn intense interest thanks to both their unique ability to manipulate CPL and the lower complexity required in fabrication. Herein, a reconfigurable metasurface decorated with planar magnetoplasmonic microbundle arrays of Au@Fe_xO_y core-shell nanowires (NWs) on polydimethylsiloxane film is fabricated.

Ag@Fe_3O_4 NPs and Au@Fe_xO_y (NWs) were aligned using a magnetic field to create linear nanochains and microbundles depending on the concentration of NWs. Chiroptical properties are not well recognized in NP linear arrays, whereas NW linear and microarrays exhibit remarkable CD spectra due to the external tilt angle (θ_{ex}) at the microscale, where the CD was modulated by controlling the bending curvature of the film. Also, the computational simulation demonstrates an asymmetric interaction mechanism derived from the optically anisotropic nature of the NW array. The electric field strength of the linear array of NPs, that is the thickness of the line in which the NPs are aligned, does not exhibit high asymmetric interactions from mineral interactions. However, that the both NW linear and microbundle array induced highly recognizable asymmetric distribution by LCP and RCP light, that is, symmetric disrupted metasurface, which is considered the main cause of the chirality of the experimental condition. Particularly, microbundle arrays exhibit inherent symmetry breaking at certain curvatures due to the internal skew angle (θ_{in}) from the NW skew alignment inside the microbundle at the nanoscale. Although both NP and NW appear to be 1D arrays, the magnetically induced NW assembly differs from the NP array in that it induces chirality and increases the specific CD signal. The chiroptical properties of the microbundles themselves were confirmed by MCD and simulations. These results suggest a strategy to realize spectacle lenses with circular polarizer function, and the fabricated metafilms can be a novel universal means to specifically tune the absorption of circularly polarized light and produce flexible devices for further signal enhancement in nanoantennas and biosensors.

Acknowledgements

This work was supported by the National Research Foundation (NRF) of Korea and grants funded by the Ministry of Science, ICT, and Future Planning (MSIP) of Korea (NRF-2019R1A2C2007825), and Regional Innovation Strategy (RIS) through the National Research Foundation of Korea (NRF) funded by the Ministry of Education (MOE) (2021RIS-004).

References

1. N Suzuki, Y Wang, P Elvati, Z. B Qu, K Kim, S Jiang, E Baumeister, J Lee, B Yeom, Bahng, J. H. “Chiral graphene quantum dots.” ACS nano Vol 10 (2), p 1744-1755, 2016.
2. Y. Wang, C. Zhao, J. Wang, X. Luo, L. Xie, S. Zhan, J. Kim, X. Wang, X. Liu, Y. Ying,” Wearable plasmonic -metasurface sensor for noninvasive and universal molecular fingerprint detection on biointerfaces”, Sci. Adv., Vol 7, eabe4553, 2021
3. KJ Jeong, J Gwak, C Wang Y Kim, VT Tran, and J Lee, “Chirality of Fingerprints: Novel Chiral-optical Properties due to the Pattern and Curvature of the Elastomeric Grating Meta-skin”, ACS Nano, Vol. 16, p 6103-6110, 2022
4.
5. J Gwak, HQ Nguyen, KJ Jeong, Y Kim, SJ Park, Y Choi, M Goddati. M, L.T.Tufa, Z Tang, J Lee, “Reconfigurable Metasurface of Magnetoplasmonic Microbundle Array for Chiral Signal Enhancing” Adv. Opt. Mater., 2202104, 2022.

Giant Magnetoimpedance effect at GHz frequencies in amorphous microwires

V. Zhukova[1,2,3], M. Ipatov[1,2], P. Corte-Leon[1,2,3], J.M. Blanco[2,3] and A. Zhukov[1,2,3,4]

[1] Dpto. de Polímeros y Materiales Avanzados, University of Basque Country, UPV/EHU, San Sebastian, Spain

[2] Dpto. de Fisica Aplicada, EIG, University of Basque Country, UPV/EHU, San Sebastian, Spain

[3] EHU Quantum Center, University of the Basque Country, UPV/EHU, Spain.

[4]IKERBASQUE, San Sebastian and Bilbao, Spain

*corresponding author: valentina.zhukova@ehu.es

Abstract: We studied Giant magnetoimpedance (GMI) effect and magnetic properties of various Co-rich amorphous microwires. We measured magnetic field dependences of the GMI ratio up to GHz frequency range and observed quite high GMI ratio in studied thin magnetic microwires even at GHz frequencies. We observed different values of the magnetic anisotropy field obtained from the hysteresis loops and the impedance curves. Observed dependences can be explained considering different magnetic anisotropy in the surface layers and in the inner part of metallic nucleus and skin depth effect. Features of high frequency GMI effect have been analyzed using FMR-like approximation.

Applications of Giant magnetoimpedance, GMI, typically observed in soft magnetic materials, have attracted considerable attention owing to extremely high sensitivity of the GMI effect to low magnetic field. Among soft magnetic materials, thin ferromagnetic amorphous microwires (typically of about 10 μm in diameter) are considered as the most promising materials owing to outstanding soft magnetic properties, highest GMI effect and reduced dimensions suitable for microsensor applications [1,2]. Comparison of various magnetic field sensors shows that magnetic sensors using GMI effect of amorphous microwires present a number of advantages such as cheap technology, excellent magnetic field resolution and low sensor dimensions [2].

Recently, much attention has been paid to the studies of the GMI effect at GHZ frequencies owing to the recent tendency in miniaturization of magnetic field sensors [2,3]. The thinnest soft magnetic microwires can be produced by so-called Tailor-Ulitovsky method allowing fabrication of glass-coated microwires with metallic nucleus diameter, d, from 0.05 to 100 μm and total diameter, D, from 5 to 120 μm.

We present our last results on the GMI effect of thin amorphous magnetically soft Co-rich microwires suitable for creation of microsensors based on high frequency GMI effect.

We studied magneto impedance effect in Co- rich microwires at frequencies up to 4 GHz using specially designed micro-strip sample holder and S_{11} reflection coefficient obtained using the vector network analyzer.

Experimentally measured dependencies of impedance, Z on magnetic field H for several Co-rich microwires with vanishing magnetostriction coefficient: $Co_{67.7}Fe_{4.3}Ni_{1.6}Si_{11.2}B_{12.4}Mo_{1.25}C_{1.55}$(d $\approx$10μm, D=13.8 μm), $Co_{69.2}Fe_{3.6}Ni_1B_{12.5}Si_{11}Mo_{1.5}C_{1.2}$ (d=22.8μm; D=23.2μm) present considerable influence of magnetic field on sample impedance up at GHz frequency. Additionally, the magnetic field of maximum shifts to the higher field region with increasing of the frequency, f. But, at GHz frequencies the magnetic fields corresponding to the impedance maximum, H_m, are much higher than the magnetic anisotropy field. Therefore we must assume that studied samples are magnetically saturated when exhibit an impedance maximum at GHz frequency range. Such discrepancy between the H_m -values and magnetic anisotropy field can be explained considering different magnetic anisotropy in the surface layers and in the inner part of metallic nucleus and skin depth effect.

For interpretation of observed frequency dependence of impedance this behavior we paid attention on the fundamental link between ferromagnetic resonance, FMR and GMI [2,3].

Thus the saturation magnetization, M_s, can be estimated from this approach using the equation:

$$M_s = 0.805x10^{-9}\, df_0^2/dH \qquad (1)$$

where f_0 is the resonant frequency and H is the applied magnetic field. Previously we already got quite reasonable M_s values for lower frequencies considering this link between the GMI effect and FMR [4].

For studied samples and for GHz range we obtained linear fit of the square of the resonance frequency, f_0, on applied field. Some deviation has been observed only in low-field region. The origin of this deviation is unclear and can be related with low field magnetization process.

Concluding, studies of magnetic properties and GMI effect of amorphous Co-Fe rich microwires reveals that they present considerable GMI effect at GHz frequencies. Magnetic field dependences of GMI effect are affected by the microwires composition and geometry. We discussed observed experimental dependences considering both different magnetic structure, saturation magnetization and magnetic anisotropy in the bulk and near the surface and close analogy between giant magnetoimpedance and ferromagnetic resonance. Features of high frequency GMI effect can be described using FMR-like approximation.

References

[1] Phan, M.-H., Peng, H.-X. “Giant magnetoimpedance materials: Fundamentals and applications”, Prog.Mater. Science vol. 53, 323–420, 2008

[2] Zhukov, A., Corte-Leon, P., Gonzalez-Legarreta, L., Ipatov, M., Blanco, J.M., Gonzalez, A., Zhukova, V. “Advanced functional magnetic microwires for technological applications”, J. Phys. D: Appl. Phys., vol. 55, 253003, 2002.

[3] Ménard, D., Britel, M., Ciureanu, P. and Yelon,A. “Giant magnetoimpedance in a cylindrical conductor,” J. Appl. Phys., vol. 84, 2805–2814, 1998.

[4] Zhukov, A., Ipatov, M., Garcia, C., Churyukanova, M., Kaloshkin, S., Zhukova, V. “From Manipulation of Giant Magnetoimpedance in Thin Wires to Industrial Applications”, J. Supercond. Nov. Magn., vol. 26(4) 1045-1054, 2013.

Casimir Force Between Pasteur Materials

Zixuan Dai[1], Qingdong Jiang[1]

[1] *Tsung-Dao Lee Institute and School of Physics and Astronomy, Shanghai Jiao Tong University, Shanghai 200240, China*

Abstract Both theoretical and experimental interest in achieving repulsive Casimir force increases in recent years. A well-known paper demonstrated that the Casimir force between two objects is always attractive if the parity symmetry is preserved. In this paper, we calculate the Casimir force between two parallel Pasteur materials and show that the sign of the Casimir force can be modified by breaking parity symmetry.

Casimir effect is one of the famous manifestations of quantum fluctuation. In 1948, Casimir proposed that attractive forces exists between two uncharged, parallel perfect metal plates [1], which is given by

$$F_c = -\frac{\pi^2 \hbar c A}{240 d^3} \tag{1}$$

Here d is the distance between the two plates, A is the area of the plates, c is the speed of light and $\hbar$ is the Planck constant. To achieve the repulsive Casimir force, materials with different optical properties [2–6] and different geometries [7–10] have been investigated. Specifically, Oded Kenneth and Israel Klich proved that "the Casimir force between two bodies related by reflection is always attractive" [11], which suggests that chiral materials may lead to repulsive Casimir force [12, 13].

In our paper, we calculate the Casimir force between two uncharged, parallel Pasteur materials. Pasteur materials are linear isotropic chiral materials with constitutive relations

$$\begin{aligned} \mathbf{D} &= \epsilon \mathbf{E} - i\kappa\sqrt{\epsilon_0 \mu_0}\mathbf{H} \\ \mathbf{B} &= \mu \mathbf{H} + i\kappa\sqrt{\epsilon_0 \mu_0}\mathbf{E} \end{aligned} \tag{2}$$

Here κ is the chirality parameter which characterizes how strong the material breaks the parity symmetry. Our results show that the sign of the Casimir force can be modified by tuning κ.

Our work shows how Casimir force changes with the chirality parameter. The results would be very useful for designing nano-devices and give a hint on understanding how parity symmetry would affect the sign of the Casimir force, which has both theoretical value and promising application potential.

References

[1] H. B. G. Casimir. On the Attraction Between Two Perfectly Conducting Plates. *Indag. Math.*, 10:261–263, 1948.

[2] G. Metalidis and P. Bruno. Magnetic casimir effect. *Phys. Rev. A*, 66:062102, Dec 2002.

[3] Giuseppe Bimonte. Casimir effect between superconductors. *Phys. Rev. A*, 99:052507, May 2019.

[4] F. S. S. Rosa, D. A. R. Dalvit, and P. W. Milonni. Casimir interactions for anisotropic magnetodielectric metamaterials. *Phys. Rev. A*, 78:032117, Sep 2008.

[5] Adolfo G. Grushin and Alberto Cortijo. Tunable casimir repulsion with three-dimensional topological insulators. *Phys. Rev. Lett.*, 106:020403, Jan 2011.

[6] Justin H. Wilson, Andrew A. Allocca, and Victor Galitski. Repulsive casimir force between weyl semimetals. *Phys. Rev. B*, 91:235115, Jun 2015.

[7] Ho Bun Chan, Vladimir A. Aksyuk, Rafael N. Kleiman, David J. Bishop, and Federico Capasso. Quantum mechanical actuation of microelectromechanical systems by the casimir force. *Science*, 291:1941 – 1944, 2001.

[8] U. Mohideen and Anushree Roy. Precision measurement of the casimir force from 0.1 to $0.9\mu m$. *Phys. Rev. Lett.*, 81:4549–4552, Nov 1998.

[9] T. Emig, N. Graham, R. L. Jaffe, and M. Kardar. Casimir forces between compact objects: The scalar case. *Phys. Rev. D*, 77:025005, Jan 2008.

[10] M. Brown-Hayes, D. A. R. Dalvit, F. D. Mazzitelli, W. J. Kim, and R. Onofrio. Towards a precision measurement of the casimir force in a cylinder-plane geometry. *Phys. Rev. A*, 72:052102, Nov 2005.

[11] Oded Kenneth and Israel Klich. Opposites attract: A theorem about the casimir force. *Phys. Rev. Lett.*, 97:160401, Oct 2006.

[12] R. Zhao, J. Zhou, Th. Koschny, E. N. Economou, and C. M. Soukoulis. Repulsive casimir force in chiral metamaterials. *Phys. Rev. Lett.*, 103:103602, Sep 2009.

[13] Qing-Dong Jiang and Frank Wilczek. Chiral casimir forces: Repulsive, enhanced, tunable. *Phys. Rev. B*, 99:125403, Mar 2019.

Phononics and acoustic metamaterials

META 2023, PARIS - FRANCE, JULY 18 – 21, 2023

Tailoring MIMO transfer of sound using reflective reconfigurable intelligent surfaces

Hongkuan Zhang[1], Qiyuan Wang[1], Guancong Ma[1*]

[1]Department of Physics, Hong Kong Baptist University, Hong Kong
[*]Corresponding author: phgcma@hkbu.edu.hk

Abstract: Acoustic signals emitted by multiple sources in a room are mixed together due to reverberation, resulting in a loss of intelligibility of speech. Here, we demonstrate that the acoustic channel matrix among multiple inputs and outputs can be controlled with reflective reconfigurable intelligent surfaces by the mean of wavefield shaping. We show how 2×2 and 4×2 channels can be customized almost at will. This research has many potential applications, including scenarios such as enhanced indoor speech communications and recognition.

In recent years, wavefield shaping in disordered systems has garnered considerable attention[1–3]. Reverberant environments are typical wave-disorder systems. Acoustic signals from different sources interfere and mix, eventually becoming indistinguishable. Here, we experimentally demonstrate a method based on a channel matrix and wavefield shaping to tame the effect of disorder for achieving multiple-input and multiple-output (MIMO) acoustic communications.

In our experiments, a loudspeaker array represents the speakers, and a microphone array represents the listeners, as shown in Fig.1(a). A channel matrix is used to describe how the signals travel from the loudspeakers to the microphones. In the Fourier domain, this can be written as $\boldsymbol{R}(f) = \boldsymbol{H}(f) \cdot \boldsymbol{S}(f)$, where $\boldsymbol{R}$ and $\boldsymbol{S}$ denote receiving signals and transmitting signals at frequency f, respectively. The channel matrix $\boldsymbol{H}$ has complex-valued entries h_{ij} that describe the channel gain from the loudspeaker to the microphone. A 2×2 channel matrix corresponds to the situation with two speakers (loudspeakers) and two listeners (microphones). Our target is to eliminate cross-talks between speakers and listeners so that listener 1(2) only hears speaker 1(2). Mathematically, this means the reduction of the off-diagonal components of the channel matrix while maintaining the effective rank of $\boldsymbol{H}$. The objective function can be expressed as

$$F(f) = w[\boldsymbol{H}(f)] + |\mathrm{rank}[\boldsymbol{H}(f)] - \mathrm{erank}[\boldsymbol{H}(f)]| \quad (1)$$

where $w = \sum_{i\neq j}|h_{ij}(f)| \,/\, \sum_{i=j}|h_{ij}(f)|$ is the ratio between the off-diagonal part and the diagonal part of the channel matrix, which is called as the weight factor of channel matrix in this paper. The symbols $\mathrm{rank}[\cdot]$ and $\mathrm{erank}[\cdot]$ denote the rank and the effective rank of a matrix, respectively. The effective rank[4,5] acts as a measure of the transmission among different channels and can be defined as $\mathrm{erank}[\boldsymbol{H}] = \exp\left(-\sum_{k=0}^{n} p_k \ln p_k\right)$, where $p_k = \sigma_k/(\sum_i \sigma_i)$ is the normalized singular values of the channel matrix $\boldsymbol{H}$. Normally, if the energy is concentrated only in one channel, the effective rank is smaller (close to 1). Conversely, if and only if the energy is evenly distributed among all channels, the effective rank takes the maximum value which is equal to $\mathrm{rank}[\boldsymbol{H}]$.

We use a 200-unit reflective reconfigurable intelligent surface to control the disordered sound field, as shown in Fig.1(a). Each unit is an electrically tunable Helmholtz resonator capable of changing the reflected phase over a wide frequency range of 1050-1750 Hz. We obtain each entry in the channel matrix by measuring the complex transfer function between the loudspeakers and the microphones. Then we calculate the objective function with Eq. (1) and use it as feedback to guide the optimization. Figure 2(b) shows the result of the 2×2 channels, wherein the off-diagonal entries are indeed suppressed. Figures 2(c, d) show the effect of optimization on acoustic

communications. Two loudspeakers independently and simultaneously emit two different pulses, signal 1 and 2. Before the optimization, it is seen that both microphones can pick up the two signals, whereas after the optimization, microphone 1(2) can only pick up the signal emitted by speaker 1(2). In other words, the two channels are completely independent and cross-talks are completely eliminated.

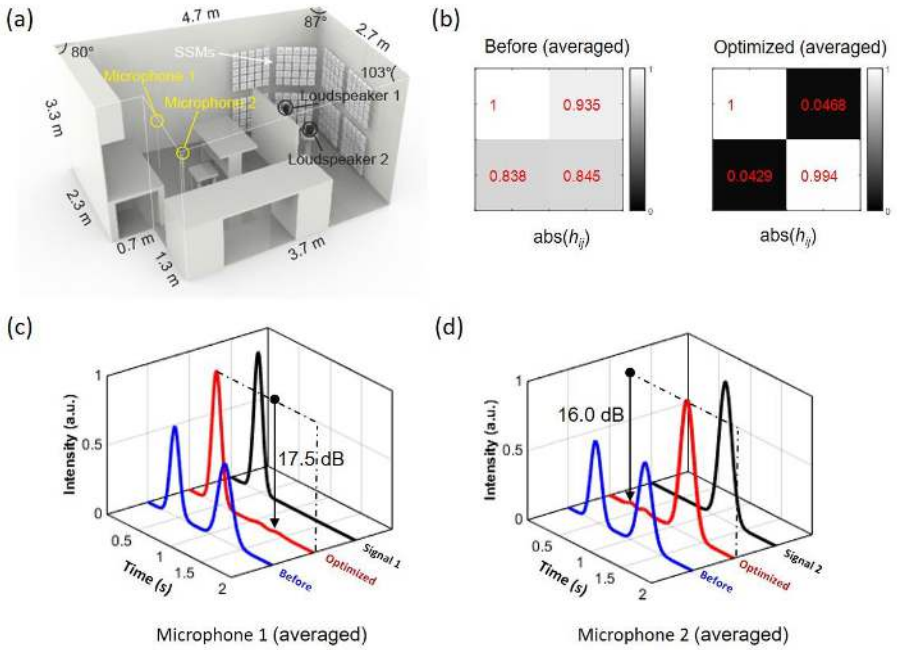


Fig. 1. (a) The room and experimental setup. (b) The channel matrices of 40 independent realizations at 1300 Hz before (left) and after (right) optimization. (c) and (d) show the averaged time-domain signal envelopes of 40 realizations received by microphones 1 and 2, respectively. The blue, red, and black lines represent the envelope of the received signal before optimization, the received signal after optimization, and the signals sent by the loudspeakers, respectively.

Acknowledgments. This work was supported by the National Natural Science Foundation of China (11922416) and the Hong Kong Research Grants Council (RFS2223-2S01, 12302420, 12300419, 12301822).

References

1. Cao, H., Mosk, A. P. & Rotter, S. “Shaping the propagation of light in complex media.” Nat Phys 18, 994–1007, 2022.
2. Bertolotti, J. & Katz, O. “Imaging in complex media. Nat Phys 18, 1008–1017, 2022.
3. Gigan, S. “Imaging and computing with disorder.” Nat Phys 18, 980–985, 2022.
4. Roy, O. & Vetterli, M. “The Effective Rank: a Measure of Effective Dimensionality.” in 606–610 (IEEE, 2007).
5. del Hougne, P., Fink, M. & Lerosey, G. “Optimally diverse communication channels in disordered environments with tuned randomness.” Nature Electronics 2, 36–41, 2019.

Subwavelength broadband perfect absorption for unidimensional open-duct problems

Y. Meng[1*], V. Romero-García[2], G. Gabard[1], J.-P. Groby[1], C. Bricault[3], and S. Goudé[3]

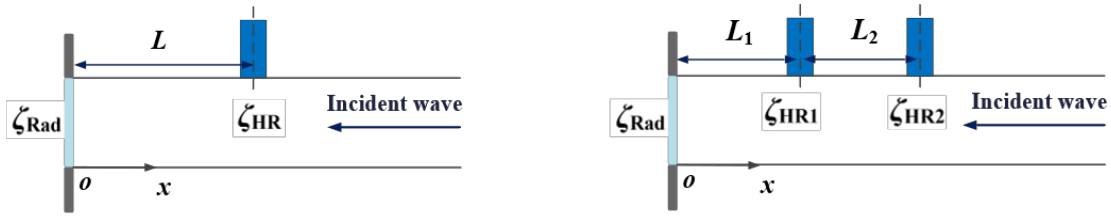
[1]Laboratoire d'Acoustique de l'Université du Mans (LAUM), UMR CNRS 6613, Institut d'Acoustique - Graduate School (IA-GS), CNRS, Le Mans Université, France.
[2]Instituto Universitario de Matemática Pura y Aplicada (IUMPA), Departamento de Matemática Aplicada, Universitat Politècnica de València, Camino de Vera, s/n 46022 València, Spain.
[3]Vibrations and Acoustics Laboratory, Valeo Thermal Systems, 78321 La Verrière, France
[*]corresponding author: Y. Meng (yang.meng@univ-lemans.fr)

Abstract: This work presents a general design methodology of metamaterial absorbers made of arrays of Helmholtz resonators for open-duct problems, which is encountered in broad practical applications. By using a single point scatterer, it is insufficient to attenuate both the reflected and radiated waves; a frequency-dependent maximum absorption exists and is derived analytically. To go beyond this absorption bound and achieve perfect absorption, at least two point scatterers are necessary. Specific designs are provided and validated both numerically and experimentally.

The absorption of both reflected and radiated acoustic waves by using monopolar point scatterers in the unidimensional (1D) open-duct problem is studied in this work. The absorption coefficient is defined as

$$\alpha = 1 - E_{\mathrm{Ref}} - E_{\mathrm{Rad}}\,. \tag{1}$$

where E_{Ref} and E_{Rad} are the reflection and radiation energies normalized by the incidence energy, respectively.



(a) (b)

Figure 1: Schematic illustrations of metamaterials made of point scatterers in the 1D open-duct problem: (a) Single point scatterer. (b) Two coupled point scatterers.

In the case that a single point scatterer is used, which is illustrated in Figure 1(a), the maximum absorption coefficient is derived as

$$\alpha_{\max} = \frac{1}{2}\left[1 + \sqrt{\frac{\left(\theta_{\mathrm{Rad}} - 1\right)^2 + \chi_{\mathrm{Rad}}^2}{\left(\theta_{\mathrm{Rad}} + 1\right)^2 + \chi_{\mathrm{Rad}}^2}}\right]. \tag{2}$$

which is in general frequency dependent and less than unity. Note that in the 1D problem, the acoustic response of the open end can be modelled by the specific radiation impedance [1] $\zeta_{\mathrm{Rad}} = \theta_{\mathrm{Rad}} + \mathrm{i}\chi_{\mathrm{Rad}}$ under the $\mathrm{e}^{\mathrm{i}\omega t}$ convention. To achieve $\alpha_{\max}$ at a single frequency, two conditions are necessary: (1) the scatterer provides the optimal impedance ζ_{opt} and (2) the distance between the scatterer and the open end is the optimal value L_{opt}. In contrast, to achieve perfect absorption ($\alpha = 1$), at least two point scatterers are needed as illustrated in Figure 1(b). Moreover, it is required that the scatterers should achieve the optimal impedance values:

$$\begin{cases} \zeta_{\mathrm{HR1}} = 0 \\ \zeta_{\mathrm{HR2}} = -\mathrm{i}\sin\left(k_0 L_2\right)\mathrm{e}^{\mathrm{i}k_0 L_2} \end{cases}. \tag{3}$$

The above definition (Eq. (1)) and results (Eqs. (2) and (3)) in the open-duct problem are direct generalizations of the 1D reflection [2] and transmission [3,4] problems. The reflection or transmission problem corresponds to the special case when the boundary impedance ζ_{Rad} approaches to infinity or 1+0i, respectively.

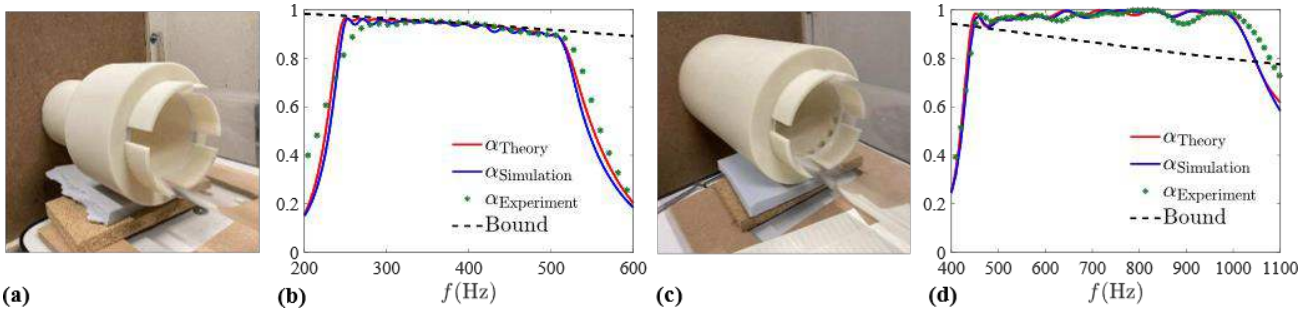


Figure 2: Single-point-scatterer metamaterial for broadband maximum absorption: (a) Sample working from 250 Hz to 500 Hz. (b) Absorption coefficient of the sample: comparison of the theory, simulation, and measurement. Coupled-point-scatterer metamaterial for broadband perfect absorption: (c) Sample working from 450 Hz to 1000 Hz. (d) Absorption coefficient of the sample: comparison of the theory, simulation, and measurement.

To realize $\alpha_{\max}$ and perfect absorption as well, we propose a general design strategy, in which monopolar point scatterers are employed. A circular waveguide (whose radius is 5 cm) with an open end in the baffled wall is considered. Arrays of Helmholtz resonators in parallel with the waveguide, i.e., in both the circumferential and the wave directions, are used to play the roles of the point scatterers. As predicted by Eq. (2), the maximum absorption is close to perfect in the low frequency range. Specifically, for this circular waveguide, $\alpha_{\max} \geq 0.9$ when $f \leq 500$ Hz. Thus, a compact and efficient absorber is realized by utilizing this property with a single point scatterer made of detuned Helmholtz resonators, which possesses deep subwavelength size and achieves broadband (250 Hz to 500 Hz) maximum absorption as shown in Figures 2(a) and 2(b). In contrast, coupled point scatterers are necessary to break the absorption bound and thus to achieve perfect absorption. A specific design is provided with numerical and experimental validations over the frequency band 450 Hz to 1000 Hz as shown in Figures 2(c) and 2(d).

Acknowledgements

All the authors gratefully acknowledge the support of Valeo. J.-P. G. and V. R.-G. would like to acknowledge the support of the ANR-RGC METARoom project (ANR-18-CE08-0021).

References

1. Kinsler, L.E., Frey, A.R., Coppens, A.B., and Sanders, J.V., "Fundamentals of acoustics," John Wiley & Sons, 2000.
2. Huang, S., Fang, X., Wang, X., Assouar, B., Cheng, Q., and Li, Y. "Acoustic perfect absorbers via Helmholtz resonators with embedded apertures," J. Acoust. Soc. Am., Vol. 145, No. 1: 254-262, 2019.
3. Merkel, A., Theocharis, G., Richoux, O., Romero-García, V., and Pagneux, V. "Control of acoustic absorption in one-dimensional scattering by resonant scatterers," Appl. Phys. Lett., Vol. 107, No. 24: 244102, 2015.
4. Jiménez, N., Romero-García, V., Pagneux, V., and Groby, J.-P. "Rainbow-trapping absorbers: Broadband, perfect and asymmetric sound absorption by subwavelength panels for transmission problems," Sci. Rep., Vol. 7, No. 1: 13595, 2017.

Strain-gradient-driven and magnetoelectric operation with order parameters in Cr_2O_3

O. V. Pylypovskyi[1,2*]

[1]Helmholtz-Zentrum Dresden-Rossendorf e.V. 01328 Dresden, Germany
[2]Kyiv Academic University, 03142 Kyiv, Ukraine
[*]corresponding author: o.pylypovskyi@hzdr.de

Abstract: Progress in computing technologies enforces an active search for novel materials, assuring low-power and high-speed operations. One of prospective materials for such needs is Cr_2O_3. Here, we discuss access to the order parameters and properties of antiferromagnetic domain walls related to the possibility of electric operations on them, as well as fundamental and technological perspectives of the recently accessed flexomagnetism in thin Cr_2O_3 films.

Strong technological need in low-power and high-speed solid-state elements of electronic devices brings attention to antiferromagnets. Being usually used as a supplementary parts of ferromagnet-based devices, this class of materials offers a wide range of phenomena related to the crystal symmetry and spin-orbit torques. Among them, Cr_2O_3 is of special interest because of easy-axis anisotropy and room-temperature magnetoelectric effect [1]. The latter gives a possibility to manipulate the primary magnetic order parameter $\boldsymbol{L}$ by electric field. In this way, magnetoelectric cooling through the Neel temperature T_N with spatially varying magnetic field allows to set the domain wall in a Cr_2O_3 single crystal. It was demonstrated, that this domain wall can be moved by the laser spot and can be pinned or deflected by the surface topography of the sample. Stable geometric bends of the domain wall mimicking an elastic ribbon enable a possibility to design a memory unit cell [2].

While distinguishing of the oppositely ordered domains separated by 180º domain walls by imaging could be complicated, anomalous Hall effect in Pt capping layer of a Cr_2O_3 sample is a powerful tool to access the net sublattice magnetization. Combining with the linear magnetoelectric effect, this gives a possibility for the completely electric operation with direction of $\boldsymbol{L}$, where the hysteresis behavior necessary for the memory storage appears due to bias of the gate voltage associated with the defect-induced magnetic moment [3]. Thin Cr_2O_3 films typically have a complex grain structure whose landscape has a correlation with antiferromagnetic domains in equilibrium because of domain wall pinning on defects. However, defect structure can be effectively controlled by the deposition and annealing temperatures, while the magnetoelectric effect is preserved even for the random orientation of single grains [4].

Low bulk T_N of about 35ºC is the key limiting factor for direct technological use of Cr_2O_3. There are theoretical predictions and experimental observations that the internal strain can rise T_N giving wider operational temperature range [5]. In addition to the average strain of order of 3% enhancing T_N, up to 100 ºC, epitaxially grown thin Cr_2O_3 films can also possess sizeable strain gradient of order up to 0.1%/nm. This enables flexomagnetic response of the film, resulting in the additional net magnetization consisting of two terms. The ordinary flexomagnetic moment is directly produced by the strain and is uniform within the film plane. The observed strain gradient also induces gradient of T_N along the film thickness z and respective scaling of $\boldsymbol{L}$ with z. The latter produces an uncompensated magnetization aligned with $\boldsymbol{L}$ and therefore accessible via stray fields measurements [6].

Magnetoelectric Cr_2O_3 is a prospective material platform for energy-consuming devices, where access to the primary antiferromagnetic order parameter can be done via electric fields. Furthermore, despite weak ferromagnetism by itself is forbidden in this material, inhomogeneous strain enables non-zero magnetization and graded Neel temperature in film interior, which provides additional degrees of freedom in design of antiferromagnetic racetracks and sub-THz magnonic waveguides.

References

1. Yan, H., Feng, Z., Qin, P. et al, "Electric-field-controlled antiferromagnetic spintronic devices,", Adv. Mater. Vol. 32, No. 12, 1905603, 2020; Spaldin, N. A., "Analogy between the magnetic dipole moment and the surface of a magnetoelectric and the electric charge at the surface of a ferroelectric,", JETP, Vol. 132, 493, 2021.
2. Hedrich, N., Wagner, K., Pylypovskyi O. V. et al. "Nanoscale mechanics of antiferromagnetic domain walls,", Nat. Phys., Vol. 17, No. 5, 574-577, 2021.
3. Kosub, T., Kopte, M., Hühne, R. et al., "Purely antiferromagnetic magnetoelectric random access memory," Nat. Comm., Vol. 8, 13985, 2017.
4. Veremchuk, I., Liedke, M. O., Makushko, P. et al. "Defect nanostructure and ist impact on magnetism of α-Cr_2O_3 thin films," Small, Vol. 18, 2201228, 2022; Veremchuk, I., Makushko, P., Hedrich, N. et al. "Magnetism and magnetoelectricisty of textured polycrystalline bulk Cr_2O_3 sintered in conditions far out of equlirbium," ACS Appl. El. Mater., Vol. 4, No. 6 2943-2952, 2022.
5. Mu, S., Wysocki, A. L., Belashchenko, K. D., "Effect of substitutional doping on the Neel temperature of Cr_2O_3," Phys. Rev. B Vol. 87, 054435 2013; Street, M., Echtenkamp, W., Komesu, T. et al. "Increasing the Neel temperature of magnetoelectric chromia for voltage-controlled spintronics," Appl. Phys. Lett., Vol. 104, 222402, 2014; Kota, Y., Yoshimori, Y., Imamura, H. et al. "Enhancement of magnetoelectric operating temperature in compressed Cr_2O_3 under hydrostatic pressure," Appl. Phys. Lett. Vol. 110, No. 4, 042902, 2017.
6. Makushko, P., Kosub, T., Pylypovskyi, O. V. et al., "Flexomagnetism and vertically graded Neel temperature of antiferromagnetic Cr_2O_3 thin films," Nat. Comm., Vol. 13, 6745, 2022.

Backscattering reduction in a twisted water wave channel

S. Kucher[1*], A. Koźluk[2], P. Petitjeans[1], A. Maurel[3] and V. Pagneux[4]

[1]Laboratoire de Physique et Mécanique des Milieux Hétérogènes, ESPCI-PSL, CNRS, Sorbonne Université, Université Paris Cité, 75005 Paris, France
[2]Institute of Aeronautics and Applied Mechanics, Warsaw University of Technology, 00-665 Warsaw, Poland
[3]Institut Langevin, ESPCI-PSL, CNRS, 75005 Paris, France
[4]Laboratoire d'Acoustique de l'Université du Maine, CNRS, 72085 Le Mans, France
[*]corresponding author: samantha.kucher@espci.fr

Abstract: We study experimentally and numerically how to reduce the backscattering of water waves in a channel with multiple turns. We show that it is possible to achieve enhanced transmission in such geometries, in agreement with a recent theoretical prediction. In order to avoid the reflection that naturally arises at each turn of the waveguide, we used an anisotropic metamaterial made of closely-spaced thin vertical plates.

In the last decade, there has been a theoretical effort [1-3] as well as an experimental one [4, 5] on using gratings with a subwavelength structure to obtain a broadband wave shifting. Recently, it has been shown [6] that the exact solution to the problem of an array of inclined infinitely thin parallel plates occupying a region of finite width yields total transmission for all wavenumbers when the inclination of the plates is opposed to the incident wave direction.

In the present study, we show experimentally a broadband backscattering reduction through an array of vertical surface piercing thin plates with a perpendicular angle with respect to the incident wave. We performed experiments in a waveguide that undergoes a twist at 90° and then continues in a direction parallel to the first section, as shown in Figure 1. In an empty channel (i.e. without the plate-array metamaterial), the transmission coefficient decreases with the frequency; it only reaches high values at the resonances. However, the addition of an anisotropic metamaterial not only reduces the backscattering but also allows for an enhanced transmission. It is important to emphasize that this effect occurs for all frequencies below the cut-off frequency, without relying on resonant phenomena.

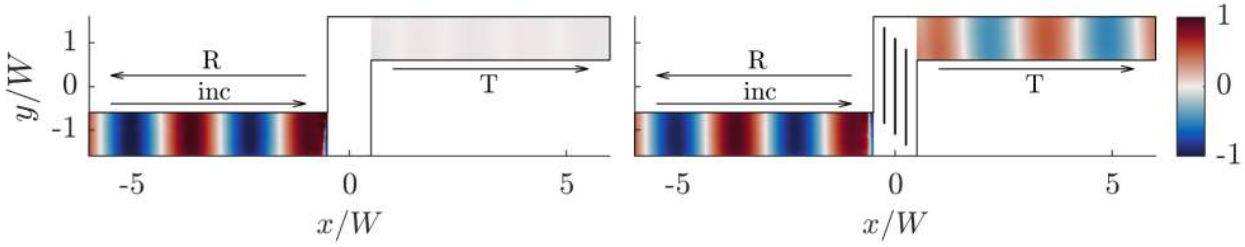


Figure 1. Experimental result: real part of the measured free surface deformation filtered at the forcing frequency for $kW = 9\pi/10$ (normalized), for a configuration without (left) and with (right) the plate array metamaterial, showing the directions of the incident, reflected and transmitted waves.

We first studied numerically the effect of the ratio between the length of the twist and the width W of the channel, proposing a 1D model analogous to a Fabry-Perot interferometer. Based on this study, we chose to work with a twist of length $3.2W$, because it is the largest ratio where we only see one

resonance (it should be reminded that we are looking for a broadband effect, regardless of resonant phenomena). Since the plates that form the metamaterial have a finite thickness, we addressed its influence on the reflection and transmission coefficients. We then decided to fix the thickness at $0.02W$ in order to have a small reflection and at the same time be large enough to perform experiments.

Experiments were performed in a 3 m long channel of width $W = 0.10$ m, with a water depth of 0.05 m, using the Fourier Transform Profilometry method [7] to measure the free surface deformation. We took measurements in a wide range of frequencies below the cut-off frequency, changing the number of plates that constitute the metamaterial, always maintaining the space between the plates smaller than the wavelength. We observed a significant backscattering reduction, providing empirical evidence to the theoretical predictions made by [6] and exploring its capabilities in terms of an experimental realization.

References

1. Alù, A., D'Aguanno, G., Mattiucci, N. and M. J. Bloemer. "Plasmonic Brewster angle: Broadband extraordinary transmission through optical gratings," Phys. Rev. Lett., Vol. 106, No. 12, 1-4, 2011.

2. Maurel, A., Félix, S. and J. F. Mercier. "Enhanced transmission through gratings: Structural and geometrical effects," Phys. Rev. B, Vol. 88, No. 11, 1-5, 2013.

3. Norris A. N. and X. Su. "Enhanced acoustic transmission through a slanted grating," Comptes Rendus - Mécanique, Vol. 343, No. 12, 622-634, 2015.

4. Wei, P., Liu, F., Liang, Z., Xu, Y., Chu, S. T. and J. Li. "An acoustic beam shifter with enhanced transmission using perforated metamaterials," Europhys. Lett., Vol. 109, No.1, 14004, 2015.

5. Berraquero, C. P., Maurel, A., Petitjeans, P. and V. Pagneux. "Experimental realization of a water-wave metamaterial shifter," Phys. Rev. E, Vol. 88, No. 5, 1-5, 2013.

6. Porter, R. "Plate arrays as a perfectly-transmitting negative-refraction metamaterial," Wave Motion, Vol. 100, 102673, 2021.

7. Cobelli, P.J., Maurel, A., Pagneux, V. and P. Petitjeans. "Global measurement of water waves by Fourier transform profilometry," Exp Fluids, Vol. 46, 1037–1047, 2009.

META 2023, PARIS - FRANCE, JULY 18 – 21, 2023

How to steer acoustic waves in a random medium in a programmable way?

A. O. Krushynska[1] and M. van Hecke[2,3]

[1] Engineering and Technology Institute Groningen (ENTEG), Faculty of Science and Engineering, University of Groningen, Nijenborgh 4, 9747 AG Groningen, The Netherlands
[2]AMOLF, Science Park 104, 1098 XG Amsterdam, The Netherlands
[3]Huygens-Kamerlingh Onnes Lab, Leiden University, 2300 RA Leiden, The Netherlands
*corresponding author: a.o.krushynska@rug.nl

Abstract: Recently emerged aperiodic textured metamaterials have opened up routes to multi-functional and programmable functionalities. Such possibilities have, however, been explored mainly in quasi-static regimes. Here, we show that the "tuning-by-pruning" strategy enables realizing multi-frequency steering in random elastic networks thus showing a way to the rational design of a new class of programmable acoustic metamaterials.

Metamaterials open exciting venues for unprecedented manipulation of mechanical characteristics and control of acoustic waves. Recently, discrete pruning of random nearly-isostatic networks has enabled the simultaneous optimize two static mechanical properties – the shear and bulk modulus [1] and evolving networks with an "allosteric" response, where static forcing at location A yields a response localized at a distant location B without a traceable load path [2]. Disordered networks constitute an attractive design space for exploring programmable functionality [3]. Here, we apply the discrete pruning strategy to control the wave dynamics of random mass-spring networks and aim at achieving multichannel wave steering. For this, we choose wave frequency as a canonical control parameter that naturally leads to intricate design questions and opportunities.

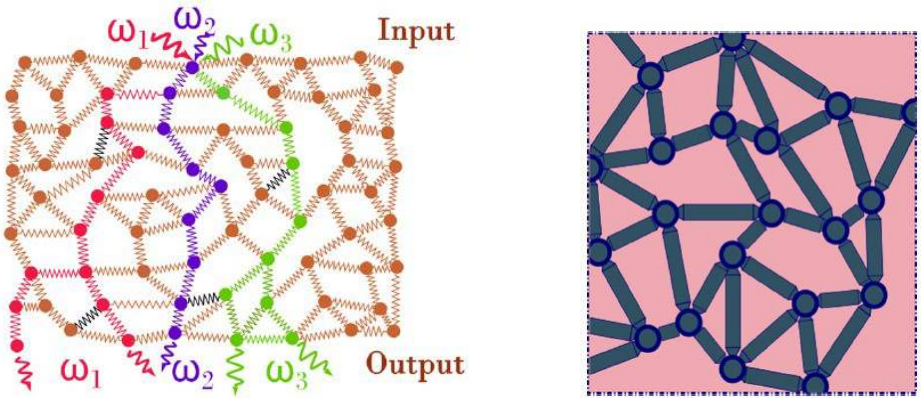


Fig.1 (left) Schematics of the expected functionality: exciting the input node of a rationally pruned network directs the vibration energy toward the output nodes depending on the excitation frequency. (right) Sketch of possible practical realization.

We consider mass-spring systems. Given n output channels and m harmonic excitations of unit amplitude and frequency $\{\omega_m\}$, how close can we approach target amplitudes $\{A_n^m\}$ with a network consisting of k springs (Fig. 1, left)? How many independent patterns ("capacity of the network") as functions of k, m or n are possible to create the foundation for the computer design of pluripotent networks?

Here, we analyze cases when m preselected frequencies (m=1,2,3) yield l on/off (1/0) normalized target amplitude patterns at n outputs for two-dimensional networks with 5x5, 7x7, … 27x27 masses. We use a greedy

pruning algorithm that removes one spring at each step which yields a minimal value to a cost function. The cost function is defined as the sum of squares of differences between the actual and target amplitudes at the outputs. Note that in the dynamic regime, such pruning is more computationally expensive as compared to previously analyzed strategies for static properties [1, 2]. In the latter case, the target function can be expressed as a sum over springs so that springs can be removed independently reducing computational costs. In our systems, the removal of a spring modifies the eigenmodes that require recalculating the cost function at each step.

We have shown that rational pruning allows controlling vibration properties of disordered networks by pruning a small number of springs (less than 10%). The pruned configurations do not show discernible paths but enable steering acoustic energy to targeted nodes at pre-defined frequencies. We observe that the number of springs that are required to be pruned increases with more stringent design objectives such as larger contrast of amplitudes at outputs or more outputs, as can be expected. For a given target functionality, the number of pruned springs increases linearly with the number of masses, so the fraction of pruned springs diminishes with this number. This suggests that larger systems allow for even more functionalities to be integrated.

Our results demonstrate that pruning is a viable strategy to realize multi-objective optimization in disordered spring-based metamaterials. Further studies are required to verify the obtained results experimentally, e.g., by testing systems as shown in Fig. 1 (right) and to extend the pruning strategy to three-dimensional network configurations.

A.K. acknowledges the Center for Information Technology of the Faculty of Science and Engineering, University of Groningen for their support and for providing access to the Peregrine high-performance computing cluster.

References

1. Goodrich, C. P., A.J. Liu and S. R. Nagel "The principle of independent bond-level response: tuning by pruning to exploit disorder for global behavior," Phys. Rev. Lett., Vol. 114, 225501, 2015.
2. Rocks, J.W., N. Pashine, I. Bischofberger, C.P. Goodrich, A.J. Liu and S.R. Nagel, "Designing allostery-inspired response in mechanical networks," Proc. Nat. Acad. Sci. U.S.A., Vol. 114, 2520-2525, 2017.
3. Florijn, B., C. Coulais and M. van Hecke "Programmable mechanical metamaterials," Phys. Rev. Lett., Vol. 113, 175503, 2014.
4. Krushynska, A. O. and M. van Hecke "Multi-frequency acoustic steering in rationally pruned disordered networks," arXiv preprint, arXiv:2212.12274, 2022.

META 2023, PARIS - FRANCE, JULY 18 – 21, 2023

Control of wave propagation in networks of gyro-elastic discrete strips

G. Carta[1*], M. J. Nieves[2], and M. Brun[1]

[1]Department of Mechanical, Chemical and Materials Engineering, University of Cagliari, Italy
[2]School of Computer Science and Mathematics, Keele University, UK
[*]corresponding author: giorgio_carta@unica.it

Abstract: We present a novel mechanical network, which can guide the elastic waves generated by an external loading towards any of its endpoints, that can be selected *a priori*. The proposed *Mechanical Switching Network* (*MSN*) is made of an arrangement of intersecting strips, possessing a lattice structure where the nodes are connected to gyroscopic spinners. This innovative system can be useful in engineering applications, where the control of energy propagation plays a crucial role.

The system under investigation, named *Mechanical Switching Network* (*MSN*), is a network of lattice strips with different orientations. The micro-structure, shown in Figure 1(a), consists of a triangular array of point masses connected by elastic links and attached to gyroscopic spinners, which couple the in-plane displacement components of the masses. The gyroscopic spinners are characterised by a quantity, denoted by Ω^* and referred to as "effective gyricity", that is given by the sum of the spinner's initial precession and spin rates and that remains constant during the motion.

In the time-harmonic regime, the vector problem is solved analytically by writing the governing equations of the particles inside the bulk and at the upper and lower free boundaries, as described in [1] for the case without gyroscopic spinners. The dispersion curves for the periodic strip exhibit a semi-infinite band-gap at higher frequencies and their number is equal to twice the number of the lattice rows. In the transient regime, the formulation is based on the use of Laplace transform and discrete Fourier transform [2]; in this case, the presence of an applied load has been taken into account.

The response in the time-harmonic and transient regimes of the MSN to an external source is determined numerically, by constructing a finite element model in *Comsol Multiphysics* (version 5.6). An example is shown in Figure 1(b), where the total displacement field is plotted. The external loading is represented by a time-harmonic horizontal force, indicated by an arrow and labelled as "S", while the four endpoints are denoted by "A" to "D". Adaptive Absorbing Layers are introduced near the ends of the MSN branches, in order to avoid reflections at the boundaries.

In Figure 1(b), the effective gyricity in each strip is selected such that waves are forced to propagate to the endpoint C. It is found that more than 96% of the energy coming from the external source is channelled towards the chosen endpoint. We point out that wave propagation can be diverted to any of the other endpoints by tuning the effective gyricity in each branch (see [2] for further results). The preferential directionality of the MSN is due to the non-reciprocal behaviour induced by gyroscopic spinners, which was formally proved in [3] and demonstrated with numerical simulations in [4] in relation to Rayleigh waves.

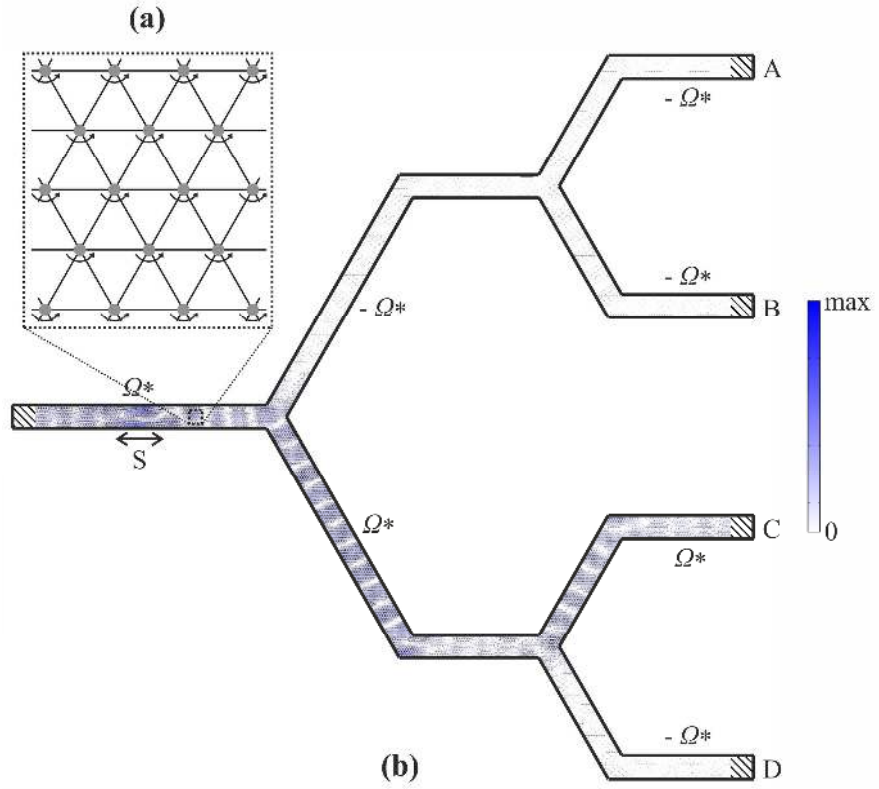


Figure 1. *Mechanical Switching Network* (*MSN*): (a) detail of a branch of the system, characterised by a lattice structure whose nodes are connected to gyroscopic spinners (circular arrows); (b) wave propagation induced by an external source S (arrow) and channelled to endpoint C by properly choosing the effective gyricity Ω^* in each branch (the dashed regions near the ends of the network indicate Adaptive Absorbing Layers).

We envisage that his work can lead to innovative engineering applications in Micro-mechanical and Signal Processing Systems, where control and tunability of wave propagation play an important role.

G.C. and M.B.'s work has been performed under the auspices of GNFM-INDAM. M.J.N. gratefully acknowledges the support of the EU H2020 grant MSCA-RISE-2020-101008140-EffectFact.

References

1. Carta, G., M. J. Nieves and M. Brun, “Lamb waves in discrete homogeneous and heterogeneous systems: Dispersion properties, asymptotics and non-symmetric wave propagation,” Eur. J. Mech. A Solids, 104695, 2022.
2. Carta, G., M. J. Nieves and M. Brun, “Forcing the silence of the Lamb waves: Uni-directional propagation in structured gyro-elastic strips and networks,” *submitted to* Eur. J. Mech. A Solids, 2023.
3. Nieves, M. J., G. Carta, V. Pagneux and M. Brun, “Rayleigh waves in micro-structured elastic systems: Non-reciprocity and energy symmetry breaking,” Int. J. Eng. Sci., Vol. 156, 103365, 2020.
4. Nieves, M. J., G. Carta, V. Pagneux and M. Brun, “Directional Control of Rayleigh Wave Propagation in an Elastic Lattice by Gyroscopic Effects,” Front. Mater., Vol. 7, 602960, 2021.

META 2023, PARIS - FRANCE, JULY 18 – 21, 2023

A nonlinear acoustic topological system through active control

X. Guo[1], L. Jezequel[2], M. Padlewski[1], H. Lissek[1], P. Delplace[2] and R. Fleury[3]

[1] Laboratoire de Traitement des Signaux LTS2, Ecole Polytechnique Fédérale de Lausanne, 1015 Lausanne, Switzerland.
[2]Univ Lyon, ENS de Lyon, CNRS, Laboratoire de Physique, F-69342 Lyon, France.
[3]Laboratory of Wave Engineering, Ecole Polytechnique Fédérale de Lausanne, 1015 Lausanne, Switzerland.

[*]corresponding romain.fleury@epfl.ch

Abstract: Here by actively controlling electroacoustic resonators, we implement a one-dimensional nonlinear topological system. We demonstrated theoretically, numerically, and experimentally that by adding nonlinearity, the edge state can be preserved at the same frequency as the linear case, provided that the chiral symmetry is satisfied. A good agreement has been found between theoretical, numerical, and experimental results. Our active control approach shows great potential for exploring different types of systems at the intersection of non-linear physics and other fields.

Active control is an efficient means to tailor the physical properties of the materials. By assignment of a specified electrical current sent to a loudspeaker, one can modify its impedance in a prescribed manner [1]. In our work, we use such a feedback control loop to design active unit cells, and then build a one-dimensional topological lattice. We first apply linear control to generate linear edge states, then we combine it with nonlinear control to study the evolution of the edge state generated. Our exploration starts from theoretical work on the nonlinear Su–Schrieffer–Heeger model, then we demonstrate with simulation and experiments that in the nonlinear cases, by satisfying the chiral symmetry, the edge state can be preserved at the same frequency as the linear case, which in agreement with the conclusions of the theoretical topology work of L. Jezequel and P. Delplace [2].

References

1. E. Rivet, S. Karkar, and H. Lissek. “Broadband Low-Frequency Electroacoustic Absorbers Through Hybrid Sensor-/Shunt-Based Impedance Control,” IEEE Trans. Control Syst. Technol., Vol. 25, No. 1, 63–72, 2017.
2. L. Jezequel and P. Delplace, “Nonlinear edge modes from topological one-dimensional lattices,” Physis. Rev. B, Vol. 105, No. 3, 035410, 2022.

META 2023, PARIS - FRANCE, JULY 18 – 21, 2023

Deep learning models for acoustic wave scatterings

W. W. Amhed[1], M. Farhat[1], P. Y. Chen[2], X. L. Zhang[3], and Y. Wu[1*]

[1]King Abdullah University of Science and Technology (KAUST), Thuwal, 23955-6900, Saudi Arabia
[2]University of Illinois at Chicago, Chicago, IL60607, United States of America
[3] University of Notre Dame, Notre Dame, IN 46556, United States of America
[*]corresponding author: ying.wu@kaust.edu.sa

Abstract: We develop deep learning models based on discriminative and generative networks to solve the forward and inverse acoustic scattering problems and show how these models benefit solving the inverse design process by eliminating the non-unique solution space. We demonstrate examples of using the developed deep learning models for designing broadband acoustic cloaks and arbitrarily-shape acoustic object recognition for underwater applications

The conventional modeling of wave-media interactions is based on analytical and numerical schemes, which often rely on hit and trial modeling of physical variables or physics-informed optimization for 'on demand' scattering properties. In general, these schemes are computationally expensive, and are slow especially for complex systems involving a design space with large degrees of freedom. On the other hand, with the blossoms of artificial intelligence, models that can capture the underlying correlation between various physical quantities and streamline the inverse design process provide completely different tools for the study of wave-media interaction. Recently, data driven approaches were on the main stream of research due to their ability to solve a wide range of physical problems with unprecedented speed and accuracy[1]. Despite of this progress, there have been limited efforts to using deep learning techniques to learn input-output mappings with diverse designs and inverse design insights. In this work, novel deep learning models are developed for the design of broadband acoustic cloak and arbitrary object recognition in water. As a surrogate physical model, discriminative neural networks are designed for forward process of one-to-one mapping. However, generative neural networks based on variational inference and adversarial learning are designed for the inverse process of one-to-many mapping, where the fundamental issue of nonuniqueness is addressed by learning the latent distribution of data structures.

In the first example, we demonstrate deterministic and probabilistic deep learning models for inverse design of broadband acoustic cloak. Acoustic cloaks, making an object invisible for sound waves, are usually build from artificially structured acoustic metamaterials. The realization of metamaterial-based cloak faces multiple challenges, such as stringent requirements on the material parameters and narrow operating bandwidth. To address these issues, we propose a design of acoustic cloak with a four-layer core-shell configuration driven by machine learning. The performance of the system is quantified by the ratio of total scattering cross-section (TSCS) spectra for the cloaked object and the bare object, computed using transfer matrix method (TMM). To achieve broadband invisibility, we first train a forward neural network (FNN) to model the relation between the design and response space using a set of training data. Once trained, the pretrained FNN is cascaded behind the inverse network forming a probabilistic encoder-decoder-like structure to capture the underlying physics to generate a variety of design parameters for one desired spectral response and uncovering the sensitivity of the design parameters on the cloaking effect [2].

In the second example, we show a generative deep learning approach for shape recognition of arbitrary objects from phaseless acoustic scattering data. Shape recognition, which relies on inverse scattering, has a wide range of applications, such as sonar detection, remote sensing, underwater imaging, and nondestructive testing. For underwater objects, however, accurate shape recognition is challenging because of high nonlinearity, large background index contrast, and one-to-many mapping in the solution space. Here, we consider a 2D arbitrarily-shaped steel scatterer submerged in water and propose a latent space to learn the nonlinear mapping between acoustic objects and its far-field scattering patterns once illuminated. The non-unique solution space is eliminated by training the probalistic networks with multi-frequency phaseless far-field amplitudes. The scatterer is discretized as a pixel-based binary image, which different indices representing different materials. A commercial software based on finite-element, COMSOL Multiphysics, is used to simulate the far-field patterns of random geometries at five different frequencies across the full angular range. The proposed deep-learning model employs an adversarial autoencoder as a training method for Generator, which generates geometric patterns from the latent distribution of arbitrary-shaped objects. The inverse neural network predicts the 2D object with the matrix of 64 × 64 for the given multi-frequency far-field scattering amplitudes [3]. The approach is generic and readily extended to design complex and random geometries of three-dimensional space structures and other physical systems.

Acknowledgements: the work described in this summary is supported by King Abdullah University of Science and Technology Baseline research fund Bas/01/1626-01-01 and AI initiative fund.

References

1. Jiang J, Chen M, Fan J. A, Deep neural networks for the evaluation and design of photonic devices . Nat Rev Mater 6, 679–700, 2021
2. Ahmed W. W, Farhat M, Zhang X, and Wu Y, Deterministic and probabilistic deep learning models for inverse design of broadband acoustic cloak. Phys Rev Res, *3*(1): 013142, 2021
3. Ahmed W. W, Farhat M, Chen P.-Y, Zhang X, Wu Y, A Generative deep learning approach for shape recognition of arbitrary objects from phaseless acoustic scattering data Adv. Intell. Sys. 2200260 2023

META 2023, PARIS - FRANCE, JULY 18 – 21, 2023

Wave reflection, transmission and antireflection layers at a temporal boundary using a Shive wave machine

M. Tomoda[1*], T. Omiya[1], H. Takeda[1], O. Matsuda[1] and O. B. Wright[2,3]

[1]Faculty of Engineering, Hokkaido University, Sapporo 060-8628, Japan
[2]Hokkaido University, Sapporo 060-0808, Japan
[3]Graduate School of Engineering, Osaka University, Osaka 565-0871, Japan
[*]Corresponding author: mtomoda@eng.hokudai.ac.jp

Abstract: We demonstrate wave reflections at temporal boundaries, at which physical constants change suddenly, by use of a one-dimensional mechanical metamaterial in the form of a Shive wave machine. We also demonstrate a temporal antireflection layer by temporal impedance matching, that makes use of an appropriate intermediate temporal layer.

Wave can reflect and transmit at spatial boundaries between two homogeneous media. Waves also reflect and transmit at temporal boundaries. To make temporal boundaries, the physical parameters of the whole medium should be changed suddenly, on a scale much faster than the time for propagation through the region of study. Because of the difficulty of making such clear temporal boundaries, there are few experiments to directly investigate reflected waves at temporal boundaries. An experiment with temporal boundaries on a water surface using a change in the effective gravitational constant has been reported [1]. Recently, an experiment for the temporal reflections at temporal boundaries on a transmission-line metamaterial is reported [2].

Here we follow the reflection and transmission at temporal boundaries for the case of a simple and readily visible one-dimensional (1D) system. The key idea is, by use of a Shive wave machine [3,4], to make the wave speed of the whole medium change suddenly. This allows the investigation of the wave propagation with the naked eye or by use of a video camera, using a system constructed with inexpensive mechanical parts.

To realize wave reflection phenomena at a temporal boundary, we construct a Shive wave machine that uses 5 wires and 95 rods (Figure 1). The central wire goes through the center of gravity of each rod and supports the rods. Two inside wires are arranged symmetrically about the center, which allows torsional motion to be transferred from rod to rod as the wave propagates. Two outside wires, with a similar function, are also arranged symmetrically and can be pulled by a stepping motor, controlled by a computer, in order to change the wire tension and hence the wave phase velocity. The rods are square cross-section brass bars ($320 \times 6 \times 6$ mm) arranged with a 20-mm lattice constant. The motion of the wave machine is recorded by four cameras with a commercial motion-capture system (OptiTrack). We have thereby recorded reflected waves at a temporal boundary, and also realized a temporal antireflection layer by adding an

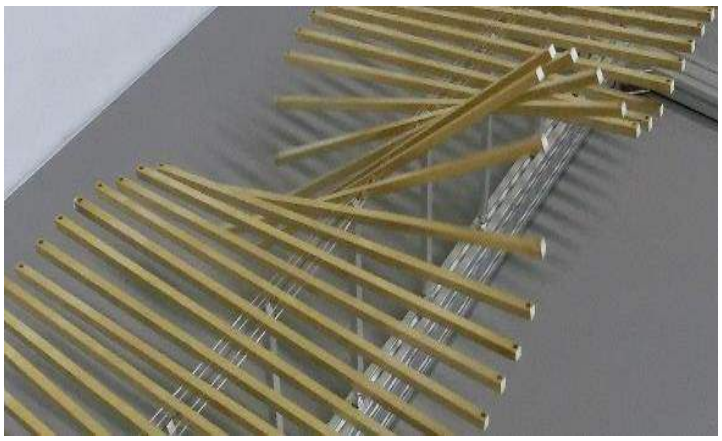


Figure 1. Photograph of the wave machine.

appropriate intermediate temporal layer [5].

In future, it should be possible to demonstrate the wave physics of time-dependent media and space-time metamaterials, for example by involving phenomena such as amplification, wave shaping or frequency transformation [6,7].

This work was supported by JSPS KAKENHI Grant Numbers 22H01930, 21H05020, and 19H05619.

References

1. V. Bacot, M. Labousse, A. Eddi, M. Fink and E. Fort. “Time reversal and holography with spacetime transformations,” Nat. Phys., Vol. 12, 972–977, 2016.
2. H. Moussa, G. Xu, S. Yin, E. Galiffi, Y. Ra’di and A. Alú, “Observation of temporal reflection and broadband frequency translation at photonic time interfaces,” Nat. Phys., 2023. https://doi.org/10.1038/s41567-023-01975-y
3. J. Shive, “Similarities in Wave Behavior,” Am. J. Phys., Vol. 32, 571, 1964.
4. R. Madrid, A. Gonzalez and G. M. Irwin, “Gravitational dispersion in a torsional wave machine,” Am. J. Phys.. Vol. 82, 1134-1141, 2014.
5. V. Pacheco-Peña and N. Engheta, “Antireflection temporal coatings.” Optica Vol. 7, 323-331. 2020.
6. C. Caloz and Z. -L. Deck-Léger, “Spacetime Metamaterials—Part I: General Concepts,” IEEE Trans. Anten. Propag. Vol. 68, 1569-1582, 2020.
7. C. Caloz and Z. -L. Deck-Léger, “Spacetime Metamaterials—Part II: Theory and Applications,” IEEE Trans. Anten. Propag. Vol. 68, 1583-1598, 2020.

META 2023, PARIS - FRANCE, JULY 18 – 21, 2023

Quasi-Bound States in the Continuum for Acoustic and Elastic Waves

Marc Martí-Sabaté[1] , Junfei Li[2], Bahram Djafari-Rouhani[3], , Steven Cummer[2], Daniel Torrent[1*]

[1]Institut de Noves Tecnologies de la Imatge (INIT), Universitat Jaume I, 12071 Castelló de la Plana, Spain

[2] Department of Electrical and Computer Engineering,7 Duke University, Durham, North Carolina 27708, USA

[3]IEMN, University of Lille, Cité Scientifique, 59650 Villeneuve d'Ascq, France

Abstract: We study the localization of flexural and acoustic waves in metasurfaces by means of clusters of scatterers. We show that when the scatterers are placed regularly in the perimeter of a circumference the structure forms a resonator which quality factor grows up exponentially with the number of scatterers. This allows the realization of high-quality resonant cavities whose quality factor can be easily tailored and, consequently, its interaction with the continuum. These modes, also named quasi-bound states in the continuum or QBICs, are robust against small perturbations in the geometry of the cluster, being therefore an excellent platform for the design of efficient structures for wave-trapping devices. Numerical experiments are performed for elastic waves in thin elastic plates and acoustic waves trapped atop a metasurface, and an experimental validation of the latter is also presented.

Acoustic and elastic resonators are indispensable structures for all type of devices devoted to the control of the energy carried out of these waves. Bound states in the continuum (BICs) offer a route for the realization of high-quality resonant cavities, since although in principle these modes cannot couple to free propagating waves, structures based on them can be used for the design of excellent resonators presenting finite lifetimes which interact weakly with the continuum.

In this work we study the realization of mechanical resonators for acoustic and elastic waves. First, we consider the propagation of flexural waves in thin elastic plates, latter we study acoustic waves trapped atop a structured metasurface. The geometry analyzed for both systems consists in clusters of scatterers regularly placed along the perimeter of a polygon. We show that in the limit of an infinite number of scatterers this structure forms a cavity with a set of resonances with an infinite quality factor, obtaining therefore a perfect BIC. However, having a finite number of scatterers allows for a finite quality factor which grows up exponentially with the number of scatterers in the cluster. The robustness of these modes is analyzed numerically performing perturbations to the geometry of the cluster, showing that while the peak of the resonance remains unchanged the quality factor can be reduced significantly.

Numerical simulations and experimental realizations support our findings, showing that this work opens a path towards the design of easy-to-tailor acoustic cavities.

References

[1] Martí-Sabaté, M., Djafari-Rouhani, B., & Torrent, D. (2023). Bound states in the continuum in circular clusters of scatterers. Physical Review Research, 5(1), 013131.

META 2023, PARIS - FRANCE, JULY 18 – 21, 2023

Latent symmetry in acoustic wave systems

M. Röntgen[1*], C. V. Morfonios[2], P. Schmelcher[2,3], and V. Pagneux[1]

[1] Laboratoire d'Acoustique de l'Université du Mans,
Unite Mixte de Recherche 6613, Centre National de la Recherche Scientifique, Avenue O. Messiaen, F-72085 Le Mans Cedex 9, France,
[*]corresponding author: malte.rontgen@univ-lemans.fr
[2] Zentrum für optische Quantentechnologien, Universität Hamburg, Luruper Chaussee 149, 22761 Hamburg, Germany,
[3] The Hamburg Centre for Ultrafast Imaging, Universität Hamburg, Luruper Chaussee 149, 22761 Hamburg, Germany

Abstract: A central characteristic of a reflection-symmetric wave system is the definite parity of its eigenmodes. In this talk, we will show that such parity of all eigenmodes, however, can also occur in asymmetric systems. To this end, we equip acoustic waveguide networks with so-called latent symmetries, that is, symmetries that become apparent only after a dimensional reduction of the underlying setup. Besides providing a systematic construction principle for such latently symmetric networks, we also explore their scattering properties.

META 2023, PARIS - FRANCE, JULY 18 – 21, 2023

Meso-scale analysis of non-periodic and periodic discrete flexural waveguides

M. J. Nieves[1] **and A.B. Movchan**[2]

[1]School of Computing and Mathematics, Keele University, UK
[2]Department of Mathematical Sciences, University of Liverpool, UK
[*]corresponding author: m.nieves@keele.ac.uk

Abstract: The dynamic behavior of asymmetric flexural systems, involving a master beam attached to a non-periodic collection of flexural resonators, is discussed. The resonators couple longitudinal and flexural responses of the master beam. Its response is described via Green's functions, with intensities determined from an algebraic system embedding interactions of individual resonators. For infinite periodic waveguides, we derive an effective model called the generalized Rayleigh beam that supports flexural-longitudinal wave coupling and is efficient in regimes not typically encountered in homogenisation.

META 2023, PARIS - FRANCE, JULY 18 – 21, 2023

A pathway to lossless non-reciprocal scattering based on synchronization

N. Noiray
CAPS Laboratory, Department of Mechanical and Process Engineering, ETH Zürich, 8092 Zürich, Switzerland
noirayn@ethz.ch

Abstract: Non-reciprocal transmission of information across large periodic networks of resonators is often hindered by their intrinsic dissipation. As a remedy to these irreversible losses, we propose to equip the resonators of these metamaterials with negative resistance elements and with suitable damping nonlinearities, such that they exhibit self-sustained oscillations. Lossless or amplified non-reciprocal scattering at each of these resonators can then be achieved, thanks to the synchronization between the natural radiation of the self-oscillating mode and the incident waves. A theoretical framework is derived in analogy to the temporal coupled-mode theory, and aero-acoustic realizations of this tunable concept are achieved by using flow-induced whistling of cavities, such as in [1].

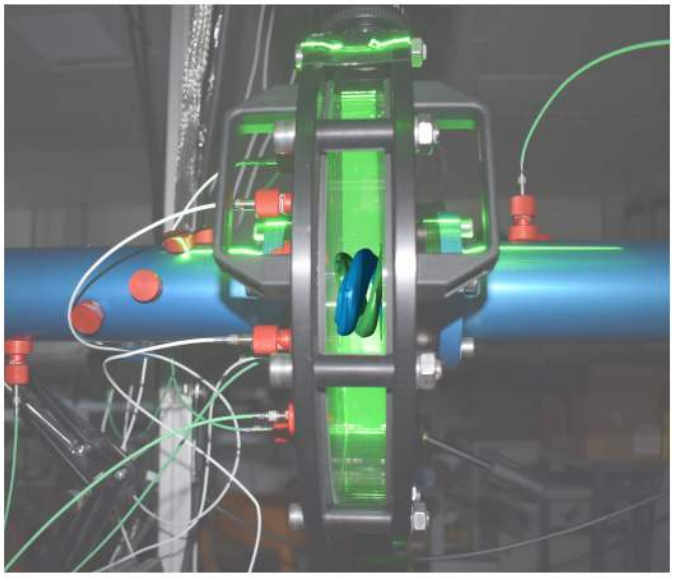


Figure 1: Experiment for the aeroacoustic realization of lossless non-reciprocal scattering based on the synchronization of incident waves with a limit cycle. The coherent flow structures at the cavity opening, obtained with stereoscopic particle image velocimetry, have been superimposed to the picture of the setup.

Reference

1. Pedergnana, T. and Noiray, N., “Superradiant Scattering from Nonlinear Wave-Mode Coupling”, arXiv:2206.10423.

Topologically invisible defects in chiral mirror lattices

Antonin Coutant,[1,*] Li-Yang Zheng,[2] Vassos Achilleos,[3]
Olivier Richoux,[3] Georgios Theocharis,[3] and Vincent Pagneux[3]

[1] *Aix Marseille Univ., CNRS, Centrale Marseille, LMA UMR 7031, Marseille, France*
[2] *School of Science, Shenzhen Campus of Sun Yat-sen University, Shenzhen, China*
[3] *Laboratoire d'Acoustique de l'Université du Mans (LAUM), UMR 6613, Institut d'Acoustique - Graduate School (IA-GS), CNRS, Avenue O. Messiaen, F-72085 Le Mans Cedex 9, France*

Abstract: The hallmark of topological phases in periodic materials is the existence of localized modes on the edges that are immune to backscattering. However, in the context of classical waves such as in photonics or acoustics, total immunity to backscattering has never been achieved so far. In this work, we show how to obtain perfect transmission and invisibility of topological edge waves over defects or disorder by exploiting a combination of chiral and mirror symmetry.

The main result of this work [1] is the following. Let us consider a periodic system that possesses commuting chiral and mirror symmetries, and such that there is a single pair of propagating modes at zero energy ($E = 0$). Then, the transmission across any defect or disorder that preserves both symmetries is either zero or unity. Moreover, it is possible to define topological indices of the defect such that if the indices are zero, then the (complex) transmission coefficient is 1.

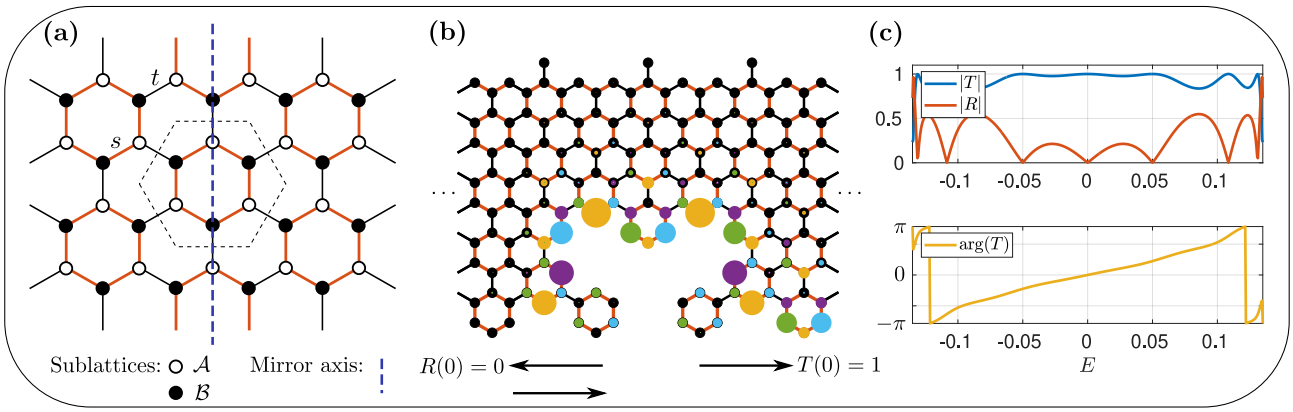


Figure 1: Topological invisibility across defects in Kekulé lattices. (a) Kekule model. (b) Scattering solutions at $\varepsilon = 0$ on the different defects. Circle radii give the field absolute value, and colors show the phase: due to the symmetries of the problem, the phase is either 0 (yellow), $\pi/2$ (green), π (purple) or $-\pi/2$ (cyan). We took $s = 0.25$, $t = 0.5$ and work with the complex energy $\varepsilon + i\nu$. (c) Illustration of perfect transmission in a chiral and mirror symmetric ribbon.

We illustrate this result in the context of the Kekule model. It is a lattice model governed by the Hamiltonian $H = \sum_{i,j} t_{ij} \hat{a}_i^\dagger a_j$ on a honeycomb lattice. The t_{ij} are the hopping coefficients and $\hat{a}_j$ the annihilation operator on site j. The hopping coefficient are modulated so as to preserve the hexagonal symmetry of the system: unit cells (molecules) are made of six sites on a hexagon, and intracell hoppings s differ from extracell hoppings t, as shown in Fig. 1-(a). This model is chiral symmetric: the lattice can be split into two sublattices $\mathcal{A}$ and $\mathcal{B}$ such that by defining the chiral operation $\Gamma = \mathrm{diag}(-\mathbf{1}_\mathcal{A}, \mathbf{1}_\mathcal{B})$, we have $\Gamma H + H\Gamma = 0$. Moreover, it also has

*Electronic address: coutant@lma.cnrs-mrs.fr

several mirror symmetries, that is, there is a mirror operation M such that: $MH - HM = 0$. Those whose axis pass through lattice sites commute with Γ.

Along an edge invariant by mirror symmetry, topological edge waves can be generated. These edge waves are protected by a pair of mirror winding numbers, a topological invariant protecting not only the existence of edge waves but also a Dirac point at $E = 0$ [2]. For instance, for molecular zigzag edges (lower edge in Fig. 1-(b)), the system is topological when $s < t$. Usually, when going from edge waves of a semi-infinite (half-plane) configuration, a mini-gap opens in their dispersion relation, due to the evanescent coupling between the upper and lower edges. Our first result [1] is that by building a lower molecular zigzag edge and an upper partially bearded edge, the Dirac point at $E = 0$ is maintained exactly (it is symmetry protected). Considering such a ribbon with a defect, for E such that only edge waves are propagating (including $E = 0$ and its vicinity), a scattering solution is asymptotically a superposition of an incident wave, a reflected wave, and a transmitted one. This defines the (complex) reflection $R(E)$ and transmission $T(E)$ coefficients (see Fig. 1-(b)). Now, using the symmetries Γ, M and energy conservation, we showed that either $T(0) = 0$ or $T(0) = \pm 1$. Moreover, any defect made of missing or added molecules and/or modified hopping (this includes a slab of chiral mirror disorder) has trivial topological indices. As a result, they are completely invisible:

$$T(0) = 1. \tag{1}$$

This means that not only the energy is fully transmitted, but also that no phase shift is induced by the defect. To confirm this, we solve the ribbon scattering problem numerically using a transfer matrix formalism [1]. The scattering solution and scattering coefficients are shown in Fig. 1-(b-c) for a defect satisfying the previous conditions.

We also propose an acoustic setup to implement this effect with high accuracy. It consists in a network of acoustic waveguides (e.g. hollow tubes) connected on a honeycomb lattice. The waveguide all have the same length L and are much longer than wide. The system is then described by an effective Hamiltonian with hoppings directly proportional to the cross-section of the corresponding tube, and an effective energy $E = \cos(kL)$ with k the natural acoustic wavenumber. The topological invisibility is shown numerically by solving the Helmholtz equation with COMSOL, see Fig. 2.

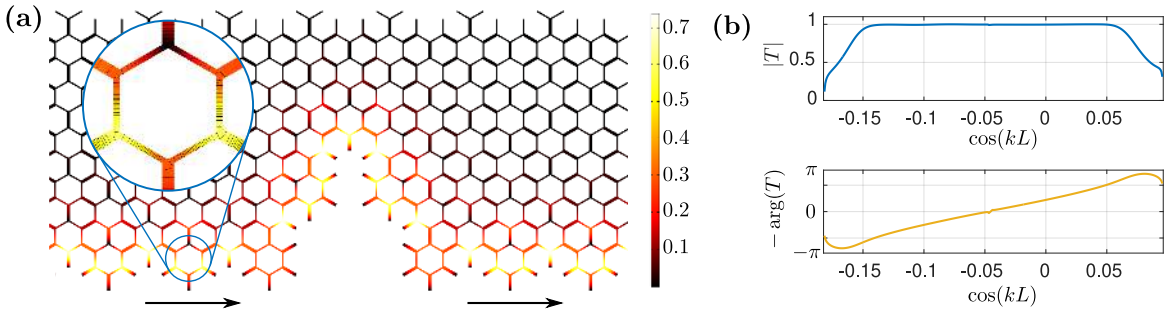


Figure 2: Finite element simulations of the 2D Helmholtz equation in a Kekulé network. We took tubes with $L = 40$, $\sigma_s = 4$ and $\sigma_t = 8$ (hence $s = 0.25$, $t = 0.5$). (a) Scattering solution. (b) Transmission coefficient (modulus and phase).

[1] A. Coutant, L. Zheng, V. Achilleos, O. Richoux, G. Theocharis, and V. Pagneux, "Topologically invisible defects in chiral mirror lattices," arXiv:2303.02029 [cond-mat.mes-hall].

[2] T. Kariyado and X. Hu, "Topological states characterized by mirror winding numbers in graphene with bond modulation," *Scientific reports* **7** no. 1, (2017) 1–8.

META 2023, PARIS - FRANCE, JULY 18 – 21, 2023

A solution to cloaking with Willis materials

P. Brucks, H. Nassar *

[1]Department of Mechanical & Aerospace Engineering, University of Missouri, U.S.
*corresponding author: nassarh@missouri.edu

Abstract: Willis elasticity is shown to be a particular microcontinuum field theory where the kinematic enrichment has been eliminated in favor of the macroscopic displacement field. The result is somewhat disappointing: it means that Willis elasticity encompasses no wave phenomena that are not already within the reach of generalized elasticity. That said, the gained insight allows to solve the longstanding problem of elastodynamic cloaking with Willis materials. In particular, the Willis materials useful for cloaking are resolved into mechanical lattices.

"Willis elasticity" is an elasticity theory where stress is coupled to velocity and momentum is coupled to strain through a typically weak "Willis coupling" tensor. The original application of Willis elasticity, by J. R. Willis, was to the effective dynamic modeling of random composites.[1] Interest in the theory was renewed when it was discovered by Milton, Briane and Willis that Willis-elastic materials can be used for elastodynamic cloaking purposes.[2] In that setup, the transformation method provides the constitutive properties needed to achieve cloaking. The difficulty resides in architecting the underlying microstructure, often a gradient of metamaterials, whose effective behavior matches the properties of the cloak. This problem of inverse design remained unsolved due to a poor understanding of the microstructure-property relationships of the Willis coupling. Here, the main contribution is to propose a solution to this problem, i.e., to provide the first architectures that produce a strong passive Willis coupling with a clear and rational set of microstructure-property relationships. The main insight that enabled this discovery is the realization that Willis elasticity is equivalent to a particular microcontinuum field theory (i) with a kinematic enrichment such that (ii) the micro-velocities are inertially coupled to the macro-velocity. Upon elimination of the kinematic enrichment in favor of the macro-displacement, the inertial coupling re-emerges as a Willis coupling (as if by Schur completion). The insight provides a clear view of the architectures that are suitable for cloaking applications: (i) the kinematic enrichment is achieved in architectures with soft deformation modes, e.g., in isostatic lattices with uninterrupted fibers running through the whole lattice;[3] (ii) the inertial coupling is achieved by offsetting the center of mass of a unit cell. Numerical simulations and proofs based on leading-order asymptotics are presented.

Work supported by the NSF under CAREER award No. CMMI-2045881.

References

1. Willis, J. R. Dynamics of composites. in *Continuum Micromechanics* (ed. Suquet, P.) 265–290 (Springer-Verlag New York, Inc., 1997).
2. Milton, G. W., Briane, M. & Willis, J. R. On cloaking for elasticity and physical equations with a transformation invariant form. *New J Phys* **8**, 248–267 (2006).
3. Nassar, H., Chen, H. & Huang, G. L. Microtwist elasticity : A continuum approach to zero modes and topological polarization in Kagome lattices. *J Mech Phys Solids* **144**, 104107 (2020).

Novel photonic materials enabled by crystal growth

D. A. Pawlak[1,2,3*], P. Paszke[1,2], P. Piotrowski[1,2], M. Tomczyk[1,2], K. Sadecka[1], K. Bandopadhay[1], K. Markus[1], H. B. Surma[1], A. Materna[1], J. Toudert[1], A. Bellardini[4], and C. Sibilia[4]

[1]ENSEMBLE[3] Centre of Excellence, Poland
[2]Faculty of Chemistry, University of Warsaw, Poland
[3]Lukasiewicz Research Network - Institute of Microelectronics and Photonics, Poland
[4]University of Rome "La Sapienza", 16 A. Scarpa, Rome, 00161, Italy
[*]corresponding author: Dorota.Anna.Pawlak@ensemble3.eu

Abstract: We will demonstrate how to utilize the crystal growth methods for manufacturing of novel composite materials for various applications, especially photonics (metamaterials, plasmonic materials), topological insulators, energy conversion. We will focus on two novel bottom-up manufacturing methods: (i) method based on directionally-grown self-organized eutectic structures; and (ii) NanoParticles Direct Doping meth-od (NPDD) based on directional solidification of dielectric matrices doped with various nanoparticles.

Recently, we proposed the idea of utilizing directional solidification as a method for manufacturing metamaterials [1] and plasmonic materials [2]. We develop two methods: (i) method based on directionally-grown self-organized eutectic structures [3-5]; and (ii) NanoParticles Direct Doping method (NPDD) based on directional solidification of dielectric matrices doped with various nanoparticles [6-8]. In both of these methods we can easily use all available resonant phenomena to develop materials with unusual electromagnetic properties. Utilizing described above methods we demonstrated: (i) volumetric eutectic-based material with localized surface plasmon resonance at visible wavelengths [9-10]; (ii) enhanced luminescence and up-conversion processes in the eutectic material exhibiting LSPR and co-doped with erbium ions [6]; (iii) volumetric matrix-nanoparticles-based materials with plasmonic resonances at visible [6, 11] and IR wavelengths based on silver (Ag), antimony-tin-oxide (ATO) and titanium nitride nanoparticles (TiN); (iv) matrix-nanoparticles-based composite with enhanced photoluminescence at the telecommunication frequency of 1.5 μm; (v) material with subwavelength transmission at IR frequencies [12]; (vi) narrow band filter and polarizer [13-14]; (vii) surface enhanced Raman scattering in a bulk eutectic material enabling enhancement of selected Raman modes [15], (viii) materials with enhanced Faraday effect; (ix) materials for photoanodes in photoelectrochemical cells for generation of hydrogen [16-17], (x) topological insulator heterostructures.

Acknowledgements: The authors thank the ENSEMBLE3 Project carried within the International Research Agendas Programme (MAB/2020/14) of the Foundation for Polish Science co-financed by the European Union under the European Regional Development Fund and the Teaming Horizon 2020 programme of the European Commission (GA No. 857543) for supporting this work.

References

1. Smith, D. R., J. B. Pendry, and M. C. K. Wiltshireet, "Metamaterials and negative refractive index," Science, Vol. 305, No. 5685, 788–792, 2004; A. M. Urbas, et al., J. Optics, Vol. 18, 093005, 2016.
2. Barnes, W. L., A. Dereux and T. W. Ebbesen, "Surface plasmon subwavelength optics," Nature, Vol. 424, No. 6950, 824–830, 2003

3. Pawlak, D. A., K. Kolodziejak, S. Turczyński, J. Kisielewski, K. Rozniatowski, R. Diduszko, M. Kaczkan and M. Malinowski, "Self-Organized, Rodlike, Micrometer-Scale Microstructure of $Tb_3Sc_2Al_3O_{12}$−$TbScO_3$:Pr Eutectic," Chem. Mater., Vol. 18, No. 9, 2450–2457, 2006.
4. Pawlak, D. A., K. Kolodziejak, K. Rozniatowski, R. Diduszko, M. Kaczkan, M. Malinowski, M. Piersa, J. Kisielewski and T. Lukasiewicz, "$PrAlO_3$−$PrAl_{11}O_{18}$ Eutectic: Its Microstructure and Spectroscopic Properties," Crystal Growth & Design, Vol. 8, No. 4, 1243–1249, 2008.
5. Pawlak, D. A., S. Turczynski, M. Gajc, K. Kolodziejak, R. Diduszko, K. Rozniatowski, J. Smalc and I. Vendik, "How Far Are We from Making Metamaterials by Self-Organization? The Microstructure of Highly Anisotropic Particles with an SRR-Like Geometry," Adv. Funct. Mat., Vol. 20, No. 7, 1116–1124, 2010.
6. Gajc, M., H. B. Surma, A. Klos, K. Sadecka, K. Orlinski, A. E. Nikolaenko, K. Zdunek and D. A. Pawlak, "Nanoparticle Direct Doping: Novel Method for Manufacturing Three-Dimensional Bulk Plasmonic Nanocomposites," Adv. Funct. Mat., Vol. 23, No. 27, 3443–3451, 2013.
7. Nowaczynski, R., M. Gajc, H. B. Surma, P. Osewski, A. Strzep, W. Ryba-Romanowski and D. A. Pawlak, "Manufacturing of Volumetric Glass–Based Composites with Single- and Double-QD Doping," PPSC, Vol. 36, No. 1, 1800124, 2019.
8. Gajc, M., H. B. Surma and D. A. Pawlak, "Optically-active metastable defects in volumetric nanoplasmonic composites," Sci. Rep., Vol. 8, 13425, 2018.
9. Sadecka, K., M. Gajc, K. Orlinski, H. B. Surma, A. Klos, I. Jozwik-Biala, K. Sobczak, P. Dluzewski, J. Toudert and D. A. Pawlak, "When Eutectics Meet Plasmonics: Nanoplasmonic, Volumetric, Self-Organized, Silver-Based Eutectic," Adv. Opt. Mat., Vol. 3, No. 3, 381–389, 2015.
10. Sadecka, K., J. Toudert, H. B. Surma and D. A. Pawlak, "Temperature and atmosphere tunability of the nanoplasmonic resonance of a volumetric eutectic-based Bi_2O_3-Ag metamaterial," Opt. Express, Vol. 23, No. 15, 19098–19111, 2015.
11. https://www.facebook.com/fmlaboratory/videos/608375495898423/ – demonstration of the plasmonic resonance in materials obtained by NanoParticle Direct Doping method.
12. Myroshnychenko, V., A. Stefanski, A. Manjavacas, M. Kafesaki, R. I. Merino, V. M. Orera, D. A. Pawlak and F. J. García de Abajo, "Interacting plasmon and phonon polaritons in aligned nano- and microwires," Opt. Express, Vol. 20, No. 10, 10879–10887, 2012.
13. Osewski, P., A. Belardini, M. Centini, C. Valagiannopoulos, G. Leahu, R. Li Voti, M. Tomczyk, A. Alù, D. A. Pawlak and C. Sibilia, "New Self-Organization Route to Tunable Narrowband Optical Filters and Polarizers Demonstrated with ZnO–$ZnWO_4$ Eutectic Composite," Adv. Opt. Mater., Vol. 8, No. 7, 1901617, 2020.
14. Petronijevic, E., M. Tomczyk, A. Belardini, P. Osewski, P. Piotrowski, M. Centini, G. Leahu, R. Li Voti, D. A. Pawlak, C. Sibilia, M. Larciprete, "Surprising Eutectics: Enhanced Properties of ZnO-$ZnWO_4$ from Visible to MIR," Adv. Mater., 2206005, 2022.
15. Szlachetko, K., P. Piotrowski, K. Sadecka, P. Osewski, D. Kasprowicz and D. A. Pawlak, "Selective surface-enhanced Raman scattering in a bulk nanoplasmonic Bi_2O_3-Ag eutectic composite," Nanophotonics, Vol. 9, No. 14, 4307, 2020.
16. Wysmulek, K., J. Sar, P. Osewski, K. Orlinski, K. Kolodziejak, A. Trenczek-Zajac, M. Radecka and D. A. Pawlak, "A $SrTiO_3$-TiO_2 eutectic composite as a stable photoanode material for photoelectrochemical hydrogen production," Appl. Catalysis B: Environ., Vol. 206, 538–546, 2017.
17. Kolodziejak, K., J. Sar, K. Wysmulek, P. Osewski, M. Warczak, A. Sadkowski, M. Radecka and D. A. Pawlak, "When eutectic composites meet photoelectrochemistry – Highly stable and efficient UV–visible hybrid photoanodes," J. Catalysis, Vol. 352, 93–101, 2017.

State of the art on the recovery of mechanical energy in the city: The role of seismic metamaterials

S. Brûlé[1*], S. Enoch[1], and S. Guenneau[3]

[1] Aix-Marseille Université, CNRS, Centrale Marseille, Institut Fresnel, 13013 Marseille, France
[2] The Blackett Laboratory, Imperial College, SW7 2AZ, London, United Kingdom
[*]corresponding author: stephan.brule@yahoo.com

Abstract: Studies on structured soils, including seismic metamaterials, have shown the existence of complex wave phenomena within and around the structured zone. Seismic protection in conjunction with invisibility cloak has led to the emerging research area of seismic energy harvesting with seismic metamaterials. In this fast-developing niche, it is a question of evaluating the zones of energy concentration and deciding on the interest of valuing them by placing piezoelectric energy sensors. The article presents what is already being done and shows the interest of seismic metamaterials in this context.

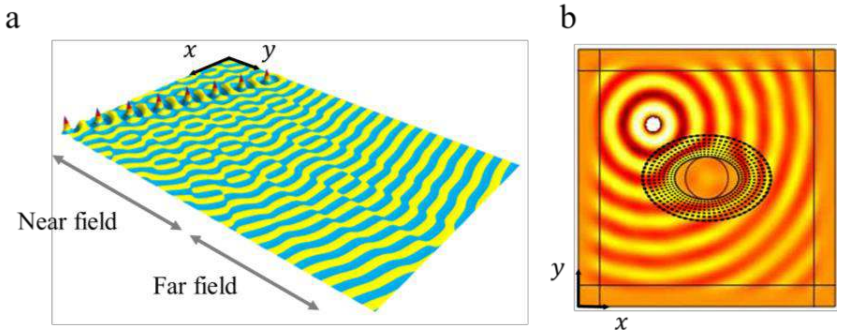


Figure 1: The zone of interest in seismicity of structured soils is the near field around the device (a) and inside the device itself, for instance an arena reminiscent of an invisibility cloak (b).

Soil dynamics as well as science of seismic metamaterials have led to the identification of materials or assemblies of materials with contrasting mechanical properties and local modes. The coupling of buildings such as surface resonators with structured soils constitutes an opportunity for development in the trapping of mechanical energy. In the era of energy transition, any source of free energy represents an interest [1-3]. The measurements show that the near field is the area of interest (Figure 1). Questions remain and technical obstacles have to be overcome. Nevertheless, applications such as podo-electric sidewalks using the kinetic energy of passers-by to produce local lighting is an encouraging avenue.

We return to the results obtained on structured soils under ambient seismic noise and under urban noise and we qualify the energy emitted by different civil engineering structures. In Figure 2 we present the case of a building which generates vibrations in its immediate environment [4].

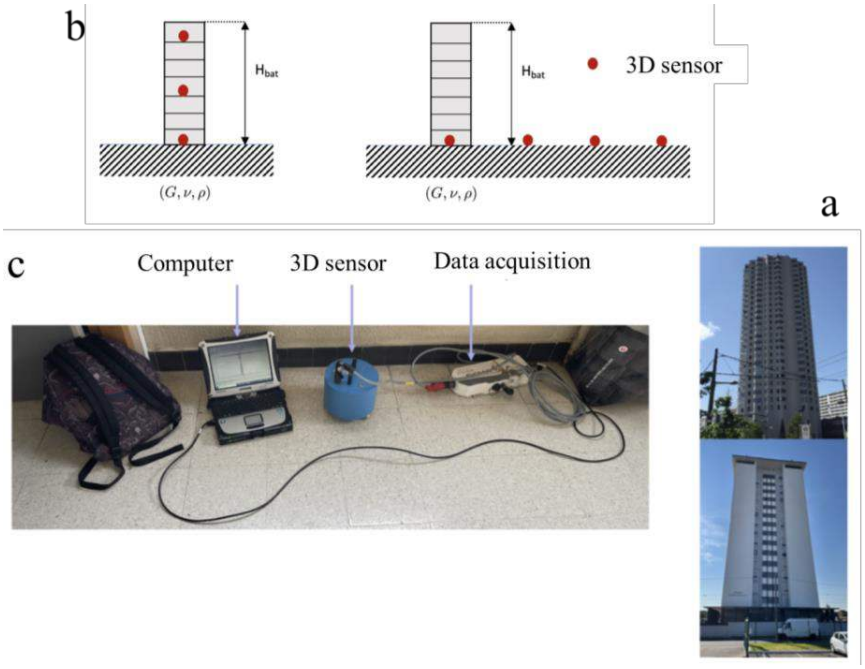


Figure 2: Instrumented buildings (a). Principle of measurement with location of 3D sensors (red dots) inside the building and on the ground surface away from the structure (b). The device for the acquisition of seismic ambient noise measurements (c).

References

1. Brûlé, S., S. Enoch and S. Guenneau, "Emergence of Seismic Metamaterials: Current State and Future Perspective," Phys. lett., A. 384 (1), 2020.
2. Brûlé S. and S. Guenneau, "Past, present and future of seismic metamaterials: experiments on soil dynamics, cloaking, large scale analogue computer and space–time modulations," C. R. Phys. 21, n°7-8, pp. 767-785, 2020.
3. Brûlé, S., S. Enoch and S. Guenneau, "Cloaking of bulk and surface mechanical waves," Proceedings Volume 12130, Metamaterials XIII; 121300D. Event: SPIE Photonics Europe, 2022, Strasbourg, France.
4. Rodet J., S. Brûlé, Ph. Gueguen, B. Tauzin, O. Coutant, V. Lanticq, R. Rollet, J. Granger, O. Depret, "Fibres optiques, sismologie et géotechnique pour ville intelligente : le projet DASARA à Lyon," 11ème JNGG 2022, 28-30 juin 2022, Lyon, France. pp. 917-925, 2022.

Tunable topological protection from auxeticity and nonlinearity

M. Morvaridi[1], **F. Bosia**[1], **M. Brun**[2*], **V.F. Dal Poggetto**[3], **A.S. Gliozzi**[1], **M. Miniaci**[4], **N. M. Pugno**[3,5], **G. Carta**[2]

[1] Department of Applied Science and Technology, Politecnico di Torino, 10129 Torino, Italy

[2] Department of Mechanical, Chemical and Materials Engineering, University of Cagliari, 09123 Cagliari, Italy

[3] Laboratory for Bioinspired, Bionic, Nano, Meta Materials and Mechanics, Department of Civil, Environmental and Mechanical Engineering, University of Trento, Trento, 38123, Italy

[4] CNRS, Univ. Lille, Ecole Centrale, ISEN, Univ. Valenciennes, IEMN - UMR 8520, Lille, France

[5] School of Engineering and Materials Science, Queen Mary University of London, London, E1 4NS, UK

[*]corresponding author: mbrun@uncica.it

Abstract: the dynamic response of an elastic porous material with a periodic distribution of elongated holes is considered[1]. The presence of the cuts makes the effective behavior auxetic and guarantees the presence of multiple Dirac points in the dispersion diagram.

By perturbing the length of half of the cuts and mirroring the structure on the opposite side of an interface, topologically protected edge modes have been showed numerically (see Figure 1). Such modes are associated with a Chern number close to 0.5. Auxeticity plays a fundamental role on the presence of such topologically protected modes, which are not present when the internal morphology is such that the effective Poisson's ratio is positive.

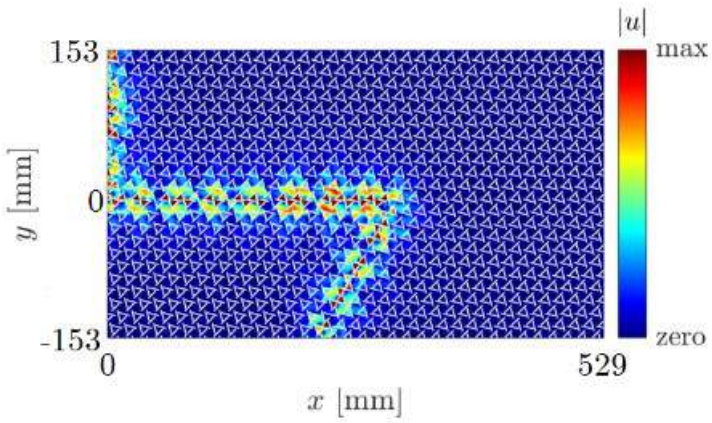


Figure 1. Topologically protected mode propagating along an interface with a sharp angle.

The dynamic response can be tuned by applying a large deformation. In such a case, the lower edge mode can be annihilated, while the upper mode can be moved at different frequencies. In addition, the possibility to activate edge modes in disjointed portion of the interface is shown.

Acknowledgements

M. Mor., V.F.D.P., M. Min., N.M.P., A.S.G. and F.B. are supported by the European Commission H2020

FET Open “Boheme” grant no. 863179. G.C. and M.B.’s work has been performed under the auspices of GNFM-INDAM..

References

1. G. Carta, M. Brun, and A. Baldi, Design of a Porous Material with Isotropic Negative Poisson’s Ratio, Mechanics of Materials 97, 67-75 (2016).

Design, fabrication and performance assessment of an acoustic focusing metamaterial lens

Feng Qin[1*], Jie Zhang[1] and Bruce W. Drinkwater[1]
[1]Department of Mechanical Engineering, University of Bristol, Bristol BS8 1TR, United Kingdom
[*]corresponding author: feng.qin@bristol.ac.uk

Abstract: we describe a procedure to design and assess an acoustic focusing metamaterial lens operating at 40kHz. The lens is based on a square unit cell containing a cross-shaped feature. The design procedure involves using the retrieval method to calculate the unit cell size and lay out, and a time delay approach to focus an acoustic wave. The designed lens was manufactured from ABS using a 3D printer and this paper carefully considers the fabrication limitations. The performance of the lens was assessed experimentally on artificial flaws, and this shows the potential for application in the non-destructive testing field.

Metamaterials are artificial components composed of subwavelength sized units which have inhomogeneous material properties. These unconventional material properties can be achieved by, for example, changing the geometry and layout of metamaterial units. In this paper, we manufacture a metamaterial lens using a cross-shape unit cell[1] and a number of layers. We first use the retrieval method[2] to evaluate the effective refractive index and impedance for a range of unit cells geometries in a finite element model. The lens is then designed using well-known ray theories, the required phase delay found and the unit cells selected to achieve a specified focused acoustic beam.

The contribution of this paper is to explore how to optimize the manufacture of this lens. Key objectives here are to reduce the cost of manufacture and this means using rapid manufacturing techniques such as 3D printing. This in turn leads us to select the largest possible unit cell size which means that the metamaterial is not truly homogenous and so has some unusual properties, for example the unit cell performance is affected by it neighbors which can no longer be considered identical. We explore how lenses can be built in this regime. We also explore how to design a unit cell that is relatively insensitive to manufacturing errors, as this enables us to manufacture the lens at low cost with a medium-quality 3D printer. Finally, the optimally designed lens was manufactured, and the experimental validation performed as shown in Figure 1. The focusing ability of this lens was such that it was capable of detecting flaws in plate-like structures with high resolution.

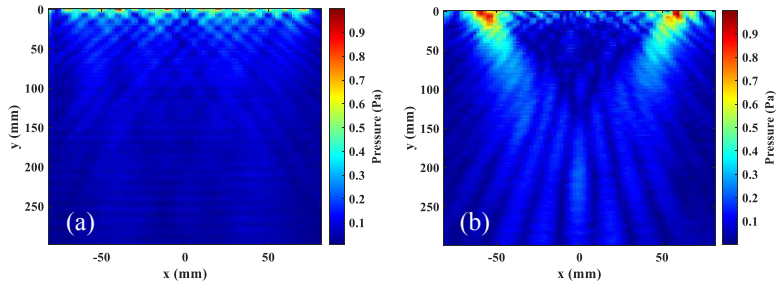


Fig. 1 Measured acoustic field of (a) the transducer array and (b) the transducer array with proposed lens

This work is supported by China Scholarship Council and EPSRC Centre for Doctoral Training in Future

Innovation in Non-Destructive Evaluation.

References

1. Zigoneanu, Lucian, Bogdan-Ioan Popa, and Steven A. Cummer. "Design and measurements of a broadband two-dimensional acoustic lens." Physical Review B. 84(2): 024305, 2011.
2. Fokin, Vladimir, et al. "Method for retrieving effective properties of locally resonant acoustic metamaterials." Physical review B. 76(14): 144302, 2007.

META 2023, PARIS - FRANCE, JULY 18 – 21, 2023

Acoustic metagratings: From principle to applications

Jun Mei

South China University of Technology, China
*corresponding author: phjunmei@scut.edu.cn

Abstract: Wavelength-thick metagratings for airborne and waterborne sound are highly desirable in various application scenarios. In this talk, we present a class of metagratings with which distinct and switchable wave manipulation functionalities, such as extraordinary transmission, total reflection, and abnormal reflection can be achieved through a single acoustic grating. Simultaneous and high-efficiency control over both reflected and transmitted waves is achieved through a systematic design approach in which wave diffraction theory and intelligent optimization algorithms are concurrently utilized.

For many industrial applications related with airborne and waterborne sound, steerable and controllable transport of acoustic signals along preferred directions is highly demanded. It is also desired that the wave front can be manipulated by a planar acoustic device, and it would be even better if such a device has a structure as simple as possible and a steering efficiency as high as possible. To meet these demands, we construct the metagratings with iron cylinders only, which are probably the simplest element of structure in two-dimensions (2D), not only making them considerably simpler to synthesize than conventional metasurfaces, but also significantly lowering fabrication demands.

Furthermore, we want to design customized metagratings that can fulfill the desired wave-front manipulation requirement, aiming to solve the inverse-design problem that scientists and engineers are constantly encountering in practical applications. Through diffraction analysis and a genetic-algorithm-assisted optimization process, we propose a powerful inverse-design approach that can faithfully and promptly produce desired wave-front manipulation effects. Various wave-diffraction functionalities, including perfect beam splitting, anomalous reflection and transmission, retroreflection, and highly asymmetric transmission response are unambiguously demonstrated with unitary efficiency.

References

1. L. Fan and J. Mei, “Metagratings for Waterborne Sound: Various Functionalities Enabled by an Efficient Inverse Design Approach, Phys. Rev. Appl. 14, 044003 (2020).
2. L. Fan and J. Mei, “Acoustic Metagrating Circulators: Nonreciprocal, Robust, and Tunable Manipulation with Unitary Efficiency”, Phys. Rev. Appl. 15, 064002 (2021).
3. L. Fan and J. Mei, “Multifunctional Waterborne Acoustic Metagratings: From Extraordinary Transmission to Total and Abnormal Reflection”, Phys. Rev. Appl. 16, 044029 (2021).
4. Z. Du and J. Mei, “Metagrating-based acoustic wavelength division multiplexing enabled by deterministic and probabilistic deep learning models”, Phys. Rev. Res. 4, 033165 (2022).

META 2023, PARIS - FRANCE, JULY 18 – 21, 2023

Exceptional points and skin modes in non-Hermitian elastic phononic beams

Y. Jin[1], R. Cai[2,3], W. Zhong[1], T. Rabczuk[4], X. Zhuang[2,5], Y Pennec[3], and B. Djafari-Rouhani[3*]

[1]School of Aerospace Engineering and Applied Mechanics, Tongji University, 200092 Shanghai, China

[2]Department of Geotechnical Engineering, College of Civil Engineering, Tongji University, 200092 Shanghai, China

[3]IEMN, UMR CNRS 8520, Département de Physique, Université de Lille, 59655 Villeneuve d'Ascq, France

[4]Institute of Structural Mechanics, Bauhaus-Universität Weimar, 99423 Weimar, Germany

[3]IOP, Department of Mathematics and Physics, Leibniz University Hannover, 30167 Hannover, Germany

[*]corresponding author: bahram.djafari-rouhani@univ-lille.fr

Abstract: Exceptional points and skin effect are two hallmarks of non-Hermitian systems combining gain and loss. We demonstrate these phenomena for flexural waves in phononic beams based on applied forces with feedback control. The non-Hermiticity is realized either by means of applying piezoelectric patches on top of the beam or by using a periodic beam made of piezoelectric materials operating as sensor and actuator. We highlight the applications of exceptional points for enhanced sensitivity and of skin modes for energy harvesting.

Non-Hermitian systems containing loss and gain elements have attracted a great deal of interest due to the discovery of several new phenomena such as invisibility, cloaking, enhanced sensing associated with exceptional points or skin effect. In this work, we are interested by the last two aspects that we shall demonstrate for elastic flexural waves propagating in a finite or a periodic beam.

Non-Hermitian systems satisfying the parity-time (PT) symmetry by a balance between gain and loss exhibit real eigenvalues with a transition at the exceptional point where the eigenvalues and eigenfunctions coalesce before a change of the spectrum from pure real to complex conjugate. We show this phenomenon[1] for flexural waves on the geometry shown in Fig. 1(a) constituted by a finite beam supporting two pillars. The gain and loss are respectively achieved by the application of appropriate forces with feedbacks at the points 1-2 and 3-4 by means of small piezoelectric patches. Figure 1(b) and (c) illustrate the evolution of the real and imaginary parts of the eigenfrequencies as a function of a parameter γ representing the strength of the feedback forces[1]. When this parameter is fixed at the position of the exceptional point, the introduction of a small perturbation, such as the addition of a mass m on the beam, gives rise to a splitting of the degenerated eigenfrequency. This is revealed by the appearance of two peaks in the frequency response as shown in Fig. 1(d). The splitting between the two peaks behaves as the square root of the perturbation which corresponds to an enhanced sensitivity and makes the exceptional point attractive for the purpose of sensing in presence of very small perturbations.

In another configuration of the applied forces with feedback control, this structure can exhibit the skin effect[1]. The latter reflects the localization of all bulk modes in a specific frequency region at a given boundary of the structure with an unconventional bulk-boundary correspondence. We have shown the localization of an incident wave towards one end of the beam whatever the position of the source in the beam. Such a skin mode is very efficient for energy harvesting[1] by attaching a piezoelectric patch at the location of the mode.

We have also studied the skin effect in a periodic phononic beam[2] containing piezoelectric elements which play the role of sensor and actuator in each unit cell to achieve the feedback control (Fig. 2(a)). By implementing effective gain and loss in the infinite beam, the band structure exhibits complex dispersion curves. For a given

wavevector, a positive or negative value of the imaginary part of the frequency means a wave attenuation or amplification, which is at the origin of the skin effect. Also, for two opposite wavevectors, the real and imaginary parts of the frequencies (Re(f) and Im(f)) are respectively equal and opposite which means a non-reciprocity in the attenuation/amplification. In Fig. (3(b), we illustrate the winding of the complex eigenfrequencies when the wavevector sweeps the one-dimensional Brillouin zone. Then, Fig. 3(c) illustrates the skin effect for selected frequencies in the consecutive bands of the infinite crystal. The sign of Im(f) defines the side of the structure (left or right) where the mode is localized whereas the magnitude of Im(f) indicates the degree of confinement.

Currently, our work is being extended to a two-dimensional lattice where the control of feedback forces allows not only to demonstrate the skin effect but also to realize a reconfigurable localization by appropriately distributing the applied forces.

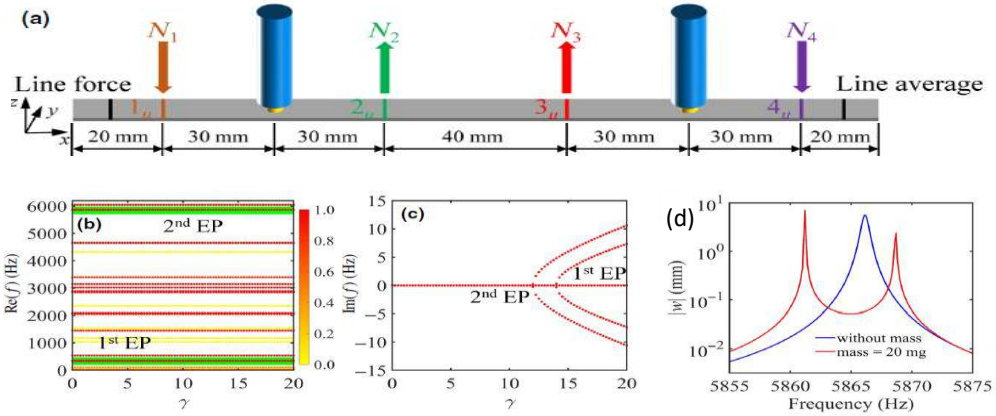


Figure 1 (a) Schematic of the metabeam with feedback control applied forces realizing gain and loss and the PT symmetry condition. (b), (c) Real and imaginary parts of the eigenfrequencies as a function of the feedback parameter γ. (d) Frequency response at the exceptional point without and with a mass perturbation.

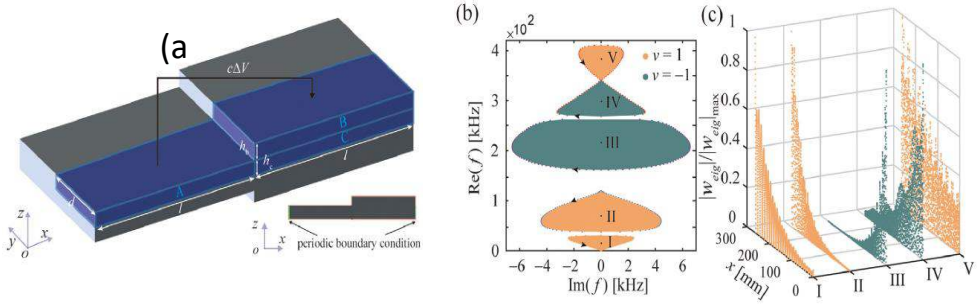


Figure 2 (a) Schematic of the piezoelectric phononic beam unit cell with feedback control. Block A is a sensor to detect the potential difference ΔV between the upper and lower surfaces generated by vibrations whereas block B is an actuator converting the electric potential difference cΔV to mechanical signals. (b) Projection of the complex dispersion band on the complex eigenfrequency plane. The orange and green loops with anticlockwise and clockwise arrows correspond to the winding numbers ν=1 and ν=-1 respectively. (c) Normalized vertical displacement component of the skin modes in a beam consisting of 44 unit cells at the eigenfrequencies of the dots shown in (b).

References

1. R. Cai, Y. Jin, T. Rabczuk, Y. Pennec, B. Djafari-Rouhani, X. Zhuang, Phys. Rev. Appl. 18 (1), 014067, 2022.
2. Y. Jin, W. Zhong, R. Cai, X. Zhuang, Y. Pennec, B. Djafari-Rouhani, Appl. Phys. Lett. 121 (2), 022202, 2022.

Long-time dynamics of one-dimensional topological lattice models

B. Many Manda[1*] **and G. Theocharis**[1]

[1] Laboratoire d'Acoustique de l'Université du Mans (LAUM), UMR 6613, Institut d'Acoustique - Graduate School (IA-GS), CNRS, Le Mans Université, France
[*]corresponding author: bertin.many_manda@univ-lemans.fr

Abstract: We consider a Su-Schrieffer-Heeger chain of oscillators. In the periodic and nonlinear regimes, we show that the dynamics of unstable nonlinear topological edge states leads to the thermalization of the entire lattice due mode interactions and chaos. Furthermore in the linear and disordered limit, the long-time dynamics of localized wave-packets is able to characterize the transition between two different topological phases. The latter feature is lost in the presence of nonlinearity once again due to mode interactions and chaos.

We consider a mechanical lattice analog of the Su-Shrieffer-Heeger (SSH) tight-binding lattice [1] with Klein-Gordon-type nonlinearity. We perform the nonlinear continuations of the linear topological edge mode and obtain a family of topological nonlinear states localized at the edge of the chain. These objects can be stable or unstable depending on the sign and strength of the nonlinearity and seem to radiate a portion of their energy (mass) in short-time scales, whenever they are unstable. Nevertheless, because a strong component of their shapes is derived from the linear topological edge mode, their long-time dynamics remains unclear. By performing long-time and high accuracy numerical simulations, computing observables such as the entropy, participation ratio and maximal Lyapunov exponent of the system, we show that the delocalization of unstable nonlinear topological edge states results in the thermalization of the entire lattice due to chaos and mode interactions. In addition, stable nonlinear topological edge states also reach the same fate, but pass a critical strength of perturbation [2].

We also study a disordered variant of the standard SSH model. We look at the connection between the system's topological phases and long-time dynamics of initially localized wave-packets in the bulk of the chain. We demonstrate using theory and numerical simulations that the transition between two different topological phases is characterized by an anomalous subdiffusion of the bulk wave-packet, in contrast to its (Anderson) localization within these topological phases. This anomalous spreading is characterized by a growth of the wave-packet's moments pass a critical order, following logarithmic laws in time. Nevertheless, in the presence of nonlinearity this feature is lost once again due to chaos and mode interactions. Since the two latter processes constitute the leading mechanisms of wave-packet dynamics, we find at all strengths of nonlinearity a wave-packet spreading characterized by moments following power laws of time in all orders, in the whole system's parameter space [3].

Since several works are carried out in the static regime of topological systems, our work emphasizes the importance of modes interactions and chaos in the dynamics of nonlinear topological lattices which must be studied in order to define reliable topological indicators.

References

1. Su, W. P, Schrieffer J. R. and Heeger A. J. "Solitons in Polyacetylene," Phys. Rev. Lett., Vol. 44, 1698, 1979.
2. Many Manda B., Chaunsali R., Theocharis G. and Skokos Ch., "Nonlinear topological edge states: From dynamic delocalization to thermalization," Phys. Rev. B, Vol. 105, 104308, 2022.
3. Many Manda B., Achilleos V., Richoux O., Skokos Ch. and Theocharis G., "Wave-packet spreading in the disordered and nonlinear Su-Schrieffer-Heeger chain," Submitted, e-print: arXiv:2212.06235, 2023.

Airborne Transverse Sound: from Spin-Orbit Interactions to Circular Dichroism

Shubo Wang[1,2*], **Qing Tong**[1], **and Guancong Ma**[3†]

[1]Department of Physics, City University of Hong Kong, Hong Kong, China
[2]City University of Hong Kong Shenzhen Research Institute, Guangdong, China
[3]Department of Physics, Hong Kong Baptist University, Hong Kong, China
[*]corresponding author: shubwang@cityu.edu.hk
[†]corresponding author: phgcma@hkbu.edu.hk

Abstract: In this talk, I will report our study about a new type of sound wave—airborne transverse sound. The transverse sound carries both spin and orbital angular momentum, and the spin-orbit interactions can give rise to novel phenomena that cannot be found in conventional acoustic systems, such as the negative refraction induced by acoustic activity and the spin-dependent vortex generation in sound scattering. We also demonstrate the acoustic circular dichroism associated with the interaction of circularly polarized transverse sound with chiral structures.

It is commonly believed that airborne sound is a longitudinal wave carrying no spin. Thus, many intriguing phenomena associated with spin, such as spin-orbit interactions, cannot be found in acoustic systems. We demonstrate that airborne sound can become a transverse wave when artificial transversality is introduced by using a micropolar metamaterial composed of acoustic dipolar resonators [1]. We show that the transverse sound carries spin-1 and possesses totally 6 degrees of freedom same as a three-dimensional transverse vector wave. This allows the realization of acoustic spin-orbit interactions in both momentum space and real space, leading to counter-intuitive phenomena such as chirality-dependent negative refraction and spin-dependent acoustic vortex generation. Our study deepens the fundamental understanding of sound waves and opens a new avenue to sound manipulations beyond the conventional scalar degree of freedom.

We further demonstrate a novel phenomenon of acoustic Circular dichroism (CD) associated with the interaction of circularly polarized transverse sound with a chiral metamaterial [2]. We find that the effect is negligible in the lossy metamaterial with C_4 rotational symmetry but is strongly enhanced in the C_2-symmetric system with inhomogeneous loss. The CD phenomenon can be well understood by analyzing the metamaterial's complex band structure and the quality factors of its eigenmodes. The enhanced CD in the C2-symmetric system is attributed to the polarization bandgaps and the non-Hermitian exceptional points appearing near the Brillouin-zone center and boundaries. The results provide new mechanisms for chiral sound-matter interactions with potential applications in the manipulations of acoustic angular momentum and acoustic sensing of chiral structures.

This work was supported by the Research Grants Council of the Hong Kong SAR, China (Nos. CityU 21302018 and C6013-18G) and the National Natural Science Foundation of China (Nos. 11922416 and 11802256).

References

1. Wang, S., G. Zhang, X. Wang, Q. Tong, J. Li and G. Ma, “Spin-orbit interactions of transverse sound”. Nat. Commun. 12, 6125, 2021.
2. Tong, Q., J. Li, and S. Wang, “Acoustic circular dichroism in a three-dimensional chiral metamaterial”, arXiv:2301.02526, 2023.

META 2023, PARIS - FRANCE, JULY 18 – 21, 2023

Study on acoustic metasurface controlling phase of transmitted waves

Jia-Hong Sun* and Ching-Yun Chang

Department of Mechanical Engineering, Chang Gung University, Taiwan
* jhsun@mail.cgu.edu.tw

Abstract: This paper studied the acoustic metasurface with microstructures that can control the phase of sound waves passing through it. The microstructures were designed to have a proper phase delay and a high transmission coefficient. After designing the structure properly, acoustic metasurfaces that control refraction angles, focus sounds, and diffuse waves were constructed. The work included design, fabrication of specimens, and experiments. This study is valuable for the development of acoustic metasurface applications.

Metamaterials are materials consisting of some special artificial microstructures, and the ones with microstructures arranged only on the surface are called the metasurface. Acoustic metasurface was currently studied to control the reflection, transmission, and absorption of sound[1-4]. In these applications, controlling the phase shift of sound by using metasurfaces is a potential topic. Controlling phase shift can realize deflecting the directions of the reflected wave or the transmitting wave; thus, the corresponding sound field characteristics can be altered. For example, a Schroeder diffuser is defined by wells with different depths to have the non-uniform phases of the reflected wave[4]. Some metasurfaces that control transmitted waves' phase were reported[1,3], but further applications wait. Thus in this paper, we studied the microstructure for controlling the phase shift of sound that passes through the microstructure and further applications.

A channel is the fundamental part of the microstructure that allows sounds to pass through a metasurface. This study used coiling channels introduced in reference 4 to control the phase delay. The coil channels defined paths with different lengths, thus delaying the incident wave and shifting the output's relative phase. The open channels are embedded in a rectangular cuboid with a square cross-section area. Considering the fabrication of specimens, the microstructures were designed for 40 kHz sound. The finite-element method (COMSOL Multiphysics) was used to calculate the sound pressure fields of waves passing the coiling channel, and the channel topology was designed to have a phase delay of 0, $\pi/8$, ..., $15\pi/8$, respectively. Meanwhile, with a square side of a half wavelength (λ), transmitted wave amplitudes are over 97%. These cuboids with a channel were defined as the basic units.

The functional metasurfaces were then constructed by combining the units with different phase delays in space. An array of linear increasing phase delay units can steer the direction of the incident wave when it passes the metasurface, as shown in Fig. 1(a). A focusing acoustic lens was also simulated, as shown in Fig. 1(b). By setting the basic units in the proper location, the plane wave passing the lens reaches the focal point (the focal length is 5λ in this case) in phase. Further, we also designed a diffuser for transmitting waves according to the principle of Schroeder diffusers. The units were redefined for 7- and 11-step phase delay in 2π, and the calculated pressure fields behind the lens showed no more synchronous.

These results showed that the coiling channels are feasible to control phase delay and keep a high transmission coefficient. Metasurfaces consisting of the units showed the potential applications of beam steering control, energy focusing, and noise diffusion. The study is expected to be valuable in building acoustics and sound control.

Acknowledgements： The authors gratefully thank the financial support from Ministry of Science and Technology, Taiwan (MOST 110-2221-E-182-046).

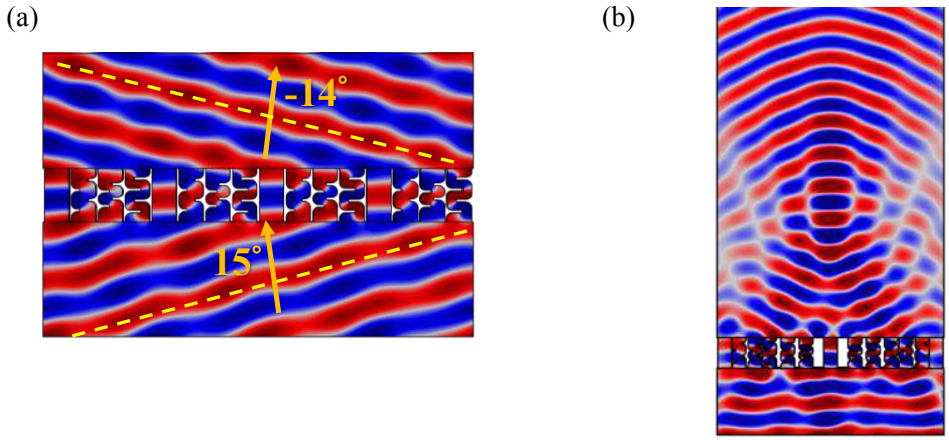


Fig 1. The sound pressure fields of plane waves passing functional metasurface.
(a) beam steering, and (b) focusing.

References

1. B. Assouar, et al., “Acoustic metasurfaces,” Nature Reviews Materials, Vol. 3, 460-472, 2018.
2. Y. Li, et al., “Reflected wavefront manipulation based on ultrathin planar acoustic metasurfaces,” Scientific Reports, Vol. 3(1), No. 2546, 2013.
3. G. Memoli, et al., “Metamaterial bricks and quantization of meta-surfaces,” Nature Communications, Vol. 8(1), No. 14608, 2017.
4. M. R. Schroeder, “Diffuse sound reflection by maximum−length sequences,” The Jour-nal of the Acoustical Society of America, Vol. 57, 149-150, 1975.

Aiming of water waves in a time-varying metabathymetry

M. Koukouraki[1*], A. Maurel[2], P. Petitjeans[1], V. Pagneux[3]

[1]Laboratoire de Physique et de Mécanique des Milieux Hétérogènes, ESPCI, Paris, France
[2]Institut Langevin, ESPCI, Paris, France
[3]Laboratoire d'Acoustique de l' Université du Mans, Le Mans, France
*magdalini.koukouraki@espci.fr

Abstract: We investigate both analytically and numerically the two-dimensional propagation of shallow water waves over a time-varying medium, which switches from isotropic to anisotropic at a given time. The anisotropy is established with the abrupt appearance of a plate array at the fluid bottom, which changes the effective water depth in each direction in the long-wavelength limit. Depending on the wavenumber angle incident on the plate array, the angle of the energy flow will change, allowing us to deflect the wave.

Time-varying metamaterials is a rapidly growing research field which provides the perfect playground for controlling wave propagation. Motivated by the study of Pacheco-Peña et al. [1], where temporal waveguides were designed for electromagnetic waves, we propose here a water-wave analog. By changing the water depth everywhere in space at a given time, the water wave velocity is modified in time. In addition, when the medium is switched from isotropic (homogeneous depth) to anisotropic (different effective depth in the x and y direction), one can deflect the wave since the angle of the energy flow θ_S is different than the angle of the wave vector θ. A schematic representation of such a deviation is depicted in Figure 1a). Note that isotropic time variation of the water wave speed has been already explored in [2] and [3].

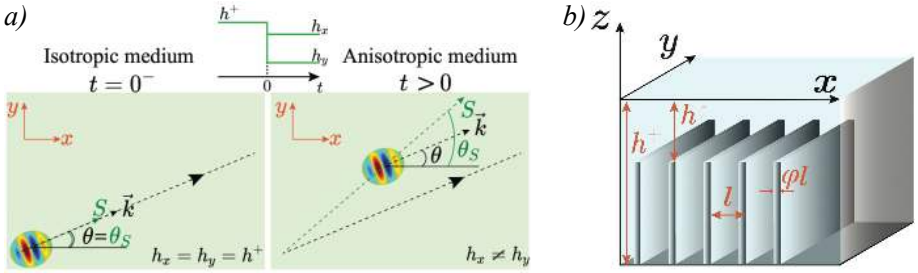


Figure 1:a) Wave packet deviation from its initial trajectory due to the anisotropy introduced at t=0. b) Representation of the plate array at the fluid depth.

As was demonstrated in [4], a structured bathymetry can create an anisotropic medium for water waves in the long wavelength approximation. In that case, an effective two-dimensional wave equation has been derived (see ref. [4],[5]):

$$\eta_{tt} = g\nabla\cdot(\mathrm{h}\nabla\eta), \quad \mathrm{h} = \begin{pmatrix} h_x & 0 \\ 0 & h_y \end{pmatrix}, \qquad (1)$$

where $h_x < \langle h^{-1}\rangle^{-1}, h_y = \langle h\rangle^{-1}, \langle h\rangle = \varphi h^- + (1-\varphi)h^+$, with h^+, h^-, φ defined in Figure 1b). When the medium is modified in time, rather than in space, and the switch occurs much faster than the wave period, the wave "sees" a time interface from which it is partly reflected and partly transmitted. One can easily demonstrate that the reflection R and transmission T coefficients are given from the expressions (see ref. [1]),

$$R = \frac{\omega_1-\omega_0}{2\omega_1}, \quad T = \frac{\omega_1+\omega_0}{2\omega_1}, \qquad (2)$$

with $\omega_0 = k\sqrt{gh^+}, \omega_1 = k\sqrt{g(h_x\cos^2\theta + h_y\sin^2\theta)}$, while the angle of energy flow θ_S is found to be

$$\theta_S = \tan^{-1}\left(\tan(\theta)\frac{h_y}{h_x}\right). \qquad (3)$$

By allowing h to depend on time, Eq. (1) can be solved numerically, where at t=0 we pass from h^+ to (h_x, h_y). Thus, numerical results are obtained for the scattering coefficients as a function of the incident angle, which show good agreement with our theoretical predictions (see Figure 2a). In Figure 2b we illustrate the maximum wave packet deviation, for the case where l=0.8cm, φ=0.0625, h^+=2cm, h^-=0.5cm, f_0=6Hz, $\theta=\theta m$.

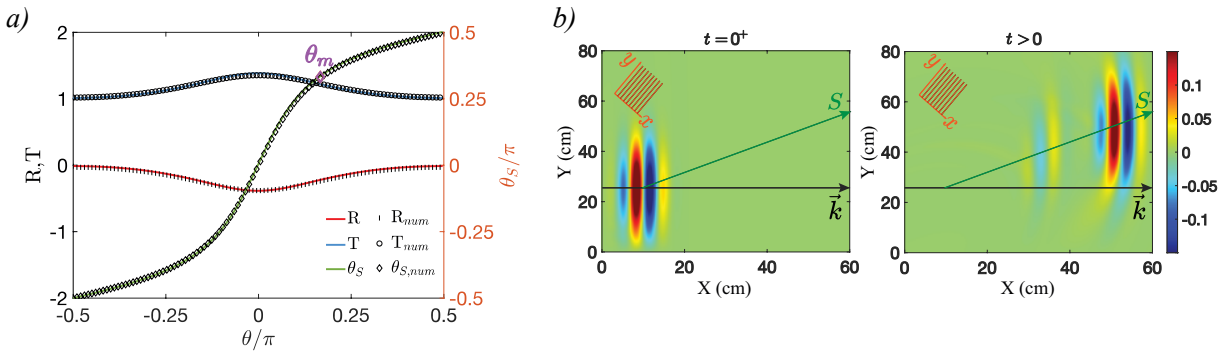


Figure 2:a) R, T and θ_S as a function of θ along with their analytical expressions (2) and (3). b) Wave packet deviation for the case where $\theta=\theta m=\pi/6$.

Finally, the ongoing part of this study is to experimentally verify our proposed theory. For this purpose, we have designed an experimental setup which allows the plate array to be suddenly lifted at the fluid bottom. Figure 3 shows the plate array right before and right after the switch. This set-up is currently under test.

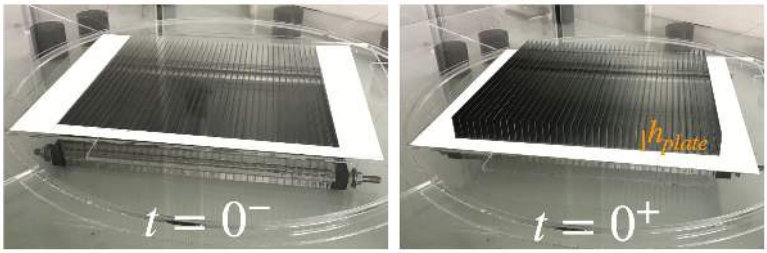


Figure 3: Fluid bottom inside the water tank before and after lifting the plate array.

References

1. Pacheco-Peña, V. and N. Engheta, "Temporal aiming", Light Sci. Appl., Vol. 9, No. 1, 129, 2020.
2. Bacot, V., M. Larousse, A. Eddi, M. Fink and E. Fort, "Time reversal and holography with spacetime transformations", Nat. Phys., Vol. 12, No. 10, 972-977, 2016.
3. Apffel, B. and E. Fort, "Frequency conversion cascade by crossing multiple space and time interfaces", Phys. Rev. Lett., Vol. 128, No. 6, 064501, 2022.
4. Maurel, A., J.J. Marigo, P. Cobelli, P. Petitjeans, and V. Pagneux, "Revisiting the anisotropy of metamaterials for water waves", Phys. Rev. B, Vol. 96, No. 13, 134310, 2017.
5. Maurel, A., K. Pham and J.J Marigo, "Scattering of gravity waves by a periodically structured ridge of finite extent", J. Fluid Mech., Vol. 871, 350-376, 2019.

META 2023, PARIS - FRANCE, JULY 18 – 21, 2023

Invariance of the transmitted field in a periodic waveguide

E. Salemeh*, S. Félix and V. Pagneux

Laboratoire d'Acoustique de l'Université du Mans LAUM – UMR CNRS 6613, France
elie.salemeh@univ-lemans.fr*

Abstract: A characteristic of the localized regime in a disordered medium is the insensitivity of the transmitted speckle pattern to the incident wave. We show that a similar phenomenon is possible in an ordered, periodic medium, when the wave is mainly carried by a dominant Bloch mode. The work presented aims to characterize this phenomenon in the case of propagation in a periodic acoustic waveguide.

Among the many striking wave phenomena that arise in disordered media and explain undiminished interest in this field of wave physics over decades [1, 2] the single channel regime is quite remarkable. Since the ratio between successive transmission eigenvalues (TEVs) is large in the localized regime, the first (largest) one dominates all others, hence the corresponding eigenchannel in the transmission problem. A consequence is that "*the speckle pattern of the transmitted intensity is literally frozen*", that is, at a given frequency, the speckle pattern is independent of the incidence conditions. Note that it was experimentally evidenced (as well as the crystallization of the TEVs) by Shi and Genack with microwaves [3] and later numerically investigated in optics in a two-dimensional medium, and used to probe Anderson localization in a single configuration of this medium [4]. Although this phenomenon is understood as being characteristic of the localized transport, the medium-induced reduction of the transmission problem to a rank-1 matrix is not intrinsically related to disorder and can be observed in other contexts, in particular in regular media. In this work, we show that the transmitted pattern through a periodic medium, though complex, can be *frozen* under proper conditions. The first condition corresponds to a frequency located in a bang gap in the periodic medium: no Bloch-Floquet mode is propagating. This case is similar to the case of localized transport: a single channel dominates the transmission. An example of such an evanescent transmission is shown in [Figure 1(a)].

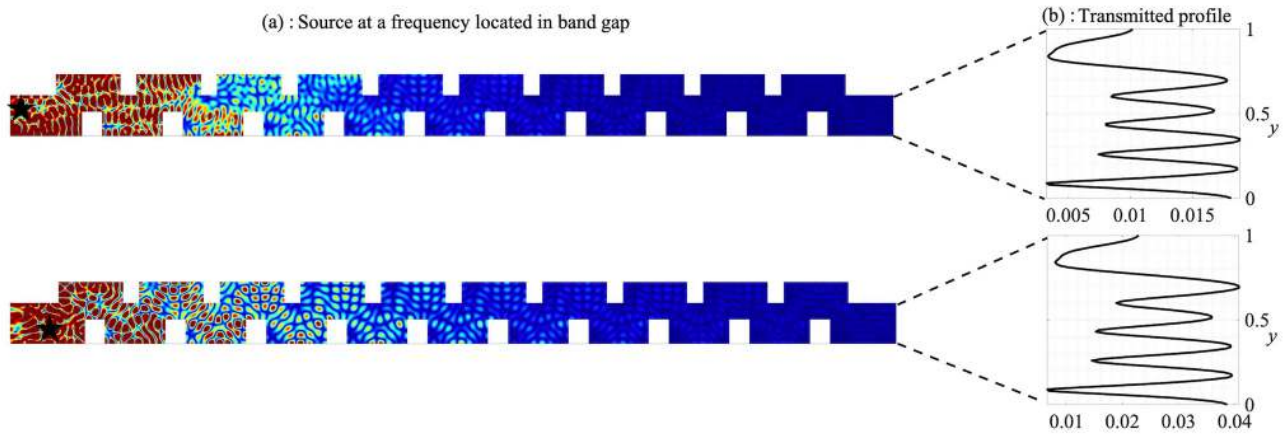


Figure 1 (a) Normalized absolute value of the field in a periodic wave guide which is excited by a source at two different positions at a frequency located in a band gap. (b) Comparison of the absolute value of the transmitted profile.

A point source (★) at a frequency located in a band gap is located in the left lead at two different positions. While the excitation, hence the incident wave, is modified from one case to the other, the pattern of the transmitted field is almost the same [Figure 1(b)].
Computing the wavefield (solution of the Helmholtz equation) in the whole waveguide allows us to go further than the only analysis of

the transmitted pattern. We can already observe the strong decrease of the amplitude but, above all, the progressive freezing of the wave pattern as we move away from the source. Thus, the transmission in a band gap of a periodic waveguide displays characteristics which, although resulting from different mechanisms, are similar to those of a Anderson-localized medium, and therefore lead to the freezing of the wave pattern.

However, the periodic system makes possible another regime of single channel transport, which cannot be observed in the disordered case. This is the case where the first TEV dominate all others without being itself small, this case corresponds to a frequency located in a region when a single Bloch-Floquet mode is propagating. It is then possible to freeze the transmitted pattern, without the counterpart of having a very low energy transmission. An example of freezing of a propagating field is shown in [Figure 2].

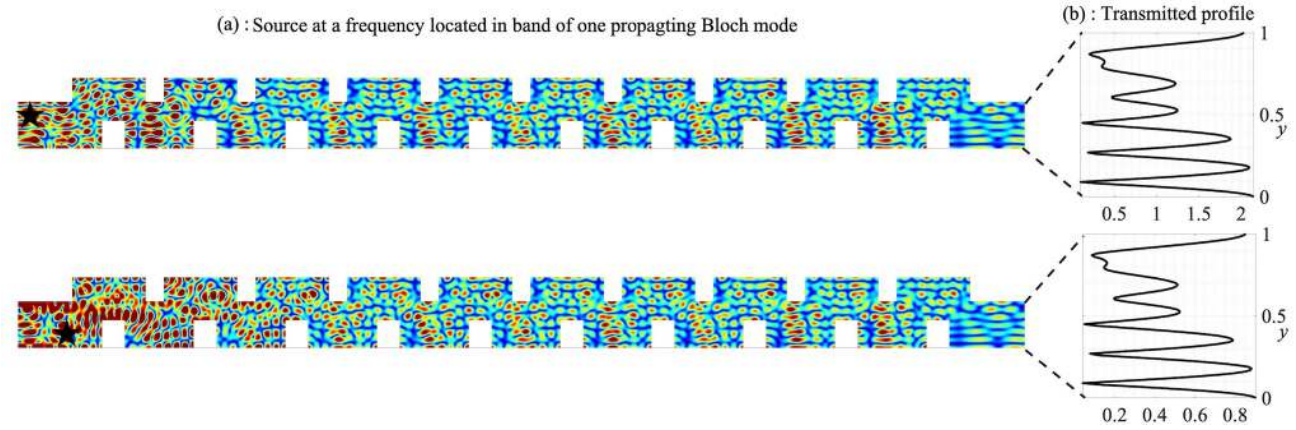


Figure 2 (a) Normalized absolute value of the field in a periodic wave guide which is excited by a source at two different positions at a frequency located in a band of one propagating Bloch mode. (b) Comparison of the absolute value of the transmitted profile.

References

[1] Rotter S. and Gigan S., "Light fields in complex media: Mesoscopic scattering meets wave control," Rev. Mod. Phys., vol. 89, p. 015005, 2017.

[2] Beenaker C.W., "Random-matrix theory of quantum transport," Rev. Mod. Phys., vol. 57, p. 731, 1997.

[3] Shi Z. and Genack A. Z., "Transmission eigenvalues and the bare conductance in the crossover to Anderson localization," Phys. rev. Lett., vol. 108, p. 043901, 2012.

[4] Leseur O., Pierrat R., Sáenz J. and Carminati R., "Probing two-dimensional Anderson localization without statistics," Phys. Rev. A, vol. 90, p. 053827, 2014.

Bottom-up approaches, new fabrication routes and ENSEMBLE3

Alignment of quantum rods for single- and multi-layered luminescence-based circular polarization convertors

Y. Okazaki[1*], H. Shimizu[1], K. Nakamura[1], S. Kubota[1], K. Hachiya[1], and T. Sagawa[1]

[1]Graduate School of Energy Science, Kyoto University, Japan
[*]corresponding author: okazaki.yutaka.8c@kyoto-u.ac.jp

Abstract: Orientation of anisotropic nanoparticles in macroscopic materials have a great potential for the generation and maximization of optical properties such as polarization. Here, we demonstrate an approach for the generation of circularly polarized (CP) light with high purity and high light intensity by luminescence-based CP convertors composed of one-dimensionally aligned quantum rods composite films and retardation film.

Circularly polarized (CP) light is recently attracting worldwide interest because of its irradiation effect on the promotion of plant growth[1] and on the enhancement of photovoltaic energy conversion efficiency[2,3]. However, despite remarkable recent progress in CP light generation, the trade-off relationship between light intensity and polarization degree of CP light remains an important issue. In this presentation, we introduce a new approach for creating CP light with high purity and high light intensity by converting linearly polarized luminescence (LPL) using luminescence-based CP convertor[4].

In our approach, LPL material play an important role to determine the performance such as light intensity, polarization degree, and spectral pattern. In this study, we selected CdSe/CdS core/shell quantum rods (QRs) as highly emissive LPL source. When the QRs was incorporated into transparent elastic polymer such as poly(ethylene-*co*-vinyl acetate) (EVA), the QRs were easily aligned in one-direction by uniaxial stretching of the QR/EVA composite film. The degree of linear polarization in the emission process ($P_{\text{LP-lum}}$) showed maximum value (0.68) when the stretching ratio of QR/EVA composite film was over 6. On the other hands, the degree of linear polarization in the absorption process ($P_{\text{LP-Abs}} = 0.28$) was clearly smaller than that in the emission process ($P_{\text{LP-lum}} = 0.68$). These phenomena could be explained by the different origin of linear polarization. Namely, linear polarization in absorption process mainly originates from dielectric effect based on the morphological anisotropy of QRs (aspect ratio: 5.1), whereas linear polarization in emission process is mainly derived from quantum confinement effect based on the QRs width (ave. 4.9 nm) of being smaller than the exciton size (10.6-10.8 nm)[5,6].

When the obtained LPL film was laminated on the quarter-wave film, with the angles between polarization plane of LPL and fast-axis of quarter-wave film were -45˚ and +45˚, left-handed (LH-) and right-handed (RH-) CP light were produced, respectively. No significant difference was observed in the light intensity and spectral pattern even after lamination. The degree of circular polarization (P_{CP}) of both LH- and RH- CP light (0.66) was similar to the $P_{\text{LP-lum}}$ value (0.68), indicating that the polarization degree of LPL was directly converted to the polarization degree of CP light. Such a large P_{CP} value with keeping the original emission intensity and the spectral pattern was also provided from other-colored CP convertors.

In this presentation, we will also discuss about multiplexing of optical information by multilayer-type luminescence-based CP light convertor consisting of various LPL films composed of different color-emissive QRs.

References

1. Lkhamkhuu, E., K. Zikihara, H. Katsura, S. Tokutomi, T. Hosokawa, Y. Usami, M. Ichihashi, J. Yamaguchi, and K. Monde “Effect of circularly polarized light on germination, hypocotyl elongation and biomass production of Arabidopsis and lettuce: Involvement of phytochrome B,” Plant Biotechnol., Vol. 37, No. 1, 57–67, 2020.
2. Qin, W., H. Xu, and B. Hu “Effects of spin states on photovoltaic actions in organo-metal halide perovskite solar cells based on circularly polarized photoexcitation,” ACS Photonics, Vol. 4, No. 11, 2821–2827, 2017.
3. Wei, M., X. Hao, A. B. Saxena, W. Qin, and S. Xie “Optical helicity-manipulated photocurrents and photovoltages in organic solar cells,” J. Phys Chem. C, Vol. 122, No. 23, 12566–12571, 2018.
4. Okazaki, Y., M. Kimura, K. Hachiya, and T. Sagawa “Luminescence-based circular polarization convertors: polarization conversion of linearly polarized photoluminescence from one-dimensionally aligned quantum rods using retardation films,” J. Mater. Chem. C, Vol. 11, No. 3, 935–942, 2023.
5. Kyhm, K., J.H. Kim, S.M. Kim and H. Yang “Gain dynamics and excitonic transition in CdSe colloidal quantum dots,” Opt. Mater., Vol. 30, No. 1, 158–160, 2007.
6. Babentsov, V., and F. Sizov “Defects in quantum dots of IIB-VI semiconductors,” Opto-Electron. Rev., Vol. 16, No. 3, 208–225, 2008.

DNA identification using surface-enhanced Raman spectroscopy

A. Kowalczyk[1], A. M. Nowicka[1], J. Krajczewski[1], A. Michałowska[1], E. Pyrak[1], A. Kowalik[2], J. L. Weyher[3], I. Dzięcielewski[3], M. Chłopek[2], S. Góźdź[2], and A. Kudelski[1*]

[1]Faculty of Chemistry, University of Warsaw, Poland
[2]Holy Cross Cancer Center, Poland
[3]Institute of High Pressure Physics of the Polish Academy of Science, Poland
[*]corresponding author: akudel@chem.uw.edu.pl

Abstract: The DNA biosensors are powerful tools in the gene mutation or pathogens detection. That is why there are a lot of DNA detection strategies and methods. Here we present the insight on a slightly overlooked DNA detection technique, surface-enhanced Raman scattering (SERS) spectroscopy. We analyse how to construct more efficient sandwich-type SERS biosensor for DNA identification. A new SERS strategy for the gene mutation identification based on rearrangement of alkanethiols linker and blocking chains is also presented.

The deoxyribonucleic acid (DNA) is the carrier of genetic information for all living organisms. Even a small mutation in its structure can lead to the development of a serious disease. Therefore, many scientists are working on developing fast, sensitive and precise methods for detecting specific DNA fragments. A very promising method for detecting and identifying many compounds, including DNA,[1-3] is surface-enhanced Raman scattering (SERS). The essence of SERS phenomenon is very large increase in the efficiency of the Raman signal generation (in some cases by 7-8 orders of magnitude on average, and locally even by 10-12 orders of magnitude) for molecules located at or near the surface of certain nano-plasmonic structures.

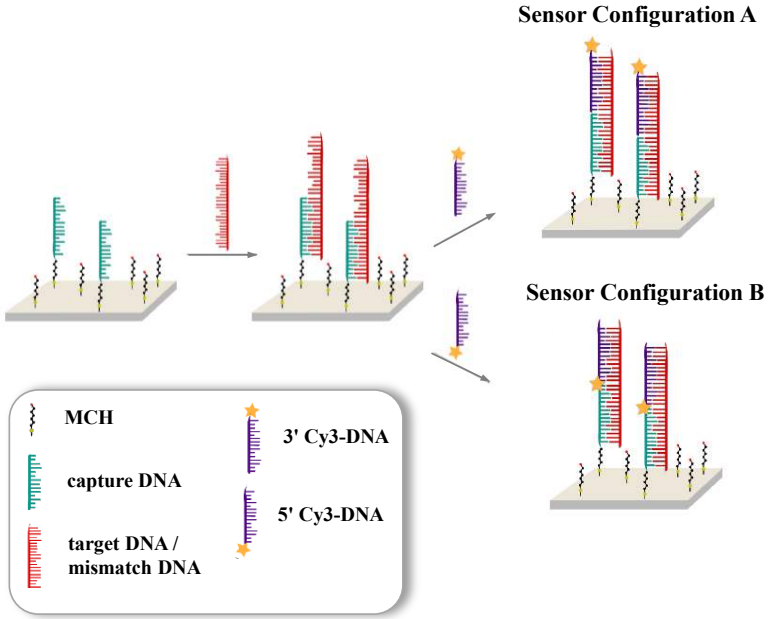


Figure 1. Scheme of the construction of sandwich-type SERS sensors for DNA detection: in configuration with Raman reporter "outside" the double-stranded DNA and with Raman reporter "inside" the double-stranded DNA.

In this work, we decided to determine how various modifications of one of the most frequently used SERS DNA sensors (so-called sandwich-type sensors - see Figure 1)[1,2] can affect the intensity of the SERS signal generated. We tested: attaching a Raman reporter moiety (chromophore) at various places of the reporter DNA chain; SERS substrates from various plasmonic metals, and the use of DNA chains with some mismatches. We hope that our results will help in the construction of more sensitive and effective sandwich-type SERS DNA sensors.

Moreover, we also developed a new SERS method of DNA detection based on the hybridization-induced (in the presence of target DNA) conformation change (*gauche* → *trans*) of alkanethiols adsorbed on the metal surface between the attached DNA strands and on the conformation change of the alkanethiol linker chain modifying the capture DNA (see Figure 2). The new DNA SERS (bio)sensor has been tested on 17 clinical samples and is characterized by the low detection limit at the level of pg μL^{-1}, wide analytical range from ca 7 pg μL^{-1} to ca. 70 ng μL^{-1} and high selectivity.

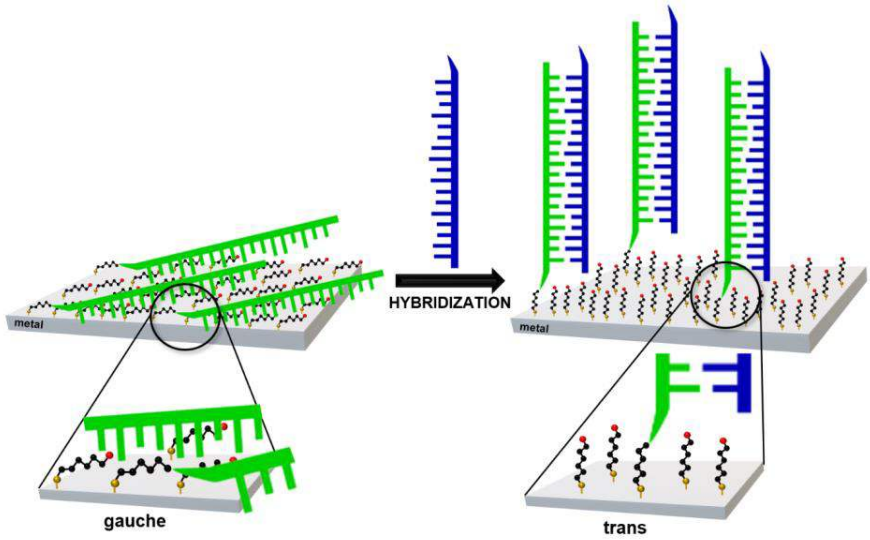


Figure 2. Scheme of the procedure of the modification of SERS substrates by DNA fragments and induced by the DNA hybridization change of the average structure of the metal–S–C–C chain.

Acknowledgements: This work was financed out of funds of the National Science Centre, Poland, No. 2019/35/B/ST4/02752.

References

1. He, Y., Su, S., Xu, T., Zhong, Y., Zapien, J. A., Li, J., Fan, C. and Lee, S.-T., "Silicon nanowires-based highly-efficient SERS-active platform for ultrasensitive DNA detection," Nano Today, Vol. 6, No. 2, 122–130, 2011.
2. He, S., Liu, K.-K., Su, S., Yan, J., Mao, X., Wang, D., He, Y., Li, L.-J., Song, S. and Fan, C., "Graphene-based high-efficiency surface-enhanced Raman scattering-active platform for sensitive and multiplex DNA detection," Anal. Chem. Vol. 84, No. 10, 4622–4627, 2012.
3. Michałowska, A., Gajda, A., Kowalczyk, A., Weyher, J. L., Nowicka, A. M. and Kudelski, A., "Surface-enhanced Raman scattering used to study the structure of layers formed on metal surfaces from single-stranded DNA and 6-mercaptohexan-1-ol: influence of hybridization with the complementary DNA and influence of the metal substrate," RSC Adv., Vol. 12, No. 54, 35192–35198, 2022.

META 2023, PARIS - FRANCE, JULY 18 – 21, 2023

Review of Remote Epitaxy and Blue Spectral Intensity Enhancement Using Surface Plasmon Resonance

Jun Hee Choi*, Kiho Kong, Eunsung Lee, Joo Hun Han, Jung Hun Park, Nakhyun Kim, Jinjoo Park, Joosung Kim, Dong Chul Shin, Sunil Kim

Compound Semiconductor TU, Samsung Advanced Institute of Technology, Samsung Electronics, Suwon 16676, Republic of Korea

*corresponding author, E-mail: joonie.choi@samsung.com

Abstract: We review remote epitaxy potentially coupled with pixelated InGaN LEDs via ion implantation for micro displays for augmented reality. Next, we discuss the degree of blue light enhancement in low-efficiency CdS/ZnS core/shell quantum dot (QD) light emitters using Ag/dielectric surface plasmon resonator.

First, we briefly review remote epitaxy for reduction of defect density for developing red InGaN LEDs as shown in Figure 1 [1]. The remote epitaxy can be coupled into tailored ion implantation pixelation (TIIP) for pixelating InGaN based micro-LEDs (μLEDs). Owing to the planar geometry, TIIP pixelation is readily incorporated into high-resolution pixel-driving circuits in high-ppi μLED displays for AR glasses [2-4].

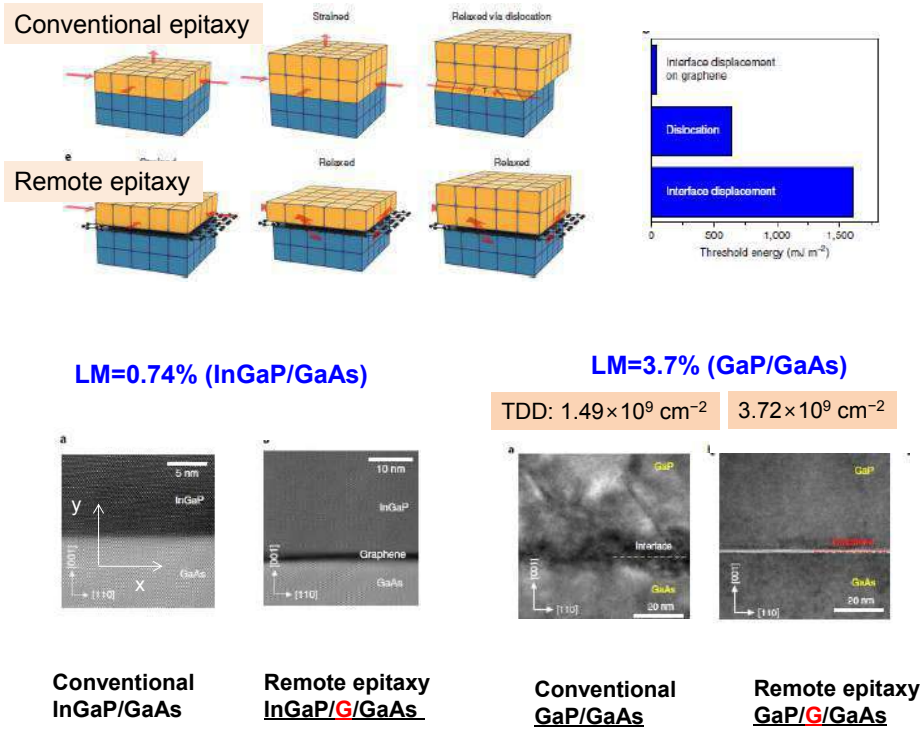


Figure 1. Schematic of remote epitaxy for reducing dislocation density [1].

Next, we discuss the light enhancement by surface plasmon resonance (SPR), a kind of energy recycling, i.e., the useless energy (the energy in the non-radiative recombination process normally wasted away in the form of heat) can be relevantly transferred to SPR with minimized charge transfer, then transferred by SPR propagation,

and finally out-coupled to light through nano-sized protrusions [5]. Therefore, in case of light emitter with quantum efficiency of unity, SPR rather acts as a loss mechanism [6]. The frequency (ω) or wavelength (λ) for SPR is determined by the equation;

$\varepsilon_{m,\,real}(\omega) + \varepsilon_d(\omega) = 0$

By selecting different combinations of metal/dielectric, the resonance frequency can be modulated: $\lambda(Ag/Si_3N_4) \sim 470$ nm, $\lambda(Ag/Al_2O_3) \sim 540$ nm, $\lambda(Au/SiO_2) \sim 520$ nm, $\lambda(Au/Al_2O_3) \sim 630$ nm, and $\lambda(Au/HfO_2) \sim 800$ nm. Finally, we investigate SPR in core/shell CdS/ZnS blue QDs on Ag/Si_3N_4 which is suitable for blue-light enhancement ($\lambda(Ag/Si_3N_4) \sim 470$ nm). The charge and energy transfer mechanism between QDs and QD and Ag is illustrated in left panel of Figure 2 [7]. From multi-layer-QD experiment, the effective distance of light enhancement by SPR is about 5 layers of QDs (30-40 nm). We suggest the optimum structure of light enhancement by SPR in right panel of Figure 1.

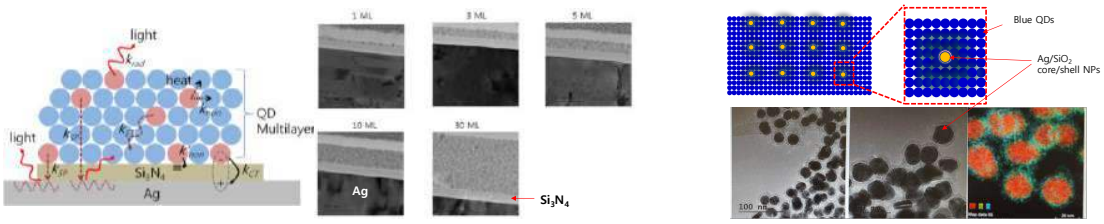


Figure 2. Diagram showing energy and charge transfer between QDs or to plasmonic structure in multi-layer QD and Optimized SPR structure for PL emission

References

1. S. H. Bae et al. “Graphene-assisted spontaneous relaxation towards dislocation-free heteroepitaxy”, Nature Nanotechnology 15, 272–276, 2020.
2. J. H. Choi et al. “Nearly single-crystalline GaN light-emitting diodes on amorphous glass substrates”, Nat. Photon. 5, 763–769, 2011.
3. J. H. Choi et al. “Fully flexible GaN light-emitting diodes through nanovoidmediated transfer”, Adv. Opt. Mater. 2, 267-274, 2014.
4. J. H. Choi et al. “Electrically driven mid-submicrometre pixelation of InGaN micro-light-emitting diode displays for augmented-reality glasses”, Nat. Photon. 15, 449–455, 2021.
5. K. Okamoto et al. “Surface plasmon enhanced spontaneous emission rate of InGaN⁄GaN quantum wells probed by time-resolved photoluminescence spectroscopy”, Appl. Phys. Lett. 87; 071102, 2005.
6. A. P. Edwards et al. “Plasmonic nanogaps for broadband and large spontaneous emission rate enhancement”, J. Appl. Phys. 115; 053101, 2014.
7. T. Shin et al. “ Exciton Recombination, Energy-, and Charge Transfer in Single-and Multilayer Quantum-Dot Films on Silver Plasmonic Resonators”, *Scientific reports* 6 ; 26204, 2016.

META 2023, PARIS - FRANCE, JULY 18 – 21, 2023

In situ growth: Bottom-up wet-chemical preparation of plasmonic gold nanostructures on substrates

G. A. Vinnacombe-Willson[1,*]

[1]BioNanoPlasmonics Laboratory, CIC biomaGUNE, Basque Research and Technology Alliance (BRTA), 20014 Donostia-San Sebastián, Spain
[*]corresponding author: gvinnacombe@cicbiomagune.es

Abstract: We present an unconventional *in situ* growth approach where bottom-up wet-chemical synthesis is used to synthesize plasmonic gold nanoparticles (AuNPs) directly on substrates, rather than in colloidal suspension. This *in situ* growth technique was implemented to prepare anisotropic AuNPs on various materials. Furthermore, we show that combining *in situ* growth and soft lithography opens the doors for the preparation of plasmonic arrays with collective plasmonic responses and tuneable optical properties.

Over the last few decades, developments in bottom-up colloidal nanofabrication have enabled the preparation of colloidal gold nanoparticles (AuNPs) with precisely tailored chemical and physical properties.[1] In this work, rather than forming AuNPs in colloidal suspension, we adapt bottom-up wet chemical synthesis to instead form plasmonic nanostructures directly on substrates for straightforward fabrication of plasmonic materials (**Figure 1**).[1-2] While the *in situ* growth approach appears intuitive, further improvement of the fundamental synthetic understanding of this class of techniques is required to elevate it to the same robustness and versatility as conventional colloidal synthesis.

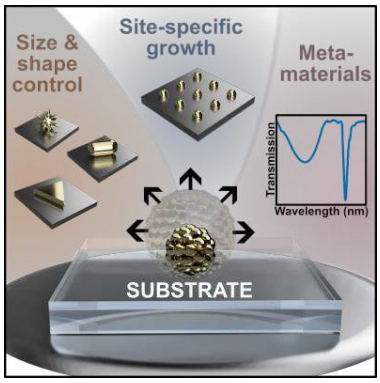


Figure 1. Schematic showing substrate bottom-up formation of gold nanoparticles.

In this work, we utilize *in situ* growth to form nanospheres and nanostars, demonstrating that the size and shape of the particles can be controlled by modulating the chemical composition of the growth solution.[2] We then combined *in situ* growth with a soft-lithographic method based on thermal nanoimprint lithography, which does not require specialized equipment nor clean-room sample preparation, to fabricate plasmonic arrays. The resulting arrays can be prepared with different periodicities, therefore exhibiting tuneable lattice plasmon resonances in the visible and near-infrared with quality factors >20.

Beyond plasmonic arrays, the *in situ* growth can be a useful approach for the fabrication of hybrid plasmonic materials with biomedical applications. For instance, plasmonic nanoparticle-decorated hydrogels can be used as matrices for 3D *in vitro* tumor models, whereby the integrated nanoparticles function to monitor the microenvironment of embedded or seeded cancer cells *via* surface-enhanced Raman scattering (SERS)-based sensing.[4] Towards this goal, we performed proof of concept tests interrogating shape control *in situ* on hydrogels.

Ultimately, we show that the creation of chemical contrast *via* surface functionalization with strong reductants can assist in controlling and directing the growth of AuNPs specifically on the substrate. Moreover, changing the chemical composition of the growth solution, while paying special attention to reducing secondary colloidal nucleation, which competes with substrate growth is key for controlling nanoparticle size and shape. Overall, continued development of *in situ* growth protocols constitutes an exciting synthetic opportunity for fabricating plasmonic materials for potential application in catalysis, optoelectronics, and as biomedical platforms.[5]

Acknowledgements
This work is supported by the European Research Council (ERC-AdG 4D-bioSERS #787510).

References

1. Liz-Marzán, L. Colloidal Synthesis of Plasmonic Nanometals; CRC Press, 2020.
2. Vinnacombe-Willson, G. A., *et. al.*, "Surface Lattice Plasmon Resonances by Direct In Situ Substrate Growth of Gold Nanoparticles in Ordered Arrays," *Adv. Mater*. Vol. 34, No. 37, 2205330-2205341, 2022.
3. Vinnacombe-Willson, G. A., *et. al.*, "In Situ Shape Control of Thermoplasmonic Gold Nanostars on Oxide Substrates for Hyperthermia-Mediated Cell Detachment." *ACS Cent. Sci.* Vol. 6, No. 11, 2105–2116, 2020.
4. Plou, J. *et al.* "Nanocomposite Scaffolds for Monitoring of Drug Diffusion in Three-Dimensional Cell Environments by Surface-Enhanced Raman Spectroscopy." *Nano Lett.* Vol. 21, No. 20, 8785–8793, 2021.
5. Neal, R. D., *et al.*, "Substrate-Immobilized Noble Metal Nanoplates: a Review of Their Synthesis, Assembly, and Application." *J. Mater. Chem. C* Vol. 9, 12974-13012, 2021.

META 2023, PARIS - FRANCE, JULY 18 – 21, 2023

Self-organization of eutectic two-phase composites: insights from phase-field simulations

M. Plapp[1*]

[1]Laboratoire de Physique de la Matière Condensée, CNRS, Ecole polytechnique, Institut Polytechnique de Paris, 91120 Palaiseau, France
[*]corresponding author: mathis.plapp@polytechnique.edu

Abstract: The crystallization of eutectic alloys yields composites in which the two solid phases are arranged in regular lamellar or rod microstructures. Those are created by a pattern-formation process at the solid-liquid interface which results from the interplay of capillary effects and diffusion. I will review several insights obtained by phase-field modeling on the effect of interphase boundary anisotropy on the emergence of lamellar patterns, the influence of transverse temperature gradients, and the transition from lamellar to rod patterns.

The crystallization of a liquid close to its eutectic composition leads to the simultaneous growth of two distinct solid phases of different compositions. The interplay between chemical diffusion in the liquid and capillary effects created by the surface energies of interfaces and interphase boundaries leads to the emergence of a characteristic length scale [1]. The most frequently observed microstructural patterns are alternating lamellar platelets of the two phases, or rods of the minority phase embedded in a matrix of the majority phase. However, many other and more complicated structures have been observed, in particular for substances with facetted solid-liquid interfaces. The idea was put forward [2] to use this capability of spontaneous structuration as a route for large-scale bottom-up fabrication of metamaterials. In this perspective, the self-organization must take place in a well-controlled manner, which requires a good fundamental understanding of the pattern-formation dynamics.

Phase-field models have emerged since three decades as the numerical method of choice for the study of microstructural pattern formation during solidification. In the phase-field approach, interfaces and boundaries are implicitly described by auxiliary scalar fields, the so-called phase-fields. The equations of motion of those fields are coupled to the relevant transport equations, such as diffusion of chemical species, and the coupled model can be derived from a free-energy functional using the thermodynamics of irreversible processes. The resulting set of partial differential equations can be solved using standard numerical methods.

Phase-field models have been used by many groups to investigate eutectic patterns. I will highlight several of our own findings that shed light on observations made in experiments. For example, we have shown that anisotropy of the solid-solid interphase boundaries is crucial for the emergence of lamellar patterns in extended systems [3]. Without anisotropy, lamellae can still be created by the presence of a transverse temperature gradient; otherwise, labyrinth-like two-phase patterns prevail [4]. Large-scale variations in concentration in the liquid can create transitions between lamellae and rods that are mediated by a propagative lamellae breakup instability [5]. Finally, the competition of this instability with a lateral temperature gradient can be used to obtain controlled transitions between lamellae and rods [6].

References

1. K. A. Jackson, J. D. Hunt, “Lamellar and Rod Eutectic Growth”, Transactions of the Metallurgical Society of AIME, Vol. 236, 1129-1142, 1966.
2. D. A. Pawlak *et al*., “How far are we from making metamaterials by self-organization? The microstructure of highly anisotropuc particles with an SRR-like geometry,” Adv. Funct. Mater., Vol. 20, 1116-1124, 2010.
3. S. Ghosh, M. PLapp, “Influence of interphase boundary anisotropy on bulk eutectic solidification microstructures,” Acta Mater. Vol. 140, 140-148, 2017.
4. M. Perrut, A. Parisi, S. Akamatsu, S. Bottin-Rousseau, G. Faivre, M. Plapp, “Role of transverse temperature gradients in the generation of lamellar eutectic solidification patterns,” Acta Mater. Vol. 58 1761-1769, 2010.
5. A. Parisi, M. Plapp, “Defects and multistability in eutectic solidification patterns,” Europhysics Lett. Vol 90 (2010), 26010, 2010.
6. S. Akamatsu et al., “In situ experiments in microgravity and phase-field simulations of the lamellar-to-rod transition during eutectic growth,” Comptes Rendus Mécanique, Vol. 142, 2023.

META 2023, PARIS - FRANCE, JULY 18 – 21, 2023

Non-resonant enhancement of photoluminescence based on metallic nanocubes

M. Khaywah[1, 2], A. Potdevin[2], F. Réveret[2], R. Mahiou[2], Y. Ouerdane[3], A. Désert[4], S. Parola[4], G. Chadeyron[2], E. Centeno[1] , R. Smaali[1] and A. Moreau[1,*]

[1]Université Clermont Auvergne, Clermont Auvergne INP, CNRS, Institut Pascal, F-63000 Clermont–Ferrand, France

[2]Université Clermont Auvergne, Clermont Auvergne INP, CNRS, ICCF, F-63000 Clermont–Ferrand, France

[3] Laboratoire Hubert Curien, UMR CNRS 5516, Université Jean Monnet, Saint-Etienne, France

[4] Ecole Normale Supérieure de Lyon, CNRS, Univ. Lyon 1, Laboratoire de Chimie (UMR 5182), Lyon, France

[*]corresponding author: antoine.moreau@uca.fr

Abstract: Metallic nanoparticles are well know for their resonant response, usually associated with Purcell effect and losses. We show here that a very large and broadband enhancement can be reached using metallic nanoparticles far from resonance. The density of nanoparticles is critical and needs to be well controlled to maximize the efficiency.

Many devices include photoluminescent layers (for lighting or sensing typically[1]) which have to be optically excited and generate light than has then to be extracted from the layer. Metallic nanoparticles can provide such an enhancement typically because they can help couple light in, present a large Purcell effect when they resonate, and can enhance light extraction. Since such particles constitute very good absorbers at resonance, the overall efficiency at resonance can be disappointing. In addition, leveraging the Purcell effect means putting nanoparticles very close to emitters. Another path would be to use metallic nanoparticles as non-resonant scatterers only at the surface of the material and to focus on the enhancement of in-coupling, with the excitation of guided modes and out-coupling of light, but giving up on Purcell effect. However, coupling efficiently a large number of guided modes requires to be able to control the density of scatterers: too many of them and the structure is reflecting or absorbing, while a lower density is associated to a lower efficiency. Using carefully designed experiments, we have shown that unexpectedly large enhancement can be reached and provide a physical analysis of the phenomenon[2]. A rule of thumb would be to keep, between nanoparticles, distances that are close to the effective wavelength of guided modes inside the luminescent layer. Such a versatile technique is likely to be useful for many devices.

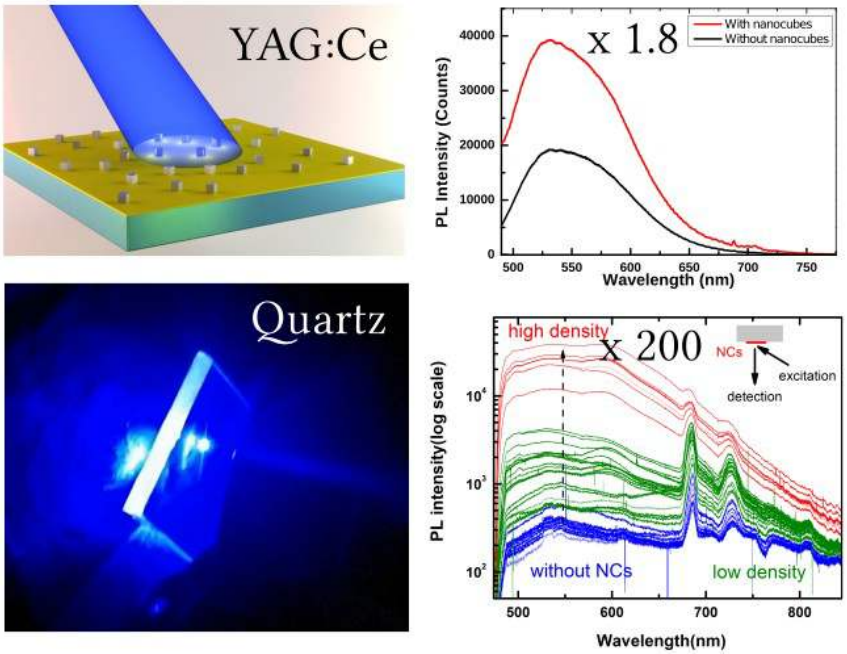


Figure 1: (top left) Artistic view of the nanocubes spread on a luminescent layer of YAG:Ce (in yellow) (top right) photoluminescence enhancement in the case of a YAG:Ce layer (bottom left) quartz slab illuminated using a blue laser showing an enhanced coupling of guided modes and (bottom right) the corresponding luminescence enhancement.

Funding. This work was sponsored by a public grant overseen by the French National Agency as part of the "Investissements d'Avenir" through the IMobS3 Laboratory of Excellence (ANR-10-LABX-0016) and the IDEX-ISITE initiative CAP 20-25 (ANR-16-IDEX-0001), project Metalum. A.M. is an Academy CAP 20-25 chair holder. This work was supported by grants from the framework of the CPER DEFI MMASYF project. The authors thank the European Regional Development Fund and the Auvergne Rhône-Alpes Region funding the project.

References

1. Zhmakin, A. I. "Enhancement of light extraction from light emitting diodes". **Phys. Rep.** Vol. 498, 189–241, 2011.
2. Khaywah, M., Potdevin, A., Réveret, F., Mahiou, R., Ouerdane, Y., Désert, A., ... & Moreau, A. (2021). Large and Versatile Plasmonic Enhancement of Photoluminescence Using Colloidal Metallic Nanocubes. **The Journal of Physical Chemistry C**, Vol. 125, No. 14, 7780-7790, 2021.

META 2023, PARIS - FRANCE, JULY 18 – 21, 2023

Fabrication and properties of GaAs Tamm plasmon confined light emitting diodes

Joel Bellessa[1*], Vincent Toanen[1], Clémentine Symonds[1], Jean-Michel Benoit[1], Alban Gassenq[1], Aristide Lemaitre[2]

[1] Univ Lyon, Université Claude Bernard Lyon 1, CNRS, Institut Lumière Matière, F-69622, Villeurbanne, France
[2] Université Paris-Saclay, CNRS, Centre de Nanosciences et de Nanotechnologies, 91120, Palaiseau, France
[*]corresponding author: joel.bellessa@univ-lyon1.fr

Abstract: A fabrication process of Ag/GaAs Tamm emitting devices will be described. As the maximum electric field of the Tamm mode is close to the surface, the fabrication of the devices requires a special procedure to maintain their emissive properties. For Tamm structures of 5µm diameter, mode confinement appears in the diode emission with energy discretization [1]. The observation of the electrically excited emission of a Tamm structure is an important step towards the exploitation of Tamm structures for novel optical devices.

Tamm plasmon modes appear at the interface between a metallic film and a Bragg mirror and exhibit properties of both cavity modes and plasmons [2]. Their main interest lies in the surface character of the mode, which allows the integration into sources of geometries ranging from simple disks [3] to complex metal metasurfaces [4]. As the field maximum is close to the surface, the metal micro/nano-structuration controls the properties of the source such as its directivity or polarization [5].

To exploit the advantages described above, electrically excited devices have to be fabricated. But the micro-structuration of a surface mode is a technological issue that is not present in the usual emitting devices. Indeed, the first few nanometres of the structure must be preserved and requires the development of specific processes.

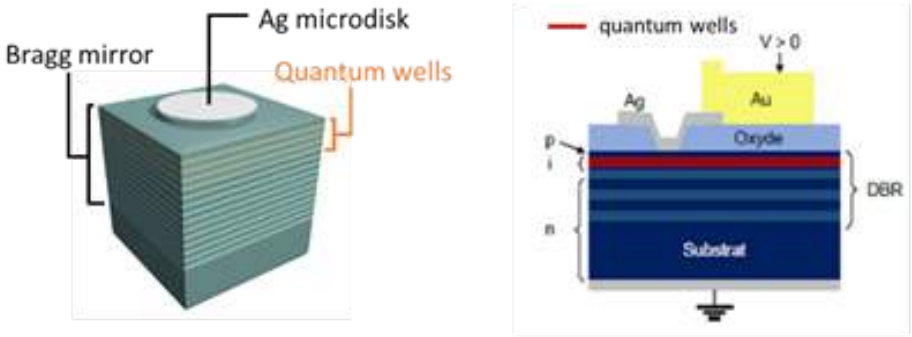


Fig. 1 a) Tamm confined principle b) Layout of the Tamm plasmon diode

The semiconductor part of the structure is constituted by a GaAs/$Ga_{0.9}Al_{0.1}As$ Distributed Bragg Reflector (DBR) grown by Molecular Beam Epitaxy. The last layer of this DBR is formed by a 3λ/4 GaAs film

comprising 6 $In_{0.15}Ga_{0.85}As$/GaAs quantum wells located at the two maxima of the electric field. To leave the thickness of the semiconductor unchanged in the emitting region, a fabrication based on pulsed laser deposition and lift off has been used.

The electroluminescence of fabricated structures follows the dispersion of the Tamm mode, showing that it occurs predominately in the Tamm mode. For a diode of 5 µm diameter, the emission dispersion shows an energy discretization characteristic of 3D confinement. The emission spatial intensity profile extracted from experiments can be superposed with the spatial profile of a HE_{11} mode.

The demonstration of the electrically excited emission of Tamm structure is a key point toward the exploitation of their versatility for confined lasers or sources with unconventional polarisation.

References

1. O. Gazzano, S.M. de Vasconcellos, K. Gauthron, C. Symonds, J. Bloch, P. Voisin, J. Bellessa, A. Lemaitre and P. Senellart. *Phys. Rev. Lett.* **107**, 247402 (2011).
2. M. Kaliteevski, I. Iorsh, S. Brand, R.A. Abram, J.M. Chamberlain, A. Kavokin and I.A. Shelykh. *Phys. Rev. B* **76**, 165415 (2007).
3. C. Symonds, G. Lheureux, J.P. Hugonin, J.J. Greffet, J. Laverdant, G. Brucoli, A. Lemaitre, P. Senellart and J. Bellessa. *Nano Lett.* **13**, 3179 (2013).
4. S. Azzini, G. Lheureux, C. Symonds, J.M. Benoit, P. Senellart, A. Lemaitre, J.J. Greffet, C. Blanchard, C. Sauvan and J. Bellessa. ACS Photon. 3, 1776 (2016).
5. L. Ferrier L., H.S. Nguyen, C. Jamois , L. Berguiga, C. Symonds, J. Bellessa, T. Benyattou, APL Photonics, 4, 106101 (2019)

META 2023, PARIS - FRANCE, JULY 18 – 21, 2023

Bioinspired Colorimetric Metasurfaces for Next Generation, On-Chip Imaging of Tissue Microstructure

P. Kirya,[1] Z. Haddadin,[1] D. Shah,[1] L. Phillips,[1] O. Aisagbonhi,[1] and L. V. Poulikakos[1,*]

[1]University of California, San Diego, California, United States
[*]corresponding author: lpoulikakos@ucsd.edu

Abstract: This work introduces a new class of bioinspired 3D-architected metasurfaces which enable the quantitative, colorimetric visualization of tissue microstructure for a variety of fiber-affecting diseases encompassing organ fibrosis, heart disease, neurodegenerative disease or various cancers.

The origin and progression of a variety of leading health challenges, encompassing Alzheimer's disease, heart disease, fibrosis and cancer, are directly linked to changes in the presence and orientation of fibrous matter in biological tissue. Fibrous biological tissue exhibits distinct anisotropic optical properties, which can be leveraged for selective imaging. However, these naturally occurring light-matter interactions are inherently weak, posing barriers to their visualization in a clinically translatable manner. Existing imaging techniques which visualize the fibrous properties of biological matter face challenges in complexity, cost, destructiveness, or precision. Thus, innovation in imaging technology of fibrous tissue with facile clinical implementation is urgently needed.

To address this challenge, we develop a new class of anisotropic, colorimetric metasurfaces to selectively visualize disease-relevant fiber density and orientation in biological tissue. We draw inspiration from iridescent structural color which is abundant in nature, arising in the saturated blues of the Morpho butterfly wing or the greens of jeweled beetle shells. At the micrometer scale and smaller, these naturally occurring, three-dimensionally (3D)-architected photonic crystals are composed of ordered, geometrically anisotropic features which exhibit distinct interactions with light at varying angles of incidence or polarization state. Due to their 3D hierarchical architecture, these nature-derived systems are unique sources of polarization-sensitive structural color with high color purity and brightness. Here, we use two-photon lithography to fabricate multilayer grating structures which surpass the polarization-sensitive colorimetric response attainable in nature. Bringing additive manufacturing to the regime of visible light-matter interactions, we implement our colorimetric metasurfaces as a next-generation tissue microstructure imaging technology. Starting with the example of breast cancer diagnostics, we then expand our view to the rich palette of fiber-affecting diseases where metasurfaces hold great potential to achieve rapid, precise and low-cost tissue diagnostics with facile clinical implementation.

The authors gratefully acknowledge funding from the Beckman Young Investigator Program, the American Cancer Society, the Moores Cancer Center and the UCSD MRSEC.

META 2023, PARIS - FRANCE, JULY 18 – 21, 2023

Tailoring Anisotropies in NIR-plasmonic Semiconductor Nanocrystals

Jisoo Oh[1], Yannis Cheref[1], Capucine Cleret de Langavant[1], Louise Daugas[1], Florian Lochon[2], Alexandre Baron[2], Thierry Gacoin[1*], and Jongwook Kim[1*]

[1]Laboratoire de Physique de la Matière Condensée, CNRS, École Polytechnique, Institut Polytechnique de Paris, France
[2]Univ. Bordeaux, CNRS, Centre de Recherche Paul Pascal, UMR5031, France

[*]corresponding author: jong-wook.kim@polytechnique.edu

Abstract: Doped semiconductor nanocrystals represent an emerging class of materials that host localized surface plasmon resonance (LSPR). Their wide spectral range (from visible to the entire IR regions) and post-synthetic tunability through doping promise new plasmon-assisted active optical materials and devices. Recent studies discovered various semiconductor species that perform efficient LSPR. However, the nanocrystals' structural impact on their LSPR remain poorly explored.

This presentation illustrates how multiple structural factors can be synergistically tuned to promote novel LSPR properties that are unseen from metal hosts. For instance, hexagonal cesium-doped tungsten oxide (Cs_xWO_{3-y}) nanocrystals exhibit crystalline anisotropy that causes a strong LSPR band-splitting into two distinct and intense peaks [1]. We combine this property with the well-known shape anisotropy of plasmonic nanoparticles to tune the multimodal LSPR bands [2]. For this, we exquisitely control the synthesis of Cs_xWO_{3-y} and achieved their variable shape aspect ratio across a widely extended range from 0.2 (platelets) to 20 (rods) [3]. With this large structural tunability, the spectral range of LSPR peaks covers the entire near-infrared region and beyond (750~4000 nm). Moreover, the LSPR response of these highly anisotropic nanocrystals can be post-synthetically and reversibly tuned by inducing LSPR coupling effects in their self-assembled structures [4]. We demonstrate how this tunable LSPR can be used to design window NIR-shields for energy-saving applications [5].

References

1. Jongwook Kim et al, "The interplay of shape and crystalline anisotropies in plasmonic semiconductor nanocrystals" Nano Letters, Vol. 15, No. 8, 5574–5579, 2016.
2. Yannis Cheref et al, "Dual-band LSPR of tungsten bronze nanocrystals tunable over NIR and SWIR ranges" Chem. Mater., Vol. 34, No. 21, 9795–9802, 2022.
3. Jisoo Oh et al, "Extending the shape tunability of plasmonic Cs_xWO_{3-y} nanocrystals" *In preparation*.
4. Capucine Cleret de Langavant et al, "Dual-band LSPR coupling in oriented assemblies of doped metal oxide nanocrystals" *In preparation*.
5. Louise Daugas et al, "Investigation of LSPR coupling effects toward the rational design of Cs_xWO_{3-y}-based solar NIR filtering coatings" Adv. Funct. Mater., *In review*.

Scalable self-assembled plasmonic metamaterials: fabrication and application

A. Zaleska*, F. Lotti, A. Krasavin, W. Dickson and A.V. Zayats

King's College London, Department of Physics and London Centre for Nanotechnology,
Strand, WC2R 2LS, London, UK
*corresponding author: anastasiia.zaleska@kcl.ac.uk

Abstract: The integration of plasmonic effects into metamaterial architectures presents exciting opportunities to design and develop new metamaterials with desired optical properties of plasmonic metal nanostructures with different geometries, shapes and sizes. In this talk will overview fabrication and optical characterisation of large-area plasmonic metamaterials based on arrays of hybrid plasmonic nanotubes and nanorods and their applications in nonlinear optics and sensing. The structural and material degrees of freedom allow such metamaterials to find a wide range of applications in nanophotonics, opto-electronics, optical filters, sensing and photocatalysis.

Plasmonic nanostructures possess unique intrinsic optical properties including a strong resonant enhancement and confinement of the local electric field. Spectral tunability of these resonances can be achieved throughout the ultraviolet to infrared via the geometry (size and shape), surrounding media and the inherent properties of the plasmonic material from which it is made from. In this talk will be overview fabrication and optical characterisation of scalable self-assembled plasmonic metamaterials based on arrays of hybrid plasmonic nanotubes and nanorods with optical properties controlled by structural and material degrees of freedom, and their various applications.

The self-assembled fabrication approach based on the anodic aluminium oxide (AAO) template method was chosen for its ability to inexpensively create subwavelength arrays of designed plasmonic nanoparticles with large surface areas. This highly controllable, facile and inexpensive fabrication technique allows for various nanostructures of different shapes and dimensions with a high uniformity and reproducibility. This allows to control the geometrical parameters of the materials with nanometric precision and illustrate the resultant spectrally tunable plasmonic behaviour, well described by numerical simulations.

Metamaterials based on plasmonic nanorods, nanotubes, core-shell coaxials, as well as hybrid plasmonic-dielectric architectures for exquisite control of optical field localisation and strong-matter interactions were developed (Fig. 1). To harness fully functionalities of the nanorod based metamaterials, they should be illuminated at oblique incidence to access all the optical modes of the metamaterial. Plasmonic nanotubes-based metamaterials are free from this restriction and also provide the increased surface area for absorbing a large number of molecules. Advantageously, the core-shell cylindrical architecture allows the functional properties of the core to be exploited in combination with the plasmonic properties of the surrounding material and can play a role in carrier extraction for reactive plasmonic applications.

The advantages of such metamaterials have been demonstrated for bio- and gas sensing, nonlinear optics, controlling spontaneous emission, nanoscale light sources and memristors. As the examples of the emerging applications, we will discuss the metamaterials designed to maximise their potential for hot-carrier plasmonic applications, metamaterial-based spectrally selective filters and nonlinear intensity limiters. For the former applications, implementation of gold/nickel-oxide core-shell metamaterials as an optical sensor for the detection

of acetone, copper metamaterials in the plasmon enhanced photo-electrochemical reduction of CO_2 will be discussed in detail.

Large scale plasmonic and hybrid dielectric-plasmonic metamaterials provide wealth of opportunities for designing spectral position of the resonant response, tuneable spatial localisation of the electromagnetic field and the related advantages in the applications in nanophotonics, nonlinear optics, opto-electronics, sensing and photochemistry.

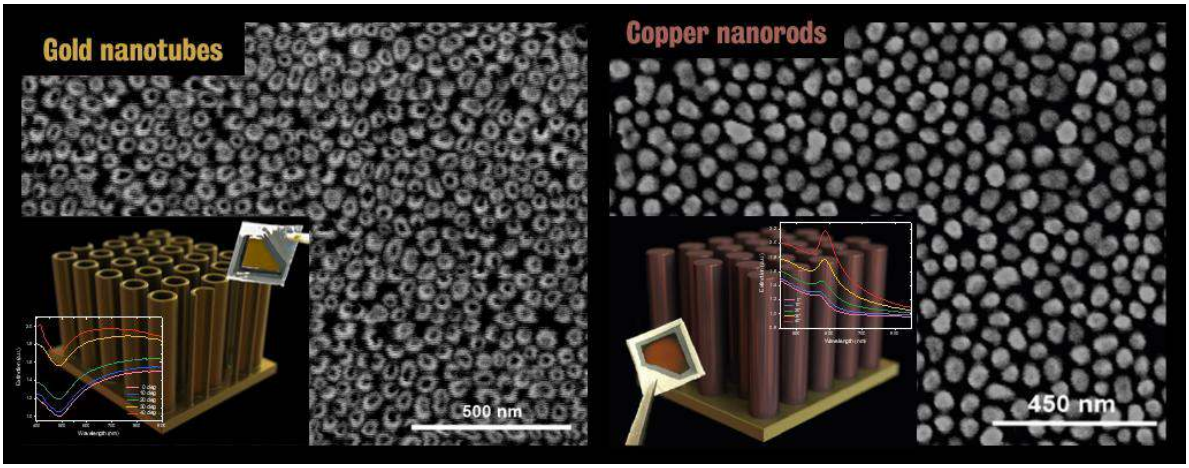


Figure 1. Scalable gold and copper plasmonic metamaterials. Top-view SEM images of an array of gold nanotubes (left) and copper nanorods (right) exposed in air on a glass substrate. Insets, a photograph of the sample with a schematic and its extinction spectrum obtained in the transmission for various angles of incidence of the TM-polarised light.

This work was supported by the EPSRC CPLAS project (EP/W017075/1).

References

1. Wang P., Krasavin A.V., Liu L., Jiang Y., Li Z., Guo X., Tong L., and Zayats A.V. "Molecular Plasmonics with Metamaterials", Chem. Rev., Vol. 122, No. 19, 15031-15081, 2022.
2. Wang P., Nasir M.E., Krasavin A.V., Dickson W., Jiang Y., and Zayats A.V. "Plasmonic Metamaterials for Nanochemistry and Sensing", Acc. Chem. Res., Vol. 52, No. 11, 3018–3028, 2019.
3. Wang P., Nasir M.E., Krasavin A.V., Dickson W., and Zayats A.V. "Optoelectronic Synapses Based on Hot-Electron-Induced Chemical Processes", Nano Lett., Vol. 20, No. 3, 1536–1541, 2020.
4. Wells B.M., Lotti F., Nasir M.E., Zayats A.V. and Podolskyi V.A. "Angle-insensitive plasmonic nanorod metamaterial-based band-pass optical filters", Optics Express, Vol. 29, No. 8, 11562, 2021.
5. Nasir M.E., Krasavin A.V., Córdova-Castro R.M., McPolin C.P.T., Bouillard J.-S. G., Wang P., and Zayats A.V. "Mode Engineering in Large Arrays of Coupled Plasmonic–Dielectric Nanoantennas", Adv. Opt. Materials, Vol. 9, 2001467, 2021.
6. Ginzburg P., Roth D., Nasir M.E., Segovia Olvera P., Krasavin A.V., Levitt J., Hirvonen L.M., Wells B., Suhling K., Richards D., Podolskiy V.A., and Zayats A.V., "Spontaneous emission in nonlocal materials", Light: Science and Applications, Vol. 6, No. 6, e16273, 2017.

META 2023, PARIS - FRANCE, JULY 18 – 21, 2023

Escaping the flatland: fabrication and application of volume metamaterials

T. Pertsch[1,2,3]

[1]Friedrich Schiller University Jena, Abbe Center of Photonics, Institute of Applied Physics, Albert-Einstein-Straße 15, 07745 Jena, Germany

[2]Fraunhofer Institute for Applied Optics and Precision Engineering, Albert-Einstein-Straße 7, Jena 07745, Germany

[3]Max Planck School of Photonics, Hans Knöll Straße 1, 07745 Jena, Germany

thomas.pertsch@uni-jena.de

Abstract: While it appeared that metasurfaces offer almost unlimited functionality, volume metamaterials may provide advantages in specific applications. In this presentation I will give an overview on the limits and perspectives of the research field of volume metamaterials, which governed the meta-research in its beginning, but later was outperformed by the advances in metasurfaces. However, new nanotechnologies bring the dream of a real meta-volume in reach.

Refractive and also diffractive optical systems are designed mostly based on classical bulk optical materials. However, the dispersion properties of these materials usually restrict the optical system design quite severely. Materials being constructed from nanosized building blocks supporting resonances in the targeted wavelength range, therefore offer a viable perspective to extend the degrees of freedom in optical system design processes considerable. These so, called metamaterials have long been investigated in their 2D equivalent, the so-called metasurfaces, where just a single layer of resonant nanoscatterers, the so-called metaatoms, controls the transmission and reflection of light. While this proved to be a quite powerful concept, it naturally has its limitations, since it allows to control only the local state of light and diffraction happens in the homogeneous space surrounding the metasurfaces, following the classical rules of diffraction in homogeneous space. Extending the metasurfaces to 3D volumes or metamaterial, would offer the perspective of controlling the diffraction itself and was therefore heavily investigated for many years. However, technological limitations rendered this field quite unpractical.

Metamaterials from densely packed scatterers could be realized by top-down or bottom-up techniques. However, while top-down techniques offer unprecedented control over the achievable geometries of metaatoms, they suffer from being limited to planar and periodic structures. In contrast, materials made with bottom-up techniques do not have such disadvantages, but unfortunately, they offer little control over the geometries that can be achieved for the metaatoms. Recently, we have introduced a nanofabrication strategy that combines these both approaches and therefore brings volume metamaterials into reach. In our approach a large number of metaatoms is fabricated by a standard lithography method on the surface of a planar substrate. By detaching the metaatoms from the substrate and reassembling them into a volume form, a bulk metamaterial containing densely packed and randomly arranged metaatoms is obtained. The fabrication of an isotropic metamaterial from these scatterers with a strong electrical and magnetic response is therefore feasible and opens up new possibilities for the production of artificial materials with tailorable optical properties in bulk form, but more importantly also on arbitrarily shaped surfaces.

When such composite nanomaterials should be introduced into the design processes for optical systems, their specific material properties, which renders them differently from classical bulk materials, must be considered.

Most prominently, these materials might suffer from considerable scattering. Hence, we have investigated this aspect and showed, that despite the presence of scattering, thin elements, like diffractive optical lenses can be constructed from such materials and might offer application advantages, like full chromatic correction.

References

1. D. Werdehausen, S. Burger, I. Staude, T. Pertsch, and M. Decker, "Dispersion-engineered nanocomposites enable achromatic diffractive optical elements," Optica 6, 1031-1038 (2019).
2. D. Werdehausen, I. Staude, S. Burger, J. Petschulat, T. Scharf, T. Pertsch, and M. Decker, "Design rules for customizable optical materials based on nanocomposites," Opt. Mater. Express 8, 3456-3469 (2018).
3. K. Dietrich, M. Zilk, M. Steglich, T. Siefke, U. Hübner, T. Pertsch, C. Rockstuhl, A. Tünnermann, and E. ‐ B. Kley, "Merging top ‐ down and bottom ‐ up approaches to fabricate artificial photonic nanomaterials with a deterministic electric and magnetic response," Adv. Funct. Mater. 30, 1905722 (2020).
4. D. Werdehausen, S. Burger, I. Staude, T. Pertsch, and M. Decker, "Flat optics in high numerical aperture broadband imaging systems," Journal of Optics 22, 065607 (2020).
5. D. Werdehausen, X. G. Santiago, S. Burger, I. Staude, T. Pertsch, C. Rockstuhl, and M. Decker, "Modelling optical materials at the single scatterer level - The transition from homogeneous to heterogeneous materials," Advanced Theory and Simulations 3, 2000192 (2020).
6. D. Werdehausen, S. Burger, I. Staude, T. Pertsch, and M. Decker, "General design formalism for highly efficient flat optics for broadband applications," Opt. Express 28, 6452-6468 (2020).

Novel surface interactions of 2D TMDs with different bacteria and virus models

Manjot Singh

University of Naples, Federico II, Italy
*corresponding author: manjot.singh@unina.it

Abstract: graphene) have attracted increasing interest and attention from the various scientific fields such as catalysis, energy storage, sensors, coatings and biomedicine, due to their unique physicochemical properties. Particularly, in biomedical applications, the high-aspect ratio sheet-like structures such as transition metal dichalcogenides (2D TMDs) have been widely studied to understand the biological and environmental interactions of these novel nanomaterials on account of their biocompatibility, stability and multifunctionality. To fulfil this aim, green fabrication routes, now-a-days have become a mainstream approach from the sustainable research point of view worldwide. In view of this, we extensively studied the surface interactions of pure water based exfoliated 2D MoS2 (belonging to the family of 2D TMDs) and graphene oxide nanosheets with a gram-negative bacterium, Escherichia coli, and a gram-positive bacterium, Staphylococcus aureus. Both the materials were also utilized to study their antiviral action towards the Herpes simplex virus type-1 (HSV-1). The obtained results showed different bactericidal impacts as well as very novel and surprising antiviral action of one nanomaterial over the other. Experimental results were also interpreted by using a simple kinetic model based on the Derjaguin-Landau-Verwey-Overbeek theory. On the other hand, among various theranostic platforms, magnetic resonance imaging (MRI)-based nanoprobes (contrast agents CA) have attracted increasing attention, with high selectivity using CAs, amplifying the T1 or T2 signal from the imaging. To this aim, we conjugated manganese oxide nanosheets with water-based iron oxide nanoparticles, based on an eco-friendly fabrication technique, to study their relaxivity properties in phantom applications.

META 2023, PARIS - FRANCE, JULY 18 – 21, 2023

Tailoring Surface Reflectance Using Self-Assembled Block Copolymer Nanopatterns

G.S. Doerk[1*] and C.T. Black[1]

[1]Center for Functional Nanomaterials, Brookhaven National Laboratory, U.S.A.
[*]corresponding author: gdoerk@bnl.gov

Abstract: This talk will discuss how thin film block copolymer self-assembly provides an alternative to nanolithography for engineering surface reflectance of visible light. Using existing nanofabrication infrastructure, we demonstrate near-ideal, omnidirectional, broadband antireflection in nanotextured silicon and glass. Furthermore, we use polymer blends that assemble with periodicities exceeding 200 nm to create resonant, reflective structural color. Using ultraviolet crosslinking-modified thermal reflow to locally tune pattern feature sizes, we fabricate hierarchical patterns for self-assembled metasurfaces with customizable reflectance.

By leveraging the existing infrastructure for nanofabrication, the use of metasurfaces comprising nanopattern arrays presents a potent method for engineering reflectance of visible light with a straightforward path to device integration. However, employing traditional nanolithography methods (e.g., electron beam lithography) precludes their use for applications requiring large areas, high-throughput, and low cost. Thin film block copolymer (BCP) self-assembly offers a promising alternative approach to create subwavelength, periodic nanopatterns that is compatible with common nanofabrication techniques [1]. In this talk, we summarize demonstrations by our group using BCP nanopatterning to tailor surface reflectivity.

In the first example, we show how combining hexagonal BCP nanopatterns with selective inorganic infiltration [2] and reactive ion etching can be used to fabricate wafer-scale arrays of conical nanotextures (~50 nm pitch). By acting as an effective medium with an ideal gradient refractive index, these nanotextured surfaces reduce reflectance to < 1% across the entire visible spectrum, which persists to incidence angles > 50°. This broadband, omnidirectional antireflection improves silicon photovoltaic efficiency [3] and renders glass "invisible" [4].

Second, we show how blending ultrahigh molecular weight block copolymers with very short homopolymer plasticizers can overcome sluggish ordering kinetics to assemble patterns with periodicities exceeding 200 nm [5]. Transferring these patterns into silicon yields reflective structural color based on electromagnetic resonances in the individual features (i.e., electric dipole, magnetic dipole, cavity). Furthermore, thermal reflow modulated through ultraviolet crosslinking can be used to locally tune feature sizes within large-area nanopatterns, generating hierarchical nanopatterns with customizable visible light reflection, exemplified in patternable structural color [6].

This research used the Materials Synthesis and Characterization Facility and the Nanofabrication Facility at the Center for Functional Nanomaterials (CFN), and the Soft Matter Interfaces (SMI) beamline at the National Synchrotron Light Source II (NSLS-II), which are U.S. Department of Energy Office of Science User Facilities at Brookhaven National Laboratory under contract no. DE-SC0012704. G.D. acknowledges support from the Department of Energy Early Career Research Program.

References

[1] A. A. Kulkarni and G. Doerk, *Thin Film Block Copolymer Self-Assembly for Nanophotonics*, Nanotechnology **33**, 292001 (2022).

[2] A. Subramanian, G. Doerk, K. Kisslinger, D. H. Yi, R. B. Grubbs, and C.-Y. Nam, *Three-Dimensional Electroactive ZnO Nanomesh Directly Derived from Hierarchically Self-Assembled Block Copolymer Thin Films*, Nanoscale **11**, 9533 (2019).

[3] A. Rahman, A. Ashraf, H. Xin, X. Tong, P. Sutter, M. D. Eisaman, and C. T. Black, *Sub-50-Nm Self-Assembled Nanotextures for Enhanced Broadband Antireflection in Silicon Solar Cells.*, Nature Communications **6**, 5963 (2015).

[4] A. C. Liapis, A. Rahman, and C. T. Black, *Self-Assembled Nanotextures Impart Broadband Transparency to Glass Windows and Solar Cell Encapsulants*, Applied Physics Letters **111**, 183901 (2017).

[5] G. S. Doerk, R. Li, M. Fukuto, and K. G. Yager, *Wet Brush Homopolymers as "Smart Solvents" for Rapid, Large Period Block Copolymer Thin Film Self-Assembly*, Macromolecules **53**, 1098 (2020).

[6] A. A. Kulkarni and G. S. Doerk, *Hierarchical, Self-Assembled Metasurfaces via Exposure-Controlled Reflow of Block Copolymer-Derived Nanopatterns*, ACS Appl. Mater. Interfaces **14**, 27466 (2022).

META 2023, PARIS - FRANCE, JULY 18 – 21, 2023

Self-assembled hexagonal array or correlated disorder plasmonic metasurfaces: optical properties comparison

Gil Cardoso[1], Frédéric Hamouda[1], Vy Yam[1], Béatrice Dagens[1,*]

[1] Université Paris-Saclay, CNRS, Centre de Nanosciences et de Nanotechnologies, 91120, Palaiseau, France

[*]corresponding author: beatrice.dagens@c2n.upsaclay.fr

Abstract: plasmonic metasurfaces have been fabricated following two different approaches in order to deliver large area devices for augmented reality systems. Their optical properties are compared at different levels: the contribution of the plasmonic nanostructures arrangement is evaluated thanks to the metasurfaces structure factors, the physical properties are assessed through optical transmission and reflection measurements, and finally the whole metasurfaces are macroscopically tested in a head-up display.

Metasurfaces based on plasmonic nanoparticles (NP) on glass substrates are of great interest for transparent displays [1] or for augmented reality (AR) applications [2]: they functionalize transparent plates to have high reflectivity at specific wavelengths (blue, green, red) by choosing the size and shape of the NPs, while preserving good transparency over the whole visible range (i.e. without scattering or diffraction effects) through an appropriate spatial arrangement of NPs [2]. However, the design of these metasurfaces must also be compatible with the fabrication of large surfaces. Self-assembly of nanoobjects is an efficient bottom-up approach to create nanostructured metasurface on large areas. Nevertheless, despite high deposition quality, arrangement defaults appear which can have a significant impact on the global optical properties of the metasurface. In order to develop transparent semi-reflective plates for AR systems, we compare here large-area metasurfaces with self-assembled patterns with those with correlated disorder patterns well controlled by electron lithography: we consider and discuss as well NPs spatial arrangement impact as plasmonic resonance effects on their global optical properties. We also propose and evaluate a combination of bottom-up and top-down approaches to better control final optical properties.

Fabrication: targeted plasmonic nanostructures constituting the metasurface are nanorods made of silver with typical dimensions of 100 to 200 nm diameter and 30 nm thickness, for operation in the visible range. We consider two samples fabricated with different approaches. The first sample, used as a reference, is made of high-quality correlated disorder nanostructuration obtained on 1 cm² thanks to electron beam lithography followed by a lift-off of silver [2]. The second sample is realized using soft UV nanoimprint lithography (soft UV-NIL), with an original process to fabricate the nanostructured PDMS (polydimethylsiloxane) stamp: in order to circumvent limitations observed with usual PDMS molding [3], we have developed a new approach which enables at the same time large area pattern definition by 200nm diameter polystyrene nanospheres (PS-NS) self-assembly, and PDMS stamp nanostructuration by RIE etching [4], as schematized in Figure 1. Thanks to arrangement breakings, the whole hexagonal compact arrangement appears as globally isotropic.

Optical transmission and reflection are performed on the both metasurfaces by using an ellipsometric setup, in order to determine their spectral filtering capabilities. Figure 2 shows that the enhanced reflection wavelength of the P polarization is near 640 nm for the ‘e-beam sample’, and near 720 nm for the ‘self-assembly sample’, when the incident angle is around 45°. Additionally the spectra of the latter are significantly broaden and attenuated, revealing the size dispersion of the plasmonic NPs.

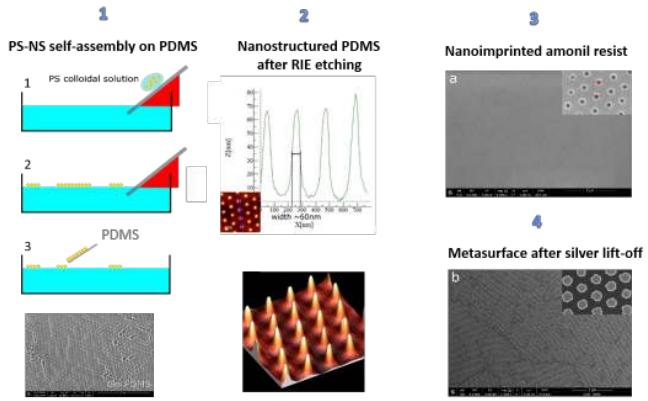


Fig. 1. Self-assembly based metasurface fabrication: (1) PDMS stamp fabricated by self-assembly and (2) RIE etching; (3) Nanoimprint process and (4) silver lift-off to generate the final metasurface.

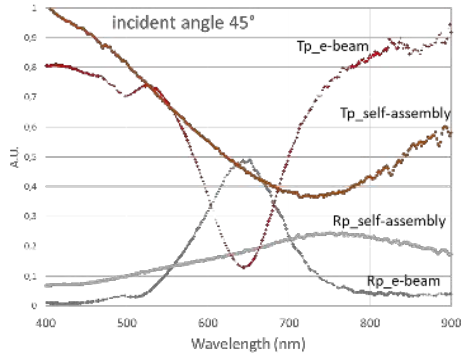


Fig. 2. Optical transmission and reflection spectra for polarization p measured on the both metasurfaces with an incident angle of 45°.

Structure factor: functionalized plate transparency quality can be numerically evaluated by the structure factor of the metasurfaces. The structure factor S(q) represents the optical response of the structure as a function of spatial frequencies q, without the influence of NPs resonance. In order to minimize diffraction and diffusion effects induced by spatial arrangement, the value of S(q) must be zero in the q range corresponding to usual observation conditions of the metasurface. In Figure 3 we calculate the structure factors using a computer vision program analyzing SEM images of the fabricated metasurfaces ((a),(b)) and of a numerically modified arrangement based on correlated disorder (c) to reduce NP density. Considering the observation range, the self-assembled metasurface with sub-wavelength period seems to be more robust in terms of transparency quality, and the spatial density reduction can be easily performed by choosing appropriate microstructuration.

These results will be presented in details, as well as the final performance of the both metasurface on a head-up display system.

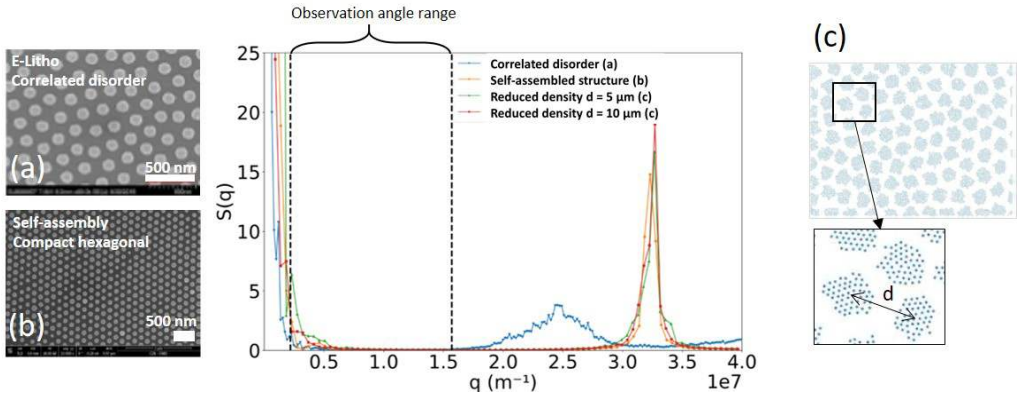


Fig. 3. Factor structure of large area metasurface made of silver nanorods, fabricated (a) by e-beam lithography with correlated disorder arrangement (average distance ~274nm) [2], (b) by self-assembly and nanoimprint (period 200nm) [4], (c) possibly followed by spatial density reduction in a correlated disorder arrangement.

This work was done with the technical support of the French cleanroom network RENATECH.

References

1. Saito, K. & Tatsuma, T., "A transparent projection screen based on plasmonic Ag nanocubes," Nanoscale 7 20365–8, 2015.
2. Bertin, H., *et al*., "Correlated Disordered Plasmonic Nanostructures Arrays for Augmented Reality," ACS Phot. 5, 2661–2668, 2018.
3. Koo, N., et al, "The fabrication of a flexible mold for high resolution soft ultraviolet nanoimprint lithography," Nanotechnology 19 225304, 2008.
4. Cardoso, G., et al, "Improved PDMS mold fabrication by direct etch with nanosphere self-assembly mask for Soft UV-NIL subwavelength metasurfaces fabrication," Microelec. Eng. 258 111755, 2022.

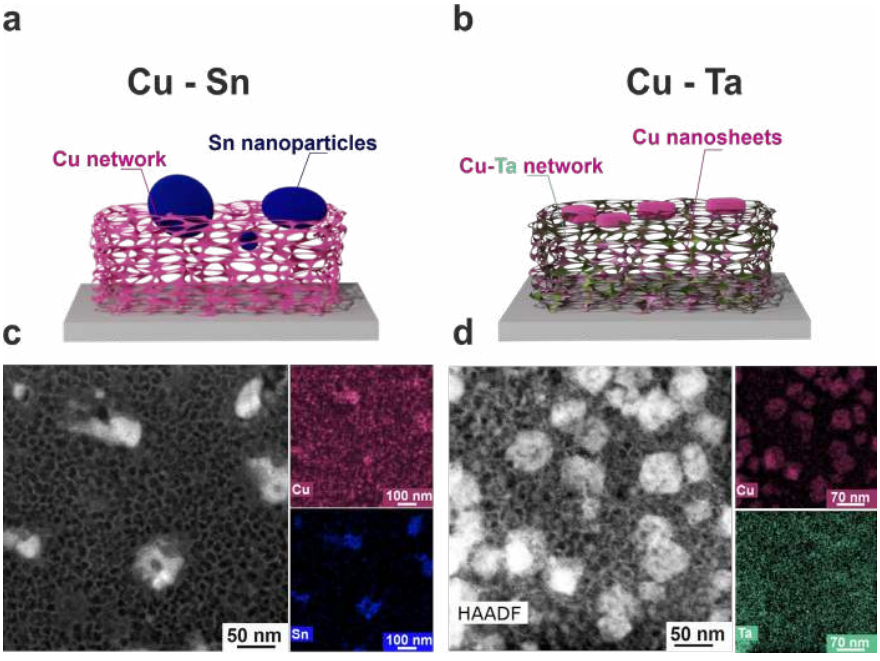
Designing Mode Coupling in Two-Phase Metamaterials made by Sequential Self-Assembly

Jelena Wohlwend[1], Georg Haberfehlner[2], Ralph Spolenak[1] and Henning Galinski[1]

[1]ETH Zürich, Switzerland
[2]TU Graz, Austria
*corresponding author: jelena.wohlwend@mat.ethz.ch

Abstract: Design and fabrication of large-area metamaterials is an on-going challenge. Here, we demonstrate how a sequence of self-assembly processes can be used to design and fabricate large-area two-phase metamaterials. These two-phase metamaterials consist of a disordered nanometric network and nanoparticles or nanosheets, which can be readily designed by chemical engineering. Using energy electron loss spectroscopy, we probe the plasmonic environment and coupling between the two phases, confirming energy exchange with the nanoparticle modes and localized "hot spots" of the network.

Self-assembled metamaterials are scalable and can, due to their often disordered structure, give rise to unique properties unattainably by ordered systems[1]. Despite their enormous potential as a platform for energy materials, disordered metamaterials are often limited to single phase systems, and complex multi-phase metamaterials have scarcely been explored. We propose a novel path to fabricate two-phase disordered network metamaterials: sequential self-assembly (phase separation during deposition followed by chemical dealloying). The resulting metamaterial consist of a disordered network[2] with embedded nanoparticles of different shapes and chemistries, shown in Figure 1.



Figures 1: Two Phase Metamaterials. (a) & (b) Schematic illustration of Cu-Sn and Cu-Ta two phase metamaterials, (c) & (d) HAADF micrographs and elemental distribution maps showing a Cu based disordered network with randomly distributed Sn NPs and a Cu-Ta based disordered network with randomly distributed Cu nanosheets respectively.

Interestingly, the different two-phase metamaterials, shown in Figure 1 a and b, can be achieved by a simple change in initial chemistry during deposition. To map the plasmonic environment of these two-phase metamaterials we take advantage of the high-spatial and high-energy resolution of electron energy loss spectroscopy (EELS). Inhomogeneous localization of light in the network is observed, concurrent with dipolar and higher-order localized surface plasmon modes in the nanoparticles. Thereby, we show that through chemical engineering during the sequential self-assembly, we are able to engineer the interaction, i. e. mode coupling between the disordered network and the nanoparticle. Since the chemistry in these metamaterials can be readily controlled, our approach can serve as a versatile platform to design materials for plasmonic catalysis and energy conversion.

Acknowledgements

This project has been funded in part by the European Union's Horizon 2020 research and innovation programme under grant agreement No 823717 – ESTEEM3.

References

1. Mao, P., Liu, C., Song, F. *et al.* Manipulating disordered plasmonic systems by external cavity with transition from broadband absorption to reconfigurable reflection. *Nat Commun* **11**, 1538 (2020).
2. Wohlwend, J., Sologubenko, A. S., Döbeli, M. , Galinski, H. and Spolenak R. "Chemical Engineering of Disordered Network Metamaterials" Nano Letters 2022 22 (2), 853-859

META 2023, PARIS - FRANCE, JULY 18 – 21, 2023

Direct Fabrication of Plasmonic Nanoantennas onto Tapered Optical Nanofibers with Electron Beam Induced Deposition for Enhanced Single Photon Emission

A. Balena[1,2,*], C. Ding[2], M. D'Amato[2], M.F. Kashif[1], F. Pisano[1], M. Pisanello[3], G. De Marzo[1], M. De Vittorio[1,4,#], A. Bramati[2,#] and F. Pisanello[1,#].

[1]Istituto Italiano di Tecnologia - Center for Biomolecular Nanotechnologies, Italy
[2]Laboratoire Kastler Brossel, Sorbonne Université, CNRS, ENS-PSL Research University, Collège de France, France
[3]Optogenix s.r.l., Italy
[4]Università del Salento – Dipartimento di Ingegneria dell'Innovazione, Italy
[#]These authors jointly supervised the work
[*]Corresponding author: antonio.balena@iit.it

Abstract: In this work, we introduce a bottom-up fabrication approach based on Electron Beam Induced Deposition to directly fabricate plasmonic nanoantennas onto the surface of tapered optical nanofibers. The structures are optically characterized by measuring the scattering from a propagating Near Infrared laser beam and a supercontinuum beam. The results, along with numerical predictions, suggest that the fabricated structures can enhance the single photon emission properties of room temperature solid-state emitters.

Quantum emitters are of great interest for various applications in quantum photonics, sensing, and information processing, as they can produce on-demand single photons with high purity and brightness and sub-nanosecond lifetimes. Different material systems have been examined as potential options for single photon sources (SPS)[1-3], including single atoms, ions, and solid-state emitters such as organic molecules, color centers in diamonds, and quantum dots. Colloidal solid-state emitters, which have simple fabrication and can operate at room temperature, have a lifetime of the order of tens of nanoseconds and face challenges in efficiently extracting their photon emissions, which hinder their practical application. Therefore, integrating SPS into photonic circuits requires specific experimental arrangements, and optical nanofibers (ONFs)[4], which have a subwavelength diameter and strong evanescent field, offer a promising input/output platform.

To further improve the performance of quantum emitters and the efficiency of single photon collection, coupling with plasmonic nanostructures has been proposed[5]. Indeed, integrating SPS with plasmonic resonances in metallic low Q cavities provides a strong enhancement of the radiative rate of the emitter while acting as a redirecting element for the radiative pattern. However, deterministic methods to fabricate single nanostructures or complex geometries directly on the ONF are not currently available, nor have been proposed. The techniques employed to realize an integrated SPS/ONF plasmonic system are based on separate or simultaneous drop-casting of the plasmonic particle and emitter, introducing a high degree of uncertainty in the positioning and orientation of the nanostructures on the ONF, as well as the reciprocal positioning with respect to the SPS. As a result, these methods fail to ensure the best coupling between the resonator and the ONF.

Here we introduce a *bottom-up* Electron Beam Induced Deposition (EBID) fabrication approach to directly pattern plasmonic nanoantennas onto ONFs, enabling sub-10 nm control over the position and the geometry of the realized structures. A specific aspect of the fabrication process is the exploitation of deliberate beam defocusing, obtained by controlled blurring of the beam during the exposure: this is needed to reduce the electron flux over the exposed area, thus reducing the mechanical pressure exerted by the beam onto the ONF, that otherwise would prevent the correct result of the nanopatterning. In general, blurring of the beam is considered a detrimental condition for nanofabrication, but instead in this work this strategy has been used to

enable the patterning on these specific substrates, that are suspended, dielectric, and nanometric samples, while maintaining practically unaltered the composition of the nanostructure.

To optically characterize the properties of the interaction between the evanescent field guided by the ONF and a single nanopillar or two nanopillars separated by a nanogap (nanoantenna, ***Figure 1.a***), we measured the degree of polarization scattered light from a Near Infrared 785 nm laser beam. Two experimental configurations were investigated to measure how the intensity of the scattered light depends on the input polarization (***Figure 1.b***) and how, by fixing the input polarization of the beam, the light scattered from the structures is polarized. Moreover, we measured the spectral differences in the scattering of a supercontinuum laser from the two geometries, highlighting a red shift of the scattered signal for the nanoantenna configuration. The experimental results were confirmed by Finite Differences Time Domain (FTDT) numerical simulations, which also showed the redirecting effect on the radiative field, which is routed towards the collection channel represented by the ONF. These results showed how our approach presents a promising alternative to top-down fabrication methods for plasmonic nanostructures, such as quantum dot SPS coupled with drop-casted gold nanorods on a ONF system. Overall, this work represents a promising way to enhance light-matter interactions and improve the performances of quantum emitters, while promoting a more efficient collection channel via the ONF.

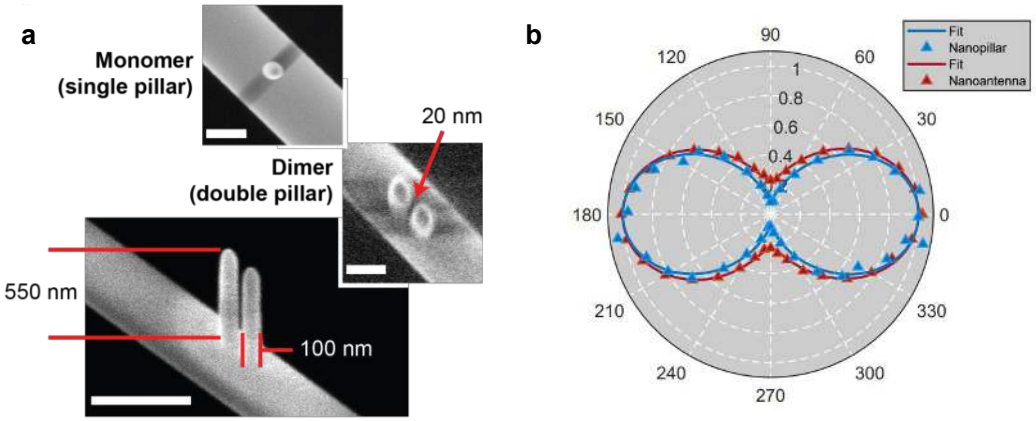


Figure 1.a) *Examples of nanostructures fabricated on a ONF using the proposed approach. The scale bar for the tilt-view SEM image is 500 nm, while for the top-view SEM image is 200 nm.* ***b)*** *Dependence of the scattered signal intensity from the EBID Nanostructures on the polarization orientation at the ONF entrance.*

References

1. Chatterjee A., Stevenson P., De Franceschi S., Morello A., de Leon N. and Kuemmeth F. "Semiconductor Qubits In Practice," Nat. Rev. Phys., Vol. 3, 157-177, 2021.
2. Kjaergaard M., Schwartz M. E., Braumüller J., Krantz P., Wang J. I.-J. and Gustavsson S., Oliver W. D, "Superconducting Qubits: Current State of Play," Annu. Rev. Condens. Matter Phys, Vol. 11, 369–95, 2020.
3. H. J. Kimble, "The quantum internet," Nature Vol. 453, 1023–1030, 2008.
4. Pierini S., D'Amato M., Goyal M., Glorieux Q., Giacobino E., Lhuillier E., Couteau C. and Bramati A., "Highly photo-stable Perovskite nanocubes: towards integrated single photon sources based on tapered nanofibers," ACS photonics, Vol. 7, No. 8, 2265–2272, 2020.
5. Hugall J.T., Singh A. and van Hulst N.F., "Plasmonic Cavity Coupling," ACS Photonics, Vol. 5, No. 1, 43–53, 2018.

META 2023, PARIS - FRANCE, JULY 18 – 21, 2023

3D Topological Insulators and Eutectics at a crossroad

K. Bandopadhyay[1*], A. Materna[1], K. Markus[1], M. Buza[2], C. Chen[3], P. Piotrowski[4], A. Barinov[5], F. Murakamia[6], M. Tonouchi[6], Y. Chen[3], D. A. Pawlak[1, 2, 4]

[1] ENSEMBLE[3] Centre of Excellence, Wolczynska 133, 01-919 Warsaw, Poland
[2] Łukasiewicz Research Network – Institute of Microelectronics and Photonics, Wolczynska 133, 01-919 Warsaw, Poland
[3] Department of Physics, Clarendon Laboratory, University of Oxford, Oxford OX1 3PU, UK
[4] Chemistry Dept. University of Warsaw, Pasteura 1, 02-093 Warsaw, Poland
[5] Elettra-Sincrotrone Trieste, Trieste, Basovizza 34149, Italy
[6] Institute of Laser Engineering, Osaka University, 2-6 Yamada-oka, Suita, Osaka 565-0871, Japan

[*]corresponding author: kingshuk.bandopadhyay@ensemble3.eu

Abstract: Three-dimensional topological insulators attract a great deal of interest due to their potential use of the topologically protected gapless surface states in topological spintronics and quantum computation [1]. However, challenges such as the high sensitivity of the surface states to the atmosphere, the low surface-to-volume ratio, and the need for various material heterojunctions currently limit the application of these materials [2]. Here, we report the successful fabrication of the topological insulator heterostructures by an easy, fast, and single-step process, which could meet all those challenges and pave the way for exploring other exotic phenomena shortly. Utilizing directional solidification different topological insulator-based eutectic composites were produced, where two crystalline phases are combined in a structured form with joined interfaces. The material exhibits lamellar micro/nanostructures with atomically smooth interfaces. The existence of the metallic surface states and the formation of the *p-n* junction have been confirmed through specific characterization methods.

The authors thank ENSEMBLE[3] Project (MAB/2020/14) which is carried out within the International Research Agendas Programme (IRAP) of the Foundation for Polish Science co-financed by the European Union under the European Regional Development Fund and Teaming Horizon 2020 programme (GA. No. 857543) of the European Commission; the TEAM/2016-3/29 Grant within the TEAM program of the Foundation for Polish Science co-financed by the European Union under the European Regional Development Fund.

References

1. Pesin, D. and A. H. MacDonald, “Spintronics and pseudospintronics in graphene and topological insulators” Nat Mater 11, 409-416 (2012)
2. Kong, D., J. J. Cha, K. Lai, H. Peng, J. G. Analytis, S. Meister, Y. Chen, H.-J. Zhang, I. R. Fisher, Z.-X. Shen and Y. Cui, “Rapid Surface Oxidation as a Source of Surface Degradation Factor for Bi_2Se_3” ACS Nano 5, 4698-4703 (2011)

Dynamic plasmonics based on conducting polymers

S. Chen[1*] and M. P. Jonsson[1]

[1] Laboratory of Organic Electronics, Department of Science and Technology, Linkoping University, Norrkoping SE 602 74, Sweden

[*]corresponding author: shangzhi.chen@liu.se

Abstract: Plasmonics based on conventional metals are broadly used for biosensing and optoelectronic devices, but suffer from limited optical tunability. We recently demonstrated conducting polymers as a new category of plasmonic materials exhibiting excellent optical tunability. In this talk, I will briefly introduce the emergence, current status, and future prospects of using conducting polymers for dynamic plasmonics.

Metal nanostructures are key elements in nano-optics due to their intense resonant interaction with light *via* plasmonic charge oscillation. However, they suffer from limited tunability due to the fixed optical properties of metals. By contrast, conducting polymers, a new category of organic conductors, exhibit excellent tunability and were recently introduced for dynamic plasmonic antennas. We revealed that nanoantennas based on conducting polymers show clear dipolar plasmonic resonance and sustain reversible tuning *via* chemical and electrochemical approaches[1,2]. In this talk, I will present our latest progress of conducting polymer nanoantennas made through colloidal lithography and their applications for dynamic optical systems[3].

Acknowledgements: financial support from Kunt and Alice Wallenberg Foundation, the Swedish Research Council (VR, No. 2020-00287 and 2022-00211), the Swedish Foundation for Strategic Research (SSF), and the Swedish Government Strategic Research Area in Materials Science on Functional Materials at Linkoping University (Faculty Grant SFO-Mat-LiU No. 2009 00971).

References

1. Chen, S., Kang, E. S. H., Shiran Chaharsoughi, M., Stanishev, V., Kuhne, P., Sun, H., Wang, C., Fahlman, M., Fabiano, S., Darakchieva, V., and Jonson, M. P. “Conductive polymer nanoantennas for dynamic organic plasmonics”, *Nat. Nanotechnol.*, Vol. 15, No. 1, 35-40, 2020.
2. Karki, A., Cincotti, G., Chen, S., Stanishev, V., Darakchieva, V., Wang, C., Fahlman, M., and Jonsson, M. P., “Electrical tuning of plasmonic conducting polymer nanoantennas”, *Adv. Mater.*, Vol. 34, No. 13, 2107272, 2022.
3. Chen, S. and Jonsson, M. P., “Dynamic conducting polymer plasmonics and metasurfaces”, *ACS Photonics*, accepted.

META 2023, PARIS - FRANCE, JULY 18 – 21, 2023

Bottom-up fabrication of 2D MoS_2: from thermochromic sensing to hyperbolic metamaterials.

Jose L. Ocana-Pujol[1*], Ramon Camilo Dominguez Ordonez[1], Christof Vockenhuber[2], Ralph Spolenak[1] and Henning Galinski[1*]

[1]Laboratory for Nanometallurgy, ETH Zurich, Switzerland
[2]Laboratory of Ion Physics, ETH Zurich, Switzerland
[*]corresponding author: joseo@ethz.ch

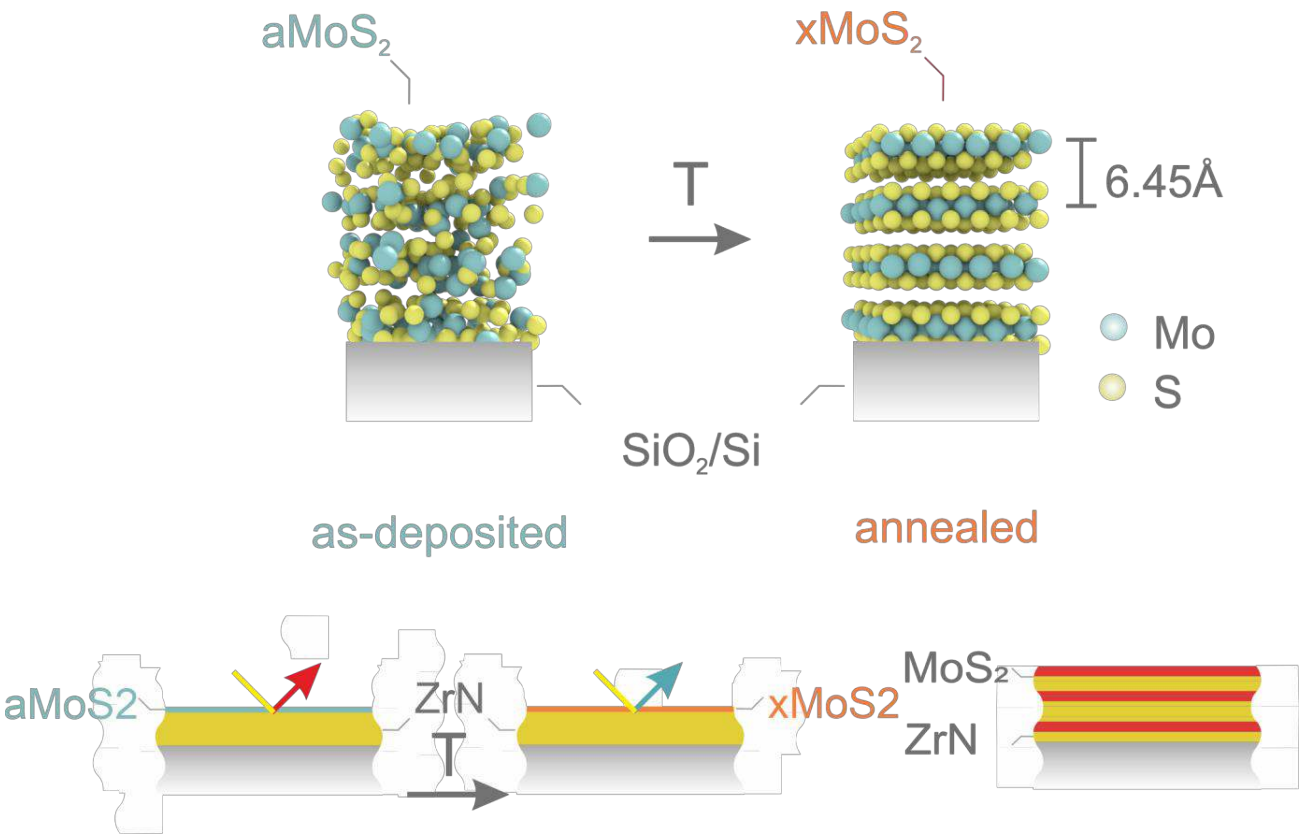
Abstract: MoS_2 has been extensively researched ever since the discovery of its thickness-tunable properties. However, its applicability is still limited by fabrication constraints and its integration with other materials. We present a bottom-up fabrication route enabling large-area synthesis of bulk and 2D MoS_2. We demonstrate how a thermochromic sensor can be used to track the thickness and the mechanical, electrical and optical properties. To showcase the precise control on the fabrication conditions, we fabricate a large-area hyperbolic metamaterial containing 2D- MoS_2.

From computers to energy harvesting, the utilization of semiconductor materials and the management of their electrical and optical properties have played a critical role in the advancement of society during the past century. Silicon, in particular, has been the backbone of semiconductor technology, and our enhanced capacity to process it has led to the ongoing reduction of device feature sizes, resulting in devices with ever-increasing capabilities and speeds. However, the push for even smaller devices has hit some major obstacles as silicon technology reaches its fundamental physical limits.

In this context, MoS_2, a semiconductor transition metal dichalcogenide, has emerged as a potential next-generation semiconductor. Unlike other 2D materials, MoS_2 is a natural material formed by earth-abundant elements and is currently used in industry due to its mechanical properties, which originate in its crystal structure, in which layers are held together by weak van der Waals forces. This weak interlayer bonding allows for thickness-tunable electrical and optical properties, making MoS_2 a promising candidate for replacing silicon in the development of future semiconductor devices. Proposed applications of MoS_2 include transistors, light-emitting diodes, and catalysis [1].

However, applications of MoS_2 have been hindered by the difficulty of processing MoS_2 into high-quality thin films and device structures. Exfoliation and chemical vapor deposition, the two most prevalent processes used to generate MoS_2 films, generally result in non-uniform coverage and can only produce crystalline MoS_2. The ability to control the synthesis of large-scale MoS_2 is therefore crucial to become a widely adopted standard semiconductor material, as is the ability to combine MoS_2 with different materials to create new device architectures [2].

Here, we present a two-step fabrication method for MoS_2 thin films. By using magnetron sputtering, it is possible to produce the material on an industrial scale, deposit it over a great variety of substrates, and study both the amorphous and crystalline forms of the material. We investigate the structural and functional properties of magnetron sputtered MoS_2 using a combination of optical and electrical characterization with scanning and electron microscopy, nanoindentation, X-ray diffraction, and Rutherford back scattering.



We demonstrate that continuous amorphous MoS_2 with thicknesses as low as 1 nm can be deposited and then crystallized by thermal annealing into horizontally layered MoS_2 with optical properties comparable to those found in the literature.We exploit the change in the optical properties of MoS_2 upon crystallization to build a thermochromic sensing platform. The presence of a metallic reflector underneath the semiconductor enables the detection of small changes in the optical properties down to the order of 1% using strong interference [3]. Here, we use zirconium nitride as an inert metallic reflector that does not react with MoS_2 at annealing temperatures < 485°C. We further use this material combination to realize a multilayered hyperbolic metamaterial. Control over the ratio between the two constituents and their thickness is demonstrated by comparing the experimental results with simulations. Our results showcase how this 2-step bottom-up fabrication route opens the door to wafer-scale photonic applications incorporating 2D MoS_2.

References

1. Ganatra, R.; Zhang, Q. Few-Layer MoS2: A Promising Layered Semiconductor. ACS Nano **2014**, 8 (5), 4074–4099. https://doi.org/10.1021/nn405938z.
2. Krbal, M.; Prokop, V.; Kononov, A. A.; Pereira, J. R.; Mistrik, J.; Kolobov, A. V.; Fons, P. J.; Saito, Y.; Hatayama, S.; Shuang, Y.; Sutou, Y.; Rozhkov, S. A.; Stellhorn, J. R.; Hayakawa, S.; Pis, I.; Bondino, F. Amorphous-to-Crystal Transition in Quasi-Two-Dimensional MoS2: Implications for 2D Electronic Devices. *ACS Appl. Nano Mater.* **2021**, *4* (9), 8834–8844. https://doi.org/10.1021/acsanm.1c01504.
3. Galinski, H.; Leutenegger, D.; Amberg, M.; Krogh, F.; Schnabel, V.; Heuberger, M.; Spolenak, R.; Hegemann, D. Functional Coatings on High-Performance Polymer Fibers for Smart Sensing. *Advanced Functional Materials* **2020**, *30* (14), 1910555. https://doi.org/10.1002/adfm.201910555.

META 2023, PARIS - FRANCE, JULY 18 – 21, 2023

Plasmonic Metasurfaces of Self-assembled Gold Nanoparticle Superlattices with Tunable Sub-nanometer Gaps

Bin Lu[1*], Karol Vegso[2], Simon Mičky[2], Christian Ritz[1], Michal Bodik[1], Yuriy Fedoryshyn[3], Peter Siffalovic[2], Andreas Stemmer[1]

[1] Nanotechnology Group, ETH Zürich, Säumerstasse 4, CH-8803 Rüschlikon, Switzerland.

[2] Institute of Physics SAS, Dubravska cesta 9, 84511 Bratislava, Slovakia.

[3] Institute of Electromagnetic Fields, ETH Zürich, Gloriastrasse 35, CH-8092 Zürich, Switzerland.
[*]corresponding author: lubinlu@ethz.ch

Abstract: We developed centimeter scale metasurfaces of self-assembled monolayer gold nanoparticle (GNP) superlattices. Through ligand exchange, the interparticle gap distance was actively tuned from 2.4 to 0 nm. The *in-situ* reflectance spectra of the GNP metasurfaces showed a monotonously red-shifted bonding dipolar plasmon (BDP) mode of enhanced intensity upon diminishing interparticle gaps until 0.2 nm. The deposited GNP metasurfaces on SiO_2/Si wafer showed tunable effective refractive index, where the maximal real part exceeded 5.

Plasmonic capacitive coupling in nanogaps promotes light-matter interaction via strong electromagnetic field confinement and enhancement. However, it has been shown that quantum effects, e.g., nonlocal screening and electron tunneling, can limit the maximal achievable local field enhancement [1]. Previous studies on various binary plasmonic systems showed a threshold of 0.5-1.1 nm gap distance as onset of a weakening BDP mode [1-3], whereas investigation into the plasmonic metasurfaces remains scarce. Recent theoretical simulation suggested a substantially reduced threshold of quantum limit in the plasmonic metasurface compared to the binary systems [4]. Experimental demonstration of plasmonic metasurfaces with tunable periodic sub-nanometer gaps remains yet an untackled task.

Here, we obtained large scale (cm^2) hexagonal close-packed GNP monolayers via interfacial self-assembling method, reaching micrometer scale single domain size. In combination with a free-floating ligand exchange process, the interparticle gap distances of GNP superlattices can be precisely controlled from 2.4 to 0 nm. When substituting the native oleylamine (OAm) ligands by ethanedithiols (C2DTs), the gap distance reduced from 1.4 to 0.2 nm. The *in-situ* reflectance spectra of the GNP metasurface acquired during ligand exchange (Figure 1a) shows a monotonously red-shifted BDP mode, with increasing peak intensity and width, upon diminishing interparticle gaps. We determined the effective refractive index of deposited GNP metasurfaces on SiO_2/Si wafer from ellipsometry measurements. The effective refractive index can be actively tuned depending on the gap distance and constituent, where maximum of the real part can exceed 5 at 0.2 nm gap distance, as shown in Figure 1b. The results of reflectance and ellipsometry measurements indicate a continuously enhanced plasmonic capacitive coupling in GNP metasurfaces of hexagonally periodic nanogaps down to 0.2 nm gap distance, allowing extreme field confinement and enhancement.

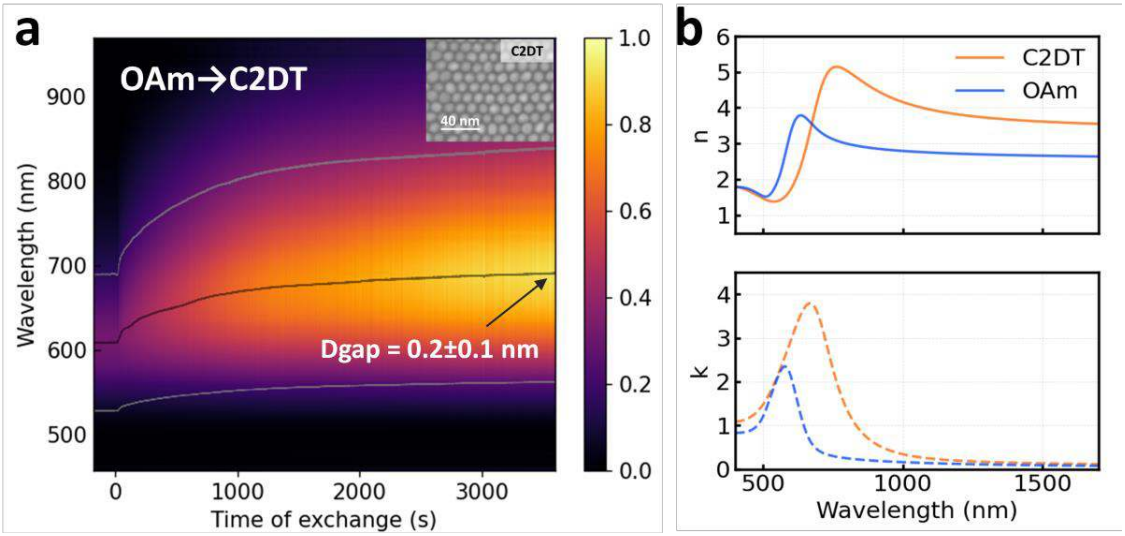


Figure 1. (a) Reflectance spectra measured *in-situ* on a GNP metasurface during ligand exchange with C2DT, launched ~0 s (insert, a high resolution SEM image of the GNP metasurface after ligand exchange). (b) The effective real, n, and imaginary, k, refractive index of the GNP metasurface with OAm and C2DT capping, respectively.

References

1. Zhu, W., Esteban, R., Borisov, A.G., Baumberg, J.J., Nordlander, P., Lezec, H.J., Aizpurua, J. and Crozier, K.B., "Quantum mechanical effects in plasmonic structures with subnanometre gaps." *Nat. Commun.*, Vol. 7, No. 1, 1-14, 2016.
2. Jung, H., Cha, H., Lee, D. and Yoon, S., "Bridging the nanogap with light: continuous tuning of plasmon coupling between gold nanoparticles." *ACS Nano*, Vol. 9, No. 12, 12292-12300, 2015.
3. Zhang, C., Li, D., Zhang, G., Wang, X., Mao, L., Gan, Q., Ding, T. and Xu, H., "Switching plasmonic nanogaps between classical and quantum regimes with supramolecular interactions." *Sci. Adv.*, Vol. 8, No. 5, eabj9752, 2022.
4. Takeuchi, T., Noda, M. and Yabana, K., "Operation of quantum plasmonic metasurfaces using electron transport through subnanometer gaps." *ACS Photonics*, Vol. 6, No. 10, 2517-2522, 2019.

Light-matter interaction on a chip

META 2023, PARIS - FRANCE, JULY 18 – 21, 2023

Efficient grating coupling strategies for silicon photonics

P. Petropoulos[1*], V. Vitali[1, 2], T. Domínguez Bucio[1], F.Y. Gardes[1], and C. Lacava[2]

[1]Optoelectronics Research Centre, University of Southampton, Southampton SO17 1BJ, United Kingdom
[2]Electrical, Computer and Biomedical Engineering Department, University of Pavia, Pavia 27100, Italy
[*]corresponding author: pp@orc.soton.ac.uk

Abstract: We discuss techniques for optimizing the coupling efficiency between optical fibers and silicon photonic waveguides through the use of back-end-of-line CMOS-compatible grating couplers.

Silicon photonics has enjoyed tremendous progress in recent years, offering exciting opportunities for miniaturizing the footprint of optical components and enabling the implementation of complete systems on chip. Its adoption has already transformed communications, sensing, nonlinear optics, as well as quantum technologies. A prevalent challenge however, remains the efficient coupling between optical fibers and silicon photonic waveguides. Among the two options available, edge coupling is admittedly the most efficient, especially when combined with suitable taper designs, which may vary in degree of sophistication. Edge coupling however, requires precise alignment, which might be an impediment when the manufacturability of a large number of devices is considered. Conversely, grating couplers that direct light off-plane offer an attractive alternative and performance that is acceptable for most applications.

A challenge associated with achieving a high coupling efficiency in grating coupler designs, relates to controlling the directionality of the gratings. To address this, several works have embedded metallic mirrors or distributed Bragg reflectors in the substrate of the wafer. By reflecting stray waves that would otherwise travel towards the bottom of the substrate and redirecting them towards the surface of the chip, these reflectors facilitate their recapture. Even though an effective solution, the implementation of back-reflectors may require the adoption of non-CMOS compatible materials in the fabrication, which can be prohibitive in certain environments. The work we discuss in this presentation, aims at maximizing the coupling efficiency of grating couplers by combining strategies that aim at: optimizing the apodization of gratings, so that the mode of the diffracted beam closely resembles that of the optical fiber [1]; adopting a dual-level grating design, which breaks the symmetry of the structure and contributes towards increasing its directionality [2]; and finally, combining two different materials to the same effect [3]. We will present the predicted performance of such designs, as well as experimental results that represent the state-of-the-art for gratings without the use of any back-reflectors. A -0.8-dB coupling efficiency for a grating written in the 220-nm silicon photonic platform is reported.

This research was funded by the UK's EPSRC through grant EP/T007303/1 "Silicon-rich silicon nitride Nonlinear Integrated Photonic ciRcuits & Systems (juNIPeRS)".

References

1. R. Marchetti et al., "High-efficiency grating-couplers: demonstration of a new design strategy," Scientific Reports, vol. 7, no. 1, p. 16670, 2017.
2. V. Vitali, T. Domínguez Bucio, C. Lacava, R. Marchetti, L. Mastronardi, T. Rutirawut, G. Churchill, J. Faneca, J.C.

Gates, F.Y. Gardes, and P. Petropoulos, “Dual-Level Silicon Grating Coupler with a Record -0.8 dB Coupling Efficiency”, presented in CLEO’2023, paper SM2G.8.

3. V. Vitali, C. Lacava, T. Domínguez Bucio, F. Y. Gardes, and P. Petropoulos, "Highly efficient dual-level grating couplers for silicon nitride photonics," Scientific Reports, vol. 12, no. 1, p. 15436, 2022.

Generation of spatial rogue waves in a Q-switched Nd:YAG laser

R. Navitskaya[1,2], I. Stashkevitch[1], S. Derevyanko[2*], and A. Karabchevsky[2]

[1]Faculty of Physics, Belarusian State University, 4 Nezalezhnasti Avenue, 220030 Minsk, Belarus
[2]School of Electrical and Computer Engineering, Ben-Gurion University of the Negev, Beer Sheva, Israel
[*]corresponding author: stasd@bgu.ac.il

Abstract: The generation of spatial rogue waves is demonstrated in a Q-switched Nd:YAG laser operating in a low-power regime under low Kerr nonlinearity. We investigate the dependence of rogue waves' statistics on the laser mode configuration. We show that spatial rogue waves can emerge when the lasing takes place at a large number of high-order transverse modes, while high Kerr or saturable absorption nonlinearity is not a necessary factor for their formation.

Spatial rogue waves are rare events that represent tightly focused spots in the transverse cross-section of the beam with extremely high intensities. They represent a particular case of general class of rogue waves (RWs) – extreme events that emerge and disappear spontaneously, and can be observed in different optical systems [1].

The exact mechanisms leading to the formation of spatial rogue waves are still under investigation. One of them concerns with the active role of nonlinearity. Typically, RWs are observed in optical systems with high medium nonlinearity, e.g. in fibers or lasers operating in a high-power regime with considerable Kerr nonlinearity or with intracavity saturable absorbers [1]. However, there are examples of purely linear optical systems that exhibit RWs generation. In such systems, RWs can be generated in the case of inhomogeneity and granularity of the beam profile [2], thus indicating the importance of spatial effects and modal dynamics. Spontaneous coupling of transverse laser modes possibly assisted by the longitudinal mode-locking can lead to the formation of complex output beam patterns with filamentary structure dynamically changing in time [3, 4]. In the extreme cases, the intensities of individual filaments can be high enough to damage the laser crystal or optical elements in the cavity [5].

Here, we demonstrate experimentally the generation of spatial RWs in a multimode Nd:YAG laser operating in the active and passive Q-switch regime [4,6]. The observed rogue wave statistics depend on the transverse mode configuration, as illustrated for example in Figure 1 for the laser generation in the active Q-switch regime. Thus, the spatial RWs were generated when a large number of high-order transverse modes were involved in the lasing (Figure 1b), while in the case of a smaller number of lasing modes with lower order the rogue wave generation was not observed (Figure 1a).

In addition, we performed a number of experiments for different pump powers to investigate the effect of Kerr nonlinearity on the properties of spatial RWs for the case of the laser operation below the self-focusing limit. In these experiments, the Nd:YAG laser was actively Q-switched without a saturable absorber in the cavity. We obtained the generation of spatial RWs under different pump powers corresponding to the output Q-switched pulse energies from 9 to 20 mJ [6]. The observed RWs had similar statistics and properties independent on the pump power. These results confirm that high Kerr nonlinearity or saturable absorption nonlinearity is not the main factor leading to the spatial rogue wave generation in a multimode solid-state laser.

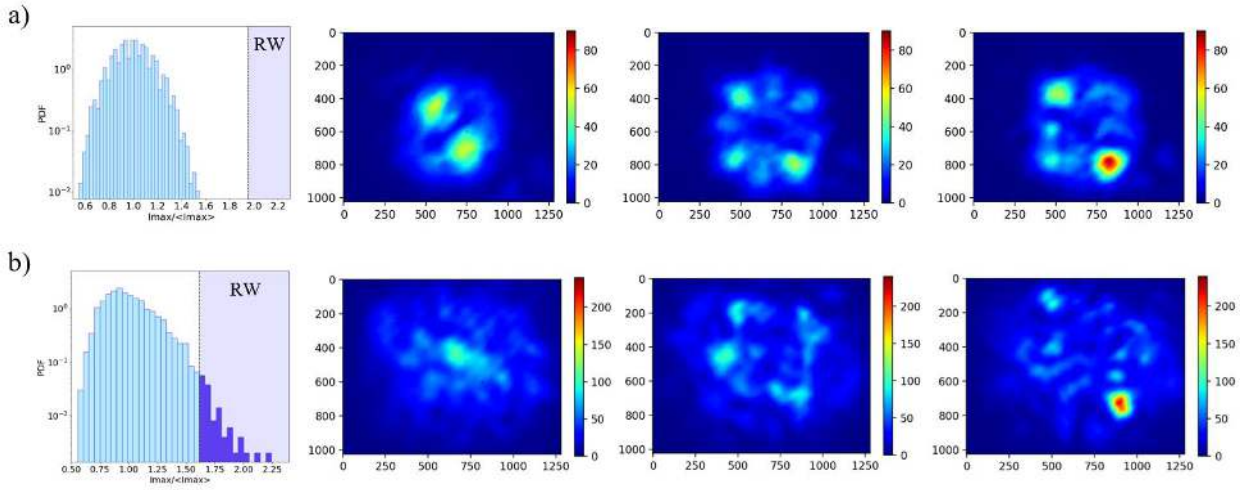


Figure 1. Statistics of pulse-to-pulse peak intensity over the transverse intensity profile and example output beam profiles for different laser mode configurations: a) small number of lasing modes with low order (spatial RWs are not observed); b) large number of high-order modes (the rightmost figure corresponds to a spatial rogue wave). The rogue wave limit is shown as a boundary of the shaded region in the statistics plots.

References

1. Akhmediev, N. et al., "Roadmap on optical rogue waves and extreme events", J. Opt.. **18**, 063001, 2016.
2. Arecchi, F., U. Bortolozzo, A. Montina, and S. Residori, "Granularity and inhomogeneity are the joint generators of optical rogue waves", Phys. Rev. Lett. **106**, 153901, 2011.
3. Encinas-Sanz, F., S. Melle, and O. G. Calderon, "Time-resolved dynamics of two-dimensional transverse patterns in broad area lasers", Phys. Rev. Lett, **93**, 21, 213904, 2004.
4. Navitskaya, R., I. Stashkevich, S. Derevyanko, and A. Karabchevsky, "Spatial rogue waves in the actively Q-switched Nd:YAG laser under low Kerr nonlinearity", Opt. Express **30**, 37076-37084, 2022.
5. Arisholm, G., "Self-focusing and optical damage in a diode-pumped neodymium laser", OSA TOPS, Vol. 10, Advanced Solid State Lasers (Optical Society of America, 1997).
6. Navitskaya, R., I. Stashkevich, S. Derevyanko, and A. Karabchevsky, "Experimental demonstration of spatial rogue waves in the passively Q-switched Nd:YAG laser", Opt. Lett. 46, 3773-3776, 2021.

Integrated Photonics for Machine Learning Assisted Signal Processing

I. Alamgir[1], L. Di Lauro[1], C. Mazoukh[1], S. Sciara[1], B. Fischer[1], A. Aadhi[1], A. Eshaghi[2], B.E. Little[3], S.T. Chu[4], D.J. Moss[5], R. Morandotti[1*]

[1]Institut national de la recherche scientifique (INRS-EMT), Canada
[2]Huawei Technologies Canada, Canada
[3]QXP Technology, Inc, China
[4]City University of Hong Kong, China
[5]Optical Sciences Centre, Swinburne University of Technology, Australia
[*]corresponding author: roberto.morandotti@inrs.ca

Integrated photonics offers unique devices and platforms for the development of cutting-edge technologies that allow for low-latency and ultra-fast signal processing, while utilizing established fabrication techniques and exploiting conventional fiber telecom networks. However, optimization of complex photonic integrated circuits is a challenging task due to their many degrees of freedom and fabrication imperfection, requiring intense design and numerical modeling. To overcome these challenges, machine learning-based smart optimization techniques can be incorporated with reconfigurable photonic circuits, thus allowing the widespread enhancement of the device functionality beyond the capabilities of traditional applications. Our group has previously demonstrated the effectiveness of this approach in both the temporal and spectral degrees of freedom by tailoring the shape of picosecond waveforms [1] and supercontinuum generation [2], respectively.

In this work, we propose the use of machine learning-based autonomous optimization techniques for the generation and arbitrary tailoring of the spectral shape, bandwidth, and repetition rate of an integrated micro-ring resonator-based optical frequency comb [3]. This technique has the potential to achieve increased comb efficiency, high repeatability, and reduced generation time. Additionally, this approach is translatable to micro-ring resonators of any geometry and composition, making it promising in telecommunication applications such as frequency synthesis and coherent parallel optical communication.

Furthermore, the small footprints (μm-nm), low power (milliwatts) consumption, and compatibility of our integrated platforms with fiber telecom infrastructures align our research with the need for new low carbon emission technologies and improvements of interconnected systems. In this regard, our research can pave the way for the advancement of artificial intelligence-assisted signal processing devices and encoding techniques for ultra-dense data transmission protocols compatible with 5G and upcoming 6G networks. Additionally, our results will strengthen the role of cross-disciplinary research between nonlinear/integrated photonics and artificial intelligence.

References

1. Fischer, B., Chemnitz, M., MacLellan, B., Roztocki, P., Helsten, R., Wetzel B., Little, B. E., Chu, S. T., Moss, D. J., Azaña. J., and Morandotti, R., "Autonomous on-chip interferometry for reconfigurable optical waveform generation," Optica, Vol. 8, No. 10, 101268-1276, 2021.
2. Wetzel, B., Kues, M., Roztocki, P., Reimer, C., Godin, P., Rowley, M., Little, B. E., Chu, S. T., Viktorov, E. A., Moss, D. J., Pasquazi, A., Peccianti, M., Morandotti, R., "Customizing supercontinuum generation via on-chip adaptive temporal pulse-splitting", Nature Communications, Vol. 9, 4884, 2018.
3. Xu, X., Tan, M., Corcoran, B., Wu, J., Boes, A., Nguyen, T. G., Chu, S. T., Little, B. E., Hicks, D. G., Morandotti, R., Mitchell, A., Moss, D. J., "11 TOPS photonic convolutional accelerator for optical neural networks", Nature Vol. 589, 44–51, 2021.

Wafer-scale fabrication of metasurfaces for infrared and energy applications

O.L. Muskens[1*], K. Sun[1*], C. Wheeler[1,2], J. J. Ou[1], and C. H. de Groot[2]

[1]Physics & Astronomy, Faculty of Engineering and Physical Sciences, University of Southampton, UK
[2] Electronics & Computer Science, Faculty of Engineering and Physical Sciences, University of Southampton, UK
[*]corresponding author: O.Muskens@soton.ac.uk

Abstract: We present results on the development of up to 200 mm full-wafer fabrication of mid-infrared metasurfaces for a variety of applications in energy, defence & space, including AZO and W:VO_2 thermal control metasurfaces, and silicon meta-lenses fabricated using deep-UV lithography.

Functional metasurfaces combine expertise in advanced materials, state-of-the-art nanofabrication, and sophisticated design. In recent years, our team has worked on different aspects in a variety of projects and here I will provide examples toward scalable metasurface technology using wafer-scale production level tools.

In the domain of advanced materials capabilities our work has focused on a number of tunable and switchable oxides that can be deposited reproducibly and with high accuracy using Atomic Layer Deposition. This includes transparent conducting oxides for infrared plasmonics and metasurfaces using Al-doped ZnO, where doping levels can be tuned not only by Al-doping, but importantly through oxygen plasma treatment.[1] We have demonstrated ability of precise lateral patterning of doping profiles with resolution better than 100nm, which can be used to define infrared metasurfaces through local doping in an otherwise completely planar structure. Wafer-scale fabrication of infrared metal oxide metasurface was demonstrated to achieve a dual band control over the spectral response in the mid and long-wave infrared.[2]

We have also reported the first demonstration of 200mm wafer-scale fabrication of tungsten-doped vanadium dioxide (W:VO_2) using atomic layer deposition, showing room-temperature insulator-to-metal phase transition.[3] This capability opens up a wide range of new applications in integration of non-volatile switching in metasurfaces and integrated photonics, with potential applications in communications, optical data processing and, thermal control coatings for energy applications.[4]

Parts of the presented work were done with the support from EPSRC, Dstl, and Horizon 2020.

References

1. Sun, K., W. Xiao, S. Ye, N. Kalfagiannis, K. S. Kiang, C. H. de Groot, O. L. Muskens, “Embedded metal oxide plasmonics using local plasma oxidation of AZO for planar metasurfaces,” Adv. Mater. 2001534, 2020.
2. Sun, K., E. Vassos, X. Yan, C. Wheeler, J. Churm, P. R. Wiecha, S. A. Gregory, A. Feresidis, C. H. de Groot, O. L. Muskens, “Wafer-Scale 200 mm Metal Oxide Infrared Metasurface with Tailored Differential Emissivity Response in the Atmospheric Windows,” Adv. Optical Mater. 2200452, 2022.
3. Sun, K., C. Wheeler, J. A. Hillier, S. Ye, I. Zeimpekis, A. Urbani, N. Kalfagiannis, O. L. Muskens, C. H. de Groot, Room Temperature Phase Transition of W-Doped VO2 by Atomic Layer Deposition on 200 mm Si Wafers and Flexible Substrates, Adv. Optical Mater. 2201326, 2022.
4. Sun, K., W. Xiao, C. Wheeler, M. Simeoni, A. Urbani, M. Gaspari, S. Mengali, C.H. de Groot, O. L. Muskens, VO_2 metasurface smart thermal emitter with high visual transparency for passive radiative cooling regulation in space and terrestrial applications, Nanophotonics 11, 4101-4114 (2022)

META 2023, PARIS - FRANCE, JULY 18 – 21, 2023

Anapole metallic nanostructures for metarsurface applications

Emadeldeen Hassan[1], **Andrey B. Evlyukhin**[2*], **Antonio Calà Lesina**[3]

[1] Department of Applied Physics and Electronics, Umeå University, SE-901 87 Umeå, Sweden,

and Department of Electronics and Electrical Communications, Menoufia University, Menouf 32952, Egypt

[2] Institute of Quantum Optics, and Cluster of Excellence PhoenixD, Leibniz University Hannover, 30167 Hannover, Germany

[3] Hannover Centre for Optical Technologies, Institute for Transport and Automation Technology (Faculty of Mechanical Engineering), and Cluster of Excellence PhoenixD, Leibniz University Hannover, 30167 Hannover, Germany

*Presenting author: evlyukhin@iqo.uni-hannover.de

Abstract: Anapole states are broadly investigated in nanophotonics for their ability to provide field enhancement and transparency. While low extinction has been achieved in dielectric nanoparticles due to the absence of intrinsic losses, in the case of plasmonic nanostructures this is still elusive. In this talk, we will present recent findings on anapole states in planar plasmonic nanostructures that were optimized for near-field energy enhancement using a topology optimization approach. The optimized structures exhibit an anapole state with characteristic properties in the visible regime including weak absorption, high near-field enhancement outside the structure, and strong suppression of scattering. We use our multipole analysis to explain both the near-field and the far-field features of the anapole state possessed by the nanostructures. Because of the low inter-coupling at the anapole state, the nanostructures act as individual meta-atoms that preserve their optical response even when used in highly packed metasurfaces and metamaterials. Due to their transparency while providing field enhancement, anapoles might be combined with waveguides in integrated optical platforms to unlock advanced functionalities for sensing, nonlinear optics, and optical information processing.

META 2023, PARIS - FRANCE, JULY 18 – 21, 2023

Emission enhancement of erbium in a reverse nanofocusing waveguide

N. A. Güsken[1,2*], M. Fu[1], M. Zapf[3], M.P. Nielsen[1,4], P. Dichtl[1], R. Röder[3], A. S. Clark[1,5], S. A. Maier[1,6], C. Ronning[3] and R. F Oulton[1*]

1Department of Physics, Imperial College London, Prince Consort Road, London SW7 2AZ, UK
2Department of Materials Science and Engineering, Stanford University, Stanford, CA 94305, USA
3Friedrich-Schiller-Universität Jena, Max-Wien-Platz 1, 07743 Jena, Germany
4School of Photovoltaics and Renewable Energy Engineering, UNSW Sydney, Kensington, NSW 2052, Australia
5Quantum Engineering Technology Labs, University of Bristol, BS8 1UB, UK
6Monash University School of Physics and Astronomy, Clayton, VIC 3800, Australia
*Corresponding authors: ngusken@stanford.edu, r.oulton@imperial.ac.uk

Abstract: We report emission enhancement of Er3+-ions across the telecommunications C-band in a single plasmonic waveguide based on the Purcell effect. Our gap waveguide uses a reverse nanofocusing approach to efficiently enhance, extract and guide emission from the nanoscale to a photonic waveguide while keeping plasmonic losses at a minimum. A large and broadband Purcell enhancement allows us to resolve Stark-split electric dipole transitions. Simultaneous enhancement of multiple quantum states is of great interest for photonic and quantum networks.

The influence of a local electromagnetic environment on light-matter interaction offers a route to realise faster and brighter light sources with associated control over the quantum states of light and matter. Mastering this control is especially important in sensing and quantum technologies [1] when working with low photon numbers and single emitters such as isolated molecules [2–4], quantum dots [5] and atoms [6], all of which inherently interact particularly weakly with light.

Optical cavities localize light in both frequency, quantified by the cavity quality factor, Q, and space, quantified by a mode volume, V_m, to accelerate luminescence by the Purcell factor, $F_p = 3\lambda^3 Q/(4\pi^2 n^3 V_m)$, where λ is the optical wavelength and n is the refractive index. This has proven to be incredibly effective; however, comes at the price of requiring innovative ways to tune and match both cavity and emitter frequency as well as the restriction of access to a single electronic transition at a time. A promising alternative is to couple luminescence into a single highly confined optical waveguide mode [7–9]. Now the mode's confinement area, A_m and group velocity, v_g, determine the Purcell factor, $F_p = 3c\lambda^2/(4\pi n^2 v_g A_m)$ [10], while the continuum of modes provides tuning-free enhancement across a broad frequency range [11]. This in principle should provide simultaneous access to multiple electronic transitions at distinct energies [12]. Although slow light propagation in photonic crystal waveguides shows excellent Purcell enhancement, their bandwidth-delay product limit prohibits broadband operation. Thus, plasmonic waveguides are especially promising as they offer large bandwidth sub-wavelength confinement without excessive dispersion.

Here we report both the enhancement and efficient guided mode extraction of dipole luminescence using reverse nanofocusing from a nanoplasmonic waveguide coupled to a buried photonic waveguide. We demonstrate this using technologically relevant Er3+ ions on a hybrid silicon plasmonic waveguide platform. Our reverse

nanofocusing device gives rise to 300-fold shorter Er3+ ion emission lifetimes accompanied by an enhancement of >338x in luminescence efficiency when compared to non-plasmonic control devices. Efficient collection of the enhanced luminescence is achieved by exploiting photonic to plasmonic nanofocusing methods, but in reverse. All plasmonic devices were found to produce more photons than photonic control devices. The extraordinary enhancements of this system are further underpinned by the observation of multiple enhanced Stark-split electric dipole transitions across the Er3+ telecommunications emission band. This demonstrates the capability to strongly dress multiple atomic transitions simultaneously using a one-dimensional mode continuum at room temperature.

This work was supported by the EPSRC Reactive Plasmonics Programme (EP/M013812/1), UK Quantum Hub in Quantum Imaging (EP/T00097X/1) and the Leverhulme Trust (RPG-2016-064). Deutsche Forschungsgemeinschaft (DFG) supported this work within the frame of the collaborative research center CRC 1375 “Nonlinear optics down to atomic scales (NOA)”, project C5. S.A.M. additionally acknowledges the Lee-Lucas Chair in Physics. This project has received funding from the European Union’s Horizon 2020 research and innovation programme under a Marie Skłodowska-Curie Fellowship (grant agreement no. 844591, M.F.). N.A.G likes to thank the German National Academy of Sciences Leopoldina for their support via the Leopoldina Postdoctoral Fellowship (LPDS2020-12).

References

1. Uppu, R., Midolo, L., Zhou, X., Carolan, J. & Lodahl, P. “Quantum-dot-based deterministic photon–emitter interfaces for scalable photonic quantum technology.” Nat Nanotechnol, Vol. 16, 1308–1317, 2021.
2. Chikkaraddy, R. et al. “Single-molecule strong coupling at room temperature in plasmonic nanocavities.” Nature, Vol. 535, 127–130, 2016.
3. Akselrod, G. M. et al. “Probing the mechanisms of large Purcell enhancement in plasmonic nanoantennas.” Nat Photonics 8, 835–840, 2014.
4. Toninelli, C. et al. “Single organic molecules for photonic quantum technologies.” Nat Mater. 20, 1615–1628. 2021.
5. Akimov, A. v. et al. “Generation of single optical plasmons in metallic nanowires coupled to quantum dots.” Nature 450, 402–406, 2007.
6. Yin, C. et al. Optical addressing of an individual erbium ion in silicon. Nature 497, 91–94 (2013).
7. Jun, Y. C., Pala, R. & Brongersma, M. L. Strong modification of quantum dot spontaneous emission via gap plasmon coupling in metal nanoslits. Journal of Physical Chemistry C 114, 7269–7273 (2010).
8. Jun, Y. C., Kekatpure, R. D., White, J. S. & Brongersma, M. L. Nonresonant enhancement of spontaneous emission in metal-dielectric-metal plasmon waveguide structures. Phys Rev B Condens Matter Mater Phys 78, 1–4 (2008).
9. Grandi, S. et al. Hybrid plasmonic waveguide coupling of photons from a single molecule. APL Photonics 4, (2019).
10. Oulton, R. F., Bartal, G., Pile, D. F. P. & Zhang, X. Confinement and propagation characteristics of subwavelength plasmonic modes. New J Phys 10, 105018 (2008).
11. Veronis, G. & Fan, S. Modes of Subwavelength Plasmonic Slot Waveguides. Journal of Lightwave Technology 25, 2511–2521 (2007).
12. Kolchin, P., Oulton, R. F. & Zhang, X. Nonlinear Quantum Optics in a Waveguide: Distinct Single Photons Strongly Interacting at the Single Atom Level. Phys Rev Lett 106, 113601 (2011).

Simulation of Plasmonic Absorption Interplays in Hybridized Semiconductor/Metal Nanostructures

Atefeh Habibpourmoghadam[1*], Wenyong Xie[1], Antonio Calà Lesina[1]

[1]Hannover Centre for Optical Technologies, Institute for Transport and Automation Technology (Faculty of Mechanical Engineering), and Cluster of Excellence PhoenixD, Leibniz University Hannover, 30167 Hannover, Germany

[*]corresponding author: atefeh.habibpoor@hot.uni-hannover.de

Abstract: In low intensity regime, the plasmonic response of hybridized nanostructures can be seen as the linear combination of each constituent's response. However, the surface plasmon resonance (SPR) at the interface between two materials, can further modify the absorption cross-section of a hybridized nanostructure. We numerically studied the optical response of hybridized nanostructures made from metal (i.e., gold) and highly doped semiconductor (i.e., copper sulfide) both in the static and transient regimes, and we will present the unconventional response of such a system.

Amongst various copper chalcogenide combinations (Cu2-xS), copper sulfide (CuS) can offer multiple advantages, such as low toxicity, and higher stability due to oxidation in air [1]. In hybridized nanostructures (see Figure. 1) made of CuS and gold (Au), charge carriers transfer can happen from Au to CuS at the interface which can change the overall optical properties of the system [2]. In addition to permittivity tensor, this mechanism can also modify electronic band gap at their interface [1]. Dual plasmonic response in Au/CuS nanostructures were experimentally investigated with transient absorption spectroscopy (TAS) [3]. Here, we provide theoretical insight to explain the optical response of these dual plasmonic hybridized nanostructures, which are not yet fully understood. Through numerical modeling, we found that Au/CuS hybrid nanostructures show unusual absorption properties due to their asymmetric geometry, which enables strong coupling between their constituents due to the excitation of plasmonic modes located at their common interface. Numerical modeling was performed both in the static and transient optical regimes. In the static regime – similarly to a conventional Mie-type calculation under linearly polarized plane wave – the total response can be understood as the linear combination of resonant modes attributed solely to the Au and CuS counterparts, with a slight spectral shift correction due to the coupling.

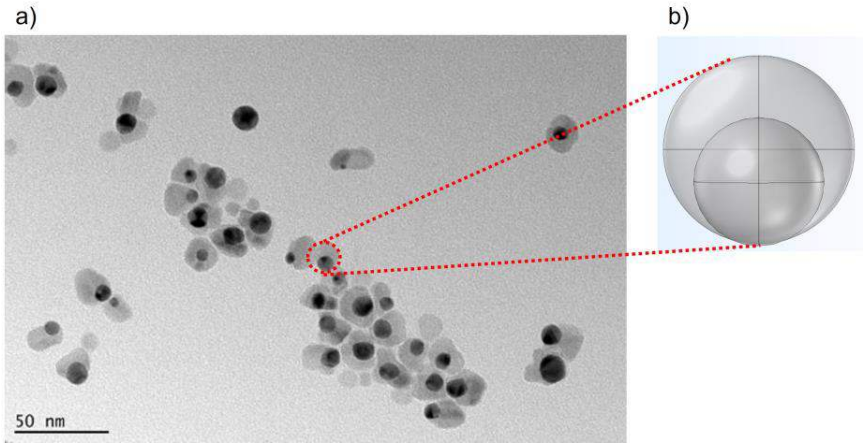


Figure 1. a) Transmission electron microscopy (TEM) image of colloidal distribution of Au/CuS nanoparticles in toluene (adapted from Ref. [3]), b) corresponding simulation configuration.

In the transient regime, a pump-probe simulation was performed as a function of delay between pump and probe signals. The experimental transient absorption results were reproduced with good accuracy, and the origin of such response identified. More details will be discussed during the talk.

References

1. Córdova-Castro, R. M., Casavola, M., Van Schilfgaarde, M., Krasavin, A. V., Green, M. A., Richards, D., & Zayats, A. V. "Anisotropic plasmonic CuS nanocrystals as a natural electronic material with hyperbolic optical dispersion". ACS nano, Vol. 13, No. 6, 6550-6560, 2019.
2. Kim, Y., Park, K. Y., Jang, D. M., Song, Y. M., Kim, H. S., Cho, Y. J., ... & Park, J. "Synthesis of Au− Cu2S core− shell nanocrystals and their photocatalytic and electrocatalytic activity". The Journal of Physical Chemistry C, Vol. 114, No. 50, 22141-22146, 2010.
3. Bessel, P., Niebur, A., Kranz, D., Lauth, J., & Dorfs, D. "Probing Bidirectional Plasmon-Plasmon Coupling-Induced Hot Charge Carriers in Dual Plasmonic Au/CuS Nanocrystals". Small, 2206379, 2022.

Green-Extraction of Graphene from Natural Mineral Shungite

A. Novikova[1*], and A. Karabchevsky[1]

[1]School of Electrical and Computer Engineering, Ben-Gurion University of the Negev, Beer-Sheva 8410501, Israel
[*]corresponding author: novikoan@post.bgu.ac.il

Abstract: With the increasing demand for graphene, the need for a simple, fast, efficient, low-stage and environmentally safe method of its production also increases. In our work, we used physical ultrasound treatment without the addition of surfactants to extract graphene films from a mineral of shungite. From our study of the structures of the resulting graphene, we see that they have the form of films with a surface length of 200 nm with a graphene structure with a hexagonal center and a lattice pitch of 0.335 nm.

We investigated two regions of shungite, as illustrated in Figure 1a,d, and conducted EDS analysis on each region. Our results indicate that the completely dark areas in region 1 (Fig. 1b) and 21 (Fig. 1e) are composed entirely of carbon. Conversely, region 2 (Fig. 1c) and 21 (Fig. 1f) is composed of carbon containing impurities, including low concentrations of oxygen, silicon, aluminum, nickel, iron, and vanadium.

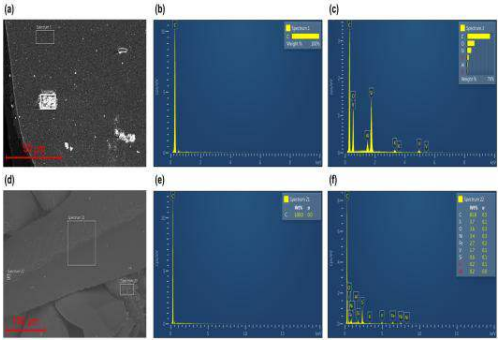


Figure 1. Scanning electron microscopy with EDS image of shungite particles: (a) first-selected sample study areas, chemical composition of area spectrum (b) 1, (c) 2, (d) second-selected sample study areas, chemical composition of area spectrum (e) 20 and (f)21.

Next, we characterized the surfaces of samples processed from shungite with a carbon concentration of 100%.

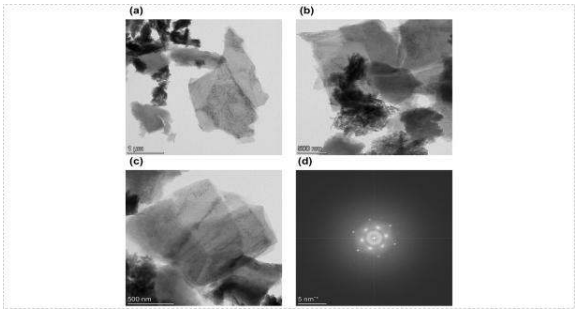


Figure 2. TEM images of sonicated shungite sample at magnifications of (a) x13,500, (b) x35,000 and (c) x22,000. (d) Fast Fourier transform pattern of sonicated shungite sample.

Transmission electron microscopy (TEM) images of a sonicated shungite sample (Fig. 2a-c) reveal the formation of thin films with a high specific surface area. For a sample with a carbon concentration of 98%, the particles have collapsed into thin monolayers. The fast Fourier transform pattern [1, 2] of the resulting films exhibits a symmetrical hexagonal pattern characteristic of primary graphene (Fig. 2d).

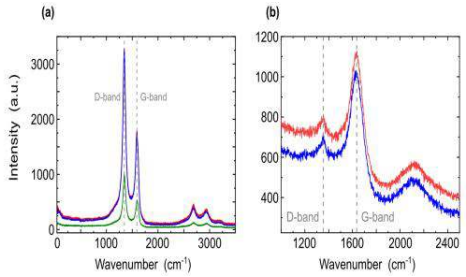


Figure 3. Raman spectra of natural shungite (a) before and (b) after sonication

Raman spectra of natural shungite from the different regions investigated (Fig. 3a) reveal the presence of a G-band at 1600 cm^{-1}, indicating the tangential stretching vibrations of sp2-bonded carbon atoms in the hexagonal graphene planes[3,4]. A D-band at 1330 cm^{-1}, indicating diamond-like sp3 bonds, corresponds to the amorphous structural state of carbon (graphite), indicating that the main allotrope of carbon in natural shungite rock is graphite. However, in Raman spectra of sonicated shungite samples (Fig. 3b), the graphene-related G-band shows increased intensity, with a corresponding decrease in the graphite-related D-band. No obvious second-order peaks appear in the spectra.

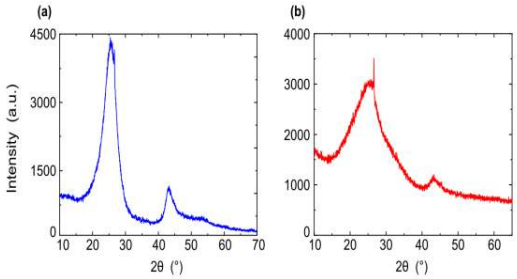


Figure 4. X-ray spectra of shungite sample (a) before, and (b) after sonication.

Figure 4 shows the X-ray spectra of shungite before and after ultrasound treatment. For the sample before sonication (Fig. 4a), wide spectra at 26.5° refer to graphite-like carbon, as well as a secondary peak at 42°, 44°, corresponding to the hexagonal structure. Here 26.5° is the angle of the base plane of centered graphene and the lattice pitch of 0.335 nm. Figure 4b shows X-ray spectra after ultrasound treatment. The positions of the peaks are located at 26.5°, 42° and 44°. The vertex is 26.5°, increased compared to the peak before processing, which means that the carbon peak can be interpreted as a decrease in the size of the coherent scattering region along the c axis in stacked graphene layers. The peak is 44° is more intense than that of shungite before ultrasound treatment, which means that the size of the hexagonal structure has been increased. Our results show that graphene films were obtained from shungite using green-extraction methods.

We acknowledged DIEGO project ERA-NET, Ministry of Energy, Grant No. 221-11-032 for funding the research.

References

1. Soler-Crespo, R.A., Mao, L., Wen, J., Nguyen, H.T., Zhang, X., Wei, X., Huang, J., Nguyen, S.T. and Espinosa, H.D. “Atomically thin polymer layer enhances toughness of graphene oxide monolayers,” Matter, 1(2), 369–388, 2019.
2. Akinwande, D., Brennan, C.J., Bunch, J.S., Egberts, P., Felts, J.R., Gao, H. and Huang, R. “A review on mechanics and mechanical properties of 2D materials-Graphene and beyond,” Extrem. Mech. Lett., 13, 42–77, 2017.
3. Novikova, A. and Karabchevsky, A. “Green Extraction of Graphene from Natural Mineral Shungite,” Nanomaterials, 12(24), 4356, 2022.
4. Novikova A., Katiyi, A., Halstuch, A. and Karabchevsky, A. “Green-Graphene Protective Overlayer on Optical Microfibers: Prolongs the Device Lifetime,” Nanomaterials, 12(17), 2915, 2022.

Plasmonic Nanomaterials for Bio-diagnostics, Environmental Monitoring and Food Safety

META 2023, PARIS - FRANCE, JULY 18 – 21, 2023

Plasmonic Metasurface for Enhanced Infrared Spectroscopy: a method to monitor protein denaturation

Valentina Di Meo [1], Gennaro Sanità [1], Massimo Moccia [2], Alessio Crescitelli [1], Annalisa Lamberti [3], Vincenzo Galdi [2], Ivo Rendina [1] and Emanuela Esposito [1*]

[1] National Research Council-Institute of Applied Sciences and Intelligent Systems-Unit of Naples, Italy
[2] Fields and Wave Labs, Dept. of Engineering, University of Sannio, Benevento, Italy
[3] Department of Molecular Medicine and Medical Biotechnology, University of Naples "Federico II", Naples, Italy
[*]corresponding author: emanuela.esposito@cnr.it

Abstract: Surface-Enhanced InfraRed Absorption (SEIRA) spectroscopy is a powerful tool to overcome the limitation offered by the standard IR spectroscopy in the case of very small amount of analyte to be detected.
Our platform relies on a plasmonic metasurface engineered to exhibit different resonances covering the infrared region of the electromagnetic spectrum (EM). In the present work, the resonances are matched to the vibrational modes of the Amide groups, to demonstrate the ability of such device to monitor a denaturation biological process over a dehydrated monolayer of protein A, with an estimated detection limit of about 3 fmol of molecules.

SEIRA spectroscopy is a powerful method for the structural determination of molecules in biological samples in a univocal, non-destructive, and label-free way, which relies on plasmonic metasurfaces (MSs) at very low concentration and with small MW [1]. Molecular vibration frequencies essentially depend on the arrangement of the atoms, as well as the strength of the involved chemical bonds, which renders this technique a valuable tool for the investigation of proteins' structure, molecular mechanisms underlying protein reactions, as well as protein folding, unfolding and misfolding [2]. MSs are composed of two-dimensional periodic arrays of sub-wavelength metallic elements (also called nanoantennas, NAs) laid on a dielectric substrate. The optical response of an MS can be tailored across the EM spectrum by varying the shape, size, and metal film thickness of each NA, as well as the array periodicity. When MSs are resonantly coupled with the incoming EM radiation, the field can be strongly confined and enhanced around the NAs and into the gaps between them; this yields a several order of magnitude amplification of the vibrational modes of nearby molecules, which in turn enables spectroscopic characterizations with unprecedented sensitivity. Especially for low concentrations of the analyte, it is crucial that the field hotspots occur consistently and homogeneously across the MS, so that the probability of enhanced light-matter interaction is maximized.
The development of our proposed sensing platform revolves around four main lines: EM modeling and design, fabrication, biofunctionalization, and IR characterization. Our design procedure relies on a preliminary parametric study, in which we extensively explore the geometrical parameter space and identify possible resonances of interest. For the inverse design, i.e., the synthesis of a resonance with desired position and line-width, we start from a coarse initial guess from the computed codebooks, and progressively fine-tune the parameters. We adopted an innovative design based on a multiresonant MS made of different pixels (covering an area of 500 x 500 μm^2) characterized by different designs, in order to exhibit resonances covering the wavenumber range 1500 – 2100

cm^{-1} related to Amide groups I and II (i.e., 4.8 – 6.7 μm in wavelength) [3]. This requires reliable and reproducible nanofabrication approaches [4]. The proposed multiresonant MS is fabricated on a 10 x 10 mm^2 float-zone silicon chip by means of electron beam lithography and lift-off processes [4]. In the present work, we take a further step and apply SEIRA spectroscopy to probe the denaturation of a protein monolayer. All pixels are biofunctionalized with Protein A (PA) by using dithiobis(succinimidyl propionate) (DSP) taken as a sample model, following a precise protocol [5] and after the characterization of their absorption SEIRA spectra they follow a PA denaturation protocol and their SEIRA spectra are acquired. The comparison between the native state and the denatured state of the PA is showed in Figure 1 through the related SEIRA spectra. We can determine changes in the Amide I and Amide II vibration coupled modes. In the region 1665 – 1650 cm^{-1}, we estimate a red-shift of 9 cm^{-1} for the Amide I band, which is frequently interpreted in terms of structural changes of α-helical structures. Moreover, we estimate a red-shift of 10 cm^{-1} for the Amide II vibration coupled modes [5]. These red-shifts are mainly due to the breaking of hydrogen bonds, which can result in insurmountable barriers to refolding. Thanks to the large surface field enhancement and the precise methods of surface chemistry, we are able to demonstrate that SEIRA spectroscopy can provide real-time, high-sensitivity, label-free methods for monitoring the protein unfolding in a simpler and cheaper fashion, against traditional experimental methods which are expensive and complicated to use.

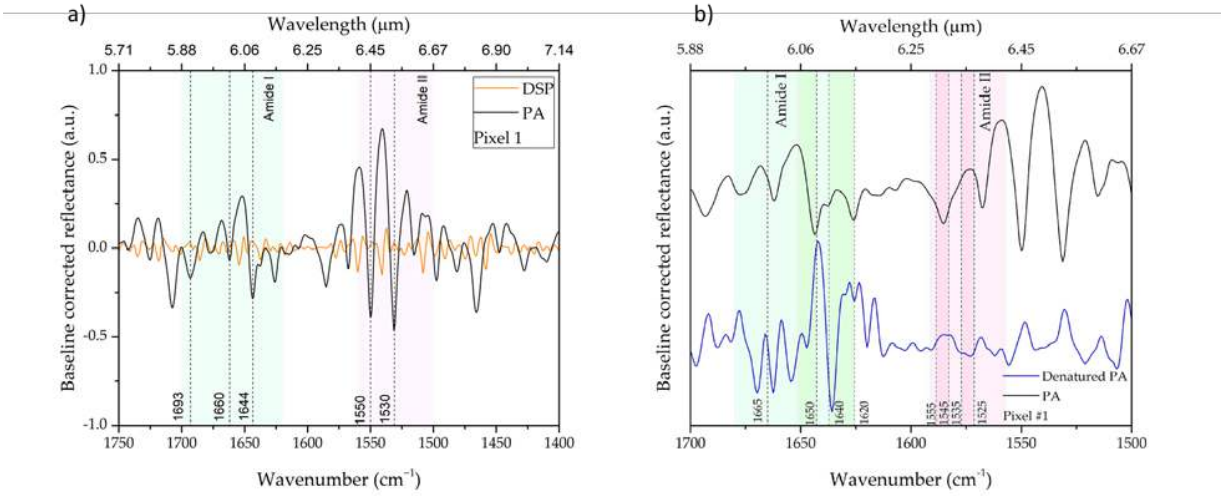


Figure 1: SEIRA reflectance spectra: a) orange curve refers to the spectrum acquired after the DSP incubation, while black curve refers to the reflectance response after the PA layer binding; b) comparison between the SEIRA spectrum of native PA (black curve) and of the denatured PA (blue curve) [5].

References

1. John-Herpin A.; Tittl A.; Kühner L.; Richter F.; Huang S. H.; Shvets G.; Oh S-H.; Altug H.; Adv. Mater. 2022, 2110163, DOI: 10.1002/adma.202110163.
2. Barth A.; Biochim. Biophys. Acta-Bioenerg. 2007, 1767, 1073–1101, doi.org/10.1016/j.bbabio.2007.06.004.
3. Di Meo V.; Crescitelli A.; Moccia M.; Sandomenico A.; Cusano A.M.; Portaccio M.; Lepore M.; Galdi V., Esposito E.; Nanophotonics 2020, 9(12), 3921-3930, doi: 10.1515/nanoph-2020-0103.
4. Di Meo, V.; Caporale, A.; Crescitelli, A.; et al.; Sens. Actuators B Chem. 2019, 286, 600–607, doi: 10.1016/j.snb.2019.02.014.
5. Di Meo, V.; Moccia, M.; Sanità, G.; et al.; Biosensors 2022, 12(5), 530; https://doi.org/10.3390/bios12070530.

META 2023, PARIS - FRANCE, JULY 18 – 21, 2023

Development of a hybrid plasmonic/photonic nanoscale strategy for multi-level anti-counterfeit labels in the framework of food safety

V. Caligiuri[*,1,2], A. Patra[1,3], M. P. De Santo[1,2], A. Forestiero[4], G. Papuzzo[4], D. M. Aceti[5], G. E. Lio[6], R. Barberi[1,2] and A. De Luca[*,1,2]

[1] Department of Physics, University of Calabria, via P. Bucci, 31C, 87036, Rende (CS), Italy
[2] CNR-Nanotec UOS Rende, via P. Bucci, 31D, 87036, Rende (CS), Italy
[3] Istituto Italiano di Tecnologia, via Morego 30, 16163 Genova (GE), Italy
[4] CNR-ICAR, Institute for High Performance and Networking, via P. Bucci 8-9c, 87036 Rende (CS), Italy
[5] Institute of Electronics, Bulgarian Academy of Sciences, 72, Tsarigradsko Chaussee blvd., 1784 Sofia, Bulgaria
[6] CNR-INO and LENS, Via Nello Carrara, 1 - 50019, Sesto Fiorentino, Firenze (FI), Italy

[*]corresponding authors: vincenzo.caligiuri@unical.it; antonio.deluca@unical.it

Abstract: Innovative goods authentication strategies are of fundamental importance considering the increasing counterfeiting levels. We propose a hybrid plasmonic/photonic multilayered structure working as a three-level strong Physical Unclonable Function. Our approach combines a functional nanostructured surface, a resonant response and a unique chromatic signature together in one single device. The proposed architectures could also be used as an irreversible and quantitative temperature exposure label in the framework of food safety. They are inexpensive, scalable and can be deposited over different substrates.

The Organization for Economic Co-operation and Development (OECD) certified that the trade in counterfeit goods is rapidly increasing. New technologies and approaches are, therefore, required. In this respect, a great promise is held by the so-called Physical Unclonable Functions (PUFs).[1] PUFs are physical signatures whose intrinsic unpredictability produces a unique and unclonable response to a specific challenge. PUFs owe their specifics to unavoidable randomness in fabrication processes, over which the manufacturer has no control. In this respect, micro- and nano-fabrication processes represent the ideal framework where to look for user-independent randomness. On the other hand, good-labeling approaches based on colors and iridescence proved their validity in countless applications. The emerging technological framework of plasmonics allows to unify these two approaches. At the nanoscale, indeed, plasmonics is synonym of "color", even though a specific tint results from an optical resonance, rather than a pigment.[2] Here, we propose a hybrid photonic/plasmonic system as a three-levels strong PUF.[3] The proposed plasmonic architecture, sketched in Fig. 1a, provides three different authentication levels: (i) chromatic (Fig. 1b), (ii) spectral (Fig. 1c), and (iii) morphological (Fig. 1d). The technological core of the idea lies in silver nano-islands (Ag-NIs) obtained by depositing Ag layers below their percolation threshold, via a DC

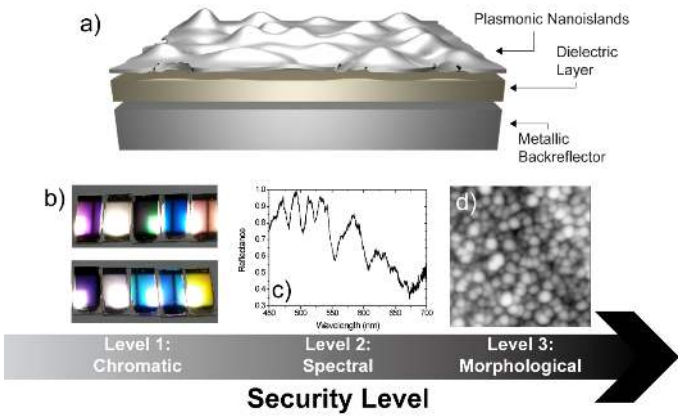


Figure 1 - a) Sketch of the Plasmonic PUF architecture. b) Chromatic and lightness effect (Level 1 - chromatic signature). c) Typical spectral response of a sample resembling the architecture shown in a). (Level 2 - spectral signature) d) Ag-NIs morphology revealed via AFM analysis (Level 3 - nanoscale morphological signature).

magnetron sputtering technique. Such a procedure allows to obtain Ag nanoclusters whose density and size depend on the sputtering deposition parameters, but whose spatial disposition and clustering is random. Ag-NIs unify a marked chromatic response with a peculiar plasmonic behavior. We demonstrate that, when used as the top layer in a multilayered configuration involving also metal/insulator/metal (MIM) resonators, the interplay between photonic cavity resonances and plasmonic modes gives rise to a glaring and distinct chromatic response. Such a property, combined with a marked iridescence, gives rise to a unique chromatic response, that cannot be reproduced by commercial paints, representing the first level of authentication of the proposed PUF. These chromatic properties stem from the spectrally rich optical response of the proposed architecture (Fig. 1c), which we characterized both by sophisticated ellipsometric measurements and by using the LED flash lamp of a smartphone in a simple spectroscopic setup. In the end, the strongest and most innovative authentication level is given by the morphological fingerprint, which is constituted by the spatial disposition of Ag-NIs (Fig. 1d). The morphology of a precise area of the patterned sample surface has been investigated through Atomic Force Microscopy (AFM) measurements and registered as a fingerprint to be compared with those of different areas by an imaging recognition algorithm. We found that the number of tags recognized by comparing two images of the same area acquired through two different AFM measurements is 2 orders of magnitude larger than the number of tags recognized by comparing AFM measurements belonging to two different areas of the patterned surface. In the end, we demonstrate that our plasmonic PUF could work as a thermal exposure label. We show, indeed, that, when the sample is exposed to temperatures higher than a certain threshold, its color and optical response change dramatically and irreversibly in a deterministic and quantitatively measurable way.

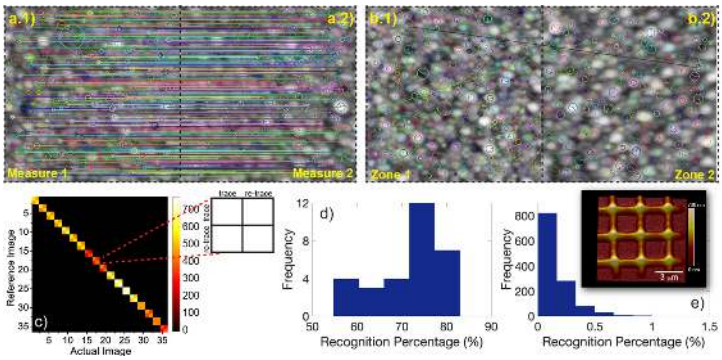


Figure 2 - Comparison between (a.1) trace and (a.2) re-trace AFM measure of the same area. (b.1, b.2) Comparison between AFM measurements of two different areas. c) Score-Match matrix representing all the possible comparisons between all the analyzed areas. d) Histogram of the distribution of the comparison between AFM images belonging to the same area together with to (e) that belonging to comparisons of AFM measurements of different areas. In the inset, AFM measure of a portion of the 3x3 µm grid into which the surface of a Ag-NIs layer has been divided.

The authors acknowledge the Project DEMETRA, “Development of MatErial and TRAcking technologies for the safety of food”, PON ARS01_00401, for the financial support.

References

1. Gao, Y.; Al-Sarawi, S. F.; Abbott, D. Physical Unclonable Functions. Nature Electronics. Nature Research February 1, 2020, pp 81–91.
2. Song, M.; Wang, D.; Peana, S.; Choudhury, S.; Nyga, P.; Kudyshev, Z. A.; Yu, H.; Boltasseva, A.; Shalaev, V. M.; Kildishev, A. v. Colors with Plasmonic Nanostructures: A Full-Spectrum Review. Applied Physics Reviews. American Institute of Physics Inc. December 1, 2019, p 041308.
3. V. Caligiuri, A. Patra, M. P. De Santo, A. Forestiero, G. Papuzzo, D. M. Aceti, G. E. Lio, R. Barberi, and A De Luca*, “Hybrid Plasmonic/Photonic Nanoscale Strategy for Multilevel Anticounterfeit Labels” - ACS Appl. Mater. Interfaces 2021, 13, 41, 49172–49183

META 2023, PARIS - FRANCE, JULY 18 – 21, 2023

Plasmonic Metasurfaces for Enhanced Spectrochemical Tissue Diagnostics

S. Rosas[1], K. A. Schoeller[3,4], E. Chang[3,4], H. Mei[2], M. A. Kats[2], K. W. Eliceiri[1], X. Zhao[3,4], and F. Yesilkoy[1*]

[1]Department of Biomedical Engineering, University of Wisconsin-Madison, Madison, WI, USA
[2]Department of Electrical and Computer Engineering, University of Wisconsin-Madison, Madison, WI, USA
[3]Department of Neuroscience, University of Wisconsin-Madison, Madison, WI, USA
[4]Waisman Center, University of Wisconsin-Madison, Madison, WI, USA
[*]corresponding author: filiz.yesilkoy@wisc.edu

Abstract: Label-free and nondestructive mid-infrared (MIR) vibrational hyperspectral imaging is emerging as an important biomedical tissue analysis tool. However, the chemically complex and heterogeneous composition of tissue specimens limit analytical performance of conventional MIR spectral histopathology. We introduce an advanced MIR spectrochemical tissue imaging modality using plasmonic metasurfaces supporting strong surface-localized electromagnetic fields to capture quantitative molecular maps of large-area brain tissue sections. Our surface-enhanced chemical imaging method is well-suited to impact translational biomedical research and diagnostic clinical histopathology.

Developing sensitive and specific analytical tools to capture the sub-wavelength biomolecular information within the complex biological media using light is one of the main challenges of the biophotonics field. Label-free and nondestructive MIR vibrational spectroscopic imaging (MIRSI) is emerging as an ex-vivo digital tissue analysis tool that can provide spatially resolved biochemical information. Thus far, many reports have shown its prospects targeting diagnostics of a large cohort of diseases [1,2]. However, the chemically complex and spatially heterogeneous composition of tissue specimens and the inherently weak interaction of infrared light with biomolecules limit the analytical performance of MIRSI hindering its potential impacts on the biomedical sciences.

In this work [3], we present plasmonic metasurface-enhanced MIR spectral imaging (SE-MIRSI) as an advanced label-free chemical tissue-imaging method (Fig. 1). We demonstrate MIR spectroscopy of murine brain tissue sections, interrogating nanoscale thicknesses over large areas using engineered photonic substrates and a hyperspectral imaging microscope with illumination from four tunable QCLs (Fig. 1a). To satisfy the critical requirement of multiplexed molecular fingerprint analysis of SE-MIRSI, we developed polarization-tunable multi-resonant plasmonic metasurfaces that enhance light-matter interactions in sub-wavelength volumes over our target spectral range of 950–1800 cm^{-1} (Fig. 1b). We reveal how tissue morphology affects quantitative chemical analysis by comparing absorbance from numerous vibrational bands, measured from murine brain tissue sections of different thicknesses, ranging from 20 μm to 80 μm, mounted on standard CaF_2 substrates and plasmonic metasurfaces. We show that SE-MIRSI is not affected by bulk morphological properties of complex tissue samples because the absorption is constrained to the plasmonic hotspots: nanoscale volumes with strong enhancement of the electric field intensity (~1.4×10^3). We also show that SE-MIRSI can detect fine spectral details corresponding to protein backbone structures, as well as other important biomolecules, such as glycogen, nucleic acids, proteins, and lipids (Fig. 1 c). Finally, we show that SE-MIRSI enables chemical analysis of ultrathin brain tissue regions, which are not otherwise detectable on standard substrates, underscoring the high analytical sensitivity of our approach. Our method, for the first time,

addresses a well-known quantitative analysis limitation of infrared absorption spectroscopy by decoupling chemical and morphological properties and enabling highly sensitive and chemically selective analysis of complex and heterogeneous biosamples. Our chemical imaging method is versatile and can be used to study any tissue type with potential applications in fundamental research and clinical histopathology.

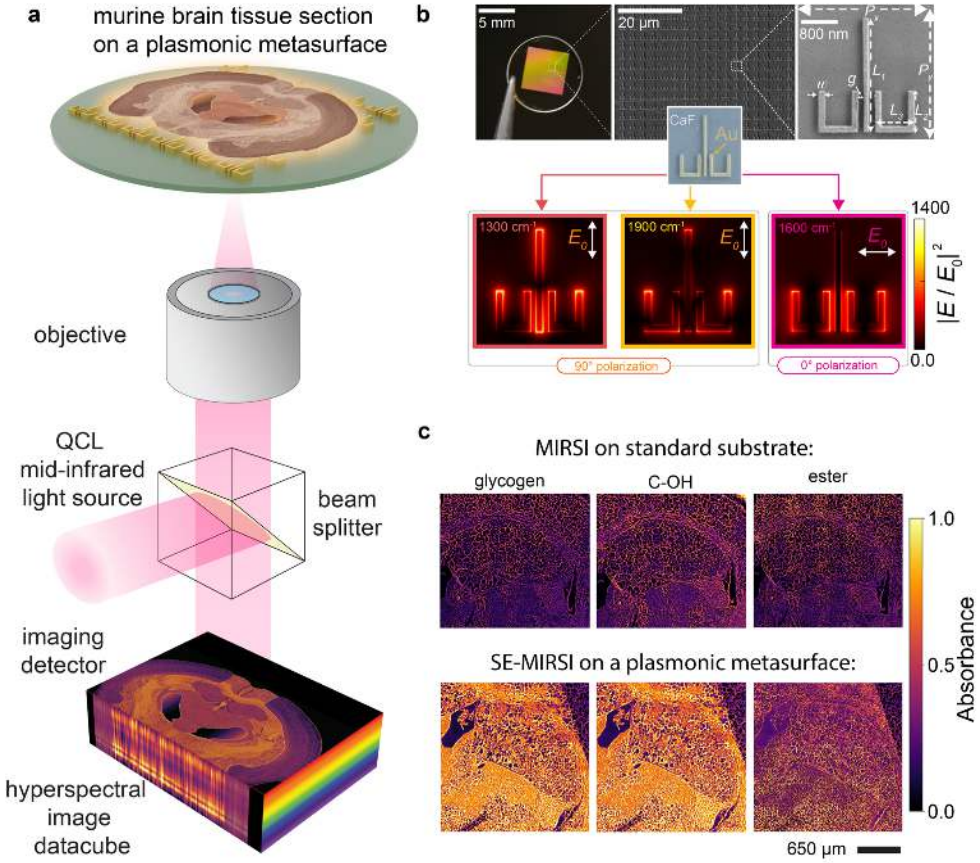


Figure 1: Surface-enhanced mid-infrared spectral imaging of tissues (SE-MIRSI). a, Schematic of the tunable quantum cascade laser (QCL)-based mid-IR spectral imaging system. Hyperspectral datacubes are acquired using a microbolometer focal-plane detector array while sweeping the illumination wavenumber across the mid-IR fingerprint spectral range of 950 to 1,800 cm^{-1}. **b**, Photographs show a plasmonic metasurface chip fabricated over a 5.5 mm × 5.5 mm area on a CaF_2 substrate, SEM images show an array of metaunits consisting of ulu-shaped Au nanostructures supporting polarization-multiplexed multi-resonance modes for broadband spectral coverage. Simulation generated images show the E-field enhancement pattern in a unit cell for orthogonal polarizations. **c**, MIRSI and SE-MIRSI of murine brain tissue section at different wavenumbers corresponding to absorption bands of functional groups present in endogenous biomolecules such as glycogens, nucleic acids, proteins, and lipids.

References

1. Schwaighofer, A. *et al.* Beyond Fourier Transform Infrared Spectroscopy: External Cavity Quantum Cascade Laser-Based Mid-infrared Transmission Spectroscopy of …. *Anal. Chem.* **90**, 7072–7079 (2018)
2. Tiwari, S. *et al.* Infrared Spectroscopic Imaging Visualizes a Prognostic Extracellular Matrix- Related Signature in Breast Cancer. *Sci Rep* **10**, 5442 (2020).
3. Rosas, S. et al. Metasurface-enhanced mid-infrared spectrochemical imaging of tissues (2023), doi:10.48550/arXiv.2301.05884.

META 2023, PARIS - FRANCE, JULY 18 – 21, 2023

Plasmon Resonances in Ga Nanoparticles and Plasmonic Antennas for Biosensing

M. Horák[1*], V. Čalkovský[1], V. Křápek[1], J. A. Riley[2], V. Pacheco-Peña[2], J. Mach[1], and T. Šikola[1]

[1]Brno University of Technology, Brno, Czech Republic
[2]Newcastle University, Newcastle Upon Tyne, United Kingdom
[*]Corresponding author: michal.horak2@ceitec.vutbr.cz

Abstract: We present a study of biocompatible gallium nanoparticles using STEM-EELS on a single particle level showing that they support plasmon resonances in the ultraviolet to visible spectral region. Moreover, we introduce a study of complementary plasmonic antennas designed using Babinet's principle and demonstrate spectral changes in the localized surface plasmons resonances when introducing variations in the parameters of a nearby dielectric analyte.

Localized surface plasmons (LSP) are self-sustained collective oscillations of free electrons in metal nano- and microstructures coupled to the local electromagnetic field. The mapping of LSP resonances with high spatial and energy resolution is necessary to understand their origin and properties. Scanning transmission electron microscopy (STEM) combined with electron energy loss spectroscopy (EELS) has become a standard technique to map LSP resonances in individual nanoparticles with a nanometer spatial and good energy (in our case 0.1 eV) resolution [1]. In this contribution, we will discuss LSP resonances in biocompatible gallium nanoparticles and we will explore the use of Babinet's principle in plasmonics for sensing.

Gallium is commonly known as a metal with a melting temperature of 29.7 °C. It is non-toxic and rather friendly to the environment. It has several solid-state phases which enable a variety of phase-changing systems which are under investigation. The bulk plasmon energy of gallium is 13.7 eV and it has in the liquid phase no interband transitions in a wide region from ultraviolet to infrared, which makes it an ideal plasmonic candidate. We have explored the plasmonic nature of its nanoparticles and shown that its plasmon resonances can be tuned from the ultraviolet to the visible spectral region by simply changing the size of the nanoparticle [2].

Babinet's principle originates in the wave theory of light and analysis of diffraction. Moreover, it is a classical EM theory that considers perfect electric conductions. In plasmonics, it relates the properties of a planar plasmonic antenna (particle) and a complementary aperture in a thin metal film of the same size and shape. In particular, the energies of LSP resonances in both antennas shall be identical and the corresponding near fields shall be complementary with the electric field distribution of the solid antenna corresponding to the magnetic field distribution of the complementary aperture [3–5]. This link allows studying the magnetic near field, for example, by measuring the electric near field by EELS in the complementary structure [6].

In this communication, we make use of Babinet's principle to design and demonstrate the performance of plasmonic sensors. We will explore the dimers of gold nanodiscs and the dimers of disc-shaped apertures in a gold film. Our recent efforts to understand their performance in terms of LSP resonances span from numerical to experimental demonstrations. We will also discuss the potential of these plasmonic nanostructures to be used as sensors by observing spectral variations of their LSP resonances depending on the thickness and refractive index of a dielectric analyte introduced on/into the plasmonic structure [7].

Numerical and experimental, studies of complementary plasmonic antennas designed using Babinet's principle will be presented. Spectral changes in the localized surface plasmons resonances will be demonstrated when introducing variations in the parameters of a nearby dielectric analyte.

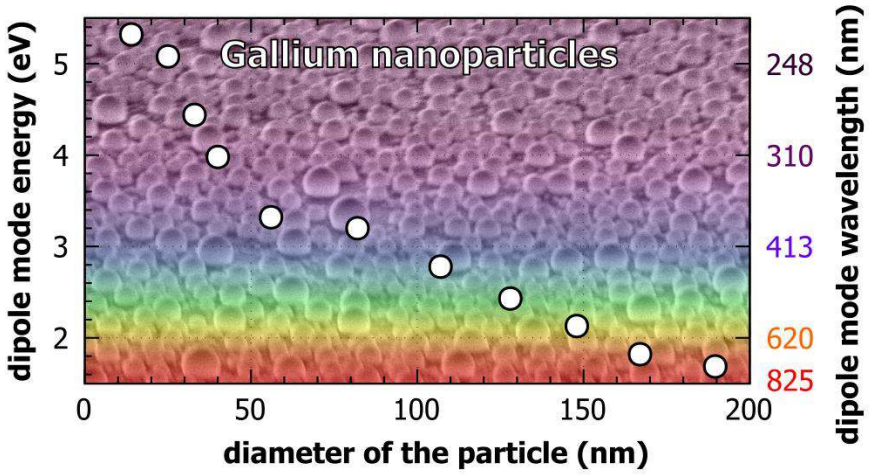


Figure 1: Energy of the dipole LSP mode in a set of gallium nanoparticles as a function of the diameter of the nanoparticle covering the spectral region from ultraviolet across visible to near-infrared.

This research has been supported by GACR (22-04859S) and MEYS CR (CzechNanoLab, LM2018110).

References

1. Horák, M. and T. Šikola "Influence of experimental conditions on localized surface plasmon resonances measurement by electron energy loss spectroscopy," Ultramicroscopy, Vol. 216, 113044, 2020.
2. Horák, M., Čalkovský, V., Mach, J., Křápek, V., and T. Šikola "Plasmonic properties of individual gallium nanoparticles," J. Phys. Chem. Lett., 2023.
3. Horák, M., Křápek, V., Hrtoň, M., Konečná, A., Ligmajer, F., Stöger-Pollach, M., Šamořil, T., Paták, A., Édes, Z., Metelka, O., Babocký, J. and T. Šikola "Limits of Babinet's principle for solid and hollow plasmonic antennas," Sci. Rep., Vol. 9, 4004, 2019.
4. Hrtoň, M., Konečná, A., Horák, M., Šikola, T. and V. Křápek, "Plasmonic Antennas with Electric, Magnetic, and Electromagnetic Hot Spots Based on Babinet's Principle," Phys. Rev. Appl., Vol. 13, 054045, 2020.
5. Křápek, V., Konečná, A., Horák, M., Ligmajer, F., Stöger-Pollach, M., Hrtoň, M., Babocký, J. and T. Šikola "Independent engineering of individual plasmon modes in plasmonic dimers with conductive and capacitive coupling," Nanophotonics, Vol. 9, 623–632, 2020.
6. Horák, M., Křápek, V., Hrtoň, M., Konečná, A., Ligmajer, F., Stöger-Pollach, M. and T. Šikola " Magnetic near field imaging with electron energy loss spectroscopy based on Babinet's principle," Microsc. Microanal., Vol. 26, No. S2, 2628–2630, 2020.
7. Riley, J. A., Horák, M., Křápek, V. and V. Pacheco-Peña, "Complementary plasmonic sensors," In preparation, 2023.

META 2023, PARIS - FRANCE, JULY 18 – 21, 2023

Plasmonic metamolecular units for biological analytes investigation

M. Rippa[1*], V. Marchesano[1], A. Vestri[1], D. Sagnelli[1], L. Zhou[1], G. Fusco[2], J. Zyss[3], J. Zhou[4], and L. Petti[1]

[1]Institute of Applied Sciences and Intelligent Systems of CNR, 80072 Pozzuoli, Italy
[2]Istituto Zooprofilattico Sperimentale del Mezzogiorno, Portici 80055, Italy
[3]LUMIN Laboratory and Institut d'Alembert, Ecole Normale Supérieure Paris-Saclay, CNRS, Université Paris-Saclay, 91190 Gif-sur-Yvette, France
[4]Institute of Photonics, Faculty of Science, Ningbo University, Ningbo, People's Republic of China
*corresponding author: m.rippa@isasi.cnr.it

Abstract: The study of novel plasmonic nanopatterns are of great interest for different applications including biological investigation and sensing. In this work we design, fabricate and characterize periodic arrangements of a novel metamolecular cell based on gold nanoelements. We tested their SERS performance analyzing different analytes among which a SARS-CoV-2 (COVID-19) Spike Antibody. Our results suggest that these plasmonic patterns are promising to develop nanodevices for the analysis of biological samples.

Development of nanostructures based on plasmonic functionalities is of great interest for a range of applications including optoelectronic devices, sensing and platforms to improve the performance in spectroscopic measurements [1, 2]. The ability to manipulate and control visible and infrared light using nanopatterns based on different geometries of metallic elements has been used to realize displays, filters, and anti-counterfeiting and sensing systems with unique and outstanding properties [3, 4]. In case of biological applications, many nanoscale systems based on gold nanoelements have been designed and tested in several research works for the study and detection of various kinds of biological analytes, giving appreciable results [5-7]. Plasmonic properties associated to the nanostructure can be tuned by changing the size and the shape of the nanoparticles or the periodicity or, more in general, the geometry of the nanopattern. These features are key to many applications aiming at signal enhancement and low threshold sensing. In this work we present a study of periodic arrangements of novel plasmonic metamolecular unit cells made of triangular nanoelements. Their plasmonic properties were firstly analyzed through numerical simulations using the finite element method (FEM) approach and their size were optimized appropriately, Successively, the nanostructures analyzed were fabricated using electron beam lithography technique (EBL) that allows to create patterns with high repeatability and accuracy. Morphological analysis was realized by Scanning Electron Microscopy (SEM) and their plasmonic properties were studied and compared using experimental set-up for Localized Surface Plasmon Resonance (LSPR) and Surface Enhanced Raman Spectroscopy (SERS) measurements. We finally tested the sensing performance of our nanostructures by detecting both Norovirus and a Spike Antibody SARS-CoV-2 (COVID-19) obtaining its

molecular fingerprint and developing some functionalization strategies for both of them on the surface of the nanopatterns under consideration. The experimental activities were realized in the frame of the projects "SERSCov-Advanced Nanobiosensing platforms for diagnostics and POC surveillance" funded by POR Campania FESR 2014/2020 (CUP B53C22003100002) and "H2OSafety-Design and development of environmental sensors for the research of microbiological and chemical contaminants hazardous to health" funded by the National Fund Sviluppo e Coesione (FSC) Proof of Concepts projects (POC01_00109).

Our preliminary results suggest that the considered plasmon nanopatterns are promising for the development of devices for rapid, label-free and high-sensitivity detection of biological analytes and, moreover, they can be integrated with other on-chip chemical/biological devices to realize portable points-care-tools.

References

1. Mejía-Salazar, J. R.; Oliveira, O. N., Jr. "Plasmonic Biosensing (focus review)". Chem. Rev., Vol. 118, 10617−10625, 2018.
2. Rippa, M., Sagnelli, D., Vestri, A., Marchesano, V., Munari, B., Carnicelli, D., Varrone, E., Brigotti, M., Tozzoli, R., Montalbano, M., Morabito, S., Zhou, J., Zyss, J. and Petti, L. Plasmonic Metasurfaces for Specific SERS Detection of Shiga Toxins. ACS Appl. Mater. Interfaces, Vol. 14, 4, 4969–4979, 2022.
3. Caligiuri, V., De Sio, L., Petti, L., Capasso, R., Rippa, M., Maglione, M. G., Tabiryan, N., Umeton, C. Electro-/All-Optical Light Extraction in Gold Photonic Quasi-crystals Layered with Photosensitive Liquid Crystals. Adv. Opt. Mater., Vol. 2, 950−955, 2014.
4. Barbillon, G. Plasmonics and its Applications. Materials; Vol. 12, 9, 1502, 2019.
5. Rippa, M., Castagna, R., Zhou, J., Paradiso, R., Borriello, G., Bobeico, E., Petti, L. Dodecagonal plasmonic quasicrystals for phagebased biosensing. Nanotechnology, Vol. 29, 405501, 2018
6. Mosier-Boss, P. Review on SERS of Bacteria. Biosensors, Vol. 7, 51, 2017.
7. Sonntag, M.D., Klingsporn, J.M., Zrimsek, A.B., Sharma, B., Ruvuna, L.K., Van Duyne, R.P. Molecular plasmonics for nanoscale spectroscopy. Chem. Soc. Rev., Vol. 43, 1230–47, 2014.

META 2023, PARIS - FRANCE, JULY 18 – 21, 2023

Development of plasmonic platforms for sensitive and selective detection of macromolecules for food-quality assessment and environmental monitoring

G. Rusciano[1*]

[1] *Department of Physics "E.Pancini, University of Naples "Federico II"* - Naples, Italy.
[*]corresponding author: giulia.rusciano@unina.it

Abstract: Surface-Enhanced Raman Spectroscopy is a powerful analytical technique which allows high sensitivity and chemical specificity thanks to the fingerprint character of Raman spectra. Herein, we present the development of novel silver-based SERS substrates endowed with relevant plasmonic performances and their use for the detection of species of environmental interest (Polycyclic Aromatic Hydrocarbons) and relevant for food-quality monitoring (melamine and lipopolysaccharides).

Nanostructures supporting surface plasmon resonance (SPR) have been widely used for sensing and biosensing applications, being at the base of different techniques, including surface-enhanced Raman spectroscopy (SERS). In the last years, SERS has attracted a high interest for the effective detection of analytes across a wide range of scientific and technological fields. Alongside the label-free nature and molecular specificity deriving from the chemical fingerprint character of Raman spectroscopy, SERS can benefit of the great amplification of Raman signals for molecules in close proximity of proper plasmonic nanostructures, allowing even the single-molecule detection. The amplification is mainly due to the excitation of the localized surface plasmon resonances (LSPRs), which originates from the resonant collective oscillation of conduction electrons on noble metal nanostructured surfaces. Since the SERS substrate plays a key role, that explains the efforts are still underway for the development of nanostructured films that are easy to produce, reproducible and with high Enhancement Factor (EF), being the latter typically of the order of 10^4-10^8.

In this work, a novel approach has been followed to fabricate highly porous SERS substrates: the process consists of three steps, schematically depicted in Fig. 1, and described in detail in [1]. In the first step, a cleaned glass coverslip (15x15 mm^2) is sequentially coated with 3 nm Cr, 10 nm Au and 30 nm Ag by magnetron sputtering. The Cr/Au bilayer assures a high adhesion of Ag layer to the underlying layer. In a second step, the substrate is exposed to an inductively coupled plasma (ICP) in synthetic air atmosphere (power = 18W, p = 0.4Torr, exposure time = 90 s). As a matter of fact, the reactive oxygen species produced in the discharge give rise to the morphological evolution of the surface metal through complex surface physics mechanisms, which leads to a high porous nano-patter, resembling to a coral-like structure (Fig.1(b)). While oxygen is crucial for nanopattering, it gives rise to the oxidation of the material which reduces its plasmonic properties. Therefore, in a third step the substrate is exposed to a further ICP treatment but using Argon as gas process (exposure time = 50 s). This step has revealed very effective in the removal of oxide layer by preserving the pristine nanotexture. Globally, our protocol produces substrates with an excellent spatial reproducibility, EF larger than 10^7, and a broad-band optical response in the Vis-NIR spectral range, which enables Raman band amplification even at wavelengths quite far from the Raman probe wavelenght.

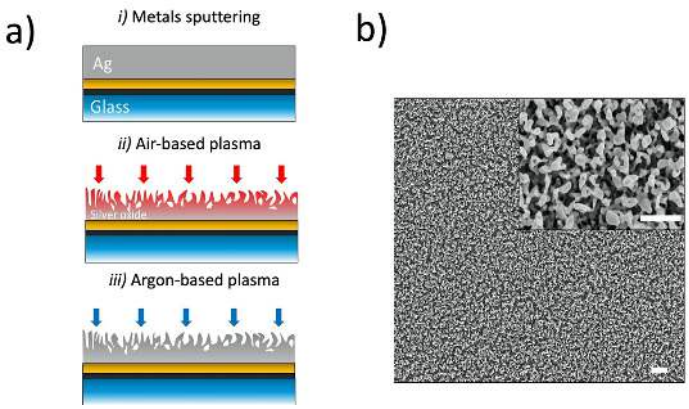


Figure 1: a) Schematic representation of the SERS substrates fabrication process. b) SEM image of SERS substrate (scale bar=1 μm). The inset shows the magnification of the SEM image (scale bar=500 nm).

These substrates have been successfully employed for the detection of chemical species relevant for the environment and food safety. Among these, of particular importance for environmental issues are Polycyclic aromatic hydrocarbons (PAHs), cancerogenesys species mainly originating from the incomplete combustion of fossil fuels. Despite the apolar nature of the PAH, our substrates are able to detect them in water without any functionalization of the surface, reaching a limit of detection (LOD) of ~ 20 nM for pyrene (PYR) [2].That because, the nanoporous nature combines a high density of hotspots with the capacity to trap PAH molecules through not covalent bonding, facilitating their adhesion to the metallic surface. In perspective, our outcomes demonstrate the high potentiality of our approach for chemical sensing and environmental control applications.

Our SERS substrates have also been used for the detection of lipopolysaccharides (LPS) in complex matrices. LPS are macromolecules consisting of lipidic and polysaccharide groups that are bacterial toxins. They are released by bacterial cells when they integrate. In order to assure a selective LPS detection in complex environment, our substrate was coated with an LPS antibody (Ab@c-SERS). LPS was revealed by the analysis of the slight modification of the antibody Raman bands. Interestingly, a detection limit of a few ng/mL was achieved.

Finally, SERS studies have been done for the detection of melamine, a toxic, nitrogen-rich chemical used for adhesives and glues but also illegally added to foodstuff (such as milk for infant) to increase apparently the protein content.

References

1. Capaccio, A., Sasso, A., Rusciano, G. “A simple and reliable approach for the fabrication of nanoporous silver patterns for surface-enhanced Raman spectroscopy applications”, Sci Rep., Vol. 11, No 1, 22295, 2021.
2. Capaccio, A., Sasso, A., Rusciano, G. “Feasibility of SERS-Active Porous Ag Substrates for the Effective Detection of Pyrene in Water” *Sensors* Vol. No *22*, 2764, 2022.

Optical metasurfaces with hybrid TE-TM collective resonances for spectroscopic applications

R. Kolkowski[1*] **and A. Shevchenko**[1]

[1]Department of Applied Physics, Aalto University, P.O.Box 13500, Aalto FI-00076, Finland
[*]corresponding author: radoslaw.kolkowski@aalto.fi

Abstract: Due to their narrow spectral bands, collective resonances of periodic metasurfaces are of growing interest in many areas of photonics. Here, we investigate collective resonances that emerge from coupling between TE and TM modes via plasmonic nanoparticles in a metasurface-based slab waveguide. We show that these hybrid resonances can provide high local field enhancement and high quality factors, which makes such plasmonic-photonic metasurfaces especially promising for applications in spectroscopic sensing and detection.

Optical resonances are essential for many photonic applications, such as spectroscopy, metrology, laser technology, nonlinear optics, etc. The quality factor Q is directly related to spectral width, $\Delta\omega$, of the resonance, or the damping rate γ ($Q = \omega/\Delta\omega = \omega/2\gamma$). Periodic metasurfaces can support high-Q resonances known as Surface Lattice Resonances (SLRs)[1] which result from multiple scattering of light by periodically arranged structural units of the metasurface (meta-atoms).[2] Of particular interest are dark SLRs, such as those that form quasi-bound states in the continuum (quasi-BICs).[3] Their coupling to external radiation can be controlled by tuning the symmetry of the structure towards a desired tradeoff between a high excitation efficiency and a low radiative loss.

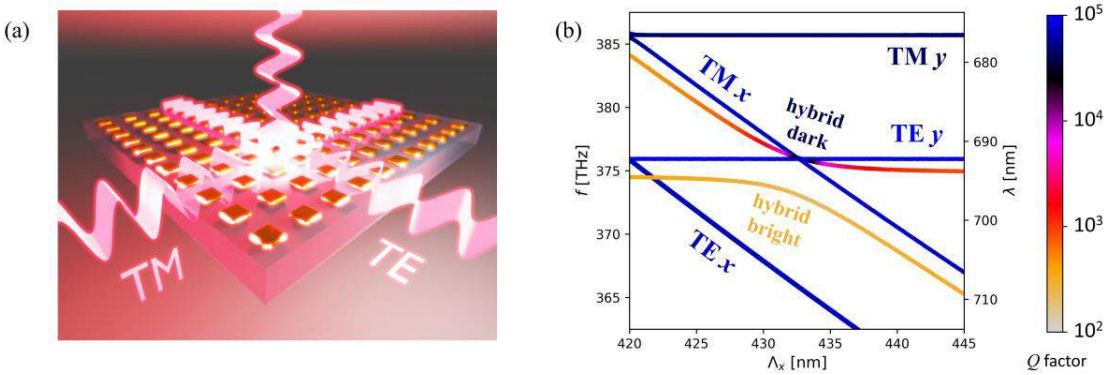


Fig. 1. (a) Illustration of a metasurface (a slab waveguide coupled to a plasmonic nanoantenna array) supporting hybrid TE-TM resonances. (b) Eigenmodes of a metasurface at normal incidence ($k_x = k_y = 0$) with varying lattice period Λ_x and fixed $\Lambda_y = 420$ nm, calculated using COMSOL Multiphysics.

In this work, we consider periodic metasurfaces on a slab waveguide in which multiple scattering is mediated by the guided modes of the waveguide.[4] In the absence of nano-scatterers, the waveguide supports mutually orthogonal TE and TM modes. These modes can be efficiently mixed by periodically arranged nano-scatterers on the waveguide surface. The nano-scatterers give rise to SLRs with band edges at the 2nd Bragg condition (resonant wavelength $\lambda_{res} = \Lambda n_{eff}$, where Λ is the lattice period and n_{eff} is the effective mode index). These SLRs can be excited by light at normal incidence. The resonance condition along a given lattice direction is different for TE and TM modes due to their different mode indices ($n_{TE} \neq n_{TM}$). However, by tuning the

periodicity Λ independently along the two orthogonal lattice directions (Λ_x and Λ_y), the resonance conditions for the TE and TM modes can be matched (e.g., $\Lambda_y n_{TE} = \Lambda_x n_{TM}$). Figure 1(b) shows the anti-crossing of TE and TM resonances in the presence of resonant nano-scatterers (gold nanoparticles) creating two hybrid TE-TM resonances: a red-shifted low-Q bright resonance and a blue-shifted high-Q dark resonance. The latter forms accidental degeneracies with completely dark modes whose field profiles "avoid" the nano-scatters. Near the degeneracies, the Q factor of the hybrid TE-TM resonance is boosted even further. At the same time, the local field enhancement at the nanoparticle surface and inside the waveguide remains relatively strong, as can be seen in Fig. 2(a). In addition, the field profile, shown in Fig. 2(b), does not resemble any of the conventional modes, but constitutes a mixture of the TE and TM modes.

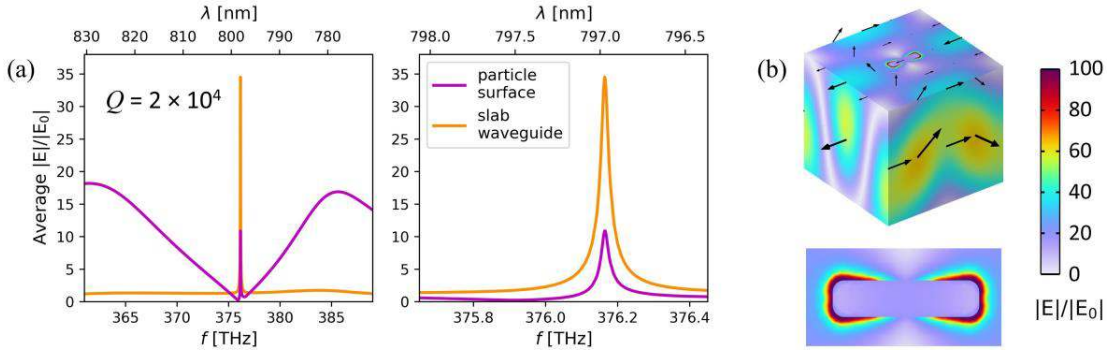


Fig. 2. (a) Spectra of the average field enhancement at the surface of a gold nanoparticle (magenta) and inside the waveguide (orange) under normal incidence illumination for $\Lambda_x = 432$ nm and $\Lambda_y = 420$ nm. The dark hybrid resonance at 376.2 THz exhibits $Q = 2\times10^4$. (b) On-resonance electric field distribution inside the waveguide and around the particle. Calculations are done using COMSOL Multiphysics.

Because of a high Q factor and strong field enhancement, the TE-TM collective resonances presented above can be used in spectroscopy, especially surface-enhanced Raman spectroscopy. Moreover, the mechanisms underlying their formation are very general, enabling one to choose a proper material platform and optimize the metasurface design for specific purposes. Experimental realization of such metasurfaces is one of the current goals of our ongoing research.

The authors acknowledge the support of the Academy of Finland (Grants No. 347449 and 353758) and the Flagship of Photonics Research and Innovation (PREIN) funded by the Academy of Finland (Grant No. 320167). For computational resources, the authors acknowledge the Aalto University School of Science "Science-IT" project and CSC – IT Center for Science, Finland.

References

1. Kravets, V. G., *et al.*, "Plasmonic Surface Lattice Resonances: A Review of Properties and Applications," Chem. Rev., Vol. 118, No. 12, 5912–5951, 2018.
2. Vaskin, A., *et al.*, "Light-emitting metasurfaces," Nanophotonics, Vol. 8, No. 7, 1151–1198, 2019.
3. Koshelev, K., *et al.*, "Asymmetric Metasurfaces with High-Q Resonances Governed by Bound States in the Continuum," Phys. Rev. Lett., Vol. 121, No. 19, 193903, 2018.
4. Christ, A., *et al.*, "Waveguide-Plasmon Polaritons: Strong Coupling of Photonic and Electronic Resonances in a Metallic Photonic Crystal Slab," Phys. Rev. Lett., Vol. 91, No. 18, 183901, 2003.

Plasmonic sensing for application in food science and eco/nanotoxicology

Duncan S. Sutherland[1]

[1]Interdisciplinary Nanoscience Center (iNANO), Aarhus University, Aarhus, Denmark

corresponding author, E-mail: duncan@inano.au.dk

Abstract:

Nanosized sensors based on the local refractive index sensitivity of plasmonic nanostructures can be applied to study interactions occurring at biointerfaces relevant for understanding proteins interactions in eco and nanotoxicology and in food science. Different functionalized plasmonic sensor designs will be described to study bio-interactions. Projects include detection of contaminants in milk via refractive index sensors and SERS, quantification of astringency in wine and the study of protein coronas in nanotoxicology.

Summary:

Metallic nanostructures supporting plasmon resonances are proposed and applied as enabling materials for bio and chemical sensors. Refractive index sensing structures at structures with appropriate functionalization can be applied for detection of molecules and bacteria through specific interactions [1,2]. For some applications such as in the food area, non-specific interactions or aggregate interactions from many different poorly specific interactions are responsible for important and measureable effects (such as sensations) requiring mimicking interfaces to provide useful sensing function. Measuring of astringency in foods and wines is complicated process typically carried out by panels of tasters and develops over the lifetime of the food. Here quantifying of specific (bio)molecules does not typically give a measure of the effect since it is an aggregate effect from many components. Plasmonic sensors can be used as multifunctional sensors allowing both refractive index measures and other spectral readouts. Here different plasmonic elements will be described as well as functionalization with biomolecules or molecular imprinted polymers to allow the study of both specific and non-specific interactions.

Examples of sensor development and designs relevant for food science and eco and nanotoxicology will be given. The first will relate to quantifying astringency in wine. Quantification of interactions of polyphenols with saliva proteins can be carried out via refractive index readout and correlated to conformational change of the proteins which are the initial steps in the sensations caused by astringency [1]. Approaches to capture biomimetic saliva coatings via MIPs allow both the classification of wines but also the study the role of individual polyphenol components from wine in causing astringency [3]. A second example will involve detection of contaminants in milk either bacteria (s. aureus) via aptamer functionalized plasmonic disk refractive index sensors [4] or disk/crescent cavity nanostructures for SERS detection of antibiotics, A last example with show quantification of protein and biotransformations relevant for nano and ecotoxicology where weak and strong interactions of proteins at different sites of silver nanocubes are studied via plasmon resonances [5] and related to biotransformations altering nanoparticle cytotoxicity [6].

. (1)

This work was funded by grants from the Danish research council (FTP and FNU) and the Portuguese research council

References

1. J.R.L. Guerreiro, M. Frederiksen, V.E. Bochenkov, V De Freitas, M.G.F Sales, D.S.Sutherland, Multifunctional biosensor based on Localized Surface Plasmon Resonance for monitoring small molecule-protein interaction, ACS Nano 8: 7958-7967, 2014
2. H. Baccar, M.B. Mejri, I. Hafaiedh, T. Ktari, M. Aouni, A. Abdelghani, Surface plasmon resonance immunosensor for bacteria detection, Talanta 82: 810-4, 2010
3. J.R.L. Guerreiro, V.E. Bochenkov, K. Runager, H. Aslan, M. Dong, J.J. Enghild, V. De Freitas, M.G.F. Sales, D.S. Sutherland, Molecular imprinting of complex matrices at localized surface plasmon resonance biosensors for screening of global interactions of polyphenols and proteins, ACS Sensors 1: 258-264, 2016
4. H. Khateb, G. Klös, R. L. Meyer and D. S. Sutherland "Development of a label-free LSPR-Apta sensor for Staphylococcus aureus detection" ACS Applied Bio Materials 5: 3066–3077 2020
5. T. Miclaus, V.E. Bochenkov, R. Ogaki, K.A. Howard, D.S. Sutherland "Spatial Mapping and Quantification of Soft and Hard Protein Coronas at Silver Nanocubes, Nano Letters 14: 2086-2093, 2016
6. T. Miclaus, C. Beer, J. Chevalier, C Scavenius, V.E. Bochenkov, J.J. Enghild, D.S. Sutherland "Dynamic protein corona revealed as a modulator of nanoparticle sulphidation in vitro, Nature Communications 7: 11770, 2016

Nanoplasmonic sensing of food product and neurochemistry

J.-F. Masson[1], F. M. Lastname[1*], and F. M. Lastname[2]

[1] Université de Montréal, Canada
[*]corresponding author: jf.masson@umontreal.ca

Abstract: This presentation will introduce our research activities in plasmonic nanobiosensing, where we use metallic nanoparticles to develop LSPR and SERS sensors for a series of applications. This paper will highlight our latest developments for sensing off-flavors in maple syrup and neurotransmitters involved in neurochemical processes.

Our research lies in the areas of plasmonic materials, low-fouling surface chemistry and instrumental design for biosensing. This presentation will focus on applying these concepts for several classes of sensors, such as for monitoring off flavors in maple syrups and our recent development of sensors for in tissue measurement of neurotransmitters. In the first example, AuNP were optimized to aggregate in presence of maple sap or syrup presenting off flavors. The sensor was tested with more than 30,000 maple syrups in the lab and at the maple sugar shacks by producers (Figure 1). In a second embodiment of our research, we are currently exploring the concept of optophysiology using plasmonic nanopipettes for monitoring living cell secretion events. Due to the lack of analytical techniques for detecting metabolites near living cells, developing tools to monitor cell secretion events remains a challenge to overcome in chemical analysis. Plasmonic nanopipettes were developed based on the decoration of patch clamp nanocapillaries with Au nanoparticles (Figure 2). The plasmonic nanopipette is thus competent for dynamic SERS measurements in the liquid environment near cells. We combine this technique with machine learning to identify spectral differences in analytes and in different conditions. This nanobiosensor was tested with the detection of small metabolites near living cells and of neurotransmitters released by neurons.

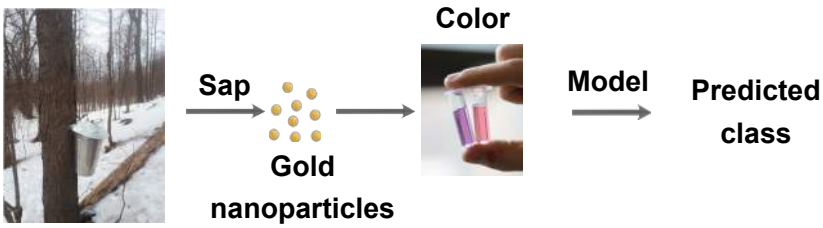


Figure 1. Concept of a maple syrup / maple sap plasmonic text to predict the commercial grade of the maple syrup.

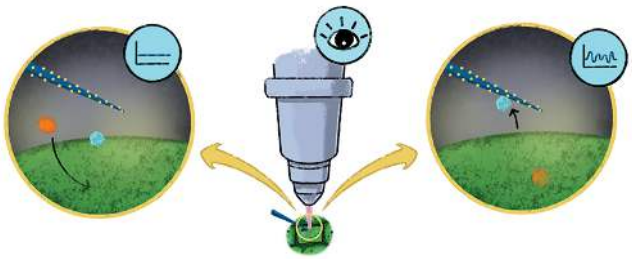


Figure 2. SERS optophysiology: a plasmonic nanofiber is placed in proximity of cells/neurons and detects metabolites/neurotransmitters with SERS. Machine learning is applied to extract molecular information from SERS.

Optomechanical disk resonators for real-time environmental monitoring and single-nanoparticle detection

E. Sentre-Arribas[1], Eduardo Gil-Santos[1*], O. Malvar[1], J. J. Ruz[1], S. Sbarra[2], L. Waquier[2], A. Lemaître[3], M. S. van der Heiden[4], R. K. Altmann[4], D. Papanastasiou[5], D. Kounadis[5], I. Panagiotopoulos[5], I. Favero[2], M. Calleja[1] and J. Tamayo[1]

[1]Bionanomechanics Lab, Instituto de Micro y Nanotecnología, IMN-CNM (CSIC), Spain.
[2] Matériaux et Phénomènes Quantiques, CNRS, Université Paris-Cité, France.
[3]Centre des Nanosciences et Nanotechnologies, CNRS, Université Paris-Saclay, France
[4]Netherlands Organization for Applied Scientific Research (TNO), the Netherlands.
[5]Fasmatech Science and Technology, Greece.
[*]Corresponding author: eduardo.gil@csic.es

Abstract: Optomechanical resonators have been successfully applied on a variety of sensing applications. Here we propose combining the optical and mechanical signals provided by this kind of devices, in order to increase their sensitivity and reliability. In particular, we use nano-optomechanical disks fabricated out of GaAs. They support high quality optical and mechanical modes that allow for high accuracy measurements. First, we apply the dual sensing technique for monitoring environmental changes. Then, we focus on the detection of single nanoparticles.

Over the last years, optomechanical resonators have stood out in terms of sensing since they exploit both optical and mechanical modes, combining the extraordinary sensitivity of optical resonator sensors and the reliability of mechanical ones. Here we use optomechanical resonators for two different sensing applications: environmental monitoring and nanoparticle detection. In particular, we employ semiconductor disk resonators fabricated out of GaAs. Optically, disk resonators support the so called whispering gallery modes (WGMs), which couple very efficiently with a particular family of mechanical modes, the radial breathing modes (RBMs) (Figure 1) [1].

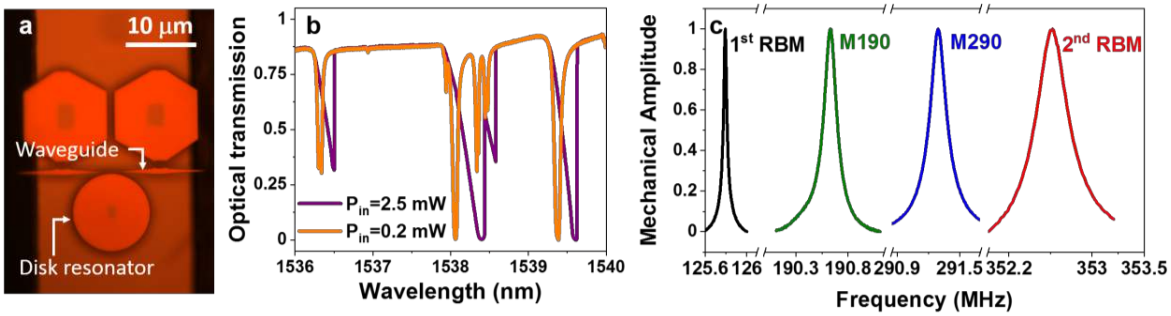


Figure 1: Optical and mechanical resonant modes. a*. Optical microscope image of a GaAs disk resonator of radius 11 μm and thickness 200 nm, together with its integrated waveguide and supporting structures.* ***b****. WGMs of the disk measured at different input powers: 2.5 mW (purple) and 0.2 mW (orange).* ***c****. Mechanical spectrum measured at 2.5 mW. Specifically, it shows the resonances associated to the 1st and 2nd RBMs (black and red) and two other in-plane modes labeled as M190 and M290 (green and blue).*

The in-plane nature of the motion associated to RBMs provides them excellent assests when operating in air, and even, in liquids [2]. For monitoring environmental changes, we employ a disk of 2.5 μm in radius and 320 nm in thickness. Figure 2 shows their optical and mechanical response to temperature and humidity changes. Taken into account the Allan variance, we demonstrate very high resolution reaching 1 mK and 0.1%, respectively. Notably, combining optical and mechanical sensing, enables disentangling temperature and humidity effects [3]. For nanoparticle (NP) detection experiments, in order to increase the capture area and, thus, the efficiency, we employed

disks having 11 μm in radius and 200 nm in thickness. Figure 3 shows the optical and mechanical response of a device, when a single polystyrene nanoparticle (70 nm in radius) is adsorbed. The dual sensing approach allows accessing the NP optical and mechanical properties [4].

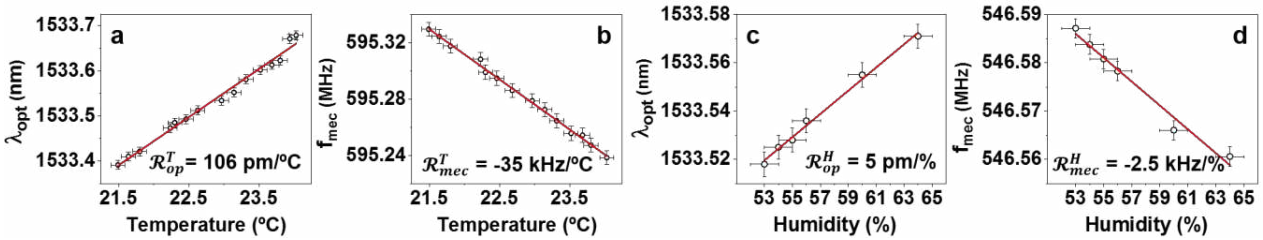


Figure 2: Environmental monitoring. ***a****. Optical resonant wavelength and* ***b****. mechanical resonant frequency of the 1st RBM as a function of temperature, at constant relative humidity 55%.* ***c****. Optical resonant wavelength of the same WGM and* ***d****. mechanical resonant frequency of the 1st RBM as a function of humidity, at constant relative temperature 23ºC.*

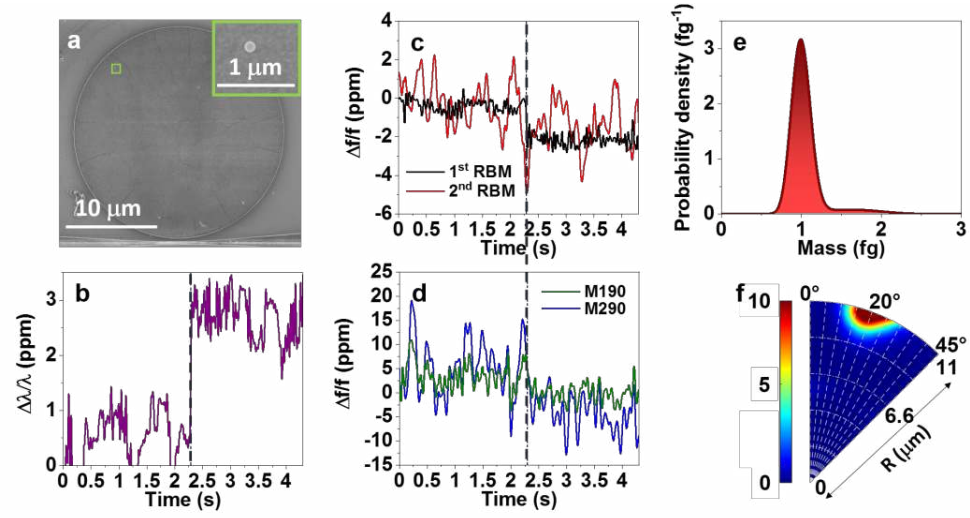


Figure 3: Single NP detection. ***a****. Scanning electron microscope image of a disk resonator with an adsorbed polystyrene NP (70 nm in radius).* ***b****. Relative optical wavelength shift and* ***c****.* ***d****. relative mechanical frequency shifts induced by the NP adsorption.* ***e****. Calculated mass and* ***f****. adsorption position probability spectra.*

Acknowledgements: Work produced with the support of a 2021 Leonardo Grant for Researchers and Cultural Creators, BBVA Foundation. The Foundation takes no responsibility for the opinions, statements and contents of this project, which are entirely the responsibility of its authors. E.G.S. acknowledges financial support by the Spanish Science and Innovation Ministry through the Ramón y Cajal grant RYC2019-026626-I. Also supported by the European Union's Horizon 2020 Research and Innovation Program under Grant Agreement No. 731868-VIRUSCAN. We acknowledge the service from the Micro and Nanofabrication Laboratory and X-SEM laboratory at IMN-CNM funded by the Comunidad de Madrid (Project S2018/NMT-4291 TEC2SPACE) and by MINECO (Project CSIC12-4E-1794 with support from FEDER, FSE).

References

1. L. Ding, et al. "Wavelength-sized GaAs optomechanical resonators with gigahertz frequency". Applied Physics Letters, 98, 113108 (2011).
2. E. Gil-Santos, et. al. "High-frequency nano-optomechanical disk resonators in liquids". Nature Nanotechnology, 10, 810 (2015).
3. E. Sentre-Arribas, et. al. "Simultaneous optical and mechanical sensing based on nano-optomechanical disks". *In preparation.*
4. O. Malvar, et al. "Multifrequency nanomechanical mass spectrometer prototype for measuring viral particle using optomechanical disk resonators". To be published in 2023 IEEE 36th International Conference on MEMS.

Optical pushing of plasmonic nanoparticles for high-sensitivity spectroscopy of molecules and nanoplastics

M.G. Donato[1], S. Bernatova[2], M. Kizovsky[2], A. Foti[1], J. Jezek[2], O. Samek[2], O. M. Marago[1], P. Zemanek[2] and P. G. Gucciardi[1]

[1]CNR – IPCF, Istituto per I Processi Chimico-Fisici, Viale F. Stagno D'Alcontres 37, I-98158 Messina, Italy
[2] Institute of Scientific Instruments, Czech Academy of Sciences, Brno, Czech Republic
*corresponding author: maria.donato@cnr.it

Abstract: Optical forces can be used to trap, manipulate and push micro and nanoparticles. In this work we will discuss the realization of aggregates of plasmonic nanoparticles by optical pushing, aiming at the high-sensitivity sensing of biomolecules and microplastics.

High-sensitivity detection of contaminants is an important task in fields such food safety and environmental monitoring. In this work, it will be shown how optical [1] and thermophoretic forces [2] can be exploited to create aggregates of plasmonic nanoparticles directly in liquid environment on flat [3] and curved surfaces [4] of different nature [5], in short times (tens of seconds) and without special preparation. The aggregates are active sites for the Surface Enhanced Raman Spectroscopy of proteins and toxins [6], decreasing their ordinary Raman limit of detection in solution by several orders of magnitude. Moreover, thermal gradients due to the heating of the plasmonic aggregates induces thermophoretic fluxes, which concentrate the microplastics dispersed in the liquid and improve their detection [7].

The authors acknowledge support from the Czech Academy of Sciences, project MSM100652101 and from the projects MERLIN-MICROPLASTIQUE (agreement 17/1212947B), ASI-INAF n.2018-16-HH.0 "SPACE Tweezers," MSCA ITN (ETN) project "Active Matter," COST Action CA20101 - Plastics monitoRIng detectiOn RemedIaTion recoverY (PRIORITY), and from the European Union (NextGeneration EU), through the MUR-PNRR project SAMOTHRACE (ECS00000022)

References

1. P. H. Jones, et al., Optical Tweezers: Principles and Applications; Cambridge University Press: Cambridge, 2015
2. G. Baffou et al., "Applications and challenges of thermoplasmonics", Nat. Mater., Vol 19, 946-958, 2020.
3. B. Fazio et al., "SERS detection of Biomolecules at Physiological pH via aggregation of Gold Nanorods mediated by Optical Forces and Plasmonic Heating." Sci. Rep., Vol. 6, pp. 26952, 2016
4. M. G. Donato, et al., "Optical Force Decoration of 3D Microstructures with Plasmonic Particles," Opt. Lett., Vol. 43, pp. 5170−5173, 2018
5. A. Foti et al. "Optically induced aggregation by radiation pressure of gold nanorods on graphene for SERS detection of biomolecules", Eur. Phys. J. Plus, Vol. 136, p. 30, 2021
6. A. Foti et al. "Optical aggregation of gold nanoparticles for SERS detection of proteins and toxins in liquid environment: Towards ultrasensitive and selective detection", Materials, Vol. 11, p. 440, 2018
7. S. Bernatova et al., "Optical force aggregation of gold nanoparticles as a tool to fabrication a multifunctional sensor," Proc. SPIE 12502, 22nd Polish-Slovak-Czech Optical Conference on Wave and Quantum Aspects of Contemporary Optics, 125020U (12 December 2022)

Portable Microfluidic Plasmonic Chip for Fast Real-Time Cardiac Troponin I Biomarker Detection

A. Campu[1], I. Muresan[1], M. Potara[1], D. R. Lazar[2,3], F. L. Lazar[4], S. Cainap[2,5], D. Maniu[1,6], S. Astilean[1,6] and M. Focsan[1*]

[1]Nanobiophotonics and Laser Microspectroscopy Center, Interdisciplinary Research Institute in Bio-Nano-Sciences, Babes-Bolyai University, Treboniu Laurian No. 42, 400271 Cluj-Napoca, Romania
[2] Department of Paediatric Cardiology, Paediatric Clinic No. 2, Emergency County Hospital for Children, Crisan No. 3 – 5, 400124 Cluj-Napoca, Romania
[3] 11th Department of Medical Oncology, University of Medicine and Pharmacology "Iuliu Hatieganu", Republicii No. 34 – 36, 400171 Cluj-Napoca, Romania
[4] Medical Clinic No. 1, University of Medicine and Pharmacology "Iuliu Hatieganu", Victor Babes No. 8, 400012 Cluj-Napoca, Romania
[5] Department of Mother & Child, University of Medicine and Pharmacology "Iuliu Hatieganu", Louis Pasteur No. 4, 400349 Cluj-Napoca, Romania
[6] Biomolecular Physics Department, Faculty of Physics, Babes-Bolyai University, Mihail Kogalniceanu No. 1, 400084 Cluj-Napoca, Romania
[*]corresponding author: monica.iosin@ubbcluj.ro

Abstract: Acute myocardial infarction is the most serious cardiovascular illness; threatening human lives for decades. Its fast diagnosis can considerably improve the patient's prognosis as well as survival, thus a great amount of effort is directed to the development of biosensing technologies, which are able to efficiently and accurately detect the cardiac troponin biomarkers, the gold standard in detecting myocardial injury. Therefore, we developed a microfluidic plasmonic chip for the fast and accurate real-time detection of the cardiac troponin I biomarker.

Specifically, the fabrication of a plasmonic nanoplatform is based on immobilized gold nanobipyramids, which exhibits optical and thermoplasmonic properties that favour a multimodal localized surface plasmon resonance (LSPR) & surface enhanced Raman spectroscopy (SERS) & thermal detection of the cTnI biomarker. The plasmonic nanoplatform is characterized in terms of LSPR and SERS sensitivity and the thermoplasmonic performance is evaluated. Based on a sandwich-like immunoassay, the "proof-of-concept" LSPR-SERS-thermal detection of the cTnI in simulated conditions is evidenced. Furthermore, after the integration of the plasmonic nanoplatform in a microfluidic channel, the determination of the cTnI in real plasma samples is successfully realized and compared with a conventional high-sensitivity clinical assay proving good correlation. Thus, the proposed portable and miniaturized microfluidic plasmonic chip is validated for clinical applications supporting the further transfer to clinical settings for the early diagnosis of cardiac diseases and progress of personalized medicine.

Acknowledgements: This work was supported by CNCS-UEFISCDI Romania, under the project number PN-III-P2-2.1-PED-2019-3345.

Numerical optimization of the optical scattering response of plasmonic nanostructures

Sven Burger[12*], Fridtjof Betz[1], Felix Binkowski[1], Martin Hammerschmidt[12], Lilli Kuen[12], Phillip Manley[12], Matthias Plock[1], Phillip-Immanuel Schneider[12], Ivan Sekulic[12], Lin Zschiedrich[12*]

[1]Zuse Institute Berlin, D- 14195 Berlin, Germany
[2]JCMwave GmbH, Bolivarallee 22, D-14050 Berlin, Germany
https://www.zib.de/cno
*corresponding author: burger@zib.de

Abstract: We discuss numerical simulation and optimization methods and their application to models of optical light scattering from plasmonic nanostructures. Agreement between experimental results and corresponding numerical results is discussed for various settings.

Modern fabrication methods allow to fabricate plasmonic nanostructures at high accuracies. This in principle allows for highly efficient plasmonic devices in which electromagnetic field energy may be concentrated to very small volumes. Results from theoretical physics provide models which accurately describe physical processes in complex setups. However, in order to reach efficient designs which optimize specific interactions, numerical simulations and optimizations are frequently used, as these can be applied to arbitrary geometrical settings, are significantly easier to realize than experimental optimization setups, and may provide additional insight.

In this contribution we will discuss numerical simulation methods and machine learning based optimization algorithms (1,2) which have recently been developed in our group. In particular, hp finite element methods and Bayesian optimization based on Gaussian processes will be discussed. We will discuss recent applications of these methods to various nanoplasmonic and nanophotonic settings. These include nanoplasmonic, chiral and achiral setups for sensing, photo-chemistry, and photovoltaics (3-8). We will in particular focus on chiral interactions in plasmonic setups assembled by DNA-origami.

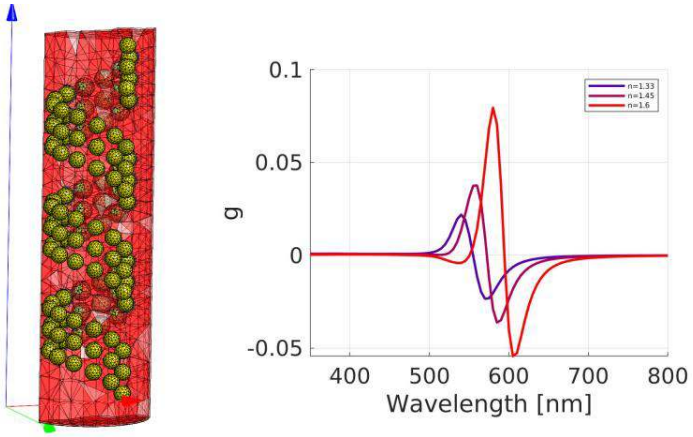


Figure: (Left) Visualization of a FEM model of a chiral arrangement of plasmonic nanoparticles. (Right) Wavelength-dependent chiral response (g-factor) for varied refractive index of the background material (blue: n=1.33, purple: n=1.45, red: n=1.6), obtained in numerical simulations.

Funded by the Deutsche Forschungsgemeinschaft (DFG, German Research Foundation) under Germany´s Excellence Strategy (MATH+, EXC-2046/1, project ID: 390685689). This project has received funding from the EMPIR programme co-financed by the Participating States and from the European Union's Horizon 2020 research and innovation programme (20IND04, 20FUN02, 20FUN05). This project has received funding from the German Federal Ministry of Education and Research (BMBF Forschungscampus MODAL, project number 05M20ZBM).

References

1. M. Plock, et al., Adv. Theory Simul. 5, 2200112 (2022)
2. F. Binkowski, et al., Commun. Phys. 5, 202 (2022)
3. K. Martens, et al., ACS Nano 16, 16143 (2022)
4. K. Martens, et al., Nat. Commun. 12, 2025 (2021)
5. S. Rej, et al., Nano Energy 104, 107989 (2022)
6. M. Dass, et al., Mater. Adv. 3, 3438 (2022)
7. F. Binkowski, et al., ACS Photon. 8, 1243 (2021)
8. P. Tillmann, et al., Opt. Express 29, 22517 (2021)

META 2023, PARIS - FRANCE, JULY 18 – 21, 2023

Mass customized optical metasurfaces

A. Kristensen*

[1]DTU Health Tech, Technical University of Denmark, DK-2800 Kongens Lyngby

*corresponding author: akri@dtu.dk

Abstract: Fabrication costs may limit applications of optical metasurfaces. This may be addressed by mass customization where identical metasurfaces or meta-film templates are manufactured by low-cost replication techniques, such as nanoimprint lithography, and differentiated for specific optical functionality by post-processing. High resolution and high throughput structural color prints as well as transparent flat optical elements are demonstrated.

This paper describes up-scalable fabrication of optical metasurfaces for ink-free color decoration and flat optics by post-processing homogenous template surfaces [1].

Our optical metasurfaces are based on the concepts of both localized surface plasmon resonances (LSPR) [2,3] and high-index dielectrics [4] compatible with technologies for high volume manufactured plastic products [5]. The optical metasurfaces are formed by nanoimprinting a surface texture comprising nanoscale cylinders. By subsequent deposition of a thin film of metal or high index dielectric, isolated nano-disks are formed on top of the cylinders, while a continuous film is formed on the substrate surface in between the cylinders. The nano-scale disks and corresponding holes in the continuous film form optical resonators. The master-original for the square-centimeter nano-texture is realized by means fast e-beam writing [6]. The nanotextured plasmonic metasurface may be covered with a transparent protective coating, which can withstand the daily life handling.

Laser post-writing can modify disks and holes, and hence the optical resonances [4,7]. Laser pulses induce transient local heat generation that leads to melting and reshaping of the imprinted nanostructures. This enables flexible definition and alignment of optical components on high volume manufactured plastic products [8]. Our approach offers a printing speed of 1 ns per pixel (in raster scan), resolution up to 127,000 dots per inch (DPI) and power consumption down to 0.3 nJ per pixel.

A cost-effective and lithography-free method for printing optical meta-films was also demonstrated [9]. It is based on resonant absorption of laser light in an optical cavity formed by a multilayer structure of ultrathin metal and dielectric coatings. A nearly perfect light absorption is obtained via interferometric control of absorption and operating around a critical coupling condition. Controlled by the laser power, the surface undergoes a structural transition from random, semi-periodic, and periodic to amorphous patterns with nanoscale precision. The reliability, upscaling, and subwavelength resolution of this approach are demonstrated by realizing metasurfaces for structural colors, optical holograms, and diffractive optical elements.

This work was in part supported via the EC funded project ODYSSEY (Grant agreement ID: 951899).

References

1. Zhu, X. et al, “Digital resonant laser printing: Bridging nanophotonic science and consumer products”, Nano Today, Vol. 19, 7-10, 2018.

2. Clausen, J. S. et al., “Plasmonic metasurfaces for coloration of plastic consumer products”, Nano Lett., Vol. 14, No. 8, 4499-4504, 2014.
3. Kristensen, A. et al., ”Plasmonic colour generation”, Nat. Rev. Mat., Vol. 2, 16088, No. 1, 2017.
4. Zhu, X. et al., “Resonant laser printing of structural colors on high-index dielectric metasurfaces”, Sci. Adv., Vol. 3, No. 5, 2017.
5. Højlund-Nielsen, E. et al., “Plasmonic colors: Toward mass production of metasur- faces”, Adv. Mat. Technol., Vol. 1, No. 7, 1600054, 2016.
6. Højlund-Nielsen, E. et al., “Single-spot e-beam lithography for defining large arrays of nano-holes”, Microel. Eng., Vol.121, 104-107, 2014.
7. Zhu, X. et al., "Plasmonic colour laser printing", Nat. Nanotechnol., Vol. 11, No. 4, 325-329, 2016.
8. Carstensen, M. S. et al., “Holographic resonant laser printing of metasurfaces using plasmonic template", ACS Photonics, Vol. 5, No. 5, 2018.
9. Zhu, X. et al., “Resonant Laser Printing of Optical Metasurfaces”, Nano Lett., Vol. 22, No. 7, 2786–2792, 2022.

Bright-field imaging of nanoscale bioparticles with Gire-Tournois photonic platform

Young Min Song

[1]Electrical Engineering and Computer Science, Gwangju Institute of Science and Technology, Gwangju 61005, Korea
[*]corresponding author: ymsong@gist.ac.kr

Abstract: we propose a novel approach to quantify nano-sized bioparticles by combining nanophotonics and deep learning (DL). We employed Gires-Tournois (GT) resonators as an immunosensor platform functionalized with antigen-specific antibodies without labelling or amplification. Based on the GT resonator, nanoscale bioparticles are dynamically detected and the number of particles is inferred from optical microscope images by a convolutional neural network as a vision-based DL model.

Biological imaging techniques have revolutionized the field of biomedical research by enabling the visualization and quantification of biological tissues. Various imaging modalities have been developed to achieve high resolution and accurate quantitation, including confocal microscopy, two-photon fluorescence, second harmonic generation, Raman spectroscopy, Fourier-transform microscopy, and electron microscopy. While these techniques have been successful in advancing biomedical research, their widespread use is limited by the need for sophisticated equipment and professional expertise. Recently, advanced nanophotonic technologies have been developed for microscale cell imaging applications such as colorimetric histology and ptychographic phase microscopy by utilizing plasmonic-based nanostructures. Moreover, nanophotonic sensors based on surface-enhanced Raman scattering (SERS) and surface plasmon resonance (SPR) have been studied by signal-based approach rather than imaging techniques. Meanwhile, recent advances in artificial intelligence have also revolutionized biomedical research, with machine learning and deep learning (DL) algorithms offering new opportunities for image classification, computer vision, and natural language processing. Specifically, the subfield of machine learning has seen significant growth in recent years, with convolutional neural networks (CNNs) demonstrating superior object categorization skills that model human vision. Although these algorithms have been successfully applied to various biomedical applications including biopotential signals and cell counting, they have not yet been properly applied to nanoscale bioparticles such as viruses and proteins.

Here, we present an intuitive method for quantifying nanoscale bioparticles by leveraging the fields of nanophotonics and DL. The Gires-Tournois (GT) resonator composed of three thin films, aimed at a 100-nm-diameter SiO_2 nanosphere, facilitates dynamic colorimetric sensing[1-2]. The DL model, which is trained with diverse structures of nanoparticle (NP) clusters with ground truth density maps from the scanning electron microscopy (SEM) images, infers the effective number of NPs in the optical microscopy (OM) images. The GT resonator was functionalized with an antigen-specific antibody, enabling utilization as an immunosensor without labeling and amplification. Therefore, viral NPs can be counted through the commercial bright-field microscope without any accessories. In addition, the DL model was trained with further hard negative samples to filter out irrelevant information and obtain only the desired data. We confirmed that our system showed the comparative limit of detection (LoD) with existing diagnostics. Also, the pre-trained model is applied to the diverse sizes of analytes in the range of zoonotic viruses using transfer learning with high transferability. We expect that this biosensing system could be deployed as a screening diagnosis in preparation for emerging viruses, saving time

and costs in clinical applications.

Acknowledgements: This work was supported by the GIST Research Institute (GRI) RISE, GIST-MIT Research Collaboration, Startup Acceleration Center, and AI-based GIST Research Scientist Project through a grant funded by the GIST and National Research Foundation of Korea (NRF) funded by the Ministry of Science and ICT (2022M3H4A1A02085336, 2020R1A2C2004983, 2021M3H4A1A04086552).

References

1. Yoo, Y. J. et al. Gires–Tournois Immunoassay Platform for Label-Free Bright-Field Imaging and Facile Quantification of Bioparticles. Advanced Materials 34, 2110003 (2022).
2. Kang, J., Yoo, Y. J., Ko, J. H., Mahmud, A. A. & Song, Y. M. Trilayered Gires-Tournois Resonator with Ultrasensitive Slow-Light Condition for Colorimetric Detection of Bioparticles. Nanomaterials 13 (2023).

META 2023, PARIS - FRANCE, JULY 18 – 21, 2023

Plasmonics on neural implants

F. Pisano[1], L. Collard[1], D. Zheng[1], A. Balena[1], B. Spagnolo[1], M. Bianco[1], L. Piscopo[1,2], M.S. Andriani[1,2], C. Montinaro[1,2], F. Tantussi[4], A. D'Orazio[3], F. De Angelis[4], M. Valiente[5], L. De La Prida[6], M. Grande[3], M. De Vittorio[1,2,+], F. Pisanello[1,+,*]

[1] Istituto Italiano di Tecnologia, Center For Biomolecular Nanotechnologies, Lecce, Italy
[2] Dipartimento di Ingegneria dell'Innovazione, Università del Salento, Lecce, Italy.
[3] Dipartimento di Ingegneria Elettrica e dell'Informazione Politecnico di Bari, Bari, Italy
[4] Istituto Italiano di Tecnologia, Via Morego 30, 16163, Genova, Italy
[5] Brain Metastasis Group, Spanish National Cancer Research Center (CNIO), Madrid, Spain
[6] Instituto Cajal, CSIC, Madrid, Spain

[*]corresponding author: ferruccio.pisanello@iit.it

Abstract: The advent of optical neural interfaces in neuroscience research has boosted the scientific community to devise novel methods and systems to interrogate brain cells and neural circuits. A promising approach relies in the use of light-matter, for both sensing and triggering neural activity. In this presentation we will describe our technology to fabricate different types of plasmonic structures on an optical neural implant, for enhanced bio-sensing, beam-manipulation and opto-thermal heat delivery in the brain.

Optical methods to control and monitor neural activity represent one of the most diffused techniques in neuroscience labs to study functional connectivity in the living mouse brain. However, the brain tissue is characterized by a high scattering coefficient and a therefore a very short photons free path, making sub-cortical regions very challenging to reach for microscopy-based methods. This has boosted the development of implantable optical neural interfaces, which represent a promising paradigm to both control and monitor neural activity with high spatio-temporal specificity. In this framework, the interest of the scientific community has recently put its spotlight on the possibility to use light-matter interactions to communicate with brain cells, aiming at increasing the number of functionalities that can be integrated in a single device. Surface plasmon polaritons represent a promising candidate for this aim, since they allow to establish a peculiar interaction between light radiation and conduction electrons to implement both triggering and sensing capabilities.

We will present our approach to generate surface plasmon polaritons (SPP) on different types of implantable fiber optics. This is obtained by exploiting the peculiar features of multimode optical fibers (MMF) to control how guided modes couple to plasmonic resonances, for enhanced bio-sensing, beam-manipulation and opto-thermal heat delivery in the brain.

Firstly, we will describe the tapered optical fibers (TF) technology. A TF is a step-index MMF gently tapered for a few millimeters down to a tip smaller than 1μm in diameter [1]. This peculiar shape reduces tissue invasiveness with respect to standard optical fibers, and it has the unique features of generating a widely-extended non-planar surface on which guided modes can interact with nanometric structures conformally laying around the waveguide [2]. To fabricate plasmonic structures on the non-planar surface of the taper, we have employed both top-down and bottom-up nanomachining. Focused ion beam milling (FIB) was used to obtain sub-diffraction apertures on a metal thin film and generate extraordinary optical transmission to control the spectral and angular patterns of optical transmission [3]. Non-planar repeated dewetting was instead employed to obtain sub-10nm plasmonic hotspot and perform sensing of neurotransmitters through surface

enhanced Raman spectroscopy, down to a detection limit of 10^{-7} M for both dopamine and serotonin [4]. An alternative method to control how guided modes interact with nanostructures fabricated at the terminal end of an optical fiber, relies in using wavefront shaping. In the second part of the talk we will describe how phase-only spatial light modulators at the input of a flat-cleaved MMF can be used to control the workpoint of the coupled system in the dispersion diagram [5], paving the way toward multifunctional plasmonic neural interfaces.

References

1. Filippo Pisano, Marco Pisanello, S. J. Lee, J. Lee, Emanuela Maglie, Antonio Balena, Leonardo Sileo, Barbara Spagnolo, Marco Bianco, M. Hyun, M. De Vittorio, Bernardo L. Sabatini, Ferruccio Pisanello, "Depth-resolved fiber photometry with a single tapered optical fiber implant" Nature Methods **16**, 1185 (2019)
2. Spagnolo B., Balena A., Peixoto R.T., Pisanello M., Sileo L., Bianco M., Rizzo A., Pisano F., Qualtieri A., Lofrumento D.D., De Nuccio F., Assad J.A., Sabatini B.L., De Vittorio M., Pisanello F. **"**Tapered fibertrodes for optoelectrical neural interfacing in small brain volumes with reduced artefacts" Nature Materials 21, 826 (2022)
3. Pisano F., Kashif M. F., Balena A., Pisanello M., De Angelis F., de la Prida L. M., Valiente M., D'Orazio A., De Vittorio M., Grande M., Pisanello F. "Plasmonics on a Neural Implant: Engineering Light–Matter Interactions on the Nonplanar Surface of Tapered Optical" Advanced Optical Materials **10**, 2101649 (2022)
4. Zheng D., Pisano F., Collard L., Balena A., Pisanello M., Spagnolo B., Mach-Batlle R., Tantussi F., Carbone L., De Angelis F., Valiente M., De La Prida L., Ciracì C, De Vittorio M., Pisanello F., "Toward Plasmonic Neural Probes: SERS Detection of Neurotransmitters through Gold Nanoislands-decorated Tapered Optical fibers with sub-10 nm Gaps" Advanced Materials in press https://doi.org/10.1002/adma.202200902
5. Collard L., Pisano F., Zheng D., Balena A., Kashif M. F., Pisanello M., D'orazio A., De La Prida L.M., Ciracì C., Grande M., De Vittorio M., Pisanello F. **"**Holographic Manipulation of Nanostructured Fiber Optics Enables Spatially-Resolved, Reconfigurable Optical Control of Plasmonic Local Field Enhancement and SERS" Small **18** 2200975 (2022)

META 2023, PARIS - FRANCE, JULY 18 – 21, 2023

Nanophotonics for biosensing: development of optical platforms for high sensitivity and specificity

G. Palermo
Department of Physics, NLHT-Lab, University of Calabria and CNR-NANOTEC Istituto di Nanotecnologia, 87036 Rende, Italy
*corresponding author: giovanna.palermo@unical.it

Abstract: Plasmonics is a branch of optics that deals with the study of surface plasmons. These plasmons can be used to manipulate light at the nanoscale, allowing for the development of novel devices for applications in sensing, imaging, and information processing. One important application of plasmonics is the development of plasmonic biosensors, which can detect and quantify the presence of molecules as biomarkers with high sensitivity and specificity.

It is well known that pathological tissues release a whole series of compounds into the vascular system, such as circulating DNA, extracellular vesicles, proteins, metabolites and so on. Going for early detection of these analytes in blood or other body fluids could allow to detect a disease when it is really in an early stage, giving the possibility to intervene promptly.

For this reason, it is necessary to develop sensing platforms capable of detecting very small concentrations of analyte, that are of the order of femtomolar or even in the attomolar range.

Plasmonic metasurfaces play a key role in the development of the next-generation nanophotonic biosensors, which can detect and quantify the presence of molecules with high sensitivity and specificity. The metal surface is typically patterned with nanoscale features, such as nanoparticles or nanoholes, that can support surface plasmons.

These sensors work by measuring the changes in the plasmon resonance of a metal surface caused by the binding of analyte molecules. The shift in plasmon resonance can be measured using various optical techniques, such as reflectance or transmission spectroscopy, and can be used to detect and quantify the presence of analyte molecules.

The highest sensitivity for a plasmonic biosensor can be achieved by optimizing the design of the sensor to maximize the interaction between the analyte molecules and the plasmonic field. Our research group addresses this challenge by developing next-generation nanophotonic biosensors based on surface plasmons and metamaterials.

In this talk, I will present some of our recent efforts in these directions [1-4]. I will show how the sensitivity of a plasmonic biosensor can be influenced by the design of the sensor surface, such as the density, the size, and shape of the metal nanostructures on the surface.

I will describe ultra-compact, rapid, and low-cost nanophotonic microarrays and their use for early disease diagnostics in real-world settings. I will also highlight chiral plasmonic metasurface that can improve the sensitivity of biosensors by using specialized CD techniques, such as resonance-enhanced CD or surface plasmon-coupled CD, which can enhance the signal-to-noise ratio and improve the detection limit.

The author acknowledges financial support from the “NLHT - Nanoscience Laboratory for Human Technologies” (POR Calabria FESR-FSE 14/20).

References

1. Palermo, G., Rippa, M., Conti, Y., Vestri, A., Castagna, R., Fusco, G., ... & Petti, L. (2021). Plasmonic metasurfaces based on pyramidal nanoholes for high-efficiency SERS biosensing. ACS applied materials & interfaces, 13(36), 43715-43725.
2. Guglielmelli, A., Nicoletta, G., Valente, L., Palermo, G., & Strangi, G. (2022). Numerical Modeling of 3D Chiral Metasurfaces for Sensing Applications. Crystals, 12(12), 1804.
3. Lininger, A., Palermo, G., Guglielmelli, A., Nicoletta, G., Goel, M., Hinczewski, M., & Strangi, G. (2022). Chirality in light–matter interaction. Adv. Mater, 2107325.
4. Palermo, G., Lio, G. E., Esposito, M., Ricciardi, L., Manoccio, M., Tasco, V., ... & Strangi, G. (2020). Biomolecular sensing at the interface between chiral metasurfaces and hyperbolic metamaterials. ACS applied materials & interfaces, 12(27), 30181-30188.

META 2023, PARIS - FRANCE, JULY 18 – 21, 2023

Plasmonic nanomaterials for detection and degradation of pesticedes.

A. Guglielmelli[1,*], **R. Mazzei**[2], **G. Palermo**[1], **P. Strangi**[1], **L. Giorno**[2] **and T. Poerio**[2,*]

[1]Department of Physics, NLHT-Lab, University of Calabria and Institute of Nanotechnology (CNR-NANOTEC), 87036 Rende, Italy
[2]Institute on Membrane Technology (CNR-ITM), Via P. Bucci 17/c, 87036 Rende (CS), Italy

[*]corresponding authors: alexa.guglielmelli@unical.it, t.poerio@itm.cnr.it

Abstract: Organophosphate pesticides are neurotoxic chemical compounds, widespread in the environment due to agricultural and domestic use. They are a major cause of cancer and some neurological diseases such as Alzheimer's and Parkinson's. Their detection in food and in the environment requires complex and expensive equipment and highly specialized operators. This has sparked growing interest in developing multifunctional platforms that can both detect and detoxify these hazardous agents. In this work we present a Poly (dimethylsiloxane) - gold nanoparticles composite thin film for detection and degradation of organophosphorus neurotoxins.

Pesticides are widely employed in agriculture to manage pests and increase productivity to address the rising demand for food, but they are equally hazardous to species that are not their intended targets, including humans. [1] Therefore the development of highly sensitive, stable, and responsive detection technology for such toxic agents is crucial for environmental and public health protection.

Polymer composites with embedded metal nanoparticles (NPs) can offer an ideal solution for detection purposes, by converting chemical or biomolecular information into a physically readable signal. The surrounding environment sensing ability of the plasmonic NPs can be exploited, while the polymer matrix holds and stabilizes the NPs allowing the loading of small molecules. Polydimethylsiloxane (PDMS) is an appealing polymeric matrix in this context, thanks to its properties, including chemical inertness, biocompatibility, mechanical flexibility and stability, optical transparency in the VIS and UV region, and most importantly, its simplicity of processing. AuNPs can be used in optical sensors thanks to the localized surface plasmon resonance (LSPR) phenomenon, the collective oscillations of delocalized electrons in response to an external electric field, by measuring changes in the refractive index of the surrounding media with high sensitivity. [2] The fabricated nanocomposite film was suitably functionalized to maximize the adsorption and at the same time trigger the degradation of the organophosphate pesticide (OP). For this reason, the enzyme phosphotriesterase was used, which can bind and detoxify OP and toxic chemical agents from the same class of chemical compound.

The obtained PDMS-AuNPs film was fully characterized. The loading and hosting ability of the PDMS-AuNPs film was tested by using a fluorescent dye as a model system. The LSPR sensing performances of the nanocomposite films were tested by systematic monitoring the UV-Vis spectroscopic signal from the AuNPs.

The presented PDMS-AuNPs has shown promising sensing responses, and could be easily integrated in microfluidic chip to perform the accurate detection of low concentrations OP neurotoxins in environmental samples.

The authors would like to thank POR Calabria FESR-FSE 2014/2020 for the financial support to the SmartMatter project in the ERA.NET Call 2019, and the “NLHT - Nanoscience Laboratory for Human Technologies” project.

References

1. Kumaran, A., et al. "Biosensors for detection of organophosphate pesticides: Current technologies and future directives." Microchem. J., Vol. 178, 107420, 2022.
2. Dissanayake, N. M., et al. "Highly sensitive plasmonic metal nanoparticle-based sensors for the detection of organophosphorus pesticides." Talanta 200, 218-227, 2019.

META 2023, PARIS - FRANCE, JULY 18 – 21, 2023

Nanophotonic biosensors based on bound state in continuum

V. Mocella, S. Romano, G. Zito, and I. Rendina

National Research Council, Institute of Applied Sciences and Intelligent Systems "Eduardo Caianiello"

Italy

*corresponding author: ivo.rendina@cnr.it

Abstract: In this communication, an overview of the applications of nanophotonic biosensors based on bound state in continuum is reported. Perspective exploitation of this new class of devices is also discussed.

In recent years, the use of Bound States in Continuum (BICs) in optical sensing applications is rapidly growing [1]. BICs are a type of resonant state that exists within a continuum of radiative modes, meaning that they are bound to the structure in which they exist but are not coupled to the external radiation. This unique property has made BICs a topic of significant interest in the photonics community. In particular, BIC-based sensors have shown exceptional sensitivity thanks to their high-quality factors that enhance the signal-to-noise ratio and provide a higher detection limit compared to conventional resonant sensors. Furthermore, these sensors have a great selectivity, which is due to the ability to tune the BIC wavelength to the desired sensing targets [3].

Our group has shown interesting potential application of BIC-based biosensors in detecting and quantifying various bio-molecules, including proteins, DNA [4], cancer cells [3], and toxins in food and environment [4]. An overview of such applications, developed in our laboratories, will be presented, with a particular emphasis on future perspectives, including the integration of BICs in microfluidic platforms, which can also enable the detection of multiple analytes in a single device.

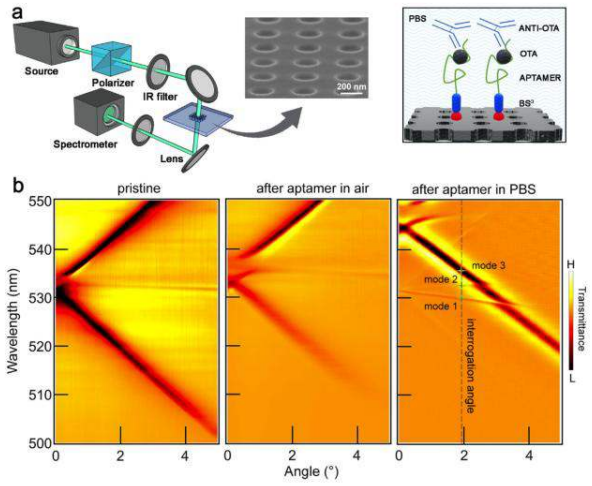


Figure 1. a. Layout of the sensing setup, with SEM image of the sensing area and a schematics of the surface functionalization. b. TE-dispersion bands along $\boldsymbol{\Gamma} - \boldsymbol{X}$ direction reconstructed from S-polarized transmittance spectra.

References

1. S. Romano, G. Zito, S. Torino, G. Calafiore, E. Penzo, G. Coppola, S. Cabrini, I. Rendina, and Vito Mocella "Label-Free Sensing of Ultralow-Weight Molecules with All-Dielectric Metasurfaces Supporting Bound States in the Continuum", Photon. Res. 6, 726, 2018.
2. S. Romano, M. Mangini, E. Penzo, *et al.* "Ultrasensitive Surface Refractive Index Imaging Based on Quasi-Bound States in the Continuum", ACS Nano 14, 15417, 2020.
3. S. Romano, G. Zito, S. N. L. Yépez, S. Cabrini, E. Penzo, G. Coppola, I. Rendina, and Vito Mocella "Tuning the Exponential Sensitivity of a Bound-State-in-Continuum Optical Sensor", Opt. Exp. 27, 18776, 2019.
4. G. Zito *et al.* "Label-Free DNA Biosensing by Topological Light Confinement", Nanophotonics-Berlin 10, 4279, 2021.
5. C. Schiattarella *et al.* "High-Q photonic aptasensor based on avoided crossing bound states in the continuum and trace detection of ochratoxin A", Biosens Bioelectron X 12, 100262, 2022.

META 2023, PARIS - FRANCE, JULY 18 – 21, 2023

Plasmonic biosensors for biomedical applications

T. Špringer, M. Bocková, J. Slabý, E Hemmerová, J Homola*
Institute of Photonics and Electronics of the Czech Academy of Sciences, Czech Republic
*corresponding author: homola@ufe.cz

Abstract: Optical biosensors hold potential for applications in numerous important areas. Herein, we discuss the main challenges in developing plasmonic biosensors for applications in biomedicine and present selected advances in biosensor research that aim to address these challenges. We cover advances in plasmonic nanostructures, sensor instrumentation, transport of target molecules in microfluidic systems, functional coatings, and detection assays. We also highlight applications of plasmonic biosensors related to the investigation of biomolecular interactions related to Alzheimer's disease and diagnosis of Myelodysplastic syndromes.

Au/Ag SERS active substrate for broader wavelength excitation.

Sebin Augustine[1,2*], Mahesh Saini[1], Sooraj KP[1], Mukesh Ranjan[1,2]

[1]Institute for Plasma Research, Gandhinagar-382428, India

[2]Homi Bhabha National Institute, Anushaktinagar, Mumbai-400094, Maharashtra, India

[*]corresponding author: sebin.augustine@ipr.res.in

Abstract: We present a two-stage process for developing dense Au-coated Ag nanoparticle arrays on ion-beam patterned nano-rippled Si substrates for broader range Surface Enhanced Raman Spectroscopy (SERS). These substrates show LSPR excitation in a broader wavelength range and good enhancement for 532 and 785 nm lasers. Results are qualitatively compared with FDTD simulations where the effect of interparticle gap and Au/Ag layer thickness on their SERS enhancement is explored.

The SERS enhancement strongly depends on the excitation laser and LSPR wavelength. A substrate shows maximum enhancement when excitation frequency matches the LSPR wavelength [1]. Therefore, developing a substrate that shows a broad LSPR region is important. Recent progress in nanoparticles grown on ripples produced using low-energy ion sources shows good control over the tunability of the LSPR active region [2][3]. However, a substrate with good sensitivity for all wavelengths, from visible to infrared, must be addressed. In this work, we deposited ordered Au/Ag nanoparticle (NPs) arrays on low energy-produced rippled Si substrates [4]. The produced substrates show good SERS enhancement for 532 nm and 785 nm lasers.

In particular, nanoscale ripple patterns are fabricated on Si surfaces by irradiating 300 eV Ar ion beams for a fluence of 5×10^{18} ions cm^{-2}[5]. Following this, using e-beam evaporation, Ag-NPs are deposited on rippled Si substrates at an oblique angle of 70° to produce ordered arrays of Ag-NPs. Further, a capping layer of Au is deposited on Ag-NPs using magnetron sputtering. The wavelength and amplitude of rippled Si are analyzed using atomic force microscopy (AFM), as shown in ***Figure 1***(a). The average wavelength of the ripple patterns is ~28 nm. The size of Ag-NPs and Au capping thickness is varied to optimize the SERS efficiency. SEM micrograph of optimized arrays of Au/Ag-NPs is shown in ***Figure 1***(b). It is observed that with increasing thickness of the Au capping layer, the interparticle gap of Au/Ag-NPs starts decreasing, and finally, they are merged to make bigger NPs. STEM images confirm the presence of Au as a capping layer on Ag-NPs. For instance, ***Figure 1*** (c-f) shows the elemental mapping of Si, Ag, Au, and all together, confirming the Au capping on top of Ag-NPs. Further, the effect of Au coating on the optical response of Ag-NPs is studied using FDTD simulations, and it is observed that the LSPR peak is red-shifted after Au deposition. The simulated spectral response for the maximum electric field between two NPs along the ripple direction is depicted in ***Figure 2*** (a). The spectral response of Ag-NP arrays exhibits an LSPR peak at ~540 nm suggesting their activity for 532 nm laser excitation. Similarly, Au-NP arrays are suitable for 785 nm laser excitation due to the LSPR peak appearing at ~625 nm. On the other hand, Au/Ag-NP arrays can show excellent SERS efficiency for both laser excitations due to the presence of doubly LSPR peaks at ~525 nm and ~650 nm. Moreover, the maximum *E*-field is observed to be 16 Vm^{-1} for Au/Ag-NP arrays along the ripple patterns, which is ~2.5 times higher than bare Ag- or Au-NPs. Optical reflection measurement of Au/Ag-NPs along and across the ripple patterns also exhibits LSPR[***Figure 2*** (b)]. Using crystal violet dye as a probing molecule, SERS efficiency is examined, and it is observed that Au/Ag-NP arrays show excellent SERS enhancement for a 532 nm laser, which is comparable to the SERS enhancement of Ag-NP arrays. However, for 785 nm laser excitation, SERS sensitivity is very low for Ag-NP arrays, which is significantly enhanced for Au/Ag-NPs [***Figure 2***(c)]. The optimized SERS substrate

shows good spatial uniformity (RSD below 10%) with a detection limit of 100 pM and 100 nM for 532 and 785 nm lasers, respectively. A SERS enhancement factor of the order of 10^5 is observed for the 532 nm laser and 10^4 for the 785 nm laser. Thus, this study results in an optimized Au-coated Ag-NP arrays-based SERS substrate for excellent sensitivity in a wide range of laser excitations.

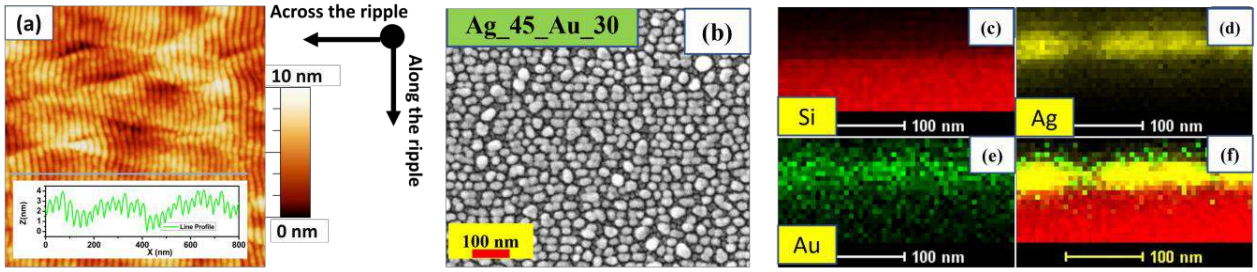


Figure 1: (a) AFM image of ripple nanostructure produced on Si substrate. (b) SEM analysis of Optimized Au/Ag substrate

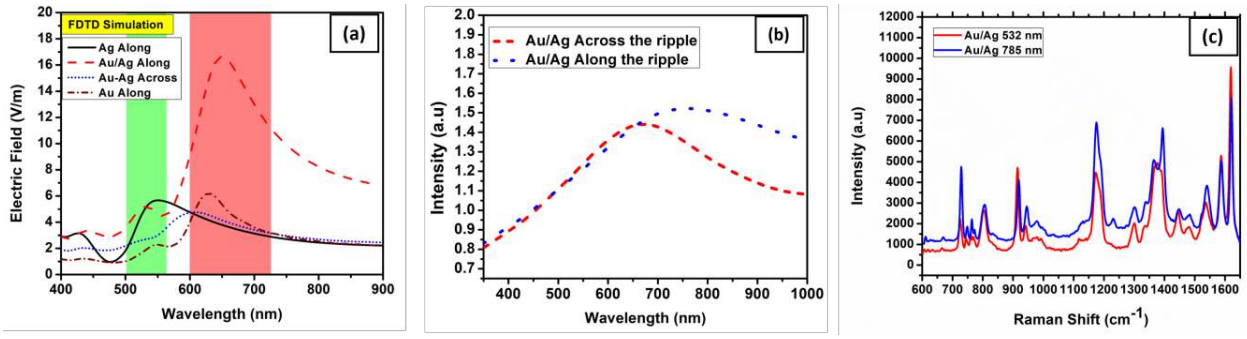


Figure 2: (a) Spectral electric field response in between adjacent NPs (b) Reflection spectrum of Au/Ag substrate (c) SERS spectra of CV molecules measured using Au/Ag substrate.

References

[1] E. C. Le Ru and P. G. Etchegoin, "Chapter 4 - SERS enhancement factors and related topics," E. C. Le Ru and P. G. B. T.-P. of S.-E. R. S. Etchegoin, Eds. Amsterdam: Elsevier, 2009, pp. 185–264.

[2] M. Saini, S. Augustine, M. Ranjan, and T. Som, "In-plane optical anisotropy and SERS detection efficiency of self-organized gold nanoparticles on silicon nanoripples: Roles of growth angle and postgrowth annealing," *Appl. Surf. Sci.*, vol. 512, no. February, p. 145703, 2020, doi: 10.1016/j.apsusc.2020.145703.

[3] M. Ranjan and S. Facsko, "Anisotropic surface enhanced Raman scattering in nanoparticle and nanowire arrays," vol. 485307, 2012, doi: 10.1088/0957-4484/23/48/485307.

[4] S. Augustine *et al.*, "Au/Ag SERS active substrate for broader wavelength excitation," *Opt. Mater. (Amst).*, vol. 135, no. November 2022, p. 113319, 2023, doi: 10.1016/j.optmat.2022.113319.

[5] S. Augustine, K. P. Sooraj, V. Pachchigar, C. Murali Krishna, and M. Ranjan, "SERS based detection of Dichlorvos pesticide using silver nanoparticles arrays: Influence of array wavelength/amplitude," *Appl. Surf. Sci.*, vol. 544, p. 148878, 2021, doi: https://doi.org/10.1016/j.apsusc.2020.148878.

Nanophotonic chiral sensing: How does it actually work?

S. Both,[1] S. F. Almousa,[2] H. Giessen,[1] E. A. Muljarov,[2] D. Shakirova,[3] and T. Weiss[1,3,*]

[1]4th Physics Institute, University of Stuttgart and Research Center SCoPE, Pfaffenwaldring 57, 70569 Stuttgart, Germany
[2]Cardiff University, School of Physics and Astronomy, The Parade, CF24 3AA, Cardiff, UK
[3]Institute of Physics, University of Graz, and NAWI Graz, Universitätsplatz 5, 8010 Graz, Austria
[*]corresponding author: thomas.weiss@uni-graz.at

Abstract: We present a general and rigorous theory of chiral light-matter interactions in arbitrary optical resonators. Our theory describes the chiral interaction as a perturbation of the resonant states, also known as quasi-normal modes. We observe two dominant contributions: A chirality-induced resonance shift and changes in the modes' excitation and emission efficiencies. Our theory brings new and deep insights for tailoring and enhancing the chiral light-matter interactions. Furthermore, it allows to predict spectra much more efficiently in comparison to conventional approaches.

Detecting the handedness of chiral molecules is of utmost importance for chemical, biological, and pharmaceutical applications, since the handedness of a molecule determines its interaction with the environment. This includes chemical interactions as well as the interaction with light. Hence, it is possible to determine the handedness of chiral molecules by optical measurements, but the chiroptical response of such molecules is usually rather weak. Therefore, conventional approaches require using large numbers of chiral molecules.

Plasmonic nanoantennas and other nanophotonic resonators can enhance the chiroptical response. We have recently shown that the electromagnetic enhancement of the circular dichroism, which is the difference in absorption of left- and right-handed circularly polarized light, can be as high as three orders of magnitude [1]. Hence, plasmon-enhanced circular dichroism spectroscopy yields a promising approach for determining the handedness of even few molecules. However, little was known about the underlying enhancement mechanisms.

We close this gap and provide a theoretical understanding of chiral light-matter interaction that is based on the expansion of the nanophotonic response in terms of resonant states [2]. More specifically, we treat the chiral interaction as a small perturbation, which yields explicit expressions for the changes of the near- and far-field properties. Our theory reveals several contributions to the resonant enhancement of that interaction. The first one is a change in the excitation and emission efficiencies of the resonant states, which requires a coplanarity of the incident field and the dominant field components at the location of the chiral medium. The second one is a chirality-induced resonance shift, which surprisingly only occurs in chiral

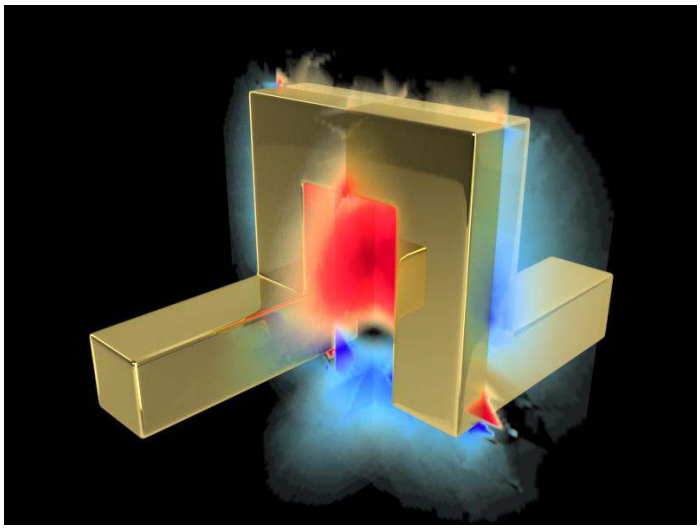


Figure 1. Local resonance shift per volume near a plasmonic nanoantenna. Positive/negative shifts (red/blue) require parallel/antiparallel electric and magnetic near fields [2].

spatial arrangements of the resonator and the chiral medium. We demonstrate that this contribution can be enhanced if we tailor the resonant electromagnetic near fields such that the electric and magnetic field components are either parallel or antiparallel, as in the case of the local optical chirality [3], see figure 1. The third contribution is based on an interplay of nearly degenerate resonant states. We find that this requires a thorough tailoring of the resonator geometry. In the perturbation regime, there is also a non-resonant contribution, which, however, is – as all higher-order contributions – usually negligible. Furthermore, only odd orders of perturbation theory allow for a handedness discrimination. Finally, we show that the coupling of quasi-degenerate modes can allow for a boost in sensitivity.

Hence, our theory allows for analyzing the different electromagnetic contributions to chiral light-matter interaction and for gaining a better understanding of resonantly enhanced chiroptical spectroscopy. Finally, it should be noted that our theory is not limited to chiroptical spectroscopy but can be applied to any sort of optical sensor that traces changes of the electromagnetic response such as the refractive index of an analyte material [4, 5].

We acknowledge support from the Deutsche Forschungsgemeinschaft (DFG) via the priority program SPP 1834 “Tailored disorder” as well as the individual DFG research grant WE 5815/5-1.

References

1. M. L. Nesterov, X. Yin, M. Schäferling, H. Giessen, and T. Weiss, “The role of plasmon-generated near fields for enhanced circular dichroism spectroscopy,” ACS Photonics 3, 578-583, 2016.
2. S. Both, M. Schäferling, F. Sterl, E. A. Muljarov, H. Giessen, and T. Weiss, “Nanophotonic chiral sensing: How does it actually work?” ACS Nano **16**, 5284-5291, 2022.
3. Y. Tang and A. E. Cohen, “Optical chirality and its interaction with matter,” Phys. Rev. Lett. 104, 163901, 2010.
4. S. Both and T. Weiss, “Resonant states and their role in nanophotonics,” Semicond. Sci. Technol. 37, 013002, 2022.
5. S. F. Almousa and E. A. Muljarov, “Exact theory and approximations for optical resonators in a changing external medium,” Phys. Rev. B **107**, L081401 (2021).

Coherent control of absorption in structured materials

META 2023, PARIS - FRANCE, JULY 18 – 21, 2023

High-Fidelity Reprogrammable Signal Processors Built Off the Anti-Laser

Philipp del Hougne

Univ Rennes, CNRS, IETR—UMR 6164, F-35000 Rennes, France
philipp.del-hougne@univ-rennes1.fr

Abstract: Achieving high-fidelity reflectionless (as opposed to merely low-reflection) excitation of complex scattering structures at specific frequencies is notoriously difficult, in particular if the frequency of operation is supposed to be reconfigured during runtime. We demonstrate that the combination of (i) overmoded systems with (ii) a massive amount of tunable degrees of freedom (provided by a programmable metasurface) enables high-fidelity reprogrammable reflectionless excitation of complex structures. Building on this technique, we demonstrate reprogrammable analog signal differentiation and reflectionless signal routing.

The reflectionless excitation of an arbitrarily complex scattering structure at a frequency ω_0 is possible if the system's scattering matrix $S(\omega_0)$, or a filtered version $R(\omega_0)$ thereof, has a zero eigenvalue [1]. If $S(\omega_0)$ has a zero eigenvalue, injecting the corresponding eigenvector yields coherent perfect absorption of the incident radiation [2]. This phenomenon is also referred to as "anti-laser" because it is the time-reverse of lasing at threshold; however, reflectionless excitation is compatible with steady-state operation in linear systems whereas lasing requires non-linear effects to respect energy conservation.

In general, neither S nor R can be expected to have any real-valued zero, let alone at the desired real frequency ω_0. Many groups have carefully designed simple scattering structures involving a single or few resonances in order to impose a real-valued zero at a desired frequency. However, such approaches are vulnerable to fabrication inaccuracies and environmental perturbations, and they lack in-situ reconfigurability. Adding one or a few tunable degrees of freedom (DoFs) to such structures allows one to tune the zero's position, however, there is in general no guarantee whatsoever that the zero remains on the real frequency axis upon tuning, and indeed it usually drifts away.

We have taken a presumably unexpected approach to overcome these difficulties that differs in two ways from the conventional approach outlined above since we work with:

1) an overmoded scattering enclosure with many modes instead of a single-mode or few-mode system.
2) a massive parametrization (100s of programmable-metasurface DoFs) instead of zero, one or few DoFs.

Thereby, we are able to achieve unprecedented fidelity (we reach reflected powers below -70 dB) and unprecedented flexibility (we can arbitrarily redefine ω_0 in situ) in imposing a reflection zero at a desired frequency [3].

After demonstrating how this technique can enable **physical-layer security in wireless backscatter communications** [3], we leverage this technique to implement challenging signal processing tasks in the analog domain:

1) First, we demonstrate high-fidelity **reprogrammable analog signal differentiation** with experimental in situ observations [4]. Moreover, thanks to the linearity of the wave equation, we can parallelize this wave-based mathematical operation by simultaneously imposing real-valued zeros at multiple distinct

frequencies [4].

2) Second, we demonstrate **reflectionless programmable signal routing** [5]. Here, in addition to suppressing the reflection, we must satisfy additional constraints such as transmission of the injected signal to specific ports and not to others. We report experimental in situ observations of reflectionless wavelength demultiplexing and other functionalities. Our reflectionless signal router can be reprogrammed both with respect to its operating frequencies and to its routing functionality [5]. Reflectionless signal routers remove the risk that reflected-power echoes pose for non-linear components like amplifiers in RF and nanophotonic networks, and thereby they remove the need for the to-date customary approach of preventing reflected-power echoes with isolators or in-line attenuators.

P.d.H. acknowledges funding from the CNRS prématuration program (project “MetaFilt”).

References

[1] W. R. Sweeney, C. W. Hsu, and A. D. Stone, “Theory of reflectionless scattering modes,” *Phys. Rev. A*, vol. 102, no. 6, p. 063511, Dec. 2020.

[2] Y. D. Chong, L. Ge, H. Cao, and A. D. Stone, “Coherent Perfect Absorbers: Time-Reversed Lasers,” *Phys. Rev. Lett.*, vol. 105, no. 5, Art. no. 5, Jul. 2010.

[3] M. F. Imani, D. R. Smith, and P. del Hougne, “Perfect Absorption in a Disordered Medium with Programmable Meta-Atom Inclusions,” *Adv. Funct. Mater.*, vol. 30, Art. no. 30, 2020.

[4] J. Sol, D. R. Smith, and P. del Hougne, “Meta-programmable analog differentiator,” *Nat. Commun.*, vol. 13, no. 1, p. 1713, Mar. 2022.

[5] J. Sol, A. Alhulaymi, A. D. Stone, and P. del Hougne, “Reflectionless programmable signal routers,” *Sci. Adv.*, vol. 9, no. 4, p. eadf0323, Jan. 2023.

META 2023, PARIS - FRANCE, JULY 18 – 21, 2023

Quantum and thermal aspects of coherent perfect absorption

I. Liberal[1*]

[1]Department of Electrical, Electronic and Communications Engineering, Institute of Smart Cities (ISC), Public University of Navarre (UPNA), 31006 Pamplona, Spain
[*]corresponding author: inigo.liberal@unavarra.es

Abstract: Coherent perfect absorption (CPA) is an interference phenomena that allows for linear photon-photon interactions, an abstract concept that can be implemented in multiple technological platforms including metasurfaces, photonic integrated circuits and plasmonics. In our talk, we will discuss quantum and thermal aspects of CPA including quantum states transformations, noise-management and the design of optical amplifiers with a reduced noise factor, as well as the practical implementation of those concepts within an integrated photonics setup.

Coherent perfect absorption (CPA) is an interference process where the proper combination of several input signals cancels out all output signals, leading to complete but phase dependent absorption [1-2]. Experimental demonstrations of CPA include technological platforms such as thin-films and metasurfaces [3-4], photonic integrated circuits [5-6] and plasmonic devices [7], laying a fertile ground for exploring applications in the fields of linear photon-photon interaction for all-optical data processing [8], sensing and quantum optics [9]. While the multiple aspects of CPA in linear optical devices have been actively investigated, quantum and thermal phenomena associated with CPA have received less attention.

In our talk, we will review our latest results on quantum and thermal aspects of CPA. In recent works [10-11], we reviewed quantum states transformations enabled by CPA, including single-photon CPA, two-photon nonlinear absorption, coherent absorption of N00N states, and absorption and manipulation of coherence in squeezed coherent states of light. Moreover, we demonstrated that by using an integrated photonics Wilkinson power divider (WPD), such transformations can be implemented in optical networks with a smaller footprint and a reduced number of elements. We pushed forward the design of a pure silicon-on-insulator (SOI) WPD, which harness radiative losses to provide a WPD response [10]. However, the concept could also be implemented in plasmonic CPA systems [6-7], providing even a smaller footprint and mitigating potential coupling to other elements of the network.

Finally, we have recently investigated the noise performance of active optical networks containing CPA elements [12]. Our analysis uncovered a number of noise cancellation effects that lead to an improvement of the noise performance. In particular, we found that it is possible to design optical amplifiers whose noise factor beat the conventional (G-1)/G expression, where G is the noise of the amplifier [12].

I.L. acknowledges support from Ramón y Cajal fellow-ship RYC2018-024123-I and project RTI2018-093714-301J-I00 sponsoredby MCIU/AEI/FEDER/UE, and ERC Starting Grant 94850.

References

1. Y. Chong, L. Ge, H. Cao, and A. D. Stone, Coherent perfect absorbers: time-reversed lasers, Phys. Rev. Lett. 105, 053901 (2010).

2. D. G. Baranov, A. Krasnok, T. Shegai, A. Alú, and Y. Chong, Coherent perfect absorbers: linear control of light with light, Nat. Rev. Mater. 2, 1 (2017).
3. W. Wan, Y. Chong, L. Ge, H. Noh, A. D. Stone, and H. Cao, Time-reversed lasing and interferometric control of absorption, Science 331, 889 (2011).
4. W. Zhu, F. Xiao, M. Kang, and M. Premaratne, Coherent perfect absorption in an all-dielectric metasurface, Appl. Phys. Lett. 108, 121901 (2016).
5. A. Espinosa-Soria, E. Pinilla-Cienfuegos, F. J. Díaz-Fernández, A. Griol, J. Martí, and A. Martínez, Coherent control of a plasmonic nanoantenna integrated on a silicon chip, ACS Photonics 5, 2712 (2018).
6. S. Zanotto, F. Bianco, V. Miseikis, D. Convertino, C. Coletti, and A. Tredicucci, Coherent absorption of light by graphene and other optically conducting surfaces in realistic on-substrate configurations, APL Photonics 2, 016101 (2017).
7. M. J. Jung, C. Han, J. W. Yoon, and S. H. Song, Temperature and gain tuning of plasmonic coherent perfect absorbers, Opt. Express 23, 19837 (2015).
8. J. Zhang, K. F. MacDonald, and N. I. Zheludev, Controlling light-with-light without nonlinearity, Light: Science & Applications 1, e18 (2012).
9. A. N. Vetlugin, Coherent perfect absorption of quantum light, Phys. Rev. A 104, 013716 (2021).
10. O. Hernández, A. Ortega-Gomez, M. Bravo and I. Liberal, Quantum interference in Wilkinson power dividers. Laser & Photonics Reviews, 16(8), 2200095 (2022).
11. O. Hernández and I. Liberal, Generalized approach to quantum interference in lossy N-port devices via a singular value decomposition, Optics Express 30, 31267 (2022).
12. A. Ortega-Gómez, O. Hernández, D. Oña, Carlos Biurrun-Quel, C. del Río and I. Liberal, Noise cancellation effects in integrated photonics with Wilkinson power dividers, Under review (2023).

META 2023, PARIS - FRANCE, JULY 18 – 21, 2023

A Massively Degenerate Coherent Perfect Absorber

Y. Slobodkin[2†], G. Weinberg[2†], H. Hörner[1†], K. Pichler[1], S. Rotter[1*] and O. Katz[2*]

[1]Institute for Theoretical Physics, Vienna University of Technology (TU Wien), Austria
[2]Applied Physics Department, Hebrew University of Jerusalem, Israel
[*]corresponding authors: stefan.rotter@tuwien.ac.at; orik@mail.huji.ac.at
[†]These authors contributed equally to this work

Abstract: In the field of non-Hermitian photonics it is a well-established concept that a time-reversed laser acts as a 'coherent perfect absorber' (CPA). However, CPAs are usually limited to a single, judiciously shaped wavefront (`mode'). Here, we demonstrate how this limitation can be overcome by time-reversing a 'degenerate cavity laser', based on a cavity that self-images any incident light-field onto itself. Placing a weak, critically-coupled absorber into this cavity, ensures that any incoming wavefront is absorbed with close to perfect efficiency.

While light is readily absorbed by thick materials that we perceive as black, thin and weakly absorbing media are inherently far less efficient in capturing incoming radiation and converting it into heat or other forms of energy. A well-known strategy to make even such weakly dissipative substances strongly absorbing is to embed them into a resonant structure. At the so-called 'critical coupling condition', where the coupling strength to such a resonator is exactly balanced with the internal dissipation, the incoming field gets perfectly absorbed with no energy being back-reflected from the resonator. The price one pays for this interferometric enhancement of absorption is a severe restriction on the properties of the incoming field for which this critical coupling condition can actually be satisfied [1, 2]. In other words, at the critical coupling condition, only a single, suitably adjusted wavefront (or spatial mode) gets 'coherently perfectly absorbed'. While this required wavefront adjustment opens up the possibility to control the absorption process interferometrically, it also comes with the severe limitation that, apart from the correctly matched input wavefront, all of the possibly many other modes are only weakly absorbed due to the different interference patterns they create.

In our paper [3], we demonstrate how to entirely eliminate the limitation of the number of perfectly absorbed modes in a CPA. Our design principle for a corresponding multi-mode CPA is based on the insight that 'coherent perfect absorption' formally corresponds to the time-reverse of laser emission at the first lasing threshold. In the aim to create a device that can perfectly absorb arbitrary combinations of incoming modes interferometrically, one thus needs to time-reverse a laser that emits all of these modes in parallel. Such a laser, indeed, exists, and is known under the name of a 'degenerate cavity laser'. The degeneracy of modes in such a cavity is based on the special feature that the field on either one of the two outer cavity mirrors is self-imaged onto itself after one cavity round-trip. This is realized in a straightforward fashion by placing two lenses in an imaging telescope configuration inside the cavity (Fig. 1), ensuring coherent perfect absorption of any combination of modes, regardless of their relative phases (Fig. 2). Such a robust absorption mechanism presents an important advantage to a large number of potential applications.

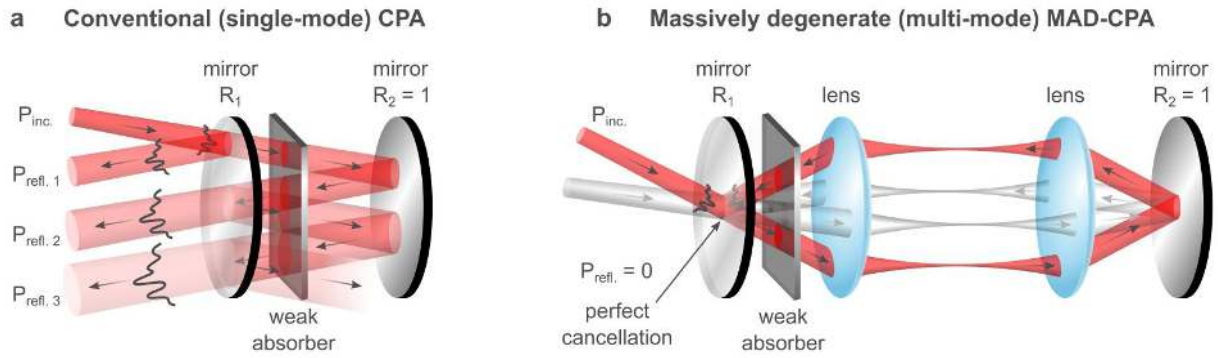


Figure 1: Concept of a massively degenerate coherent perfect absorber (MAD-CPA) for arbitrary wavefronts. ***(a)*** *A conventional (single-mode) CPA is composed of a weak absorber placed between two flat mirrors. While perfect absorption can be achieved for a normal-incident plane-wave via destructive interference of reflections, any other incoming mode, such as the simple tilted beam shown, results in multiple reflections that cannot destructively interfere.* ***(b)*** *In contrast, the massively degenerate multi-mode CPA can perfectly absorb any complex incident wavefront. This is achieved by placing the weak absorber in a degenerate (self-imaging) cavity, realized here by a conventional cavity with two lenses in a telescopic arrangement. In such a degenerate cavity, any complex input field impinging on the front cavity-mirror (R1) is self-imaged onto itself after each cavity round-trip: all reflections from the multiple cavity round-trips show perfect destructive interference with the outer reflection from the front cavity-mirror (here shown for two incoming beams at different angles), leading to perfect absorption of light in the weak absorber.*

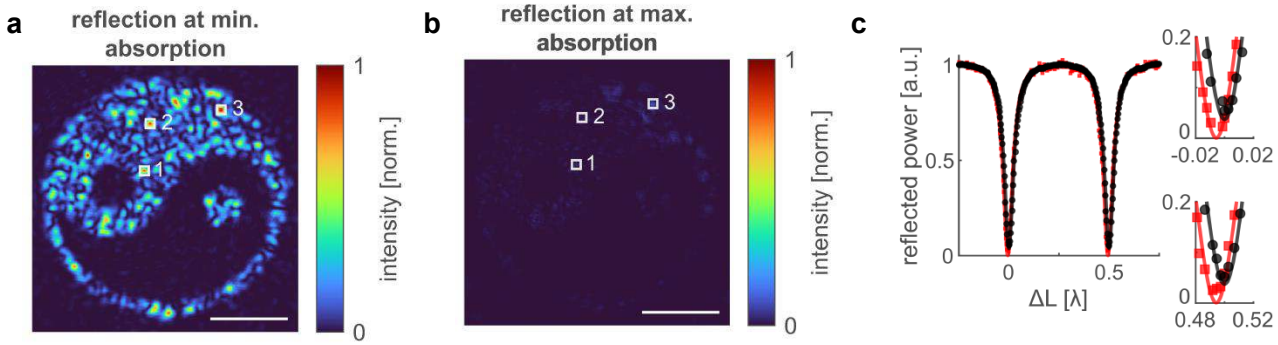


Figure 2: Results for a complex input field in the form of a speckled Yin-Yang symbol composed of > 1000 modes. ***(a)*** *Measured reflected intensity distribution when the cavity length is tuned for minimal, and* ***(b)*** *for maximum absorption, showing near perfect absorption of all input modes.* ***(c)*** *Total back-reflected power as a function of the cavity length (black dots) and for the reflected power of one individual mode (red squares) together with the numerical prediction for the total reflected power for a 100-modes input, considering the residual reflection of the lenses (black and red lines)*

References

1. Chong, Y. D., Ge, L., Cao, H. and Stone, A. D., “Coherent Perfect Absorbers: Time-Reversed Lasers”, Phys. Rev. Lett., Vol. 105, No. 5, 053901, 2010.
2. Baranov, D.G., Krasnok, A., Shegai, T., Alù, A., Chong, Y.: “Coherent perfect absorbers: linear control of light with light”, Nat. Rev. Mater. Vol. 2(12), 1-14, 2017.
3. Slobodkin, Y., Weinberg, G., Hörner, H., Pichler, K., Rotter, S., and Katz, O., “Massively degenerate coherent perfect absorber for arbitrary wavefronts”, Science, Vol. 377, No. 6609, 995–998, 2022.

Coherent Retroreflector, Coherent Asymmetric Absorber, and Bianisotropy Emulation using Coherent Illumination

F. S. Cuesta, M. S. Mirmoosa, and S. A. Tretyakov*

Department of Electronics and Nanoengineering, Aalto University

P.O. Box 15500, FI-00076, Aalto, Finland

*corresponding author: sergei.tretyakov @ aalto.fi

Abstract: In this presentation we will review our recent works on using advanced interference phenomena to realize various effects in extremely thin metasurfaces.

The phenomenon of wave interference, discovered by Thomas Young, is in the core of the wave theory of light, developed by Fresnel and Huygens. Many effects due to wave interference in bulk media and in thin films are known for a long time. In recent years, coherent illumination of extremely thin lossy sheets was considered in [1], with two features highlighted: first, a possibility to absorb all incident power in a layer of negligible thickness and, second, an (obvious) possibility to change the response to one of the illuminating waves by changing the phase or amplitude of the other one. In this talk, we present a review of how coherent illuminations of purposely designed metasurfaces can bring novel, unusual, and useful properties. First, we will discuss coherent effects in non-uniform sheets and show how the incident power coming from coherent sources can be channeled towards non-specular directions in coherent retroreflectors [2]. If absorption is present, a sheet under coherent illumination can behave as a reflector or as an absorber depending on the angle of incidence, as presented in Fig. 1(a) [3]. Next, we will discuss possibilities to emulate bianisotropy effects (for example, omega coupling or chiral response) in simple isotropic metasurfaces. Such applications of coherent illuminations are illustrated in Fig. 1(b), where a single non-bianisotropic sheet can emulate asymmetric reflections under adequate coherent illuminations [4].

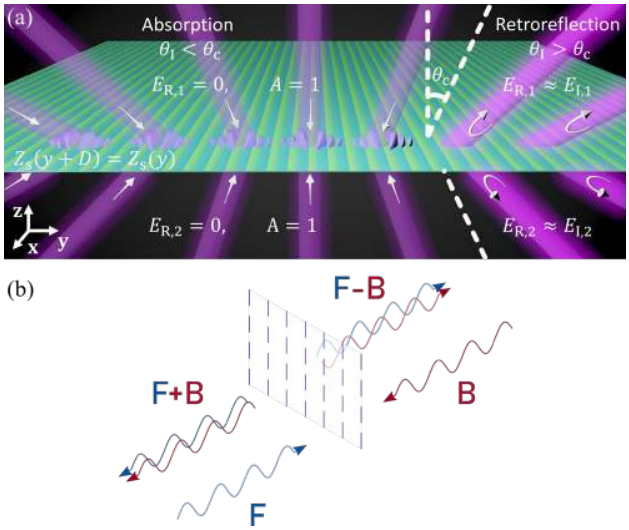


Figure 1. (a) A thin sheet can behave either as an absorber or a reflector by controlling the incidence angle of a coherent source. (b) A single non-bianisotropic sheet can replicate omega-coupling scattering under coherent illumination.

References

1. Zhang, J., K. F. MacDonald, and N. I. Zheludev, “Controlling light-with-light without nonlinearity,” Light. Sci. Appl., Vol. 1, No. 7, e18, 2012.
2. Cuesta, F. S. G. A. Ptitcyn, M. S. Mirmoosa, and S. A. Tretyakov, “Coherent retroreflective metasurfaces,” Phys. Rev. Research, Vol. 3, L032025, 2021.
3. Cuesta, F. S., A. D. Kuznetsov, G. A. Ptitcyn, X. Wang, and S. A. Tretyakov, “Coherent asymmetric absorbers,” Phys. Rev. Applied, Vol. 17, 024066, 2022.
4. Cuesta, F. S., M. S. Mirmoosa, and S. A. Tretyakov, “Emulating bianisotropic coupling through coherent illumination,” Phys. Rev. B, Vol. 107, 035145, 2023.

Nontrivial application of coherent quantum absorption

A. N. Vetlugin[1,2*], R. Guo[1,2], S. Dong[1,3], F. Martinelli[1,2], C. Soci[1,2,3], and N. I. Zheludev[1,2,4]

[1] Centre for Disruptive Photonic Technologies, TPI, Nanyang Technological University, 637371 Singapore
[2] Division of Physics and Applied Physics, School of Physical and Mathematical Sciences, Nanyang Technological University, 637371 Singapore
[3] School of Electrical and Electronic Engineering, Nanyang Technological University, 639798 Singapore
[4] Optoelectronics Research Centre & Centre for Photonic Metamaterials, University of Southampton, Southampton SO17 1BJ, UK
[*]a.vetlugin@ntu.edu.sg

Abstract: The interference of quantum light on a thin absorber (e.g., a metasurface) leads to non-trivial phenomena such as single-photon Zeno and two-photon anti-Hong-Ou-Mandel effects with applications in light detection, communication, and metrology.

Common wisdom tells us that absorption is detrimental to the quantum properties of light and, accordingly, absorption is generally avoided as much as possible. Nevertheless, this rule has exceptions, with coherent absorption of quantum light being a bright example. The uniqueness of quantum coherent absorption relies on its selectivity: while some quantum states are effectively coupled to dissipative channels and are completely absorbed, other states are immune to absorption passing through the absorber without any changes. This mechanism provides a fruitful recipe: blend the properties of the absorber with different quantum states of light to unveil novel aspects of light absorption [1].

Here, we first consider the interference of single-photon states on a thin absorber [2]. In this experiment, the level of absorption depends not only on the relation between the absorber properties and the quantum state of the photon but also on the disclosure of which-path information. In the spirit of conventional single-photon interference on a lossless beamsplitter, which-path information destroys coherent control of absorption.

By exploiting the sensitivity of the absorber to the photon quantum state, we build a quantum state filter, a basic module of quantum experiments, and demonstrate a single-photon switching function of such a filter [3]. Discussion of quantum coherent absorption in terms of quantum states transformation opens the window for replicating this phenomenon on other quantum systems: as an example, we perform modeling of the quantum coherent absorption experiment using the transmon, a superconducting charge qubit of the IBM quantum computer [4].

One of the striking features of quantum coherent absorption is that may turn a probabilistic traveling wave absorption into a deterministic standing wave absorption. Deterministic light absorption is a must-have in numerous applications based on light-matter interaction. For instance, by treating the quantum network consisting of coherence-preserving quantum nodes as a *distributed* absorber, we show that a single photon can be deterministically absorbed within the network generating entanglement between the nodes [5]. Another application benefiting from efficient light absorption is quantum light detection. We demonstrate that distributed coherent absorption in multiple detecting layers, like superconducting nanowire single-photon detectors, allows efficient and photon-number resolving detection of quantum light, which is free of the limitations of conventional multiplexing schemes [6].

By distributing the absorption in time, rather than in space, we show that strong single-cycle coherent absorption is not equivalent to the multiple weak absorption cycles. A bizarre theoretical limit of an infinite number of absorption cycles, where the absorption of each cycle is infinitesimal suggests that absorption becomes zero despite the infinite number of absorption cycles. “Absorption is an illusion” – the ancient Greek philosopher Zeno would conclude. The proof-of-principal experiment of a few-cycle Zeno absorption experiment is presented.

Compared to single-photon states, multi-photon states of light provide even more flexibility in how light may interact with the dissipative channels of the absorber. Here, we consider the coherent absorption of entangled photons. While the conventional interference on a lossless beamsplitter – the prominent Hong-Ou-Mandel effect, results in the coalescence of bosonic particles and anti-coalescence of fermionic particles, the interference on a coherent absorber completely reverses the outcome. In the

experiment, we observe that entangled photons with symmetric spatial wavefunction (“bosonic” type) anti-coalesce and photons with anti-symmetric spatial wavefunction (“fermionic” type) exhibit coalescent-like behavior – the anti-Hong-Ou-Mandel interference takes place [7].

When one photon from the entangled pair interrogates the absorber, the absorption process can be controlled non-locally, for instance, via the geometric phase of the second remote photon from the pair. We report on the observation of such non-local control through the two-photon correlation measurements and discuss how it can be used in quantum metrology applications.

Finally, we briefly outline some general features of coherent effects in quantum light absorption, their origin, and how they would affect the absorption of other, more complex quantum states of light.

References

1. Vetlugin, A. N. “Coherent perfect absorption of quantum light,” Phys. Rev. A Vol. 104, 013716, 2021.
2. Roger, T., Vezzoli, S., Bolduc, E., Valente, J., Heitz, J. J. F., Jeffers, J., Soci, C., Leach, J., Couteau, C., Zheludev, N. I., Faccio, D., “Coherent perfect absorption in deeply subwavelength films in the single-photon regime,” Nat. Commun. Vol. 6, 7031, 2015.
3. Yanikgonul, S., Guo, R., Xomalis, A., Vetlugin, A. N., Adamo, G.., Soci, C., Zheludev, N. I. “Phase stabilization of a coherent fiber network by single-photon counting,” Opt. Lett. Vol. 45, 2740, 2020.
4. Vetlugin, A. N., Soci, C., Zheludev, N. I. “Modeling quantum light interference on a quantum computer,” Appl. Phys. Lett. Vol. 121, 104001, 2022.
5. Vetlugin, A. N., Guo, R., Soci, C., Zheludev, N. I. “Deterministic generation of entanglement in a quantum network by coherent absorption of a single photon,” Phys. Rev. A Vol. 106, 012402, 2022.
6. Vetlugin, A. N., Martinelli, F., Dong, S., Soci, C. “Photon number resolution without optical mode multiplication,” Nanophotonics, 2023.
7. Vetlugin, A. N., Guo, R., Soci, C., Zheludev, N. I. “Anti-Hong–Ou–Mandel interference by coherent perfect absorption of entangled photons,” New J. Phys. Vol. 24, 122001, 2022.

META 2023, PARIS - FRANCE, JULY 18 – 21, 2023

Non-Hermitian Wavefront shaping and Optical Limiting

T. Kottos

Wave Transport in Complex Systems Lab, Department of Physics, Wesleyan UniversityUSA
*corresponding author: tkottos@wesleyan.edu

Abstract: The underlying mathematical structures of non-Hermitian wave physics have inspired several recent applications. Among them are wavefront shaping protocols for efficient energy deposition at lossy targets and optical limiters based on lossy non-linear defects. An example of the first category is the coherent perfect absorption while of the second is the exceptional-point based photonic limiter. We shall explain the intimate connection between these two seemingly different concepts and present our experimental results that highlight the underlying mechanisms.

The development of non-Hermitian optics has led to new avenues for the manipulation of light transport. Examples include PT-symmetric photonics, hypersensitive sensors, unidirectional invisibility, non-reciprocal Bloch oscillations, Coherent perfect absorption, optical limiters and more.

Coherent perfect absorption (CPA) is a multichannel waveform shaping protocol which leads to a complete extinction of a monochromatic radiation when it enters a weakly lossy cavity. The scheme has been initially proposed in the framework of classical optics, as the time-reversed process of a laser. It relies on wave interference effects that entrap the incident radiation inside the lossy cavity, leading to its complete absorption. Subsequent studies nicely demonstrated the CPA implementation, beyond the original platform of optics, spanning all areas of classical wave physics ranging from microwave and RF to acoustics. In all above-mentioned cases, the CPA protocol demonstrated a narrow, resonant-based, (perfect) absorption with very sharp characteristics around the frequency of perfect absorbance. Obviously, addressing this ``deficiency" will open-up a whole new range of possibilities for the CPA scheme including solar photovoltaic or stealth applications. Importantly, the scheme was considering only linear scattering processes.

Here we analyze CPAs in two settings. The first one is associated with a CPA occurring at a chaotic cavity with one localized lossy target embedded inside. The second paradigm is involving nonlinear lossy elements. We show that in both cases CPA is still an effective protocol of targeted energy deposition despite the loss of hidden or geometrical symmetries and/or scale invariance (in the presence of nonlinear processes). In the latter case, we will show that CPA can be turned, using the incident field power as a control parameter, to a (relatively) broad-band phenomenon when the coupling of the system to the interrogating antennas is properly tuned. We have traced this broadband effect to the existence of exceptional point degeneracies (EPD) occurring in the spectrum of the zeros of the scattering matrix.

At the second part of the talk, we shall introduce a class of optical limiters based on concepts borrowed from non-Hermitian defect theory. We shall contrast this class of limiters to a novel proposal that utilizes EPDs in the spectrum of an auxiliary wave-operator (AWO) that describes a scattering process of completely transparent modes (TM). We will show that these modes can be utilized for the design of a non-resonant reflective photonic limiter in the visible range. The analysis of the AWO reveals that the formation of the TM-EPDs is a consequence of a “hidden” parity-time (PT) symmetry that characterizes this operator when the input and output channels are interpreted as effective radiative gain/loss. For low power incident radiation near the TM-EPD

frequency, the transmittance acquires a (near-)unity, flat-top lineshape. When the incident power increases, a self-induced permittivity variation enforces an explicit PT-symmetry violation of the AWO, which results in a destruction of the TM-EPD and an abrupt increase of reflectance to (near)-unity values.

We acknowledge partial support from Simons Foundation grant no MPI 733698 and from NSF grant no ECCS 2148318 (RINGS program).

References

1. L. Chen, T. Kottos, S. Anlage, "Perfect absorption in complex scattering systems with or without hidden symmetries," Nature Communications, Vol. 11, 5826, 2020.
2. S. Suwunnarat, Y. Tang, M. Reisner, F. Mortessagne, U. Kuhl, T. Kottos, "Non-linear coherent perfect absorption in the proximity of exceptional points," Communications Physics, Vol. 5, 5, 2022.
3. F. Riboli, R. Kononchuk, F. Tommasi, A. Boschetti, S. Suwunnarat, I. Anisimov, I. Vitebskiy, D. S. Wiersma, S. Cavalieri, T. Kottos, A. A. Chabanov, "Optical Limietr based on PT-symmetry Breaking of Reflectionless Modes," submitted, 2023.

META 2023, PARIS - FRANCE, JULY 18 – 21, 2023

Quantum Coherent Absorption of Squeezed Light

A. Ü. C. Hardal[1], D. Pandey[1], S. Xiao[1,2,3], and M. Wubs[1,2,3*]

[1]Department of Electrical and Photonics Engineering, Technical University of Denmark, 2800 Kgs. Lyngby, Denmark

[2]Center for Nanostructured Graphene, Technical University of Denmark, 2800 Kgs. Lyngby Denmark

[3]NanoPhoton—Center for Nanophotonics, Technical University of Denmark, 2800 Kgs. Lyngby, Denmark

[*]corresponding author: mwubs@dtu.dk

Abstract: Two identical squeezed coherent states at the input ports of a 50% absorbing beam splitter do not show coherent perfect absorption (CPA). All coherence is lost, though, since at the output ports entangled squeezed vacuum states emerge. Remarkably, this output state is a pure state, although produced by a lossy device. Therefore this CPA gate could become a new tool for continuous-variable quantum state preparation. Moreover, for graphene multilayers engineered for CPA, we discuss the effects of interlayer separation.

We study coherent absorption of squeezed light by a 50% absorbing beam splitter [1]. Identical coherent states at the input ports of such a beam splitter lead to coherent perfect absorption (CPA): the output state is the vacuum state. Not so for identical pairs of squeezed coherent states, we find. We make a distinction between the loss of coherence and the loss of intensity, and show that corresponding absorption coefficients for quantum coherence and for intensity are different. This CPA gate has further intriguing properties: two identical but otherwise arbitrary incoming squeezed coherent states leave all of their coherence and half of their squeezing behind in the beam splitter, producing a pure entangled squeezed vacuum state as the output. This output state of light is not entangled with the lossy beam splitter by which it was produced. This surprising result may make the CPA gate a new tool for continuous-variable quantum state preparation.

Next we analyze absorbing beam splitters made by layers of graphene [2]. To achieve the 50% absorption needed for the CPA gate described above, we are in the "difficult" regime where we need more than a few layers of graphene on the one hand, but we are not necessarily in the bulk graphite limit either. To understand the absorption of a few layers of graphene, one typically uses the transfer matrix approach and neglects their subnanometer interlayer separation. Continuing to neglect this separation results in upper bounds to the absorption by graphene multilayers of 50%, exactly the value needed for coherent perfect absorption (CPA). This upper limit is only reached for real-valued sheet conductivities, and for pristine graphene the finite number of layers that would be required to attain this maximum is fixed by the fine structure constant. We show however that for the thicker multilayers needed to engineer 50% absorption, realistic interlayer separations need to be taken into account, in which case the upper bounds to the absorption at a finite number of layers no longer exist. More generally, more reliable predictions of the absorption by multilayer Van der Waals crystals suitable for CPA can be obtained if their subnanometer interlayer separations are carefully accounted for.

References

1. Hardal, A. Ü. C. and M. Wubs, "Quantum coherent absorption of squeezed light", Optica, Vol. 6, No. 2, 181–189, 2019.
2. Pandey, D., S. Xiao and M. Wubs, "Graphene multilayers for coherent perfect absorption: effects of interlayer separation", Opt. Express, Vol. 30, No. 25, 44504–44517, 2022.

META 2023, PARIS - FRANCE, JULY 18 – 21, 2023

Many-body Quantum Metasurfaces with Coherent Perfect Absorption with PT Symmetry Breaking

Kyle Ballantine[1] **and Janne Ruostekoski**[1*]

[1]Department of Physics, Lancaster University, Lancaster LA1 4YB, United Kingdom
[*]corresponding author: j.ruostekoski@lancaster.ac.uk

Abstract: We theoretically show how a quantum metasurface of atoms can undergo coherent perfect absorption with an effective parity-time (PT) symmetry and non-exponential decay. The effective symmetry is achieved in delocalized collective excitation eigenmodes. These modes coalesce at exceptional points (EPs), evidenced by the emergence of coherent perfect absorption (CPA) where coherent incoming light is perfectly absorbed and scattered only incoherently. The system is versatile and can be modified for single-photon absorption and quantum storage.

Atomic physics technology provides a variety of approaches for trapping closely spaced atoms in arrays with single-site control and unit occupancy per site. For cold atoms with subwavelength spacing, the light-mediated interactions can be very strong due to resonant light undergoing multiple scattering between the atoms, when the realization of strong collective coupling in large resonator arrays of metasurfaces typically requires special arrangements. The first measurements of the transmitted light through an optical lattice of atoms have now been performed that demonstrate subradiant resonance narrowing where the entire lattice responds as a coherent collective entity.

Here we analyze a quantum-photonic surface formed by a single layer of atoms in an array with light mediating strong cooperative many-body interactions. We show how delocalized collective excitation eigenmodes can exhibit an effective PT symmetry and non-exponential decay. This effective symmetry is achieved in a passive system without gain by balancing the scattering of a bright mode with the loss from a subradiant dark mode. These modes coalesce at EPs, evidenced by the emergence of CPA where coherent incoming light is perfectly absorbed and scattered only incoherently.

By controlling atomic level shifts, a collective analogue of electromagnetically-induced transparency (EIT) can be constructed by coupling light dominantly only to two uniform collective excitation modes: a ‘bright mode’, with atomic dipoles coherently oscillating in phase in the plane of the array, and a ‘dark mode’, with the dipoles oscillating in phase perpendicular to the plane. As in a standard independent-atom EIT, the bright and dark modes couple strongly and weakly to radiation, respectively. However, here the microscopic origin of the dark mode is not single-atom interference, but collective many-body subradiance. We show that by balancing the loss of the dark mode with the scattering of the bright mode, the system becomes invariant to PT reversal. The collective eigenmodes of the system, which are linear combinations of the in-plane and out-of-plane modes, can then coalesce at the EPs, leading to spontaneous breaking of the PT symmetry of the eigenvectors, realizing CPA.

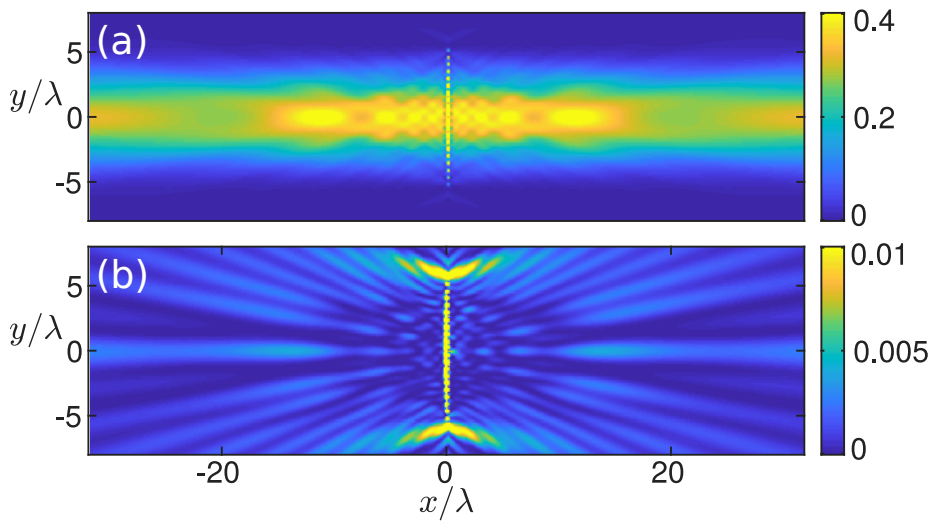


Figure 1: Spatial dependence of intensity for reflecting and CPA phases for a 20×20 atom array on the yz plane at x = 0. We show the total outgoing coherently scattered light intensity (a) in the absence of CA and (b) in the presence of CPA. The atomic arrays are illuminated by Gaussian laser beams propagating from both directions.

By generalizing the model for a bilayer lattice, we can show how the system can be used for single-photon absorption and quantum storage. The excitation can be stored in a subradiant state, transferred coherently between different subradiant states, and released, again in an arbitrary combination of highly collimated forward and backward propagating components. We explain the directionality of single and bilayer arrays by a symmetry analysis based on the scattering parities of different multipole radiation components of collective excitations.

References

1. Ballantine, K. E. and Ruostekoski, J. “Parity-time symmetry and coherent perfect absorption in a cooperative atom response,” Nanophotonics, Vol. 10, No. 4, 1357–1366, 2021.
2. Ballantine, K. E. and Ruostekoski, J. “Unidirectional absorption, storage, and emission of single photons in a collectively responding bilayer atomic array,” Phys. Rev. Research, Vol. 4, 033200, 2022.

META 2023, PARIS - FRANCE, JULY 18 – 21, 2023

Multipolar Coherent Amplification of Chiroptical Scattering and Absorption from a Magnetoelectric Core-shell Nanoparticle

Hsin-Yu Wu[1,2,*] **and Frank Vollmer**[1,2]

[1]Living Systems Institute, University of Exeter, United Kingdom
[2]Department of Physics and Astronomy, University of Exeter, United Kingdom
[*]corresponding author: h.wu@exeter.ac.uk

Abstract: We analytically and numerically demonstrate multipolar coherent amplification of chiroptical responses in the near-infrared wavelength regime via a magnetoelectric core-shell nanoparticle encapsulated in a monolayered optically-active substance. The proposed achiral core-shell nanoparticles can simultaneously support both multipolar electric and magnetic resonances, and thus collaboratively interact with the electric and magnetic components of the incident radiation, which enhances chiroptical signals at specific resonances in the presence of monolayered chiral substances and enables effective molecular chirality sensing at the nanoscale.

Plasmonic and dielectric nanostructures and nanoparticles are attractive in many fields of science and technology, and promising nanoscale tools for detection and analysis of the chirality (handedness) of molecules. Their optical, electronic/magnetic transition properties and resonant frequencies can be easily tuned and tailored by engineering the geometrical parameters to exhibit the desired near-field enhancement and far-field interference for achieving sensitive and reliable chirality sensing. Numerous approaches have been demonstrated, such as chiral and achiral planar nanoarrays/nanolattices, metasurfaces and nanoaggregates, for separation and identification of enantiomers at the specific resonant modes. Among them, the structurally achiral arrangements are highly preferable because each building block does not contribute to unwanted background signals so that the absolute measurement of chiral signals become feasible [1]. Although yielding decent enhancement in chiroptical signals, most of these chiral-sensing schemes only support either electric or magnetic resonances (or one is more dominant than the other). They have not taken into account the fact that the interaction of light with the chiral medium significantly relies on the coexistence of magnetic and electric, i.e. magnetoelectric, coupling implicitly implied by the bi-isotropic constitutive relations [2]. Therefore, the abovementioned chiroptical enhancements are limited since the effect of magnetoelectric coupling on the optical chirality is largely ignored and neglected. In this invited talk, we proposed a hybrid core-shell nanosphere composed of a metallic core and a dielectric shell to amplify the magnetoelectric interactions between the incident radiation and the multipolar electric and magnetic resonances of the nanosphere capped with a chiral monolayer. We derive analytically and verify numerically expressions that provide insight to the enhancement mechanism of the magnetoelectric coupling. The results of our work pave the way for use of achiral core-shell nanoparticles to efficiently boost the background-free chiroptical responses.

The authors acknowledge funding from the European Research Council under an H2020-FET open grant (ULTRACHIRAL, ID: 737071) and EPSRC (EP/T002875/1).

References

1. Wu H-Y, Vollmer F. Enhanced chiroptical responses through coherent perfect absorption in a parity-time symmetric system. *Communications Physics* 2022, **5**(1).

2. Lindell IV, Sihvola AH, Tretyakov SA, Viltanen AJ. *Electromagnetic Waves in Chiral and Bi-Isotropic Media*. Artech House Publishers, 1994.

META 2023, PARIS - FRANCE, JULY 18 – 21, 2023

Beyond CPA: A General Theory of Reflectionless Scattering

A. Douglas Stone[1*], W. R. Sweeney[1], C.-W. Hsu[2], A. Alhulaymi[1] and P. Del Hougne[3]

[1]Dept of Applied Physics and Yale Quantum Institute, Yale University, USA
[2]Viterbi School of Engineering, University of Southern Califorinia, USA
[3]Univ. Rennes, CNRS, IETR-UMR Rennes, France
[*]corresponding author: douglas.stone@yale.edu

Abstract: Coherent Perfect Absorption is one form of reflectionless scattering, involving transduction of an adapted input field. We present a general theory of reflectionless scattering, which includes CPA, based on choosing a subset of input channels and requiring no backscattering into them. We show that infinitely many such solutions exist at complex frequency, can be calculated efficiently, and can be made accessible via tuning a single structural parameter. Optimization of a parameterized structure can achieve high quality signal routing.

The discovery of Coherent Perfect Absorption (CPA) or time-reversed lasing drew attention to the existence of special non-scattering solutions of any linear wave equation, which exist in the complex frequency (ω) plane, and are the time reverse of the resonances (purely outgoing solutions of the wave equation). When gain is added to the system, a resonance can reach the real frequency axis, corresponding to the threshold for lasing in a single mode; conversely when equivalent loss is added, the incoming solution has a real frequency, corresponding to perfect trapping and absorption (or transduction). But this is true only for a specific input wavefront, adapted to the scattering structure, which is the time-reverse of the lasing mode. In the scattering matrix description, the input wavefront must be an eigenvector of the S-matrix with eigenvalue zero. The existence of such reflectionless input waves is guaranteed by the analytic structure of the scattering matrix, although they will only lead to a steady-state harmonic solution if the loss of the structure is carefully tuned. Often in wave physics, and particularly in electromagnetic systems, one is interested not in transduction of input signals, but in suppressing reflection and routing signals into chosen output channels. It is natural to ask if such solutions also exist and are robustly present as are the CPA solutions. In recent work we have shown that indeed any linear wave impedance matching problem can be framed in the a manner similar to CPA, and can also be shown to have infinitely many discrete solutions at complex ω, which can be tuned to the real axis (steady-state) with a single tuning parameter, leading to narrow-band resonant perfect impedance matching [1]. We refer to the complex reflectionless solutions as R-zeros, and the steady-state solutions as Reflectionless Scattering Modes (RSMs), in analogy to the terminology of lasing modes.

These R-zeros and RSMs exist independent of the complexity of the scattering structure (as long as it is finite) and of whether it is in free-space or accessed by guided waves. One of the insights from the theory is that reflectionless scattering is only possible if all the input channels are filled and coherently excited; similar to CPA only a special wavefront is scattered without reflection. The reflectionless scattering condition for the input modes mathematically implies that a submatrix of the scattering matrix has an eigenvector with eigenvalue equal to zero. One can show that each choice of submatrix (i.e. of input channels) leads to discrete complex solutions with spectra distinct from each other and from the resonances or zeros of the full scattering matrix. Importantly, these solutions can be

tuned to the real axis using structural or geometric parameters, without the necessity of using loss or gain, because the reflectionless condition does not inherently violate flux conservation. In the case of a single input channel with an isolated high Q resonance, this concept reduces to the familiar notion of critical coupling, but importantly it is exact and still valid when resonances overlap and the structure is relatively open, or highly damped. Finally, calculating the R-zeros of a particular structure is not significantly more difficult than calculating its resonances and in many cases can be implemented via a modification of the method of perfectly-matched layers (PML). Importantly one does not have to calculate the S-matrix and the relevant submatrix for many frequencies and search for solutions; a single computation yields the R-zeros over a wide bandwidth. In principle one doesn't need to compute the S-matrix at all, although typically this is helpful to do.

Once reflectionless states are found, it is very interesting to try to optimize or functionalize the states for routing functions. The reflectionless boundary conditions do not imply any constraint on the output field distribution, so one needs to build an optimization search on top of it to perform non-random forward scattering of the wavefront. Recently we have done exactly such a study in a massively parameterized microwave cavity with a reconfigurable metasurface [2]. We found that we could implement a demultiplexer with almost 40db of discrimination in such a system, as well as achieving other interesting routing functions which I will review in this talk. A simple example of such routing is shown in Fig. 1 below.

In addition to reviewing the structure and applications of the theory of RSMs, I will discuss the consequences of Parity-Time and other symmetries on the R-zero spectrum and the properties of exceptional points in the RSM spectrum.

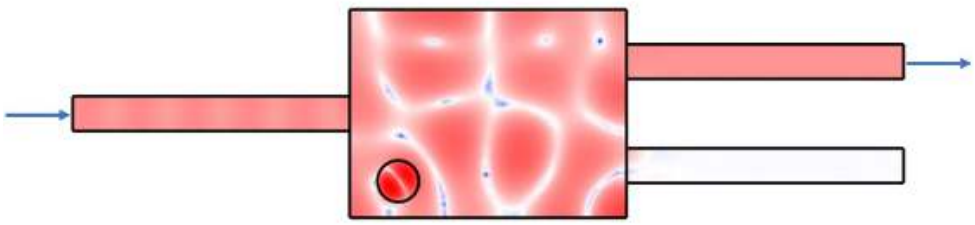


Fig. 1: Simulation of the field for reflectionless routing of a microwave signal into the upper output waveguide in a cavity with a scattering center, based on optimization of the scatterer location.

ADS acknowledges support for this work from the National Science Foundation and the Simons Foundation.

References

1. Theory of Reflectionless Scattering Modes", William R. Sweeney, Chia Wei Hsu, and A. Douglas Stone, Phys. Rev. A, 2020, https://link.aps.org/doi/10.1103/PhysRevA.102.063511
2. "Reflectionless Programmable Signal Routers", J. Sol, A. Alhulaymi, A. D. Stone and P. del Hougne. Science Advances, 25 Jan 2023, Vol 9, Issue 4, DOI: 10.1126/sciadv.adf0323

Controlling wave phases and absorption in curved space for light

Y. Liu*(刘泱杰), Z. K. Xiong, Z. Mao and B. Zhou
School of Physics, Hubei University, Wuhan 430062, P. R. China
* corresponding author: yangjie@hubu.edu.cn

Abstract: In this contribution, we present a general methodology to manipulate the amplitude of an electromagnetic wave in a pre-defined way, without introducing any scattering. This leads to a whole class of isotropic spatially varying permittivity and permeability profiles that are invisible to incident waves. The theory is illustrated through various numerical examples, including the non-magnetic case. Also some new work on manipulating the wave phases and absorption of emission via multipole expansion is included in the hope to develop this methodology further.

Transformation optics [1, 2] is a powerful analytic tool to design impedance-matched material, which gives rise to scattering-free wave solutions up to designer's will. However, this method inevitably requires the material parameter to be anisotropic, which complicates its manufacturing process. Therefore, an isotropic material to achieve the required wave solution may solve this issue. We will demonstrate a method to design isotropic material parameters in an optical inverse problem. We will start from vectorial Helmholtz equations [3] and show how one can find some exact wave solution in a corresponding inhomogeneous medium, where light wave and medium come in pairs. After that we exploit further the idea to seek the pair of wave solution and material parameters: spatial profiles of permittivity and permeability.

We demonstrate examples of how to control wave front [4, 5]– whether maintaining it or varying it at our will. Our method is a general analytic tool to avoid unwanted scattering due to gradient-index profile of materials.

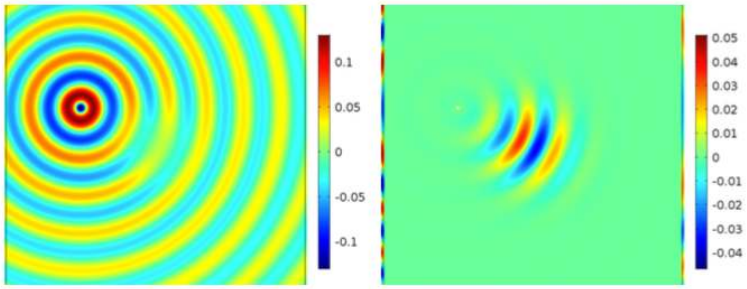


Fig. 1 An example of invisible materials for also a cylindrical wave.

Furthermore, we also demonstrate examples of how to control wave front in accurate way, and of an invisible current source which gives zero far fields at all.

Acknowledgments
We are sponsored by Natural Science Foundation of China [NSFC11804087], Lanzhou Center for Theoretical Physics [NSFC12047501], Department of Science and Technology [2022CFB553, 2022CFB012, 2018CFB148, 2020CFB266];

Educational Commission of Hubei Province [T2020001,Q20201006,Q20211008] and Hubei University [X202210512039, 030-017643].

References

1. U. Leonhardt, “Optical conformal mapping,” Science 312, 1777–1780 (2006).
2. J. B. Pendry, “Controlling electromagnetic fields,” Science 312, 1780–1782 (2006).
3. T. G. Philbin, “Making geometrical optics exact,” Journal of Modern Optics pp. 1–6 (2014).
4. Y. Liu, B. Vial, S. A. R. Horsley, T. G. Philbin, and Y. Hao, “Direct manipulation of wave amplitude and phase through inverse design of isotropic media,” New Journal of Physics 19, 73,010 (2017).
5. B. Vial, Y. Liu, S. A. R. Horsley, T. G. Philbin, and Y. Hao, “A class of invisible inhomogeneous media and the control of electromagnetic waves,” Physical Review B 94, 245,119 (2016).

META 2023, PARIS - FRANCE, JULY 18 – 21, 2023

Optical control of collective states in 1D ordered atomic chains beyond the linear regime

N. Fayard[1*], I. Ferrier-Barbut[1], A. Browaeys[1] and J.-J Greffet[1]

[1]Université Paris Saclay, Institut d'Optique Graduate School, France

[*]nikos.fayard@institutoptique.fr

Abstract: Driven by the need to develop new atom-photon platforms, people recently replaced cavities by large arrays of cold atoms that can support superradiant or subradiant collective states. In practice subradiant states are decoupled from radiation with constitutes a hurdle to most applications. In this work, we study a protocol that enables the deterministic coupling to subradiant modes in subwavelength atoms arrays.

Recently, a new scheme based on the local control of the transition frequency of atoms with light shifts has been proposed to store and manipulate single photon using the subradiant modes of a 2D array [1]. Motivated by the possibility to implement those idea with ongoing experiment using Sr, Yb or Dy, we study theoretically a similar protocol for 1D atomic chain [2]. More precisely, we propose a method to:

1. Excite the most superradiant singly-excited state of the chain from the far field
2. Transfer the excitation to the most subradiant state using a position varying detuning (PVD)
3. Store the excitation
4. Emit the excitation in the desired superradiant mode of the chain, thus controlling its frequency, emission rate and pattern.

In particular, we show that doubly-excited states follow a similar trajectory than singly-excited states. We thus demonstrate that they can be coherently transferred from superradiant to subradiant states, opening the way to the optical access of their entanglement.

References

1. Rubies-Bigorda, O., Walther, V., Patti, T. L., & Yelin, S. F. (2022). Photon control and coherent interactions via lattice dark states in atomic arrays. *Physical Review Research*, *4*(1), 013110.
2. Fayard, N., Ferrier-Barbut, I., Browaeys, A., & Greffet, J. J. (2022). Optical control of collective states in 1D ordered atomic chains beyond the linear regime. *arXiv preprint arXiv:2212.13022*.

Chiroptical phenomena

META 2023, PARIS - FRANCE, JULY 18 – 21, 2023

Computational implementation of the hyper-Rayleigh scattering optical activity: theory, symmetry considerations and quantum chemistry applications

A. Bonvicini* **and B. Champagne**

Theoretical Chemistry Laboratory, Unit of Theoretical and Structural Physical Chemistry, Namur Institute of Structured Matter, University of Namur, B-5000 Namur, Belgium
*corresponding author: andrea.bonvicini@unamur.be

Abstract: We performed the first computational implementation of the hyper-Rayleigh scattering optical activity (HRS-OA) spectroscopy, a nonlinear chiroptical method theoretically predicted by D. Andrews and T. Thirunamanchandran in 1979 [1]. Recent experiments on silver nanohelices and on molecular oligoamide foldamers confirmed this chiroptical phenomenon [2, 3]. Moreover, the measured circular differential scattering ratios make the HRS-OA a promising method for application in chiral discrimination problems due to its high sensitivity compared to other linear chiroptical methods like electronic circular dichroism.

This work reports on the first computational quantum-chemistry implementation of the hyper-Rayleigh scattering optical activity (HRS-OA) spectroscopy [1] which has been experimentally confirmed only recently [2,3]. First, from the basics of the theory, which is based on quantum electrodynamics, the equations for the simulation of the differential scattering ratios of HRS-OA are re-derived; in particular, the symmetry of the polarization and molecular tensors involved, the associated response functions of the latter, and the origin-invariance of the theory for exact wavefunctions are discussed. Then, for the first time, computations of HRS-OA quantities are presented and analyzed. They have been enacted on prototypical chiral organic molecules (methyloxirane, carvone) at the time-dependent density functional theory (TDDFT) level, using a broad range of atomic orbital basis sets. In particular, i) we analyzed the basis set convergence, demonstrating that converged results require basis sets with both diffuse and polarization functions, ii) we discussed the relative amplitudes of the 6 contributions to the differential scattering ratios, and iii) we studied the effects of origin-dependence and derived the expression of the tensor shifts. Our computations show the ability of HRS-OA as a nonlinear chiroptical method, able to distinguish between the enantiomers of the same chiral molecule.

A. B. and B. C. thank F.R.S. - FNRS (Nonlinear chiroptics project) GRANT n° T.0025.22.

A. B. and B. C. thank Prof. Vincent Rodriguez, Prof. Céline Olivier, Prof. Kain Forbes, and Prof. David Andrews for helpful discussions on HRS-OA.

References

1. Andrews, D. L. and T. Thirunamachandran, “Hyper−Raman scattering by chiral molecules”, J. Chem. Phys., Vol. 70, 1027-1030, 1979.
2. Collins, J. *et al.*, “First Observation of Optical Activity in Hyper-Rayleigh Scattering”, Phys. Rev. X, Vol. 9, 011024, 2019.
3. Verreault, D. *et al.*, “Hyper-Rayleigh Scattering as a New Chiroptical Method: Uncovering the Nonlinear Optical Activity of Aromatic Oligoamide Foldamers”, J. Am. Chem. Soc., Vol. 142, 257-263, 2020.

Maximum Chirality Achieved with Resonant Dielectric Metastructures

M.V. Gorkunov[1*], A.A. Antonov[1], D.G. Baranov[2], and Y.S. Kivshar[3]

[1] Shubnikov Institute of Crystallography, FSRC "Crystallography and Photonics"
Russian Academy of Sciences, Moscow 119333, Russia
[2] Center for Photonics and 2D Materials, Moscow Institute of Physics and Technology,
Dolgoprudny 141700, Russia
[3] Nonlinear Physics Centre, Research School of Physics, Australian National University,
Canberra ACT 2601, Australia
[*]corresponding author: gorkunov@crys.ras.ru

Abstract: Resonant dielectric metastructures provide a game-changing platform for chiral optics: maximum-chiral metasurfaces are transparent to waves of a particular circular polarization and strongly interact with waves of the opposite polarization. High-quality chiral resonances enhance selectively diverse nonlinear optical transformations of circularly polarized light. Stacking chiral and achiral metasurfaces and mirrors one can build optical cavities which selectively detect/emit chiral light and open a door to chiral polaritonics and chiral electromagnetic vacuum prospectively facilitating chiral chemistry.

Chiral dielectric metasurfaces – planar subwavelength arrays of elements made of highly refracting transparent materials shaped to break the mirror symmetry – manifest unprecedentedly strong optical chirality approaching the fundamental limits [1-3]. Taking the advantage of controlled coupling of photonic bound states in the continuum (BICs) with free-space light, one can create quasi-BIC-metasurfaces with *maximum optical chirality* that are transparent to waves of one circular polarization and resonantly block their counterparts. In particular, rotationally symmetric quasi-BIC-metasurfaces, built as arrays of dimers of dielectric bars, can be maximum chiral absorbers [1]. Asymmetric arrays are capable of even better and purer maximum chirality, if their quasi-BIC eigenstate is decoupled from one circular polarization. Such quasi-BICs can be hosted by subwavelength-periodic square lattices of relatively simple unit cells containing pairs of dielectric bars of different height. Millimeter-scale ceramic bars arranged in this way fully transmit microwaves of one circular polarization and reflect the others [2]. Recent nanotechnology advances allow fabricating similarly designed arrays of silicon bars demonstrating maximum optical chirality in the near infrared range [3].

Generally, high quality factor resonances underpinned by quasi-BICs of metasurfaces amplify near electric fields and enhance numerous nonlinear-optical phenomena. For maximum-chiral metasurfaces, the circular polarization selectivity of excitation and emission of the quasi-BICs pave the way for various nonlinear-optical transformations of circularly polarized light waves. In particular, we consider how *circularly polarized high-harmonic* wave can be generated if its wavelength is matched to a chiral quasi-BIC. Alternatively, one can pump a metasurface at a chiral quasi-BIC wavelength and achieve *giant high-harmonic circular dichroism*. By comparing such processes we conclude that the best efficiency and chiral selectivity can be realized when several interacting waves are matched to chiral quasi-BICs, and, in the absence of rotational symmetry, arbitrary nonlinear co-polarized and cross-polarized chiral light transformations become possible.

All the flat-optical chiral components can be combined in *chiral cavities* supporting helical eigenmodes – standing waves with uniform chirality density. Here, apart from the geometrically chiral variants, also achiral structures, e.g., planar mirror-symmetric metasurfaces, selectively reflecting one circular polarization and transmitting the opposite while reversing its helicity, are also very useful [4]. We analyze different types of

metacavities built as stacked pairs of maximum chiral and/or mirror-symmetric metasurfaces and conclude that there are several combinations supporting helical Fabry-Perot eigenstates coupled to normally incident/outgoing circularly polarized waves. Such cavities have broad prospects for efficient generation and sensitive detection of chiral light as well as for its chiral nonlinear conversion. By expanding the set of tools for chiral light-matter interactions, they open a door to chiral polaritonics and chiral electromagnetic vacuum prospectively facilitating chiral chemistry [5].

Finally, we analyze simpler cavities consisting of a metasurface and an ordinary metal mirror. While it is unclear how they could sustain chiral cavity modes at normal incidence, there are clear advantages of such arrangements operating in oblique directions. In such a case, the metasurface may even lack intrinsic structural chirality but exhibit instead strong resonant extrinsic optical chirality. Then stacking an achiral metasurface, built as a square array of silicon triangular prisms, with an ordinary metal mirror creates a cavity selectively coupled to obliquely propagating circularly polarized free-space waves. This allows designing ultracompact chiral light sources based on thin layers of electroluminescent material confined inside such cavities [6].

Support from the Russian Science Foundation (project 23-42-00091) is gratefully acknowledged.

References

1. Gorkunov, M. V., A. A. Antonov, and Y. S. Kivshar, "Metasurfaces with maximum chirality empowered by bound states in the continuum," Phys. Rev. Lett., Vol. 125, No. 9, p. 093903, 2020.
2. Gorkunov, M. V., A. A. Antonov, V. R. Tuz, A. S. Kupriianov, and Y. S. Kivshar, "Bound states in the continuum underpin near‐lossless maximum chirality in dielectric metasurfaces," Adv. Optical Mater., Vol. 9, No. 19, p. 2100797, 2021.
3. Kühner, L., F. J. Wendisch, A. A. Antonov, J. Bürger, L. Hüttenhofer, L. de S. Menezes, S. A. Maier, M. V. Gorkunov, Y.S. Kivshar, and A. Tittl, "Unlocking the out-of-plane dimension for photonic bound states in the continuum to achieve maximum optical chirality," arXiv:2210.05339, 2022. http://arxiv.org/abs/2210.05339
4. Voronin, K, A. S. Taradin, M. V. Gorkunov, and D. G. Baranov, "Single-handedness chiral optical cavities," ACS Photonics, Vol. 9, No. 8, pp. 2652–2659, 2022.
5. Baranov, D. G., C. Schäfer, and M. V. Gorkunov, "Towards chiral polaritons," arXiv:2212.13090, 2022. http://arxiv.org/abs/2212.13090
6. Kim, S., S-C. An, Y. Kim, Y. S. Shin, A. A. Antonov, I. C. Seo, B. H. Woo, Y. Lim, M. V. Gorkunov, Y. S. Kivshar, J. Y. Kim, and Y. C. Jun, "Chiral electroluminescence from thin-film perovskite metacavities," arXiv:2302.05241, 2023. http://arxiv.org/abs/2302.05241

META 2023, PARIS - FRANCE, JULY 18 – 21, 2023

Signature of the Chiral Tensor Elements of the First Hyperpolarizability in Metallic Nanoparticles in Hyper Rayleigh Scattering Experiments

Z. Behel, M. Slemp, K. Matczyszyn,[2] S. Parola[3] and P.F. Brevet[1*]

[1]*Institut Lumière Matière, UMR CNRS 5306 and University Claude Bernard Lyon 1, F-69622 Villeurbanne, France*
[2]*Institute of Advanced Materials, Faculty of Chemistry, Wroclaw University of Science and Technology, Wroclaw, Poland.*
[3]*Laboratoire de Chimie, UMR CNRS 5182, École Normale Supérieure de Lyon and Université Claude Bernard Lyon 1, F-69364 Lyon, France*

[*]corresponding author: pfbrevet@univ-lyon1.fr

Abstract: We report the use of polarization resolved hyper Rayleigh scattering to identify the chiral elements of the first hyperpolarizability tensor of small metallic nanoparticles. This operation is performed in gold nanoparticles ensemble measurements directly in liquid suspensions using an elliptically polarized fundamental beam. Several nanoparticle shapes are discussed and directions towards single nanoparticle measurements proposed.

Quantitative characterization of the physical properties of nano-objects with dimensions much smaller than the wavelength of light is still a great demand in the nanosciences, notably in view of developing probes and sensors [1]. This is routinely achieved when these nano-objects are supported onto substrates using microscopy-based methods such as Scanning or Transmission electronic microscopy (SEM or TEM). These methods indeed provide morphological parameters of nano-objects with great accuracy. A full description of a sample containing a large number of these nano-objects requires though TEM images in a large number, something that may not be easily achievable. However, in absence of substrate, the problem remains acute and challenging. This is notably the case for liquid solutions where the nano-objects are not supported and undergoing Brownian motion. Characterization of these nano-objects is on high demand due to the large variety of the physical properties that they may be shown by the nano-object ensemble as the result of bottom-up chemical syntheses. An example is the case of the nano-object size or shape that may undergo large deviations from the ensemble distribution average quantities.

Optical methods have thus been proposed to the determination of the linear properties of metallic nanoparticles, in particular the determination of their extinction cross sections, notably using UV-visible extinction spectroscopy on large ensembles. More recently, nonlinear optical methods have appeared with advantages, as the first hyperpolarizability, effectively the cross-section for second harmonic generation, namely the process whereby two photons at a fundamental energy are converted into one photon at the sum energy, scales with the

surface rather than the volume as it is the case with linear extinction for metallic gold or silver nanoparticles [2]. With nanoparticles randomly dispersed in a liquid suspension, an incoherent SHG signal can indeed be observed. This method is known as hyper Rayleigh scattering (HRS), due to the orientation fluctuations of the particles in the medium [3]. Such a technique has been extensively used to determine the first hyperpolarizability of molecules and more recently nanoparticles at the ensemble level.

In this work, the HRS method is employed using polarization analysis of both the fundamental and harmonic light to get fine details on the morphology of the nanoparticles [4]. Using elliptical light, it possible to access fine details of the nonlinear response, and in particular several tensor elements of first hyperpolarizability associated with chiral responses. This operation is performed on spherical gold nanoparticles in aqueous suspensions as it is demonstrated that these nanoparticles do not retain any specific symmetry because their shape is not perfect. Some specific shapes are then discussed in view of observing the signature of chirality with this method. Finally, some issues are discussed in order to aim to perform these measurements on single nanoparticle [5].

References

1. Butet J., Brevet P.F., Martin O.J.F., Optical Second Harmonic Generation in Plasmonic Nanostructures: From Fundamental Principles to Advanced Applications, *ACS Nano* (2015) 9, 10545.
2. Butet J., Maurice A., Bergmann E., Bachelier G., Russier-Antoine I., Ray C., Bonhomme O., Jonin C., Benichou E., Brevet P.F., Second Harmonic Generation with Metallic Nanoparticles in Metal Nanostructures for Photonics, Eds. C.B. de Araujo and L. Reyes Pires Kassab, Elsevier, Amsterdam, 2018
3. Clays K., Persoons A., Hyper-Rayleigh Scattering in Solution, *Phys. Rev. Lett.* (1991) 66, 2980.
4. Duboisset J., Brevet P.F., Second Harmonic Scattering-Defined Topological Classes for Nano-Objects, *J. Phys. Chem.* C, 123, 25303, 2009.
5. Duboisset J., Russier-Antoine I., Benichou E., Bachelier G., Jonin C., Brevet P.F., Single Metallic Nanoparticle Sensitivity with Hyper Rayleigh Scattering, *J. Phys. Chem. C,* 113, 13477, 2009.

Transition Metal Nitride and Oxide Thin Films for Chiral Structures: Spectral and Environmental Applicability

R. Bower and P. K. Petrov*

Department of Materials, Imperial College London, Royal School of Mines, Exhibition Road, London, SW7 2AZ, U.K.
*corresponding author: p.petrov@imperial.ac.uk

Abstract: Refractory plasmonic thin film materials are of interest for the development of chiral structures due to their increased thermal stability when compared to gold and silver. Transition metal nitride and oxide thin films have been highlighted as promising alternative materials, offering both strong plasmonic and thermal performance. In this work, we analyse the stability of both the structural and optical response of various plasmonic thin films and individual nanodiscs of various diameters subjected to elevated temperature conditions in the air.

Chiral plasmonic structures combine the chiral properties of materials with the plasmonic properties of metals, leading to a wide range of potential applications in a wide range of fields, including sensing, spectroscopy, and photonics. [1]. Chiral plasmonic structures that require high operational temperatures have been of particular interest in recent years, because, at elevated temperatures, the chirality of these structures can be altered, leading to changes in their behaviour. However, typical plasmonic materials such as gold, silver and copper are unsuitable for such high-temperature applications, due to their poor thermal stability. Refractory plasmonic materials are therefore of increasing importance, presenting the potential to improve the performance and operational lifetimes of the chiral plasmonic structures at high-temperature.

In this work, the temperature stability of thin films of W, Mo, Ti, TiN, TiON, Ag, Au, and $SrRuO_3$ are investigated to assess their viability for robust refractory plasmonic applications as well as the nanostructured plasmonic materials at the level of individual nanodiscs, tracing both the shape modification and the optical response modification of the same nanostructure utilizing cathodoluminescence (CL) spectroscopy.

Films ranging in thickness from 50 - 180 nm are deposited using various deposition methods, before characterisation using AFM, XRD, spectroscopic ellipsometry, and DC resistivity. Measurements are conducted before and after annealing in air at temperatures ranging from 300 - 1000° C for one hour, to establish the maximum cycling temperature and potential longevity at the temperature for each material. It is found that SrRuO3 retains metallic behaviour after annealing at 800° C, however, importantly, the optical properties of TiN and TiON are degraded as a result of oxidation. Nevertheless, both TiN and TiON may be better suited than Au or SRO for high-temperature applications operating under vacuum conditions.

Finally, Figure 1 provides an overview of the operational limits for each of the materials under investigation. The observed maximum operating temperature in air (i.e. the annealing temperature after which metallic behaviour was lost) for each material is plotted against the plasma frequency as reported in the literature. In general, it appears oxide materials such as SRO exhibit superior stability in the air than pure metals and TiN.[2]

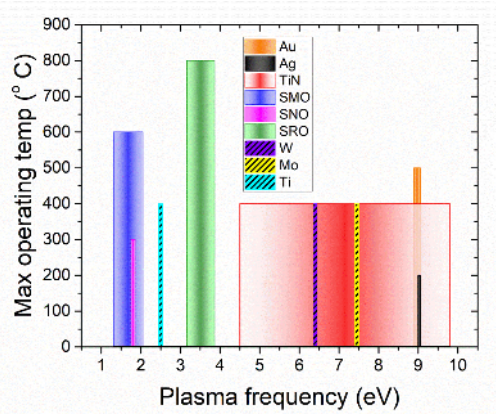


Figure 1 Spectral and temperature applicability of the investigated materials. [2]

In contrast to smooth plasmonic films, for which primarily the modification of the optical constants with annealing is important, for nanostructures, both morphology and optical constants can be modified at high temperatures. The electron beam of the CL microscope can be readily used to directly excite plasmonic modes with nanoscale resolution. Collection of the light emitted upon excitation can be used to identify plasmon resonances and hybrid modes, and also allows for the polarization and angular emission profile to be resolved [3,4]. Here, we compare the thermal stability of single nanoscale titanium nitride and gold discs, patterned on silicon substrates. Samples are annealed in the air for 30 min each at temperatures ranging from 150 °C to 325 °C. Following each annealing stage, CL spectra and SEM images are collected to assess variations in the optical response and disc morphology. Experimental spectral data for the CL response of plasmonic discs are supplemented by simulations, identifying the excited plasmonic modes and confirming the oxidation-related mechanism of the change in the optical response of TiN nanodiscs with the annealing temperature. SEM imaging and CL spectroscopy indicate that although TiN displays superior thermal stability in comparison with Au when considering morphological changes and disc deformation, deterioration in the optical properties of both materials occurs at comparable temperatures. The degradation of individual discs occurs at significantly lower temperatures than previously reported for plasmonic thin films.[5]

From these results, it is apparent that oxidation of TMNs remains a limitation to the integration of TiN components within plasmonic devices to be used in ambient conditions. However, we suggest that TiN could display improved performance compared to gold when used in inert or vacuum environments.

This work was financially supported by the Engineering and Physical Sciences Research Council (EPSRC) grant “Robust manufacturable antibacterial surfaces enabled by superhard plasmon-enhanced photocatalytic materials (ROMANS)” EP/W012197/1 and by the Henry Royce Institute through EPSRC grant EP/R00661X/1.

References

1. M J Urban, C Shen, X-T Kong, C Zhu, A O Govorov, Q Wang, M Hentschel, and N Liu, “Chiral Plasmonic Nanostructures Enabled by Bottom-Up Approaches” *Annu. Rev. Phys. Chem*. 70, 275–99, 2019.
2. Wells M, Bower R, Kilmurray B, Zou B, Mihai AP, GOBALAKRICHENANE G, Alford NM, Oulton RFM, Cohen L, Maier SA, Zayats A, and Petrov PK., “Temperature stability of thin film refractory plasmonic materials”, *Optics Express*, Vol: 12, 15726-15744, 2018
3. E. J. R. Vesseur, J. Aizpurua, T. Coenen, A. Reyes-Coronado, P. E. Batson, and A. Polman, "Plasmonic excitation and manipulation with an electron beam," MRS Bulletin 37, 752-760, 2012
4. T. Coenen, and N. M. Haegel, "Cathodoluminescence for the 21st century: Learning more from light," Applied Physics Reviews 4, 031103, 2017.
5. R Bower, CPT McPolin, AV Krasavin, AV Zayats, and PK Petrov, “Temperature stability of individual plasmonic Au and TiN nanodiscs”, *Optical Materials Express* 12 (9), 3471-3479, 2022

META 2023, PARIS - FRANCE, JULY 18 – 21, 2023

Photogalvanics of chiral topological insulator metamaterials

A. M. Dubrovkin[1,2], G. Adamo[1,2], N. I. Zheludev[1,2,3], and C. Soci[1,2*]

[1]Centre for Disruptive Photonic Technologies, TPI, Nanyang Technological University, Singapore
[2]School of Physical and Mathematical Sciences, Nanyang Technological University, Singapore
[3]Optoelectronics Research Centre and Centre for Photonic Metamaterials, University of Southampton, UK
[*]corresponding author: csoci@ntu.edu.sg

Abstract: Confinement of electromagnetic fields at the subwavelength scale allows engineering light-matter interactions in topological materials, providing new avenues to access nontrivial features of their electronic band structure [1]. It has been shown that nanostructures carved on the surface of topological insulator crystals deeply affect the response of their surface states, as probed by optical near-field imaging [2] and by light helicity dependent photocurrents induced by the circular photogalvanic effect [3]. Here we report deeply subwavelength nanoimaging of light helicity dependent photocurrents and their local texture in pristine and artificially nanostructured topological insulator crystals. To map the local surface photocurrents, which are typically overshadowed by the bulk electron contribution, we used $Bi_{1.5}Sb_{0.5}Te_{1.8}Se_{1.2}$ (BSTS) crystals known for their extremely high surface-to-bulk conductivity ratio [4] and developed a new differential photocurrent nanoimaging technique, built on the platform of a scattering-type scanning near-field optical microscope (s-SNOM). Deeply nanoscale resolution is achieved by higher harmonic demodulation of the polarization dependent photocurrent signal at the s-SNOM tip tapping frequency. While the helicity-dependent photocurrent distribution is found to be fairly homogeneous over the flat areas of the BSTS device far from the electrodes, patterning of the topological crystal surface with enantiomeric spirals generates local hot-spots where the photocurrent response is significantly enhanced, embedded into deeply subwavelength spatial textures. Numerical simulations accounting for the optical absorption and the spin angular momentum of the optical field suggest a link between the quantum spin Hall effect of light in the nearfield of the chiral nanostructures and the local photocurrents generated on the surface of the topological insulator. A new, direct probe of the effect of nanostructuring on the local distribution of circular photogalvanic surface currents, helicity dependent photocurrent nanoscopy unlocks the understanding and exploitation of spin-mediated light-matter interactions in in topological insulator metamaterials.

References

1. H.N.S. Krishnamoorthy, G. Adamo, A.M. Dubrovkin, C. Soci, Topological insulator metamaterials, *Chemical Reviews* (2023).
2. A.M. Dubrovkin, G. Adamo, J. Yin, L. Wang, C. Soci, Q.J. Wang, N.I. Zheludev, Visible range plasmonic modes on topological insulator nanostructures, *Adv. Opt. Mat.* 5, 1600768 (2017).
3. X. Sun, G. Adamo, M. Eginligil, H.N.S. Krishnamoorthy, N.I. Zheludev, C. Soci, Topological insulator metamaterial with giant circular photogalvanic effect, *Science Advances* 7, eabe5748 (2021).
4. L. Wang B. Xia, P. Ren, A. Sulaev, L. Liu, S.Q. Shen, Indications of surface-dominated transport in single crystalline nanoflake devices of topological insulator $Bi_{1.5}Sb_{0.5}Te_{1.8}Se_{1.2}$, *Physical Review B* 87, 085442 (2013).

Multifunctional Chiral Meta-Platform for Dynamic Spin-Encoded Phase Multiplexing

Hafiz Saad Khaliq[1], Junhwa Seong[2], Asad Nauman[1], Jae-Won Lee[1], Jung-Yeop Shin[1], Junsuk Rho[2,3] and Hak Rin Kim[1, 4*]

[1]School of Electronic and Electrical Engineering, Kyungpook National University, Daegu 41566, Republic of Korea

[2]Department of Mechanical Engineering, Pohang University of Science and Technology (POSTECH), Pohang 37673, Republic of Korea

[3]Department of Chemical Engineering, Pohang University of Science and Technology (POSTECH), Pohang 37673, Republic of Korea

[4]School of Electronics Engineering, Kyungpook National University, Daegu 41566, Republic of Korea
[*]Corresponding author: rinney@knu.ac.kr

Abstract: Recently, chiral metasurfaces have been designed for numerous applications in flat optics and photonics, specifically in encrypted displays, imaging, and sensing. Here, we proposed a reflective multifunctional dielectric chiral metasurface integrated with liquid crystal modulator incorporating the ability for spin-encoded phase multiplexing based on the dynamic switching of input and output polarization of visible light. Moreover, the chiral meta-platform reproduces two distinct phase profiles with simultaneous control on its cross and co-polarized component for one-handedness of incident circularly polarized light.

Previously, numerous meta-platforms based on plasmonic and dielectric nanostructures were presented with simultaneous control on amplitude, polarization, and phase for promising applications in data encryption, quantum information processing, holographic displays, bio-imaging, etc [1]. However, dielectric metasurfaces with low losses emerged as efficient and compact solutions for integrated optical systems. Meanwhile, multiplexing and multifunctionality in the metasurfaces created more versatile meta-devices for the aforementioned applications. Metasurfaces with integrated functionality and combining multiple-phase modulation techniques have been presented for hologram multiplexing and spin-dependent wavefront shaping [2]. Although such meta-platforms provide multiplexing of multiple phase information, they cost efficiency due to the phase distortion and require additional optical components to distinguish encoded information.

In polarization optics, chiral metasurfaces have recently gained significant attention due to their unique way of interaction with light [3-5]. This work proposed a unique strategy to incorporate multiple-phase information in a single dielectric chiral structure. The proposed chiral metasurface can encode two distinct phase information using the geometric phase modulation technique compared to the conventional chiral geometries, which can embed just one phase profile. The building block of the meta-platform comprises the carefully optimized pair of hydrogenated amorphous silicon (a-Si:H) based achiral unit atoms to introduce chirality in the visible regime. Apart from chirality inclusion, the building block included extra degree of freedom to encode more than one phase information using geometric phase modulation technique. The proposed chiral meta-platform illuminated with one-handedness of circularly polarized light reproduces two distinct spin-selective phase information with output polarization control using liquid crystal (LC) modulator. The schematic art of the working principle of the designed multifunctional chiral meta-platform is depicted in Figure 1. In our opinion, such multifunctionality and multiplexing in chiral metasurfaces can pave the way for numerous applications in the healthcare sector for bio-imaging, media for polarization-encrypted displays, communication, and data encryption.

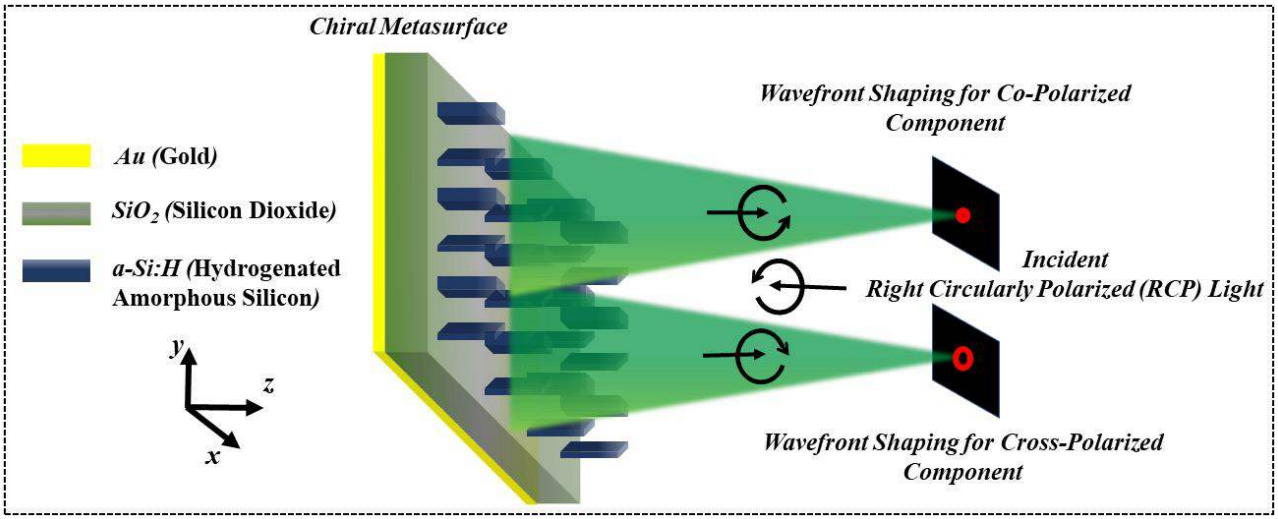


Figure 1. The artistic view of the working principle of the proposed multifunctional chiral meta-platform. The distinct wavefront shaping is depicted based on the handedness of output.

Acknowledgment: This work is supported by the Electronic Parts Industry Technology Innovation Program (20016297, Development of variable focus lens-based industrial augmented reality device and operating system technology for worker safety in industrial sites) funded By the Ministry of Trade, Industry & Energy (MOTIE, Korea).

References

1. Hsiao, H.-H.; Chu, C. H.; Tsai, D. P. Fundamentals and Applications of Metasurfaces, Small Methods. 1, 1600064, 2017.
2. Xiong, B.; Deng, L.; Peng, R.; Liu, Y. Controlling the degrees of freedom in metasurface designs for multi-functional optical devices. Nanoscale Adv., 1, 3786, 2019.
3. Naeem, T.; Kim, J.; Khaliq, H. S.; Seong, J.; Chani, M. T. S.; Tauqeer, T.; Mehmood, M. Q.; Massoud, Y.; Rho, J. Dynamic Chiral Metasurfaces for Broadband Phase-Gradient Holographic Displays. Adv Opt. Mater, 2023.
4. Khaliq, H. S.; Kim, J.; Naeem, T.; Riaz, K.; Badloe, T.; Seong, J.; Akbar, J.; Zubair, M.; Mehmood, M. Q.; Massoud, Y.; Rho, J. Broadband Chiro-Optical Effects for Futuristic Meta-Holographic Displays. Adv Opt Mater, 10 (22), 2022.
5. Khaliq, H. S.; Kim, I.; Kim, J.; Oh, D. K.; Zubair, M.; Riaz, K.; Mehmood, M. Q.; Rho, J. Manifesting Simultaneous Optical Spin Conservation and Spin Isolation in Diatomic Metasurfaces. Adv. Optical Mater. 9, 2002002, 2021.

META 2023, PARIS - FRANCE, JULY 18 – 21, 2023

Strong broadband circular dichroism in chiral plasmonic woodpiles

B. Abdennadher[1], R. Iseli[1], U. Steiner[1], and M. Saba[1*]

[1]Adolphe Merkle Institute, Chemin des Verdiers 4, 1700 Fribourg, Switzerland
[*]corresponding author: matthias.saba@unifr.ch

Abstract: Chiral woodpile structures are well known to boost chiro-optical effects. We here demonstrate that light scattering at a chiral plasmonic woodpile, which is structured on the order of the wavelength of the light, can be well understood by considering its fundamental evanescent Floquet states. In particular, we report a broadband circular polarization bandgap in the complex band structure between 3 and 4 μm wavelength, yielding a strong and broadband circular dichroism. Our findings could pave the way for an ultra-broadband circularly polarized thermal source.

Electromagnetic wave propagation in traditional metamaterials with a deeply sub-wavelength structure is typically well understood through homogenization and associated effective parameters [1]. On the other hand, wave propagation in lossless photonic crystals, structured on the order of the wavelength, is generally best characterized through the photonic bandstructure [2]. An extension of the classical Bloch waves to evanescent Floquet states, and an associated bandstructure with complex-valued wave number allows to fully characterize light propagation in finite material slabs (**Figure 1**) and thus provides a quantitative translation between material modes and experimentally observed scattering parameters [3]. By semi-analytically calculating the evanescent Floquet states of a layered chiral plasmonic woodpile using a standard transfer matrix method, we show that the woodpile gives rise to a large *plasmonic* bandgap for one circular polarization, with gap-to-midgap ratio of more than 2/7 [4]. This bandgap is typically found close to, but below the first Wood anomaly of the woodpile. Even considering the fundamental Floquet modes only allows surprisingly accurate predictions on the scattering parameters of a woodpile slab, which gives rise to a strong and broadband circular dichroism and thus enables circular polarized thermal emission with high enantiopurity of the emitted light.

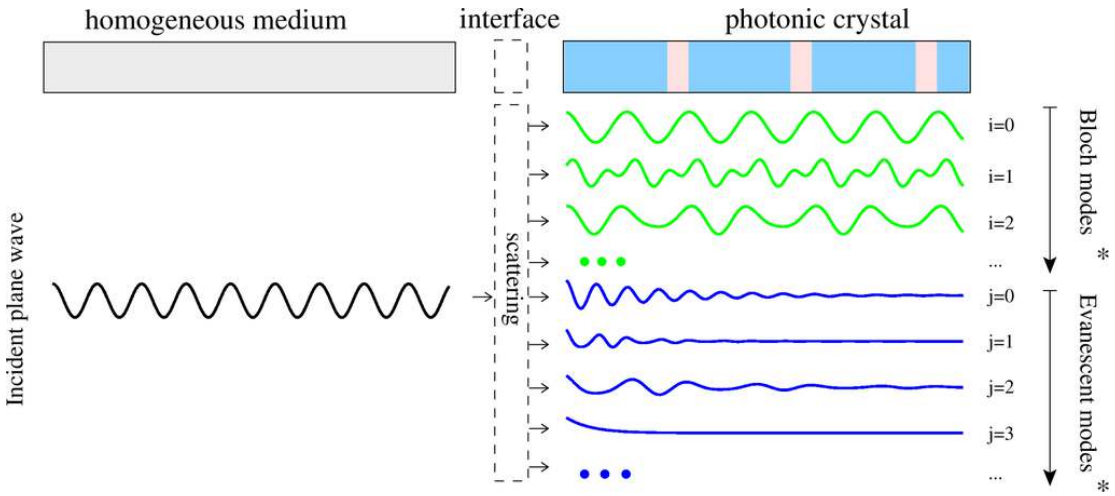


Figure 1 Mock illustration of a plane wave exciting a semi-infinite slab of a periodic material hosting a countably infinite number of evanescent Floquet modes.

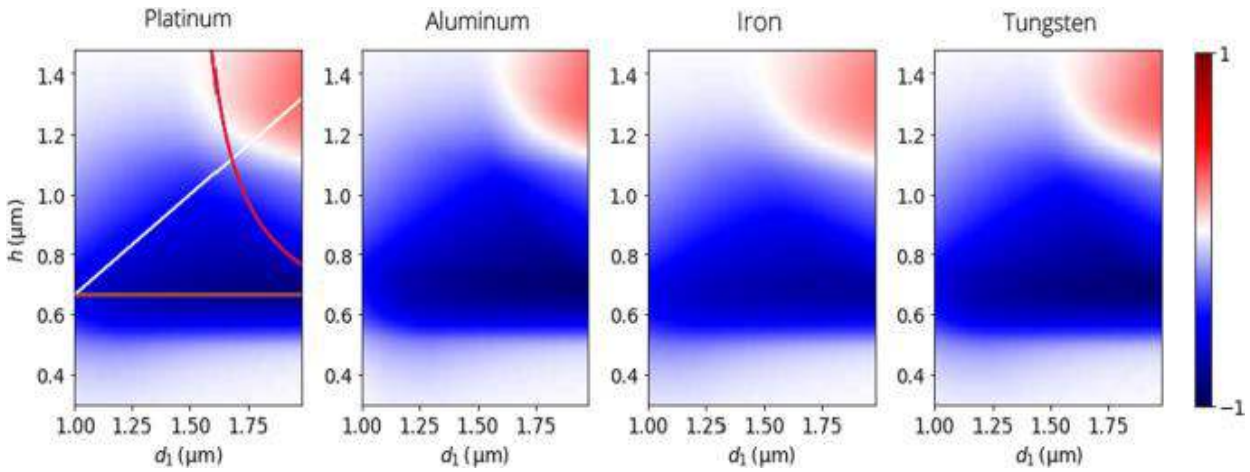


Figure 2 Heatmap of average circular dichroism (defined as absolute difference in absorptivity between right and left circularly polarized light, averaged over a spectral range between 3 and 4 μm wavelength) for a hexagonal plasmonic woodpile made of four different metals. The circular dichroism is shown to mainly depend on two geometrical parameters: the layer height h (one third of the chiral pitch), and the thickness of the air region between metallic bars in each layer d_1. The lines in the platinum figure indicate the theoretically predicted boundaries of the region of large circular dichroism.

At mid-infrared frequencies (we focus on the optical transparency window between 3 and 4 μm wavelength), due to the small size of the effective skin-depth compared to the structural lengths, the circular polarized bandgap is largely independent of the plasmonic metal and exists within a large region in the geometrical parameter space of the structure (**Figure 2**). Employing a Bouligand approximation [5] of the woodpile structure, we develop analytical expressions for the boundary of the region of large broadband circular dichroism, which agree well with the full model. The Bouligand model thus not only explains the shape and large size of the parameter space region of high circular dichroism, but further provides general design principles to optimize the latter. Our findings suggest that hexagonal plasmonic woodpiles structured on the order of the wavelength of the light are an ideal platform to build a circularly polarized thermal source. First, their performance is insensitive to structural variations and thus fabrication imperfections or high temperatures. Additionally, the frequency region of large circular dichroism is not only broadband, but close to the first Wood anomaly. The relative frequency, scaled by the lattice constant, is therefore twice a high as in comparable high-index photonic crystal structures, and thus easing the requirements of the feature size of top-down fabrication techniques, such as two-photon polymerization.

References

1. Engheta, N. and Ziolkowski, R.W. “Metamaterials: Physics and Engineering Explorations,” Wiley, New York, 2006.
2. Joannopoulos, J.D., Johnson, S.G. and Winn, J.N. “Photonic Crystals: Molding the Flow of Light,” 2nd edition, Princeton University Press, Princeton, 2011.
3. Saba, M. and Schröder-Turk, G.E. “Bloch modes and evanescent modes of photonic crystals: weak form solutions based on accurate interface triangulation.” Crystals Vol. 5, No. 1, 14–44, 2015.
4. Abdennadher, B., Iseli, R., Steiner, U. and Saba, M. “Broadband circular dichroism in chiral plasmonic woodpiles,” Applied Physics A, Vol. 129, No. 229, 2023.
5. Bouligand, Y. “Twisted fibrous arrangements in biological materials and cholesteric mesophases,” Tissue Cell, Vol. 4, No. 2, 189–217, 1972.

BSW-based transducer for surface mode polarization control

E. Mogni[1], G. Pellegrini[2], J. Gil-Rostra[3], F. Yubero[3], G. Simone[1,4], S. Fossati[5], J. Dostálek[5,6], R. Martínez Vázquez[7], R. Osellame[7], M. Celebrano[1*], M. Finazzi[1] and P. Biagioni[1]

[1]Politecnico di Milano, Dipartimento di Fisica, 20133 Milano, Italy
[2]Università degli studi di Pavia, Dipartimento di Fisica, 27100 Pavia, Italy
[3]CSIC-Universidad de Sevilla, Instituto de Ciencia de Materiales de Sevilla, 41092 Sevilla, Spain
[4]Northwestern Polytechnical University, School of Mechanical Engineering, Xi'an Shaanxi, People's Rebublic of China
[5]AIT-Austrian Institute of Technology GmbH, Biosenso Technologies, Tulln an der Donau, Austria
[6]Czech Academy of Sciences, FZU-Institute of Physiscs, Prague, Czech Republic
[7]Istituto di Fotonica e Nanotecnologie (IFN)-CNR, 20133 Milano, Italy
*Corresponding author: michele.celebrano@polimi.it

Abstract: We manufacture and evaluate the optical performance of a novel optical transducer that allows uniform surface-enhanced fields for sensing through the excitation of Bloch Surface Waves (BSWs). The aim is to attain the coherent superposition of TE and TM dispersion relations of BSWs that is essential to provide "superchiral" fields over a wide spectral range (down to the UV). The resulting BSW-based transducer paves the way to the implementation of polarization-resolved surface-enhanced techniques.

Bloch Surface waves (BSWs) can be supported at the surface of truncated one-dimensional photonic crystals (1DPCs). Thanks to the high sensitivity to the local refractive index where they propagate, BSW-based transducers are widely used for sensing analytes [1-3].

A further step in surface-enhanced spectroscopies using BSWs is the control over the polarization, which can be attained by engineering the overlap between the dispersion relations of the transverse electric (TE) and the transverse magnetic (TM) eigenmodes that can be sustained by these truncated 1DPCs. In fact, the resonant wavelength of the modes can be tuned by a proper design of the 1DPC, acting on the materials (i.e. the refractive index) and the thicknesses of the layers.

For example, the surface-enhanced study of oriented molecules anchored to the 1DPC surface could be approached via differential TE-TM reflectivity measurements, as customarily done in standard attenuated total internal reflection spectroscopy [4]. More specifically, the superposition of the TE and TM modes enables linear and circular dichroism (CD) spectroscopies. CD, in particular, is gaining more and more importance due to the wide applications in chemistry, biology, medicine and pharmacology [5]. In general, CD signals are very weak if compared to those standard absorption spectroscopies so, recently, novel "superchiral" approaches have been introduced to enhance the CD signal by engineering the optical chirality of the electromagnetic field with the use of nanostructured systems [6]. In this framework, both metallic and dielectric approaches are used [7,8]. We recently proposed a BSW-based transducer that allows for the generation of "superchiral" surface waves [2]. Here we manufacture and evaluate the optical response of alternative simplified design of the 1DPC reducing the number of layers while keeping similar polarization performance.

The BSW-based transducer is a truncated 1DPC grown by reactive magnetron sputtering and made by 2 periods of alternating layers of SiO_2 (low refractive index) and Ta_2O_5 (high refractive index) terminated with an additional low-index layer incorporating a high refractive index inclusion. The optical performance of this BSW-based transducer was monitored in water using a fluidic cell realized using a polymeric double-side tape with the fluidic chamber cut by femtosecond laser micromachining. The top layer is a fused silica slide that

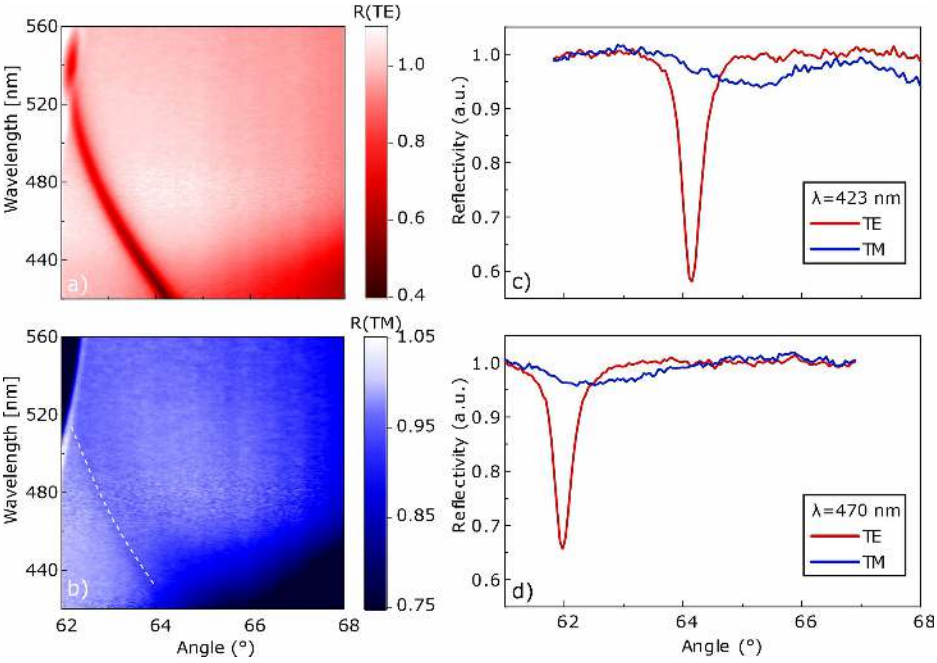


Figure 1. Experimental reflectivity (R) maps for a) TE illumination and b) TM illumination when the surface is immersed in water. The dispersive TE and TM modes are visible as dips in the reflectivity maps. Experimental angular plot for a wavelength equal to c) 423 nm and d) 470 nm.

contains the housing to plug the fluidic tubes. Experimental demonstration of the superposition in energy and momentum of the TE and TM modes can be assessed by reflectance measurements performed on the BSW-based transducer with the fluidic chamber filled with water. The modes are visible as dips in the corresponding reflectivity maps (Figure 1) evaluated for TE and TM illumination (panels a and b, respectively). Panels c) and d) include representative angular plots at specific wavelengths. It can be observed that, while the TE mode is narrow and sharp, the TM mode is broader and weaker but still recognizable, allowing experimental confirmation of the mode superposition. Upon increasing the wavelength, the excitation angle of the modes decreases, approaching the onset of total internal reflection.

The reported overlap of the TE and TM modes paves the way to the employment of such a BSW-transducer for surface-enhanced polarization-sensitive spectroscopies in the visible-UV range and more generally to the implementation of polarization-resolved surface-enhanced techniques, such as enhanced CD spectroscopy.

This work was partially supported by the Grant PON ARS01_00906 “TITAN - Nanotecnologie per l’immunoterapia dei tumori”, funded by FESR in the framework of PON “Ricerca e Innovazione” 2014 -2020 - Azione II - OS 1.b).

References

1. A. Sinibaldi, et al., Sensors and Actuators B 174, 292-298 (2012)
2. G. Pellegrini, M. Finazzi, M. Celebrano, L. Duò, P. Biagioni, Phys. Rev. B 95, 241402 (2017)
3. F. Giorgis, E. Descrovi, C. Summonte, L. Dominici, F. Michelotti, Optics Express 18, 8087-8093 (2010)
4. L. Fornasari, et al., Appl. Phys. Lett 105, 053303 (2014)
5. P. Ferenci, Aliment Pharmacol Ther 19, 157-165 (2004)
6. Y. Tang, A. E. Cohen, Phys. Rev. Lett. 104, 163901 (2020)
7. F. Mattioli, et al., ACS Photonics 7, 2672-2681 (2020)
8. M. L. Solomon, J. Hu, M. Lawrence, A. García-Etxarri, J. A. Dionne, ACS Photonics 6, 43-49 (2019)

Circular dichroism in plasmonic array of elliptical nanoholes with square lattice

H. Ali[1*], E. Petronijevic[2], G. Pellegrini [1], C. Sibilia[2], L.C. Andreani[1]

[1] University of Pavia, Department of Physics, I-27100, Pavia, Italy
[2] Sapienza University of Rome, Department S.B.A.I, I-00161, Rome, Italy
[*]hanan.ali01@universitadipavia.it

Abstract: We numerically studied the chiral properties of square 2D elliptic nanohole arrays in three different metallic metasurfaces (Ag, Au, and Al), from the near-infrared to the ultraviolet spectral range. Circular dichroism arises in absorption spectra at the same wavelength region of extraordinary optical transmission. We elucidate the physical origin of absorption CD and we optimize the CD as a function of the geometrical parameters of the structure. The results suggest interesting applications for chiral biomolecule sensing.

Altering the electromagnetic properties at the nanoscale can be efficiently achieved by means of specially engineered metasurfaces. Particularly, when the symmetry of the metasurface is broken, its interaction with circularly polarized light can be controlled. Different absorption of left and right circular polarization is called circular dichroism (CD). Metasurfaces able to generate large CD are very interesting for both fundamental science and applications regarding ultrasensitive chiral molecule detection. Furthermore, it was recently shown that high-quality chiral metasurface samples can be created by using low-cost nanosphere lithography combined with tilted metal deposition [1]. In this work, we theoretically study CD in square arrays of elliptical nanoholes etched in thin metallic layers (Au, Ag, Al) on a glass substrate. Fig.1 shows the metasurface structure used in our study at a normal incident on top of the surface. Transmission spectra display the well-known phenomenon of extraordinary transmission (EOT) from sub-wavelength hole arrays in a metal.

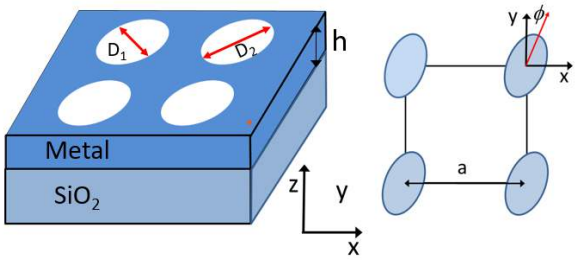


Fig.1. Scheme of the proposed structures studied in this work

The optical properties of elliptic nanoholes are numerically investigated by using two methods, 3D Finite Difference Time Domain (FDTD) simulation using Lumerical Ansys and Bloch-mode scattering matrix method in the open-source software known as Emustack [2]. To ensure convergence, we performed a comparison of the two methods. We calculate the optical spectra for circularly polarized light (RCP, LCP) to define the CD in absorption as

$$CD = (A_{LCP} - A_{RCP})/(A_{LCP} + A_{RCP}).$$

Results

We investigated chiral properties of square 2D elliptic nanohole arrays in three different metallic metasurfaces made of Ag, Au, and Al, from the near-infrared to the ultraviolet spectral range. The Elliptical NanoHole Array with tilted holes on a glass substrate is an intrinsically chiral lattice, giving rise to circular dichroism which is closely related to extraordinary optical transmission through the nanoholes, and it is resonantly enhanced at absorption peaks due to Surface Plasmon Polariton resonances at the metal/glass and metal/air interfaces. The elliptical shape of the nanoholes

splits the absorption peaks at each SPP resonance, while tilting of the nanohole axis produces an unbalance between the fields originating from linear polarizations along the long and short axes: they sum up with a phase delay of -90° (LCP) or +90° (RCP), ending up in a CD for tilted holes and explaining the strongly dispersive features of CD spectra. We then performed a full optimization on the geometry parameters, leading to substantial CD values (|CD|max > 50%) for silver and gold leading to suitable use in visible or near-IR, and (|CD|max > 40%) for aluminum leading to suitable use in the visible and ultraviolet (Fig.2). The CD resonance wavelengths have a minor dependence on the ellipse parameters, as they follow from a lattice effect, and can be effectively tuned via the lattice constant.

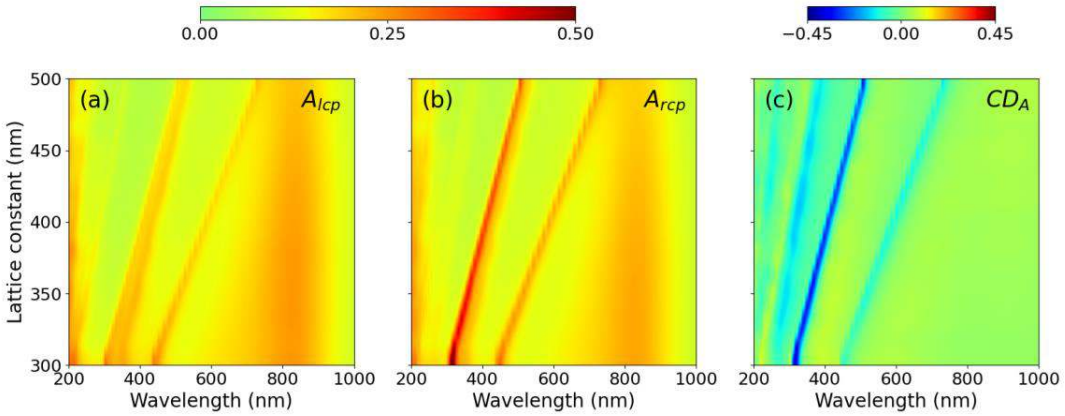


Fig. 2. (a) Absorption spectra for LCP, (b) absorption spectra for RCP, (c) CD in absorption for an Al film of thickness t=100 nm as a function of lattice constant a, keeping constant values D_1/a=0.5565, D_2/a=1, ϕ=20.95°.

The benchmark of the two computational electromagnetic tools EMUstack and FDTD leads to a good agreement of the spectra and supports the reliability of the results. Plasmonic metasurfaces made of an Al film stands up as a promising candidate to achieve large |CD| in the near-UV region, possibly with the addition of a thin oxide layer to prevent oxidation of the top surface. Absorption and CD spectra of Al films at wavelengths below the interband transition display a number of features that arise from folded SPP modes. These findings can be further pursued for deeper investigations of plasmonic light-matter coupling, as well as for applications to chiral sensing of biomolecules with resonances in the visible or near-UV spectral range.

Acknowledgments

This research was partly supported by the Italian Ministry of Education and Research (MIUR) through 2017 PRIN project 2017MP7F8F-004 “NOMEN”.

References

1. Petronijevic, E., G. Leahu, R. Li Voti., A. Belardini, C. Scian, N. Michieli, T. Cesca, G. Mattei, and C. Sibilia, “Photo-acoustic detection of chirality in metal-polystyrene metasurfaces,” *Appl. Phys. Lett.*, vol.114, p. 053101, 2019.
2. Sturmberg, B.C.P., K. B. Dossou, F. J. Lawrence, C. G. Poulton, R. C. McPhedran, C. M de Sterke, L. C. Botten, “EMUstack: An open-source route to insightful electromagnetic computation via the Bloch mode scattering matrix method,” Comp. *Phys. Commun., vol.* 202, p.276, 2016.

META 2023, PARIS - FRANCE, JULY 18 – 21, 2023

A characterization method for an achiral magnetic photonic antenna with arbitrary excitation

L. Cui[1], X. Yang[1], C. Schwob[1], M. Mivelle[1], B. Gallas[1*]

[1]Sorbonne Université, CNRS, Institut des NanoSciences de Paris, INSP, F-75005 Paris, France
[*]corresponding authors: bruno.gallas@insp.jussieu.fr

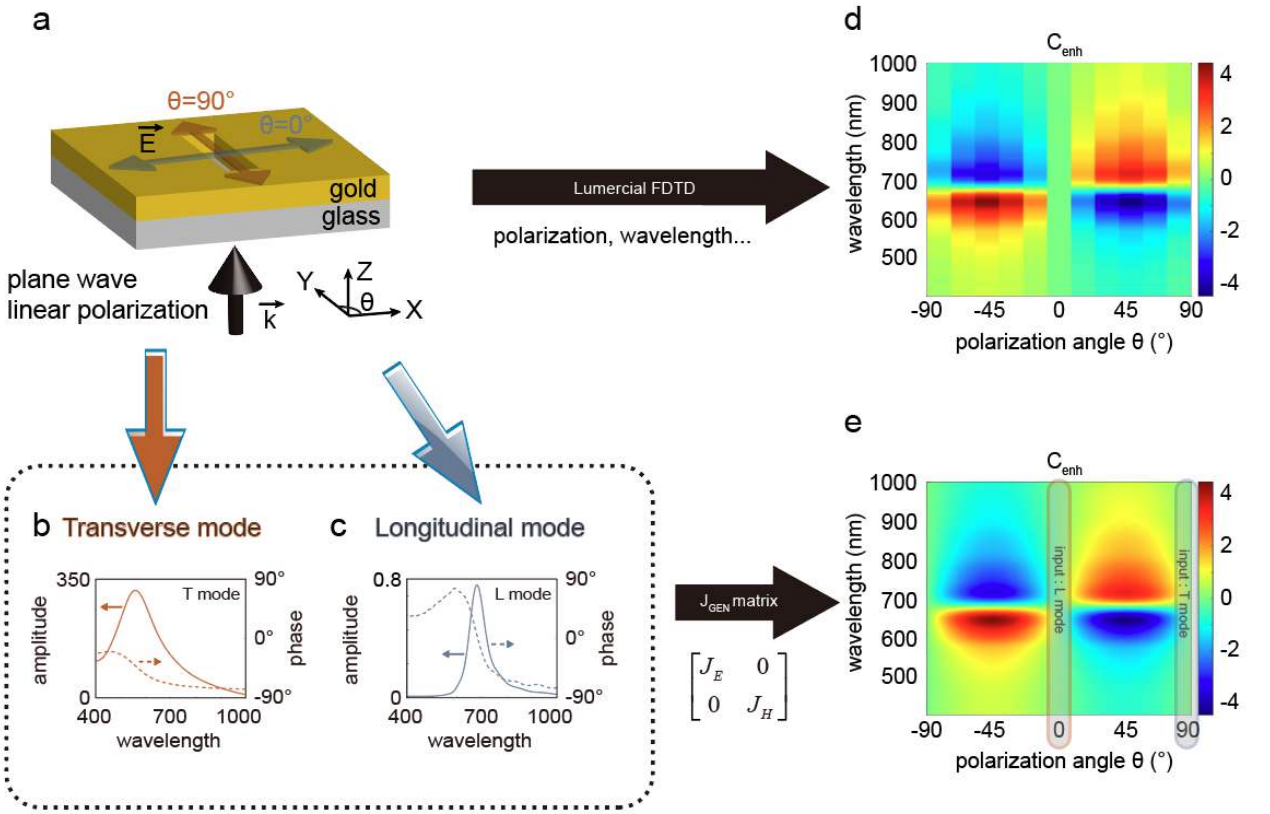
Abstract: The interaction between chiral materials and light at the nanoscale, can be controlled and optimized by using nano-antenna. However, understanding the properties of the near field of a nano-antenna requires extensive numerical simulations where the polarization and excitation wavelength can be varied. We propose a matrix method based on the Jones decomposition of the polarization to evaluate the vectorial properties of the electromagnetic near field of an antenna.

Many physical quantities allow for characterizing the interaction between chiral materials and light at the nanoscale, including chirality density, spin density, ellipticity. By generating superchiral light, nanophotonics has brought innovative solutions to reduce the detection volume and increase the sensitivity. We have already shown numerically that an achiral plasmonic resonator based on a rectangular nanoslit could be described as a magnetic dipole and was behaving as a tunable nanosource of purely superchiral light[1] (Figure 1 (a)). Here we show that the knowledge of the nearfield for the transverse (T) and longitudinal (L) modes is enough to optimize the illumination conditions that yield the best chiral properties of the nearfield for all the polarization of excitation possible.

In order to explore systematically and efficiently the properties of chiroptical phenomena, like chirality density and ellipticity, we propose a mathematical matrix method which provides an alternative tool for the search for a specific superchiral field or circular polarization near field. In this method, the local field was related to the incident field through a generalized Jones matrix J_{GEN}. This matrix contains the information about both the electric and the magnetic field of light so that $J_{GEN} = \begin{bmatrix} J_E & 0 \\ 0 & J_H \end{bmatrix}$. The 2x2 submatrix J_E is defined by $\boldsymbol{E}_{loc} = J_E \boldsymbol{E}_{inc}$ with $\mathbf{E}_{loc}$ and $\mathbf{E}_{inc}$ the local and incident fields, respectively. After decomposition of the electric fields on the (x,y) coordinates, the elements of J_E were obtained as $J_E = \begin{bmatrix} J_E^{xx} & J_E^{xy} \\ J_E^{yx} & J_E^{yy} \end{bmatrix}$. A similar treatment was performed for the elements of J_H with the magnetic fields.

The incident and local fields were obtained from numerical simulations (FDTD, Lumerical) only performed for incident illuminations linearly polarized along x and y. Figure 1 (b) (c) present the spectral dependence of the amplitude of the total electric field and phase of the radiation electric field in the center of the nanoslit for incident light polarized along x and y exciting the longitudinal and transverse modes of the nanoslit. These two illumination conditions were sufficient for the determination of the elements of J_E and J_H. The knowledge of J_{GEN} allowed then for the calculation of any electromagnetic property of the light in the center of the nanoslit for any incident polarized or wavelength. This was illustrated in the case of the angular dependence of the chirality density, defined as $C = -\frac{\varepsilon_0 \mu_0 \omega}{2} Im(\boldsymbol{E}^*.\boldsymbol{H})$, in the nanoslit (Figure 1 (e)). These calculated values can be compared with the numerical FDTD simulation results presented in Figure 1(d). This method not only reproduces the simulation results accurately, but also can quickly give feedback on the chiral properties for any polarization state or

wavelength, opening the way to the optimization of the illumination conditions for any (or combination of any) goal: chirality density as well ellipticity, electric and magnetic energies.



Figures 1 (a) 3D representation of the rectangular nanoslit in a thin gold layer of 40 nm. The vector **k** represents the direction of propagation of the linearly polarized incident plane wave, and θ, the angle of this polarization with respect to the nanoslit transverse axis (Ox). (b) Transverse mode and (c) longitudinal mode spectral responses of the amplitude and phase obtained for θ = 90° and 0°. (d) Variations of C_{enh} as a function of the incident polarization angle θ and wavelength in the center of the nanoslit obtained from FDTD simulations (angle θ step by 15°). C_{enh} defined as $C/|C_{cpl}|$, with C_{cpl} the chirality density of a circularly polarized light, without the aperture, carrying the same power as the linearly polarized excitation impinging on the nanoslit. (e) Variations of C_{enh} as a function of the incident polarization angle θ and wavelength calculated using the J_{GEN} matrix.

References

1. Cui, L., Yang, X., Reynier, B., Schwob, C., Bidault, S., and Gallas, B., & Mivelle, M. “An achiral magnetic photonic antenna as a tunable nanosource of superchiral light.,” https://doi.org/10.48550/arXiv.2301.11044

Resonant Optics - Fundamentals and Applications

META 2023, PARIS - FRANCE, JULY 18 – 21, 2023

Microstar cavities: Ray-wave correspondence in the semiclassical regime

J. Kullig[1*] and J. Wiersig[1]

[1]Institut für Physik, Otto-von-Guericke-Universität Magdeburg, Magdeburg, Germany
[*]corresponding author: julius.kullig@ovgu.de

Abstract: Microstar cavities confine light in a star-shaped quasi-two-dimensional microcavity via successive perfect transmissions through the dielectric interface under Brewster's angle. Therefore, beam splitting effects are avoided and ray orbits without intensity loss are formed. We investigate the correspondence between the ray dynamics and the long-lived modes of the electromagnetic field in the semiclassical regime. A difference between clockwise and counter-clockwise propagation in traced back to nonlinear resonance chains in phase space.

A traditional whispering-gallery cavity confines light via total internal reflection at the dielectric interface. However, in 2020 the authors proposed a novel concept for the light confinement in a microstar cavity that completely avoids any kind of reflection [1]. The star-shaped cavity with $\nu>2$ spikes is designed by fixing the opening angle of the spikes to

$$a=\frac{\nu-2}{2\nu}\pi \qquad (1)$$

and the refractive index of the cavity to

$$n=\frac{1+\sin\left(\pi/\nu\right)}{\cos\left(\pi/\nu\right)}. \qquad (2)$$

Under these conditions a transverse electric polarized ray is guided along a periodic orbit that successively leaves and re-enters the cavity without loss of intensity as all the transmissions occur under Brewster's angle. The periodic orbit can be stabilized further by a slight focusing deformation of the microstar boundary, see Fig. 1a.

A convenient method to describe the dynamics in such systems is a phase-space representation. Here, the position and angle θ of rays that cross the x-axis are tracked, see Fig. 1b. For the deformed microstar the dynamics generates a regular region with a resonance chain in the phase space as shown in Fig. 1c. On the other hand, the boundary deformation of the microstar leads to a slight nonuniform loss in the generated regular phase-space region. The interplay of the loss gradient and the nonlinear resonance chain then leads to an interesting difference between clockwise (CW) and counter-clockwise (CCW) propagating rays (illustrated by blue and red arrows in Fig. 1b) [2]. The difference between both propagation directions can be analyzed by constructing classical eigenstates of the dynamics from the so-called Frobenius-Perron operator [2,3].

Additionally, full numerical wave simulations are performed to compute the optical modes in the microstar cavity. In consistency, the long-lived modes typically follow the classical orbit as shown in Fig. 1d. A further comparison can be done by a Husimi representation that projects the

modes into the phase space (not shown). It is demonstrated that in the semiclassical regime the modes localize on the classical phase-space structures of the regular region and, furthermore, have a similar difference between their CW and CCW components as the classical Frobenius-Perron operator eigenstates. Our work shows that microstar cavities are interesting systems to study ray-wave correspondence with unexpected phenomena as time-reversal symmetry can be naturally broken by a difference in CW and CCW ray propagation.

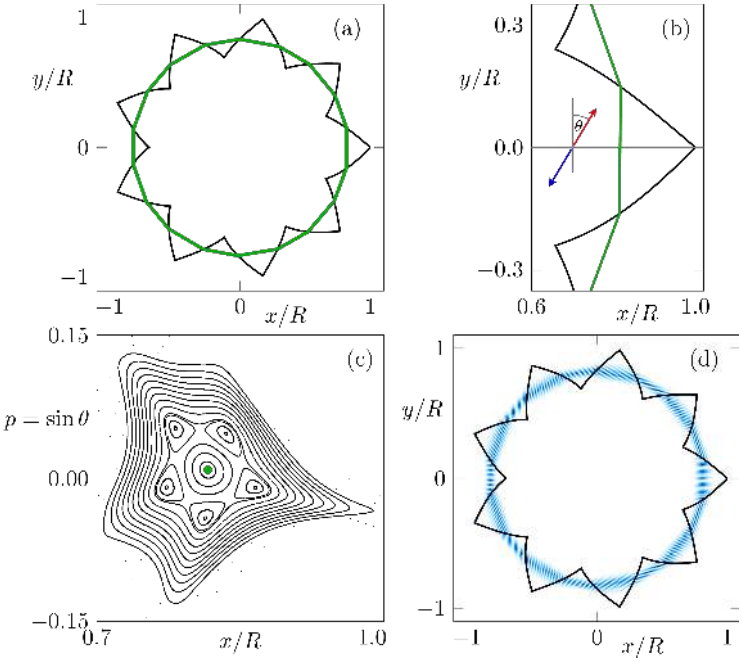


Figure 1: The green curve shows a periodic orbit in the deformed (black curve) microstar cavity. (b) Magnification of (a). (c) Phase space portrait of CCW propagating rays. The periodic orbit is marked as green dot. (d) Intensity pattern of a long-lived optical mode.

References

1. Kullig, J., X. Jiang, L. Yang, and J. Wiersig, “Microstar cavities: An alternative concept for the confinement of light”, Phys. Rev. Research 2 , 012072(R), 2020.
2. Kullig, J. and J. Wiersig, “Ray–Wave Correspondence in Microstar Cavities”, Entropy 24, 1614, 2022.
3. Kullig, J. and J. Wiersig, “Frobenius–Perron eigenstates in deformed microdisk cavities: non-Hermitian physics and asymmetric backscattering in ray dynamics”, New J. Phys. 18, 015005, 2016.

Resonant Photonic Galleries of Dielectric Particles

N. S. Solodovchenko[1], M. E. Bochkarev[1], K. B. Samusev[1,2], and M. F. Limonov[1,2*]

[1]Department of Physics and Engineering, ITMO University, St. Petersburg, 197101, Russia
[2]Ioffe Institute, St. Petersburg 194021, Russia
[*]corresponding author: m.limonov@metalab.ifmo.ru

Abstract: An original picture of photonic resonances in single dielectric particles (cylinder, ring, split ring, cuboid) is presented. The basic result is the separation of low-frequency scattering spectra into short galleries that start with a broad Fabry-Perot band and continue with narrow longitudinal modes. The existence of individual resonant galleries leads to the appearance of entire galleries of bound states in the continuum, in contrast to the repeatedly observed single bound states, and also to the appearance of exceptional points.

The modification of physical properties determined by topological transitions is the subject of intensive research in various fields of physics, and optical properties are no exception. Between the most famous elementary resonators, two topological transitions can be distinguished, namely, from a disk to a ring with a rectangular cross section and further to a split ring. Of interest is another transformation of the structure, although not accompanied by a change in topology, namely, the transition from a split ring to a cuboid. Thus, we obtain an interesting sequence for analyzing the modification of optical properties: disk → ring → split ring → cuboid.

To describe the photonic properties of dielectric resonators in the three-dimensional general case, we used numerical calculations that provide key information about the optical spectrum with resonant eigenmode frequencies (eigenvalues), field distribution (corresponding eigenfunctions), and mode *Q*-factors. In three-dimensional resonators, the eigenfunctions can be characterized by azimuthal (*m*), radial (*r)*, and axial (*z*) indices forming an ordered triple (*m, r, z*). We compared the results of our calculations with the experimental results obtained on ceramic samples with a high permittivity and low material losses in the gigahertz range. The results are based on an analysis of the low-frequency region of the spectra, where all spectral features can be unambiguously interpreted, including the Mie and Fabry-Perot resonances.

We have established that the topological transition from a disk to a ring with a rectangular cross section leads to a fundamental rearrangement of the photonic spectrum. The disk spectrum is characterized by an infinite set of equidistant whispering gallery modes. The low-frequency spectrum of the ring is divided into separate short galleries, each of which begins with a broad transverse Fabry-Perot resonance between two pairs of opposite walls of the ring and continues with a set of equidistant azimuthal high-Q resonances modes. By tuning the geometrical parameters of the ring, a structure with alternating broad transverse Fabry-Perot resonances in the strict sequence Lorentz – Fano – Lorentz – Fano –… was determined [1]. The Fano resonances [2] lead the galleries with even radial photonic indices, and the Lorentzian resonances lead the galleries with odd radial indices. The results of a study of the optical scattering spectra at a topological transition between a dielectric ring and a split ring are of no less interest. We observed a strong orientational dependence of the spectra as the angle of incidence of the plane wave on the ring relative to the slit varied.

Recently, bound states in the continuum (BIC) have been of great interest, which are characterized by exceptionally high Q-factors, which in theory reach infinity [3]. We studied the properties of BIC, which is

described by the Friedrich – Wintgen model [4], during the transition from a homogeneous dielectric cylinder to a ring with narrow walls with a gradual increase in the inner diameter [5,6]. Friedrich–Wintgen's BICs arise from two interacting resonances via a radiation continuum due to appropriate tailoring of the structural parameters. The results demonstrate a transition from BIC in the strong-coupling regime to BIC in the weak-coupling regime, which manifests itself in the transition from avoided crossing to photonic branches crossing.

However, the greatest interest from our point of view is the discovery of galleries of BICs, which, as far as we know, have not been observed before. Different photonic galleries of a ring with a rectangular cross section have different dependences on structural parameters; therefore, when the ring geometry changes, regions of anticrossing of entire galleries appear, which corresponds to the formation of BIC galleries by the Friedrich – Wintgen mechanism. We also discuss the eigen-solutions of non-Hermitian systems with emphasis on the presence of exceptional points (EPs) [7,8], where we observe the coalesce of two resonant modes with mutual coupling. In this case, the BIC mode switches from the high-frequency branch to the low-frequency branch.

This work was funded by the Russian Science Foundation (Project No. 23-12-00114).

References

1. Solodovechenko, N., M. Sidorenko, T. Seidov, I. Popov, E. Nenasheva, K. Samusev and M. Limonov, "Cascades of Fano resonances in light scattering by dielectric particles," Mater. Today, Vol. 60, 169-78, 2022.
2. Limonov, M. F., "Fano resonance for applications," Adv. Opt. Photon., Vol. 13, No. 3, 703-771, 2021.
3. Hsu, C. W., B. Zhen, A. D. Stone, J. D. Joannopoulos and M. Soljacic, ''Bound states in the continuum,'' Nat. Rev. Mater., Vol. 1, pp. 1−13, 2016.
4. Friedrich H. and D. Wintgen, ''Interfering resonances and bound states in the continuum,'' Phys. Rev. A, Vol. 32, 3231-3242, 1985.
5. Solodovchenko, N., K. Samusev, D. Bochek and M. Limonov, "Bound states in the continuum in strong-coupling and weak-coupling regimes under the cylinder – ring transition, " Nanophotonics, Vol. 10, 0351, 2021.
6. Bochek, D. V., N. S. Solodovchenko, D. A. Yavsin, A. B. Pevtsov, K. B. Samusev and M. F. Limonov, "Bound states in the continuum versus material losses: Ge2Sb2Te5 as an example," Phys. Rev. B, Vol. 105, 165425, 2022.
7. Miri M.-A. and A. Alù, "Exceptional points in optics and photonics," Science Vol. 363, eaar7709, 2019.
8. Kikkawa, R., N. Munehiro and Y. Kadoya, "Bound states in the continuum and exceptional points in dielectric waveguide equipped with a metal grating", New J. Phys. Vol. 22, 073029, 2020.

Plasmonic nanocavities: From resonant modes to semi-persistent sub-radiant states

A. Demetriadou[1*]

[1]School of Physics and Astronomy, University of Birmingham, Birmingham, B15 2TT, United Kingdom
[*]corresponding author: a.demetriadou@bham.ac.uk

Abstract: Plasmonic nanocavities have the ability to significantly confine and enhance light, while at the same time efficiently radiate energy to the far-field. Due to these properties, unprecedented light-matter interactions have been realised at room temperature. In this talk, I will present the complex set of plasmonic modes supported by extreme plasmonic nanocavities, their impact on the excitation and radiative properties of the antenna, and how these properties can lead to generating sub-radiant entangled states between two or more quantum emitters.

Plasmonic nanocavities have gaps between two metallic nano-structures of just 1-2 nm, and have been used in the past few years to reach the light-matter strong coupling regime between molecular emitters and plasmons at room temperature [1,2]. One of the most common designs is the nanoparticle assembled on a mirror (NPoM) configurations (see fig.1). The extremely small gap between the two metallic structures, gives rise to a complex set of modes, each with a different field profile and radiative properties. Hence, a cavity is created that supports many different photonic modes that all simultaneously interact with all the quantum emitters (QEs) in the cavity.

Using an auxiliary-field eigenvalue method, we obtain the quasi-normal modes (QNM) [3] of the system. Although so far, theoretically plasmonic nanocavities were studied assuming that they are spherical (or truncated) nanoparticles on a mirror (fig.1A), in reality 'spherical' nanoparticles acquire three common polyhedral shapes during their synthesis: (i) cuboctahedron, (ii) rhombicuboctahedron and (iii) decahedron (seen in fig.1B-D).

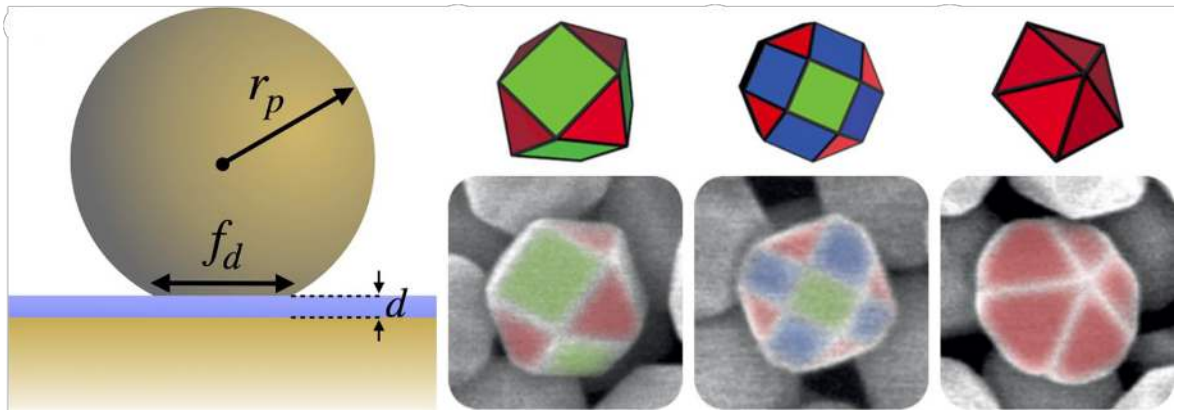


Figure 1: The nanoparticle-on-mirror (NPoM) configuration, and the three common shapes that spherical nanoparticles acquire during their synthesis.

The QNM mode expansion provides a complete description of the plasmonic modes in such nanocavities, and we show that the shape and symmetry of these plasmonic nanocavities dominate both their near- and far-field response, with intricate and rich optical behavior, both in the near- and far-field. We also show that the same nanoparticle shape gives very different results when assembled on the mirror with a different facet, even if the facet shape and size (i.e. geometry of the cavity) are identical.

The extreme light confinement in plasmonic nanocavities has opened the fascinating prospect of controlling

quantum matter with light, and ultimately generating quantum states at room temperature, avoiding the complex and cumbersome experimental methods required at cryogenic temperatures. We consider two (or more) quantum emitters residing in a NPoM nanocavity, and show that semi-persistent sub-radiant states emerge [4]. With a quantum electrodynamics description for an open cavity, we obtain both its quantum dynamics of the system (see figure 2) and the quantum extinction cross section:

$$\langle \sigma_ext \rangle = -\sqrt{\kappa_{in}}\,\frac{(\alpha\langle a^{\dagger}\rangle + \alpha^{*}\langle a\rangle)}{c|\alpha|^{2}}$$

where $\sqrt{\kappa_{in}}$ is the rate that energy couples into the system by a monochromatic source, α is the amplitude of the coherent state defined by the incident source's photon flux $c|\alpha|^2$ and $\{a, a^{\dagger}\}$ are the bosonic creation and annihilation operators.

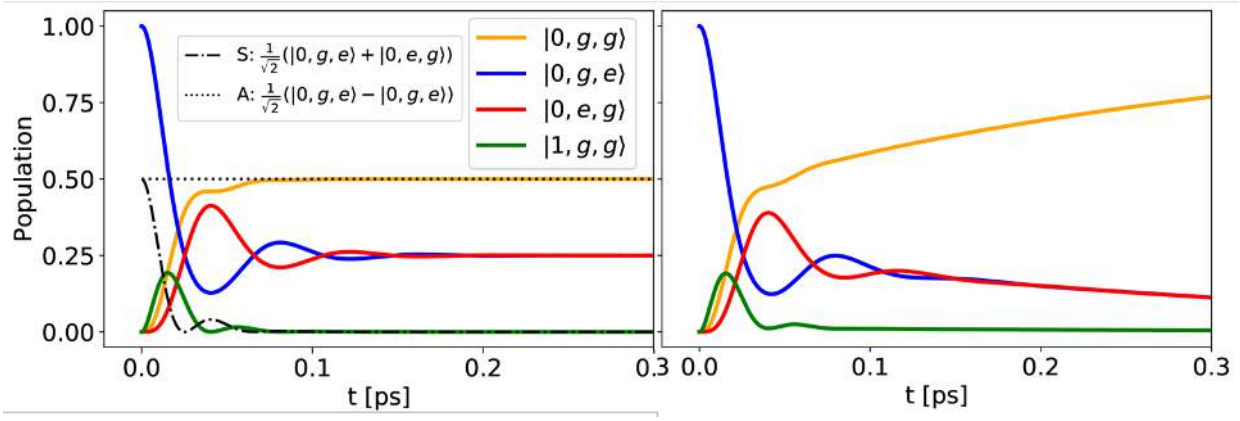


Figure 2: The quantum dynamics of two emitters in NPoM when (left) the emitters have no inherent loss and (right) with inherent loss.

The quantum dynamics of two or more quantum emitters placed in a plasmonic nanocavity, and reveal persistent sub-radiant states formed between them (shown in figure 2). Although the Rabi oscillations between the plasmon and emitters decay very fast (~within few tens of fsec), these sub-radiant states persist for up to 100fsec, depending on the inherent non-radiative losses of the molecular emitters chosen. Additionally, the quantum extinction cross section allows us to theoretically predict experimental observables, and in fact in the absence of quantum emitters reduces to the classical behavior of the plasmonic nanocavity.

AD would like to acknowledge support from the Royal Society and EPSRC.

References

1. Chikkaraddy, R., de Nijs, B., Benz, F., Barrow, S.J., Scherman, OA, Rosta, E., Demetriadou, A. *et al.*, "Single-molecule strong coupling at room temperature in plasmonic nanocavities", Nature, Vol. 535, 127-130, 2016.
2. Zengin, G., Wersäll, M., Nilsson, S., *et al.*, "Realizing Strong Light-Matter Interactions between Single-Nanoparticle Plasmons and Molecular Excitons at Ambient Conditions", Physical Review Letters, 114, 157401, 2015.
3. Bedingfield, K., Elliot, E., Gisdakis, A., Kongsuwan, N., Baumberg, JJ., Demetriadou, A., "Symmetry and shape on the plasmonic behaviour of nanocavities", arXiv:2210.05587, 2023.
4. Bedingfield, K, Yuen, B., Demetriadou, A., "Sub-radiant entanglement of quantum emitters in palsmonic nanocavities", 2023, submitted

Predicting nonlinear optical scattering with physics-driven neural networks

C. Gigli[1*], A. Saba[1], A.B. Ayoub[1], and D. Psaltis[1]

[1] Optics Laboratory, École polytechnique fédérale de Lausanne, CH-1015, Lausanne, Switzerland

[*]corresponding author: carlo.gigli@epfl.ch

Abstract: We present a physics informed deep neural network trained on Maxwell's equations, hence we named it MaxwellNet, which can act as a surrogate of numerical solvers and reduce computational times of three orders of magnitude compared to commercial software packages. Beyond demonstrating the possibility of studying linear and nonlinear scattering in presence of optical kerr effect, we show how this approach facilitates the inverse design of optical components with size comparable with light wavelength for which full wave simulations are normally required.

Deep neural networks are emerging as promising surrogates of nonlinear numerical solvers for their ability to map complex functions as the relation coupling material properties, geometry, and electromagnetic sources to scattered fields. These tools offer two advantages when compared to commercially available software packages: 1) they are naturally implemented to exploit the full computational power of GPUs and they don't require the inversion of very large matrices to predict solutions of Maxwell's equations which boost the calculation velocity of orders of magnitudes, 2) the gradients of the field predictions with respect to the given inputs can be easily and rapidly computed through backpropagation algorithms, making of them a well suited tool for inverse design. Here we propose to use a U-Net architecture to map the relationship between arbitrary refractive index distributions and the scattered field evaluated on the same grid for a fixed excitation source. In common data driven approaches, this process requires the creation of a large dataset of input-output pairs pre-computed with a numerical solver. Conversely, we propose to avoid the burden of dataset preparation by training the network directly on Maxwell's equations, see Fig. 1. We use the residual of Maxwell's equation as the proper physical loss to adjust the weights of network during the training. The electric and magnetic fields are discretized on the staggered Yee grid and the curl of fields is computed using the same approach as in finite differences frequency domain.

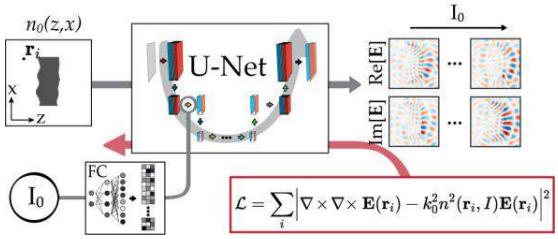


Figure 1 Tunable MaxwellNet with respect to incident power predicting optical Kerr scattering. Grey (red) arrows denote forward (backward) propagation. The model is based on a U-Net architecture taking in input the 2D refractive distribution of the material in the zx-plane $n(z, x)$ and returning the complex scattered field. By changing the incident beam intensity I_0, the weights of specific convolutional layers in the U-Net architecture are tuned so that the physical loss is simultaneously minimized for different working powers.

This work complement a previous demonstration on the implementation of MaxwellNet for predicting linear scattering from arbitrary refractive index distributions[1]. We focus here on the possibility to extend the method to

the prediction of optical scattering in presence of optical kerr effect. On one side this problem is much harder to simulate with commercial solvers and usually requires iterative approaches, and on the other it is of central interest in the photonic community to introduce an all-optical control mechanism to realize ultrafast switches.
If the central U-Net structure can correctly infer linear scattering problems, we do expect that by adjusting some of its weights it is also possible to model the intensity dependent index due to optical kerr effect. For this purpose, we introduce a second block which takes as an input the incident power and returns the kernels used in one convolutional layer in the encoding branch of the core U-Net[2].
As a proof of concept, we used the trained model for the shape optimization of 2D aspheric microlenses with focal properties resilient to power variations. The solution of the inverse problem in this case equals to find the best set of geometrical parameters (radius of curvature and conical constant of the two interfaces, and thickness of the lens) for which the field is focused at a distance $z_f = 14\,\mu m$ from the lens both for low and high incident powers , see Fig.2a. The adjustable weights of MaxwellNet allow to evaluate the objective function to optimize, in this case the field intensity at $z_f = 14\,\mu m$, at multiple powers and update the geometrical parameters accordingly. Fig.2b shows two major outcomes of the present work: 1) the possibility of performing thousands of fields evaluations and backpropagations in a short time, 2) the possibility to track the physical loss during the optimization process to ensure that the network predictions remain accurate and do not diverge to unphysical results. Fig.2c finally shows the field evaluation along the optical axis at low and high powers for the optimized structure which minimizes the field variations around the focal spot for different working conditions.

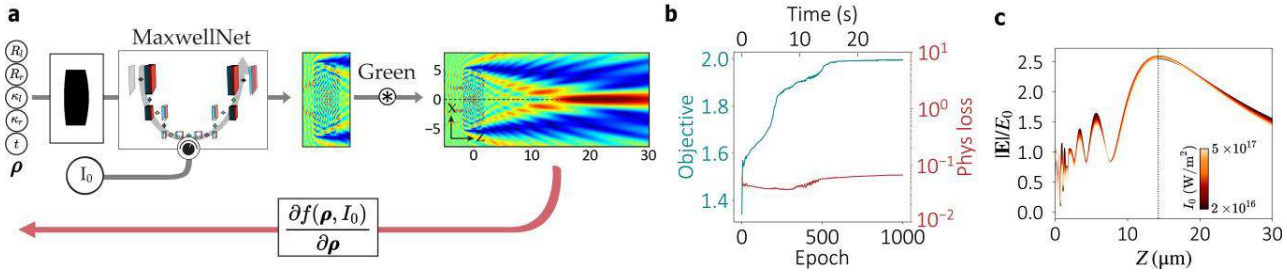


Figure 2 Lens design with MaxwellNet. (a) Sketch of the optimization algorithm. An initial lens design defined by the geometrical parameters ρ is provided to the trained MaxwellNet model which returns the total field |E|. We use Green convolution the retrieve the field amplitude close at the focal plane which constitutes the objective function *f* to maximize. The derivatives of *f* with respect to ρ are computed through backpropagation and we iterate until convergence. (b) Evaluation of the objective function (left axis) and physical loss (right axis) for the optimization of a lens focusing at $z = 14\mu m$ on the optical axis. (c) Normalized field amplitude profile along the optical axis predicted with MaxwellNet for 20 different intensities.

In conclusion, we provided a demonstration of a neural network trained on Maxwell's equations for intensity dependent refractive index distributions which can be used in conjunction with traditional numerical solvers for both speed up electromagnetic simulations and offer a new alternative for the inverse design of optical devices.

References

1. J. Lim and D. Psaltis, "MaxwellNet: Physics-driven deep neural network training based on Maxwell's equations," APL Photonics **7**(011301), 1–10 (2022).

2. C. Gigli et al., “Predicting nonlinear optical scattering with physics-driven neural networks,” APL Photonics **(accepted)** (2023).

Polarization Singularities in Optical Near Fields: Topology and Chirality

Shubo Wang[1,2*], **Jie Peng**[1], **Shiqi Jia**[1], **and Ruo-Yang Zhang**[3]

[1]Department of Physics, City University of Hong Kong, Hong Kong, China
[2]City University of Hong Kong Shenzhen Research Institute, Guangdong, China
[3]Department of Physics, The Hong Kong University of Science and Technology, Hong Kong, China
[*]corresponding author: shubwang@cityu.edu.hk

Abstract: In this talk, I will discuss polarization singularities emerging in the near fields of optical structures. I will show that simple optical structures can generate rich configurations of polarization singularities with intriguing topological and chiral properties. These properties are subtly related to the topology and symmetry of the structures and provide new degrees of freedom for light manipulations and new mechanisms for chiral light-matter interactions.

Polarization singularities are topological defects in the spatial distribution of light's polarization ellipses. They can emerge in various optical systems such as light scattering by small particles [1]. In two-dimensional systems such as photonic crystal slabs, they are intimately related to the boundary states in the continuum. In three-dimensional space, polarization singularities can give rise to interesting polarization configurations such as Möbius strips. We theoretically investigate the polarization singularities generated by simple optical structures (e.g., sphere and torus), and we explored their applications in chiral discrimination and optical force manipulation of small particles.

We find that the nontrivial topology of an optical structure ensures the birth of polarization singularities in the near fields, and bounds their spatial morphologies characterized by topological indexes [2]. The topological indexes of these singularities satisfy $\sum_{\mathbf{r}_s} I_{\mathrm{pl}}(\mathbf{r}_s) = \chi(M)$, where $I_{\mathrm{pl}}(\mathbf{r}_s)$ denotes the index of the polarization singularity at $\mathbf{r}_s$ and $\chi(M)$ denotes the Euler characteristic of the optical structure M. For example, a torus and a sphere will induce different polarization singularities with different total indices. This is decided by their different genus, i.e., torus has one "hole" while sphere has no "hole". In addition, introducing extra spatial symmetries can give rise to higher-order polarization singularities with intriguing polarization configurations inaccessible with conventional optical structures. By mapping the polarization singularities to non-Hermitian exceptional points, we provide a complete framework to understand their invariant properties in spatial evolutions (merging, bifurcation, and topological transitions).

We apply the chiral properties of polarization singularities in chiral discrimination [3]. Chiral discrimination is usually limited by the weak chiral response of enantiomers and the high complexity of the detection methods. We use the C lines (i.e., lines of polarization singularities) emerged in light scattering by a metal sphere to detect small chiral particles. The C lines carry optical chirality since they are intrinsically circularly polarized, and the optical chirality is strongly enhanced in the near fields. We calculated the absorption dissymmetry of the chiral particles at different positions on the C lines. It is found that the absorption dissymmetry can be much larger than that induced by circularly polarized plane-wave excitation, and it strongly depends on the anisotropy of the helices.

We also explore the application of polarization singularities in optical force manipulation of small particles [4]. Near-field optical forces are crucial to on-chip optical manipulations of small particles and molecules. We simulated the optical force and torque on small particles induced by the polarization singularities of a gold cylinder. It is found that the scattering near fields of the cylinder give rise to both electric and magnetic C lines. The chirality

of the C lines can induce complex optical force and torque on small particles, which manifest dramatic spatial variations in the near field region. The optical force and torque provide rich degrees of freedom for manipulating small particles in subwavelength scale.

Our study uncovers the subtle connections between the topological properties of optical near fields and the topology of optical structures. The novel properties of polarization singularities can find broad applications in chiral light-matter interactions, chiral quantum optics, optical sensing and metrology, etc. The study can also be extended to other classical waves such as sound waves.

This work was supported by the Research Grants Council of the Hong Kong Special Administrative Region, China (Nos. CityU 11306019, C6013-18G, and AoE/P-502/20) and the National Natural Science Foundation of China (No. 11904306).

References

1. Peng, J., W. Liu, and S. Wang, "Polarization singularities in light scattering by small particles", Physical Review A 103, 023520, 2021.
2. Peng, J., R.-Y. Zhang, S. Jia, W. Liu and S. Wang. "Topological near fields generated by topological structures," Science Advances 8, eabq0910, 2022.
3. Jia, S., J. Peng, Y. Cheng and S. Wang, "Chiral discrimination by polarization singularities of a metal sphere", Physical Review A 105, 033513, 2022.
4. Peng, J., S. Jia, C. Zhang, and S. Wang, "Optical force and torque on small particles induced by polarization singularities", Optics Express 30, 16489, 2022.

META 2023, PARIS - FRANCE, JULY 18 – 21, 2023

Computing partial derivatives of quasinormal modes

Felix Binkowski[1*], Fridtjof Betz[1], Martin Hammerschmidt[2], Philipp-Immanuel Schneider[2], Lin Zschiedrich[2], and Sven Burger[1,2]

[1]Zuse Institute Berlin, Germany
[2]JCMwave GmbH, Germany
[*]corresponding author: binkowski@zib.de

Abstract: We present an approach to compute partial derivatives of eigenfrequencies corresponding to quasinormal modes using Riesz projections. The approach is based on contour integration with direct differentiation enabling an efficient numerical realization.

The knowledge on the partial derivatives of eigenfrequencies, the so-called sensitivities, is essential for fabrication of nanophotonic devices with a high quality factor [1], which is given by the scaled ratio of the real and imaginary parts of the corresponding eigenfrequency. Furthermore, the sensitivities are important for the numerical simulation of such nanoresonators since the accuracies of the eigenfrequencies are strongly influenced by their sensitivities. In this contribution, we review an approach, proposed in Ref. [2], for computing sensitivities of eigenfrequencies corresponding to quasinormal modes. The approach is based on Riesz projections, i.e., contour integrals. The contour integrals are computed by solving Maxwell's equations with a source term enabling an efficient numerical realization based on direct differentiation of the scattering solutions to Maxwell's equations. We apply the approach to compute the eigenfrequency sensitivities of a nanophotonic resonator [3] with respect to several shape parameters of the resonator. It is demonstrated that our approach allows partial derivatives to be computed with significantly less computational effort than is required by a standard approach.

We acknowledge funding by the Deutsche Forschungsgemeinschaft (DFG, German Research Foundation) under Germany's Excellence Strategy - The Berlin Mathematics Research Center MATH+ (EXC-2046/1, project ID: 390685689) and the German Federal Ministry of Education and Research (BMBF Forschungscampus MODAL, project 05M20ZBM). This project has received funding from the EMPIR program co-financed by the Participating States and from the European Union's Horizon 2020 research and innovation program (project 20FUN02 POLIGHT).

References

1. Wu, T., Gurioli, M., and Lalanne, P. Nanoscale light confinement: The Q's and V's. ACS Photonics 8, 1522 (2021).
2. Binkowski, F., Betz, F., Hammerschmidt, M. et al. Computation of eigenfrequency sensitivities using Riesz projections for efficient optimization of nanophotonic resonators. Commun. Phys. 5, 202 (2022).
3. Koshelev, K., Kruk, S., Melik-Gaykazyan, E. et al. Subwavelength dielectric resonators for nonlinear nanophotonics. Science 367, 288 (2020).

Quasi-normal mode expansions of resonant scattering responses

J.T. Zimmerling[1*], and R.F. Remis[2]

[1]Uppsala Universitet, Department of Information Technology, Scientific Computing, Sweden
[2]Delft University of Technology, The Netherlands
[*]corresponding author: jorn.zimmerling@it.uu.se

Abstract: Electromagnetic field interactions with photonic resonators can be efficiently modeled using Quasi Normal Mode (QNM) expansions, especially near a resonator, where low-order expansions are often sufficient. However, we are often interested in the electromagnetic field far away from a resonator. Since QNMs diverge with increasing distance from the resonator, a straightforward QNM expansion of the field is not possible. Here, we propose a formulation that allows for field evaluations at arbitrary distances, using only QNM expansions inside a resonator.

Effect modelling and computation of electromagnetic responses of resonators is an important problem when designing photonic resonators. We are interested in modeling such responses for (possibly dispersive) electromagnetic resonators. Let $\boldsymbol{x}$ denote the position vector and let s denote the complex Laplace frequency. The electromagnetic field is excited by the distant volumetric electric current source $\boldsymbol{J}^{\mathrm{src}}(\boldsymbol{x}, s)$ supported in the domain Ω_{src}. The electric field is then measured using the volumetric receiver $\boldsymbol{J}^{\mathrm{rec}}(\boldsymbol{x}, s)$ supported in Ω_{rec}. In this contribution we are interested in the response $D(s)$ given by the interaction integral

$$D(s) = \int_{\mathbf{x}\in\Omega_{\mathrm{rec}}} \boldsymbol{J}^{\mathrm{rec}}(\boldsymbol{x}, s) \cdot \boldsymbol{E}(\boldsymbol{x}, s)\, \mathrm{d}V.$$

A (possibly dispersive) resonator characterized by the contrast current $\boldsymbol{J}^{\mathrm{sc}} = \chi\mathbf{E}$ is placed far from the support of the source and receiver and is embedded into a background medium. The support of the contrast is denoted by Ω_{sc}. The configuration is illustrated in Figure 1.

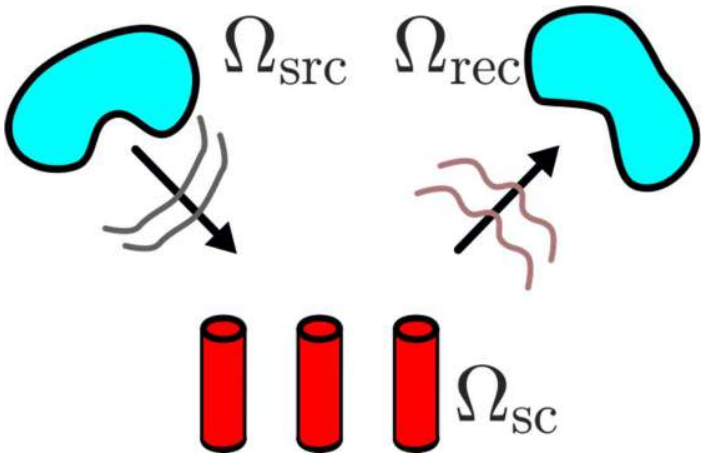


Figure 1: Illustration of a scattering problem where the electromagnetic response of a resonant configuration is of interest.

Let $\boldsymbol{G}(\boldsymbol{x}, \boldsymbol{x}', s)$ denote the Greens tensor of the configuration, then the response can be succinctly written as

$$d(s) = \int_{x \in \Omega_{\mathrm{rec}}} \boldsymbol{J}^{\mathrm{rec}}(\boldsymbol{x}, s) \cdot \int_{\boldsymbol{x}' \in \Omega_{\mathrm{src}}} \boldsymbol{G}(\boldsymbol{x}, \boldsymbol{x}', s) \cdot \boldsymbol{J}^{\mathrm{src}}(\boldsymbol{x}, s) \mathrm{d}V' \, \mathrm{d}V. \quad (1)$$

A common technique to approximate this response especially in the field of plasmonics or nano-photonics is to use so-called Quasi-Normal Mode (QNM) expansions. The Green function is essentially approximated using a few of its eigenfunctions which correspond to the resonance fields of the configuration [2,3,4]. To compute these QNMs multiple efficient numerical methods exists [review paper]. Unfortunately, since the resonator is embedded in an open system with radiation to infinity, the QNM fields diverge far from the resonators. Outside the resonator these fields are not complete, and a straightforward expansion is not possible.

Approaches to still be able to approximate field responses exist in [6,7,1] where the fields are regularized, via for instance the Dyson equation or causality principle. In this contribution we take a different path and rewrite the integral equation (1), using scattered field formalisms such that the Green function is only integrated over the domain Ω_{sc}. In this domain the QMNs form a good approximation space such that QNM expansions are successful in giving low-order description of the electromagnetic field response. We will present numerical examples to illustrate our formalism.

References

[1] B. Gralak and M. Abdelrahman, "Completeness and divergence-free behavior of the quasi-normal modes using causality principle," *The International Photonics and Optoelectronics Meeting (POEM), OSA Technical Digest (Optica Publishing Group, 2018)*, paper OT4A.36. (2018)

[2] Lalanne, P., Yan, W., Vynck, K., Sauvan, C., and Hugonin, J.-P. "Light interaction with photonic and plasmonic resonances," *Laser & Photonics Reviews*, page 1700113, (2018)

[3] F. Zolla, A. Nicolet, and G. Demesy,"Photonics in highly dispersive media: the exact modal expansion," *Opt. Lett.*, 43(23):5813–5816, (2018)

[4] C. Sauvan, J. P. Hugonin, I. S. Maksymov, and P. Lalanne, "Theory of the spontaneous optical emission of nanosize photonic and plasmon resonators," *Phys. Rev. Lett.*, 110:237401, (2013)

[5] P. Lalanne, W. Yan, A. Gras, C. Sauvan, J.-P. Hugonin, M. Besbes, G. Demésy, M. D. Truong, B. Gralak, F. Zolla, A. Nicolet, F. Binkowski, L. Zschiedrich, S. Burger, J. Zimmerling, R. Remis, P. Urbach, H. T. Liu, and T. Weiss, "Quasinormal mode solvers for resonators with dispersive materials," *J. Opt. Soc. Am.* A36, 686-704, (2019)

[6] M. Kamandar Dezfouli and S. Hughes, "Regularized quasinormal modes for plasmonic resonators and open cavities," Phys. Rev. B 97, 115302 (2018)

[7] R.-C. Ge, P. T. Kristensen, J. F. Young, and S. Hughes, "Quasinormal mode approach to modelling light-emission and propagation in nanoplasmonics," New J. Phys. 16, 113048 (2014).

META 2023, PARIS - FRANCE, JULY 18 – 21, 2023

Optomechanics of Quasi-Bound States in the Continuum of Dielectric Metasurfaces

S. Zanotto[1*]

[1]CNR—Istituto di Nanoscienze, and NEST - Scuola Normale Superiore, Piazza San Silvestro 12, Pisa 56217, Italy

[*]corresponding author: simone.zanotto@nano.cnr.it

Abstract: Quasi-Bound States in the Continuum (Q-BICs) are here investigated by means of optomechanic spectroscopy. With this technique, the metasurface is driven into motion according to its mechanical eigenstates, and the time-dependent optical transmission is detected and demodulated at the mechanical frequency. Here we show that this method allows to reveal fine features of Q-BICs hardly observable with conventional spectroscopy. In addition, we believe that our work opens interesting technological perspectives for high-quality factor metasurface-based optical modulators.

Quasi-Bound States in the Continuum are currently a topic of intense investigation due to their unique property of being high-quality resonances with macroscopic (i.e., spatially extended over multiple wavelength) mode sizes. Meanwhile, Q-BICs have typically a large angular dispersion, which make them interesting for Fourier-space image processing. These features are both interesting and challenging: from one side Q-BICs are highly sensitive to perturbation and hence relevant for sensing, low-threshold lasing etc., from the other side they are difficult to detect and to fabricate with reproducibility. In our study, we have considered a slab metasurface based on a silicon holey membrane (Fig. 1d-e), that, according to common practice in fabrication technology, is realized on a silicon bulk carrier wafer through SiO_2 underetching. In this kind of sample, two Fabry-Pérot processes occur: one in the air spacer immediately below the metasurface, and another in the carrier wafer. The latter has a typical free spectral range comparable to the Q-BIC linewidth, making the direct detection of the Q_BIC through ordinary optical spectroscopy (i.e., transmission, reflection) challenging (Fig. 1a).

We thus leveraged on the optomechanical interaction intrinsic in the fact that the metasurface membrane is free to oscillate with drum-like modes, that in our case fall in the MHz range. By an ordinary lock-in type measurement, we detected the modulated transmittance, that shows the notable behavior illustrated in Fig. 1b. Here, the signature of the Q-BIC is much stronger than before, thus allowing a clearer and safer indentification of the optical resonance position and strength. What is more, relying to a coupled-mode model, it is possible to retrieve the static optical signal that would have originated from the metasurface alone, in absence of the multiple Fabry-Pérot resonances (Fig. 1c).

Our result is thus twofold: from one side it delineates a procedure to disembed the spectral signature of Q-BICs in typical slab-spacer-wafer platforms; from the other it defines a prototype for light modulators operating at MHz frequencies. Interestingly, those modulators can implement peculiar angular dispersions, and polarization response [2], all in a lossless fully dielectric environment.

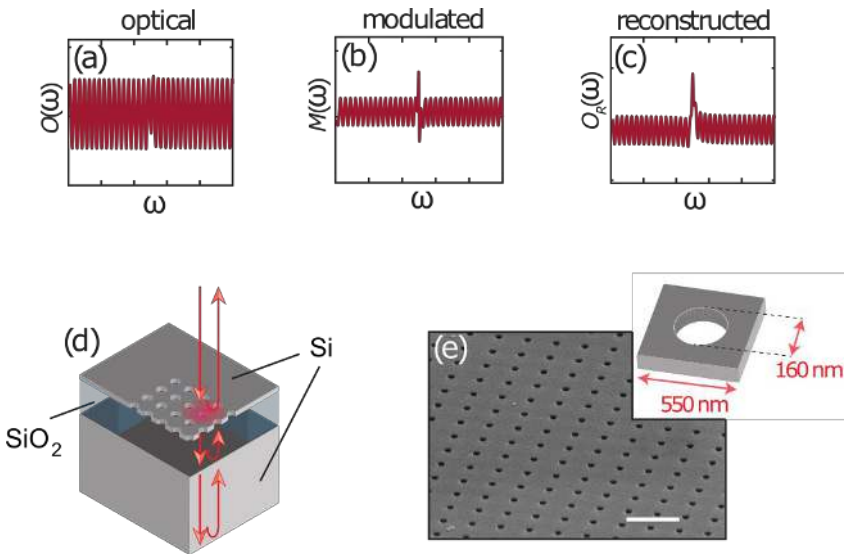


Figure 1: Schematic illustration of the modulation and reconstruction of optical Q-BIC resonances through optomechanical effect. The optomechanical interaction takes place since the metasurface membrane (d, e) is free to move out-of-plane, being constrained through underetched SiO_2 only at the sample edges. (a) Direct optical spectrum (i.e., transmission or reflection) This contains strong Fabry-Pérot contributes from the Si substrate. (b) Modulated optical signal detected e.g. through a lock-in when the membrane is moving. (c) Reconstructed Q-BIC resonances, following elaboration of the spectrum in (b).

References

1. Zanotto, S., Conte, G., Bellieres, L. C., Griol, A., Navarro-Urrios, D., Tredicucci, A., Martìnez, A., and Pitanti, A. "Optomechanical Modulation Spectroscopy of Bound States in the Continuum in a Dielectric Metasurface," Physical Review Applied, **17** (4), 044033 (2022).
2. Zanotto, S., Tredicucci, A., Navarro-Urrios, D., Cecchini, M., Biasiol, G., Mencarelli, D., Pierantoni, L., and Pitanti, A. "Optomechanics of chiral dielectric metasurfaces," Advanced Optical Materials, **8**(4), 1901507 (2020).

Photon-Pair Generation in Resonant Dielectric Nanostructures

Maximilian A. Weissflog[1,2,*]

[1]Institute of Applied Physics, Abbe Center of Photonics, Friedrich Schiller University Jena, Albert-Einstein-Str. 15, 07745 Jena, Germany
[2]Max Planck School of Photonics, Hans-Knöll-Str. 1, 07745 Jena, Germany
[*]corresponding author: maximilian.weissflog@uni-jena.de

Abstract: Resonant nonlinear nanostructures are evolving into a versatile platform for the generation of entangled photon-pairs with engineered properties. The talk will discuss recent advances in the theoretical description and experimental control of quantum photon-pair states, particularly the generation of maximally polarization entangled Bell states in single nanoresonators as well as spatial tuning of pair-emission in a nonlocal Lithium Niobate metasurface.

Photon-pairs are a crucial resource for many applications relying on quantum optical effects such as quantum communication, imaging, sensing and computing. While entangled photon-pairs were so far mainly generated via spontaneous parametric down-conversion (SPDC) in bulk-optical nonlinear components, recently resonant photonic nanostructures have been introduced as a new platform for SPDC [1,2]. The high degree of control on e.g. the polarization of classical nonlinearly generated emission from nanoresonators [3] suggests that they could in principle be further developed into sources of polarization entangled two-photon states. However, the large number of degrees of freedom in highly multimodal and open nanocavities made a formal description and design of entangled photon-pair sources challenging so far.

The talk will discuss how this issue is solved by combining a Green's function (GF) formalism that can handle SPDC in radiative or lossy systems [4] with an expansion of the GF into a limited number of quasinormal modes (QNMs) of the nanoresonator. Using this new approach, it can be shown that already simple nanoresonator geometries such as a single AlGaAs nanocylinder can generate maximally polarization entangled Bell states, revealing the intricate connection between resonant modes, nonlinear susceptibility tensor and the photon-pair detection configuration.

Next to the polarization degree of freedom, also the spatial emission properties of photon-pairs can be efficiently controlled in resonant nanoscale SPDC sources. Based on a metasurface consisting of a SiO2-grating on a Lithium Niobate thin film, I will show that the strong angular dispersion of the supported nonlocal guided mode resonances [5] can be used to continuously tune the emission angle of frequency-degenerate photon pairs by changing the SPDC excitation wavelength. Furthermore, our recent experiments prove that such a metasurface allows generation of entangled photon-pairs simultaneously in transmission, reflection and counter-propagating configuration.

In sum, I will discuss our recent progress in the development of a theoretical framework as well as experiments for photon pair-generation in resonant nanostructures with emphasis on the generation of polarization entangled states and spatial emission control.

References

1. Santiago-Cruz, T., Fedotova, A., Sultanov, M., Weissflog, M. A. *et al.*, "Photon Pairs from Resonant Metasurfaces," Nano Lett., Vol. 21, No. 10, 4423–4429, 2021.
2. Santiago-Cruz, T. *et al.*, "Resonant metasurfaces for generating complex quantum states," Science, vol. 377, no. 6609, 991–995, 2022.
3. Weissflog, M. A. *et al.*, "Far-Field Polarization Engineering from Nonlinear Nanoresonators," Laser Photonics Rev., vol. 16, no. 12, 2200183, 2022.
4. Poddubny, A. N., Iorsh, I. V., and Sukhorukov A. A., "Generation of Photon-Plasmon Quantum States in Nonlinear Hyperbolic Metamaterials," Phys. Rev. Lett., vol. 117, no. 12, 123901, 2016.
5. Zhang, J. *et al.*, "Spatially entangled photon pairs from lithium niobate nonlocal metasurfaces," Sci. Adv., vol. 8, no. 30, eabq4240, 2022.

Light scattering and dipole emission in resonant periodic structures

L. Zschiedrich[1*], F. Binkowski[2], P. Manley[1], M. Hammerschmidt[1], P.-I. Schneider[1], and S. Burger[1,2]

[1]JCMwave GmbH, Germany
[2]Zuse-Institute-Berlin, Germany
[*]corresponding author: lin.zschiedrich@jcmwave.com

Abstract: We address the numerical computation of the emission and radiation of an isolated dipole within a laterally periodic structure such as a photonic crystal, a light emitting device or a meta lens. We utilize the Bloch-Floquet transform and its inverse to represent the solution as an integration of Bloch-periodic sub-solutions over the Brillouin zone. Due to the appearance of trapped modes and Wood anomalies this integration is numerically very challenging.

The emission and radiation of a dipole is highly influenced by its surrounding. State-of-the-art solvers are capable to deal with isolated dipoles placed within a finite computational domain of an arbitrary geometry and with a stratified background as the exterior space. For the treatment of a periodic environment we apply the Bloch-Floquet transform [1]. Then, for each point in the Brillouin zone it is required to solve a problem on the unit cell with a Bloch-periodic dipole as a source. Numerically, one encounters two major challenges. Firstly, the singularity of the dipole solution requires to split the field into a semi-analytical part comprising the singular field and a smooth correction field feasible for a numerical discretization. However, even the semi-analytical solution of a Bloch-periodic dipole is delicate to compute [2]. We therefore propose an alternative approach which only relies on the analytic solution for a dipole in homogeneous or stratified background and which perfectly fits into our Finite-Element framework. Secondly, to gain the overall solution we need to integrate over the Brillouin zone. We will show that arising resonances due trapped modes within the periodic structures renders this integration extremely costly. To mitigate the numerical efforts we apply an adaptive integration scheme.

Acknowledgments

We acknowledge funding by the Deutsche Forschungsgemeinschaft (DFG, German Research Foundation) under Germany's Excellence Strategy - The Berlin Mathematics Research Center MATH+ (EXC-2046/1, project ID: 390685689). This project is partially funded by the German Federal Ministry of Education and Research (BMBF, project number 01IS20080A, SiM4diM).

References

1. Zschiedrich, L, Greiner, H, et al. “Numerical analysis of nanostructures for enhanced light extraction from OLEDs,” Proc. SPIE, Vol. 8641, 86410B (2013)
2. Moroz, A., “Quasi-periodic Green’s functions of the Helmholtz and Laplace equations,” J. Phys. A: Math. Gen. 39, 11247 (2006).

Towards a highly directional hybrid Mie-Tamm optical cavity for high-performance single-photon sources

J. M. Llorens[1*], A. Nowak[2], J. M. Ulloa[3], and B. Alén[1]

[1]Instituto de Micro y Nanotecnología, IMN-CNM, CSIC (CEI UAM+CSIC) Isaac Newton, 8, E-28760, Tres Cantos, Madrid, Spain

[2]g2-Zero S.L., Calle de las Dos Doncellas 6, Getafe, Madrid, Spain

[3]Institute for Optoelectronics Systems and Microtechnology (ISOM), Universidad Politécnica de Madrid, Avda. Complutense 30, 28040, Madrid, Spain

[*]corresponding author: jose.llorens@csic.es

Abstract: We propose a Mie-Tamm optical cavity structure (MTOCS) that can enhance the photon flux of a quantum emitter above 3 GHz within a small numerical aperture collection cone. Our design uses a nested cavity system in which the quantum emitter's emission is coupled to an extended Tamm mode through Mie resonances supported by a nanocylinder. This approach enables highly efficient light-matter interactions in nanophotonic systems, making it suitable for single-photon sources.

To achieve high-performance true single-photon sources, on-demand emission at rates exceeding the GHz regime is required. However, current semiconductor technologies face limitations due to the difficulty of extracting photons from the semiconductor, which is caused by the high refractive index of the host material. In our study, we analyze single-photon emitters that are embedded in a cylinder, which is defined vertically by a bottom distributed Bragg reflector (DBR) and a top metallic mirror, and laterally by dielectric confinement with a low refractive index layer (Figure 1(a))[1]. The goal is to optimize the flux and collection efficiency of single photons at the substrate-air interface. By doing so, we can utilize the top metallic mirror as an electrical contact to switch the single-photon emitter on and off, or to tune its properties. This design, combined with an embedded excitation source underneath, could potentially enable the creation of a monolithic electrically-driven and tunable single-photon source.[2]

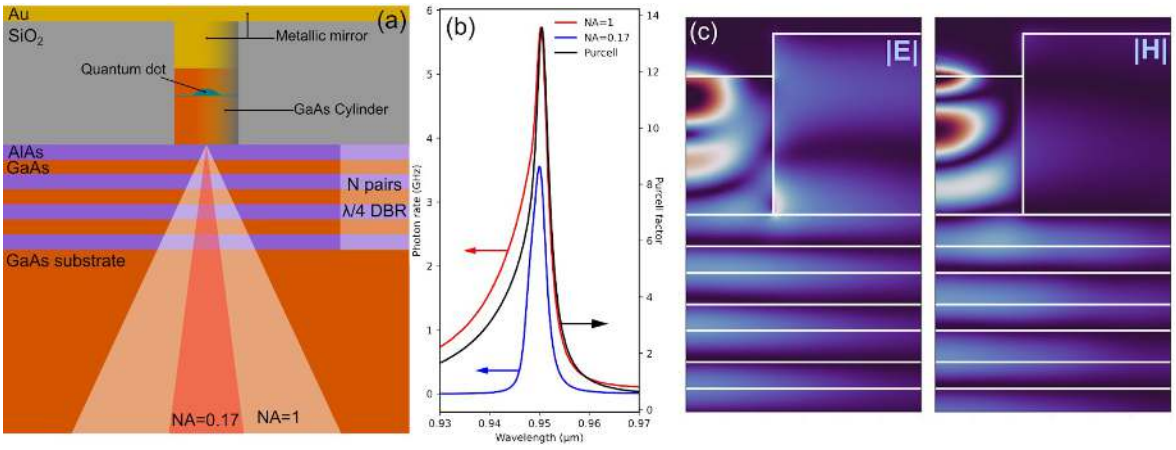


Figure 1. (a) Scheme of the MTOCS where the main elements are identified and two extraction cones of different NA are illustrated (not to scale). (b) Photon extraction rate in GHz (assuming a radiative lifetime of 1 ns) for the two NAs indicated

before and the Purcell factor. (c) Electric and magnetic field modulus at resonance showing the excitation of a Mie-resonance together with the planar front-wave in the DBR explaining the coupling between the cavities and the high directionality of the proposal.

To demonstrate the potential of our design on GaAs technology, we have chosen a specific configuration in which the substrate is made of GaAs and the dielectric layer as SiO_2, the distributed Bragg reflector (DBR) is composed of AlAs/GaAs bilayers, and the quantum emitter is an InAs quantum dot. Our analysis demonstrates that the proposed system is capable of achieving a photon emission rate of more than 3 GHz, collecting within a very narrow numerical aperture (NA) of 0.17 (as shown in Figure 1(b)). At the critical angle (NA=1), the emission rate can be larger than 5 GHz. We will present a detailed analysis of the different modes involved in enhancing the emission rate and directionality of the proposed nanocavity design. Additionally, we will explore potential modifications to the geometry that could reduce off-axis scattering and simplify the fabrication process and show the advances on the physical realization of the TMOC. We are currently in the process of fabricating a single-photon source based on the proposed TMCO design, and we will present our latest results on the device fabrication.

This work is supported by the following grants: European Union's Horizon 2020 research and innovation programme under the Marie Sklodowska-Curie grant agreement No 956548, project Quantimony; project 20FUN05 SEQUME, which has received funding from the EMPIR programme co-financed by the Participating States and from the European Union's Horizon 2020 research and innovation programme; the Agencia Estatal de Investigación (AEI) grant PID2019-106088RB-C31; and the CSIC Interdisciplinary Thematic Platform (PTI+) on Quantum Technologies (PTI-QTEP+).

References

1. Llorens, J.M., and Alén, B. "Inverse Design of a Hybrid Mie-Tamm Photonic Structure as a Highly Directional Gigahertz Single-Photon Source," Phys. Rev. Appl., Accepted 2023. arXiv:2202.05032.
2. Alén, B., Fuster, D., González, Y. and González, L., "Device for emitting single photons or entangled photon pairs," (EP3361516B1, 2017-02-08).

META 2023, PARIS - FRANCE, JULY 18 – 21, 2023

Calculating resonant states in optical systems: Exact theory and approximations

E. A. Muljarov

School of Physics and Astronomy, Cardiff University, Cardiff CF24 3AA, United Kingdom

*corresponding author: Egor.Muljarov@astro.cf.ac.uk

This talk will focus on recent advances of the resonant-state expansion (RSE) - a rigorous theory of optical resonances in open systems [1,2], allowing their accurate calculation and intuitive understanding. New achievements include variations of the RSE aiming to enhance its efficiency and reach, as well as some useful approximations following from the RSE, including single-mode and first-order approximations [3,4], for treating homogeneous and inhomogeneous perturbations, both inside and outside the optical systems.

References

1. E. A. Muljarov, W. Langbein, and R. Zimmermann, Brillouin-Wigner perturbation theory in open electromagnetic systems, Europhys. Lett. **92**, 50010 (2010).
2. M. B. Doost, W. Langbein, and E. A. Muljarov, Resonant-state expansion applied to three-dimensional open optical systems, Phys. Rev. A **90**, 013834 (2014).
3. S. F. Almousa and E. A. Muljarov, Exact theory and approximations for optical resonators in a changing external medium, Phys. Rev. B **107**, L081401 (2023).
4. Z. Sztranyovszky, W. Langbein, and E. A. Muljarov, First-order perturbation theory of eigenmodes for systems with interfaces, Phys. Rev. Research **5**, 013209 (2023).

Bound-State-in-the-Continuum Resonances in Monolithic Cavities on a Substrate

Cindy Péralle[1], Sushanth Kini Manjeshwar[2], Anastasiia Ciers[2], Witlef Wieczorek[2], and Philippe Tassin[1]

[1]Department of Physics, Chalmers University of Technology, 412 96 Gothenburg, Sweden
[2]Department of Microtechnology and Nanoscience, Chalmers University of Technology, 412 96 Gothenburg, Sweden

Abstract: We present a strategy to find photonic cavities with bound-state-in-the-continuum resonances that can be fabricated with planar fabrication methods on a substrate.

Due to their low mass and high reflectivity, photonic-crystal membranes are excellent candidates for vibrating end mirrors in optomechanical cavities. Cavities with photonic-crystal membranes can support a quasi-bound state in the continuum (BIC), i.e., a resonance exhibiting an optical quality factor only limited by dissipative loss. Such cavities promise to access new regimes in optomechanics [1], e.g., the single-photon strong-coupling regime for applications in precision sensing [2] and quantum information processing [3]. However, previously proposed designs turned out to be difficult to fabricate with state-of-the-art nanolithography techniques. Furthermore, it is difficult to find new nanophotonic structures with a bound state in the continuum, in particular if a substrate breaks the mirror symmetry of the cavity.

In this contribution, we will present our work on designing a new monolithic cavity on a substrate exhibiting a bound state in the continuum and, in the process, we will reveal a design methodology to turn cavities with an in-plane mirror plane into a cavity on a substrate.

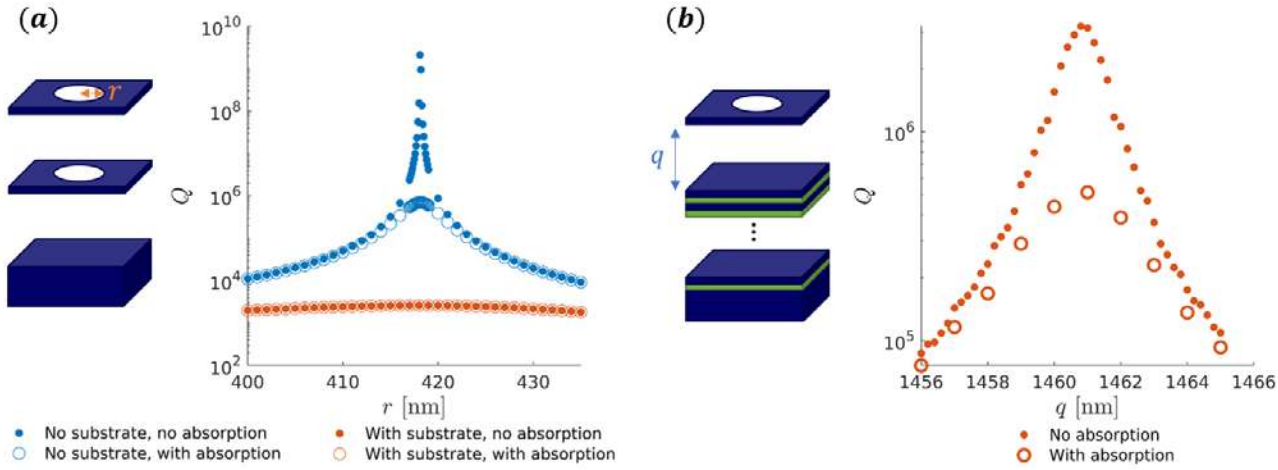


Figure 1: (a) Schematic of a cavity formed by two identical 2D photonic-crystal membranes and its quality factor around a BIC as a function of the hole radius r, without (blue) and with (orange) substrate, with (dots) and without (empty circles) material absorption. (b) Schematic of a cavity formed by one 2D photonic-crystal membrane and a DBR deposited on a substrate and its quality factor around a BIC as a function of the cavity length q, with (blue) and without (orange) material absorption.

We start from a cavity formed by two identical membranes patterned with cylindrical holes arranged in a square lattice in GaAs; such a cavity is known to exhibit a bound state in the continuum [1], but only when floating in air. For practical reasons, a substrate must be introduced close to the cavity. Unfortunately, a substrate allows light to escape the cavity through diffraction orders in the substrate, resulting in a radiative loss channel and destroying the bound state in the continuum.

In order to counter this effect, we propose a new design, illustrated in Fig. 1(b), replacing one of the photonic-crystal membranes by a DBR, specifically designed to reflect both the 0^{th} and 1^{st} orders of diffraction from the above 2D photonic-crystal membrane at a convenient wavelength of 1525nm. This design is derived from the previous cavity with two photonic-crystal membranes by taking advantage of the mirror symmetry plane in the original cavity. This allows us to preserve the bound state in the continuum and, at the same time, also eliminates the need to carefully align two patterned membranes. Indeed, in Fig. 1(b), we see that our new cavity again has a high quality factor. After an optimization process, we predict quality factors reaching about $5\times10_5$ when material absorption is included in the model. By eliminating the radiative loss channels through the substrate and making the system also easier to fabricate, our new design allows for a more practical observation of an optomechanical cavity exhibiting a bound state in the continuum.

We acknowledge support from the Chalmers Excellence Initiative Nano and from the Swedish Research Council under Grant No. 2020-05284. The numerical calculations and ANN training were performed on resources provided by the Swedish National Infrastructure for Computing (SNIC) at the Chalmers Centre for Computational Science and Engineering (C3SE), partially funded by the Swedish Research Council under Grant No. 2018-05973.

References

1. J. M. Fitzgerald, S. K. Manjeshwar, W. Wieczorek, and P. Tassin, “Cavity optomechanics with photonic bound states in the continuum,” Phys. Rev. Research, Vol. 3, 013131, 2021.
2. B.-B. Li, L. Ou, Y. Lei, and Y.-C. Liu, “Cavity optomechanical sensing,” Nanophotonics, Vol. 10, No. 10, 2799, 2021.
3. C. Galland, N. Sangouard, N. Piro, N. Gisin, and T. J. Kippenberg, “Heralded single-phonon preparation, storage, and readout in cavity optomechanics,” Phys. Rev. Lett., Vol. 112, 143602, 2014.

META 2023, PARIS - FRANCE, JULY 18 – 21, 2023

Quantum confinement effects in atomic-scale polaritons

F. Javier García de Abajo[1,2*]

[1] ICFO-Institut de Ciencies Fotoniques, The Barcelona Institute of Science and Technology, Barcelona, Spain
[2] ICREA-Institució Catalana de Recerca i Estudis Avançats, Barcelona, Spain
[*] javier.garciadeabajo@nanophotonics.es

Abstract: We discuss the prospects to observe quantum confinement effects in different types of optical excitations supported by systems ranging from single molecules to nanostructures. In contrast to plexitons, where the hybridization of a plasmonic mode and a fermionic excitation leads to a deviation from the uniform energy spacing in the bosonic ladder, we consider optical nonlinearities at the level of a single quantum. Practical implementations and applications are also discussed.

In this presentation, we discuss the prospects to observe quantum confinement effects in different types of optical excitations supported by systems ranging from single molecules to nanostructures. In contrast to plexitons, where the hybridization of a plasmonic mode and a fermionic excitation leads to a deviation from the uniform energy spacing in the bosonic ladder, we consider optical nonlinearities at the level of a single quantum. Practical implementations and applications are also discussed in systems that comprise plasmons in ultrathin metals[1,2] and quantum-phase materials,[3] excitons in transition metal dichalcogenides, and phonon polaritons in ionic insulators.[4]

References

1. Z. M. Abd El-Fattah et al., “Plasmonics in atomically thin crystalline silver films,” ACS Nano 13, 7771, 2019.
2. V. Mkhitaryan et al. (in preparation).
3. V. Di Giulio et al., Nat. Commun. “An image interaction approach to quantum-phase engineering of two-dimensional materials,” 13, 5175, 2022.
4. F. Iyikanat et al., “Nonlinear tunable vibrational response in hexagonal boron nitride,” ACS Nano 15, 13415, 2021.

META 2023, PARIS - FRANCE, JULY 18 – 21, 2023

Nanolasers: Dynamics and Phase Locking

Yeshaiahu (Shaya) Fainman, Sizhu Jiang, Suruj Deka and Athena Pan
Department of Electrical and Computer Engineering, University of California San Diego, La Jolla, CA, 92093-0407 USA
*corresponding author: fainman@ece.ucsd.edu

Abstract: We discuss nanoscale metal-dielectric-semiconductor resonant gain geometries to create a new type of light emitters focusing on three key aspects: second order intensity correlation characterizations, direct modulation and coupled nanolasers dynamics.

Introduction: Nanolasers have attracted considerable attention in the past two decades due to their advantageous characteristics such as ultrasmall footprint, lower power consumption, and high-speed operation that can benefit a plethora of applications. While most studies so far have been focused on individual lasers, the next phase would be applying these nanolasers in an array form for various applications, including imaging, biosensing, orbital angular momentum generation, virtual and augmented reality, and Lidar systems. We present the past and on-going research on nanolasers that is conducted in our group at UCSD, starting from the study on individual nanolasers to coupled nanolasers towards the realization of nanolaser array. Specifically, we discuss design of optically and electrically pumped nanolasers together with the second order intensity correlation characterization technique that helps to define the lasing threshold and different operating regimes of nanolasers when the conventional measurement is inadequate. We then discuss the wavelength tunability and intensity modulation of nanolasers followed by the studies on the phase-locking condition of nanolasers supported by experimental demonstration of mode selection in coupled nanolasers.

Design and characterization of nanolasers: Room-temperature optically pumped MDNLs that are subwavelength in all three dimensions have been demonstrated a decade ago [1]. In this design, metal cladding is used to provide the 3D optical confinement, and dielectric shield reduces the optical mode overlap with the lossy metal and thus lowers the lasing threshold. Thresholdless coaxial nanolasers have also been demonstrated in [2] with the light-in light-out curve (L-L curve) showing vanishing of a kink in the curve suggesting that the spontaneous emission (SpE) factor β approaches unity. To make nanolasers more useful for practical on-chip application, we experimentally demonstrate in [3], a new CW electrically pumped (e-pumped) nanolaser. For high energy efficiency and fast modulation speed nanolasers with a high spontaneous emission factor β are desirable, but their threshold characterization with traditional methods are not challanging. We developed a novel method to characterize the coherence properties of high-β nanolasers employing second-order intensity correlation ($g^2(\tau)$) [4]. Specifically, other than the height of the $g^2(0)$ peak as reported in the literature, it is first reported in [4] that the $g^2(\tau)$ pulse width also changes as a function of the pump intensity. The measurement technique is applied to a MDNL with β=0.25 and demonstrate that the SpE, ASE, and lasing regime can be fully characterized. We show that $g^2(\tau)$ pulse width shrinks below and near the threshold and broadens above the threshold when nanosecond pump pulses are employed.

Phase-locking in nanolasers: Understanding the phase-locking stability and the nonlinear dynamics of coupled nanolasers is essential for generating phase-locked laser arrays for high-power and steerable optical beam generation. Theoretical analysis of such laterally coupled lasers have been vastly investigated previously. However, these studies overlooked the effect of β, which is not-negligible for nanoscale lasers. In [5], we

reported the theoretical effects of varying β on the stability of phase-locking, with varying pump rates and frequency detuning considered. The stable and unstable regimes of the coupled lasers are identified through a bifurcation analysis over the coupled laser rate equations, with the details given in [5]. To demonstrate stable in-phase locking in nanolasers, we start with two coupled nanolasers that serve as a building block in laser array. The simulation results of simply arranging the two nanolasers next to each other show that the out-of-phase mode always have higher quality factor and lower lasing threshold. In our most recent work [6], we investigate addition of a coupling bridge in between two MDNLs, and study stability of in-phase and out-of-phase locking of such designs with the corresponding supermodes. We show that by controlling the length and the width of the bridge, we can control the resonance frequencies and the quality factors of the two supermodes, and thus obtain a coupling coefficient that supports an in-phase or out-of-phase locking modes.

We acknowledge partial support of NSF, ARO, DARPA, and ASML/Cymer Corporation.

References

1. M. P. Nezhad et al., “Room-temperature subwavelength metallo-dielectric lasers”, Nature Photon, vol 4, 2010, pp. 395-399
2. M. Khajavikhan et al., "Thresholdless nanoscale coaxial lasers," Nature Photon, vol. 482, no. 7384, 2012, pp. 204-207.
3. C.-Y. Fang et al., "Lasing action in low-resistance nanolasers based on tunnel junctions," Opt. Lett., vol. 44, no. 15, 2019, pp. 3669-3672.
4. S. H. Pan et al. , "Dynamic hysteresis in a coherent high-β nanolaser," Optica, vol. 3, no. 11, 2016, pp. 1260-1265.
5. S. Jiang et al., “Effects of High-β on Phase-Locking Stability and Tunability in Laterally Coupled Lasers”, IEEE JOURNAL OF SELECTED TOPICS IN QUANTUM ELECTRONICS, Vol. 28, Issue 1, Article 1800312
6. S. Jiang, et al., “Experimental Demonstration of Mode Selection in Bridge-Coupled Metallo-Dielectric Nanolasers,” Optics Letters, vol. 46, no. 23, 2021

Resonantly confining light in air: The dielectric Mie voids

M. Hamidi,[1] K. Koshelev,[2] M. Hentschel,[3] A. Canós-Valero,[1] Y. Kivshar,[2] H. Giessen,[3] and T. Weiss[1,3,*]

[1] Institute of Physics, University of Graz, and NAWI Graz, Universitätsplatz 5, 8010 Graz, Austria
[2]Nonlinear Physics Centre, Research School of Physics, Australian National University, Canberra, Australia,
[3]4th Physics Institute, University of Stuttgart and Research Center SCoPE, Pfaffenwaldring 57, 70569 Stuttgart, Germany
[*]corresponding author: thomas.weiss@uni-graz.at

Abstract: Manipulating light at the nanoscale has become a central challenge in photonic metastructures, resonant metasurfaces, nanoscale optical sensors, and many more, and it is largely based on resonant light confinement in dispersive and lossy metals and dielectrics. We present the theoretical framework for resonantly confining light in air surrounded by high-index dielectrics and compare it with experiments. This confinement works down to the ultraviolet and can be understood to some extent via a generalization of the Babinet's principle to dielectrics.

In a recent publication [1], we demonstrated that individual voids embedded in high-index dielectric host materials support localized resonant modes with exceptional optical properties. Due to the confinement in air, the modes do not suffer from the loss and dispersion of the dielectric host medium. We show theoretically that the modes demonstrate highly local properties in the near- and far-field, which makes them non-interacting while arranged in lattices. The Mie void modes in dispersive dielectric materials, e.g., silicon, possess large quality factors, which become comparable or larger than that for silicon resonant nanoparticles in the visible and UV. We experimentally realize resonant Mie voids by focused ion beam milling into bulk silicon wafers and experimentally demonstrate resonant light confinement from visible down to the UV spectral range at 265 nm (4.68 eV). We further utilize the bright, intense, and naturalistic colours for nanoscale colour printing employing individual Mie voids as individual pixels.

It might be tempting to attribute the observed phenomena to the well-known Babinet's principle [2]. However, a straightforward application of this principle is not possible for connecting Mie voids to conventional dielectric resonators as their inverse structures. The reason is that Babinet's principle is an approximation for perfect electric conductors in the limit of infinitesimally thin films. Yet, we find that a generalization of this principle to dielectrics allows us to infer properties of Mie voids from those of their inverse counterparts. This provides design rules for achieving certain optical responses, which can be even extended to magnetic materials.

The concept of Mie voids paves the way towards the operation of functional high-index metasurfaces into the blue and UV spectral range, while the combination of resonant dielectric Mie voids with dielectric nanoparticles will more than double the parameter space for the future design of metasurfaces and other micro- and nanoscale optical elements. This extension will enable novel antenna and structure designs, which benefit from the full access to the modal field inside the void as well as the nearly free choice of the high-index material for novel sensing and active manipulation strategies.

We acknowledge support from the Deutsche Forschungsgemeinschaft (DFG) via the GRK 2642 as well as the individual DFG research grant WE 5815/5-1.

References

1. M. Hentschel, K. Koshelev, F. Sterl, S. Both, J. Karst, L. Shamsafar, T. Weiss, Y. Kivshar, and H. Giessen, "Dielectric Mie voids: Confining light in air," Light: Science & Applications **12**, 3 (2023).
2. M. Born and E. Wolf, *Principles of Optics*, 1999, Cambridge University Press, Cambridge.

META 2023, PARIS - FRANCE, JULY 18 – 21, 2023

Design and Simulation of Large-Scale Metalenses

J. Niegemann[1*], D. Huynh[2], F. Gomez[1], D. McGuire[1], and J. Pond[1]

[1]Ansys Canada Ltd., Canada
[2]Ansys Germany GmbH, Germany
[*]corresponding author: jens.niegemann@ansys.com

Abstract: One of the biggest challenges in the characterization of meta-atoms is the large parameter space that needs to be explored. To design realistic metalenses, we usually need to characterize the individual meta-atoms by frequency, angles of incidence, polarization, and often multiple geometric parameters. Here, we present our approach to quickly construct large databases of meta-atoms. In addition, we demonstrate how such a database can then be used to efficiently simulate centimeter-sized meta-lenses.

Metalenses consist of carefully arranged meta-atoms with sub-wavelength structures. By adjusting and optimizing the geometry of these individual elements, we can tailor the phase, amplitude, and polarization of the transmitted (or reflected) light. Over the past few years, substantial progress was made in the simulation and manufacturing of metalenses [1] which has generated large interest from both academia and industry. However, the design and optimization of centimeter-sized meta-lenses remains challenging and there still is a need for improved simulation approaches.

In this presentation, we will first discuss and compare different numerical methods to characterize and optimize meta-atoms. In particular, we will consider the respective strengths and weaknesses of the finite-difference time-domain (FDTD) method and the rigorous coupled-wave analysis (RCWA) approach. Then, we will discuss our approach for constructing databases of meta-atoms which store the local amplitude, phase and polarization information of a specific unit cell as a function of frequency, angles of incidence, polarization, and multiple geometric parameters. To efficiently cover this parameter space, we make use of adaptive surrogate models. Finally, we also discuss how to use these databases to enable the fast but accurate simulation of large-scale metalenses in optical systems using raytracing.

References

1. Y. He, B. Song and J. Tang, “Optical metalenses: fundamentals, dispersion manipulation, and applications,” Front. Optoelectron. Vol. 15, No. 24, 2022.

META 2023, PARIS - FRANCE, JULY 18 – 21, 2023

Engineered Solid-State Quantum-Light Sources for Quantum Networking

Tobias Heindel[1]

[1]Institute of Solid State Physics, Technische Universität Berlin, Berlin, Germany
[*]corresponding author: tobias.heindel@tu-berlin.de

Abstract: In this talk I present our recent progress in the field of solid-state quantum light sources for applications in quantum networking. In this context I present recent advances in the numerical optimization and fabrication of quantum light sources, designed for the direct coupling to single-mode optical fibers, and their application in quantum communication testbeds operating at wavelengths around 800, 1300, and 1550 nm.

In recent years, tremendous progress has been achieved in the engineering of solid-state-based quantum light sources. In this context, semiconductor quantum dots (QDs) are among the most promising candidates for implementations of quantum information [1]. In my talk, I will present recent progress in this field, ultimately striving towards quantum networks at global scales. I will discuss the development of novel building blocks, including fiber-pigtailed quantum devices [2,3] and plug&play benchtop single-photon quantum key distribution (QKD) systems [4], to be assembled in local quantum communication networks in Berlin city, but also in inter-city links. I show how to optimize and certify the performance of QKD systems [5] and report on our recent efforts in transferring our knowledge to advanced protocols, different technology platforms (e.g. quantum emitters in 2D materials [6]), and telecom C-band wavelengths suitable for long-haul quantum communication [7]. Not least, a deep dive into coherent optical control experiments on quantum emitters reveals important implications for the realization of quantum-secured data links [8], thereby building the bridge from fundamental quantum optics to secure data communication exploiting photonic quantum technologies. Assembling these building blocks to functional multi-partite quantum networks is a grand challenge in quantum technologies which is tackled in my group.

Many people contributed to this work, including my group members L. Rickert, T. Gao, D. Vajner, K. Kaymazlar, M. Lach, N. Kewitz as well as the many team members of collaborating groups - I would like to express my gratitude to all of them. We further acknowledge financial support by the German Federal Ministry of Education and Research (BMBF) via the project “QuSecure” (Grant No. 13N14876), the BMBF joint project “tubLAN Q.0” (Grant No. 16KISQ087K), and the Einstein Foundation via the Einstein Research Unit “Quantum Devices”.

References

1. D. A. Vajner et al., Advanced Quantum Technologies 2100116, (2022) Review Article
2. L. Rickert et al., Optics Express 27, 36824 (2019)
3. L. Rickert et al., Applied Physics Letters 119, 131104 (2021)
4. T. Gao et al., Applied Physics Reviews 9, 011412 (2022)
5. T. Kupko et al., npj Quantum Information 6, 29 (2020)
6. T. Gao et al., npj 2D Materials & Applications 7, 4 (2023)
7. P. Holewa, E. Zięba-Ostój, D. Vajner et al., manuscript in-preparation (2023)
8. Y. Karli, D. Vajner et al., manuscript in-preparation (2023)

MAN: A freeware to compute and analysis modes of resonators

T. Wu[1*], D. Arrivault [1], W. Yan[2], and P. Lalanne[1]

[1] LP2N, Institut d'Optique Graduate School, CNRS, France
[2] Westlake Institute for Advanced Study, China
[*]corresponding author: tong.wu@institutoptique.fr

Abstract: In this talk, we introduce MAN (Modal Analysis of Nanoresonators) a software with many open scripts, which computes and normalizes the quasinormal modes (QNMs) of electromagnetic resonators.

Introduction: In this talk, we present MAN [1-2], an open-source software that uses the QNM basis for analyzing the response of virtually any resonators or antennas, be they composed of dispersive, anisotropic, or non-reciprocal materials, or operated at high (optical and near-IR waves) or low (RF waves) frequencies. MAN is conceived to educatively help the user analyze the physics of electromagnetic resonators towards the identification of the dominant QNMs to speed up the simulation of resonant structures and offer physical transparency in the design.

Result: Figure 1 shows the structure of the software. MAN is the result of a collective effort over the last decade. It gathers two solvers, QNMPole [3] and QNMEig [4], which have already acquired a good reputation as can be seen from the number of citations of the referent publications [3-4] or software downloads [2]. QNMEig provides a comprehensive interface to the commercial software COMSOL Multiphysics; QNMPole can be used with any software capable of solving Maxwell equations in the frequency domain. MAN additionally features many toolboxes that illustrate how to use the software for analyzing various emblematic geometries with a superposition of QNMs, therein providing a transparent interpretation of the physics.

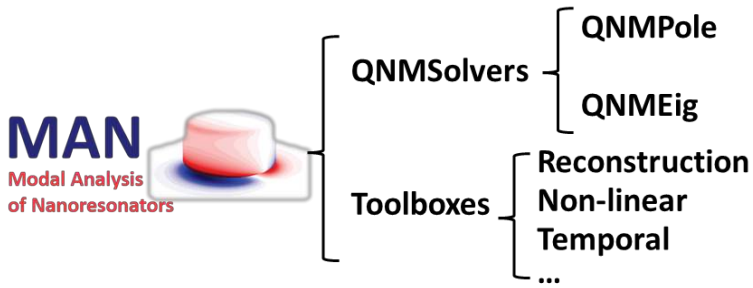


Fig. 1. Structure of MAN

References

1. Wu, T., Arrivault, D., Yan, W., Lalanne, P. "Modal analysis of electromagnetic resonators: User guide for the MAN program," Comput. Phys. Commun., Vol. 284, 108627, 2023.
2. DOI: https://doi.org/10.5281/zenodo.7400937
3. Bai, Q., Perrin, M., Sauvan, C., Hugonin, J.-P., Lalanne, P., "Efficient and intuitive method for the analysis of light scattering by a resonant nanostructure," Opt. Express, Vol. 21, 27371, 2013.
4. Yan, W., Faggiani, R., Lalanne, P., "Rigorous modal analysis of plasmonic nanoresonators." Phys. Rev. B, Vol. 97, 205422, 2018.

META 2023, PARIS - FRANCE, JULY 18 – 21, 2023

Complex $\chi^{(3)}$ of polyaniline and silver nanoparticle metafluids

G. Leo[1], G. Guercio[1], M. Lafitte[2], V. Ponsinet[2], O. Mondain-Monval[2], and A. Baron[2]

[1] Matériaux et Phénomènes Quantiques, Université Paris Cité, 10 rue A. Domon et L. Duquet, 75013 Paris, France

[2] Univ. Bordeaux, CNRS, CRPP, UMR 5031, F-33600 Pessac, France

*corresponding author: g.leo@u-paris.fr

Designing new materials is crucial for nonlinear nanophotonics, where strong local field enhancements are sought after in sub-wavelength structures. Since transparent optical materials are typically weakly nonlinear, special interest is currently directed at artificial composites that combine nonlinear media where the local field enhancement is provided by plasmonic nanoparticles.

In the context of nanoscale materials engineering, polymers have been studied as possible candidates for all-optical devices because of their relatively large $\chi^{(3)}$ susceptibility and fast response time. In particular, a significant effort has been devoted in understanding the properties of polyaniline (PANI), which also exhibits excellent environmental stability [1].

In this work, we measured the intensity-dependent complex refractive index of ethanol-based solutions with PANI and Ag nanoparticles via Z-scan [2], being motivated by their potential exploitation in all-optically controlled solid-state meta-lenses and ultrathin variable absorbers.

By moving a thin $\chi^{(3)}$ sample in and out of the focus of an intense coherent beam, the Z-scan trace is retrieved via the modulation of the transmittance through an iris placed after the sample. This enables to evaluate the real part of the refractive index, $\mathrm{Re}[n(I)] = n_0 + n_2 I$, which self-focuses or self-defocuses the Gaussian beam due to the optical Kerr effect. The imaginary part of $n(I)$ can also be inferred by completely opening the iris, which provides the two-photon-absorption coefficient β_2.

Our measurements were performed with 150 fs coherent pulses provided by an Amplitude Mango optical parametric amplifier at $\lambda = 400$ nm, where Ag nanoparticles exhibit a strong plasmonic resonance. Two different solutions in ethanol were characterized: with 2.3×10^{-6} mol/L of PANI, and 5.5×10^{13} Ag nanoparticles/L. In the former case, we found $n_2 = -4.4 \times 10^{-14}\mathrm{cm}^2/\mathrm{W}$ and $\beta_2 = -0.53$ cm/GW.

These results are promising towards the demonstration of solid-state Ag-PANI metasurfaces on a transparent substrate, which is currently under way.

1. D. V. Petrov et al., “Nonlinear-optical properties of a poly(vinyl alcohol)–polyaniline interpenetrating polymer network”, Opt. Letters 20, 554 (1995).
2. M. Sheik-Bahae et al., “Sensitive measurement of optical nonlinearities using a single beam”, IEEE J. Quantum Electron. 26, 760 (1990).

META 2023, PARIS - FRANCE, JULY 18 – 21, 2023

Quasi-Normal Mode Expansion in Unbounded Photonic structures: Perfectly Matched Layers (PML) vs. Bayliss-Turkel (BT) Absorbing Boundary Condition

G. Demésy[1], A. Nicolet[1*], and F. Zolla[1]

[1]Aix Marseille Univ, CNRS, Centrale Marseille, Institut Fresnel, Marseille, France

[*]corresponding author: andre.nicolet@fresnel.fr

Abstract: This paper compares truncation methods, i.e. Perfectly Matched Layers (PML) vs. Bayliss-Turkel (BT) Absorbing Boundary Condition (ABC), of unbounded domains for their performance in the quasi-normal mode expansions involving a continuous spectrum.

The quasi-normal mode expansion has received a lot of attention in the last decade[1,2] and is now well understood for very general problems that may involve very general types of dispersive materials[3]. The main remaining pitfall is the treatment of the continuous spectrum associated with unbounded domains. For the direct scattering problems, the perfectly matched layers (PML) [3] have proved to be a very efficient tool. However, they are not always satisfactory for modal expansion problems: they can give good approximations to the leaky modes but the numerical representation of the continuous spectrum they provide can be a source of numerical inaccuracies. An alternative approach is to use absorbing boundary conditions (ABC). At first order, the simple impedance condition (Robin condition) is too simple, but higher order approximations such as the Bayliss-Turkel (BT) condition[4] are very interesting alternatives as it will be shown in numerical examples.

References

1. Sauvan, C., Wu, T., Zarouf, R., Muljarov, E. A. and Lalanne, P, “Normalization, orthogonality, and completeness of quasinormal modes of open systems: the case of electromagnetism”, Optics Express, 2022.
2. Binkowski, F., Zschiedrich, L., Hammerschmidt, M. and Burger S., “Modal analysis for nanoplasmonics with nonlocal material properties”, Phys. Rev. B 100, 155406, 2019.
3. Truong, M.D., Nicolet, A., Demésy, G. and Zolla, F., Continuous family of exact Dispersive Quasi-Normal Modal (DQNM) expansions for dispersive photonic structures, Optics express 28 (20), 29016-29032, 2020.
4. Berenger, J. “A perfectly matched layer for the absorption of electromagnetic waves.”, J. Comput. Phys. , pp. 185–200, 1994.
5. Bayliss, A., Gunzburger, M. and Turkel, E. “Boundary Conditions for the Numerical Solution of Elliptic Equations in Exterior Regions”, SIAM Journal on Applied Mathematics, 42, 430–451, 1982.

Exploiting and Engineering non-Hermiticity in Photonics

M.Gurioli[1*], N. Granchi[1,2], and F. Intonti[1,2]

[1]Department of Physics and Astronomy, University of Florence, Italy
[2]European Laboratory for Non-linear Spectroscopy, University of Florence, Italy
[*]corresponding author: massimo.gurioli@unifi.it

Abstract: The non-Hermiticity is an unavoidable feature of any photonics system based on sound models and experiments. It has been used for mapping and optimizing the Q factor of photonic modes. Here we discuss its exploitation for engineering three effects: i) exciton light traps via radiative Lamb shift, ii) Purcell effect beyond the dipole approximation and iii) shaping the Fano LDOS via engineering the cavity losses.

At the basis of many relevant photonic accomplishments is the control of the lineshape and spatial extension of the photonic local density of states (LDOS) and consequently the manipulation of any light-matter interaction process. The so-called Purcell effect, i.e. the enhancement of the spontaneous emission rate is controlled by the quality factor (Q) and the modal volume (V) of the microresonators [1]. Important progress has been achieved on the description of photonics as a non-Hermitian open system by means of quasi normal modes (QNMs) with complex eigenvalues, which has led to deep modification of the common picture for V [2]. The complex-valued character of V, with its imaginary part linked to the non-Hermitian nature of open systems, is now established and experimentally confirmed [3,4]. At the same time, non-Lorentzian LDOS lineshapes have been experimentally observed even in carefully designed photonic systems displaying relatively low optical losses [5]. More recently, the map of the imaginary part of the modal volume has been used for driving the optimization of the in-plane and out-of-plane Q factor of any photonic modes [6].

In this contribution we review three recent achievements where the complex modal volume is engineered and exploited: i) enhancement and control of the Lamb Shift for exciton light trapping [7], ii) tailoring the CDOS for shaping the Purcell effect beyond the dipole approximation [8] and iii) controlling the in-plane losses for shaping the Fano LDOS [9].

Acknowledgements: fundamental contributions to the presented items have been done by Philippe Lalanne, Rémi Carminati, Guillermo Arregui and Andrea Fiore.

References

1. Purcell E. M., “Spontaneous emission probabilities at radio frequencies” Phys. Rev. ,Vol. 69, 681, 1949
2. Wu T., Gurioli M., Lalanne Ph. “Nanoscale Light Confinement: the Q’s and V’s” ACS photonics, Vol.8, No. 6, 1522-1538, 2021
3. Cognée K.G., Wei Yan, La China F., Balestri D., Intonti F., Gurioli M., Koenderink A.F., Lalanne Ph., “Mapping complex mode volumes with cavity perturbation theory”, Optica, Vol.6, No.3, 269-273, 2019
4. Caselli N., Wu T., Arregui G., Granchi N., Intonti F., Lalanne Ph., Gurioli M., “Near-field imaging of magnetic complex mode volume”, ACS photonics, Vol.8, No. 5, 1258-1263, 2021
5. Pellegrino D., Balestri D., Granchi N., Ciardi M., Intonti F., Pagliano F., Silov A.Y., Otten FW, Wu T., Vynck K., Lalanne Ph, Fiore A., Gurioli M., “Non-Lorentzian local density of states in coupled photonic crystal cavities probed by

near-and far-field emission", Phys. Rev. Lett.,Vol. 124, No. 12, 123902, 2020
6. Granchi N., private communications
7. Gurioli M., "Vacuum Field Photonic Trap for Excitons", Adv. Quantum Tech., Vol. 4, No. 7, 2100046, 2021
8. Carminati R., Gurioli M., "Purcell effect with extended sources: the role of the cross density of states" Opt. Express, Vol. 30, No. 10, 16174-16183, 2022
9. Gurioli M., to be submitted

Double helical plasmonic antennas for enhanced chiroptical interactions

A. Tsarapkin[1], S. Jürgensen[2], Th. Feichtner[3], K. Mackosz[4], V. Deinhart[1], I. Utke[4], S. Reich[2], and K. Höflich[1*]

[1]Ferdinand-Braun-Institut gGmbH, Leibniz-Institut für Höchstfrequenztechnik, Germany
[2]Freie Universität Berlin, Germany
[3]University of Würzburg, Germany
[4]Empa - Swiss Federal Laboratories for Materials Science and Technology, Switzerland
[*]corresponding author: katja.hoeflich@fbh-berlin.de

Chiral plasmonic nanostructures can play a crucial role in quantum optics and sensing, as they combine extremely enhanced electromagnetic near-fields with a strong sensitivity to the handedness of far-field radiation. Here we study the excitation of plasmonic double helices theoretically and experimentally in the visible and near-infrared regime. Full-field numerical modelling reveals the presence of several resonant plasmonic modes that can be selectively excited by left and right circularly polarized light. All observed modes are similar to those of a single helix, but show an overall stronger response. The mode symmetry of double helices corresponds to an antisymmetric charge distri- bution of straight two wire waveguides. The full description of the excitation mechanism is provided by extending our analytical model for single helices [1] by taking the near-field coupling of the two helical wires into account.

The helices are directly written with a focused electron beam [2,3]. The technique is based on electron-induced dissociation of a gaseous precursor in the vacuum chamber of an electron microscope and allows single-step 3D printing of complex geometries. The optical response of the helices is characterized by confocal transmission spectroscopy. This work is funded by German Research Foundation under grant no. HO 5461/3-1.

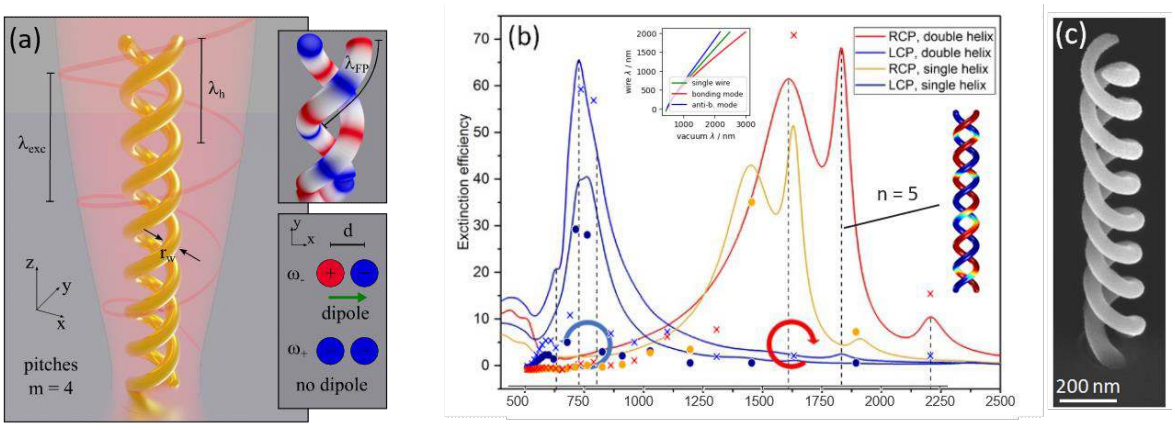


Figure: (a) Artistic sketch denoting the important geometrical quantities; (b) comparison of full-field modeling to the extended analytical model; (c) scanning electron micrograph of experimentally realized double helical antenna.

References

1. Höflich, K. et al. “Resonant behavior of a single plasmonic helix,” Optica, Vol. 6, 1098–1105, 2019.
2. Höflich, K. et al. “The direct writing of plasmonic gold nanostructures by electron-beam-induced deposition,” Adv. Mater., Vol. 23, 2657–2661, 2011.
3. Haverkamp, C. et al. “Plasmonic gold helices for the visible range fabricated by oxygen plasma purification of electron beam induced deposits,” Nanotech., Vol. 28, 55303, 2017.

Tailored local fields for nonlinear optics, strong coupling and chiral recoil forces

Bert Hecht[1*], Jessica Meier[1], Luka Zurak[1], Rene Kullock[1], Andrea Locatelli[2], Daniel Friedrich[1], Jin Qin[1], Tommaso Tufarelli[3], Benedikt Schurr[1], Thorsten Feichtner[1]

[1]Nano-Optics & Biophotonics group, Experimental Physics 5, Physics Institute, University of Würzburg, Am Hubland, D-97074 Würzburg, Germany
[2]Department of Information Engineering, University of Brescia, Italy
[3]School of Mathematical Sciences and Centre for the Mathematics and Theoretical Physics of Quantum Non-Equilibrium Systems, University of Nottingham, Nottingham, NG7 2RD, United Kingdom
[*]corresponding author: hecht@phhysik.uni-wuerzburg.de

Abstract: The precision afforded by He-ion beam milling on monocrystalline gold and silver flakes presents an opportunity to tailor local fields at an unprecedented level of 1nm. This method enables the fabrication of intricate structural details, which can be used to create nanoresonators and antennas with unique properties. We leverage these capabilities to create devices that exhibit local symmetry breaking, ultrasmall mode volumes, and precise chiral scattering.

In a first project we exploit the capabilities of He-io beam milling to fabricate resonant optical antennas exhibiting a global antisymmetric mode, which causes very high field enhancement in the gap. We then locally break the symmetry of the antenna hotspot to efficiently generate second harmonic radiation by switching of the silencing effect (see Fig. 1).

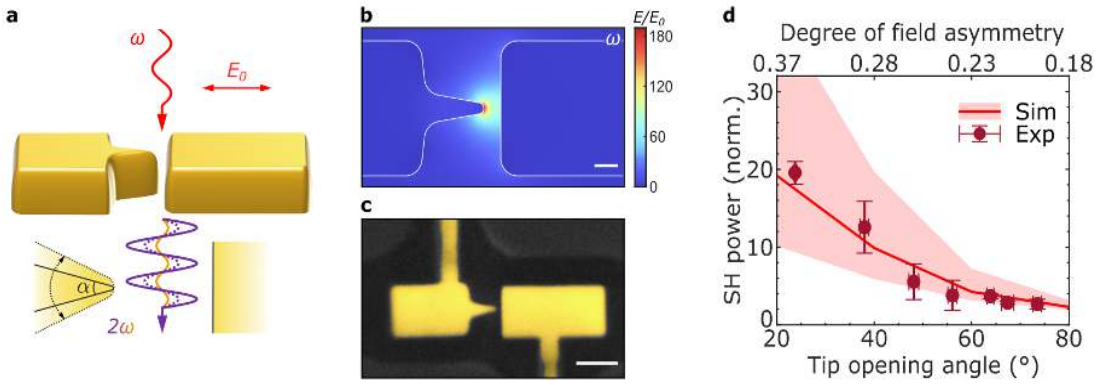


Fig. 1: Effect of local symmetry breaking on the SHG process in gold nanoantennas. a, Scheme of the SHG process from an asymmetric-gap antenna. b, Linear field enhancement plot. Scale bar, 10 nm. c, Scanning electron micrograph of an asymmetric-gap antenna with tip apex radius of 3 nm and gap size of 8 nm. Scale bar, 50 nm. d, Tuning SHG emission by variation of the local degree of asymmetry.

In a second application we fabricate plasmonic nanoslit resonators with very small modal volumes to achieve strong coupling at ambient conditions To match the transition energy of single quantum dots to the nanoresonators we exploit a photoactivated, oxygen-driven blueshift of the quantum dot emission to tune its photoluminescence spectrum. As a result, we observe complete anticrossing spectra at ambient conditions (see Fig. 2).

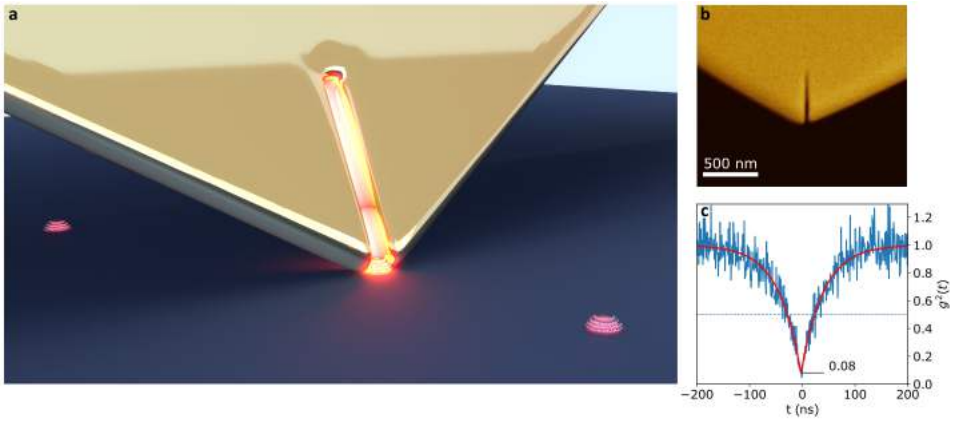


Fig. 2: A gold microplatelet scanning plasmonic nanoresonator in close contact to a quantum dot (artistic representation). b SEM image of a fabricated PNR. c 2nd-order autocorrelation function, $g^{(2)}$, of an individual QD.

Finally, we present light-driven microdrones, which can be steered in 2D in all degrees of freedom by means of plasmonic nanomotors (see Fig. 3). These motors are optical antennas which resonantly scatter unfocused circular polarized light into specific directions. This results in photon recoil forces which driven the microdrones.

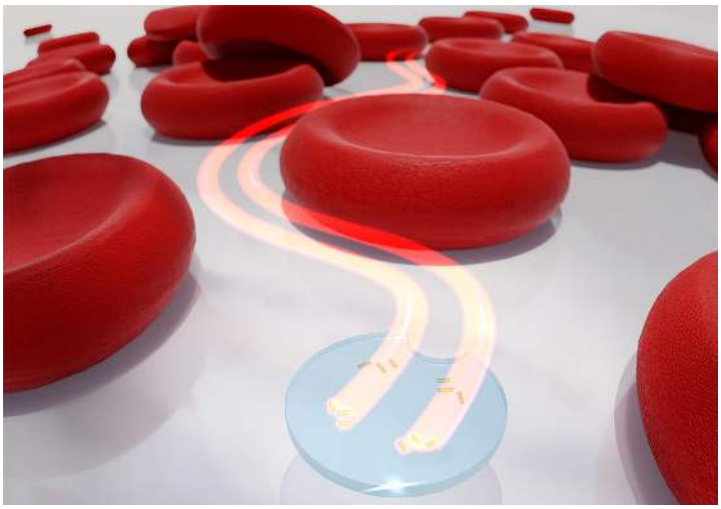


Fig. 3: A gold microplatelet scanning plasmonic nanoresonator in close contact to a quantum dot (artistic representation). b SEM image of a fabricated PNR. c 2nd-order autocorrelation function, g2, of an individual QD.

References

1. Meier, J., Zurak, L., Locatelli, A., Feichtner, T., Kullock, R. and Hecht, B. “Second harmonic generation from plasmonic hotspots by controlled local symmetry breaking,” submitted (2023), arXiv:2210.14105.
2. Groß, H., Hamm, J. M., Tufarelli, T., Hess, O. & Hecht, B. “Near-field strong coupling of single quantum dots,” Science Advances 4 (3), eaar4906 (2018).
3. Wu, X., Ehehalt, R., Razinskas, G. Feictner, T., Qin, J. and Hecht, B. “Light-driven microdrones,“ Nat. Nanotechnol. 17, 477–484 (2022). https://doi.org/10.1038/s41565-022-01099-z

META 2023, PARIS - FRANCE, JULY 18 – 21, 2023

Self-assembled DNA-origami inverse diamond lattice with a photonic band gap in the UV

Gregor Posnjak[1*], Xin Yin[1], Paul Butler[2], Oliver Bienek[2], Mihir Dass[1], Ian Sharp[2], and Tim Liedl[1]

[1]Ludwig-Maximilian-Universität München, Germany
[2]Walter Schottky Institute, Technical University Munich, Germany

[*]corresponding author: gregor.posnjak@lmu.de

Abstract: Inverse diamond lattice is a potential photonic crystal that was predicted to show one of the widest and most robust photonic band gaps. We designed DNA origami-based self-assembling tetrapod structures which crystalize into an inverse diamond lattice with a periodicity of 170 nm. After chemically depositing silica and titania on the diamond structure we observe tunable reflection bands in the UV which are in good agreement with theoretical predictions of photonic properties of the system.

Photonic crystals are optical analogues of semiconductors, where the periodic modulation of the dielectric constant prevents photons with energies within certain ranges to propagate through the material [1]. This so-called photonic band gap is determined by the symmetry of the structure, its periodicity and the contrast between the regions of high and low dielectric constant. While there have been many realizations of different types of photonic crystals, materials with a direction independent, complete photonic band gap at visible wavelengths have been notoriously difficult to manufacture. One of the prime candidates for such a structure is the inverse diamond structure which is a diamond lattice where all the lattice points are connected to their nearest neighbors with rods [2,3]. Many different approaches for assembling such a structure at periodicities comparable to visible wavelengths have been proposed but realizing it has been proven difficult [4].

Here we demonstrate inverse diamond lattice assembly based on DNA origami-designed building blocks. DNA origami is a nanotechnology, which uses the predictable sequence-dependent binding of DNA strands to form objects of different shapes and functionalities [5,6]. We use it to design a self-assembled tetrapod building block, which we can polymerize into a 3D lattice. By carefully controlling the interactions between the individual tetrapods we can crystalize them into inverse diamond lattices with 170 nm lattice constant (Figure 1a). These crystals serve as the scaffolds on which we can deposit different materials. To manufacture the photonic crystals we first use wet chemistry to deposit a layer of silica that increases the structural stability during drying. On the dried crystal we deposit titania to increase the refractive index of the structure to open up the photonic band gap. We characterize the optical properties of the titania-coated crystals by measuring the reflected light spectra where we observe a reflection band in the UV region, the position and width of which depends on the thickness of the titania coating. The measurements show good agreement with simulations of the photonic properties of the structure (Figure 1b).

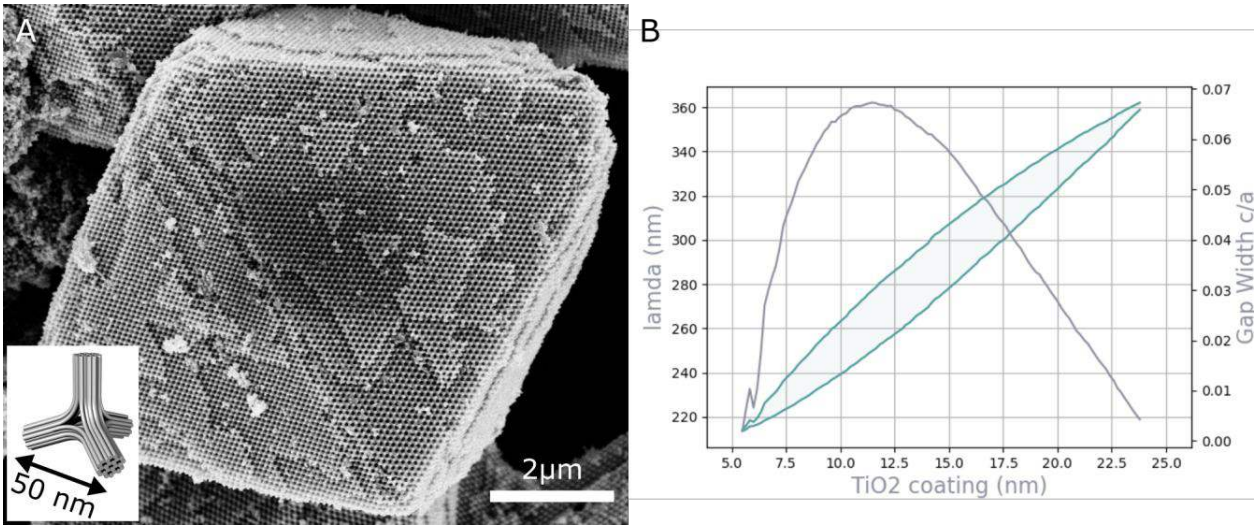


Figure 1. Left: Silica-coated diamond lattice with 170 nm periodicity. Inset: model of the DNA origami tetrapod building block. Right: The photonic bandgap opens in the UV and red-shifts with the increase of the titania thickness. Simulated with MPB [7] (http://ab-initio.mit.edu/mpb).

References

1. Yablonovitch, E. "Photonic Crystals: Semiconductors of light," Sci. Am., Vol. 285, 46-55, 2001.
2. Park, S. H., H. Park, K. Hur and S. Lee, "Design of DNA Origami Diamond Photonic Crystals," ACS Appl. Bio Mater., Vol. 3, No. 1,747-756, 2020.
3. Cersonsky, R. K., J. Antonaglia, B. D. Dice and S. C. Glotzer, "The diversity of three-dimensional photonic crystals," Nat. Commun., Vol. 12, 2543, 2021.
4. He, M., et al. "Colloidal diamond," Nature, Vol.585, 524-529, 2020.
5. Rothemund, P. W. K. "Folding DNA to create nanoscale shapes and patterns," Nature, Vol. 440, No. 7082, 297-302, 2006.
6. Dietz, H., S. M. Douglas and W. M. Shih, "Folding DNA into twisted and curved nanoscale shapes," Science, Vol. 325, No. 5941, 725-730, 2009.
7. Johnson, S. G. and J. D. Joannopoulos, "Block-iterative frequency-domain methods for Maxwell's equations in a planewave basis," Opt. Express, Vol. 8, 173-190, 2001.

META 2023, PARIS - FRANCE, JULY 18 – 21, 2023

Photonic resonances in next-level metrology and precision experiments

S. Kroker[1,2,3*], B. Bodermann[3], J. Dickmann[1,2], T. Käseberg[3], M. Gaedtke[1,2], S. Sauer[1,2], T. Siefke[4]

[1]Technische Universität Braunschweig, Institut für Halbleitertechnik, Hans-Sommer-Str. 66, 38106 Braunschweig, Germany
[2]Technische Universität Braunschweig, LENA Laboratory for Emerging Nanometrology, Langer Kamp 6 a/b, 38106 Braunschweig, Germany
[3]Physikalisch-Technische Bundesanstalt, Bundesallee 100, 38116 Braunschweig, Germany
[4]Friedrich-Schiller-Universität, Institute of Applied Physics, Albert-Einstein-Str. 7, 07747 Jena, Germany

[*]corresponding author: s.kroker@tu-braunschweig.de

Photonic resonances are a viable mechanism to shape and switch the properties of light. Besides that, they allow tailoring light-matter interaction, opening new pathways in next-level optical metrology and precision experiments. Applications range from non-invasive nanometrology beyond conventional diffraction limits to compact and robust sensors and the world's most stable optical atomic clocks. This contribution provides an overview of selected metrological applications of photonic resonances and the most important physical properties to achieve optimum measurement precision.

Funded by the Deutsche Forschungsgemeinschaft (DFG, German Research Foundation) under Germany's Excellence Strategy—EXC-2123 QuantumFrontiers—390837967. J.D. and S.K., B.B., T.K also acknowledge partial support by European Association of National Metrology Institutes. These projects (20FUN08 NEXTLASERS and 20FUN02 PoLight) have received funding from the EMPIR programme co-financed by the Participating States and from the European Union's Horizon 2020 research and innovation programme.

META 2023, PARIS - FRANCE, JULY 18 – 21, 2023

Non-Abelian gauge fields for non-Hermitian systems

Yi Yang
Department of Physics, The University of Hong Kong, Hong Kong, China
*corresponding author: yiyg@hku.hk

Abstract: Non-Abelian gauge fields are versatile tools for synthesizing topological phenomena but have so far been mostly studied in Hermitian systems. We study them in non-Hermitian systems via a generalized Hatano--Nelson model with imbalanced non-Abelian hopping. Despite lacking gauge flux in one dimension, non-Abelian gauge fields create rich non-Hermitian topological consequences. Under only nearest-neighbor coupling, non-Abelian gauge fields enable Hopf-link bulk braiding topology, whose phase transition accompanies the emergence of exceptional points (EPs). At both ends of an open chain, non-Abelian gauge fields lead to the simultaneous presence of non-Hermitian skin modes, whose population can be effectively tuned. We present concrete optical realizations based on synthetic dimensions in driven ring resonators.

Auto-differentiable Computational Photonics and its application to optimization

B. Vial[1*] and Y. Hao[2]

[1]Department of Mathematics, Imperial College London, United Kingdom
[2]School of Electronic Engineering and Computer Science, Queen Mary University of London, United Kingdom
[*]corresponding author: b.vial@imperial.ac.uk

Abstract: We present the development of numerical methods for the resolution of Maxwell's equations implemented using open source libraries. All of them are endowed with automatic differentiation capabilities and typical inverse design examples using topology optimization will be presented.

In recent years, technological advances in nanofabrication have opened up new applications in the field of nanophotonics. To engineer and develop novel functionalities, rigorous and efficient numerical methods are required. In parallel, tremendous advances in algorithmic differentiation, in part pushed by the intensive development of machine learning and artificial intelligence, has made possible large-scale optimization of devices with a few extra modifications of the underlying code. In the past two decades, gradient-based topology optimization (TO) has become a widely used tool in computational electromagnetism and has allowed the inverse design of a broad range of devices such as invisibility cloaks, metamaterials and metasurfaces to name a few.

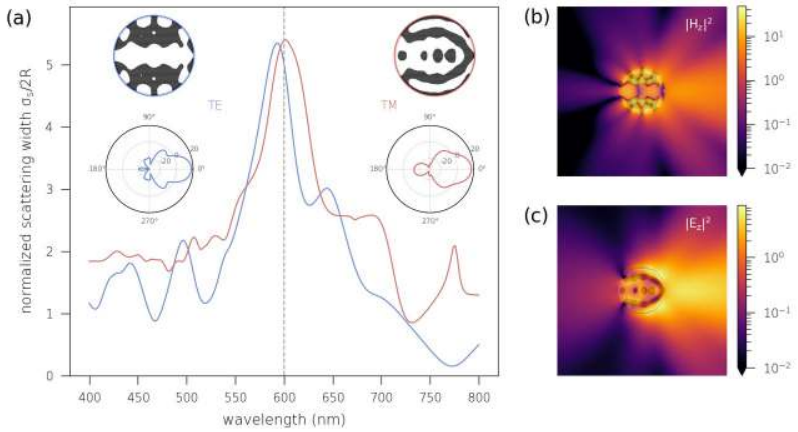


Figure 1: Optimized superscattering nanorods. (a): normalized scattering width as a function of the wavelength of the incident light (blue: TE polarization, red: TM polarization). The insets at the top show the optimized dielectric distribution (white for SiO2 and black for Si), and the bottom insets are the radiation patterns for the normalized scattering width, in dB. The field maps on the right panels show the square norm of the fields at the target wavelength λ_0=600 nm. (b): $|Hz|^2$ for TE polarization. (c): $|Ez|^2$ for TM polarization.

I will present the development of software libraries with automatic differentiation capabilities

[1]: a finite element method (FEM)-based code for 2D scattering problems, an implementation of the Fourier modal method (FMM) for stacked bi-periodic structures, and a plane wave expansion method (PWEM) to compute the eigenmodes of 2D photonic crystals. After describing the methods and the automatic differentiation [2] and topology optimization tools [3], we give examples of application for each: the design of supperscattering structures with the FEM, of a metasurface optimized to transmit maximally in a given diffraction order with the FMM, and maximization of bandgap and dispersion engineering in dielectric photonic crystals using the PWEM.

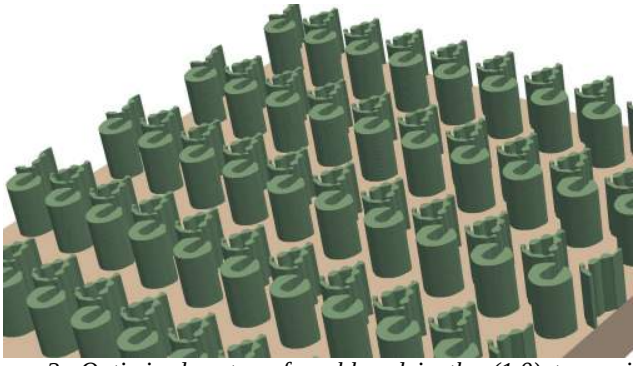


Figure 2: Optimized metasurface blazed in the (1,0) transmitted order for both polarizations using the FMM.

The availability of open-source codes for solving Maxwell's equations is of paramout importance in the growing field of metamaterials and photonics. Indeed, free software, besides being low cost, has many advantages such as being portable, customizable, and vendor-independent. Our implementation of the three numerical methods commonly used in photonics is freely available as Python packages: https://gyptis.gitlab.io (FEM), https://nannos.gitlab.io (FMM) and https://protis.gitlab.io (PWEM). In addition, the integration of automatic differentiability in our implementation makes the calculation of gradients with respect to inputs straightforward. As illustrated in this study, it allows the inverse design of photonic structures and metamaterials with improved performances or to explore intriguing effects such as supperscattering, polarization-tolerant blazed metasurfaces, or photonic crystals with large bandgaps and dispersion engineering.

This work was funded by the Engineering and Physical Sciences Research Council (EPSRC), UK, under grants (EP/N010493/1) and (EP/R035393/1).

References

1. Vial, B. and Hao, Y., “Open-Source Computational Photonics with Auto Differentiable Topology Optimization,” Mathematics, Vol. 10, No. 20, 3912, 2022.
2. Corliss, G., Faure, C., Griewank, A., Hascoet L. and Naumann, U., “Automatic Differentiation of Algorithms: From Simulation to Optimization,” Springer: Berlin/Heidelberg, Germany, 2013.
3. Bendsoe, M.P. and Sigmund, O., “Topology Optimization: Theory, Methods, and Applications,” Springer: Berlin/Heidelberg, Germany, 2013.

Tailoring resonant interactions in suspensions of disordered particles to achieve near zero reflection

C. Blanchard[1,*], **T. Guerra**[1], **J. P. Hugonin**[2], and **O. Rozenbaum**[1]

[1]CNRS, CEMHTI UPR3079, Univ. Orléans, F-45071 Orléans, France
[2]Institut d'Optique Graduate School, CNRS, Université Paris-Saclay, 91127 Palaiseau, France
[*]corresponding author: cedric.blanchard@cnrs-orleans.fr

Abstract: We take advantage of the cooperative effects that take place in a suspension of randomly distributed nanoparticles to inhibit the reflection of an electromagnetic radiation incident on it. The strategy consists in coupling resonant and lossless particles. In a counterintuitive manner, the near zero reflection phenomenon relies here on particles which have the ability to strongly scatter light when they are considered individually.

The control of electromagnetic radiations has been prompted, in the last decades, by the combination of an increasing understanding of light/matter interaction in photonic materials and the maturation of nanofabrication techniques. In this context, a lot of attention has been put on systems with a well-defined structuration, either horizontal (photonic crystals, metasurfaces, etc.) or vertical (e.g., stratified media). Since the former is periodic and the latter is characterized by a refractive index which is a function of one Cartesian coordinate only, they can be classified as ordered media.

Despite appealing ease of fabrication, much less attention has been paid to disordered inhomogeneous media as a means to the control of electromagnetic radiation. This is probably due to the fact that a system of subwavelength particles, for instance, can be considered at first sight as merely homogeneous [1], with no special capabilities for the tailoring of the electromagnetic fields and hence unable to achieve competitive functional properties.

In this contribution, we are interested in suspensions of nanoparticles that are randomly distributed. We numerically show a design rule for a many-particle structure that allows to inhibit the reflection of a radiation that impinges on it, without specially design the incident waveform for this purpose [2].

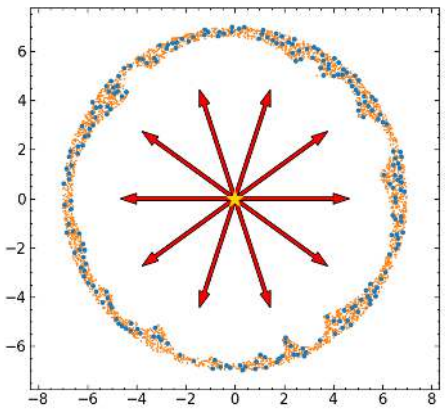
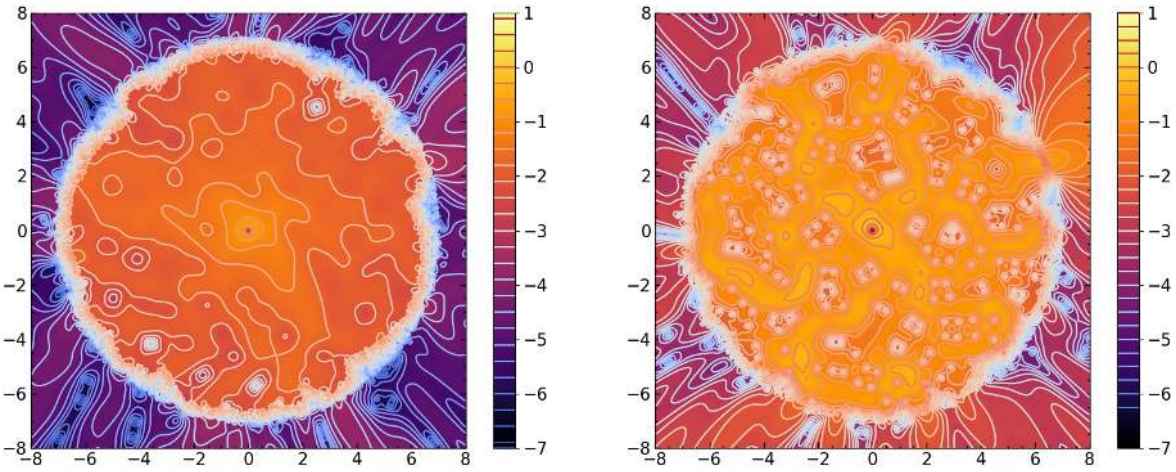


Figure 1: A disordered inhomogeneous medium: polydisperse nanoparticles arranged in the form of a shell. A point source is located at the center.

By exciting an individual particle near its resonance, it is theoretically possible to ensure high absorption cross section values. But when put in interaction with other resonating particles, absorption naturally tends to decrease because the multiple resonances that occur in the structure overlap. In other words, we are no longer in an ideal situation with a well-isolated resonance and, as a result, it is difficult to prevent a many-particle structure from reflecting part of the incident field. To circumvent this issue, we propose here a strategy that consists in incorporating lossless particles into the system of resonant particles.

Fig. 1 displays a cavity delimited by a system of particles, which overall constitutes a shell with irregular shape. A point source radiating isotropically at wavelength $\lambda = 2$ µm is located in the cavity. In Fig. 2(a) are plotted the contour lines of the Poynting vector (with logarithmic scale) after



(a) Optimized configuration (b) $n = 2 + i$

Figure 2: Contour plot of the Poynting vector in a many-particle core-shell structure which is illuminated by a point source.

optimization of the volume fraction, size and constitution of the particles. The energy flux is strongly absorbed in the shell and almost no energy escapes the structure despite the subwavelength thickness of the shell. In contrast, highly lossy particles of refractive index $n = 2 + i$ [3] with the same spatial distribution do not provide the same performance; it is plain from Fig. 2(b) that more energy escapes the structure, while the isolines are strongly perturbed in the cavity, indicating a greater amount of reflection at the inner interface of the shell.

In order to quantitatively calculate the degree to which the system is able to absorb energy, we have also arranged the polydisperse nanoparticles in the form of a large slab illuminated by a planewave. The reflectance is below few percent. In comparison, the reflectance before incorporating the lossless particles was about 20%.

Acknowledgment: This work has been founded by the French National Research Agency (ANR) through the "Jeunes Chercheuses et Jeunes Chercheurs" program (project: OUTWARDS, ID: ANR 19-CE05-0021).

References

[1] T. Guerra, D. De Sousa Meneses, J.-P. Hugonin, and C. Blanchard, "Unconventional Electromagnetic Response of Strongly Coupled Nanoparticles in the Thermal Infrared Region: Link with Effective Medium Properties and Incoherent Fields," Part. Part. Syst. Charact., 39(3), 2100245, 2022.

[2] D. G. Baranov, A. Krasnok, T. Shegai, A. Alù, and Y. Chong, "Coherent perfect absorbers: linear control of light with light," Nat. Rev. Mater., 2(12), 1–14, 2017.

[3] D. W. Mackowski, "Calculation of total cross sections of multiple-sphere clusters," J. Opt. Soc. Am. A, 11(11), 2851–2861, 1994.

Quasinormal Mode Theory for Nanoscale Electromagnetism informed with the Feibelman's d-Parameter Treatment

Qiang Zhou[1,2], **Pu Zhang**[1,2], **and Xue-Wen Chen**[1,2*]

[1]School of Physics and Wuhan National Laboratory for Optoelectronics, Huazhong University of Science and Technology, Wuhan, People's Republic of China
[2]Wuhan Institute of Quantum Technology, Wuhan, People's Republic of China
[*]corresponding author: xuewen_chen@hust.edu.cn

Abstract: We report a self-consistent quasinormal mode theory for nanometer scale electromagnetism where the possible nonlocal and quantum effects are treated through the Feibelman's *d*-parameters. With the frequency-dependent *d*-parameters to describe the quantum surface responses, which are reminiscent of the permittivity function, we formulate the source-free Maxwell's equations into a generalized linear eigenvalue problem to define the quasinormal modes. We then construct an orthonormal relation for the modes and consequently unlock the powerful toolbox of modal analysis.

The research field of nano-optics has flourished along with the development of concepts and techniques to shrink light to scales well below the diffraction limit. The subwavelength confinement primarily results from the plasmonic resonances in metal nanostructures. To capture the physics of such scenarios, *e.g.,* deciphering the optical eigen-modes [1, 2, 3], the nonlocal and quantum effects of the conduction electrons need to be treated properly. A trending approach in recent years is to leverage the Feibelman's *d*-parameters [4, 5] to account for the major quantum responses at metal surface. A rigorous quasinormal mode theory compatible with the *d*-parameter treatment thus would be elusive.

In the *d*-parameter treatment, the quantum responses manifest macroscopically as an effective surface current $\mathbf{K}$ and surface polarization $\mathbf{\Pi}$, which are approximated in the leading order as

$$\mathbf{K} = i\omega d_{\parallel}(\omega)[\![\varepsilon(\omega)]\!]\,\mathbf{E}_{\parallel}, \qquad \mathbf{\Pi} = d_{\perp}(\omega)[\![\varepsilon^{-1}(\omega)]\!]\,\mathbf{D}_{\perp}, \tag{1}$$

where the time convention $\exp(-i\omega t)$ is assumed. $\varepsilon(\omega)$ is the permittivity in bulk domains. We have adopted $[\![f]\!] = f^{+} - f^{-}$ to denote a difference across surface, and the notation $\perp/\parallel$ to denote the normal/parallel component of a vector. $\mathbf{K}$ and $\mathbf{\Pi}$ feed back to Maxwell's equations as secondary sources and consistently modify the overall optical responses. Since $d_{\parallel}$ is negligible in most situations with charge-neutral interfaces, we assume $d_{\parallel} = 0$ and focus on the surface polarization $\mathbf{\Pi}$ and the effective surface response function $f(\omega) = d_{\perp}(\omega)[\![\varepsilon^{-1}(\omega)]\!]$. Noticing that $f(\omega)$ is bounded at $\omega = 0$ and ∞, we may expand it over the simple poles $\widetilde{\omega}_{\beta}$ as

$$f(\omega) = \sum_{\beta=0}^{N} f_{\beta} \frac{\widetilde{\omega}_{\beta}}{\omega - \widetilde{\omega}_{\beta}}. \tag{2}$$

A pseudopole $\widetilde{\omega}_0 = 0$ is formally introduced for conciseness of expression. Thereupon, we introduce for each pole an auxiliary surface polarization $\mathbf{\Pi}_{\beta} = \omega\mathbf{D}_{\perp}/(\omega - \widetilde{\omega}_{\beta})$, with the constraint $\sum_{\beta=0}^{N} f_{\beta}\mathbf{\Pi}_{\beta} = \mathbf{\Pi}$. The surface response then is linearized regarding the frequency ω, with $(\omega - \widetilde{\omega}_{\beta})\mathbf{\Pi}_{\beta} = \omega\mathbf{D}_{\perp}$. Assuming that the metal is described by the Drude-

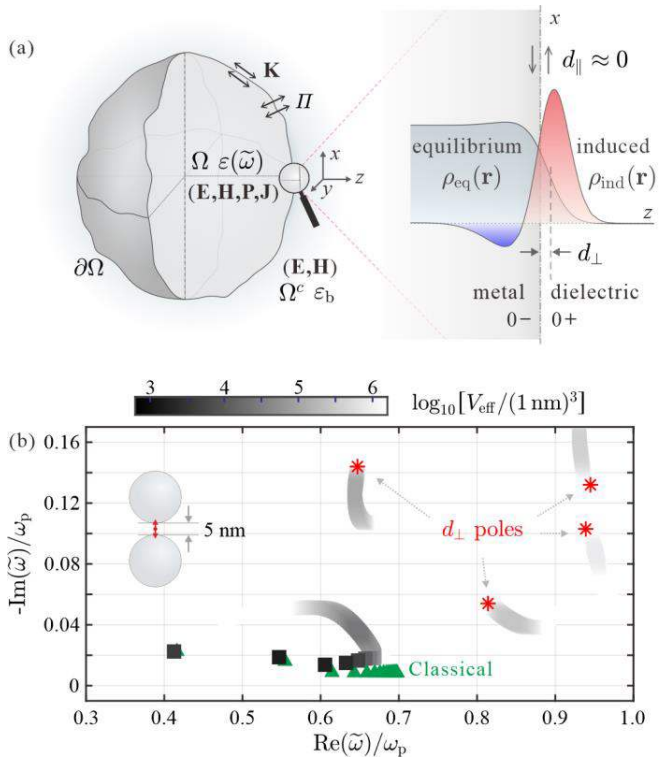


Fig. 1. Quasinormal mode analysis informed with the Feibelman's *d*-parameter treatment.

Lorentz model, the responses in bulk domains can also be linearized by introducing the auxiliary polarization $\mathbf{P}$ and the corresponding current density $\mathbf{J}$ [6]. In terms of the electromagnetic fields $\mathbf{E}$, $\mathbf{H}$, and the auxiliary fields $\mathbf{P}$, $\mathbf{J}$, $\mathbf{\Pi}_\beta$, the source-free Maxwell's equation can finally be formulated as a volume-surface composite linear eigenvalue problem, which set the stage for quasinormal mode analysis [3]. The orthonormalization relation of the modes then can be derived basing on the generalized Lorentz reciprocity, and validated by the reconstruction of the full numerical results through modal contributions. Such a quasinormal mode theory would facilitate the establishment of a general theoretical framework for nanometer scale electromagnetism

References

1. Q. Zhou, P. Zhang, and X.-W. Chen, "General framework of canonical quasinormal mode analysis for extreme nano-optics," Phys. Rev. Lett., 127, 267401 (2021).
2. W. Li, Q. Zhou, P. Zhang, and X.-W. Chen, "Direct electro plasmonic and optic modulation via a nanoscopic electron reservoir," Phys. Rev. Lett., 128, 217401 (2022).
3. Q. Zhou., P. Zhang, and X.-W. Chen, "Quasinormal mode theory for nanoscale electromagnetism informed by quantum surface response," Phys. Rev. B, 105, 125419 (2022).
4. F. J. Feibelman., "Surface electromagnetic fields," Prog. Surf. Sci., 12, 287-407 (1982).
5. Y. Yang, D. Zhu, W. Yan, A. Agarwal, M. Zheng, J. D. Joannopoulos, P. Lalanne, T. Christensen, K. K. Berggren, and M. Soljačić "A general theoretical and experimental framework for nanoscale electromagnetism," Nature, 576, 248-252, (2019).
6. W. Yan, R. Faggiani, and Philippe Lalanne, "Rigorous modal analysis of plasmonic nanoresonators," Phys. Rev. B, 97, 205422 (2018).

META 2023, PARIS - FRANCE, JULY 18 – 21, 2023

Quasi normal mode perturbation theory to achieve Q factor optimization of resonances in disordered photonic systems

N. Granchi[1*], F.Intonti[1], M. Gurioli[1] and G. Arregui[2]

[1]Department of Physics and Astronomy and LENS, University of Florence, Sesto Fiorentino (FI), Italy
[2]Department of Electrical and Photonics Engineering, DTU Electro, Denmark
[*]corresponding author: granchi@lens.unifi.it

Abstract: The optimization of the quality factor (Q) of photonic resonators is of great importance for applications exploiting both ordered and disordered systems. Here we propose a gradient-based automated optimization approach to maximize the Q of optical resonances in ordered and disordered dielectric slabs which uses first-order non-hermitian perturbation theory. By applying our method to optimize a selected Anderson mode in a random design exhibiting a Q-factor of 200, a new mode displaying $Q = 10^5$ is generated.

Photonic crystal cavities nowadays are the most widespread and versatile devices conceived to mold the flow of light at the nanoscale. They offer a versatile platform to study classical and quantum light-matter interaction in fields such as cavity quantum electrodynamics, non-linear optics, and cavity optomechanics. In parallel, other photonic systems, based on random distributions of point scatterers, have emerged and proposed as complementary alternative to ordered photonics [1]. They have been investigated for their basic physical insights, such as Anderson localization, and envisioned for several applications, due to their capability of exhibiting a higher spectral and spatial density of modes in a small spatial domain with respect to their ordered counterparts [1]. Conversely, the main disadvantage, mainly in purely random photonic systems operating at telecom wavelengths, is represented by the low Q factors that Anderson modes exhibits (typically ≈ 200). While the problem of Q factor optimization of photonic crystal cavities have been accomplished widely and successfully [2,3], in the case of Anderson modes localized in random structures, further complicated by the lack of an in-plane photonic band gap, it has never been addressed.

Here, we propose a gradient-based automated optimization approach to maximize the Q of a selected Anderson mode supported by a dielectric slab randomly patterned with air holes (Fig.1a). The method uses the theoretical framework of quasinormal modes (QNMs) [4] and relies on first-order non-hermitian perturbation theory to efficiently compute the gradients of Q relative to arbitrary material boundary displacements. Given its first order nature, the method requires only the calculation of the complex eigenfrequency and field profile of the QNM of interest. The optimization process, which determines a shift in the position of all holes in the structure (Fig.1b) to produce a Q-factor enhancement from 200 to 10^5 as well as a negligible average wavelength shift (Fig.1c). By monitoring the spatial distribution of the mode along the optimization we observe the mode central location and spatial distribution to change dramatically (Fig.1d), with a final spatial localization comparable with the one achieved in engineered photonic-crystal cavities ($Q/V \approx 10^6$ μm^{-3}). Our result might be relevant for the employment of random structures for lasing an sensing applications and constitute an important step toward the full engineering of the random photonic platform.

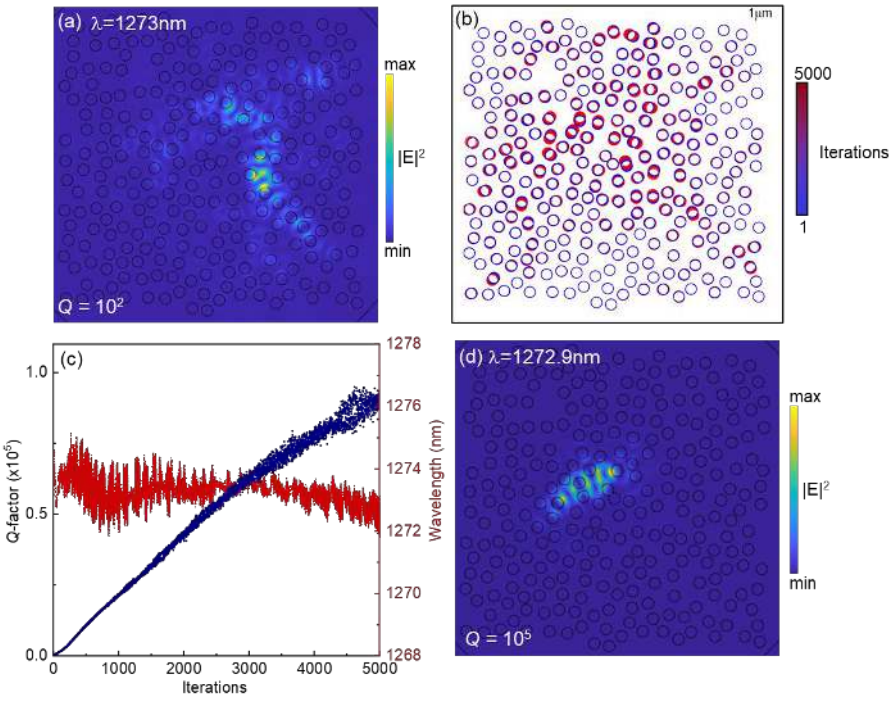


Figure 1: Results of the optimization process applied to a random design with slab thickness d=180 nm and air holes of radius r=110nm. (a) FEM Electric field intensity maps of the Anderson mode in the initial configuration; (b) Evolution of the position of all holes in the random design from the initial configuration (red) to the final one (blue). (c) Evolution of the resonant wavelength and quality factor of the Anderson mode for all iterations of the optimization process. (d) FEM Electric field intensity maps of the Anderson mode in the final configuration.

References

1. Balestri, D., Petruzzella, M., Checcucci, S., Intonti, F., Caselli, N., Sgrignuoli, F., van Otten, F. W. M., Fiore, A., and Gurioli, M., "Mechanical and electric control of photonic modes in random dielectrics", Adv. Mater., 31, 1807274, 2019.
2. Akahane, Y., Asano, T., Song, BS. And Noda, S., "High-Q photonic nanocavity in a two-dimensional photonic crystal", Nature 425, 944–947, 2003.
3. Sekoguchi, H., Takahashi, Y., Asano, T. and Noda, S., "Photonic crystal nanocavity with a Q-factor of ~9 million", Opt. Express 22, 916-924, 2014.
4. Lalanne, P., Yan, W., Vynck, K., Sauvan, C., Hugonin, J.P., "Light interaction with photonic and plasmonic resonances", Laser and Photonics Review, 12, 1700113, 2018.

Anisotropic Light Scattering from Tunable Self-Assembled Submicron Resonators

M. Lafitte[1], R. Dwivedi[1,2], R. Elancheliyan[1], P. Barois[1], A. Baron[1], O. Mondain-Monval[1], V. Ponsinet[1*]

[1] Univ. Bordeaux, CNRS, Centre de Recherche Paul Pascal, UMR 5031, Pessac, France

[2] ENSEMBLE3 Centre of Excellence, Wolczynska 133, 01-919 Warsaw, Poland

[*]corresponding author: virginie.ponsinet@crpp.cnrs.fr

Abstract: Metamaterials rely on assembled artificial optical resonators, having strong interactions with light and presenting local field enhancements. This presentation aims at pointing out how colloid-based chemical engineering offers exciting routes to tailor the optical response, including polarizabilities and scattering diagram of nanoresonators.

Strong magnetic resonances, which when spectrally superposable with the electric resonances, are the cornerstone for achieving Huygens scatterers, were previously obtained with complex colloidal nanoresonators [1, 2]. We show that densely-packed spherical colloidal clusters of metallic nanoparticles present such properties. These colloidal clusters have garnered a lot of interest recently, because they involve localized resonant inclusions that are assembled into a Mie resonator. This multiscale resonant nature provides a lot of leverage in the engineering of the spectral scattering characteristics of the resonators.

We synthesized clusters of gold or silver nanoparticles using an emulsion-based formulation approach. This fabrication technique involves emulsification of an aqueous suspension of plasmonic nanoparticles in an oil phase, followed by controlled drying of the aqueous droplets. The structural control of the as-synthesized clusters, produced in large numbers, is demonstrated with microscopy and Xray scattering techniques. Each cluster comprises a few hundreds or thousands of nanoparticles, depending on the formulation parameters.

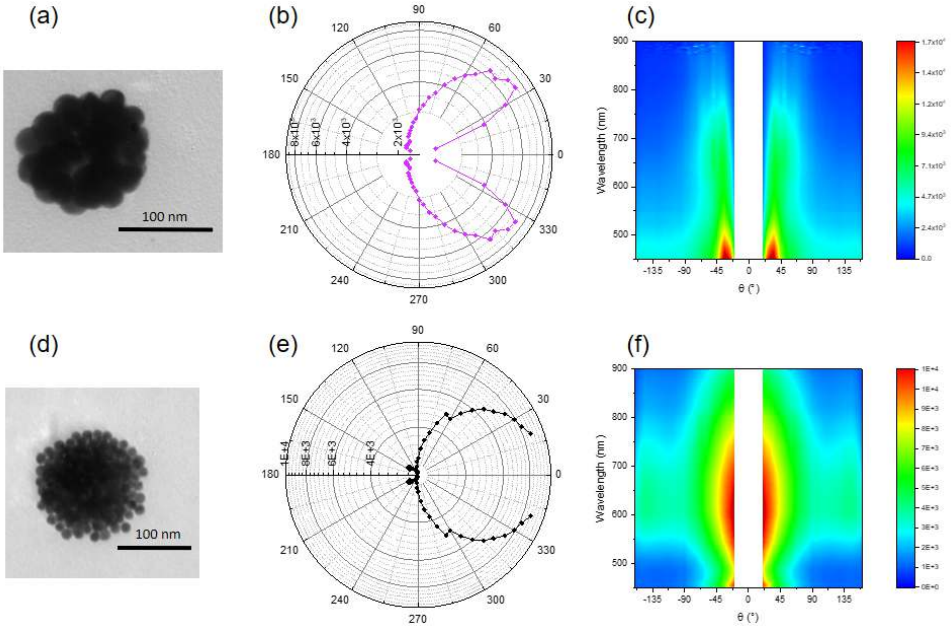


Fig 1. TEM images of a representative **(a)** Ag-cluster and (**d**) Au-cluster. Scale bars are 100 nm. Logarithmic polar plot of the experimental differential scattering cross-section for (**b**) Ag-clusters at wavelength

662 nm and (**e**) Au-clusters at wavelength 751 nm. Lines are guides for the eye. Experimental scattering color pattern representing the differential scattering cross-section values of (**c**) Ag-PVP clusters and (**f**) Au-clusters as a function of the scattering angle θ and of the wavelength λ. Measures were only made for positive values of θ but we assumed that differential cross-section values are identical for θ and -θ. All differential scattering cross-section values are represented in nm^2 per steradian units.

Using polarization-resolved multi-angle light scattering measurements, we conducted a comprehensive angular and spectroscopic determination of the complex colloid optical resonant scattering in the visible wavelength range [3]. We report on the clear experimental evidence of strong optical magnetic resonances and directional anisotropic scattering patterns (see Fig. 1). High-precision T-matrix computations were performed to described the object scattering while taking into account strong interparticle couplings and spatial dispersion effects within the colloids.

Our findings crucially show that the electric and magnetic resonances as well as the scattering patterns can be tuned by adjusting the inner cluster structure, modifying simple parameters of the fabrication method.

We acknowledge the help of A. Bentaleb for Xray scattering study, and of E. Nativ-Roth and O. Regev for Cryo-TEM imaging.

References

1. Aradian, A., Barois, P., Mondain-Monval, O., Ponsinet, V., and A. Baron, "The bottom-up approach toward artificial optical magnetism in metastructures" in Hybrid Flatland Metastructures, Ed R. Caputo and G.E. Lio (New York, NY: AIP Publishing), Ch 3, pp 3-1–3-28, 2021
2. Lermusiaux, L., Many, V., Barois, P., Ponsinet, V., Ravaine, S., Duguet, E., Tréguer-Delapierre, M., and A. Baron "Toward Huygens' sources with dodecahedral plasmonic clusters" Nano Lett. 21 2046–52, 2021
3. Elanchelyian, R., Dézert, R., Castano, S., Bentaleb, A., Nativ-Roth, E., Regev, O., Barois, P., Baron, A., Mondain-Monval, O., and V. Ponsinet, "Tailored self-assembled nanocolloidal Huygens scatterers in the visible," Nanoscale, Vol. 12, No. 47, 24177-24187, 2020, DOI:10.1039/D0NR05788F

Purcell Enhanced Intrinsic Linear and Nonlinear Optical Responses in Colloidal Dielectric Resonators

Jeanne Heintz, Gauthier Roubaud, Samuel Grésillon, and Sébastien Bidault*

Institut Langevin, ESPCI Paris, Université PSL, CNRS, 75005 Paris, France
*corresponding author: sebastien.bidault@espci.fr

Abstract: We demonstrate an enhancement of the intrinsic linear and nonlinear spontaneous emission from silicon and gallium phosphide-based resonators by a conjunction of scattering, luminescence lifetime and nonlinear spectroscopies at the single particle level.

Subwavelength resonators featuring highly confined and enhanced electromagnetic fields are a versatile photonic platform to optimize light-matter interactions at the nanoscale thanks to the Purcell effect. Dielectric resonators made of high-index semiconductors are an exciting alternative to plasmonic systems by readily enhancing the magnetic component of light and by providing these enhancement effects in the core of the resonator while introducing negligible ohmic losses [1]. Dielectric resonators have thus been engineered to optimize spontaneous emission from extrinsic emitters, either based on electric [2] or magnetic [3] dipolar transition dipoles, but also to inhibit it [4].

In this work, we evidence how enhanced electromagnetic fields in the core of semiconductor-based resonators can be exploited to optimize their intrinsic linear (spontaneous emission) and nonlinear optical responses (multiphoton luminescence and harmonic generation). In particular, we develop new nanofabrication techniques based on mechanical grinding and laser-based melting to produce colloidal resonators made of silicon or gallium phosphide (Fig. 1-a). By performing in parallel linear and nonlinear single nanostructure spectroscopy, we demonstrate how geometrical resonances allow an improvement of multiphoton absorption and harmonic generation by several orders of magnitude while also providing Purcell-enhanced spontaneous emission. In particular, multiphoton luminescence peaks measured in Si resonators spectrally match their electric dipolar and quadrupolar modes (Fig. 1-b). Furthermore, luminescence lifetime and spectral measurements on single GaP resonators provide a direct evidence of Purcell-enhanced radiative emission from this low-quantum yield indirect semiconductor (Fig. 1-c).

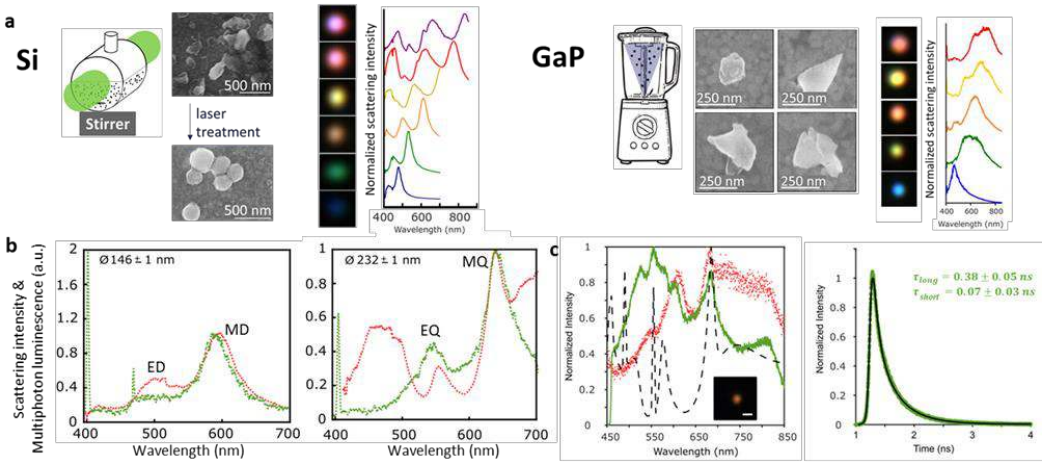


Figure 1: Si- and GaP-based resonators (a) featuring Purcell-enhanced multiphoton (b) or linear (c) emission.

References

1. Bidault, S. et al., J. Appl. Phys. 126, 094104 (2019).
2. Regmi, R. et al., Nano Lett. 16, 5143 (2016).
3. Sanz-Paz, M. et al., Nano Lett. 18, 3481 (2018).
4. Bouchet, D. et al., Phys. Rev. Applied 6, 064016 (2016)

Generalized Lorentz Model and Quasinormal Mode theory for Nonlocal Media

Xue-Wen Chen[*1,2]

[1]School of Physics and Wuhan National Laboratory for Optoelectronics, Huazhong University of Science and Technology, Wuhan, China.
[2]Wuhan Institute of Quantum Technology, Wuhan, China.
[*]corresponding author: xuewen_chen@hust.edu.cn

Abstract: Studies of extremely confined optical field down to (sub)nanoscale have been one forefront of optical physics. The related optical phenomena should be understood with the consideration of complex nonlocal effects, which pose a difficult hurdle for constructing a quasinormal mode theory. Here we introduce a generalized Lorentz model to describe the nonlocal effects, then provide a procedure to orthonormalize the quasinormal modes, establishing a general modal theory. Our theory enables drawing the mode evolution path during the quantum tunneling process.

Extreme nano-optics is one forefront of optical physics and has attracted enormous attention. In recent years, experimental demonstrations develop from the observation of nonlocal effects [1-2], quantum tunneling phenomena [3] to the discovery and application of extremely localized fields [4-5]. Along this line of research, the field of nano-optics enters a new regime, where classical local treatment of nanomaterials becomes invalid. As an example, metallic gaps of a few nanometers or smaller exhibit significant nonclassical effects from electron nonlocality, spillover at metal surfaces, Landau damping, and quantum tunneling. Since the optical response and light-matter interaction often can be conceptualized by the properties of a few modes [6], a proper mode analysis theory is essential to the burgeoning field of extreme nano-optics. However, the above mentioned complex nonlocal responses and quantum effects pose a difficult hurdle for constructing a canonical quasinormal mode (QNM) theory in such situations.

In this work, we develop a general theoretical framework of canonical QNM analysis with applicability to materials showing various kinds of nonlocal and quantum effects in the situation of extreme nano-optics, where classical local description of materials' optical response fails. Specifically, we creatively propose a generalized Lorentz Model to describe various nonlocal media, formulate source-free Maxwell equations for nonlocal media as a linear eigenvalue problem for modal analysis and derive a canonical orthonormal relation for the QNMs [7-8]. Moreover, the theory enables intuitively visualization of optical responses in quantum tunneling regime in terms of mode evolution for the first time. The framework established in this work entitles nano-optics to a powerful semi-analytical rigorous treatment of complex (sub)nanoscale structures.

We acknowledge partial financial support from the National Natural Science Foundation of China (Grants No. 9215011 and No. 11874166).

References

1. J. A. Scholl, A. L. Koh, and J. A. Dionne, "Quantum plasmon resonances of individual metallic nanoparticles", Nature 483,421 (2012).
2. C. Ciracì, R. T. Hill, J. J. Mock, Y. Urzhumov, A. I. Fernández-Domínguez, S. A. Maier, J. B. Pendry, A.Chilkoti, and D. R. Smith, "Probing the Ultimate Limits of Plasmonic Enhancement", Science 337, 1072 (2012).

3. K. J. Savage, M. M. Hawkeye, R. Esteban, A. G. Borisov, J. Aizpurua, and J. J. Baumberg,, “Revealing the quantum regime in tunnelling plasmonics”, Nature 491, 574 (2012).
4. F. Benz, M. K. Schmidt, A. Dreismann, R. Chikkaraddy, Y. Zhang, A. Demetriadou, C. Carnegie, H. Ohadi, B. de Nijs, R. Esteban, J. Aizpurua, and J. J. Baumberg, “Single-molecule optomechanics in “picocavities” ”, Science 354, 726(2016).
5. B. Yang, G. Chen, A. Ghafoor, Y. Zhang, Y. Zhang, Y. Zhang, Y. Luo, J. Yang, V. Sandoghdar, J. Aizpurua, Z. Dong, and J. G. Hou, “Sub-nanometre resolution in single-molecule photoluminescence imaging”, Nature Photonics 14, 693 (2020).
6. W. Yan, R. Faggiani, and P. Lalanne, “Rigorous modal analysis of plasmonic nanoresonators”, Phys. Rev. B 97, 205422 (2018).
7. Q. Zhou, P. Zhang, X.-W. Chen, “General framework of canonical quasinormal mode analysis for extreme nano-optics”, *Phys. Rev. Lett.* 127, 267401 (2021).
8. Q. Zhou, P. Zhang, X.-W. Chen, “Quasinormal mode theory for nanoscale electromagnetism informed by quantum surface response”, Phys. Rev. B 105, 125419 (2022).

META 2023, PARIS - FRANCE, JULY 18 – 21, 2023

Resonances in doubly anisotropic, high-index nanoplatelets

Bingying You[1,2], Tom T. C. Sistermans[1,2], and Alberto G. Curto[1,2*]

[1] Photonics Research Group, Ghent University-imec, Ghent, Belgium

[2] Center for Nano- and Biophotonics, Ghent University, Ghent, Belgium

[*]Corresponding Author: Alberto.Curto@UGent.be

Abstract: Optical anisotropy plays a crucial role in the manipulation of light. Its strength is, however, limited to low values in conventional materials. Transition metal dichalcogenides possess both high refractive index and high birefringence due to their layered structure. Here we investigate optical resonances in nanoplatelets with both geometrical and refractive index anisotropies. A multipole expansion allows us to analyze their distinct influence on magnetic and electric resonances. Nanoplatelets thus create new opportunities to control light scattering and emission.

Anisotropy is the basis for a variety of bulk optical components, including polarizers, wave plates, modulators, and phase-matching elements. The constituting material's birefringence, Δn, determines the device size and performance. Thus, a large birefringence is beneficial because it leads to more compact and efficient devices. However, currently used materials such as inorganic solids like calcite and liquid crystals possess a relatively small birefringence with typical values of refractive index difference below 0.4. As a result, natural materials with giant anisotropy ($\Delta n > 1$) are in growing demand both for scientific and industrial purposes.

Transition metal dichalcogenides are promising birefringent materials due to their layered van der Waals structure, which naturally leads to a large intrinsic birefringence above unity. In particular, molybdenum disulfide (MoS_2) possesses the highest birefringence of all natural materials in the near infrared. Such a high birefringence is possible because of the presence of strong excitons, which endow MoS_2 with a high in-plane refractive index above 4.5 and makes it possible to have higher out-of-plane index contrast than lower index dielectrics. A high refractive index also enables the existence Mie-type resonances in MoS_2 nanostructures for enhancing and controlling light-matter interaction.

Here, we study the optical resonances sustained by nanoplatelets (thin nanodisks) made of high refractive index material with high optical anisotropy. Nanoplatelets have both geometrical and refractive index anisotropies . They sustain electric and magnetic multipolar resonances. We investigate the distinct impact of changes in height and birefringence on the tunability of the different resonances. We use a multipolar analysis to understand the influence of anisotropy on each resonance. We find that magnetic dipole resonances are particularly sensitive to changes in the material anisotropy. Due to their double anisotropy, nanoplatelets also show a strong dependence of their optical response on the direction of plane wave illumination. We relate the nature of the resonances under illumination with the same electric or magnetic field polarization and different directions of incidence and consider the impact of retardation effects. Finally, we show that nanoplatelets can also control the polarization and directionality of dipolar sources such as fluorescent molecules due to the preferential excitation of in-plane resonances.

In summary, we have studied high-refractive-index nanoplatelets with intrinsic out-of-plane anisotropy and large birefringence. These nanoresonators exhibit a rich variety of electric and magnetic multipolar resonances that are sensitive to geometry and anisotropy in distinct and different ways. We envision that films consisting of disordered but

oriented nanoplatelets could be used to enhance and direct light scattering and light emission, with applications in light-emitting devices and random lasers.

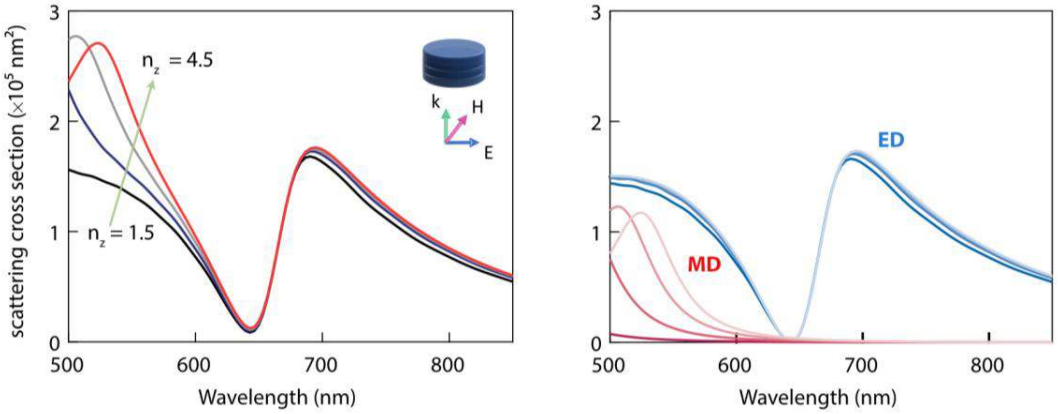


Figure 1. Resonances in high refractive index, birefringent nanoplatelets. Left: Scattering cross section resonances that depend on the optical anisotropy of the nanoplatelet material. Right: Multipolar decomposition of the resonances for different anisotropy values, indicating that the magnetic dipole (MD) resonance is more sensitive to birefringence than the electric dipole (ED) features.

References

1. Ermolaev, G. A., D. V. Grudinin, Y. V. Stebunov, K. V. Voronin, V. G. Kravets, J. Duan, A. B. Mazitov, G. I. Tselikov, A. Bylinkin, D. I. Yakubovsky, S. M. Novikov, D. G. Baranov, A. Y. Nikitin, I. A. Kruglov, T. Shegai, P. A. González, A. N. Grigorenko, A. V. Arsenin, K. S. Novoselov and V. S. Volkov, "Giant optical anisotropy in transition metal dichalcogenides for next-generation photonics," Nature Communication, Vol. 12, No. 854, 2021.
2. Verre, R., D. G. Baranov, B. Munkhbat, J. Cuadra, M. Käll, and T. Shegai, "Transition metal dichalcogenide nanodisks as high-index dielectric Mie nanoresonators," Nature Nanotechnology, Vol. 14, 679-683, 2019.
3. Munkhbat B., P. Wróbel, T. J. Antosiewicz and T. Shegai, "Optical Constants of Several Multilayer Transition Metal Dichalcogenides Measured by Spectroscopic Ellipsometry in the 300−1700 nm Range: High Index, Anisotropy, and Hyperbolicity," ACS Photonics, Vol. 9, No.7, 2398-2407, 2022.

Analog optical differentiation using metal-dielectric layered structures

A. I. Kashapov[1,2], L. L. Doskolovich[1,2*], E. A. Bezus[1,2], N. V. Golovastikov[1,2] and D. A. Bykov[1,2]

[1]Image Processing Systems Institute – Branch of the Federal Scientific Research Centre "Crystallography and Photonics" of Russian Academy of Sciences, 151 Molodogvardeyskaya st., Samara 443001, Russia
[2]Samara National Research University, 34 Moskovskoye shosse, Samara 443086, Russia
[*]corresponding author: leonid@ipsiras.ru

Abstract: Design and investigation of nanophotonic structures for the optical implementation of different differential operators have attracted considerable attention in recent years. In this work, we present the optical computation of the Laplace operator of the profile of a three-dimensional optical beam incident on a resonant metal-dielectric layered structure composed of two metal-dielectric-metal structures, which, in turn, consist of an upper metal layer, a dielectric layer, and a lower metal layer.

Optical differentiation is a powerful technique that has the ability to extract valuable information about the spatial distribution of optical signals or the rate of change of an optical signal over time. That makes it an essential tool for researchers in a wide range of fields, including imaging, microscopy, and optical communication. Differentiation of optical signals can be achieved using various methods including resonant diffraction gratings (photonic crystal slabs), layered structures, and microresonators.

The resonant diffractive structure considered in this work consists of seven alternating metal (m) and dielectric (d) layers in the following order: "m-d-m-d-m-d-m" (see the inset in Fig. 1a). In [1], a numerical method was developed for designing such multilayer structures possessing a second-order reflection zero. Investigation of the optical properties of the considered metal-dielectric structures has shown that the quantity of the independent parameters of the structure, such as the materials of the layers, the thickness of the lower layer (which determines the thickness of the other layers), the angle of incidence of the beam, and the central frequency, allows us to fulfill the conditions for the optical computation of various differential operators [2].

As an example, let us consider a structure designed for the optical computation of the Laplace operator. The configuration of the structure is shown in Table 1. The developed structure enables optically computing the Laplace operator at oblique incidence (in the presented example, at an incidence angle of 36 degrees).

Layer material	Au	SiO_2	Ag	SiO_2	Ag	TiO_2	Au
Layer thickness, nm	10.0	132.3	8.6	52.2	33.6	74.4	105.0

Table. 1. Layer thicknesses of the considered metal-dielectric structure

Figure 1a shows the profile of the incident linearly polarized beam, which is an Hermite–Gaussian beam of the order (1, 0) with the x-component of the electric field $E_{x.inc}(x_{\text{inc}}, y_{\text{inc}}) = H_{1,0}(\sqrt{2}x_{\text{inc}}/\sigma, \sqrt{2}y_{\text{inc}}/\sigma)\exp(-x_{\text{inc}}^2/\sigma^2 - y_{\text{inc}}^2/\sigma^2)$, where $H_{m,n}(x,y)$ is the Hermite

polynomial and $\sigma = 20\ \mu m$ is the beam width. Figure 1b shows the reflected beam profile calculated numerically using the enhanced transmittance matrix approach [3], which corresponds to the Laplacian of the incident beam profile with a high accuracy (the normalized RMSD of the rigorously calculated reflected beam profile from its analytical representation amounts to only 0.61 %).

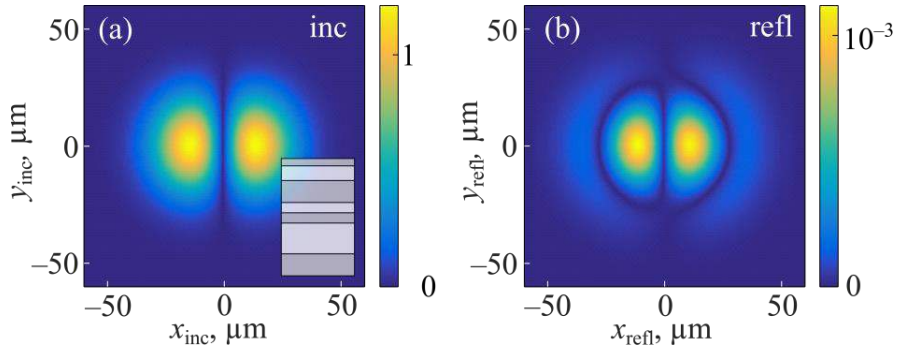


Fig. 1. Profiles of the incident (a) and reflected (b) beams. The MDM structure is shown in the inset to (a).

In conclusion, it was shown that the designed structure enables high-accuracy optical computation of the Laplace operator of the profile of the incident optical beam. The presented structure can also be used in image processing for optical edge detection. It is also worth noting that layered metal-dielectric structures provide an opportunity to optically compute other differential operators including temporal and spatial derivatives of various orders.

This work was funded by the Russian Science Foundation (project 19-19-00514, design and investigation of the metal-dielectric structures for analog optical differentiation) and by the Ministry of Science and Higher Education of the Russian Federation (State assignment to the FSRC “Crystallography and Photonics” RAS, implementation of the numerical simulation software).

References

1. Doskolovich, L. L., A. I. Kashapov, E.A. Bezus and D.A. Bykov, “Optical properties of cascaded metal-dielectric-metal structures and their application to the differentiation of optical signals,” Photonics Nanostructures — Fundam. Appl., Vol. 52, Art. No. 101069, 2022.
2. Doskolovich, L. L., A. I. Kashapov, E.A. Bezus and D.A. Bykov, “Spatiotemporal optical differentiation and vortex generation with metal-dielectric-metal multilayers,” Phys. Rev. A, Vol. 106, No. 3, Art. No. 033523, 2022.
3. Moharam, M. G., D. A. Pommet, E.B. Grann and T.K. Gaylord, “Stable implementation of the rigorous coupled-wave analysis for surface-relief gratings: enhanced transmittance matrix approach,” J. Opt. Soc. Am. A, Vol. 12, No. 5, 1077–1086, 1995.

Optical properties of resonant gratings with spatially varying period

D. A. Bykov[1,2], E. A. Bezus[1,2], A. I. Kashapov[1,2], A. A. Morozov[1,2], V. V. Podlipnov[1,2], and L. L. Doskolovich[1,2*]

[1]Image Processing Systems Institute — Branch of the Federal Scientific Research Centre "Crystallography and Photonics" of Russian Academy of Sciences, 151 Molodogvardeyskaya st., Samara 443001, Russia
[2]Samara National Research University, 34 Moskovskoye shosse, Samara 443086, Russia
[*]corresponding author: leonid@ipsiras.ru

Abstract: We study guided-mode resonant gratings with the period linearly changing along the periodicity direction. At relatively small period change rates, such structures are used as linearly varying filters. However, when designing compact filters, the period change rate increases, which results in the appearance of multiple resonant peaks. We study this effect numerically and experimentally. We also develop a coupled-mode theory describing the optical properties of the investigated structures and providing a very good agreement with the simulation results.

Investigation of the resonant properties of subwavelength diffraction gratings continuously attracts considerable research interest [1]. The most important application of resonant gratings (RG) is in narrowband optical filters. In the design of spectrometric systems, one is required to divide the incident radiation into a large number of spectral channels. Spectral filters for such systems can be created by utilizing resonant structures with the parameters varying along a certain spatial dimension. This enables filtering different wavelengths in different areas of the structure. Such filters are usually referred to as linearly variable filters (LVFs). Along with the most well-known type of LVFs, namely, Bragg gratings with a wedged central layer, RGs with the period varying along the periodicity direction represent another promising LVF type [2, 3]. In addition to the application in spectrometers, gratings with varying parameters are also promising for refractive index sensing.

In this work, we investigated a guided-mode RG with the period varying linearly as $d(x) = d_0 + \alpha x$, where $\alpha = 2.5 \cdot 10^{-4}$ is the period change rate. The geometry of the studied structure is shown in Fig. 1; the parameters are presented in the figure caption. Such a grating was fabricated using e-beam lithography in a PMMA layer deposited on a TiO_2 thin film. The substrate and superstrate were fused silica and free space, respectively.

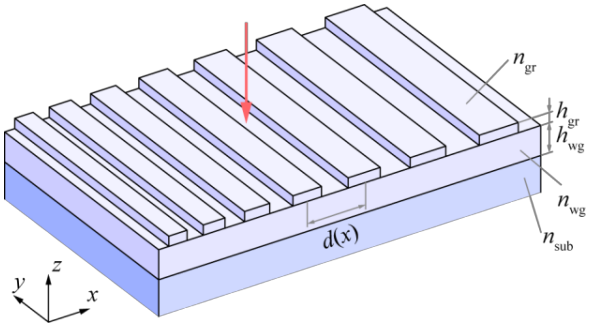


Fig. 1. Geometry of the guided-mode resonant grating with linearly varying period. Parameters: grating thickness $h_{gr} = 300\,\text{nm}$, grating fill-factor $f = 1/2$, grating period $d_0 = 330\,\text{nm}$, waveguide layer thickness $h_{wg} = 130\,\text{nm}$.

The measured reflected field distribution is presented in Fig. 2a. Its normalized averaged cross-sections are shown in Fig. 2b for three different wavelengths. One can see that instead of a single resonant peak with a spectrally-dependent position (as it is predicted by the local periodic approximation), several "secondary" peaks appear to the left and to the right to the central peak [3]. The magnitude and spacing of these peaks depend on the period change rate α. When α tends to zero, the secondary peaks disappear and the resonance acquires a conventional Lorentzian line shape.

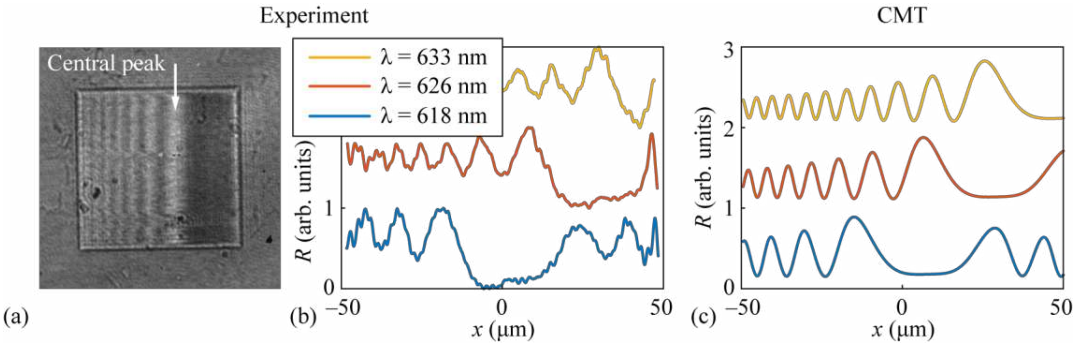


Fig. 2. Measured reflected field distribution (a) at $\lambda = 626$ nm and its normalized averaged cross-sections (b) at the wavelengths $\lambda = 633$ nm (upper lines), $\lambda = 626$ nm (middle lines), and $\lambda = 618$ nm (lower lines). The lines are vertically offset for clarity. Reflected field distributions predicted by the coupled-mode theory at the same wavelengths (c).

To explain the appearance of the secondary peaks evident in Figs. 1a and 1b, we developed a coupled mode theory with varying parameters. This theory describes the coupling of two counter-propagating modes of the waveguide layer and allows one to calculate the reflected and transmitted field distributions along the structure at a given wavelength of a normally incident plane wave. The CMT predictions shown in Fig. 2c are in good agreement with the experimental results. We also performed rigorous electromagnetic simulations using Fourier modal method [4] with the super-period approach (not presented here for the sake of brevity), the results of which are also in very good agreement with the CMT predictions.

This work was funded by the Russian Science Foundation project 22-12-00120.

References

1. Zhou, W., D. Zhao, Y.-C. Shuai, H. Yang, S. Chuwongin, A. Chadha, J.-H. Seo, K. X. Wang, V. Liu, Z. Ma and S. Fan, "Progress in 2D photonic crystal Fano resonance photonics," Prog. Quantum Electron., Vol. 38, P. 1, 2014.
2. Hsiung, C.-T and C.-S. Huang, "Refractive index sensor based on a gradient grating period guided-mode resonance," IEEE Photon. Technol. Lett., Vol. 31, 253–256, 2019.
3. Bykov, D. A., E.A. Bezus, A.A. Morozov, V.V. Podlipnov and L.L. Doskolovich, "Optical properties of guided-mode resonant gratings with linearly varying period," Phys. Rev. A, Vol. 106, Art. No. 053524, 2022.
4. Moharam, M. G., D. A. Pommet, E.B. Grann and T.K. Gaylord, "Stable implementation of the rigorous coupled-wave analysis for surface-relief gratings: enhanced transmittance matrix approach," J. Opt. Soc. Am. A, Vol. 12, No. 5, 1077–1086, 1995.

Bound states in the continuum in the waveguide structure covered by the 2D-rectangular plasmonic lattice

S. I. Pavlov[1*], S. A. Dyakov[2], D. P. Markov[1], S. A. Grudinkin[1], N. A. Feoktistov[1] and A. B. Pevtsov[1]

[1]Ioffe Institute, Russia
[2]Skolkovo Institute of Science and Technology, Russia
[*]corresponding author: Pavlov_Sergey@mail.ioffe.ru

Abstract: In this work, we study the optical properties of the a-$Si_{0.65}C_{0.35}$:H-based planar waveguide structure covered by a 2D array of gold nanodisks. The rectangular lattice of nanodisks allows controlling the wavelength of the TE and TM guided modes resonances separately and the single nanodisk size supports localized plasmon resonance. We show that the structure possesses different types of BICs which are the result of the interaction of guided modes and single-particle resonances.

The control of light propagation and localization at the subwavelength scale is of great interest due to the possibility of tailoring light-matter interaction. Traditionally, the utmost localization and enhancement of the electromagnetic field have been associated with plasmonic resonances in metallic nanostructures. However, material absorption in the metal shrinks the advantages of plasmonic effects.

Recently it was shown that in structures combining plasmonic and photonic resonances bound states in the continuum (BICs) can occur [1]. Since BICs are theoretically perfectly non-radiating modes, the use of their properties to metal-based nanostructures is promising for plasmonic Q-factor improvement.

In this work, we studied the optical properties of the structure consisting of a waveguide luminescent layer covered by the gold nanodiscs array. A plasmonic array arranged in the 2D lattice provides coupling of light to quasi-guided modes [2] while the size of a single nanodisk supports localized plasmon resonance.

The waveguide layer was created from the a-$Si_{0.65}C_{0.35}$:H film with the thickness of 150 nm deposited on a silica substrate by plasma-enhanced chemical vapor deposition (PECVD). The film composition with a specified C/Si ratio corresponds to a refractive index of approximately 2.5 and the photoluminescence peak maximum at 725 nm.

The array of gold disks was created on top of the waveguide layer by the e-beam lithography. The rectangular lattice allows to control of the wavelength of the quasi-guided resonances attributed to TE and TM guided modes separately. The periods of the lattice were 340x370 nm providing overlapping of the modes at the Γ-point (normal incidence of the light). The disk's diameter of 100 nm was chosen to adjust the LPR wavelength to the luminescence peak maximum.

To examine the resonant modes of the structure we performed angle-resolved reflection and photoluminescence spectra measurements by the Fourier-imaging spectroscopy method. Theoretical analysis of the optical response of the structure included numerical calculations of the structure’s eigenmodes and angle-resolved spectra performed by a Fourier modal method in the scattering matrix form [3].

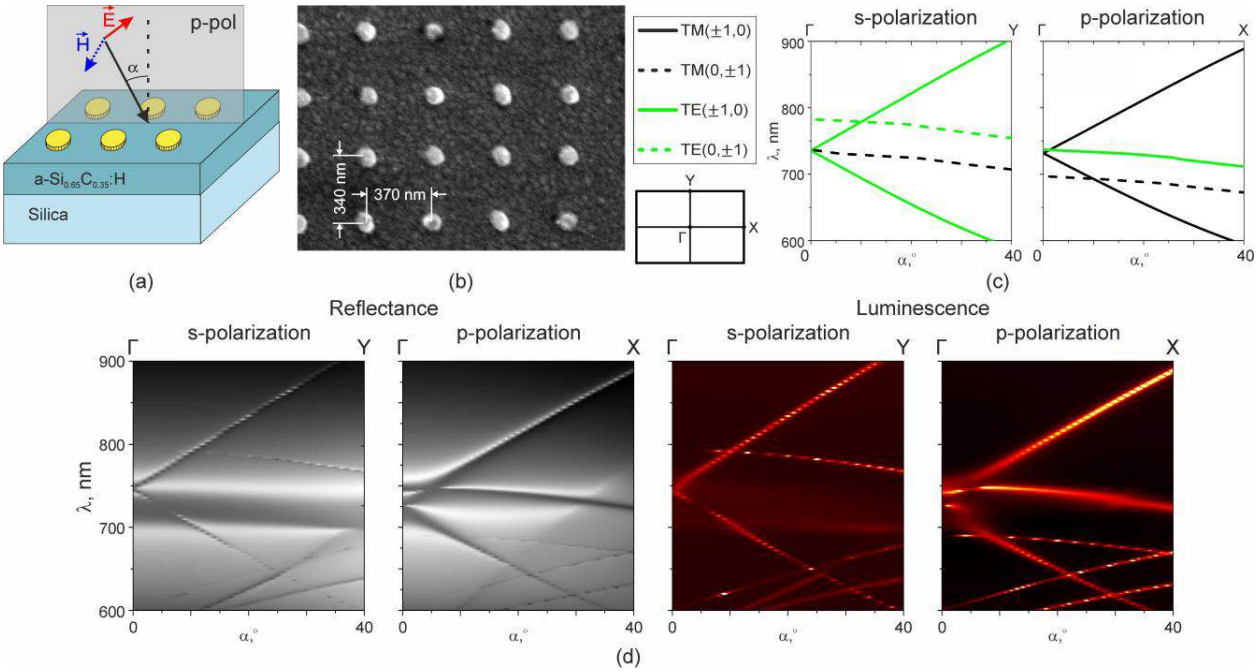


Figure 1. (a) Schematic view of the structure. (b) SEM top view image of the 2D array of the gold nanodisks. (c) Waveguide modes dispersion curves. (d) Angle-resolved spectral maps of the reflectance and photoluminescence calculated for the structure.

As a result, in the angle-resolved spectral maps, we observed features attributed to specific guided modes dispersion curves. Interaction of the quasi-guided and plasmon resonances leads to the polaritonic states formation. The anticrossing behavior is a clear evidence of the coupling between modes while the vanishing of the resonant lines at particular points indicates the formation of a bound state. The analysis of the results has shown that different types of BICs are present in the structure. These are symmetry-protected BICs at the normal incidence angle and accidental (Friedrich–Wintgen) BICs at the off-Γ points.

References

1. Azzam, S. I., Shalaev V. M., Boltasseva A. and Kildishev A. V.,"Formation of Bound States in the Continuum in Hybrid Plasmonic-Photonic Systems", Phys. Rev. Lett., Vol. 121, 253901, 2018.
2. Linden, S., Kuhl, J., Giessen, H., "Controlling the Interaction between Light and Gold Nanoparticles: Selective Suppression of Extinction", Phys. Rev. Lett., Vol. 86, 4688, 2001.
3. Moharam, M. G., Grann, E. B., Pommet, D. A. and Gaylord T. K., "Formulation for stable and efficient implementation of the rigorous coupled-wave analysis of binary gratings", J. Opt. Soc. Am. A, Vol. 12, No. 5, 1068, 1995.

Metamaterials and Metasurfaces for Medical and Healthcare Applications

Super-Resolution Ultrasonic Cellular Imaging by Localization of Meta-Nanodroplets

Chengzhi Shi, PhD
Assistant Professor
George W. Woodruff School of Mechanical Engineering
Georgia Institute of Technology

Abstract

The ability to image cellular structures and morphology in deep tissues in vivo is essential for the fundamental study of developmental cell biology and physiology. Traditional cellular imaging techniques rely on imaging cells embedded in planar slices using histological staining ex vivo. Confocal and two photon microscopy techniques enable 3D reconstruction of cells in vivo, but are limited to superficial layers within several hundred micrometers of depth. Ultrasound imaging, on the other hand, has been safely used for decades to observe organ structures and behaviors deep in the body in vivo. However, the resolution of ultrasound imaging is typically limited to the wavelength scale (about 100 μm for 15 MHz) due to the diffraction limit, which can hardly be used to visualize microscale cellular structures. In this work, we used phase-transitioning perfluorocarbon meta-nanodroplets to break the diffraction limit. A pumping ultrasound at 3 MHz is used to stochastically activate the meta-nanodroplets and a 15 MHz probe ultrasound is used to reconstruct the image over time, which achieved 8.9 μm resolution. These meta-nanodroplets can be micro-injected into single cells via patch clamping technique for cellular imaging. Our work will pave the way towards ultrasonic cellular imaging in deep tissue in vivo, which will be essential for fundamental biological studies.

META 2023, PARIS - FRANCE, JULY 18 – 21, 2023

Metamaterial Antenna for High Field MRI

Anton Nikulin[1], Benoit Larrat[2], Djamel Berrahou[4], Alexandre Vignaud [2], Redha Abdeddaim [3], and Abdelwaheb Ourir [1], Julien de Rosny [1*]

1 Institut Langevin, ESPCI Paris, CNRS, PSL University, 1 rue Jussieu, 75005 Paris, France

2 CEA, DRF, JOLIOT, NeuroSpin, Université Paris-Saclay, 91191 Gif-sur-Yvette Cedex, France

3 Aix Marseille University, CNRS, Centrale Marseille, Institut Fresnel, Marseille, France

4 Multiwave Imaging, Marseille, France

*corresponding author: julien.derosny@espci.fr

Abstract: A general approach based on cylindrical metasurface is proposed to design antennas for high field magnetic resonance imaging. It is applied to create two volume coils dedicated to brain imaging at 7T with a large aperture on the top. The first prototype is dedicated to preclinical imaging of rodent brain while the second one is committed for clinical application. Both prototypes have been tested in-vivo. Then, this approach combined to phase conjugation processing allows to control the magnetic field distribution.

Magnetic Resonance Imaging is unique tool for medical diagnosis. It is based on the Larmor precession of nuclear spin under strong static magnetic field. Because Larmor frequency belongs to the radiofrequency domain, antennas are required to excite the nuclear spins and probe their relaxation. Birdcage antennas introduced in 1985[1] are the most common antenna used to operate over an entire volume such as for brain imaging. Actually, such an antenna is composed of cylindrical periodic arrangement of *N* conductive legs which are connected at the extremity by conductive rungs. In order that the fundamental mode this structure resonate at the Larmor frequency, inductive and capacitive lumped elements are inserted. This design is very similar to a metamaterial transmission line that is closed on itself [2] composed of *N* unit cells. The wave propagation on the metasurface can be modeled thanks to the transmission matrix formalism that relates the input voltage and current to the output ones by the way of the 2x2 transmission matrix T:

$$\begin{pmatrix} U_2 \\ I_2 \end{pmatrix} = T \begin{pmatrix} U_1 \\ I_1 \end{pmatrix}$$

The eigenmodes of a loss-less transmission matrix are characterized by their self-impedance Z_0 ($Z_0 = \pm 2\sqrt{Z_1 Z_2 + Z_1^2}$) and their phase shift $\delta\theta$ ($\cos(\delta\theta) = 1 - 2Z_1/Z_2$). Actually because of the inductive coupling between legs, an effective inductance should be taken into account in the expressin of Z_2. In order to generate a magnetic field that couples with the nuclear spins, the antenna should be able to generate 2 circularly polarized magnetic field B1+ in transmit mode and B1- in receive mode. This condition only occurs if $\delta\theta$ fits the angular distance between the 2 legs and the line impedance of the metasurface is constant. We first use this approach to propose two birdcages with a large aperture. The small "opencage" (Fig. 1a and b) is dedicated to a preclinal 7T MRI[3] and the large one (Fig1c and d) to clinical 7T MRI[4]. The quality of the results obtained in-vivo and ex-vivo are as good as the ones provided by classical birdcages (see Fig. 2)

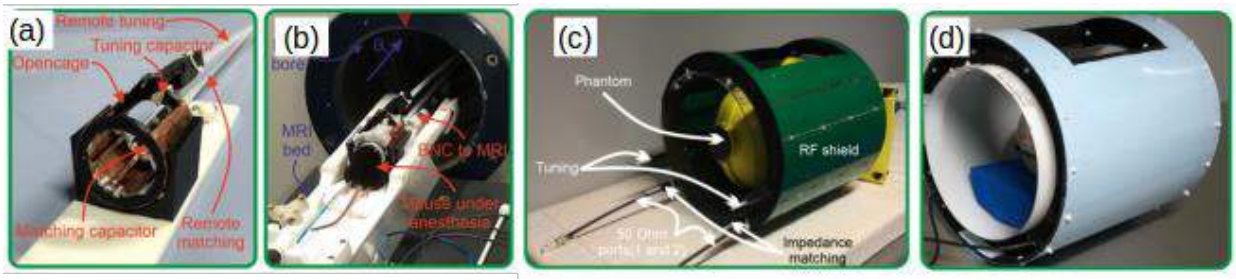


Figure 2: Photographies of the preclinical open-cage devoted to rodent brain imaging [(a) and (b)] and the clinical device dedicated to human brain imaging [(c) and (d)].

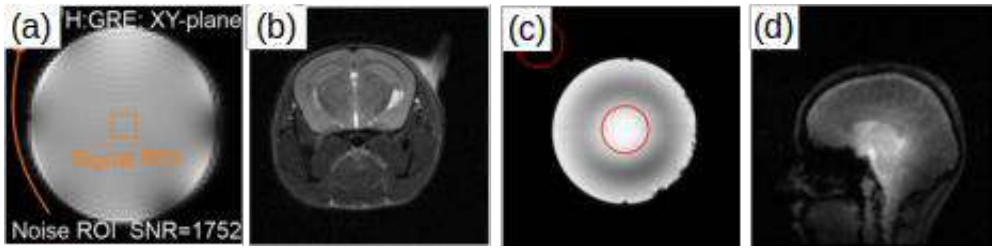


Figure 3: Magnetic resonance images obtained with the preclinical open-cage of a phantom cylinder (a) and of rodent head (b). Magnetic resonance images obtained with the clinical open-cage of a phantom cylinder (c) and of the head of a volunteer (d).

Both prototypes where tested ex-vivo and in-vivo. Finally, we combine the principle of phase conjugation and the metamaterial approach in order to shift the maximum of the magnetic field off the center axis. This approach is tested with phantom in a 17.2T preclinical MRI with a 3D printed prototype (see Fig. 3a). One image obtained when only one port is fed is shown in Fig. 3c. It qualitatively corresponds to the expected map resulting for the simulation.

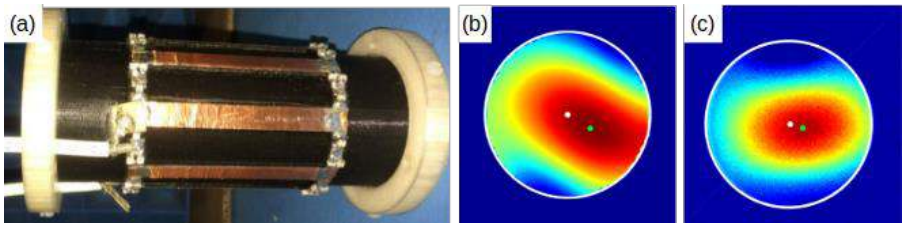


Figure 3: Magnetic resonance images obtained with the preclinical open-cage of a phantom cylinder (a) and of rodent head (b). Magnetic resonance images obtained with the clinical open-cage of a phantom cylinder (c) and of the head of a volunteer (d).

This project has received funding from the European Union's Horizon 2020 research and innovation program under Grant Agreement No. 736937.

References

1. CE Hayes, WA Edelstein, JF Schenck, OM Mueller, and M Eash, "An efficient, highly homogeneous radiofrequency coil for whole-body NMR imaging at 1.5 T", Journal of Magnetic Resonance, Vol 63, No 3, 622–628, 1985.
2. Christophe Caloz and Tatsuo. Itoh. "Electromagnetic metamaterials : transmission line theory and microwave applications : the engineering approach", John Wiley & Sons, 2006.
3. A Nikulin, J De Rosny, K Haliot, B Larrat, A Ourir, "Opencage radio frequency coil for magnetic resonance imaging", Applied Physics Letters, Vol 114, No 5, 053503, 2019.
4. AV Nikulin, A Vignaud, NI Avdievich, D Berrahou, J de Rosny, A Ourir, "Open birdcage coil for head imaging at 7T", Magnetic Resonance in Medicine, Vol 86, No 4, 2290-2300, 2021

Enhancing the performance of antennas for biomedical applications with inverse-designed nonlocal-inspired metamaterials

Dimitrios C. Tzarouchis[1*], Maria Koutsoupidou[1], Dionisios Rompolas[1], Ioannis Sotiriou[1], Efthymios Kallos[2], and Panagiotis Kosmas[1*]

[1]Meta Materials Europe, Ap. Pavlou 10a, Marousi, 15123, Greece

[2]Meta Materials Inc., QMB Innovation Centre, 42 New Road, E1 2AX, UK

[*]corresponding authors: {dimitrios.tzarouchis, panagiotis.kosmas}@metamaterial.com

Abstract: In this work, we introduce a nonlocal-inspired metamaterial that enhances the performance metrics of antennae used in biomedical applications, such as glucose sensing and other applications.

Since its conception, the paradigm of metamaterials has continuously delivered a novel design approach with many applications in energy control and harvesting[1]. These paradigms have been exploited for specific biomedical applications with promising results[2]. In this domain, recent works on metamaterials shed light on a particular category of nonlocal metamaterials. While local metamaterials transversely vary, their nonlocal counterparts are typically transversely homogenous while they typically can be longitudinally inhomogeneous[3]. A characteristic example is a stack of dielectric layers with proper permittivity recently used as spaceplates and for enhancing the performance of optical and lensing systems[3]. Interestingly, nonlocal metamaterials share many similarities with the broader category of grated refractive index (GRIN) lenses often encountered in microwave engineering. Finally, inverse design in metamaterial research offers new possibilities by expanding the available design space of microwave components, such as antennas for conventional and unconventional functionalities[4]. Therefore, adopting nonlocal metamaterials principles and inverse design for specific biomedical applications is an obvious pathway. Biosensing, bioimaging, and telemetry usually require an antenna design with an extremely sensitive response and a compact and robust setup to operate close to or inside a highly lossy medium that is the human body[5].

This work introduces the design methodology for a non-local-inspired metamaterial for antenna enhancement. First, we assume a region typically given by the application requirements. This is the space where the unknown nonlocal-inspired metamaterial will be placed. In principle, this slab consists of a continuous inhomogeneous permittivity profile. We then discretize this in the longitudinal direction in slices of unknown permittivity and width. At this stage, we inverse design the desired profile (ε, width) that yields desirable~~specific~~ goals/constraints using standard optimization technics, such as a genetic algorithm. Then, assuming a given set of thicknesses and permittivities, we proceed to the implementation phase. The slabs can be implemented via chemical[6,7] or metamaterial[1] synthesis approaches in this phase. Chemical synthesis is the process where the desired permittivity and thickness are chemically/mechanically achieved. The metamaterial synthesis follows the metamaterial design principles, where effective permittivity emerges from the properly designed constituents. Each methodology has its advantages, especially in terms of robustness and manufacturability.

For example, we demonstrate the case of an antenna array (4 patches) specially designed for a K-band (37GHz) sensor for biomedical applications. The enhancement of the performance of such an antenna is evident with the usage of a thin layer of desired profiles (permittivities and widths). These layers are subsequently implemented via properly designed metamaterials. ~~We note that this~~This inverse-design nonlocal-inspired design approach

essentially expands other typical design approaches, such as the design of matching layers or GRIN lenses to enhance antenna systems.

References

1. Nader Engheta and R. W. Ziolkowski, "A positive future for double-negative metamaterials," in *IEEE Transactions on Microwave Theory and Techniques*, vol. 53, no. 4, pp. 1535-1556, April 2005, doi: 10.1109/TMTT.2005.845188
2. Paul, S., Tiwari, N. K., & Akhtar, M. J. (2022). Design of Highly Directive GRIN MS Lens Integrated DFHA for Deep Tissue Biomedical Imaging. *IEEE Transactions on Antennas and Propagation*. https://doi.org/10.1109/TAP.2022.3222808
3. Shastri, K., & Monticone, F. (2023). "Nonlocal flat optics." *Nature Photonics* (Vol. 17, Issue 1, pp. 36–47). Nature Research. https://doi.org/10.1038/s41566-022-01098-5
4. Molesky, S., Lin, Z., Piggott, A. Y., Jin, W., Vucković, J., & Rodriguez, A. W. (2018). "Inverse design in nanophotonics." *Nature Photonics* (Vol. 12, Issue 11, pp. 659–670). Nature Publishing Group https://doi.org/10.1038/s41566-018-0246-9
5. Kaur, G., Kaur, A., Toor, G.K. *et al.* (2015). "Antennas for biomedical applications." *Biomed. Eng. Lett.* **5**, 203–212. https://doi.org/10.1007/s13534-015-0193-z
6. Lazebnik, M., Madsen, E. L., Frank, G. R., & Hagness, S. C. (2005). Tissue-mimicking phantom materials for narrowband and ultrawideband microwave applications. Physics in Medicine & Biology, 50(18), 4245. https://iopscience.iop.org/article/10.1088/0031-9155/50/18/001
7. Otterskog, M., Petrovic, N., & Risman, P. O. (2016, October). A multi-layered head phantom for microwave investigations of brain hemorrhages. In 2016 IEEE Conference on Antenna Measurements & Applications (CAMA) (pp. 1-3). IEEE. https://ieeexplore.ieee.org/abstract/document/7815764

The benefit of reconfigurable metamaterials in Magnetic Resonance Imaging

M. Günther[1,2*], E. Stoja[3], S. Konstandin[1], T. Bertuch[3], J. Müller[2] and D. Philipp[1,2]

[1]Fraunhofer MEVIS, Bremen, Germany
[2]Faculty of Physics, University of Bremen, Germany
[3]Fraunhofer FHR, Wachtberg, Germany

[*]corresponding author: matthias.guenther@mevis.fraunhofer.de

Abstract: Reconfigurable Metamaterials introduce manifold degrees of freedom into MRI to overcome limitations of present technological capabilities. Reconfigurability in this respect does not only include tailored and controllable spatial sensitivity profiles w.r.t. the interaction with incident fields, but also the precise control in the time domain. The state of the art and various use-cases of static, dynamic, reconfigurable, and interactive metamaterials as well as control strategies are shown. Applications range from SNR enhancement to spatial encoding patterns for reduced gradient fields.

Magnetic Resonance Imaging (MRI) is a powerful, non-invasive, and indispensable medical imaging modality. The involved technology has been improved for decades and state-of-the-art imaging makes use of i) advanced hardware components such as multi-channel, tailored Tx/Rx coils, and ii) modern software solutions such as vendor-independent pulse sequence design frameworks [6] and AI-based image reconstruction strategies. MRI is an essential part of clinical diagnostics and therapy control due to the variety of tissue contrasts. However, physiological limitations hamper technically possible advancements. A prime example is peripheral nerve stimulation caused by the gradient field switching that sets clear limits on the imaging speed. Whilst higher static B_0 fields of 7 T and beyond may also improve the signal-to-noise-ratio (SNR), they are related to higher costs and come with other disadvantages such as standing waves in the field-of-view at the same time.

The use of **Metamaterials** (MTMs) in the field of MRI is a recent development that offers a great potential to overcome some of the aforementioned limitations. Standard applications of MTMs in MRI are the SNR enhancement, imaging speed-up, and field homogenization [1-3]. MTMs may even outperform local, conventional Rx coils in specific applications when used in combination with an MRI scanner's integrated body coil [1,3]. A similar impact is seen in the field of bio-electronic in general [4]. However, the full potential of MTM-based solutions can only be unleashed if reconfigurable designs are employed in combination with advanced control and optimization paradigms. True **reconfigurability** means active, spatio-temporal control of a metamaterial's sensitivity profile, i.e., the tailored interaction with incident fields in its vicinity, which may also vary over time. In contrast, a static MTM always reacts in the same way to excitations and a dynamic one may be sensitive to, e.g., the imaging phase in MRI as demonstrated in [2,3,5]. A MTM that allows for, at least, fine-tuning of its resonance frequency exhibits a very low degree of reconfigurability [3]. In this case, patient- or vendor-specific adaptions become possible and such a design must be considered the bare minimum for meaningful applications. Control and optimization, down to the unit cell scale, must include MRI scanner synchronization and a wireless interface to manipulate the MTM before and during an MRI scan.

In Fig. 1, an MRI-tested prototype for a wirelessly reconfigurable (in one dimension) metasurface is shown. The use of digital capacitors (dcaps) in combination with a low-power microcontroller allows to interface the MTM via BLE even during an MRI scan. The same figure also shows an example of a tunable and dynamic

MTM that uses a dcap and a crossed diode pair. It allows to i) fine-tune the resonance and ii) react autonomously to the incident power level such that in Tx there is no recognizable effect whilst in Rx the SNR is enhanced significantly, c.f. [3].

Advanced, three-dimensional, reconfigurable MTMs in the future will allow for more dynamical use-cases such as spatial signal encoding via time-dependent resonant patterns, realization of virtual coil channels in Tx/Rx, electronic focusing, flexible designs of wireless coils that benefit imaging efficiency and patient comfort. Necessary developments will be outlined, which include, e.g., the embedding into a sequence development framework such as GammaStar [6], or the optimization and image reconstruction via AI-based tools.

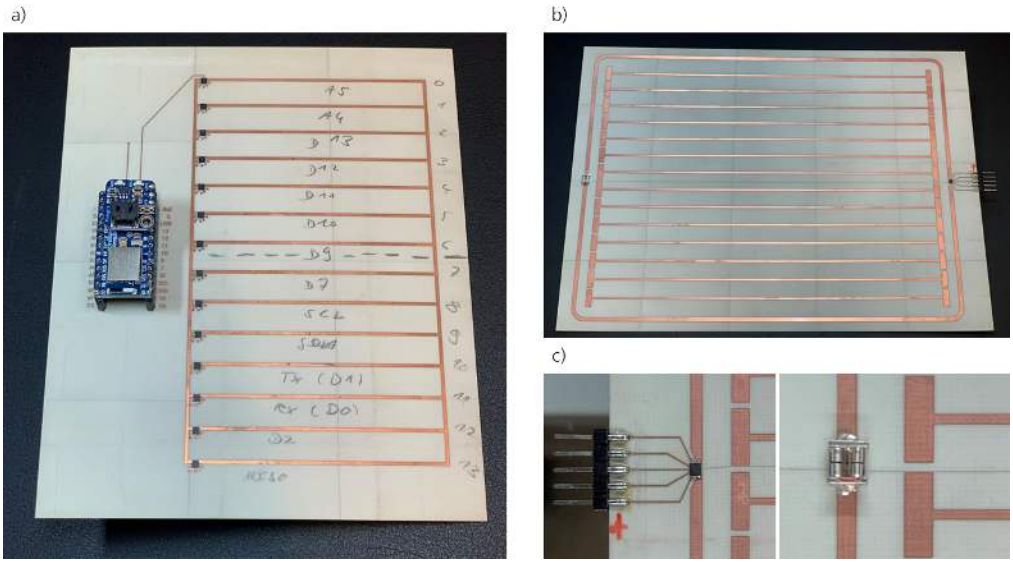


Figure 1 Prototypes of reconfigurable MTMs manufactured at Fraunhofer MEVIS. A 14-dcap, one-dimensional MTM with embedded microcontroller (a) allows for spatio-temporal, BLE-based control. A tunable, smart MTM allows for resonance frequency adjustments and automatic Tx detuning (b) via a dcap and crossed diode pair (c), respectively.

Funding by the Fraunhofer Society (Grant No. MAVO 142-600555) and the University of Bremen Research Alliance UBRA (project Meta^{N}) is gratefully acknowledged. Simulations and design iterations were partly performed using Sim4Life by ZMT [7].

References

1. Shchelokova AV, van den Berg CAT, Dobrykh DA, et al. Volumetric wireless coil based on periodically coupled split-loop resonators for clinical wrist imaging. Magn Reson Med. 2018;80:1726–1737.
2. Zhao X, Duan G, Wu K et al. Intelligent Metamaterials Based on Nonlinearity for Magnetic Resonance Imaging. Adv. Mater. 2019, 31, 1905461
3. Stoja E, Konstandin S, Philipp D et al. Improving magnetic resonance imaging with smart and thin metasurfaces. Sci Rep 11, 16179 (2021)
4. Li Z, Tian X, Qiu CW. et al. Metasurfaces for bioelectronics and healthcare. Nat Electron 4, 382–391 (2021)
5. Slobozhanyuk AP, Shchelokova AV, Dobrykh DA et al. Detunable Wire Metasurface for Applications in Magnetic Resonance Imaging. Bulletin of the Russian Academy of Sciences: Physics, 86, S216-S221 (2022)
6. Fraunhofer MEVIS, gammaSTAR. https://gamma-star.mevis.fraunhofer.de.
7. ZMT, Sim4Life. http://www.zmt.swiss/sim4life/

Comparison between a highly sensitive H-shape Terahertz metasurface absorber and an EIT-like terahertz Metasurface for refractive index biosensing

Tomas Pires , University of Glasgow

Ruobin Han, University of Glasgow

Shohreh Nourinovin, University of Glasgow

Hasan Abbas, University of Glasgow

Akram Alomainy, Queen Mary University

Muhammad Ali Imran, University of Glasgow

Qammer Abbasi, University of Glasgow

James Watt School of Engineering

Department of Electronic Engineering

Abstract- Achieving higher sensitivity in THz metasurfaces requires a larger Q-factor to minimize losses. EIT-like and perfect absorber metasurface can reduce losses and gain higher sensitivity. Here, we designed a novel THz absorber metasurface and its EIT-like counterpart and compared their sensing performance. Using EM simulation and varying the sample's refractive index, a theoretical sensitivity of 842GHz/RIU and 560GHz/RIU achieved for absorber and EIT-like metasurface, respectively. These findings validate the effectiveness of both biosensors, with absorbers showing greater potential for biosensing.

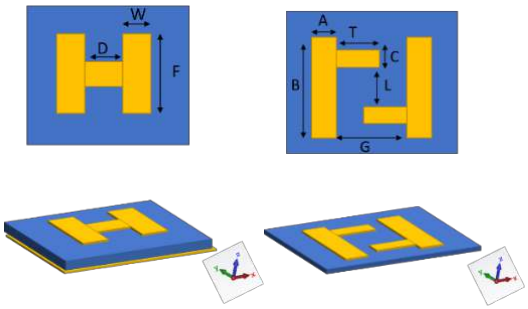


Figure 1 H- Shape metasurface absorber (on the left) with 200nm Aluminum layer for electrode and ground and Polymide Substrate with 5um thickness. With Dimensions W=15um;F=60um and D=25um. H-shape EIT-like Metasurface with 200nm aluminum layer. With Dimensions A=15um, B=60um,L=20um,T=22um,C=10um, G=25um (on the right)

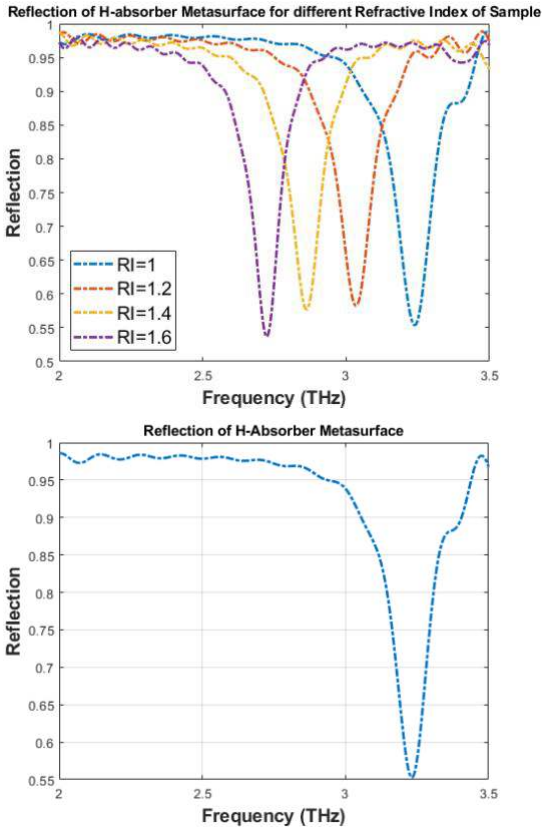


Figure 2 Reflection of H-absorber metasurface with changing refractive index(1-1.6) of a 13um thick sample (on the top), Reflection of H-shape absorber without sample (on the bottom).

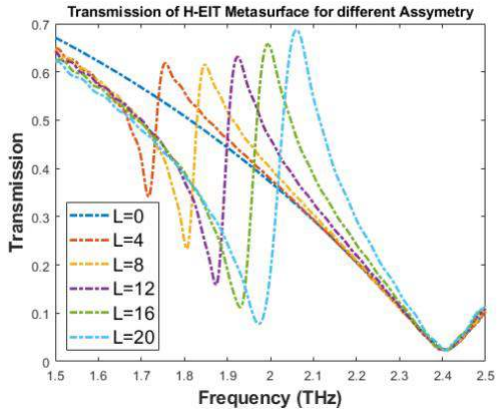
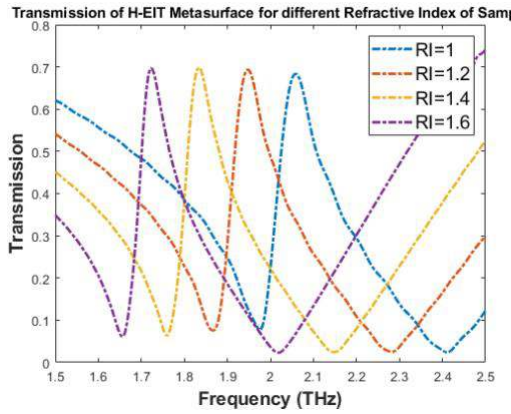


Figure 3 Transmission of H-EIT-like metasurface for assymetry degrees varying from L= 0 to L=20um



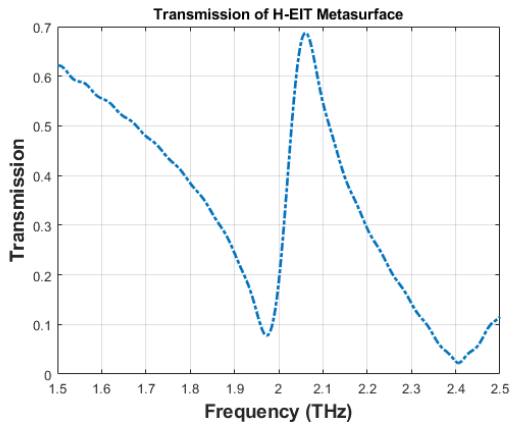


Figure 4 Transmission of EIT-like Metasurface with a 13um thick sample varying its refractive index from 1 to 1.6 (on the top) and transmission of EIT-like Metasurface without sample (on the bottom)

Table 1 Sensing Performance Characteristics comparison of both H-shape metasurface absorber and EIT-like Metasurface

Metasurface	Resonant Frequency (THz)	FWHM (GHz)	Sensitivity (GHz/RIU)	Q-Factor
EIT	2.1	150	560	14
Absorber	3.25	134	842	24.25

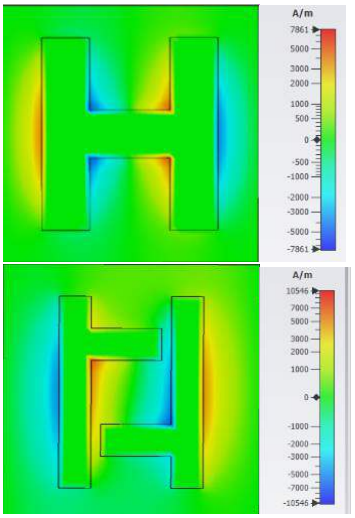


Figure 5 Magnetic Field distribution of both H-shape metasurface absorber (on the top) and EIT-like Metasurface (on the bottom).

References:

[1] X. Yan, T. Li, G. Ma, J. Gao, T. Wang, H. Yao, M. Yang, L. Liang,
J. Li, J. Li *et al.*, "Ultra-sensitive dirac-point-based biosensing on terahertz metasurfaces comprising patterned graphene and perovskites," *Photonics Research*, vol. 10, no. 2, pp. 280–288, 2022.

[2] V. Fedotov, M. Rose, S. Prosvirnin, N. Papasimakis, and N. Zheludev, "Sharp trapped-mode resonances in planar metamaterials with a broken structural symmetry," *Physical review letters*, vol. 99, no. 14, p. 147401,2007.

[3] N. Liu, L. Langguth, T. Weiss, J. Kästel, M. Fleischhauer, T. Pfau, and H. Giessen, "Plasmonic analogue of electromagnetically induced transparency at the drude damping limit," *Nature materials*, vol. 8,no. 9, pp. 758–762, 2009.

[4] L. Cong, M. Manjappa, N. Xu, I. Al-Naib, W. Zhang, and R. Singh, "Fano resonances in terahertz metasurfaces: a figure of merit optimiza- tion," *Advanced Optical Materials*, vol. 3, no. 11, pp. 1537–1543, 2015.

[5] J. Wang, C. Fan, J. He, P. Ding, E. Liang, and Q. Xue, "Double fano resonances due to interplay of electric and magnetic plasmon modes in planar plasmonic structure with high sensing sensitivity," *Optics express*, vol. 21, no. 2, pp. 2236–2244, 2013.

[6] Z. Zhang, H. Ding, X. Yan, L. Liang, D. Wei, M. Wang, Q. Yang, and
J. Yao, "Sensitive detection of cancer cell apoptosis based on the non- bianisotropic metamaterials biosensors in terahertz frequency," *OpticalMaterials Express*, vol. 8, no. 3, pp. 659–667, 2018.

[7] vol. 3, no. 6, pp. 772–782, 2013.

[8] S. Nourinovin and A. Alomainy, "A Terahertz Metasurface for Thin Film Biosensing," 2022 IEEE MTT-S International Microwave Biomedical Conference (IMBioC), Suzhou, China, 2022, pp. 236-238, doi: 10.1109/IMBioC52515.2022.9790176.

[9] Wang, Yang, et al. "Experimental Analysis and Comparison between Cross-Shaped Metamaterial Absorber and Its Complementary Structure." Microwave and Optical Technology Letters, vol. 61, no. 4, 2019, pp. 930–936., https://doi.org/10.1002/mop.31666.

Metasurface Pads for body imaging at 3T

Marc Dubois[3], Stefan Enoch[1], David Bendahan[2], Redha Abdeddaim[1]
[1]Aix-Marseille Universite, CNRS, Centrale Marseille, Institut Marseille Imaging, Institut Fresnel
[2]Aix-Marseille Universite, CNRS, Center for Magnetic Resonance in Biology and Medicine,
[3]Multiwave Imaging

3T MR scanners are popular in a clinical context, offering higher SNR compared to the widely deployed 1.5T. Higher field strength leads to shorter scanning times or higher resolution images. However, when 3T MRI is used to image large cross-sectional areas such as the abdomen, thorax, or spinal cord, inhomogeneities in the radiofrequency (RF) field appears and can affect the image quality [1]. On that basis, alternatives are needed if one intends to scan large central body parts at 3T.

Both high dielectric pads and high permittivity ceramics blocks have been used as efficient solutions with the aim of mitigating RF inhomogeneities [2] [3]. However, ceramic materials are very limited in terms of dimensions.

Here, original metasurface pads are presented as an alternative approach to mitigate RF inhomogeneities. Several designs which can be integrated within standard MRI equipment will be presented with a particular attention dedicated to field penetration efficiency and safety in the field of whole-body imaging.

Acknowledgements: This work has been supported by the FET-OPEN M-CUBE Project (grant #736937) and the Excellence Initiative of Aix-Marseille University - A*MIDEX, a french “Investissements d’Avenir” programme under Multiwave chair of Medical Imaging.

1. Dietrich, O, et al. Eur J Radiol 2008; 65:29–35.
2. Webb, AG, et al. Magnetic Resonance Materials in Physics, Biology and Medicine 2022; 1-20.
3. Koolstra, K, et al., Magnetic Resonance in Medicine 2018; 79: 1192-1199.

Metamaterials for 7T Ultra High Field MRI

Redha Abdeddaim[1], Marc Dubois[2], Stefan Enoch[1]
[1]Aix-Marseille Universite, CNRS, Centrale Marseille, Institut Marseille Imaging, Institut Fresnel, [2]Multiwave Imaging

Ultra-high field MRI head coils are characterized by a specific B1+ magnetic field distribution leading to signal and contrast inhomogeneities over the image in relevant regions of interest such as the temporal lobes of the brain and the cerebellum[1]. This issue has been previously targeted by different passive RF shimming approaches such as high permittivity dielectric pads or metamaterials[2].

Passive RF shimming is based on the insertion of passive structures between the subject and the coil. Devices such as high-permittivity dielectric pads or metamaterials have been assayed as potential solutions. These structures are inductively coupled to the main transmit RF coil. Induced currents (displacement or conduction currents) can generate a secondary RF field that redistributes the initial B1+ field. In the present study, we present how metamaterials can improve the B1+ field over each temporal lobe without deterioration of the RF performances in other brain areas and with minimal impact on patient comfort[3]. Different shapes and types of metamaterials will be presented and compared in order to identify the optimal configuration considering the targeted field intensity increase[4].

Acknowledgements: This work has been supported by the FET-OPEN M-CUBE Project (grant #736937), the FET-OPEN MRI PADS launchpad Project (grant #850506), the FET-PROACT M-ONE (project grant #952106), the Excellence Initiative of Aix-Marseille University - A*MIDEX, a french “Investissements d’Avenir” programme under Multiwave chair of Medical Imaging.

1- Webb, A. G. (2011). Dielectric materials in magnetic resonance. Concepts in magnetic resonance part A, 38(4), 148-184.
2- Webb, A., Shchelokova, A., Slobozhanyuk, A., Zivkovic, I., & Schmidt, R. (2022). Novel materials in magnetic resonance imaging: high permittivity ceramics, metamaterials, metasurfaces and artificial dielectrics. Magnetic Resonance Materials in Physics, Biology and Medicine, 35(6), 875-894.
3- Dubois, M., Leroi, L., Raolison, Z., Abdeddaim, R., Antonakakis, T., De Rosny, J., ... & Enoch, S. (2018). Kerker effect in ultrahigh-field magnetic resonance imaging. Physical Review X, 8(3), 031083.
4- Gomez, T. S. V., Dubois, M., Rustomji, K., Georget, E., Antonakakis, T., Vignaud, A., ... & Abdeddaim, R. (2022). Hilbert fractal inspired dipoles for passive RF shimming in ultra-high field MRI. Photonics and Nanostructures-Fundamentals and Applications, 48, 100988.

META 2023, PARIS - FRANCE, JULY 18 – 21, 2023

Segmentation of individual muscles in MR images from patients with neuromuscular diseases

D. BEN DAHAN

Aix Marseille Université, CNRS, CRMBM UMR 7339, Faculté de Médecine de la Timone, 27 Bd. J. Moulin, 13005 Marseille-France

Abstract : Segmentation methods developed at CRMBM for the semi or fully automatic delineation of individual muscles in MR Images will be presented and the corresponding performances will be discussed.

Neuromuscular Diseases (NMDs) are genetic disorders progressively affecting nerves and/or muscles thereby leading to a loss of motor function (1). From an MRI perspective, the contrast available between fat and water is very useful to assess and possibly quantify the severity of the fat infiltration occurring throughout these disorders and to follow-up the corresponding natural history. Rather counter-intuitively, this fat infiltration largely differs among patients with a given disorder and even among different muscles within a given patient. On that basis, the assessment of MRI changes in NMD patients should be combined to methods allowing to delineate individual muscles from 3D datasets. The MSK research group at CRMBM has developed over the last few years semi-supervised and fully automated approaches with the aim of segmenting individual muscles from 3D MRI datasets and use the corresponding labels to compute specific biomarkers values within e ach label. As part of the presentation, we will show that the different methods are very sensitive to fat infiltration and will illustrate the accuracy of the quantified biomarkers with the different methods.

On the design, control, and AI-driven optimization of reconfigurable metamaterials for Magnetic Resonance Imaging

D. Philipp[1,2*], E. Stoja[3], S. Konstandin[1], T. Bertuch[3], J. Müller[2], M. V. Schmidt[1], and M. Günther[1,2]

[1]Fraunhofer MEVIS, Bremen, Germany
[2]Faculty of Physics, University of Bremen, Germany
[3]Fraunhofer FHR, Wachtberg, Germany

[*]corresponding author: dennis.philipp@mevis.fraunhofer.de

Abstract: Reconfigurable metamaterials offer the possibility to drastically improve various metrics in Magnetic Resonance Imaging. Among those are, e.g., speed, efficiency and local signal-to-noise ratio. To extremize a given target function, suitable optimization strategies must be followed. Here we report on the design of first prototypes, including their functionality, wireless control and conventional as well as AI-driven optimization. Simulations, on-bench measurements, deep learning optimization results, and MRI scans are shown to demonstrate a proof-of-principle.

Magnetic Resonance Imaging (MRI) is a powerful, non-invasive, and indispensable medical imaging modality. **Reconfigurable metamaterials** (MTMs) introduce many degrees of freedom that allow to lift the imaging performance to the next level and overcome some technological limitations. MTMs have become increasingly popular in MRI for a variety of applications. Specifically, they have been utilized for the signal-to-noise-ratio (SNR) enhancement in standard MRI scans [1-3] and may even have superior performance to conventional Rx coils [1,2]. However, all realizations presented in the available literature offer only a very low degree of reconfigurability, if any. In particular, resonance frequency fine-tuning must be ensured to cope with vendor-dependent and patient-specific effects. Manual tuning strategies are too far from clinical use and, thus, only a digital and wireless control shall be employed, ideally supplemented by an on-board logic.

In Fig. 1, a one-dimensional MTM prototype is shown that resembles a low-pass open birdcage coil design and includes N = 14 digital capacitors (dcaps) which can be individually controlled via Bluetooth (BLE) from a host device. A dedicated user interface allows to easily change the MTM's momentary configuration, which is verified by on-bench measurements and MRI scans. To optimize a target function, e.g., SNR in a region of interest, or a predefined field profile, conventional as well as AI-based optimization strategies can be followed. Possible applications are magnetic field shaping (electronic on-demand focusing or shielding of medical devices), the realization of virtual coil channels, and patient-specific imaging approaches. A desired field profile may be the result of many different sets of parameters and the inverse problem must be tackled.

Deep Learning (DL) approaches are especially well-suited for solving such non-linear optimization tasks. To overcome the inverse problem, a well-trained neural network can be used to find an appropriate set of parameters. On-bench as well as MRI tests will be reported on and results of the DL-based optimization using measurement and simulation data will be shown with a focus on generic field shaping capabilities. In Fig. 2, simulations results for a next-generation, two-dimensional prototype are shown, which is optimized for the purpose of local SNR enhancement. Analytical models assist in the design and complement numerical methods.

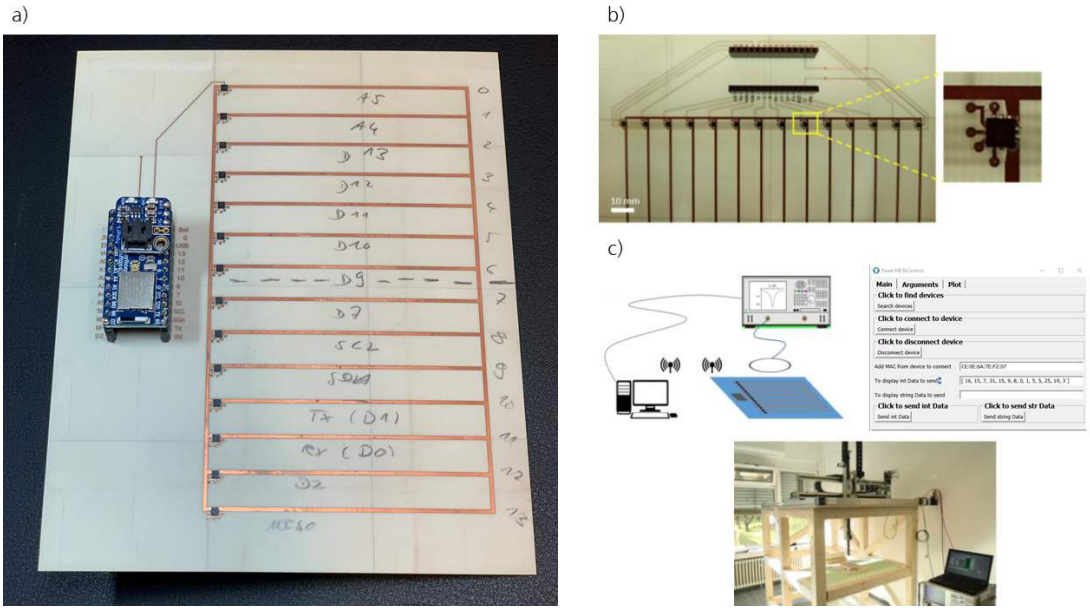


Figure 1 Prototype of a reconfigurable MTM manufactured at Fraunhofer MEVIS. A 14-dcap, one-dimensional MTM with embedded microcontroller (a) allows for spatio-temporal, BLE-based control. Connection traces are manufactured on the back-side of the PCB (b) and the BLE connection to a computer allows to individually control all dcaps from a dedicated user interface during on-bench measurements (c).

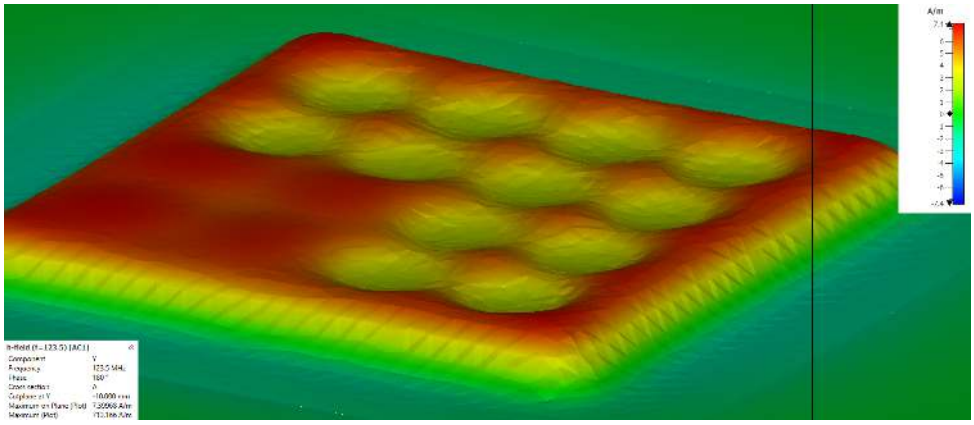


Figure 2 Exemplary magnetic field shaping with a two-dimensional, reconfigurable MTM based on 4x4 split ring resonator unit cells.

Funding by the Fraunhofer Society (Grant No. MAVO 142-600555) and the University of Bremen Research Alliance UBRA (project Meta^{N}) is gratefully acknowledged. Simulations and design iterations were partly performed using Sim4Life by ZMT [4].

References

1. Shchelokova AV, van den Berg CAT, Dobrykh DA, et al. Volumetric wireless coil based on periodically coupled split-loop resonators for clinical wrist imaging. Magn Reson Med. 2018;80:1726–1737.
2. Stoja E, Konstandin S, Philipp D et al. Improving magnetic resonance imaging with smart and thin metasurfaces. Sci Rep 11, 16179
3. Slobozhanyuk AP, Shchelokova AV, Dobrykh DA et al. Detunable Wire Metasurface for Applications in Magnetic Resonance Imaging. Bulletin of the Russian Academy of Sciences: Physics, 86, S216-S221 (2022)
4. ZMT, Sim4Life. http://www.zmt.swiss/sim4life/

Boosting received magnetic field (B_1^-) strength using wearable metasurface-based add-ons for 1.5T MRIs

Jegyasu Gupta[1, *], Tanmay Bhowmik[1], Ratnajit Bhattacharjee[1], and Debabrata Sikdar[1]

[1]Department of Electronics and Electrical Engineering, Indian Institute of Technology Guwahati, Guwahati 781039, Assam, India

[*]Corresponding author: jegyasu19@iitg.ac.in

Abstract: Magnetic resonance imaging (MRI) is a popular non-invasive diagnostic technique for examining human body tissues and organs. Metasurfaces have the ability to boost the received magnetic field (B_1^-) locally inside an MRI scanner. However, the metasurfaces reported in the literature for 1.5T MRI are not flexible enough to conform around different shapes of the subject's body parts undergoing scan. Here, we present a wearable metasurface-based "add-on" comprising copper-based apertures for boosting B_1^- in the region-of-interest (ROI) for 1.5T MRI.

Introduction: Magnetic resonance imaging (MRI) is a popular clinical diagnostic tool that uses non-ionizing radiation to ensure the safety of patients undergoing scans. In MRI, the image resolution depends on the received magnetic field (B_1^-) which can be increased by boosting the applied static magnetic (B_0) inside the MRI scanners [1]. However, this leads to an increased RF power deposition *i.e.* specific absorption rate (SAR) inside the body tissues which could cause safety concerns for patients with metallic implants and demand costly state-of-the-art hardware installation $[2-3]$. Metasurfaces or 2D metamaterials, whose electromagnetic properties and near-field distribution can be tailored by engineering their sub-wavelength unit cells, have shown potential in boosting the received magnetic field of 1.5T MRI scanners [4]. Several metamaterial designs based on split-ring resonators, swiss rolls, and wire-based resonators have been reported so far to enhance B_1^- for 1.5T MRI systems [5]. However, due to their large physical dimensions, the utilization of the reported metamaterial designs in clinical MRI applications is limited $[6-7]$. Further, these reported metasurfaces, for boosting the B_1^- of 1.5T MRI, are not flexible enough to cover different body parts such as head, legs, *etc*. undergoing scan $[6-8]$. This manuscript proposes a wearable (conformably attachable) metasurface-based add-on comprising copper apertures on a polyimide substrate for enhancing magnetic field localization inside a curved phantom mimicking human properties.

Design: The unit cell of the proposed metasurface comprises a polyimide substrate (of thickness $h = 1$ mm) sandwiched between the complementary bowtie-based aperture and square patch, as shown in Fig. 1(a). The design parameters of

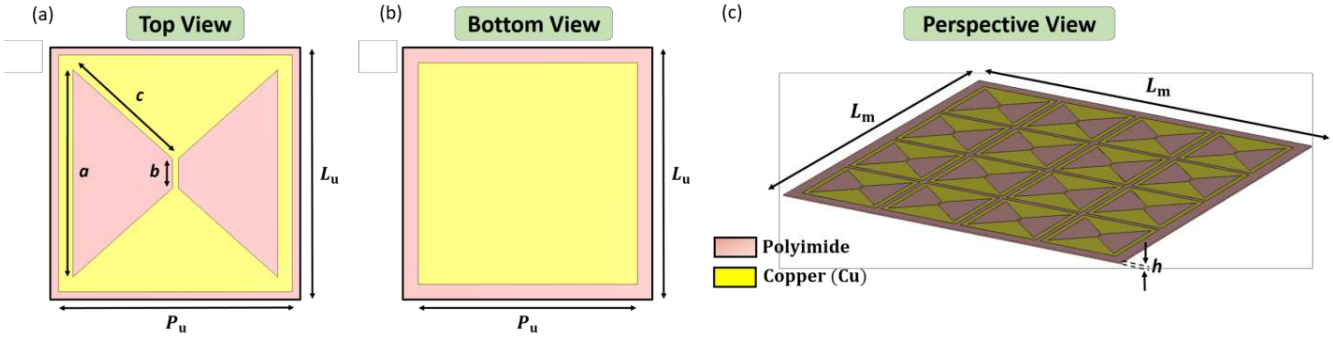


Fig.1.(a) Top (b) Bottom and (c) Perspective views of the proposed metasurface-based add-on with copper apertures on a flexible polyimide substrate.

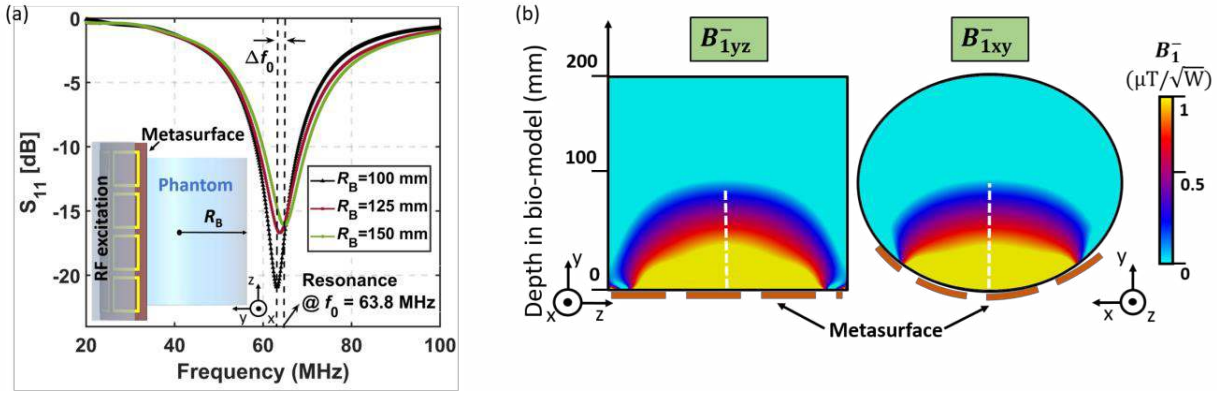


Fig.2. (a) Frequency response of the reflection coefficient of the metasurface in the scanning setup (inset), when excited by a quadrature-fed RF loop coil. (b) Received magnetic flux density (B_1^-) along (b) yz and xy plane with the metasurface at the bottom of phantom (with $R_B = 150$ mm).

complementary bowtie patch are: $a = 70$ mm, $b = 10$ mm, $c = 70$ mm, $P_u = 70$ mm, and $L_u = 80$ mm. The thickness of both copper patches on the top and bottom of the metasurface's substrate is 0.035 mm. A 4×4 array of unit cells (with dimensions $L_m \times L_m = 340$ mm $\times 340$ mm) is considered for the numerical analysis to study the enhancement in the received magnetic field inside a human properties mimicking phantom.

Results and Discussion: The metasurface is wrapped around the cylindrical phantoms of different bending radii ($R_B =$ 100 mm, 125 mm, and 150 mm), which mimics different human body parts. S-parameters are extracted from the simulation setup for the resonance analysis of metasurface in differently bent states, as shown in Fig.2(a). There is a very nominal shift ($\Delta f_0 \leq 2$MHz) in the resonating frequency ($f_0 = 63.8$ MHz) of the metasurface for various bend radii with a return loss $>$ 15 dB at f_0 for the radii. The circulating currents (*i.e.* magnetic dipoles) are generated on the resonating copper apertures of the metasurface by the magnetic flux of the RF loop coil. This significantly boosts the received magnetic field (B_1^-) inside the phantom ($R_B =$ 150 mm), as can be seen in Fig. 2(b).

Conclusion: We present a design of a wearable and body-conformal metasurface-based 'add-on', which can be wrapped around different body parts (with different curvatures) going inside the clinical MRI scanners. This will enable enhancement in received magnetic field in the region undergoing scan, leading to an enhancement in the quality of MR images.

Acknowledgments: This work is supported by MoE (PMRF) and iHUB DivyaSampark, IIT Roorkee (Project TIH/RP/05), Govt. of India.

References

1. Redpath, T W, "Signal-to-noise ratio in MRI," Brit. J. Radiol., 71(847), 704-707, 1998.
2. Ladd, M E *et al*. "Pros and cons of ultra-high-field MRI/MRS for human application," Prog. Nucl. Magn. Reson. Spectro.,109 1-50, 2018.
3. Geethanath, S. *et al*. "Accessible magnetic resonance imaging: a review," J. Magn. Reson. Imag., 49(7), pp.e65-e77, 2019.
4. Chen, H. T. *et al*. "A review of metasurfaces: physics and applications," Rep. Prog. Phys., 79(7), p.076401, 2016.
5. Padilla, W. J. "Imaging with metamaterials," Nat. Rev. Phys., 4(2), pp.85-100, 2022.
6. Gupta, J *et al*. "Thin-Wire Array based Resonator for Targeted Clinical 1.5 T Magnetic Resonance Imaging," In 2022 IEEE Photon. Confer. (IPC) 1-2, 2022.
7. Das, P. *et al*. "A thin metallo-dielectric stacked metamaterial as "add-on" for magnetic field enhancement in clinical MRI," J. Appl. Phys., 132(11), p.114901, 2022.
8. Webb, A. *et al*. "Novel materials in magnetic resonance imaging: high permittivity ceramics, metamaterials, metasurfaces and artificial dielectrics," Mag. Reson. Mater. in Phys., Biol. and Med., pp.1-20, 2022.

New Trends in Topological Matematerials

META 2023, PARIS - FRANCE, JULY 18 – 21, 2023

Topological singular points and skin modes in asymmetric dielectric structures

M. Notomi[1,2,3], T. Yoda[2], and Y. Moritake[1]

[1]Department of Physics, Faculty of Science, Tokyo Institute of Technology, Japan
[2]NTT Basic Research Laboratories, Nippon Telegraph and Telephone Corporation, Japan
[3]Nanophotonics Center, Nippon Telegraph and Telephone Corporation, Japan
*corresponding author: notomi@phys.titech.ac.jp

Abstract: We investigate how one can control topological and non-Hermitian properties by manipulating the symmetry of dielectric structures. First, we show one can create and annihilate various topological singular points starting from the topological charge of high-symmetry points or exceptional points by breaking the symmetry. Second, we demonstrate that the reciprocal non-Hermitian effect appears in simple uniform media by breaking the symmetry of the dielectric tensor.

Recently, various intriguing and non-trivial properties have been found in topological and non-Hermitian photonics. Many of these properties result from breaking the intrinsic symmetries of initial structures. In this talk, we investigate how one can manage topological and non-Hermitian properties, such as topological charges and the non-Hermitian skin effect by manipulating the spatial symmetry.

Among various topological properties of photonic crystals, we are interested in topological polarization singularity, which appears in the far-field radiation field from photonic crystals. This singularity is described by the topological charge which is derived from vectorial properties of eigenmodes in photonic crystals. Hence, this topological property does not have a counterpart in topological physics in solid-state materials governed by scalar wavefunctions. Generally, topological singular points exist at high-symmetry points in the reciprocal lattice of photonic crystals. If one breaks the intrinsic symmetry of this initial highly-symmetric photonic crystals, various non-trivial topological singular points can be generated and these points can be moved away from high-symmetry points in the reciprocal space. We previously demonstrated that non-trivial off-Γ BICs (bound states in the continuum) and circularly-polarized singular points can be generated from a trivial BIC at Γ point by breaking the C_6 rotational symmetry of the triangular lattice [1]. In this talk we extend this idea to other examples including the case starting from Dirac points in the C_6 symmetry. We will also show experimental results with fabricated photonic crystal slabs.

Next, we investigate a topological charge in non-Hermitian photonic crystals. As well known, non-Hermitian photonic crystals exhibit exceptional points (EPs) in the reciprocal space. Although it is well known that EPs appear for PT-symmetric structures, EPs can appear when the spatial symmetry of the imaginary effective refractive index (Im n) is broken. EP exhibits topological properties described by the vorticity defined by the phase rotation of the complex eigenfrequency. Employing graphene-loaded C_4 square-lattice photonic crystals, we show that the topological charge can be generated from the EP by breaking the spatial symmetry of Im n, and one can further manipulate generation and annihilation processes of EPs and topological singular points by breaking the spatial symmetry of Re n.

Lastly, we investigate non-Hermitian skin effect in dielectric media. Although the non-Hermitian skin effect has been mostly discussed in non-reciprocal discrete systems described by the tight binding model, recently, the non-Hermitian skin effect has been confirmed in reciprocal non-Hermitian photonic crystals which cannot be

expressed by the tight binding model. In the case for non-Hermitian photonic crystals, it is important to break the symmetry of the crystal structure itself [2] or of the dielectric tensor [3] to realize the skin effect. Here we show that the non-Hermitian skin effect appears even for uniform media without any crystal lattice if the dielectric tensor has a certain asymmetry and gain or loss component. We will discuss the relationship between the symmetry and this novel skin effect.

Acknowledgements

We acknowledge K. Tanaka, M. Ono, E. Kuramochi, S. Otsuka, S. Suzuki, and T. Honda for invaluable contribution. This work was supported by Japan Society for the Promotion of Science (KAKENHI JP 20H05641).

References

1. T. Yoda and M. Notomi, "Generation and Annihilation of Topologically Protected Bound States in the Continuum and Circularly Polarized States by Symmetry Breaking", Phys. Rev. Lett. 125, 053902 (2020).
2. J. Zhong, K. Wang, Y. Park, V. Asadchy, C. C. Wojcik, A. Dutt, and S. Fan, "Nontrivial point-gap topology and non-Hermitian skin effect in photonic crystals", Phys. Rev. B104, 125416 (2021).
3. K. Yokomizo, T. Yoda and S. Murakami, "Non-Hermitian waves in a continuous periodic model and application to photonic crystals", Phys. Rev. Research. 4, 023089 (2022).

3D Magnetic Topological Photonic Crystals

Baile Zhang[1, 2‡]

[1]Division of Physics and Applied Physics, School of Physical and Mathematical Sciences,
Nanyang Technological University, Singapore 637371, Singapore
[2]Centre for Disruptive Photonic Technologies, Nanyang Technological University, Singapore 637371, Singapore
corresponding authors: ‡blzhang@ntu.edu.sg

Abstract: More than a decade ago, topological photonics emerged with the discovery of the first photonic topological insulator, which was a two-dimensional (2D) periodic lattice of gyromagnetic rods or a magnetic photonic crystal. Although electronic topological insulators were successfully generalized from 2D to three-dimensional (3D) in the past decade, the development of 3D photonic topological insulators has been highly challenging. In this talk, we present some of our recent research on 3D magnetic topological photonic crystals.

The field of topological photonics [1] investigates a novel class of photonic states that exhibit topological protection, similar to the behavior of electrons in topological quantum matter. This field began a decade ago with the realization of the first photonic topological insulator, a periodic lattice of gyromagnetic rods or a magnetic photonic crystal [2]. This achievement marked the first demonstration of the Chern insulator phase [3], even before its condensed-matter realization [4], highlighting the benefits of using photonic crystals for demonstrating challenging physics.

The generalization of topological insulators from 2D to 3D was a remarkable breakthrough in topological physics, upgrading topological states from edge states to surface states [5,6]. However, the realization of their photonic analogues in 3D, known as 3D photonic topological insulators, remains extremely challenging, with only a few realizations to date [7]. Recent studies in condensed matter systems have offered new avenues for exploration in magnetic topological insulators and magnetic topological semimetals. It is thus of particular interest to explore the potential of 3D magnetic topological photonic crystals [8].

In this talk, I will present some of our recent studies on three-dimensional (3D) magnetic topological photonic crystals.

References

1. Ozawa, T., H. M. Price, A. Amo, N. Goldman, M. Hafezi, L. Lu, M. C. Rechtsman, D. Schuster, J. Simon, O. Zilberberg and I. Carusotto, “Topological Photonics,” Rev. Mod. Phys., Vol. 91, 015006, 2019.
2. Wang, Z., Y. D. Chong, J. D. Joannopoulos and M. Soljacic, “Observation of Unidirectional Backscattering-Immune Topological Electromagnetic States,” Nature, Vol. 461, 772, 2009.
3. F. D. Haldane, “Model for a quantum Hall effect without Landau levels: condensed-matter realization of the ‘parity anomaly’,” Phys. Rev. Lett., Vol. 61, 2015, 1988.
4. C.-Z. Chang, J. Zhang, X. Feng, J. Shen, Z. Zhang, M. Guo, K. Li, Y. Ou, P. Wei, L.-L. Wang, Z.-Q. Ji, Y. Feng, S. Ji, X. Chen, J. Jia, X. Dai, Z. Fang, S.-C. Zhang, K. He, Y. Wang, L. Lu, X.-C. Ma, and Q.-K. Xue, “Experimental observation of the quantum anomalous Hall effect in a magnetic topological insulator,” Science, Vol. 340, 167, 2013.
5. M. Z. Hasan and C. L. Kane, “Colloquium: topological insulators,” Rev. Mod. Phys., Vol. 82, 3045, 2010.

6. X. L. Qi and S. C. Zhang, “Topological insulators and superconductors,” Rev. Mod. Phys., Vol. 83, 1057, 2011.
7. Y. Yang, Z. Gao, H. Xue, L. Zhang, M. He, Z. Yang, R. Singh, Y. Chong, B. Zhang, and H. Chen, “Realization of a three-dimensional photonic topological insulator,” Nature, Vol. 565, 622, 2019.
8. G.-G. Liu, Z. Gao, Q. Wang, X. Xi, Y.-H. Hu, M. Wang, C. Liu, X. Lin, L. Deng, S. A. Yang, P. Zhou, Y. Yang, Y. Chong, and B. Zhang, “Topological Chern vectors in three-dimensional photonic crystals,” Nature, Vol. 609, 925, 2022.

META 2023, PARIS - FRANCE, JULY 18 – 21, 2023

Florian Marquardt

[1]Max Planck Institute for the Science of Light, Germany
[2]Friedrich-Alexander-Universität Erlangen-Nürnberg, Germany
[*]corresponding author: florian.marquardt@mpl.mpg.de

Title:

Topological Transport in a Nanoscale Optomechanical Array

Abstract:

I will present the results of a recent theory-experiment collaboration with the lab of Oskar Painter at Caltech [Nat. Comms, 13, 3476 (2022)]. We were able to design and realize the largest optomechanical array to date, using a new concept that we term a multiscale optomechanical crystal. We engineered it to produce a phononic topological metamaterial at the nanoscale, exploiting the Valley Hall effect. Thanks to the sensitivity of optomechanical measurements, we were able, for the first time, to measure the topologically protected transport of thermal excitations. This experiment paves the way towards unlocking the full toolbox of optomechanics for the field of nanoscale topological phonon transport.

META 2023, PARIS - FRANCE, JULY 18 – 21, 2023

Topological Thouless Pumping in Photonic Time Crystals

Xiang Ni[1,2], Shixiong Yin[1,3], Huanan Li[1,4] and Andrea Alù[*1,,3,5]

[1]Photonics Initiative, Advanced Science Research Center, City University of New York, New York, NY 10031, USA
[2]School of Physics and Electronics, Central South University, Changsha, Hunan 410083, China
[3]Department of Electrical Engineering, City College of The City University of New York, New York 10031, USA
[4]School of Physics, Nankai University, Tianjin 300071, China
[5]Physics Program, Graduate Center, City University of New York, New York, NY 10016, USA
[*]corresponding author: aalu@gc.cuny.edu

Abstract: We study the exotic behaviors and topological phases of photonic time crystals (PTCs) and emulate their Integer Quantum-Hall Effect in parameter space. By exploiting the eigenvalue approach of frequency vs. momentum, we verify their quantized topological invariant and disclose topological edge states at temporal boundary. To experimentally disclose their edge bands, we propose a simple approach of scattering parameters at a dedicated time relating them to the eigenmodes. We also reveal exclusive features of PTCs not observed in spatial counterpart.

Topological photonic crystals have been investigated intensively owing to their unusual topological properties like the robust edge modes immune from the backscattering, enabling opportunity for useful applications in classical and quantum optics[1]. Meanwhile, the photonic time crystals (PTCs), the analogs of spatial photonic crystals, are created by enforcing periodic temporal switching on parameters of the media. It is out of curiosity whether topological phenomena in photonic crystals can be similarly observed in PTCs. Two groups have recently inspected the topological aspects of photonic/phononic time crystals by studying 1D spatially homogenous and temporally alternative media which emulates the Su-Schrieffer–Heeger(SSH) models in the time domain[2,3], the disorder PTCs were also studied and some interesting phenomena related to temporal Anderson localization were disclosed[4,5].

Here, we study the extreme wave phenomena and topological properties of PTCs analogy to IQHEs. We develop the frequency vs. momentum approach to efficiently study the eigenstates of PTCs and topological properties of large temporal systems like photonic time quasicrystals, and prove their temporal Chern numbers, calculated from eigenstates of Floquet effective Hamiltonian, are integer quantized. To verify the bulk-edge correspondence, we generate the temporal trivial boundaries by creating switching event with large permittivity right after PTCs. As a result, the band structures of such temporal heterojunctions display gapless edge bands in the momentum bandgaps, of which the eigenstates are localized at the temporal interfaces between PTCs and TCSs. To measure the dispersion of topological edge states via the external excitation, we compare two measurement schemes and record the scattering parameters after the switching events from PTCs to TCSs or from TCSs to PTCs, and only the latter precisely captures the temporal edge bands crossing the momentum bandgap of the bulk bands, which is a unique feature for PTCs. Finally, we demonstrate the temporal topological Thouless pumping on multiple periods of PTCs, and show the transition behaviors of excited waves from the left temporal boundary, to the bulk and to the right temporal boundary. Due to the causality relation, topological edge states exhibit temporal localization on the second or later period depending on their Floquet Bloch phase, which is another exceptional feature not found in their spatial counterparts. Our findings are confirmed by full-wave simulations, and the results provide new avenues for studying topological properties of time-varying

media and enable interesting functionalities of PTCs beyond the spatial counterparts. The simple yet rich temporal models can be expediently implemented in the state-of-art photonic experiment.

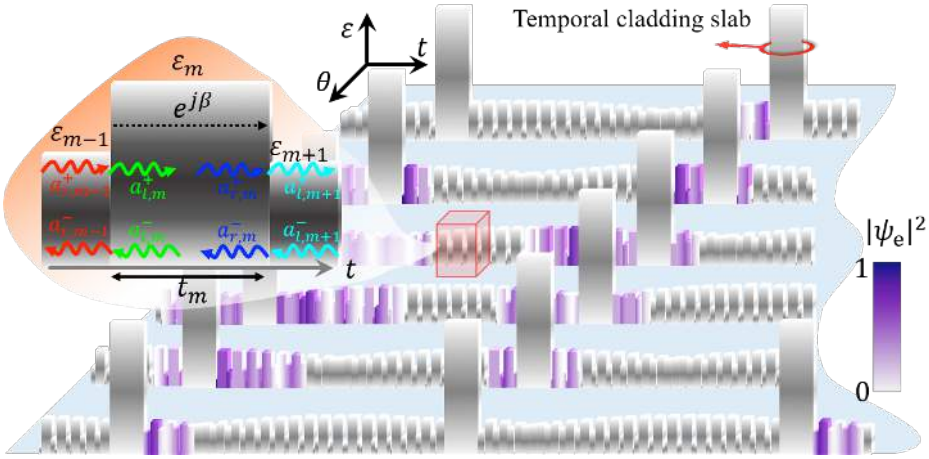


Figure 1: schematics of photonic time crystals (PTCs) with permittivity ε_m and time step δt_m modulated as a function of time slab index m and phason parameter θ accordingly. The temporal cladding slabs (TCSs) with a large permittivity ε_{tcs} act as the trivial regime next to PTCs (not to scale). The color of the pillars represents the magnitudes of edge wave functions $|\psi_e|^2$ evolving with θ, and exhibit period doubling oscillation in the time domain due to properties of Floquet Bloch waves. Inset shows forward and backward waves at different temporal interfaces formed by various time slabs. The propagation phase accumulated in each time slab is made the same and denoted as β.

References

1. T. Ozawa et al., "Topological photonics," Rev. Mod. Phys., Vol. 91, 015006, 2019.
2. E. Lustig, Y. Sharabi, and M. Segev, "Topological aspects of photonic time crystals," Optica, Vol. 5, 1390-1395, 2018.
3. M. Oudich, Y. Deng, M. Tao, and Y. Jing, "Space-time phononic crystals with anomalous topological edge states," Phys. Rev. Research, Vol. 1, 033069, 2019.
4. R. Carminati, H. Chen, R. Pierrat, and B. Shapiro, "Universal Statistics of Waves in a Random Time-Varying Medium," Phys. Rev. Lett. Vol. 127, 094101, 2021.
5. Y. Sharabi, E. Lustig, and M. Segev, "Disordered Photonic Time Crystals," Phys. Rev. Lett. Vol. 126, 163902, 2021.

Hyperbolic topological states with first-order and higher-order Chern numbers

W. X. Zhang *, and X. D. Zhang

Key Laboratory of advanced optoelectronic quantum architecture and measurements of Ministry of Education, Beijing Key Laboratory of Nanophotonics & Ultrafine Optoelectronic Systems, School of Physics, Beijing Institute of Technology, 100081, Beijing, China
*corresponding author: zhangwx@bit.edu.cn

Abstract: The exploration of novel topological physics is one of the most fascinating frontiers in recent years. So far, most studies on topological states have focused on systems in Euclidean space. Here, we report on the construction of various topological phases in hyperbolic space, which is non-Euclidean space with constant negative curvature. We firstly reveal the boundary-dominated Chern topological states in hyperbolic spaces. Moreover, based on the unique property of non-Abelian Fuchsian translation group, the 2D hyperbolic topological states with non-zero second-order Chern numbers are constructed. These exotic hyperbolic topological states have been experimentally observed by electric circuit networks.

The discovery of novel topological states has served as a major branch in physics and material sciences. To date, most of the established topological states have been employed in Euclidean systems. Recently, the experimental realization of the hyperbolic lattice with a constant negative curvature has attracted much attention. Here, we demonstrate both in theory and experiment that exotic topological states with first-order and higher-order Chern numbers can exist in hyperbolic space [1, 2].

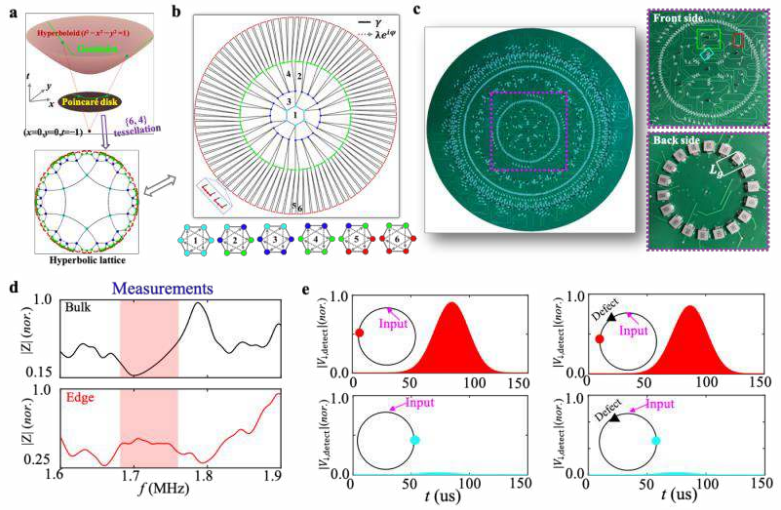


Fig. 1. Lattice model and electric circuits of hyperbolic Chern insulators.

1. Boundary-dominated topological states of hyperbolic Chern insulators. We extend the Haldane model originally defined in Euclidean space to the hyperbolic lattice {6, 4}. It is noted that the property of hyperbolic tight-binding lattice model depends on the connection of all vertices, and is regardless of the configuration of vertices. Hence, the hyperbolic lattice could also be illustrated by arranging the vertices in the form of quasi-concentric rings, and maintaining the connection of all vertices unchanged. In this case, the finite hyperbolic lattice {6, 4} with a sixfold rotation invariance in Poincaré disk (shown in Fig. 1a) is equivalent to the successive quasi-concentric rings with L=4 layers, as shown in Fig. 1b. For clarity, we mark lattice sites in the first, second, third and fourth layers by cyan, blue,

green and red dots, respectively. By introducing nearest-neighbor (NN) hoppings and direction-dependent next-nearest-neighbor (NNN) hoppings in each hexagon, the hyperbolic Haldane model is achieved. Detailed coupling patterns in hexagons composed of lattice sites from different layers are illustrated in right insets of Fig. 1b, where solid lines and dashed arrow lines correspond to NN hoppings and NNN hoppings, respectively. We numerically demonstrate that such a hyperbolic Haldane model possesses non-trivial real space Chern numbers and boundary-dominated one-way topological edge states. In experiments, we design hyperbolic Chern circuits to observe the hyperbolic Chern topological states. Fig. 1c illustrates the photograph image of the fabricated circuit sample with L=3. The front and back sides of enlarged views (enclosed the pink dashed block) and the schematic diagram of NN and NNN couplings are plotted in right insets. Based on the site-resolved impedance responses and dynamics of voltage packets, as shown in Fig. 1d, the boundary-dominated hyperbolic topological states have been observed.

2. Hyperbolic band topology with second Chern numbers. Motivated by the hyperbolic band theory, the hyperbolic topological band insulators with non-trivial first Chern numbers have been theoretically created. Here, we construct the hyperbolic topological band insulator with nontrivial second-order Chern numbers. Fig. 2a illustrates the Bravais lattice of designed hyperbolic model in a Poincaré disk, where the translational symmetry of a {8,8} hyperbolic tiling exists. Each unit cell (enclosed by the pink block), which is the fundamental tile in 2D hyperbolic space, contains four sublattice sites, as marked by colored dots in bottom inset. The infinite hyperbolic model can be constructed by tiling the 2D hyperbolic space with the unit cell along eight translational directions, which are marked by colored arrows. The inter-cell coupling patterns along these directions are illustrated in four subplots of Fig. 2b. Following the hyperbolic band theory, our proposed lattice model in 2D hyperbolic space can be described in the momentum space. In particular, we can equip inter-cell couplings of the hyperbolic unit cell with twisted boundary conditions along four translation directions, where the $U(1)$ phase factors e^{ikj} (j=1, 2, 3, 4) along eight directions are introduced. We find that such a model sustains non-trivial second-order Chern numbers. In experiments, we design and fabricate hyperbolic circuit networks with twelve units to observe the hyperbolic band topology with second Chern numbers. Fig. 2c illustrates the photograph image of the fabricated circuit sample. Based on the site-resolved impedance measurements, the non-trivial hyperbolic edge states with non-trivial second-order Chern numbers have been observed.

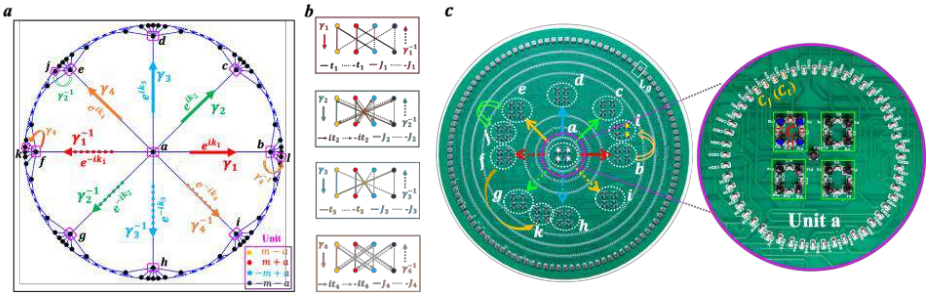


Fig. 2. Lattice model and electric circuits of hyperbolic band topology with second Chern numbers.

References

1. Zhang, W. X. et. al "Observation of novel topological states in hyperbolic lattices," Nature Communications, Vol. 13, 2937, 2022.
2. Zhang, W. X. et. al " Hyperbolic band topology with non-trivial second Chern numbers," Nature Communications, Vol. 14, 1083, 2023.

META 2023, PARIS - FRANCE, JULY 18 – 21, 2023

Optical holography and coding based on topological light field in real space

L. J. Kong, and X. D. Zhang*

Key Laboratory of advanced optoelectronic quantum architecture and measurements of Ministry of Education, Beijing Key Laboratory of Nanophotonics & Ultrafine Optoelectronic Systems, School of Physics, Beijing Institute of Technology, 100081, Beijing, China
*corresponding author: zhangxd@bit.edu.cn

Abstract: Optical knots and links have attracted great attention because of their exotic topological characteristics. Recent investigations have shown that the information encoding based on optical knots could possess robust features against external perturbations. However, as a superior coding scheme, it is also necessary to achieve a high capacity, which is hard to be fulfilled by existing knot-carriers owing to the limit number of associated topological invariants. Thus, how to realize the knot-based information coding with a high capacity is a key problem to be solved. Here, we create a type of nested vortex knot, and show that it can be used to fulfill the robust information coding with a high capacity assisted by a large number of intrinsic topological invariants. In experiments, we design and fabricate metasurface holograms to generate light fields sustaining different kinds of nested vortex links. In addition, we introduce optical topological structures into holographic technology and establish a new topological holographic coding. We verify the feasibility of the high-capacity coding scheme based on topological optical knots in experiment.

The research on topological properties has received extensive attention. In addition to the research on the topological characteristics in momentum space, the topological structure light fields and acoustic fields in real space, such as knot and link, have also attracted great attention because of their exotic topological characteristics [1–3]. Recent investigations have shown that the information encoding based on optical knots could possess robust features against external perturbations [4]. However, the capacity in this topological coding scheme based on the optical framed knots is very limited. Here, we theoretically propose and experimentally create the nested vortex knots in light fields to construct a topological coding scheme with high capacity. In addition, we introduce optical topological structures into holographic technology, demonstrate an entirely new concept of optical topological holography and establish a new topological holographic coding [5].

1. The theory of constructing nested vortex knots and links and coding scheme. We theoretically designed a nested knotted structure contains multiple topological invariants. As an example, a nested three-strand braid with twisted three times is shown in Fig. 1a. It contains three strands marked by green, red and blue. In order to show it more clearly, an enlarged view of the starting end plane is shown in Fig. 1b. The braid with a radius of r_1 is called the first-generation braid. Then, each strand with a radius of r_2 contains a sub-braid (called the second-generation braid, which is composed of three twined sub-strands). Similarly, each sub-strand with a radius of r_3 contains a sub-sub-braid (the third-generation braid, composed of three twined sub-sub-strands). Keep going in this way, we can finally construct a general nested braid structure with a fractal-like geometry. Finally, the nested link (as shown in Fig. 1c) can be obtained by using stereographic projection.

2. Coding scheme based on the nested knots and links. As shown in Fig. 1a, the braid structure corresponding to this new nested knot can contain multiple zero lines at different generation. And every zero line contains a topological invariant - the winding number $w_{\mathbf{M}_i}$. Using these topological invariants as information carriers, we design a high-capacity topological coding scheme. First of all, Alice, the sender of the message, converts the

message into a set of numbers $\{w_{\mathbf{M}_i}\}$ by using a certain program, and calculates the total values of winding numbers, W. Then, Alice chooses a positive integer α, assigns prime numbers $p_{\mathbf{M}_i}$ to the winding number $w_{\mathbf{M}_i}$, and calculates β as

$$\beta = \prod_{i=1}^{i=n} \left[\prod_{m_1=1}^{m_1=N_1} \prod_{m_2=1}^{m_2=N_2} \cdots \prod_{m_i=1}^{m_i=N_i} p_{\mathbf{M}_i}^{\left(\alpha^{w_{\mathbf{M}_i}} - W\right)} \right].$$

At the same time, a nested knotted structure (N_k) is generated, the set of winding numbers is exactly the $\{w_{\mathbf{M}_i}\}$. Then, Alice sends the pair of numbers (α, β) and the N_k to Bob in real time. After receiving these, Bob computes $\mathbb{N}_{\alpha,\beta}(W)$ with its definition, decodes the $\{w_{\mathbf{M}_i}\}$ by using prime factorization, and obtains the Alice's message.

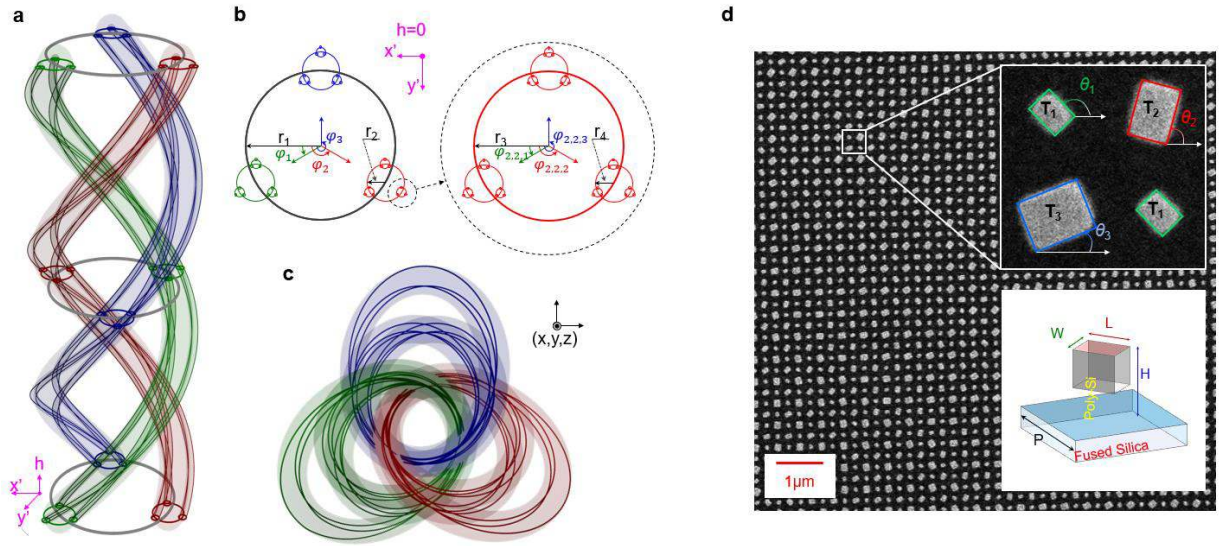


Figure 1. A nested three-strand braid with twisted three times (a, b, c) and the designed metasurface (d).

3. The Experimental demonstration. Compared with the knotted or linked structures generated previously, the nested knotted and linked structures are more complicated. Therefore, it is very difficult to construct nested knots at a single wavelength. In order to solve this problem, we design a metasurface hologram (as shown in Fig. 1d) to precisely manipulate the phase singularity of the light field at three frequencies, and experimentally realized all-optical nested knots. Furthermore, we also demonstrate both theoretically and experimentally topological holography and robust information storage with optical knots and links.

1. M. R. Dennis, R. P. King, B. Jack, K. O'Holleran, and M. J. Padgett, Nat. Phys. 6(2), 118 (2010).
2. H. Larocque, D. Sugic, D. Mortimer, A. J. Taylor, R. Fickler, R. W. Boyd, M. R. Dennis, and E. Karimi, Nat. Phys. 14(11), 1079 (2018).
3. H. Zhang, W. Zhang, Y. Liao, X. Zhou, J. Li, G. Hu, and X. Zhang, Nat. Commun. 11(1), 3956 (2020).
4. H. Larocque, A. D'Errico, M. F. Ferrer-Garcia, A. Carmi, E. Cohen, and E. Karimi, Nat. Commun. 11(1), 5119 (2020).
5. L.-J. Kong, W. Zhang, P. Li, X. Guo, J. Zhang, F. Zhang, J. Zhao, and X. Zhang, Nat. Commun. 13(1), 2705 (2022).

Experimental observation of the bulk-edge correspondence in anomalous-Chern topological insulators in a synthetic photonic lattice

Rabih El Sokhen[1], Albert F. Adiyatullin[1], Álvaro Gómez de Leon[2], Stéphane Randoux[1], Pierre Delplace[3], Alberto Amo[1*]

[1] Univ. Lille, CNRS, UMR 8523 – PhLAM – Physique des Lasers Atomes et Mol´ecules, F-59000 Lille, France
[2] Institute of Fundamental Physics IFF-CSIC, Calle Serrano 113b, 28006 Madrid, Spain
[3] ENS de Lyon, CNRS, Laboratoire de Physique (UMR CNRS 5672), F-69342 Lyon, France
[*]corresponding author: alberto.amo-garcia@univ-lille.fr

Abstract: Coupled fibre rings implement synthetic multiplexed lattices for light pulses with great flexibility to study fundamental topological properties. We measure both the intensity and the phase of the eigenvectors in a two dimensional two bands model and we extract the Berry curvature and the Chern number of the bands across topological phase transitions. The measured topological indices match perfectly the observed number of edge states in each gap at an interface, and the expected value of the Rudner invariant.

Anomalous topological insulators are paradigmatic examples of lattice systems whose topological properties arise from periodic modulations in time. The periodic driving of the lattice gives rise to a spectrum of modes that is not only periodic in space but also in quasienergy. This feature opens the possibility of having bands with topological chiral edge states traversing the gap while showing trivial Chern indices [1]. Despite the fundamental importance of these topological phases, simultaneous measurement of the anomalous bulk invariants and the presence of topological edge states has been hindered due to the stringent experimental constraints to access global and local properties in the same system.

Using a two-dimensional synthetic lattice implemented in a coupled fibre ring setup, we provide an experimental verification of the bulk-edge correspondence in anomalous and Chern topological insulators. The two band system we implement for light pulses is characterised by trivial and nontrivial Chern numbers. Using a heterodyne detection technique [2] we measure both the intensity and the phase of the eigenvectors, and we extract the Berry curvature and the Chern number of the bands. By inspecting the local changes of the Berry curvature at a topological phase transition we also measure the winding number characterising the anomalous phases. The measured topological indices match perfectly the observed number of edge states in each gap when an interface with vacuum is engineered in the experiment. These experimental observations are well described by an extension of the Rudner invariant [1] and provide the first experimental verification of the Bulk edge correspondance in Floquet-Chern insulators.

References

1. M. S. Rudner, N. H. Lindner, E. Berg, and M. Levin, “Anomalous Edge States and the Bulk-Edge Correspon- dence for Periodically Driven Two-Dimensional Systems”, Phys. Rev. X Vol. 3, 31005, 2013
2. C. Lechevalier, C. Evain, P. Suret, F. Copie, A. Amo, and S. Randoux, “Single-shot measurement of the photonic band structure in a fiber-based Floquet-Bloch lattice”, Commun. Phys. Vol. 4, 243, 2021.

META 2023, PARIS - FRANCE, JULY 18 – 21, 2023

Topological transport of GHz surface acoustic wave

Y. Nii and Y. Onose

[1]Institute of Materials Research, Tohoku university, Japan
*corresponding author: yoichi.nii.c1@tohoku.ac.jp

Abstract: Implementation of topological concept to phonon could have large impact on sound manipulation since novel features including low-dissipation, localization, and unidirectionality could be involved. Intensive studies have realized various topological acoustic waveguides, but most of the demonstrations are limited to kHz to MHz soundwaves. Here, we experimentally show GHz topological surface acoustic waves (SAW) using a nano-scaled phononic device and novel imaging technique. Our realization can be useful for superior SAW device for microwave communication.

In the last decade, the topological properties in condensed matters have been attracting much attention. The basic physics of topological insulators, Weyl semimetals, and topological superconductors have been extensively studied. The application to quantum computation or novel spintronic application has been considered.

The topological concept is now extended also to rather classic waves such as acoustic waves [1]. By constructing an artificial periodic structure denoted as phononic crystal, the topological nature such as low-dissipation, localization, and unidirectionality can be implemented to the acoustic waves. Despite their efforts, however, most experiments have remained limited to airborne sound at kHz region or elastic waves at MHz region [1]. There are two reasons for this: The most critical reason would be the increased difficulty of fabricating the sub-micron scaled device. The other reason would be high frequency measurement with high spatial resolution. Especially for GHz sounds, one cannot use classical probes such as microphone and also optical ones because the required spatial resolution is smaller than 1 μm, which is below the diffraction limit of visible light. However, it seems important to realize topological acoustic properties at these high frequencies, especially in the GHz range, since these microwave frequencies are compatible with commercial telecommunication applications. In addition, surface acoustic wave (SAW) devices with GHz working frequency are becoming increasingly important for the development of quantum technologies [2] such as quantum transduction among disparate systems and quantum control of SAW.

In this paper, we show that the topological nature can be introduced to GHz SAW device composed of a piezoelectric substrate with nano-scaled surface patterning by pillars [3]. By means of scanning microwave impedance microscopy, we directly visualized frequency dependence of the nano-scaled acoustic dynamics operating at GHz range and found acoustic edge mode when the frequency is within the band gap, consistent with the topological nature. The realization of a topological waveguide in a simple pillar structure on a substrate might pave a new path to the development of topological SAW devices for a wide range of usages such as quantum computing, sensing and communication applications.

This work is supported by JSPS KAKENHI (JP20K03828, JP 21H01036, JP 22H04461) and PRESTO (JPMJPR19L6).

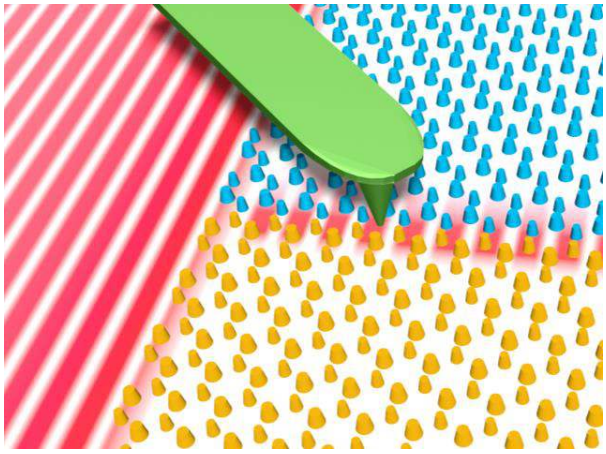


Fig. 1. Imaging of a GHz topological surface acoustic wave by scanning probe microscopy. Periodic contrast represents surface acoustic wave propagating into the phononic crystal. The dynamics at GHz range was directly visualized by scanning probe technique.

References

1. Zhang, X., Xiao, M., Cheng, Y., Lu, M. and Christensen, J., Commun. Phys. 1, 97 (2018)
2. Satzinger, K. J., Zhong, Y. P., Chang, H.-S., Peairs, G. A., Bienfait, A., Chou, Ming-Han., Cleland, A. Y., Conner, C. R., Dumur, É., Grebel, J. *et al.*, "Quantum control of surface acoustic-wave phonons", Nature 563, 661 (2018)
3. Nii, Y. and Onose, Y., "Imaging an Acoustic Topological Edge Mode on a Patterned Substrate with Microwave Impedance Microscopy", Phys. Rev. Applied., **19**, 014001 (2023)

META 2023, PARIS - FRANCE, JULY 18 – 21, 2023

Non-Hermitian topological light manipulations in integrated waveguide lattices

Wange Song[1*], Luqi Yuan[2], Shining Zhu[1], and Tao Li[1*]

[1]College of Engineering and Applied Sciences, Nanjing University, Nanjing, 210093, China
[2]State Key Laboratory of Advanced Optical Communication Systems and Networks, School of Physics and Astronomy, Shanghai Jiao Tong University, Shanghai 200240, China
[*]corresponding author: songwange@nju.edu.cn, taoli@nju.edu.cn

Abstract: Non-Hermitian photonics has established entirely new ways for flexible control of light, which has sparked considerable interest in connection with topological physics. Here, we propose a new concept of *non-Hermitian synthetic dimension* and reveal its capability in manipulating the topological states, e.g., zero and Floquet π states. Significantly, we unveil new types of high-dimensional Weyl states hidden in this non-Hermitian dimension. We anticipate our integrated photonics platform to reveal more complex non-Hermitian topology in the future.

Topological photonics has successfully opened up a new degree of freedom for light manipulations. Recently, the study of high-dimensional topological effects by *synthetic dimension* has sparked considerable interest. Compared with the existing construction of synthetic dimensions in the Hermitian systems, the introduction of non-Hermitian parameters will increase the dimension of the system and is expected to form a new topological phase of matter. Here, I would like to show two fascinating examples demonstrated in integrated silicon waveguide platforms. One is the recovery of topological zero/π modes in static/driven systems from topologically trivial lattices by non-Hermitian synthetic modulations [1,2]. Such a non-Hermitian potential is further extended as a new synthetic dimension in another example. By carefully modulating the loss arrangement in the waveguides, new Weyl interface states were successfully observed in optical regimes [3]. They significantly originate from the *non-Hermitian order* transition, which are quite different from many previous interface modes caused by the *topological order* transition. Our works enrich non-Hermitian topological physics, which would possibly stimulate more interesting phenomena beyond this.

References

1. Song, W., et al., “Breakup and recovery of topological zero modes in finite non-Hermitian optical lattices,” Phys. Rev. Lett. Vol. 123, 165701, 2019.
2. Wu, S., et al., “Floquet π mode engineering in non-Hermitian waveguide lattices,” Phys. Rev. Research Vol. 3, 023211, 2021.
3. Song, W., et al. “Observation of Weyl interface states in non-Hermitian synthetic photonic systems,” Phys. Rev. Lett. Vol. 130, 043803, 2023.

Beam Trajectory Steering by Distorted Photonic Crystals

K. Kitamura[1, 2*], J. Hashizume[1], Y. Kawamoto[1], A. Onishi[1] and H. Kitagawa[1]

[1] Kyoto Institute of Technology, JAPAN

2 Japan Science and Technology Agency PREST, JAPAN

[*]corresponding author: kyoko@kit.ac.jp

Abstract: We show beam trajectory bending, meandering, bifurcating and beam splitting by distorted photonic crystals which possess adiabatic change (lattice distortion) in photonic crystal lattice properties.

A Photonic crystal (PC) is an artificial material that is constructed by periodically arranging two or more dielectric media with different relative permittivity. Due to such periodicity, PCs possess a photonic band structure that controls the group velocity of light waves and that lead exotic beam trajectory such as negative refraction and superprism effect. Recently, we defined a PC that exhibits adiabatic change (lattice distortion) in the lattice constant as a distorted PC (DPC). In contract to the above-mentioned effects, even in isotropic dispersion region (low-frequency range), the light trajectory can be bent in DPCs. Some specific examples of schematic DPCs and beam trajectories in their DPCs are shown in Fig. 1. Although all DPCs maintain the averaged refractive index in the unit cells homogeneously, the beam trajectories show bending (Fig. 1 (f)), meandering (Fig. 1 (g)), bifurcating and beam splitting (Fig. 1 (h)), in contrast to the straight trajectory in non-distorted (normal) PC (Fig. 1 (e)). These beam trajectory steering effects can evaluate from the viewpoints of differential geometry [1] and adiabatic change of equi-frequency contours [2-3]. Since no spatial varies of refractive index, these light propagation controls using lattice distortion will be new approach in the fields of transformation optics. Details will be reported at the conference.

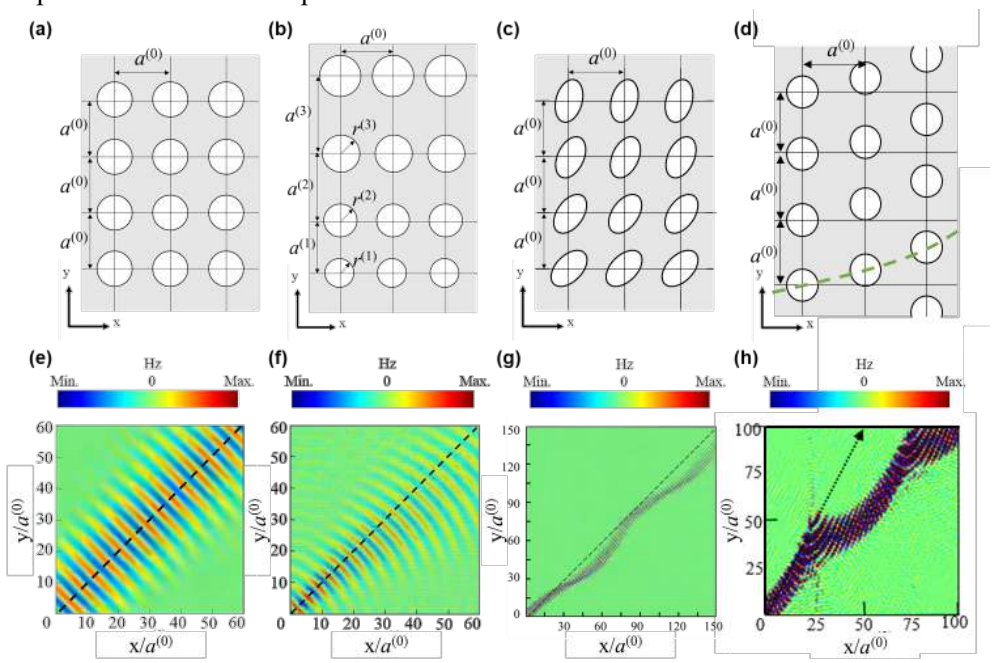


Fig. 1 (a)-(d) Schematic lattice-points arrangements of the DPCs based on a square-lattice PC. (a) non-distorted PC, (b) position-(lattice constant-) DPC, (c) shape-DPC, (d) slip-DPC. (e)-(h) Numerical simulation results of light trajectory (H_z-polarization, frequency is 0.2 $c/a^{(0)}$). (e), (f), (g), (h) correspond to the structures of (a), (b), (c), (d) respectively.

References

1. Kitagawa, H, K. Nanjyo, and K. Kitamura, “Effective field theory for distorted photonic crystals,” Phys. Rev. A 103(6) 063506 (2021).
2. Nanjyo, K, H. Kitagawa, D. Headland, M. Fujita, and K. Kitamura, “Steering of beam trajectory by distorted photonic crystals,” arXiv:2110.05729.
3. Honda, M, K. Nanjyo, J. Hashizume, H. Kitagawa and K. Kitamura, “Beam Trajectory Bending and Meandering by Distorted Photonic Crystal” The 15th Pacific Rim Conference on Lasers and Electro-Optics, CFP8I-04 (2022).

Filling anomalies and chiral winding numbers in higher-order topological metamaterials

Wladimir A. Benalcazar[1,*]

[1] *Department of Physics, Emory University*

(Dated: March 17, 2023)

Abstract

I will present the classification of topological bands in one- and two-dimensional crystalline metamaterials based on "filling anomalies" and their accompanying "symmetry indicator invariants." I will first show how this classification facilitates the diagnosis of metamaterial analogs of obstructed atomic limits, fragile phases, and stable topological phases that include bands with Dirac points and Chern numbers. Then, I will present phases outside of that classification; these are chiral-symmetric higher-order topological phases whose invariants, "multiple chiral numbers," indicate the number of degenerate mid-gap states at each corner. Finally, I will show an experimental realization of such a phase in an acoustic metamaterial.

* benalcazar@emory.edu

META 2023, PARIS - FRANCE, JULY 18 – 21, 2023

Adiabatic topological photonics

Anton Vakulenko[1], Svetlana Kiriushechkina[1], Daria Smirnova[2], Sriram Guddala[1], Filipp Komissarenko[1], Andrea Alù[1,3], Monica Allen[4], Jeffery Allen[4], and Alexander B. Khanikaev[1,3*]

[1]Electrical Engineering and Physics, The City College of New York (USA), New York, NY 10031, USA

[2]Research School of Physics, The Australian National University, Canberra ACT 2601, Australia

[3]Physics Program, Graduate Center of the City University of New York, New York, NY 10016, USA

[4]Air Force Research Laboratory, Munitions Directorate, Eglin AFB, USA.

[*]corresponding author: akhanikaev@ccny.cuny.edu

Abstract: We introduce the concept of adiabatic topological photonic structures, which allows us to overcome many of the limitations of topological photonic metasurfaces. Adiabatic variation of the mass terms at the domain walls makes topological boundary modes less sensitive to details of the lattice, perceiving the structure as an effectively homogeneous Dirac metasurface. As the result, the modes exhibit longer radiative lifetime and propagation distance, while retaining their topological resilience.

Topological phases of matter represent a new realm of physics that has been attracting significant attention across diverse fields, from inherently quantum systems (e.g., condensed matter and lattices of trapped ions) to purely classical photonic and acoustic metamaterials. In the context of photonics, topological phases offer resilience to defects and disorder and bring novel opportunities to control light with pseudo-spin degrees of freedom. However, topological photonic systems can suffer from limitations associated with their bosonic nature, including partial breakdown of topological properties due to their symmetry-protected origin and radiative leakage. In this article, we introduce the concept of adiabatic topological photonic interfaces, which helps to overcome many of these issues. We demonstrate theoretically and confirm experimentally that adiabatic topological metasurfaces with slowly varying synthetic gauge fields significantly improve trapping of optical modes, and also offer excellent guiding features in both spin-Hall and valley-Hall topological photonic structures, which are the most commonly used in the design of symmetry- protected topological devices. Adiabatic variation of the mass terms at the domain walls leads to the delocalization of topological boundary modes, which makes them less sensitive to details of the lattice, perceiving the structure as an effectively homogeneous Dirac metasurface [1]. As the result, the modes showcase enhanced bandgap crossing behavior, longer radiative lifetime, and propagation distance, while retaining their topological resilience. At the same time, localized modes trapped due to the 2D variation of the mass term [2] exhibit high quality factors and controllable radiative properties, which, along with non-zero angular momentum of their far field, makes them of great interest for applications.

References

1. S. Kiriushechkina, S., Vakulenko, A., Smirnova, D., Guddala, S., Komissarenko, F., Allen, M., Allen, J., and Khanikaev, A. B., Spin-Full Guided Modes in Photonic Dirac Metasurfaces, (arXiv:2211.00701 – Photonic Dirac Waveguides), Nature Nanotech. (2023) (in press).
2. Chen, K., Komissarenko, F., Smirnova, D., Vakulenko, A., Kiriushechkina, S., Volkovskaya, I., Guddala, S., Menon, V., Alù, A., and Khanikaev, A. B., Photonic cavities within Dirac metasurfaces with spatially varying mass, Science Advances (2023) (in press).

Nanophotonic structures to control propagation, emission and topological behavior of light

Ganapathi Subramania

Semiconductor materials and device sciences, Sandia National Laboratories,

Albuquerque, NM 87185

Abstract: This work describes controlling light propagation, emission and topological behavior of light using seminconductor based nanophotonic structures.

Controlling light at the scale of few wavelengths of is enabled by nanophotonic structures such as photonic crystals, metamaterials and metasurfaces and have emerged as key components in modern photonics. With suitable design these nanophotonic structures offer new capabilities as well as versatility in controlling various aspects such as light-propagation, polarization, emission, photon statistics, topological property etc. greatly influencing chipscale photonics. The talk will cover research carried out along with my colleagues at Sandia using nanophotonic architectures. This will include work on light emission and lasing from III-nitride based photonic crystals, and dynamic index modulation and nanofabrication control with electrochemical and photolectrochemical etching[1-3]. Furthermore, we will discuss topologically non-trivial photonic structures[4] that exhibit one-way scatter-free light transport and their implementation in silicon-on-insulator material that can have important applications in optical and quantum communications.

Sandia National Laboratories is a multimission laboratory managed and operated by National Technology & Engineering Solutions of Sandia, LLC, a wholly owned subsidiary of Honeywell International Inc., for the U.S. Department of Energy's National Nuclear Security Administration under contract DE-NA0003525. The views expressed in the article do not necessarily represent the views of the U.S. Department of Energy or the United States Government.

References:

[1] P. D. Anderson, A. J. Fischer, D. D. Koleske, B. P. Gunning, and G. Subramania, "III-nitride photonic crystal emitters by selective photoelectrochemical etching of heterogeneous quantum well structures," *Optical Materials Express,* vol. 8, no. 11, pp. 3543-3550, 2018/11/01 2018, doi: 10.1364/OME.8.003543.

[2] A. J. Fischer, P. D. Anderson, D. D. Koleske, and G. Subramania, "Deterministic Placement of Quantum-Size Controlled Quantum Dots for Seamless Top-Down Integration," *ACS Photonics,* vol. 4, no. 9, pp. 2165-2170, 2017/09/20 2017, doi: 10.1021/acsphotonics.7b00774.

[3] X. Xiao *et al.*, "Quantum-Size-Controlled Photoelectrochemical Fabrication of Epitaxial InGaN Quantum Dots," *Nano Lett.,* vol. 14, no. 10, pp. 5616-5620, 2014/10/08 2014, doi: 10.1021/nl502151k.

[4] P. D. Anderson and G. Subramania, "Unidirectional edge states in topological honeycomb-lattice membrane photonic crystals," *Optics Express,* vol. 25, no. 19, pp. 23293-23301, 2017/09/18 2017, doi: 10.1364/OE.25.023293.

META 2023, PARIS - FRANCE, JULY 18 – 21, 2023

Harness Light with Spinor Wavefunction

Xiao Hu*

International Center for Materials Nanoarchitectonics (MANA), National Institute for Materials Science (NIMS), Japan
*corresponding author: Hu.Xiao@nims.go.jp

Abstract: Dirac dispersions are associated with spin degree of freedom. Electromagnetic modes in honeycomb photonic crystals exhibiting Dirac-type frequency dispersions are characterized by synthetic spin and described in terms of spinor wavefunctions. We show that spinor wavefunctions can be exploited for harnessing light and achieving novel features.

Honeycomb structures host Dirac-type energy and/or frequency dispersions where spin degree of freedom appears with spinor wavefunctions [1]. It was shown that deforming the honeycomb structure in a semiconductor photonic crystal in ways respecting C_{6v} symmetry, one opens gaps at Γ point in the Dirac-type dispersion accompanied by a p-d band inversion, where the frequency difference between p and d modes defines the Dirac mass. The structure with negative Dirac mass (p-mode with higher frequency) constitutes a photonic analogue of quantum spin Hall effect [2].

Unlike the case of electron with spin as an intrinsic property, the photon spinor wavefunctions with basis formed by the p and d modes are defined in real space, which yields a unique interference between the two spinor components. In this talk, I discuss how this real-space spinor wavefunction works for the topological interface propagations in semiconductor topological photonic crystals [3], in parallel to the seminal Jackiw-Rebbi soliton solution for s=1/2 fermionic field. I then show that one can harness the topological waveguide mode in terms of the light spinor compatible with nanofabricated photonic crystal structures. As another interesting example, I reveal how the light spinor wavefunction can be explored for realizing a high-performance topological cavity surface emission laser (TCSEL) with frequency slightly below the lower band edge [4,5].

This work is supported by JST CREST (No. JPMJCR18T4).

References

1. H.-M. Weng, R. Yu, X. Hu, X. Dai and Z. Fang: “Quantum anomalous Hall effect and topological electronic states”, Adv. Phys. **64**, 227 (2015).
2. L.-H. Wu and X. Hu: “A scheme for achieving topological photonic crystal by using dielectric material”, Phys. Rev. Lett. **114**, 223901 (2015).
3. Y.-T. Yang, Y.-F. Xu, T. Xu, H.-X. Wang, J.-H. Jiang, X. Hu and Z.-H. Hang: “Visualization of unidirectional optical wave guide using topological photonic crystals made of dielectric material”, Phys. Rev. Lett. **120**, 217401 (2018).
4. Z.-K. Shao, H.-Z. Chen, S. Wang, X.-R. Mao, Z.-Q. Yang, S.-L. Wang, X.-X. Wang, X. Hu and R.-M. Ma: “A high-performance topological bulk laser based on band-inversion-induced reflection”, Nat. Nanotechnol. **15**, 67 (2020).
5. H. Huang, X.-X. Wang, T. Kariyado and X. Hu: submitted (2023).

Topological photonic integrated circuits for controlling optical vortex signal

T. Amemiya[1*], H. Kagami[1], S. Okada[1], I. Sakamoto[1], N. Nishiyama[1], and X. Hu[2]

[1]Department of Electrical and Electronic Engineering, Tokyo Institute of Technology, Tokyo 152-8552, Japan,
[2]WPI-MANA, National Institute for Materials Science, Ibaraki 305-0044, Japan
[*]corresponding author: amemiya.t.ab@m.titech.ac.jp

Abstract: Topological photonics brings the concept of mathematical topology into the field of optics, which allows us to systematically handle information derived from the topology of light, such as optical spin and orbital angular momentum. In this talk, starting from the concept of topological photonic integrated circuits, we describe analytical methods, fabrication technology, and its application to optical circuits.

1. Introduction

Tracing the topology of electronic systems in topological insulators and Weyl semimetals into photon systems is called 'topological photonics' and has rapidly progressed in recent years [1]. In particular, for a typical photonic structure in which multiple dielectrics having C_6 symmetry are arranged in a honeycomb lattice, unprecedented optical phenomena can be realized because the unit cell has a higher degree of freedom in that configuration than that of a conventional photonic crystal whose unit cell comprises one dielectric. The most well-known phenomenon of topological photonics is the topological edge state which enables the propagation of optical vortices in optical circuits. Therefore, by replacing a part of the conventional optical circuit with a topological photonics system, we aim to realizing various controls of optical vortex signal in the photonic integrated circuit (TPICs: Topological Photonic Integrated Circuits) [2-5]. Since the optical vortex carries information on the helical cycle of the wave front, it is attracting attention as a key technology for high-capacity transmission.

2. Infrared photonic band microscope for high-speed measurement of topological photonic crystal

In the field of topological photonics, it is well known that the ℤ2 topology is expressed by using photonic structures consisting of a honeycomb lattice of unit cells, where the dielectrics are arranged with C_{6v} symmetry [6]. In the above structure, interaction is required not only between unit cells but also inside them. Thus, these systems require extremely fine structural design and fabrication compared to conventional photonic crystals. This is particularly noticeable in the optical communication band, which is considered as the most useful application area for these systems.

In this study, we developed and commercialized an infrared photonic band microscope based on hyperspectral Fourier image spectroscopy (Fig. 1) [7-9]. Developed microscope obtained a Fourier image for each wavelength

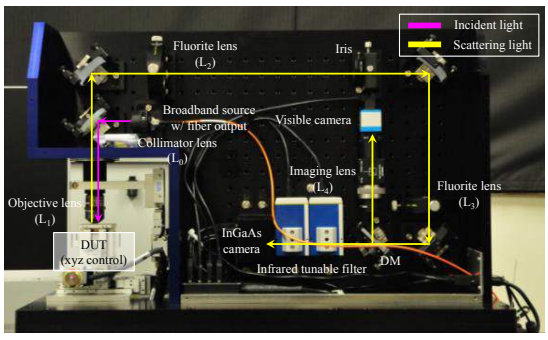


Fig. 1. Configuration of photonic band microscope.

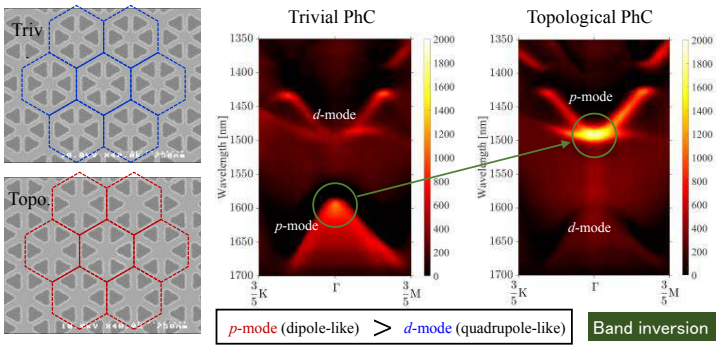


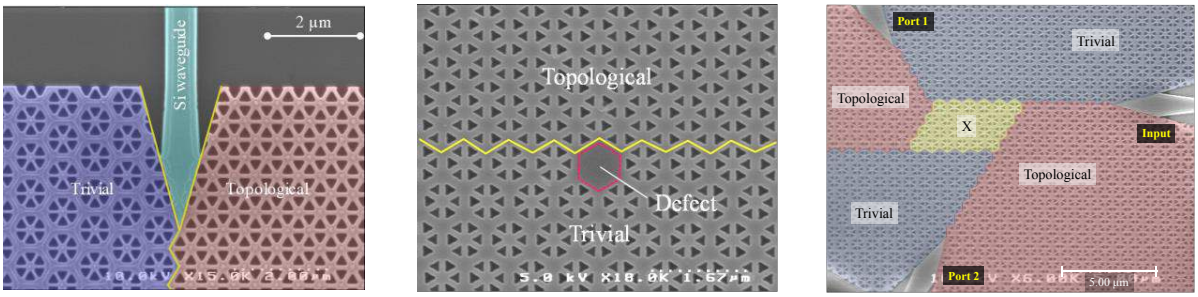
Fig. 2. Measured photonic band of two topological PhC with different topology

by using infrared hyperspectral imaging, following which it reconstructed a photonic band diagram based on these images. Figure 2 shows measured photonic band of two topological photonic crystals with different topology. Photonic band gap was observed at the wavelength of 1.55 μm near the Γ point for both photonic crystals. The intensities of the upper and lower band gap edges close to the Γ point are reversed. In general, the reflection intensity of the *d*-wave in the electromagnetic mode tends to be weaker than that of the *p*-wave [X]. Therefore, the experimental results show that the electromagnetic modes of the *p*-wave and *d*-wave are band inverted, which suggests the expression of different topologies.

3. Each element for constructing TPICs

Toward the topological photonic integrated circuits (TPICs), we have proposed the following four basic components. They are: (i) topological waveguide for propagating optical vortex signals with a specific charge number [2]; (ii) topological mode converter to realize highly efficient horizontal coupling from a normal waveguide to a topological waveguide (Fig. 3a) [3]; (iii) topological vertical coupler to realize highly efficient coupling from free space to a topological waveguide (Fig. 3b) [4]; (iv) topological splitter for branching optical vortex signals (Fig. 3c) [5]. The day's presentation will touch on all of the above, but this paper will focus specifically on the topological splitter.

Figure 3c illustrates the operating principles of topological splitter using the ℤ2 topological photonic phase. The device consists of five domains, namely, the two trivial photonic domains, two topological photonic domains, and a variable photonic domain (domain X). Here, we consider controlling the intensity ratio of the optical vortex signal emitted from output 1 and 2 by arranging a suitable photonic structure in the central domain X. When the trivial photonic structure or topological photonic structure was arranged in the domain X, the input was directly connected to each output through a topological edge state waveguide, and the optical vortex signal was output only to port 1 or port 2. Furthermore, when a zero-bandgap photonic structure—where all electromagnetic modes are degenerated in the center of the Brillouin zone—was arranged in the domain X, the intensity ratio of the optical vortex signal emitted from output 1 and 2 approached 1:1.



(a) (b) (c)

Fig. 3. Scanning electron microscope images of basic components for TPICs. (a) Topological mode converter. (b) Topological vertical coupler. (c) Topological splitter.

References

1. T. Ozawa *et al.*, *Rev. Mod. Phys.* **91**, 015006 (2019).
2. H. Kagami, T. Amemiya, S. Okada, Y. Wang, N. Nishiyama, X. Hu, *Optics Letters* **47**, 2190 (2022).
3. H. Kagami, T. Amemiya, S. Okada, N. Nishiyama, and X. Hu, *Opt. Express* **28**, 33619 (2020).
4. H. Kagami, T. Amemiya, S. Okada, N. Nishiyama, X. Hu, *Optics Express* **29**, 32755 (2021).
5. S. Okada *et al.*, Proc. *The Conference on Lasers and Electro-Optics 2020* (CLEO 2020), JW2A.38 (2020).
6. L.-H. Wu and X. Hu, *Phys. Rev. Lett.* **114**, 223901 (2015).
7. T. Amemiya, S. Okada, H. Kagami, N. Nishiyama, Y. Yao, K. Sakoda, X. Hu, *Optics Letters* **47**, 2430 (2022).
8. S. Okada, T. Amemiya, H. Kagami, Y. Wang, N. Nishiyama, X. Hu, *J. Opt. Soc. Am. B* **39**, 2464 (2022).
9. https://www.tokyoinst.co.jp/en/products/detail/photonic_band_diagram_microscope/TTA01/index.html

META 2023, PARIS - FRANCE, JULY 18 – 21, 2023

High-throughput generation of topological metamaterials

S. D. Huber

[1]AInsitut for Theoretical Physics, ETH Zurich, CH-8093 Zürich
sebastian.huber@phys.ethz.ch

Abstract: There is a wide range of design principles for topological metamaterials. All the indices characterizing of such topological materials also have a correspondence in terms of crystalline symmetries. In this framework, all metamaterials fall under the category of fragile topological insulators. Here we present an algorithm how to find fragile topological bands in two spatial dimensions. We generate all possible fragile bands, up to several ten-thousand structures per unique class and perform a statistical analysis of the so-obtain topological metamaterials.

Crystalline topological insulators can be described using the framework of topological quantum chemistry: Using band induction, all *trivial* bands can be exhaustively tabulated [1]. Using this table, one can in turn test any band-structure: If it is not in the table of trivial bands it has to be topological. Amongst those, there are two classes: strong and fragile ones, where in the absence of spin-orbit interactions for spin-1/2 particles, only the latter can be realized. In fact also those fragile ones have been tabulated for two spatial dimensions [2]. In other words: there exists a list all possible physically realizable two-dimensional topological insulator states for classical systems.

We devise a search algorithm to find all of these states. Using an advanced evolution algorithm, the Covariance Matrix Adaptation Evolution Strategy (CMA-ES) we find up to several ten thousands samples for each possible topological band systems. We perform a statistical analysis on their relative frequency, their topological content, as well as their surface physics.

With this tool we allow for on-demand large-throughput searches for topological bands, tailored to specific applications.

References

1. Bradlyn, B. et al. “Topological Quantum Chemistry”, Nature, 547, 298, 2017
2. Song, Z.-D. et al. “Twisted bulk-boundary correspondence of fragile topology,” Science, 367, 794, 2017

Probing bulk topology of one dimensional synthetic frequency lattice

Greta Villa[1,2], Iacopo Carusotto[3], and Tomoki Ozawa[2*]

[1] Department of Physics, University of Konstanz, D-78464 Konstanz, Germany
[2]Advanced Institute for Materials Research, Tohoku University, Japan
[3]Pitaevskii BEC Center, INO-CNR and Dipartimento di Fisica, Università di Trento I-38123 Trento, Italy
[*]corresponding author: tomoki.ozawa.d8@tohoku.ac.jp

Abstract: Ways to effectively realize lattice models utilizing a frequency degree of freedom of photonic resonators as an effective "synthetic" dimension have been actively studied in photonic community. Since the frequency degrees of freedom is used as a spatial degree of freedom in realizing lattices, its conjugate variable, which is time, plays a role analogous to momentum. We propose how to detect the bulk topological invariant of one-dimensional topological lattices in such a synthetic frequency lattice in the presence of losses.

Synthetic dimensions provide a unique way to realize various lattice models in photonic setups by using non-spatial degrees of freedom as dimensions [1-3]. Recently, of particular interest in photonic community is the synthetic frequency lattice where frequency modes of resonators span a synthetic dimension which can be exploited to realize topological lattice models [4,5]. Topological lattice models are lattices whose energy eigenstates in momentum space exhibit nontrivial shape, or topology [6].

In a synthetic frequency dimension, an equivalent of momentum space is time. Although bulk energy band in a synthetic frequency dimension has been experimentally measured [7,8], it is still unclear how one can detect bulk topological number in such situations, in particular in the presence of inevitable losses of photons.

In this talk, we propose some methods to detect the bulk topological invariant of one dimensional topological models along a synthetic frequency dimension in the presence of a chiral symmetry. We show that a clear signature of bulk topological number, i.e. the winding number, can be obtained by looking at an analog of the mean chiral displacement [9] in driven-dissipative setups.

T. O. acknowledges support from JSPS KAKENHI Grant No. JP20H01845, JST PRESTO Grant No. JPMJPR19L2, and JST CREST Grant No. JP- MJCR19T1.

References

1. Yuan, L., Q. Lin. M. Xiao, and S. Fan, "Synthetic dimension in photonics" Optica **5**, 1396-1405 (2018).
2. Ozawa, T. and H. M. Price, "Topological quantum matter in synthetic dimensions," Nat. Rev. Phys. **1**, 349–357 (2019).
3. Lustig, E. and M. Segev, "Topological photonics in synthetic dimensions. Adv Opt Photonics 13, 426 (2021).
4. Ozawa, T., H. M. Price, N. Goldman, O. Zilberberg, and I. Carusotto, "Synthetic dimensions in integrated photonics: From optical isolation to four-dimensional quantum Hall physics," Phys. Rev. A **93**, 043827–17 (2016).
5. Yuan, L., Y. Shi, and S. Fan, "Photonic gauge potential in a system with a synthetic frequency dimension," Opt. Lett., **41**, 741 (2016).
6. Ozawa, T. et al. "Topological photonics," Rev. Mod. Phys. **91**, 015006 (2019).
7. Dutt, A. et al. "Experimental band structure spectroscopy along a synthetic dimension," Nat. Comm. **10**, 3122 (2019).
8. Balčytis, A., T. Ozawa, Y. Ota, S. Iwamoto, J. Maeda, T. Baba, "Synthetic dimension band structures on a Si CMOS photonic platform," Science Adv. **8**, eabk0468 (2022).
9. Cardano, F. et al., "Detection of Zak phases and topological invariants in a chiral quantum walk of twisted photons," Nat. Comm. **8**, 15516 (2017).

Photonic Bimorphic Floquet Topological Insulators

Julius Beck[1*], Georgios G. Pyrialakos[2,3*], Matthias Heinrich[1], Lukas J. Maczewsky[1], Mercedeh Khajavikhan[4], Nikolaos V. Kantartzis[3], Alexander Szameit[1] and Demetrios N. Christodoulides[2]

[1] Institute for physics, University Rostock, Albert-Einstein-Str. 23, 18059 Rostock, Germany.
[2]College of Optics & Photonics-CREOL, University of Central Florida, Orlando, Florida 32816, USA.
[3]Department of Electrical and Computer Engineering, Aristotle University of Thessaloniki, GR-54124 Thessaloniki, Greece.
[4]Ming Hsieh Department of Electrical and Computer Engineering, University of Southern California, Los Angeles, CA, USA.
*equal contribution
Contact: julius.beck@uni-rostock.de

Abstract: We introduce a novel class of Floquet topological insulators simultaneously hosting Chern-type and anomalous edge states. The driving mechanism is implemented using laser-written waveguides arranged in a chained honeycomb lattice, allowing us to observe its different chiral edge states.

Floquet topological phases in photonic lattices [1] are typically realized by helical modulation [2] or the imposition of discrete coupling protocols [3,4]. In this work, a new method that allows for the distinct characteristics of these approaches to coexist while overcoming technical limitations such as curvature losses by virtue of entirely straight waveguides is presented and experimentally demonstrated. Our driving scheme leverages interstitial sites whose on-site potential

$$\mathrm{V}_j(t) = 1 + \sin\left(\frac{2\pi t}{T} + \frac{2\pi j}{3}\right) \quad j \in \{1,2,3\}, \tag{1}$$

is sinusoidally modulated with a Floquet period T and systematically phase-shifted counterclockwise in steps of $2\,\pi/3$ around the primary sites of a conventional honeycomb lattice (s. Fig. 1a) [5]. In this vein, chirality is induced while preserving the sublattice symmetry. In the static case ($V_j = 0$), the band structure comprises two copies of the conventional honeycomb spectra symmetrically arranged around a zero-energy degenerate flat band that hosts compact and localized states (CLS) exclusively residing on the interstitial sites. In the presence of the Floquet drive, two additional band gaps emerge at the Dirac points (s. Fig. 1b), giving rise to conventional Chern-type edge states as evidenced by the nontrivial Chern numbers $\mathcal{C}$ of the adjacent bands. Crucially, at the same time, a second type of chiral states bifurcate from the flat band. In accordance with their anomalous nature, they are described by winding numbers $\mathcal{W} = 1$.

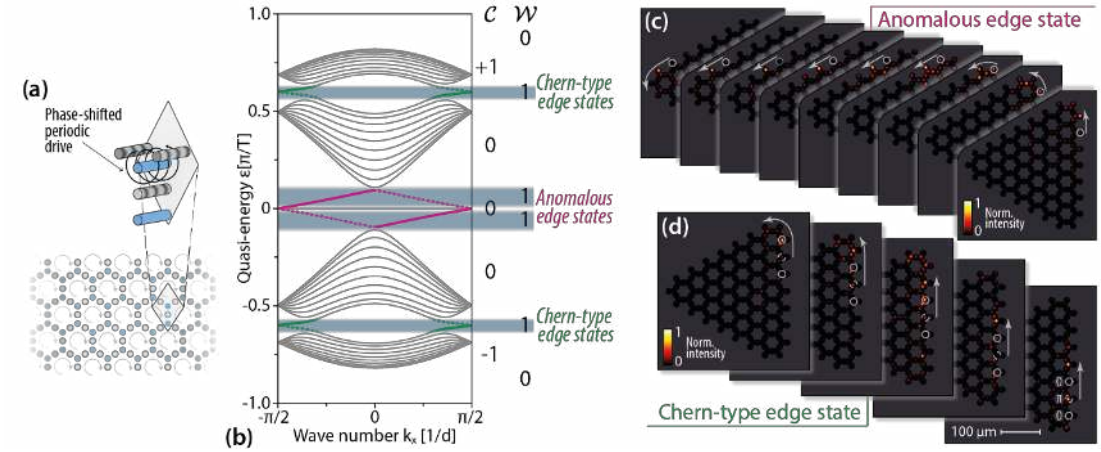


Fig. 1: Chain-driven honeycomb lattice. (a) The chained honeycomb lattice comprises interstitial sites (grey), that are sinusoidally modulated in their onsite potential and placed between adjacent principal elements (blue). (b) The Floquet drive creates bandgaps at the Dirac points, inducing a non-trivial topology (Winding number of blue shaded gaps becomes $\mathcal{W} = 1$) and coexisting Chern-type and anomalous boundary states emerge. (c,d) Both edge states propagate around corners along the edge in a protected fashion.

In order to experimentally study the propagation dynamics in this system, we implement the chain-driven honeycomb structure in femtosecond laser-written waveguide lattices [7], where the light evolution is described by a Schrödinger-type equation in which the refractive index profiles of the individual waveguides act as potential wells of the lattice atoms. In this vein, the on-site potential is directly related to the effective refractive index contrast each waveguide, allowing for it to be modulated at will along the propagation coordinate *z* that takes the role of time by appropriate changes to the writing speed. By injecting light into the encircled sites depicted in Fig. 1 c,d, the helical states were populated and their protected edge propagation around the corners was observed. In this vein, the dispersive nature of the Chern-type and compactness of the anomalous edge state are demonstrated.

In addition to the the helical states, the fraction of the flat band that persists in the driven lattice can be populated in the form of quasi-CLS in the bulk. This correspondence opens up the possibility to set the light in motion by exciting the anomalous chiral state, to temporarily trap it with high efficiency in CLS by suspending the modulation of the interstitial sites at an appropriate time, and resuming it as desired to allow the wave packet to continue along its way. The presented Floquet mechanism is general, and can be applied to other lattice geometries and any topological platform that allows for a control of the on-site potential.

References

1. T. Kitagawa, E. Berg, M. Rudner, and E. Demler, "Topological characterization of periodically driven quantum systems," Phys. Rev. B **82**, (2010).
2. M. C. Rechtsman, J. M. Zeuner, Y. Plotnik, Y. Lumer, D. Podolsky, F. Dreisow, S. Nolte, M. Segev, and A. Szameit, "Photonic Floquet topological insulators," Nature **496**, 196–200 (2013).
3. L. J. Maczewsky, J. M. Zeuner, S. Nolte, and A. Szameit, "Observation of photonic anomalous Floquet topological insulators," Nat. Commun. **8**, 13756 (2017).
4. S. Mukherjee, A. Spracklen, M. Valiente, E. Andersson, P. Öhberg, N. Goldman, and R. R. Thomson, "Experimental observation of anomalous topological edge modes in a slowly driven photonic lattice," Nat. Commun. **8**, 13918 (2017).
5. G. G. Pyrialakos, J. Beck, M. Heinrich, L. J. Maczewsky, N. V. Kantartzis, M. Khajavikhan, A. Szameit and D. N. Christodoulides, "Bimorphic Floquet topological insulators," Nat. Mater. **21**, 634–639 (2022).
6. A. Szameit and S. Nolte, "Discrete optics in femtosecond-laserwritten photonic structures," J. Phys. B At. Mol. Opt. Phys. **43**, (2010).

Surface states in double diamond nodal line photonic crystals

Haedong Park and Sang Soon Oh*

School of Physics and Astronomy, Cardiff University, Cardiff CF24 3AA, United Kingdom
*corresponding author: ohs2@cardiff.ac.uk

Abstract: We theoretically observe photonic surface states related to nodal lines in the momentum space. First, we demonstrate nodal lines' phase transition by a structural deformation of dielectric photonic crystals. We also calculate the Zak phases using them. Finally, we show the surface states in our photonic crystals.

Since the discovery of the topological insulator [1], most studies have focused on the proposal of crystal structures that exhibit topological phases. The prosed crystal structures include metallic [2], photonic [3], and acoustic [4] crystals. The topological phases are closely related to degeneracies such as the Dirac [5] and Weyl points [6] and nodal lines [7]. However, there have been relatively few studies on boundary states associated with nodal lines. Although drumhead surface states have been observed, the surface states driven by multiple nodal lines have not been explored.

This study explores the photonic surface states using the nodal line photonic crystals. We adopt a dielectric and anisotropic double diamond structure, introduced in Ref. [3]. This double diamond crystal exhibits a nodal link (the most famous shape among the nodal lines) in the momentum space. Next, we apply a structural deformation. The deformation drives the phase transitions of nodal lines so that the nodal link transforms to another shape. We analyze its topological nature using the following Euler class, an integer topological invariant [8-10]:

$$\chi_{mn}(\mathcal{D}) = \frac{1}{2\pi}\left[\int_{\mathcal{D}} \mathrm{Eu}^{mn} dk_a dk_b - \oint_{\partial\mathcal{D}} \mathbf{a}(\mathbf{k}) \cdot d\mathbf{k}\right] \quad (1)$$

where $\mathrm{Eu}^{mn}(\mathbf{k}) = \langle \nabla_{\mathbf{k}} u_{\mathbf{k}}^m | \times | \nabla_{\mathbf{k}} u_{\mathbf{k}}^n \rangle$ is the Euler form and $\mathbf{a}(\mathbf{k}) = \langle u_{\mathbf{k}}^m | \nabla_{\mathbf{k}} u_{\mathbf{k}}^n \rangle$ is the Euler connection. We also calculate the Zak phase for the nodal lines' situation from the following Wilson loop:

$$\mathcal{W}_{pq}(C) = \mathcal{P} \exp\left[i \int_C \langle u_{qk} | i\nabla_k | u_{pk} \rangle \cdot d\boldsymbol{k}\right] \quad (2)$$

Based on the above information, we search the surface states of the photonic array that consists of many double diamond unit cells. The array is periodic along the two lattice vectors. Along the remaining direction, the array is finite and terminated by the perfectly electric conductor (PEC) boundaries. We believe this study will provide a new insight on topologically protected modes in multigap systems and widen the scope of topological physics to electromagnetic waves in three-dimensional photonic crystals.

References

1. Hasan, M. Z. and C. L. Kane, "*Colloquium*: Topological insulators," Rev. Mod. Phys., Vol. 82, 2010.
2. Bouhon, A., Wu, Q., Slager, R.-J., Weng, H., Yazyev and O. V., Bzdušek, T., "Non-Abelian reciprocal braiding of Weyl points and its manifestation in ZrTe," Nat. Phys., Vol. 16, 1137–1143, 2020.
3. Park, H., Wong, S., Zhang, X. and Oh, S. S., "Non-Abelian charged nodal links in a dielectric photonic crystal," ACS Photonics, Vol. 8, 2746–2754, 2021.

4. Park, H., S. Wong, A. Bouhon, R.-J. Slager, S. S. Oh, “Topological phase transitions of non-Abelian charged nodal lines in spring-mass systems,” Phys. Rev. B, Vol. 105, 2022.
5. Wong, S., M. Saba, O. Hess, S. S. Oh, “Gapless unidirectional photonic transport using all-dielectric kagome lattices,” Phys. Rev. Res., Vol. 2, 2020.
6. Park, H., S. Lee, “Double Gyroids for Frequency-Isolated Weyl Points in the Visible Regime and Interference Lithographic Design,” ACS Photonics, Vol. 7, 1577-1585, 2020.
7. Park, H., W. Gao, X. Zhang, S. S. Oh, “Nodal lines in momentum space: topological invariants and recent realizations in photonic and other systems,” Nanophotonics, 11, 2779-2801, 2022.
8. Jiang, B., Bouhon, A., Lin, Z.-K., Zhou, X., Hou, B., Li, F., Slager, R.-J. and Jiang, J.-H., “Experimental observation of non-Abelian topological acoustic semimetals and their phase transitions,” Nat. Phys. Vol. 17, 1239–1246, 2021.
9. Bouhon, A., Wu, Q., Slager, R.-J., Weng, H., Yazyev and O. V., Bzdušek, T., “Non-Abelian reciprocal braiding of Weyl points and its manifestation in ZrTe,” Nat. Phys., Vol. 16, 1137–1143, 2020.
10. Ünal, F. N., Bouhon A. and Slager, R.-J., “Topological Euler Class as a Dynamical Observable in Optical Lattices,” Phys. Rev. Lett., vol. 125, p. 053601, 2020.

Laser based on Bound States in the Continuum in the Ultraviolet Region

Mu-Hsin Chen[1], Di Xing[1], Vin-Cent Su[2], Yang-Chun Lee[1], Ya-Lun Ho[1*], and Jean-Jacques Delaunay[1*]

[1]School of Engineering, The University of Tokyo, Japan
[2]Department of Electric Engineering, National United University, Taiwan
[*]corresponding author: yalunho@g.ecc.u-tokyo.ac.jp; jean@mech.t.u-tokyo.ac.jp

Abstract

Bound states in the continuum (BICs) in optical systems have been utilized to achieve resonant modes with high quality-factors (Q) as BIC modes provide strong light confinement by suppressing out-of-plane radiative losses. In recent years, BICs have been applied in various fields, including nonlinear optics, sensing, and lasing in the visible or near-infrared region. Here, we report a laser based on symmetry-protected BIC with single-mode ultraviolet (UV) emission and a small full-width at half-maximum (FWHM) of 0.10 nm.

1. Introduction:

Optical bound states in the continuum (BICs) existing in sub-diffraction periodic structures such as photonic crystals are special modes in which light is in completely localized states without radiating to the far field. By fully suppressing radiative losses, light confinement with extremely high-quality factors (Q) of near infinity is likely to be achieved for infinitely extending periodic structures. For real devices with only finite spaces, quasi-BIC modes can still support optical modes with relatively high Q when compared to typical diffraction-coupled band-edge modes. Thus, quasi-BICs have been utilized to build passive devices in the form of metasurfaces or photonic elements. In recent years, lasers based on quasi-BICs within the near-infrared (NIR) or the visible region have also been reported. Due to the advantages of BIC in light confinement, BIC-based lasers can support narrow-linewidth lasing with out-of-plane emission while the devices' sizes remain small. However, ultraviolet (UV) microlasers based on BICs have not been reported. Since tiny UV light sources hold important applications in various fields, including high-resolution bio-imaging, laser therapy, spectroscopy, and lithography, UV microlasers with narrow linewidths and highly directional emissions are strongly desired.

2. Results and Discussion:

Here, we demonstrate a UV laser based on BICs consisting of a one-dimensional (1-D) periodic line-and-space structure, which is made up of a patterned electron beam (e-beam) resist, on top of a standard GaN thin film. The proposed periodic resist structure supporting a quasi-BIC mode can be directly fabricated by a single-step e-beam lithography process. With the strong light confinement provided by the quasi-BIC mode, a single-mode UV lasing action at around 376.5 nm with a small full-width at half-maximum (FWHM) of 0.10 nm was observed when the system is pumped by a 355-nm pulsed laser. Such a lasing linewidth is among the narrowest in the reported GaN-based single-mode UV microlasers. Also, the laser exhibits highly directional out-of-plane emission as the collected far-field emission pattern shows a low beam divergence of 1.5˚. Furthermore, the wavelength of lasing emission was found controllable over a wide range with a resolution of 0.45 nm per step by adjusting the structure period (Λ) and operating temperature (T). It is noted that lasing can be achieved at 383 K, exhibiting the potential for applications under high-T environments. Lastly, this work discussed the effect of the laser size on the lasing threshold. The threshold of the fabricated lasers was found to grow as the laser size was shrunk, and no more stable lasing can be achieved for samples having a side length smaller than 8 μm.

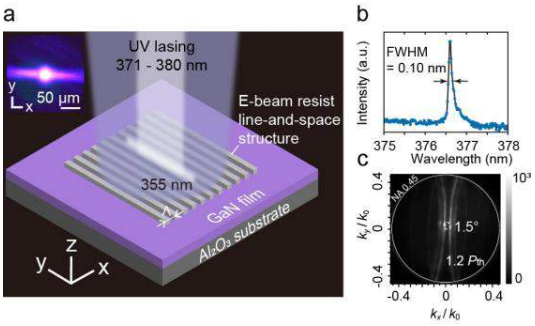


Figure 1. Ultraviolet laser based on bound states in the continuum. (a) The schematic of the proposed laser. The inset shows the optical image when lasing occurs. (b) The emission spectrum of lasing. (c) The far-field emission pattern of lasing.

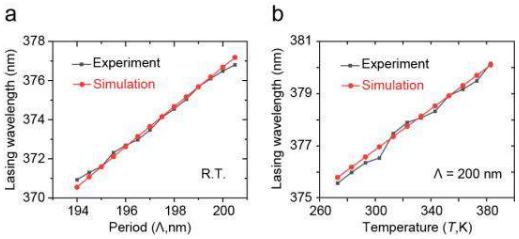


Figure 2. Sub-nm wavelength control of lasing achieved by adjusting the (a) structure period (Λ) or (b) operation temperature (*T*).

3. Conclusions:

With the superior mode properties of BICs, the presented BIC-based UV laser can support single-mode lasing with an extra narrow linewidth and highly directional emissions. Additionally, the achieved wavelength control can be useful in photochemical, analytical, or spectroscopic applications. We envision this work to pave the way for BIC-based active devices in the UV region.

Acknowledgement

This work was supported by JSPS KAKENHI (JP20H02197, JP21H01383, JP21J11825, JP20F40045) and the Ministry of Science and Technology, Taiwan (110-2221-E-239-026-MY3). This work was supported by "Advanced Research Infrastructure for Materials and Nanotechnology in Japan (ARIM)" of the Ministry of Education, Culture, Sports, Science and Technology (MEXT). Proposal Number JPMXP1222UT1026. M.-H. Chen acknowledges the fellowship from WINGS-QSTEP.

References

1. Hsu, C. W., Zhen, B., Lee, J., Chua, S.-L., Johnson, S. G., Joannopoulos J. D., Soljačić M. "Observation of trapped light within the radiation continuum," Nature, Vol. 499, 188–191, 2013.
2. Hsu, C. W., Zhen, B., Stone, A. D., Joannopoulos, J. D., Soljačić, M. "Bound states in the continuum," Nature Review Materials, Vol. 1, 16048, 2016.
3. Kodigala, A., Lepetit, T., Gu, Q., Bahari, B., Fainman, Y., Kanté, B. "Lasing action from photonic bound states in continuum," Nature, Vol. 541, 196–199, 2017.
4. Huang, C., Zhang, C., Xiao, S., Wang, Y., Fan, Y., Liu, Y., Zhang, N., Qu, G., Ji, H., Han, J., Ge, L., Kivshar, Y., Song, Q. "Ultrafast control of vortex microlasers," Science, Vol. 367, No. 6481, 1018–1021, 2020.
5. Wang, Y., Fan, Y., Zhang, X., Tang, H., Song, Q., Han, J. "Highly controllable etchless perovskite microlasers based on bound states in the continuum," ACS Nano, Vol. 15, No. 4, 7386–7391, 2021.

Topological corner states in photonic bilayer square lattice with π flux

Natsuko Ishida[1*], Motohiko Ezawa[2], Guangtai Lu[1], Wenbo Lin[3], Yasutomo Ota[1,4], Yasuhiko Arakawa[5], and Satoshi Iwamoto[1,5,6]

[1] Research Center for Advanced Science and Technology, The University of Tokyo, Japan
[2] Department of Applied Physics, The University of Tokyo, Japan
[3] Komaba Institute for Science (KIS), The University of Tokyo, Japan
[4] Research Center for Department of Applied Physics and Physico-Informatics, Keio University, Japan
[5] Institute for Nano Quantum Information Electronics, The University of Tokyo, Japan
[6] Institute of Industrial Science, The University of Tokyo, Japan
[*]corresponding author: n-ishida@iis.u-tokyo.ac.jp

Abstract: We analyzed a bilayer photonic structure consisting of two topologically distinct square lattices with π flux by using a tight-binding model. In the weak interlayer coupling regime, a topological corner state exists at each corner of the finite bilayer lattice, while it disappears when the coupling strength exceeds a critical value, indicating the occurrence of a topological phase transition induced by the interlayer coupling. This phenomenon could be applicable to control light localization in bilayer photonics systems.

Topological photonics [1] can provide novel approaches for controlling light, gathering great attention. In addition to a conventional topological insulator, a higher-order topological insulator (HOTI) has been discovered which hosts topological states two or more dimensions lower than the system [2]. A 2D HOTI can support 0D corner states besides 1D edge states and the topological corner states have been investigated in various kinds of 2D photonic platform [3,4,5]. Optical cavities based on the topological corner states have been applied to nanocavity lasers [6], nonlinear optics [7], and cavity QED experiments [8]. The platform for exploring photonic corner states has recently been extended to multilayer systems such as bilayer photonic graphene [9]. On the other hand, a bilayer structure stacking 2D photonic HOTI has not been discussed yet as a possible platform. In this work, we consider a stack of two π-flux square lattices based on the Benalcazar–Bernevig–Hughes (BBH) model [2], which describes a photonic quadrupole topological insulator, recently realized using an array of ring resonators [10]. Our calculations demonstrate that tuning the interlayer coupling strength induces a phase transition and controls the emergence and disappearance of topological corner states.

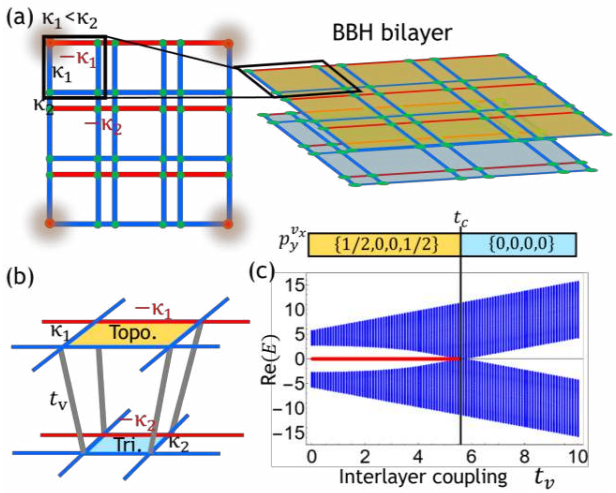


Figure 1: (a) A finite 2D BBH layer where κ_1 and κ_2 denote the intra- and inter-cell coupling strengths. Blue and red bonds represent the positive and negative couplings, respectively. Corner states appear when $\kappa_1 < \kappa_2$. (b) A unit cell of bilayer system where the top and bottom layers are topological and trivial, respectively. (c) Energy spectrum for the bilayer system. Red line corresponds to four corner states at E=0. The polarization is depicted in the above with a critical interlayer coupling t_c. Parameters are chosen as κ_1=1, κ_2=3 and N=20.

In the BBH model, π flux is inserted by introducing the negative coupling, as shown with the red bond in Fig. 1 (a). We vertically stack topologically distinct layers by considering the coupling between vertical nearest neighbor sites t_v. Fig. 1 (b) shows a unit cell of the finite bilayer lattice, where the top and bottom layers are

topological and trivial, respectively. Each layer is a 2D lattice consisting of $N \times N$ sites. In Fig. 1(c), we show the energy spectrum when t_v is varied. Red line corresponds to four corner states which locate dominantly at each corner of the topological layer. In the weak interlayer coupling regime, the corner states exist at E=0, while they disappear when t_v exceeds a critical value $t_c = \sqrt{2}(\kappa_1 + \kappa_2)$. Sudden disappearance of the corner states implies a possible non-trivial phase transition by increasing interlayer coupling.

The nested Wilson loop gives the bulk topological invariant of the BBH model [7]. Here, we adapt this formalism to the bilayer system and discuss the possible non-trivial boundary associated with t_v. The polarizations are obtained as follows:

$$p_y^{v_x^{\pm}} = -\frac{i}{2\pi}\frac{1}{N_x}\sum_{k_x}\log[\tilde{W}^{\pm}_{y,k_x}] \qquad (1)$$

where $\tilde{W}^{\pm}_{y,k_x}$ is a nested Wilson loop. The bilayer system has four pairs of doubly degenerate bands. By adapting the Wilson loop, the non-degenerate Wannier bands are obtained from four occupied bands (Fig.2). After calculating the nested Wilson loop, we obtain polarizations as p_y={1/2, 0, 0, 1/2} for $t_v < t_c$ and p_y= {0, 0, 0, 0} for $t_v > t_c$. The polarizations change when t_v exceeds t_c, which is in agreement with our results on the disappearance of corner states in the finite system. Note that similar topological phase transitions are observed in trilayer BBH systems.

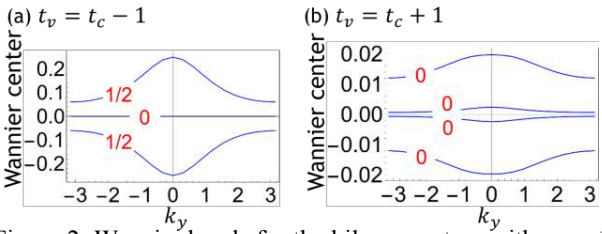


Figure 2: Wannier bands for the bilayer system with κ_1=1 and κ_2=3. The numbers in red represent the polarization. (a) Two bands have quantized polarization for $t_v < t_c$. (b) All four bands have zero quadrupole moment for $t_v > t_c$.

In summary, we analyzed a bilayer structure by stacking two topologically distinct lattices and found a phase transition induced by the interlayer coupling. We believe that our work provides a new insight on controlling light localization in multilayer photonics systems.

Acknowledgements: This work was partially supported by JSPS KAKENHI (Grant No. JP21J40088), CREST, JST (Grant No. JPMJCR20T2 and No. JPMJCR19T1), and the Grants-in-Aid for Scientific Research from MEXT KAKENHI (Grants No. 22H01994 and No. 22H00298).

References

1. Ozawa, T., et al., "Topological photonics", Rev. Mod. Phys. **91**, 015006, 2019.
2. Benalcazar, W. A., Bernevig, B.A., and Hughes, T. L., "Quantized electric multipole insulators", Science, **357**, 61, 2017.
3. Ota, Y., et al., "Photonic crystal nanocavity based on a topological corner state", Optica **6**, 786, 2019.
4. Chen, X-D., et al., "Direct Observation of Corner States in Second-Order Topological Photonic Crystal Slabs", Phys. Rev. Lett. **122**, 233902, 2019.
5. Li, M., et al., "Higher-order topological states in photonic kagome crystals with long-range interactions", Nat. Photonics **14**, 89, 2020.
6. Zhang, W., et al., "Low-threshold topological nanolasers based on the second-order corner state", Light Sci. Appl. **9**, 109, 2020.
7. Kirsch, M.S., et al., "Nonlinear second-order photonic topological insulators", Nat. Phys. **17**, 995, 2021.
8. Xie, X., et al., "Cavity Quantum Electrodynamics with Second-Order Topological Corner State", Laser Photonics Rev. **14**, 1900425, 2020.
9. Oudich, M., et al., "Photonic analog of bilayer graphene", Phys. Rev. B **103**, 214311, 2021.
10. Mittal, S., et al., "Photonic quadrupole topological phases", Nat. Photonics, **13**, 692, 2019.

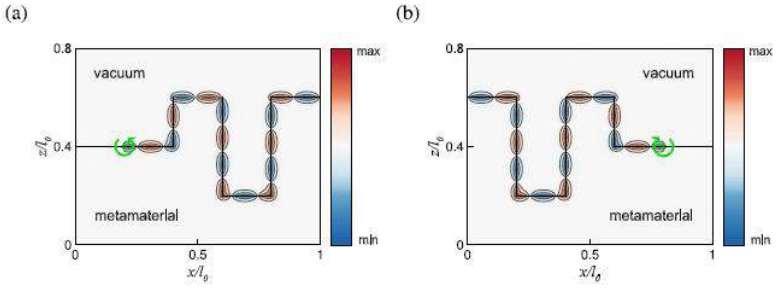
Photonic topological phases in pseudochiral metamaterials

Ruey-Lin Chern* **and Ti-Jung Hsu**

Institute of Applied Mechanics, National Taiwan University, Taiwan
*corresponding author: chernrl@ntu.edu.tw

Abstract: We investigate the photonic topological phases in pseudochiral metamaterials characterized by magnetoelectric tensors with symmetric off-diagonal chirality components. The underlying medium is considered a photonic analogue of the type-II Weyl semimetal featured with two pairs of tilted Weyl cones in the frequency-wave vector space. Surface modes at the interface between vacuum and the pseudochiral metamaterial exist in their common gap in the wave vector space, which form two pairs of crossing surface sheets that are symmetric about the transverse axes.

In this study, bulk modes of the pseudochiral metamaterials are represented by two decoupled quadratic equations as a certain symmetry of the material parameters is included. When the 'spin'-degenerate condition [1] is satisfied, the bulk modes are featured with two pairs of Weyl cones symmetrically displaced in the frequency-wave vector space. The electromagnetic duality allows for the photonic system to be decoupled as two subsystems for the hybrid modes defined as the linear combinations of electric and magnetic fields. By introducing the pseudospin states as the basis for the hybrid modes, the photonic system can be described by a pair of spin-orbit Hamiltonians with spin 1 [2,3] that respect the fermionic-like pseudo time-reversal symmetry. The topological properties of the photonic system are determined by the nonzero spin Chern numbers calculated from the eigenfields of the Hamiltonians. Surface modes at the interface between vacuum and the pseudochiral metamaterial exist in their common gap in the wave vector space, which are analytically formulated by algebraic equations. In particular, the surface modes are tangent to both the vacuum light cone and the Weyl cones, which form two pairs of crossing surface sheets in the frequency-wave vector space. At the Weyl frequency, the surface modes that connect the Weyl points form four Fermi arc-like states as line segments. The topological features of the pseudochiral metamaterials are illustrated with the robust transport of surface modes at an irregular boundary, which are able to bend around sharp corners without backscattering, as shown in the following figure.



References

1. Khanikaev, A. B. et al. Photonic topological insulators. Nat. Mater. **12**, 233–239 (2013).
2. Fang, A., Zhang, Z. Q., Louie, S. G. and Chan, C. T. Klein tunneling and supercollimation of pseudospin-1 electromagnetic waves. Phys. Rev. B **93**, 035422 (2016).
3. Yu, Y. Z., Kuo, C. Y., Chern, R. L. and Chan, C. T. Photonic topological semimetals in bianisotropic metamaterials. Sci. Rep. **9**, 18312 (2019).

Generation and applications of textured photonics fields

Nanofemto vectorial texturing of electromagnetic fields by spin-orbit interaction of light

H. Petek[1*], A. Ghosh[1], S. Yang[1], and Y. Dai[1,2]

[1]University of Pittsburgh, USA
[2]Southern University of Science and Technology, China
[*]corresponding author: petek@pitt.edu

Abstract: The excitation laser polarization and coupling geometry metastructures define the spin-orbit interaction of surface plasmon polaritons at metal-vacuum interfaces. We image the topological plasmonic fields by photoemission electron microscopy with nanometer spatial and femtosecond temporal resolution, to deduce the generated space-time spin textures of plasmonic vortex fields and how they can dress the space-time invariance of matter.

The polarization of optical fields interacting with lithographically structured metasurfaces defines the polarization structure and focusing of surface plasmon polariton (SPP) fields at metal-vacuum interfaces.[1-5] As the evanescent SPP waves propagate, their spin angular momentum (SAM) is locked transversely to their propagation vector k giving them a chiral property, where changing the sign of k, changes the sign of SAM.

Given this spin-momentum locking, as SPP fields propagate and form standing waves, they create field and spin phase discontinuities that can globally be defined as plasmonic vortices.[5] We image the space-time evolution of plasmonic vortices by performing interferometric time-resolved two-photon photoemission electron microscopy.[6] Nonlinear two-photon photoemission of electron spatial distributions from silver/vacuum interfaces are imaged with electron optics. Movies of the SPP propagation at the local speed of light, with sub-wavelength spatial resolution and ~100 as/frame time-step advance are obtained by interference between phase correlated SPP and time-delayed optical probe fields enabling us to stop plasmonic fields in space and time to perform their attosecond phase-correlated imaging.[1] The vortex fields appear as geometrical structures, where near PHz fields at vortex cores become stationary in space, and their periodic oscillation is converted into PHz field rotation. The consequent electromagnetic spin acquires bianisotropic textures that can mimic those of magnetic monopoles, and their fields can break spatially and temporally the time-reversal symmetry.

As an example of plasmonic vortex fields, in Figure 1, we show calculated spatial field distribution that are generated by SPP coupling structures with triangular, square, pentagonal, ...N-gon, to circular symmetry. The figure shows the S3 stokes polarization parameter with the contrasting colors signifying the opposite sign, when circularly polarized light interacts with the N-gon coupling structures. The textures evolve from ordered periodic 3-, 4-, and 6-gon structures that tile the two-dimensional space, to ordered aperiodic quasicrystalline structures, and eventually evolve to a circular structure where the central polygon with the N-gon symmetry acquires a meron, or half-skyrmion topological charge.[1] As N increases, the central meron becomes surrounded by an oppositely charged meron, which together form of a skyrmion texture for a circular structure.

We explore different ways to generate plasmonic vortices that host topological spin textures, and explore how they evolve in space and time. While the supporting plasmonic material silver is not topological, the plasmonic fields can transiently impose space-time bianisotropy, or couple to topological materials in their nearfield. The ability to impose bianisotropy by plasmonic fields enables us to explore the rich physics of ultrafast structured

light. Beyond microscopy, the structured light in vortex form provides insights into the cosmological structure formation.[1]

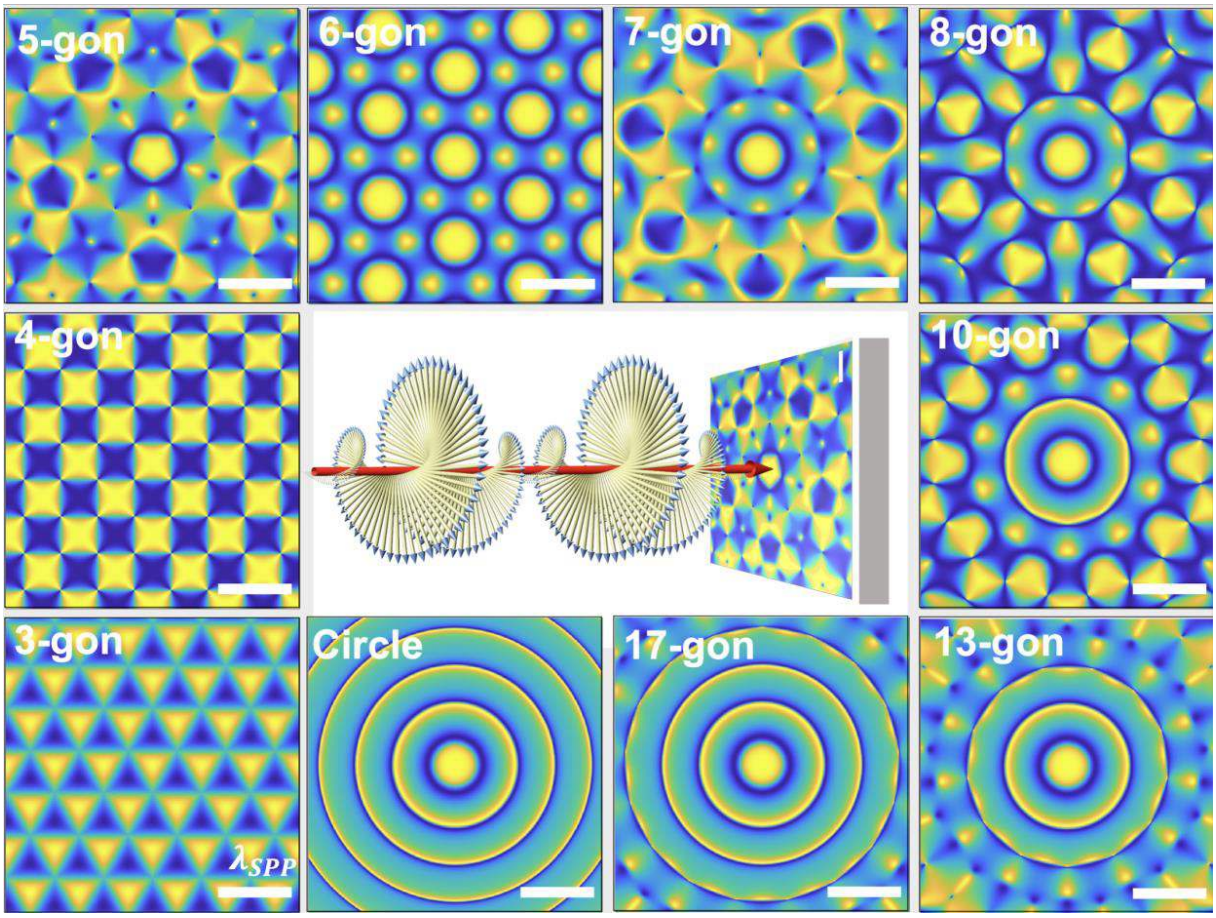


Figure 1. Figure 1. The calculated Stokes S_3 parameter of SPP fields with spin-orbit coupling defined by circular polarization and N-gon symmetry. The center is a schematic of the experimental technique.

References

[1] Dai, Y., Zhou, Z., Ghosh, A., Mong, R.S.K., Kubo, A., Huang, C.-B., & Petek, H. Plasmonic topological quasiparticle on the nanometre and femtosecond scales. *Nature* **588**, 616-619 (2020).

[2] Dai, Y., Zhou, Z., Ghosh, A., Yang, S., Huang, C.-B., & Petek, H. Ultrafast nanofemto photoemission electron microscopy of vectorial plasmonic fields. *MRS Bulletin* **46**, 738-746 (2021).

[3] Ghosh, A., Yang, S., Dai, Y., Zhou, Z., Wang, T., Huang, C.-B., & Petek, H. A topological lattice of plasmonic merons. *Applied Physics Reviews* **8**, 041413 (2021).

[4] Dai, Y., Zhou, Z., Ghosh, A., Kapoor, K., Dąbrowski, M., Kubo, A., Huang, C.-B., & Petek, H. Ultrafast microscopy of a twisted plasmonic spin skyrmion. *Applied Physics Reviews* **9**, 011420 (2022).

[5] Ghosh, A., Yang, S., Dai, Y., & Petek, H. The Spin Texture Topology of Polygonal Plasmon Fields. *ACS Photonics* **10**, 13-23 (2023).

[6] Dąbrowski, M., Dai, Y., & Petek, H. Ultrafast Photoemission Electron Microscopy: Imaging Plasmons in Space and Time. *Chem. Rev.* **120**, 6247-6287 (2020).

Tailoring vortex light sources with planar optical devices

M. de Oliveira[1,2*], M. Piccardo[1], and A. Ambrosio[1]

[1]Center for Nano Science and Technology, Fondazione Istituto Italiano di Tecnologia, Milan, Italy
[2]Physics Department, Politecnico di Milano, Milan, Italy
[*]corresponding author: michael.almeida@iit.it

Abstract: The generation of vortex light beams, carrying orbital angular momentum (OAM), has seen a shift from using bulky optics to subwavelength structured planar devices. Here, we look at how planar devices are pushing the boundaries in generating complex light fields, from high-purity vortex beams to the dynamic topologies of vortex arrays tailored directly at the source. We will see how multiplexing OAM with other degrees-of-freedom, in particular space-time beams, has the potential to enable exciting insights and applications in optics.

The notion of integrating many degrees of freedom to form complex structured light fields holds untapped promise, from the generation of classical and quantum states of light, the exploitation of linear and nonlinear light-matter interactions, to the advancement of applications in microscopy, spectroscopy, holography, and communication [1]. To realize the full potential of structured light, advanced manipulation of each optical mode is required, among which, metasurfaces are one of the most powerful platforms. They are planar nanostructured materials implementing a spatially varying optical response that allows to mold the light wavefront in amplitude, phase, and polarization. These devices offer unprecedented control in generating vortex beams with large topological charge and high mode purity, a necessity if one wants to take advantage of the infinite Hilbert space offered by vortex beams [2].

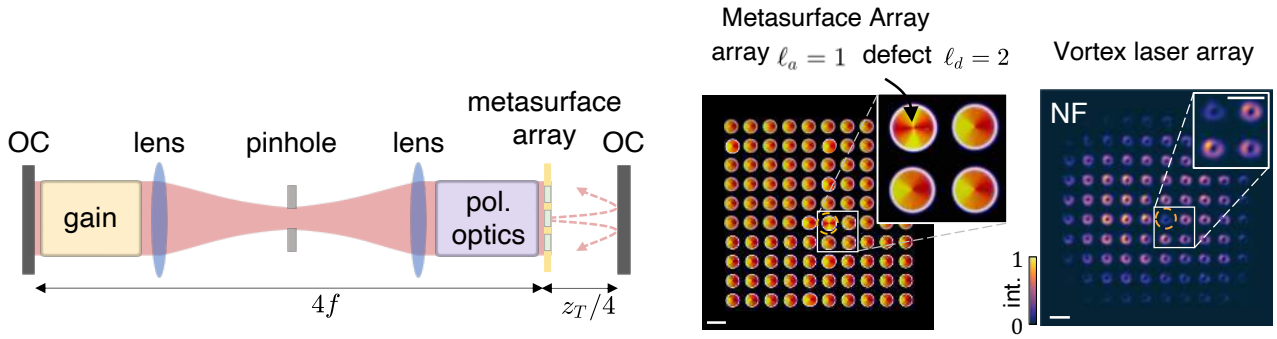


Figure 1: Schematic of a metasurface laser cavity. An array of 100 metasurfaces used to impart spin-orbit transformations inside the laser cavity. Generated array of coupled vortex lasers showing the topological charge of the 'defect' device being healed to that of the topological charge of the array.

Different from reshaping a conventional "Gaussian" laser beam, some applications could benefit from the inherent dynamic complexities of light structured directly at the source. By placing an array of metasurface devices inside a laser cavity resonator, combining non-Hermitian coupling, we can mix the vortices and couple. By allowing the modes to dynamically evolve in a resonator system, we realize a platform to explore complex topological transformations and collective vortex effects at the source. In this regard, we have demonstrated a

coupled laser cavity in which a hundred metasurfaces create an optical vortex array, allowing for OAM tuning (despite the static nature of the metasurfaces) and built-in robustness leading to the self-healing of topological defects, thanks to the iterative nature of the system and a fine balance of gain and loss [3].

On the other hand, the recent push toward multimode photonics opens one of the most prolific optical frontiers, with space-time beams offering enormous potential when coupled with OAM. Here, the goal is to structure not only the spatial transverse profile of the beam, but also the frequency, by tailoring the topological-spectral correlations of the light source. To this end, we structure femtosecond optical parametric amplified pulses using a Fourier space-time shaper based on flat diffractive axicons. The system offers complete control over the broadband topological content of the ultrashort pulses, with tuning of the topological-spectral correlations providing control over the chirality, orbital radius, number of intertwined helices and their dynamics, enabling new applications in ultrafast technology.

This work was financially supported by the European Research Council (ERC) under the European Union's Horizon 2020 research and innovation programme "METAmorphoses", grant agreement no. 817794, and by Fondazione Cariplo, grant no. 2019-3923.

References

1. Forbes, A., de Oliveira, M. and Dennis, M. R. "Structured light," Nat. Photonics, 15, 253−262, 2021.
2. de Oliveira, M., Piccardo, M., Eslami, S., Aglieri, V., Toma, A., and Ambrosio, A. "Radially and azimuthally pure vortex beams from phase-amplitude metasurfaces," ACS Photonics, 10, 1, 290–297, 2022.
3. Piccardo, M., de Oliveira, M., Toma, A., Aglieri, V., Forbes, A., and Ambrosio, A. "Vortex laser arrays with topological charge control and self-healing of defects," Nat. Photonics 16, 359–365 2022.

Photonic N00N-sates with spatially structured photons

M. Hiekkamäki[1], R. F. Barros[1], M. Ornigotti[1], and R. Fickler[1*]

[1]Tampere University, Photonics Laboratory, Physics Unit, Tampere, FI-33720, Finland
[*]corresponding author: robert.fickler@tuni.fi

Abstract: We study photonic N00N with spatially structured photons, i.e. quantum states where N photons are in a superposition between two orthogonal spatial modes. Using these states, we can show angular super-resolution measurements when implement through modes with a twisted transverse phase front. When realized with radially structured modes, the states allow us to study the Gouy phase anomaly in the quantum domain, its benefits in longitudinal sensing, and its fundamental importance in gaining a deeper understanding multi-photon quantum states.

Shaping the transverse structure of quantum light has attracted a lot of attention in quantum photonics ranging from fundamental studies to quantum information applications. A powerful way to describe any spatial structure in the paraxial limit are orthogonal transverse spatial modes e.g. Laguerre-Gauss modes. Amongst many other things, such modes show interesting features like a theoretically unbound quanta of orbital angular momentum (OAM) per single photon related to a twisted phase structure. Moreover, structured photons serve as a versatile testbed for the study of novel complex quantum states [1].

In this presentation talk, I will show some of the key areas of the application of structured photons in quantum photonics and introduce advanced schemes of spatial-mode modulation leading to the generation of photonic N00N states with transverse spatial modes. The latter describes quantum states where N photons are in an extremal superposition between two orthogonal modes, i.e $\frac{1}{\sqrt{2}}(|N0\rangle+|N0\rangle)$. Our results show that such states when realized with OAM modes, i.e. twisted N00N states, can be used to achieve super resolving angle measurements that scale with the photon number N as well as the OAM quanta, as shown in Fig. 1 a) [2].

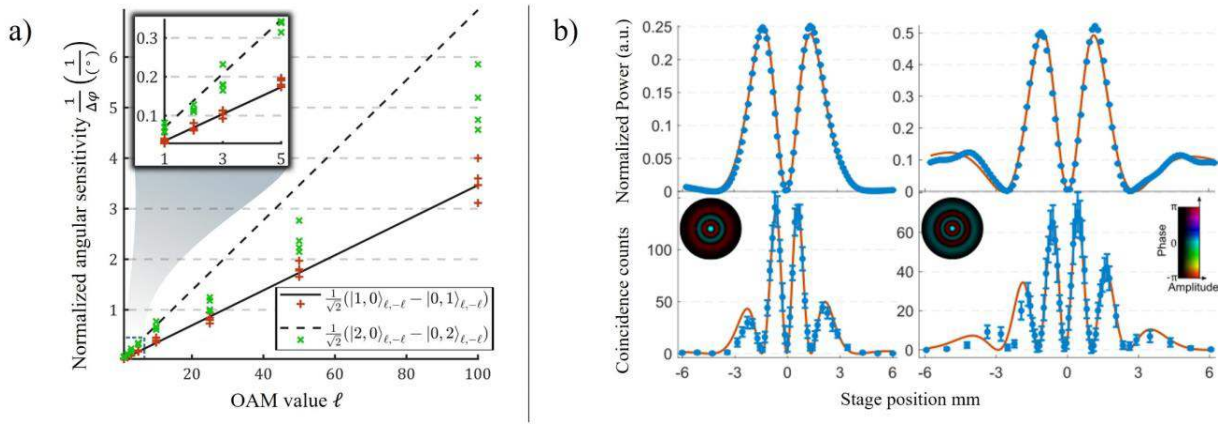


Fig. 1: a) Twisted N00N states show increased angular sensitivities for larger OAM values and for two-photons (green) compared to single photons (red). The plotted lines show the theoretically expected behavior. b) Experimentally recorded data of the Gouy phase's effect on radial mode superpositions between a Gaussian and radial mode of order 3 (left) and order 4 (right). The top row shows the classical behavior, the bottom row shows the effects of the quantum Gouy phase for N00N states using the same pair of modes for both cases.

In addition, we studied spatial mode N00N states in connection to a fundamental wave phenomenon, the so-called Gouy phase anomaly. It describes the anomalous phase delay of transversely confined waves when propagating through a focus. When probing it in quantum domain, i.e. when probing the quantum Gouy phase we find that it behaves different from classical light waves in terms of phase evolution as well as spatial mode order (see Fig.1 b). We further provided a few more insights, such as a nice corollary to Feng and Winful's proposition on the origin of the Gouy phase [3] by linking the speeding up of the quantum Gouy phase to an increasing spread in the transverse momentum of the state. Finally, our results show that radial mode NOON states can open up the possibility for supersensitive measurements of longitudinal displacement and highlight that the so-called photonic de Broglie wavelength is not sufficient for describing the behavior of photon number states [4].

Hence, the presented findings show an example of how engineering the quantum state and transverse-spatial profile of a set of photons can lead to quantum enhanced measurement precisions as well as gaining a deeper understanding of fundamental features of quantum light.

The authors acknowledge the support of the Academy of Finland (decisions 301820, 308596, 332399) and the Photonics Research and Innovation Flagship (PREIN - decision 320165) and support from the Doctoral School of Tampere University and the Magnus Ehrnrooth foundation through its graduate student scholarship.

References

1. Erhard, M., Fickler, R., Krenn, M., Zeilinger, A., „Twisted photons: new quantum perspectives in high dimensions." Light: Science & Applications, 7(3), 17146-17146, 2018
2. Hiekkamäki, M., Bouchard, F., Fickler, R., "Photonic Angular Superresolution Using Twisted N00N States"' Phys. Rev. Lett. 127, 263601, 2021
3. Feng, S., Winful, H. G., "Physical origin of the Gouy phase shift," Opt. Lett. 26, 485-487, 2001
4. Hiekkamäki, M., Barros, R. F., Ornigotti, M., Fickler, R., "Observation of the quantum Gouy phase," Nature Photonics 16, 828-833, 2022.

Novel Effects in Propagation and Absorption of Optical Vortices

Andrei Afanasev*

The George Washington University, Washington, DC 20052, USA

**corresponding author: afanas@gwu.edu*

Abstract: We present new theoretical results on twisted-light propagation and absorption by atomic matter. We demonstrate several effects arising due to the presence of the phase singularity on the propagating wave front: (a) Novel polarization states of optically polarized atoms (b) Enhanced quantum recoil, and (d)Nondivergent polarization features of divergent beams. Possible applications of the above effects will be discussed.

OCIS codes: (270.0270) Quantum Optics; (260.6042) Singular Optics; (050.4865) Optical Vortices

Ability of the twisted light to transfer combined optical spin and orbital angular momentum to atomic excitations was demonstrated experimentally with cold trapped ions [1]. Previously [2] we derived quantum selection rules that describe atomic transitions caused by twisted photons and in subsequent experiments [3] demonstrated dependence of angular-momentum selection rules on atom's position with respect to the phase singularity of the wave front.

The verified selection rules thus allow to predict optical polarization of atoms that absorb the twisted light [4]. We show that the longitudinal electric fields of the vortex play an important role especially in the case of anti-aligned spin and orbital angular momenta of the beam.

Next, we address the problem of determining the physically correct definition of the momentum and angular momentum densities in a spatially structured electromagnetic field, given that the expressions are not the same when one uses the canonical energy-momentum tensor instead of the symmetric Belinfante energy-momentum tensor in electrodynamics. This has important consequences for the interaction of matter with structured light, for example, with optical vortices and would give drastically different results for forces and angular momenta induced on small test objects. We show, with numerical estimates of the size of the effects, situations where the canonical and symmetrized forms induce very different torques or (superkick) recoil momenta on small objects or atomic rotors [5].

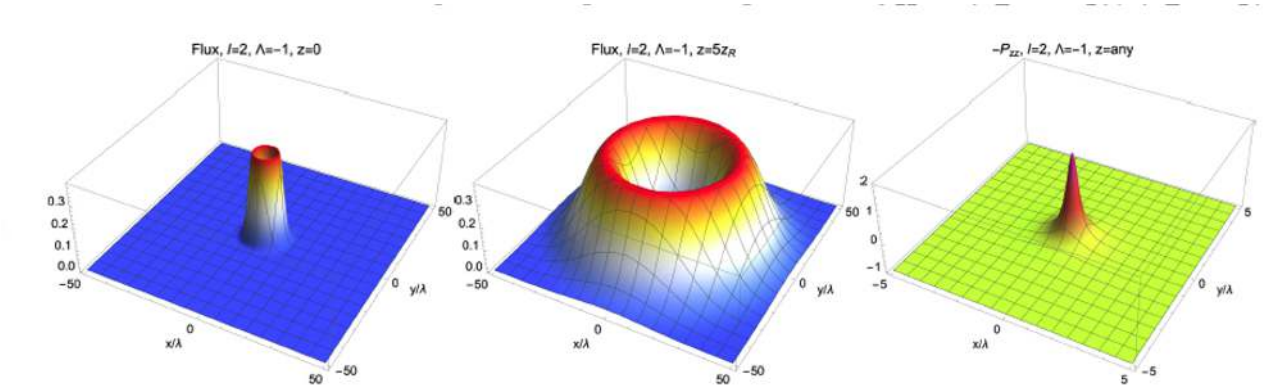


Figure 1. Non-diffractive behavior of polarization in an optical vortex beam (Laguerre Gauss) propagating in free space, having a topological charge l=2 and spin-helicity $\Lambda = -1$. Shown is the transverse-plane profile of energy density in beam's focus (z=0, left plot) that expands during propagation due to diffraction (z=five Raleigh lengths, middle plot), while the polarization parameter p_{zz} remains independent of propagation distance (right plot).

Finally, we demonstrate, both analytically and with simulations, that certain polarization features of optical vortex beams maintain constant transverse spatial dimensions independently of beam divergence due to diffraction. These polarization features appear in the vicinity of the phase singularity and are associated with the presence of longitudinal electric fields. The predicted effect may prove important in metrology and high-resolution imaging applications. In Figure 1, we compare transverse profile of the energy density for the optical vortex beam and a polarization parameter p_{zz} that measures relative contribution of longitudinal (along beam's axis) and transverse electric fields defined as [4,6]

$$p_{zz} = \frac{|E_\perp|^2 - 2|E_z|^2}{|E_\perp|^2 + |E_z|^2}.$$

The results of the calculation are shown in Figure 1, indicating a non-diffractive behavior of the polarization feature while the intensity profile of the beam expands during propagation because of diffraction. The demonstrated effect allows one to pinpoint the position of a phase singularity with subwavelength accuracy independently of the size of a beam spot.

Acknowledgements. This work was supported by US ARO Awards W911NF-19-1-0022 and W911NF-23-1-0085.

References

[1] Schmiegelow, C.T., Schulz, J., Kaufmann, H. et al., "Transfer of optical orbital angular momentum to a bound electron", Nature Comm. **7**, 12998 (2016).

[2] Afanasev, A., Carlson, C.E., and Mukherjee, A., "Off-axis excitation of hydrogen-like atoms by twisted photons," Phys. Rev. A **88**, 033841 (2013).

[3] Afanasev, A., Carlson, C.E., Schmiegelow, C.T. et al., "Experimental verification of position-dependent angular-momentum selection rules for absorption of twisted light by a bound electron", New J. Phys. **20**, 023032 (2018).

[4] Afanasev, A., Carlson, C.E., and Wang, H., "Polarization transfer from the twisted light to an atom", J. Opt. **22**, 054001 (2020).

[5] Afanasev, A., Carlson, C. E., & Mukherjee, A. (2022). Superkicks and the photon angular and linear momentum density. Phys. Rev. A **105**, L061503 (2022).

[6] Afanasev, A., Kingsley-Smith, J. J., Rodríguez-Fortuño, F. J., and Zayats, A. V. "Nondiffractive three-dimensional polarization features of optical vortex beams", Advanced Photonics Nexus **2**, 026001 (2023).

META 2023, PARIS - FRANCE, JULY 18 – 21, 2023

Generation of Extreme-Ultraviolet structured fields with the seeded Free Electron Laser FERMI, and applications in atomic and molecular physics.

C. Callegari

Elettra – Sincrotrone Trieste, Italy
carlo.callegari@elettra.eu

Abstract: Free Electron Lasers are the most powerful light source presently available in the EUV and x-ray range; they allow the time-resolved study of atoms, molecules and condensed matter with chemical sensitivity. A seeded, modular design adds the possibility to generate fields with differing properties (wavelength, polarization, phase), and to combine them coherently. Applications range from sub-attosecond resolution in photoionization processes, to the generation and control of attosecond pulse trains, to the excitation or probing of chiral observables.

First demonstrated (and still of great practical interest) in the infrared [1], Free Electron Lasers (FELs) are of greatest interest where few or no alternatives are available to produce intense, ultrashort light pulses: at short wavelengths. Most of the existing FELs of the latter class are based on the Self Amplified Spontaneous Emission (SASE) process, with limited control on the longitudinal coherence properties of the pulse, much less on the precise structure of the pulse field [2]. The Free Electron laser FERMI in Trieste is based on a seeded design [3] that—along with the independent control of the resonant wavelength, phase, and polarization, of each radiator module—allows the generation and coherent superposition of fields with differing properties, such as wavelength [4], polarization [5], phase [6], and ultimately to the generation (with known limitations) of customized fields.

In this work I will summarize the technical aspects of generating such fields at FERMI, their limitations, and their main applications in the realm of atomic and molecular physics; I will then report on selected recent results concerning: the (post-processing) synchronization with an independent infrared field [7]; the study of photoionization processes by Optical Angular Momentum light beams [8]; the generation of exotic polarization states [9].

The results originate from the joint effort of many international laboratories and of a large number of researchers, whose work is gratefully acknowledged.

References

1. Elias, L. R., W. M. Fairbank, J. M. J. Madey, H. A. Schwettman and T. I. Smith, “Observation of Stimulated Emission of Radiation by Relativistic Electrons in a Spatially Periodic Transverse Magnetic Field,” Phys. Rev. Lett., Vol. 36, No. 13, 717–720, 1976.
2. Callegari, C., A. N. Grum-Grzhimailo, K. L. Ishikawa, K. C. Prince, G. Sansone and K. Ueda, “Atomic, molecular and optical physics applications of longitudinally coherent and narrow bandwidth Free-Electron Lasers,” Phys. Rep., Vol. 904, 1–59, 2021.

3. Allaria, E., et al., “Highly coherent and stable pulses from the FERMI seeded free-electron laser in the extreme ultraviolet,” Nat. Photon., Vol. 6, No. 10, 699–704, 2012. Allaria E., et al., “Two-stage seeded soft-X-ray free-electron laser,” Nat. Photon., Vol. 7, No. 11, 913–918, 2013.
4. Prince, K.C., et al., “Coherent control with a short-wavelength free-electron laser,” Nat. Photon., Vol. 10, No 3, 176–179, 2016. Maroju, P. K., et al., “Attosecond pulse shaping using a seeded free-electron laser,” Nature, Vol. 578, No. 7795, 386–391, 2020.
5. Ferrari, E., et al., “Single Shot Polarization Characterization of XUV FEL Pulses from Crossed Polarized Undulators,” Sci. Rep., Vol. 5, 13531, 2015.
6. Gauthier, D., et al., “Generation of Phase-Locked Pulses from a Seeded Free-Electron Laser,” Phys. Rev. Lett., Vol. 116, 024801, 2016. Wituscheck, A. et al., “Tracking attosecond electronic coherences using phase-manipulated extreme ultraviolet pulses,” Nat. Commun., Vol. 11, No. 1, 883, 2020. Gauthier, D., et al., “Chirped pulse amplification in an extreme-ultraviolet free-electron laser,” Nat. Commun., Vol. 7, 13688, 2016.
7. Maroju, P.K., et al., “Attosecond coherent control of electronic wave packets in two-colour photoionization using a novel timing tool for seeded free-electron laser,” Nat. Photon., Vol. 17, 200–207, 2023.
8. De Ninno, G., et al., “Photoelectric effect with a twist,” Nat. Photon., Vol. 14, No. 9, 554–558, 2020. Wätzel, J., et al., “Light-Induced Magnetization at the Nanoscale,” Phys. Rev. Lett., Vol. 128, No. 15, 157205, 2022.
9. Rebernik Ribič, P., et al., in preparation, 2023.

META 2023, PARIS - FRANCE, JULY 18 – 21, 2023

High efficiency interface between multi-mode and single-mode fibers

O. Korichi[1*], M. Hiekkamäki [1], and Fickler[1]

[1] Photonics Laboratory, Physics Unit, Tampere University, Tampere FI-33720, Finland
[*]corresponding author: Oussama.korichi@tuni.fi

Abstract: A new method for interfacing MMFs with SMFs is presented using a multi-plane light conversion scheme, achieving coupling efficiencies of 30% to 70%, for MMFs with core diameters up to 200 μ m, with only three phase modulations. We also investigate the influence of resolution on coupling efficiencies for field reconstruction and MPLC, and we show that commercial wavefront sensors and deformable mirrors can auto-correct in the kilohertz regime to establish an MMF-SMF interface.

Multi-mode fibers (MMFs) and Single-mode fibers (SMFs) are widely used in communication networks. Choosing to utilize either MMFs or SMFs depends on many factors. For example, in applications that require distances of up to 500 m - 600 m, MMFs are the practical choice in terms of cost. Beyond that, SMFs are necessary due to the modal dispersion in MMFs [1]. Hence, a device for efficiently interfacing an MMF with an SMF would be beneficial to optical telecommunication.

In this work, we present a method capable of achieving this interfacing between an MMF and SMF using a multi-plane light conversion scheme (MPLC) [2]. With our method, and discluding the losses in the optics, we demonstrate that only 3 phase modulations, realized with a single spatial light modulator (SLM), are enough to achieve MMF to SMF coupling efficiencies of 72% ± 7%, 60% ± 3%, 50% ± 4%, and 29% ± 3%, using MMFs with core diameters of 8.2 µm, 25 µm, 50 µm, and 200 µm, respectively [3].

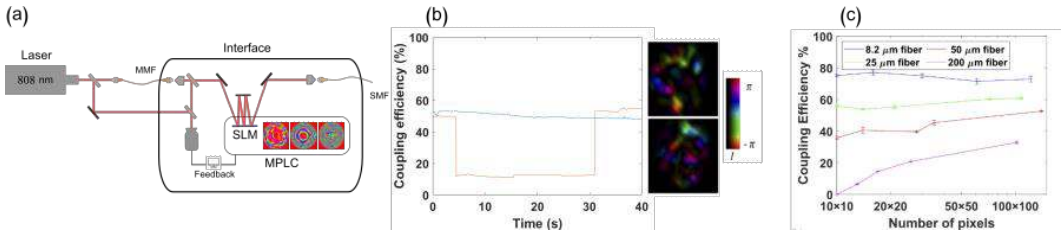


Fig. 1 (a) Sketch of the experimental setup for efficient MMF to SMF coupling using an MPLC implemented with an SLM. (b) Stability of coupling efficiency without disturbance (blue) and automatized correction after a strong deformation of an MMF with 50 µm of core diameter (orange). The insets on the right correspond to the complex field before (top) and after (bottom) the deformations (c) SMF coupling efficiencies after the mode transformation for different MMFs and resolutions of the reconstructed field. The efficiencies were obtained from 200 measurements within a time frame of 35 s, and the errors represent the standard deviation of the respective dataset.

In the experiment, we sent an 808 nm laser into an MMF and reconstructed the complex transverse amplitude of the output field from an interferogram [4]. We then used the obtained full field information to calculate the 3 phase modulation screens with wavefront matching [5]. The phase screens were optimized to transform the multi-mode field into the Eigenmode of the SMF, i.e., a Gaussian beam profile, such that the

transformed field could be efficiently coupled into the SMF (see Fig. 1a). Because the field reconstruction, as well as the mode transformation, were updated in real-time, the obtained coupling efficiency remains stable even if the output field of the MMF changes entirely, for example through strong deformation of the fiber (see Fig. 1b). We additionally tested the influence of the resolutions for both, the field reconstruction and MPLC system, on the coupling efficiencies. The former is shown in Fig. 1c. For both, we found that commercially available devices with increased speed and efficiency, such as wavefront sensors and deformable mirrors, would be enough to establish an MMF to SMF interface working in the kHz-regime.

The presented method might find applications in optical telecommunication and could also be adapted to correct for very strong atmospheric disturbances in long distance free space communication.

References

1. Peng, G. D. (Ed.). (2019). Handbook of Optical Fibers. Berlin/Heidelberg, Germany: Springer.
2. Labroille, G., Denolle, B., Jian, P., Genevaux, P., Treps, N., & Morizur, J. F. (2014). Efficient and mode selective spatial mode multiplexer based on multi-plane light conversion. Optics express, 22(13), 15599-15607.
3. Korichi, O., Hiekkamäki, M. and Fickler, R., 2023. High-efficiency interface between multi-mode and single-mode fibers. Optics Letters, 48(4), pp.1000-1003.
4. Takeda, M., Ina, H., & Kobayashi, S. (1982). Fourier-transform method of fringe-pattern analysis for computer-based topography and interferometry. J. Opt. Soc. Am. , 72(1), 156-160.
5. Fontaine, N. K., Ryf, R., Chen, H., Neilson, D. T., Kim, K., & Carpenter, J. (2019). Laguerre-Gaussian mode sorter. Nature communications, 10(1), 1-7

Thermal plasmonics and metamaterials for sustainable society

Quasi-resonance of surface plasmons for near-infrared sensitivity improvement of silicon image sensor

A. Ono[1,2*], T. Yoshinaga[1], K. Hashimoto[1], and N. Teranishi[2]

[1]Graduate School of Integrated Science and Technology, Shizuoka University, Japan
[2]Research Institute of Electronics, Shizuoka University, Japan
[*]corresponding author: ono.atsushi@shizuoka.ac.jp

Abstract: We proposed quasi-resonant mode of surface plasmons with metal grating which diffracts incident photons to a large diffraction angle of nearly 90 degrees with high efficiency. The quasi-resonance of surface plasmons were applied to improve the near-infrared sensitivity of silicon image sensor. Metal grating was fabricated on the top of silicon sensor and the trench was embedded by a metal for the pixel separation. The diffracted light repeats reflection at metal-filled trench. The effective absorption length was extended in silicon.

The enhanced electric field by surface plasmon resonance has been applied in surface enhanced Raman scattering, fluorescence enhancement, photovoltaics, and so on. Most of the approaches in plasmonics have been considered to utilize the strong electric field enhancement on the metal surface. Here, we applied quasi-resonance of surface plasmons to improve the silicon absorption efficiency in near-infrared wavelength region [1, 2]. Silicon absorption efficiency is low in near-infrared wavelength region due to its band gap at the wavelength of 1100 nm. A thicker silicon absorption layer improves the absorption efficiency, but degrades the image recognition due to the crosstalk between pixels. Therefore, near-infrared sensitivity improvement for silicon image sensor without thick layer is one of the significant issues to be applied in time-of-flight imaging, night monitoring, and biological tissue imaging. Yokogawa *et al*. have been proposed and demonstrated extension of the effective absorption length in silicon using pyramid arrays and SiO_2 trench [3]. They improved 1.8 times sensitivity at 850 nm wavelength. Here, we proposed plasmonic diffraction to extend the effective absorption length in silicon. The target wavelength was selected at 940 nm, which was used for many applications in near-infrared sensing. Our proposed plasmonic image sensor was constructed by silver gratings on the silicon absorption layer and silver trenches for the pixel isolation (Fig.1).

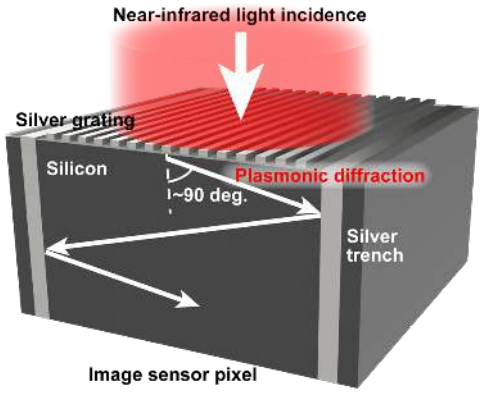


Figure 1. Schematic diagram of silicon based plasmonic image sensor with silver grating and silver trench

We found that near-infrared light incidence was diffracted with nearly 90 degrees in silicon side by silver gratings under the quasi-resonance of surface plasmons. The diffracted light propagates back and forth in silicon absorption layer by the reflection at the silver trenches. The effective propagation length was extended by this diffraction propagation, resulting in the absorption enhancement of the limited thickness of silicon absorption layer. Figure 2 shows the electric field intensity distribution of the cross-sectional view in silicon with silver grating on the top surface. In the silver grating period with 265 nm, width 230 nm, and height 85 nm, the incident near-infrared light was efficiently diffracted to the silicon side with high diffraction angle of approximately 80 degrees. The enhanced electric filed was observed at the interface between silver grating and silicon by surface plasmon excitation. In FDTD simulation, the diffraction efficiency was achieved to 49.7%. This plasmonic diffraction contributes to absorption enhancement because of the effective propagation length extension. By setting the silver trench as the isolation between pixels and the reflection mirror for the diffracted light, the incident photons were confined in silicon. Further devising the sensor configuration, we have clarified in simulation that absorption of silicon was enhanced to 53.5% in a limited thickness of 3 μm, which was an 8.2-fold enhancement compared to the bare silicon. Plasmonic image sensor dramatically improved the sensitivity in near-infrared and has a potential to be applied in near-infrared sensing.

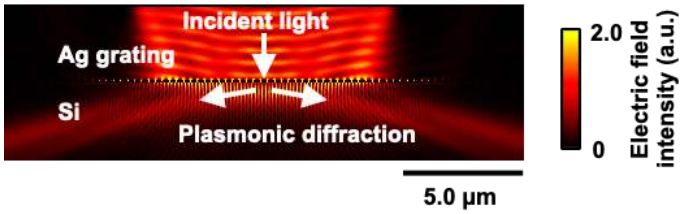


Figure 2. Electric field intensity distribution under quasi-resonance of surface plasmon

References

1. A. Ono, K. Hashimoto, and N. Teranishi, “Near-infrared sensitivity improvement by plasmonic diffraction for a silicon image sensor with deep trench isolation filled with highly reflective metal,” Opt. Express, Vol. 29, No. 14, 21313–21319, 2021.
2. T. Yoshinaga, K. Hashimoto, N. Teranishi, and A. Ono, “Photon confinement in a silicon cavity of an image sensor by plasmonic diffraction for near-infrared absorption enhancement,” Opt. Express, Vol. 30, No. 20, 35516–35525, 2022.
3. S. Yokogawa, I. Oshiyama, H. Ikeda, Y. Ebiko, T. Hirano, S. Saito, T. Oinoue, Y. Hagimoto, and H. Iwamoto, “IR sensitivity enhancement of CMOS image sensor with diffractive light trapping pixels,” Sci. Rep., Vol. 7, No. 1, 3832, 2017.

Optical magnetic field distribution imaging using a single-gap, crescent-shaped metal split-ring resonator

T. Okamoto[1*], **K. Takabatake**[2], **K. Yamaguchi**[1], **M. Haraguchi**[1]

[1] Institute of Post-LED Photonics, Tokushima University, Japan
[2] Graduate School of Science and Technology, Tokushima University, Japan
[*]corresponding author: toshi-okamoto@tokushima-u.ac.jp

Abstract: When a previously invisible physical quantity becomes observable, it opens the way to the discovery and elucidation of new physical phenomena. This has advanced science and technology, spread to various fields, and contributed to the development of society. Since the interaction between the optical magnetic field and matter is small, the optical magnetic field has not been observed. We have enabled optical magnetic field imaging by utilizing the magnetoelectric effect of single-gap split-ring resonator(SRR) that exhibits magnetic resonance at optical wavelengths.

Most of the optical responses in natural materials are caused by interactions with optical electric fields. Therefore, even if there is a place where the optical magnetic field is peculiarly strong, it cannot be detected directly. So, we have never seen the distribution of the optical magnetic field. If we can see the distribution of the optical magnetic field, what can we learn? For example, one would see the presence of loop currents (oscillating at high frequencies). Possibly, we may also see non-radiative electric quadrupole modes that occur in nanostructures. It may also contribute to elucidating the interaction between photons and phonons, which has recently attracted attention.

In our research, we proposed and demonstrated a method for observing the optical magnetic field distribution. We fabricated a large number of single-gap crescent-shaped gold SRRs with a diameter of around 100 nm on a glass substrate using Nanosphere Lithography.[1] White light was incident on a SRR arranged on the bottom surface of the prism in the arrangement shown in Fig.1(a). TE polarized light was incident at 45 degrees, which is the total internal reflection condition. The scattered light spectra of single isolated SRR are shown in Fig.1 (b). The spectral peak of the Ey polarization of the same component as the incident light was a wavelength of around 700 nm. This peak means the electric dipole in the same direction as the incident light was excited by the localized surface plasmon resonance of SRR. On the other hand, the scattered light of Ex polarized component different from the incident light appeared in the wavelength around 900 and 600 nm. In the case of

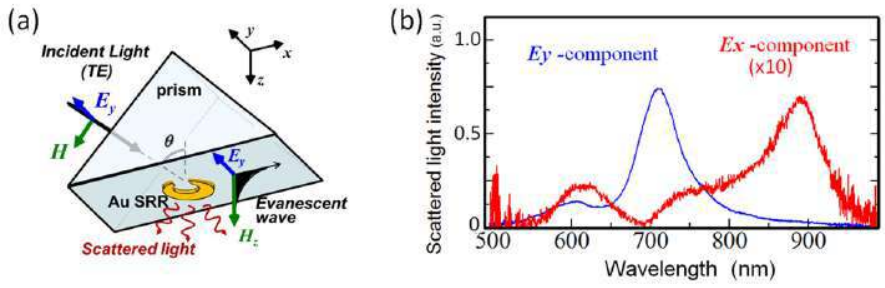


Fig.1 Experimental setup(a) and scattered light spectra of a single SRR(b)

oblique incidence, the incident magnetic field penetrates the single-gap SRR structure, and a magnetic resonance mode is excited in which a loop current flows in the ring of SRR. At that time, the loop current is thought to induce an oscillating current component perpendicular to the axis of symmetry, that is, an electric dipole in the x-direction due to the imperfect symmetry of the SRR structure, resulting in Ex-polarized scattered light. That is, when there is an optical magnetic field (Hy) perpendicular to the plane of the single-gap SRR, an electric dipole (x direction) perpendicular to the symmetry axis of the SRR is generated. Such a phenomenon is called the magnetoelectric effect.[2] We thought that this effect of single-gap SRR could be used for local magnetic field intensity monitoring and spatial distribution imaging. In order to demonstrate this, we fabricated a metasurface in which single-gap silver SRRs are densely arranged two-dimensionally[3] and photographed the scattered light intensity distribution at the magnetic resonance wavelength. For the optical magnetic field distribution used for the demonstration, interference fringes with a period of 367 nm created by two-beam interference were used. The interference fringes of the optical magnetic field and the optical electric field were designed so that the brightness was reversed. As a result of the experiment, Figure 2 was obtained, and the expected interference fringes were observed. This proves that optical magnetic field distribution imaging is possible.

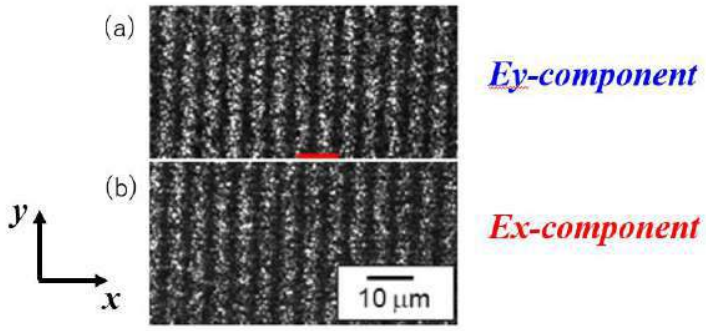


Fig.2 Scattered light image from SRR metasurface.
(a) Ey polarization component, (b) Ex polarization component.

This work was supported by JSPS KAKENHI Grant Numbers JP18K19024, JP18H01902.

References

1. T. Okamoto, et al., "Visible near-infrared light scattering of single silver split-ring structure made by nanosphere lithography," Opt. Exp., Vol. 19, No. 8, 7068–7076, 2011.
2. I. Sersic, et al., "Magnetoelectric point scattering theory for metamaterial scatterers", Phys. Rev. B 83, 245102-1-12, 2011.
3. K. Tanikawa, T. Okamoto et al., "Fabrication of peelable thin films containing crescent-shaped split-ring resonators for three-dimensional optical metamaterials," Opt. Mat. Exp., Vol. 7, No. 1, 1–7, 2017.

Fabrication of metasurfaces for heat-shielding windows and 6G communications and investigation of the possibility of near-infrared reflection control by movable thin films

Y. Kanamori [1*]

[1] Tohoku University, Japan
[*]corresponding author: ykanamori@tohoku.ac.jp

Abstract: Metasurfaces for heat-shield windows which transmit visible wavelengths and reflect near-infrared (NIR) wavelengths for sun light were designed and fabricated. Transmittance of terahertz waves assumed for 6G communications was measured. Moreover, by combining the metasurfaces with movable thin-films, reflectance switchable filters that could change reflectance at NIR wavelengths whereas there was little change in visible wavelengths were designed. It can be expected to be used as smart glasses that control transmittance of the thermal wavelengths in summer and winter.

Metasurfaces have attracted attention as novel artificial materials having exotic optical characteristics academically, but also as practical usages [1-3]. Localized surface plasmon resonance on metasurfaces produces reflection peaks at the resonant wavelengths. Since the optical properties of metasurfaces depend on their shapes, or the refractive index of material existing within the surface plasmon polaritons distance range of metasurface, tunable metasurfaces based on micro-electromechanical systems technologies have been studied intensively in recent years [4,5].

In this study, visible-transparent and NIR reflective metasurfaces by designing their resonant wavelengths in the NIR region while maintaining high transmittance in the visible region are fabricated. The metasurfaces function as heat shielding filters and lead to energy saving. Moreover, by combining the metasurfaces with movable thin-films, reflectance switchable filters that can change reflectance at NIR wavelengths whereas there is little change in visible wavelengths are designed. It can be expected to be used as smart glasses that control transmittance of the thermal wavelengths in summer and winter.

Figure 1 shows a unit structure of metasurfaces. A cross-shaped Al structure is formed on an SiO_2 substrate. Here, l, w, h, and Λ are length, width, height, and period of the unit structure, respectively. h and Λ are fixed to be 60 and 450 nm, respectively. By making cross-shaped structures, there are no polarization dependence at a normal incident angle.

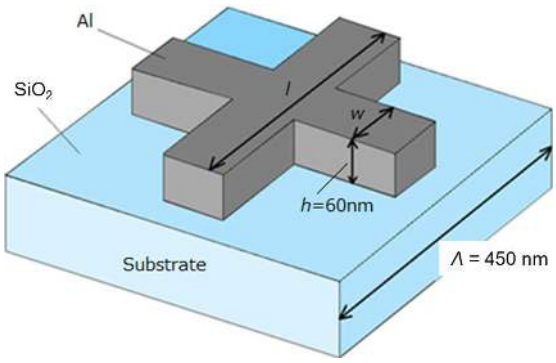


Figure 1: Unit structure of metasurfaces.

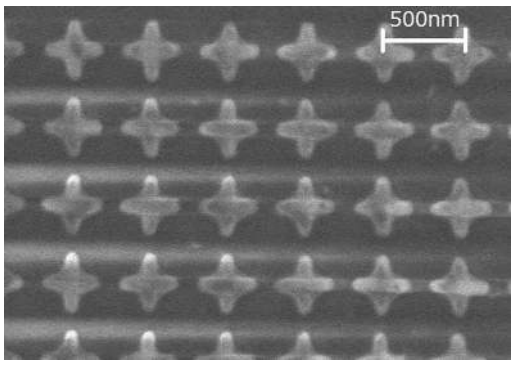


Figure 2: An SEM image of fabricated metasurface.

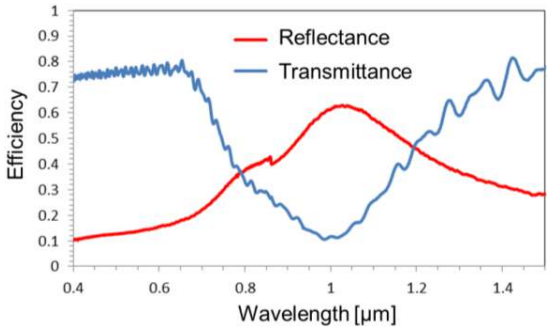


Figure 3: Measured spectra of the metasurface.

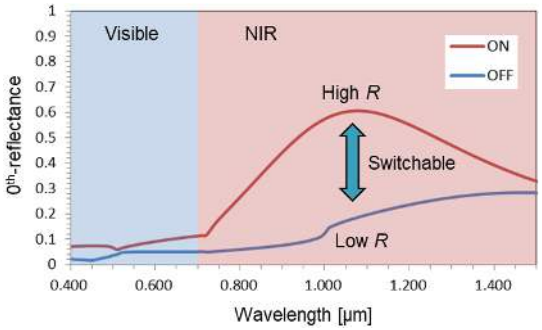


Figure 4: Calculated reflectance.

In fabrication, firstly, Al was deposited on a cleaned SiO_2 substrate, followed by electron beam lithography. Next, plasma etching was carried out. Finally, residual resist was removed.

A scanning electron microscope (SEM) photograph of fabricated metasurface is shown in Fig. 2. It is confirmed that the crossed structures which consist of Al are arranged on the SiO_2 substrate.

Figure 3 shows the measured transmittance and reflectance spectra of fabricated metasurface from visible to NIR wavelengths. At the visible wavelengths from 400 to 700 nm, uniform transmittance over 70% is maintained. At the NIR wavelengths larger than 700 nm in Fig. 3, the maximum reflectance of 62% is obtained at the resonant wavelength around 1.0 μm. In addition, high transmittance of terahertz wave (>50%) in the frequency range of 0.2-1 THz was achieved, which is suitable for applications in 6G communications.

Figure 4 shows calculated 0^{th}-ordered reflectance, based on rigorous coupled-wave analysis. ON and OFF indicated in Fig. 4 show high and low reflectance (R) at NIR wavelengths, respectively. By contacting a high refractive index plate consisting of silicon nitride on the metasurface, reflectance characteristics are switched from ON to OFF.

In conclusions, the metasurfaces that transmit visible wavelengths and reflect NIR wavelengths were designed and fabricated, successfully. The maximum reflectance of 62% was obtained at wavelengths around 1.0 μm, whereas uniform transmittance over 70% was maintained in the visible region. It was confirmed that reflectance in NIR region were switched from high to low one by contacting a high refractive index plate consisting of silicon nitride on the metasurface, on calculations. A part of this research was supported by JST, CREST Grant No. JPMJCR2102, Japan. A part of this research was performed in Micro/Nano-Machining Research and Education Center, Tohoku University.

References

1. Y. Kanamori, D. Ema, and K. Hane, “Miniature spectroscopes with two-dimensional guided-mode resonant metal grating filters integrated on a photodiode array”, Materials, Vol. 11, 1924, 2018.
2. Y. Kanamori, T. Shimizu, S.-I. Nomura, and K. Hane, “Fabrication of refractive index sensors using polarization independent metamaterial and their application to chemical concentration measurement and DNA detection”, Electron. Comm. Jpn., Vol. 102, 34-40, 2019.
3. T. Shimizu, H. Sai, Y. Kanamori, and K. Hane, “Transmissive plasmonic color filters with built-in Si photodiodes”, IEEJ Trans. Sens. Micromachines, Vol. 137, 134-139, 2017.
4. Y. Kanamori, R. Hokari, and K. Hane, “MEMS for plasmon control of optical metamaterials”, IEEE J. Sel. Top. Quantum Electron., Vol. 21, 2701410, 2015.
5. J.-Y. Ou, E. Plum, J. Zhang, and N. I. Zheludev, “An electromechanically reconfigurable plasmonic metamaterial operating in the near-infrared”, Nat. Nanotechnol., Vol. 8, 252-255, 2013.

Si Plasmonic MEMS device for infrared sensing

M. Oshita, E. A. Abadi, T. Kan*

The University of Electro-Communications, JAPAN
*corresponding author: tetsuokan@uec.ac.jp

Abstract: When a metallic structure is formed on a semiconductor surface, the hot electrons in the metal excited by surface plasmon resonance (SPR) are extracted as an electric current. This method makes it possible to measure SPR by electric current in spacially limited situations. This sensing method can thus be integrated into MEMS (Micro Electro Mechanical Systems) to create attractive devices.

SPR is a collective resonance of free electrons on a metal surface in contact with a dielectric. When the light incident on a metal structure satisfies the SPR matching condition, the incident light couples to the free electron resonant vibration on the metal surface (Fig. 1(a)). Since the resonance mode changes depending on the metal geometry, a device can operate for specific wavelengths and polarizations. Furthermore, suppose the metallic structure is formed on a semiconductor. In that case, a Schottky barrier is formed at the metal-semiconductor interface, allowing hot electrons to be injected into the semiconductor and extracted as a current, enabling electrical readout of SPR (Fig. 1(b)). Furthermore, since the Schottky barrier height can be tuned lower than the silicon band gap, infrared detection becomes possible on a silicon device.

The authors have developed an infrared photodetector with metallic nanostructures embedded in Si. Copper nano blocks were embedded in the bottom of nanoholes on a silicon substrate (Fig. 1(c)). The block forms a Schottky junction with the surrounding silicon (Si), and hot electrons are injected into silicon by localized SPR induced by incident light irradiation. Copper forms a Schottky barrier of Φ_B = 0.65 eV with n-type silicon, so infrared photodetection is possible. In a device consisting of a 1000 nm periodic lattice of nanoholes with an

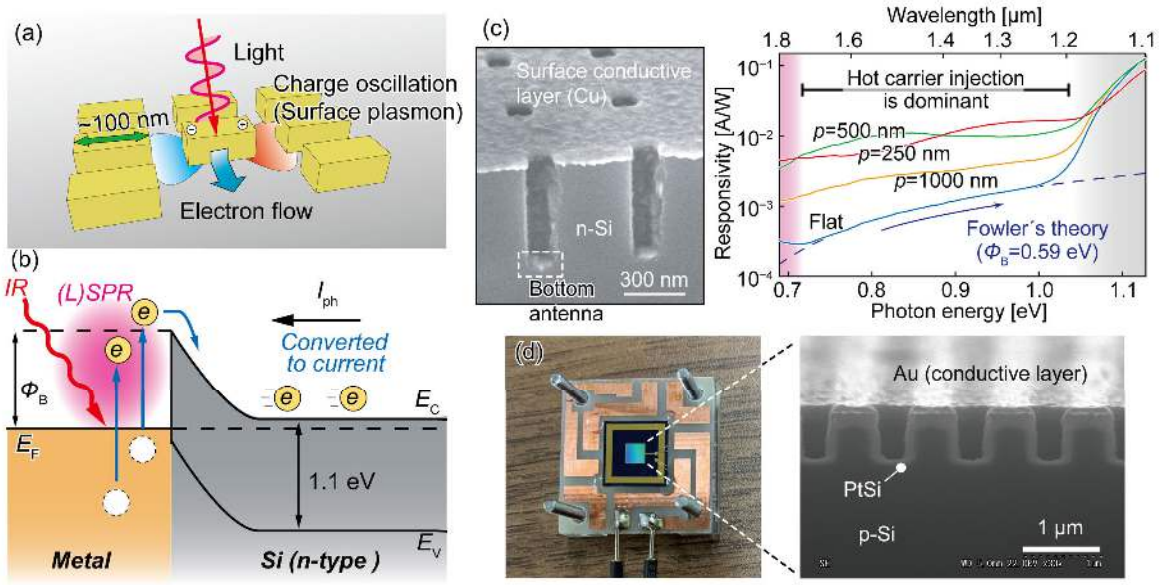


Fig. 1 Surface plasmon assisted infrared photodetection, (a) a device concept, (b) the Schottky barrier and photodetection mechanism, (c) buried nanoantennas for near-infrared photodetection[1], and (d) an mid-infrared photodetector[2].

aperture width of 150 nm, a sensitivity of more than 1 mA/W has been obtained down to a wavelength of 1.76 μm[1]. Furthermore, by changing the metal to a silicide (PtSi) presenting Φ_B = 0.28 eV with a p-type Si, it became possible to extend the measurable wavelength to mid-infrared, 3.4 μm[2]. Moreover, the spectrum measurement can be performed using a diffraction grating. Since SPR occurs at a unique angle of incidence for each wavelength on the grating, the angular current waveforms present peaks at a different angle depending on the wavelength (Fig. 2(a)). When the current is measured while scanning the incident angle, current waveforms become a superposition of each wavelength contribution composing the incident light (Fig. 2(b)). If the angular sensitivity spectrum for each wavelength is obtained in advance, the spectrum of the incident light can be reconstructed from this angular current waveform[3]. This measurement requires scanning the device angle relative to the incident light, and the angle scanning function can be integrated into a small device with MEMS technology[4]. Thus the spectral measurement is completed simply by irradiating light onto the small MEMS device. Integrating SPR with silicon MEMS can open up new fields of infrared sensing.

Acknowledgment: This research was financially funded by IMRA Japan Co., Ltd. and NEDO, Japan. EB lithography was performed in Takeda CR of d.lab, the University of Tokyo, Japan. Microfabrication was performed in a CR of the Division of Advanced Research Facilities (DARF) of the Coordinated Center for UEC Research Facilities of the University of Electro-Communications, Tokyo, Japan.

References

1. S. Yasunaga *et al.*, *Advanced Materials Interfaces* 7, 2001039 (2020)
2. M. Shiraishi, D. Noda, R. Ohta, and T. Kan, *Appl. Opt.* 61, 3987-3996 (2022)
3. M. Oshita, H. Takahashi, Y. Ajiki and T. Kan, *ACS Photonics* 7, 673-679 (2020)
4. M. Oshita, S. Saito, T. Kan, *Microsystems & Nanoengineering* (in press)

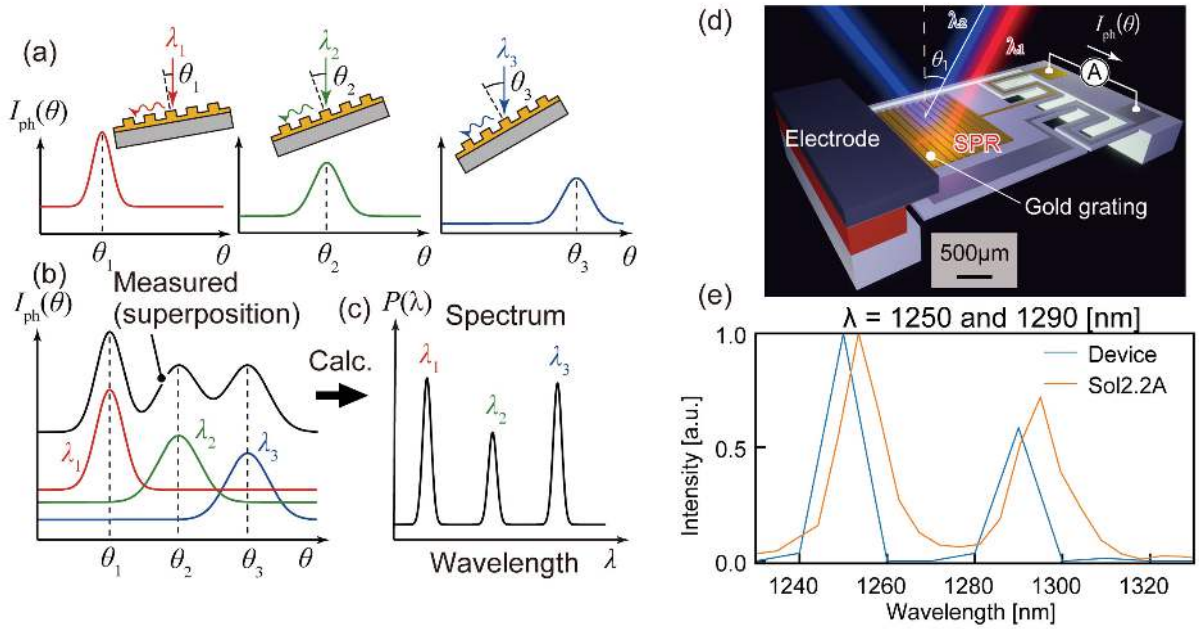


Fig. 2 Spectroscopy using a grating plasmonic photodetector, (a) angular photoresponses, (b) a response for multi-wavelength incidence, (c) derivation of the spectrum, and (d)(e) a MEMS cantilever-type plasmonic photodetector and the spectrum obtained using the device[3, 4].

META 2023, PARIS - FRANCE, JULY 18 – 21, 2023

Material systems for metamaterial based selective thermal emitters

M. Eich[1,2*], G.V. Krishnamurthy[2], M. Störmer[2], A. Yu. Petrov[1,2]

[1]Institute of Optical and Electronic Materials, Hamburg University of Technology, Germany
[2]Institute of Photoelectrochemistry, Helmholtz-Zentrum Hereon, Geesthacht, Germany
[*]corresponding author: m.eich@tuhh.de

Abstract: High temperature stable thin film multilayers of metal and dielectric materials are important as selective emitters for thermophotovoltaics (TPV). We will present structured material systems from W, Ir, and HfO_2 and discuss degradation mechanisms.

Since the total radiated power of a thermal emitter scales with the fourth power of temperature, it is beneficial to realize structured material systems which not only provide selective emission, thus avoiding the emission of unwanted photons, but also stay stable at very high temperatures well above 1000 deg C. We are discussing the influence of phase stability of the dielectric constituent, agglomeration of the metallic constituent along with oxidation mechanisms and countermeasures to prevent such oxidation. In particular, Ir is promising as an oxidation-stable plasmonic material for TPV applications.

References

1. P. N. Dyachenko, S. Molesky, A. Yu Petrov, M. Störmer, T. Krekeler, S. Lang, M. Ritter, Z. Jacob and M.Eich, “Controlling thermal emission with refractory epsilon-near-zero metamaterials via topological transitions,” Nature Communications. **7,** 11809 (2016).
2. M. Chirumamilla, G. Vaidhyanathan, K. Knopp, T. Krekeler, M. Graf, D. Jalas, M. Ritter, M. Störmer, A. Yu Petrov, and M Eich, “Metamaterial emitter for thermophotovoltaics stable up to 1400 °C” Scientific Reports **9**, 7241 (2019).
3. M. Chirumamilla, *et al.* Thermal stability of tungsten based metamaterial emitter under medium vacuum and inert gas conditions. *Sci. Rep.* **10**, 3605 (2020).
4. G.V. Krishnamurthy, M. Chirumamilla, S.S. Rout, K.P. Furlan, T. Krekeler, M. Ritter, H.-W. Becker, A.Y. Petrov, M. Eich and M. Störmer: Structural degradation of tungsten sandwiched in hafnia layers determined by in-situ XRD up to 1520 °C. Scientific Reports **11**, 3330 (2021)

Spectrally selective infrared emitters enabled by 1D metamaterials

Yongkang Gong and Sang Soon Oh*

School of Physics and Astronomy, Cardiff University, Cardiff CF24 3AA, United Kingdom
*corresponding author: ohs2@cardiff.ac.uk

Abstract: We propose a new type of integrated and electrically controlled infrared emitter that exploits 1D dielectric/metallic multilayers. We design a multilayer system with a large photonic bandgap at the visible wavelengths and negligible reflection at the infrared wavelengths. Here, we experimentally demonstrate significantly enhanced emission at the broad infrared wavelengths of 1.4–14μm as well as strongly suppressed emission in the visible region.

Infrared (IR) emitters have been used for gas sensing in numerous applications such as detection of explosive or toxic gases, indoor/outdoor air quality monitoring, and medical diagnosis. Mid-IR thermal emitters based on metamaterials, especially with refractory metamaterials [1], have become popular due to their ability to generate thermal radiation with near-unity emissivity at arbitrary infrared wavelengths. We have recently demonstrated novel broadband and narrowband mid-Infrared metamaterial thermal emitters [2-4].

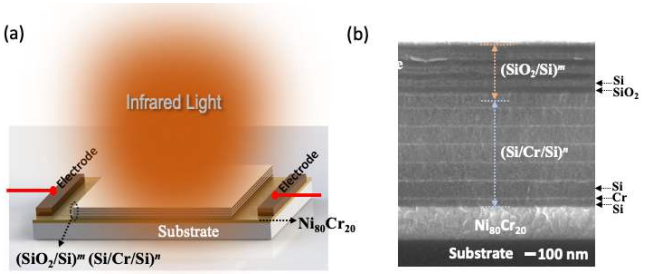


Figure 1 (a) Schematic of the IR emitter device (b) The thickness of each Si (SiO_2) layer in the $(SiO_2/Si)^m$ is 40 nm (100 nm), and the thickness of each Si (Cr) layer in the $(Si/Cr/Si)^n$ is 100 nm (4 nm); the number of periods m and n are 4 and 6, and the thickness of the $Ni_{80}Cr_{20}$ layer and the substrate is 300 nm and 0.5 mm, respectively. Adapted from Ref. [5].

In this work, we design a structure consisting of a 1D photonic crystal of and 1D metal/dielectric multilayer to suppress the emission at the visible wavelengths and enhance the emission at the infrared. As shown in Fig. 1, we stack $(Si/Cr/Si)^n$ and (SiO_2/Si) successively on top of a $Ni_{80}Cr_{20}$ nanolayer-deposited quartz substrate. After determining the thicknesses based of the transfer-matrix-method calculations, the designed structures have been fabricated using e-beam evaporation. Then, the emission property of the electrically heated devices was characterized using Fourier-transform infrared spectroscopy (FTIR) and grating spectrometer. Our experimental results show the averaged emissivity as high as ~0.81 over a broad infrared wavelength range of 1.4–14 μm and the averaged emissivity as low as ~0.07 at visible wavelengths of 0.45–0.75 μm.

We believe that the proposed high-efficiency thermal emitters will pave the way toward integrated infrared light source platforms for various thermal-photonic applications and provide a novel alternative for cost-effective, compact, low glare, and energy-efficient infrared heating.

References

1. W. Li, et al., “Refractory Plasmonics with Titanium Nitride: Broadband Metamaterial Absorber,” Adv. Mater., 26, 7959–7965 (2014).
2. Y. Gong, et al., “Highly efficient and broadband mid-infrared metamaterial thermal emitter for optical gas sensing," Opt. Lett. 42, 4537-4540 (2017)
3. Y. Gong, et al., “Coherent emission of light using stacked gratings,” Phys. Rev. B, 87, 205121 (2013).
4. A. Pusch, et al., "A highly efficient CMOS nanoplasmonic crystal enhanced slow-wave thermal emitter improves infrared gas-sensing devices." Scientific reports 5, 17451 (2015).
5. Y. Gong, K. Li, N. Copner, H. Liu, M. Zhao, B. Zhang, A. Pusch, D. L. Huffaker, and S. S. Oh, Integrated and Spectrally Selective Thermal Emitters Enabled by Layered Metamaterials, Nanophotonics 10, 1285 (2021).

META 2023, PARIS - FRANCE, JULY 18 – 21, 2023

Dynamic emissivity modulating thermoregulating fabric using metallic particles

M. G. Abebe[1*], G. Rosolen[1], and B. Maes[1]

[1]Micro- and Nanophotonic Materials Group, Research Institute for Materials Science and Engineering, University of Mons, 20 Place du Parc, B-7000 Mons, Belgium

[*]corresponding author: mulunehgeremew.abebe@umons.ac.be

Abstract: Maintaining comfort using photonic thermal management textiles can potentially decrease the energy cost for heating and cooling in residential and office buildings. We propose a thermoregulating fabric comprised of a high emissivity bottom layer and a metal-particle polymer composite on top to modulate emissivity and provide dynamic and passive thermal comfort. With detailed numerical modeling we demonstrate a wide dynamic ambient setpoint temperature window of ∼7.25 °C, with the wearer staying comfortable in the range between 18.5 and 25.75 °C. This thermoregulating performance indicates a vital energy-saving potential and paves the way to a more sustainable society.

As humanity starts to experience the consequences of climate change, addressing the global energy crisis provides us with a significant challenge. Surprisingly, more than half of our energy consumption goes to the heating and cooling of large empty spaces in residential and commercial buildings [1]. Therefore, passive personal thermal management, which creates a localized thermal regulation, can become critical to lower consumption and guarantee a sustainable future. Recently, micro-photonic driven local thermal management in textiles has captivated attention. Since radiative transfer accounts for around 50% of heat dissipation from the human body, a proper photonic thermal management strategy allows one to design passive temperature-regulating textiles. Previously we have shown a static state-of-the-art emissivity switch fabric design based on the Janus-yarn concept [2]. However, this fabric requires mechanical flipping to switch between cooling and heating modes.

Here we propose a metal-particle dynamic emissivity switch textile for dual-mode temperature regulation, using the fabrics' outer surface emissivity modulation. The fabric is constituted of a highly emissive bottom layer and a low emissive composite layer on top, which is thermo-mechanically dynamic (Fig. 1a). The top layer is made from a temperature-sensitive shape-memory polymer matrix with equal-sized metal particles (copper) uniformly dispersed, while the bottom layer is composed of carbon black. The proposed design operates in two modes, heating and cooling. When the ambient is cold, the fabric is in heating mode, and the polymer shrinks; thus, the volume fraction of the metal particles increases, resulting in high scattering and reflection, leading to a low effective emissivity of the fabric's surface [see Fig. 1a (I)]—subsequently, strong radiative heat emission to the ambient. When the ambient is hot, the fabric is in cooling mode; the polymer expands, allowing the low-emissive shape-memory polymer based top layer to stretch; as a result, the volume fraction of metal particles decreases [see Fig. 1a (II)]. This decrease substantially lowers radiation scattering and increases the fabric's emissivity, therefore facilitating more radiative heat transfer from the human body to the ambient. By introducing an optimized copper particle, one can achieve an effective emissivity contrast of about 0.65, which translates to a wide ambient setpoint window.

To model the fabric design, we first use electromagnetic wave theory (i.e., extended Lorenz-Mie solutions) to calculate the optical properties of a single metallic microsphere, such as scattering phase function, scattering

efficiency, and absorption efficiency. Second, we calculate the effective radiative properties of a particle cloud uniformly dispersed in a polymer matrix (effective scattering and absorption coefficients). Third, we investigate the radiative transfer analysis of a particulate medium using a collision-based forward Monte Carlo method. Finally, we implement the radiative parameters (emissivity) retrieved from the Monte Carlo calculations in the thermal model to retrieve the ambient setpoint temperature [3].

Figure 1b plots spectral emissivity for two specific cases, volume fraction f_v = 0.01 and 0.1, respectively, which we associate with the cooling and heating mode. In cooling mode (f_v = 0.01, blue line), we observe a very high spectral emissivity; therefore, the fabric is almost a perfect emitter for all the interesting wavelengths. In heating mode (f_v = 0.1, dark red line), the spectral emissivity is low over the entire human body emissivity spectral range (light blue background surface plot). It is clear that a low volume fraction results in high emissivity, and high volume fraction results in substantially decreased emissivity. This result is directly related to the metal particle cloud's effective scattering coefficient, which increases with volume fraction. The emissivity dependence on the volume fraction delivers the expected dynamic temperature regulation property of the proposed fabric. Heat transfer analysis shows that the design achieves a minimum setpoint of 18.5 °C to provide heating and the highest setpoint of 25.75 °C to provide cooling (Fig. 1c). The minimum setpoint corresponds to the emissivity of 0.27, where f_v = 0.1. On the other hand, the highest setpoint corresponds to an emissivity of 0.93, where f_v < 0.01.

Overall, we propose a dual-mode fabric design for personal thermal management using a multilayer approach by incorporating metallic particles to deliver emissivity modulation. The dynamic switching is achieved via a shape memory polymer matrix that responds to environmental changes. This design provides thermal comfort in a setpoint window of about 7.25°C.

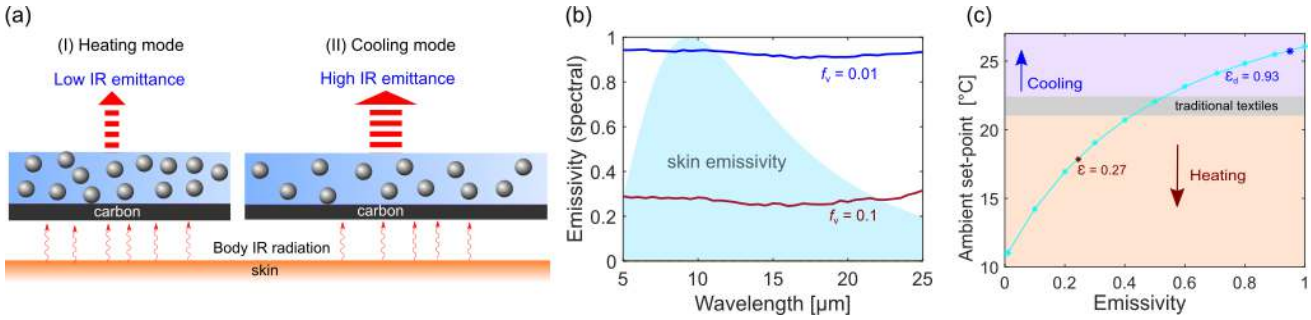


Figure 1. (a) Schematic illustration of fabric design working principle with dual mode operation. (b) Spectral emissivity for f_v = 0.01 and 0.1. (c) Ambient setpoint temperature of the design as a function of emissivity.

We acknowledge support from the INTERREG PHOTONITEX and ARC-21/25 UMONS2 projects.

References

1. Walther, G.-R., Post, E., et al., "Ecological responses to recent climate change," Nature 416(6879), 389 (2002).
2. Abebe, M. G., De Corte, A., Rosolen, G., and Maes, B., "Janus-yarn fabric for dual-mode radiative heat management," Phys. Rev. Appl 16(5), 054013 (2021).
3. Abebe, M. G., Rosolen, G., Odent, J., Raquez, J.-M., and Maes, B., "A dynamic passive thermoregulation fabric using metallic microparticles," Nanoscale 14, 1421–1431 (2022).

Zero-dimensional thermal light emitters in the infrared based on silicon microspheres

R. Fenollosa[1*], F. Ramiro-Manzano[1], M. Garín[2] and F. Meseguer[1]

[1]Instituto Universitario de Tecnología Química, CSIC-UPV, Universitat Politècnica de València, Spain

[2]GR-MECAMAT, Universitat de Vic, Spain

[*]corresponding author: rfenollo@ter.upv.es

Abstract: Silicon microspheres with 2-3 μm in diameter, heated by means of a blue laser, at temperatures from 500 to 700 ºC emit light in the infrared with pronounced peaks that are associated with their Mie resonances. The emission occurs through the lowest order modes in the mid-infrared where the intensity can surpass the black body limit because the optical absorption cross section is larger than the geometric one.

The development of photonic circuitry in the mid-infrared constitutes a very promising technological niche, yet it is still in its infancy. In this context, light sources with appropriate performance are essential elements. Here, we show a light source based on a silicon microsphere and its thermal emission. The microsphere can reach a high temperature, near 700 ºC, when it is irradiated by a blue laser, λ = 405 nm, at a moderate power, P= 5mW. This process is relatively fast,[1] with characteristic excitation and decay times of the order of 10 μs, and it yields light radiation in the infrared with interesting spectral features. Instead of a broad emission, a silicon microsphere shows pronounced peaks that are associated with their Mie resonances. We have studied this phenomenon in two spectral regions of technological interest: in the mid-infrared where the fingerprint of most molecules appears, and in the near infrared, around the telecommunication wavelengths. Figure 1 shows such spectrum (black curve) in the mid infrared for a microsphere with 2080 nm in diameter, heated at 660 ºC.

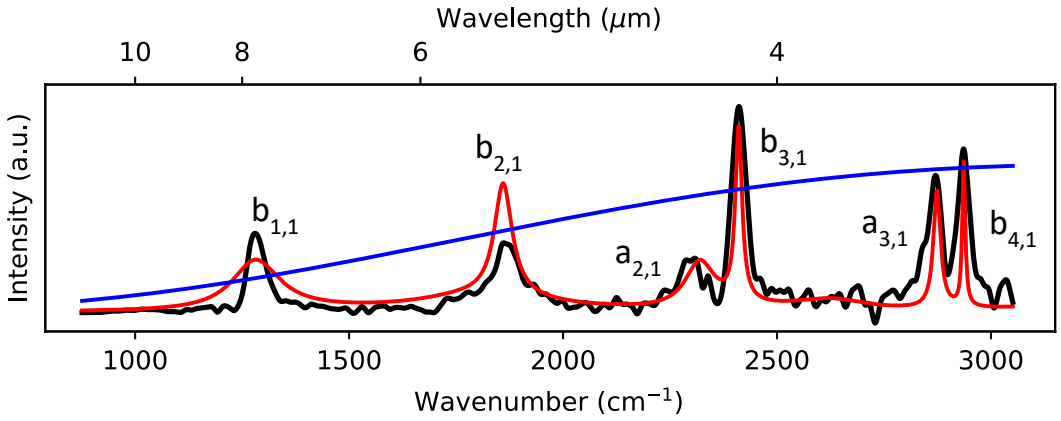


Figure 1: Measured thermal emission spectrum (black line) of a silicon microsphere with 2080 nm in diameter. The red curve corresponds to a fit to equation (1) with a fitted temperature of 660 ºC. The blue line is the calculated emission of a black body that has an area equal to the geometric projected area of the microsphere. The modes associated with each peak are indicated.[2]

The spectrum of figure 1 could be fitted (red curve) to the following equation:

$$I = \frac{2\pi hc^2}{\lambda^5 exp\left(\frac{hc}{\lambda kT}-1\right)}\, e \qquad (1)$$

that corresponds to the Planck equation of the black body emission modulated by the emissivity factor, *e*, where in this case *e* equals to the absorption efficiency of the microcavity defined by the particle. This allows identifying the resonances, that have been indicated besides their corresponding peaks with the usual nomenclature for transverse electric (b's) and transverse magnetic (a's) modes.[3] These are the lowest order modes. In addition, because the absorption efficiency is larger than one, the emission surpasses the Planck limit (blue curve) for the black body for some resonances.

Besides the mid-infrared, where the lowest order modes appear and where the sub-wavelength character in the three dimensions manifests, the light emission in the near infrared region shows as well pronounced peaks associated with Mie resonances. In this region we have found resonances with a quality factor of 400. In addition, we have demonstrated their wavelength tunability with temperature as figure 2 shows for a 3595 nm in diameter microsphere.[1]

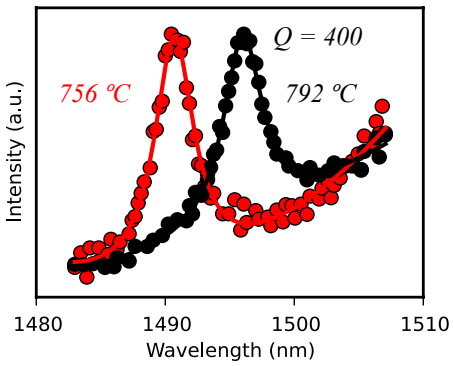


Figure 2: Measured $b_{10,5}$ resonance of a 3595 nm diameter silicon microsphere at two different indicated temperatures.[1]

This work was supported by several projects of the Spanish Ministry of Economy and Competitiveness: Severo Ochoa program for Centers of Excellence CEX2021-001230-S and PLEC2021-007576.

References

1. R. Fenollosa, F. Ramiro-Manzano, M. Garín, R. Alcubilla, "Thermal Emission of Silicon at Near-Infrared Frequencies Mediated by Mie Resonances" ACS Photonics, 34, 3174–3179, 2019.
2. R. Fenollosa, F. Ramiro-Manzano, M. Garín, F. Meseguer, "Silicon Microspheres for Super-Planckian Light Sources in the Mid Infrared", submitted to Adv. Optical Mater.
3. R. Fenollosa, F. Meseguer, M. Tymczenko, "Silicon Colloids: From Microcavities to Photonic Sponges" Adv. Mater. 20, 95-98, 2008.

META 2023, PARIS - FRANCE, JULY 18 – 21, 2023

Refractory metamaterials for tuning thermal emission at high temperature

A. Nzie[1,2,4], S. Sayegh[3,4], O. Rozenbaum[2,4], M. Bechelany[3] and Q. Flamant[1,4*]

[1] Saint-Gobain Research Provence, 550 Rue Alphonse Jauffret, 84300, Cavaillon, France
[2] CEMTHI, UPR 3079, CNRS, 1D avenue de la Recherche Scientifique, 45071, Orléans, France
[3] Institut Européen des Membranes (IEM), UMR 5635, Univ Montpellier, CNRS, ENSCM, Place Eugène Bataillon, 34095, Montpellier, France
[4] Laboratoire Commun Canopée, CNRS / Université de Lorraine / Saint-Gobain, Orléans / Nancy / Cavaillon / Paris, France
[*]Corresponding author: Quentin.flamant@saint-gobain.com

Abstract: Metamaterials provide an accrued flexibility for tuning thermal emission but their resistance to high temperature is limited. So far, the few attempts to realize refractory metamaterial emitters relied on materials that are prone to oxidation which limits their operating temperature in air. In this work, we show how using innovative fabrication approaches and making the proper choice for associating a conducting and a dielectric material allows elaborating metamaterials with tunable emissivity that can operate in air at temperatures exceeding 1000°C.

At high temperature, thermal radiation accounts for a large part of the heat transfer. Therefore, the ability to tune thermal emission is paramount to improve energy efficiency when heating and cooling. It is also one of the keys for converting efficiently heat into electricity in a thermophotovoltaic system.

Electromagnetic properties of natural materials are mainly determined by their chemical composition. The metamaterial approach provides additional degrees of freedom for tailoring these properties by playing on the internal structure. This accrued flexibility is of particular interest for the design of thermal emitters: it allows full spectral control and impedance matching with free space, thereby maximizing the emission for a chosen wavelength range [1].

Unfortunately, most existing metamaterials rely on metals with a low melting point such as gold or silver. So far, the attempts to realize refractory metamaterial emitters relied either on refractory metals (e.g. Ta, Mo, W) or on nitrides (e.g. TiN, AlN, ZrN) [2, 3]. These materials do have high melting points but are prone to oxidation which limits their operating temperature in air [2, 4].

In 2013, Molesky et al. proposed a new approach to design selective emitters by engineering the poles and the zeros of the dielectric function of a hyperbolic metamaterial [5]. This theoretical paper served as a basis for several experimental implementations, the most successful one consisting of alternating layers of tungsten and hafnia [6], which were shown to be stable up to 1400°C under high vacuum [4]. However, in air the emitter still oxides and degrades above 1000 °C.

In this presentation, we will show how using innovative fabrication approaches and making the proper choice for associating a conducting and a dielectric material allows elaborating refractory metamaterials with tunable emissivity in the near infrared (NIR) that can operate in air at temperatures exceeding 1000°C.

References

1. Landy, N.I., Sajuyigbe, S., Mock, J.J., Smith, D.R. and Padilla, W.J., Perfect metamaterial absorber, Phys Rev Lett, 2008. DOI: 10.1103/PhysRevLett.100.2074021064–1076, 1986.
2. Chirumamilla, M., Chirumamilla, A., Yang, Y., Roberts, A.S., Kristensen, P.K., Chaudhuri, K., Boltasseva, A., Sutherland, D.S., Bozhevolnyi, S.I. and Pedersen, K., Large-Area Ultrabroadband Absorber for Solar Thermophotovoltaics Based on 3D Titanium Nitride Nanopillars, Advanced Optical Materials, 2017. DOI: 10.1002/adom.201700552
3. Chirumamilla, M., Krishnamurthy, G.V., Rout, S.S., Ritter, M., Stormer, M., Petrov, A.Y. and Eich, M., Thermal stability of tungsten based metamaterial emitter under medium vacuum and inert gas conditions, Sci Rep, 2020. DOI: 10.1038/s41598-020-60419-2
4. Chirumamilla, M., Krishnamurthy, G.V., Knopp, K., Krekeler, T., Graf, M., Jalas, D., Ritter, M., Stormer, M., Petrov, A.Y. and Eich, M., Metamaterial emitter for thermophotovoltaics stable up to 1400 degrees C, Sci Rep, 2019. DOI: 10.1038/s41598-019-43640-6
5. Molesky, S., Dewalt, C.J. and Jacob, Z., High temperature epsilon-near-zero and epsilon-near-pole metamaterial emitters for thermophotovoltaics, Opt Express, 2013. DOI: 10.1364/OE.21.000A96
6. Dyachenko, P.N., Molesky, S., Petrov, A.Y., Stormer, M., Krekeler, T., Lang, S., Ritter, M., Jacob, Z. and Eich, M., Controlling thermal emission with refractory epsilon-near-zero metamaterials via topological transitions, Nat Commun, 2016. DOI: 10.1038/ncomms11809

Perfect Absorbers and Photothermal Control of Light by Single Crystalline Silicon Metasurface

J. Takahara[1,2*]

[1] Graduate School of Engineering, Osaka University, Japan
[2] Photonics Center, Graduate School of Engineering, Osaka University, Japan
[*]corresponding author: takahara@ap.eng.osaka-u.ac.jp

Abstract: Perfect absorbers (PAs) play crucial roles for energy saving towards sustainable society. Recently, all-dielectric PA metasurfaces have been demonstrated by degenerate critical coupling. In this talk, I present recent progress of our studies about single-crystalline silicon metasurface PAs operating from visible to near-infrared region by using electric/magnetic dipoles, quadrupoles excited in silicon Mie resonators. In addition, I demonstrate scattering control of light by photothermal effects in Huygens' metasurface.

A perfect absorber (PA) is one of the promising devices for energy saving towards sustainable society. This is because PAs achieve mutual energy conversion between heat and light with 100% efficiency [1]. In recent years, many kinds of plasmonic PAs have been proposed and demonstrated. Metal-free (non-plasmonic), all-dielectric PAs can be realized by degenerate critical coupling (DCC) [2]. In DCC condition, Electric Dipole (ED) and Magnetic Dipole (MD) modes in Mie resonator with mirror symmetry co-exist in Huygens' metasurface (HMS). In addition, radiative loss (γ) and intrinsic loss (ohmic loss) (δ) of two modes must be matched. For this reason, the wavelength of PA depends on δ of the material. We demonstrated that the wavelength of PAs can be tuned from visible to near-IR by controlling γ and δ by using embedded Mie resonators in silicon (Si) metasurface [3,4].

In this talk, I present recent progress of our studies about single-crystalline silicon (c-Si) metasurface PAs operating with wide-range of wavelength by DCC using electric/magnetic dipoles, quadrupoles excited in Mie resonators. In addition, I demonstrate scattering control of light beam by photothermal effect in the c-Si PA.

Figure shows schematic view of the PA based on embedded Si Huygens' metasurface and the concept of DCC. We are able to achieve PA at any wavelength in principle by tuning refractive index of surrounding dielectric medium (n) as well as intrinsic loss of a cap layer (e.g. amorphous Si (a-Si)), because DCC condition ($\gamma = \delta$) can be satisfied at any wavelength if the cap layer is lossy at the wavelength.

In addition, we propose and demonstrate experimentally all-optical switching device by using photothermal effect of the PAs of Huygens' metasurface. All-optical switching (on/off) effect can be observed in 1/10 power rather than the non-PA metasurface [5]. Photothermal effects in Mie resonators pave a new pathway to efficient all-optical switching in low power consumption.

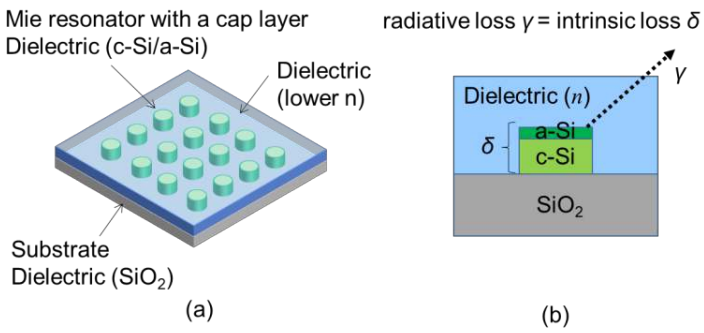


Figure (a) Schematic view of PA based on embedded Si Huygens' metasurface and (b) the concept of DCC.

The part of this study was supported by the Japan Society for the Promotion of Science (JSPS) KAKENHI Grant No. JP22K18987 and Research grant by Support Center for Advanced Telecommunications Technology Research (SCAT).

References

1. Toyoda H., K. Kimino, A. Kawano and J. Takahara, “Incandescent Light Bulbs Based on a Refractory Metasurface”, Photonics, Vol. 6, No. 4, 105, 2019.
2. Ming X., X. Liu, L. Sun, and W.J. Padilla, “Degenerate critical coupling in all-dielectric metasurface absorbers,” Opt. Express Vol. 25, No.20, 24658-24669, 2017.
3. Xu R. and J. Takahara, "Radiative loss control of an embedded silicon perfect absorber in the visible region," Opt. Lett. Vol. 46, No. 4, 805-808, 2021.
4. Rongyang Xu and J. Takahara, "All-dielectric perfect absorber based on quadrupole modes," Opt. Lett. Vol. 46, No. 15, 3596-3599, 2021.
5. Nishida K., K. Sasai, R. Xu, T-H. Yen, Y-L. Tang, J. Takahara, S-W. Chu, "All-optical scattering control in an all-dielectric quasi-perfect absorbing Huygens’ metasurface," Nanophotonics Vol. 12, No. 1, 139–146, 2023.

Transition Metal Nitride Metasurface Broadband Absorbers for Plasmon-Enhanced Solar-Driven Hydrogen Evolution

Yu-Jung Lu*[1,2]

[1]*Research Center for Applied Sciences, Academia Sinica, Taipei 11529, Taiwan*

[2]*Department of Physics, National Taiwan University, Taipei 10617, Taiwan*

*corresponding author: yujunglu@gate.sinica.edu.tw

Abstract: We demonstrate the plasmon-enhanced visible-light-driven hydrogen production from water using a polymer photocatalyst integrated with a TiN metasurface absorber. A 300 % increase in the hydrogen evolution rate was observed due to the LSPR that enhances the rates of light absorption, carrier separation, and hot-carrier transfer in polymer photocatalysts.

Broadband perfect absorbers in the visible region have attracted considerable attention in many fields, especially in solar thermophotovoltaic and energy harvesting systems. However, developing light absorbers with high absorptivity, thermal stability, and a broad bandwidth remains a great challenge. Here, we theoretically and experimentally demonstrate that a titanium nitride metasurface absorber exhibits broadband absorption with an average absorption of more than 92 % over a wavelength range of 400 nm to 750 nm. The increase in absorption is attributed to the localized surface plasmon resonance (LSPR). We demonstrate the plasmon-enhanced visible-light-driven hydrogen production from water using a polymer photocatalyst integrated with a TiN metasurface absorber, as shown in Figure 1. A 300 % increase in the hydrogen evolution rate was observed due to the LSPR that enhances the rates of light absorption, carrier separation, and hot-carrier transfer in polymer photocatalysts.[1] These results enable a new approach to preparing high-efficiency solar energy harvesting systems. The concept is extensible to other types of photocatalysts, such as 2D materials. In the end, we will also discuss the outlook for refractory metasurface in applications of solar energy harvesting systems.[1,2]

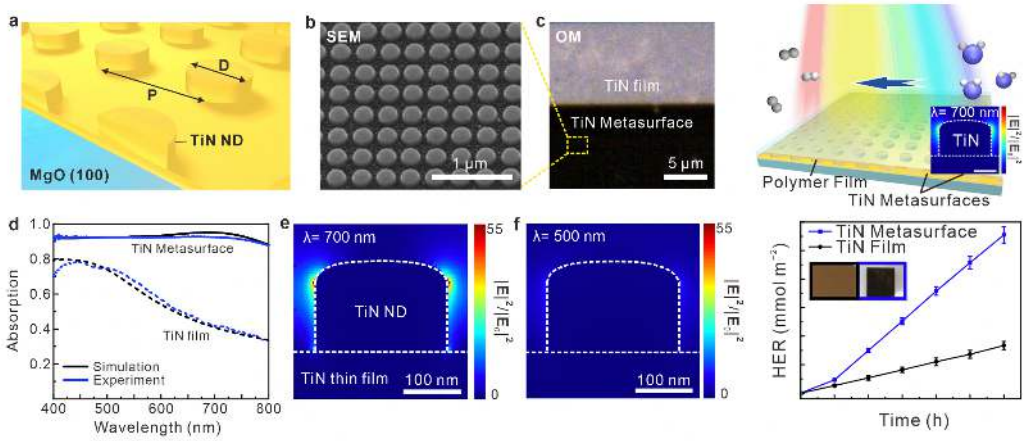


Figure 1. Plasmon-enhanced visible-light-driven production of hydrogen production from water using a TiN plasmonic metasurface absorber.

References

[1]. M-J Yu, C-L Chang, H-Y Lan, Z-Y Chiao, Y-C Chen, H W H. Lee, Y-C Chang, S-W Chang, T. Tanaka, V. Tung, H-H Chou*, and Y-J Lu*, Plasmon-Enhanced Solar-Driven Hydrogen Evolution Using Titanium Nitride Metasurface Broadband Absorbers. ACS Photonics 8, 3125-3132 (2021).

[2]. Z-Y Chiao, Y-C Chen, J-W Chen, Y-C Chu, J-W Yang, T-Y Peng, W-R Syong, H W H. Lee, S- W Chu, and Y-J Lu*, Full-Color Generation Enabled by Refractory Plasmonic Crystals. Nanophotonics 11, 2891-2899 (2022)

A Sustainable Power Scavenger Using Zebra-Inspired In-Plane Radiative Cooler/Heater

S. -Y. Heo[1], and Y. M. Song[1,2*]

[1]Country School of Electrical Engineering and Computer Science, Gwangju Institute of Science and Technology (GIST), 123 Cheomdangwagi-ro, Buk-gu, Gwangju, 61005, Republic of Korea
[2] Artificial Intelligence (AI) Graduate School, Gwangju Institute of Science and Technology (GIST), 123 Cheomdangwagi-ro, Buk-gu, Gwangju, 61005, Republic of Korea
[*]corresponding author: ymsong@gist.ac.kr

Abstract: A typical thermoelectric generators (TEGs) employ complex out-of-plane configurations, which often require additional thermal insulation components to preserve the temperature difference across the TEG. However, this can result in rigid and bulky configuration. In this study, we came up with a new TEG that is environmentally friendly and soft to the touch. It uses a pattern inspired by the stripes of a zebra to create a large temperature difference, making it a good option for future energy systems.

A thermoelectric generator (TEG) provides electrical power with thermal gradient. A key challenge in the development of TEG is making large temperature gradient through the device and miniaturization [1]. A conventional thermoelectric generator (TEG) involve a selective emitter with high IR emissivity to form the cool region at the TEG, while the bottom side is heated by ambient surroundings or solar energy with extended structures. However, a conventional TEG typically has the heating and cooling area in the direction of out-of-plane, matching the natural direction of heat flow, which requires additional thermal insulation components to preserve the temperature difference across the TEG [2]. Consequently, such TEGs can become bulky and complex, hindering their integration with other system components. Furthermore, As the size of the device reduces, so does its thickness, making it challenging to maintain a significant temperature differential between its upper and lower surfaces.

In this study, we present a novel approach for creating a large-area, in-plane thermoelectric generator (TEG) inspired by the zebra pattern, which maintains a significant temperature differential even in the horizontal direction. The TEG's heating region employs solar absorption, whereas the cooling region utilizes passive radiative cooling to optimize the temperature contrast between the two regions. Maintaining the temperature difference horizontally enables the TEG to be compact and stretchable. (Fig. 1A) The device is biodegradable, addressing the environmental impact. (Fig. 1B)

Fig. 1C illustrates an exploded view of stretchable, scalable, sustainable power scavenger using zebra pattern, consisting of a radiative modulator (top layer) and TEG (bottom layer). The proposed system comprises a microfiber membrane made of Poly(lactide-co-ε-caprolactone) (PLCL), which is coated with distinct patterns of poly(3,4-ethylenedioxythiophene)-poly(styrenesulfonate) (PEDOT:PSS) functioning as radiative heating and cooling elements. During the daytime, the TEG sustains the temperature gradient through infrared (IR) radiation and solar reflection in cooling region and IR reflection and solar absorption in the heating region. Even at night, the device maintains the temperature difference due to the cooling and heating regions responding oppositely to the IR radiation. (Fig. 1D)

To demonstrate the proof-of-concept, we measured the real-time outdoor power generation of the energy-harvesting system equipped with the radiation modulator, as shown in Fig. 2. The TEG produced a

maximum temperature gradient of approximately 17℃ between the black and white regions, resulting in a maximum power density of roughly 0.006 mW/m^2.

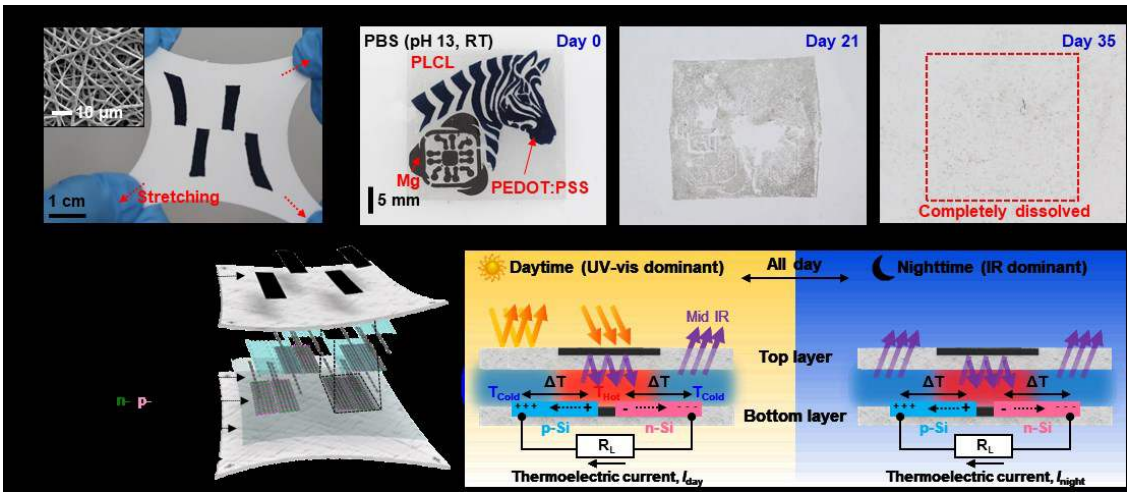


Figure 1. (A) A picture demonstrating stretching of a sustainable power scavenger using zebra-inspired in-plane radiative cooler/heater. The inset shows SEM image of the radiation modulator. (B) A series of dissolution images of a PLCL/PEDOT:PSS membrane and Mg film device, in PBS solution (pH 13) at room temperature. (C) A schematic view of (top layer) radiation modulator inspired by the stripes of a zebra and (bottom layer) thermoelectric generator (TEG) that are oriented in-plane direction of the device. (D) Cooling (white area) and heating (black area) mechanism of the device that sustain its temperature difference in two color region by 24 hours.

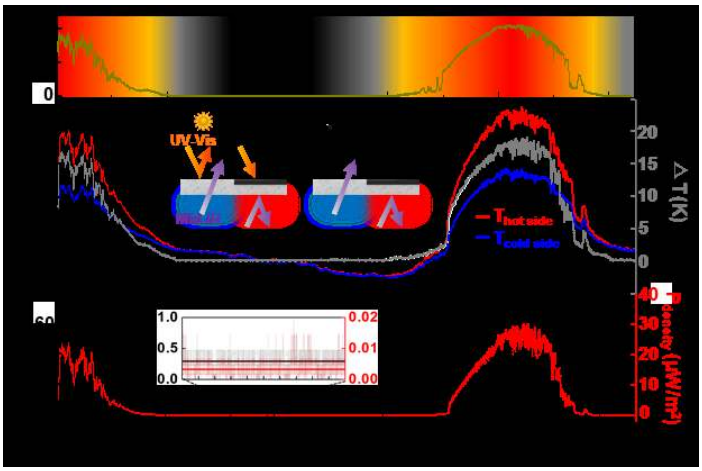


Figure 2. Measured solar irradiance(Isolar), hot and cold side temperature(T), open circuit voltage (Voc), generated power(P) density.

References

1. Nan, Kewang, et al. "Compliant and stretchable thermoelectric coils for energy harvesting in miniature flexible devices." Science Advances 4.11 (2018): eaau5849.
2. Han, Won Bae, et al. "Zebra-inspired stretchable, biodegradable radiation modulator for all-day sustainable energy harvesters." Science Advances 9.5 (2023): eadf5883.

META 2023, PARIS - FRANCE, JULY 18 – 21, 2023

Realization of true perfect absorber metasurfaces

Y. Nishijima[1*]

[1] Department of Electrical and Computer Engineering, Graduate School of Engineering, Yokohama National University, 79-5 Tokiwadai, Hodogaya-ku, Yokohama, 240-8501, Japan

[*]corresponding author: nishijima-yoshiaki-sp@ynu.ac.jp

Abstract: We have realized true perfect absorption with midinfrared metasurfaces by numerical simulation and experimental measurements. To realize this feature, we noticed that the controlling of absorption and scattering in metasurface.

Realization of perfect absorption is desirable in the field of photo-thermal, photo-voltaic energy conversion. Especially radiation absorption in metal-insulator-metal (MIM) metasurface, which generally consist of a metal back-plate, dielectric layer, and a metal nano-structure, is currently applied for realizing a great variety of efficient photo-thermal energy converter designs. Such converters also show significant promise in the mid-infrared (IR) wavelength range, where they are used as both IR radiation sources as well as detectors, notably for applications in optical sensing of volatile organic compounds (VOCs)[1-3].

In most studies, the absorbance A exhibited by a MIM metasurface is among its most important properties implicitly treated as $A = I - R$, where I is total incident energy on the sample ($I = 1$ in the normalized presentation), whereas R is the reflectance. The metal back plate is understood as a reflector with negligible transmittance owing to its considerable thickness (Typically, thickness $t > 200$ nm of Au thickness is used as back ground metal). Hence, the scattered portion of radiation energy S is either ignored or not explicitly accounted for, since it is assumed to be incorporated in R or and is distributed among them[4].

However, the origin of plasmon resonance comes from scattering of light by metal nano structures. The absorption part will become the loss of the resonance. Therefore, it is natural to put the scattering as optical power balance equation as $I = A + R + T + S$. Due to a zero transmittance $T=0$ of the MIM metasurface, both R and S manifest as a backward reflection of light. Therefore, it is difficult to identify the true A and S from reflection measurement in experiments, it corresponds to the extinction, $Ext = A + S$.

One of the evidences of this scattering effects can bee seen in thermal radiation measurements. Figure 1 shows reflection spectra and thermal radiation spectra of MIM metasurface with different disc diameter. When the parameters of metasurface, such as thickness and permittivity of insulator layer, disc diameter, periodicity and resonance wavelength, metasurface realized perfect ant reflection R~0 (PAR). However, even such PAR condition, the radiation is reached around 60 ~ 70% and they did not reach to the perfect radiation (PR, Rad ~ 100%). According to the Kirchhoff's thermal law of radiation (absorption coefficient □ = radiation coefficient □), Absorption portion is directly equal to the radiation portion. Therefore, we concluded that PAR condition is not equal to the perfect absorption (PA), and the reflection measurements cannot identify PAR and PA.

In the presentation, we demonstrate the quantitatively analyzed the scattering effects by numerical modeling as well as fabrication and characterization of MIM metasurface. We observed the considerable effect backwards scattering has on the optical response of metasurface. Also, there is further room for improvement in removing the specular reflection of metasurface, guided by detailed FDTD analysis. Light scattering under

slanted incidence is the next required step for analysis of MIM response and can be achieved at a quantitative level using FDTD modeling. Also, we will show that it is possible to increase the PA and PR condition with using of nano-thin layers of metals with strong absorbance such as Cr, and high absorption plasmonic metal, AgAuCuPdPt high entropy alloy as new plasmonic materials.

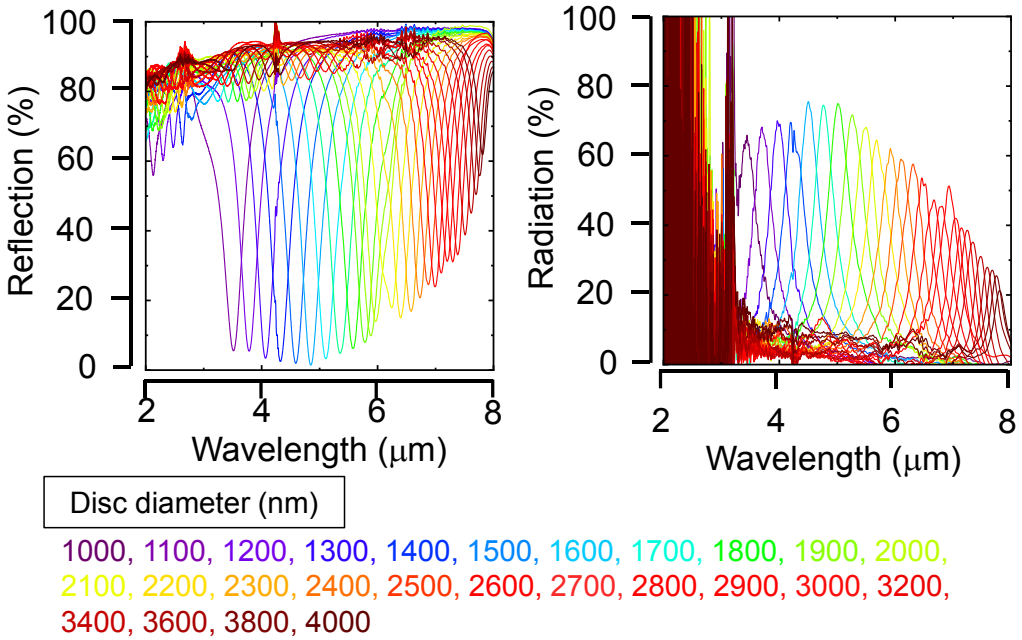


Figure 1: absorption and thermal radiation of metasurfaces with Au-SiO_2-Au nanodisc.

References

1. Y. Nishijima, S. Morimoto, A. Balčytis, T. Hashizume, R. Matsubara, A. Kubono, N. To, M. Ryu, J. Morikawa, and S. Juodkazis, "Coupling of molecular vibration and metasurface modes for efficient mid-infrared emission," J. Mater. Chem. C, 10, 451-462, (2022).
2. Y. Nishijima, S. Juodkazis, "Control of Vibration-Metasurface Coupling at the Mid-Infrared Spectral Window for Inorganic Thermal Emitters," Bull. Chem. Soc. Jpn, 95, 1411-1418, (2022).
3. Y. Nishijima, S. Juodkazis, "The Tunable Coupling between Metasurface and Molecular Vibration towards the Platform of Spectral Analysis," Bull. Chem. Soc. Jpn, 95, 1318-1324, (2022).
4. Y. Nishijima, N. To, A. Balčytis, and S. Juodkazis, "Absorption and scattering in perfect thermal radiation absorber-emitter metasurfaces," 30, 4058-4070 (2022).

Non-radiative cooling materials with high transparency

H. TT. Tam, M. Toma, and K. Kajikawa*

Tokyo Institute of Technology, Japan
*corresponding author: kajikawa@ee.e.titech.ac.jp

Abstract: Transparent non-radiative materials (non-RC) materials were investigated. The temperature reduction was measured for a glass plate covered with ITO, DMD, or Ag nanowire. It was found that the temperature reduction was negligible when exposed to the sky, whereas the samples were transparent in the visible wavelength region. The results show that these materials can be used for non-RC materials.

Radiative cooling (RC) releases heat into the universe through black-body radiation. This research field has recently attracted much attention because RC can refrigerate objects without using electricity [1]. However, there are some cases in which RC is a hindrance. For example, the surface of a car's windshield freezes on a sunny morning because the glass shows a relatively high RC performance. The windshield is sometimes covered with a cloth at midnight to prevent a freeze.

We investigated transparent "non-radiative materials (non-RC)" materials in this research. Glass plates coated with ITO (Indium Tin Oxide), DMD (dielectric/metal/dielectric: AZO(Aluminum-doped Zinc Oxide)/Ag/AZO), and AgNWs (silver nanowires) were examined. They are transparent in the visible region and have high reflectivity in the mid-infrared region. The RC measurements were performed in both in-house and in-field setups. The temperature reduction, $\Delta T = T_{amb} - T_{samp}$, was measured in both cases, where T_{amb} and T_{samp} are the temperatures of the ambient and the sample, respectively.

The temperature reduction measured in the field was negligible for ITO and DMD, whereas that for a glass plate was 1.5 K. The reduction for AgNW was 0.3 K, which is lower than that of a glass plate. These results show they can be used as non-RC materials.

References

1. Raman, A. P., Anoma, M. A., Zhu, L., Rephaeli, E., and Fan, S., “Passive radiative cooling below ambient air temperature under direct sunlight”, Nature, Vol. 515, 540-544, 2014.

New trends in opto-magnetism and magneto-optics

META 2023, PARIS - FRANCE, JULY 18 – 21, 2023

Twisted light affects ultrafast demagnetization

E. Prinz[1*], J. Hoefer[1], B. Stadtmüller[1,2], and M. Aeschlimann[1]

[1]Department of Physics and Research Center OPTIMAS, RPTU Kaiserslautern-Landau, Erwin-Schrödinger-Straße 46, 67663 Kaiserslautern, Germany
[2]Institute of Physics, Johannes Gutenberg University Mainz, Staudingerweg 7, 55128 Mainz, Germany
[*]corresponding author: eprinz@rptu.de

Abstract: High-intensity ultrashort laser pulses can destroy the magnetic order of ferromagnetic thin films on the femtosecond timescale. It is still an open question if the angular momentum of light can support this effect. For the material nickel, it has been shown that the spin of light only has a negligible influence. However, in our work, we experimentally demonstrate that photonic orbital angular momentum (OAM) affects the ultrafast demagnetization dynamics of a thin nickel film within the first hundreds of femtoseconds.

Optical fields can carry an orbital angular momentum (OAM) of $L = l\hbar$ with the OAM quantum number $l \in \mathbb{Z}$. Since its discovery in 1992 [1], there have been various applications of light with additional OAM, such as quantum entanglement, micromanipulation, communication, and microscopy [2].

Our research explores the potential impact of the OAM of light (often referred to as twisted light) on laser-induced ultrafast demagnetization of ferromagnetic materials. In this field, the question of how the angular momentum is conserved during the optically induced loss of magnetic order has not yet been fully answered. It has been shown that the spin angular momentum of light does not affect ultrafast demagnetization in ferromagnetic thin films such as Ni [3, 4]. However, pumping such a system with photons carrying OAM offers the potential to provide new insights, not only into the dissipation of angular momentum in the material but also into the interaction of optical OAM with matter in general.

We investigate ultrafast demagnetization of a thin nickel film induced by OAM light with time-resolved magneto-optic Kerr-effect measurements. We observed peculiar demagnetization dynamics that have so far not been observed for light without OAM: depending on the excitation geometry, the photonic OAM either supports (speeds up) or obstructs (slows down) the demagnetization process. Furthermore, we discovered that this effect occurs faster for higher OAM orders [5].

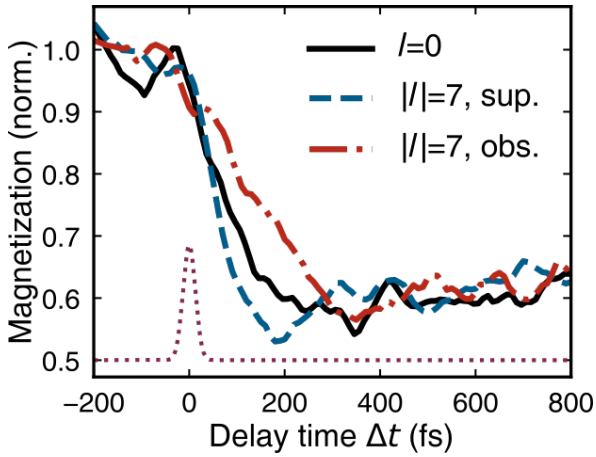


Figure 1: Demagnetization of the sample after irradiation of a pump pulse with $|l| = 7$ in the supporting (dashed line) and the obstructing (dash-dotted line) geometry in comparison to demagnetization with an $l = 0$ (solid line) beam. For better visualization, the data was smoothed. The dotted curve visualizes the pump pulse duration.

Acknowledgments: E. Prinz and J. Hoefer would like to thank Martin Stiehl, Simon Häuser, Stephan Wust, and Paul Herrgen for support with the experimental setup. The experimental work was funded by the Deutsche Forschungsgemeinschaft (DFG, German Research Foundation) - TRR 173 - 268565370 Spin + X: spin in its collective environment (Projects A08 and B03). B. Stadtmüller acknowledges financial support from the Dynamics and Topology Center funded by the State of Rhineland Palatinate.

References

1. Allen, L., M. W. Beijersbergen, R. J. C. Spreeuw, and J. P. Woerdman "Orbital angular momentum of light and the transformation of Laguerre-Gaussian laser modes," Phys. Rev. A, Vol. 45, 8185–8189, 1992.
2. Shen, Y., X. Wang, Z. Xie, C. Min, X. Fu, Q. Liu, M. Gong, and X. Yuan, "Optical vortices 30 years on: OAM manipulation from topological charge to multiple singularities," Light: Science & Applications, Vol. 8, No.1, 1–29, 2019.
3. Koopmans, B., M. van Kampen, J. T. Kohlhepp, and W. J. M. de Jonge, "Ultrafast Magneto-Optics in Nickel: Magnetism or Optics?," Phys. Rev. Lett., Vol. 85, 844–847, 2000.
4. Dalla-Longa, F., J. T. Kohlhepp, W. J. M. de Jonge, and B. Koopmans, "Influence of photon angular momentum on ultrafast demagnetization in nickel," Phys. Rev. B, Vol. 75, 224431, 2007.
5. Prinz, E., B. Stadtmüller, and M. Aeschlimann, "Twisted light affects ultrafast demagnetization," arXiv:2206.07502, 2022.

META 2023, PARIS - FRANCE, JULY 18 – 21, 2023

Magnetoplasmonics beyond metals: the case of plasmonic Transparent Conductive Oxide Nanocrystals

A. Gabbani[1*]

[1]Department of Chemistry and Industrial Chemistry, University of Pisa, Pisa, Italy

[*]corresponding author: alessio.gabbani@dcci.unipi.it

Abstract: In this contribution we show the potentiality of Transparent Conductive Oxide (TCOs) nanocrystals (NCs) for magnetoplasmonics, giving a proof-of-concept demonstration of their excellent performance in field-modulated refractometric sensing. Moreover, we demonstrate the ability of magneto-optical spectroscopy to accurately extract carrier parameters in this novel class of plasmonic materials, widely employed in plasmonics and optoelectronics.

Active modulation of the plasmonic resonance with an external tool enables a significant improvement of plasmon-based sensors and optical devices.[1] The use of magnetic fields to modulate plasmons presents several advantages: it is fast, easy to implement in devices, and fully reversible as it does not damage or modify the plasmonic material. However, achieving large magnetic modulation of the plasmonic resonance without broadening the optical response represents a great challenge in material choice for magnetoplasmonics, limiting the application in real-life devices. Indeed, noble metal nanocrystals (NCs) have sharp optical resonances, but weak magneto-optical signal, proportional to the cyclotron frequency (ω_C) [2]; on the other hand, nickel ferromagnetic nanodisks [3] or hybrid bimetallic nanostructures [4] have large magnetic modulation, while suffering from the high optical losses of the magnetic metal, thus broadening the plasmonic resonance.

To overcome such limitations, we propose a paradigm shift in material choice, employing plasmonic TCO NCs. Such NCs are able to support a plasmonic resonance in the infrared, due to the free carrier density introduced through aliovalent doping, and are promising materials for several optoelectronic applications spanning from smart windows[5] to infrared thermoplasmonics[6] and redox sensors[7]. Here, we employed two classes of TCOs NCs: Indium Tin Oxide (ITO) and F- and In^{3+} doped CdO (FICO), prepared by chemical synthesis with an average size around 10 nm. FICO NCs show up to 40-fold enhancement of the magnetoplasmonic response compared to Au NCs, detected through Magnetic Circular Dichroism (MCD). Such enhancement is due to the lower mass (m*) of free carriers in TCOs with respect to most metals, which in turn increase ω_C, combined with a reduced plasmon line width.[8]

Employing colloidal dispersions of TCO NCs in a proof of concept field-modulated refractometric sensing experiment we achieved a superior refractive index sensitivity with respect to metal-based magnetoplasmonic systems reported in the literature (Figure 1) [2-4]. Our approach challenges the current state of the art of plasmonic refractometric sensing [9], with the advantage of not requiring curve fitting but simply tracking a change in magneto-optical signal at a fixed wavelength. Considering that non-magnetic TCOs have been used in our work, a further improvement is potentially achievable incorporating TCOs in hybrid magnetic-plasmonic nanostructures, or introducing magnetic dopants in TCO NCs.

Finally, we demonstrate how the use of magneto-optical spectroscopy can be important to extract accurately free carrier parameters (density and effective mass) in this novel class of plasmonic materials. The latter is

quite important as carrier density in TCOs can be tuned across a wide range (from 10^{18} to 10^{21} carriers/cm^3), this affecting their optical and conductive properties. Indeed, conventional approaches to extract the carrier density rely on the fitting of the extinction spectrum, and the use of literature values of the carrier effective mass, which are generally measured independently on films or bulk materials.[10] Conversely, we propose a novel approach based on the simultaneous fitting of the extinction and MCD spectra to extract the carrier density and effective mass directly on the colloidal dispersion of the NCs. We believe that the proposed approach will contribute to shed light on the modification of free carrier parameters with synthetic or post-synthetic (photo-chemical or electrochemical) doping in plasmonic doped semiconductor NCs.

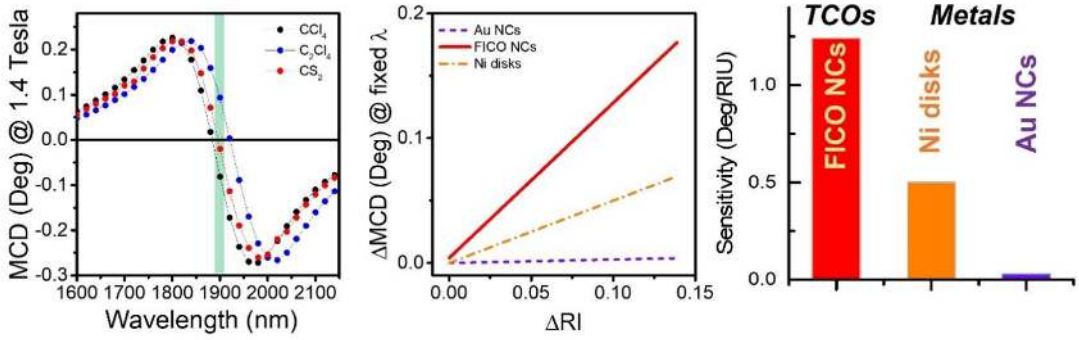


Figure 1: a) MCD of FICO NCs in three different solvents; b) MCD signal at fixed wavelength as a function of the solvent refractive index (RI) variation; c) RI magneto-optical sensitivity for FICO NCs compared with gold and nickel nanostructures.

References

1. N. Jiang et al., "Active Plasmonics: Principles, Structures, and Applications", Chem. Rev, Vol. 118, 3054−3099, 2018.
2. A. Gabbani et al., "Magneto-optical methods for magnetoplasmonics in noble metal nanostructures", Vol. 129, 211101, 2021.
3. N. Maccaferri et al., "Ultrasensitive and label-free molecular-level detection enabled by light phase control in magnetoplasmonic nanoantennas", Nat. Commun., 6, 6150, 2015.
4. J. B. Gonzàlez-Diàz et al., "Plasmonic Au/Co/Au nanosandwiches with enhanced magneto-optical activity", Small, 4, 202-205, 2008.
5. E. L. Runnerstrom et al., "Nanostructured electrochromic smart windows: traditional materials and NIR-selective plasmonic nanocrystals", Chem. Commun., 50, 10555, 2014.
6. A. Mazzotta et al., "Invisible Thermoplasmonic Indium Tin Oxide Nanoparticle Ink for Anti-counterfeiting Applications" ACS Appl. Mater. Interfaces, 14,35276, 2022.
7. R. J. Mendelsberg et al., "Dispersible Plasmonic Doped Metal Oxide Nanocrystal Sensors that Optically Track Redox Reactions in Aqueous Media with Single-Electron Sensitivity", Adv. Optical Mater. 3, 1293–1300, 2015.
8. A. Gabbani et al., "Magnetoplasmonics beyond Metals: Ultrahigh Sensing Performance in Transparent Conductive Oxide Nanocrystals", Nano Lett., 22, 22, 9036–9044, 2022.
9. M. Svedendahl et al., "Refractometric Sensing Using Propagating versus Localized Surface Plasmons: A Direct Comparison", Nano Letters, 9, 4428-4433, 2009.
10. R.J. Mendelsberg et al., "Understanding the Plasmon Resonance in Ensembles of Degenerately Doped Semiconductor Nanocrystals", J. Phys. Chem. C, 116, 12226−12231, 2012

Nanoscale and ultrafast magnetophotonics

A. Dmitriev[1]

[1]Department of Physics, University of Gothenburg, Gothenburg, Sweden
alexd@physics.gu.se

Abstract: Nanoscale magnetophotonics unites the concepts from magnetism (switching, storage, steering) with light (energy, information, photochemistry) at the nanoscale [1]. Our own exploration of this merger started some 10 years ago by conceiving nanoscale optical and magnetic antennas with magneto-optical properties dependent on optical resonances [2]. Today I highlight our recent work, were we employ plasmon nanoantennas to either funnel electromagnetic energy into ferrimagnetic films at the nanoscale assisting the demagnetization [3], or construct hybrid plasmon-ferrimagnet nanoantennas for that [4]. The produced architectures could also serve as the conceptually new high-resolution light incidence direction sensors or a platform with multistate demagnetization, potentially opening up for nanomagnetic neuromorphic-like ultrafast systems. We also show how adding nanoplasmonics allows to 'see' single molecule magnets with spectroscopy at ambient conditions [5]. Finally, I discuss a very intriguing prospect of 'spilling' materials properties (like electronic interband transition) outside the actual material by strongly coupling electronic and optical resonances in ferromagnetic Ni [6].

References

[1] N. Maccaferri et al., Nanoscale magnetophotonics, ***J. Appl. Phys.***, 127, 080903 (2020).

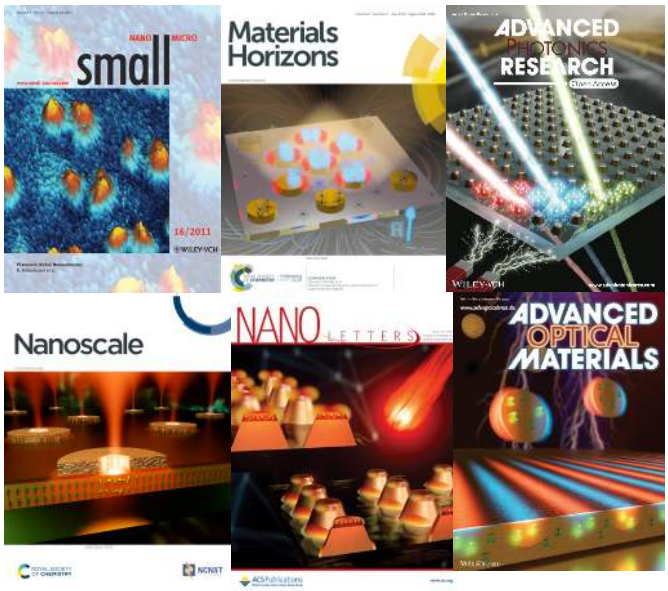
[2] J. Chen et al., ***Small*** 7, 2341 (2011) *(journal cover)*; V. Bonanni et al., ***Nano Lett.*** 11, 5333 (2011).

[3] K. Mishra et al., ***Nanoscale*** 13, 19367 (2021) *(journal cover).*

[4] R. M. Rowan-Robinson et al., ***Adv. Photon. Research*** 2100119 (2021) *(journal cover);* K. Mishra et al., Ultrafast demagnetization control in magnetophotonic surface crystals, ***Nano Lett.*** 22, 9773 (2022) *(journal cover).*

[5] F. Pineider et al., ***Mater. Horiz.***, 6, 1148 (2019) *(journal cover).*

[6] A. Assadillayev et al., Nanoscale engineering of optical strong coupling inside metals, ***Adv. Optical Mater.*** 11, 2201971 (2022) *(journal cover).*



META 2023, PARIS - FRANCE, JULY 18 – 21, 2023

Magneto-Optical Light-Matter interactions in Weyl Semimetals

D. Cheskis[1*]

[1]Physics Department, Faculty of Natural Sciences, Ariel University, Israel

[*]corresponding author: dimach@ariel.ac.il

Abstract:

We present in this work is an experimental study of topological semimetals. This work was focused on studying the behavior of the type I $Co_3Sn_2S_2$ Weyl semimetals. Primarily, we are interested in magneto-optical measurements of these materials. Due to the effect of chiral anomaly, it is expected that the angle between electric and magnetic fields due to the term E*B [1] leads to the specific impacts in Weyl semimetals. In particular, it has been claimed that the chiral anomaly results in a charge imbalance between the Weyl nodes. In Weyl semimetals, the dielectric tensor receives a specific form [2] that allows observing chiral anomaly via magneto-optical Kerr effect. Such studies have been performed for Cd_3As_2 crystals under an external magnetic field, and the outcome of the chiral anomaly was measured by magneto-optical methods. We are demonstrating our first results for $Co_3Sn_2S_2$ crystals. To the best of our knowledge, such a study was not performed in these materials.

References

1. D. Cheskis, "Magneto-optical tools to study effects in Dirac and Weyl semimetals", Symmetry, 12(9), 1412, 2020.
2. P. Hosur and X. L. Qi, "Tunable circular dichroism due to the chiral anomaly in Weyl semimetals", Phys. Rev. B, 91(8), 081106, 2015.

META 2023, PARIS - FRANCE, JULY 18 – 21, 2023

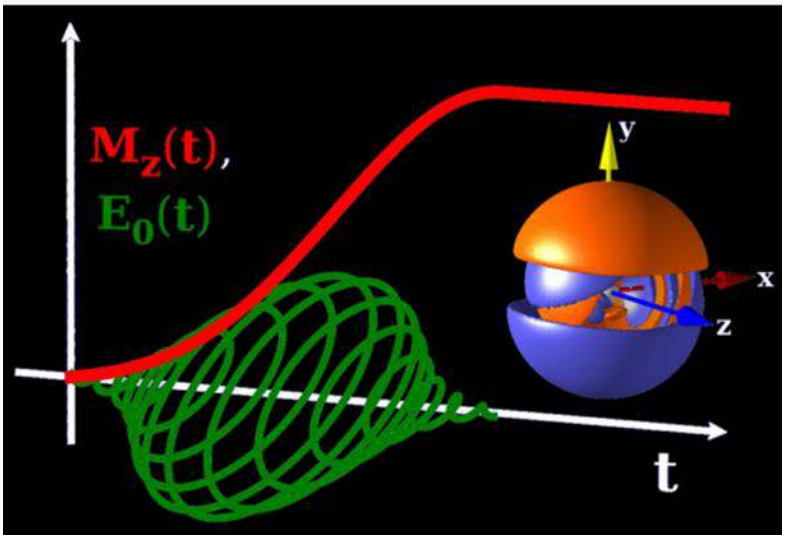
Ultrafast Driving of Orbital Magnetism in Metallic Nanoparticles using Circularly Polarized Light

P. -A. Hervieux[1], R. Sinha-Roy[2], J. Hurst[1], and G. Manfredi[1]

[1]Université de Strasbourg and CNRS, IPCMS, Strasbourg, France
[2]Université Claude Bernard and CNRS, ILM, Lyon, France
*corresponding author: hervieux@unistra.fr

Abstract: The angular momentum transfer of circularly polarized light to a metal nanoparticle is studied using the time-dependent density functional theory in the real time formulation. It is found that the induced magnetic moment is maximal at the surface plasmon frequency of the nanoparticle, showing that it is a resonant plasmonic effect.

Transfer of angular momentum from helicity-controlled laser fields to a nonmagnetic electronic system can lead to the creation of magnetization [1]. The underlying mechanism in metallic nanoparticles is based on the inverse Faraday effect and has been studied using different theoretical approaches [2]. In this work, the dynamics using an orbital-based quantum-mechanical method within a many-body theoretical framework is investigated [3]. To this end, the real-time formulation of time-dependent, density-functional theory is used to study induced orbital magnetism in metallic nanoparticles excited by circularly polarized light. The nanoparticles are described by a spherical jellium model on a real-space grid. The polarized laser field gives rise to an angular momentum and, hence, a magnetic moment, which is maximum at the surface plasmon frequency of the nanoparticle, revealing that this is a resonant plasmonic effect. The primary contribution to the magnetic moment comes from surface currents generated by the plasmonic field, although some bulk contributions due to the quantum-mechanical nature of the system (Friedel oscillations) still persist. We compare several nanoparticles of K, Na, and Au having the same size and excited at their respective plasmon frequencies and show that the generated magnetic moment per energy pumped into the system is maximum for K and minimum for Au. A similar trend is observed for nanoparticles of the same chemical species but different sizes.



References

1. Cheng O. H.-C., Son D.H., Sheldon, M. “Light-induced magnetism in plasmonic gold nanoparticles,” Nat. Photonics Vol. 14, 365, 2020.
2. Hurst J., Oppeneer P.M., Manfredi G. and Hervieux P.-A. “Magnetic moment generation in small gold nanoparticles via plasmonic inverse Faraday effect,” Phys. Rev. B vol. 98, 134439, 2018.
3. Sinha-Roy R., Hurst J., Manfredi G. and Hervieux P.-A. “Driving Orbital Magnetism in Metallic Nanoparticles Through Circularly Polarized Light: A Real-Time TDDFT Study,” ACS Photonics vol. 7, No. 9, 2429, 2020.

META 2023, PARIS - FRANCE, JULY 18 – 21, 2023

Optics and THz for ultrafast magnetization manipulation in ferro and ferrimagnetic systems

J. Gorchon[1]

[1]Institut Jean Lamour, CNRS, Université de Lorraine, 54000 France

Abstract: Controlling magnetization at ultrafast timescales has always been a major challenge and objective both for applications and fundamental aspects. In recent times, new methods that enable ultrafast magnetization reversal exploiting different stimuli, ranging from optics, to ultrafast on-chip current pulses, have been demonstrated. Moreover, some of these methods enable control of simple archetypal ferromagnetic systems. In this talk I will present some of these methods and will discuss various of the physical mechanisms playing a role.

Spin-transport, and the resulting spin-torques when spins are injected into a magnetic material, allow us to control the magnetization direction in magnetic devices electrically. We can use, for example, the spin-transfer torque effect [1,2] to reverse the magnetization of a magnet within nanoseconds. Such method has paved the way for applications such as spin-transfer-torque magnetoresistive random access memory (STT-MRAM). However, current-induced STT switching below a few hundred picoseconds with low power consumption while maintaining high thermal stability is challenging.

At our lab in IJL we are working on two different approaches to exploit spin transfer effects at ultrafast timescales. The first consists on using picosecond-wide charge current pulses (in the THz range) generated via photoconductive switches, to induce spin-orbit torques on magnetic layers [3,4]. The second approach focuses on the use of optical absorption to drive sub-picosecond spin currents in spin-valve structures [5,6] (see Fig1). We have recently shown, that both of these methods allow for ultrafast control of various archetypal out-of-plane magnetized ferromagnetic and/or ferrimagnetic layers. The mechanisms at play bridge concepts from ultrafast magnetism and conventional spintronics, enabling surprising dynamics.



Figure 1: A fully ferromagnetic spin-valve being excited by a femtosecond laser pulse can have its free layer reversed under no application of any magnetic field. We attribute the reversal to spin currents generated during the heating of the layers.

References

1. J. C. Slonczewski, Journal of Magnetism and Magnetic Materials **159**, L1–L7 (1996).
2. L. Berger, Phys. Rev. B **54**, 9353–9358 (1996).
3. K. Jhuria et al., Nature Electronics **3**, 680–686 (2020)
4. D. Polley et al., submitted
5. Q. Remy et al., Nature Communications **14**, 445 (2023)
6. J. Igarashi et al., Nature Materials (2023)

META 2023, PARIS - FRANCE, JULY 18 – 21, 2023

Amplification of magneto-optical activity via plasmonic modes hybridization

P. Vavassori[1,2*], Terunori Kaihara[1], and Pablo Rodriguez-Suarez[1]

[1]CIC nanoGUNE BRTA, Donostia–San Sebastian 20018, Spain
[2] IKERBASQUE, Basque Foundation for Science, Bilbao 48013, Spain
[*]corresponding author: p.vavassori@nanogune.eu

Abstract: We explore magnetoplasmonic-disk/plasmonic-ring nanocavities to achieve free-space light excitation and hybridization of multipolar modes. We show that the enhanced tunability and linewidth sharpening of Fano resonances in metasurfaces made of periodic arrangements of such hybridized magnetoplasmonic nanocavities produce a large amplification of the magneto-optical response together with the control of reflectance (Kerr configuration) and transmittance (Faraday configuration).

Magneto-optical (MO) effects are widely used in studying technologically relevant magnetic materials as well as to realize optical devices exploiting non-reciprocal propagation of light. The continuously developing field of magnetoplasmonics merges the concepts from plasmonics and magneto-optics to realize novel phenomena and functionalities for the manipulation of light at the nanoscale [1-4]. Owing to the intertwined optical and magneto-optical properties, magnetoplasmonics offers a versatile toolbox for actively tunable optical ultrathin surfaces and metasurfaces [5-7]. Enhancing magneto-optical effects is crucial for size reduction of key photonic devices based on non-reciprocal propagation of light and to enable active nanophotonics. Most studies focused on the amplification of the MO response produced by the excitation of localized dipolar plasmonic resonances (LPRs) in metallic magneto-plasmonic nanostructures. For a circular disk-like magneto-plasmonic nanoantenna, incident radiation of proper wavelength excites a primary LPR. When the nanoantenna is magnetized by the application of a magnetic field (H), a second LPR is induced by the inherent MO activity. This second MO-induced LPR (MOLPR) is driven by the primary LPR and is directed orthogonally to both H and the LPR. The ratio between the orthogonal radiating electric dipoles corresponding to the MOLPR and the LPR determines the magnetic-field induced polarization change of scattered light [1]. The amplitude of the electric dipole of the LPR is enhanced by the quality factor Q of the resonance with respect to the electric dipole induced in a continuous film. For typical metallic constituents Q can be up to 10 in the visible/near-infrared spectral range. Interestingly, the amplitude of the electric dipole of the MOLPR is enhanced by a factor Q^2 (i.e., up to 100) with respect to film or bulk magnetic material counterparts. This is because the MOLPR is a LPR resonance (Q-enhancement) not directly driven by the incident electromagnetic field but by the Q-enhanced primary LPR. This Q^2-enhancement of the MOLPR represents the limit for the maximum achievable amplification of the MO activity with respect to the film counterpart. However, polarization of re-emitted light is determined by the ratio between the MOLPR and LPR. Therefore, the simultaneous excitation of the LPR and MOLPR limits the maximum achievable enhancement of magnetic-field activated change in polarization to only a factor of Q, as observed experimentally [1-2], given that the LPR increases the reflectance. This Q-times enhancement of the MO activity represents a sort of fundamental upper limit that cannot be overcome using dipolar LPRs, hindering the practical applications of magnetoplasmonics to active nanophotonics and flat-optics

Recently, we disclosed and demonstrated an approach that exploits dark plasmons to achieve an unprecedented amplification of MO activity [8]. We designed and realized a symmetry broken

non-concentric magnetoplasmonic-disk/plasmonic-ring nanocavity fabricated by e-beam lithography. The broken symmetry enables the free-space light excitation of dark multipolar modes in the plasmonic-nanoring and their hybridization with the dipolar plasmonic resonance of the magnetoplasmonic nanoantenna. Such hybridization gives rise to a multipolar Fano resonance that, when excited, increases the reflectivity by a factor substantially lower than Q resulting in a large amplification of the magneto-optic response of the nanocavity, which is now approaching the Q^2-enhancement, namely the limit for the maximum achievable MO activity amplification. Such large amplification is explained as due to the peculiar and enhanced electrodynamics of the nanocavity, yielding to a large magnetically activated and radiant MOLPR driven by the intense but low-radiant multipolar Fano resonance mode [8]. It was anticipated in Ref. [8] that the concept proposed is general with prospects for even higher enhancements via optimization of the nanocavity design. In this study, we present a different nanocavity design that would allow overcoming several of the limiting constraints of the original design, that is a concentric arrangement of the noble-metal nanoring with an embedded hybrid noble-metal/ferromagnetic disk. In this design, an intense, sharp, and low-radiant Fano mode is produced by the hybridization of the dipolar mode of the disk and the dipolar bonding mode of the ring. The electrodynamics arising from the strong coupling between these two dipolar modes produces an exceptionally enhanced radiant MOLPR and allows for a broad control of the reflectance and transmittance to achieve a large amplification of the MO response both in reflection and transmission.

The authors acknowledge support from the Spanish Ministry of Science, Innovation and Universities under the Maria de Maeztu Units of Excellence Programme (grant n. CEX2020-001038-M) and the Spanish Ministry of Science and Innovation via the project n. PID2021-123943NB-I00 (MCIN/FEDER). T.K. acknowledges support via the European Union's Horizon 2020 Research and Innovation Programme under the Marie Słodowska-Curie Grant Agreement n. 101029928 (MANACOLIPO).

References

1. Maccaferri, N., et al., "Tuning the Magneto-Optical Response of Nanosize Ferromagnetic Ni Disks Using the Phase of Localized Plasmons", Phys. Rev. Lett., Vol. 111, 167401 (2013).
2. Lodewijks, K., et al., "Magnetoplasmonic Design Rules for Active Magneto-Optics", Nano Lett. Vol. 14, 702-714 (2014).
3. Kimel, A., et al., "The 2022 magneto-optics roadmap", Journal of Physics D: Applied Physics, Vol. 55, 463003 (2022).
4. Maccaferri, N., A. Gabbani, F. Pineider, T. Kaihara, T. Tapani1, and P. Vavassori, "Magnetoplasmonics in confined geometries: current challenges and future opportunities", Appl. Phys. Lett., in press, https://doi.org/10.1063/5.0045281.
5. Maccaferri, N., et al., "Ultrasensitive and label-free molecular-level detection enabled by light phase control in magnetoplasmonic nanoantennas", Nature Commun., Vol. 6, 6150 (2015).
6. Maccaferri, N, et al., "Anisotropic nanoantenna-based magnetoplasmonic crystals for highly enhanced and tunable magneto-optical activity", Nano Lett., Vol. 16, 2533-2542 (2016).
7. Zubritskaya, I., et al., "Magnetic control of the chiroptical plasmonic surfaces", Nano Lett. Vol. 18, 302 (2018).
8. López-Ortega, A., et al., "Enhanced magnetic modulation of light polarization exploiting hybridization with multipolar dark plasmons in magnetoplasmonic nanocavities", Light Sci. Appl. Vol. 9, 49 (2020).

META 2023, PARIS - FRANCE, JULY 18 – 21, 2023

Magnetic Helicoidal Dichroism with XUV Light Carrying Orbital Angular Momentum

M. Fanciulli[1, 2], M. Pancaldi[3], E. Pedersoli[3], M. Vimal[1], D. Bresteau[1], M. Luttmann[1], D. De Angelis[3], P. R. Ribic[3], B. Rösner[4], C. David[4], C. Spezzani[3], M. Manfredda[3], R. Sousa[5], I.-L. Prejbeanu[5], L. Vila[5], B. Dieny[5], G. De Ninno[3,6], F. Capotondi[3], M. Sacchi[7,8], and T. Ruchon[1†]

[1]LIDYL, Université Paris-Saclay, CEA, CNRS, 91191 Gif-sur-Yvette, France

[2]Laboratoire de Physique des Matériaux et Surfaces, CY Cergy Paris Université, 95031 Cergy-Pontoise, France

[3]Elettra-Sincrotrone Trieste S.C.p.A., 34149 Basovizza, Trieste, Italy

[4]Paul Scherrer Institut, 5232 Villigen, Switzerland

[5]IRIG-SPINTEC, Université Grenoble Alpes, CNRS, CEA, Grenoble INP, 38000 Grenoble, France

[6]Laboratory of Quantum Optics, University of Nova Gorica, 5001 Nova Gorica, Slovenia

[7]Institut des NanoSciences de Paris, CNRS, Sorbonne Université, 75005 Paris, France

[8]Synchrotron SOLEIL, L'Orme des Merisiers, Saint-Aubin, B.P.48, 91192 Gif-sur-Yvette, France

[†]corresponding author: Thierry.ruchon@cea.fr

Abstract: We report magnetic helicoidal dichroism (MHD) in the interaction between XUV beams carrying orbital angular momentum (OAM) and magnetic vortices. It appears as a differential intensity profile of beams with OAM, reflected off magnetic structures with opposite curling sense. The results match theoretical predictions and confirm the potential of MHD for studying laser-triggered ultrafast dynamics in complex magnetic materials.

After finding many applications in the visible range, OAM beams with XUV wavelengths and ultra-short pulse duration, in the femtosecond to attosecond ranges, became available recently at high-harmonic generation (HHG) [3, 4] and free-electron laser (FEL) sources [6], widening considerably their application range. However, it has thus far found very scarce applications for magneto-optics, which rather harnesses the spin angular momentum of light to investigate and control magnetization, through the Faraday and Kerr effects [5].

Recently, we analysed theoretically the interaction of OAM beams with magnetic structures featuring non-uniform magnetization, in particular of XUV beams with magnetic vortices consisting of a curling in-plane magnetization [1]. We predicted that the far field intensity profile encodes the vortex symmetry in a way that depends on the sign and value of the topological charge ℓ, an effect deriving from the inhomogeneous modification of the

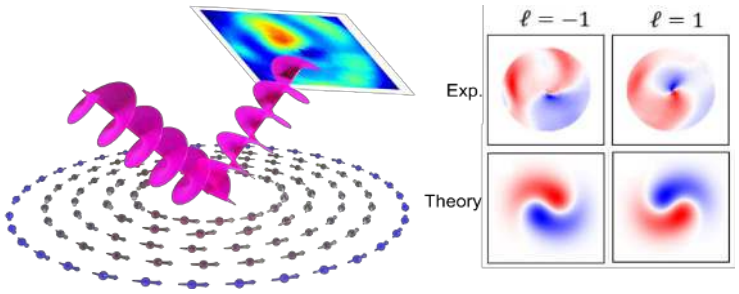


Figure 1. (Left) Experimental sketch for the observation of magnetic helicoidal dichroism. (Right panel) Differences between the images acquired for two opposite curling senses of the magnetic vortex, showing a typical 2D chiral structure, which depends on the incoming orbital angular momentum (top). Theoretical result (bottom).

regular reflectivity coefficients by the local magnetization. We named this effect Magnetic Helicoidal Dichroism (MHD). As for magnetic circular dichroism, MHD can be observed by inverting the sign of either the orbital momentum or of the magnetization, i.e. by switching the handedness of either the light helicoidal wavefront, or of the magnetic vortex.

In this contribution we report on the first experimental evidence of MHD (Fig. 1) obtained at the DiProI station of the FERMI free-electron laser source by measuring the scattered intensity from an Fe-Ni-alloy dot forming a magnetic vortex. The photon energy of the ˜100 fs long pulses was set to 52.8 eV (˜23 nm wavelength) in order to match the Fe 3p→3d core resonance, enhancing magneto-optical effects at XUV wavelengths and providing element selectivity. The scattered intensity data, collected as a function of ℓ and of the magnetic vortex winding sense, compared well to theoretical model predictions [2]. The match between theory and experiments confirms the potential of the new toolset provided by MHD for studying complex magnetic structures and, in particular, for addressing their laser-triggered ultrafast dynamics.

Understanding the interaction of OAM-light with a magnetic vortex has many potential interests. At the fundamental level, it allows to observe a new kind of dichroism, to study the role of photon spin-orbit coupling mediated by magnetization, as well as to explore new possibilities of angular momentum transfer between light and matter. In terms of applications, MHD in reflection can be exploited as a new spectroscopic tool joining the family of magnetic dichroism techniques. For their symmetry and size, magnetic vortices can be considered as an ideal benchmark sample to explore the interaction with OAM beams; moreover, given their rich dynamical response in the ultrafast domain, they are promising structure for light manipulation of the magnetization topology.

References

[1] M. Fanciulli, D. Bresteau, M. Vimal, M. Luttmann, M. Sacchi, and T. Ruchon. Electromagnetic theory of helicoidal dichroism in reflection from magnetic structures. *Physical Review A*, 103 (1), jan 2021. doi: 10.1103/physreva.103.013501.

[2] M. Fanciulli, et al., Observation of magnetic helicoidal dichroism with extreme ultraviolet light vortices. *Physical Review Letters*, 128 (7): 077401, 2022. doi: 10.1103/physrevlett.128.077401.

[3] D. Gauthier, et al., Tunable orbital angular momentum in high-harmonic generation. *Nature Communications*, 8: 14971, apr 2017. doi: 10.1038/ncomms14971.

[4] R. Géneaux, A. Camper, T. Auguste, O. Gobert, J. Caillat, R. Taïeb, and T. Ruchon. Synthesis and characterization of attosecond light vortices in the extreme ultraviolet. *Nature Communications*, 7: 12583, Aug 2016. ISSN 2041-1723. doi: 10.1038/ncomms12583. URL http://dx.doi.org/10.1038/-ncomms12583.

[5] A. Kimel, et al., The 2022 magneto-optics roadmap. 55 (46): 463003. doi: 10.1088/1361-6463/ac8da0.

[6] P. R. Ribic, et al., Extreme-ultraviolet vortices from a free-electron laser. *Physical Review X*, 7 (3), aug 2017. doi: 10.1103/physrevx.7.031036.

META 2023, PARIS - FRANCE, JULY 18 – 21, 2023

Ultrafast control of spins using resonant light excitation

D. Afanasiev

Radboud University, Nijmegen, The Netherlands
d.afanasiev@science.ru.nl

Abstract: I will discuss how light can be used to control magnetism: fundamental magnetic interactions, magnetic phase transitions, and highly nonlocal spin dynamics. I will particularly concentrate on nonthermal means to control magnetism when the photon energy of light is tuned precisely in resonance with optical resonance, e.g., lattice, orbitals, or electron excitation, carrying a direct impact on the ordered spins.

For many years, the central goal of condensed matter physics has been to understand and describe naturally occurring phenomena, both in macroscopic and microscopic terms. Over the past decades, a new paradigm emerged, which is to experimentally realize and control new states of matter that are not found in nature. Alongside answering fundamental scientific questions, control over and knowledge of potential ‘exotic’ phases also holds promise to create a new and radically different generation of data processing devices.

Ultrashort pulses of light are especially appealing in this sense as they allow to create strongly nonequilibrium transient states of matter with properties that are often not even available in the equilibrium. Light-induced superconductivity, metal-to-insulator transitions, and light-driven Floquet engineering are to name a few. Here I will discuss how light can be used to control magnetism: fundamental magnetic interactions, magnetic phase transitions, and highly nonlocal spin dynamics. I will particularly concentrate on nonthermal means to control magnetism when the photon energy of light is tuned precisely in resonance with optical resonance, e.g., lattice, orbitals, or electron excitation, carrying a direct impact on the ordered spins.

Structured ultrafast electric and magnetic fields by design

H. Petek[1*], A. Ghosh[1], S. Yang[1], and Y. Dai[1,2]

[1]University of Pittsburgh, USA
[2]Southern University of Science and Technology, China
[*]corresponding author: petek@pitt.edu

Abstract: We investigate the electric and magnetic fields in space and time when circularly polarized light interacting with a metal-dielectric interface is structured to generate single, periodic, and quasiperiodic topological vortex arrays. We image the space-time correlations of such fields by ultrafast photoemission electron microscopy. The structured fields interact with matter through electric dipole and magnetic dipole interactions. These interactions can overlap in space and time to drive magnetoelectric responses in topologically trivial and nontrivial matter.

The geometry of metastructures and circular polarization of light can generate topological plasmonic fields, that can have exotic interactions with matter as compared to plane wave optical fields.[1-5] By defining the orbital angular momentum of light, we design the spin-orbit interaction of surface plasmon polaritons leading to the plasmonic vortex generation. The structure of such fields varies according to the orbital angular momentum that is defined by geometry of SPP launching causing the fields to focus on $\lambda_{SPP}/2$ length scale (~250 nm). We generate movies of SPP fields as they evolve on sub-optical cycle time and sub-wavelength spatial scales by interferometric time-resolved two-photon photoemission electron microscopy.[6] Of particular interest is to image the spatial variation of isotropic (e.g. electric dipole) and bianisotropic (magnetoelectric) responses of matter within the fields of plasmonic vortices. The local field textures can locally observe and define time-parity conserving processes and break the time-parity conservation in materials that are exposed to their nearfield. Such fields are predicted to exist at the vortex that forms a plasmonic spin skyrmion texture (Figure 1). We will describe the magnetoelectric imaging of material responses by design of structured fields in plasmonic vortices.

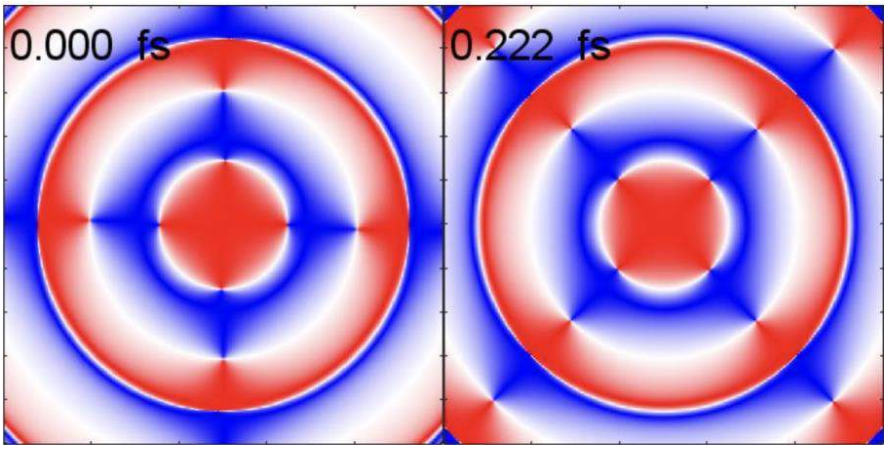


Figure 1. The calculated fields of a plasmonic skyrmion where blue and red designate instantaneous regions of isotropic and bianisotropic interactions, respectively. The two frames represent advance of 0.222 fs of 566 THz plasmonic field. The lateral dimension of the center meron (half-skyrmion; red) region is 260 nm.

References

[1] Dai, Y., Zhou, Z., Ghosh, A., Mong, R.S.K., Kubo, A., Huang, C.-B., & Petek, H. Plasmonic topological quasiparticle on the nanometre and femtosecond scales. *Nature* **588**, 616-619 (2020).

[2] Dai, Y., Zhou, Z., Ghosh, A., Yang, S., Huang, C.-B., & Petek, H. Ultrafast nanofemto photoemission electron microscopy of vectorial plasmonic fields. *MRS Bulletin* **46**, 738-746 (2021).

[3] Ghosh, A., Yang, S., Dai, Y., Zhou, Z., Wang, T., Huang, C.-B., & Petek, H. A topological lattice of plasmonic merons. *Applied Physics Reviews* **8**, 041413 (2021).

[4] Dai, Y., Zhou, Z., Ghosh, A., Kapoor, K., Dąbrowski, M., Kubo, A., Huang, C.-B., & Petek, H. Ultrafast microscopy of a twisted plasmonic spin skyrmion. *Applied Physics Reviews* **9**, 011420 (2022).

[5] Ghosh, A., Yang, S., Dai, Y., & Petek, H. The Spin Texture Topology of Polygonal Plasmon Fields. *ACS Photonics* **10**, 13-23 (2023).

[6] Dąbrowski, M., Dai, Y., & Petek, H. Ultrafast Photoemission Electron Microscopy: Imaging Plasmons in Space and Time. *Chem. Rev.* **120**, 6247-6287 (2020).

Microwaves and millimeter waves applications of metamaterials and metasurfaces for the real world

META 2023, PARIS - FRANCE, JULY 18 – 21, 2023

Deep learning-driven all-optical operations utilizing metasurfaces

Zihan Zhao[1], Yue Wang[1], and Xumin Ding[1*]

[1] Advanced Microscopy and Instrumentation Research Center, School of Instrumentation Science and Engineering, Harbin Institute of Technology, Harbin 150080, China
[*]xuminding@hit.edu.cn

Abstract: In this paper, a novel compact trigonometric function operator based on the metasurface is proposed. Such an operator, which consists of a simple P-B (Pancharatnam-Berry) phase metasurface, can implement the four basic trigonometric operations (sine, cosine, tangent, and cotangent functions) at ultra-high speed with low power consumption, providing a feasible way to achieve a universal photonic computing chip.

Photonic computing has attracted great interest from researchers due to its remarkable advantages in terms of computing speed and power performance. Such an EM-wave-based computing strategy avoids analog-to-digital conversion and allows ultra-high-speed massively parallel operations, which has been proven to have great potential in temporal integration and differentiation[1,2], Hilbert transformation[3], spatial differentiators[4]. In recent years, the emergence and rise of metamaterials bring new developments to photonic computing, breaking through the limitations of traditional lens-based computing systems in terms of size and aberration. Compared to conventional Fourier-based optical computing devices, metasurfaces can achieve modulation of the EM profile within the sub-wavelength thickness, which facilitates the miniaturization of photonic signal processors in volume. The superiority of such a metasurface-based optical computing strategy has been demonstrated in various optical signal processing scenarios, such as spatial differentiation, integration, and convolution[5-7], Laplacian operation[8], image processing[9].

However, previous metasurface-based photonic computing systems mainly focus on spatial time and frequency domain operations, while lack of the solutions for optical function operations with specifc numerical inputs. As one family of the basic mathematical operations, trigonometric operations lie at the core position in the field of communication and signal processing. Conventional devices used to perform trigonometric operations, such as field-programmable gate array (FPGA) and digital signal processors (DSPs), are usually based on electronic components which result in low speed, high power consumption, and inevitable complexity. Nowadays, exponentially growing communication data and information need to be processed and stored in real-time, which poses a tough challenge to conventional electron-based operations. Therefore, a disruptive solution for numerical trigonometric operations is highly desired. To this end, we designed a trigonometric operator driven by an all-optical diffraction neural network, as shown in Figure 1. Here, different patterns of planar input light signals are designed as inputs to the network and the information is passed to the hidden layer which is mapped by a metasurface in the way of scattering. Finally, the output result will be presented on the output layer with the designed output pattern representing different values. Our design features several attractive advantages: Firstly, we achieve EM-based basic trigonometric operations under specific input values and the optimized visualized outputs allow clear and recognizable operation results. Besides, only one hidden layer is utilized in the diffractive neural network under the proposed composite input mode strategy, which considerably reduces the resources and time required to train the network and improves integration with other photonic systems. The proposed solution has been theoretically and experimentally verified to accurately perform the four

basic trigonometric operations and has great potential for applications in the field of ultra-high-speed signal processing and communication.

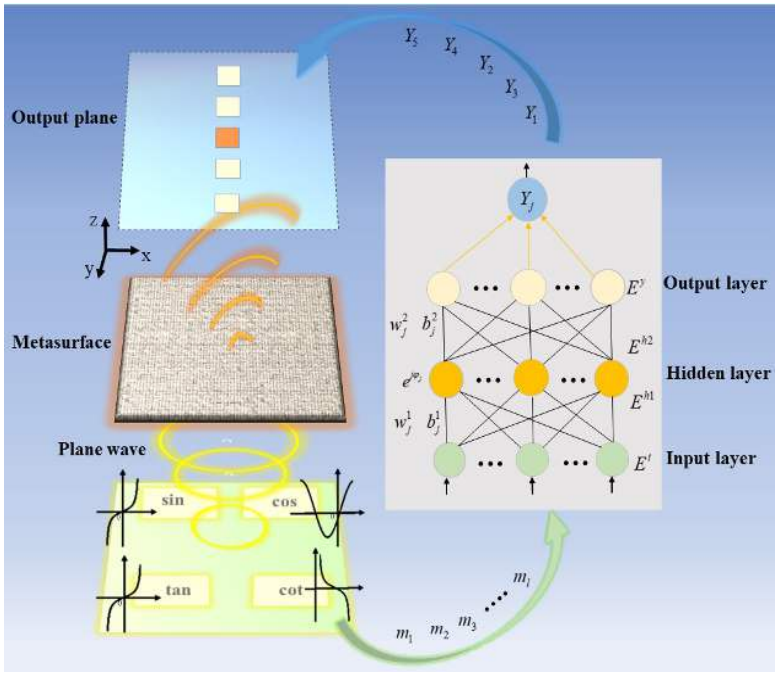


Figure 1. The conceptual representation of the designed optical trigonometric operator.

References

1. R. Slav´ık, Y. Park, N. Ayotte, S. Doucet, T. J. Ahn, S. LaRochelle, et al. “Photonic temporal integrator for all-optical computing,” Opt. Express, Vol. 16, No. 22, 18202-18214, 2008.
2. M. Michalska, J. Swiderski, M. Mamajek, “Arbitrary pulse shaping in erdoped fiber amplifiers possibilities and limitations,” Opt Laser Technol, Vol. 60, 8-13, 2014.
3. R. Ashrafi, M. R. Dizaji, L. R. Cortés, J. Zhang, J. Yao, J. Azaña, et al. “Time-delay to intensity mapping based on a second-order optical integrator: application to optical arbitrary waveform generation,” Opt. Express, Vol. 23, No. 12, 16209–16223, 2015.
4. D. Pérez, I. Gasulla, L. Crudgington, D. J. Thomson, A. Z. Khokhar, L. Ke, et al. “Multipurpose silicon photonics signal processor core,” Nat. Commun, Vol. 8, No. 1, 636, 2017.
5. T. Zhu, Y. Zhou, Y. Lou, H. Ye, M. Qiu, Z. Ruan, et al. “Plasmonic computing of spatial differentiation,” Nat Commun, Vol. 8, No. 1, 15391, 2017.
6. S. Y. Zuo, Y. Tian, Q. Wei, Y. Cheng, X. Liu, “Acoustic analog computing based on a refective metasurface with decoupled modulation of phase and amplitude,” J Appl Phys, Vol. 123, No. 9, 091704, 2018.
7. W. Fu, D. Zhao, Z. Li, S. Liu, C. Tian, K. Huang, “Ultracompact meta-imagers for arbitrary all-optical convolution,” Light Sci. Appl, Vol. 11 No. 1, 62, 2022.
8. H. Kwon, D. Sounas, A. Cordaro, A. Polman, A. Alù, “Nonlocal metasurfaces for optical signal processing,” Phys. Rev. Lett, Vol. 121, No. 17, 173004, 2018.
9. P. Huo, C. Zhang, W. Zhu, M. Liu, S. Zhang, S. Zhang, T. Xu, “Photonic spin-multiplex-ing metasurface for switchable spiral phase contrast imaging,” Nano Lett, Vol. 20, No. 4, 2791-2798, 2020.

META 2023, PARIS - FRANCE, JULY 18 – 21, 2023

Emulating Fast-Fading Rician Wireless Environments with Electronically Adjustable K-Factors in a Programmable-Metasurface-Stirred Reverberation Chamber

Ismail Ahmed[†], Matthieu Davy, Philippe Besnier, and Philipp del Hougne[*]

Univ Rennes, INSA Rennes, CNRS, IETR-UMR 6164, F-35000 Rennes, France

[†]presenting author
[*]corresponding author: philipp.del-hougne@univ-rennes1.fr

Abstract: Experimentally emulating the wireless test environments typically considered in signal processing can be challenging, especially for MIMO communications under Rician fast-fading if the K-factor is supposed to be adjustable. We demonstrate experimentally that electronic stirring of a reverberation chamber with a programmable metasurface conveniently enables the implementation of such channel conditions. We carefully characterize the precision with which a desired K-factor can be implemented simultaneously across multiple antenna pairs.

The signal-processing literature routinely assumes certain statistical properties of the wireless radio environment but experimentally emulating these conditions for real-life tests is often challenging. Consider the case of a wireless channel with fast Rician fading. In a single-input single-output (SISO) scenario, this can be emulated by pointing two horn antennas at each other inside a reverberation chamber; rotating a mode stirrer can yield different realizations and varying the horn antennas' separation can be used to adjust the Rician K-factor. However, note that the use of horn antennas implies that the unstirred field component is largely dominated by the line-of-sight (LOS) path, which is a special case of what happens in general, namely that the unstirred component includes the LOS path as well as significant multi-bounce paths that did not encounter the stirrer [1], [2]. In any case, this approach involving horn antennas does not trivially extend to multiple-input multiple-output (MIMO) scenarios, let alone to timely MIMO scenarios involving reconfigurable intelligent surfaces (RISs) that assist the wireless system. One possibility to emulate Rician fading for a MIMO scenario is to use omnidirectional antennas in combination with mechanical mode stirrers whose physical size would have to be adjusted every time that a different K-factor is supposed to be emulated. However, such an approach appears to be very cumbersome in practice.

A potential solution to overcome the above restrictions and limitations lies in the use of electronic stirring by partially reconfiguring the boundary conditions of the reverberation chamber with random configurations of a programmable metasurface. This idea was first proposed in [3] and the first experimental implementation of a programmable-metasurface stirred wireless channel was reported (in a context of wireless localization) in [4]. Subsequent work has characterized the statistical properties of the stirred field (i.e., *not* of the physical field which would be the sum of the unstirred and stirred fields) [5], by subtracting the unstirred field in post-processing. There has, to the best of our knowledge, not been any experimental study on implementing Rician fast fading with adjustable K-factor for generic wireless scenarios (involving MIMO, etc.), where the K-factor is adjusted by using only a subset of all available meta-atoms. Note that the programmable metasurface is used in order to setup the wireless test environment here, rather than as part of the wireless communications network that is under the wireless system engineer's control.

In this presentation, we report our experimental results on emulating fast-fading Rician conditions with electronically adjustable K-factor for a 4×4 MIMO wireless system based on omnidirectional dipole antennas. We carefully evaluate the K-factor [6], and how it depends on the number of utilized meta-atoms. We also check how for a given number of utilized meta-atoms the K-factor fluctuates across different antenna pairs. We find that these fluctuations are substantial, essentially because the unstirred component (since it is not dominated by the LOS) is itself a random variable. This phenomenon is not specific to our method of electronic stirring, but has seemingly not been clearly documented even in the case of mechanical stirring.

The authors acknowledge funding from the Rennes Métropole acquisition d'équipements scientifiques program (project "SRI"), the European Union's European Regional Development Fund, and the French region of Brittany and Rennes Métropole through the contrats de plan État-Région program (project "SOPHIE/STIC & Ondes").

References

[1] J.-H. Yeh, T. M. Antonsen, E. Ott, and S. M. Anlage, "First-principles model of time-dependent variations in transmission through a fluctuating scattering environment," *Phys. Rev. E*, vol. 85, no. 1, Art. no. 1, Jan. 2012.

[2] A. Rabault, L. Le Magoarou, J. Sol, G. C. Alexandropoulos, N. Shlezinger, H. V. Poor, and P. del Hougne, "On the Tacit Linearity Assumption in Common Cascaded Models of RIS-Parametrized Wireless Channels," *arXiv:2302.04993*, Feb. 2023.

[3] M. Klingler, "Dispositif et procédé de brassage électromagnétique dans une chambre réverbérante à brassage de modes," Patent FR 2 887 337, 2005

[4] P. del Hougne, M. F. Imani, M. Fink, D. R. Smith, and G. Lerosey, "Precise Localization of Multiple Noncooperative Objects in a Disordered Cavity by Wave Front Shaping," *Phys. Rev. Lett.*, vol. 121, no. 6, Art. no. 6, Aug. 2018.

[5] J.-B. Gros, P. del Hougne, and G. Lerosey, "Tuning a regular cavity to wave chaos with metasurface-reconfigurable walls," *Phys. Rev. A*, vol. 101, no. 6, Art. no. 6, Jun. 2020.

[6] C. Lemoine, E. Amador, and P. Besnier, "On the K-Factor Estimation for Rician Channel Simulated in Reverberation Chamber," *IEEE Trans. Antennas Propag.*, vol. 59, no. 3, pp. 1003–1012, Mar. 2011.

META 2023, PARIS - FRANCE, JULY 18 – 21, 2023

Intelligent Surfaces for Wireless Communications: Living at the Interface of Electromagnetic and Communication Theories

Marco Di Renzo
Universit\é Paris-Saclay, CNRS, CentraleSupélec, Laboratoire des Signaux et Systèmes
3 Rue Joliot-Curie, 91192 Gif-sur-Yvette, France
marco.di-renzo@universite-paris-saclay.fr

Abstract: We discuss the emerging field of reconfigurable and holographic metasurfaces for wireless.

In wireless communications, the term intelligent surface is referred to a planar metamaterial structure that is capable of generating an arbitrary current density distribution, so as to ensure the highest flexibility in generating a specified electromagnetic field and in shaping the propagation of the electromagnetic waves in large-scale networks. This presentation is aimed to report the latest research advances on analytical modeling, evaluating the ultimate performance limits, and optimizing intelligent surfaces for application to wireless communications, with focus on the synergies between electromagnetic and communication theories.

References

1. M. Di Renzo, A. Zappone, M. Debbah, M.-S. Alouini, C. Yuen, J. de Rosny, and S. A. Tretyakov, "Smart radio environments empowered by reconfigurable intelligent surfaces: How it works, state of research, and the road ahead", IEEE J. Sel. Areas Commun., vol. 38, no. 11, pp. 2450-2525, Nov. 2020.
2. M. Di Renzo, A. Ahmed, A. Zappone, V. Galdi, G. Gradoni, M. Moccia, and G. Castaldi, "Digital reconfigurable intelligent surfaces: On the impact of realistic reradiation models", arXiv, 2022. [Online]. Available: https://arxiv.org/abs/2205.09799.
3. C. Pan, G. Zhou, K. Zhi, S. Hong, T. Wu, Y. Pan, H. Ren, M. Di Renzo, A. L. Swindlehurst, R. Zhang, and A. Y. Zhang, "An overview of signal processing techniques for RIS/IRS-aided wireless systems", IEEE J. Sel. Topics Signal Process., vol. 16, no. 5, pp. 883-917, Aug. 2022.
4. M. Di Renzo, F. H. Danufane, and S. Tretyakov, "Communication models for reconfigurable intelligent surfaces: From surface electromagnetics to wireless networks optimization", Proc. of the IEEE, vol. 110, no. 9, pp. 1164-1209, Sep. 2022.
5. F. H. Danufane, M. Di Renzo, J. de Rosny, and S. Tretyakov, "On the path-loss of reconfigurable intelligent surfaces: An approach based on Green's theorem applied to vector fields", IEEE Trans. Commun., vol. 69, no. 8, pp. 5573-5592, Aug. 2021.
6. G. Gradoni and M. Di Renzo, "End-to-end mutual coupling aware communication model for reconfigurable intelligent surfaces: An electromagnetic-compliant approach based on mutual impedances", IEEE Wireless Commun. Lett., vol. 10, no. 5, pp. 938-942, 2021.

Metagratings for wavefronts manipulation: Theory and design

Z. Tan[1,2], J. Yi[1], B. Ratni[2], and S. N. Burokur[2*]

[1]School of Information and Communication Engineering, Xi'an Jiaotong University, Xi'an 710049, China
[2]LEME, UPL, Univ Paris Nanterre, 92410 Ville d'Avray, France
[*]corresponding author: sburokur@parisnanterre.fr

Abstract: Metagratings, structures composed of sparsely arranged load-impedance wires, are exploited to tailor and manipulate diffracted beams. Here, we focus on planar reflective-type metagratings where reflected diffracted orders are controlled.

Metagratings have been introduced in 2017 by Y. Ra'di et al. [1]. These structures consist of an array of wires arranged periodically and structured on a small scale with respect to the wavelength such that it is possible to introduce an effective linear (electric or magnetic) impedance. On the other hand, in the perpendicular direction, the distances are of the order of the wavelength. The properties of these wires are periodically repeated with a period generally greater than the wavelength, thus defining an elementary "supercell", which allows propagative diffracted orders.

By engineering judiciously the load impedance of the wires, the diffraction orders can be accurately controlled for various functionalities. Generally, the load impedance is a complex quantity, with a real part that can be active or lossy, and a reactive part that can be capacitive or inductive. Concerning the real part, we restrict ourselves to a positive or null value to avoid the complex realization of active circuits.

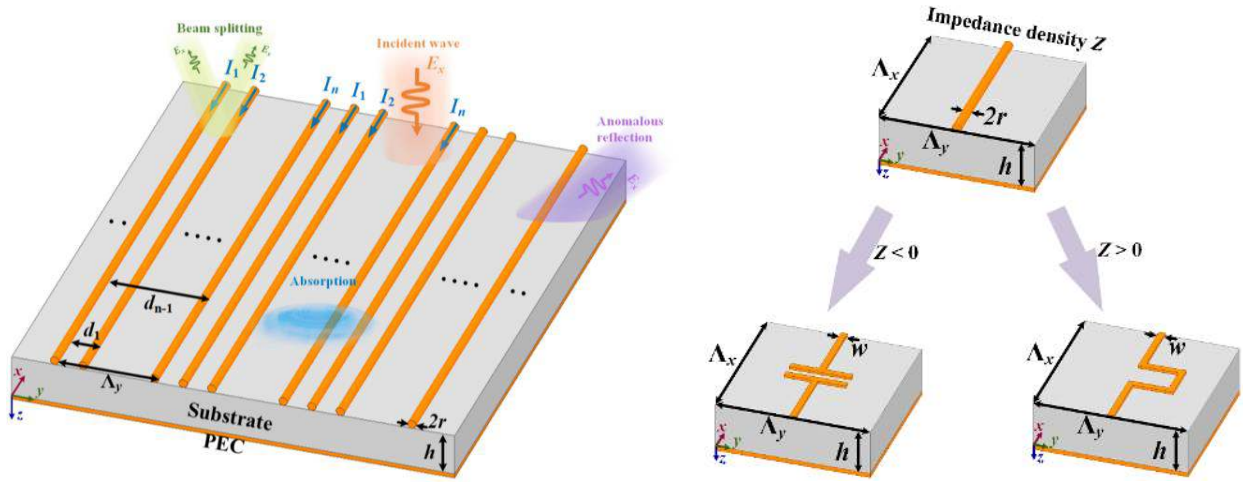


Figure 1. The physical system of the metagratings: a periodic array of cylindrical wires placed on a PEC-backed dielectric substrate. The array is illuminated by a TE-polarized plane wave. The elementary meta-atom of the metagrating is a cylindrical wire with a reactive impedance density *Z*. For negative *Z*, a microstrip capacitor is used and when *Z* is positive, a microstrip inductor is used to achieve the desired impedance density.

The schematic of a planar reflective-type metagrating is shown in Fig. 1. In the presence of the grounded

substrate, the excitation field takes the following form:

$$E_x^{exc}(y, z \le -h) = E_{inc}\left[e^{-ik_0(z+h)} + R_0 e^{ik_0(z+h)}\right] e^{-ik_0 \sin(\theta_{inc})y} \quad (1)$$

where $R_0 = \left[i\tan(k_s h) - \frac{\eta_0}{\eta_s}\right] / \left[i\tan(k_s h) + \frac{\eta_0}{\eta_s}\right]$ is the reflection coefficient of the incident wave, with $k_0 = \omega\sqrt{\mu_0\varepsilon_0}$, $\eta_0 = \sqrt{\mu_0/\varepsilon_0}$, $k_s = \omega\sqrt{\mu_s\varepsilon_s}$ and $\eta_s = \sqrt{\mu_s/\varepsilon_s}$. The radiated field in free space is then written as:

$$E_x(y, z \le h) = -\frac{k_0\eta_0}{2\Lambda_y} \sum_{m=-\infty}^{\infty} \frac{1+R_m}{\beta_m} \sum_{q=1}^{n} I_q e^{j\xi_m d_{q-1}} e^{-j\xi_m y} e^{-j\beta_m |z+h|} \quad (2)$$

where $d_{n\text{-}1}$ is the distance between n^{th} wire and 1st wire in one period ($d_0 = 0$), $\xi_m = 2\pi m/\Lambda_y$ and $\beta_m = \sqrt{k_0^2 - \xi_m^2}$ are the transverse component and longitudinal component of the m^{th} mode wavenumber in air, and $R_m = \left[j\tan(\beta_m' h) - \beta_m'/\beta_m\right] / \left[j\tan(\beta_m' h) + \beta_m'/\beta_m\right]$ is the reflection coefficient of the m^{th} mode, with $\beta_m' = \sqrt{k_s^2 - \xi_m^2}$.

Using the metagrating concept, functionalities related to antennas can be considered. For the implementation, considering that the imaginary part of the load-impedance density calculated can be positive or negative, microstrip inductor or capacitor structure are used to design the meta-atoms. The structure of the considered meta-atoms are shown in Fig. 1(b). For such simple microstrip structures, analytical formulations exist to calculate the load impedances. However, such analytical models have to be completed with a phenomenological scaling parameter by means of 3D full-wave simulations of an entire supercell. On the other hand, the LPA method described in [2], can also be applied to design metagratings in the "unit cell by unit cell" manner.

Using the above methodology, metagratings can be judiciously designed for different applications, such as beam steering, beam-splitting and absorbers [3-5], as schematically illustrated in Fig. 1(a).

Z. Tan acknowledges funding from the Chinese Scholarship Council (No. 202206280099).

References

1. Ra'di, Y., D. L. Sounas and A. Alù, "Metagratings: beyond the limits of graded metasurfaces for wave front control," Phys. Rev. Lett., Vol. 119, No. 6, 067404, 2017.
2. Popov, V., M. Yakovleva, F. Boust, J.-L. Pelouard, F. Pardo and S. N. Burokur, "Designing metagratings via local periodic approximation: from microwaves to infrared," Phys. Rev. Appl., Vol. 11, No. 4, 044054, 2019.
3. Tan, Z., J. Yi, Q. Cheng and S. N. Burokur, "Design of perfect absorber based on metagratings: theory and experiment," IEEE Trans. Antennas Propag., Vol. 71, No. 2, 1832–1842, 2023.
4. Tan, Z., J. Yi, S. Wang, X. Chen and S. N. Burokur, "Closed-form analytical design of a beamforming reflective metagrating with a relatively low number of meta-atoms," Opt. Mater. Express, Vol. 13, No. 3, 624-635, 2023.
5. Tan, Z., J. Yi, X. Chen, M. Lin, Z. H. Jiang, D. Werner and S. N. Burokur, "Fully analytical design of dual-wire PCB metagratings for beam steering and splitting," IEEE Trans. Antennas Propag., in press, doi: 10.1109/TAP.2023.3243729, 2023.

Modulated metasurface antennas and arrays for millimeter wave and sub-terahertz applications

D. González Ovejero[1*], J. Taillieu[1,2], C. Bilitos[1], R. Sauleau[1], and O. de Sagazan[1]
[1]Univ Rennes, CNRS, Institut d'Électronique et des Technologies du numéRique (IETR), UMR 6164, 35000 Rennes, France.
[2]Univ Rennes, CNRS, Institut FOTON – UMR 6082, F-35000 Rennes, France
[*]corresponding author: david.gonzalez-ovejero@univ-rennes.fr

Abstract: This summary presents the application of modulated metasurfaces in millimeter wave and sub-terahertz antenna systems. We succinctly show that by adopting metasurfaces as array element, one may mitigate some of the challenges found in large phased arrays with a limited field of view and concurrently enhance the gain bandwidth of modulated metasurfaces antennas with a single port.

The advent of future wireless networks beyond 5G has fostered the interest in millimeter and sub-terahertz (sub-THz) frequency bands, which will allow one to benefit from large unlicensed bandwidths and thus satisfy the need for higher data rates [1]. However, to make the most of such large bandwidths, one has to compensate the free space path loss (FSPL), which is proportional to the carrier's frequency and typically burdens the link budget as one approaches sub-THz bands [2]. Moreover, the generation of power at room temperature in the sub-THz gap is also challenging. Therefore, high-gain antennas radiating narrow pencil beams must be adopted. Typical architectures consist of scalar horns used as focal source for large reflector and lens systems [3]. Although efficient and wideband, such architectures are bulky and difficult to adopt in a paradigm that foresees the massive deployment of small cells. As opposed to electrically large reflectors and lenses, we target low-profile and light-weight architectures that can provide similar gains without imposing a toll on the relative bandwidth. This summary discusses the use of modulated metasurfaces (MTSs) [4]-[5] for the efficient transformation of guided modes into directive radiation in the millimeter-wave and sub-THz ranges.

In modulated MTSs, a dominantly transverse magnetic (TM) surface wave (SW) is typically excited on an inductive impedance plane. It has been shown that one can gradually radiate the SW power by periodically modulating such impedance boundary condition (IBC) [6]. This effect has been successfully exploited to design high-gain antennas capable of providing multiple beams [7], dual-polarization [8], and dual-band [9] operation [9]. Their main drawback is a relatively narrow bandwidth (BW) in gain, which has so far precluded their use for broadband applications (wideband sensing, 5G communications, etc.). The relative -3dB gain fractional BW ($\Delta f/f_0$, with f_0 being the center frequency and Δf the total BW) of modulated MTS antennas with circular shape is equal to [10],

$$B = \Delta f / f_0 = 1.2\left(v_g / c\right)\left(\lambda_0 / a\right) \tag{1}$$

where c is the speed of light in vacuum, a is the antenna radius, λ_0 is the free-space wavelength at f_0, and v_g is the SW group velocity at f_0. Practical values of $\Delta f/f_0$ may vary between 3.5% and 12% when the radius goes from $17\lambda_0$ to $5\lambda_0$ for v_g/c =0.5. On the other hand, the aperture gain G in absence of losses (directivity) is given by

$$G = \left(2\pi a / \lambda_0\right)^2 \left(a / \lambda_0\right) / \left(a / \lambda_0 + 2\right) \tag{2}$$

Combining the latter expressions the product between fractional bandwidth and gain can be approximately written as $G\times B$=47.37$(v_g/c)(a/\lambda_0)^2/(a/\lambda_0+2)$. On this basis, and assuming that v_g is fixed and according to (1), we

will show that one can increase the BW without impacting the gain (G) by dividing the total aperture into sub-apertures with smaller radius, each one fed by its own source. Second, grating lobes (repetitions of the main lobe related to the spacing between sources) can be avoided by the combined action of an aperiodic tiling of the aperture [11] and appropriately tailoring the element pattern of each sub-aperture. Compared to other approaches for broadband operation [12], the aperiodic tiling of the plane presents the advantage of allowing one to steer the beam over a limited field of view (FoV).

Acknowledgements: This work has received support from the French National Research Agency (ANR) through the project AROMA with reference ANR-22-CE24-0013, and from the French Government through the Labex CominLabs Excellence Laboratory, managed by ANR in the Investing for the Future Program under Reference ANR-10-LABX-07-01.

References

1. T. S. Rappaport *et al.*, "Wireless communications and applications above 100 GHz: Opportunities and challenges for 6G and beyond," *IEEE Access*, vol. 7, pp. 78 729–78 757, 2019.
2. T. Nagatsuma, G. Ducournau, and C. C. Renaud, "Advances in terahertz communications accelerated by photonics," *Nature Photon.*, vol. 10, no. 6, pp. 371–379, Junc. 2016.
3. S. Koenig, D. Lopez-Diaz, J. Antes et al., "Wireless sub-THz communication system with high data rate," *Nature Photon.*, vol. 7, no. 12, pp. 977–981, Dec. 2013.
4. B. H. Fong, J. S. Colburn, J. J. Ottusch, J. L. Visher and D. F. Sievenpiper, "Scalar and Tensor Holographic Artificial Impedance Surfaces," *IEEE Trans. Antennas Propag.*, vol. 58, no. 10, pp. 3212-3221, Oct. 2010.
5. M. Faenzi *et al.*, "Metasurface antennas: New models, applications and realizations," *Sci. Rep.*, vol. 9, p. 10178, Jul. 2019.
6. A. Oliner and A. Hessel, "Guided waves on sinusoidally-modulated reactance surfaces," *IRE Trans Antennas Propag.*, 7(5), 201-208 (1959).
7. D. González-Ovejero, G. Minatti, G. Chattopadhyay and S. Maci, "Multibeam by metasurface antennas," *IEEE Trans. Antennas Propag.*, vol. 65, no. 6, pp. 2923-2930, Jun. 2017.
8. A. T. Pereda et al., "Experimental validation of a Ku-band dual-circularly polarized metasurface antenna," *IEEE Trans. Antennas Propag.*, vol. 66, no. 3, pp. 1153-1159, Mar. 2018.
9. M. Faenzi, D. González-Ovejero, and S. Maci, "Overlapped and sequential metasurface modulations for bi-chromatic beams generation", *Appl. Phys. Lett.*, vol. 118, pp. 181902, 2021.
10. G. Minatti, M. Faenzi, M. Sabbadini, and S. Maci, "Bandwidth of gain in metasurface antennas," *IEEE Trans. Antennas Propag.*, 65(6), 2836-2842 (2017).
11. V. Pierro, V. Galdi, G. Castaldi, I. M. Pinto, and L. B. Felsen, "Radiation properties of planar antenna arrays based on certain categories of aperiodic tilings," *IEEE Trans. Antennas Propag.*, 53, 635–644 (2005).
12. M. Faenzi, D. González-Ovejero and S. Maci, "Flat gain broad-band metasurface antennas," *IEEE Trans. Antennas Propag.*, vol. 69, no. 4, pp. 1942-1951, Apr. 2021.

Perfect Control of Diffraction Patterns with Phase Gradient Metasurfaces

Yuxiang Wang,[1] Kuang Zhang[1],Guohui Yang, [1], Shah Nawaz Burokur and Qun Wu,[1]

[1]Department of Microwave Engineering, Harbin Institute of Technology, Harbin 150001, China
[2] LEME, UPL, Univ Paris Nanterre, Ville d'Avray, F92410, France
*corresponding author: zhangkuang@hit.edu.cn and sburokur@parisnanterre.fr

Abstract: Most studies on PGM focus only on single diffraction order. Multiple beams are still in the same order, and energy carried by different beams cannot be controlled. Here we propose a general method to perfectly control diffraction patterns based on a multi-beam phase gradient metasurface. An analytical solution for arbitrarily controlling diffraction beams is derived, the generation and energy distribution in high order diffraction beams can be achieved.

Considering a simple one-dimensional scenario where metasurface carries a spatial phase distribution along one direction located at $z = 0$ plane. When illuminated by a plane wave at an angle θ_{in}, the scattered beam will be composed of several diffraction orders, which are scattered in different directions. The response of the unit cells is the superposition of all beams. The intensity on the metasurface can be expressed as:

$$P_{meta}(x_i) = \left|R_{meta}(x_i)\right|^2 = \sum_{m=-n}^{n} \left|a_m\right|^2 + \sum_{\substack{p,\, q=-n \\ p\neq q}}^{n} \left|a_p\right|\left|a_q\right| \cos\left(2\pi\left(\frac{px_i}{L_p} - \frac{qx_i}{L_q}\right) + \phi_q - \phi_p\right) \tag{1}$$

where p and q represent arbitrary diffraction orders. We set the former term as unit energy and the latter term as 0. Obviously, it is satisfied for a single diffracted beam. Then, we consider the case when two diffracted orders are excited. When the period and number of the unit cells are same for both orders, the relationship between the diffracted orders and the discrete points is derived as:

$$\left|p - q\right| = \frac{s}{2}, \quad \phi_p - \phi_q = \frac{\pi}{2} + \pi b \tag{2}$$

where s is the number of unit cells in a period and b is arbitrary integer. The equation is only applicable for two beams with opposite diffractions. Since the equation does not limit the energy relationship between the beams, the energy of the different beams can be independently controlled. Fig. 1 shows the measured far-field energy distribution of two cases, which are +1st and -1st diffraction orders sharing an energy ratio of 1:2 and +2nd and -3rd diffraction orders sharing an energy ratio of 1:3. Both energy distributions of simulation and measurement show good agreement with the preset value, validating the proposed method that provides a new way to design multi-beam antennas and that has significance in wireless communication applications.

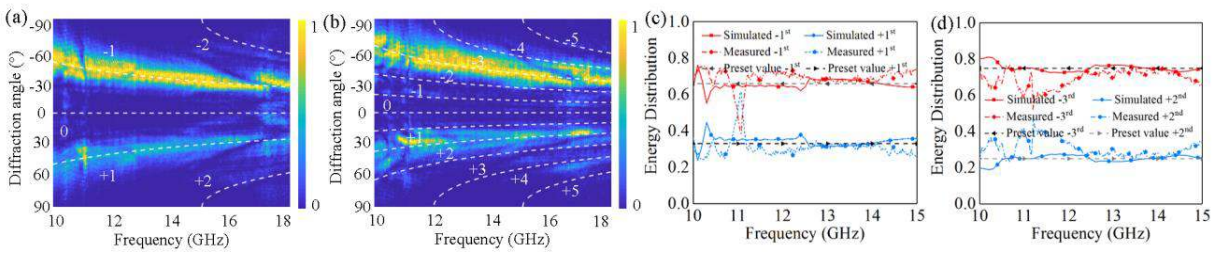


Figure 1. The measurement results, where (a) and (b) are normalized intensity of two cases, (c) and (d) are corresponding intensity comparison in the desired channels.

META 2023, PARIS - FRANCE, JULY 18 – 21, 2023

Holographic Metasurfaces for Wireless Communications and Extended Reality

A. Pitilakis[1,2*], O. Tsilipakos[3,4], A. C. Tasolamprou[4], A. Tsioliaridou[1], T. V. Yioultsis[2], N. V. Kantartzis[2], D. Manessis[5], G. Kenanakis[4], S. Ioannidis[1,6], M. Kafesaki[4,7], and C. Liaskos[1,8]

[1] Institute of Computer Science, Foundation for Research and Technology Hellas, 71110 Heraklion, Greece
[2] School of Electrical and Computer Engineering, Aristotle University of Thessaloniki, 54124 Thessaloniki, Greece
[3] Theoretical and Physical Chemistry Institute, National Hellenic Research Foundation, 11635 Athens, Greece
[4] Institute of Electronic Structure and Laser, Foundation for Research and Technology Hellas, 71110 Heraklion, Greece
[5] Department of System Integration & Interconnection Technologies, Fraunhofer IZM, 13355 Berlin, Germany
[6] School of Electrical & Computer Engineering, Technical University of Crete, 73100 Chania, Greece
[7] Department of Materials Science and Technology, University of Crete, 70013, Heraklion, Greece
[8] Computer Science and Engineering Department, University of Ioannina, 45110 Ioannina, Greece
[*]corresponding author: alexpiti@ece.auth.gr

Abstract: We present our progress in developing tunable metasurfaces for microwave holographic imaging and for its application to wireless communications and virtual/augmented reality (VR/AR). Our methodology starts from the analysis of ideal metasurface apertures and moves to tunable static prototypes designed for fabrication with cost-effective techniques, e.g., 3D printing or conductive inks. We envision to translate the proof-of-concept study, and associated devices, to printed circuit board technology, implementing practical reconfigurable metaholograms for wireless communications and VR/AR.

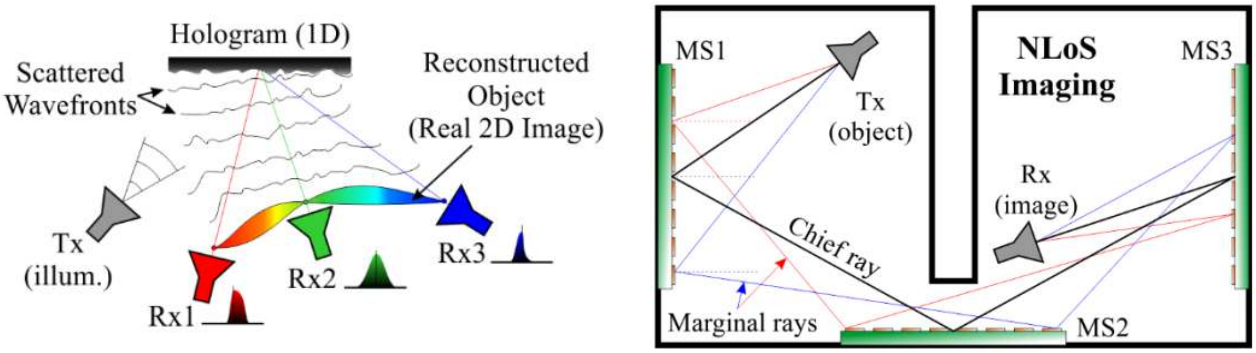
The reconfigurable intelligent surface (RIS) archetype has recently gained traction, as an abstract electrically tunable aperture that can filter and manipulate the scattering of wavefronts in ways transcending the elementary geometric optics prescriptions, i.e., the standard laws of reflection and refraction. Metasurfaces (MSs), ultrathin sheets with subwavelength-sized resonators on their exposed face, are the physical implementations of RISs. Varactor or PIN-diode assembled printed-circuit boards (PCBs) are currently the go-to technology for microwave and mmWave band devices. This operation mode means that, by electrically tuning the microwave value of the loading element (varactor or diode), we can tune the equivalent reactance of a metasurface, i.e., tune its resonance to the desired frequency, polarization, and direction of scattering. This enables tunable functionalities such as perfect absorption, anomalous reflection (steering), focusing/imaging, and holography.

In this work we cast MSs as holograms [1], i.e., as devices storing phase and amplitude profiles that, when illuminated with a specific wavefront, can re-construct real images of the stored objects in 3D space, by coherent interference. For wireless communications, holography can be considered as the 3D extension of beam forming: In the latter we direct beams to desired directions in the farfield (so we have only two dimensions, the θ_{el} and φ_{az} angles), whereas in holography we can focus an arbitrary wavefront to any point or scatter/diffract it anywhere in 3D space, Fig 1(a). Envisioning widely deployed reconfigurable metaholograms, e.g., covering all the walls of a room, essentially implements a programmable wireless environment (PWE) in a rigorous and holistic way, i.e., overcoming the limitations of geometric optics approximations (neglect of near-field effects etc.). This framework enables us to design and optimize practical applications that are sensitive to power considerations and real-world "non-ideality", e.g., non-line of sight links, interference, obstructions, fabrication imperfections, fading, etc.

Back/front hauling of information for extended reality (XR) devices, a portmanteau for both virtual and augmented reality (VR/AR), is an application that stands to benefit from holographic metasurface imaging: Immersive interaction between remote users in an XR world is currently limited by latency, mostly imposed by

digital signal processing and by traversing multiple OSI (Open Systems Interconnection model) layers. To overcome this hurdle, we are developing a system where a PWE, enabled by reconfigurable metaholograms, can record the wavefronts scattered from the source object, in real-time, and then reconstruct (image) them in a remote location; the transmission happens at the speed of light, either over-the-air (for small distances) or over fiber (for larger distances). Reconfigurable metasurfaces play a twin role in this system: (i) on the source location, they operate as a distributed imaging lens, i.e., gathering all the rays scattered from the illuminated object, and focusing them onto a microwave imager; (ii) on the remote location, they operate as a distributed projection lens, i.e., scattering the reference beam in such a way so that a real 3D image of the source object is formed.

The aim/scope of our work can be broken down in three parts: Firstly, we develop the theoretical framework for holographic imaging in arbitrary environments, Fig. 1(b), assuming a set of ideal reconfigurable metasurfaces, both in the "imaging lens" and in the "projection lens" configuration; from this framework, we extract performance metrics related to sharpness and quality of object-image formation etc. Subsequently, we design and manufacture static but cost-effective metahologram boards, using additive manufacturing (3D printing) and/or conductive inks, for an experimental proof of concept. Lastly, we develop designs for reconfigurable boards in PCB technology [3].



(a) (b)

Figure 1. (a) Abstract off-axis holographic 2D projection by illuminating a reflective 1D hologram with the reference coherent source Tx. The real image of the reconstructed object is the twisted ribbon, where colors represent frequencies. In a wireless communications analogy, the hologram is focusing the broadband signal from Tx to three receivers, each at a different band. (b) Three MSs implementing a non-line of sight (NLoS) link by conjugate point-object/image formation on the Tx-Rx antennas; each of the three MSs aperture is custom phase-profiled, as can be seen by the anomalous reflections of the chief and marginal rays across MS1.

Acknowledgement: This work was funded by the Foundation for Research and Technology - Hellas (FORTH) via the Theodore Papazoglou synergy grant 2022 – Project WISAR.

References

1. Li, L., *et al.*, "Electromagnetic reprogrammable coding-metasurface holograms," Nature Communications, vol. 8, no. 1, 2017. [URL]
2. Liaskos, C., *et al.*, "XR-RF Imaging Enabled by Software-Defined Metasurfaces and Machine Learning: Foundational Vision, Technologies and Challenges," IEEE Access, vol. 10, pp. 119841–119862, 2022. [URL]
3. Pitilakis, A., *et al.*, "Multifunctional Metasurface Architecture for Amplitude, Polarization and Wave-Front Control," Physical Review Applied, vol. 17, no. 6., 2022. [URL]

A Dual Polarized Metagrating to Manipulate Wavefronts

W. Zhou[1], **L. N. Zhu** [1], **and J. Yi**[2*]

[1] School of Telecommunication Engineering, Xidian University, China

[2] School of Information and Communication Engineering, Xi'an Jiaotong University, Xi'an 710049, China

[*]corresponding author: jianjia.yi@xjtu.edu.cn

Abstract: Metagratings (MGs), which are sparse arrangements of subwavelength polarizable particles (meta-atoms), have demonstrated efficient realization of various electromagnetic functions in recent years. Here, we proposed a dual polarized metagrating which can independently control dual polarized waves.

The metagrating is derived from the periodic grating whose periodic constant is smaller than the working wavelength [1]. Unlike traditional grating, the period of metagrating is larger than the working wavelength. Based on the coupling behavior of periodic structure and the scattering modulation characteristics of the meta atoms, mg can improve the efficiency of the regulatory beam by using periodic Bragg scattering, thus avoiding the efficiency reduction and energy loss caused by the phase discretization of the metasurface.

Dual-polarized MG can effectively deflect *x* and *y* polarized incident waves, which is rarely seen in the literature and mainly depends on numerical optimization of the whole large period or typical MG design methods [2]. Based on the theory of line current [3] and referring to the structure of the metasurface, polarization-insensitive, dual-polarized cross-shaped structure metagrating is proposed which can independently control the *x*- and *y*-polarized wave.

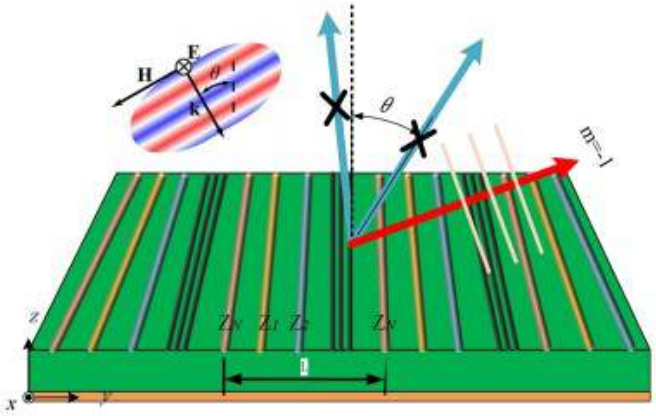


Figure 1. The physical system of the metagratings: a periodic array of thin loaded wires (represented by color cylinders) placed on a PEC-backed dielectric substrate. The array is excited by a TE-polarized plane wave, and has the functions of anomalous reflection.

Figure 1 shows the equivalent line current model of metagratings. When the plane wave illuminated on metagrating at the angle θ_{in}, its electric field expression is

$$E_x^{(in)}(y, z \le -h) = e^{-j\beta_0 z - jk\sin|\theta| y} \tag{1}$$

Since the period of the illuminated structure is L, the scattered field can be represented as a superposition of

plane waves:

$$E_x(y,z) = -\frac{k\eta}{4}\sum_{q=1}^{N}\sum_{n=-\infty}^{\infty} I_q e^{-jk\sin[\theta]nL} H_0^{(2)}\left[k\sqrt{(y-nL-(q-1)d)^2+z^2}\right] \tag{2}$$

Then, each polarization line current is excited in a thin wire characterized by its input-impedance Z_{in} and load-impedance densities Z_q. Ohm's law gives the relation between Z_{in}, Z_q and I_q:

$$Z_q I_q = E_q^{(exc)} - Z_{in} I_q - \sum_{p=1}^{N} Z_{qp}^m I_p \tag{3}$$

Thus, by setting up the specific impedance distribution of mg, the expected scattered electric field can be obtained.

In this paper, we design a cross structure mg which can respond to *x*- and *y*-polarized waves separately. The first MG has an impedance distribution of [-2.45j, -6.59j, -4.01j, -3.18j] along the *x* direction and the same impedance distribution along the *y* direction. It can realize single beam diffraction with different polarization wave incident. The second MG has an impedance distribution of [-2.45j, -6.59j, -4.01j, -3.18j] along the *x* direction and [-3.57j, -2.45j, -8.62j, -2.27j] along the *y* direction. It can realize single beam diffraction under *x*-polarized wave incidence and beam splitting under *y*-polarized wave incidence.

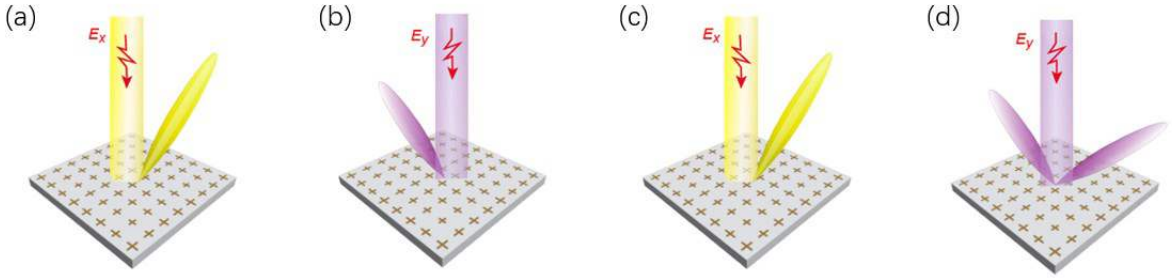


Figure 2. Functional diagram of two MGs. (a) The wavefront control for the first MG under *x*-polarized incidence. (b) The wavefront control for the first MG under *y*-polarized incidence. (c) The wavefront control for the second MG under *x*-polarized incidence. (d) The wavefront control for the second MG under *y*-polarized incidence.

The designed dual-polarized mg has great potential in multi-channel information processing, dynamic dual-polarized antennas and radar systems.

References

1. D. Sell, J. Yang, S. Doshay, R. Yang, and J. A. Fan, "Large angle, multi-functional metagratings based on freeform multi-mode geometries," Nano Letters, vol.7, pp. 3752-3757, 2017.
2. O. Rabinovich and A. Epstein, "Dual-Polarized All-Metallic Metagratings for Perfect Anomalous Reflection," Phys. Rev. Applied, vol. 14, no. 6, p. 064028, Dec. 2020.
3. V. Popov, F. Boust, and S. N. Burokur, "Controlling Diffraction Patterns with Metagratings," Phys. Rev. Applied, vol. 10, no. 1, p. 011002, Jul. 2018.

META 2023, PARIS - FRANCE, JULY 18 – 21, 2023

Composite based metasurface for surface wave excitation in HF band

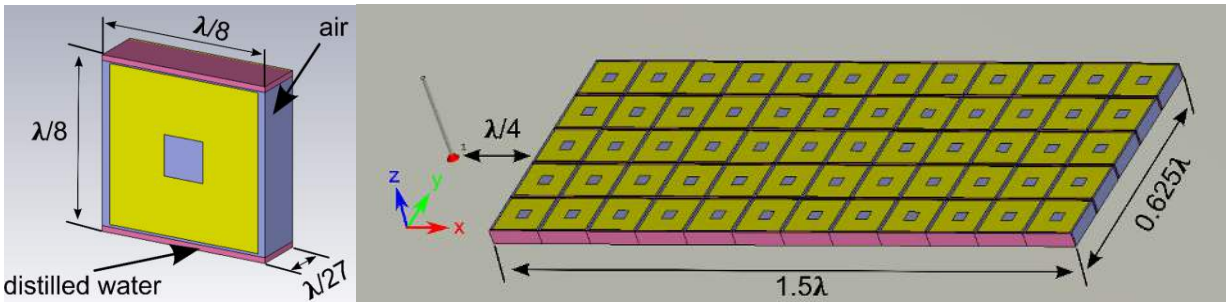
G. Briand[1*], A. Barka[1], and S. N. Burokur[2]

[1]ONERA/DEMR, Université de Toulouse, France
[2]LEME, UPL, Univ Paris Nanterre, F92410 Ville d'Avray, France
[*]corresponding author: gildas.briand@onera.fr

Abstract: This paper describes the design of a low profile inductive surface for High Frequency Surface Wave Radars (HFSWR) in HF-band. We discuss about reducing the thickness of the metasurface by designing an adapted dielectric support. The metasurface is then exploited to highly increase the electric field near the ground when illuminated by a quarter-wave monopole in TM polarization. This enhancement of the electric field is necessary in order to excite a surface wave.

Being able to detect ships up to 200 nautical miles, High Frequency Surface Wave Radars (HFSWR) constitute a major asset for maritime surveillance of Exclusive Economic Zone (EEZ), which is an area up to 200 nautical miles from coastal baseline where a sovereign state has special rights such as fishing and oil extraction exclusivity. ONERA, the French Aerospace Lab, has been developing radars (Graves, Nostradamus) and more specifically HFSWR for several years. First, an installation has been successfully tested [1], but interferences due to sky waves reflecting on ionosphere have been acknowledged [2]. Later, a metamaterial structure placed in front of the emitting antenna has been proposed in order to reduce ionospheric sky wave interferences and to increase the propagating energy near the ground in the forward direction [3, 4]. However, it has been observed that the structure is too high, typically $\lambda/10$ (3 m at 10 MHz), to withstand strong sea winds and due to regulation in protected natural area. A reduced profile metasurface of height $\lambda/30$ designed on a Rogers TMM6 substrate has been proposed and tested in the L-band at about 1.1 GHz [5]. Here, we make a step forward to design a new surface wave exciting structure that is compact and realizable in HF-band.

The metasurface is composed of resonant square metal rings printed on a dielectric substrate. The transposition of the previously designed L-band metasurface to the HF-band would require a very large size of the commercial Rogers TMM6 dielectric substrate, which is unrealizable in practice. Hence, it is highly desirable to find a natural material that has similar properties to the TMM6 substrate. We thus propose a composite material based on air and distilled water.

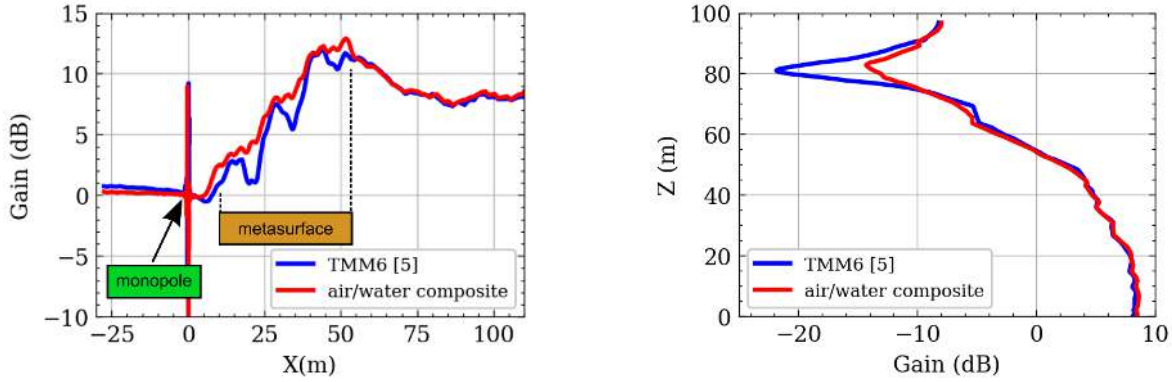


(a) (b)

Figure 1. (a) Unit cell designed using a composite dielectric material made of air and distilled water. (b) HF-band metasurface-based antenna.

Different designs of dielectrics, based on the shape of the composite and the materials used, can be considered. Their dielectric properties are obtained using the Nicholson-Ross-Weir parameter extraction method. An example of such design is made of 90% of air in distilled water to obtain an effective permittivity $\varepsilon_{eff} = 6$, see Fig. 1(a). An analytical study of the unit-cell using transmission line theory allows to tune the shape of the dielectric to get the desired inductive behaviour [5].

The performance of the metasurface is evaluated thanks to the vertically radiated electric field $E_{metasurface}$. The gain of the metasurface antenna is defined as $Gain = 20\log10\left(\frac{E_{metasurface}}{E_{inc}}\right)$, where E_{inc} is the amplitude of the electric field radiated by the monopole source. A gain enhancement of more than 10 dB (Fig. 2(a)) is observed at the extremity of the metasurface and most of the field is located at ground level (Z=0) (Fig. 2(b)), which is mandatory to excite a surface wave.



(a) (b)

Figure 2. (a) Simulated gain of the SIS and the novel composite metasurface at 10MHz along a line in the horizontal plane. (b) Simulated gain of the SIS and the novel composite metasurface at 10MHz along a line in the vertical plane.

This work is co-funded by the French Ministry of Defense (DGA/AID) and ONERA.

References

1. M. Menelle, G. Auffray, et F. Jangal, « Full digital High Frequency Surface Wave Radar: French trials in the biscay bay », in 2008 International Conference on Radar, Adelaide
2. M. J. Abi Akl, F. Jangal, M. Darces, et M. Helier, « Modelling the ionospheric effects in HF radar long term integration », in 2016 10th European Conference on Antennas and Propagation (EuCAP), Davos, Switzerland
3. F. Jangal, N. Bourey, M. Darces, F. Issac, et M. Hélier, « Observation of Zenneck-Like Waves over a Metasurface Designed for Launching HF Radar Surface Wave », International Journal of Antennas and Propagation, vol. 2016, p. 1-5, 2016
4. Q. Herbette, N. Bourey, M. Menelle, M. Darces, S. Saillant, et M. Helier, « Using a 3D metamaterial to enhance surface wave propagation in HF band », in 2021 15th European Conference on Antennas and Propagation (EuCAP), Dusseldorf, Germany
5. A. Barka, D. Prost, « Low-profile inductive metasurface for surface wave excitation in L-band: design, manufacture and electromagnetic infrared measurements », AEM, vol. 11, n° 2, p. 49-53, june 2022

A Compact, Quad-Band, and Wideband Antenna Using Triple-Band AMC

Rafael Gonçalves Licursi de Mello*, Anne Claire Lepage, and Xavier Begaud

LTCI, Télécom Paris, Institut Polytechnique de Paris, 91120 Palaiseau, France
*corresponding author: E-mail: rafael.licursi@ieee.org

Abstract

We present a compact antenna with stable, unidirectional, high-gain radiation patterns to cover the standards 5G/4G/Wi-Fi 2.4/5/6E and X-band communications. The operating frequency bands are 2.4–2.7, 3.4–3.8, 5.17–6.45, and 8.0–12.0 GHz. The thickness is $0.09\lambda_l$ and the aperture size is $0.51 \times 0.65\ \lambda_l^2$, where λ_l is the wavelength at the lowest frequency. To achieve the desired performance, we exploit both the in-band and out-of-band operation modes of a triple-band artificial magnetic conductor (AMC) illuminated by a grooved bow-tie radiating element surrounded by a metal ring.

1. Introduction

Modern Telecommunications are defined by the operation of multiple standards in parallel, which is pushing the employed components and systems towards a multiband and wideband technology. This paradigm represents a challenge in the antenna field because obtaining stable, unidirectional, high-gain radiation patterns in multiple, wide bands using a single antenna is not trivial.

In this work, we present a compact antenna with directive radiation patterns operating in the frequency bands 2.4–2.7, 3.4–3.8, 5.17–6.45, and 8.0–12.0 GHz appropriate to cover the standards 5G/4G/Wi-Fi 2.4/5/6E and X-band communications.

This quad-band antenna exploits both the in-band behavior of a triple-band artificial magnetic conductor (AMC), when it mimics a perfect magnetic conductor (PMC), and its out-of-band behavior, when it emulates a perfect electric conductor (PEC). This idea is represented in Fig. 1.

A wideband radiating element providing stable radiation patterns with maxima at each broadside direction in the addressed bands should be used as the radiating element. By choosing a spacing h_{refl} between the radiating element and the AMC that is about a quarter-wavelength distance in the highest band, which implies an electric distance much smaller than a wavelength for the lowest band, it is possible to achieve a stable, unidirectional, high-gain pattern in a triple-band operation with wide bandwidths covering the addressed standards.

In essence, this idea was already presented and validated in [1] with the design, fabrication, and measurement of a triple-band antenna with a dual-band AMC for the 5G/4G and Wi-Fi 2.4/5/6E standards. In [2], we extended the multiband reflection scheme to also handle the X-band, and the broadside gain of a spiral radiating element was considerably enhanced. The spiral radiating element is circularly polarized. Its current distribution follows a quasi-circular pattern and is not appropriate to illuminate an AMC with a cartesian arrangement [3]. For this reason, although [2] validates the multiband reflection scheme, the cross-polarization level and the flatness in the gain curve are not satisfactory.

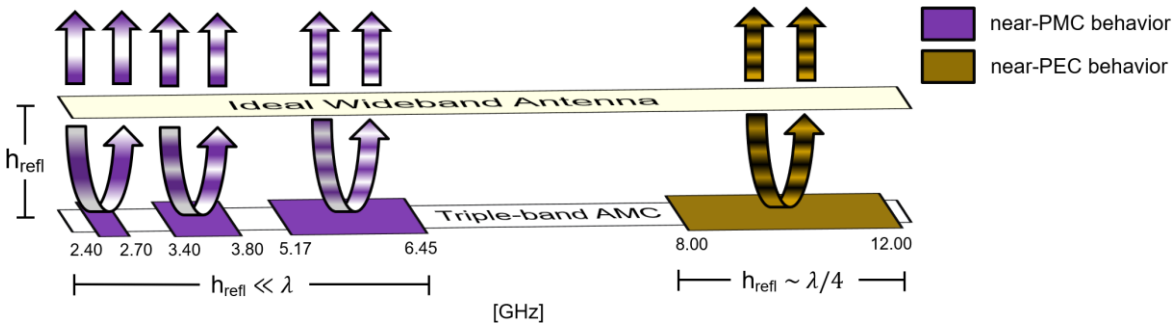
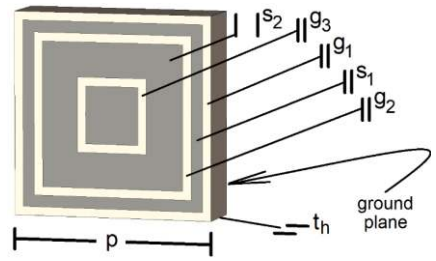


Fig. 1. Working principle: the triple-band AMC works as a near-PMC reflector around three resonances and as a near-PEC reflector far from resonances.

In this work, a grooved bow-tie radiating element [4], whose polarization is linear, is surrounded by a ring so that an appropriate bandwidth is achieved to cover the whole frequency range from 2.4 to 12.0 GHz. As such, the AMC can be properly illuminated by the radiating element in all the addressed bands. Results simulated with CST Studio Suite show that the proposed antenna provides unidirectional, high-gain patterns with maxima at the broadside direction associated to reasonable levels of cross-polarization and front-to-back ratios for all the addressed bands.

2. Materials and Methods

For the AMC, we use a unit cell with three square slots. This unit cell is designed to obtain the behavior of a perfect magnetic conductor (PMC) in three frequencies close to each other, where resonances occur with a reflection coefficient phase $\varphi_r = 0°$. Far from resonances, φ_r asymptotically goes to ±180° and a behavior close to the perfect electric conductor (PEC) is obtained. Fig. 2 depicts such unit cell.



Parameters

g_1	0.55 mm
g_2	0.30 mm
g_3	0.25 mm
s_1	0.25 mm
s_2	2.00 mm
t_h	4.90 mm
p	17.5 mm

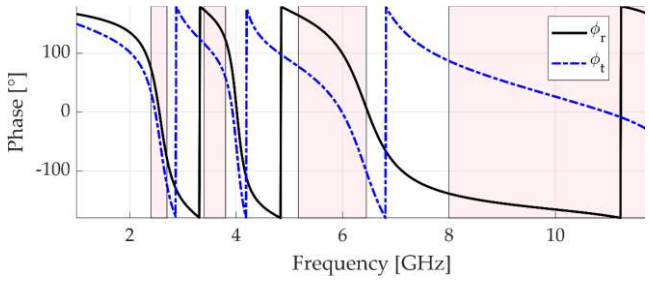
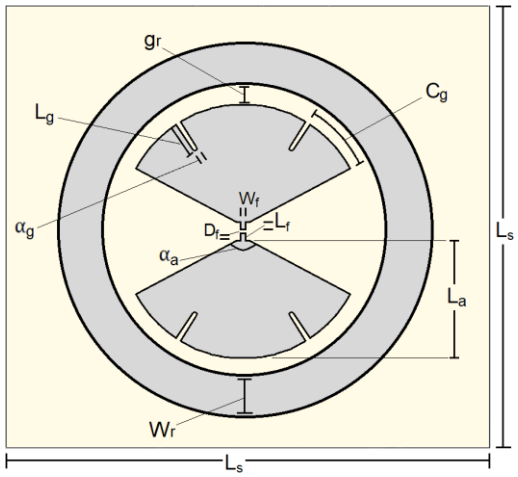


Fig. 2. Simulated unit cell, its parameters, and its reflection coefficient phase φ_r. The phase difference φ_t between the direct and reflected electric fields in the plane $h_{refl} =$ 7.5 mm is also shown.

It was shown in [5] that constructive interferences occur between the direct and reflected electric fields at the broadside direction when $-120° < \varphi_t < +120°$, where $\varphi_t = \varphi_r + \varphi_p$ is the phase difference between both fields, $\varphi_p = -2kh_{refl}$ is the phase delay due to the round trip between the radiating element and the reflector, and k is the wavenumber.

We first design the AMC unit cell using a methodology similar to those of [1], to obtain the desired φ_t range in all the bands. The transient solver of CST Studio Suite is set for an infinite structure, using PEC and PMC boundary conditions, as proposed in [6]. A quarter wavelength at the central frequency of the highest band (10.0 GHz) is 7.5 mm. Fig. 2 also shows the parameters of this first unit cell, as well as its reflection coefficient φ_r and the phase difference φ_t between direct and reflected electric fields in a plane distance 7.5 mm from the unit cell. The substrate relative permittivity is $\varepsilon_r = 2.34$, and the loss tangent is $\tan\delta = 0.0013$. The addressed bands are colored, and the condition $-120° < \varphi_t < +120°$ is met in all of them.

Next, a radiating element presenting stable radiation patterns with maxima at each broadside direction in the addressed bands is designed. The element consists of a grooved bow-tie [4] surrounded by a metal ring (Fig. 3).



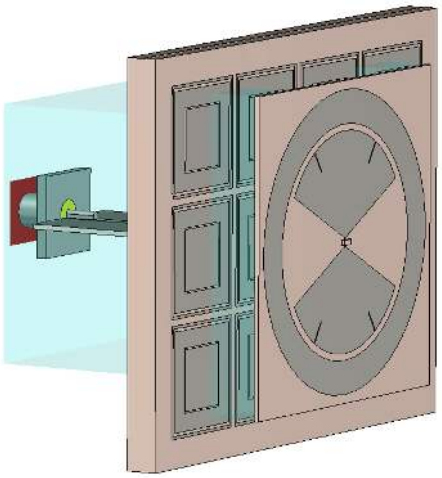
Parameters

ε_r	2.2	W_f	0.32 mm
$\tan\delta$	0.0009	D_f	0.76 mm
L_s	49.6 mm	L_g	3.7 mm
t_s	0.76 mm	α_g	0.69°
L_a	16.1 mm	C_g	30.0°
α_a	124.4°	g_r	2.0 mm
L_f	0.42 mm	W_r	10.0 mm

Fig. 3. Simulated grooved bow-tie with ring and its parameters.

The substrate presents a thickness $t_s = 0.76$ mm, relative permittivity $\varepsilon_r = 2.2$, and loss tangent $\tan\delta = 0.0009$. This antenna is first simulated alone with a discrete port whose reference impedance is $Z_{ref} = 151\ \Omega$. Its parameters are also shown in Fig. 3.

The AMC and the grooved bow-tie with ring are joined in a single device. As such, an optimization with full-wave simulations that consider the actual incidence of waves over the finite AMC can be done. The AMC has 3×4 unit cells, resulting in an aperture size of $62.9 \times 81.2\ \text{mm}^2$, that is, $0.51 \times 0.65\ \lambda_l^2$, where λ_l is the wavelength at the lowest operating frequency (2.4 GHz). A taper balun similar to the one used in [7] allows the feeding of the structure with a waveguide port over a 50-Ω SMA connector. Foam bricks ensure mechanical stability. The final structure is illustrated in Fig. 4.



New AMC parameters

g_1	0.52 mm
g_2	0.45 mm
g_3	0.25 mm
s_1	0.45 mm
s_2	2.75 mm
t_h	5.00 mm
p	18.3 mm

Fig. 4. Complete device with grooved bow-tie with ring and AMC. The AMC new parameters are also listed.

After the optimization, we used in the AMC unit cell the new parameters shown in Fig. 4. Further, a spacing $h_{refl} = 5.0$ mm was adopted. As such, the final device presents a total thickness 10.76 mm, which represents $0.09\lambda_l$. The balun in this work was used only to allow a future measurement of the structure in an anechoic chamber using a 50-Ω SMA connector. Hence, it was not considered in this calculation. In a real application, the feeding of the antenna would occur through a balun integrated in a board parallel to the antenna ground plane.

3. Results

The simulated results for the radiating element without and with the AMC are shown in Fig. 5. In terms of broadside realized gain, the introduction of the AMC provides an enhancement of up to 2.8 dB in the first band (2.4–2.7 GHz). In the second band (3.4–3.8 GHz), the improvement is up to 3.3 dB. In the third (5.17–6.45 GHz), it is up to 5.7 dB. On the other hand, in the fourth band (8.0–12.0 GHz), an enhancement of up to 4.2 dB occurs in the first half of the band, but a deterioration of up to 1.9 dB is seen in the second half, specifically from 10.5 GHz.

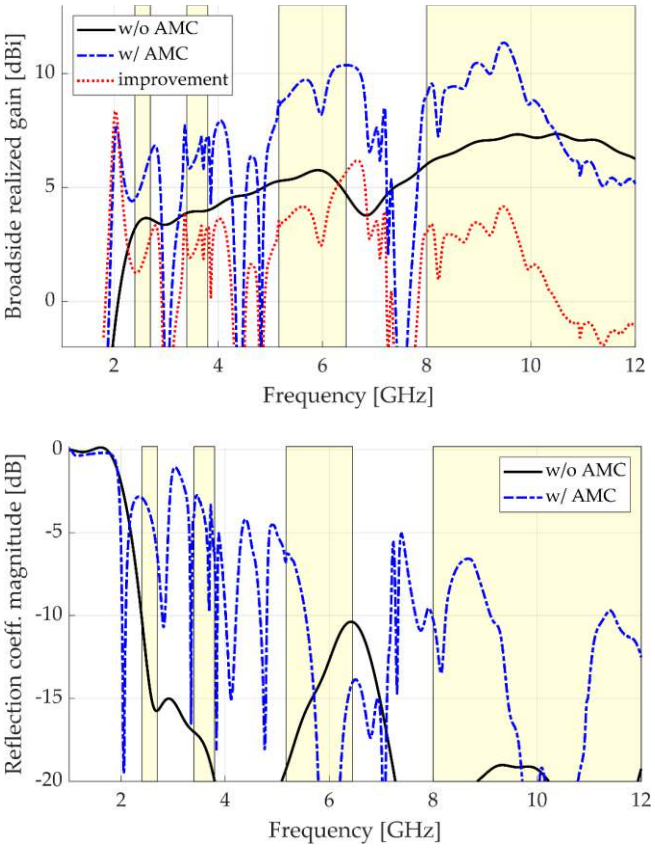


Fig. 5. Simulated broadside realized gain and reflection coefficient magnitude of the grooved bow-tie with ring, without and with the triple-band AMC.

Concerning the reflection coefficient, its magnitude is degraded in all the bands, which indicates that the proposed technique requires the design of a multiband impedance matching network. This network is considered out of the scope of this work to avoid losing focus on the advantages of the multiband reflection scheme.

Fig. 6 shows both E- and H-planes normalized radiation patterns of the grooved bow-tie with ring and AMC at the center frequency of each band. We can see that all the patterns are directive, with maximum radiation at the broadside direction. In the H-plane, the cross-polarization levels are -19.5, -23.1, -23.9, and -17.6 dB respectively for each band, whereas in the E-plane they are all negligeable. In the H-plane, the beamwidth is respectively 79°, 71°, 69°, and 43°. In the E-plane, the beamwidth is 80°, 69°, 54°, and 98°. The front-to-back ratios are 14.3, 26.3, 13.1, and 12.7 dB, respectively.

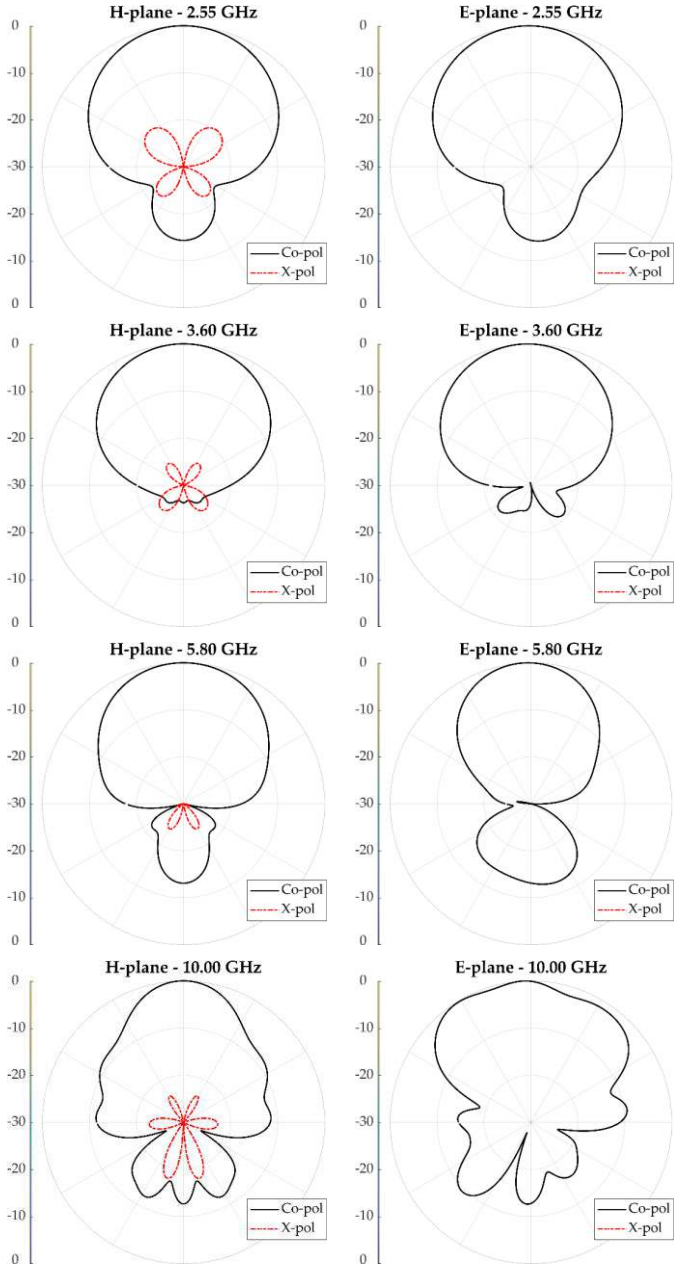


Fig. 6. Simulated normalized radiation patterns of the complete device in the center frequency of each addressed band.

4. Conclusions

We presented a compact, quad-band antenna with directive radiation patterns operating in the frequency bands 2.4–2.7, 3.4–3.8, 5.17–6.45, and 8.0–12.0 GHz appropriate to cover the standards 5G/4G/Wi-Fi 2.4/5/6E and X-band communications. Both the in-band and out-of-band operation of a triple-band AMC illuminated by a grooved bow-tie antenna shape surrounded by a ring were exploited to this end.

The results showed that the multiband reflection scheme enabled by the AMC provided a considerable improvement of the broadside realized gain in comparison to the radiating element alone, with unidirectional radiation patterns and reasonable levels of cross-polarization and front-to-back ratios in all the addressed bands.

The device is compact, with an aperture size of $0.51 \times 0.65\ \lambda_l^2$, and a thickness of $0.09\lambda_l$. However, the proposed approach requires a multiband impedance matching network to provide reflection coefficient magnitudes that could be acceptable in most of the applications.

Acknowledgements

This work has received funding from the National Council for Scientific and Technological Development (CNPq-Brazil), grant no. 201760/2018-5.

References

[1] R. Gonçalves Licursi de Mello, A. C. Lepage, X. Begaud, A Low-Profile, Triple-Band, and Wideband Antenna Using Dual-band AMC, *Sensors* 23: 1–19, 2023. https://doi.org/10.3390/s23041920

[2] R. Gonçalves Licursi de Mello, A. C. Lepage, X. Begaud, Réflecteur multibande à métamatériaux, *Proc. Journées Scientifiques URSI France*, Palaiseau, France, pp. 1–2, 2022.

[3] M. Grelier, C. Djoma, M. Jousset, S. Mallégol, A. C. Lepage, X. Begaud, Axial ratio improvement of an Archimedean spiral antenna over a radial AMC reflector, *Appl. Phys. A* 109: 1081–1086, 2012. https://doi.org/10.1007/s00339-012-7401-9

[4] R. Gonçalves Licursi de Mello, A. C. Lepage, X. Begaud, The bow-tie antenna: Performance limitations and improvements, *IET Microw. Antennas Propag.* 16: 1–12, 2022. https://doi.org/10.1049/mia2.12242

[5] C. Djoma, M. Jousset, A. C. Lepage, S. Mallégol, C. Renard, X. Begaud, Maximal Bandwidth of an Archimedean Spiral Antenna Above a Reflector, *IEEE Antennas Wirel. Propag. Lett.* 13: 333–336, 2014. https://doi.org/10.1109/LAWP.2014.2303858

[6] F. Linot, R. Cousin, X. Begaud, M. Soiron, Design and measurement of high impedance surface, *Proc. 4th Euro. Conf. Ant. Prop.*, Barcelona, Spain, pp. 1–4, 2010.

[7] M. Vahdani, X. Begaud, A directive ultra wideband sinuous slot antenna, *Proc. 1st European Conf. on Ant. and Prop.*, Nice, France, 06 Nov. 2006, pp. 1–6. https://doi.org/10.1109/EUCAP.2006.4584965

Design and measurement of an oblique wide-angle metamaterial absorber for RF space applications

A.C. Lepage[1*], X. Begaud[1], O. Rance[1], K. Elis[2], and N. Capet[2]

[1]LTCI, Télécom Paris, Institut Polytechnique de Paris, 91120 Palaiseau, France
[2]Centre National d'Etudes Spatiales, 31400 Toulouse, France
[*]corresponding author: anne-claire.lepage@telecom-paris.fr

Abstract: The paper deals with the design, realization and measurement of a lightweight electromagnetic metamaterial absorber for space applications operating on the [2 GHz, 2.3 GHz] frequency band, under oblique incidence from 35° to 65°.

Nowadays the satellites are getting more and more multifunctional leading to the presence of numerous antennas on the platform. The latter are generally close to each other which may cause interference and thus degraded performances. One solution is to cover some critical areas of the platform with absorbing material [1,2]. However, these areas are generally illuminated with an oblique incidence over a wide angular range which makes the design of the absorber very challenging with the constraints of space applications.
Thanks to their numerous design parameters, metamaterial absorbers appear as a promising solution [3]. Thus it has been demonstrated that metamaterial absorbers enable low-profile and low-mass structures [3]. Some feature a wide angular range but are optimized at normal incidence [4-7]. The question of oblique incidence is addressed in [8]. But gathering oblique incidence and wide angular range remains challenging.
In the present scenario, as the position of the antennas is known, it is possible to divide the absorber surface into smaller parts, each one operating with respect to the incoming angle, and thus reducing the angular range as shown on Figure 1. This concept was first proposed in [9]. The geometry of the unit cell has been studied in [10-11].

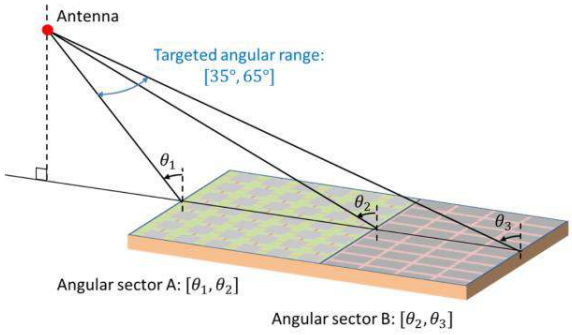


Figure 1: Concept of multi-sectoral absorber.

In this work, we present a sectoral metamaterial absorber for the angular range [35°, 65°] comprising two different sectors. A specific measurement setup has been developed to demonstrate that the whole structure effectively behaves as expected. Particular attention has also been paid on the post-processing of the measurements. Finally, the absorber achieves a measured reflection coefficient inferior to −11.5 dB, corresponding to an absorptivity above 0.965, over the 14% frequency band for [2 GHz, 2.3 GHz] for TE and TM polarizations over the targeted angular range.

References

1. Martel, C., B. Gabard, F. Boust, V. Gobin and K. Elis, "A metamaterial electromagnetic wave absorber based on resistive films for micro-satellite spatial applications," In Proceedings of the 2018 IEEE Int. Symp. on Antennas and Propagation USNC/URSI National Radio Science Meeting, Boston, MA, USA, 8–13 July 2018, pp. 441–442.
2. Delfini, A., M. Albano, A. Vricella, F. Santoni, G. Rubini, R. Pastore and M. Marchetti, "Advanced radar absorbing ceramic-based materials for multifunctional applications in space environment," Materials, Vol. 11, 1730, 2018.
3. Engheta, N., "Thin absorbing screens using metamaterial surfaces," In Proceedings of the IEEE Antennas and Propagation Society International Symposium, San Antonio, TX, USA, 16–21 June 2002, pp. 392–395.
4. Lee, D., J.G. Hwang, D. Lim, T. Hara and S. Lim, "Incident angle- and polarization-insensitive metamaterial absorber using circular sectors, " Sci. Rep., Vol. 6, 27155, 2016.
5. Wang, J., R. Yang, J. Tian, X. Chen and W.A. Zhang, "A dual-band absorber with wide-angle and polarization insensitivity, " IEEE Antennas Wirel. Propag. Lett., Vol. 17, 1242–1246, 2018.
6. Kalraiya, S., R.K. Chaudhary and M.A. Abdalla, "Design and analysis of polarization independent conformal wideband metamaterial absorber using resistor loaded sector shaped resonators, " J. Appl. Phys., Vol. 125, 134904, 2019.
7. Nguyen, T.T. and S. Lim, "Wide incidence angle-insensitive metamaterial absorber for both TE and TM polarization using eight-circular-sector, " Sci. Rep., Vol. 7, 3204, 2017.
8. Munk, B.A., P. Munk and J. Pryor, "On designing jaumann and circuit analog absorbers (CA absorbers) for oblique angle of incidence," IEEE Trans. Antennas Propag., Vol. 55, 186–193, 2007.
9. Capet, N., Y.C.P. Ballesteros, A.C. Lepage, J. Sarrazin and X. Begaud, "Multi-Sector Absorbing Method and Device. U.S. Patent WO2015136121, 17 September 2015.
10. Pinto, Y., J. Sarrazin, A.C. Lepage, X. Begaud and N. Capet, "Design and measurement of a thin and light absorbing material for space applications," App. Phys. A, Vol. 115, 541–545, 2014.
11. Pinto, Y., J. Sarrazin, A.C. Lepage, X. Begaud and N. Capet, "Resistive high-impedance surfaces (RHIS) as absorbers for oblique incidence electromagnetic waves," Appl. Phys. A, Vol. 117, 693–697, 2014.

META 2023, PARIS - FRANCE, JULY 18 – 21, 2023

Transparent Passive Reflector for Coverage Enhancement in 5G Millimeter Wave

Konstantinos Dovelos[1], Panagiotis Kosmas[1], Efthymios Kallos [2], and Ragip Pala[2]

[1] Meta Materials Europe, Ap. Pavlou 10, 15123, Marousi, Athens, Greece

[2] Meta Materials Inc., QMB Innovation Centre, 42 New Road, E1 2AX, UK

[3] Meta Materials Inc, 5880 W. Las Positas Blvd, Suite 37, Pleasanton, CA 94588, USA

[*]corresponding author: kostis.dovelos@metamaterial.com

Abstract: In this work, we propose transparent passive reflectors installed on windows to boost the millimeter wave signal quality in non-line-of-sight scenarios. The transparent passive reflectors are based on a structured metal mesh called NANOWEB, which exhibits exceptionally high conductivity and optical transmissivity. Ray tracing simulations were conducted for an L-shaped office building using commercial software. Numerical results showcase that NANOWEB-made reflectors can effectively eliminate dead spots, hence rendering them an appealing alternative to conventional opaque metallic reflectors.

Fifth generation (5G) cellular networks are expected to offer multi-gigabit data rates over the millimeter wave (mmWave) band, spanning from 24 to 40 GHz [1]. Despite the abundance of unutilized spectrum beyond the sub-6 GHz band, mmWave signals suffer from high propagation losses and are susceptible to obstruction. This can lead to poor radio coverage in non-line-of-sight (NLoS) scenarios, such as dense urban and indoor propagation environments [2]. To surmount this limitation, it is customary to deploy many base stations and active repeaters (i.e., network densification) in a geographical area.

On the other hand, the advent of metamaterials has recently led to the concept of smart reflecting surfaces, which can passively redirect the impinging signals toward desired directions [3]. Thus, reflecting surfaces could be a power-efficient alternative to typical active relays for coverage enhancement. To this end, transparent reflecting surfaces have attracted the interest of both academia and industry, mainly because they can cover windows and exteriors of buildings without blocking visible light. Existing transparent conductive films such as those made by indium tin oxide (ITO), however, have several drawbacks, including poor mechanical stability and low optical transmissivity versus electrical conductivity [4]. In this work, we rely on the conductive film called NANOWEB, which is a structured mesh of submicron metal wires [5]. This structure results in superior optical and electrical properties compared to other solutions, hence making it ideal for transparent reflectors of high efficiency.

For the performance assessment, we considered a realistic office environment with NANOWEB-made reflectors on its windows. Simulations were carried out by Altair's commercially available WinProp ray-tracing software. Extensive numerical results suggest that the use of passive reflectors can significantly improve the signal quality and achievable data rate in various NLoS locations at 28 GHz. Passive reflectors could therefore play a key role in the successful deployment of mmWave indoor networks, and our presentation will discuss multiple scenarios where their deployment can be beneficial.

Acknowledgements: This study is part of a joint project with Altair Engineering Inc., which has conducted the numerical simulations using its WinProp software.

References

[1] Xiao, M., *et al*., "Millimeter wave communications for future mobile networks," *IEEE J. Sel. Areas Commun*., vol. 35, no. 9, pp. 1909-1935, 2017.

[2] Rappaport, T. S., Xing, Y., MacCartney, G. R., Molisch, A. F., Mellios, E., and Zhang, J., "Overview of millimeter wave communications for fifth-generation (5G) wireless networks—with a focus on propagation models," *IEEE Trans. Antennas Propag.*, vol. 65, no. 12, pp. 6213-6230, 2017.

[3] Di Renzo, M., *et al*., "Smart radio environments empowered by reconfigurable intelligent surfaces: How it works, state of research, and the road ahead," *IEEE J. Sel. Areas Commun*., vol. 38, no. 11, pp. 2450-2525, 2020.

[4] Silva, Z. J., Valenta, C. R., and Durgin, G. D., "Optically transparent antennas: A survey of transparent microwave conductor performance and applications," *IEEE Antennas Propag. Mag.*, vol. 63, no. 1, pp. 27-39, 2021.

[5] Saha, S. C., *et al*., "An optically transparent antenna for digital TV reception using nanoweb sub-micron wire mesh," *IEEE AP-S/URSI*, Denver, CO, USA, 2022, pp. 375-376.

META 2023, PARIS - FRANCE, JULY 18 – 21, 2023

GRIN Lens Design by Defining Phase Function and Using Optical Path Rescaling

H. Eskandari[1,2*], M. Shokooh-Saremi[1], W. Whittow[2], and T. Tyc[3]

[1]Department of Electrical Engineering, Ferdowsi University of Mashhad, Mashhad, Iran
[2]Wolfson School of Mechanical, Electrical and Manufacturing Engineering, Loughborough University, Loughborough, U.K.
[3]Institute of Theoretical Physics and Astrophysics, Faculty of Science, Masaryk University, Brno, Czech Republic
[*]Corresponding author: H.eskandari@lboro.ac.uk

Abstract: In this paper, the phase function inside a graded index dielectric is directly defined using a closed-form formula to create a rotationally symmetric lens antenna. To maintain the refractive index within realistic limits, the refractive index is modified by the optical path rescaling method. An exemplar lens antenna provides a 2 dB improvement over the Luneburg lens at 10 GHz of the same length. The lens has a maximum refractive index of 2 and a side-lobe level of -25 dB.

All-dielectric lens antennas provide a low-loss, wide-band solution and aid in achieving excellent directivity while maintaining a compact structure. The rapid development of fabrication technology has brought graded index (GRIN) solutions to the spotlight. GRIN lens antennas provide good matching and have shown the capacity to give wide bandwidths. The Luneburg lens [1] is a standard GRIN lens capable of producing scanning directional beams. This lens is often large, and a low-profile lens antenna can be built for single-beam applications. Geometrical optics (GO) and Transformation optics (TO) are the two most prevalent GRIN lens antenna design methodologies in the literature. In the latest GO-based lens antenna design, a rectangular GRIN slab is positioned in front of a point source to progressively flatten the cylindrical phase fronts [2,3]. The two-dimensional (2D) refractive index is computed in such that a ray travelling down the optical axis arrives in phase at the aperture, with the ray entering the lens obliquely. The design formula is established on the assumption that rays within the slab propagate exclusively along the optical axis, which eventually results in a phase error [2,3]. Additionally, TO has been used in the design of lens antennas and the material complexity of the transformation-optical devices is dependent on the mapping utilized. It has been shown that employing a (quasi) conformal transformation yields a GRIN dielectric medium [4-6]. When improving directivity is the intention, reflections are an inherent part of TO. The aperture's refractive index is not uniform, and reflections occur at air-lens interface. Moreover, in regions of the design domain where the mapping expands the space, the refractive index falls below unity [5]. Recently, the optical path rescaling approach has been offered as a viable remedy for this flaw [6].

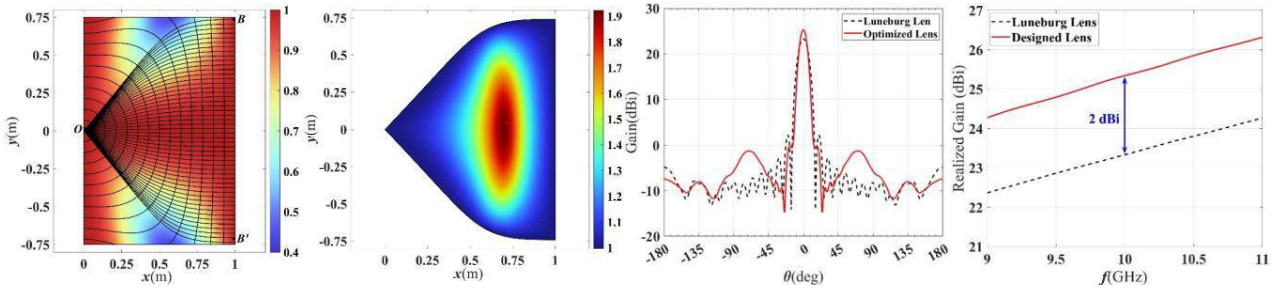
In the first step, we propose a mathematical formula for describing the phase function. This closed-form phase function formula satisfies the problem's constraints without making any unnecessary assumptions. It generates a refractive index of one at the source and the aperture, while producing a semi-circular phase front near the source and a flat phase front near the aperture.

Based on the principles of geometrical optics, the phase function of a region of space, defines the ray trajectories and the refractive index. The ray trajectories are aligned with the phase gradient and the refractive index is the absolute value of the phase gradient [1]. Now consider a 2D space within the x-y plane. Consider a point source radiating cylindrical waves from the coordinate system origin. Suppose a GRIN medium is located within $0 \leq x \leq 1$ that gradually flattens the cylindrical phase front emanating from the origin and traversing toward x=1. The phase function $S(x,y)$ of such device can be described as follows:

$$S(x,y)=rf(x)+x(1-f(x)) \tag{1}$$

where r equals $(x^2+y^2)^{1/2}$, and $f(x)$ is a suitable polynomial series. The above function must satisfy the boundary conditions of the problem. The refractive index should equal one near the source and near the aperture at x=1. Also, the phase contours should resemble cylindrical shapes near the source and should change to flattened contours near the aperture. It can be shown that having $f(x)=(2x+1)(x-1)^2$ in Eq. 1 satisfies these conditions. Figure 1(a) shows the phase function contours, the corresponding refractive index, and the ray trajectories for 50 rays. It can be seen from Fig. 1(a) that the refractive index for the regions above and below the optical axis is below one. This issue is resolved using the optical path rescaling method inside the *OAA'O* region [6]. The modified refractive index is depicted in Fig. 1(b) which is above one everywhere having a maximum value of less than two.

The designed lens antenna in Fig.1 (b) is simulated as a rotationally symmetric lens antenna in the X-band using CST. The Luneburg lens antenna with the refractive index formula of $n=(2-x^2-y^2)^{1/2}$ is chosen as the reference. Both lenses share the same length of 5 λ for λ=3 mm at the center frequency of 10 GHz. Both cases are aligned such that the optical axis is along the z-axis. The feed is a standard circular waveguide with a diameter of 23.83 mm, covering the 9–11 GHz range. The realized gain versus θ is plotted in the ϕ=0 plane for both cases in Fig. 1(c) at the center frequency of 10 GHz. The designed lens has side-lobe level (SLL) values of -25 dB compared to -21 dB for the Luneburg lens. The peak gain is increased from 23.3 dBi with the Luneburg lens to 25.4 dBi. The maximum realized gain value for both cases is plotted within the 9<f<11 GHz band in Fig.1 (d).



(a) (b) (c) (d)

Figure 1- Refractive index profile of (a) initial lens with defined phase function in Eq. 1 and (b) modified lens using optical path rescaling. (c) The realized gain patterns of the reference Luneburg and the modified lens in the ϕ=0 plane, and (d) the peak realized gain versus frequency fed with a standard circular waveguide.

This work was funded by EPSRC Grant 'ANISAT' EP/S030301/1. Also, it was supported by a postdoctoral fellowship from Iran's National Elites Foundation and Ferdowsi University of Mashhad (No. FUM-34832).

References

1. Luneburg, R. "Mathematical Theory of Optics," University of California Press, 1964.
2. Zhang, N., W. X. Jiang, H. F. Ma, W. X. Tang and T. J. Cui, "Compact high-performance lens antenna based on impedance-matching gradient index metamaterials," IEEE TAP, Vol. 67, No. 2, 1323–1328, 2019.
3. Papathanasopoulos, A., Y. Rahmat-Samii, N. C. Garcia and J. D. Chisum, "A novel collapsible flat-layered metamaterial gradient refractive-index lens antenna," IEEE TAP, Vol. 68, No. 3, 312–1321, 2020.
4. Leonhardt, U. "Optical conformal mapping," Science, Vol. 312, No. 5781, 1777–1780, 2006.
5. Aghanejad, I., H. Abiri and A. Yahaghi, "Design of high-gain lens antenna by gradient-index metamaterials using transformation optics," IEEE TAP, Vol. 60, No. 9, 4074–4081, 2012.
6. Eskandari, H. and T. Tyc, "Controlling refractive index of transformation optics devices via optical path rescaling," Scientific Reports, Vol. 9, No. 1, 1–12, 2019.

META 2023, PARIS - FRANCE, JULY 18 – 21, 2023

Time-varying OAM beams generation by a metasurface

Jingxin Zhang[1], **Peixing Li**[2], **Ray C. C. Cheung**[2], **Alex M. H. Wong**[2,3*], **and Jensen Li**[1*]

[1] Department of Physics, The Hong Kong University of Science and Technology, Clear Water Bay, Hong Kong, China
[2] Department of Electrical Engineering, City University of Hong Kong, Hong Kong, China
[3] State Key Laboratory of Terahertz and Millimeter Waves, City University of Hong Kong, Hong Kong, China
*corresponding author: alex.mh.wong@cityu.edu.hk, jensenli@ust.hk

Abstract: We demonstrate the use of a space-time-coding digital metasurface operating in the microwave regime to experimentally generate various modes of time-varying orbital angular momentum (OAM) beams. By developing a time-domain field mapping technique, we are able to observe the generated time-varying OAM. Moreover, we explore an additional higher-order twist in the wavefront structure of time-varying OAM beams based on the flexible programmability of the metasurface. These proposed time-varying OAM beams hold potential for applications in communication and particle manipulation.

The orbital angular momentum (OAM) is the component of angular momentum of Electromagnetic (EM) waves that is associated with a helical or twisted wavefront, and the helical modes are characterized by topological charge l. The recent demonstration of extreme-ultraviolet beams with time-varying OAM realized by high harmonic generation has opened new opportunities for quantum excitation control and particle manipulation [1]. However, such an approach is not easily scalable to other frequency regimes and is not flexible enough for the exploration of other time-varying OAM modes. The recently proposed space-time-coding digital metasurface with powerful and flexible programmability of space-time modulation provides us an alternative approach to generate the time-varying OAM beams and further unlock their full potential [2].

In our work, we experimentally construct and observe time-varying OAM beams using a space-time-coding digital metasurface in the microwave regime. We divide the metasurface into 8 independent azimuthal sectors for reflection phase modulation. The space-time modulation scheme is designed as in Fig. 1(b), where the coding digits "1" to "8" represent the reflection phase from 0° to 315° in every 45° and the phase distributions at different time layers result in a time-varying topological charge $l(t)$. Then a time-varying OAM beam with topological charge $l(t)$ varying in $0,\ 1,\ 2,\ 3,\ 4(-4),\ -3,\ -2,\ -1$ periodically in time is generated as shown in Fig. 1(a). Due to the flexible programmability of the metasurface, we can generate different modes of the time-varying OAM beams by adding a time-dependent initial phase in each time layer. In Fig. 1(b), the designed zero phase (coding digit "1") positions marked by the black stars lead to a higher-order twist in the wavefront structure of the time-varying OAM beam. Such a higher-order twist can be described by a winding number w and regarded as an additional degree of freedom in constructing the time-varying OAM beams, which can be used in structured light construction, information encoding, and the rotational Doppler effect.

For experimental demonstration of the time-varying OAM beams generated by the space-time-coding digital metasurface, we directly map the time-varying OAM field including amplitude and phase patterns at various instants of time. A scanning probe and a reference probe are used to measure the time-domain scattering parameters at different positions in the near field. The results from the reference probe can be used to align the time-domain signals probed at different positions. After the synchronization process, we obtain the measured near-field amplitude and phase patterns of the time-varying OAM beams at different instants of time in one period as seen

in Fig. 1(c), showing the time-varying topological charge $l(t)$ in consecutive integer values. The change of OAM is clearly observable in the phase patterns as the spiral fringes vary in time. In addition, the OAM spectrum analysis is performed using OAM mode decomposition on the measured field patterns, demonstrating the high mode purity of the generated time-varying OAM and the designed higher-order twist in the wavefront structure.

In summary, we have experimentally generated time-varying OAM beams by a space-time-coding digital metasurface in the microwave regime. Different modes of time-varying OAM beams can be generated by designing a high-order twist in wavefront structure. We develop a time-domain field mapping technique to dynamically map the time-varying OAM field patterns and evaluate them by performing the OAM spectrum analysis. Our proposed time-varying OAM beams provide new routes in in communication and particle manipulation

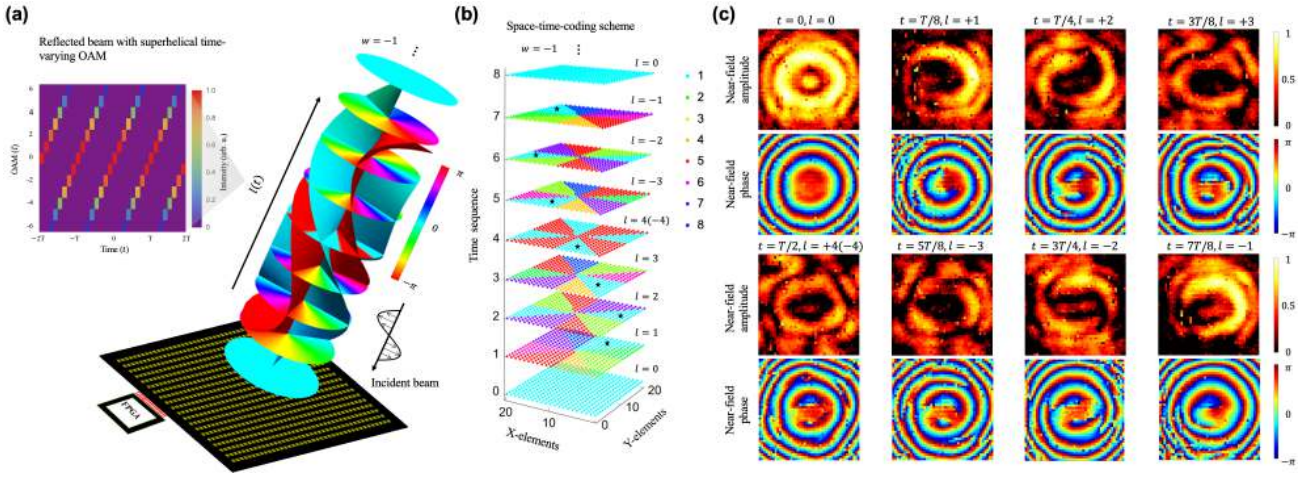


Figure 1. Time-varying OAM beam generation and experimental results. (a) The schematic of time-varying OAM beam generation by a space-time-coding digital metasuraface. (b) The space-time coding scheme of the metasurface. (c) The measured amplitude and phase patterns of the generated time-varying OAM at different instants of time.

Acknowledgment: This work is supported by the Hong Kong Research Grants Council with project number R6015-18 and C6012-20G.

References

1. Rego, L., K. M. Dorney and N. J. Brooks, "Generation of extreme-ultraviolet beams with time-varying orbital angular momentum," Science, Vol. 364, No. 6447, eaaw9486, 2019.
2. Zhang, L., X. Chen, and S. Liu, "Space-time-coding digital metasurfaces," Nat. Commun., Vol. 9, No. 1, 1–11, 2018.
3. Zhang, J., P. Li, and J. Li, "Generation of superhelical time-varying OAM beam with space-time-coding digital metasurface," arXiv:2210.06941, 2022.

A Non-Interleaved Bidirectional Janus Metasurface with Full-Space Scattering Channels

Guanyu Shang[1], Zihan Zhao[1], and Xumin Ding[1*]

[1] Advanced Microscopy and Instrumentation Research Center, School of Instrumentation Science and Engineering, Harbin Institute of Technology, Harbin 150080, China
[*]xuminding@hit.edu.cn

Abstract: Our metasurface with broken mirror symmetry can fully exploit four independent information channels under opposite propagation directions. A series of proof-of-concept is constructed to validity of our methodology, and the simulations and experimental results further show that the proposed non-interleaved bidirectional metasurface can provide an attractive platform for various applications, ranging from structured light conversion, optical imaging, multifunctional optical information processing and others.

Metasurface, composed of two-dimensional artificial meta-atoms, offers the complete control of light, including amplitude [1-3], phase and polarization [7-9] within a platform of various merits such as thinness, easy fabrication and low loss, compared to conventional optical elements. A plethora of exciting applications are demonstrated, such as optical vortex beam generation, energy absorption beam deflection and all-optical image processing, just to name a few. The demand to process the increased information loads with more compact devices in modern optics calls for multifunctional metasurfaces. For instance, the transmission-type metasurface can perform the multiplexing of wavelength, polarization, angle and angular momentum of light, thus enriching the information processing capabilities. Recently, the capacity limit of a single transmissive metasurface as characterized with the Jones matrix has been demonstrated[36], which leads to a natural question of whether one can further add more capacity atop it. To answer this, we note such claims only hold true under the assumption of a metasurface working in half-space, either in reflection or transmission sides, while leaving full-space scattering channels overlooked.

Herein, we demonstrate a transmission-reflection-integrated Janus metasurface, supporting independent functions in both reflection and transmission channels with different incident directions at the same frequency. Importantly, meta-atoms with multilayer composites have broken mirror symmetry, which allows different transmission performances propagating in opposite directions for our demonstrated extreme wave manipulations. Besides, all meta-atoms contribute to the scattering, thus free of segmented or interleaved arrangement (Figures 1a and 1b) and suggesting the full utilization of the metasurface. As a proof of concept, for the forward and backward propagations of the y-polarized incidence, co-polarized reflection and cross-polarized transmission channels in two directions can be independent control and produce four different holographic imaging effects with broken mirror symmetry (Figure 1c). Moreover, protected by reciprocity, the reflected cross-polarized component can show the same holography with the transmitted cross-polarized component when propagation direction changes, suggesting six concurrent operation channels in our designs. Our Janus metasurface with the integration of multifunctional channels in full spaces suggests a new regime of meta-devices with high function capacity and compactness, of great potential in information encryption, optical anti-counterfeiting and others.

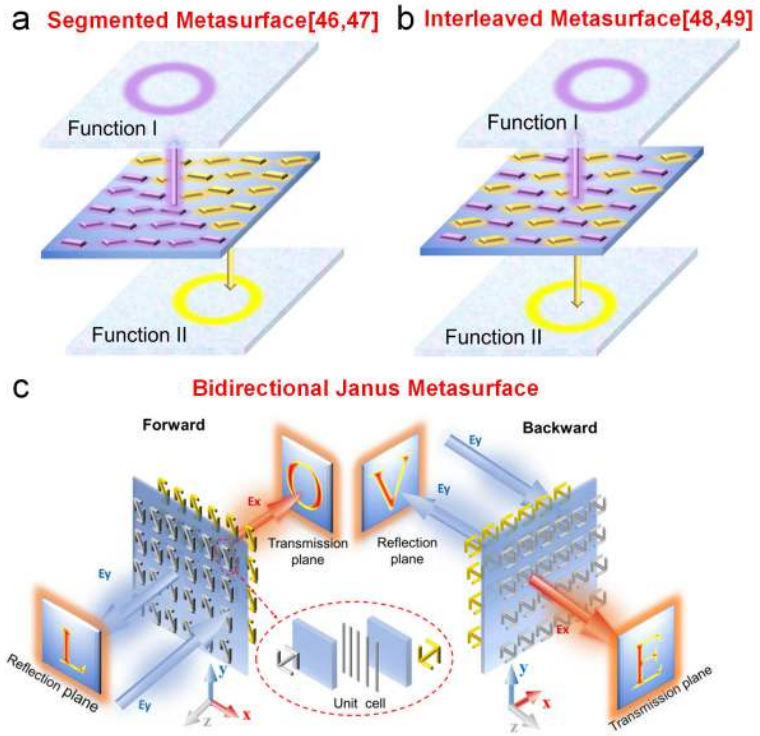


Figure 1. Schematic diagram of the multifunctional metasurface. (a) Illustration of the segmented metasurface. (b) Illustration of the interleaved metasurface. (c) Schematic illustration of the proposed non-interleaved multifunctional metasurface.

References

1. Y. Mu, M. Zheng, J. Qi, et al., "A large field-of-view metasurface for complex-amplitude hologram breaking numerical aperture limitation," Nanophotonics, Vol, 9, No. 16, 4749-4759, 2020.
2. R. Y. Wu, L. Bao, L. W. Wu, et al., "Independent Control of Copolarized Amplitude and Phase Responses via Anisotropic Metasurfaces," Advanced Optical Materials, Vol. 8, No. 11, 1902126, 2020.
3. K. Fan, Y. Jonathan, Y. Suen, et al., "All-dielectric metasurface absorbers for uncooled terahertz imaging," Optica, Vol. 4, No. 6, 601-604. 2017.
4. G. Shang, H. Li, Z. Wang, et al., "Coding metasurface holography with polarization-multiplexed functionality," Journal of Applied Physics, Vol. 129, No. 3, 035304, 2021.
5. K. Zhang, Y. Yuan, X. Ding, et al., "Polarization‐Engineered Noninterleaved Metasurface for Integer and Fractional Orbital Angular Momentum Multiplexing," Laser & Photonics Reviews, Vol. 15, No. 1, 2000351, 2020.
6. P. C. Wu, W. Zhu, Z. X. Shen, et al., "Broadband Wide-Angle Multifunctional Polarization Converter via Liquid-Metal-Based Metasurface," Advanced Optical Materials, Vol. 5, No. 7, 1600938, 2017.
7. Y. Bao, L. Wen, Q. Chen, et al., "Toward the capacity limit of 2D planar Jones matrix with a single-layer metasurface," Science advances, Vol. 7, No. 25, eabh0365, 2021.

META 2023, PARIS - FRANCE, JULY 18 – 21, 2023

Reconfigurable Intelligent Surface as MIMO

S. Droulias[1*] and A. Alexiou[1]

[1]Department of Digital Systems, University of Piraeus, Piraeus 18534, Greece

[*]corresponding author: sdroulias@unipi.gr

Abstract: The Reconfigurable Intelligent Surface (RIS) is often treated either as a collection of point scatterers with properties similar to antennas in an equivalent MIMO communication link or as a continuous radiating surface, which is subsequently discretized. In this work we investigate the connection between the two approaches, we analytically find the factor that renders them equivalent and we demonstrate our findings with examples of RIS elements modeled as antennas with commonly used radiation patterns and properties consistent with antenna theory.

A Reconfigurable Intelligent Surface (RIS) redirects and possibly modifies the properties of incident waves, with the aim to restore non-line-of-sight communication links. Usually, the RIS is treated as a continuous radiating surface or sheet that locally satisfies the boundary conditions, ensuring that an incident plane wave is reflected towards the desired direction [1,2]. Alternatively, due to the inherently discrete nature of the RIS elements, it is more natural to treat the RIS as a planar distribution of scatterers and, in particular, point scatterers that bear the properties of conventional antennas, such as gain and directivity [3-5]. Because the former approach involves a continuous radiating sheet of infinite extent that is subsequently discretized, the question is how well the local RIS elements retain the properties prescribed by the continuous infinite radiating sheet upon discretization and what is the effect of the finite RIS size. Because the latter approach involves the collective response of individual scatterers, therefore by definition implementing a finite-sized RIS, the question is how well the properties of the individual antenna-like scatterers can reproduce the actual field radiated from the RIS.

In this work, we demonstrate the equivalence between the two approaches. We analyze each approach separately and we find the connection between the two, on the basis that they must both account for elements with the same properties, i.e. polarizabilities, guaranteeing the same scattered wave. We investigate how the properties of the continuous sheet are related to the properties of point scatterers that bear characteristics consistent with the antenna theory, and we discuss commonly used models in recent theoretical works. We find that, overall, the treatment of the RIS as point scatterers may overestimate the scattered field and, therefore, a correction factor must be taken into account. By analyzing the correction factor by means of realistic radiation patterns, we demonstrate how the RIS performance is affected by design properties of the RIS elements, such as gain, directivity and inter-element coupling, and we discuss the implications on the predicted power at the receiver.

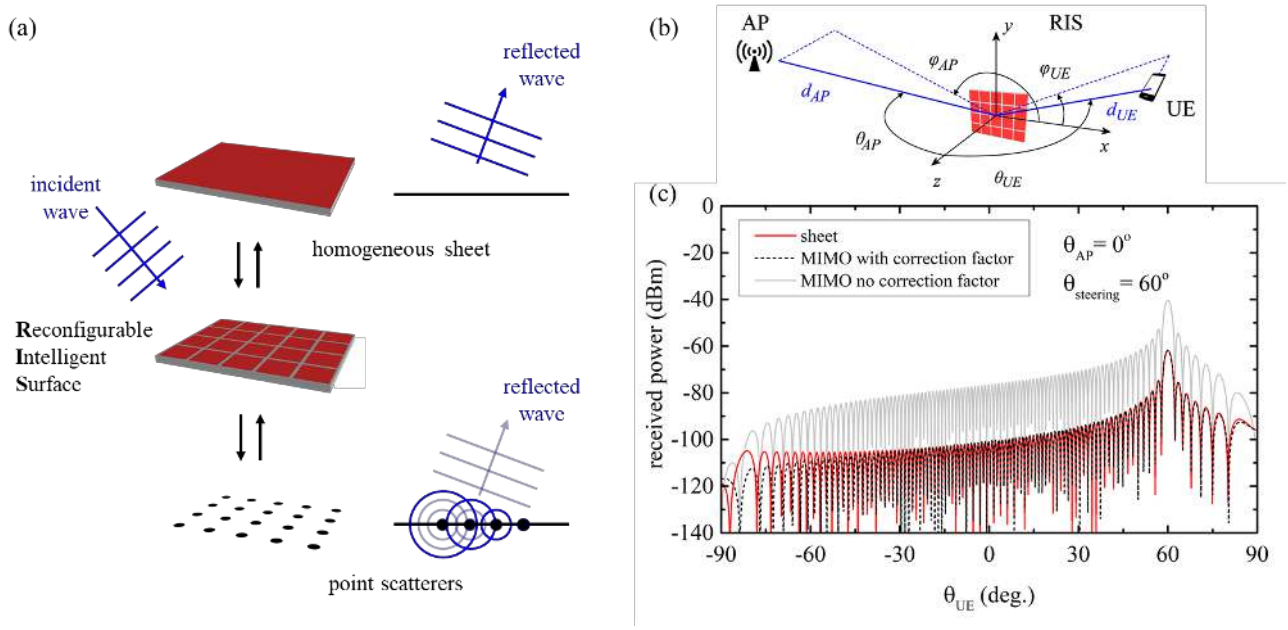


Figure 1. RIS as sheet and MIMO. (a) Schematic representation of a RIS steering an incident wave towards a prescribed direction. The RIS can be analyzed as a homogeneous radiating sheet or, equivalently, as a distribution of point scatterers that bear the properties of conventional antennas. (b) System model of RIS-aided link, illustrating the positions and relative angles between the Access Point (AP), RIS and User Equipment (UE). (c) Equivalence between the sheet and MIMO model for RIS elements modeled as antennas with radiation pattern $U_0(\theta,\varphi) = \cos^2\theta$ and properties consistent with antenna theory. The AP transmitts a TE-polarized wave with amplitude 1 V/m, which impinges normally on a lossless RIS ($\theta_{AP} = 0^o$). The RIS steers the wave on the xz plane at angle $\theta_{steering} = 60^o$, maximizing the received power when $\theta_{UE} = 60^o$. Without the correction factor (solid gray line) the antenna model overestimates the analytically predicted power (solid red line); the sheet-MIMO equivalence is restored upon incorporating the correction factor (dashed black line). The RIS is operating at 150 GHz and consists of 250×250 elements with periodicity $\lambda/5$, forming a reflecting surface of total size 10 × 10 cm^2. The received power is calculated at distance 20 m from the RIS, as a function of the angle θ_{UE} that marks the UE position.

Acknowledgements

This work has received funding from the European Commission's Horizon 2020 research and innovation programme ARIADNE under grant agreement No. 871464.

References

1. Tang, W. et al., "Wireless Communications With Reconfigurable Intelligent Surface: Path Loss Modeling and Experimental Measurement," in IEEE Transactions on Wireless Communications, vol. 20, no. 1, 421-439, 2021.
2. Boulogeorgos, A. -A. A. and Alexiou, A., "Coverage Analysis of Reconfigurable Intelligent Surface Assisted THz Wireless Systems," in IEEE Open Journal of Vehicular Technology, vol. 2, 94-110, 2021.
3. Dovelos, K. et al., "Electromagnetic Modeling of Holographic Intelligent Reflecting Surfaces at Terahertz Bands," 2021 55th Asilomar Conference on Signals, Systems, and Computers, Pacific Grove, CA, USA, 415-420, 2021.
4. Stratidakis, G., Droulias, S. and Alexiou, A., "Analytical performance assessment of beamforming efficiency in reconfigurable intelligent surface-aided links," IEEE Access, vol. 9, 115 922–115 931, 2021.
5. Di Renzo, M., Danufane, F. H. and Tretyakov, S., "Communication Models for Reconfigurable Intelligent Surfaces: From Surface Electromagnetics to Wireless Networks Optimization," in Proceedings of the IEEE, vol. 110, no. 9,1164-1209, 2022

Cross-wavelength Metasurface Based on Carbon Nanotubes

Jin Zhang[1*], Peng Liu[1], and Zhipei Sun[1]

[1]QTF Centre of Excellence, Department of Electronics and Nanoengineering, Aalto University, FI-02150 Espoo, Finland.
[*]Corresponding author: jin.zhang@aalto.fi

Abstract: Multifunctional metasurfaces have garnered significant interest from both academia and industry in the past decade. However, achieving cross-wavelength functionalities remains a challenge due to the strong dispersion of passive materials. In this study, we propose a novel concept of cross-wavelength metasurface that integrates various functionalities with multispectral channels. As proof of concept, we demonstrate optical transparency, Thz diffusion and microwave selectivity simultaneously in a carbon nanotube based metasurface through a laser micromachining technique.

Metasurfaces, which are a new class of subwavelength ultrathin flat components, have brought disruptive innovations to the electromagnetic and nanophotonic fields[1]. Despite of the maturing developments of customized metasurfaces in specific scenarios, limited working wavelength and fixed wave-manipulation emerge as the common defects. To overcome these challenges, cross-wavelength metasurfaces with multispectral capability have been proposed to expand the engineering space for processing concurrent tasks in different channels . However, the interaction of nanostructures between long and short wavelength has not been fully underutilized, resulting in a vacuum region in the terahertz band between microwave and optical regions. To our knowledge, a real cross-wavelength multifunctional metasurface has not been achieved thus far.To address this, we propose a new mechanism for achieving multi-functionalities across the whole frequency band, including microwave, THz and optical region, using interacted layered metasurfaces based on carbon nanotubes (CNT). T The conceptual features of the designed metasurface are pictorially depicted by covering the window of a car (Fig. 1A), offering the challenging compatibility for optical transparency, THz diffusion and microwave selectivity simultaneously. The schematic view in Fig. 1B shows that it is composed of a five-layered stack including a CNT coding array as the top layer, a 175μm-thick transparent polycarbonate spacer as the second layer, a CNT patch structure as the third layer, a 2mm-thick transparent quartz substrate as the fourth layer, and the CNT fishnet structures as the bottom layer. The CNT is made of transparent double-walled carbon nanotubes doped by AuCl3. This selection of materials ensures high transmission of visible light in the assembled metasurface.

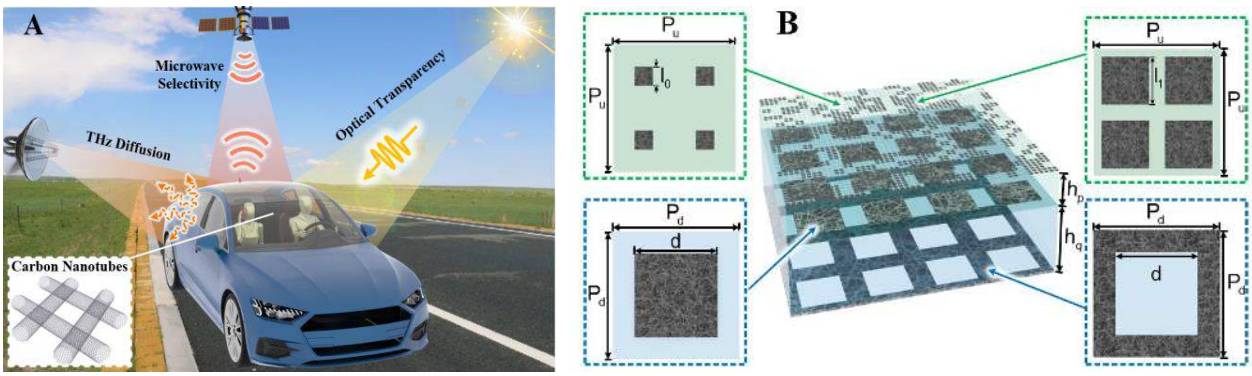


Figure 1 (A) Conceptual features and (B) schematic depiction of the cross-wavelength metasurface.

We start the design by engineering the electromagnetic response for microwave selectivity. Figure 2A gives a schematic representation of the unit cell of proposed metasurface and its physical mechanism can be demonstrated by the equivalent circuit model (ECM) shown in Figure 2B, where Z_p and Z_f represent the characteristic impedance of the CNT patch and fishnet structures, respectively. We plot the reflection and transmission spectra in Figure.2C, which shows the good agreement between simulated and calculated results. It is seen that the reflection amplitude was minimized to about -45 dB, while the transmission reached its maximum value at 7 GHz. This demonstrated that the proposed metasurface formed a selective electromagnetic window in the microwave region, which only allowed the transmission of EM waves at specific frequencies and reflected other noise waves. Next, we demonstrated the performance of the proposed metasurface in terms of THz diffusion, as shown in Figure 3. The metasurface was divided into three parts: the THz coding array providing 1 bit phase random distribution, the polycarbonate (PC) and quartz layers acting as dielectric layers, and the CNT patch/fishnet structures reflecting all the incident THz waves. By optimizing the metasurface using genetic algorithm, we were able to achieve diffuse scattering, as shown in Figure 3B and C, thereby demonstrating the effectiveness of the design.

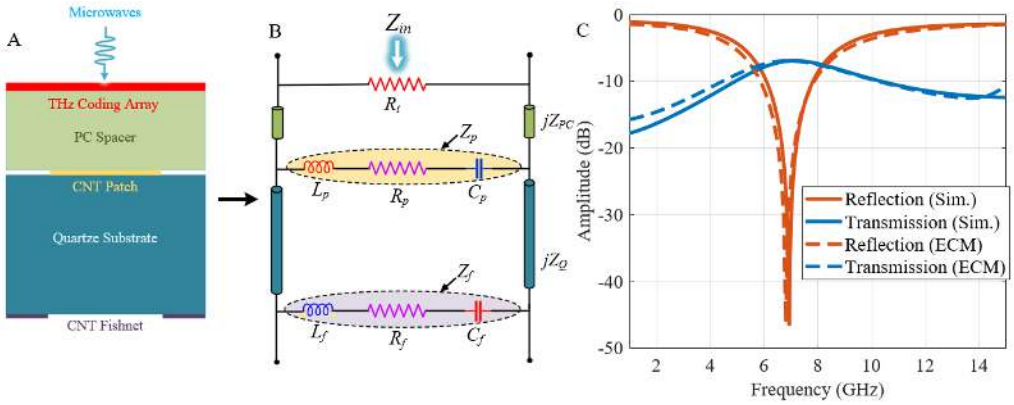


Figure 2 (A) Unit cell schematic and (B) equivalent circuit model of the proposed metaasurface. (C) Reflection and transmission spectra at microwave frequencies.

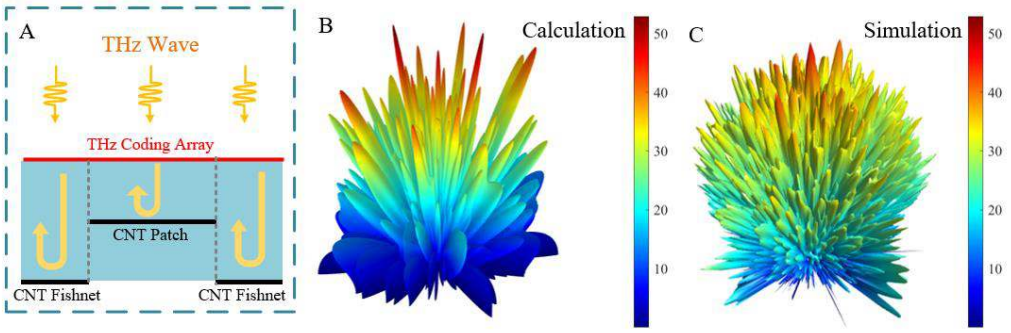


Figure 3 (A) Schematic of the proposed metasurface. (B) Calculated and (C) simulated far-field patterns at 0.84THz.

References

1. Yu N. and Capasso, F., "Flat optics with designer metasurfaces," *Nat. Mater.* Vol. 13, 139–150, 2014.
2. Liu, H., et al., "Enhanced high-harmonic generation from an all-dielectric metasurface," *Nat. Phys.*, Vol. 14, No. 10, 1006-1010, 2018.
3. Xu, S., et al. "Cross-wavelength invisibility integrated with various invisibility tactics," *Sci. Adv.*, Vol. 6, No. 39, eabb3755, 2020.

Classical and Quantum Phononics

Single electron spin dynamics in a two-electron double quantum dot under a nonequilibrium phonon environment

K. Kuroyama[1,2,*], S. Matsuo[2], S. Yabunaka[3], S. R. Valentin[4], A. Ludwig[4], A. D. Wieck[4], Y. Tokura[5], and S. Tarucha[2]

[1]Institute of Industrial Science, The University of Tokyo, Japan
[2]Center of Emergence Material (CEMS), RIKEN, Japan
[3]Kyushu University, Japan
[4]Ruhr-Universität Bochum, Germany,
[5]University of Tsukuba, Japan,
[*]corresponding author: kuroyama@iis.u-tokyo.ac.jp

Abstract:
We have experimentally studied the charge-spin cooperative dynamics of two-electron states in a GaAs double quantum dot (DQD), which are driven in a nonequilibrium phonon environment created by a nearby QD-based phonon source. The spin-flip rates increase remarkably, which is explained by the simultaneous action of the spin-orbit and electron-phonon interactions. Furthermore, we found the imbalance of the occupation probabilities between antiparallel/parallel spin states, which is explained by the thermal nonequilibrium of the phonon environment in the DQD.

Thermodynamics in quantum mesoscopic systems has long been studied as one of the central concepts in solid-state physics. In particular, temperature gradients over mesoscopic structures have realized various kinds of thermodynamic functions such as heat engines and heat valves, which are useful for improvements of thermoelectric conversion and heat control by electrical means in mesoscopic devices. For the demonstration of a heat engine in nano-structure devices, a semiconductor quantum dot (QD) is recognized as one of the best platforms because a dot can be coupled to the multiple electron reservoirs with the different electron temperatures. However, none of QD-based heat engines discussed in previous studies is driven by heat reservoirs at different lattice temperatures. This is probably because a lattice temperature gradient over a few hundred nanometer distances, order of a QD size is technically difficult to be created. A QD-based local phonon source has already been utilized to study phonon-assisted electron tunneling in the Coulomb blockade QD but not yet the effects of thermodynamics [1].

In this work, we concentrated on both the charge and spin dynamics of two-electron states in a GaAs lateral double QD (DQD), that are driven by a nonequilibrium phonon environment created by a QD-based phonon source located at the one side of the DQD (see Fig. 1(a) for the sample geometry) [2]. Note that the maximum energy of the phonon is determined by the applied bias voltage as eV_{PS}. The DQD is adjusted in such a way that the ground states of the (1,1) and (0,2) charge states are resonant, and the possible spin states in the resonant DQD are depicted in the diagram in Fig. 1(b). To discuss the phonon-induced charge-spin dynamics at a single electron level, we implement a real-time charge sensing technique using a nearby QD, which is combined with the Pauli spin blockade effect of a DQD. Thereby, we count the number of the spin-flip tunneling events in the two-electron DQD set in the spin blockade regime under phonon radiation. Our experimental results show that the spin-flip rate remarkably increases when the irradiated phonon energy exceeds the lowest excitation energy in the DQD (see Fig. 2(a)). The increase in the spin-flip rate can be explained by the phonon-mediated inter-dot tunneling process and the intra-dot spin-flip process involving the excited states (see Processes I and II illustrated in Fig. 2(b), respectively). Furthermore, we discovered the significant imbalance in the occupation probabilities between the antiparallel and parallel spin configurations of the (1,1) charge state (see Fig.

2(c)). These experimentally observed behaviors of the spin dynamics are successfully reproduced by our recent theoretical calculations, which take into account the spin-orbit and electron-phonon interactions in the DQD under the nonequilibrium phonon environment. Our theoretical calculation indicates that the imbalance of the occupation probability between parallel and anti-parallel spin configurations shown in Ref. [2] is created not just by the phonon temperature increase but the phonon temperature gradient in the DQD system.

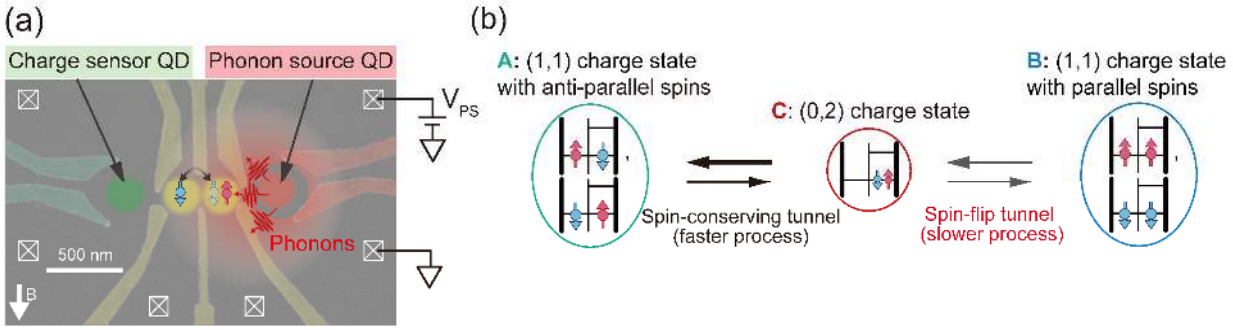


Fig. 1. (a) Geometrical configuration of our GaAs DQD sample. The DQD is formed on the two yellow circles, and the charge sensor is placed on the left green circle. The phonon source locates on the right red circle, on which the DC bias voltage V_{PS} is applied. (b) Transition diagram in a resonant two-electron DQD. States A and C (B and C) are connected by the spin-conserving (spin-flip) tunneling processes.

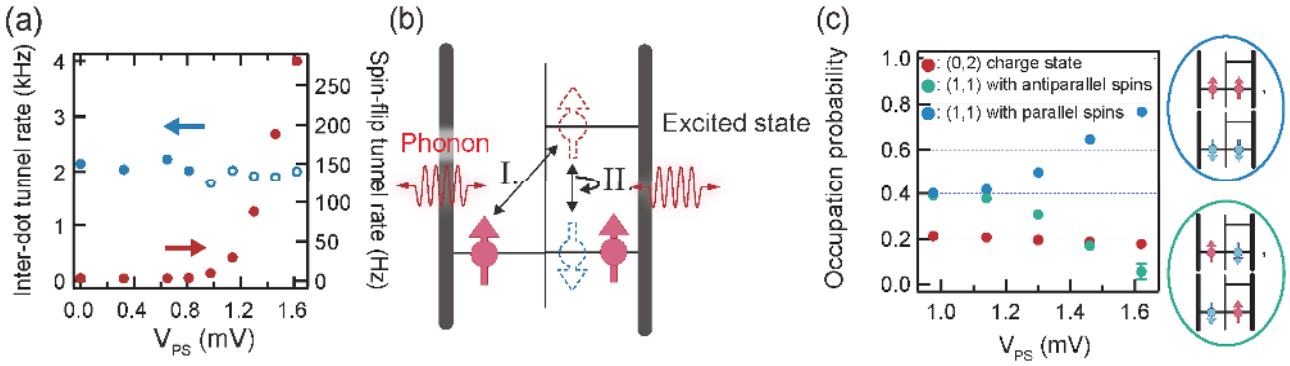


Fig. 2. (a) Spin-conserving inter-dot tunnel rate from state C to A (blue) and the spin-flip tunnel rate from state B to C (red) plotted as a function of V_{PS}. (b) Energy level diagram in a DQD, which explains the phonon-induced spin-flip tunneling process involving the excited state. (c) Occupation probabilities of the (0,2) charge state and anti-parallel and parallel spin states of the (1,1) charge state, plotted by red, green, and blue dots, respectively. For the (1,1) charge state, as V_{PS} is larger, the occupation probability of parallel spin configurations increases, while that of anti-parallel spin configurations decreases.

References

[1] G. Granger, D. Taubert, C. E. Young, L. Gaudreau, A. Kam, S. A. Studenikin, P. Zawadzki, D. Harbusch, D. Schuh, W. Wegscheider, Z. R. Wasilewski, A. A. Clerk, S. Ludwig, and A. S. Sachrajda, Nature Physics volume 8, pages522–527, 2012.

[2] K. Kuroyama, S. Matsuo, J. Muramoto, S. Yabunaka, S. R. Valentin, A. Ludwig, A. D. Wieck, Y. Tokura, and S. Tarucha, Physical Review Letter 129, 095901, 2022.

META 2023, PARIS - FRANCE, JULY 18 – 21, 2023

Quantum interference of electron-phonon coupled states in semiconductors using phase-locked femtosecond pulses

K. G. Nakamura[1,2*], I. Takagi[1,2], Y. Kayanuma[1,3]

[1]Laboratory for Materials and Structures, Institute of Innovative Research, Tokyo Institute of Technology, Japan

[2]Department of Materials Science and Engineering, Tokyo Institute of Technology, Japan

[3]Graduate School of Science, Osaka Metropolitan University, Japan

[*]corresponding author: nakamura@msl.titech.ac.jp

Abstract: Electronic and phononic coherence has been studied in an n-type GaAs crystal using transient reflection measurements with relatively phase-locked femtosecond pulses at 90 K. The interference fringes due to electronic and phononic coherence are observed in the coherent phonon amplitude as a function of pump-pump delays. The collapse and revival feature was observed in electronic coherence and well represented in the theoretical calculations. The electronic decoherence time was estimated to be 23 ±0.3 fs.

Quantum coherence, which enables a superposition state, is one of the most important features of quantum mechanics. Quantum coherence persits in an isolated system but disappears rapidly in condensed matter. Quantitative values of the decoherence time and the decoherence mechanism in condensed matter are still well understood. We are investigating the quantum coherence, in particular electronic and phononic coherence, in semiconductors by developing ultrafast quantum-path interferometry.

We have studied quantum interference (electronic and phononic coherence) between electron-phonon coupled states in n-type GaAs (001) excited by relatively phase-locked femtosecond pulses through changes in transient reflectivity. The sample is doped with Si at a donor concentration of 1.0×10^{18} cm^{-3} and placed in a cryostat. The pulse width is approximately 60 fs (full width at half maximum). The central energy of the pulse is 1.55 eV, slightly above the GaAs bandgap. The delay (τ) between two pump pulses was controlled with a step of approximately 300 attoseconds by using a home-built Michelson-type interferometer. At the fixed τ, a reflectivity change as a function of a pump-probe delay (T) shows a damped oscillation with ~114 fs and ~128 fs spacing, which are attributed to the longitudinal optical (LO) phonon at 8.8 THz and the LO phonon-plasmon coupling (LOPC) at 7.8 THz, respectively [1]. The 8.8 THz oscillation represents phononic coherence, and the decoherence time is estimated from its decay behavior to be 3.4 ps at 90 K. The amplitude of the LO phonon is determined from the Fourier transformed spectrum.

The LO phonon amplitude ($A(\tau)$) as a function of the pump-pump delay τ shows fringes with ~2.7 and ~114 intervals in the parallel polarized condition (Fig. 1 (a)). The sample temperature is set to be 90 K. The fast and slow fringes are due to electronic and phononic coherence, respectively. The electronic coherence continues longer than the pump-pulse duration and exhibits a collapse and revival feature characteristic of the impulsive stimulated Raman scattering (ISRS) pathway [1]. At 45 degrees condition (Fig. 1 (b)), both the fast and slow fringes are observed and the additional splitting feature is found on the fast fringe pattern [2]. On the other hand, in the perpendicularly polarized condition (90 degrees, Fig. 1 (c)), only the slow fringe is observed [3].

We have constructed a simple quantum mechanical model for the generation of LO phonons by double-pulse excitation [4]. In the model, the system consists of two electronic bands and a harmonic oscillator for phonons.

The Raman tensor is used for the electron-phonon coupling. We use a dipole interaction between the system and optical pulses (classical electric field) and the rotating wave approximation. The time evolution of the system is calculated via a quantum master equation with second order perturbation. Theoretical calculations using ISRS paths give good agreement with the experimental data for three polarized conditions. The fast fringe corresponding to the electronic coherence is due to the ISRS path in which photo-excitation and de-excitation are induced by pump 1 and 2, respectively. On the other hand, the slow fringe corresponding to phononic coherence is due to interference between coherent phonons induced by each pump 1 and pump 2 (photoexcitation and de-excitation occur within one pulse). In addition, the calculation predicts that the splitting in the collapse and revival feature of electronic coherence at the 45-degree condition depends on the electronic decoherence time. From the splitting, the electronic decoherence time is estimated to be 23 ±0.3 fs in n-GaAs at 90 K.

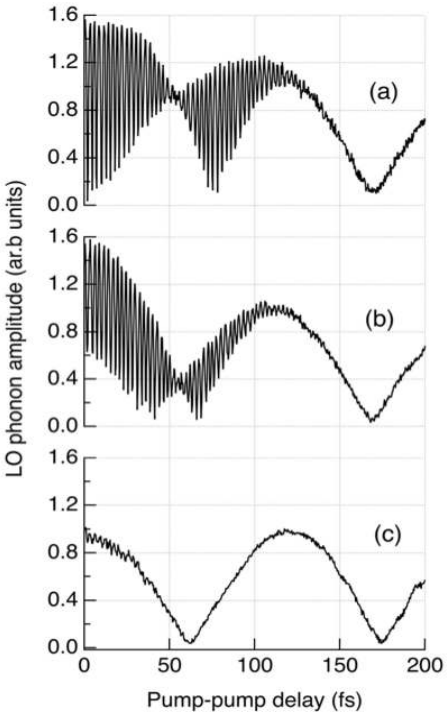


Fig. 1 LO phonon amplitude as a function of pump-pump delay at relative polarization angle of (a) 0, (b) 45, and (c) 90 degrees. Sample temperature is 90 K.

Acknowledgements: This work is supported by JSPS KAKENHI 19K22141, 21K18904, 22J23231, and 22H01984, and by Design & Engineering by Joint Inverse Innovation for Materials Architecture, MEXT, and MSL corporative research project.

References

1. Nakamura, K. G., K. Yokota, Y. Okuda, R. Kase, T. Kitashima, Y. Mishima, Y. Shikano, and Y. Kayanuma, “Ultrafast quantum-path interferometry revealing the generation processes of coherent phonons”, Phys. Rev. B, Vol. 99, 180301(R), 2019.
2. Takagi, I., Y. Kayanuma, and K. G. Nakamura (to be published).
3. Matsumoto, M., T. Kitashima, T. Maruhashi, I. Takagi, Y. Kayanuma, and K. G. Nakamura, “Coherent control of optical phonons in GaAs by relative-phase-locked optical pulses under perpendicular polarized conditions” Solid State Commun., Vol. 327, 114215, 2021.
4. Takagi, I., Y. Kayanuma, and K. G. Nakamura, “Theory for coherent control of longitudinal optical phonons in GaAs using polarized optical pulse with relative phase locking” Phys. Rev. B, Vol. 104, 134201, 2021.

Generation of entangled electron-photon-phonon states in nanocavity-QED systems

M. Tokman[1], M. Erukhimova, Q. Chen[2], and A. Belyanin[2*]

[1]Department of Electrical and Electronic Engineering, Ariel University, Israel
[2]Department of Physics & Astronomy, Texas A&M University, USA
[*]corresponding author: belyanin@tamu.edu

Abstract: Many molecular, quantum-dot, and optomechanical nanocavity-QED systems demonstrate strong nonlinear interactions between electrons, photons, and phonon modes. We show that such systems can be described by a universal model in the vicinity of the nonlinear resonance involving all three degrees of freedom. We solve the nonperturbative quantum dynamics in the strong-coupling regime, taking into account quantization, dissipation, and fluctuations of all fields. Strong coupling at the nonlinear resonance leads to tripartite quantum entanglement and distinct emission spectra.

Nonlinear optical interactions acquire qualitatively new features in the strong-coupling regime of cavity QED, especially when utilizing an extreme field localization achievable in nanophotonic cavities. The dynamics becomes especially interesting when the strong coupling regime is realized at the nonlinear resonance between three or more degrees of freedom. One possible example where it can be realized is a molecule or an ensemble of molecules in a plasmonic nanocavity, when molecular vibrations modulate the electron transition frequency. This coupling is typically introduced via the Huang-Rhys theory and is often used to describe not only molecules but also the effect of phonons on the coupling of a quantum dot or an optically active defect to the cavity field. When the strength of such a nonlinear three-wave interaction is higher than the dissipation rates, entangled electron-photon-phonon states of GHZ type are formed. Another route to the nonlinear resonance is cavity optomechanics, where mechanical oscillations of a cavity parameter modulate the frequency of the photon cavity mode. We show how these very different physical models of electron-photon-vibrational coupling can be mapped onto the universal parametric Hamiltonian, independently on the specific physical mechanism of coupling. When solving for the quantum dynamics we include the effects of dissipation and fluctuations for all degrees of freedom. The effects of the phonon reservoir lead to qualitatively new features and rich multi-peak structure in both photon and phonon emission spectra at the nonlinear resonance that are not present in the standard Rabi oscillations regime.

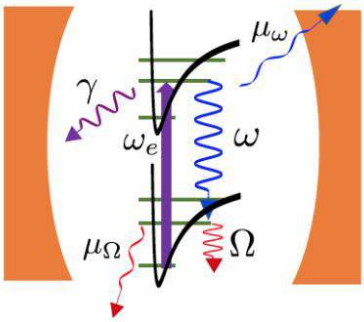


Figure 1. A sketch of the nonlinear resonance for a molecule in a cavity showing the nonlinear parametric decay of the electron excitation at frequency ω_e into a cavity mode photon at frequency ω and a phonon of a given vibrational mode at frequency Ω.

References

1. Tokman, M., M. Erukhimova, Q. Chen, and A. Belyanin, The universal model of strong coupling at the nonlinear parametric resonance in open cavity-QED systems, Phys. Rev. A, Vol. 105, 053707, 2022.
2. Tokman, M., M. Erukhimova, Y. Wang, Q. Chen, and A. Belyanin, Generation and dynamics of entangled fermion-photon-phonon states in nanocavities, Nanophotonics, Vol. 10, 491, 2021.

Engineering optomechanical and nonlinear effects in nanostructured silicon photonics

P. Nuño Ruano[1], J. Zhang[1,2], T. T. D. Dinh[1], D. González-Andrade[1], X. Le Roux[1], M. Montesinos-Ballester[1], C. Lafforgue[1], D. Medina-Quiroz[1], D. Benedikovic[3], P. Cheben[2], S. Edmond[1], E. Herth[1], D. Bouville[1], N. D. Lanzillotti-Kimura[1], D. Marris-Morini[1], E. Cassan[1], L. Vivien[1], and C. Alonso-Ramos[1]

[1] *Université Paris-Saclay, CNRS, Centre de Nanosciences et de Nanotechnologies, Palaiseau, France*
[2] *National Research Council Canada, Ottawa, Canada*
[3] *University Science Park, University of Zilina, Zilina, Slovakia*

Abstract: Periodic subwavelength silicon patterning opens new degrees of freedom to control the propagation of light and sound in silicon photonic circuits. In this invited presentation, we will show our most recent results on leveraging silicon nanostructuration for optomechanical and nonlinear applications.

Brillouin scattering, i.e. the nonlinear interaction between optical and mechanical fields inside a material, has generated great scientific interest for its numerous applications in communications, sensing and quantum technologies. However, efficient Brillouin interactions require simultaneous confinement of optical and mechanical modes. Such optomechanical confinement is challenging in SOI waveguides due to a strong phonon leakage towards the silica cladding. On the other hand, the absorption of the silica cladding for wavelengths above 3.5 μm limits the use of the silicon-on-insulator (SOI) technology in the mid-infrared.

Since their first demonstration in silicon photonics [1,2], subwavelength-grating metamaterials [3, 4] have been used as a powerful tool for overcoming performance limitations of conventional silicon photonic devices. Furthermore, periodically patterning silicon with a subwavelength pitch opens new degrees of freedom to control the propagation of light and sound in silicon photonic circuits with unprecedented flexibility. In this invited presentation, we will show our most recent results on the use of subwavelength nanostructuration to control photons and phonons in integrated silicon waveguides [5,6]. We will also present the supercotinuum generation in the near-IR and mid-IR with suspended silicon waveguides [7].

These results open exciting new perspectives to exploit nonlinear and optomechanical effects with scalable silicon photonics technology, having great potential for applications in optical and wireless communications, radar, sensing, metrology and quantum technologies.

References

1. P. Cheben, D-X. Xu, S. Janz, and A. Densmore, "Subwavelength waveguide grating for mode conversion and light coupling in integrated optics," Opt. Express 14(11), pp. 4695-4702 (2016).
2. P. Cheben, P. J. Bock, J. H. Schmid, J. Lapointe, S. Janz, D.-X. Xu, A. Densmore, A. Delage, B. Lamontagne, and T. J. Hall, "Refractive index engineering with subwavelength gratings for efficient microphotonic couplers and planar waveguide multiplexers," Opt. Lett. 35(15), pp. 2526-2528 (2010).
3. P. Cheben, R. Halir, J. H. Schmid, H. A. Atwater, and D. R. Smith, "Subwavelength integrated photonics," Nature 560, pp. 565-572 (2018).
4. R. Halir, A. Ortega-Moñux , D. Benedikovic, G. Z. Mashaovich, J. G. Wangüemert-Pérez, J. H. Schmid, I. Molina-Fernández, and P. Cheben, "Subwavelength-grating metamaterial structures for silicon photonic devices," Proc. IEEE 106(12), pp. 2144-2157 (2018).
5. J. Zhang, P. Nuño Ruano, X. Le Roux, M. Montesinos-Ballester, D. Marris-Morini, E. Cassan, L. Vivien, N. D. Lanzillotti-Kimura, and C. Alonso Ramos, "Subwavelength control of photons and phonons in release-free silicon optomechanical resonators," ACS Photonics 9(12), pp. 3855-3862 (2022).
6. P. Nuño Ruano, J. Zhang, D. Melati, D. González-Andrade, X. Le Roux, E. Cassan, D. Marris-Morini, L. Vivien, N. D. Lanzillotti-Kimura, C. Alonso-Ramos, "Genetic optimization of Brillouin scattering gain in subwavelength-structured silicon membrane waveguides," Opt. Laser Technol. 161, p. 109130 (2023).
7. C. Lafforgue, M. Montesinos-Ballester, T.T.D. Dinh, X. Le Roux, E. Cassan, D. Marris-Morini, C. Alonso-

Ramos, L. Vivien, “Supercontinuum generation in silicon photonics platforms,” Photonics Res., Vol. 10, No. 3, A43-A56, 2022.

META 2023, PARIS - FRANCE, JULY 18 – 21, 2023

Nano-optomechanical systems for ultrasensitive mass measurement

W. K. Hiebert[1,2*], C. Thrideep[2], M. Belov[1], J. Westwood-Bachman[1,2], S. K. Roy[1,2,3], M. P. Maksymowych[1,2], V. T. K. Sauer[1,2], T. S. Lee[1], T. Firdous[1,2], A. Venkatasubramanian[1,2], A. Kobryn[1]

[1] Nanotechnology Research Centre, National Research Council of Canada, 11421 Saskatchewan Drive, Edmonton, T6G 2M9, Canada

[2] Department of Physics, University of Alberta, Edmonton T6G 2E1, Canada

[3] Department of Physics, Chittagong University of Engineering and Technology (CUET), Chittagong-4349, Bangladesh

[*]corresponding author: Wayne.Hiebert@nrc-cnrc.gc.ca

Abstract: Nano-optomechanical systems (NOMS) are developed to explore the ultimate limits of sensitivity in mass sensing. Fabricated using silicon-on-insulator and typical integrated photonics process flows, we use NOMS chips for directly sensing miniscule mass levels in gas chromatography and in mass spectrometry as well as for performing sub-millidegree resolved temperature sensing. We have a vision for achieving single atomic mass unit mass sensitivity resolution in air and room temperature.

Nano-optomechanical systems have been deployed as the mass sensing element in niche applications of mass spectrometry [1] and gas chromatography [2]. Using racetrack optical resonators in silicon-on-insulator coupled to doubly clamped mechanical beams, we were able to demonstrate that the intrinsic sensitivity of a thermomechanically limited NOMS resonant sensing system is independent of mechanical damping [3]. We have explored the nonlinearity limitations in NOMS, both taking advantage of it for optomechanical spring effect sensing [4], and designing around it to extend the linear range of device operation [5, 6]. Taking advantage of optomechanical numerical modeling that combines the coupling of two optical field colors and mechanical response, we were able to locate and exploit a null in optomechanical nonlinearity at a specific optical cavity detuning in order to increase linear operation range in one of our NOMS devices. The increased linear range led to our most recent demonstrated sensitivity level of 83 yg (yocto = 10-24) or about 50 atomic mass units [7]. Our current project develops slot-mode waveguides with photonic crystal cavities and phononic crystal mechanical elements for enhancement in both optical and mechanical quality factors. This will enhance the optomechanical coupling and the frequency stability which will allow size-down-scaling of cantilever beams and the potential of single Dalton mass sensitivity levels.

References

1. Sansa M., *et al.,* "Optomechanical mass spectrometry," Nature Communications 11, 3781 (2020).
2. Venkatasubramanian, A., Sauer, V. T. K., Roy, S. K., Xia, M., Wishart, D. S., Hiebert, W. K., "Nano-Optomechanical Systems for Gas Chromatography," Nano Letters. 16(11): 6975-6981 (2016).
3. Roy, S. K., Sauer, V. T. K., Westwood-Bachman, J. N., Venkatasubramanian, A., Hiebert, W. K., "Improving mechanical sensor performance through larger damping," Science **360**, eaar5220 (2018).
4. Maksymowych, M. P., Westwood-Bachman, J. N., Venkatasubramanian, A., Hiebert, W. K., "Optomechanical spring enhanced mass sensing," Appl. Phys. Lett. 115 101103 (2019).
5. Westwood-Bachman, J. N., Maksymowych, M. P., Van, V., Hiebert, W. K., "Transduction of large optomechanical amplitudes with racetrack-loaded Mach-Zehnder interferometers," Optics Express 28, 21835 (2020).
6. Westwood-Bachman, J. N., Lee, T. S., Hiebert, W. K., "Efficient actuation design for optomechanical sensors," Optics

Express 29, 32349 (2020).

7. Westwood-Bachman, J. N., Firdous, T., Kobryn, A. E., Belov, M., Hiebert, W. K., “Isolation of optomechanical nonlinearities in nanomechanical cantilevers,” Physical Review A **105**, 053517 (2022).

Diamond X-band Optomechanical Crystals

E. Zohari[1, 2, 3], W. El-Sayed[2], J. E. Losby[2, 3], G. O. Luiz[4], and P. E. Barclay[2,3*]
[1]Department of Physics, University of Alberta, Edmonton, Alberta, T6G 2E1, Canada
[2]Institute for Quantum Science and Technology, University of Calgary, Calgary, AB, T2N 1N4, Canada
[3]Nanotechnology Research Centre, National Research Council, Edmonton, AB, T6G 2M9, Canada
[4]nanoFAB Centre, University of Alberta, Edmonton, AB, T6G 2V4, Canada
[*]pbarclay@ucalgary.ca

Abstract: We demonstrate single-crystal diamond optomechanical crystal cavities that support ~ 200 THz optical modes co-localized with high-frequency 10 GHz acoustic modes. Their measured optomechanical coupling $g_0/2\pi > 200$ kHz is extracted through optomechanical back action measurements.

Cavity optomechanics integrates mechanical resonators within optical cavities, enhancing the coupling of light and the motion of mechanical resonator [1]. Mechanical resonators interact with a wide range of physical systems, making them a critical element of sensing and quantum transduction technologies by connecting a mechanical degree of freedom to other physical systems. The performance of these systems is enhanced by integrating mechanical resonators directly within optical cavities, which confine photons and phonons to small mode volumes.

Diamond is a promising material for hybrid quantum systems due to its extraordinary optical, thermal, and mechanical properties and the presence of accessible colour center defects for spin-qubit applications. Optomechanical crystal (OMC) devices fabricated from diamond can be used as quantum transducers that bypass the need for spin-optical transitions.

Thanks to advances in diamond nanofabrication techniques, cavity optomechanical devices can be realized from single crystal diamond (SCD). OMC cavities fabricated using angle etching [2] and membrane thinning [3] have enabled coherent optomechanical coupling to mechanical resonances with frequencies of 5.5 to 9.5 GHz. Here we use quasi-isotropic etching for the first time to fabricate OMC cavities in single-crystal diamond, and show that they confine optical and high-frequency mechanical modes coupled via radiation pressure. Using these devices, we characterize the optomechanical coupling to 10.2 GHz modes - the highest frequency acoustic mode measured in SCD to date.

Diamond optomechanical crystal demonstrated in this work is designed to support co-localized optical and mechanical modes, and unlike previously studied angle-etched devices, have rectangular cross-section and was fabricated using a quasi-isotropic etch process adopted from Khanaliloo *et al.* [4]. Simulated normalized transverse electric (TE-like) field of the localized optical mode and mechanical displacement profiles of the mechanical breathing modes are shown in Fig. 2(a).

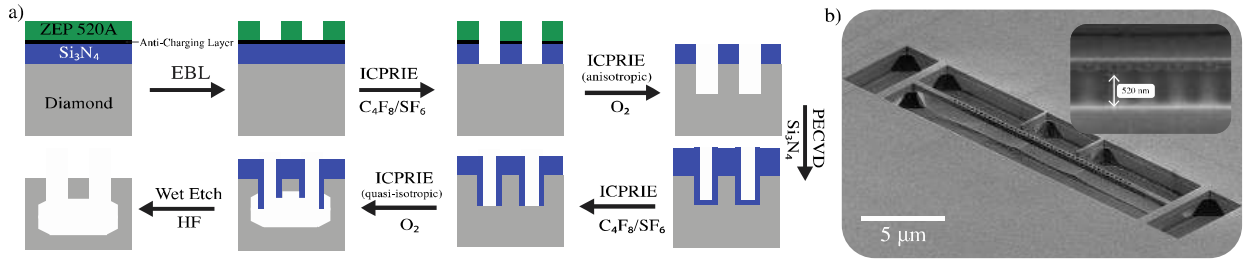


Figure 1. Fabricated diamond optomechanical crystals. (a) Fabrication process flow using high temperature plasma quasi-isotropic undercut etch. (b) Tilted scanning electron microscope (SEM) images of 1-dimensional OMC defined by air holes and zoomed-in view of the defect region (inset).

In the experimental setup, light is coupled into the OMC via a dimpled fibre taper. The transmitted light from the device is split into two outputs for optical and mechanical spectroscopy measurements. Figure 2(b) displays both the optical transmission and measured mechanical spectra as a function of input laser wavelength. A Lorentzian fit of the optical spectrum gives a measured total optical decay rate of 10.16 GHz corresponding to an optical Q-factor of $Q_O = 3.05\times10^4$ centered at $\lambda_0 = 1575.25$ nm. Mechanical spectroscopy was performed by analyzing the RF spectrum of the photodetector light using a real-

time signal analyzer (RSA). As the laser is tuned onto the side of the optical resonance, thermomechanically driven motion of the mechanical mode at 10.178 GHz with quality factor of $Q_m = 9.05\times10^2$ is transduced.

To characterize optomechanical coupling, Fig. 2(c) plots the measured mechanical linewidth of the mechanical breathing mode, collected under laser detuning $\Delta = \pm\omega_m$ as a function of the intracavity photon number (n_{cav}). The mean value extracted from the Γ_{red} and Γ_{blue} data yields an intrinsic mechanical linewidth of $\Gamma_i/2\pi = 11.25$ MHz. Figure 2(d) demonstrates the calculated optomechanically induced damping $\Gamma_{OM} = \Gamma_{red} - \Gamma_i$, plotted versus intracavity photon number (n_{cav}). A linear fit yields $g_0/2\pi = 229.9$ kHz. With a blue-detuned input field by the mechanical frequency and sufficiently high power, the effective mechanical line-width, Γ_m, goes to zero, and we are able to excite the mechanical mode into self-induced oscillations (i.e. phonon lasing) shown in Fig. 2(e).

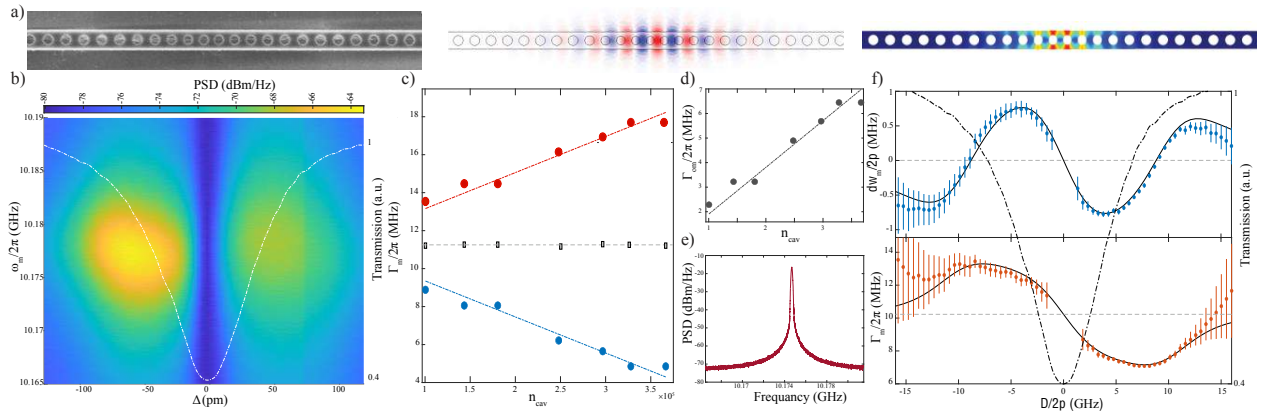


Figure 2. Diamond OMC optical and mechanical spectroscopy of the acoustic breathing mode. (a) Top-view SEM image of the device, normalized optical mode, and mechanical displacement profile of the mechanical mode. (b) The acoustic breathing mode's power spectral density (PSD) and normalized optical transmission (white path) plotted versus input laser detuning from the optical cavity resonance. (c) Measured mechanical linewidths at $\Delta = \pm\omega_m$ plotted versus n_{cav}. (d) Calculated optomechanically induced damping (Γ_{OM}). (e) Self-induced oscillation (i.e. phonon lasing) of the mechanical mode. (f) Optically amplified mechanical loss and spring shift in mechanical frequency measured as a function of laser detuning. Large error bars in regions far from cavity resonance are due to low amplitude mechanical mode resulting from the low number of cavity photons, yielding more uncertainty in the fit.

The optically amplified mechanical loss rate and optical spring shift in the mechanical frequency were also measured as a function of laser detuning. Figure 2(f) displays the experimentally derived optical damping and springing curves for the diamond OMC acoustic breathing mode. Estimates for the intrinsic mechanical damping of $\Gamma_i/2\pi = 10.23$ and 10.18 MHz and the single-photon optomechanical coupling rate of $g_0/2\pi = 192.0$ and 195.8 kHz can be extracted from this data.

In summary, we reported demonstration of a high-frequency diamond OMC cavity fabricated using quasi-isotropic etching. Optomechanical coupling in these devices will allow cooperativity > 1 for an intracavity photon population on the order of 10^5. The demonstrated device is a promising platform for reaching much larger cooperativities by operating at cryogenic temperatures where mechanical dissipation will decrease. The high-frequency mechanical mode of this device makes it less susceptible to decoherence due to its low thermal phonon population. These features open the door to demonstrating quantum optomechanical applications.

References

1. Aspelmeyer, M., T. J. Kippenberg, and F. Marquardt. "Cavity optomechanics," Reviews of Modern Physics 86.4 (2014): 1391.
2. Burek, M. J., et al. "Diamond optomechanical crystals." Optica 3.12 (2016): 1404-1411.
3. Cady, J, V., et al. "Diamond optomechanical crystals with embedded nitrogen-vacancy centers." Quantum Science and Technology 4.2 (2019): 024009.
4. Khanaliloo, B., et al. "Single-crystal diamond nanobeam waveguide optomechanics." Physical Review X 5.4 (2015): 041051.

META 2023, PARIS - FRANCE, JULY 18 – 21, 2023

Optomechanics in the microwave regime: leveraging strong non-linearities for cooling

David Zoepfl[1,2], Lukas Eng[1,2], Olivier-Michel Tardif[3], Étienne Pilon[3], Laurence Mercier-Coderre[3], David Tran[3], Gerhard Kirchmair[1,2], Mathieu Juan[3]

[1]University of Innsbruck (Austria)

[2]Austrian Academy of Sciences (Austria)

[3]Institut Quantique and Département de Physique, Université de Sherbrooke, Sherbrooke, Québec, J1K 2R1 (Canada)
*corresponding author: Mathieu.Juan@USherbrooke.ca

Abstract: Departing from traditional optomechanics, the integration of microwave circuits offers substantial nonlinearities that can be effectively harnessed for enhanced coupling between microwave and mechanical systems. In this work, we show that a mechanical system can be strongly coupled to a microwave circuit, enabling cavity cooling with one microwave photon in average. In addition, the strong Kerr non-linearity of the circuit can be leveraged to further increase the cooling efficiency compared to what is achievable with a linear system. Since mechanical systems can also be efficiently coupled to optical fields, mechanical interfaces can be used to realize transduction of quantum information between the microwave and optics domains.

Applications of phonon-electron devices for microwave frequency signal processing

Matt Eichenfield

Sandia National Labs, USA
*corresponding author, E-mail: eichenfield@arizona.edu

Abstract

Devices that allow controllable interactions between electrons and phonons—acoustoelectric devices—have undergone a resurgence of interest in the last 8 years due to rapid advanced in heterogeneous integration of piezoelectric materials and semiconductors. Here, I will describe some of the novel devices and systems that are emerging from this field. I will discuss my group's work demonstrating devices such as phononic amplifiers, mixers, switches, and others. Finally, I will discuss the prospects of these devices for insertion into wireless technologies both existing and future, as well as novel applications.

META 2023, PARIS - FRANCE, JULY 18 – 21, 2023

Photonic Implementation of Non-Adiabatic Holonomies for Quantum Computing

V. Neef, J. Pinske, M. Heinrich, S. Scheel, A. Szameit*

Institute for physics, University of Rostock, Albert-Einstein-Str. 23, 18059 Rostock, Germany
*corresponding author: alexander.szameit@uni-rostock.de

Abstract: We present the experimental realization of non-adiabatic holonomies in integrated quantum optics. Implementing quantum gates solely by means of non-Abelian geometric phases increases stability and reduces the need for quantum error correction. We use femtosecond laser-written waveguides and to realize topologically protected single-qubit gates as well as gate sequences, and verify their performance by means of heralded single-photon measurements. Our findings pave the way towards a holonomic architecture for quantum computers.

Implementing quantum gates as non-Abelian holonomies, a class of topologically protected unitary operators, is a particularly promising paradigm for the design of intrinsically stable quantum computers[1]. In contrast to dynamical phases, which record the passage of time, the geometric phase accumulated by a quantum system propagating through a Hilbert space $\mathcal{H}$ depends exclusively on its path. A famous example of such a quantity is the Berry-Pancharatnam phase[2,3], which is Abelian and belongs to the one dimensional unitary group $\mathrm{U}(1)$. In general, however, geometric phases can exhibit arbitrary dimensionality. Wilczek and Zee introduced the idea of multi-dimensional, non-Abelian geometric phases – so called holonomies[4]. Anandan later lifted the requirement of adiabaticity to create truly time-independent holonomies[5]. Non-adiabatic holonomies rely on a subspace $\mathcal{H}_{\mathrm{geo}}$ of the Hilbert space which is spanned by states $\{|\Phi_k\rangle\}_k$ fulfilling $\langle\Phi_k|\widehat{H}|\Phi_j\rangle = 0$, where $\widehat{H}$ is the system's Hamiltonian. Restricting the propagation to $\mathcal{H}_{\mathrm{geo}}$ ensures parallel transport and, thus, a purely geometric phase (see Fig. 1a). Crucially, the states $\{|\Phi_k\rangle\}_k$ are no longer instantaneous eigenstates of the Hamiltonian[6,7].

Quantum optics constitutes a particularly versatile platform for quantum information processing and the construction of non-adiabatic holonomic quantum computers: Not only does it readily enable the desired integration and miniaturization, the bosonic nature of photons also conveniently allows for multiple excitations of the same bosonic mode[8,9].

Our system consists of three waveguides (L, C, R) fabricated by femto-second laser direct inscription[10]. In this planar geometry, direct coupling between the outer channels L and R is effectively suppressed, while each of them interacts with the central site C via the couplings κ_{L} and κ_{R}, respectively. Pairs of indistinguishable photons from a Type-I SPDC source allow for heralded coincidence measurements with a set of avalanche photo diodes (APDs). Exciting the three-waveguide structure with a single photon creates a two-dimensional geometric subspace $\mathcal{H}_{\mathrm{geo}}$. Under a cyclic evolution through $\mathcal{H}_{\mathrm{geo}}$ a two-dimensional non-adiabatic holonomy $\widehat{U}$ can therefore be realized. Parametrizing the couplings[6,7] as $\kappa_{\mathrm{L}}(z) = \Omega(z)\sin\left(\theta/2\right)\mathrm{e}^{\mathrm{i}\phi}$ and $\kappa_{\mathrm{R}}(z) = \Omega(z)\cos\left(\theta/2\right)$ with constant weights (defined through θ and ϕ) and an envelope function $\Omega(z)$, the cyclicity condition simplifies to $\int_{z_{\mathrm{i}}}^{z_{\mathrm{f}}}\Omega(z)\,\mathrm{d}z = \pi$. The resulting holonomy[11]

$$\widehat{U} = \begin{pmatrix} \cos\theta & -\mathrm{e}^{-\mathrm{i}\phi}\sin\theta \\ -\mathrm{e}^{\mathrm{i}\phi}\sin\theta & -\cos\theta \end{pmatrix}$$

belongs to the group $\mathrm{U}(2)$ and acts as a single-qubit gate for the dual-rail encoded qubit $|0\rangle_{\mathrm{logic}} = |1_{\mathrm{L}}0_{\mathrm{R}}0_{\mathrm{C}}\rangle$,

$|1\rangle_{\text{logic}} = |0_L 1_R 0_C\rangle$. A dense subset of the symmetry group can be created using two successive non-commuting holonomies[8,11]. Interestingly, and in contrast to the adiabatic approach, real-valued couplings ($\phi = 0$) already suffice to realize such non-commuting holonomies. As a proof of principle, we experimentally realize two prominent quantum gates, Pauli-X and Hadamard, up to a global phase. Figure 1b depicts the waveguide structure for the Hadamard gate ($\theta = 3\ \pi/4$), where $\Omega(z)$ was chosen such that the waveguides L and R approach C along a cosinusoidal path, followed by a straight section, and finally are separated once more by another cosine segment. To ensure a smooth transition to a standard fiber array, additional cosine-shaped fanning sections were implemented at the beginning and end of the chip. Due to its inherent symmetry, no fanning section is needed for the Pauli-X gate ($\theta = \pi/2$). The measured probabilities of the Hadamard gate are depicted in Fig. 1c. We find an average fidelity between theoretically expected probabilities and measurement of $\bar{F} = (99.2 \pm 0.2)\%$ for the Hadamard gate and $\bar{F} = (99.1 \pm 1.0)\%$ for the Pauli-X gate, showcasing the high accuracy of our quantum-optical realization of non-adiabatic holonomic quantum gates. We experimentally prove the non-Abelian nature of the quantum gates and realize the *QP penny flipover*[12], a quantum algorithm from quantum game theory. Our findings pave the way towards universal holonomic quantum computing.

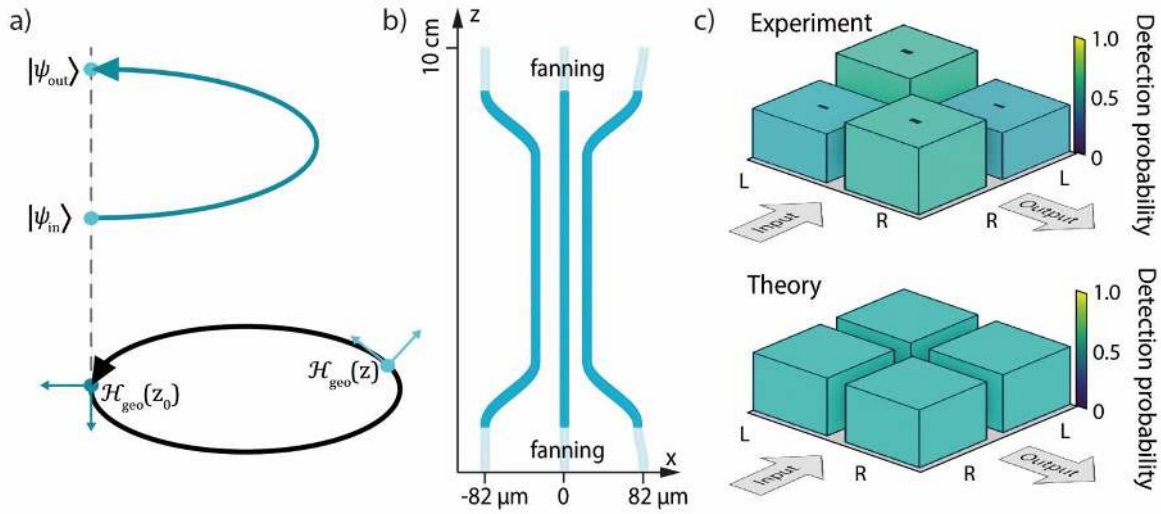


Figure 1: a) Schematic illustration of a non-adiabatic holonomy. The geometric subspace $\mathcal{H}_{\text{geo}}$ (spanned by non-dynamical states) is time dependent (bottom layer). In input state $|\psi_{\text{in}}\rangle$, prepared inside the initial geometric subspace, will be transformed into an output state $|\psi_{\text{out}}\rangle$, that also lies inside the initial geometric subspace. **b)** Waveguide-based implementation of the non-adiabatic holonomic Hadamard gate. **c)** Experimental results and theoretical predictions for the probability distributions of a Hadamard gate.

1. Zanardi, P. & Rasetti, M. *Phys. Lett. A* **264**, 94–99 (1999).
2. Berry, M. V. *Proc. R. Soc. London* **392**, 45–57 (1984).
3. Pancharatnam, S. *Proc. Indian Acad. Sci. - Sect. A* **44**, 247–262 (1956).
4. Wilczek, F. & Zee, A. *Phys. Rev. Lett.* **52**, 2111–2114 (1984).
5. Anandan, J. *Phys. Lett. A* **133**, 171–175 (1988).
6. Sjöqvist, E. *et al. New J. Phys.* **14**, 103035 (2012).
7. Abdumalikov, A. A. *et al. Nature* **496**, 482–485 (2013).
8. Pinske, J., Teuber, L. & Scheel, S. *Phys. Rev. A* **101**, 062314 (2020).
9. Neef, V. *et al. Nat. Phys.* **19**, 30–34 (2023).
10. Szameit, A. & Nolte, S. *J. Phys. B At. Mol. Opt. Phys.* **43**, 163001 (2010).
11. Pinske, J. & Scheel, S. *Phys. Rev. Res.* **4**, 1–10 (2022).
12. Meyer, D. A. *Phys. Rev. Lett.* **82**, 1052–1055 (1999).

Quantum explorations and applications of phonon-electron interactions

Matt Eichenfield

Sandia National Labs, USA
*corresponding author, E-mail: eichenfield@arizona.edu

Abstract

Interactions between electrons and phonons are being vigorously explored for their utility in RF signal processing, sensing, and more. However, these devices are almost entirely unexplored in the quantum regime. Here, I will describe our recent work theoretically and experimentally exploring quantum electron-phonon interactions and how they can be applied to fundamental studies of materials and quantum information science.

META 2023, PARIS - FRANCE, JULY 18 – 21, 2023

Thermalization and condensation of light waves: Wave turbulence theory and experiments in multimode optical fibers

K. Baudin[1], J. Garnier[2], N. Berti[1], A. Fusaro[3], K. Krupa[4], L. Zanaglia[5], C. Michel[5], V. Doya[5], G. Millot[1], A. Picozzi[1]

[1]Laboratoire Interdisciplinaire Carnot de Bourgogne, CNRS, Université de Bourgogne, Dijon, France
[2] CMAP, CNRS, Ecole Polytechnique, Institut Polytechnique de Paris, 91128 Palaiseau Cedex, France
[3] CEA, DAM, DIF, F-91297 Arpajon Cedex, France
[4] Institute of Physical Chemistry Polish Academy of Sciences, Warsaw, Poland
[5] Université Côte d'Azur, CNRS, Institut de Physique de Nice, Nice, France
[*]corresponding author: Antonio.Picozzi@u-bourgogne.fr

Abstract: We review recent progress on the experimental observation of light thermalization to the Rayleigh-Jeans equilibrium in multimode optical fibers. We develop a nonequilibrium thermodynamic description of light thermalization on the basis of the wave turbulence theory by taking into account the impact of disorder (weak and strong random mode coupling), which is inherent to light propagation in multimode optical fibers. The analysis reveals that weak disorder increases the rate of thermalization to equilibrium, whereas strong disorder can inhibit light thermalization.

Different studies on wave turbulence revealed that purely classical waves can exhibit a process of condensation that originates from the thermalization of the waves toward the Rayleigh-Jeans (RJ) equilibrium distribution [1,2]. Although this phenomenon of condensation of classical waves differs from the quantum Bose-Einstein condensation, the underlying mathematical origin is formally analogous because of the common singular behavior (vanishing denominator) of the equilibrium Bose distribution for quantum particles and the equilibrium Rayleigh-Jeans distribution for classical waves [1]. However, the observation of condensation of optical waves in a conservative (e.g., cavity-less) configuration is hindered by the prohibitive large propagation lengths required to achieve RJ thermalization. Recently, the observation of the RJ condensation and thermalization of light waves has been reported in multimode optical fibers [3-5].

The experiments are based on a phenomenon of spatial beam cleaning recently discovered in multimode optical fibers [6-8]. As a matter of fact, light propagation in multimode optical fibers is affected by a structural disorder of the material. We have formulated a wave turbulence kinetic description of the random waves that account for the presence of structural disorder. The theory unveils a significant acceleration of the process of thermalization and condensation that is induced by the disorder [9]. This fast process of condensation can explain the effect of spatial beam cleaning as a consequence of the macroscopic population of the fundamental mode of the fiber.

Our experiments in multimode fibers evidence the transition to light condensation: By decreasing the kinetic energy ('temperature') below the critical value, we observe a transition from the incoherent thermal RJ distribution to wave condensation [3]. The experimental results show that the chemical potential reaches the lowest energy level at the critical value of the energy to condensation, which leads to the macroscopic population of the fundamental mode of the optical fiber. The condensate fraction across the transition to condensation is in quantitative agreement with the RJ theory. We have also characterized the thermodynamics [10] of classical

condensation through the analysis of the specific heat: In opposition to quantum Bose-Einstein condensation, the heat capacity takes a constant value in the condensed state and tends to vanish above the transition in the normal state [3]. More recently, RJ thermalization has been extended to non-Hermitian optical lattices [11] or by including the conservation of orbital angular momentum [12-13].

We will present recent developments about the development of a wave turbulence theory accounting for the impact of strong disorder [14]. The theory unveils the interplay of disorder and nonlinearity. It reveals that a nonequilibrium process of condensation and thermalization can take place in the regime where disorder effects dominate over nonlinear effects. We validate the theory by numerical simulations of the nonlinear Schrödinger equation and the derived kinetic equation, which are found in quantitative agreement without using adjustable parameters. Experiments realized in multimode optical fibers with an applied external stress evidence the process of thermalization in the presence of strong disorder [14].

Finally, we report the recent observation of Rayleigh-Jeans thermalization to negative temperature equilibrium states through its propagation in a multimode optical fiber [15]. The bounded energy spectrum of the optical fiber enables negative temperature equilibriums with high energy levels (high order fiber modes) more populated than low energy levels (low order modes). Our experiments show that negative temperature speckle beams are featured, in average, by a non-monotonous radial intensity profile [15]. Bringing negative temperatures to the field of optics opens the door to the investigation of fundamental issues of negative temperature states in a flexible experimental environment [10].

References:

[1] C. Connaughton, C. Josserand, A. Picozzi, Y. Pomeau, S. Rica, PRL 95, 263901 (2005)

[2] P. Aschieri, J. Garnier, C. Michel, V. Doya, A. Picozzi, PRA 83, 033838 (2011)

[3] K. Baudin, A. Fusaro, K. Krupa, J. Garnier, S. Rica, G. Millot, A. Picozzi, PRL 125, 244101 (2020)

[4] H. Pourbeyram, P. Sidorenko, F. Wu, L. Wright, D. Christodoulides, F. Wise, Nature Physics 18, 685 (2022)

[5] F. Mangini, M. Gervaziev, M. Ferraro, D. S. Kharenko, M. Zitelli, Y. Sun, V. Couderc, E.V. Podivilov, S. A. Babin, and S. Wabnitz, Optics Express 30, 10850 (2022)

[6] K. Krupa, K. Krupa, A. Tonello, B.M. Shalaby, M. Fabert, A. Barthélémy, G. Millot, S. Wabnitz, V. Couderc, Nature Photonics 11, 237 (2017)

[7] L.G. Wright, Z. Liu, D.A. Nolan, M.-J. Li, D.N. Christodoulides, F.W. Wise, Nature Photonics 10, 771 (2016)

[8] E. Podivilov F. Mangini, O.S. Sidelnikov, M. Ferraro, M. Gervaziev, D.S. Kharenko, M. Zitelli, M.P. Fedoruk, S.A. Babin, S. Wabnitz, PRL 122, 103902 (2019)

[9] A. Fusaro, J. Garnier, K. Krupa, G. Millot, A. Picozzi, PRL 122, 123902 (2019)

[10] F. O. Wu, A.U. Hassan, D.N. Christodoulides, Nature Photonics 13, 776 (2019)

[11] G. G. Pyrialakos, H. Ren, P.S. Jung, M. Khajavikhan, D.N. Christodoulides, PRL 128, 213901 (2022)

[12] F.O. Wu, Q. Zhong, H. Ren, P.S. Jung, K.G. Makris, D.N. Christodoulides, PRL 128, 123901 (2022)

[13] E.V. Podivilov, F. Mangini, O.S. Sidelnikov, M. Ferraro, M. Gervaziev, D.S. Kharenko, M. Zitelli, M.P. Fedoruk, S.A. Babin, S. Wabnitz, PRL 128, 243901 (2022)

[14] N. Berti, K. Baudin, A. Fusaro, G. Millot, A. Picozzi, J. Garnier, PRL 129, 063901 (2022)

[15] K. Baudin, J. Garnier, A. Fusaro, N. Berti, C. Michel, K. Krupa, G. Millot, A. Picozzi, PRL 130, 063801 (2023)

Thermalization of weakly non-integrable Josephson junction networks

Gabriel M. Lando

Center for Theoretical Physics of Complex Systems, Institute for Basic Science, Daejeon 34126, Korea

February 17, 2023

Statistical mechanics is, in many ways, considerably more general than either classical or quantum mechanics: as long as one knows how to write a partition function, the statistical formalism can be applied. A cornerstone assumption for such generality is the ergodic hypothesis, which allows us to average over ensembles of similarly prepared systems rather than time. This is definitely not true for integrable systems, in which motion is always confined to lower-dimensional submanifolds and, therefore, thermalization is never achieved. It is then natural to wonder how thermalization is suppressed as a system approaches an integrable limit: Is integrability reached through an universal mechanism? How long does it take? Does it happen isotropically?

In this talk I will expand on results previously published by our group, namely that there appear to be two main pathways towards integrability, each with markedly distinguishable features. While previous investigations were focused on abstract discrete unitary maps, I will present results obtained for one- and two-dimensional networks with hundred(s) of coupled Josephson junctions. Such a generalization from maps to high-dimensional Hamiltonian systems is quite a formidable computational task, some aspects of which I will also briefly expose in the presentation.

META 2023, PARIS - FRANCE, JULY 18 – 21, 2023

Diffusion without Spreading of Wavepackets in Nonlinear Lattices with linear Anderson Localization

Serge AUBRY
Laboratoire Léon Brillouin, CEA Saclay, 91191-Gif-sur-Yvette, France
*serge.aubry91@gmail.com

Abstract:
We discuss the long time behavior of a finite energy wave packet in nonlinear Hamiltonians on infinite lattices at arbitrary dimension, exhibiting linear Anderson localization. Early numerical studies suggested a subdiffusive behavior of the wave packets in such models. However, strong arguments both mathematical and numerical, suggest for infinite models that small amplitude wave packets may generate stationary quasiperiodic solutions (KAM tori) almost indistinguishable from linear wave packets. The probability of this event is non vanishing at small enough amplitude and goes to unity at amplitude zero. Most other wave packets (non KAM tori) are chaotic (as well as in finite size systems).

We propose a modified Boltzmann statistics for wave packets based on the Arnold diffusion conjecture (recently partially proven) which should be valid in generic models. The consequence is that the probability that a chaotic wave packet spreads to zero amplitude is zero. It must always remain focused around one or few chaotic spots which wander randomly over the whole system and generate subdiffusion. Moreover, it can be rigorously proven in a large class of so-called Ding Dong models (where the nonlinearities are replaced by hard core potentials) that spreading is impossible for any initial wave packet despite subdiffusion has been also numerically observed in some of these models.

,

References

1. S. Aubry, ArXiv:2212.05771 [cond-mat.dis-nn]

META 2023, PARIS - FRANCE, JULY 18 – 21, 2023

Thermodynamics and pressure of composite multimoded optical systems

N.K. Efremidis[1,2*] and D.N. Christodoulides[3]

[1]Department of Mathematics and Applied Mathematics, University of Crete, Heraklion 70013 Crete, Greece.
[2]Institute of Applied and Computational Mathematics, Foundation for Research and Technology-Hellas (FORTH), Heraklion 70013 Crete, Greece.
[3]Ming Hsieh Department of Electrical and Computer Engineering, University of Southern California, Los Angeles, California 90089, USA.
[*]corresponding author: nefrem@uoc.gr

Abstract: We investigate the thermodynamic behavior of composite optical systems. Each component is associated with a different color or polarization and the components are coupled via nonlinear interactions. In a manifestation of Le Chatelier's principle, we find that depending on the type of the nonlinearity, such systems thermalize to different final states. In addition, we compute the partial optomechanical pressure of each component, whereas the total pressure is the direct sum of the partial pressures (Dalton's law).

A thermodynamic theory for optical systems has recently been developed [1]. It predicts that optical systems can reach thermal equilibrium in the form of a Reyleigh-Jeans distribution. This theory can have important consequences in multimoded optical settings explaining, for example, phenomena, such as beam self-cleaning in multimode fibers [2,3]. The resulting Rayleigh-Jeans distribution can also be derived using a grand-canonical approach [4,5], and can be extended to include additional system parameters [5]. Such parameters are particularly important, in the formulation and derivation of the actual optomechanical pressure that is applied under thermal equilibrium conditions [6].

Here, we examine the statistical mechanics of composite optical settings using a grand canonical statistical approach. In principle, we can have Γ different components, that can be different colors or different polarizations. For simplicity, we assume that each component has the same number of supermodes M. The linear systems are then coupled through their nonlinear interactions to a single nonlinear Hamiltonian. The linear part of the Hamiltonian can be written as

$$H = \sum_{l=0}^{M} \sum_{\gamma=1}^{\Gamma} \frac{\varepsilon_\gamma^{(l)} n_\gamma^{(l)}}{\omega_\gamma}$$

where γ denotes the component associated with frequency ω_γ, and $\varepsilon_\gamma^{(l)}, n_\gamma^{(l)}$ is the propagation constant and the power occupation number of the lth mode of the γ component. The number of power conservation laws depends on the type of the nonlinearity. For example, in the case of two components, a cubic nonlinearity results to self-phase and cross-phase modulations and thus to two conservation laws $N_\gamma = \sum_l n_\gamma^{(l)}, \gamma = 1,2$. On the other hand, for second harmonic generation, due to the power exchange between the fundamental and the second harmonic, we have only one conservation law $N = \sum_\gamma \sum_l n_\gamma^{(l)}$.

Interestingly, independently of the number of power conservation laws, the system has a unique temperature.

However, for each power conservation law, an associated chemical potential gives rise to a different Rayleigh-Jeans distribution. Thus, depending on the type of the nonlinearity, the same initial condition can get thermalized to a different final state, depending on these conservation laws. A resulting Le Chatelier's principle determines the equilibrium state for the partial power of each component. We also compute the optomechanical pressure that is applied to the system. In particular, for each the pressure due to the γ component can be written as

$$p_\gamma = -\sum_{l=1}^{M} \frac{n_\gamma^{(l)} M}{\omega_\gamma} \left(\frac{\partial \varepsilon_\gamma^{(l)}}{\partial L} \right)_M$$

where L is the transverse size of the system. The total optomechanical pressure is the sum of the partial pressures a manifestation of Dalton's law.

References

1. Wu, F. O., Hassan, A. U., and Christodoulides, D. N. "Thermodynamic theory of highly multimoded nonlinear optical systems", Nat. Photonics Vol. 13, 776–782 (2019).
2. Pourbeyram, H. et al., "Direct observations of thermalization to a Rayleigh–Jeans distribution in multimode optical fibres", Nat. Phys. 18, 685–690 (2022).
3. Mangini, F. et al., "Statistical mechanics of beam self-cleaning in grin multimode optical fibers", Opt. Express 30, 10850–10865 (2022).
4. Makris, K. G., Wu, F. O., Jung, P. S., and Christodoulides, D. N., "Statistical mechanics of weakly nonlinear optical multimode gases", Opt. Lett. 45, 1651–1654 (2020).
5. Efremidis, N. K. & Christodoulides, D. N, "Fundamental entropic processes in the theory of optical thermodynamics", Phys. Rev. A 103, 043517 (2021).
6. Efremidis, N. K. & Christodoulides, D. N, "Thermodynamic optical pressures in tight-binding nonlinear multimode photonic systems", Commun. Phys.

META 2023, PARIS - FRANCE, JULY 18 – 21, 2023

Controlling optical thermalization via spectral engineering: A Kinetic Equation Approach

T. Kottos*

Wave Transport in Complex Systems Lab, Department of Physics, Wesleyan University, USA
*corresponding author: tkottos@wesleyan.edu

Abstract: We utilize a kinetic equation approach together with a nonlinear scaling theory for the analysis of optical thermalization in multimode nonlinear photonic networks. We show that spectral engineering, either via band-gap design or via disorder, molds the thermalization process and the formation of the thermal states. Further isomorphisms with the theory of spin networks reveals the existence of optical phase transitions of the thermal equilibrium states, which resemble a paramagnetic to ferromagnetic and to a spin-glass phase transition.

In physics, one often encounters problems involving a great number of interacting modes. Such problems naturally arise in statistical mechanics, hydrodynamics, matter-waves, and more. An emerging framework is in photonics, where light propagation in non-linear or disordered multimode optical structures have recently attracted a lot of attention. On the fundamental side there are many unanswered questions associated with the energy exchange between the modes and the role of the underlying spatio-temporal complexity, originating from the disorder, the network topology, the complex nonlinear intermodal interactions and mode-dependent losses. Brute force computational attempts to answer these questions are either impossible (due to the large number of degrees of freedom involved) or unsatisfactory as far as the understanding of the underlying physics that dictates the energy redistribution. At the same time, there is a pressing need from modern technologies to develop theoretical tools that will allow us to tailor the intermodal energy exchange and harvest it to our advantage. If this endeavor is successful, it will give rise to a next generation of high-power light sources, high-resolution imaging schemes, and high-speed telecommunication systems.

A prominent photonic framework where the above fundamental questions are interlinked with technological developments appear in the multi-core fibers (MCFs) and multi-mode fibers (MMFs). These systems have recently been exploited as alternatives to single mode fibers – the latter experiencing information capacity limitations, imposed by amplifier noise and fiber non-linearities. What makes multicore and multimode fibers attractive is the possibility to utilize the multiple cores/modes as extra degrees of freedom in order to carry additional information -- thus increasing the information capacity of a single fiber. Of course, MCFs and MMFs also suffer from the above-mentioned challenges (e.g. disorder-induced or/and nonlinearity-induced mode mixing). It is, therefore, imperative to develop theories that take into consideration the role of band-structures of an underlying linear structure, the potential presence of disorder and their interplay with non-linearities in the modal mixing and provide a quantitative description of light transport in such multimode photonic systems.

We have addressed these questions, by implementing a kinetic equation (KE) approach together with a newly developed scaling theory, to the optical beam propagation in such multimoded nonlinear settings. Our analysis is able to highlight the importance of spectral engineering and band-gap structures, disorder, and connectivity between the nodes of the optical nonlinear network. We have found that an engineered band-gap dispersion leads to an optical beam thermal state that is described by a generalized Rayleigh-Jeans distribution. Its formation is controlled by the size of the underlying band-gap of the linear system. The KE allows us also to evaluate the relaxation times towards

such thermal states. In case that disorder is introduced into the linear structure, the thermalization process is hindered. We have developed a universal one-parameter scaling theory that predicts an exponential suppression of the relaxation rate for increasing disorder. The one-parameter scaling variable that controls the relaxation rate, describes the resilience of spatially localized modes to form "localization" clusters against non-linear interactions which tends to desegregate them. Finally, we have shown that appropriate connectivity of the underlying linear system might lead to the presence of various phases of the optical thermal state that share similar features as the paramagnetic, ferromagnetic and spin-glass phase encountered in spin systems.

We acknowledge partial support from Simons Foundation grant no MPI 733698.

References

1. A. Y. Ramod, C. Shi, L. J. Fernandez-Alcazar, D. N. Christodoulides, T. Kottos, "Theory of localization-hindered thermalization in nonlinear multimode photonics," submitted, 2023.
2. C. Shi, T. Kottos, B. Shapiro, "Controlling Opyical beam Thermalization via Band-Gap Engineering," Phys. Rev. research, Vol. 3, 2973, 2021.
3. A. Ramod, L. Fernandez-Alcazar, T. Kottos, B. Shapiro, "Optical Phase Transitions in Photonic Networks: a Spin-System Formulation," Phys. Rev. X, Vol. 10, 031024, 2020.

Recent Advances in Non-Hermitian Photonics: Topological, Disordered and Quantum systems

The bosonic skin effect: boundary condensation in asymmetric transport

L.Garbe*, Y.Minoguchi, J.Huber, P.Rabl

Vienna Center for Quantum Science and Technology, Atominstitut, TU Wien, 1040 Vienna, Austria
*corresponding author: louis.garbe@tuwien.ac.at

Abstract: We study the incoherent transport of bosons through a one dimensional lattice with different left and right hopping rates, modelled by the asymmetric simple inclusion process (ASIP). In this unusual transport scenario, the density profile acquires a zigzag pattern near the boundary, with particle distribution alternating between thermal and Bose-condensed distributions. Furthermore, we show that the onset of this phase is closely related to the non-Hermitian skin effect and coincides with an exceptional point in the spectrum of density fluctuations.

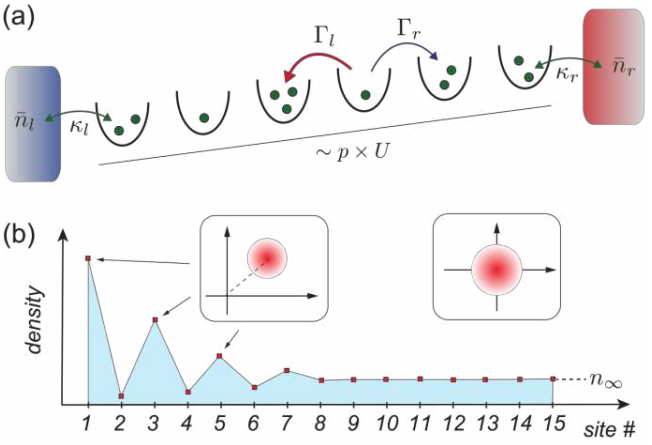


Fig 1 : (a) Sketch of our model. (b) The density acquires a zig-zag pattern, with a number distribution alternating between thermal and coherent.

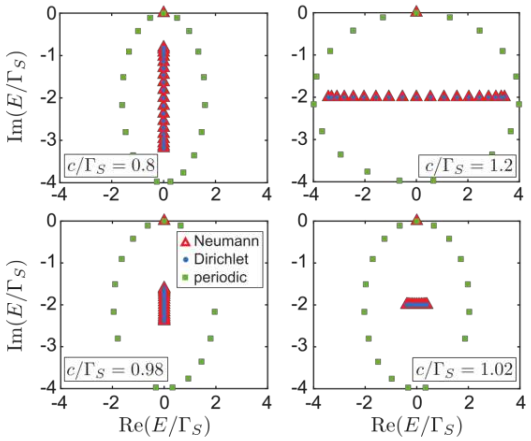


Fig 2 : Excitation spectrum of density fluctuations. The onset of the zig-zag phase coincide with an exceptional point.

We consider bosons hopping through a lattice, according to the following Lindbladian:

$$\mathcal{L} = \Gamma_r D[\hat{a}^\dagger_{p+1}\hat{a}_p] + \Gamma_l D[\hat{a}_{p+1}\hat{a}^\dagger_p]$$

with different left and right hopping rates. In this model, the probability for a boson to jump on a site already occupied is *enhanced* by bosonic bunching. This is an exemple of a so-called *inclusion* process, or ASIP. This non-linear, asymmetric transport leads to an unusual phase, where the population shows a *zig-zag pattern* near the boundary. Remarkably, although the transport is purely incoherent, every other site enters a *Bose-condensed state*, with a coherent particle distribution breaking a U(1) symmetry. We show that this boundary condensation is closely related to *the non-Hermitian skin effect*, and coïncide with an exceptional point in the excitation spectrum of density fluctuations. This effect thus establishes a direct connection between quantum transport, non-equilibrium condensation phenomena and non-Hermitian physics, which can be probed in cold-atom experiments or in systems with long-lived photonic, polaritonic or plasmonic excitations.[1]

References

1. L.Garbe, Y.Minoguchi, J.Huber, P.Rabl, arXiv:2301.11339 (2023)

META 2023, PARIS - FRANCE, JULY 18 – 21, 2023

Non-unitary boson sampling dynamics – distinguishability, complexity, and noise

K. Mochizuki[1] **and R. Hamazaki**[1*]
1Nonequilibrium Quantum Statistical Mechanics RIKEN Hakubi Research Team,
RIKEN Cluster for Pioneering Research (CPR), 2-1 Hirosawa, Wako 351-0198, Japan
2RIKEN Interdisciplinary Theoretical and Mathematical Sciences Program (iTHEMS), 2-1 Hirosawa, Wako 351-0198, Japan
[*]corresponding author: ryusuke.hamazaki@riken.jp

Abstract: We discuss nontrivial physics in boson sampling dynamics generalized to the non-unitary regime. We discover novel dynamical transitions characterized by the distinguishability of photons, which is also relevant for sampling complexity. We especially show that parity-time (PT) symmetry breaking affects the complexity of sampling the probability distribution. In particular, for a PT-broken phase, a notable dynamical transition that the boson distribution becomes distinguishable in the long time occurs, indicating the easiness of sampling bosons.

META 2023, PARIS - FRANCE, JULY 18 – 21, 2023

Extended Nielsen-Ninomiya theorem and non-Hermitian topological phenomena

Masatoshi Sato

[1]Center for Gravitational Physics and Quantum Information, Yukawa Institute for Theoretical Physics, Kyoto University, Kyoto 606-8502, Japan
msato@yukawa.kyoto-u.ac.jp

Abstract: The Nielsen-Ninomiya theorem is a fundamental theorem on chiral fermions in lattice systems. In this talk, I report an extension of the theorem in open systems, which includes the original Nielsen-Ninomiya theorem in a special limit. In contrast to the original theorem, which is a no-go theorem for bulk chiral fermions, the new theorem permits them due to bulk topology intrinsic to open systems. I will also report on applications of our theorem and predict a new type of topological phenomena.

References

1. T. Bessho, M. Sato, “Nielsen-Ninomiya Theorem with Bulk Topology: Duality in Floquet and Non-Hermitian Systems”, Phys. Rev. Lett. 127, 196404 (2021).

Continuum of Bound States in a Non-Hermitian Model

Qiang Wang[1,2*], Changyan Zhu[1], Xu Zheng[1], Haoran Xue[1], Baile Zhang[1], and Y. D. Chong[1]

[1] Nanyang Technological University, Singapore
[2]Nanjing University, China
[*]Corresponding author: q.wang@ntu.edu.sg

Abstract: In a Hermitian system, bound states have quantized energies while free states form a continuum. We demonstrate how this principle can fail in non-Hermitian systems. Certain non-Hermitian systems with imaginary momentum and Landau-type vector potential host eigenstates that we call "continuum Landau modes" (CLMs), featuring gaussian spatial envelopes and a continuum of complex energies. CLMs could be realized in 1D and 2D photonic or acoustic lattices, and have interesting behaviors such as rainbow trapping and wave funnelling.

Introduction A quantum particle in an infinite continuous space can have two kinds of energy eigenstates: the bound states with quantized energies, or spatially extended free states with continuous energies. This property has been mathematically proven based on certain assumptions, one of which is that the Hamiltonian is Hermitian [1]. Over the past two decades, there has been much progress in realizing non-Hermitian Hamiltonians, particularly in the context of photonic lattices and other synthetic structures [2,3]. Could we use such ideas to engineer non-Hermitian Hamiltonians that violate the standard dichotomy between bound states and free states? Here, we discuss non-Hermitian Hamiltonians that have localized energy eigenstates, which we call "continuum Landau modes" (CLMs), at every complex energy E. These CLMs arise from a mapping to the zero modes of a continuous family of Hermitian 2D Dirac models [4].

Continuous and Discrete Model Consider the non-Hermitian 2D Hamiltonian

$$\mathcal{H} = s_x\left[-i\frac{\partial}{\partial x} - By\right] + is_y\left[-i\frac{\partial}{\partial y} + Bx\right] \tag{1}$$

here $s_{x,y} = \pm 1$. It has eigenstates of the form

$$\psi(x,y) = C\exp\left[-\tau|\boldsymbol{r} - \boldsymbol{r_0}|^2 + i\,\boldsymbol{q}\cdot\boldsymbol{r}\right] \tag{2}$$

where C is a normalization constant, $\tau = -s_x s_y B/2$, $\boldsymbol{q} = (q_x, q_y)$ is an arbitrary real vector, and $\boldsymbol{r_0}$ is some function of $\boldsymbol{q}$ and the eigenenergy E. If $\tau > 0$, the wavefunctions are normalizable regardless of $\boldsymbol{q}$ and E, with characteristic length $l \sim B^{-1/2}$. For each $E \in C$, there is a continuum of bound states centered at different $\boldsymbol{r_0}$. We call these eigenstates CLMs as they are related to zeroth Landau level (0LL) modes of massless 2D Dirac fermions [4]. CLMs of a given energy E have a one-to-one map with the 0LL modes of a given Hermitian Dirac Hamiltonian, whose gauge is determined by E. The CLM eigenstates are thus uncountable because the gauge can be continuously varied.

The 2D lattice in Fig. 1(a) exhibits CLMs in its long-wavelength limit. The Hamiltonian is

$$\mathcal{H} = \sum_r \left[B(y - ix)a_{\boldsymbol{r}}^\dagger a_{\boldsymbol{r}} + t_x\left(a_{\boldsymbol{r}-\hat{x}}^\dagger a_{\boldsymbol{r}} + h.c.\right) + t_y\left(a_{\boldsymbol{r}-\hat{y}}^\dagger a_{\boldsymbol{r}} - h.c.\right)\right] \tag{3}$$

where $a_{\boldsymbol{r}}^\dagger$, $a_{\boldsymbol{r}}$ are creation and annihilation operators at $\boldsymbol{r} = (x,y)$(the lattice constant is set to 1, thus $x, y \in Z$), and $t_x, t_y \in R$ are hopping coefficients. $\mathcal{H}$ is manifestly non-Hermitian. In a slowly-varying envelope approximation, we find that the envelope function obeys $H_{\boldsymbol{k}}\Psi_{\boldsymbol{r}} = E\Psi_{\boldsymbol{r}}$, where to first order in spatial derivatives,

$$H_k = E_k^0 - \left[-i\mu_k\frac{\partial}{\partial x} - By\right] + i\left[-i\nu_k\frac{\partial}{\partial y} - Bx\right] \tag{4}$$

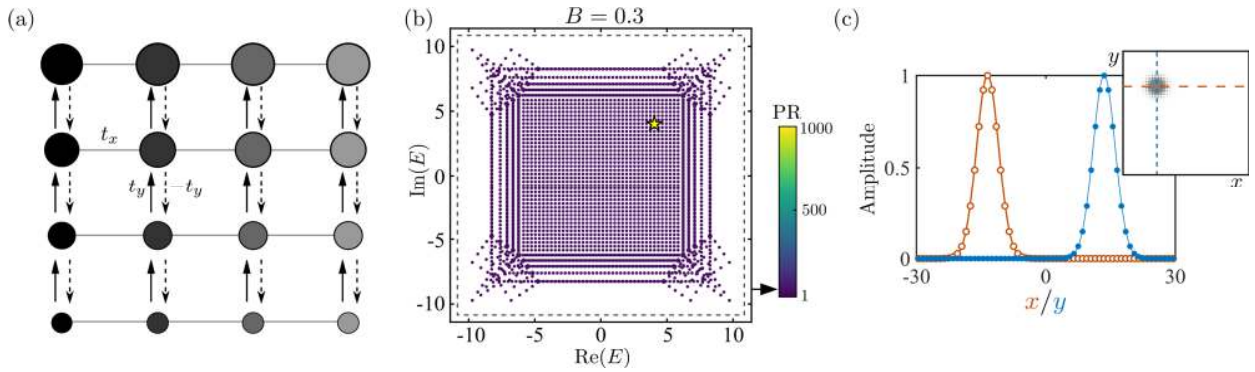


Figure 1: (a) Schematic of a square lattice with reciprocal hoppings along x (gray lines), nonreciprocal hoppings along y (black arrows), and onsite mass $m_{x,y} = B(y - ix)$ (size and darkness of the circles indicate the real and imaginary parts). (b) Complex energy spectrum for a finite lattice of size 60 × 60 with open boundary conditions, with $t_x = t_y = 1$ and $B = 0.3$. The color of each dot corresponds to the eigenstate's participation ratio (larger for less localized states). (c) Wavefunction amplitude for the eigenstate marked by a yellow star in (b). Hollow and filled circles respectively indicate the variation with x and y, along lines passing through the center of each gaussian; solid curves show the CLM predictions. Insets show the distribution in the 2D plane.

where $\mu_{\boldsymbol{k}} = 2t_x \sin k_x$ and $\nu_{\boldsymbol{k}} = 2t_y \cos k_y$. For $B/\mu_{\boldsymbol{k}} < 0, B/\nu_{\boldsymbol{k}} > 0$, there exist CLMs similar to the continuous case. If the lattice is infinite, they form a continuous set over $E \in C$. If the lattice is finite, the CLMs reduce to a band in a finite area of the complex plane, as shown in Fig. 1(b). All the eigenstates are localized, as shown in Fig. 1(c). CLMs can also occur in 1D lattices, we show one of these lattices can serve as a rainbow trap [5], whereby the response to an excitation is concentrated at a position proportional to the frequency. Another lattice can act as a wave funnel [6], concentrating an input excitation onto a boundary over a wide frequency bandwidth.

Summary Non-Hermitian Hamiltonians can violate the usual distinctions between quantized bound states and the continuum of free states. Such systems could be realized on the same platforms (e.g., photonic lattices) already being used to study other non-Hermitian phenomena. It would be interesting to explore other Hamiltonians that cause similar violations, and the physical consequences thereof.

Acknowledge This work was supported by the Singapore MOE Academic Research Fund Tier 3 Grant MOE2016-T3-1-006 and Tier 1 Grant RG148/20, and by the National Research Foundation Competitive Research Programs NRF-CRP23-2019-0005 and NRF-CRP23-2019-0007.

References

1. Teschl, G., "Mathematical methods in quantum mechanics", Grad. Stud. Math., Vol. 99, 106 (2009).
2. Bergholtz, E. J., Budich, J. C. and Kunst, F. K., "Exceptional topology of non-Hermitian systems", Rev. Mod. Phys., Vol. 93, No. 1, 015005 (2021).
3. Heiss, W. D., "The physics of exceptional points", J. Phys. A: Math. Theor., Vol. 45, No. 44, 444016 (2012).
4. Peres, N. M. R., Guinea, F., and Castro Neto, A. H., "Electronic properties of disordered two-dimensional carbon", Phys. Rev. B, Vol. 73, No. 12, 125411 (2006).
5. Tsakmakidis, K. L., Boardman, A. D., and Hess, O., "'Trapped rainbow'storage of light in metamaterials", Nature, Vol. 450, No. 7168, 397 (2007).
6. Weidemann, S., et al., "Topological funneling of light", Science Vol. 368, No. 6488, 311(2020).

META 2023, PARIS - FRANCE, JULY 18 – 21, 2023

Non-orthogonality of Bogoliubov modes and the laser linewidth

I. Amelio[1,2*], I. Carusotto[3]

[1]Center for Nonlinear Phenomena and Complex Systems, Université Libre de Bruxelles, Belgium
[2]Institute of Quantum Electronics, ETH Zurich, Switzerland
[3]INO-CNR BEC Center and Dipartimento di Fisica, Università di Trento, Italy
[*]corresponding author: ivan.amelio@ulb.be

Abstract: The non-orthogonality of Bogoliubov modes accounts for both Henry and Petermann broadening mechanisms of the laser linewidth. Applications to exceptional points, (disordered) topological lasers and polariton condensates are discussed.

For a generic semi-classical laser dynamics in the complex Ginzburg-Landau form, in Ref. 1 we develop a Bogoliubov approach for the computation of the laser emission linewidth. The main ingredients are the Goldstone mode and how fluctuations are projected into this mode, keeping into account the non-orthogonality with the other modes.
Our method provides a unifying, geometric perspective of the treatments by Henry and Petermann: both broadening mechanisms are ascribed to the non-orthogonality of the Bogoliubov modes, which live in a space with doubled degrees of freedom.

We then illustrate a few applications. Even before we discussed the general theory and its geometrical aspects, the method was in fact used to compute the diverging Petermann factor at the exceptional point of a phonon laser (Ref. 2).

Then, in Ref. 3 we developed the approach in full generality to study the Petermann factor of topological lasers. Since the edge mode of a 2D Harper-Hofstadter model is also present at the Hamiltonian level, when saturable gain is introduced and the system lases, the distortion of the the edge mode can be very small and the Petermann factor close to 1. This is a fundamental result, demonstrating that topological lasers can emit in a highly coherent manner. When disorder is considered, our formulas also hold and the linewidth will decrease for small systems. Notice that for very long edges, Bogoliubov theory eventually breaks down and Kardar-Parisi-Zhang physics sets in and disorder can increase coherence!

Finally, the method allows to study the interplay of drive-dissipation, interactions and spatial inhomogeneity typical of polariton condensates (Ref. 1). The traditional theory of the Henry and Petermann factors (the latter comes from a linear analysis of the system close to threshold) is found to fail dramatically in the presence of sizable polariton-polariton interactions, which deform the condensate shape. In particular, also in a strong confining potential, the intrinsically multi-mode nature of the density fluctuations has to be considered in order to describe quantitatively Henry-like phase diffusion.

I. C. acknowledges financial support from the H2020-FETFLAG-2018-2020 project "PhoQuS" (n.820392), and from the Provincia Autonoma di Trento.

References

1. Amelio, I and I. Carusotto, "Theory of the coherence of topological lasers," Phys. Rev. X, Vol. 10, No. 4, 041060, 2020.
2. Zhang J. et al., "A phonon laser operating at an exceptional point," Nat. Photonics, Vol. 12, 479-484, 2018.
3. Amelio, I and I. Carusotto, "Bogoliubov theory of the linewidth and application to polariton condensates," Phys. Rev. A, Vol. 105, No. 2, 023527, 2022.

Non-Hermitian quantum optics in cold atomic ensembles

Georgios A. Siviloglou* and J. F. Chen

Southern University of Science and Technology, Shenzhen, 518055, Guangdong, China
corresponding author: siviloglouga@sustech.edu.cn

Abstract: In this talk, we will introduce a quantum non-Hermitian interface between photons and atoms. A tunable interaction between photonic and magnonic modes is established, and probing non-Hermitian dynamics at the single quantum level is achieved. We demonstrate experimentally quantum interference between two distinct bosonic excitations, and that their tendency to bunch together can be altered by hermiticity.

In an ideal quantum memory, single photons can be stored as single quanta of atomic spin coherence and, in turn, coherence can be converted back to photons. This conversion can be represented by a linear and unitary beamsplitter operation which mixes two different bosonic modes. If the beamsplitting operation can become non-Hermitian, as in the case of a cold atomic ensemble [1], photon bunching can be switched to antibunching.

In our experiments, we demonstrate that controlling the dissipation in an atom-photon interface alters the statistics of quantum interference [2]. The degree of hermiticity is controlled by the detuning of two lasers interacting in laser cooled gas of atomic rubidium. The standard Hong-Ou-Mandel dip is thus reversed, and, in stark contrast, a bump of enhanced coincidence is observed as shown in Figure 1.

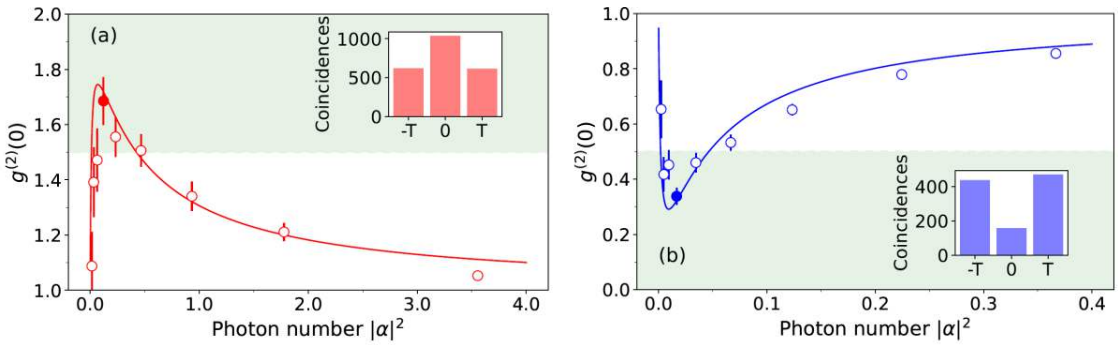


Figure 1: Second-order correlation function as a function of average photon number. Observation of (a) fermionic antibunching, and (b) bosonic bunching between atomic and photonic excitations. Green shading indicates the classically forbidden regions.

This work is supported by the National Natural Science Foundation of China (NSFC) through Grants No. 12074171, No. 12074168, No. 92265109 and No. 12204227; the Guangdong Provincial Key Laboratory (Grant No. 2019B121203002); and the Guangdong projects under Grant No. 2022B1515020096 and No. 516 2019ZT08X324.

References

1. Wen, R., C.-L. Zou, X. Zhu, P. Chen, Z. Y. Ou, J. F. Chen and W. Zhang, "Non-Hermitian magnon-photon interference in an atomic ensemble," Phys. Rev. Lett. 122, 253602, 2019.
2. Wang, X., J. Wang, Z. Ren, R. Wen, C.-L. Zou, G. A. Siviloglou and J. F. Chen, "Quantum interference between photons and single quanta of stored atomic coherence," Phys. Rev. Lett. 128, 083605, 2022.

META 2023, PARIS - FRANCE, JULY 18 – 21, 2023

Observation of tailored non-Hermiticity induced transparency and photonic constant-intensity waves in optical mesh lattices

A. Steinfurth[1], I. Krešić[2], S. Weidemann[1], M. Kremer[1], K. G. Makris[3,4], M. Heinrich[1], S. Rotter[2], and A. Szameit[1*]

[1]Institute for Physics, University of Rostock, A.-Einstein-Str. 23, DE-18059 Rostock, Germany
[2]Institute of Theoretical Physics, Vienna University of Technology, Vienna A-1040, Austria
[2]Physics Department, University of Crete, GR-71003 Heraklion, Greece
[2]Institute of Electronic Structure and Laser, FORTH, GR-71110 Heraklion, Greece
[*]email: alexander.szameit@uni-rostock.de

Abstract: While light waves propagating through inhomogeneous media are typically subject to scattering, non-Hermitian settings allow for these processes to be suppressed by an appropriately tailored complex refracted index. Along these lines, we leverage the additional degrees of freedom presented by gain and loss in optical mesh lattices to observe photonic constant-intensity waves and induced transparency.

When light waves propagate through inhomogeneous media, local scattering and subsequent interference affect both amplitude and phase, giving rise to complex speckle patterns. It has recently been proposed that these distortions can be suppressed by generalizing the initial Hermitian medium to a non-Hermitian system by judiciously adding gain and loss [1,2] (Fig. 1a). While the viability of the underlying concept has been demonstrated for acoustic waves [3], we here present the first all-optical realization in photonic mesh lattices implemented via coupled fiber-loops [4].

Fundamentally, a complex inhomogeneous medium is defined by two degrees of freedom at each point: The real part of the refractive index, and its imaginary part encoding local amplification or damping. In conjunction, both components of the complex refractive index govern the phase and amplitude of propagating waves. Harnessing the tunability of these parameters allows one to synthesize inhomogeneous media in which any distortion due to scattering and subsequent interference is entirely cancelled. Along similar lines, our conceptual framework enables us to tailor the optical properties of non-Hermitian systems to support the propagation of waveforms with (in principle) any desired intensity distribution. To experimentally observe these features, we employ pulse propagation of light in coupled optical fiber-loops (Fig. 1(b) top) [5]. The time-multiplexed pulse dynamics readily map onto a mesh lattice with one spatial and one temporal dimension (Fig. 1(b) bottom), while the desired non-Hermitian characteristics of the lattice sites are implemented with phase- and amplitude modulation that directly address the real and imaginary part of the optical potential for any given lattice site, respectively.

In this vein, we demonstrate here for the first time an optical realization of constant-intensity waves [6] (Fig. 1c) with preserved amplitudes and phases during the propagation through potentials with static disorder. The stark difference between conventional Hermitian systems and our tailored complex inhomogeneous media demonstrates the efficiency of our technique, which is fundamentally based on the direct relation between the wave solution and the medium's optical characteristics [2]. Similarly, any desired propagation pattern can be preserved in an inhomogeneous environment by a time-dependent potential, e.g. for the discrete diffraction pattern known from quantum random walks [7] (Fig. 1d). We anticipate our findings to drive future developments in scattering-free wave propagation or phase-amplitude selective transmission, e.g. for secure communications.

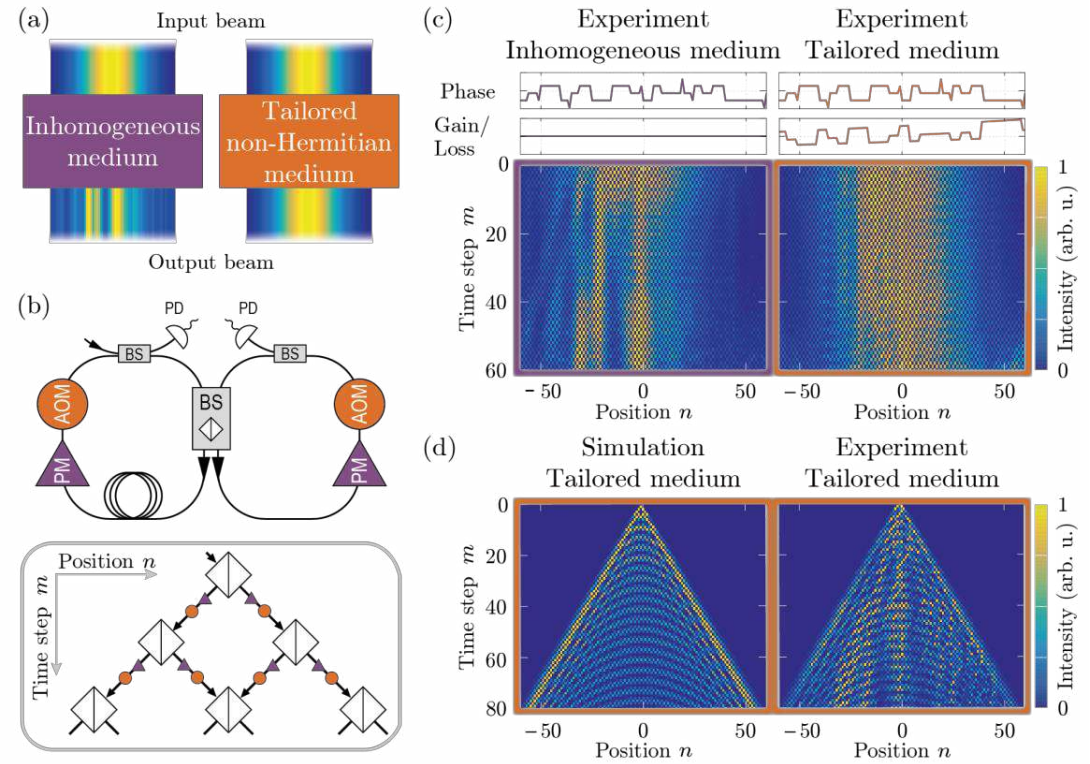


Figure 1: (a) Wave packet distortions in inhomogeneous media can be suppressed by tailored non-Hermiticity. (b) Fiber-loop-based optical mesh lattices employ phase-modulators (PM), beam splitters (BS) and acousto-optical modulators (AOM) in each loop to control the complex potential landscape (top). The time-multiplexed light evolution is recorded by photo detectors (PD) can be mapped onto a 1D lattice (bottom). (c) Compensation of scattering and diffraction for a Gaussian envelope by a time-independent tailored medium (right) versus a conventional inhomogeneous medium (left). (d) Simulation (left) and experimental data (right) of the compensation of scattering for discrete diffraction associated with a homogeneous lattice in an inhomogeneous setting.

References

1. K. G. Makris, A. Brandstötter, P. Ambichl, Z. H. Musslimani, and S. Rotter, "Wave propagation through disordered media without backscattering and intensity variations", Light Sci Appl 6, e17035 (2017).
2. K. G. Makris, I. Krešić, A. Brandstötter, and S. Rotter, "Scattering-free channels of invisibility across non-Hermitian media", Optica 7, 619 (2020).
3. E. Rivet, A. Brandstötter, K. G. Makris, H. Lissek, S. Rotter, and R. Fleury, "Constant-pressure sound waves in non-Hermitian disordered media", Nature Phys. 14, 942 (2018).
4. A. Steinfurth, I. Krešić, S. Weidemann, M. Kremer, K. G. Makris, M. Heinrich, S. Rotter, and A. Szameit, "Observation of photonic constant-intensity waves and induced transparency in tailored non-Hermitian lattices", Sci. Adv. 8, eabl7412 (2022).
5. A. Schreiber, K. N. Cassemiro, V. Potoček, A. Gábris, P. J. Mosley, E. Andersson, I. Jex, and Ch. Silberhorn, "Photons Walking the Line: A Quantum Walk with Adjustable Coin Operations", Phys Rev Lett 104, 050502 (2010).
6. K. G. Makris, Z. H. Musslimani, D. N. Christodoulides, and S. Rotter, "Constant-intensity waves and their modulation instability in non-Hermitian potentials", Nat Commun 6, 7257 (2015).
7. Y. Aharonov, L. Davidovich, and N. Zagury, "Quantum random walks", Phys Rev A 48, 1687 (1993).

META 2023, PARIS - FRANCE, JULY 18 – 21, 2023

Observation-dependent enhancement and suppression of two-photon coincidences by tailored losses

M. Ehrhardt*, M. Heinrich, and A. Szameit

University of Rostock, Institute for Physics, Albert-Einstein-Str. 23, 18059 Rostock, Germany
*corresponding author: max.ehrhardt@uni-rostock.de

Abstract: We investigate the Hong-Ou-Mandel interference of photon pairs in birefringent waveguides with polarization-dependent losses. Depending on the detection basis, we show seamless tunability all the way from enhancement to full suppression of indistinguishable photons.

The Hong-Ou-Mandel (HOM) effect [1] is perhaps the most well-known consequence of two-photon interference, where a pair of indistinguishable photons interferes destructively on a balanced beam splitter. As a result, the photons bunch together in either one of the two output ports, ideally reducing the coincidence rate to zero. Notably, the introduction of non-trivial losses can change this behavior in various ways. For example, parity-time symmetric conditions in an optical coupler have been shown to systematically shift the conditions for fully destructive quantum interference from balanced to unbalanced [2]. Similarly, a lossy beam splitter can actually cause an enhancement of coincidence rates for indistinguishable photons (compared to distinguishable photons), represented by a peak in the HOM experiment [3-5], that is generally associated with fermionic anti-bunching behavior.

In our work, we experimentally demonstrate that bosonic HOM dip characteristics are retained even in the case of a loss-induced peak. To this end, we implement nontrivial losses in a birefringent waveguide via coupling the waveguide to a reservoir (Fig. 1A) with polarization-dependent hopping rates $c_{H/V}$ for horizontal and vertical polarization, respectively. The target waveguide itself represents a polarization coupler [6] that performs polarization oscillation with the rate $\Delta\beta$ (mismatch between horizontal/vertical propagation constants), periodically transferring intensity between the diagonal $|D\rangle$ and antidiagonal $|A\rangle$ polarization states, respectively. Fig. 1B shows the influence of the sink: In addition to the global loss rate of $2\overline{c}$, the difference in the polarization-dependent coupling $\Delta c=c_H-c_V$ to the sink (exemplified in Fig. 1C) yields an imaginary part of the hopping rate. In our experiments, we launch photon pairs with one photon in the state $|D\rangle$ and the other one in the state $|A\rangle$. The experimental setup (Fig. 1D) is used to record the resulting HOM pattern in different observation bases as shown in Fig. 1E: The observed peak with a visibility of 0.541±0.009 in AD-basis is seamlessly transformed into a dip with a visibility of 0.93±0.05 in the horizontal/vertical (HV)-basis by rotating the observation basis.

In conclusion, we presented a nontrivial loss implementation in a polarization coupler. This system serves to combine intrinsically bosonic statistics of the two-photon input state and an enhanced survival probability of indistinguishable photon pairs [7]. As consequence, switching between HOM pattern with dip and peak characteristics is enabled by changing the observation basis.

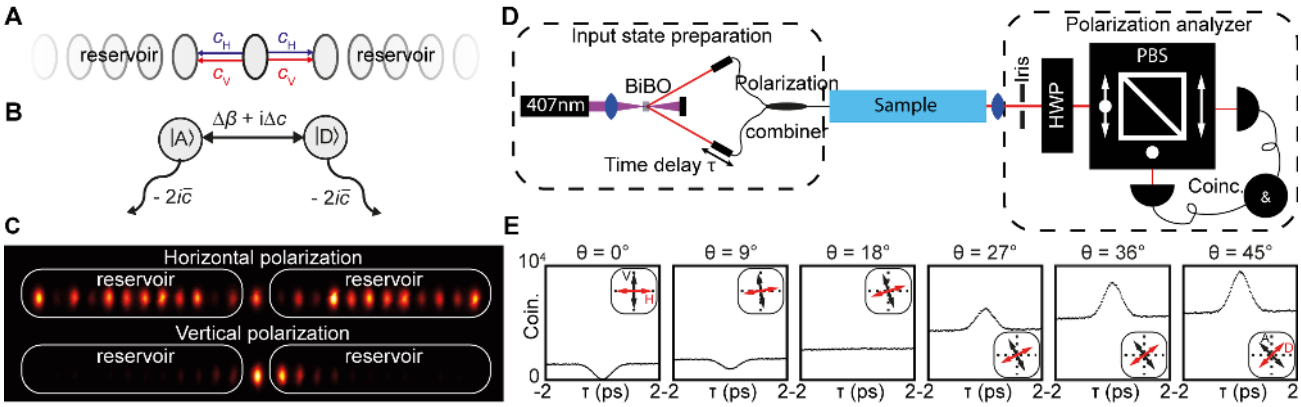


Figure 1. HOM experiment in a lossy polarization coupler. (**A**) A birefringent optical input and target waveguide is coupled to two sinks consisting of a long linear array of tightly coupled waveguides. Polarization-dependent coupling strengths c_H and c_V between the horizontal and vertical (fast/slow principle) axes of the main waveguide and the first waveguide of the sink implement (**B**) a non-trivial loss distribution for photons launched and observed diagonally $|D\rangle$ and antidiagonally $|A\rangle$ towards the HV-frame of reference. (**C**) Intensity distribution of the output after z=15 cm observed with a CCD camera when the central waveguide is illuminated at λ=814 nm. For an excitation in the horizontal polarization only 4.5% intensity remain in the main waveguide, whereas 48.3% remain for the vertical polarization. (**D**) Photon pairs are created via spontaneous parametric down conversion and coupled into a polarization combiner that launches one photon in the state $|A\rangle$ in the main waveguide whereas the other one is launched in the state $|A\rangle$. After the subsequent propagation in the sample, the remaining photons in the target waveguide are analyzed with a polarization beam splitter (PBS). The photons detected with Avalanche photo diodes at the PBS' transmitting and reflecting port, record coincidences in the horizontal/vertical (HV) and antidiagonal/diagonal (AD) polarization basis adjusted via the half-wave plate's (HWP) principal axes orientation. (**E**) HOM patterns recorded in different polarization bases.

References

1. C. K. Hong, Z. Y. Ou, and L. Mandel, "Measurement of subpicosecond time intervals between two photons by interference," Phys. Rev. Lett., vol. 59, no. 18, 2044–2046, 1987.
2. F. Klauck, L. Teuber, M. Ornigotti, M. Heinrich, S. Scheel, and A. Szameit, "Observation of PT-symmetric quantum interference," Nat. Photonics, vol. 13, no. 12, 883–887, 2019.
3. T. A. W. Wolterink, R. Uppu, G. Ctistis, W. L. Vos, K.-J. Boller, and P. W. H. Pinkse, "Programmable two-photon quantum interference in 10^3 channels in opaque scattering media," Phys. Rev. A, vol. 93, no. 5, 53817, 2016.
4. B. Vest et al., "Anti-coalescence of bosons on a lossy beam splitter," Science., vol. 356, no. 6345, 1373–1376, 2017.
5. Q. Li, W. Bao, Z. Nie, Y. Xia, Y. Xue, Y. Wang, S. Yang & X. Zhang, "A non-unitary metasurface enables continuous control of quantum photon–photon interactions from bosonic to fermionic," Nat. Photonics, vol. 15, no. 4, 267–271, 2021.
6. M. Ehrhardt, R. Keil, L. J. Maczewsky, C. Dittel, M. Heinrich, and A. Szameit, "Exploring complex graphs using three-dimensional quantum walks of correlated photons," Sci. Adv., vol. 7, no. 9, eabc5266, 2021.
7. A. Crespi, L. Sansoni, G. Della Valle, A. Ciamei, R. Ramponi, F. Sciarrino, P. Mataloni, S. Longhi, and R. Osellame, "Particle statistics affects quantum decay and Fano interference," Phys. Rev. Lett., vol. 114, no. 9, 090201 (2015).

META 2023, PARIS - FRANCE, JULY 18 – 21, 2023

Compressibility and fluctuations of an optical quantum gas

J. Schmitt

Institute of Applied Physics, University of Bonn, Wegelerstr. 8, 53115 Bonn, Germany
email: schmitt@iap.uni-bonn.de

Abstract: Quantum gases of atoms, exciton-polaritons, and photons provide a test bed for many-body physics under both in- and out-of-equilibrium settings. Experimental control over dimensionality, potentials, or the coupling to reservoirs offers wide possibilities to explore phases of matter, for example, by probing susceptibilities, as the compressibility. For gases of material particles, studies of the mechanical response are well established; for optical quantum gases, they have so far remained elusive. In my talk, I will discuss experimental work demonstrating a measurement of the compressibility of a two-dimensional quantum gas of photons in a box potential inside a dye-filled microcavity, from which we obtain the equation of state for the optical medium [1]. Upon entering the quantum degenerate regime, the density response to an external force sharply increases, hinting at a highly compressible Bose gas. In other recent work, we have demonstrated a non-Hermitian phase transition of an open photon Bose-Einstein condensate, which is revealed by an exceptional point in the fluctuation dynamics [2, 3].

References

1. E. Busley, L. Espert Miranda, A. Redmann, C. Kurtscheid, K. Karkihalli Umesh, F. Vewinger, M. Weitz, and J. Schmitt, Compressibility and the equation of state of an optical quantum gas, *Science* **375**, 1403–1406 (2022)
2. F. E. Oeztuerk, T. Lappe, G. Hellmann, J. Schmitt, J. Klaers, F. Vewinger, J. Kroha, and M. Weitz, Observation of a Non-Hermitian Phase Transition in a Photonic Quantum Gas, *Science* **372**, 88–91 (2021)
3. F. E. Oeztuerk, F. Vewinger, M. Weitz, and J. Schmitt, Fluctuation-dissipation relation for a Bose-Einstein condensate of photons, *Phys. Rev. Lett.* **130**, 033602 (2023)

Stability of Non-Hermitian Hamiltonians with Different Periodicities Using Floquet Theory

Avadh Saxena[1], Julia Cen[1], and Yogesh N. Joglekar[2]

[1]Theoretical Division, Los Alamos National Lab, USA
[2]Department of Physics, Indiana University-Purdue University Indianapolis, USA

By using Floquet theory Hermitian Hamiltonians with time-periodic coefficients can be readily analyzed. They have been extensively used for engineering Floquet Hamiltonians in standard quantum simulators. When generalized to non-Hermitian Hamiltonians, time-periodicity provides important means to engineer the landscape of Floquet quasi-energies across the complex plane. Here, we study two-level non-Hermitian Hamiltonians with coefficients that have different periodicities by invoking Floquet theory [1]. Both parity-time or PT-symmetric and anti-PT (or APT)-symmetric Hamiltonians are considered. Using analytical as well as numerical calculations we obtain the regions of stability, defined by real Floquet quasi-energies and contours of exceptional point (EP) degeneracies. We then extend our analysis to investigate the phases that accompany these cyclic changes. Our results demonstrate that time-periodic, non-Hermitian Hamiltonians generate a truly rich landscape of stable and unstable regions, particularly when compared with single-drive models.

[1] J. Cen, Y. N. Joglekar, and A. Saxena, arXiv:2301:06255

Classifying topological solitons using local markers

S. Wong[1*], T. A. Loring[2], and A. Cerjan[1]

[1]Center for Integrated Nanotechnologies, Sandia National Laboratories, Albuquerque, New Mexico 87185, USA
[2]Department of Mathematics and Statistics, University of New Mexico, Albuquerque, New Mexico 87131, USA
[*]corresponding author: stewong@sandia.gov

Abstract: Due to the local nature of the nonlinearities in nonlinear photonic topological insulators, attempts to describe its topology using traditional band structure approaches are not suitable. Here, we propose to use the so-called spectral localizer, which allows us to define local topological invariants such as a local Chern number. Using the nonlinear Haldane model with on-site Kerr terms, we show that the soliton can creates topological interfaces inside the lattice.

In recent years, photonic topological insulators (PTIs) have gained substantial interest due to their promise to improve current photonics devices with their topologically protected edge states **[1]**. At high optical power, it becomes natural to consider nonlinear PTIs. However, the topological characterization of the solitons, so far, has been relying on a band structure formalism **[2]**, which does not fully account for the nonlinear phenomena due to the local nature of the nonlinearities. Here, we present a general framework for classifying topological solitons using local markers that is applicable to topology of any dimension in the ten Altland-Zirnbauer classes **[6]**. As these local markers can be calculated entirely from the system's real-space properties, and without projecting into an occupied subspace, they can be directly applied to non-linear systems. Finally, we illustrate this general framework using a Haldane lattice with on-site Kerr terms.

Compared to traditional topological descriptions that rely upon a system's Bloch eigenstates to characterize its topology, the spectral localizer takes an operator-based approach. This approach can be seen as the real-space analogue to topological quantum chemistry, namely by looking for obstructions that prohibit continuing the system to an atomic limit **[3]**. For a two-dimensional system, the localizer can be defined as **[4]**:

$$L_{\lambda=(x,y,E)}(X,Y,H) = \begin{pmatrix} (H-E) & \kappa(X-x)-i\kappa(Y-y) \\ \kappa(X-x)+i\kappa(Y-y) & -(H-E) \end{pmatrix}, \quad (1)$$

where H is the Hamiltonian matrix considered, X, Y are the position operators that are diagonal matrices indexing the position of the sites, and $\lambda = (x, y, E)$ is to be seen as an input for the local probing of the topology in space (x,y) and energy (E). κ is a hyperparameter that makes the units consistent between the position and Hamiltonian matrices. The localizer framework shares similar features as the band structure approach. Indeed, its spectrum $\sigma(L_\lambda)$ can heuristically be understood as a real-space, local analogue of the bulk bands. For the 2D system in class A **[6]**, the spectral localizer can be used to find the local Chern number **[4]** defined as:

$$C_{L,\lambda} = \frac{1}{2} sig(L_\lambda(X,Y,H)), \quad (2)$$

where $sig(M)$ is the signature of the matrix M, i.e., the number of positive eigenvalues minus the number of negative ones, and for which the local Chern number can only change through a gap closing of the localizer spectrum, namely when $\min(|\sigma(L_\lambda)|) = 0$. The topological robustness can then be represented by its localizer gap $\Delta L_\lambda := \min(\sigma(L_\lambda))$.

As an example for describing the topology in nonlinear PTIs, we consider the nonlinear Haldane lattice **[5]**, with the lattice geometry as shown in Fig. 1(a). The lattice is characterized by a (next) nearest neighbor coupling

t_1 ($t_2/t_1 = 0.5$), an inversion-symmetry-breaking on-site term $M/t_1 = 0.3 * 3\sqrt{3}$, a time-reversal-symmetry-breaking Haldane flux $\phi = \pi/2$, and on-site Kerr terms $g|c_n|^2$ with $|c_n|^2$ being the intensity at the given site n. Given the above parameters, the linear lattice (g = 0) is in the topologically non-trivial phase which is given by the condition $|M/t_2| < 3\sqrt{3}\,|\sin\phi|$. Here, we consider a nonlinear mode ψ_{NL} [Fig. 1(a)] obtained by numerical continuation of the linear mode at energy $E/t_1 = 1.28$, by first increasing the Kerr coefficient $g/t_1 = 0 \rightarrow 3$, then by increasing the total power $\|\psi_{NL}\|^2 = 1 \rightarrow 7.8$. The obtained nonlinear Hamiltonian matrix $H(\psi_{NL})$ is then used to calculate the localizer [Eq.1-2] at $E/t_1 = E_{NL}/t_1 = 1.028$. Figure 1(b) plots the local Chern number obtained across the whole lattice, directly revealing the real-space picture of the topology of the system. There is a topological interface at the edge of the lattice as expected from the lattice being in the topological non-trivial phase. However, the system also reverts to a trivial topological phase in two locations in its interior where the strength of the soliton results in strong on-site energies, yielding another pair of topological interfaces. This shows the topological nature of the obtained soliton, which is self-sustained by the topological edge states created at the topological interface. By looking at the localizer spectrum $\sigma(L_\lambda)$ [Fig. 1(c)], one can also quantify the robustness of the topological soliton to be $\Delta L_\lambda/\Delta E = 2.7\%$, with ΔE being the bulk band gap in the linear lattice. This shows that the nonlinear mode is weakly protected in case of perturbation $\|\delta H\|$ of the order of 2.7% of bulk band gap.

To conclude, using a real-space picture of the topology of the system, we demonstrate the topological origin of a given soliton mode as well as its topological robustness against disorder.

This work is part-funded by Sandia National Laboratories (SNL). SNL is managed and operated by NTESS under DOE NNSA contract DE-NA0003525.

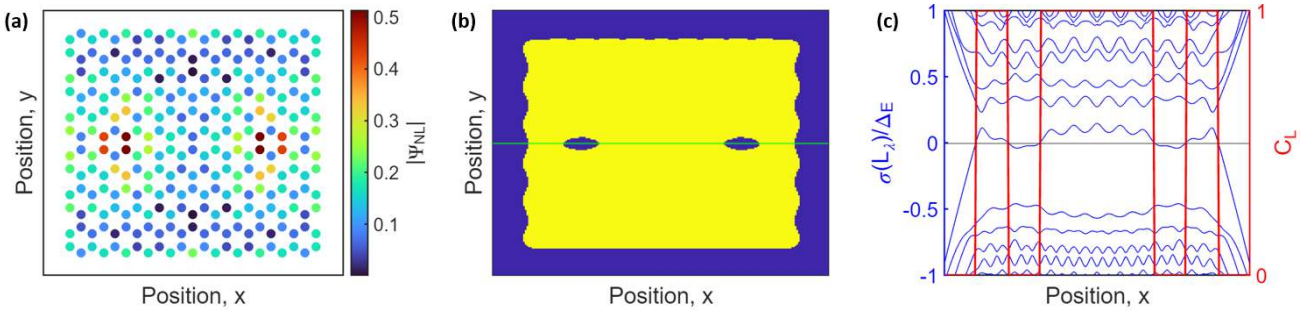


Figure 1: (a) Field profile of the soliton $|\psi_{NL}|$. (b) Local Chern number C_L across the lattice (and outside the lattice). Yellow (purple) region correspond to $C_L = 1$ ($C_L = 0$). (c) Spectrum of the localizer normalized to bulk band gap $\sigma(L_\lambda)/\Delta E$ and the local Chern number C_L along the green line in panel (b). For panels (b) and (c), $E = E_{NL} = 1.028t_1$ and $\kappa = 2.2$ has been used.

References

1. Ozawa T., Price H. M., Amo A., et al, "Topological photonics", Rev. Mod. Phys. 91, 015006 (2019).
2. Smirnova D., Leykam D., Chong Y.D., et al., "Nonlinear topological photonics", Appl. Phys. Rev. 7, 021306, (2020).
3. Loring T. A., "K-theory and pseudospectra for topological insulators", Ann. Phys. 356, 383-416, (2015).
4. Cerjan A. and Loring T. A., "Local invariants identify topology in metals and gapless systems", Phys. Rev. B. 106, 064109, (2022).
5. Haldane F. D. M., "Model for a quantum Hall effect without Landau levels: Condensed-matter realization of the "parity anomaly", Phys. Rev. Lett. 61, 2015 (1988).
6. Altland A. and Zirnbauer, M. R., "Nonstandard symmetry classes in mesoscopic normal-superconducting hybrid structures", Phys. Rev. B 55, 1142, (1997).

META 2023, PARIS - FRANCE, JULY 18 – 21, 2023

Experimentally realizable *PT* phase transitions in reflectionless quantum scattering

M. B. Soley[1*], C. M. Bender[2*], and A. D. Stone[3]

[1]University of Wisconsin-Madison, USA
[2]Washington University, St. Louis, USA
[3]Yale University, USA
[*]corresponding author: msoley@wisc.edu

Abstract: We demonstrate theoretically that *PT*-symmetry behaviors could be measured in fundamental Schrödinger quantum mechanics via standard cold-atom experiments. Whereas *PT* symmetry-breaking has previously only been measured for classical wave equations or open quantum systems with complex potentials and inherent information loss, we identify spontaneous *PT*-symmetry breaking in a novel family of purely real, experimentally realizable quantum potentials, $V(x)=-|x|^p$ for real p. The results encourage the search for quantum *PT* symmetry behaviors and the development of quantum *PT* symmetry technologies.

PT (parity-time reversal) symmetry has seen great success in optics, with applications from lasing and sensing to wireless power transfer. Despite *PT* symmetry's promise in quantum mechanics, the only quantum *PT*-symmetry experiments have been for open systems with complex potentials, which entail inherent information loss. We introduce a novel class of purely real potentials ($V(x)=-|x|^p$ for real p truncated to constant energy beyond the region $-L\leq x\leq L$) that makes *PT* symmetry experimentally realizable in fundamental quantum mechanics. We show these potentials make possible the measurement of quantum *PT* symmetry behaviors, including spontaneous *PT*-symmetry breaking, in standard cold-atom experiments with programmable traps [1].

In particular, we consider the curious case of weakly bound states in upside-down *PT*-symmetry potentials. Upside-down *PT*-symmetry potentials of the form $V(x)=-x^p$ for $p=2,4,6\ldots$ at first appear not to support bound states, as the potentials tend towards minus infinity at large distances from the origin. Yet, consideration of the complex Schrödinger equation indicates the potentials in fact support an infinite set of weakly bound states [2,3,4]. Straightforward implementation of the potential in fundamental Schrödinger quantum mechanics is not possible, as the potentials are both infinite-length and unbounded in energy. In contrast, the aforementioned novel class of potentials are finite in length and bounded in energy, and therefore are amenable to elementary quantum scattering experiments. Inspired by ref. [3], we hypothesize that reflectionless states in these potentials reproduce the weakly-bound states for sufficiently large L. We identify these states by applying the general theory of reflectionless scattering mode (RSM) theory from optics [5,6] to quantum mechanics for the first time.

We find the novel class of potentials reproduces the eigenvalues and eigenstates of the upside-down *PT*-symmetric potentials to high accuracy. The RSM energies agree with the analytic eigenvalues with up to 7-8 digits to arbitrarily high energy and are robust to various models of experimental error over wide ranges of noise strengths. Likewise, the RSM wavefunctions exhibit all the expected behaviors of the eigenstates, including a symmetric probability density, oscillatory behavior, and subexponential decay.

Importantly, we find the novel class of potentials enables measurement of spontaneous *PT*-symmetry breaking in fundamental quantum mechanics for the first time. Previously, spontaneous quantum *PT*-symmetry breaking has been seen for the analytic continuations of the upside-down *PT*-symmetric potentials, $V(x)=x^2(ix)^\varepsilon$ and $V(x)=x^4(ix)^\varepsilon$ [2,4]. However, these potentials are inherently complex except at even integer values of ε. Instead,

we consider the novel class of purely real potentials for varying p. We find the class in fact exhibits all phases of *PT* symmetry: The fully-broken phase appears for $p \leq 2$, a mixed phase appears for $2<p<4$, and an unbroken phase appears for $p \leq 2$. In addition, the quantum phase transitions are accompanied by a "smoking-gun" of *PT*-symmetry breaking: the reflection coefficient transitions from a quadratic to quartic reflection coefficient lineshape at clear exceptional points.

Preliminary results indicate that implementation of the proposed quantum system is well within reach of today's experimental cold-atom approaches. The required energy and length scales are commensurate with readily reachable ultracold temperatures for Bose-Einstein condensates of alkali atoms, and the potentials can be readily produced with techniques such as Digital Micromirror Devices (DMD) and holographic methods. These results suggest the proposed system can be straightforwardly implemented in cold-atom experiments with programmable traps and calls for further search for *PT* symmetry behaviors in fundamental quantum cold-atom systems.

Acknowledgements: The authors would like to thank E. J. Heller for discussions and Yale Quantum Institute Postdoctoral Fellowship, Simons Collaboration on Extreme Wave Phenomena Based on Symmetries, Alexander von Humboldt Foundation, and the UK Engineering and Physical Sciences Research Council (EPSRC) grant at King's College London for financial support.

References

1. Soley, M. B., Bender, C. M., Stone, A. D. "Experimentally-realizable *PT* phase transitions in reflectionless quantum scattering," arXiv:2209.05426, 2022.
2. Bender, C. M., Boettcher, S. "Real Spectra in Non-Hermitian Hamiltonians Having *PT* Symmetry," Phys. Rev. Lett., Vol. 80, No. 24, 5243, 1998.
3. Bender, C. M., Gianfreda, M. "Scattering off *PT*-symmetric upside-down potentials," Phys. Rev. A, Vol. 98, No. 5, 052118, 2018.
4. Bender, C. M. "Making sense of non-Hermitian Hamiltonians," Rep. Prog. Phys., Vol. 70, No. 6, 947-1018, 2007.
5. Sweeney, W. R., Hsu, C. W., Stone, A. D., Phys. Rev. A, "Theory of reflectionless scattering modes," Vol. 10, No. 6, 063511, 2020.
6. Stone, A. D., Sweeney, W. R., Hsu, C. W., Wisal, K., Wang, Z. "Reflectionless excitation of arbitrary photonic structures: a general theory," Nanophoton.,Vol. 10, No. 1, 343-360, 2021.

META 2023, PARIS - FRANCE, JULY 18 – 21, 2023

Restoration of the non-Hermitian bulk-boundary correspondence via topological amplification

M. Brunelli[1*], C. C. Wanjura[2], A. Nunnenkamp[3]

[1]Department of Physics, University of Basel, Klingelbergstrasse 82, 4056 Basel, Switzerland

[2]Cavendish Laboratory, University of Cambridge, Cambridge CB3 0HE, United Kingdom

[3]Faculty of Physics, University of Vienna, Boltzmanngasse 5, 1090 Vienna, Austria

[*]corresponding author: matteo.brunelli@unibas.ch

Abstract: Starting from an open quantum system description of driven-dissipative arrays of cavities, I show how to restore the bulk-boundary correspondence for the most paradigmatic class of non-Hermitian lattice Hamiltonians, namely those involving a single complex band, and how this links to topological amplification.

Non-Hermitian (NH) lattice Hamiltonians display a unique kind of energy gap and extreme sensitivity to changes of boundary conditions—the so-called NH skin effect. Due to the NH skin effect, the separation between edge and bulk states is blurred and the bulk-boundary correspondence in its conventional form breaks down [1]. Despite considerable efforts to accommodate the NH skin effect into a modified bulk-boundary correspondence, a formulation for point-gapped spectra has remained elusive.

In this contribution, I will show how to restore the bulk-boundary correspondence for the most paradigmatic class of NH lattice models, namely single-band models without symmetries [2]. This is achieved by presenting an alternative route to the classification of NH topological phases, where the focus is shifted (i) from effective NH Hamiltonians to NH Hamiltonians obtained from the unconditional dynamics of driven-dissipative arrays of cavities, and (ii) from the eigen-decomposition to the singular value decomposition as the main tool for studying their bandstructure.

The class of NH Hamiltonians that reveal the bulk-boundary correspondence are unconditional NH Hamiltonians which do not neglect quantum jumps altogether but instead retain a contribution from fluctuation-dissipation processes by averaging over the quantum state of the system. Concretely, the desired NH Hamiltonian is implemented in one-dimensional driven-dissipative cavity arrays, in which Hermiticity-breaking terms—in the form of non-reciprocal hopping amplitudes, gain and loss—are explicitly modelled via coupling to (engineered and non-engineered) reservoirs. I will show that this approach introduces extra constraints to the NH Hamiltonian, neglected so far, which determine the following major changes to the topological characterization: First, the complex spectrum is not invariant under complex energy shifts, which removes the arbitrariness in the definition of the topological invariant. Second, topologically non-trivial Hamiltonians are only a strict subset of those with a point gap; this implies that the NH skin effect does not have a topological origin. Third, topological phase transitions are accompanied by the closure of a real-valued gap, defined in terms of the singular values.

I will then show how to reinstate the bulk-boundary correspondence in terms of the singular value decomposition, instead of the eigen-decomposition, and explain its physical significance. The NH bulk-boundary correspondence takes the following simple form: *An integer value* $\nu \in \mathbb{Z}$ *of the winding number defined on the complex spectrum of the system under periodic boundary conditions corresponds to* $|\nu|$ *exponentially small*

singular values associated with singular vectors that are exponentially localized at the system's edge under open boundary conditions and vice versa; the sign of ν *determines at which edge the vectors localize*. Non-trivial topology manifests as directional amplification with gain exponential in system size, which is the hallmark of NH topology [3]. I will explain the physical relevance of this peculiar behaviour.

References

1. E. J. Bergholtz, J. C. Budich, and F. K. Kunst, Rev. Mod. Phys. 93, 015005 (2021).
2. M. Brunelli, C. C. Wanjura, and A. Nunnenkamp, arXiv:2207.12427 (2022).
3. C. C. Wanjura, M. Brunelli, and A. Nunnenkamp, Nature Communications 11, 3149 (2020).

Non-Hermitian dispersive hydrodynamics and Riemann problems

Sathyanarayanan Chandramouli[1*], Nicholas Ossi[1], Ziad H. Musslimani[1] and Konstantinos G. Makris[2,3]

[1]Florida State University, Tallahassee, Florida 32306, United States of America
[2] Institute of Electronic Structure and Laser (IESL), Foundation for Research and Technology - Hellas (FORTH), 71110 Heraklion, Greece **and** [3]ICTP, Department of Physics, University of Crete, 71003, Heraklion, Greece
[*]corresponding author: sc17n@fsu.edu

Abstract: Dispersive hydrodynamics (DH) is the study of nonlinear dispersive wave dynamics in fluid-like media. A fundamental problem in DH corresponds to studying the dynamics of a Riemann problem: a step-like initial condition connecting two constant amplitude states. Constant-intensity waves can exist in non-Hermitian optical media (while generally absent in Hermitian inhomogeneous environments). Thus, we can define and study the notion of non-Hermitian dispersive hydrodynamics and its associated Riemann problems in both ordered and disordered optical media for the first time.

The last decade or so has witnessed an intense interest in the general area of dispersive hydrodynamics and its associated Riemann problems [1]. Central to this effort is the investigation into the structure and formation of dispersive shock waves. Much of the research done along these lines has revolved around nonlinear wave propagation inside a homogeneous and conservative medium, where the total power or integrated density is time-independent. Extensions to scenarios involving weak dissipation have however been proposed and studied, with the KdV-Burger's equation being a prototypical test bed model. On the other hand, certain nonlinear wave phenomena (such as DSW) can occur in a spatially non-uniform media, as is the case, for example, in Bose-Einstein condensate flows [1] and optical waveguide arrays [2] and resonant fluid flows over variable topography [3], to name a few. Often, the interplay between dissipation and inhomogeneity lead to the formation of novel multi-scale wave excitations (for example, in polariton condensate flows: [4]). Generally speaking, in inhomogeneous media (conservative or dissipative) plane waves of constant amplitude are no longer viable. This in turn leads to the fundamental question as to how one can formulate and study dispersive hydrodynamics through the lens of Riemann problems. An equally important related issue is the effect of non-Hermiticity (that manifests itself in the gain-loss distribution) on wave breaking. In this paper, leveraging on the new concept of non-Hermitian constant intensity waves, originally proposed in [5] (additional references [6],[7]), we develop a general framework within which non-Hermitian dispersive hydrodynamics and its associated non-Hermitian, Riemann problems can be studied.

Our starting point is the NLS equation with external Wadati potential

$$i\psi_t + \frac{1}{2}\psi_{xx} + \frac{1}{2}(w^2(x) - iw'(x))\psi - |\psi|^2\psi = 0 - - - (1),$$

where $w(x) = \theta'(x)$. Eq. (1) supports a one-parameter (ρ_0) family of constant intensity solutions of the form

$$\psi_{CI}(x,t) = \sqrt{\rho_0}e^{i(\theta(x) - \rho_0 t)} - - - (2)$$

Eq. (1) also governs the dynamics of a dispersive "fluid", which can be seen by considering the polar representation

$$\psi(x,t) = \sqrt{\rho(x,t)}\exp\left(i\phi(x,t)\right), \text{ where } u(x,t) = \phi_x - - - (3),$$

that when inserted into (1) yields the system

$$\rho_t + (\rho u)_x = \rho w'(x) - - - (4)$$
$$(\rho u)_t + (\rho u^2 + \mathsf{P} + R)_x = w'(u + w)\rho - - - (5)$$

This system with reaction terms thus governs wave intensity and momentum dynamics in active media with gain

and loss. Here, $\mathsf{P} \equiv \rho^2/2$ and $R \equiv -\frac{1}{4}\rho(\ln\rho)_{xx}$.These hydrodynamic equations possess source terms that are proportional to the imaginary and real parts of the external potential respectively. These additional new terms give rise to a host of new nonlinear wave patterns that do not exist in bulk media. This hydrodynamic system also conserves a “modified" hydrodynamic momentum density

$$\big(\rho(u-w)\big)_t + \big(\rho(u-w)u + \mathsf{P} + R\big)_x = 0 \quad ---(6)$$

while also admitting constant intensity hydrodynamic backgrounds (Eq.(2)).

Within this setting, we thus formulated for the first time a three-parameter family of (non) centered Riemann problems for Eq. (1) that connect two exact and modulationally stable CI states

$$\psi(x,0) = \begin{cases} \sqrt{\rho_0^{(1)}}\exp(i\theta(x)), & \text{as } x < x_0, \\ \sqrt{\rho_0^{(2)}}\exp(i\theta(x)), & \text{as } x > x_0, \end{cases} \quad ---(7)$$

where x_0 (the location of the step) is an additional parameter influencing the dynamics of the non-centered Riemann problems. The long-time evolutions of these non-Hermitian Riemann problems reveal rich dynamics [8], particularly due to the loss of space-translational and reflection symmetries.

Acknowledgements: Sathyanarayanan Chandramouli and Nicholas Ossi would like to thank Dr. Mark Hoefer, Dr. Gennady El, Dr. Patrick Sprenger, and Dr. Panayotis Kevrekidis for the insightful discussions. Special thanks to the Isaac Newton Institute for the hospitality extended to SC and NJO during the dispersive hydrodynamics workshop, where a part of this work was presented.

References

1. Gennady A El and Mark A Hoefer. Dispersive shock waves and modulation theory. Physica D: Nonlinear Phenomena, 333:11–65, 2016.

2. Shu Jia, Wenjie Wan, and Jason W Fleischer. Dispersive shock waves in nonlinear arrays. Physical review letters, 99(22):223901, 2007.

3. Roger HJ Grimshaw and Noel F Smyth. Resonant flow of a stratified fluid over topography. Journal of Fluid Mechanics, 169:429–464, 1986

4. Alberto Amo, Daniele Sanvitto, Fabrice P Laussy, Dario Ballarini, Elena del Valle, *et al*. Collective fluid dynamics of a polariton condensate in a semiconductor microcavity. Nature, 457(7227):291–295, 2009.

5. Konstantinos G Makris, Ziad H Musslimani, Demetrios N Christodoulides, and Stefan Rotter. Constant-intensity waves and their modulation instability in non-hermitian potentials. Nature Communications, 6(1):1– 7, 2015.

6. Nicholas Ossi, Sathyanarayanan Chandramouli, Ziad H Musslimani, and Konstantinos G Makris. Topological constant-intensity waves. Optics Letters, 47(4):1001–1004, 2022.

7. Dmitry A Zezyulin. Nonlinear schrödinger equations with amplitude-dependent wadati potentials. Physical Review E, 106(5):054209, 2022.

8. Sathyanarayanan Chandramouli, Nicholas Ossi, Ziad H Musslimani, and Konstantinos G Makris. Non-Hermitian dispersive hydrodynamics and Riemann problems. *Under review*.

META 2023, PARIS - FRANCE, JULY 18 – 21, 2023

Models and other phenomena in photonic Chern insulator systems

Mark J. Ablowitz[1], **Justin T. Cole**[2*], **and Sean D. Nixon**[1]

[1]University of Colorado, Boulder USA
[2]University of Colorado, Colorado Springs USA
[*]corresponding author: jcole13@uccs.edu

Abstract: Methods for deriving discrete models of Chern insulators in photonic lattices will be discussed. In particular, honeycomb lattices in Floquet longitudinally driven and magneto-optical systems are found to described by similar asymptotic models, namely the Haldane model. The second half of the talk will focus on some recent results. Spiral wave solutions and how to generate them will be discussed. In addition, a phase-induced switching effect along interface boundaries will be discussed.

META 2023, PARIS - FRANCE, JULY 18 – 21, 2023

Exceptional robustness of anomalous topological scattering network

Z. Zhang[1*], P. Delplace[2], and R. Fleury[1]

[1] Laboratory of Wave Engineering, School of Electrical Engineering, EPFL, Station 11, 1015 Lausanne, Switzerland
[2] Ens de Lyon, CNRS, Laboratoire de physique, F-69342 Lyon, France
[*]corresponding author: zhe.zhang@epfl.ch

Abstract: Robustness against defects and disorder is one of the most appealing properties of topological insulators. However, such topological resilience typically collapses when the level of disorder is beyond the magnitude of the band gap. Here, we address this problem by exploring the anomalous topological insulator in non-reciprocal scattering networks, whose edge transport survives strong disorder, and even thrives in the absence of periodicity in very amorphous cases. We experimentally confirm such exceptional robustness on microwave scattering networks.

References

1. Zhang, Zhe, Pierre Delplace, and Romain Fleury. "Anomalous topological waves in strongly amorphous scattering networks." Science Advances (2023).
2. Zhang, Zhe, Pierre Delplace, and Romain Fleury. "Superior robustness of anomalous non-reciprocal topological edge states." Nature 598.7880 (2021): 293-297.

Topological framework for directional amplification in driven-dissipative cavity arrays

C. C. Wanjura[1*], M. Brunelli[2], and A. Nunnenkamp[3]

[1]Max Planck Institute for the Science of Light, Erlangen, Germany
[2]University of Basel, Switzerland
[3]University of Vienna, Austria
[*]corresponding author: clara.wanjura@mpl.mpg.de

Abstract:
We present a unifying framework based on non-Hermitian topology to understand non-reciprocity and directional amplification in driven-dissipative cavity arrays. Specifically, there is a one-to-one correspondence between non-trivial non-Hermitian topology defined on the spectrum of the dynamic matrix and regimes of directional amplification, in which the end-to-end gain grows exponentially in system size. The distance between complex spectrum and origin (size of the point gap) determines the amount of tolerated disorder which makes topological, directional amplification extremely robust against disorder.

Directional amplification, in which signals are selectively amplified depending on their propagation direction, has attracted much attention as key resource for applications, including quantum information processing. Recently, several, physically very different, directional amplifiers have been proposed and realized in the lab. Here, we present a unifying framework based on non-Hermitian topology to understand non-reciprocity and directional amplification in driven-dissipative cavity chains [1-2].

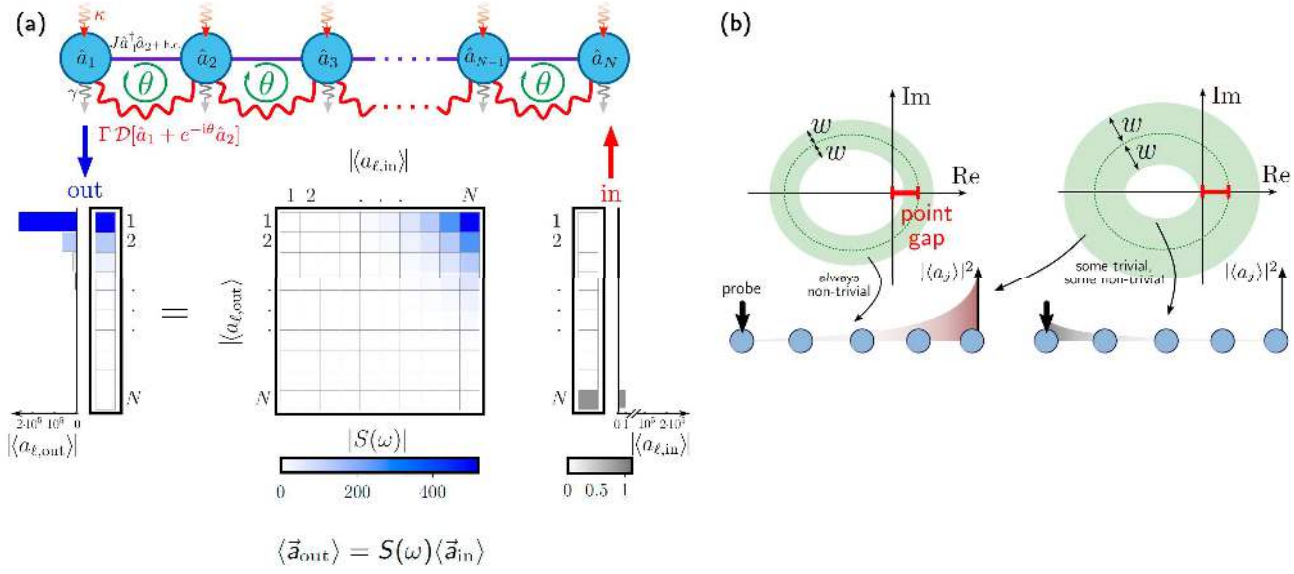


Figure 1. Topological, directional amplification in a driven-dissipative chain. (a) In topologically non-trivial regimes, input signals are amplified from one end to the other but suppressed in the reverse [1]. (b) The amount of tolerated disorder w is set by the distance of the complex spectrum from the origin (size of the point gap) [2]. If the disorder strength is smaller than the size of the point gap, any disordered realization will display directional amplification and the robustness is guaranteed; if the disorder strength exceeds the size of the point gap, robustness against disorder is not guaranteed and the directional amplification may be lost.

We consider translational-invariant bosonic systems in which nearest-neighbours are coupled through bi-linear Hamiltonian terms and non-local dissipators [1], e.g. Figure 1 (a). All modes are subject to decay and possibly incoherent pumping. The system is furthermore coupled to input-output waveguides at rate γ which allows to probe the scattering response of the system. This gives rise to equations of motion of the form $\langle \dot{a}_j \rangle = \sum_\ell H_{j,\ell} \langle a_\ell \rangle - \sqrt{\gamma} \langle a_{\ell,\mathrm{in}} \rangle$ in which $\langle a_\ell \rangle$ denotes the mean cavity field of the ℓth mode, H is the non-Hermitian dynamic matrix and $\langle a_{\ell,\mathrm{in}} \rangle$ the probe field incident on the ℓth site. The scattering matrix $S(\omega) = \mathbb{I} + \gamma(\mathrm{i}\omega\mathbb{I} + H)^{-1}$ encodes the system response to this probe relating input to output fields $\langle a_{j,\mathrm{out}} \rangle = \sum_\ell S_{j,\ell}(\omega) \langle a_{\ell,\mathrm{in}} \rangle$. $|S(\omega)|^{\mathrm{T}} \neq |S(\omega)|$ implies non-reciprocity, since transmission in forward and backward direction differ, while $\left|S_{j,\ell}(\omega)\right| > 1$ implies amplification with the gain $\mathcal{G}(\omega) \equiv |S(\omega)|^2$.

We define a winding number as topological invariant on the complex spectrum $H(k)$ of the dynamic matrix under periodic boundary conditions in reciprocal space which counts the number of times $H(k)$ encircles the origin. Moving from periodic to open boundary conditions, we have shown that there is a one-to-one correspondence between a non-zero winding number and regimes of directional amplification, in which the end-to-end gain grows exponentially with the number of cavities [1]. Specifically, we derived an analytic expression for the scattering matrix in topologically non-trivial regimes [1]

$$S(\omega) \cong \overbrace{\sqrt{\mathcal{G}(\omega)} \sum_{j,\ell} f(j,\ell)\, |j\rangle\langle\ell|}^{\text{directional amplification}} + \overbrace{\begin{pmatrix} \text{PBC} \\ \text{background} \end{pmatrix}}^{\ll \mathcal{G}(\omega)} + \begin{pmatrix} \text{exponentially} \\ \text{small correction} \end{pmatrix}$$

in which the gain $\mathcal{G}(\omega) \propto e^{\alpha N}$ ($\alpha > 1$) grows exponentially with the number of sites N. The function $f(j,\ell)$ shapes the scattering matrix leading to a dominant matrix corner resulting in directional end-to-end gain, see Figure 1 (a). The transmission in the reverse direction, the reverse gain $\bar{\mathcal{G}}(\omega)$, is exponentially suppressed, $\bar{\mathcal{G}}(\omega) \propto e^{-\alpha N}$, and at the exceptional point $\bar{\mathcal{G}}(\omega) = 0$ exactly. Parameter regimes achieving directional amplification can be elegantly obtained from a topological 'phase diagram' [1].

Realistic systems are always subject to disorder. However, we have shown that topological, directional amplification is extremely robust against disorder [2]. Indeed, the separation between the complex spectrum and the origin (the size of the point gap) determines the amount of tolerated disorder, see Fig. 1 (b). Furthermore, we have shown that the zero reverse gain associated with exceptional points remains exactly zero in the presence of arbitrary on-site disorder.

On a practical level, our work unifies existing proposals for both phase-preserving and phase-sensitive directional amplifiers and provides a guiding principle for the design of novel multimode directional amplifiers that can be implemented with state-of-the-art platforms such as superconducting circuits, optomechanics, photonic crystals and nanocavity arrays. On a fundamental level, our framework predicts immediate physical and observable consequences for a topological invariant closing the gap between theory and experiment since non-Hermitian winding numbers are otherwise difficult to extract.

Acknowledgements: We acknowledge funding received from the Winton Programme for the Physics of Sustainability, EPSRC (Project Reference EP/R513180/1), the Royal Society, and the European Union's Horizon 2020 research and innovation programme under Grant No. 732894 (FET Proactive HOT).

References

1. Wanjura, C.C., Brunelli, M. and Nunnenkamp, A. "Topological framework for directional amplification in driven-dissipative cavity arrays," *Nat Commun* **11**, 3149, 2020.
2. Wanjura, C.C., Brunelli, M. and Nunnenkamp, A. "Correspondence between Non-Hermitian Topology and Directional Amplification in the Presence of Disorder," Phys. Rev. Lett. 127, 213601 2021.

META 2023, PARIS - FRANCE, JULY 18 – 21, 2023

Non-Hermitian optical design by coordinate transformations and mapping

I. Kresic[1,*], K. G. Makris[2], A. Brandstötter[1], U. Leonhardt[3] and S. Rotter[1]

[1]Technical University of Vienna (TU Wien), Austria
[2]University of Crete, Greece
[3]Weizmann Institute of Science, Israel
[*]corresponding author: ivor.kresic@tuwien.ac.at

Abstract: Coordinate transformations have been a powerful tool for design of metamaterial optical structures during the last 15 years [1]. In this talk I will discuss our recent research about theoretical methodologies for creating non-Hermitian transparent materials [2], invisibility cloaks [3], and light confinement [4], by coordinate transformations and mapping of electromagnetic field solutions.

Waves typically propagate very differently through homogeneous medium than through an inhomogeneous medium such as complex dielectric structures. In the first part of the talk I will present the surprising result that wave solutions in two-dimensional free space can be mapped to a solution inside a suitably designed non-Hermitian potential landscape, such that both solutions share the same spatial distribution of their wave intensity [2]. This protocol naturally enables the design of structures with broadband unidirectional invisibility for which outgoing waves are indistinguishable from those of free space.

In disordered media, multiple scattering prevents the application of conventional approaches for the design of light fields with desired properties. This is because any local change to such a medium typically affects these fields in a non-local and complicated fashion. By modifying the above theoretical methodology we devised a procedure for tailoring an inhomogeneous 1D Hermitian dielectric index distribution that allows us to control the intensity profile of an incoming light field purely locally, that is, with little or no influence on the field profile outside of a designated region of interest [4].

Transformation of coordinates is a versatile tool to mold the flow of light, enabling a host of astonishing phenomena such as optical cloaking with metamaterials. Moving away from the usual restriction that links isotropic materials with conformal transformations, we have shown how nonconformal distortions of optical space are intimately connected to the complex refractive index distribution of an isotropic non-Hermitian medium [3]. Remarkably, this insight can be used to circumvent the material requirement of working with refractive indices below unity, which limits the applications of transformation optics. We apply our approach to design a broadband unidirectional dielectric cloak, which relies on nonconformal coordinate transformations to tailor the non-Hermitian refractive index profile around a cloaked object. Our insights bridge the fields of two-dimensional transformation optics and non-Hermitian photonics.

References

1. J. B. Pendry, A. Aubry, D. R. Smith and S. A. Maier, “Transformation Optics and Subwavelength Control of Light”, Science **337**, 6094 (2012).
2. K.G. Makris, I. Krešić, A. Brandstötter and S. Rotter, “Scattering-free channels of invisibility across non-Hermitian media”, Optica **7**, 619–623 (2020).
3. I. Krešić, K. G. Makris, U. Leonhardt and S. Rotter, “Transforming space with non-Hermitian dielectrics”, Phys. Rev.

Lett. **128**, 183901 (2022).

4. I. Krešić, K. G. Makris and S. Rotter, “Light confinement by local index tailoring in inhomogeneous dielectrics”, Laser and Photonic Rev. **15**, 2100115 (2021).

META 2023, PARIS - FRANCE, JULY 18 – 21, 2023

Graph parity-time symmetry for bipartite graphs and system stability analysis

H. Benisty[1,2*], L. A. Moreno-Rodriguez[3] C. T. Martinez-Martinez,[4] and J. A. Mendez-Bermudez,[3]

[1]Laboratoire Charles Fabry, Institut d'Optique Graduate School, CNRS, Univ. Paris Saclay, Palaiseau, France
[2]Université de Paris, LIED, CNRS UMR 8236, 75013 Paris, France
[3]Instituto de Física, Benemérita Universidad Autónoma de Puebla, Apartado Postal J-48, Puebla 72570, Mexico
[4]Universidad Autónoma de Guerrero, Centro Acapulco CP 39610, Acapulco de Juárez, Guerrero, Mexico
[*]corresponding author: henri.benisty@institutoptique.fr

Abstract: We investigate the eigenvalues of random matrices depicting a set of gain and loss systems that are coupled to each other, forming a bipartite graph that exhibits parity-time symmetry. It has significance for complex systems e.g. in the sense of May's instability and the consequences of the "circular law" of eigenvalues distribution and disordered nanolasers. Regions of real spectra in (connectivity, gain/loss) space are outlined. A new feature is a simple angle dependence of eigenvalue distribution in a parametric plane.

Random matrices and their eigenvalues are known as a key tool for stability analysis of large systems, since R.E. May well-known proposal in 1972, that large systems become unstable as the disc occupied by the relevant eigenvalues grows and pushes some eigenvalues in the unstable part of the complex plane in a marginal stability analysis. On the other hand, a renewed approach to open coupled systems has taken place with parity-time symmetry, whereby coupling could force eigenvalues to be real (in the unbroken phase) in spite of uncoupled elements having gain and loss, provided that parity-time (PT) symmetry holds (gain <–> loss under a space symmetry).

Combining earlier knowledge from binary bipartite networks [1], studies on random graphs with gain and loss [2], and studies of non-bipartite PT-symmetric graphs [3], we address here the case of bipartite graphs having parity-time symmetry. Fig.1(a) gives an example of size N=10 (5+5 nodes), and the PT-symmetry holds due to the same topology of edges for 12345 and ABCDE, causing the adjacency matrix in Fig.1(b) to exhibit a pattern with two anti-diagonal N/2 block matrices transposed of each other. The two parameters are the connectivity (fraction of nonzero edges) α and the gain-loss parameter γ on the diagonal.

The relevance to real system with multiple gain and loss elements is emerging in nanophotonics [4]. More generally, the issue of the stability of specific complex systems ensuring e.g. those ensuring transfer of energy from one subgraph to the other could benefit from these studies.

The typical results that we have explored are the fraction of eigenvalues that are real (or imaginary) as a function of N, α and γ, Fig.1(c), for which relatively simple but nontrivial laws emerge, requiring fractional power laws. See ref. [5] for more details.

Another kind of result of possible interest is the eigenvalue distribution density, not in the complex plane, but in the [γ,Re(λ)] plane: It appears to be a combination of what the circular law would predict along the ordinate, Re(λ) at $\gamma=0$ here, and a simple trigonometric function of the local angle of this plane, thus $\psi = \mathrm{atan}(\mathrm{Re}(\lambda)/\gamma)$.

We thus hope to get a set of analytical tools as well as other accurate parametric trends by numerical studies, so as to pave the way to the understanding of a broad series of complex open system with a view to their stability criteria.

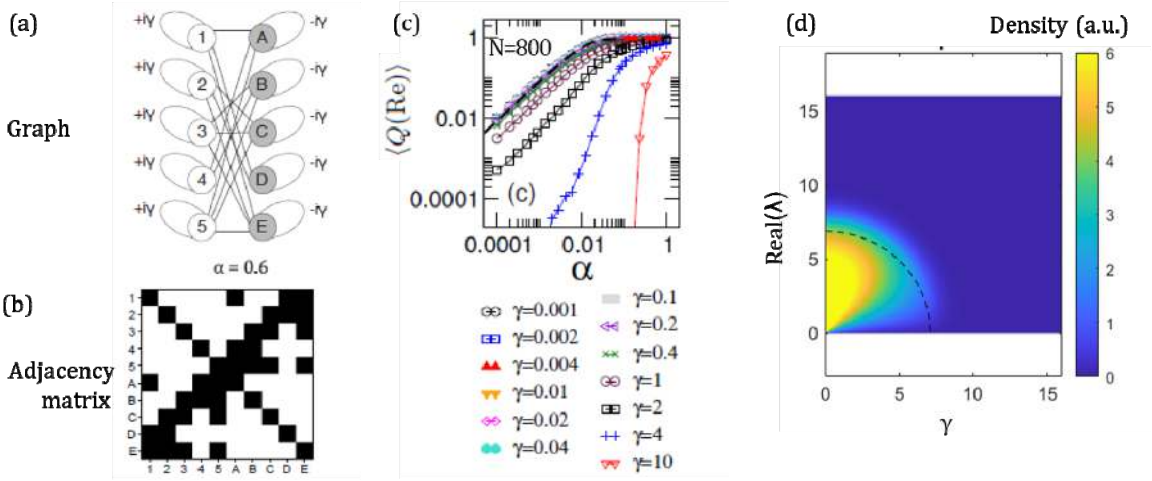


Fig.1 (a) Example of bipartite graph of size 10 with 5 gain + 5 loss elements, with PT symmetry with connectivity α=0.6; (b) corresponding adjacency matrix (1=black) ; (c) fraction of real eigenvalues vs $\log_{10}(\alpha)$ for several γ values; (d) statistical density distribution of eigenvalues in the [γ, Re(α)] plane for a large matrix, with a circle law indicated.

J.A.M.-B. acknowledges support from CONACyT (Grant No. 286633), CONACyT-Fronteras (Grant No. 425854), VIEP-BUAP (Grant No. 100405811-VIEP2022), and Laboratorio Nacional de Supercómputo del Sureste de México (Grant No. 02201007C), Mexico.

References

1. Martinez-Martinez, C. T., J. A. Mendez-Bermudez, Y.Moreno, J. J. Pineda-Pineda, and J. M. Sigarreta, “Spectral and localization properties of random bipartite graphs,” Chaos Soliton Fract. Vol. X, No. 3, 100021(1–9), 2019.
2. Martinez-Martinez, C. T. and J. A. Mendez-Bermudez, “Information entropy of tight-binding random networks with losses and gain: Scaling and universality,” Entropy Vol. 21, No. 21, 86, 2019.
3. Benisty, H. and C. Goupil “Configuration barrier towards parity-time symmetry in randomly connected mesoscopic sets on a graph”, Eur. Phys. J. B, Vol. 93, 192(1–14), 2020.
4. Gaio, M. D., Saxena, J. Bertolotti, D. Pisignano, A.Camposeo and R. Sapienza, “A nanophotonic laser on a graph” Nat. Commun. Vol. 10, 226(1–7), 2019.
5. Moreno-Rodriguez, L.A., C. T. Martinez-Martinez, J. A. Mendez-Bermudez and Henri Benisty, “Stability mapping of bipartite tight-binding graphs with losses and gain”, arXiv:2212.13642v1, 2022.

META 2023, PARIS - FRANCE, JULY 18 – 21, 2023

Electrically injected first-order gratings broken Parity-Time symmetry DFB lasers: insight on device design rules and experimental results

Y. Liang[1], Q. Gaimard[1], J.R. Coudevylle[1], A. Garreau[3], A. Wilk[3], O. Delorme[3] H. Benisty[2], A. Ramdane[1], and A. Lupu[1*]

[1]Centre de Nanosciences et de Nanotechnologies, CNRS, Université Paris-Saclay, Palaiseau, 91120, France

[2]Laboratoire Charles Fabry de l'Institut d'Optique LCFIO, Université Paris-Saclay, Palaiseau, 91120, France

[3]III-V Lab, 1 avenue Augustin Fresnel, 91767 Palaiseau Cedex, France
[*]corresponding author: anatole.lupu@c2n.upsaclay.fr

Abstract: We address the problem of the optimal design of first-order Parity-Time symmetric Bragg grating for the distributed feedback laser diodes operation. It is shown that the optimal design grating is not the exceptional point where the perfect unidirectional reflectivity condition is met. It is rather the design corresponding to the broken Parity-Time symmetry phase where the reflection asymmetry is still playing in important role. We also present experimental results on the electrically injected DFB lasers based on such design.

The advent of Parity-Time symmetry in photonics benefited from an important interest to this topic that sparkled a plethora of experimental demonstrations of related physical effects. This work represents an attempt to apply the concept of PT-symmetry to practical mature complex devices, in particular to the design and fabrication of an electrically injected single frequency DFB laser. The main interest of applying the concept of PT-symmetry to DFB lasers is to take advantage of two characteristics that improve the single-frequency behavior by the simultaneous presence of index modulation and losses. Fig. 1 represents the principle of complex coupling with gratings made up of physically separate components which are seen as two (complex) additive contributions by the mode of the waveguide. The presence of the index-modulated grating ensures a lower threshold injection current, while the presence of losses improves the laser emission mode discrimination mechanism and makes single-frequency operation more robust [1,2]. Moreover, according to several theoretical works, the one-way reflection characteristic of the Parity-Time symmetry should make the laser more robust with respect to online optical feedback.

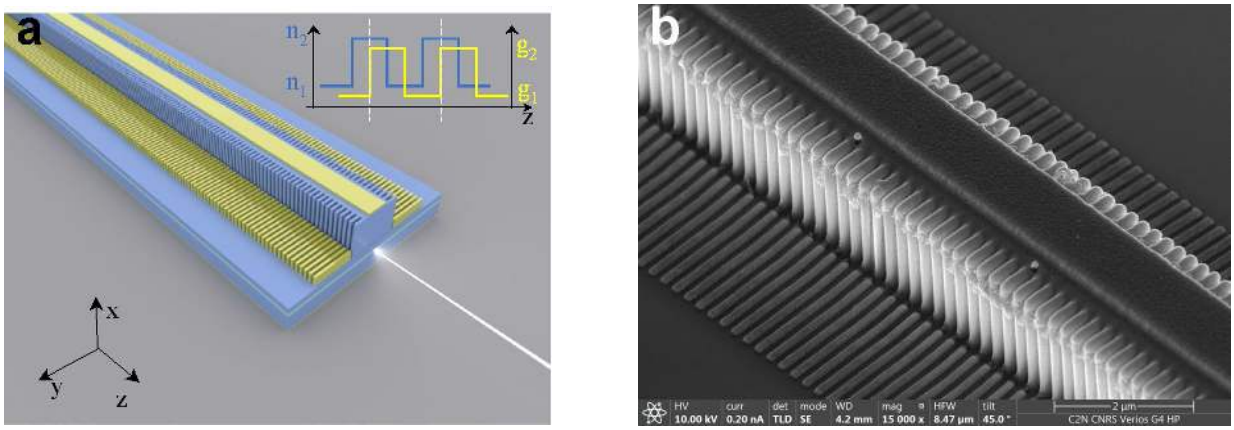


Fig.1. a) Sketch of PT-symmetric DFB laser, blue (dielectric) and yellow (metallic) gratings are shown; the inset depicts the condition for PT-symmetric potential. b) SEM side view of a fabricated first-order broken PT-symmetry DFB laser.

Our modeling results show that optimal operation of these complex coupled DFB lasers requires careful management of the imaginary part of the index profile to avoid excessive losses leading to increased threshold current and reduced power. It turns out that, as a rule, the modulation of the imaginary part of the index profile must be approximately three to four times lower compared to the modulation of the real part of the index profile. Such a complex index profile Bragg grating corresponds to the PT-symmetry broken condition (the associated added imaginary terms being off-diagonal). Nevertheless, the asymmetry in the reflection coefficient leading to the appearance of an additional narrow-band gain discrimination mechanism [1] still plays a beneficial role leading to more robust single-frequency operation. An additional improvement of this mechanism allowing to decrease even more the threshold current and to increase the emitted power could be obtained by using an AR/HR coating whose asymmetry is matched to that of the Bragg grating with a complex profile [2].

Experimental results for electrically injected uncoated DFB lasers with a first order PT-symmetry broken Bragg grating are shown in Fig. 2. As can be seen, the threshold current is less than 20mA while the output power at 100mA injection current is about 13mW. This presents a very noticeable improvement over the third-order PT-symmetry-broken DFB lasers that we reported earlier [1]. Further improvement in output power can be achieved by increasing the injection current up to 300 mA, but this requires mounting the fabricated lasers on heat sink mounts. Work along this direction is ongoing.

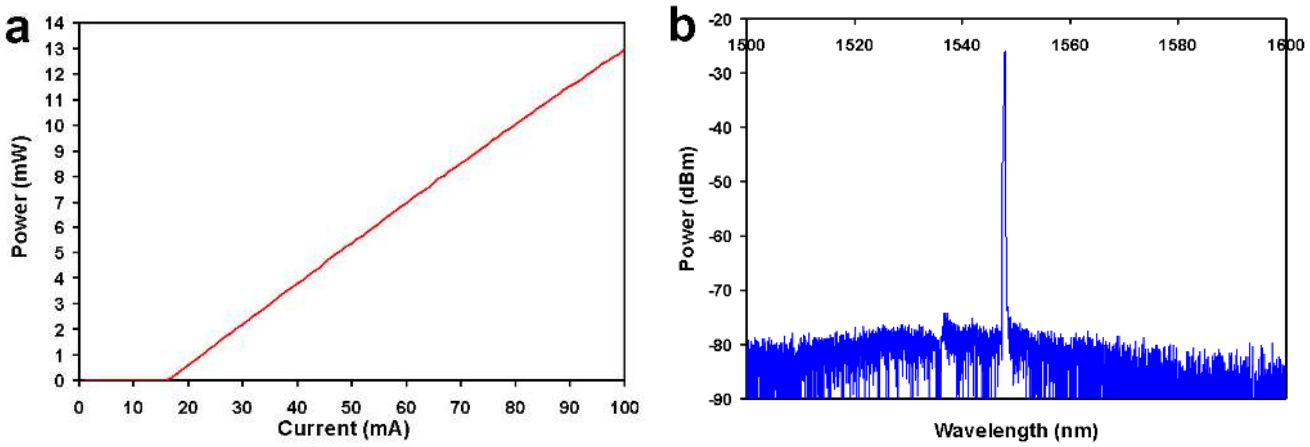


Fig. 2 Typical a) Light–current characteristic; b) Emission spectrum for first-order broken PT-symmetry DFB lasers.

Acknowledgements

This work was funded by the French Agence Nationale pour la Recherche (project "PARTISYMO", contract number N° ANR-18-CE24-0024-01) and partially supported by the French network RENATECH and C2N cleanroom staff and facilities. Funding by the China Scholarship Council is acknowledged by Y. Liang.

References

1. V. Brac de la Perrière, Q. Gaimard, H. Benisty, A. Ramdane, A. Lupu, "Electrically injected parity-time symmetric DFB lasers for telecom applications," Nanophotonics 10, 1309-1317 (2021).
2. H. Benisty, V. Brac de la Perrière, A. Ramdane, A. Lupu, "Parity-time Symmetric gratings in 1550 nm Distributed-Feedback lasers diodes: insight on device design rules," J. Opt. Soc. Am. B 38, C168-C174 (2021).

Experimental observation of lasing over Anderson-localized modes at exceptional points using quantum echoes

Sushil Mujumdar[1], **and Krishna Joshi**[1]

[1]Nano-optics and Mesoscopic Optics Laboratory, Tata Institute for Fundamental Research, Mumbai, India
[*]corresponding author: mujumdar@tifr.res.in; sumujumdar@gmail.com

Abstract: We report experimental observation of Anderson-localized lasing modes in quasi-one-dimensional disordered systems over exceptional points. The non-Hermitian system comprised linear arrays of coupled microresonators in which a lasing material provided gain, while free-space scattering in the open system provided loss. Using a probabilistic search over a massive sample space of Anderson-localized modes, we identified exceptional points by tracing the vanishing quantum echo between coupled modes. The spectral lineshape analysis confirmed a second-order exceptional point.

Exceptional points[1] are intriguing spectral degeneracies in non-Hermitian systems at which two or more eigenvalues coalesce simultaneously with the coalescence of associated eigenfunctions. EPs signify singularities at which the eigenvalues and eigenfunctions of non-Hermitian matrices cannot be described analytically[2]. This seemingly abstract construct has been demonstrated to bear a significant impact on the performance of photonic systems. Hitherto, typical photonic systems operated at exceptional points involved coupled resonators or coupled waveguides, whose parameters are chosen with prior knowledge of the systemic behavior. One of the parameters, usually gain or loss, is then tuned gradually to hit a magnitude where the PT symmetry is broken. Such a process, however, is untenable in a mesoscopic disordered system, wherein the physical configuration is randomly organized, and is apriori nondeterministic. Therefore, hitherto, despite theoretical proposals[3], there are no experimental reports of exceptional points in disordered or localizing systems.

Our approach involves a statistical route towards EPs, in which we realize a massive sample space of about 15000 Anderson localizing configurations. This is enabled by our experimental setup wherein a linear array of coupled microresonators realized in a dynamic manner is periodically interrogated by a pulsed laser, wherein every individual laser pulse illuminates a different configuration. The diagnostic apparatus was built to *simultaneously* measure the spatial, spectral and temporal signatures of modes for every configuration. The temporal measurements played a critical part of revealing quantum echoes representing oscillations of energy between the coupled modes, akin to Rabi oscillations in two-level systems[4]. This measurement is vital because it sifts out coupled modes from various accidental spectral peaks that mimic a doublet. Subsequent analysis of the vanishing quantum echo, accompanied by simultaneous coalescence of eigenvalues and eigenvectors leads to the identification of exceptional points. Further, spectral lineshape analyses confirm the second-order nature of these exceptional points[5].

We acknowledge funding from the Department of Atomic Energy, Government of India, and the Swarnajayanti Fellowship from the Department of Science and Technology, Government of India.

References

1. Miri, M.-A., Alù, A. “Exceptional points in optics and photonics,” Science 363(6422), 7709, 2019.
2. Heiss, W. “The physics of exceptional points.” Journal of Physics A: Mathematical and Theoretical 45(44), 444016,

2012.

3. Bachelard, N., Schumer, A., Kumar, B., Garay, C., Arlandis, J., Touzani, R., Sebbah, P. “Coalescence of Anderson-localized modes at an exceptional point in 2d random media” Optics Express 30(11), 18098–18107, 2022.
4. Dietz, B., Friedrich, T., Metz, J., Miski-Oglu, M., Richter, A., Schaefer, F.,Stafford, C. “Rabi oscillations at exceptional points in microwave billiards,” Physical Review E 75(2), 027201, 2007.
5. Joshi, K., and Mujumdar, S, arxiv:2301.06532.

Level statistics and Anderson localization transitions of non-Hermitian systems with exceptional points

Chen Wang[1]*

[1]Center for Joint Quantum Studies and Department of Physics, School of Science, Tianjin University, Tianjin 300350, China

*corresponding author: physcwang@tju.edu.cn

Abstract: In this talk, I will discuss some recent progress in the understanding of level statistics of non-Hermitian Hamiltonians. These include 1) Poisson level statistics of extended states of non-Hermitian metals [1]; 2) A new universal level spacing distribution, which displays linear level repulsion, for exceptional points of disordered non-Hermitian systems [2].

Open systems are described by non-Hermitian Hamiltonians and have drawn increasing attention in recent years due to their academic interest, importance, and relevance to reality. Unlike Hermitian Hamiltonians, whose eigenenergies are real, the eigenenergies of non-Hermitian Hamiltonians are, in principle, complex numbers. The real parts of eigenenergies are interpreted as quasi-particle energies, and the imaginary parts are the inverse of quasi-particle lifetimes.

It is known that the level-spacing distribution for random Hermitian Hamiltonian is a fundamental quantity that reveals the underlying physics. For example, level repulsion is a general principle in Hermitian quantum physics, which prevents two extended states from having the same energy and gives rise to the well-known Wigner-Dyson distributions for the normalized nearest-neighbor energy-level spacing [3]. Differently, for non-Hermitian systems, a pioneering work by Grobe, Haake, and Sommers shows that the nearest-neighbor level spacing distributions are the so-called Ginibre distributions, where the three Gaussian Ginibre (orthogonal, unitary, and symplectic) ensembles display a universally cubic level repulsion [4].

We revisit the level statistics of non-Hermitian systems by focusing on a different question: What is the distribution of the quasi-particle energies, i.e., the real part of eigenenergies, of extended states? To this end, we first show that an Anderson localization transition can happen in either preserved time-reversal-symmetry or broken disordered non-Hermitian Hamiltonians. Then, we find that the nearest-neighbor quasi-particle energies follow the Wigner-Dyson distribution if the non-Hermiticity is much smaller than the mean level spacing of quasi-particle energies. If the meaning level spacing of the quasi-particle energies is much smaller than the non-Hermiticity, we observe a universal Poisson distribution, which is universally true for the Anderson insulators whose energy eigenstates do not overlap with each other. Our results thus provide a unified picture for recently discovered “level attraction” in various systems and a theoretical basis for manipulating quasi-particle energy levels.

Besides, we also study the level statistics of complex eigenenergies of some non-Hermitian systems with exceptional points. The widely accepted Ginibre distributions are no longer applicable in our models. In the symmetry-protected or symmetry-broken phases, where the eigenenergies are real or come in complex-conjugate pairs, respectively, the nearest-neighbor level spacing distributions follow the Wigner-Dyson distributions. Here, time-reversal symmetry plays a

significant role in determining the degree of level repulsion. Near the exceptional points, we observe some new distributions, which depend on symmetries for small sizes but become a universal distribution for large sizes. In both cases, they display a universal linear level repulsion rather than the universal cubic level repulsion of the Ginibre distributions.

In conclusion, the general Wigner-Dyson distribution of energy level spacing of extended states in Hermitian systems is replaced by the Poisson distribution for quasi-particle level spacing of non-Hermitian disordered metals. This is a surprising result since Poisson distribution is only valid for highly localized states in Hermitian systems. Furthermore, the level repulsion of states near exceptional points is universally linear, rather than the cubic level repulsion of the Ginibre distributions. This recent progress shows that the level-statistics problem for non-Hermitian systems is far from fully solved.

Acknowledgements. This work is supported by the National Natural Science Foundation of China (Grants No. 11704061 and No.11974296) and Hong Kong RGC (Grants No. 16300522 and No. 16302321).

References:

[1] C. Wang and X. R. Wang, Phys. Rev. B **101**, 165114 (2020).
[2] C. Wang and X. R. Wang, Phys. Rev. B **106**, L081118 (2022).
[3] M. L. Mehta, Random Matrices (Elsevier, Amsterdam, 2004).
[4] F. Haake, Quantum Signatures of Chaos (Springer Science & Business Media, New York, 2010), Vol. 54.

META 2023, PARIS - FRANCE, JULY 18 – 21, 2023

Enhanced avionic sensing based on Wigner's cusp anomalies

R. Kononchuk[1], J. Feinberg[2*], J. Knee[1] and T. Kottos[1]

[1]Wave Transport in Complex Systems Lab, Dept. of Physics, Wesleyan Univ. Middletown, CT 06459, USA
[2]Department of Physics, University of Haifa, Mt. Carmel, Haifa 31905, Israel
[*]corresponding author: jfeinberg@univ.haifa.ac.il

Abstract: Sensors typically detect small perturbations by measuring their effects on a physical observable in the linear response regime. As it turns out, once linear resonse is abandoned, new opportunities emerge. A prominent example is resonant systems operating near Nth-order exceptional point degeneracies (EPD), where a small perturbation $\varepsilon \ll 1$ activates an inherently sublinear response $\sim \varepsilon^{1/N} \gg \varepsilon$ in resonant splitting. Here we propose an alternative sublinear optomechanical sensing scheme that is rooted in Wigner's cusp anomalies (WCA), first discussed in the framework of nuclear reactions: a frequency-dependent square-root singularity of the differential scattering cross section around the energy threshold of a newly openened channel, which we use to amplify small perturbations. WCA hypersensitivity can be applied in a variety of sensing applications, besides optomechanical accelerometry focused on in this talk. Our WCA platforms are compact, do not require judicious arrangement of active elements (unlike EPD platforms), and if chosen, can be cavity free.

References

1. Kononchuk, R., Feinberg, J., Knee, J. And Kottos, T. "Enhanced avionic sensing based on Wigner's cusp anomalies," Sci. Adv. 2021; **7** :eabg8118.

META 2023, PARIS - FRANCE, JULY 18 – 21, 2023

Emergence of non-Hermitian dynamics in a quantum gas leading to a self-driven topological pump

A.Baumgärtner

[1]ETH Zürich

The time evolution of a driven quantum system can be strongly affected by dissipation. Although this mainly implies that the system relaxes to a steady state, in some cases it can lead to the appearance of new phases and trigger emergent dynamics. In our experiment, we study a Bose-Einstein condensate dispersively coupled to a high finesse optical resonator. The cavity is populated by scattering photons from a transverse drive illuminating the atoms. The sum of the drive and the self-consistent intracavity field provides a topological band structure. When the dissipative and coherent timescales are comparable, we find a regime of persistent oscillations where the cavity field does not reach a steady state: The emergence of an exceptional point. In this regime the atoms experience a potential that periodically deforms itself, even in the absence of an external time-dependent drive. Consequently, the dynamic lattice triggers topological pumping [1]. We show complementary measurements of the light field and of the atomic transport, proving the connection between the non-stationarity and the topological pumping and further investigate the emergence of the dynamics with various spectroscopic techniques.

References

1. Dreon D, Baumgärtner A, Li X, Hertlein S, Esslinger T & Donner T: Self-oscillating pump in a topological dissipative atom–cavity system. Nature 608, 494–498 (2022)

Non-Hermitian microresonators at an Exceptional Point

Riccardo Franchi[1*], Stefano Biasi[1], and Lorenzo Pavesi[2]

[1]Nanoscience Laboratory, Department of Physics, University of Trento, 38123 Trento, Italy
[*]corresponding author: riccardo.franchi@unitn.it

Abstract: In this work, we present a new integrated structure operating at an exceptional point consisting of an infinity-shaped microresonator twice coupled to a bus waveguide. Its improved sensing performance is reported as well as its high variability of output spectra. Finally, an experimental method for individually exciting supermodes of resonant Hermitian and non-Hermitian structures is presented.

The study of non-Hermitian systems has found great interest in recent years. In particular, the discovery of PT-symmetric non-Hermitian systems [1] and the special non-Hermitian degeneracies called exceptional points (EPs) have stimulated the study of new systems. The features of exceptional points have been used in various applications through the realization of devices such as sensors, unidirectional lasers, unidirectional reflectors, and non-reciprocal optical components exhibiting a violation of the Lorentz reciprocity theorem. In these realizations, integrated optics may be the disruptive technology thanks to the advantage of miniaturization and the ease of implementation of loss, gain and asymmetric coupling.

Here, we report the study of a new integrated device called the infinity-loop microresonator (ILMR) [2]. The ILMR operates at an EP and consists of an infinity-shaped waveguide twice coupled to a bus waveguide. Its shape allows high tunability of the transmission and reflection spectra as a function of the two couplings with the bus waveguide while remaining at an EP. We show how this device is able to increase the sensitivity to a backscattering perturbation compared to a standard microring resonator. In addition to increasing the sensitivity due to the characteristic square root EP trend [3], using both the transmission spectrum and the sum of the transmission and reflection spectra, the ILMR is able to avoid the region of insensitivity typically found at small perturbations. Finally, an experimental method for individually exciting the supermodes of a Hermitian or non-Hermitian resonator system is presented. It is based on a simultaneous and coherent excitation of a system from both sides. By properly tuning both the intensity and the relative phase between the two input fields, one can directly measure the real and imaginary parts of the eigenvalues from the output spectrum [4]. This allows the quality factor of a resonant system to be defined even in the presence of a resonant doublet.

References

1. C. M. Bender and S. Boettcher, “Real Spectra in Non-Hermitian Hamiltonians Having PT Symmetry,” Phys. Rev. Lett., vol. 80, no. 24, pp. 5243–5246, Jun. 1998, doi: 10.1103/PhysRevLett.80.5243.
2. R. Franchi, S. Biasi, D. Piciocchi, and L. Pavesi, “The Infinity-loop microresonator: a new integrated photonic structure working at an exceptional point.” arXiv, Feb. 02, 2023. doi: 10.48550/arXiv.2302.01108.
3. W. Chen, Ş. Kaya Özdemir, G. Zhao, J. Wiersig, and L. Yang, “Exceptional points enhance sensing in an optical microcavity,” Nature, vol. 548, no. 7666, Art. no. 7666, Aug. 2017, doi: 10.1038/nature23281.
4. S. Biasi, R. Franchi, F. Mione, and L. Pavesi, “Interferometric method to estimate the eigenvalues of a non-Hermitian two-level optical system,” Photonics Res., vol. 10, no. 4, p. 1134, Apr. 2022, doi: 10.1364/PRJ.450402.

META 2023, PARIS - FRANCE, JULY 18 – 21, 2023

Non-Hermitian topological disclination defect in a valley-Hall sonic lattice

J. I. Martínez[1], R. Pernas-Salomón[2*], Penglin Gao[3,4], M. Kadic[1], and J. Christensen[5]

[1] Institut FEMTO-ST, CNRS, Université Bourgogne Franche-Comté, 25030 Besancon, France
[2]Department of Physics, Universidad Carlos III de Madrid, Avda. Universidad, 30, 28911 Leganés, Madrid, Spain
[3]State Key Laboratory of Mechanical System and Vibration, Shanghai Jiao Tong University, Shanghai, 200240, China
[4]Institute of Vibration, Shock and Noise, Shanghai Jiao Tong University, Shanghai, 200240, China
[5]IMDEA Materials Institute, Calle Eric Kandel, 2, 28906 Getafe, Madrid, Spain
[*]corresponding author: rpernas@fis.uc3m.es

Abstract: In this contribution we focus on topological defects that are local kinks or obstructions in an order parameter field where domain walls, superconductor vortices or dislocations are few of many prominent examples. Topological bound states can form around these defects much in the same way edge and surface states bind to one- and two-dimensional interfaces, respectively. Here, we discuss both numerical and experimental advanced in the context of topological acoustics, where a man-made lattice hosting a topological nontrivial phase is realized with added real-space lattice distortion and non-Hermiticity.

META 2023, PARIS - FRANCE, JULY 18 – 21, 2023

Non-Hermitian resonant energy transfer

A. Novitsky[1,2], F. Morozko[1,3], D.V. Novitsky[4], and A. Karabchevsky[3*]
[1]Belarusian State University, Minsk, Belarus
[2]ITMO University, St. Petersburg, Russia
[3]School of Electrical and Computer Engineering, Ben-Gurion University of the Negev, Beer-Sheva, Israel
[4]B. I. Stepanov Institute of Physics, NAS of Belarus, Minsk, Belarus.
[*]corresponding author: alinak@bgu.ac.il

Abstract: Non-Hermiticity exhibits an excellent platform to achieve new insights in physics and technology. Here we discuss the influence of non-Hermitian environments on emission properties of a dipole. Using the perturbation theory, we reveal that resonant energy transfer between donor and acceptor molecules strongly enhances at the exceptional point. Our results are essential for nanooptical applications including light energy transport and signal processing on a chip.

Introduction

Parity-time (PT) symmetry and non-Hermiticity is a remarkable tool for tailoring light-matter interaction. It has been already achieved advantageous behaviors in scattering, lasing, coherent perfect absorption, wireless power transfer, etc. Therefore, this topic is under a close attention from the photonic community.

Non-Hermitian physics initiated by Bender and Boettcher [1] in relation to quantum mechanics was extended to optics due to possibility to associate a Hamiltonian with an optical system [2,3]. The optical non-Hermitian Hamiltonians including PT-symmetric ones then can have real eigenvalues. By changing system's parameters one is able to reach an exceptional point, in which sets of both eigenvalues and eigenvectors coalesce. The physics in vicinity of exceptional points is rich and can be analyzed from mode, topology and symmetry points of view. Many prospective applications of non-Hermitian systems as CPA-lasing and sensing are related to the behaviors near exceptional points [4]. In the particular case of a PT-symmetric system exceptional points separate PT-symmetric and broken-PT-symmetric states. Here we deal with some nanophotonic issues, namely, resonance energy transfer and spontaneous emission of dipoles interacting with non-Hermitian systems. In order to describe the system in vicinity of higher-order exceptional points we develop the appropriate perturbation theory.

Results

We consider a generic system described by the non-Hermitian Hamiltonian as a sum of unperturbed and perturbed parts [an example of such a system is shown in Fig. 1(a)]. The unperturbed Hamiltonian corresponds to that at the exceptional point, while the perturbed Hamiltonian is proportional to the small perturbation parameter ε. In the perturbation series for eigenvalues and eigenvectors the leading terms are proportional to $\varepsilon^{1/n}$, where n is the order of the exceptional point. Owing to the perturbation the degeneracy available at the exceptional point is lifted and we can generally determine the eigenvalues in two non-Hermitian phases corresponding to $\varepsilon<0$ and $\varepsilon>0$ [5]. We demonstrate such a behavior in Fig. 1(b) for PT-symmetric system possessing a second-order exceptional point at $\varepsilon=0$. Green's function as a Mittag-Leffler expansion can be also presented through the perturbation parameter ε. The Green function is indispensable for finding the local density of states and resonance energy transfer.

Using the perturbation theory, we can find the eigenfrequencies of the modes and compare the results with a numerical simulation. The degenerate eigenfrequency of unperturbed modes is generally a complex number $\omega_0 = \omega_0' + i\omega_0''$, the imaginary part of which determines decaying properties (both radiation and non-radiation) of the modes. When the decay is small, the local density of states and, therefore, the Purcell factor can increase at the

exceptional point [6]. Otherwise, the exceptional point does not affect the local density of states. It was confirmed in numerical and analytical calculations of the Purcell factor for the system of two coupled PT-symmetric rectangular waveguides [7]. The resonant energy transfer in a non-Hermitian system can be characterized by a spectral function $T(\omega)$ maximizing at the exceptional point. As it is seen in Fig. 1(c), the spectral function rapidly grows with the order of exceptional point. The increase of $T(\omega)$ with the order n is shown in [5] as a result of numerical simulation for mirror-assisted system of coupled resonators.

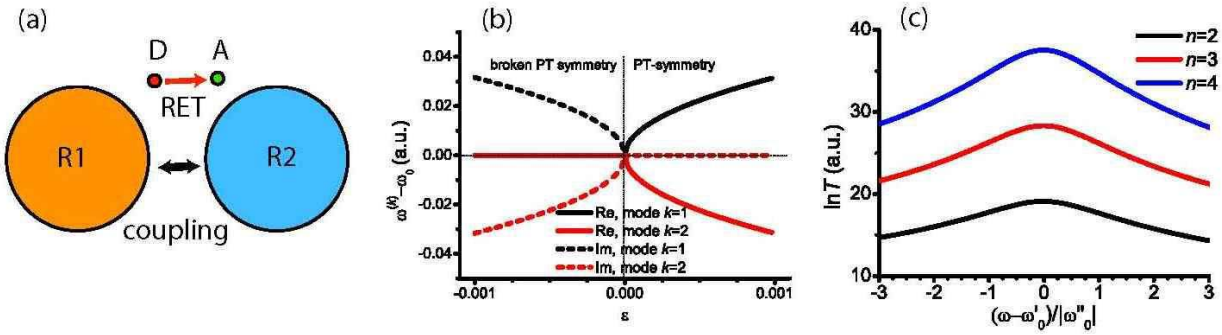


Figure 1. (a) Non-Hermitian system of coupled resonators to enhance resonance energy transfer (RET) between donor (D) and acceptor (A) molecules. (b) Departure of the eigenfrequencies $\omega^{(k)}$ of modes k from the degenerate frequency ω_0 as function of the perturbation parameter ε (order of exceptional point n=2). (c) Frequency dependence of spectral function $T(\omega)$ of the RET for different orders n of exceptional points.

To sum up, exploiting the developed perturbation theory near a higher-order exceptional point we have determined the closed-form frequency dependences of the local density of states and resonance energy transfer. Our results may find application for tailoring response of non-Hermitian systems at the nanoscale.

Acknowledgements

A.K. acknowledges the support of EU ERA-NET, Ministry of Energy, Grant No. 221-11-032. A.N. thanks Russian Science Foundation (Project No. 21-12-00383) for calculation of higher-order EPs.

References

1. Bender, C. M. and S. Boettcher, "Real Spectra in Non-Hermitian Hamiltonians Having PT Symmetry," Phys. Rev. Lett., Vol. 80, 5243-5247, 1998.
2. Feng, L., R. El-Ganainy and L. Ge, "Non-Hermitian photonics based on parity-time symmetry," Nat. Photon., Vol. 11, 752-762, 2017.
3. El-Ganainy, R., K.G. Makris, M. Khajavikhan, Z.H. Musslimani, S. Rotter and D.N. Christodoulides, "Non-Hermitian physics and PT symmetry," Nat. Phys., Vol. 14, 11-19, 2018.
4. Miri, M.-A. and A. Alù, "Exceptional points in optics and photonics," Science, Vol. 363, eaar7709, 2019.
5. Novitsky, A., F. Morozko, D. Gao, L. Gao, A. Karabchevsky and D.V. Novitsky, "Resonance energy transfer near higher-order exceptional points of non-Hermitian Hamiltonians," Phys. Rev. B, Vol. 106, 195410, 2022.
6. Khanbekyan, M. and J. Wiersig, "Decay suppression of spontaneous emission of a single emitter in a high-Q cavity at exceptional points," Phys. Rev. Res., Vol. 2, 023375, 2020.
7. Morozko, F., A. Novitsky and A. Karabchevsky, "Modal Purcell factor in PT-symmetric waveguides," Phys. Rev. B, Vol. 102, 155303, 2020.

A Hermitian Bypass to the non-Hermitian Quantum Theory

Tanmoy Das
Department of Physics, Indian Institute of Science, Bangalore 560012

tnmydas@iisc.ac.in

Conservation laws are an idealization of real-world problems, and hence the demand to develop non-Hermitian (NH) quantum theory is growing. The NH quantum theory suffers from various ill-defined properties and singularities. Here we construct a unified approach, applicable to all NH operators, by constructing a Hilbert space of a suitably designed Hermitian operator and expanding the NH Hilbert space on this basis. This way, the singularities are transported to the expansion parameters while the basis states remain well-defined. We developed a well-defined time-independent quantum theory of the generic NH Hamiltonians and exhibited several representative examples and applications.

META 2023, PARIS - FRANCE, JULY 18 – 21, 2023

Non-Hermitian modulations for stabilization of VCSEL, EEL and EEL arrays

R.Herrero[1*], S.B.Ivars[1], M.Botey[1], K.Staliunas[1,2,3]

[1] Universitat Politecnica Catalunya, Dep. de Fisica, Rambla Sant Nebridi 22, 08222, Terrassa (Barcelona) Spain

[2]ICREA, Passeig Lluís Companys 23, 08010, Barcelona, Spain

[3] Vilnius University, Faculty of Physics, Laser Research Center, Sauletekio Ave. 10, 10223, Vilnius, Lithuania
[*]corresponding author: ramon.herrero@upc.edu

Abstract: Semiconductor lasers and laser arrays emit temporally unstable and low spatial quality beams associated to intrinsic dynamical spatiotemporal instabilities. We propose the simultaneous modulations of refractive index and gain-loss generating non-Hermitian potentials as a stabilization mechanism. The proposed spatiotemporal modulations are introduced by directly acting on field and carriers. The stabilization is based on the stabilization of specific stationary solutions or on field localization. Stabilization is shown for VCSELs, EELs and EEL arrays.

Semiconductor lasers, like Vertical-Cavity Surface Emitting Lasers (VCSELs) and Edge Emitting Lasers (EELs) with flat mirrors lack from transverse mode selection to guarantee a Gaussian mode emission, developing turbulent behaviors and unstable emitted beams. The instability is primarily due to the intrinsic modulation instability (MI) of the homogeneous solution and is dramatically enhanced by nonlinear destabilizing effects such as self-focusing and filamentation when pump power is increased.

Periodic non-Hermitian potentials were proposed for the control of turbulence by changing the dispersion relation to suppress the MI in some general models and specifically in optical systems where such potential corresponds to simultaneous periodic modulations of refractive index and gain-loss [1]. Aside, Parity-Time (PT) symmetries that includes phase-shifts between the real and imaginary parts of the potential have been proposed for the light control [2]. More recently, periodic space-time potentials with temporal PT-symmetry, have been applied in general models like the Complex Ginzburg-Landau Equation (CGLE) for the turbulence reduction and stabilization of the homogeneous solution [3,4].

Here, we summarize two different manners for the stabilization of laser emission with non-Hermitian potentials differing from the usual stabilization of the homogeneous solution. The first is the non-homogeneous but stable laser emission in new transverse solutions generated by the introduction of a transverse non-Hermitian periodic modulation with in-phase real and imaginary parts. This technique stabilizes specific new stationary solutions emerging when the modulation amplitude is large enough. We analytically and numerically investigate such stabilization way in general models like the CGLE and in VCSELs, see Fig.1 a [5].

The second is based on the symmetry breaking of the coupling in the transverse direction induced by non-Hermitian potentials with a phase-shift between real and imaginary parts. The induced coupling asymmetry achieves its maximum for phase-shifts corresponding to PT-symmetries. The combination of such potentials with axial symmetries lead to field concentration and stabilization. Such non-Hermitian potentials with radial symmetry in VCSELs can induce unidirectional inward radial mode coupling allowing to an axial concentration of the energy generated in the whole active region, avoiding turbulent behavior and generating narrow bright beams even below threshold [6]. The stabilization of EELs and EEL arrays by field localization involves a

transverse multimode field in a long cavity and showing temporal dynamics. Taking advantage of the different time scales of the cavity round trip time and carrier's relaxation time a 2D+1 spatiotemporal model for these class B lasers is developed to characterize the stabilization by field localization [7,8]. Temporal stabilization with spatially redistributed light emission can be achieved in EEL arrays by particular shifts between electrodes (green) and laser waveguides (brown), see Fig.1 d.

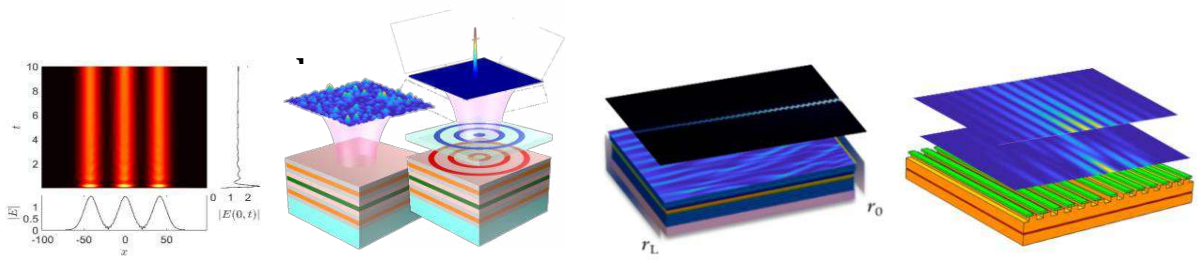


Figure 1: a) Transient to the stable solution induced by a symmetric non-Hermitian potential for a 1D VCSEL. Intensity distributions showing stable and localized (turbulent) behaviors with (without) axisymmetric phase-shifted non-Hermitian potentials for b) 2D VCSELs, c) single broad area EELs and d) EEL arrays.

This work was supported by the Government of Spain through grants IJCI-2016-27752, MTM2016-75963-P, FIS2015-71559-P and Severo Ochoa CEX2019-000910-S; by Generalitat de Catalunya; CERCA; Fundació Cellex; and Fundació Mir-Puig. K.S acknowledges European Social Fund (project No 09.3.3- LMT-K712-17-0016) under grant agreement with the Research Council of Lithuania (LMTLT).

References

1. W. W. Ahmed, S. Kumar, R. Herrero, M. Botey, M. Radziunas, and K. Staliunas, "Stabilization of broad-area semiconductor laser sources by simultaneous index and pump modulations." Optics letters 43.11, 2511-2514, 2018.
2. Rüter, C. E., Makris, K. G., El-Ganainy, R., Christodoulides, D. N., Segev, M., & Kip, D. "Observation of parity–time symmetry in optics," Nature physics, 6(3), 192-195. 2010.
3. Ivars, S. B., Botey, M., Herrero, R., Staliunas, K. "Optical turbulence control by non-Hermitian potentials," Physical Review A, 105(3), 033510, 2022.
4. Ivars, S. B., Botey, M., Herrero, R., Staliunas, K., "Non-Hermitian control of optical turbulence in systems with fractional dispersion," Chaos, Solitons & Fractals, 165, 112774, 2022.
5. Ivars, S. B., Botey, M., Herrero, R., & Staliunas, K. "Stabilisation of spatially periodic states by non-Hermitian potentials," Chaos, Solitons & Fractals, 168, 113089, 2023.
6. Ahmed, W. W., et al. "Stabilization of flat-mirror vertical-external-cavity surface-emitting lasers by spatiotemporal modulation of the pump profile." Physical Review A 92.4, 043829, 2015.
7. Pardell, J. M., Herrero, R., Botey, M., Staliunas, K. "Stabilized narrow-beam emission from broad-area semiconductor lasers," Physical Review A, 101(3), 033833, 2020.
8. Pardell, J. M., Herrero, R., Botey, M., Staliunas, K., "Non-Hermitian arrangement for stable semiconductor laser arrays," Optics express, 29(15), 23997-24009, 2021.

Time-Refraction Optics at Single Cycle Modulation

Ohad Segal[1†*] ,Eran Lustig[2†], Soham Saha[3,4], Eliyahu Bordo[1], Sarah N. Chowdhury[3], Yonatan Sharabi[1], Avner Fleischer[5], Mustafa Ozlu[3,4], Alexandra Boltasseva[3,4], Oren Cohen[1], Vladimir M. Shalaev[3,4] and Mordechai Segev[1]

[1]Physics Department and Solid State Institute, Technion-Israel Institute of Technology, Haifa, Israel
[2]Ginzton Laboratory and Department of Electrical Engineering, Stanford University, Stanford, California 94305, USA
[3]Elmore Family School of Electrical and Computer Engineering, and Purdue Quantum Science and Engineering Institute, Purdue University, West Lafayette, IN, USA
[4]Birck Nanotechnology Center, Purdue University, West Lafayette, IN 47907, USA
[5]School of Chemistry, Tel Aviv University, Israel
[†]These authors contributed equally to this work
*corresponding author: ohadse@campus.technion.ac.il

Abstract: We present an experimental study of optical time-refraction in single-cycle time-interfaces. Specifically, we study the propagation of a probe pulse through a sample undergoing large refractive index changes induced by an intense ultra-short modulator pulse. © 2023 The Author(s)

Large and fast modulations of the macroscopic electromagnetic (EM) properties of materials can have far reaching consequences [1–6]. Unlike low amplitude modulation or slow modulation in time, in cases where the macroscopic response is large and fast enough - even a single "step" modulation can result in dramatic changes [7].

When a wave propagating in a medium experiences a sudden change in the real part of the refractive index $\boldsymbol{n(t)}$, it undergoes two fundamental process - time refraction, and time reflection [8]. In this process of temporal modulation of the EM properties of the medium, the energy of the propagating wave ("probe") is not conserved, but when the medium is homogeneous the wave momentum (wave-vector) is conserved. Consequently, when the refractive index is increased abruptly the spectrum of the wave undergoes a red-shift, and when the index is decreased the spectrum undergoes a blue-shift. broadband frequency translation through time refraction has been recently observed in experiments [9,10], but time-reflection was thus far demonstrated only with water waves [11] and very recently with microwaves [12]. The lack of energy conservation in such time-modulated EM media implies the scattered wave may even be more energetic than the incident one [13], and can lead to tremendous amplification of waves by the modulation. Such time boundaries may also be used for applications such as antireflection temporal coatings [14], extreme energy transformations [15], inverse prisms [16], temporal aiming [17] and fundamental physics as well [18–22]. Concatenating several time-modulations periodically can lead to the formation of wide momentum gaps and the system functions as a Photonic Time-Crystal (PTC) [2,3,23,24]. The gaps in momentum of a PTC, where the temporal frequency is complex, can lead to broadband parametric amplification, and can interact with the emission of radiation by free electrons [25], atoms [4] and classical dipoles [4]. All of these rely on the ability to induce time-interfaces: very large changes in the EM properties of materials occurring at single-cycle rates.

Here, we explore the physics of time-refraction induced by a large 1-2 cycles modulation of the EM properties in Epsilon Near Zero (ENZ) materials.

Conventional nonlinear optics enables material response that is instantaneous but very small in the optical regime, and hence cannot be used for our purpose. On the other hand, recent progress with transparent conductors enables large optically-induced response in the optical regime. Thus, to induce significant time-refraction in the single-cycle regime, we create a moving time-boundary that occurs as fast as the time-period of the propagating wave, with a refractive index change of the order of $\boldsymbol{\Delta n \sim 0.5}$. Crucially, the material remains relatively transparent despite the huge relative index change, which allows us to explore new physics. The time-refraction we observe exhibits two frequency shifts induced by the index modulation. The first is a red-shift from the instantaneous rise in the refractive index. We demonstrate, for the first time, that this large refractive index change can occur within the single cycle regime. We do that by varying the duration of the modulation pulse between 30fs down to 6fs, and observe the corresponding decrease in the response time directly. The second frequency shift we observe is the blue shift associated with the relaxation (decrease) of the refractive index of the material back to its original value. We observe a large blue shift of a duration similar to that of the red shift. This implies that the relaxation process of the electrons back to their original energies (bottom of conduction band) occurs within ultrashort time scales, contrary to the expected relaxation of hot electrons in transparent conductors, which relies on coupling to phonons and takes hundreds of femtoseconds.

It is essential to analyze the transmitted pulse measurements of Fig.1B as a function of the modulator width. In Fig. 1C we plot the wavelength shifts of the mean wavelength vs. modulator-probe delay. These wavelength shifts show clear dependence on the modulator width both in rise time and in the magnitude of the red-shift. This conforms with the understanding that the refractive index change occurs because the material absorbs the modulator light, which excites conduction electrons to higher energies in the conduction band. Since absorption is an induced transition process, it is fundamentally instantaneous, hence it was expected that the rise of the refractive index would follow the accumulation of energy absorbed in the material. That is

$$\frac{d}{dt}\Delta\varepsilon(\mathrm{t}) \approx \mathrm{I_{mod}}(\mathrm{t}) - \frac{1}{T_{Decay}}\Delta\varepsilon(\mathrm{t}), \qquad \mathrm{n(t)} = \mathrm{Re}\left\{\sqrt{\varepsilon_{I_{mod}=0} + \Delta\varepsilon(\mathrm{t})}\right\} \tag{1}$$

Where $I_{mod}(t)$ is the time-dependent intensity of the modulator pulse in proper units, $\varepsilon_{I_{mod}=0}$ is the ambient (unmodulated) permittivity of the TCO slab and t=0 is defined when the modulator starts entering the sample. Since in our setup we probe the index change with a probe pulse, the refractive index response appearing in our measurements is a convolution of the index response and the temporal envelope of the probe pulse. In Fig. 1D we present the amount of refractive index change occurring within a single

cycle of the temporal period of the probe, as calculated from the mean wavelength shift shown in Fig. 1C and described by Eq. 1. For the shortest modulator width, we estimate that the refractive index of the sample is varied by ~0.12 within a single cycle of the probe wave.

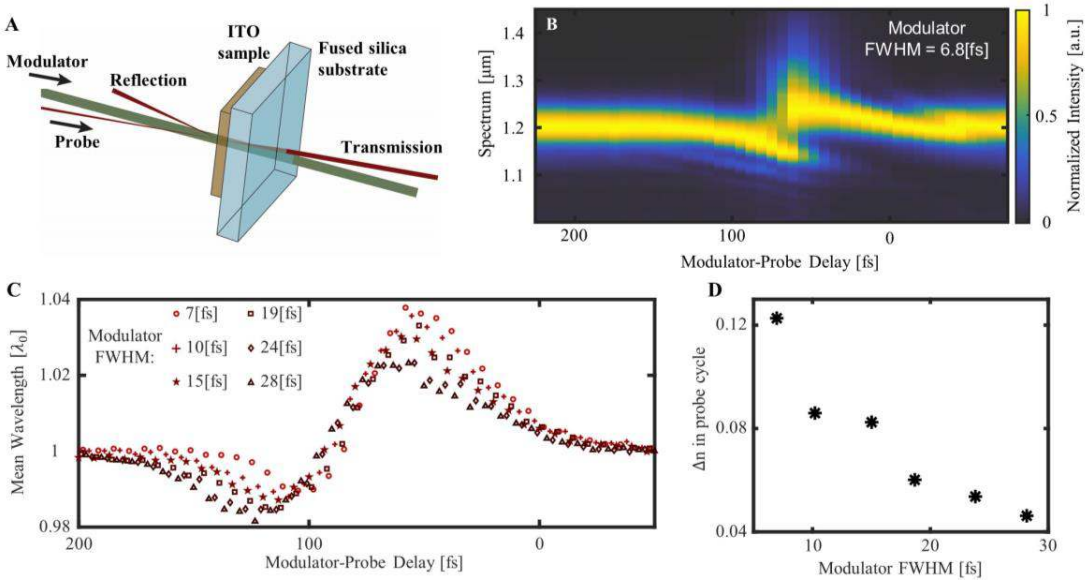


Figure 1: (A) Schematics of the modulator – probe setup. The modulator is a pulsed optical beam at 800nm (mean) wavelength, compressed to different pulse widths through a hollow core fiber system, illuminating a 700 micrometers diameter region of the sample. The probe beam is a 40fsec pulse at mean wavelength of 1200nm. The modulator and probe are synchronized to arrive at the TCO sample at controlled delays. The intensity and spectrum of the transmitted probe and the intensity of the reflected probe are measured. (B) Spectrogram of the probe pulse transmitted through the sample, for modulator pulse of the temporal width (FWHM) of 6.8[fs]. Negative delays (right side of the plot) correspond to the probe pulse passing through the sample before the modulator arrives. Each spectrum of the spectrogram is normalized individually. (C) Mean wavelength of the transmitted probe pulse vs modulator-probe delay, for different modulator pulse widths. Zero delay is arbitrarily set when 20% red-shift change is achieved for each modulator width. The rise time for red-shift appears to decrease with the modulator width, while the maximal shift increases. (D) The maximal refractive index change occurring within a single cycle of the probe temporal period vs the modulator width. Each data point is obtained using eq.1 and fitting the rise of the red-shift in Fig. 1C to erf function convolved with the probe envelope.

To conclude, we experimentally studied a new regime in which a pulse propagates in a material whose refractive index undergoes very large variations (~0.5) on the single cycle time scale while maintaining transparency. We find that the response time to large index variations can be extremely fast (few femtoseconds), and, unexpectedly, the relaxation seems to be on similar time scales. Our findings, especially the very fast relaxation of the variation in the refractive index in ITO, pave the way for observing new phenomena involving time refraction and reflection, photonic time crystals, and many other effects related to time boundaries.

[1] F. R. Morgenthaler, IRE Trans. Microw. Theory Tech., 6, 2, 167–172, (1958).
[2] P. Halevi, J. H. Abundis-Patiño, and J. R. Zurita-Sánchez, Opt. Express, 20, 5, 5586–5600, (2012).
[3] E. Lustig, Y. Sharabi, and M. Segev, Optica, 5, 11, 1390, (2018).
[4] M. Lyubarov, Y. Lumer, A. Dikopoltsev, E. Lustig, Y. Sharabi, and M. Segev, Science, 377, 6604, 425–428, (2022).
[5] A. Shaltout, A. Kildishev, and V. Shalaev, Opt. Mater. Express, 5, 11, 2459–2467, (2015).
[6] A. M. Shaltout, J. Fang, A. V. Kildishev, and V. M. Shalaev, Conf. Lasers Electro-Optics, FM1D.4, (2016).
[7] J. Mendonca, Theory of Photon Acceleration. Boca Raton: CRC Press, (2000).
[8] J. T. Mendonça and P. K. Shukla, Phys. Scr., 65, 2, 160–163, (2002).
[9] Y. Zhou et al., Nat. Commun., 11, 1, 1–7, (2020).
[10] A. M. Shaltout et al., 2016 Conf. Lasers Electro-Optics, FF2D.6, (2016).
[11] V. Bacot, M. Labousse, A. Eddi, M. Fink, and E. Fort, Nat. Phys., 12, 10, 972–977, (2016).
[12] H. Moussa, G. Xu, S. Yin, E. Galiffi, Y. Radi, and A. Alù, arXiv, (2022).
[13] D. Holberg and K. Kunz, IEEE Trans. Antennas Propag., 14, 2, 183–194, (1966).
[14] V. Pacheco-Peña and N. Engheta, Optica, 7, 4, 323–331, (2020).
[15] H. Li, S. Yin, E. Galiffi, and A. Alù, Phys. Rev. Lett., 127, 15, (2021).
[16] A. Akbarzadeh, N. Chamanara, and C. Caloz, Opt. Lett., 43, 14, 3297–3300, (2018).
[17] V. Pacheco-Peña and N. Engheta, Light Sci. Appl., 9, 1, 129, (2020).
[18] Y. Sharabi, E. Lustig, and M. Segev, Phys. Rev. Lett., 126, 16, 163902, (2021).
[19] V. Pacheco-Peña and N. Engheta, Phys. Rev. B, 104, 21, 214308, (2021).
[20] Y. Sharabi, E. Lustig, A. Dikopoltsev, Y. Lumer, and M. Segev, Opt., 9, 6, 585–592, (2022).
[21] B. Apffel, S. Wildeman, A. Eddi, and E. Fort, Phys. Rev. Lett., 128, 9, 94503, (2022).
[22] B. Apffel and E. Fort, Phys. Rev. Lett., 128, 6, (2022).
[23] F. Biancalana, A. Amann, A. V. Uskov, and E. P. O'Reilly, Phys. Rev. E - Stat. Nonlinear, Soft Matter Phys., 75, 4, 046607, (2007).
[24] X. Wang, M. S. Mirmoosa, V. S. Asadchy, C. Rockstuhl, S. Fan, and S. A. Tretyakov, arXiv, (2022).
[25] A. Dikopoltsev et al., Proc. Natl. Acad. Sci. U. S. A., 119, 6, e2119705119, (2022).

META 2023, PARIS - FRANCE, JULY 18 – 21, 2023

Statics and Dynamics of non-Hermitian Many-body Localization

Arijeet Pal

University College London, UK
*corresponding author: a.pal@ucl.ac.uk

Abstract: Many-body localized phases retain memory of their initial conditions and have been shown to exist in disordered interacting systems with unitary dynamics. The stability of the localized phase due to the breakdown of unitarity is of relevance to experiments when coupling to the environment. Motivated by this, we investigate the impact of non-Hermitian perturbations on many-body localization in the interacting Hatano-Nelson model which breaks unitarity via asymmetric hopping. We study the impact on eigenstates and dynamics due to the non-Hermiticity.

META 2023, PARIS - FRANCE, JULY 18 – 21, 2023

Reflectionless Scattering in Disordered Media: exceptional points and anti-reflection structures

Matthieu Davy[1*], Clément Ferise[1], Michael Horodynski[2], Matthias Kühmayer[2], Stefan Rotter[2], Simon Félix[3] and Vincent Pagneux[3]

[1] Univ. Rennes, CNRS, IETR (Institut d'Electronique et des Technologies du numéRique), UMR–6164, F–35000 Rennes, France
[2] Institute for Theoretical Physics, Vienna University of Technology (TU Wien), A–1040 Vienna, Austria
[3] Laboratoire d'Acoustique de l'Université du Mans (LAUM), UMR 6613, Institut d'Acoustique - Graduate School (IA-GS), CNRS, Le Mans Université, France
[*]corresponding author: matthieu.davy@univ-rennes1.fr

Abstract: Reflectionless (RL) states that are eigenfunctions of a non-Hermitian operator enable reflectionless coupling of light to a scattering sample. Here, we first observe exceptional points of RL states obtained by tuning the scattering strength in symmetric scattering samples. Then, instead of using wavefront shaping techniques, we will show that we can design anti-reflection structures for perfect transmission through disordered medium for any incident wavefront.

The transmission of waves through disordered media is ordinarily frustrated by multiple scattering within the medium. The average transmission is typically small when the sample length is much larger than the transport mean free path. However, as illustrated by the existence of open channels with perfect transmission, it is possible to find states of no reflection at the input at specific frequencies even in random media. In this talk, we will first discuss the related concept of reflectionless (RL) states [1,2]. Similarly to the poles of the scattering matrix, RL eigenvalues are eigenvalues of a non-Hermitian operator based on the wave equation. For this operator, the incoming channels are modelled with gain and outgoing channels with losses. When a RL eigenvalue is tuned to the real axis, a state with zero reflection and therefore perfect transmission in non-absorbing samples is obtained. Interesting properties arise in symmetric samples because the reflectionless operator is parity-time symmetric. Two real RL eigenvalues can coalesce at an exceptional points (EP) when the scattering strength is tuned symmetrically [2]. We experimentally observe such EPs in a multimirror Fabry-Perot system and then a complex cavity [3]. A clear signature of an EP is the broadening of the reflection lineshape. Our theoretical work are fully confirmed by measurements in the microwave range.

Using the framework of RL states, we will show that the transmission through an obstacle can be greatly enhanced by positioning new scattering elements in front or behind it. A symmetric disorder placed on each side of a barrier can indeed enhance transmission through the barrier over a broad frequency range [4] as a result of the PT-symmetric property of the RL operator. Finally, we will demonstrate that a structureless medium can even be made fully transmitting to all incoming wavefronts at a single frequency by placing a customized complementary medium in front of it [5]. The matrix generalization of the critical coupling condition between the two structures leads to the presence of a high-order diabolic point of RL states. Unlike open channels that are restricted to properly engineered wavefronts, any incoming wave is fully transmitted when the anti-reflection structure is placed. The design of the anti-reflection structure is realized numerically and the results are verified

experimentally. We render electromagnetic waveguides fully transmitting in spite of several dozen scattering elements being placed inside of them.

References

1. Dhia, A.-S. B.-B., L. Chesnel, et al., "Trapped modes and reflectionless modes as eigenfunctions of the same spectral problem." Proc. R. Soc. A 474(2213): 20180050, 2018.
2. Sweeney, W. R., C. W. Hsu, et al., "Theory of reflectionless scattering modes." Phys. Rev. A 102(6): 063511, 2020.
3. C. Ferise, P. Del Hougne, S. Félix, V. Pagneux, and M. Davy, "Exceptional Points of P T-Symmetric Reflectionless States in Complex Scattering Systems," Physical Review Letters, vol. 128, p. 203904, 2022.
4. M. Davy, C. Ferise, É. Chéron, S. Félix, and V. Pagneux, "Experimental evidence of enhanced broadband transmission in disordered systems with mirror symmetry," Appl. Phys. Lett., vol. 119, p. 141104, 2021.
5. M. Horodynski, M. Kühmayer, C. Ferise, S. Rotter, and M. Davy, "Anti-reflection structure for perfect transmission through complex media," Nature, vol. 607, pp. 281-286, 2022/07/01 2022.

META 2023, PARIS - FRANCE, JULY 18 – 21, 2023

Sensitivity and robustness in non-Hermitian topological lattices

I. Komis[1,2*], D. Kaltsas[2,3], S. Xia[4], H. Buljan[4,5], Z. Chen[4,6], and K. G. Makris[2,3]

[1]Humboldt -Universität zu Berlin, Institut für Physik, AG Theoretische Optik & Photonik, D-12489 Berlin, Germany
[2]Institute of Electronic Structure and Laser (IESL) – FORTH, Heraklion, 71110, Greece
[3]ITCP-Physics Department, University of Crete, Heraklion, 70013, Greece
[4]The MOE Key Laboratory of Weak-Light Nonlinear Photonics, TEDA Applied Physics Institute and School of Physics, Nankai University, Tianjin 300457, China
[5]Department of Physics, Faculty of Science, University of Zagreb, Bijenička c. 32, 10000 Zagreb, Croatia
[6]Department of Physics and Astronomy, San Francisco State University, California 94132, USA
[*]corresponding author: ikomis@physics.uoc.gr

Abstract: Higher order exceptional points (sensitivity) and topological protection (robustness) are two antagonistic effects. We examine their interplay on the prototypical non-Hermitian SSH lattice in terms of pseudospectra theory and its geometric features.

In the context of non-Hermitian topological photonics, we examine the interplay between robustness (due to topology) and sensitivity (due to non-Hermiticity) in the prototypical system of a non-Hermitian Su-Schrieffer-Heeger (NHSSH) lattice around the underlying exceptional points (EPs) [1,2]. In order to systematically examine the lattice sensitivity, we provide a mathematical framework ideal for non-Hermitian systems, that is the complex and structured pseudospectra theory [3,4,5,6,7,8]. In particular, we consider three different lattices, namely an infinite, a finite and a hetero structure of two NHSSH lattices (see Fig. 1). The intricate relation between the lattice symmetry and the symmetries of the perturbations is revealed based on pseudospectra [3,4]. Our starting point is the prototypical SSH model, in the context of coupled mode theory. More specifically, the lattices that we consider are schematically depicted in Fig. 1. The coupling constants are denoted by c_1 and c_2 for intra- and inter-cell coupling, respectively. The global gain-loss amplitude of each waveguide channel is described by the parameter γ, and thus making the whole system non-Hermitian. Regarding the case of an interface SSH lattice, we consider two SSH chains that are connected with an extra channel at the interface that has a tunable gain/loss amplitude γ_0.

In the vast majority of previous studies, the sensitivity of a non-Hermitian system under external perturbations was analyzed using the semi-analytical techniques based on perturbation theory, for systems of usually small number of waveguides. For lattices of our type such an approach is rather problematic and is not easily applicable, since we do have to use different versions of perturbation theory depending how close we are at the underlying EPs, and with very limited types of perturbation strengths. Therefore we introduce an alternative and general computational framework based on pseudospectra [3].

Our results for the three NHSSH lattices, are shown in Fig. 1. The red dots represent the spectrum and the yellow dots the corresponding pseudospectra. As we can see, the corresponding pseudospectra are extended patterns on the complex plane, and their size is related to the sensitivity of the lattice. In particular, the eigenstates close to the gap closing point are most sensitive and these away from that gap are more robust. The geometrical size of the main lobe of the complex pseudospectrum as a function of the perturbation strength ε has a square-root and cubic-root dependence, that are characteristics signatures of the EP2 and EP3, respectively, for small values of the perturbation strengths.

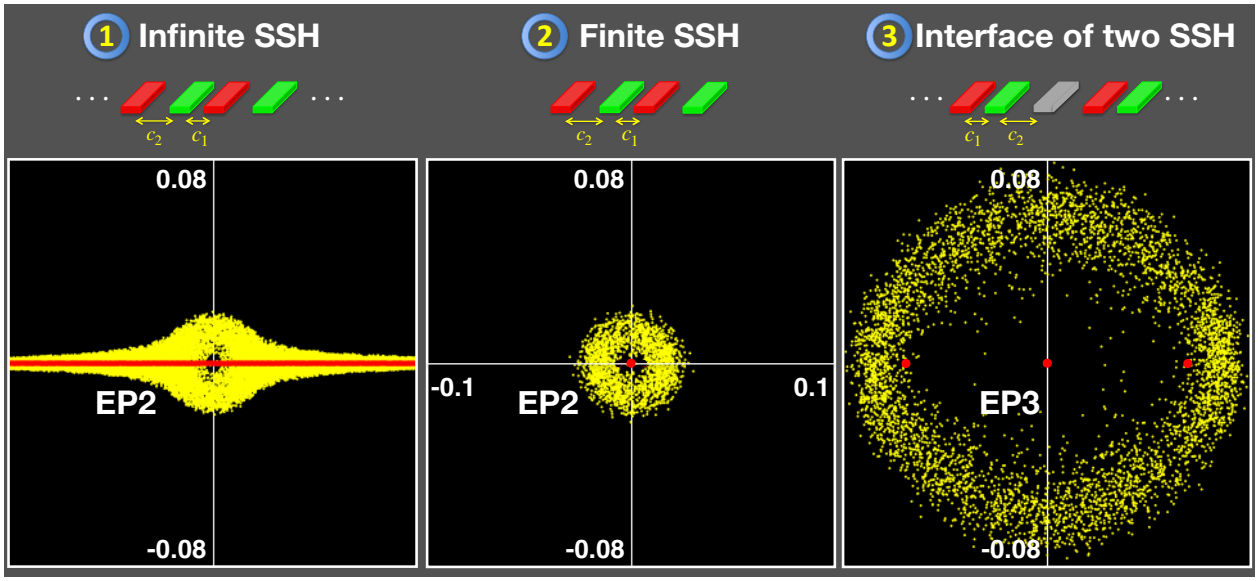


Figure 1: Complex unstructured pseudospectra around the EPs of the three NHSSH lattices: infinite (left), finite (center, N=80) for $\gamma = 2$, and interface (right, N=81) for $\gamma = 2.0159$ and $\gamma_0 = 0$. In all cases $c_1=3$ and $c_2=1$. On the top row the red, green and gray colors illustrate the gainy, lossy, and neutral waveguide, respectively. On the bottom row, the modes that form the EPs (conventional spectra, red dots) and corresponding 0.0001-pseudospectra (1000 realizations-yellow dots), for the three lattices are presented on the complex plane. We have to note here that in the interface lattice, at the red dot at [0,0] three eigenvalues coalesce. We do not show the edge states of the finite SSH, which are located at [0, ± 2i] and the associated perturbations of the order $\varepsilon/2$.

In conclusion, our results highlight the fundamental question of the interplay between ultrasensitivity and topological protection in the unique framework of pseudospectrum theory and may provide insight for the study of other lattices of non-Hermitian topological physics.

Acknowledgements: This project was funded by the European Research Council (ERC- Consolidator) under the grant agreement No. 101045135 (Beyond Anderson).

References

1. S. Xia, D. Kaltsas, D. Song, I. Komis, J. Xu, A. Szameit, H. Buljan, K. G. Makris, and Z. Chen, Science **372**, 72 (2021).
2. I. Komis, D. Kaltsas, S. Xia, H. Buljan, Z. Chen, and K. G. Makris, Phys. Rev. Research **4**, 043219 (2022).
3. L. N. Trefethen and M. Embree, Spectra and Pseudospectra, (Princeton University Press, 2005).
4. L.N. Trefethen, A.E. Trefethen, S.C. Reddy and T.A. Driscoll, Science **261**, 578 (1993).
5. L. N. Trefethen, SIAM Rev. **39**, 383 (1997).
6. L. N. Trefethen, Acta Num. **8**, 247 (1999).
7. K. G. Makris, L. Ge, and H. E. Türeci, Phys. Rev. X **4**, 041044 (2014).
8. K. G. Makris, Phys. Rev. E **104**, 054218 (2021).

META 2023, PARIS - FRANCE, JULY 18 – 21, 2023

Physical limitations on the observability of non-Hermitian effects in passive systems

H. Schomerus[1] *

[1]Department of Physics, Lancaster, University, UK
*corresponding author: h.schomerus@lancaster.ac.uk

Abstract: I contrast fundamental limitations on the physical observability of non-Hermitian effects in passive and active non-Hermitian systems. While active systems suffer from noise, passive systems are limited by causality, which can be reformulated in terms of constraints on the experimentally observed density of states. Applied to paradigmatic effects, it turns out that signatures of exceptional points and the non-Hermitian skin effect become hidden.

Active elements appear to be critical in experimental realization and observations of paradigmatic non-Hermitian phenomena, such as the non-Hermitian skin effect and the squared-Lorentzian line shape at an exceptional point. As such systems consume energy and suffer from noise that violates the exact implementation of topologically relevant symmetries, passive realizations appear desirable. Here, I establish fundamental limits on this objective that relate constraints from causality to the experimental protocol of determining the density of states [1]. In the density of states, the non-Hermitian skin effect turns out to be completely hidden, while the squared Lorentzian only appears as a background effect of limited contrast (Fig. 1).

Theoretically, the key insight is utilizing an appropriately generalized time-delay operator to link the causality constraints with the experimental protocol to determine the density of states. Practically, the constraints can then be formulated directly in terms of the microscopic model, as earlier established via spectral considerations [2]. Conceptually, the strong link between a fundamental concept and a key experimental observable provides a new perspective on analogous constraints on the spectral features and response in active and passive non-Hermitian systems [3-7].

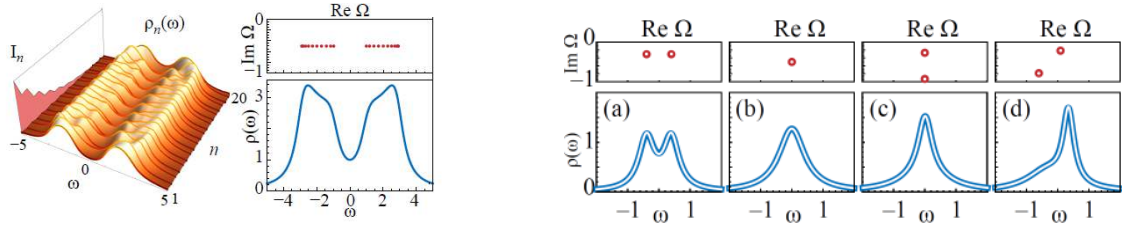


Fig. 1 Left: Local and global density of states ρ in a non-reciprocal non-Hermitian system with open boundaries. The eigenfunctions display the non-Hermitian skin effect (see intensity profile I_n), but this is not reflected in the local density of states. Right: Density of states of a passive system passing through an exceptional point. In striking contrast to active systems, right at the exceptional point (second panel) the density of states is a normal Lorentzian. For both systems, the red dots show the position of states in the complex frequency plane.

References

1. H. Schomerus, "Fundamental constraints on the observability of non-Hermitian effects in passive systems," Phys. Rev. A 106, 063509 (2022).
2. J. Wiersig, "Nonorthogonality constraints in open quantum and wave systems, " Phys. Rev. Res. 1, 033182 (2019).
3. H. Schomerus, "Quantum Noise and Self-Sustained Radiation of PT-Symmetric Systems, " Phys. Rev. Lett. 104, 233601 (2010).
4. G. Yoo, H.-S. Sim, and H. Schomerus, "Quantum noise and mode nonorthogonality in non-Hermitian PT-symmetric optical resonators, " Phys. Rev. A 84, 063833 (2011).
5. H. Schomerus, "Nonreciprocal response theory of non-Hermitian mechanical metamaterials: Response phase transition from the skin effect of zero modes", Phys. Rev. Research 2, 013058 (2020).
6. J. Wiersig, "Distance between exceptional points and diabolic points and its implication for the response strength of non-Hermitian systems," Phys. Rev. Res. 4, 033179 (2022).
7. A. Hashemi, K. Busch, D. N. Christodoulides, S. K. Ozdemir, and R. El-Ganainy, "Linear response theory of open systems with exceptional points, " Nat. Commun. 13, 3281 (2022).

Pseudomagnetic suppression of non-Hermitian skin effect

H. T. Teo[1], S. Mandal[1], Y. Long[1*], H. Xue[1†], and B. Zhang[1, 2‡]

[1]Division of Physics and Applied Physics, School of Physical and Mathematical Sciences, Nanyang Technological University, Singapore 637371, Singapore
[2]Centre for Disruptive Photonic Technologies, Nanyang Technological University, Singapore 637371, Singapore
corresponding authors: *yang.long@ntu.edu.sg, †haoran001@e.ntu.edu.sg, ‡blzhang@ntu.edu.sg

Abstract: Inspired by previous work on magnetic suppression, we demonstrate that a pseudomagnetic field can also suppress non-Hermitian skin effect using a two-dimensional tight-binding lattice. By increasing pseudomagnetic field, the skin modes are pushed into the bulk, accompanied by the reduction of skin topological area and the restoration of Landau levels. Our results provide a new route to localization control and could be useful in classical wave devices that are able to host non-Hermitian skin effect but inert to magnetic fields.

Nontrivial point gap topology that is unique to non-Hermitian physics has led to the non-Hermitian skin effect (NHSE), where most of eigenstates accumulate at the boundaries. Contrary to NHSE, pseudomagnetic fields (PMFs) which are constructed from spatially varying artificial gauge fields can induce Landau levels and associated bulk-localized modes in magnetic-free systems. Considering both localization mechanisms, how will NHSE and PMF interact if they are present in a single system? Recent theoretical studies show that magnetic fields can lead to a suppression of the NHSE: with an increasing magnetic field, the skin modes are gradually pushed into the bulk [1, 2]. Compared to magnetic field that interacts with charged systems, current platforms for realizing the NHSE are mostly magnetically inert. This separation in physical systems poses a challenge in utilizing the competition between the NHSE and magnetic field.

Instead of a real magnetic field, we show that a PMF can also suppress the NHSE in this work. As illustrated in Fig. 1, we construct a two-dimensional lattice model with both NHSE and a PMF, induced by nonreciprocal hoppings and inhomogeneous hoppings, respectively. The NHSE can occur in either x or y direction, depending on directions of nonreciprocal hoppings. The PMF is applied via y dependent J_1 hoppings, thus generating a spatially uniform PMF that is directly proportional to η:

$$J_1(y) = J_2 + 2t\cos\left[\frac{1}{2}\left(\frac{\pi}{2} - \frac{2\pi y}{N_y}\eta\right)\right], \tag{1}$$

When NHSE is along x-direction, we demonstrate the suppression via calculation of skin topological area S_1, which is the weighted sum of winding number $w(E_0)$ in the complex energy E_0 plane:

$$w(E_0) = \frac{1}{2\pi i}\int_{-\pi}^{\pi} dk_x \frac{d}{dk_x}\log\det\left(\mathcal{H}(k_x) - E_0\right), \tag{2}$$

As shown in Fig. 2, the reduction of S_1 signifies the overall weakening of $w(E_0)$, therefore elucidating the suppression of NHSE from its topological origin.

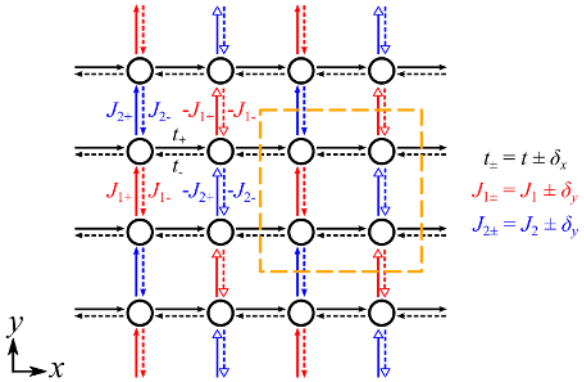


FIG. 1. Illustration of the lattice model. The solid and dashed arrows denote hoppings along opposite directions, with the colors indicating different hopping strengths. Due to the presence of negative hoppings, there is a π gauge flux per plaquette. The yellow dashed box denotes the unit cell.

On the other hand, by starting from y directional NHSE, we demonstrate the suppression via calculations of skin mode profiles and Landau level spectrum as depicted in Fig. 3. The suppression is prominent for energies within the first few Landau levels, where the effective theory of the PMF stays valid. In addition to the transition from skin mode to Landau mode, the zero-energy eigenstate even shows a sublattice polarization that captures the states of different origins at distinct sublattices, thus highlighting its uniqueness in PMF systems.

As a result, our model can be directly mapped to realistic physical settings in photonic, acoustic and circuit systems, therefore paving a novel way to localization control for classical wave devices. In future works, it would be desired to further apply the tunable skin modes found here to various classical wave devices, especially in optical systems where active control of localization and nonlinear effects can be studied.

This work is supported by Singapore Ministry of Education Academic Research Fund Tier 3 under Grant No. MOE2016-T3-1-006.

References

1. M. Lu, X.-X. Zhang, and M. Franz, "Magnetic suppression of non-Hermitian skin effects," Phys. Rev. Lett., Vol. 127, No. 25, 256402, 2021.

2. K. Shao, Z.-T. Cai, H. Geng, W. Chen, and D. Y. Xing, "Cyclotron quantization and mirror-time transition on nonreciprocal lattices," Phys. Rev. B, Vol. 106, No. 8, L081402, 2022.

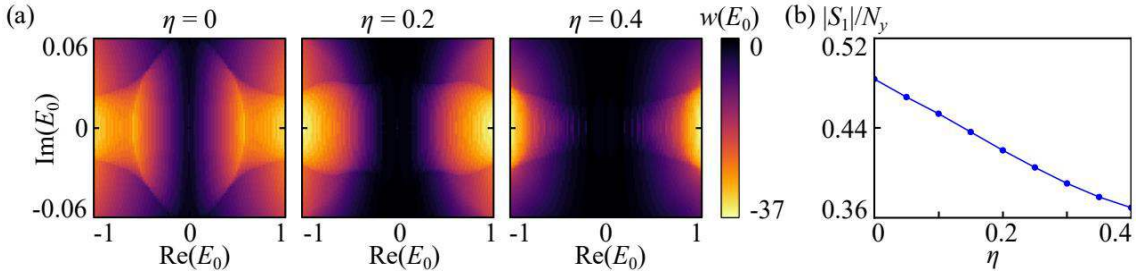


FIG. 2. (a) Plots of winding number $w(E_0)$ against PMF indicator η in the complex reference energy plane [Re(E_0), Im(E_0)] at (δ_x, δ_y) = (0.05, 0). The color indicates the magnitude of winding number $w(E_0)$ obtained from a strip of N_y cells along y direction, but infinite along x direction. (b) Skin topological area per unit cell S_1/N_y as a function of PMF indicator η, computed in a similar supercell as panel (a).

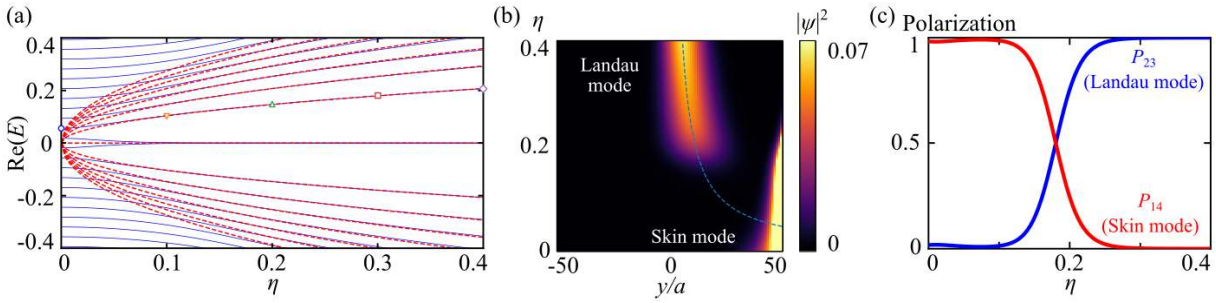


FIG. 3. (a) Real part of the energy spectrum as a function of η at the $k_x = \pi/2$ valley and fixed non-Hermitian components (δ_x, δ_y) = (0, 0.05). Landau levels of lower orders in the Hermitian limit are included as red dashed lines that agree with computed spectrum at large PMFs. (b) Spatial variation of the eigenstate characterized by zero energy at different PMFs with fixed δ_y, showing a transition from skin mode to bulk-localized zeroth Landau mode as theoretically predicted by its center (blue curve). (c) Sublattice polarization of the eigenstate in panel (b). P_{14} and P_{23} quantify the probability distributions which concentrate at each pair of the sublattices respectively, at the same time quantifying the dominance of skin mode and Landau mode at different η.

Probing the spatial and temporal decay of quasimodes in non-Hermitian Vogel spirals via localization maps

***M. Prado[1], F. Sgrignuoli[2], Y. Chen[2], L. Dal Negro[2,3,4], F. A. Pinheiro[1]**

[1]Instituto de Física, Universidade Federal do Rio de Janeiro, Rio de Janeiro-RJ, 21941-972, Brazil
[2]Department of Electrical and Computer Engineering, Boston University, Boston, Massachusetts, 02215, USA
[3]Division of Material Science & Engineering, Boston University, Boston, Massachusetts, 02446, USA
[4]Department of Physics, Boston University, Boston, Massachusetts, 02215, USA
[*]corresponding author: mvap@pos.if.ufrj.br

Abstract: We investigate the temporal and spatial properties of the quasimodes of non-Hermitian Vogel spiral planar arrays. The analysis of the localization maps reveals that optical quasimodes with three types of spatial decay coexist in these deterministic aperiodic structures: exponential, Gaussian and power-law decay. On average, the Gaussian ones are found to be the most spatially and temporally localized. In addition, our results provide the first direct demonstration of critical quasimodes in Vogel spirals.

Aperiodic metamaterials, whose structural order lie in between periodic and disordered media, have emerged as an alternative photonic platform [1-3]. Among them, Vogel spirals stand out as prominent examples due to being generated by simple, deterministic mathematical rules and to their unusual optical properties [1,2,4]. They consist of planar arrays of scatterers (*e.g.*, dielectric or metallic nanoparticles) whose positions in polar coordinates are given by $r_n = a_0\sqrt{n}$, $\theta_n = \alpha n$, where $n = 1, 2, 3, ...$ The scaling factor a_0 determines the average interparticle separation, while the divergence angle α allows interpolating the structural properties between short-range correlated amorphous systems and uncorrelated random ones.

Remarkably, a transition to light localization has been predicted to occur in non-Hermitian (*i.e.*, open) Vogel spiral arrays [4], despite the fact that Anderson localization of light for randomly distributed dipoles does not occur in 3D [5]. In this work we investigate the spatial and temporal localization properties of Vogel spirals. Their quasimodes ψ_n are obtained using the Green's matrix method [2,4,5]. The spatial decay of the quasimodes are characterized by the localization maps [6]. The analysis consists of calculating their normalized participation ratios $q_n = \mathrm{PR}_n/N$ and structural entropies, which are defined as

$$S_{str_n} = -\sum_{i=1}^{N}|\psi_n(i)|^2 \ln|\psi_n(i)|^2 - \ln \mathrm{PR}_n \quad (1)$$

The relation between these two quantities allows us to predict the existence of quasimodes of arbitrary types of spatial decay by comparing the results to the corresponding references curves [6]. Furthermore, we access information regarding the temporal localization of each quasimode by determining its normalized decay rate g_n, that quantifies modal overlap [5].

In Figure 1 the localization maps for four types of Vogel spirals (*i.e.*, different divergence angles α) are shown. The maps reveal that these arrays support a rich variety of localized quasimodes. In particular, we verify the coexistence of modes with exponential, Gaussian, and power-law decay, as indicated by the reference

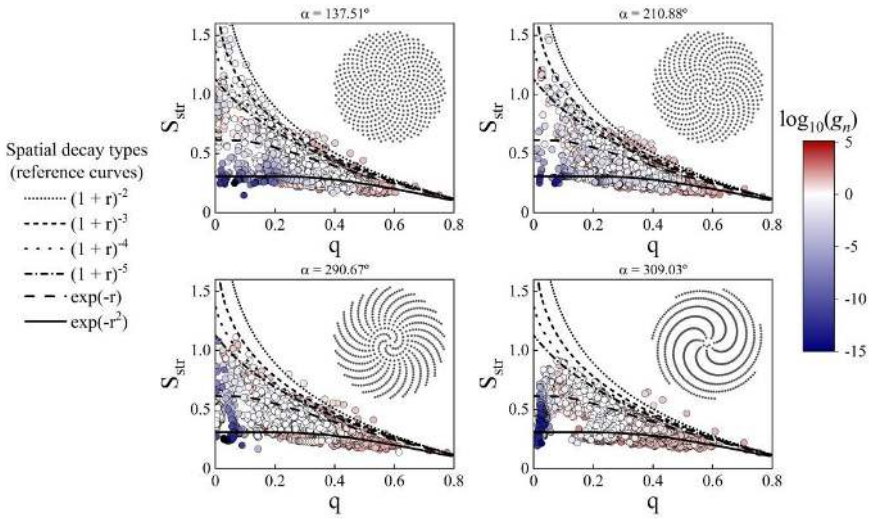


Figure 1. Localization maps: structural entropy S_{str} as a function of the normalized participation ratio q of all quasimodes of different Vogel spiral arrays (depicted in the insets) with $N = 5000$ point scatterers and optical density $\rho\lambda^2 = 30$. The maps are color coded according to the $\log_{10}$ values of the normalized decay rate g_n.

curves. Modes with exponential decay are usually associated with Anderson localization in disordered systems, but here we show that they can also exist in deterministic aperiodic Vogel spirals. Nonetheless, we find that, on average, the quasimodes with Guassian decay are not only the most spatially localized (smallest participation ratios) but also the most temporally localized (smallest decay rates, for which $g_n \ll 1$). In addition, the localization maps show that quasimodes with power-law decay do exist in Vogel spirals, with a broad range of spatial extents. These modes, known as critical modes, typically exist in aperiodic systems and were believed to occur in Vogel spirals, but had not been directly demonstrated so far [1,2,4].

M.P. and F.A.P. acknowledge CNPq, CAPES, and FAPERJ for financial support. L.D.N. acknowledges the support from the Army Research Laboratory under Cooperative Agreement No. W911NF-12-2-0023.

References

1. Dal Negro, L., Waves in Complex Media. Cambridge: Cambridge University Press, 2022.
2. Prado, M., F. Sgrignuoli, Y. Chen, L. Dal Negro, and F. A. Pinheiro, “Structural entropy and spatial decay of quasimodes in Vogel spirals”, Phys. Rev. B, Vol. 104, No. 18, 184204, 2021.
3. Dal Negro, L., Y. Zhu, Y. Chen, M. Prado, and F. A. Pinheiro, “Wave localization in number-theoretic landscapes”, Phys. Rev. B, Vol. 106, No. 22, 2242003, 2022.
4. Sgrignuoli, F., R. Wang, F. A. Pinheiro, and L. Dal Negro, “Localization of scattering resonances in aperiodic Vogel spirals”, Phys. Rev. B, Vol. 99, No. 10, 104202, 2019.
5. Skipetrov, S. E., “Finite-size scaling analysis of localization transition for scalar waves in a three-dimensional ensemble of resonant point scatterers”, Phys. Rev. B, Vol. 94, No. 6, 064202, 2016.
6. Pipek, J. and I. Varga, “Universal classification scheme for the spatial-localization properties of one-particle states in finite, d-dimensional systems”, Phys. Rev. A, Vol. 46, No. 6, 3148-3163, 1992.

Engineering localised modes via drive and dissipation in photonic lattices

O. Jamadi[1], B. Real[1], K. Sawicki[2], C. Hainaut[1], A. González-Tudela[3], N. Pernet[4], I. Sagnes[4], M. Morassi[4], A. Lemaître[4], L. Le Gratiet[4], A. Harouri[4], S. Ravets[4], J. Bloch[4], and A. Amo[1*]

[1] Univ. Lille, CNRS, UMR 8523 – PhLAM – Physique des Lasers Atomes et Mol´ecules, F-59000 Lille, France
[2] Institute of Experimental Physics, Faculty of Physics, University of Warsaw, Pasteura St. 5, 02-093 Warsaw, Poland
[3] Institute of Fundamental Physics IFF-CSIC, Calle Serrano 113b, 28006 Madrid, Spain
[4] Université Paris-Saclay, CNRS, Centre de Nanosciences et de Nanotechnologies, 91120, Palaiseau, France
[*]corresponding author: alberto.amo-garcia@univ-lille.fr

Abstract: An efficient strategy to design localized modes in photonic structures is to use the interplay of constructive and destructive interference in periodic photonic lattices. Here, we show experimentally that in lattices of lossy resonators, the addition of external optical drives with a controlled phase enlarges the possibilities of manipulating interference effects and allows for the design of novel types of localized modes with footprints down to a single site.

The engineering of localised modes in photonic structures is one of the main targets of modern photonics. An efficient strategy to design these modes is to use the interplay of constructive and destructive interference in periodic photonic lattices. This mechanism is at the origin of defect modes in photonic bandgaps, bound states in the continuum and compact localised states in flat bands. In this presentation we show that in lattices of lossy resonators made of coupled semiconductor micropillars, the addition of external optical drives with controlled phase enlarges the possibilities of manipulating interference effects and allows designing novel types of localised modes [1]. We show that light can be localised down to a single site of a photonic lattice in a fully reconfigurable manner. We use the technique to engineer dissipative solitons in topological gaps [2].

The localized modes reported here are fully reconfigurable and have the potentiality of enhancing nonlinear effects and of controlling light–matter interactions with single site resolution

References

1. O. Jamadi, B. Real, K. Sawicki, C. Hainaut, A. González-Tudela, N. Pernet, I. Sagnes, M. Morassi, A. Lemaître, L. Le Gratiet, A. Harouri, S. Ravets, J. Bloch, and A. Amo, "Reconfigurable photon localization by coherent drive and dissipation in photonic lattices," Optica Vol. 9, 706, 2022.
2. N. Pernet, P. St-Jean, D. D. Solnyshkov, G. Malpuech, N. Carlon Zambon, Q. Fontaine, B. Real, O. Jamadi, A. Lemaître, M. Morassi, L. Le Gratiet, T. Baptiste, A. Harouri, I. Sagnes, A. Amo, S. Ravets, and J. Bloch, "Gap solitons in a one-dimensional driven-dissipative topological lattice," Nat. Phys. Vol. 18, 678–684, 2022.

META 2023, PARIS - FRANCE, JULY 18 – 21, 2023

Non-Hermitian Spin-Hall Effect in Topological Metasurfaces

Svetlana Kiriushechkina[1], Anton Vakulenko[1], Daria Smirnova[2], Sriram Guddala[1], Filipp Komissarenko[1], Monica Allen[3], Jeffery Allen[3], Alexander B. Khanikaev[1*]

[1]Electrical Engineering and Physics, The City College of New York (USA), New York, NY 10031, USA
[2]Research School of Physics, The Australian National University, Canberra ACT 2601, Australia
[3]Air Force Research Laboratory, Munitions Directorate, Eglin AFB, USA
[*]corresponding author: akhanikaev@ccny.cuny.edu

Abstract: We demonstrate that, for suitable trapping one-dimensional Dirac potentials, there exist guided modes exhibiting spin-dependent field distributions, which may give rise to their different coupling efficiency to the radiative continuum or light-matter coupling properties. For leaky open Dirac metasurfaces this should manifest in different transport and radiative properties of modes of opposite spin – the non-Hermitian spin-Hall effect. We use silicon nanophotonic metasurfaces that support pseudo-spin degree of freedom as a testing platform to experimentally confirm such spin-dependent non-Hermitian properties of spin-full photonic Dirac waveguides.

The Dirac equation is a paradigmatic model that describes a range of intriguing properties of relativistic spin-½ particles, from the existence of antiparticles to Klein tunneling. However, the Dirac-like equations have found application far beyond the original scope and have been used to comprehend the properties of graphene and topological phases of matter. In the field of photonics, the opportunity to emulate Dirac physics has also enabled topological photonic insulators. In this work, we demonstrate that judiciously engineered synthetic potentials in photonic Dirac systems can offer physical properties beyond both the elementary/quasi-particles' and topological realms. Specifically, we introduce a new class of optical "Dirac waveguides", whose guided electromagnetic modes are endowed with pseudo-spin degree of freedom. When combined with the ability to engineer synthetic gauge potentials acting on it, the pseudo-spin enables control over the guided modes which is unattainable in conventional optical waveguides. In particular, we use silicon nanophotonic metasurfaces supporting pseudo-spin degree of freedom as a testing platform to predict and experimentally confirm a spin-full nature of the photonic Dirac waveguides. We also demonstrate that, for suitable trapping potentials, the guided modes exhibit spin-dependent field distributions, which gives rise to their distinct transport and radiative properties. Thereby, the Dirac waveguides manifest spin-dependent radiative lifetimes – the non-Hermitian spin-Hall effect – and open new avenues for spin-multiplexing, controlling characteristics of guided optical modes, and tuning light-matter interactions with photonic pseudo-spins.

The demonstrated pseudo-spin-dependent trapping and guiding of light opens a completely new direction for applications of photonic pseudo-spins, beyond topological concepts. We anticipate that the spin-full nature of the modes will find its use in on-chip quantum photonic devices where quantum information could be encoded by a photonic pseudo-spin. The spin-dependent field distributions and quality factors of the modes can also be used for selective (e.g., polarization dependent) control of

light-matter interactions on a photonic chip, which envisions novel design principles of polaritonic, active, and nonlinear photonic devices.

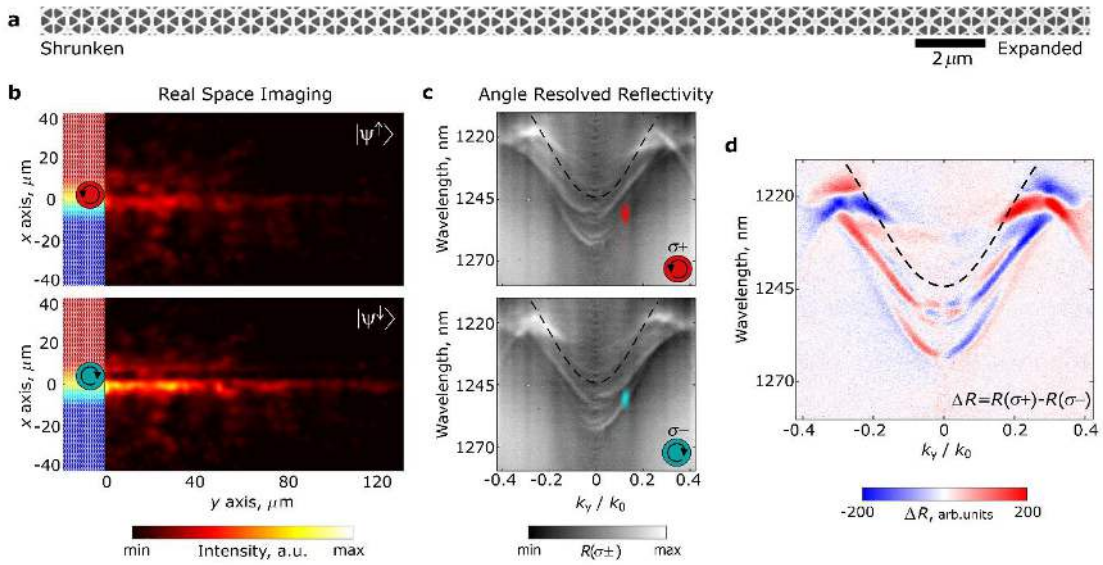


Figure 1. Experimental results evidencing pseudo-spin polarized transport and non-Hermitian spin-Hall effect in the Dirac meta-waveguide. a, SEM image of a cross-section of the Dirac meta-waveguide with antisymmetric mass term distribution. **b**, Real-space images of the spectrally and momentum-space filtered excitations of the lowest upper-frequency (positive energy) guided modes of the Dirac meta-waveguide, driven by left (top panel) and right (bottom panel) circularly polarized light for selective excitation of pseudo-spin-up and pseudo-spin-down modes, respectively. Non-Hermitian spin-Hall effect manifests in differing excitation efficiencies and propagation lengths for two guided modes of opposite pseudo-spins. **c**, Fourier-plane images of the Dirac meta-waveguide in the reflection geometry showing dispersion of the upper guided and bulk pseudo-spin-up and pseudo-spin-down modes. The colored dots indicate positions of spectral and momentum filtering for the real-space image in **a**. **d**, Differential reflectivity spectra evidencing contrast in excitation and leakage of the guided modes of opposite pseudo-spins.

References

1. S. Kiriushechkina, S., Vakulenko, A., Smirnova, D., Guddala, S., Komissarenko, F., Allen, M., Allen, J., and Khanikaev, A. B., Spin-Full Guided Modes in Photonic Dirac Metasurfaces, (arXiv:2211.00701 – Photonic Dirac Waveguides), Nature Nanotech. (2023) (in press).
2. Chen, K., Komissarenko, F., Smirnova, D., Vakulenko, A., Kiriushechkina, S., Volkovskaya, I., Guddala, S., Menon, V., Alù, A., and Khanikaev, A. B., Photonic cavities within Dirac metasurfaces with spatially varying mass, Science Advances (2023) (in press).

META 2023, PARIS - FRANCE, JULY 18 – 21, 2023

Higher order exceptional points in photonic lattices

Dimitrios Kaltsas[1,2], Ioannis Komis[2,3], and Konstantinos G. Makris[1,2]
[1]ITCP-Physics Department, University of Crete, Heraklion, 71003, Greece
[2]Institute of Electronic Structure and Laser (IESL) – FORTH, Heraklion, 71110, Greece
[3]Humboldt -Universität zu Berlin, Institut für Physik, AG Theoretische Optik & Photonik, D-12489 Berlin, Germany
corresponding author: dkaltsas@physics.uoc.gr

Abstract: Higher order exceptional points (HEPs), are unique characteristic degeneracies of non-Hermitian systems. We provide a systematic method for constructing infinite optical lattices that exhibit HEPs. The spectral properties-sensitivity of these lattices around HEPs is investigated in terms of pseudospectra theory, along with the topological character of the corresponding bands. Recent results concerning conservation laws in non-Hermitian systems and their relation to HEPs, will also be presented.

Open systems under the effect of dissipation and/or amplification, are effectively described by non-Hermitian Hamiltonians. One of their most important features is the existence of unique non-Hermitian degeneracies [1] or exceptional points [2], where two or more eigenvalues and eigenvectors coalesce for particular values of the system's parameters. One special class of non-Hermitian Hamiltonians are these that respect parity-time (PT)-symmetry. In the past years, in the context of non-Hermitian photonics [3] various PT-symmetric systems with higher order exceptional points have been experimentally demonstrated and used to design ultra sensitive sensors [4]. However these exceptional points are usually studied in finite lattices of few elements. In the first part of the talk, we will present a systematic methodology of constructing infinite one-dimensional optical lattices that exhibit higher order exceptional points. The appropriate gain-loss distribution is determined analytically for HEP's of various orders. In the second part of our talk, we will present the pseudospectra [5, 6] of the associated infinite lattices around the HEP's and relate them to the lattice's sensitivity to external perturbations. At the end, we are going to discuss recent results regarding the existence of conservation laws in non-Hermitian systems.

Let us start by considering one dimensional trimerized lattices, that are described by the following 3-by-3 bulk momentum Hamiltonian of the form:

$$H=\begin{bmatrix} i\gamma & t_1 & t_2 e^{ik} \\ t_1 & 0 & t_1 \\ t_2 e^{-ik} & t_1 & -i\gamma \end{bmatrix} \qquad (1)$$

This matrix describes a three-cell periodic lattice where γ, t_1, t_2 are real and k is the Bloch wavenumber $k \in [-\pi, \pi)$. For, $k=\pi/2$ the three values of the propagation eigenvalues λ are equal to zero and the eigenvectors coalesce. Indeed we can show that this is an HEP of order three, meaning EP3. Note that although we only consider the bulk momentum Hamiltonian that exhibits an EPN with N=3, this method can be generalized to derive a lattice with an EPN from a suitable N-by-N bulk momentum Hamiltonian.

Our computational results for N=3, and coupling constants $t_1=1$ and $t_2=2$ are shown in Fig.1. In particular the real and imaginary parts of the three bands versus the gain-loss amplitude, γ are shown in Fig.1 (a), (b), respectively. We have also analyzed the sensitivity of the system to external perturbations by using pseudospectra methods [5, 6]. More specifically, by adding a random matrix E such that $\|E\| < \varepsilon$ -where $\| \cdot \|$ denotes the norm of the matrix- to the bulk momentum Hamiltonian, and calculating the union of all the resulted spectra, we get a pattern in the complex plane, called pseudospectrum (Fig.1(c)). The blue dots are the pseudoeigenvalues of an ensemble of 1000 perturbed bulk momentum Hamiltonians, for $\varepsilon = 2 \cdot 10^{-3}$. The red dots are the actual eigenvalues that form the EP3. Finally, in Fig. 1(d) we numerically evaluate the pseudospectral abscissa A_ε, that provides a measure of the sensitivity of the lattice for different values of ε [6]. The slope of the linear fit is $\approx 1/3$, which is a characteristic signature of an EP3 [2, 4]. We have also

extended our methodology to higher orders and thus constructing lattices that exhibit EP4 and EP7.

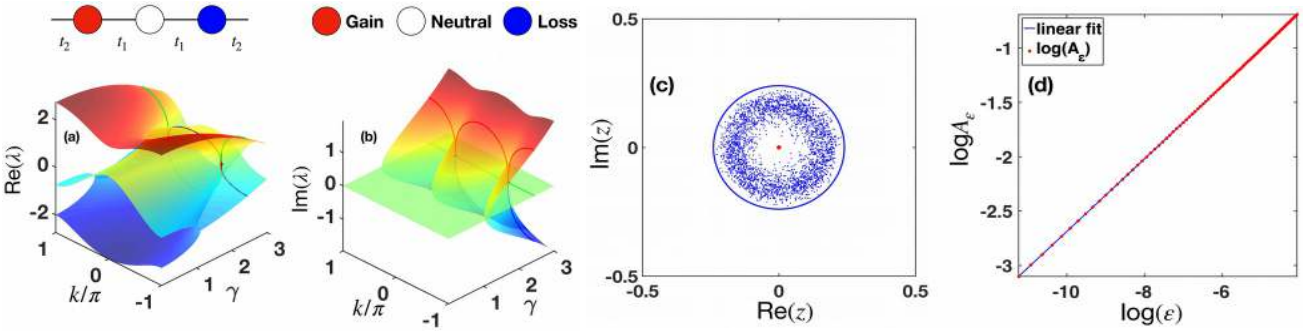


Figure 1: Bandstructure and sensitivity of the system. The values of the coupling coefficients have been chosen to be t_1=1 and t_2=2. (a), (b) Real Re(λ) and imaginary Im(λ) part of the three bands vs the Bloch wavenumber k/π and vs the gain/loss amplitude γ, respectively. (c) The red dots are the exact three eigenvalues that form the EP3 in the complex plane. The blue dots denote the pseudospectrum for $\varepsilon = 2 \cdot 10^{-3}$. The solid blue line is the pseudospectrum calculated by a singular value decomposition method [6]. (d) Pseudospectral abscissa A_ε for different values of ε, in logarithmic scale. The slope is 1/3, as is expected for an EP3.

In conclusion, we have introduced a systematic method [7] to construct infinite optical lattices that exhibit EPs of higher order. In particular, we have considered trimerized and tetramerized non-Hermitian lattices that exhibit EP3 and EP4, respectively. Our methodology is quite general and can be applied to even higher orders (we have numerically verified our method up to N=7). Notice that the corresponding finite lattices with periodic boundary conditions, exhibit the same HEPs, thus making our results relevant to experimental realizations. Our novel complex lattices are directly related to non-Hermitian optics and topological physics, since on the one hand they can be used to implement ultra sensitive sensors and on the other hand, can be used to identify new topological phases in the complex plane.

Acknowledgments: This project was funded by the European Research Council (ERC-Consolidator) under the grant agreement No. 101045135 (Beyond_Anderson).

References

1. M. V. Berry, "Physics of nonhermitian degeneracies", Czechoslovak J. Phys. **54**, 1039 (2004).
2. J. Wiersig, "Enhancing the sensitivity of frequency and energy splitting detection by using exceptional points: application to microcavity sensors for single-particle detection", Phys. Rev. Lett., **112**, 203901 (2014).
3. R. El-Ganainy, K.G. Makris, M. Khajavikhan, Z.H. Musslimani, S. Rotter, and D. N. Christodoulides, "'Non-Hermitian physics and PT symmetry" Nat. Phys. **14**, 11 (2018).
4. H. Hodaei, A. U. Hassan, S. Wittek, H. Garcia-Gracia, R.El-Ganainy, D. N. Christodoulides, and M. Khajavikhan, "Enhanced sensitivity at higher-order exceptional points", Nature **548**, 187 (2017).
5. K. G. Makris, L. Ge, and H. E. Tureci, "Anomalous transient amplification of waves in non-normal photonic media", Phys. Rev. X **4**, 041044 (2014).
6. K. G. Makris, "Transient growth and dissipative exceptional points", Phys. Rev. E **104**, 054218 (2021).
7. D. Kaltsas, I. Komis and K. G. Makris, "Higher order exceptional points in infinite lattices", Opt. Lett. **47**, 4447 (2021).

Metasurfaces for Nonlinear and Ultrafast Nanophotonics

META 2023, PARIS - FRANCE, JULY 18 – 21, 2023

Broadband control of topological-spectral correlations in space-time beams

Marco Piccardo[1*], Michael de Oliveira[1,2], Veronica R. Policht[2], Mattia Russo[2], Benedetto Ardini[2], Matteo Corti[2], Gianluca Valentini[2], Jorge Vieira[3], Cristian Manzoni[4], Giulio Cerullo[2], and Antonio Ambrosio[1*]

[1] Center for Nano Science and Technology, Fondazione Istituto Italiano di Tecnologia, Milan, Italy
[2] Physics Department, Politecnico di Milano, Milan, Italy
[3] Instituto Superior Técnico, Universidade de Lisboa, Lisbon, Portugal
[4] Institute for Photonics and Nanotechnology, Consiglio Nazionale delle Ricerche, Milan, Italy
[*]corresponding author: piccardo@g.harvard.edu; antonio.ambrosio@iit.it

Abstract: We introduce shaping and characterization methods for femtosecond space-time beams with broadband correlations between their topological charges (up to L=80) and spectral frequencies (covering nearly 50% of the visible spectrum).

The synthesis of ultrashort wave packets with simultaneously tailored spatial and temporal properties has seen tremendous advances in recent years [1], following progress in both wavefront and pulse shaping. This is part of a more general trend towards multimodal photonics [2], in which more and more degrees of freedom of light are combined together to attain unprecedented light fields. In the realm of space-time beams, of particular interest are wave packets carrying orbital angular momentum (OAM) with a topological charge ℓ. Many fascinating demonstrations of these beams have appeared so far, including time-varying OAM beams [3, 4], spatiotemporal optical vortices with transverse OAM [5], light coils [6, 7], and revolving-rotating beams [8]. Most of these schemes, however, were limited to small topological charges and/or narrow spectral bandwidths. By changing the geometry of our Fourier space-time synthesizer and fabricating custom grayscale optical phase plates, we demonstrate here the shaping of space-time wave packets with correlations between a wide band of topological charges, with values up to $\ell = 80$, and spectral frequencies covering nearly 50% of the visible spectrum. The broadband nature of these correlations brings unprecedented capability in the tailoring of OAM-carrying space-time beams on a femtosecond scale.

We characterize [9] this new family of space-time beams both by means of an established technique based on axis interference and cross-correlation, as well as by introducing a spatially-resolved spectral method. The latter relies on the combination of two interferometers, a temporal one based on the translating-wedge-based identical pulses encoding system (TWINS) [10] and a spatial one based on off-axis interference. This provides a temporal interferogram for every pixel of the camera from which we can obtain spectral interference images and carry out off-axis digital holography. As a result, we obtain a hypercube with the intensity and phase of the spectral components of the shaped femtosecond pulse. This allows us to experimentally characterize the topological-spectral correlation, which is observed to closely follow our design.

With our technique we can generate both separable and nonseparable space-time beams carrying OAM. The first one corresponds to a separable pulsed vortex, in which all spectral frequencies carry the same topological charge, $\ell = 40$. On the other hand, the second light field can have the profile of a light coil [6] (or helical wave packet) and exhibit an azimuthally-dependent pulse arrival time. We use this technique to generate a variety of space-time beams with both linear and nonlinear topological-spectral correlations. The former allow us to control the chirality, orbital radius, intertwining and multiplexing of helical wave packets,

while the latter allow us to manipulate their dynamics. We foresee that our space-time shaping method will find its use in several applications allowing: the transfer of OAM to matter, such as in Raman-active media at the core of laser- plasma accelerators; the imaging of ultrafast electronic processes, thanks to the mapping of time to space carried out by these wave packets; and the increase of the capacity of optical communication channels, thanks to OAM-frequency division multiplexing.

References

1. M. Yessenov, L. A. Hall, K. L. Schepler, and A. F. Abouraddy, "Space-time wave packets," Adv. Opt. Photon. 14, 455–570 (2022).
2. M. Piccardo, V. Ginis, A. Forbes, S. Mahler, A. A. Friesem, N. Davidson, H. Ren, A. H. Dorrah, F. Capasso, F. T. Dullo, B. S. Ahluwalia, A. Ambrosio, S. Gigan, N. Treps, M. Hiekkam¨aki, R. Fickler, M. Kues, D. Moss, R. Morandotti, J. Riemensberger, T. J. Kippenberg, J. Faist, G. Scalari, N. Picqu´e, T. W. H¨ansch, G. Cerullo, C. Manzoni, L. A. Lugiato, M. Brambilla, L. Columbo, A. Gatti, F. Prati, A. Shiri, A. F. Abouraddy, A. Alu, E. Galiffi, J. B. Pendry, and P. A. Huidobro, "Roadmap on multimode light shaping," J. Opt. 24, 013001 (2022).
3. L. Rego, K. M. Dorney, N. J. Brooks, Q. L. Nguyen, C.-T. Liao, J. San Roman, D. E. Couch, A. Liu, E. Pisanty, M. Lewenstein, L. Plaja, H. C. Kapteyn, M. M. Murnane, and C. Hernandez-Garcia, "Generation of extreme-ultraviolet beams with time-varying orbital angular momentum," Science 364, eaaw9486 (2019).
4. D. Cruz-Delgado, S. Yerolatsitis, N. K. Fontaine, D. N. Christodoulides, R. Amezcua-Correa, and M. A. Bandres, "Synthesis of ultrafast wavepackets with tailored spatiotemporal properties," Nat. Photonics 16, 686–691 (2022).
5. A. Chong, C. Wan, J. Chen, and Q. Zhan, "Generation of spatiotemporal optical vortices with controllable transverse orbital angular momentum," Nat. Photonics 14, 350–354 (2020).
6. G. Pariente and F. Quere, "Spatio-temporal light springs: extended encoding of orbital angular momentum in ultrashort pulses," Opt. Lett. 40, 2037–2040 (2015).
7. L. Chen, W. Zhu, P. Huo, J. Song, H. J. Lezec, T. Xu, and A. Agrawal, "Synthesizing ultrafast optical pulses with arbitrary spatiotemporal control," Sci. Adv. 8, eabq8314 (2022).
8. Z. Zhao, H. Song, R. Zhang, K. Pang, C. Liu, H. Song, A. Almaiman, K. Manukyan, H. Zhou, B. Lynn, R. W. Boyd, M. Tur, and A. E. Willner, "Dynamic spatiotemporal beams that combine two independent and controllable orbital-angular-momenta using multiple optical-frequency-comb lines," Nat. Commun. 11, 4099 (2020).
9. S. W. Jolly, O. Gobert, and F. Quere, "Spatio-temporal characterization of ultrashort laser beams: a tutorial," J. Opt. 22, 103501 (2020).
10. A. Perri, B. E. Nogueira de Faria, D. C. T. Ferreira, D. Comelli, G. Valentini, F. Preda, D. Polli, A. M. de Paula, G. Cerullo, and C. Manzoni, "Hyperspectral imaging with a TWINS birefringent interferometer," Opt. Express 27, 15956–15967 (2019).

Third-order Infrared Upconversion Imaging with Silicon Metasurfaces

Ze Zheng [1], Lei Xu [1]*, Lujun Huang [2,3], Daria Smirnova [4], Khosro Zangeneh Kamali [4], Arman Yousefi [1], Fu Deng [5], Rocio Camacho-Morales [4], Cuifeng Ying [1], Andrey E. Miroshnichenko [2], Dragomir N. Neshev[4], Mohsen Rahmani [1]*

[1] Advanced Optics and Photonics Laboratory, Department of Engineering, School of Science & Technology, Nottingham Trent University, NG11 8NS, UK;

[2] School of Engineering and Information Technology, University of New South Wales, Canberra, ACT 2600, Australia;

[3] School of Physics and Electronic Science, East China Normal University, Shanghai, 200241, China

[4] ARC Centre of Excellence for Transformative Meta-Optical Systems (TMOS), Research School of Physics, The Australian National University, Canberra, ACT 2601, Australia;

[5] Department of Physics, Hong Kong University of Science and Technology, Kowloon, Hong Kong, SAR, China

*corresponding author: mohsen.rahmani@ntu.ac.uk

Abstract: We experimentally demonstrated the near-infrared to visible imaging, based on the third-order generation processes, by designing a silicon membrane metasurface supporting symmetry-protected bound states in the continuum.

Nonlinear nanophotonics has been attracting tremendous attention due to its vast applications in sensing, optical microscopy, and quantum photon source generation. Nonlinear metasurfaces have been recognised as a potential substitute for commercial infrared (IR) imaging and spectroscopy detectors because of their superiority of being ultra-compact and containing fewer components for signal conversion [1]. Here, we propose silicon membrane metasurfaces with smaller unit-cell sizes (Fig. 1a) to enhance local light confinement and to increase the conversion efficiency and spatial resolution of the third-harmonic generation (THG) in IR imaging applications [2].

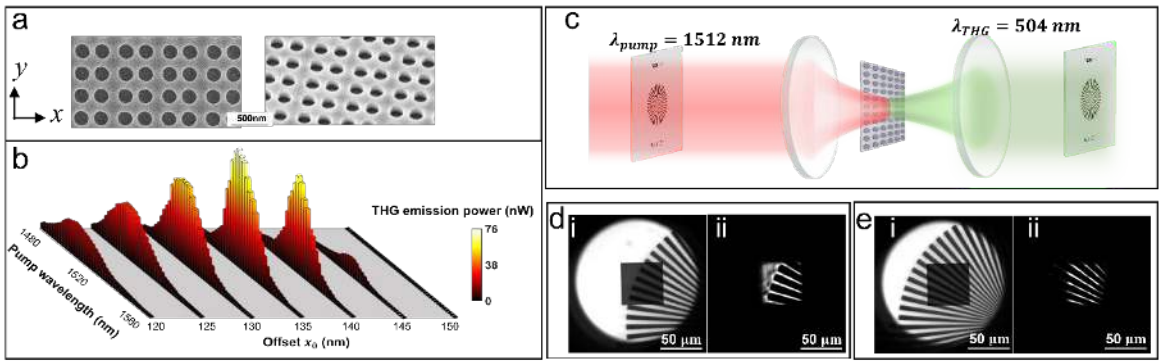


Fig. 1 (a) SEM image of the fabricated metasurface sample. (b) Experimentally measured THG spectra of the samples with different offset x0. The offset x0 is defined as the distance from the center of one hole to the midline of the unit (with a dimer hole) along the x direction. (c) Schematic of THG imaging based on Si membrane metasurfaces. The near-IR signal passes through the target, then is converted into the visible signal via the metasurfaces, forming the target image on the CCD camera. (d, e) The images of the target and the metasurfaces under (i) white light source illumination. (ii) Transformed visible images of the target via membrane metasurfaces under NIR light illumination.

We theoretically and experimentally demonstrate the formation of different types of bound states in the continuum (BIC) from silicon dimer-hole membrane metasurfaces to achieve nanoscale light manipulation with strong electromagnetic field confinement. By tuning the gap between the two holes, the symmetry-protected BICs can be transformed into quasi-BICs with a tuneable Q-factor, which can directly affect the conversion efficiency (see Fig. 1b). We experimentally obtained a significant THG enhancement near the resonance, leading to a conversion efficiency of 3.6×10^{-6} under a pump peak intensity of 1.0 GW/cm^2. Importantly, compared to classical metasurfaces composed of the periodic arrangement of nanoparticles, our silicon membrane metasurface supports resonances with a smaller unit-cell size and a larger mode volume, providing a powerful platform for nonlinear imaging applications. Figures 1c-e demonstrate the ability of THG imaging with our designed metasurface. Under a pump at a wavelength of 1512 nm, an image of the NBS 1963A resolution target is formed by the focal lens onto the metasurface (see Fig 1c). The pattern of the overlapping area between the image of the target and the metasurface, shown in Fig. 1d and e, can be clearly converted to visible images at a wavelength of 504 nm. The quasi-BIC metasurface significantly boosted the THG emission intensity as compared to the silicon slab area (the dark background), where our camera can detect no sizeable nonlinear emission.

In summary, we experimentally demonstrated the conversion of the invisible image to the visible based on the THG process with the designed silicon metasurface. Our results suggest a new paradigm for realising efficient nonlinear photonics metadevices and extending the applications of nonlinear nanoscale photonics to new types of imaging technologies.

Acknowledgement

L.X. and M.R. acknowledge support from the UK Research and Innovation Future Leaders Fellowship (MR/T040513/1). The authors acknowledge the use of NTU High Performance Computing cluster Hamilton, and the Australian National Fabrication Facility (ANFF), the ACT Node.

References

1. Camacho-Morales, R., Xu, L., Dimitrov, et al. “Infrared upconversion imaging in nonlinear metasurfaces”. Advanced Photonics Vol 3, No. 3, 036002. 2021.
2. Zheng, Z., L. Xu, L. Huang, D. Smirnova, et al, Third-harmonic generation and imaging with resonant Si membrane metasurface, submitted.

Generation of Quantum Entanglement from a Nonlinear Metasurface and Its Application in Quantum Imaging

Jinyong Ma[1], Jihua Zhang[1], Marcus Cai[1], Rocio Camacho Morales[1], Lei Xu[2], Jinliang Ren[1], Yuxin Jiang[1], Tongmiao Fan[1], Matthew Parry[1], Dragomir N. Neshev[1], Andrey A. Sukhorukov[1]

[1] *ARC Centre of Excellence for Transformative Meta-Optical Systems (TMOS), Research School of Physics, The Australian National University, Canberra, ACT 2601, Australia*

[2] *Advanced Optics and Photonics Laboratory, Department of Engineering, School of Science and Technology, Nottingham Trent University, Nottingham, NG11 8NS, UK*

Abstract: We demonstrate experimentally that a strongly enhanced generation of spatially entangled photon pairs can be achieved from metasurfaces supporting nonlocal double resonances at the signal and idler wavelengths, and reveal that multiplexed metagratings featuring different orientations allow the engineering of bi-photon polarization states and optically controllable generation of arbitrary polarization qutrits. Furthermore, leveraging the exceptional capabilities of the metasurface, we present a combined quantum ghost and scanning imaging protocol allowing 2D imaging with a 1D detector array.

Quantum entanglement underpins a broad range of fundamental physical effects [1] and serves as an essential resource in various applications. In optics, the most common source of entangled photons is based on the spontaneous parametric down-conversion (SPDC) process in quadratically nonlinear materials. Dramatic enhancements of nonlinear light-matter interactions were achieved in nanofabricated structures with subwavelength thickness known as metasurfaces [2], which are also bringing advances to the field of quantum optics [3, 4]. The generation with metasurfaces of photons entangled in spatial and polarization degrees of freedom and their applications are currently active research topics.

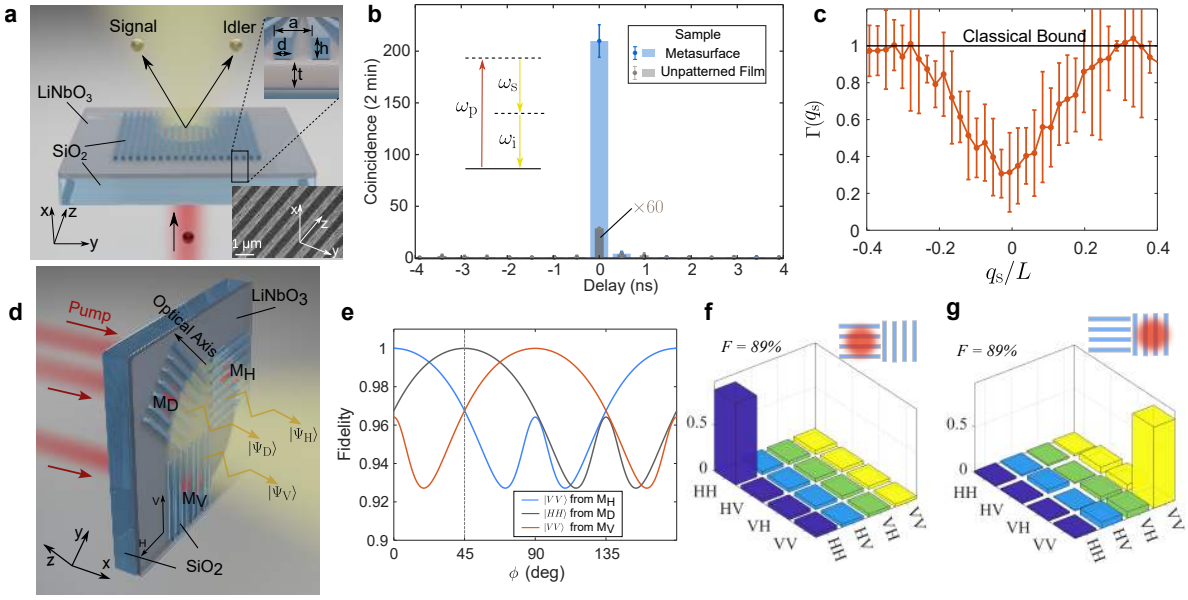


Fig. 1. a Sketch of spatially entangled signal and idler photons generation from a $LiNbO_3$ thin film covered by a SiO_2 metagrating and pumped by a continuous laser. Inset shows the SEM image of the metasurface. **b** Coincidence histograms of SPDC from metasurface and unpatterned film. **c** Violation of Cauchy-Schwartz inequality for values below the classical bound. **d** Sketch of generation of polarization-entangled photon pairs with multiplexed metagratings (M_H, M_V, and M_D) in a metasurface. **e** Fidelity of polarization states generated from metagratings vs. optical axis orientation angle ϕ. **f-g** Experimentally reconstructed density matrix of polarization state from metagratings M_H and M_V.

Here we report the experimental generation of spatially entangled photon pairs through SPDC from a metasurface incorporating a lithium niobate nonlinear thin film of 300 nm thickness [5], see Fig. 1**a**. We measure the correlations of photon pairs and identify their spatial anti-bunching through violation of the classical Cauchy-Schwartz inequality [Fig. 1**c**], witnessing the presence of multi-mode entanglement. Simultaneously, the photon-pair rate is strongly enhanced by 450 times as compared to unpatterned films [Fig. 1**b**] due to high-quality-factor resonances.

Additionally, we present an original approach for engineering photon polarization states with a nonlinear metasurface and preparing polarization Bell states and qutrits with arbitrary amplitude and phase, thereby overcoming the fundamental limitation of an unpatterned nonlinear crystal. We develop a single metasurface incorporating multiplexed linear metagratings with different orientations, as sketched in Fig. 1**d**. Since each metagrating selectively

enhances the generation of photon pairs that are linearly polarized along the grating direction (see Fig. 1**e**), one can produce desired polarization states by controlling the grating orientation, unrestricted by the form of quadratic susceptibility tensor in unpatterned nonlinear materials. As an example, we fabricate two orthogonal metagratings oriented at $\pm 45^\circ$ from the optical axis of $LiNbO_3$. The experimental reconstruction of the density matrix confirms the polarization state engineering of photon pairs with metagrating orientations (Fig. 1**f**-**g**).

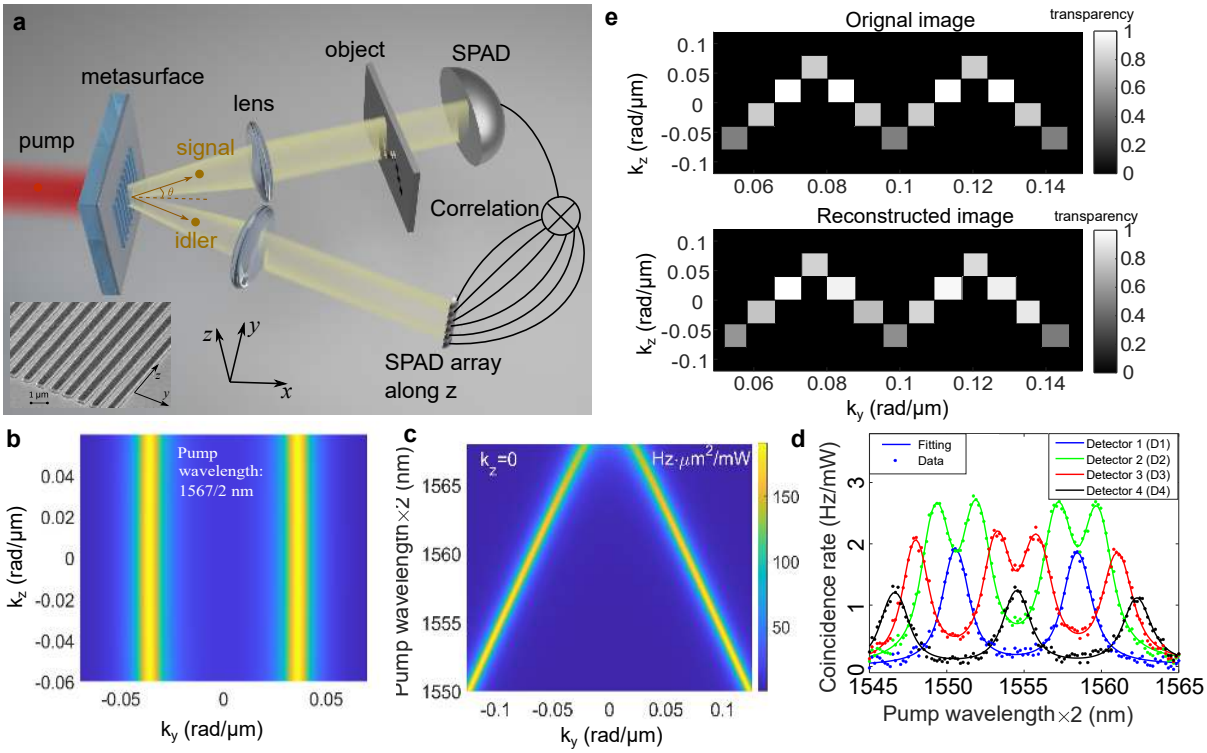


Fig. 2. a Quantum imaging system based on nonlinear lithium niobate metasurface photon-pair source. **b** Simulated emission pattern of photon pairs at a pump wavelength of $1567/2$ nm. **c** Predicted tunability of the photon emission along k_y via the pump wavelength. **d** Simulated coincidences with a four-detector array in the 'idler' arm, for the 'M' shape object in the 'signal' arm. **e** Comparison of the original (top) and reconstructed (bottom) object images.

Furthermore, using the unique benefits of the fabricated metasurface shown in Fig. 1**a**, we reveal, for the first time to our knowledge, the practical potential of quantum imaging, facilitating an efficiently combined ghost and all-optical scanning imaging protocol. The schematic setup is represented in Fig. 2**a**, where the metasurface generates spatially entangled signal and idler photons, featuring two unique properties: (i) the photon emission is narrow in y- yet broad in z-direction (Fig. 2**b**) and (ii) the emission angle in y-direction can be all-optically scanned by simply tuning the pump beam wavelength (Fig. 2**c**). Using these features, we can image an object placed in the 'signal' arm. A single-photon bucket detector and a 1D array of detectors are put in the 'signal' and 'idler' arms respectively, allowing ghost imaging in the z-direction and all-optical scanning in the y-direction. Considering an 'M'-shape object as an example, we simulate the correlations between the 1D detector array and the bucket detector across a range of pump wavelengths (Fig. 2**d**). We use the correlations data to perform the full reconstruction of the 2D object image, which closely reproduces the original pattern (Fig. 2**e**). We also verified that the reconstruction is robust under experimental conditions [5], accounting for measurement noise and fabricated metasurface dimensions.

These results pave the way towards miniaturization of various quantum devices by incorporating ultra-thin metasurfaces functioning as room-temperature sources of quantum-entangled photons, opening the door to various applications including quantum imaging.

References

[1] R. Horodecki and et al., "Quantum entanglement," Rev. Mod. Phys. **81**, 865 (2009).

[2] A. H. Dorrah and F. Capasso, "Tunable structured light with flat optics," Science **376**, 367 (2022).

[3] T. Santiago-Cruz, A. Fedotova, V. Sultanov, M. A. Weissflog, D. Arslan, M. Younesi, T. Pertsch, I. Staude, F. Setzpfandt, and M. Chekhova, "Photon pairs from resonant metasurfaces," Nano Lett. **21**, 4423 (2021).

[4] T. Santiago-Cruz, S. D. Gennaro, O. Mitrofanov, S. Addamane, J. Reno, I. Brener, and M. V. Chekhova, "Resonant metasurfaces for generating complex quantum states," Science **377**, 991 (2022).

[5] J. H. Zhang, J. Y. Ma, M. Parry, M. Cai, R. Camacho-Morales, L. Xu, D. N. Neshev, and A. A. Sukhorukov, "Spatially entangled photon pairs from lithium niobate nonlocal metasurfaces," Sci. Adv. **8**, eabq4240 (2022).

Piezoelectric MEMS-empowered dynamic optical metasurfaces

Fei Ding

Centre for Nano Optics, University of Southern Denmark, Campusvej 55, DK-5230 Odense, Denmark
*corresponding author: feid@mci.sdu.dk

Abstract: We have demonstrated an electrical-driven micro-electro-mechanical (MEMS) empowered dynamic optical metasurface platform for dynamic polarization control with high modulation efficiencies and fast speed by leveraging the commercially available piezoelectric MEMS technique.

Metasurfaces have attracted increasing attention due to their unprecedented capabilities of molding classical light, thus promising potential applications in integrated photonics with ultracompact footprints and multiple functionalities [1]. Despite significant progress, most existing metadevices to date are passive and lack real-time dynamic modulation post-fabrication. Therefore, it is highly desirable to realize tunable metasurfaces with functionalities actively controlled by applying external stimuli, which are promising for more intelligent and adaptive systems. In this talk, I will talk about a piezoelectric MEMS-empowered dynamic metasurface waveplate with high polarization conversion efficiencies (~ 75%), broadband operation (~ 100 nm near the operating wavelength of 800 nm), fast responses (< 0.4 ms) and full-range birefringence control that enables complete encircling Poincaré sphere along trajectories [2].

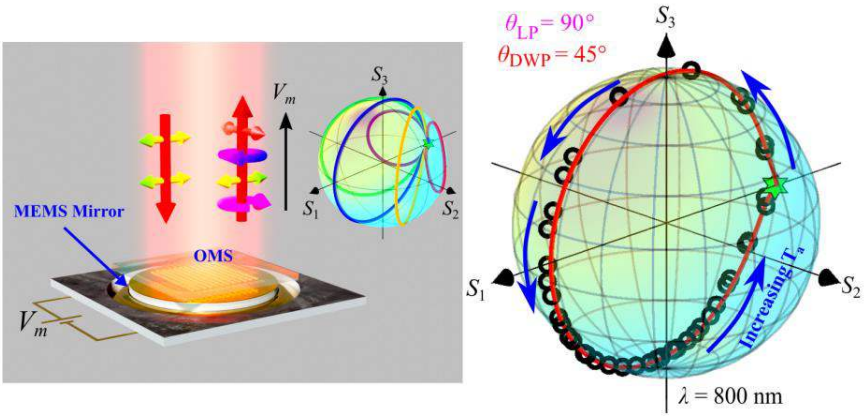


Fig. 1. Schematic of the dynamic waveplate component consisting of an optical metasurface (OMS) on a glass substrate, mounted on a movable (MEMS) mirror.

This work was supported by Danmarks Frie Forskningsfond (1134-00010B) and Villum Fonden (grant no. 37372).

References

1. F. Ding, A. Pors, and S. I. Bozhevolnyi, “Gradient metasurfaces: a review of fundamentals and applications,” Rep Prog Phys. 81,026401 (2018).
2. C. Meng, P. C. V. Thrane, F. Ding, and S. I. Bozhevolnyi, “Full-range birefringence control with piezoelectric MEMS-based metasurfaces”, Nat. Commun. 13, 2071 (2022).

META 2023, PARIS - FRANCE, JULY 18 – 21, 2023

Ultrafast nanophotonics of subwavelength semiconductor resonators beyond the perturbative regime

Anton Rudenko[1*], Anastasiia Zalogina[2,3], Jerome V. Moloney[1], Yuri Kivshar[2], and Sergey Kruk[2]

[1]Arizona Center for Mathematical Sciences and College of Optical Sciences,
University of Arizona, Tucson, Arizona 85721, USA

[2]Nonlinear Physics Center, Research School of Physics, Australian National University, Canberra ACT 2601, Australia

[3]Research School of Biological Sciences, The University of Adelaide, Adelaide SA 5005
[*]corresponding author: antmipt@gmail.com

Abstract: Subwavelength resonators can enhance nonlinear optical response of laser-excited semiconductors by several orders of magnitude, provide ideal conditions for accessing and exploring qualitatively new physics beyond the perturbative regime, and serve as nanoscale sources for nonlinear frequency conversion. Nonperturbative generation of higher harmonics can be observed in a single subwavelength resonator supporting bound states in the continuum excited by an ultrashort mid-infrared laser beam. Our experimental observations are supported by numerical simulations based on nonperturbative model for electronic excitation.

Since decades, the optical physicists have been interested in quadratic and cubic nonlinear optical responses of materials and the methods to enhance and to control over the nonlinearity. High-intensity ultrashort laser pulses in ultraviolet/near-infrared wavelength range suited well for this purpose, albeit the high-order harmonics were mainly generated in laser-induced plasmas in gases and ablation plasma plumes, but not in bulk solids. The observation of non-perturbative high-order spectra, spanning up to the 25th harmonic, in ZnO bulk crystal by applying high-intensity mid-infrared laser [1] has opened new opportunities, as well as encouraged for new theoretical insights to describe the electronic excitation and harmonic generation beyond perturbation theory.

Simultaneously, subwavelength nanostructures were extensively used to enhance further the nonlinear optical response, starting from plasmonic gratings and bowtie antennas to confine the electric fields at the nanoscale and directing towards semiconductor nanostructures of high refractive index, supporting high-Q resonances, exhibiting comparable nonlinearity but having lower absorption losses. A considerable improvement of nonlinear conversion efficiency was provided by resonant metasurfaces, consisting of periodic arrangement of meta-atoms, supporting Mie, collective lattice and Fano resonances, and, most recently, bound states in the continuum [2].

Recent experiments on high-order harmonics benefit from both state-of-the-art concepts, exploring the ultrashort excitation of resonant semiconductor nanostructures with high-intensity mid-infrared laser pulses [3-5]. However, the sizes of the metasurfaces have remained relatively large in the two lateral dimensions. A novel concept to overcome this limitation by using a single subwavelength AlGaAs resonator, hosting quasi-bound states in the continuum mode, has been proposed in our recent work, enabling to generate harmonic spectra up to the 7th harmonic [6]. High-order harmonics show clear signatures of non-perturbative behavior such as weaker power law scaling than expected from the perturbative theory.

We support our findings by implementing a full-vector Maxwell-based approach with a nonlinear current, describing the response of photo-excited carriers. The calculated high harmonics spectra are enhanced by several

orders of magnitude comparing to the unstructured sample, non-resonant geometry or off-resonant laser irradiation conditions. Our simulations indicate that the nanoscale confinement of electron plasma inside subwavelength resonator is at the origin of pronounced non-perturbative odd harmonics. We have analyzed the contributions of the photo-excited carriers (non-perturbative origins) and of the cascaded frequency mixing of 2nd and 3rd harmonics alone (perturbative origins) and reveal that in our settings the odd-order harmonics are favored over the even-order harmonics.

Combining metaphotonics and nonlinear optics, extending to quantum optics of semiconductors to describe both optical and electronic properties beyond the perturbative regime, would be a next challenging step, opening up new perspectives for selective control over the generated harmonics and their polarization state and for ultrafast optical switching and resonance tuning at the nanoscale.

Acknowledgements. Australian Research Council (DE210100679, DP210101292), Samsung Research Funding and Incubation Center of Samsung Electronics (SRFC-MA2001-01), Air Force Office for Scientific Research under awards no. FA9550-19-1-0032 and FA9550-21-1-0463.

References

1. S. Ghimire, A. D. Dichiara, E. Sistrunk, P. Agostini, L. F. Dimauro, and D. A. Reis, "Observation of high-order harmonic generation in a bulk crystal," *Nat. Phys.*, vol. 7, no. 2, pp. 138–141, 2011.
2. V. Zubyuk, L. Carletti, M. Shcherbakov, and S. Kruk, "Resonant dielectric metasurfaces in strong optical fields," *APL Mater.*, vol. 9, no. 6, p. 060701, 2021.
3. H. Liu, C. Guo, G. Vampa, J. L. Zhang, T. Sarmiento, M. Xiao, P. H. Bucksbaum, J. Vuckovic, S. Fan, and D. A. Reis, "Enhanced high-harmonic generation from an all-dielectric metasurface," *Nat. Phys.*, vol. 14, no. 10, pp. 1006–1010, 2018.
4. M. R. Shcherbakov, H. Zhang, M. Tripepi, G. Sartorello, N. Talisa, A. AlShafey, Z. Fan, J. Twardowski, L.A. Krivitsky, A. I. Kuznetsov, E. Chowdhury, and G. Shvets, "Generation of even and odd high harmonics in resonant metasurfaces using single and multiple ultra-intense laser pulses," *Nat. Commun.*, vol. 12, 4185, pp. 1-6, 2021.
5. G. Zograf, K. Koshelev, A. Zalogina, V. Korolev, R. Hollinger, D.-Y. Choi, M. Zuerch, C. Spielmann, B. Luther-Davies, D. Kartashov, S. V. Makarov, S. S. Kruk, and Y. Kivshar, "High-Harmonic Generation from Resonant Dielectric Metasurfaces Empowered by Bound States in the Continuum," *ACS Photonics*, vol. 9, no. 2, pp. 567–574, 2022.
6. A. Zalogina, L. Carletti, A. Rudenko, J. V. Moloney, A. Tripathi, H.-C. Lee, I. Shadrivov, H.-G. Park, Y. Kivshar, and S. Kruk, "Observation of high-harmonic generation from a subwavelength dielectric resonator," *Sci. Adv.*, 2023.

META 2023, PARIS - FRANCE, JULY 18 – 21, 2023

Reconfigurable nonlinear dielectric metasurfaces

D. Rocco[1*], L. Carletti[1], M. Gandolfi[1], A. Zilli[2], M. Celebrano[2], M. Finazzi[2], U. Arregui Leon[2], A. Ferraro[3], R. Caputo[3], G. Leo[4], G. Della Valle[2] and C. De Angelis[1]

[1]Department of Information Engineering, University of Brescia, Italy
[2]Department of Physics, Politecnico di Milano, Italy
[3]Department of Physics, University of Calabria, Italy
[4]Laboratoire MPQ, Université de Paris, France
[*]corresponding author: davide.rocco@unibs.it

Abstract: High refractive index metasurfaces represent a promising research area of nanophotonics and light–matter interaction at the nanoscale. In this work, we report our recent progress concerning tunable nonlinear dielectric metasurfaces. We discuss the main physical phenomena enabling the dynamic control of the nonlinear process and compares the temporal dynamics of the different adopted approaches.

Dielectric and semiconductor nanostructures emerged as excellent candidates for nanophotonic applications. The possibility to engineer their radiated fields and the capability to govern the polarization of the emitted light with very low losses compared to metallic nanodevices, in the near-infrared and visible region of the electromagnetic spectrum, have gained significant attention in the nanophotonic community [1].

In this regard, the resonant enhancement of the fields inside semiconductor resonators has been already proved to enhance nonlinear frequency generation. III-V semiconductors such as Gallium Arsenide (GaAs) or Aluminum Gallium Arsenide (AlGaAs) show remarkably high even-order susceptibilities due to the broken central symmetry in their crystal structures. Notably, AlGaAs exhibits a direct gap which increases with the Aluminum molar fraction, enabling two-photons absorption free operation around the third communication window. As a result, efficient harmonic generation of the second order from AlGaAs nano-platforms was recently demonstrated in different static scenarios [2]. However, in several applications including modulators, tunable imaging and active beam shaping, a reconfigurable behavior of the emitted nonlinear signal is desirable.

In this work, we will discuss several promising approaches to dynamically tune the emitted nonlinear signal coming from AlGaAs metasurfaces, including liquid crystal infiltration and exploitation of opto-thermal effects [3, 4]. Finally, we will discuss our newest achievements concerning difference frequency generation in such kind of platforms [5].

References

1. Kuznetsov, A. I., A.E. Miroshnichenko, M.L. Brongersma, Y.S. Kivshar and B. Luk'yanchuk "Optically resonant dielectric nanostructures," Science, Vol. 354, No. 6314, 1064–1076, aag2472, 2016.
2. Gili, V. F., L. Carletti, A. Locatelli, D. Rocco, M. Finazzi, L. Ghirardini, I. Favero, C. Gomez, A. Lemaitre, M. Celebrano, C. De Angelis, and G. Leo, "Monolithic AlGaAs second-harmonic nanoantennas," Opt. Express, Vol. 24, No. 14, 15965–15971, 2016.

3. Rocco, D, A. Zilli, A. Ferraro, A. Borne, V. Vinel, G. Leo, A. Lemaitre, C. Zucchetti, M. Celebrano, R. Caputo, C. De Angelis and M. Finazzi, “Tunable second harmonic generation by an all-dielectric diffractive metasurface embedded in liquid crystals,” New Journal of Physics, Vol. 24, No. 4, 045002, 2022.
4. Rocco, D., M. Gandolfi, A. Tognazzi, O. Pashina, G. Zograf, K. Frizyuk, C. Gigli, G. Leo, S. Makarov, M. Petrov, and C. De Angelis, “Opto-themally controlled beam steering in nonlinear all-dielectric metastructures,” Opt. Express, Vol. 29, No. 23, 37128-37139, 2021.
5. Leon, Unai Arregui, D. Rocco, L. Carletti, M. Peccianti, S. Maci, G. Della Valle, and C. De Angelis, “THz-photonics transceivers by all-dielectric phono-polariton nonlinear nanoantennas,” Scientific Reports, Vol. 12, No. 1, 4590, 2022.

Photon-pair generation in thin-film materials

Frank Setzpfandt[1,2,*]

[1]Institute of Applied Physics, Abbe Center of Photonics, Friedrich Schiller University Jena, Albert-Einstein-Str. 15, 07745 Jena, Germany
[2]Fraunhofer Institute of Applied Optics and Precision Mechanics IOF, Albert-Einstein-Str. 7, 07745 Jena, Germany
[*]corresponding author: f.setzpfandt@uni-jena.de

Abstract: Thin films of artificially designed materials, e.g. by nanostructuring, are enticing systems for the generation of photon pairs by nonlinear frequency conversion. They can enable control of many properties of the generated photons, as the polarization, spectrum, and propagation direction. The talk will discuss recent results, in particular steps towards the control of the polarization degree of freedom.

Photon-pairs have evolved as a critical resource for quantum technologies, and many applications in quantum communication, imaging, sensing and computing are based on using such quantum states with judiciously designed properties. For many applications, sources of photon pairs are still based on bulk nonlinear crystals, which due to the need for phase matching enable efficient generation only in limited parameter ranges. In the last years, it was demonstrated that also thin films of second-order nonlinear materials can serve as sources of photons pairs by spontaneous parametric down conversion (SPDC), without the need to achieve phase matching [1]. Structuring these films into resonant metasurfaces enhances the generation efficiency while providing a large number of degrees of freedom for controlling the properties of the generated pairs through the geometry of the nanoresonators [2, 3].

For controlling the polarization of the generated pairs, with the aim of realizing polarization-entangled photon pairs, in particular resonant structures made from III-V semiconductors seem promising [4], as their nonlinear tensor couples all polarization components. The talk will discuss recent experiments and simulations that highlight this potential in sum-frequency generation, a classical inverse process to SPDC, which allows to accurately predict the properties of the photon-pairs generated in SPDC.

Alternatively to using the geometry of resonant metasurfaces to control the polarization properties of photon pairs, one can also use materials with specifically chosen nonlinear tensor structures to achieve particular states. One material class with very peculiar nonlinear properties are transition metal dichalcogenides (TMDC), which tensor structure only couples the two in-plane polarization due to the two-dimensional nature of the layered material. Recently, TMDCs became available that conserve the second-order nonlinearity also for crystals with thicknesses in the range of several tens of nm, such that efficient nonlinear interactions can be achieved [5]. I will discuss our progress towards photon-pair generation in such materials.

References

1. C. Okoth et al. "Microscale generation of entangled photons without momentum conservation." Physical Review Letters 123, 263602 (2019).
2. Santiago-Cruz, T., Fedotova, A., Sultanov, M., Weissflog, M. A. et al., “Photon Pairs from Resonant Metasurfaces,” Nano Lett., Vol. 21, No. 10, 4423–4429, 2021.
3. T. Santiago-Cruz et al, "Resonant metasurfaces for generating complex quantum states," Science 377, 991 (2022).
4. Weissflog, M. A. et al., “Far-Field Polarization Engineering from Nonlinear Nanoresonators,” Laser Photonics Rev. 16,

2200183 (2022).
5. X. Xu et al. "Towards compact phase-matched and waveguided nonlinear optics in atomically layered semiconductors." Nature Photonics 16, 698 (2022)

K-space engineering in nonlinear metasurfaces

D. de Ceglia[1,2], and C. De Angelis[1,2,*]
[1]Department of Information Engineering, University of Brescia, Italy
[2]Istituto Nazionale di Ottica, Consiglio Nazionale delle Ricerche, Via Branze, 45, Brescia, 25123, Italy
[*]corresponding author: costantino.deangelis@unibs.it

Abstract: Flat optics has been recently unveiled as a powerful platform to perform data processing in real-time, and with small footprint [1, 2, 3]. So far, these explorations have been limited to linear optics, while arguably the most impactful operations stem from nonlinear processing of the incoming signals. In this context, here we add a new twist and depth to analog optical computing: we demonstrate that nonlinear phenomena combined with engineered nonlocality in flat-optics devices can be leveraged to synthesize Volterra kernels able to perform complex operations on incoming images in real-time.

Metasurfaces have already introduced a paradigm shift for nonlinear optics enabling stronger nonlinearities in thin films and manipulation of the nonlinearly-generated wavefront [4, 5, 6]. In this framework, here we show that it is possible to exploit nonlocal nonlinearities as a powerful tool for analog computing with light waves. We show that using nonlinear nonlocality in flat optics we can realize analog image processing with previously not accessible functionalities. By exploring the simple scenario of a uniform χ_2 thin sheet, we demonstrate edge detection operation with exciting potentials. In our proposed nonlinear flat-optics solution, the non-resonant nature of the nonlinear interaction involved in image processing allows edge detection over a broadband spectrum with ultra–high contrast and superior resilience to noise.

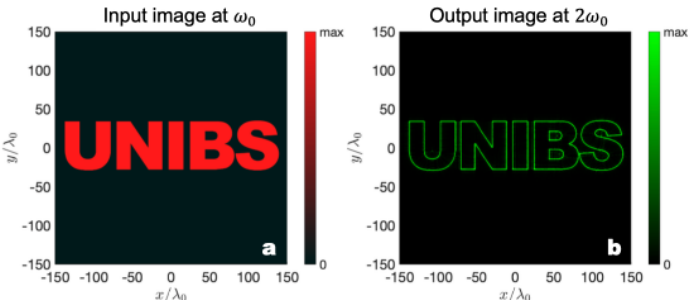


Figure 1: Edge detection with a nonlinear thin film

Our results indicate that Volterra kernels of nonlinear nonlocal flat optics can open new opportunities in applications such as image processing, item recognition for computer vision, and high-contrast, high-resolution microscopy.

References

1. Solli, D.R., Jalali, B., Nature Photonics 9(11), 704–706 (2015).
2. Silva, A., Monticone, F., Castaldi, G., Galdi, V., Alù, A., Engheta, N., Science 343(6167), 160–163 (2014).
3. Overvig, A., Alù, A., Laser & Photonics Reviews 16(8), 2100633 (2022).
4. Vabishchevich, P., Kivshar, Y., Photon. Res. 11, B50-B64 (2023)
5. Schlickriede, C., Waterman, N., Reineke, B., Georgi, P., Li, G., Zhang, S., Zentgraf, T., Advanced Materials 30(8), 1703843 (2018).
6. Gigli, C., Marino, G., Artioli, A., Rocco, D., De Angelis, C., Claudon, J., Gerard, J.-M., Leo, G., Optica 8(2), 269–276 (2021).

META 2023, PARIS - FRANCE, JULY 18 – 21, 2023

From light to heat: electronic dynamics and photothermal effects in engineered metasurfaces

A. Schirato[1,2], Y. Zhao[3,4,5], P. Dongare[1,5,6] , J. Cunha[7], L. Mascaretti[8], M. Maiuri[2,9], G. Cerullo[2,9,10], R. Proietti Zaccaria[11,12], A. Naldoni[8,13], G. Della Valle[2,9,10], N. Halas[1,3,5,6,14] , P. Nordlander[1,3,5,6] and A. Alabastri[1,5,6*]

[1] Department of Electrical and Computer Engineering, Rice University, Houston, Texas, United States; [2]Dipartimento di Fisica, Politecnico di Milano, Italy; [3]Department of Physics and Astronomy, Rice University, Houston, Texas, United States; [4]Applied Physics Graduate Program, Rice University, Houston, Texas, United States; [5]Laboratory for Nanophotonics, Rice University, Houston, Texas, United States; [6] Nanosystems Engineering Research Center for Nanotechnology-Enabled Water Treatment (NEWT), Rice University, Houston, Texas, United States; [7]International Iberian Nanotechnology Laboratory – INL, Braga, Portugal; [8]Czech Advanced Technology and Research Institute, Regional Centre of Advanced Technologies and Materials, Palacký University, Olomouc, Czech Republic; [9]Istituto di Fotonica e Nanotecnologie, CNR, Italy; [10]Istituto Nazionale di Fisica Nucleare, Milano, Italy; [11]Istituto Italiano di Tecnologia, Genova, Italy; [12]Cixi Institute of Biomedical Engineering, China; [13]Department of Chemistry and NIS Centre, University of Turin, Turin, Italy; [14]Department of Chemistry, Rice University, Houston, Texas, United States;
[*]corresponding author: alabastri@rice.edu

Abstract: Light can interact with nanostructured materials giving rise to several physical phenomena, including enhanced electric fields, generation of high energy carriers and heat dissipation. These effects can be manipulated by engineering such materials into optical metasurfaces where the shape, material and arrangement of the meta-atoms, the metasurface building blocks, can be modified depending on the application. This talk reports recent results where nanoscale optical metasurfaces are utilized in diverse systems, targeting extreme electromagnetic energy focusing, light rectification or steam generation.

Conductive nanoparticles interact with electromagnetic radiation through highly confined electronic oscillations named plasmons. Following a series of events, plasmons decay, losing their energy to electron-hole pairs and, eventually, to the particles' lattice as heat, increasing their temperature [1].

Plasmonic oscillations display large field enhancements that can be utilized to redirect radiation at nanoscale locations. Recently we have implemented an optothermal design where metallic bowties antennas connected to a heat sink funnel electromagnetic energy into small thermally insulated and poorly absorptive reactors. Thanks to the antenna plasmonic properties and reactor insulation, the system displayed dramatic thermal gradients, even leading to the reactors melting while leaving the antennas at relatively lower temperatures. The concept paves the way to realizing photothermally asymmetric systems where absorbing elements stay cool while electromagnetically hidden structures heat up [2].

The approach shows particular promise because the capability to generate heat in subwavelength regions can lead to thermal hot spots, improving the efficiency of nonlinear processes. For example, we have shown how water desalination is a nonlinear optical process benefitting from high-temperature regions of limited size with respect to homogeneous thermal landscapes, both achievable with the same input power, showing how light absorption engineering can positively affect thermal processes [3].

In this context, we have recently demonstrated how topologically optimized dielectric metasurfaces can

attain extremely large field enhancements in ultra-confined regions, potentially improving the efficiency of nonlinear optical processes, even at the cost of rejecting part of the input power [4]. Besides light steering, a critical requirement for photothermal processes is the efficient light-heat conversion at the base of the temperature increase. By utilizing arrays of TiN nanocavities, we have achieved the dissipation of about 90% of the solar spectrum within ~250 nm only thick substrates [5], paving the way to ultrathin optothermal devices.

There are applications, however, where heat dissipation is detrimental, and hot carriers should be harnessed before their thermalization. We have shown how the spatial distribution of out-of-equilibrium carriers excited by plasmon decay can be utilized, before their decay, to control the optical properties of nanostructures at the ~ps timescale [6,7]. Additionally, we proved that tapered conical nanoantennas could be fabricated in a point-contact metal-insulator-metal configuration to increase the hot electron extraction process close to the visible by orders of magnitude [8]. While the efficiency of such a light rectification process remains low, our work points to the key role that hot carrier management plays in energy applications.

This work acknowledges support from the National Science Foundation (NSF) under grant no. IIP-1941227

References

1. J. Cunha, T.-L. Guo, G. Della Valle, A. N. Koya, R. Proietti Zaccaria and A. Alabastri*, Controlling Light, Heat, and Vibrations in Plasmonics and Phononics, Advanced Optical Materials, 2001225, (2020)
2. P. D. Dongare, Y. Zhao, D. Renard, J. Yang, O. Neumann, J. Metz, L. Yuan, A. Alabastri*, P. Nordlander* and N. J. Halas*, A 3D Plasmonic Antenna-Reactor for Nanoscale Thermal Hotspots and Gradients, ACS Nano, 15, 5, pp. 8761-8769, (2021)
3. P. Dongare*, A. Alabastri*, O. Neumann, P. Nordlander and N. Halas, Solar thermal desalination as a nonlinear optical process, PNAS, 116(27), pp. 13182-13187 (2019)
4. Y. Zhao, m. Zhang, A. Alabastri* and P. Nordlander*, Fast Topology Optimization for Near-Field Focusing All-Dielectric Metasurfaces Using the Discrete Dipole Approximation, ACS Nano, 16, 11, 18951–18958, (2022)
5. L. Mascaretti, A. Schirato, R. Zboril, S. Kment, P. Schmuki, A. Alabastri* and Alberto Naldoni*, Solar steam generation on scalable ultrathin thermoplasmonic TiN nanocavity arrays, Nano Energy, 83, 105828, (2021)
6. A. Schirato, M. Maiuri, A. Toma, S. Fugattini, R. Proietti Zaccaria, P. Laporta, P. Nordlander, G. Cerullo, A. Alabastri* and G. Della Valle*, Transient optical symmetry breaking for ultrafast broadband dichroism in plasmonic metasurfaces, Nature Photonics, 14, 723-727 (2020)
7. A. Schirato, A. Mazzanti, R. Proietti Zaccaria, P. Nordlander, A. Alabastri* and G. Della Valle*, All-Optically Reconfigurable Plasmonic Metagrating for Ultrafast Diffraction Management
8. R. Mupparapu, J. Cunha, F. Tantussi, A. Jacassi, L. Summerer, M. Patrini, A. Giugni, L. Maserati, A. Alabastri*, D. Garoli, R. Proietti Zaccaria*, High-Frequency Light Rectification by Nanoscale Plasmonic Conical Antenna in Point-Contact-Insulator-Metal Architecture, Advanced Energy Materials, 12 (15), 2103785, (2022)

Quantum optical metasurfaces: new avenues for generating and engineering entangled photons

T. Santiago-Cruz[1,2*]

[1]Max Planck Institute for the Science of Light, Staudtstr. 2, 91058 Erlangen, Germany
[2]Friedrich-Alexander-Universität Erlangen-Nürnberg, Staudtstr. 7/B2, 91058 Erlangen, Germany
[*]corresponding author: jose-tomas.santiago@mpl.mpg.de

Abstract: Quantum optical metasurfaces are outperforming their bulk counterparts in terms of multifunctionality. In this talk, I show how quasi bound states in the continuum resonances in semiconductor metasurfaces can be used to engineer entangled photons in several degrees of freedoms, such as frequency and direction of emission.

Optical metasurfaces are playing an essential role in the development of subwavelength-scale devices with multifunctional operation. By exploiting high quality factor resonances, such as quasi bound states in the continuum (qBIC), metasurfaces can enhance nonlinear effects such as harmonics generation, or spontaneous effects like photoluminescence emission from quantum dots. Another promising direction for qBIC resonant metasurfaces in quantum optics is the spontaneous emission of entangled photons. One way to generate entangled photons is via spontaneous parametric down-conversion (SPDC), where a higher-energy photon splits into two lower-energy photons (called signal (s) and idler (i)) upon interaction with a second-order nonlinear material. The three interacting photons (pump, signal and idler) fulfill energy conservation. Here, I am going to discuss our new results on photon pair generation via SPDC driven by qBIC resonances in quantum optical metasurfaces (QOM).

In the first work, we used symmetry-broken GaAs metasurfaces featuring two quasi-BIC resonances in the IR infrared range, as shown by the white light transmittance in Figure 1A (top and central panels). These resonances have different multipolar contributions. The resonance at 1359.4 nm is of electric dipole (ED-qBIC) origin, and resonance at 1429.4 nm has a magnetic dipole (MD-qBIC) electric field distribution [1]. When the QOM is pumped at 725.4 nm, it emits frequency-degenerate photon pairs in the forward direction, as shown in Figure 1A (bottom panel). The outer peaks (see yellow vertical lines) correspond to an SPDC process driven by the ED-qBIC resonance, and the inner peaks (see blue vertical lines) to another SPDC process driven by the MD-qBIC resonance. Because of energy conservation, the QOM emits one photon of a pair at the resonance wavelength (either ED- or MD-qBIC), and the conjugate sister photon is emitted at the wavelength that conserves energy given the pump wavelength. By adjusting the pump wavelength or the resonance wavelength, the QOM can emit frequency-degenerate or non-degenerate photon pairs [1]. This multicolor emission of photon pairs is scalable with the number of resonances in the QOM. For further details see Ref. [1].

In the second work, again we exploited quasi-BIC resonances in GaP metasurfaces. The QOM under study exhibits a resonance at 1184 nm, as shown by the white light transmittance in Figure 1B (top). A principal difference between the GaAs and GaP metasurfaces is that in the former, the resonances appear as peaks in the white light transmission spectrum, while in the latter, the resonance appears as a dip in the spectrum. We pumped the GaP metasurface with a laser centred at 594 nm, and measured the spectrum of the photon pairs emitted in the forward-backward directions, i.e., we collected one photon of the pair in the forward direction, while its conjugate photon is detected backwards, in this way, we perform forward-backward two-photon correlation measurements.

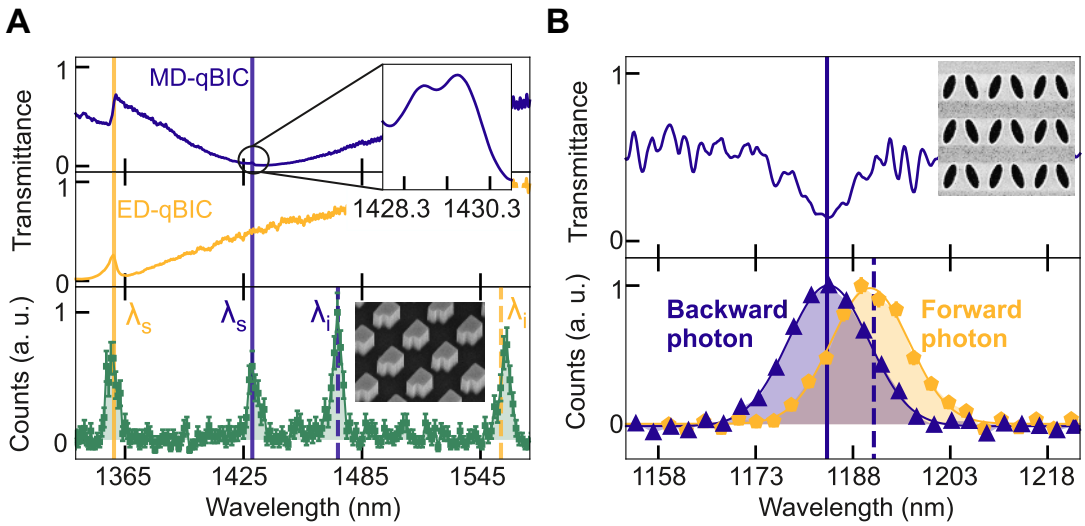


Figure 1. (**A**) White light transmittance (top and central panels) measured in the GaAs metasurface (inset in the bottom panel shows a scanning electron micrograph (SEM)), featuring two qBIC resonances (blue and yellow solid vertical lines). The bottom panel shows the spectrum of the photon pairs emitted by the QOM. The dashed vertical lines indicate the wavelength of the partner photons to the ED-qBIC (yellow) and MD-qBIC (blue) resonant photons. (**B**) White light transmittance (top panel) measured in the GaP metasurface (inset shows an SEM) showing a qBIC resonance at 1184 nm (solid vertical line). The blue and yellow points in bottom panel show the spectrum of photons emitted in the backward and forward directions, respectively. The dashed vertical line indicates the wavelength of the conjugate photon to the resonant one.

The yellow and blue points in Figure 1B (bottom) show the spectrum of the photon emitted in the forward and backward direction, respectively. The QOM metasurface emits frequency non-degenerate photon pairs, where the photon generated by the resonance is emitted in the backward direction, while its conjugate photon is emitted in the forward direction, that is, the QOM demultiplexes the emission of the photon pair, both in direction of emission and wavelength. For further details see Ref. [2].

In summary, our works show that metasurfaces are promising platforms for quantum optical applications. Both features shown here cannot be achieved in standard bulk crystals. The QOMs not only generate photon pairs but also engineer their spectral and spatial properties. The GaAs QOM can be used for the generation of linear graph states [1], while the GaP QOM can be used in applications where heralding one of the photons is crucial.

References

1. Santiago-Cruz, T., Gennaro, S. D., et al., “Resonant metasurfaces for generating complex quantum states,” Science, 377 991-995, 2022.
2. Son, C., Sultanov, V., et al., “Photon pairs bidirectionally emitted from a resonant metasurface,” Nanoscale, 15, 2567–2572, 2023.

Stimulated Emission Tomography of Spontaneous Four Wave Mixing from a Metasurface

J. Yang[1], P. Dichtl[1], J. Florez[1], N. Gemmel[1], S. D. Gennaro[1], X. Xiao, C. C. Phillips[1], A. Clark[1,2], and R. F. Oulton[1*]

[1] Department of Physics, Imperial College London, SW7 2AZ, United Kingdom
[2] Department of Electrical and Electronic Engineering, University of Bristol, BS8 1FD, United Kingdom
*corresponding author: r.oulton@imperial.ac.uk

Abstract: We apply stimulated emission tomography (SET) to assess the ability of individual nanoantennas and their metasurface arrays to generate correlated photon pairs via spontaneous four-wave mixing (SFWM). Following the SET framework, we characterize SFWM by studying four-wave mixing (FWM), producing maps of joint spectral density (JSD) to characterize the bi-photon state. Although a much weaker process than parametric down conversion, SFWM from metasurfaces produces similar photon production rates, and brings the advantage of wider choice of nonlinear materials.

Plasmonic and dielectric nanoparticles have been used extensively for nonlinear optical frequency mixing in recent years due to their broadband field enhancement and the large ultrafast nonlinearities they offer [1,2,3]. Through careful design of the particle resonances and shapes, bespoke nonlinear optical responses can be achieved, such as a second-order response in a non-centrosymmetric arrangement of Au nanoparticles. The control of the nonlinear output can be maximised when arranging the nanoparticles in a metasurface for harnessing the power of designer 'flat optics' with capabilities such as frequency- and polarisation-dependent routing of photons. However, while many proof-of-principle studies have been published on classical coherent frequency mixing of multiple beams, the practical aspects of spontaneous photon pair generation rates in metasurfaces and a comparison with conventional photon pair sources is rarely addressed.

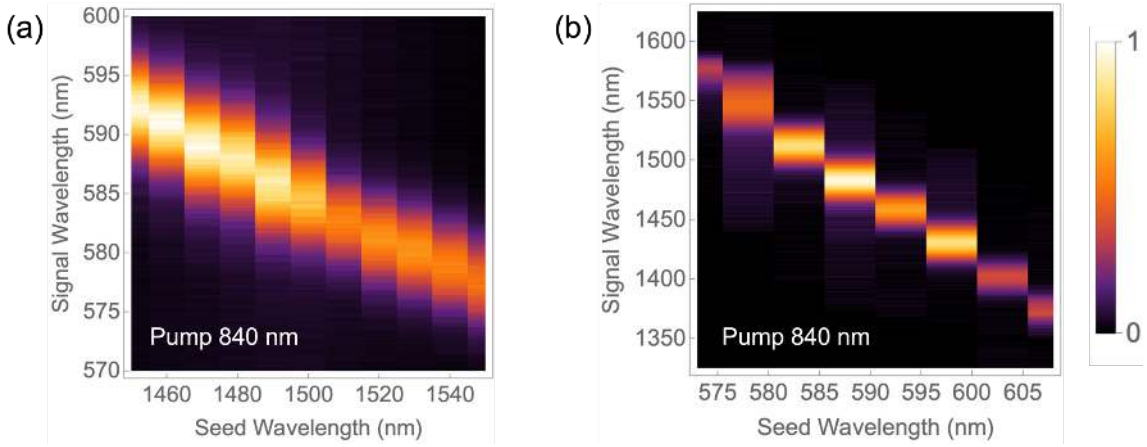


Figure 1. Joint Spectral Density maps for (a) up-conversion and (b) down-conversion Four Wave Mixing spanning 580 nm to 1500 nm.

Here, we apply the Stimulated Emission Tomography (SET) technique to frequency mixing in plasmonic nanoantennae to quantify their expected performance as novel wavelength-agile correlated photon pair sources. Introduced by Liscidini and Sipe [4], SET conveniently enables characterises photon pair generation by studying the corresponding stimulated process, thus bridging the gap between nonlinear optics and quantum optics. We first introduce our sample [5] and setup and explain how the numbers of stimulating and generated photons are determined in our experiment. Next, the classical frequency mixing efficiencies and the estimated spontaneous photon pair generation rates are presented. Below the damage threshold of the particles, we find a generation efficiency for spontaneous parametric down conversion approaching 1 photon pair per second per nanoparticle. This analysis is followed by a characterisation of Joint Spectral Density (JSD), (example shown in Fig. 1) allows us to quantify the spectral entanglement of the biphoton output. Here, the SET technique provides increased spectral resolution, limited only by the spectral width of the stimulating beam, compared to an SPDC experiment with spectrally resolved coincidence measurements. Our sample does not yet offer the ability to directly detect spectrally correlated photons, however, with our experimental capabilities we would be able to easily characterise any of a variety of candidate nonlinear metasurfaces. The paper closes with perspectives on applications as wavelength-agile pair sources for quantum imaging in previously inaccessible wavelength ranges.

This work was supported by the EPSRC Reactive Plasmonics Programme (EP/M013812/1), UK Quantum Hub in Quantum Imaging (EP/T00097X/1) and the Leverhulme Trust.

References

1. Kauranen, M. and Zayats, A. “Nonlinear Plasmonics,” Nature Photonics, **6**, 737–748, 2012.
2. Rahmani, M. et al, “Nonlinear frequency conversion in optical nanoantennas and metasurfaces: materials evolution and fabrication,” Opto-Electronic Advances 1, 180021, 2018.
3. Koshelev, K., “Subwavelength dielectric resonators for nonlinear nanophotonics,” Science, 367, 288-292, 2020.
4. Liscidini, M., and Sipe, J. E., “Stimulated Emission Tomography,” Physical Review Letters, Vol. 111, 193602, 2013.
5. Gennaro, S. D., Rahmani, M., Giannini, V. Aouani, H., Sidiropoulos, T. P. H., Navarro-Cia, M., Maier, S. A. and Oulton, R. F., “The Interplay of Symmetry and Scattering Phase in Second Harmonic Generation from Gold Nanoantennas,” Nano Letters, Vol. 16, 5278-5285, 2016.

Combining plasmonic nanostructures and diamond for emission of electrons using visible light.

P. O'Keeffe[1, *], G. Ammirati[2], A. Bellucci[3], V. Campanari[2], D. Catone[2], F. Martelli[4], M. Mastellone[3], S. Orlanducci[5], A. Paladini[1], R. Polini[3,5], F. Toschi[2], D. M. Trucchi[3], S. Turchini[2], V. Valentini[3]

[1]Istituto di Struttura della Materia-CNR (ISM-CNR), EuroFEL Support Laboratory (EFSL), 00015 Monterotondo Scalo, Italy.
[2]Istituto di Struttura della Materia-CNR (ISM-CNR), EuroFEL Support Laboratory (EFSL), 100 Via del Fosso del Cavaliere, 00133 Rome, Italy.
[3]Istituto di Struttura della Materia-CNR (ISM-CNR), DiaTHEMA Lab, 00015 Monterotondo Scalo, Italy.
[4]CNR-IMM, Area della Ricerca di Roma Tor Vergata, 100 Via del Fosso del Cavaliere, 00133 Rome, Italy
[5]Dipartimento di Scienze e Tecnologie Chimiche, Università di Roma "Tor Vergata", Via della Ricerca Scientifica, 1, 00133 Roma, Italy.
[*]corresponding author: patrick.okeeffe@ism.cnr.it

Abstract: The aim of this work is to exploit the negative electron affinity of the surface of hydrogenated diamond combined with the excitation of conduction band electrons to induce emission of electrons following the interaction with visible light. Diamond is a very wide band gap semiconductor and therefore interacts weakly with visible light. However, we show that by combining plasmonic nanoparticles with diamond it is possible to excite electrons into the conduction band of the diamond through a multistep process involving at least two visible light photons.

Combining plasmonic metal nanoparticles with wide bandgap semiconductor materials has been demonstrated to be an effective way to sensitise these materials to sub bandgap light.[1] This is often used as a strategy improve the photocatalytic properties of these materials.

In this work we focus our efforts on diamond as it has the very interesting property of having a negative electron affinity at its surface when it is hydrogenated. The result is that when electrons are excited into the conduction band in the vicinity of a diamond/vacuum or, indeed, a diamond/water interface they are ejected from the diamond into the vacuum or water. This property can lead to numerous useful applications such as a cold cathode or as a clean source of solvated electrons. The problem is that diamond has a band gap of 5.5 eV and therefore this process only works with VUV light ($\lambda < 213$ nm).

We have fabricated two separate systems based on the combination of plasmonic nanoparticles with diamond which show that the exciting the plasmonic resonance of the metal nanoparticles can lead to a strong enhancement of the emission of electrons from the diamond surface. The process is demonstrated using an array of nanoparticles embedded below the surface of a thin film of diamond for the emission of electrons into vacuum using visible light. The increased electron emission efficiency was verified by photoemission and photoconducibility measurements. Initial attempts with Aluminium as the plasmonic material were not successful[2] while successive fabrication using silver showed the required properties. The results allow us to hypothesise metasurfaces with properties which could optimise the efficiency of the process. Furthermore, a second system involving nanodiamonds coupled with gold nanoparticles in acqueous solution has been shown to be source of solvated electrons following interaction with visible light. In this case the presence of solvated electrons was verified by using an ultrafast pump-probe experiment in which a visible light pump was used to

excite the plasmon resonance of the gold nanoparticles while the white light probe was used to optically detect the formation of the solvated electron in the first picoseconds after the excitation.

Based on the details of the above measurements we propose a mechanism to explain the results which initially involves the excitation of an electron into empty defect states followed by a second step in which the electron is excited from the defect state into the conduction band.

References

1. D. Catone, L. Di Mario, F. Martelli, P. O'Keeffe, A. Paladini, J.S. Pelli Cresi, A.K. Sivan, L. Tian, F. Toschi, S. Turchini "Ultrafast optical spectroscopy of semiconducting and plasmonic nanostructures and their hybrids." Nanotechnology, Vol. 32, 025703, 2020.
2. A. Bellucci, V. Campanari, M. Mastellone, P. O'Keeffe, A. Paladini, R. Polini, D.M. Trucchi, "Optical characteristics of nanostructured aluminium/diamond composite systems in the visible range," Diamond and Related Materials, Vol. 132,109669, 2023.

Ultrafast optical switching in Si-metasurfaces for wireless and space optical communication

K. Ch. Georgiev[1], A. A. Trifonov[1,3], K. Z. Kamali[2], D. Neshev[1,2]
G. Crotti[4], G. D. Valle[4], L.S.Petrov[1],I. Ch. Buchvarov[1]*

[1.] John Atanasoff Center for Bio and Nano Photonics (JAC BNP), Sofia, Bulgaria
Physics Department, Sofia Univesrsity "St. Kl.Ohridski", 5 James Bourchier Blvd, Sofia, Bulgaria
[2.] ARC Centre of Excellence for Transformative Meta-Optical Systems (TMOS), Dept. of Electronics Materials Engineering, Research School of Physics, Australian National University, ACT 2601, Australia.
[4.] Department of Physics - Politecnico di Milano, 20133 Milano, Italy
*corresponding author: ivan.buchvarov@phys.uni-sofia.bg

Abstract: We demonstrate ultra-fast all-optical switching based on the implementation of a metasurface-based laser dichroic mirror design. The crystalline silicon metasurfaces with 100 nm thickness on sapphire substrates are fabricated using established processes in Si-semiconductor industry. Under weak-pump excitation, relative transmittance changes of up to 100% are possible for characteristic times ranging from 25 to 120 ps. A carrier-driven absolute amplitude modulation of over 72% is observed at 102-120 ps relaxation times. A CW 1030 nm laser's beam modulation for free space communication is verified in a laboratory environment.

Novel optical switching [1,2] and wavelength conversion[3]based on optical-metasurfaces have showed a lot of promise for ultra-fast modulation of light. However the total transmission modulation in such all-optical processes has remained low so far, in the range of a few percentages. High-quality factor metasurfaces made of robust materials are necessary to boost the modulation contrast to the levels (70-90 %) necessary for practical use for wireless and free space communication. Here, we show an incredibly high-contrast and quick-responding of transmission modulation of the silicon optical metasurface. The interference of a radiative electric dipole and a non-radiative, asymmetric bound-state in the continuous (BIC) channel results in a kink-type transmission response in our metasurface design[4]. With a few tens of picoseconds of temporal response, we show absolute transmission modulation of over 72% that is driven by carrier injection in the crystalline silicon metasurface.

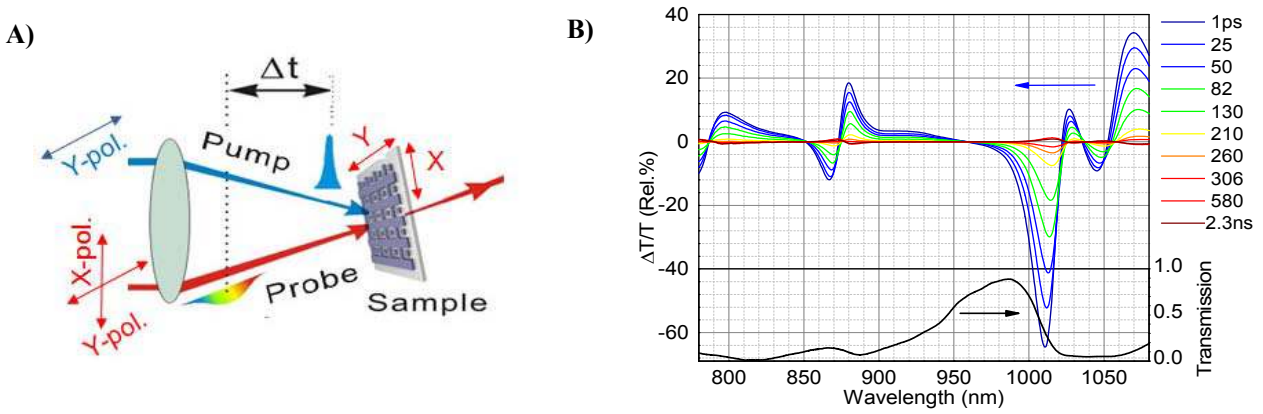


Figure 1. A) Schematic of the ultra-fast time-modulation based on a pump-probe Q-boosting time variant resonator. B) Transmission spectrum (black curve) and relative transmission modulation after pumping with 41 kW pump power and intensity of 1GW/cm^2 .
The metasurface is fabricated from a crystalline silicon on a sapphire substrate. It has periodicity of 500 nm and a thickness of 100 nm,

Figure 1. The metasurface is characterised via pump-probe spectroscopy, Fig.1(a), where a 170 fs pump beam at 520 nm excites the sample and generates free carriers in the silicon. A broad-spectrum probe beam is used to test the metasurface transmission at different time delays. The relative and absolute change of transmission spectra at different delay are depicted with coloured curves on Fig. 1(b). The two kinetics of the positive and negative maximum, Fig. 1(d), show that the relaxation of the induced charge carriers is predominantly characterized by a time constant about 102 ps (at 108nm) and 120 ps at 1012 nm respectively. Transmission spectra with a pump-probe delay of +3ps with and without pump, respectively are shown on Fig.2B. The highest depth of modulation (purple, differential spectrum) is -72% at around 990 nm. The modification of a CW 1030 nm laser's beam for free space communication has been verified in a lab setting using the same sample.

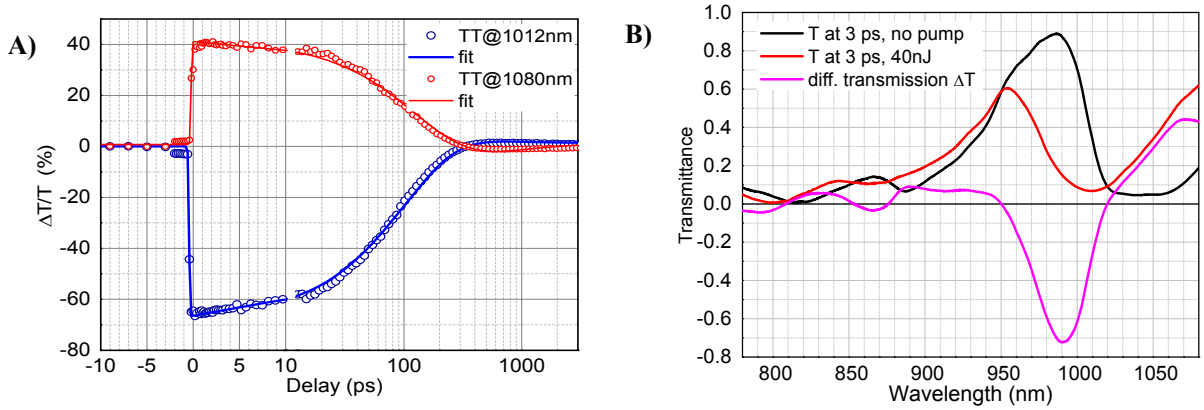


Figure 2. A) Transient dynamics at wavelengths of 1012 nm (blue circles) and 1080 nm (red circles). The time response for relaxation of the carrier injection obtained from exponential fit (solid lines) is 120 ps. B) Transmission spectra at pump-probe delay of +3ps with no pump (black) and with 245 kW pump power and intensity of 6 GW/cm^2 (red curve). Differential spectrum (purple) shows maximal depth of modulation of -72% at ca. 990nm

In summary, we demonstrate a record-high ultra-fast transmission modulation in silicon metasurfaces with BIC kink-type high-Q transmission. Our results open new opportunities for all-optical high-contrast switching in resonant metasurfaces.

This work is part of the METAFAST project (no. 899673) funded by the European Union's Horizon 2020 and HEPHAESTUS grant (DO1-307) of the Bulgarian National Roadmap for Research Infrastructure funded by Ministry of Education and Science of Republic of Bulgaria.

References

1. Shcherbakov, M. R., Vabishchevich, P. P., Shorokhov, A. S., Chong, K. E., Choi, D.-Y., Staude, I., Miroshnichenko, A. E., Neshev, D. N., Fedyanin, A. A., Kivshar, Y. S., "Ultrafast All-Optical Switching with Magnetic Resonances in Nonlinear Dielectric Nanostructures" Vol. 15**,** 6985, 2015.
2. Della Valle, G., Hopkins, B., Ganzer, L., Stoll, T., Rahmani, M., Longhi, S., Kivshar, Y. S., De Angelis, C., Neshev, D. N., Cerullo, G., "Nonlinear Anisotropic Dielectric Metasurfaces for Ultrafast Nanophotonics" Vol. 4**,** 2129, 2017.
3. Shcherbakov, M. R., Werner, K., Fan, Z., Talisa, N., Chowdhury, E., Shvets, G., "Photon acceleration and tunable broadband harmonics generation in nonlinear time-dependent metasurfaces" Vol. 10**,** 1345, 2019.
4. Georgiev, K., Kamali, K. Z., Xu, L., Rahmani, M., Miroshnichenko, A., Neshev, D., Buchvarov, I., "Metasurface Dichroic Mirrors: Application to Low Quantum Defect Lasers", Proc. SPIE ca_4_5 (2021).

META 2023, PARIS - FRANCE, JULY 18 – 21, 2023

Two-Dimensional Electronic Spectroscopy of Strong Exciton-Surface Plasmon Polariton Coupling

Christoph Lienau[1]

[1]Institute of Physics and Center for Nanoscale Dynamics (CeNaD), University of Oldenburg, 26129 Oldenburg
*corresponding author: christoph.lienau@uol.de

Abstract: Strong exciton-plasmon-couplings are investigated using two-dimensional electronic spectroscopy, revealing Rabi oscillations of polariton cross-peaks and accessing two-quantum excitations. Coherent population oscillations between excitons that are strongly and weakly coupled to the plasmonic field are demonstrated.

The creation of hybrid light-matter systems due to strong coupling is of major current interest for material science and to steer chemical reactions [1–3]. Of special interest are dipolar interactions between molecular excitons (X) and plasmonic resonators, such as surface plasmon polaritons (SPP) [4]. Sufficiently strong coupling to vacuum field fluctuations allows for the coherent flow of energy between X and SPP, i.e. Rabi oscillations, forming new hybridized upper (UP) and lower (LP) polariton states.

Here, we explore these strong coupling phenomena and especially their dynamics for the first time using two-dimensional electronic spectroscopy (2DES). We demonstrate strong coupling by revealing coherently oscillating cross-peaks" in the 2DES and demonstrate a new coherent transport phenomenon: Plasmon fields drive coherent exciton population oscillations between distant two distant exciton sites.

For this, we investigate the polariton dynamics of a prototypical system for X-SPP coupling, a periodic gold slit array coated with a 10-nm-thick squaraine-based J-aggregated thinfilm (Fig.1a) [5, 6]. The linear reflectivity of the sample shows an avoided crossing between UP and LP branches of the dispersion relation arising from strong X-SPP coupling (Fig. 1b) and an additional, angle-independent UX peak, usually explained by "uncoupled" excitons sitting outside the regions of high field-enhancements.

To probe the coherent dynamics of the system we performed a series of 2DES experiments at different angles of the dispersion relation. Fig.1b-c show the results for an angle of incidence of $\theta = 27°$. Dispersive resonances at the UX and LP energy, arising from a blue-shifted excited state absorption, give access to two-quantum excitations of the coupled system. The extracted one- and two-quantum dispersion relations are depicted in Fig. 1e. Dynamics of diagonal and cross peaks show pronounced Rabi oscillations, whose corresponding energy matches the 2DES peak splittings. The analysis of the data (Fig.1f) reveals that the dynamics of the strongly coupled system are not only governed by the anticipated UP-LP Rabi oscillations. Most prominently, the observed oscillations match the peak splittings between the UX and LP, thus indicating that the "uncoupled" excitons play a major role in the coherent dynamics.

Our findings can be understood by considering the effect of of SPP fields on the excitons distributions. For this, it is important that the relevant in-plane components of the SPP fields, driving the coupling to the excitons, are strongly enhanced inside the slits, yet have a finite value in between the slits. Thus, only those excitons residing indside slits can undergo strong X-SPP coupling, enabled by sufficiently strong local field enhancements. Those "uncoupled" excitons that sit between the slits, instead, couple only weakly couple to the same SPP mode. Hence, their energetic positions are basically unaffected by X-SPP coupling even although they can still exchange energy with the plasmon field. This is a three-level scenario that is reminiscent of lambda-type systems in atomic physics for which coherent, light-driven population transfer processes are already known. In our case, we demonstrate that the plasmon drives coherent population oscillations between the strongly-coupled excitons,

spatially confined to the slit regions and spatially distant "uncoupled excitons" that reside between at slits, separated by a few hundreds of nanometers from the two strongly-coupled excitons. It is this coherent populations transfer that gives rise to the pronounced Rabi oscillations probed in 2DES. We further support this conclusion by quantitative density matrix and Frenkel exciton model simulations.

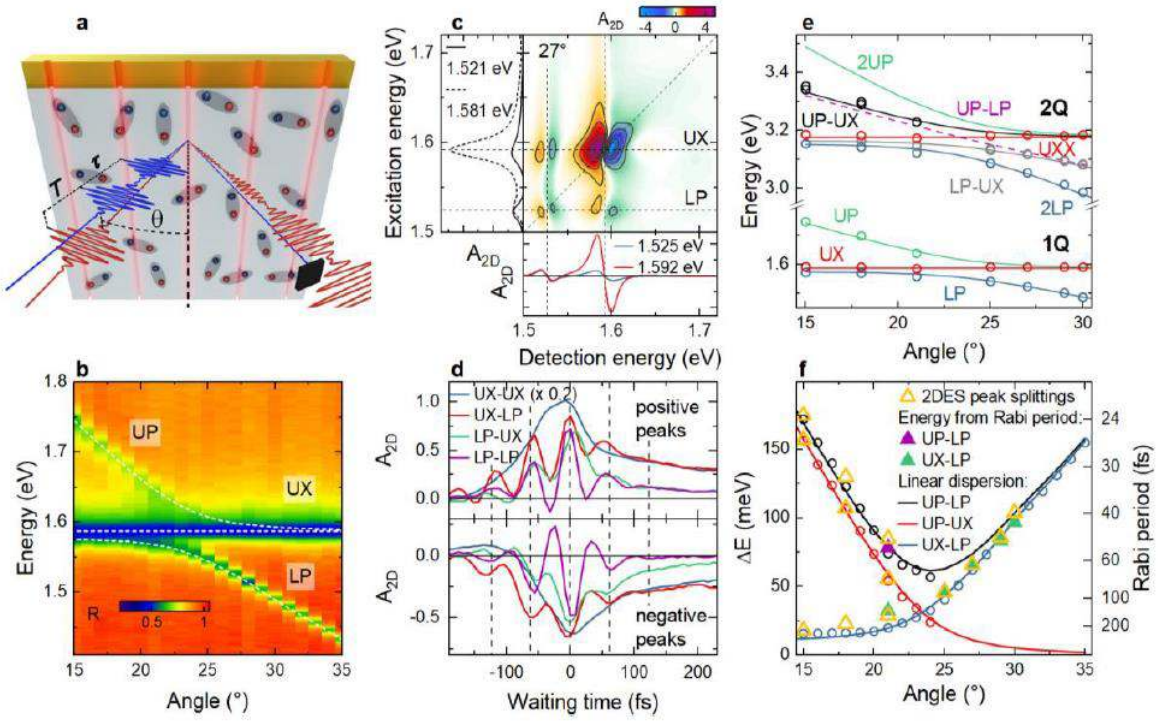


Fig. Sample geometry of the J-aggregate coated gold slit grating. b) Angle-resolved linear reflectivity (θ) of the strongly coupled X-SPP system. "Uncoupled" excitons (UX) appear 1.6 eV. c) Absorptive 2DES map at waiting time 0 fs and θ = 27°. Dispersive peaks arise from the superposition of one-quantum transitions and excited state absorption into two-quantum states. d) Peak dynamics in c) showing pronounced Rabi oscillations with a period of ~65 fs, matching the UX-LP energy splitting. e) One- and two-quantum dispersion relations f) Energetic splittings from the linear (circles) and 2DES measurements (triangles). The observed Rabi periods do match the energy difference between UX and LP and reflect coherent population oscillations between locally distant exciton sites driven by the plasmon field.

Our 2DES study thus not only provides the first observation of coherent Rabi oscillations due to strong couplings but also indicates a new pathway for coherent, plasmon-driven long-distance energy transfer in hybrid nanostructures.

References

1. Thomas, A. et al., "Tilting a ground-state reactivity landscape by vibrational strong coupling," Science 363, 615, 2019.
2. Gu B. and Mukamel S., "Optical-Cavity Manipulation of Conical Intersections and Singlet Fission in Pentacene Dimers," Journal of Physical Chemistry Letters 12, 2052, 2021.
3. Timmer, D. et al., "Charge Delocalization and Vibronic Couplings in Quadrupolar Squaraine Dyes," J. Am. Chem. Soc. 144 , 19150, 2022.
4. Quenzel, T. et al., "Plasmon-Enhanced Exciton Delocalization in Squaraine-Type Molecular Aggregates," ACS Nano 16, 4693, 2022.

META 2023, PARIS - FRANCE, JULY 18 – 21, 2023

Modelling and Inverse Design of Complex Nanophotonic Systems

L. Ramunno[1*]

[1]Department of Physics and Nexus for Quantum Technologies Institute, Canada
[*]corresponding author: lramunno@uottawa.ca

Abstract: Numerical modelling provides an important tool for understanding light matter interaction in complex nanoscale systems, teasing out most relevant underlying phenomena in very complex scenarios and providing a platform for inverse design. This talk will focus on recent examples of nanophotonics simulations from our group with complex response (*e.g.,* nonlocal and nonlinear plasmonics, and nonlinear ENZ materials for active nanophotonics), as well optimizing the response of time varying materials by inverse designing the incident light.

.

All-optical routing of upconverted light by dielectric metasurfaces through coherent control

A. Di Francescantonio[1], A. Zilli[1], D. Rocco[2], F. Conti[1], V. Vinel[3], A. Borne[3], M. Morassi[4], A. Lemaître[4], P. Biagioni[1], L. Duò[1], C. De Angelis[2], G. Leo[3], M. Finazzi[1], M. Celebrano[1*]

[1]Physics Department, Politecnico di Milano, Piazza Leonardo Da Vinci 32, 20133 Milano, Italy.
[2]Department of Information Engineering, University of Brescia, Via Branze 38, 25123 Brescia, Italy.
[3]Université de Paris, CNRS, Laboratoire Matériaux et Phénomènes Quantiques, 75013 Paris, France
[4]Centre de Nanosciences et de Nanotechnologies, CNRS, Université Paris-Saclay, 91120 Palaiseau, France
*Corresponding author: michele.celebrano@polimi.it

Abstract: We achieve all-optical switching of the upconverted light in periodic dielectric metasurfaces through a $\omega + 2\omega$ pump scheme. Exploiting the pump pulse phase as tuning knob, upconversion is switched between diffraction orders with efficiency >90%. Polarization of the pump beams and of the emitted light can is also employed to route the upconverted light among different sets of diffraction orders. We envision the proposed approach as an effective approach to upconvert and steer telecom photons into visible detection paths.

Frequency upconversion of near-infrared photons to the visible range is strategical for information technology, as it can provide an alternative for the read out of telecom signals using efficient silicon-based detectors. Light upconversion is a nonlinear process mediated by matter that consists in the interaction of either energy-degenerate photons, such as in second-harmonic and third-harmonic generation (THG), or photons with different energies, such as in sum-frequency generation (SFG). We recently investigated frequency upconversion in both plasmonic and dielectric nanoantennas [1,2]. Thanks to the adopted dual-beam pump scheme, where an ultrashort pulse (ω) at telecom wavelength (λ = 1551 nm) impinges on the sample along with its frequency-doubled replica (2ω), THG and SFG are degenerate in energy. This, along with coherence, enables the interference between the processes. Yet, we found that in individual nanoantennas symmetry plays a major role in enhancing/suppressing the interference between SFG and THG. By tuning the relative phase between the two

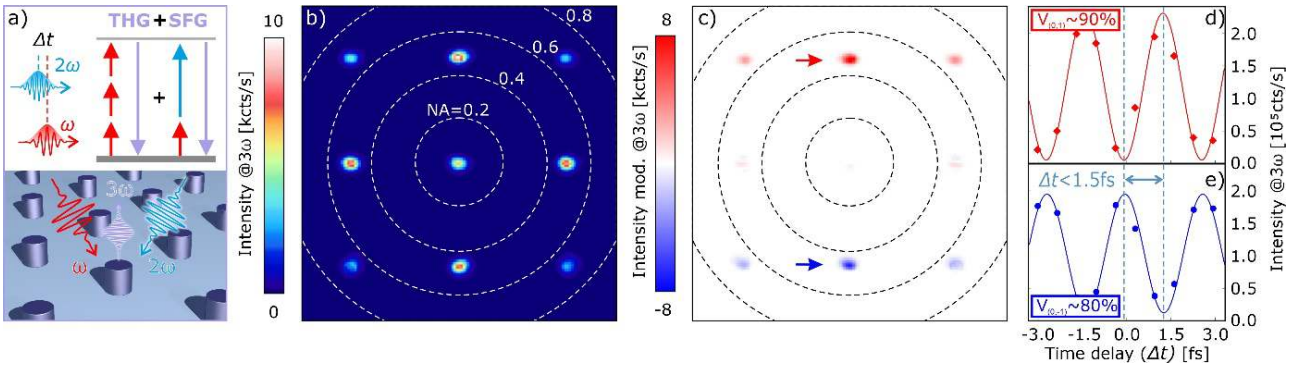


Fig. 1 a) Scheme of the dual beam pumping for upconversion (top) and pictorial description of the AlGaAs metasurface excitation and emission. b) Back focal plane (BFP) map of the upconverted light (SFG+THG) emission by the metasurfaces. The first order diffraction lobes appear at a NA=λ/p = 517 nm/1100 nm = 0.47, where p is the array periodicity. c) Modulation of the upconversion evaluated as the difference between the BFP maps acquired at about 1.5 fs delay between the pump pulses (see dashed lines in panels d and e). d) and e) Upconversion intensity of the (0,1) and (0,-1) orders of the metasurface (red and blue arrows, respectively) demonstrating switching with visibility V up to 90% and switching times of about 1.5 *fs*.

impinging pulses, we performed all-optical switching of upconverted light with efficiency > 50% in asymmetric plasmonic antennas [2].

Optical metasurfaces are rapidly emerging as flexible, ultrathin and multi-functional platforms to manipulate light [3]. Recently, they were also applied to efficient nonlinear light conversion and steering [4]. Here, by applying the above dual-beam pump scheme to a periodic AlGaAs metasurfaces (Fig. 1a), we attain all-optical switching of the upconverted telecom photons in the visible range as in [1,2]. This is attained thanks to the symmetry-breaking induced in the detection and obtained by tuning the metasurface diffraction with respect to the meta-atom nonlinear emission in the Fourier plane. Using the relative phase between the pump pulses as a tuning knob, we could steer the upconverted radiation among different metasurface diffraction orders (see Fig. 1b and c) with an efficiency up to 90% (see Fig. 1d). This is attained by engineering the nonlinear emission of the individual meta-atoms along with the metasurface diffraction in the Fourier space to maximize the interference between SFG and THG in specific *k*-space directions. We also demonstrate that the polarization state of both pump and emission allows to reconfigure the switching between different sets of diffraction orders.

Notably, we reach an overall conversion efficiency $\beta = P^{3\omega}/P^{2\omega}P^{\omega} > 10^{-5}W^{-1}$ at relatively low pump peak intensities (10 MW/cm^2). The proposed approach can be envisioned as an all-optical method to route upconverted telecom photons into various detection channels. The combination of the interferometric and nonlinear character of the emitted light could be also extremely appealing for applications to nonlinear sensing.

Acknowledgements

The authors acknowledge financial support from the European Union's Horizon 2020 Research and Innovation program "METAFAST" (Grant Agreement No. 899673) and from the Italian Ministry of University and Research through the PRIN project NOMEN (2017MP7F8F).

References

[1] A. Zilli, D. Rocco, M. Finazzi, A. Di Francescantonio, L. Duò, C. Gigli, G. Marino, G. Leo, C. De Angelis, M. Celebrano
"Frequency Tripling via Sum-Frequency Generation at the Nanoscale" ACS Photonics **8**, 1175-1182 (2021).

[2] A. Di Francescantonio, A. Locatelli, X. Wu, A. Zilli, T. Feichtner, P. Biagioni, L. Duò, D. Rocco, C. De Angelis, M. Celebrano, B. Hecht, M. Finazzi "Coherent Control of the Nonlinear Emission of Single Plasmonic Nanoantennas by Dual-Beam Pumping"
Adv. Opt. Mat. **2200757**, 1-8 (2022).

[3] W. T. Chen, A. Y. Zhu, F. Capasso, "Flat Optics with Dispersion-Engineered Metasurfaces". Nat. Rev. Mater. **5**, 604–620 (2020).

[4] L. Carletti, A. Zilli, F. Moia, A. Toma, M. Finazzi, C. De Angelis, D. N. Neshev, M. Celebrano "Steering and Encoding the Polarization of the Second Harmonic in the Visible with a Monolithic LiNbO3 Metasurface" ACS Photonics **8**, 731-737 (2021).

META 2023, PARIS - FRANCE, JULY 18 – 21, 2023

Ultrafast optical control of nonlinear dielectric nanoantennas

E. A. A. Pogna[1*], M. Celebrano[2], A. Mazzanti[2], L. Ghirardini[2], L. Carletti[3], G. Marino[4], A. Schirato[2], D. Viola[2], P. Laporta[2], C. De Angelis[3], G. Leo[4], G. Cerullo[2], M. Finazzi[2], and G. Della Valle[2]

[1] Istituto di Fotonica e Nanotecnologie, Consiglio Nazionale delle Ricerche, P.zza L. da Vinci 32, 20133 Milano, Italy
[2]Dipartimento di Fisica, Politecnico di Milano, I-20133 Milano, Italy;
[3]Dipartimento di Ingegneria dell'Informazione, Università di Brescia, I-25123 Brescia, Italy
[4] Matériaux et Phénomènes Quantiques, Université de Paris & CNRS, F-75013 Paris, France;
[*]corresponding author: evaariannaaurelia.pogna@cnr.it

Abstract: Efficient ultrafast reconfiguration of the second-harmonic generation of AlGaAs nonlinear nanoantennas operating at 1550 nm telecom wavelength, is achieved by ultrafast interband photoexcitation with femtosecond visible pulses. The combination of broadband transient transmittivity, time-revolved second harmonic generation, and nonlinear optics nanoscale modeling, allows to track the ultrafast modulation of the second harmonic signal, into the nanoscale charge carrier dynamics at the base of a giant permittivity change at the semiconducting band edge.

Strong non-linear optical effects can be demonstrated, exploiting the enhancement of light-matter interaction in subwavelength nanostructures based on media with high nonlinear susceptibility. High-refractive index dielectrics are promising material platforms for nonlinear nanophotonics in the visible and near-infrared ranges. They enable large field enhancement via multiple Mie scattering resonances, that can be tuned controlling the geometrical parameters of the nanoantennas. Remarkably, dielectrics nanoantennas benefit from reduced Ohmic losses compared to metallic nanostructures.

Conventional semiconductors have been explored for fabricating nonlinear dielectric nanoantennas operating both in transmission and in reflection configuration. Amongst these, GaAs is particularly promising because of the direct near-infrared bandgap of the material (1.422eV/872nm at room temperature), enabling efficient excitation with visible light. Moreover, fine-tuning of the semiconducting bandgap can be achieved by controlling the Al and Ga concentration in AlGaAs.

Here, we discuss the ultrafast control of the linear and nonlinear optical response of dielectric nanoantennas based on AlGaAs, exploiting photoexcitation with femtosecond visible pulses [1-2].

First, we investigate the transient optical response of $Al_{0.18}Ga_{0.82}As$ nanopillars with multiple Mie resonances. To this aim, we apply a combination of broadband transient reflectivity measurements and nonlinear optics nanoscale modeling, to follow the simultaneous modulation of four distinct resonances in the range 650-1150 nm, after the above bandgap photoexcitation with a 400nm pump pulse, see Figure 1a-b [1].

We observe a build-up of the transient reflectivity signal, which is attributed to the ambipolar diffusion of the photo-generated electron hole pairs inside the nanopillar. While, the relaxation dynamics exhibi a picosecond component driven by the interplay of intraband transitions, i.e. the Drude plasma response, and the Pauli blocking of interband transition induced by the pump absorption.

Remarkably, the investigated dynamics of the dielectric nanoantennas preside over large permittivity modulation, which is expected to affect the nonlinear optical response of the nanoantennas.

Here, we propose an efficient configuration for ultrafast control of the second harmonic generation (SHG) of the AlGaAs nanoantennas, see Figure 1c-d, exploiting the giant modulation to the dielectric permittivity expected at the semiconductor band edge, after photoexcitation with femtosecond visible pulses.

We demonstrate intense (up to 6%) modulation of the SHG of $Al_{0.18}Ga_{0.82}As$ nanopillar [2] by the time-resolved SHG experiment, with the fundamental at 1500nm telecom wavelength, and the second harmonic signal at 775 nm, at a pronounced scattering resonance. A control pulse at 500nm, is used to photo inject charge carriers and induce an intense modulation of the dielectric permittivity. Interestingly, the photoexcitation, can either quench or enhance the SHG signal depending on the nanopillar radius. The SHG shows buildup dynamics which we attribute to the ambipolar diffusion of the photogenerated electron−hole pairs, occurring in a few picoseconds. The efficient nonradiative recombination of the carriers, which in the nanopillar is favored by the the higher surface-to-volume, is then driving the decay of the SHG signal, in a few tens of picoseconds.

In conclusion, we demonstrate the active control of the reflectivity and of the second-order nonlinearities of dielectric nanoantennas by ultrafast optical excitation, opening intriguing application perspectives for light manipulation in ultra-compact configurations. The understanding of the nanoscale dynamics, appears crucial for the design of novel nonlinear nanophotonics devices based on optically reconfigurable multiresonant nanoantennas. Large modulation of other nonlinear optical effects is expected, including difference-frequency generation for spontaneous parametric down conversion, to be exploited in optically controlled nanosource of entangled photons, for quantum applications.

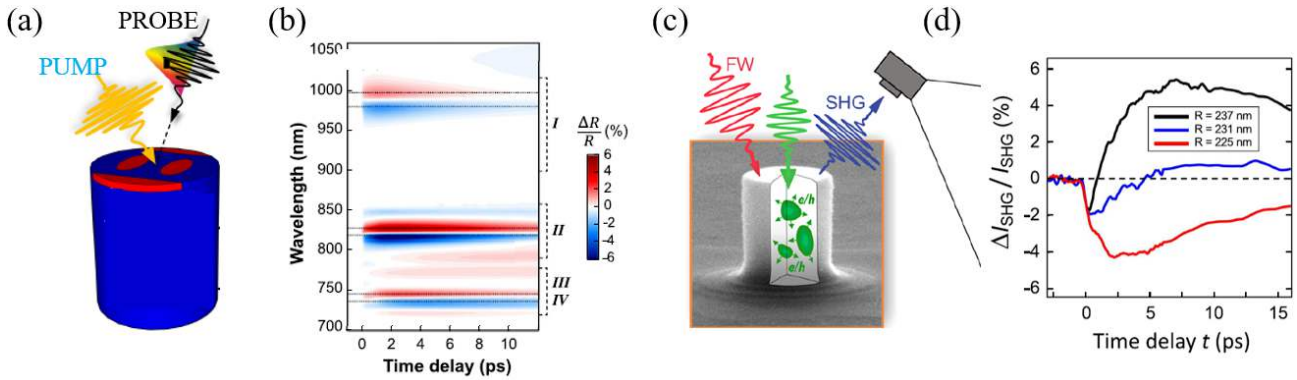


Figure 1. a) Sketch of the broadband transient reflectivity ΔR/R experiment on a $Al_{0.18}Ga_{0.82}As$ nanopillar excited with 400nm-150fs pump pulse, and monitored with a broadband probe pulse; b) transient reflectivity ΔR/R of a pillar of radius R=243 nm, showing the simultaneous modulation of four Mie resonances labelled with roman numbers; c) sketch of the time-resolved SHG experiment on individual $Al_{0.18}Ga_{0.82}As$ nanopillar excited with 500 nm pulses; d) SHG signal as a function of the time delay after the photoexcitation for pillar of different radius R. A-b are readapted from Ref. 1, c-d are readapted from Ref. 2.

References

1. Mazzanti, A. and Pogna, E.A.A et al., "All-Optical Modulation with Dielectric Nanoantennas: Multiresonant Control and Ultrafast Spatial Inhomogeneities," Small Sci., Vol. 1, 2000079, 2021.
2. Pogna, E. A. A. and Celebrano, M. and Mazzanti A. et al., "Ultrafast, All Optically Reconfigurable, Nonlinear Nanoantenna," ACS Nano, Vol. 15 No. 7 11150–11157, 2021.

Disentangling the ultrafast optical response of Titanium Nitride

S. Rotta Loria[1]*, B. R. Bricchi[2], A. Schirato[1,3], L. Mascaretti[4], C. Mancarella[2], A. Naldoni[4,5], A. Li Bassi[2,6], G. Della Valle[1,7] and M. Zavelani-Rossi[7,8]

[1]Dipartimento di Fisica, Politecnico di Milano, Piazza Leonardo da Vinci 32, 20133 Milano, Italy
[2]Dipartimento di Energia, Laboratorio Materiali Micro e Nanostrutturati, Politecnico di Milano, 20133 Milano, Italy
[3]Istituto Italiano di Tecnologia, 16163 Genova, Italy
[4]Czech Advanced Technology and Research Institute, Regional Centre of Advanced Technologies and Materials, Palacký University Olomouc, Šlechtitelů 27, 77900 Olomouc, Czech Republic
[5]Department of Chemistry and NIS Centre, University of Turin, Turin 10125, Italy
[6]Center for Nano Science and Technology - IIT@PoliMi, Via Giovanni Pascoli 70/3, 20133 Milano, Italy
[7]IFN-CNR piazza L. da Vinci 32, 20133 Milano, Italy
[8]Dipartimento di Energia, Politecnico di Milano, via G. Ponzio 34/3, 20133 Milano, Italy
*silvia.rotta@polimi.it

Abstract:
In the last decade, Titanium Nitride has emerged as an alternative plasmonic material to noble metals, thanks to its refractory properties and a carrier-lattice thermalization time much faster (< 100 fs), with respect to e.g. gold (~ 1 ps). In this work, we provide a numerical model to unfold TiN ultrafast nonlinear optical response, on a broad spectral range. The calculations are validated on a 200 nm-thick TiN film on glass.

Titanium Nitride (TiN) has gained notable interest in the last decade due to its refractory nature, CMOS- and bio-compatibility, interband losses lower than gold in the visible range, and a tunable permittivity when varying the synthesis parameters [1,2]. Regarding TiN transient optical response, the electron-phonon coupling in this material was found to be much stronger than in typical plasmonic media, such as noble metals. Indeed, the relaxation of out-of-equilibrium hot electrons following ultrafast photoexcitation takes place in less than 100 fs, one order of magnitude faster than, e.g., in gold (~ 1 ps) [3,4]. However, a comprehensive study of TiN nonlinear optical response upon excitation with fs-pulses is still missing. This represents a major lack when thinking about exploiting TiN as a new material for ultrafast plasmonic devices.

In this work, starting from the inhomogeneous Two-Temperature Model [5], we first assess the carrier and lattice temperature increase following the ultrashort photoexcitation of a 200 nm-thick TiN film. Then, considering one interband transition and an isotropic and parabolic band structure, we connect the increase in the carrier temperature to the variation of the interband contribution to the material's permittivity. For what concerns the modulation of the intraband (Drude) part of the permittivity, we prove it to be due both to the increase in the carriers' scattering with phonons and to the onset of thermoelastic effects in the TiN film. To validate the theoretical calculations, we perform ultrafast pump-probe spectroscopy on a 200 nm-thick TiN film on glass by monitoring its transient reflectivity, with ~ 100 fs temporal resolution, 500 nm pump and broadband (320 -550 nm) probe. The main results are shown in Figure 1 a)-d). The theoretical calculations are able to accurately reproduce the experimental pump-probe measurement. Our model also enables us to disentangle the interband and Drude contributions to the permittivity variation, and we demonstrate that the modulation of interband transitions plays a key role in TiN nonlinear optical response. Indeed, without considering it, we completely miss the ultrafast features (< 150 fs) in the transient reflectivity ($\Delta R/R$), as shown in Figure 1e)-f).
As such, thanks to the combination of ultrafast pump-probe spectroscopy measurements and semi-classical modelling, we are indeed able to unfold the origin of the ultrafast nonlinearities in TiN. Moreover, our model

represents a powerful tool to make predictions on TiN transient response of more complex structures, such as TiN nanostructures and metasurfaces. This paves the way for the engineering and development of new TiN devices for ultrafast plasmonics applications, such as the all optical modulation of light.

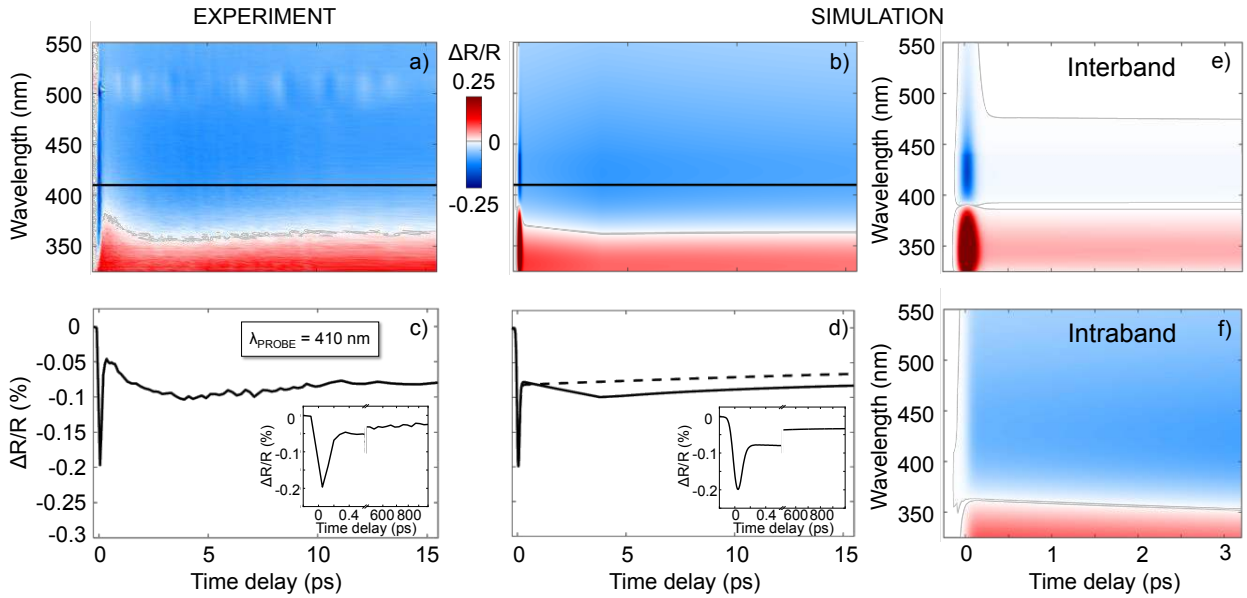


Figure 1. Experimental a) and Theoretical b) pump-probe map of the TiN film, with the corresponding dynamics: c) experimental, d) theoretical at 410 nm. ΔR/R is the transient reflectivity signal. The insets in figures 1 c)-d) show a zoom in the dynamics in the first 600 fs and from 500 ps to 1 ns. e-f) Pump-probe map (theoretical) showing the disentanglement of c) interband and d) intraband contributions to the modulation of permittivity.

The authors acknowledge the METAFAST project that received funding from the European Union Horizon 2020 Research and Innovation programme under Grant Agreement No.899673. This work reflects only author view and the European Commission is not responsible for any use that may be made of the information it contains.

References

1. Reddy H., Guler U., Kudyshev Z., Kildishev A. V., Shalaev V. M. and Boltasseva A., "Temperature-Dependent Optical Properties of Plasmonic Titanium Nitride Thin Films" ACS Photonics, Vol. 4, No. 6, 1413-1420, 2017.
2. Kharitonov, A. V. and Kharintsev, S. S., "Tunable optical materials for multi-resonant plasmonics: from TiN to TiON [Invited]" Opt. Mater. Vol. 10, No. 2, 513–531, 2020.
3. Dal Forno S. and Lischner J., "Electron-phonon coupling and hot electron thermalization in titanium nitride" Phys. Rev. Mater., Vol. 3, No. 11, 115203-115211, 2019.
4. Diroll B. T., Saha S., Shalaev V. M., Boltasseva A. and Schaller R. D., "Broadband Ultrafast Dynamics of Refractory Metals: TiN and ZrN" Adv. Opt. Mater., Vol. 8, No. 19, 2000652, 2020.
5. Allen, P. B., "Theory of thermal relaxation of electrons in metals" Phys. Rev. Lett., Vol. 59, No. 13, 1460–1463, 1987.

Ultrafast Polarization Control via All-Optical Modulation in Anisotropic Metasurfaces

G. Crotti[1,2*], M. Akturk[1], A. Schirato[1], V. Vinel[8], R. Proietti Zaccaria[2,3], M. Maiuri[1,4], A. A. Trifonov[5], I. C. Buchvarov[5,6], D. N. Neshev[7], G. Leo[8], G. Cerullo[1,4], and G. Della Valle[1,4,9*]

[1]Department of Physics - Politecnico di Milano, 20133 Milano, Italy
[2]Istituto Italiano di Tecnologia, 16163, Genova, Italy
[3]Cixi Institute of Biomedical Engineering, Ningbo Institute of Industrial Technology, Chinese Academy of Sciences, Ningbo 315201, China
[4]IFN – Consiglio Nazionale Delle Ricerche, 20133, Milan, Italy
[5]John Atanasoff Center for Bio and Nano Photonics (JAC BNP), 1164 Sofia, Bulgaria
[6]Faculty of Physics, St. Kliment Ohridski University of Sofia, 5 James Bourchier Boulevard, 1164 Sofia, Bulgaria
[7]ARC Centre of Excellence for Transformative Meta-Optical Systems (TMOS), Research School of Physics, Australian National University, Acton, ACT 2601, Australia.
[8]Laboratoire Matériaux et Phénomènes Quantiques, MPQ UMR 7162, Université de Paris, CNRS, 75013, Paris, France
[9]INFN - Sezione di Milano, I-20133 Milano, Italy
[*]corresponding author: giulia1.crotti@polimi.it, giuseppe.dellavalle@polimi.it

Abstract: Sub-picosecond polarization control is a fundamental functionality for several applications, from information encoding to probing of chemical systems such as chiral molecules. We present an all-optically reconfigurable AlGaAs metasurface, showing giant dichroism modulation upon investigation via ultrafast pump-probe spectroscopy. By combining modelling of carriers excitation and relaxation processes with full-wave electromagnetic simulations, we can attribute the relevant transient features to pump-induced band-filling effect, opening a gain region in the spectral range of a sharp resonance of the structure.

Active control of light polarization in the THz speed regime is a highly desirable and challenging goal in Photonics. Indeed, the ability to master this functionality would allow the development of novel free-space optical links for telecommunications [1], as well as the implementation of innovative techniques to manipulate material processes [2] or to probe polarization-sensitive systems as chiral molecules [3] in a time-resolved fashion. To this aim, all-optical paradigms present several advantages, also having the potential to exceed the fundamental limitations of electronics, and have been employed on a variety of platforms [4,5,6]. Metasurfaces are the ideal candidates for the implementation of devices working in such schemes; as planar collections of nanoresonators, compactly arranged, they are both tunable and convenient for integrated applications.

Within this context, we present an anisotropic metasurface of AlGaAs nanowires on top of a GaAs-AlOx substrate, working in reflection. Anisotropy in the metasurface plane entails a strongly dichroic optical response in static conditions, which is in fact evident in the unperturbed reflection spectra for the two in-plane polarizations. We experimentally demonstrate a giant modulation of such dichroic properties via ultrafast pump-probe spectroscopy, using a low-moderate level of excitation (pump fluence ~70 $\mu J/cm^2$) with respect to values reported in literature: specifically, we obtain a peak value of differential reflectivity of almost 470% for probe polarized along the periodicity direction ('TM'), with comparatively negligible, yet remarkable modulation (up to ~60%) for probe polarization parallel to the wires ('TE').

To provide a clearcut interpretation of these results, we construct a modelling approach based on a segregated, multi-step procedure [7,8]. We first consider the physical processes presiding over relaxation of

electron-hole pairs photogenerated in the semiconductor nanowires, by employing the so-called three-temperature model (3TM). The latter is a rate equation model which describes the evolution of internal degrees of freedom: electron-hole pairs density in the skin depth of the nanustructure and in its bulk, and lattice temperature.

In turn, each of these quantities is responsible for a transient modification of permittivity, $\Delta\varepsilon$, through three mechanisms: a Drude effect, accounting for intraband transisitions; band-filling, relative to interband transitions and consisting of a saturation of absorption channels at photon energies near the AlGaAs bandgap; thermo-optics processes. Permittivity variation then entails a modified optical response with respect to unperturbed conditions, which we describe with full-wave electromagnetic simulations.

Our modelling strategy is able to capture the transient dynamics of the optical signal qualitatively and quantitatively. Moreover, it reveals that a pivotal role is played by band-filling effect, dominating $\Delta\varepsilon$ near the AlGaAs bandgap (~750 nm), so that the resulting modulated permittivity $\varepsilon + \Delta\varepsilon$ presents a *negative* imaginary part in a narrow spectral band comprised between 735 nm and 750 nm. This is the fingerprint of the opening of a gain window, precisely in the region of a resonant mode of the structure for the TM polarization. It is specifically this interplay of phenomena which enables the surge of the huge differential reflection signal.

These results unveil a new promising route to employ direct-gap semiconductor platforms for the ultrafast control of light polarization near the bandgap region; they pave the way for the design of novel resonant structures, specifically engineered to exploit the band-filling induced gain window.

This work is part of the METAFAST project (no. 899673) funded by the EU H2020 program.

References

1. Wang J., J.-Y. Yang, I. M. Fazal, N. Ahmed, Y. Yan, H. Huang, Y. Ren, Y. Yue, S. Dolinar, M. Tur and A. E. Willner, "Terabit free-space data transmission employing orbital angular momentum multiplexing", Nat. Photon., Vol. 6, No. 7, 488-496, 2012.
2. Först, M., C. Manzoni, S. Kaiser, Y. Tomioka, Y. Tokura, R. Merlin and A. Cavalleri, "Nonlinear phononics as an ultrafast route to lattice control," Nat. Phys., Vol. 7, No. 11, 854–856, 2011.
3. Bradshaw, D. S., J. M. Leeder, M. M. Coles and D. L. Andrews, "Signatures of material and optical chirality: Origins and measures," Chem. Phys. Lett., Vol. 626, 106-110, 2015.
4. Nicholls, L. H., F. J. Rodríguez-Fortuño, M. E. Nasir, R. M. Córdova-Castro, N. Olivier, G. A. Wurtz and A. V. Zayats, "Ultrafast synthesis and switching of light polarization in nonlinear anisotropic metamaterials," Nat. Photon., Vol. 11, No. 10, 628–633, 2017.
5. Yang, Y., K. Kelley, E. Sachet, S. Campione, T. S. Luk, J.-P. Maria, M. B. Sinclair, and I. Brener, "Femtosecond optical polarization switching using a cadmium oxide-based perfect absorber," Nat. Photon., Vol. 11, No. 6, 390–395, 2017.
6. Schirato, A., M. Maiuri, A. Toma, S. Fugattini, R. Proietti Zaccaria, P. Laporta, P. Nordlander, G. Cerullo, A. Alabastri and G. Della Valle, "Transient optical symmetry breaking for ultrafast broadband dichroism in plasmonic metasurfaces," Nat. Photon., Vol. 14, No. 12, 723–727, 2020.
7. Mazzanti, A., E. A. A. Pogna, L. Ghirardini, M. Celebrano, A. Schirato, G. Marino, A. Lemaítre, M. Finazzi, C. De Angelis, G. Leo, G. Cerullo and G. Della Valle, "All-optical modulation with dielectric nanoantennas: Multiresonant control and ultrafast spatial inhomogeneities," Small Sci., Vol. 1, No. 7, 2000079, 2021.
8. Pogna, E. A. A., M. Celebrano, A. Mazzanti, L. Ghirardini, L. Carletti, G. Marino, A. Schirato, D. Viola, P. Laporta, C. De Angelis, G. Leo, G. Cerullo, M. Finazzi and G. Della Valle, "Ultrafast, all optically reconfigurable, nonlinear Nanoantenna," ACS Nano, Vol. 15, No. 7, 11150–11157, 2021.

META 2023, PARIS - FRANCE, JULY 18 – 21, 2023

All-Optical Modulation of Birefringence in Nonlinear All-Dielectric Metasurfaces

M. Akturk[1*], G. Crotti[1,2] A. Schirato[1], Vincent Vinel[8], R. Proietti Zaccaria[2,3], A. A. Trifonov[5], I. C. Buchvarov[5,6], D. N. Neshev[7], G. Leo[8], M. Maiuri[1,4], G. Della Valle[1,4,9*], G. Cerullo[1,4]

[1]Department of Physics - Politecnico di Milano, 20133 Milano, Italy
[2]Istituto Italiano di Tecnologia, 16163, Genova, Italy
[3]Cixi Institute of Biomedical Engineering, Ningbo Institute of Industrial Technology, Chinese Academy of Sciences, Ningbo 315201, China
[4]IFN – Consiglio Nazionale Delle Ricerche, 20133, Milan, Italy
[5]John Atanasoff Center for Bio and Nano Photonics (JAC BNP), 1164 Sofia, Bulgaria
[6]Faculty of Physics, St. Kliment Ohridski University of Sofia, 5 James Bourchier Boulevard, 1164 Sofia, Bulgaria
[7]ARC Centre of Excellence for Transformative Meta-Optical Systems (TMOS), Research School of Physics, Australian National University, Acton, ACT 2601, Australia.
[8]Laboratoire Matériaux et Phénomènes Quantiques, MPQ UMR 7162, Université de Paris, CNRS, 75013, Paris, France
[9]INFN - Sezione di Milano, I-20133 Milano, Italy
[*] mert.akturk@polimi.it, giuseppe.dellavalle@polimi.it

Abstract: Steering the polarization of light at an ultrafast speed is a crucial functionality for a plethora of applications, including free-space optical links for high-speed information processing and recording. Nonlinear metamaterials have recently been developed for ultrafast manipulation of light polarization by all-optical means (i.e., upon excitation by a femtosecond control pulse). Here, we demonstrate strong birefringence features in a reconfigurable, anisotropic AlGaAs metasurface, achieving more than 90° rotation of the polarization ellipse at a few picosecond timescales.

One of the fundamental characteristics of light is its polarization state. Controlling light polarization on the ultrafast timescale may enable a wide range of applications in numerous systems, ranging from chemical complexes, spin precession to lattice vibrations [1,2,3]. The state-of-the-art polarizing components (i.e., polarizers and waveplates) are either passive or suffer from the intrinsic limits of electronic (GHz) modulation speed [4]. To achieve dynamical polarization control in the THz speed regime, one promising approach involves the design of reconfigurable and all-optical schemes utilizing anisotropic thin nanostructures such as metamaterials, in which optical pumping could induce a transient modulation of static dichroism and birefringence [5].

Within this framework, we present an anisotropic AlGaAs nanowire metasurface fabricated on top of a GaAs-AlOx substrate, operating in reflection mode. We experimentally demonstrate remarkably efficient ultrafast birefringence features via ultrafast pump-probe spectroscopy Specifically, we observed up to 90° rotation of the polarization state around the 750 nm wavelength, sitting near the bandgap of the AlGaAs, and up to 120° rotation at 790 nm.

For the realization of the ultrafast transient birefringence experiment, the polarimetric pump-probe data are recorded using polarized probe pulses and controlling the polarization outcome at the detector. Specifically, the incident pump beam (400 nm) is linearly polarized perpendicular to the nanowires, while the polarization of the broadband probe beam is rotated 45° clockwise with respect to the pump polarization by utilizing a combination of a half-wave plate and a linear polarizer, illuminating the sample almost at a normal incidence (θ = 7°). At the detection, to determine the polarization state of the reflected probe beam, we utilized a quarter-wave plate and a fixed polarizer which is set to the same transmission axis of the first polarizer used for the input probe beam, i.e. at 45° with respect to the pump polarization. The fast-axis of the quarter-waveplate is aligned parallel with the wires and then rotated to a different angle (β) for each set of measurements. The reflected probe intensity is then recorded as a function of probe wavelength and the time delay between pump and probe pulses. The 2D differential reflectivity maps for the two different angles (β) of the quarter-waveplate ($\Delta\beta$ = 60°) are

depicted in figure 1, indicating strong modulations of the polarization components around 750 nm spectral region associated with the rotation of the polarization ellipse.

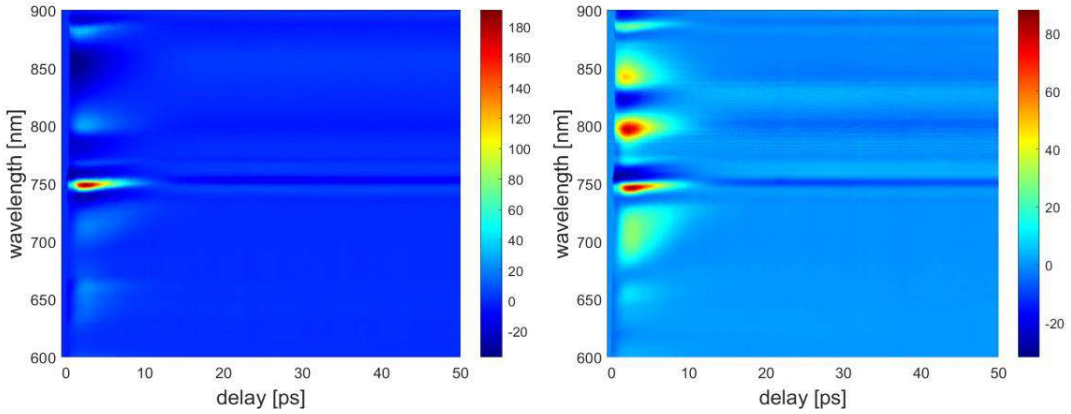


Figure 1: Pump-probe transient reflection maps recorded at different angular positions of quarter waveplate ($\Delta\beta = 60°$).

By using these sets of dynamic and static reflection measurements, we can retrieve the Stokes parameters of the probe light reflected by the metasurface and reconstruct the corresponding polarization ellipses as shown in figure 2. We observed complex dynamics within the spectral window near the bandgap (750 nm) and at longer wavelengths (790 nm).

Our results indicate in a clearcut way the potential of direct-gap semiconductor platforms for all-optical birefringence modulation and pave the way for the development of high-performance, reconfigurable metasurfaces, featuring extended-state birefringent resonances for the ultrafast control of light polarization.

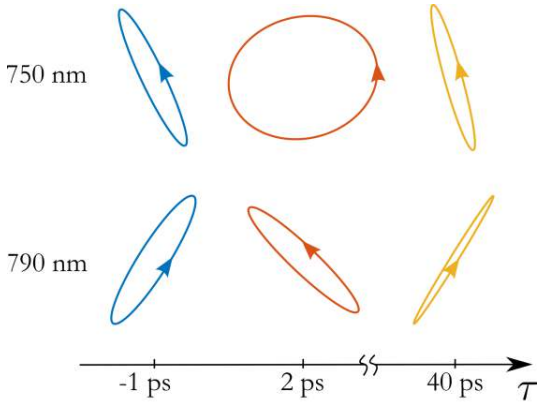


Figure 2: Dynamical polarization ellipse reconstruction at two different wavelengths evaluated for three selected pump-probe delays.

This work is part of the METAFAST project that received funding from the European Union Horizon 2020 Research and Innovation program under grant agreement no. 899673.

References

1. Fleischer, S., Zhou, Y., Field, R. W. & Nelson, K. A. Molecular orientation and alignment by intense single-cycle THz pulses. Phys. Rev. Lett. 107, 163603 (2011).
2. Först, M. et al, "Nonlinear phononics as an ultrafast route to lattice control," Nat. Phys., Vol. 7, No. 11, 854–856, 2011.
3. Kampfrath, T. et al., "Coherent terahertz control of antiferromagnetic spin waves," Nat. Photon. 5, 31–34, 2011.
4. Yang, Y. et al., "Femtosecond optical polarization switching using a cadmium oxide-based perfect absorber," Nat. Photon., Vol. 11, No. 6, 390–395, 2017.
5. Della Valle, G. et al., "Nonlinear anisotropic dielectric metasurfaces for ultrafast nanophotonics," ACS Photonics, Vol. 4, No. 9, 2129–2136, 2017.

Tensorial artificial optical nonlinearity in dielectric metasurfaces

F. Yue[1], N. Montaut[1], F. Riminucci[2], G. Balistreri[1*], A. Toma[3], R. Piccoli[1,4], S. Cabrini[2], R. Morandotti[1], L. Razzari[1]

[1]Institut National de la Recherche Scientifique, Centre Énergie Matériaux Télécommunications (INRS-EMT), 1650 Boulevard Lionel-Boulet, Varennes, Quebec, J3X 1P7, Canada
[2]Molecular Foundry, Lawrence Berkeley National Laboratory, One Cyclotron Road, Berkeley, California, 94720, USA
[3]Istituto Italiano di Tecnologia, Via Morego 30, Genova, 16163, Italy
[4]Politecnico di Milano, Department of Physics, Piazza Leonardo da Vinci 32, I-20133, Milano, Italy
[*]corresponding author: giacomo.balistreri@inrs.ca

Abstract: We report on the development of an analytical expression for the description of the artificial third-order nonlinearity induced in an amorphous-silicon based metasurface, which takes into account the polarization states of the interacting light fields. Based on this model, we retrieve the tensorial values of the nonlinear susceptibility by measuring the third harmonic generation efficiency of a dielectric metasurface composed of rectangularly-shaped amorphous silicon elements.

Introduction

Recently, dielectric metasurfaces, two-dimensional arrays of subwavelength elements, called meta-atoms, have been extensively employed to tailor nonlinear interactions without being restricted by phase-matching requirements[1]. It has been shown that dielectric metasurfaces can enhance the nonlinear conversion efficiency when compared to a film of the same material with the same thickness[2]. Despite this interest, a complete description of the artificial nonlinearity in meta-atoms is still missing. In this work, we derive an analytical expression to describe third-harmonic generation (THG) via the artificial third-order nonlinearity originating from the meta-atom symmetry, with an emphasis on the polarization states of the fundamental and generated third-harmonic fields. By exploiting this description, the tensor elements of the artificial nonlinearity of a test-bed amorphous silicon (a-Si) metasurface are experimentally retrieved from the THG conversion efficiency. The presented theoretical analysis and experimental results allow for the design of functional nonlinear metasurface devices for various applications, from nonlinear imaging to novel sources of nonclassical light.

Theory and experimental characterization

The sample under test is an array of rectangular blocks, which belongs to the orthorhombic crystal class, also referred to as C_2 (twofold in-plane rotational symmetry)[3]. The nonlinear polarization density, P, of the THG process is proportional to the third-order susceptibility matrix, $M^{(3)}$, of the corresponding crystal class. In our case, the incident light is polarized along the x-y plane and propagates in the z-direction (i.e., $E_z = 0$). As such, the z polarization can be omitted, so that $M^{(3)} = \begin{pmatrix} \chi_{11} & 0 & \chi_{18} & 0 \\ 0 & \chi_{22} & 0 & \chi_{29} \end{pmatrix}$. Using Ansys Lumerical® software, we designed an a-Si metasurface (on a silica substrate) so that no dipole resonances would occur close to our input wavelength, i.e., λ_f = 1596 nm. The geometric parameters obtained from this numerical study are as follows: L = 420 nm, W = 160 nm, H = 425 nm, and D = 520 nm (see inset of Fig 1b). The sample was then fabricated via e-beam lithography and characterized by means of a tunable femtosecond pulsed-laser source. The THG power was measured using a silicon-based photodiode paired with a lock-in amplifier. The setup (see Fig. 1a) also included a THG imaging module, comprising focusing lenses. We measured the metasurface linear transmission in the telecom band (see Fig. 1b) for input horizontally- (H) and vertically-polarized (V) light. The metasurface shows a high

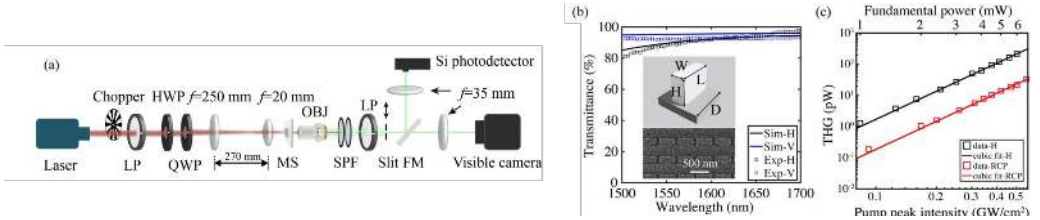


Figure 1. (a) Experimental setup for the characterization of the metasurface. LP: linear polarizer, HWP: half-wave plate, QWP: quarter-wave plate, MS: metasurface, SPF: short-pass filter; OBJ: objective, FM: flip mirror. (b) Simulated (solid curves) and measured (squares) linear transmittance for horizontal (with respect to the meta-atom long axis, black curve) and vertical (blue curve) input light. In the inset, a scanning electron microscopy image of the metasurface is shown, together with a schematic of a meta-atom. (c) Powe scaling measurements. Solid lines represent cubic fit curves while square markers are associated with the experimental data for horizontally- (black) and circularly- (red) polarized input light.

measured and simulated transmittance (> 92%), which confirms its off-resonance response at the target fundamental wavelength. We also investigated the dependence of the THG power on the fundamental peak intensity in the case of horizontally- and circularly (right handedness, RCP) polarized lights (see Fig. 1c). Both measurements show a good agreement with a cubic fit, as expected from the THG process. Finally, we retrieved the nonlinear tensor elements by quantifying the THG conversion efficiency for various input polarizations: 1) H-polarized fundamental light (η_{P1}); 2) V-polarized light (η_{P2}); 3) RCP light with an output linear polarizer set to H (η_{P3}) and V (η_{P4}). The conversion efficiency is evaluated as the ratio between the intensities of the THG and fundamental beams. The corresponding tensor elements could be found via the following relationships:

$$\chi_{11} = G\sqrt{\eta_{P1}};\ \chi_{22} = G\sqrt{\eta_{P2}};\ \left|\frac{\chi_{11}-3\chi_{18}}{2\sqrt{2}}\right| = G\sqrt{\eta_{P3}};\ \left|\frac{\chi_{22}-3\chi_{29}}{2\sqrt{2}}\right| = G\sqrt{\eta_{P4}}, \quad (1)$$

Where $G = \frac{2\varepsilon_0 c\lambda_f\sqrt{n_{3\omega}n_{\omega}^3}}{\sqrt[4]{3}\pi l I_{\omega} sinc\left(\frac{\Delta kl}{2}\right)}$, ε_0 is the vacuum dielectric permittivity, c the vacuum speed of light, l the meta-atom thickness, Δk the wave-vector mismatch, $n_{3\omega}$ and n_{ω} the refractive indices at ω and 3ω, respectively, and I_{ω} the input beam intensity. The retrieved tensor elements are hence estimated to be: $\chi_{11} = 7.9 * 10^{-18}\, m^2/V^2$; $\chi_{22} = 7.42 * 10^{-19}\, m^2/V^2$; $\chi_{18} = 4.67 * 10^{-19}\, m^2/V^2$; $\chi_{29} = 1.38 * 10^{-18} m^2/V^2$. It is worth stressing that, for a uniform a-Si film, $\chi_{18} = \chi_{29} = \chi_{11}/3$, and that THG is forbidden for circularly polarized light (see Eq. 1), while $\chi_{11} = \chi_{22}$. This further highlights the artificial nature of THG in the metasurface.

In conclusion, we have developed a mathematical description for the THG process in rectangularly-shaped meta-atoms and estimated their artificial optical nonlinearity by taking into account their geometrical features and symmetry. We have also designed and fabricated an a-Si metasurface to characterize its THG properties and retrieve the values of its artificial susceptibility tensor. The presented model represents a useful and convenient approach to develop novel metasurface platforms for nonlinear photonic manipulations.

References

1. Litchinitser N. M. and Sun, J., "Optical meta-atoms: Going linear", Science, Vol. 350, 1033-1034 (2015).
2. Liu B, Sain B., Reineke B., Zhao R., Meier C., Huang L., Jiang Y., and Zentgraf T., "Nonlinear wavefront control by geometric-phase dielectric metasurface: influence of mode field and rotational symmetry", Adv. Opt. Mater., Vol. 8, 1902050 (2020).
3. Li G., Chen S., Pholchai N., Reineke B., Wong P.W.H., Pun E.Y.B, Cheah K.W., Zentgraf T., and Zhang S., "Continuous control of the nonlinearity phase for harmonic generation", Nat. Mat., Vol 14, 607-612 (2015).

META 2023, PARIS - FRANCE, JULY 18 – 21, 2023

Metasurface Design with Robust Resonances for Nonlinear Photonics

G. Q. Moretti[1], B. Tilmann[2], A. Tittl[2], E. Cortés[2], S. Maier[2,3,4], A. V. Bragas[1], and G. Grinblat[1*]

[1]Departamento de Física, FCEN, IFIBA-CONICET, Universidad de Buenos Aires, Argentina
[2]Chair in Hybrid Nanosystems, Nanoinstitute Munich, Faculty of Physics, Ludwig-Maximilians-Universität, Germany
[3]School of Physics and Astronomy, Monash University, Australia
[4]Department of Physics, Imperial College London, United Kingdom
[*]corresponding author: grinblat@df.uba.ar

Abstract: A metasurface of Gallium Phosphide on glass with a robust design enables high-quality factor (Q) modes, arising from the concept of quasi bound states in the continuum (QBICs). The high enhancement of the incident electric field is used to compute the nonlinear second harmonic (SH) fields in a non-perturbative approach, yielding a theoretical maximum conversion efficiency of 0.5%. Preliminary experimental results will be presented.

Bound States in the Continuum (BICs) are inaccessible modes with eigen-energies embedded in the radiation continuum. The phenomenon was first introduced in quantum mechanics, but its formalism can be expanded to many systems with wave-like behavior, such as the interaction of light with structures in the nanoscale. In principle, a BIC cannot be coupled to external radiation. A symmetry-protected BIC, however, can be accessed by adding a defect that breaks a certain symmetry, thus becoming a quasi-BIC or QBIC [1]. Because of its conception as a purely bound state, periodic structures, like metasurfaces, were a starting point for its study with electromagnetic waves. Many designs have been proposed and experimentally studied in recent years [2], with quality factors in the range of 10^2 to 10^5.

In this work, we propose a novel design [3] of a GaP metasurface with a very high-quality factor and a robust design. Its properties come from the relatively large dimensions of the added defect and its behavior when increasing the asymmetry. In figure 1A, the unit cell composing the metasurface can be seen in the top panel, and a schematic showing the electric field's direction at the resonance is shown. The design consists of two elliptical cylinders with an extra cylinder that acts as a coupler to form the QBIC. When the coupler is at the positions marked with an 'x' (or the dashed sections at the bottom of 1A), the system has reflection symmetry in the y-direction. When the coupler is then displaced a distance Δy, a QBIC can be excited. In general, for small asymmetries the quality factor of the resonance depends on the inverse square of the asymmetry parameter. In figure 1B we show how the relationship holds for displacements up to 40 nm with a coupler diameter of 80 nm. It is also interesting to note how the quality factor does not monotonically decrease, and a region of stability appears between the two extremes. This is a novel behavior in QBIC dielectric metasurfaces and shows that it is possible to obtain strong resonances (Q between 10^3 to 10^5) without fine-tuning the geometry.

To check the performance of the metasurface in nonlinear applications, we computed the SHG efficiency for a selected geometry with a Q of 4×10^5, whose electric field distribution can be seen in the top inset of figure 1B. The simulations were done with non-perturbative approximations, two extra terms were added to the linear polarization inside the material, pump depletion and optical Kerr effect, which depend on the second and third-order nonlinear susceptibilities, respectively. These terms are relevant because of the high-intensity fields that arise even with low excitation powers (1 to 10 mW to excite a large area of 10 to 30 μm^2). In these conditions, the SH fields and the intensity-dependent refractive index are no longer negligible. The theoretical maximum efficiency with all effects considered is 0.5 %, which is higher than the previously reported value of

0.2 % [4] in the same regime and shows further room for improvement from the maximum achieved experimentally of 2×10^{-5} % at similar pump intensities [5].

Figure 1C shows some preliminary samples fabricated using this design on silicon. GaP metasurfaces are currently being made and experimental results will be presented. We believe that the presented metasurface would bring new record-breaking efficiencies for nonlinear light generation processes.

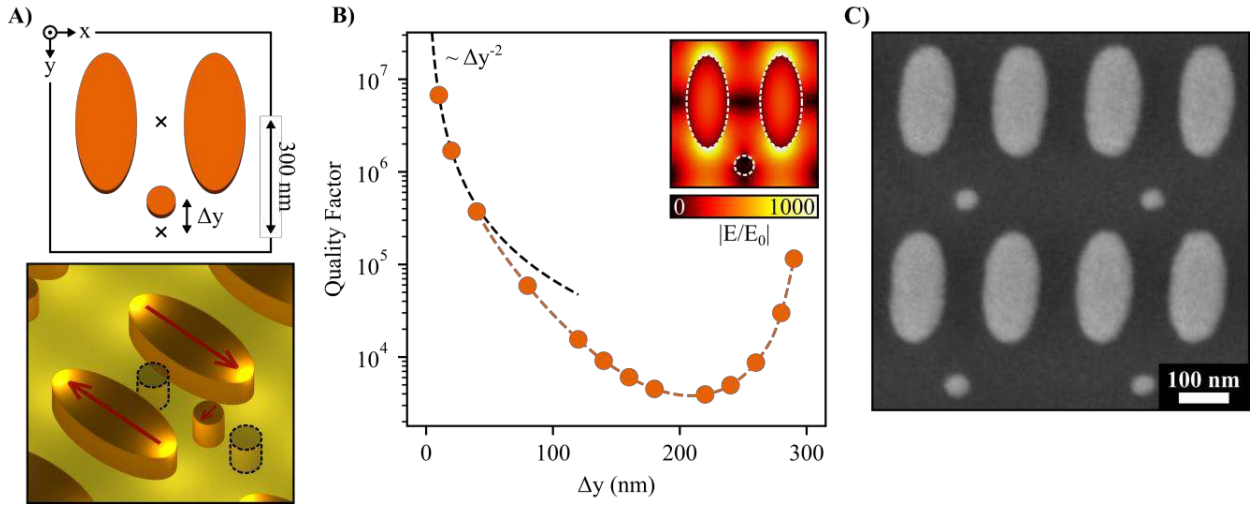


Figure 1. A) In the top panel the unit cell conforming the metasurface can be seen. A schematic of the electric field's direction at the resonance is shown at the bottom. B) Quality factor of the mode as a function of the coupler displacement. In the top inset the electric field enhancement for Δy = 40 nm. C) SEM image of fabricated metasurface with a coupler diameter of 40 nm

This work was partially supported by PICT 2017-2534, PICT 2019-01886, PIP 112 201301 00619, PIP 112 202001 01465, UBACyT Proyecto 20020170100432BA, and UBACyT Proyecto 20020190200296BA and from the Deutsche Forschungsgemeinschaft (DFG, German Research Foundation) under Germany's Excellence Strategy – EXC 2089/1 – 390776260.

References

1. Hsu C. W., B. Zhen, A. D. Stone, J. D. Joannopoulos and M. Soljačić, "Bound States in the Continuum," Nat. Rev. Mater, Vol 1, 16048, 2016
2. Koshelev K., S. Lepeshov, M. Liu, A. Bogdanov. And Y. Kivshar, "Asymmetric Metasurfaces with High-Q Resonances Governed by Bound States in the Continuum," Phys. rev. Lett., Vol. 121, 193903, 2018.
3. Moretti G. Q., A. Tittl, E. Cortés, S. A. Maier, A. V. Bragas and G. Grinblat, "Introducing a Symmetry-Breaking Coupler into a Dielectric Metasurface Enables Robust High-Q Quasi-BICs," Adv. Photonics Res., Vol. 3, No. 12, 2200111, 2022.
4. Ning T., X. Li, Z. Zhang, Y. Huo, Q. Yue, L. Zhao and Y. Gao, "Ultimate Conversion Efficiency of Second Harmonic Generation in All-dielectric Resonators of Quasi-BICs in Consideration of Nonlinear Refraction of Dielectrics" Opt. Express, Vol. 29, No. 11, 17286-17294, 2021.
5. Anthur A. P., H. Zhang, R. Paniagua-Dominguez, D. A. Kalashnikov, S. T. Ha, T. W. W. Maß, A. I. Kuznetsov and L. Krivitsky "Continuous Wave Second Harmonic Generation Enabled by Quasi-Bound-States in the Continuum on Gallium Phosphide Metasurfaces" Nano Lett., Vol. 20, No. 12, 8745–8751, 2020.

Ultrafast modulation of surface plasmon dispersion in metallic bilayers by hot non-equilibrium electrons

A. Avdizhiyan[1*], A. Stupakiewicz[1], and I. Razdolski[1]

[1]Faculty of Physics, University of Białystok, Poland
[*]corresponding author: a.avdizhiyan@uwb.edu.pl

Abstract: Employing back pump-front probe spectroscopy to Fe/Au bilayers, we investigate an indirect manipulation of the surface plasmon dispersion at the remote Au/air interface. The absorption peak of the surface plasmon resonance experiences a shift at the femtosecond timescale, highlighting the role of hot nonequilibrium electrons for ultrafast plasmonics.

Active plasmonics, a rapidly developing branch of modern nanophotonics, aims at controlling collective excitations of free charges at metallic interfaces. Its growth is fueled by the quest for light localization and manipulation at the nanoscale, opening pathways to novel optical devices [1]. Conventional ways of modulation of the surface plasmon dispersion entail the use of femtosecond laser pulses which are operative on the ultrashort timescale [2]. However, direct irradiation of the plasmonic interface with high-power optical pulses inevitably leads to significant heating, resulting in an increased energy dissipation.

In this work, we employ an indirect optical excitation to control the surface plasmon dispersion at a remote interface. As a model system, we use a Fe/Au metallic bilayer in which an efficient laser-induced injection of spin-polarized non-thermal electrons was demonstrated [3]. In a back pump-front probe experimental configuration with 50 fs temporal resolution, we study the impact of the pump-induced hot electron injection from Fe on the surface plasmon dispersion at the Au/air interface. A plasmonic grating at the Au surface enabled the excitation of a propagating plasmon-polariton mode with a free-space probe radiation. The thickness of the Au layer is sufficiently large (70 nm in total: 35 nm solid Au and 35 nm grating depth) to exclude the direct optical excitation of the electrons in Au in the vicinity of the surface. The grating periodicity of 460 nm results in the excitation of the surface plasmon-polariton at an incidence angle of 45 degrees around 790 nm wavelength. The reflected probe radiation is registered with a spectroscopic camera allowing for the wavelength-resolved analysis of the plasmonic impact of the laser-induced hot electron injection.

The main result of our work is presented in Figure 1. It is seen that the pump-induced injection primarily results in antisymmetric variations of the optical reflectivity around the plasmon resonance at few hundred fs pump-probe delays. On the contrary, symmetric variations are suppressed. As such, we conclude that the injection of non-thermal electrons mainly results in a shift of the resonance, while leaving the quality factor unperturbed. This is a striking contrast to the direct laser irradiation which often results in deteriorating of the resonance quality factors due to the ultrafast heating of the electronic subsystem. Further, the lifetime of the effect resides on the subpicosecond timescale, in agreement with the estimated lifetime of the non-thermal electron population in Au. We then discuss physical mechanisms of the electron dynamics resulting in the plasmon resonance shift upon non-thermal electron injection. Our results demonstrate high promise of the novel

approach towards ultrafast active plasmonics based on non-thermal electrons.

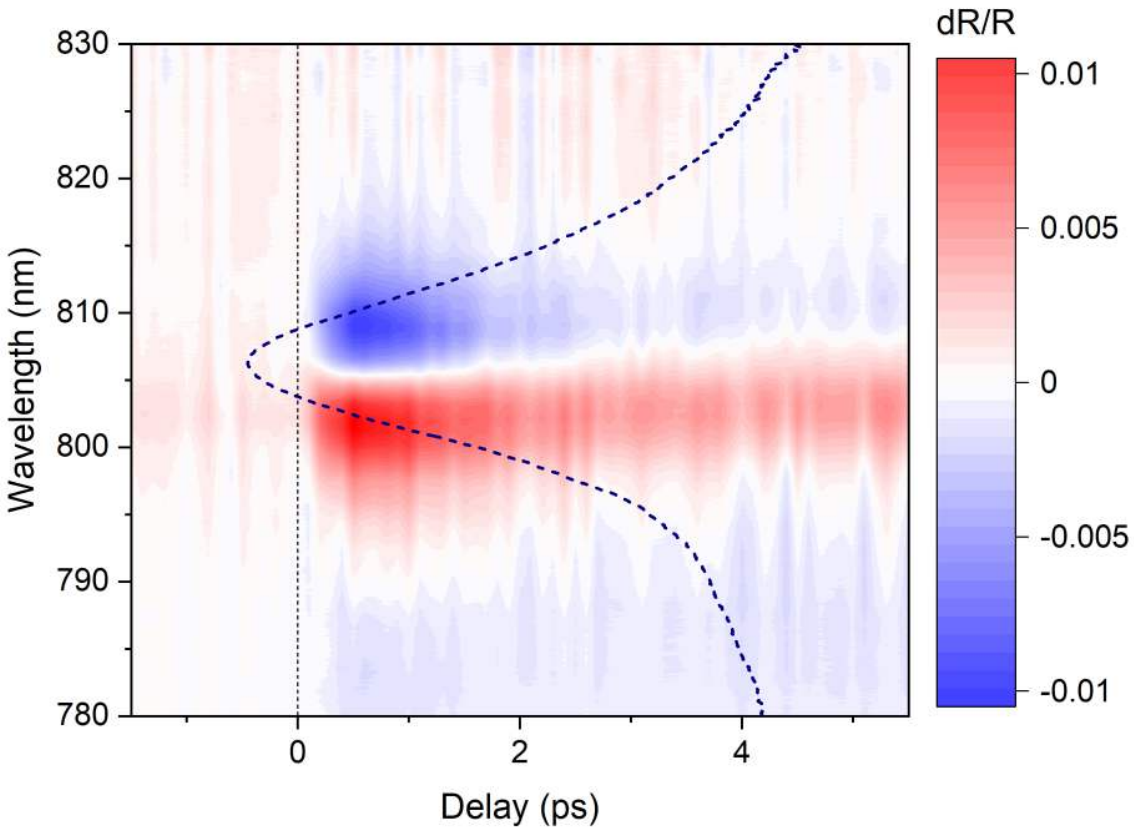


Figure 1. SPP back pump – front probe spectroscopy of a Fe/Au bilayer with a plasmonic grating. The figure shows variations dR/R by wavelength from the delay time between the pumping and probing pulses. The dashed line indicates the resonant surface plasmon-polariton excitation in the equilibrium state (at negative delays).

This work was supported by the National Science Center of Poland (NCN) under the OPUS-18 funding scheme.

References

1. Barnes W. L., Dereux A. et. al., “Surface plasmon subwavelength optics”, Nature (London) 424, 824, 2005.
2. MacDonald K. F., Samson Z. L. et. al., “Ultrafast active plasmonics”, Nature Photonics 3, 55, 2009.
3. Alekhin A. and Razdolski I. et al,“Femtosecond spin current pulses generated by the non-thermal spin-dependent Seebeck effect and interacting with ferromagnets in spin valves”, Phys. Rev. Lett. 119, 017202, 2017.

Advanced Computational Electromagnetics for the Analysis and Design of Nanophotonic Devices

Modeling the Acousto-Plasmonic Coupling: Raman Energy Density Framework

N. Large[1*], Montaño-Priede[1], and A. Mlayah[2]

[1]Department of Physics and Astronomy, University of Texas at San Antonio, United States
[2]Laboratoire d'Analyse et d'Architecture des Systèmes, CNRS – Université de Toulouse, France
[*]corresponding author: Nicolas.Large@utsa.edu

Abstract: We present a theoretical study of the interactions between confined acoustic phonons and localized surface plasmons (LSPs) in the framework of acoustic Raman scattering. By using the Fermi golden rule we introduce a new physical quantity, the Raman energy density (RED), which is a local quantity that serves as a tool for the study of resonant Raman scattering mediated by LSPs in nanoparticles. The RED represents the electromagnetic energy density excited by the Raman probe and modulated by the phonons.

Most of the studies focusing on metallic nanoparticles consider them as static bodies at rest. However, localized surface plasmons (LSPs) can be temporally modulated by acoustic vibrations, also known as acoustic phonons, naturally present in the nanomaterial and surrounding environment. Very recently, there has been a renewed interest on the modulation effect of the LSPs by (opto)mechanical modes and elastic waves [1-6]. Such high-frequency (GHz-THz) modulation can be used to increase detection and sensing accuracy of nano-objects and molecules. For instance, these vibrating nanoparticles, acting as simple optomechanical nanoresonators, can be seen as nanoscale analogs to quartz crystal microbalances. Acoustic-phonons Raman scattering is a very effective, high-precision, and non-invasive technique for nanometrology. It uses the acoustic vibrations as local probes to determine sizes and distances at the nanoscale with very high accuracy. However, the effectiveness of this technique is directly related to the knowledge of the interaction mechanisms between electrons (plasmons) and phonons (acoustic vibrations). Therefore, it is necessary to know what are the vibrational modes sustained by a given nanostructure (amplitude, frequency, symmetry) and know how they interact with the LSPs to completely determine the Raman efficiencies and selection rules.

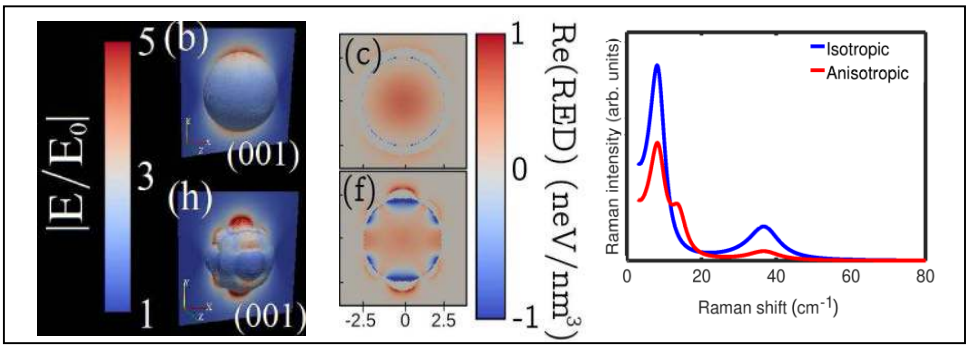


Fig. 1 Left: Isotropic (l=0) and Anisotropic (A_{1g}) breathing acoustic mode of a AuNP modulating the near electric field induced par the dipolar localized surface plasmon (LSP). **Center**: Raman energy density (RED) resulting from the interaction of the l=0 and A_{1g} vibration mode with the dipole LSP. **Right**: Calculated acoustic Raman spectra for the isotropic and anisotropic nanoparticles.

Here, we investigate the dynamic properties of metallic nanoparticles by focusing on the interaction between confined acoustic vibrations and LSPs (**Fig. 1, left**) [5, 7]. The dynamic properties of LSPs are responsible for the transient optical absorption modulation, that can be observed in time-resolved transient absorption experiments [6], and for the acoustic SERS effect [4], We describe the resonant Raman scattering process using a new approach based on a single direct acousto-plasmonic interaction process described by Fermi golden rule [7]. Within this framework, we introduce a new physical quantity, namely, the Raman energy density (RED; **Fig. 1, center**). Similarly to the Raman-Brillouin electronic density (RBED) introduced in semiconducting nanostructures [8, 9], the RED allows for studying and monitoring the acousto-plasmonic Raman scattering in the near-field. We modeled the acousto-plasmonic interaction by implementing vibrational dynamics (resonant ultrasound method, RUS), into electrodynamic calculations (discrete dipole approximation, DDA). We used this methodology to compute the acoustic Raman spectra (**Fig. 1, right**) and investigate the interaction between LSPs and (an)isotropic acoustic vibrations, thus leading to the full determination of Raman efficiencies and selection rules. We show that the RED (**Fig. 1, center**), which can be mapped in the near-field for each vibration mode, correlates the far-field Raman scattering (**Fig. 1, right**) to the local acousto-plasmonic hot spots (**Fig. 1, left**), provides a deeper understanding of the Raman scattering process (*e.g.*, Raman selection rules), and serves to study the acousto-plasmonic coupling of complex nanostructures.

This work received financial support from the Office of Naval Research (ONR) under Grant No. N00014-21-1-2729 and the NanoX Grant No. ANR-17-EURE-0009 in the framework of the “Programme des Investissements d’Avenir.”

References

1. A. Ahmed, M. Pelton, and J. R. Guest, "Understanding How Acoustic Vibrations Modulate the Optical Response of Plasmonic Metal Nanoparticles," ACS Nano **11**, 9360-9369 (2017).
2. O. Saison-Francioso, G. Lévêque, and A. Akjouj, "Numerical Modeling of Acousto–Plasmonic Coupling in Metallic Nanoparticles," J. Phys. Chem. C **124**, 12120-12133 (2020).
3. K. O’Brien, N. D. Lanzillotti-Kimura, J. Rho, H. Suchowski, X. Yin, and X. Zhang, "Ultrafast acousto-plasmonic control and sensing in complex nanostructures," Nat. Comm. **5**, 4042-4042 (2014).
4. S. Tripathy, R. Marty, V. K. Lin, S. L. Teo, E. Ye, A. Arbouet, L. Saviot, C. Girard, M. Y. Han, and A. Mlayah, "Acousto-Plasmonic and Surface-Enhanced Raman Scattering Properties of Coupled Gold Nanospheres/Nanodisk Trimers," Nano Lett. **11**, 431-437 (2011).
5. N. Large, L. Saviot, J. Margueritat, J. Gonzalo, C. N. Afonso, A. Arbouet, P. Langot, A. Mlayah, and J. Aizpurua, "Acousto-plasmonic hot spots in metallic nano-objects," Nano Lett. **9**, 3732 (2009).
6. W. M. Deacon, A. Lombardi, F. Benz, Y. del Valle-Inclan Redondo, R. Chikkaraddy, B. de Nijs, M.-E. Kleemann, J. Mertens, and J. J. Baumberg, "Interrogating Nanojunctions Using Ultraconfined Acoustoplasmonic Coupling," Phys. Rev. Lett. **119**, 023901 (2017).
7. J. L. Montaño-Priede, A. Mlayah, and N. Large, "Raman energy density in the context of acoustoplasmonics," Phys. Rev. B **106**, 165425 (2022).
8. N. Large, J. R. Huntzinger, J. Aizpurua, B. Jusserand, and A. Mlayah, "Raman-Brillouin electronic density in short period superlattices," Phys. Rev. B **82**, 075310-075318 (2010).
9. A. Mlayah, J.-R. Huntzinger, and N. Large, "Raman-Brillouin light scattering in low-dimensional systems: Photoelastic model versus quantum model," Phys. Rev. B **75**, 245303-245303 (2007).

META 2023, PARIS - FRANCE, JULY 18 – 21, 2023

Heat transfer modelling in the crossover regime between conduction and radiation

M. Gómez Viloria[1], P. Ben-Abdallah[1], and R. Messina[1*]

[1]Laboratoire Charles Fabry, Laboratoire Charles Fabry, Institut d'optique,

CNRS, UMR 8501, Université Paris-Saclay, 91127 Palaiseau, France

[*]corresponding author: riccardo.messina@institutoptique.fr

Abstract: We analyze the heat transfer between two metals separated by a vacuum gap in the extreme near-field regime, in which tunneling photons, phonons and electrons are expected to play a role. We quantify the relative contribution of these carriers with respect to the separation distance and the applied bias voltage. Our results emphasize some inconsistencies in recent experimental results about heat exchanges in extreme near-field regime and set a roadmap for future experiments.

The theoretical framework of Fluctuational ElectroDynamics (FED) [1] describes the near field radiative heat transfer for separation distances below the thermal wavelength (some microns at ambient temperature). In this distance regime the heat flow between two solids at different temperatures can exceed the far field limit by several orders of magnitude, in particular when the bodies exchanging heat support surface resonant modes, such as surface phonon-polaritons or surface plasmons [2].

At even smaller distances, in the so-called extreme near field (distances in the nanometer range and below) the physics is expected to change radically. Interestingly, two recent scanning thermal microscopy (SThM) experiments [3,4], approaching gold tips to gold substrates, reached apparently opposite conclusions. While one of them shows large deviations from FED for separation distances of few nanometers, the other one shows no deviations from FED even at sub-nanometer gaps, where acoustic phonons and electrons are expected to contribute as further channels to the heat exchange.

Here we introduce a theoretical framework to investigate the heat transfer mediated by photons, phonons and electrons between two metallic bodies. We quantify the role of electron tunnelling currents [5] by paying attention to the role played by the shape of the electronic barrier in the presence of electron-electron screening interactions [6,7]. Using an approach based on the elastic theory [8-10], we address the role of acoustic phonons coupled through the van der Waals and the electrostatic forces. Finally, we employ FED [1] to study the role played by photons, by taking into account the contribution of non-local effects [11,12].

This theoretical work allows us to outline the relative weight of the different carriers with respect to the separation distance, and to highlight the crucial role played by the external bias voltage on the heat flux carried by the three types of carriers [13]. We also demonstrate that depending on the sign of this bias, electrons can either heat up the cold body or pump heat from it by Nottingham effect.

References

1. Polder, D. and van Hove, M., "Theory of Radiative Heat Transfer between Closely Spaced Bodies", Phys. Rev. B **4**, 10 (1971)
2. Joulain, K., Mulet, J.-P., Marquier, F., Carminati, R. and Greffet, J.-J., "Surface electromagnetic waves thermally excited: Radiative heat transfer, coherence properties and Casimir forces revisited in the near field", Surf. Sci. Rep. **57**, 59 (2005)
3. Kloppstech, K. et al., "Giant heat transfer in the crossover regime between conduction and radiation", Nat. Commun. **8**,

14475 (2017)
4. Cui, L. et al., “Study of radiative heat transfer in Ångström- and nanometre-sized gaps”, Nat. Commun. **8**, 14479 (2017)
5. Simmons, J. G., “Generalized Formula for the Electric Tunnel Effect between Similar Electrodes Separated by a Thin Insulating Film”, J. Appl. Phys **34**, 1793 (1963)
6. Gabovich, A. M., Il’chenko, L. G., Pashitskii, E. A. and Romanov, Yu. A., “Electrostatic energy and screened charge interaction near the surface of metals with different Fermi surface shape”, Surf. Sci. **13**, 179 (1980)
7. Il’chenko, L. G. and Goraychuk, T. V., “Role of the image forces potential in the formation of the potential barrier between closely spaced metals”, Surf. Sci. **478**, 169 (2001).
8. Pendry, J. B., Sasihithlu, K. and Craster, R. V., “Phonon-assisted heat transfer between vacuum-separated surfaces”, Phys. Rev. B **94**, 075414 (2016)
9. A. I. Volokitin, “Effect of Resonant Photon Emission in Radiative Heat Transfer and Generation”, JETP Lett. **110**, 397 (2019)
10. A. I. Volokitin, “Effect of an Electric Field in the Heat Transfer between Metals in the Extreme Near Field”, J. Phys.: Condens. Matter **32**, 215001 (2020)
11. Ford, G. W. and Weber, W. H., “Electromagnetic interactions of molecules with metal surfaces”, Phys. Rep. **113**, 195 (1984)
12. Chapuis P.-O. et al., “Effects of spatial dispersion in near-field radiative heat transfer between two parallel metallic surfaces”, Phys. Rev. B **77**, 035431 (2008)
13. Gómez Viloria, M., Guo, Y., Merabia, S., Ben-Abdallah, P. and Messina, R., “Heat transfer in the extreme near-field regime between metallic bodies”, preprint arXiv: 2212.03073 (2022)

META 2023, PARIS - FRANCE, JULY 18 – 21, 2023

Strategies to Tailor Thermal Properties of Metamaterials: Perforation and Amorphisation

K. Termentzidis[1]

[1]CETHIL Laboratory UMR5008, CNRS, INSA of Lyon, France
[*]corresponding author: konstantinos.termentzidis@insa-lyon.fr

Abstract: The rapid development of fabrication techniques enables the elaboration of new class of materials with tailor thermal properties. The thermal metamaterials are intelligently designed artificial structures with which one can engineer heat energy as the thermal conductivity becomes an extrinsic property. Here several theoretical and experimental examples of thermal metamaterials using the strategies of perforation and amorphisation will be presented.

The thermal conductivity of pristine bulk materials is an intrinsic physical property of the material and it cannot be controlled. With the nanostructuration, one can design materials with extrinsic thermal properties. The so called thermal metamaterials enable us to manipulate heat flow, with aim to propose thermal functional devices [1]. Among them, Phononic Crystals (CR) rise interesting fundamental questions and promising applications in thermal management and thermoelectricity. Recently, important new physical insights proposed in the literature concerning heat flux manipulation based in new phenomena such as: coherent effect, hydrodynamics, phonon focusing, thermal shielding, concentration, or even inversion [2]. Here, the impact of purposed amorphisation, perforation and the existence of native oxides (that arise on samples in presence of air) located at the membranes surfaces or around patterned holes on the thermal conductivity will be analyzed using atomistic simulations.

When the characteristic sizes of metamaterials with perforated holes, or amorphous inclusions are of the order of the mean free path of the heat carriers, here the phonons, all structural details should be taken into account. In this regime, the heat flux becomes very sensitive to atomic scale engineering as the creation of holes, the neck distances, the alignment of holes, the orientation of defects and surfaces/interfaces [3,4,5]. The aformentioned PC are considered 2D nanostructures. Adding complexity, there are also three-dimensional (3D) metamaterials as nanowire networks. These nanostructured materials are potential metastructures for nanoelectronics and thermoelectric applications. The 2D and 3D nanowire networks are a new class of nanoarchitectured materials have interesting physical properties due to their low mass density and their high surface-to-volume ratio. We will show that the thermal conductivity of these networks decreases in increasing the distance between the nodes [6]. This effect is much more pronounced in 3D networks due to increased porosity, surface-to-volume ratio, and the enhanced backscattering at 3D nodes compared to 2D nodes. We propose a model to

estimate the thermal resistance related to the 2D and 3D interconnections in order to provide an analytic description of thermal conductivity of such nanowire networks; the latter is in good agreement with molecular dynamic results. The backscattering processes in the nodes increase the thermal resistance by a factor of 5 compared to simple nanowires.

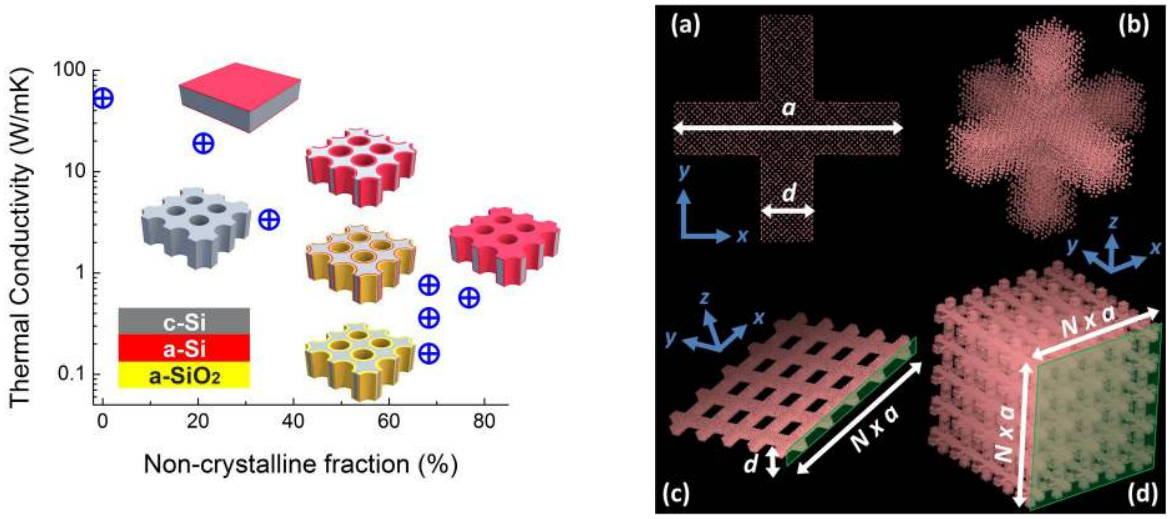


Figure: (Left) Thermal conductivity of phononic crystals and the impact of perforation and amorphisation. (Right) 2D and 3D nanowire networks.

Acknowledgements: All coauthors and collegues who contributed in these results.

References

1. Wang J., Dai G., Huang J., “Thermal Metamaterial: Fundamental, Application, and Outlook”, Science 23, 101637 (2020).
2. Naratana S and Sato Y. “Heat Flux Manipulation with Engineered Thermal Materials”, Phys. Rev. Lett. 108, 214303 (2012)
3. Verdier M., Lacroix D., Didenko S., Robillard J-F., Lampin E., Bah T. and Termentzidis K., “Influence of amorphous layers on the thermal conductivity of phononic crystals” K., Phys. Rev. B 97, 115435 (2018).
4. Verdier M., Anufriev R., Ramiere A., Termentzidis K. and Lacroix D., “Thermal conductivity of phononic membranes with aligned and staggered lattices of holes at room and low temperatures”, Phys. Rev. B 95, 205438 (2017).
5. Verdier M., Lacroix D. and Termentzidis K., “Heat transport in phononic-like membranes: Modeling and comparison with modulated nano-wires”, Int. J. Heat and Mass Transfer 114, 550 (2017)
6. Verdier M., Lacroix D. and Termentzidis K., “Thermal transport in two- and three-dimensional nanowire networks”, Phys. Rev. B 98, 155434 (2018).

META 2023, PARIS - FRANCE, JULY 18 – 21, 2023

Nanostructures for Photocatalysis - From regular to dendritic Architectures

Christin David

Friedrich-Schiller Universität Jena, Institute of Condensed Matter Theory and Optics, 07743 Jena, Germany
Abbe Center of Photonics, 07745 Jena, Germany
*corresponding author: christin.david@uni-jena.de

Abstract: We discuss the opportunity to design switchable nanostructures for enhanced selectivity in photocatalytic reactions. While we can tailor regular nanostructures in active metasurfaces to manipulate light in the desired way, irregular nanostructure platforms as obtained from self-organized growth of dendritic nanoarchitectures offer a high density of hot-spots with a wealth of spectral features. We present numerical calculations assessing optical and thermal properties of such structures as well as estimating light-induced electron transfer mechanisms to nearby molecules.

Complex nanostructured matter is of great interest for spectroscopy, biochemical sensors, microscopy and (photo-)catalysis [1]. They show high tunability of spatial and spectral properties, boosting energy conversion efficiency with high local fields or improving absorption through directional scattering. Surface roughness poses a major challenge to theoretical methods aiming at accurately describing realistic experimental situations [2].

We study the structure-performance relationship in nanostructured architectures for nanophotonic applications from regular thin-walled TiO2 and TiN nanotubular pillars [3, 4] to self-organized dendritic structures made from gold [5]. The possible enhancement of reaction and transport rates due to a large surface area, strong electron confinement and short diffusion paths make them highly interesting for energy conversion platforms [6,7]. A further advantage for use in bionanotechnology, catalysis and related fields is the biocompatibility of the employed materials. Self-assembled nanostructures are favorable with view to their fabrication costs in a highly competitive industry.

The emergence and density of hot-spots is studied in dendritic structures and applied in SERS and photoreduction experiments on methylene blue (MB) [5]. Interestingly, a high hot-spot density does not guarantee a high catalytic yield but is more favorable in SERS measurements. For the catalytic experiments, a uniform distribution of similar hot-spots through more homogeneous feature sizes yields better results. We support experimental findings with numerical calculations using Boundary Element Method (BEM) for dendritic structures, Fourier Modal Method (FMM) for regular structures and also give an overview over our most recent contributions to modeling optical response from rough and irregular nanostructures [2-5]. Furthermore, we consider local temperature effects [8] and calculate electron transition rates from local dipole-dipole coupling as well as electron injection [9].

The author acknowledges funding by the Deutsche Forschungsgemeinschaft DFG through the IRTG 2675 META-ACTIVE, GEPRIS n° 437527638.

References

1. A. V. Akimov, A. J. Neukirch, and O. V. Prezhdo, Chem. Rev. 113(6), 4496–4565 (2013).
2. M. Dehghani and C. David, Nanomaterials 11(1), 113 (2021).
3. C. David, Materials (12), 1332 (2019).
4. I. H. Öner, C. David, C. J. Querebillo, I. M. Weidinger, and K. H. Ly, Sensors 22(2), 487 (2022).
5. Z. Fusco, A. Riaz, C. David, F. Beck, Adv. Mater. Interfaces 2202236 (2022).
6. J. Schneider, M. Matsuoka, M. Takeuchi, J. Zhang, Y. Horiuchi, M. Anpo, and D. W. Bahnemann, Chem. Rev. 114(19), 9919–9986 (2014).
7. K. Awazu, M. Fujimaki, C. Rockstuhl, J. Tominaga, H. Murakami, Y. Ohki, N. Yoshida, and T. Watanabe, J. Am. Chem. Soc. 130(5), 1676–1680 (2008).
8. J. Jahng, B. Kim, and E. S. Lee, Physical Review B 106, 155424 (2022).
9. J. B. Khurgin, A. Petrov, M. Eich, and A. V. Uskov, ACS Photonics 8(7), 2041–2049, (2021).

META 2023, PARIS - FRANCE, JULY 18 – 21, 2023

Smart Sensing and Spectroscopy using Thermal Emission

Yuzhe Xiao[1]

[1]Department of Physics, The University of North Texas, USA
[*]corresponding author: yuzhe.xiao@unt.edu

Abstract:

Thermal emission is a ubiquitous phenomenon where hot objects radiate energy as electromagnetic waves. I will first introduce a new metrology method—depth thermography—that can measure the temperature distributions of an object at different depths, based on the light thermally emitted from that object. Then, I will introduce a new spectroscopic technique—Planck spectroscopy—that measures the spectral emissivity of an object using only a temperature-controlled stage and a detector, without any wavelength-selective components such as prisms, gratings, or interferometers.

Nanophotonic scintillators for enhanced x-ray detection and imaging

Charles Roques-Carmes[1,2]

[1]Research Laboratory of Electronics, Massachusetts Institute of Technology, Cambridge MA 02139, USA
[2]Ginzton Laboratory, Stanford University, Stanford University, Stanford CA 94305, USA
[*]corresponding author: chrc@mit.edu

Abstract: Scintillators are materials that emit light in the form of spontaneous emission when pumped by high-energy particles, such as x-rays. We demonstrate that several concepts in nanophotonics, such as out-coupling and Purcell enhancements, can enhance and shape scintillation light. We then discuss possible applications of such "nanophotonic scintillators" (consisting in the integration of scintillator materials into nanophotonic structures) in enhancing the resolution and detection efficiency of x-ray imaging systems.

Bombardment of materials by high-energy particles (e.g., electrons, x- and γ-ray photons) often leads to light emission, known generally as scintillation. Scintillation is ubiquitous and enjoys widespread applications in many areas such as medical imaging, x-ray non-destructive inspection, night vision, electron microscopy, and high-energy particle detectors. A large body of research focuses on finding new materials optimized for brighter, faster, and more controlled scintillation. Recent results have proposed scintillation enhancement relying on photonic effects, either by enhancing the rate of spontaneous emission [1, 2], or through improved light extraction [3].

Here, we develop a general framework based on integrating nanophotonic structures into scintillators to enhance their emission, which we coin "nanophotonic scintillators" [4]. To start, we develop a unified and *ab initio* theory of nanophotonic scintillators that accounts for the key aspects of scintillation: the energy loss by high-energy particles, as well as the light emission by non-equilibrium electrons in arbitrary nanostructured optical systems. This theoretical framework allows us, for the first time, to experimentally demonstrate nearly an order-of-magnitude enhancement of scintillation in x-ray-induced scintillation, through improved light extraction from bulk scintillators. Our theory also allows the discovery of structures that could eventually achieve orders-of-magnitude scintillation enhancement and shaping of scintillation's optical properties (e.g. angular, spectral, polarization), in addition to the end-to-end imaging optimization of nanophotonic scintillators integrated into imaging systems [5]. We show that inverse-designed nanophotonic scintillators could enable the development of a new class of brighter, faster, and higher-resolution scintillators with tailored and optimized imaging performances.

References

1. Kurman et al., "Kurman, Yaniv, et al. "Photonic-crystal scintillators: Molding the flow of light to enhance X-ray and γ-ray detection." *Phys. Rev. Lett.* 125.4 (2020): 040801.
2. Kurman et al, "Purcell-enhanced x-ray scintillation", preprint available at arXiv:2302.01300 (2023)
3. Knapitsch et al., "Review on photonic crystal coatings for scintillators," *Int. J. Mod. Phys. A*, 29, 30 (2015)
4. Roques-Carmes, et al., "A framework for scintillation in nanophotonics", *Science*, 375.6583 (2022) : eabm9293
5. Shultzman et al., "Optimization of nanophotonic scintillators for imaging", *Adv. Opt. Mater.*, in press (2023)

A multimode quasi-normal mode framework for nonlinear harmonic generation with 2D materials

Thomas Christopoulos[1,2*], Emmanouil E. Kriezis[1], and Odysseas Tsilipakos[2*]
[1]School of Electrical and Computer Engineering, Aristotle University of Thessaloniki, GR-54124 Thessaloniki, Greece
[2]Theoretical and Physical Chemistry Institute, National Hellenic Research Foundation, GR-11635 Athens, Greece
[*]corresponding authors: cthomasa@ece.auth.gr, otsilipakos@eie.gr

Abstract: In this work, we present a multimode framework for linear and nonlinear modal calculations in non-Hermitian systems comprising 2D materials. The framework is based on the ability to appropriately expand both the linear and nonlinear responses of a resonant cavity in terms of the supported quasi-normal modes. Through numerical simulations, we find that the proposed framework is efficient and extremely accurate, even when complex contemporary photonic systems incorporating 2D materials are involved.

Non-Hermitian cavities, i.e., resonant systems with radiation leakage and resistive loss, support quasi-normal modes (QNMs), whose properties are not as well-defined as those of normal modes supported by Hermitian systems. QNMs exhibit interesting but cumbersome properties, with the most notable being the unphysical spatial exponential divergence of the field components outside the resonant cavity, complicating the process of their normalization. Lately, the study of QNMs has produced very interesting results by providing the appropriate normalization needed to regularize this mode divergence [1-2]. In effect, this important fact led to the development of elegant techniques to reconstruct the full linear spectrum of a system using the QNMs it supports [3]. However, the study of expansions that additionally include nonlinear interactions received much less attention [4-5]. Additionally, although the methods presented thus far cover a wide range of material configurations (dielectric and plasmonic scatterers and metasurfaces, photonic crystals, etc.), none has focused on the contemporary family of 2D materials (e.g., graphene, transition metal dichalcogenides, black phosphorus, etc.) which, among others, possess unique nonlinear properties. In this work, we present such a complete methodology, beginning from the careful introduction of 2D materials in the linear QNMs framework through their natural representation as infinitesimally thin layers and subsequently progressing to additionally include their nonlinear properties through the demonstration of the third harmonic generation effect [5]. We also rigorously take into account material dispersion by expanding the established finite-element method using appropriate surface auxiliary fields [3,5]. Thus, we successfully provide with the proper normalization that correctly captures the full complexity of 2D materials including infinitesimal thickness, dispersion, loss, and anisotropy, applicable either in linear or nonlinear systems.

The developed nonlinear multimode framework is validated through two indicative resonant structures comprising graphene [Fig. 1(a)], i.e., the most prominent 2D material. Graphene supports tightly confined surface plasmons in the THz regime, whose tight confinement further enhances its inherent strong nonlinear response. The first example that is examined consists of a single graphene strip lying on a glass substrate. The second is a metasurface made of periodically arranged graphene strips on a metal-backed substrate to operate in reflection. The response (both linear and nonlinear) of the two systems is studied using the developed QNMs framework and validated through (nonlinear) full-wave simulations. The results of Fig. 1(b-e) show that excellent agreement is achieved between the two methods both in the linear and nonlinear regimes and even under oblique incidence.

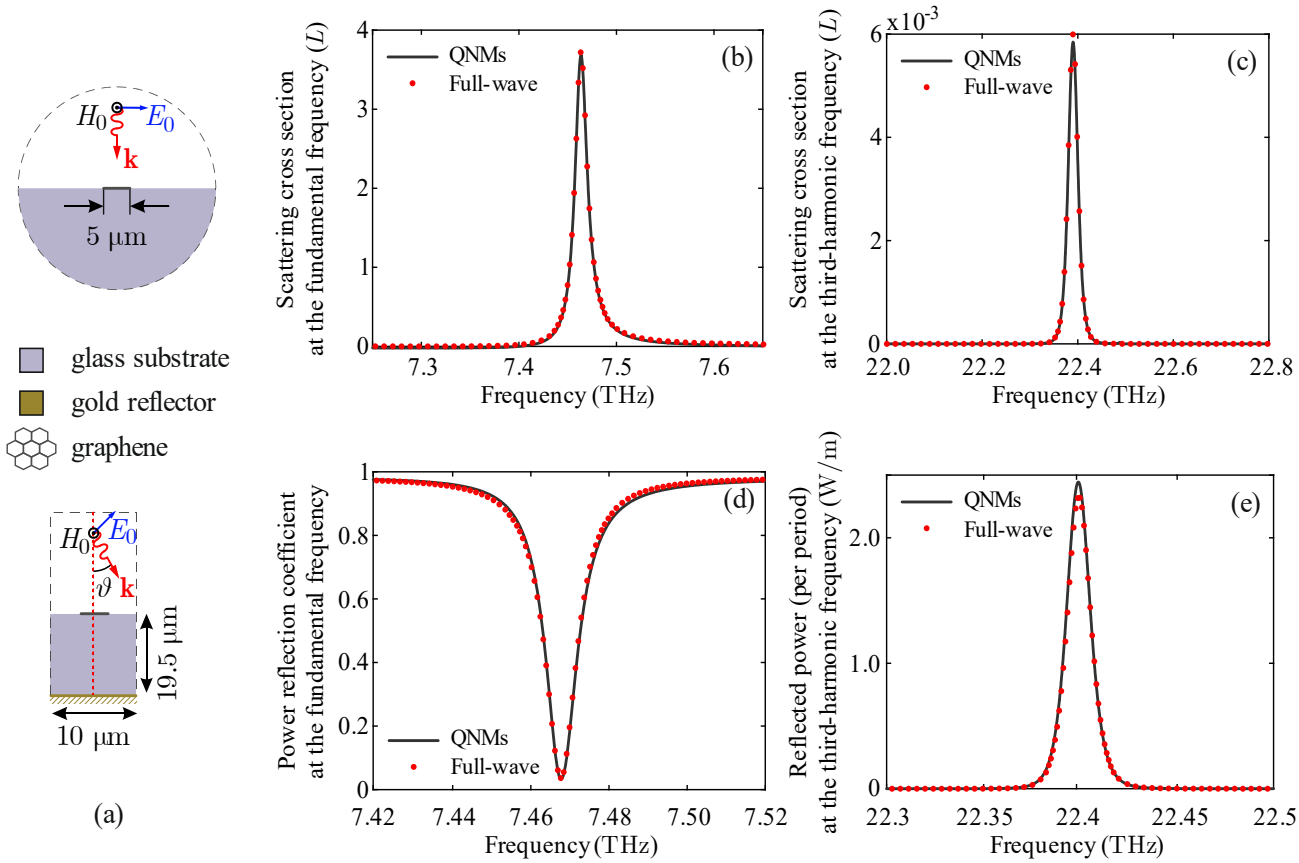


FIGURE 1. (a) The two considered structures comprising graphene on a glass substrate. (b) Linear and (c) nonlinear response (scattering cross-section) of a single graphene strip under normal incidence. (d) Linear and (e) nonlinear response (power reflection coefficient and reflected power, respectively) of a graphene metasurface under oblique incidence ($\theta=20^o$). QNM expansion (solid lines) and full-wave simulations (red point markers) show excellent agreement in both cases.

This work was supported by the Hellenic Foundation for Research and Innovation (H.F.R.I.) under the "2nd Call for H.F.R.I. Research Projects to support Post-doctoral Researchers" (Project Number: 916, PHOTOSURF).

References

1. P. Lalanne, W. Yan, K. Vynck, C. Sauvan, and J. P. Hugonin, "Light interaction with photonic and plasmonic resonances," Laser Photonics Rev, Vol. 12, 1700113, 2018.
2. S. Both and T. Weiss, "Resonant states and their role in nanophotonics," Semicond Sci Tech, Vol. 37, 013002, 2022.
3. W. Yan, R. Faggiani, and P. Lalanne, "Rigorous modal analysis of plasmonic nanoresonators," Phys Rev B, Vol. 97, 205422, 2018.
4. C. Gigli, T. Wu, G. Marino, A. Borne, G. Leo, and P. Lalanne, "Quasinormal-mode non-Hermitian modeling and design in nonlinear nano-optics," ACS Photonics, Vol. 7, No. 5, 1197-1205, 2020.
5. T. Christopoulos, E. E. Kriezis, and O. Tsilipakos, "Multimode non-Hermitian framework for third harmonic generation in nonlinear photonic systems comprising two-dimensional materials," Phys Rev B, Vol. 107, 035413, 2023.

META 2023, PARIS - FRANCE, JULY 18 – 21, 2023

Green's tensor inverse design of light-matter interactions

R. Bennett[1]

[1]University of Glasgow, United Kingdom
[*]corresponding author: robert.bennett@glasgow.ac.uk

Abstract: Effective designs for photonic elements are usually found through a combination of intuition, symmetry and previous experience. By contrast, inverse design allows (locally) optimal geometries to be algorithmically discovered, often leading to much higher performance than structures designed by hand [1]. Originating in fluid dynamics, inverse design techniques are finding new applications across quantum optics and (nano-) photonics. In this talk I will outline a very general approach towards inverse design that concerns itself only with the electromagnetic dyadic Green's tensor of a particular scattering geometry [2]. Significant reductions of computational overhead are achieved by using the adjoint method, which is naturally built into the formalism through the symmetry properties of the Green's tensor. This approach allows inverse design methods to be applied to a whole family of surface-dependent light-matter interactions in a unified and consistent way, opening up new routes to optimisation of, for example, Casimir-Polder forces, resonant energy transfer [2], environment-induced coherence [3], helicity structures [4], dielectric cloaks [5] and non-local response of metasurfaces [6], among others.

The author acknowledges financial support from the UK Research and Innovation Council (UKRI) grants EP/W016486/1 and EP/V048449/1

References

1. Molesky, S., et al. "Inverse design in nanophotonics" Nat. Photonics **12**, 659-670, (2018).
2. Bennett, R., Buhmann, S. Y., "Inverse design of light–matter interactions in macroscopic QED" New J. Phys. **22**, 093014, (2020).
3. Bennett, R., "Inverse design of environment-induced coherence" Phys. Rev. A. **103**, 013706 (2021)
4. Kilianski, R., Bennett R., "Inverse design of arbitrary optical helicity patterns" arXiv optics 2211.15295 (2022)
5. A. Miguel-Torcal et al., "Inverse-designed dielectric cloaks for entanglement generation" Nanophotonics **11**(19): 4387–4395 (2022)
6. Capers, J.P. et al., "Designing the collective non-local responses of metasurfaces" Comms Phys Vol **4** 209 (2021)

META 2023, PARIS - FRANCE, JULY 18 – 21, 2023

Efficient computation of EM scattering from a dielectric cylinder partially covered with a graphene strip.

Y. Jeyar[1*], B. Guizal[1], and M. Antezza[1,2]

[1]Laboratoire Charles Coulomb (L2C), UMR 5221 CNRS-Université de Montpellier, F-34095 Montpellier, France

[2]Institut Universitaire de France, 1 rue Descartes, Paris Cedex 05 F-75231, France

[*]Corresponding author: Youssef.jeyar@umontpellier.fr

Abstract: We present a numerical approach for the solution of EM scattering from a dielectric cylinder partially covered with graphene. It is based on a classical Fourier-Bessel expansion of the fields inside and outside the cylinder to which we apply the ad-hoc boundary conditions in the presence of graphene. Due to the singular nature of the electric field at the ends of the graphene sheet, we introduce auxiliary boundary conditions to better take this reality into ac- count. The result is a very simple and very efficient method allowing the study of diffraction from such structures.

1 Introduction

Diffraction of electromagnetic waves from circular cylinders is rather a simple and classical problem [1]. In this situation, the incoming and outgoing fields can be represented in terms of circular waves expressed through Fourier-Bessel expansions. All the channels are independent from each other because of the circular symmetry and homogeneity of the cylinder. However, when this cylinder is partially covered with a sheet of graphene, this breaks the symmetry and homogeneity at the level of the surface and then all the channels can be mixed up thus leading to interesting physical phenomena. Under this situation, the boundary conditions lead to an algebraic system linking the outgoing amplitudes of the fields to the incoming ones. This system may be singular in the case of transverse magnetic polarization (TM: the magnetic field is parallel to the direction of invariance of the cylinder). This is due to the singularities of the tangential component of the electric field at the ends of the graphene sheet. One way of solving this issue is to use a supplementary expression of this field right at the level of the circumference of the cylinder in terms of Local Basis Functions (LBFs) able to reproduce the singularities [2].

2 Results

Figure 1 shows the geometry of the diffraction problem where a plane wave (wavelength λ) is impinging on a circular cylinder (radius R and dielectric permittivity ε_r) partially covered by a graphene (conductivity σ). As already said in the introduction, this problem of diffraction can be solved through the expansion of the fields in terms of Fourier- Bessel modes. This will be called the classical method. It turns out that under TM polarization there are some singularities of the tangential electric field that cause slow convergence of the computations. This problem is handled through the introduction of LBFs that possess the same singularities of the field.

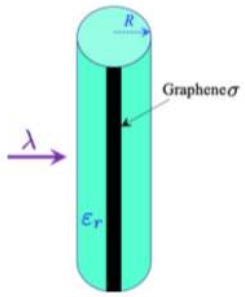


Figure 1. Sketch of the diffraction problem under consideration: an electromagnetic plane wave hits the covered dielectric cylinder under classical diffraction.

Figure 2 shows the scattering efficiency versus the wavelength, obtained with the classical method and with the LBFs method. It can be clearly seen that the LBFs method converges rapidly as compared to the classical one. For the LBFs method the number of modes necessary to achieve convergence (stabilization of the fourth digit for example) is very low about: 40 modes contrary to the classical method where even more than 150 modes do not give the same results.

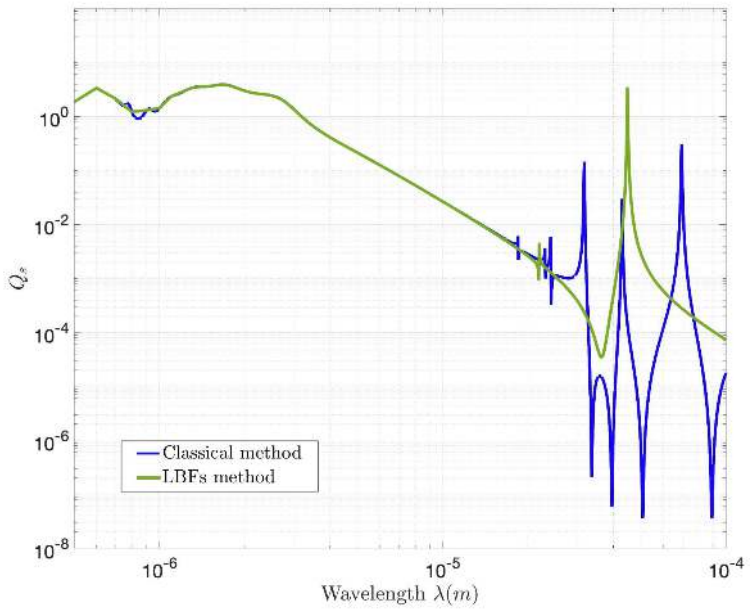


Figure 2. Scattering efficiency *Qs* of cylinder of radius $R = 0.5\mu m$ and permittivity $\varepsilon_r = 3.9$ immersed in air, a graphene sheet of chemical potential $\mu = 0.5$ eV and $T = 300$ K

References

1. Kong, J.A., Electromagnetic Wave Theory (Wiley,1986) 782
2. Hwang, Ruey-Bing, Scientific Reports 10, 12855 1 (2020)

META 2023, PARIS - FRANCE, JULY 18 – 21, 2023

Improving Photonic Crystal Waveguide Simulation Efficiency: A Journey from 3D approaches to Deep Neural Networks

C. F. Schwahn[1], S. A. Schulz[1]

[1]SUPA, School of Physics and Astronomy, University of St Andrews, St Andrews, UK
*corresponding author: sas35@st-andrews.ac.uk

Abstract: In this paper, we summarize the historical and recent contributions of our group to the development of accurate and efficient simulation and design methods for Photonic crystal waveguides. This will look at the use of ensemble average properties for the calculation of propagation loss, 2-dimensional approximations and finally optimization and machine learning techniques. Here we demonstrate the same accuracy as full 3D simulations with a 7-orders of magnitude reduction in the calculation time, to the sub-ms per design range.

The properties of slow light Photonic crystal (PhC) waveguides are fully controlled by their design parameters, such as the lattice period, hole radius or shifts of individual rows of holes [1]. Thus designing such devices seems like a straightforward task – all that needs to be done is to solve Maxwell's equations using appropriate boundary conditions and the appropriate refractive index distribution. However, this picture belittles the complexity of this task.

To accurately predict the properties we would need to solve Maxwell's equations with a deep-subwavelength resolution – typically 10 or more grid points per wavelength – in 3D, resulting in simulations that take multiple CPI/GPU hours per device. Combined with the fact that we need to optimize over a large design space (e.g. figure 1 indicates a 7-dimensional design space) the device design quickly becomes prohibitively complex, severely limiting the use of PhC waveguides.

During this talk, I will focus on both historical and recent developments in the field of PhC waveguide simulations, resulting in highly accurate and efficient simulation methods. We will consider the 7-dimensional design space shown in figure 1. It consists of the hole radius of the background lattice (r_0), row-wise variations of the hole radius of the first three rows (r_1-r_3) and row-wise shifts of the first three rows of holes perpendicular to the waveguide (s_1-s_3).

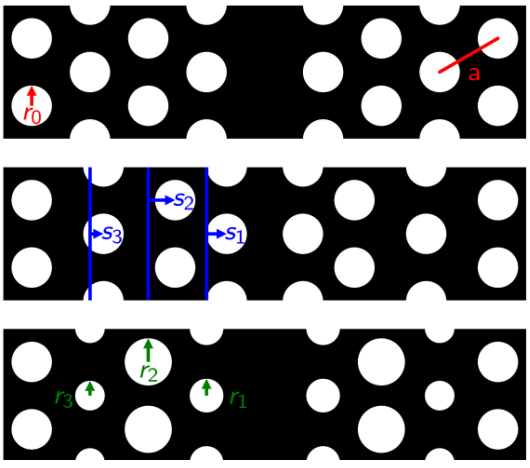


Figure 1: Schematic of a Photonic crystal waveguide with 7 design parameters (r_0, r_1, r_2,

The historical overview will begin with the traditional approach of solving Maxwell's equations or simplified wave equations in 3D [2], before moving on to 2-d approximation methods, that reduce the design space and hence grid volume [3]. These methods have enabled optimization methods [4] and eventually machine learning approaches [5,6]. These latest developments allow us to simulate the optical properties of PhC waveguides not in CPU hours but on a sub-ms timescale. This paves the way

towards the rapid and fast exploration of the design space. Our Neural Network based approach has an absolute mean error of only 0.3% compared to the MIT Photonics Band solver (better than the accuracy achieved with modern fabrication methods), with a 7-orders of magnitude reduction in the simulation time.

Acknowledgements
S. A. Schulz acknowledges funding from EPSRC through grant [EP/V029975/1].

References

1. Schulz, S. A. and L. O'Faolain and D. M. Beggs and T. P. White and A. Melloni and T. F. Krauss "Dispersion engineered slow light in photonic crystals: a comparison" *Journal of Optics* **12**, 104004 (2015).
2. Johnson, S.G. and J. D. Joannopoulos "Block-iterative frequency-domain methods for Maxwell's equations in a planewave basis " *Optics Express* **8**, 173 (2001).
3. Schulz, S. A. amd A. H. Park and J. Upham and R. W. Boyd "Beyond the effective index method: improved accuracy for 2D simulations of photonic crystal waveguides " *Journal of Optics* **17**, 075006 (2015).
4. Billings, S and S. A. Schulz and J. Upham and R. W. Boyd "Application-tailored optimisation of photonic crystal waveguides " *Journal of Optics* **18**, 115005 (2016).
5. Hirotami, K. and R. Shiratori and T. Baba "Si photonic crystal slow-light waveguides optimized through informatics technology" *Optics Letters* **46**, 4422 (2021).
6. C.F. Schwahn & S. A. Schulz "Accurate and Efficient Prediction of Photonic Crystal Waveguide Bandstructures using Neural Networks" *under review.*

META 2023, PARIS - FRANCE, JULY 18 – 21, 2023

Modeling and Applications of Nonlocal Asymmetric Metasurfaces

K. Achouri[1*], S. Boroviks[1], and O. JF Martin[1]

[1]Swiss Federal Institute of Technology in Lausanne (EPFL), Switzerland
[*]corresponding author: karim.achouri@epfl.ch

Abstract: The concept of nonlocal metasurfaces has recently emerged to overcome the limitations of local metasurfaces in terms of efficiency and diversify their functionalities. To better exploit the potential of nonlocal metasurfaces, we have developed a general modeling framework that includes nonlocal interactions. Based on this model, we show the connection between nonlocality and the metasurface spatial symmetries. Finally, we provide several examples highlighting the advantages and related applications of nonlocal metasurfaces.

Nonlocality in electromagnetism, often alternatively called spatial dispersion, refers to an extended distance between an excitation and the response that it induces in a nonlocal medium. In practice, most conventional optical or electromagnetic media are spatially local due to the simple nature of their structure. However, this is generally not the case of metamaterials and metasurfaces that often exhibit non-negligible nonlocal interactions between their complex scattering particles [1,8].

Historically, these nonlocal interactions have often been considered undesirable as they were considered detrimental in many applications due their strong dependence on the direction of light propagation. However, it now appears that nonlocality presents a major advantage which is that, in contrast to temporal dispersion, it is not restricted by causality. While temporal dispersion must obey the Kramers-Kronig relations implying that a change in the response of a medium leads to an increase of its loss, nonlocal effects may be leveraged without inducing additional loss and thus do not impair the efficiency of the system. This suggests that highly efficient operations may be performed with nonlocal metasurfaces.

In this work, we present a general approach for modeling nonlocal metasurfaces. This modeling approach is based on the concept of the generalized sheet transition conditions that have been extensively used to design dipolar metasurfaces [2]. We will show how this model may be extended to include multipolar contributions, which includes nonlocal effects. We will also discuss how nonlocal interactions are intimately related to the spatial symmetries of the lattice and scattering particles of metamaterial structures [3].

Finally, we will present several examples of metamaterials where nonlocal interactions play an essential role. A selection of such examples is illustrated in Fig. 1. The case of perfect (i.e., fully efficient) refraction and reflection is depicted in Fig. 1a, where such operations respectively require bianisotropy (a type of nonlocal response) or nonlocal energy transport [2,4]. In Fig. 1b, we show that an asymmetric plasmonic metasurface may be used to generate asymmetric second-harmonic generation [5]. This unconventional effect stems from nonlocal interactions in both linear and nonlinear regimes. The last example shown in Fig. 1c shows that a longitudinal optical torque may be induced by illuminating a helical-shaped nanoparticle with a normally incident plane wave [6,7]. In this case, note that the particle is *not* geometrically chiral, however it nonetheless exhibits a pseudochiral response that originates from multipolar nonlocal effects [3,6,7].

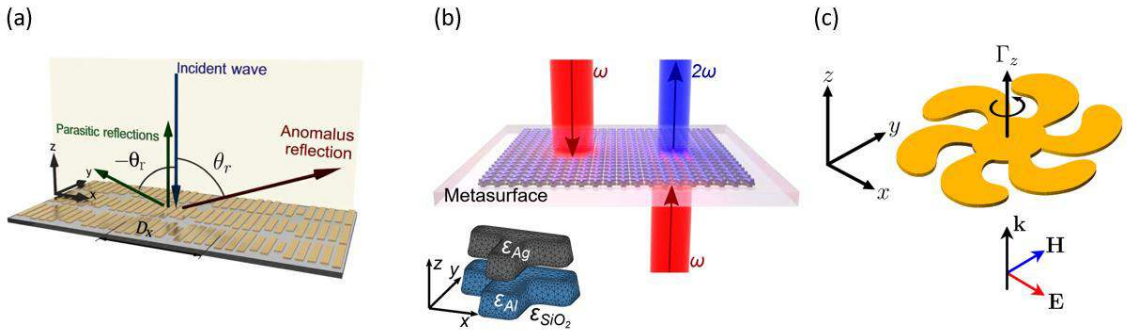


Figure 1. Examples of applications of nonlocal metasurfaces. (a) Perfect refraction and reflection [4]. (b) Asymmetric second-harmonic generation [5]. (c) Optical torque induced by multipolar pseudochirality [6,7].

Acknowledgement

We gratefully acknowledge funding from the Swiss National Science Foundation (project PZ00P2_193221).

References

1. C. Simovski. Composite Media with Weak Spatial Dispersion. Jenny Stanford Publishing, 2018.
2. K. Achouri, and C. Caloz. Electromagnetic Metasurfaces: Theory and Applications. John Wiley & Sons, 2021.
3. K. Achouri, V. Tiukuvaara, and O. JF Martin. "Spatial Symmetries in Multipolar Metasurfaces: From Asymmetric Angular Transmittance to Multipolar Extrinsic Chirality." arXiv preprint arXiv:2208.12504 (2022).
4. A. Díaz-Rubio, V. S. Asadchy, A. Elsakka, and S. A. Tretyakov. "From the generalized reflection law to the realization of perfect anomalous reflectors." Science advances 3.8 (2017): e1602714.
5. Boroviks, S., Kiselev, A., Achouri, K., & Martin, O. J. (2023). Demonstration of a plasmonic nonlinear pseudo-diode. arXiv preprint arXiv:2302.03409.
6. M. Chung, K. Achouri, and O. JF Martin. "Optically driven nano-motors designed by machine learning." Optical Trapping and Optical Micromanipulation XIX. SPIE, 2022.
7. M. Riccardi, A. Kiselev, K. Achouri, and O. JF Martin. "Multipolar expansions for scattering and optical force calculations beyond the long wavelength approximation." Physical Review B 106.11 (2022): 115428.
8. Overvig, A., Alù, A., “Diffractive Nonlocal Metasurfaces”. Laser & Photonics Reviews 2022, 16, 2100633.

An overview of spatial spectral methods with complex-plane deformations for the representation of waves in homogeneous and layered media without absorbing boundary conditions

R. J. Dilz[1*] **and M. C. van Beurden**[1]

[1]Eindhoven University of Technology, The Netherlands
[*]corresponding author: r.dilz@tue.nl

Abstract: The prevention of reflections from the edge of the computational domain is a challenge in computational electromagnetics. Although ways exist to absorb/negate such reflections, we recently proposed an entirely different strategy. Based on a representation in the spectral domain, we analytically represent waves on the entirety of space, but with accuracy focused only on a certain region. Therefore, we can employ formulations without worrying about boundary conditions. We show several examples of this technique, including simulations in layered media.

In the past, several methods have been developed for the computation of electromagnetic fields that employ a Fourier transform of the spatial dimension(s). An important reason for employing the spectral domain is that the Green function for electromagnetic scattering can be expressed easily in it. Especially for layered media this is true, since an analytical expression for the Green function is only available in the spectral domain, and a spatial-domain Green function can only be computed through tedious Sommerfeld integrals [1]. Additionally, spatial derivatives are more easily represented in the spectral domain.

Examples of computational methods include the Fourier Modal Method [2], which uses (truncated) analytic expressions within layers and then couples these layers with each other by employing the layer-boundary conditions. Another example is the spectral domain volume integral equation in [3]. Here, analytical expressions for reflection and transmission coefficients are employed to incorporate the boundary conditions. However, both these methods have in common that they are usually employed for periodically repeating structures.

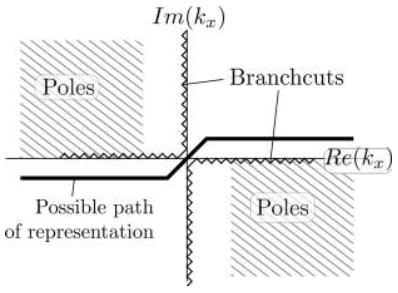


Figure 1: Typical locations of poles and branch cuts for layered media

One reason that spectral-domain methods are usually employed for periodically repeating scatterers is that employing a simple Fourier-series discretization then leads to simple and fast algorithms. However, the generalization to aperiodic scatterers is challenging. Absorbing boundaries can help to mitigate waves that travel over the unit-cell-boundary [4], but these can lead to numerical instabilities. Fully aperiodic discretization methods that are compatible with Fourier transforms exist, e.g. Gabor frames [5] and Hermite-interpolations [6]. Still the behavior of both Green function and fields are difficult, since radiation/guided waves can extend to infinity in the spatial domain. In the spectral domain, this is represented by branch cuts and poles.

In Figure 1 we indicate the location of such poles and branch cuts for a typical reflection coefficient of a layered-medium stack – a function that is typically required to be represented in a computational method for layered media. As long as the full stack is made of passive materials, the poles and branch points will always be a certain range away from the origin, and will not exceed a range from the origin on the real k-axis. To efficiently discretize this singular behavior is hard, especially when using discretizations that are meant for continuous functions, such as is the case with discretizations that work well in both spatial and spectral domain.

We solve this issue by representing electromagnetic fields and Green functions on a deformed contour in the complex plane [6,7,9]. This contour then circumvents the poles and branch cuts, so that all desired quantities can be properly discretized. However, the contour does represent fields in the numerically unstable regions of the complex plane that represent gain-media. In [8, Chapter 9] we have shown that a stable representation can always be reached, when the deformation contour is chosen smartly, depending on the size of the simulation domain. Several formulations for complex-plane path deformations have been developed.

We will show the current status of our ongoing research and show some examples of cases relevant to the meta-materials community.

References

1. Hochman, A. & Leviatan, Y. "A Numerical Methodology for Efficient Evaluation of 2D Sommerfield Integral in the Dielectric Half-Space Problem," IEEE-TAP, Vol. 58, No. 2, 413–431, 2010.
2. M. G. Moharam and T. K. Gaylord, "Rigorous coupled-wave analysis of planar-grating diffraction," J. Opt. Soc. Am A., Vol. 71, 811–818, 1981.
3. van Beurden, M. C., "Fast convergence with spectral volume integral Equation for crossed block-shaped gratings with improved material interface conditions," J. Opt. Soc. Am A., Vol. 28, 2269–2278, 2011.
4. Pisarenco, M.; Maubach, J.; Setija, I. & Mattheij, R., "Aperiodic Fourier modal method in contrast-field formulation for simulation of scattering from finite structures," J. Opt. Soc. Am A., Vol. 27, 2423–2431, 2010.
5. Feichtinger, H. G. & Strohmer, T., "Gabor Analysis and Algorithms: Theory and Applications," *Birkhauser*, 1998.
6. Dilz, R. J. & van Beurden, M. C., "A Hermite-interpolation discretization for the spatial spectral integral equation method in multilayered media," PIER B, No. 80, 37–57, 2018.
7. Dilz, R. J. & van Beurden, M. C., "An efficient complex spectral path formulation for simulating the 2D TE scattering Problem in a layered medium using Gabor frames," PIER B, No. 80, 37–57, 2018.
8. Dilz, R. J., "A spatial spectral integral equation solver for electromagnetic scattering in dielectric layered media," PhD Thesis, Eindhoven University of Technology, 2017.
9. Michalski, K. A. & Mosig, J. R., "Efficient computation of Sommerfeld integral tails – methods and algorithms ," J. Electromagn. Waves Appl., Vol. 30, No. 3, 281-317, 2016.

META 2023, PARIS - FRANCE, JULY 18 – 21, 2023

Effect of top metallic contacts on radiation transfer and conversion efficiency for near-field thermophotovoltaics

K. Austry[1], **Y. Jeyar**[1], **M. Luo**[1], **B. Guizal**[1], **R. Messina**[2], **R. Vaillon**[3], **and M. Antezza**[1,4]

[1] Laboratoire Charles Coulomb (L2C), Université de Montpellier, CNRS, Montpellier 34095, France

[2] Université Paris-Saclay, Institut d'Optique Graduate School, CNRS, Laboratoire Charles Fabry, 91127, Palaiseau, France

[3] IES, Univ Montpellier, CNRS, Montpellier, France

[4] Institut Universitaire de France, 1 rue Descartes, F-75231 Paris Cedex 05, France

Abstract: Design of the metallic contact grid at the front side of thermophotovoltaic cells is critical. In particular, in the near field, the effect of this metallic grid can be tremendous both in terms of optical and electrical (resistive) losses. However, this effect has been theoretically either discarded or studied by means of extremely simplified models (like shadowing methods, consisting in just ignoring the fraction of the cell surface covered by metal).

Our study, based on a rigorous approach, investigates the real influence of the front metal contact grid. By modelling this grid by a metallic grating, we show that it can significantly affect the electrical power generated by the cell. Quantitative and qualitative analyses indicate behaviors which are quite different from those predicted by previous simplistic approaches.

By using the fluctuational electrodynamics framework, we first solve the full electromagnetic problem of a metallic grating in the presence of a cell and an emitter. Then we derive the emitted/absorbed radiation in the nanophotonic structure (including all multiple electromagnetic wave reflections involving the grating, the cell and the emitter) and electrical power production in the thermophotovoltaic cell.

Similarly to a previous work [1], we consider a doped-silicon emitter at 800 K which irradiates on an indium arsenide p-n junction cell kept at 300 K. A gold grating is set above the cell spaced at 100 nm from the emitter in order to observe the influence of the height of this body on the emitter-cell near-field heat transfer (see Fig. 1).

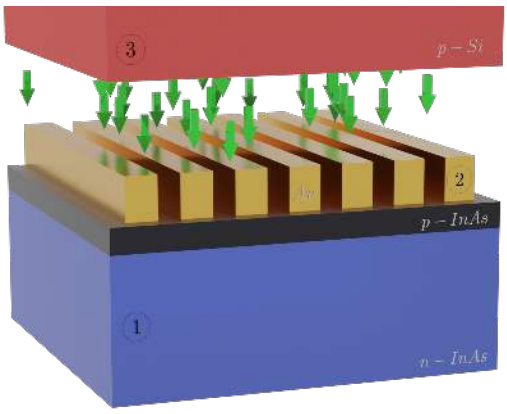


Figure 1: The configuration studied is a doped-silicon emitter which irradiates at 800 K on a TPV cell made of indium arsenide, kept at 300 K and covered by a gold grating.

A plane-wave decomposition is carried out for the incoming and outcoming waves of each body in a stationary regime. With the scattering matrix approach [2,3,4], we are able to compute the reflection and transmission coefficients in order to determine the net heat flux absorbed and the electrical power generated by the cell, in this three-body configuration.

Near-field regime allows evanescent waves to contribute, and this happens here in the presence of a grating which opens new heat transfer channels. To tackle the grating periodicity, we use a Fourier modal method (FMM) to evaluate the reflection and transmission coefficients. We need high-order Fourier modes in order to face the abrupt transition of the dielectric permittivity at the metallic-vacuum interfaces within the grating. To reach a faster convergence when calculating the grating reflection and transmission coefficients, we combine the FMM with the adaptative spatial resolution (ASR) [4]. By performing a change of coordinates, this method allows to densify the sampling around the critical region of the grating and get convergence much more rapidly. This is a crucial ingredient in order to have a fast and reliable converging code that must perform a three-dimensional integral over the mode quantum numbers, necessitating evaluation of millions of reflection and transmission matrices.

We first show that the presence of a grating increases the generated electrical power with respect to a cell without grating, and this for grating heights smaller than 1 micron. We also show that the previous over-simplified theoretical method considering a simple shadowing effect underestimates the generated electrical power by around one order of magnitude.

Concerning the TPV conversion efficiency, it is defined as the ratio of the electrical power generated by the cell to the net radiative power absorbed by the cell and the grating. We find that the presence of the metallic grating can reduce the TPV efficiency in a considerable way.

Our results suggest that rigourous approaches considering properly the impact of a metallic contact grid at the front of cells in near-field thermophotovoltaic devices are absolutely required in order to make accurate predictions of both electrical power and conversion efficiency.

References

1. D. Milovich, J. Villa, E. Antolin, A. Datas, A. Marti, R. Vaillon, and M. Francoeur, “Design of an indium arsenide cell for near-field thermophotovoltaic devices”, J. Photonics for Energy 10, 025503, 2020
2. R. Messina, and M. Antezza, “Scattering-matrix approach to Casimir-Lifshitz force and heat transfer out of thermal equilibrium between arbitrary bodies”, Phys. Rev. A 84, 042102, 2011
3. R. Messina, and M. Antezza, “Casimir-Lifshitz force out of thermal equilibrium and heat transfer between arbitrary bodies”, Europhys. Lett. 95, 61002, 2011
4. R. Messina, and M. Antezza, “Three-body radiative heat transfer and Casimir-Lifshitz force out of thermal equilibrium for arbitrary bodies”, Phys. Rev. A 89, 052104, 2014
5. R. Messina, A. Noto, B. Guizal, and M. Antezza, “Radiative heat transfer between metallic gratings using adaptative spatial resolution”, Phys. Rev. B 95, 125404, 2017

Acknowledgements

We thank Prof. M. Francoeur (McGill University) for participating to the discussions that led to the initiation of this research work. Financial support by CNRS-INSIS (project-team TREE) is acknowledged.

Inverse design of dispersive optical nanostructures and tunable metasurfaces

Antonio Calà Lesina[1*]

[1]Hannover Centre for Optical Technologies, Institute for Transport and Automation Technology (Faculty of Mechanical Engineering), and Cluster of Excellence PhoenixD, Leibniz University Hannover, 30167 Hannover, Germany
[*]corresponding author: antonio.calalesina@hot.uni-hannover.de

Abstract: Inverse design techniques hold the promise to uncover free-form nanophotonic structures in 3D with shapes beyond human intuition and novel optical functionalities. This talk focuses on our recent work on large-scale topology optimization of dispersive materials, anapole states in plasmonic nanostructures for transparent metasurfaces and metamaterials, and inverse design of tunable metasurfaces while accounting for the tuning mechanism.

Advances in computing capabilities and numerical methods, such as the finite-difference time-domain (FDTD) and finite-element methods (FEM), have recently empowered the design of nanophotonic devices [1]. By exploring large design spaces one can find solutions to complex optimization problems, but also discover new conceptual free-form designs. However, exploring large parameter spaces is computationally challenging. Techniques such as parameters sweep or stochastic optimization methods, e.g., genetic algorithms, are only suitable to handle problems with few design parameters, and therefore only useful when a good initial guess is known. Deep learning algorithms are emerging as a promising option for nanophotonics inverse design, but they require prohibitively large data sets for training. Topology optimization (TopOpt) is a robust inverse design technique which produces solutions far beyond human intuition and other optimization methods. Typically, TopOpt problems are solved using gradient-based optimization methods, where the gradient of the objective function with respect to the design variables is computed using efficient techniques such as the adjoint method, which only requires two simulations [2].

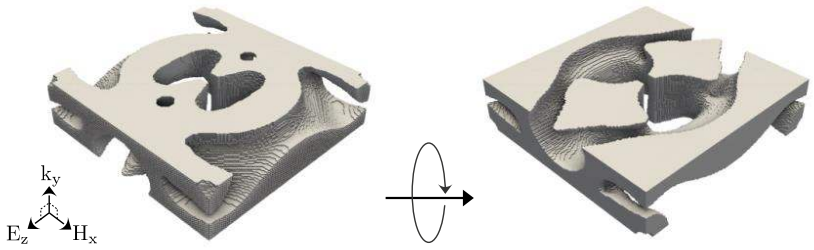


Figure 1: High-index dispersive dielectric nanostructures designed via topology optimization [credit: J. Gedeon].

My team develops and maintains an in-house parallel 3D FDTD Maxwell solver, which has been used for over a decade on supercomputers in Italy, Canada and Germany. The solver is parallelized with the message passing interface (MPI) and exhibits nearly linear scalability tested up to 16k cores [3]. Our software allows us to simulate large-scale devices that are intractable with commercial (Ansys Lumerical FDTD) and open-source (MEEP) software packages. Performing free-form optimization employing high-performance computing (HPC) has revolutionized many engineering disciplines, where new conceptual designs were obtained [4]. My team is focusing on TopOpt techniques combined with HPC to address the urgent need both in research and industry to make the numerical tools for the inverse design of large-scale free-form nanophotonic systems in 3D more scalable and efficient. In my talk, I will present our recent results on the inverse design of large-scale nanostructures and

metasurfaces in 3D, focusing on:

- Time-domain topology optimization of 3D metallic and dielectric dispersive nanoantennas with broadband optical response. A high-index dielectric nanostructure optimized in 3D for broadband field enhancement is presented in Fig. 1.
- Novel plasmonic nanostructures with anapole states for highly packed transparent metasurfaces and metamaterials, which may find application in nonlinear optics, lasing and sensing.
- Inverse design of tunable metasurfaces, where the tuning mechanism is taken into account during the optimization process.

References

[1] S. Molesky et al., Nature Photonics 12(11): 659–670, 2018. doi: 10.1038/s41566-018-0246-9

[2] E. Hassan et al., Optics Express 30(11): 19557, 2022. doi: 10.1364/OE.458080

[3] A. Calà Lesina et al., Optics Express 23(8): 10481, 2015. doi: 10.1364/OE.23.010481

[4] N. Aage et al., Nature 550(7674): 84–86, 2017. doi: 10.1038/nature23911

META 2023, PARIS - FRANCE, JULY 18 – 21, 2023

Energy Efficient Back-to-Back Neural Networks to Design Photonic Devices

Ergun Simsek

Department of Computer Science and Electrical Engineering,
University of Maryland Baltimore County, Baltimore, MD 21250, USA
simsek@umbc.edu

Abstract: By solving the drift-diffusion equations on nonuniform spatial and temporal grids, where the broadband modulations are defined with window functions, the computation time can be reduced by two orders of magnitude. This significant reduction enables the simulation of thousands of photodetectors within a few hours, allowing for the creation of a large database. This dataset is then used to train energy-efficient back-to-back neural networks that can successfully design photodetectors based on the desired phase noise, quantum efficiency, and bandwidth.

Photonic and optoelectronic devices, which are typically designed with numerical solvers, exhibit complex and nonlinear behavior. Machine learning algorithms can help design these devices more efficiently, but they require a large amount of data to learn and make accurate predictions. Therefore, a fast numerical solver is essential to create a large enough dataset.

In this work, we achieve this goal by developing a new drift-diffusion equation solver that is two orders of magnitude faster than traditional solvers, allowing us to study both group IV and III-V photodetectors. The significant reduction in simulation time was made possible by implementing non-uniform time-stepping [1] and utilizing window functions as broadband modulations [2].

In [3], we demonstrate two important findings regarding the prediction of photodetector performance metrics with neural networks. Firstly, traditional fully-connected neural networks can predict these metrics with a high level of accuracy (97%). Secondly, neural networks that are designed based on the physical principles and characteristics of the photodetectors can achieve even higher prediction accuracy (99%) while using fewer neurons and consuming less energy. The neural network architecture depicted in the left half of Fig. 1 uses multiple layers to pair the parameters of each photodetector layer, inform the decoder network about the interfaces separating the layers, mimic the current transport among neighboring layers, and teach the decoder about the specific order and bi-directional interactions between these paired inputs. Additional layers are then used to perform the regression of the device performance metrics.

In this work, we employ a similar strategy to design an energy-efficient back-to-back neural network. The encoder network is identical to the one used in our previous study [3], while the decoder network is almost a symmetric copy, with the exception that clustering is performed in the last neural network layer instead of regression. In this direction, each parameter is allowed to be one of the 201 pre-defined unique values. For instance, there are 201 unique thickness values that can be assigned to each photodetector layer, ranging from 10 nm to 2000 nm in increments of 10 nm. Similarly, there are 201 doping levels that can be assigned to these layers, which are logarithmically distributed between 10^{14} cm^{-3} and 10^{19} cm^{-3}.

The encoder network is asked to determine the parameters of the designs for phase noise levels ranging from –170 dBc/Hz to –180 dBc/Hz, quantum efficiency between 0.1 and 0.2, and bandwidth between 5 GHz and 20 GHz. These designs are subsequently analyzed using a solver for drift-diffusion equations. The resulting metrics are found to be very similar to the desired metrics.

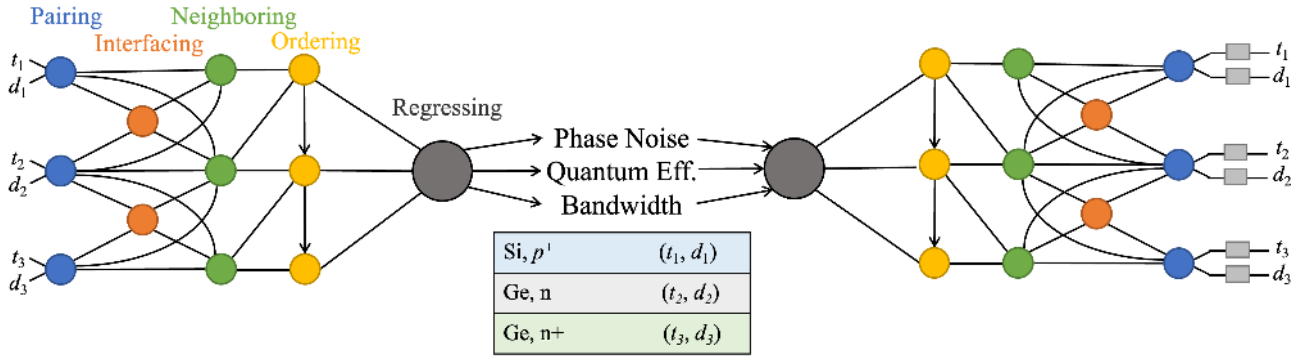


Figure 1 An illustration of energy-efficient the back-to-back neural network specifically designed (i) to learn from device parameters (layer thicknesses and doping levels) to predict performance metrics (phase noise, quantum efficiency, and bandwidth) and (ii) to design a photodetector for the desired set of device metrics. In the middle, a 3-layer Si-Ge photodetector is illustrated, where t_i and d_i are the layer thickness and doping levels for the i^{th} layer, where i = 1, 2, 3.

In order to comprehend the reasoning behind the proposed back-to-back neural network's successful device design capabilities, we conducted an investigation into the relationship between the inputs and outputs. At the conference, we will discuss this in detail and elaborate on our findings. Briefly, we were able to identify the influence of each design parameter on the device's performance metrics. Additionally, we noticed that phase noise, quantum efficiency, and bandwidth result in almost a flat surface in three dimensions, as illustrated in Figure 2. This provides a clear visualization of the trade-offs and limitations that are present.

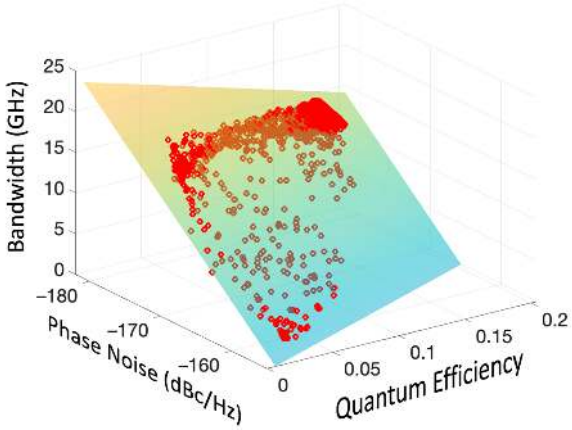


Figure 2 Phase noise, quantum efficiency, and bandwidth of the Si-Ge photodetectors form almost a flat surface.

References

1. Simsek, E., *et al.*, "Non-Uniform Time-Stepping for Fast Simulation of Photodetectors Under High-Peak-Power, Ultra-Short Optical Pulses," 22nd Int. Conf. on Num. Sim. of Optoelec. Dev., Sept. 12–16, 2022.
2. Simsek, E., *et al.*, "Efficient and Accurate Calculation of Photodetector RF Output Power," 2022 IEEE Photonics Conference (IPC), Vancouver, Canada, November 13 – 17, 2022.
3. Simsek, E., *et al.*, "Designing Photodetectors with Machine Learning," Advanced Photonics Conference, Novel Optical Materials and Applications, Maastricht, Netherlands, July 24–28, 2022.

META 2023, PARIS - FRANCE, JULY 18 – 21, 2023

The Fourier Modal Method simplified for crossed subwavelength gratings

B. Guizal[1*]

[1]Laboratoire Charles Coulomb (L2C), UMR 5221 CNRS- Université de Montpellier, F-34095 Montpellier, France
[*]corresponding author: brahim.guizal@umontpellier.fr@institution.edu

Abstract: We present a simplification of the Fourier Modal Method (FMM) for crossed gratings with subwavelength heights. We show that in this case it is possible to compute the scattering matrix of the structure without solving the eigenvalue problem which is the most expensive computational part of the FMM algorithm. This approach is very efficient and thus suitable for periodic metasurfaces.

The Fourier Modal Method[1] is one of the most versatile and efficient methods for modeling diffraction from gratings. This is why it is suitable for modeling metasurfaces based on crossed binary gratings. The problem with this approach is that for metallic structures, it is necessary to truncate the Fourier series representing the fields to a high order implying the use of large matrices (especially in the case of crossed gratings). This is very demanding from the computational point of view because the heart of the FMM is based on the solution of an eigenvalue problem. This later has a cost scaling with the third power of the dimension of the matrices in play. This can be a severe limitation and hinder the use of the FMM.

On the other hand, an interesting class of metasurfaces is made of gratings with subwavelength heights. In this special case, it is possible (via a Taylor series expansion of the phase propagation matrix) to simplify the FMM is such a way that it is no longer needed to solve any eigenvalue problem. This proves to be very efficient in reducing the computational cost.

After recalling the principle of the FMM and the details of the corresponding algorithm, I will show how the assumption of subwavelength height leads to a simplified scattering matrix where there is no need to solve any eigenvalue problem. Numerical examples will be presented to support this new algorithm.

References

1. L. Li, “New formulation of the Fourier Modal Method for crossed surface-relief gratings,” J. Opt. Soc. Am. A 14, 2758-2767, 1997.

META 2023, PARIS - FRANCE, JULY 18 – 21, 2023

Enhanced and Tunable Kerr effect on InSb/graphene hybrid magnetoplasmonic structure at Terahertz waves

M. Ben Rhouma[1*], K. Edee[2], and B. Guizal[3]

[1] ESYCOM lab, Univ Gustave Eiffel, CNRS UMR 9007, F-77454 Marne-la-Vallee, France
[2]Université Clermont Auvergne, Institut Pascal, BP 10448, F-63000 Clermont-Ferrand, France, CNRS, UMR 6602, France
[3]Laboratoire Charles Coulomb (L2C), UMR 5221 CNRS-Université de Montpellier, F-34095 Montpellier, France
[*]corresponding author: maha.ben-rhouma@univ-eiffel.fr

Abstract: In this work, we propose a novel hybrid magneto-plasmonic structure based on graphene and doped InSb to enhance the magneto-optical Kerr effect at terahertz frequencies. The structure is composed of a 1D periodic doped InSb inlayed between a metallic backgate and a dielectric/doped graphene sheet . By computing the optical response of this structure, we show an enhanced and large Kerr rotation in a wide range of THz frequencies compared to that induced by a single graphene sheet and/or a doped magnetized InSb .

Magneto-optical (MO) effects such as Faraday and Kerr effects are phenomena referring to changes in the polarisation state of light after interacting with a magnetic material and describe the interaction between optical and magnetic materials, which plays a fundamental role in the technological applications, such as optical isolators and magnetic sensors. The ability to enhance MO effects is then crucial for designing several devices. One way to achieve that is to combine plasmonics and magnetics to give rise to the magnetoplasmonics field which became, recently, an active topic of research.

Graphene magneto-plasmonics, the research area that combines magnetic and plasmonic properties of graphene, has attracted considerable interest in recent years, thanks to the unique and unusual properties of the surface magnetoplasmons supported by graphene [1]. These properties have been exploited to design many tunable plasmonic nonreciprocal devices in the terahertz regime which became attractive for its benefits in various applications such as medical imaging, biological studies, space exploration, communications and security. Doped InSb has been recently exploited in magneto-plasmonic devices for the terahertz range as a potential MO material and showed interesting magneto-plasmonic properties in this frequency range. In this work, we propose to combine the interesting properties of both materials in the THz regime by hybridizing their surface magnetoplasmons which give rise to a large and enhanced magneto-optical effect. The studied structure consists of a 1D periodic doped InSb inlayed between a metallic backgate and a dielectric/doped graphene sheet and an external static magnetic field can be applied. We compute the magneto-optical spectra with the Polynomial Modal Method (PMM) and study the magneto-optical Kerr effect on such structures. We show an enhanced and large Kerr rotation in a wide range of THz frequencies compared to that induced by a single graphene sheet and/or a doped magnetized InSb. It is found that the underlying mechanism is due to the hybrid plasmonic waveguide guided modes resulting from the strong coupling between the graphene surface magneto-plasmons (GSMP) and the surface magneto-plasmons across the InSb. Moreover, calculation results demonstrate that this large Kerr rotation can be tuned by optimizing the graphene properties and structure parameters such as the graphene fermi level and the applied magnetic field. Our findings may offer a promising way in the design of new THz magneto-optical devices.

References

1. Jun Guo, Xiaoyu Dai, Yuanjiang Xiang, and Dingyuan Tang , "Excitation of graphene magneto-plasmons in terahertz range and giant Kerr rotation", Journal of Applied Physics 125, 013102 (2019)

Ray Tracing Model for Non-Rotationally Symmetric Geodesic Lens Antennas with Full Beam Scanning Range in the Azimuthal Plane

S. Clendinning[1*], O. Zetterstrom[1], F. Mesa[2], and O. Quevedo-Teruel[1]

[1]Division of Electromagnetic Engineering and Fusion Science, KTH Royal Institute of Technology, Sweden
[2]Department of Applied Physics 1, Universidad de Sevilla, Spain
[*]corresponding author: saclendi@kth.se

Abstract: This presentation discusses a ray tracing model developed to determine the radiation pattern of geodesic lens antennas with non-rotationally symmetric footprints, where the geometry of the lens is defined using spline functions. The shape of this footprint and lens height profile can be modified by changing parameters in the defined functions. The code features a significant modification to work previously published by the authors to account for the non-rotationally symmetric design. The model runs significantly faster than commercially available software.

Lenses are very useful when integrated with antennas as they can be used to manipulate a wave front propagating through the lens to have attractive features. This manipulation is dependent on the shape of the lens, the refractive index profile or both. Graded refractive index (GRIN) lenses that are rotationally symmetric, for example the Luneburg lens, are of high interest as they are capable of beam scanning over a large range. The Luneburg lens is particularly of interest as it can generate a planar wave front from a point source [1-5]. This planar wave translates to a directive beam, which is a feature desirable for 5G/6G, satellite communications or radars. An inherent disadvantage of rotationally symmetric lenses is their size. This can be reduced through the introduction of a mirror plane, reducing the lens size by half but also reducing the scanning range by half [2], or by introducing a compression along a single axis [3]. A further reduction in profile size (that maintains scanning range) can be achieved by defining the profile footprint with a desired shape then applying a modified GRIN to this.

The GRIN medium can be implemented using a range of techniques such as with dielectrics [1] or a quasi-periodic structure such as metallic pins [4]. Another option is to use the geodesic form where the graded refractive index is replicated using parallel curved metallic plates [3, 5]. The plates follow a height profile that replicates the optical path length that the wavefront traverses and the Poynting vector direction at the lens aperture that is present in the GRIN equivalent. In a geodesic Luneburg-like lens, the height profile (z) is a function of the lens radius (ρ) and follows approximately the hyper-elliptic form,

$$z = h_0(1 - \rho^p)^{\frac{1}{q}} \qquad (1)$$

where h_0, p and q are design parameters which modify the profile shape [3]. There are no known closed-form expressions to determine the required height profile for non-rotationally symmetric cases analytically, and hence a convenient strategy must be used to optimize the height profile in these cases. Geodesic lenses can be modelled using commercial software, e.g. in CST Microwave Studio, however this is often computationally expensive. This is particularly problematic when optimizing the profile or exploring new arrangements (such as non-rotationally symmetric cases) where many simulation runs are required, thus motivating the development of

a ray tracing model. We will present an example of a non-rotationally symmetric case designed using a ray tracing model, which has been verified using full wave simulations. This code follows a similar technique to works previously reported by the authors, however a significant modification has been applied into how the lens is meshed and how the lens is fed.

The ray tracing model to be presented can be broken into 3 steps. Firstly, geometric optics is used to determine the trajectory of rays through the lens. The outline of the lens footprint is defined using a spline function. It is this step that differentiates this presentation from our previous work [3, 5]. The desired height profile is then applied and meshed using polar coordinates. As a result of Fermat's principle and the homogenous refractive index profile between the conductive plates, the shortest physical distance (the geodesic) is equivalent to the optical path taken by the rays. The python library *gdist* is used in conjunction with the mesh to determine the ray trajectory through the lens [3]. The second step assumes that power is conserved along each ray tube to approximate the amplitude distribution at the lens aperture (ray tube theory). As an adequate assumption of the E-field pattern of the source is imposed, an additional comparison of the ray separation close to the source and at the lens aperture provides the amplitude distribution at the aperture. The radiation of the lens aperture is then assumed to be equivalent to that of an array of radiating dipoles (one for each ray) with amplitudes following this amplitude distribution obtained from ray tube theory. The excitation phase of each dipole is given by the travelled optical path length for the corresponding ray. The number of dipoles/rays must be sufficient for the result to converge. The final step combines the contribution of each of these 'target-dipoles' to generate the far-field radiation pattern using Kirchhoff's diffraction formula.

The resulting ray tracing model is capable of calculating a far-field radiation pattern that fits well with those determined from full-wave simulation, however with a significantly shorter run-time. This allows for the exploration of structures that would be highly inconvenient to investigate using commercial software only.

This work was supported by the Office of Naval Research (ONR), under project N62909-20-1-2040. The views and conclusions contained herein are those of the authors only and should not be interpreted as representing those of ONR, the U.S. Navy or the U.S. Government. The contribution of F. Mesa has been supported by the Grant PID2020-116739GB-I00 funded by MCIN/AEI/10.13039/501100011033.

References

1. Di Falco, A., S. C. Kehr and U. Leonhardt "Luneburg lens in silicon photonics," Opt- Express, Vol. 19, 5156–5162, 2011.
2. Zetterstrom, O., N. J. G. Fonseca and O. Quevedo-Teruel, "Compact half-Luneburg lens antenna based on a glide-symmetric dielectric structure," IEEE AWPL, Vol. 21, No. 11, 2283–2287, 2022.
3. Liao Q, N. J. Fonseca, M. Camacho, A. Palomares-Caballero, F. Mesa and O. Quevedo-Teruel, "Ray-tracing model for generalized geodesic lens multiple beam antennas," IEEE TAP, in press, 2023.
4. Nie, B., H. Lu, T. Skaik, Y. Liu and Y. Wang, "A 3D-printed sub-terahertz metallic surface-wave Luneburg lens multibeam antenna," IEEE TTHz, in press, 2023.
5. Clendinning, S., F. Mesa and O. Quevedo-Teruel, "Ray-tracing model for elliptical half-geodesic lens antennas," ISAP 2022, Sydney, Australia, Oct. 31- Nov. 3, 2022.

META 2023, PARIS - FRANCE, JULY 18 – 21, 2023

Numerical methods for topological polaritonics

I. Septembre[1*], C. Leblanc[1], D. D. Solnyshkov[1], and G. Malpuech[1]

[1]Institut Pascal, Université Clermont Auvergne, CNRS, INP, France
[2]Author Affiliation, Country
[*]corresponding author: ismael.septembre@uca.fr

Abstract: Exciton-polaritons represent an exciting platform for the implementation of topological photonics. In the field of polaritonics, we use the paraxial approximation which allows mapping the Helmholtz equation to the Schrödinger equation. We use this to model microcavities with or without patterning and observe topological effects. We use this in polariton waveguides and demonstrate polariton Bose-Einstein condensation.

Exciton-polaritons are part-light, part-matter quasiparticles that can be described in the simplest case using the strongly-coupled oscillator model.

First, I will present our works on guided polaritons. We use FEM (Finite Element Method) calculations to compute the dispersion of photonic modes in a photonic crystal hosting unidirectional topological interface states. We show that a triangular photonic crystal slab has the same topology as a staggered honeycomb photonic crystal slab but with a giant advantage in the calculation time and experimental feasibility. The coupling of the photonic modes to the excitonic resonance can be made by two methods. The first one can be fully implemented in FEM calculations by taking into account the excitonic resonance in the dielectric permittivity tensor. The second one is more efficient and consists in calculating the photonic modes and then using the coupled oscillators model. We then show that FDTD (Finite-Difference Time-Domain) calculations can simulate the propagation of topological interface states between two photonic crystals with different symmetries, and we probe their unidirectionality [1].

Thanks to the large quantization wavevector in the growth direction, photonic modes in the microcavities can be described using the paraxial approximation. Interacting polaritons are thus described by the non-linear Schrödinger equation (also called the Gross-Pitaevskii equation), which is simpler to solve than Maxwell equations. This is a very powerful tool, which allows simulation of the spatial dynamics and even the relaxation of macroscopically populated states of exciton-polaritons and their Bose-Einstein condensation. Continuing our study of the topological structures, we use the photonic dispersion of a photonic crystal to demonstrate Bose-Einstein condensation of exciton-polaritons. The photonic mode is tuned to a bound state in the continuum leading to a dispersion of the radiative losses which are null at the bound state and grow quadratically with the wave vector. This loss profile facilitates reaching the condition for polariton Bose-Einstein condensation, as demonstrated using the non-linear Schrödinger equation taking into account the dispersion of real and imaginary parts of the photonic modes calculated by FEM and the strong coupling with the exciton.

In the last part, I will elaborate on our works on microcavities. We first describe the phenomenon of Andreev reflection on a polaritonic superfluid (analogue of optical parametric oscillations with a phase-conjugating mirror), using the non-linear Schrödinger equation [2,3]. We then show that it is possible to simulate numerically the Gross-Pitaevskii equation to observe parametric amplification of topological interface states [3]. We study numerically the possibility to form a polaritonic analogue of a multi-terminal Josephson junction using the Bogoliubov-de Gennes formalism derived from the non-linear Schrödinger equation [4]. We

show that it can lead to topological singularities (Weyl nodes) in arbitrary large, and we study both 3D and 4D parameter space that we can approximate by an effective Hamiltonian which facilitates the calculations.

This research was supported by the ANR Labex GaNext (ANR-11-LABX-0014), the ANR program "Investissements d'Avenir" through the IDEX-ISITE initiative 16-IDEX-0001 (CAP 20-25), the ANR project "NEWAVE" (ANR-21-CE24-0019) and the European Union's Horizon 2020 program, through a FET Open research and innovation action under the grant agreement No. 964770 (TopoLight).

References

1. I. Septembre, C. Leblanc, L. Hermet, H. S. Nguyen, X. Letartre, D. D. Solnyshkov, and G. Malpuech., "Design of a room-temperature topological exciton-polariton laser in a ZnO/TiO_2-photonic crystal slab," arXiv:2212.11563 (2022)
2. I. Septembre, S. V. Koniakhin, J. S. Meyer, D. D. Solnyshkov, and G. Malpuech., "Parametric amplification of topological interface states in synthetic Andreev bands," *Phys. Rev. B* **103**, 214504 (2021)
3. I. Septembre, D. D. Solnyshkov, and G. Malpuech., "Angular-dependent Andreev reflection on a polaritonic superfluid", arXiv:2212.04874 (2022)
4. I. Septembre, J. S. Meyer, D. D. Solnyshkov, and G. Malpuech., "Weyl singularities in polaritonic multi-terminal Josephson junctions", arXiv:2212.04874 (2022)

Analyzing Invisibility using a Nonlinear Eigenvalue Formulation

Zitao Mai and Ya Yan Lu*

Department of Mathematics, City University of Hong Kong, Hong Kong
*corresponding author, E-mail: mayylu@cityu.edu.hk

Abstract

For some incident plane waves, the waves reflected by a lossless periodic structure may be identical (in the far field) to the waves reflected by a perfectly electric (or magnetic) conductor. The periodic structure is thus invisible with respect to these incident waves. We propose an efficient method for computing such special incident waves, based on a nonlinear eigenvalue formalation and a contour-integral method.

1. Introduction

When a time-harmonic plane wave impinges upon a periodic structure (such as a diffraction grating), reflected and transmitted waves are generated. Mathematically, this leads to a boundary value problem (BVP), where the frequency and the wavevector of the incident wave are given. If the periodic structure is lossless and backed by a perfectly electric (or magnetic) conductor (PEC or PMC), there are only reflected waves. If there is only a single propagating diffraction order, the reflected wave in the far field is a plane wave with a fixed wavevector. In some cases, the (far field) reflected wave of the periodic structure is identical to the wave reflected by a PEC (or PMC) for the same incident wave. In that case, the periodic structure is *invisible* with respect to the incident wave. For a given periodic structure, it is of interest to find all such incident waves. The standard approach is to search the frequency and wavevector of the incident waves iteratively, but it is not efficient and unreliable.

For a linear operator A, the standard eigenvalue problem $Av = \lambda v$ is linear, if A does not depend on the eigenvalue λ. We formulate the invisibility problem for periodic structures as a nonlinear eigenvalue problem (NEV)

$$A(\omega)v = 0, \tag{1}$$

where A is an operator depending on the angular frequency ω and a wavenumber β, but we consider β as given and ω as the unknown eigenvalue, such that Eq. (1) has a nonzero solution v. When A depends on ω analytically, the NEV can be solved by the contour-integral method [1,2]. An important advantage of the contour-integral method is its robustness. All eigenvalues inside a contour (in the complex plane of ω) are determined, and no initial guesses are needed.

2. Theory

We consider a lossless 2D structure given by a dielectric function $\epsilon(x, y)$ that is invariant in z, periodic in x with period L, and bounded between $y = 0$ and $y = h$. The structure is on a PEC (or PMC) given in $y < 0$, and the medium above (i.e., $y > h$) is air. For a transverse electric (TE) incident wave

$$u^{(i)} = e^{i[\alpha_0 x - \beta_0 (y-h)]}, \quad y > h, \tag{2}$$

where α_0 is real, $\beta_0 = \sqrt{k_0^2 - \alpha_0^2}$ is positive, and $k_0 = \omega/c$ is the free space wavenumber, the wave reflected by the periodic structure can be written as

$$u^{(r)} = \sum_{m=-\infty}^{+\infty} R_m e^{i[\alpha_m x + \beta_m (y-h)]}, \quad y > h, \tag{3}$$

where $\alpha_m = \alpha_0 + 2m\pi/L$, $\beta_m = (k_0^2 - \alpha_m^2)^{1/2}$. If k_0 satisfies $k_0 < 2\pi/L - |\alpha_0|$, then for all $m \neq 0$, β_m is pure imaginary. In that case, $u^{(r)}$ is asymptotically a single plane wave $R_0 e^{i[\alpha_0 x + \beta_0 (y-h)]}$ as $y \to +\infty$. For the same incident wave, if there is a PEC (or PMC) at $y = h$, the reflected wave is exactly $R_* e^{i[\alpha_0 x + \beta_0 (y-h)]}$, where $R_* = -1$ or 1. If $R_0 = R_*$, then the periodic structure is invisible with respect to this incident wave.

The governing equation for the total field u is the Helmholtz equation $\partial_x^2 u + \partial_y^2 u + k_0^2 \epsilon(x,y) u = 0$. In the rectangular domain Ω given by $0 < x < L$ and $0 < y < h$, if u at $y = h$ is known, we can solve the Helmholtz equation with a PEC (or PMC) boundary condition at $y = 0$, and quasi-periodic conditions $u(L,y) = e^{i\alpha_0 L} u(0,y)$ and $\partial_x u(L,y) = e^{i\alpha_0 L} \partial_x u(0,y)$, and we can evaluate the y derivative of the solution at $y = h$. This leads to a linear operator Λ_0 satisfying

$$\left.\frac{\partial u}{\partial y}\right|_{y=h} = \Lambda_0 u|_{y=h}. \tag{4}$$

On the other hand, from Eq. (3), we can define an operator Λ_1, such that $\partial_y u^{(r)} = \Lambda_1 u^{(r)}$. More precisely, Λ_1 is a linear operator satisfying $\Lambda_1 e^{i\alpha_m x} = i\beta_m e^{i\alpha_m x}$ for all m. Moreover, since $u = u^{(i)} + u^{(r)}$ for $y > h$, and $u^{(i)}$ is given in Eq. (2), we have

$$\left.\frac{\partial u}{\partial y}\right|_{y=h} = \Lambda_1 u|_{y=h} + f, \tag{5}$$

where f is related to $u^{(i)}$. Combining Eqs. (4) and (5), we obtain

$$(\Lambda_0 - \Lambda_1) u|_{y=h} = f. \tag{6}$$

The above is a reformulation of the diffraction problem as a linear equation for total field u on the line segment given by $y = h$ and $0 < x < L$. To impose the invisibility condition $R_0 = R_*$, we notice that

$$u(x,h) = (1 + R_*) e^{i\alpha_0 x} + \sum_{m \neq 0} R_m e^{i\alpha_m x}. \tag{7}$$

Therefore, we have a linear functional B satisfying

$$B u|_{y=h} = \frac{1}{L} \int_0^L u(x,h) e^{-i\alpha_0 x} dx = 1 + R_*. \tag{8}$$

We can re-write Eqs. (5) and (8) as

$$\begin{bmatrix} \Lambda_0 - \Lambda_1 & -f \\ B & 0 \end{bmatrix} \begin{bmatrix} u|_{y=h} \\ 1 \end{bmatrix} = \begin{bmatrix} 0 \\ 0 \end{bmatrix}. \tag{9}$$

If the interval $(0, L)$ is discretized by N points, then $u|_{y=h} = u(x,h)$ becomes a column vector of length N, Λ_0 and Λ_1 are approximated by $N \times N$ matrices, B is approximated by a $1 \times N$ matrix, f is approximated by an $N \times 1$ matrix, and the right hand side in Eq. (9) is a column vector of length $N + 1$. This leads to the NEV Eq. (1), where A is an $(N+1) \times (N+1)$ matrix.

3. Conclusion

The NEV Eq. (1) can be solved by the contour-integral method which is robust and efficient. In a previous work [3], we have formulated diffraction anomalies, such as zero reflection, zero transmission and total absorption, as NEVs, and applied the contour-integral method. In this paper, we formulate an invisibility problem as an NEV and demonstrate the efficiency of the approach by numerical examples.

Acknowledgement

The work is partially supported by the Research Grants Council of Hong Kong Special Administrative Region, China (Grant No. CityU 11304619).

References

[1] J. Asakura, T. Sakurai, H. Tadano, T. Ikegami, and K. Kimura, A numerical method for nonlinear eigenvalue problems using contour integrals, *JSIAM Letters* 1: 52-55, 2009.

[2] W.-J. Beyn, An integral method for solving nonlinear eigenvalue problems, *Linear Algebra and its Applications* 436: 3839-3863, 2012.

[3] Z. Mai and Y. Y. Lu, Computing diffraction anomalies as nonlinear eigenvalue problems, *Physical Review E* 106: 035204, 2022.

META 2023, PARIS - FRANCE, JULY 18 – 21, 2023

Local-rational models for the adaptive frequency sampling of nanophotonic simulations

F. Ferranti*[1], D. Peumans[2]
[1]Department of Applied Physics and Photonics, Brussels Photonics group, Vrije Universiteit Brussel, Belgium
[2]Department of Fundamental Electricity and Instrumentation, Vrije Universiteit Brussel, Belgium
*corresponding author: francesco.ferranti@vub.be

Abstract: Electromagnetic (EM) simulation tools are necessary tools for the design of nanophotonic devices (or systems). The frequency-domain behavior of these devices can become quite complex, for example due to delay phenomena, and the presence of multiple (anti-)resonances. Performing EM computations with an EM solver can be a computationally complex task that is time-consuming and resource demanding. Complementary time- and frequency-domain EM solvers exist that provide insight and understanding into optical and EM phenomena.

In this work, we focus on frequency-domain EM solvers. The computation of the device's behavior at each frequency (wavelength) sample of interest can be computationally expensive. Undersampling potentially leads to an inaccurate description of the EM behavior, as valuable behavior characteristics such as (anti-)resonances and coupling effects can be partly identified or even missed. On the other hand, oversampling leads to a waste of computational resources.

Adaptive frequency sampling (AFS) algorithms can be used to prevent under/oversampling by automatically selecting a minimal set of frequencies, in such a way that each frequency sample contains as much valuable information as possible about a nanophotonic device's behavior [1]. This work investigates a novel AFS algorithm based on a local rational modeling (LRM) technique. LRM techniques [2] can greatly mitigate issues associated to the model order selection when rational models are used to drive the AFS process. By only focusing on a small sub-band around a specific center frequency, the local dynamic variations can be more easily modeled by a low-order model. Once all the local rational models are obtained after the first iteration, consecutive iterations only need to update the models around those frequencies that are affected by the inclusion of new frequency samples. LRM techniques are also suitable for parallel computing. Numerical results will be shown during the talk to validate this novel AFS technique.

Acknowledgements: This work was supported by the Methusalem and Hercules foundations, the OZR of the Vrije Universiteit Brussel (VUB), and the Strategic Research Program of the VUB (SRP-19).

References

[1] F. Ferranti, "Feature-based machine learning for the efficient design of nanophotonic structures", Photonics and Nanostructures - Fundamentals and Applications, Volume 52, 2022.

[2] D. Peumans, R. Pintelon, J. Lataire and G. Vandersteen, "Frequency Response Function Measurements of Multivariable Systems via Local Rational Modeling," IEEE Transactions on Instrumentation and Measurement, vol. 70, pp. 1-9, 2021.

META 2023, PARIS - FRANCE, JULY 18 – 21, 2023

Enhanced photoluminescence of ZnO nanowire coatings and gratings

E. Centeno[1*], Aubry Martin [2,3], Michel Langlet[3], Audrey Potdevin[2*], François Réveret[2], Rafik Smaali[1], Elena Kachan, Yves Jourlin[4], Geneviève Chadeyron[2]

[1]Université Clermont Auvergne, Clermont Auvergne INP, CNRS, Clermont-Ferrand, France

[2]Université Clermont Auvergne, CNRS, Clermont Auvergne INP, ICCF, F-63000 Clermont–Ferrand

[3]Université Grenoble Alpes, CNRS, Grenoble INP, LMGP, 38000 Grenoble, France

[4]Université de Lyon, Laboratoire Hubert Curien, UMR 5516, Université Jean Monnet, Saint-Etienne, France

[*]corresponding authors: emmanuel.centeno@uca.fr, audrey.potdevin@sigma-clermont.fr

Abstract: We study the light emission mechanisms of coatings and gratings made of ZnO nanowire (NWs) elaborated with a soft chemistry approach, Fig. 1(a-c). The latter architecture relies on the photo-imprinting of a sol-gel ZnO-based photosensitive seed layer combined with the subsequent localized hydrothermal growth of ZnO NWs [1]. Standard and angle-resolved photoluminescence measurements performed on both kinds of structures reveal that the grating structuration increases the NWs emission by a factor up to 2 and directionally extracts the red radiation of light. Our electromagnetic simulations based on an effective model theory and on the resolution of the eigen modes highlight that the NWs ribbons act as coupled microcavities that boost the ZnO emission thanks to light localization and diffractive mechanisms. The photoluminescence of the ZnO NWs is also simulated with a semi-classical approach based on Maxwell-Bloch equations and the finite-difference time-domain (FDTD) algorithm [2], Fig. 1d. The light extraction efficiencies for NWs coatings and gratings are calculated when a structural disorder is included to reproduce the random aspect of the set of NWs.

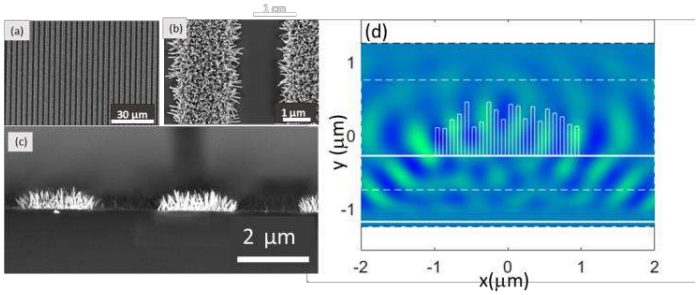


Figure 1: (a-c) SEM images from a top and perspective view of ZnO NWs grating on a quartz substrate. (d) Map of the emitted electric field calculated around 600 nm with the FDTD algorithm.

Our numerical study shows that the optical properties of these structures result from a competition between the structural disorder and the periodic structuring. These specific features could be exploited in applications where specific spatial extraction is useful such as anti-counterfeiting marking.

This work was supported by the French “Agence Nationale de la Recherche” for its financial support in the frame of the ANR SMARtLEDs project (ANR-19-CE08-0001).

References

1. N. Amara, A. Martin, A. Potdevin, D. Riassetto, M. Messaoud, F. Réveret, G. Chadeyron, J. Bouaziz, M. Langlet, Journal of Alloys and Compounds **842**, 155708 (2020).
2. M. Fang, Z. Huang, E. I. Wei, C. M. Soukoulis, IEEE Transactions on Nanotechnology **20**, 543 (2021).

Time-Varying Photonics

Matias Koivurova[1,2], Charles W. Robson[2], and Marco Ornigotti[2]
1 Tampere Institute for Advanced Study, Tampere University, 33100 Tampere, Finland
2 Faculty of Engineering and Natural Sciences, Tampere University, 33720 Tampere, Finland
Contact: matias.koivurova@tuni.fi

Keywords: Time-varying materials, relativity, momentum, arrow of time

Recently, time-varying media has risen as a new paradigm in photonics [1], which implicitly allows waves to experience *longitudinal acceleration*. However, such accelerating waves are *not* a solution of the standard wave equation. To study such waves rigorously, we have derived the accelerating wave equation in 1+1 dimensions,

$$\frac{\partial^2 f(x,t)}{\partial t^2} = c(t)^2 \frac{\partial^2 f(x,t)}{\partial x^2} - \dot{c}(t)\frac{\partial f(x,t)}{\partial x}, \tag{1}$$

where $f(x,t)$ is the wave, $c(t)$ is the time dependent speed of the wave, and $\dot{c}(t)$ is the acceleration. If we choose c_0 as the (constant) vacuum speed of light, and write the speed variations as a modulation to the vacuum speed, such that $c(t) = c_0/n(t)$, we can find the general plane wave solution to the accelerating wave equation as in

$$f(x,t) = A\exp(i\omega t' - ikx) + B\exp(i\omega t' + ikx). \tag{2}$$

Here, A and B are amplitude coefficients and $k = \omega/c_0$ is the wavenumber. Moreover, we have defined an *intrinsic* time for the electric field as $t' = \int n(t)^{-1}dt$, which is the time experienced by the wave. Intriguingly, this is fully equivalent to the definition of proper time in general relativity [2]. In other words, if we allow waves to accelerate, they exhibit properties that have natural parallels in the theory of relativity, such as *time dilation* and *length contraction*. To test this framework, we investigated simple refraction problems, as well as the more exotic disordered photonic time crystal [3]. Our results are entirely consistent with earlier studies, and our formulation can be used to model time-varying materials, as well as material interfaces *without* boundary conditions (i.e. our solutions are analytical and continuous over the whole domain).

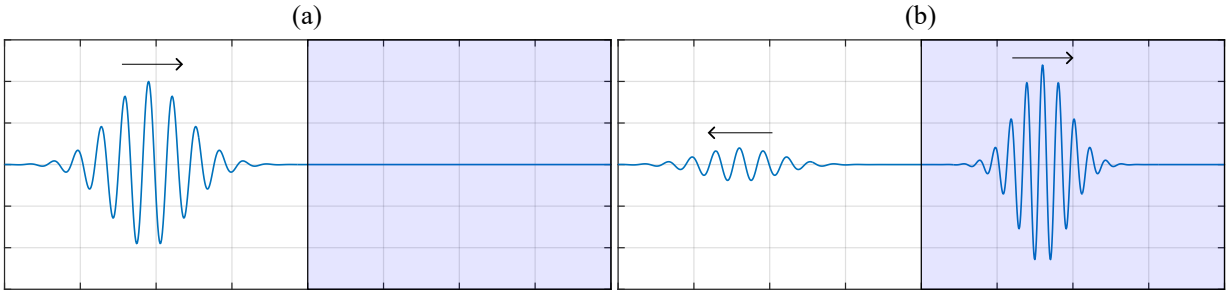


Figure 1: Electric field at an interface, as seen in the laboratory frame. (a) Gaussian pulse incident on a dielectric, travelling from left to right (indicated by right pointing arrow), (b) the reflected pulse (leftarrow) and the transmitted pulse (right arrow). This pulse was analytically simulated with continuous functions. The wavenumber of light does *not* change inside the dielectric, but rather, the pulse experiences length contraction.

Lastly, we have gained important new insight into two long-standing problems in physics: the Abraham–Minkowski controversy and the arrow of time. To be more specific, by considering the effects of longitudinal acceleration, the Abraham–Minkowski controversy can be solved without dividing the overall momentum to wave and material portions. Moreover, the accelerating wave equation allows only solutions with a positive time, thus establishing a preferred temporal direction and shedding light on the microscopic arrow of time. Note that this is distinct from the thermodynamic (macroscopic) arrow of time.

1. E. Galiffi et al., Adv. Photon. **4**, 014002 (2022).
2. L. D. Landau and E. M. Lifshitz, *The Classical theory of Fields* (Butterworth-Heinemann, 1975).
3. Y. Sharabi, E. Lustig, and M. Segev, Phys. Rev. Lett. **126**, 163902 (2021).

META 2023, PARIS - FRANCE, JULY 18 – 21, 2023

Deep Learning and Optimization for Efficient and Robust Nanophotonic Design

S. D. Campbell, R. P. Jenkins, P. L. Werner, and D. H. Werner

The Pennsylvania State University, Department of Electrical Engineering, University Park, PA 16802 USA
*corresponding author: sawyer@psu.edu

Abstract: Nanophotonic device design requires efficient full-wave solvers and optimization techniques. To this end, deep learning shows promise for improving both forward- and inverse-design aspects of such problems. Meanwhile, multiobjective and topology optimization approaches have proven successful in realizing highly performant freeform nanophotonic devices with tailored functionalities. Combining deep learning with advanced optimization techniques gives designers beyond state-of-the-art tools for realizing extremely efficient nanophotonic device design cycles.

Deep learning (DL) techniques have seen tremendous interest in recent years within the greater electromagnetics and optical communities for their potential to accelerate both forward- and inverse-design problems [1], [2]. Several studies have trained deep neural networks (DNNs) to act as sophisticated surrogate models (*i.e.*, black boxes) to replace the forward modelling component in nanophotonic design problems. This can lead to tremendous time savings by eliminating the need for expensive full-wave simulations (*e.g.*, those based on FDTD or FEM methods). To this end, we developed a cascaded two-stage DNN based on U-Net and CNN (convolutional neural network) topologies to assist in the multiobjective optimization of nanophotonic meta-devices that are resilient to common fabrication uncertainties during E-beam lithography and other conventional manufacturing techniques [3]. At the same time, we have developed techniques that enforce minimum size constraints including for both positive and negative features (*i.e.*, widths and gaps/voids) which can be directly integrated with our freeform metasurface synthesis techniques and DNN framework [4].

Meanwhile, optimization techniques exist in parallel to DL and are equally important to nanophotonic design [5]. Generally, these algorithms are judged according to their convergence statistics with particular emphasis on the number of iterations required to meet a desired cost (or fitness) value and the variance of final cost values achieved when starting from random seeds. To this end, topology optimization (TO) is an extremely popular gradient-based technique for freeform nanophotonic device design. TO is commonly employed to simultaneously adjust the permittivity of each voxel in an array that comprises the space where the nanophotonic structure may exist [6], [7]. Since we usually desire binary (*i.e.*, two-material, usually dielectric and air) 2.5D planar nanophotonic devices, the permittivity gradients in vertically-aligned voxels are often averaged so as to maintain a fixed permittivity throughout. Meanwhile, binary-coercion techniques are employed to enforce adjacent voxel pillars to a fixed permittivity value. However, these compromises can degrade convergence behavior which can lead to inefficiencies if many trials are needed to achieve a desired performance goal. To improve upon these compromises, we demonstrated how the multi-gradient can lead to a better choice of gradient to follow than conventional averaging and accelerate TO convergence two-fold [8].

Acknowledgment

This research was supported in part by DARPA EXTREME (contract HR00111720032).

References

[1] P. R. Wiecha and O. L. Muskens, “Deep Learning Meets Nanophotonics: A Generalized Accurate Predictor for Near Fields and Far Fields of Arbitrary 3D Nanostructures,” *Nano Lett.*, vol. 20, no. 1, pp. 329–338, Jan. 2020, doi: 10.1021/acs.nanolett.9b03971.

[2] W. Ma, Z. Liu, Z. A. Kudyshev, A. Boltasseva, W. Cai, and Y. Liu, “Deep Learning for the Design of Photonic Structures,” *Nat. Photonics*, vol. 15, no. 2, Art. no. 2, Feb. 2021, doi: 10.1038/s41566-020-0685-y.

[3] R. P. Jenkins, S. D. Campbell, and D. H. Werner, “Establishing Exhaustive Metasurface Robustness Against Fabrication Uncertainties Through Deep Learning,” *Nanophotonics*, vol. 10, no. 18, pp. 4497–4509, Dec. 2021, doi: 10.1515/nanoph-2021-0428.

[4] E. B. Whiting, S. D. Campbell, L. Kang, and D. H. Werner, “Meta-atom Library Generation via an Efficient Multi-objective Shape Optimization Method,” *Opt. Express,* vol. 28, no. 16, pp. 24229–24242, Aug. 2020, doi: 10.1364/OE.398332.

[5] S. D. Campbell, D. Sell, R. P. Jenkins, E. B. Whiting, J. A. Fan, and D. H. Werner, “Review of Numerical Optimization Techniques for Meta-device Design [Invited],” *Opt. Mater. Express*, vol. 9, no. 4, p. 1842, Apr. 2019, doi: 10.1364/OME.9.001842.

[6] J. S. Jensen and O. Sigmund, “Topology Optimization for Nano-photonics,” *Laser & Photonics Reviews*, vol. 5, no. 2, pp. 308–321, 2011, doi: 10.1002/lpor.201000014.

[7] T. Phan *et al.*, “High-efficiency, Large-area, Topology-optimized Metasurfaces,” *Light Sci. Appl.*, vol. 8, no. 1, Art. no. 1, May 2019, doi: 10.1038/s41377-019-0159-5.

[8] R. P. Jenkins, E. B. Whiting, S. D. Campbell, and D. H. Werner, “Improved Convergence in Planar Nanophotonic Topology Optimization via the Multigradient,” *Photonics and Nanostructures - Fundamentals and Applications*, vol. 52, p. 101067, Dec. 2022, doi: 10.1016/j.photonics.2022.101067.

META 2023, PARIS - FRANCE, JULY 18 – 21, 2023

Chiral nanophotonic waveguides for spin-based quantum optical devices

Hamidreza Siampour,[1,2,§,*] Christopher O'Rourke,[1] Alistair J. Brash,[1] Maxim N. Makhonin,[1] René Dost,[1] Dominic J. Hallett,[1] Edmund Clarke,[3] Pallavi K. Patil,[3] Maurice S. Skolnick,[1] A. Mark Fox[1]

[1]Department of Physics and Astronomy, University of Sheffield, Hicks Building, Sheffield S3 7RH, UK
[2]Cavendish Laboratory, University of Cambridge, J. J. Thomson Avenue, Cambridge CB3 0HE, UK
[3]EPSRC National Epitaxy Facility, Department of Electronic and Electrical Engineering, University of Sheffield, Sheffield S1 3JD, UK
[§]Current address: School of Mathematics and Physics, Queen's University Belfast, University Road, Belfast BT7 1NN, UK
[*]corresponding author: h.siampour@qub.ac.uk

Abstract: We present a symmetry-broken nanophotonic waveguide platform with embedded quantum dots (QDs) that enables both Purcell-enhanced emission and strong chiral coupling.

The confinement of the light in nanophotonic waveguides enables chiral coupling between the spin of the quantum emitter and the helicity of the waveguide mode with a near-unity directionality to left- or right-propagating modes. We present a symmetry-broken waveguide platform with embedded quantum dots (QDs) that enables both Purcell-enhanced emission and strong chiral coupling. We observe record high Purcell factors for both non-chirally-coupled and chirally-coupled quantum dots emitting in the slow-light spectral region of a glide-plane photonic crystal waveguide (PCW).[1] For the non-chirally-coupled dot, we use a quasi-resonant phonon-sideband excitation scheme to eliminate slow internal relaxation and achieve an extremely large radiative decay rate of 17±2 ns^{-1} (60±6 ps lifetime), corresponding to a 20±2 fold Purcell enhancement. We also observe chiral routing of spin-carrying photons from a QD near a chiral point with a 5±1 fold Purcell factor, substantially outperforming previous demonstrations with nanobeam[2], nanofiber[3], and PCWs[4-6]. Together, these results constitute significant progress towards reaching the threshold for scalable chiral networks relying on chiral quantum optics.

This work was funded by the Engineering and Physical Sciences Research Council (EPSRC) UK Programme Grants EP/N031776/1 and EP/V026496/1. A.J.B. acknowledges support from the EPSRC UK Quantum Technology Fellowship EP/W027909/1.

References

1. Siampour, H. *et al.* Observation of large spontaneous emission rate enhancement of quantum dots in a broken-symmetry slow-light waveguide. *npj Quantum Inf* **9**, 15 (2023)
2. Coles, R. J. *et al.* Chirality of nanophotonic waveguide with embedded quantum emitter for unidirectional spin transfer. *Nature Communications* **7**, 11183 (2016).
3. Mitsch, R., Sayrin, C., Albrecht, B., Schneeweiss, P. & Rauschenbeutel, A. Quantum state-controlled directional spontaneous emission of photons into a nanophotonic waveguide. *Nature Communications* **5**, 5713 (2014).
4. Söllner, I. *et al.* Deterministic photon–emitter coupling in chiral photonic circuits. *Nature Nanotechnology* **10**, 775 (2015).
5. Scarpelli, L. *et al.* 99% beta factor and directional coupling of quantum dots to fast light in photonic crystal waveguides determined by spectral imaging. *Physical Review B* **100**, 035311 (2019).
6. Østfeldt, F. T. *et al.* On-Demand Source of Dual-Rail Photon Pairs Based on Chiral Interaction in a Nanophotonic Waveguide. *PRX Quantum* **3**, 020363 (2022).

META 2023, PARIS - FRANCE, JULY 18 – 21, 2023

Multifunctional metasurface optics for imaging and sensing

Fan Yang[1], Hung-I Lin[1], Juejun Hu[1] and Tian Gu[2*]

[1]Department of Materials Science and Engineering, Massachusetts Institute of Technology, USA

[1]Materials Research Laboratory, Massachusetts Institute of Technology, USA

[*]corresponding author: gutian@mit.edu

Abstract: Optical metasurfaces, planar subwavelength nanoantenna arrays with the singular ability to sculpt wavefront in almost arbitrary manners, are poised to become a powerful tool enabling compact and high-performance optics. Multifunctional metasurfaces, whose optical response vary according to the operation conditions, further allow a plurality of new functionalities unattainable with traditional optical approaches. In this talk, we discuss multifunctional meta-optics designs and demonstrations in imaging and sensing applications.

META 2023, PARIS - FRANCE, JULY 18 – 21, 2023

Towards cm-scale full-wave metasurface simulation and design

O. D. Miller[1,*]

[1]ADepartment of Applied Physics and Energy Sciences Institute, Yale University, New Haven, CT, United States
[*]corresponding author: owen.miller@yale.edu

Abstract: Simulating the full wave dynamics of centimeter-scale metasurfaces is beyond the capabilities of finite-difference and finite-element solvers, yet is necessary for reaching the ultimate limits of functionality and performance. In this talk, I describe our fast direct integral-equation solver that can accurately and efficiently simulate cylindrical metasurfaces tens of thousands of wavelengths in diameter. We demonstrate its capabilities with the successful inverse design of a high-efficiency, high-NA, cm-scale metalens.

Fabrication-Conscious Inverse Design of Single-Material Variable-Index Multilayer Films (Invited)

Omer Yesilyurt[1-3], Samuel Peana[1-3], Vahagn Mkhitaryan[1-3], Karthik Pagadala[1-3], Vladimir Shalaev[1-3], Alexandra Boltasseva[1-3], Alexander V. Kildishev[*,1-3]

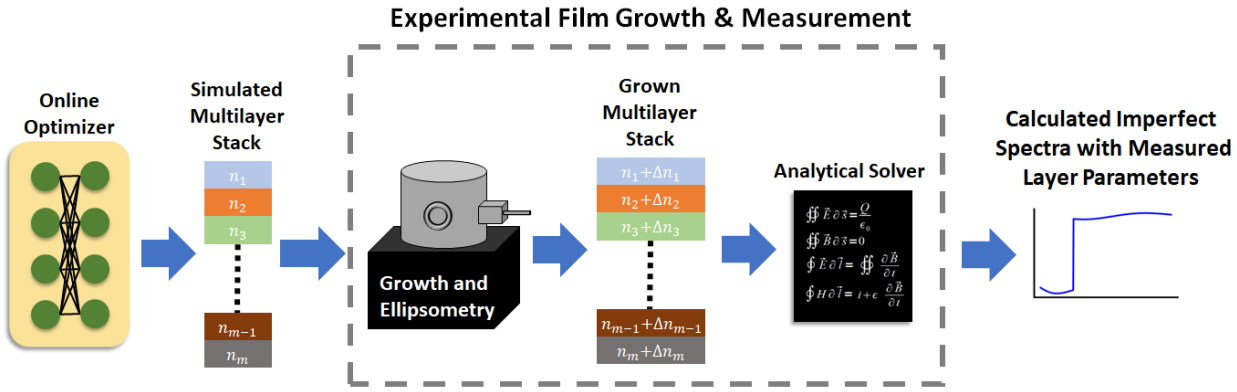
[1]Birck Nanotechnology Center, Purdue University, West Lafayette, IN 47907, USA

[2]School of Electrical and Computer Engineering, Purdue University, West Lafayette, IN 47907, USA

[3]Quantum Science Center, a National Quantum Information Science Research Center of the U.S. Department of Energy, Oak Ridge, TN 37931, USA

[*]Email: kildishev@purdue.edu

Abstract: We developed a neural network-based inverse-design technique for the design of single-material multilayer optical devices. Such devices are made of one material and the growth parameters are varied to achieve different refractive indices at each layer. The inverse design method explored is computationally efficient and capable of designing devices consisting of several hundred layers. If systemic fabrication imperfections are introduced during training the resulting designs account for the non-idealities of the growth process while still yielding sufficiently high performance.



We demonstrate a neural network based inverse design technique based on a differentiable analytical solver for the design of single-material multilayer planar film devices [1]. Such devices are created by varying the growth conditions of a single monolithic film during its growth. This results in controllable variations of the refractive index allowing for multilayer devices such as filters, anti-reflective coatings, and a variety of other optical devices to be realized [2,3]. As there is only one material in the device there are no multi-material interfaces leading to superior mechanical, optical, and thermal properties [2,4,5]. However, modelling the growth conditions, particularly dynamic growth conditions, is challenging. In this work as can be seen in the figure (adapted from [1]) the "Online Optimizer" is a fully connected neural network which is trained to take a seed multilayer film stack and modify it to produce an optimized film stack. In the first stage of the optimization, we bypass the growth and ellipsometry and assume that the growth was perfect. The analytical solver used (Transfer Matrix Method) is differentiable, as a result the training of the neural network can be done by backpropagating the error between the target and realized spectra through it. This contributes to dramatically improving the convergence of the method and allows for efficient design even for devices with several hundred layers. The training of the "Online Optimizer" is repeated until the error between the designed stack transmission spectra and target spectra converges to a minimum. Similar neural network based design methods have been recently explored for metasurfaces, and multilayer films with discrete materials [6–8].

Additionally, as mentioned previously, imperfections during the growth, multilayer effects, and other non-ideal factors will be present as imperfections in any experimentally realized device. Even minor imperfections in layer thicknesses and refractive indices can dramatically affect the resulting transmission and reflection spectra of the device. To account for this a second stage of training is initiated taking the optimized neural network as a starting point. In the proposed method, the design produced by the neural network is experimentally grown with in situ ellipsometry providing information as to the deviation in both thickness and refractive index of each grown layer. The measured stack is then simulated using the analytical solver. This allows for backpropagation through the solver to update the neural network weights. The result of this second stage of training is that the retrained neural network will produce material stacks which are designed to compensate for systemic errors occurring during the growth of the device. The efficacy of this approach was explored by simulating a variety of possible fabrication imperfections and demonstrating that the resulting design after training perfectly compensated for the simulated imperfections.

In summary, in this work we explored a neural network based inverse design technique capable of producing highly optimized single-material multilayer film devices with arbitrary target transmission/reflection spectra. Furthermore, we developed a method for utilizing this architecture to optimize the growth of these devices to compensate for the complex systemic imperfections introduced during growth. We believe this approach provides a path for the design and optimization of complex single material multilayered devices.

This work is supported by the US Department of Energy (DOE), Office of Science through the Quantum Science Center (QSC), a National Quantum Information Science Research Center and National Science (ML Algorithm Development) Foundation award 2029553-ECCS and Purdue ECE Elmore Emerging Frontiers Center "The Crossroads of Quantum and AI."

References

[1] O. Yesilyurt, S. Peana, V. Mkhitaryan, K. Pagadala, V. M. Shalaev, A. V. Kildishev, and A. Boltasseva, *Fabrication-Conscious Neural Network Based Inverse Design of Single-Material Variable-Index Multilayer Films:*, Nanophotonics **12**, 993 (2023).

[2] R. Vernhes, O. Zabeida, J. E. Klemberg-Sapieha, and L. Martinu, *Single-Material Inhomogeneous Optical Filters Based on Microstructural Gradients in Plasma-Deposited Silicon Nitride*, Appl. Opt., AO **43**, 97 (2004).

[3] H. Szymanowski, K. Olesko, J. Kowalski, M. Fijalkowski, M. Gazicki-Lipman, and A. Sobczyk-Guzenda, *Thin SiNC/SiOC Coatings with a Gradient of Refractive Index Deposited from Organosilicon Precursor*, Coatings **10**, 8 (2020).

[4] D. Rats, D. Poitras, J. M. Soro, L. Martinu, and J. von Stebut, *Mechanical Properties of Plasma-Deposited Silicon-Based Inhomogeneous Optical Coatings*, Surface and Coatings Technology **111**, 220 (1999).

[5] M. F. Ouellette, R. V. Lang, K. L. Yan, R. W. Bertram, R. S. Owles, and D. Vincent, *Experimental Studies of Inhomogeneous Coatings for Optical Applications*, Journal of Vacuum Science & Technology A: Vacuum, Surfaces, and Films **9**, 1188 (1998).

[6] J. Jiang and J. A. Fan, *Global Optimization of Dielectric Metasurfaces Using a Physics-Driven Neural Network*, Nano Lett. **19**, 5366 (2019).

[7] L. Gao et al., *Optics and Nonlinear Buckling Mechanics in Large-Area, Highly Stretchable Arrays of Plasmonic Nanostructures*, ACS Nano **9**, 5968 (2015).

[8] J. Jiang and J. A. Fan, *Multiobjective and Categorical Global Optimization of Photonic Structures Based on ResNet Generative Neural Networks:*, Nanophotonics **10**, 361 (2021).

Efficient Design of 2D Slanted Gratings using Polynomial Modal Method

K. Edee[1*], G. Granet[1] and P. Bonnet[1]

[1] Université Clermont Auvergne, INP, CNRS, Institut Pascal, F-63000 Clermont-Ferrand, France
[*]corresponding author: kofi.edee@uca.fr

Abstract: We present an efficient approach to design 2D gratings using the polynomial modal method (PMM). The PMM is a rigorous modal method based on orthogonal and modified polynomials, as proposed by [1]. By utilizing the covariant form of Maxwell's equations, we accurately account for boundary conditions. We demonstrate the effectiveness of our method through several relevant numerical examples.

Slanted gratings, which exhibit a non-vertical profile, have garnered significant attention due to their unique electromagnetic properties and potential applications including optical communication, sensing, and energy harvesting , polarization control, and enhanced light-matter interactions [1-3]. These non-standard grating structures, where the grating patterns profile are intentionally tilted or exhibit a slanted profile, can manipulate the polarization state of incident light and introduce specific diffraction characteristics that are unattainable with conventional gratings. Accurate calculation of the electromagnetic diffraction in slanted gratings is essential to optimize their design and improve their performance in practical implementations.

Traditionally, Fourier modal method (FMM) also called, rigorous coupled-wave analysis (RCWA) [4-8], and finite-difference time-domain (FDTD) methods [9] have been used to investigate the electromagnetic properties of grating structures. However, these methods can be computationally demanding and may not always provide an efficient solution, particularly for complex or high-aspect-ratio slanted gratings. Therefore, alternative approaches that offer improved computational efficiency and accuracy are desirable for studying the electromagnetic field behavior in these structures.

Here, we present a polynomial modal method-based [10-13] approach to solve the 2D slanted grating problem. This method is based on orthogonal and modified polynomials.
To meticulously account for boundary conditions, the covariant form of Maxwell's equations is used. The resulting metric tensor is no more diagonal, making it intricate to apply factorization rules in the FMM/RCWA framework. Nonetheless, the PMM does not require these rules, simplifying the computation process.

We use the PMM to design 2D gratings and demonstrate its efficiency through several pertinent numerical examples. These examples reveal that the PMM can accurately predict the diffraction efficiency and other properties of the designed gratings while reducing computational complexity in comparison to traditional methods.

References:

[1] H. Kogelnik, "Coupled wave theory for thick hologram gratings," Bell System Technical Journal, vol. 48, no. 9, pp. 2909-2947, 1969.

[2] J. A. Polo Jr., and T. A. Leskova, "Slanted surface-relief diffraction gratings: modeling and analysis," Opt. Lett., vol. 29, no. 23, pp. 2784-2786, 2004.

[3] S. R. Park, C. J. Lee, Y. M. Sung, and H. S. Lee, "Slanted grating couplers for efficiently coupling light between waveguides and single-mode fibers," Opt. Express, vol. 26, no. 19, pp. 24874-24889, 2018.

[4] K. Knop "Rigorous diffraction theory for transmission phase gratings with deep rectangular grooves," J. Opt. Soc. Am. A, 1978, **68**, 1206-1210

[5] M. G. Moharam, D. A. Pommet, E. B. Grann, and T. K. Gaylord, "Stable implementation of the rigorous coupled-wave analysis for surface-relief gratings: enhanced transmittance matrix approach," J. Opt. Soc. Am. A, vol. 12, no. 5, pp. 1077-1086, 1995.

[6] G. Granet and B. Guizal "Efficient implementation of the coupled-wave method for metallic lamellar gratings in TM polarization," J. Opt. Soc. Am. A, 1996, **13**, 1019-1023

[7] P. Lalanne and G. M. Morris "Highly improved convergence of the coupled-wave method for TM polarization," J. Opt. Soc. Am. A **13**, 779-784 (1996)

[8] L. Li "Use of Fourier series in the analysis of discontinuous periodic structures," J. Opt. Soc. Am. A, 19996, **13**, 1870-1876 (1996)

[9] A. Taflove and S. C. Hagness, Computational Electrodynamics: The Finite-Difference Time-Domain Method, 3rd ed. Norwood, MA: Artech House, 2005.

[10] K. Edee, I. Fenniche, G. Granet, B. Guizal "Modal method based on subsectional Gegenbauer polynomial expansion for lamellar gratings: weighting function, convergence and stability," PIER, 2013, **133** 17-35.

[11] K. Edee, B. Guizal "Modal method based on subsectional Gegenbauer polynomial expansion for nonperiodic structures: complex coordinates implementation," J. Opt. Soc. Am. A, 2013,**30**, 631-639.

[12] K. Edee, J.-P. Plumey "Numerical scheme for the modal method based on subsectional Gegenbauer polynomial expansion: application to biperiodic binary grating," J. Opt. Soc. Am. A, 2015, **31**, 402-410.

[13] K. Edee, J.-P. Plumey, B. Guizal "Unified Numerical Formalism of Modal Methods in Computational Electromagnetics and Latest Advances: Applications in Plasmonics" Elsevier, Advances in Imaging and Electron Physics, 2016, **197**, chapter 2.

Photonic crystal design targeting room temperature operation of GaN-based ridge polariton laser

V. Develay[1*], L. Doyenette[1], C. Brimont[1], G. Malpuech[2], J. Zúñiga-Pérez[3,4], S. Bouchoule[5], T. Guillet[1]

[1]Laboratoire Charles Coulomb (L2C), Université de Montpellier, CNRS, Montpellier, France

[2]Université Clermont Auvergne, CNRS, Institut Pascal, Clermont-Ferrand, France

[3]UCA, CNRS, CRHEA, Rue de Greogry, 06560 Valbonne, France

[4]MajuLab, International Research Laboratory IRL 3654, CNRS, Université Côte d'Azur, Sorbonne Université, National University of Singapore, Nanyang Technological University, Singapore

[5]Centre de Nanosciences et de Nanotechnologies, Université Paris-Saclay, CNRS, France

[*]corresponding author: valentin.develay@umontpellier.fr

Abstract: We simulate a structured GaN waveguide with EigenMode simulation (EME) and optimize the geometrical parameter of this structure in order to control its emission energy. Those simulations reveal the impact of the decrease of GaN thickness on the Rabi splitting and the photonic gap as well as the optimal filling factor range in order to have large photonic gap. These results contribute to the realization of photonic crystal laser ridge at room temperature.

Polariton in microcavities are one of the main actual research field in polaritonics. The recent development of waveguide polariton lasers open a new range of possibilities in optoelectronics. Wide gap semiconductor such as ZnO and GaN are used in order to maintain the strong coupling regime up to room temperature thanks to their strong exciton binding energies (E_X=25 meV for the GaN) and large oscillator strength [1]. Polariton laser at room temperature has already been demonstrated in a ZnO waveguide in a cavity formed by cracks [2]. Recently, H.Souissi *et al.* demonstrated a CW polariton laser in a GaN ridge with distributed bragg reflectors [3]. The study of this Fabry-Perot cavity reveals unconventional properties compared to conventional ridge lasers, such as the loss of reciprocity between the loss and gain process in the cavity and the diminution of the pump size required to operates in the laser regime (15% of the cavity length). Similarly, polariton laser has also been evidenced in GaN/AlGaN microrings [3].

Yet, in the GaN ridge laser [3,4], competition between the laser emission and the relaxation of the condensate along-side the lower polariton branch leads to a quick increase of the threshold with the temperature as well as a significant redshift of the laser emission. This phenomenon is worsened by the absence of ground state in GaN waveguide [3]. The implementation of a photonic crystal onto a waveguide (Fig 1a) could overcome this difficulty and provide a solution to have a better control over laser emission.

Indeed, based on the result of EigenMode Expansion (EME) Simulation [5], we proposed a design of structured waveguide composed of an etched TiO_2 surface, a GaN Core and an AlGaN lower cladding, in which we reveal the formation of a potential minimum in the waveguide dispersion (upper blue curve Fig 1b). By comparison, the dispersion of a GaN planar polariton waveguide has no ground state (orange and green curve, with or without TiO_2 top cladding, Fig. 1b). The dispersion in a 1D photonic crystal slab is simulated with dispersive TiO_2 and GaN refractive indices which take into account the excitonic effect with an Elliott-Tanguy model [1]. The optimization of the geometrical parameters is of a paramount importance in order to obtain a

large Rabi splitting, manifestation of the strong coupling regime, as well as a large photonic gap, allowing an effective selection of the lasing polariton mode. GaN thickness decrease induces a diminution of the Rabi splitting (blue curve Fig 1c) and an increase of the photonic gap (black curve Fig 1c). The variation of the filling factor (ff) leads to an optimal ff range of 60 to 85% (Fig 1d), preserving an 80 meV Rabi splitting as well as a 30 meV photonic bandgap. For a laser emission at 3.44 eV [3], a 69nm period is required, which imposes an etching width of the TiO_2 surface between 10 and 30 nm in order to have a reasonably large photonic gap, which is very challenging in terms of technological realization. This photonic crystal waveguide design is a step towards the experimental realization of low threshold GaN laser operating in the strong coupling regime at room temperature.

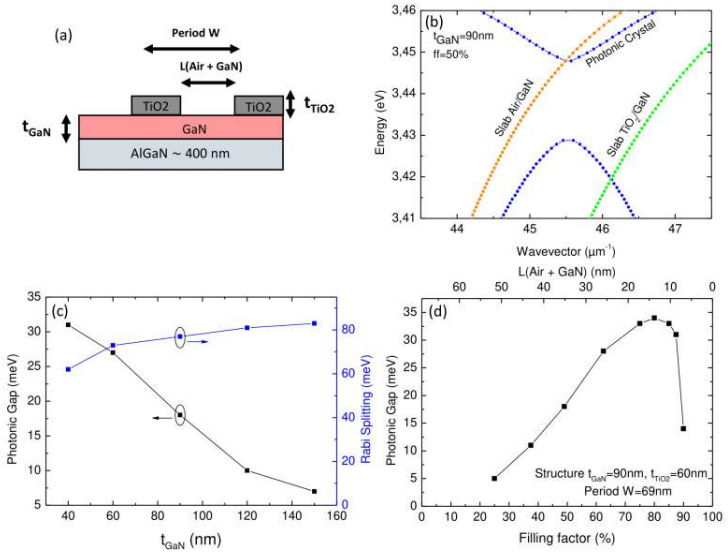


Figure 1: (a) Photonic crystal waveguide (ff = 1 – L(Air+GaN)/W), (b) Polariton dispersion for a given set of parameters (t_{GaN}=90nm, f_{TiO2}=60nm, W=68.9nm, ff=50%), (c) Rabi splitting vs GaN thickness vs Photonic Gap, (d) Photonic gap vs of the filling factor

Acknowledgements: The authors acknowledge fundings from the French National Research Agency (ANR-16-CE24-0021-03, ANR-11LABX-0014, ANR 21-CE24-0019-01), the French Renatech network and the Region Occitanie (ALDOCT-001065)

REFERENCES

1. C. Brimont *et al*, "Strong Coupling of Exciton-Polaritons in a Bulk GaN Planar Waveguide: Quantifying the Coupling Strength", *Phys. Rev. Appl.* **14**, 054060, 2020.
2. O. Jamadi *et al*, "Edge-emitting polariton laser and amplifier bases on a ZnO waveguide", *Light: Sci & Appl* **7**, 82, 2018.
3. H. Souissi *et al*, "Ridge polariton laser: different from a semiconductor edge-emitting laser", *Phys. Rev. Appl.* **18**, 044029, 2022.
4. A. Delphan *et al*, "Polariton lasing in AlGaN microring with GaN/AlGaN quantum wells", *APL Photonics* **8**, 021302, 2023.
5. P. Bientsman and R.Baets, "Optical modelling of photonic crystals and VCSELs using eigenmode expansion and perfectly matched layers", *Optical and Quantum Electronics* **33** , 327-341, 2001.

META 2023, PARIS - FRANCE, JULY 18 – 21, 2023

Quantum Hydrodynamic Theory for Plasmonics: a Computational Perspective

C. Ciracì[1,*], M. Castriotta[1], H. Baghramyan[1], M. Khalid[2], F. della Sala[1,3]

[1]Center for Biomolecular Nanotechnologies, Istituto Italiano di Tecnologia (IIT), Italy

[2]Institute of Nanotechnology (CNR-Nanotec), Italy

[3]Institute for Microelectronics and Microsystems, (CNR-IMM), Italy

[*]corresponding author: cristian.ciraci@iit.it

Abstract: In this talk, we discuss the computational aspects of the quantum hydrodynamic theory (QHT). We review the theoretical basis of the QHT and discuss the numerical methods used to solve the QHT and discuss the challenges associated and applications.

A reliable way to theoretically describe and numerically model optical properties of plasmonic nanostructures with different length scales requires methods beyond classical electromagnetism. In this context, it becomes very important to develop simulation techniques to take into account quantum microscopic features at the scale of billions of atoms.

The quantum hydrodynamic theory (QHT) is a powerful approach to study the behavior of plasmons in metallic nanostructures, as it incorporates the nonlocal behavior of the electron response by including the electron pressure, electron spill-out and tunneling effects [1, 2]. This method allows to explore light-matter interactions in extreme scenarios in which microscopic features can strongly affect the macroscopic optical response. However, the QHT requires solving a set of coupled partial differential equations in region that goes from a fraction of a nanometer to few microns, which makes it computationally challenging.

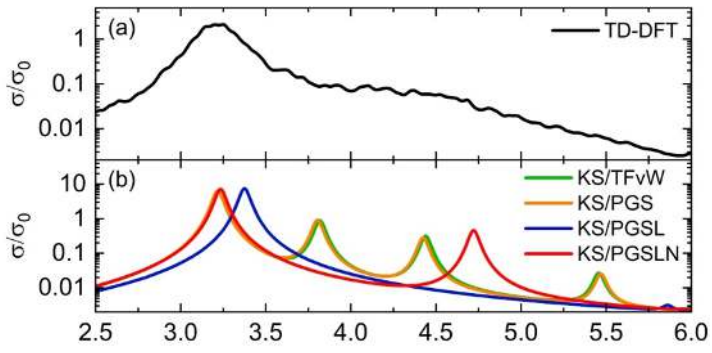


Figure 1: Na jellium sphere with $N_e = 1074$ electrons: absorption cross section normalized to σ_0 geometrical cross section as obtained from (a) TD-DFT, and (b) several QHT approximations.

In this talk, we discuss some of the computational aspects of the QHT. We first review the theoretical basis of the QHT and explore some applications, including photon emission [3], strong-coupling [4] and nonlinear optics [5]. We describe the numerical methods used to solve the QHT and discuss the challenges associated with simulating plasmonic systems. Finally, we point out the limitations of conventional functionals in QHT and propose possible corrections [6,7]. We introduce a more general QHT method accounting for kinetic energy contributions depending on the Laplacian of the electronic density, thus, beyond the gradient-only dependence of the Thomas-Fermi and von Weizsäcker functional (see Figure 1).

References

1. C. Ciracì and F. Della Sala, Phys. Rev. B **93**, 205405 (2016).
2. G. Toscano, *et al.*, Nat. Commun. **6**, 7132 (2015).
3. H. M. Baghramyan and C. Ciracì, Nanophotonics **11**, 2473–2482 (2022).
4. C. Ciracì, R. Jurga, M. Khalid and F. Dell Sala, Nanophotonics **8**, 1821–1833 (2019).
5. C. Ciracì, Phys. Rev. B **95**, 245434 (2017).
6. M. Khalid and C. Ciracì, Commun. Phys. **3**, 214 (2020).
7. H. M. Baghramyan, F. Della Sala and C. Ciracì, Phys. Rev. X **11**, 011049 (2021).

Radiative heat exchange driven by acoustic modes between two solids at the atomic scale

M. Gómez Viloria*, R. Messina, and P. Ben-Abdallah

Laboratoire Charles Fabry, Institut d'Optique, CNRS, UMR 8501,

Université Paris-Saclay, 2 Avenue Augustin Fresnel, 91127 Palaiseau Cedex, France

*corresponding author: mauricio.gomez-viloria@institutoptique.fr

Abstract: When two solids are separated by a vacuum gap of smaller thickness than the wavelength of acoustic phonons, the latter can tunnel across the gap. We show that the acoustic modes in polar crystals can also significantly contribute, at atomic scale, to the nonlocal optical response of the material. We investigate the radiative heat transfer between two slabs of polar materials separated by vacuum gaps of atomic thickness and highlight the strong contribution of these modes at cryogenic temperatures.

In the near field (for separation distances smaller than the thermal wavelength, of the order of some microns at ambient temperature), the radiative heat flow between two solids at different temperatures can exceed the blackbody limit by several orders of magnitude. Furthermore, at the atomic scale, close to contact, the vibrational modes of the crystal lattice are expected to play an important role in the heat exchange. While the contribution of acoustic phonons tunneling due to Van der Waals forces and electrostatic interactions near the surface has been investigated [1–5], the radiative contribution of the acoustic modes has been neglected so far. Under the local assumption (wavevector $\mathbf{k} \approx 0$), optical modes are independent from the acoustic modes, and are the sole responsible for the thermal radiation for distances larger than a few nanometers. However at subnanometer distances, the electromagnetic response of solids is nonlocal ($\mathbf{k} \neq 0$) and both acoustic and optical modes are coupled, contributing together to the radiative heat exchange. In order to demonstrate the role of this contribution, we calculate [6] the nonlocal dielectric permittivity of magnesium oxide (MgO) using molecular dynamics. In conjunction with fluctuational electrodynamics calculations, we are able to highlight the role of radiation between two solids produced by acoustic modes compared to the expected results from the local theory. We show that this additional contribution can become the dominant channel for radiative heat exchanges at atomic scale in the cryogenic regime (below 100 K). Since the acoustic vibration modes can be excited with the help of piezoelectric transducers, our work opens the possibility to the control of radiative heat exchanges at atomic scale using external mechanical actuation.

References

[1] V. Chiloyan, J. Garg, K. Esfarjani, and G. Chen. Transition from near-field thermal radiation to phonon heat conduction at sub-nanometre gaps. *Nat. Commun.*, 6(1):6755, 2015. doi:10.1038/ncomms7755.

[2] J. B. Pendry, K. Sasihithlu, and R. V. Craster. Phonon-assisted heat transfer between vacuum-separated surfaces. *Phys. Rev. B*, 94(7):075414, 2016. doi:10.1103/PhysRevB.94.075414.

[3] A. I. Volokitin. Effect of an electric field in the heat transfer between metals in the extreme near field. *JETP Lett.*, 109:749–754, 2019. doi:10.1134/S0021364019180103.

[4] Y. Guo, C. Adessi, M. Cobian, and S. Merabia. Atomistic simulation of phonon heat transport across metallic vacuum nanogaps. *Phys. Rev. B*, 106(8), 2022. doi:10.1103/PhysRevB.106.085403.

[5] M. Gómez Viloria, Y. Guo, S. Merabia, P. Ben-Abdallah, and R. Messina. Heat transfer in the extreme near-field regime between metallic bodies. *(preprint)*, 2022. doi:10.48550/arXiv.2212.03073.

[6] M. Gómez Viloria, Y. Guo, S. Merabia, R. Messina, and P. Ben-Abdallah. Radiative heat exchange driven by the acoustic vibration modes between two solids at the atomic scale. *(preprint)*, 2023. doi:10.48550/arXiv.2302.00520.

Nonlinear generation of vortex beams on optical metasurfaces

L. Coudrat[1], K. Moratis[1], P. Filloux[1], R. Tanos[2], J. Claudon[2], J.-M. Gerard[2], A. Degiron[1], G. Leo[1]

[1] Laboratoire Matériaux et Phénomènes Quantiques, Université Paris Cité, France
[2] Université Grenoble Alpes, CEA, IRIG, PHELIQS, Grenoble, France
*corresponding author: g.leo@u-paris.fr

Abstract: The generation of vortex beams is a field of research with an important impact on both fundamental and applied physics. [1] In this work, we show our recent results on the generation of second-harmonic vortex beams with a dielectric nonlinear optical metasurface.

Recently, the rise of interest for nanophotonics and flat-optics [2] has spurred the demonstration of meta-holograms that can create Laguerre-Gauss beams with ultrathin devices. [3] Flat optics also showed its potential in the nonlinear regime. [4] Plasmonic MS were the first to perform wavefront shaping in connection with second harmonic generation (SHG), albeit with low conversion efficiency and huge dissipation in the near-infrared (near-IR) range. [5] Later, based on silicon-on-insulator (SOI) platform, nonlinear wavefront shaping was demonstrated with third-harmonic-generation (THG), based on the $\chi^{(3)}$ of silicon. [6]

Here we generate second harmonic (SH) beams carrying non-zero orbital angular momentum (OAM) via a dielectric $\chi^{(2)}$ metasurface, with SH generation and phase control being achieved at the level of single meta-atoms. The related lookup-table-based meta-hologram has a fork-like phase profile that steers a vortex beam of topological charge |5| in the first diffraction order, with good agreement between analytical and experimental results. The optical vortices studied experimentally in this work are characterized in three dimensions, by following the related singularity along a straight line perpendicular to the metasurface. However, it is also possible to generate more complex beam topologies. More precisely, we can shape light beams into several zero-intensity loops that are knotted or linked [8,9].

References

1. D. L. Andrews, "Structured Light and Its Applications", Elsevier Science (2008).
2. N. Yu, P. Genevet, M. A. Kats, F. Aieta, J. P. Tetienne, F. Capasso, and Z. Gaburro, "Light Propagation with Phase Discontinuities: Generalized Laws of Reflection and Refraction", Science 334, 333 (2011).
3. X. Wang, Z. Nie, Y. Liang, J. Wang, T. Li and B. Jia, "Recent advances on optical vortex generation", Nanophotonics 7, 1533 (2018).
4. C. De Angelis, G. Leo, D. Neshev, "Nonlinear Meta-Optics", CRC Press (2020).
5. S. Keren-Zur, O. Avayu, L. Michaeli, and T. Ellenbogen, "Nonlinear Beam Shaping with Plasmonic Metasurfaces", ACS Photonics 3 117 (2016).
6. C. Schlickriede, S. Kruk, L. Wang, B. Sain, Y. Kivshar, T. Zentgraf, "Nonlinear Imaging with All-Dielectric Metasurfaces", Nano Lett. 20, 4370 (2020).
7. C. Gigli, G. Marino, A. Artioli, D. Rocco, C. De Angelis, J. Claudon, J.M. Gérard, G. Leo, "Tensorial phase control in nonlinear meta-optics", Optica 8, 269 (2021).
8. M. R. Dennis, R. P. King, B. Jack, K. O'Holleran, M. J. Padgett, "Isolated optical vortex knots", Nat. Phys 6, 2 (2010).
9. L. Wang, W. Zhang, H. Yin, and X. Zhang, "Ultrasmall Optical Vortex Knots Generated by Spin-Selective Metasurface Holograms", Adv. Opt. Mater. 7, 1900263 (2019).

DNA nanotechnologies for photonics and sensing

Interfacing quantum emitters and plasmonic resonators with DNA

Jeanne Heintz[1], Claudia Corti[1], Sylvie Marguet[2], Gaëtan Bellot[2], and Sébastien Bidault[1*]
[1]Institut Langevin, ESPCI Paris, Université PSL, CNRS, France
[2]CEA Saclay, IRAMIS, NIMBE, Gif-sur-Yvette, France
[3]CBS - Centre de Biochimie Structurale, CNRS, INSERM, Montpellier, France
[*]corresponding author: sebastien.bidault@espci.fr

Abstract: We discuss how DNA templates can be engineered as smart building materials to associate quantum emitters and plasmonic resonators and to maximize light-matter interactions at room temperature.

Light-matter interactions in condensed media at room-temperature are fundamentally limited by electron-phonon coupling. For instance, while the excitation cross-section of an isolated atom, or of a single quantum emitter at cryogenic temperatures, can reach one half of the wavelength of light squared (meaning that more than 50% of incoming photons will interact for a diffraction-limited excitation); this value is reduced by 6 orders of magnitude for a fluorescent molecule or for a colloidal quantum dot at room temperature because of homogeneous phonon broadening. In order to render the exceptional optical properties of single quantum systems (such as single-photon emission and nonlinearities) efficiently accessible at room temperature and in condensed media, it is essential to enhance and optimize these interaction cross-sections.

Over the last decade, gold nanostructures have shown amazing promise towards this goal thanks to their ability to enhance optical fields by several orders of magnitude in deeply sub-wavelength volumes. However, the nanoscale dimensions of these field enhancements mean that it is extremely difficult to address them in a controlled and reproducible way. To this end, we exploit DNA molecules to create plasmonic resonators with a control over both their nanoscale dimensions and their chemical environment. Using this strategy, we were able to enhance single-photon emission from fluorescent molecules by more than two orders of magnitude in a weak-coupling regime [1,2] and to reach a strong-coupling regime between a plasmonic resonator and 5 organic molecules (figure 1), albeit with low reproducibility [3]. We propose the DNA-based assembly of dimers of plasmonic nanocubes in order to provide reproducible single-molecule strong coupling [4] and to make the coherent interaction of light with single quantum emitters feasible at room temperature.

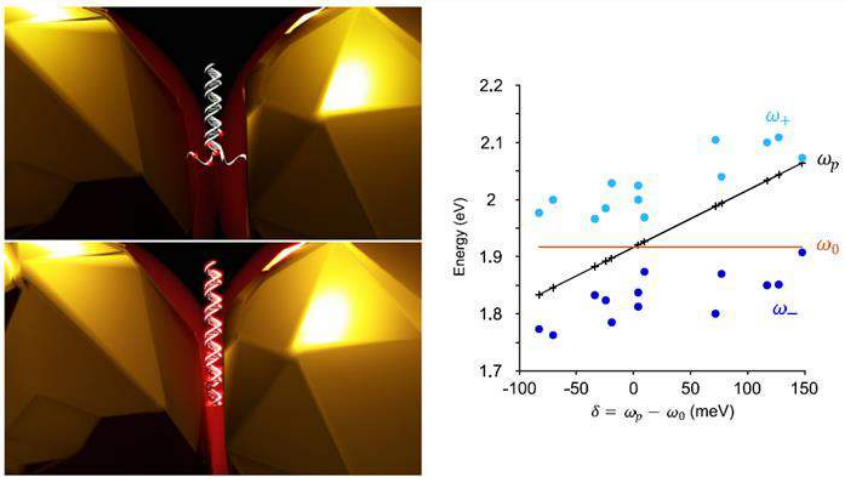


Figure 1: Representation of 5 fluorescent molecules placed in the hotspot of a gold particle dimer using DNA and distribution of eigenenergies in strongly coupled nanostructures exhibiting an anti-crossing behavior.

References

1. Busson, M. P. et al., Nat. Commun. 2012, 3, 962.
2. Bidault, S. et al., ACS Nano 2016, 10, 4806.
3. Heintz, J. et al., ACS Nano 2021, 15, 14732.
4. Heintz, J. et al., J. Phys. Chem. Lett. 2022, 13, 11996.

META 2023, PARIS - FRANCE, JULY 18 – 21, 2023

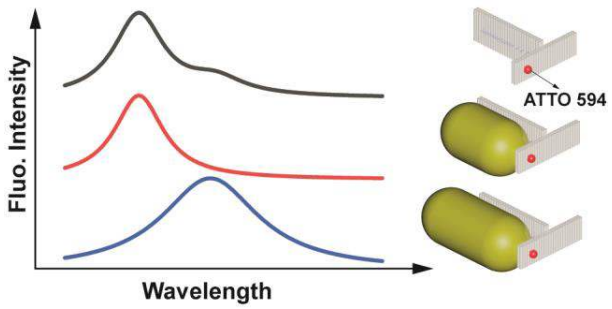
DNA origami assembled nanoantennas for manipulating single-molecule spectral emission

M. Sanz-Paz[1*], F. Zhu[1], N. Bruder[1], K. Kolataj[1], M. Pilo-Pais[1], A. Fernandez-Dominguez[2], and G. P. Acuna[1]

[1]Department of Physics, University of Fribourg, Chemin du Musée 3, Fribourg CH-1700, Switzerland
[2]Departamento de Física Teórica de la Materia Condensada and Condensed Matter Physics Center (IFIMAC), Universidad Autónoma de Madrid, E-28049 Madrid, Spain
[*]corresponding author: maria.sanz@unifr.ch

Abstract: Optical antennas have been widely used for manipulating single-molecule emission properties, including intensity and decay rates, and thus for affecting lifetime, polarization, spectrum, or directivity. Here, we make use of DNA origami as a breadboard to precisely position a single emitter in the vicinity of a single gold nanorod and study their interaction with high accuracy. We show, that we can affect the spectrum of a single fluorophore depending on its relative position and spectral overlap with the gold nanorod.

Optical nanoantennas can affect the decay rates of nearby emitters by modifying the local density of photonic states around them [1,2]. In the weak-coupling limit, and according to the Fermi's Golden Rule, the emission spectrum of a dye is given by the energy of all the possible radiative transitions weighted by the probability of each of them to occur. By engineering the resonance of a nanoantenna, one can selectively enhance specific vibronic transitions of a dye molecule, thus shaping its emission spectrum [3]. Since interactions between emitters and nanoantennas are known to be position dependent, we make here use of DNA origami [4,5] to precisely place an individual dye at different positions around a gold nanorod. We show how this relative position between the nanorod and the emitter affects the emission spectrum of the latter [6]. In particular, we observe the appearance of a second fluorescence peak whose wavelength and intensity are correlated with the fundamental plasmonic resonance of the nanorod, which we extract from its photoluminescence spectrum [7] and will depend on the nanorod's dimensions. This second peak results from the selective enhancement of transitions to different vibrational levels of the excitonic ground state, whose energies are in resonance with the plasmonic one. Finally, we show how this reshaping of the fluorescence spectrum can be used to experimentally determine the wavelength-dependent radiative decay rate enhancement.



Sketch of the experimental configuration, showing the fluorescence emission reshaping experienced by a single fluorophore in the presence of a nanorod, in a way that depends on the dimensions of the latter.

References

1. Novotny, L., and van Hulst, N. "Antennas for Light," *Nat. Photonics*, *5*, 83–90, 2011.
2. Anger, P., Bharadwaj, P., and Novotny, L. "Enhancement and Quenching of Single-Molecule Fluorescence," *Phys. Rev. Lett.*, 96, 113002, 2006
3. Ringler, M., Schwemer, A., Wunderlich, M., Nichtl, A., Kürzinger, K., Klar, T. A., and Feldmann, J. "Shaping Emission Spectra of Fluorescent Molecules with Single Plasmonic Nanoresonators," *Phys. Rev. Lett.*, 100, 20, 1– 4, 2008
4. Rothemund, P. W. K. "Folding DNA to create nanoscale shapes and patterns," *Nature*, 440, 297–302, 2006
5. Pilo-Pais, M., Acuna, G. P., Tinnefeld, P., and Liedl, T. "Sculpting Light by Arranging Optical Components with DNA Nanostructures," *MRS Bull*, 42, 12, 936–942, 2017
6. Saemisch, L., Liebel, M., and van Hulst, N. F. "Control of Vibronic Transition Rates by Resonant Single-Molecule-Nanoantenna Coupling," *Nano Lett.*, 20, 6, 4537–4542, 2020
7. Cai, Y.Y., Liu, J.G., Tauzin, L.J., Sung, E., Zhang, H., Joplin, A., Chang, W.-S., Nordlander, P., and Link, S. "Photoluminescence of Gold Nanorods: Purcell Effect Enhanced Emission from Hot Carriers," *ACS Nano* 12, 2, 976–985, 2018

DNA Precision Placement Allows for Studying and Exploiting Energy Transfer beyond the Classical FRET Limit

M. Chiriboga[1], C. M. Green[1], D. Mathur[2], Y. Kim[3], J. S. Melinger[4], I.L. Medintz[1], and S. A. Díaz[1*]

[1]Center for Bio/Molecular Science and Engineering Code 6900, U.S. Naval Research Laboratory, United States of America
[2] Department of Chemistry, Case Western Reserve University, United States of America
[3]Center for Materials Physics and Technology Code 6390, U.S. Naval Research Laboratory, United States of America
[4]Electronic Science and Technology Division Code 6800, U.S. Naval Research Laboratory, United States of America
[*]corresponding author: sebastian.diaz@nrl.navy.mil

Abstract: DNA nanotechnology allows for nm precision positioning of moieties, be these organic dyes, or inorganic nanoparticles. Using this we can study and exploit energy transfer beyond the classic FRET limit in manners that are not available with other methodologies. Using DNA bricks and organic dyes we have demonstrated point-to-plane transfer and its r^{-4} dependence we also exploited DNA origami for positioning of semiconductor quantum dots and plasmonic gold nanoparticles to investigate nanosurface energy transfer (NSET).

The most common use of Förster resonance energy transfer (FRET) is the interaction of a single dipole-dipole pair, i.e. between a single D(onor) and A(cceptor). In this case the FRET efficiency decays with the D-A distance (r_{DA}) to the sixth power. This makes FRET a powerful tool for determining nanoscale changes in position or orientation. Yet, similar dipole-dipole interaction mechanisms can be imagined in much more complex systems, such as interactions where the dipole of a D is interacting with an A surface, which can be either molecular or continuous. In these cases the mathematical models can change drastically, for example changing the r_{DA} dependence from r^{-6} to r^{-4}. To undertake molecular energy transfer studies, nm control of positioning is required due to the large changes in efficiency on that scale. DNA nanotechnology provides that capability through well-characterized bioconjugation strategies in combination with designable and modular 2-D and 3-D nanostructures.

Through the use of DNA bricks 3-D nanostructures which incorporate five two-dimensional planes with each controllably having 1 to 12 copies of five different D, A, or intermediary organic dyes we were able to access clear signatures of sheet regime FRET, also described as point-to-plane transfer (See Figure 1), which accesses r^{-4} transfer efficiencies.[1] Nanostructure characterization, steady-state and time-resolved spectroscopic data, along with molecular dynamics modeling and numerical simulations, allowed us to compare experimental energy transfer efficiencies to theoretical expectations.

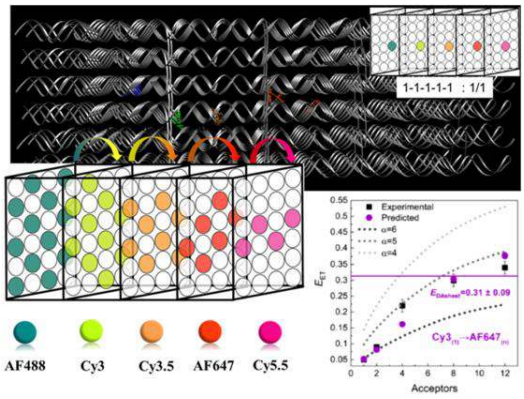


Figure 1: (Top) Chimera schematic of DNA brick with a single dye per plane. (Bottom) Cartoon demonstrating the variation of dyes that can be placed in each plane. Comparison of experimental and theoretical prediction of energy transfer as a function of the number of acceptors in a plane. Adapted from Reference 1.

In a complimentary approach, we are utilizing 2-D DNA origami to look at the energy transfer between a QD and a single dye A and compare that with a single gold nanoparticle (AuNP) A. We utilize a histag peptide-peptide nucleic acid hybrid approach to efficiently conjugate the QD to the DNA origami (See Figure 2).[2] The intent is to distinguish between the traditional FRET mechanism of energy transfer and nanosurface energy transfer (NSET), also known as dipole–metal plane coupling, that is theorized to occur between a QD and AuNP.[3] We aim to deposit the structures into films which can then be cryogenically cooled down to as low as 4 K to vary the transfer efficiency without varying the r_{DA} which should allow us to distinguish whether r^{-6} (FRET) or r^{-4} (NSET) or something in between is occuring.

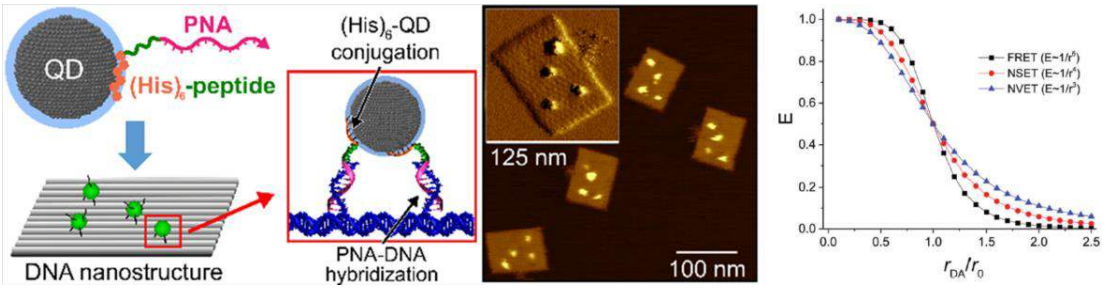


Figure 2: (Left) Schematic of histag peptide-peptide nucleic acid QD capture. (Middle) AFM images of QD captured onto DNA breadboard. (Right) Comparison of energy transfer mechanism efficiency as a function of distance. Adapted from References 2 and 3.

The authors gratefully acknowledge the Office of Naval Research, the U. S. Naval Research Laboratory (NRL), and the NRL-Nanosciences Institute.

References

1. Mathur, D. et al "Understanding Förster Resonance Energy Transfer in the Sheet Regime with DNA Brick-Based Dye Networks," ACS Nano, Vol. 15, No. 10, 16452–16468, 2021.
2. Green, C. M., et al, "Direct and Efficient Conjugation of Quantum Dots to DNA Nanostructures with Peptide-PNA," ACS Nano, Vol. 15, No. 5, 9101-9110, 2021.
3. Díaz, S. A., et al, "Understanding Energy Transfer with Luminescent Gold Nanoclusters: A Promising New Transduction Modality for Biorelated Applications," J. Mater. Chem. B, Vol. 5, No. 39, 7907-7926, 2017.

DNA-origami-based plasmonic assemblies with tailored stimuli and optical responses

A. Kuzyk[1*], M-K. Nguyen[1], J. Ryssy[1], J. Loo[1], R. Klajn[2], P. Albella[3], Y. Huang[1]

[1]Department of Neuroscience and Biomedical Engineering, School of Science, Aalto University, Finland
[2]Department of Organic Chemistry, Weizmann Institute of Science, Israel
3 University of Cantabria, Spain
[*]corresponding author: anton.kuzyk@aalto.fi

Abstract: The DNA origami technique has emerged as one of the most versatile bottom-up nanofabrication methods. In this talk I will discuss our recent results related to application of DNA origami for fabrication of plasmonic systems with novel stimuli and optical responses. Specifically, we will present fabrication of i) light-responsive dynamic plasmonic assemblies with easily regulated steady out-of-equilibrium states[1]; ii) chiral plasmonic systems with visually detectable reconfigurable optical activity; iii) metal shells with tailored complex morphologies and optical responses within near-infrared transparency window(s).

References

1. Ryssy, J *et al.* "Light-Responsive Dynamic DNA-Origami-Based Plasmonic Assemblies," Angew. Chem. Int. Ed. Vol 60, No. 11, 5859-5863, 2021

Colloidal Silicon Nanospheres as Building Blocks for Photonic Applications

H. Sugimoto[1*]

[1]Department of Electrical and Electronic Engineering, Graduate School of Engineering at Kobe University, Japan
[*]corresponding author: sugimoto@eedept.kobe-u.ac.jp

Abstract: Low-loss optical nanoantennas made of high index dielectrics have attracted much attention as an alternative to plasmonic antennas that often suffer from losses of noble metals. Here, we develop Mie resonant crystalline Si nanospheres in the size range of 100-300 nm dispersible in solution. Monodisperse colloidal Mie resonators not only exhibit vivid colors but also act as colloidal metamaterial (i. e., meta-fluids) that have advantages in solution-based fabrication of thin film optical devices. In addition, colloidal dispersions of Si nanospheres enable the formation of functional nanoantennas for enhanced light matter interactions using printing and self-assembly technologies.

Dielectric nanoparticles exhibit electric and magnetic Mie resonances and provide opportunities for manipulating and enhancing the light-matter interactions. The dielectric nanoantennas have been usually fabricated by electron beam lithographically on the solid substrate and thus the applicability of the solution based assembly techniques have been limited compared to the plasmonic counterparts since gold and silver colloids that are commercially available.

In this talk, we present development of colloidal dispersion of perfectly spherical silicon nanoparticles dispersible in alcohol by thermal disproportionation of silicon monoxide at very high temperature (>1450°C) followed by chemical etching. We also developed monodisperse silicon nanoparticles by applying density gradient centrifugation process for the size separation.[1-4] Figure 1a shows the solution in which different sized silicon nanoparticles are dispersed. The solutions exhibit bright scattering colors depending on nanoparticles sizes. TEM image in Fig. 1b shows the monodisperse silicon nanoparticles with highly spherical shapes. In addition, Figure 1c demonstrates high crystallinity of the particle. We show fundamental properties of the silicon nanoparticles including directional scattering and fluorescence enhancement by exploiting magnetic Purcell effect of Mie resonances.[5-7]

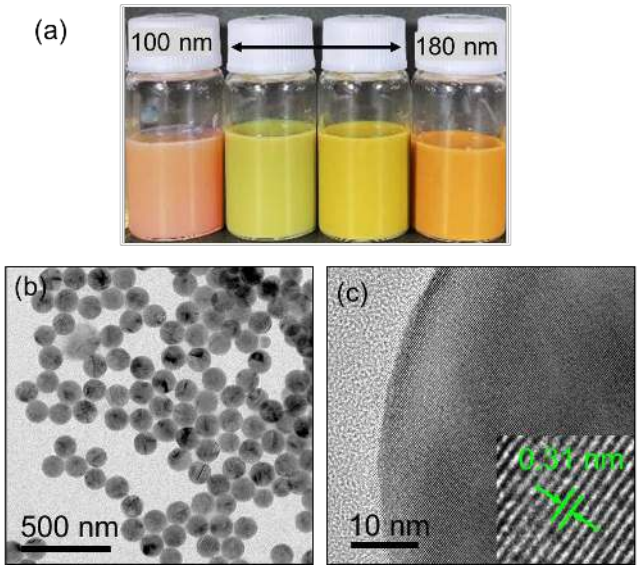


Figure 1. Dual nanoantennas. Helicity of incident light is preserved at Kerker condition of dielectric nanoantennas.

In this work, we also introduce the assembly of the silicon nanoparticles.[8] By properly assembling high index nanoparticles, the optical response can be tailored via the near field coupling between nanoparticles. The coupling provides accessible electric and magnetic hot spots in an assembly, and modulates the directionality of the light scattering. We develop a process to fabricate linear and zigzag arrays of silicon nanoparticles by using a

template assisted capillary assembly method. From angle and polarization resolved scattering spectroscopy, we show that coupling of the electric dipole and magnetic dipole resonances between nanoparticles strongly modifies the scattering spectra. The results demonstrate the potential of the silicon nanoparticles for development of functional optical nanoantennas by employing further sophisticated assembly techniques by using DNAs.

References

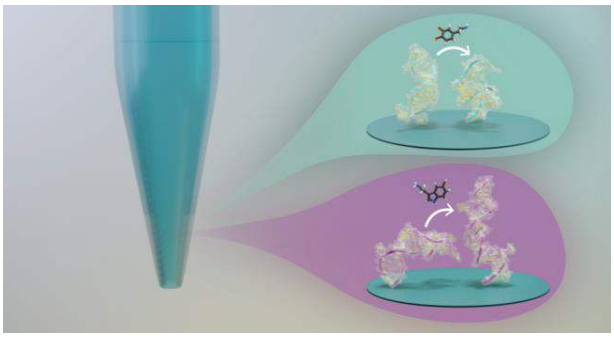
1. Sugimoto, H, *et al.*, "Mie Resonator Color Inks of Monodispersed and Perfectly Spherical Crystalline Silicon Nanoparticles", Advanced Optical Materials, Vol. 8, Issue 12, 2000033, 2020.
2. Hinamoto, T *et al.*, "Colloidal Solutions of Silicon Nanospheres toward All-Dielectric Optical Metafluids", Nano Letters, Vol. 20, Issue 10, 7737-7743, 2020.
3. Sugimoto, H, Fujii, M, "Colloidal Mie Resonators for All-Dielectric Meta-Optics", Advanced Photonics Research, Vol. 2, Issue 4, 2000111, 2021.
4. Sugimoto, H, Fujii, M, "Colloidal Mie Resonant Silicon Nanoparticles", Nanotechnology, Topical Review, Vol. 32, Number 45, 452001, 2021.
5. Sugimoto, H, Fujii, M, "Magnetic Purcell Enhancement by Magnetic Quadrupole Resonance of Dielectric Nanosphere Antenna", ACS Photonics, Vol. 8, Issue 6, 1794, 2021.
6. Shinomiya, H, *et al.*, "Enhanced Light Emission from Monolayer MoS2 by Doubly Resonant Spherical Si Nanoantennas", ACS Photonics, Vol. 9, Issue 5, 1741-1747, 2022.
7. Adachi, M, *et al.*, "Fluorophore-Decorated Mie Resonant Silicon Nanosphere for Scattering/Fluorescence Dual-Mode Imaging", Small, 2207318, 2023.
8. Negoro, H, *et al.*, "Template-Assisted Self-Assembly of Colloidal Silicon Nanoparticles for All-Dielectric Nanoantenna", Advanced Optical Materials, Vol. 10, Issue 8, 2102750, 2022.

Neurotransmitter Sensing *via* Ionic Flux Modulation Through Aptamer Conformational Rearrangement

Annina Stuber[1], Ali Douaki[2], Julian Hengsteler[1], Denis Buckingham[1], Dmitry Momotenko[3], Denis Garoli[2], and Nako Nakatsuka[1]

1. Laboratory of Biosensors and Bioelectronics, Institute for Biomedical Engineering, ETH Zürich, CH-8092, Switzerland
2. Instituto Italiano di Tecnologia, Via Morego 30, 16163, Genova, Italy
3. Department of Chemistry, Carl von Ossietzky University of Oldenburg, Oldenburg D-26129, Germany

Abstract: Aptamers are artificially engineered DNA sequences which can change their conformation upon the binding of their specific target. Aptamers immobilized inside of a nanopore regulate ionic flux through target recognition, as the conformation switch rearranges the corona of charge density within the orifice. Gaining mechanistic insight into these dynamic nano-systems would enable the development and tailoring of new methods for small-molecule sensing. We have explored the link between aptamer conformation and signal modulation both experimental and theoretically.



Summary: In this work, we immobilized dopamine-specific aptamers inside of nano-scaled orifices. We then demonstrated that the binding of dopamine modulates the ionic flux antipodally when compared to the target specific response of nanopipettes functionalized with serotonin specific aptamers [1], even though both neurotransmitters have the same charge. We identified the opposite conformational changes upon analyte capture as being responsible for the distinctive signal behaviors, supported by combining experimental quartz crystal microbalance with dissipation monitoring results with theoretical finite element method and molecular dynamic simulations. Our investigations improve our understanding of the complex interactions occurring in confined nanoscale environments and have the possibility of driving further innovations in bioinspired nanopore technologies for small molecule sensing.

Acknowledgements: The authors thank Prof. Janos Vörös for helpful discussions. A.S. and N. N. thank the ETH Zürich research grant (ETH-13 21-2) and A.D. and D.G. the European Union under the Horizon 2020 Program, FET-Open: DNA-FAIRYLIGHTS, Grant Agreement No. 964995. A.D. also thanks Walter Rocchia for the access to the computation

facility. D.M. acknowledges the financial support from the European Research Council (ERC) under the European Union's Horizon 2020 research and innovation program (Grant Agreement 948238).

References:

1. Nakatsuka, N., Faillétaz, A., Eggemann, D., Forro, C., Vörös, J., Momotenko, D., "Aptamer Conformational Change Enables Serotonin Biosensing with Nanopipettes" Anal. Chem. Vol. 93, No.8, 4033–4041, 2021.

META 2023, PARIS - FRANCE, JULY 18 – 21, 2023

Probing fast dynamics of single DNA molecules in real-time using plasmon-enhanced fluorescence

S. Nooteboom[1], K. Okholm[2], V. Lamberti[1], B. Oomen[1], S. Dey[1], D. Sutherland[2], and P. Zijlstra[1]

[1]Eindhoven University of Technology, Department of Applied Physics, The Netherlands

2 iNANO Center, Aarhus University, Denmark

[*]corresponding author: p.zijlstra@tue.nl

Abstract: Plasmon-enhanced fluorescence provides an attractive avenue toward single-molecule studies, providing high sensitivity and superior signal-to-noise ratio. I will describe our recent efforts in this field, focusing on the use of plasmon-enhanced fluorescence to reveal single-molecule DNA dynamics on microsecond timescales and in real-time.

Biomolecules such as DNA are at the basis of all processes in living organisms. These molecules exhibit intra- and intermolecular interactions on timescales from nanoseconds to hours. Understanding such mechanisms is key to solving problems in many fields including diagnostics and molecular biology. Typically, these mechanisms are studied using single-molecule fluorescence,[1] a powerful technique that allows for the observation of real-time biomolecular dynamics while revealing spatial and temporal heterogeneity. However, the brightness and photon budget of the required fluorophores are limited by saturation and bleaching, prohibiting direct observation of sub-ms processes in most cases.[2] Methods based on optical tweezers have better time resolution, but are not force-free.[3]

In this work, we optimize the size and shape of nanoantennas based on gold nanorods[4] to harvest millions of photons per second from a single fluorophore coupled to the antenna. This provides superior signals compared to free space fluorophores, and dramatically increases the signal-to-noise ratio at short timescales. Using methods based on DNA-PAINT,[5] we study the dynamics of very short complementarity regions and Holliday junctions in real-time with microsecond integration times.

References

1. Bandyopadhyay, D.; Mishra, P. P. (2021). Front. Mol. Biosci., 8 (September), 1–18.
2. Ha, T.; Tinnefeld, P. (2012). Annu. Rev. Phys. Chem., 63 (1), 595–617.
3. Neupane, K.; Foster, D. A. N.; Dee, D. R.; Yu, H.; Wang, F.; Woodside, M. T. (2016). Science, 352 (6282), 239–242.
4. Wang, Y.; Horáček, M.; Zijlstra, P. (2020). J. Phys. Chem. Lett., 11, 1962–1969.
5. Nooteboom, S. W.; Wang, Y.; Dey, S.; Zijlstra, P. (2022). Small, 18 (31), 2201602.

Colorimetric sensing with hybrid gold-DNA origami nanostructures

Claudia Corti[1]*, Elise Gayet [1], Nesrine Aissaoui [2], Sylvie Marguet [3], Gaetan Bellot[2], Sébastien Bidault[1]

[1] Institut Langevin, ESPCI Paris, Université PSL, CNRS, Paris, France
[2]CBS - Centre de Biochimie Structurale, CNRS, INSERM, Montpellier, France
[3] CEA Saclay, Univ. Paris-Saclay, IRAMIS, NIMBE, Gif-sur-Yvette, France
*corresponding author: claudia.corti@espci.fr

Abstract: We develop a colorimetric sensing platform compatible with single-molecule detection by assembling gold-nanosphere dimers on a Y-shaped 3D DNA origami that acts as a nanoscale actuator in response to specific stimuli.

DNA origamis are a flexible platform to produce nanostructures that shift their morphology when interacting with specific target molecules, such as DNA/RNA strands, proteins, or specific cations [1]. To translate the conformational changes of a DNA origami in colorimetric information, we exploit the nanoscale dependence of plasmon coupling between two gold nanospheres. Dark-field microscopy allows us to monitor such nanoscale distance changes on a color camera [2,3]. The design of our Y-shaped 3D DNA origami (Fig. 1-a) features an active site, whose conformation can be tuned by hybridizing specific DNA single strands (Fig. 1-b), and two arms on which gold nanospheres are attached. The overall morphology of the hybrid nanostructure is governed by the geometry of the DNA origami but also by steric and electrostatic repulsion between gold nanospheres. We observe that the difference in conformation of the active site is only visible in the optical response of the nanostructures for high ionic strengths, when these steric and electrostatic repulsions are reduced.
One-step colorimetric sensing of DNA single strands is achieved at high ionic strengths by using a strand displacement reaction (Fig. 1-c). These measurements are carried out both by performing single-nanostructure scattering spectroscopy (Fig. 1-d) and by monitoring the hue of single dimers in dark-field images (Fig. 1-e), obtaining similar statistical responses. These results open exciting perspectives for the colorimetric sensing of individual DNA strands on a color camera.

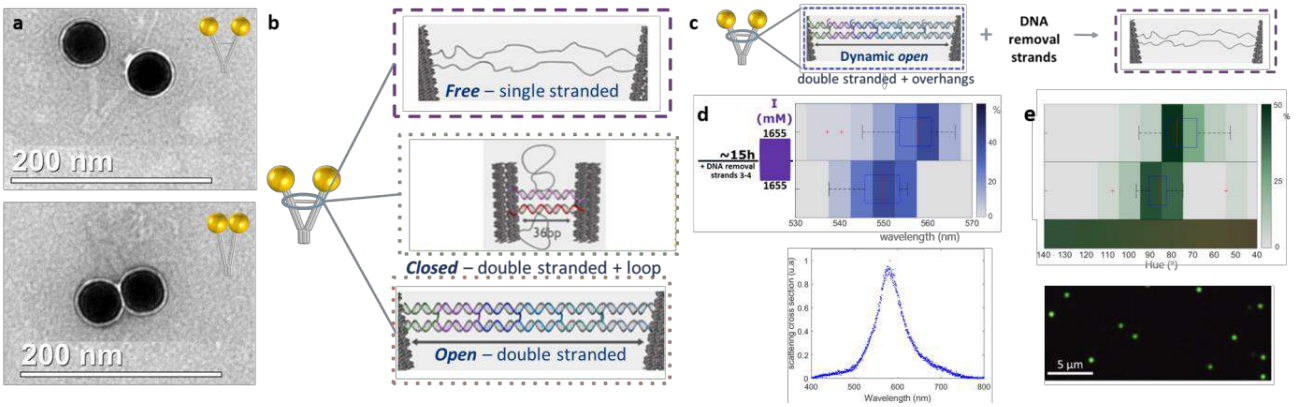


Figure 1: (a) EM images with negative staining of 40nm gold particle dimers with DNA origami in open (top) and closed (bottom) conformations. (b) Schemes of the different conformations of the active site. (c) Strand-displacement reaction monitored by (d) single-nanostructure scattering spectroscopy and (e) colorimetric sensing. (d) Distributions of resonance wavelength (top) obtained from single-nanostructure scattering spectra (bottom). (e) Distributions of maximum hue value of single-nanostructures (top), retrieved from a dark-field color-camera image (bottom).

References

[1] Y. Ke et al. 2016. Nat. Commun. 7:10935.

[2] L. Lermusiaux et al. 2015. ACS Nano 9:978.

[3] L. Lermusiaux et al. 2018. Langmuir 34:14946.

Superconducting Josephson classical and quantum metamaterials

META 2023, PARIS - FRANCE, JULY 18 – 21, 2023

Slowing down microwave photons in a superconducting quantum metamaterial

A. V. Ustinov*

Physics Institute, Karlsruhe Institute of Technology, Germany
*corresponding author: ustinov@kit.edu

Abstract: Progress in quantum information processing leads to a rising demand for devices to control the propagation of electromagnetic wave pulses and to ultimately realize a universal and efficient quantum memory. While in recent years significant progress has been made to realize slow light and quantum memories with atoms at optical frequencies, superconducting circuits in the microwave domain still lack such devices. We present an overview of our recent experiments with arrays of eight frequency-tunable superconducting qubits coupled to a one-dimensional waveguide.

Waveguide quantum electrodynamics offers a wide range of possibilities to effectively engineer interactions between artificial atoms via a one-dimensional open waveguide. While these interactions have been experimentally studied in the few qubit limit, it is relevant to demonstrate the collective properties of such systems for larger arrays of qubits in a metamaterial configuration. We will present our recent results of experimental study a metamaterial made of eight superconducting transmon qubits with local frequency control. By consecutively bringing the qubits to a common resonance frequency we observe the super- and sub-radiant states, as well as the emergence of a bandgap [1].

Making use of the quantum nonlinearity of qubits coupled to the mode continuum of a waveguide, we demonstrate formation of a transparency window in the bandgap region of the ensemble. We also experimentally demonstrate slowing down electromagnetic waves in this qubit array. Time-resolved experiments show electromagnetic wave group velocities reduced by a factor of about 1500 in the single-photon regime [2]. We analyze two complementary approaches, one relying on dressed states of the Autler–Townes splitting and the other based on a tailored dispersion profile using the qubits frequency tunability. Depending on the method used, the speed of light can be controlled with an additional microwave tone or an effective qubit detuning.

Our findings demonstrate high flexibility of superconducting circuits to realize custom band structures and open the door to microwave dispersion engineering in the quantum regime.

This work has received funding from European Union’s Horizon 2020 Research and Innovation Programme under Grant Agreement No. 863313 (SUPERGALAX).

References

1. Brehm, J. D., Poddubny A. N., Stehli, A., Wolz, T., Rotzinger, H., Ustinov, A. V. npj Quantum Materials, Vol. 6, No. 1, 10 (2021).
2. Brehm, J. D., Gebauer, R., Stehli, A., Poddubny, A. N., Sander, O., Rotzinger, H., Ustinov, A. V. Appl. Phys. Lett., Vol. 121, No. 20, 204001 (2022).

Quantum Analogues of Dissipative Circuit Elements

A. M. Zagoskin[1]

[1]Department of Physics, Loughborough University, UK
*a.zagoskin@lboro.ac.uk

Abstract: Quantum analogues of non-dissipative circuit elements, that is, structures which can exist in a coherent superposition of states with different values of inductance or capacitance, are readily realized using superconducting qubits. Here I show the possibility of the existence of quantum analogues of dissipative circuit elements, which demonstrate superpositions of states with different resistances or memristances.

A circuit containing a superconducting quantum bit can demonstrate a quantum contribution to its (inverse) inductance [1] or capacitance [2] dependent on the qubit state. One can therefore speak of full quantum analogues of inductance and capacitance, that is, non-dissipative circuit elements which can be in a superposition of states with different values of these parameters [3].



Figure 1 (reproduced from [3]). A quantum point contact in a 2D electron gas controlled by a qubit near the pinching point can be considered as a 1D conductor interrupted by a scatterer. The transparency of the contact is controlled by the quantum state $|j\rangle$ *of the qubit.*

The situation may seem qualitatively different for quantum analogues of dissipative circuit elements (resistors and memristors) [4]. Indeed, the dissipation inherent in these elements would seem to destroy all quantum coherence between the superposed states, so that the best one can hope for is observing random fluctuations between two values of resistance or memristance [5,6].

The discussion of coherent superposition of states in quantum memristors requires a more technical approach (see Ref.[7]). Here we restrict ourselves to the case of quantum resistors and argue that quantum superpositions of states with different resistances are possible, e.g., in the situation of Fig.1. Here the region which determines the conductance is spatially separated from the regions where the corresponding dissipation occurs. Therefore the superposition lifetime can exist at least on the scale of the electron travel time $\tau \sim l/v$. The actual lifetime of a superposition can exceed this minimum for small enough voltages across the system, since the decoherence rate of the qubit controlling the point contact is (see [8]) $\Gamma = -\frac{eV}{h}\ln|t_0 t_1^* + r_0 r_1^*|$.

Here $t_{0,1}$ and $r_{0,1}$ are the transmission and reflection amplitudes of the contact in the corresponding quantum states. The quantum conductance of the system is thus

$$\hat{G} = \frac{e^2}{h}\left(|t_0|^2|0\rangle\langle 0| + |t_1|^2|1\rangle\langle 1|\right) = G_0|0\rangle\langle 0| + G_1|1\rangle\langle 1|,$$

similar to the expressions for quantum inductance and capacitance.

The realization of fully quantum analogues of all four classical circuit elements will simplify the design and advance the development of quantum metamaterial-based devices, such as detectors, antennas and neural networks.

I am grateful to C. Huggins, A. Balanov, S. Saveliev and P. Navez for stimulating discussions. This research was supported by the European Union's Horizon 2020 Research and Innovation Program under Grant Agreement No. 863313 (SUPERGALAX).

References

1. Greenberg, Ya.S., A. Izmalkov, M. Grajcar et al. Phys. Rev. B, Vol. 66, 214525, 2002.
2. Sillanpää, M.A., T. Lehtinen, A. Paila et al. Phys. Rev. Lett., Vol. 95, 206806, 2005.
3. Zagoskin, A.M. "Quantum Engineering: Theory and Design of Quantum Coherent Structures". Cambridge University Press, 2011.
4. Chua, L. IEEE Trans. on Circuit Theory, Vol. 18, 507, 1971.
5. Kumar, S., F. Cardenas-Lopez, N. Hegade et al. Phys. Rev. A, Vol. 104, 062605, 2021.
6. Spagnolo, M., J. Morris, S. Piacentini et al. Nature Photonics, Vol. 16, 318-323, 2022.
7. Huggins, C., S. Savel'ev, A. Balanov and A. Zagoskin. arXiv:2203.13044, 2022 (EPJ B, in press).
8. Averin, D.V., and E.V. Sukhorukov. Phys. Rev. Lett. Vol. 95, 126803, 2005.

META 2023, PARIS - FRANCE, JULY 18 – 21, 2023

Improved Method for Characterizing Resonance Quality Factor in Superconducting Resonators

Martin Weides
James Watt School of Engineering and Centre for Quantum Technology, University of Glasgow, Glasgow, G12 8QQ, UK
Martin.Weides@glasgow.ac.uk

Abstract: We present a study on tunable Fano-type resonances in a superconducting coplanar cavity coupled to multiple artificial atoms [1,2]. By applying bias current through nearby control lines, the shape of the measured cavity transmission can be continuously tuned, exhibiting Fano-type resonances with a dispersive shift that can be observed as a peak or a dip. We demonstrate how the heating of the environment can invert the line shape of the cavity, and how this Fano-peak inversion is possible due to a tunable interference between a microwave transmission through a background and through the cavity. We also discuss how the background transmission can be accounted for by Jaynes-Cummings type models via modified boundary conditions.
Additionally, we investigate the characterization of material losses in superconducting resonators, using a combination of simulation and experiment to determine the reliability of a fitting algorithm for separating internal and coupling quality factors of the resonance quality factor [3,4]. We propose a novel measurement protocol to reduce fitting errors and mitigate the influence of the measurement background on fit results.
Our findings provide insights into the tunability and manipulation of Fano-type resonances in superconducting quantum devices and can be generalized for other resonance systems beyond superconducting resonators.

References

1. [1] Phys. Rev. A 99, 063804 (2019)
2. [2] Phys. Rev. Applied 14, 024025 (2020)
3. [3] Review of Scientific Instruments 86, 024706 (2015)
4. [4] arXiv:2301.06364

META 2023, PARIS - FRANCE, JULY 18 – 21, 2023

Development of high temperature superconducting terahertz emitters

T. Kashiwagi[1*], S. Nakagawa[1,2], R. Kikuchi[1], S. Yamada[1], Y. Enomoto[1], Y. Yamauchi[1], H. Nakao[3], S. Ishida[2], H. Eisaki[2], T. Mochiku[4], M. Tsujimoto[5] and H. Minami[1]

[1]Graduate School of Pure & Applied Sciences, University of Tsukuba, 1-1-1 Tennodai, Tsukuba, Ibaraki 305-8573, Japan.
[2]Research Institute for Advanced Electronics and Photonics, National Institute of Advanced Industrial Science and Technology (AIST), 1-1-1 Umezono, Tsukuba, Ibaraki 305-8568, Japan
[3]Photon Factory, Institute of Materials Structure Science, High Energy Accelerator Research Organization (KEK), Tsukuba, Ibaraki 305-0801, Japan
[4]National Institute for Materials Science (NIMS), 1-2-1 Sengen, Tsukuba, Ibaraki 305-0047, Japan
[5]Research Center for Emerging Computing Technologies, National Institute of Advanced Industrial Science and Technology (AIST), Central2, 1-1-1 Umezono, Tsukuba, Ibaraki 305-8568, Japan
[*]corresponding author: kashiwagi@ims.tsukuba.ac.jp

Abstract: To obtain high performance THz-waves emitting devices made by single crystals of high temperature superconductor $Bi_2Sr_2CaCu_2O_{8+\delta}$(Bi2212), an understanding of the device characteristics based on the material characteristics would be an important issue. In principle, electric characteristics of the intrinsic Josephson junctions (IJJs) constructed in Bi2212 crystals strongly depend on the crystal conditions such as carrier concentrations, crystal defects, quality of atomic scale of Josephson junctions. We have studied material and device characteristics of Bi2212 crystals prepared with different annealing conditions.

THz-waves emitters based on the ac Josephson effect have been developed using a single crystal of high-T_c superconductor $Bi_2Sr_2CaCu_2O_{8+\delta}$ (abbreviated as Bi2212)[1]. Single crystals of Bi2212 consist of insulating Bi_2O_2 layers and superconducting CuO_2 layers stacking alternately along the crystallographic *c*-axis and these stacks are known as intrinsic Josephson junctions (IJJs)[2]. THz-waves can be obtained by processing Bi2212 single crystals into mesa structures and applying dc bias voltages across the IJJs[1]. It is noted that the device characteristics are summarized in the several review papers[3]. Most previous research has primarily focused on their emitting characteristics, although some studies have investigated the device characteristics of emitters under different annealing conditions and substitution effects. Recent advancements in knowledge and fabrication techniques have enabled us to study the device characteristics connected with the material properties of the compound. In this study, we prepared Bi2212 crystals with different oxygen contents δ, and compared the crystal characteristics and device characteristics in order to obtain further understanding of the role of excess oxygen δ for the device.

$Bi_{2+x}Sr_{2-x}CaCu_2O_{8+\delta}$ single crystals prepared with nominal composition ratios of Bi/Sr = 2.15/1.85 (x = 0.15) were grown using a floating zone furnace. The grown crystals were cut into square shapes with several mm^2. Then, to adjust oxygen contents δ of the crystals, they were annealed either under 0.2%-O_2 gas flow at 650°C or under N_2 gas flow at 600°C. At the end of the annealing process, the crystals were quenched to stabilize oxygen contents in the crystals. To fabricate a Bi2212 crystal chip for a THz-emitter, a wet etching method was used[4]. After that, these chips were assembled as Bi2212 THz-waves emitters using a sandwich structure developed in our group[5].

As for the characterization of the fabricated crystal chips, X-ray diffraction was performed with ω and θ-2θ scan to evaluate the homogeneity of the crystals and the lattice constants. A four-circle diffractometer was used at BL-4C in Photon Factory, High Energy Accelerator Research Organization (KEK). The incident X-ray energy was set to be 8.8 keV through a Si(111) double-crystal monochromator.

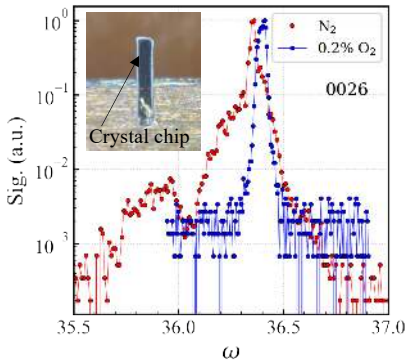


Fig.1 ω scan plot for the crystal chips. Inset displays an optical photograph of the sample.

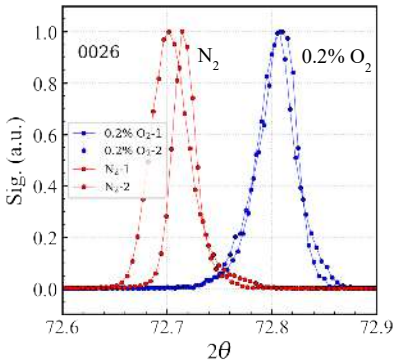


Fig. 2 θ-2θ scan plot for the crystal chips.

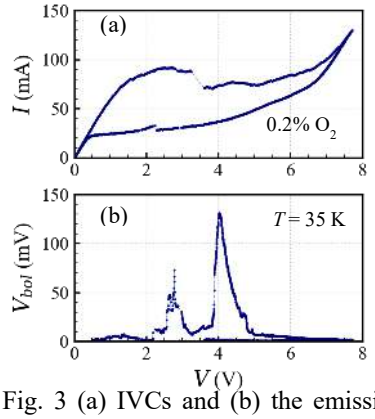


Fig. 3 (a) IVCs and (b) the emission intensities detected by the bolometer at 35 K.

As for the characterization of the Bi2212 THz-emitters, the fabricated devices were mounted on a cold finger of a helium-flow type of cryostat (Oxford Instruments, CF1104) equipped with optical windows. The electrical characteristics of the devices were measured using a conventional two-terminal method. An InSb hot-electron bolometer (HEB) (QMC Instruments, QFI/2BI) was used to detect the electro-magnetic waves from the devices.

The inset of Fig. 1 displays an optical photograph of a 0.2%-O_2-annealed crystal chip with the dimensions of ~65×390×6 μm^3. Figure 1 shows typical ω-scan plots measured around 0026 for the 0.2%-O_2-annealed and the N_2-annealed samples. The data were normalized by the values of the maximum peak intensities of the scans. In this case, the curve profile suggests that the crystal homogeneity of the 0.2%-O_2-annealed sample is higher than that of the N_2-annealed one. It is noted that the curve profile seems to depend on the crystal chips. Figure 2 shows the θ-2θ scan plots measured around 0026 for the samples. We measured two samples for each annealing conditions. The plot indicates that the lattice constant of the c-axis becomes longer with decrease of the oxygen contents of the crystal. The difference of the lattice constant and the carrier density would be reflected in the device characteristics. For the device characteristics, a clear THz emission was only observed from the 0.2%-O_2-annealed crystal chip. Figure 3 (a) and (b) display the current-voltage characteristics (IVCs) and the applied bias voltage dependence of the emission intensities detected the bolometer (V_{bol}) for the 0.2%-O_2-annealed one at 35 K. The clear emission is observed at around 4 V (35 mA). In the conference, we will discuss relationships between the device and material characteristics in detail.

References

1. L. Ozyuzer, *et al.* "Emission of Coherent THz Radiation from Superconductors," Science, Vol. 318, 1291-1293, 2007.
2. R. Kleiner, F. Steinmeyer, G. Kunkel, and P. Müller, "Intrinsic Josephson effects in $Bi_2Sr_2CaCu_2O_8$ single crystals," Phys. Rev. Lett. Vol. 68, 2394, 1992.
3. U. Welp, K. Kadowaki, and R. Kleiner, "Superconducting emitters of THz radiation," Nat. Photon. Vol. 7, 702-710, 2013., I. Kakeya, and H. Wang, "Terahertz-wave emission from Bi2212 intrinsic Josephson junctions: a review on recent progress," Supercond. Sci. Technol. Vol. 29, 073001, 2016., R. Kleiner & H.B. Wang, "Terahertz emission from $Bi_2Sr_2CaCu_2O_{8+\delta}$ intrinsic Josephson junction stacks," J. Appl. Phys. Vol. 126, 171101, 2019., K. Delfanazari *et al.*, "Integrated, Portable, Tunable, and Coherent Terahertz Sources and Sensitive Detectors Based on Layered Superconductors," Proc. IEEE Vol. 108, 721-734, 2020.
4. T. Imai *et al.*, "Investigation of wet etching solutions and method for thicker stand alone type of mesa structures of Bi2212 single crystals," Jpn. J. Appl. Phys. Vol.60, 126501, 2021.
5. T. Kashiwagi *et al.*, "Efficient Fabrication of Intrinsic-Josephson-Junction Terahertz Oscillators with Greatly Reduced Self-Heating Effects," Phys. Rev. Applied Vol.4, 054018, 2015.

Ultrastrongly coupled THz metasurfaces: from large arrays to single meta-atom spectroscopy

G. Scalari[1*], E. Jöchl[1], S. Rajabali[1], S. Markmann[1], E. Cortese[2], S. DeLiberato[2], M. Beck[1], J. Faist[1]

[1] *Institute for Quantum Electronics, ETH Zürich, Zürich, Switzerland*
[2] *School of Physics and Astronomy, University of Southampton, Southampton, UK*
[*]corresponding author: gscalari@ethz.ch

Abstract: We will present experiments on ultrastrongly coupled, strongly subwavelength resonators in arrays down to single element. We will discuss the limitations of the planar resonators approach when employing extremely subwavelength gaps and we will present the new developments towards single-object, few electrons ultrastrongly coupled systems.

Sub-wavelength electromagnetic field localization is a central theme in photonic research, as it allows sensing capabilities as well as increasing the light-matter coupling strength. Recently, the strong and ultrastrong light-matter coupling regime [1] in the THz range with split-ring resonators coupled to magnetoplasmons [2] has been widely investigated, achieving successive world-records for the largest light-matter coupling ever achieved. Ever-shrinking resonators have allowed to approach the regime of few electrons strong coupling, in which single-dipole properties can be modified by the vacuum field [3].

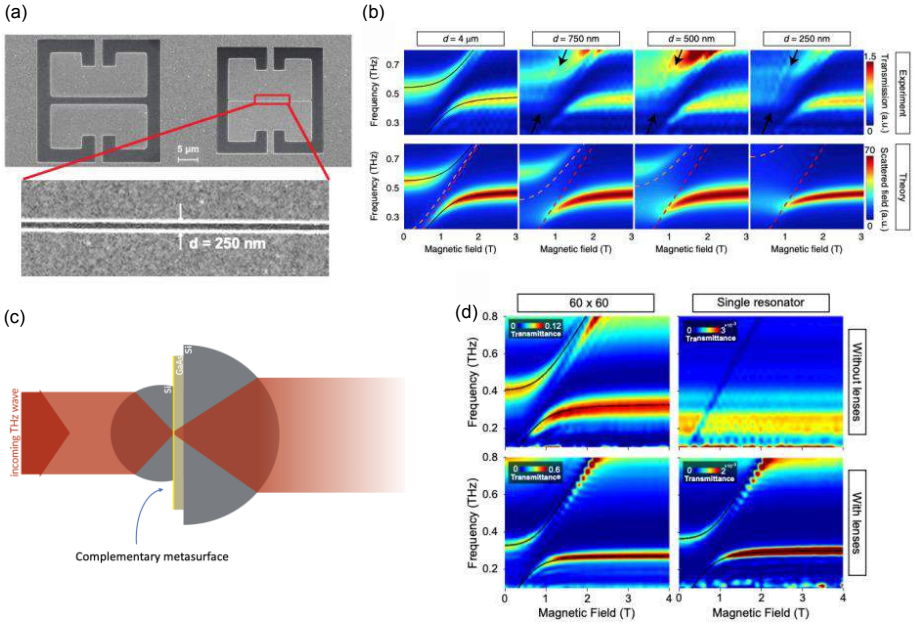


Figure 1: (a) SEM image of two cSrr , one with 2um gap and one with 250-nm gap. (b) Top row: transmission of cSrrs coupled to the Landau level transition in 2DEG versus magnetic field for four different gap sizes, d. black arrows indicate an additional feature that corresponds to $f = 1.6 \times \omega c/2\pi$, and the black solid lines are fitted LP and UP. bottom row: the calculated scattered field for different gap feature sizes, d (same as the gap sizes of the experiment results). (c) Schematic of the immersion lenses setup. (d) Transmission measurements without (top row) and with the aSIL configuration (bottom row) for a 2D array of 60 × 60 cSRRs (left column) and a single resonator (right column). The black solid lines are the fitted LP and UP using the Hopfield model.

Using our Landau polariton platform [2], we will discuss, using theoretically and experimentally, the existence of a limit to the possibility of arbitrarily increasing electromagnetic confinement in polaritonic systems. Strongly sub-wavelength fields can excite a continuum of high-momenta propagative magnetoplasmons [4] when planar resonators with sub-micrometric gaps are employed (Fig.1 (a)). This leads to leading to the emergence of nonlocal polaritonic effects, as certain polaritonic features disappear and the system enters in the regime of discrete-to-continuum strong coupling(Fig.1b). Particularly, the upper branch progressively disappears as the resonator's gap is reduced. Theoretical analysis including non-local effects displays that the frequency of the polaritonic resonances becomes complex, as the continuum of plasma waves irreversibly absorbs photons, even neglecting intrinsic plasmonic and photonic losses. The physics is akin to the one found in Landau damping, where in our case energy is dissipated generating plasma waves and not free electron–hole pairs.

We will as well discuss experiments reporting spectroscopy of a single, ultrastrongly coupled, highly subwavelength complementary resonator (cSRR) operating at 300 GHz. By using a combination of immersion lenses (Fig.1 c, asymmetric Silicon immersion lens aSIL) and THz-TDS , we unravel the linewidth dependence of planar metamaterials as a function of the meta-atom number indicating quenching of the superradiance. On these grounds, we investigate ultrastrongly coupled Landau polaritons at the single resonator level (Fig.1 d) [5], reaching ultrastrong coupling normalized ratio $\frac{\Omega}{\omega} = 0.6$. We will as well discuss the THz spectroscopy of micron-sized, exfoliated 2D materials.

References

[1] Forn-Diaz, P., et al., Rev. Mod. Phys.91, 025005 (2019)

[2] Scalari, G. et al., Science, 335, 1323–1326 (2012)

[3] R Chikkaraddy et al., Nature 535 (7610), 127-130 (2016)

[4] S. Rajabali, E. Cortese, M. Beck, S. De Liberato, J. Faist and G Scalari, Nat. Phot, (2021)

[5] S. Rajabali, S. Markmann, E. Jöchl, M.Beck, C. Lehner, W. Wegscheider, J. Faist and G Scalari, Nat. Commm., 13 (1), 1-8 (2022)

Josephson terahertz plasmonics with layered superconductor microcavity arrays

S. Kalhor[1], **Sergey Savel'ev**[2], **K. Delfanazari**[1*]

[1] Electronics and Nanoscale Engineering Division, James Watt School of Engineering, University of Glasgow, Glasgow G12 8QQ, United Kingdom
[2]Department of Physics, Loughborough University, Loughborough, UK
[*]Corresponding author: kaveh.delfanazari@glasgow.ac.uk

Abstract: To engineer the ultrastrong light-matter interaction between Josephson plasma waves (JPWs) and terahertz (THz) radiation for manipulation of cavity quantum electrodynamic (cQED), we propose an array of deeply subwavelength micro-cavities composed of high-temperature superconductor BSCCO. We confirm the ultrastrong coupling of the JPWs and THz radiation by observing anti-crossing behaviour in the reflection spectra of the array in the superconducting regime. The proposed metamaterial could be useful in the development of THz cQED, coherent emitters, sensitive detectors, and tunable bolometers.

Terahertz (THz) radiation has become increasingly important for both practical applications such as high-speed wireless communications and fundamental scientific research, such as studying superconducting condensates in layered high-temperature superconductors. $Bi_2Sr_2CaCu_2O_{8+\delta}$ (BSCCO) is a particularly important high-temperature superconductor (HTS) due to its intrinsic Josephson junctions (IJJs), which are the building blocks of coherent and continuous solid-state THz IJJ emitters [1]. The Josephson plasma waves (JPWs), resulting from the coupling of the c-axis Josephson current with electromagnetic (EM) waves, have diverse applications, from slowing down light to converting continuous THz radiation into short pulses in the nonlinear regime [2]. The strong-light matter coupling between the JPWs and THz EM waves can be beneficial for boosting the radiated power of IJJ emitters.

This paper proposes an array of microcavities, each composed of a high-temperature superconducting BSCCO thin film sandwiched between two silicon films. The substrate of the cavity arrays is a layer of gold with a thickness of 500 nm, and each cavity is covered with a thin layer of gold (200 nm thick), as shown in the inset of Figure 1 (a). The BSCCO thin film is a c-axis oriented superconductor with a c-axis dielectric function of $\varepsilon_c(\omega) = \varepsilon_\infty\left(1 - \omega_p^2/\omega^2\right)$ where $\varepsilon_\infty = 12$. The cavity array has a subwavelength spacing of P=100 μm, and the distance between two gold patches is kept constant at 1200 nm.

Here, the THz wave is normally incident on the structure. Above the transition temperature (T_c), the Josephson plasma frequency ω_p is zero and approaches a value of 0.67 at T=20 K. For a cavity width of w=67.3 μm, the cavity resonance frequency $f_c = c/2w\sqrt{\varepsilon_{eff}}$ is equal to the Josephson plasma frequency. ε_{eff} is the effective permittivity of the cavity. The reflection spectra of the device show a single dip at a frequency of 0.67 THz for this cavity width (as shown in Figure 1 (b)). However, when a BSCCO film with a thickness of 225 nm is inserted into the cavity, two dips are observed in the reflection spectra. The frequency splitting between these two dips is 0.29 THz.

Three weak, strong, and ultrastrong coupling regimes between THz EM waves and Josephson plasmon can be

defined. The splitting in resonance frequency is representative of strong coupling. The minimum value of splitting (so-called Rabi frequency) between two dips is obtained by tuning the cavity frequency (i.e. cavity width) around the value of Josephson frequency [3]. The coupling is in the ultrastrong regime when the normalized Rabi frequency, which is the Rabi frequency divided by cavity frequency, is not negligible compared to one. Our study shows that the normalized Rabi frequency is 0.29 for a BSCCO thickness of 200 nm, indicating ultrastrong coupling. It increases to 0.87 for a BSCCO thickness of 800 nm [3].

Further study on the thermal characteristic of the normalized Rabi frequency shows that this quantity is not dependent on temperature below T_c. However, approaching T_c leads to weak coupling, and no splitting is observed. Overall, our proposed array of microcavities demonstrates ultrastrong coupling between JPWs and THz EM waves, which can be beneficial for boosting the radiated power of coherent emitters and the development of sensitive BSCCO THz detectors.

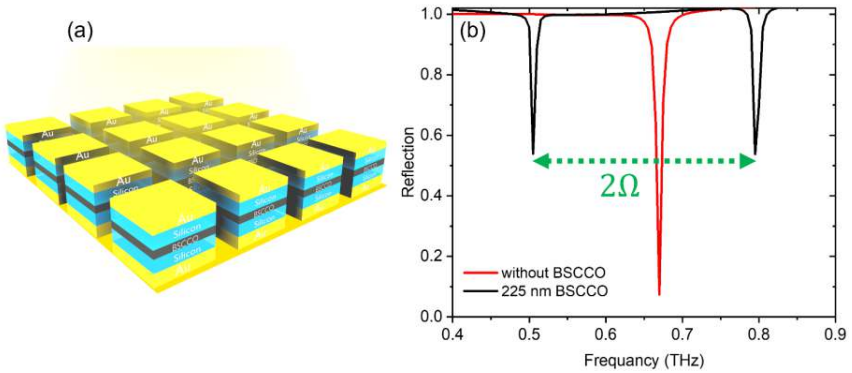


Figure 1: (a) Array of subwavelength microcavities composed of gold/silicon/BSCCO/silicon/gold layers. (b) The reflection spectra of the device with a cavity width of w=67.3 μm. when there is no superconductor (red line) and a superconductor with a thickness of 225 nm is between two silicon films. Here the temperature is T=20 K where $\omega_p = 0.67$ THz.

The authors acknowledge the Royal Society for the funding support.

References

1. K. Delfanazari, R. A. Klemm, H. J. Joyce, D. A. Ritchie, and K. Kadowaki, “Integrated, Portable, Tunable, and Coherent Terahertz Sources and Sensitive Detectors Based on Layered Superconductors" *Proc. IEEE*, vol. 108, no. 5, pp. 721-734, 2020
2. S. Savel'ev, A. L. Rakhmanov, V. A. Yampol'skii, and F. Nori, “Analogues of nonlinear optics using terahertz Josephson plasma waves in layered superconductors" *Nat. Phys.*, vol. 2, no. 8, pp. 521–525, 2006
3. S. Kalhor, S. Savel'ev, and K. Delfanazari, “Engineering ultrastrong coupling between Josephson plasmon polaritons and subwavelength microcavity arrays in silicon/van der Waals layered superconductor heterostructure for terahertz hybrid circuit cavity quantum electrodynamics" *Phys. Rev. B*, vol. 106, no. 24, p. 245140, 2022

META 2023, PARIS - FRANCE, JULY 18 – 21, 2023

Creation and annihilation of Josephson vortex loops in a Junction with nanopillar

G. R. Berdiyorov[1], M. V. Milosevic[2], F. Kusmartsev[3], F. M. Peeters[2], S. Savel'ev[3*]

[1] Qatar Environment and Energy Research Institute, Qatar Foundation, P.O.B. 5825, Doha, Qatar

[2] Departement Fysica, Universiteit Antwerpen, Groenenborgerlaan 171, B-2020 Antwerpen, Belgium

[3]Department of Physics, Loughborough University, Loughborough, UK
[*]Corresponding author: S.Saveliev@lboro.ac.uk

Abstract: We consider a Josephson Junction with nanoengineered pillars connecting its two banks. Josephson vortices are generated by the applied magnetic field applied and are driven by the applied current flowing through the junction. If pillar is large enough, the vortices cannot pass through it and go around it, forming a loop behind. The evolution of the loops depends on the Josephson coupling and external conditions and usually results in multiple creations and annihilations of the loops.

Mutual interaction of vortices and Josephson plasma waves in Josephson structures offers an unprecedented level of control of electromagnetic field waves, which are in much needed THz frequency range [1]. Josephson vortices can be used to generate THz radiation [2], to form tuneable photonic crystals [3], to guide THz waves [4, 5], or to manipulate them [6] utilizing natural nonlinearity of Josephson junctions or even to generate a quanta of THz radiation [7]. Therefore, superconducting THz devices can provide an alternative to more conventional THz systems.

Here, we discuss how nanoengineered single Josephson junction can be used to generate Josephson vortex loops. Creation and annihilation of such loops can be used as to emit THz radiation. Moreover, when loops are created, they can be stable inside the junction as they trapped by pillars connecting superconducting banks of the junction. Therefore, the system can be used as a storage of THz radiation (THz battery) or as a memory element for computing at THz frequency range.

To simulate creation and annihilation of Josephson loop, we used time-dependent Ginsburg Landau equations with Josephson coupling at the junction [8]. Superconducting banks of the junction are also connected by cylindrical pillars made of the same materials as the banks or superconducting material with slightly different superconducting critical temperature, which helps us to switch on and off barrier provided by superconducting pillars. Detailed of our extended simulations are published in [8] where different evolution and annihilation of Josephson vortex loops are considered.

Figures 1 (a-h) show the simples possible case of a simulated 4 pillar sample at steady state creation-annihilation cycle of Josephson vortex loop. In Fig. a, a vortex shown by dark blue colour enters the sample with two vortex loops trapped by the right column of the pillars. The current pushes the vortex to go round the two pillars, which initially had with no loops Fig. 1 b-d. The two vortex loops formed behind the vortex (Fig. 1 e) when it passes the left two pillars and approaches the right two pillars pushing the vortex loops at the right pillars, as a result, collapsing these loops (Fig. 1f). Them the vortex circumvents the right pillars (Fig. 1 g) and escapes the sample, leaving two new vortex loops formed arounf the right pillars (Fig 1h), while the new vortex entering the sample forces the two loops at the left pillars to collapsed. This process continues if the applied current is constant, however, if the current is switched of at moment shown in Fig. 1e, the system relaxed at the state Fig. 1j with four loops and the vortex trapped between pillars. However, if the current is switched of at the moment (h), the system is relaxed to the state (i) with four pillars and no vortex

between loops. Switching the system at other time moments can result in diverse vortex-loop configurations. These states can be used both for computational memory and storage of THz radiation energy.

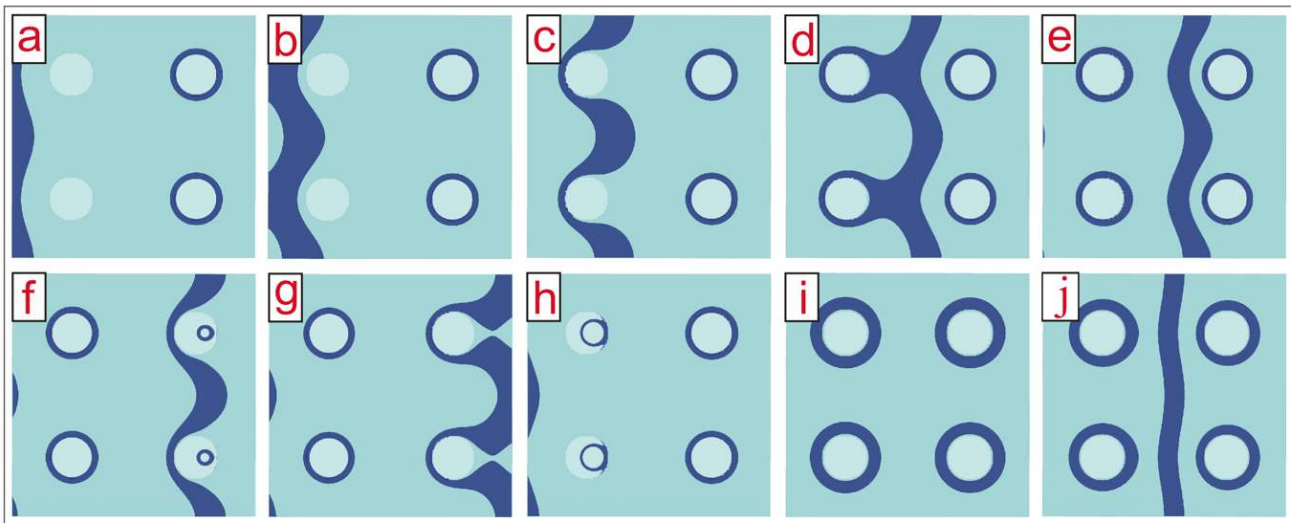


Figure 1: (a-h) Evolution of vortices and vortex loops at a constant applied magnetic field and DC current; (i) and (j) represent the steady states of the system if the applied current is switched off at the moment (h) and (e), respectively.

References

1. S. Savel'ev, V.A. Yampol'skii, A.L. Rakhmanov, F. Nori, Terahertz Josephson plasma waves in layered superconductors: spectrum, generation, nonlinear and quantum phenomena, Report on Progress in Physics 73, 026501 (2010).

2. S. Savel'ev, V. Yampol'skii, A. Rakhmanov, F. Nori, Generation of tunable Terahertz out-of-plane radiation using Josephson vortices in modulated layered superconductors, *Phys. Rev. B* **72**, 144515 (2005).

3. S. Savel'ev, A.L. Rakhmanov, F. Nori, Using Josephson vortex lattices to control THz radiation:

tunable transparency and THz photonic crystals, *Phys. Rev. Lett.* **94**, 157004 (2005).

4. D.R. Gulevich, F.V. Kusmartsev, S. Savel'ev, V.A. Yampol'skii, F. Nori, Shape waves in 2D Josephson junctions: Exact solutions and time dilation, *Phys. Rev. Lett.* **101**, 127002 (2008).

5. S. Savel'ev, V.A. Yampol'skii, A.L. Rakhmanov, F. Nori, Layered superconductors as nonlinear waveguides for terahertz waves, *Phys. Rev. B* **75**, 184503 (2007).

6. S. Savel'ev, A. L. Rakhmanov, V. A. Yampol'skii, and F. Nori, "Analogues of nonlinear optics using terahertz Josephson plasma waves in layered superconductors" *Nat. Phys.*, vol. 2, no. 8, pp. 521–525, 2006

7. S. Savel'ev, A.L. Rakhmanov, F. Nori, Quantum Terahertz Electrodynamics and Macroscopic Quantum Tunneling in Layered Superconductors, *Phys. Rev. Lett.* **98**, 077002 (2007).

8 G. R. Berdiyorov, M. V. Milošević, F. Kusmartsev, F. M. Peeters, S. Savel'ev, Josephson vortex loops in nanostructured Josephson junctions, *Scientific Reports* **8**, 2733 (2018).

Quantum electrodynamics of non-demolition detection of single microwave photon by superconducting qubit array

P. Navez

Loughborough University, Epinal Way Loughborough, Leicestershire LE11 3T, UK

Summary

Single particle detection is one of the most fundamental issues in quantum me-chanics as it addresses the question of quantum measurement. An accurate quantum description of a detector would avoid the use of the Born's rule (or von Neumann postulate) about the probabilities of different outcomes, leading to the controversial interpretation of the collapse of the wave packet or the Schrodinger's cat. In addition, it leads to applications standing from precise weak microwave signal measurement to the detections of axions, that are hypo-thetical particles predicted in the standard model of elementary particles and which become photons when passing through a magnetic field.

In this talk, we apply consistently the formalism of quantum electrodynamics and we developed a comprehensive theoretical framework describing the inter-action of single microwave photons with an array of superconducting transmon qubits in a waveguide cavity resonator [1]. In particular, we analyse the effects of microwave photons on the array's response to a weak probe signal exciting the resonator. The study reveals that a high quality factor cavities provide better spectral resolution of the response, while cavities with moderate quality factor allow better sensitivity for a single photon detection. Remarkably, our analysis showed that a single-photon signal can be detected by even a sole qubit in cavity under the realistic range of system parameters. We also discuss how quantum properties of the microwave radiation and electrodynamical properties of resonators affect the probe response of qubits' array and, how the interaction between the qubits improve the detection by reaching a noise level close the Heisenberg lowest bound limit [2]. Our results provide an efficient theoretical background for informing the development and design of quantum devices con-sisting of arrays of qubits, especially for those using a cavity where an explicit expression for the transmission or reflection is required.

Our results is used for the interpretation of the experiments done within the EU-SUPERGALAX consortium. Preliminary measurements show the influence of an external power on the transmission spectrum [3] in accordance with the theory [1].

References

[1] P. Navez et al., J. Appl. Phys. **133**, 104401 (2023)

[2] P. Navez et al., Phys. Rev. B **103**, 064503 (2021)

[3] C. Gatti et al., *Coherent Quantum Network of Superconduct-ing Qubits as a Highly Sensitive Detector of Single Microwave Photons for Searching of Galactic Axions*, (submitted in IEEE-TAS)

Metamaterials Meeting Industry

META 2023, PARIS - FRANCE, JULY 18 – 21, 2023

Modelling hot carrier generation in large metallic nanoparticles

Johannes Lischner[1*]

[1]Department of Materials, Imperial College London, United Kingdom
[*]corresponding author: j.lischner@imperial.ac.uk

Abstract: Localized surface plasmons in metallic nanoparticles give rise to very strong light absorption. The decay of these excitations results in the generation of energetic or "hot" electrons and holes which can be harvested and harnessed for applications in photovoltaics, photocatalysis and light sensing. To optimize hot carrier production in devices, a detailed theoretical understanding of the relevant microscopic processes, including light-matter interactions, plasmon decay and hot electron thermalization, is needed. In my talk, I will describe a material-specific theory of hot-carrier generation in metallic nanoparticles which combines a classical description of the electromagnetic radiation with large-scale atomistic quantum-mechanical simulations. I will present results for hot carrier distributions in spherical nanoparticles of gold, silver and copper and discuss the relative importance of interband and intraband transitions as function of nanoparticle size. Finally, I will describe results for more complex systems, such as core-shell nanoparticles or "reactor" systems in which small catalytic nanoparticles are adsorbed to a larger plasmonic nanoparticles.

META 2023, PARIS - FRANCE, JULY 18 – 21, 2023

Dynamic plasmonics and optics with organic conducting polymers

Magnus Jonsson

Organic Photonics and Nanooptics group, Laboratory of Organic Electronics, Department of Science and Technology, Linköping University, Sweden

E-mail: magnus.jonsson@liu.se

Abstract: My group is interested in developing novel ways to control light and heat using organic materials like conducting polymers and cellulose. Applications include tuneable nanooptical metasurfaces, reflective color displays and energy-regulating optical materials. In particular, we recently introduced conducting polymers as a new materials platform for dynamically tuneable plasmonics.[1] By contrast to static nanoantennas made of traditional metals, the optical response of the polymeric antennas can be repeatedly turned off and on again by varying the redox state of the polymer, which reversibly switches the material between optically metallic and dielectric states in the near infrared and infrared ranges.[1-4] I will then demonstrate how the same type of conducting polymers offers novel means for forming dynamically tuneable structurally colored materials,[5,6] with anticipated use for reflective labels and electronic readers in color. If time allows, I hope to also introduce our latest works on radiative cooling, including electrical tuning at ambient conditions, structurally colored cooling systems, and integration with ionic thermoelectric devices.[7-9]

1. *Conductive polymer nanoantennas for dynamic organic plasmonics*. S. Chen et al. **Nature Nanotechnology** 2020, 15, 35-40.
2. *Electrical Tuning of Plasmonic Conducting Polymer Nanoantennas*. A. Karki et al. **Advanced Materials** 2022, 34, 13, 2107172
3. *Doped Semiconducting Polymer Nanoantennas for Tunable Organic Plasmonics*. A. Karki et al. **Communications Materials** 2022, 2022, 3, 48
4. *Dynamic conducting polymer plasmonics and metasurfaces.* S. Chen and M. P. Jonsson. **ACS Photonics** 2023, accepted
5. *Dynamically tuneable reflective structural colouration with electroactive conducting polymer nanocavities.* S. Rossi et al. **Advanced Materials** 2021, 33, 40, 2105004
6. *Tunable structural color images by UV-patterned conducting polymer nanofilms on metal surfaces*. S. Chen et al. **Advanced Materials** 2021, 33, 33, 2102451
7. *Electrical Tuning of Radiative Cooling at Ambient Conditions*
   D. Banerjee et al. **Cell Reports Physical Science** 2023, in press
8. *Structurally Colored Cellulose Nanocrystal films as Trans-Reflective Radiative Coolers*. R. Shanker et al. **ACS Nano** 2022, 16, 7, 10156-10162
9. *Cellulose-based Radiative Cooling and Solar Heating Powers Ionic Thermoelectrics*
   M. Liao et al. **Advanced Science** 2022, in press

META 2023, PARIS - FRANCE, JULY 18 – 21, 2023

Surface Susceptibility Synthesis of Spatially Dispersive Metasurfaces

J. Dugan[1*], T. J. Smy[1], F. Monticone[2], and S. Gupta

[1]Carleton University, Canada
[2]Cornell University, USA
[*]corresponding author: jordandugan@cmail.carleton.ca

Abstract: We propose a simple method to synthesize and obtain a zero thickness sheet boundary condition of a spatially dispersive (SD) metasurface to achieve desired wave transformations operations specified in the spatial frequency domain. We demonstrate the proposed method by synthesizing a space-plate as an example, using zero-thickness sheet description of a Huygens' metasurface in terms of angle-dependent surface susceptibilities.

Recently, there has been a lot of interest in nonlocal, or spatially dispersive metasurfaces, where the induced polarizations on the unit-cells are strongly dependent on the fields over an extended region across the surface. These surfaces have found applications in wave-based computing [1] as well as in shrinking optical systems [2], for instance, thereby greatly expanding the wave transformation capabilities compared to what is currently beenachieved using purely local metasurfaces. Recently, a computationally efficient method for modeling these surfaces has been proposed whereby the metasurface is modeled as a zero thickness sheet characterized by angle-dependent surface susceptibilities and the fields around the surface satisfy the generalized sheet transition conditions (GSTCs) [3]. If these surface susceptibilities take the form of a rational polynomial, they can be implemented as spatial boundary conditions in standard numerical methods [4]. While these works have focused on the field analysis of SD metasurfaces, the focus of this paper is the synthesis of surface susceptibilities to achieve desired field transformations in the spatial frequency domain. This is in contrast to synthesis methods currently restricted to local metasurfaces only [5]. To demonstrate the procedure to synthesize a 2D metasurface in the y − z plane to achieve a desired reflection R(k_y) and transmission T(k_y) response, let us assume TE Polarization, and a Huygens' metasurface configuration, which consists of orthogonal tangential electric and magnetic susceptibilities only. These susceptibilities, assuming the surface is described by the GSTCs, take the following form:

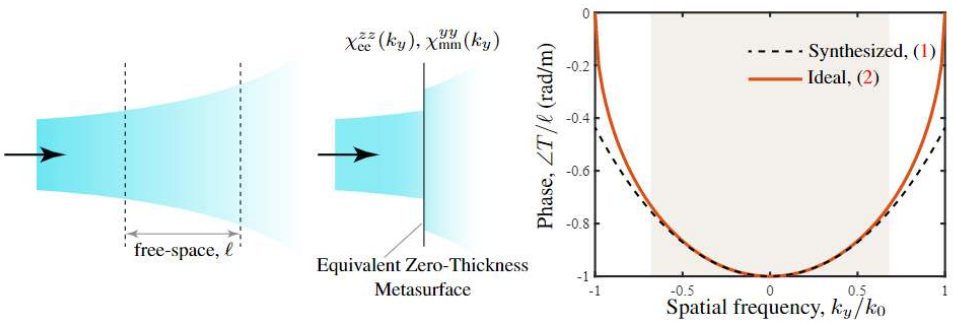


Figure 1: Phase response of a free space body of length ℓ and of the synthesized space-plate in the spatial frequency domain, where the space-plate is represented as an equivalent zero thickness sheet model.

$$\chi_{\mathrm{ee}}^{zz}(k_y) = \frac{2j\sqrt{k_0^2 - k_y^2}\left(-1 + R(k_y) + T(k_y)\right)}{k_0^2\left(1 + R(k_y) + T(k_y)\right)} \approx \frac{\sum_{m=0}^{\infty} a_m\, k_y^m}{\sum_{n=0}^{\infty} b_n\, k_y^n} \tag{1a}$$

$$\chi_{\mathrm{mm}}^{yy}(k_y) = \frac{-2j\left(1 - T(k_y) + R(k_y)\right)}{\sqrt{k_0^2 - k_y^2}\left(1 - R(k_y) + T(k_y)\right)} \approx \frac{\sum_{m=0}^{\infty} c_m\, k_y^m}{\sum_{n=0}^{\infty} d_n\, k_y^n}, \tag{1b}$$

where k_y is the transverse wave vector, and the surface susceptibilities are to be approximated as rational polynomial functions for simple integration with standard numerical full-wave solvers. This is achieved by inverse Fourier transforming the GSTCs with the incorporation of (1), which converts the polynomial terms to spatial field derivatives, and thus the corresponding spatial boundary conditions. To apply this method, consider a metasurface to compress free space (also known as a space-plate), as illustrated in Fig. 1. Such an ideal surface has zero reflection (i.e., R = 0) and a transmission coefficient given by:

$$T(k_y) = \exp\left(-j\ell\sqrt{k_0^2 - k_y^2}\right), \tag{2}$$

where ℓ is the length of free space we are attempting to compress. This needs to be substituted in (1) to obtain the surface susceptibilities to construct the zero thickness sheet boundary condition. To obtain the desired polynomial form of the susceptibilities, T (ky) can be expressed in an alternate all-pass filter form as

$$T = \frac{1 - j\xi}{1 + j\xi}, \quad \text{where } \xi = -\tan\left(\frac{-j\ell\sqrt{k_0^2 - k_y^2}}{2}\right) \tag{3}$$

This all-pass form ensures the magnitude of the transmission response ensures unity magnitude for all k_y. Taking a 2nd order Taylor expansion of ξ with respect to k_y, substituting T into (1) and then taking a 2nd order Taylor expansion of the radical terms yields the final set of rational polynomial susceptibilities that can now be integrated into standard numerical methods. Fig. 1 shows one example, where we see that in the paraxial regime, the phase shift produced by the synthesized susceptibilities provides an excellent match with the ideal space-plate response with the quality of the match deteriorating for large values of k_y. In future works, we will integrate the synthesized susceptibilities in the full-wave numerical solvers to demonstrate their operation directly in the space-domain, as well as explore the mapping between the synthesized susceptibilities and the physical unit cell structures to practically implement the synthesized SD metasurfaces. The proposed synthesis method thus represents an important theoretical technique to analyze SD metasurfaces and evaluate their fundamental performance limits.

References

1. Zangeneh-Nejad, F., D. L. Sounas, A. Alu and R. Fleury “Analogue computing with metamaterials,” Nat Rev Mater, Vol. 6, No. 3, 207–225, 2021.
2. Chen, A. and F. Monticone, "Dielectric Nonlocal Metasurfaces for Fully Solid-State Ultrathin Optical Systems,” ACS Photonics, Vol. 8, No. 5, 1439–1447, 2021.
3. Rahmeier J. G. N, T. J. Smy, J. Dugan and S. Gupta, “Part I -Spatially Dispersive Metasurfaces: Zero Thickness Surface Susceptibilities \& Extended GSTCs,” IEEE Trans. Antennas Propag., Early Access, 2022.
4. Smy T. J, J. G. N. Rahmeier, J. Dugan and S. Gupta, “Part II -Spatially Dispersive Metasurfaces: IE-GSTC-SD Field Solver with Extended GSTCs,” IEEE Trans. Antennas Propag., Early Access, 2022.
5. Achouri, K., M. A. Salem and C. Caloz, "General Metasurface Synthesis Based on Susceptibility Tensors,” IEEE Trans. Antennas Propag., Vol. 63, No. 7, pp. 2977-2991, 2015.

Time-resolved NIR to Visible Upconversion Luminescence from Single $NaYF_4:Yb^{3+},Tm^{3+}$ Nanoparticles on Plasmonic Nanowire Composites

K.Y. Chiok[1], A. Haghizadeh[1], A. Ahmed[1], A. Baride[2], R.B. Anderson[1], S. May[2], S. Smith[1]

[1]South Dakota School of Mines and Technology, Rapid City, South Dakota, USA
[2]University of South Dakota,Vermillion, South Dakota, USA

Corresponding author email: Steve_Smith@mailaps.org

Abstract: We use single particle spectroscopic imaging and statistical analysis to assess the plasmonic enhancement of NIR-to-visible upconversion luminescence (UCL) from single β-$NaYF_4:Yb^{3+}:Tm^{3+}$ upconverting nanoparticles (UCNPs) coupled to random arrangements of Ag nanowires supported on glass substrates, termed nanowire composites (NWCs). By examining the effects at the single particle level, and accumulating a statistical sampling of single particle emitters, both on and off the plasmonic substrates studied, we obtain a statistical description of UCL emission enhancement in the Tm-doped UCNPs and map out the statistical distribution of excitation and luminescence enhancement on the plasmonic substrates. We use both wide field and confocal scanning spectroscopic imaging of single UCNPs on and off the plasmonic substrates in combination with energy and time resolved spectroscopy, and compare these results to a coupled rate equation analysis to elucidate the energy transfer upconversion enhancement mechanisms. The results obtained are compared to Finite Difference Time Domain (FDTD) calculations of the fields near the plasmonic substrate.

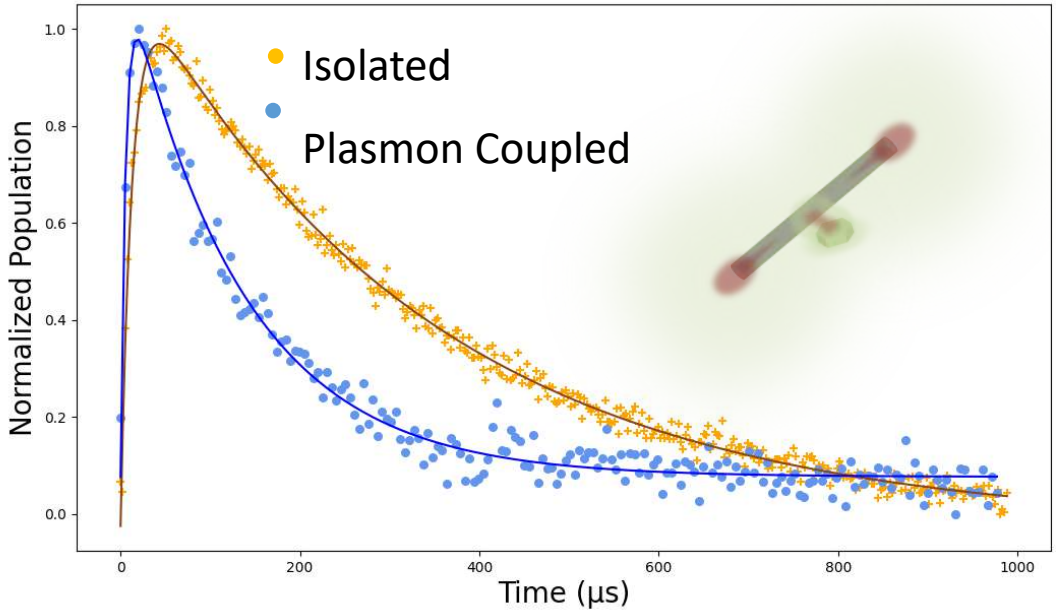


Figure: Single particle luminescence decay of isolated and plasmon-coupled upconverting nanoparticle.

References:

(1) Fisher, J.; Zhao, B.; Lin, C.; Berry, M. T.; May, P. S.; Smith, S. Spectroscopic Imaging and Power Dependence of NIR to Visible Upconversion Luminescence from $NaYF_4:Yb^{3+},Er^{3+}$.. . *J. Phys. Chem. C* 2015, *119*, 24976–24982.
(2) Hor, A.; Luu, Q.; May, P.; Berry, M.; Smith, S. Non-Linear Density Dependent Upconversion Luminescence of β-$NaYF_4$: Yb^{3+} : Er^{3+} Nanoparticles on Random Ag Nanowire Aggregates. *MRS Adv.* 2016, *1*, 2677–2682.
(3) M. Y. Hossan, A. Hor, Q. Luu, S. J. Smith, P. S. May, and M. T. Berry, "Explaining the Nanoscale Effect in the Upconversion Dynamics of β-$NaYF_4Yb^{3+},Er^{3+}$ … Nanocrystals," *J. Phys. Chem. C*, 2017 vol. 121, pp. 16592–16606.

META 2023, PARIS - FRANCE, JULY 18 – 21, 2023

Topological Trapped-Rainbow and Nonreciprocal Guides Beyond the Time-Bandwidth Limit

Konstantinos Baskourelos and Kosmas L. Tsakmakidis
Section of Condensed Matter Physics, Department of Physics, National and Kapodistrian University of Athens, Greece
Author e-mail address: ktsakmakidis@phys.uoa.gr

Abstract: Topologically protected wave transport has recently emerged as an effective means to address a recurring problem hampering the field of 'slow light' for the past two decades: Its keen sensitivity to disorders and structural imperfections. With it, there has been renewed interest in efforts to overcome the delay-time–bandwidth limitation usually characterizing slow-light devices, on occasion thought to be a 'fundamental limit'. Our talk will overview latest developments and point out important new functionalities that overcoming the limit can enable.

1. Introduction

It has recently been realized[1-3] that nonreciprocity and topology – both, important even in the usual light regime of integrated optoelectronic and photonic structures – are particularly crucial in the slow- and stopped-light regime, with a number of recent works having elucidated that they both play a key role for attaining prolonged *and* broadband (i.e., T-B unlimited) light localization in topological, terminated[1] or 'rainbow trapping'[4], structures (see Fig. 1). In the latter approach, use can be made of the concept of synthetic dimensions.

A synthetic dimension in graded 'rainbow trapping' structures can be constructed[4] by exploiting a translational degree of freedom – e.g., inside the unit cell of a two-dimensional chirped photonic crystal waveguide. The translational grading (tapering) gives rise to a nontrivial topology in the synthetic dimension, which in turn results to robustly localized (stopped) surface states where different frequencies are localized at different positions along the guide ('rainbow principle', see Fig. 1c).

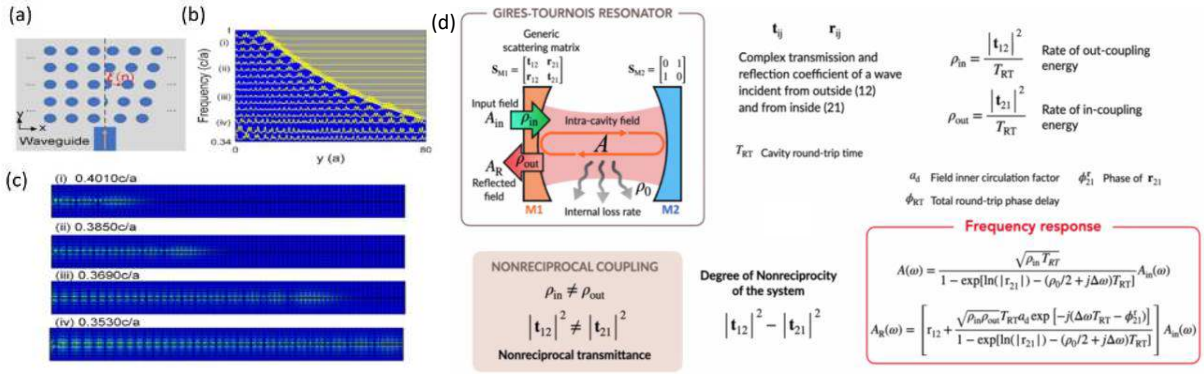


Fig. 1. (a) Schematic diagram of a topological 'trapped rainbow' structure, with light coupled-in using a dielectric waveguide. (b) Normalized energy density distributions along the interface shown in (a). The blue and gray parts are regions of existence and nonexistence of interface modes. (c) Different light frequencies are rigorously stopped and trapped at different positions along the topological guide of (a). (d) General schematic of a nonreciprocal cavity, along with the main definitions used for the analysis of its time-bandwidth product and intra-cavity power.

Such ‘topological trapped rainbows’ can rigorously stop and localize states of different frequencies at different positions along a topological waveguide, controlled by the tuning of the spatial modulation of the states’ group velocity. For photonic crystal structures, in particular, the operation frequency as well as the bandwidth of the topological trapped rainbow can be tuned by controlling the band gap of the photonic crystal, and is completely decoupled from the storage (stopping) time. This topological principle can be applied to photonic crystals of any symmetry and material composition, so long as a complete band gap exists.

In terminated topological structures forming nonreciprocal cavities[1-3], on the other hand, wave propagation is halted by the use of a terminating metallic layer (not by reducing v_g to zero), where back-reflections and scattering are prevented owing to the topological design of the structure.

2. Enabled applications and outlook

As has recently been established[5], the degree to which the limit can be exceeded exactly corresponds to the degree to which light power increases inside a device. Thus, devices operating beyond the limit will be uniquely positioned to enhance optical nonlinearities or achieve ultrafast active control. The nonlinear interactions can here be greatly enhanced due to the compression of the local energy density as a *broadband* pulse is decelerated inside the device.

The enhancement of nonlinearities can be large enough to produce measurable effects due to single-photon input fields[6-9] – an effect already well-established even for T-B limited slow-light devices. There is a principal way a single-photon nonlinearity could here be useful: As a source of single (e.g., Foch-state) photons with controllable spatio-temporal characteristics.

Further envisaged applications of beyond-the-limit slow and stopped light, the regime where the density of states and the Purcell factor dramatically increase[6], would be ultralow-light-level all-optical switching, enhanced chiral nanobiosensing, optical micro-combs, and enhanced spontaneous emission rates – appealing for fast light-emitting diodes (nano-LEDs), with an ultimate goal of attaining spontaneous emission rates faster than around 50 GHz, so that LEDs could become faster than lasers[7]. All devices relying on strong light-matter interactions would benefit from the above regime because, as explained before, the degree to which the T-B limit is exceeded exactly corresponds to the degree to which power inside a device increases[5], thereby potentially enabling unprecedented capabilities in the fields of metamaterials, nanophotonics and nonlinear optics – both, classical and quantum ones.

4. References

[1] K. L. Tsakmakidis, *et al*., “Breaking Lorentz reciprocity to overcome the time-bandwidth limit in physics and engineering", *Science* **356**, 1260 (2017).

[2] K. L. Tsakmakidis, Y. You, T. Stefański, and L. Shen, "Nonreciprocal cavities and the time-bandwidth limit: comment," *Optica* **7**, 1097 (2020), DOI: https://doi.org/10.1364/OPTICA.384840.

[3] K. L. Tsakmakidis, K. Baskourelos, and T. P. Stefański, “Topological, nonreciprocal, and multiresonant slow light beyond the time-bandwidth limit,” *Appl. Phys. Lett.* **119**, 190501 (2021), DOI: 10.1063/5.0068285. (invited / Featured)

[4] C. Lu, C. Wang, M. Xiao, *et al*., “Topological rainbow concentrator based on synthetic dimension,” *Phys. Rev. Lett.* **126**, 113902 (2021).

[5] I. Cardea, D. Grassani, J. Upham, *et al*., Unconventional time-bandwidth performance of resonant cavities with nonreciprocal coupling,” *Phys. Rev. A* **103**, 013716 (2021).

[6] K. L. Tsakmakidis, O. Hess, R. W. Boyd, and X. Zhang, “Ultraslow waves on the nanoscale,” *Science* **358**, eaan5196 (2017).

[7] K. L. Tsakmakidis, R. W. Boyd, E. Yablonovitch, and X. Zhang, "Large spontaneous-emission enhancements in metallic nanostructures: towards LEDs faster than lasers", *Opt. Express* **24**, 17916-17927 (2016).

[8] K. L. Tsakmakidis, "Stopped-light nanolasing in optical magic-angle graphene," *Nature Nanotechnol.* (2021), DOI: 10.1038/s41565-021-00960-x.

[9] O. Hess and K. L. Tsakmakidis, "Metamaterials with quantum gain", *Science* **339**, 654 (2013).

From synthesis to assembly: a Silicon based metasurface fabrication

Juan Xin[1], Wajdi Chaabani[1], Julien Proust[1] and Jérôme Plain[1*]

[1] Lumière, nanomatériaux et nanotechnologie (L2n), CNRS EMR 7004 & Université de Technologie de Troyes, 12 rue Marie Curie, 10004 Troyes Cedex, France

[*]Corresponding author: jerome.plain@utt.fr

Abstract: In this study, we present a simple method to fabricate silicon nanoparticles from wafer chips. This technique allows to obtain nanoparticles of relatively homogeneous size and showing Mie resonances in the visible range. The second result that we will present is an assembly technique based on the use of the capillarity force and allowing the obtaining of metasurfaces from silicon nanoparticles.

There are many ways to fabricate nanoparticles allowing to have optical properties at nanometric scales. For example, top-down approaches based on electron lithography have as main drawbacks the cost and time of fabrication. On the other hand, bottom-up approaches are less expensive but do not allow easy organization to obtain metasurfaces. Thus, it is necessary to combine the two types of approaches to associate a low-cost synthesis technique with a lithography technique.

In our synthesis technique, we simply grind bulk silicon to obtain nanoparticles[1]. This technique allows us to obtain in solution Si nanoparticles with a diameter ranging from 80 nm to about 250 nm. By centrifugation steps, it is possible to obtain a final mean size of about 120 nm ± 20 nm. Dark field and corresponding SEM images are shown for individual nanoparticles in Figure 1.

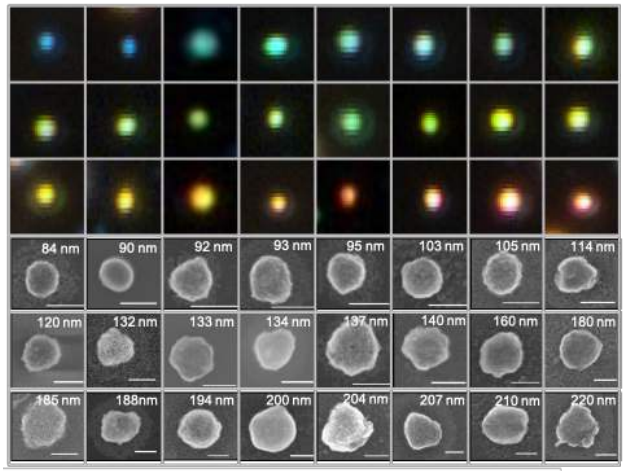


Figure 1. Up. Dark field images of Si nanoparticles. Down. Corresponding SEM images.

The second step allows to deposit the nanoparticles in a pattern obtained by electronic lithography. This technique, based on the assistance of capillary forces, allows to obtain large surfaces from a colloidal solution of nanoparticles. Figure 2 shows nanoparticles of two different sizes distributed on a complex pattern.

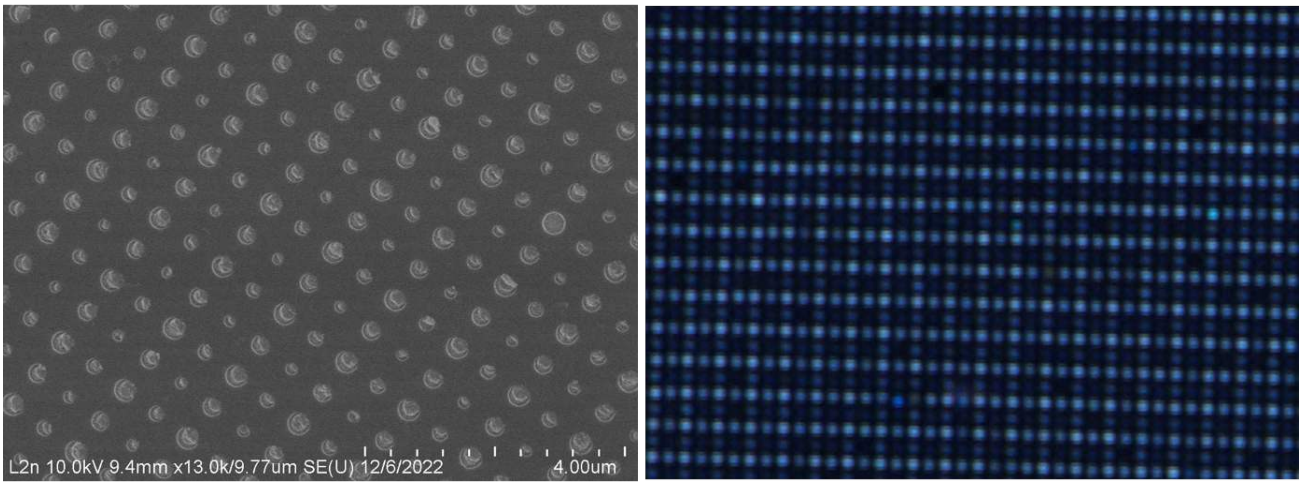


Figure 2. Left. SEM images of Si nanoparticles arranged on a complex pattern. Right. Corresponding Dark field images of Si based metasurface.

We have demonstrated that it is possible to organize naonaoparticles obtained in solution on a surface using a technique that is relatively simple to implement and compatible with all nano-lithography techniques.

References

(1) Chaabani W., Proust J., Movsesyan A., Beal J., Baudrion A-L., Adam P-M., Chehaidar A., and Plain J., Large-Scale and Low-Cost Fabrication of Silicon Mie Resonators ACSnano 2019,13 4199-4208

Acknowledgment: Samples were fabricated in the Nanomat platform (www.nanomat.eu). The authors acknowledge support from the French Agence Nationale de la Recherche (ANR) under grant NOSE (ANR-21-CE39-0014). This work was done within the framework of the Graduate School NANO-PHOT (École Universitaire de Recherche, grant ANR-18-EURE-0013). JX thanks the China Scholarship Council (CSC), (contract 202208070142) for the financial support.

META 2023, PARIS - FRANCE, JULY 18 – 21, 2023

The effect of periodically corrugated substrate on SERS anisotropy of organic molecules

E.T. Mathew[1], J. Jenczyk[1], Z. Miłosz[1] , W. Andrzejewska[1], M. Lewandowski[1], M. Wiesner[1,2,*]

[1] NanoBioMedicalCentre, Adam Mickiewicz University, Wszechnicy Piastowskiej 3, 61-614 Poznań, Poland
[2] Faculty of Physics, Adam Mickiewicz University, Uniwersytetu Poznańskiego 2, 61-614 Poznań, Poland
[*]Corresponding author: mwiesner@amu.edu.pl

Abstract:
Periodically corrugated Au/α-Al_2O_3 plasmonic substrates were used for surface enhanced Raman spectroscopy of thiophenol molecules. The results showed a strong dependence of the intensity of the Raman peaks of thiophenol molecules on the value of the period of corrugation and the angle between the polarization of the laser beam and the corrugation vector.

The dielectric-metal interface is a system that enhances the response of light-exited molecules when deposited on metallic surface. This enhancement can be observed in Raman light scattering as the surface enhanced Raman scattering (SERS) effect. A plasmonic substrate consisting of periodically-corrugated sapphire surface coated with a thin layer of metal creates a periodic modulation in the surface plasmon resonance (SPR) of the material. It results in the formation of surface plasmon polaritons (SPPs) that can be tailored to specific wavelengths of light. This modulation can also result in the formation of a photonic bandgap [1,2]. Results of our studies showed an additional effect of the corrugation on Raman spectra collected from organic molecules deposited onto corrugated metallic surface.

The Raman spectroscopy was used to investigate the effect of corrugation on the SERS (Fig. 1a) of organic molecules (thiophenol) deposited onto the plasmonic substrate (Au on M-cut α-Al_2O_3). The substrate consisted of periodically-arranged sapphire rows coated with a 10 nm-thick gold layer (Fig. 1b). Periods of nanostructures were ranging from 170 nm till 450 nm. The 785 nm laser wavelength was used to illuminate the thiophenol.

The sample was rotated and an angle between laser polarization and the corrugation vector was determined (Fig. 1a and 1d). Collected Raman spectra of thiophenol revealed several characteristic peaks (Figure 1c).

Analysis of the results showed the existence of dependencies of thiophenol Raman peaks intensities:

1. on the angle between the direction of polarization and the corrugation vector (Fig. 1d.),
2. on the period of corrugated substrate (Fig. 1d.).

The results showed that the strongest Raman intensity is observed along the corrugation vector, whereas the smallest intensity is in the direction perpendicular to the corrugation vector. Moreover, Raman intensities increase with the period of corrugation up to 270 nm. For larger periods, the intensity decreases. Such behavior could be explained with the use of the model discussed in Ref.3 showing that at selected frequencies a SPP damping changes nonlinearly as a function of corrugation dimensions.

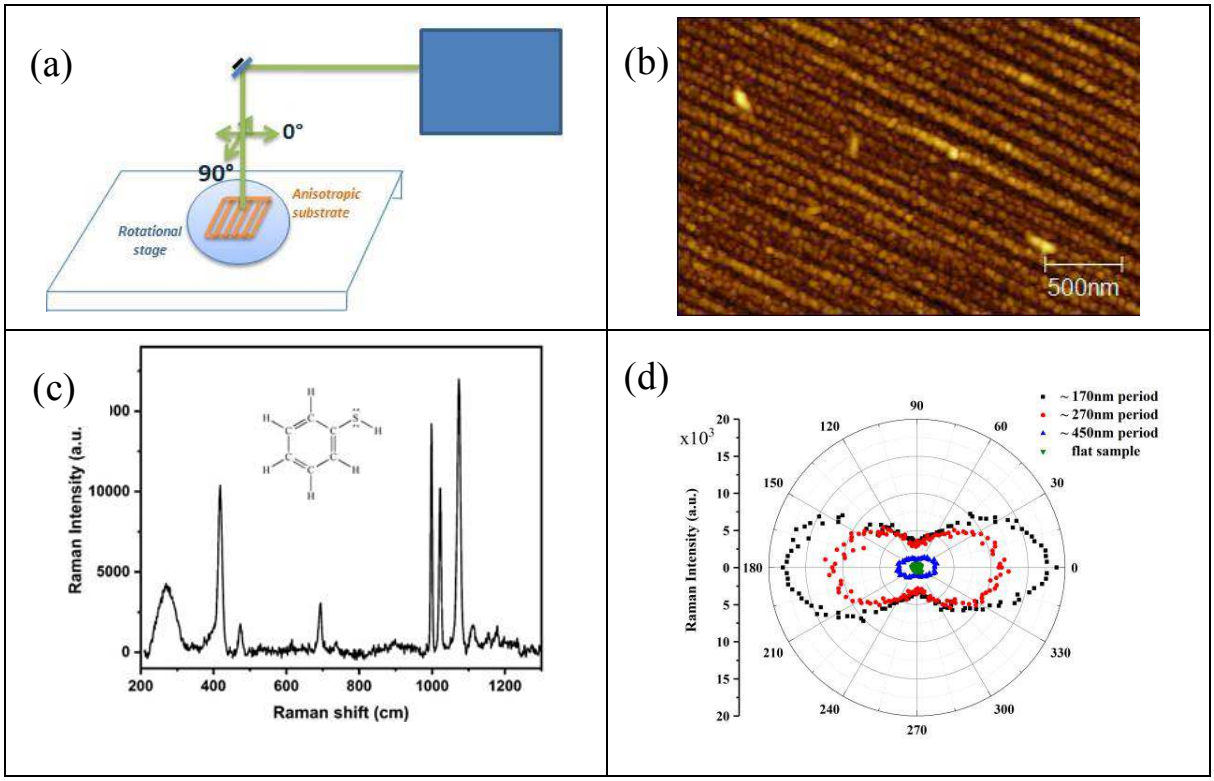


Figure 1. Schematic of measurements geometry (a). Raman spectrum of thiophenol (b). AFM image of corrugated sapphire coated with a 10 nm-thick Au layer (c). Period and angle dependency of Raman intensity of the thiophenol peak at 1072 cm^{-1} (the angle was determined between the corrugation direction and the laser beam polarization) (d).

References

[1] Barnes W. L., Preist T. W., Kitson S. C., Sambles J. R., Cotter N. P. K., Nash D. J., "Photonic gaps in the dispersion of surface plasmons on gratings," Phys. Rev. B, Vol. 51, No. 16, 11164, 1995.

[2] Barnes W., Preist T., Kitson S., Sambles J., "Physical origin of photonic energy gaps in the propagation of surface plasmons on gratings," Phys. Rev. B, Vol. 54, No. 9, 6227, 1996.

[3] Ioannidis T., Gric T., Rafailov E., "Surface plasmon polariton waves propagation at the boundary of graphene based metamaterial and corrugated metal in THz range," Opt. Quantum Electron., Vol. 52, No. 1, 1, 2020.

Acknowledgments

The studies were performed within the LaSensA project carried out under the M-ERA.NET 2 scheme (European Union's Horizon 2020 research and innovation programme, grant No. 685451) and co-funded by the Research Council of Lithuania (LMTLT), agreement No. S-M-ERA.NET-21-2, the National Science Centre of Poland, project No. 2020/02/Y/ST5/00086, and the Saxon State Ministry for Science, Culture and Tourism (Germany), grant No. 100577922, as well as from the tax funds on the basis of the budget passed by the Saxon state parliament.

Bio-Inspired Nanophotonics

META 2023, PARIS - FRANCE, JULY 18 – 21, 2023

Bioinspired coating for bird-safe glazing optimised for avian and human vision

S. R. Mouchet[1,2*], R. Wauters[1], E. Haye[1], S. Lucas[1], and O. Deparis[1]

[1]Department of Physics and Namur Institute of Structured Matter (NISM), University of Namur, Rue de Bruxelles 61, 5000 Namur, Belgium
[2]School of Physics, University of Exeter, Stocker Road, Exeter EX4 4QL, UK
[*]corresponding author: sebastien.mouchet@unamur.be

Abstract: Bird-window collisions often lead to the death of the bird and damage to the window. However, many animals, including birds, can perceive UV light. Many species have hence developed visual communication in this wavelength range, for instance, thanks to photonic structures. Such structures allowed us to design a new UV-reflecting multilayered coating for bird-safe glazing, through a bioinspiration approach. This coating was optimised for bird and human visual perception.

Every year, billions of birds collide with windows, often resulting in their death, as well as in significant material damage. Some manufacturers developed UV-reflective coatings for bird-safe glazing. These coatings are often visible to the human eye over a wide range of viewing angles. In addition, the bird perception of these glazings is usually not considered in depth when developing such selectively reflective devices. However, many animal species, including birds and insects, have developed a wide variety of photonic structures active in the UV due to their perception of light in this range of the electromagnetic spectrum [1]. These structures, optimised during evolution by natural selection, allow us to elaborate new concepts of optimised coatings for selective reflection in the UV and to develop bird-safe glazing through a bioinspiration approach [1]. We developed a bird-safe coating for flat glass panels and polymers that exploits the difference of light perception between humans and birds. This coating consists of a periodic multilayer of metal oxide layers deposited on soda-lime glass substrates by Physical Vapour Deposition (PVD) with patterns. The optical response of the multilayer was numerically designed in terms of morphology and material composition, through a multi-objective optimisation, using human and avian colour perception models. Such a coating deposited on a window makes the window bird-safe, while preserving the aesthetics of the window. The deposited pattern is invisible to human eyes but strongly reflects in the UV range.

Acknowledgements

SRM was supported by the Belgian National Fund for Scientific Research (FRS-FNRS) (91400/1.B.309.18F), the Maturation Fund of the Walloon Region, and a BEWARE Fellowship (Convention n°2110034) of the Walloon Region (Marie Skłodowska-Curie Actions of the European Union - COFUND - contract~847587), as a Postdoctoral Researcher.

References

1. Mouchet, S. R. and O. Deparis, Natural Photonics & Bioinspiration, Boston: Artech House, 2021.

META 2023, PARIS - FRANCE, JULY 18 – 21, 2023

Cross-reactive plasmonic arrays as optical tastebuds

Justin R. Sperling [1], William J. Peveler [2], Alasdair W. Clark* [1]
[1]James Watt School of Engineering, University of Glasgow, Glasgow, United Kingdom
[2] School of Chemistry, University of Glasgow, Glasgow, United Kingdom

*corresponding author: Alasdair.clark@glasgow.ac.uk

Abstract: We present a cross-reactive nanoplasmonic sensor capable of identifying and classifying complex liquid mixtures. Analogous to biological tastebuds, our plasmonic sensor shows promise in a variety of industrial applications as a simple, rapid quality control measure.

There are a variety of analytical tools that are used in the beverage industry for quality control. Typically, these tools are large, expensive, and are not compatible with real-time, in-line monitoring (e.g. gas chromatography mass spectrometry). On the other end of the scale are human tasters who can be trained to recognize impurities within batches of product, but who, due to the nature of human taste, are prone to giving inconsistent scores. As such, there is the need for simple, real-time sensory tools that can be deployed within production facilities as quality control systems; tools which, ideally, could also provide "taste" scores analogous to those provided by human testers. Here, we present a nano-scale optical tastebud system that may fit these requirements.

Our artificial tastebud arrays are composed of millions plasmonic nanostructures, each approximately 100nm x 100nm. Made from Au and Al, these tastebuds provide a plasmonic response (a colour shift in their resonance condition) that is highly dependent on the refractive index of their immediate surroundings. Through specific surface modification we segregate, within the nanoscale sensing volume of the structures, the molecular components of the liquids introduced to the tastebuds. By modifying different arrays of tastebuds with different chemical groups, we can ensure each array probes a different family of components within the liquid. By comparing the resonance shifts from each array we generate a unique statistical score for each mixture. We believe that this development may lead to both portable and in-line devices for applications in beverage production, counterfeit detection, and environmental monitoring.

META 2023, PARIS - FRANCE, JULY 18 – 21, 2023

Effective refractive index determination and light propagation mechanisms in natural scattering media

D. T. Meiers[1*] and G. von Freymann[1,2]

[1]Physics Department and Research Center OPTIMAS, RPTU Kaiserslautern-Landau, 67663 Kaiserslautern, Germany
[2]Fraunhofer Institute for Industrial Mathematics ITWM, 67663 Kaiserslautern, Germany
[*]corresponding author: dmeiers@rptu.de

Abstract: We present a new mixing rule for calculating the effective refractive index beyond the limit of small particles; a restriction found in common effective medium approaches such as the Maxwell-Garnett or Bruggeman theory. Subsequently, these findings are used to distinguish the diffusive and coherent portion of light transport in ultrathin, strongly scattering white beetle scales. It is shown that weakly localized random photonic modes contribute about one third of the overall scattered light, revealing their significance for the brilliant whiteness.

1. Introduction

The interaction of electromagnetic waves with disordered media is ubiquitous in nature, which can be for example observed as vivid structural coloration of various insects, fishes, algae etc. [1]. However, due to the random local arrangements a full description of the light transport on the microscopic scale is in general impossible and an effective medium approach is used instead. Such a description requires the determination of an effective refractive index, which is often done applying the Maxwell-Garnett (MG) or Bruggeman (BG) theory. While both theories are simple to use, they are restricted to grains much smaller than the wavelength of light, which is infrequently fulfilled for natural disordered materials. Using finite-difference time-domain (FDTD) simulations, we systematically investigate the effect of the sphere size on the effective refractive index. Based on the simulation results a new mixing rule is derived, which is capable to correctly describe the effective refractive index of sphere packings composed of large particles [2].
In addition, it is shown that this mixing rule can be also applied for interconnected random structures such as the complex chitin network found in the scales of the white beetle *Cyphochilus*. These scales are of particular interest, since they belong to the strongest scattering structures based on low refractive index materials. While previous studies related the strong scattering to solely diffusive light transport [3], here we find a significant contribution of coherent light scattering by using time and spatially resolved coherent light scattering spectroscopy measurements and accompanying simulations [4].

2. Results

Applying the condition that the forward scattering amplitude of a spherical region of the composite medium vanishes once the background index matches the effective refractive index, FDTD simulations are used to investigate the influence of the sphere size. For dielectric spheres embedded in a dielectric host, it is found that for small sphere sizes the results of the MG theory are obtained. However, with increasing sphere size the results start to deviate from the MG theory, with larger discrepancy at higher refractive index contrasts. In all cases it is observed that a parabola can be fitted to the results in good accordance. Finding a simple empirical formula for

the coefficients of the parabola yields a new, simple mixing rule for large particles. This mixing rule clearly outperforms the prediction of the MG and BG theory, as shown in Fig. 1a.

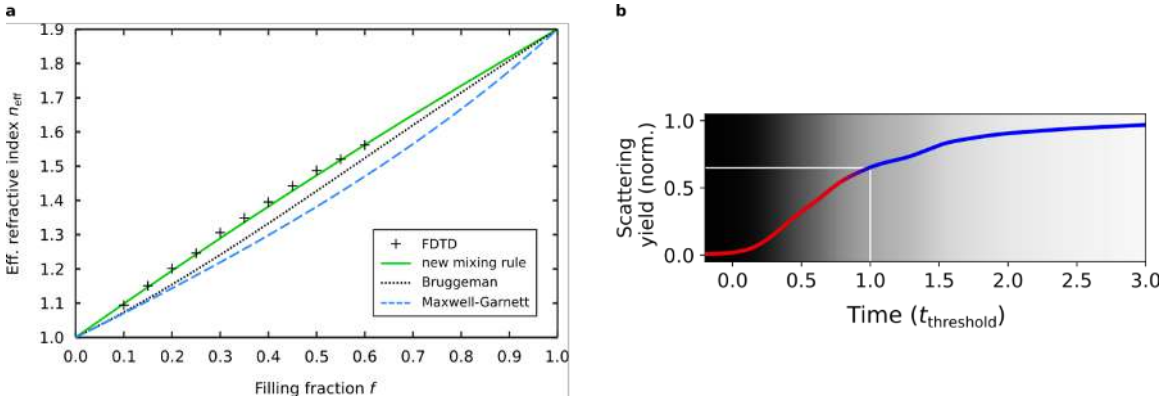


Figure 1: **a**, Comparison of the predictions of the new mixing rule for large particles, the MG and the BG mixing rule with the effective refractive index of a sphere packing, yielded by FDTD simulations. The sphere packing is composed of spheres with a refractive index of 1.9 and a sphere diameter of 380 nm which is not small with respect to the used wavelength of 700 nm. Adapted from [2].**b**, Accumulated scattering yield of the white beetle scales over time. The threshold time $t = 1$ marks the point where the scattering behavior changes from diffusive (red curve) to weak localization assisted (blue). The background shading represents the color impression of the scale over time. Adapted from [4].

Using the mixing rule to determine the effective refractive index of the beetle scales, typical lifetime of diffusive transported light inside the scales is calculated. It is found that this lifetime matches well with the point where the transport behavior changes qualitatively as observed in experiments and simulations. Thereby, the transport at early times is dominated by diffusion while for late times leakage from weakly localized random photonic modes is mainly contributing to the scattered light. Since the portion of this coherent light scattering phenomenon is about one third of the total scattered light, coherent light scattering plays a crucial role for the efficient scattering exhibited by the scales as well as their brilliant whiteness. This can be also discerned in Fig. 1b, revealing that the scales would rather appear gray than white if the coherent light transport would be missing.

Acknowledgements

We gratefully acknowledge financial support from the German research foundation DFG within the priority program SPP1839 “Tailored Disorder”.

References

1. M. Rothammer, C.Zollfrank, K. Busch, and G. von Freymann,“Tailored Disorder in Photonics: Learning from Nature,” Adv. Opt. Mater., Vol. 9, No. 19, 2100787, 2021.
2. D. T. Meiers and G. von Freymann, “New Mixing Rule for Calculating the Effective Refractive Index Beyond the Limit of Small Particles,” (in preparation),2023.
3. M. Burresi, L. Cortese, L. Pattelli, M. Kolle, P. Vukusic, D. S. Wiersma, U. Steiner, and S. Vignolini, “Bright-White Beetle Scales Optimise Multiple Scattering of Light,” Sci. Rep., Vol. 4, No. 1, 6075, 2014.
4. R. C. R. Pompe, D. T. Meiers, W. Pfeiffer, and G. von Freymann, “Weak localization enhanced ultrathin scattering media,” Adv. Opt. Mater., Vol. 10, No. 18, 2200700, 2022.

META 2023, PARIS - FRANCE, JULY 18 – 21, 2023

Transparent and Durable Dust-Repellent Coatings for Photonics Application

Pritha Sarkar[1], **and Kausik Mukhopadhyay**[1,2*]

[1]Materials Science Engineering, University of Central Florida. Orlando, FL. USA
[2]Advanced Materials Processing and Analysis Center, University of Central Florida. Orlando, FL. USA
[*]Corresponding author: kausik@ucf.edu

Abstract: Currently, there is no coating system that can repel dust, is resistant to UV radiation, and can withstand subzero temperatures to deter serious surface, operational and bodily threats in defense, space, and planetary missions. Such risks not only affect the crew but also damage equipment, on-board instruments, sensors, thermal switches, lens, solar and electronic panels. In this talk, we will present a case study of an optically transparent, solid- and liquid-repellent 'omniphobic' coating (SLRC) developed in our lab with exceptional mechanical durability that can tackle dust mitigation issues for a wide range of solids (regolith, dust, debris, ice etc.). Anti-static, anti-reflective, UV-resistant and dust-repellent features have been designed displaying extreme-low adhesion of solids and liquids. Such SLR coatings are instrumental for a wide range of applications, including photonics.

Bio-inspired surface nanopatterning using Femtosecond Lasers and its Applications

Chunlei Guo

University of Rochester, USA
corresponding author: guo@optics.rochester.edu

Abstract: In this talk, I will introduce various technologies that have been developed in my lab, including laser-induced structural coloring and wettability alteration.

Femtosecond lasers are a powerful tool for surface structuring, enabling micro- and nano-patterning that can enhance surface functionality. In this talk, I will introduce various technologies that have been developed in my lab, including laser-induced structural coloring and wettability alteration. The resulting applications of these technologies will also be discussed. Lastly, I will also introduce our research on non-laser-based structural coloring and nanophotonics.

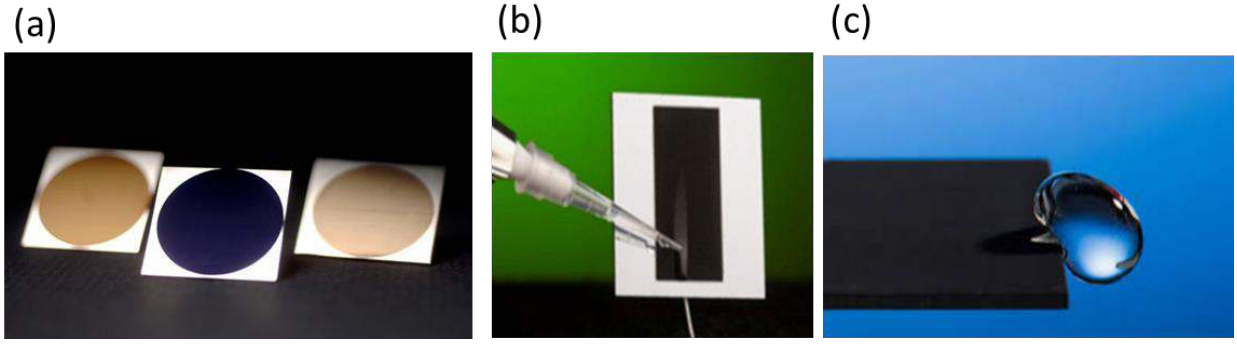


Figure 1: Femtosecond laser-induced (a) black and colored metals, (b) superwicking surface, and (c) superhydrophobic surface.

References

1. Singh, S.C. and Guo, C., EcoMat, Vol. 4, e12161, 2022.
2. Jalil, S.A., Lai, B., ElKabbash, M., Zhang, J. Singh, S.C., and Guo, C., Light: Sci. & Appl., Vol 9, 14, 2020.
3. ElKabbash, M., Letsou, T., Jalil, S.A., Hoffman, N., Zhang, J., Rutledge, J., Fann, C.-H., Hinczewski, M., Strangi, G., and Guo, C., Nat. Nanotech., Vol 16, 440, 2021.
4. Lee, K.J., Wei, R., Wang, Y., Zhang, J., Kong, W., Chamoli, S., Huang, T., Yu, W., Elkabbash, M., and Guo, C., Nat. Photonics, Vol. 17, 236, 2023.

Cuttlefish-eye inspired vision systems with high-quality imaging capabilities

Young Min Song

[1]Electrical Engineering and Computer Science, Gwangju Institute of Science and Technology, Gwangju 61005, Korea
[*]corresponding author: ymsong@gist.ac.kr

Abstract: We discuss the development of an artificial vision system inspired by the unique vision system of cuttlefish. The system compensates for uneven vertical light distribution and reduces incident lights from the top of its vertical field of view using a W-shaped pupil. The high-density belt-like pixel region of a cylindrical silicon photodiode array allows for high-acuity imaging in the region of interest. A flexible carbon nanotube polarizing film integrated into the surface of the array enables polarization-sensitive imaging, resulting in an artificial vision system that achieves high contrast and acuity under uneven light conditions.

Artificial vision is crucial for mobile robotics, particularly for self-driving cars that need to monitor their environment and detect objects to avoid collisions. High contrast and acuity imaging systems are necessary for these applications, but limited image contrast under vertically uneven illumination conditions can hinder object detectability. While drivers can physically mitigate these issues, software-based approaches are necessary for artificial vision systems. However, processing the large amount of visual information required demands high computational power and energy consumption, requiring appropriate hardware solutions.

Inspired by vision systems in nature, such as those found in aquatic and amphibious animals, various artificial vision systems have been developed [1-5]. These bio-inspired systems have unique features that enable high-performance imaging, but none have yet achieved high contrast and acuity under highly noisy conditions caused by randomly polarized sunlight. In this context, the cuttlefish, which have evolved to have a high-acuity vision system optimized for vertically uneven illumination and to detect polarized light, inspire a high-performance artificial vision for mobile robotics [6].

The unique eye structure of the cuttlefish, consisting of a W-shaped pupil, a single spherical lens, and a curved retina with a high-density belt-like photoreceptor region and polarization-sensitive photoreceptors, enables high-contrast and high-acuity vision under vertically uneven illumination conditions. Inspired by these features, an artificial vision system has been developed that compensates for uneven vertical light distribution, enables high-acuity imaging in the region of interest, and maintains an average degree of polarization for polarization-sensitive imaging. By integrating these optical and electronic components, the developed system can balance uneven light distribution while achieving high contrast and acuity, making it a promising candidate for high-performance artificial vision in mobile robotics.

Acknowledgements: This work was supported by the National Research Foundation (NRF) of Korea (2017M3D1A1039288/2018R1A4A1025623).

References

1. G. J. Lee et al., Bioinspired artificial eyes: Optic components, digital cameras, and visual prostheses, Adv. Funct. Mater. 28, 1705202 (2018).
2. M. S. Kim et al., Bio-inspired artificial vision and neuromorphic image processing devices, Adv. Mater. Technol.

2100144 (2021).
3. Y. M. Song et al., Digital cameras with designs inspired by the Arthropod eye, Nature 497, 95 (2013).
4. M. S. Kim et al., An aquatic vision inspired camera based on a monocentric lens and a silicon nanorod photodiode array, Nat. Electron. 3, 546 (2020).
5. M. Lee et al., An amphibious artificial vision system with a panoramic visual field, Nat. Electron. 5, 452 (2022).
6. M. Kim et al., Cuttlefish-eye-inspired artificial vision for high-quality imaging under uneven illumination conditions, Sci. Robot. 8, eade4698 (2023)

META 2023, PARIS - FRANCE, JULY 18 – 21, 2023

Quasi-ordered photonic structures colour the bluespotted ribbontail ray

J. Bouchat[1], F. Cortesi[2], K. Cheney[2,3], P. Vukusic[4], N. Justin Marshall[2], O. Deparis[1], and S. R. Mouchet[1,2,4*]

[1]Department of Physics and Namur Institute of Structured Matter (NISM), University of Namur, Rue de Bruxelles 61, 5000 Namur, Belgium
[2]Queensland Brain Institute, The University of Queensland, Brisbane 4072, Queensland, Australia
[3]School of Biological Sciences, The University of Queensland, Brisbane 4072, Queensland, Australia
[4]School of Physics, University of Exeter, Stocker Road, Exeter EX4 4QL, UK
[*]corresponding author: sebastien.mouchet@unamur.be

Abstract: Due to the scarcity of blue colour exhibited by natural organisms, highlighting the underlying this colour mechanisms is always very impactful for the understanding of the natural world. In this research, the colour of the blue rounded spots occurring in the skin of *Taeniura lymma* stingray was unveiled by a combination of experimental and numerical techniques. Our results demonstrated that this blue colour arises from coherent scattering in quasi-ordered photonic structures occurring in the skin of this stingray.

Blue is often described as the rarest colour in natural organisms [1]. Elucidating the underlying mechanism(s) giving rise to such a hue is always very impactful for the understanding of the natural world in which human beings live. In this research, the colour of the blue rounded spots occurring in the skin of the bluespotted ribbontail ray *Taeniura lymma* was unveiled by a combination of experimental and numerical techniques. Histological observations were carried out with optical, fluorescence and transmission electron microscopies. Optical characterisations were performed by spectrometry and microspectrofluorimetry. Numerical simulations were based on two-dimensional fast Fourier transforms of electron micrographs of the observed structures and Benedek's theory relating Fourier transform of spatial variation in refractive index to the intensity of coherent scattering [2]. Our results demonstrated that the blue colour of this ray arises from coherent scattering in quasi-ordered photonic structures occurring in the skin of this animal. This type of structures made of collagen fibres is mostly unknown in marine species. In addition, structural blue colours had never been reported in elasmobranches.



Figure 1. The blue spots occurring in the integuments of *T. lymma* arise from quasi-ordered photonic structures. Photograph by Taken reproduced from https://pixabay.com/photos/ray-stingray-fish-sea-ocean-539788/

Acknowledgements

SRM was supported by the Belgian National Fund for Scientific Research (FRS-FNRS) (91400/1.B.309.18F), the Maturation Fund of the Walloon Region, and a BEWARE Fellowship (Convention n°2110034) of the Walloon Region (Marie Skłodowska-Curie Actions of the European Union - COFUND - contract~847587), as a Postdoctoral Researcher.

References

1. Mouchet, S. R. and O. Deparis, Natural Photonics & Bioinspiration, Boston: Artech House, 2021.
2. Benedek, G. B., "Theory of Transparency of the Eye," Applied Optics, Vol. 10, No. 3, 459-473, 1971.

SERS Detection of Neurotransmitters through Gold Nanoislands-Decorated Tapered Optical Fibers

D. Zheng[1, *], F. Pisano[1], L. Collard[1], A. Balena[1], M. Pisanello[1], B. Spagnolo[1], L. Piscopo[1,2], C. Ciracì[1], M. D. Vittorio[1,2, *, †], F. Pisanello[1, *, †]

[1] Istituto Italiano di Tecnologia, Center for Biomolecular Nanotechnologies, Arnesano, LE 73010, Italy
[2] Dipartimento di Ingegneria Dell'Innovazione, Università del Salento, Lecce 73100, Italy
[*] Corresponding authors: di.zheng@iit.it, massimo.devittorio@iit.it, ferruccio.pisanello@iit.it
[†]These authors contributed equally to this work

Abstract: In this report, we introduce a non-planar repeated dewetting approach to fabricate gold nanoislands (NIs), uniformly distributed on the wide and highly curved surface of tapered fiber (TF). Through-TF measurements show that the device can achieve a limit of detection in aqueous solution of 10^{-7} M for rhodamine 6G and 10^{-5} M for serotonin and dopamine at near-infrared wavelengths. We envision our technology as a first step towards the unexplored frontier of in-vivo label-free plasmonic neural interface.

Optogenetics has stimulated the development of optical neural interfaces. However, the field largely replies on exogenous fluorescent indicators, which is an indirect way to investigate the biological system and may even alter the native state of the system[1]. Thus, the neuroscience field would highly benefit from label-free approaches to investigate the central neural systems. Surface-enhanced Raman spectroscopy (SERS) is a promising, highly sensitive and label-free approach to detect biomolecules. However, bringing SERS into the deep brain regions requires a specific design to integrate plasmonic structures with minimally invasive neural probes that provide enough sensitivity to detect neurochemicals in a physiological environment.

Here, we introduce a novel non-planar repeated dewetting approach (npRDW)[2] to obtain uniformly distributed gold nanoislands (NIs), decorated along and around the entire highly curved surface of a tapered optical fiber (TF). The fabrication approach is schematically shown in Figure1a. The SEM inspections (Figure1b) of the fabricated NIs-TF device show a uniform NIs coverage until the very tip. The experimental configuration for measuring the limit of detection (LOD) through the tapered fiber (TF) is schematically shown in Figure1c. The results show the NIs-TFs probe have a LOD of 10^{-7} M for aqueous solutions of rhodamine 6G (R6G), and 10^{-5} M for serotonin and dopamine in the near-infrared region. The obtained LOD for neurotransmitters surpasses the current report for SERS-active TF detecting dopamine employing the same configuration (excitation and collection field guided in the same waveguide) by two orders of magnitude[3], and is compatible with the upper bound level of concentrations for neurotransmitters, measured to be in the tens of μM range for both dopamine and serotonin[4,5]. We believe that the highly sensitive SERS detection of the NIs-TFs probe offers opportunities to explore neurotransmitters' dynamics in vivo.

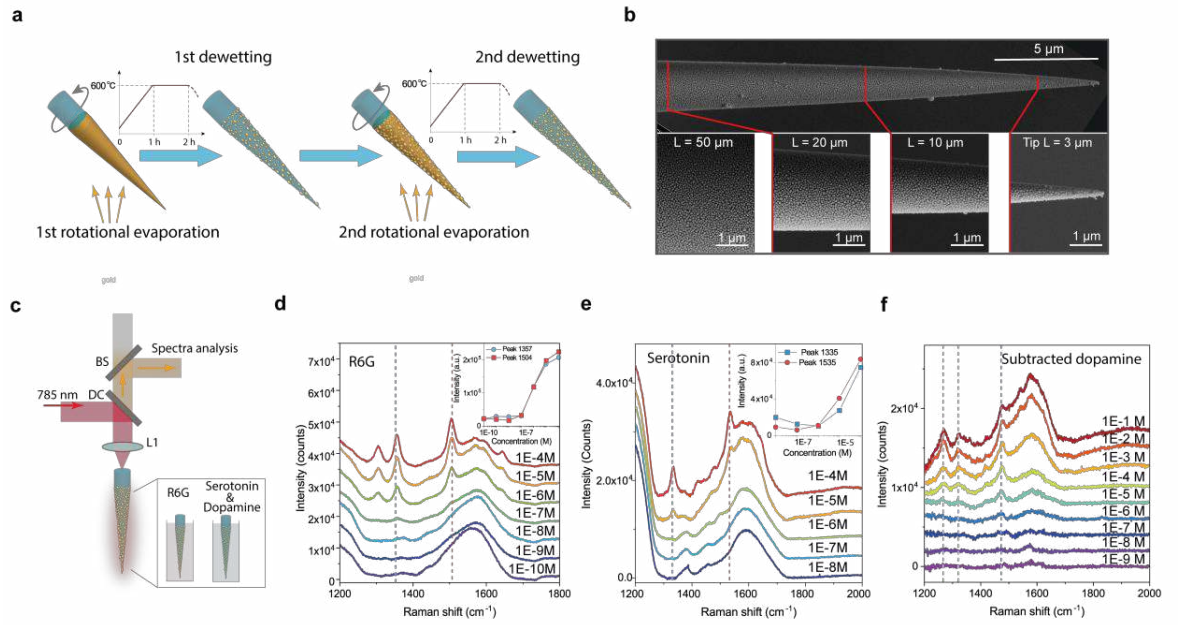


Figure1 (a) Schematic illustration of fabrication procedures of npRDW TF. (b) SEM inspections on the very tip of the NI-TF probe. (c) The configuration of LOD experiment for R6G, serotonin and dopamine. (d-f) Spectra response for NIs-TF detecting R6G, serotonin and silica background subtracted dopamine. Figures modified from ref.1.

References

1. Opilik, L., Schmid, T. & Zenobi, R. Modern Raman Imaging: Vibrational Spectroscopy on the Micrometer and Nanometer Scales. *Annual Rev. Anal. Chem.* **6**, 379–398 (2013).
2. Zheng, D. *et al.* Toward Plasmonic Neural Probes: SERS Detection of Neurotransmitters through Gold Nanoislands-decorated Tapered Optical fibers with sub-10 nm Gaps. *Advanced Materials*, 2200902 (2022).
3. Volkan, M., Stokes, D. L. & Vo-Dinh, T. Surface-Enhanced Raman of Dopamine and Neurotransmitters Using Sol-Gel Substrates and Polymer-Coated Fiber-Optic Probes. *Applied Spectroscopy* **54**, 1842–1848 (2000).
4. Patriarchi, T. *et al.* Ultrafast neuronal imaging of dopamine dynamics with designed genetically encoded sensors. *Science* **360**, eaat4422 (2018).
5. Wan, J. *et al.* A genetically encoded sensor for measuring serotonin dynamics. *Nat Neurosci* **24**, 746–752 (2021).

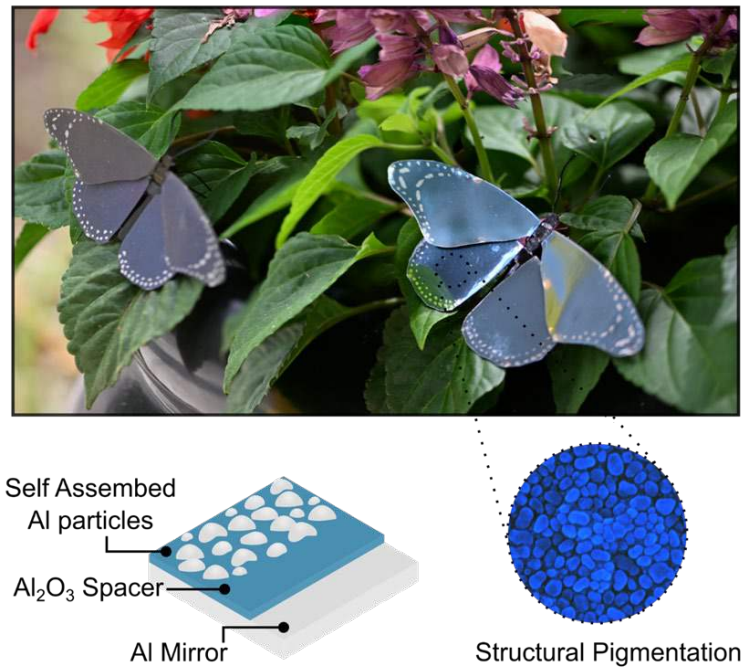
META 2023, PARIS - FRANCE, JULY 18 – 21, 2023

Ultralight, Energy Saving Plasmonic Structural Color Paint

P. Cencillo-Abad[1], D. Chanda[1,2,3*]

[1]NanoScience Technology Center, University of Central Florida, USA
[2]Department of Physics, University of Central Florida, USA
[3]CREOL, The College of Optics and Photonics, University of Central Florida, USA
[*]corresponding author: Debashis.Chanda@ucf.edu

Abstract: In recent years, various nanoengineered structures have been suggested as substitutes for chemical colorants. Nevertheless, many suffer from limited color-palette, angle sensitivity, and are incompatible with industrial production requirements. Here, we introduce a technique for structural coloring that overcomes these constraints by exploiting the hybridization of self-assembled nanoparticles with an ultrathin cavity. Our technique provides a flexible foundation for producing an ultralight plasmonic paint that is eco-friendly and large-scale compatible, bridging the gap between proof-of-concept and industrial applications.



Demonstration of purely structural color based large scale butterflies and paints – A subwavelength plasmonic cavity formed by a self-assembly of metallic nanoislands on top of an oxide-coated mirror, generates color by selectively absorbing certain wavelengths and strongly back-reflecting other..

Summary: Commercial paints rely on the use of molecules that selectively absorb photons matching their electronic transitions. However, these chemicals have low resolution, are environmentally unstable, and can be toxic and polluting. In recent times, nanostructured materials have been suggested as potential alternatives for coloring. These engineered materials control the scattering and reflection of incident light to create color without the need for harmful chemicals. Nevertheless, they often lack saturation, offer a limited color palette, are difficult to integrate with industrial standards, and suffer from severe angle and polarization sensitivity.

Here, we report an approach to structural coloration that exploits the plasmonic resonances that arise naturally from the interaction of light with a random array of metallic islands at visible frequencies. These self-assembled nanoislands, grown using conventional thin film techniques, are placed near a mirror to create a strong hybridization of localized plasmon and subwavelength cavity modes. This results in a single resonance with minimal angular and polarization dispersion and over 90% reflectance at certain wavelengths. Crucially, the optical response of these nanostructures can be easily adjusted across the entire visible spectrum through simple changes in geometrical parameters to achieve a full color range. Fabricating the structures through large-scale techniques we produce stand-alone paints that are ready to be transferred onto any substrate. Remarkably, the platform offers full coloration with a single layer of pigment, with an unbeatable surface density of 0.4 g/m^2, making it the lightest paint in the world. Overall, our plasmonic structural color provides a non-toxic, fade-resistant, and environmentally friendly coloring solution that bridges the gap from proof-of-concept to real-world industrial applications.

Acknowledgements This work at University of Central Florida was supported by National Science Foundation Grant #ECCS-1920840. P.C.A. acknowledges the support from the UCF Preeminent Postdoctoral Fellowship Program (P3).

META 2023, PARIS - FRANCE, JULY 18 – 21, 2023

Plasmonic Colors – Valuable Members of the Structured Colors Family

Samuel Peana[1-3], Sarah Chowdhury[1-2], Ludmila Prokopeva[1-2], and Alexander V. Kildishev[*,1-2]

[1]Birck Nanotechnology Center, Purdue University, West Lafayette, IN 47907, USA

[2]School of Electrical and Computer Engineering, Purdue University, West Lafayette, IN 47907, USA

[3]Quantum Science Center, a National Quantum Information Science Research Center of the U.S. Department of Energy, Oak Ridge, TN 37931, USA

[*]Email: kildishev@purdue.edu

Abstract: We review the accomplishments and motivations behind the development of plasmonic structural colors, overview the highlights of recent works, and provide a perspective on this field's colorful and bright future going forward. In particular, for perspective, we will review the current application space for plasmonic colors, from displays to sensors. Furthermore, we provide a overview on the different manufacturing processes of various plasmonic color films proposed to produce products at industrial scales.

The development of plasmonic structural colors began centuries ago, with plasmonic colors being used in stained glass. These beautiful vibrant colors result from localized surface plasmon resonances of nanoparticles embedded in the glass. The fact that the some of the oldest stained-glass windows in the world found in the Bavarian Augsburg Cathedral were constructed in approximately 900 years ago and still retain their original beautiful colors speaks to many of the advantages of plasmonic colors [1]. They can be constructed to be extremely durable, made of common environmentally friendly materials, and produce a variety of beautiful colors.

As nanofabrication techniques became common, various engineered nano-plasmonic antenna designs became common. These resulted in an explosion in the variety of plasmonic structural color systems, including, gratings [2] and periodic arrays of metallic nano-antenna [3], subwavelength nanohole arrays [4], surface relief metasurfaces [5], and hybrid nanohole/disc arrays [6], and dye free plasmonic structural paints [7].

Additionally, unlike stained glass, plasmonic nano-antenna systems can be engineered to exhibit very particular responses to their environment, this has led to a large number of tunable metasurfaces based on a number of physical processes, including polarization tuning [5,8], electrical tuning [9,10], temperature tunability [11], one-time laser tuning [12], chemical tuning [13], mechanical tuning [14], and finally the rapidly developing field of micro/nano-electromechanical (MEMS/NEMS) tunable colors [15]. MEMS/NEMS and electrical tunability is envisioned to allow for a future of bright, wide-angle visible, high-resolution retro-reflective displays. Since retro-reflective displays use light from the environment for illumination, they are in principle more energy efficient than current light-emitting display technologies, such as liquid crystal or light-emitting diode displays. They are also in principle more visible in direct sunlight. Indeed, many of the possible applications of such displays have been pioneered by e-ink display technology.

Additionally, the same sensitivity to the environment that allows for tunability has also resulted in various applications for colorimetric sensing. Plasmonic structural colors can also be made sensitive to refractive index environment, angle, and strain allowing for sensitive colorimetric sensing of all of these quantities [8,14,16,17]. There are a variety of other applications of the inherently high resolution, tunability, and robustness of plasmonic structural colors in various fields such as security, information storage, steganography, and other areas where plasmonic colors can prove to be an effective solution [18].

Plasmonic structural colors colors are part of a visually striking field, and in this work we will overview

some of the most exciting past achievements in this field, recent and present research, and provide a view on future work in this field. We will emphasize the exploding application space for such plasmonic colors and overview common manufacturing techniques and how they can be applied to solve problems at scale across the application space now and in the future.

References

[1] R. K. Moore, *Stained Glass*, in *The Encyclopedia of Christian Civilization* (John Wiley & Sons, Ltd, 2011).

[2] T. Xu, Y.-K. Wu, X. Luo, and L. J. Guo, *Plasmonic Nanoresonators for High-Resolution Colour Filtering and Spectral Imaging*, Nat. Commun. **1**, 1 (2010).

[3] A. S. Roberts, A. Pors, O. Albrektsen, and S. I. Bozhevolnyi, *Subwavelength Plasmonic Color Printing Protected for Ambient Use*, Nano Lett. **14**, 783 (2014).

[4] F. Cheng, J. Gao, T. S. Luk, and X. Yang, *Structural Color Printing Based on Plasmonic Metasurfaces of Perfect Light Absorption*, Sci. Rep. **5**, 1 (2015).

[5] M. Song, L. Feng, P. Huo, M. Liu, C. Huang, F. Yan, Y. Lu, and T. Xu, *Versatile Full-Colour Nanopainting Enabled by a Pixelated Plasmonic Metasurface*, Nat. Nanotechnol. **18**, 1 (2023).

[6] M. Song, D. Wang, S. Peana, S. Choudhury, P. Nyga, Z. A. Kudyshev, H. Yu, A. Boltasseva, V. M. Shalaev, and A. V. Kildishev, *Colors with Plasmonic Nanostructures: A Full-Spectrum Review*, Appl. Phys. Rev. **6**, 041308 (2019).

[7] P. Cencillo-Abad, D. Franklin, P. Mastranzo-Ortega, J. Sanchez-Mondragon, and D. Chanda, *Ultralight Plasmonic Structural Color Paint*, Sci. Adv. **9**, eadf7207 (2023).

[8] M. Song, X. Li, M. Pu, Y. Guo, K. Liu, H. Yu, X. Ma, and X. Luo, *Color Display and Encryption with a Plasmonic Polarizing Metamirror*, Nanophotonics **7**, 323 (2018).

[9] K. Xiong, G. Emilsson, A. Maziz, X. Yang, L. Shao, E. W. H. Jager, and A. B. Dahlin, *Plasmonic Metasurfaces with Conjugated Polymers for Flexible Electronic Paper in Color*, Adv. Mater. **28**, 9956 (2016).

[10] D. Franklin, R. Frank, S.-T. Wu, and D. Chanda, *Actively Addressed Single Pixel Full-Colour Plasmonic Display*, Nat. Commun. **8**, 15209 (2017).

[11] F.-Z. Shu, F.-F. Yu, R.-W. Peng, Y.-Y. Zhu, B. Xiong, R.-H. Fan, Z.-H. Wang, Y. Liu, and M. Wang, *Dynamic Plasmonic Color Generation Based on Phase Transition of Vanadium Dioxide*, Adv. Opt. Mater. **6**, 1700939 (2018).

[12] S. N. Chowdhury, P. Nyga, Z. A. Kudyshev, E. Garcia Bravo, A. S. Lagutchev, A. V. Kildishev, V. M. Shalaev, and A. Boltasseva, *Lithography-Free Plasmonic Color Printing with Femtosecond Laser on Semicontinuous Silver Films*, ACS Photonics **8**, 521 (2021).

[13] X. Duan, S. Kamin, and N. Liu, *Dynamic Plasmonic Colour Display*, Nat. Commun. **8**, 1 (2017).

[14] M. L. Tseng, J. Yang, M. Semmlinger, C. Zhang, P. Nordlander, and N. J. Halas, *Two-Dimensional Active Tuning of an Aluminum Plasmonic Array for Full-Spectrum Response*, Nano Lett. **17**, 6034 (2017).

[15] Z. Han, C. Frydendahl, N. Mazurski, and U. Levy, *MEMS Cantilever–Controlled Plasmonic Colors for Sustainable Optical Displays*, Sci. Adv. **8**, eabn0889 (2022).

[16] N. S. King, L. Liu, X. Yang, B. Cerjan, H. O. Everitt, P. Nordlander, and N. J. Halas, *Fano Resonant Aluminum Nanoclusters for Plasmonic Colorimetric Sensing*, ACS Nano **9**, 10628 (2015).

[17] F. Lütolf, D. Casari, and B. Gallinet, *Low-Cost and Large-Area Strain Sensors Based on Plasmonic Fano Resonances*, Adv. Opt. Mater. **4**, 715 (2016).

[18] M. Song, D. Wang, Z. A. Kudyshev, Y. Xuan, Z. Wang, A. Boltasseva, V. M. Shalaev, and A. V. Kildishev, *Enabling Optical Steganography, Data Storage, and Encryption with Plasmonic Colors*, Laser Photonics Rev. **15**, 2000343 (2021).

Parity-Time and quasi-normal modes in Photonics, Plasmonics, Acoustics

META 2023, PARIS - FRANCE, JULY 18 – 21, 2023

Acoustic nonreciprocity in a linear viscous medium with broken *P* symmetry

A. Krokhin[1*], H. Heo[2], A. Neogi[3], Yu. Zubov[1], and E. Walker[4]

[1]Department of Physics, University of North Texas, P.O. Box 311427, Denton, Texas 76203, USA
[2]Penn State University, 201 Applied Science Bldg, University Park, PA 16802, USA
[3]University of Electronic Science and Technology of China, Chengdu 611731, China
[4]Echonovus Inc., 1800 South Loop 288 STE 396 #234, Denton, Texas 76205, USA
[*]corresponding author: arkady@unt.edu

Abstract: Acoustic transmission through arbitrary arrangement of scatterers possesses Rayleigh reciprocal symmetry with respect to switch of emitter and receiver at points *A* and *B*, $p_A(\mathbf{r}_B) = p_B(\mathbf{r}_A)$. Velocity field does not possess the same reciprocal symmetry if the system of scatterers does not have reflection symmetry (*P* symmetry). Here we show that in a viscous fluid lack of reciprocal symmetry for velocity leads to different dissipated energy for forward and backward propagation, thus making acoustic propagation truly nonreciprocal.

Wave propagation in a viscous fluid is an irreversible process since it is accompanied by entropy production. While viscous dissipation breaks time-reversal symmetry (*T* symmetry), which is the necessary condition for nonreciprocity, it is commonly believed that viscosity is not a factor for nonreciprocity. This is due to the fact that reciprocity of pressure is compatible with viscosity. The velocities obtained from the Navier-Stokes equation in general case form a vortex field. The vorticity, however, does not contribute to pressure, which depends only on the potential part of the field of velocities, $p(\mathbf{r}) \sim \nabla \cdot \mathbf{v}$, as it follows from the linearized continuity equation. Therefore, the Rayleigh reciprocal symmetry for pressure remains valid even in a viscous fluid. Asymmetry in velocity field, $\mathbf{v}_A(\mathbf{r}_B) \neq \mathbf{v}_B(\mathbf{r}_A)$ cannot be a manifestation of nonreciprocity in *ideal* fluid since fluid dynamics is time reversible. If now the viscosity factor is "switched on" different distribution of velocities in the forward and backward propagation generates different amount of dissipative losses. As a result, the difference in intensities $I_A(r_B) - I_B(r_A)$ acquires a truly nonreciprocal dissipation-induced part. Of course, if the distribution of scatterers between points *A* and *B* is mirror symmetrical the viscous losses become equal. Then, propagation of sound becomes reciprocal while remaining irreversible. Thus, broken *PT* symmetry is the necessary condition for acoustic nonreciprocity.

Numerical simulations were performed for a rigid cylindrical scatterer of diameter 6.35 mm imbedded in a fluid with viscosity η and density ρ, Fig. 1. The upper half of the cylinder (along arc DAC) is not flat. It is covered by square tips of size σ. This roughness breaks *P* symmetry but it does not affect much the scattering cross-section if $\sigma \ll \lambda$. At the same time, it strongly affects the velocity field within the narrow boundary layer $\delta = \sqrt{2\eta/\rho\omega}$ where dissipation occurs. The emitter and receiver were placed 5 mm away from the center at the symmetrical points *A* and *B*. Numerical solutions using the Navier-Stokes equation were obtained for $\sigma = 10$ and 100 μm at frequency 565 kHz that corresponds to the wavelength in water $\lambda = 2.6$ mm. Viscosity of the fluid was changed from 0 to $\eta = 60\,\eta_{water}$. Nonreciprocity for pressure is characterized by $\Delta_p = \frac{2(p_A(B) - p_B(A))}{p_A(B) + p_B(A)}$, which is plotted as a function of normalized viscosity η/η_{water} in Fig. 1a. The numerical values for Δ_p presented in Fig. 1a are very small for both amplitudes of roughness and they do not grow with viscosity. This suggests that pressure remains reciprocal even in a very viscous fluid. The graph in Fig. 1b clearly demonstrates that nonreciprocity $\Delta_v(\eta)$ for modulus of velocity, which exists even for acoustic mode in ideal fluid $\eta = 0$, grows

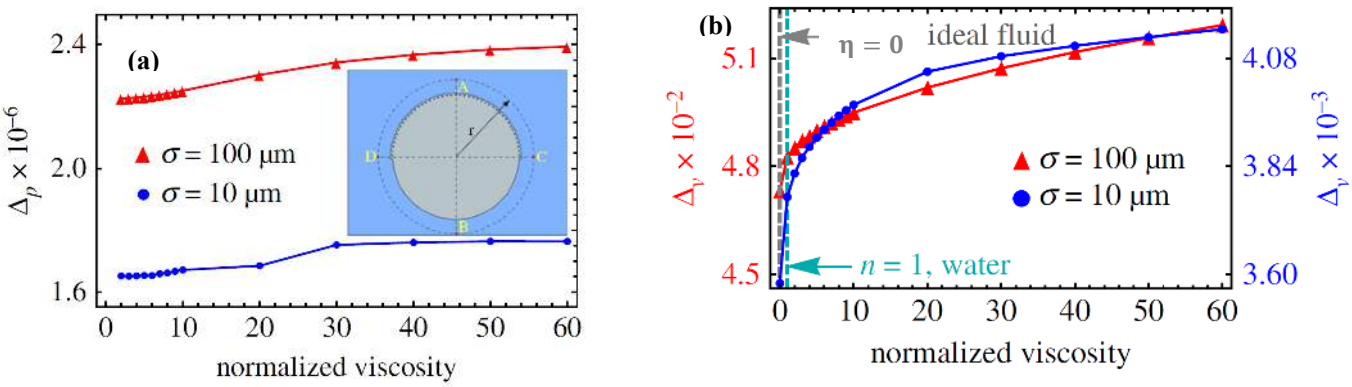


Fig. 1. Nonreciprocity for (a) pressure, Δ_p and (b) modulus of velocity versus normalized viscosity η/η_{water}. The left (right) vertical axis in (b) is for roughness $\sigma = 100$ (10) μm. The graphs demonstrate reciprocal behavior of pressure and strongly nonreciprocal behavior of velocity [1].

fast with η. The difference $\Delta_v(\eta) - \Delta_v(\eta = 0)$ is the part of nonreciprocity caused solely by viscosity. This part scales as $\sqrt{\eta}$ according to the scaling of viscous losses in the boundary layer δ.

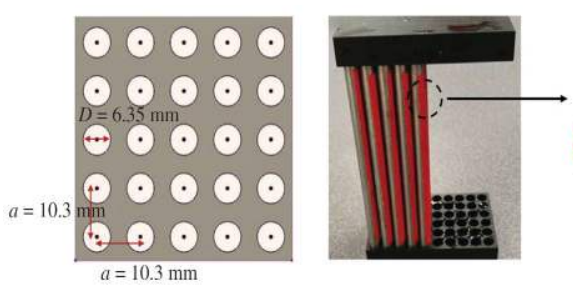


Fig. 3. The cross-section view of the phononic crystal. Rough part of cylindrical surface is highlighted in red.

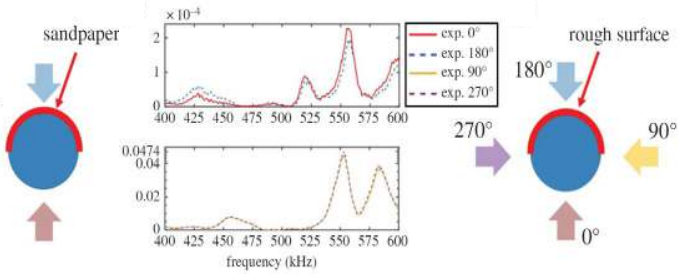


Fig. 4. Experimental transmission spectra along asymmetric (upper panel) and symmetric (lower panel) directions.

A phononic crystal used for experimental demonstration [1] of the effects of asymmetry and non-reciprocity is shown in Fig. 3. Stainless steel rods (D = 6.35 mm) were arranged in a square lattice with period a = 10.30 mm. Half of the cylindrical surface of each rod was covered by a sandpaper representing a scatterer with broken P symmetry (σ = 1.36 μm) along the direction 0° ↔ 180°. The measure of non-reciprocity does not remain constant in Fig. 4 (upper panel) but changes and even alternates its sign with frequency. At the same time, all the spectra measured along the P-symmetric direction 90° ↔ 270° are reciprocal (lower panel). Nonreciprocal transmission through a phononic crystal with strongly asymmetric scatterers was experimentally measured in Ref. [3].

This work was supported by the National Science Foundation under EFRI grant no. 1741677.

References

1. Heo, H., E. Walker, Y. Zubov, D. Shymkiv, D. Wages, A. Krokhin, T.-Y. Choi and A. Neogi, "Non-reciprocal acoustics in a viscous environment," Proc. R. Soc. A, Vol. 476, 20200657 2020.
2. Walker, E., A. Neogi, A. Bozhko, Yu. Zubov, J. Arriaga, H. Heo, J. Ju and A. A. Krokhin, "Nonreciprocal linear transmission of sound in a viscous environment with broken P symmetry" Phys. Rev. Lett., Vol. 120, 204501, 2018.

META 2023, PARIS - FRANCE, JULY 18 - 21, 2023

Spectral response at hierarchically-constructed exceptional points

Jan Wiersig*

Institut für Physik, Otto-von-Guericke-Universität Magdeburg, D-39016 Magdeburg, Germany
*corresponding author: jan.wiersig@ovgu.de

Abstract: Non-Hermitian degeneracies, so-called exceptional points, have attracted considerable attention in photonics, plasmonics, and acoustics. One way to implement exceptional points of higher order is the scheme of hierarchical construction. We derive explicit formulas for the spectral response at such higher-order exceptional points.

At an exceptional point (EP) of order n exactly n eigenvalues and the corresponding eigenstates of a non-Hermitian Hamiltonian coalesce [1]. Several peculiar and counterintuitive properties of such non-Hermitian degeneracies have been studied in particular in optics and photonics [2]. EPs exhibit a strong spectral response to perturbations: when a Hamiltonian $\hat{H}$ at an EP of order n and eigenvalue E_{EP} is subjected to a perturbation,

$$\hat{\mathcal{H}} = \hat{H} + \varepsilon \hat{H}_1 \,, \tag{1}$$

then the resulting energy (or frequency) splittings are generically proportional to the n-th root of the small perturbation parameter $\varepsilon > 0$ [1]. These splittings are considerably larger than the linear splittings at conventional degeneracies. Importantly, for fixed order n the resulting splittings still depend on the perturbation and the internal structure of the EP. Their contributions can be separated for generic perturbations in the inequality [3]

$$|E_j - E_{\mathrm{EP}}|^n \le \varepsilon ||\hat{H}_1||_2 \, \xi \,, \tag{2}$$

where E_j are the eigenvalues of the perturbed $n \times n$ Hamiltonian matrix (1), $||\cdot||_2$ is the spectral matrix norm, $\xi := ||\hat{N}^{n-1}||_2$ is the spectral response strength, and $\hat{N} := \hat{H} - E_{\mathrm{EP}}\mathbb{1}$ is the traceless part of the unperturbed Hamiltonian.

An EP with large ξ has potentially a strong response to perturbations which makes it attractive for sensing applications [4]. However, this comes at a price, namely the delicate fine tuning of experimental parameters, in particular for higher-order EPs. A robust method to obtain higher-order EPs is the hierarchical construction [5]. In this scheme two subsystems with $n \times n$ Hamiltonians $\hat{H}_{\mathrm{a}}$ and $\hat{H}_{\mathrm{b}}$, each at an EP of order n with the same eigenvalue E_{EP}, are coupled in a unidirectional way,

$$\hat{H} = \begin{pmatrix} \hat{H}_{\mathrm{a}} & 0 \\ \hat{K} & \hat{H}_{\mathrm{b}} \end{pmatrix} . \tag{3}$$

For a generic $n \times n$ coupling matrix $\hat{K}$ the Hamiltonian of the composed system $\hat{H}$ has an EP of order $2n$.

We generalize this scheme to include also two EPs of different order n_{a} and n_{b} and determine the spectral response strength of the resulting EP of higher order $n_{\mathrm{a}} + n_{\mathrm{b}}$ to be [6]

$$\xi = ||\hat{N}_{\mathrm{b}}^{n_{\mathrm{b}}-1} \hat{K} \hat{N}_{\mathrm{a}}^{n_{\mathrm{a}}-1}||_2 \,, \tag{4}$$

with $\hat{N}_{\mathrm{a}}$ and $\hat{N}_{\mathrm{b}}$ being the traceless parts of $\hat{H}_{\mathrm{a}}$ and $\hat{H}_{\mathrm{b}}$. The spectral response strength ξ can be written in terms of the spectral response strengths ξ_{a} and ξ_{b} of the two subsystems as

$$\xi = \xi_{\mathrm{a}} \xi_{\mathrm{b}} |\langle \widetilde{j_{\mathrm{b},n_{\mathrm{b}}}} | \hat{K} | \psi_{\mathrm{EPa}} \rangle| \,. \tag{5}$$

Here, $|\psi_{\mathrm{EPa}}\rangle$ is the eigenvector of $\hat{H}_{\mathrm{a}}$ and $|\widetilde{j_{\mathrm{b},n_{\mathrm{b}}}}\rangle$ is the normalized last Jordan vector of $\hat{H}_{\mathrm{b}}$. Equation (5) provides a

possibility to design the unidirectional coupling in order to maximize the spectral response at the resulting higher-order EP. For fixed properties of the original lower-order EPs and fixed total coupling strength, measured e.g. by $||\hat{K}||_2$, the coupling matrix $\hat{K}$ can be chosen such that $|\langle\widetilde{j_{\mathrm{b},n_\mathrm{b}}}|\hat{K}|\psi_{\mathrm{EPa}}\rangle|$ is maximized. We also derive an easy to calculate upper bound

$$\xi \leq \xi_\mathrm{a}\xi_\mathrm{b}||\hat{K}||_2 \,. \tag{6}$$

Figure 1 shows as example the unidirectional coupling of a parity-time ($\mathcal{PT}$) symmetric dimer to a $\mathcal{PT}$-symmetric trimer. The parameters are chosen such that the former is at an EP of order $n_\mathrm{a} = 2$ and the latter at an EP of order $n_\mathrm{b} = 3$. The two subsystems are coupled in a unidirectional manner from the gainy cavity of the dimer to the gainy cavity of the trimer resulting in an EP of order $n_\mathrm{a} + n_\mathrm{b} = 5$. Such a scenario can be realized experimentally by replacing the single-mode cavities by microrings supporting clockwise and counterclockwise traveling modes and couple them via a conventional optical waveguide [6]. The spectral response strength of the dimer (trimer) is $\xi_\mathrm{a} = 2g_\mathrm{a}$ ($\xi_\mathrm{b} = 4g_\mathrm{b}^2$) [3]. From Eq. (4) or (5) one calculates

$$\xi = \sqrt{8}|k|g_\mathrm{a}g_\mathrm{b}^2 \,, \tag{7}$$

which shows how the coupling strengths have to be chosen in order to obtain a strong spectral response at this hierarchically-constructed EP of order 5.

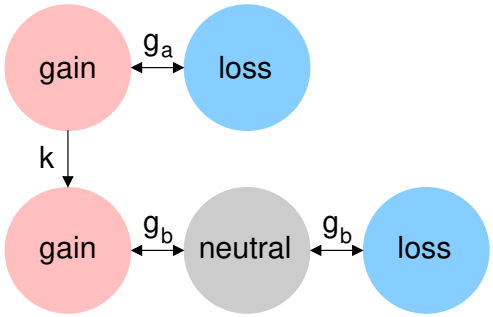


Figure 1: Illustration of the unidirectionally-coupled $\mathcal{PT}$-symmetric dimer and trimer at an EP of order 5. Each disk represents a single-mode cavity. The cavities are coupled horizontally in a symmetric fashion with coupling strengths $g_\mathrm{a} > 0$ and $g_\mathrm{b} > 0$. The vertical coupling is unidirectional with strength $|k|$.

We have presented an explicit formula for the spectral response strength of hierarchically-constructed higher-order EPs. The response strength is a measure of the quality of the EP and is relevant for the design of EP-based devices. We have related this quantity to the spectral response strengths of the individual subsystems. The analysis presented here also serves as a first step towards a more general theory of mode coupling at and near EPs.

References

1. T. Kato, *Perturbation Theory for Linear Operators*. New York: Springer, 1966.

2. M.-A. Miri and A. Alù, "Exceptional points in optics and photonics," *Science*, vol. 363, no. 6422, p. eaar7709, 2019.

3. J. Wiersig, "Response strengths of open systems at exceptional points," *Phys. Rev. Res.*, vol. 4, p. 023121, 2022.

4. W. Chen, Ş. K. Özdemir, G. Zhao, J. Wiersig, and L. Yang, "Exceptional points enhance sensing in an optical microcavity," *Nature (London)*, vol. 548, pp. 192–196, 2017.

5. Q. Zhong, J. Kou, Ş. K. Özdemir, and R. El-Ganainy, "Hierarchical construction of higher-order exceptional points," *Phys. Rev. Lett.*, vol. 125, p. 203602, 2020.

6. J. Wiersig, "Revisiting the hierarchical construction of higher-order exceptional points," *Phys. Rev. A*, vol. 106, p. 063526, 2022.

Efficient analysis and design of edge states

H. Schomerus[1] *

[1]Department of Physics, Lancaster, University, UK
*corresponding author: h.schomerus@lancaster.ac.uk

Abstract: I describe an efficient approach that allows to design edge states at arbitrary energies. In this approach, edge states are mapped onto unstable fixed points of a non-linear map, which can be directly determined from microscopic coupled-mode descriptions. The approach can make effective use of topological symmetries, but also applies to non-Hermitian and nonreciprocal systems.

Edge and interface states are central to our understanding of topological systems. I show how one can directly determine interface configurations that support edge states at a given energy or frequency. In paradigmatic systems, the underlying equations can be approached analytically, allowing, for instance, to determine a symmetry-breaking edge potential that fixes an edge state in a Su-Schrieffer-Heeger (SSH) chain at a predetermined energy (see Fig. 1). As shown in Fig. 2, the approach also applies to higher-dimensional edges, allowing to design unconventional edge dispersion relations in the complex energy plane.

The design framework rests on a simple real-space renormalization approach that reformulates the quantization condition of these states as a powerful fixed-point condition [1]. Using these fixed points, one then directly obtains the required interface data. Besides its practical utility, this approach provides a completely novel perspective on the formation of such states, clearly separating the roles of symmetries in the bulk and at the interface. As the approach holds for non-Hermitian and non-reciprocal systems, it also gives novel insights into the non-Hermitian skin effect. Conceptually, the approach also highlights the interplay of left and right eigenstates, whose separate roles features physically, e.g., in sensors.

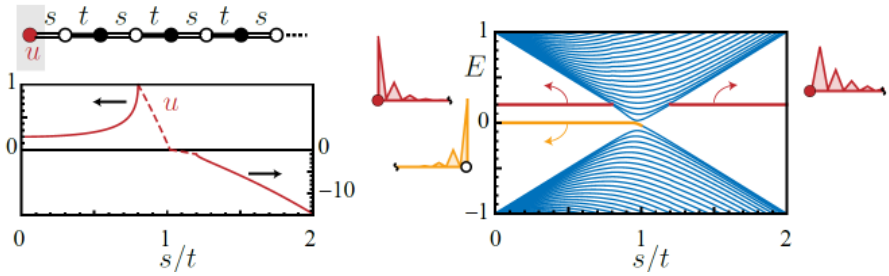


Fig. 1 Design and implementation of a symmetry-breaking edge state in a Su-Schrieffer-Heeger (SSH) chain, illustrated here for target energy E=0.2. This is achieved by using a symmetry-breaking edge potential u, which can be determined analytically (left panel). Implemented in a finite chain (right panel), the desired edge state (red) appears whenever its energy is inside the gap, possibly coexisting with a conventional edge state at the other edge (yellow).

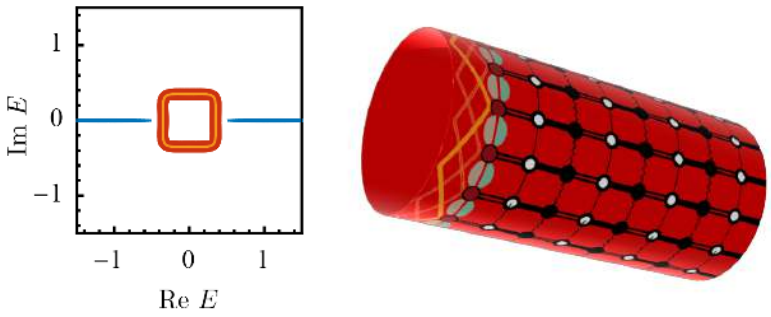


Fig. 2 Design and implementation of a dispersion relation approximating a square in the complex energy plane. The target dispersion is shown in yellow, the actually obtained dispersion is shown in red (with additional extended bulk states shown in blue). The sketch on the right illustrates the implementation of the system on a cylinder. The edge is configured with couplings that follow from a simple condition. The bulk consists of ladders made out of SSH chains.

References

1. H. Schomerus, "Universal renormalization approach to the analysis and design of Hermitian and non-Hermitian interfaces," arXiv:2208.14626 (2022).

Shaping the Topological States

Hamidreza Ramezani[1*], Elnaz Hamdarsi[1], Cem Yuce[2], Prineha Narang[3]

[1]Department of Physics and Astronomy, University of Texas Rio Grande Valley, Edinburg, TX 78539, USA

[2]Department of Physics, Eskisehir Technical University, Eskisehir, Turkey

[3]College of Letters and Science, University of California, Los Angeles, CA 90095, USA
[*]corresponding author: hamidreza.ramezani@utrgv.edu

Abstract: Topological zero-modes are known to be localized at the interface between two structures with different topology. Here using the degree of non-Hermiticity and using non-unitary and yet similarity transformation we lift this property and design zero-modes that are not necessarily localized. Our proposed approach paves the way for designing topologically protected states that potentially could be used for far field imaging and sensing.

The study of the topological system is by now well-established and both Hermitian and non-Hermitian systems are addressed fairly in the literature [1]. The major concept in topological lattices is the existence of a so-called zero-mode that its eigenenergy is robust against disorder and its corresponding field distribution is mainly localized at the interface of the lattice. Specifically, in 1D localization occurs at the edge and in 2D while along the interface of the edge of the structure, the topological mode can provide transport, perpendicular to the edge the topological state is localized. This localization creates a barrier for practical applications of topological modes as in many systems the mode requires to be extended. An example of such an application is far-field sensing and imaging.

Thus, it is essential to find a universal approach that allows for engineering the shape of topologically protected zero-modes. Here we will show that using a similarity transformation we can engineer a non-Hermitian structure and obtain a topologically protected zero-mode with any desired field distribution. It is important to notice that the actual lattice with an engineered topological state might not have any obvious symmetry that allows describing the topological properties of the system. Furthermore, although the engineered structure is non-Hermitian, its spectrum remains real as its corresponding Hamiltonian is obtained from acting a similarity transformation on the Hamiltonian of a Hermitian topological system. Despite the existence of the real spectrum, the non-Hermiticity of the engineered Hamiltonian can lead to the skin effect in the engineered structure such that all the bulk eigenmodes become exponentially localized on one side of the structure.

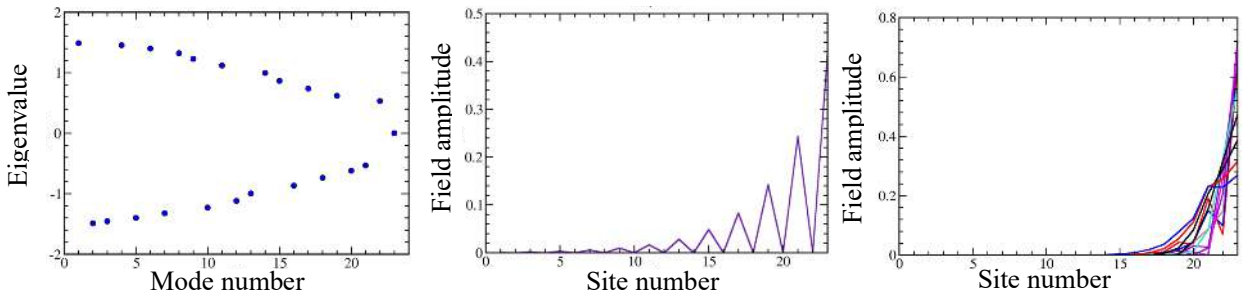


Figure 1. (a) Spectrum of the engineered lattice, (b) Flipped zero mode, (c) Skin states.

An example of engineered zero-mode is given in Fig. (1b) in which a flipped edge state is depicted. The engineered lattice with N number of sites has a non-Hermitian Hamiltonian that is given by non-unitary and yet

similarity transformation $H = AH_{SSH}A^{-1}$ in which H_{SSH} is a $N \times N$ matrix associated with the Hamiltonian of a system that is given by the well celebrated Su-Schrieffer-Heeger (SSH) Hamiltonian and is expected to have an edge state localized at the left side of the lattice. Furthermore, A is a $N \times N$ diagonal matrix. The diagonal element a_{nn} $(n = 1, \ldots, N)$ of A is given by the $a_{nn} = f_n$ with $f_n = f_{n-1} + f_{n-2}$, $f_1 = 1$ and $f_2 = 2$. We note that, a_{nn} is generated by the Fibonacci sequence. The similarity transformation that we used here makes sure that the two Hamiltonian H_{SSH} and H have the same spectrum even H is a non-Hermitian Hamiltonian. The spectrum of H is shown in Fig.(1a). As expected, we observe that both Hamiltonians have a zero-mode. However, the mode profile associated with the zero-mode of the Hamiltonian H_{SSH} is localized at the left side as we mentioned before while H has a zero-mode profile that is localized at the right side of the engineered lattice. We further, observe that the spectrum of the non-Hermitian Hamiltonian H depicts the so-called skin effect in which all the extended states are localized at one side of the lattice. This is shown in Fig.(1c).

By choosing a different function rather than the one we used in the previous example we can obtain other desired zero-modes not only in 1D but even in 2D. Figures (2a,b) are examples of such engineered zero-mode profiles. Specifically, in Fig. (2a) we have a zero-mode that is extended [2] all over the lattice while Fig.(2b) shows a zero-mode localized in the center of a 2D lattice.

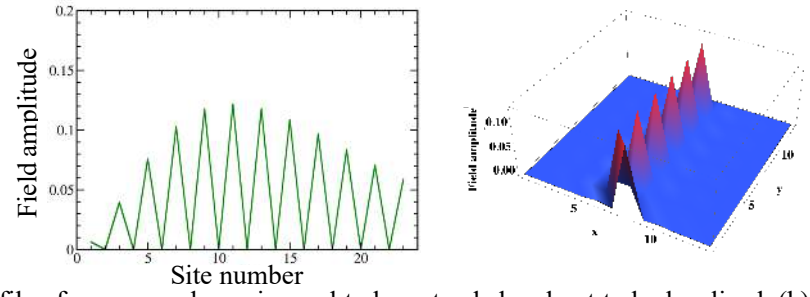


Figure 2. (a) Field profile of a zero-mode engineered to be extended and not to be localized. (b) Mode profile of a zero-mode associated with a 2D engineered structure that is localized at the center of the lattice and not at the edge.

Conclusion: We have shown that using a similarity transformation we can tune the shape of a zero-mode such that is no longer necessarily localized at one edge. This idea is not limited to 1D and can be extended to 2D as well. Our results can pave the way for designing topological devices that are working based on specific mode profiles, this includes far-field imaging, switches, gates, etc.

HR. acknowledge the support by the Army Research Office Grant No. W911NF-20-1-0276 and NSF Grant Nos. PHY-2012172. HR. and PN. acknowledge the support by NSF OMA-2231387.

References

1. Ozawa, T., et al., "Topological photonics," Rev. Mod. Phys., 91, 015006, 2019.
2. Ferdous, J., et al., "Observation of Robust Zero Energy Extended States," arXiv preprint arXiv:2205.02181 (2022).

Parity-time symmetric waveguides with tailored dipoles and chiral features

A. De Corte[1], M. Besbes[2], H. Benisty[2], B. Maes[1*]

[1]Micro- and Nanophotonic Materials Group, Research Institute for Materials Science and Engineering, University of Mons, 20 Place du Parc, B-7000 Mons, Belgium

[2]Laboratoire Charles Fabry, Institut d'Optique Graduate School, CNRS, Univ. Paris Saclay, 2 Av. Augustin Fresnel, 91127 Palaiseau Cedex, France

[*]corresponding author: bjorn.maes@umons.ac.be

Abstract: We extend the standard coupled waveguide system with balanced gain and loss for PT-symmetry, in order to exploit and tailor the exceptional points. First, we place an electric dipole source between the waveguides, to create a contrast between wave propagation on both sides of the dipole by controlling its polarization. Secondly, we study the influence of chirality on the guided modes, by inserting a chiral material in the waveguide gap. We observe a strong chiral impact at degeneracies, and interesting avoided crossings at exceptional points arise.

Parity-time (PT) symmetry is the focus of various research projects due to its unique properties. [1] A standard photonic structure for PT-symmetry concerns coupled waveguides, one made of a gain material and the other with an equal amount of loss. The imaginary part of the refractive index in the waveguides defines the gain/loss parameter γ, that determines the operating regime: PT-symmetric when the two modes propagate without gain or loss, and PT-broken when one mode is amplified and the other decays. The transition between these two regimes occurs at the exceptional point (EP). On the one hand, we tailor an electric dipole source to the features of PT guided modes to create a contrast between wave propagation on both sides of the dipole. [2] On the other hand, we study the influence of chirality on these modes by inserting a chiral material in the gap between the waveguides.

Coupling a circularly or elliptically polarized electric dipole to a single waveguide can lead to directional excitation of waveguide modes. [3] This directionality is lost if the dipole is at the center of coupled waveguides but can be restored by taking advantage of the unique characteristics of PT modes. We place an electric dipole in the center of the air layer separating two PT-symmetric slab waveguides (fig. 1(a)). This setup is numerically simulated using an eigenmode expansion Maxwell equations' solver (CAMFR).

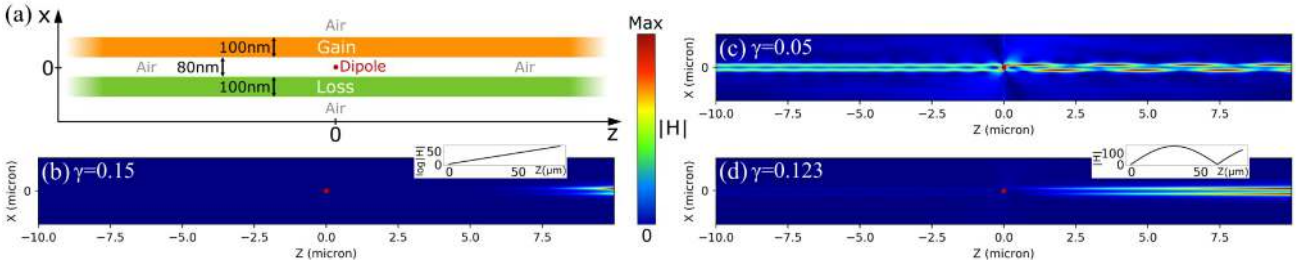


Figure 1 - (a) PT-symmetric coupled waveguides, infinite in the z direction. The dipole is at the red dot. (b-d) Magnetic field absolute value in the structure for various γ. The insets show the value at x=0. The value of the gain/loss parameter at the EP for our structure is γ_{EP} = 0.123.

For each γ, we search for the electric dipole that excites only one mode on one of the sides of the dipole. In the PT-broken regime ($\gamma > \gamma_{EP}$=0.1231 – fig. 1(b)), we choose to cancel the gain mode on the left, making the field considerably smaller than on the right side, as the gain mode on the right increases the field

exponentially. In the PT-symmetric regime ($\gamma \leq 0.1231$ – fig. 1(c,d)), one of the two propagating supermodes of the structure is removed on the left which produces a uniform field profile, while exciting both modes on the right causes a beating (fig. 1(c)). As γ increases, the beating pattern on the right side elongates until γ reaches the EP, where it is infinitely long (fig. 1(d) shows a close situation). Moreover, each of these contrasts can be switched between left and right by adapting the dipole polarization, which can be useful in integrated photonics applications.

Instead of a dipole, we then introduce a chiral material in the gap between PT-symmetric rectangular waveguides (fig. 2(a)). We simulate this setup with the finite element method using the SimPhotonics software, a Matlab Toolbox developed at the Laboratoire Charles Fabry. The gain/loss parameter is varied to explore the different regimes. The width of the gap is tuned to obtain desired features in the mode dispersion. We observe that chirality has the most effect on the modes when their dispersions cross, i.e., when they are degenerate. When the gap is narrow and achiral, the fundamental modes cross: a quasi-TM mode and the quasi-TE symmetric mode. An anticrossing appears between these modes when chirality is introduced in the gap (fig. 2(b)). An intermediate situation can be obtained for medium gaps: the TM-mode crosses the EP for an achiral gap, so chirality prompts a trimodal interaction that generates a complex, hybrid dispersion (fig.2(c)). For a larger gap, the quasi-TM mode crosses the antisymmetric TE-mode of a PT fork, leading to a `symmetry recovery' zone (an `inverted' EP, fig.2(d)).

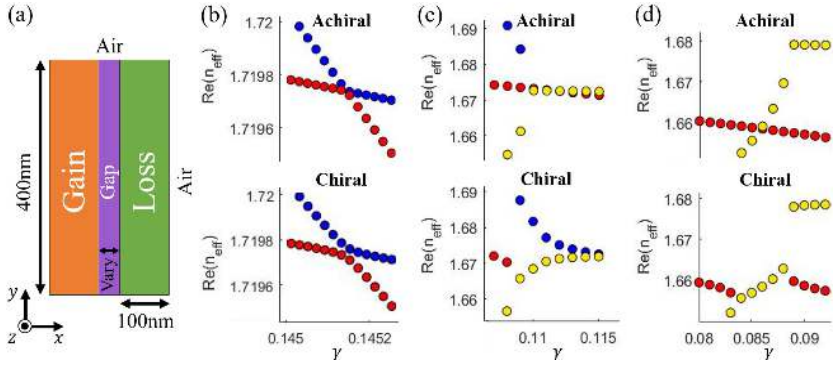


Figure 2 - (a) PT-symmetric rectangular waveguides and chiral gap, infinite along *z*. (b-d) Dispersion with an achiral (top) or chiral (bottom) gap, with width (b) 12nm, (c) 32nm, or (d) 44nm.

In the end, by using an adequate dipole coupled to PT-waveguides, a contrast in the mode excitation can be obtained between both sides, which can be exploited in integrated photonic structures. Furthermore, introducing a chiral material in the gap results in noticeable and rich avoided crossing patterns, which could be exploited in integrated chiral sensing applications.

This work benefits from the support of the French Community of Belgium with the financing of a FRIA grant.

References

1. Feng, L., R. El-Ganainy and L. Ge, "Non-Hermitian photonics based on parity-time symmetry," Nat. Photonics, Vol. 11, 752-762, 2017.
2. De Corte, A. and B. Maes, "Tailoring of electric dipoles for highly directional propagation in parity-time-symmetric waveguides", Phys. Rev. A, Vol. 10, No. 023509, 2022.
3. Picardi, M. F., A. V. Zayats and F. J. Rodríguez-Fortuño, "Janus and Huygens Dipoles: Near-Field Directionality Beyond Spin-Momentum Locking," Phys. Rev. Lett., Vol. 120, No. 117402, 2018.

META 2023, Paris - France, July 18 – 21, 2023

Stabilizing topological transport in a non-Hermitian optomechanical system

J. R. Lane[1*], C. Guria[1], V. Chavva [2], T. D. Montalvo [1], H. Ribeiro[2], and J. G. E. Harris[1,3,4]

[1]Department of Physics, Yale University, USA
[2]University of Massachusetts Lowell, USA
[3]Department of Applied Physics, Yale University, USA
[4]Yale Quantum Institute, Yale University, USA
[*]corresponding author: justin.lane@yale.edu

Abstract: When a non-Hermitian system is tuned around a loop in Hamiltonian parameter space, its complex eigenvalues trace out a braid that depends only on how the loop encloses the space of exceptional points (EPs). While in principle adiabatic loops could be used to execute braid operations, long-time dynamics is dominated by gain-loss imbalance and adiabatic evolution breaks down. We discuss experimental progress speeding up adiabatic operations encircling EPs by optomechanically tuning two nearly-degenerate vibrational modes of a SiN membrane.

META 2023, PARIS - FRANCE, JULY 18 – 21, 2023

Maximally transmitted states in non-Hermitian photonics

K. G. Makris[1,2]

[1]*ITCP-Physics Department, University of Crete, Heraklion, 71003, Greece*

[2]*Institute of Electronic Structure and Laser (IESL) FORTH, Heraklion, 71110, Greece*

[*]corresponding author: makris@physics.uoc.gr

Abstract: In the context of non-Hermitian photonics we present recent results regarding structured wavefronts that are maximally transmitted through a complex medium. We investigate dissipative optical lattices with gain and non-Hermitian multimode optical fibers. In both cases we present a unified framework of description that reveals the common features of these optimal states. Connection to Anderson localization, scattering eigenchannels, phase conjugation and imaging will be also discussed.

Dissipation due to the inherent material losses has been always considered as an obstacle. However, based on the notion of parity-time (PT)-symmetry, that was recently introduced in the context of optical physics [1], such synthetic structures can utilize loss as an advantage in many applications [2,3]. Here in the context of non-Hermitian optics, we introduce the concept of non-Hermitian power eigenchannels [4] based on singular value decomposition of the associated propagator [5,6].

The first part of the talk is devoted to dissipative waveguide arrays with sparse gain with symmetric or not coupling coefficients. The effect of uncorrelated disorder and noise, is systematically investigated. In this case, despite the Anderson localization of all eigenstates, the system exhibits counter-intuitive propagation by quantized jumps between states located around distant sites [7, 8]. Such a novel effect was recent experimentally demonstrated in optical fiber loop networks. The relevance of this type of transport to the corresponding power eigenchannels will be discussed.

In the second part of the talk, we will present recent results regarding maximally transmitted states in non-Hermitian multimode fibers. Connections to phase conjugation and imaging applications will also be presented.

Our methodology can be applied to any non-Hermitian system that contains complex elements with loss-gain, or exhibits an asymmetry induced non-Hermiticity and thus exploits the meaning of wave transport in complex open systems.

Acknowledgements: This project was funded by the European Research Council (ERC- Consolidator) under the grant agreement No. 101045135 (Beyond Anderson).

References

1. K. G. Makris, R. El-Ganainy, D. N. Christodoulides, Z. H. Musslimani, ”Beam dynamics in PT symmetric optical lattices”, Phys. Rev. Lett. 100, 103904 (2008).
2. R. El-Ganainy, K. G. Makris, M. Khajavikhan, Z. H. Musslimani, S. Rotter and D. N. Christodoulides, ”Non-Hermitian physics and PT symmetry”, Nat. Phys. **14**, 11 (2018).
3. S. Xia, D. Kaltsas, D. Song, I. Komis, J. Xu, A. Szameit, H. Buljan, K.G. Makris, and Z. Chen, "Nonlinear tuning of PT symmetry and non-Hermitian topological states", Science **372** 72 (2021).
4. K.G. Makris and D. Psaltis, CLEO Conference, California, US, 2023.
5. K.G. Makris, L. Ge, and H.E. Türeci, "Anomalous transient amplification of waves in non-normal photonic media" Phys. Rev. X. **4**, 041044. (2014).
6. K. G. Makris, "Transient growth and dissipative exceptional points", Phys. Rev. E **104**, 054218 (2021).
7. A. Tzortzakakis, K. G. Makris, A. Szameit, and E. N. Economou, "Transport and spectral features in non-Hermitian open systems", Phys. Rev. Res. **3**, 013208 (2021).
8. A. Leventis, K. G. Makris, and E. N. Economou, "Non-Hermitian jumps in disordered lattices", Phys. Rev. B **106**, 064205 (2022).

META 2023, PARIS - FRANCE, JULY 18 – 21, 2023

Switching between topological edge states in nanophotonic structures using phase-change materials

G. Veronis[1], Y. Huang[2], and Y. Shen[3]

[1]Lousiana State University, USA
[2]Central South University, China
[2]Sun Yat-Sen University, China

Abstract: We introduce non-Hermitian plasmonic waveguide-cavity structures based on the Aubry-Andre-Harper model to realize switching between right and left topological edge states using the phase-change material $Ge_2Sb_2Te_5$ (GST).

We introduce non-Hermitian plasmonic waveguide-cavity structures based on the Aubry-Andre-Harper model to realize switching between right and left topological edge states using the phase-change material $Ge_2Sb_2Te_5$ (GST). We show that switching between the crystalline and amorphous phases of GST leads to a shift of the dispersion relation of the optimized structure so that a right topological edge state for the crystalline phase, and a left topological edge state for the amorphous phase occur at the same frequency. Thus, we realize switching between right and left topological edge states at that frequency by switching between the crystalline and amorphous phases of GST. We also find that the right and left topological edge states in the optimized structure are robust in the presence of disorder. Topological edge states in one-dimensional photonic systems are important for applications in sensing, nonlinear optics, and optical diodes. Our results could lead to the development of compact reconfigurable photonic devices based on such topological edge states.

Exceptional-point sensing with a quantum interferometer

Wai Chun Wong[1] and Jensen Li[1,2*]

[1]Department of Physics, The Hong Kong University of Science and Technology, Clear Water Bay, Hong Kong, China
[2]IAS Center for Quantum Technologies, The Hong Kong University of Science and Technology, Clear Water Bay, Hong Kong, China
[*]corresponding author: jensenli@ust.hk

Abstract

We demonstrate the existence of exceptional points (EPs) in dual-beam SU(1,1) interferometers and show EPs are linked to both high signal and low noise. For a multistage variant, EPs of the overall input-output matrix form multiple bands of high signal-to-noise ratio (SNR) which separate into two phases by EPs of the transfer matrix of a repeating unit. Our investigations demonstrate the possibility of EP sensing in lossless nonlinear quantum systems and the significance of EPs in quantum interferometers.

1. Introduction

Recently, non-Hermitian systems and EPs have attracted many attention for their implementation in the quantum realm. For instance, chiral quantum state conversions have been experimentally observed in a cold atom system [1]. Regarding the regime of quantum EP sensing, the way to setup a quantum EP sensor is still unclear. Nevertheless, it has been suggested to use lossless (Hermitian) systems with nonlinear interactions (e.g. a parametric amplifier), instead of material gain and loss, to construct non-Hermitian dynamics so that the quantum noise can be much smaller to tackle current problem of noise in EP sensors. Meanwhile, nonlinear interactions in parametric amplifiers are already useful in constructing quantum interferometers which raises the question of whether these lossless interferometers can also capture a quantum EP.

2. EP in quantum interferometers

An example SU(1,1) dual-beam interferometer is shown in fig. 1(a) where parametric amplifiers (PAs) are used to replace the beam splitters in the classical Mach–Zehnder interferometer. The observables quadrature amplitudes before and after this interferometer are therefore related by [2]:

$$\begin{pmatrix} \hat{X}_2^+(\theta_{\text{out}}) \\ \hat{Y}_2^+(\theta_{\text{out}}) \end{pmatrix} = S(\phi) \begin{pmatrix} \hat{X}_0^+(\theta_{\text{in}}) \\ \hat{Y}_0^+(\theta_{\text{in}}) \end{pmatrix}, \qquad (1)$$

where $\hat{X}_n^+(\theta) = \frac{1}{\sqrt{2}}(\hat{a}_n^\dagger + \hat{b}_n^\dagger)e^{i\theta} + \frac{1}{\sqrt{2}}(\hat{a}_n + \hat{b}_n)e^{-i\theta}$ and $\hat{Y}_n^+(\theta) = \hat{X}_n^+(\theta + \pi/2)$. By tuning the parameters within the interferometer $S(\phi)$ can exhibit EP. Furthermore, if we choose $\theta_{in} + \theta_{out} = \pi/2$, this matrix $S(\phi)$ has an analogy to scattering matrices in PT-symmetric systems, for instance, EP occurs as zero at an off-diagonal element of $S(\phi)$, reminiscent of unidirectional zero reflection. To quantify the sensing performance of this EP sensor we evaluate the noise and signal-to-noise ratio in Fig. 1 (b) and (c), with respectively. Here the noise is given by the quantum fluctuations $\Delta^2\hat{Y}_2^+ = \langle \hat{Y}_2^{+2} \rangle - \langle \hat{Y}_2^+ \rangle^2$ and the signal is given by

$$\text{SNR} = \frac{\left(\frac{d}{d\phi}\langle \hat{Y}_2^+ \rangle\right)^2}{\Delta^2\hat{Y}_2^+}.$$

We found that the noise is preserved as the white dashed line (indicating EP condition) and the solid black line (indicating noise preserving condition) completely overlaps with each other. For SNR in Fig. 1(c), we observe the SNR is generally higher in the low noise region near EP lines. Compared to the original sensing scheme for the interferometer [3], our EP scheme has an SNR ratio of approximately 90% of the highest theoretically possible value.

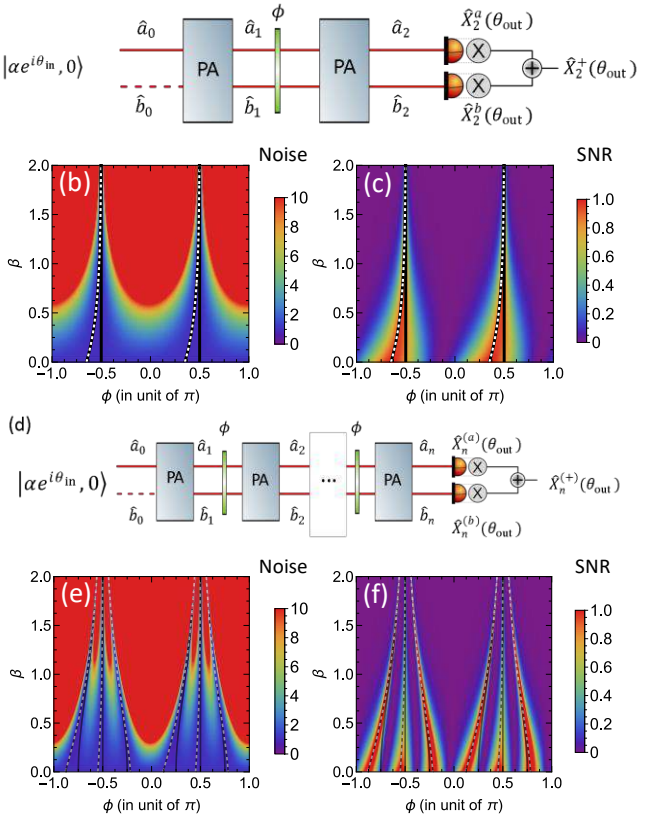


Figure 1. (a) Schematic of a dual-beam SU(1,1) interferometer. (b) noise and (c) SNR of this interferometer when measuring $\hat{Y}_2^+(\theta_{out})$ with an input coherent state $|\alpha e^{i\theta_{\text{in}}}, 0\rangle$. Here $\theta_{out} = 0.425\pi$ and $\theta_{in} = \pi/2 - \theta_{out}$. Black curves denote the noise is being preserved in the interferometer, i.e. $\Delta^2\hat{Y}_2^+ = \Delta^2\hat{Y}_0^+ = 1$. White dashed curve represents the EP. SNR are normalized by

$2|\alpha|^2 e^{4\beta}$ (d) Schematics of a multistage dual-beam SU(1,1) interferometer. (b,c) same as (a) with 4-stages i.e., totally 4 PAs. SNR are renormalized by $|\alpha|^2 n^2 e^{4\beta}$ for n stages interferometer

A variant of multistage dual-beam SU(1,1) interferometer is shown in fig. 1 (d) with increased numbers of PAs. We also found that the noise is preserved here and SNR is generally higher near EP lines indicate our EP sensing scheme extends to the multistage setting. Fig. 2(a) shows the eigenvalues of the transfer matrix U_{unit} of a single repeating unit consisting of one phase object and one PA as

$$U_{unit} = \begin{pmatrix} G & g \\ g & G \end{pmatrix} \begin{pmatrix} \exp(i\phi) & 0 \\ 0 & \exp(-i\phi) \end{pmatrix}.$$

where $G = \cosh\beta$ and $g = \sinh\beta$ with β controlling the gain of PAs, ϕ is the phase objected to be sense. this matrix indeed undergoes a phase transition at EP and two phases directly affect the SNR in Fig. 2(b) which shows the SNR for n-stage interferometers. Here SNR forms two phases separated by the EPs of U_{unit}. One phase has highly oscillating behaviour in SNR when U_{unit} is in the PT-symmetric phase ($\lambda_1 = \lambda_2^*$). While SNR has no such oscillations when U_{unit} is in the PT-broken phase ($\lambda_1 = 1/\lambda_2$).

3. Conclusion

We presented a dual-beam SU(1,1) interferometer as a platform for obtaining a quantum exceptional point (EP) We found out the signal is amplified while the quantum fluctuation noise is preserved at this EP. Numerical results showed that the sensitivity in terms of signal-to-noise ratio (SNR) will attain its maximum around the quantum EP of the overall input-output relation matrix. Additionally, our investigation of a multistage variant of the SU(1,1) interferometer indicate that the EP sensing scheme extends to this setting since the preserving property is universal across the number of stages. Finally, we have found that the EP of the overall input-output relation matrix for an increasing number of stages separate into two phases, which are identified by the EPs of the transfer matrix of a single stage.

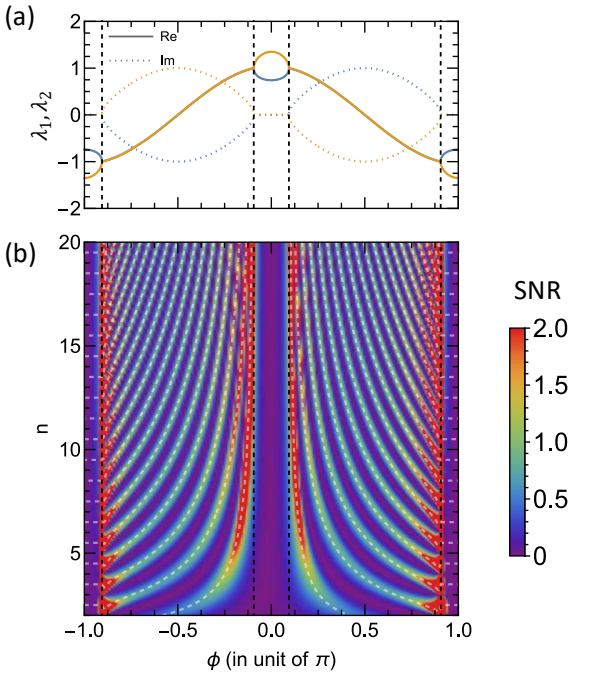


Figure 2. (a) Eigenvalues of U_{unit}. (b) SNR of n-stages interferometer with respect to the stages number n and operation point ϕ using the same EP sensing scheme as in Fig. 1 (e-f)

4. Acknowledgements

This work is supported by the Hong Kong RGC grant 16304520.

[1] Z. Ren, D. Liu, E. Zhao, C. He, K. K. Pak, J. Li, and G.-B. Jo, Chiral Control of Quantum States in Non-Hermitian Spin–Orbit-Coupled Fermions, Nat. Phys. 18, 385 (2022).

[2] W. C. Wong, and J. Li, Exceptional-point sensing with a quantum interferometer, New J. Phys. (in press)

[3] J. Li, Y. Liu, L. Cui, N. Huo, S. M. Assad, X. Li, and Z. Y. Ou, Joint Measurement of Multiple Noncommuting Parameters, Phys. Rev. A 97, 052127 (2018).

META 2023, PARIS - FRANCE, JULY 18 – 21, 2023

Landau-Zener transitions through a pair of higher order exceptional points

E. M. Graefe[1*], S. Malzard[1,2], and R. Melanathuru[1]

[1]Department of Mathematics, Imperial College London, United Kingdom
[2]Alan Turing Institute, United Kingdom
[*]corresponding author: e.m.graefe@ic.ac.uk

Abstract: We study the Landau-Zener type transition probabilities between the asymptotic states of a PT-symmetric non-Hermitian N-level Landau-Zener with two exceptional points of order N. The system is Hermitian for asymptotically large times, and has purely imaginary eigenvalues between the exceptional points. The transition probabilities show a characteristic binomial behaviour, which, in the adiabatic limit, are given by the ratios of binomial coefficients. This behaviour can be understood via the eigenvector structure, despite the breakdown of adiabaticity typical for non-Hermitian systems.

We consider a non-Hermitian N-level generalisation of the Landau-Zener scenario, described by a time-dependent Hamiltonian of the form

$$\hat{H} = -2\alpha t \hat{J}_z + 2\mathrm{i}\gamma \hat{J}_x \ ,$$

Where $\alpha, \gamma \in \mathbb{R}$ and $\hat{J}_j$ denote angular momentum operators. In an N-dimensional representation, this system has N-th order exceptional points at $|\alpha t| = |\gamma|$. At large positive and negative times the eigenvectors are the standard angular momentum basis. We consider the asymptotic relative (re-normalised) populations of the eigenstates at $t \to +\infty$ assuming the system was in an eigenstate at $t \to -\infty$. Using the SU(2) structure of the system we derive an analytic expression for these populations, and show that in the adiabatic limit $\alpha \to 0$ they are given by

$$P_{jk} \to \frac{1}{2^n} \binom{n}{k} \ .$$

We show how this can be understood from the overlaps of the adiabatic eigenvectors close to the exceptional point.

References

1. Rishindra Melanathuru , Simon Malzard , and Eva-Maria Graefe, “Landau-Zener transitions through a pair of higher-order exceptional points”, Phys. Rev. A 106, 012208, 2022

Dispersion curves of guided modes in a $\mathcal{PT}$ symmetric waveguide

N. Zhang[1*] **and Y. Y. Lu**[1]

[1]Department of Mathematics, City University of Hong Kong, Hong Kong, China
*corresponding author: nzhang234-c@my.cityu.edu.hk

Abstract: In this paper, we analyze dispersion curves of guided modes in a two-layer $\mathcal{PT}$ symmetric slab waveguide. It is shown that the total number of cutoff points and dispersion curves is always finite. As the imaginary part of the dielectric constant is increased, the lowest dispersion curve always exists but other dispersion curves degenerate into points on the light line and then disappear. Interestingly, the dispersive curves are not always tangential to the light line.

We consider a two-layer $\mathcal{PT}$ symmetric slab waveguide surrounded by air as shown in Fig. 1 [1]. The structure is perpendicular to the z axis, the relative dielectric function ε has a nonzero imaginary part and satisfies $\varepsilon(z) = \overline{\varepsilon}(-z)$. The transverse electric (TE) guided mode has an electric field component $E_x = \mathrm{Re}[u(z)\exp(i\beta y - \omega t)]$, where β is the propagation constant, $\omega = k_0 c$ is the angular frequency, and k_0 is the free space wavenumber [2]. We consider real β, k_0 and $|\beta| > k_0$. The dispersion curves are connected with the light line at the cutoff points [3, 4].

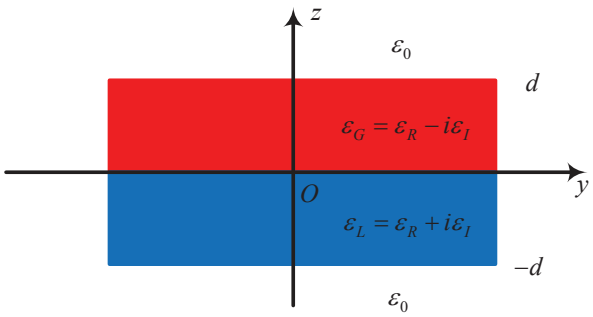


Figure 1: A two-layer $\mathcal{PT}$ symmetric slab waveguide with thickness $h = 2d$ surrounded by air. ε is the relative dielectric constant and $\varepsilon_0 = 1$. ε_R and ε_I are constants.

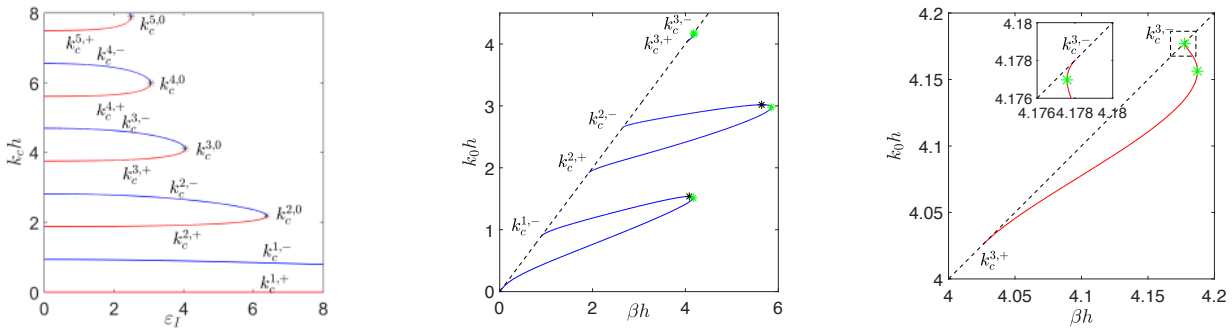


Figure 2: Left: The cutoff wavenumbers for different ε_I. Middle: The dispersion curves for $\varepsilon_I = 4$. Right. Two second order EPs $dk_0/d\beta = \infty$ exist in the 3rd dispersion curve for $\varepsilon_I = 4$. Green * represent EPs.

As shown in Fig. 2 for $\varepsilon_R = 12.25$, each dispersion curve originates from two dispersion curves of the slab waveguide with $\varepsilon_I = 0$. The total number of cutoff points is finite for $\varepsilon_I > 0$. This implies that the number of dispersion curves is also finite as shown in the middle panel of Fig. 2. On the 3rd dispersion curve, there exist 2 exceptional points (EPs) satisfying $dk_0/d\beta = \infty$ as shown in the right panel of Fig. 2.

From Fig. 3, we can see that the lowest dispersion curve exists for any ε_I. As ε_I is increased, all other dispersion curves will degenerate into points and then disappear. At a special value of ε_I, the dispersion curve is not tangential to the light line. This is a distinguished feature of the $\mathcal{PT}$ symmetric waveguide.

On each dispersion curve, there could exist 2 exceptional points (EPs) satisfying $dk_0/d\beta = \infty$ as shown in the panel (b) of Fig. 3. But as ε_I is increased, they merge into a third order EP and then disappear as shown in panels (b) and (d) of Fig. 3.

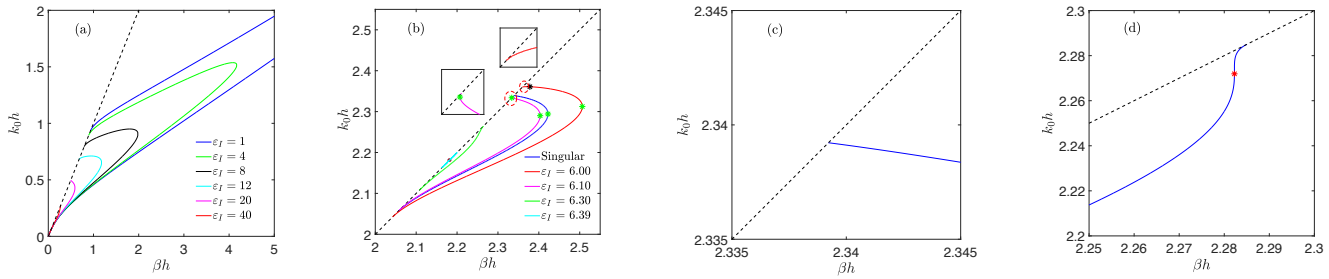


Figure 3: (a). The lowest dispersion curve for different ε_I. (b). The 2nd dispersion curve for different ε_I. (c). The local behavior of the 2nd dispersion curve when the dispersion curve is not tangential to the light line. (d). The 2nd dispersion curve when a third order EP appear. The third order EP is denoted by red *.

References

1. Nolting, H. P., Sztefka, G., Grawert, M., and Ctyroky, J., "Wave propagation in a waveguide with a balance of gain and loss," in Integrated Photonics Research, 1996.
2. El-Ganainy, R., Makris, K. G., Christodoulides, D. N., and Musslimani, Z. H., "Theory of coupled optical $\mathcal{PT}$- symmetric structures," Opt. Lett., Vol. 32, No. 17, 2632–2634, 2007.
3. Klaiman, S., Günther, U., and Moiseyev, N., "Visualization of branch points in $\mathcal{PT}$ -symmetric waveguides," Phys. Rev. Lett., Vol. 101, 080402, 2008. ,
4. Rüter, C., Makris, K. G., El-Ganainy, R., Christodoulides, D. N., Segev, M., and Kip, D., "Observation of parity–time symmetry in optics," Nat. Phys., Vol. 6, 47, 2010.

Scanning Quantum Interference across PT-symmetry Breaking

F.Klauck[1*], T.A.W. Wolterink[1], M. Heinrich[1] and A. Szameit[1]

[1] Universität Rostock, Institute of Physics, A.-Einstein-Str.23, D-18057 Rostock, Germany
[*]corresponding author: friederike.klauck@uni-rostock.de

Abstract: In PT-symmetric systems, losses dramatically alter the quantum correlations of interfering photons. We study lossy directional couplers with increasing loss values beyond the PT-symmetry breaking point and observe the impact of this transition on the two-photon dynamics. Upon entering the PT-broken phase, the visibility of the Hong-Ou-Mandel interference decreases.

With their conceptual description of Parity-Time (PT) symmetry [1] , Bender and Boettcher inaugurated a new field of studies with fascinating implications on topology [2] and exceptional point dynamics [3], to name a few. Typically, PT-symmetric Hamiltonians exhibit real eigenvalues below a certain threshold, whereas above, the PT-symmetry is spontaneously broken as the eigenvalue spectrum becomes complex. Entirely passive configurations based solely on differential losses [4] allow the physics of PT symmetry to be faithfully carried over to a quantum-optical context [5] and explored therein [6]. Here we study the ways in which the relative proportion of losses systematically impacts the characteristics of quantum correlations between interfering photons by analyzing the two-photon correlations in PT-symmetric directional couplers.

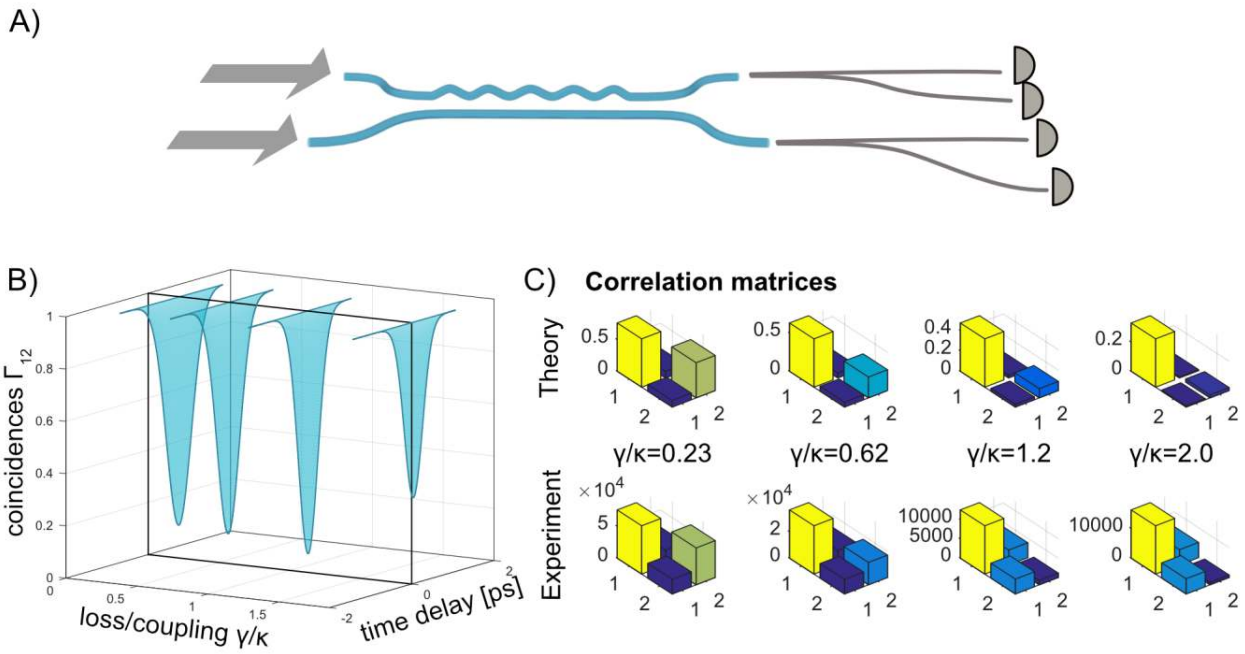


Figure 1. A) Indistinguishable photon pairs are launched into the waveguide structure of the PT-symmetric coupler, the output is routed through 50/50 fiber beam splitters and detected using avalanche photo diodes. B) Hong-Ou-Mandel dips measured in PT-symmetric couplers for increasing loss, up to PT-symmetry breaking. C) Measurement of the full correlation matrix for the PT-symmetric couplers and corresponding analytical solution of the two-photon correlation.

Our system (Fig.1 A)) consists of two waveguides whose interaction is described by a coupling coefficient κ. As one of the waveguides exhibits a loss γ, the PT symmetry breaking threshold is found at $\gamma = 2\ \kappa$. For our studies, we implemented a set of such lossy couplers with fixed coupling coefficient and identical interaction lengths for different loss values, ranging from the conventional Hermitian case ($\gamma = 0$) up to and above the PT-symmetry breaking point at $\gamma/\kappa = 2.0$. We probed these systems by injecting pairs of indistinguishable photons, followed by coincidence measurements with click detectors to record the two-photon correlation matrices at the output, as shown in the lower row of Fig. 1 C). Based on our experimental parameters and the analytical solution of the full correlation matrix [6], the theoretical curves depicted above are retrieved. Subsequently, we tuned the time delay between the incident photons to record the corresponding Hong-Ou-Mandel interference curves in Fig. 1B).

Our studies show that increasing losses in the PT-symmetric coupler gradually decrease the visibility of the quantum interference in a Hong-Ou Mandel experiment, potentially below the value of 50%, without actually impacting the quantum nature of the system. This also manifests itself in a systematic reshaping of the correlation matrix (Fig. 1C)).

References

1. C. M. Bender and S. Boettcher, "Real Spectra in Non-Hermitian Hamiltonians Having PT Symmetry," Phys. Rev. Lett. **80**, 5243–5246, 1998.
2. R. M. C. Weimann S., Kremer M., Plotnik Y, Lumer Y, NolteS, Makris K G, Segev M and S. A, "Topologically protected bound states in photonic parity–time-symmetric crystals," Nat. Mater. **16**, 433–438, 2017.
3. K. Özdemir, S. Rotter, F. Nori, and L. Yang, "Parity–time symmetry and exceptional points in photonics," Nat. Mater. **18**, 783-798, 2019.
4. M. Ornigotti and A. Szameit, "Quasi PT-symmetry in passive photonic lattices," J. Opt. **16**, 65501 (2014).
5. S. Scheel and A. Szameit, "PT -symmetric photonic quantum systems with gain and loss do not exist," EPL **122**, 34001, 2018.
6. F. Klauck, L. Teuber, M. Ornigotti, M. Heinrich, S. Scheel, and A. Szameit, "Observation of PT-symmetric quantum interference," Nat. Photonics **13**, 883-887, 2019.

Symmetry-protected topological exceptional chain

Xiaohan Cui[1], Ruo-yang Zhang[1], Guancong Ma[2], and C. T. Chan[1*]
[1]Department of Physics, Hong Kong University of Science and Technology, Clear Water Bay, Kowloon, Hong Kong, China
[2]Department of Physics, Hong Kong Baptist University, Kowloon Tong, Hong Kong, China
[*]corresponding author: phchan@ust.hk

Abstract: We studied the exceptional chains (ECs) in non-Hermitian systems and the symmetries that secure their stability. By assigning orientations to exceptional lines (ELs), we analyzed the robustness of ECs via establishing a source-free principle for ELs. The principle leads to the discovery of three mechanisms for stabilizing the junction of ELs. The observation of these exotic ECs is demonstrated through numerical simulations in photonic crystals and experimental observations in coupled active oscillators.

In 3D non-Hermitian systems, the EPs can form stable exceptional lines (ELs) or more striking geometric features such as knots and links in the momentum space without any symmetry. However, as another typical EL configuration, the exceptional chains (ECs), formed by several connected ELs, have a fundamental difference from other EL morphologies, i.e., the existence and stability of ECs demand symmetry protection. We revealed that the complex eigenenergy braiding around an EL can assign a positive orientation to the EL. Via generalizing the Fermion doubling theorem of EPs to arbitrarily oriented and closed surfaces, we establish the source-free principle of the directed ELs, implying that if several ELs flow into a junction, the same number of ELs must outflow from the junction. As an immediate application, this principle, when combined with certain non-Hermitian spatiotemporal symmetries, can ensure the robust formation of ECs from several directed ELs.

We also uncover that by incorporating the Hermitian-adjoint into account as a new dimension, the non-Hermitian crystalline systems are generalized, and we propose three symmetry-based mechanisms that can stabilize different types of ECs with distinct local morphologies and topological features. In addition, we designed non-Hermitian photonic crystals (PCs) to illustrate our ideas of symmetry-protected ECs. Through numerical simulations, three typical ECs are observed in the PCs, hence confirming the applicability of our theory for general full-wave systems.

Our theory also applies to other systems such as mechanical oscillators. We designed and implemented a non-Hermitian mechanical model to exhibit ECs in a three-dimensional synthetic parameter space while being protected by symmetries.

In short, we established the source-free principle of directed ELs and showed that the source-free principle together with symmetry constraints are two crucial conditions for the formation of ECs. Based on this idea, a comprehensive theory has been developed to construct ECs of diverse local morphologies. Furthermore, we experimentally observed the symmetry-protected EC in crafted nonreciprocally coupled mechanical oscillators.

Acknowledgements: We acknowledge support from Research Grants Council (RGC) Hong Kong and the Croucher Foundation.

Quantum exceptional points of metasurfaces

Wai Chun Wong[1], Hong Liang[1], Kai Ming Lau[1], Tsz Kit Yung[1], Bei Zeng[1,2] and Jensen Li[1,2*]

[1]Department of Physics, The Hong Kong University of Science and Technology, Clear Water Bay, Hong Kong, China
[2]IAS Center for Quantum Technologies, The Hong Kong University of Science and Technology, Clear Water Bay, Hong Kong, China
[*]corresponding author: jensenli@ust.hk

Abstract

We develop an approach to map the quantum optical scattering of linear dissipative metasurfaces to Liouvillian dynamics, based on the effective Hamiltonian of the metasurfaces in a fictitious time. Our approach enables us to specify the generalized eigenspace of the Liouvillian superoperator, allowing us to analytically obtain the input-output relationship of the density matrix and the photon transition probabilities. This work facilitates the straightforward modeling of non-Hermitian metasurfaces in the quantum regime, directly from the specification of classical scattering matrix.

1. Introduction

The capability of manipulating scattering from metasurfaces enables many applications including quantum tomography, and entangled state preparation [1, 2]. Classically, non-Hermitian and topological systems are already under active research using metamaterial structures as building blocks [3] making non-Hermitian or lossy metasurfaces a possible candidate as a versatile platform in quantum optics.

2. Scattering at EP by Lindblad moment equation

Starting from a classical scattering of a linear dissipative metasurface given by scatting matrix S, one can describe the input-output relationship of density matrices by adding loss channels to the system as in the left route in Fig. 1. We find another equivalent method as shown in the right route in fig. 1 by mapping the input-output relationship to an equivalent Liouvillian dynamics evolve in fictitious time τ given by

$$\frac{d\hat{M}(\tau)}{d\tau} = \mathcal{L}'\hat{M}(\tau) = -i\left(\hat{H}_{\text{eff}}\hat{M}(\tau) - \hat{M}(\tau)\hat{H}_{\text{eff}}^{\dagger}\right) \quad (1)$$

with the effective Hamiltonian operator $\hat{H}_{\text{eff}}$ defined as:

$$\hat{H}_{\text{eff}} \triangleq \Sigma_{ij}(i\log(S))_{ij}\hat{a}_i^{\dagger}\hat{a}_j$$

where moment matrix $\hat{M}$ is equivalent to density matrix on another basis [4]. With this equation, we first design a bianisotropic metasurface with two gold bars in a unit cell that can capture a classical EP in Fig. 2 (a). Classical EP happen at $\Delta\gamma = 0$ as shown in Fig. 2 (b-c). The quantum EP of this metasurface is probed using Eq. (1). Using this approach all photon transition probabilities can be obtained analytically in terms of classical scattering matrix elements. For example, the photon transition probabilities at EP ($\Delta\gamma = 0$) for pure state input are summarized in Fig. 2 (d). Figure 3 (a,b) shows the evolution of the eigenvalues of $\mathcal{L}'$ when $\Delta\gamma$ scans across the classical EP at $\Delta\gamma = 0$ and at this moment all eigenvalues of $\mathcal{L}'$ all degenerate indicating that Eq. (1) promotes the classical EP at S to quantum EP in $\mathcal{L}'$.

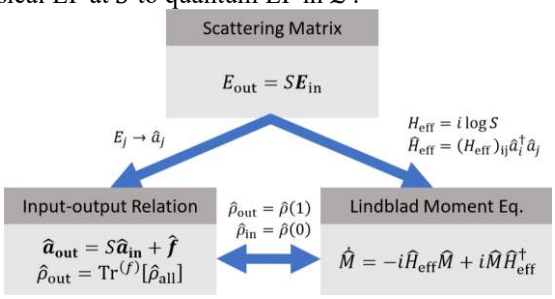


Figure 1. The left route is the standard dilation approach with ancilla modes added to represent absorption channels. The right route is the mapped Lindblad moment equation propagating photon moment matrix from fictitious time $\tau = 0$ to 1.

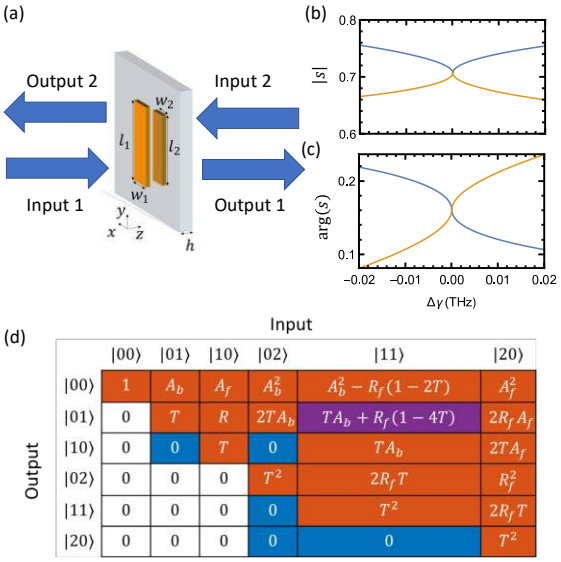


Figure 2. (a) Schematic of a classical EP capturing metasurface. (b,c) Eigenvalues of scattering matrix S of matersurface in (a) when extra material loss $\Delta\gamma$ is added. The two branches are colored as blue and orange. At $\Delta\gamma = 0$ there is an EP where two eigenvalues coalesce. (d) Photon transition probabilities at EP in terms of scattering matrix elements with transmission $T = |t|^2$, forward reflection $R_f = |r_f|^2$, forward absorption $A_f = 1 - T - R_f$ and backward absorption $A_b = 1 - T$ here the metasurface give unidirectional zero reflection $r_b = 0$ at EP.

The generalized eigenspace is summarized in Fig. 3(c), where each block represents a set of general eigenmatrices with the same eigenvalue. The squares represent individual general eigenmatrices, and multiple squares are grouped together to form a row, indicating they belong to the same Jordan chain. The arrows in Fig. 3(c) illustrate the flow of data, such as the density matrix or moment matrix decomposed into the eigenbasis, during propagation at quantum EPs. When the representation is changed from $\hat{\rho}$ to $\widehat{M}$ or vice versa, the data flow is shown by the blue arrows. Propagation of the moment matrix $\widehat{M}$ is governed by the Lindblad moment equation in Eq. (1), and the flow of data is indicated by the blue arrows. An example of propagating the state $\hat{\rho} = \frac{1}{2}(|2,0\rangle + i|1,0\rangle)(\langle 2,0| - i\langle 1,0|)$ is provided in Fig. 3(d), where the color represents the decomposition coefficient in the eigenbasis for the input and output $\hat{\rho}$ and $\widehat{M}$.

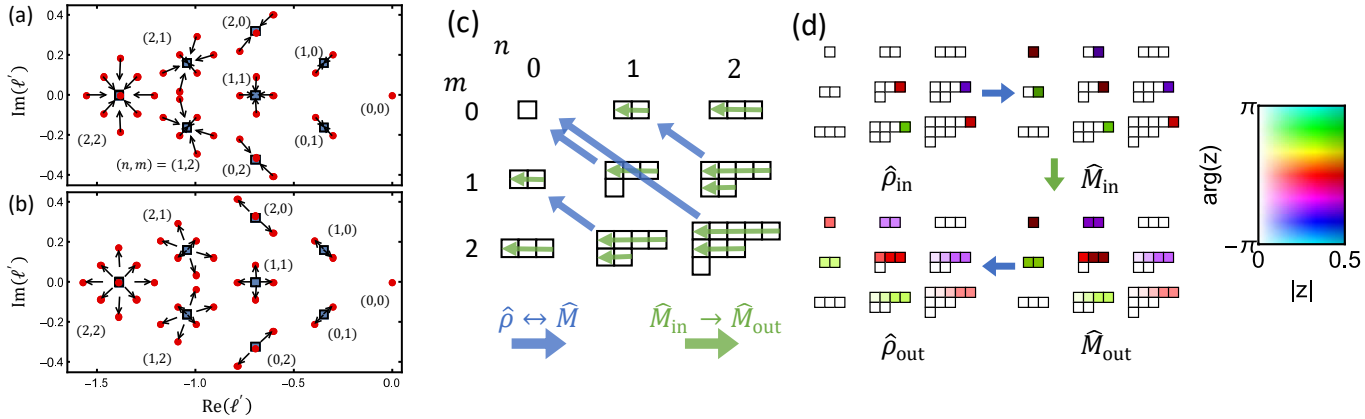


Figure 3. (a,b) The eigenvalues ℓ' of the Liouvillian superoperator $\mathcal{L}'$ as red dots for (a) $\Delta\gamma = -0.009$ THz, (b) $\Delta\gamma = 0.009$ THz, and blue squares for $\Delta\gamma = 0$ in both (a) and (b). Arrows represent the trajectory of the eigenvalues when $\Delta\gamma$ is increasing. (c) The flow of information when states are propagating at EP in the eigen-moment basis. Blue arrows represent the effect of changing representation $\hat{\rho} \leftrightarrow \widehat{M}$. Green arrows represent the effect of propagation $\widehat{M}_{in} \rightarrow \widehat{M}_{out}$. (b) States transformation of input $\hat{\rho} = \frac{1}{2}(|2,0\rangle + i|1,0\rangle)(\langle 2,0| - i\langle 1,0|)$. The colors in each square represent the complex coefficient of the corresponding eigen-moment in decomposing either density matrix $\hat{\rho}$ or moment matrix $\widehat{M}$.

3. Conclusion

In this work, we have established a model for quantum scattering from a lossy metasurface as a Lindblad master equation in a fictitious time. This approach enables us to form a complete eigen-moment basis to describe the propagation of the photon density matrix through a change of representation. The numerical examples presented in this study provide insight into the characterization of quantum scattering from a bianisotropic metasurface for a single polarization. These investigations pave the way for future studies on passive parity-time symmetric metasurfaces in the quantum optical regime.

4. Acknowledgements

This work is supported by the Hong Kong RGC grant 16304020, 16304520 and C6013-18G.

[1] K. Wang, J. G. Titchener, S. S. Kruk, L. Xu, H.-P. Chung, M. Parry, I. I. Kravchenko, Y.-H. Chen, A. S. Solntsev, Y. S. Kivshar, D. N. Neshev, and A. A. Sukhorukov, Quantum Metasurface for Multiphoton Interference and State Reconstruction, Science 361, 1104 (2018).

[2] Liang, H., et.al., 2021. One-sided destructive quantum interference from an exceptional-point-based metasurface. Physical Review A, 104(6), p.063710.

[3] Gorlach, M.A., Ni, X., Smirnova, D.A. et al. Far-field probing of leaky topological states in all-dielectric metasurfaces. Nat Commun 9, 909 (2018).

[4] Wong, W.C. , Lau, K.M., Liang, H., Yung, T.K., Zeng, B. and Li, J., 2022. Quantum optics of lossy metasurfaces: Propagating the photon-moment matrix by the semiclassical Liouvillian. Physical Review A, 106(1), p.013503.

META 2023, PARIS - FRANCE, JULY 18 – 21, 2023

A Coherent Perfect Absorber for Arbitrary Wavefronts

Y. Slobodkin[2†], G. Weinberg[2†], H. Hörner[1†], K. Pichler[1], S. Rotter[1*] and O. Katz[2*]

[1]Institute for Theoretical Physics, Vienna University of Technology (TU Wien), Austria
[2]Applied Physics Department, Hebrew University of Jerusalem, Israel
[*]corresponding authors: stefan.rotter@tuwien.ac.at; orik@mail.huji.ac.at
[†]These authors contributed equally to this work

Abstract: The concept of a 'coherent perfect absorber' (CPA) as a time-reversed laser is well-known in the domain of non-Hermitian photonics. However, conventional CPAs are usually limited to perfectly absorbing only a single, carefully shaped wavefront (`mode'). Apart from the correctly matched input wavefront, all of the possibly many other modes are only weakly absorbed. We have now overcome this limitation by creating a 'massively degenerate coherent perfect absorber' (MAD-CPA) that can absorb any complex input field with near-perfect efficiency.

It is easy to achieve efficient light absorption with thick materials. But thin materials with a low absorption factor are much less effective at transforming incident radiation into other forms of energy, such as heat. One method of addressing this problem is embedding the weak-absorbing material into a resonant structure. At the 'critical coupling condition', where the coupling strength to the resonator is balanced with the internal dissipation, the incoming field is perfectly absorbed, with no energy reflected back from the resonator. However, there is a severe limitation to this method: the incoming field must have a judiciously shaped wavefront in order to satisfy the critical coupling condition [1, 2]. In other words, only a single incoming wavefront, or spatial mode, can be "coherently perfectly absorbed". Although this allows for interference-based control of the absorption process, other modes are only weakly absorbed due to the different interference patterns they produce.

We can successfully demonstrate both in theory and by experimental implementation how to eliminate this constraint on the number of perfectly absorbed modes in a coherent perfect absorber (CPA) [3]. Our multi-mode CPA for arbitrary wavefronts is based on the notion that "coherent perfect absorption" is equivalent to time-reversing a laser operating at the first lasing threshold. Therefore, to achieve a device that can completely absorb *any* combination of incoming modes through interference, it is necessary to create a time-revered laser that emits *all* of these modes simultaneously. It turns out that such a laser already exists, and is known as a 'degenerate cavity laser'. The degeneracy of modes in such a cavity is based on the special feature that the field on either one of the two outer cavity mirrors is self-imaged onto itself after one cavity round-trip. This achieved by placing two convex lenses inside the cavity, the first lens one focal length after the input coupling mirror, and the second lens three focal lengths after the input coupling mirror. The total length of the cavity is four focal lengths, and it is therefore often referred to as '4f-cavity' (Fig. 1). With this configuration, we can ensure coherent perfect absorption of any combination of modes, regardless of their relative phases (Fig. 2). This robust absorption mechanism promises to be highly advantageous for numerous potential applications.

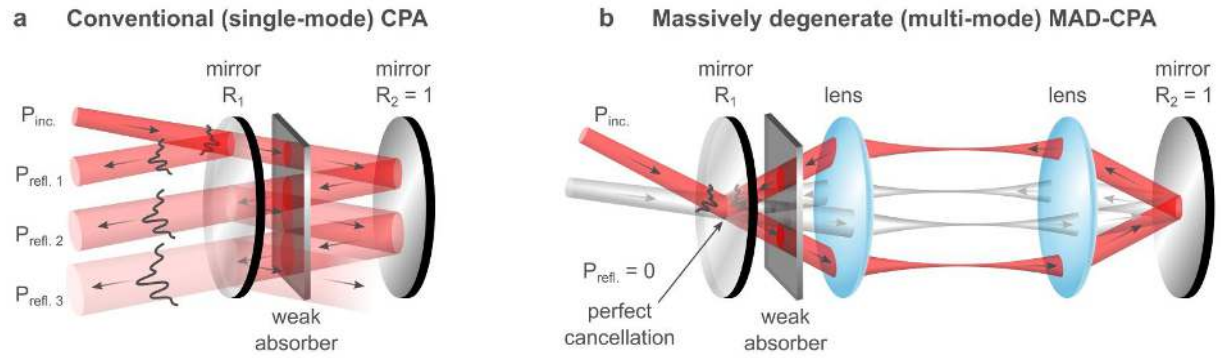


***Figure 1**: **Concept of a massively degenerate coherent perfect absorber (MAD-CPA) capable of absorbing arbitrary wavefronts.** **(a)** In a conventional CPA, a weak absorber is positioned between two flat mirrors. While destructive interference can lead to perfect absorption of a normal-incident plane-wave, any other incoming mode, such as the tilted beam shown, results in multiple reflections that cannot destructively interfere. **(b)** In contrast, the multi-mode MAD-CPA can perfectly absorb any complex incident wavefront. This is accomplished by placing the weak absorber in a degenerate (self-imaging) cavity, which is realized in this case by a conventional cavity with two lenses arranged telescopically. In such a degenerate cavity, any complex input field incident on the front cavity-mirror (R1) is self-imaged onto itself after each cavity round-trip. All reflections from the multiple cavity round-trips show perfect destructive interference with the outer reflection from the front cavity-mirror (as shown for two incoming beams at different angles), leading to perfect absorption of light in the weak absorber.*

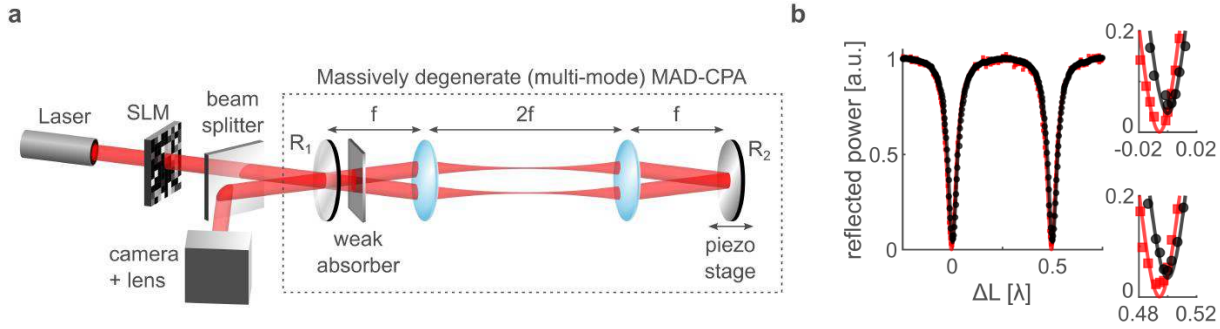


***Figure 2:** **(a)** Setup: Complex input fields are injected into a degenerate cavity that contains a critically-coupled weak absorber, using a computer-controlled SLM, illuminated by a wavelength-stabilized laser. The spatial intensity distribution of the reflected light is measured by a camera. Coherent perfect absorption is achieved by tuning the cavity length to be resonant with the laser wavelength. **(b)** Experimental results for a speckled Yin-Yang symbol with over 1000 modes as the complex input field. The back-reflected power is plotted as a function of cavity length, with black dots indicating the total reflected power and red squares representing the reflected power of one individual mode. The numerical prediction for the total reflected power of a 100-mode input, considering the residual reflection of the lenses, is shown with black and red lines.*

References

1. Chong, Y. D., Ge, L., Cao, H. and Stone, A. D., "Coherent Perfect Absorbers: Time-Reversed Lasers", Phys. Rev. Lett., Vol. 105, No. 5, 053901, 2010.
2. Baranov, D.G., Krasnok, A., Shegai, T., Alù, A., Chong, Y.: "Coherent perfect absorbers: linear control of light with light", Nat. Rev. Mater. Vol. 2(12), 1-14, 2017.
3. Slobodkin, Y., Weinberg, G., Hörner, H., Pichler, K., Rotter, S., and Katz, O., "Massively degenerate coherent perfect absorber for arbitrary wavefronts", Science, Vol. 377, No. 6609, 995–998, 2022.

Photon production in cavity: Quasinormal modes as a tool for quantum dynamics

M. Federico[1*] and H. R. Jauslin[1]

[1]Laboratoire Interdisciplinaire Carnot de Bourgogne, CNRS – Université de Bourgogne, UMR 6303, BP 47870, 21078 Dijon, France

[*]corresponding author: maxime.federico@u-bourgogne.fr

Abstract: We discuss the construction of a model using quasinormal modes (QNMs) to describe the production of single-photons inside a leaky cavity. Our approach is based on the fact that photon's dynamics is given by Maxwell's equations. By taking advantage of this property, we construct a hybrid basis made of truncated QNMs inside the cavity and completed with any other basis outside. The completeness allows to write a quantum Hamiltonian interacting with an emitter expressed with creation-annihilation operators directly on QNMs.

Single-photons are of great interest in the race towards quantum technologies since they can be used as qubits. Their production on demand is already well mastered experimentally, for instance through cavity quantum electrodynamics schemes [1]. However, the theoretical models describing such systems are often based either on normal modes or on a continuum of modes [1,2]. These two approaches feature some drawbacks: normal mode models require the addition of phenomenological parameters to let photons escape from the cavity while a continuum of modes prevents to consider only a finite number of modes to describe the interaction with an emitter. We thus want to develop a third option (see Figure 1) using the concept of quasinormal modes (QNMs) [3,4] that are particular solutions of the wave equation with outgoing boundary conditions. They are promising objects since they form a discrete set and already contain the information about the interface of the resonator.

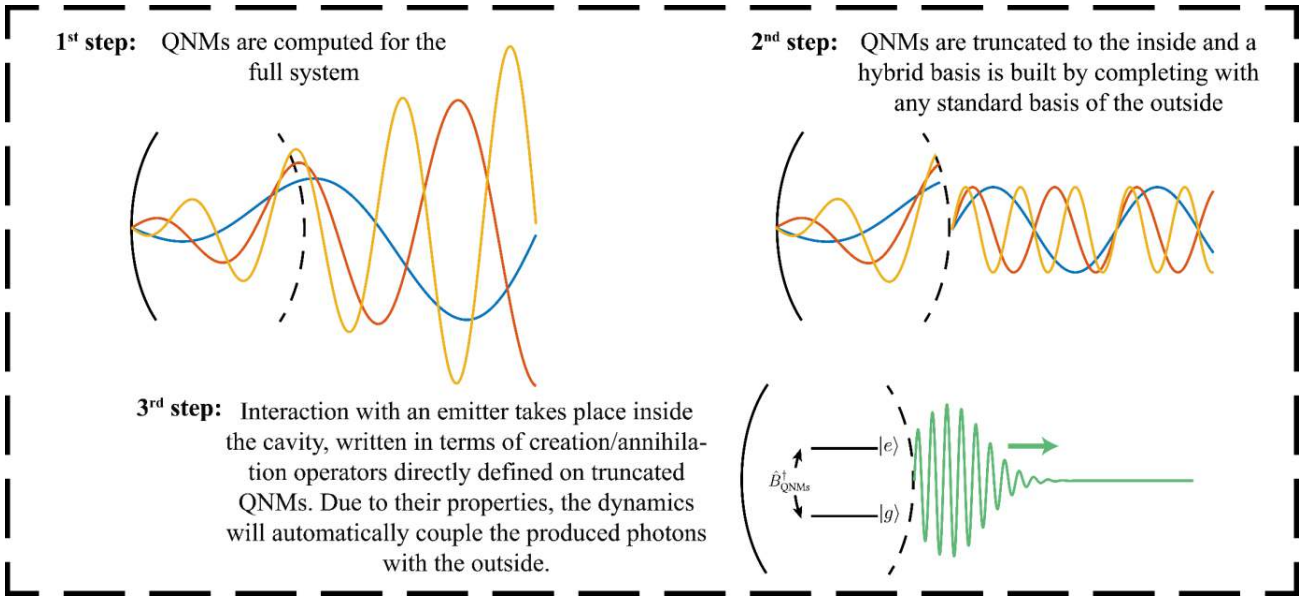


Figure 1: Schematic showing the step-by-step construction of a quantum model using quasinormal modes to describe photon's production in leaky cavity.

To be able to use QNMs (that are classical solutions of the wave equation), to describe photons (that are quantum excitations of the electromagnetic field), we want to take advantage of the particular description of photon's dynamics. Indeed, although they are quantum objects, photons are carried by classical solutions of Maxwell's equation i.e. if one considers a single-photon (described by the action of a bosonic creation operator onto the vacuum state of a Fock space $\mathbb{F}(\mathcal{H})$ as $|1_\psi\rangle = \hat{B}_\psi^\dagger|\emptyset\rangle$, where ψ is any element of the one-quantum subspace $\mathbb{F}_1 = \mathcal{H}$), the time evolution of such state is given by $|1_\psi(t)\rangle = \hat{B}_{\psi(t)}^\dagger|\emptyset\rangle$, where $\psi(t)$ is a solution of the classical Maxwell equations [5]. And since Maxwell's equations can be rewritten in terms of a wave equation, QNMs could in principle be used to describe the dynamics of a single-photon. The only constraint about the classical solution is that it should belong to the one-quantum subspace $\mathbb{F}_1$ i.e. to the Hilbert space of square integrable functions $\mathcal{H}$.

A well-known property of QNMs, which causes some difficulties, is that they diverge for positions far from the cavity [3,4], meaning that they cannot belong to $\mathcal{H}$. However, one can take advantage of the particular setup in which they are used that is, in our case, a cavity embedded either in vacuum or in a passive dielectric medium such as an optical fiber that collects the produced photons. Indeed, for these media, the dynamics given by Maxwell's equations is known and is very simple: a translation outward the cavity at the speed of light in the medium. One therefore only needs to use QNMs inside the cavity at initial time since the dynamics for later time will be directly given by the translation outward the cavity of the QNMs at the interface. Moreover, QNMs are known to form a complete basis inside the cavity [3,4] which allows us to construct a hybrid basis made of QNMs inside and of any other basis of $\mathcal{H}$ outside. Such a basis can then be used in the quantum formalism to have a quantum description using the concept of QNMs but without following the Green function quantization nor defining regularized QNMs outside the cavity [6].

The power of this model lies in the use of truncated QNMs which are thus automatically in $\mathcal{H}$. Then, the interaction with a single emitter can be described as a coupling with QNMs only because everything happens within the cavity. Finally, the dynamics will naturally link the inside with the outside due to the leakage properties of QNMs. Such model drastically reduces the dimensionality of the problem since one can choose only QNMs that are resonant with the single-emitter and for the outside part, the model will create only states that are propagating outward the cavity.

References

[1] Kuhn, A. and D. Ljunggren, “Cavity-based single-photon sources”, Contemp. Phys., Vol. 51, No. 4, 289–313, 2010.

[2] S. M. Dutra, “Cavity Quantum Electrodynamics” John Wiley & Sons, 2004.

[3] Ching, E. S. C., P. T. Leung, A. M. van der Brink, W. M. Suen, S. S. Tong and K. Young, “Quasinormal-mode expansion for waves in open systems”, Rev. Mod. Phys., Vol. 70, No. 4, 1545–1554, 1998.

[4] Sauvan, C., J. P. Hugonin, I. S. Maksymov, and P. Lalanne, “Theory of the spontaneous optical emission of nanosize photonic and plasmon resonators”, Phys. Rev. Lett., Vol. 110, No. 23, 237401, 2013.

[5] Federico, M., V. Dorier, S. Guérin, and H. R. Jauslin, “Space-time propagation of photon pulses in dielectric media, illustrations with beam splitters”, J. Phys. B-At. Mol. Opt., Vol. 55 No. 17, 174002, 2022.

[6] Franke, S., S. Hughes, M. K. Dezfouli, P. T. Kristensen, K. Busch, A. Knorr, and M. Richter, “Quantization of quasinormal modes for open cavities and plasmonic cavity quantum electrodynamics”, Phys. Rev. Lett., Vol. 122 No. 21, 213901, 2019.

Machine learning for metamaterials and metasurfaces

Deep learning based inverse design: Neural adjoint for free-form geometries

P. R. Wiecha[1], A. Khaireh-Walieh[1], T. Radford[2], A. Politi[2], O. L. Muskens[2]

[1]LAAS-CNRS, Université de Toulouse, 31000 Toulouse, France
[2]Physics and Astronomy, Faculty of Engineering and Physical Sciences, University of Southampton, Southampton, UK
*corresponding author: pwiecha@laas.fr

Abstract: I will give an overview over the most important inverse design techniques techniques, will discuss respective drawbacks and advantages, while discussing also potential dangers and risks, that come with data-driven techniques in a general picture. Particular focus will be spent on the neural adjoint method and its variations.

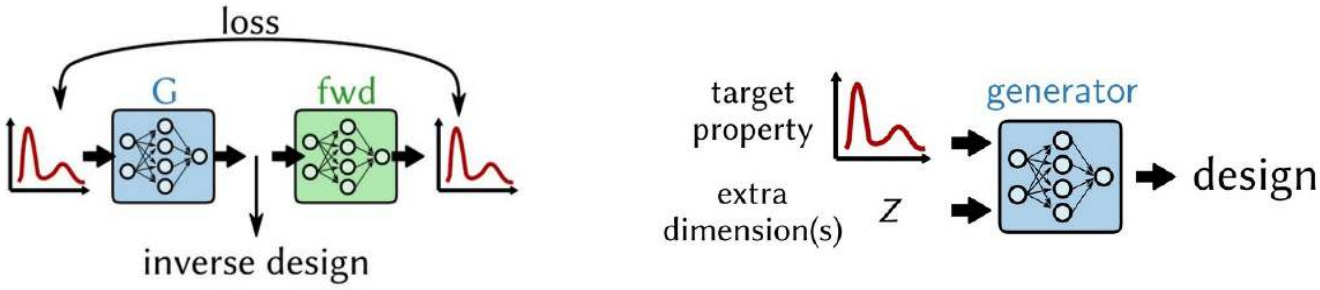


Fig.1 Left: Tandem inverse design network; right: latent space based inverse network concept

Artificial intelligence and in particular deep learning (DL) has proven in recent years to provide powerful numerical methods for various fields of research. DL is particularly interesting for inverse design tasks which mostly cannot be solved with analytical or direct approaches [1]. Often, very cost-intensive, iterative solvers are used. For nano-photonics inverse design, various deep learning methods have been proposed and benchmarked in the recent past [2]. Frequently used methods are the so-called tandem network (Fig 1, left), or latent space method (Fig 1 right), such as conditional variational autoencoders (cVAE) and conditional generative adversarial networks (cGANs). However all of those methods do not perform an optimization of the design to a given task, but rather match the physical property approximately with the design target. As a result, the inverse designed systems often roughly match the desired functionality, while it would be physically possible to achieve better performance.

The recently proposed neural adjoint (NA) method [4,5] is a deep learning based approach which actually optimizes the target functionality by using a forward network as fast differentiable surrogate, to optimize many random geometries concurrently via gradient descent (Fig 2). It has been shown, that at the cost of an increased computational budget, the NA is in fact delivering superior designs compared to one-shot methods like the tandem [2].

A major subtlety in NA is to constrain the geometry with an additional design loss, since feed-forward neural networks are weak in extrapolation tasks. While this is straightforward in multilayer

perceptron (MLP) networks [4,5], it is a significant challenge for convolutional neural networks, taking free-form geometries as input. The problem can be circumvented by an additional, pre-trained, generator network that maps the free-form design to a latent space, the latter being optimized by the NA. By constraining the latent-space during optimization using an additional KL loss, we obtain robust and stable inverse design results. Furthermore, the design-generator can implicitly incorporate further constraints such as fabrication accuracy

I will give an overview over the most important inverse design techniques techniques, will discuss respective drawbacks and advantages, while discussing also potential dangers and risks, that come with data-driven techniques in a general picture.

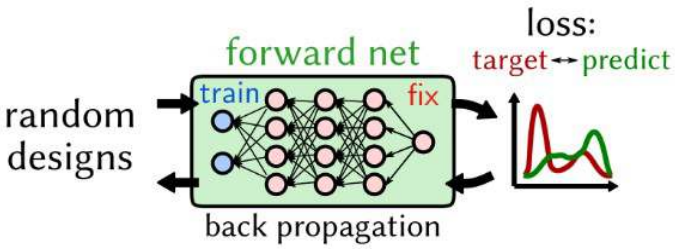


Fig.2 The neural adjoint (NA) method uses a pre-trained forward neural network as ultra-fast, differentiable surrogate for gradient-based, stochastic optimization.

References

1. Wiecha, et al. Deep learning in nano-photonics: inverse design and beyond. Photonics Research 9, B182 (2021)
2. Ren, S. et al. Inverse deep learning methods and benchmarks for artificial electromagnetic material design. Nanoscale 14, 3958–3969 (2022)
3. Estrada-Real et al. Inverse design with flexible design targets via deep learning, PNFA 52, 101066 (2022)
4. Jiang, L. et al. Neural network enabled metasurface design for phase manipulation. Opt. Express 29, 2521–2528 (2021)
5. Deng, Y., Ren, S., Fan, K., Malof, J. M. & Padilla, W. J. Neural-adjoint method for the inverse design of all-dielectric metasurfaces. Opt. Express 29, 7526–7534 (2021)

META 2023, PARIS - FRANCE, JULY 18 – 21, 2023

Digital Twins for Generic Radio Environments Parametrized by Reconfigurable Intelligent Surfaces: Physics-Based vs. Physics-Agnostic Surrogate Models

Hugo Prod'homme[†] and Philipp del Hougne[*]

Univ Rennes, CNRS, IETR—UMR 6164, F-35000 Rennes, France

[†]presenting author
[*]corresponding author: philipp.del-hougne@univ-rennes1.fr

Abstract: Optimizing the configuration of reconfigurable intelligent surfaces (RISs) in generic (potentially complex-scattering) radio environments for a desired communications or sensing functionality is challenging because of the non-linear manner in which the RIS impacts the wireless channel. The availability of a learned surrogate forward model of the mapping from RIS configuration to wireless channel can substantially facilitate the optimization problem. Here, we explore different approaches (physics-based vs. physics-agnostic) to learning such digital twins.

The ability to control the wireless radio environment via programmable metasurfaces (often referred to as RIS) constitutes a paradigm shift because the system engineer can now not only control the input signals but also the wireless channel itself. However, while the wireless channel is a linear input-output relation, its dependence on the RIS configuration is in general non-linear [1], [2]. This "structural non-linearity", largely overlooked by the signal-processing community to date, originates from proximity-induced mutual coupling between close-by RIS elements and reverberation-induced long-range correlations among all RIS elements. The non-linear dependence of the wireless channel on the RIS configuration constitutes a substantial challenge for optimizing the RIS configuration.

In this presentation, we will explore the feasibility of learning digital twins of the physical system that act as surrogate forward model, i.e., that map the RIS configuration to the experimentally observed wireless channel. We will explore a variety of surrogate models, ranging from a blind (completely physics-agnostic) model, via various hybrid intermediate steps, to a fully physics-based model. We compare the fidelity with which these models can approximate the experimental reality, and we explain what physical parameters of the experimental setting determine the difficulty with which surrogate models can be learned. We validate our techniques both based on the physics-compliant channel model PhysFad [1] as well as various experimental data sets.

P.d.H. acknowledges funding from the CNRS prématuration program (project "MetaFilt").

References

[1] R. Faqiri, C. Saigre-Tardif, G. C. Alexandropoulos, N. Shlezinger, M. F. Imani, and P. del Hougne, "PhysFad: Physics-Based End-to-End Channel Modeling of RIS-Parametrized Environments With Adjustable Fading," *IEEE Trans. Wireless Commun.*, vol. 22, no. 1, pp. 580–595, Jan. 2023.

[2] A. Rabault, L. Le Magoarou, J. Sol, G. C. Alexandropoulos, N. Shlezinger, H. V. Poor, and P. del Hougne, "On the Tacit Linearity Assumption in Common Cascaded Models of RIS-Parametrized Wireless Channels," *arXiv:2302.04993*, Feb. 2023.

Exploring Multiple Network Architectures to Solve Selected Challenges in Computational Nanophotonics

Y. Augenstein[1], L. Kuhn[1], T. Repän[2], and C. Rockstuhl[1,3*]

[1] Institute of Theoretical Solid State Physics, Karlsruhe Institute of Technology, Germany
[2] Institute of Physics, University of Tartu, Estonia
[3] Institute of Nanotechnology, Karlsruhe Institute of Technology, Germany
[*]corresponding author: carsten.rockstuhl@kit.edu

Abstract: We present our most recent contributions to explore the use of different architectures for artificial neural networks to simulate the interaction of light with nanostructured materials. Among others, we exploit graph neural networks to substitute a finite-difference time-domain scheme and Fourier neural operators as surrogate solvers for electromagnetic scattering problems. For the latter, we highlight the opportunity to solve tasks in the context of the inverse design of free-form scatterers with an optical response on demand.

Methods and techniques from the field of computer science, and especially from the field of machine learning, currently penetrate optics and photonics and are explored for selected purposes. While multiple networks were studied for designing specific nanophotonic devices [1, 2], we explore from a slightly different perspective the use of particular architectures of artificial neural networks for the more general task of solving Maxwell's equations or replacing traditional techniques to simulate the interaction of light with nanostructured photonic materials.

One example of the latter would be the finite-difference time-domain (FDTD) method, where simulations are made by discretizing Maxwell's equations in space and time on a grid and evolving an initial field through a given spatial domain using a leap-frog-scheme. In our work, we have been using graph neural networks (GNN) for the same purpose. By representing the electromagnetic field distribution as a graph, we successfully train a GNN to propagate the field for a fixed time step. Despite relatively small domain sizes in training, our GNN can extrapolate to arbitrarily large domains while preserving high prediction accuracy. Additionally, our approach works on square grids, the backbone of any FDTD, but also on arbitrary unstructured meshes. Hence, this GNN architecture opens novel opportunities to bypass a notorious shortcoming of the traditional FDTD approach.

On the other hand, we introduce a Fourier neural operator network as a surrogate solver for Maxwell's equations. The FNO is not a general-purpose Maxwell solver but requires a set of structures and their scattering response as training data. The model is trained on a diverse set of free-form electromagnetic scatterers, and we compare its performance to a state-of-the-art convolutional architecture (UNet). We show that FNO requires significantly fewer data to reach the same accuracy as UNet. Further, we show the inverse design of free-form three-dimensional optical elements using our pre-trained model. We obtain feasible devices while achieving a significant speedup over conventional means for inverse design. The model is geared to predict structures feasible for fabrication with additive manufacturing technologies. The FNO makes it possible to design structures with disparate objective functions and is, in that sense, a general-purpose tool.

References

1. Repän, T., Y. Augenstein, and C. Rockstuhl, "Exploiting geometric biases in inverse nano-optical problems using artificial neural networks," Opt. Express Vol. 30, 45375, 2022
2. Kuhn, L., T. Repän, and C. Rockstuhl „Inverse design of core-shell particles with discrete material classes using neural networks," Sci. Rep. Vol. 12 19019, (2022)

Deep-Neural-Network for Meta-Lens Image Reconstruction

Yunxi Dong[1*], Bowen Zheng[1], Sensong An[1], Hang Li[1], Hong Tang[1], Yi Huang[1], Mohammad Haerinia[1], and Hualiang Zhang[1*]

[1]ECE Dept., University of Massachusetts Lowell, Lowell, Massachusetts, USA
*corresponding authors, E-mail: Yunxi_dong@student.uml.edu, hualiang_zhang@uml.edu

Abstract: We have proposed a deep learning (DL) approach for reconstructing images taken through meta-lenses. We trained a deep neural network (DNN) that can recover the chromatic aberration of meta-lens imaging. The invented DNN can be used to restore images taken from different focusing distances. The designed DNN model achieved high fidelity computationally and great meta-lens imaging performance.

1. Introduction

Metasurfaces are capable of controlling wavefronts with compact size and flat shape, which have great potential to replace conventional refractive optical components [1-4]. For example, metasurfaces can work as meta-lens in visible light with a hyperbolical phase design. However due to inherent dispersive behavior of metasurfaces, meta-lens imaging can experience strong chromatic dispersion. Various approaches [1-4] have been proposed in recent years to solve this problem.

In this paper, we proposed a novel Deep Learning (DL) method to solve the chromatic dispersion of meta-lens imaging. We used a modified U-Net [5] structure DL network to correct the image color and reconstruct the image to its original quality. With this fully trained network, we could process a single image in less than 1 second with high fidelity.

2. Meta-Lens Imaging Reconstruction

To restore the image color, we designed our model based on the U-Net model [5,6]. In addition to the original U-Net model, we add more skip connections between different convolutional blocks to capture more color features and avoid model degradation. The detailed network architecture is shown in Fig. 1. The encoder and decoder blocks consist of several convolutional and upsampling layers. The dashed lines between blocks represent exemplar skip connections we added to our DL model's encoder and decoder blocks.

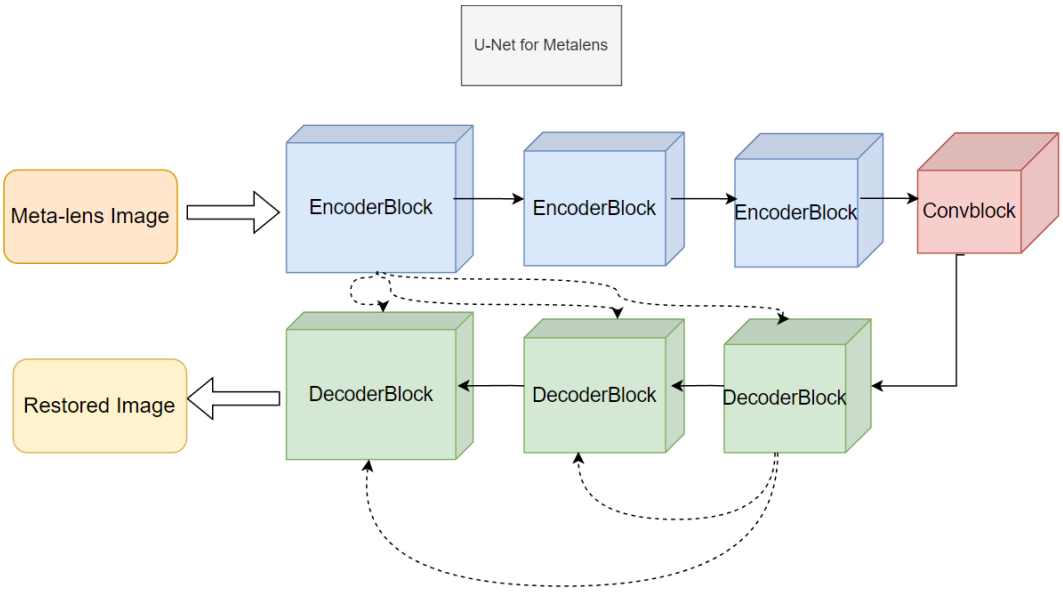


Fig. 1. General architecture of the proposed network.

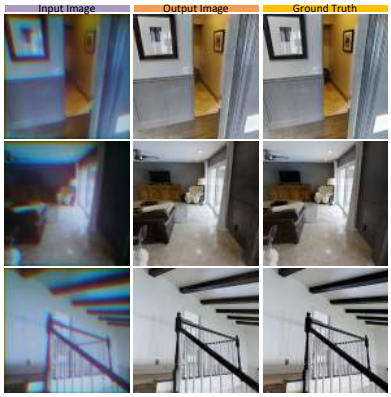


Fig. 2. Examples of image reconstruction using the proposed network.

After hundreds of epochs of training, our DL model can eliminate chromatic dispersion from meta-lens imaging with losing texture details. A few examples are shown in Fig. 2. It is found that, with this model, we can efficiently process any meta-lens imaging in a short time with promising quality.

3. Meta-lens Design and Imaging Setup

The proposed meta-lens is fabricated on silicon-on-Sapphire (SOS) wafers. Meta-atoms are formed by silicon cylindrical pillars with various diameters to achieve different phase responses. The total phase coverage exceeded 360° across the operating wavelength range.

The targeted wavelength of the meta-lens is 560nm, so that at such wavelength, all the meta-atoms achieved at least 80% transmission efficiency. Photos of the fabricated meta-lens are shown in Fig. 3. This meta-lens has a diameter of 1mm, and the focal length is set to be 5mm.

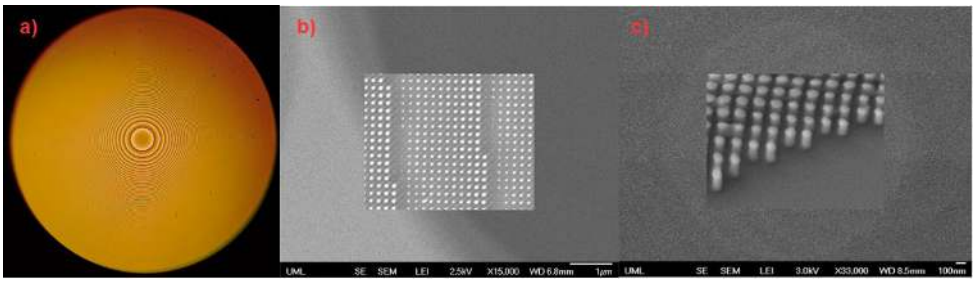


Fig. 3. a) The photo of whole fabricated meta-lens. b) SEM photo of the fabricated meta-lens (top view). c) SEM photo of the fabricated meta-lens (tilted view at the edge).

References

1. S. Wang, P. C. Wu, V.-C. Su, Y.-C. Lai, M.-K. Chen, H. Y. Kuo, B. H. Chen, Y. H. Chen, T.-T. Huang, J.-H. Wang, R.-M. Lin, C.-H. Kuan, T. Li, Z. Wang, S. Zhu, and D. P. Tsai, "A broadband achromatic metalens in the visible," Nature Nanotechnology, vol. 13, no. 3, pp. 227–232, 2018.
2. W. T. Chen, A. Y. Zhu, V. Sanjeev, M. Khorasaninejad, Z. Shi, E. Lee, and F. Capasso, "A broadband achromatic metalens for focusing and imaging in the visible," Nature Nanotechnology, vol. 13, no. 3, pp. 220–226, 2018.
3. M. Khorasaninejad, Z. Shi, A. Y. Zhu, W. T. Chen, V. Sanjeev, A. Zaidi, and F. Capasso, "Achromatic metalens over 60 nm bandwidth in the visible and Metalens with reverse chromatic dispersion," Nano Letters, vol. 17, no. 3, pp. 1819–1824, 2017.
4. W. Ma, F. Cheng, and Y. Liu, "Deep-learning-enabled on-demand design of chiral metamaterials," *ACS nano,* vol. 12, no. 6, pp. 6326-6334, 2018.
5. O. Ronneberger, P. Fischer, and T. Brox, "U-Net: Convolutional Networks for Biomedical Image Segmentation," Lecture Notes in Computer Science, pp. 234–241, 2015.
6. Y. Liu, C. Zhang, T. Kou, Y. Li, and J. Shen, "End-to-end computational optics with a singlet lens for large depth-of-field imaging," Optics Express, vol. 29, no. 18, p. 28530, 2021.

META 2023, PARIS - FRANCE, JULY 18 – 21, 2023

Normalization flows for designing metasurfaces

Kebin Fan[1*], Jia-Qi Yang[1], Yu-Cheng Xu[1], Jingbo Wu[1], Caihong Zhang[1], De-Chuan Zhan[1], Biaobing Jin[1], and Willie J. Padilla[2]

[1]Nanjing University, Nanjing, China

[2]Duke University, Durham, NC 27708,USA
[*]corresponding author: kebin.fan@nju.edu.cn

Abstract: Training data are very expensive for metasurface designs using deep-learning based methods. To achieve data efficiency, we introduced normalization flows to inversely design metasurfaces through learning the probabilistic distribution of the data. To explore the distribution efficiently, we proposed a prior shaping method to re-weight the data based on their fitness to the design target. Through implementing the algorithm, we obtained an emitter with in-band emittance efficiency close to 99%. Our results present a new route for designing metasurfaces inversely.

Deep learning techniques have triggered new perspectives not only for our daily life, but also for science exploration and engineering designs. To achieve functional metasurface with better performance, various machine learning algorithms have been investigated, such as generative adversarial networks (GANs), variational auto-encoders (VAEs), adversarial auto-encoders (AAEs), and the neural adjoint (NA). [1-4] To better explore the data and model the probability of data distribution with respect to the design target, we propose conditional probabilistic learning – specifically a normalizing flow (NF) method – for inverse design. In recent literature, the normalizing flow architecture has also been termed invertible neural networks (INNs) [5], which can be trained with exact log-likelihood, which leads to better convergence and performance. We also proposed a novel prior reshaping (PR) method to explore the feasible design parameter space more efficiently, which can be adjusted freely with a hyperparameter τ without re-generating new data. Using the NF-based inverse design, we successfully designed an Nb-based emitter working for GaSb with nearly 100% in-band efficiency. We also experimentally show that the normalizing flow model trained on a large-scale dataset can be transferred by only using a few new data. Using only 5% of the original data, we inversely designed an emitter working for InGaAsSb with in-band efficiency up to 99.7%. And the correlation between the design variables and the latent parameters provides excellent interpretation for the underline physics. Our results indicate that this method can be used to generate feasible design variables and enables sampling from different prior data distribution efficiently without re-simulation. Our proposed method is not limited to the demonstrated metasurface emitters, and may also be applied to other design problems in photonics, plasmonics, materials, and mechanics.

This work is supported by National Natural Science Foundation of China (62275118), the Fundamental Research Funds for the Central Universities, and Research fund for Jiangsu Key Laboratory of Advanced Techniques for Manipulating Electromagnetic Waves.

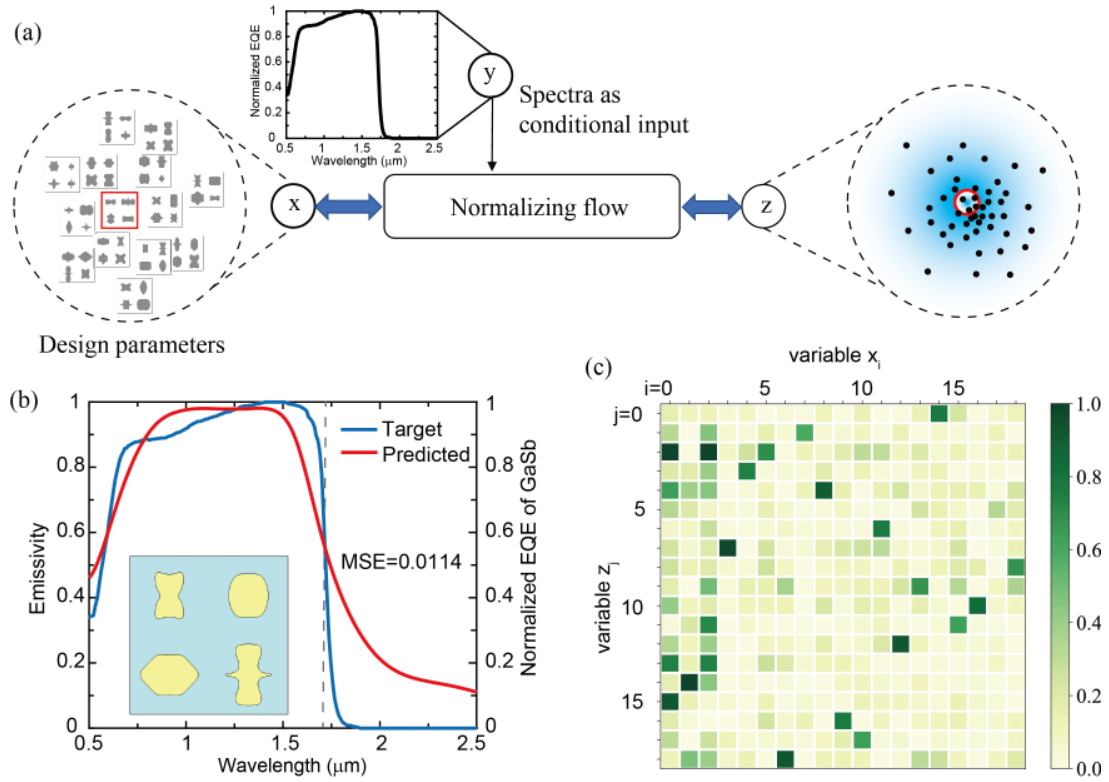


Figure 1 (a) The model architecture of a normalizing flow (NF). Given the design target y as input, the NF model can perform bidirectional transformation between design parameter x and latent variable z. (b) The comparison between the emissivity (left ordinate) obtained from the inverse design (red curve) and the target (blue curve), which is the normalized EQE (nEQE) of GaSb (right ordinate). The inset shows the structure obtained from inverse design. (c) Correlation strength between latent variable z_j and design parameter x_i.

References

1. Liu, Z.; Zhu, D.; Rodrigues, S. P.; Lee, K.-T.; Cai, W. Generative model for the inverse design of metasurfaces. Nano letters 2018, 18, 6570–6576.
2. Ma, W.; Cheng, F.; Xu, Y.; Wen, Q.; Liu, Y. Probabilistic representation and inverse design of metamaterials based on a deep generative model with semi-supervised learning strategy. Advanced Materials 2019, 31, 1901111.
3. Kudyshev, Z. A.; Kildishev, A. V.; Shalaev, V. M.; Boltasseva, A. Machine-learning-assisted metasurface design for high-efficiency thermal emitter optimization. Applied Physics Reviews 2020, 7, 021407.
4. Deng, Y.; Ren, S.; Fan, K.; Malof, J. M.; Padilla, W. J. Neural-adjoint method for the inverse design of all-dielectric metasurfaces. Optics Express 2021, 29, 7526–7534.
5. Kobyzev, I.; Prince, S. J. D.; Brubaker, M. A. Normalizing Flows: An Introduction and Review of Current Methods. IEEE Trans. Pattern Anal. Mach. Intell. 2021, 43, 3964–3979.

META 2023, PARIS - FRANCE, JULY 18 – 21, 2023

Adaptive physics-driven neural networks for electromagnetic inverse problems and design of ultracompact diffractive devices

L. Dal Negro[1,2,3*], Y. Zhu[2], and R. Riganti[3]

[1]Department of Electrical & Computer Engineering and Photonics Center, Boston University, USA
[2]Division of Materials Science & Engineering, Boston University, USA
[3]Department of Physics, Boston University, USA
[*]corresponding author: dalnegro@bu.edu

Abstract: We present a robust computational framework that combines artificial neural network architectures with scattering and wave transport physics for the inverse design of ultracompact diffractive devices and for the inverse solution of high-dimensional integro-differential problems of relevance to optoelectronic and metamaterial technologies. Specifically, we develop and test different adaptive learning strategies that provide enhanced accuracy and scalability for the design and discovery of novel nanophotonic and metamaterial devices.

There is a growing interest in developing deep learning (DL) and artificial intelligence (AI) algorithms for electromagnetic wave engineering and metamaterials design. These rapidly emerging approaches include training artificial neural networks (ANNs) to solve inverse problems and parameter estimation in complex photonic environments [1,2]. Although successfully demonstrated at solving several inverse design problems, traditional DL methods are essentially data-driven techniques requiring time-consuming training steps that use massive datasets. Moreover, in order to improve on purely data-driven methods, it is also important to constrain and regularize them leveraging on the underlying physics of the investigated problems. Here we discuss our approaches to build a robust framework that efficiently integrates powerful ANN architectures and the physical laws that fundamentally constrain the wave scattering and parameter retrieval inverse-problems for metamaterials and nano-optical devices. In particular, we introduce and discuss adaptive learning methods based on diffractive optical networks (a-DONs) for the inverse-design of ultracompact spectroscopic imaging devices [3,4] as well as physics-informed neural networks (a-PINNs) for complex electromagnetic inverse scattering and radiative transfer problems [5,6,10]. The flexible a-DONs approach builds on diffractive optical networks that naturally combine optical diffraction physics and deep learning capabilities [7-9]. In our work, we demonstrate the inverse design of two-layer focusing devices that selectively focus incident radiation over well-separated spectral bands at desired distances, achieving focusing efficiencies beyond the limit of single-layer diffractive optical elements (DOEs). Moreover, we engineer the angular dispersion and steering behavior of broadband incident radiation across predefined focal trajectories achieving nanometer spectral resolution in diffractive devices with $L = 100\ \mu$m side length and $f = 300\ \mu$m focal length across the visible spectrum. We also address the fabrication and characterization of the designed devices using multi-level lithography and doublet metasurface technology, potentially enabling single-shot focusing spectrometers with customized focal trajectories for applications to ultracompact spectroscopic imaging and lensless microscopy. Finally, we discuss our recent work on the development and testing of adaptive PINNs methods for the accurate solution of complex forward and inverse problems in electromagnetic scattering and radiative transfer theory. We introduce a-PINNs architectures for the inverse solution of high-dimensional integro-differential transport problems of relevance to optoelectronic devices and metamaterials technologies. In particular, we demonstrate efficient parameter estimation in coupled

conductive-radiative systems and discuss applications to the inverse design of heat transfer in nano-devices with engineered thermal properties [10]. Our work shows that a-PINNs possess the flexibility, accuracy, and noise robustness required to become a powerful design approach for inverse scattering and the non-local homogenization of multi-scale optoelectronic devices and metamaterials.

We acknowledge the support from National Science Foundation (ECCS-2015700) and from the US Army Research Office (W911NF-22-2-0158).

References

1. W. Ma, Z. Liu, Z. A. Kudyshev, A. Boltasseva, W. Cai, Y. Liu, "Deep learning of the design of photonics structures", Nat. Photonics Vol. 15, No. 2, 77-90, 2021.
2. Z. Liu, D. Zhu, L. Raju, W. Cai, "Tackling Photonic Inverse Design with Machine Learning", Adv. Sci., Vol. 8, No. 5, 2002923, 2021.
3. Y. Chen, Y. Zhu, W. A. Britton, and L. Dal Negro, "Inverse design of ultracompact multi-focal optical devices by diffractive neural networks", Opt. Lett., Vol. 47, No. 11, 2842-2845, 2022.
4. Y. Zhu, Y. Chen, and L. Dal Negro, "Design of ultracompact broadband focusing spectrometers based on diffractive optical networks", Opt. Lett., Vol. 47, No. 24, 6309-6312, 2022.
5. Y. Chen, L. Lu, G. E. Karniadakis, and L. Dal Negro, "Physics-informed neural networks for inverse problems in nano-optics and metamaterials", Opt. Express, Vol. 28, No. 8, 11618-11633, 2020.
6. Y. Chen and L. Dal Negro, "Physics-informed neural networks for imaging and parameter retrieval of photonic nanostructures from near-field data", APL Photonics, Vol. 7, No. 1, 010802, 2022.
7. X. Lin, Y. Rivenson, N. T. Yardimci, M. Veli, Y. Luo, M. Jarrahi, and A. Ozcan, "All-optical machine learning using diffractive deep neural networks", Science, Vol. 361, No. 6406, 1004-1008, 2018.
8. Y. Luo, D. Mengu, N. T. Yardimci, Y. Rivenson, M. Veli, M. Jarrahi, A. Ozcan, "Design of task-specific optical systems using broadband diffractive neural networks", Light: Sci. Appl., Vol. 8, No. 1, 112, 2019.
9. M. Veli, D. Mengu, N. T. Yardimci, Y. Luo, J. Li, Y. Rivenson, M. Jarrahi, and A. Ozcan, "Terahertz pulse shaping using diffractive surfaces", Nat. Commun., Vol. 12, No. 1, 37, 2021.
10. R. Riganti and L. Dal Negro, "Physics-Informed Adaptive Learning for Complex Radiative Transport Problems", in preparation, 2022.

META 2023, PARIS - FRANCE, JULY 18 – 21, 2023

Importance of Metric Learning and Manifold Learning in Knowledge Discovery and Inverse Design of Nanophotonic Structures

Mohammadreza Zandehshahvar, Muliang Zhu, Mohammad Hadigheh Javani, and Ali Adibi*

School of Electrical and Computer Engineering
Georgia Institute of Technology
Atlanta, GA 30332-0250
*Corresponding author: adibi@ece.gatech.edu

Abstract: We discuss the importance of manifold-learning algorithms in reducing the dimensionality of the nanophotonic design problems while enabling the better visualization of their input-output relation. This can be helpful in forming least complex structures for a given response while also uncovering subtle details about the physics of light-matter interaction. We also show the importance of metric learning in the efficacy of the manifold-learning algorithms and empowering them to distinguish different classes of responses while preserving important response features.

Nanophotonics structures have a wide range of applications in different disciplines from virtual reality and lens design to computing thanks to their unique features and capabilities in manipulating light spatially, temporally, and spectrally. The recent advances in fabrication technologies have enabled the design of structures with more degrees of freedom compared to the past. This makes the inverse design of such structures more challenging and yet more important than ever.

The gradient-based inverse-design techniques such as topology optimization and adjoint optimization have been on the forefront of the inverse design in nanophotonics and shown promising performance on the design of different classes of structures over the past few years. However, since these methods rely on an electromagnetic (EM) solver at each iteration, they can become computationally extensive in the cases that the forward problem and its gradient cannot be calculated efficiently, and the inverse design needs to be solved repeatedly for different solutions. These methods also cannot provide insight about the hidden patterns in the data and are not easy to interpret.

More recently, machine-learning (ML) approaches have been extensively employed for the inverse design in nanophotonics thanks to their unique features in processing high-dimensional data. These methods mainly use a set of training data that is generated using EM solvers to learn the mapping between the input (i.e., the design space) and the output (i.e., the response space) and use the surrogate model to solve the inverse design with far less computation. These approaches have been applied to different classes of structures including binary structures, thin films, multi-layered structures, metasurfaces, etc.

In addition to the utilization of ML methods for inverse design, they have been used for knowledge discovery and uncovering hidden patterns of the high-dimensional data in these structures. Reducing the dimensionality and visualization of the data in the lower-dimensional space can facilitate the interpretation of the results and understanding the role of design parameters.

In this work, we present a manifold-learning approach for efficient inverse design and knowledge discovery in nanophotonics. We use this approach for understanding the range of responses in a class of nanostructures with different geometric complexities and study the role of design parameters. We also present a new approach for metric learning to define new metrics (i.e., similarity measure) that are well-suited for nanophotonics applications. We show how this approach can result in a better representation of the data in the embedding space (i.e., low-dimensional space or latent space).

META 2023, PARIS - FRANCE, JULY 18 – 21, 2023

Multipolar Resonance Engineering Using Machine Learning

Wenhao Li,[1] Hooman Barati Sedeh,[1] Willie J. Padilla,[1] Jordan Malof,[2] and Natalia M. Litchinitser[1]

[1]Duke University, USA
[2]University of Montana, USA
[*]corresponding author: natalia.litchinitser@duke.edu

Abstract: We developed machine learning models to predict the multipolar resonances and electric field distributions of all-dielectric meta-atoms. Machine learning method is also used for inverse designing meta-atoms based on the desired multipolar resonances.

Machine learning methods have been widely used in subwavelength photonic structure designs since they are capable of solving the non-intuitive and nonlinear relationship between subwavelength structures and their optical responses and are significantly faster than the traditional numerical simulation methods. However, in the inverse design problems, machine learning models usually serve as black boxes which take the desired spectrum as an input to predict the shape of meta-atoms without elucidating the physics behind it. This makes the machine learning method difficult to apply when designing structures aimed at performing complicated functions. At the same time, the multipole expansion of the scattering cross sections, i.e. multipolar resonances, has been instrumental in analyzing and designing meta-atoms. In this work, we developed forward prediction models to discover hidden relationships between scattering behavior and the shapes/optical properties of meta-atoms, and an inverse design model to reconstruct the meta-atoms having desired properties under the guidance of multipole expansion theory. We discuss several linear and nonlinear optics examples of applications that are likely to be enabled by the developed multipolar resonances guided machine learning approach.

Meta-Atom Design for a Highly-Sensitive Liquid Sensor

Kazunori Serita, Luwei Zheng, Kazuki Hara, and Masayoshi Tonouchi

Institute of Laser Engineering, Osaka University, Suita, Osaka, 5650871 JAPAN
*corresponding author: tonouchi.masayoshi.ile@osaka-u.ac.jp

Abstract: We propose new type of a highly-sensitive liquid sensor. Terahertz (THz) point source was combined with a few arrays of meta-atoms, and reflection type THz-TDS was developed. The design of the meta-atoms and configuration of the array were studied to enhance the sensitivity.

The femtosecond laser pulses are focused in a GaAs wafer from the backside and, by adjusting the focus near the surface, a point THz source is formed. Combining with a few arrays of meta-atoms, the highly-sensitive sensor for liquid biopsy can be developed in a reflection mode (Fig.1). However, a variety of meta-atom design should be considered. In the present work, we examine the some types of meta-materials design, and evaluated their performance experimentally with the point source as indicated in Fig.2.

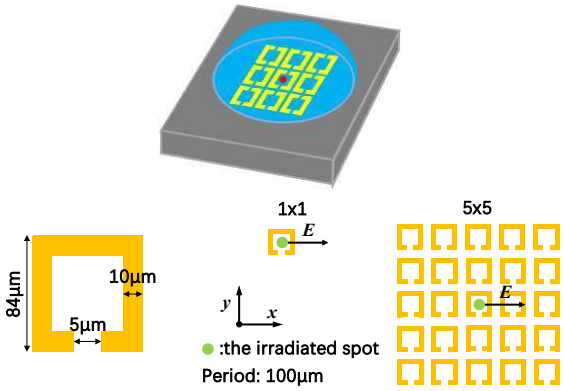


Fig. 1 Schematic of solution sensing using the arrays of meta-atoms and the configurations of meta-atoms.

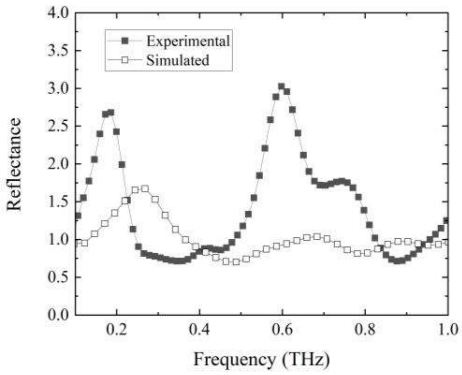


Fig.2 THz reflectance of arrayed meta-atoms.

In the presentation, we will report the optimization of the design of the meta-atom and its array configuration for highly-sensitive liquid biopsy.

Acknowledgements: This work is supported by JSPS KAKENHI JP20K20536, JP21H01392, Fusion Oriented REsearch for disruptive Science and Technology JPMJFR2029, and China Scholarship Council (Grant No. 202206170007).

References

1. K. Serita et al., "Direct measurements of terahertz meta-atoms with near-field emission of terahertz waves," Journal of Infrared, Millimeter, and Terahertz Waves, vol.38, pp.1107-1119, 2017.
2. K. Serita et al., "Terahertz microfluidic chips sensitivity-enhanced with a few arrays of meta-atoms," APL Photonics, vol.3, p.051603, 2018.
3. K. Serita et al., "A terahertz-microfluidic chip with a few arrays of asymmetric meta-atoms for the ultra-trace sensing of solutions." Photonics, Vol.6, p.12, 2019.
4. K. Serita et al., "I-design terahertz microfluidic chip for attomole-level sensing," Journal of Physics: Photonics, vol.4, p.034005, 2022.

Broadband invisibility cloaking design of concentric multilayered cylindrical metamaterials based on genetic algorithm

Tomoya Momose, Mana Toma, and Kotaro Kajikawa*

Tokyo Institute of Technology, Japan
*corresponding author: kajikawa@ee.e.titech.ac.jp

Abstract: A computational approach to design a cloaking medium is presented on the basis of the genetic algorithm (GA). The cloaking target is a dielectric cylinder with a diameter of 1 μm, and the cloaking medium is multilayered cylindrical layers with a thickness of 0.5 μm. The cloaking performance designed by the GA is much better than that designed on the basis of the transformation optics and the effective medium approximation.

Introduction

Invisibility cloaking is a technique to make a cloaking target invisible. A cloaking design is based on the transformation optics proposed by Pendry *et al* [1]. In this method, the cloaking medium is designed so that light detours the target. But this method is impractical in the optical frequency range because it requires the cloaking medium with anisotropy and magnetic response. Cai *et al*. proposed the cloaking medium with no magnetic response [2] by modifying the expression of the transformation optics. Huang *et al*. replaced this medium with a concentric multilayered cylindrical metamaterial, using the effective medium approximation, alternating the layers with high and low dielectric constants to generate effective-medium layers [3]. However, the cloaking performance is not sufficient. Our approach delivers the optimal cloaking structure by performing the GA calculations by assuming a stacked structure with high and low dielectric constant layers.

Methods

The designed structure is shown in Figure 1. This structure consists of a cylinder (dielectric constant ε_0 : 9, radius r_0 : 500 nm) covered with 26 layers of cloaking medium (thickness of one layer: about 19.23 nm, total thickness: 500 nm). TE polarized light (perpendicular to the long axis of the cylindrical medium) was incident to the medium. The dielectric constant of each layer was determined so that the scattering cross section (C_{sca}) is small in the wavelength range of 400 - 700 nm. The dielectric constant was investigated in the range of 0 - 1 for odd layers and 1 - 30 for even layers, counting from the center. The parameters were set as follows: the size of tournament selection as 3, the probability of two-point crossover as 50%, the probability of calling the mutation subroutine as 20%, the probability of each gene mutating when the mutation subroutine was called as 5%, the number of individuals as 500, and the number of generations as 320. Then, 60 trials were performed with different random number seeds to find the solution with the smallest scattering cross-section.

Results

To compare the cloaking performance, the following evaluation function was introduced.

$$\text{Evaluation value} = \frac{\sum_{\lambda=400}^{700} C_{\mathrm{sca(cloaked)}}}{\sum_{\lambda=400}^{700} C_{\mathrm{sca(target\ only)}}} \tag{1}$$

Figure 2 shows that the cloaking performance of the medium designed by our approach is better than that obtained

by the previous approach [3]. It also shows that the 26-layer cloaking medium exhibits the most broadband invisibility among those designed by the GA. The scattering cross-section with the 26-layer cloaking medium was reduced to about 4.8% on average in the optical wavelength range (400-700 nm) compared to the case without the cloaking medium. Figure 3 shows the magnetic field for the target-only case obtained by FDTD simulation at a wavelength of 540 nm. Figure 4 shows it for the case of the target covered with 26 layers of cloaking medium. It shows that invisibility cloaking was achieved using our GA approach.

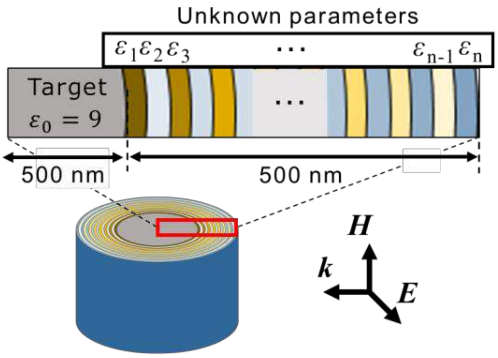


Figure 1. Optical geometry of the multilayered cylinder.

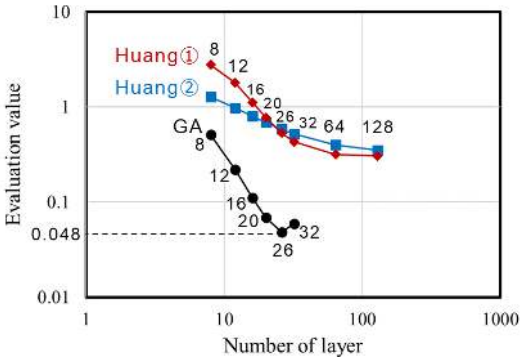


Figure 2. Evaluation value for broadband cloaking.

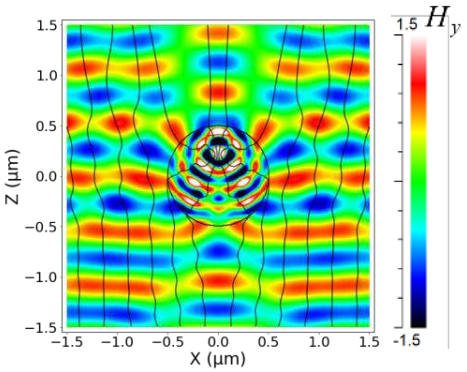


Figure 3. Magnetic field H_y of the target only.

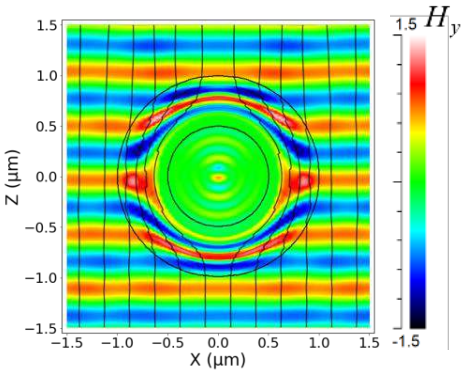


Figure 4. Magnetic field H_y of the cloaked target.

This work was partially supported by a Grant-in-Aid for Scientific Research (19H02624) from the Japan Society for the Promotion of Science. T.M. acknowledges the financial support by the program of the establishment of university fellowships towards the creation of science technology innovation of JST, Grant Number JPMJFS2112.

References

1. J. B. Pendry, D. Schurig, and D. R. Smith, “Controlling electromagnetic fields,” Science, Vol. 312, 1780–1782, 2006.
2. W. Cai, U. K. Chettiar, A. V. Kildishev, and V. M. Shalaev, “Optical cloaking with metamaterials,” Nat. Photonics, Vol. 1, 224–227, 2007.
3. Y. Huang, Y. Feng, and T. Jiang, “Electromagnetic cloaking by layered structure of homogeneous isotropic materials,” Opt. Express, Vol. 15, 11133–11141, 2007.

Enabling the inverse design of metasurfaces at the unit cell and the supercell level using neural network approaches for industrial applications

Konstantinos Dovelos[1], Evangelos Galaris[1], Vasiliki Vardakastani[1], Panagiotis Kosmas[1*], and Dimitrios C. Tzarouchis[1*]

[1] Meta Metamaterials Europe, Ap. Pavlou 10, 15123, Marousi, Athens, Greece
[*]corresponding authors: {panagiotis.kosmas,dimitrios.tzarouchis}@metamaterial.com

Abstract: In this work, we report a general methodology for the inverse design of metasurfaces at the unit cell and supercell level, using a combination of commercial software (FDFD) and a neural network approach, all controlled by a properly designed software wrapper in Python. This automated scheme can be used to develop metasurfaces with on-demand performance and functionalities for industrial applications.

Metasurfaces or intelligent surfaces are ubiquitous applications of applied electromagnetics and metamaterials that carry the momentum of transforming modern antenna systems from energy harvesting and telecommunications to biomedical devices and optics[1]. Many intuitive analytical/semi-analytical approaches have been used to design metasurfaces, delivering many exciting designs[1]. However, the design process for on-demand metasurfaces is a challenging task. It requires excellent knowledge of available libraries and procedures, often not easily adaptable from the available literature (reproducibility) and for different frequency ranges (scalability). Moreover, metasurfaces for industrial applications require robustness, high efficiency, specific frequency bands, and other quite strict modalities. In other words, real-world engineering metasurfaces entail a much more cumbersome process than the one usually found in academic research. To this end, inverse design is an excellent tool that explores a much larger design set, i.e., the set of non-intuitive geometries and designs[1-6] adding extra degrees of complexity and manufacturing constraints.

Here we describe a general methodological approach to develop a robust metasurface design pipeline for various functionalities, requirements, and constraints. To this end, the talk will present a broad methodological approach that utilizes standard commercial e/m simulation software, e.g., CST Microwave Studio (Dassault Systemes), combined with an appropriate tailored custom-made wrapper software code (Python). The automated process enables the usage of (any) commercially available software and, therefore, expands their optimization/inverse-design modalities.

By means of example, we start by assuming a given design goal, such as designing a metasurface absorber with three different absorption bands, and specific manufacturing constraints, such as realizing it with a flexible transparent material operating at the microwave regime. We then program the wrapper to reproduce thousands of randomized results with these specifications. These results are fed as the training set to a specifically designed neural network. While the procedural pipeline can be considered trivial, the process is redesigned to accommodate metrics such as high efficiency, accuracy, and manufacturing processes, dictated by industrial-level applications. The integrability of such a tool with the overall design manufacturing process via the Python interface makes it an ideal candidate for block design schemes and other custom design options.

Acknowledgments: This work is part of the "*Metamaterial Products to Protect from Electromagnetic Radiation - PROPILEA*" project with ID 16971 - OPS TA 5149205.

References

1. Tsilipakos, O., Tasolamprou, A. C., Pitilakis, A., Liu, F., Wang, X., Mirmoosa, M. S., Tzarouchis, D. C., Abadal, S., Taghvaee, H., Liaskos, C., Tsioliaridou, A., Georgiou, J., Cabellos-Aparicio, A., Alarcón, E., Ioannidis, S., Pitsillides, A., Akyildiz, I. F., Kantartzis, N. V., Economou, E. N., … Tretyakov, S. (2020). "Toward Intelligent Metasurfaces: The Progress from Globally Tunable Metasurfaces to Software-Defined Metasurfaces with an Embedded Network of Controllers". *Advanced Optical Materials*, *2000783*. https://doi.org/10.1002/adom.202000783
2. Nikkhah, V., Tzarouchis, D. C., Hoorfar, A., & Engheta, N. (2022). "Inverse-Designed Metastructures Together with Reconfigurable Couplers to Compute Forward Scattering." *ACS Photonics*. https://doi.org/10.1021/acsphotonics.2c00373
3. Pestourie, R., Yao, W., Kanté, B., & Johnson, S. G. (2022). "Efficient inverse design of large-area metasurfaces for incoherent light" *ACS Photonics*. https://doi.org/10.1021/acsphotonics.2c01015
4. Molesky, S., Lin, Z., Piggott, A. Y., Jin, W., Vucković, J., & Rodriguez, A. W. (2018). Inverse design in nanophotonics. In *Nature Photonics* (Vol. 12, Issue 11, pp. 659–670). Nature Publishing Group. https://doi.org/10.1038/s41566-018-0246-9
5. Deng, Y., Ren, S., Fan, K., Malof, J. M., & Padilla, W. J. (2021). "Neural-adjoint method for the inverse design of all-dielectric metasurfaces." *Optics Express*, *29*(5), 7526. https://doi.org/10.1364/oe.419138

Metasurfaces for light control emission

Universal light encoders: artificial intelligent hardware for nanoscale light control

A. Fratalocchi[1]

[1]Primalight, Faculty of Electrical and Computer Engineering, KAUST, Thuwal, Saudi Arabia
*corresponding author: andrea.fratalocchi@kaust.edu.sa

Abstract: Universal light encoders represent a new generation of metasurface that implements hardware machine learning for controlling light propagation. In this talk, I will review the fundamentals and application of this technology in various areas, ranging from the inverse design of ultra-flat optical components to Hyplex™ , an innovative camera for acquiring and processing high-resolution hyperspectral videos in real-time at 30 frames per second.

In this invited talk, I will summarize recent research results in the field of universal light encoders. These components represent a particular class of metasurfaces implementing optical hardware feedforward neural networks that can universally approximate any user-defined input-output function. In the first series of applications, I will discuss the exploitation of this technology to implement ultra-flat (60 nm thick) optical components for vectorial light control with near-unity experimental efficiencies in the visible. In the second part, I will discuss a new area of research that focuses on the implementation in the hardware of software machine learning concepts for various applications in machine vision. I will summarize the fundamentals of Hyplex™, a new hyperspectral technology platform that allows the acquisition and processing of high-resolution videos in real-time for a broad spectrum of applications, including remote sensing, medical diagnosis, precision agriculture, and security.

References

1. Getman, F., Makarenko, M., Burguete-Lopez, A. *et al.* Broadband vectorial ultrathin optics with experimental efficiency up to 99% in the visible region via universal approximators. *Light Sci Appl* **10**, 47 (2021). https://doi.org/10.1038/s41377-021-00489-7
2. Makarenko, M., Wang, Q., Burguete-Lopez, A., Getman, F. and Fratalocchi, A. (2021), Robust and Scalable Flat-Optics on Flexible Substrates via Evolutionary Neural Networks. Adv. Intell. Syst., 3: 2170075. https://doi.org/10.1002/aisy.202170075
3. Makarenko, M., Burguete-Lopez, A., Wang, Q., Getman, F., Giancola, S., Ghanem, B., & Fratalocchi, A. (2022). Real-time Hyperspectral Imaging in Hardware via Trained Metasurface Encoders. 2022 IEEE/CVF Conference on Computer Vision and Pattern Recognition (CVPR). https://doi.org/10.1109/cvpr52688.2022.01236. DOI: 10.1109/CVPR52688.2022.01236 Handle: 10754/676851

All-dielectric metasurfaces for enhancing and tuning the emission of quantum emitters

A. Barreda[1,2,3*], C. Zou[1,2,4], A. Sinelnik[1,2], E. Menshikov[5], I. Sinev[5], T. Pertsch[2,6], and I. Staude[1,2]

[1]Friedrich Schiller University Jena, Institute of Solid State Physics, Max-Wien-Platz 1, 07743 Jena, Germany

[2]Friedrich Schiller University Jena, Institute of Applied Physics, Abbe Center of Photonics, Albert-Einstein-Str. 15, 07745 Jena, Germany

[3]Dep. Tecnología Electrónica, Universidad Carlos III de Madrid, Avda. Universidad, 30., 28911 Leganés, Madrid, Spain

[4]Institute of Microelectronics, Chinese Academy of Sciences, Beitucheng West Road 3, Chaoyang District, Beijing, China

[5]School of Physics and Engineering, ITMO University, 191002 Lomonosova st. 9, St. Petersburg, Russia

[6]Fraunhofer Institute for Applied Optics and Precision Engineering, Albert Einstein Str. 7, 07745 Jena, Germany

[*]corresponding author: angela.barreda@uni-jena.de

Abstract: All-dielectric metasurfaces have been proposed to enhance the emission of electric and magnetic quantum emitters via engineering of high-quality factor optical modes. The excitation of quasi-bound states in the continuum can offer high *Q*-factors in symmetry-broken metasurfaces. However, in most designs, the emission wavelengths are fixed by the geometric parameters of the metasurface. Here, we propose to use phase-change materials to tune the emission of light-emitting metasurfaces supporting quasi-bounds states in the continuum in the telecom spectral range. This work may find applications for tunable spectral shaping, dynamic wavefront shaping, tunable filters, or sensors.

The development of efficient quantum emitters is key in photonic quantum technologies. All-dielectric metasurfaces have been vastly investigated in the last years with the aim of improving the efficiency of quantum emitters. On the one hand, the directionality properties of the dielectric nanoparticles can redirect the emitted radiation towards the detector used in the experiment, improving the radiation collection [1]. On the other hand, the electromagnetic energy confinement inside the nanoresonators that conform the metasurface can increase the emission of electric or magnetic quantum emitters located in the hot-spots [2]. In order to boost the *Q*-factor of the structure, the possibility of exciting quasi-bound states in the continuum (quasi-BIC) has been proposed [3].

BIC are dark modes, which cannot couple to the incident radiation or, equivalently, emit radiation, showing an infinite *Q*-factor. However, BIC resonances are just a mathematical concept, which cannot be attained experimentally. In fact, in experimental demonstrations, the BIC is converted in a leaky mode known as quasi-BIC. This mode is characterized by a narrow asymmetric Fano resonance (high *Q*-factor) [4]. Different kinds of BICs can be distinguished depending on the origin of radiation suppression. In metasurfaces, symmetry-protected BIC can be achieved due to the spatial symmetry of the mode not being compatible with the symmetry of the radiating waves. By breaking the symmetry of the metasurface, it is possible to open a radiation channel through which the radiation of the mode can be coupled to the incident radiation, giving rise to the quasi-BIC resonance [3].

In spite of the high *Q*-factor that can be achieved in all-dielectric metasurfaces, for certain applications, their utility is limited due to the band emission being fixed by the geometry of the design. To avoid this constraint, phase-change materials or liquid crystals can be used [5].

In this work, we analyze different phase change materials ($Ge_2Sb_2Te_5$ and Sb_2Se_3) to tune the emission of a quasi-BIC mode excited in the telecom band. In particular, we analyze a silicon metasurface composed of two

asymmetric nanobars. A thin layer of the considered phase-change material is placed on top of each resonator. Fig. 1a shows a scheme of the unit cell of the metasurface.

In the amorphous state, a quasi-BIC for both $Ge_2Sb_2Te_5$ and Sb_2Se_3 is observed. However, for the crystalline state, the quasi-BIC is only attained for Sb_2Se_3. This is due to the high losses of $Ge_2Sb_2Te_5$ in the crystalline state. Fig. 1b depicts a comparison of the transmission spectra of the Si metasurface combined with Sb_2Se_3 for the amorphous and crystalline states. A 58-nm spectral shift is attained. In addition, two important features are observed: for the crystalline state the amplitude and *Q*-factor of the quasi-BIC resonance decrease due to the absorption rise. However, it is still possible to observe moderately high *Q*-factors for the quasi-BIC resonance in the crystalline phase.

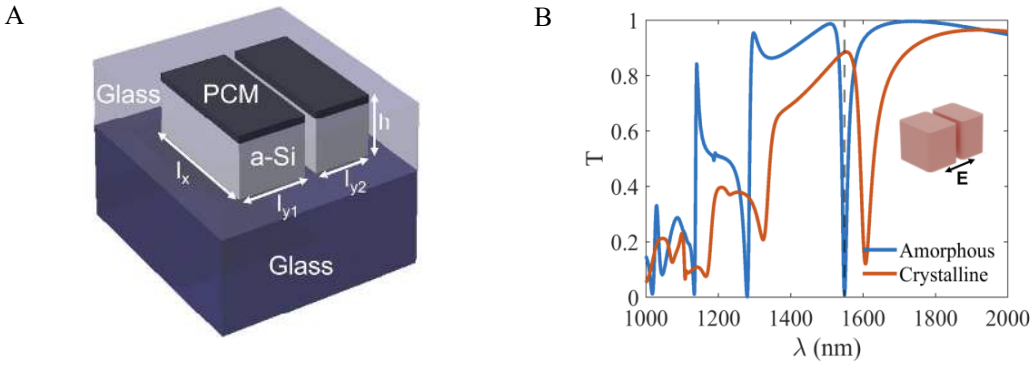


Figure 1. (A) Scheme of the unit cell of the asymmetric metasurface. (B) Trasmission spectra for the silicon metasurfaces combined with Sb_2Se_3. The inset indicates the polarization direction of the incident radiation with respect to the unit cell of the metasurface.

Acknowledgements

The authors thank the financial support of the German Research Foundation (DFG) under the framework of the International Research Training Group (IRTG) 2675 "META-ACTIVE".

References

1. García-Etxarri, A. *et al*., "Strong magnetic response of submicron Silicon particles in the infrared," Opt. Express, Vol. 19, 4815-4826, 2011.
2. Bakker, R. M., *et al*., "Magnetic and Electric Hotspots with Silicon Nanodimers," Nano Lett., Vol. 15, No. 3, 2137-2142, 2015.
3. Koshelev, K., Bogdanov, A. and Kivshar, Y., "Meta-optics and bound states in the continuum," Sci. Bull. Vol. 64, No. 12, 836–842, 2019.
4. Sadrieva, Z. F. *et al*., "Transition from optical bound states in the continuum to leaky resonances: Role of substrate and roughness," ACS Photonics, Vol. 4, No. 4, 723–727, 2017.
5. Barreda, A. *et al*., "Tuning and switching effects of quasi-BIC states combining phase change materials with all-dielectric metasurfaces," Opt. Mater. Express, Vol. 12, No. 8, 3132-3142, 2022.

META 2023, PARIS - FRANCE, JULY 18 – 21, 2023

Electroluminescent Metasurface Light Emitting Diodes (Invited)

Jon A. Schuller

Electrical and Computer Engineering Department, UC Santa Barbara, USA
corresponding author: jonschuller@ucsb.edu

Abstract: Recent demonstrations of metasurface mediated photoluminescence[1-10] highlight their potential for future device implementation. However, phased array electroluminescent metasurface devices have not previously been realized. Here, we demonstrate GaN-based quantum well LEDs where light is generated within an integrated metasurface architecture. In addition to demonstrating directional and focused electroluminescence, we describe how previous photoluminescent metasurfaces must be modified to incorporate device functionality, and show that metasurface LEDs can add new functionality without negatively impacting device brightness or efficiency.

This work was supported by the Office of Naval Research (Grant # N00014−22−1−2337).

References

1. Langguth, L., Schokker, A. H., Guo, K. & Koenderink, A. F. Plasmonic phase-gradient metasurface for spontaneous emission control. *Phys. Rev. B* **92**, 205401 (2015).
2. Yuan, S. *et al*. Strong photoluminescence enhancement in all-dielectric Fano metasurface with high quality factor. *ACS Nano* **11,** 10704−10711 (2017).
3. Capretti, A, Lesage, A. & Gregorkiewicz, T. Integrating quantum dots and dielectric Mie resonators: a hierarchical metamaterial inheriting the best of both. *ACS Photonics* **4**, 2187−2196 (2017).
4. S. Liu *et al*. Light-emitting metasurfaces: simultaneous control of spontaneous emission and far-field radiation. *Nano Lett.* **18**, 6906-6914 (2018).
5. Vaskin, A., Kolkowski, R., Koenderink, A. F., Staude, I. Light-emitting metasurfaces. *Nanophotonics* **8**, 1151–1198 (2019).
6. Bucher, T. *et al*. Tailoring photoluminescence from MoS2 monolayers by Mie-resonant metasurfaces. *ACS Photonics* **6**, 1002−1009 (2019).
7. Khaidarov, E. *et al*. Control of LED emission with functional dielectric metasurfaces. *Laser Photonics Rev*. **14**, 1900235 (2019).
8. Iyer, P.P. *et al*. Unidirectional luminescence from InGaN/GaN quantum-well metasurfaces. *Nat. Photonics* **14**, 543-548 (2020).
9. Mohtashami, Y. *et al.* Light-emitting metalenses and meta-axicons for focusing and beaming of spontaneous emission. *Nat Commun* **12**, 3591 (2021).
10. Heki, L. *et al.* Designing highly directional luminescent phased-array metasurfaces with reciprocity-based simulations. *ACS Omega* **7**, 22477–22483 (2022).

META 2023, PARIS - FRANCE, JULY 18 – 21, 2023

Amplifying nanophotonic lattices

A. Femius Koenderink

Department of Physics of Information in Matter & Center for Nanophotonics, AMOLF, Science Park 104, 1098XG The Netherlands

f.koenderink@amolf.nl

Abstract: Recent theory for scattering lattices with spatially distributed loss and gain point at the potential for topological and pseudochiral bandstructure physics. At the same time, these systems are quite different from true tight-binding systems, owing to long-range dipole dipole coupling, and diffraction channels. We study plasmonic realisations in a femtosecond pump probe set up that provides single-shot imaging, k-space mapping and photonic band structure mapping I will present experiments on diffractive and significantly sub-diffractive amplifying and lasing nanophotonic lattices.

Theory in context of PT-symmetry for plasmonic realizations of honeycomb, and Kagomé nanophotonic lattices with loss and gain that are spatially distributed point at the potential for topological and pseudochiral bandstructure physics in this system. At the same time, these systems are quite different from true tight-binding systems, such as coupled-waveguide realizations of topological bandstructires in photonics. This difference owes to long-range dipole dipole coupling, retardation effects, and the presence of radiation loss via diffraction channels. Motivated by these prospects, our group commissioned a set up for femto-second pump-probe studies on amplifying metasufaces, using white-light supercontinuum probe pulses in a high-NA microscope suited for simultaneously imaging real-space and k-space fluorescence, plasmon array lasing, as well as nonlinear reflectivity for samples that are, e.g., pumped into gain. Thereby we aim to reveal changes in metasurface bandstructure as function of optically pumped gain. While we ultimately aim to study lattices with spatially distributed loss and gain – for instance introduced by shaping the pump beam with a spatial light modulator –I will present results on homogeneously pumped lattices, which present diffractive plasmon array lasing behavior.

Plasmon antenna lattices enjoy a long history in the domain of fluorescence control, SERS, sensing and plasmon lasers, due to the combination of high Q and strong field enhancement that occur by virtue of diffractive resonances. While diffractive plasmon array lasers of various symmetries have been widely studied before, I will show that single-shot real-space and Fourier-space imaging gives a detailed view in hitherto unstudied physics in these systems, such as spontaneous symmetry breaking, and the singular polarization nature of lasing in K-point modes. To reach the regime of predicted topological and pseudochiral bandstructure physics it is necessary to move away from diffractive lattices, instead accessing subdiffractive periodicities, where strong near-field interactions between meta-atoms push the array bandstructure well beyond the light line. We will present an approach to access this band structure in optical experiments on basis of auxiliary periodicities in a supercell geometry to perturbatively cause band structure folding. This approach provides far-field access to guided modes, and we demonstrate lasing also in subdiffractive lattices. As an outlook we will discuss work from our group on how fluorescence and lasing in these systems could be harnessed for solid-state lighting, considering some of the challenges that integration of light emitting metasurfaces with practical devices present.

META 2023, PARIS - FRANCE, JULY 18 – 21, 2023

Topological exciton-polaritons in metasurfaces integrated with transition metal dichalcogenides

Ivan Sinev[1,2], Mengyao Li[3,4,5], Fedor Benimetskiy[6], Tatiana Ivanova[2], Svetlana Kiriushechkina[3], Anton Vakulenko[3], Sriram Guddala[3,4], Dmitry Krizhanovskii[6], A. Alu[3,5,7] Anton Samusev[8], Alexander Khanikaev[3,4,5]

[1]Institute of Bioengineering, École Polytechnique Fédérale de Lausanne (EPFL), Lausanne, Switzerland

[2]Department of Physics and Engineering, ITMO University, St. Petersburg, Russia

[3]Department of Electrical Engineering, City College of New York, New York, USA

[4]Physics Department, City College of New York, New York, USA

[5]Physics Program, Graduate Center of the City University of New York, New York, USA

[6]Department of Physics and Astronomy, University of Sheffield, Sheffield S3 7RH, UK

[7]Photonics Initiative, Advanced Science Research Center, City University of New York, New York, USA

[8]Experimentelle Physik II, Technical University of Dortmund, Dortmund, Germany
[*]corresponding author: ivan.sinev@epfl.ch

Abstract: In the last few years, polaritonic metasurfaces were established as a viable alternative to vertical cavities for realization of strong light-matter interaction regimes that in turn enable unique nonlinear and quantum phenomena. We explore topological exciton polaritons which are formed in a suitably engineered all-dielectric topological photonic metasurface coupled to transition metal dichalcogenide monolayers. We experimentally observe the transition of topological charge from photonic to polaritonic bands with the onset of strong coupling regime and demonstrate one-way spin-polarized edge topological polaritons.

One of the recently emerged research directions in the already mature field of topological photonics is aimed at expanding the developed concepts towards systems with strong light-matter interaction. This opens the possibilities for creation and control of exotic quasiparticles – topological polaritons. The first topolaritonic system characterized by a 2D topological invariant was demonstrated in GaAs quantum well lattices [1] for the case of broken time-reversal symmetry induced by magnetic field. Here, we realize topological polaritonic spin-Hall phase that does not require magnetic field in a topological metasurface based on planar Si photonic structure strongly coupled to excitons in transition metal dichalcogenides (TMD) monolayers. We experimentally demonstrate the transfer of topological charge from photonic to polaritonic mode, one-way propagation of the edge topological polaritons and conservation of valley polarization of the emission.

Our structure represents a Si photonic metasurface with a honeycomb shrink-expand lattice design [2,3] (Fig. 1a). We adjust it to support leaky topological edge modes near the exciton frequencies in $MoSe_2$ or WSe_2 (1.65 eV and 1.74 eV at 7K, respectively). To realize the transition to topological polariton regime, we transfer TMD monolayer on top of the metasurface together with thin hBN layers. We then measure the angle-resolved differential reflectivity spectra to reveal that the onset of strong coupling regime leads to the topological charge transfer from bulk photonic band to the newly formed upper polaritonic band (Fig. 1b). The change of the dispersion of the edge modes in strong coupling regime confirms their polaritonic nature.

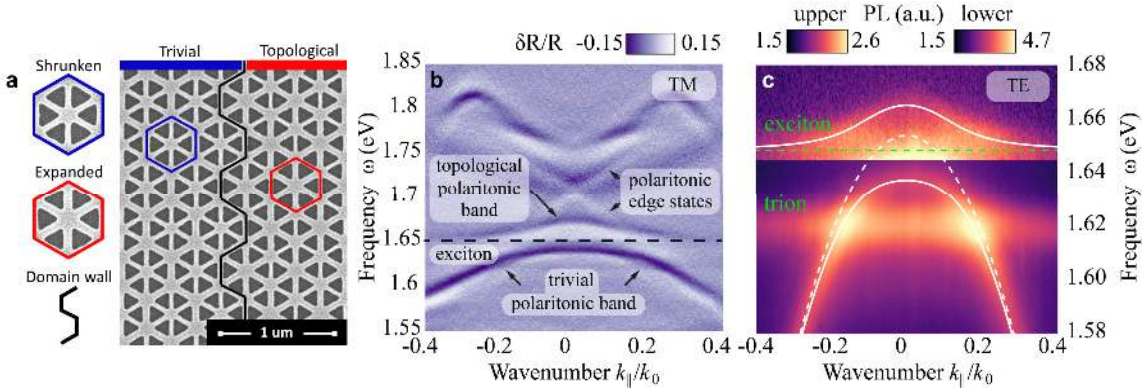


Fig. 1 (a) SEM image of the domain wall of the silicon topological metasurface based on the shrink-expand design. (b) Angle-resolved differential reflectivity measured from the domain wall of a metasurface coupled with a MoSe2 monolayer. (c) Angle-resolved PL spectra for TE polarization fitted with a coupled oscillator model.

We further extract the parameters of strong coupling regime from the angle-resolved photoluminescence spectra (Fig. 1c) and demonstrate one-way propagation of polaritonic topological edge modes for resonant excitation. Finally, we explore the possibilities of valley polarization transport with edge states for the sample coupled to a WSe_2 monolayer.

References

1. Klembt, S. Harder, T. H., Egorov, O. A., Winkler, K., Ge, R., Bandres, M. A., Emmerling, M., Worschech, L., Liew, T. C. H., Segev, M., Schneider, C. and Höfling, S. “Exciton-polariton topological insulator” Nature Vol. 562, 552–556, 2018.
2. Yang, Y., Xu, Y. F., Xu, T., Wang, H.-X., Jiang, J.-H., Hu, X., and Hang, Z. H. “Visualization of a unidirectional electromagnetic waveguide using topological photonic crystals made of dielectric materials” Phys. Rev. Lett. Vol. 120, 217401, 2018.
3. Liu, W., Hwang, M., Ji, Z., Wang, Y., Modi, G., Agarwal, R. “Z2 photonic topological insulators in the visible wavelength range for robust nanoscale photonics” Nano Lett., Vol. 20, No. 2, 1329-1335, 2020.

Nonlinear generation and detection of valleys in atomically thin semiconductors

P. Herrmann[1], S. Klimmer[1], T. Lettau[2], M. Monfared[2], I. Staude[1], I. Paradisanos[3], U. Peschel[2], G. Soavi[1*]

[1]Institute of Solid State Physics, Friedrich Schiller University Jena, Germany
[2]Institute of Condensed Matter Theory and Optics, Friedrich Schiller University Jena, Germany
[3]Institute of Electronic Structure and Laser, Foundation for Research and Technology, Crete, Greece
[*]corresponding author: giancarlo.soavi@uni-jena.de

Abstract: We show ultrafast and coherent write and read states for valleytronic operations in an atomically thin semiconductor. We assign the write state to the generation of a valley imbalance by coherent optical Stark shift induced by off-resonance below gap excitation. The read state is enabled by the sensitivity of second harmonic generation to changes in the material symmetry, triggered by the valley imbalance.

Light is the ideal candidate to realize devices operating with high speed and low consumption thanks to all-optical operations [1]. A promising approach in this direction is based on valleytronics using two-dimensional transition metal dichalcogenides (TMDs): TMD monolayers are direct gap semiconductors with two energetically degenerate but non-equivalent valleys in the K and K' points of the Brillouin zone. The valleys can be selectively excited (write) in an all-optical fashion, because light of opposite helicity couples to opposite valleys, while their detection (read) was so far mostly based on polarization-resolved photoluminescence (PL). However, this approach has two main drawbacks: (1) it detects an averaged light emission over a time-scale that is much longer compared to the valley and spin lifetimes; (2) it is intrinsically a destructive method, which measures the valley polarization (VP) only after light emission. Nonlinear optics [2], and in particular second harmonic generation (SHG), overcomes these disadvantages and provides an ultrafast and non-destructive method for the detection of the VP in TMDs. The presence of a VP breaks time-reversal symmetry and leads to new terms in the nonlinear optical susceptibility. In this seminar, I will discuss our recent results, where we simultaneously pump (write) and probe (read) the VP in WSe_2 with one single elliptically polarized ultra-short pulse. We probe the VP using polarization dependent SHG measurements at different values of the fundamental wavelength and find that resonant SHG at the *1s* exciton state is the most sensitive probe of the VP. In addition, we show that, in the case of below gap excitation, the VP is generated by ultrafast coherent optical Stark-shift, which is valley selective in TMDs [3]. Thus, this work provides direct evidence of ultrafast and all-optical coherent generation and detection of valleys in atomically thin semiconductors.

This work was funded by the Deutsche Forschungsgemeinschaft (DFG, German Research Foundation) through the Collaborative Research Center (CRC) 1375 "NOA" projects B5 (G.S.), B2 (I.S.) and A2 (U.P.), and the International Research Training Group (IRTG) 2675 "Meta-ACTIVE", project number 437527638, subproject A4 (G.S. and I.S.).

References

1. Klimmer, S., *et al.*, "All-optical polarization and amplitude modulation of second-harmonic generation in atomically thin semiconductors", Nat. Photon., Vol. 15, 837-842, 2021.
2. Dogadov, *et al.*, "Parametric Nonlinear Optics with Layered Materials and Related Heterostructures", Laser Photonics Rev., Vol. 16, 2100726, 2022.
3. Sie, E. J., *et al.*, "Large, valley-exclusive Bloch-Siegert shift in monolayer WS_2", Science, Vol. 355, 1066-1069, 2017.

META 2023, PARIS - FRANCE, JULY 18 – 21, 2023

Approaching the thin-film absorption limit with monolayer semiconductor superlattices

Sara A. Elrafei[1], Lennart M. Heijnen[1], Rasmus H. Godiksen [1], Alberto G. Curto[1,2,3*]

[1] Department of Applied Physics and Eindhoven Hendrik Casimir Institute, Eindhoven University of Technology, Eindhoven, The Netherlands

[2] Photonics Research Group, Ghent University-imec, Ghent, Belgium

[3] Center for Nano- and Biophotonics, Ghent University, Ghent, Belgium

[*]Corresponding author: Alberto.Curto@UGent.be

Abstract: Strongly absorbing materials are needed for nanoscale optoelectronics and strong light-matter coupling applications. The absorption limit of ultrathin films is 50%. The strong excitonic resonance in monolayer WS_2 provides 16% absorptance. Here we demonstrate that monolayer WS_2 superlattices provide higher absorption while preserving the exciton emission. We show that an artificial superlattice structure increases absorptance to 37%. Our results put forward superlattices as a platform for developing novel two-dimensional semiconductor devices.

Strong light absorption in ultrathin materials plays a vital role in variety of applications including light detection, waveguiding, and modulation. One relatively new class of strongly absorbing materials is that of atomically thin materials. Transition metal dichalcogenides (TMDs), such as tungsten disulfide (WS_2) and molybdenum diselenide ($MoSe_2$) possess unique optical properties. Bulk TMDs consist of weakly bound atomically thin layers and stable monolayers can be easily prepared through exfoliation. Compared to other growth methods such as chemical vapor deposition (CVD), exfoliation provides the highest exciton quality for the strongest absorption and narrowest linewidth.

Monolayer TMDs, despite being less than one nanometer thick, show an exceptionally strong absorption of light: absorption of sunlight up to 5-10% has been observed in TMDs monolayer, an order of magnitude larger than GaAs or Si of comparable thickness[1]. The strong interaction of light with TMDs monolayers has potential advantages in atomically thin devices. The combination of strong absorption and the ability to tune the excitonic resonances through doping enables their use in nanoscale optical elements such as atomically thin photodetectors[2], modulators[3], and lenses[4]. TMD monolayers can also be used to create atomically thin mirrors that are promising for a range of uses, including spatial light modulators, active metasurfaces, and active cavity control[5]. In addition, the high oscillator strengths and sharp resonances of excitons in these materials can enable reaching the regime of strong light-matter coupling and the manipulation of light via surface exciton-polaritons[6,7].

Here, we create WS_2 monolayer-based structures to approach the fundamental thin-film absorption limit of 50%. We demonstrate three simple methods to obtain stronger absorption than that of monolayer WS_2. Different superlattice structures of WS_2 monolayers result in an increased light absorption, while also preserving the exciton emission and quality. We characterize these structures using transmission and photoluminescence spectroscopy. Additionally, we employ hyperspectral imaging to gain insight into the spatial variations of exciton properties.

We start with simple structures containing two monolayers separated by a spacer to retain the optical properties of the individual monolayers. However, such structures prove to have coupling between layers that is difficult to control reliably and results in absorption reduction. Instead, we demonstrate the use of a molecular spacer to construct stable stacked bilayers. Finally, we fabricate higher-order superlattices with an increased number of layers using Al_2O_3 as a thin dielectric spacer to approach the thin-film absorption limit in a more scalable process.

Our work puts forward the potential of monolayer superlattices as a flexible platform for developing novel two-dimensional nanophotonic devices. As the superlattice fabrication process relies on simple methods, such superabsorbing materials are posed to have an impact on a variety of fields.

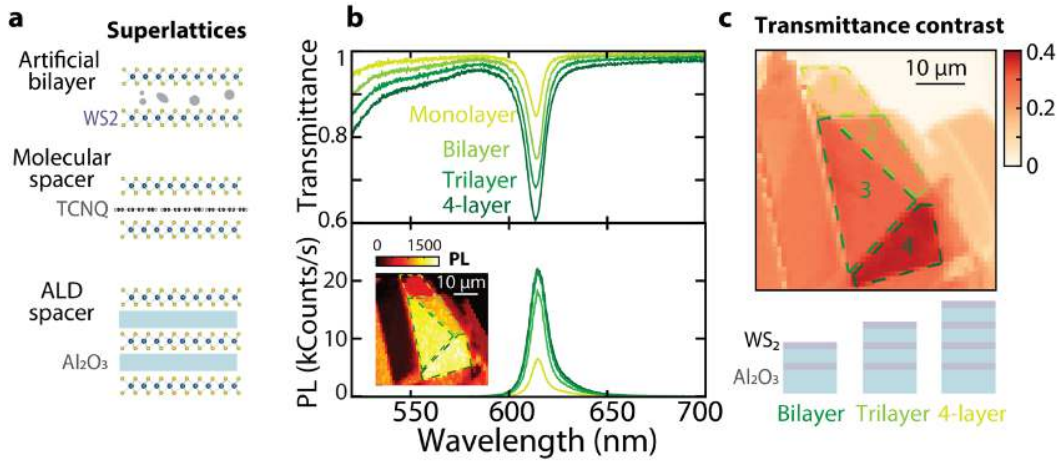


Figure 1 | Stacking of monolayers WS_2 (Superlattices) provides higher absorption with preserving the exciton emission. a, Artificial stacking of monolayers WS_2 with small spacer approaches the ultra-thin film absorption limit. b, Transmittance and PL spectra of superlattice with alternating layers of monolayer WS_2 and Al_2O_3 using atomic layer deposition. c, Hyperspectral imaging displaying the transmittance contrast at the A exciton peak of the different regions.

References

1. Bernardi, M., Palummo, M. & Grossman, J. C. Extraordinary sunlight absorption and one nanometer thick photovoltaics using two-dimensional monolayer materials. *Nano Lett.* **13**, 3664–3670 (2013).
2. Kang, D. H. *et al.* High-Performance Transition Metal Dichalcogenide Photodetectors Enhanced by Self-Assembled Monolayer Doping. *Adv. Funct. Mater.* **25**, 4219–4227 (2015).
3. Datta, I. *et al.* Low-loss composite photonic platform based on 2D semiconductor monolayers. *Nat. Photonics* **14**, 256–262 (2020).
4. van de Groep, J. *et al.* Exciton resonance tuning of an atomically thin lens. *Nat. Photonics* **14**, 426–430 (2020).
5. Back, P., Zeytinoglu, S., Ijaz, A., Kroner, M. & Imamoğlu, A. Realization of an Electrically Tunable Narrow-Bandwidth Atomically Thin Mirror Using Monolayer MoSe2. *Phys. Rev. Lett.* **120**, 1–5 (2018).
6. Hu, F. & Fei, Z. Recent Progress on Exciton Polaritons in Layered Transition-Metal Dichalcogenides. *Adv. Opt. Mater.* **8**, 1–16 (2020).
7. Wang, S. *et al.* Limits to Strong Coupling of Excitons in Multilayer WS 2 with Collective Plasmonic Resonances. *ACS Photonics* **6**, 286–293 (2019).

META 2023, PARIS - FRANCE, JULY 18 – 21, 2023

Capturing near-field circular dichroism enhancements from far-field measurements

Jorge Olmos-Trigo[1,2*], Jon Lasa-Alonso[1,2], Iker Gomez-Viloria[2], Gabriel Molina-Terriza[1,2,3] and Aitzol García-Etxarri[1,2]

[1]Donostia International Physics Center, Paseo Manuel de Lardizabal 4, 20018 Donostia-San Sebastian, Spain.
[2]Centro de Física de Materiales, Paseo Manuel de Lardizabal 5, 20018 Donostia-San Sebastian, Spain.
[3]IKERBASQUE, Basque Foundation for Science, María Díaz de Haro 3, 48013 Bilbao, Spain.

[*]corresponding author: jolmostrigo@gmail.com

Abstract: We present an exact multipolar expansion of f_{CD}, which can be used to deduce the integrated near-field CD enhancements of chiral molecules in the presence of scatterers under general illumination conditions. Our analytical findings reveal that the near-field f_{CD} factor is related to magnitudes that can be computed in the far-field, such as the scattering cross-section and the helicity expectation value. We demonstrate that in the case of lossless cylindrically symmetric samples, the near-field f_{CD} factor can be experimentally inferred from only two far-field measurements.

Molecular Circular dichroism (CD) spectroscopy faces significant limitations due to the inherent weakness of chiroptical light-matter interactions [1]. In this view, resonant optical antennas constitute a promising solution to this problem since they can be tuned to increase the CD enhancement factor, f_{CD}, a magnitude describing the electromagnetic near-field enhancement of scatterers [2] associated with a given helicity [3, 4] (Fig. 1).

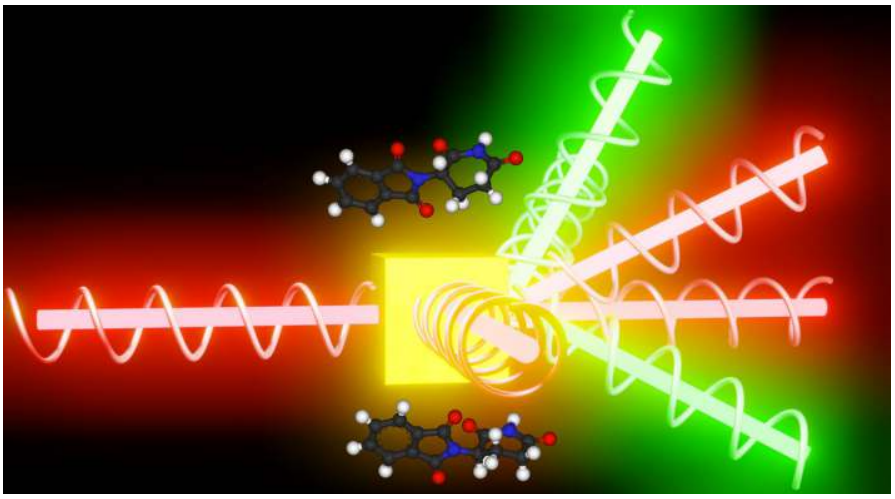


Fig. 1: Scattering process in which an incident field with well-defined helicity (red beam with σ = +1) impinges on an achiral antenna, represented by a glossy cube. Both R-and-S Thalidomide enantiomers are also depicted close to the achiral antenna.

However and in the context of CD enhancements, researchers rely exclusively on numerical methods to design enhanced chiral sensing devices as capturing the vector character of the near-field contribution can be challenging. In this work, we derive an exact multipolar expansion of f_{CD}, which is valid to deduce the integrated near-field CD enhancements of chiral molecules in the presence of scatterers of any size and shape under general illumination conditions [6]. From our analytical results, we show that f_{CD} is proportional to the scattering cross-section and the helicity expectation value, which are experimentally measurable magnitudes in the far-field. In addition to this, we also show that for lossless and cylindrically symmetric scatterers, it is possible to infer the f_{CD} factor only with two far-field measurements: the scattering cross-section and the helicity density at specific scattering angles. Our results pave the way for experimental verification and characterization of building blocks for CD enhancement from far-field measurements, and thus, may give rise to novel developments in the field of chiral light-matter interaction

References

1. Tang, Yiqiao, and Adam E. Cohen. “Optical chirality and its interaction with matter”, Physical Review Letters, PRL, Vol. 104, No. 16, 163901, 2010.

2. Aitzol García-Etxarri and Jennifer A. Dionne, “Surface-enhanced circular dichroism spectroscopy mediated by nonchiral nanoantennas”. Physical Review B, PRB, Vol 87, No 23, 235409, 2013.

3. Florian Graf, Joshua Feis, Xavier Garcia-Santiago, Martin Wegener, Carsten Rockstuhl, and Ivan Fernandez-Corbaton, “Achiral, Helicity Preserving, and Resonant Structures for Enhanced Sensing of Chiral Molecules”, ACS Photonics, Vol. 6, No. 2, 482-491, 2019.

4. Jon Lasa-Alonso, Diego Romero Abujetas, Álvaro Nodar, Jennifer A. Dionne, Juan José Sáenz, Gabriel Molina-Terriza, Javier Aizpurua, and Aitzol García-Etxarri, "Surface-enhanced circular dichroism spectroscopy on periodic dual nanostructures.", ACS Photonics, Vol 7, No 11, 2978-2986, 2020.

5. Jorge Olmos-Trigo, Jon Lasa-Alonso, Iker Gómez-Viloria, Gabriel Molina-Terriza, Aitzol García-Etxarri, “Capturing near-field circular dichroism enhancements from far-field measurements”. arXiv:2301.01248v1 2023.

META 2023, PARIS - FRANCE, JULY 18 – 21, 2023

Optical nanostructures for boosting fluorescence from magnetic dipolar transitions

A. Bashiri[1,2*], M. Rikers[1,2,5], A. Vaskin[2], K. Tanaka[1,2,4], A. Barreda[1,2], M. Steinert[2], DY. Choi[5], T. Pertsch[1,2,3,4], I. Staude[1,2,4]

[1]Friedrich Schiller University Jena, Institute of Solid-State Physics, Germany
[2]Friedrich Schiller University Jena, Institute of Applied Physics, Germany
[3]Fraunhofer-Institute of Applied Optics and Precision Engineering IOF, Germany
[4]Max Planck School of Photonics, Germany
[5]Australian National University, Australia
[*]corresponding author: Ayesheh.bashiri@uni-jena.de

Abstract: Trivalent lanthanides naturally offer strong magnetic dipole (MD) transition due to the selection rule forbidden electric dipole (ED) transition. This inspires the investigation of different nanophotonic platforms for efficiently modifying the magnetic nature of light. Here, we introduce high-index all-dielectric nanostructures including Mie-resonant silicon (Si) nanocylinder metasurfaces, broken symmetry titanium dioxide (TiO_2) metasurfaces supporting high Q-factor resonances, and an efficient fabrication process for deterministic coupling of the fluorophores to the hotspot of the Si dimers.

MD transitions in a quantum system are typically negligible at the optical frequency range since their transition rates are usually up to 5 orders of magnitude weaker than allowed ED transition rates. However, lanthanide ions, such as Eu^{3+}, exhibit MD transition with a comparable strength to ED transitions, which makes them a proper candidate for magnetic light-matter interaction studies. Eu^{3+} ions possess a strong MD transition at 590 nm ($^5D_0 \rightarrow {}^7F_1$) and several ED transitions including the most dominant one at 610 nm ($^5D_0 \rightarrow {}^7F_2$) [1].
High index all-dielectric nanostructures supporting multipolar electric and magnetic Mie-resonances are versatile platforms for both spectral and spatial tailoring of spontaneous emission from coupled emitters as they provide low absorption loss, high radiation efficiency, and substantial radiative decay rate enhancement [2]. A particularly interesting case are metasurfaces with a slightly broken in-plane symmetry that exhibit quasi-bound state in continuum (BIC) modes characterized by sharp, high quality (Q) factor resonances. Such a system can thus offer a strong fluorescence enhancement and emission directionality of the coupled emitters [3]. Efficiently enhancement of the emission from nanoscale emitters integrated with the photonic nanostructures requires a precise coupling of the emitters to the electromagnetic near-field hotspots of the nanostructure. Therefore, developing optimal methods of fabrication of fluorophore-embedded nanostructures that allow for the deterministic placement and immobilization of the emitters is particularly important. Here, we summarize our studies on three different platforms based on high index all-dielectric nanostructures for tailoring the MD transition of Eu^{3+} at 590 nm. In the first work [4], spontaneous emission enhancement of Eu^{3+} ions using Mie-resonant Si nanocylinder metasurfaces was experimentally demonstrated. Metasurfaces were fabricated featuring different nanocylinder radii, so that their strong quadrupolar Mie-resonances swept over the spectral range of Eu^{3+} electric and magnetic dipole transition bands. Then, they were covered by a thin layer of a $Eu(TTA)_3L18$ containing polymer and excited at λ = 325 nm. The emission was collected using a 0.4NA objective. Figure 1a shows the scanning electron micrograph (SEM) of the focused ion beam (FIB) cross section of the coated metasurface and Figure 1b demonstrates the systematic change of the enhancement ratio of emission via MD and ED transition channels as G_{590}/G_{610}, reaching the maximum of 1.12. This verifies that Mie-resonant all-dielectric metasurfaces allow for selective enhancement of the MD over ED emission for a proper choice of the metasurface

geometry. The next work was dedicated to design, fabrication, and characterization of Mie-resonant metasurfaces composed of broken symmetry TiO_2 nanoparticles, that support high Q-factor resonances at 590 nm, corresponding to the MD transition of Eu^{3+}. A top-view SEM image of the fabricated sample is shown in Figure 1c. The sample was spin-coated with a resist film (PMMA) containing $Eu(TTA)_3$. The fluorescence properties and emission directionality of the coated sample were characterized by fluorescence spectroscopy and back focal plane (BFP) imaging, respectively. Using a 0.1NA collective objective in fluorescence spectroscopy, as illustrated in Figure 1d, a brightness enhancement of up to 15.5 for the MD transition and an enhancement ratio of $G_{590}/G_{610} = 8.7$ were achieved. Also, Figure 1e show the measured BFP images using a 0.6NA objective. The results illustrate that the designed broken symmetry metasurface allows for the strong fluorescence enhancement for near-zero polar angles as well as selective routing of the MD transition of the coupled Eu^{3+} ions. In the last work, deterministic fabrication of Eu^{3+} embedded nanostructures with the minimal number of steps, for localizing the MD emitters in the hotspot of a Si dimer was represented. The sample was spin-coated with the mixture of an electron beam resist (ma-N2401) with $Eu(TTA)_3$ with a final thickness of ~80 nm. Then, the film was exposed using electron beam lithography (EBL) and developed. The SEM image of the fabricated hybrid system is shown in Figure 1f. This fabrication process allows for the precise control over the shape and size of the resulting fluorescent structures with a resolution of ~100 nm. Figure 1g shows that the fluorescence from Eu^{3+} embedded in resist is robust for the exposure doses up to 500 $\mu C.cm^{-2}$. In conclusion, our results offer novel possibilities toward spectrally and spatially tailoring the MD-dominated spontaneous emission, thus allowing to exploit magnetic component of light which is essential for applications such as chiral sensing [5].

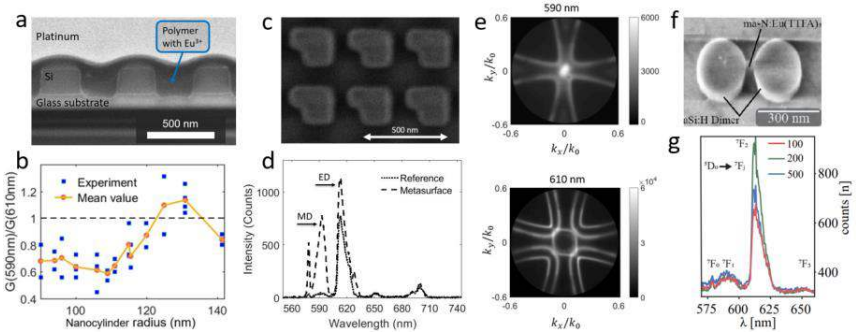


Figure 1. (a) SEM image of the FIB cross section of the coated metasurface. (b) Emission enhancement ratio G_{590}/G_{610} as a function of the nanocylinder radius. (a) and (b) Reproduced with permission [4]. Copyright 2019, American Chemical Society. (c) A top-view SEM image of fabricated broken symmetry TiO_2 metasurface. (d) and (e) the fluorescence spectra and measured BFP images of the Eu^{3+} doped PMMA coated metasurface shown in (c), respectively. (f) SEM image of the fabricated hybrid system of the Eu^{3+}- resist and Si dimers. (e) The fluorescence spectra of the Eu^{3+}- resist after exposure with a dose of 100, 200, and 500 $\mu C.cm^{-2}$.

References

1. Taminiau, T. H. et al.,"Quantifying the magnetic nature of light emission" Nat. Commun,Vol. 3, No. 1, 10.1038, 2012.
2. Staude, I. et al., "Metamaterial-inspired silicon nanophotonics," Nat. Photonics, Vol. 11, No. 5, 10.1038, 2017.
3. Liu, S. et al., "Light-Emitting Metasurfaces: Simultaneous Control of Spontaneous Emission and Far-Field Radiation" Nano Lett., Vol. 18, No. 11, 10.1021, 2018.
4. Vaskin, A. et al., "Manipulation of Magnetic Dipole Emission from Eu^{3+} with Mie-Resonant Dielectric Metasurfaces," Nano Lett., Vol. 19, No. 2, 10.1021, 2019.
5. Ho, C.-S. et al., "Enhancing Enantioselective Absorption Using Dielectric Nanospheres," Nano Lett., Vol. 4, No. 2, 10.1021, 2017.

META 2023, PARIS - FRANCE, JULY 18 – 21, 2023

Engineering spatial dispersion in metasurfaces through materials dispersion

S. Boroviks, A. Kiselev, Ch. Santschi, K. Achouri, and O.J.F. Martin*

Nanophotonics and Metrology Laboratory, Swiss Federal Institute of Technology Lausanne (EPFL), Switzerland
*corresponding author: olivier.martin@epfl.ch

Abstract: Although metasurfaces are intrinsically planar objects, geometrical variations in the third – out-of-plane – direction are becoming instrumental to engineer exotic optical responses. Unfortunately, such complex three-dimensional meta-atoms are extremely difficult to fabricate at the nanoscale. Here, we demonstrate that similar optical responses are amenable to simple geometries that include different materials, thus paving the way for a new class of hybrid metasurfaces.

Metasurfaces have appeared very naturally as the field of metamaterials strived to evolve toward the visible part of the spectrum and technology challenges emerged. Whilst it is possible to fabricate intricate three-dimensional (3D) meta-atoms that operate at microwave frequencies,[1] this becomes extremely difficult at optical frequencies, where their dimensions should be in the order of 100s of nanometers. The reason being that 3D nanofabrication is still in its infancy and it is very hard to control nanostructures' shapes in all three directions, especially throughout the depth of a material.[2] Fortunately, planar technologies are very well developed, and it is possible to manufacture a broad variety of nanostructures with different lateral shapes and materials on a two-dimensional (2D) substrate, to fabricate a metasurface.[3]

Although metasurfaces are in principle flat and 2D, it is emerging now that variations outside of their 2D plane can enable specific phenomena at optical wavelengths. This is the case for example to achieve arbitrary beam-steering with maximum efficiency,[4] to enable the excitation of multipolar resonances to better control scattering properties,[5] or even to produce exotic effects such as asymmetric responses in the linear or nonlinear regimes.[6] This novel development toward 3D meta-atoms is quite challenging from a technological point of view, especially when geometrical variations are required in the out-of-plane direction, as illustrated in Fig. 1(a).

In this presentation, we will demonstrate that a similar optical response can be achieved from heterogeneous nanostructures with a more regular shape, but composed of different materials, Fig. 1(b).

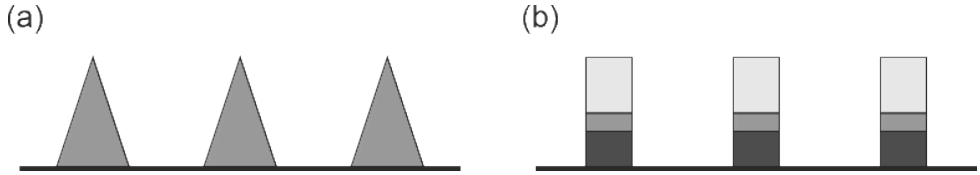


Figure 1: (a) 3D homogeneous meta-atoms made from a single material with geometrical variations in the out-of-plane direction can be replaced with (b) simpler geometries that incorporate different materials and are much easier to fabricate at the nanoscale.

A similar response between these two very different meta-atoms can be obtained by controlling the various multipolar contributions that arise in both systems. For example, among the two materials families used in nanophotonics, the fundamental mode for metal nanostructures is electric, while that for dielectric nanostructures

is magnetic and heterogeneous meta-atoms that mix both materials have a very rich electromagnetic response.[7] Two such metasurfaces built from heterogeneous meta-atoms are illustrated in Fig. 2: a combination of dielectric and plasmonic materials produces extremely narrow spectral features that can be used for sensing, Fig. 2(a).[8] A combination of two different plasmonic metals exhibits an asymmetric nonlinear response that depends on the illumination direction, akin to an optical diode.[6] These exotic optical responses originate from the spatial dispersion in the out-of-plane direction of the metasurfaces, which – in this case – does not occur through complicated geometrical variations as in Fig. 1(a), but through a mere combination of different materials.

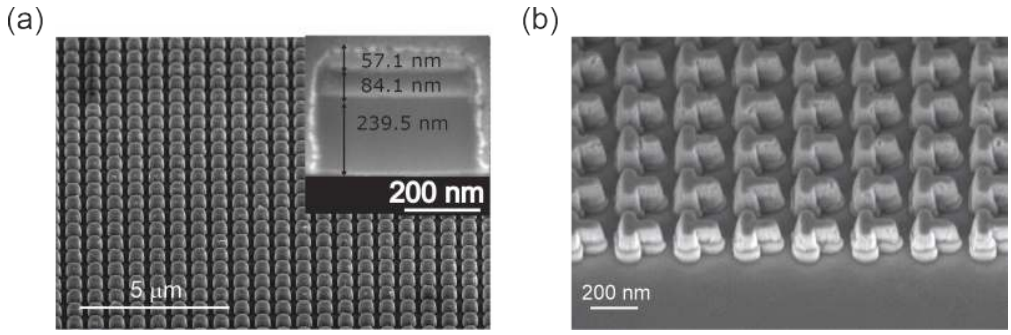


Figure 2: Two examples of metasurfaces built with heterogeneous meta-atoms that achieve similar functionalities as homogeneous nanostructures with a more complicated geometry: (a) cylindrical meta-atoms built from Si, SiO_2 and Al; (b) T-shaped meta-atoms built from Al, SiO_2 and Ag.

References

1. P. Gay-Balmaz and O.J.F. Martin, "Efficient isotropic magnetic resonators," Appl. Phys. Lett., Vol. 81, 939-941 (2002).
2. H. Zhao, *et al.*, "Nanofabrication approaches for functional three-dimensional architectures," Nano Today, Vol. 30, 100825 (2020).
3. B. Abasahl, Ch. Santschi, T.V. Raziman and O.J.F. Martin, "Fabrication of plasmonic structures with well-controlled nanometric features: a comparison between lift-off and ion beam etching," Nanotechnology, Vol. 32, 475202 (2021).
4. K. Achouri and C. Caloz, Electromagnetic metasurfaces: Theory and applications (Wiley-IEEE Press: Hoboken, NJ, 2021).
5. K. Achouri, V. Tiukuvaara and O.J.F. Martin, "Spatial symmetries in multipolar metasurfaces: From asymmetric angular transmittance to multipolar extrinsic chirality," arXiv:2208.12504 (2022).
6. S. Boroviks, A. Kiselev, K. Achouri and O.J.F. Martin, "Demonstration of a plasmonic nonlinear pseudo-diode," arXiv:2302.03409 (2023).
7. D. Ray, A. Kiselev and O.J.F. Martin, "Multipolar scattering analysis of hybrid metal-dielectric nanostructures," Opt. Express, Vol. 29, 24056-24067 (2021).
8. D. Ray, T.V. Raziman, Ch. Santschi, D. Etezadi, H. Altug and O.J.F. Martin, "Hybrid metal-dielectric metasurfaces for refractive index sensing," Nano Lett., Vol. 20, 8752-8759 (2020).

META 2023, PARIS - FRANCE, JULY 18 – 21, 2023

Exploiting light-matter interactions to realize selective artificial photosynthesis

Z. Fusco[1], C. David[2], F. J. Beck[1]

[1]School of Engineering, College of Engineering and Computer Science, Australian National University, Acton, ACT 2601, Australia

[2]Institute of Condensed Matter Theory and Optics, Abbe Center of Photonics, Friedrich Schiller University of Jena, Max-Wien-Platz 1, 7743 Jena, Germany

*corresponding author: fiona.beck@anu.edu.edu

Abstract: Artificial photosynthesis of carbon dioxide, using water as the reducing agent and sunlight to drive the reaction, has the potential to provide renewable fuels at scale. Key challenges in the field are realizing product selectivity and enhancing yields. Our work aims to exploit the strong, confined near fields and hot carriers generated at specific energies by suitably designed plasmonic nanostructures to control chemical reaction pathways. We focus on understanding underlying mechanisms and developing scalable plasmonic substrates with suitable resonances.

Photocatalytic processes mediated by strong, tunable, plasmonic resonances have the potential to provide optical control of chemical reactions. It is well known that plasmonic resonances can be induced and sensitively controlled by modifying the geometry of sub-wavelength metal nanostructures, as well as their composition and the optical properties of their surroundings. Molecules can couple with these resonant optical modes, through either electron or photon transfer (fig 1a), driving reactions and activating bonds to initiate particular reaction pathways.

The mechanism of plasmonically-mediated reactions has been the subject of lively debate in the field. Our work employs a practical approach to exploring the underlying mechanisms of plasmonic control of reactions, and distinguishing between thermal and optical driven chemistry[1]. We focus on a model system comprised of methylene blue (MB) adsorbed on random arrays of gold nanoparticles. Methylene-blue can undergo a transformation to thionine which can be monitored *in-situ* using surface enhanced Raman spectroscopy (SERS) (fig 1b). By varying the average size of the nanoparticles in the disordered arrays, the wavelength of the excitation of plasmonic resonances, and the incident power, we are able to explore the dependence of the reaction yield on the excited plasmonic resonances. We couple these experiments with rigorous theoretical analysis of the photothermal induced temperature increase, the induced near-fields, and the generation of hot-electrons in the plasmonic array. In doing so, we can infer that the reaction is primarily driven by enhanced optical near-fields and transfer of hot-carriers. This is an important result, as it suggests that such reactions can be optically controlled.

Practical application of artificial photosynthesis will require scalable, stable photocatalysts in continuous flow reactors[2]. To progress towards this goal, we demonstrate plasmonic photocatalysts based on complex 3D metallic nanostructures electrodeposited over centimeter scales on commercial electrode materials[3]. The resulting substrates are coated in dense arrays of hierarchical, gold dendrites. Using cathodoluminescence (CL) measurements, we map the plasmonic 'hot-spots' excited on these substrates, revealing the spatial and spectral distribution of the plasmonic resonances excited on such structures (fig 1c). We are able to qualitatively reproduce the variety of CL spectra observed experimentally by simulating simplified conical and triangular geometries using boundary element method (BEM) (implemented in the freely available MNPBEM toolbox). By doing so we were able to conclude that 1) the optical properties of the hot-spots are determined by the local

geometry, rather than the overall interconnected sample morphology; and 2) there is a clear correlation between the tip shape and the spectral and spatial distribution of the plasmonic resonances and corresponding hot-spots. These insights offer the potential to design scalable plasmonic substrates, engineered to selectively drive chemical reactions.

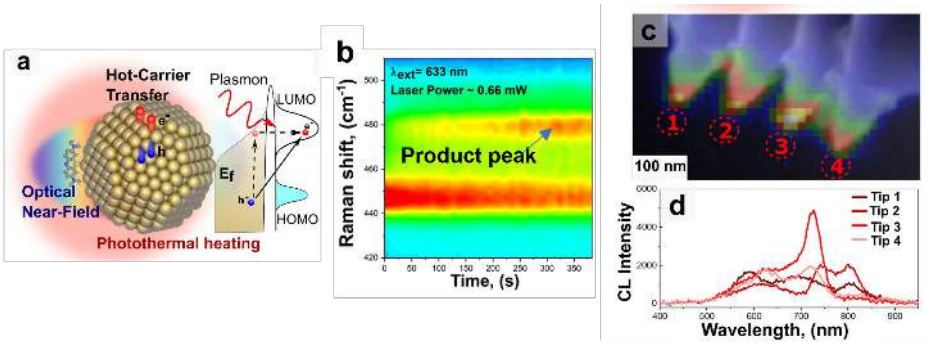


Figure 1. a) Illustration of possible mechanisms for transferring energy from plasmonic resonances to adsorbates. b) Time evolution of SERS spectra. c) Cathodoluminescence mapping of plasmonic resonances on gold dendritic structures

The insights from the studies discussed above are combined to progress towards practical plasmonic catalytic substrates for selective, solar-driven, renewable fuel production. The conversion of carbon dioxide to valuable hydrocarbons is a complex, multistep process requiring multiple electron and proton transfers which can proceed through several different radical intermediates[4]. The existence of multiple, branching, and co-existing reaction pathways can lead to a variety of different produce – some much more valuable than others. Selectively producing desired products is an ongoing challenge. Our ongoing work focuses on harnessing the strong, confined, optical near fields and energetic hot carriers generated by the dendritic structures to drive gas-phase CO_2 photoreduction. Preliminary results have demonstrated 57% selectivity for desirable double-carbon bond (C_2) hydrocarbons under 1-sun illumination.

Acknowledgments: *The authors acknowledge the financial support by the Australian Research Council, through the Discovery Early Career Researcher Award DE180100383 awarded to FJ Beck and the International Research Training Group IRTG 2675: META-ACTIVE.*

References

1. Fusco, Z., K. Catchpole, and F.J. Beck, *Investigation of the mechanisms of plasmon-mediated photocatalysis: synergistic contribution of near-field and charge transfer effects.* Journal of Materials Chemistry C, 2022.
2. Cortés, E., et al., *Challenges in Plasmonic Catalysis.* ACS Nano, 2020. **14**(12): p. 16202-16219.
3. Fusco, Z., et al., *Cathodoluminescence Spectroscopy of Complex Dendritic Au Architectures for Application in Plasmon‐Mediated Photocatalysis and as SERS Substrates.* Advanced Materials Interfaces, 2022: p. 2202236.
4. Habisreutinger, S.N., L. Schmidt-Mende, and J.K. Stolarczyk, *Photocatalytic Reduction of CO2 on TiO2 and Other Semiconductors.* Angewandte Chemie-International Edition, 2013. **52**(29): p. 7372-7408.

Multifunctional Optical Surfaces with Ultrathin Materials and Nano-structuring

J. Arrés Chillón[1,*], D. Martinez-Cercos[1], C. Graham[1], A. Mezzadrelli[1], I. Karadzhov[1], W. Senaratne[2], R. Bellman[2], D. Thelen[2], P. Mazumder[2] and V. Pruneri[1,3].

[1]ICFO-Institut de Ciencies Fotoniques, The Barcelona Institute of Science and Technology, 08860, Barcelona, Spain.
[2]Corning Research and Development Corporation, Sullivan Park, Corning, New York 14831, United States.
[3]ICREA-Institució Catalana de Recerca i Estudis Avançats, Passeig Lluís Companys, 23, 08010 Barcelona, Spain.
*corresponding author: javierarres@icfo.eu

Abstract: A wide range of optical and optoelectronic applications requires surfaces with specific properties, such as optical and electrical tunability, self-cleaning and cooling, antimicrobial properties, etc. In this talk, we will review recent efforts from our group in developing optical surfaces with unique properties based on ultrathin materials and nano-structuring. In particular, we will describe the use of ultrathin metals films (UTMF), dewetted nano-particles (DNPs), scalable nano-patterning for transparent electrodes, transparent antimicrobial glass for display applications, optical windows and infrared sensing.

UTMFs are emerging as game-changing optoelectronic materials for many applications in transparent electronics and plasmonic meta-surfaces. For practical use of UTMFs, transparent dielectric substrates and large-scale fabrication are desirable which require physical vapor deposition (PVD) techniques. However, if no measures are taken, metal PVD onto dielectric substrates typically results in an island like structure at the initial stage, and only show long-range connectivity (percolation) at mass equivalent thicknesses ≥5 nm. We show that by using a fully transparent seed layer of copper oxide (CuO) for subsequent Ag and Au UTMF growth, percolation is achieved at thicknesses close to 1nm. We will then explore possible optoelectronic applications, such as infra-red reflector or plasmonic resonant structures. In these, the UTMF's properties are continuously tuned and reconfigured by surface electrolyte electrical gating, which is only possible due to their small thickness. The results demonstrate the potential applications of UTMFs in reconfigurable and tunable devices such as smart-windows and plasmonic bio-sensing.

Scalable DNPs (i.e. large area fabrication of randomly distributed nano-particles on a surface) are of great interest for industrial applications. As example, metal DNPs can be used as a mask to pattern glass surfaces (SiO_2) via reactive ion etching (RIE), allowing the fabrication of large area nanopillars and nanoholes, which has shown unpreceded optical properties such as anti-reflection and increased transparency, as well as self-cleaning properties. Moreover, when large nanopillars are fabricated, surface phonon polaritons (SPhP) on glass can be excited i.e. increase the optical emissivity in the infrared (IR) , allowing the use of these surfaces for passive radiative cooling (PRC). We also exploit the antimicrobial properties of surfaces starting from copper (Cu) UTMFs by demonstrating their effectiveness to kill viruses and bacteria.

Enhanced light-matter interaction in a hollow nanocuboid metasurface supporting delocalised quasi-BIC modes

J.F. Algorri[1,2,3*], P. Roldán-Varona[1,2,3], L. Rodríguez-Cobo[2], J.M. López-Higuera[1,2,3], and D. C. Zografopoulos[4]

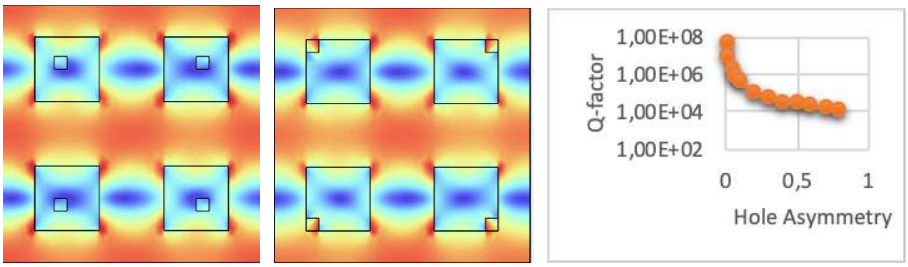
[1]Photonics Engineering Group, Universidad de Cantabria, 39005, Santander, Spain
[2]CIBER-bbn, Instituto de Salud Carlos III, 28029, Madrid, Spain
[3]Instituto de Investigación Sanitaria Valdecilla (IDIVAL), 39011, Santander, Spain
[4]Consiglio Nazionale delle Ricerche, Istituto per la Microelettronica e Microsistemi, 00133 Rome

[*]algorrijf@unican.es

Abstract: The two main problems of dielectric metasurfaces for sensing based on enhanced light-matter interaction are that resonances are mainly localised inside the resonator volume and experimental Q-factors are very limited. We investigate a dielectric metasurface supporting delocalised modes based on quasi-bound states in the continuum (qBICs) to address these issues. The metasurface comprises a periodic array of silicon hollow nanocuboids patterned on a glass substrate. The resonance stems from the excitation of a symmetry-protected qBIC mode, accessed by perturbing the arrangement of the nanocuboid holes. Thanks to the variation of the unit cell with a cluster of 4 hollow nanocuboids, delocalised modes with ultra-high Q-factor are produced.

Bound States in the Continuum (BICs) are a unique class of optical modes localised within a photonic structure and immune to radiative losses [1]. Metasurfaces, which are two-dimensional arrays of subwavelength scatterers, have emerged as a promising platform for engineering BICs. In these structures, symmetry-protected BICs are eigenmodes situated above the light cone, possessing different symmetries than the incoming wave, rendering them unexcitable within the continuum of radiation modes. By introducing some kind of perturbation, pure BICs transform into quasi-BICs with a finite lifetime, narrow linewidth and arbitrarily high radiative Q-factor. Indeed, quasi-BICs have been intensely investigated in dielectric metasurfaces with symmetry breaking, such as by introducing geometrical asymmetry or using anisotropic materials [2]. Although in most cases the resonant near fields are mainly confined to the interior of the high-index subwavelength scatterers, thus providing limited light-matter interaction with the surrounding material, it is still feasible to achieve interaction at the interface, allowing for biosensing and integration with 2D materials [3], as well as in slotted regions [4]. Furthermore, it has been recently reported that asymmetric dielectric particles arranged in clusters can be used to achieve greater flexibility in obtaining the desired near-field configuration [5] and enhancing the sensing capabilities for refractometry [6]. The operation principle in the latter case is based on plasmon-like surface waves, which are delocalised over a wide area to provide a large interaction volume with the matter but are excited in an all-dielectric structure.

In this work, we investigate a dielectric metasurface supporting delocalised quasi-BIC modes. The metasurface comprises a periodic array of hollow nanocuboids patterned on a glass substrate and designed to produce ultra-high Q-factor delocalised resonances. The authors previously demonstrated this structure for toroidal responses [7-9], but now, the cluster arrangement has advanced features. The device in Figure 1 consists of a periodic array of silicon hollow nanocuboids patterned on glass (silica). As observed, the electrical field is mainly located outside the resonator volume at the telecommunication wavelength of 1.55 μm.



(a) (b) (c)

Figure 1. qBIC mode electrical profile for two different hole asymmetries (a) 20% and (b) 80% (it has to be taken into account that the hole is 20% of the total cuboid width). (c) Q factor as a function of the hole asymmetry.

The proposed hole symmetry-breaking mechanism has several advantages: normal coupling, polarisation independency, ultra-high radiative Q-factor (minimum 10^4) and delocalised field confinement. Furthermore, this kind of metasurface paves the way for different applications in which light-matter interaction is critical, e.g. refractometric sensing and spectroscopy.

Funding

J. F.A. received funding from Ministerio de Ciencia, Innovación y Universidades of Spain under Juan de la Cierva-Incorporación grant and he also acknowledges the support of the project (PID2019-107270RB-C21/AEI/10.13039/501100011033) funded by Agencia Estatal de Investigación. D.C.Z. acknowledges the support of the CNR-FAPESP biennial (2022–2023) bilateral project StReAM “Strongly Resonant All-dielectric Metasurfaces based on quasi-dark and toroidal modes”.

References

1. C. Hsu, B. Zhen, A. Stone et al. Bound states in the continuum. Nat Rev Mater 1, 16048,2016.
2. N. Bernhardt et al., Quasi-BIC Resonant Enhancement of Second-Harmonic Generation in WS2 Monolayers, Nano Lett. 20, 5309–5314, 2020.
3. J. Gomis-Bresco et al. Anisotropy-induced photonic bound states in the continuum. Nature Photon 11, 232–236, 2017.
4. J. F. Algorri, F. Dell’Olio, P. Roldán-Varona, L. Rodríguez- Cobo, J. M. López-Higuera, J. M. Sánchez-Pena and D. C. Zografopoulos, Opt. Express 29, 10374, 2021.
5. A. S. Kupriiannov, K. L. Domina, V. V. Khardikov, A. B. Evlyukhin, and V. R. Tuz, "Homogeneous enhancement of near-fields in all-dielectric metasurfaces with cluster-based unit cells," Opt. Lett. 45, 1527-1530, 2020.
6. D. C. Zografopoulos and V. Dmitriev, Quasi-Dark Resonances in Silicon Metasurface for Refractometric Sensing and Tunable Notch Filtering, J. Lightwave Technol. 39, 6985–6993, 2021.
7. J. F. Algorri, D.C. Zografopoulos, A. Ferraro, B. García-Camara, R. Beccherelli, J.M. Sanchez-Pena, Ultrahigh-Quality Factor Resonant Dielectric Metasurfaces Based on Hollow Nanocuboids. Opt. Express 27 (5), 6320 2019.
8. J. F. Algorri, D. C. Zografopoulos, A. Ferraro, B. García-Camara, R. Vergaz, R. Beccherelli, J. M. Sanchez-Pena, Anapole Modes in Hollow Nanocuboid Dielectric Metasurfaces for Refractometric Sensing. Nanomaterials, 9 (1), 1−13, 2019.
9. J.Jeong et al. High Quality Factor Toroidal Resonances in Dielectric Metasurfaces, ACS Photonics 7 (7), 1699-1707 2020.

META 2023, PARIS - FRANCE, JULY 18 – 21, 2023

Structure dependent photoluminescence of colloidal PbS quantum dots in low refractive index dielectric 3D infrared metamaterials

Angelos Xomalis [1], Lorenzo J. A. Ferraresi [2,3], Oriol P. de G. Busquests [1], Krzysztof Maćkosz [1], Dmitry N. Dirin [2], Ivo Utke [1], Johann Michler [1], Maksym V. Kovalenko [2,4], Jakob Schwiedrzik [1], and Ivan Shorubalko [3]

[1] Laboratory for Mechanics of Materials and Nanostructures, Empa, Swiss Federal Laboratories for Materials Science and Technology, Thun, Switzerland

[2] Institute of Inorganic Chemistry, Department of Chemistry and Applied Biosciences, ETH Zürich, Zürich, Switzerland

[3] Laboratory for Transport at Nanoscale Interfaces, Empa, Swiss Federal Laboratories for Materials Science and Technology, Dübendorf, Switzerland

[4] Laboratory for Thin Films and Photovoltaics, Empa, Swiss Federal Laboratories for Materials Science and Technology, Dübendorf, Switzerland

Angelos.Xomalis@empa.ch

Abstract: Colloidal quantum dots (QDs) have been extensively used for their size dependent optoelectronic properties resulting in broadband detection of electromagnetic radiation. Conventionally photoluminescence (PL) enhancement requires plasmonic structures or high refractive index dielectric metamaterials. We report on a 1600% structure dependent PL enhancement with the aid of low refractive index ZnO coated laser-printable 3D infrared (IR) metamaterials. The metamaterial structure is used to enhance interaction between light and PbS QDs. Our findings shed light on conformal QD coating over complex surfaces of 3D structures, and open new avenues in the use of QDs for optoelectronic and nanophotonic applications.

I. INTRODUCTION

Quantum dots (QDs) find extensive applications in optoelectronic devices. Detection of electromagnetic radiation for example, particularly in near-infrared (NIR) and shortwave-IR, has relevant potential, for example thanks to the biological window between 700-1400nm, where tissues show reduced absorption offering the opportunity for noninvasive monitoring [1]. For the realization of such wearable and miniaturized devices, there are several limitations currently. First, QDs-based devices mainly concern coating of flat surfaces however, curved and bendable substrates for such applications is a critical need. Further, small fingerprint optoelectronic devices are ideal for not invasive and cost-effective applications, and processing issue point to the reduction of layers' thicknesses. Reducing the overall size of such architectures leads to reduced light interaction with the 'active' medium of the device, minimizing the detected signals.

In this work, we show how conformal QDs coating of 3D structures is possible overcoming geometrical restrictions and how miniaturizing the active-photonic area leads to higher photoluminescence (PL) signal compared to normal QDs films due to optical resonances of laser-printable structures. Our recent results open up new directions for designing optoelectronic devices beyond 2D geometries as well as a broader range for materials selection necessary for applications ranging from energy harvesting and light emission to photocatalysis and biosensing [2-3].

II. STRUCTURE FABRICATION, ZNO COATING AND QDS DEPOSITION

For the fabrication of 3D metamaterials, we use direct laser writing (DLW) and specifically multi-photon polymerization allowing fabrication of features with resolution as high as 100nm. Here we use a conventional nanoprinter (Nanoscribe Photonic Professional GT) with Ti:Sapphire femtosecond laser at a center wavelength of780 nm, 25 kW peak power, 100 fs

pulse duration, and 80 MHz repetition rate. For achieving high-resolution features, we use a 63x (1.4NA) oil-immersion objective and IP-Dip photoresist (Nanoscribe) in dip-in laser lithography mode on standard Si wafer (Fig. 1a). For achieving optical resonances at wavelength of interest, we use a standard woodpile-like geometry with periodicities of 1.0, 1.1 and 1.2μm and overall size of 70x70μm^2. The structures periodicity chosen carefully to provide an optical resonance within the excitonic peak of the QDs.

Polymeric structures have relative low refractive index (~1.4), thus challenging to facilitate optical resonances. To increase the refractive index, 80nm of ZnO (~1.7) is deposited in a custom-built atomic layer deposition (ALD) system using diethyl zinc (DEZ) precursor and water (H_2O) co-reactant. The optimal deposition temperature for the ZnO created by DEZ/H_2O is still ambiguous compared to other precursor recipes. The temperature chosen was 50°C for the reactor walls and the sample, and room temperature for the reservoir. Such lowering of the temperature is possible thanks to the high reactivity of DEZ. Moreover, the deposition parameters were 0.1s for precursor pulse, 1s for exposure and 90s for the purge in both cases (DEZ and H_2O). The precursor pulse and the purge were executed with 15sccm and 100sccm argon flows, respectively. Using transmission electronic microscope (TEM), we determine the thickness of the ZnO layer (80nm) and calculate the growth per cycle (GPC) of about 0.12 Å/cycle allowing coating with extreme sub-nm resolution (Fig. 1b).

PbS QDs have been synthesised following the method from Hines et al. [4] with slight modification, obtaining a final dispersion of 5nm particles absorbing at 1380nm, capped with oleic acid ligands in octane at a concentration of 40mg/mL. QDs are carried to a nitrogen glovebox and deposited as synthesised via spin coating at 2000rpm for 30s, and annealed at 75°C for 30s, obtaining a conformal layer of 70nm onto 3D ZnO structures (Fig. 1c). After deposition, the excitonic peak of QDs is red-shifted to 1435nm.

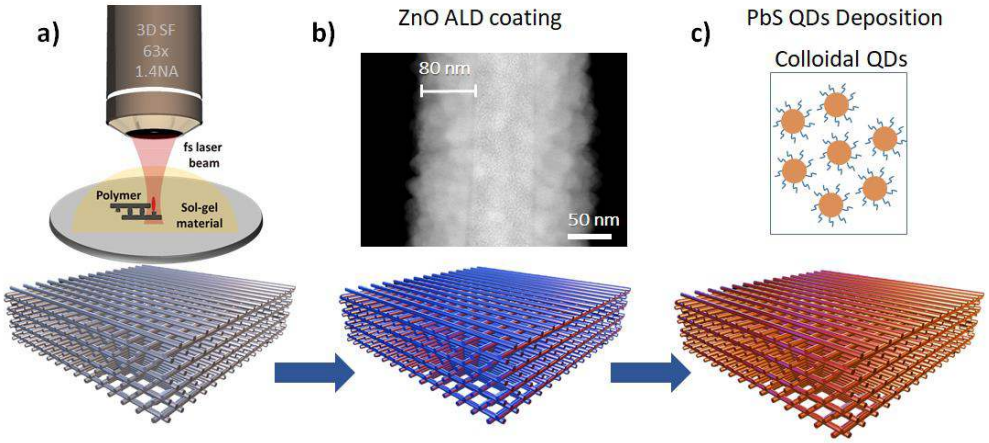


Fig. 1. 3D laser-processed metamaterials. a) Nanoscale 3D fabrication of woodpile structures via multi-photon polymerization. b) Atomic-layer deposition (ALD) conformal coating with 80nm of ZnO. c) Deposition of PbS quantum dots (QDs) with an excitonic peak at wavelength of 1435 nm.

III. Nanoscale Photoluminescence Measurements

To evaluate performance of the 3D laser-printed structures, we perform PL nanoscale measurements. First, we obtain PL maps centered at the excitonic peak of PbS QDs (1435nm) with pump laser centered at a wavelength of 640 nm (Fig. 2b). Woodpile structures show extreme PL enhancement compared to QDs film on Si. The PL enhancement is even high enough to identify the exact position of the woodpile structures (see Fig. 2a-b). PL signals is increasing with periodicity, as expected, due to the optical resonance of the 1.2μm structure that is 'closer' to excitonic peak of the QDs. To understand this better, we perform wavelength resolved measurements for the QDs film and woodpiles) with pump laser centered at a wavelength of 785 nm. While PL of QDs film is relative low, it increases with periodicity dramatically resulting in almost 1600% higher PbS PL signal (Fig. 2c). Inset shows PL *vs* periodicity for clarity.

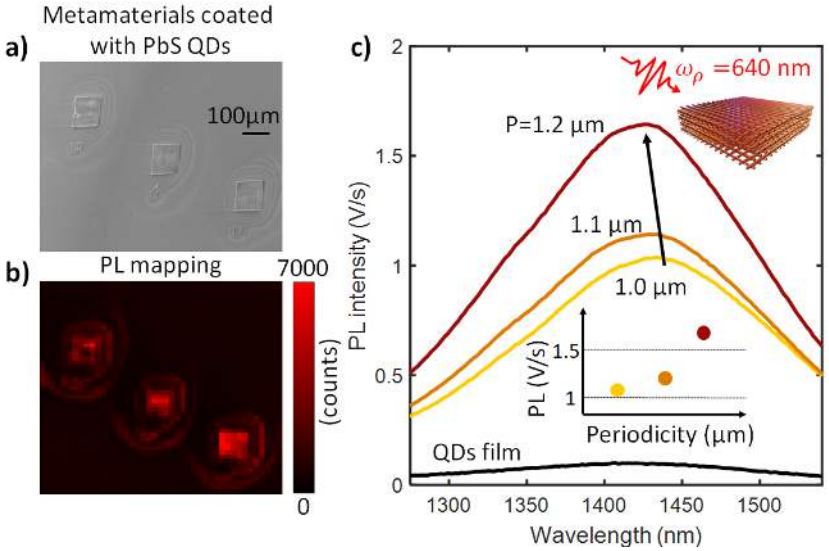


Fig. 2. Low refractive index 3D metamaterials for structure dependent QDs PL enhancement. a) Scanning electron microscope image of the QDs coated metamaterials. b) PL mapping (ω_P=785nm) shows extreme signal boosting on the dielectric IR photonic structures compared to the QDs film on Si. c) Wavelength-resolved PL for different metamaterial periodicities. Insets show the laser pump wavelength of 640nm and periodicity dependent PL enhancement.

IV. Conclusion

Here we show how QDs conformal coatings can be achieved over 3D structures overcoming current geometrical deposition restrictions. Furthermore, low refractive index dielectric laser-printable IR metamaterials boost PL of PbS QDs resulting in an increase of about 1600% compared to QDs film. This makes a wide materials collection beyond the standard plasmonic or high refractive index dielectrics available for nanoscale optoelectronic and photonic applications.

Acknowledgement

We acknowledge support from Empa internal funding call (IRC 2021).

References

[1] G. Kara, S. Bolat, K. Sharma, M.J. Grotevent, D.N. Dirin, D. Bachmann, R. Furrer, L.F. Boesel, Y.E. Romanyuk, R. M. Rossi, M. V. Kovalenko, M. Calame, I. Shorubalko, "Conformal Integration of an Inkjet-Printed PbS QDs-Graphene IR Photodetector on a Polymer Optical Fiber," *Adv. Mater. Technol.*, 2201922, 2023.

[2] A. Xomalis, X. Zheng, R. Chikkaraddy, Z. Koczor-Benda, E. Miele, E. Rosta, G.A.E. Vandenbosch, A. Martínez, J.J. Baumberg, "Detecting Mid-infrared Light by Molecular Frequency Upconversion in Dual-wavelength Nanoantennas," *Science.,* 374, 6572, 1268, 2021.

[3] A. Xomalis, O. Tsilipakos, M. Manousidaki, O. Busquets, G. Kenanakis, S. Tzortzakis, M. Farsari, C.M. Soukoulis, E.N. Economou, M. Kafesaki, "Enhanced Refractive Index Sensing with Direction-Selective Three-Dimensional Infrared Metamaterials," *ACS Appl. Opt. Mater*., 1, 1, 10, 2023.

[4] M.A. Hines and G.D. Scholes "Colloidal PbS Nanocrystals with Size-Tunable Near-Infrared Emission: Observation of Post-Synthesis Self-Narrowing of the Particle Size Distribution," *Adv. Mater.*, 15. 1844, 2003.

META 2023, PARIS - FRANCE, JULY 18 – 21, 2023

Nonlinear dielectric metasurfaces for infrared imaging and light sources

Dragomir Neshev
ARC Centre of Excellence for Transformative Meta-Optical Systems (TMOS), Department of Electronic Material Engineering, Research School of Physics, Australian National University, Canberra, Australia
*corresponding author: Dragomir.Neshev@anu.edu.au

Abstract: We review the recent achievements of nonlinear frequency conversion in dielectric metasurfaces and show the different strategies for optimization of the nonlinearity enhancement. We further review the important applications of such nonlinear metasurfaces for infrared imaging and novel photon sources.

Nonlinear optical phenomena are central to a myriad of applications in light sources and microscopy. Nonlinear optical effects, such as harmonic generation, frequency mixing and spontaneous parametric down conversion (SPDC) are fundamentally enhanced in materials with a high refractive index, as well as by the presence of a resonant photonic environment. These conditions have triggered a quest for nonlinearity enhancement in nanoscale resonators of high refractive index, where resonant dielectric metasurfaces play a key role. However, the applicability of high-index single-crystal metasurfaces for enhanced nonlinear light matter interactions has remained limited. This is hindered by several factors, including low conversion efficiency, difficulties in the fabrication of nanostructures from high-index crystalline materials, as well as by the diffractive nature of the emitted nonlinear light.

Here we discuss the recent advances in the field of nonlinear metasurfaces for enhancement of nonlinear frequency conversion, including second harmonic generation, sum-frequency generation and third harmonic generation. We present how the resonant effects of bound states in the continuum together with free-form optimization techniques for optimization of the mode overlaps inside the metasurfaces can significantly enhance the nonlinear conversion. In particular, we explore different materials platforms, including III-V semiconductors, single-crystal transition-metal-dichalcogenide (TMDC) and lithium niobate metasurfaces. We further present possible applications of nonlinear metasurfaces for nonlinear infrared imaging and non-classical photon sources.

Light source engineering of directive photoluminescent metasurfaces with the local Kirchhoff's law

E. Bailly[1], **J.-P. Hugonin**[1], **B. Vest**[1], **J.-J. Greffet**[1*]
[1]Universite Paris-Saclay, Institut d'Optique Graduate School, CNRS, Laboratoire Charles Fabry, 91127, Palaiseau, France
[*]corresponding author: jean-jacques.greffet@institutoptique.fr

Abstract: Light-emitting metasurfaces are nanostructured surfaces covered with emitters. The interaction between emitters and the metasurface enables a precise control of the emission properties. In practice, devices can be designed exploiting a reciprocity picture given by the local Kirchhoff's law [1]. The emission features can be derived from the absorption features. In this presentation, we report on the whole process of quantitative design, fabrication and characterization of devices made on nanoplatelets deposited on a 2D metallic grating, providing highly directional photoluminescence.

Light-emitting metasurfaces are devices consisting of a nanostructured surface covered with dense ensemble of emitters. In the standard model, the emitters are considered as a collection of electric dipoles randomly oriented inside the structure, whose contribution can be added incoherently [2]. This approach however does not account for modifications of the spectrum influenced by temperature and pumping conditions and cannot predict the intensity of the emitted signal. Here, we present an alternative procedure to model emission by light-emitting metasurfaces, using a generalized Kirchhoff's law formalism [1], as the product of a local absorptivity rate by a Planckian exponential contribution depending on the temperature and the photon chemical potential. Thanks to this formalism, we were able to design a directive photoluminescent metasurface made of nanoplatelets on a 2D silver grating with absorption computations. The fabrication and characterization of this source are in great agreement with the theory. In particular, the photoluminescent emission can be retrieved numerically with a Brendel-Bormann model of permittivity for the nanoplatelets [3]. Figure 1 presents the experimental results of the photoluminescence signal obtained as a function of the energy and parallel wave vector (Fig. 1b), for a non-polarized light. The radiation pattern is given in Fig. 1c for the nanoplatelets on top of the silver grating (red line) at the wavelength corresponding to the maximum of emission (black dotted line in Fig 1b), compared to the emission of the nanoplatelets on top of an untextured silver substrate (blue line). The metasurface leads to a directive emission in a 30° cone at half maximum.

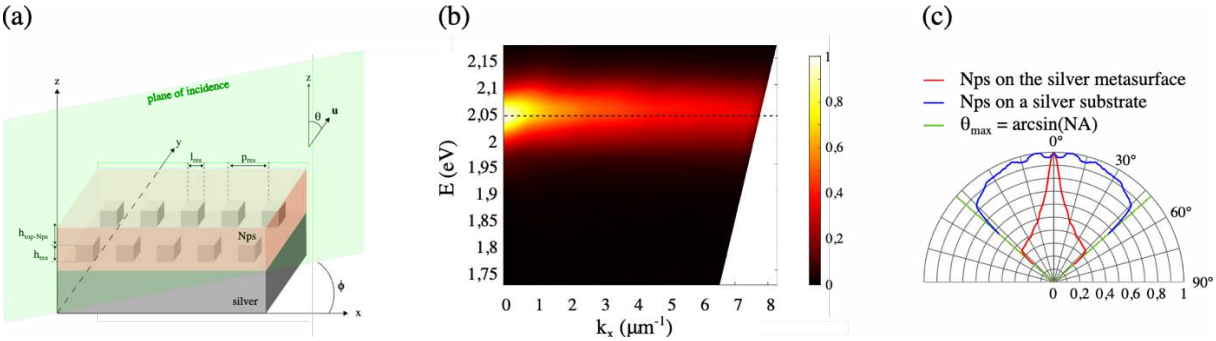


Fig. 1 : Directive photoluminescent metasurface. (a) Schematic diagram of the metasurface, made of nanoplatelets (Nps) located on top of a 2D silver grating. The parameters of the metasurface are h_{res} = 100 nm, l_{res} = 460 nm, p_{res} = 600 nm, $h_{top\text{-}Nps}$ = 6 nm. (b) Normalized photoluminescent emission as a function of the energy E and parallel wave vector $k_x = k_0 \sin(\theta)$, for ϕ=0°. (c) Radiation pattern of the photoluminescent emission at the maximum value of emission represented by the horizontal dotted line of figure b, in presence of the metasurface (red line) or without (blue line). The emission is limited by the numerical aperture of our objective, NA = 0.75 (green line).

Acknowledgement: This work is supported by the French National Agency (ANR) (ANR-17-CE24-0046).

References

[1] J.-J. Greffet, P. Bouchon, G. Brucoli, and F. Marquier, “Light Emission by Nonequilibrium Bodies: Local Kirchhoff Law”, Phys. Rev. X **8**, 21008 (2018)
[2] A. Vaskin, J. Bohn, K. E. Chong, T. Bucher, M. Zilk, D.-Y. Choi, D. N. Neshev, Y. S. Kivshar, T. Pertsch, and I. Staude, “Directional and spectral shaping of light emission with mie-resonant silicon nanoantenna arrays,” ACS Photonics **5**(4), 1359–1364 (2018).
[3] E. Bailly, K. Chevrier, C. Perez de la Vega, J.-P. Hugonin, Y. De Wilde, V. Krachmalnicoff, B. Vest, and J.-J. Greffet. “Method to measure the refractive index for photoluminescence modelling”, Opt. Mater. Express, **12**(7) :2772–2781, Jul 2022.

Stick-and-play nanoantenna stickers to control photoluminescence

S. Murai*, T-Y. Lo, K. Tanaka

Department of Material Chemistry, Graduate School of Engineering, Kyoto University, Japan
*Corresponding author: murai@dipole7.kuic.kyoto-u.ac.jp

Abstract: Nanoantenna stickers, where the periodic array of nanoparticles is embedded in an elastomer film, can be easily attached to and detached from the surface of target materials and work as nanoantenna to control light. The stickers can be fabricated by nanoimprint lithography followed by a transfer process. We make stickers consisting of the nanoantenna made of aluminum, silver, silicon or titania embedded in polydimethylsiloxane, and demonstrate a photoluminescence outcoupling by placing a sticker on luminous layers.

Periodic arrays of metallic nanoparticles act as nanoantennas to control light at the interface. Although the combination of a variety of functional materials with nanoantennas should open a rich scientific research field, the application degree of freedom is limited severely by the fabrication process. We developed a "nanoantenna sticker" that can be stuck on any surface and gives control over in- and outcoupling of light. The stickers consist of the nanoantenna made of aluminum, silver, silicon or titania embedded in polydimethylsiloxane. We demonstrate a photoluminescence outcoupling by placing a sticker on the luminescent layers: the emission pattern is modulated both spatially and spectrally in a way defined by the nanoantenna sticker. The sticker is useful for enhancing optical response from many different surfaces including those that are incompatible with the nanofabrication processes and should help the integration of nanoantennas into functional devices.

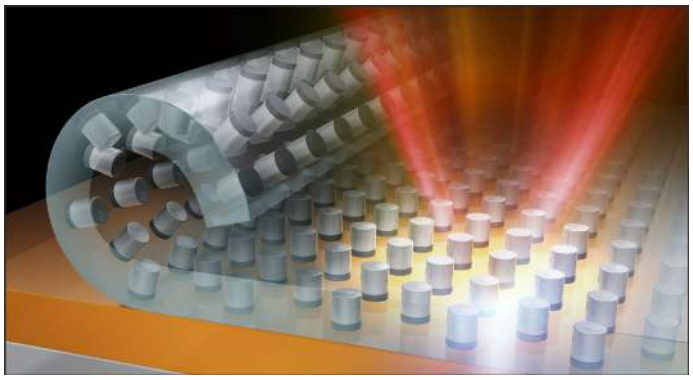


Fig. 1: Sketch of the nanoantenna sticker on a phosphor layer, radiating photoluminescence with a directionality. The nanoantenna sticker is flexible and can be attached to any clean surfaces.

We acknowledge financial support from MEXT (Kekanhi 22K18884, 22H01776), Izumi Science and Technology Foundation, Casio Science Promotion Foundation and The Futaba Foundation.

References

1. Agata, K. et al., “Stick-and-play metasurfaces for directional light outcoupling,” *Appl. Phys. Lett*. **118**, (2021) 021110
2. Lo, T-Y. et al, “Silver nanoantenna stickers for photoluminescence control,” *ACS Appl. Opt. Mater.* accepted (2023)

META 2023, PARIS - FRANCE, JULY 18 – 21, 2023

Reciprocity Violation in Time-Modulated Structures for Enhanced Optical Heating

V. M. Levkovskaya[1], A. V. Kharitonov[1*], and S. S. Kharintsev[1]

[1]Insitute of Physics, Kazan Federal University, Russian Federation
[*]corresponding author: antonharitonov@gmail.com

Abstract: In recent years, resonant nanostructures have been demonstrated that are capable of absorbing >99% of incident light in the wide spectral range. However, the photo-heating efficiency observed in these structures is low, which is due to processes of heat diffusion and thermal radiation. These processes can be substantially suppressed by violating the reciprocity. For this purpose, we propose thermophotonic nanostructures, whose optical and thermal properties are simultaneously modulated in time.

Highly efficient local heating plays a crucial role in many applications, such as thermophotovoltaics, photothermal therapy etc. For this purpose, nanostructures are typically used, which absorb the incident light and then convert it into the heat. As a result, one can obtain a nanosized heat source. In recent years, resonant nanostructures have been demonstrated that a capable of absorbing more than 99% of the incident light. However, the photoheating temperature observed in such structures is typically low: on the order of tens of degrees. This is due to the heat dissipation through the two main mechanisms, such as heat diffusion and thermal radiation. In general, these processes are difficult to control since they obey the Lorentz reciprocity principle. In this article, we propose an approach that allows to break the reciprocity for heat diffusion and thermal radiation. The approach is based on the use of time-varying media [1,2].

Kirchhoff's law for thermal radiation states that the absorptivity of a body is equal to its emissivity. Therefore, if the nanostructure absorbs light with high efficiency, then it will also efficiently lose the absorbed energy upon heating. One of the ways to break the reciprocity is the use of magneto-optical materials [3]. However, this requires sufficiently strong magnetic fields on the order of 1 T, which hinders the practical applications.

The heat diffusion rate, according to the heat equation, can be decreased by reducing the thermal diffusivity. This can be done by using the appropriate material. The disadvantage of this approach is the limited set of existing materials. Breaking the reciprocity [4] may potentially lead to the situation, in which the heat does not flow in one or more directions, even in a material with high thermal conductivity.

This work is devoted to the development of an approach for reciprocity breaking in thermphotonic nanostructures. Our approach is based on the use of time-varying media, i.e., media whose parameters are modulated in the time domain. For the case of optical processes, the dielectric permittivity is modulated. For the case of heat diffusion, the thermal conductivity, density or heat capacity are the parameters that can be modulated to achieve a desired functionality. We carried out numerical simulations in order to investigate the propagation of electromagnetic waves (heat flow) in media, which is spatially uniform, but has a temporal inhomogeneity. For this purpose a finite element method was used. We investigated the effect of parameters of the temporal inhomogeneity (switching speed, depth and profile) on the asymmetry in light (heat) propagation. It is shown that in time-varying media the violation of the Kirchhoff's law takes place only in the presence of losses. For the case of heat diffusion, the reciprocity breaking requires simultaneous modulation of two parameters. This stems from to the continuity equation.

Thus, time-varying media provides new opportunities for boosting the light-to-heat conversion in nanostructures. The development of non-reciprocal devices is of great importance for many applications, including radiative heating/cooling, wireless power transfer, and ultrafast information processing.

This work has been supported by the Kazan Federal University Strategic Academic Leadership Program (PRIORITY-2030).

References

1. Sounas, Dimitrios L., and Andrea Alù. "Non-reciprocal photonics based on time modulation." Nature Photonics Vol. 11, No. 12, 774-783, 2017.
2. Ghanekar, Alok, et al. "Violation of Kirchhoff's Law of Thermal Radiation with Space–Time Modulated Grating." ACS Photonics Vol. 9, No. 4, 1157-1164, 2022.
3. Liu, Tianji, et al. "Thermal photonics with broken symmetries." eLight Vol. 2, No. 1, 25, 2022.
4. Li, Jiaxin, et al. "Reciprocity of thermal diffusion in time-modulated systems." Nature Communications Vol. 13, No. 1, 167, 2022.

Quantum Light Emitters and Photonic Heterogeneous Integration

Heterogeneous III-V on Diamond Nanophotonics for Quantum Nodes based on Defects in Diamond

A. Abulnaga[1*], S. Karg[1], D. Huang[1,2], A. Pakpour-Tabrizi[1], Z. Zhang[1,3], and N. P. de Leon[1]

[1]Department of Electrical and Computer Engineering, Princeton University, USA
[2]Current: Institute of Materials Research and Engineering, Agency for Science, Technology and Research, Singapore
[3]Current: Department of Electrical Engineering and Computer Sciences, University of California Berkeley, USA
[*]Corresponding author: alex.abulnaga@princeton.edu

Abstract: We describe a heterogeneously integrated, on-chip, III-V on diamond platform designed for color centers in diamond that circumvents the need for etching the diamond substrate. Through evanescent coupling to defects near the surface of diamond, the platform will enable Purcell enhancement and efficient frequency conversion to the telecommunication C-band.

Color centers in diamond combine optical addressability with long spin coherence times, making them promising candidates for repeater-based quantum networks [1]. However, currently known platforms suffer from either degraded optical coherence when incorporated into nanophotonic devices [2, 3], or limited electron spin coherence times of milliseconds combined with the requirement to work at millikelvin temperatures [4]. The recently reported SiV0 center in diamond has the potential to overcome many of these challenges [5, 6]. The unique combination of stable optical transitions and long spin coherence times at liquid helium temperature makes the SiV0 center an attractive building block for nodes in quantum networks. One proposal for enhancing the entanglement generation rate in color-center-based quantum networks is to integrate color centers with nanophotonic devices. Optical cavities greatly enhance atom-photon interaction, which improves spin readout and spin-photon entanglement fidelity. Furthermore, nanophotonic devices can enable other functionality such as on-chip quantum frequency conversion (QFC), which is key to achieving long-distance quantum communication. Monolithic fabrication techniques of diamond nanophotonic cavities require milling or etching bulk single crystal diamond. A promising method to mitigate the constraints imposed by diamond nanofabrication is heterogeneous integration of diamond and a separate device layer material. The photonic device is fabricated in a high-index photonic layer on top of the diamond substrate such that photons can evanescently couple to color centers that are close to the diamond surface (Fig.1).

We present a platform for integrating III-V nanophotonic devices with SiV0 centers [7]. One-dimensional photonic crystal cavities enhance the optical emission from single SiV0 centers, and the emission can then be routed on-chip to a microresonator-based frequency converter using a four-wave mixing Bragg scattering (FWM-BS) scheme. In contrast to previous demonstrations, our design does not require etching into the diamond, avoiding deleterious effects on the color center. We report on recent experimental progress towards fabricating these photonic structures and integrating them with SiV0 defects in diamond.

This work was supported by the DOE Center for Quantum Advantage (DE-SC0012704), DARPA (D18AP00047), the NSF (1640959 and DMR-1420541), and the Air Force (FA9550-17-0158). A. A. was supported by the Natural Sciences and Engineering Research Council of Canada. (PGSD3 - 545932 – 2020).

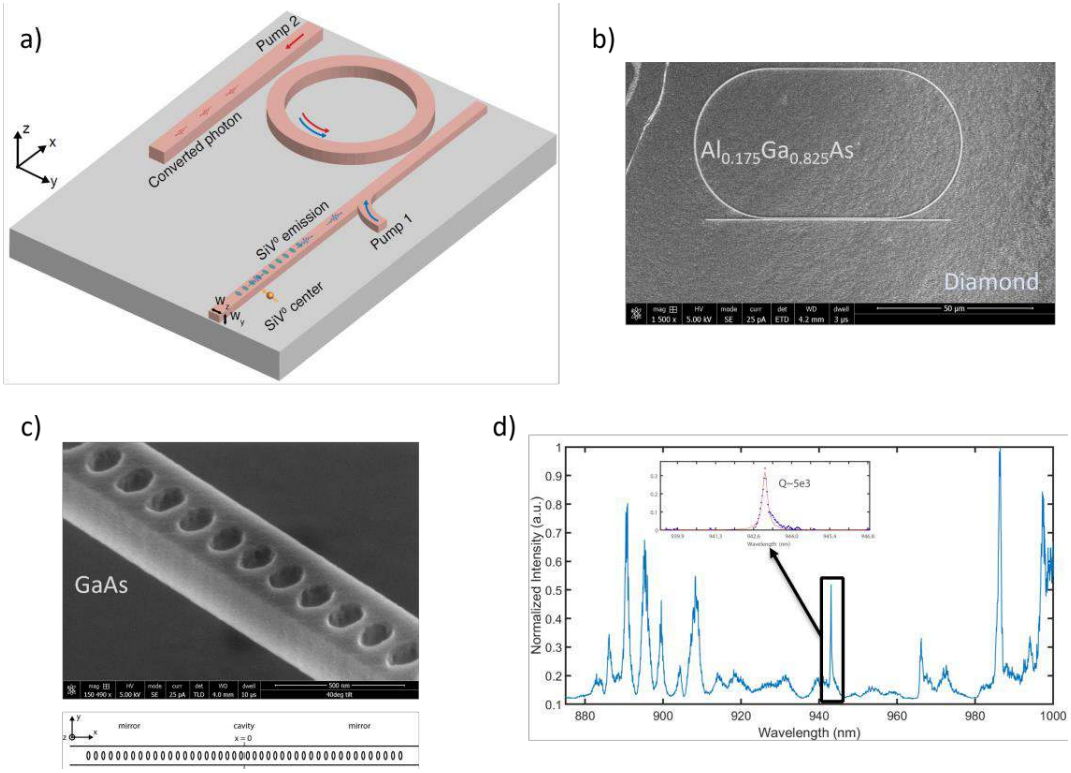


Figure 1. a) Proposed III-V on diamond nanophotonic platform for Purcell-enhanced coupling and quantum frequency conversion of SiV^0 defects in diamond. b) Fabricated $Al_{0.175}Ga_{0.825}As$-on-Diamond microring resonator. c) Fabricated GaAs photonic crystal cavity suspended in air. d) Transmission spectrum of the cavity, showing a resonance with Q~5e3 in air.

References

1. M. Atatüre, D. Englund, N. Vamivakas, S.-Y. Lee, and J. Wrachtrup, “Material platforms for spin-based photonic quantum technologies,” Nat. Rev. Mater. 3, 38–51 (2018).
2. Y. Chu, N. P. de Leon, B. J. Shields, B. Hausmann, R. Evans, E. Togan, M. J. Burek, M. Markham, A. Stacey, A. S. Zibrov, A. Yacoby, D. J. Twitchen, M. Loncar, H. Park, P. Maletinsky, and M. D. Lukin, “Coherent optical transitions in implanted nitrogen vacancy centers,” Nano letters 14, 1982–1986 (2014).
3. M. Ruf, M. IJspeert, S. van Dam, N. de Jong, H. van den Berg, G. Evers, and R. Hanson, “Optically coherent nitrogen-vacancy centers in micrometer-thin etched diamond membranes,” Nano Lett. 19, 3987–3992 (2019).
4. D. D. Sukachev, A. Sipahigil, C. T. Nguyen, M. K. Bhaskar, R. E. Evans, F. Jelezko, and M. D. Lukin, “Silicon-vacancy spin qubit in diamond: a quantum memory exceeding 10 ms with single-shot state readout,” Phys. Rev. Lett. 119, 223602 (2017).
5. B. C. Rose, D. Huang, Z.-H. Zhang, P. Stevenson, A. M. Tyryshkin, S. Sangtawesin, S. Srinivasan, L. Loudin, M. L. Markham, A. M. Edmonds, D. J. Twitchen, S. A. Lyon, and N. P. de Leon, “Observation of an environmentally insensitive solid-state spin defect in diamond,” Science 361, 60–63 (2018).
6. Z.-H. Zhang, P. Stevenson, G. Thiering, B. C. Rose, D. Huang, A. M. Edmonds, M. L. Markham, S. A. Lyon, A. Gali, and N. P. de Leon, “Optically detected magnetic resonance in neutral silicon vacancy centers in diamond via bound exciton states,” Phys. Rev. Lett. 125, 237402 (2020).
7. D. Huang, A. Abulnaga, S. Welinski, M. Raha, J. D. Thompson, and N. P. de Leon, "Hybrid III-V diamond photonic platform for quantum nodes based on neutral silicon vacancy centers in diamond," Opt. Express 29, 9174-9189 (2021)

Plug & play quantum light sources with fiber-integrated quantum emitters

W. B. Jeon and J.-H. Kim*

[1] Department of Physics, Ulsan National Institute of Science and Technology, Republic of Korea
*jehyungkim@unist.ac.kr

Abstract: We demonstrate a highly efficient fiber-interfacing photonic device that directly launches single photons from quantum dots into a standard FC/PC-connectorized single-mode fiber. An optimally designed hole-based circular Bragg grating produces an ultra-narrow vertical beam whose emission angle matches the small numerical aperture of a single-mode fiber. The heterogeneously integrated fiber–quantum dot system enables the compact plug-and-play operation of single photons from a source to a detector with high coupling efficiency and long-term stability.

The future quantum photonic system requires the integration of highly reliable quantum light sources with low-loss optical channels as well as highly efficient single-photon detectors. Interfacing quantum dots with fiber optics opens the door for quantum networks that transmit quantum information over long distances and create remote entanglements between separated quantum systems. The primary challenge when connecting quantum emitters to fiber channels is the large mismatch in spatial field profiles of the dipole emission and the fiber mode. Several different approaches have been proposed for achieving high coupling efficiency between a quantum dot and a single-mode fiber, including integration of micro-optics and adiabatic coupling. However, they lack practicality and long-term reliability.

Here, we present efficient and compact plug-and-play single-photon sources based on hole-based circular Bragg gratings (hole-CBGs). Compared to conventional ring-based circular Bragg gratings, a newly designed hole-CBGs produces an ultra-narrow vertical beam whose emission angle matches the small numerical aperture of a single-mode fiber (Fig.1 (a)). The advantages of hole-CBGs come from several factors. First, according to the effective medium theory, hole patterns lower the refractive index contrast between air and matter (InP) than ring-CBGs. A smooth refractive index gradient in hole-CBGs enlarges the spatial mode size, resulting in a narrow divergence in momentum space. Moreover, hole-CBGs optimize the optical mode in both the radial and axial directions, whereas ring-CBGs optimize the structure parameter only in the radial direction. This additional degree of freedom enables further optimization of constructive and destructive interferences, resulting in highly enhanced vertical emission and suppressed higher-order diffraction. In the numerical simulation, the integrated hole-CBGs on a single-mode fiber (SMF28) can couple single photons more than 60%.

To implement a fiber-integrated single-photon source, we fabricated hole-CBGs on a telecom-emitting InAs/InP quantum dot membrane. Using a pick-and-place technique, the fabricated hole-CBGs were precisely integrated into the core of a single-mode fiber (Fig,1 (d)). The integrated fiber–QD system successfully demonstrated the efficient and reliable transmission of single photons into an all-fiber coupled system from a source to a detector without any optical alignment. The results represent a major step toward the practical and reliable transmission of quantum light across a fiber network.

References

1. Jeon, W. B., Moon, J. S., Kim,K.-Y., Ko, Y.-H., Richardson, C. J. K. Waks, E., Kim, J.-H., “Plug-and-play single-photon devices with efficient fiber-quantum dot interface",”Adv. Quantum. Technol. 2200022 (2022)

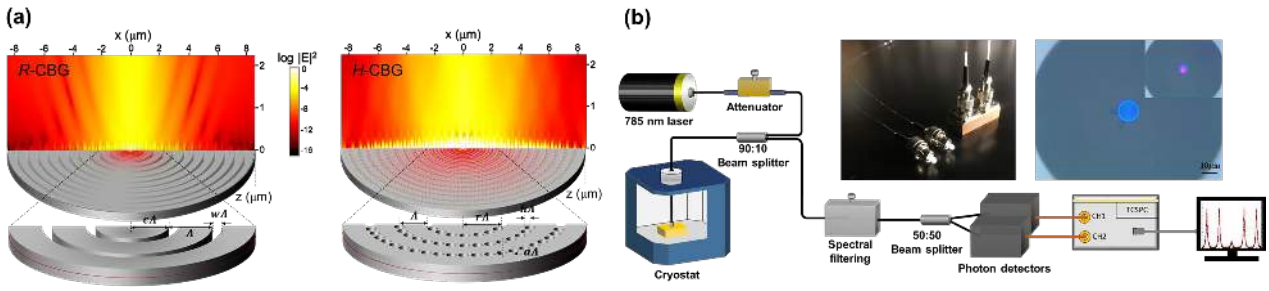


Fig. 1 (a) Cross-sectional intensity profiles and schematics of (left) ring-based and (right) hole-based circular Bragg gratings (CBGs) (b) Schematic of all-fiber integrated single-photon system. Inset: Photo image of a plug-and-play single-photon device and the integrated hole-CBG device at the core of a single-mode fiber.

META 2023, PARIS - FRANCE, JULY 18 – 21, 2023

Spin and level structure of positioned sulfur vacancies in MoS_2 acting as quantum emitters

A.W. Holleitner[1*]

[1]Walter Schottky Institute, TU Munich, Germany
[*]holleitner@wsi.tum.de

Abstract: We report on the level structure of single vacancies in monolayer MoS_2 and WS_2 which are generated by the help of a helium ion microscope at a lateral accuracy of <10nm. The vacancies turn out to be quantum emitters in the near-infrared electromagnetic regime. Moreover, we demonstrate the absorption characteristics of the defect emitters measured by utilizing both a cavity enhanced detection scheme and a highly sensitive photocurrent tunneling spectroscopy.

Summary: In our endeavor to explore atomistic quantum emitters in 2D materials, we report on the deterministic generation of optically active defects in monolayer MoS_2 and WS_2, which can act as single photon emitters [1-3]. The defects are generated by the help of a helium ion microscope on a lateral scale <10nm, and they can be attributed to single sulfur vacancies [4,5]. Based on high-field magneto-photoluminescence experiments, we demonstrate how to lift the spin-degeneracy of the involved defect states [6]. The results highlight that defects in 2D semiconductors may be utilized as spin-photon interfaces in quantum technologies even at zero magnetic field. In the last part, we highlight our recent experiments on the absorption characteristics of the sulfur vacancies by utilizing both, a cavity enhanced photonic detection scheme [7] and a highly sensitive photocurrent tunneling spectroscopy down to a single defect.

We acknowledge the very fruitful collaboration with J. Finley, K. Müller, A. Stier, and C. Kastl and financial support by the Munich Quantum Valley, MCQST, and e-conversion.

References

1. J. Klein et al. “Site-selectively generated photon emitters in monolayer MoS_2 via local helium ion irradiation”, Nature Comm. 10, 2755 (2019).
2. J. Klein, L. Sigl et al. “Engineering the Luminescence and Generation of Individual Defect Emitters in Atomically Thin MoS_2”, ACS Photonics 8, 2 (2021).
3. A. Micevic, et al, “On-demand generation of optically active defects in monolayer WS_2 by a focused helium ion beam”, Appl. Phys. Lett. 121, 183101 (2022).
4. E. Mitterreiter, et al. “Atomistic Positioning of Defects in Helium Ion Treated Single-Layer MoS_2”, Nano Letters. 20, 6, 4437 (2020).
5. E. Mitterreiter, et al. “The role of chalcogen vacancies for atomic defect emission in MoS_2”, Nature Comm. 12, 1-8 (2021).
6. A. Hötger et al. “Spin-defect characteristics of single sulfur vacancies in monolayer MoS_2”, NPG 2D materials and applications, accepted (2023).
7. F. Sigger et al. “Ultra-Sensitive Extinction Measurements of Optically Active Defects in Monolayer MoS_2”, J. Phys. Chem. 13, 10291 (2022).

META 2023, PARIS - FRANCE, JULY 18 – 21, 2023

Modeling exciton dynamics behind single-phonon emission by interacting solid-state defects

A. Piryatinski

Theoretical Division, Los Alamos National Laboratory, USA
*corresponding author: apiryat@lanl.gov

Abstract: We discuss an open quantum system approach to model exciton dynamics within coupled multi-level states facilitating the spontaneous emission of quantum photons. Our goal is to establish a connection between statistics of emitted photons quantified by the two-photon correlation functions $g^{(2)}$, typically measured via the Hanbury Brown and Twiss (HBT) interferometry, and associated dynamics of the excitons. We apply these techniques to interpret experimental studies of single-photon emission properties of DNA-functionalized single-wall carbon nanotubes and indented MoS_2-WSe_2 2D layered heterostructures.

Ideally, a single photon emitter can be described by an isolated two-level system subject to incoherent pumping and radiative decay resulting in the production of single photons. However, the electronic structure of solid-state defects deviates from the two-level system by a manifold of interacting exciton states that includes spectrally separated bright states, dark states, and the band exciton states. Furthermore, the defect environmental fluctuations result in a broad variety of relaxation timescales, i.e., the exciton transfer and nonradiative decay rates. In this complex situation interpretation of experimentally measured two-photon correlation functions $g^{(2)}$, relies on the modeling of the exciton dynamics within multi-level state manifolds.

We approach this problem by implementing an open quantum system approach. Specifically, we describe the exciton states interacting with each other and the environmental bath using the reduced density operator, ρ. Its time evolution is governed by the following Liouville-Lindblad equation

$$\partial_\tau \hat{\rho}(\tau) = \frac{i}{\hbar}\left[\widehat{H}, \hat{\rho}(\tau)\right] + \sum_{\hat{C}_\uparrow} \widehat{D}_{\hat{C}_\uparrow}[\hat{\rho}(\tau)] + \sum_{\hat{C}_\downarrow} \widehat{D}_{\hat{C}_\downarrow}[\hat{\rho}(\tau)]. \quad (1)$$

Here, the first term on the right-hand side describes the defect's coherent dynamics governed by the exciton Hamiltonian $\widehat{H}$. The second term is a sum of all pathways for the incoherent excitation (irreversible energy pump) each defined by a set of collapse operators $\hat{C}_\uparrow$. The last term describes the dissipation pathways defined by a set of collapse operators $\hat{C}_\downarrow$. In Eq. (1), the Lindblad superoperator is

$$\widehat{D}_{\hat{C}}[\hat{\rho}] = \hat{C}\hat{\rho}\hat{C}^\dagger - \frac{1}{2}(\hat{C}^\dagger\hat{C}\hat{\rho} + \hat{\rho}\hat{C}^\dagger\hat{C}). \quad (2)$$

Leveraged by the quantum computational package QuTiP,[1] we developed a computational code for solving Eqs. (1) and (2) for an arbitrary multi-level system with the excitation and relaxation rates encoded into the collapse operators. With the help of the quantum regression theorem,[2] obtained trajectories for the density operator are used to evaluate the two-time exciton correlation functions

$$G^{(2)}_{ij}(t,\tau) = Tr\{\hat{\rho}\,\hat{b}_i^\dagger(t)\hat{b}_j^\dagger(t+\tau)\hat{b}_j(t+\tau)\hat{b}_i(t)\}, \quad (3)$$

where $\hat{b}_i$ and $\hat{b}_j$ are the ladder operators for defects *i* and *j*. Armed with these correlation functions, we can model the two-photon correlation function $g^{(2)}$ in the continuous-wave (CW) and impulsive excitation regimes. For the coupled defect states emitting quantum photons, this methodology provides us with a complete set of two-photon auto-correlation, $g_{i,i}^{(2)}$, and cross-correlation, $g_{i,j}^{(2)}$ functions.

We have applied this methodology to gain insights into the features of the auto-correlation and cross-correlation functions measured, using both CW and impulsive HBT interferometry, from coupled quantum defects in the DNA-functionalized carbon nanotubes[3] and indented MoS_2-WSe_2 layered heterostructures.[4] In Figure 1A, we show schematics of quantum defects created via chemical bonding between DNA segments wrapped around a (6, 5) single-walled carbon nanotube. Adopting a two-defect model interacting via the exciton band, we explained features of the experimentally measured (dots) CW defect total correlation function (panel B), spectrally filtered auto-correlation function of each defect (panels C and D), and the cross-correlation function of the defects (panel E). Our model fit is shown by solid lines. Each defect emits photons through the spontaneous decay of optically active two levels. This explains the strong anti-bunching at zero delay times in panels B-D. The bunching observed in the same panels for non-zero delay times is a signature of the dark (shelving) states. Most interesting is the behavior of the cross-correlation function in panel D. As our modeling confirmed, a sharp dip at zero delay time is a signature of the interaction between the defects via the exciton band. In general, we demonstrated the importance of the cross-correlation functions to carry unique signatures of the defect interaction mechanisms. Our further analysis (not shown in Fig. 1) reveals connections between histograms obtained in the impulsive and CW HBT measurements. Finally, theoretical modeling of the impulsive $g^{(2)}$ in MoS_2-WSe_2 layered heterostructures showed good agreement with the experiment and pointed towards the existence of long-lived, ~1 μs, dark states coupled to the optically active quantum defects.

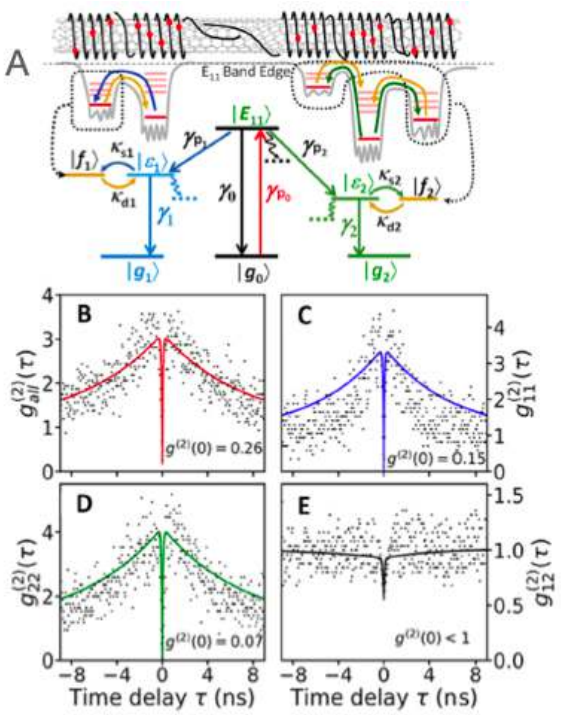


Figure 1

Acknowledgments: This work was partially performed at the Center for Integrated Nanotechnologies, an Office of Science User Facility operated by the U.S. Department of Energy (DOE) Office of Science. Los Alamos National Laboratory (LANL). The funding has been provided by the Laboratory Directed Research and Development (LDRD) program under the grants 20200104DR and 20220047DR.

References

1. J. R. Johansson, P. D. Nation, and F. Nori: "QuTiP 2: A Python framework for the dynamics of open quantum systems.", Comp. Phys. Comm. Vol. 184, No 4 1234-1240, 2013; "QuTiP: An open-source Python framework for the dynamics of open quantum systems.", Comp. Phys. Comm. Vol. 183, No8, 1760–1772 2012.
2. R. Loudon, *The quantum theory of light* (OUP Oxford, 2000).
3. Y. Zheng, Y. Kim, A. C. Jones, G. Olinger, E. R. Bittner, S. M. Bachilo, S. K. Doorn, R B. Weisman, A. Piryatinski, H. Htoon, "Quantum light emission from coupled defect states in DNA-functionalized carbon nanotubes", ACS Nano Vol. 15, No 6, 10406-10414, 2021.
4. H. Zhao, L. Zhu, X. Li, V. Chandrasekaran, J. K. Baldwin, M. T. Pettes, A. Piryatinski, L. Yang, H. Htoon, "Manipulating interlyer excitons for ultra-pure near-infrared quantum light generation", Phys. Rev. Lett. (under review). arXiv preprint arXiv:2205.02472.

Efficient outcoupling of light from single-photon emitters in 2D materials

R. Bratschitsch[1*]

[1]Institute of Physics and Center for Nanotechnology, University of Münster, Germany
[*]corresponding author: Rudolf.Bratschitsch@uni-muenster.de

Abstract: We demonstrate how single photons originating from 2D materials can be efficiently collected and routed either on a photonic chip or beamed into the far field. For on-chip coupling, we deposit GaSe crystals with embedded single-photon emitters onto silicon nitride rib waveguides. For efficient far-field collection, we 3D-print elliptical polymer microlenses on an array of hBN nanocrystals hosting single-photon emitters.

Single-photon sources are crucial components for building quantum networks and communications. Recently, single-photon sources in 2D materials have emerged as robust solid-state quantum light emitters [1]. Promising materials include transition metal dichalcogenides, such as WSe_2 or $MoTe_2$, transition metal monochalcogenides (e.g. GaSe), and also hexagonal boron nitride (hBN). For collecting and making use of single photons emitted from these 2D materials, different strategies can be envisioned, whether the photons are needed on-chip or in free space.

Interestingly, nonclassical light is commonly coupled onto photonic chips from the outside, because presently only few integrated single-photon sources exist. In my talk, I will present waveguide-coupled single-photon emitters in the layered semiconductor gallium selenide (Fig. 1, left) as promising on-chip sources [2]. GaSe crystals with a thickness below 100 nm are placed on Si_3N_4 rib or slot waveguides, resulting in a modified mode structure efficient for light coupling. Using optical excitation from within the silicon nitride waveguide, we find nonclassicality of generated photons routed on the photonic chip. Thus, our work provides an easy-to implement and robust light source for integrated photonic quantum technology.

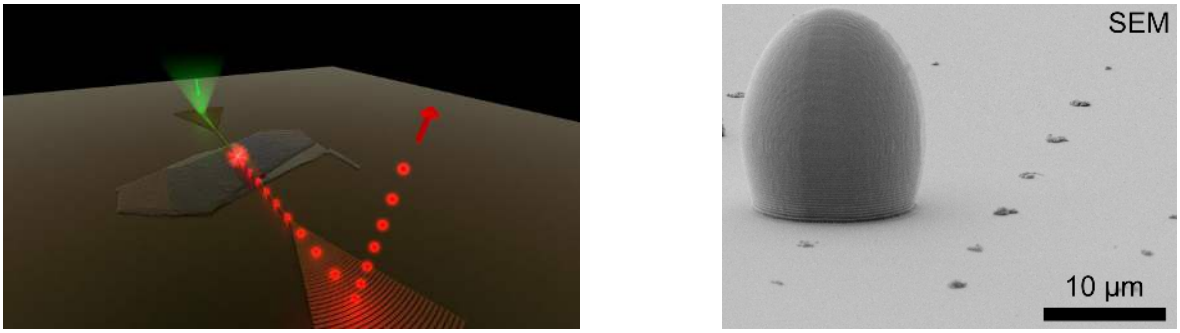


Figure 1. (left) Artistic impression of an on-chip single-photon source based on a GaSe crystal placed on a linear silicon nitride waveguide. To verify its operation, light used for excitation of the emitter is coupled into the waveguide with a grating coupler. Single photons are routed in the waveguide on-chip and are detected at the second grating coupler. (right) Scanning electron microscopy (SEM) image of an elliptical polymer microlens 3D-printed on a hBN nanocrystal.

Coupling light into the far-field calls for different methods. Ideally, the emitted light is collimated. In

contrast, expensive and bulky collection optics, such as objective lenses with a high numerical aperture are widely used today to collect the light emitted under high angles. We present polymer microlenses, which are 3D-printed directly on 2D single-photon emitters. We use commercially available hexagonal boron nitride (hBN) nanocrystals, which host the emitters. First, a regular array of hBN nanocrystals is created (Fig. 1, right) using capillary assembly [3]. Then, we 3D-print elliptical polymer microlenses with direct laser writing onto hBN nanocrystals, which host emitters. An ultra-low-fluorescence polymer ensures that negligible background luminescence is added to the single-photon stream. The light emission is efficiently collimated to angles below 5°, while the emission of the in-plane dipole in the 2D material without the microlens occurs mostly under high angles. The small angle of emission of the new single-photon source allows for using collection lenses with very low numerical apertures of NA > 0.06, including optical fibers.

In conclusion, we have demonstrated two efficient methods to efficiently harvest single photons from 2D materials, rendering these single-photon sources highly promising for quantum optics and photonic quantum technologies.

References

1. Michaelis de Vasconcellos, S., Wigger, D., Wurstbauer, U., Holleitner, A. W., Bratschitsch, R., Kuhn, T. "Single-photon emitters in layered van der Waals materials," phys. stat. sol (b), Vol. 259, 2100566, 2022.
2. Tonndorf, P., Del Pozo-Zamudio, O., Gruhler, N., Kern, J., Schmidt, R., Dmitriev, A. I., Bakhtinov, A. P. Tartakovskii, A. I., Pernice, W. H. P., Michaelis de Vasconcellos, S., Bratschitsch, R., "On-chip waveguide coupling of a layered semiconductor single-photon source," Nano Lett., Vol. 17, 5446, 2017.
3. Preuß, J. A., Rudi, E., Kern, J., Schmidt, R., Bratschitsch, R., Michaelis de Vasconcellos, S., "Assembly of large hBN nanocrystal arrays for quantum light emission," 2D Materials, Vol. 8, 035005, 2021.
4. Preuß, J. A., Gehring, H., Schmidt, R., Jin, L., Wendland, D., Kern, J., Pernice, W. H. P., Michaelis de Vasconcellos, S., Bratschitsch R., "Low-divergence hBN single-photon source with a 3D-printed low-fluorescence elliptical polymer microlens," Nano Lett., Vol 23, 407, 2023.

META 2023, PARIS - FRANCE, JULY 18 – 21, 2023

Nanometric axial localization of color centers in hexagonal boron nitride flakes

Pankaj K. Jha

Quantum Technology Laboratory ⟨Q | T | L⟩, Department of Electrical Engineering and Computer Science, Syracuse University, Syracuse, NY, USA
*Corresponding author: pkjha@syr.edu

Abstract: Novel materials are the backbone of next-generation quantum technologies. In this talk, color centers in hexagonal boron nitride, will be discussed as a promising candidate for single photon sources at room temperature. Nanometric axial localization of these color centers with 3D characterization of their dipole orientation will be highlighted.

Quantum emitters are the building blocks of photonic quantum technologies. Discovery of bright quantum light emission at room temperature from point defects in hexagonal boron nitride (*h*BN) has introduced a promising candidate for single photon emitter (SPEs) [1,2]. Owing to 2D nature of the host material, these SPEs offer easier integration with photonic structures and minimal loss due to refractive index mismatch. To date, emission characteristics of *h*BN quantum emitters in multi-layered flakes are superior to those in monolayer and few-layered flakes. However, the exact location of any quantum emitter within the thickness of a multi-layered flake remains unknown due to the random nature of defect formation. Determining the exact location and 3D orientation of their dipole moment is critical for quantum applications.

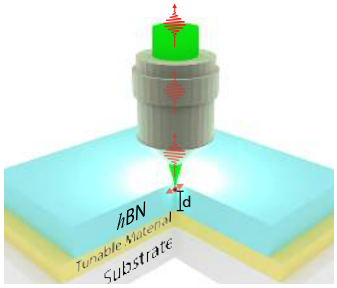


Fig 1: Extracting axial position *d* using a nanophotonic interface.

In this talk, I will discuss a tunable nanophotonic platform which can be employed to extract the axial position of quantum emitters in a multi-layered *h*BN with nanometer-scale accuracy while also determining their full dipolar orientation [3]. We leverage the sharp change in complex refractive index of vanadium dioxide (VO_2), a phase change material, at room temperature to tailor the optical environment and induce a highly sensitive, axial distance-dependent decay rate of a quantum emitter located in the vicinity of the *h*BN/VO_2 interface. Using our approach, we were able to locate several quantum emitters at a distance of ~ 20 nm from the surface of VO_2 with axial position uncertainty (full width) down to ~ 7 nm. Such accurate measurement of *h*BN quantum emitter's location and 3D orientation together with advances in precise transfer and stacking of 2D materials, interfacing with engineered interfaces (4-6) would offer unprecedented opportunities for both fundamental physics advances and quantum photonic technologies.

References

1. Tran T. T. *et al.*, "Quantum emission from hexagonal boron nitride monolayers", Nat. Nanotechnol. 11, 37 (2016).
2. Caldwell J. D. *et al.*, "Photonics with hexagonal boron nitride," Nat. Rev. Mater. 4, 552 (2019).
3. Jha P. K. *et al.*, "Nanoscale axial position and orientation measurement of hexagonal boron nitride quantum emitters using a tunable nanophotonic environment," Nanotechnology 33, 015001 (2012).
4. Yang F. *et al.,* A hybrid coupler for directing quantum light emission with high radiative Purcell enhancement to a dielectric metasurface lens," J. Appl. Phys. 130, 163103 (2021).
5. Jha P. K. *et al.*, "Metasurface-enabled remote quantum interference," Phys. Rev. Lett. 115, 025501 (2015).
6. Jha P. K. *et al.*, "Metasurface-mediated quantum entanglement," ACS Photonics 5, 971 (2017).

META 2023, PARIS - FRANCE, JULY 18 – 21, 2023

Carbon nanotubes and atomically thin materials integrated with silicon photonic crystal nanocavities

Y. K. Kato[1,2*]

[1]Nanoscale Quantum Photonics Laboratory, RIKEN Cluster for Pioneering Research, Saitama 351-0198, Japan
[2]Quantum Optoelectronics Research Team, RIKEN Center for Advanced Photonics, Saitama 351-0198, Japan
[*]corresponding author: yuichiro.kato@riken.jp

Abstract: Excitons in carbon nanotubes exhibit single photon emission at room temperature, and their telecommunication wavelength emission make them ideal for integration with silicon photonics. We have recently developed a transfer process utilizing anthracene crystals which allows for deterministic coupling of a nanotube emitter to a cavity. The same transfer process can be used to integrate atomically thin materials with the cavities, offering opportunities for manipulation of the photonic structures.

Electron-hole pairs form tightly-bound excitons in carbon nanotubes due to limited screening of the Coulomb interaction, and these stable excitonic states exhibit single photon emission at room temperature. Furthermore, they are ideal for integration with silicon photonics as their emission is in the telecommunication wavelength range [1,2]. In pristine air-suspended nanotubes, efficient exciton-exciton annihilation leads to antibunching [3], and cavity quantum electrodynamical effects can be utilized by coupling to silicon photonic crystal nanobeam cavities [4]. Functionalizing the nanotubes with organic molecules [5,6] should further enhance their performance. To overcome the low device yields with the probabilistic approach, we have developed a transfer process which allows for deterministic coupling of a nanotube emitter to a cavity [7]. Single-crystalline anthracene is used as a medium which readily sublimes by mild heating, leaving behind clean nanotubes and thus enabling bright photoluminescence. We are able to position nanotubes of a desired chirality with a sub-micron accuracy under in-situ optical monitoring. The anthracene assisted transfer process can also be used to integrate atomically thin materials with the nanobeam cavities to manipulate their properties [8]. With atomically precise thickness over a macroscopic area, few-layer flakes give rise to quantization of the mode shifts.

Work partly supported by JSPS (KAKENHI JP20H02558), MIC (SCOPE JP191503001), and MEXT (Nanotechnology Platform JPMXP09F20UT0053, JPMXP09F20UT0057, JPMXP09F21UT0009). We thank the Advanced Manufacturing Support Team at RIKEN for technical assistance.

References

1. A. Ishii, X. He, N. F. Hartmann, H. Machiya, H. Htoon, S. K. Doorn, Y. K. Kato, “Enhanced single photon emission from carbon nanotube dopant states coupled to silicon microcavities,” Nano Lett. 18, 3873 (2018).
2. D. Yamashita, H. Machiya, K. Otsuka, A. Ishii, Y. K. Kato “Waveguide coupled cavity-enhanced light emission from individual carbon nanotubes,” APL Photonics 6, 031302 (2021).
3. A. Ishii, T. Uda, Y. K. Kato, “Room-temperature single-photon emission from micrometer-long air-suspended carbon nanotubes,” Phys. Rev. Applied 8, 054039 (2017).
4. H. Machiya, D. Yamashita, A. Ishii, Y. K. Kato, “Evidence for near-unity radiative quantum efficiency of bright excitons in carbon nanotubes from the Purcell effect,” Phys. Rev. Research 4, L022011 (2022).

5. Z. Li, K. Otsuka, D. Yamashita, D. Kozawa, Y. K. Kato, “Quantum emission assisted by energy landscape modification in pentacene-decorated carbon nanotubes,” ACS Photonics 8, 2367 (2021).
6. D. Kozawa, X. Wu, A. Ishii, J. Fortner, K. Otsuka, R. Xiang, T. Inoue, S. Maruyama, Y-H. Wang, Y. K. Kato, “Formation of organic color centers in air-suspended carbon nanotubes using vapor-phase reaction,” Nat. Commun. 13, 2814 (2022).
7. K. Otsuka, N. Fang, D. Yamashita, T. Taniguchi, K. Watanabe, Y. K. Kato, “Deterministic transfer of optical-quality carbon nanotubes for atomically defined technology,” Nat. Commun. 12, 3138 (2021).
8. N. Fang, D. Yamashita, S. Fujii, K. Otsuka, T. Taniguchi, K. Watanabe, K. Nagashio, Y. K. Kato, “Quantization of mode shifts in nanocavities integrated with atomically thin sheets,” Adv. Opt. Mater. 10, 2200538 (2022).

Stimulated Emission from a Three-Level Quantum Ladder System

E. Schöll[1], B. Jonas[1,2], F. Sbresny[2], L. Hanschke[1,2], D. Heinze[1], P. Kallert[1], T. Langer[1], W. Rauhaus[2], B. Scaparra[2], K. Boos[2], E. Zubizarreta Casalengua[3], H. Riedl[2], E. del Valle[3], D. Reuter[1], S. Schumacher[1], J. J. Finley[2], A. Zrenner[1], K. Müller[2], and K. D. Jöns[1,*]

[1]Institute for Photonic Quantum Systems, Center for Optoelectronics and Photonics, and Department of Physics, Paderborn University, Paderborn, Germany
[2]Walter Schottky Institute and MCQST, TUM Munich, Munich, Germany
[3]Departamento de Física Teórica de la Materia Condensada, Universidad Autónoma de Madrid, 28049 Madrid, Spain
[*]corresponding author: klaus.joens@upb.de

Abstract: We investigate 3-level quantum ladder systems in optically active quantum dots and use additional stimulation lasers to tailor the emitted photons properties. We are able to realize highly indistinguishable photons and the on-demand generation of frequency tuned single-photons with polarization control.

With the advent of the second quantum revolution, striving for real-world applications of photonic quantum technologies, enormous efforts have been made to develop and optimize the necessary building blocks, in particular quantum light source. In recent years, epitaxial semiconductor quantum dots have made substantial progress as suitable quantum emitters.

One big advantage of quantum dots is their biexciton-exciton cascade forming a 3-level quantum ladder system commonly used to generate entangled photon pairs. However, the cascaded emission typically hinders the generation of highly indistinguishable photons, due to the intrinsic time correlation of the cascade [1]. To overcome this challenge, we proposed to use tailored Purcell enhancement to change the life time ratio between the exciton and biexciton states. The realization of such nanostructured cavities is technologically very demanding but to experimentally proof the concept we artificially reduced the biexciton excited state life time using a depopulating control laser [2]. With this technique we were able to restore the degree of indistinguishability to the level of the strictly resonantly excited exciton case. The benefit of using the two-photon excitation of the cascade plus a depopulating control laser is that we not only restore the degree of indistinguishability but also maintain the lower multi-photon emission stemming from the two-photon excitation of the cascade. Thus our scheme combines the advantages of strictly resonant excitation of the exciton (high indistinguishability) and two-photon excitation of the cascade (low multi-photon emission).

Furthermore, we are able to detune the control laser to use a virtual state for the realization of a stimulated spontaneous down-conversion process [3]. This process, which can also be explained in the dressed state picture, enables the on-demand generation of frequency tuned single-photons with polarization control. Based on our theoretical framework, we expect that the efficiency and tuning range of the down-conversion process can be vastly improved by the employment of cavities with high Purcell-factor.

References

1. E. Schöll and L. Schweickert et al., „Crux of using the cascaded emission of a three-level quantum ladder system to generate indistinguishable photons," Phys. Rev. Lett. 125, 233605 (2020).
2. F. Sbresny and L. Hanschke et al., "Stimulated generation of indistinguishable single photons from a quantum ladder system," Phys. Rev. Lett. 128, 093603 (2022).
3. B. Jonas et al., "Nonlinear down-conversion in a single quantum dot," Nature Communications 13, 1387 (2022).

META 2023, PARIS - FRANCE, JULY 18 – 21, 2023

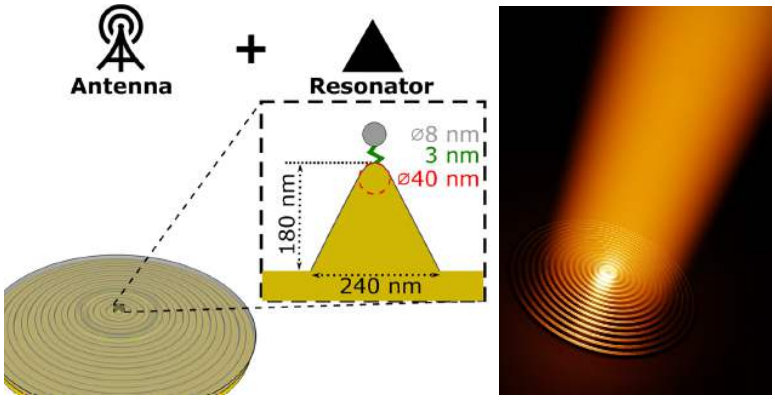
Room-temperature ultrabright single photon sources based on colloidal quantum dots on directional resonator-antennas: towards high dimensional encoding of photonic qudits

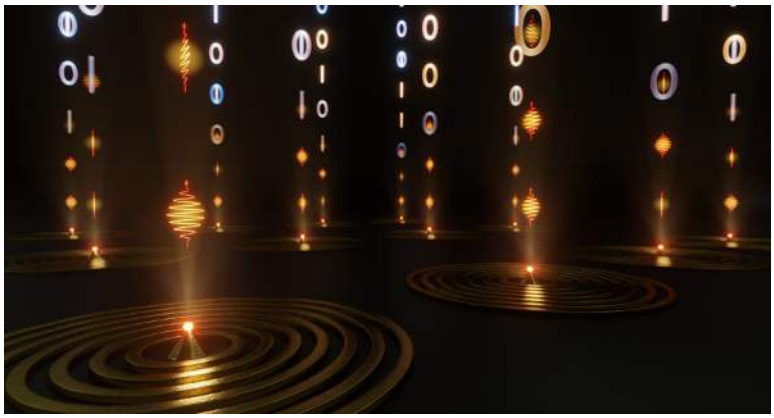
Ronen Rapaport[1, 2,*]

[1]*Racah Institute of Physics, The Hebrew University of Jerusalem, Jerusalem 9190401, Israel*
[2]*The Center for Nanoscience and Nanotechnology, The Hebrew University of Jerusalem, Jerusalem 9190401, Israel*
[*]*ronen.rapaport@mail.huji.ac.il*

Abstract: we present a novel approach that overcomes the outstanding challenge of the rate-directionality tradeoff of monolithic single photon sources operating at room temperature, and demonstrate ultrabright, highly directional single photon sources based on colloidal quantum dots positioned on a hybrid nano-resonator – antenna device, that can be used for both free-space and fiber applications. We also demostrate methods for encoding high-dimensional qudits on the different spatial degrees of freedom of the photons emitted from these sources.

Deterministic GHz-rate single photon sources at room-temperature would be essential components for various quantum applications. However, both the slow intrinsic decay rate and the omnidirectional emission of typical quantum emitters are two obstacles towards achieving such a goal which are hard to overcome simultaneously. We solve this challenge by a novel hybrid approach, using a complex monolithic photonic resonator constructed of a gold nanocone responsible for the rate enhancement, enclosed by a circular Bragg antenna for emission directionality [1,2]. A repeatable process accurately binds giant colloidal quantum dots that show blinkingless emission which is stable over hours, to the tip of the antenna-embedded nanocone. As a result we achieve simultaneous >20-fold emission rate enhancement and record-high directionality leading to an increase in the observed brightness by a factor as large as 450 (80) into an NA = 0.22 (0.5). We project that these miniaturised on-chip devices can reach photon rates approaching 1.4×10^8 single photons/second thus enabling ultrafast light-matter interfaces for quantum technologies at ambient conditions.





We further demostrate a significant progress towards a practical plug-and-play single photon source with an antenna device which allows back optical pumping of the quantum dots and a front directional single photon emission with high single photon purity and an almost unity colllection efficiency [3-6], as well as a direct coupling to a fiber without any coupling optics.

Finally, we show two distinct methods for encoding high-dimentional quantum information on the spatial degrees of freedom of the emitted photons. The first method takes advantage of the radial polarization nature of the emitted photons from the resoator-antenna device to encode information on mutually unbiased hybrid polarization modes. The second method utilizes spatial light modulators to encode information on the spatial orbital angular momentum states of the unpolarized photons emitted from the quantum dot.

Keywords: *Single photon sources, quantum dots, quantum optics, quantum information, plasmonics, colloidal nanocrystals, colloidal quantum dots*

References

[1] Hamza Abudayyeh and Ronen Rapaport, *Quantum Sci. Technol.* **2** 034004 (2017)
[2] Abudayyeh et al., *ACS Nano* 15, 11, 17384 (2021)
[3] Abudayyeh et al., *APL Photonics* 6, 036109 (2021)
[4] Abudayyeh et al., *ACS Photonics* 6, 446 (2019)
[5] Livneh et al., *Nanoletters* 16, 2527 (2016)
[6] Waltrich et al., *New Journal of Physics* 23, 113022 (2021)

Biography

Ronen Rapaport is a Professor at the Racah Institute of Physics at the Hebrew University of Jerusalem, Israel (HUJI). Ronen has received his PhD in Physics from the Technion, Israel in 2001, where he studied the physics of exciton polaritons. Ronen then became a principle investigator (MTS) at the Optical Physics department, Bell Laboratories, where he conducted research in various fields related to quantum nano-structures of semiconductors until 2007. Ronen is heading the Nanophotonics of quantum structures Lab at HUJI, with research efforts ranging from many-body quantum physics of excitons and polaritons in low dimensional quantum structures, to light-matter coupling of quantum emitters and nano-optical devices.

Generating Quantum Emitters in 2D Semiconductors Using UV Light

Xuedan Ma
Argonne National Laboratory
xuedanma@anl.gov

The controlled creation of quantum photon sources in two-dimensional transition metal dichalcogenides (TMDs) has attracted considerable interest primarily due to the unique characteristics of TMDs. Studies have discovered that both local strain modification[1] and ion beam irradiation[2] are viable approaches for creating quantum defects that are capable of single photon emission.

In this work, we report an alternative approach for generating quantum photon sources in TMDs utilizing easily accessible UV light.[3] This method leverages two recent findings: the small formation energies (a few eV) of chalcogen vacancies in this group of materials,[4] and the association of such chalcogen vacancies with single photon emitters.[5] By irradiating MoS_2 monolayers in vacuum with UV light, we discover quantum defects capable of single photon emission can be created. The success of this approach relies critically on the irradiation environment: only defects that are generated in vacuum exhibit single photon emission characteristics, whereas those created in air do not support single photon emission. Combining the optical features of the UV-induced defects with density functional theory calculations, we attribute the quantum defects generated in vacuum to pristine sulfur vacancies, whereas those in air to oxygen-passivated defects. These findings suggest that energies provided by UV photons are sufficient for creating quantum emitters in TMDs.

We acknowledge support from the Center for Molecular Quantum Transduction, an Energy Frontier Research Center funded by the U.S. Department of Energy, Office of Science, Office of Basic Energy Sciences, under award no. DE-SC0021314, National Science Foundation DMR Program under award no. DMR-1905990, and U.S. Department of Energy, Office of Science, National Quantum Information Science Research Centers. Work performed at the Center for Nanoscale Materials, a U.S. Department of Energy Office of Science User Facility, was supported by the U.S. DOE, Office of Basic Energy Sciences, under Contract No. DE-AC02-06CH11357.

References

1. Branny et al, Nat. Commun. 2017, 8, 15053; Palacios-Berraquero et al. Nat. Commun. 2017, 8, 15093
2. Klien et al. Nat. Commun. 2019, 10, 2755
3. Wang et al. ACS Nano 2022, 21240
4. Liu et al. Appl. Phys. Lett. 2013, 103, 183113
5. Mitterreiter et al. Nat. Commun. 2021, 12, 3822

META 2023, PARIS - FRANCE, JULY 18 – 21, 2023

Low Energy Focused Ion Beam Implantation

Michael Titze[1], Jonathan D. Poplawsky[2], Barney Doyle[1], Edward Bielejec[1], Alex Belianinov[1]

[1]Sandia National Laboratories, USA
[2]Center for Nanophase Materials, Oak Ridge National Laboratory, USA
*corresponding author: mictitz@sandia.gov

Abstract: We performed 1-2 keV focused Au implants into Si, in which the depth was validated by atom-probe tomography. We show that identical results are achievable by either lowering the column voltage, or decelerating ions using bias – while maintaining nanoscale spatial resolution. Furthermore, our data reveal that standard implant modeling overestimates experimental depth by 4.7× and 3.8× at 1 and 2 keV respectively. Finally, we demonstrate how our results pave a way to eV-scale implantation energies, while maintaining high spatial resolution.

Technological scaling towards smaller devices and shallower junctions requires decreasing ion energy. In parallel, the integration of novel materials necessitates additional ion species. Lastly, integration of 2D materials requires ion implantation to deterministically target single atomic layers, at precise location[1]. Focused ion beams (FIB) have demonstrated the ability of targeting nanoscale features, and using liquid metal alloy ion sources, a variety of ion species is available with isotopic resolution, required for QIS applications due to precise control over implanted ion hyperfine coupling. Here, we address the gap of low energy and precise positioning of exotic ion species by combining a multi-species FIB with a biased sample holder to allow implantation at 1 keV enabling a path towards implantation at eV-scale energies. The results of implantation by low source energy are compared to those using the biased plate and show agreement in ion range and straggle.

We use a 35 kV Raith VELION to implant Au. The ion landing energy is determined by both the source voltage and the bias plate voltage Fig. 1(a). We implant at V_S = 1,2,5 kV with the biased plate held at V_P = 0,0,4 kV leading to ion landing energies of 1, 2, and 1 keV, respectively.

The implants are assessed by atom-probe tomography (APT), a highly depth sensitive technique, although sample requirements are stringent. Commercially available pre-sharpened Si tips were used as the substrate for Au ion implantation for the APT experiment. As-received tips were first be pre-dulled in the APT setup using voltage mode and stopping at 5 kV to increase the top surface area because as-received tips consist only of a few unit cells at the surface. A scanning electron microscope image of a pre-dulled tip is shown in Fig. 1(b) with the original tip shape denoted by the white lines. APT is ideal for this measurement because it is a three-dimensional projection microscope equipped with a time-of-flight mass spectrometer that is capable of Å depth resolution (z). The resulting implant depth reconstruction of a tip is shown in Fig. 1(c). The datapoints are the measured Au concentration with different implant condition. Blue points correspond to V_S = 1 kV, V_P = 0 V, E = 1 keV, magenta points are V_S = 2 kV, V_P = 0 V, E = 2 keV, and red points denote V_S = 5 kV, V_P = 4 kV, E = 1 keV. The dashed lines are Gaussian fits to the data. Additionally, the results from Stopping and Range of Ions in Matter (SRIM) simulation are shown as the cyan (green) curves for E = 1 (2) keV, respectively. Notably, SRIM overestimates the range of ions by 4.7×, and 3.8×, at 1 and 2 keV, respectively. This discrepancy is explained by SRIM not considering multiple collisions, which are a significant stopping mechanism at low energy[2].

Lastly, we assess the feasibility of focused low energy implantation, required for devices. For this, we simulate a simplified version of the FIB in SIMION, consisting of a collimated beam being focused by an Einzel lens. The

optimal focus solution obtained at V_S = 5 kV, V_P = 0 kV, E = 5 keV is found to be a spot with 60 nm diameter. Then, the same focusing solution is used but V_P is increased to 4 kV, such that E = 1 keV, similar to the experiment performed in Fig. 1(a). Since refocusing of the beam using the biased plate may not be feasible due to the low ion energy leading to low secondary electron yield and the biased plate attracting any secondary electrons, we believe this to be a reasonable estimate of the best achievable spot size using this technique. We find that the ion beam diverges to form a 500 nm beam spot on the sample. However, by refocusing the Einzel lens our SIMION simulations shows we can obtain an 80 nm spot by changing the Einzel lens voltage by only 0.74 %.

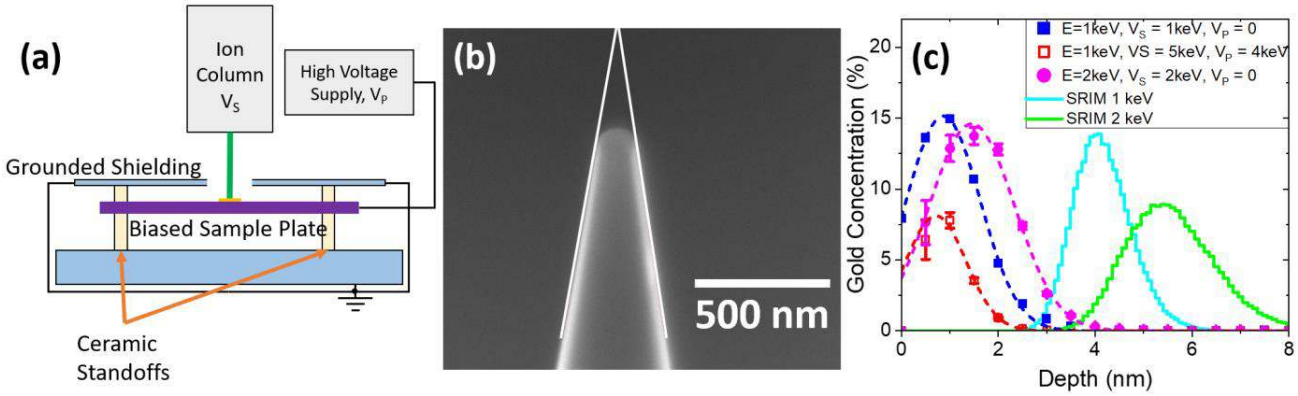


Figure 1(a) Schematic of the low energy focused ion implantation setup. The ion column produces ions at energy $q \times V_S$ where q is the ion charge state and V_S is the source voltage. The high voltage plate decelerates ions such that the ion landing energy $E = q \times (V_S - V_P)$. (b) Dulled APT tip used for measuring implant depth. The original tip shape is denoted by the white lines. (c) Measured implant depth using APT (points) and Gaussian fit (dashed lines). The corresponding ion landing energy SRIM simulations are shown as the solid lines.

In conclusion, we have implanted Au ions at landing energies of 1 and 2 keV and verified the implant depth using APT. Our results show the implant depth at 1 keV is 0.8 nm and at 2 keV it is 1.45 nm. SRIM simulations are found to be inadequate at these ions energies, overestimating the implant depth by 4.7× and 3.8× at 1 and 2 keV, respectively requiring more involved treatment of the modeling of low energy implantation. We also present a focusing solution of the decelerated ions using SIMION, showing a 60 nm beam spot can be achieved for 5 keV Au ions while a 1 keV ion may be focused to a 80 nm spot size.

Acknowledgements

This work was performed, in part, at the Center for Integrated Nanotechnologies, an Office of Science User Facility operated for the U.S. Department of Energy (DOE) Office of Science. Sandia National Laboratories is a multimission laboratory managed and operated by National Technology & Engineering Solutions of Sandia, LLC, a wholly owned subsidiary of Honeywell International, Inc., for the U.S. DOE's National Nuclear Security Administration under contract DE-NA-0003525. APT research was supported by the Center for Nanophase Materials Sciences (CNMS), which is a US Department of Energy, Office of Science User Facility at Oak Ridge National Laboratory. The views expressed in the article do not necessarily represent the views of the U.S. DOE or the United States Government.

References

1. Kang, S. et al., "Highly enhanced Ferroelectricity in HfO2 based Ferroelectric Thin Film by Ligh Ion Bombardment", Science, Vol. 376, No. 6594, 731-738 (2022)
2. Hofsäss, H. and Stegmaier, A., "Binary collision approximation simulations of ion solid interaction without the concept of surface binding energies", Nucl. Instr. Meth. B, Vol. 517, 49-62 (2022)

META 2023, PARIS - FRANCE, JULY 18 – 21, 2023

Integrated Quantum Dot Optomechanics

M. Weiß[1,2], D. Wigger[3,4], D. D. Bühler[5], E. D. S. Nysten[1,2], M. Choquer[6], M. Lienhart[2,7], B. Mayer[1,2], A. Vogele[2], A. Crespo-Povedo[8], K. Müller[9], J. J. Finley[7], A. Rastelli[10], T. Kuhn[11], P. Machnikowski[3], M. M. de Lima Jr.[5], P. V. Santos[8], G. Moody[6], H. J. Krenner[1,2,*]

[1]Physikalisches Institut, Universität Münster, Münster, Germany
[2]Lehrstuhl für Experimentalphysik I, Universität Augsburg, Augsburg, Germany
[3]Department of Theoretical Physics, Wrocław University of Science and Technology, Wrocław, Poland
[4]School of Physics, Trinity College Dublin, Dublin, Ireland
[5]Materials Science Institute (ICMUV), Universitat de València, València, Spain
[6]Electrical and Computer Engineering, University of California Santa Barbara, Santa Barbara CA, United States
[7]Walter Schottky Institut, School of Natural Sciences, TU München, Garching, Germany
[8]Paul-Drude-Institut für Festkörperelektronik, Berlin, Germany.
[9]Walter Schottky Institut, School of Computation, Information and Technology, TU München, Garching, Germany
[10]Institute of Semiconductor and Solid State Physics, Johannes Kepler Universität Linz, Linz, Austria
[11]Institut für Festkörpertheorie, Universität Münster, Münster, Germany
[*]corresponding author: krenner@uni-muenster.de

Abstract: Elastic waves and phonons are an indispensable resource for radio frequency signal processing. Recently, elastic waves have been recognized as versatile transducers between dissimilar quantum systems for hybrid quantum technologies. Here show recent advances including piezo-optomechanical wave mixing by a single quantum dot, acoustically regulated single photon emission or dynamic routing of on-chip generated single photons. Finally, we highlight how the governing acousto-optic interactions can be deliberately enhanced in heterogeneously integrated devices and nanophononic devices.

Over the past decades, innovation for radically new devices was mostly driven by controlling electrons and photons: microelectronics (electrons) and photonics (photons) revolutionized our everyday life. Today, Surface Acoustic Waves (SAWs) and other types of elastic waves are one of the only very few phononic technologies of industrial relevance. Acoustic radio frequency filters, for instance, are integral parts of wireless devices and SAWs find applications in life sciences and microfluidics for sensing and mixing of tiny amounts of liquids (1). In fundamental and applied research, these “nanoquakes on a chip” provide an extremely useful and versatile tool for massively parallel addressing a broad variety of nanosystems at radio frequencies via strong acousto-mechanical and acousto-electric couplings.

In this presentation, we highlight our recent advances towards the realization of hybrid phononic quantum technologies. We synergistically couple single quantum emitters in the form of III-V compound semiconductor quantum dots (QDs), laser photons and phonons in the form of nanoscale sound waves and demonstrate several key functionalities required for hybrid quantum technologies. Specific examples include the deliberate coherent control of optically active quantum dots and their coupling to light by the SAW’s coherent acoustic field. The coherent optomechanical coupling gives rise to wave mixing between optical photons and GHz phonons by the optical dipole of the quantum dot (2). Moreover, QDs embedded in integrated photonic structures enable precisely triggered single photon generation by dynamic modulation of the Purcell-effect (3) or single photon routing at GHz frequencies in a SAW-modulated integrated Mach-Zehnder interferometer (4). Finally, we show

that these concepts can be transferred to a hybrid architecture comprising epitaxial QD membranes heterogeneously integrated onto $LiNbO_3$ (5,6). This novel class of devices combines the superior optical properties of semiconductor QDs and strong piezoelectricity of $LiNbO_3$ for efficient on-chip optomechanical quantum transduction, ultimately in the limit of single quanta.

This work is supported in parts by Deutsche Forschungsgemeinschaft (DFG, German Research Foundation) under Grant 465136867 (QUASAR).

References

1. Delsing, P. et al., "2019 surface acoustic wave roadmap," J. Phys. D: Appl. Phys., Vol. 52, 353001, 2019.
2. Weiß, M. et al., "Optomechanical wave mixing by a single quantum dot," Optica, Vol. 8, 291, 2021.
3. Weiß, M. et al., "Surface acoustic wave regulated single photon emission from a coupled quantum dot–nanocavity system," Appl. Phys. Lett., Vol. 109, 033105, 2016
4. Bühler, D. D. et al., "On-chip generation and dynamic piezo-optomechanical rotation of single photons," Nat. Commun., Vol. 13, 6998, 2022
5. Nysten E. D. S. et al., "A hybrid (Al)GaAs-$LiNbO_3$ surface acoustic wave resonator for cavity quantum dot optomechanics," Appl. Phys. Lett., Vol. 117, 122106, 2020
6. Lienhart, M. et al., "Heterogeneous integration of superconducting thin films and epitaxial semiconductor heterostructures with Lithium Niobate," preprint: arXiv:2302.02712, 2023

META 2023, PARIS - FRANCE, JULY 18 – 21, 2023

Indistinguishable telecom-band single photons from a coupled cavity-nanotube system at room temperature

L. Husel[1], J. Trapp[1], M. Nutz[1,2], M. Förg[1,2], J. Noé[1,2], T. Hümmer[1,2], P. Wang[3], J. Wu[3], Y.-H. Wang[3], D. Hunger[4] and A. Högele[1,5*]

[1]Fakultät für Physik, Munich Quantum Center, and Center for NanoScience (CeNS), Ludwig-Maximilians-Universität, Geschwister-Scholl-Platz 1, 80539 München, Germany

[2]Qlibri GmbH, Maistr. 67, 80337 München, Germany

[3]Department of Chemistry and Biochemistry, University of Maryland, 8051 Regent Drive, College Park, Maryland 20742, United States

[4]Karlsruher Institut für Technologie, Physikalisches Institut, Institut für Quanten Materialien und Technologien, Wolfgang-Gaede-Str. 1, 76131 Karlsruhe, Germany

[5]Munich Center for Quantum Science and Technology (MCQST), Schellingtr. 4, 80799 Munich, Germany

[*]corresponding author: alexander.hoegele@lmu.de

Carbon nanotubes have emerged as solid-state sources of quantum light for advances in quantum photonic technologies [1]. In particular, luminescent quantum defects in carbon nanotubes with deep exciton-localizing potentials are known to exhibit highly non-classical correlations in photon emission statistics up to room temperature [2] with emission wavelengths that can be tailored to the telecom band [3]. Here, we report successful incorporation of luminescent quantum defects with room-temperature telecom-band single-photon emission into a fiber-based open microcavity [4] and report the characteristics of the coupled system in the regime of incoherent good cavity coupling [5].

References

1. He, X., H. Htoon, S. K. Doorn, W. H. P. Pernice, F. Pyatkov, R. Krupke, A. Jeantet, Y. Chassagneux, and C. Voisin, Carbon nanotubes as emerging quantum-light sources, Nature Materials 17, 663, 2018.
2. Ma, X., N. F. Hartmann, J. K. S. Baldwin, S. K. Doorn, and H. Htoon, Room-temperature single-photon generation from solitary dopants of carbon nanotubes, Nature Nanotechnology 10, 671, 2015.
3. X. He, N. F. Hartmann, X. Ma, Y. Kim, R. Ihly, J. L. Blackburn, W. Gao, J. Kono, Y. Yomogida, A. Hirano, T. Tanaka, H. Kataura, H. Htoon, and S. K. Doorn, Tunable room-temperature single-photon emission at telecom wavelengths from sp3 defects in carbon nanotubes, Nature Photonics 11, 577, 2017.
4. Hunger, D. et al. A fiber fabry–perot cavity with high finesse, New Journal of Physics 12, 065038, 2010.
5. Auffèves, A., J.-M. Gérard, and J.-P. Poizat, Pure emitter dephasing: A resource for advanced solid-state single-photon sources, Physical Review A 79, 053838, 2009.

Hybrid high-Q nanocavities for 2D materials and their heterostructures

C. Qian[1,*], V. Villafañe[1], P.Soubelet[1], A. Hötger[1], T.Taniguchi[2], K. Watanabe[3], N. P. Wilson[1], A. V. Stier[1], A. W. Holleitner[1], and J. J. Finley[1,†]

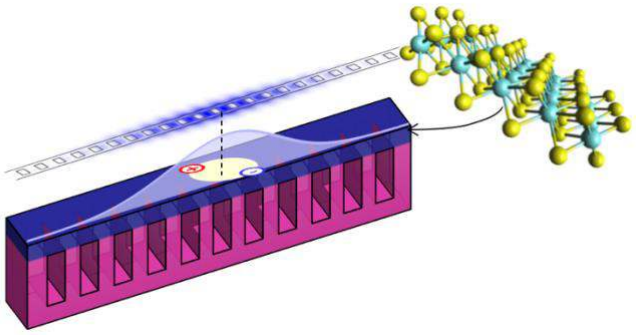
1 Walter Schottky Institut and Physik Department, Technische Universität München, Am Coulombwall 4, 85748 Garching, German

2 International Center for Materials Nanoarchitectonics, National Institute for Materials Science, 1-1 Namiki, Tsukuba 305-0044, Japan

3 Research Center for Functional Materials, National Institute for Materials Science, 1-1 Namiki, Tsukuba 305-0044, Japan

ABSTRACT: 2D semiconductors such as transition metal dichalcogenides (TMDs) and defects in hBN are ideally suited for solid-state cavity quantum electrodynamics (cQED) investigations. The exciton binding energies in TMDs are very strongly bound and emission linewidths close to the homogeneous limit when monolayers, hetero- and homo-bilayers are suitably encapsulated by hexagonal boron nitride (hBN). In addition, 2D-heterostructures can be readily attached to a wide range of substrates, making them ideally suited for solid-state cQED experiments with heterogeneous integration.

In this contribution, we describe our recent investigations of the heterogeneous integration of 2D materials onto novel Si_3N_4 nanobeam optical cavities [1-5]. Such zip-tie nanobeam optical resonators host ultra-high $Q > 10^4 - 10^5$ cavity modes and allow us to explore novel light-matter and multimodal *vibronic – phonon – photon* couplings mediated by electronic excitations. For hBN-encapsulated MoS_2 monolayers, we observe a nonmonotonic temperature dependence of the cavity-trion interaction strength, consistent with the nonlocal light-matter interactions in which the extent of the centre-of-mass wave function is comparable to the cavity mode volume in space [1]. For $MoSe_2$ homo-bilayers [2], we study the twist-dependent moiré coupling. For small angles, we find a pronounced redshift of the K−K and Γ−K excitons, an effect that we trace to the underlying moiré pattern. Studies of thick hBN layers coupled to ziptie cavities reveal intriguing dynamics: For example, we identify the zero phonon line transition of charged boron vacancies (V_B^-) [3,4] and observe a novel tripartite coupling between the cavity photonic modes, lattice phonon and nanobeam vibrational modes. The fingerprint for this tripartite coupling is a pronounced asymmetry in the emission spectrum for cavities with Q-factor above a threshold of ~10^4. Similar asymmetries are not observed for cavities without V_B^- centers, or lower Q-cavities. To explain our findings, we model the system with phonon-induced light-matter coupling and compare it to the Jaynes-Cummings model for usual emitters. Our results reveal that the multipartite interplay arises during the light-matter coupling of V_B^- centers, illustrating that it is phonon-induced, rather than caused by the thermal population of phonon modes. Our results indicate how different photon (V_B^- emission, cavity photonic) and phonon (V_B^- phonon, cavity mechanical) modes provides a novel system to interface spin defects, photons and phonons in condensed matter systems.



[1] C. Qian et al. Phys. Rev. Lett. **128**, 237403 (2022)
[2] V. Villafane et al. Phys. Rev. Lett. 130, 026901, (2022)
[3] C. Qian et al. arXiv 2210.00150, to appear in Phys. Rev. Lett. (2023)
[4] C. Qian et al. Nano Lett, 22, 13, 5137–5142, (2022)
[5] R. Rizzato et al. arXiv 2212.12816 (2023)

META 2023, PARIS - FRANCE, JULY 18 – 21, 2023

Exciton photophysics in $MoSe_2$-WSe_2 Moiré hetero-bilayers

Arnab Barman Ray[1], Arunabh Mukherjee[1], Liangyu Qiu[1], Sefaattin Tongay[2], Anthony Nickolas Vamivakas[1]

[1]*The Institue of Optics, University of Rochester, Rochester 14627, New York, USA*

[2]*Arizona State University, 1151 S Forest Ave, Tempe, AZ 85281, USA*

abarmanr@ur.rochester.edu

Abstract: *: The stacking of 2D materials in Moiré heterobilayers provide a novel platform to study intra and interlayer excitons. Of interest for quantum science is the bilayers exhibit a natural and periodic trapping potential that enables a spatially periodic array of programmable quantum emitters. In this talk we discuss the $MoSe_2$-WSe_2 system. The atomically sharp interface between the two monolayers creates an effective type-2 heterojunction that allows ultrafast charge transfer and the existence of trapped interlayer excitons upon optical excitation. Our work investigates and elucidates the nature of the quantum emitter ensemble in these materials. We demonstrate the existence of valley coherence for trapped trions, excitons, and biexcitons. Our results contribute to an understanding of trapped excitonic species in these systems and how they may be utilized for quantum information storage.*

A. Observation of Valley Coherence

Moiré excitons represent a new paradigm in exciton photophysics and should inherit some photophysical properties from the constituent monolayer materials[1-5]. One characteristic, excitonic valley coherence, is well-studied in monolayer transition metal dichalcogenides [6-8]. In this work, we use low-temperature polarization resolved micro-photoluminescence (PL) spectroscopy to characterize interlayer exciton valley coherence in H-type $MoSe_2$/WSe_2 Moiré hetero-bilayers.

In Figure 1, an exemplary data set on valley coherence is presented. The valley coherence is measured as a function of the laser illumination wavelength. To access the valley coherence, linearly polarized laser excitation excites the sample excitons. PL with a polarization oriented parallel (perpendicular) to the excitation direction is measured. From the recorded spectrum, the degree of valley is calculated by taking the difference between the measured spectra over their sum. The left panel of Fig. 1 and middle panel of Fig. 1 presents the recorded parallel and perpendicular spectra for an excitation wavelength of 725 nm and 705 nm. In the right panel of Fig. 1 the spectral variation of the valley coherence is shown. Similar to the degree of valley polarization [9-11], the A-exciton resonances of both $MoSe_2$ and WSe_2 lead to larger amounts of observed valley coherence.

We note that on average the observed degree of valley coherence found in the sample (~10%) is less than that reported for monolayers. This can be attributed to the spatial nonuniformity in PL we have seen across the interlayer region. In certain sample locations we did observe valley coherence of ~ 50%, but it was not the average observed behavior.

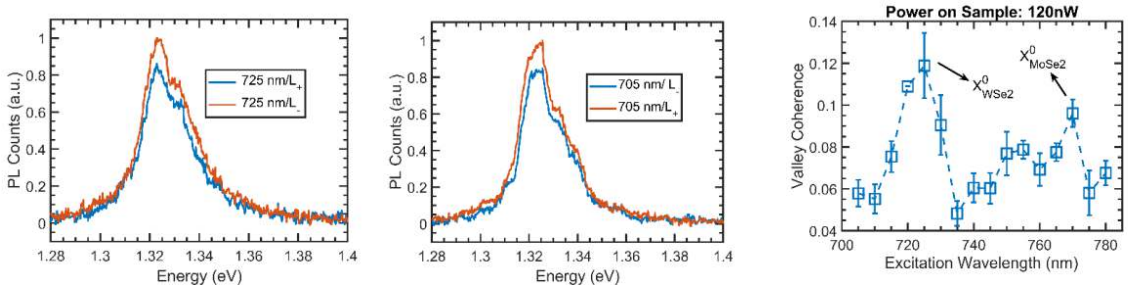


Figure 1 PL from interlayer excitons showing different intensities for parallel-polarized (L_+) and perpendicularly-polarized(L_-) emission. The left panel is for 725 nm excitation and the right panel is for 705 nm excitation. Both data sets exhibit valley coherence. Right panel is the variation observed in valley coherence as a function of excitation wavelength. For all data the excitation laser powers is kept at 120 nW.

Acknowledgments

This work was supported by AFOSR FA9550-19-1-0074 from the Cornell Center for Materials Research with funding from the NSF MRSEC program (DMR-1719875). The authors would also like to thank UR Nano, the nano-fabrication facility at the University of Rochester where some of the work was carried out.

References

1. C. Jin et al., "Observation of moiré excitons in WSe2/WS2 heterostructure superlattices," Nature, vol. 567, no. 7746, pp. 76-80, 2019/03/01 2019, doi: 10.1038/s41586-019-0976-y.
2. M. Förg et al., "Moiré excitons in MoSe2-WSe2 heterobilayers and heterotrilayers," Nature Communications, vol. 12, no. 1, p. 1656, 2021/03/12 2021, doi: 10.1038/s41467-021-21822-z.
3. H. Yu, G.-B. Liu, J. Tang, X. Xu, and W. Yao, "Moire excitons: From programmable quantum emitter arrays to spin-orbit coupled artificial lattices," Science Advances, vol. 3, no. 11, p. e1701696, 2017, doi: doi:10.1126/sciadv.1701696.
4. K. L. Seyler et al., "Signatures of moiré-trapped valley excitons in MoSe2/WSe2 heterobilayers," Nature, vol. 567, no. 7746, pp. 66-70, 2019/03/01 2019, doi: 10.1038/s41586-019-0957-1.
5. K. F. Mak and J. Shan, "Semiconductor moiré materials," Nature Nanotechnology, vol. 17, no. 7, pp. 686-695, 2022/07/01 2022, doi: 10.1038/s41565-022-01165-6.
6. K. Hao et al., "Direct measurement of exciton valley coherence in monolayer WSe2," Nature Physics, vol. 12, no. 7, pp. 677-682, 2016/07/01 2016, doi: 10.1038/nphys3674.
7. A. M. Jones et al., "Optical generation of excitonic valley coherence in monolayer WSe2," Nature Nanotechnology, vol. 8, no. 9, pp. 634-638, 2013/09/01 2013, doi: 10.1038/nnano.2013.151.
8. A. Ciarrocchi, D. Unuchek, A. Avsar, K. Watanabe, T. Taniguchi, and A. Kis, "Polarization switching and electrical control of interlayer excitons in two-dimensional van der Waals heterostructures," Nature Photonics, vol. 13, no. 2, pp. 131-136, 2019/02/01 2019, doi: 10.1038/s41566-018-0325-y.
9. W. Li, X. Lu, S. Dubey, L. Devenica, and A. Srivastava, "Dipolar interactions between localized interlayer excitons in van der Waals heterostructures," Nature Materials, vol. 19, no. 6, pp. 624-629, 2020/06/01 2020, doi: 10.1038/s41563-020-0661-4.
10. S. K. Behura, A. Miranda, S. Nayak, K. Johnson, P. Das, and N. R. Pradhan, "Moiré physics in twisted van der Waals heterostructures of 2D materials," Emergent Materials, vol. 4, no. 4, pp. 813-826, 2021/08/01 2021, doi: 10.1007/s42247-021-00270-x.
11. L. Zhang et al., "Highly valley-polarized singlet and triplet interlayer excitons in van der Waals heterostructure," Physical Review B, vol. 100, no. 4, p. 041402, 07/03/ 2019, doi: 10.1103/PhysRevB.100.041402.

META 2023, PARIS - FRANCE, JULY 18 – 21, 2023

From flask to devices: Exceptionally functional colloidal quantum emitters and deterministic integration

E. Dolgopolova,[1] E. G. Bowes,[1] R. Rapaport,[2] A. Piryatinski,[3] H. Htoon,[1] and J. A. Hollingsworth[1*]

[1]Materials Physics & Applications Division: Center for Integrated Nanotechnologies, Los Alamos National Laboratory, New Mexico 87545, USA

[2]Racah Institute of Physics, The Hebrew University of Jerusalem, Jerusalem 9190401, Israel

[3]Theoretical Division: Physics of Condensed Matter and Complex Systems, Los Alamos National Laboratory, New Mexico 87545, USA

[*]corresponding author: jenn@lanl.gov

Abstract: Colloidal quantum dots (cQDs) synthesized in simple laboratory flasks are finding real-world applications in demanding technologies from displays and lighting to photovoltaics and photodetectors. In the future, cQDs may be the basis for single-photon devices in quantum networks. Beyond quantum-size control, we pursue an expanded "structural toolbox" to synthetically engineer new quantum emitters with optimal photophysical properties.[1-8] Taking advantage of their solution-phase processibility, we demonstrate deterministic, direct-write placement of the quantum emitters into photonic and plasmonic platforms using scanning-probe techniques.[9,10]

New cQDs and other nanocrystalline semiconductor quantum emitters continue to be discovered. Here, I will describe our efforts using two strategies to identify and control quantum optical properties in new/optimized systems: (1) solution-phase chemistry to "nanoengineer" all aspects of the nanocrystal via a deep understanding of synthesis-nanostructure-property relationships (Figure. 1a-c) and (2) deterministic integration of quantum emitters with nanoplasmonic/photonic structures via a scanning-probe technique (Figure 1d).

Recently, we demonstrated through designed shell growth PbS/CdS core/shell cQDs that could deliver single photons in the telecom O and S bands at room-temperature, obtaining single-emitter spectra at this elevated temperature for the first time.[1] Two shell-growth methods—cation exchange and successive ionic layer adsorption and reaction (SILAR)—were employed to prepare cQD heterostructures with shells of 2–16 monolayers, allowing us to identify the shell properties responsible for enhanced stability. With collaborators we have since rectified the inherently slow photon-delivery rate characteristic of Pb-chalcogenide cQDs by integration with nanoplasmonic antenna—demonstrating >2000-fold rate enhancement with retention of non-blinking/non-photobleaching behavior.

Deterministic emitter-photonic/plasmonic integration has been aided by our development of a three-step reading-inking-writing approach using dip-pen nanolithography (DPN).[9,10] First, atomic force microscopy (AFM) images of a nanostructured surface are obtained that serve as a "topography map" to guide writing of liquid ink. The DPN "ink" comprises gQDs suspended in a solvent, e.g., *o*-dichlorobenzene. Systematic analyses of factors influencing deposition rate—dwell time, ink-substrate contact angle and ink volume—were assessed for flat substrates and pushed to small (sub-500 nm) feature sizes.[9] This knowledge was subsequently translated to the 3-step writing process to deposit cQDs onto photonic or plasmonic nanostructures, now down to the single-QD level.[10] Overall, the results lay the groundwork for expanded use of nanocrystal liquid inks and DPN for fabrication of multi-component nanostructures that are challenging to create using traditional lithographic techniques.

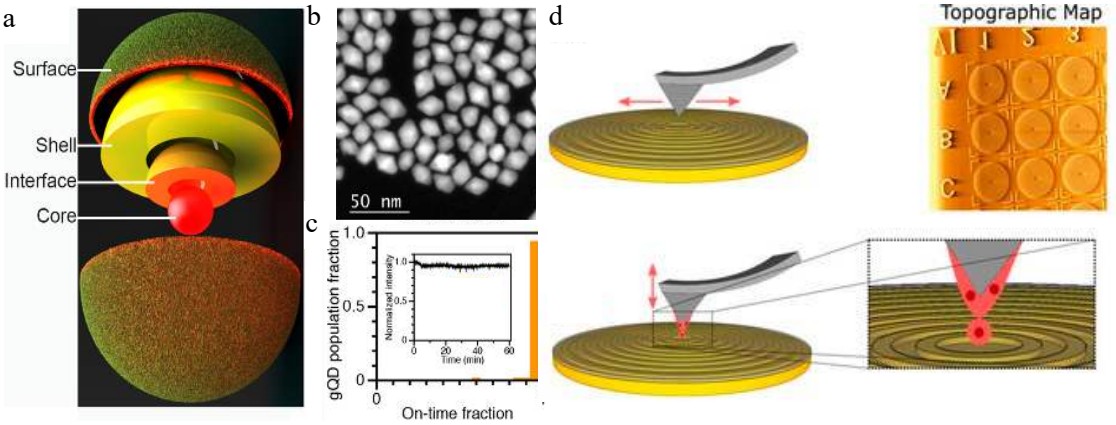


Figure 1. (a) Schematic illustration of the components of a core/shell QD from the inside out. Whether a spherical QD or some other shape, these components must be synthetically controlled to obtain ideal single-photon emission. **(b)** High-angle annular dark-field (HAADF-STEM) image of CdSe/CdS "giant" QDs (gQDs), the prototype gQD.[8] **(c)** On-time fraction as a function of CdSe/CdS gQD population fraction under high pump-fluence widefield excitation and collection conditions (1 W/mm^2, 405 nm continuous-wave excitation, room-temperature), demonstrating non-blinking behavior—*a key attribute for an on-demand quantum emitter that has now been extended from the blue-green to the full telecommunications window*.[1-7] Inset shows non-photobleaching over a long observation time (1 h). **(d)** Precision additive nanofabrication via dip-pen nanolithography (from Ref. 10): **(top)** An AFM scan of the area of interest is conducted; right panel shows an actual image of the scanning of an antenna array comprising hybrid metal–dielectric bullseye antennas. **(bottom)** AFM writing tip is wetted, and a droplet of dilute QD suspension is placed at the center of each bullseye structure (guided by the image created in the first step), leaving behind a single QD or a small cluster with ~25% success rate, far exceeding random distribution approaches.

References

1. Krishnamurthy, S. et al., "PbS/CdS Quantum Dot Room-Temperature Single-Emitter Spectroscopy Reaches the Telecom O and S Bands via an Engineered Stability," ACS Nano, Vol. 15, No. 1, 575-587, 2021.
2. McBride, J. R. et al., "Role of shell composition and morphology in achieving single-emitter photostability for green-emitting "giant" quantum dots," J. Chem. Phys. Vol. 152, 124713-1-11, 2020.
3. Dennis, A. M. et al., "Role of Interface Chemistry in Opening New Radiative Pathways in InP/CdSe Giant Quantum Dots with Blinking-Suppressed Two-Color Emission," Adv. Funct. Mater. Vol. 29, No. 37, 1809111-1-10, 2019.
4. Hanson, C. J. et al., "Giant PbSe/CdSe/CdSe Quantum Dots: Crystal-Structure-Defined Ultrastable Near-Infrared Photoluminescence from Single Nanocrystals," J. Am. Chem. Soc. Vol. 139, No. 32, 11081-11088, 2017.
5. Mishra, N. et al., "Using shape to turn off blinking for two-colour multiexciton emission in CdSe/CdS tetrapods," Nature Commun. Vol. 8, 15083-1-9, 2017.
6. Dennis, A. M. et al., "Suppressed Blinking and Auger Recombination in Near-Infrared Type-II InP/CdS Nanocrystal Quantum Dots," Nano Lett., Vol. 12, No. 11, 5545-5551, 2012.
7. Ghosh, Y. et al., "New Insights into the Complexities of Shell Growth and the Strong Influence of Particle Volume in Nonblinking "Giant" Core/Shell Nanocrystal Quantum Dots," J. Am. Chem. Soc. Vol. 134, No. 23, 9634-9643, 2012.
8. Chen, Y. et al., "Giant" Multishell CdSe Nanocrystal Quantum Dots with Suppressed Blinking," J. Am. Chem. Soc. Vol. 130, No. 15, 5026-5027, 2008.
9. Dawood, F. et al., "The Role of Liquid Ink Transport in the Direct Placement of Quantum Dot Emitters onto Sub-Micrometer Antennas by Dip-Pen Nanolithography," Small, Vol. 14, No. 31, 1801503-1-10, 2018.
10. Abudayyeh, H. et al., Single Photon Sources with Near Unity Collection Efficiencies by Deterministic Placement of Quantum Dots in Nanoantennas," APL Photonics Vol. 6, 036109-1-7, 2021.

META 2023, PARIS - FRANCE, JULY 18 – 21, 2023

Localized Dipolar Excitons in 2D Semiconductors for Quantum Sensing of Correlated Electrons

A. Srivastava[1*]

[1]Emory University, USA

[*]corresponding author: ajit.srivastava@emory.edu

Abstract: We report localized dipolar excitons as high-resolution quantum sensors of generalized Wigner crystals in $WSe_2/MoSe_2/WSe_2$ heterotrilayer.

Atomically thin materials, such as graphene and transitional metal dichalcogenides (TMDs), are at the forefront of research in materials physics. This is largely due to the ease with which they can be combined into artificially engineered heterostructures that exhibit emergent electronic and optical properties. Enhanced Coulomb interactions in the truly 2D limit, reduced kinetic energy of electrons in moiré heterostructures and the presence of nontrivial quantum geometry is a perfect recipe for strongly correlated and topological electronic phases. Moreover, strong light-matter coupling results in stable optically excited quasiparticles such as excitons and their neutral and charged complexes. Furthermore, moiré heterostructures present a unique opportunity to study the interplay of correlated electrons and excitons. While electronic phases have garnered a lot of attention, many-body correlated phases of interacting optical excitations remain poorly studied. These out-of-equilibrium quantum phases could also serve as sources of exotic light.

In this talk, I will begin by highlighting some unique properties of excitons in TMDs. Next, I will show how trapped dipolar excitons can serve as high-resolution quantum sensors of correlated electronic phenomena[1]. Finally, I will talk about our recent efforts to engineer the internal structure of excitons to tune the strength and sign of excitonic interactions[2] as a step towards realizing on-demand quantum matter in a driven-dissipative setting.

References

1. Li *et al*., “Local Sensing of Correlated Electrons in Dual-moiré Heterostructures using Dipolar Excitons”, *arXiv: 2111.09440*
2. Lastname, Li et al., “Quadrupolar excitons in a tunnel-coupled van der Waals heterotrilayer”, arXiv: 2208.05490.

Site Controlled Integration of SiN/SiO_2 Single Photon Emitters with a Topologically-Optimized Coupler

Samuel Peana[1-3,*], Omer Yesilyurt[1-3], Zachariah O. Martin[1-3], Alexander Senichev[1-3], Vahagn Mkhitaryan[1-3], Alexei S. Lagutchev[1,3], Alexandra Boltasseva[1-3], [3]Alexander V. Kildishev[1-3], and Vladimir M. Shalaev[1-3]

[1]Birck Nanotechnology Center and School of ECE, Purdue University, West Lafayette, IN 47907, USA

[2]Purdue Quantum Science and Engineering Institute, Purdue University, West Lafayette, IN 47907, USA

[3]Quantum Science Center, a National Quantum Information Science Research Center of the U.S. Department of Energy, Oak Ridge, TN 37931, USA

[*]Email: speana@purdue.edu

Abstract: We demonstrate the first site-controlled integration of an SiN/SiO2 single photon emitter (SPE) with a topology optimized coupler. Previously our group demonstrated the large scale fabrication of such emitters in nanopillars with high yield (67%). This work leverages this fabrication process to allow for the large-scale integration of such nanopillar SPEs with complex nanophotonic devices such as topology optimized couplers. This is a major step on the path towards wafer-scale fabrication of quantum-photonic circuitry with precisely integrated SPEs.

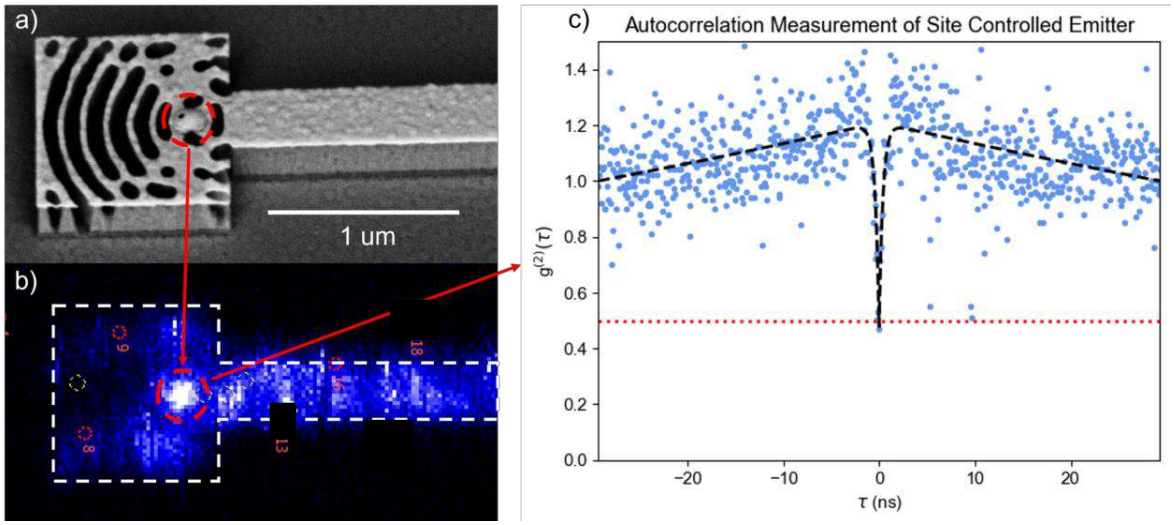


Figure 1 a) A scanning electron microscopy image of a fabricated TO coupler. The red circled bump is the location of the nanopillar hosting the SPE. **b)** A photoluminescence image of a similar structure, the red circled bright spot is the location of the embedded SPE, **c)** An autocorrelation measurement with the Hansbury-Brown-Twiss setup showing a dip at 0 of 0.47 indicating that the bright spot is hosting a SPE.

For photonic quantum information systems and technology (QIST), photons are the basic information-carrying units. One of the major approaches for generating single photons useful for QIST application is the application of solid-state single-photon sources – mechanically stable, bright, on-demand, and potentially ultra-compact sources of indistinguishable photons. However, integrating such emitters into nanophotonic structures is generally very challenging, both from a design and fabrication point of view [1–4]. One of the challenges is to efficiently channel the SPE light into nanophotonic circuitry with high efficiency [1–4].

We will briefly overview an adjoint topology optimization scheme used to design high-efficiency couplers [5]. This technique is computationally tested for coupling light emitted by an hBN SPE into a single-mode on-chip

silicon nitride (SiN) waveguide.

Recently, a new type of SPEs occurring at the interface between SiN/SiO_2 was discovered. They have proven to be bright, stable, and, most importantly, native to SiN [6], making its integration with SiN circuitry much more straightforward and monolithic. We demonstrated some initial integration of such emitters with on-chip waveguides and developed a novel technique for the site-controlled fabrication of SiN/SiO_2 emitters achieving 67% yield with an estimated lateral placement accuracy < ±85nm [7]. The approach includes fabricating SiN/SiO_2 nanopillars followed by thermal processing. Since the emitters are defined lithographically, multi-mask alignment techniques can create other structures aligned with the SPE-filled nanopillars. This is leveraged to align TO couplers and other nanophotonic elements with SPE-containing nanopillars. The scanning electron microscopy (SEM) image (figure 1a) shows the TO coupler etched around the emitter. The emitter is visible as the red circled bump where the emitter is encased in the SiN layer forming the TO coupler and waveguide. Figure 1b depicts an image of a similar structure using a custom-built scanning confocal photoluminescence setup at room temperature. As expected, the red-circled bright spot in the photoluminescence image is right at the SPE location. Finally, $g_2(0)$ measurement with a typical Hanbury-Brow-Twiss setup at room temperature confirms that the emission originates from an SPE with a $g_2(0)$ of 0.47.

In conclusion, we will briefly overview a technique for designing TO couplers. We also discuss the large-scale production of such couplers with precisely integrated SiN/SiO_2 SPEs leveraging a novel site-controlled fabrication technique. The method allows for high yield and precision alignment of such SPEs with complex nanophotonic elements such as TO couplers. As a proof of concept, we demonstrate the successful integration of such site-controlled emitters with TO couplers. Future work will involve further optimization and customization of the TO techniques to leverage and enhance this exciting industrially-scalable method of integrating SPEs with nanophotonic circuitry.

This work is supported by the U.S. Department of Energy (DOE), Office of Science through the Quantum Science Center (QSC), and the National Science Foundation Award 2015025-ECCS.

References

[1] J.-H. Kim, S. Aghaeimeibodi, J. Carolan, D. Englund, and E. Waks, *Hybrid Integration Methods for On-Chip Quantum Photonics*, Optica **7**, 291 (2020).

[2] M. Kianinia, Z.-Q. Xu, M. Toth, and I. Aharonovich, *Quantum Emitters in 2D Materials: Emitter Engineering, Photophysics, and Integration in Photonic Nanostructures*, Appl. Phys. Rev. **9**, 011306 (2022).

[3] S. I. Azzam, K. Parto, and G. Moody, *Prospects and Challenges of Quantum Emitters in 2D Materials*, Appl. Phys. Lett. **118**, 240502 (2021).

[4] F. Lenzini, N. Gruhler, N. Walter, and W. H. P. Pernice, *Diamond as a Platform for Integrated Quantum Photonics*, Adv. Quantum Technol. **1**, 1800061 (2018).

[5] O. Yesilyurt, Z. A. Kudyshev, A. Boltasseva, V. M. Shalaev, and A. V. Kildishev, *Efficient Topology-Optimized Couplers for On-Chip Single-Photon Sources*, ACS Photonics **8**, 3061 (2021).

[6] A. Senichev, Z. O. Martin, S. Peana, D. Sychev, X. Xu, A. S. Lagutchev, A. Boltasseva, and V. M. Shalaev, *Room-Temperature Single-Photon Emitters in Silicon Nitride*, Sci. Adv. **7**, eabj0627 (2021).

[7] S. Peana, O. Yesilyurt, A. Senichev, Z. O. Martin, V. Mkhitaryan, A. S. Lagutchev, A. Boltasseva, and V. M. Shalaev, *Large Scale Site-Controlled Fabrication of Single Photon Emitters in Silicon Nitride Nanopillars*, in *Frontiers in Optics + Laser Science 2022 (FIO, LS) (2022), Paper FTh3E.1* (Optica Publishing Group, 2022), p. FTh3E.1.

META 2023, PARIS - FRANCE, JULY 18 – 21, 2023

Two-photon interference from a position-controlled quantum emitter in hexagonal boron nitride

C. Fournier[1*], S. Roux[1,2], A. Pierret[3], M. Rosticher[3], S. Buil[1], J. Barjon[1], J.-P. Hermier[1], A. Delteil[1]

[1] Université Paris-Saclay, UVSQ, CNRS, GEMaC, 78000, Versailles, France
[2] Laboratoire d'étude des microstructures - LEM, UMR 104, CNRS-ONERA, Université Paris-Saclay, France
[3] LPENS - Laboratoire de physique de l'ENS - ENS Paris, France
[*]corresponding author: clarisse.fournier@uvsq.fr

Abstract: We investigate two-photon interference of a quantum emitter generated in hexagonal boron nitride (hBN) using an electron beam. We measure the correlations of zero-phonon-line photons in a Hong-Ou-Mandel (HOM) interferometer under non-resonant excitation. We find that the emitted photons exhibit a partial indistinguishability of 0.56 ± 0.11 in a 3 ns time window, after accounting for imperfect emitter purity. With this result, we provide the first demonstration of photon indistinguishability from a 2D material quantum emitter.

In the context of photonic quantum information science, hexagonal boron nitride (hBN) has emerged as a very promising material. The two-dimensional character of hBN renders it attractive for the realisation of compact heterostructures and integrated photonic devices. Moreover, this wide-gap material has been shown to host single-photon emitters (SPEs) with appealing optical properties in the red and near infrared regions[1]. However, the deep defects initially observed in hBN suffer from the wide distribution of their emission wavelength and, in most cases, a random spatial location[2,3]. These limitations hinder the scalability of the system for applications.

Recently, a new family of quantum emitters has been observed in hBN – a class of blue-emitting colour centres that have appealing properties[4,5,6]. We demonstrate deterministic positioning of these SPEs with reproducible emission wavelengths, based on irradiation with an electron beam[5,7]. The SPEs are locally activated in exfoliated hBN flakes using a focused electron beam and subsequently characterised using microphotoluminescence (fig. 1,2). They exhibit narrow linewidths at low temperature and a drastically reduced ensemble distribution of their emission wavelength ($\Delta\lambda < 1$ nm) (fig. 3). Individual emitters display low $g^{(2)}(0)$ as well as high and stable count rates. Moreover, emission is observed up to room temperature.

Finally, we investigate two-photon interference between consecutively emitted photons based on the Hong-Ou-Mandel effect. We use coherent photons from the zero-phonon-line that are obtained under non-resonant excitation. This measurement leads to a sizeable degree of indistinguishability[8] of 0.56 ± 0.11 in a 3 ns time window, after accounting for imperfect emitter purity (fig. 4). The dependence of the HOM visibility on the width of the post-selection time window allows us to estimate the dephasing time of the emitter to be ~ 1.7 ns. This is the first observation of photon indistinguishability from a 2D material quantum emitter and opens the way to the use of these SPEs for quantum information applications.

Our results suggest new avenues towards top-down realisation of integrated quantum optical devices based on indistinguishable single photon sources in hBN.

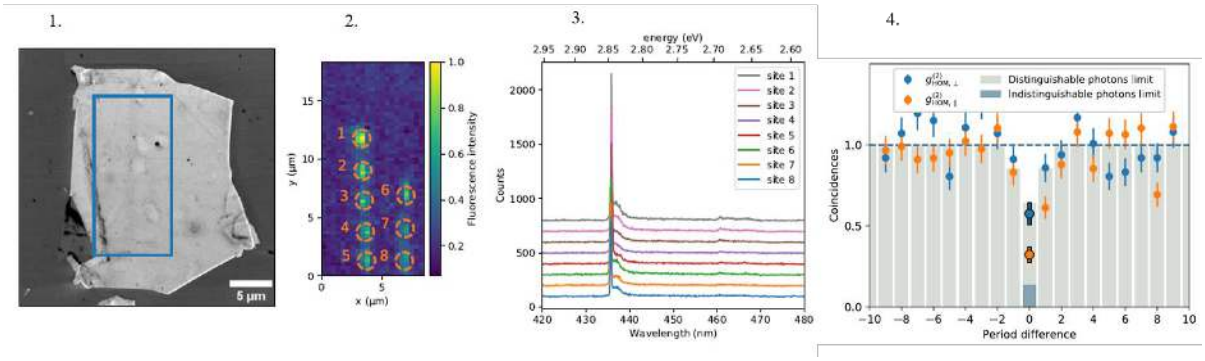


Figure 1. hBN flake with eight irradiation sites. Figure 2. Corresponding confocal map. Figure 3. Corresponding spectra, displaying reduced statistical dispersion of the emission wavelength. Figure 4. Photon correlations with a signature of Hong-Ou-Mandel effect between consecutive photons.

This work is supported by the French Agence Nationale de la Recherche (ANR) under reference ANR-21-CE47-0004-01 (E-SCAPE project). This work also received funding from the European Union's Horizon 2020 research and innovation program under Grant No. 881603 (Graphene Flagship Core 3).

References

1. Tran, T.T., K. Bray, M. J. Ford, M. Toth and I. Aharonovich, “Quantum emission from hexagonal boron nitride monolayers”, Nature Nanotech. Vol. 11, No. 1, 37-41, 2016.
2. Jungwirth, N. R., B.Calderon, Y. Ji, M. G. Spencer, M. E. Flatté and G. D. Fuchs, “Temperature dependence of wavelength selectable zero-phonon emission from single defects in hexagonal boron nitride”, Nano Lett. Vol. 16, No. 10, 6052-6057, 2016.
3. Chejanovsky, N., M. Rezai, F. Paolucci, Y. Kim, T. Rendler, W. Rouabeh, F. Fávaro de Oliveira, P. Herlinger, A. Denisenko, S. Yang, I. Gerhardt, A. Finkler, J. H. Smet, and J. Wrachtrup “Structural attributes and photodynamics of visible spectrum quantum emitters in hexagonal boron nitride”, Nano Lett. Vol. 16, No. 11, 7037-7045, 2016.
4. Shevitski, B., S. M. Gilbert, C. T. Chen, C. Kastl, E. S. Barnard, E. Wong, D. F. Ogletree, K. Watanabe, T. Taniguchi, A. Zettl, and S. Aloni , “Blue-light-emitting color centers in high-quality hexagonal boron nitride”, Phys. Rev. B, Vol. 100, No. 15, 155419, 2019.
5. Fournier, C., A. Plaud, S. Roux, A. Pierret, M. Rosticher, K. Watanabe, T. Taniguchi, S. Buil, X. Quélin, J. Barjon, J-P. Hermier, and A. Delteil,” Position-controlled quantum emitters with reproducible emission wavelength in hexagonal boron nitride”, Nature Commun. Vol. 12, No. 1, 3779, 2021.
6. Gale, A., C. Li, Y. Chen, K. Watanabe, T. Taniguchi, I. Aharonovich and M. Toth, “Site-specific fabrication of blue quantum emitters in hexagonal boron nitride”, ACS Photonics, Vol. 9, No. 6, 2170-2177, 2022.
7. Roux*, S., C. Fournier*, K. Watanabe, T. Taniguchi, J-P. Hermier, J. Barjon and A. Delteil, “Cathodoluminescence monitoring of quantum emitter activation in hexagonal boron nitride”, Appl. Phys. Lett., Vol. 121, No. 18, 184002, 2022.
8. Fournier, C., S. Roux, K. Watanabe, T. Taniguchi, S. Buil, J. Barjon, J-P. Hermier and A. Delteil, “Two-photon interference from a quantum emitter in hexagonal boron nitride”, arXiv:2210.05590, 2022.

Activation of a quantum emitter in a hBN waveguide for integrated quantum photonics

Domitille Gérard[1], Michael Rosticher[2], Stéphanie Buil[1], Jean-Pierre Hermier[1], Julien Barjon[1], Aymeric Delteil[1*]

[1] Université Paris-Saclay, UVSQ, CNRS, GEMaC, 78000, Versailles, France.
[2]Laboratoire de Physique de l'École Normale Supérieure, ENS, Université PSL, CNRS, Sorbonne Université, Université de Paris, 75005 Paris, France
*aymeric.delteil@usvq.fr

Abstract: We created single-photon sources that are directly integrated into a monolithic hBN (hexagonal Boron Nitride) waveguide. The color centers are locally activated using an electron beam and emit photons at 436 nm that couple to the guided mode and can be collected after having crossed the waveguide. Such structure would be the starting point for designing a nanophotonic circuit.

Single-photon emitters in hexagonal boron nitride are promising candidates for applications in integrated quantum nanophotonics. One requirement for creating quantum photonic circuits is to find a way to couple a quantum emitter to the guided mode of a photonic waveguide. Several structures have already been developped, including hybrid integration of a quantum dot on a silicon waveguide [1], or etching of a monolithic waveguide around previously created color centers [2,3].

Here we propose a protocol that starts with the fabrication of the waveguide by performing electron beam lithography on an exfoliated hBN flake. Then we integrate a quantum emitter within the waveguide by electron irradiation. Indeed this technique enables position-controlled activation of defects that emit single photons at 436 nm [4,5,6]. Previous studies on these color centers have shown that they display high and stable count rates, good single-photon purity and coherence properties that allow indistinguishability between the emitted photons [7,8].

After irradiation the waveguides are studied with a confocal microscope at room temperature. The emitters are spotted along the waveguide and their photophysical properties are determined using usual photon-counting techniques. Then, the excitation path is decoupled from the collection path in two different manners. First, the excitation laser is sent at one end of the waveguide, couples to the guided mode and excites the emitters along the waveguide. We collect directly from one color center the photoluminescence that is emitted in the far-field. The other configuration consists in exciting a defect directly and collecting its single-photon emission at one end of the waveguide to evaluate the efficiency of the coupling to the guided mode. The second-order auto-correlation histograms reveal a good preservation of the source's antibunching whether the excitation or photoluminescence photons couple to the waveguide.

Extending and building from this prototype would enable to design integrated quantum photonic circuits in the

frame of applied quantum information science.

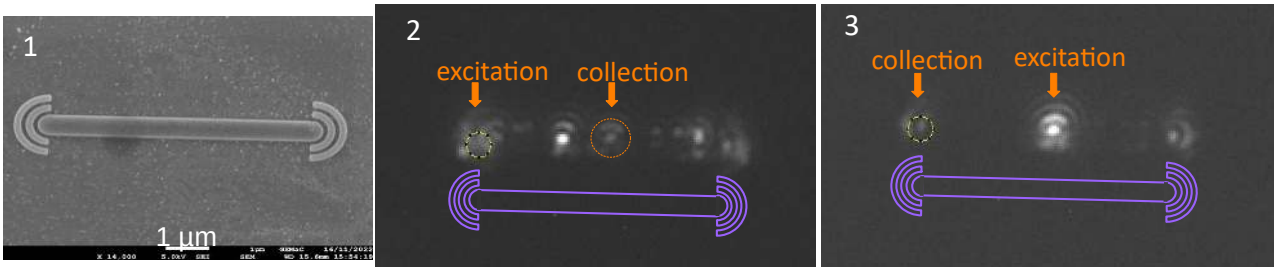


Figure 1 : SEM image of a hBN waveguide. **Figure 2 :** CCD image showing the emitters along the waveguide (white spots) when the are excited by a 405nm laser passing through the waveguide. The reflected light of the excitation is suppressed by a pass-band filter. A scheme of the waveguide in purple was added under the actual waveguide. **Figure 3 :** CCD image showing the photoluminescence of one single-photon emitter that is directly excited, after filtering to suppress the excitation light. The photons that coupled to the guided mode appear at both ends of the waveguide.

This work is supported by the French Agence Nationale de la Recherche (ANR) under reference ANR-21-CE47-0004-01 (E-SCAPE project). This work also received funding from the European Union's Horizon 2020 research and innovation program under Grant No. 881603 (Graphene Flagship Core 3). K.W. and T.T. acknowledge support from JSPS KAKENHI (Grant Numbers 19H05790, 20H00354 and 21H05233)

References

1. Kim, J. H., S. Aghaeimeibodi, C. J. K. Richardson, R. P. Leavitt, D. Englund and E. Waks, "Hybrid integration of solid-state quantum emitters on a silicon photonic chip", Nano Lett., Vol 17, No. 12, 7394-7400, 2017.

2. Li, C., J. E. Fröch, M. Nonahal, T. N. Tran, M. Toth, S. Kim and I. Aharonovich, "Integration of hBN quantum emitters in monolithically fabricated waveguides", ACS Photonics, Vol. 8, No. 10, 2966-2972, 2021.

3. Senichev, A., S. Peana, Z. O. Martin, O. Yesilyurt, D. Sychev, A. S. Lagutchev, A. Boltasseva and V. M. Shalaev, "Silicon nitride waveguides with intrinsic single-photon emitters for integrated quantum photonics", ACS Photonics, Vol. 9, No. 10, 3357-3365, 2022

4. Gale, A., C. Li, Y. Chen, K. Watanabe, T. Taniguchi, I. Aharonovich, M. Toth, " Site-specific fabrication of blue quantum emitters in hexagonal boron nitride", ACS Photonics, Vol. 9, No 6., 2170-2177, 2022.

5. Shevitski, B., S. M. Gilbert, C. T. Chen, C. Kastl, E. S. Barnard, E. Wong, D. F. Ogletree, K. Watanabe, T. Taniguchi, A. Shettl and S. Aloni, "Blue-light-emitting color centers in high-quality hexagonal boron nitride", Phys. Rev. B, Vol. 100, No. 15, 155419, 2019.

6. Roux, S., C. Fournier, K. Watanebe, T. Taniguchi, J. P. Hermier, J. Barjon and A. Delteil, "Cathodoluminescence monitoring of quantum emitter activation in hexagonal boron nitride", Appl. Phys. Lett., Vol. 121, No.18, 184002, 2022.

7. Fournier, C., A. Plaud, S. Roux, A. Pierret, M. Rosticher, K. Watanabe, T. Taniguchi, S. Buil, X. Quélin, J. Barjon, J. P. Hermier and A. Delteil, "Position-controlled quantum emitters with reproducible emission wavelength in hexagonal boron nitride", Nat Commun, vol. 12, No. 1, 3779

8. Fournier, C., S. Roux, K. Watanabe, T. Taniguchi, S. Buil, J. Barjon, J. P. Hermier and A. Delteil, "Two-photon interference from a quantum emitter in hexagonal boron nitride", arχiv preprint arχiv:2210.05590, 2022.

Dynamic control of emission from quantum emitters embedded in ultra thin ENZ media

Arun M[1] **and Joy Mitra**[2]

School of Physics, Indian Institute of Science Education and Research, Thiruvananthapuram, Kerala, India
*corresponding author: itsmearun18@iisertvm.ac.in

Abstract: Controlling light-matter interactions at the nanoscale has been the basis of most of the active plasmonic, photonic and optoelectronic systems. The ability to tailor emission from quantum emitters by tuning the optical parameters of an epsilon near zero (ENZ) material environment around is both of fundamental and applied interest. The understandings provide newer degrees of freedom in controlling and trapping fields within confined regions and in designing opto-mechanical systems, which may be exploited for quantum information processing.

Understanding the interactions between quantum emitters (QE) such as quantum dots or dye molecules, and resonant cavity has been a norm in cavity quantum electrodynamics (QED) with a commensurate body of work to comprehend its fundamental aspects. In parallel, immense technological advancement has leveraged associated phenomena in lasing, cavity opto-mechanics, dielectric micro-cavities, single-photon nonlinearities, photonic systems, etc. [1,2]. While light-matter interaction is weak in general, its is significantly more interesting with the ENZ materials [3]. In these materials the real part of dielectric permittivity goes to zero at the ENZ wavelength (λ_{ENZ}). Close to this λ_{ENZ} the non-trivial properties are evidenced such as enhanced nonlinear optical response in the otherwise linear media, slow light etc. [4,5] The materials of study in this work is Indium Tin Oxide (ITO), these are widely used transparent conducting oxide having the ENZ region in the near IR. In this work we study the far-field emission of a point dipole embedded within a thin-film of ITO backed with a metal substrate using finite element method (FEM). This simulations were carried out by using the wave optics module in COMSOL© Multiphysics. The geometry is as shown in figure 1a and the red gradient cone depicts the emission from the point dipole. A small area of ITO around the center of the embedded dipole is electrostatically gated using a very thin gate electrode. Electrostatic gating can dynamically modulate the carrier density locally, which in turn shifts the plasmonic frequency and λ_{ENZ}, thus changing the refractive index of ITO. [5] Here, we exploit the fact that, emission from a quantum emitter buried in 10 nm thick ENZ material is quenched if the emission wavelength matches the ENZ wavelength (λ_{ENZ}) of the material. This stems from the fundamental understanding that for a lossless ENZ material at the λ_{ENZ} its refractive index ($n + ik$) is zero, which only sustains non-radiative modes in the ENZ media. While finite solutions for the electric field exists in this media, its impedance and the associated wavelength diverges as $n \to 0$, quenching the magnetic field that kills radiation. Real systems are not loss less thus the radiative modes are only partially quenched.

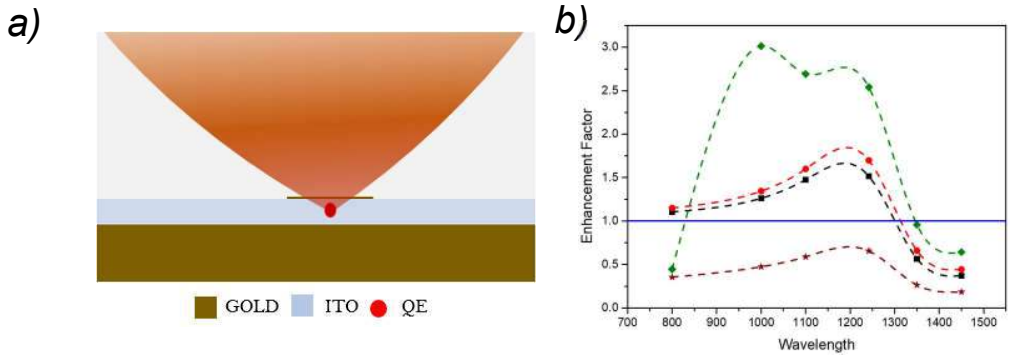


Figure 1: (a) Schematic of the dipole embedded in a thin-film of ITO. (b) Far field power enhancement factor increases as ITO becomes more dielectric.

Figure 1b plots the calculated far field emission intensity of a quantum dipole emitter embedded in the center of 20nm pattered ITO film. As such the ITO is specified to have ENZ wavelength of 1245 nm. Upon activation of the gate bias the far field radiation enhances in the local ITO is depleted of carriers i.e. the ENZ wavelength is shifted to the IR above 1500 nm. Conversely, the far field radiation quenches if the local ITO is rendered metallic by accumulation of charge carriers via positive gate bias.

Acknowledgments
JM acknowledges financial support from SERB, Govt. of India (CRG/2019/004965), UGC-UKIERI 184-16/ 2017 (IC), and the Royal Academy of Engineering, Newton Bhabha Fund, UK (IAPPI 77). AM acknowledges IISER Thiruvananthapuram for the doctoral fellowship and research facilities.

References
1. Chang, D. E., Sørensen, A. S., Demler, E. A., & Lukin, M. D. (2007). A single-photon transistor using nanoscale surface plasmons. Nature physics, 3(11), 807-812.
2. McKeever, J., Boca, A., Boozer, A. D., Buck, J. R., & Kimble, H. J. (2003). Experimental realization of a one-atom laser in the regime of strong coupling. Nature, 425(6955), 268-271.
3. Liberal, I., & Engheta, N. (2016). Nonradiating and radiating modes excited by quantum emitters in open epsilon-near-zero cavities. Science advances, 2(10), e1600987.
4. Reshef, O., De Leon, I., Alam, M. Z., & Boyd, R. W. (2019). Nonlinear optical effects in epsilon-near-zero media. Nature Reviews Materials, 4(8), 535-551.
5. Johns, Ben, Navas Meleth Puthoor, Harikrishnan Gopalakrishnan, Akhileshwar Mishra, Ravi Pant, and J. Mitra. "Epsilon-near-zero response in indium tin oxide thin films: Octave span tuning and IR plasmonics." Journal of Applied Physics 127, no. 4 (2020): 043102.

Exotic Meta-media â€“ Time-dependent, Nonlocal and Other Novel Responses

META 2023, PARIS - FRANCE, JULY 18 – 21, 2023

Manifestations of thermal hysteresis in theoretical studies of Mie scattering, columnar thin films, and surface-plasmon-polariton wave propagation

Tom G. Mackay[1,2*], Tran V. Son[3], Alain Haché[4], Waleed I. Waseer[2,5,6], and Akhlesh Lakhtakia[2]

[1]School of Mathematics and Maxwell Institute for Mathematical Sciences, University of Edinburgh, Edinburgh EH9 3FD, UK

[2]NanoMM - Nanoengineered Metamaterials Group, Department of Engineering Science and Mechanics, Pennsylvania State University, University Park, PA 16802-6812, USA

[3]Department of Physics, Concordia University, Montreal H3G 1M8, Canada

[4]Département de physique et d'astronomie, Université de Moncton, E1A 8T1, Canada

[5]Department of Electronics, Quaid-i-Azam University Islamabad, Islamabad, Pakistan

[5]Department of Electrical and Computer Engineering, COMSATS University Islamabad, Islamabad, Pakistan

[*]corresponding author: T.Mackay@ed.ac.uk

Abstract: The crystal structure of vanadium dioxide is monoclinic at temperatures below 58°C and tetragonal at temperatures above 72°C. Both monoclinic and tetragonal crystals exist at temperatures in the range (58°C, 72°C). Monoclinic vanadium dioxide is a dissipative insulator. Tetragonal vanadium dioxide is a dissipative insulator only at free-space wavelengths less than 1100 nm; at longer free-space wavelengths it is a plasmonic metal. The monoclinic–tetragonal transition is reversible but hysteretic. Manifestations of this thermal hysteresis were found in theoretical studies of (i) scattering by vanadium dioxide spheres; (ii) constitutive parameters of columnar thin films made from vanadium dioxide; and (iii) surface-plasmon-polariton waves propagating at a silver-vanadium dioxide interface.

The prospect of thermally controlling the dielectric properties of materials, metamaterials, and metasurfaces is attractive for numerous applications involving reconfigurable and multifunctional devices [1]. In particular, vanadium dioxide (VO_2) looks promising in this context as it exhibits a thermally induced, hysteretic phase change over the temperature range (58°C, 72°C) [2]. While VO_2 is electromagnetically isotropic and characterized by its (complex-valued) relative permittivity ε_{VO2}, its crystal structure is monoclinic at temperatures below 58°C and tetragonal at temperatures above 72°C [3]. Both monoclinic and tetragonal crystals exist at temperatures in the range (58°C, 72°C). Tetragonal vanadium dioxide is a dissipative insulator only for $\lambda_0 < 1100$ nm, where λ_0 is the free-space wavelength; at longer free-space wavelengths, it is a plasmonic metal. At a fixed free-space wavelength, the value of ε_{VO2} for monoclinic VO_2 differs from its value for tetragonal VO_2. The transition from monoclinic VO_2 to tetragonal VO_2 can be achieved by heating, and the transition from tetragonal VO_2 to monoclinic VO_2 can be achieved by cooling. For temperatures in the range (58°C, 72°C), the value of ε_{VO2} depends on whether VO_2 was heated up or cooled down to reach that temperature [4].

Manifestations of thermal hysteresis in the monoclinic–tetragonal transition for VO_2 were investigated in the following three theoretical studies:

(i) The extinction, total scattering, absorption, radiation-pressure, back-scattering, and forward-scattering

efficiencies of a VO_2 sphere were calculated [5]. Manifestations of thermal hysteresis were found in (a) the forward-scattering, back-scattering, and absorption efficiencies for $\lambda_0 < 1100$ nm, and (b) the forward-scattering, back-scattering, total scattering, and absorption efficiencies for $\lambda_0 > 1100$ nm.

(ii) The Bruggeman homogenization formalism was used to numerically investigate the dielectric properties of a columnar thin film (CTF) made from VO_2 [6]. For visible and near-infrared wavelengths, the CTF is electromagnetically equivalent to a homogeneous orthorhombic material. The anisotropy revealed through the eigenvalues of the CTF's relative permittivity dyadic, and the anisotropy of the associated hysteresis, were investigated in relation to temperature for CTFs of different porosities and columnar cross sections. For $\lambda_0 = 800$ nm, the CTF is a dissipative dielectric material that exhibits temperature-dependent anisotropy and anisotropic hysteresis. In contrast, for $\lambda_0 = 1550$ nm, the CTF can be a dissipative dielectric material, a hyperbolic material or a metal-like material, depending on the temperature and the porosity of the CTF.

(iii) The propagation of surface-plasmon-polariton (SPP) waves at the planar interface of a metal and VO_2 impregnated with a combination of active dyes was numerically investigated [7]. Depending upon the volume fraction of VO_2, either attenuation or amplification of the SPP waves may be achieved, the degree of attenuation or amplification being strongly dependent on both the temperature and whether the temperature is increasing or decreasing.

Acknowledgments: TGM was supported by EPSRC (grant number EP/V046322/1). AL was supported by the US National Science Foundation (grant number DMS-1619901) as well as the Charles Godfrey Binder Endowment at Penn State.

References

1. Wang, Q., Rogers, E.T., Gholipour, B., Wang, C.-M., Yuan, G., Teng, J., and Zheludev, N.I. "Optically reconfigurable metasurfaces and photonic devices based on phase change materials," Nat. Photon., Vol. 10, 60-65, 2016.
2. Cueff, S., John, J., Zhang, Z., Parra, J., Sun, J., Orobtchouk, R., Ramanathan, S., and Sanchis, P., "VO_2 nanophotonics," APL Photon., Vol. 5, 110901, 2020.
3. Morin, F.J., "Oxides which show a metal-to-insulator transition at the Néel temperature," Phys. Rev. Lett., Vol. 3, 34-36, 1959.
4. Cormier, P., Son, T.V., Thibodeau, J., Doucet, A., Truong, V.-V., and Haché, A., "Vanadium dioxide as a material to control light polarization in the visible and near infrared," Opt. Commun. Vol. 382, 80-85, 2017.
5. Lakhtakia, A., Mackay, T.G., and Waseer, W.I., "Thermal hysteresis in scattering by VO_2 spheres," J. Opt. Soc. Am. B, Vol. 39, 1921–1928, 2022.
6. Mackay, T.G. and Lakhtakia, A., "Towards morphologically induced anisotropy in thermally hysteretic dielectric properties of vanadium dioxide," AIP Advances, Vol. 12, 105026, 2022.
7. Mackay, T.G., Son, T.V., Haché, A., and Lakhtakia, A., "Thermal hysteresis in amplification and attenuation of surface-plasmon-polariton waves," (submitted for publication).

META 2023, PARIS - FRANCE, JULY 18 – 21, 2023

Temporal boundaries in electromagnetic materials

J. Gratus[1,2,*], R. Seviour[3], P. Kinsler[1,2,4], D. A.Jaroszynski[5] and S. Balakrishnan[3]

[1]Department of Physics, Lancaster University, Lancaster LA1 4YB, United Kingdom
[2]The Cockcroft Institute, Sci-Tech Daresbury, Daresbury WA4 4AD, United Kingdom
[3]University of Huddersfield, Huddersfield HD1 1JB, United Kingdom
[4]Department of Physics, Imperial College London, Prince Consort Road, London SW7 2AZ, United Kingdom
[5]Department of Physics, SUPA and University of Strathclyde, Glasgow G4 0NG, United Kingdom
[*]corresponding author: j.gratus@lancaster.ac.uk

Abstract: Temporally modulated optical media have amazing potential to amplify signals. Here we investigate the behaviour of temporal boundaries, and show that traditional approaches that assume constant dielectric properties, with loss incorporated as an imaginary part, necessarily lead to unphysical solutions. Furthermore, although physically reasonable predictions can be recovered with a narrowband approximation, we show that appropriate models should use materials with a temporal response and dispersive behaviour. We indicate recent experiential demonstrating temporal boundaries.

A very exciting new concept is time dependent media, where abrupt changes in permittivity can create a temporal boundary. Boundaries play a key role in many physical models; they provide initial and final states in dynamical systems, constrain analytic solutions in confined systems, and represent transitions between different modes of operation. We show [1] that modelling loss using a constant complex permittivity and permeability is physically incompatible with a temporal boundary. Such models can lead to unphysical post-boundary solutions that grow exponentially, despite being applied to passive and lossy materials; or fields may become complex-valued despite being real-valued before.

To see this consider the simple scenario with vacuum constitutive relations before the the time bounty and a constant complex permittivity $\varepsilon\in\boldsymbol{C}$. An initial propagating wave of the form

$$E_x(t,z)=E_0\exp(-\omega t+ikz)$$

where $c_0 k=\omega_a$. By imposing the the boundary conditions $[\boldsymbol{E}]=0$ and $[\boldsymbol{B}]=0$ we obtain the solution after the time boundary as

$$E_x(t,z)=g_1 e^{ik_c(-c_R t+z)}e^{kc_I t}+g_2 e^{ik(-c_R t-z)}e^{kc_I t}+g_3 e^{ik(c_R t-z)}e^{-kc_I t}+g_4 e^{ik(c_R t+z)}e^{-kc_I t}$$

where $c_R+i\,c_I=c_0(\varepsilon_c\mu_0)^{-1/2}$ and $\omega_c=k(\varepsilon_c\mu_0/c_0)^{1/2}$. Now we have $C_I\neq 0$, so *E* increases exponentially with time *despite* this being a lossy medium. Clearly this is physically invalid, so the constant complex CR model has *failed*. This has a crucial significance for

any technology relying on temporal boundaries.

We propose two methods to avoid this unphysical result. The first is to use a narrowband approximation, which requires two permativities. The second is to consider full dynamical models of permittivity.

To examine the predicted behaviour of electromagentic waves in time dependent media, we have constructed an time dependent metamaterial, from sub-wavelength active components. In the experiment an externally applied DC current to the material dynamically changes the permittivity. Preliminary results indicate that in some frequency regimes it behaves as expected, producing a time mirror, whereas at other frequency there are unexpected results.

References

1. J. Gratus, R. Seviour, P. Kinsler, and D. A.Jaroszynski, 2021 *New J. Phys.* **23** 083032

Solution generation in electrodynamics

Robert T. Thompson[1*] and Martin W. McCall[2]
[1]*Rhea Space Activity, Washington DC, USA*
[2]*Department of Physics, Imperial College London, UK*
*rtthompson.phd@gmail.com

Abstract: The transformation approach can be understood as a method of solution generation. We discuss solution generation in electrodynamics and seek to develop a systematic approach to identifying mechanisms for generating non-trivial electromagnetic field solutions.

We take as our starting point the electromagnetic vector potential 1-form $\boldsymbol{A}$ and the field strength tensor $\boldsymbol{F} = d\boldsymbol{A}$. Maxwell's homogeneous equations $d\boldsymbol{F} = 0$ follow directly from the fact that $d^2\omega = 0$ for any scalar-valued differential form ω. The inhomogeneous equations $d \star \boldsymbol{F} = \boldsymbol{J}$ follow from a variation of the Yang-Mills action. Separating $\boldsymbol{J} = \boldsymbol{J}_{free} + \boldsymbol{J}_{bound}$, we can find a particular solution $\boldsymbol{P}$ that satisfies $d \star \boldsymbol{P} = \boldsymbol{J}_{bound}$. Absorbing a sign, we can write $d \star (\boldsymbol{F} + \boldsymbol{P}) = \boldsymbol{J}_{free}$. In macroscopically neutral media, polarizations arise in response to the free solution $\boldsymbol{F}$ (a combination of homogeneous and particular solutions to the free charge source), thus we expand $\boldsymbol{P}$ in terms of $\boldsymbol{F}$

$$\boldsymbol{P} = \boldsymbol{\xi}(\boldsymbol{F}) + \boldsymbol{\Xi}(\boldsymbol{d} \star \boldsymbol{F}) + \boldsymbol{\Lambda}(\boldsymbol{F} \wedge \boldsymbol{F}) + \cdots. \tag{1}$$

The precise form of $\boldsymbol{P}$ requires a physical model. Here we merely write down some possible terms that are in keeping with exterior calculus. Notice that there is no term dependent on $d\boldsymbol{F}$ since $d\boldsymbol{F} = 0$.

A. Solution generation in the vacuum

The general covariance of Maxwell's equations follows directly from the commutativity of the exterior derivative with diffeomorphisms. In other words, given a coordinate transformation ϕ, and its associated action on the tangent space $\psi = d\phi$, then, with an abuse of notation whereby we let ψ also denote the action of ϕ on products of the tangent space, e.g. $\psi(\boldsymbol{F}) = \psi_\alpha^\mu \psi_\beta^\nu F_{\mu\nu}$

$$\psi(d\boldsymbol{F}) = d\psi(\boldsymbol{F}) = 0, \quad \text{and} \quad \psi(d \star \boldsymbol{F}) = d\big(\psi \star \psi^{-1}\psi(\boldsymbol{F})\big) = \psi(\boldsymbol{J}) \tag{2}$$

preserves the form of Maxwell's equations in different coordinate systems. On the other hand, the game is slightly different if one is interested in generating new vacuum solutions from a given initial solution, rather than a coordinate transformation. Given the initial solution $\boldsymbol{F}$, we suppose that $\boldsymbol{F'} = \Lambda(\boldsymbol{F})$ is a new vacuum solution for some transformation Λ, and we wish to know what conditions Λ must satisfy such that $\boldsymbol{F'}$ is in fact a solution to Maxwell's equations. In other words, we must find conditions on Λ such that $d\boldsymbol{F'} = d\Lambda(\boldsymbol{F}) = 0$, and $d \star \boldsymbol{F} = d \star \Lambda(\boldsymbol{F}) = 0$ are true. From the first equation, we see that Λ must commute with the exterior derivative so that $\Lambda(d\boldsymbol{F}) = 0$, which will be satisfied since $d\boldsymbol{F} = 0$ for the seed solution $\boldsymbol{F}$. Similarly, we must be able to demonstrate that the second equation can put into the form $\Lambda(d \star \boldsymbol{F}) = 0$. Since we have already required that Λ and d commute, this requirement is equivalent to $\star\,\Lambda(\boldsymbol{F}) = \Lambda(\star\,\boldsymbol{F})$. By linearity, Λ must therefore preserve the Hodge $\star$ on 2-forms

$$\Lambda \star \Lambda^{-1} = \star \tag{3}$$

Which leads to the condition $\Lambda_\mu^\alpha \Lambda_\nu^\beta g^{\mu\nu} = \pm\sqrt{\det(\Lambda)}\, g^{\alpha\beta}$. Remarkably, we started by looking for constraints on the allowable transformations of the *field* and found a condition with respect to the space-time *metric*. At any space-time point $\boldsymbol{x}$ the metric may be put into the Minkowski form, so local Lorentz transformations with determinant ±1 are valid, as are conformal transformations of the form $\Lambda = \boldsymbol{\Omega I}$. This is a compact derivation of well-known results [1–3].

B. Generation of more arbitrary solutions

We are not constrained to generate just vacuum solutions. Linear transformation optics supposes we begin with the seed solution $\boldsymbol{F}$ within an initial linear dielectric $\boldsymbol{\chi}$, satisfying $d\boldsymbol{F} = 0$ and $d \star$

$\boldsymbol{\chi F} = 0$ with $\boldsymbol{F}$ and $\boldsymbol{\chi}$ complex. Let $\boldsymbol{F'} = \Lambda(\boldsymbol{F})$ where Λ is a (complex) transformation that commutes with the exterior derivative such that $d\boldsymbol{F'} = d\Lambda(\boldsymbol{F}) = \Lambda(d\boldsymbol{F}) = 0$ is satisfied. We demand that $\boldsymbol{F'}$is a valid solution to Maxwell's equations in some non-vacuum but again linear medium $\boldsymbol{\chi'}$. In this case the inhomogeneous equation for the primed field is $d \star \boldsymbol{\chi'}\boldsymbol{F'} = d \star \boldsymbol{\chi'}\Lambda(\boldsymbol{F}) = 0$, which, similarly to the vacuum case, will be true if $d \star \boldsymbol{\chi'}\Lambda(\boldsymbol{F}) = d\Lambda(\star\, \boldsymbol{\chi F}) = 0$. As before, we are not changing coordinates but rather generating new solutions. So the coordinates and space-time are unchanged, which means that $\star$ must again be preserved, but this time we have the freedom to modify $\boldsymbol{\chi'}$ to support the new field. Thus, it may be quickly determined that for any given Λ that commutes with the exterior derivative, $\Lambda(\boldsymbol{F})$ will be a solution as long as

$$\boldsymbol{\chi'} = - \star \Lambda \star \boldsymbol{\chi}\Lambda^{-1} \tag{4}$$

which we already knew from transformation optics, and which immediately recovers the vacuum condition Eq. (3) when $\boldsymbol{\chi'} = \boldsymbol{\chi} = \boldsymbol{\chi}_{vac}$.

However, the linearity of $\boldsymbol{\chi'}$ turns out to be a consequence of demanding that Λ be the pullback of a manifold diffeomorphism. By relaxing the assumptions on linearity, we may start with a slightly different point of view, one where we haven't imposed a model on the bound charges. Then it is possible to systematically consider the effect of more general solution generating transformations by studying (in the case of no free charges)

$$d \star (\boldsymbol{F'} + \boldsymbol{P'}) = d \star ((\Lambda(\boldsymbol{F}) + \boldsymbol{P'}(\Lambda(\boldsymbol{F}))) = 0. \tag{5}$$

C. Bundle map automorphisms

Given a point p on manifold M, the associated tangent space $T_p(M)$ is a vector space. The collection of all tangent spaces for all points on the manifold is the tangent (vector) bundle TM. The tangent bundle is itself a manifold, and a point on the tangent bundle is given by the pair $(p, \boldsymbol{v})$ with $p \in M, \boldsymbol{v} \in T_p(M)$. Given a diffeomorphism $f: M \to N$ between two manifolds M and N, one can find a map $f^*: T_p(M) \to T_{f(p)}N$ between tangent spaces. Hence the pair

$$(f, f^*): TM \to TN, \tag{6a}$$

$$(p, \boldsymbol{v}) \mapsto (f(p), f^*(\boldsymbol{v})) \tag{6b}$$

defines a map between bundles. However, there is no requirement that a bundle map be formulated this way, and the map $\Lambda: T_p(M) \to T_q(N)$ can be defined independently from the map identifying p and q, so the pushforward is a special case of bundle map. In particular, suppose we define an automorphism of the bundle by

$$(id, \Lambda): TM \to TM, \tag{7a}$$

$$(p, \boldsymbol{v}) \mapsto (p, \Lambda(\boldsymbol{v})). \tag{7b}$$

This bundle map is similar to a "frame transformation" of the tangent space; for example when one wants to formulate equations relative to a tetrad field. One can show that this bundle map will preserve Maxwell's equations *iff* $d\Lambda = 0$. Bundle maps are a class of transformations that has not been well-studied in transformations optics [4–6]. I will discuss the combination of these more general types of transformations with the approach of Eq. (5).

References

[1] H. Bateman, Proc. London Math. Soc. **s2-8**, 223 (1910).
[2] E. Cunningham, Proc. London Math. Soc. **s2-8**, 77 (1910).
[3] T. Fulton, F. Rohrlich, and L. Witten, Rev. Mod. Phys. **34**, 442 (1962).
[4] S. A. Tretyakov, I. S. Nefedov, and P. Alitalo, New J. Phys. **10**, 115028 (2008).
[5] R. T. Thompson and M. Fathi, Phys. Rev. A **92**, 013834 (2015).
[6] Y. Zhang, L. Shi, R.-Y. Zhang, J. Duan, J. Ng, C. T. Chan, and K. H. Fung, Phys. Rev. Lett. **122**, 200201 (2019).

Spatial dispersion with Mathieu's equation for EM generation and particle acceleration

J. Gratus[1,2], **T. Boyd**[1,2], **S.S. Siaber**[1,2] **S.P. Jamison**[1,2] **and R. Seviour**[3]

March 17, 2023

[1]Lancaster University, Physics department, Lancaster LA1 4YB, UK
[2]The Cockcroft Institute, Sci-Tech Daresbury, Daresbury WA4 4AD, UK
[3]University of Huddersfield, Huddersfield HD1 1JB, United Kingdom
corresponding author, e-mail: s.siaber@lancaster.ac.uk

Abstract **– Corrugated waveguides can be modelled as a spatially dispersive media. By varying the structure we can make the electric field obey Mathieu's equation. This is utilised to tailor the dispersion relation to match phase and group velocity of the waves to the particle beam. These corrugated structures can be used as slow wave structures to either produce EM fields or accelerate charged particles.**

I. Introduction

One of the reasons to design artificial structures in electromagnetism is creating an electro-magnetic dispersion relation with certain useful properties. One of the desirable features, for either electromagnetic radiation generation or charged particle acceleration structures, is dispersion relation having a point where phase and group velocities are the same. Moreover, a range of frequencies at which phase and group velocities are very close is even more desirable. This, as we show below, can occur in a medium, plasma frequency of which is varied periodically; and is also achievable in a relatively simple corrugated waveguide.

To simplify analytical study system's dispersion relation it is convenient to consider periodic systems that can be described by Mathieu equation. This enables us to easily calculate the dispersion relation, for example as given by figure 2. The longitudinal component of the electric field $E_z(t,z)$ along the centre of waveguide can be modelled as a 1-dimensional medium with spatial dispersion, which is also spatially dependent.

II. Spatial dispersion and Mathieu's equation

We choose corrugation profile of the waveguide in the form $\mathcal{L}_x(z) = \left(L_0^{-2} + 2L_z^{-2}\, p_x^{-2}\, q\, \cos(2\,\pi\, L_z^{-1}\, z)\right)^{-1/2}$. The guide height $\mathcal{L}_x(z)$ oscillates non-sinusoidally around the central height L_0. For physical solutions $\mathcal{L}_x(z) > 0$, we require $2\,q < L_0^{-2}\, L_z^2$. The Mathieu parameter q effectively defines the corrugation depth. For small corrugation with $q\, L_0^2\, L_z^{-2} \ll 1$ the undulations take a simple sinusoidal form $\mathcal{L}_x(z) \approx L_0 - L_0^3\, L_z^{-2}\, q\, \cos(2\,\pi\, L_z^{-1}\, z)$

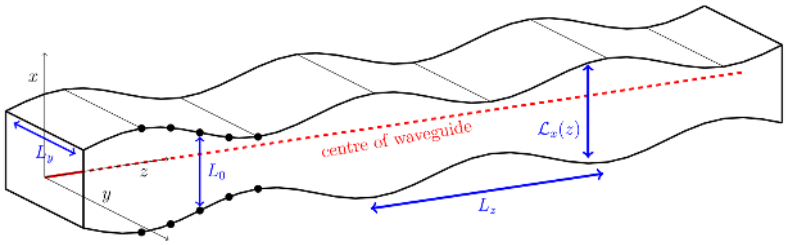


Fig. 1: Corrugated Wave Guide

This profile shape leads to longitudinal field of a transversal magnetic mode $\mathrm{TM}_{p_x p_y}$ (p_x and p_y are odd integers) to be in the form

$$E_z\left(\vec{r},\omega\right) = E_\perp(x,y)\left[\left(\frac{\pi p_x}{\mathcal{L}_x(z)}\right)^2 + \left(\frac{\pi p_y}{L_y}\right)^2\right]\phi\left(\frac{\pi z}{L_z}|a,q\right), \tag{1}$$

Here $\phi\left(\xi|a,q\right)$ is a solution of the Mathieu equation $\phi''\left(\xi\right) + \left(a - 2q\cos(2\xi)\right)\phi\left(\xi\right) = 0$, and $a = L_z^2\left(c^{-2}\pi^{-2}\omega^2 - p_x^2 L_0^{-2} - p_y^2 L_y^{-2}\right) = \hat{\omega}^2 - \hat{\omega}_c^2$.

For a given TM mode we can reduce the propagation of the electromagnetic waves to one dimensional problem of propagation through spatially variying the susceptibility $\chi(\omega, z)$of the effective medium by choosing an appropriate $\chi(\omega, z)$ in the polarisation equation

$$\frac{\partial^2 E_z(z,\omega)}{\partial z^2} - \frac{\omega^2}{c^2} E_z(z,\omega) = \frac{\omega^2}{\epsilon_0 c^2} P_z(z,\omega), \quad \Leftrightarrow \quad \frac{\partial^2 E_z(z,\omega)}{\partial z^2} = -\left(\frac{\omega^2}{c^2} + \frac{\omega^2}{c^2}\chi(\omega, z)\right) E_z(z,\omega) \quad (2)$$

Alternative formulation of material properties can be done using spatially varied plasma frequency ω_P of the material. Thin wire medium, studied in [1-4], is an example of such system with spatial variation of plasma frequency along z as: $\omega_P^2(z) = \omega_c^2 + 2\,\Lambda\,\cos\left(\frac{2\,z}{L_z}\right)$; longitudinal field in the medium E_z obeys an equation:

$$\beta^2\, c^2\, \frac{d^2 E_z}{dz^2} + \left(\omega^2 - \omega_p^2\right) E_z = 0 \quad (3)$$

Since the solutions to Mathieu's equation are known, we can use them to find parameters a, q, $\hat{\omega}$, and $\hat{k}$ such that the optimal wave-particle interaction can take place. For example in figure 2 where we see that the phase and group velocities are matched at an inflection point - leading to extended interaction range.

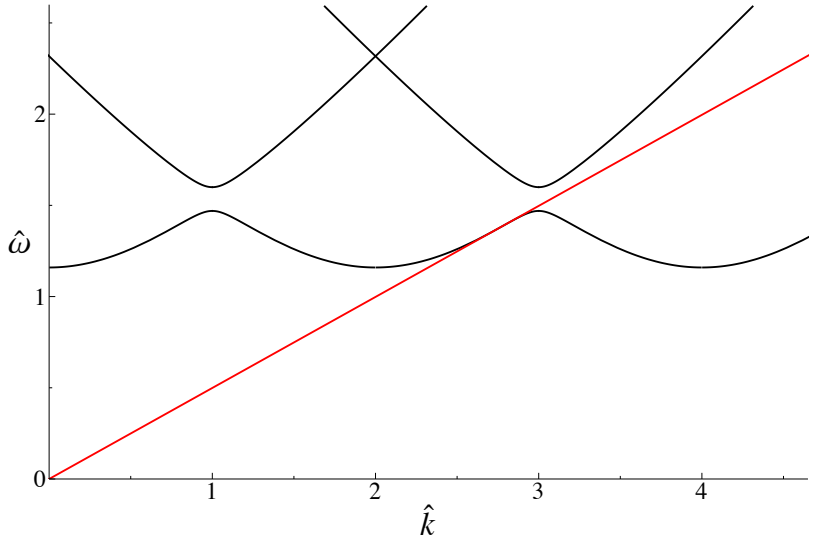


Fig. 2: Dispersion relation for scaled frequency $\hat{\omega}$ versus scaled wavevector $\hat{k}$, for Mathieu's parameters $q = 0.2$ $a = \hat{\omega}^2 - \hat{\omega}_c^2$ where $\hat{\omega}_c = 1.168$. For these values the phase and group velocities are approximately equal. Both correspond to a beam travelling at about 0.5c

III. Conclusion

We have shown how to use Mathieu's equation and a spatially dispersive model of the medium to predict the dispersion relation for a corrugated structure, and tailor them to a preferred wave-particle interaction.

We have compared corresponding modes can then be checked by running a full numerical simulation with the corrugated structure.

Acknowledgement

JG, TB, SSS and SPJ acknowledge support provided by STFC (Cockcroft Institute, ST/V001612/1 and ST/P002056/1). JG acknowledge EPSRC (Lab in a Bubble, EP/N028694/1). RS thanks AFOSR (FA8655-20-1-7002).

References

[1] J. Gratus, M. McCormack "Spatially dispersive inhomogeneous electromagnetic media with periodic structure" *Journal of Optics* 17 (2), 025105 (2015)

[2] J. Gratus, P. Kinsler, R. Letizia, T. Boyd "Electromagnetic mode profile shaping in waveguides" *Applied Physics A* 123 (1), 108 (2017)

[3] T. Boyd, J. Gratus, P. Kinsler, R. Letizia "Customizing longitudinal electric field profiles using spatial dispersion in dielectric wire arrays" Optics express 26 (3), 2478-2494 (2018)

[4] T. Boyd, J. Gratus, P. Kinsler, R. Letizia, R. Seviour "Mode profile shaping in wire media: Towards an experimental verification" *Applied Sciences* Vol 8 (8), 1276 (2018)

META 2023, PARIS - FRANCE, JULY 18 – 21, 2023

Twisting an optomechanical cavity

Daigo Oue[1,2,3*] **and Mamoru Matsuo**[1,4,5]

[1]Kavli Institute for Theoretical Sciences, University of Chinese Academy of Sciences, China
[2]Instituto Superior Técnico, University of Lisbon, Portugal
[3]Department of Physics, Imperial College London, United Kingdom
[4]CAS Center for Excellence in Topological Quantum Computation, University of Chinese Academy of Sciences, China
[5]Advanced Science Research Center, Japan Atomic Energy Agency, Japan
[*]corresponding author: daigo.oue@gmail.com

Abstract: In this presentation, we show introducing birefringence in an optomechanical cavity breaks the rotational symmetry and induces two nondegenerate modes: ordinary and extraordinary rays. Mechanically twisting the cavity mixes the two modes and modulates the electromagnetic energy. Consequently, we find that the two optical modes behave as an effective two-level system which is coupled with torsional mechanical oscillation. We can also find the torsional oscillation can be resonantly driven by optically pumping the cavity.

Light is far from mechanical rotation and vibration in the frequency domain; thus, the optical and mechanical systems cannot resonantly interact with each other. That was why transporting linear momenta between optical and mechanical degrees of freedom was inefficient as experimentally investigated by Nichols and Hull a long time ago [1].

Recently, it has been realized that light and quantized mechanical vibration are coupled with one another by confining both of them in the same 'optomechanical' cavity [2]. There are various types of optomechanical cavities, including a micro-disk resonator [3], a periodic photonic structure [4], a suspended membrane in an optical cavity [5], a levitated particle in a cavity [6]. All of these examples are about the coupling of light with linear mechanical oscillation, and, to the best of our knowledge, it has never been studied that with torsional oscillation in solid-state materials.

In this presentation, based on our recent paper [7], we show breaking rotational symmetry in an optomechanical cavity produces the interaction between optical fields and torsional mechanical oscillation. Our key to break the symmetry is filling the cavity with a birefringent medium which induces uniaxial anisotropy and thus two nondegenerate optical modes: ordinary and extraordinary rays. If the cavity is mechanically twisted, the two modes are mixed, and the electromagnetic energy is modulated. Following the standard quantization procedure of the electromagnetic energy as well as mechanical energy, we can find that the two optical modes can be regarded as an effective two-level system interacting with torsional mechanical oscillation. We can also find the torsional oscillation can be resonantly driven by optically pumping the cavity.

Our setup comprised two mirrors and a uniaxial filling medium, which support two orthogonal eigenmodes: ordinary and extraordinary rays. Mechanical twisting of the medium induces position-dependent anisotropy (Figure 1).

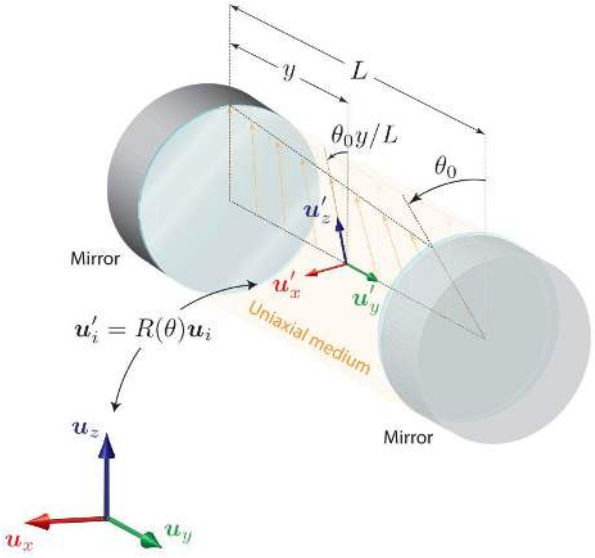


Figure 1.: uniaxial medium filling a cavity. The twisting induces position-dependent anisotropy.

Applying a coordinate transformation maps the inhomogeneous anisotropic medium to a homogeneous one and provides the interaction energy between the twisting and two optical modes in the cavity. Due to this rotational nature, the interaction becomes an angular-momentum-exchange type, through which we can optically pump mechanical torsional motion [7].

Acknowledgements. This work was supported by the Priority Program of Chinese Academy of Sciences and Japan Society for the Promotion of Science KAKENHI. D.O. acknowledges supports from the President's PhD Scholarships at Imperial College London and Japan Society for the Promotion of Science Overseas Research Fellowships.

References

1. E. F. Nichols and G. F. Hull "The pressure due to radiation," Proc. Am. Acad. Arts Sci. Vol. 38, 559, 1903; Phys. Rev. (Series I), Vol. 17, 26, 1903.
2. M. Aspelmeyer, T. J. Kippenberg and F. Marquardt, "Cavity optomechanics," Rev. Mod. Phys., Vol. 86, 1391 2014.
3. E. Verhagen, S. Deléglise, S. Weis, A. Schliesser, and T. J. Kippenberg, "Quantum-coherent coupling of a mechanical oscillator to an optical cavity mode," Nature (London) Vol. 482, 63, 2012.
4. M. Eichenfield, J. Chan, R. M. Camacho, K. J. Vahala, and O. Painter, "Optomechanical crystals," Nature (London), Vol. 462, 78, 2009.
5. D. J. Wilson, C. A. Regal, S. B. Papp, and H. J. Kimble, "Cavity Optomechanics with Stoichiometric SiN Films," Phys. Rev. Lett., Vol. 103, 207204(R), 2009.
6. D. E. Chang, C. Regal, S. Papp, D. Wilson, J. Ye, O. Painter, H. J. Kimble, and P. Zoller, "Cavity opto-mechanics using an optically levitated nanosphere," Proc. Natl. Acad. Sci. USA, Vol. 107, 1005, 2010.
7. Oue, D and Matsuo, M "Twisting an optomechanical cavity," Phys. Rev. A, Vol. 106, No. 4, L041501, 2022.

Time-varying fundamental acoustic equations

R. Picó[1*], J. Redondo[1], and V. J. Sánchez Morcillo[1]

[1]Instituto de Investigación para la Gestión Integrada de Zonas Costeras,
Universitat Politècnica de València,
Paranimf 1, Grau de Gandia, Spain
*rpico@fis.upv.es

Abstract: The basic equations of acoustics are developed for a purely time-varying medium. The linear non-invariant continuity equation is established by considering the time dependence of the mass density and the adiabatic bulk modulus. A parametric study is carried out to consider the influence of the terms in the equation. Numerical simulations using the Finite-Differences Time-Domain (FDTD) method show the peculiarities of these wave phenomena in different scenarios for time-varying parameters of the medium in specific acoustic systems.

Applications such as unidirectional amplification [1-2], frequency conversion [3] and non-reciprocal transmission [4] are supported by spatiotemporal modulated metamaterials in incredibly diverse ways. Metamaterials have been used to modulate material properties in time to increase the degrees of freedom in wave control. In particular, they have been used in acoustics for sound diffusers [5], diffraction gratings [6], metasurfaces [7] and spatiotemporal sonic crystals [8].

In the following, we derive the basic first-order linear equations of acoustics by assuming that the properties of the medium depend on time but not on space. Thus, we consider here a purely time-varying medium. If we assume that the non-linear terms are negligible, Euler's equation can be linearised as follows:

$$\rho_0(t)\frac{\partial \vec{u}(\vec{r},t)}{\partial t} + \nabla p(\vec{r},t) = 0, \tag{1}$$

where ρ_0 is the equilibrium density, $\vec{u}$ the particle velocity and p the acoustic pressure. This equation applies to small amplitude acoustic processes. The other linear equation is the exact continuity equation [9] is:

$$\frac{\partial \rho}{\partial t} + \nabla\left(\rho_0(t)\vec{u}(\vec{r},t)\right) = 0, \tag{2}$$

where $\rho = \rho_0(1+s)$ is the instantaneous density, ρ_0 is the equilibrium density and s is the condensation. If we develop the partial derivative of time we get:

$$\frac{\partial \rho_0(t)}{\partial t}(1+s(\vec{r},t)) + \rho_0(t)\frac{\partial s(\vec{r},t)}{\partial t} + \rho_0(t)\nabla\vec{u}(\vec{r},t) = 0. \tag{3}$$

If we assume small concentrations $|s| << 1$, that is $|\rho - \rho_0| << \rho_0$, and pressure-concentration linear relationship $p(\vec{r},t) = B(t)\cdot s(\vec{r},t)$, the continuity equation with time-varying parameters can be written as:

$$\frac{\partial \rho_0(t)}{\partial t} + \rho_0(t)\frac{\partial}{\partial t}\left(\frac{p(\vec{r},t)}{B(t)}\right) + \rho_0(t)\nabla\vec{u}(\vec{r},t) = 0. \tag{4}$$

To obtain the wave equation (second order equations), one performs the partial derivative of time of (4) and the gradient of (1) and gets:

$$\frac{\partial^2 \rho_0(t)}{\partial t^2} - \frac{\partial \rho_0(t)}{\partial t}\frac{p(\vec{r},t)}{B(t)} + \rho_0(t)\frac{\partial^2}{\partial t^2}\left(\frac{p(\vec{r},t)}{B(t)}\right) - \Delta p(\vec{r},t) = 0. \quad (5)$$

If ρ_0 and B are assumed to be invariant, the first and second terms of (5) vanish and we obtain the well-known wave equation:

$$\frac{\partial^2}{\partial t^2} p(\vec{r},t) - \frac{1}{c^2}\Delta p(\vec{r},t) = 0, \quad (6)$$

where $c = \sqrt{B/\rho_0}$ is the speed of waves.

By replacing the derivatives with central difference approximations in equations (1) and (4), these can be transformed into updating equations to obtain a FDTD leapfrog scheme. In this way, we can perform numerical simulations of one-dimensional media with time-varying parameters:

$$u\left(x+\Delta x, t+\frac{\Delta t}{2}\right) = u\left(x+\Delta x, t-\frac{\Delta t}{2}\right) - \frac{1}{\rho_0(t)}\left(p\left(x+\frac{\Delta x}{2}, t+\Delta t\right) - p\left(x-\frac{\Delta x}{2}, t+\Delta t\right)\right)\frac{\Delta t}{\Delta x}, \quad (7)$$

and

$$p\left(x+\frac{\Delta x}{2}, t+\Delta t\right) = p\left(x+\frac{\Delta x}{2}, t\right)\left(1+\Delta t\left(\frac{B(t+\Delta t)}{B(t)}-1\right)\right) - B(t)\left(u_x\left(x+\Delta x, t+\frac{\Delta t}{2}\right) - u_x\left(x, t+\frac{\Delta t}{2}\right)\right)\frac{\Delta t}{\Delta x} - B(t)\left(\frac{\rho(t+\Delta t)}{\rho(t)}-1\right) \quad (8)$$

References

1. Koutserimpas, T. T. & Fleury, R., "Nonreciprocal gain in non-Hermitian time-Floquet systems. Phys. Rev. Lett. Vol. 120, 087401, 2018.
2. Wen, X., Zhu, X., Fan, A., Tam, W. Y., Zhu, J., Wu, H. W., and Li, J, "Unidirectional amplification with acoustic non-Hermitian space− time varying metamaterial", Commun., Vol. 5(1), No. 18, 2022.
3. Zhao, J. et al., "Programmable time-domain digital-coding metasurface for non-linear harmonic manipulation and new wireless communication systems,". Natl Sci. Rev. Vol. 6, 231–238, 2019.
4. Sounas, D. L. and Alù, A., "Non-reciprocal photonics based on time modulation," Nat. Photonics Vol. 11, 774–783, 2017.
5. Kang, J., and Haberman, M. R., "Sound diffusion with spatiotemporally modulated acoustic metasurfaces," Appl. Phys. Lett., Vol. 121, No. 18, 181703, 2022.
6. Pham, K., and Maurel, A. Diffraction grating with space-time modulation. J. Comput., Vol. 469, No. 111528, 2022
7. Fakheri, M. H., Rajabalipanah, H., and Abdolali, A., "Spatiotemporal binary acoustic metasurfaces," Phys. Rev. Appl., Vol. 16(2), No. 024062, 2021.
8. Psiachos, D., and Sigalas, M. M., "Band-gap tuning in two-dimensional spatiotemporal phononic crystals,". Phys. Rev. Appl., Vol. 15(1), No. 014022, 2021.
9. Lesniewski, P. J. "Linear time domain model of the acoustic potential field,". J. Acous., Vol. 112 No. 2, 385–394, 2002.

Time-varying metasurfaces for parametric amplification of electromagnetic waves

F. V. Kovalev* **and I. V. Shadrivov**

ARC Centre of Excellence for Transformative Meta-Optical Systems (TMOS),
Research School of Physics, The Australian National University, Canberra ACT 2601, Australia
*corresponding author: fedor.kovalev@anu.edu.au

Abstract: We propose and study a time-varying metasurface for parametric amplification of electromagnetic waves. We found that our subwavelength thin metasurface can provide amplification of up to 10 dB and analysed its stability. The proposed amplification principle can be used for electromagnetic waves in the radio, microwave and subterahertz range and is limited by the properties of modern varactor diodes.

Time-varying metasurfaces give us access to many non-trivial physical effects. They can shift the frequency of the radiation, steer electromagnetic beams, control parametric waves in the scattered field and exhibit nonreciprocity, meaning that electromagnetic waves are transmitted through the metasurface differently depending on the direction of incidence [1]. The higher the modulation rate, the more interesting effects can be achieved. When it becomes comparable to the frequency of an electromagnetic wave, it is possible to have complete control over light both in space and time [2].

Recently, several research groups used different methods to amplify incident radiation with the help of metasurfaces. They utilised active substrates, used parametric rotation of the anisotropy of surface susceptibility, permittivity modulation, or integration of power amplifiers and transistors. Parametric amplification in left-handed transmission line media and metamaterial waveguides was studied almost two decades ago [3], but these methods have not yet been applied to amplification of free-space propagating electromagnetic waves. Parametric amplification techniques are used in electronic circuits and optics. In particular, they became the leading technology for ultralow-noise microwave measurements in quantum computing.

In this work, we propose a new approach to electromagnetic wave amplification using time-varying metasurfaces. Each meta-atom of the developed metasurface acts as a parametric amplifier based on a split-ring resonator (SRR) with variable capacitance. By applying the appropriately modulated voltage to the embedded varactors in each SRR we can change its capacitance with the pump frequency according to the following periodic law:

$$C(t) = C_0\left[1 + \beta\cos\left(\omega_p t + \varphi_p\right)\right] \quad (1)$$

where C_0 – the medium capacitance, $\beta = \Delta C/C$ – the parametric modulation coefficient, ΔC – the amplitude of the parametric modulation, $\omega_p \approx 2\omega_s$ – the parametric modulation frequency, ω_s – the incident electromagnetic wave frequency, φ_p – the phase of the parametric modulation.

We use numerical simulations to model the three-dimensional geometry along with a nonlinear circuit simulation of a real variable capacitance diode and an appropriate biasing network. We studied various regimes of operation of the system and found that we could achieve a significant gain of more than 10 dB. The gain can be controlled by the parameters of the modulation. We studied the instability threshold for this system and our model shows excellent agreement with the results of numerical simulations. The instability threshold corresponds to a change in the resonance frequency of the circuit equal to its bandwidth.

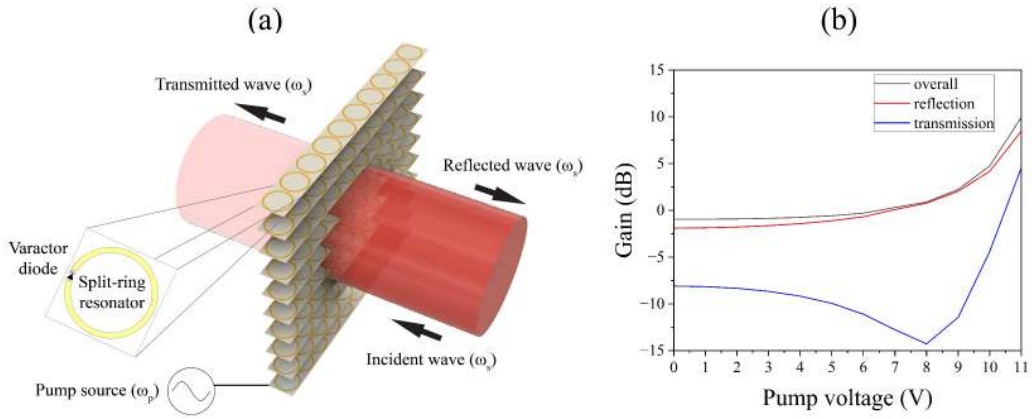


Figure 1. The proposed time-varying metasurface with the pump source connected electrically (a) and dependence of the gain on the pump amplitude (b).

We considered two different pump schemes: applying the parametric modulation electrically (Fig. 1a) and inducing the currents in SRRs at $\omega_p \approx 2\omega_s$ by the incident electromagnetic wave (Fig. 2a). The gain increases with increasing the parametric pump amplitude and ΔC in both cases, as shown in Fig. 1b and Fig. 2b.

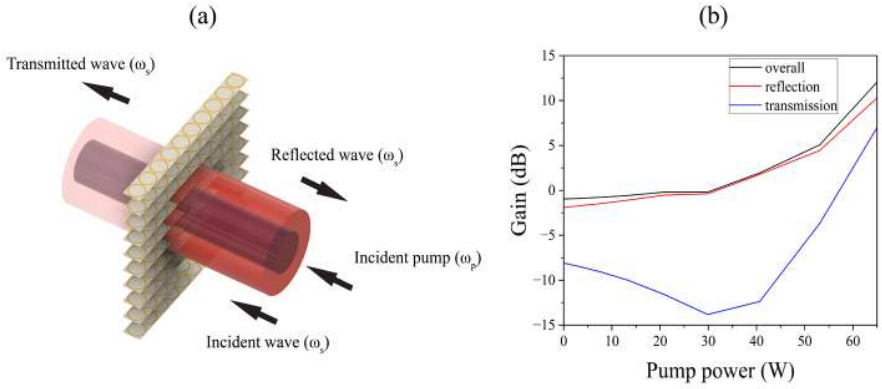


Figure 2. The proposed time-varying metasurface with the external pump source (a) and dependence of the gain on the incident pump power (b).

We anticipate that the proposed structure also be able to provide spatial control of amplified waves using spatially inhomogeneous amplification. Such integration of several functionalities can be useful in a range of applications; for example, in multifunctional and programmable antenna radomes or repeaters on the ground and in orbit that can reflect and amplify incident signals.

References

1. Liu, M., Powell, D. A., Zarate, Y. & Shadrivov, I. V. “Huygens’ Metadevices for Parametric Waves,” Phys. Rev. X 8, 031077, 2018.
2. Galiffi, E. et al. “Photonics of time-varying media,” Adv. Photon. 4, 2022.
3. Kozyrev, A. B., Kim, H. & van der Weide, D. W. “Parametric amplification in left-handed transmission line media,” Appl. Phys. Lett. 88, 264101, 2006.

META 2023, PARIS - FRANCE, JULY 18 – 21, 2023

The operator theory of dispersive time varying media

S. A. R. Horsley[1*]

[1]School of Physics and Astronomy, University of Exeter, Stocker Road, Exeter, EX4 4QL UK
[*]corresponding author: s.horsley@exeter.ac.uk

Abstract: The theory of dispersive, time varying materials is challenging: the material response is both externally modulated, and depends on the history of the field. I will explain a new approach, where the optical 'constants' (refractive index etc.) become operators. I will show the resulting theory predicts spectrally tailored 'eigenpulses' of modulated materials and matches well with numerical simulations. Finally I will illustrate connections with the ABC problem of non-local media and also discuss some surprising connections with quantum mechanics.

Some fascinating wave physics has been discovered through considering materials with properties that vary in time. In the simplest case, an instantaneous change in the refractive index causes a wave to reflect without any spatial boundary, through making a transition to a negative frequency. However, in all experiments to date, the refractive index has neither been changed instantaneously, nor without depending on frequency (e.g. [1-3]). This presents a theoretical challenge: what is the best way of describing wave propagation in a dispersive time varying material?

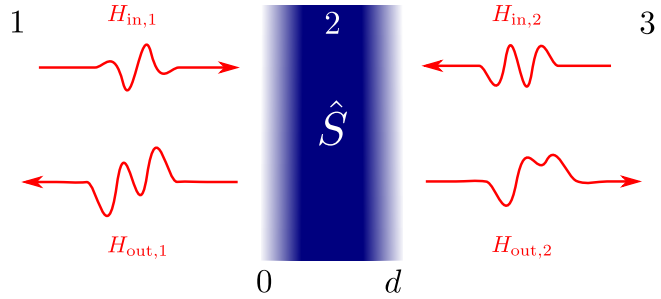


Figure 1: *Scattering from a time varying dispersive medium:* The scattering operator $\hat{S}$ acts on the incident spectra $H_{\mathrm{in},1/2}$ to give the output spectra. We compute $\hat{S}$ through describing the permittivity via Eq. (2), and find its eigenvectors, which represent the special pulses with a spectrum that is unchanged by the medium.

Here I shall discuss our attempt to solve this problem, where arbitrary dispersion and time variation are modeled through letting the common constants of electromagnetism (refractive index, wave-number, impedance etc.) become operators [4]. To see how this works, consider the displacement field in a dispersive time varying material

$$D(t)=\int_{-\infty}^{t}\epsilon(t,t-t')E(t')dt' \qquad (1)$$

If we attempt to write this in the frequency domain through inserting the Fourier representation of the electric field, we are prevented by the explicit time dependence of the permittivity. However, in the frequency domain the time variable is equivalent to a frequency derivative, allowing us to write (1) in the form

$$D(\omega)=\hat{\epsilon}(i\partial_\omega,\omega)E(\omega) \qquad (2)$$

We can numerically construct this operator through e.g. using a finite difference approximation to the frequency derivative and evaluating the permittivity as a function of a matrix argument. Following this line of argument, all quantities involving the permittivity (e.g. the wave number) become operators but otherwise we can treat the problem like an ordinary frequency domain one. Inside a time modulated material the field then takes the familiar form $E(x,\omega)=\exp(i\hat{K}x)A_{+(\omega)}+\exp(-i\hat{K}x)A_{-(\omega)}$.

Using this approach I shall show we can derive semi-analytic expressions for the scattering from a arbitrarily time varying slab. In addition to comparing this approach to existing numerical and analytical techniques, we find that the eigenfunctions of these operators represent pulses (eigenpulses) that do not change their spectra after interaction with the time-varying, dispersive material (see Fig. 2). Furthermore, the poles of these operators represent the non-time harmonic bound states of the system, the time varying medium analogue of surface plasmons. Finally I shall demonstrate the application of this theory to problems of quantum emission in time varying media, taking the particular example of a moving grating [5] where we can compare our method with fully analytic results.

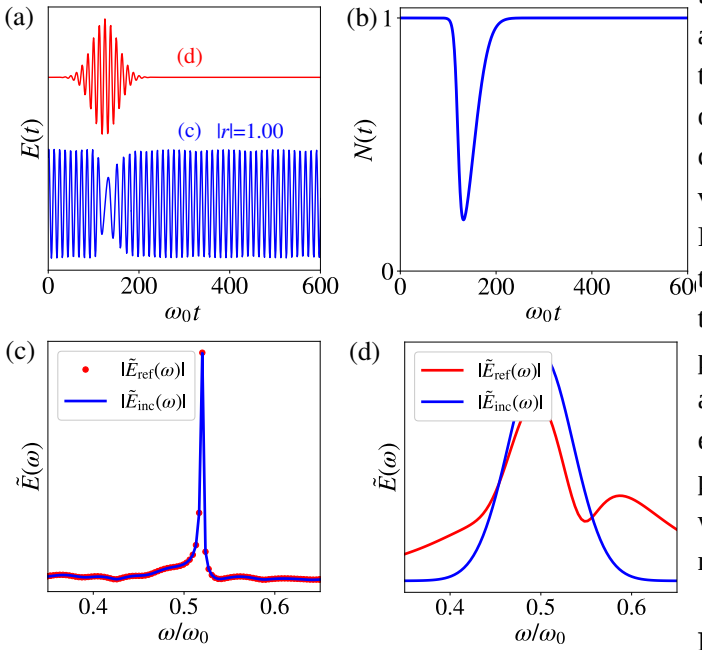


Figure 2: *Eigenpulses of a time varying dispersive medium:* (a) we compare the scattering of two pulses incident onto a metal with the time dependent carrier density shown in (b). (c) shows the incident and reflected spectrum of an eigenpulse, illustrating the medium acts as a mirror, while (d) shows the effect on a Gaussian pulse, which is reshaped.

SARH acknowledges the Royal Society and TATA (URF\R\21103)

References

[1] E. Galiffi, R. Tirole, S. Yin, H. Li, S. Vezzoli, P. A. Huidobro, M. G. Silveirinha, R. Sapienza, A. Alu, and J. B. Pendry "*Photonics of Time-Varying Media*" *Adv. Phot.* **4**, 014002 (2022).

[2] J. Bohn, T. S. Luk, C. Tollerton, S. W. Hutchings, I. Brener, S. A. R. Horsley, W. L. Barnes, and E. Hendry "*All Optical Switching of an epsilon-near-zero plasmon resonance in Indium Tin Oxide*" *Nat. Comm.* **12**, 1017 (2021)

[3] J. Bohn, T. Shan. Luk, S. A. R. Horsley, and E. Hendry "*Spatiotemporal refraction of light in an epsilon-near-zero indium tin oxide layer: frequency shifting effects arising from interfaces*" *Optica* **8**,6 1532 (2021)

[4] S. A. R. Horsley, E. Galiffi, and Y.-T. Wang "*Eigenpulses of dispersive time-varying media*" arXiv:2208.11778 (2022)

[5] S. A. R. Horsley and J. B. Pendry "*Time varying gratings model Hawking radiation*" arXiv:2302.04066 (2023)

META 2023, PARIS - FRANCE, JULY 18 – 21, 2023

Surface plasmon polaritons are not polaritons, and not plasmons either

Antoine Moreau[1]

[1]Université Clermont Auvergne, Clermont Auvergne INP, CNRS, Institut Pascal, F-63000 Clermont–Ferrand, France

[*]corresponding author: antoine.moreau@uca.fr

Abstract: Recent interest in the study of spatial dispersion has brought forward some difficulties in the way the community has named physical objects for decades, sometimes describing electromagnetic guided modes using a vocabulary coming from solid state physics and quantum mechanics. While changing our habits now may not be the best idea, it could be interesting to clarify a few points: the guided mode that we call now a surface plasmon polariton (SPP) has not always been called so, and its properties do not match with those of the polariton, nor on those the plasmon as defined by the solid state community. Understanding why not sheds light on the way spatial dispersion has an influence on "surface plasma oscillations" and why this may be important in the future.

Ten years ago, an experiment has renewed in the community of photonics, the interest for the study of spatial dispersion, also called non-locality[1]. In metals, the repulsion between electrons, which cannot be taken into account in the framework of the Drude model, makes the optical response of the jellium intrinsically non-local. Taking into account this phenomenon means taking into account another wave inside the jellium, considered as a plasma: the Langmuir wave, the corresponding quantum being the actual plasmon[2]. At the edges of a plasma, a surface wave, initially called "surface plasma oscillation" and that we call today an SPP can be excited. This solution of Maxwell's equations is completely transverse, while the plasmons correspond to a purely longitudinal solution. Ironically enough, we now have to call plasmons "bulk" to distinguish them from the surface plasmon. We underline that there is no conversion, inside the metal, from the transverse to the longitudinal wave and thus no coupling mechanism which would characterize a polariton. When light is able to couple to vibration degrees or to generate excitons, true surface polaritons can be supported by the interface. But the mechanism is very different from the SPP. The negativity of the permittivity is, in that case, linked to this coupling mechanism while in a jellium the negative permittivity is due to the Drude model in the framework of which no true plasmon can propagate. Or course, things are never simple, so that a more accurate description of a SPP taking into account spatial dispersion shows that there is a small longitudinal component accompanying the wave[2] – this small component being able to bring dramatic changes to the dispersion curbe of the mode[3]. We will try, in this talk, to sort things out – and to pinpoint when in history, shifts in the vocabulary of the community occurred[4].

We would finally like to underline that, while this discussion has been for decades focused on metals, highly doped semi-conductors are probably the materials for which such a discussion is the most illuminating – especially for epsilon-near-zero materials, for which spatial dispersion has to be undoubtedly taken into account.

References

1. Ciracì, C., Hill, R. T., Mock, J. J., Urzhumov, Y., Fernández-Domínguez, A. I., Maier, S. A., ... & Smith, D. R. (2012) Probing the ultimate limits of plasmonic enhancement. *Science*, *337*(6098), 1072-1074.
2. Moreau, A., Ciraci, C., & Smith, D. R. (2013). Impact of nonlocal response on metallodielectric multilayers and optical patch antennas. *Physical Review B*, *87*(4), 045401.
3. Pitelet, A., Schmitt, N., Loukrezis, D., Scheid, C., De Gersem, H., Ciracì, C., ... & Moreau, A. (2019). Influence of spatial dispersion on surface plasmons, nanoparticles, and grating couplers. *Journal of the Optical Society of America B*, *36*(11), 2989.
4. Burstein, E., Chen, W. P., Chen, Y. J., & Hartstein, A. (1974). Surface polaritons—propagating electromagnetic modes at interfaces. *Journal of Vacuum Science and Technology*, *11*(6), 1004-1019.

META 2023, PARIS - FRANCE, JULY 18 – 21, 2023

Metamaterials with Temporal Inhomogeneity for Analog Optical Computing

A. V. Kharitonov[1*], A. I. Minibaev[1], and S. S. Kharintsev[1]

[1]Department of Optics and Nanophotonics, Institute of Physics, Kazan Federal University, Russian Federation
[*]corresponding author: antvharitonov@kpfu.ru

Abstract: In recent years, there has been a growing interest in metamaterials that a capable of performing mathematical operations on the optical signals. However, this concept requires a complicated distribution of spatial inhomogeneities, which hinders its practical applications. Here, we propose an approach for analog optical computing using spatially uniform systems. For this purpose, we leverage novel regimes of light-matter interactions arising in time-varying media. The target operation is achieved by controlling the Fourier amplitudes through the effect of wave amplification/attenuation.

The ability to perform ultrafast and energy-efficient computing is of key importance for the development of cutting-edge technologies. However, widely used integrated electronic circuits are reaching their physical limitations [1] and, therefore, they cannot meet the growing demands for computing performance. New platforms and physical approaches are needed to outperform existing computers. Analog optical computers have recently attracted renewed interest as an alternative to digital electronic computers []. These devices, in their modern form, are artificial materials – metamaterials – that can perform mathematical operations and even solve integro-differential equations [2, 3]. Computational metamaterials provide opportunities for real-time processing of large amounts of data using on-chip architectures.

Computational metamaterials modulate the optical field so that the output signal is the result of performing a mathematical operation on the input signal. This functionality is achieved by suitably designing the metamaterial's building blocks. However, this concept requires a complicated distribution of spatial inhomogeneities, which hampers its practical applications. Here, we show that analog wave-based computing can be performed using spatially uniform systems. For this purpose, we exploit the properties of time-varying media. Time-varying media is a class of artificial materials that are spatially uniform, but has inhomogeneities in the time domain [4]. The latter means that one of the parameters of the medium, e.g., dielectric permittivity, is modulated in time. This can be implemented by means of external influence. Time-modulated structures have attracted a great fundamental and practical interest due to recent observations of fascinating wave phenomena [4].

The underlying principle of our computing system is that a linear mathematical operation on the spatial profile can be described as a kernel, which operates on the incident momentum spectrum [3]. The desired kernel is imprinted on the spatially uniform structure by suitably tailoring its temporal inhomogeneity. For this purpose, we exploit the effect of energy non-conservation in time-modulated systems. This effect allowed to control the Fourier components of the signal through wave amplification/attenuation. Using numerical simulations we investigated the process of light interaction with a time-modulated slab. Simulations were carried out by means of commercially available 3D electromagnetic solver (COMSOL Multiphysics). We calculated the transmission (T) and reflection (R) coefficients for various incident angles and various parameters of temporal inhomogeneity (switching time, modulation depth and switching profile of the refractive index). R and T coefficients reflect the efficiency of light conversion in time-modulated systems. The obtained results allowed us to optimize the

parameters of the temporal inhomogeneity in order to realize the desired mathematical operation. The resulting material represents a filter of spatial frequencies with suitably designed optical transfer function.

The computational metamaterials based on time-varying media open up novel opportunities for designing and practical implementation of analog optical computers with simple spatial configuration and extended functionalities.

This work was supported by grant no. 22-72-00091 of the Russian Science Foundation, https://grant.rscf.ru/site/user/forms?number=22-72-00091.

References

1. Caulfield, H. J. and S. Dolev, "Why future supercomputing requires optics," Nat. Photonics, Vol. 4, 261–263, 2010.
2. Silva, A., F. Monticone, G. Castaldi, V. Galdi, A. Alù and N. Engheta, "Performing mathematical operations with metamaterials," Science, Vol. 343, No. 6167, 160–163, 2014.
3. Goh, H. and A. Alù, "Nonlocal scatterer for compact wave-based analog computing," Phys. Rev. Lett., Vol. 128, 073201, 2022.
4. Galiffi, E., R. Tirole, S. Yin, H. Li, S. Vezzoli, P. A. Huidobro, M. G. Silveirinha, R. Sapienza, A. Alù and J.B. Pendry, "Photonics of time-varying media," Adv. Photonics, Vol. 4, No. 1, 014002, 2022.

Nanophotonics in Biomedical Applications

META 2023, PARIS - FRANCE, JULY 18 – 21, 2023

Holographic control of plasmonic structures on the distal facet of multimode optical fibers

Liam Collard[*,1], Filippo Pisano[1], Di Zheng[1], Antonio Balena[1], Linda Piscopo[1,2], Muhammad Fayyaz Kashif[1],Marco Pisanello[1], Liset M de la Prida[3], Cristian Ciraci[1], Marco Grande[4],Massimo De Vittorio[*,†,1,2],Ferruccio Pisanello[*,†,1]

[1] Center for Biomolecular Nanotechnologies, Istituto Italiano di Tecnologia, Arnesano, LE ,73010, Italy

[2]Dipartimento di Ingegneria Dell'Innovazione, Università del Salento, Lecce, 73100, Italy

[3]Instituto Cajal, CSIC, Ave Doctor Arce, Madrid, 28002, Spain

[4]Dipartimento di Ingegneria Elettrica e dell'Informazione, Politecnico di Bari, Bari, 70125, Italy

[*]Corresponding author: liam.collard@iit.it
† These authors jointly supervised this work

Abstract: Plasmonic fiber tips have attracted considerable research interest from a broad range of perspectives. However, they have been hindered by the turbidity of the fiber combined with the resonant properties of the nanostructures. By applying wavefront shaping, we show that either a sub-region or entire plasmonic structure can be holographically activated. We have applied this method to a wide range of plasmonic structures including periodic nanostructures for EOT and sub-diffraction beam formation and nanoislands for Surface Enhanced Raman Spectroscopy (SERS).

The tip of a multimode optical fiber (MMF) has emerged as a natural candidate to host plasmonic structures as it is miniaturized and inherently light coupled. This has enabled a set of applications across a wide range of fields including enhanced sensing[1], integrated phase shift/beam steering[2] and second harmonic generation[3]. However, these technologies have been limited by the turbidity of the MMF that scrambles the structured input light over the entire core thus limiting the optical control of the plasmonic effects through the fiber.

Here, we propose to use a wavefront shaping technique to reveal links between input light and the mode coupling with the plasmonic resonances through the turbid MMF[4]. In particular we show that the optical transmission may be confined to a focal spot of few micrometers on the plasmonic fiber facet,limited only by the fiber numerical aperture. The wavefront shaping technique enables us to generate a re-configurable spot scanning the fiber facet or to activate an entire plasmonic structure.

We have investigated two intrinsically different classes of plasmonic structures: periodic nano-structures milled on the fiber facet by focused ion beam milling (top-down) and gold nanoislands grown on the fiber by a dewetting procedure (bottom-up). The periodic nanostructures exhibit well-defined transmission properties known as the extraordinary optical transmission (EOT) and are also well suited to generate beams with sub-diffraction features. The nanoislands, instead, exhibit broad resonances and are well suited to enhanced sensing via SERS. This opens up the possibility to host a variety of plasmonic structures on the tip of a MMF, potentially enabling multi-functional, and hyperspectral plasmonic fiber optic sensing.

The optical setup used to focus light through a plasmonic fiber optic is shown in 1a. Prior to transmission through the fiber, a spatial light modulator (SLM) was used to pre-shape the laser light (633 nm) to generate reconfigurable foci at the output. Both the surface of the output facet and its angular output were monitored on CCD2 and CCD3. Inelastically backscattered light collected by the fiber was sent to the spectrometer (SF).

To fabricate plasmonic structures, firstly a thin layer of gold (ranging from 5-100 nm) was evaporated onto the facet of an optical fiber, then the fiber was transferred to either the FIB for milling or furnace for dewetting.

Firstly nanohole arrays were milled on the facet of fiber. Panel 1c shows how each nanohole array may be holographically activated with the SLM, the foci were found to have diameter in the vicinity of the diffraction limit (approx. 3.5 um). On closer inspection with a higher NA objective collecting from the plasmonic facet we found clear evidence of sub-diffraction beam formation, leading us to conclude that the combination of periodic nanostructures and wavefront shaping show great potential for super resolution imaging through a MMF.

The final panel shows a focused spot on the nanoisland annealed surface. Benzenethiol molecules (BT) were functionalized to the facet and SERS spectra were collected through the fiber. The spectra are a convolution of both the silica background from the fiber and the BT molecule SERS signal, with prominent peaks as shown in panel 1d. Both components are of similar intensity, which marks a clear enhancement when compared with our Raman through blank fiber experiments.

Due to the diverse application of plasmonic fiber optics, the ability to confine light to a sub-region of the plasmonic facet could lead to a number of new applications. In particular, we envisage that the ability to perform sub diffraction beam formation, and enhanced sensing at the fiber tip in a reconfigurable manner will lead to a new generation of high sensitivity, multifunctional, plasmonic endoscopes potentially hosting a range of nano-photonic structures.

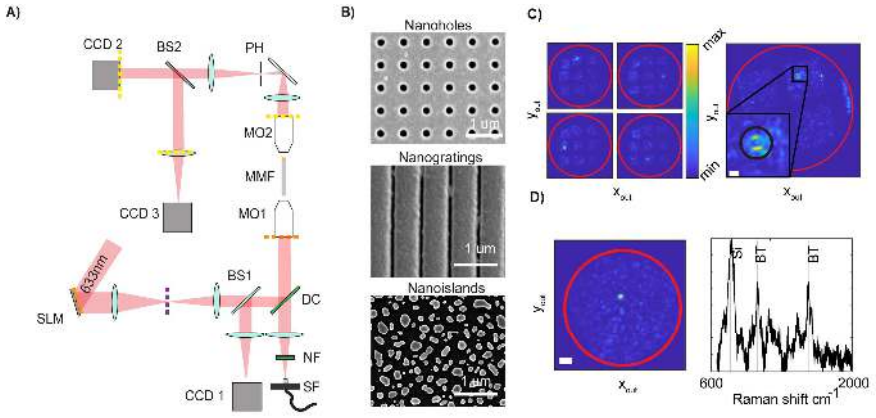


Figure 1. A) The optical train used to shape light through plasmonic fiber optics SLM- spatial light modulator, BS – beam splitter, CCD – charged coupling device, DC – dichroic mirror, MO1 – microscope objective, MMF – multimode fiber, PH- pinhole, SF- spectrometer fiber. B) SEM micrographs of three types of plasmonic structures fabricated on the facet of a multimode fiber. C) Holographic activation of nanohole arrays on the tip of a MMF. D) Spatially resolved SERS of BT molecules through the fiber.

References

[1] Smythe, E. J., Dickey, M. D., Bao, J., Whitesides, G. M. and Capasso, F., "Optical antenna arrays on a fiber facet for in situ surface-enhanced Raman scattering detection," Nano Lett. **9**(3), 1132–1138 (2009).

[2] Principe, M., Consales, M., Micco, A., Crescitelli, A., Castaldi, G., Esposito, E., La Ferrara, V., Cutolo, A., Galdi, V. and Cusano, A., "Optical fiber meta-tips," Light Sci. Appl. **6**(3), e16226–e16226 (2017).

[3] Xu, J., Plum, E., Savinov, V. and Zheludev, N. I., "Second harmonic generation in amorphous silicon-on-silica metamaterial," APL Photonics **6**(3), 36110 (2021).

[4] Collard, L., Pisano, F., Zheng, D., Balena, A., Kashif, M. F., Pisanello, M., D'Orazio, A., de la Prida, L. M., Ciracì, C., Grande, M., De Vittorio, M. and Pisanello, F., "Holographic Manipulation of Nanostructured Fiber Optics Enables Spatially-Resolved, Reconfigurable Optical Control of Plasmonic Local Field Enhancement and SERS," Small, 2200975 (2022).

Inversely design a phase mask for an extended depth of focus through adjoint optimization

Huade Mao[1], Jiqiang Kang[1,2], and Kenneth K.Y. Wong[1,2*]

[1]Department of Electrical and Electronic Engineering, The University of Hong Kong, Hong Kong, China
[2]Advanced Biomedical Instrumentation Centre, Hong Kong Science Park, Hong Kong, China
[*]corresponding author: kywong@eee.hku.hk

Abstract: We present an adjoint optimization method to inversely design a phase mask for an extended depth of focus. It reduces computation burden and has a promising application in optical imaging.

In optical imaging field, extended depth of focus (EDOF) demonstrates great importance in improving imaging depth and resolution [1]. In this regard, Bessel beam and Airy beam has been frequently adopted as a penetration beam due to their diffraction-free features [2]. However, such features come with high-energy side lobes, which will cause background noise and photobleaching [2]. Therefore, the community spends huge efforts in designing different optical devices, e.g. metasurface [3], phase mask [4], to achieve an EDOF with reduced side lobes. However, the forward process, e.g. phase mask designing, may pose high computation burden [2] but lead to a decreased focusing efficiency [3]. Recently, some inverse design methods have been applied in metasurface designing [5]. However, the research on inversely designing a phase mask for an EDOF is very limited.

Here, we present an adjoint optimization method to deliver a phase mask so as to achieve an EDOF. The phase mask could be easily accomplished through a spatial light modulator (SLM) or metasurface. The EDOF will empower optical imaging with a higher resolution and signal-to-noise ratio (SNR) compared to Bessel beam.

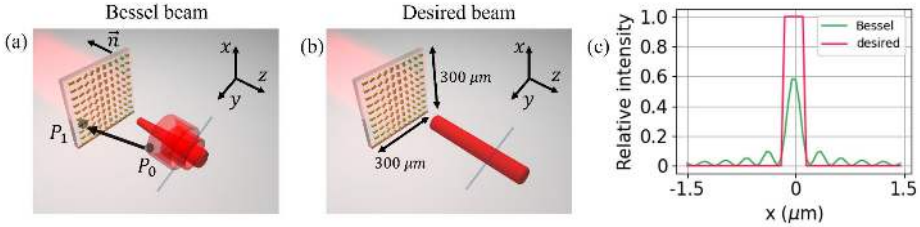


Figure 1. Schematic demonstration of the beam profile. (a) Bessel beam intensity distribution. (b) Desired beam intensity distribution without side lobes. (c) Intensity at a cross section.

Figure 1 presents our schematic setup. The size of the metasurface is 300×300 μm^2. The wavelength is 532 nm. Each pixel has a size of 250×250 nm^2. For a given phase mask $U(\vec{r})$, we can have its far-field radiation $U(P_0)$ through Fresnel-Kirchhoff formula $U(P_0)=\frac{1}{j\cdot 2\lambda}\int \frac{exp(jkr_{01})}{r_{01}}\cdot U(\vec{r})\cdot\cos(\vec{n},\overrightarrow{r_{01}})dS$, where $\overrightarrow{r_{01}}$ points from the field to the phase mask, λ is the wavelength and k is the wavenumber. It can be written in a nonlinear matrix form $g(v,p)=A_{nl}(p)v-b(p)=0$, where v is the field value, and p is the tunable phase modulation.

Here, we initialize the phase profile $p(x,y)$ for Bessel beam generation. Then, we use the adjoint optimization to update the phase pattern. We firstly propose a desired focus field I_0. The objective function we want to minimize is $f(v,p)=\sum_{x,z} abs(I_0-U)$, where U is the far-field intensity distribution during iteration.For each pixel on the phase mask, we apply a gradient descent updating rule, which is $p_{i+1}:=p_i-\frac{df}{dp_i}$. The gradient on each pixel can be obtained through only two adjoint simulation. The adjoint simulation is solving

the following equation of $\left(\frac{\partial g}{\partial v}\right)^T \cdot \lambda = -\left(\frac{\partial f}{\partial v}\right)^T$. The gradient can be readily calculated from this adjoint simulation as $\frac{df}{dp} = \frac{\partial f}{\partial p} + \lambda^T \cdot \frac{\partial g}{\partial p}$. In the end, we output the phase mask when the objective function is lower than threshold.

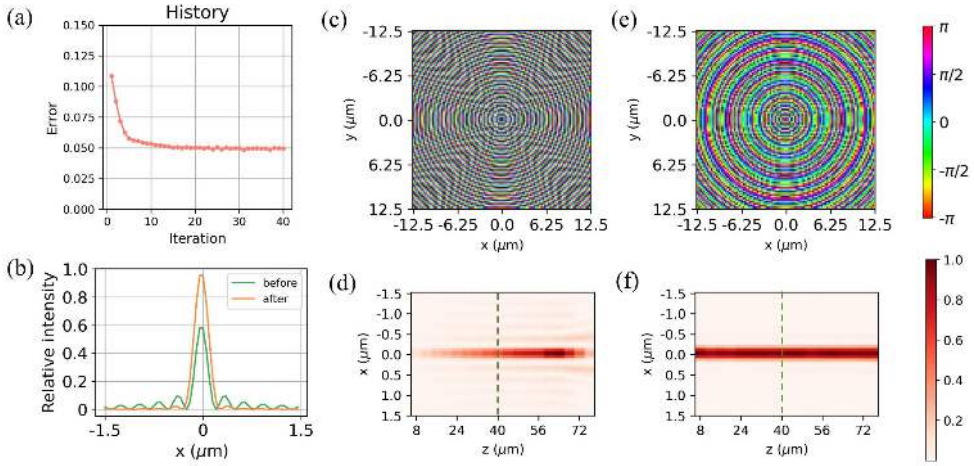


Figure 2. (a) Optimization history. (b) Intensity distribution at z-axis distance of 40 μm displayed in (d) and (f) before and after optimization. (c) Initial phase mask. (d) Initial intensity distribution. (e) Optimized phase mask. (f) Optimized intensity distribution.

The optimization result is shown in Figure 2. After optimization, the far-field focus has been greatly improved with a reduced side lobe in Figure 2(f). In Figure 2(a), the error is defined as the deviation from the desired intensity averaged across pixels. During the iteration, the error has been lowered from 10.84% to 4.90%. Once optimized, the phase mask can be uploaded to SLM or fabricated into a metasurface. It shows a great potential in an enhanced biomedical tissue imaging.

Acknowledgment: Research Grants Council of the Hong Kong Special Administrative Region of China (HKU 17210522, HKU C7074-21G, HKU 17205321, HKU 17200219, HKU 17209018, CityU T42-103/16-N) and Health@InnoHK program of the Innovation and Technology Commission of the Hong Kong SAR Government.

References

1. E. Bayati, R. Pestourie, S. Colburn, Z. Lin, S.G. Johnson, A. Majumdar, "Inverse Designed Metalenses with Extended Depth of Focus", ACS Photonics, Vol. 7, No. 4, 873-878, 2020.

2. G. Di Domenico, G. Ruocco, C. Colosi, E. DelRe, G. Antonacci, "Cancellation of Bessel beam side lobes for high-contrast light sheet microscopy", Sci. Rep., Vol. 8, No. 1, 17178, 2018.

3. L. Huang, J. Whitehead, S. Colburn, A. Majumdar, "Design and analysis of extended depth of focus metalenses for achromatic computational imaging", Photonics Res, Vol. 8, No. 10, 1613-1623, 2020.

4. J. Zhao, Y. Winetraub, L. Du, A. Van Vleck, K. Ichimura, C. Huang, S.Z. Aasi, K.Y. Sarin, A. de la Zerda, "Flexible method for generating needle-shaped beams and its application in optical coherence tomography", Optica, Vol. 9, No. 8, 859-867, 2022.

5. M. Mansouree, A. McClung, S. Samudrala, A. Arbabi, "Large-Scale Parametrized Metasurface Design Using Adjoint Optimization", ACS Photonics, Vol. 8, No. 2, 455-463, 2021.

META 2023, PARIS - FRANCE, JULY 18 – 21, 2023

Plasmonic infrared sensor aided with artificial intelligence and immunoassay for structural protein biomarker-based neurodegenerative disease detection

D. Kavungal[1], P. Magalhães [2], S.T. Kumar [2], R. Kolla [2], H.A. Lashuel[2*] and H. Altug[1*]

[1]Institute of Bioengineering, EPFL, Switzerland

[2]Brain Mind Institute, EPFL, Switzerland

[*]Corresponding author: hilal.lashuel@epfl.ch, hatice.altug@epfl.ch

Abstract: We introduce an infrared metasurface sensor based on plasmonic surface-enhanced infrared absorption spectroscopy combined with immunoassay, which detects alpha-synuclein, an early structural biomarker protein for Parkinson's disease with clinical specificity and identifies its different structural species using their unique spectroscopic signals. Unprecedentedly, we augmented the sensor with Deep Neural Network, enabling quantitative differentiation of aSyn aggregates. Capable of multiplexing and retrieving aggregate absorbance from complex biomatrix, our sensor shows promise for PD diagnosis, disease progression monitoring, and drug efficacy assessment.

Parkinson's disease (PD) is the fastest-growing neurodegenerative disorder with devastating consequences on patients' health and quality of life. Yet, there is neither a cure that can thwart the progression of the disease nor any diagnostic method for early detection and disease progression monitoring. The structural misfolding of protein biomarker: alpha-synuclein (aSyn) from its physiologically disordered or alpha-helix form into beta-sheet enriched fibrillar aggregates *via* intermediary oligomers is an early event in PD progression (Fig. 1A) [1]. For the first time, we will present a plasmonic surface enhanced infrared absorption (SEIRA) spectroscopy-based sensor combined with immunoassay and custom-made microfluidics (ImmunoSEIRA), which detects aSyn with clinically relevant specificity in real-time and distinguishes its different structural species using their unique infrared absorption spectra. This structural biomarker-based detection scheme involves a plasmonic chip combined with PDMS-based microfluidic channels in a backside measurement configuration (Fig. 1B). Sensor is immobilized with antibodies for specific capture of aSyn species (Fig. 1C). The plasmonic nanorod array design on the chip is tuned to resonate around the infrared amide absorption bands of proteins (1500-1700 cm^{-1}), thereby collecting enhanced absorption spectra of the captured aSyn (Fig.1D). Among this, the Amide I band (1600-1700 cm^{-1}) can provide quantitative information on the different secondary structure motifs that are present differently in each structural species of aSyn (Fig.1E). Thus, this method helps to identify and classify aSyn monomers from the pathological species of oligomers and fibrils based on their unique spectral response, which forms the basis of our structural biomarker-based detection [2] (Fig.1F).

Unprecedently, by combining ImmunoSEIRA with Deep Neural Network (DNN), we show the ability to quantitatively predict the individual presence of aggregates, i.e., oligomers and fibrils from mixed aSyn aggregate samples [2] (Fig.2). This is not achievable by any other existing methods and assays. The DNN-aided ImmunoSEIRA analysis is substantial for obtaining the quantitative presence of different aggregate species of the same protein biomarker in patient body fluids for accurate and timely diagnosis and to differentiate PD from other synucleopathies. We will also present other results showing the multiplexing aspect of the sensor to monitor different protein biomarkers at the same time, along with its capability to retrieve the protein signature in the presence of human cerebrospinal fluid. These results bring our sensor one step closer to clinical standards for PD diagnosis with future applications, including disease progression assessment, patient stratification, and aSyn-targeted drug engagement studies.

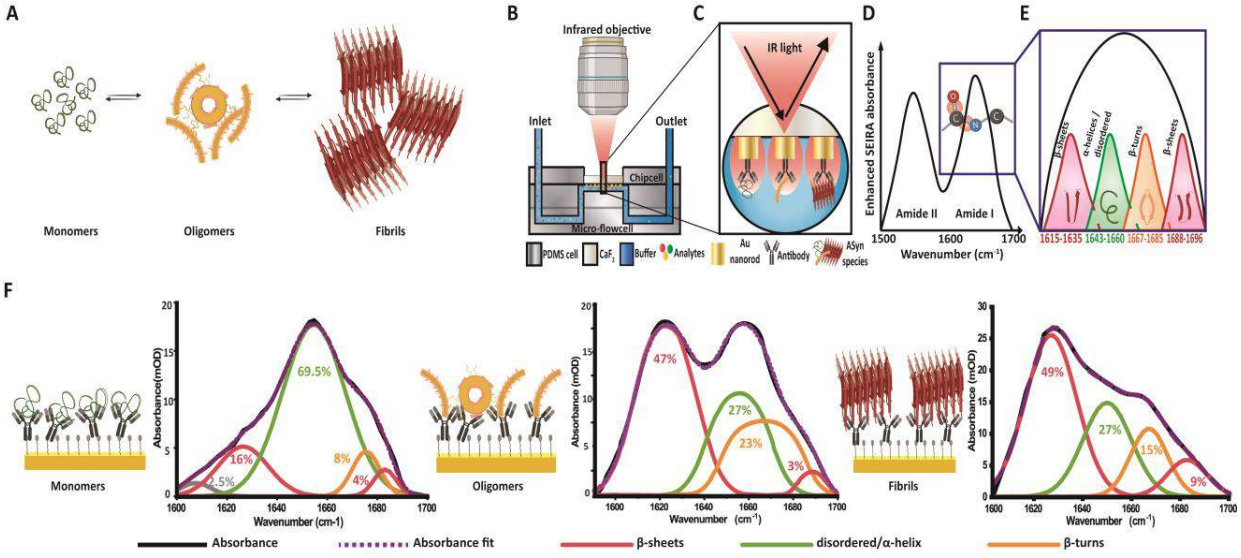


Figure 1. (A) Scheme showing aggregation of unstructured aSyn monomers into beta-sheet enriched fibrillary aggregates through intermediary oligomeric species (B) Structural biomarker-based detection scheme involving a plasmonic chip combined with PDMS-based microfluidic channels in a backside measurement SEIRA configuration (C) Immunoassay combined SEIRA (ImmunoSEIRA) for specific capture of aSyn protein species (D) Collection of enhanced SEIRA signal from aSyn protein amide absorption bands (E) Presence of different secondary structure motifs present in the protein extracted from the Amide I band based on distinct sub-bands (F) SEIRA enhanced absorbances of aSyn monomers, oligomers, and fibrils with their corresponding retrieved percentage presence of secondary structures.

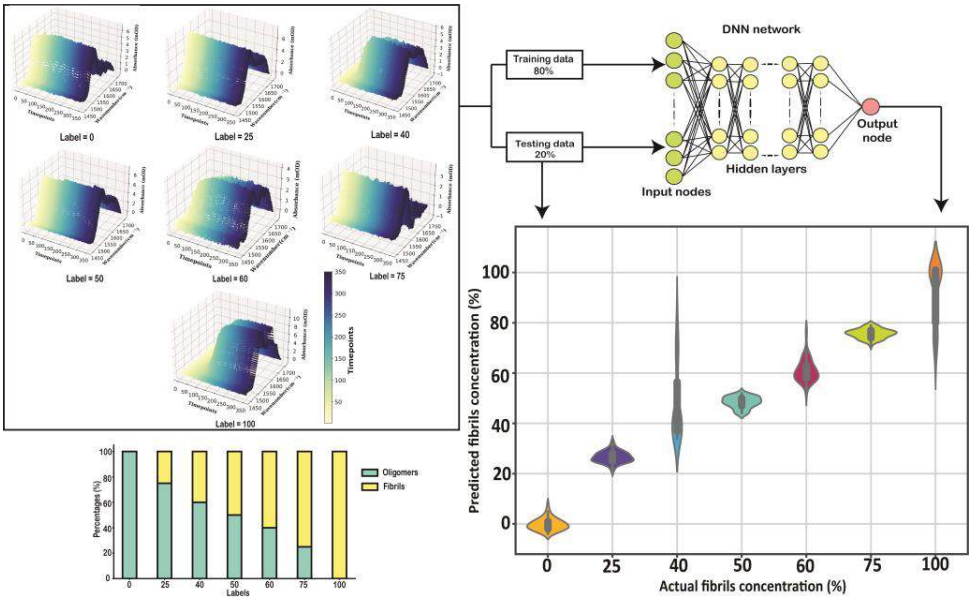


Fig. 2: 3D absorbance profile of different aggregate mixture samples, as mentioned in the stacked bar plot collected using the ImmunoSEIRA setup with labels corresponding to the percentage presence of fibrils, forms the entire dataset. This is split into training (80%) and testing (20%) datasets. The output produced by the trained DNN network shown in the violin plot compared with the actual output shows excellent accuracy of the network in predicting the individual presence of oligomers and fibrils in a mixture.

References

1. Magalhães, P. and H. A. Lashuel, "Opportunities and challenges of alpha-synuclein as a potential biomarker for Parkinson's disease and other synucleinopathies," Npj Park. Dis., vol. 8, no. 1, Art. no. 1, Jul. 2022
2. Kavungal, D., P. Magalhães, S.T. Kumar, R.Kolla, H. A. Lashuel, H.Altug, "Artificial intelligence coupled plasmonic infrared sensor for the detection of structural protein biomarkers in neurodegenerative diseases" (submitted, *Sci. Adv.*)

META 2023, PARIS - FRANCE, JULY 18 – 21, 2023

LSPR sensors with antiadhesive layer made of DNA: nanostructure pitch study

R. Trojanowicz[1], A. Vestri[2], M. Rippa[2], J. Zyss[3], K. Matczyszyn[4] and L. Petti[2*]

[1]Université Paris-Saclay, CEA, CNRS, SPEC, France
[2]Institute of Applied Sciences and Intelligent Systems "E. Caianiello" of CNR, Italy
[3] Laboratoire de Photonique Quantique et Moleculaire, Institut d'Alembert, ENS Cachan, France
[4] Advanced Materials Engineering and Modelling Group, Faculty of Chemistry, Wroclaw University of Science and Technology, Poland
[*]corresponding author: lucia.petti@isasi.cnr.it

Abstract: Sensors based on Localized Surface Plasmon Resonance (LSPR) reach impressive detection limits, however their fabrication in most cases is time-consuming and costly. In this work, we immobilized LSPR sensor with antiadhesive layer that allows detection of analyte through shift of the resonance and it subsequent recovery to initial LSPR peak position. Immobilization on 4 sensors from the same pattern family (Achiral Octupolar) with different pitch is performed to investigate what role nanostructure dimensions play in sensor's response.

Ideal LSPR sensor for biomedical application should be rapid, reusable (or inexpensive) and specific (low cross-sensitivity to typical contaminants). Developing such a device is a long and complicated process. Moreover, biomolecules such as DNA have size comparable to sensing volume of nanostructure which can't be neglected.

In our recently published paper [1], we have reported protocol for creating DNA antiadhesive layer for LSPR sensors fabricated with Electron Beam Lithography. Its reusability was shown by performing 13 measurements of analyte at various concentration, each one followed by washing (recovery protocol) – measurement protocol in Figure 1. Calibration curve was constructed and limit od detection (LOD) of 105 ng/ml was calculated. Standard deviation of LSPR peak after recovery was equal to 711 ± 2 nm, proving that recovery outcome is repeatable, therefore antiadhesive layer remains intact.

Subsequently, to find optimal nanostructure, immobilization is done on 4 sensors – each of Achiral Octupolar pattern but with a pitch of 25 nm, 50 nm, 100 nm and 263 nm. As analyte A we use 1 μg/ml sodium salt salmon dsDNA in deionized water (~2000 bp, salt/DNA 5% mass concentration) and as analyte B (B1, B2, B3) we use 1 μg/ml dsDNA of specific molecular weight (546 bp, 1064 bp and 1614 bp) in 100 mM Tris buffer and 10 mM $MgCl_2$. All analytes contain molecule of interest but of various size and with other solutes present.

Achiral Octupolar 25 yielded LSPR shift of 16 ± 4 nm and 46 ± 2 nm for analyte A and analyte B (average of B1, B2, B3), respectively. As we increase pitch of Achiral Octupolar structure to 263 nm the difference becomes negligible – down to shifts of 25 ± 5 nm and 32 ± 4 nm for analyte A and B, respectively. For all Achiral Octupolar structures solutions B1-B3 yield similar shifts. Therefore variations in molecular weight within 546 bp-1614 bp do not change sensor's response. Shift of LSPR resonance peak is linear with refractive index change, which was also verified for Achiral Octupolar family [2]. Ratio of shifts between solution A and B yields 2,88 and 1,28 for pitch of 25 nm and 263 nm, respectively. Those results indicate clearly a pitch effect response beyond each structure's inherent sensitivity to refractive index change.

Simultaneously, difference between LSPR shifts of analyte B and A decreases as pitch increases – 30 nm, 17 nm, 12 nm and 7 nm for dimensions of 25 nm, 50 nm, 100 nm and 263 nm, respectively. Ionic strength of solution affects DNA persistence length [3]. We hypothesize that sensor with 25 nm pitch gives much larger

response to analyte B as Mg^{2+} changes DNA persistence length, allowing it to penetrate more efficiently into sensing volume. For pitch of 263 nm, analyte A and B can both reach sensing volume with a comparable efficiency, regardless of Mg^{2+} presence.

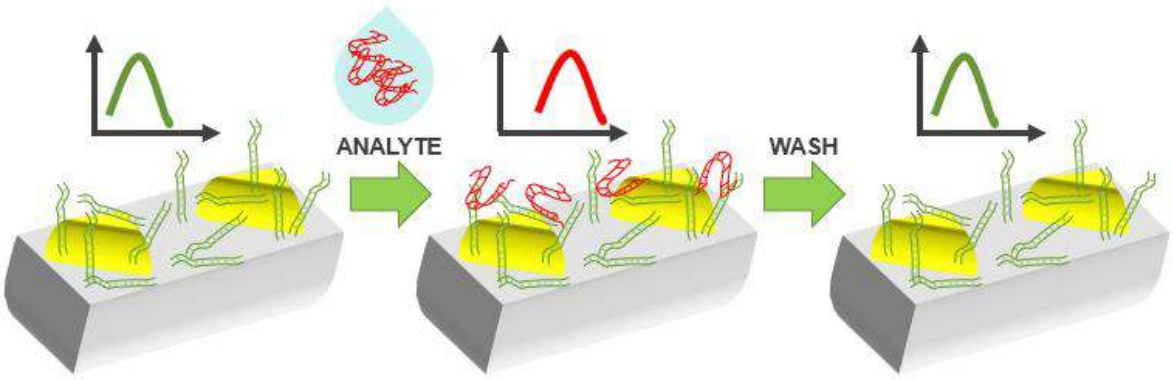


Figure 1. Scheme of measurement protocol: immobilized sensor with given LSPR peak position (left), analyte deposition and LSPR peak shift observation (centre) and recovery back to initial LSPR (right).

Using DNA solutions with relatively small concentration of other solutes allows successful sensor recovery. In order to manipulate well DNA persistence length, high concentration of buffers and salts is required. Unfortunately, they also reduce reusability of the protective layer. Currently, we are working on developing recovery protocol that could tackle that problem. In perspective, we hope to take advantage of the pitch-analyte interplay to develop multiplex sensor calibrated for typical solutes present in DNA samples. Such sensor could offer a full lab-on-chip functionality.

This work was funded by PNR 2015−2020 (POC01_00109), PULSE-COM (Grant agreement No 863227) and Erasmus+.

References

1. Trojanowicz, R., Vestri, A., Rippa, M., Zyss, J., Matczyszyn, K. and Petti, L., “DNA Antiadhesive Layer for Reusable Plasmonic Sensors: Nanostructure Pitch Effect,” ACS Omega, Vol. 36, No. 7, 31682–31690, 2022.
2. Rippa, M., Castagna, R., Brandi, S., Fusco, G., Monini, M., Chen, D., Zhou, J., Zyss, J. and Petti, L., “Octupolar Plasmonic Nanosensor Based on Ordered Arrays of Triangular Au Nanopillars for Selective Rotavirus Detection,” ACS Appl. Nano Mater., Vol. 3, No. 5, 4837–4844, 2020.
3. Brunet, A., Tardin, C., Salome, L., Rousseau, P., Destainville, N., Manghi, M., “Dependence of DNA Persistence Length on Ionic Strength of Solutions with Monovalent and Divalent Salts: A Joint Theory–Experiment Study” Macromolecules, Vol. 48, No. 11, 3641–3652, 2015.

New materials for photonics (Graphene, MoS2, WS2, etc)

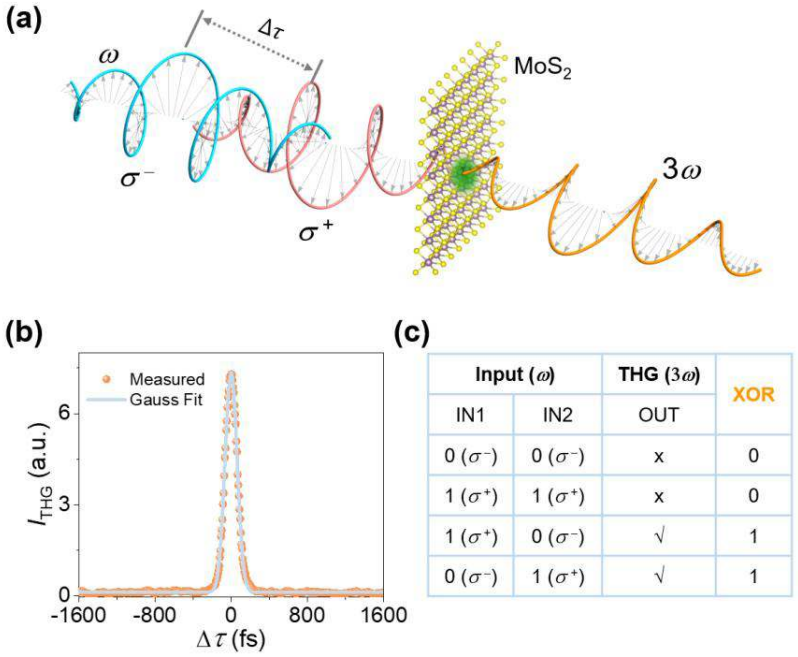
Chirality nonlinear optics enabled modulator and logic gates

Yi Zhang[1,2*], Juan Arias Muñoz,[1,2] and Zhipei Sun[1,2]

[1]Department of Electronics and Nanoengineering, Aalto University, Espoo 02150, Finland
[2]QTF Centre of Excellence, Department of Applied Physics, Aalto University, Espoo 02150, Finland
[*]corresponding author: yi.1.zhang@aalto.fi

Abstract: Ultrafast (<~130 fs) chirality all-optical modulators and various chirality logic gates with chirality nonlinear optics in monolayer semiconductors are demonstrated.

Chiral light, referring to left-handed (σ^-) and right-handed (σ^+) circularly polarized light, has been extensively studied both in linear optics [1] and nonlinear optics [2]. Recently, intrinsic chiral coupling effect in nanostructures (e.g., nanofiber and photonic waveguide) due to the spin-momentum locking in evanescent waves has been revealed for nanophotonics and quantum optics applications [3,4]. Here we demonstrate an ultrafast (<~130 fs) chirality all-optical gate and logic gates with chiral THG in monolayer semiconductors.



Input (ω)		THG (3ω)	XOR
IN1	IN2	OUT	
0 (σ^-)	0 (σ^-)	x	0
1 (σ^+)	1 (σ^+)	x	0
1 (σ^+)	0 (σ^-)	√	1
0 (σ^-)	1 (σ^+)	√	1

Figure 1. **Chirality nonlinear optics in monolayer MoS_2. (a)** Schematic illustration of chirality THG process in monolayer MoS_2. **(b)** Illustration of an ultrafast optical gate enable by chiral THG when the two opposite circularly polarized pump beams are employed. **(c)** The truth table of the chirality XOR logic gate based on the chiral THG.

Figure 1(a) shows the chiral third harmonic generation (THG) in monolayer MoS_2. The chiral THG effect is defined as the presence or absence of THG signal when the two fundamental waves possess opposite or identical circular polarization, which is since THG cannot be generated by a circularly polarized pump beam [5]. By controlling the time delay between the two oppositely polarized pump beams (~1560 nm), an ultrafast gate is demonstrated as shown in Fig. 1 (b) [6]. The operation speed (~130 fs) of the ultrafast gate is only limited by the pulse duration of the pump beam (~81 fs). Note that this ultrafast gate also provides an easy solution for

characterizing the pulse width of the fundamental wave due to the lift of strict symmetry breaking requirement as that in the $\chi_{(2)}$ nonlinear process. Figure 1(c) shows the truth table of the chirality XOR logic gate based on the chiral THG, where the two incident beams with different chirality, i.e., σ^- or σ^+ circular polarization, are synchronized in the time domain (i.e., $\Delta\tau$=0) and defined as input logic 0 or 1, the presence and absence of output THG signal is defined as logic output 1/0. By changing the chirality of the incident beams with waveplates, other chirality logic gates, such as XNOR, NOR, AND, OR, and NAND, can also be constructed as previous demonstrated with nonlinear optics [7]. With the electrically tunable THG in graphene [8], it is feasible to realize the electrical reconfigurable chirality logic gates, which is promising for next-generation mixed and hybrid computing technology.

In conclusion, we have demonstrated two prominent all-optical functions based on chiral THG in monolayer MoS_2. The relaxed phase matching limitation in nonlinear effect of monolayer materials implies broad working bandwidth, ultrafast, and on-chip devices possiblities. These demonstrated devices provide a promising all-optical approach for emerging nano-photonics applications based on chiral nonlinear effects.

Acknowledgment The authors acknowledge the financial support from the Academy of Finland (grants: 333099, 314810, 333982, 336144 and 336818), the Academy of Finland Flagship Programme (320167, PREIN), the European Union's Horizon research and innovation program (Grant agreement No. 101067269, ChirLog: 965124, FEMTOCHIP), the EU H2020-MSCA-RISE-872049 (IPN-Bio), and ERC grant (834742).

References

1. A. J., Miles, et. al., "Tools and methods for circular dichroism spectroscopy of proteins: A tutorial review". Chem. Soc. Rev. **50**, 8400 (2021).
2. O. Neufeld, et. al., "Optical chirality in nonlinear optics: application to high harmonic generation". Phys. Rev. Lett. **120**, 133206 (2018).
3. T. V. Mechelen, et. al., "Universal spin-momentum locking of evanescent waves". Optica, **3**, 118 (2016).
4. P. Lodahl, et al., "Chiral quantum optics". Nature, **541**, 473 (2017).
5. J. Cheng, et. al., "Chiral selection rules for multi-photon processes in 2D honeycomb materials". Opt. Lett. **44**, 2141 (2019).
6. Y. Zhang, et. al., "Coherent modulation of chiral nonlinear optics with crystal symmetry", Light Sci. Appl., **11**, 216 (2022).
7. Y. Zhang, et. al., "Chirality logic gates", Sci. adv. **8**, eabq8246 (2022).
8. T. Jiang, et al., "Gate-tunable third-order nonlinear optical response of massless Dirac fermions in graphene", Nat. Photon., **12**, 430 (201).

META 2023, PARIS - FRANCE, JULY 18 – 21, 2023

Layer-Dependent Optical Properties of 2D CrI_3 from Monolayer to Mesoscale Mapped by Hyperspectral Imaging

F. Ramiro-Manzano[1,2*], M. Galbiati[2*], J. J. Pérez Grau[2], F. Cantos-Prieto[2], J. Meseguer-Sánchez[2], I. Kosic[2], F. Mione[2], A. Cantarero[2], D. Soriano[3,4] and E. Navarro-Moratalla[2*]

[1] Instituto de Tecnología Química, Universitat Politècnica de València - Consejo Superior de Investigaciones Científicas (UPV-CSIC), Avd. de los Naranjos s/n, 46022, Valencia, Spain
[2]Instituto de Ciencia Molecular, Universitat de València, Calle Catedrático José Beltrán Martínez 2, 46980, Paterna, Spain
[3]Information Engineering Department, University of Pisa, Via Caruso 16, 56122, Pisa, Italy.
[4]Departamento de Física Aplicada, Universidad de Alicante, 03690, San Vicente del Raspeig, Alicante, Spain.
[*]corresponding authors: ferraman@fis.upv.es, marta.galbiati@uv.es, efren.navarro@uv.es

Abstract: Understanding the optical properties of 2D magnetic materials in relation to the number of layers is crucial for their application in photonics research. In this study, we investigate the modulation of the optical properties of CrI_3 across different thicknesses ranging from single layer to hundreds of layers. Our findings reveal a crossover in the modulation of optical properties at the mesoscale, which aligns with the thickness range at which the low-temperature magnetic properties of CrI_3 changes from antiferromagnetic to ferromagnetic.

Magnetic 2D materials have garnered substantial interest from both fundamental groundbreaking studies[1] and their potential applications[2]. The posiblity to create ultra-thin magnetic devices allows new chances to overcome the limitations of magnetic-enabled microelectronics and integrated photonics. An essential step[3] towards integrating these materials into photonic devices is to understand their optical properties as a function of the number of layers, from bulk down to the monolayer limit, which is still missing. In this study, we employed a hyperspectral imaging technique to acquire visible transmittance spectra of numerous CrI_3 flakes. These flakes whose thicknesses ranges from monolayer to more than 100 layers, were obtained by mechanically exfoliating bulk crystals onto standard microscopy glass slides. To prevent degradation, the samples were encapsulated with a coverslip that was sealed using a thermoplastic material. The hyperspectral imaging was performed employing a modified transmittance microscope. Here, the illuminating light comes from a bespoke monochromator which allowed to select the excitation wavelength. By sweeping the wavelength from 430 nm (2.9 eV) to 720 nm (1.7 eV) in increments of 1 nm, transmission images of several regions of interest in the samples were acquired at room temperature. For this purpose, the optical microscope was equipped with a monochrome CMOS camera, which was specifically chosen for its high linear range and low noise, enabling accurate quantitative analysis of even thin layers in the visible range. This wide-field method enhances the reliability of data under the same experimental conditions by acquiring images containing different samples and background. Regarding the data analysis, multiple spectra of different thickness flakes have been fitted simultaneously[4] to a transmittance model for increasing the accuracy of the results. We consider our experimental system as a basic Fabry-Pérot cavity formed by a stack of three layers and two interfaces. Here, the dielectric function of CrI_3 is assumed to follow a Lorentzian-based model composed by two oscillators whose parameters include a dependency with the sample thickness. Among other examined alternatives, the measuring method based on transmittance, the minimum multilayer system composed of air-CrI_3-glass and the simultaneous fitting process have been chosen to obtain robust and accurate results. Figure 1a presents the spectral changes of the minimum dip positions of the transmittance spectra, and Figure 1b displays the imaginary part of the dielectric function extracted from the

simultaneous fitting process. Rather than observing two thickness regimes (corresponding to few-layer and bulk thickness), an intermediate multi-layer regime shows a distinct behavior. Specifically, a crossover in the modulation of optical properties can be observed at the mesoscale. This peculiarity coincides with the thickness range in which the low-temperature magnetic properties of CrI3 changes from antiferromagnetic to ferromagnetic[2].

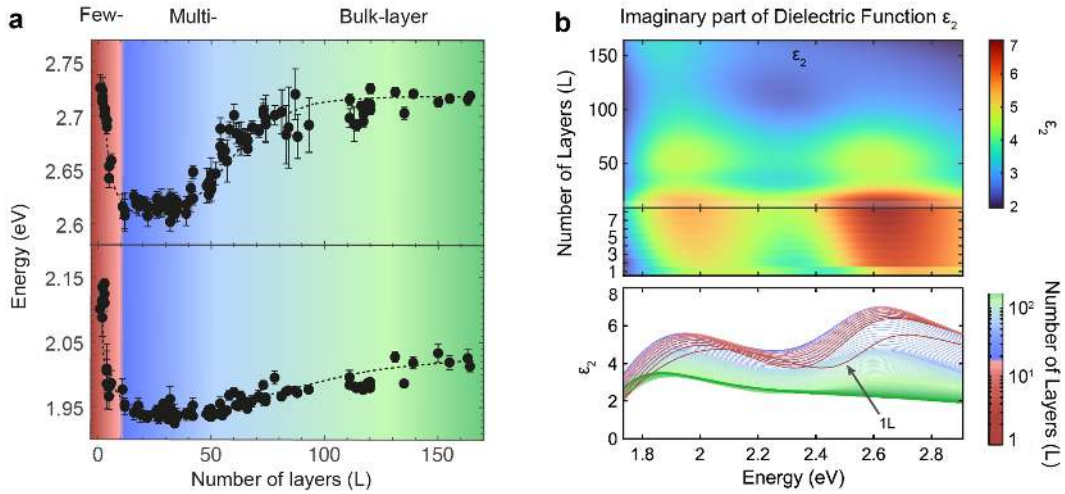


Figure 1. (a) Few-layer, multilayer and bulk thickness regimes are depicted according to the low (bottom panel) and high (top panel) energy transmittance minima experimentally measured. Markers display experimental data while the dotted lines are guides to the eye. (b) Evolution of the imaginary part of the dielectric functions (ε_2) in CrI_3 as a function of the number of layers. ε_2 is represented by way of colourmaps (top panel) and line plots (bottom panel).

Acknowledgements

F.R.M. Contributed equally to this work. FRM acknowledges MICINN and CISC for financial support from Ayudas de Incorporación de Científicos Titulares de Turno Libre de la Oferta de Empleo Público 2018/2019 No. 202280I200 and MICINN from Proyectos de Generación de conocimiento, No. PID2021-123163OB-I00. ENM and MG acknowledge the MICINN and the European Union NextGenerationEU for financial support from the Ramon y Cajal program (Grant No. RYC2018-024736-I and No. RYC2021-034609-I). FCP also acknowledges the MICINN for the FPU program (Grant No. FPU17/01587).

References

1. Huang, B., Clark, G., Navarro-Moratalla, E. et al. “Layer-dependent ferromagnetism in a van der Waals crystal down to the monolayer limit,” Nature Vol. 546, 270–273, 2017
2. Sun, Z., Yi, Y., Song, T. et al. “Giant nonreciprocal second-harmonic generation from antiferromagnetic bilayer CrI3,” Nature Vol. 572, 497–501, 2019
3. Li M., Biswas S., Hail C.U., and Atwater H.A., “Refractive Index Modulation in Monolayer Molybdenum Diselenide,“ *Nano Letters 21* (18), 7602-7608, 2021
4. Biasi S., Ramiro-Manzano, F., Turri, F. et al., "Hermitian and Non-Hermitian Mode Coupling in a Microdisk Resonator Due to Stochastic Surface Roughness Scattering," IEEE Photonics J. Vol. 11, No. 2, 6101114, 2019

META 2023, PARIS - FRANCE, JULY 18 – 21, 2023

Radiative suppression of exciton-exciton annihilation in a two-dimensional semiconductor

Luca Sortino[1*], Merve Gülmüs[1], Benjamin Tilmann[1], Leonardo de S. Menezes[1,2], Stefan A. Maier[3,4, 1]

[1] Chair in Hybrid Nanosystems, Faculty of Physics, Ludwig-Maximilians-Universität München, 80539 Munich, Germany
[2] Departamento de Física, Universidade Federal de Pernambuco, 50670-901 Recife-PE, Brazil
[3] School of Physics and Astronomy, Monash University, Clayton, Victoria 3800, Australia
[4] The Blackett Laboratory, Department of Physics, Imperial College London, London, SW7 2BW, United Kingdom
*corresponding author: luca.sortino@lmu.de

Abstract: Exciton-exciton annihilation (EEA) processes are a fundamental limit for the efficiency of two-dimensional (2D) semiconductors. Here, we demonstrate suppressed EEA by enhancing light-matter interaction in hybrid 2D-dielectric nanophotonic platforms, by coupling excitons in a transition metal dichalcogenide (TMDC) WS_2 monolayer with optical Mie resonances in gallium phosphide (GaP) dielectric nanoantennas. From their ultrafast dynamics, we show reduced EEA processes, even under high exciton density, demonstrating the potential of all-dielectric nanoantennas for low-power integrated nanophotonic devices based on 2D semiconductors.

2D semiconductors, such as TMDCs, exhibit exceptional optical properties governed by strongly bound excitons, opening novel opportunities for engineering light-matter interaction at the nanoscale. However, their in-plane confinement leads to large rates of Auger-type non-radiative EEA processes, even at relatively low exciton densities, which sets a fundamental limit for their applications [1]. Here, we demonstrate EEA processes can be suppressed via enhancement of light-matter interaction in hybrid 2D-dielectric nanophotonic platforms [2,3]. We achieve this by coupling excitons in a TMDC monolayer of WS_2 with optical Mie resonances in GaP dielectric nanoantennas. We observe intermediate light-matter coupling regime between excitons and nanoantennas, as well as photoluminescence enhancement factors above 10^2. Probing the ultrafast dynamic via pump-probe spectroscopy reveals suppressed EEA processes for coupled excitons (Figure 1a). Owing to the increased radiative recombination rate, we observe reduced EEA processes, even under a high exciton density > 10^{13} cm^{-2}, as evidenced by the absence of the onset of a bimolecular recombination process ascribed to EEA [4]. For uncoupled monolayers, we observe the expected onset under fluences above 10 $\mu J/cm^{-2}$ (Figure 1b). We extracted EEA coefficients in the order of 10^{-3}, compared to 10^{-2} for uncoupled monolayers, as well as absorption enhancement of 5.6 and Purcell factor of 4.5. Our results highlight all-dielectric nanoantennas as a promising plaform for hybrid nanophotonics with 2D materials, paving the way to the realization of higher quantum efficiencies and larger exciton densities, towards low-power integrated nanophotonic devices based on atomically thin semiconductors

References

[1] Y. Yu, et al. “Fundamental limits of exciton-exciton annihilation for light emission in transition metal dichalcogenide monolayers” Physical Review B, **93(20)**, 201111 (2016)

[2] L. Sortino, et al. “Enhanced light-matter interaction in an atomically thin semiconductor coupled with dielectric nano-antennas” Nat. Commun. **10**, 5119 (2019)

[3] L. Sortino, et al. “Bright single photon emitters with enhanced quantum efficiency in a two-dimensional semiconductor coupled with dielectric nano-antennas” Nat. Commun. **12**, 6063 (2021)

[4] D. Sun, et al. “Observation of Rapid Exciton–Exciton Annihilation in Monolayer Molybdenum Disulfide” Nano Letters, **14(10)**, 5625–5629 (2014)

Atomically thin waveguides for photonics with 2D light waves

M. Lee[1*], H. Hong[2], J. Yu[2], F. Mujid[2], A. Ye[3], C. Liang[3], and J. Park[2,3,4]

[1]Department of Materials Science and Engineering, Seoul National University, 08826 Seoul, Korea
[2]Department of Chemistry, University of Chicago, Chicago, IL 60637, USA
[3]Pritzker School of Molecular Engineering, University of Chicago, Chicago, IL 60637, USA
[4]James Franck Institute, University of Chicago, Chicago, IL 60637, USA
[*]corresponding author: myungjae@snu.ac.kr

Abstract: Monolayer MoS_2 films can be used as a high-index core to support guided modes and create slab waveguides. These waveguides can guide light waves for millimeter-scale propagation lengths across a broad range of wavelengths, including the visible and near-infrared regions. The guided wave exhibits significantly reduced light momentum in the out-of-plane direction compared to its momentum along the waveguiding plane, indicating the guiding of 2D light waves.

We have developed an atomically thin waveguide that can guide visible and near-infrared light waves over millimeter lengths [1]. The waveguide is constructed by growing a monolayer MoS_2 film on fused silica substrate using metal organic chemical vapor deposition [2], and then embedding it in an index-matched liquid environment. This results in a slab waveguide with an atomically thin core layer embedded in semi-infinite symmetric claddings. The waveguide is excited using a free-space laser beam in an edge-on configuration where the beam is incident on the edge of the waveguide with a beam trajectory nearly parallel to the waveguiding plane. Wide-field microscopy is used to investigate the light-field intensity on the film, which exhibits a field profile that starts from the edge of the MoS_2 film and gradually decays as it propagates.

Our study confirms that the atomically thin MoS_2 waveguide supports an optical mode that starts at the edge of the film and gradually decays as it travels along the film. We found that for near-infrared light with photon energies lower than the bandgap energy of MoS_2, the propagation loss of observed modes is less than 1 dB/mm, which corresponds to millimeter-scale propagation length as predicted by theoretical investigation [3]. The waveguide is capable of taking light only with near-zero out-of-plane momenta as confirmed by the angle-resolved in-coupling efficiency measurement that couples the free-space laser beam into the guided mode by adjusting the relative angle between the incident beam and the waveguide. This result indicates that the atomically thin waveguide wave may generate light waves that have 2D dispersion with greatly suppressed out-of-plane momentum broadening. We believe this waveguide has the potential to enable the development of novel photonic devices and systems for taking advantage of the 2D light waves.

References

1. Lee, M., Hong, H., Yu, J., Mujid, F., Ye, A., Liang, C. and Park, J. Unpublished work.
2. Kang, K., Xie, S., Huang, L., Han, Y., Huang, P. Y., Mak, K. F., Kim, C.-J., Muller, D. and Park, J. “High-mobility three-atom-thick semiconducting films with wafer-scale homogeneity,” Nature, Vol. 520, 656–660, 2015.
3. Khurgin, J. B. “Two-dimensional exciton-polariton-light guiding by transition metal dichalcogenide monolayers,” Optica, Vol. 2, No. 8, 740–742, 2015.

S Vacancies-Triggered High SERS Activity of MoS_2 for Ultrasensitive Detection of Trace Diclofenac

Y. N. Quan [1*], X. J. Huang[1], and W. Q. Liu[1]

[1] University of Science and Technology of China Hefei 230031, P. R. China
*corresponding author: qyn2022@mail.ustc.edu.cn

Abstract: Recently, non-metallic surface-enhanced Raman scattering (SERS) substrates such as MoS_2 have developed rapidly due to the photo-induced charge transfer characteristics. However, the low SERS activity of intrinsic MoS_2 has hindered its application in SERS. Here, a high SERS active MoS_2 substrate based on sulfur vacancy (V_S) excitation is proposed, which aims to enhance SERS effect by regulating the structure of V_S. The research results show that V_S-MoS_2 can accurately perceive the nanomolar concentration of diclofenac in the actual water environment.

The preparation process of V_S-MoS_2 substrate is shown in Figure 1. First, the micro-nano MoS_2 flowers with abundant folds were synthesized by hydrothermal method, and then the MoS_2 with different degrees of defects was obtained by controlled annealing in a high temperature furnace (temperature controlled at 400-1000 ℃). V_S-MoS_2 presents a large number of adsorption and active sites that facilitate its effective binding to probe molecules (such as diclofenac). Therefore, based on the exploration and analysis of corresponding Raman signals, combined with other structural characterizations, the optimal conditions for regulating the S-vacancy in MoS_2 can be screened out, so as to obtain the optimal V_S-MoS_2 substrate for the SERS detection of diclofenac.

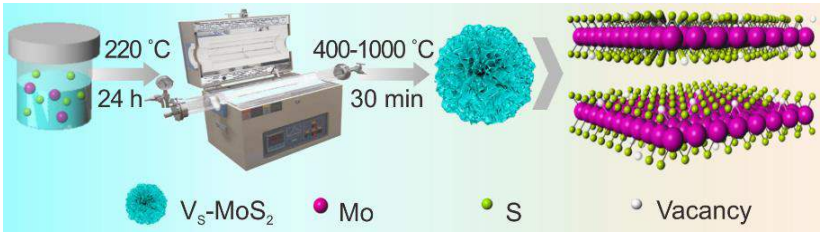


Figure 1. Schematic illustration of the synthesis of V_S-MoS_2.

The V_S-MoS_2 substrate was characterized by LABRAM HR800 Raman system equipped with 532 nm excitation wavelength. As shown in Figure 2a, the unannealed MoS_2 exhibits two first-order Raman modes, E^1_{2g} and A_{1g}, at 375.7 and 402.9 cm^{-1}, respectively. Studies have shown that the position of E^1_{2g} mode varies with the change of strain or interlayer van der Waals forces, while the peak position of A_{1g} is related to electron-phonon interaction [1]. It can be seen from the figure that the E^1_{2g} and A_{1g} peaks of MoS_2 annealed at 400 and 600℃ are roughly in the same position, which is caused by their insensitivity to electron density, strain and interlayer van der Waals forces. However, when the annealing temperature rises to 800 ℃, the positions of these two peaks appear obvious redshift, which is due to the high temperature calcination destroying the local S-Mo-S bond in MoS_2, resulting in a large number of S vacancies. As the temperature continues to rise (1000 ℃), the peak shift of the two decreases, which is because a large number of S vacancies lead to the change of the restoring force constant of the system or the chemical adsorption of foreign molecules. In addition, studies have shown that the full width at half maximum (FWHM) of Raman peaks is determined by crystallinity and charge density, and will broaden with the increase of vacancy density [2]. Both E^1_{2g} and A_{1g} peaks broaden first and then narrow with the increase of annealing temperature, which again shows that MoS_2 calcined at 800 ℃ has the most abundant

vacancies. After annealing at 1000 ℃, the reason for the decrease of the FWHM of the Raman peak may be that the adsorbed foreign molecules occupy some vacancies. Generally speaking, the specific surface area of the substrate materials was one of the important factors affecting SERS response. The larger the specific surface area is, the more adsorption/active sites are, the more significant the enrichment effect is, which is more conducive to the adsorption of the molecules to be tested. Figure 2b shows the N_2 adsorption and desorption isotherms of MoS_2 and V_S-MoS_2-800. The specific surface area of V_S-MoS_2-800 (29.83 $m^2 \cdot g^{-1}$) is significantly larger than that of MoS_2 (5.85 $m^2 \cdot g^{-1}$). Lattice fracture and dislocation are caused by the generation of S vacancy and the fracture of local Mo-S bond. The stress generated by this phenomenon makes the surface of the sample rougher, the specific surface area increases, and the enrichment effect is enhanced, which is conducive to the enrichment of probe molecules.

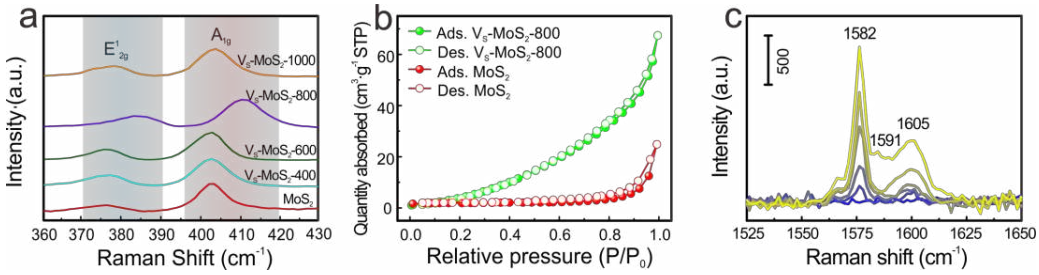


Figure 2. a) Raman spectra of MoS_2, MoS_2-400, MoS_2-600, MoS_2-800 and MoS_2-1000, respectively. b) N_2 adsorption-desorption isotherms of MoS_2 and MoS_2-800. c) SERS response of diclofenac in the concentration range from 10^{-4} M to 10^{-9} M in the real water samples.

Further, this work used V_S-MoS_2-800 sample with excellent enrichment ability as SERS substrate to detect diclofenac, an antibiotic environmental pollutant. Practicality is one of the difficulties that need to be overcome for the highly sensitive SERS substrate in recent years. We took the real water sample from Dongpu Reservoir (Hefei, China) to simulate the actual detection environment, and explored the actual detection ability and anti-interference ability of the V_S-MoS_2-800 substrate. Figure 2c shows the SERS spectra of diclofenac at different concentrations (10^{-4}-10^{-9} M) in real water samples collected using V_S-MoS_2-800 as the substrate. Three characteristic peaks in the range of 1525-1650 cm^{-1} were analyzed. Among them, the characteristic peak at 1582 cm^{-1} corresponds to the asymmetric stretching vibration of $O_1C_8O_2$, the peak at 1591 cm^{-1} corresponds to the stretching vibration of dichlorobenzene ring, and the peak at 1605 cm^{-1} is caused by the stretching vibration of phenylacetic acid ring. It was found that characteristic peaks at 1582 and 1605 cm^{-1} could still be identified when the concentration of diclofenac was as low as 10^{-8} M. The results of this experiment (33.8 ng/L) were far lower than the environmental quality standard for diclofenac in inland waters listed (100 ng/L) in the Water Framework Directive (2013/39/EU) [3]. This work has realized the SERS analysis of diclofenac residues in real water samples, and is expected to play a huge potential in practical applications such as water pollution control and detection.

References

1. Kim, H.J., Kim, D., Jung, S., Bae, M.H., Yun, Y.J., Yi, S.N., Yu, J.S., Kim, J.H. and Ha, D.H. “Changes in the Raman spectra of monolayer MoS_2 upon thermal annealing,” J. Raman Spectrosc., Vol. 34, No. 12, 1938-1944, 2018.
2. Mignuzzi, S., Pollard, A.J., Bonini, N., Brennan, B., Gilmore, I.S., Pimenta, M.A., Richards, D. and Roy, D., “Effect of disorder on Raman scattering of single-layer MoS_2,” Phys. Rev. B, Vol. 91, No. 19, 195411, 2015.
3. Vieno, N. and Sillanpaa, M., “Fate of diclofenac in municipal wastewater treatment plant - a review,” Environ. Int., Vol. 69, 28–39, 2014.

META 2023, PARIS - FRANCE, JULY 18 – 21, 2023

Mesoporous g-C_3N_4/TiO_2 photonic film with a chiral nematic structure: slow photonic effect inducing improved H_2 generation

M. Johar[1], C. Wang[1], and M. N. Ghazzal[1*]

[1]Institut de Chimie Physique, UMR 8000 CNRS, Université Paris-Saclay, 91405 Orsay, France

[*]corresponding author: mohamed-nawfal.ghazzal@universite-paris-saclay.fr

Abstract: Photocatalysis is one of the ideal approaches to address the energy crisis. Graphitic carbon nitride (g-C_3N_4) is a promising photocatalyst that attracts attention due to its unique properties. However, its photocatalytic activity remains low due to high photogenerated charges recombination and low absorption factor. Therefore, massive efforts have been undertaken to solve these problems. This presentation proposes a fabrication of a bioinspired photonic crystal SiO_2/g-C_3N_4/TiO_2 film with a chiral-nematic structure to enhance the photocatalytic activity of g-C_3N_4.

Summary: Energy crises have flashed in the last few decades. Different materials and technologies were developed to convert solar light into usable energy, such as photovoltaic solar cells, H_2 generation, and CO_2 reduction. However, these technologies suffer from poor energy-conversion efficiency due to low optical-absorption coefficients and quantum-conversion yield of the currently developed materials. Photocatalysis is one of the promising sustainable processes to convert solar energy into chemical fuel under a mild reaction. Different semiconductors were used as photocatalysts, such as TiO_2, Fe_2O_3, WO_3 etc. However, most semiconductors share common problems, which are high recombination of charge carriers and low absorption factor directly affecting their photocatalytic efficiencies.

Among the reported photocatalysts, g-C_3N_4 shows interesting properties and promising photocatalytic activity. It is a metal-free semiconductor formed by the stacking of g-C_3N_4 layers consisting of tri-s-triazine units linked by amino groups. This photocatalyst has a moderate band gap of 2.7 eV, corresponding to the visible range, with potential band edge of the conduction band (CB) and valence band (VB) at -1.4 eV and 1.3 eV, respectively, favorable to performing water splitting. g-C_3N_4 is known for its high chemical stability, low cost, nontoxicity, appropriate band structure, and facile synthesis. However, g-C_3N_4 exhibits high photogenerated charge recombination and low absorption factor.[1] Different strategies have been developed to improve the photocatalytic activities of g-C_3N_4, including chemical modification, exfoliation into nanosheets, and fabrication of heterojunctions[2–4]. Even if these strategies enabled the enhancement of the photocatalytic of g-C_3N_4, the efficiency for photon conversion and the spatial separation for photogenerated charges carries of g-C_3N_4 is still limited. In this work, we designed a bioinspired photocatalyst with a photonic structure using cellulose nanocrystals as biotemplate seems to be a promising strategy.[5–7] The films showed iridescent color and Bragg peak reflection, which were tuned by controlling the sol formulation, see Figure 1. The films were characterized using UV-vis spectroscopy, scanning electron microscopy (SEM), Scanning transmission electron microscopy (STEM), X-ray photoelectron spectroscopy (XPS), and then the photocatalytic activity was evaluated for H_2 generation under Xenon lamp illumination. The results demonstrate that the structure can be controlled by the adjusting the formulation of the sol and thus the optical properties and the position of the Bragg peak reflection. We found that adjusting the Bragg position affect directly the photocatalytic performance of the photocatalyst for H_2 generation.

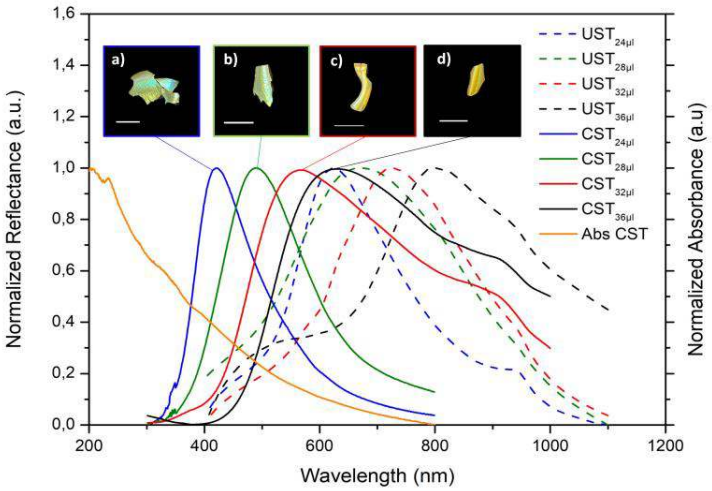


Figure 1. UV-vis reflectance spectra for calcined and hybrid films showing variable Bragg peaks as well as the absorption spectra for Mesoporous photonic g-C_3N_4/TiO_2. Photographic images of chiral nematic C_3N_4/SiO_2/ TiO_2 films a) CST-$_{24µl}$ b) CST-$_{28µl}$ c) CST-$_{32µl}$ d) CST-$_{36µl}$. UST is an abbreviation for the precursors used: Urea/TMOS/TAA (before calcination) and CST corresponds to g-$C_3N_4/SiO_2/TiO_2$ (after calcination).

Acknowledgements: Masa Johar acknowledges all collaborators: François Brisset for SEM analysis, Diana Dragoe for XPS analysis, and Marie-Claire Schanne-Klein for the access to the polarized microscope, as well as Campus France and An-Najah National University for their joint scholarship.

References

1. Qi, K., Liu, S. & Zada, A. Graphitic carbon nitride, a polymer photocatalyst. *J. Taiwan Inst. Chem. Eng.* **109**, 111–123, 2020
2. Stroyuk, O., Raievska, O. & Zahn, D. R. T. Graphitic carbon nitride nanotubes: a new material for emerging applications. *RSC Adv.* **10**, No. 56, 34059–34087, 2020
3. Rahman, M., Davey, K. & Qiao, S. Counteracting Blueshift Optical Absorption and Maximizing Photon Harvest in Carbon Nitride Nanosheet Photocatalyst. *Small* **13**, No. 23, 1700376, 2017
4. Lin, W. *et al.* Bioinspired Mesoporous Chiral Nematic Graphitic Carbon Nitride Photocatalysts modulated by Polarized Light. *ChemSusChem* **11**, No.1, 114–119, 2018
5. Wang, C. *et al.* A sol–gel biotemplating route with cellulose nanocrystals to design a photocatalyst for improving hydrogen generation. *J. Mater. Chem. A* **8**, No. 21, 10779–10786, 2020
6. Gesesse, G. D. *et al.* Enhanced Photogenerated Charge Carriers and Photocatalytic Activity of Biotemplated Mesoporous TiO_2 Films with a Chiral Nematic Structure. *Chem. Mater.* **31**, No. 13, 4851–4863, 2019
7. Wang, C., Paineau, E., Remita, H. & Ghazzal, M. N. Cellulose Nanocrystals in Spherical Titania-Sol Microdroplet: From Dynamic Self-Assembly to Nanostructured TiO_x/C Microsphere Synthesis. *Chem. Mater.* **33**, No. 17, 6925–6933, 2021.

Non-Unity Magnetic Permeability in 2D Hybrid Organic/Inorganic Perovskites

J. A. Schuller[1*], R. A. DeCrescent[2], R.M. Kennard[3], and M. L. Chabinyc[3]

[1]Electrical and Computer Engineering Department, UC Santa Barbara, USA
[2]National Institute for Standards and Technology Boulder Laboratories, USA
[3]Materials Science and Engineering Department, Sheffield University, United Kingdom
[*]corresponding author: jonschuller@ucsb.edu

Abstract: Atomic-scale material optical properties are universally described within the electric dipole approximation—bulk optical frequency light-matter interactions are assumed to arise solely from electric dipoles interacting with electric fields. This inability of matter to interact with optical frequency magnetic fields led to the advent of metamaterials. Atomic-scale optical magnetism represent an unrealized frontier in optical materials. Here, we demonstrate in 2D Hybrid Organic/Inorganic Perovskites the only known example of an atomic scale non-unity optical frequency magnetic permeability.

At optical frequencies and atomic length scales quantum mechanical light-matter interactions are inherently non-magnetic. Linear and nonlinear processes are treated in the electric dipole (ED) approximation and assumed to be driven purely by the *electric* field component of light. The lack of intrinsic optical magnetism—i.e., deriving from atomic-scale magnetic dipoles (MD)—led to the advent of metamaterials[1] wherein artificial optical magnetism is engineered at the mesoscale (~ λ/5). Metamaterials phenomena such as negative refractive index[2,3], "perfect" lensing[4,5], and electromagnetic cloaking[6,7] have captivated the imagination of scientists and laypeople alike. Here, I describe our recent discovery of atomic-scale optical magnetism in 2D Layered Hybrid Organic/Inorganic Perovskites (2D HOIPs). First, I briefly detail our use of momentum-resolved optical spectroscopy to demonstrate magnetic dipole (MD) light emission originating from self-trapped excitons[8,9]. Subsequently, I describe a series of optical experiments that demonstrate a non-unity optical frequency magnetic permeability in a 2D HOIP[10]—the only known material with bulk atomic-scale optical magnetism (Fig. 1).

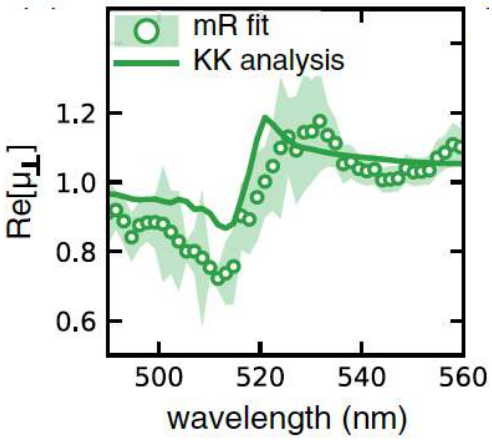


Figure 1. Real part of the magnetic permeability from a 2D HOIP. Solid markers represent experimental values determined from unconstrained momentum-resolved reflectometry measurements. The filled color region represents the standard deviationa cross all measurements. The solid line is determined from a Kramers-Kronig transformation of the measured imaginary part of the magnetic permeability.

All optical measurement, analysis, theory, and instrument design were supported by the National Science Foundation (DMR-2004093). Sample growth was supported by the U.S. Department of Energy, Office of Science, Basic Energy Sciences, under Award No. DESC-0012541.

References

1. Cui, T.J., Smith, D.R. and Liu, R., 2010. *Metamaterials* (p. 1). Boston, MA, USA:: springer.
2. Smith, D.R., Pendry, J.B. and Wiltshire, M.C., 2004. Metamaterials and negative refractive index. *Science*, *305*(5685), pp.788-792.
3. Soukoulis, C.M., Linden, S. and Wegener, M., 2007. Negative refractive index at optical wavelengths. *Science*, *315*(5808), pp.47-49.
4. Pendry, J.B., 2000. Negative refraction makes a perfect lens. *Physical review letters*, *85*(18), p.3966.
5. Merlin, R., 2007. Radiationless electromagnetic interference: evanescent-field lenses and perfect focusing. *Science*, *317*(5840), pp.927-929.
6. Schurig, D., Mock, J.J., Justice, B.J., Cummer, S.A., Pendry, J.B., Starr, A.F. and Smith, D.R., 2006. Metamaterial electromagnetic cloak at microwave frequencies. *Science*, *314*(5801), pp.977-980.
7. Chen, H., Wu, B.I., Zhang, B. and Kong, J.A., 2007. Electromagnetic wave interactions with a metamaterial cloak. *Physical Review Letters*, *99*(6), p.063903
8. DeCrescent, R.A., Venkatesan, N.R., Dahlman, C.J., Kennard, R.M., Zhang, X., Li, W., Du, X., Chabinyc, M.L., Zia, R. and Schuller, J.A., 2020. Bright magnetic dipole radiation from two-dimensional lead-halide perovskites. *Science advances*, *6*(6), p.eaay4900.
9. DeCrescent, R.A., Du, X., Kennard, R.M., Venkatesan, N.R., Dahlman, C.J., Chabinyc, M.L. and Schuller, J.A., 2020. Even-Parity Self-Trapped Excitons Lead to Magnetic Dipole Radiation in Two-Dimensional Lead Halide Perovskites. *ACS nano*, *14*(7), pp.8958-8968.
10. DeCrescent, R.A., Kennard, R.M., Chabinyc, M.L. and Schuller, J.A., 2021. Optical-Frequency Magnetic Polarizability in a Layered Semiconductor. *Physical Review Letters*, *127*(17), p.173604.

Flexible Interdigitated Pd/ZnO-SWCNT/Pd Ultraviolet Photodetectors.

M. R. Sabity, and Ghusoon M. Ali*

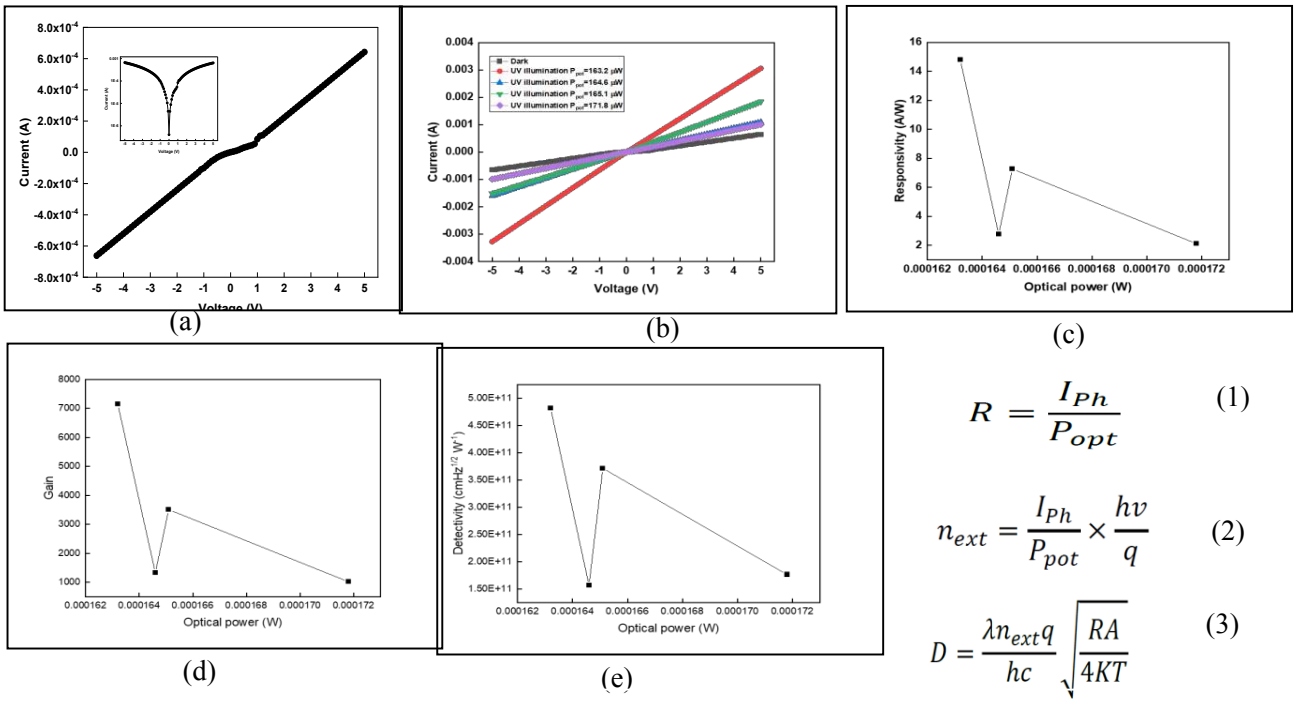
Electrical Engineering Department, Mustansiriyah University, Baghdad, Iraq
*corresponding author: eng.ghusoon_ali@uomustansiriyah.edu.iq, eema1002@uomustansiriyah.edu.iq

Abstract: Recently, flexible electronic and optoelectronic devices have gotten excessive attention because of their role in wearable technology. This work successfully fabricates Pd/ZnO-SWCNT/Pd flexible interdigitated photodetector. Hydrothermal growth of ZnO thin films was used. A device's I-V characteristics were evaluated in both dark and UV light environments over a voltage range of -5 to 5 V. The barrier heights for the fabricated devices were 0.765 eV, while the ideality factors were 1.84. The responsivity was found to be 14.8 A/W, the device exhibited gain.

Introduction: Flexible electronics is a new type of electronic device that has mechanical capabilities. To make such electrical devices, the components and materials must be pliable in multiple directions, stretchable, and shrinkable [1]. Photodetectors (PDs) have found use in a wide range of industrial and military applications due to their ability to convert incident light into charge carriers via the photoelectric effect. The elasticity of flexible photodetectors versus PDs on rigid substrates has inspired a variety of new applications, including wearable electronics, e-skin, smart fabrics, and electronic eye cameras, among others [2-4]. The UV photodetectors cut off wavelength at 400 nm. Wide band gap (WBG) semiconductors have attracted substantial attention for the detection of UV wavelengths, afforded by the correlation of their band gap energies [4]. Zinc oxide (ZnO) stands out inorganic material among wideband potential candidates for UV photodetectors fabrication. ZnO has gotten a lot of attention as a semiconductor material with a direct bandgap of 3.20-3.37 eV and a significant exciton binding energy of 60 meV at 25℃. The seed layer affect the ZnO nanostructured growth. Here we use the single-walled carbon nanotubes (SWCNTs) as a seed layer to enhance the orientation and crystallinity of the ZnO nanorods. SWCNTs can be thought of as a perfect sheet of graphene rolled up into a cylinder, with the hexagonal rings touching and fitting together perfectly [3]. In this work, Pd/ZnO-SWCNT/Pd flexible interdigitated MSM UV photodetector has been fabricated, characterized and studied.

Result and Discussion: The I-V characteristics of the ZnO-SWCNT-based MSM PDs in the dark as shown in Fig. 1 (a), governed by the thermionic emission. It is possible to calculate the saturation current I_S from I-V characteristics by extrapolating the dark current and setting the voltage to zero. The extracted saturation currents for devices were found to be 3.62×10^{-7} A. The computed barrier height from thermionic theory is 0.765 eV. The value of the ideality factor of Pd/ZnO-SWCNT/Pd is found to be 1.84). ZnO-SWCNT thin film-based devices were constructed, tested, and evaluated under UV irradiation (254 nm) at varying optical power levels (from 163.2 to 171.8 µW). Equation (1) [5] describes the photodiode's responsivity that connects the photocurrent (I_{ph}) to the optical power (P_{opt}) Fig.1 (b) illustrate the dark and illumination current under different UV level. The maximum responsivity for the fabricated devices at optical power 163.2 µW is 14.8 A/W as shown in Fig. 1 (c). Using the external quantum efficiency Equation (2) to calculate the O/E conversion efficiency [4]. As shown in Fig.2 .(d), the MSM highest EQE is 7160 (gain) at 163 µW. Equation (3) may be used to get the voltage-dependent detectivity value. From Fig. 2 (e), the detectivity begins to

increase at 163.2 μW and reaches maximum values at 164.6 μW, are $4.82\times10^{11} cmHz^{1/2}W^{-1}$ after which it decreases to $1.77\times10^{11}\ cmHz^{1/2}\,W^{-1}$ at 165 μW.



$$R = \frac{I_{Ph}}{P_{opt}} \qquad (1)$$

$$n_{ext} = \frac{I_{Ph}}{P_{pot}} \times \frac{h\nu}{q} \qquad (2)$$

$$D = \frac{\lambda n_{ext} q}{hc}\sqrt{\frac{RA}{4KT}} \qquad (3)$$

Figure 1. (a) I-V characteristics, (b)I-V under dark and illumination conditions, (c) Responsivity, (d) Gain, and (e) Detectivity

Conclusions: In conclusion, simply fabricated flexible interdigitated MSM PD ZnO-SWCNT on a PET/ITO substrate. Based on the findings of dark I-V measurements, it is evident PD performs like a conventional MSM. The actual barriers heights are lower than their theoretical values. The existence of elevated surface charges or a nonhomogeneous barrier may cause the estimated and ideal barrier height values to diverge. The performance characteristics responsivity of 14.8 A/W A/W , detectivity of $4.82\times10^{11} cmH^{1/2}W^{-1}$, with a high gain of 7160.

References

[1] K. J. Baeg and J. Lee, "Flexible electronic systems on plastic substrates and textiles for smart wearable technologies," *Advanced Materials Technologies,* vol. 5, no. 7, p. 2000071, 2020.

[2] Y. Wang *et al.*, "Organic crystalline materials in flexible electronics," *Chemical Society Reviews,* vol. 48, no. 6, pp. 1492-1530, 2019.

[3] J. Abraham, "Functionalization of carbon nanotubes," Friedrich-Alexander-Universität Erlangen-Nürnberg (FAU), 2005.

[4] P. Sahatiya, S. S. Jones, P. T. Gomathi, and S. Badhulika, "Flexible substrate based 2D ZnO (n)/graphene (p) rectifying junction as enhanced broadband photodetector using strain modulation," *2D Materials,* vol. 4, no. 2, p. 025053, 2017, doi: https://doi.org/10.1088/2053-1583/aa6534.

[5] G. M. Ali and P. Chakrabarti, "ZnO-based interdigitated MSM and MISIM ultraviolet photodetectors," *Journal of Physics D: Applied Physics,* vol. 43, no. 41, p. 415103, 2010.

Metal-insulator transition in vanadium dioxide studied by analytical transmission electron microscopy

M. Horák[1], J. Krpenský[1,2], J. Planer[1], P. Kepič[1], J. Kabát[1], T. Šikola[1], A. Konečná[1], and V. Křápek[1]

[1] Brno University of Technology, Brno, Czech Republic
[2]CIC nanoGUNE, Donostia-San Sebastián, Spain
[*]Corresponding author: michal.horak2@ceitec.vutbr.cz

Abstract: We present a comprehensive study of vanadium dioxide, a phase-changing material relevant for active plasmonics and optical metasurfaces, using analytical scanning transmission electron microscopy combined with in-situ heating. A combination of imaging, diffraction, and spectroscopy with nanometer spatial resolution allowed us to locally correlate the optical properties with applied temperature and local variations in stoichiometry. We observed a reduction of the oxide for sample thickness below 30 nm and the formation of nanoparticles at elevated temperatures.

Vanadium dioxide is a phase-changing material with a low transition temperature (around 67 °C) with a dielectric low-temperature and metallic high-temperature phase. Due to the proximity of its transition temperature to the room temperature, VO_2 is a promising candidate for applications in photonics including fast optical switching or tunable optical metasurfaces [1]. Moreover, it was shown that VO_2 is biocompatible [2], which open a way to design a temperature-driven plasmonic biosensor. However, the nature of the metal-insulator transition in VO_2 is not yet fully understood, with the Mott transition and Peierls transition being the most considered scenarios.In this contribution, we present a comprehensive study of vanadium dioxide using analytical scanning transmission electron microscopy (STEM) combined with in-situ heating. A combination of imaging, diffraction, and spectroscopy with nanometer spatial resolution allowed us to locally correlate the optical properties of VO_2 with applied temperature and local variations in stoichiometry.

First, we fabricated a thin layer of VO_2 by evaporation and verified the presence of metal-insulator transition by ellipsometry. Next, we fabricated lamellas by focused ion beam milling. Energy-dispersive X-ray spectroscopy revealed a rather homogeneous composition with only discernible contamination by Ga ions implanted during the milling. High-angle annular dark field (HAADF) STEM imaging revealed pronounced structural inhomogeneity – a porous and polycrystalline character of the examined lamella. A thinned part of the lamella has been examined by core-loss and low-loss electron energy loss spectroscopy (EELS) at temperatures well below and above the transition, and the experimental loss spectra were interpreted by ab-initio simulations and by comparison with literature [3,4]. We observed that the thin part of the lamella is dominated by reduced vanadium oxides (VO, V_2O_3) and exhibit no switching. This fact presents an important limit for the fabrication of VO2 nanostructures. The thicker parts of the lamella are dominated by VO_2 and exhibit signatures of thermal-induced switching (Fig. 1). Second, we fabricated thin layers of VO_2 by atomic layer deposition. One of them was further recrystalized into nanoparticles. Investigation of such nanoparticles revealed signatures of thermal-induced switching in the low-loss EELS (Fig. 2).

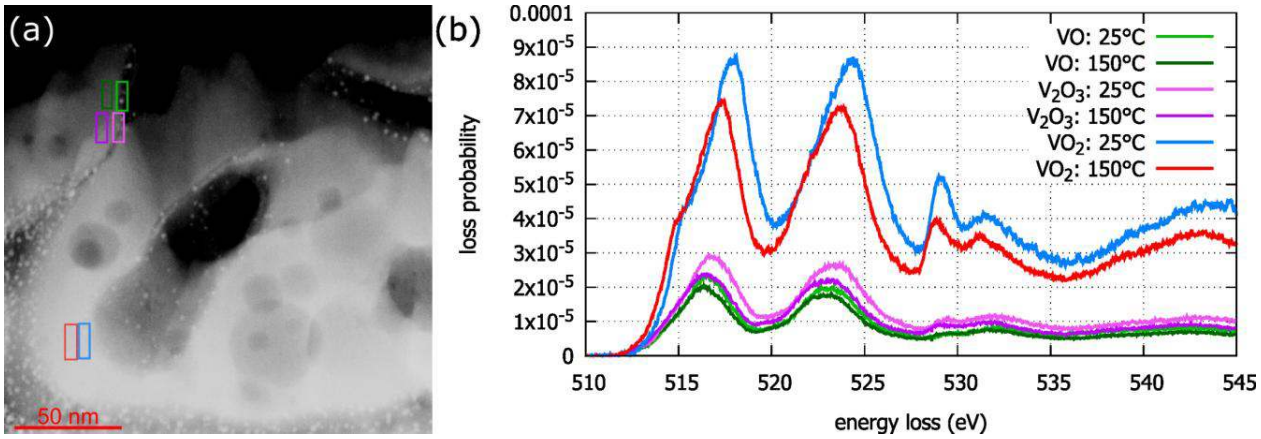


Figure 1: (a) STEM-HAADF micrograph of VO_X lamella reveals its porous character. (b) Core-loss EELS obtained from marked positions. The spectra from the thin part of the lamella are attributed to VO (green) and V_2O_3 (magenta) and do not change with the temperature. The spectra from the thicker part are attributed to VO_2 (blue and red) and exhibit possible changes with the temperature.

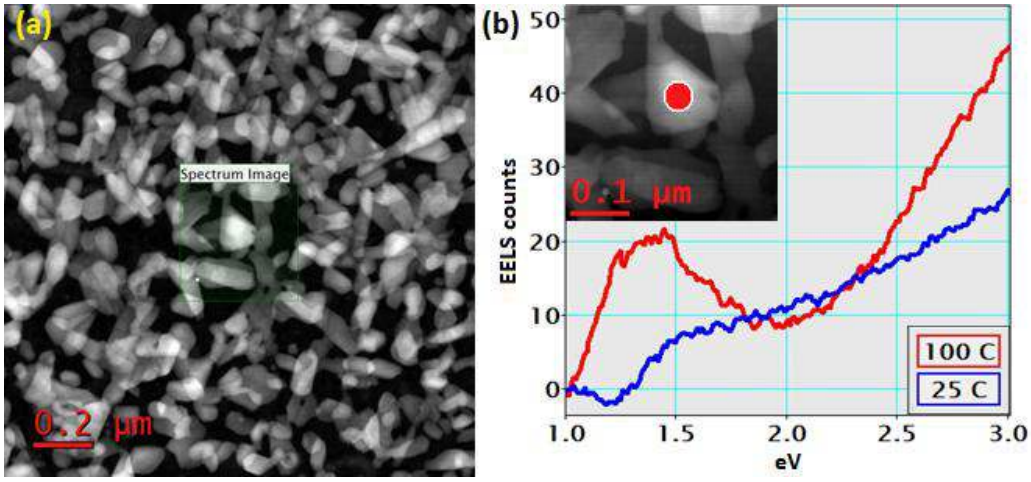


Figure 2: (a) STEM-HAADF micrograph of VO_2 nanoparticles, (b) Low-loss EELS of one nanoparticle at room temperature (dielectric phase) and at 100°C (metallic phase).

This research has been supported by GACR (22-04859S) and MEYS CR (CzechNanoLab, LM2018110).

References

1. Kepič, P., Ligmajer, F., Hrtoň, M., Ren, H., Menezes, L. S., Maier, S. A. and T. Šikola, "Optically Tunable Mie Resonance VO_2 Nanoantennas for Metasurfaces in the Visible," ACS Photonics, Vol. 8, No. 4, 1048–1057, 2021.
2. Guo, J., Zhou, H., Wang, J., Liu, W., Cheng, M., Peng, X., Qin, H., Wei, J., Jin, P., Li, J. and X. Zhang, "Nano vanadium dioxide films deposited on biomedical titanium: a novel approach for simultaneously enhanced osteogenic and antibacterial effects," Artif. Cells Nanomed. Biotechnol., Vol. 46, No. sup2, 58–74, 2018.
3. Hebert, C., Willinger, M., Su, D.S., Pongratz, P., Schattschneider, P. and R. Schlögl, "Oxygen K-edge in vanadium oxides: simulations and experiments," Eur. Phys. J. B, Vol. 28, 407–414, 2002.
4. Li, X., Gloter, A., Gu, H., Luo, J., Cao, X., Jina, P. and C. Colliex, "Discovery of nanoscale reduced surfaces and interfaces in VO2 thin films as a unique case of prewetting," Scripta Materialia, Vol. 78–79, 41–44, 2014.

META 2023, PARIS - FRANCE, JULY 18 – 21, 2023

Fabrication of Mie-resonant nanostructures using laser annealing for highly sensitive fluorescence spectroscopy

T. Fukuta[1], R. Kato[1, 2], T. Tanaka[1, 2], and T. Yano[1, 2*]

[1]Institute of Post-LED Photonics, Tokushima University, Tokushima, Japan
[2]Innovative Photon Manipulation Research Team & Metamaterials Laboratory, RIKEN, Saitama, Japan
[*]corresponding author: yano.takaaki@tokushima-u.ac.jp

Abstract: High refractive index dielectric nanoparticles have gained considerable attention as an alternative to plasmonic nanoparticles. In this study, we developed a new method for producing Mie resonant silicon nanoparticles using laser annealing, and were able to control the Mie resonance wavelength across the entire visible region by adjusting the laser annealing conditions. The Mie resonant Si nanoparticles were then utilized to enhance the fluorescence of analytes in their vicinity.

Dielectric nanoparticles with a high refractive index and low energy losses have attracted much attention as a new visible light resonance medium to replace plasmonic nanoparticles. The electric and magnetic multipoles excited in dielectric nanoparticles enable the manipulation of light at the nanoscale and exhibit high electromagnetic field enhancement effects. In this study, we developed a practical method to fabricate silicon (Si) nanoparticles with Mie resonances in the visible region over a large area on a substrate by laser annealing, as schematically shown in Fig. 1a.

Laser annealing was performed by focusing a CW laser with a wavelength of 532 nm on a Si thin film deposited on a glass substrate. Figure 1b shows a dark-field optical image of the laser-annealed Si substrate, exhibiting strong green scattering color over the entire irradiated area. SEM observations and dark-field scattering spectrum measurements revealed that Si nanoparticles with a diameter of about 150 nm were produced by the annealing effect in the laser irradiation area (as shown in inset of Fig. 1b) and had a Mie resonance mode near 530 nm. The size of the Si nanoparticles was controlled by the laser annealing conditions (irradiation time and power density), enabling us to tune the Mie resonance wavelength in the entire visible region. Finally, the Si nanoparticles were utilized to enhance fluorescence of dye molecules with an excitation wavelength close to the Mie resonance wavelength, resulting in two-order-of-magnitude fluorescence enhancement in the vicinity of the Si nanoparticles (Fig. 1c).

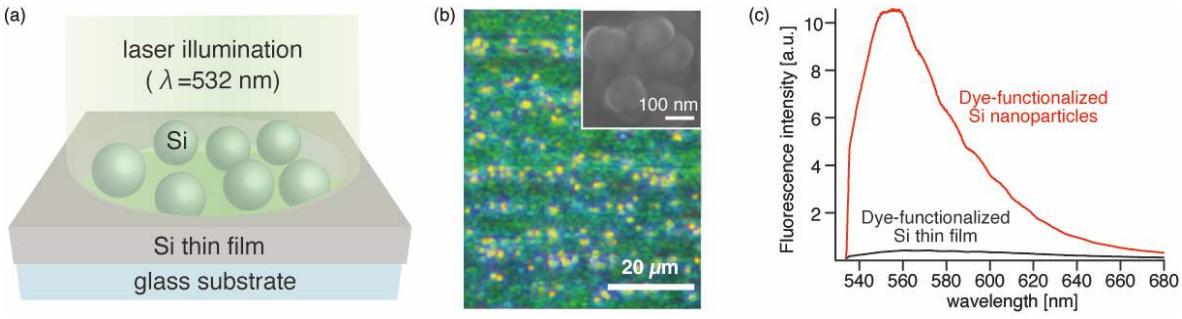


Figure 1 (a) Schematic of fabricating Si nanoparticles by laser annealing of a Si thin film. (b) Dark-field optical image of the laser-annealed Si substrate. The inset shows an SEM image of the annealed substrate, indicating formation of spherical nanoparticles. (c) Fluorescence spectra of dye-functionalized Si nanoparticles and Si thin film.

Graphene-based plasmonic nanostructures for efficient SERS detection of odor molecules

S. Ozeki[1], R. Kato[1, 2], T. Tanaka[1, 2], and T. Yano[1, 2*]

[1]Institute of Post-LED Photonics, Tokushima University, Tokushima, Japan
[2]Innovative Photon Manipulation Research Team & Metamaterials Laboratory, RIKEN, Saitama, Japan
[*]corresponding author: yano.takaaki@tokushima-u.ac.jp

Abstract: Graphene-based plasmonic nanostructures were investigated for highly sensitive Raman detection of odor molecules. Odor molecules with aromatic benzene rings were preferentially adsorbed on graphene through π-π stacking in the proximity of metallic nanostructures. Raman enhancement factor varied significantly depending on the number of graphene layer, and the highest enhancement was obtained for the monolayer graphene substrate due to the strongest field confinement in the vicinity of metallic nanostructures.

Optical detection of odor molecules is of great importance for healthcare monitoring. Among various analytical tools, surface-enhanced Raman scattering (SERS), in which strong electromagnetic field is generated in the vicinity of the metallic nanostructures and enhances Raman scattering of molecules near metallic nanostructures, is a promising technique for detecting odor molecules with high sensitivity, down to the single-molecule level. However, it is challenging to capture the SERS signal of odor molecules because they do not directly adsorb onto metallic surfaces. Here, we propose to utilize graphene-based metallic nanostructures as a SERS substrate where odor molecules are selectively adsorbed on graphene through π-π stacking in the proximity of metallic nanostructures, as schematically shown in Fig. 1(a).

Graphene-based metallic nanostructures were fabricated by depositing 8 nm-thick silver (Ag) layer on mechanically-exfoliated monolayer (1L) graphene using thermal evaporation. Figure 1(b) shows an atomic force microscope (AFM) image of the Ag-deposited graphene substrate, exhibiting Ag nanograins with nanometric separation distance. More interestingly, the size and the separation distance of the nanograins varied significantly depending on the number of graphene layers. To investigate the layer-number-dependence of plasmonic Raman enhancement, 4-aminothiophenol (4-ATP) molecules were adsorbed on the Ag nanograins deposited on 1L, 2L, and 3L graphene, respectively. Figure 1(c) shows SERS spectra of 4-ATP measured on the substrates with different number of graphene layers. The SERS intensity was significantly dependent on the layer number, and the highest Raman enhancement was obtained for the 1L graphene. This is because the separation gap distance of Ag nanograins decreased as the layer number decreases, resulting in the highest field-confinement of -enhancement at the small gap for the 1L graphene substrate. Finally, SERS measurement of odor molecules were demonstrated using the 1L-graphene-based substrate.

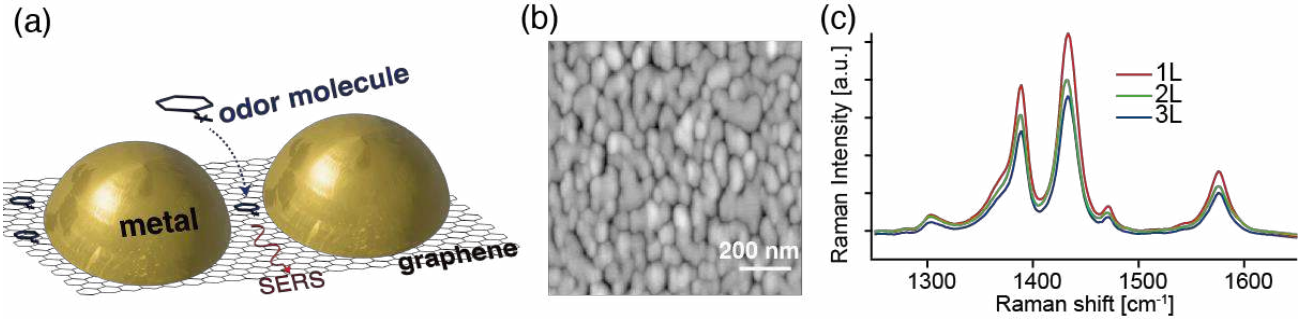


Figure 1 (a) schematic of graphene-based SERS substrate, (b) AFM image of silver nanograins formed on 1L graphene, (c) layer-number-dependent SERS spectra of 4-ATP monolayer.

META 2023, PARIS - FRANCE, JULY 18 – 21, 2023

Twist-tunable polaritonic nanoresonators in a van der Waals crystal

O. G. Matveeva[1†], A. I. F. Tresguerres-Mata[2†], R. V. Kirtaev[1], K. V. Voronin[1], J. Taboada-Gutiérrez[2,3], C. Lanza-García[2], J. Duan[2,3], J. Martín-Sánchez[2,3], V. S. Volkov[4], P. Alonso-González[2,3*], A. Y. Nikitin[1,5*]

[1]Donostia International Physics Center (DIPC), Donostia/San Sebastián 20018, Spain

[2]Department of Physics, University of Oviedo, Oviedo 33006, Spain.

[3]Center of Research on Nanomaterials and Nanotechnology, CINN (CSIC-Universidad de Oviedo), El Entrego 33940, Spain.

[4]XPANCEO, Bayan Business Center, DIP, 607-0406, Dubai, UAE

[5]IKERBASQUE, Basque Foundation for Science, Bilbao 48013, Spain.

*alexey@dipc.org pabloalonso@uniovi.es

† These authors contributed equally to this work.

Abstract: We introduce a class of nanoresonators that incorporate a new degree of freedom: twist tuning. To achieve this result, we place a pristine slab of the van der Waals α-MoO_3 crystal on an array of metallic ribbons. This sample design based on electromagnetic engineering, allows the definition of α-MoO_3 nanoresonators with low losses (Q up to 200) and enables a broad spectral tuning of the polaritonic resonances (up to 32 cm^{-1}) by an in-plane rotation (from 0 to 45º).

Thin uniaxial and biaxial vdW crystal slabs have recently emerged as an extremely attractive playground for manipulating light on deeply subwavelength scale[1-4]. Here, we design an array of in-plane anisotropic resonators by placing a continuous (pristine) thin biaxial vdW crystal slab α-MoO_3 on top of a grating (Figure 1) formed by metal ribbons. In the areas above the ribbons, the refractive index of the PhPs supported by the slab changes, so that PhPs can bounce back and forth between the boundaries of these areas, forming resonant modes. We characterize our refractive index engineered PhP resonators by both the far-field Fourier-Transform IR spectroscopy (FTIR) and near-field scattering type scanning near-field optical microscopy (s-SNOM), disentangling the resonant PhP modes from the experimental data with the help of the theoretical analysis. By rotating the α-MoO_3 slab above the grating, we demonstrate tuneability of the PhP resonances, and reconstruct the isofrequency curves of the PhP modes.

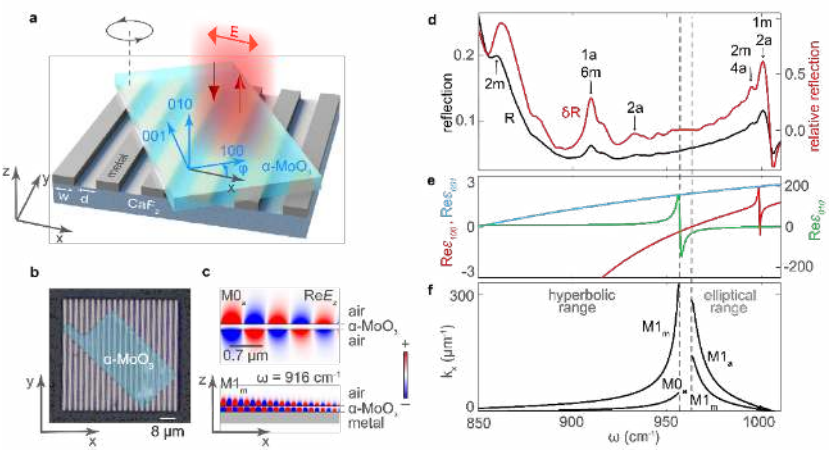


Figure 1 | PhPs nanoresonators in α-MoO_3 defined by placing a pristine α-MoO_3 slab on metallic ribbons. **a**, Schematics of the studied structure that allows defining the nanoresonators by "electromagnetic engineering" and controlling them by a twist angle, φ. The inset shows the AFM profile of the metal grating. **b**, False-color optical image (top view) of the sample consisting of a 110 nm-thick α-MoO_3 slab placed on a 50 nm-thick metal grating. **c**, Simulated field distributions of the M0 and M1 PhPs modes in the α-MoO_3/air (top) and α-MoO_3/metal (bottom) regions. **d**, Relative far-field reflection spectrum of the PhPs nanoresonators for φ = 0º. The subscripts "a" and "m" indicate the PhPs resonances originated in the α-MoO_3/air and α-MoO_3/metal regions, respectively. **e**, Real part of the dielectric permittivity tensor components as a function of ω. f, Calculated dispersion of the M1 and M0 modes shown in (**c**).

References

1. Yuan, Z. "Extremely Confined Acoustic Phonon Polaritons in Monolayer-hBN/Metal Heterostructures for Strong Light-Matter Interactions," Acs Photonics 7, 2610-2617, 2020.
2. Alfaro-Mozaz, F. J. "Deeply subwavelength phonon-polaritonic crystal made of a van der Waals material," Nature Communications 10, 7, 2019.
3. Taboada-Gutiérrez, J. "Broad spectral tuning of ultra-low-loss polaritons in a van der Waals crystal by intercalation," Nature Materials 19, 964, 2020.
4. Ma, W. L. "In-plane anisotropic and ultra-low-loss polaritons in a natural van der Waals crystal," Nature 562, 557, 2018.

Acknowledgments

The authors acknowledge Irene Dolado López for her advice and assistance in the Au gratings fabrication. A.I.F.T.-M. and J.T.-G. acknowledge support through the Severo Ochoa program from the Government of the Principality of Asturias (nos. PA-21-PF-BP20-117 and PA-18-PF-BP17-126, respectively). J.M.-S. acknowledges financial support from the Ramón y Cajal Program of the Government of Spain and FSE (RYC2018-026196-I), and the Spanish Ministry of Science and Innovation (State Plan for Scientific and Technical Research and Innovation grant number PID2019-110308GA-I00/AEI/10.13039/501100011033). P.A.-G. acknowledges support from the European Research Council under starting grant no. 715496, 2DNANOPTICA and the Spanish Ministry of Science and Innovation (State Plan for Scientific and Technical Research and Innovation grant number PID2019-111156GB-I00). A.Y.N. acknowledges the Spanish Ministry of Science and Innovation (grants MAT201788358-C3-3-R and PID2020-115221GB-C42) and the Basque Department of Education (grant PIBA-2020-1-0014). This project has been supported by Asturias FICYT under grant AYUD/2021/51185 with the support of FEDER funds. This work is produced with the support of a 2022 Leonardo Grant for Researchers in Physics, BBVA Foundation. The Foundation takes no responsibility for the opinions, statements and contents of this project, which are entirely the responsibility of its authors.

META 2023, PARIS - FRANCE, JULY 18 – 21, 2023

Fluctuation imaging of nanoscale disorder in monolayer semiconductors

Tom T. C. Sistermans[1,2,3], **Rasmus H. Godiksen**[1], **Alberto G. Curto**[1,2,3*]

[1] Department of Applied Physics and Eindhoven Hendrik Casimir Institute, Eindhoven University of Technology, Eindhoven, The Netherlands

[2] Photonics Research Group, Ghent University-imec, Ghent, Belgium

[3] Center for Nano- and Biophotonics, Ghent University, Ghent, Belgium

[*]Corresponding Author: Alberto.Curto@UGent.be

Abstract: We show that monolayer semiconductors, a rising material family in photonics and electronics, can exhibit noise-like, localized fluctuations in their fluorescence. Inspired by a superresolution technique, we use imaging to show that the fluctuation strength depends on the monolayer's nanoscopic environment. Fluctuation imaging, a fast and simple method, can thus be used for quality control throughout a manufacturing process flow to quantify and map disorder. Our results are relevant for the integration of monolayer semiconductors into nanophotonic devices and metasurfaces.

Two-dimensional semiconductors are promising materials for the fields of electronics, optoelectronics, and photonics. Monolayer transition-metal dichalcogenides (TMDs) are particularly interesting because they host excitons that dominate the optical properties even at room temperature. The exciton electric field extends outside the monolayer rendering it sensitive to the surroundings. Together with other effects like charge transfer, interaction with the local environment makes excitonic fluorescence potentially unstable over time[1,2]. The fluctuations in the fluorescence depend thus on disorder in the monolayer, which is generally detrimental for devices[3].

Here, we adapt a fluctuation-based super-resolution technique to image the localized exciton fluctuation strength in monolayer TMDs[4]. Fluctuation imaging shows fluctuating spots on a stable monolayer. We correlate the presence of localized fluctuations with features in atomic force microscopy (AFM) height scans. We compare different TMDs and substrates to test the role of different material combinations in these fluctuations. To gain more insight into the disorder behind these fluctuations, we employ hyperspectral mapping. Furthermore, we evaluate a thermal annealing process as a method to clean the monolayers and evaluate their fluctuations before and after cleaning.

To conclude, fluctuation imaging is a simple technique that can be used in any camera-based fluorescence microscope. Our results show that fluctuation imaging reports features that would take a longer time to characterize using more complex equipment such as AFM or hyperspectral imaging. It is, therefore, a promising method for fast evaluation of the quality of monolayer semiconductors and their interfaces with other materials, including nanostructures such as metasurfaces or nanophotonic devices.

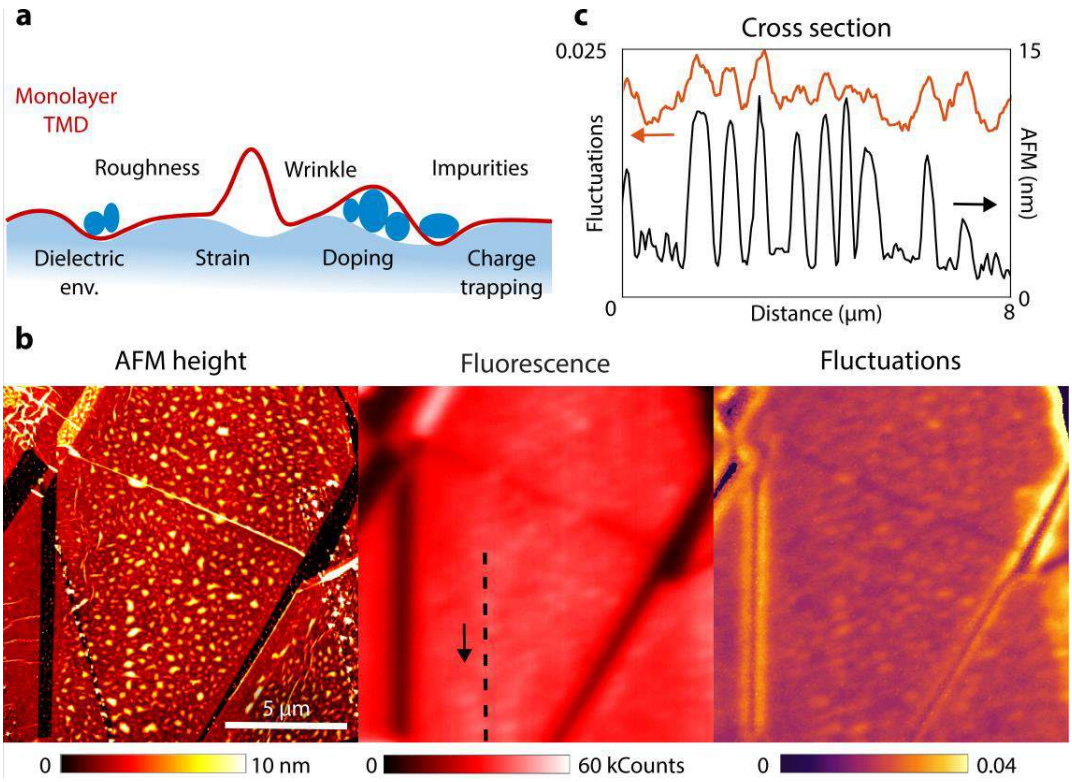


Figure 1. Fluctuation imaging of disorder in monolayer WS_2. a, Physical origin of disorder in a monolayer and its effects. b, Monolayer WS_2 imaged with AFM, fluorescence intensity, and fluctuation imaging, showing the presence of disorder. c, Cross-section along the dashed line in (b) showing the correlation between fluctuations and disorder measured by AFM.

Acknowledgements. This work was financially supported by the European Research Council (ERC) under the European Union's Horizon 2020 Research and Innovation Program (Grant Agreement 948804, CHANSON).

References

1. Xu, W., Liu, W., Schmidt, J. et al. "Correlated fluorescence blinking in two-dimensional semiconductor heterostructures," *Nature*, Vol. 541, No. 7635, 62–67, 2017.
2. Hjelmgart Godiksen, R., Wang, S.; Raziman, T. V., Guimaräes, M., Rivas, J. and Curto, A. "Correlated Exciton Fluctuations in a Two-Dimensional Semiconductor on a Metal," *Nano Lett*, Vol. 20, No. 7, 4829-4836, 2020.
3. Raja, A., Waldecker, L., Zipfel, J. et al. "Dielectric disorder in two-dimensional materials," *Nat. Nanotechnol*. Vol.14, No. 9, 832–837, 2019.
4. Dertinger, T., Colyer, R., Iyer, G., Weiss, S. and Enderlein, J. "Fast, background-free, 3D super-resolution optical fluctuation imaging (SOFI)," *PNAS*, Vol. 106, No. 52, 22287–22292, 2009.

Towards Graphene-comprising Waveguide Resonators for Kerr Comb Generation in the Non-Perturbative Electrodynamic Nonlinearity Regime

Alexandros Pitilakis[1*] and Emmanouil. E. Kriezis[1]

[1] School of Electrical and Computer Engineering, Aristotle University of Thessaloniki, 54124 Thessaloniki, Greece
[*]Corresponding author: alexpiti@ece.auth.gr

Abstract: We present a study of Kerr microcombs generated by CW pumping of graphene-comprising silicon nitride waveguide ring resonators in the NIR. Our resonator is designed to access the dissipative cavity soliton regime under the combined effect of defocusing nonlinearity from graphene and normal group velocity dispersion (GVD) from a slot waveguide, properly accounting for the wideband dispersion of all waveguide parameters. We then proceed to study the effect of non-perturbative graphene nonlinearity on comb formation and efficiency.

Optical frequency combs can be efficiently generated in small travelling wave resonators made of dispersive materials with third order (Kerr-like) nonlinearity [1]. The most frequently used resonators are bulk whispering-galleries (e.g., magnesium fluoride micropillars) designed for very high Q-factors and critically coupled to optical fibers. As practical applications shift towards integrated optics, waveguide ring resonator (WRR) Kerr combs have also appeared, underpinned by the same principles but also requiring for redesign to exploit the stronger light-matter interaction in integrated nanophotonics. To that end, graphene is a novel optical material that can enrich integrated WRR Kerr combs with its electro-optic tunability of its dispersion [2] and nonlinearity [3], controlled by tuning its chemical potential μ_c. Recent studies have shown that when graphene interacts with high electric field intensities, like the ones that can develop in high-Q photonic resonators, its nonlinearity transcends from a perturbative third order to a non-perturbative photoconductivity regime [3]; the latter is characterized by both self-focusing or defocusing refraction, depending on μ_c, and a deep saturation of its absorption as intensity increases. In this work, we investigate these features, i.e., the intensity- and μ_c-dependent electrodynamic nonlinearity, and exploit them for Kerr comb formation, while rigorously accounting for the frequency dispersion of all properties.

To model the Kerr comb formation, we use the Lugiato-Lefever equation (LLE) framework, in the two-timescale arrangement, that monitors the total electric field inside the cavity. The LLE can be considered as a driven, damped, and detuned variant of the nonlinear Schrödinger equation (NLSE) typically used to model pulse propagation along nonlinear waveguides [3]. The LLE, following the variable notation of [1], is:

$$t_R \frac{\partial E(t,\tau)}{\partial t} = L\left[-\frac{\alpha}{2} + i\sum_{n\geq 2}\frac{\beta_n}{n!}\left(i\frac{\partial}{\partial \tau}\right)^n + i\gamma|E|^2\right]E(t,\tau) + \left(-\frac{\theta}{2} - i\delta_0\right)E(t,\tau) + \sqrt{\theta}E_{in}, \quad (1)$$

where $E(t,\tau)$ is the E-field amplitude inside the resonator (fast-time: τ) as the slow-time (t) progresses. The dispersion of the two Q-factors (α and θ), the nonlinear parameter (γ), and β, are incorporated in the LLE.

For the WRR, we consider a graphene monolayer-clad air-slot design, formed by two rails of silicon nitride on insulator (SNOI), transparent down to the visible range; the slot design was chosen for its normal GVD, a prerequisite for soliton formation under the defocusing nonlinearity of graphene in the μ_c range considered. The waveguide cross-section, inset of Fig. 1(a) [800 nm $\times$ 500 nm SNOI rails separated by a 50 nm slot], was tuned for operation in $\lambda_0 = [1.1,2.3]$ μm, i.e., in an octave span around 1.55 μm. The frequency and μ_c dispersion of the waveguide parameters is depicted in Fig. 1(a)-(c); for this preliminary study, we used standard linear and third-order surface conductivity formulas for graphene, at room temperature and assuming regular quality samples

(τ_{intra} = 20 fs). We tune graphene at μ_c = 0.5 eV, as an optimal compromise between attenuation and nonlinearity, and set the WRR round-trip at L = 100 μm for a pump power $|E_{in}|^2$ = 10 W. Using the LLE, we slowly detune the pump frequency through the 1.55 μm resonance, from −10 to +50 GHz, acquiring a 50 THz (quarter octave) comb, Fig. 1(d). Due to the non-negligible high-order dispersion of the waveguide, the produced soliton is stable but highly dispersive in the fast time frame. Nevertheless, all the Kerr comb regimes are traversed, Fig. 1(d)-(e): modulation instability (MI), chaos, unstable/breather solitons, and stable phase-locked cavity solitons.

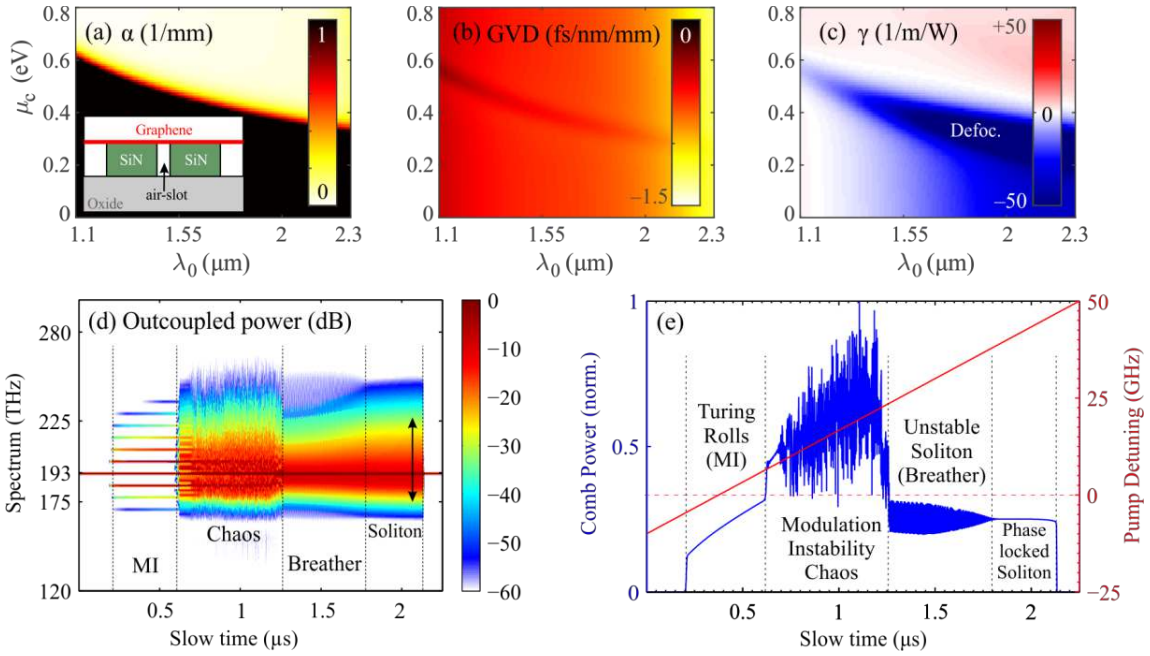


Figure 1. Frequency and μ_c dispersion of the waveguide (a) attenuation, (b) GVD, and (c) nonlinear parameter. The FSR=1.48 THz Kerr comb's (d) outcoupled spectrum and (e) total power, as the pump frequency is detuned.

These results provide encouraging evidence that graphene-comprising WRRs can indeed produce adequately wide Kerr combs in the NIR whereas graphene's tunability can be used not only to control the dispersion [2] but also the nonlinearity and intrinsic Q-factor in a non-trivial way. Our next endeavor will be to study Kerr comb formation under graphene's non-perturbative electrodynamic nonlinearity [3], that could potentially offer improved efficiency owing to the combination of saturable absorption and high nonlinear refraction.

Acknowledgement: The research work was supported by the Hellenic Foundation for Research and Innovation (H.F.R.I.) under the "First Call for H.F.R.I. Research Projects to support Faculty members and Researchers and the procurement of high-cost research equipment grant."' (Project Number: HFRI-FM17-2086)

References

1. Pasquazi, A., *et al.*, "Micro-combs: A novel generation of optical sources," Phys. Rep., Vol. 729, pp. 1–81, 2018. [URL]
2. Yao, B., *et al.*, "Gate-tunable frequency combs in graphene–nitride microresonators," Nature, Vol. 558, No. 7710, pp. 410–414, 2018. [URL]
3. Pitilakis, A. and E.E. Kriezis, "Ultrafast pulse propagation in graphene-comprising nanophotonic waveguides considering nonperturbative electrodynamic nonlinearity," JOSA B, Vol. 39, No. 10, pp. 2723-2734, 2022. [URL]

Non-linear Optical Properties Investigation on the Colloidal WS_2 nanosheets

Y. Zhao[1], M. Fröhlich[1], O. Strolka[1], T. Parker[1], J. Lauth[1], A. J. Meixner[1] and D. Zhang[1*]

[1]Institute of Physical and Theoretical Chemistry, Eberhard-Karls University Tuebingen, Germany
[*]corresponding author: dai.zhang@uni-tuebingen.de

Abstract: The relationship between the local structure and optical properties of colloidal WS_2 nanosheets is studied by nonlinear confocal microscopy. Experimental results show that individual WS_2 nanosheets have higher second harmonic signal intensity and shorter fluorescence lifetimes compared to those of clusters, which could be attributed to the different optical properties of monolayers and multilayers.

In the relationship between the optical properties of two-dimensional transition metal dichalcogenides (2D-TMDCs) materials and their local structural properties, especially syntheses process and layer numbers are important since the features could exhibit optoelectronic properties that are significantly different from bulk materials[1, 2]. With the help of Fluorescence Lifetime Imaging (FLIM) technique, the photoluminescence distribution and intensity from 2D-TMDCs can be clearly characterized due to its deeper analysis of the emission properties of nanoscale sample, as it reveals both intensities and photoluminescence lifetimes in space. The optical Second Harmonic Generation (SHG) process is a promising tool since it performs strong sensitivity to the local structural properties of nonlinear optical materials, which usually characterizes the irregularities in the layers of 2D-TMDCs materials[3, 4]. For colloidal 2D-TMDCs which are prepared by wet-chemical syntheses, are becoming rapidly popular, and representing promising prospects in the application of scalable and nanoscale devices. Therefore, further investigation on the optical properties of colloidal 2D-TMDCs should be carried out since previous studies sparsely provide reports on the layer-dependent characterization.

Here, colloidal WS_2 nanosheets prepared by wet-chemical syntheses are applied for local optical properties measurement. Detailed synthesis information can be found in the previous work[5]. Fluorescence lifetime imaging is supported by FLIM microscopy system with pulsed laser excited at 750 nm and oil-immersed objective (numerical aperture = 1.4).

The preliminary working progress is shown in Figure. 1. The nanosheets show significant SHG signal compared to the large cluster which has much weaker resonance intensity in Figure. 1a. In Figure. 1b, the two-photon photoluminescence image also displays similar features on the intensity distribution, for the nanosheets they show higher intensity which contributes to find valuable regions for further investigation on SHG detection with femtosecond pulsed laser. The FLIM images Figure 1c and 1d, which are collected from different regions, represent notable short lifetime from nanosheets. The distribution difference agrees to the description in literature very well[6], that the monolayers of WS_2 nanosheets have shorter fluorescence lifetime than that of the multilayers.

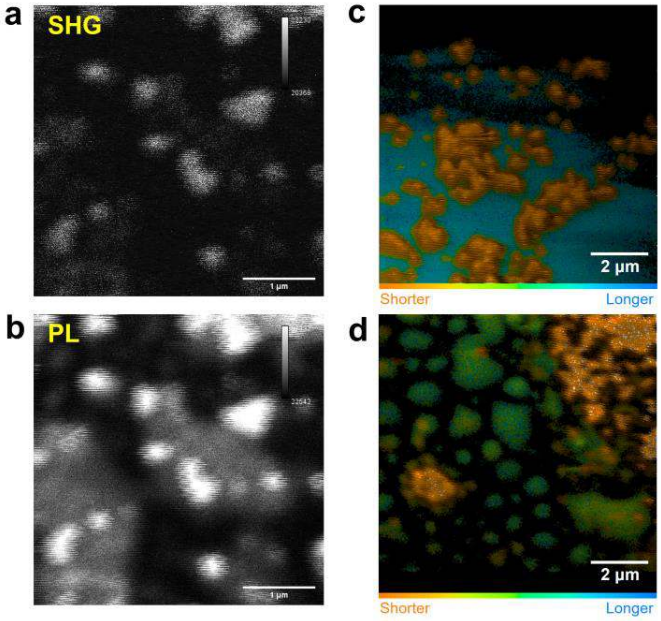


Figure 1. Second harmonic, photoluminescence and fluorescence lifetime signals collected from FLIM microscopy system. a) Second harmonic signal distribution of WS_2 nanosheets collected with 750 nm pulsed laser; b) Photoluminescence signal distribution of WS_2 nanosheets collected with 750 nm pulsed laser; c) and d) Emission FLIM of the WS_2 nanosheets between the detection range 509 and 594 nm.

Acknowledgements: This work was financially supported by the German Research Foundation (Nos. ZH 279/13-1 and ME 1600/21-1), and the Chinese Scholarship Council (CSC).

References

1. Onga, M., Y. Zhang, T. Ideue and Y. Iwasa, "Exciton Hall effect in monolayer MoS_2," Nat. Mater., Vol. 16, 1193–1197, 2017.
2. Zhao Y.C., P. Miao, E. Jack, H.Y. Hu, X. X. Wang, T. Heumueller, Y. Hou, G. J. Matt, A. Osvet, Y. T. Chen, M. Tarrago, D. de Ligny, T. Przybilla, P. Denninger, J. Will, J.Y. Zhang, X. F. Tang, N. Li, C.L. He, A.L. Pan, A.J. Meixner, E. Spiecker, D. Zhang, C.J. Brabec, "Strain-activated light-induced halide segregation in mixed-halide perovskite solids," Nat. Commun., Vol. 11, 6328, 2020.
3. Miao P., Y. T. Chen, L. Pan, A. Horneber, K. Greulich, T. Chassé, H. Peisert, P. M. Adam, P. Xu, A. J. Meixner, D. Zhang, "Inhomogeneous defect distribution of triangular WS_2 monolayer revealed by surface-enhanced and tip-enhanced Raman and photoluminescence spectroscopy," J. Chem. Phys., Vol. 156, 034702, 2022.
4. Pan L., P. Miao, A. Horneber, A. J. Meixner, P. M. Adam, D. Zhang, "Revealing local structural properties of an atomically thin $MoSe_2$ surface using optical microscopy," Beilstein J. Nanotechnol., Vol. 13, 572–581, 2022.
5. Frauendorf, A. P., A. Niebur, L. Harms, S. Shree, B. Urbaszek, M. Oestreich, J. Hübner and J. Lauth, "Room temperature micro-photoluminescence studies of colloidal WS_2 nanosheets," J. Phys. Chem. C, Vol. 125, 18841–18848, 2021.
6. Barker, S. E., S. Wang, R. H. Godiksen, G. W. Castellanos, M. Berghuis, T. V. Raziman, A. G. Curto and J. G. Rivas, "Preserving the emission lifetime and efficiency of a monolayer semiconductor upon transfer," Adv. Opt. Mater., 201900351, 2019.

Enhanced As(III) detection under near-neutral conditions: Synergistic effect of boosted adsorption by oxygen vacancies and valence cycle over activated Au NPs loaded on $FeCoO_x$ nanosheets

Cong-Cong Huang[1*], Xing-Jiu Huang[1], and Meng Yang[2]

[1] Department of Materials Science and Engineering, University of Science and Technology of China, Hefei 230026, China
[2] Key Laboratory of Environmental Optics and Technology, And Environmental Materials and Pollution Control Laboratory, Institute of Solid State Physics, HFIPS, China
*corresponding author: hcc1998@mail.ustc.edu.cn

Abstract:

As(III) has always been detected in acidic environments while the unstable modified nanomaterials under this case may lead to unreliable results. Herein, $FeCoO_x$ nanosheets with oxygen vacancies were employed to stabilize even activate Au NPs for enhancing As(III) detection under mild conditions. The sensitivity of 1.45 μA ppb^{-1} with a detection limit of 0.27 ppb were obtained. This study reveals synergistic effect of the defects and valence cycles on catalytic performance, also gives guidelines for constructing electrochemical sensing interface.

Summary:

Electrochemical method is one of the most traditional technologies for detecting the highly toxic pollutant of As(III) since the efficient redox reaction under acidic conditions[1]. However, the decomposition and agglomeration of metal nanoparticles in the strong acid solution leads to poor reproducibility as well as low precision of the results, which seriously limited the practical applications[2]. Hence, improving the stability for sensitive electrocatalysis of As(III) under mild conditions is still an intractable and indispensable problem. In this work, functionalized nanosheets with rich oxygen vacancies named Au NPs/ $FeCoO_x$ were synthesized to minimize the aggregation of Au NPs and provide abundant sites for As(III) adsorption due to the huge surface area. The square wave anodic stripping voltammetry (SWASV) technique was adopted to detect As(III) under optimal conditions while getting rid of the dependence on the strong acidic substrate and the sensitivity of 1.45 μA ppb^{-1} was obtained. A detection limit (3σ method) of 0.27 ppb in this work meets the maximum concentration in drinking water set by the World Health Organization. In addition, the tests of reproducibility, stability, anti-interference detection of Cu(II), and concrete analysis of real water samples were also conducted, all of which achieved satisfactory results, indicating the potential application of the proposed method. The possible mechanism of Au NPs/$FeCoO_x$ nanosheets enhanced detection of As(III) was proposed in Fig. 1. It was found that the large specific surface area of the nanosheets and the introduced oxygen vacancies provided abundant active sites for As(III) adsorption, as well as stabilized Au NPs to ensure the ideal electrocatalytic activity of uniformly dispersed Au NPs. Besides, the process of electron transfer from Fe sites to Au sites activated Au NPs to promote the reduction of As(III). What's more, the valence cycle of Fe(II)/(III) and Co(II)/(III) synergistically improved the electrochemical performance towards As(III). This work not only parsing the excellent electrochemical performance for synergistic effect of the defects and valence cycles, but also provide new insights into the design

of nanomaterials with excellent adsorption capacity and electrocatalytic activity to achieve effective detection of heavy metal pollutants.

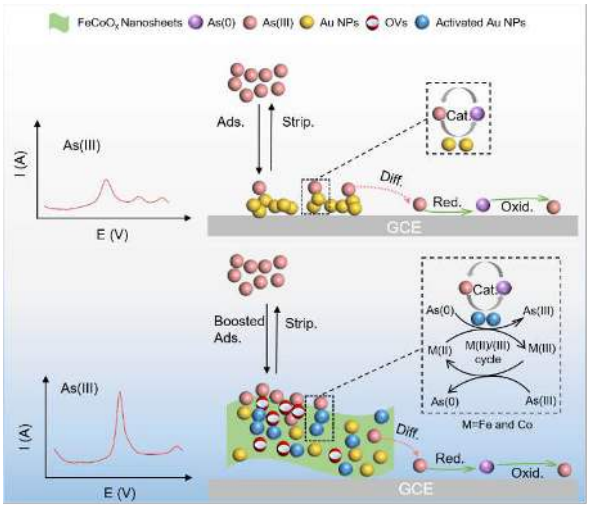


Fig. 1. Schematic of electrochemical detection of As(III) by SWASV method on Au NPs/FeCoOx nanosheets: boosted adsorption of As(III) and activated Au NPs by valence cycle for enhanced electrochemical performance, compared to that of Au NPs.

References

[1] S. Kempahanumakkagari, A. Deep, K.-H. Kim, S.K. Kailasa, H.-O. Yoon, Nanomaterial-based electrochemical sensors for arsenic - A review, Biosens. Bioelectron., 95(2017) 106-116.

[2] H. Hu, B. Xie, Y. Lu, J. Zhu, Advances in electrochemical detection electrodes for As(III), Nanomaterials, 12(2022) 781.

Acknowledgements

This work was supported by the National Natural Science Foundation of China (22204166, 22206187), the Youth Innovation Promotion Association of CAS (2023469), the National Key R&D Program of China (2021YFB3201400), the Key R&D Program of Anhui Province (202104i07020006, 202104i07020011), the Postdoctoral Researcher Funding Project of Anhui Province (2021B528), the HFIPS Director’s Fund, Grant No., YZJJ202102, YZJJZX202019, and YZJJ2022QN26, the special project (SXHZ202003) of Science and Technology Cooperation between Fuyang Municipal People’s Government and Fuyang Normal University.

Optical antennas and plasmonics-based devices

META 2023, PARIS - FRANCE, JULY 18 – 21, 2023

Improved Control over Multipole Excitations in Multi-Shelled Particles Leads to Higher Directivity Scattering

S. Min[1*] and J. Shin[1]

[1]Department of Materials Science and Engineering, Korea Advanced Institute of Science and Technology, Republic of Korea

[*]corresponding author: seokhwan.min@kaist.ac.kr

Abstract: Directional scattering has been studied for decades since the discovery of the Kerker conditions. Numerous studies on superdirective scattering have found that the collective interference of a large number of modes is a crucial factor. In this study, we show that multiple shells are required for the independent control of such an extended number of multipole modes. Furthermore, we use a topology nucleation method tailored to layered systems to design particles with high scattering directivities in the visible wavelengths.

Multi-shell particles and cylinders have a special importance in photonics due to its increased geometric complexity compared to homogeneous particles. When designing traditional homogeneous or core-shell particles, one only has access to at most four degrees of freedom: two layer thicknesses and two refractive indices. On the other hand, there are many more multipole modes in the particle, especially in the Mie scattering regime ($x \approx 1$), with significant excitation strength whose amplitudes and phases can be freely designed. Thus, it is evident that more shells, and therefore, more design parameters, are needed for better control over the large number of multipole modes. The collective interference of a large number of multipoles with specific amplitudes and phases can lead to many interesting optical phenomena such as superdirective scattering [1–2], superscattering [3–4], and super-absorption [5–6].

Despite the benefits of increasing the number of shells, it also significantly raises the design complexity of the particle. This complexity is exacerbated by the fact that there are three different types of parameters for a typical multi-shell particle: (1) layer thickness, which is continuous, (2) materials, which is discrete, and (3) the number of layers, which is related to particle topology. Optimization methods that can handle all three variable types simultaneously are conspicuously absent in the literature, particularly since most studies opt to fix the particle topology throughout the optimization process [7–10]. In our study, we use a topology nucleation approach to design multi-shell, lossless directional scatterers with high directivity values in the visible wavelengths (Fig. 1). Notably, to ensure that the designed particles are experimentally realizable, we restrict the material permittivities to those of existing dielectrics; namely, SiO_2 and TiO_2.

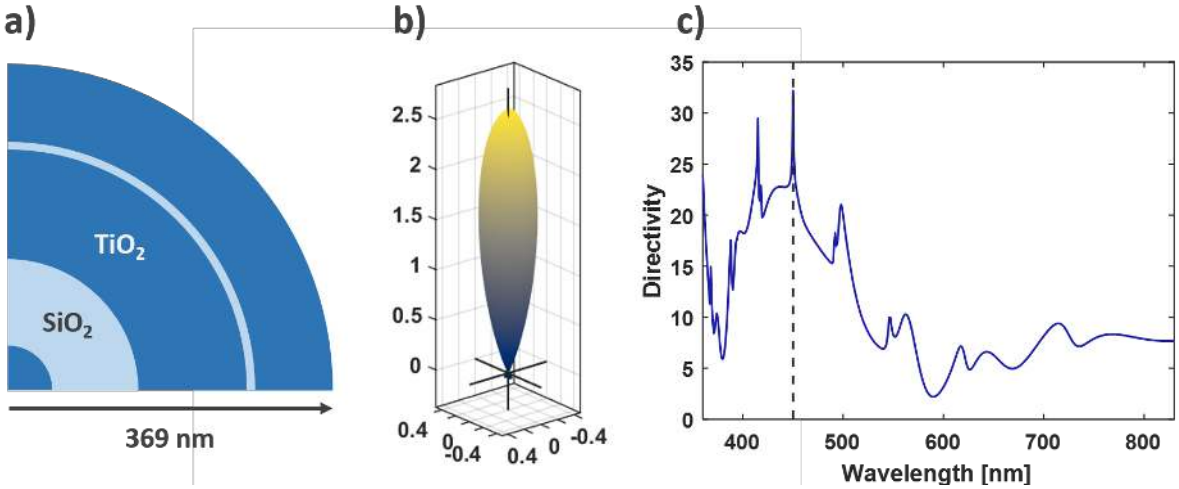


Figure 1. Example optimization result for directional scattering at 450 nm. **a)** Optimized particle geometry. **b)** Three-dimensional plot of the scattering phase function. Light is incident from the *–z* direction. **c)** Forward directivity as a function of wavelength. A sharp peak can be seen at the target wavelength.

The authors S. Min and J. Shin received funding from the National Research Foundation of the Republic of Korea (2018M3D1A1058998).

References

1. Sushencev, I., A. Shcherbakov, K. Ladutenko and P. Belov. "Superdirective dielectric spherical multilayer antennae," Proc. IEEE Int. Conf. Microw. Antennas Commun. Electron. Syst. (COMCAS), 1–3, 2019.
2. Gaponenko, R., A. Moroz, I. Rasskazov, K. Ladutenko, A. Shcherbakov and P. Belov, "Harnessing superdirectivity in dielectric spherical multilayer antennas," Phys. Rev. B, Vol. 104, No. 19, 195406, 2021.
3. Ruan, Z. and S. Fan, "Superscattering of Light from Subwavelength Nanostructures," Phys. Rev. Lett., Vol. 105, No. 1, 013901, 2010.
4. Ruan, Z. and S. Fan, "Design of subwavelength superscattering nanospheres," Appl. Phys. Lett., Vol. 98, No. 4, 043101, 2011.
5. Ladutenko, K., P. Belov, O. Peña-Rodríguez, A. Mirzaei, A. Miroshnichenko and I. Shadrivov, "Superabsorption of light by nanoparticles," Nanoscale, Vol. 7, No. 45, 18897–18901, 2015.
6. Grigoriev, V., N. Bonod, J. Wenger and B. Stout, "Optimizing Nanoparticle Designs for Ideal Absorption of Light," ACS Photonics, Vol. 2, No. 2, 263–270, 2015.
7. Paria, D., C. Zhang and I. Barman, "Towards rational design and optimization of near-field enhancement and spectral tenability of hybrid core-shell plasmonic nanoprobes," Sci. Rep., Vol. 9, 16071, 2019.
8. Huang, Y., Z. Zhen, Y. Shen, C. Min and G. Veronis, "Optimization of photonic nanojets generated by multilayer microcylinders with a genetic algorithm," Opt. Express, Vol. 27, No. 2, 1310–1325, 2019.
9. Ladutenko, K., O. Peña-Rodríguez, I. Melchakova, I. Yagupov and P. Belov, "Reduction of scattering using thin all-dielectric shells designed by stochastic optimizer," J. Appl. Phys., Vol. 116, No. 18, 184508, 2014.
10. So, S., J. Mun and J. Rho, "Simultaneous Inverse Design of Materials and Structures via Deep Learning: Demonstration of Dipole Resonance Engineering Using Core-Shell Nanoparticles," ACS Appl. Mater. Interfaces, Vol. 11, No. 27, 24264–24268, 2019.

Plasmonic addressing structure

M. Crouzier[1,3*], V. Yam[1*], G. Magno[2], T. Lopez[3] and B. Dagens[1]

[1]*Université Paris-Saclay, CNRS, Centre de Nanosciences et de Nanotechnologies, 91120, Palaiseau, France*

[2]*Department of Electrical and Information Engineering, Polytechnic University of Bari, Via Orabona, 4, 70125, Bari, Italy*

[3] *Stellantis, Centre technique de Vélizy, 78140 Vélizy-Villacoublay, France*

[*]marius.crouzier@c2n.upsaclay.fr

Abstract: We present here a new structure allowing for independent addressing of sub-micrometric area. Plasmonic chains are deposited above a waveguide array. The coupling between the chains and the waveguides is numerically analyzed. This structure could have applications in various domains, from holography with reconfigurable metasurfaces to biotechnology with lab-on-chip structure.

Pixel pitch is critical for achieving high-resolution holograms with a large viewing angle. Today, spatial light modulators (SLM) based on Liquid-Crystal on Silicon (LCOS) technology are used to make dynamic holograms. However, it does not enable downsizing the pixel pitch under 1µm [1,2]. On the other hand, metasurface based on optical resonators can reach such a pixel pitch. Nevertheless, the remaining challenge of metasurface is reconfigurability. Phase change materials seem to be a promising way to achieve reconfiguration. It was shown that it was possible to enable reconfigurability over the entire metasurface by controlling the temperature [3]. Solutions to reconfigure each meta-atom independently have been realized in the IR range using a free-space system [4]. Here, our structure is integrated and could help to achieve reconfigurability in the visible range.

We have focused on a new all-optical addressing principle based on silicon-guided optics coupled to plasmonic nanoparticles (NPs). The target structure is composed of a matrix of single-mode rectangular silicon waveguides (height h=220 nm and width l=500 nm). This matrix is encapsulated in HSQ resist and is relying on a SiO2 box. Each intersection of sub-micrometric size is functionalized by chains of elliptical gold NPs where each pair of perpendicular chains forms the base of a pixel. TE modes propagated in silicon waveguides can efficiently couple to plasmonic chains [5] and generate sub-wavelength hot spots on some NPs [5]. The wavelength range studied here is near-infrared (1200-1650nm).

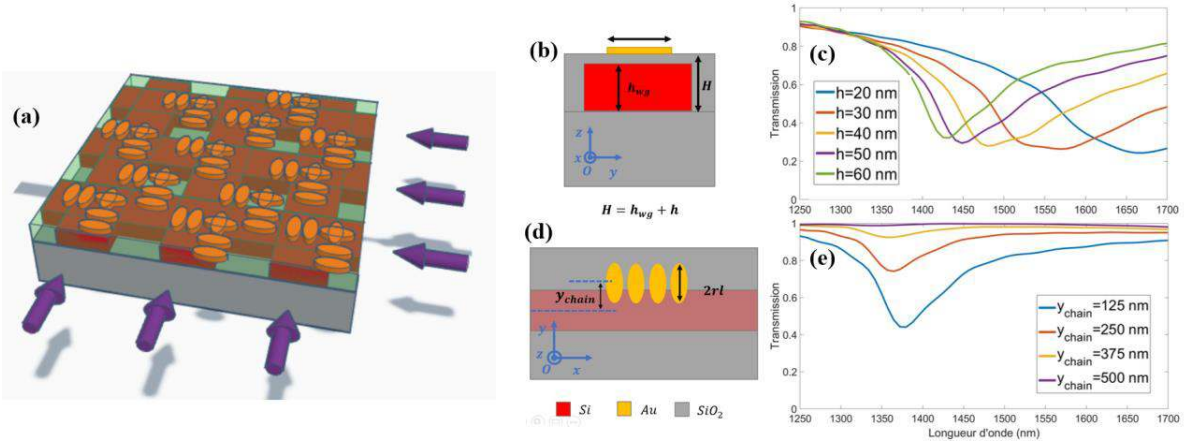


Figure 1. (a) Schematized global structure. (b, d) Simulated structure. TE mode transmission for different height of SiO_2 (c) and for different lateral alignment (e).

We use FDTD simulation to analyze the chain's plasmonic excitation in different configurations. In Fig.2, we analyze the effect of encapsulation height, showing a decrease in the coupling strength with a height beyond 50 nm. Simulations were also used to define lateral alignment tolerance allowed by the encapsulation.

The independent addressing principle is based on the geometry dependence of the plasmonic resonance wavelength. Each chain will have NPs with different size or shape on one waveguide, allowing it to have a specific wavelength resonance. Then, to select the chain to excite, one needs to inject the wavelength corresponding to its resonance in the waveguide.

To this end, we numerically determine the minimum nanoparticle's radius difference between two chains to ensure that two spectrally separated resonance is at least 30 nm. Then, we simulate two potential pixels at the intersection of two silicon guides where two couples of identical perpendicular chains are placed so that the last nanoparticles of each chain form a cross at the intersection (Fig.2b-d). The pixel pitch is 600nm. The NPs size of each couple of chains is different, leading to different resonance wavelengths. Thus, the pixel to be addressed can be selected by propagating the relevant, exciting wavelength in both perpendicular waveguides simultaneously.

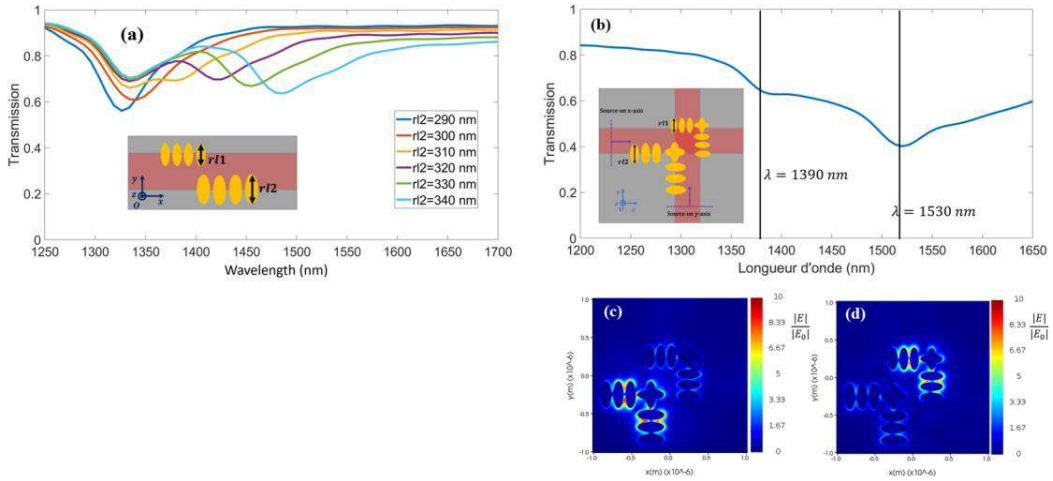


Figure 2. (a) TE mode transmission for different NP ellipse major axis rl2 of one chain whereas the NP size of the other is constant. (b) X-axis TE mode transmission. (c) Electric field module at λ=1390 nm, and (d) at λ=1530 nm

This design could also be used for other applications such as optical trap for lab-on-chip structure. We will show that the flexibility of chains positions allows different arrangements of nanoparticles to be created without being limited by the width of the guide, leading to a greater variety of optical traps or pixels on a dense waveguide array.

References

1. Choi et al., "Evolution of spatial light modulator for high-definition digital holography", C. S. ETRI Journal, 41(1), 23-31, 2019.
2. Y. Isomae et al., "Alignment control of liquid crystals in a 1.0-μm-pitch spatial light modulator by lattice-shaped dielectric wall structure" J. Soc. Inf. Disp., vol. 27, no 4, p. 251-258 (2019)
3. Shu, F et al. "Dynamic Plasmonic Color Generation Based on Phase Transition of Vanadium Dioxide", *Adv. Opt. Mater*, 6, 1700939, 2018.
4. Leitis, A. et al, "All-Dielectric Programmable Huygens' Metasurfaces". *Adv. Funct. Mater.* 30, 1910259, 2020.
5. Février, M et al., "Giant Coupling Effect between Metal Nanoparticle Chain and Optical Waveguide," Nano Lett., 12 (2), p. 1032-1037, (2012)

Room-temperature waveguide-coupled plasmonic crystal lasers on GaAs substrate

Y. T. Tsai, Y. H. Wu, C. C. Wu, and S. D. Lin*

Institute of Electronics, National Yang Ming Chiao Tung University, Taiwan.
*corresponding author: sdlin@nycu.edu.tw

Abstract: Semiconductor-based 2-D plasmonic crystal lasers (PCLs) has been studied in this work. The waveguide mode coupling with the surface plasmonic mode plays an essential role in these GaAs-based PCLs. The cooperation of the dielectric layers and the metallic nano-pillar array gives the needed resonant mode of high-quality factor. The polarization-dependent two-wavelength lasing in the PCLs with a rectangular lattice has been demonstrated at room temperature.

Due to their easy fabrication, small divergence angle and wide tuning range of lasing wavelength, semiconductor-based plasmonic crystal lasers (PCLs) have received increasing attentions [1-2]. Recently, the PCLs lasing at and above room temperature have been achieved and a very wide tuning range in lasing wavelengths has been reported [3-4]. Although these results were exciting and could lead to realizing plasmonic laser diodes, the underlying reason for enabling successful lasing remains unclear.

The sample structure illustrated in Fig. 1 was grown by molecular beam epitaxy. The photoluminescence from the four InGaAs/GaAs quantum wells (QWs) had the peak around 985 nm. The full-structure, 3-D FDTD simulations on the unit cell shown in Fig. 2 have been performed. For a square lattice with a period of 260 nm, the simulated transmission spectra in Fig. 3 indicates a high-Q mode ~897 nm. The electric field distribution in Fig. 4 tells that the resonant mode is formed by the coupling between the surface plasmonic mode and the waveguide mode and the strong electric field at the InGaAs QWs gives a high confinement factor needed for lasing. Experimental L-L curves in Fig. 5 and lasing spectra in Fig. 6 for the square-lattice devices with the period of 260-280 nm evidence the successful lasing at room temperature. The inset in Fig. 6 indicate a divergence angle of ~ 2.4^{o}. For PCLs with rectangular lattice, the simulation results in Fig. 7 predict a polarization-dependent behavior, which has been confirmed with our measurements shown in Fig. 8. The two-wavelength lasing due to the different periods in two directions has been observed.

In conclusion, the room-temperature 2-D PCLs have been investigated by simulation and experiment. The waveguide mode effect on PCL operation is the key for room temperature lasing. The rectangular lattice devices exhibited a two-wavelength polarization-dependent lasing, which is consistent with our simulation results.

The authors thank the help from the CNST/ NFC at NYCU, the discussions with Profs. S. T. Yen and G. Lin, and the support from NSTC under grants No. 111-2221-E-A49-141-MY3 and No. 111-2124-M-A49-007.

References

1. F. van Beijnum, et al., “Surface plasmon lasing observed in metal hole arrays,” Phys. Rev. Lett. Vol. 110, p. 206802, 2013.
2. E. W. de Vos, et al., “Surface plasmon laser with two hole arrays as cavity mirrors,” Optica Vol. 6, pp. 92-95, 2019.
3. S.-H. Kim, et al., “Broadband surface plasmon lasing in one-dimensional metallic gratings on semiconductor,” Sci. Rep. Vol. 7, p. 7907, 2017.
4. K.-Y. Huang, et al., “Two-dimensional plasmonic crystal surface emitting lasers with gain medium of InGaAs/GaAs quantum wells,” CLEO 2020 STu4M.6, 2020.

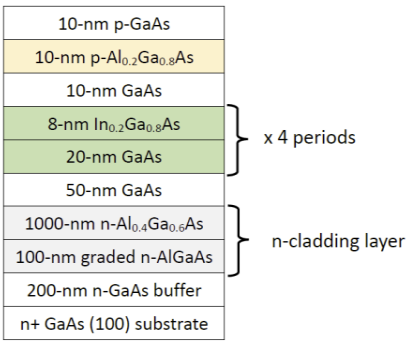


Fig. 1 Schematic sample structure.

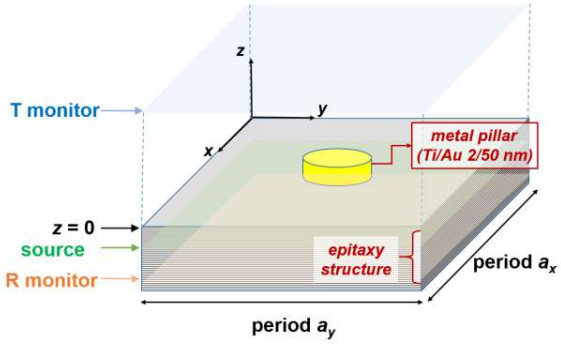


Fig. 2 Unit cell schematic for simulation.

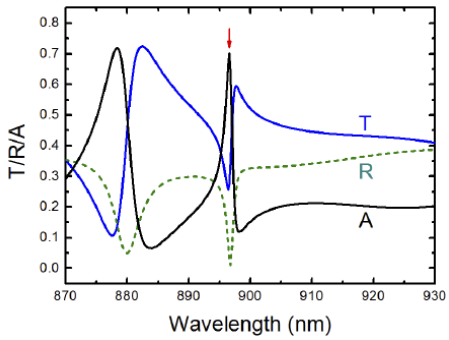


Fig. 3 Simulated Transmission/Reflection/Absorption spectra.

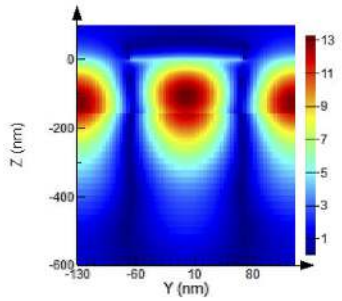


Fig. 4 Cross-sectional E-filed profile for the mode at 879 nm.

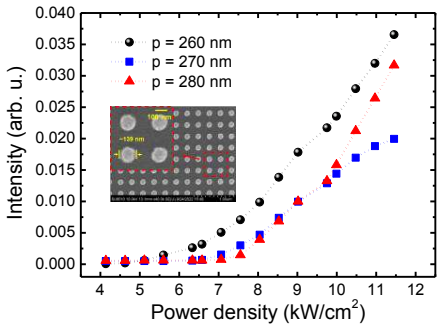


Fig. 5 Transmission spectra for a rectangulart lattice device.

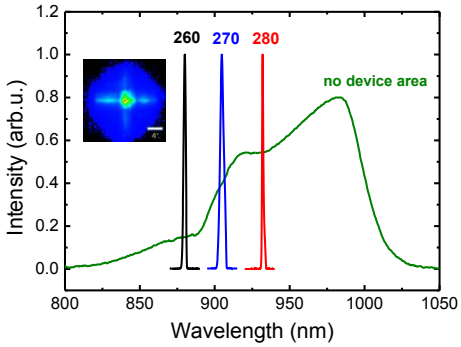


Fig. 6 Lasing spectra from the rectangular lattice device.

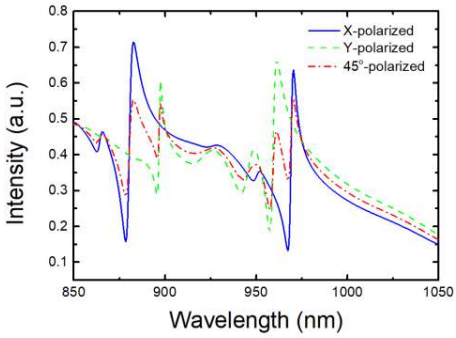


Fig. 7 Transmission spectra for a rectangulart lattice device.

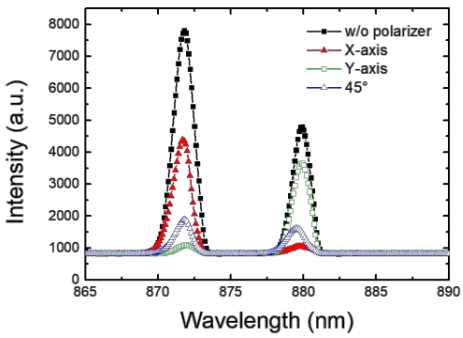


Fig. 8 Lasing spectra from the rectangular lattice device.

META 2023, PARIS - FRANCE, JULY 18 – 21, 2023

Electrical excitation of surface plasmon polaritons with a nanoantenna tunneling junction

Delphine Pommier[1], Cheng Zhang[2], Yunhe Lai[3], Eric Le Moal[4], Christophe Sauvan[2], Jean-Jacques Greffet[2], Jianfang Wang[3], Elizabeth Boer-Duchemin[4*]

[1]Thales Research and Technology, Antony, France
[2]Laboratoire Charles Fabry, Institut d'Optique Graduate School, Université Paris-Saclay, Palaiseau, France
[3]Department of Physics, Chinese University of Hong Kong, Hong Kong, China
[4]Institut des Sciences Moléculaires d'Orsay, Université Paris-Saclay, Orsay, France
[*]corresponding author: Elizabeth.Boer-Duchemin@universite-paris-saclay.fr

Abstract: We use the tunneling junction between a nanoantenna and a gold film to electrically excite propagating surface plasmons. The nanoantenna consists of a gold nanocube that is separated from a thin Au film by an insulating molecular layer. A novel method for completing the electrical circuit between the nanoantenna and gold film using an atomic force microscope is developed. Thanks to numerical modeling, the nanoantenna modes exciting the SPPs are identified as gap modes or hybridized gap and antenna modes.

Using a nanoantenna to control the emission properties of light (such as the intensity, direction and spectrum) is an active field[1]. The use of a tunneling junction as a nanoscale electrical source of photons[2-4] and surface plasmon polaritons (SPPs)[5-6] is also extremely promising. In this work, we combine a nanoantenna and a tunneling junction in order to locally and electrically excite propagating surface plasmons and light.

The sample consists of chemically synthesized gold nanocubes (~50-nm side length) separated from a thin (50-nm) Au film by a molecular layer (~1 nm) as shown schematically in Fig. 1a. When a conducting AFM tip is used to apply a potential difference between the nanoantenna and gold film, a tunneling current flows between the cube and substrate. The inelastic component of this current excites the available optical modes of the system. In particular, these include gap modes in the tunneling junction which locally increase the electromagnetic density of states, and an antenna mode which may be engineered to efficiently couple to the propagating SPP modes on the film. The light emitted from the excited SPPs is then detected through the transparent substrate in a leakage radiation microscopy configuration.

Figure 1b depicts the resulting spectrum in such an experiment. Two distinct peaks may be seen which, thanks to numerical modeling [7], may be identified as arising from specific gap modes or hybridized gap and antenna modes (see insets to Fig. 1b). The ability to interrogate individual nano-antennas and the theoretical comprehension of the nano-antenna junction system lead to system optimization, an enhanced excitation efficiency and the ability to control the SPP spectrum. These results will also lead to the development of new electrical nanosources of surface plasmon polaritons and light.

This work was supported by the French National Research Agency (ANR) projects "Intelplan" (ANR-15-CE24-0020) and "ChiC" (ANR-21-CE09-0038). C.Z. acknowledges support from the Safran-IOGS chair on Ultimate Photonics (Ph.D. fellowship).

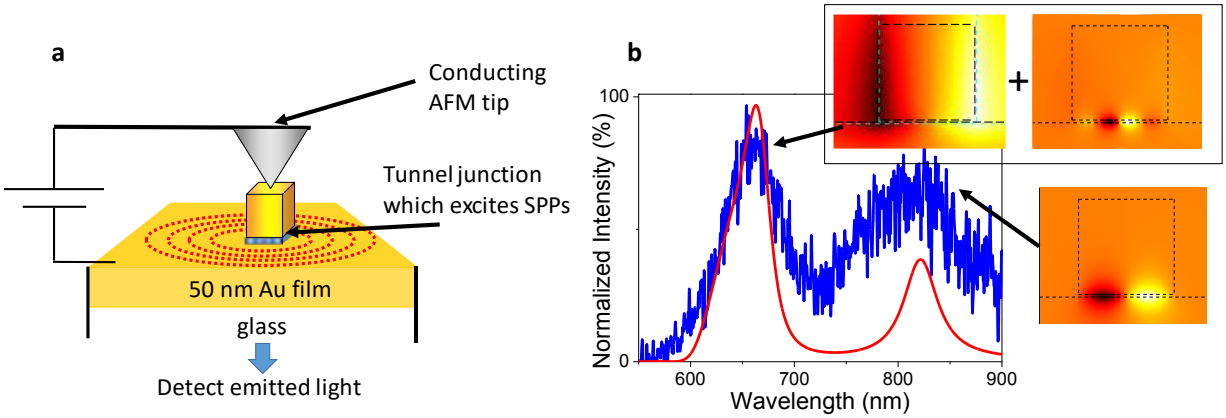


Figure 1: a. Schematic of the experiment. A molecular layer between a nanocube antenna and a gold film acts as a tunneling junction when a voltage is applied via a conducting AFM tip. Light from the resulting SPPs is detected through the transparent substrate. b. Experimental (blue) and simulated (red) spectrum resulting from the electrical excitation of a nano-antenna junction. Insets: Maps of the *y*-component of the magnetic field in the *xz*-plane (perpendicular to the interface) show the presence of a gap mode, or of a gap + antenna mode.

References

1. Novotny, L. and van Hulst, N. 2011. *Nat. Photonics*, 5, 83-90.
2. Kern, J., Kullock, R., Prangsma, J., Emmerling, M., Kamp, M., Hecht, B., 2015. *Nat. Photonics*, 9, 582−586.
3. Qian, H., Hsu, S.-W., Gurunatha, K., Riley, C. T., Zhao, J., Lu, D., Tao, A. R., Liu, Z., 2018. *Nat. Photonics*, 12, 485−488.
4. Parzefall, M., Szabó, Á., Taniguchi, T., Watanabe, K., Luisier, M., Novotny, L., 2019. *Nat. Commun*. 10, 292.
5. Du, W., Wang, T., Chu, H.-S., Nijhuis, C. A., 2017. *Nat. Photonics* 11, 623−627.
6. Zhang C., Hugonin J.-P., Coutrot A.-L., Sauvan C., Marquier F., Greffet J.-J., 2019. *Nat. Commun*. 10, 4949.
7. Zhang C., Hugonin J.-P., Greffet J.-J., Sauvan C., 2019. *ACS Photonics* 6, 2788.

Visible range active metasurface device fabrication and characterization

Y. H. Kim*, K. H. Choi, C. S. Hwang, J. H. Yang, J. Y. Kim, J. Moon, J. H. Choi

Electronics and Telecommunications Research Institute, Korea

*corresponding author: yhakim@etri.re.kr

Abstract: We fabricated a visible range active metasurface device with Mo/AlO/ITO/AZO/Ag/AZO/AlO/Mo layers and explained its working principle as interacting coupled gap plasmons modes. The metasurface device showed peculiar reflectivity modulation characteristics as a function of incoming electric polarizations, Mo antenna's pitch/space, and applied electric voltage polarity.

For the metaverse era, a realistic and embedding three-dimensional display is a necessary item for online communication. Among competing three-dimensional displays, many researchers believe that the ultimate winner will be a holographic display if high quality and ultrawide visual angle are guaranteed. Metasurface device is an ideal candidate for the holographic display because it can control both amplitude and phase of the light and narrow down the pixel pitch of the display under visible wavelength.

Recently, amplitude, phase, and polarization modulations are fancy research items and many researchers suggested innovative ideas theoretically and experimentally [1]. But the fabricated metasurface devices usually resides in infrared wavelength due to the limitation of small refractive index change in the visible wavelength.

In the paper, we designed the coupled gap plasmon active metasurface device with Mo/AlO/ITO/AZO/Ag/AZO/AlO/Mo layers and fabricated using e-beam lithography as shown in figure 1. During the metasurface device manufacturing, the AZO (aluminum doped zinc oxide) layer is so important to stabilize the silver layer. The FDTD simulation shows the enhanced electric field on the ITO layer due to the gap plasmon generation. Figure 2 shows the modulation characteristics according to the variation of Mo antenna's pitch/space. As the pitch was increased, the resonant dip showed redshift, but the space showed the blue shift. Figure 3 shows the reflectivity variation as a function of the applied voltage. Even though its change is small, it showed different reflectivity modulation with the different voltage polarity. We checked the hologram generation with the fabricated device.

This work was supported by the National Research Foundation of Korea (NRF-2021M3H4A1A04086553).

References

1 Chang T et al., "Universal metasurfaces for comlete linear control of coherent linear control of coherent light transmission", Advanced Materials., 2204085, 2022.

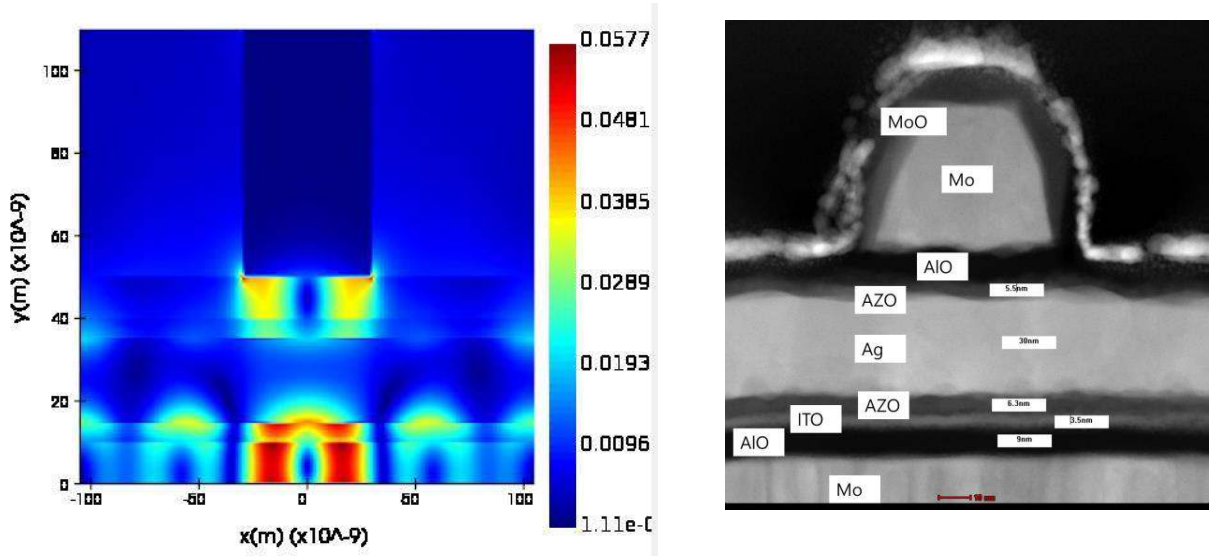


Figure 1. FDTD simulation and fabricated visible range active metasurface device.

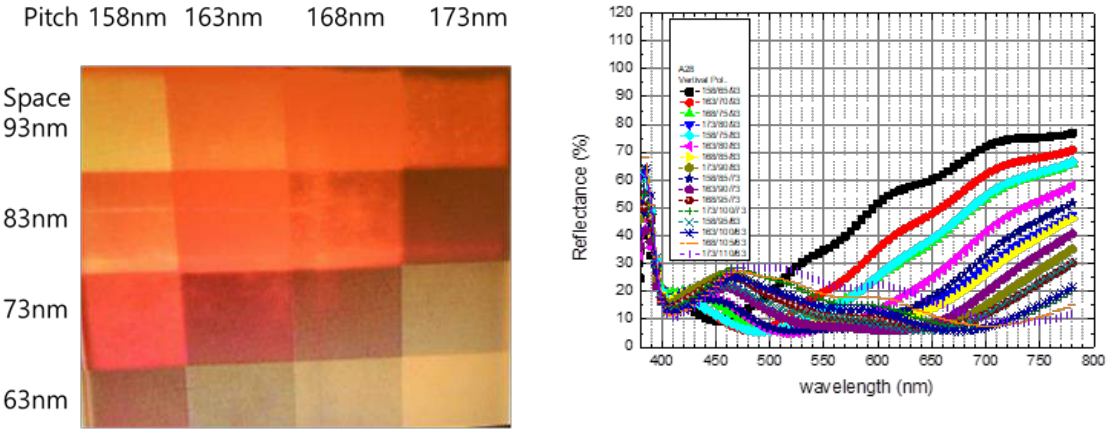


Figure 2 Color change and reflectivity modulation of active metasurface device as a function of Mo antenna's width/space.

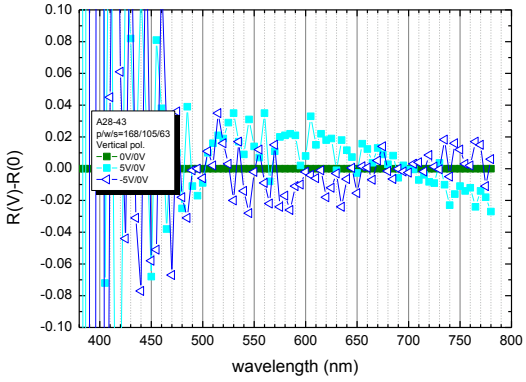


Figure 3. Reflectivity change of active metasurface device as a function of applied voltage.

Plasmonically-enhanced phase-change integrated photonic memory device

J. Song[1*], I. Bente[2], W.H.P. Pernice[2,3], H. Bhaskaran[4], and C. D. Wright[1],

[1]Centre for Metamaterial Research and Innovation, University of Exeter, UK
[2]Institute of Physics, University of Münster, Heisenbergstr. 11, 48149 Münster, Germany
[3]Kirchhoff-Institute for Physics, Heidelberg University, Im Neuenheimer Feld 227, 69120 Heidelberg, Germany
[4]Department of Materials, University of Oxford, Oxford OX1 3PH, UK
[*]corresponding author: J.Song2@exeter.ac.uk

Abstract: We explore the potential for the realization of fast, energy-efficient photonic memory and computing devices arising from the combination of the energy-efficient silicon nitride platform, the sub-wavelength light-squeezing and field-enhancing capability of plasmonic resonant structures, and the intrinsic tuneability brought by chalcogenide phase-change materials. We concentrate on designs that should be readily manufactured, comprising plasmonic dimer-bar nanoantenna deposited on top of a phase-change cell, itself deposited on top of an integrated photonic waveguide.

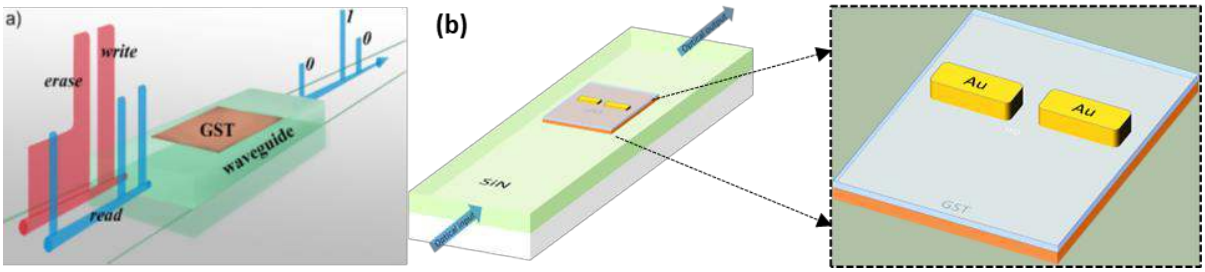


Fig. 1. Integrated phase-change photonic memory, configuration and operation schematic. (a) The conventional configuration with a GST cell on top the waveguide. (b) The proposed plasmonically-enhanced configuration.

Integrated phase-change photonic memory devices offer a novel route to non-volatile storage and computing. Such devices generally consist of integrated waveguide structures onto which are fabricated small phase-change memory cells (e.g., $Ge_2Sb_2Te_5$, or GST), as shown in Fig. 1(a). In the drive to reduce switching energies and increase switching speeds, plasmonic enhancement of the interaction of the propagating mode with the phase-change cell has been proposed [1,2]. Here we explore further this concept of plasmonic enhancement, concentrating on device designs with relatively simple architectures that lend themselves to easy manufacture.

As shown in Fig. 1(b), our proposed plasmonic device consists of a SiN ridge waveguide (1200 nm x 334 nm) fabricated on top of a SiO_2 substrate. A gold plasmonic nanoantenna is deposited on top of a 500 x 500 nm GST patch of 10 nm thickness. The nanoantenna employs a dimer-bar configuration, each bar here being 40 nm wide and 30 nm thick. The gap between each bar is either 40 nm or (for easier fabrication) 80 nm, and each vertical corner of the bar is rounded (curvature radius of 10 nm) to reflect fabrication realities. Since gold tends to diffuse easily with chalcogenides, resulting in adverse changes in the latter's optical and electrical properties, a 5 nm ITO layer is deposited on top of the GST patch as a barrier layer to eliminate the diffusion. The basic operating concept of the device, shown in Fig. 1(b), employs of the nanoantenna's capability to maintain a localized plasmonic resonance by coupling with the optical mode propagating in the waveguide. This plasmonic resonance results in a very strong enhancement of the electric field in the gap region, as compared to the conventional integrated phase-change photonic cell [1]. Such enhancement increases the interaction between the

phase-change cell and propagating light significantly, so improving switching energies and speeds. We here analyse the proposed concept via finite element modelling (FEM) method in the COMSOL package and fabricate test devices using e-beam lithography.

Exemplar simulation results of the device optical performance are shown in Fig. 2, for a range of dimer bar lengths and excitation wavelengths. The transmission contrast of the devices confirms that both GST amorphous and crystalline states exhibit distinguishable resonance features, with a peak contrast of around 22% for bar lengths of 165 nm at 1550 nm wavelength. This contrast is around double that of the conventional device of Fig. 1(a). This is a direct result of the substantial electric field enhancement in the nanogap resulting from the plasmonic resonance. The insertion loss, see Fig. 2(b), of our plasmonically-enhanced design was also found to be acceptable, with a value of approximatively -0.3 dB at the 165 nm bar length.

(a) (b) (c)

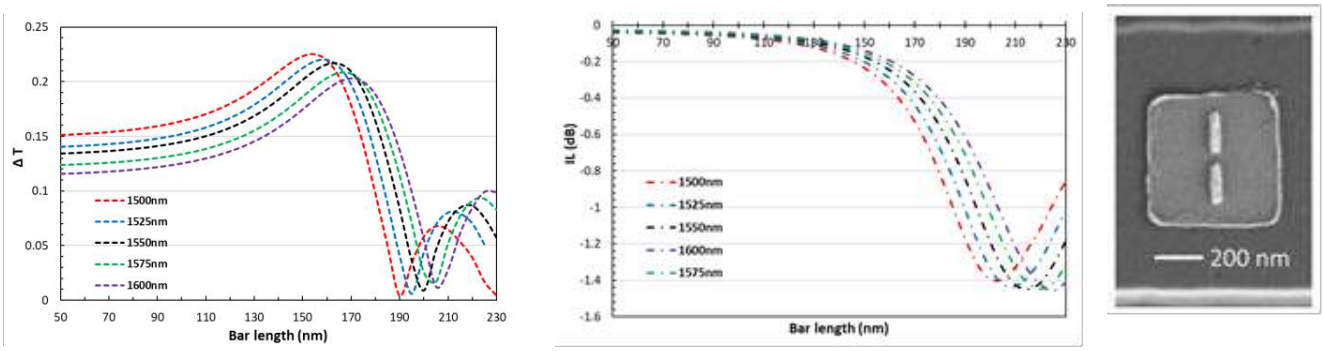


Fig. 2. (a) Simulated optical contrast as a function of dimer bar length for the plasmonic cell architecture shown in Fig. 1(b). (b) Simulated insertion loss as a function of bar length. (c) Experimentally fabricated plasmonically enhanced device.

The fabrication of our proposed plasmonically-enhanced phase-change photonic device designs has also been achieved, with a typical as-fabricated device shown in Fig. 2(c). Experimental characterization results will be compared to simulation predictions and devices further optimized.

Acknowledgments

The authors acknowledge funding via the H2020 project PHOENICS (Grant No. 101017237).

References

1. E. Gemo et al., “Plasmonically-enhanced all-optical integrated phase-change memory”, Optics Express, Vol.27, No. 17, 24724-24738, 2019.
2. E. Gemo et al., “A plasmonically enhanced route to faster and more energy-efficient phase-change integrated photonic memory and computing devices”, Journal of Applied Physics, Vol. 129, 110902-1, 2021.

META 2023, PARIS - FRANCE, JULY 18 – 21, 2023

Plasmon-mediated wavelength-selective photoactuation for multi-directional soft robots

Dong-Jin Lee[1,3], and Dae Yu Kim[1,2,3*]

[1]Inha Research Institute for Aerospace Medicine, Inha University, Incheon 22212, Republic of Korea
[2]Electrical Engineering, College of Engineering, Inha University, Incheon 22212, Republic of Korea
[3]Center for Sensor Systems, Inha University, Incheon 22212, Republic of Korea

[*]Corresponding author: dyukim@inha.ac.kr

Abstract: Light-driven soft actuators have been gaining attention in soft robots, although the challenges of accurately and reversibly modulating in various directions remains. Here we present a strategy for wavelength-selective photoactuation based on Au nanorod/reduced graphene oxide nanocomposites. The plasmonic characteristic of Au nanorods can induce strong photothermal conversion at different wavelengths depending on the aspect ratio of that. The reduced graphene oxides have high thermal conductivity and negative coefficients of thermal expansion, leading to significant bending in bilayer configurations.

Stimuli-responsive actuator, which can convert energy into mechanical motion, have been intensively attracted for leading-edge applications such as micro-electromechanical systems, microrobotics, and sensors [1-3]. Many researchers have performed for developing artificial smart actuators enabled by heat, humidity, electric, magnetism, and light. Of the various environmental stimuli, light is a clean and safe energy with the unique properties of omnipresence, high spatial and temporal resolution, and degrees of control freedom including wavelength, polarization, and intensity [4]. Photothermal effect is a primary mechanism of light-driven actuators, and induces the thermal expansion, leading to deformation in a multi-layer configuration with different a coefficient of thermal expansions (CTEs).

In this study, we propose a strategy of making a wavelength-selective photoactuation system capable of carrying out multi-directional movement, which is based on selective photothermal heating in multi-layer structured actuator consisting of flexible substrates and Au nanorod (NR)/reduced graphene oxide (rGO) nanocomposites. The surface plasmon resonance characteristic of Au NRs can bring about intense photothermal conversion at different wavelengths in visible and near-infrared range depending on the aspect ratio of that. The rGO have high thermal conductivity (~1500 $Wm^{-1}K^{-1}$) and negative CTEs (~0.77×10^{-6} K^{-1}), leading to significant bending due to the mismatch between the deformations between flexible substrates and rGO layers.

Figure 1 shows the strategy for wavelength-selective photoactuation based on Au nanorod/reduced graphene oxide nanocomposites. Figure 1(a) shows the schematic of the absorption spectra depending on the aspect ratio of Au NRs. Au NRs have the plasmonic resonance in visible and near-infrared region, and the plasmonic resonance can be modulated by control of aspect ratio of Au NRs. The soft actuators with multi-layer configurations are fabricated by inkjet printing process using Au nanorod/reduced graphene oxide nanocomposite inks as shown in Figure 1(b).

Au NRs in aqueous suspension are obtained by seed-mediated synthesis according to previous report [5]. Figure 2 shows the morphological and the optical characteristics of the Au NRs with the aspect ratio of 1. The average diameter and plasmonic resonance of the Au NRs with the aspect ratio of 1 are 34.7±3.6 nm and ~528 nm, respectively.

In a follow-up study, we examine the plasmonic property of Au NRs/rGO nanocomposite inks, and

investigate the effect of light illumination intensity and wavelength selectivity on photoactuation response.

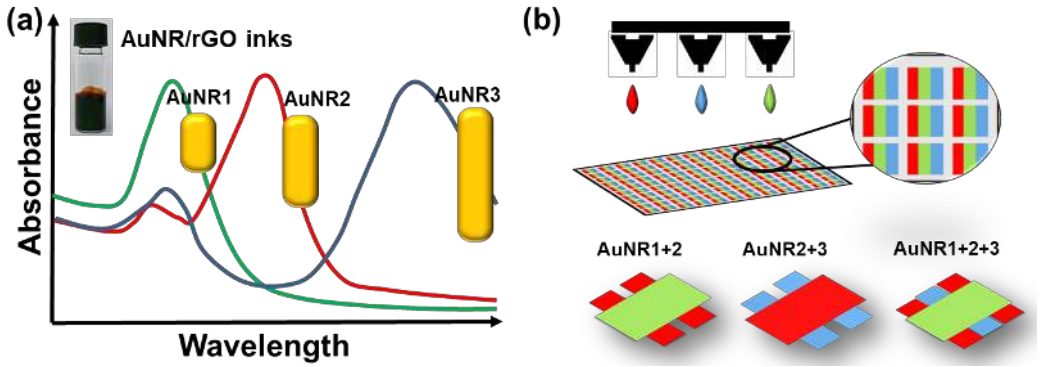


Figure 1. Strategy for wavelength-selective photoactuation based on Au nanorod/reduced graphene oxide nanocomposites. (a) Schematic of the absorption spectra depending on the aspect ratio of Au NRs. (b) Schematic of the multi-layered soft actuators fabricated by inkjet printing process.

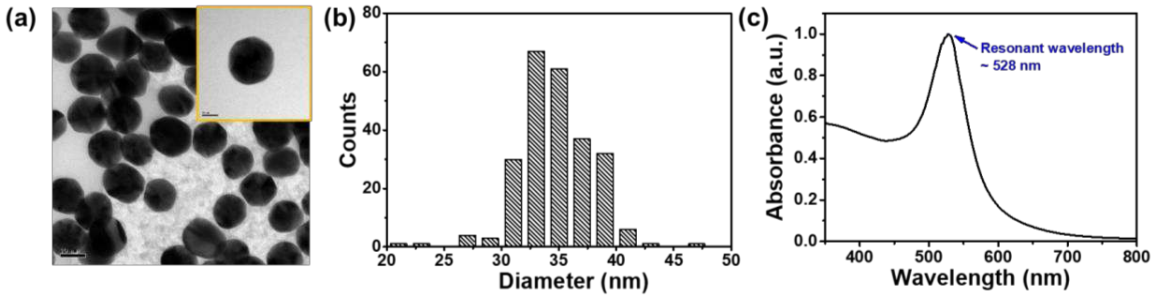


Figure 2. Morphological and the optical characteristics of the Au NRs. TEM images (a), size distribution (b), and (c) UV-vis spectrum of Au NR with the aspect ratio of 1.

Acknowledgements

This research was supported by Basic Science Research Program through the National Research Foundation of Korea (NRF) funded by the Ministry of Education (2018R1A6A1A03025523 and 2020R1I1A1A01075317). This research was supported by the Korean Medical Device Development Fund grant funded by the Korea government (the Ministry of Science and ICT, the Ministry of Trade, Industry and Energy, the Ministry of Health & Welfare, the Ministry of Food and Drug Safety) (KMDF_PR_20200901_0026).

References

1. I. Apsite, Salehi, S., Ionov, L., "Materials for Smart Soft Actuator Systems," Chem Rev, vol. 122, pp. 1349-1415, 2022.
2. X. D. Wang, N. D. Jiao, S. Tung, and L. Q. Liu, "Photoresponsive Graphene Composite Bilayer Actuator for Soft Robots," Acs Applied Materials & Interfaces, vol. 11, no. 33, pp. 30290-30299, 2019.
3. Z. Zhang, Y. Wang, Q. Wang, and L. Shang, "Smart Film Actuators for Biomedical Applications," Small, p. 2105116, 2022.
4. J. Xiao, Zhou, T., Yao, N., Ma, S., Pan, C., Wang, P., Fu, H., Liu, H., Pan, J., Yu, L., Wang, S., Yang, W., Tong, L., Zhang, L., "Optical fibre taper-enabled waveguide photoactuators," Nat Commun, vol. 13, no. 1, p. 363, 2022.
5. A. Chhatre, R. Thaokar, and A. Mehra, "Formation of Gold Nanorods by Seeded Growth: Mechanisms and Modeling," Crystal Growth & Design, vol. 18, no. 6, pp. 3269-3282, 2018.

META 2023, PARIS - FRANCE, JULY 18 – 21, 2023

Controlling Förster Resonance Energy Transfer in Plasmonic Nanopatch Antennas

Abdullah O. Hamza[1,2], Francesco N. Viscomi[1], Jean-Sebastien G. Bouillard[1], and Ali M. Adawi[1,*]
[1]Department of Physics and Mathematics and G. W. Gray Centre for Advanced Materials, University of Hull, HU6 7RX Hull, U.K.
[2]Department of Physics, College of Science, Salahaddin University, Erbil, Iraq
[*]corresponding author: a.adawi@hull.ac.uk

Abstract: Successful control of Förster resonance energy transfer (FRET) through the engineering of the local density of states (LDOS) will allow us to develop novel strategies to fully exploit this phenomenon in key enabling technologies. Here we present an experimental and theoretical study on the effect of LDOS on the FRET rate and efficeny in plasmonic nanopatch antennas. Our results reveal that FRET rate is linearly dependent on LDOS and LDOS plays an important part in controlling FRET efficiency and range.

Förster resonance energy transfer (FRET) is a fundamental phenomenon in photosynthesis and is of increasing importance for the development and enhancement of a wide range of optoelectronic devices, including color-tuning LEDs and lasers, light harvesting, sensing systems, and quantum computing. Successful control of FRET will allow us to develop novel strategies to fully exploit this phenomenon in these key enabling technologies.

In this work, we present an experimental and theoretical study on the effect of the local density of optical states (LDOS) on the FRET rate and efficiency using plasmonic nanopatch antennas formed between a plasmonic nanoparticle and an extended metallic film. Our results reveal that LDOS plays an important part in controlling both FRET rate and efficiency. By tuning the nanoparticle size and material, we show that the FRET rate is directly dependent on the LDOS of the nanopatch antennas. We also found that plasmonic nanopatch antennas can be utilised to extend the FRET range over 200 nm while keeping the FRET efficiency over 0.38, with efficiency enhancement factor of ~10^3 with respect to homogeneous environment. Our findings contribute to the ongoing debate about the relation between the FRET process and the LDOS, as well as directly impacting the development of novel FRET based light harvesting and sensing devices.

ACKNOWLEDGMENT

This work was supported by the UK EPSRC through Grant EP/L025078/1 and the EU Horizon 2020 research and innovation programme under grant number 861950, project POSEIDON. We also acknowledge the Viper High Performance Computing facility of the University of Hull and its support team. We thank Stuart Harris at Zeon Chemicals Europe Ltd for the gift of the Zeonex polymer.

Hybrid Dielectric-Plasmonic Nanoantenna with Multiresonances for Subwavelength Photon Sources

Emmanuel Lassalle[1,*], Pavel A. Dmitriev[1], Lu Ding[1], Darren C. J. Neo[1], Vytautas Valuckas[1], Ramon Paniagua-Dominguez[1], Joel K. W. Yang[1,2], Hilmi V. Demir[3,4], and Arseniy I. Kuznetsov[1]

[1] *Institute of Materials Research and Engineering, A*STAR (Agency for Science, Technology and Research), 2 Fusionopolis Way, #08-03 Innovis, 138634 Singapore*

[2] *Singapore University of Technology and Design, 8 Somapah Road, 487372 Singapore*

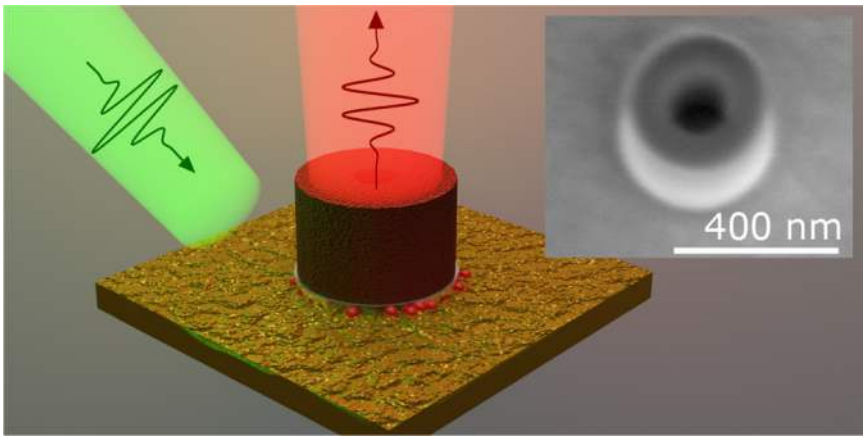
[3] *LUMINOUS! Centre of Excellence for Semiconductor Lighting and Displays, School of Electrical and Electronic Engineering, Nanyang Technological University, Singapore 639798, Singapore*

[4] *Department of Electrical and Electronics Engineering, Department of Physics, UNAM – Institute of Materials Science and Nanotechnology, Bilkent University, Ankara 06800, Turkey*

[*] *corresponding author: emmanuel_lassalle@imre.a-star.edu.sg*

Abstract: In this talk, we propose and demonstrate single subwavelength hybrid dielectric-plasmonic optical nanoantennas coupled to localized quantum dot emitters that constitute efficient and bright unidirectional photon sources under optical pumping. To achieve this, we devised a silicon nanoring sitting on a gold mirror with a 10 nm gap in-between, where an assembly of colloidal quantum dots is embedded, and obtain experimentally total fluorescence enhancement up to 600-fold, due to high radiative efficiency.

Hybrid dielectric-plasmonic optical nanoantennas have been recently put forward to mitigate the losses encountered in all-plasmonic nanostructures [1]. Here, we report on one of the first few experimental demonstrations of a subwavelength single hybrid dielectric-plasmonic optical nanoantenna coupled to localised quantum dot emitters, that constitutes an efficient and bright unidirectional photon source under optical pumping. To achieve this, we use a subwavelength silicon nanoring sitting on a metallic (gold) mirror with a 10 nm gap in-between, where an assembly of quantum dots is embedded. Such a structure presents the advantage of supporting two classes of modes, "gap" plasmon modes [2] and "antenna" (radiative) modes [3], to which the quantum dots can efficiently couple for the dual purpose of enhancing the absorption of the optical pump, and for out-coupling the light into the far-field with high directionality, respectively. Moreover, an almost independent control of the resonance spectral positions is achieved by a simple tuning of geometrical parameters such as the ring outer and inner diameters, which is not possible with other, simpler, nanoparticle-on-mirror antennas [4]. We obtain total enhancement factors of the fluorescence of the assembly of emitters up to 600-fold, simultaneously with a directional emission of the photoluminescence into a cone of $\pm 17°$ in the upward direction [5].



References

1. A. Barreda, F. Vitale, A. E. Minovich, C. Ronning, and I. Staude, "Applications of Hybrid Metal-Dielectric Nanostructures: State of the Art", *Advanced Photonics Research* **3**, 2100286 (2022).

2. Y. Yang, O. D. Miller, T. Christensen, J. D. Joannopoulos, and M. Soljacic, "Low-loss plasmonic dielectric nanoresonators", *Nano Letters* **17**, 3238–3245 (2017).
3. J. Yik, P. Bai, Z. Liu, C. E. Png, Y. H. Fu, and A. I. Kuznetsov, "Antenna, antenna array, and methods of forming the same", International Publication Number: WO2020171771A1 (Aug. 2020).
4. G. M. Akselrod, C. Argyropoulos, T. B. Hoang, C. Ciraci, C. Fang, J. Huang, D. R. Smith, and M. H. Mikkelsen, "Probing the mechanisms of large Purcell enhancement in plasmonic nanoantennas", *Nature Photonics* **8**, 835–840 (2014).
5. P. A. Dmitriev, E. Lassalle, L. Ding, D. C. J. Neo, V. Valuckas, R. Paniagua-Dominguez, J. K. W. Yang, H. V. Demir, and A. I. Kuznetsov, "Hybrid dielectric-plasmonic nanoantenna with multiresonances for subwavelength photon sources", *ACS Photonics*, DOI: 10.1021/acsphotonics.2c01332 (online publication 22 Feb. 2023).

META 2023, PARIS - FRANCE, JULY 18 – 21, 2023

Tailoring Nanowire Lasing Modes via Coupling to Metal Gratings

F. Vitale[1*], D. Repp[2], T. Siefke[2], U. Zeitner[2,3], U. Peschel[4], T. Pertsch[2] and C. Ronning[1]

[1]Institute of Solid State Physics, Friedrich Schiller University Jena, Max-Wien-Platz 1, 07743 Jena, Germany

[2]Institute of Applied Physics, Abbe Center of Photonics, Friedrich Schiller University Jena, Albert-Einstein-Straße 15, 07745 Jena, Germany

[3]Fraunhofer Institute for Applied Optics and Precision Engineering, Albert-Einstein-Straße 7, 07745 Jena, Germany

[4]Institute of Condensed Matter Theory and Solid State Optics, Friedrich Schiller University Jena, Max-Wien-Platz 1, Jena 07743, Germany

[*]corresponding author: francesco.vitale@uni-jena.de

Abstract: In this study, we proposed a lasing mode selection scheme based on distributed feedback, achieved via the external nano-manipulation of single zinc oxide nanowires onto an aluminum grating. By orienting the nano-cavity perpendicular to the ridge direction, we identified an additional peak in the emission spectrum on the low-energy side of the gain envelope. As a consequence of the fulfillment of the Bragg condition, such a peak was attributed to a novel hybrid mode dominating the mode competition.

Tailoring the emission of plasmonic nanowire-based lasers represents one of the major challenges in the field of nanoplasmonics, given the envisaged integration of such devices into on-chip all-optical circuits[1]. In this work, we made use of a mechanical nano-manipulation approach, to study the effects of a metal grating[2,3], characterized by geometrical parameters tailored to the lasing emission wavelength, on the lasing properties of semiconductor nanowire-based plasmonic lasers. Namely, the same nanowire could be manipulated and "switched" among different configurations: from placed on dielectric/metal substrates (planar plasmonic configuration) to overlaid on metal gratings (nanowire-metal grating configuration) at different orientations with respect to the ridges. The optical characterization of single nanowires in a given configuration was measured by focusing the emission from an ns-pulsed, low-repetition-rate, frequency-tripled Nd:YAG laser onto the sample mounted into a liquid He flow cryostat. To explain the emergence of the additional peak in the low-energy side of the PL spectrum (visible in Figure 1a) for the $\vartheta \approx 90°$ on-grating configuration, we performed active lasing simulations using the software Lumerical. To this end, the geometrical parameters, extracted from the SEM cross-section of the "fenced" grating (shown in Fig. 1c), were used. The simulation results show that the excitation of surface plasmon polaritons at the fences enhances the mode confinement[3]: this, in turn, leads to a large modal mismatch between the "fence-coupled mode" supported by the parts of the nanowire in contact with the metal, and the "fence-uncoupled mode" supported by the free-standing parts. This results in a resonator feedback of about 50% (excluding the end-facet reflectance) even for a small number of periods (N = 40), as shown in Figure 1(d). Thus, for an orientation of the nanowire perpendicular to the grating ridges, the experimental and theoretical results showed that the lasing action is dominated by a hybrid mode, which is supported by its effective coupling with the localized plasmon polaritons at the fence edges.

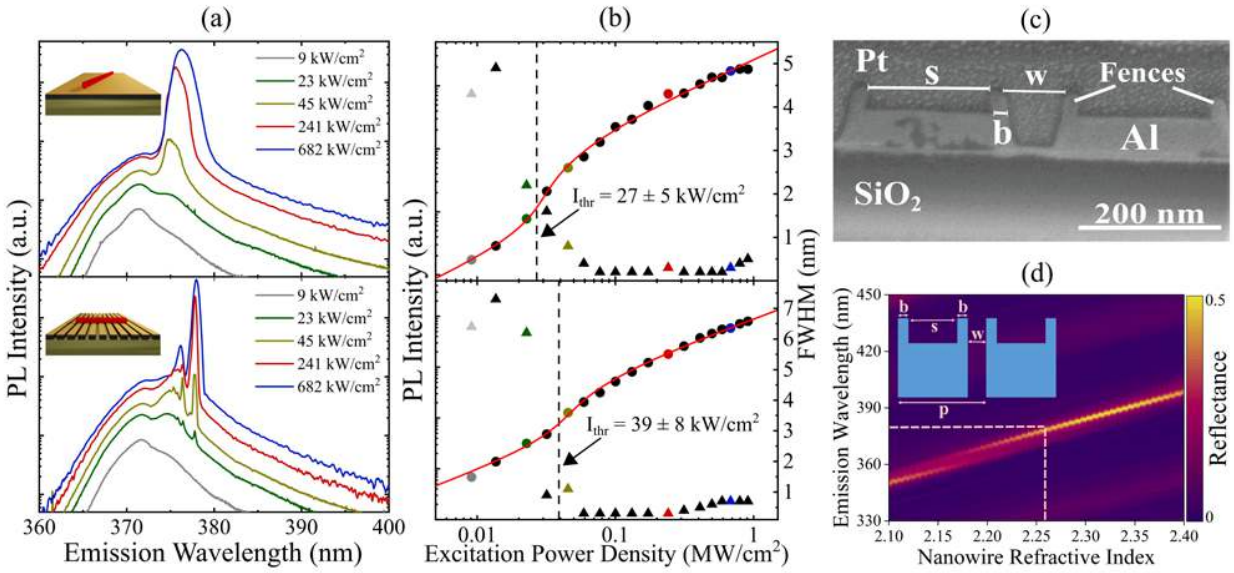


FIGURE 1: (a) PL spectra of the planar (top panel) and nanowire-grating (bottom panel) configurations acquired for different pump power densities at 150 K; the NW was oriented perpendicular to the ridge direction $\vartheta \approx 90^\circ$. (b) Corresponding light-in-light-out curves (circles) of the emission intensity and spectral width trends (triangles) of the emission for the planar (top panel) and nanowire-grating (bottom panel) configurations, as a function of the excitation power density. The dashed lines indicate the respective lasing thresholds estimated by fitting the experimental data points with an adapted multimode lasing model. (c) SEM cross-section of an Al grating with a nominal pitch p = 300 nm and fill factor FF = 0.3. (d) Simulated reflectance of the "fenced" Al grating (sketched in the inset) for the lasing mode as a function of the wavelength and nanowire index. The intersection point of the dashed white lines indicates the reflectance at λ = 378 nm for the corresponding material index value (n_{ZnO} = 2.26).

The authors acknowledge the financial support by the CRC 1375 "NOA–Nonlinear optics down to atomic scales" funded by the Deutsche Forschungsgemeinschaft (DFG).

References

1. Fukuda, Mitsuo, et al. "Feasibility of plasmonic circuits in nanophotonics." IEEE Access 8 (2020): 142495-142506.
2. Cheng, Pi-Ju, et al. "High-performance plasmonic nanolasers with a nanotrench defect cavity for sensing applications." Acs Photonics 5.7 (2018): 2638-2644.
3. Chou, Yu-Hsun, et al. "Ultracompact pseudowedge plasmonic lasers and laser arrays." Nano letters 18.2 (2018): 747-753.

META 2023, PARIS - FRANCE, JULY 18 – 21, 2023

Near unity Raman β-factor of surface enhanced Raman scattering in a waveguide

M. Fu[1], M. P. dS. P. Mota[1], X Xiao[1], A Jacassi[1], N. A. Güsken[1], Y. Chen[1], H. Xiao[1], Y. Li[1,2], A. Riaz[1], S. A. Maier[1,3], R. F. Oulton[1,*]

[1]Blackett Laboratory, Imperial College London, Prince Consort Road, London SW7 2BZ, UK
[2]School of Microelectronics, Southern University of Science and Technology, Shenzhen 518055, China
[3] Nanoinstitute Munich, Faculty of Physics, Ludwig-Maximilians-Universität München, 80539 Munich, Germany
* corresponding author: r.oulton@imperial.ac.uk

Abstract: We show that SERS from monolayer 4-Aminothiophenol (4-ATP) bonded to a plasmonic gap waveguide is directed into a single mode with >99% efficiency. Although sacrificing a confinement dimension, we find a 10^3x SERS enhancement across a broad spectral range, enabled by the plasmonic waveguide's larger sensing volume and non-resonant waveguide mode. Waveguide-SERS (W-SERS) is bright enough to image Raman transport across the waveguides. This exposes the roles of nanofocusing, the Purcell effect and the spontaneous Raman scattering factor, or Raman β-factor.

To enhance the Raman scattering efficiency of light by molecules, various enhancement techniques relying on either stimulated or surface enhanced Raman scattering (SERS) have been developed [1-9]. Since the first SERS signal observed from pyridine adsorbed on a roughened silver electrode in 1973, various types of nanostructures for SERS have been designed, for instance, rough metallic surfaces, nanoparticles, and metallic tips. Remarkable enhancement of Raman scattering efficiency has been achieved by using those SERS techniques, but they are either limited by the poor control of the scattered light, narrow bandwidth of the resonance frequency, or restricted area of field enhancement.

In this talk, we present a unique plasmonic waveguide approach to Raman scattering enhancement with precise control of both the incident light intensity and the scattered Raman light [1]. Raman scattering is enhanced in a plasmonic waveguide via two mechanisms. Firstly, the local intensity of the pump light is increase by efficient nano-focussing into a plasmonic slot waveguide with approximately 30% coupling efficiency. Secondly, within the optically confined slot waveguide environment, molecules experience increased local vacuum fluctuations. Since the waveguide presents both nano-focussing and confinement over a broad spectral range, it provides a broadband Raman enhancement.

In particular, we report directional broadband Raman scattering of light by 4-Aminothiophenol (4-ATP) molecules which are chemically bound as a single molecular layer onto well designed plasmonic slot waveguide. The waveguides are decorated with optical antennas that allow light to couple in and out of the slot waveguide with 30% efficiency, evaluated experimentally. Since we observe strong Raman signals from these waveguide, we have been able to spatially resolve the coupling in of the excitation laser and coupling out of Raman scattering. This enables us to precisely investigate how the scattered Raman photons of molecules couple into the waveguide, propagate and couple out via the antennas. In this way, we have experimentally determined the spontaneous Raman beta factor in a plasmonic waveguide for the first time. We have demonstrated that 99% of the Raman photons are coupled into the waveguide and coupled out through the antenna pairs of the waveguide.

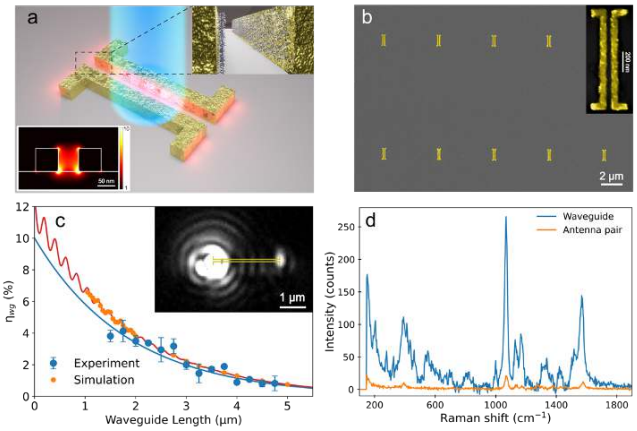


Figure 1. a) Schematic of the plasmonic waveguide bonded with 4-Aminothiophenol (4-ATP) molecules. b) Scanning electron microscopic image of the waveguide. c) The waveguide coupling efficiency was measured by focused excitation on the waveguide's antennas and compared with theory. d) Comparison of Raman spectra from an antenna coupled waveguide and a single antenna. Both spectra were recorded at 400 µW power, and 10 s integration. The waveguide SERS sample shows a 10-fold enhancement relative to the antenna alone.

The high Raman beta-factor is due to the largely enhanced spontaneous Raman scattering rate into the waveguide mode. The enhancement mechanism can be understood analogously to fluorescence emission enhanced by the Purcell effect, which is due to increased vacuum fluctuations and increased density of states. While Raman scattering in highly localised metallic hotspots offer high enhancement factors for a few molecules, here, a plasmonic waveguide offers predictable broadband enhancement for many molecules with a greatly improved interaction volume compared to other SERS approaches.

This work was supported by the EPSRC Reactive Plasmonics Programme (EP/M013812/1), UK Quantum Hub in Quantum Imaging (EP/T00097X/1) and the Leverhulme Trust. This project has received funding from the European Union's Horizon 2020 research and innovation programme under the Marie Skłodowska-Curie grant agreement No 844591.

References

1. Fu et al, "Near-unity Raman β-factor of surface-enhanced Raman scattering in a waveguide" Nature Nanotech., Vol. 17, 1251–1257, 2022.
2. Hümmer, T. et al. "Cavity-enhanced Raman microscopy of individual carbon nanotubes," Nat. Commun., Vol. 7, 12155, 2016.
3. Dhakal, A. et al., "Nanophotonic Waveguide Enhanced Raman Spectroscopy of Biological Submonolayers." ACS Photonics, Vol. 3, 2141–2149, 2016.
4. Holmstrom, S. A. et al., "Trace gas Raman spectroscopy using functionalized waveguides." Optica, Vol. 3, 891–896 2016.
5. Eslami, S. & Palomba, S., "Integrated enhanced Raman scattering: a review." Nano Converg., Vol. 8, 41, 2021.
6. Ettabib, M. A. et al., "Waveguide Enhanced Raman Spectroscopy for Biosensing: A Review." ACS Sens., Vol. 6, 2025–2045, 2021.
7. Wong, H. M. K., Dezfouli, M. K., Sun, L., Hughes, S. & Helmy, A. S., "Nanoscale plasmonic slot waveguides for enhanced Raman spectroscopy." Phys. Rev. B, Vol. 98, 085124, 2018.
8. Turk, N. et al., "Comparison of Free-Space and Waveguide-Based SERS Platforms." Nanomater., 9, E1401, 2019.
9. Raza, A. et al. ALD assisted nanoplasmonic slot waveguide for on-chip enhanced Raman spectroscopy. APL Photonics 3, 116105, 2018.

META 2023, PARIS - FRANCE, JULY 18 – 21, 2023

A Terahertz Lens Antenna Array Design for Beam Steering in Time-Domain

A.C. Songur[1], A.O. Sakin[1], H.A. Gunes[1], B. Akcay[1] and, M. Unlu[1*]

[1] Dept. of Electrical and Electronics Engineering, TOBB University of Economics and Technology, 06510 Ankara, Turkey

[*]corresponding author: munlu@etu.edu.tr

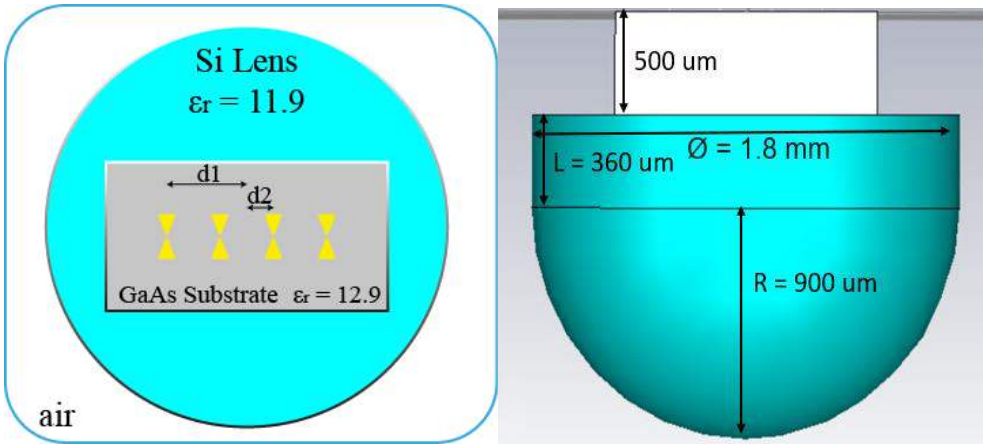
Abstract: In this paper, a terahertz switched antenna array allowing beam steering between ±30° in the time-domain for 0.8-2 THz band has been designed. A silicon lens is utilized, which also allows a time-domain steering range between ±30° and is custom-developed as an extended-hemispherical lens, and the elements of the antenna array consist of broadband bowtie antennas. The far-field terahertz radiation has been successfully obtained in terms of time-domain performance criteria.

Terahertz waves exhibit several unique attributes that other bands cannot, since electromagnetic waves in the terahertz frequency band have some characteristics of both RF frequencies and optical frequency waves. To efficiently use terahertz waves in next-generation communication systems, it is imperative to develop efficient terahertz sources and detectors. However, the development of terahertz sources and detectors showing high performance is currently one of the most challenging topics of terahertz research since in these photoconductive antenna (PCA) systems, the optical-to-electrical conversion is inefficient [1]. As a remedy to the power loss problem in PCAs, it is critical to design high-gain antennas and antenna arrays. In addition to the antenna array design, high-performance terahertz lens designs are required to augment the terahertz power radiated by the PCA array. The beam-steering capability of terahertz PCA arrays, on the other hand, is critical for the deployment of terahertz sources in next-generation communication systems. Thus, the terahertz lens antenna array to be designed is crucial not only for enhancing terahertz radiation effectively but also for beam steering [2].

Furthermore, short-pulsed signals with high bandwidth are used in terahertz PCA excitation. Hence, the characterization of antennas and lenses in the classical frequency domain loses its functionality. Purely time-domain characterization of antenna arrays and lenses is substantially more efficient than the former. To the authors' best knowledge, a lens photoconductive antenna array capable of beam steering at terahertz frequencies in the time-domain has not been presented in the literature.

In this study, a terahertz-switched lens antenna array capable of beam steering between ±30° in the time-domain has been developed for 0.8-2 THz band. The silicon lens, capable of effective time-domain steering between ±30°, has been custom designed as an extended-hemispherical lens, and the elements of the antenna array consist of broadband bowtie antennas. Successful far-field time-domain terahertz radiation was obtained, similar to what the authors demonstrated in a previous single terahertz time-domain antenna study [3]. In Figure 1, the proposed time-domain terahertz switch lens array and its dimensions are given. In Figure 2, the time-domain far-field radiation result indicating successful 30° steering is given.

Extended-hemispherical lens design for beam-steering mostly follows the thin lens approximation which associates the focal length of a thin lens to the scan angle of the lens. The extension height, denoted by "L" in Figure 1.b, can be interpreted as the effective focal length of a thin lens [4]. The steering angle depends on the geometrical parameters of the lens (“L” and “R” in Figure 1.b) as well as the positioning of array elements with respect to the lens center (“d1” and “d2” in Figure 1.a).



(a) **(b)**

Figure 1. The designed lens switched-array and its dimensions **(a)** Top view **(b)** Side view

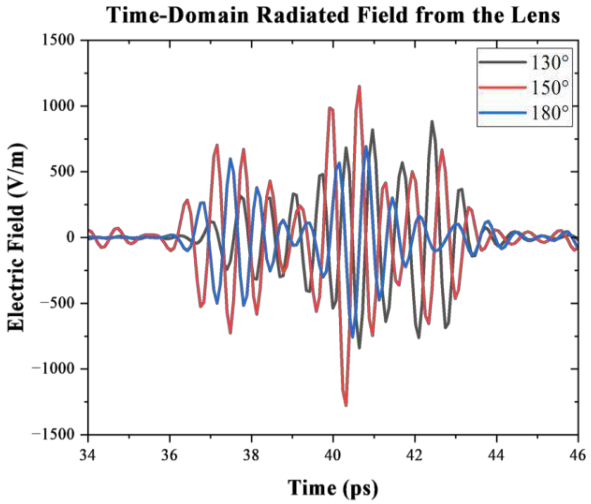


Figure 2. The time-domain far-field radiation of the lensed antenna when the antenna with the distance "d1" to the origin is active in Figure 1.a (maximum radiation towards 150°, indicating a 30° steering)

Acknowledgement

All authors acknowledge TUBITAK for their support with the project number: 119E501. A.C. Songur, A.O. Sakin, H.A. Gunes, and B. Akcay acknowledge the support of TUBITAK BIDEB 2210A grant.

References

1. Zhong, S. "Progress in terahertz nondestructive testing: A review." Frontiers of Mechanical Engineering, Vol. 14, 273-281, 2019.
2. Fu, X., F. Yang, C. Liu, X. Wu, and T. J. Cui, "Terahertz beam steering technologies: from phased arrays to field-programmable metasurfaces." Advanced optical materials, Vol. 8, No. 3, 1900628, 2020.
3. Songur, A. C., and M. Ünlü, "Comparison of time-domain antenna performances for the terahertz photoconductive sources and detectors" Terahertz Photonics II, Vol. 12134, 90-96, 2022.
4. Frid, H. "Closed-form relation between the scan angle and feed position for extended hemispherical lenses based on ray tracing." IEEE Antennas and Wireless Propagation Letters, Vol. 15, 1963-1966, 2016.

META 2023, PARIS - FRANCE, JULY 18 – 21, 2023

A Terahertz Time-Domain Antenna Array based on a Parametric Study

A.C. Songur[1], A.O. Sakin[1], B. Akcay[1], H. A. Gunes[1] and, M. Unlu[1*]

[1] Dept. of Electrical and Electronics Engineering, TOBB University of Economics and Technology, 06510 Ankara, Turkey

[*]corresponding author: munlu@etu.edu.tr

Abstract: In this paper, the design parameters are examined in detail for the terahertz photoconductive antenna arrays operating in the terahertz frequency region, which is one of the most important band candidates for future communication systems, and a 1x4 wide-band time-domain bowtie antenna array providing 30° steering is designed for 0.8-2 THz band. This study is entirely realized in the time-domain to process the broadband terahertz pulsed signals more efficiently.

The terahertz band is classified as the frequency range between 0.3 THz and 10 THz in the electromagnetic spectrum, corresponding between the microwave and infrared parts of the spectrum. Effective THz sources and detectors must be developed for terahertz applications. Terahertz photoconductive antennas (PCA) combined with photonic integrated circuits (PICs), particularly those based on metamaterial topological structures can be critical for advanced communication systems [1-2]. In this context, it is critical to construct broadband antennas that can be compatible with ultra-wide bandwidths of THz pulsed signals. THz antenna arrays, which are to be developed for beam steering applications that are compatible with next-generation communication systems, also gain importance within this frame of reference [3]. On the other hand, because THz pulsed signals are inherently broadband, it is essential to design these antenna arrays in the time-domain, and thus THz ultrawide-band pulses include multiple frequency components, antenna characterization in the frequency domain loses its effectiveness. Instead, conducting direct time-domain characterization is substantial for processing these signals more efficiently. The concept of time-domain analysis of THz antennas has previously been presented in our study where the 3D time-domain solver has been validated using the time-domain analytical approach [4]. The time-domain analytical approach was previously presented at lower frequencies for short-dipole antennas [5]. The preceding single-element work is adapted to the time-domain antenna array in this study.

We first propose a parametric-comprehensive study in this paper which we expect will be pertinent for future time-domain THz antenna array designs. We investigate the effect of spacing, element length, steering angle, and observation angle on the time-domain maximum electric-field radiation emitted by the antenna array within this framework. We also offer a study of a time-domain THz PCA array system capable of beam steering and present a THz time-domain wideband 1x4 bowtie antenna array, whose performance is enhanced with a custom design. Further, it is aimed to provide a 30° steering for the purpose of communication applications. Such an antenna array can be used in both high-power transmission and steering applications using effective compatible optical lasers and substrates in a photoconductive antenna system. Therefore, it is also critical to employ a suitable laser (e.g., 1550 nm ultra-short-pulsed laser) and a substrate with a properly grown active layer (e.g., InGaAs) to obtain the maximum efficiency from the THz PCA array system.

In Figure 1, a summary of the parametric study is given. The 1x4 bowtie antenna array, designed in the light of the parametric study, is also given in the right-bottom inset, and the resulting time-domain radiated field, maximum towards 150° meaning 30° steering, from the array is given the left-bottom inset in Figure 1.

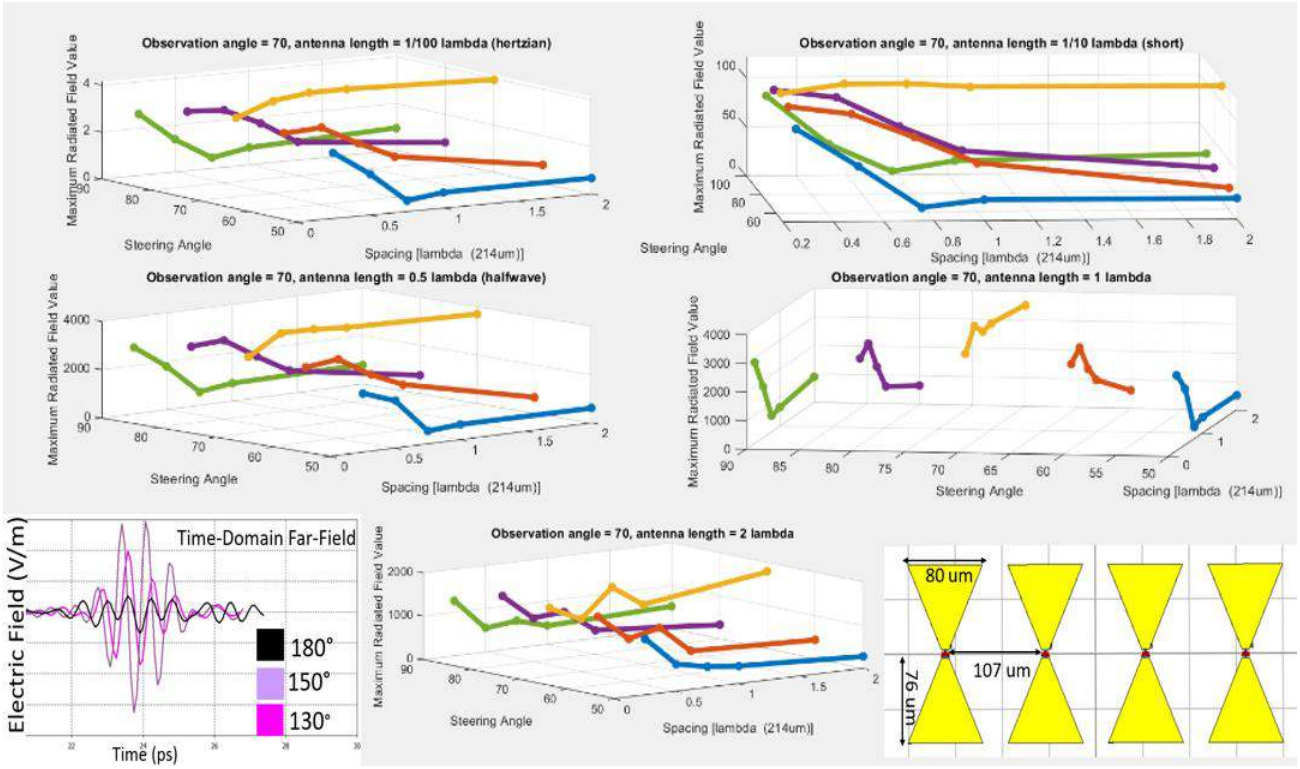


Figure 1. The effect of antenna length variation (0.01 λ to 2 λ) and spacing (0.25 λ to 2 λ) variation on the time-domain maximum radiated field (V/m) under 70° steering (insets: the designed 1x4 bowtie antenna array and the resulting radiated electric-field in the time-domain)

Acknowledgement

All authors acknowledge TUBITAK for their support with the project number: 119E501. A.C. Songur, A.O. Sakin, H.A. Gunes, and B. Akcay acknowledge the support of TUBITAK BIDEB 2210A grant.

References

1. Fu, X., F. Yang, C. Liu, X. Wu, and T. J. Cui, "Terahertz beam steering technologies: from phased arrays to field-programmable metasurfaces." Advanced optical materials, Vol. 8, No. 3, 1900628, 2020.
2. Xie, J., W. Ye, L. Zhou, X. Guo, X. Zang, L. Chen, and Y. Zhu "A review on terahertz technologies accelerated by silicon photonics." Nanomaterials, Vol. 11, No. 7, 1646, 2021.
3. Boulogeorgos, A. A. A., J. M. Jornet, and A. Alexiou. "Directional terahertz communication systems for 6G: Fact check." IEEE Vehicular Technology Magazine, Vol. 16, No. 4, 68-77, 2021.
4. Songur, A. C., and M. Ünlü, “Comparison of time-domain antenna performances for the terahertz photoconductive sources and detectors” Terahertz Photonics II, Vol. 12134, 90-96, 2022.
5. Shlivinski, A., E. Heyman, and R. Kastner. "Antenna characterization in the time domain." IEEE transactions on antennas and propagation, Vol. 45, No. 7, 1140-1149, 1997.

Realization of electromagnetically-induced transparency in the mid-infrared with symmetry-broken metamaterials

The Linh Pham[1,*], Fei Han[1,2], Kacper Pilarczyk[1], Joris Van de Vondel[1], Niels Verellen[2], Thanh Tung Nguyen[3] and Ewald Janssens[1]

[1] Quantum Solid State Physics, Department of Physics and Astronomy, KU Leuven, Leuven, Belgium
[2] IMEC, 3001 Leuven, Belgium
[3] Institute of Materials Science and Graduate University of Science and Technology, Vietnam Academy of Science and Technology, Hanoi, Vietnam
[*]corresponding author: thelinh.pham@kuleuven.be

Abstract: A low-profile metamaterial structure is designed to achieve an analogue of electromagnetically-induced transparency (EIT) in the mid-infrared regime. By breaking the symmetry of the gold resonator, a transmission window occurs around 8.5 μm, instead of a reflectance peak as in the symmetric configuration. The EIT behavior was investigated using near-field distribution analytics and confirmed by microfabrication and FTIR spectroscopy. Based on the EIT effect, the realization of strong dispersion and high Q-factor resonance metamaterials is the first step to the development of sensing devices or optical modulators that we are focusing.

1. Introduction

"Metamaterial" (MM) was introduced in the 2000s and has gained popularity in recent years. Simply put, it is a branch of artificial structure in which properties can be predesigned by quasi-atoms and their arrangement in a subwavelength quasi-lattice and described by effective medium theory [1]. In this study, we proposed a simple structure, in which the symmetry-breaking approach allowed us to achieve the so-called electromagnetically-induced transparency (EIT) effect in the mid-infrared region (see Figure 1). This effect was first observed in the field of quantum mechanics, where two highly coherent optical sources (e.g., lasers) are used simultaneously (as pump and probe fields) to interact with multiple-quantum-state materials [2]. Interestingly, it can be mimicked in metamaterials using multi-resonant metamaterials with individual resonances tuned as bright and dark states (see Figure 1c). The effective medium theory was also used to compute the group index and group delay of a propagating wave. After confirming the effect, we fabricated the sample and characterized its optical spectrum to demonstrate its dependability. The reflectance spectra obtained from Fourier-transform Infrared spectroscopy (FTIR) spectroscopy match well with the simulations.

2. Methodology

Firstly, we optimized the MM structure through simulations of its optical spectra using CST Suite Studio with the finite element method. Then MMs were fabricated using electron beam lithography (EBL) to pattern the MM design, followed by molecular beam epitaxy (MBE) to deposit 5 nm platinum and 50 nm gold, before finishing with a lift-off procedure. FTIR spectroscopy (Vertex 80V) was used to measure the reflectance of the sample before and after the plasma treatment process for characterization.

3. Results

We investigated the reflectivity of EIT-MM in symmetric and asymmetric configurations under different polarization mid-IR sources (TE and TM modes) in both simulation and experiment (Figure 2). The reflection dip in TE mode seen at 8.8 μm for the asymmetric configuration corresponds to the EIT transmission window. Because the symmetry of the TM mode is protected along the electric field direction, the reflectivity in both symmetric and asymmetric structures is nearly unchanged. The slight difference in resonant frequencies between

simulation and experiment could be caused by fabrication tolerance and measurement conditions.

4. Conclusion and outlook

In this study, we have proposed and demonstrated a simple approach to achieve an analogue of the intriguing EIT phenomenon. Following the realization in this study, we can now dig deeper into the nature of EIT effect, by using more profound characterization, such as ultrafast laser stimulation and time-resolved studies on short time scales. Then, the time delay due to the dispersion or near-field enhancement caused by high Q-factor resonance can be best understood and utilized. In sensing applications, the former characteristic will enhance the interaction of light with molecular vibrations, especially in the mid-infrared regime, and can be used in surface-enhanced IR absorption (SEIRA) spectroscopy [3] and surface-enhanced Raman spectroscopy (SERS) substrates [4].

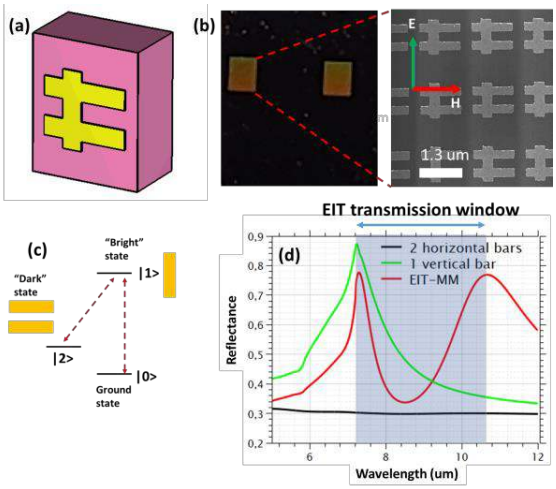


Figure 1. (a) EIT-MM unit cell design; (b) Fabricated sample with gold resonator on silicon wafer; (c) Three-level transition scheme of the EIT effect, (d) Simulated reflectance of individual resonators and EIT-MM in TE mode.

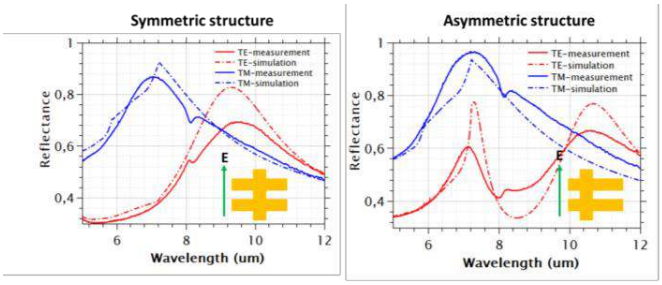


Figure 2. EIT-MM with symmetric and asymmetric geometry, under TM and TE excitation (the direction of **E** field in both insets corresponding to TE mode).

References

1. B. A. Slovick et al., “Generalized effective-medium theory for metamaterials”, Phys. Rev. B 89, 155118 (2014).
2. M. Fleischhauer et al., “Electromagnetically induced transparency: Optics in coherent media”, Rev. Mod. Phys. 77 633–73 (2005).
3. T. Tanaka et al., “Nanostructure-enhanced infrared spectroscopy”, Nanophotonics., 11(11): 2541–2561 (2022).
4. S. Ren et al., "Surface-enhanced Raman scattering from an electromagnetic induced transparency substrate for the determination of hepatocellular carcinoma," Opt. Express 30, 12387-12396 (2022)

Actively Real-time Controllable Metal-Graphene Hybrid Metasurfaces

Fei Han[1,2*], Bart Raes[1], The Linh Pham[1], Nguyen Thanh Tung[3], Xuezhi Zheng[4], Guy A. E. Vandenbosch[4], Joris van de Vondel[1], Niels Verellen[2,1], Ewald Janssens[1]

[1]Quantum Solid-State Physics, Department of Physics and Astronomy, KU Leuven, 3001 Leuven, Belgium
[2]IMEC, 3001 Leuven, Belgium
[3]Institute of Materials Science, Vietnam Academy of Science and Technology, Hanoi, Vietnam
[4]WaveCoRE research group, ESAT, KU Leuven, 3001 Leuven, Belgium
[*]corresponding author: fei.han@kuleuven.be

Abstract: We report on actively controllable metasurfaces by in-situ electrostatic doping of graphene. A resonance tuning of 0.40 um is demonstrated around 7.06 um, allowing for more efficient optoelectronic devices operating under ambient conditions.

Metasurfaces are artificial two-dimensional materials with a periodic pattern of subwavelength-scaled structures, the meta-atoms. Metasurfaces can control the properties (amplitude, phase, polarization and momentum [1]) of the light with which they interact. However, conventional metasurfaces currently made are "passive'', i.e. fixed by the geometric design, and cannot be "actively'' controlled by an external stimulus of thermal, electrical, mechanical, or optical origin [2,3]. In modern photonics, it is highly desirable to develop real-time actively controllable metasurfaces for advanced applications. It has been proved that graphene can be integrated to the nanogaps of metallic plasmonic antennas and leads to the broad tuning of the antenna optical resonance [4]. So far, graphene tunable metasurfaces have been studied without in-situ monitoring of the graphene doping level [5], which is difficult to control in ambient conditions [6]. Here, we experimentally demonstrate electro-optic tuning of a mid-infrared plasmonic resonance using a graphene field effect transistor. The charge carrier concentration of graphene is controlled by a back gate voltage and the electronic transport characteristics are measured with the four-terminal circuit. At the same time, the optical tunability is measured by Fourier-transform infrared spectroscopy (FTIR).

The devices shown in Figure 1a and b consist of a monolayer graphene sheet which was grown by chemical vapor deposition and transferred onto a SiO_2/p^{++} doped Si layer [7]. Reactive ion etching was used to remove unnecessary graphene and the resulting pattern is a rectangular graphene sheet. A plasmonic antenna array was fabricated on the graphene sheet by electron beam lithography (EBL), followed by molecular beam epitaxy (MBE) of 10 nm platinum and 30 nm gold, and lift-off. Also source, drain and four other contacts (10 nm titanium and 200 nm gold) were deposited on top of the graphene sheet by EBL and MBE. For the as-fabricated graphene field effect transistor (GFET), the charge neutral point (CNP) is at -5 V (Figure 1c). The insets show graphene's dispersion relation, where the shaded areas represent the level filling. The reflectance of the hybrid metasurfaces is calculated by the FDTD simulations (Lumerical Solutions, Inc.).

We used in-situ current-voltage (I-V) measurements in the FTIR setup to study the reflectivity of the device for different gate voltages, ranging from -100 V to 100 V. The conductance of graphene is measured in-situ. As shown in Figure 2a (simulation) and b (measurement), the resonance wavelength of the zero-bias system at 7.06 μm could be blue shifted to 6.64 μm by an -100 V applied gate voltage. This shift is due to an increased graphene charge carrier concentration, resulting in a decrease of the real part of graphene permittivity. Figure 2c shows the resonance wavelength as a function of the back gate voltage in both simulations and measurements. A maximum reflectance modulation of ~ 8% is achieved when the device is in resonance, corresponding to the reduced ratio of

the dip reflectance from 60 V to -100 V (Figure 2d). The results are promising for novel on-chip biosensors in the mid-infrared range, as well as for on-chip optical modulators.

We have demonstrated a broad tuning of the resonance of electro-optic metasurfaces based on a GFET configuration. Our four-terminal measurement circuit offers in-situ monitoring of the graphene Fermi level, while obtaining the optical spectrum with FTIR. We anticipate that the combination of a high switching speed and a high Q resonance will not only make graphene metasurfaces suitable for biosensing application, but also provide a perfect platform for efficient optical modulation.

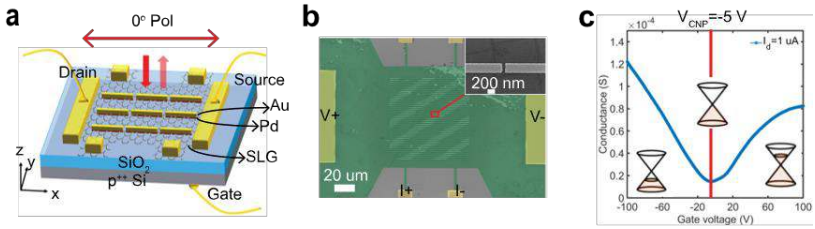


Figure 1. Device configuration and experimental results of a paired nanoantenna array on top of graphene. (a) The schematic of the tunable plasmonic device based on the four-terminal measurement circuits. The material stacks (Au, Pd, graphene, SiO_2 and P^{++} doped Si) are marked with arrows. (b) Scanning electron microscope (SEM) image of the device and a zoomed-in view of the nanoantenna array (antenna length 1.8 um, gap size 80 nm, vertical period 1.8 um). (c) Measured graphene-metal conductance as a function of back gate voltage. The CNP is marked with the vertical red solid line at -5 V.

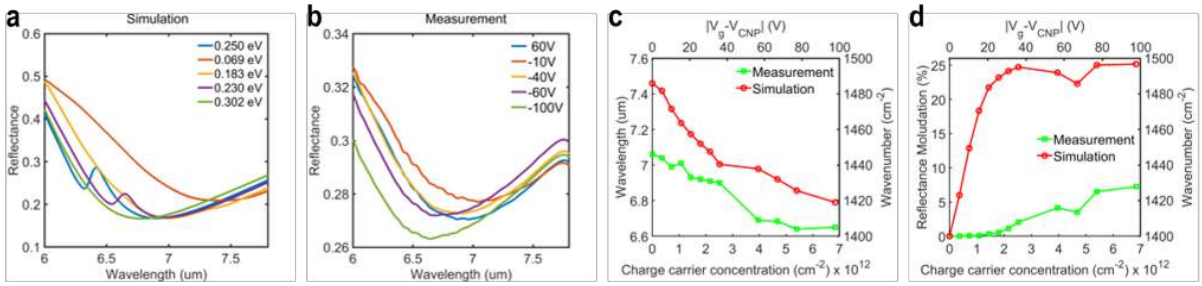


Figure 2. (a) Simulated reflectance as a function of the Fermi energy, which can be tuned by the gate voltage. (b) FTIR measured reflectance from an antenna as a function of the back gate voltage. Color coding is such the Fermi level energies in a correspond to the gate voltages in b. (c) Simulated (red open circle) and measured (green solid square) reflectance dip wavelength. (d) Reflectance on resonance as a function of the gate voltage and the charge carrier concentration. V_g is the back gate voltage, and V_{CNP} is the gate voltage at the charge neutral point during the FTIR spectroscopy measurement.

Acknowledgements

Funding by the China Scholarship Council (CSC) is acknowledged by F. Han.

References

1. Yu, N. et al. “Flat optics with designer metasurfaces,” Nat. Mater., Vol. 13, No. 2, 139-150, 2014.
2. Tittl, A. et al. “A switchable mid-infrared plasmonic perfect absorber with multispectral thermal imaging capability,” Adv. Mater., Vol. 27, No. 31, 4597-4603, 2015.
3. Chen, K. et al. “Infrared Aluminum Metamaterial Perfect Absorbers for Plasmon-Enhanced Infrared Spectroscopy,” Adv. Funct. Mater., Vol. 25, No. 42, 6637-6643, 2015.
4. Yao, Y. et al. “Electrically Tunable Metasurface Perfect Absorbers for Ultrathin Mid-Infrared Optical Modulators,” Nano Lett., Vol. 14, No. 11, 6526-6532, 2014.
5. Dabidian, N. et al. “Electrical Switching of Infrared Light Using Graphene Integration with Plasmonic Fano Resonant Metasurfaces,” ACS Photon., Vol. 2, No. 2, 216-227, 2015.
6. Böttcher, S. et al. “Adsorption of Water and Ammonia on Graphene: Evidence for Chemisorption from X-ray Absorption Spectra,” J. Phys. Chem. Lett., Vol. 8, No. 15, 3668-3672, 2017.
7. J. Scheerder, J. E. et al. “Electronic detection of oxygen adsorption and size-specific doping of few-atom gold clusters on graphene,” Adv. Mater. Interfaces, Vol. 5, No. 24, 1801274, 2018.

Optical characterization of polymer-based Fresnel zone plate probe structures combined with hyperbolic metamaterial by means of SNOM

P. Micek[1*], A. Belosludtsev[2] D. Pudiš[1], D. Pawlak[3], P. Gašo[1], M. Goraus[1]

[1]Dpt. of Physics, University of Zilina, Slovakia
Center for Physical Sciences and Technology, Vilnius, Lithuania
[2]Ensemble[3], Centre of Excellence, Warsaw, Poland
[*]corresponding author: micek@fyzika.uniza.sk

Abstract: This paper presents a novel design of a polymer-based 3D FZP near-field probe with sub-wavelength resolution and significant optical field enhancement with the possibility of implementation of such a device onto the optical fiber

Herein we aimed to optically characterize and compare the near-field emission of a 2D and 3D fresnel zone plate (FZP) structures using both numerical simulation and experimental setup of conventional near-field scanning optical microscope using metal-coated fiber-based pulled probe. The overall conceptualization is based on the fresnel zone plate (FZP) design, where each individual zone influences the phase of the transmitted wave so that they interfere constructively at a given distance of the focal plane [1-2]. The main input parameters characterizing a FZP are its diameter, the focal length, the refractive index of the structure and the incident wavelength. These parameters directly influence the radius of each zone according to equation

$$r_k = \sqrt{\frac{k\lambda_0 f}{n} + \frac{k^2\lambda_0^2}{4n^2}},$$

where k is the integer number, λ_0 is the incident wavelength in vacuum, f is the focal length of the FZP, and n is the index of refraction. The overall design is shown in Fig.1.

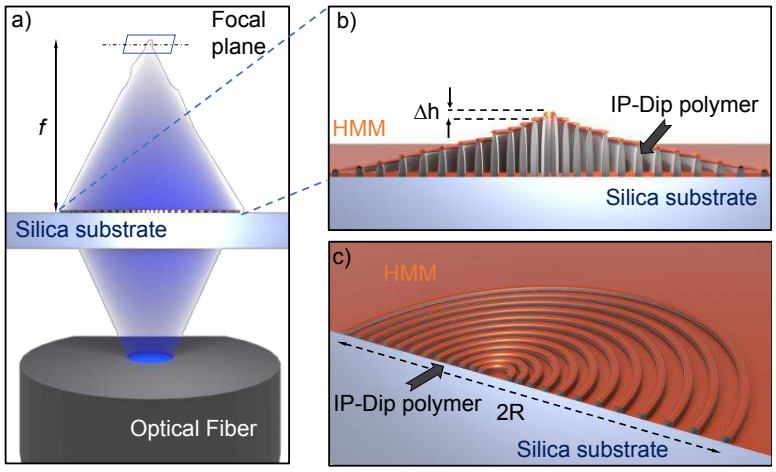


Figure 1: Schematics of the 2D fresnel zone plate design with its a) working principle, b) a simulation of the Poyinting vector distribution at the x-z plane of the 2D fresnel zone plane antenna, c) schematic of the structure physical parameters, with 2R depicting the diameter of the FZP antenna.

The implying structure was designed for λ_0= 420nm, focal length of 300 nm and refractive index of the IP-Dip polymer n= 1,53. The total number of the FZP zones was chosen to be 11, in order to address the previous

documented results of the efficiency gain of FZPs with higher number of zones. The diameter of the whole structure is 12.15 μm, indicated in Fig. 1 c) as the distance 2R, while the height of each individual zone is 760 nm with the HMM included. It is also worth to mention, that we chose to design the structure without the innermost first zone to avoid the effect of undesirable polymerization of the IP-Dip forming a 3D defect documented in our previous study [3]. Fig. 2 documents the topography of both designs as well as the result of the near-field characterization by NSOM.

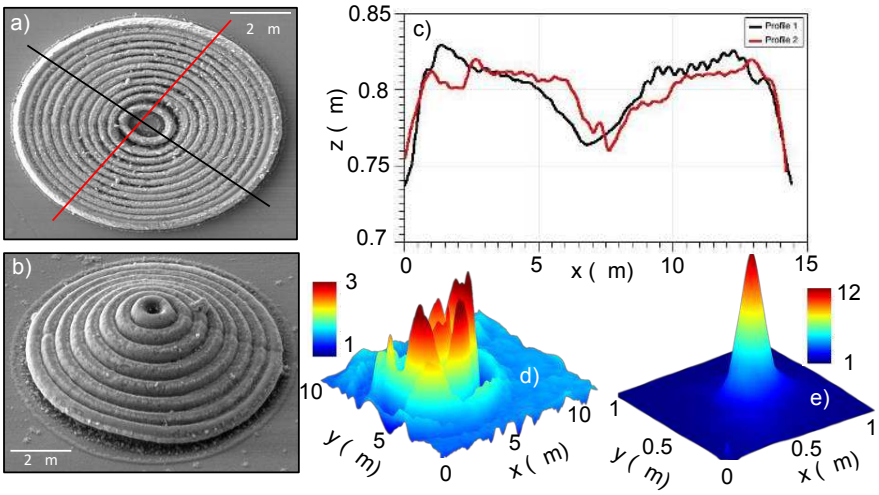


Figure 2: Experimental results of the a) AFM topography measurement of the 2D FZP, b) SEM of the 3D FZP, c) Surface profile lines depicted from a), d) NSOM measurement of the 2D FZP taken above the surface, e) NSOM map of the 3D FZP measured at the apex of the aperture. The color-scale depicts the intensity of the electric field enhancement with respect to the source

The SEM images show clear distinguishable features of the FZPs, however the spacers between the zones are partially filled out after the HMM deposition. It is worth to mention that for the 3D design, the deposition resulted in the formation of subwavelength aperture with diameter of 300 nm, resulting in the suppression of the side-lobes and enhancement of the central peak with FWHM of 0.6λ making a great candidate for a fiber-integration and further optical characterization. Such a probe would prove to be an excellent near-field characterization tool implemented on an optical fiber tip, tuning fork or a cantilever for SNOM.

The authors thank the ‘‘ENSEMBLE3 – Centre of Excellence for nanophotonics, advanced materials and novel crystal growth- based technologies’’ project (GA No. MAB/2020/14) carried out within the International Research Agendas programme of the Foundation for Polish Science co-financed by the European Union under the European Regional Development Fund and the European Union’s Horizon 2020 research and innovation programme Teaming for Excellence (GA. No. 857543) for the support of this work.

References

[1] E. Minerbi, S. Keren-Zur, and T. Ellenbogen, “Nonlinear Metasurface Fresnel Zone Plates for Terahertz Generation and Manipulation,” *Nano Lett*, vol. 19, no. 9, 2019, doi: 10.1021/acs.nanolett.9b01970.

[2] J. Baine, J. Tang, and X. Li, “Polarization-independent metasurface lens based on binary phase fresnel zone plate,” *Nanomaterials*, vol. 10, no. 8, pp. 1–9, Aug. 2020, doi: 10.3390/nano10081467.

[3] P. Micek, D. Pudis, P. Gaso, J. Durisova, and D. Jandura, “Microring zone structure for near-field probes,” *Coatings*, vol. 11, no. 11, Nov. 2021, doi: 10.3390/coatings11111363.

META 2023, PARIS - FRANCE, JULY 18 – 21, 2023

Enhancement of a single molecule triplet depopulation rate by a dielectric nanoantenna

R. Trojanowicz[1], S. Vassant[1*], F. Charra[1]
[1]Université Paris-Saclay, CEA, CNRS, SPEC, 91191, Gif-sur-Yvette, France
[*]corresponding author: simon.vassant@cea.fr

Abstract: In this work, we investigate the effect of a dielectric nanoantenna on a single Terrylene molecule's photon statistics. Nanoantenna increases the excitation intensity and local density of optical states (LDOS), affecting the rates at play in the fluorescence process. Compared to its plasmonic analog, a dielectric antenna introduces low background and no quenching. Experiments show that the nanoantenna increases the efficiency of pumping the lowest-energy triplet state into higher-level triplets by excitation field concentration.

Terrylene in p-terphenyl is a perfect host-guest system for single molecule and nano-antenna studies. Using simple spin-coating one can produce thin films down to sub-30 nm with fluorophores of well-defined orientation that are photostable for hours [1]. Previous studies proved that Terrylene in p-terphenyl has a power-dependent effective triplet lifetime due to additional decay channel such as pumping triplets to higher levels and reversed intersystem crossing (rISC) [2,3]. The influence of a dielectric nanoantenna on the singlet rate was previously reported [4], but to our knowledge, its influence on the intersystem crossing rate and on the triplet depopulation rate are not reported yet.

As dielectric nanoantenna, we use pulled glass fiber with sub-100 nm radius of curvature in Scanning Probe Microscopy configuration (Figure 1. left). We use an inverted microscope coupled to a Hanbury-Brown-Twiss detection scheme with Time-Correlated Single Photon Counting to extract all the rates at play in the photon emission process of single Terrylene molecule, and observe in particular how the presence of the nanoantenna affects the triplet depopulation rate. We perform 3 experiments on each molecule: Terrylene alone (pre-approached), Terrylene with nanoatenna (approached) and again Terrylene alone (post-approached) as nanoantenna effect should be reversible in nature – Figure 1, right.

Terrylene is modeled as 3 level system to extract molecular rates. Via a linear fit of the triplet depopulation power-dependence $k_{31}(P)$ intercept and slope can be extracted – power-independent component corresponds to T1-S0 transition and power-dependent component corresponds to pumping higher triplet states and subsequent rISC.

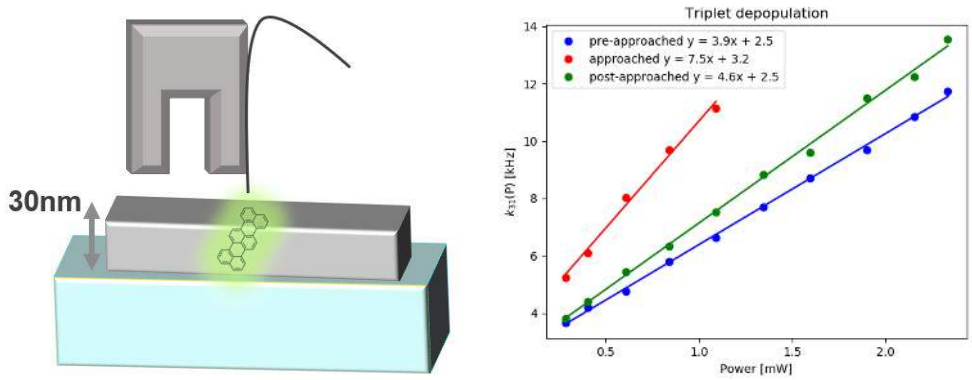


Figure 1. Scheme of set-up: tuning fork with a nanoantenna (glued pulled optical fiber) working in shear-force mode above sub-30 nm thin film of p-terphenyl doped with Terrylene molecules (left). Power-dependence of triplet depopulation rate (k_{31}) for the same molecule with nanoantenna pre-, post- and approached (right).

Across population, we observe around 2-fold reduction in lifetime due to change in LDOS. Power-dependent component in k_{31} and excitation rate k_{12} have similar enhancements of around 2. This indicates an excitation field concentration by the nanoantenna. Small differences between enhancements of these two rates may imply slight misalignment of singlet and triplet transition dipole moments in space. Effect on power-independent component in k_{31} and k_{23} are very small with dispersion across molecules. In some cases, measurements have a slight pre-/post-approach hysteresis that indicates a small modification in those rates (Figure 1, right). This highlights the importance of our measurement protocol as changes in rates can originate from modification of molecule environment by the scanning probe, rather than from nanoantenna effect itself.

This work in funded by the ''Controlled influence of a Plasmonic nano-antenna on a single molecule Instersystem Crossing Rate'' (PlasmonISC; ANR-19-CE09-0009) project.

References

1. Pfab, R.J., Zimmermann, J., Hettich, C., Gerhardt, I., Renn, A. and Sandoghdar, V, "Aligned terrylene molecules in a spin-coated ultrathin crystalline film of p-terphenyl" Chem. Phys. Lett., Vol. 387, 490–495, 2004.
2. Fleury, L., Segura, J.-M., Zumofen, G., Hecht, B. and Wild, U., '' Nonclassical Photon Statistics in Single-Molecule Fluorescence at Room Temperature'' Phys. Rev. Lett, Vol. 84, No. 10, 1148-1151, 2000.
3. Banasiewicz, M., Morawski, O., Wiącek, D. and Kozankiewicz, B., "Triplet population and depopulation rates of single terrylene molecules in p-terphenyl crystal" Chem. Phys. Lett, Vol. 414, No. 4-6, 374–377, 2005.
4. Kühn, S., and Sandoghdar V., "Modification of single molecule fluorescence by a scanning probe", Appl. Phys. B, Vol. 84, 211-217, 2006.

Multiresonant nano-optical trap of Rayleigh particles with coaxial plasmonic apertures

Hipólito A. Arredondo Champi[1,2*], Rina H. Bustamante[1], Daniel R. Cornejo[2], Walter J. Salcedo[1] and José Roberto Castilho Piqueira[3]

[1]Electronic Systems Engineering Department, Polytechnic School of the University of São Paulo, 05508-900, São Paulo, SP, Brazil

[2]Department of Physics of Materials and Mechanics, Institute of Physics of the University of São Paulo, 05508-090, São Paulo, SP, Brazil

[3]Telecommunication and Control Engineering Department, Polytechnic School of the University of São Paulo, 05508-900, São Paulo, SP, Brazil

[*]corresponding author: radeemdlb@usp.br or hyppolite88@gmail.com

Abstract: Resonant nano-optical tweezers based on dielectric, plasmonic and metamaterial nanostructures have been recently proposed to overcome the diffraction limit imposed by conventional optical tweezers. As a result of this innovative approach, it was possible to reduce the confinement volume of the trap (nanometer scale), increase the intensity of the gradient force, and decrease the power of the incident light. However, local and multiresonant isotropic confinement of nanoparticles (NPs), the size limit of the captured NP in the sense of Rayleigh scattering theory, and the modeling of realistic PNOs with the mentioned characteristics still remain major challenges. In this paper, using electromagnetic modeling (FDTD simulations) and dipole approximation, we proposed a multiresonant nano-optical tweezer based on coaxial plasmonic nanoapertures with the ability to trap small nanoparticles smaller than 5 nm.

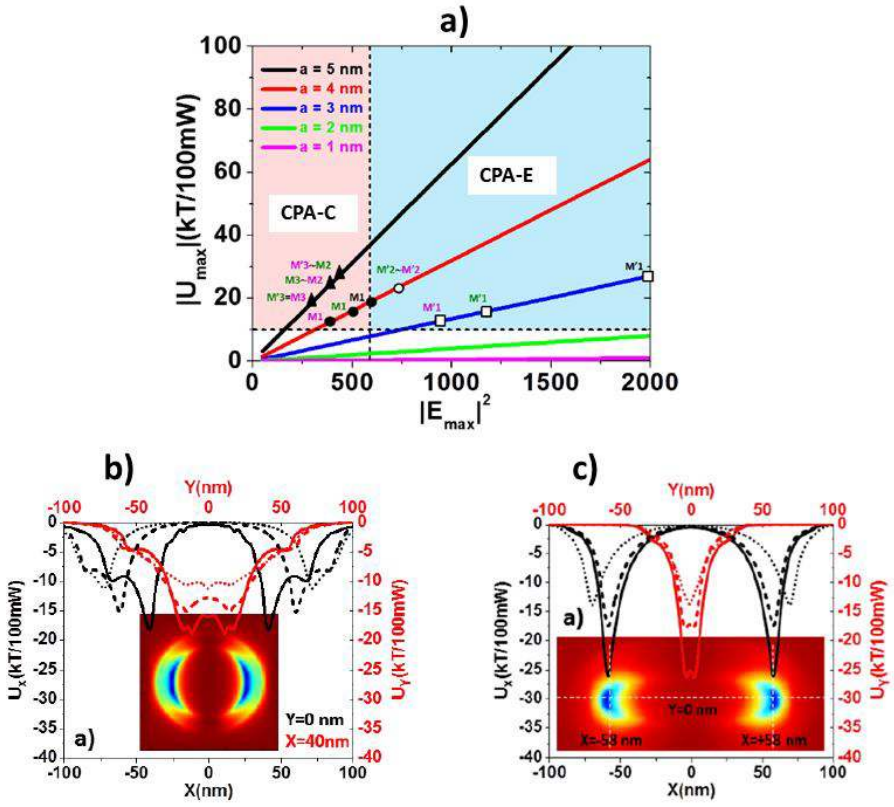


Figure 1

The first theoretical design of an optical tweezer using localized surface plasmons was independently reported by Novotny [1] and Martin [2]. After this proposal of nanoplasmonic optical trapping, many other theoretical and experimental works were developed replacing metallic nanostructures with more complex structures [3-5]. In this sense, a local and stable trapping (via surface plasmons) of Rayleigh particles with diameters up to 10 nm was possible. However, plasmonic optical tweezers for nanoparticles with diameters smaller than 3 nm still face many technical challenges [3,6,7].

Figure 1(a) shows the linear relationship between the absolute value of the minimum optical potential, $|U_{min}|$, and the maximum electric field enhancement factor, $|\mathbf{E}_{max}|^2$, for spherical proteins with radii of 1, 2, 3, 4 and 5 nm. The propagating modes M1 (dipole resonance), M2 (quadrupole resonance) and M3 (sextupolar resonance) belong to a coaxial plasmonic aperture with cylindrical symmetry (CPA-C), whereas the modes M'1, M'2 and M'3 belong to a coaxial plasmonic aperture with elliptical symmetry (CPA-E). Note that Figure 1(a) has been divided into two regions separated by the factor $|E|^2 = 600$ which corresponds to the upper limit of near-field enhancement generated by a CPA-C. Above 600, with an upper limit of 2000, corresponds to a CPA-E.

Figure 1(a) shows the transverse optical potentials U_X and U_Y along the X-axis (for Y = 0) and the Y-axis (for X = ±X0 nm), respectively, for three CAPs-C. The optical potentials were calculated for proteins of 4 nm radius using the M1s modes: CAPs-C1 with $|E|^2 = 600$ and $\lambda_1 = 755$ nm; CAPs-C2 with $|E|^2 = 500$ $\lambda_1 = 900$ nm and CAPs-C3 with $|E|^2 = 340$ and $\lambda_1 = 1027$ nm. These tweezers with two potential wells have an optical potential depth between -17kT/100mW and -11kT/100mW enough to trap proteins of 4 nm radius when the particle approaches the regions of high near-field enhancement.

Finally, in order to show the efficiency of CPAs-E as optical tweezers, Figure 1(c) shows the results of optical trapping of a 3 nm radius protein using the M'1s resonant plasmonic modes of three CPAs-E with eccentricity of 0.9: CAPs-E1 with $|E|^2 = 2000$ and $\lambda_1 = 809$ nm; CAPs-E2 with $|E|^2 = 1200$ and $\lambda_1 = 935$ nm and CAPs-E3 with $|E|^2 = 900$ and $\lambda_1 = 1030$ nm. As can be seen, the X component of the double optical potential, U_X, corresponds to the greater near-field intensification (~2000) and presents a greater depth $U_X = -27$kT/100 mW with a full-width at half-maximum of 10 nm, which indicates a high stability and a high confinement of the protein at the ends of the elliptical nanoaperture.

References

1. NOVOTNY L., BIAN R. X. and XIE X. S. Theory of Nanometric Optical Tweezers, Phys. Rev. Lett. 79, 645, 1997.
2. MARTIN O. J. F., GIRARD C. Controlling and tuning strong optical field gradients at a local probe microscope tip apex, Appl. Phys. Lett. 70, 705, 1997.
3. SALEH A. A. E. and DIONNE, J. A. Toward efficient optical trapping of sub-10 nm particles with coaxial plasmonic apertures, Nano Lett. 12, 5581-5586, 2012.
4. SALEH A. A. E. et al. Grating-flanked plasmonic coaxial apertures for efficient fiber optical tweezers, Optics Express 24, 20593-20603, 2016.
5. YOON, S. J. et al. Nonfluorescent nanoscopic monitoring of a single trapped nanoparticle via nonlinear point sources, Nature Communications 9, 2218, 2018.
6. ZHAN, C. et al. Single-Molecule Plasmonic Optical Trapping, Matter 3, 1-11, 2020.
7. DANESH M. et al. Monolayer Conveyoc for Stably Trapping and Transporting Sub-1 nm Particles, Laser Photonic Rev. 14, 2000030, 2020.

Photothermal and photoelectric nanophotonics

Overcoming color limitation of sub-ambient radiative cooler for full-color expression

Suwan Jeon[1,2], Soomin Son[3], Seokhwan Min[1], Hyeonjin Park[1], Heon Lee[3*], and Jonghwa Shin[1*]

[1]Department of Materials Science and Engineering (DMSE), Korea Advanced Institute of Science and Technology (KAIST), Republic of Korea
[2]Department of Nano Mechanics, Korea Institute of Machinery & Materials (KIMM), Republic of Korea
[3]Department of Material Science and Engineering (DMSE), Korea University, Republic of Korea
[*]corresponding author: heonlee@korea.ac.kr, qubit@kaist.ac.kr

Abstract: The lack of color diversity is the fundamental problem inherent in the radiative cooling system, which raises practical issues of eye safety, light pollution, and aesthetics. In this work, we show a breakthrough for colored radiative cooling by experimentally demonstrating that sub-ambient cooling under direct sunlight is possible for all colors, including black. The key principle is thermal non-equilibrium between color and cooling parts, which can potentially serve as a new avenue for radiative cooling applications requiring diverse color expression.

In recent years, radiative cooling has emerged as a promising approach to alleviate power consumption driven by cooling demand, with no carbon emission. Despite intensifying interest in the carbon-free cooling system, the lack of color diversity is a critical obstacle for outdoor applications of radiative cooling to commercial buildings and residential houses; because the ultra-bright appearance (mostly in white [1], or silvery colors [2]) of current radiative cooling materials raises questions of eye safety, light pollution, and aesthetics. Based on similar concerns, several countries have already banned the use of highly reflecting materials in buildings [3], which makes current radiative cooling materials and schemes inapplicable.

Here, we propose a novel radiative cooling system, recently published in Ref. 4, that can express arbitrary colors while being cooled below the ambient temperature during all daytime. Experimentally, we present that radiative cooling systems with dark colors (black and red) absorbing solar power over 640 Wm^{-2} (which far exceeds the fundamental cutoff of ~110 Wm^{-2}) reach sub-ambient temperatures with the average cooling over 3.5 K in the daytime. We emphasize that the thermal effect of atmospheric non-radiation, which normally serves as heating, is flipped in our case to improve sub-ambient cooling performance.

This counter-intuitive result is possible by separating the color and cooling parts and inducing non-equilibrium between them (Fig. 1). In our system, the thermal emitter releases radiative heat toward the outer space while being decoupled from the sunlight by the color part. The middle part is composed of high thermal resistive material, which allows a steep temperature gradient. Due to this non-equilibrium configuration, the thermal emitter can maintain a sub-ambient temperature even under the perfect solar absorption condition of the color part, unlike the previous isothermal emitter.

Building upon theoretical study for non-equilibrium systems, we built colored radiative cooling systems for black and red (Fig. 2). The color part is optimally designed as a multi-layer stacking composed of germanium and zinc sulfide on a germanium substrate. The cooling part is designed with PDMS and Al foil, which works as a broadband emitter. These two parts are separated by a thermal-resistive wall that is mostly filled with air. The outdoor measurement results show that, as expected, the emitters with black and red exteriors cool by an average of 3.7 K and 3.5 K compared to daytime ambient temperature.

Further examination of the same principle [4] also confirms the feasibility of other colors (e.g., blue, green,

cyan, magenta, and yellow) and the reliability of the experimental results over a longer period (~ 3 days). Based on reproducible and consistent cooling results with diverse exterior colors, we envision that our work would be a complete and general solution to practical applications that require both carbon-free cooling and aesthetics.

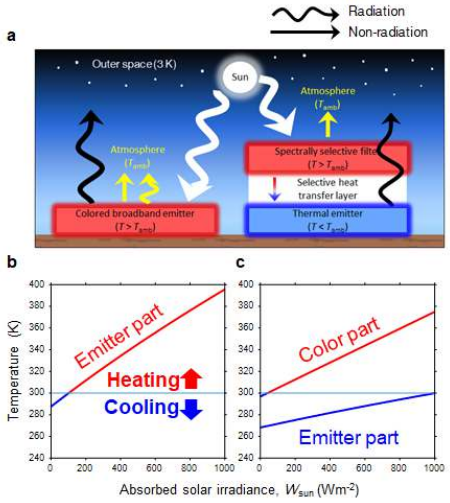


Figure 1. Colored radiative cooling system. (**a**) Schematic of the radiative cooler for isothermal and non-isothermal design, in which radiatively and non-radiatively interact with the surroundings. The steady-state temperature of (**b**) isothermal design and (**c**) non-isothermal design depending on the absorbed solar irradiance.

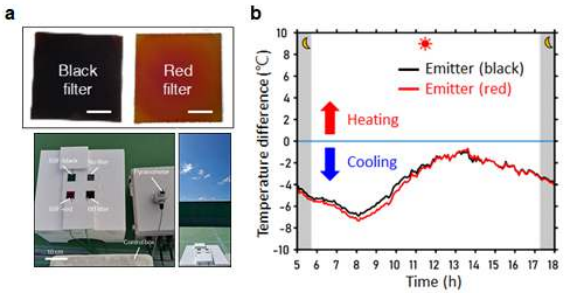


Figure 2. Outdoor measurement results. (**a**) Photographic images for spectrally selective filters colored in black and red, and for measurement setup. (**b**) Measured temperatures of the thermal emitter compared to the ambient temperature.

Acknowledgements: This work was supported by the National Research Foundation of Korea (NRF) Grant funded by the Korea government (MSIT) (Nos. 2018M3D1A1058998, 2021R1A2C2008687, and 2020R1A2C3006382) and by the Nano Material Technology Development Program of Ministry of Science and ICT (2022M3H4A1A02046445).

References

1. A. P. Raman, M. A. Anoma, L. Zhu, E. Rephaeli, S. Fan. “Passive radiative cooling below ambient air temperature under direct sunlight”, Nature, Vol. 515, No. 7528, 540–544, 2014.
2. J. Kou, Z. Jurado, Z. Chen, S. Fan, A. J. Minnich. “Daytime radiative cooling using near-black infrared emitters”, ACS Photonics, Vol. 4, No. 3, 626–630, 2017.
3. City of Singapore, Building Control Act - Chapter 29, https://sso.agc.gov.sg/SL/BCA1989-S666-2003.
4. S. Jeon, S. Son, S. Min, H. Park, H. Lee, & J. Shin. “Daylong Sub-Ambient Radiative Cooling with Full-Color Exterior Based on Thermal Radiation and Solar Decoupling”. Advanced Optical Materials, 2202129, 2022.

Surface absorbers for thermomechanical bolometers

B. Bertoni[1]*, L. Vicarelli[2], S. Zanotto[2]*,
S. Roddaro[1,2], A. Tredicucci, and A. Pitanti[2]

[1]Dipartimento di Fisica, Università di Pisa, Largo B. Pontecorvo 3, Pisa, Italy
[2]NEST Lab., CNR Istituto Nanoscienze, piazza San Silvestro 12, Pisa, Italy
* b.bertoni@studenti.unipi.it , simone.zanotto@nano.cnr.it

Thermomechanical bolometers based on high-quality mechanical resonators are a promising technology for broadband light detection. Further functionalities can be added by controlling the absorption spectrum of the devices. To this end, we embedded (almost-) 2D layers, minimally impacting the mechanical quality while, at the same time, offering strong absorbance. Further layer patterning could grant resonant absorption, for hyperspectral imaging or polarization sensitive detection.

Thermomechanical bolometers (TB) detect radiation by measuring the thermal shift in the resonant frequency of a microresonator when heated up trough light absorption [1]. The main shift contributions come from thermal expansion and tensile stress reduction of the materials constituting the suspended mechanical resonator, granting for room-temperature operation of the devices. Here, as a further progress, we will introduce smart absorbers, capable of enhancing thermomechanical detection without impacting on the mechanical quality of the resonator. Weightless and stiff 2D materials, which can also be patterned for complex light control, are the perfect candidates to this end.

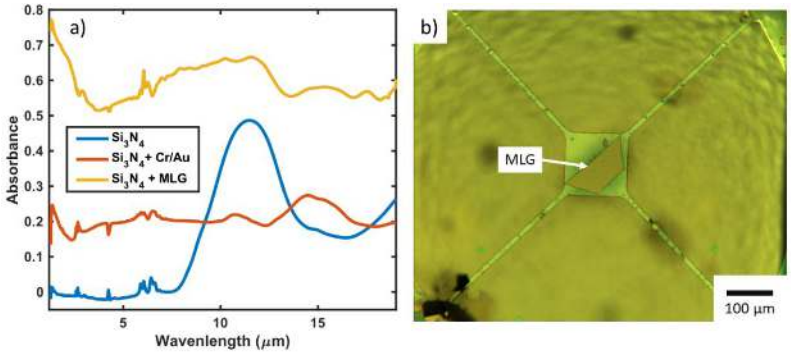


Figure 1: a) Absorbance of bare, Cr/Au and MLG coated Si_3N_4 membranes. b) Microscope image of a graphene flake on a Si_3N_4 trampoline

We considered multi-layer graphene (MLG) obtained from graphite mechanical exfoliation with the 'Scotch tape method' [2] as a first candidate. We prepared a set of homogeneous, 300 nm thick, silicon nitride membranes covering some of them with a 3/15 nm Cr/Au film. Furthermore, we successfully transferred MLG onto some of them, using a PMMA/PVA vector, as detailed in [3]. The membrane absorbance in the mid-infrared range was measured via FTIR spectroscopy and reported in Fig.1a. While the bare Si_3N_4 material gives a sharp absorption peak around 11 μm wavelength (with negligible absorption elsewhere), the metal film shows a flat absorbance

of about 20% in the investigated spectral region. Conversely, MLG exhibits large and broad absorbance, up to 60% in the whole frequency range. Promising, the MLG can also be transferred on patterned membranes, which constitute the core device for thermomechanical bolometers. The microscope image of Fig. 1b shows, as an example, a roughly 100 μm x 50 μm MLG flake deposited on the central plate of a trampoline resonator. While the main limit of exfoliation lies in the non-deterministic nature of available thickness and size of the flakes, other techniques based on pyrolyzed polymers [4] can overcome this issue and grant for reliable and large-scale fabrication.

An intriguing possibility of further optimization considers a complex patterning of the smart absorbers. By defining an artificial surface with the introduction of subwavelength and periodic scattering centers (metasurface), it is possible to implement selective absorption, creating hyperspectral detectors. More complex geometries can give rise to new functionalities. Chiral scatterers couple preferentially with selected polarization state of light and can be employed for polarimetry based on selective absorption [5]. As described in the sketch of Fig. 2, an interesting scenario would see the use of polarization sensitive TBs, which could respond to circular right polarization while being insensitive to illumination with circular left one.

With the technological possibility of electrical read-out, large scale fabrication and video rate operation, arrays based on TBs with smart absorbers could realize a promising technology for field applications requiring detection of mid- and far-infrared light, with use in security, healthcare and quality control.

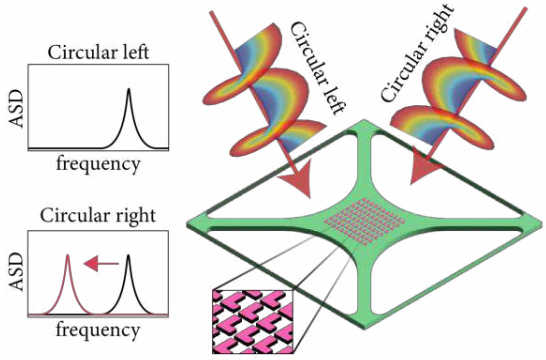


Figure 2: Perspective for metasurface-based thermomechanical bolometers.

References

1. Vicarelli, L., A. Tredicucci and A. Pitanti, "Micromechanical bolometers for subterahertz detection at room temperature", *ACS Photonics*, 9, 2, 360–367, 2022.
2. Novoselov, K. S., D. Jiang, F. Schedin, T. J. Booth, V. V. Khotkevich, S. V. Morozov, and A. K. Geim, "Two-dimensional atomic crystals", *PNAS*, 102, 30, 10451–10453, 2005.
3. Giambastiani, D., C. Tommasi , F. Bianco, F. Fabbri , C. Coletti , A. Tredicucci, A. Pitanti , and S. Roddaro, "Strain-engineered wrinkles on graphene using polymeric actuators", *Phys. Rev. Applied*, 18, 024069, 2022.
4. Kaplas, T. and P. Kuzhir, "Ultra-thin pyrocarbon films as a versatile coating material", *Nanoscale Res. Lett.*, 12, 121, 2017
5. Zanotto, S., A. Tredicucci, D. Navarro-Urrios, M. Cecchini, G. Biasiol, D. Mencarelli, L. Pierantoni, and A. Pitanti, "Optomechanics of Chiral Dielectric Metasurfaces", *Adv.OpticalMater.*, 8, 4, 1901507, 2020.

Designing tunable, broadband absorber/emitter using epsilon near zero media

Sraboni Dey* **and J. Mitra**

School of Physics, Indian Institute of Science Education and Research, Thiruvananthapuram, India-695551
*corresponding author: srabonidey20@iisertvm.ac.in

Abstract: Customizing the optical response of surfaces, using subwavelength thick coatings is an area of topical interest. The advent of novel materials like ENZ materials along with the capability of nanostructuring has enabled realization of new design strategies to control absorption/emission properties over broad spectral ranges. We present a straightforward design using a multilayer ITO/SiO_2/Au coating which shows wide-angle absorption over tunable broadband regimes.

Introduction

Recently, perfect broadband absorption and emission have drawn significant attention in optical devices. Engineered metal-insulator-metal (MIM) structures, gratings, meta-materials [1], etc. have been shown to be crucial in tailoring different aspects of emission including directionality and spectral efficiency with applications in various fields, from solar energy harvesting to photo-thermal cooling [2]. Further, the advent of nanofabrication tools has provided novel pathways to engineer coatings with periodic subwavelength structures and thickness that result in highly isotropic optical responses, over broad spectral ranges. Evidently, the choice of materials plays an integral role in effecting such control and epsilon-near-zero (ENZ) materials has been at the forefront of research in the area. ENZ materials undergo optical dielectric to metal transition at a particular wavelength known as the ENZ wavelength (λ_{ENZ}) at which the real part of permittivity goes to zero [4,5]. Phenomena like perfect absorption, strong electric field enhancements and giant optical nonlinearities are realized in this regime [3], which can be harnessed to enable selective light absorption and emission.

In this work, we have discussed a straightforward approach to simulate a broadband absorber/emitter employing a 200 nm bi-layer coating of dielectric (SiO_2) on metal (Au) on a transparent glass (NBK7) substrate, decorated with a grating of an ENZ material (ITO). The results show that the system has above 90% absorption in the wavelength window 1310 - 2125 nm and very low absorptance of ~ 10% elsewhere. The coating design is shown to be elemental in achieving the desired absorption/emission spectral response that is independent of the angle from 0° - 60°. Further, the absorption window can be tuned to higher wavelengths leveraging the tunable λ_{ENZ} of ITO.

Results and Discussions

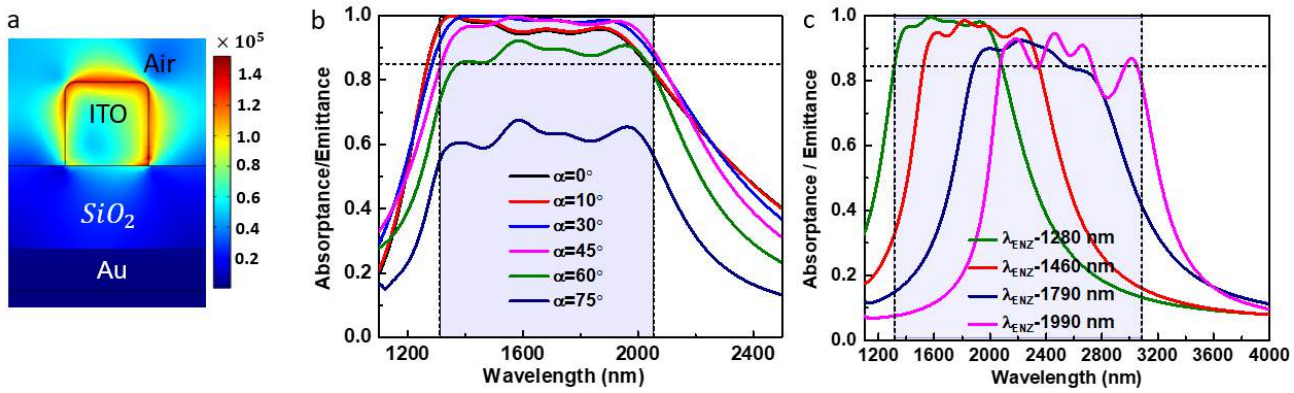


Figure 1: (a) Simulated electric field at λ=1450 nm, (b) Simulated absorptance spectra for different angles of incidence (0º, 10º, 30°, 45°, 60º, 75°), b. Simulated absorptance spectra for the broadband absorber system for different λ_{ENZ} (1280 nm, 1460 nm, 1790 nm, 1990 nm) of ITO at 45° oblique angle of incidence.

The multilayer structure optimization and the simulations were conducted using a finite element method solver in COMSOL® Multiphysics 5.3a. The structure consists of a periodic array of ITO nano-ridges on the top and gold as the back reflector separated by a SiO_2 layer as shown in Fig 1a. The optical properties of ITO can be modeled using the Drude model that connects the λ_{ENZ} with the electron density in ITO, which can be reversibly controlled by various means [4]. Figure 1b shows the simulated spectral response for the multilayer structure for ITO with λ_{ENZ} = 1280 nm, that is very weakly dependent on the angle of incidence or emission, between 0 - 60º. The strong absorption, selectively in the 1310 - 2125 nm wavelength range is understood to be brought about by the plasmonic response of the ITO nano-ridge array in its metallic regime, facilitated by the refractive index contrast provided by the underlying SiO_2/Au layers. To obtain a comprehensive picture of the phenomena, the λ_{ENZ} of ITO was changed to 1460nm, 1790 nm, and 1990 nm, the response for which is shown in figure 1c. Evidently, the multilayer supports a high absorption/emission spectral window (~ 800 nm) that is readily tunable in the near IR regime and is potentially elemental in various photo-thermal applications.

Acknowledgments

JM acknowledges financial support from SERB, Govt. of India (CRG/2019/004965). SD acknowledges DST INSPIRE for the doctoral fellowship and IISER Thiruvananthapuram for the research facilities.

References

1. Landy, N. I., Sajuyigbe, S., Mock, J. J., Smith, D. R., & Padilla, W. J. Perfect metamaterial absorber. *Physical Review Letters*, *100*(20), 1–4,2008.
2. Sergeant, N. P., Agrawal, M., & Peumans, P. High-performance solar-selective absorbers using coated sub-wavelength gratings. *Optics Express*, *18*(6), 5525, 2008.
3. Vassant, S., Archambault, A., Marquier, F., Pardo, F., Gennser, U., Cavanna, A., Pelouard, J. L., & Greffet, J. J. Epsilon-near-zero mode for active optoelectronic devices. *Physical Review Letters*, *109*(23), 1–5, 2012.
4. Johns, B., Puthoor, N. M., Gopalakrishnan, H., Mishra, A., Pant, R., & Mitra, J. Epsilon-near-zero response in indium tin oxide thin films: Octave span tuning and IR plasmonics. *Journal of Applied Physics*, *127*(4),2020.
5. Johns, B., Chattopadhyay, S., & Mitra, J. Tailoring Infrared Absorption and Thermal Emission with Ultrathin-film Interferences in Epsilon-Near-Zero Media. *Adv Photonics Research*, *2100153*, 1–9, 2022.

Plasmon-enhanced photovoltaics, photocatalysis, and solar fuels

META 2023, PARIS - FRANCE, JULY 18 – 21, 2023

Pd nanoparticles as Visible and near-IR plasmonic catalysts

Y. Yokota*, A. Fujita and M. Abe

Sophia Univ., Japan
*corresponding author: y_yokota@sophia.ac.jp

Abstract: Pd nanoparticles are used as catalysts for organic chemical reactions and exhibit higher catalytic activity than commercial Pd catalysts. In this study, we have prepared Pd nanoparticles by liquid-phase synthesis and and investigated their optical properties. The optical properties of Pd nanoparticles depending on shape and size, and the reaction kinetics of model reactions were compared.

Transition metal Pd nanoparticles exhibit high catalytic activity in coupling reactions to their large surface area and can store hydrogen on their surface[1), 2)]. Noble metal nanoparticles interact with light to induce localized surface plasmon resonance (LSPR), which is affected by the type of metal. The effect on LSPR is related to the dielectric in the bulk metal, with the real part of the dielectric being less negative than in gold or silver. Although Pd nanoparticles have weaker LSPR electric field enhancement, the new plasmon-enhanced fields, which are characteristic of Pd, have potential applications in photocatalysis and energy storage and conversion. In this study, Pd nanocubes (PdNCs) were synthesized in the liquid phase and their plasmon optical properties were investigated. The kinetics of the p-nitrophenol reduction reaction was also compared as a model reaction.

PdNCs were synthesized seed-mediated method. The morphology of PdNCs was observed by Scanning electron microscopy (SEM). The synthesized PdNCs were dispersed in aqueous solution, and the absorption spectra were measured with an ultraviolet-visible spectrophotometer. The synthesized PdNCs were used as a catalyst for the reduction of *p*-nitrophenol in aqueous solution with an excess of $NaBH_4$. The reaction was carried out in the dark and under Xe lamp irradiation (wavelength: 440 nm-740 nm).

Fig. 1(a) and 1(b) show SEM images of the synthesized PdNCs with CTAB and PVP, respectively. When CTAB was used as a protector of nanocubes, the average side length was 61 nm. In addition to the cubes, about 16% of the Pd nanorods were also formed. The average side length of PdNCs with PVP was 55 nm and a larger percentage of rounded cubes were formed than PdNCs with CTAB. The absorbance of PdNCs in aqueous solution is shown in Fig. 1(c). PdNCs with PVP have a single peak at 380 nm. Multiple plasmon resonance peaks were observed for PdNCs with CTAB; the peak around 400 nm is from the cube and the peak at 520 nm is from the long axis of the nanorods.

Fig. 2 shows the time-dependent absorption spectra of p-nitrophenol reduction catalyzed by PdNC synthesized in the dark. p-Nitrophenol becomes *p*-nitrophenoxide ion due to the addition of $NaBH_4$ and stirring, and the reaction time is 0 s. Because the solution is an aqueous solution with pH above 10, p-nitrophenol becomes p-nitrophenoxide ion and has an absorption peak at a wavelength of 400 nm with an absorption peak at 400 nm. The peak decreased with reaction time when PdNS of either surfactant was used as a catalyst. In the case of CTAB, the peak at 300 nm increased, while in the case of PVP, an absorption peak at 310 nm appeared at 240 s reaction time, and its intensity decreased with time with a blue shift, until a peak at 300 nm appeared at the end of the reaction. The peak of 310 nm is derived from the reaction intermediate, *p*-hydroxylaminophenol. The *p*-nitrophenol reduction reaction can be regarded as a pseudo-

first-order reaction, and the rate constants were determined from the slope of the approximate straight line. The reaction rate constants of PdNS with PVP were little changed by dark and light irradiation. In the case of CTAB, the value of the reaction rate constant was about three times larger under light irradiation than in the dark. The results of reduction reactions at different reaction temperatures will also be presented on the same day.

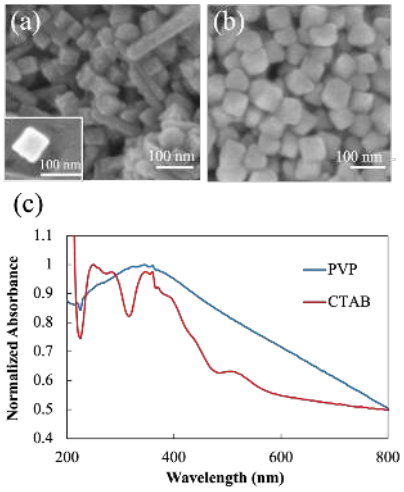


Fig. 1 SEM images of PdNCs with (a)CTAB and (b)PVP. (c) Absorption spectra of PdNCa dispersed in aqueous solution.

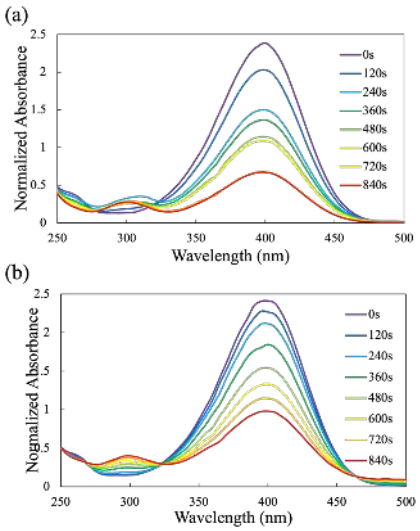


Fig. 2 SEM images of PdNCs with (a)CTAB and (b)PVP. (c) Absorption spectra of PdNCa dispersed in aqueous solution.

References

1. F. Wang, et al., “Porous Single-Crystalline Palladium Nanoparticles with High Catalytic Activities”, Angew. Chem. Int. Ed., Vol. 51, No. 20, 4872 –4876, 2012.
2. L. J. T. Metzroth et al., “Accelerating Hydrogen Absorption and Desorption Rates in Palladium Nanocubes with an Ultrathin Surface Modification,” Nano Lett., Vol. 21, No. 21, 9131–9137, 2021.

META 2023, PARIS - FRANCE, JULY 18 – 21, 2023

Cathodoluminescence spectroscopy of Au dendritic structures for photocatalysis applications

Z. Fusco[1], A. Riaz[1], C. David[2], F. J. Beck[1]

[1]School of Engineering, College of Engineering and Computer Science, Australian National University, Acton, ACT 2601, Australia

[2]Institute of Condensed Matter Theory and Optics, Abbe Center of Photonics, Friedrich Schiller University of Jena, Max-Wien-Platz 1, 7743 Jena, Germany

*corresponding authors: zelio.fusco@anu.edu.au, fiona.beck@anu.edu.edu

Abstract: Metallic nanostructures supporting plasmonic resonances offer potential for efficient spectroscopy and photocatalysis. Here, we fabricate hierarchical Au dendrites and map their plasmonic properties using cathodoluminescence spectroscopy. We demonstrate a controllable hot-spot density and show a correlation between the spatial and spectral distribution of resonances and their morphology. Their performance as both SERS substrates and as photocatalysts is investigated, revealing large SERS enhancements with high hot-spot density and high photocatalytic yields with low hot-spot density. These findings provide insights for the rational design of plasmonic architectures for various applications.

The field of plasmonics has emerged as a promising platform for enhancing light-matter interactions, offering the potential to manipulate light at the nanoscale with unprecedented precision. In particular, metallic nanostructures with complex three-dimensional geometries, have attracted significant attention due to their large surface areas, broadband absorption and multiple resonances, making them attractive candidates for a variety of applications, including photocatalysis and spectroscopy[1].

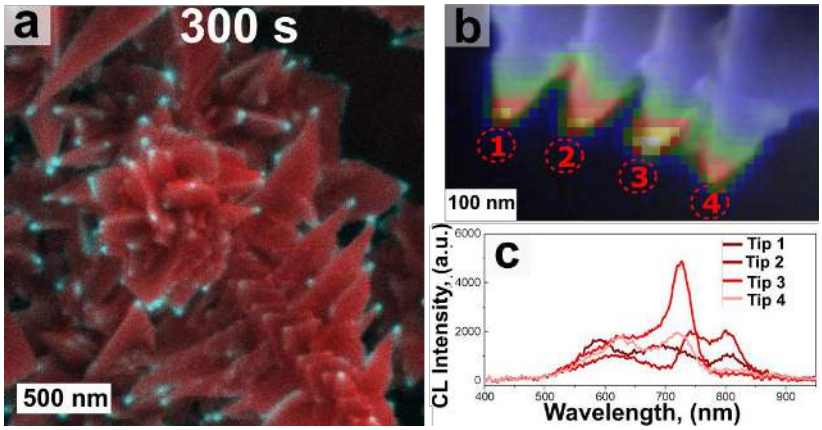


Figure 1. a) CL emission superimposed on the image of a 3D Au dendritic structure. b-c) Panchromatic CL map and spectral distribution of CL emission of a Au dendritic structure, respectively.

In this study, we mapped the spatial and spectral distribution of plasmon hot-spots in 3D complex Au structures with nanometric resolution, using cathodoluminescence (CL) spectroscopy[2]. Hierarchical Au dendrites were deposited over centimeter-scale conductive substrates by a single-step electrodeposition technique, which allows statistical control of the morphology by modifying the electrodeposition time. The resulting structures had self-similar properties, high curvature regions, and multibranched architectures that result in broadband visible and near-infrared absorption. These structures support a multitude of plasmon resonances in the wavelength range of 400–900 nm, which strongly correlate with the local morphology of the network. We demonstrate that

the hot-spot density correlates with morphology, increasing by more than threefold as the deposition time increased from 100 to 400 s. Boundary element method simulations on simplified geometries supported the experimental results and showed that the plasmon modes supported by the complex morphologies are determined by the details of the local geometry of sharp features.

We studied the performance of these dendrites as surface-enhanced Raman scattering (SERS) substrates for the detection of parts-per-million concentration of methylene blue (MB) and as photocatalysts, by monitoring the N-demethylation reaction of MB. Architectures with higher hot-spot density resulted in better SERS detection, while a lower hot-spot density led to improved reaction yields, indicating that the hot-spot density alone is not sufficient to optimize the photocatalytic performance of plasmonic substrates. This highlights the importance of considering the spectral distribution of plasmon resonances in the design of plasmonic architectures for photocatalysis, which can modify the hot electron generation efficiency.

Building on the insights gained from our investigation of hierarchical Au dendrites in promoting the N-demethylation reaction, we are exploring the possibility of these structures for achieving selective CO_2 photoreduction. In summary, supported by experimental results and theoretical analysis, this work provide insights for the rational design and realization of efficient and selective plasmon-mediated photocatalysis.

Acknowledgments: *The authors acknowledge the financial support by the Australian Research Council, through the Discovery Early Career Researcher Award DE180100383 awarded to FJ Beck and the International Research Training Group IRTG 2675: META-ACTIVE.*

References

1. Ron, R., M.S. Zielinski, and A. Salomon, *Cathodoluminescence Nanoscopy of 3D Plasmonic Networks.* Nano Letters, 2020. **20**(11): p. 8205-8211.
2. Fusco, Z., et al., *Cathodoluminescence Spectroscopy of Complex Dendritic Au Architectures for Application in Plasmon-Mediated Photocatalysis and as SERS Substrates.* Advanced Materials Interfaces, 2023. **10**(3): p. 2202236.

Synergistic Photonic and Morphology Design of Solar Powered Redox Cells

Jiaming Ma[1], Kiseok Oh[1], Giulia Tagliabue[1]*

[1] Laboratory of Nanoscience for Energy Technologies (LNET), STI, École Polytechnique Fédérale de Lausanne, 1015 Lausanne, Switzerland

*corresponding author: giulia.tagliabue@epfl.ch

Abstract

Solar powered redox cells (SPRC) offer compelling opportunities for large-scale and long-term storage of solar-energy and have thus attracted increasing attention[1-3]. Yet, to date, photoelectrodes suffer from poor light absorption and limited charge transport [4,5]. While efforts have primarily focused on heterostructure engineering, the potential of synergistic morphology and photonic design has not been carefully investigated. In our work, we study the wavelength-dependent effects of light-absorption and charge transfer characteristics on the performance of gold decorated TiO2-based SPRC photoanodes operating with RFB-compatible redox couples[6]. On one hand, engineering nm-scale TiO_2 semiconductor can increase the light absorption because of its good light scattering property and maximize charge carrier collection as the semiconductor size is comparable to the charge carrier mean free path. On the other hand, metallic nanostructure supporting plasmon resonances can help overcome light-absorption limitations and suppress charge recombination due to it acting as intermedia between semiconductors and hot charge carries. Using an in-depth optical and photoelectrochemical characterization of Au/TiO2 based SPRCs, including IPCE and IQE measurements, we are able to disentangle the roles of charge generation, charge transport and charge collection in these photoanodes. Ultimately, we demonstrate that the synergistic effect of nm-scale semiconductor and plasmonic design can greatly improve optical and photoelectrochemical performance.

More specifically, we report an in-situ directly growing TiO_2 nanotubes on FTO substrate with plasmonic Au nanoparticles coating. The nanotubes have an ultrathin thickness (10 nm) with length range from 1.2 -1.5 um, which possess more electrode/electrolyte interface and higher electrochemical active surface area, as well as creating more sites for plasmonic structure. Benefiting from its morphology, the charge transfer distance in those nanotubes is comparable to the mean free path of electrons, which can enhance the photo-generated carrier separation. Meanwhile, the plasmonic Au nanoparticles not only provide extra light absorption in visible range but also enhance the catalytic activity across the whole spectrum, thus improving incident photon to current efficiency. In particular, we achieve a high photocurrent at 0.098 mA/cm^2 with an interior stability during long time photo-charging process in an H-cell under no bias. The incident photon to current efficiency (IPCE) is also superior to non-modified TiO_2 showing a high value of 54.7%, indicating the role of plasmonic nanoparticles in SPRC. This design is expected to be a potential candidate for the rechargeable solar-energy technologies such as solar redox flow batteries.

Reference

1. Cao, L., Skyllas-Kazacos, M. & Wang, D.-W. Solar Redox Flow Batteries: Mechanism, Design, and Measurement. Adv. Sustain. Syst. 2, 1800031 (2018).

2. Zhou, Y. et al. Efficient Solar Energy Harvesting and Storage through a Robust Photocatalyst Driving Reversible Redox Reactions. Adv. Mater. 30, 1802294 (2018).

3. Azevedo, J. et al. Unbiased solar energy storage: Photoelectrochemical redox flow battery. Nano Energy 22, 396–405 (2016).

4. Zeng, Q. et al. Integrated Photorechargeable Energy Storage System: Next-Generation Power Source Driving the Future. Adv. Energy Mater. 10, 1903930 (2020).

5. Li, W. & Jin, S. Design Principles and Developments of Integrated Solar Flow Batteries. Acc. Chem. Res. 53, 2611–2621 (2020).

6. Ma, J., Oh, K., Tagliabue, G. Understanding Wavelength-Dependent Synergies between Morphology and Photonic Design in TiO2-Based Solar Powered Redox Cells, JPhysChem C, 127, 1, 11–21 (2023).

Layer transfer of multispectral plasmonic absorbers onto graphene for enhanced selective photo-absorption

H. S. Park[1,2], G. W. Hwang[1], J. K. Park[1], J. Y. Kwak[1], D. S. Jeong[2], and K.-S. Lee[1*]

[1]Center for Neuromorphic Engineering, Korea Institute of Science and Technology, Seoul 02792, Korea
[2]Department of Materials Science and Engineering, Hanyang University, Seoul 04762, Korea
[*]corresponding author: kslee21@kist.re.kr

Abstract: In this study, we demonstrate a high-quality transfer method for a multi-periodic array of plasmonic nanodiscs onto a graphene monolayer by carefully adjusting the surface tension of a water-ethanol mixture. Our analysis using optical microscopy, scanning electron microscopy, and optical spectrum measurements revealed little difference compared to those formed by direct patterning. We observed multispectral selective enhancement of photo-absorption at resonant wavelengths corresponding to each period of the plasmonic absorber array.

The lithographic fabrication of plasmonic nanostructures on graphene hindered by the lack of interfacial chemical bonding, and may even cause surface damage and contamination, leading to the deterioration of their functionality. Layer transfer technique offers a great alternative to this issue. However, the hydrophobic nature of graphene surface requires careful consideration of interfacial wetting properties to prevent bursting or defect formation during the drying process, and to obtain uniformly transferred plasmonic nanostructures over a large area. We used a water-ethanol mixture as a transfer liquid in the convention PMMA support wet transfer method to improve the wettability on the graphene layer by reducing the surface tension of the liquid. We found that the optimum condition was achieved with approximately 0.3 moles of ethanol, and any additional amount of ethanol would cause the PMMA film to sink. Figure 1 compares photographs of layer-transferred plasmonic nanodiscs arrays on hydrophobic Si substrates using deionized water (a) and a 0.3 mole ethanol-water mixture. Optical microscopy images before PMMA support layer removal are shown in (b) and (f), while (c) and (g) display the images after removal.

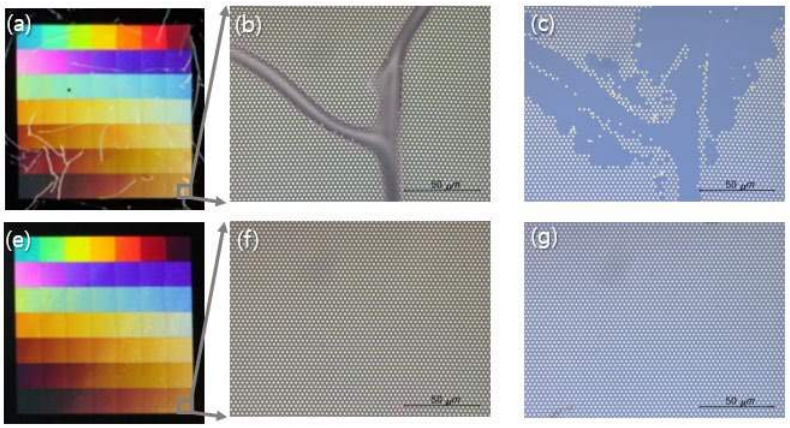


Fig. 1. Photographic images of multispectral plasmonic nanodiscs absorbers layer-transferred onto Si substrates using deionized water (a) and a 0.3 mole ethanol-water mixture (e), along with optical microscope images before (b, f) and after (c, g) PMMA support layer removal.

Using the optimum condition, a multi-periodic array of plasmonic nanodiscs was transferred onto a Si substrate coated with a graphene monolayer, and the optical absorption spectra were compared between samples with and without graphene layer inserted between the nanodiscs and Si substrate. Figure 2 shows the relative optical absorption ratio profiles depending on the period of the nanodiscs array, which confirms a significant enhancement of light-graphene interaction facilitated by the plasmonic selective absorbers at each resonant wavelength. These results are expected to contribute to the development of spectral-selective optoelectronic detectors and devices based on graphene.

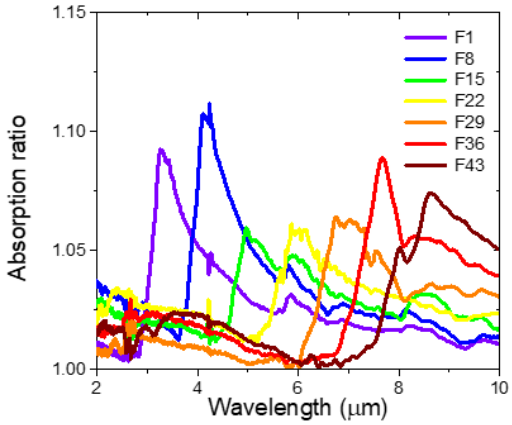


Fig. 2. The measured optical absorption ratio profiles of graphene with multispectral plasmonic selective absorbers layer transferred onto it.

This work was supported by an institutional program grant (2E32261) from Korea Institute of Science and Technology.

References

1. T. J. Echtermeyer, L. Britnell, P. K. Jasnos, A. Lombardo, R. V. Gorbachev, A. N. Grigorenko, A. K. Geim, A. C. Ferrari, and K. S. Novoselov, “Strong plasmonic enhancement of photovoltage in graphene,” Nat. Comm., Vol. 2, 458, 2011.
2. Y. Yao, R. Shankar, P. Rauter, Y. Song, J. Kong, M. Loncar, and F. Capasso, “High-responsivity mid-infrared graphene detectors with antenna-enhanced photocarrier generation and collection,” Nano Lett., Vol. 14, No. 7, 3749–3754, 2014.
3. H. H. Kim, S. K. Lee, S. G. Lee, E. Lee, and K. Cho, “Wetting-assisted crack- and wrinkle-free transfer of wafer-scale graphene onto arbitrary substrates over a wide range of surface energies,” Adv. Funct. Mater., Vol. 26, No. 13, 2070–2077, 2016.

Plasmonics and nano-optics

Artificial intelligence-based refractive index sensing achieving atto-mol detection limit

N. Li[1], Q. Wang[1], Z. He[1], A. B. Lopez[1], F. Xiang[1] and A. Fratalocchi[1*]

King Abdullah University of Science and Technology (KAUST), Thuwal 23955-6900, Saudi Arabia
*corresponding author: andrea.fratalocchi@kaust.edu.sa

Abstract: This study implements an ultrasensitive platform technology that integrates a wet-chemistry scalable sensor with optical artificial intelligence hardware attached to a conventional monochrome camera. The system extracts sensing features in the optical hardware, enabling accurate quantification of glucose concentration with a detection limit as low as 10^{-20} mol/L. The results improve the current state-of-the-art by six orders of magnitude. The system does not require an electrochemical workstation and works in real-time.

Refractive index (RI) sensing attracts considerable interest in the analysis of blood components [1], DNA [2], proteins [3], cancerous cells [4], virus and bacteria [5]. Traditionally, RI sensors measure refractive index variation via localized spectral features, such as frequency shift or width changes in resonances [6]. This approach, while straightforward to implement, suffers from the effects of noise and does not allow to reach detection limits comparable to chemical techniques [7]. For example, in the detection of glucose, which is essential in detecting heart failure, diabetes, and other metabolic syndromes [8], the best RI-based results reach the detection limit of 10^{-6} mol/L [9]. Conversely, enzymatic can detect glucose at levels as low as 1×10^{-13} mol/L with a GOx/ZnONPs-[EMIM][Otf]/ESM sensing platform [10] and 4.2×10^{-14} mol/L with a CuONPs/Ni-foam sensing platform [11], respectively.

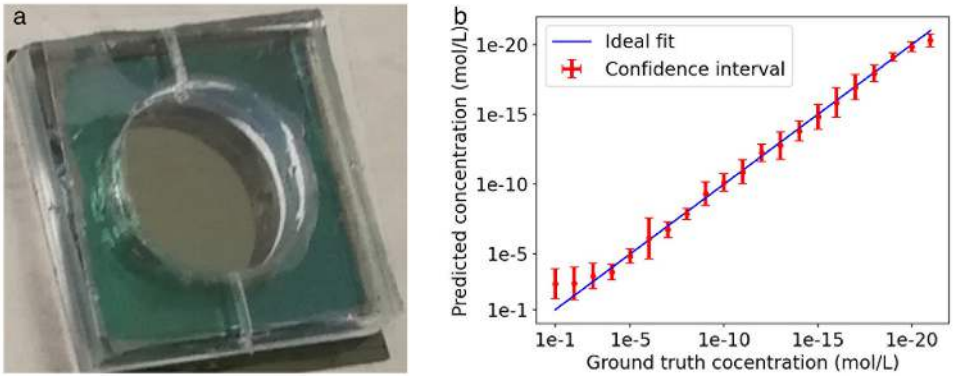


Figure 1: (a) A fabricated optical RI sensor. (b) Prediction results on a test dataset, including 20 different glucose concentrations varying from 10^{-1} mol/L to 10^{-20} mol/L. The presented confidence interval is magnified by 30 times for better visualization.

This work implements an ultrasensitive detection framework by integrating RI sensors with artificial intelligence (AI) optical hardware into a monochrome camera. The hardware comprises inversely designed metasurface encoders [12], which extract sparse spectral features that train a regression model. We fabricate the

sensor via wet chemistry, expandable up to 4 inches. Figure 1a shows a picture of a manufactured device. The sensor includes a structured silicon substrate covered by golf film and a top cover glass that confines the incident light on the substrate. The semi-enclosed container used in our system automatically removes invisible residue after each measurement, making it possible to reuse the container and collect large-scale datasets for subsequent training of the AI models. Figure 1b depicts the sensitivity of this system in determining glucose concentration, achieving detection resolutions as low as 10^{-20} mol/L, the lowest reported for this analyte to date. Our regression network shows high measuring accuracy with an R^2 value of 0.9648.

References

1. V. S. Chaudhary, D. Kumar, G. P. Mishra, S. Sharma, and S. Kumar, "Plasmonic biosensor with gold and titanium dioxide immobilized on photonic crystal fiber for blood composition detection," IEEE Sens. J., 22, 8474–8481, 2022.
2. M. S. Rahman, M. S. Anower, M. R. Hasan, M. B. Hossain, and M. I. Haque, "Design and numerical analysis of highly sensitiveau-mos2-graphene based hybrid surface plasmon resonance biosensor," Opt. Commun., 396, 36–43, 2017.
3. W. Wang, Z. Mai, Y. Chen, J. Wang, L. Li, Q. Su, X. Li, and X. Hong, "A label-free fiber optic spr biosensor for specific detection of c-reactive protein," Sci. Rep., 7, 16904, 2017.
4. R. Singh, S. Kumar, F.-Z. Liu, C. Shuang, B. Zhang, R. Jha, and B. K. Kaushik, "Etched multicore fiber sensor using copper oxide and gold nanoparticles decorated graphene oxide structure for cancer cells detection," Biosens. Bioelectron., 168, 112557, 2020.
5. A. Kumar, P. Verma, and P. Jindal, "Surface plasmon resonance biosensor based on a d-shaped photonic crystal fiber using ti3c2tx mxene material," Opt. Mater., 128, 112397, 2022.
6. Y. Xu, P. Bai, X. Zhou, Y. Akimov, C. E. Png, L.-K. Ang, W. Knoll, and L. Wu, "Optical refractive index sensors with plasmonic and photonic structures: promising and inconvenient truth," Adv. Opt. Mater., 7, 1801433, 2019.
7. B. Liu, S. Chen, J. Zhang, X. Yao, J. Zhong, H. Lin, T. Huang, Z. Yang, J. Zhu, S. Liu et al., "A plasmonic sensor array with ultrahigh figures of merit and resonance linewidths down to 3 nm," Adv. Mater., 30, 1706031, 2018.
8. T. B. Horwich and G. C. Fonarow, "Glucose, obesity, metabolic syndrome, and diabetes: relevance to incidence of heart failure," J. Am. Coll. Cardio., 55, 283–293, 2010.
9. J. Kim, M. Kim, M.-S. Lee, K. Kim, S. Ji, Y.-T. Kim, J. Park, K. Na, K.-H. Bae, H. Kyun Kim et al., "Wearable smart sensor systems integrated on soft contact lenses for wireless ocular diagnostics," Nat. commun., 8, 14997, 2017.
10. B. N. Aini, S. Siddiquee, K. Ampon, K. F. Rodrigues, and S. Suryani, "Development of glucose biosensor based on zno nanoparticles film and glucose oxidase-immobilized eggshell membrane," Sens. Bio-Sens. Res., 4, 46–56, 2015.
11. M. A. Kamyabi, M. Moharramnezhad, and N. Hajari, "Silica template as a morphology-controlling factor for attachment of cuo nanoparticles on 3d-ni-foam as a new enzyme-free electrochemiluminescence probe for glucose detection," J. Electrochem. Soc., 168, 037506, 2021.
12. F. Getman, M. Makarenko, A. Burguete-Lopez, and A. Fratalocchi, "Broadband vectorial ultrathin optics with experimental efficiency up to 99% in the visible region via universal approximators," Light Sci. Appl., 10, 47, 2021.

Effect of Mirror Quality on the Optical Properties of Nanoparticle-on-Mirror Plasmonic Nanocavities

Z. X. Wang[1*], A. V. Krasavin[2] and P. Wang[1]

[1]State Key Laboratory of Modern Optical Instrumentation, College of Optical Science and Engineering, Zhejiang University, Hangzhou 310027, China
[2]Department of Physics and London Centre for Nanotechnology, London WC2R 2LS, UK
[*]Corresponding author: iswzx@zju.edu.cn

Abstract: As an important part of nanoparticle-on-mirror (NPoM) plasmonic nanocavities, metal mirrors play an important role in determining the optical properties of the nanocavities and their application performance. Here, we experimentally study the effect of mirror quality (e.g., surface morphology, crystalline quality) on optical properties of NPoM nanocavities including nanosphere-on-mirror (NSoM) and nanocube-on-mirror (NCoM) designs, which improve the understanding of optical properties of the nanocavity and provide guidelines for the design of nanocavity-based devices with optimized performance for practical applications.

Plasmonic nanocavities based on metal nanoparticle-on-mirror (NPoM) nanostructures, have attracted extensive research interest due to their ability of extreme optical field localization and enhancement. They provide an intriguing platfrom for the study of light-matter interactions at the nanoscale and have enabled a series of breakthroughs in nanophotonic research and applications[1,2]. They are usually fabricated using deposited polycrystalline metal films with a rough surface or template-stripped polycrystalline metal films with a very smooth surface as the mirrors[1,2]. Recently, we have employed chemically grown single-crystalline gold microflakes (GMFs) as the metal mirror[3], providing NPoM nanocavities with significantly reduced loss. Because of the strong confinement of optical fields in the nanoscale gap, the optical property of NPoM nanocavities is very sensitive to the nanoscale morphology of the gap as well as the crystalline quality of the bottom metal mirror. A small change in the gap morphology induced by a rough mirror surface may result in a significant variation of the spectral position of the plasmonic resonances. Meanwhile, the scattering of electrons by surface roughness and numerous grain boundaries can cause a significant optical loss and resonance broadening. Therefore, it is highly required to investigate how the mirror quality affects the optical response of NPoM nanocavities. Here we systematically investigate the effect of mirror quality on the optical properties of plasmonic NPoM nanocavities including nanosphere-on-mirror (NSoM) and nanocube-on-mirror (NCoM) nanocavities[4].

Polycrystalline sputtered gold films (SGFs), template-stripped gold films (TSGFs) and single-crystalline gold microflakes (GMFs) were employed as the mirrors. Firstly, the structural and dielectric properties of the three kinds of gold films were investigated. Their surface quality and crystal structure were characterized. Besides, their dielectric functions were measured and compared for subsequent simulation verification. Then, the scattering intensities, quality factors, peak wavelengths of the plasmonic modes of NSoM and NCoM nanocavities formed on these mirrors were compared and analyzed. Due to the greatly improved surface roughness that can minimize the fluctuation in the gap morphology, the scattering spectra of NSoM and NCoM nanocavities formed on smooth TSGFs and GMFs have a better cavity-to-cavity homogeneity than those formed on rough SGFs. Furthermore, there is an obvious difference in the average peak wavelengths of resonance modes

of NSoM and NCoM nanocavities formed on different gold films, which can be attributed to the difference in their dielectric functions and surface qualities. And this is well reproduced by theoretical calculations based on the measured dielectric functions of the gold films. Moreover, due to the improvement in the surface smoothness and crystalline quality from SGF to TSGF and GMF, there is an increase in the quality factors and scattering intensities of the resonance modes for nanocavities formed on the corresponding films due to the reduced loss. This research deepens the understanding of the nanocavity properties and provides a guideline for the realization of high-performance nanocavities for practical applications.

In conclusion, we have demonstrated both experimentally and theoretically that the mirror quality has a significant effect on the optical property of NPoM nanocavities. Surface roughness of the metal mirrors can introduce significant change in the gap morphology, resulting in a poor cavity-to-cavity homogeneity of the optical response as well as a shift in the peak wavelength of resonance mode compared with nanocavities formed on smooth mirror. Overall, single-crystalline GMFs provide a fascinating platform for the construction of high-quality (low-loss and high cavity-to-cavity homogeneity) NPoM nanocavities, especially when the mirror thickness is further decreased, compared with deteriorated film quality for SGFs and TSGFs. However, for the construction of large-scale nanocavity arrays, TSGFs are recommended due to the limited lateral size (several hundred micrometers) of GMFs.

This research was supported by the National Natural Science Foundation of China (62075195, 1200433 and 92150302), Fundamental Research Funds for the Central Universities (226-2022-00147), EPSRC (UK), grant number EP/W017075/1, and the ERC iCOMM Project (No. 789340).

References

1. J. J. Baumberg, J. Aizpurua, M. H. Mikkelsen and D. R. Smith, Extreme nanophotonics from ultrathin metallic gap, Nat. Mater. 18, 668-678, 2019.
2. G. C. Li, Q. Zhang, S. A. Maier and D. Y. Lei, Plasmonic particle-on-film nanocavities: a versatile platform for plasmon-enhanced spectroscopy and photochemistry, Nanophotonics, 7, 1865–1889, 2018.
3. L. F. Liu, A. V. Krasavin, J. S. Zheng, Y. B. Tong, P. Wang, X. F. Wu, B. Hecht, C. X. Y. Pan, J. L. Li, X. Guo, A. V. Zayats and L. M. Tong, Atomically smooth single-crystalline platform for low-loss plasmonic nanocavities, Nano Lett., 22, 1786–1794, 2022.
4. Z. X. Wang, L. F. Liu, D. Zhang, A. V. Krasavin, J. S. Zheng, C. X. Y. Pan, E. X. He, Z. F. Wang, S. C. A. Zhong, Z. Y. Li, M. X. Ren, X. Guo, A. V. Zayats, L. M. Tong and P. Wang, Effect of mirror quality on optical response of nanoparticle-on-mirror plasmonic nanocavities, Adv. Opt. Mater. 11, 2201914, 2023.

META 2023, PARIS - FRANCE, JULY 18 – 21, 2023

Stark Effect Control of the Scattering Properties of Plasmonic Nanogaps

Donatello Pagnotto, Alina Muravitskaya, David M. Benoit, Jean-Sebastien G. Bouillard, and Ali M. Adawi*

Department of Physics and G. W. Gray Centre for Advanced Materials, University of Hull, Hull HU6 7RX, United Kingdom.
*corresponding author: a.adawi@hull.ac.uk

Abstract: The development of actively tunable plasmonic nanostructures enables real-time and on-demand enhancement of optical signals. This is an essential requirement for a wide range of applications such as sensing and nanophotonic devices. Here we show that by modifying the transition energies of a material via the application of an electric field, the Stark effect offers practical approach to realise nano-scattering sources with high integration potential and a direct method to probe the excitonic properties of semiconducting materials on the nanoscale.

In this work, we report on the use of the Stark effect to control the scattering response of a plasmonic nanogap formed between a silver nanoparticle and an extended silver film separated by a 20 nm thin layer of the organic semiconductor PQT-12. The constructed plasmonic device can be utilised as an electrically tuned multiband nano-scattering source. Both observed plasmonic modes are red-shifted with electric field according to a quadratic Stark shift, providing a promising way for achieving electrically tuned plasmonic devices for active nanopixels and real-time sensing applications. In addition, our approach allows one to experimentally determine the polarizability of the semiconductor material embedded in the nanogap region, offering a new approach to interrogate the excitonic properties of semiconductor materials at the nanoscale.

ACKNOWLEDGMENT

We acknowledge the University of Hull for financial support through a PhD scholarship. This work was supported by the EU Horizon 2020 research and innovation programme under grant number 861950, project POSEIDON. We also acknowledge the Viper High Performance Computing facility of the University of Hull and its support team.

Microscopic Theory of Tip-Enhanced Nonlinear Raman Scattering with Self-Consistent Nonlocal Response

H. Ikagawa[1*], M. Tamura[1,2], T. Yokoyama[1] and H. Ishihara[1]

[1]Department of Materials Engineering Science, Osaka University, Japan
[2]Research Institute for Light-induced Acceleration System, Osaka Metropolitan University, Japan
[*]corresponding author: ikagawa.h@opt.mp.es.osaka-u.ac.jp

Abstract: We constructed a microscopic theory of tip-enhanced coherent anti-Stokes Raman scattering (TE-CARS) which utilizes a metallic probe tip to enhance the CARS. To describe the optical response in a mesoscopic system including a metal and sample, we self-consistently solved the Maxwell's equations and a nonlocal constitutive equation for the polarization of sample. Based on this theory, we discuss the enhancement effect and spatial resolution in the TE-CARS.

Tip-enhanced Raman Spectroscopy (TERS), a technique combined Raman spectroscopy and scanning near-field optical microscope (SNOM), has been attracting much attention due to nanoscale vibrational nanoimaging[1]. The TERS utilizes a sharp metallic probe tip to enhance and confine a near-field at the tip apex by a localized surface plasmon (LSP) on the tip. These effects allow the TERS to achieve optical sensing with high spatial resolution beyond the diffraction limit of light.

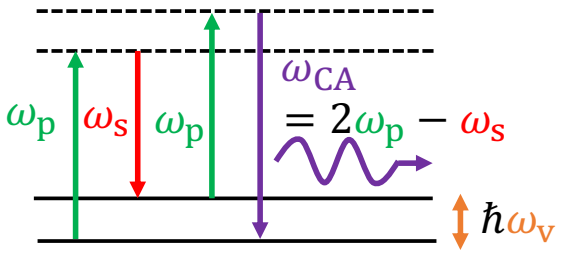


Fig. 1. Energy diagram of CARS process.

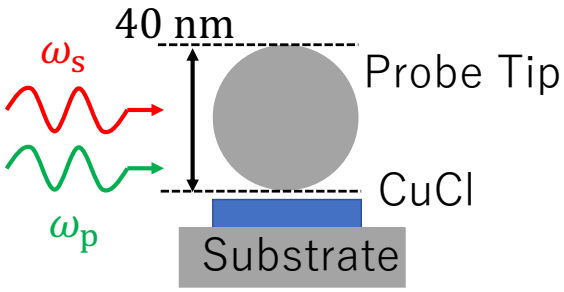


Fig. 2. Calculation model.

Furthermore, the TERS based on the nonlinear Raman scattering has been studied. Ichimura, et al., realized the tip-enhanced microscopy with the coherent anti-Stokes Raman scattering (CARS), namely, tip-enhanced CARS (TE-CARS)[2]. The CARS is a third-order nonlinear Raman scattering caused by the two incident light sources, a pump light with the frequency ω_1 and Stokes light with the frequency ω_2 $(\omega_1 > \omega_2)$, which emits the anti-Stokes light with the frequency ω_{CA} (Fig. 1). There has been an expectation that the CARS nonlinearity could contribute to improving the spatial resolution and intensity of the signal in TE-CARS. However, the detailed discussion about the nonlinear interaction in the TE-CARS has been insufficient. Therefore, we have constructed a theoretical framework to evaluate the TE-CARS, and studied the contribution of nonlinearity for the spatial resolution and intensity of the signal.

In a mesoscopic system such as the TE-CARS, the optical response reflects spatial distribution of wave functions of elementary excitations in the sample. In other words, in a sample, the polarization $\boldsymbol{P}(\boldsymbol{r},\omega)$ at a position $\boldsymbol{r}$ can be induced by the electric field $\boldsymbol{E}(\boldsymbol{r}',\omega)$ at a different position $\boldsymbol{r}' \neq \boldsymbol{r}$ nonlocally. Thus, the linear and third-order nonlinear polarizations are described as,

$$\boldsymbol{P}^{(1)}(\boldsymbol{r},\omega) = \int d\boldsymbol{r}' \boldsymbol{\chi}^{(1)}(\boldsymbol{r},\boldsymbol{r}',\omega)\boldsymbol{E}(\boldsymbol{r}',\omega), \quad (1)$$

and

$$\boldsymbol{P}^{(3)}(\boldsymbol{r},\omega) = \iiint d\boldsymbol{r}'d\boldsymbol{r}''d\boldsymbol{r}'''\boldsymbol{\chi}^{(3)}(\boldsymbol{r},\boldsymbol{r}',\boldsymbol{r}'',\boldsymbol{r}''',\omega',\omega'',\omega''')\boldsymbol{E}(\boldsymbol{r}',\omega')\boldsymbol{E}(\boldsymbol{r}'',\omega'')\boldsymbol{E}(\boldsymbol{r}''',\omega''') \quad (2)$$

respectively. $\boldsymbol{\chi}^{(1)}(\boldsymbol{r},\boldsymbol{r}',\omega)$ and $\boldsymbol{\chi}^{(3)}(\boldsymbol{r},\boldsymbol{r}',\boldsymbol{r}'',\boldsymbol{r}''',\omega',\omega'',\omega''')$ are linear and third-order nonlinear susceptibility, respectively. These susceptibilities include the information of the wave function as the nonlocality. To derive these polarization and susceptibility, we assumed the following Hamiltonian,

$$\hat{H} = \hat{H}_{\mathrm{v}} + \hat{H}_{\mathrm{ex}} + \hat{H}_{\mathrm{ex-r}} + \hat{H}_{\mathrm{ex-v}}, \quad (3)$$

$$\hat{H}_{\mathrm{v}} = \hbar\omega_{\mathrm{v}}\hat{a}^{\dagger}\hat{a},\ \ \hat{H}_{\mathrm{ex}} = \hbar\omega_{\mathrm{ex}}\hat{b}^{\dagger}\hat{b},\ \ \hat{H}_{\mathrm{ex-r}} = -\int d\boldsymbol{r}\hat{\boldsymbol{P}}(\boldsymbol{r})\cdot\boldsymbol{E}(\boldsymbol{r}),\ \ \hat{H}_{\mathrm{ex-v}} = F\hat{b}^{\dagger}\hat{b} + \mathrm{H.C.}, \quad (4)$$

where $\hat{H}_{\mathrm{v}}, \hat{H}_{\mathrm{ex}}, \hat{H}_{\mathrm{ex-r}}, \hat{H}_{\mathrm{ex-v}}$ are the Hamiltonian of the system of excitons, the system of phonons, polarization-electric field interaction, and exciton-phonon interaction, respectively. The operator $\hat{a}\ (\hat{a}^{\dagger})$ and $\hat{b}\ (\hat{b}^{\dagger})$ are the annihilation (creation) operator of phonons and excitons, respectively. The expression of polarization can be derived as an expectation value of the excitonic polarization operator $\hat{\boldsymbol{P}}(\boldsymbol{r})$ with the quantum master equation.

On the other hand, the electric field can be described as,

$$\boldsymbol{E}(\boldsymbol{r},\omega_j) = \boldsymbol{E}_{\mathrm{inc}}(\boldsymbol{r},\omega_j) + \int d\boldsymbol{r}'\boldsymbol{G}(\boldsymbol{r},\boldsymbol{r}',\omega_j)\{\boldsymbol{P}^{(1)}(\boldsymbol{r}',\omega_j) + \boldsymbol{P}_{\mathrm{bg}}(\boldsymbol{r}',\omega_j) + \boldsymbol{P}_{\mathrm{metal}}(\boldsymbol{r}',\omega_j)\}, \quad (5)$$

where $\omega_j = \omega_1, \omega_2, \omega_{\mathrm{CA}}$, $\boldsymbol{E}_{\mathrm{inc}}(\boldsymbol{r},\omega_j)$ is incident field, $\boldsymbol{G}(\boldsymbol{r},\boldsymbol{r}',\omega_j)$ is a Green's function of Maxwell's equation, $\boldsymbol{P}_{\mathrm{bg}}(\boldsymbol{r},\omega_j)$ is a background polarization of the sample, and $\boldsymbol{P}_{\mathrm{metal}}(\boldsymbol{r},\omega_j)$ is a polarization of the metal. We self-consistently solved the induced polarization and electric field at each frequency, while the equations at CARS frequency are solved with regarding the scattering field from the nonlinear polarization as the incident field, $\boldsymbol{E}_{\mathrm{inc}}(\boldsymbol{r},\omega_{\mathrm{CA}}) = \int d\boldsymbol{r}'\boldsymbol{G}(\boldsymbol{r},\boldsymbol{r}',\omega_{\mathrm{CA}})\boldsymbol{P}^{(3)}(\boldsymbol{r}',\omega_{\mathrm{CA}})$.

To evaluate the CARS spectra, we assumed the calculation model shown in Fig. 2, where the sample was located between the metal substrate and probe tip, and they were irradiated by the two light sources with the frequency of ω_1 and ω_2. We assumed that the sample was a CuCl rectangular nanoparticle and the material of metal structure was aluminum. For the elementary excitations in the CuCl, we assumed the presence of LO phonons and Z_3 excitons with the eigenenergy 3.2022 eV and 23.1 meV, respectively. Fig. 3 shows the calculated CARS power as TE-CARS signal. There was a peak of LO phonon near 190 cm^{-1}. In addition, the probe tip enhances the CARS power with an enhancement factor (EF) of nearly 10^5. Such a high EF results from the nonlinearity of the optical response. Furthermore, the scanned signal of the nanostructure can be obtained by displacing the probe tip, where the spatial resolution of TE-CARS was estimated about 4 nm also attributed to the nonlinearity. The obtained results show the advantage of TE-CARS by the nonlinearity.

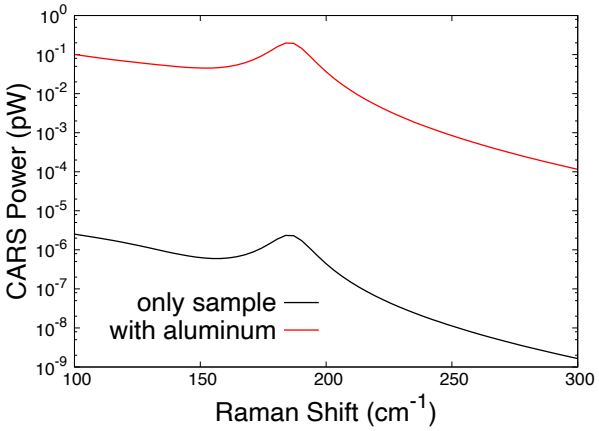


Fig. 3. CARS spectra. Black and red lines are spectrum from the CuCl nanoparticle without and with aluminum, respectively. The value of Raman shift $\omega_1 - \omega_2$ is converted into the wavenumber.

Acknowledgments: This work was supported by JSPS KAKENHI (Grant Numbers JP16H06504, JP21H05019, JP20K15196), JST-Mirai Program (Grant Numbers JPMJMI18GA and JPMJMI21G1), and JST CREST (Grant Number JPMJCR1903).

References

1. N. Hayazawa, *et. al., Opt. Commun.*, **183**, 333 (2000).
2. T. Ichimura, *et al., Appl. Phys. Lett.*, **84**, 1768 (2004).

CdZnO nanoparticles for SEIRA sensing in the mid-infrared

P. Ibañez-Romero[1], E. Martinez Castellano[1], J. Yeste[2], V. Muñoz-Sanjosé [2] , M. Montes Bajo*[1], and A. Hierro[1]

[1] ISOM, Universidad Politécnica de Madrid, Madrid, Spain
[2] Departament de Física Aplicada i Electromagnetisme, Universitat de València, Burjassot, Spain
*corresponding author: miguel.montes@upm.es

In this work we report a novel approach to resonant surface enhanced infrared absorption (SEIRA) sensing employing Cd(Zn)O nanoparticles. We provide experimental demonstration of the coupling between the localized surface plasmons supported by the nanoparticles and the narrowband absorption of PMMA resist. Our system becomes an excellent alternative to the lossy metals commonly used in the mid infrared (mid-IR) and prevents the need for complex lithographic processes for SEIRA sensing.

Resonant SEIRA allows the resonant coupling of a broadband plasmonic mode supported by a metallic micro or nanostructure and the narrowband absorption minimum of the analyte to detect. With this method, enhancements up to a factor 7 in the signal of the analyte have been reported [1]. However, most reports rely on noble metals that suffer from high losses in the mid-IR range [2], and complex lithography is required to place the plasmonic resonances at the desired wavelengths. In this study, we report a novel approach for resonant SEIRA sensing, completely free of lithography. We employ self-assembled nanoparticles (NPs) made of $Cd_{1-x}Zn_xO$ –a material characterized by its low losses in the mid-IR [3]— deposited on GaAs. The deposition on a high-refractive index substrate allows plasmonic resonances at frequencies well below the plasma frequency of the $Cd_{1-x}Zn_xO$ [3].

Resonant coupling between the localized surface plasmons (LSPs) supported by the NPs and the sharp absorption minimum presented by PMMA resist at 1730 cm^{-1} is demonstrated. This minimum corresponds to the vibrational mode of the double C=O bond of the PMMA molecule. This is a good example of one of the bonds that absorb in the so-called functional group region of the mid-IR [4], where most of the carbon-based molecules from organic chemistry have their resonances. By controlling the plasma frequency of the $Cd_{1-x}Zn_xO$ via doping or Zn alloying, we expect to target other frequencies within this region.

The samples were grown by metal organic chemical vapor deposition (MOCVD) at 300 ºC on a semi-insulating GaAs substrate. The nominal Zn percentage was set to 10% following Tamayo-Arriola *et al.* [5]. Figure 1 shows a SEM view of the surface, where a homogeneous distribution of multiple-sized, isolated NPs is shown. The plasmonic response of the samples was characterized by its transmission spectrum, obtained by Fourier transform infrared (FTIR) spectroscopy at an angle of incidence of 45º.

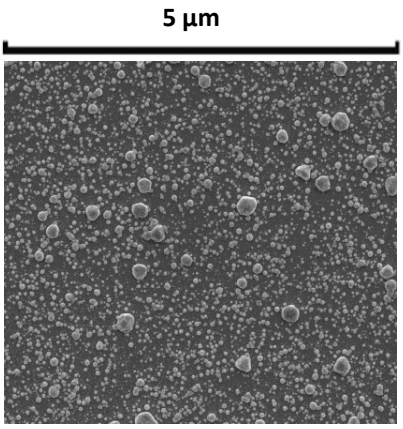


Figure 1. SEM micrography of the $Cd_{0.9}Zn_{0.1}O$ NPs on a semi-insulating GaAs substrate.

Due to the high refractive index of the substrate (n=3.3), a broad LSP resonance is found at around 1750 cm^{-1}, well below the plasma frequency of $Cd_{0.9}Zn_{0.1}O$ (~ 4000 cm^{-1}). This energy matches that of the C=O absorption in the PMMA. Figure 2 presents the transmission spectrum of a $Cd_{0.9}Zn_{0.1}O$/GaAs sample before and after the deposition of a thin layer of highly diluted PMMA. Here, the PMMA absorption band appears as a sharp, well-defined maximum in the middle of the broadband LSP. This paradoxical behavior where an absorptive mode appears as a non-symmetrical maximum is typical of this type of resonant coupling, as first described by Fano and shown in most successful SEIRA experiments [5]. Other absorptive modes of PMMA can be observed at energies below 1730 cm^{-1}, and are weakly coupled to the LSP.

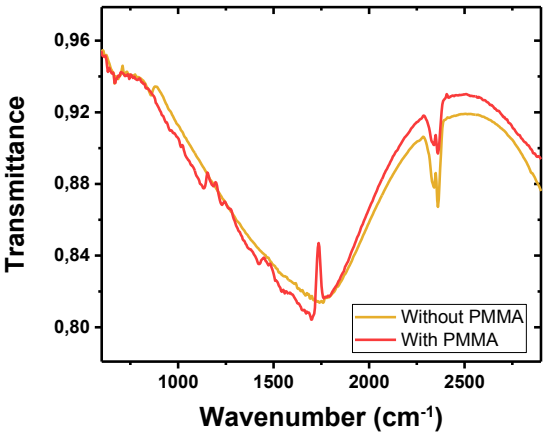


Figure 2. Transmittance spectra of the $Cd_{0.9}Zn_{0.1}O$ NPs on GaAs, with and without a layer of PMMA on top.

With these results, we have proven the resonant coupling between the LSP supported by self-assembled, lithography-free $Cd_{0.9}Zn_{0.1}O$ NPs grown on GaAs and the narrow band absorption mode presented by PMMA resist at 1730 cm^{-1}. Further optimization of NP density and size are necessary to maximize the resonant signal shown here. This approach is not restricted to Cd(Zn)O as we expect other transparent conductive oxides grown in a similar pattern to produce similar results. Different approaches to tune the SEIRA frequency across the mid-IR using Cd(Zn)O will also be addressed.

References

[1] L. V. Brown, X. Yang, K. Zhao, B. Y. Zheng, P. Nordlander, and N. J. Halas, 'Fan-Shaped Gold Nanoantennas above Reflective Substrates for Surface-Enhanced Infrared Absorption (SEIRA)', *Nano Lett*, vol. 15, no. 2, pp. 1272–1280, Feb. 2015.

[2] G. V. Naik, V. M. Shalaev, and A. Boltasseva, 'Alternative Plasmonic Materials: Beyond Gold and Silver', *Advanced Materials*, vol. 25, no. 24, pp. 3264–3294, Jun. 2013.

[3] E. M. Castellano, J. Tamayo-Arriola, M. Montes Bajo, A. Gonzalo, L, Stanojevic, J. M. Ulloa, O. Klymov, J. Yeste, S. Agouram, E. Muñoz, V. Muñoz'Sanjosé, and A. Hierro, "Self-assembled metal-oxide nanoparticles on GaAs: infrared absorption enabled by localized surface plasmons," Nanophotonics, vol. 10, no. 9, pp. 2509–2518, Jul. 2021.

[4] J. Tamayo-Arriola, A. Huerta-Barberà, M. Montes Bajo, E. Muñoz, V. Muñoz-Sanjosé, and A. Hierro, 'Rock-salt CdZnO as a transparent conductive oxide', *Appl Phys Lett*, vol. 113, no. 22, p. 222101, Nov. 2018.

[5] P. J. Larkin, *Infrared and Raman Spectroscopy*. Elsevier, 2018.

[6] F. Neubrech, C. Huck, K. Weber, A. Pucci, and H. Giessen, 'Surface-Enhanced Infrared Spectroscopy Using Resonant Nanoantennas', *Chem Rev*, vol. 117, no. 7, pp. 5110–5145, Apr. 2017.

META 2023, PARIS - FRANCE, JULY 18 – 21, 2023

Synergetic hot carrier generation due to coherent couplings of plasmon-carrier excitations and plasmon hybridization in a metallic nano-chain array

S. Inoue [1*], T. Yokoyama [1] and H. Ishihara [1,2]

[1] Graduate School of Engineering Science, Osaka Univ., Japan
[2] Center for Quantum Information and Quantum Biology, Osaka Univ., Japan
[*]corresponding author: inoue.s@opt.mp.es.osaka-u.ac.jp

Abstract: Hot carrier generation is one of the most significant issues in plasmonics and energy conversion of light. In this study, we discuss a novel mechanism of coherent energy transfer between the plasmon and carrier excitations mediated by radiative and cavity fields. In the case of metallic nano array, such coherent effects can be enhanced. We elucidated that plasmon-carrier excitations' coherence and plasmon hybridization in the array cause a synergetic effect and it could enhance the energy conversion efficiency.

Localized surface plasmon resonance (LSPR) is a key ingredient for a light-induced phenomena on nanoscale metals. A hot carrier generation is one of the most attractive phenomena by the LSPR. The hot carrier is a nonequilibrium electron distribution, where the electrons have exceeded energy more than that of thermal distribution. Then, the hot carrier can be injected to an attached semiconductor and several applications have been proposed, e.g., photovoltaics [1] and photosynthesis [2]. The LSPR induces a strong electric field near the surface of metallic nanostructures. In the array of such metallic nanostructures, the enhanced electric field causes an interaction between the plasmon excitation on the nanoscale metals and results in a hybridization of the plasmons [3]. This plasmon hybridization could enhance the hot carrier generation efficiency. Recently, X. Shi, et al., have studied an enhancement of the hot carrier generation by the design of spatial structure of electromagnetic field based on cavity structures [4].

A mechanism of the hot carrier generation has been discussed based on several relaxation and damping process theoretically [5], where the photon energy of incident light is transferred unidirectionally to the hot carrier via the LSPR. In our previous study, we have considered the radiative field induced by the plasmon excitation in a single nanostructure and discussed a coherent coupling between a collective (plasmon) excitation and individual (electron-hole pair) excitations owing to the radiative field [6], where bidirectional energy transfers could be obtained by the coherent couplings.

In this work, by imitating [4], we consider light-plasmon interactions, plasmon-plasmon interactions and novel coherent interactions between plasmon and carrier excitations like Fig. 1. We applied this minimal model to a metallic nano-chain array and investigate the relation between plasmon-carrier excitations' coherence and hot carrier generation. As a result, if we consider coherent couplings between plasmon and electron-hole pairs, a sharp behavior happens in absorption spectra at the electron-hole pair's excitation energy position (Fig. 2). In addition, looking at hot carrier generation efficiency spectra toward absorbed photon number, if plasmon-carrier excitations' coherence is absent, no features appear in spectral shapes due to only thinking incoherent carrier generation process (Fig. 3). However, thinking the coherence, we indicate that resonant peak appears and this peak increases as plasmon-plasmon interactions become bigger (Fig. 4). It indicates that plasmon-carrier excitations' coherence induces a resonant energy transfer from plasmon to electron-hole pairs, that lead to enhance the efficiency of photoelectric conversion. Moreover, hybridization of plasmon excitations as with [3] interplay with this novel

coherent coupling and it is expected that an Fano resonant-type energy transfer will occurs as the synergetic effect. This result shows the possibility to realize more efficient carrier devices only by controlling the arrangements of nano-metal structures.

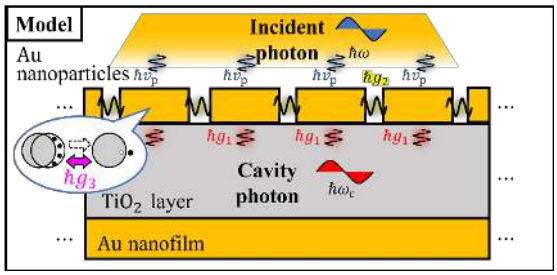


Figure 1: Model for describing coherent couplings between plasmon and electron-hole pairs via radiative field.

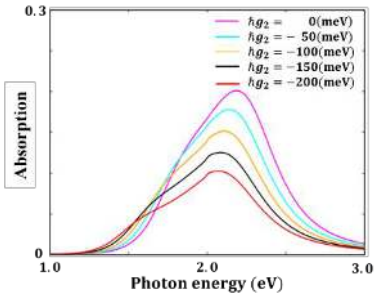


Figure 2: plasmon interactions dependence of absorption spectra.

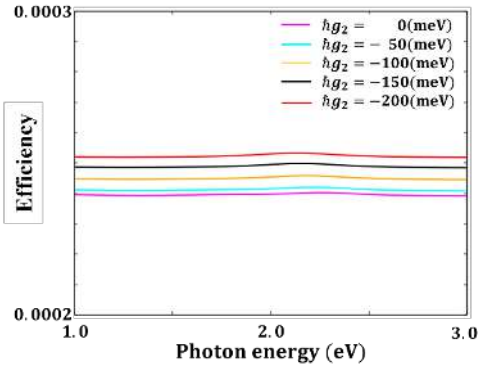


Figure 3: plasmon interactions dependence of carrier generation efficiency spectra. (Without plasmon-carrier excitations' coherence)

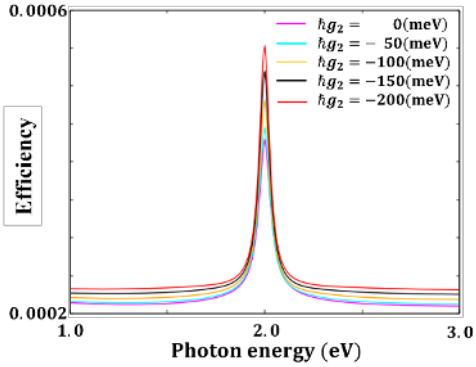


Figure 4: plasmon interactions dependence of carrier generation efficiency spectra. (With plasmon-carrier excitations' coherence)

References

1. Jang, Y. H., Y. J. Jang, S. Kim, L. N. Quan, K. Chung and D. H. Kim, "Plasmonic Solar Cells: From Rational Design to Mechanism Overview," Chem. Rev. Vol. 116, 14982-15034, 2016.
2. Ueno, K., T. Oshikiri and H. Misawa, "Plasmon-induced Water Splitting Using Metallic-Nanoparticles-Loaded Photocatalysts and Photoelectrodes," Chem. Phys. Chem. Vol. 17, 199-215, 2016.
3. Yu, H., Q. Sun, J. Yang, K. Ueno, T. Oshikiri, A. Kubo, Y. Matsuo, Q. Gong and H. Misawa, "Near-field spectral properties of coupled plasmonic nanoparticle arrays," Opt. Express Vol. 25, 6883-6894, 2017.
4. Shi, X., K. Ueno, T. Oshikiri, Q. Sun, K. Sasaki and H. Misawa, "Enhanced water splitting under modal strong coupling conditions," Nat. Nanotechnol. Vol. 13, 953-958, 2018.
5. Brongersma, M. L., N. J. Halas and P. Nordlander, "Plasmon-induced hot carrier science and technology," Nat. Nanotechnol. Vol. 10, 25-34, 2015.
6. Yokoyama, T., M. Iio, T. Kinoshita, T. Inaoka and H. Ishihara, "Comprehensive microscopic theory for coupling of individual and collective excitations via longitudinal and transverse fields," Phys. Rev. B Vol. 105, 165408, 2022.

META 2023, PARIS - FRANCE, JULY 18 – 21, 2023

Hybrid gold-(CdSe/CdS/CdZnS) nanocrystal supraparticles emission: from FRET inhibition to collective emission of a mesoscopic ensemble of NCs

V. Blondot[1], D. Gérard[1], G. Quibeuf[1], C. Arnold[1], A. Delteil[1], A. Bogicevic[2], T. Pons[2], N. Lequeux[2], J.-P. Hugonin[3], J.-J. Greffet[3], S. Buil[1], J-P. Hermier[1*]

[1]Université Paris-Saclay, UVSQ, CNRS, GEMaC, 78000, Versailles, France.

[2]Laboratoire de Physique et d'Etude des Matériaux, ESPCI-Paris, PSL Research University, CNRS UMR 8213, Sorbonne Université, 10 rue Vauquelin, 75005 Paris, France

[3]Université Paris-Saclay, Institut d'Optique Graduate School, CNRS, Laboratoire Charles Fabry, F- 91127 Palaiseau, France

[*]corresponding author: jean-pierre.hermier@uvsq.fr

Abstract: we investigate the optical properties of single self-assembled hybrid gold-CdSe/CdS/CdZnS colloidal nanocrystal supraparticles. First, spectrally time resolved photoluminescence experiments show that they exhibit Förster resonance energy transfer (FRET) that is inhibited by the gold nanoshell, in agreement with the results of numerical simulations. Next, the analysis of the intensity autocorrelation function $g^{(2)}(\tau)$ reveals that FRET combined to non radiative Auger recombination can result in photon antibunching. Bunching at short time scale related to coherent collective emission is finally reported.

Despite continuous improvements, colloidal semiconductor nanocrystals (NCs) still exhibit limitations such as residual blinking or photobleaching. The progress in chemical synthesis offers new possibilities like the realization of close-packed self assemblies of nanoemitters as well as hybrid structures consisting in colloidal fluorophores encapsulated in plasmonic resonators. Beyond the standard increase of the decay rate by Purcell effect, this new class of emitters exhibit specific optical properties due to collective emission or related to the mesoscopic number of emitters.

In this presentation, we first report the synthesis of supraparticles (SPs) consisting in compact ensembles of CdSe/CdS/CdZnS colloidal nanocrystal (NCs) with a mean diameter about 8 nm and emitting at 645 nm (FWHM = 30 nm) [1]. Briefly, the NCs are aggregated by a micro-emulsion/evaporation method before encapsulation into a silica shell (thickness = 15 nm). After its functionalization by reaction with aminosilane precursors, a gold shell (thickness = 19 nm) is then synthesized following [2]. The overall diameter of the resulting golden supraparticles (GSPs) ranges between 100 nm and 500 nm.

The optical properties of the GSPs are studied at the single particle level by spin coating few tens of µL of the solution on a glass coverslip. The optical measurements are performed between 4 K and 300 K with a confocal microscope under optical pulsed excitation. The emission is detected with a standard Hanbury Brown and Twiss setup based on two avalanche photodiodes (APDs), a standard spectrometer or an interferometer associated with an APD. The latter enables to carry out spectrally and time resolved experiments to establish a fluorescence map as a function of the wavelength and photon time emission.

As a first step, the Purcell effect as a function of the GSP diameter is measured by fitting the PL decay of several single GSPs. The variations of the decay rate with the GSP diameter (the PL decay rate is twice higher for the smallest GSPs with respect to the biggest ones) is well fitted by a multilayer spherical model based on Mie theory [3].

Interestingly, we next show that the Purcell enhancement results in the decrease of the non-radiative FRET which is commonly observed in NC aggregates (when optically excited, the smallest diameter NCs tend to

transfer non-radiatively and incoherently their energy to bigger diameter NCs) [3]. Whereas, due to FRET, the PL decay rate is highly dependent on the detection wavelength for SPs without a gold nanoshell, the difference is much less significant for the GSPs. For the smallest ones, we measured a reduction by a factor 3 of the FRET efficiency. Simultaneously, we show a reduction of the broadening of the overall emission spectrum induced by FRET [4].

The number of emitters involved in the GSP emission could also be deduced from a detailed analysis of the specific shape of the emission spectra [5]. By using a simple analytical model and numerical simulations, we demonstrate that the autocorrelation function of the emission provides simultaneously the number of bright emitters and their mean linewidth. This general method when applied specifically to single GSPs also provides the fraction of photobleached emitters by comparison with the geometric parameters of the structure.

The last part of the presentation is devoted to the opportunities opened by the inhibition of incoherent FRET processes in terms of collective emission of the NCs. By using the function $g^{(2)}(\tau)$ and its analysis with a method first used in [6], we first show that despite the mesoscopic number of emitters, antibunching, which is well modelled by a Monte Carlo simulation taking into account residual FRET and Auger processes, can be evidenced. More interestingly, we finally show that bunching at sub-ns time scale is observed for several GSPs. It corresponds to a coherent emission involving a large ensemble of NCs [7].

In conclusion, GSPs are very promising hybrid gold-NC supraparticles. Beyond their brightness and photostability, these mesoscopic systems exhibit specific emission regimes and enable to explore collective emission with colloidal structures.

Acknowledgements: this work was funded by the Agence Nationale de la Recherche in the framework of the GYN project (Grant No. ANR-17-CE24-0046).

References

1. A. Bogicevic, X. Xu, S. Buil, C. Arnold, J.-P. Hermier, T. Pons, N. Lequeux, "Synthesis and characterization of colloidal quantum dot superparticles - plasmonic gold nanoshell hybrid nanostructures", ChemRxiv-2022-1m9q5 (2022).
2. S. J. Oldenburg, R. D. Averitt, S. L. Westcott, and N. J. Halas, “Nanoengineering of optical resonances,” Chem. Phys. Lett. 288(2-4), 243–247 (1998)
3. V. Blondot, A. Bogicevic, A. Coste, C. Arnold, S. Buil, X. Quélin, T. Pons, N. Lequeux, J.-P. Hermier, "Fluorescence properties of self assembled colloidal supraparticles from CdSe/CdS/ZnS nanocrystals", New J. Phys. 22, 113026 (2020)
4. V. Blondot, C. Arnold, A. Delteil, D. Gérard, A. Bogicevic, T. Pons, N. Lequeux, J.-P. Hugonin, J.-J. Greffet, S. Buil, J-P. Hermier, "Fluorescence decay enhancement and FRET inhibition in self-assembled hybrid gold CdSe/CdS/CdZnS colloidal nanocrystal supraparticles", Opt. Exp. 31, 4454 (2023)
5. A. Delteil, V. Blondot, S. Buil, J.-P. Hermier, "First-order coherence of light emission from inhomogeneously broadened mesoscopic ensembles", Phys. Rev. B. 106, 115302 (2022)
6. C. Bradac, M. T. Johnsson, M. van Breugel, B. Q. Baragiola, R. Martin, M. L. Juan, G. K. Brennen, and T. Volz, "Room temperature spontaneous superradiance from single diamond nanocrystals," Nat. Comm. 8 1205 (2017)
7. V. Blondot, D. Gérard, G. Quibeuf, C. Arnold, A. Delteil, A. Bogicevic, T. Pons, N. Lequeux, S. Buil, J-P. Hermier, "Photon correlations in the collective emission of hybrid gold-(CdSe/CdS/CdZnS) nanocrystal supraparticles", arXiv: 2302.07538

Investigation of Terahertz SSPP Waveguides Using TRL Calibration

Y. Colak[1], M. Demircioglu[1], and M. Unlu[1]

[1]TOBB University of Economics and Technology, Turkey

Abstract: Spoof surface plasmon polaritons waveguides (SSPP WGs) have shown record-breaking performances at the terahertz frequencies to enable CMOS technologies. In this paper, we present the TRL calibration of the SSPP WGs between the 0.22 THz and 0.3 THz. We utilize the TRL calibration to extract the real loss behavior of the SSPP WGs. By designing two different length lines, we prove that the TRL calibration of SSPP WGs is internally consistent.

Surface Plasmon Polaritons (SPP), which is a commonly used concept in optical frequencies, does not exist in Microwave and Terahertz bands due to metals behave like perfect conductors instead of negatively permittivity plasmas [1]. As a solution to this, the spoof surface plasmon polariton waveguides (SSPP WGs) are presented, which is corrugated structures, and planned to be used in many areas such as near future CMOS technologies [2]. On the other hand, the real loss behavior of the SSPP WGs is not characterized due to the need of the CPW-to-SSPP WG transition circuit [3]. Moreover, TRL calibration, which takes its name from the initials of the Through-Reflect-Line standards, is a type of calibration that supports two-port connections [4]. In this paper, we present the TRL calibration of the terahertz Spoof Surface Plasmon Polariton Waveguides (THz-SSPP WGs) that operate at 0.22 THz to 0.3 THz frequencies. In order to remove systematic errors, especially the errors of the transition circuit, the TRL calibration technique is used to setup the reference plane at the device under test (DUT).

The SSPP WG structure, which consists of two-sided corrugated structures, is given in Figure 1. The entire structure consists of Coplanar Waveguide, Transition and SSPP Structure. The transition circuit is necessary for the mode conversion between the CPW and SSPP WGs. The transition circuit proposed in *Unutmaz et.al*. [5] which is named as Transition-6 is utilized in all the designs in this paper, namely thru, reflect, line calibration kits and DUTs.

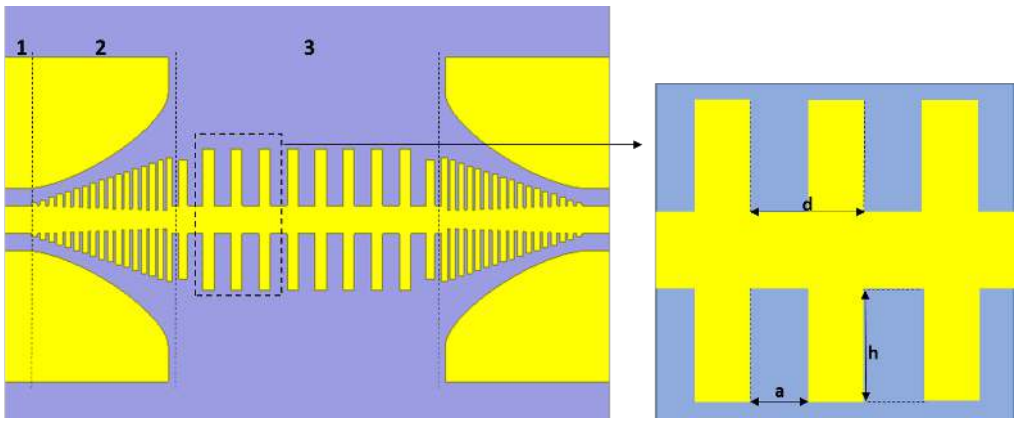
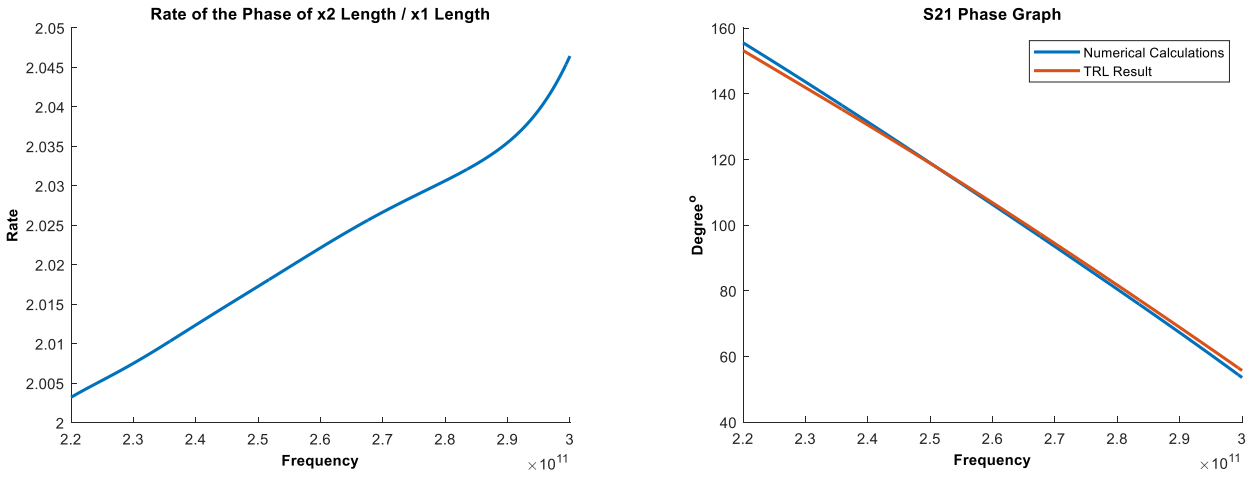


Figure 1. The schematics of SSPP WGs from top side (1) Coplanar waveguide section (2) Transition section (3) SSPP section

The ANSYS HFSS program is used for all the simulations. In simulations, Si substrate is used with ε_r=11.62

and ρ_{Si}=10 kΩ-cm and the Au metal is taken as σ_{Au}=28 MS/m. Two different DUT designs are designed with the same parameter values, the aperture (a) of 15 µm, the periodicity (d) of 25 µm, and the corrugation depth (h) of 50 µm, but in different periods. Applying the TRL calibration for the SSPP WGs, the real loss behavior of the DUTs is acquired. The phase difference between the 8 period and 16 period DUTs is presented in figure 2 (a), two times phase difference, which is theoretically expected, is obtained between both DUTs. Furthermore, by extracting the back-to-back transition from the whole SSPP WGs, numerical insertion phase is calculated and given in figure.2 (a). The insertion phase values of the TRL results and numerical calculations prove that the TRL calibration of the SSPP WGs is successful.



(a) **(b)**

Figure 2. Phase ratios of two different DUT designs after TRL calibration (a) Comparison of the phase values of DUTs obtained by numerical calculations and TRL calibration (b)

Y.C. acknowledge TUBITAK 2247-C (STAR) for their financial support. M.D acknowledges the partial support from the Scientific and Technical Research Council (TUBITAK) 2210A Grant. This work is financially supported by TUBITAK 119E489.

References

1. Lan, Y. C., & Chern, R. L. (2006). Surface plasmon-like modes on structured perfectly conducting surfaces. Optics express, 14(23), 11339-11347.
2. Huang, C. H., Lee, C. H., Hsieh, T. M., Tsao, L. C., Wu, S., Liou, J. C., ... & Fang, W. (2011). Implementation of the CMOS MEMS condenser microphone with corrugated metal diaphragm and silicon back-plate. Sensors, 11(6), 6257-6269.
3. Cinar, Y., Yildirim, S. S., Ozsahin, G., Unutmaz, M. A., & Unlu, M. (2021). Modelling terahertz spoof surface plasmon polariton waveguides using a circuit model. IEEE Transactions on Terahertz Science and Technology, 11(5), 557-565.
4. Elsherbeni, D., Jordan, L., Hutchcraft, E., Kajfez, D., & Gordon, R. K. (2008). The Design of a TRL Calibration Kit for Microstrip and its use for Measurement and Modeling of Active and Passive RF Components. The Applied Computational Electromagnetics Society Journal (ACES), 276-285.
5. Unutmaz, M. A., Ozsahin, G., Abacilar, T., & Unlu, M. (2021). Investigation of the transitions for coplanar waveguide to terahertz spoof surface plasmon polariton waveguides. IEEE Transactions on Antennas and Propagation, 70(4), 3002-3010.

Design of Subwavelength Confinement Waveguides at 1 THz Band

M. Demircioglu[1], M. A. Unutmaz[2], and M. Unlu[1*]

[1]TOBB University of Economics and Technology, Turkey
[2]Ankara Yildirim Beyazit University, Turkey
[*]corresponding author: munlu@etu.edu.tr

Abstract: In this paper, we present the design and simulation results of the Terahertz Subwavelength Confinement Waveguides (TSCW) operating at 1 THz. The design of the TSCWs includes CPW-to-TSCW transition circuits and the Spoof Surface Plasmon Polariton (SSPP)-based waveguides. The best-case simulation results exhibit return loss and insertion loss of -13.86 dB and -1.72 dB for the back-to-back (b-to-b) transition circuit and -26.5 dB and -4.66 dB for the TSCW with a total length of 267 µm at 1 THz, respectively.

The terahertz frequency range, which is between the microwave and infrared frequency bands, has unique abilities for applications such as imaging, sensing and communication [1]. Compact, on-chip and high-performance terahertz components are required in order to utilize the terahertz frequencies efficiently, one of the required terahertz components is the terahertz waveguides [2]. The Terahertz Subwavelength Confinement Waveguides (TSCW) are among the leading design methods to attain compact and high-performance waveguides [3]. Nevertheless, they are generally investigated at the sub-terahertz frequencies [3]-[5]. In this paper, we present the design steps of the CPW-to-TSCW transition and TSCW with optimum performance at 1 THz.

All the designed structures are simulated in ANSYS HFSS program. The metal is considered as Au with a conductivity of 28 MS/m and the Si substrate is taken with bulk resistivity of 10 kΩ/cm and relative permittivity of ε_r=11.62.

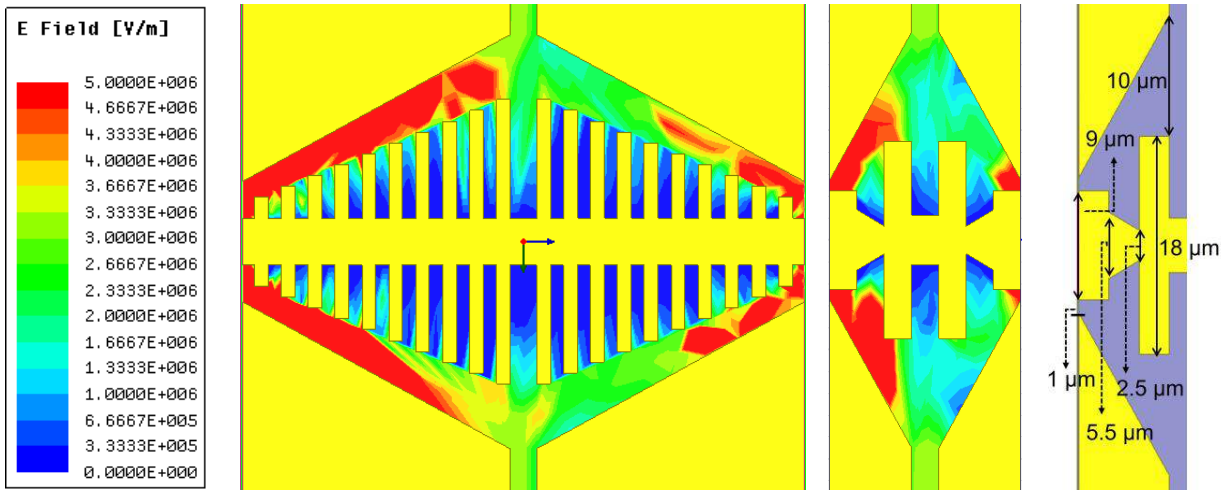
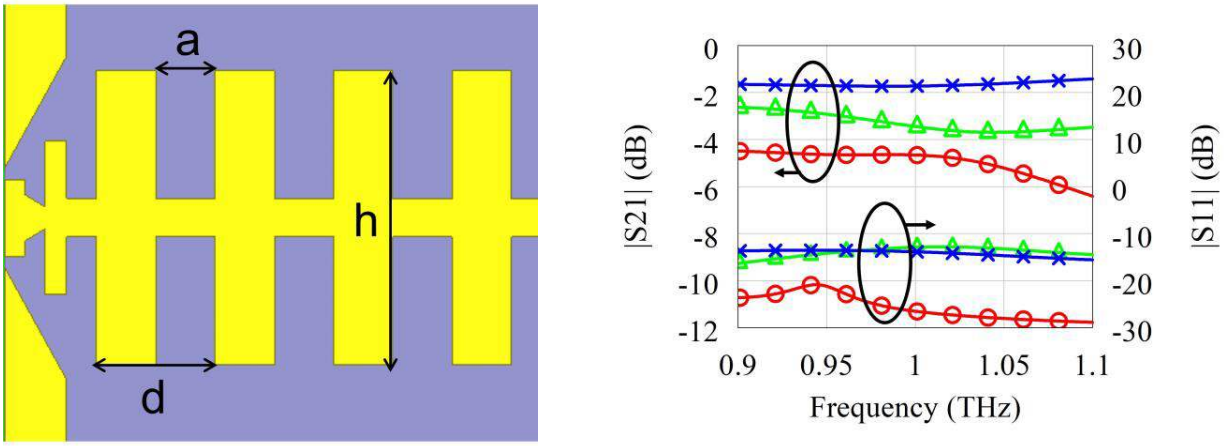


Figure 1. The electrical field distribution scale (a), electrical field distribution of TC-1 (b), electrical field distribution of TC-2 (c) and the physical lengths of TC-2 (d)

The first transition circuit (TC-1) is designed with adapting the transition circuits given in *Unutmaz. et.al.* to 1 THz [5]. The second transition circuit (TC-2) is designed from the TC-1 as analyzing the electrical field distribution and S-parameters of the simulation results. The electrical field distribution scale, electrical field

distribution of the CPW-to-TSCW transition circuits and the physical dimensions of the TC-2 are given in Figure 1. In addition to the electrical field distributions, the S-parameter results of the TC-1 and TC-2 is presented in Figure 2 and insertion losses of -3.44 dB and -1.72 dB at 1 THz, respectively. These results exhibit the advantage of TC-2 over TC-1.



(a) (b)

Figure 2. The schematic of the TSCW (a) and the S-parameter results (b) of the TC-1 (Δ), TC-2 (x) and TSCW (○)

With the TC-2, 267 µm length TSCW having a periodicity (d) of 14 µm, aperture width (a) of 7 µm and corrugation depth (h) of 15 µm is simulated. The simulation results of the TSCW are presented in Figure 2, the results show the return losses are lower than -20 dB between 0.9 THz and 1.1 THz and the insertion loss is -4.66 dB at 1 THz.

M.D acknowledges the partial support from the Scientific and Technical Research Council (TUBITAK) 2210A Grant. This work is financially supported by TUBITAK 119E489.

References

1. Mittleman, D. M. (2018). Twenty years of terahertz imaging. *Optics express*, *26*(8), 9417-9431.
2. Chiu, T. Y., & Li, C. H. (2021). Low-loss low-cost substrate-integrated waveguide and filter in GaAs IPD technology for terahertz applications. *IEEE Access*, *9*, 86346-86357.
3. Unutmaz, M. A., Ozsahin, G., & Unlu, M. (2021). Optimization of terahertz spoof surface plasmon polariton waveguides for maximum/dB performance. *Journal of Lightwave Technology*, *39*(17), 5508-5515.
4. Unutmaz, M. A., & Unlu, M. (2021). Spoof surface plasmon polariton delay lines for terahertz phase shifters. *Journal of Lightwave Technology*, *39*(10), 3187-3192.
5. Unutmaz, M. A., Ozsahin, G., Abacilar, T., & Unlu, M. (2021). Investigation of the transitions for coplanar waveguide to terahertz spoof surface plasmon polariton waveguides. *IEEE Transactions on Antennas and Propagation*, *70*(4), 3002-3010.

META 2023, PARIS - FRANCE, JULY 18 – 21, 2023

Metasurface-driven surface-enhanced infrared absorption spectroscopy for superior characterization of electrocatalytic reactions

Luca M. Berger[1‡], Malo Duportal[2‡], Leonardo de Souza Menezes[1,3], Emiliano Cortés[1], Stefan A. Maier[4,5,1], Andreas Tittl[1*], Katharina Krischer[2*]

[1]Faculty of Physics, Ludwig-Maximilian-University Munich, 80539 München, Germany

[2]Department of Physics, Technical University of Munich, 85748 Garching, Germany

[3]Departamento de Física, Universidade Federal de Pernambuco, 50670-901 Recife-PE, Brazil

[4]School of Physics and Astronomy, Monash University, Melbourne, Victoria, Australia

[5]Department of Physics, Imperial College London, SW7 2AZ London, United Kingdom

[*]corresponding author: andreas.tittl@physik.uni-muenchen.de; krischer@tum.de

Abstract: Understanding electrocatalytic processes is crucial to realize the transition toward a sustainable zero-carbon future. Surface-enhanced infrared absorption spectroscopy (SEIRAS) is a suitable method to monitor the mechanisms of these processes with chemical specificity. However, it remains difficult to detect many relevant aspects of electrochemical reactions such as short-lived intermediates. Here, we demonstrate an integrated nanophotonic-electrochemical SEIRAS platform for the *in-situ* investigation of molecular signal traces emerging during electrochemical experiments.

Working in an attenuated total internal reflection (ATR) geometry (Figure 1a), we detect *in-situ* the CO vibrational mode at 2033 cm^{-1} emerging during the electrochemical conversion of CO into CO_2 using a platinum nano-slot metasurface on a CaF_2 substrate (Figure 1b) by coupling its resonance to the molecular vibrational mode and analysing the perturbation of the intensity in reflection[1]. Pt is a catalytic material for many reactions, making this platform very useful not only for the CO oxidation reaction but also for other reactions. Nano-slots can be tuned to enhance the electric and magnetic near-fields (Figure 1c) due to the excitation of a magnetic dipole aligned parallel to the long axis of the slot.[2] We confirm the detection of adsorbed CO (Figure 1d-f) *via* the observation of the typical Stark shift and resolve a so far scarcely studied[3] effect due to the decrease of the CO coverage on the surface of platinum during the electrochemical oxidation (Figure 1e-f). Furthermore, the presence of a second peak at 2086 cm^{-1} on the spectral location of the linear vibrational mode could be attributed to the effect of the crystal orientation.

Compared to conventional unstructured platinum films, our nanophotonic-electrochemical platform delivers a 27-fold improvement of the experimentally detected characteristic absorption signals, enabling the detection of new species with weak signals, fast conversions, or low surface concentrations. By providing a deeper understanding of catalytic reactions, we anticipate our nanophotonic-electrochemical platform to open exciting perspectives for electrochemical SEIRAS, surface-enhanced Raman spectroscopy, and other fields of chemistry.

We thank Thomas Weber for his help with the temporal-coupled mode theory algorithms and Simon Stork for the platinum and titanium electron beam evaporation. This work was funded by the Deutsche Forschungsgemeinschaft (DFG, German Research Foundation) under grant numbers EXC 2089/1–390776260 (Germany′s Excellence Strategy) and TI 1063/1 (Emmy Noether Program), ERC-STG 802989 Catalight, the Bavarian program Solar Energies Go Hybrid (SolTech) and the Center for NanoScience (CeNS). S.A.M. additionally acknowledges the Lee-Lucas Chair in Physics and the EPSRC (EP/W017075/1).

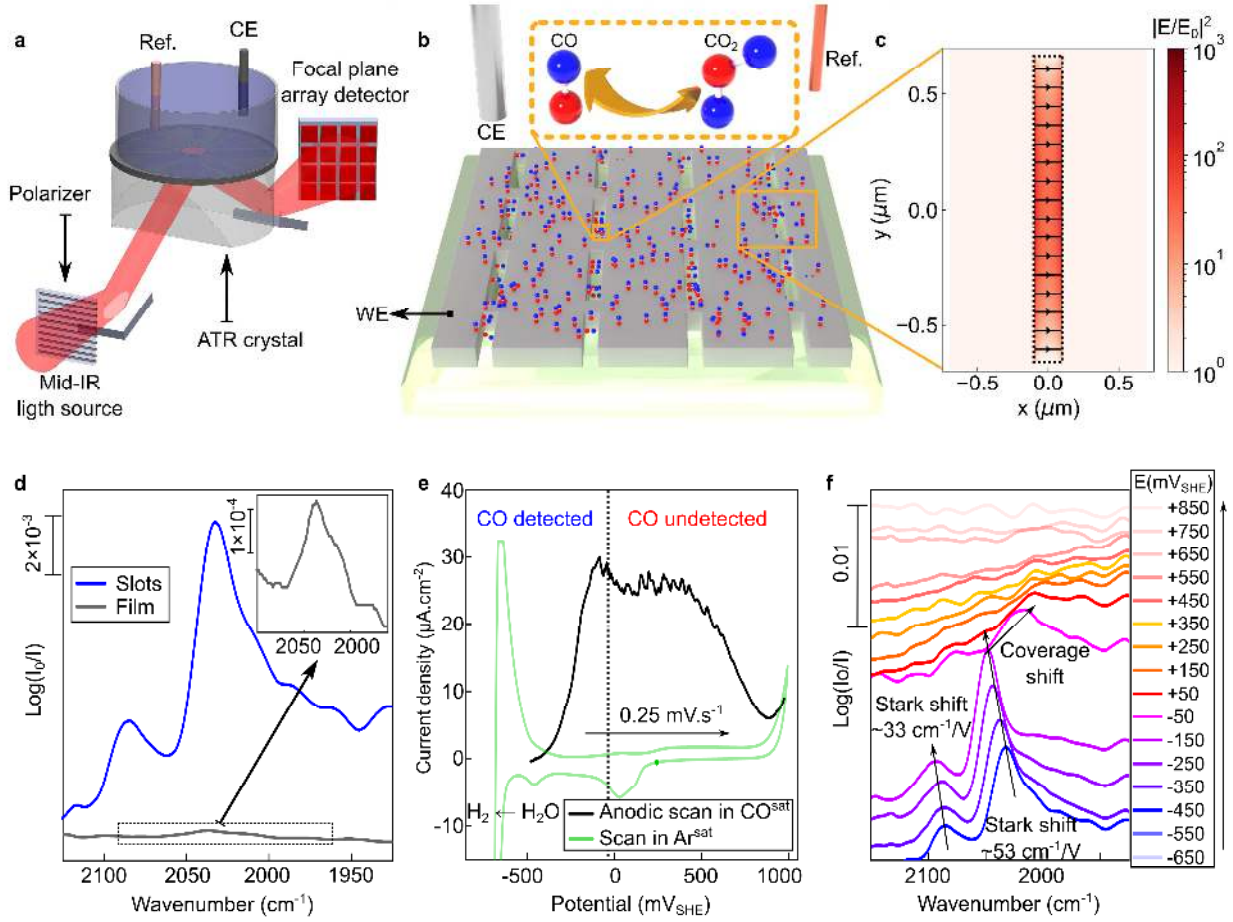


Figure 1: Schematic for the (a) ATR-SEIRAS configuration using the (b) Pt-based nano-slot metasurface for the *in-situ* integrated nanophotonic-electrochemical study of CO oxidation. As the potential between the working electrode (WE) and the reference electrode (Ref.) was swept the presence of adsorbed CO was monitored via the detection of the linear vibrational mode of CO at 2033 cm^{-1} with a Fourier transform infrared spectrometer. (c) Electric near field intensity (taken on film surface) of the unit cell including arrows (black) showing the direction of the electric field inside the slot. Comparison of CO_{linear} signals obtained in CO saturated electrolyte after 80 min of CO bubbling with a pure Pt layer (p-polarized light) and with the nanophotonic-electrochemical platform (s-polarized light). (e) Evolution of the current density with the potential during the anodic (from OCP to +1000 mV_{SHE}) in 0.5m K_2CO_3 saturated with CO at 0.25 $mV.s^{-1}$ (black line). For comparison, the green line depicts CVs in an Ar saturated electrolyte. (f) Evolution of SEIRAS spectra using s-polarized light with, the anodic scan acquired every 100 mV. Adapted from [1].

References

[1] L. M. Berger, M. Duportal, L. de S. Menezes, E. Cortés, S. A. Maier, A. Tittl, K. Krischer, "Improved in-situ characterization of electrochemical interfaces using metasurface-driven surface-enhanced infrared absorption spectroscopy," arXiv:2301.01993, 2023.

[2] C. Huck, J. Vogt, M. Sendner, D. Hengstler, F. Neubrech, and A. Pucci, "Plasmonic Enhancement of Infrared Vibrational Signals: Nanoslits versus Nanorods," *ACS Photonics*, Vol. 2, No. 10, 1489–1497, 2015.

[3] I. Villegas and M. J. Weaver, "Carbon monoxide adlayer structures on platinum (111) electrodes: A synergy between *in-situ* scanning tunneling microscopy and infrared spectroscopy," *J. Chem. Phys.*, Vol. 101, No. 2, 1648–1660, 1994.

META 2023, PARIS - FRANCE, JULY 18 – 21, 2023

A TD-DFT Approach for Polariton Chemistry:

Polaritonic and Charge Transfer Excitations in Azobenzene Photoisomerization

L. Cascino[1,2], S. Corni[3,4], and S. D'Agostino[1,2,5*]

[1]Mathematics and Physics Department "*E. De Giorgi*", University of Salento, Lecce 73100, Italy
[2]Institute of Nanotechnology, National Research Council (CNR-NANOTEC), Lecce 73100
[3]Dipartimento di Scienze Chimiche, Università di Padova, 35131 Padova, Italy
[4]CNR Istituto Nanoscienze, 41124 Modena, Italy
[5]Center for Biomolecular Nanotechnologies, Istituto Italiano di Tecnologia, Arnesano (LE) 73010
[*]corresponding author: stefania.dagostino@nanotec.cnr.it

Abstract: The desire to control the interaction between surface plasmons and quantum systems as cells, molecules, polymeric macromolecules has boosted the progress in theoretical and experimental techniques for the effective manipulation of such objects. The work here presented is somehow at the frontier between quantum chemistry and nanophotonics, providing, within the TD-DFT framework, a deeply understanding of the coupling mechanisms between the azobenzene photoswitch and a prototype plasmonic nanocluster, showing the effects of the localized plasmon on strong-coupling and charge-transfer phenomena.

Fabrication and characterization techniques are nowadays able to finely control light-matter interaction at sub-nanometer scales where classical electrodynamics fails. New theoretical frameworks able to overcome the limits of the classical vision and to fully take into account quantum mechanical effects (i.e. nonlocality, electron spill-out, charge transfer) are, thus, required. By means of a fully atomistic TDDFT approach, in this work we show how the potential energy surfaces for a photochemical system of practical interest as azobenzene, can be importantly modified by both classical electromagnetic and charge transfer effects in the presence of a metal nanostructure. Inspired by the pioneering work in 2012 by Ebbesen's group [1], polaritonic chemistry, i.e., the field caring of manipulating chemical structure and reactions through the formation of polaritons, hybrid half-light half-matter states, has become the attraction of several experimental and theoretical researches in the last few years. From a theoretical point of view, the problem of the perturbations induced on the potential energy surfaces of a molecule by photonic modes has been largely faced in the framework of Quantum Electrodynamics (QED) [2].
In this work a fully-QM scheme, based on an atomistic description in the linear response framework of the TD-DFT of both the matter and light components, is proposed to analyze a chosen isomerization pathway for an azobenzene molecule interacting with a plasmonic nanocluster put in its proximities (Fig. 1). Azobenzene represents one of the simplest photochromes able to interconvert between trans- and cis- forms. Despite its isomerization process has not yet been fully understood, numerous applications have been developed: in biomedicine, in bioimaging, in photopharmacology, etc. The metallic counterpart is a tetrahedral cluster of Ag_{20}. This choice is due to the fact that this cluster has a simple spectrum dominated by only one narrow excitation in the same spectra range of Azobenzene which can be associated to a localized plasmon [3]. Recent works have shown that the strong coupling between surface plasmon-polariton mode and excitons could lead to the formation of hybrid states, namely polaritons or plexcitons [4]. Here we show the onset of these new states for particular conditions and how these can modify the potential energy landscape of the molecule. Moreover we introduce a

new figure of merit defined *Polaritonic Index* (PI) which allow us to identify all the hybrid excitations and among them to distinguish polaritonic (Fig. 1) from charge-transfer states (Fig. 2).

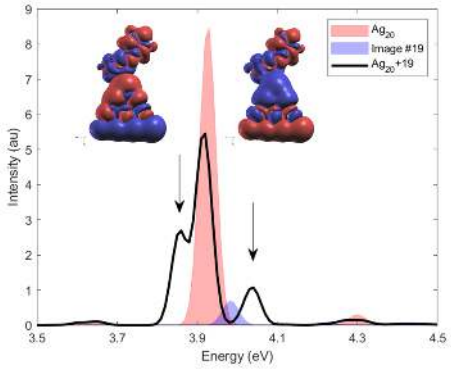


Fig. 1 Comparison between the TD-DFT absorption spectra of the isolated Ag, isomer #19 and the hybrid systems composed of Ag_{20} + isomer #19 (Gaussian broadening of 0.02 eV). Inset: transition densities of the lower and upper polaritonic states.

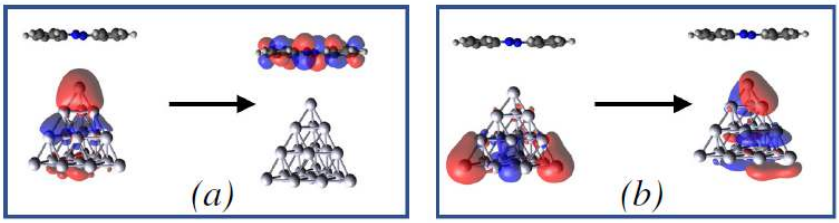


Fig. 2 First two Natural Transition Orbitals pairs for the lowest energy CT state appearing under S2.

While polaritonic states appear only in the barrier region, charge transfer excitations seem to be present along the selected isomerization pathway from trans- to cis- conformation in between S_1 and S_2, this possibly providing additional channels whose relevance is likely dependent on the relative molecule-metal distance and orientation [4]. The work has a double mission. From one side it shows how a theoretical scheme beyond classical EM descriptions is required to properly explain the physics underlying the interaction between metallic and molecular excitations. From the other one, it presents a possible scenario of plasmon-induced perturbations in the photoisomerization of a switch of practical interest, as azobenzene, opening the way to polariton chemistry applications.

References

1. Henzl, J., M. Mehlhorn, H. Gawronski, K.H. Rieder, and K. Morgenstern, "Reversible cis–trans isomerization of a single azobenzene molecule", Angew. Chem. Int, Vol. 45, No. 4, 603–606, 2006.
2. Feist, J., J. Galego, and F.J. Garcia-Vidal, "Polaritonic chemistry with organic molecules", ACS Photonics, Vol. 5, No. 1, 205-216, 2018.
3. D'Agostino, S., R. Rinaldi, G. Cuniberti and F. Della Sala, "Density functional tight binding for quantum plasmonics", J. Phys. Chem. C ., Vol. 122, No. 34, 19756– 19766, 2018.
4. Giannone, G., F. Della Sala and S. D'Agostino, "Atomistic investigation of hybrid plasmonic systems", Nanomater. Nanotechnol., Vol. 9, 1847980419856534, 2019.

Coherent coupling between the individual and collective excitations by radiative fields in nanoscale materials

T. Yokoyama[1*], M. Iio[1,2], T. Inaoka[3], and H. Ishihara[1,4]

[1]Department of Material Engineering Science, Osaka University, Japan
[2]Department of Physics and Electronics, Osaka Prefecture University, Japan
[3]Department of Physics and Earth Sciences, University of the Ryukyus, Japan
[4]Center for Quantum Information and Quantum Biology, Osaka University, Japan
[*]corresponding author: yokoyama.t.es@osaka-u.ac.jp

Abstract: Plasmon is a collective excitation by the longitudinal electron-electron interaction. The plasmon excitation radiates the transverse field. In this study, we formulate a microscopic self-consistent theory for the nonlocal electronic response and the Maxwell fields. The collective (plasmon) and individual (electron-hole pair) excitations are coupled coherently with each other by the longitudinal and transverse fields in nanostructures. This coherence means a bidirectional energy transfer between their excitations, which would provide an efficient hot carrier generation.

A light-matter interaction is one of the central subjects in physics. Plasmon is a collective excitation of electrons and provides rich applications, e.g., sensor, photovoltaics, photosynthesis, etc. The plasmon excitation is owing to the electron-electron interaction which is a part of longitudinal field. Hence electromagnetic field response due to the plasmon excitation has been discussed based on the Drude model in many studies. However, if material size is nanometer-scale, the nonlocal response due to a quantum coherence of electron wavefunctions should be significant and the phenomenological treatment must be extended. Then, the hydrodynamic Drude model has been developed [1,2], where the spatial gradient of current is incorporated into the Drude conductivity. On the other hand, for the atomic scale cluster, a microscopic description based on the first principle calculation has been developed [3], where the longitudinal component is treated with high accuracy. However, in the electromagnetic field response by the plasmons, the transverse field is induced and can cause the collective (plasmon) and individual (electron-hole pair) excitations. Therefore, for several tens to hundreds nanometer scale, a microscopic description with a self-consistent treatment of electronic response and Maxwell's equation including both the longitudinal and transverse component should be discussed [4,5].

In this study, for nanostructures, we develop the microscopic description with the self-consistent treatment of the nonlocal response and the Maxwell field [5]. In the formulation, the electronic response is described in terms of charge and current densities. The longitudinal and transverse fields are expressed by scalar and vector potentials, respectively. By this formulation, we can develop an understanding for th e collective and individual excitations based on both the longitudinal and transverse components. Our formulation reveals that the transverse field provides a coherent coupling between the

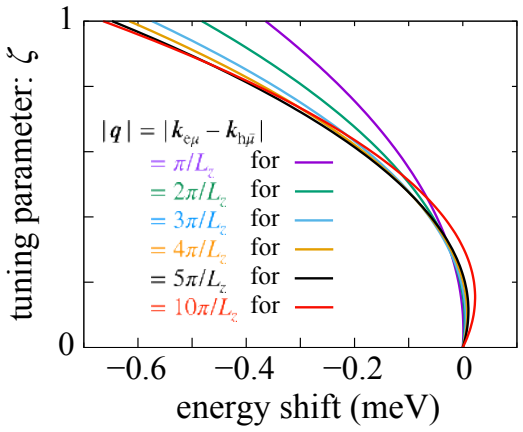


Fig. 1: Energy shift of collective excitation modulated by a tuning parameter ζ.

collective and individual excitations, which means bidirectional energy transfer between them.

Figure 1 shows energy shifts of the collective excitations by the transverse fields with small "wavenumbers" $|\boldsymbol{q}| = |\boldsymbol{k}_e - \boldsymbol{k}_h|$ of excitations in a rectangular nanoscale rod with L_z being the length of rod. Our parameter ζ tunes the contribution of transverse field, and $\zeta = 1$ ($\zeta = 0$) corresponds to full (no) contribution. We obtain finite shifts by the transverse field. As ζ approaches full contribution, the transverse field operates to lower the collective excitation energy. The shifts can be enlarged by a design of nanostructure and electromagnetic fields. Then, this result gives possibility of an enhancement of hot carrier generation due to the plasmon excitation.

Acknowledgments: T.Y. is supported by JSPS KAKENHI 18K13484 and Toyota Riken Scholar. H.I. is supported by JSPS KAKENHI 18H01151.

References

1. Svendsen, M. K., C. Wolff, A.-P. Jauho, N. A. Mortensen, and C. Tserkezis, "Role of diffusive surface scattering in nonlocal plasmonics," J. Phys.: Condens. Matter 32, 395702 2020, and related reference therein.
2. Mortensen, N. A. "Mesoscopic electrodynamics at metal surfaces - From quantum-corrected hydrodynamics to microscopic surface-response formalism," Nanophotonics Vol. 10, 2563–2616, 2021.
3. Ma, J., Z. Wang, and L.-W. Wang, "Interplay between plasmon and single-particle excitations in a metal nanocluster," Nat. Commun. Vol. 6, 10107 2015.
4. Svendsen, M. K., Y. Kurman, P. Schm idt, F. Koppens, I. Kaminer, and K. S. Thygesen, "Combining density functional theory with macroscopic QED for quantum light-matter interactions in 2D materials," Nat. Commun. Vol. 12, 2778 2021.
5. Yokoyama, T., M. Iio, T. Kinoshita, T. Inaoka and H. Ishihara, "Comprehensive microscopic theory for coupling of individual and collective excitations via longitudinal and transverse fields," Phys. Rev. B Vol. 105, 165408, 2022.

Reconfigurable Non-Volatile Silicon Photonics Using Ultralow-Loss Phase-Change Chalcogenide Sb_2Se_3

Sophie Blundell[1,2*], Daniel Lawson[1,2], David J. Thomson[1], Ioannis Zeimpekis[1], and Otto L. Muskens[2]

[1]Optoelectronics Research Centre, University of Southampton, UK
[2]School of Physics and Astronomy, University of Southampton, UK
[*]corresponding author: s.blundell@soton.ac.uk

Abstract: Antimony Selenide (Sb_2Se_3) is explored as an alternative to popular phase-change materials (PCMs), such as Ge-Sb-Te (GST), for modulation of light through silicon photonic devices. Previous investigations of Sb_2Se_3 have been limited by using thin surface films, where only the evanescent field is modulated. By creating waveguide structures where light travels directly through the PCM, greater modulation depths are achieved, resulting in a higher change in effective refractive index. Applications of this work include light routing, photomodulation and photonic computing.

We demonstrate an increased phase shift incurred for light travelling through thicker layers of Sb_2Se_3 using a novel method for increasing the modulation depth of devices. Recently, Sb_2Se_3 has gathered interest because it demonstrates very low losses at 1550nm, and due to its large refractive index contrast ($\Delta n \sim 0.77$ [1]). So far, this has only been explored for thin layers of Sb_2Se_3, which does not take advantage of the excellent matching of refractive indices between silicon and Sb_2Se_3, allowing low losses to be achieved even for large thicknesses. This is vital for creating high enough modulation to enable compact devices. By argon-ion etching into the SOI chip before then depositing the layer of Sb_2Se_3, light is modulated as it travels directly through the PCM, rather than evanescently coupling. A schematic of this method of fabrication is shown in Figure 1.

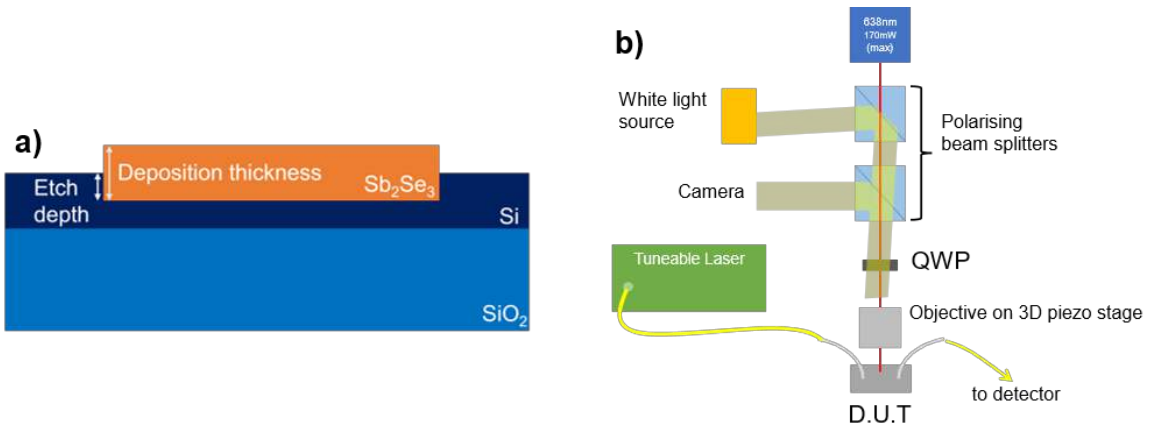


Figure 1: Demonstrating the variation in etch depth and deposition thickness of the different chips, b) diagram of switching set-up used to take data in Figure 2.

A chip was fabricated with 60nm etched out of the original sample and 80nm Sb_2Se_3 deposited into this gap. Measuring the devices on this chip with the PCM in both amorphous and crystalline (hot plate annealed) states showed a change in insertion loss.

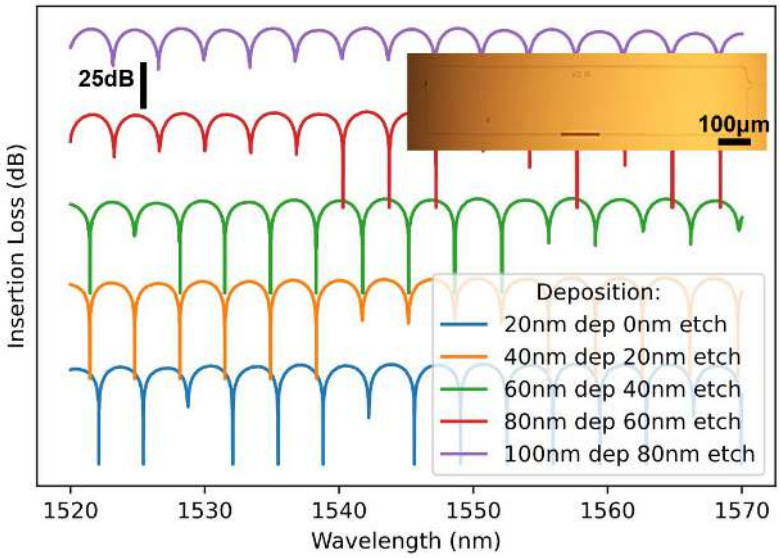


Figure 2: Spectral response of MZIs with 125µm length of Sb_2Se_3 on lower arm, vertically spaced to ease comparison between chips with differing depositions. Scale bar in y-direction of 25dB.

Further chips were fabricated with a range of etch depths and deposition thicknesses. Figure 2 shows the difference in Mach-Zehnder Interferometer (MZI) spectra found by increasing the depth of etch and subsequent deposition, demonstrating that the infiltration of Sb_2Se_3 into the device does not degrade it in the amorphous state.

This work shows the possible benefit of increasing the thickness and depth of Sb_2Se_3 used for photomodulation in SOI chips with multiple different devices. This has applications within neuromorphic computing, as a method for weighting photonic neurons. PCMs are sought after for such uses because they are capable of existing in multiple solid states that have different refractive indices, which can be switched between, thermally, electrically, or optically [2-4]. Integrating PCMs onto waveguide devices enables light travelling through the device to be directionally controlled and as such is a method for storing memories, or weighting neurons [5].

This work is funded by an EPSRC PhD studentship.

References

1. Rios, C., Du Q, Zhang Y. et al., "Ultra-compact nonvolatile photonics based on electrically reprogrammable transparent phase change materials," PhotoniX, Vol. 3, No. 26, 2022.
2. Miscuglio, M. and Sorger V. J., "Photonic tensor cores for machine learning," App. Phys. Revs., Vol. 7, No. 3, 031404 2020.
3. Wuttig, M. and Yamada, N., "Phase-change materials for rewriteable data storage," Nature Materials, Vol. 6, No. 11, 824-832, 2007.
4. Zhang, H., Yang X., Iu L. et al., "Comparison of the phase change process in a GST-loaded silicon waveguide and MMI," Opt. Express, Vol. 29, No. 3, 3503-3514, 2021.
5. Fang, Z., Zheng, J., Xu, P. et al., "Phase change material integrated silicon photonics: GST and beyond," Proc. SPIE, Vol. 11276, Optical Components and Materials XVII (2020).

High resolution plasmonic-based impedance microspectroscopy

Sidahmed A. Abayzeed

Optics and Photonics Research Group, Faculty of Engineering, University of Nottingham, University Park, Nottingham, NG7 2RD

This talk presents a novel optical imaging technique that is capable of mapping electrical impedance with submicrometric diffraction-limited resolution. The method presented is based on the widely used surface plasmon resonance imaging; an optical microscopy technology with an emerging application in label-free and non-scanning imaging of voltage. High resolution probing of electrical impedance is extremely important. For instance, it provides a way of studying electrical properties of living cells that use electrical signaling to communicate and regulate a range of physiological processes.

Measurements of electrical current and impedance is performed using plasmonic sensors that can be viewed as two-dimensional electrodes with optical readout. They are highly sensitive to external voltage. The principle of the technique is based on surface plasmon resonance that occurs due to optical excitation of electron density waves at the metal dielectric interface. Externally applied voltage alters the density of free electrons in metal surface and therefore changes the resonance position of the sensor. Gold thin film is commonly used to construct the sensing structure where sample under study is deposited or cultured in case of living cells. This metallic thin film is also used as a working electrode in combination with a proximal reference electrode. To perform impedance spectroscopy, a small alternating voltage is applied to the gold surface, against a reference electrode, resulting in a current flow across the electrolyte solution and the sample under the test. The real-time change in resonance position of the sensor is monitored that is directly proportional to the charge modulation. Voltage-modulated surface charge density varies spatially depending on the impedance of the object.

One of the major challenges of impedance imaging is that measurements are distorted by the crosstalk from the optical properties of the sample resulting in an inaccurate impedance mapping. In this talk, a correction method is presented that provides an effective way of separating the effect of optical properties and therefore produces quantitative measurements of dynamic electrical signals. The method is illustrated by mapping the impedance of Bovine Albumin Serum (BSA) patterns deposited on the gold film. BSA patterns were fabricated on the gold surface using micro-contact printing. Impedance microspectroscopy was performed by sweeping voltage between 1 and 100 Hz while computing impedance and current maps for each frequency. Local spectroscopic information was analysed using least square fitting to produce the equivalent electrical network of the sample. Within this frequency range, the surface capacitance has a dominant effect. Contrast in capacitance between the BSA and the gold background is observed. This is expected since the protein deposits have a lower static permittivity compared to the water molecules that constitute the dielectric properties of the double layer capacitor of the gold electrolyte interface. The technique shows a remarkable sensitivity being able to detect current as low as 0.1pA on a 0.5 micrometre scale. These findings demonstrate that this new impedance imaging technique is capable of revealing microscopic electrical properties with promising applications in studying cells and biomolecules.

META 2023, PARIS - FRANCE, JULY 18 – 21, 2023

Enhancing Optical Chirality Detection through Collective CD Resonance

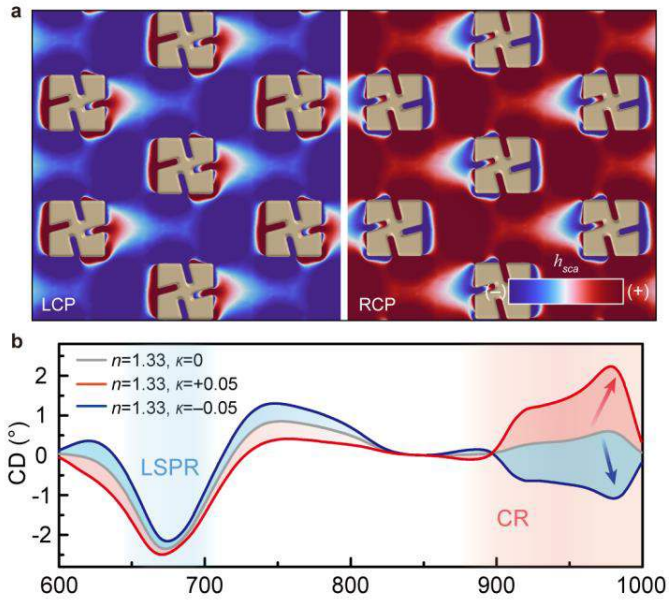
Ji-Hyeok Huh[1], Ryeong Myeong Kim[2], SeokJae Yoo[3], Tae Gyun Kim[4,5], Changwon Kim[4,5], Hyeohn Kim[2], Jeong Hyun Han[2], Nam Heon Cho[2], Yae-Chan Lim[2], Sang Won Im[2], EunJi Im[6], Jae Ryeol Jeong[7], Min Hyung Lee[7], Tae-Young Yoon[4,5], Ho-Young Lee[8], Q-Han Park[9], Ki Tae Nam[2] & Seungwoo Lee[1,6,10*]

[1]KU-KIST Graduate School of Converging Science and Technology, Korea University, Seoul, Republic of Korea.
[2]Department of Materials Science and Engineering, Seoul National University, Seoul, Republic of Korea.
[3]Department of Physics, Inha University, Incheon, Republic of Korea.
[4]School of Biological Sciences, Seoul National University, Seoul, Republic of Korea.
[5]Institute for Molecular Biology and Genetics, Seoul National University, Seoul, Republic of Korea.
[6]Department of Biomicrosystem Technology, Korea University, Seoul, Republic of Korea.
[7]Department of Applied Chemistry, Kyung Hee University, Seoul, Republic of Korea.
[8]Department of Nuclear Medicine, Seoul National University Bundang Hospital, Seongnam, Republic of Korea.
[9]Department of Physics, Korea University, Seoul, Republic of Korea.
[10]Department of Integrative Energy Engineering, Korea University, Seoul, Republic of Korea.
[*]corresponding author: seungwoo@korea.ac.kr

Abstract: Chirality discrimination plays a critical role in various scientific disciplines such as biology, chemistry, and pharmaceuticals. We propose a novel theoretical concept of collective CD resonances (CRs), which exhibit much stronger optical chiral hotspots over a broad region compared to conventional methods. As a result, we have successfully demonstrated the in situ determination of molecular chirality at the picomole level, with ultra-high sensitivity.

Determining the chirality of molecules is deemed a crucial challenge in several fields, including chemistry, biology, and pharmacology. The conventional method for analyzing molecular chirality, circular dichroism (CD), relies on measuring the difference in absorbance between two circularly polarized lights rotating in opposite directions. However, this method has the drawback of requiring a high-concentration sample and a long measurement time due to the mismatch in size between the molecules (a few Å) and light (a few 100 nm) being measured.

Since 2010, the concept of optical superchirality suggests that exposing molecules to a strong chiral optical environment leads to an enhancement of optical chiral response, and it has been established through both theoretical and experimental methods that the circular dichroism (CD) signals of chiral molecules can be significantly amplified in a chiro-optical environment[1]. Despite this, challenges in sensing at low concentrations have persisted due to the confined nature of conventional chiro-optical systems in local regions. To address this issue, we propose an extension of the traditional sensing theory, referred to as the extended chiral-sensing theory. Additionally, we seek to maximize the interaction between plane wave light and chiral molecules by incorporating the collective vibrations (CR) that occur in two-dimensional helicoid lattices, thereby enhancing the molecular CD signals[2].



Figures: Numerical simulation result of 2D helicoid crystal **a**. Spatial distribution of the $\boldsymbol{h}_{\mathbf{sca}}$ at CR mode under 60° oblique incidence of LCP (left) and RCP (right) light. The $\boldsymbol{h}_{\mathbf{sca}}$ values exhibit the same sign over the entire surface **b**. CD spectra ($\equiv T_{RCP} - T_{LCP}$) for media with $\kappa = 0$ (racemic), $\kappa < 0$ (D-molecules), and $\kappa > 0$ (L-molecules). The asymmetric shift in transmission spectra results in pronounced peak changes in CD spectra.

Acknowledgements, This research was supported by NRF-MSIT grant (2019R1A4A1028121), KU-KIST School Project, Korea University grant, NRF (2019R1A2C2004846), Basic Research Laboratory program (2022R1A4A1034315).

References

1. Tang, Y. et al., "Optical chirality and its interaction with matter," *Phys. Rev. Lett.* **104**, 163901–163904 (2010).
2. Kim. et al., "Enantioselective sensing by collective circular dichroism" *Nature* **612**, 470–476 (2022)

META 2023, PARIS - FRANCE, JULY 18 – 21, 2023

Experimental Realization of Quantum Walks near Synthetic Horizons on Photonic Lattices

C. Sheng*, R. Q. He, Y. L. Zhao, J. C Duan, Y. Wei, C. W. Sun, L.L Lu, Y. X Gong, S. N. Zhu and H. Liu

National Laboratory of Solid State Microstructures and School of Physics, Collaborative Innovation

Center of Advanced Microstructures, Nanjing University, Nanjing, Jiangsu 210093, China
*corresponding author: csheng@nju.edu.cn

Abstract: Recently, integrated photonic chips, particularly those with the aid of transformation optics, have simulated various aspects of curved spacetime. However, thus far, studying the influence of curved space on quantum entanglement on this type of platform has not yet occurred. Here, we propose and experimentally realize quantum walks of entangled photons near an emulated event horizon, resulting in a counterintuitive phenomenon of optical escape. Our study paves a tabletop platform for studying quantum entanglement in curved space.

Quantum walks (QWs), the quantum mechanics analog of classical random walks [1], are a powerful tool used in quantum computing and simulation. In contrast to classical random walks, QWs have the distinct advantages of coherent superposition and quantum interference, making them a compelling platform for simulating topological physical phenomena, constructing novel quantum algorithms, and realizing universal quantum computing. Recently, there has been an increasing interest in quantum effects in curved space [2-4] arising from quantum gravity, which is a great challenge field for unifying quantum mechanics and general relativity in modern physics. The salient example is the Hawking-Unruh effect, which has been well-emulated using a variety of quantum architectures. Nevertheless, methods to leverage the advances of QWs on photonic chips to study the quantum aspects of general relativity have rarely been investigated.

At the same time, recent years have witnessed remarkable progress in the highly efficient manipulation of electromagnetic waves on the subwavelength scale using metamaterials, as well as the production of various functional photonic architectures with unprecedented performance in integrated photonic chips. In particular, the emerging concept of transformation optics [5-6], a design method for controlling photons at a researcher's discretion, opens up unique possibilities for advancing the integration of complex functionalities in photonic circuits. Additionally, optical simulations of large-scale astrophysical phenomena using small-scale photonic chips [7]. Nevertheless, in all these experiments, simulations were carried out using either classical Gaussian or a single-photon wave packet, both of which could be explained classically. Based on this background, we propose the use of the QWs of entangled photons [8] to study quantum interference in a noninertial frame with a Rindler metric that is emulated by a nonuniform photonic lattice with the aid of transformation optics. Thus far, however, no experiments have been carried out for quantum interference of entangled photons in the emulated curved space using transformation optics.

Here, we present the first experimental observation of the QWs of entangled photons near an emulated event horizon. We exploit silicon-on-insulator (SOI) technology to fabricate a nonuniform silicon waveguide lattice with site-dependent coupling coefficients inspired by transformation optics (Fig. 1(a)). This technology can map the space around the event horizon of a Schwarzschild black hole. We find that QWs of single photons and two

indistinguishable photons exhibit optical trapping near the emulated event horizons, which is a well-known classical physical process due to the strong gravitational force of a black hole (Fig. 1(b), Fig. 1(c)). Intriguingly, for a certain type of path-entangled photon, there is a counterintuitive phenomenon of optical escape arising from quantum interference (Fig. 1(d)).

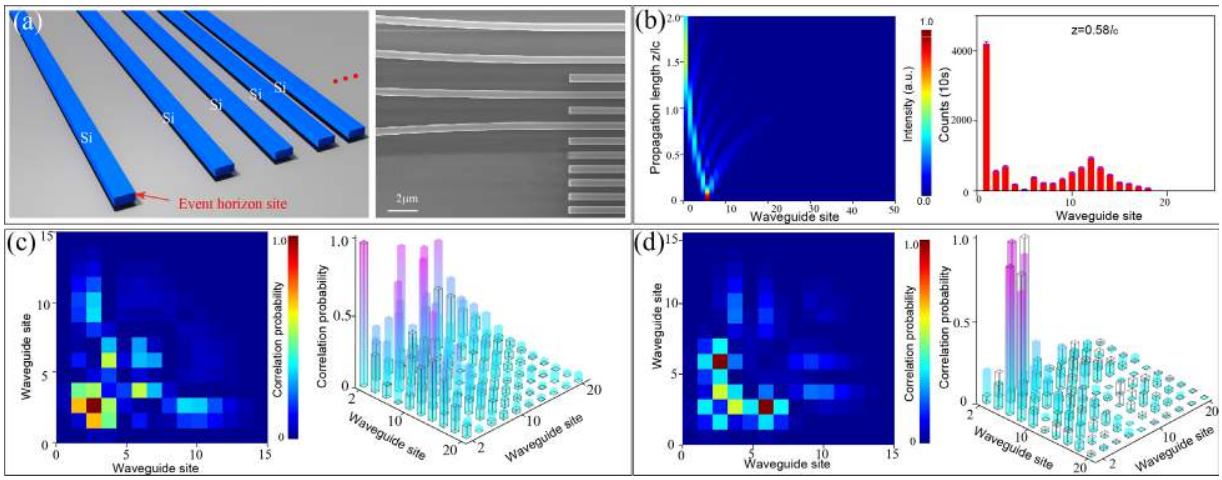


Fig.1 (a) Schematic of the nonuniform silicon lattice. (b), (c), (d) are respectively quantum walks of single photons, two indistinguishable photons and path-entangled photon.

In conclusion, we have experimentally realized the quantum walks of single photons, two indistinguishable photons, and entangled photons in the emulated event horizon using silicon photonics. To our knowledge, our work is the first to exploit silicon photonics to conduct QWs for simulating quantum effects in curved space. These types of nonuniform silicon photonic lattices inspired by transformation optics may provide a promising platform to study more challenging works about quantum mechanics and general relativity, such as the Anti-de Sitter/Conformal Field conjecture and loop quantum gravity.

References

1.Aharonov, Y., Davidovich, L. & Zagury, N. Quantum random walks. Phys. Rev. A 48, 1687-1690 (1993).

2.Di Molfetta, G., Brachet, M. & Debbasch, F. Quantum walks as massless Dirac fermions in curved space-time. Phys. Rev. A 88, 042301 (2013).

3.Arrighi, P., Facchini, S. & Forets, M. Quantum walking in curved spacetime. Quant.Info.Proc. 15, 3467-3486 (2016).

4.Wang, Y. et al. Quantum simulation of particle pair creation near the event horizon. Natl. Sci. Rev. 7, 1476-1484 (2020).

5. Pendry, J. B., Schurig, D. & Smith, D. R. Controlling electromagnetic fields. Science 312, 1780-1782 (2006).

6. Leonhardt, U. Optical conformal mapping. Science 312, 1777-1780 (2006).

7. Sheng, C., Liu, H., Wang, Y., Zhu, S. N. & Genov, D. A. Trapping light by mimicking gravitational lensing. Nat.Photon. 7, 902-906 (2013).

8. Sheng, C. et al. Simulating the escape of entangled photons from the event horizon of black holes in nonuniform optical lattices. Phys. Rev. A 103, 033703 (2021).

META 2023, PARIS - FRANCE, JULY 18 – 21, 2023

Ultrasmall and tunable TeraHertz surface plasmon cavities in the deep plasmonic regime

Ian Aupiais[1], Romain Grasset[1], Tingwen Guo[1], Dmitri Daineka[2], Javier Briatico[3], Sarah Houver[4], Luca Perfetti[1], Jean-Paul Hugonin[5], Jean-Jacques Greffet[5], Yannis Laplace[1]

[1]LSI, CEA/DRF/IRAMIS, CNRS, Ecole Polytechnique, Institut Polytechnique de Paris, Palaiseau, France

[2]LPICM, CNRS, Ecole Polytechnique, Institut Polytechnique de Paris, Palaiseau, France

[3]Unité Mixte de Physique, CNRS, Thales, Université Paris Saclay, 91767 Palaiseau, France

[4]Université Paris Cité, CNRS, Matériaux et Phénomènes Quantiques, F-75013, Paris, France

[5]Université Paris-Saclay, Institut d'Optique Graduate School, CNRS, Laboratoire Charles Fabry, 91127 Palaiseau, France

Abstract: I will discuss TeraHertz (THz) cavities exploiting the resonance of THz surface plasmons which achieve extreme plasmonic confinement of the EM-field together with a large tunability as compared to more conventional THz cavity architectures based on noble metals. Deep inside the plasmonic regime, the THz cavities exhibit strong signatures of electromagnetic nonlocality. Our work introduces a new platform for exploring nonlocal aspects in plasmonics at an unprecedentedly large, i.e. micrometer, scale and may open the door to many THz applications.

In optics, surface plasmons can provide an efficient confinement of light at visible/infrared frequencies, i.e. in the range of the plasma frequency of noble metals. On the other hand, the use of noble metals in most of the THz cavity architectures realized to date [1-5] does not harness the potential of THz surface plasmons for photon confinement. In this study, by relying on a THz plasmonic material, we manufacture THz cavities which exploit the resonance of localized THz surface plasmon modes [6].

Based on this, we demonstrate plasmonic confinement of free space THz radiation in cavities of mode volumes V_{cav} as small as $V_{cav}/\lambda_0^3 \sim 10^{-8}$ ($\lambda_0 =$ free space wavelength). We also demonstrate large temperature-tunability of the cavity resonances as compared to more conventional architectures. Finally, as the length scales of the smallest cavities manufactured become comparable to that of the microscopic degrees of freedom of the plasma, we find strong evidence supporting the onset of nonlocal EM interactions.

Our experimental results may open the door to a wide range of THz applications and will allow to explore surface plasmonic phenomena in a brand new regime of parameters and tunability that are not accessible at optical frequencies.

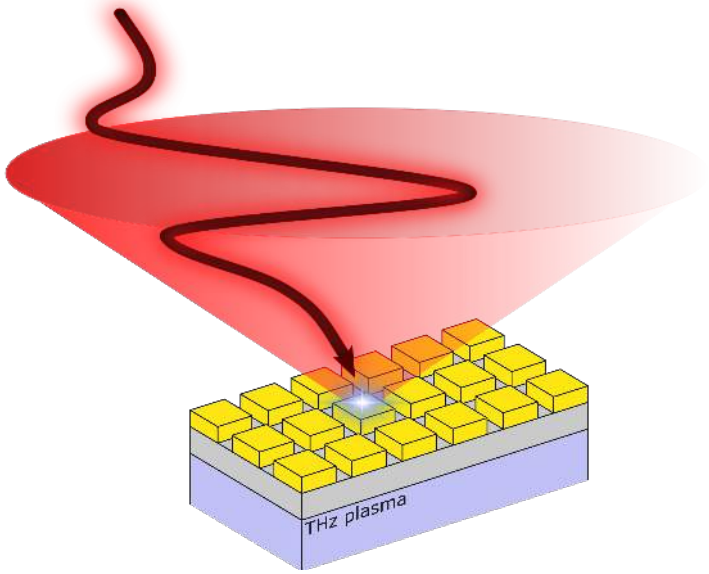


Fig 1: Sketch of THz photons getting trapped in a deeply sub-wavelength THz plasmonic cavity

Acknowledgements: this work was supported by Agence Nationale de la Recherche (grant n° ANR-17-CE30-0011-11) and Labex PALM (grant n° ANR-10-LABX-0039-PALM).

References

[1] W. J. Padilla, A. J. Taylor, C. Highstrete, M. Lee and R. D. Averitt, *Physical Review Letters,* vol. 96, p. 107401 (2006)

[2] C. Feuillet-Palma, Y. Todorov, R. Steed, A. Vasanelli, G. Biasiol, L. Sorba and C. Sirtori, *Optics Express,* vol. 20, p. 29121 (2012)

[3] C. Walther, G. Scalari, M. I. Amanti, M. Beck and J. Faist *Science,* vol. 327, p. 1495–1497 (2010)

[4] A. Mottaghizadeh, Y. Todorov, M. Cameau, D. Gacemi, A. Vasanelli and C. Sirtori, *Opt. Express,* vol. 25, p. 28718–28730 (2017)

[5] B. Paulillo, J. M. Manceau, A. Degiron, N. Zerounian, G. Beaudoin, I. Sagnes and R. Colombelli, *Opt. Express,* vol. 22, p. 21302 (2014)

[6] I. Aupiais, R. Grasset, T. Guo, D. Daineka, J. Briatico, S. Houver, L. Perfetti, J.-P. Hugonin, J.-J. Greffet, Y. Laplace (to be submitted, 2023)

Surface material dependance in tip enhanced Raman spectroscopy

Tim Parker*, Felix Schneider, Yang Zhao, Alfred J. Meixner, and Dai Zhang

Eberhard-Karls Universität Tübingen, Institute of Physical and Theoretical Chemistry, Germany
*corresponding author: tim-maikel.parker@uni-tuebingen.de

Abstract: Raman spectra may strongly be enhanced through the use of a sharp gold tip in close proximity to the samples surface. A great difference in the enhancement factor for the Raman spectra can be observed for various substrates and their surface properties.

Tip enhanced Raman spectroscopy (TERS) is a great technique to acquire optical and topological information from a large variety of samples [1,2].
In TERS a great deal of attention is paid to the tip, both to its material and geometry. The use of noble metal tips, either made of solid metal or a coating, such as gold or silver is common. The plasmonic properties of the tip must be in accordance with the incident lasers wavelength. The geometry of the tip plays a role in the enhancement of the electric field [3]. A smaller tip apex generally leads to a stronger amplification of the signal. For the probe scanning aspect of TERS, the geometry has an influence on the quality of the recorded topography.
For surface enhanced Raman spectroscopy, the surface of the sample is often reported to have a significant impact on the recorded spectra and is often varied accordingly [4-6].
The substrate on which TERS measurements are performed is often dictated by the sample of interest. In this work a dependence similar to surface enhanced measurements is investigated. The enhancement of Raman spectra is observed when the samples surface is varied.

Measurements were performed on a home built parabolic mirror scanning confocal microscope. The tip used was etched from gold wire. Tip sample distance was controlled using shear force feedback. Two different substrates were used: a glass surface and a smooth gold film.

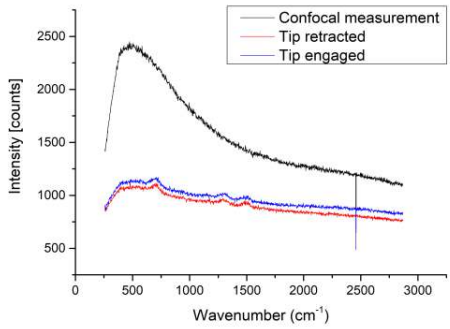


Figure 1: Comparison of confocal and TERS measurements on glass

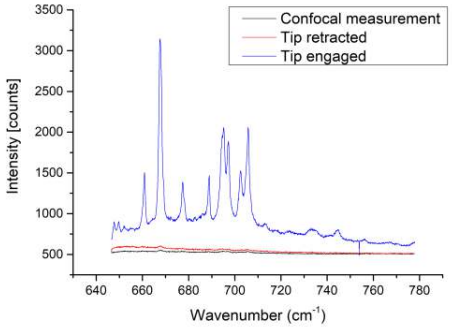


Figure 2: Comparison of confocal and TERS measurements on smooth gold

In both figures presented a clear trend can be observed. For Figure 1 which was recorded on glass very little difference can be seen with either engaged or retracted tip. A comparably low Raman enhancement can be concluded. The confocal measurement shows luminescence which is absent in the TERS spectra. For the smooth gold surface, shown in Figure 2, a very strong Raman enhancement can be seen. Additionally, the clarity of the spectrum is greatly improved, with many peaks which cannot be seen in confocal measurements becoming visible. The TERS measurement with tip retracted shows a slight increase in intensity compared to the confocal measurement. For the smooth gold film an enhancement factor of $4 \cdot 10^3$ can be calculated.

It can be concluded that for varying surfaces the TERS enhancement can be strongly different. For glass surfaces a slight enhancement of the Raman signal can be observed. For the smooth gold film, a significant increase in the Raman signal can be found.

Acknowledgement

This work was financially supported by both the German Research Foundation (Nos. ZH 279/13-1 and ME 1600/21-1) and the Chinese Scholarship Council.

References

1. Chen, Y.-T. et al. (2019) “Charge transfer and electromagnetic enhancement processes revealed in the SERS and Ters of a COPC thin film,” Nanophotonics, 8(9), pp. 1533–1546.
2. van den Berg, M. et al. (2020) “Revealing the local crystallinity of single silicon core–shell nanowires using tip-enhanced Raman spectroscopy,” Beilstein Journal of Nanotechnology, 11, pp. 1147–1156.
3. Blum, C. et al. (2014) “Tip-enhanced Raman spectroscopy - an interlaboratory reproducibility and comparison study,” Journal of Raman Spectroscopy, 45(1), pp. 22–31.
4. Abdelsalam, M.E. et al. (2005) “Electrochemical SERS at a structured gold surface,” Electrochemistry Communications, 7(7), pp. 740–744.
5. Sackrow, M. et al. (2008) “Imaging nanometre-sized hot spots on smooth au films with high-resolution tip-enhanced luminescence and Raman near-field optical microscopy,” ChemPhysChem, 9(2), pp. 316–320.
6. Zhang, D. et al. (2010) “Nanoscale spectroscopic imaging of Organic Semiconductor Films by Plasmon-Polariton coupling,” Physical Review Letters, 104(5).

Plasmonic single-nanoantennas enabling fast and nanoscale-controllable insulator-to-metal transition of VO_2

Luca Bergamini[1,2*], Bigeng Chen[3], Daniel Traviss[3], Yudong Wang[3], Cornelis H. de Groot[3], Jeffrey M. Gaskell[4], David W. Sheel[4], Nerea Zabala[1,2], Javier Aizpurua[2], and Otto L. Muskens[3]

[1]Department of Electricity and Electronics, FCT-ZTF, UPV-EHU, Bilbao 48080, Spain
[2]Materials Physics Center, CSIC-UPV/EHU and DIPC, San Sebastian 20018, Spain
[3]Physics and Astronomy, University of Southampton, Highfield, Southampton SO17 1BJ, United Kingdom
[4]Materials and Physics Research Centre, University of Salford, Manchester, M5 4WT, United Kingdom
[*]corresponding author: luca.bergamini@ehu.eus

Abstract: The VO_2 attracts wide interest for its insulator-to-metal transition when heated-up above the relatively low critical temperature of 68˚C. Plasmonic nanoantennas are known to concentrate light at the nanoscale around their surface when resonantly illuminated in the Vis-NIR. Here we show how this nanoantennas plasmonic feature can be used to steer and control a fast and nanoscaled insulator-to-metal transition in a VO_2 film. We investigated the effect of a single nanoantenna, which is the smallest unit-block.

Introduction

Gold single nanoantennas are well-known for addressing plasmon excitations when illuminated at a specific wavelength [1], giving rise to, e.g., enhanced light extinction and electromagnetic field concentration close to the antenna surface [2]. Due to these properties, plasmonic antennas are often combined with active materials, namely materials whose properties change under the application of an external stimulus, to obtain metasurfaces with enhanced optical properties [3–5]. Among phase transition materials, VO_2 is one of the most studied because its insulator-to-metal transition, induced by heating, occurs at relatively low critical temperature (68˚C).

In a previous study we showed that it is possible to originate a picosecond phase transition in a VO_2 film by using plasmonic nanoantenna lattices [5]. In this combined experiential-theoretical investigation, we show how a single plasmon nanoantenna can be used to induce and actively control the reversible phase transition in a VO_2 film down to the nanoscale [6]. The determination of the properties of the single antenna coupled to VO_2, which can be used as a building-block in nanodevices, is fundamental for the design and miniaturization of nanoscaled nonlinear optical devices and switches.

Results and Discussion

A gold single nanoantenna with size 312 nm x 105 nm x 50 nm (length x width x height) was fabricated by e-beam lithography on top of a 50 nm thick VO_2 film, which was deposited on a glass substrate. The spatial modulation microscopy (SMM) technique was used for single-antenna spectroscopy, namely to obtain the normalized spatial modulation transmission of the single antenna $(-\Delta DT/T)_{SMM}$, where ΔT is connected to the difference between the transmission of the system with and without the antenna. A pump laser (λ_{laser} = 1060 nm) illuminates the antenna-VO_2 hybrid for 10 ps with a polarization either parallel or perpendicular to the antenna length, and after 40 ps from the pump switching off, the spatial modulation transmission of the system is recorded by a probe laser characterized by a polarization parallel to the antenna length. Figure 1A shows the $(-\Delta DT/T)_{SMM}$ obtained under no pump (black curve) and a 0.6 nJ pump with polarization parallel (blue curve) and perpendicular (red curve) to the antenna length. The peak in the spectra is ascribable to the plasmon excitation in the antenna. For both polarizations the pump produces a red-shift of the peak and a decrease of the

optical response, with respect to the unpumped system, with the perpendicular pump providing more effect on the antenna response.

Numerical hybrid optical-thermal multiphysics simulations via the Finite-Element-Method were performed to obtain the theoretical normalized differential transmission with and without the antenna $(-\Delta DT/T)_{th}$. The simulated electromagnetic-illumination and heat diffusion reveal the presence, at the probing time, of hot-spots in the VO_2 around the nanoantennas where the temperature is higher than the initial one of 45˚C (yellow-to-white regions in the colormaps of Figure 1C and 1D). To obtain the $(-\Delta DT/T)_{th}$, to be compared with $(-\Delta DT/T)_{SMM}$, we changed the permittivity of the VO_2 around the nanoantenna according to the obtained temperature maps and then we calculated the optical response. For accurate results, a bi-dependent temperature-wavelength modelling of the complex permittivity of the VO_2 was developed. The theoretical results, displayed in Figure 1B, are qualitatively in agreement with the experiments, confirming that our modelling is well-suited. The red-shift of the plasmon peak for the pumped systems is due to the creation of VO_2 regions around the antenna where the permittivity decreases, even if a metallization is not reached. Even if this higher temperature is not enough to obtain a complete metallization (observed for T>90˚C), the reached value leads to a permittivity close to zero, making the system of interest for applications based on epsilon-near-zero materials. The dependence of the size, shape and position of the hot-spots on the pump polarization explains the difference observed between the blue and red curves of Figure 1A and 1B.

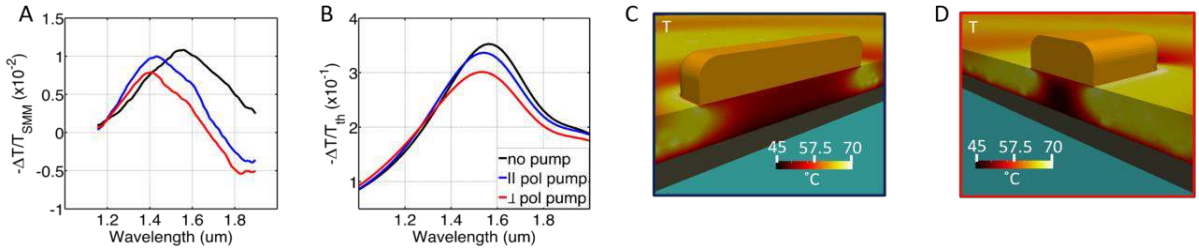


Fig. 1. (A) Measured $(-\Delta DT/T)_{SMM}$ and (B) simulated $(-\Delta DT/T)_{th}$ of the system as a function of the probe wavelength. (C, D) Colormap of the temperature in the system under pumping (C) parallel and (D) perpendicular to the antenna length.

References

1. V. Giannini, A. I. Fernández-Domínguez, S. C. Heck, and S. A. Maier, “Plasmonic nanoantennas: Fundamentals and their use in controlling the radiative properties of nanoemitters,” Chem. Rev., Vol. 111, No. 6, 3888–3912, 2011.
2. J. A. Schuller, E. S. Barnard, W. Cai, Y. C. Jun, J. S. White, and M. L. Brongersma, “Plasmonics for extreme light concentration and manipulation,” Nat. Mater., Vol. 9, No. 3, 193, 2010.
3. N. Maccaferri, L. Bergamini, M. Pancaldi, M. K. Schmidt, M. Kataja, S. v. Dijken, N. Zabala, J. Aizpurua, and P. Vavassori, “Anisotropic nanoantennabased magnetoplasmonic crystals for highly enhanced and tunable magneto-optical activity,” Nano Lett., Vol. 16, No. 4, 2533–2542, 2016.
4. G. Armelles, L. Bergamini, N. Zabala, M. U. Gonzlez, F. Garca, R. Alvaro, J. Aizpurua, and A. Cebollada, “Broad band infrared modulation using spintronicplasmonic metasurfaces,” Nanophotonics, Vol. 8, No. 10, 1847–1854, 2019.
5. O. L. Muskens, L. Bergamini, Y.Wang, J. M. Gaskell, N. Zabala, C. De Groot, D.W. Sheel, and J. Aizpurua, “Antenna-assisted picosecond control of nanoscale phase transition in vanadium dioxide,” Light Sci. Appl., Vol. 5, No. 10, e16173, 2016.
6. L. Bergamini, C. Bigeng, D. Traviss, Y. Wang, C. De Groot, J. M. Gaskell, D. W. Shee, N. Zabala, J. Aizpurua, and O. L. Muskens “Single-nanoantenna driven nanoscale control of the VO2 insulator to metal transition,” Nanophotonics, Vol. 10, No. 14, 3745–3758, 2021.

Orbit–Orbit Interaction of Light: Harnessing Vortex–Trajectory Interplay for Light Manipulation

Raghvendra P. Chaudhary[1], **Avraham Reiner**[1], **Nir Shitrit**[1*]

[1]School of Electrical and Computer Engineering, Ben-Gurion University of the Negev, Beer Sheva 8410501, Israel
[*]Corresponding author: nshitrit@bgu.ac.il

Abstract: The orbit–orbit interaction of light is the interaction between the intrinsic and extrinsic orbital angular momenta associated with optical vortex beams and varying beam trajectories, respectively. We report the orbit–orbit interaction of light in a plasmonic ellipse cavity, whose unique geometry facilitates vortex–trajectory interplay when a vortex is considered in one of the foci of the ellipse. This interaction, manifested by vortex-dependent shifts, opens a new paradigm for light manipulation by leveraging the manifold vortex states.

Light can carry three types of angular momenta: a spin angular momentum, an intrinsic orbital angular momentum (OAM), and an extrinsic OAM (1). These momenta are associated with the handedness of the circular polarization, optical vortex beams with helical phase fronts, and varying beam trajectories, respectively (1). The interplay between these momenta yields the spin–orbit interaction (SOI) of light (2), in which the spin (circular polarization) controls the spatial (orbital) degrees of freedom of light: either the extrinsic OAM (trajectory) or the intrinsic OAM (vortex). By providing a toolbox for spin-controlled light manipulations, the SOI plays a crucial role in the new reality of nano-optics. However, while the SOI of light has been studied extensively (2,3), the interaction between the intrinsic OAM and the extrinsic OAM—the orbit–orbit interaction (OOI) of light—has remained elusive. In this nontrivial interplay, the helical phase fronts of optical vortices control the spatial trajectory of light, which gives rise to vortex-dependent shifts of optical beams. Strikingly, the OOI of light significantly enhances the toolbox available for controlling light by leveraging the *manifold* OAM states for vortex-controlled light manipulation, in contrast to SOI-based light manipulation (2,3), which exploits the *binary* polarization helicity.

Here, we report the OOI of light in a plasmonic ellipse cavity, whose unique geometry facilitates the OOI when a vortex is considered in one of the foci of the ellipse. In this configuration, the OOI between the intrinsic OAM and the extrinsic OAM is achieved by the interplay between the vortex of the source and the ellipse-induced transverse shift of the source beam, positioned at one of the focal points. The OOI of light in the plasmonic ellipse cavity induces transverse vortex-dependent shifts, i.e., shifts that depend on both the vortex helicity and strength, at the second focal point (Fig. 1).

To demonstrate the OOI of light, we investigated a plasmonic cavity, defined by an ellipse Bragg grating, in which a source of intrinsic OAM is considered in one of the foci of the ellipse (Fig. 2B). The ellipse cavity was chosen due to its unique geometric property, i.e., a curve on a plane surrounding two focal points, such that for every point on the curve, the sum of the distances to the two focal points is constant. Therefore, if we place a source without an intrinsic OAM (a Gaussian beam) at one of the foci of the ellipse cavity, then, according to Fermat's principle, we expect the source to be perfectly "imaged" to the second focal point (Fig. 2B). Conversely, if the source carries an intrinsic OAM, we expect to reveal transverse vortex-dependent shifts at the

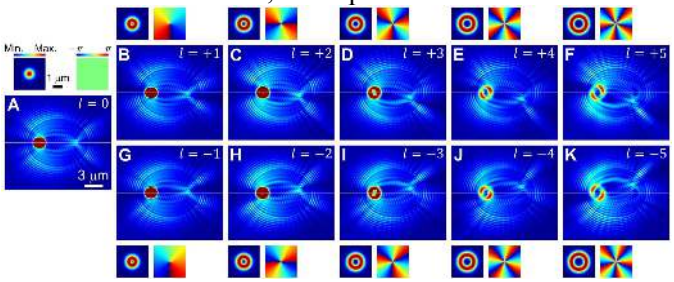


Fig. 1. Intensity and phase profiles of the Laguerre–Gaussian source beam with a topological charge l are shown in the left and right insets, respectively. (**A**) Simulated near-field intensity map of the plasmonic ellipse cavity for $l = 0$, where a transverse shift from the right focal point is not observed. (**B**–**F**) Simulated near-field intensity maps for $l = +1$ to $+5$, respectively. (**G**–**K**) Simulated near-field intensity maps for $l = -1$ to -5, respectively. The horizontal symmetry lines reveal the vortex-dependent shifts.

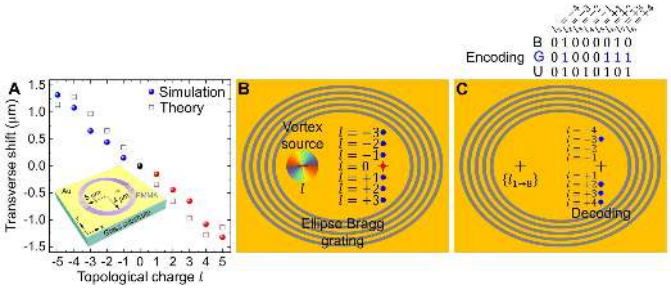


Fig. 2. (**A**) Dependence of the transverse shift on the topological charge l of the source beam. The inset shows the simulated structure. (**B**) Vortex-dependent shifts induced by the OOI of light in the plasmonic ellipse cavity. (**C**) On-chip information processing based on the OOI by encoding information (e.g., using ASCII binary strings) via the different vortex states $\{l_{1\to 8}\}$ in the superposed source beam, and decoding the information via the spatially separated vortex-dependent shifts.

second focal point (Fig. 2B). This anticipated observation is the manifestation of the OOI of light, where the helical phase fronts of optical vortices control the spatial trajectory of light. Uniquely, the geometric property of the ellipse makes it an excellent candidate to study the OOI via the interplay between the vortex of the source and the ellipse-induced transverse shift of the source beam, positioned at one of the focal points.

We performed numerical simulations to observe the vortex-dependent shifts in the plasmonic ellipse cavity by using a finite-difference time-domain algorithm to calculate the electromagnetic near fields. We considered an ellipse with semi-major and semi-minor axes of 5 μm and 4 μm, respectively (Fig. 2A, inset). To define the plasmonic ellipse cavity, we introduced an air–PMMA–gold structure to realize the ellipse Bragg grating, that defines the plasmonic ellipse cavity by encircling it and provides high reflectivity for the SPPs by satisfying the Bragg condition. For the source, we realized Laguerre–Gaussian beams carrying an intrinsic OAM determined by the topological charge of the vortex $l = 0, \pm 1, \pm 2,\ldots$—an integer representing the phase increment around the singular vortex core. We considered normally incident beams at the wavelength of 810 nm and a varying topological charge l (Fig. 1, insets). This vortex source was positioned at the left focal point of the ellipse and the incident polarization was set to be linear (zero spin angular momentum).

Figure 1 shows the simulated near-field intensity distributions of the plasmonic ellipse cavity for different topological charges l of the source. The test case of a source without a vortex, i.e., a Gaussian beam with $l = 0$, shows the expected result—the source is "imaged" to the right focal point due to the unique geometry of the ellipse (Fig. 1A). Conversely, once the vortex is introduced by the source beam, vortex-dependent shifts from the right focal point are clearly observed (Figs. 1B–1K). This observation stems from the OOI in the plasmonic ellipse cavity, which enables the interplay between the vortex of the source beam and its transverse shift, induced by the ellipse, once the source is positioned at one of the focal points. Figure 2A shows the dependence of the shift, extracted from the intensity patterns, on the topological charge of the source beam. In this effect, the shift depends on both the vortex helicity and strength, such that higher values of intrinsic OAM result in larger shifts. Moreover, we derived a theoretical wave interference model by which we calculated the vortex-dependent shifts that exhibit good agreement with the simulated results (Fig. 2A).

Owing to the inherent orthogonality of OAM beams and the linear nature of the OOI, this interplay can be harnessed to enable both the multiplexing and demultiplexing of OAM beams—which is desired for high-capacity optical communications (4). Figures 2B and 2C show a proof-of-concept demonstration for information processing via on-chip OAM demultiplexing based on the OOI by encoding information via different vortex states and decoding it via the spatially separated vortex-dependent shifts.

In summary, we report the OOI of light in a plasmonic ellipse cavity, whose unique geometry facilitates the vortex–trajectory interplay when a vortex is considered in one of the foci of the ellipse. By utilizing the multiple OAM states as a new degree of freedom in light manipulation, the OOI offers great potential for OAM-supported applications, including high-bandwidth optical communication and quantum information processing, enhanced resolution in imaging and microscopy, control of matter by optical trapping and tweezing, and many more.

References

1. Allen, L. *et al.* "*Optical Angular Momentum*," (IOP Publishing, Bristol, 2003).
2. Bliokh, K. Y. *et al.* "Spin–orbit interactions of light," Nat. Photonics, 9, 796–808, 2015.
3. Shitrit, N. *et al.* "Spin-optical metamaterial route to spin-controlled photonics," Science, 340, 724–726, 2013.
4. Wang, J. *et al.* "Terabit free-space data transmission employing orbital angular momentum multiplexing," Nat. Photonics, 6, 488–496, 2012.

Low Loss All-Oxide Plasmon-Assisted Electro-Optic Modulator

D. Fomra[1], Md. Sojib[2], V. Avrutin[2], Ü. Özgür[2], A. Agrawal[1], H. J. Lezec[1], and N. Kinsey[2]

[1]National Institute of Standards and Technology, Gaithersburg, MD 20899, USA.
[2]Department of Electrical and Computer Engineering, Virginia Commonwealth University, Richmond, VA 23284, USA.
*Corresponding Author: dnf4@nist.gov

Abstract: To address the growing need of energy efficient (~100's of fJ/bit) and high-speed (100's of GHz) optical components, we design, fabricate, and optically characterize an all-oxide ENZ plasmon-assisted modulator based on sputtered ITO and a planar Si slot waveguide. For an 8-um long device, simulations predict a low insertion loss (< 0.2 dB), a modulation depth of 9 dB, an RC-limited speed of 333 GHz, and a switching energy consumption of 480 fJ.

Telecommunications applications and technologies have rapidly evolved over recent decades, evolving from slow (kbps) point-to-point communications from between home and offices to universally connected devices. This tremendous growth has been supported by a deeper penetration of optical technologies such as fiber to home (FTTH), short distance fiber communication (within data centers), and massive parallelism. However, as 5G and millimeter-wave technologies become more ubiquitous, a growing need exists for optical components that are more energy-efficient and provide a bandwidth closer to that of the carrier wave. Indeed, current devices are limited in optical bandwidth to speeds about a thousand times slower than what can be theoretically accommodated by the carrier signal.

State-of-the-art optical modulators leverage active dielectric optical materials such as Si, Si_3N_4 or $LiNbO_3$. The relatively weak tunability of typical electro-optic materials nonlinearities, lead to devices requiring light-matter interaction lengths that limit the frequency of operation, such as long waveguide interferometers with large capacitive footprints (f ~ 1/RC) or high-quality-factor ring resonators with long ring-down times (f ~ 1/Q) [1,2]. On the other hand, plasmonic devices offer great potential for addressing some of the limitations of silicon photonics. Recent literature has demonstrated plasmonic modulators realizing speeds > 600 GHz in compact footprints (<20 μm^2) [3]. However, high insertion loss and on-state transmission efficiencies of ~10% have restricted the practicality of these devices.

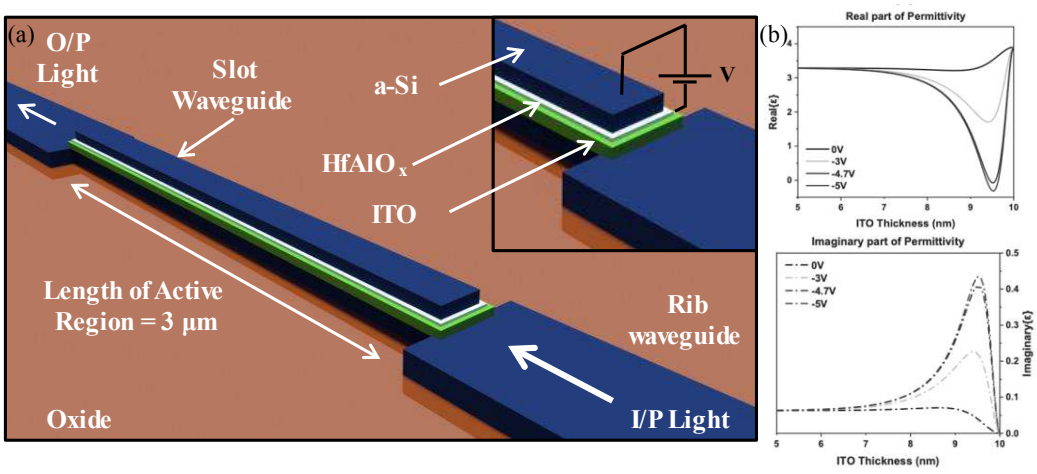


Figure 1: Proposed vertical alternative to the horizontal slot design, (b) Real and imaginary part of permittivity within ITO as a function of gate voltage and position within the ITO layer (COMSOL simulations)

To overcome the speed, transmission, and insertion-loss limitations of both dielectric and plasmonic electro-optic modulators to date, we realize a Si waveguide modulator incorporating an active layer of indium tin oxide ITO in a slot configuration, which combines the high-speed benefits of metal-based plasmonic devices with the low-loss advantages of dielectric-based photonic devices by allowing selective engagement or disengagement of a lossy plasmonic state (Fig. 1(a)). In this device, operating at a standard telecommunications wavelength of 1550 nm, electrically induced modification of the electromagnetic permittivity of the ITO in the slot enables switching of the optical mode profile in the slot between a dielectric state with high transmission ("off state") and a plasmonic state with low transmission ("on-state").

More specifically, optical switching is achieved by formation of an electron accumulation layer in the ITO under bias by a Si/Al_2O_3 gate, which takes the local electromagnetic permittivity, via change in free carrier dispersion, from an unperturbed positive "dielectric" value to a value close to zero in its real part, known as an epsilon-near-zero (ENZ) condition (Fig. 1(b)). This change leads to a radical reconfiguration of the optical mode profile due to continuity of the electric displacement vector normal to the accumulation layer, squeezing it into a quasi 2D plasmonic state and fully absorbing the propagating mode over only a few microns (Fig. 2).

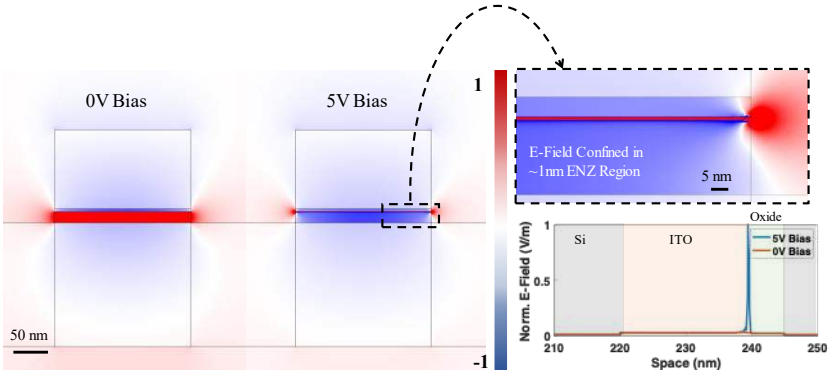


Figure 2: Simulated E-field profiles of the active region (COMSOL). At a bias of 0V, an incoming optical mode, polarized with electric field normal to the plane of the layers, occupies the full volume of a low-index slot region (consisting of ITO and Al_2O_3 gate-insulator layers), experiencing an all-dielectric environment and hence low-loss propagation. Upon application of a 5V bias, a ~1-nm thick region at the ITO/insulator interface acquires a permittivity close to 0, leading to drastic mode confinement into this narrow region (right inset), along with drastic enhancement of its electric field, increased mode losses due to increased electron-electron scattering, and drastic propagation attenuation as a result.

We will present the design, construction, and optical characterization of an ENZ plasmon-assisted modulator based on sputtered ITO and a fabrication-friendly, planar Si slot waveguide configuration, enabling well-controlled field profiles and high field enhancement without the use of lossy metal. For an 8-um long device, simulations predict a low insertion loss (< 0.2 dB), a modulation depth of 9 dB, an RC-limited speed of 333 GHz, and a switching energy consumption of 480 fJ/bit.

The authors acknowledge financial support from National Science Foundation (1808928).

References

1. M. Zhang, et.al., "Monolithic Ultrahigh-Q Lithium Niobate Microring Resonator," **4**, 1536–1537 (2017).
3. M. Ayata, et.al., "High-speed plasmonic modulator in a single metal layer," Science (1979) **358**, 630–632 (2017).

Synopsys Workshop at META 2023

Automated Inverse Design Solution for Metalenses

July 18 and 19

5:00-6:00 pm

Location: Salle des Conseils

To help researchers design metalenses easily and quickly, Synopsys has developed MetaOptic Designer, a fully automated design tool for metalenses. Based on a few inputs from designers, such as a pre-built meta-atom library and basic lens configuration, MetaOptic Designer generates an optimized design to meet all design targets.

Synopsys will introduce and demonstrate MetaOptic Designer in two workshop sessions at META 2023. On July 18, we will provide a general overview of the MetaOptic Designer optimization algorithm, followed by quick demonstrations of the tool's capability. On July 19, we will demonstrate advanced metalens applications with tips and tricks; applications will include:

- Achromatic metalens
- Wide-angle metalens
- Chiral hologram
- Reflective metalens
- Hybrid optical system with both metasurfaces and traditional refractive lenses

The workshop is free and open to all META conference attendees.

META 2023, PARIS - FRANCE, JULY 18 – 21, 2023

Photonic Band Structure Calculations of 3D Finite Nanostructured Supercrystals

N. Large[1*], J. L. Montaño-Priede[1]

[1]Department of Physics and Astronomy, University of Texas at San Antonio, United States
[*]corresponding author: Nicolas.Large@utsa.edu

Abstract: Computational modelling of plasmonic periodic structures are challenging due to their multiscale nature. Here, we developed a computational approach, based on the finite-difference time-domain method to accurately calculate the photonic band structures of finite supercrystals, accounting for both nanoscale features an overall habit of the supercrystal. We applied this new approach to 3D periodic microstructures of Au nanoparticles with cubic, spherical, and rhombic dodecahedral habits and discuss how their photonic band structures differ from those of infinite structures.

Well-structured, periodic plasmonic supercrystals possess the unique ability to retain the intrinsic properties of their building blocks but also display unique collective properties originating from interparticle coupling effects [1-4]. With the countless superlattices now synthetically realizable [4], computational methods and theoretical models play a crucial role in identifying the supercrystals that exhibit the most exciting properties. When the supercrystal lattice parameter is much smaller than the wavelength, the medium usually behaves like a uniform, continuous material, characterized by an effective dielectric permittivity and magnetic permeability, which are modelled using effective medium models. However, when the lattice parameter is comparable to the optical wavelength, the photonic band structure plays a key role. In such assemblies, the interparticle distance becomes the critical parameter that governs the collective optical properties. When the distance is larger than the wavelength of optical excitation the NPs are uncoupled and the collective optical response is the incoherent summation of individual responses of each NP constituting the assemblies. Additional photonic behaviors arise when the interparticle distance satisfies Bragg's law (*e.g.*, Rayleigh anomalies) or when multipolar interactions are involved. Finally, geometrical aspects such as the dimensionality and the habit of the supercrystal, the lattice parameter in each spatial direction, and the morphology of the NPs composing the supercrystal play a key role in defining their optical properties including (an)isotropy/birefringence [5], the emergence of Fabry-Pérot resonances and whispering gallery modes (WGM) [6], and decrease of the photonic mode lifetime.

Here, we theoretically investigate the photonic properties of 3D periodic microscale arrangements of plasmonic nanoparticles that form supercrystals, also known as plasmonic supercrystals, 3D superlattices, or plasmonic photonic crystals. To that end, we proposed a theoretical and computational approach for calculating the photonic band structures of finite supercrystals (**Fig. 1**), and investigating the effect of the habit (*i.e.*, crystal shape) and size on its photonic properties [7]. Our approach allows for accurately calculating the photonic band structures from finite-size 3D superlattices of various habits (cubic, spherical, rhombic dodecahedral) and building blocks (spheres and rods). We showed that they differ from the band structures computed for infinite structure and encompass phenomena such as the Fabry-Pérot interferences, whispering gallery modes, the decrease in photonic mode lifetime, and the formation of polaritonic bandgaps.

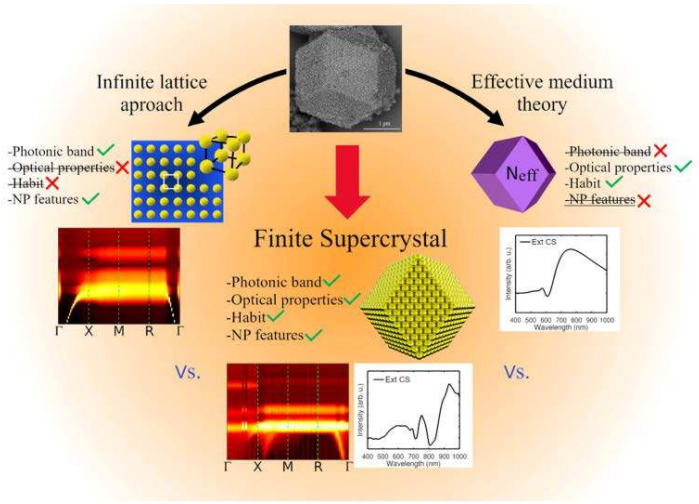


Fig. 1. Approaches to calculate the properties of photonic crystals, i.e., infinite lattice for band structure calculations, effective medium theory for optical properties like reflectance, and proposed FDTD simulation for finite supercrystals.

It is important to notice that, although this approach was applied to 3D supercrystals, it is far more general and versatile. Not only it applies to various morphology, composition, and size of the building blocks (*e.g.*, cubes, prisms …), but also to different unit cell symmetries (*e.g.*, fcc, bcc …), supercrystal habits (*e.g.*, ellipsoidal, pyramidal …), and dimensionalities of the periodic structures (*e.g.*, 1D chains, 2D arrays).

This work received financial support from the Thomas Jefferson Fund managed by the Office for Science and Technology of the Embassy of France in the United States and the FACE Foundation under grant number TJF 19_092.

References

1. C. A. Mirkin, R. L. Letsinger, R. C. Mucic, and J. J. Storhoff, "A DNA-based method for rationally assembling nanoparticles into macroscopic materials," Nature **382**, 607-609 (1996).
2. M. B. Ross, J. C. Ku, B. Lee, C. A. Mirkin, and G. C. Schatz, "Plasmonic Metallurgy Enabled by DNA," Adv. Mater. **28**, 2790-2794 (2016).
3. M. B. Ross, C. A. Mirkin, and G. C. Schatz, "Optical Properties of One-, Two-, and Three-Dimensional Arrays of Plasmonic Nanostructures," J. Phys. Chem. C **120**, 816-830 (2016).
4. D. García-Lojo, S. Núñez-Sánchez, S. Gómez-Graña, M. Grzelczak, I. Pastoriza-Santos, J. Pérez-Juste, and L. M. Liz-Marzán, "Plasmonic Supercrystals," Acc. Chem. Res. **52**, 1855-1864 (2019).
5. L. Sun, H. Lin, D. J. Park, M. R. Bourgeois, M. B. Ross, J. C. Ku, G. C. Schatz, and C. A. Mirkin, "Polarization-Dependent Optical Response in Anisotropic Nanoparticle–DNA Superlattices," Nano Lett. **17**, 2313-2318 (2017).
6. D. J. Park, C. Zhang, J. C. Ku, Y. Zhou, G. C. Schatz, and C. A. Mirkin, "Plasmonic photonic crystals realized through DNA-programmable assembly," Proc. Natl. Acad. Sci. U.S.A. **112**, 977-981 (2015).
7. J. L. Montaño-Priede, and N. Large, "Photonic band structure calculation of finite 3D superlattices in finite-difference time-domain method," Nanoscale Adv. **4**, 4589-4596 (2022).

Directional scattering by composite SiO2/Au nanoparticles

T.P.S. Kotte[1*], A.J.L. Adam[1], and H.P. Urbach[1]

[1]Delft University of Technology, the Netherlands
[*]corresponding author: t.p.s.kotte@tudelft.nl

Abstract: We show that composite nanoparticles can be designed to scatter light into a desired direction. By choosing the materials of the nanoparticle carefully, the phase of the scattered light by the different components can be controlled. This leads to constructive interference is certain directions and destructive interference in others, resulting in directional scattering obtainable for a large bandwidth. FEM simulations were used to validate the theory. Furthermore, SiO2/Au nanoparticles were fabricated and measured confirming the directional scattering.

Introduction

Most studies towards scattering by nanoparticles have focused on particles made up of a single material, where the scattering is determined by multipole resonances[1]. Combining particles of different materials allows for more degrees of freedom, which has been demonstrated for dimer and trimer structures[2,3]. However, the directional scattering by these configurations is determined by interference between their different components, acting as spatially separated point sources. Therefore, the direction of the scattered field is highly dependent on the wavelength of the light and the distance between the point sources. Thus, broadband light scattering where the scatter pattern remains constant is hard to attain. Composite nanoparticles (CNPs) could be a solution for this, as the materials are not separated.

Approach

Let us consider a linearly polarized plane wave traveling in the x-direction incident on a CNP, which is inside a homogeneous medium with permittivity ε_{med}. For now we will assume that the contrast of the particle is very low compared to the medium. In this case, we can use the Born approximation in the Lipmann-Schwinger equation to calculate the scattered field. Using a spherical coordinate system, with polar angle θ (from the z-axis) and azimuthal angle φ (from the x-axis) and some algebraic steps we get the following expression for the field scattered in the forward direction:

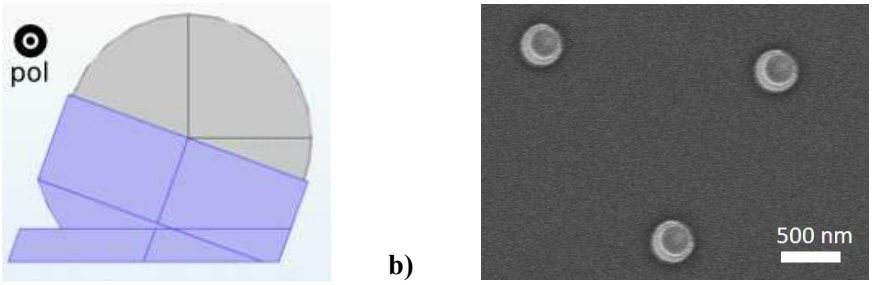
$$\bar{E}^{sc}(r,0,\pi/2) = \bar{E}_0 \frac{k^2 e^{ikr}}{4\pi r}\left[\left(\varepsilon_{\Omega_1} - \varepsilon_{med}\right)\int_{\Omega_1} d^3 r_0 + \left(\varepsilon_{\Omega_2} - \varepsilon_{med}\right)\int_{\Omega_2} d^3 r_0\right]. \quad (1)$$

Here, k is the wavenumber in the medium, ε the permittivity, E the electric field and Ω_1 and Ω_2 the volumes occupied by the different materials. From Equation 1, we see that the scattered field is determined by the volume of the materials and their permittivity. By choosing different sizes and materials, the magnitude of the scattered field can be controlled.

To investigate whether this relation holds beyond the Born approximation, a SiO2/Au CNP in air was simulated using the FEM software COMSOL. To make fabrication possible, a geometry was chosen of a spherical SiO_2 particle (with a diameter of 300 nm) with Au attached to its side (Figure 1a). The calculated scattered light intensity for incident light with a wavelength of 633 nm is shown in Figure 2a.

Samples of SiO2/Au CNPs of the same geometry were fabricated. A solution of colloid SiO2 nanospheres were deposited onto a glass wafer. Next, the sample was sputtercoated with a layer of 40 nm Au. Finally, most of

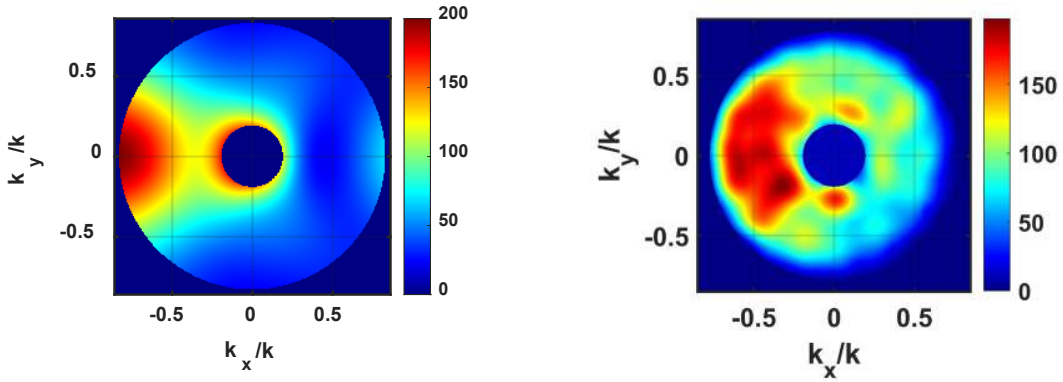
the gold was removed by ion beam etching at an angle of 20 degrees, so that only the Au in the shadow of the nanoparticle remained. The samples were inspected using a SEM, the result can be seen in Figure 1b.



a) **b)**

Figure 1: a) Geometry of the SiO2/Au CNP in the simulation. The blue part is made of Au and the grey part is made out of SiO2. The polarization of the incident light used for simulations and measurements is also indicated; **b)** SEM micrograph of three fabricated SiO2/Au CNPs

The scattering of the manufactured CNPs was measured using a transmission Fourier microscope setup using a HeNe laser as a light source with a *y*-polarization. Figure 2 shows the simulated and the measured scattering intensity produced by a single CNP in the Fourier plane. It can be seen that most of the light is scattered to the left of the particle and that the measurement corresponds to what is expected from the simulation.



a) **b)**

Figure 2. Scattered light intensity in the Fourier plane by a SiO2/Au CNP on a glass substrate with incident y-polarized light: **a)** simulated using a FEM software; **b)** experimentally measured. (arbitrary units)

Conclusion

We have shown that directional scattering can be achieved by CNPs with the right material combinations for their components. Theory and FEM simulations show that the phase differences of the scattered field caused by the material properties of the CNP are the source of the directional scattering. Subsequent experimental measurements confirm the directional scattering found by the FEM software.

Acknowledgements

We acknowledge support by NWO-TTW Perspectief program (P15-36) "Free-form scattering optics".

References

1. Fu, Y. H. et al, “Directional visible light scattering by silicon nanoparticles,” Nat.Comm., 4, 1–6. 2013.
2. G. Lu, et al, “Directional side scattering of light by a single plasmonic trimer,” Laser Phot. Rev. 9, 530–537. 2015.
3. T. Shegai, et al, “A bimetallic nanoantenna for directional colour routing,” Nat. Comm. 2. 2011.

META 2023, PARIS - FRANCE, JULY 18 – 21, 2023

Displacement trajectory of nanoparticles illuminated by pulsed photonic jet and photonic hook

M. H. Shor Peled[1], P. Maioli[2], and A. Karabchevsky[1*]

[1]School of Electrical and Computer Engineering, Ben Gurion University, Israel

[2]Institut Lumière Matière (ILM), CNRS and Université de Lyon, Villeurbanne, France

[*]corresponding author: alinak@bgu.ac.il

Abstract: We present the displacement trajectory of a gold nanoparticle under photonic nano-jet and photonic hook fields generated with an ultrashort pulsed beam. We compared the optical forces exerted on the nanoparticle under pulsed and CW illumination and calculated its displacement. We observed peculiar nanoparticle trajectories when placed in different initial positions, under pulsed light. To understand the effect, we analyzed the gradient and scattering forces. Our work stimulates the development of experimental methods for opto-mechanical manipulation.

The trapping and manipulation of particles by optical tools have been widely used in biological research and implemented in medicine [1], yet nanoscale objects cannot be manipulated by such tools due to the diffraction limit of light [2]. Therefore, achieving manipulation on the nanoscale requires auxiliary structures that generate a tightly confined electric field. Photonic nano-jets are high intensity, narrow light beams generated by dielectric structures that are subjected to illumination by a plane wave [3]. When the symmetry is broken, the generated structured light becomes curved, which is known as a photonic hook effect [4]. In this research, we report the displacement trajectory of gold nanoparticles under photonic nano-jet and hook fields generated with an ultrashort pulsed beam. The studied system is composed of a micro-cylinder and metallic mask that partially blocks the incident light and creates an asymmetric illumination [5]. We simulated the electric fields and calculated the optical forces exerted on the nanoparticle. We compared between continuous wave and pulsed illumination, and found that the forces exerted on the gold nanoparticle generated via pulsed illumination are five orders of magnitude higher and are significant enough to move the nanoparticle. We observed peculiar nanoparticle trajectories when placed in different initial positions, and found that the trajectory is not affected by input intensity. To better understand our results, we analyzed the gradient and scattering forces exerted on the nanoparticle by the photonic nano-jet and hook. Our results stimulate the development of experimental methods for the opto-mechanical manipulation of nanoparticles. Opto-mechanical manipulation opens a venue for future fundamental investigations and a range of practical applications, where accurate control over the mechanical motion of small objects is required.

The research reported in the manuscript was funded by Israel Science Foundation (ISF no. 2598/20).

References

1. Baker, James E., Ryan P. Badman, and Michelle D. Wang. "Nanophotonic trapping: precise manipulation and measurement of biomolecular arrays." Wiley Interdisciplinary Reviews: Nanomedicine and Nanobiotechnology 10.1 (2018): e1477.
2. Karabchevsky, Alina, et al. "Super-Resolution Imaging and Optomechanical Manipulation Using Optical Nanojet for Nondestructive Single-Cell Research." Advanced Photonics Research 3.2 (2022): 2100233.
3. Luk'yanchuk, Boris S., et al. "Refractive index less than two: photonic nanojets yesterday, today and tomorrow." Optical Materials Express 7.6 (2017): 1820-1847.
4. Yue, Liyang, et al. "Photonic hook: a new curved light beam." Optics letters 43.4 (2018): 771-774.
5. Minin, Igor V., …., Karabchevsky, Alina "Experimental demonstration of a tunable photonic hook by a partially illuminated dielectric microcylinder." Optics Letters 45.17 (2020): 4899-4902.

Integrated Polarization Control for Trapped-Ion Quantum Computers

G. Du[1,*], C. Grimpe[1], A. Sorokina[2,3], P. Gehrmann[2,3], E. Jordan[1], S. Sauer[2,3], S. Kroker[1,2,3] and T. Mehlstäubler[1,4,5]

[1]Physikalisch-Technische Bundesanstalt, Bundesallee 100, Braunschweig, 38116, Deutschland
[2]Institut für Halbleitertechnik, Technische Universität Braunschweig, Hans-Sommer-Str. 66, Braunschweig, 38106, Deutschland
[3]Laboratory for Emerging Nanometrology, Langer Kamp 6 a/b, Braunschweig, 38106, Deutschland
[4]Institut für Quantenoptik, Leibniz Universität Hannover, Welfengarten 1, Hannover, 30167, Deutschland
[5]Laboratorium für Nano- und Quantenengineering, Leibniz Universität Hannover, Schneiderberg 39, Hannover, 30167, Deutschland
[*]guochun.du@ptb.de

Abstract: Ion traps are a promising platform for the realization of high-fidelity quantum information processors. Integrated photonic components are important for scaling ion trap systems to large numbers of qubits. Polarization control is essential for state preparation, electron-shelving and quantum logic operations. Here, we present our work on ion traps with integrated grating couplers combined with metasurfaces as a two-layer system for the conversion of linear polarization to circular polarization.

Ion traps are one of the most promising platforms for quantum computers to solve classically intractable problems efficiently [1,2,3]. To enable scalability of these systems, integrated photonic components for guiding, manipulating and shaping laser light are essential. Polarization control is useful for state preparation, electron-shelving, and quantum logic operations.

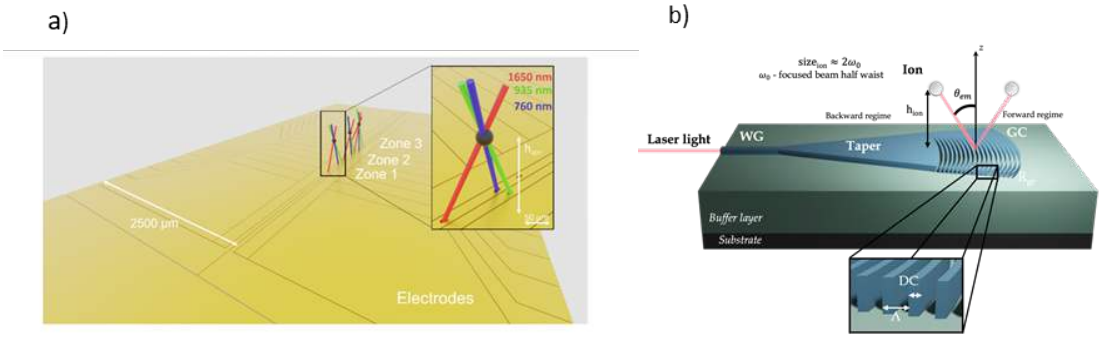


Figure 1: a) Surface ion trap with integrated photonics to control the outcoupled beams for addressing the ions (black spheres) in different trap zones; b) Waveguide – Grating coupler design scheme with forward and backward light focusing regimes.

Figure 1 a) show a photonically integrated ion trap. To guide the laser light on the chip, different passive optical elements are utilized. The light is guided to the ion via waveguides, taper and focusing grating outcouplers as shown in Figure 1 b).

Standard grating couplers only provide linear polarized light. During the past years, metasurfaces have been demonstrated to realize polarization control on chip [4, 5, 6]. In Figure 2 we present a two-layer system for

converting the linear polarization into circular polarization. The light is guided and outcoupled as indicated in Figure 1b) and a metasurface as a second layer above the grating layer is added to control the polarization.

We perform simulations of this system using LUMERICAL®. In our simulations, we take a wavelength of 760 nm as an example and select Si_3N_4 as waveguide and grating material, SiO_2 as the cladding material, while the metasurface material is selected to be Si, which provides a large refractive index contrast. The grating coupler is designed to emit the light vertically. The metasurface is composed of asymmetrically arranged rectangle elements, which generate a phase difference for the two electric field components of the light coming from the grating couplers. For a metasurface with a thickness of 500 nm, pixel size of 433 nm x 744 nm, element size of 333 nm x 100 nm, we get a circular polarized beam (phase difference is 90°).

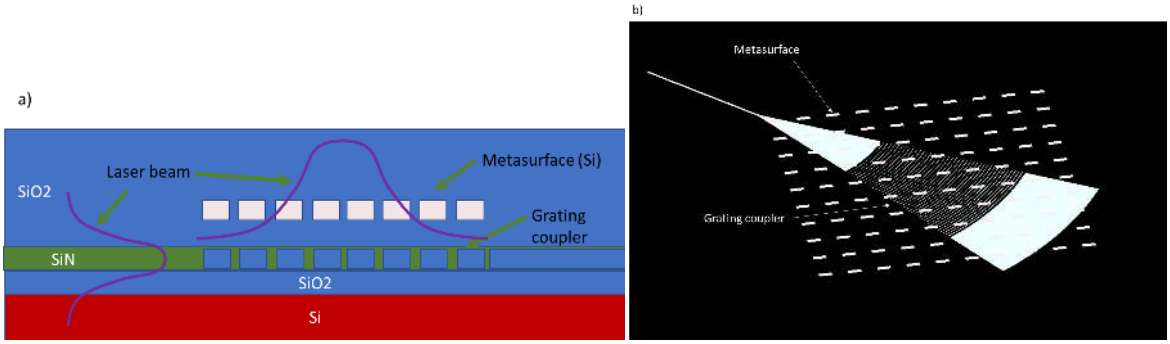


Figure 2: a) two-layer system using grating coupler combined with a metasurface to couple light out of the surface and change its polarization from linear to circular; b) 3D view of the two-layer system.

Acknowledgments: The authors gratefully acknowledge support from the Braunschweig International Graduate School of Metrology B-IGSM and the DFG Research Training Group GrK1952/1 “Metrology for Complex Nanosystems”. Furthermore, we thank the Quantum Valley Lower Saxony, ATIQ (FKZ 13N16126) and cluster of Excellence QuantumFrontiers (EXC-2123–390837967). Moreover, we thank Karan Mehta for his help, support and discussions.

References

1. C. D. Bruzewicz et al., Trapped-Ion Quantum Computing: Progress and Challenges, Appl. Phys. Rev. vol. 6, no.2, pp. 021314 (2019)
2. J. Benhelm, G. Kirchmair, C. Roos, et al. Towards fault-tolerant quantum computing with trapped ions. Nature Phys 4, 463–466 (2008)
3. B. Bauer et al. Quantum Algorithms for Quantum Chemistry and Quantum Material Science, Chemical Reviews, vol 120, no.22, pp. 12685-12717, (2020)
4. Kamali, Seyedeh Mahsa, Ehsan Arbabi, Amir Arbabi, und Andrei Faraon. „A Review of Dielectric Optical Metasurfaces for Wavefront Control“. arXiv, 25. April 2018. http://arxiv.org/abs/1804.09802.
5. Chen, Hou-Tong, Antoinette J Taylor, und Nanfang Yu. „A Review of Metasurfaces: Physics and Applications“. Reports on Progress in Physics 79, Nr. 7 (1. Juli 2016): 076401. https://doi.org/10.1088/0034-4885/79/7/076401.
6. Hu, Yueqiang, Xudong Wang, Xuhao Luo, Xiangnian Ou, Ling Li, Yiqin Chen, Ping Yang, Shuai Wang, und Huigao Duan. „All-Dielectric Metasurfaces for Polarization Manipulation: Principles and Emerging Applications“. *Nanophotonics* 9, Nr. 12 (11. September 2020): 3755–80. https://doi.org/10.1515/nanoph-2020-0220.

Vertical Injection and Wideband Grating Coupler Based on Asymmetric Grating Trenches for Higher Coupling Efficiency

Md Asaduzzaman*
School of IT and Engineering, Melbourne Institute of Technology, Melbourne, Victoria 3000, Australia
*Corresponding author: masad@mit.edu.au

Abstract: A Silicon-on-insulator (SOI) perfectly vertical fibre-to-chip grating coupler is proposed and designed based on engineered subwavelength structures. The high directionality of the coupler is achieved by implementing step gratings to realize asymmetric diffraction and by applying effective index variation with auxiliary ultra-subwavelength gratings. The proposed structure is numerically analysed by using two-dimensional Finite Difference Time Domain (2D FDTD) method and achieves 96% (-0.2 dB) coupling efficiency and 39 nm 1-dB bandwidth. This highly efficient GC is necessary to applications where coupling efficiency is critical such as photonics quantum computing.

Grating couplers (GC) are most preferred choice for light coupling between optical fibre and nanophotonic waveguides [1]. However low coupling efficiency (CE) of vertical GC [2-3] has been an active issue specially where near unity CE is highly desirable, for instance, in quantum photonics experiments. In this work, we propose a new GC structure for perfectly vertical coupling by creating asymmetric grating trenches with a combination of step and engineered subwavelength gratings that manipulate the effective refractive index to achieve higher coupling efficiency along wider wavelength range. Our proposed structure can be fabricated on standard SOI wafer using Focused Ion Beam (FIB) or few steps of etching with Electron Beam Lithography (EBL) process. Although the fabrication complexity of the structure might be relatively higher, it promises of higher CE (96%) and provides solutions to various applications, e.g. for the experiments of photonics quantum computing.

The proposed GC with secondary gratings including step gratings is simulated by 2D FDTD. The electromagnetic field distribution and CE obtained are shown in Fig.1. The light that coupled with substrate through BOX is reduced in the redesigned structure as can be seen in Fig.1 (a). The directionality of the power propagation in subwavelength grating coupler is improved significantly. With such engineered sub-wavelength grating structure, the CE of ~72% is achieved as shown in Fig.1 (b) that peak coupling efficiency occurred at 1550 nm with 1-dB bandwidth of ~ 44 nm.

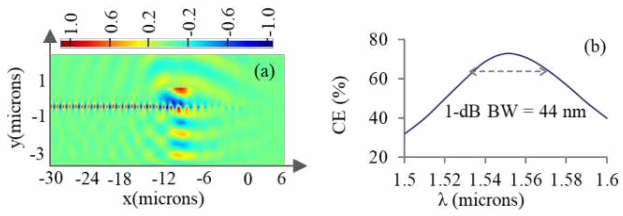


Fig. 1. (a) Electromagnetic field distribution along the grating structure and (b) coupling efficiency at wavelength range from 1500 nm to 1600 nm with centre at 1550 nm for grating coupler with secondary ultra-subwavelength grating.

Finally, the estimated coupling efficiency over the wavelength range of 1500-1600 nm for grating coupler with optimized secondary grating parameters as of in Table 1 is shown in Fig.2. The CE and BW increases with

Table 1: Optimized secondary grating parameters.

Λ_s (nm)	DC_s	w_s (nm)	w_{gs} (nm)	d_s (nm)	w_{ss} (nm)	t_s (nm)
154	0.4	62	92	15	38.6	15

the number of step gratings in the primary groove up to 4 steps and nearly saturates with higher numbers as shown in Fig. 2. Significant increment of CE can be observed from step number 1 to 4 but are similar CE for steps 4 and 5. The peak coupling efficiency of ~ 96% is achieved at wavelength of 1550 nm with 1-dB coupling bandwidth of ~39 nm for 4 step gratings in the primary groove. Although the efficiency is improved with optimized structure, the bandwidth is little lower than that of obtained in Fig.1 (b). This is due to fact that the modified effective refractive index causes lower coupling efficiency for longer wavelengths. This once again proves that there always exists compromise between coupling efficiency and coupling bandwidth in a grating coupler.

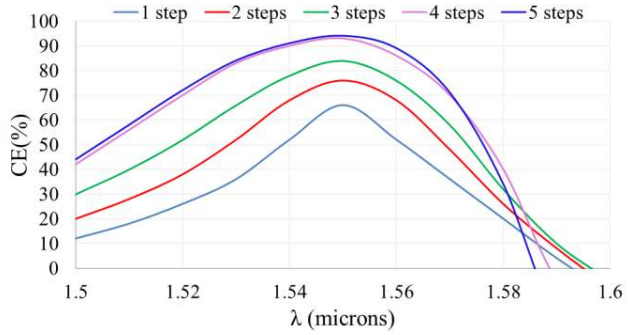


Fig. 2. Coupling efficiency vs. wavelength for optimized grating coupler with various numbers of step gratings in the primary groove.

In summary, a perfectly vertical grating coupler is proposed for light coupling between SOI waveguides and optical fibres in this work. The symmetrical propagation nature of the diffracted waves from grating is broken by incorporating asymmetric grating trenches with step gratings. The coupling efficiency of the coupler is also boosted by implementing effective index variation of the primary grating achieved by combination of auxiliary ultra-subwavelength gratings and step gratings. In this design the coupling efficiency is estimated as high as 96% (-0.2 dB) and 1-dB coupling bandwidth of 39 nm. Our proposed structure provides solutions where coupling efficiency between optical fibre and nanophotonics waveguide is critically important, for instance, experiments of the quantum photonics integrated circuits. Such efficient and broadband perfectly vertical grating couplers are also significantly advantageous in high dense photonic packaging.

References

1. Neil Na, Harel Frish, I-Wei Hsieh, Oshrit Harel, Roshan George, Assia Barkai, and Haisheng Rong, "Efficient broadband silicon-on-insulator grating coupler with low backreflection," Opt. Lett. 36, 2101-2103, 2011.
2. Zan Zhang, Xiaotao Shan, Beiju Huang, Zanyun Zhang, Chuantong Cheng, Bing Bai, Tianxi Gao, Xiaobo Xu, Lin Zhang and Hongda Chen, "Efficiency Enhanced Grating Coupler for Perfectly Vertical Fiber-to-Chip Coupling", Materials, 13, 2681, 2020.
3. Siya Wang, Yue Hong, Yuntao Zhu, Jingye Chen, Shengqian Gao, Xinlun Cai, Yaocheng Shi, Liu Liu, "Compact high-efficiency perfectly-vertical grating coupler on silicon at O band", Opt. Exp. 25, No.18, 22032-22037, 2017.

Nonlinear optical generation of photon pairs using hybrid plasmonic nanostructures

S. Mathew, G. Laurent, N. Chauvet, G. Nogues, A. Drezet and G. Bachelier*
Univ. Grenoble Alpes, CNRS, Institut Néel, 38000 Grenoble, France
corresponding author: guillaume.bachelier@neel.cnrs.fr

Abstract

With the increasing need for scaling down devices to the nanoscale, the quest for an ideal photon pair source having a high degree of brightness and purity with an ability to operate under ambient temperature has never been more relevant than it is now. Within this context, here we demonstrate a framework to evaluate photon pair generation efficiency via spontaneous parametric down conversion (SPDC) from nonlinear crystal coupled to plasmonic nanoantennas (hereby called hybrid nanostructures) and we report on the experimental advances made towards this purpose.

SPDC being a quantum process, traditional approaches to numerically evaluate it have been (i) to neglect the quantum effects by using quantum classical correspondence with the reverse process of SPDC which is sum frequency generation, (ii) to perform a Hamiltonian treatment given the known optical mode of fields at excitation and emission.

In this work, by correlating quantum fluctuations associated to signal and idler photons at emission and detector using classical Green's function we evaluate photon pair emission rate from a hybrid nanostructure under pulsed field excitation. The numerical modelling of the currents generated in the nanostructure is based on solving Maxwell's equation using finite element methods. The framework we develop here is adapted to realistic experimental setups by taking into account analytically the propagation of the generated fields through a glass substrate and collection by a microscope objective.

Additionally, we investigate the effect of plasmonic field enhancement of aluminum and gold nanoantennas on KTP crystal which is well studied from the point of view of second harmonic generation as well as the effect of absorption inherent in metals. Finally, we also explore the feasibility of experimental photon pair generation from a novel nonlinear material such as gallium phosphide and field enhancement resulting from different geometry of the plasmonic nanoantennas.

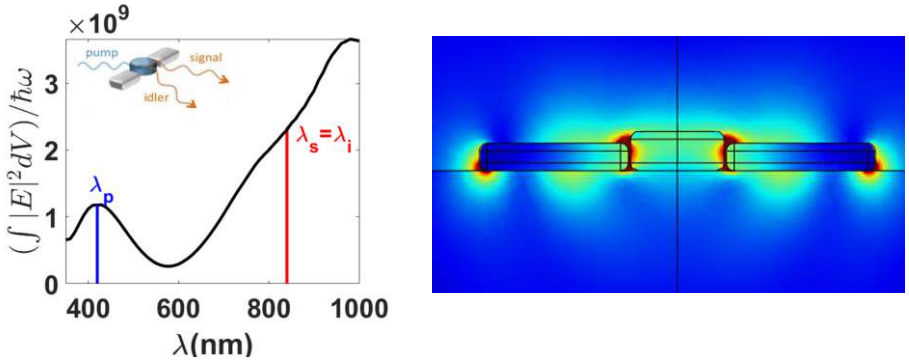


Figure 1 *Left*: Simulated energy density plot over the volume of KTP nanocrystal. *Right*: Pump electric field norm at λp = 420 nm for a hybrid structure composed of two 190 ×100×35 nm Aluminum antenna and a 120 nm wide 50 nm high

References

[1] G. Laurent et al. 'Photon-pair production at the nanoscale with hybrid nonlinear/plasmonic antennas'arxiv:1806.08702, 2018

[2] N. Chauvet et al, 'Hybrid KTP−Plasmonic Nanostructures for Enhanced Nonlinear Optics at the Nanoscale' ACS Photonics, **7, 3**, pp 665–672, 2020

[3] M. W. Mitchell, 'Parametric down-conversion from a wave-equation approach: Geometry and absolute brightness' Phys. Rev. A 79, 043835, 2009

Strain sensors based on Fano resonance in plasmomechanical system

N.Ahmidayi[1*], W. d'Orsonens[2],Th.Maurer[2], and G.Lévêque[1]

[1]Institut d'Electronique, Microélectronique et Nanotechnologie, UMR CNRS 8520, Université de Lille, 59652 Villeneuve d'Ascq, France.

[2]UTT-Université de Technologie de Troyes, 12 rue Marie Curie-Cs 42060-10004 TROES CEDEX, France.

[*]najat.ahmidayi@univ-lille.fr

Abstract: Due to their unique plasmonic and mechanical properties, plasmomechanical systems have become thoroughly investigated for strain sensing applications. The realization of strain sensors with high performance requires plasmonic resonances with high quality Factor (Q) such as Fano resonances (FR). In this respect, we have carried out an optomechanical study of a plasmomechanical system supporting FR, consisting of two gold nanoparticles (GNs), a disk and a rod, deposited on a polydimethylsiloxane (PDMS) substrate.

1. Introduction

The capability of metallic nanoparticles to generate localized surface plasmon resonances (LSPR), resulting from the interaction between the conduction electrons and the incident light, have made them choice candidates in many applications, from biosensing to solar energies.[1] In nanostructure assemblies consisting of two nanoparticles or more, the LSPR depends strongly on the interparticle spacing due to the coupling via their near-fields.[2] The possibility of exploiting this property in the realization of strain nanosensors has led to the birth of a new field in nanophotonics called plasmomechanics.[3] Rod-shaped nanoparticles are known to support plasmonic narrow dark modes which can be used, in combination with bright modes supported by other particles such as disks, to generate FR whose shape can be modified by deformation of a PDMS substrate.

2. Structure and simulation method description

The investigated structure as schematically shown in Figure 1 consists of a Au disk (R=90nm) and a rod (w=50nm and l_r=320nm) with a fixed thickness h=30nm. Displacements (ε), ranging from 0% to 20%, have been applied in opposite directions on the substrate. The structure has been illuminated by a p-polarized monochromatic planewave, propagating normally from the (-z) direction. Refractive index of PDMS is 1.4 and that of gold is taken from Johnson and Christy database.[4] Simulations have been performed using *Comsol Multiphysics* software, based on finite element method. An hyperelastic model have been used to model the PDMS based on a nearly incompressible neo-Hookean material model, and an elastic model for GNs.

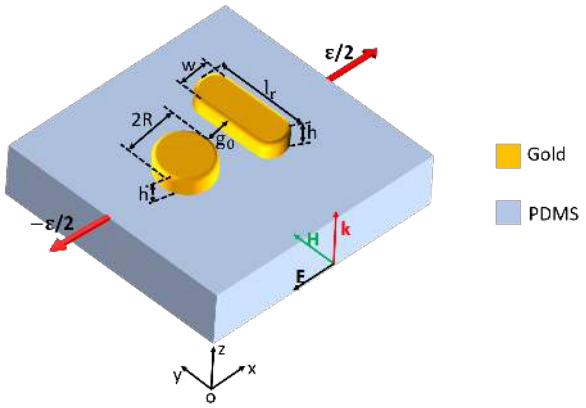


Figure 1. Schematic illustration of the investigated structure under stretching.

3. Results

When the GNs in this system are close enough (few ten nanometers) to each other, the first excited dark mode of the rod can hybridize with the bright dipole mode of the disk, leading to the formation of a bonding and an antibonding modes whose interference is at the origin of a Fano resonance profile. Figure 2 represents the evolution of the resonance maxima as a function of the applied displacements, the inset showing the FR for ε=0%. When the displacement percentage passes from 0% to 20%, the bonding mode (long wavelength maximum) exhibits a strong blue shift of 32nm while the antibonding mode shows a smaller shift in the opposite direction, of 10nm. Indeed, when the PDMS is under stretching, GNs move away from each other and the gap undergoes a dramatic amplification with a percentage higher than that of the applied strain, which causes a decoupling and a transition to weak interaction between the two modes, as it can be seen on the electric field maps, (d) and (e), where a strong amplitude decrease is observed in the gap region.

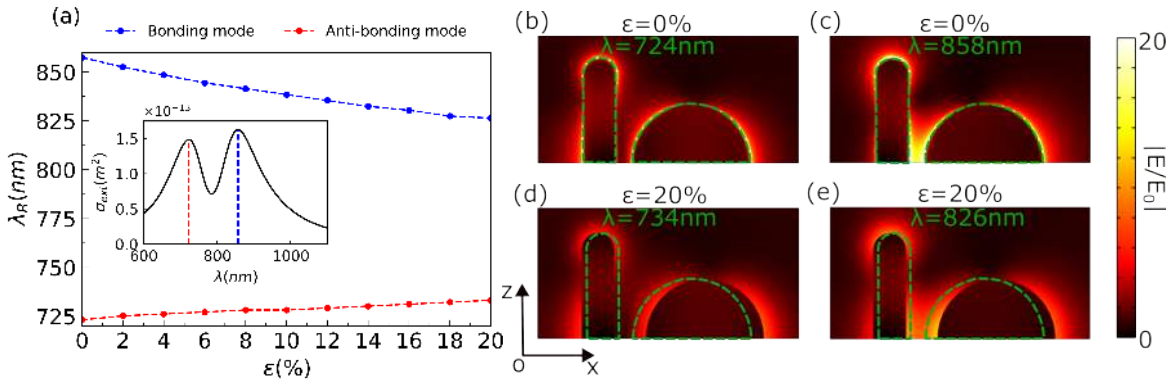


Figure 2. Calculated trend of the resonance wavelength as a function of the applied displacement ranging from 0% to 20% (a), Electric field distribution of the structure at rest and under 20% of displacement: for the antibonding mode [(b) and (d)], and for the bonding mode [(c) and (e)].

4. Conclusion

Resonance wavelength of FR shows a strong sensibility to the applied displacements due to the dramatic gap amplification. In fact, when ε=0% of strain is applied, the gap passes from g_0=25nm to g=48.6nm which corresponds to a relative gap variation of $\Delta g/g_0$=0.94 higher than the elastic variation $\Delta g/g_0$=0.2. As consequence, the proposed plasmomechanical system can be used in strain sensing applications.

References

[1] L. Wang, M. Hasanzadeh Kafshgari, et M. Meunier, « Optical Properties and Applications of Plasmonic-Metal Nanoparticles », *Advanced Functional Materials*, vol. 30, nº 51, p. 2005400, 2020, doi: 10.1002/adfm.202005400.

[2] D. Eschimèse, F. Vaurette, C. Ha, S. Arscott, T. Mélin, et G. Lévêque, « Strong and weak polarization-dependent interactions in connected and disconnected plasmonic nanostructures », *Nanoscale Adv.*, vol. 4, nº 4, p. 1173-1181, 2022, doi: 10.1039/D1NA00620G.

[3] T. Maurer *et al.*, « The beginnings of plasmomechanics: towards plasmonic strain sensors », *Front. Mater. Sci.*, vol. 9, nº 2, p. 170-177, juin 2015, doi: 10.1007/s11706-015-0290-z.

[4] P. B. Johnson et R. W. Christy, « Optical Constants of the Noble Metals », *Phys. Rev. B*, vol. 6, nº 12, p. 4370-4379, déc. 1972, doi: 10.1103/PhysRevB.6.4370.

Propagating surface plasmons for plasmonic nanocavities

A. Gisdakis[1], K. Bedingfield[1], J.J. Baumberg and A. Demetriadou[1*]

[1]School of Physics and Astronomy, University of Birmingham, Edgbaston, Birmingham, B15 2TT, UK
[2]NanoPhotonics Centre, Cavendish Laboratory, University of Cambridge, Cambridge, CB3 0HE, UK
[*] a.demetriadou@bham.ac.uk

Abstract: Recent advances have led to the realization of plasmonic nanocavities that have gaps of just 1-2 nm, and have allowed for light-matter strong coupling at room temperature. Previous studies have focused on the energy coupled to the far-field, however the energy carried out by propagating surface plasmon polaritons (SPPs) is often neglected in literature. Here we quantify the fraction of energy coupled in to SPPs and that coupled into plane waves (PWs), which carry the energy into the far-field.

Metallic nanostructures are able to confine light through localized surface plasmons. At extreme nanogaps of just 1-2 nm extraordinary light confinement occurs due to tight coupling between two plasmonic structures [1]. A geometry that has attracted considerable attention over the past few years is the nanoparticle-on-mirror (NPoM) configuration (Fig 1.a) with which light-matter strong coupling of a single molecule at ambient conditions was realized [2]. This nanocavity is made of a usually spherical nanoparticle, separated from a gold substrate by a molecular monolayer. Such optical resonators play a key role in various areas in nanophotonics, including quantum information processing, lasers, nonlinear optics and ultrasensitive biosensing [2,3].

Most studies have been focusing on the scattering and absorption properties of such nanocavities, while a few recent ones have explored the system's photonic quasinormal modes (QNMs) (see Fig 1.b) and how they couple energy to the far-field (Fig 1.c) [1]. However, the same QNMs have a propagating SPP component, bound and propagating on the metal substrate. Here, we develop different methods that allow us to quantify how each QNM couples energy into a propagating SPP, and to the far-field in the form of a plane wave (PW). Although the propagating SPP component of the QNMs has been largely ignored by the community, we find that it is in fact dominant for almost all plasmonic modes for nanocavity configurations.

We use three different approaches to analyze and quantify the propagating SPP and PW component of each plasmonic mode. We first consider the radiative decay rate (γ_{rad}) of the system, where a dipole source is placed in the centre of the nanocavity, and we identify how much energy is coupled in the SPP and PW components. However, this method is dependent on the position of the dipole source. To avoid this problem, we perform QNM numerical solutions [3], and find that the propagating SPP is launched along the same direction as the near-field enhancement (see Fig 1.d). We then consider the QNM expansion coefficients proposed in [3], which demonstrate how much an incident PW or propagating SPP couples into a specific QNM, which we integrate over all possible incident angles for both propagating SPPs and PWs:

$$A_m(\omega) = \iint \left(\frac{\tilde{\omega}_m}{\tilde{\omega}_m - \omega} \left\langle \tilde{\boldsymbol{E}}_m^* \middle| \varepsilon(\tilde{\omega}_m) - \varepsilon_b \middle| \boldsymbol{E}_{inc}(\omega, \theta, \varphi) \right\rangle_{V_{res}} + \left\langle \tilde{\boldsymbol{E}}_m^* \middle| \varepsilon_b - \varepsilon_\infty \middle| \boldsymbol{E}_{inc}(\omega, \theta, \varphi) \right\rangle_{V_{res}} \right) d\varphi \, d\theta, \quad (1)$$

where $\boldsymbol{E}_{inc}$ is the incident field, $\tilde{\boldsymbol{E}}_m$ the QNM field and V_{res} is the resonator domain, and ε_b, $\varepsilon(\tilde{\omega}_m)$ and ε_∞ are respectively the permittivity of the background medium, the resonator's permittivity at a given QNM frequency and the asymptotic permittivity of gold.

Finally, we calculate new coefficients from the QNM expansion that do not require us to consider an incident field, so are independent of the source fields. Using all three methods, we show that the propagating SPP component of the plasmonic modes in nanocavities is dominant for most modes. This means that most of the energy does not reach the far-field, but instead is launched on the metal surface as a propagating SPP.

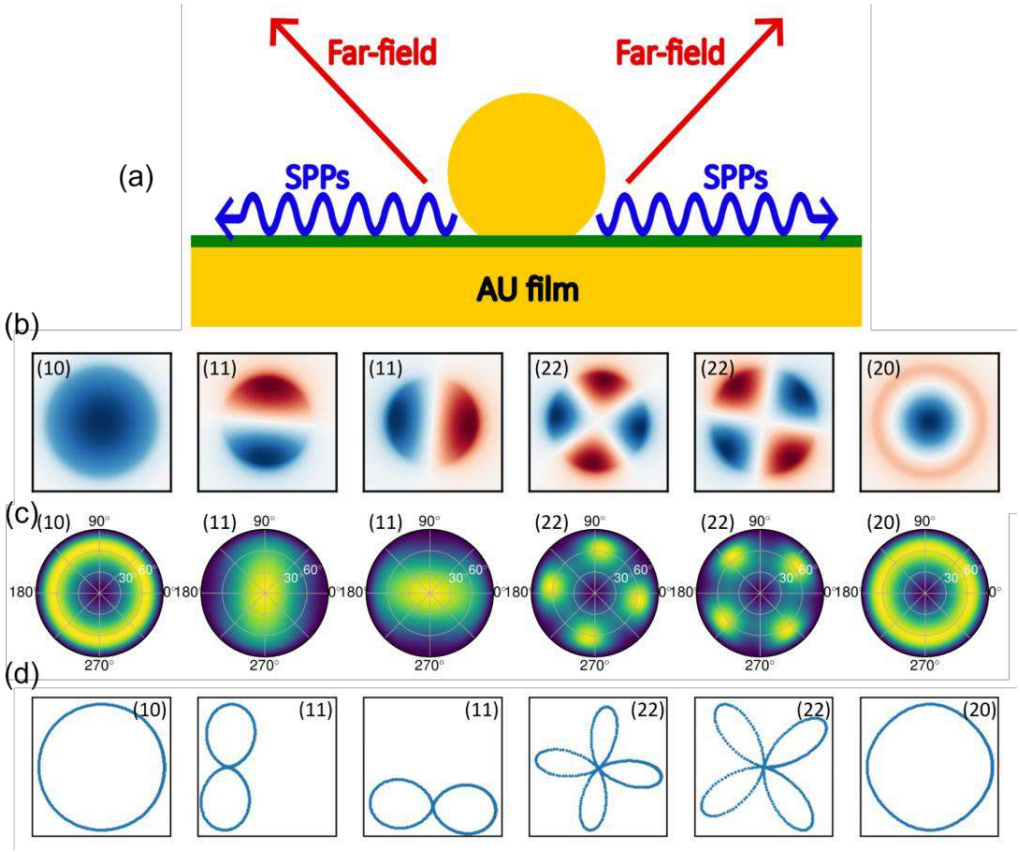


Figure 1: (a) NPoM geometry considered. (b) Normalized QNM electric fields E_z, (c) Normalized Poynting fluxes and (d) SPP radiation patterns of the first 6 QNMs.

In conclusion, we show using various methods that plasmonic nanocavities have two distinct components, a plane wave component that carries energy to the far-field and a propagating SPP component that is bound on the metal surface and dominates the nanocavity behavior.

AD gratefully acknowledges support from the Royal Society University Research Fellowship URF\R1\180097, Royal Society Research Fellows Enhancement Award RGF \EA\181038, Royal Society Research grants RGS \R1\211093 and funding from the EPSRC for the CDT in Topological Design EP/S02297X/1

References

1. N.Kongsuqwan, A. Demetriadou, M. Horton, R. Chikkaraddy, J.J. Baumberg and O. Hess ‘‘Plasmonic nanocavity modes: From near-field to far-field radiation’’, ACS Photonics, 7(2), pp. 463-471, 2020.
2. R. Chikkaraddy, B. De Nijs, F. Benz, S.J. Barrow, O.A. Scherman, E. Rosta, A. Demetriadou, P. Fox, O. Hess and J.J. Baumberg, ‘‘Single-molecule strong coupling at room temperature in plasmonic nanocavities’’, Nature, 535(7610), pp. 127-130, 2016.
3. W. Yan, R. Faggiani and P. Lalanne, ‘‘Rigorous modal analysis of plasmonic nanoresonators’’, Physical Review B, 97(20), p.205422, 2018.

META 2023, PARIS - FRANCE, JULY 18 – 21, 2023

Manipulating the Modes of Radially Symmetric Resonators

J. R. Capers[1*], D. A. Patient[1], S. J. Boyes[2], A. P. Hibbins[1] and S. A. R. Horsley[1]

[1]Department of Physics and Astronomy, University of Exeter, Stocker Road, Exeter, EX4 4QL, United Kingdom
[2]DSTL, Porton Down, Salisbury, Wiltshire, SP4 0JQ, United Kingdom
[*]corresponding author: jrc232@exeter.ac.uk

Abstract: The frequency response of a resonator is governed by the locations of its quasi-normal modes (QNMs) in the complex frequency plane. The real part of the QNM determines the resonance frequency and the imaginary part determines the width of the resonance. For applications such as energy harvesting and sensing, the ability to manipulate the frequency, linewidth and multipolar nature of resonances is key. Here, we present a simple analytical tool to control the location and polarity of radially symmetric resonators.

Many photonic devices are composed of dielectric or plasmonic resonators. The spectral properties of a resonator are governed by its geometry and the material it is made from. In many applications, such as sensing, it is desirable to have a particular character of resonance occur at a particular frequency. Currently, however, the design of resonators to have specific spectral properties involves the exploration of large parameter spaces manually [1,2]. Here we build upon the results of [3] to develop a framework that can be used to design isotropic or graded radially symmetric resonators that exhibit specific multipolar resonances at specific frequencies.

Quasi-normal modes are the complex frequency bound states of a system, corresponding to poles of the scattering matrix. Motivated by the direct connection between the location of the quasi-normal modes in the complex frequency plane and scattering properties of a resonator, we derive a method to design resonators that support quasi-normal modes at specific complex frequencies. This allows us to control the resonance frequency and linewidth of modes simultaneously, as well as the multipolar characteristic of the mode. Our method is based on the insight of Chen et al. [4], who proposed that one could approach quasi-normal mode expansions by keeping k real, but extending the permittivity ε into the complex plane. We instead treat ε as a free parameter that can be chosen in order to place a resonance at a particular location. To do this, we begin from the 2D Helmholtz equation

$$\left(\frac{\partial^2}{\partial r^2}+\frac{1}{4\,r^2}-\frac{m^2}{r^2}+k^2\varepsilon(r)\right)\psi(r)=0,$$

where we have assumed a solution of the form $\phi(r,\theta)=\psi(r)e^{i\,m\,\theta}/\sqrt{r}$ to eliminate the first derivative. Splitting the permittivity into a spatially varying part and a background $\varepsilon(r)\rightarrow\varepsilon(r)+\varepsilon_b$, we can then formulate an eigenvalue problem for the background as

$$-\frac{1}{k^2}\left(\frac{\partial^2}{\partial r^2}+\frac{1}{4\,r^2}-\frac{m^2}{r^2}+k^2\varepsilon(r)\right)\psi(r)=\varepsilon_b\,\psi(r).$$

This allows one to choose a complex k value at which one would like a mode with polarity m to occur, then find a background permittivity that can be added to the initial structure so that it supports the desired mode.

It is important to note for this to be applicable to quasi-normal modes the boundary condition on the second derivative operator must be set to correspond to an outgoing wave at the edge of the resonator. This means that at $r = a$, where a is the radius of the resonator, $\phi \propto H_m^{(1)}(kr)$, which has the asymptotic form of a plane wave.

As an example of applying this framework, we consider a 2D circular resonator of initial permittivity of $\varepsilon = 4$ and radius a = 550 nm. This supports a dipolar (m = 1) quasi-normal mode at 97 - i 21 THz. For isotropic cylinders, one can find the locations of the quasi-normal modes using many methods: analytically using Mie theory, numerically by formulating the Helmholtz equation as a matrix with the appropriate boundary conditions, or using finite element solvers such as COMSOL. Each of these methods is shown in Figure 1a). To now *move* the dipole mode to 100 – i 1 THz, our framework can be applied to find that a background shift of $\varepsilon_b = -0.046 + i\,0.483$ will facilitate this. These results are shown in Figure 1.

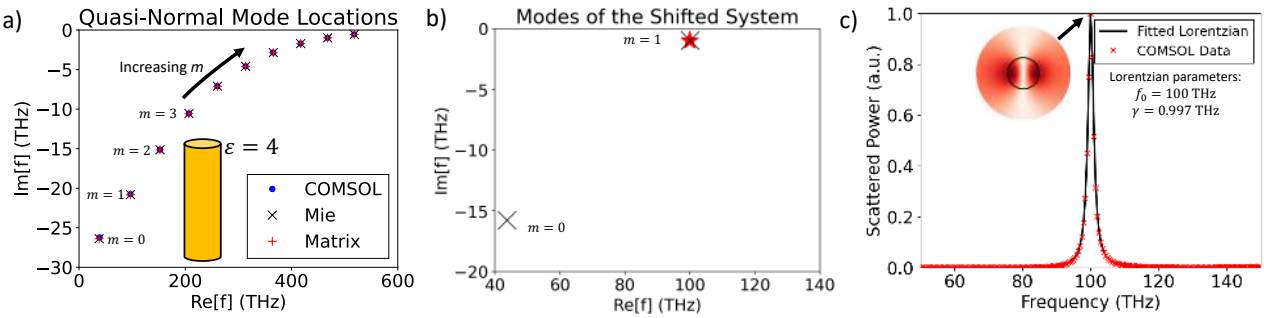


Figure 1 An example of using our framework to move the dipole resonance of a dielectric cylinder. a) the initial locations of all of the quasi-normal modes of a cylinder of permittivity $\varepsilon = 4$. The dipole (m=1) mode is at f = 96.8 – i 20.8 THz . Applying a background shift to the permittivity of the cylinder, calculated using our proposed framework, the new location of the m=1 mode is shown in b). The target frequency of 100 - i THz is shown as a red star. To verify that shifting the mode modifies the scattering behaviour of the resonator, we use COMSOL to calculate the scattered power under plane wave incidence as a function of frequency, shown in c). A clear peak is seen at the desired frequency, and with the correct width. The scattered field at 100 THz, shown in c) inset, verify that the scattering peak is indeed due to the re-located dipole mode.

We acknowledge financial support from the Engineering and Physical Sciences Research Council (EPSRC) of the United Kingdom, via the EPSRC Centre for Doctoral Training in Metamaterials (Grant No. EP/L015331/1). JRC also wishes to acknowledge financial support from Defence Science Technology Laboratory (DSTL). SARH acknowledges financial support from the Royal Society (URF\R\211033).

References

1. Wu, T., Baron, A., Lalanne, P. and Vynck, K., "Intrinsic Multipolar Contents of Nanoresonators for Tailored Scattering", Phys. Rev. A **101** 011803(R) 2020.
2. Ming, X., Sun, L., "Optimization of Broadband Perfect Absorber by Weierstrass Factorization", IEEE Photonics Journal 11 4602010 2019.
3. Capers, J. R., Patient, D. A. and Horsley, S. A. R. "Inverse Design in the Complex Plane: Manipulating Quasi-Normal Modes", Phys. Rev. A, **106** 053523 2022.
4. Chen, P. Y., Bergman, D. J., Sivan Y., "Generalizing Normal Mode Expansion of Electromagnetic Green's Tensor to Open Systems", Phys. Rev. Applied **11** 044018 2019.

Near-field seeing the colorful nano-world

Xuezhi Ma[1*], Qian Wang[1], Ming Liu[2*]

[1]Institute of Materials Research and Engineering, Agency for Science, Technology and Research (A*STAR), Singapore
[2]Department of Electrical and Computer Engineering, University of California, Riverside, CA, 92521, USA
[*]Corresponding author: maxuezhi@imre.a-star.edu.sg;
mingliu@ucr.edu;

Abstract: We reported the 6 nm spatial resolution for invisible-near IR (415nm-980nm) ultra-broadband near-field scanning optical microscope (NSOM). The NSOM provides two different channels to see the absorption and scattering spectroscopy at the same time. Using this super tool, we revealed a colorful nano-world on the sub-10nm scale. This is the first time that humans can "see" the carbon nanotube, which is well-known as one of the blackest materials, and find them colorful on the nanoscale.

Light is one of the most powerful and popular tools to interact with matters[1], such interactions are critical in quantum information processing, nano-lasing, spectroscopies, optical cavities, sensing, etc[2]. Light is also one of the most important mediums for humans to interact with the world. Light can be treated as a "ruler" to measure or see the world. However, light, especially in the visible region, has a wavelength ranging from 400 nm to 800 nm and it is too "long" to see the nanoscale world, and that is the diffraction limit[3]. One of the major tasks of the modern microscopy technique is increasing the spatial resolution by either enhancing the light-matter interaction strength or shrinking the dimension of the light source into sub-wavelength. Tip-enhanced probing techniques tried to enhance the near-field energy of light and shrink the hot spot to enhance the light-matter interaction, and the representatives include Tip-enhanced Raman Spectroscopy (TERS) and scattering-Scanning Near-field Optical Microscope (s-SNOM)[4]. Because of the requirement to filter out the large background noise, typically, interferometry is needed and thus the higher order or harmonic signal can give pure near-field signals. However, the direct signals (zero-order or first-order) signals provide much higher information and the s-SNOM cannot provide[5]. Alternatively, creating a nano-light source can intrinsically enhance the sensitivity and resolution of a microscope technique and achieve the zero-order signal. Principally, the color of light, which is determined by the frequency (*f*), is one of the intrinsic properties of photons and will not be changed in a linear process. Thus, the nano-focusing can compress the light but maintain its color. Here, we use the nano-focusing technique to compress the light volume into deep-sub-wavelength ($< \lambda/100$) and achieved the 1 nm resolution of Raman spectroscopy and 6 nm white light Near-field Scanning Optical Microscope (NSOM) absorption and scattering images[6]. To highlight that by using this super tool, we, for the first time, took a colorful picture of the single-walled carbon nanotubes (SW-CNTs), which are recognized as the darkest materials in the world. In addition, thanks to the super-resolution of both spectral and spatial, the chirality of CNTs can be distinguished from the CNT near-field color and the stress force stored in CNT can be mapped.

Figure 1 shows the details of the nano-focusing technique. Inspired by Otto's coupling configuration, which can provide up to 100% coupling efficiency to couple the light from free space into surface plasmon polariton (SPP) mode using a prism, we use the tapered single-mode optical fiber to replace the prism and couple the guided light into silver nanowire (AgNW)[7]. The light can be compressed by an adiabatic process into deep-sub-wavelength and be scattered from the sharp tip of the AgNW (Figure 1 b and c). By using this configuration, the nano-focusing efficiency was revolutionary and increased from 1%- 9% to 70%. By using this super tool, we achieved a 1 nm spatial resolution of TERS imaging in our previous work (see ref.). The configuration of the nano-focusing support ultra-broad band coupling as well. We used the normal LED, which just cost 1 dollar, to do the nano-focusing and achieved the ~5 nm focused white light source. Thanks to the ultra-confined white light source, the direct signal of bright field and dark field images are achieved with ~ 6 nm spatial resolution. To highlight that the spectral resolution is high as well, and thus it can be used to distinguish the chirality of CNTs (Figure 2b and c). This is the first time a human can direct see so small features with their intrinsic colors.

In summary, we used the nano-focusing technique to achieve colorful NSOM images with the highest-ever spatial resolution (6 nm). With this super tool, we took the first color pictures of the CNT.

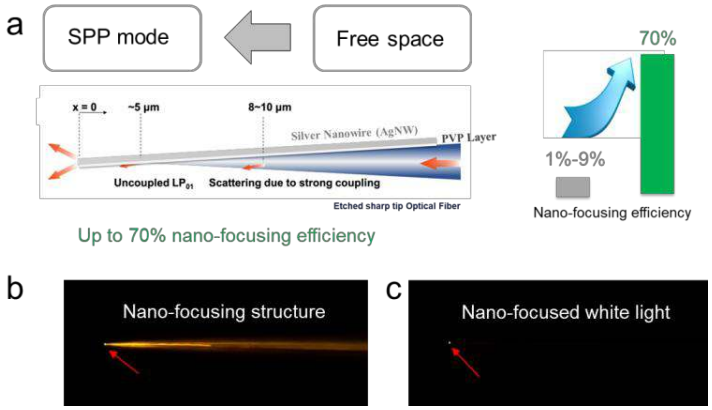


Figure 1. The details of nano-focusing. a) White light couple from a tapered single mode optical fiber into a sharp tip silver nanowire (AgNW) by Otto's coupling configuration. The nano-focusing efficiency was enhanced from 1%-9% to 70%. b) and c) show the nano white light source is scattered from the tip.

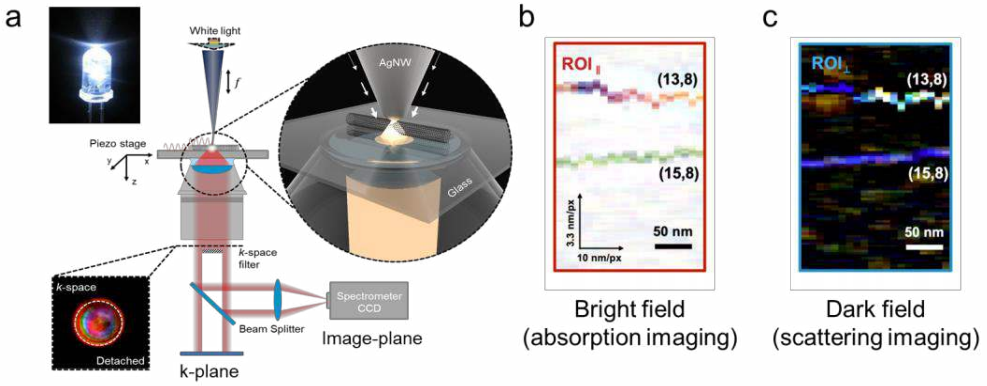


Figure 2. a) The configuration of the white-light NSOM setup. White light generated from the LED was compressed into a sub-wavelength hot spot and can interact with matters. By using a *k*-space blocker to filter out the undesired low-*k* light, the high-*k* signal with high resolution can be detected by the spectrometer in the image plane. b) and c) show the bright field and dark field of the near-field imaging to present the absorption signal and scattering signal, respectively. By using the reconstruction process, the colorful images of CNTs can be achieved.

Acknowledgments: This work was supported by the Agency for Science, Technology, and Research (A*STAR) under Career Development Fund-Seed Projects Grant No. 222D800038.

References

1 Rivera, N. & Kaminer, I. Light–matter interactions with photonic quasiparticles. *Nature Reviews Physics* **2**, 538-561 (2020).

2 Ren, H. & Maier, S. A. Nanophotonic Materials for Twisted‐Light Manipulation. *Advanced Materials*, 2106692 (2021).

3 Zalevsky, Z. Defying Abbe's law. *Nature Photonics* **7**, 593-594 (2013).

4 Kim, S. *et al.* High external-efficiency nanofocusing for lens-free near-field optical nanoscopy. *Nature Photonics* **13**, 636-643 (2019).

5 Pohl, D., Fischer, U. C. & Dürig, U. Scanning near‐field optical microscopy (SNOM). *Journal of Microscopy* **152**, 853-861 (1988).

6 Ma, X. *et al.* 6 nm super-resolution optical transmission and scattering spectroscopic imaging of carbon nanotubes using a nanometer-scale white light source. *Nature communications* **12**, 6868 (2021).

7 Akimov, Y. Optical resonances in Kretschmann and Otto configurations. *Optics letters* **43**, 1195-1198 (2018).

Supersymmetric Reshaping and Higher-Dimensional Rearrangement of Photonic Lattices

Tom A. W. Wolterink*, Matthias Heinrich, and Alexander Szameit

Institute for Physics, University of Rostock, Albert-Einstein-Straße 23, 18059 Rostock, Germany
*corresponding author: tom.wolterink@uni-rostock.de

Abstract: Self-imaging J_x photonic lattices enable perfect imaging and coherent transfer of quantum and classical states, yet their large-scale implementation remains challenging. We harness supersymmetry to engineer compacted two-dimensional systems that exhibit imaging and state transfer characteristics equivalent to one-dimensional J_x lattices and experimentally investigate their dynamics.

Evolution dynamics of wave-mechanical systems are governed by the full set of their modes and their respective eigenvalues. The key task of transferring arbitrary excitation patterns between two specific planes can therefore be accomplished by an appropriate structure of the eigenvalue spectrum. Along these lines, self-imaging is particularly effective if the spectrum is equidistantly spaced, similar to that of the harmonic oscillator. In finite-size discrete systems, the so-called J_x lattice fulfils this condition and has been employed for the perfect coherent transfer of quantum and classical states [1–3]. Yet, implementing large-scale J_x arrays remains experimentally challenging, as this class of systems relies on a precise realization of a large number of different yet finely tuned nearest-neighbor interaction strengths spanning a substantial dynamic range. To overcome these limitations, we leverage the concept of supersymmetric (SUSY) photonics [4,5] and present a method to design families of compact two-dimensional equivalent systems that inherit the spectral and key dynamic features of one-dimensional J_x arrays while requiring dramatically fewer distinct coupling values [6].

Our approach iteratively applies discrete SUSY transformations to decompose the original Hamiltonian of a J_x array, resulting in a sequence of higher-order superpartners and isolated sites. This is followed by reattachment of these sites in a series of inverse SUSY transformation steps in the orthogonal direction, thereby constructing two-dimensional arrays. The two-dimensional structure and its original one-dimensional counterpart share all their eigenvalues and will therefore exhibit similar characteristics.

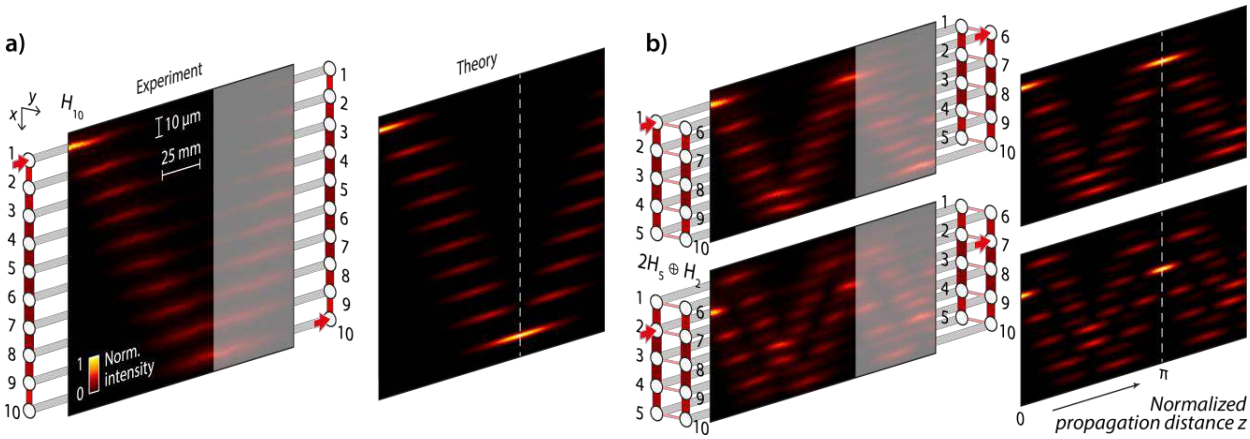


Figure 1. Measured (left) and calculated (right) evolution dynamics of light in a) a ten-waveguide J_x array and b) its two-dimensional superpartner. The initially excited and imaging target waveguides are marked by arrows. The imaging distance $z = \pi$ is indicated by semitransparent overlay (experiments) and dashed lines (simulations).

We experimentally realize these systems in arrays of evanescently coupled waveguides fabricated by femtosecond-laser direct writing and investigate their imaging properties by recording the intensity dynamics of guided light through fluorescence microscopy. We implement a conventional ten-waveguide J_x array and its two-dimensional superpartner of 5×2 sites. Figure 1 shows the observed light evolution for distinct input waveguides in each of these systems. We find that, while exhibiting systematically different dynamics in these two systems, light coalesces to the single target waveguide at the same imaging distance, demonstrating the desired perfect state transfer enabled by their identical spectra. In conclusion, our method readily allows for the design of compact self-imaging architectures with a minimum of structural parameters. By enabling increased robustness to perturbations and fabrication inaccuracies, it provides an avenue for high-fidelity coherence-maintaining state transfer in larger-scale photonic circuits.

References

1. M. Christandl, N. Datta, A. Ekert, and A. J. Landahl, "Perfect State Transfer in Quantum Spin Networks," Phys. Rev. Lett., Vol. 92, No. 18, 187902, 2004.
2. A. Perez-Leija, R. Keil, A. Kay, H. Moya-Cessa, S. Nolte, L.-C. Kwek, B. M. Rodríguez-Lara, A. Szameit, and D. N. Christodoulides, "Coherent quantum transport in photonic lattices," Phys. Rev. A, Vol. 87, No. 1, 012309, 2013.
3. A. Perez-Leija, R. Keil, H. Moya-Cessa, A. Szameit, and D. N. Christodoulides, "Perfect transfer of path-entangled photons in J_x photonic lattices," Phys. Rev. A, Vol. 87, No. 2, 022303, 2013.
4. M.-A. Miri, M. Heinrich, R. El-Ganainy, and D. N. Christodoulides, "Supersymmetric optical structures," Phys. Rev. Lett. , Vol. 110, No. 23, 233902, 2013.
5. M. Heinrich, M.-A. Miri, S. Stützer, R. El-Ganainy, S. Nolte, A. Szameit, and D. N. Christodoulides, "Supersymmetric mode converters," Nat. Commun. , Vol. 5, No. 1, 3698, 2014.
6. T.A.W. Wolterink, M. Heinrich, and A. Szameit, "Supersymmetric reshaping and higher-dimensional rearrangement of photonic lattices," arXiv:2209.12847, 2022.

META 2023, PARIS - FRANCE, JULY 18 – 21, 2023

Quasi-Dark States: A New Frontier in Light Enhancement and Control based on metasurface structures

Hicham. Mangach[1,2], Abdenbi. Bouzid[2], Younes. Achaoui[2], and Shuwen. Zeng[1,*]

[1] Light, Nanomaterials Nanotechnologies, CNRS-EMR 7004, Université de Technologie de Troyes, 10000 Troyes, France

[2] Laboratory of Optics, Information Processing, Mechanics Energetics and electronics, Department of physics, Moulay Ismail University, B.P. 11201, Zitoune, 50000 Meknes, Morocco

[*]corresponding author: shuwen.zeng@cnrs.fr

Abstract: Quasi-dark states in optical metasurfaces has a significant impact on the control of electromagnetic fields at subwavelength scales. These exceptional states, resembling bound states, have resulted in unparalleled light enhancement and a dramatic increase in the quality factor under the resonance condition. This phenomenon has been recently employed for refractometric sensing and near-field imaging. In this study, we demonstrate a hybrid metasurface without inversion symmetry, revealing a quasi-bound state in the continuum with a remarkable field enhancement at subwavelength scales.

Metasurfaces have emerged as a promising synthetic material with a finite extended constituent [1]. In fact, this subwavelength depth characteristic has proven to be a viable option in several aspects, including reducing the usage of high-consumption materials and streamlining overall manufacturing procedures, as they do not require a deep anisotropic profile akin to photonic crystals and metamaterials. Recently, these planar structures have exhibited their ability to shape the wavefronts as one can tune the structure, which leads to the emergence of a diverse range of lenses with different focus [2]. Moreover, with the optimized structure, a light-matter enhancement through the emergence of a quasi-bound state in the continuum is observed, thereby providing a novel perspective on amplifying electromagnetic intensity at a subwavelength scale. Recently, the concept of bound states in the continuum has stimulated the interest of the quantum mechanics community, as it demonstrates the mathematical possibility of high-energy electrons in a quantum wall can exhibit a localized state, commonly known as a dark state [3]. The Schrödinger equation's all-encompassing nature has bestowed upon phenomenon with versatility and ease of implementation across various disciplines, including optics, acoustics, and mechanics. Non-radiative sources, in particular, have attracted great interest due to their capacity for confining light to a nanoscale dimension. This property holds immense potential for various applications, including light enhancement at nanoscale in dielectric material with near-zero energy dissipation, in contrary to their plasmonic counterparts. Thus, the strong light confinement based on the quasi-dark state generated on the metasurface has bolstered for enhanced near field imaging, and increase of the refractometric sensitivity of optical devices [4]. Here, in this work, we have proposed a hybrid metasurface that integrates a non-centrosymmetric dimer made of Indium Tin Oxide (ITO) deposited on a Silicon Dioxide (SiO2) substrate. The unit cell has a spatial period of $\boldsymbol{a}$ and a total thickness $\boldsymbol{T}$ defined as the sum of $\boldsymbol{h1}$ and $\boldsymbol{h2}$. A detailed geometric parameters can be found in Figure 1. We have obtained the transmission and reflection amplitude at the lower and uppermost parts of the structure. These results were prompted by the impingement of y-polarized light upon its uppermost region, indicates a manifestation of significant light-matter interplay with a quality

factor of 2.6×10^7. In Figure 2, the illustrations of the calculation of the electric field norm in both the far field and near field are presented, demonstrating a strong confinement of energy associated with the emergence of quasi-bound states in the continuum under the resonance condition.

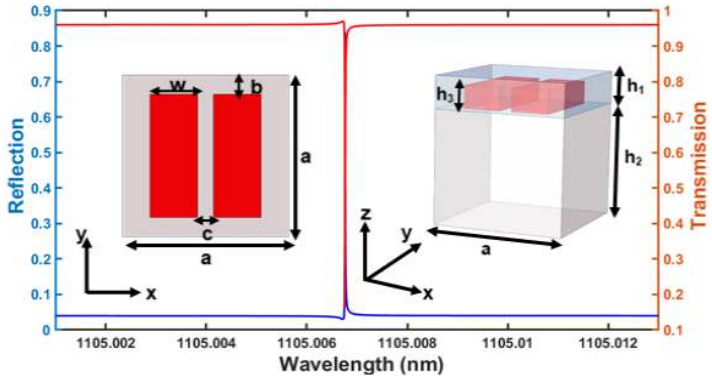


Figure 1: Schematic figure of the unit cell of our metasurface in 2D and 3D, with a variety of geometrical parameters, including: a = 750 nm, b = 95 nm, c = 70 nm, w = 210 nm, h1 = 200 nm, h2 = 700 nm and h3 = 140 nm. The transmission spectra (red curve) and reflection spectra (blue curve) of the quasi-bound state at the resonance.

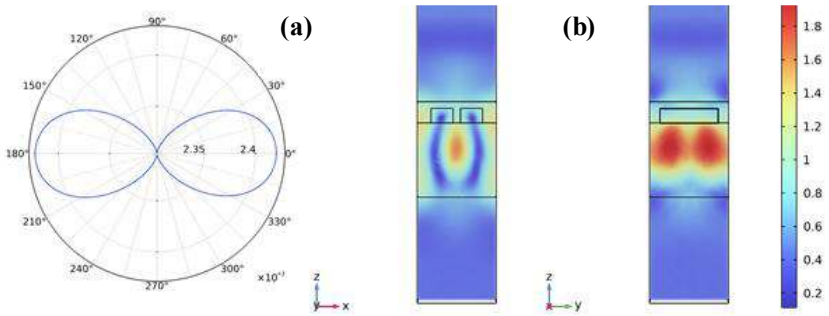


Figure 2: (a) The Far-field pattern at resonance, and (b) the Near-field distribution in (X,Z) and (Y,Z) planes, respectively.

Funding:

This work is supported under the UTT Project Stratégique NanoSPR (OPE-2022-0293), the Graduate School (Ecole Universitaire de Recherche) "NANOPHOT" (ANR-18-EURE-0013).

References

1. Lee, S. G., S. H. Kim, and C. S. Kee, "Metasurfaces with bound states in the continuum enabled by eliminating first Fourier harmonic component in lattice parameters," Physical Review Letters, 126(1), 013601, 2021.
2. Khorasaninejad, M., F. Aieta, P. Kanhaiya, M. A. Kats, P. Genevet, D. Rousso and F. Capasso, "Achromatic metasurface lens at telecommunication wavelengths," Nano letters, 15(8), 5358-5362, 2015.
3. Rybin, M., and Y. Kivshar, "Supercavity lasing," Nature, 541(7636), 164-165, 2017.
4. Wang, J., J. Kühne, T. Karamanos, C. Rockstuhl, S. A. Maier, and A. Tittl, "All-dielectric crescent metasurface sensor driven by bound states in the continuum," Advanced Functional Materials, 31(46), 2104652, 2021.

META 2023, PARIS - FRANCE, JULY 18 – 21, 2023

Imaging of Anti-ferroelectric Dark Modes in an Inverted Plasmonic Lattice

Javier Rodríguez-Álvarez[1,2,*], Amílcar Labarta[1,2], Juan Carlos Idrobo[3], Rossana Dell'Anna[4], Alessandro Cian[4], Damiano Giubertoni[4], Xavier Borrisé[5], Albert Guerrero[5], Francesc Perez-Murano[5], Arantxa Fraile Rodríguez[1,2] and Xavier Batlle[1,2]

[1] Departament de Física de la Matèria Condensada, Universitat de Barcelona, 08028 Barcelona, Spain
[2] Institut de Nanociència i Nanotecnologia (IN2UB), Barcelona, 08028, Spain
[3] Materials Science and Engineering Department, University of Washington, Seattle, WA, 98195, USA
[4] Sensors & Devices Center, FBK - Bruno Kessler Foundation, via Sommarive, 18, Povo, TN 38123 Italy
[5] Institut de Microelectrónica de Barcelona (IMB-CNM, CSIC), Bellaterra, 08193, Spain
*corresponding author: javier.rodriguez@ub.edu

Abstract: In this work an inverted plasmonic honeycomb lattice is studied by using state-of-the-art fabrication techniques, optical and electron spectroscopy, and simulations. The plasmonic lattice exhibits several bright and dark modes in the visible and near-infrared energy regime. Moreover, dark modes with anti-ferroelectric charge distributions that extent out of the unit cell of the honeycomb lattice have been experimentally found.

Plasmonic lattice nanostructures are of technological interest because of their capacity to manipulate light below the diffraction limit. Here, we present a detailed study of dark and bright modes in the visible and near-infrared energy regime of an inverted plasmonic honeycomb lattice by a combination of state-of-the-art Au+ focused ion beam lithography, optical and electron spectroscopy, and finite-difference time-domain simulations. The lattice consists of slits carved in an Au thin film, exhibiting a plethora of resonances in the visible and near-infrared ranges.

A detailed description of the charge distribution and near-field enhancement has been given by virtue of the good agreement between the electron energy loss spectroscopy (EELS) measurements, the optical measurements, and simulations. The most remarkable result is the finding of dark modes that may be caused by antiferroelectric arrangements of the slit polarizations, giving rise to charge arrangements with a unit cell four times larger than that of the original honeycomb lattice (see Figure 1b and 1e). Additionally, bright plasmonic modes exhibiting hotspots far from the metal slits are also found. The studied plasmonic resonances take place within 0.5 and 2 eV energy range, indicating that they could be suitable for a synergistic coupling with excitons in 2D transition metal dichalcogenides materials or for designing nanoscale sensing platforms based on near-field enhancement over a metallic surface. For example, the exciton energies for 2D WSe2 and MoS2 on an Au substrate, 1.75 and 1.9 eV, respectively [1], could be targeted by easily tuning manufacturing parameters such as the pitch of the lattice, thus changing the spectral position of the plasmonic resonances.

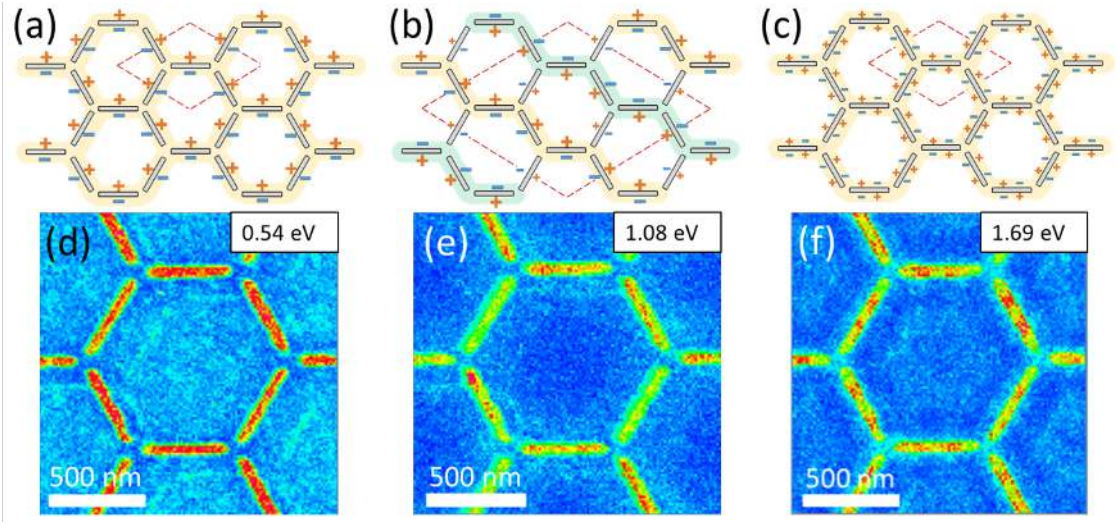


Figure 1. Plasmonic modes measured in the lattice at three different energies. (a), (b) and (c) show schematic representations of the charge distributions associated with one bright and two dark modes, respectively. Panels (d), (e) and (f) present the EELS mapping for the each of the modes depicted in the upper panels.

The authors acknowledge the financial support from Spanish MICIIN, grant number PGC2018-097789-B-I00 and PID2021-127397NB-I00, Spanish ICTS Network MICRONANOFABS and the European Union FEDER funds. The EELS measurements were supported by the CNMS, which is a U.S. Department of Energy, and using instrumentation within ORNL's Materials Characterization Core provided by UT-Batelle, LLC, under Contract No. DE-AC05-00OR22725 with the U.S. Department of Energy. Special thanks to A. Mihi group at ICMAB-CSIC for the FTIR measurements.

References

1. S, Park, et al., *2D Mater.* **2018**, *5*
2. J.Rodríguez-Álvarez, et al., *ACS Nano* (in review)

A Planar, NEMS-Based Terahertz Phase Shifter Using Subwavelength Confinement Waveguides

M. Demircioglu[1], M. A. Unutmaz[2], and M. Unlu[1*]

[1]TOBB University of Economics and Technology, Turkey
[2]Ankara Yildirim Beyazit University, Turkey
[*]corresponding author: munlu@etu.edu.tr

Abstract: In this paper, we present the Nano-Electro-Mechanical Systems (NEMS)-Based phase shifter using the Terahertz Subwavelength Confinement Waveguides (TSCW). The 90° phase difference is obtained from the OFF- and ON-states of the NEMS-based phase shifter at 0.29 THz. The measurement results of the 90° phase shifter show -4.79 dB worst-case insertion loss for the TSCW with 630 µm total length, which indicates the performances of 7.60 dB/mm and 18.8 °/dB.

The terahertz spectrum is an interesting frequency range for researchers due to the capabilities that are not achievable by the other spectrums, specifically the ultra-high data transfer rate supporting high-speed wireless communication [1]. There is an absolute necessity for compact, high-performance terahertz active and passive devices to enable high-speed communication [2]. Terahertz phase shifters are among the most required circuit elements for high-speed communication and currently have been worked on by many research groups [3]. TSCW have shown record-breaking degree per dB (°/dB) performance among all the planar terahertz phase shifters [4]. Nevertheless, they only presented theoretical records and did not present a real-time controllable phase shifters [5]. In this paper, we present the design, fabrication and the measurement of the Nano-Electro-Mechanical Systems (NEMS)-based 90° phase shifter using the Terahertz Subwavelength Confinement Waveguides (TSCW) operating at 0.29 THz. Combining the capabilities of NEMS and TSCW, a real-time controllable, miniature size and low-loss phase shifter is designed.

The NEMS switches have a perfect isolation during the OFF-state and good contact during the ON-state. The states can be controlled real-time by applying a DC voltage of 120 V. With the abilities of the TSCW, which is the effect of corrugation depth (h) on insertion phase, it provides a phase difference of 90° between the OFF- and ON-states.

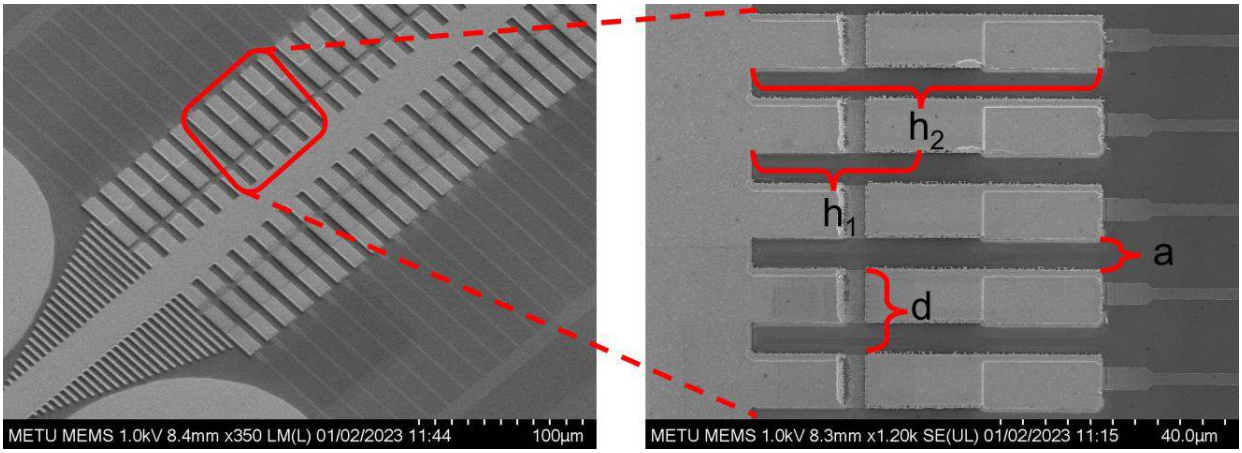
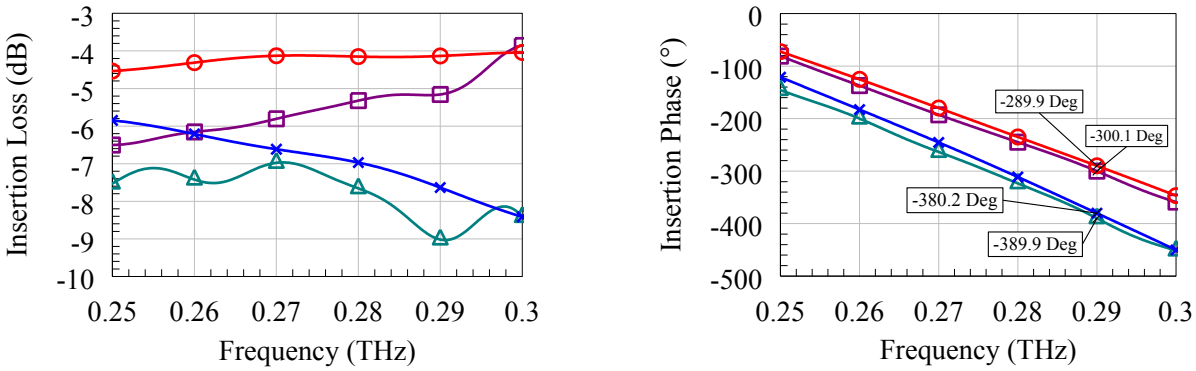


Figure 1. The SEM images of the fabricated NEMS-based phase shifters using TSCW.

Figure 1 shows the SEM images of the fabricated NEMS-based phase shifters. Corrugation depths (h_1), (h_2) show the corrugation depths of OFF- and ON-states and have 30 µm and 60 µm lengths, respectively. Additionally, the periodicity (d) and aperture width (a) are 15 µm and 5 µm, respectively.



(a) (b)

Figure 2. The insertion loss (a) and insertion phase (b) graphs for the comparison of the simulation and measurement results of OFF- (○), (□) and ON-states (x), (Δ) of the NEMS-based phase shifters, respectively.

In Figure 2, the comparison of simulated and measured S-parameter results of OFF- and ON-states are given. The simulation and measurement results exhibit a good match. The insertion losses of the OFF and ON-state are -5.16 dB and -9.02 dB at 0.29 THz. Extracting the back-to-back insertion loss of -4.23 dB, the worst-case insertion loss of -4.79 is obtained. For both simulation and measurement results 90° phase difference is obtained. The measurement results exhibit the performances of 7.60 dB/mm and 18.8 °/dB at 0.29 THz.

M.D acknowledges the partial support from the Scientific and Technical Research Council (TUBITAK) 2210A Grant. This work is financially supported by TUBITAK 119E489. The authors also acknowledge METU-MEMS Center personnel and TeraProbes, Inc. for the support during the fabrication and measurement.

References

1. Pfeiffer, U. R., Jain, R., Grzyb, J., Malz, S., Hillger, P., & Rodríguez-Vízquez, P. (2018, October). Current status of terahertz integrated circuits-from components to systems. In *2018 IEEE BiCMOS and Compound Semiconductor Integrated Circuits and Technology Symposium (BCICTS)* (pp. 1-7). IEEE.
2. Nagatsuma, T., Ducournau, G., & Renaud, C. C. (2016). Advances in terahertz communications accelerated by photonics. *Nature Photonics*, *10*(6), 371-379.
3. Zeng, H., Liang, H., Zhang, Y., Wang, L., Liang, S., Gong, S., ... & Mittleman, D. M. (2021). High-precision digital terahertz phase manipulation within a multichannel field perturbation coding chip. *Nature Photonics*, *15*(10), 751-757.
4. Unutmaz, M. A., Ozsahin, G., & Unlu, M. (2021). Optimization of terahertz spoof surface plasmon polariton waveguides for maximum/dB performance. *Journal of Lightwave Technology*, *39*(17), 5508-5515.
5. Unutmaz, M. A., & Unlu, M. (2021). Spoof surface plasmon polariton delay lines for terahertz phase shifters. *Journal of Lightwave Technology*, *39*(10), 3187-3192.

META 2023, PARIS - FRANCE, JULY 18 – 21, 2023

Coupling of semiconductor nanowire lasers to dielectric cylinders

D. Repp[1], F. Vitale[2], C. Ronning[2] and T. Pertsch[1,3]

[1]Institute of Applied Physics, Friedrich-Schiller-Universität Jena, Albert-Einstein-Str. 15, 07745 Jena, Germany

[2]Institute of Solid State Physics, Friedrich-Schiller-Universität Jena, Max-Wien-Platz 1, 07743 Jena, Germany

[3]Fraunhofer Institute of Applied Optics and Precision Engineering, Friedrich-Schiller-Universität Jena, Albert-Einstein-Str. 7, 07745 Jena, Germany

*corresponding author: daniel.repp@uni-jena.de

Abstract: We present active 3D-FDTD calculations of the field distribution and polarization of zinc oxide (ZnO) nanowires in the lasing regime coupled to dielectric cylinders. Significant coupling between nanowire and cylinder can be achieved, showing mode-specific resonance signatures when the cylinder diameter and refractive index are varied. By this modification of the nanowire lasing environment, we numerically demonstrate control of the polarization state of the lasing mode.

The lasing mode structure is calculated via the commercial FDTD software Lumerical, utilizing its built-in 4-level-2-electron system as an active lasing model. The gain profile is assumed to be spatially homogenous, which is a valid approximation when the nanowire is optically pumped in a quasi-static temporal regime. The nanowire is excited via a mode source placed perpendicular to the nanowire axis, which permits solving for different transverse field distributions. In prior work, this approach has proven useful for the study of the coupling between nanowire lasers and planar metallic substrates [1] as well as metallic gratings [2]. Here, a dielectric cylinder with a refractive index of n = 2.7 is placed close to the nanowire. Figure 1 shows a sketch of the investigated geometry. On a dielectric substrate (n = 1.4), two fundamental modes of perpendicular polarization, called the HE_{11x} and HE_{11y} modes, are excited separately and the average intensity in the cylinder is recorded and plotted in Fig. 2. Resonant coupling to whispering-gallery modes inside the cylinder is observed, independently of the nanowire size and refractive index.

In an active simulation, this knowledge is utilized by placing a nanowire on top of an aluminum substrate, separated from the nanowire by a small spacer. The nanowire is brought into contact with a cylinder tuned into resonance with the HE_{11x} mode, which would be the lasing mode if there were no cylinder. The HE_{11x} and HE_{11y} modes are excited simultaneously and the HE_{11y} mode is found to be lasing, contrary to the case where there is no cylinder. With this, it is proven possible to control the polarization of the lasing mode by placing a dielectric cylinder close to it. Since the resonance diameter of the cylinder is independent of the nanowire size, this approach paves the way towards deterministic, low-threshold excitation of Surface-Plasmon-Polaritons, which on perfect metals are surface modes mostly polarized perpendicular to the metal plane.

Acknowledgement: The authors acknowledge the financial support via projects C5 in the CRC 1375 “NOA–Nonlinear optics down to atomic scales” funded by the Deutsche Forschungsgemeinschaft (DFG) under project-ID 398816777.

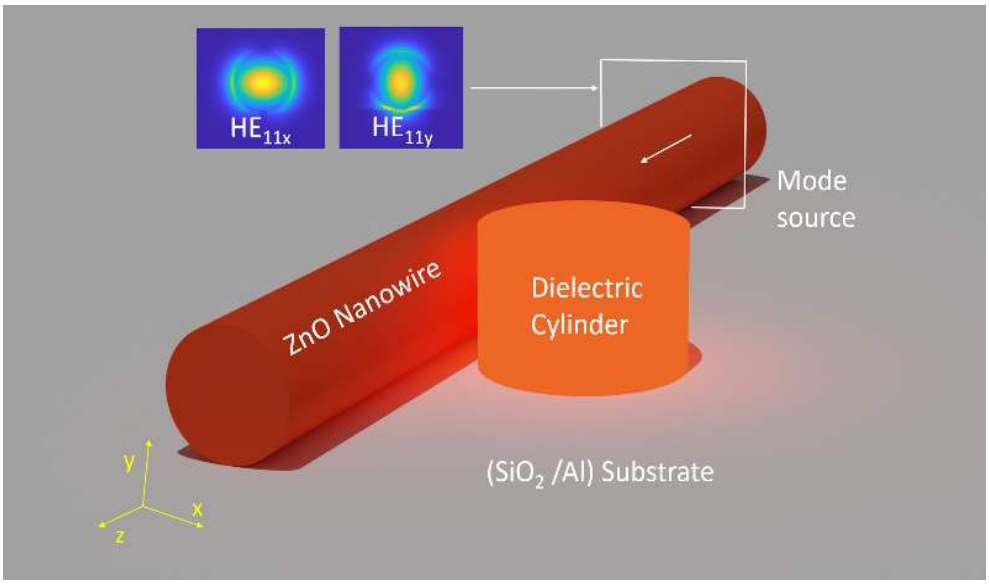


Figure 1: Sketch of the simulation geometry.

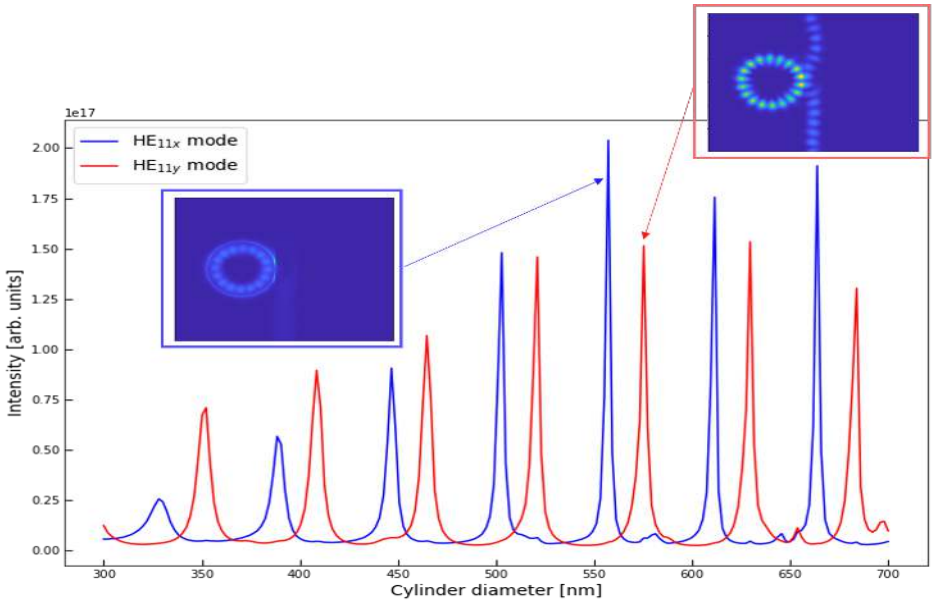


Figure 2: Integrated spectral power at a wavelength of 380nm (1 nm bandwidth) inside the cylinder, normalizer to cylinder area, in arbitrary units, for the HE11x and HE11y waveguide modes separately.

References

1. Repp, D., A. Barreda et al. "Lasing modes in ZnO nanowires coupled to planar metals," Optics Express, Vol. 31, No. 2, 3364-3378, 2023.
2. Vitale, F. and D. Repp. et al., "Tailoring Nanowire Lasing Modes via coupling to Metal Gratings," arXiv:2211-05470 (in revision at APL)

Tests for large-scale fabrication of plasmonic metasurfaces with fluorescence enhancement applications

R. Tomescu*, V. Anăstăsoaie, C. Pârvulescu, I. Mihalache, D. Cristea

National Institute for Research and Development in Microtehnologies—IMT-Bucharest,
126A, Erou Iancu Nicolae Street, 077190 Bucharest, Romania
*corresponding author: roxana.tomescu@imt.ro

Abstract: This paper presents the initial tests regarding the development of the technology process necessary to obtain large sensitive areas based on plasmonic metasurface for low-cost fluorescent biosensors. The nanostructured surfaces are attained using polystyrene nanospheres lithography and lift-off, processes that do not require high manufacturing time or cost. The test showed that the presence of the metallic nanostructures increases the fluorescence of Rhodamine 6G dispersed in a 170 nm thick PMMA film.

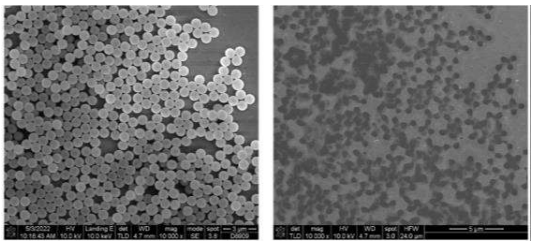
There is a constant need in the medical domain for reliable, fast and inexpensive methods for diagnostics and imaging [1]. Florescence biosensors based on metasurface structures are one of the best solutions [2]. Our aim is to develop a low-cost process suitable for large-scale fabrication of plasmonic nanostructures used to improve fluorescent emission. The process we propose allows the fabrication of metasurface platforms based on silver nanostructures on silicon obtain using polystyrene lithography and lift-off. We employed different deposition methods (spinning/droplet/immersion) and diameters for the polystyrene nanospheres (PSn) (Tabel 1) to determine the best uniformity which offers an optimal distribution of the metallic nanostructures, and consequently a significant fluorescence improvement. The silicon substrate was immersed in an aqueous based priming agent (SurPass 4000) for 2 minutes to maximize the adhesion properties, and PSn (water solution 2.5 wt%) were functionalized in a methanolic solution of Triton-X (1:400).

Table 1. Technological parameters employed in the substrate preparation and PSn deposition

No.	Substrate Functionalization	PSn deposition	PSn	No.	Substrate Functionalization	PSn deposition	PSn
S1	SurPass 4000	Spinning	880 nm	**S5**	SurPass 4000	Spinning	700 nm
S2	SurPass 4000	Spinning	940 nm	**S6**	SurPass 4000	Droplet	700 nm
S3	SurPass 4000	Spinning	700 nm	**S7**	SurPass 4000	Immersion	700 nm
S4	SurPass 4000	Spinning	850 nm	**S8**	-	Droplet	450 nm

*SurPass 4000 is an advance aqueous based priming agent which provides maximum adhesion to a wide range of substrate materials [3].

Figure 1 presents the SEM micrographs of structure S3 after silver deposition (Figure 1a) and after lift-off (Figure 1b). To investigate the improvement of R6G fluorescent intensity due to the presence of the metallic nanostructures, we deposited on top of the metasurface a 170 nm thick Rhodamine 6G (R6G) dispersed in polymethylmethacrylate (PMMA) film with a concentration of 50 µM. A fluorescence spectrometer FLS920 (Edin. Inst. Ltd, UK) was employed to perform steady-state photoluminescence emission. The excitation of $\lambda = 480$ nm was used to measure the emission/fluorescence intensity of the samples. Figure 2a shows the FL intensity spectra consisting of an emission band around 550 nm specific to the R6G thin films.

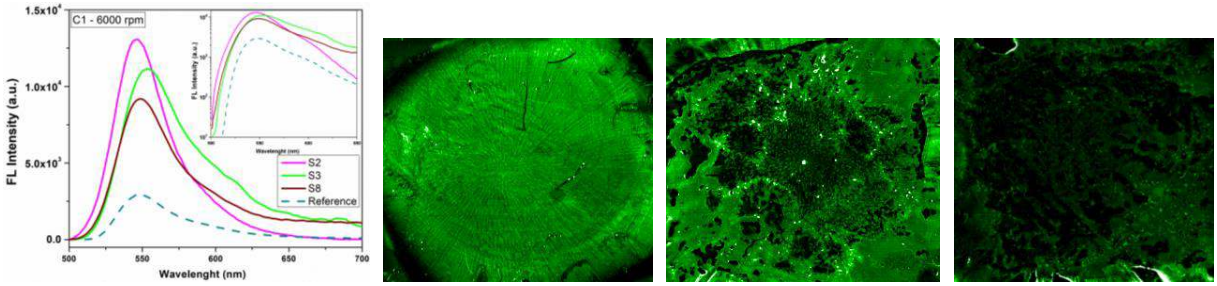


a) b)

Figure 1. SEM micrographs of S2 structure obtained: a) before lift-off; b) after lift-off

The results show a promising intensity improvement with a fluorescence enhancement factors (FLEN) between 3.1 (S8) and 4.5 (S2) (Figure 2a), depending on the distribution of the polystyrene spheres on the surface.

Also, samples' fluorescence was detected using a laser scanning confocal fluorescence system (GeneTAC UC4 Microarray Scanner, Genomic Solutions), by scanning the dices with Cy3 (532 nm) excitation laser. Figure 2 presents the images of the best samples (Figure 2b - S2 and Figure 2c - S3) and the faintest one (Figure 2d - S8).



a) b) c) d)

Figure 2. Fluorescence intensity: a) enhancement for different metasurfaces obtained on **Si** substrate; and images obtained with a laser scanning confocal fluorescence system: b) S2; c) S3; d) S8.

The results demonstrate that we can achieve a promising FLEN for R6G fluorophore up to 4.5 folds, depending on the distribution of PSn and the deposition method, and that these types of metasurfaces are useful in various biosensing applications. Our next steps are to optimize both the functionalization parameters and the deposition parameters of the polystyrene nanoparticles by employing different ratios of polystyrene solution and surfactant for the functionalization of the PSn, and deposition by progressive spinning with several steps, and also to investigate the FLEN for fluorophores with quantum efficiencies lower/equal to 0.5, (e. g.: Rose Bengal, Coumarin 153, Nile Blue, Oxazine Perchlorate 1, Crystal Violet, IR-140).

Acknowledgements: This work was supported by the Core Program of IMT-Bucharest within the National Research Development and Innovation Plan 2022-2026, carried out with the support of Romanian Ministry of Research, Innovation and Digitization, project no. 2307.

References

1. Li Z., et. al., Hybrid metasurface-based mid-infrared biosensor for simultaneous quantification and identification of monolayer protein, ACS Photonics, 6, 501–509 (2019)
2. Qu, H., et al., Recent advances of fluorescent biosensors based on cyclic signal amplification technology in biomedical detection, J Nanobiotechnol, **19**, 403, December 2021.
3. Surpass 4000 DisChem inc., Data Sheet.

Single-shot mapping of the second harmonic 3D radiation pattern by harmonic holography

S. Goldmann[1*], S. Grésillon[1], I. Izeddin[1], G. Tessier[2] and Y. De Wilde[1]

[1] Institut Langevin, ESPCI Paris, Université PSL, CNRS, 75005 Paris, France
[2] Sorbonne Université, INSERM, CNRS, Institut de la Vision, 17 rue Moreau, 75012, Paris
*corresponding author: serena.goldmann@espci.fr

Abstract: Digital holography is an imaging technique which measures both the amplitude and phase, from which the 3-dimensional electromagnetic field scattered objects can be reconstructed by digital propagation. Since Second Harmonic Generation (SHG) is a coherent process, SHG light can be used to generate interferences and holograms. We apply SHG holography to nonlinear nanostructured samples made of dielectrics or metals to obtain single-shot measurements of their second harmonic 3D radiation pattern and to map intensity and phase variations near the sample.

Digital holography is an interferometric imaging technique which can measure both the optical amplitude and phase. A digital back-propagation of this field therefore allows a 3-dimensional reconstruction of the electromagnetic field scattered by an object. We demonstrated its use in linear mode in off-axis digital holographic microscopy for the full 3-D mapping of the field scattered by single nanostructures such as nano-antennas [1] and near-field probes [2]. Since holography is an interference-based method, it can be performed at the laser illumination wavelength, but also with second harmonic generation (SHG), since the latter is a coherent process [3,4].

Here, we describe the development of a harmonic holographic microscope to map the second harmonic 3D radiation pattern in the vicinity of samples with non-zero second harmonic susceptibilities in one single-shot acquisition.
The knowledge of the scattered field (amplitude and phase) in a given plane (that of the camera) allows its reconstruction in any other plane using e.g. the angular spectrum representation of optical fields [5], and assuming propagation in homogeneous media, a process called 3D numerical back-propagation [6].

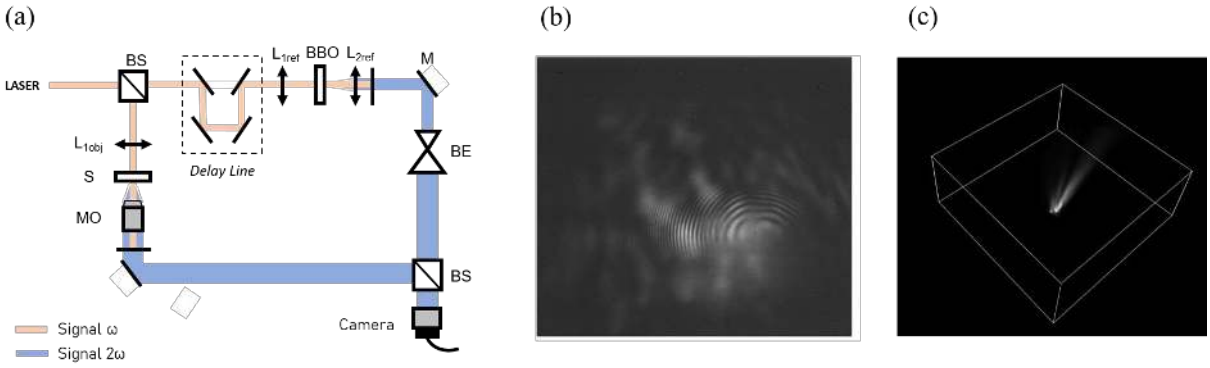


Fig 1.(a) Experimental setup schematics : BS, beam splitter ; L, lens ; MO, microscope objective ; BE, beam expander ; M, mirror ; BBO, beta-barium borate crystal ; S, sample (b) Hologram (c) 3D Reconstruction of the SH generated by a small (a few μm) BBO crystal.

In addition to providing 3D reconstruction, thus enhancing the imaging capabilities beyond those of back focal-plane imaging, the harmonic holography microscope also benefits from an amplification effect [7] since the signal from the sample is multiplied by an intense reference in the interference term, making the method particularly well suited to measure the weak SHG signals produced by metallic nanostructures [8]. The technique also benefits from the laser's short coherence length, which is 10 micrometers only with the 100 fs- source we use. The resulting coherence sectioning enables to proceed to a tomographic mapping of the sample.

After a first validation on dielectric samples made of nonlinear micro-crystals and cornea collagen, we are currently implementing it to unravel the SHG field radiated by plasmonic nano-antennas.

The authors are very grateful to Marie-Claire Shanne-Klein for stimulating discussions regarding SHG microscopy. This research is supported by the French National Research Agency (ANR-20-CE24-0021), and LABEX WIFI under references ANR-10-LABX-24 and ANR-10-IDEX-0001-02 PSL*.

References

1. Suck, S. Y.; Collin, S.; Bardou, N.; De Wilde, Y.; Tessier, G. 2011. Optics Letters, 36, 849–851
2. Rahbany, N., Izeddin, I., Krachmalnicoff, V., Carminati, R., Tessier, G., De Wilde, Y. 2018. ACS Photonics, 5, 1539-1545
3. Shaffer E., Pavillon N., Kühn J., Depeursinge C. 2009. Optics Letters, 34, 2450-2452
4. Pu Y., Centurion M., Psaltis D. 2008. Applied Optics, 47, A103-A110.
5. Novotny, L., and Hecht, B. Principles of Nano-optics. 2006. Cambridge University Press.
6. Hu, C., Field, J.J., Kelkar, V. *et al.* Harmonic optical tomography of nonlinear structures. *Nat. Photonics* 14, 564–569
7. Gross, M., Atlan, M. 2007. Optics Letters, 32, 909-911
8. Slablab, A., Le Xuan, L., Zielinski, M., De Wilde, Y., Jacques, V., Chauvat, D., Roch, J.-F., 2012. Optics Express 20, 220-227

Spectral Control of Plasmonic response and Spontaneous Emission Reinforcement from Quantum Dot near Nanoplasmonic Structures

R. Choudhary[1], and S. K. Srivastava[1,2*]

[1]Departmrnt of Physics, Indian Institute of Technology Roorkee, Roorkee-247667,India
[2] *Center for Photonics and Quantum Communication Technology*, *Indian Institute of Technology Roorkee,* Roorkee, *India*
*corresponding author: sachin.srivastava@ph.iitr.ac.in

Abstract: We show that the tuning of geometrical parameters of nanoplasmonic structures changes not only the electric field enhancement and plasmonic response but also the spontaneous emission. Spontaneous emission increases due to interaction between the quantum dot (QD) and the localized electric field in its vicinity. The spontaneous emission rate enhancement of the quantum dot follows plasmonic response of the nanoplasmonic structures. Thus, modified emission rate leads these nanostructures to have potential applications in sensing, integrated photonics, and solar energy conversion.

The coupled hybrid systems consisting of quantum dot and plasmonic nanostructures have been of interest for decades [1]. The plasmonic nanostructures confine the light below the diffraction limit [2]. Coupling between the quantum dots and localized plasmonic resonances in the nanoplasmonic structures leads to an increase in the emission rates of the quantum dots [3]. The electromagnetic near-field confinement due to localized plasmon resonance (LSPR) can lead to enhancement of the Purcell factor and thus plasmon enhanced Fluorescence (PEF) [4]. The Purcell factor is defined as the ratio between the modified (Γ_g) and free-space emission rates (Γ_0) of the quantum dot, given by [5]

$$F_P = \frac{\Gamma_g}{\Gamma_0} = \frac{3\,Q\left(\frac{\lambda}{n}\right)^3}{4\pi^2 V_0} \quad with\ V_0 = \frac{\int \varepsilon |E|^2\, dr}{\max\left(\varepsilon |E|^2\right)} \tag{1}$$

Where n is refractive index of the host medium, λ is the wavelength, Q is the quality factor of the cavity mode and V_0 is its volume.

In this work, we employed a commonly used method to calculate the Purcell factor of quantum dot put exactly at the center of the nanoparticle (NP) dimer cavities. We show that due to the localized field in the vicinity of plasmonic dimer cavities, the peak of extinction cross-section changes with the shape (sphere, cube, nanorod) and size of the plasmonic cavities leads to change the spontaneous emission rate of the quantum dot.

The schematics of plasmonic NP dimer cavities of different shapes (sphere diameter =60 nm, cube side =60 nm, nanorod length =60 nm) has been shown in Fig.1(a-c) with interparticle gap d taking surrounding medium as air. In Fig.1(d), the normalized extinction cross-section has been plotted as a function of the incident energy for each shape of the nanoparticle dimer. The resonance wavelength of plasmonic dimer cavities sphere, cube and nanorod were 532, 585, 577 nm respectively. We have optimized the spherical NP dimer for PEF based sensing application at excitation wavelength of 532 nm. The Purcell factor of the quantum dot placed at the center of the optimized plasmonic cavity (diameter=60 nm and d=6 nm) has been calculated using equation (1). A scattering resonance with Q=7.04 occurs near λ =542 nm, with 1350 times $|E|^2$ enhancement polarized along the dimer axis for the spherical NP dimer. Purcell analysis predicts a Purcell factor F_p~874. In Fig.1(e, f), the electric field profiles for spherical nanoparticle dimer have been shown at the excitation wavelength 532 nm both in absence and presence of a quantum dot (point dipole). As can be seen from Fig.1(e), the hotspot is generated between the

nanoparticles. This leads to an increase in the spontaneous emission rate of the point dipole.

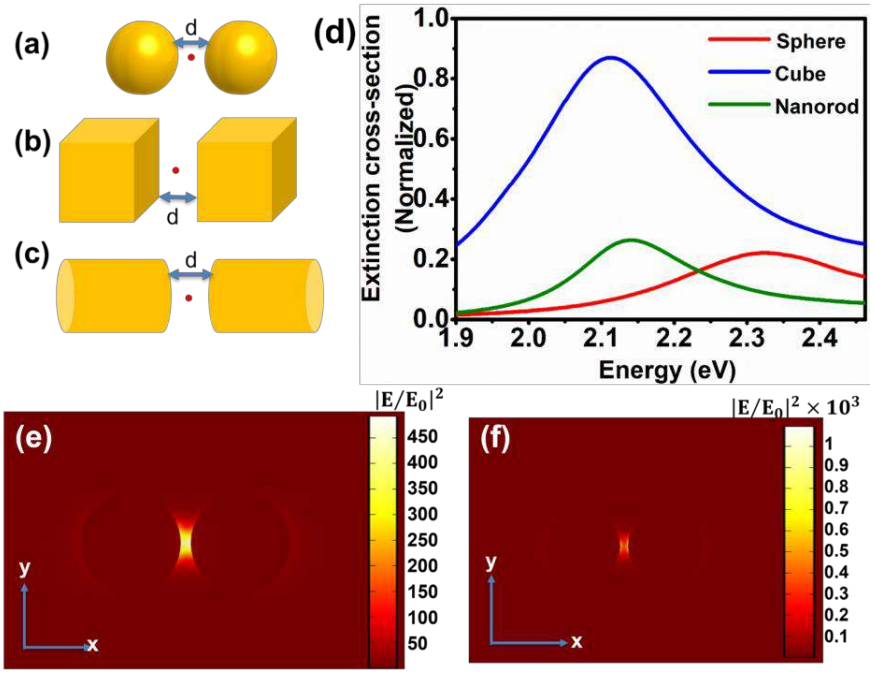


Fig.1.The schematics of the plasmonic dimers with quantum emitter (a) sphere, (b) cube, (c) nanorod respectively (d) Normalized extinction cross-section. The Electric field profiles at wavelength 532 nm in the (e) absence and (b) presence of quantum emitter (point dipole) for spherical dimer of diameter =60 nm, gap d=6 nm.

In conclusion, we have simulated plasmonic dimer cavities of different shapes (sphere, cube and nanorod) with quantum dot placed at the center. The resonance wavelength corresponding to peak extinction cross-section changes from 532 nm to 585 nm. We have optimized the spherical NP dimer cavity at the excitation wavelength of 532 nm for PEF based sensing applications. The Purcell factor F_p~874 was calculated for optimal parameters (diameter =60 nm, gap d=6 nm) for spherical NP dimer cavity.

Acknowledgements: Funding from MoE-STARS, DRDO-CARS and DST-BDTD grants are thankfully acknowledged. Riya Choudhary thanks to Council of Scientific & Industrial Research (CSIR) -India for the research fellowship.

References

1. Leng, H., Szychowski, B., Daniel, M. C., and Pelton M. "Strong coupling and induced transparency at room temperature with single quantum dots and gap plasmons," Nat. Comm., Vol. 9, No. 18, 06450-4, 2018.
2. Pelton, M., and Bryant, G., " Introduction to metal-nanoparticle plasmonics," Hoboken, NJ, John Wiley & Sons, 2013.
3. Pelton, M. "Modified spontaneous emission in nanophotonic structures," Nat. Photonics, Vol. 9, No. 7, 427–435, 2015.
4. Ringler, M., Schwemer, A., Wunderlich, M., Nichtl, A., Ku¨rzinger, K., Klar, T. A., and Feldmann, J. "Shaping Emission Spectra of Fluorescent Molecules with Single Plasmonic Nanoresonators," Phys. Rev. Lett., Vol. 100, No. 20, 203002-4, 2008.
5. Koenderink, A. F. "On the use of Purcell factors for plasmon antennas," Opt. Lett., Vol. 35, No. 24, 4208-4210, 2010.

META 2023, PARIS - FRANCE, JULY 18 – 21, 2023

Improvement of photoluminescence quality of MoS_2 monolayers by an atomic hydrogen beam

Mahan Bakhshikhah[1], Jiří Liška[1], Sayed Hossein Mirdamadi Khouzani[1], Ondřej Červinka[1], Jindřich Mach[1,2], Miroslav Kolíbal[1,2], Tomáš Šikola[1,2*]

[1]Central European Institute of Technology, Brno University of Technology, Brno, Czech Republic

[2]Institute of Physical Engineering, Faculty of Mechanical Engineering, Brno University of Technology, Brno, Czech Republic

[*]corresponding author: sikola@fme.vutbr.cz

Abstract: Thin and tiny metasurface-based flat optics based on exciton resonances can be used as the replacement for bulky optical elements to develop tuned nanophotonic structures. We present that the optical response of this type of metasurface can be enhanced by improving the photoluminescence properties of their semiconducting building blocks made of a MoS_2 monolayer by their treatment using an atomic hydrogen beam source.

1. Introduction

Metasurfaces are two-dimensional (2D) versions of metamaterials with impressive abilities to control their electromagnetic response by a properly designed flat structure consisting of specific sub-wavelength resonant scatterers. Metasurfaces with tailored wavefronts find applications at frequencies ranging from microwaves to UV, namely metasurface lenses, antennas, and optical devices (e.g., lidars, non-linear modulators) and sensors [1]. Localized surface plasmon resonances (LSPR) are caused by collective oscillations of electrons in metallic nanostructures – sub-wavelength elements, e.g., Au, Ag antennas [2], [3]and thus, naturally, their performance is hindered by strong dissipative losses (heating) in these elements. These detrimental effects are not present in Mie-type resonances [1], [4], but with LSPR–based metasurfaces, those utilizing Mie resonances show up limitations in the electrical tunability of their functionalities. With this respect, the utilization of exciton resonances represents a promising method for overcoming this problem [4]. Unlikely to bulk materials, excitons (i.e., coupled electron-hole pairs) in some 2D semiconductor materials dominate in the optical properties even at room temperature. However, a light-matter interaction with atomically thin materials such as transitional metal dichalcogenides (TMDCs) is generally weak. On top of that, even though 2D TMDCs should show more powerful photoluminescence (PL) ability in contrast to bulk counterparts, in reality, they exhibit poor luminescence quantum yield (QY) due to the defect-mediated nonradiative recombination and biexcitonic recombination at higher excitation powers. However, 2D TMDCs are generally known to be amenable to defect surface passivation by a chemical treatment using (bis(trifluoromethane) sulfonimide (TFSI)) [5] or, as we propose, by their treatment via a home-built atomic hydrogen beam source (expected QY ≥ 60% - more than 100-fold increase). Naturally, it would open ways for novel applications of metasurfaces not achievable so far. In this presentation, we report on an improvement of PL properties of a TMDCs material, namely MoS_2. Consequently, we will present the results on patterning of nanoflakes by electron beam lithography and dry etching (plasma treatment) to get an assembly of sub-wavelength building blocks of a metasurface flat optics for the dynamic wavefront control of optical beams.

2. Nanofabrication

We have prepared MoS_2 monolayered flakes by mechanical exfoliation from a bulk crystal, and they were

transfered on a fused quartz substrate. After that, we have treated the samples by a home-built atomic hydrogen beam source to verify this method for enhancement of PL properties (QY) of these flakes. Consequently, the patterning of flakes to fabricate a metasurface-based flat optics using electron beam lithography (EBL), reactive ion etching (RIE), and flake protection by a resist film (e.g., polymethyl methacrylate, PMMA) was done (Figure 1).

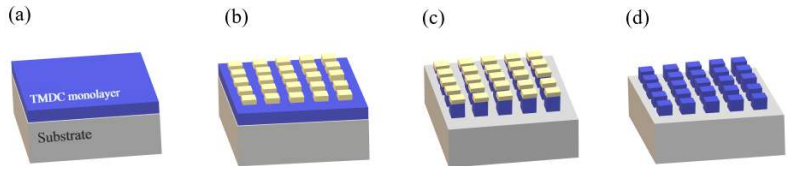


Figure 1. Nanofabrication process (patterning). (a) TMDC monolayer on a substrate (not-to-scale drawing), (b) PMMA (yellow) patterned using EBL on top of the TMDC (c) TMDC etched by RIE, (d) patterned TMDC after removing PMMA in acetone.

3. Results and discussion

The results of the MoS_2 treatment are shown in Figure 2. One can see the PL enhancement was 2-fold. This value can certainly be increased by optimization of process parameters (e.g., better aiming of the beam, proper flux density, and exposure time). Generally, the optical quality of commercially available MoS_2 flakes prepared by a CVD method is notably poorer compared to the exfoliated ones. Hence, one can anticipate a more significant improvement of in PL after the application of hydrogen atoms to them.

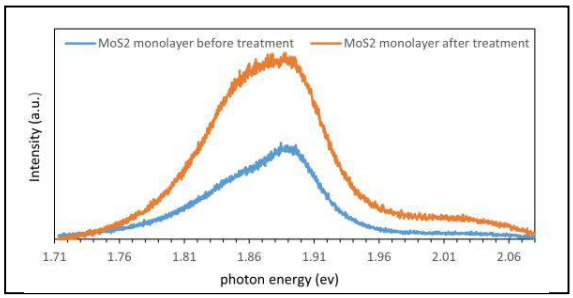


Figure 2. PL spectrum for MoS_2 monolayer before and after atomic hydrogen source treatment

4. Conclusions

We have proved that the proposed method based on the application of the atomic hydrogen beam source is capable of improving the PL of MoS_2 monolayers. In the next step, larger, commercially available MoS_2 flakes prepared by a CVD method will be tested for this method and, consequently, patterned by EBL, this would open the way to a design of more efficient metasurface devices based on atomically thin 2D layers.

Acknowledgements

This research is carried out by the Central European Institute of Technology (CEITEC) Nano Research Infrastructure and collaboration with the Institute of Physical Engineering at Brno University of Technology in the Czech Republic.

References

[1] S. S. Bukhari, J. Vardaxoglou, and W. Whittow, "A metasurfaces review: Definitions and applications," *Appl. Sci.*, vol. 9, no. 13, 2019.

[2] R. S. Kshetrimayum, "A brief intro to metamaterials," *IEEE Potentials*, vol. 23, no. 5, pp. 44–46, 2004.

[3] Y. Liu and X. Zhang, "Metamaterials: A new frontier of science and technology," *Chem. Soc. Rev.*, vol. 40, no. 5, pp. 2494–2507, 2011.

[4] T. J. Cui, S. Liu, and L. Zhang, "Information metamaterials and metasurfaces," *J. Mater. Chem. C*, vol. 5, no. 15, pp. 3644–3668, 2017.

[5] T. Mueller and E. Malic, "Exciton physics and device application of two-dimensional transition metal dichalcogenide semiconductors," *npj 2D Mater. Appl.*, vol. 2, no. 1, pp. 1–12, 2018.

META 2023, PARIS - FRANCE, JULY 18 – 21, 2023

Spin-coating Based Nanosphere Lithography

Alejandro Descalzo [1 2] *, Lu He [1 2], Teresa Madeira [1 2], Dietrich R.T. Zahn [1 2]

[1] Semiconductor Physics, Chemnitz University of Technology, D-09107 Chemnitz, Germany
[2] Center for Materials, Architectures, and Integration of Nanomembranes (MAIN), Chemnitz University of Technology, 09107 Chemnitz, Germany
*E-mail: alejandro.descalzo-ruiz@s2021.tu-chemnitz.de

Abstract: Nanosphere lithography (NSL) is a straightforward, cost-efficient technique for creating plasmonic nanostructures with high precision. This work reviews the challenge of the NSL mask preparation by spin coating. The process parameters to achieve large, well-ordered monolayer areas covered by polystyrene (PS) nanoparticles with a diameter of 400 nm over a glass substrate are discussed. The results reveal that the surface coverage increases with decreasing spin velocity and acceleration in a certain range.

Nanosphere lithography (NSL) has been used in various applications like bio/chemical sensors and light trapping in solar cells or spectroscopy [1]. Within the range of methods used for NSL, spin coating stands out for its effectivity, fastness, and flexibility in controlling the process [2]. However, the uniformity and compactness of the nanospheres depend on several interdependent parameters, and finding an optimal recipe is still a challenge [3]. This work aims at revealing the influence of spin acceleration and velocity on the mask prepared by NSL.

For this purpose, a solution of 4% weight of polystyrene (PS) nanospheres (purchased from Thermo Fisher Scientific) is deposited onto 2.5 x 2.5 cm^2 glass substrates via spin coating (WS-650Sz-23NPP Lite Single Wafer Spin coater). The substrates are pre-treated with a series of ultrasonication baths (in acetone, ethanol, and de-ionised water for 15 minutes each) followed by rinsing in ethanol to increase the wettability of the surface. The substrates are then dried with nitrogen flow. After the substrate cleaning, drops of 100 µl of the dispersed suspension are pipetted over the surface of the substrate and accelerated to specific spin velocities for 2 min. The samples are covered with gold by thermal evaporation and are analyzed by scanning electron microscopy (FEI Nove NanoSEM 200). In the first series of experiments, the spin velocity is varied while the spin acceleration is fixed at 200 rpm/s. In the second series of experiments, the spin acceleration is varied at a fixed spin velocity of 6000 rpm.

The optimal velocity is found at the lowest value (4000 rpm), at which nanospheres assemble and form large domains of well-ordered and compacted nanosphere arrays (figs. 1a,d). At a higher velocity (6000 rpm), the self-assembling of the nanospheres is weakened, leading to distorted and non-compacted areas as well as a sharp decrease in the total surface coverage (figs. 1b,e). Increasing the velocity further (8000, 10000 rpm) leaves a high percentage of the sample uncovered. At these high values, the nanospheres are mainly agglomerated at some impurities, forming small islands, in which we find some compact and uniform hexagonal nanosphere arrays (figs. 1c,f).

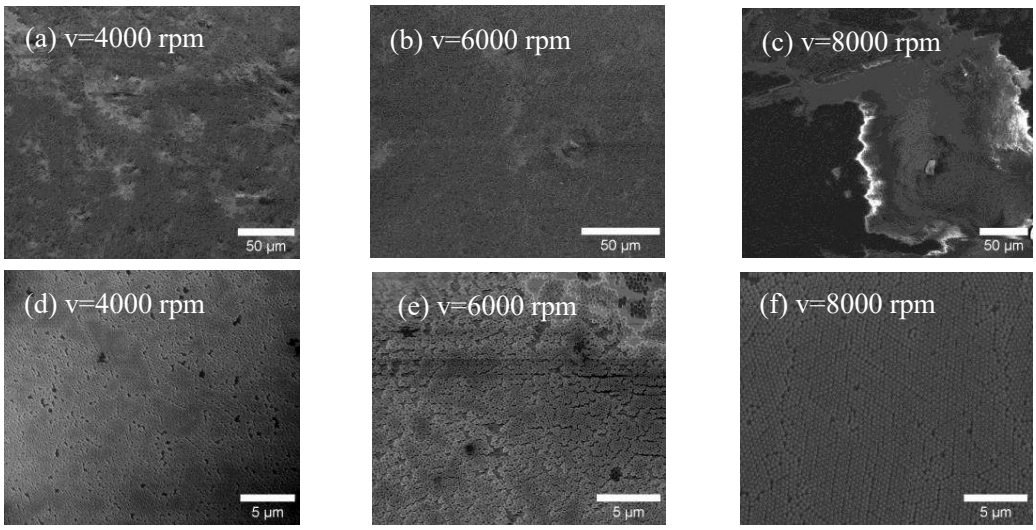


Fig. 1: SEM images of nanostructures obtained at different spin velocities: (a-c) at low magnification (d-f) at high magnification.

Considering the spin acceleration the highest total surface coverage is achieved at the lowest acceleration of 200 rpm/s while lower surface coverage is observed with increasing acceleration value (600 rpm/s, 1000 rpm/s) (figs. 2a,b).

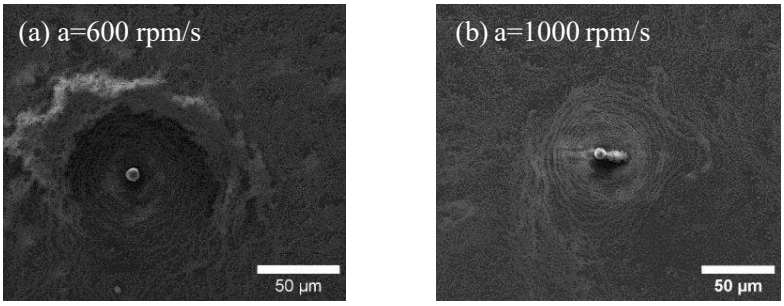


Fig. 2: SEM images of nanostructures obtained at different spin accelerations with low magnification.

In summary, spin coating at low spin velocities and accelerations is preferred to form a large hexagonal compacted nanosphere arrays. However, there is a need for fine-tuning the spin parameters for NSL.

References

1. Razaulla, T., Bekeris, M., Feng, H., Beeman, M., Nze, U., & Warren, R. “Multiple Linear Regression Modeling of Nanosphere Self-Assembly via Spin Coating”, Langmuir, 37(42), 12419–12428, 2021.
2. Song, C., Ye, B., Xu, J., Chen, J., Shi, W., Yu, C., An, C., Zhu, J., & Zhang, W. “Large-Area Nanosphere Self-Assembly Monolayers for Periodic Surface Nanostructures with Ultrasensitive and Spatially Uniform SERS Sensing”, Small, 18(8), 2022.
3. Osipov, A. A., Gagaeva, A. E., Speshilova, A. B., Endiiarova, E. v., Bespalova, P. G., Osipov, A. A., Belyanov, I. A., Tyurikov, K. S., Tyurikova, I. A., & Alexandrov, S. E. “Development of controlled nanosphere lithography technology”, *Scientific Reports*, *13*(1), 3350, 2023

META 2023, PARIS - FRANCE, JULY 18 – 21, 2023

Size-dependent Localized Surface Plasmon Resonance of Structures Prepared by Nanosphere Lithography

Milad Karami[1,2*], Lu He[1,2], Teresa I. Madeira[1,2], and Dietrich R. T. Zahn[1,2]

[1]Semiconductor Physics, Chemnitz University of Technology, D-09107 Chemnitz, Germany
[2]Center for Materials, Architectures, and Integration of Nanomembranes (MAIN), Chemnitz University of Technology, 09107 Chemnitz, Germany
[*]corresponding author: milad.karami@s2020.tu-chemnitz.de

Abstract: Nanosphere lithography (NSL), which is used to generate ordered two-dimensional periodic arrays of plasmonic nanostructures, is an inexpensive, versatile, intrinsically parallel, and high-throughput nanofabrication technique [1]. Localized surface plasmon resonances (LSPRs) produced by MNPs offer essential application opportunities in photonics, electronics, and nanotechnology [2]. The LSPR can be tuned by different methods, where changing the geometry of metal nanoparticles (MNP) provides a very diverse approach. We systematically studied the geometry dependence on LSPR produced by polystyrene beads of various sizes.

For the preparation of nanosphere monolayers a colloidal solution is first created by mixing ethanol and polystyrene nanospheres in a 1:1 volume ratio and then ultrasonicated for 10 minutes. A glass slide is then washed using acetone, ethanol, and water, followed by drying with N_2 gas to create a hydrophilic surface. Subsequently, a petri dish is filled with distilled water to facilitate the deposition of 10 µL of colloid dispersion onto the glass slide. As a result of the interfacial tension between the liquid and air, the colloid particles self-assemble into a monolayer at the water-air interface, as illustrated in Figure 1. Finally, the glass substrate is gently lifted to retrieve the monolayer of polystyrene nanospheres.

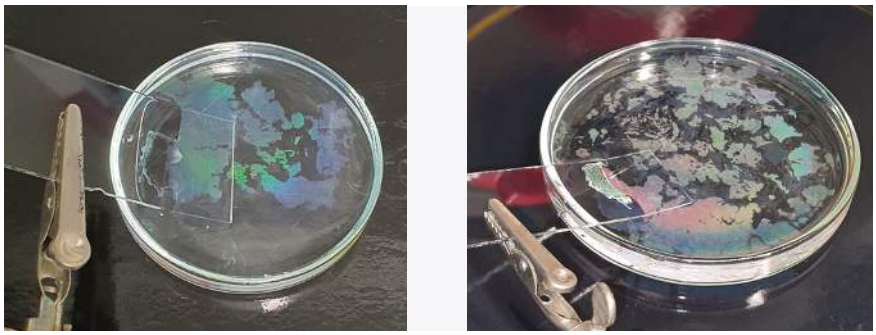


FIG. 1. Images of colloidal film at the water-air interface.

Scanning electron microscopy is used to analyze the geometry of the structures after deposition of approximately 50 nm gold layer [3]. Figure 2 displays the typical formation of monolayer of self-assembled nanospheres with a diameter of 200 nm (left) and 400 nm (right). The 200 nm nanosphere size (left) leads to well-ordered hexagonal close-packed (hcp) structures of nanospheres with some impurities. For 400 nm nanosphere size (right), the nanospheres are arranged in well-ordered hcp structures with some stacking faults.

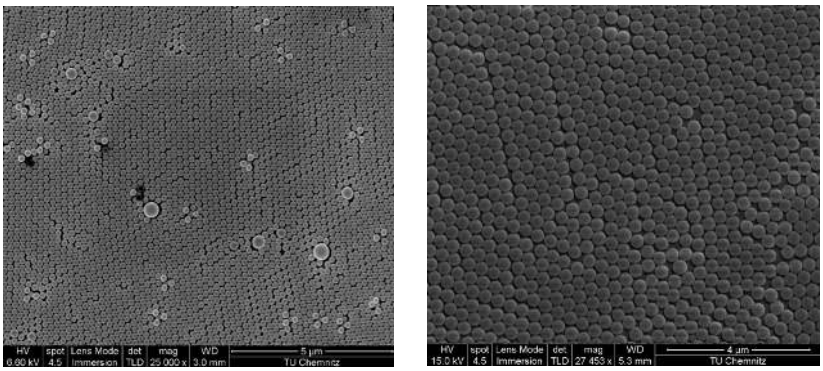


FIG. 2. SEM images of gold covered 200 nm (left) and 400 nm (right) polystyrene spheres on glass.

Theoretically, the size of the Au nanotriangles, a, which are obtained on the substrate after removing the nanospheres is directly related to the size of the polystyrene nanospheres (D) by the following expression [1,4]:

$$a = (3/2)\,(\sqrt{3} - 1 - 1/\sqrt{3})D = 0.233D \quad (1)$$

In Figure 3, the transmittance spectra for gold nanotriangle arrays fabricated using the polystyrene nanospheres are presented. The reference transmittance spectrum corresponds to the glass substrate. Examination of the spectra demonstrates that the localized surface plasmon resonance (LSPR) for a 400 nm nanosphere size occurs at 1.65 eV, while for a 200 nm size, it is observed at 1.85 eV. This finding provides evidence for the correlation between the size of the Au nanostructure and the LSPR energy, where smaller structures lead to higher LSPR energy.

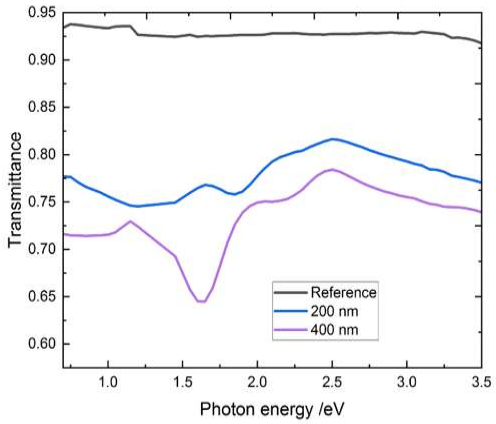


FIG. 3. Transmittance spectra of gold (Au) nanotriangles on glass as a function of polystyrene nanosphere size.

Our findings demonstrate that the localized surface plasmon resonance (LSPR) of the plasmonic nanostructures can be changed through the utilization of polystyrene nanospheres of varying sizes. This outcome holds significant potential for applications that necessitate a tunable resonance wavelength, as it enables tailored optimization of the LSPR properties to suit the specific requirements of the given application.

References

1. J.C. Hulteen, D.A. Treichel, M.T. Smith, M.L. Duval, T.R. Jensen, R.P. Van Duyne, Journal of Physical Chemistry B 103 (1999) 3854–3863.
2. M. Rahaman, S. Moras, L. He, T.I. Madeira, D.R.T. Zahn, J Appl Phys 128 (2020) 233104.
3. G.H. Chan, J. Zhao, G.C. Schatz, R.P.V. Duyne, Journal of Physical Chemistry C 112 (2008) 13958–13963.
4. A. V. Whitney, B.D. Myers, R.P. Van Duyne, Nano Lett 4 (2004) 1507–1511.

Highly directional plasmomechanic stretchable strain sensor

Asad Nauman[1], Jae-Won Lee[1], Jun-Chan Choi[2], Hafiz Saad Khaliq[1], Junkai Wang[1], and Hak-Rin Kim[1,3*]

[1]School of Electronic and Electrical Engineering, Kyungpook National University, 41566 Daegu, republic of Korea
[2]Soft Hybrid Materials Research Center, Korea Institute of Science and Technology, Seoul 02792, Korea
[3]School of Electronics, Kyungpook National University, 41566 Daegu, republic of Korea
[*]Corresponding author: rineey@knu.ac.kr

Abstract: We report asymmetric tuning of nanogap resonance between gold nanoparticles (Au NPs), deposited on anisotropically stretchable polydimethylsiloxane (PDMS) for directional strain sensing. The alternate high and low Young's modulus PDMS line patterns induce anisotropic Poisson's effect (0.45 to 0.61), resulting in direction-dependent plasmon resonance between the Au NPs. For the light polarized perpendicular to the stretching direction, the maximum absorbance peak shift of ~90.85 nm and ~39.13 nm is achieved for $\theta = 0°$ and $\theta = 90°$ direction, respectively.

Localized and coupled plasmon resonance based on metallic nanoparticles has been investigated thoroughly for promising applications in color filtering and sensing [1]. The coupled plasmonic resonance resulting in distinctive colors depends on several parameters, such as materials, their arrangement, interparticle distance, and the nanostructure's geometry [2]. Among these parameters, the mechanical substrate can reversely tune the interparticle distance [3]. However, multidirectional and broadband resonance tuning is hard to achieve based on conventional isotropic mechanical substrates. We propose a highly directional and polarization-sensitive coupled plasmon resonance between the Au NPs deposited on an anisotropic line pattered PDMS substrate with alternate high and low Young's modulus (Fig. 1a(i)). The deposited Au NPs (diameter of ~20nm) on anisotropic PDMS exhibit localized resonance initially. Meanwhile, its size was grown hydrothermally up to the diameter of ~36 nm to reduce distance between the NPs until the coupled resonance was achieved, as shown by the SEM image (inset of Fig. 1a(i)). The alternate high and low modulus line patterns of PDMS induce anisotropic Poisson's effect (width change $W_{\perp}$ perpendicular to stretching direction), which is verified using COMSOL simulations (Fig. 1a(ii)). These results show a considerable change in $W_{\perp}$ when stretched parallel to patterns ($\theta = 0°$) compared to the stretching perpendicular to the patterns ($\theta = 90°$).

When the external force is applied in $\theta = 0°$, it sharply decreases the interparticle distance between the Au NPs (Fig. 1b) along the perpendicular direction to the stretching due to high Poisson's effect. Consequently, it enhances the coupled resonance, and the maximum absorbance peak shifts from 539 nm to 629 nm as the force intensity increases from 0 N to 1.3 N for linearly polarized light perpendicular to the stretching direction. In contrast, when force is applied in $\theta = 90°$ direction, the interparticle distance is not significantly reduced perpendicular to the stretching direction since the high modulus PDMS patterns hinder the width W change$_{\perp}$ (low Poisson's ratio). This results in a comparably minor peak shift of ~39.13 nm in a range of 539 nm to 578 nm for the light polarized perpendicular to the stretching direction. Our proposed plasmomechanical structure shows a visible color shift to distinguish the deformation direction as well as the intensity of applied force which can have a significant impact in the field of wearable and stretchable sensors.

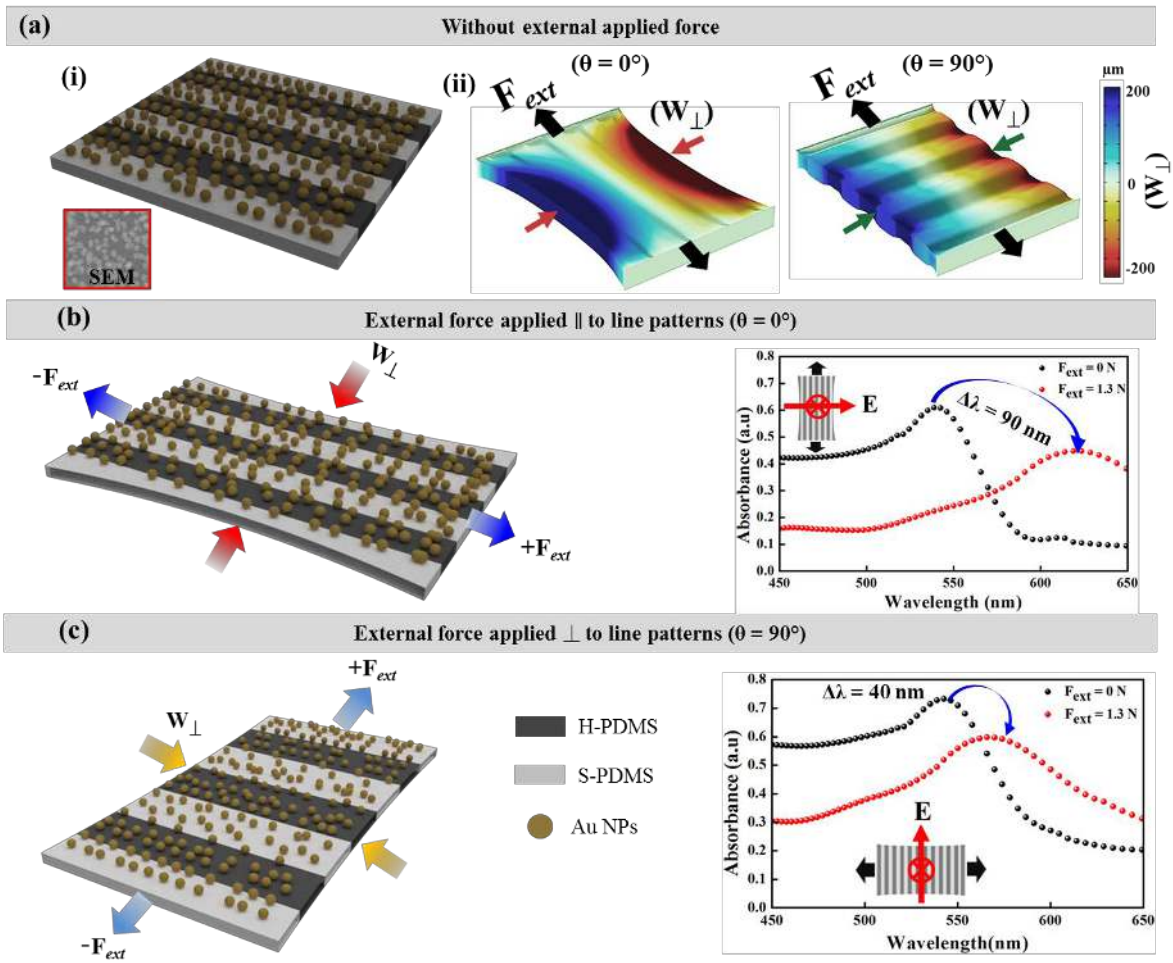


Figure1. Schematic and experimental illustrations of directional plasmomechanic strain sensor, (a) (i) shows the proposed device in its unstretched condition, inset shows scanning electron microscopy (SEM) image of Au NPs on PDMS substrate, (ii) simulated results of anisotropic Poisson's effect of the substrate for θ = 0° and θ= 90° directions, (b, c) the device structure and measured wavelength-dependent absorbance under the external force applied along θ = 0°, and θ = 90°, respectively.

Acknowledgment: This research was financially supported by the Institute of Civil Military Technology Cooperation funded by the Defense Acquisition Program Administration and Ministry of Trade, Industry and Energy of Korean government under grant No.22-CM-BD-03.

References

1. Lee, T.; Jang, J.; Jeong, H.; Rho, J. Plasmonic- and Dielectric-Based Structural Coloring: From Fundamentals to Practical Applications. Nano Converg. 5, 1–21, 2018.
2. Ghosh, S.K.; Pal, T. Interparticle Coupling Effect on the Surface Plasmon Resonance of Gold Nanoparticles: From Theory to Applications. Chem. Rev. 107, 4797–4862, 2017.
3. Tang, Z.; Wu, J.; Yu, X.; Hong, R.; Zu, X.; Lin, X.; Luo, H.; Lin, W.; Yi, G. Fabrication of Au Nanoparticle Arrays on Flexible Substrate for Tunable Localized Surface Plasmon Resonance. ACS Appl. Mater. Interfaces 2021, 13, 9281–9288.

Development of a novel optical label-free voltage sensing technique

O.G.Barajas, J. Sollini , M. G. Somekh and S.A. Abayzeed

[1]Optic and Photonics Research Group, Faculty of Engineering, University of Nottingham, United Kingdom
[*]Corresponding author: sidahmed.abayzeed2@nottingham.ac.uk

Abstract: This work presents an innovative impedance microscopy approach that promises the capability of measuring the bioelectrical properties of single cells. This optical label-free method exploits the sensitivity of metal's dielectric constant to voltage-induced changes in electron density in thin metallic films [1,2]. This can be monitored by tracking the change in intensity of optical transmission or reflection of metal [3]. This technique is a novel form of performing impedance microscopy using a simple optical configuration, which can allow exploring wide applications in studying living organisms and material characterisation.

Living organisms generate and conduct electrical signals that are critical for living functions. Retrieval of information at sub-cellular levels is critical to understanding cell bioelectrical function. However, this capability is not currently available due to the lack of appropriate imaging technology. Here, we present preliminary results towards a novel method for performing impedance microscopy using a simple optical sensing setup. To test this concept, a simple optical system was configured where the sample is illuminated using a collimated light beam, and the light transmitted through the sample is focused onto the photodiode to measure changes in light intensity. To test voltage-induced changes in light transmission, a sinusoidal voltage form with different frequencies was applied to the metal surface against a reference immersed in sodium chloride (NaCl) solution. When a voltage is applied to the metal film, a nanoscale capacitor at the metal-electrolyte interface is charged, leading to changes in electron density. The results show that we can detect voltage of 200mVpp with a modulation depth lower than $1x10^{-5}$ with a bandwidth of 10 kHz.

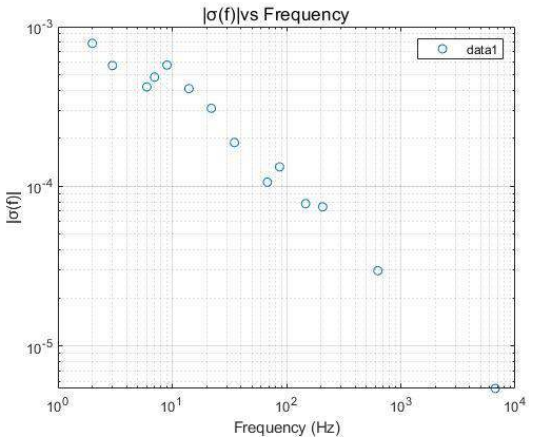


Fig.1. Change in transmitted light intensity at different frequencies in the range of 1Hz to 10 kHz in response to 200mVpp voltage signal.

References

[1] Abayzeed SA, Smith RJ, Webb KF, Somekh MG, See CW. “Sensitive detection of voltage transients using differential intensity surface plasmon resonance system”. Opt Express. 2017 Dec 11;25(25):31552-31567. doi:

10.1364/OE.25.031552.
[2] Abayzeed Sidahmed. “Plasmonic-based impedance microspectroscopy of optically heterogeneous samples”. Biomed. Opt. Express 2020, 11, 6168-6180.
[3] Yaping Shi, Shi Y, Feng G, Li X, Yang X, Ghanim AH, Ruchhoeft P, Jackson D, Mubeen S, Shan X. “Electrochemical Impedance Imaging on Conductive Surfaces”. Analytical Chemistry 2021, 93, 36, 12320-12328.

Investigation of the optical properties and the emission behavior of nanoscale Yagi-Uda antennas using nonlinear optics and back focal plane imaging

F. Schneider[1*], F. Nägele[2], A. J. Meixner[1], M. Fleischer[2], and D. Zhang[1]

[1]Institute for Physical and Theoretical Chemistry, Eberhard Karls University Tübingen, Germany
[2]Institute for Applied Physics, Eberhard Karls University Tübingen, Germany
[*]corresponding author: felix.schneider@uni-tuebingen.de

Abstract: Downscaling of conventional Yagi-Uda antennas to nanometer size provides a powerful tool to influence the behavior of visible light for optical applications. For this, the plasmonic properties of gold nanorods are combined with the geometry of the well-established Yagi-Uda antenna. The impact of the linear polarization direction on their excitation and emission behaviors is investigated in optical spectra and the k-space. Here, we demonstrate strong discrepancies between on- and off-resonance excitation.

At larger scale, antennas are commonly used all over the world to send and receive electromagnetic waves with varying wavelengths. They are engineered to be resonant for specific wavelength and frequency regions. Yagi-Uda antennas are directional antennas and are mostly used for TV signals in the MHz range. They are composed of one feed, which is the resonantly engineered heart of the antenna, with an adjacent reflector on one side and multiple directors on its other side [1] (Fig. 1). This special design allows for a precisely directed emission of radiation due to interaction of plasmonic nanostructures [2], including destructive interference on the reflector side and constructive interference on the side of the directors, resulting in strongly preferred angular emission towards the directors [3]. In this work, this principle at nanoscale size is investigated with nonlinear optics combined with k-space imaging.

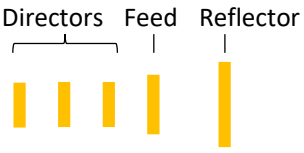


Figure 1: Geometry of a Yagi-Uda antenna



Figure 2: SEM-image of the fabricated nanoantenna

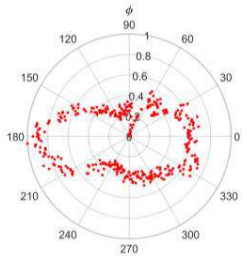


Figure 3: Emission pattern x-y-directionality on resonance

The probed Yagi-Uda antennas were manufactured as an array of gold nanorods with defined sizes and distances using microlithography techniques (Fig. 2). For the feed, the nanorod was designed to have a long axis plasmonic resonance matching the laser excitation wavelength. The Yagi-Uda antennas did not include any additional emitter, thus the observed signal is originating in the antenna itself [4]. A pulsed laser with λ = 779 nm and 40 MHz repetition frequency was focused onto the sample by a parabolic mirror with NA = 0.9986 to induce two-photon excitation processes. Second harmonic generation (SHG) and the combined signal of SHG and two-photon luminescence (2PPL) were investigated using a laser beam linearly polarized by a Glan-Taylor prism. The orientation of the linear polarization could be modified by a $\lambda/2$-waveplate to match the long axis of the antennas feed nanorod. Depending on the linear polarization direction, a strong difference in emission intensity is observed accompanied by changes to the observed emission patterns in the k-space (Fig. 3).

When the polarization direction of the laser matches the long axis of the feed nanorod (here: 90°), a strong enhancement of the SHG and 2PPL intensity is observed (Fig. 4). A gradual change of the intensity depending on the rotation of the linear polarization direction shows a good agreement with the theoretical expectations for on- and off-resonance measurements in proximity to plasmonic gold nanostructures [5]. The integrated intensity of the 2PPL is much larger than that of the SHG, which means the combined back focal plane image of SHG and 2PPL is dominated by the 2PPL signal. Preliminary experiments indicate a directionality of the nonlinear signal, which predicts that the nanoscale Yagi-Uda antenna is working properly and is suitable for use in further optical applications.

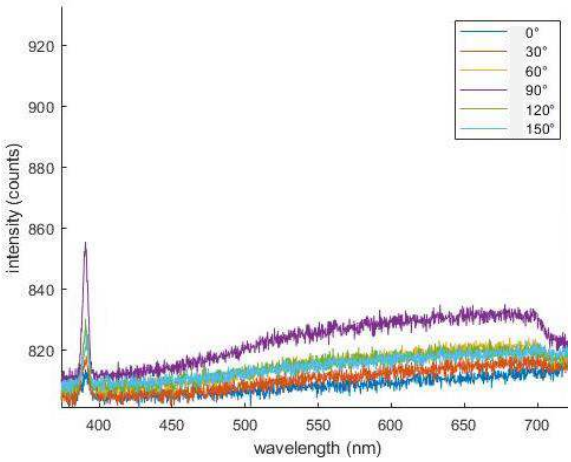


Figure 4: SHG and 2PPL intensity at different linear polarization angles

Acknowledgements: This work was financially supported by the German Research Foundation (Nos. ZH 279/13-1 and ME 1600/21-1).

References

1. Maksymov, I.S., Staude, I., Miroshnichenko, A. E., and Kivshar, Y. S., “Optical Yagi-Uda nanoantennas”, Nanoph, Vol. 1, No. 1, 2012.
2. Wang, J., Butet, J., Baudrion, A.-L., Horrer, A., Lévêque, G., Martin, O. J. F., Meixner, A. J., Fleischer, M., Adam, P.-M., Horneber, and Zhang, D., “Direct comparison of second harmonic generation and two-photon photoluminescence fom single connected gold nanodimers”, J. Phys. Chem. C, Vol. 120, No. 31, 17699 – 17710, 2016.
3. Xiong, X. Y. Z., Jiang, L. J., Sha, W. E. I.,Lo, Y. H., and Chow, W. C., “Compact nonlinear Yagi-Uda nanoantennas”, Sci. Rep., Vol. 6, 18872 – 18881, 2016.
4. Fleischer, M., Zhang, D., and Meixner, A. J., „Optically and electrically driven nanoantennas”, Beilstein J. Nanotechnol., Vol. 11, 1542 – 1545, 2020.
5. Gürdal, E., Horneber, A., Meixner, A. J., Kern, D. P., Zhang, D., and Fleischer, M., „Enhancement of the second harmonic signal of nonlinear crystals by a single metal nanoantenna”, Nanoscale, Vol. 12, 23105 – 23115, 2020.

META 2023, PARIS - FRANCE, JULY 18 – 21, 2023

High resolution impedance imaging with plasmonic nanostructures

F. Nelson[1], R.Fuentes-Dominguez[1], F. Hei[1], R. Smith[1], M. Clark[1], G. Gordon[1], S. Abayzeed[1*]

[1]Optics and Photonics Research Group, Faculty of Engineering, University of Nottingham, United Kingdom

[*]Corresponding author: Sidahmed.Abayzeed@nottingham.ac.uk

Abstract: We present a high resolution impedance microscopy technique for imaging the local electrical properties of cells in an effort to obtain an in-depth understanding of their bioelectrical functions. This information is critical to understanding aspects of cell activity such as metabolism, disease state, and cell stress. Our approach involves the investigation and utilisation of the tuneable local surface plasmon resonances (LSPR) of highly ordered nanoparticle arrays to make impedance imaging possible with spatial resolutions not achievable using pre-existing methods.

A cell can be described as an electrical system that generates and conducts electrical signals vital for living processes, but due to a lack of suitable measurement techniques there is limited knowledge as to how the electrical properties of such cells vary in space and in time. Single electrode techniques offer no spatial resolution while multi-electrode arrays find that their resolution limits arise from difficulties surrounding the density with which the increased number of electrodes can be arranged. As electrodes have grown smaller, new challenges surrounding signal-to-noise ratio, and in the case of scanning microelectrode techniques the propensity to damage samples, have driven to search for a new approach to electrophysiology at the single cell level [1].

In order to measure local impedance with the sub-micrometre resolution necessary to fully characterise the electrophysiology of individual cells, this work describes an optical approach to impedance imaging based on the local surface plasmon resonance (LSPR) of highly ordered nanoparticle arrays. Fabricated using electron beam lithography, these allow minute fluctuations in sub-microscopic charge density to be used as an indirect measurement of local impedance. Confining surface plasmons to nanoscale volumes offers the spatial resolution that conventional surface plasmon resonance sensing lacks [2], and in addition to its unrivalled spatial resolution, LSPR impedance microscopy is non-invasive, non-destructive, and has no external influence on cell behaviour nor the quantities it measures.

Here, we discuss the design, fabrication, and testing of homogeneous nanoparticle arrays for LSPR impedance imaging using several geometries including rods, discs, triangles and prisms. Based on thorough simulation of the opto-electronic properties of plasmonic nanoparticles and several analytical expressions including the scattering theories of Mie and Gans, particle dimensions have been carefully selected so as to tailor the location of LSPR according to the frequency of incident light. These simulations allow us to determine the relationship between particle geometry and the sensitivity of particle resonances to charge density variations. Validated by experiment, this information allows us to quantify sensor performance and ultimately obtain the highly localised electrical properties necessary for single-cell impedance imaging.

The plasmonic properties and local electric field enhancements associated with different particle types have been investigated and exploited in an effort to maximise sensitivity and signal quality. It is expected that this approach to impedance imaging will pave the way towards imaging the electrical properties of single cells at a length-scale not yet seen using existing techniques. With thanks to Richard Cousins and the nanoscale and microscale research centre (nmRC) for their assistance in sensor fabrication and imaging throughout this work.

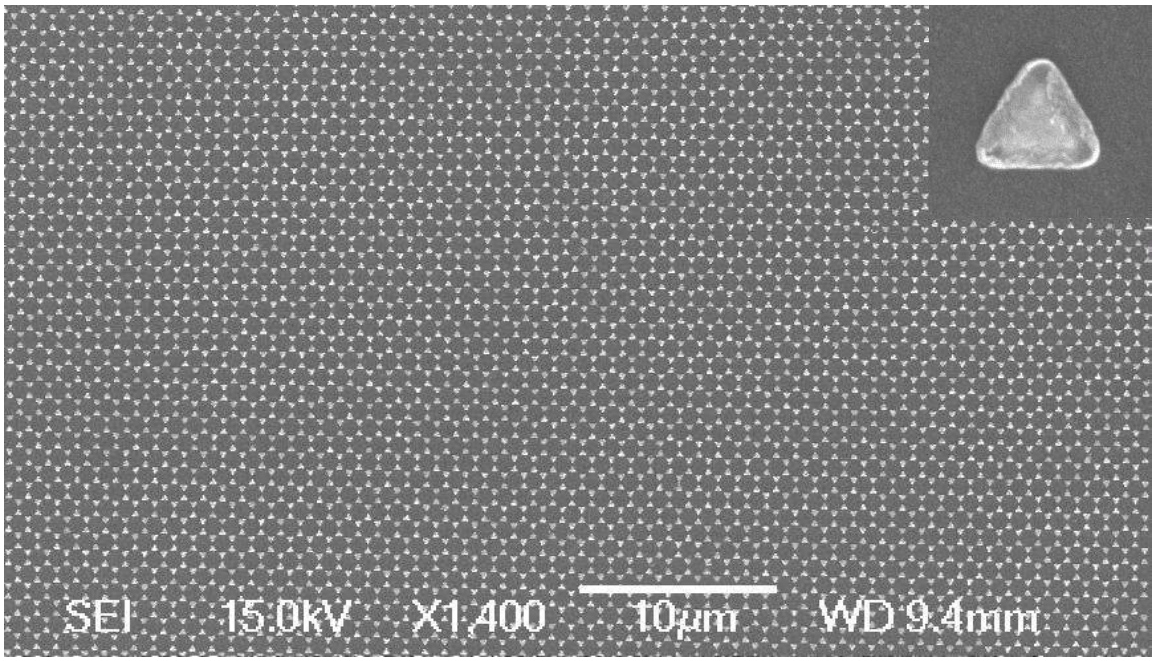


Figure 1. A representative scanning electron microscopy image of a 1cm^2 nanotriangle array prepared using electron beam lithography. Arrays comprising rods, discs, and prisms have also been fabricated with similar uniformity to investigate the geometric-dependence of LSPR and its bearing on impedance sensing. The inset shows a single nanotriangle magnified to 60,000x whose sides measure ~352nm

References

1. Schwarz, M., M. Jendrusch, and I. Constantinou, “Spatially resolved electrical impedance methods for cell and particle characterization”, *Electrophoresis*, Vol. 41, No. 10, 65–80, 2020
2. Abayzeed, S. A., R. J. Smith, K.F. Webb, M. G. Somekh, and C. W. See, “Sensitive detection of voltage transients using differential intensity surface plasmon resonance system”, Opt. Express, OE, Vol. 25, No. 25, 31552-31567, 2017

META 2023, PARIS - FRANCE, JULY 18 – 21, 2023

Quasi minimum-scattering-superabsorbed nanowires

Jeng Yi Lee[1*]

[1] 1Department of Opto-Electronic Engineering, National Dong Hwa University, Hualien 974301, Taiwan.

[*]corresponding author: jengyilee@gms.ndhu.edu.tw

Abstract: With consideration of an energy function involving scattering and power cross sections for a nanowire under a normal incidence for one polarization (either TE or TM), by using variational calculus, we propose a power diagram where can indicate all scattering properties. Without lock of scattering resonant modes with same phases and amplitudes, we design a nanowire with scattering performances having minimum-scattering superabsorption by exciting higher modes.

Understanding limitation of light-matter interaction has important applications in biological non-invasive cell-tracking, solar energy harvesting, optical sensors, enhanced single photon emission, enhanced Raman spectroscopy to name a few. Inspired by metamaterials, compact scatterers composed by multilayers with plasmonic and high indexing dielectric embedded can boost overlapping resonant modes for specific designs, such as superabsorption, superdirective nanowires, and superscattering [1, 2, 3].

In this work, by introducing an energy function with absorption and scattering cross sections as well as employing the calculus of variation, we can provide a normalized power diagram for any passive nanowire systems, beyond any specific system configurations, materials, and operating frequency, as shown in Fig. 1 (a). Here the exciting electric field is along z-axis direction (**s**- polarization) and normal incident to our nanowire systems. We find that there exists a physical boundary for scattering and absorption powers for any N-dominant resonant modes [4]. In the boundary (blue for ED (electric dipole), purple for ED and MD (magnetic dipole), green for ED, MD, and MQ (magnetic quadrupole)), the scattering systems can exhibit superscattering, superabsorption or minimum scattering superabsorption. However, we further find that when exciting more modes, its scattering boundary can wrap up that of the lower ones. This result indicates the degeneracy of power in light scattering and absorption, that two scatterers with different N dominant modes can display the same scattering and absorption cross sections.

To demonstrate this degeneracy property, in Fig. 1 (b), we design two nanowire systems, where one is made by silicon and another is made by gold (core) and silicon (shell). In the right panel of (b), by tuning outer radius a, we display its dominant scattering modes, where we can see only ED is primary scattering in silicon nanowire. However, in the gold-silicon nanowire, at a=74nm and radius ratio of 0.2, we can see the dominant modes are ED, MD, and MQ, belonging to higher excited levels. These two systems can have same absorption and scattering powers at the black stars. Next, our interest is to design a quasi-minimum-scattering superabsorbed nanowire where its scattering and absorption powers are same as the case of minimum-scattering superabsorbed nanowire [4], while its phases and amplitudes are not identical. In Fig. 1 (c), we design the nanowire by empolying gold in core with radius of 55.85nm and silicon in shell with outer radius of 132.98nm. Interestingly, we can see although the overall light scattering and absorption spectra are at the boundary, its scattering coefficients for the dominant modes are ED, MD, and MQ.

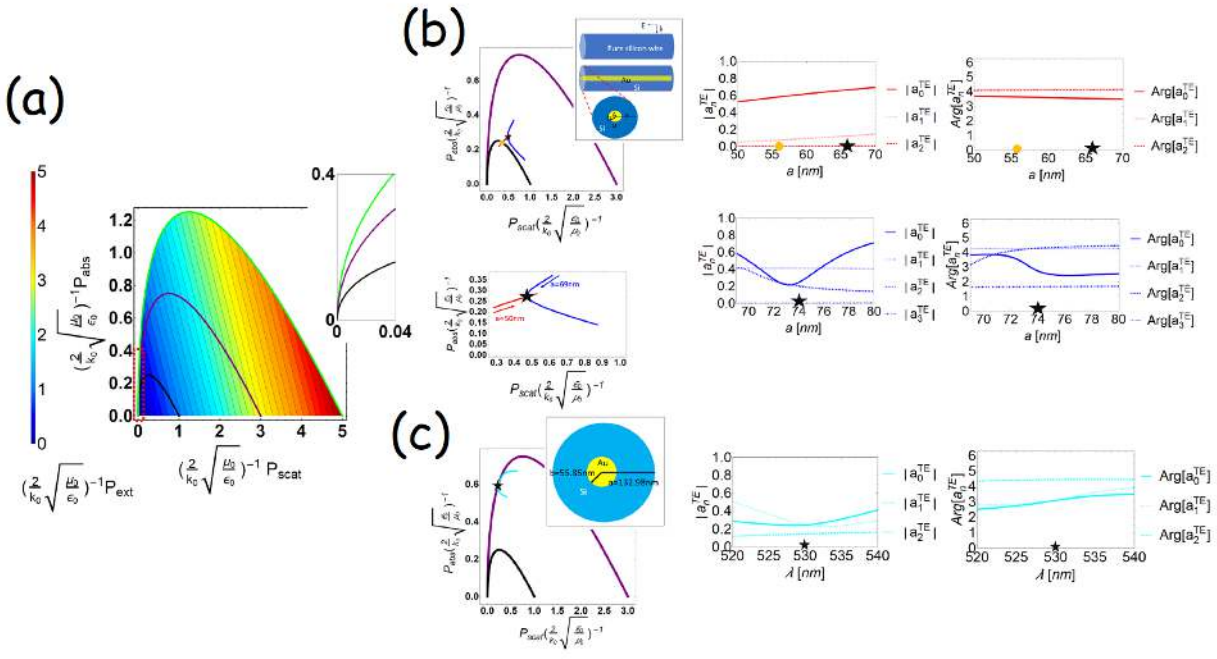


Figure 1. (a) Power diagram of absorption and scattering for any passive systems. The scattering boundary are depicted by blue line (ED), purple line (ED and MD), and green line (ED, MD, and MQ). (b) The red line in the power diagram denotes the silicon nanowire by tuning radius from 50nm to 70nm. Here the dominant mode is only ED. The blue line is, from the nanowire made of gold in core and silicon in shell, with a thickness ratio of 0.42, with respect to outer radius from 70nm to 80nm. Here the dominant modes are ED, MD, and MQ. (c) Quasi minimum-scattering-superabsorption result is achieved by the nanowire by gold in core and silicon in shell at operating wavelength of 530nm [4].

In this work, by using the concept of calculus of variation for introducing an energy function with absorption and scattering powers, we provide a power diagram to indicate all possible scattering results, beyond specific system configurations, materials, and operating wavelengths. We find the scattering and absorptions by any scatterers can exhibit degeneracy, that passive scattering systems excited by different N-level modes can have the same light scattering and absorption powers. Consequently, we design the quasi-minimum-scattering superabsorbed nanowire.

Acknowledgements: This work is partially supported by the Ministry of Science and Technology of Taiwan (107- 2112-M-259-007-MY3, 110-2112-M-259-005- and111-2112-M-259 -011 -)

References

1. Qian, Chao, et al. “Experimental observation of superscattering,” Physical review letters 122.6 (2019): 063901.
2. Arslanagić, Samel, and Richard W. Ziolkowski. “Highly subwavelength, superdirective cylindrical nanoantenna,” Physical Review Letters 120.23 (2018): 237401.
3. Estakhri, Nasim Mohammadi, and Andrea Alù. “Minimum-scattering superabsorbers,” Physical Review B 89.12 (2014): 121416.
4. Lee, Jeng Yi, Yi-Huan Chen, and Pai-Yen Chen. “Degeneracy of light scattering and absorption by a single nanowire,” Scientific Reports 11.1 (2021): 18657.

Plasmonic surface lattice resonances in 2D hexagonal arrays of Au nanoparticles

Rina H. Bustamante[1*], Hipólito A. Arredondo Champi[1,2], Daniel R. Cornejo[2], and Walter J. Salcedo[1]

[1]Electronic Systems Engineering Department, Polytechnic School of the University of São Paulo, 05508-900, São Paulo, SP, Brazil

[2]Department of Physics of Materials and Mechanics, Institute of Physics of the University of São Paulo, 05508-090, São Paulo, SP, Brazil

[*]corresponding author: rinahb@usp.br

Abstract: We have fabricated three hexagonal arrays of gold nanoparticles (Au-NPs) using template-assisted electrodeposition. The main geometric parameter that characterizes each of the hexagonal arrangements of NPs is the distance neighboring NPs. Our transmission measurements show redshifts of the plasmonic resonance as the distance between Au-NPS decreases (or increasing the diameter of the NPs). Using FDTD simulations it can be shown that the redshifts can be explained by a dipolar interference model of localized surface plasmons (or plasmonic surface lattice resonances). Our computational simulations based on the experimentally extracted parameters show an increase in near-field enhancement (27-fold in water) compared to a typical single-NP localized surface plasmon.

Figures 1(a), 1(b) and 1(c) show SEM images of ordered hexagonal arrays of Au-NPs with average diameters of 60, 75 and 85 nm, respectively. These NPs were fabricated by AC electrodeposition using porous anodic alumina as templates (1 µm thickness). The self-organizing alumina nanostructures (with average pore diameters of 90 nm and fixed interparticle distance of 110 nm) were obtained by two-step anodization using a simple electrochemical cell with two electrodes in 0.5 M $H_2C_2O_4$ at 25°C and 45 V. To increase the diameter of the nanopores we performed a 40 min etch on the anodized samples using 1 M H_3PO_4. The Au-NPs was conducted in an electrolyte containing 1 g/L $HAuCl_4{:}3H_2O$ + 30 g/L H_3BO_3, with a pH of 1.5, AC voltage of 10 V (RMS), and a frequency of 200 Hz [1].

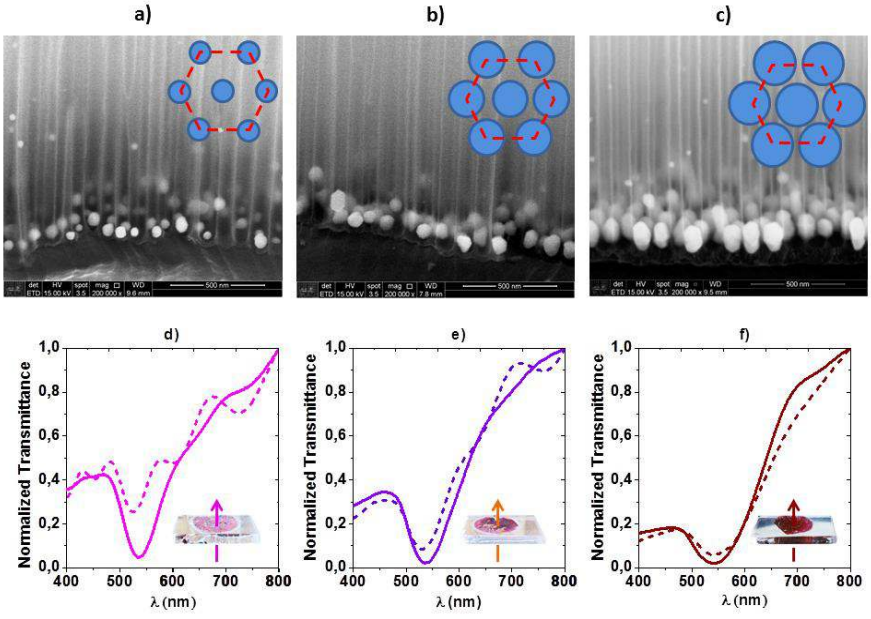


Figure 1

Figures 1(d), 1(e) and 1(f) show normalized transmission measurements (UV-Vis spectrophotometer) for the different hexagonal arrays of Au-NPs (60, 75 and 85 nm in diameter) in host media air (line dotted) and water (solid line). The insets of these figures show the Au-NPs/Al2O3 composite films on quartz sheets and the incidence of unpolarized light. In the transmission spectra we can clearly see drops in transmission (absorption peaks) due to surface plasmons in the Au-NPs. Note that the positions in the transmission drops shift to the near-infrared as the size of the Au-NPs increases (or the distance between neighboring NPs decreases). This displacement of the surface plasmon is closely related to the interaction between neighboring NPs or in other words it is an interference effect of plasmons [2].

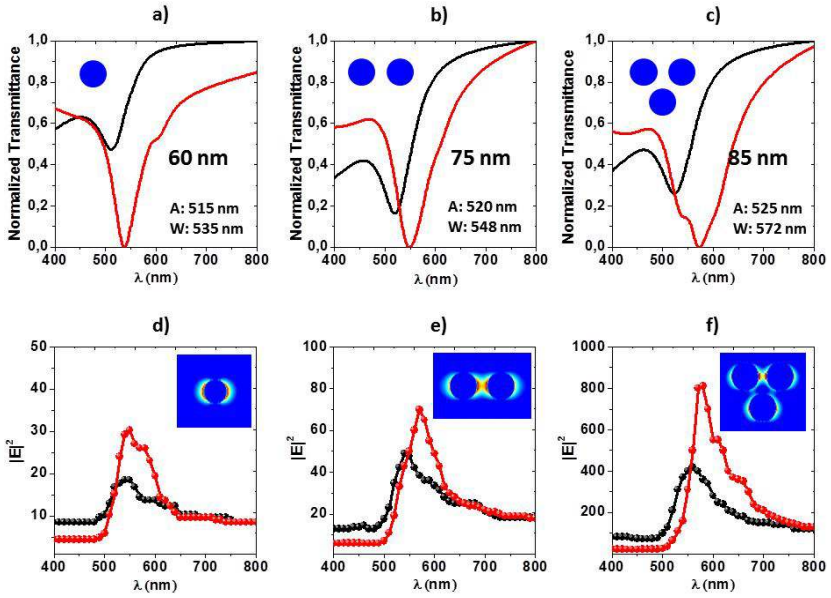


Figure 2

Figures 2(a), 2(b) and 2(c) show FDTD numerical simulations (FDTD Solutions 8.5, Lumerical Inc., Canada) of the transmission spectra for the fabricated Au-NPs arrays. In the simulations, experimental parameters such as NP diameter, distance between NPs, refractive index of the effective medium (Au-NPs/Al_2O_3 composite). To understand the effect of the displacement of the collective plasmon relative to the localized surface plasmon (LSP), we performed numerical simulations for 1, 2 and 3 NPs in mutual interaction [insets of Figures 2(a)-(c)]. The numerical results shown in Figures 2(a)-(c) are in good agreement with the experimental results for single spherical NPs (60 nm diameter), NP dimers (75 nm diameters) and NP trimers (85 nm). The effect of this plasmon coupling (LPSs interference) can be clearly noted in the electric near-field intensification that reaches a value of 800 (water host medium) for the trimers (interparticle distance of 25 nm). Higher values for near-field enhancement can be reached when the distance between NPs is less than 20 nm.

Using the lattice modes to intensify the near-field could improve the sensitivity of biosensors, increase the efficiency in plasmonic optical traps and increase the optical chirality in optical enantioseparation devices [3].

References

1. Zhan Z., and Lei Y., ACS Nano 8, 4, 3862–3868, 2014.
2. V. G. Kravets et al., Chem. Rev., 118, 5912−5951, 2018.
3. Petronijevic E. et al., Optical Materials Express 12(7), 2724-2746 (2022).

META 2023, PARIS - FRANCE, JULY 18 – 21, 2023

Metal-insulator-metal metamaterial as optoplasmonic biosensor for refractive index sensing

Z. Ayareh[1,2], D. Sutherland[2*], and M. Moradi[1]

[1] Institute of Nanoscience and Nanotechnology, University of Kashan, Kashan, 87317, Iran.

[2]Interdisciplinary Nanoscience Center (iNANO), Aarhus University, 8000 Aarhus C, Denmark.

[*]Duncan@inano.au.dk

Abstract: The optoplasmonic biosensor is a label-free sensor which has significant potential to detect biomolecules. We proposed it based on metal–insulator–metal (MIM) metamaterials utilizing the gap between two metals as a space to detect biomolecules. We fabricated Au/SiO_2/Au heterostructures using the hole-mask colloidal lithography method. In this work, the localized surface plasmon resonance was demonstrated by modifying the MIM heterostructure by etching back the insulator (SiO_2) to provide a sensing cavity. A bulk sensitivity of 285 nm/RIU was measured.

The metal-insulator-metal (MIM) metamaterials are high potential elements for the development of various novel materials, such as optoplasmonic heterostructures or highly efficient biosensors [1]. Their exceptional properties and performance rely on localized surface plasmon resonances (LSPR), i.e., spatially confined charge-density oscillations that are readily excited at optical frequencies in noble-metal structures [2]. In MIM metamaterial, LSPR waves demonstrate strong optical absorption in two plasmon peaks at a broad range of incident angles and polarizations of the incidence light [3]. After coupling of light and a MIM metamaterial, the excited LSPR modes are strongly confined in the gap between the two metals which has the potential to high optical fields enhancement and importantly, small volumes of detection which can allow high sensitivity for the detection of biomolecules. The advantage of LSPRs in MIM metamaterial is that it makes them suitable for fabricating biosensors. Herein, we present a very simple but effective approach to fabricate an improved biosensor via etching of SiO_2 to have a cavity between the two Au disks. The SiO_2 layer is introduced into the double stacked Au disk, forming Au disk/SiO_2 bridge/Au disk heterostructure. Then, part of the SiO_2 between the Au disks is removed by chemical etching, producing the nanogap between Au disks. The nanogap size can be easily and precisely tuned to nanometer scale by adjusting the thickness of SiO_2 disk and etching time. The spectroscopy results show that Au disk/SiO_2 bridge/Au disk heterostructure has a good refractive index sensitivity. This heterostructure shows good potential for MIM metamaterial fabrication and biosensor application. Hole Mask Colloidal Lithography method [4] was used to prepare MIM heterostructures. As a brief, the PMMA solution was added to the glass substrate by spin coating and baked. The three polyelectrolyte layers were then sequentially deposited. (2 wt% PEI, 2 wt% PSS, and 0.2 wt% PDDA). Finally, 0.2 wt% of polystyrene nanoparticles (200 nm diameter) were added to the samples. After removing PS nanoparticles, the mask was finalized by an O_2 plasma etching step to make holes through the PMMA layer. The TiO2 (4nm) /Ti (2nm) Au/Ti(1nm)/SiO_2/Ti(1nm)/Au disks on the glass substrate were deposited with a thickness of 20 nm for each disk (Fig1). We used TiO_2 to protect the etching of the glass substrate and Ti as an adhesion layer. To have a SiO_2 bridge we used 20% KOH solution as chemical etching and the sample has immersed in 120 s at 30℃. Optical spectra were taken of the final structures and peak shifts with refractive index made using glucose solutions (Fig 2).

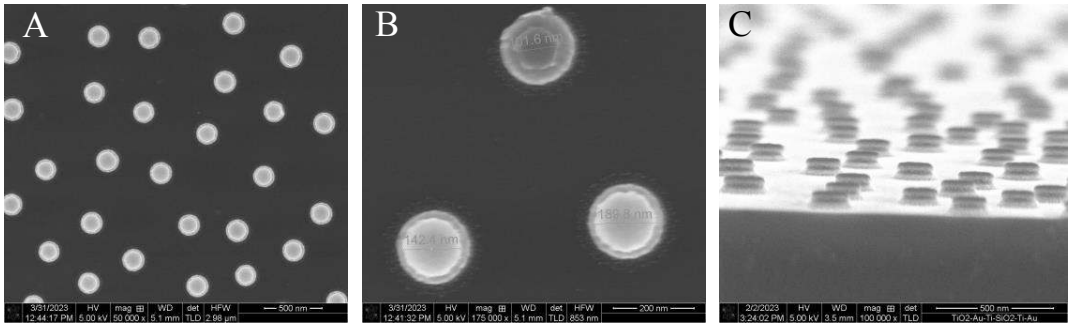


Figure 1: SEM images of Au/SiO2/Au heterostructure after etching. (A) The top of MIM (B) after removing the second Au disk to see the SiO2 bridge (C) The cross-section image of MIM heterostructure.

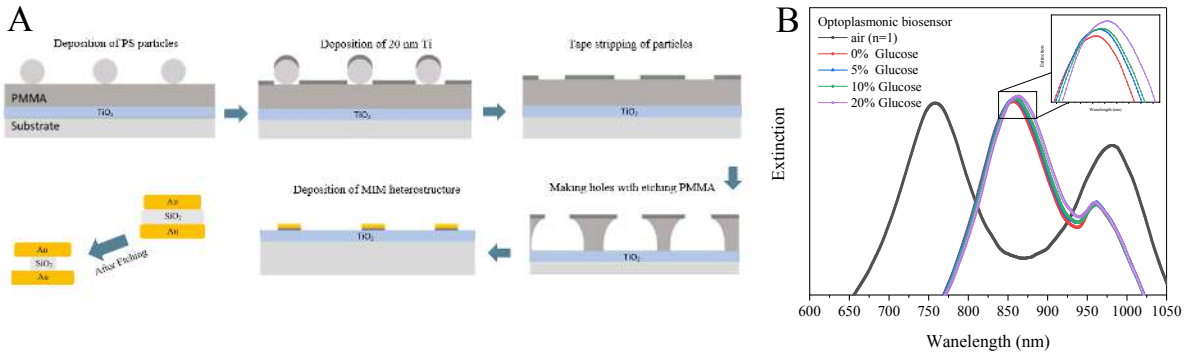


Figure 2: (A) Schematic of fabrication of MIM heterostructure on the glass substrate. (B) Extinction measurement of the optoplasmonic biosensor with different concentrations of Glucose solution using a flow cell.

In summary, we have successfully presented a simple high throughput approach to fabricate Au disk/SiO_2 bridge/Au disk heterostructure for biosensor application with two plasmon peaks at 758 nm and 980 nm. The nanogap size can be easily and precisely controlled to nanometer scale by adjusting the thickness of the SiO_2 disk and etching time. The chemical etching process could expose the strong electromagnetic field area to analytes allowing specific functionalization of the silica bridge to localize molecular recognition events in the gap. The MIM heterostructure with 20 nm height and 40 nm width gap size shows the best bulk sensitivity (285 nm/RIU).

References

1. Yamada, H., D., Kawasaki, K., Sueyoshi, H., Hisamoto and T., Endo, "Fabrication of Metal-Insulator-Metal Nanostructures Composed of Au-MgF_2-Au and Its Potential in Responding to Two Different Factors in Sample Solutions Using Individual Plasmon Modes," Micromachines, Vol. 13, 257. 2022.
2. Altug, H., SH., OH, S. A. Maier, and J. Homola, "Advances and applications of nanophotonic biosensors," Nat. Nanotechnol, Vol. 17, 5–16, 2022.
3. Chang, C. Y., H. T., Lin, M. S. Lai, *et al.*, "Flexible Localized Surface Plasmon Resonance Sensor with Metal–Insulator–Metal Nanodisks on PDMS Substrate," Sci Rep, Vol. 8, 11812, 2018.
4. Khateb, H., G., Klös, R. L. Meyer and D. S. Sutherland, "Development of a Label-Free LSPR-Apta Sensor for *Staphylococcus aureus* Detection," ACS Appl. Bio Mater., Vol. 3, No. 5, 3066-3077, 2020.

META 2023, PARIS - FRANCE, JULY 18 – 21, 2023

Curriculum Vitae

Zohreh Ayareh



- Ph.D. candidate in Nanoscience-Nanophysics Nanoscience and Nanotechnology institute, University of Kashan, Kashan, Iran.
- Guest Ph.D. student in Prof. Duncan Sutherland's team Interdisciplinary Nanoscience center, Aarhus University, Aarhus, Denmark.

Email: z.ayareh@yahoo.com
z.ayareh@inano.ac.ir

Phone: +98 9176867287
+45 50204175

Web:
https://scholar.google.ca/citations?user=V6t1s6AAAAAJ&hl=en
https://orcid.org/0000-0003-4577-861X

PROFESSIONAL INTERESTS

Combined aspects of nanophotonic and materials research applied in optical sensors, biosensors, and light management in thin-film optical devices. Analytical technologies for rapid and sensitive detection of chemical and biological species relevant to medical diagnostics.

KEY FIELDS OF EXPERTISE

Magneto optical Kerr effect, Plasmonic, Localized surface plasmon resonance, Optical sensor and biosensor, amplification strategies in UV-visible and Raman spectroscopy, Metallic nanostructures, Graphene-metal hybrid materials, Metal-Insulator-Metal sensor, Hole mask colloidal lithography, Electron beam lithography.

EDUCATION

Guest Ph.D. - Interdisciplinary Nanoscience center, Aarhus University, Denmark
September 2022 till now

Ph.D. - Institute of Nanoscience and Nanotechnology, University of Kashan, 87317 Kashan, Iran.
September 2017
Thesis: Fabrication and characterization of Optoplasmonic sensor chip: Multilayer Au nanorods/Carbon nanostructures based on refractive index to recognization of biomarkers
Supervisor: Dr. Mehradad Moradi

MS. - Institute of Nanoscience and Nanotechnology, University of Kashan,87317 Kashan, Iran.
September 2013-November 2015
Thesis: Excitation of Surface Plasmon Polariton in Magnetoplasmonic Nanostructures doped with Au Nanoparticles
Supervisor: Dr. Mehradad Moradi

BS. - Department of Physics, College of Sciences, Yasouj University, Yasouj 75914-353, Iran
September 2011-November 2015
Project: MATLAB code to solve Rashba spin-orbit coupling

PUBLICATION ACTIVITIES

1. M. Moradi, **Z. Ayareh**, S. Mahmoodi "Enhancement of magneto-optical Kerr response by LSPR in magneto

plasmonic nanostructures for biological sensor" Journal of Magnetism and Magnetic Materials, 444 (2017) 410–415.

2. **Z. Ayareh**, M. Moradi, S. Mahmoodi, "Tuning the effective parameters in (Ta/Cu/[Ni/Co]x/Ta) multilayers with perpendicular magnetic anisotropy", Physica C: Superconductivity and its applications, 549 (2018) 30-32.
3. **Z. Ayareh**, M. Moradi, "Increase of Magneto optical Kerr signal in Ta/Cu/[Ni/Co]x2/Ta structure with Localized Surface Plasmon Resonance of Gold nanoparticles", Nanomeghyas (Iranian Journal) 4(1) (2019) 65-72.

4. **Z. Ayareh**, S. Mahmoodi, M. Moradi, "Magneto-plasmonic biosensing platform for detection of glucose", optik. 178 (2019) 765-773.

5. **Z. Ayareh**, M. Moradi, "Nanoplasmonic Sensor Chip Fabricated Based on Au Nanoparticles: Effect of Graphene Oxide and Reduced Graphene Oxide", Plasmonics 17 (2022) 1437-1444.

TEACHING ASSISTANT

Courses:

Raman Spectroscopy	(Tutorial Class)
UV-Visible Spectroscopy	(Tutorial Class)
Plasmonic Biosensor	(Tutorial Class)
Fundamental of Nanomaterials	(Grader)

HONORS AND AWARDS

- Member of Iran's National Elites Foundation
- Ranked 4th among 40 students and selected as the Exceptionally student in the master's degree.
- Ranked 1st among 4 students in the PhD program.
- Achieving the sabbatical grant for 6 months to research in Aarhus university as visiting PhD student.

COMPUTER SKILLS

Engineering Software: MATLAB, MAPLE, COMSOL, LUMERICAL
Tools: Origin, Excel, Word, Power point, Photoshop, ImageJ, Gwyddion, Xpert High Score

INSTRUMENTS

Cleanroom experience, SEM, TEM, AFM, PVD (Sputtering-Thermal and Electron beam evaporation), RIE, UV-VIS spectroscopy, Raman spectroscopy, Profilometer, Vacuum furnace.

PROFESSIONAL EXPERIENCE

2014- 2nd National congress and workshops on Nanoscience & Nanotechnology - Iran
Fabrication and characterization of two-step magnetic memory by magneto-photonic crystal
M. Moradi, **Z. Ayareh**, S. M. Mohseni

2014- The International Conference on Science and Nanotechnology - Iran
Surface Plasmon Excitation in the Magneto-Plasmonic Crystal Ag/Py

Mehrdad Moradi, Davood Rezvani, **Zohreh Ayareh**, Ali Dadsetan

2015- The Annual Physics Conference of Iran on university of Mashhad
Fabrication and Analysis Nano Magneto-Photonic Crystal with Magnetization Perpendicular to the Surface
Moradi, Mehrdad; **Ayareh, Zohreh**; Mohseni, Majid

2016- The Annual Physics Conference of Iran on university of Shiraz
Performance of diagnosis of cancer progression sensors based on changing in optical refractive index
Moradi, Mehrdad; **Ayareh, Zohreh**

2017-10th International conference on Magnetic and Superconducting materials (MSM17), Sharif University of technology - Iran
Tuning the effective parameters in Ta/Cu/[Ni/Co]x/Ta multilayers with perpendicular magnetic anisotropy
Ayareh, Zohreh; Moradi, Mehrdad; Mahmoodi, Saman; Mohseni, Majid

2019- The Annual Physics Conference of Iran on university of Tabriz
Effect of surface plasmon polariton excitation on magnetic properties of Au/Co/Au structure
Ayareh, Zohreh; Moradi, Mehrdad

2019-The 26th Iranian Conference on Optics and Photonics (ICOP) and the 12th Iranian Conference on Photonics Engineering and Technology (ICPET)
Investigation of localized surface plasmon resonance and Fano resonance in Au:Ag heterodimers
Zohreh Ayareh and Mehrdad Moradi

2021-8th International E-congress on Nanosciences and Nanotechnology (ICNN) Mashhad University of Medical Sciences, Mashhad, Iran
Fabrication of LSPR sensor chip with immobilization of Au nanoparticles on the transparent substrate
Z. Ayareh, M. Moradi

2021- The Annual Physics Conference of Iran on university of Isfahan University of Technology (IUT)
Faraday rotation spectroscopy with a homemade optical setup
Moradi, Mehrdad; **Ayareh, Zohreh**; Rahimabadi, Zohreh

2021- The Annual Physics Conference of Iran
Investigation the performance of Kretschmann configuration and surface plasmon resonance for sensor application
Rahimabadi, Zohreh; Moradi, Mehrdad; **Ayareh, Zohreh**

دانشگاه کاشان
University of Kashan

In The Name of Allah

No: 16282
Date: 2023/2/20
Enc:

META conference 2023 committee,

I am writing in a recommendation and my strong support of Zohreh Ayareh, as a promising candidate to obtain your support. As her record show, she is a motivated and first-best Ph.D. student in the nanoscience and nanotechnology department at Kashan University, Iran. Zohreh has vastly worked on plasmonic material and plasmonic sensor fields. I evaluate Zohreh as a unique, dedicated, hard-working, and creative problem-solver person who actively seeks new opportunities and experiences. I am completely sure this conference can be extremely effective for her creativity. She has received a grant from her home university to spend 6 months at Aarhus university as a gest Ph.D. student, unfortunately, this budget is not enough to cover the whole cost of living in Denmark and participating in the META conference. In this case, after receiving support from the META conference, the grant can cover any remaining cost. Undoubtedly, the META's contribution would be highly appreciated. In receiving this travel grant, Zohreh will obtain an opportunity that would otherwise not be possible. If you need more information, please do not hesitate to contact me.

Sincerely

Dr. Mehrdad Moradi
University of Kashan, Iran
m.moradi@kashanu.ac.ir
+983155913216

University of Kashan
Kashan, IRAN
Post Code: 87317-53153
Tel: +98 31 5551 1114
Fax: +98 31 5551 1121
proffice@kashanu.ac.ir
www.kashanu.ac.ir

LSPR enhanced In-situ Ellipsometry as a Label-free Optical Sensing Platform

Natasha Mandal[1*], Rakesh Singh Moirangthem[2]

[1] Nanophotonics Lab, Dept. of Physics, Indian Institute of Technology (Indian School of Mines) Dhanbad, India
[2]Dept. of Physics, Manipur University, Manipur-795003, India
[*]corresponding author: natashamndl@gmail.com

Abstract: We present an efficient, highly surface-sensitive, non-invasive, label-free optical sensing platform by integrating Localized Surface Plasmon Resonance (LSPR) and Ellipsometry. We adopted a facile route of solid-state thermal dewetting for preparing a LSPR sensor chip by the formation of highly stable, partially embedded bimetallic alloy nanoparticles with an average size of 27±8 nm. The experiment was performed in in-situ mode (90°)) using our custom-built 3D printed cell setup. We obtained sensitivity of around 1870±273 °/RIU for the prepared LSPR chip.

Over the past 30 years, integrating optical techniques with other analytical methods has become progressively popular for higher sensitivity, accuracy, precise analysis, and device miniaturization. SPR, LSPR, and Ellipsometry are well-recognized optical sensing techniques due to their real-time, label-free, non-invasive, rapid detection features. The basic theory of Ellipsometry is based on the change in the polarisation state of the p- and s- polarized light after reflection from the sample's surface. It determines the film thickness, optical properties, complex refractive index, dielectric function, surface roughness, elemental composition, etc. Ellipsometry signal is measured in terms of Psi (Ψ, 0°< Ψ <90°) and Delta (Δ, -180°<Δ<+180° or 0°<Δ<360°) parameters, representing the amplitude ratio and phase difference of reflected p- and s- polarized light, respectively, and defined by the following expressions [1].

$$tan\,\Psi = \frac{|R_p|}{|R_s|} \; and \quad \Delta = \delta_p - \delta_s$$

One of the limitations encountered in in-situ Ellipsometry measurement is that incident and reflected light from the sensor surface must pass directly through the sensing medium. The detection of low molecular weight analytes is challenging in SPR/LSPR techniques. Thus, we could overcome these limitations using Ellipsometry in SPR conditions [2–4] and utilize both advantages. The LSPR-enhanced in situ-Ellipsometry method, also known as Total internal Reflection Ellipsometry (TIRE), has the potential to be a reliable, rapid, non-destructive, label-free optical sensing platform with enhanced sensitivity and lower detection limit [5]. We have prepared the highly stable LSPR sensor chip using a facile, economical, and single-step solid-state thermal dewetting method by annealing Ag_5nm/Au _5nm bimetallic film deposited on a piranha cleaned glass substrate (3cm×2cm) at 550°C (glass transition temperature brings the embeddedness of nanoparticles) for 5 hrs in air ambient. The FESEM, EDX and UV-VIS absorbance spectra at 522 nm confirmed that the shape of the nanoparticles are spherical with an average size of 27±8 nm, mostly within the size of 20-30 nm, and the content of Au and Ag elements. The performance of the LSPR chip was investigated by the bulk refractive index sensitivity measurements. The experiment was performed using our custom-built 3D printed module incorporated with the commercial Ellipsometer by exposing the LSPR chip with the 0-50% concentrations of glycerol-water solutions with refractive indices in the 1.333-1.3981 (flow rate 1ml/h, 15 mins each solution). The real-time response of Ψ at the wavelength of 586 nm and Δ at 540 nm, which correspond to the maximum sensitivity, are depicted in fig.1(d,e), and the bulk sensitivity was obtained around 1870±273 °/RIU and 274±20 °/RIU for Ψ and Δ respectively from the sensitivity plots (fig. f,g). The Δ signal is more pronounced than Ψ, a

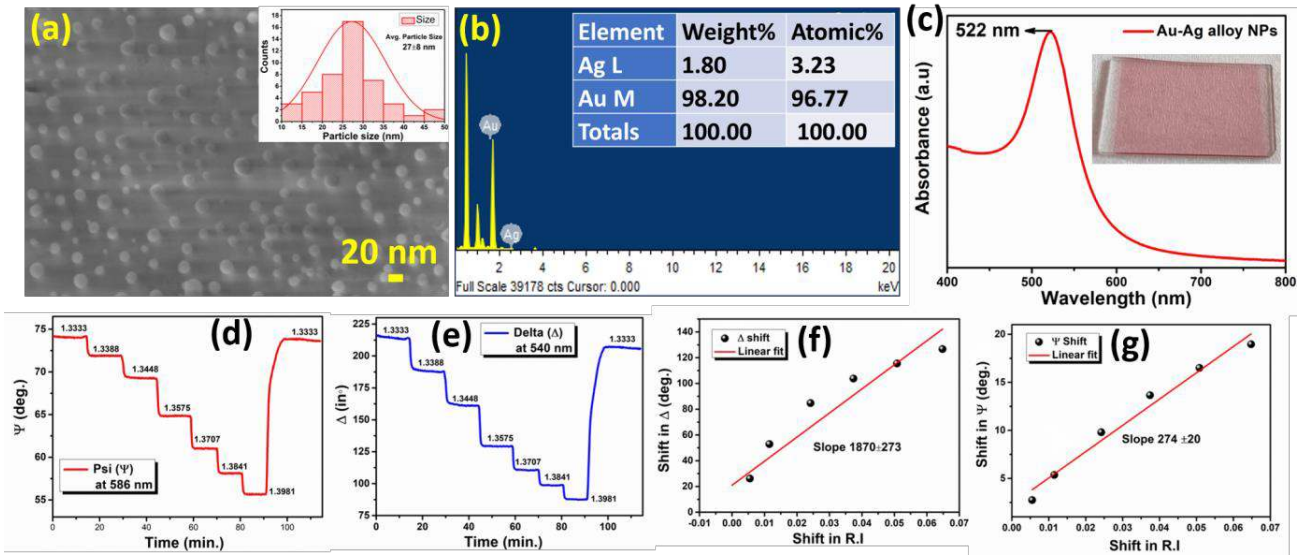


Figure 1. (a) FESEM image and inset shows the histogram plot, (b) corresponding EDX spectra, and (c) UV-VIS absorbance spectra for the prepared sensor chip. Real-time Ellipsometry response in terms of (d) Ψ, (e) Δ , and (f,g) corresponding sensitivity plots for 0-50% glycerol-water solutions.

small change in sensing media leads to a significant shift in Δ response. This integrated platform is not limited to transparent liquid analyte media. It could be explored in non-transparent or opaque gaseous media, and the sensitivity can be enhanced by several modifications (e.g., using 2D materials) of the LSPR chip. Our approach for preparing LSPR chips could be produced on a large scale at a low cost with good reproducibility, and the proposed integrated technique could be used in industrial applications.

We acknowledge the funding from the SERB-DST, India (EEQ/2017/000370).

References

[1] Moirangthem, R. S., Yaseen, M.T., Wei, P.-K, Cheng, J.-Y., Chang, Y.-C., "Enhanced localized plasmonic detections using partially-embedded gold nanoparticles and ellipsometric measurements," Biomed. Opt. Express., Vol. 3, No. 5, 899-910, 2012. https://doi.org/10.1364/boe.3.000899.

[2] Arwin, H., Poksinski, M., Johansen, K., "Enhancement in ellipsometric thin film sensitivity near surface plasmon resonance conditions," Phys. Status Solidi Appl. Mater. Sci., Vol.205,817–820. 2008. https://doi.org/10.1002/pssa.200777899.

[3] Poksinski, M., Arwin, H., "In situ monitoring of metal surfaces exposed to milk using total internal reflection ellipsometry," Sensors Actuators, B Chem., 94 (2003) 247–252. https://doi.org/10.1016/S0925-4005(03)00382-4.

[4] Arwin, H., "Is ellipsometry suitable for sensor applications?," Sensors Actuators, A Phys., Vol. 92, 43–51, 2001. https://doi.org/10.1016/S0924-4247(01)00538-6.

[5] Mandal, N., Das, A., Moirangthem, R.S., "In-situ label-free optical biosensing with plasmonic enhanced ellipsometry using partially-embedded bimetallic Ag-Au alloy nanoparticles," Sensors Actuators B Chem., Vol. 379, 133164,2023. https://doi.org/10.1016/j.snb.2022.133164.

Exploring Propagation Characteristics of Ga:ZnO Thin Films in the Epsilon-near-zero Region

Ranjeet Dwivedi[1*] and Dorota A. Pawlak[1]

[1]ENSEMBLE3 Centre of Excellence, Wolczynska 133, 01-919 Warsaw, Poland
[*]corresponding author: ranjeet.dwivedi@ensemble3.eu

Abstract: We examined the propagation characteristics of Ga:ZnO (GZO) thin films in the epsilon-near-zero (ENZ) region, revealing a novel non-radiating TM mode with strong field enhancement. We also explored a multilayer structure of GZO layers in a ZnWO4 matrix, which exhibits strong polarization selectivity and resonant absorption. The spectral location and bandwidth of absorption could be adjusted by carefully selecting the GZO layer thickness and geometrical parameters. Our results offer promising possibilities for developing ENZ-based devices with enhanced functionality and tunability.

Strong light-matter interaction in narrow region of space have many potential uses in photonic circuitry, including ultrafast switching, high harmonic generation, sensing, etc. To achieve these functionalities, transparent conducting oxides such as ITO, AZO, and GZO are often employed in photonic devices. These materials exhibit extreme field enhancement in the near-infrared region, which occurs when their permittivity approaches zero. Such materials, also called epsilon-near-zero (ENZ) materials, can be incorporated into various platforms such as meta-materials and surfaces [1], waveguides [2], and thin films [3] to create devices with a wide range of electromagnetic functionalities.

Propagation of light in ENZ thin films is characterized mainly by two modes: the radiating Berreman mode and the non-radiating ENZ mode [4–6]. The modal analysis of ENZ thin films presented in previous studies [4–6] is based on the calculation of complex frequency for a given real-valued propagation constant, which is relevant to Local Density of Optical States (LDOS) and pulsed excitation experiments. However, this analysis does not provide a complete description of modal field propagation characteristics, such as propagation length and confinement. To obtain a more comprehensive description of modal field propagation characteristics, one would need the complex propagation constant calculated at the real frequencies.

In this work, we analyze the propagation characteristics of ENZ films by solving the Helmholtz wave equation at real frequencies and calculating the complex propagation constants for ENZ layer thickness ranging between 2 - 100 nm (~ 1/600 - 1/12 of ENZ wavelength). The schematic of the considered structure is shown in Fig. 1(a), which consists of a Ga:ZnO (GZO) layer of thickness *d* surrounded by semi-infinite $ZnWO_4$ layers. We found that such a structure supports a novel non-radiating mode in the ENZ region of GZO. Such a mode has its dispersion curve lying to the left of the light line in the surrounding region (real part of effective index lower than the $ZnWO_4$ refractive index), as depicted in Fig. 1(b) and 1(c). However, the calculated electromagnetic fields display non-radiating (evanescent in the surrounding region) nature contrary to the Berreman mode. Subsequently, we studied the propagation characteristics of a multilayer structure constituting periodic array of GZO layer in $ZnWO_4$ matrix considering the modal field's excitation using the end fire coupling. Such a multilayer structure shows strong polarization selective and geometricaly tunable resonant absorption/emission. Moreover, incorporating antireflection coating at the facets of the structure empowers it to perfectly absorb the TM-polarized incident light. The spectral range of high absorption can be tuned by varying

the thickness of the GZO/ $ZnWO_4$ layer. We believe that our study will be helpful in the designing of photonic components such as modulators, sensors and other optoelectronic devices based on light absorption/emission.

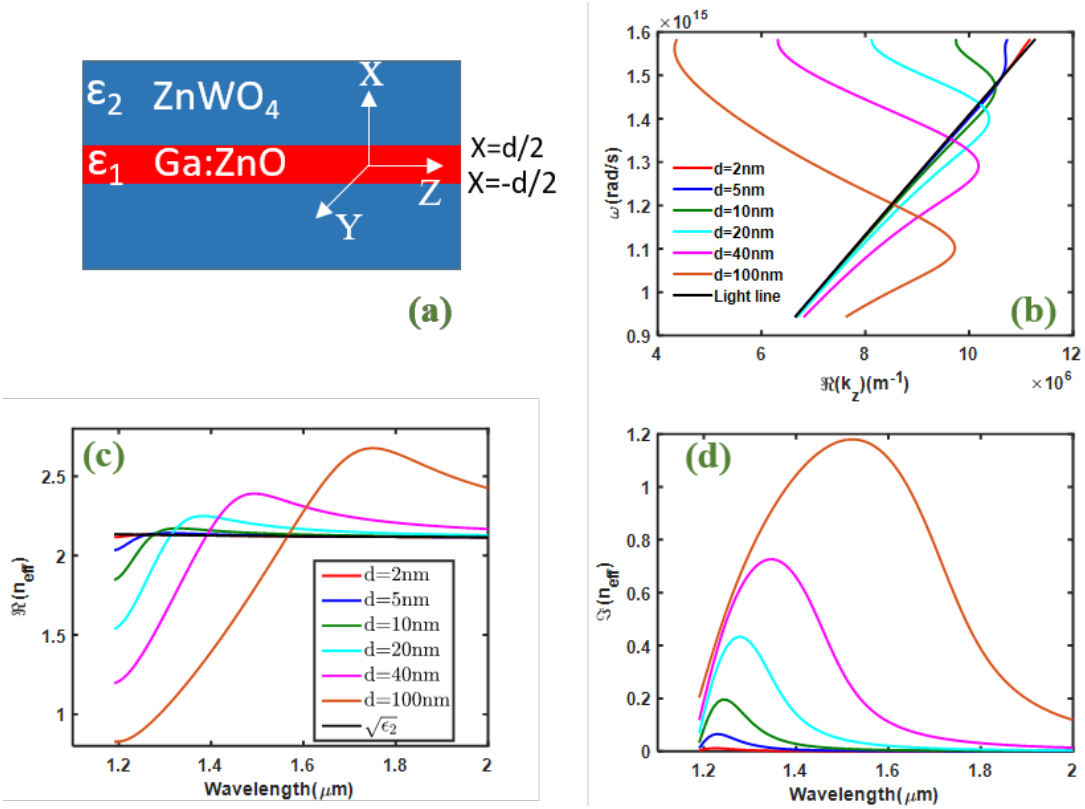


Fig. 1. (a) Schematic of the considered structure, (b) dispersion curve of the TM mode; Spectral variation of (c) real and (d) imaginary part of effective index.

This work is supported by the ENSEMBLE3 Project (MAB/2020/14) which is carried out within the International Research Agendas Programme (IRAP) of the Foundation for Polish Science co-financed by the European Union under the European Regional Development Fund and the Teaming Horizon 2020 program (GA. No. 857543) of the European Commission.

References

1. P. C. Wu, R. Sokhoyan, G. K. Shirmanesh, W. H. Cheng, and H. A. Atwater, "Near-Infrared Active Metasurface for Dynamic Polarization Conversion," Adv. Opt. Mater. **9**, (2021).
2. X. Jiang, H. Lu, Q. Li, H. Zhou, S. Zhang, and H. Zhang, "Epsilon-near-zero medium for optical switches in a monolithic waveguide chip at 1.9 μm," Nanophotonics **7**, (2018).
3. Y. Yang, K. Kelley, E. Sachet, S. Campione, T. S. Luk, J. P. Maria, M. B. Sinclair, and I. Brener, "Femtosecond optical polarization switching using a cadmium oxide-based perfect absorber," Nat. Photonics **11**, 390–395 (2017).
4. S. Campione, I. Brener, and F. Marquier, "Theory of epsilon-near-zero modes in ultrathin films," Phys. Rev. B - Condens. Matter Mater. Phys. **91**, (2015).
5. S. Vassant, J.-P. Hugonin, F. Marquier, and J.-J. Greffet, "Berreman mode and epsilon near zero mode," Opt. Express **20**, 23971 (2012).
6. S. Vassant, A. Archambault, F. Marquier, F. Pardo, U. Gennser, A. Cavanna, J. L. Pelouard, and J. J. Greffet, "Epsilon-near-zero mode for active optoelectronic devices," Phys. Rev. Lett. **109**, (2012).

META 2023, PARIS - FRANCE, JULY 18 – 21, 2023

Photonic nanojet enhanced Raman scattering: A new platform for Raman nanoscopy

Gour Mohan Das[1*], Piotr Paszke[1], Katarzyna Sadecka[1], and Dorota A. Pawlak[1,2,3]

[1]ENSEMBLE[3] Sp. z o. o. Centre of Excellence, Wólczynska 133, Warsaw 01-919, Poland
[2]Łukasiewicz–Institute of Microelectronics and Photonics, Al. Lotników 32/46, Warsaw 02-668, Poland
[3]Chemistry Department University of Warsaw, ul. Pasteura 1, Warsaw 02-093, Poland
[*]corresponding author: gourmohan.das@ensemble3.eu

Abstract: This study proposes a novel technique for enhancing Raman scattering signal using a combination of a single dielectric microsphere attached to a stem and confocal Raman microscopy. The technique involves directing laser through the glass microsphere to generate a photonic nanojet, a narrow-focused, non-evanescent, and highly intense electromagnetic beam with subwavelength lateral sizes, and obtaining Raman spectra. The method was tested on Bi_2O_3-Ag substrate, and an enhancement factor of ~90 was observed for the γ phase of Bi_2O_3.

Raman spectroscopy is a nondestructive analytical technique that is widely used in science and engineering applications for molecular identification, structural and quantitative analysis, and imaging often referred as molecular '*fingerprint*' [1]. In crystal engineering, Raman spectrum provides valuable information on the vibrational modes of the crystal lattice, which in turn provide insights into the crystal structure and composition, as well as defects, impurities, and lattice dynamics. However, there are certain limitations associated with the use of Raman spectroscopy for crystal phase determination. These include weak Raman signals, particularly for low-symmetry crystal structures or small crystals, and overlapping peaks from different crystal phases, especially for complex crystal structures or crystals with multiple phases present [2].

Herein we report a novel technique for enhancing Raman scattering signal with the combination of single dielectric optical microsphere attached with a stem and confocal Raman microscopy. In the conventional Raman scattering method, a microscopic objective lens directs laser light onto the top of the sample, and signal is collected in a back-scattering geometry. In photonic nanojet enhanced Raman scattering technique, the laser light coming from the microscopic objective lens is incident on the silica microsphere, and laser light can easily penetrate through the transparent glass microsphere and form the photonic nanojet at the shadow surface of the microsphere (the schematic is shown in figure 1a). Photonic nanojet is a narrow-focused, non-evanescent, and highly intense electromagnetic beam with subwavelength lateral sizes that emerged from the shadow side of dielectric microparticles (The generation of photonic nanojet from an optical microsphere is shown in figure 1b).

The microsphere was placed on top of Bi_2O_3-Ag substrate (an eutectic plasmon active multiphase material synthesized by micro pulling down method) using a customized manipulation system attached with the Raman spectroscopy. Raman spectra was collected with and without microsphere at the same location using similar experimental parameters (shown in figure 1c). The 826 cm^{-1} peak represents the γ phase of Bi_2O_3 while the other Raman peaks correspond to the α phase of Bi_2O_3 [3]. The enhancement is observed due to the presence of nano precipitates of γ phase of Bi_2O_3 close to Ag nanoparticles, and the further near-field enhancement of Ag nanoparticles by photonic nanojet, with an estimated enhancement factor of ~90 for the 826 cm^{-1} peak. We are confident that our developed technique will not only advance Raman nanoscopy in terms of chemical and phase

mapping but also pave a new path in vibrational spectroscopy-based optical nano-characterization.

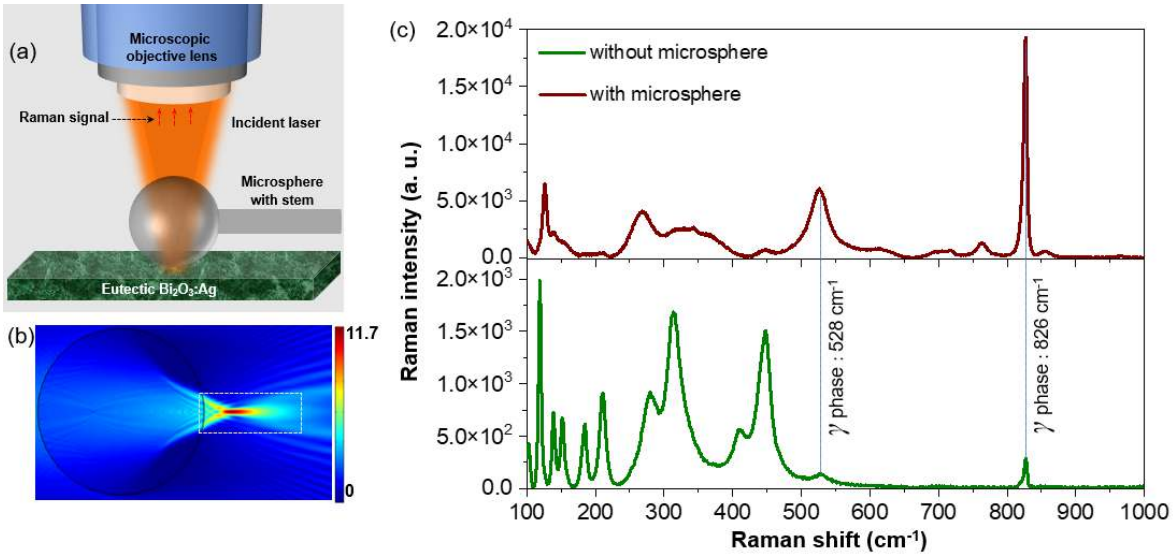


Figure: (a) Schematic of the photonic nanojet enhanced Raman scattering, (b) Numerical simulation of photonic nanojet from glass microsphere, and (c) the comparison between Raman scattering signal collected from an area of Bi_2O_3-Ag eutectic metamaterials without and with the presence of silica microsphere (enhancement factor ~ 90, excitation laser: 532 nm).

Acknowledgements: The authors thank the ENSEMBLE^3 Project carried within the Teaming for Excellence Horizon 2020 program of the European Commission (GA No. 857543), and the International Research Agendas Programme (MAB/2020/14) of the Foundation for Polish Science co-financed by the European Union under the European Regional Development Fund and Teaming Horizon 2020 program of the European Commission

References

1. Ferrari, A. C. and D. M. Basko, "Raman spectroscopy as a versatile tool for studying the properties of graphene," Nat. Nanotechnol., vol. 8, no. 4, pp. 235–246, 2013.
2. Zhang, X., Q.-H. Tan, J.-B. Wu, W. Shi, and P.-H. Tan, "Review on the Raman spectroscopy of different types of layered materials," Nanoscale, vol. 8, no. 12, pp. 6435–6450, 2016.
3. Szlachetko, K., P. Piotrowski, K. Sadecka, P. Osewski, D. Kasprowicz, and D. A. Pawlak, "Selective surface-enhanced Raman scattering in a bulk nanoplasmonic Bi2O3-Ag eutectic composite," Nanophotonics, vol. 9, no. 14, pp. 4307–4314, 2020.

Quantum and topological photonics

META 2023, PARIS - FRANCE, JULY 18 – 21, 2023

Optical control of topological and correlated electronic states

M. Hafezi[1]

[1]Joint Quantum Institute, and Quantum Technology Center, University of Maryland USA

[*]corresponding author: hafezi@umd.edu

Abstract: We discuss how quantum optical control techniques could pave a radically new way to prepare, detect and manipulate non-local and correlated electronic states. Specially, we discuss topological interplay between photons and electron and strongly correlated driven-dissipative system.

Given tremendous progress in controlling individual photons and other excitations such as spin, excitonic, phononic in solid-state systems, it is intriguing to explore whether these quantum optical control techniques could pave a radically new way to prepare, detect and manipulate non-local and correlated electronic states. After discussing several broad theoretical schemes, as the first experimental example, we report on optical and electrical tunable Bose-Fermi mixtures in hetero-bilayer systems and the observation of an excitonic Mott insulator [1]. This enables us to form strongly interacting excitons that are manifested in a large energy gap in the photoluminescence spectrum. The incompressibility of excitons is further corroborated by measuring exciton diffusion, which remains constant upon increasing pumping intensity, as opposed to the expected behavior of a weakly interacting gas of bosons, suggesting the formation of a bosonic Mott insulator. Our system provides a controllable approach to the
exploration of quantum many-body effects in the generalized Bose-Fermi-Hubbard model.

As the second experimental example, we report on the optical manipulation of quantum Hall states in graphene using twisted light. Specifically, we present a novel mechanism for such an orbital angular momentum transfer from optical vortex beams to electronic quantum Hall states [2-6]. Specifically, we identify a robust contribution to the radial photocurrent, in an annular graphene sample within the quantum Hall regime, that depends on the vorticity of light. This phenomenon can be interpreted as an optical pumping scheme, where the angular momentum of photons is transferred to electrons, generating a radial current with a polarity that is solely sensitive to the light's vorticity. Our findings offer fundamental insights into the optical probing and manipulation of quantum coherence, with wide-ranging implications for advancing quantum coherent optoelectronics.

References

1. B. Gao, D. G. Suarez-Forero, S. Sarkar, T. Huang, D. Session, M. Jalali Mehrabad, R. Ni, M. Xie, J. Vannucci, S. Mittal, K. Watanabe, T. Taniguchi, A. Imamoglu, Y. Zhou, and M. Hafezi, "Excitonic Mott insulator in a Bose-Fermi-Hubbard system of moiré WS2/WSe2 heterobilayer" arXiv, 2304:09731 (2023)
2. M. Gullans et al., Phys. Rev. B 95, 235439 (2017)
3. T. Grass et al. Phys. Rev. B 101, 155127 (2020)
4. Bin Cao et al, Phys. Rev. B 103, L241301 (2021)
5. Bin Cao et al, ACS Nano 2022, 16, 18200–18209, (2022)
6. Deric Session, M. Jalali-Mehrabad et al. in preparation.

META 2023, PARIS - FRANCE, JULY 18 – 21, 2023

Luminescence of molecular polaritons in a microcavity: non-Markovian Fano resonances, motional narrowing, and nonlinearity associated with vibronic coupling

B. D. Fainberg[1,2], **and V. Al. Osipov**[1]
[1]Faculty of Sciences, Holon Institute of Technology, Holon 58102, Israel
[2]School of Chemistry, Tel Aviv University, Tel Aviv 69978, Israel
[*]corresponding author: fainberg@hit.ac.il

Abstract: We develop a non-Markovian theory of polariton luminescence taking molecular vibrations into account. In the single-mode microcavity, our theory predicts the Fano resonances in the polariton luminescence, motional narrowing and explains experimental observations of the molecular Stokes shift in polariton fluorescence spectra in systems with strong light-matter coupling. Using the multiconfiguration Hartree approach we also derive nonlinear equations of motion for the polariton wavefunction, where vibration degrees of freedom interact with the polariton quantum field through the mean-field Hartree term.

In the last time Frenkel exciton polaritons (EPs) in organic materials and biological structures attracted considerable interest in relation to their Bose-Einstein condensation, low threshold polariton lasing, and polariton chemistry in microcavity. The concept of EPs suggests strong light-matter interaction that is supported by a considerably larger oscillator strength of organic systems compared to inorganic semiconductors. Theoretical description of EP luminescence in molecular systems is a challenge since in this case both the interaction with radiation field and electron-vibrational interaction are strong. In this work using a realistic non-Markovian theory for the description of the polariton-molecular vibrations interaction we calculate polariton luminescence in the polariton basis. To obtain the dispersion equation for the polaritons that coincides with the equation for the transverse eigenmodes of the medium, we average the Hopfield coefficients with respect to the optically active vibrations, and the polariton operators obey the Heisenberg equations [1]. We show that the frequency shift and broadening of polariton luminescence spectra strongly depend on the exciton contribution to the exciton polariton that is a function of frequency. Further we considered a single-mode microcavity (Fig.1a). It is usually believed that polariton states are formed when splitting of the upper and lower polariton branches is much larger than broadening of molecular resonances. In contrast, our non-Markovian theory [1] demonstrates the main characteristic features of the Fano resonance in the polariton luminescence (Fig.1b) associated with the characteristic "zero" frequency, at which luminescence intensity is equal to zero, and a peculiar asymmetric and ultra-sharp line shape for splitting of the upper and lower polariton branches of the same order of magnitude as inhomogeneous broadening of the molecular spectra. In addition, we predict motional narrowing of the EP luminescence spectrum in the microcavity. Our theory also enables us to consider a non-equilibrium (hot) EP luminescence.

It is worthy to note that the theory catches the effect of the Stokes shift in the polariton luminescence spectra. It can serve as a basis for the heuristic model formulated in experimental work [2] qualitatively explaining why the Stokes shift in resonant cavities filled with R6G:PMMA is larger than that in the same dye-doped films deposited on glass. Moreover, our theory explains also the luminescence spectrum

narrowing of the R6G:PMMA film in the cavity with respect to the luminescence spectrum of the same film deposited on glass [2].

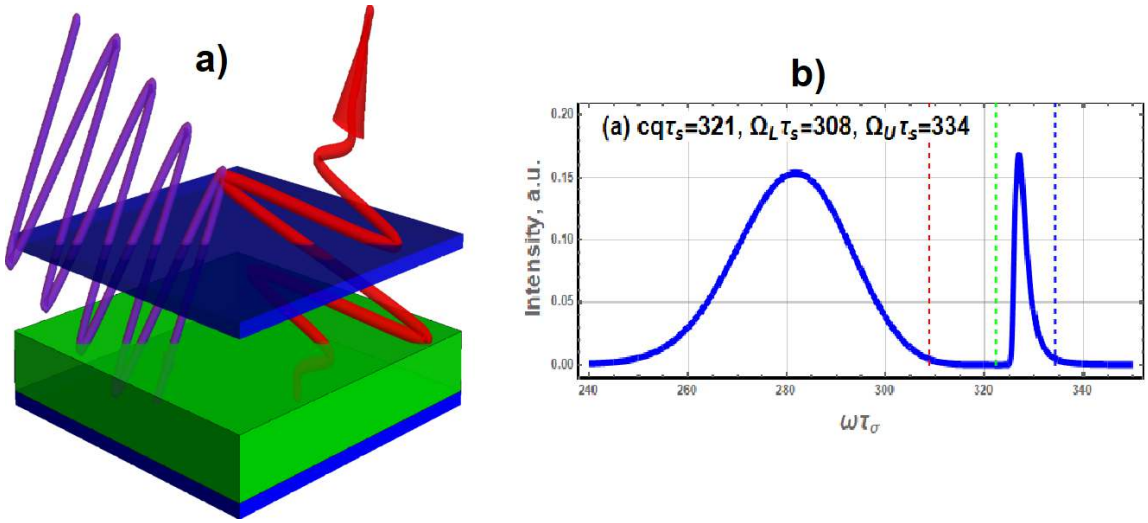


Fig.1. a) The molecular substance (green) is located between the cavity mirrors (blue) of a single-mode microcavity; the wavy arrows represent pumping (purple) and luminescence (red). b) Luminescence spectra of molecules in a single-mode cavity; the dashed lines correspond to the frequencies of the lower polariton branch (red) and the upper polariton branch (blue) and to the "zero" frequency (green).

Using the multiconfiguration Hartree approach we also derive nonlinear equations of motion for the polariton wavefunction, where vibration degrees of freedom interact with the polariton quantum field through the mean-field Hartree term [3]. We expect that the theory will lead us to new, associated with the nonlinearity, manifestations of the collective behaviour in polaritonic and similar systems, for example, mutual synchronization of interacting oscillators, oscillation death etc. [4].

Acknowledgements. The work was supported by the Ministry of Science & Technology of Israel (grant No. 79518) and the grant RA1900000633 for cooperation between the Ariel University and the Holon Institute of Technology.

References

1. Fainberg, B. D. and V. Al. Osipov, "Effects of electron-vibration interaction in polariton luminescence: non-Markovian Fano resonances and hot luminescence," *J. Phys. Chem. A*, Vol. 126, 2761–2777, 2022.
2. Tanyi, E. K., H. Thuman, N. Brown, S. Koutsares, V.A. Podolskiy, and M.A. Noginov, "Control of the Stokes Shift with Strong Coupling," *Adv. Opt. Mat.*, Vol. 5, 1600941, 2017.
3. Osipov, V. Al. and B. D. Fainberg, "Hartree Method for Molecular Polaritons," *Phys. Rev. B*, Vol. 107, 075404, 2023.
4. Pikovsky, A., M. Rosenblum, and J. Kurthsi. "Synchronization. A universal concept in nonlinear sciences." Cambridge University Press, New York, 2001.

Order-Invariant Quantum Correlations in non-Hermitian Interferometers

Tom A. W. Wolterink*, Matthias Heinrich, Stefan Scheel, and Alexander Szameit

Institute for Physics, University of Rostock, Albert-Einstein-Straße 23, 18059 Rostock, Germany
*corresponding author: tom.wolterink@uni-rostock.de

Abstract: We identify types of sequences of concatenated two-mode systems that perform distinct linear optical transformations, whereas their two-photon behavior is invariant under reversal of the order. We experimentally verify this systematic behavior in parity-time-symmetric complex interferometer arrangements of varying composition, and demonstrate that non-Hermitian quantum correlations may be preserved in counterintuitive ways even in small-scale networks.

Quantum correlations in linear optical networks are a crucial resource for quantum information processing. Correlations between multiple photons are described by the permanent of the transmission matrix of the optical network [1]. Yet, despite their central role, very few properties of permanents are known to exist and the calculation of matrix permanents remains a computationally hard problem. At large scale, this has sparked the field of boson sampling through the connection to linear optical quantum computing. However, the lack of tangible properties also affects small-scale networks, as it hinders intuitive prediction of the behavior of composite systems from their components. This especially holds for non-Hermitian systems that incorporate losses, which are known to drastically alter quantum correlations even in the simplest networks of just two modes, such as a lossy beam splitter [2,3]. Here, we systematically identify sequences of two-mode systems that perform distinct linear optical transformations, whereas their permanents remain invariant under reversal of the entire sequence's order. We experimentally verify this property by probing the two-photon correlations in parity-time (PT)-symmetric interferometers of wildly different composition.

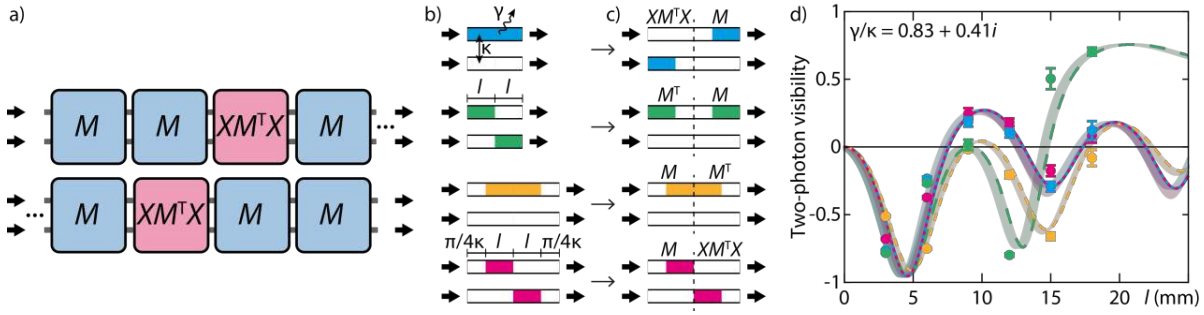


Figure 1. a) Sequences of two-mode transformations M and $XM^{\mathrm{T}}X$, concatenated in either forward or backward order, exhibit identical two-photon coincidences. b) Schematic drawing of concatenated PT-symmetric directional couplers and 50:50 directional couplers and c) their equivalent descriptions in terms of the transformation M. Color of the lossy section distinguishes the geometry. d) Measured (dots) and calculated (curves) two-photon visibility versus length.

Let us consider an arbitrary two-mode linear optical system described by its 2×2 transmission matrix M and its row-and-column-reversed transpose $XM^{\mathrm{T}}X$. When interpreting M as the transformation resulting from evolution of a time-dependent Hamiltonian $H(t)$, $XM^{\mathrm{T}}X$ corresponds to evolving $H(t)$ in reverse order while also swapping parity. Note that this is distinct from a simple time reversal, as it involves no complex conjugation. Concatenating these two systems results in different transformations $X(M^{\mathrm{T}}XM)$ or $M(XM^{\mathrm{T}}X)$, depending on the specific order. Surprisingly, their permanents turn out to be the same. Therefore, while these two sequences

show distinct behavior when probed with classical light or single photons, their two-photon behavior is identical. This peculiar effect does not arise from a trivial property of permanents and extends to longer sequences (Fig. 1(a)). As it holds for any complex matrix M, it provides a symmetry to link two-photon behavior in non-Hermitian systems.

To experimentally verify these invariant correlations, we study the two-photon behavior of interferometers consisting of multiple passive PT-symmetric directional couplers [4]. A passive PT coupler consists of two coupled waveguides of length l with coupling constant κ, one of which experiences loss at a rate γ. For $\gamma/\kappa < 2$, PT symmetry is unbroken and the Hamiltonian has real eigenvalues when viewed in the co-damped reference frame. We investigate interferometers of two concatenated passive PT couplers, either aligned with the lossy waveguide or opposite, as well as sandwiched between lossless 50:50 directional couplers on each end, as shown in Fig. 1(b). These four systems wildly differ in geometry, yet can all be described in terms of a transformation M, consisting of a 50:50 directional coupler followed by a PT coupler (Fig. 1(c)). We implement these non-Hermitian systems using evanescently coupled waveguides fabricated by femtosecond-laser direct writing and probe their two-photon behavior [5]. Figure 1(d) shows the measured visibility of the two-photon quantum interference as a function of the length of a single PT coupler. As a function of length we observe that the visibility oscillates between negative (Hong-Ou-Mandel bunching of photons) and positive (antibunching-like). Such antibunching behavior is precluded in a lossless system and can only be achieved in a non-Hermitian context. While differing in composition, the $X(M^{\mathrm{T}}XM)$ configuration indeed displays behavior identical to $M(XM^{\mathrm{T}}X)$, confirming the expectation that the permanent is preserved via their symmetry.

In summary, we have identified types of sequences of two-mode systems whose permanents remain invariant when reversing the order of the sequence, and experimentally verified these findings in PT-symmetric interferometers of varying composition by demonstrating that two-photon correlations are indeed invariant on the order. Our results emphasize that even in small two-mode systems quantum correlations may be related in ways that are a priori not obvious, which may inspire design of linear optical networks that harness non-Hermiticity for quantum information processing and sensing.

References

1. S. Scheel, “Permanents in linear optical networks,” arXiv:quant-ph/0406127, 2004.
2. S. M. Barnett, J. Jeffers, A. Gatti, and R. Loudon, “Quantum optics of lossy beam splitters,” Phys. Rev. A, Vol. 57, No. 3, 2134–2145, 1998.
3. R. Uppu, T. A. W. Wolterink, T. B. H. Tentrup, and P. W. H. Pinkse, “Quantum optics of lossy asymmetric beam splitters,” Opt. Express, Vol. 24, No. 15, 16440–16449, 2016.
4. M. Ornigotti and A. Szameit, “Quasi PT-symmetry in passive photonic lattices,” J. Opt., Vol. 16, No. 6, 065501, 2014.
5. F. Klauck, L. Teuber, M. Ornigotti, M. Heinrich, S. Scheel, and A. Szameit, “Observation of PT-symmetric quantum interference,” Nat. Photonics, Vol. 13, No. 12, 883–887, 2019.

Space-time Quantum Metasurfaces

W. J. M. Kort-Kamp[1*], A. K. Azad[1], and D. A. R. Dalvit[1]

[1]Los Alamos National Laboratory, Los Alamos, NM 87545, United States
[*]kortkamp@lanl.gov

Abstract: We introduce the concept of space-time quantum metasurfaces for arbitrary control of the spectral, spatial, and spin properties of nonclassical light using a compact photonic platform. We show that spacetime quantum metasurfaces allow on-demand tailoring of entanglement among all degrees of freedom of a single photon and that spatiotemporal modulation induces asymmetry at the fundamental level of quantum fluctuations, resulting in the generation of steered and vortex photon pairs out of the vacuum.

Demonstrations of metasurfaces in quantum photonics are based on meta-atoms whose optical properties are determined by their material composition and geometrical design, and the lack of spatiotemporal control severely limits the functionalities that state-of-the-art quantum metasurfaces can attain. At the classical level, space-time metasurfaces have been shown to provide that higher degree of control, both by reconfigurable and fully dynamic tailoring of the optical response of meta-atoms using analog and digital modulation schemes. Transitioning spatiotemporal modulation through the classical quantum divide could be critical to enable novel opportunities for flat quantum photonics. We put forward the concept of space-time quantum metasurfaces (STQMs) for spatiotemporal control of quantum light [1]. In the STQM paradigm, meta-atoms are modulated in space and time enabling manipulation of quantum light interacting with the dynamical metasurface. STQMs come in different flavors, including quantum systems such as monolayer atom arrays driven by laser pulses, quantum-classical systems such as quantum emitters embedded in modulated nanostructures, and meta-atoms made of classical or quantum materials with a driven electro-optical response. Here, we discuss examples for the last two flavors.

We first study the entanglement dynamics of a single photon as it transits through a dielectric metasurface whose permittivity is spatiotemporally modulated to create a synthetic phase for photons. The identical meta-atoms are anisotropic and are suitably rotated with respect to each other (Fig. 1, top), imprinting a Pancharatnam-Berry geometric phase in the quantum light field. When the geometric phase is a linear function of the meta-atoms' positions, it generates spin-path correlations, while a linear synthetic phase creates path-color correlations. The two correlations are intertwined through the path and the photon evolves into a state that is hyperentangled in spin, path, and color. Considering an incident linearly polarized single-photon pulse impinges on the metasurface, the probability amplitude to find the output in a state with frequency $\omega_p = \omega_0 + p\Omega$, momentum $\boldsymbol{k}_{p,q} = \boldsymbol{k}_0 + p\boldsymbol{\beta}_s + q\boldsymbol{\beta}_g$, with left/right circular polarization is

$$|c_{p,q}^{L/R}(t)|^2 = \cos^2\left(\frac{\omega_0 t\Delta\alpha}{2V_{uc}}\right) J_p^2\left(\frac{\omega_0 t\Delta\alpha}{2V_{uc}}\right)/2,$$

where V_{uc} is the volume of the unit cell and $\Delta\alpha$ the meta-atom polarizability modulation amplitude. The probability that the output photon is in a given harmonic as a function of the modulation depth is

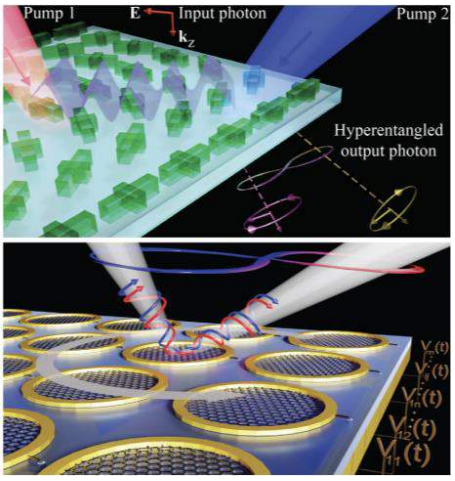


Fig. 1: *(Top) A dielectric STQM induces color-spin-path entanglement on a single photon. (Bottom) A graphene-based STQM generates entangled vortex photon pairs out of the quantum vacuum.*

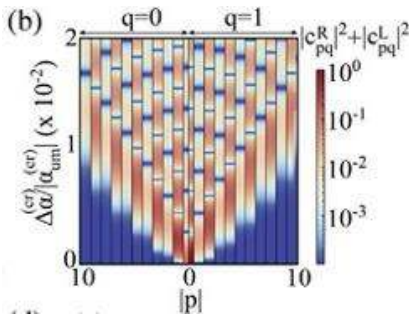


Fig. 2: *Conversion probability of an input photon into an output photon in frequency harmonic and momentum diffraction order versus polarizability modulation depth.*

shown in Fig. 2. At zero modulation, the output has the same frequency as the input and is an equal superposition of right- and left-polarized geometric-phase-kicked states. As the modulation increases, transitions to only the first few frequency and momentum harmonics occur and a larger amount of the Hilbert space is explored at large modulation depths.

We now study STQMs comprising modulated quantum materials and manipulating quantum vacuum fluctuations. We consider a graphene-disk STQM whose Fermi energy E_F is spatiotemporally modulated. The geometric phase is zero and the highly localized plasmons supported by the graphene disks [2] result in resonant enhancements of the light-matter interaction conducive to the efficient coupling of the STQM with the quantum vacuum. The STQM couples to the quantum electromagnetic field via a photon-number-nonconserving Hamiltonian that describes an analog of the dynamical Casimir effect (DCE) in which an oscillating boundary excites virtual into real photons. The STQM synthetic phase allows for a novel degree of control over the quantum vacuum, beyond previously demonstrated DCE setups: in STQMs steered and twisted DCE photons can be produced, reflecting that Lorentz reciprocity is broken at the level of quantum vacuum fluctuations. We design the metasurface to operate in the low-THz regime, and consider modulation frequencies also in the same range, which can be achieved using dynamical optical gratings and graphene's Kerr nonlinearity. We compute the rates of photon production out of the quantum vacuum using time-dependent perturbation theory. Energy conservation dictates that the photon pairs satisfy $\omega + \omega' = \Omega$. Figure 3 shows the emission rate for the linear synthetic phase as a function of momentum kick and Fermi energy. Giant photon-pair production rates on the order of 10^{12} photons/(cm^2 s) are obtained at low-THz driving frequencies and modest modulation depths.

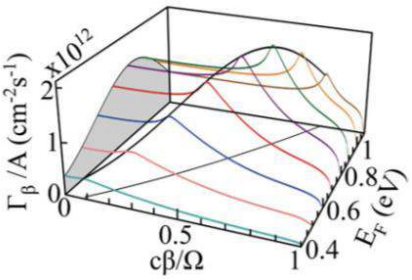


Fig. 3: *Two-photon emission rate of a graphene-based STQM versus dopintg level and linear synthetic phase gradient amplitude.*

In conclusion, we uncovered a key property of STQMs relevant for applications: On-demand reconfiguration of the synthetic phase allows dynamically tunable quantum correlations, enabling one to tailor the nature of entanglement depending on the symmetry properties of both geometric and synthetic phases. We also illustrated a second key property of STQMs with fundamental relevance: Lorentz nonreciprocity at the deepest level of vacuum fluctuations is attained through joint space and time modulations of optical properties and can be interpreted as an asymmetric quantum vacuum. Novel photonic devices potentially enabled by the proposed STQM concept include quantum emitters with reconfigurable spatial modes, quantum nonreciprocal routers and isolators for free-space photon transport in distributed quantum networks, and active quantum sensors with photon steering capabilities.

We acknowledge funding from the DARPA QUEST and the LANL LDRD program office.

References

1. Kort-Kamp, W. J. M. *et al.*, "Space-times Quantum Metasurfaces," PRL, Vol. 127, No. 10, 0430603, 2021.
2. Muniz, Y. *et al*, "Two-photon spontaneous emission in atomically thin plasmonic nanostructures", PRL, Vol. 125, 033601, 2020.

META 2023, PARIS - FRANCE, JULY 18 – 21, 2023

Photonic circuit simulation of topological arrays compared with experimental results in tantalum pentoxide

B. J. Thompson[1], R. Gibson[2*], and S. C. Badescu[2]

[1]KBR, Inc., 3725 Pentagon Blvd. Suite 210., Beavercreek, OH, 45431, USA
[2]Sensors Directorate, Air Force Research Laboratory, 2241 Avionics Circle, Wright-Patterson AFB, OH, 45433, USA
[*]corresponding author: ricky.gibson.2@us.af.mil

Abstract: A topological array composed of coupled microring resonators was simulated using passive lumped-element components. The topological bandgap is observable in the simulated spectrum, and no topological bandgap is present for a simulated trivial array which has no synthetic magnetic field phase accumulation. The material platform is oxide clad tantalum pentoxide which has low-loss performance at telecom wavelengths. The simulated transmission spectra have similar features to measured experimental arrays. This work demonstrates the capability of using rudimentary photonic circuit elements of waveguides and waveguide couplers to simulate and analyze complex topological array performance.

Topological photonic devices have similarities to bulk insulation and edge conduction of electrons in topological insulators [1-3]. These photonic devices are studied for robust light transmission even in the presence of defects. Silicon waveguide devices from photonic foundries have demonstrated topological behavior based on the integer quantum Hall Effect (QHE) [4]. Demonstrated applications are optical delay lines [3], and photon pair generation [5]. Recently the anomalous QHE has also been shown [6]. Frequency combs utilizing lower loss waveguides like SiN [7] have been proposed, and integer QHE devices have been demonstrated in tantalum pentoxide [8]. Tantalum pentoxide has a similar loss to SiN but a 3-times higher non-linearity [9].

The standard solution for simulating QHE topological arrays is using tight-binding modeling. This single-mode approximation is useful for modeling the energy transfer across the array based on coupling rates and accumulated phase shifts. It is valuable for viewing the energy distribution for a topological mode, and including disorder in site-resonators. However tight-binding simulations do not represent waveguide dispersion, group index, free spectral range, or include anti-resonant link-resonators.

Our alternate method for simulating topological array behavior was done with a commercially available photonic integrated circuit (PIC) simulation package [10] to graphically perform the transfer-matrix method (TMM). A ring resonator is represented by segmented waveguide regions and coupling regions, and an array can be constructed by coupling rings with link resonators. Waveguides were simulated using a finite-difference eigenmode (FDE) solver and waveguide coupling power transfer was simulated with finite-difference time-domain (FDTD). A synthetic magnetic field was imparted by modifying specific waveguide lengths for appropriate phase shifting. Once each component is defined by frequency dependent scatting matrix parameters, the components are assembled into an array and the transmission matrix for an entire array can be calculated. Backscatter, disorder, and array mode profiles are currently not included in these simulations. Figure 1 illustrates the transmission spectra for 10×10 arrays, a topological array with an applied phase shift and a trivial array with no phase accumulation. A flat bandgap is seen in the topological array that is not present in the trivial spectrum. Comparing with experimental results for the same modeled geometry shows the same features from the simulation, however there is more loss present in the experimental data. We believe that this work is the first use of photonic circuit modeling applied to simulate topological array behavior.

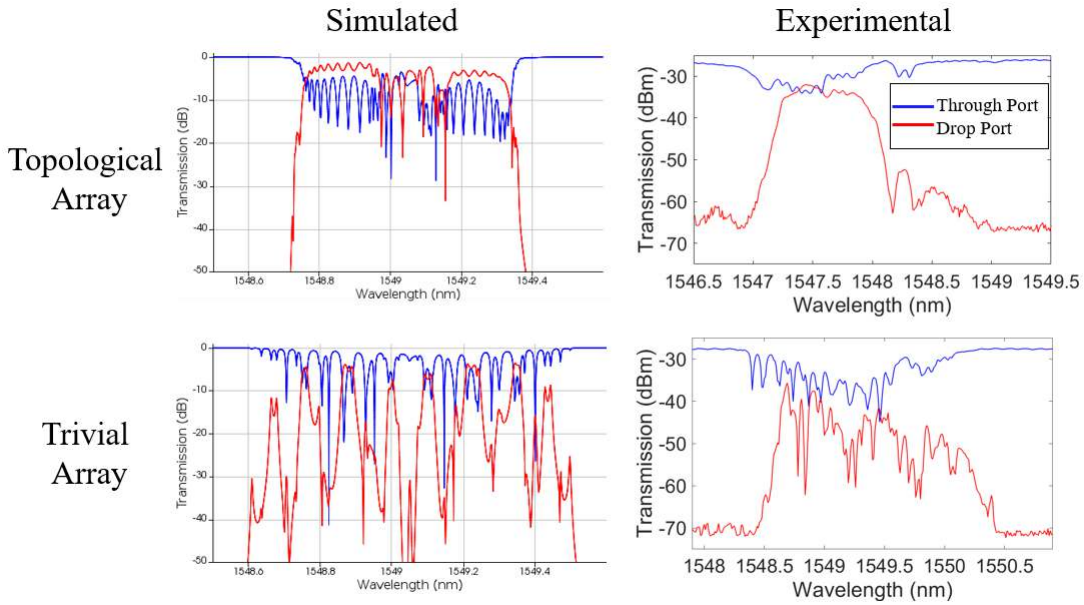


Figure 1. Simulated (left) and measured (right) transmission spectra for 10×10 topological (top) and trivial (bottom) arrays.

References

1. M. Z. Hasan and C. L. Kane, “Colloquium: Topological insulators,” Rev. Mod. Phys., Vol. 82, No. 4, pp. 3045-3067, 2010.
2. T. Ozawa, et al., “Topological photonics,” Reviews of Modern Physics, Vol. 91, No. 1, p. 015006, 2019.
3. M. Hafezi, E. A. Demler, M. D. Lukin, and J. M. Taylor, “Robust optical delay lines with topological protection,” Nature Physics, Vol. 7, No. 11, pp. 907–912, 2011.
4. M. Hafezi, S. Mittal, J. Fan, A. Migdall, and J. Taylor, “Imaging topological edge states in silicon photonics,” Nature Photonics, Vol. 7, No. 12, pp. 1001–1005, 2013.
5. S. Mittal, E. A. Goldschmidt, and M. Hafezi, “A topological source of quantum light,” Nature, Vol. 561, No. 7724, pp. 502–506, 2018.
6. S. Mittal, V. V. Orre, D. Leykam, Y. D. Chong, and M. Hafezi, “Photonic anomalous quantum hall effect,” Physical review letters, Vol. 123, No. 4, p. 043201, 2019.
7. S. Mittal, G. Moille, K. Srinivasan, Y. K. Chembo, and M. Hafezi, “Topological frequency combs and nested temporal solitons,” Nature Physics, Vol. 17, No. 10, pp. 1169–1176, 2021.
8. B. J. Thompson, R. Gibson, D. R. Carlson, and S. C. Badescu, "Topological Photonics in Low Loss Tantalum Pentoxide," in Conference on Lasers and Electro-Optics, Technical Digest Series (Optica Publishing Group, 2022), paper STu4E.3.
9. H. Jung, S.-P. Yu, D. R. Carlson, T. E. Drake, T. C. Briles, and S. B. Papp, “Tantala kerr nonlinear integrated photonics,” Optica, Vol. 8, No. 6, pp. 811–817, 2021.
10. Lumerical Inc. https://www.lumerical.com/

Disclaimer: The authors gratefully acknowledge support from the Applied Research for the Advancement of S&T Priorities program of the Office of the Under Secretary of Defense. The views and conclusions contained in this document are those of the authors and should not be interpreted as presenting the official policies or position, either expressed or implied, of the U.S. Government.

Fabrication of GaN Topological Photonic Crystals and Observation of Edge Modes in Visible Region

Yamato Takano[1*], Umito Kurabe[1], Koji Yoneta[1], Taiju Kudo[1], Mirai Akimoto[1], Takuto Honda[1], Xiao Hu[4], and Kikuchi Akihiko[1,2,3]

[1]Sophia Univ, Japan, [2]Sophia Photonics Research Center, Japan, [3]Sophia Semiconductor Research Institute, Japan

[4]WPI-MANA, National Institute for Materials Science, Japan

[*]corresponding author: kikuchi@sophia.ac.jp

Abstract: GaN-based visible range topological PhCs consisting of a honeycomb lattice of C6 symmetry triangular nanoholes were successfully fabricated by a combination of hydrogen environment anisotropic thermal etching (HEATE) and wet etching of AlInN sacrificial layer. Experimentally obtained photonic band diagram showed manifestation of topological properties such as, intensity inversion of upper- and lower-band-edge at G-point, and interfacial topological edge states. These topological properties were verified by FDTD simulation with precisely reproduced three-dimensional models.

In topological photonic crystals (PhC) [1], which introduce the concept of topology into photonic crystals (PhC), topological edge states formed at the interface of PhCs with different topologies exhibit unique propagation phenomena such as strong robustness against bending and unidirectional propagation, and are expected to be applied to various novel functional devices. Experimental verification of topological PhC is progressing rapidly in the near-infrared (NIR) wavelength region, where fabrication techniques are mature. In this study, we report the first fabrication of topological PhC using GaN, a well-known visible light emitting device material, and the successful observation of its topological properties in the visible wavelength.

The issues in GaN based visible region PhCs are the fact that the dimension of PhC is miniaturized to less than half of it in NIR and difficult processability. We fabricated GaN PhC membrane using combination process of low-damage precise GaN etching technique of hydrogen environment anisotropic thermal etching (HEATE) [2], and wet etching of AlInN sacrificial layer[3]. A model of a typical topological PhC with triangular nanoholes arranged in a deformed honeycomb lattice having C_6v symmetry and a design of a GaN-based PhC are shown in Fig.1. A 15 nm-thick SiO_2 film was deposited on the GaN (200nm)/AlInN (300nm)/GaN (4.8μm)/(0001)Al_2O_3 wafer, then hexagonal clusters consisting six triangular nanoholes with a period a_0 (=500-400 nm) were formed to expose GaN surface via conventional electron beam lithography and CF_4 dry-etching process. The cluster region where the distance R between the center of gravity of the triangular nanohole and the hexagonal cluster center is $R<a_0/3$ is a trivial PhC and that with $R>a_0/3$ is a topological PhC, and a topological edge state is formed at the boundary between two PhCs. The PhC pattern was transferred to the upper GaN layer using HEATE, and then the AlInN sacrificial layer was selectively removed by hot nitric acid wet etching to fabricate a membrane topological PhC. Fourier images of the fabricated PhC in the visible wavelength (400-730 nm) were obtained by a spectral microscope system every 1.0 or 0.4 nm, and three-dimensional (3D) photonic band diagram was constructed by stacking these images and two-dimensional band diagrams were drawn from the cross section. The observed photonic band diagrams were compared with the 3D-finite-difference time-domain calculations (3D-FDTD) simulation based on actual PhC structure to verify the occurrence of topological properties.

Fig. 2(a), (c) show the photonic band diagrams observed in the trivial and topological PhC with a_0=450 nm,

and the surface SEM images of each PhC are shown in the inset. The formation of fine triangular nanoholes with a side length of 174 nm and a radius of curvature of 15 nm at the apex was confirmed. The membrane thickness was 170 nm. The photonic band gap was confirmed at around 620 nm in both PhCs. At the Γ-point, intensity of lower-band edge is stronger for trivial PhC but that of upper-band edge is stronger for topological PhC. This intensity inversion reflects the topological property related to the inversion of the P and d modes of the out-of-plane magnetic field component at the band edge. The band structures are in good agreement with the 3D-FDTD simulation results shown in Figs. 2(b) and 2(d). Figs. 3(a), (c), and (e) show the photonic bands obtained by irradiating the boundary region between the trivial and topological PhC with linearly polarized light, right-handed polarized light, and left-handed polarized light, respectively. Fig.3(b), (d), and (f) are corresponding simulation of edge modes calculated by 3D-FDTD using a supercell. The clear edge modes depend on the polarized light were observed at the band gap wavelength and the experimental results are well reproduced by simulation.

We have successful observed topological photonic phenomena in the visible region using GaN-based materials for the first time, and the results show potential of topological PhC devices in the visible region.

References

1. L-H. Wu and X. Hu, Phys. Rev. Lett., 114 (2015) 223901.
2. R. Kita, R. Kita, T. Mizutani, H. Furuhashi, and A. Kikuchi, Jpn, J. Appl. Phys., 54 (2015) 046501.
3. K. Yoneta, K. Abe, T. Kudou, and A. Kikuchi, Jpn. J. Appl. Phys., 61 (2022) SC1078.

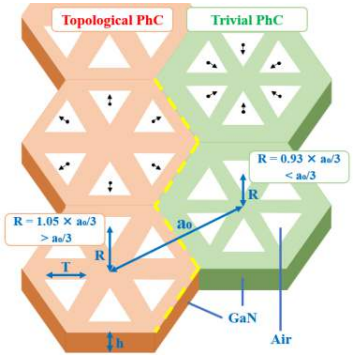


Fig.1. Schematic diagram and parameters of GaN topological and trivial PhCs membrane composed of six-membered triangular nanoholes.

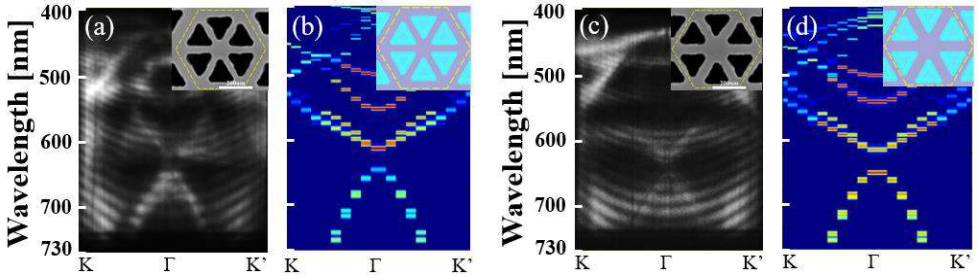


Fig.2 Photonic band diagrams of GaN-based PhC with different band topology Experimentally mesasured and numerically calculated (from FDTD) of (a,b) Trivial PhC with R values of 0.93(a_0/3) (c,d)Topological PhC with R values of 1.05(a_0/3) at a_0=450, respectively The insets show SEM images of the hexagonal clusters of the respective PhCs.

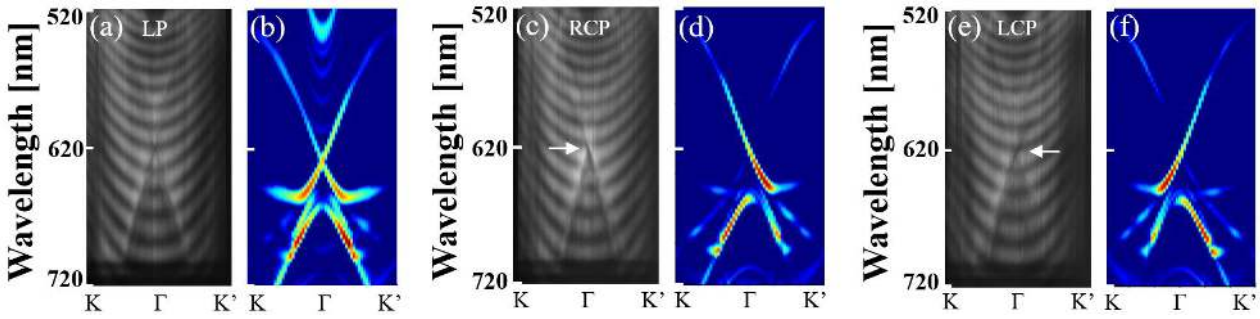


Fig.3 Magnified photonic band diagram near the photonic gap observed with injection of polaraized light Experimentally mesasured and numerically calculated (from FDTD) of (a,b) linearly (c,d) right-handed (e,f) left-handed circular polaraized light. Arrows indicate observed edge modes.

Polarization singularities and far-field optical properties in dielectric metasurfaces

L. Zagaglia[1], S. Zanotti[1], M. Minkov[2], M. Liscidini[1], D. Gerace[1], and L.C. Andreani[1*]

[1]Physics Department, University of Pavia, via Bassi 6, 27100 Pavia, Italy
[2]Flexcompute, Inc., 130 Trapelo Rd., Belmont, MA 02478, USA
[*]corresponding author: lucio.andreani@unipv.it

Abstract: We study the relation between the degree of circular polarization of eigenmodes and far-field optical properties in dielectric metasurfaces supporting Bound States in a Continuum (BICs) or with symmetry breaking leading to Circularly Polarized States (CPSs). The Stokes parameter S_3 is extracted from finite-difference time-domain (FDTD) and rigorous coupled-wave analysis (RCWA) simulations. In addition to the symmetries imposed by the lattice, the S_3 parameter has a nontrivial dependence on the wavevector, with different regimes that are manifest in the optical properties.

Photonic crystal (PhC) slabs, or periodic dielectric metasurfaces, support BICs that are not coupled to the radiation field. Such BICs lead to vortex singularities in momentum space with an integer winding number or topological charge [1]. Symmetry-protected BICs can split into CPSs with a semi-integer topological charge upon symmetry reduction [2,3]. Such polarization singularities are of current interest in the field of topological photonics and could in principle be used to tailor the polarization properties in the far field [4].

In this work, we consider a PhC with square lattice and different kinds of bases, leading to BICs and CPSs. Our goal is to explore the relation between the Stokes parameter S_3 of the eigenmodes (which measures the degree of circular polarization) and the optical properties in the far field. An example of polarization singularities is shown in Fig. 1: we consider the lowest resonance in the photonic band structure below the diffraction limit, which in the case of a circular hole displays a symmetry-protected BIC at k=0. The Stokes parameter S_3 is generally nonvanishing except along directions that correspond to symmetry planes, where the eigenmodes are linearly polarized. A nonvanishing S_3 is associated to the breaking of time-reversal symmetry in the formation of quasi-normal modes with complex eigenfrequencies. In the case of a triangular hole, the BIC splits in two CPS with $S_3=\pm1$ that appear along the [10] direction in the S_3 map.

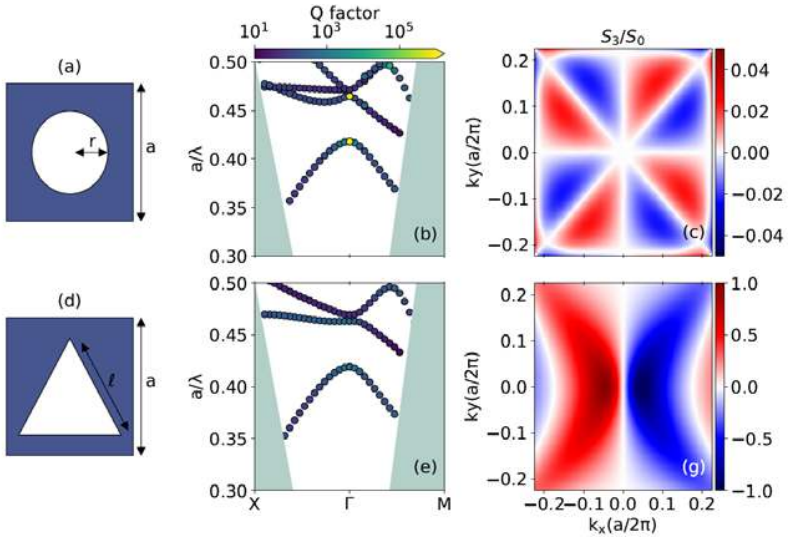


Figure 1: (a), (d) Sketch of a unit cell of a PhC slab with a square lattice of circular or triangular air holes. (b), (e) TE-like photonic band structure together with the quality factor (Q) of each resonance. (c), (g) k-space map of the normalized Stokes parameter S_3 of the lowest resonance. Parameters: photonic crystal slab of thickness d=0.3a, refractive index n=3.48, circle radius r=0.3a (b,c) or triangle side l=0.8081a (e,g) yielding the same air fill fraction in both cases.

In Fig. 2 we show an example of the relation between the far-field optical response and the properties of the eigenmodes. Reflection spectra for circularly polarized light show that around the incidence angles $\theta=\pm5°$ (which correspond to the CPSs in Fig. 1g), the incident field couples to the eigenmode only for right circular polarization (RCP) for positive θ, only for left circular polarization (LCP) for negative θ. The circular dichroism in reflectivity, $CD_R=(R_{lcp}-R_{rcp})/(R_{lcp}+R_{rcp})$, reaches ±1 at the same angles. Its dependence of the incidence angle θ corresponds very well to the behavior of the Stokes parameter S_3 extracted from FDTD and RCWA simulations.

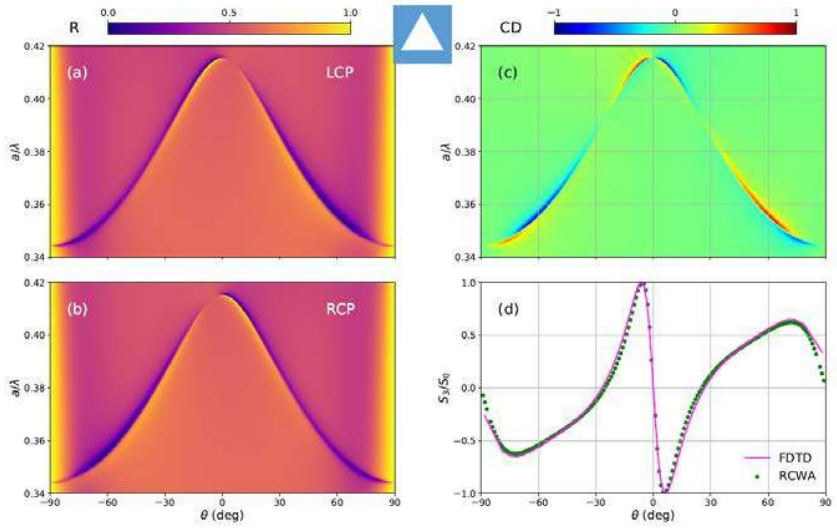


Figure 2: (a), (b) Reflectivity for left- and right-circular polarizations, (c) reflectivity CD, (d) normalized Stokes parameter S_3 of the lowest eigenmode extracted from the simulations. The results are for the square lattice PhC slab with triangular holes of Fig.1, lower panels, orientation along the [10] direction.

We further explore the relation between polarization singularities and the optical properties by considering various shapes for the holes, which continuously interpolate between a circular hole (leading to the C_{4v} point group in the square lattice) and a triangular hole (breaking the C_2 symmetry and leading to the C_{1v} point group). In general, the degree of circular polarization has a complex dependence on wavevector with sign inversions, and it is maximized close to CPS. The optical properties are found to be determined by a complex interplay between the effect of topological singularities and the direct scattering term, as follows from temporal coupled-mode theory [5]. The results may be exploited to design structures with given polarization properties.

This research was supported from the Italian Ministry of University and Research (MUR) through PRIN project 2017MP7F8F-004 “NOMEN” and through PNRR project PE0000023-NQSTI.

References

1. Zhen, B., C. W. Hsu, L. Lu, A. D. Stone, and M. Soljačić, “Topological Nature of Optical Bound States in the Continuum”, Phys. Rev. Lett., Vol. 113, 257401, 2014.
2. Liu, W., B. Wang, Y. Zhang, J. Wang, M. Zhao, F. Guan, X. Liu, L. Shi, and Jian Zi1, “Circularly Polarized States Spawning from Bound States in the Continuum”, Phys. Rev. Lett., Vol. 123, 116104, 2019.
3. Yoda, T., and M. Notomi, “Generation and Annihilation of Topologically Protected Bound States in the Continuum and Circularly Polarized States by Symmetry Breaking”, Phys. Rev. Lett., Vol. 125, 053902, 2020.
4. Chen, W., Q. Yang, Y. Chen, and W. Liu, “Extremize optical chiralities through polarization singularities,” Phys. Rev. Lett., Vol. 126, 253901 (2021).
5. Fan, S., W. Suh, and J. D. Joannopoulos, “Temporal coupled-mode theory for the Fano resonance in optical resonators,” J. Opt. Soc. Am. A, Vol. 348, 569–572 (2003).

Controlling Spontaneous Emission with Nanomaterials at the Single-Emitter Level

R. M. Cordova-Castro[1*], C. Cabriel[2], D. Jonker[3], M. Zapata-Herrera[4], A. Krasavin[5], A. Susarrey-Arce[3], R. Sapienza[6], Yannik De Wilde[2], Valentina Krachmalnicoff[2], A. Zayats[5], Ignacio Izeddin[2] and R. W. Boyd[1,7]

[1]University of Ottawa, Department of Physics, Canada

[2]Institute Langevin, ESPCI Paris, PSL University, CNRS, France

[3]University of Twente, MESA+ Institute, The Netherlands.

[4] Materials Physics Center CSIC-UPV/EHU, Spain

[5]Department of Physics, King's College London, UK.

[6] The Blackett Laboratory, Department of Physics, Imperial College London, UK.

[7]University of Rochester, Institute of Optics, USA.

*corresponding author: margoth.physics@gmail.com

Abstract: Abstract: The direct measurement of a single emitter decay rate and the simultaneous knowledge of its position is a powerful tool for the study of light-matter interaction at the nanometer scale. We use single-molecule fluorescence lifetime imaging microscopy (smFLIM) to map at the nanometer scale the decay rate enhancement of single emitters coupled to new nanomaterials platforms that significantly modified the electromagnetic environment.

Exploiting the quantum behavior of light for new or advancing existing technologies will rely on better understanding and manipulating light in the quantum regime. A necessary part of that developments must include understanding on how to control the spontaneous emission of light, process that determines how likely, how quickly and where an excited emitter will release a photon. In this work, we study how new dielectric and plasmonic structures and metamaterials platforms can manipulate the response of nearby quantum emitters, by using far-field super resolution microscopy we observe this light-matter interaction at the nanometer scale.

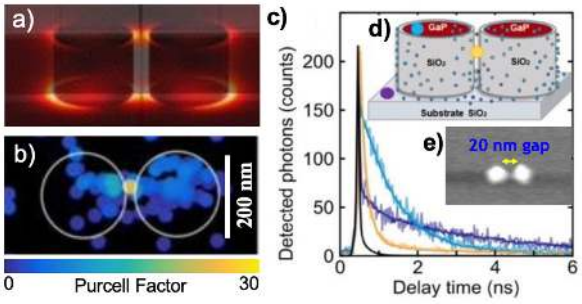


Figure 1. a) Electromagnetic field modification by a GaP nanodimer when illuminated by a 650 nm plane wave. b) Super resolved map of measured spontaneous emission lifetime of quantum emitters coupled to gap nanoantenna. c) Measured decay rate curves for single-emitter on glass substrate (purple), on top of antenna (blue) and in the 20nm gap of the dimer (yellow) as shown in d). e) Scanning Electron Microscopy of fabricated dielectric nanoantenna. The emission of the quantum emitter is divided into two detections paths; 1. The single-photon emission lifetime is measured by a single-photon avalanche diode connected to time correlating single photon counter (TCSPC) and 2. correlated with single molecule localization microscopy SMLM to image below the diffraction limit.

The principle of our research is shown in Fig. 1; when light illuminates a nanostructure, the electromagnetic field is concentrated extremely close to the particle by resonant optical modes. Quantum emitter's spontaneous emission will dramatically depend on its position near these modes. This makes the single-photon emission (SPE) rate a precise measure of location, far more accurate than the optical resolution from the same photon. In order to study at the super-resolution level, the modification of SPE with the proposed nanodevices that present unique photonics properties, we combine the Nobel prize winner single molecule super localization microscopy (SMLM) technique (used mainly for bioimaging) with Nanophotonics to unveil light-matter interaction at the nanoscale. Allowing the detection of the single-emitter position and emission rate modification with far-field microscopy without perturbing the local environment with metallic probes as previous works applying near-field scanning techniques. We show single-emitter super-resolved imaging of radiative decay rate enhancement a 20 nm gap dielectric nanoantenna, reporting the use of gallium phosphite (GaP) nanodimers for radiative decay rate enhancement (above 30 Purcell factor) at room temperature and detected at the single-emitter resolution.

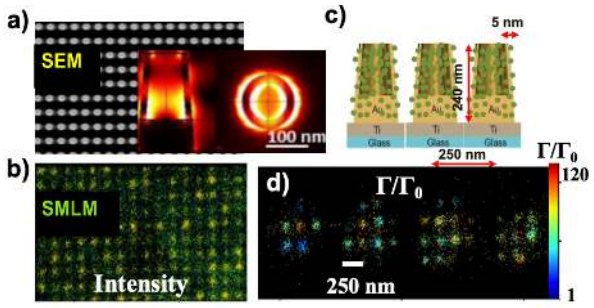


Figure 2. a) SEM images of 3D fabricated HCNPs and calculation of electromagnetic near-field modification with 3D distribution b) Measured Super-resolved image of emitters emission coupled to plasmonic modes in lattice of HCNPs. c) Representation of nanostructure dimensions with quantum emitters deposited all along separated 4 nm from Au surface. d) Measured Super-Resolved single-emitter decay rate enhancement map at room temperature.

In the contrary when placed single emitters on a square lattice hollow nanoconical pillars HCNP that presents high enhancement and 3D modification of electric field; SPE rate is modified significantly all along the material (Fig. 2). We show super resolved maps of total and radiative decay rate enhancement of quantum emitters coupled to the HCNP metamaterial at the super resolution level, with enhancement above 100. We study as well single emitters couple to hyperbolic metamaterials observed at the single-emitter resolution. We will discuss experimentally and numerically the important nanophotonics effects responsible of the modification of the quantum emitter properties in each studied material platform and how to optimize the emission depending on the wavelength and desired application. An interesting consequence of this work stems from the rate of emission being extremely position specific and enhanced at room temperature; this could have significant implications on the development of light sources capable of emitting single photons on demand at room temperature, for quantum sensing with atoms of local electric and magnetic fields, super-resolution microscopy and highly sensitive spectroscopic measurements.

References

1. R. M. Cordova-Castro, B. van Dam, A. Lauri, S. Maier, R. Sapienza, Y. de Wilde, I. izeddin and V Krachmalnicoff, "Single-Emitter Super-resolved Imaging of Radiative Decay Rate Enhancement in Dielectric Gap Nanoantennas," Nano Letters, to be published, 2023.

2. D. Jonker, Z. Jafari, J. Winczewski, C. Eyovge, J. W. Berenschot, N. R. Tas, J. G. E. Gardeniers, I. De Leon, and A. Susarrey-Arce, "A wafer-scale fabrication method for three dimensional plasmonic hollow nanopillars," Nanoscale Adv., Vol. 3, 4926–4939, 2021.

Quantum remote control of vortex beams using a metasurface

Hong Liang[1], Hammad Ahmed[2], Wing Yim Tam[1], Xianzhong Chen[2*], and Jensen Li[1*]

[1]Department of Physics, The Hong Kong University of Science and Technology, Clear Water Bay, Hong Kong, China
[2]School of Engineering and Physical Sciences, Heriot-Watt University, Edinburgh EH144AS, UK
[*]corresponding author: x.chen@hw.ac.uk, jensenli@ust.hk

Abstract: We propose and experimentally demonstrate a scheme to remotely and continuously control the vortex beam structure using polarization-entangled photon pairs together with a metasurface. With a heralding technique adopted, the spin-orbit coupling provided by the metasurface translates to a tailor-made entanglement of the orbital angular momentum and the polarization of the signal photon. Then, the polarization of the heralding photon is used to remotely control the vortex structure of the signal photon, directly manifested as a continuous orbital rotation.

Metasurfaces, with distinct capability to modulate light, have led to unprecedented applications such as beam steering [1]. One particular interest is to hybridize the polarization and orbital angular momentum (OAM) of light to generate vortex beams through spin-orbit interactions (SOI) [2]. The generated beams, carrying different OAMs, have a great potential to enhance the channel capacity in optical communication, leading to applications like OAM-encoded holograms [3]. At the same time, recent interests arise in adopting metasurfaces in quantum optics, including high-dimensional quantum sources, quantum entangled states manipulation and reconstruction [4-6]. Our work focuses on generating remotely controlled vortex beams with a geometric-phase metasurface and polarization-entangled photon pairs (heralding and signal photons). Specifically, the SOI from the metasurface entangles the OAM and polarization of the signal photons. As a result, we can select different heralding polarizations to control the vortex state of the signal photons remotely and continuously. Our demonstration using a metasurface can also be extended to more sophisticated vortex structures of the signal photon and opens a new avenue for quantum communication with increased information capacity.

Fig. 1(a) shows the proposed scheme for quantum remote control of vortex beams with a geometric-phase metasurface and a polarization-entangled photon pair (signal and heralding photons). The signal photon is sent to interact with the metasurface with SOI, while the heralding photon is sent to a polarization analyzer. The metasurface is designed to induce different OAM changes depending on the spin of the input light and hence entangles the polarization and the OAM of the signal photon. Together with the polarization entanglement between the heralding and the signal photon, the polarization of the heralding photon and the vortex structure of the signal photon are entangled as a result. Thus, the heralding detection with a rotating linear polarization will result in a rotating vortex structure of the signal photons. This control scheme can be visualized in Fig. 1(b) using the mapping between two Poincaré spheres for the heralding polarization and signal vortex state. As shown in Fig. 1(b), points with the same color on the two spheres show matching pairs of the controlling polarization and the corresponding vortex state. Specific cases located on the equator are examined and verified with experimental results.

Figs. 1(c-f) show the experimental and theoretical results for selected linear heralding polarizations, from the horizontal (H), diagonal (D), vertical (V), to antidiagonal (A) polarizations. For example, Fig. 1(c) shows the signal vortex state heralded by the photons with horizontal polarization. In this case, the signal vortex state collapses to the state $|+1\rangle - |-1\rangle$, with the normalization factor omitted, resulting in an intensity profile of two bright lobes with a horizontal dark line in between. On the other hand, using vertical photons to herald, the signal states collapse to $|+1\rangle + |-1\rangle$, with two lobes and a vertical dark line in between, as shown in Fig. 1(e). Similarly, the results with diagonal and antidiagonal heralding photons are shown in Figs. 1(d,f) with vortex states $|+1\rangle \pm i|-1\rangle$, where the "+" ("-") sign is for the D (A) polarization. Furthermore, the heralded results all have higher signal-to-noise ratios than the classical results, showing greater robustness to noise than single-photon imaging.

In conclusion, based on a geometric-phase metasurface, we experimentally demonstrate a heralding scheme, with great robustness to noise, to control vortex structures of OAM interference remotely and continuously using polarization-entangled photon pairs. Through this work, multifunctional metasurfaces further extend their applications in the quantum optical regime, providing a platform to implement quantum information processing with tailor-made vortex structures. Importantly, such a continuous heralding control of rotating orbitals provides additional dimensions in the quantum state manipulation that could benefit future quantum communication protocols.

With more complex metasurfaces, further extensions to higher OAM values, structured beams, and other degrees of freedom of light will be possible to enhance the associated information capacity in quantum communication.

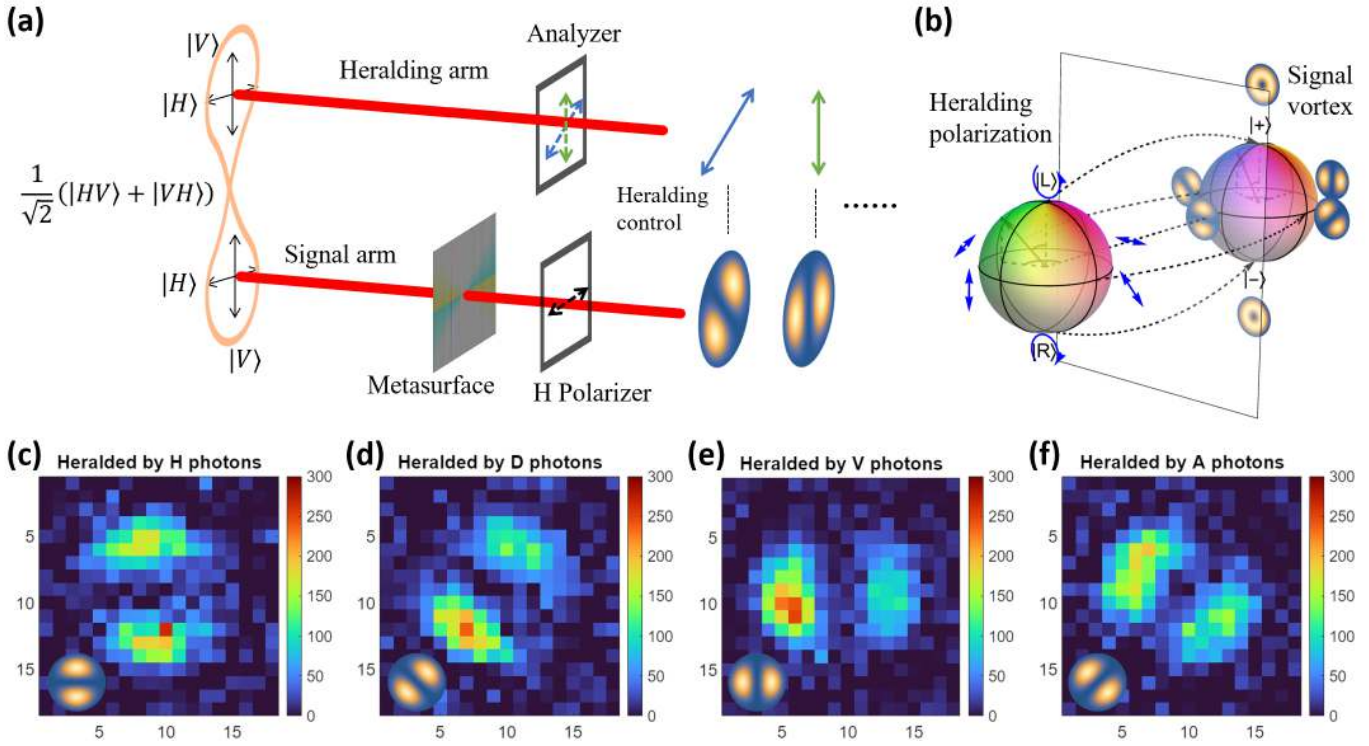


Figure 1. Quantum remote control of vortex beams. (a) Schematic for quantum remote control of vortex beams using a metasurface. (b) The remote control of signal vortex states using heralding polarizations, visualized with two corresponding Poincaré spheres. Points with the same color on the two spheres show matching pairs of the controlling polarization and the corresponding vortex state. Some specific examples are connected using dashed arrows. (c-f) Heralded images of signal vortex states shown as rotating orbitals for H, D, V, and A heralding polarizations. Lower-left insets are the theoretical predictions.

Acknowledgments

The work is supported by the Hong Kong RGC (16304020, 16306521, C6013-18G, AoEP-502/20) and by Croucher Foundation (CAS20SC01).

References

[1] N. Yu, P. Genevet, M. A. Kats, F. Aieta, J.-P. Tetienne, F. Capasso, and Z. Gaburro, *Light Propagation with Phase Discontinuities: Generalized Laws of Reflection and Refraction*, Science **334**, 333 (2011).

[2] G. Li, M. Kang, S. Chen, S. Zhang, E. Y.-B. Pun, K. W. Cheah, and J. Li, *Spin-Enabled Plasmonic Metasurfaces for Manipulating Orbital Angular Momentum of Light*, Nano Lett. **13**, 4148 (2013).

[3] H. Ren, G. Briere, X. Fang, P. Ni, R. Sawant, S. Héron, S. Chenot, S. Vézian, B. Damilano, V. Brändli, S. A. Maier, P. Genevet, *Metasurface orbital angular momentum holography*. Nat Commun. **10**, 2986 (2019).

[4] L. Li et al., *Metalens-Array–Based High-Dimensional and Multiphoton Quantum Source*, Science **368**, 1487 (2020).

[5] K. Wang et al., *Quantum Metasurface for Multiphoton Interference and State Reconstruction*, Science **361**, 1104 (2018).

[6] Z. Gao, Z. Su, Q. Song, P. Genevet, K. E. Dorfman, *Metasurface for complete measurement of polarization Bell state*. Nanophotonics (2022).

Quantum dynamics and dissipation-driven formation of entangled dark states in strongly coupled many-qubit systems in solid-state nanocavities

M. Tokman[1], A. Behne[2], B. Torres[2], M. Erukhimova, Y. Wang[2], and A. Belyanin[2*]

[1]Department of Electrical and Electronic Engineering, Ariel University, Israel
[2]Department of Physics & Astronomy, Texas A&M University, USA
[*]corresponding author: belyanin@tamu.edu

Abstract: We study quantum dynamics of many-qubit systems strongly coupled to a quantized electromagnetic field of a nanocavity in the presence of decoherence and dissipation for both fermions and cavity photons, and taking into account the nonuniform nanocavity field and the spread of qubit transition frequencies. We show that the dissipation in a cavity may drive the system into many-qubit entangled dark states that live much longer than the cavity decay time and can be used for quantum information applications.

Solid-state nanocavity QED attracted much interest as a promising platform for quantum information and quantum sensing systems; A typical scenario involves an ensemble of quantum dots, defects in crystals, or molecules, strongly coupled to a quantized electromagnetic field in a plasmonic nanocavity. The cavity field is strongly nonuniform, which makes the qubit-cavity coupling strength strongly variable from qubit to qubit. Moreover, for many popular quantum emitters, such as quantum dots, optically active point defects, excitons in semiconductor nanostructures etc., the spread of transition frequencies exceeds homogeneous linewidth, making inhomogeneous broadening the dominant source of dephasing. Any of these factors break permutation symmetry and increase the complexity of the problem. We are able to drastically simplify the analysis and obtain analytic or semi-analytic solutions for quantum dynamics of strongly coupled dissimilar qubits or multilevel fermionic systems in the presence of decoherence and dissipation for both fermions and cavity photons. This progress is made possible by applying a modified version of the stochastic Schroedinger equation at the level of Lindblad approximation. Here we will concentrate on dissipation-driven formation of highly entangled dark states that are decoupled from the cavity field and therefore live much longer than the decay time of cavity photons, even though each qubit remains strongly coupled to the cavity field. The ability to generate and control such states is an important problem for plasmonic nanocavities where the dissipation of a cavity mode is much faster than the relaxation in quantum emitters. We determine the conditions in which the formation of dark states is possible even in systems with strong inhomogeneous broadening and with energy bands.

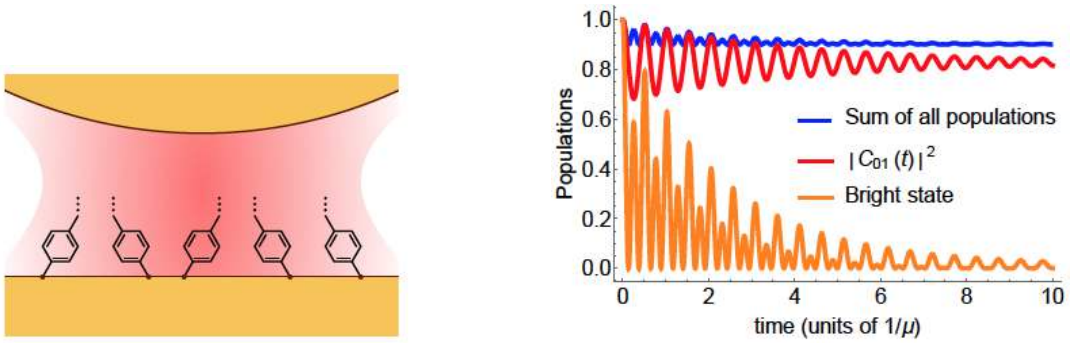


Figure 1. Left: A sketch of an ensemble of quantum emitters (e.g. quantum dots or molecules) in a strongly nonuniform field of a plasmonic nanocavity. Right: Time evolution of the populations for an ensemble of 21 qubits

in the nanocavity formed by the metallic sphere of radius 10 nm with its center located at 12 nm above the substrate. The molecules are assumed to be distributed randomly within a circle of radius 10 nm on the substrate, with the center of the circle at the cavity axis. The cavity decay time is $1/\mu$ = 20 fs. Top blue curve: The sum of the occupation probabilities of all qubits when only the qubit in the center of the cavity is excited, i.e., $C_{01}(0) = 1$; middle red curve: the occupation of the initially excited qubit; bottom orange curve: the sum of all occupation probabilities when the qubits were initially prepared in the bright state.

References

1. M. Tokman, A. Behne, B. Torres, M. Erukhimova, Y. Wang, and A. Belyanin, Dissipation-driven formation of entangled dark states in strongly-coupled inhomogeneous many-qubit systems in solid-state nanocavities, Phys. Rev. A, Vol. 107, 013721, 2023.

Prime comb lasing in a fiber ring at low temperatures

Eyal Buks,[1]

[1] *Andrew and Erna Viterbi Department of Electrical Engineering, Technion, Haifa 32000 Israel*

[*] *eyal@technion.ac.il*

Abstract: We experimentally study a fiber loop laser with an integrated Erbium doped fiber (EDF). The output optical spectrum is measured as a function of the EDF temperature. We find that below a critical temperature of about 10K the measured optical spectrum exhibits a sequence of narrow and unequally-spaced peaks. Externally injected light and filtering are employed for tuning the peaks' wavelengths. Operation of the device as an optical memory having storage time of about 20 ms is demonstrated. The multimode lasing tunability can be exploited for novel applications in the fields of sensing, communication, and quantum data storage. © 2023 The Author(s)

1. Introduction

Erbium doped fibers (EDF) are widely employed in a variety of applications. Key properties of EDF can be controlled by varying the temperature. Multimode lasing has a variety of applications in the fields of sensing, spectroscopy, signal processing and communication. Multimode lasing in the telecom band has been demonstrated by integrating an EDF cooled by liquid nitrogen into a fiber ring laser [1–3]. It has been recently proposed that EDF operating at low temperatures can be used for storing quantum information [4].

In this work we study a fiber loop laser with an integrated EDF. We measure the emitted optical spectrum as a function of the EDF temperature. Below a critical temperature of about 10 K the measured optical spectrum exhibits an unequally-spaced optical comb (USOC) made of a sequence of narrow peaks. The observed USOC and multimode lasing are attributed to intermode coupling [5]. We find that the wavelengths at which the multimode lasing occurs can be controlled by light that is externally injected into the fiber loop. The possibility of using the device under study as an optical memory is explored, and a storage time of about 20 ms is demonstrated. The USOC controllability, together with its high stability, can be exploited for facilitating novel applications in the fields of sensing, communication, and quantum data storage.

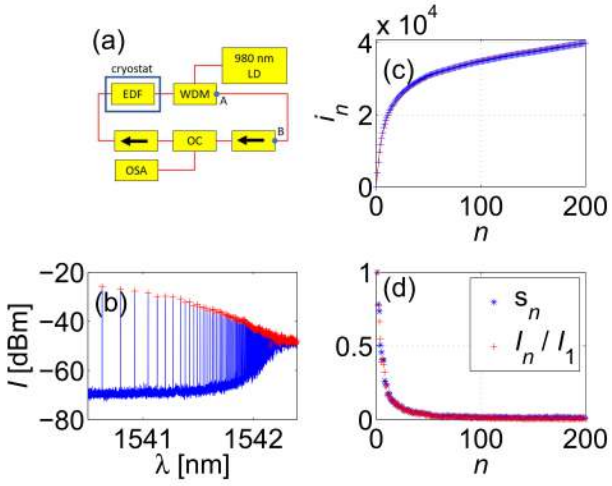
2. Experimental setup

The experimental setup is schematically depicted in Fig. 1(a). EDF having length of 20 m, absorption of 30 dB m^{-1} at 1530 nm, and mode field diameter of 6.5μm at 1550 nm, is cooled down using a cryogen free cryostat. The EDF is thermally coupled to a calibrated silicon diode serving as a thermometer, and it is pumped using a 980 nm laser diode (LD) biased with current denoted by I_{D}. The cold EDF is integrated with a room temperature fiber loop using a wavelength-division multiplexing (WDM) device. Two isolators [labeled by arrows in the sketch shown in Fig. 1(a)] and a 10:90 output coupler (OC) are integrated in the fiber loop. The loop frequency f_{L} (inverse loop period time), which is measured using a radio frequency spectrum analyzer and a photodetector, is given by $f_{\mathrm{L}} = c/(n_{\mathrm{F}} l_{\mathrm{L}}) = 4.963\,\mathrm{MHz}$, where c is the speed of light in vacuum, $n_{\mathrm{F}} = 1.45$ is the fiber refractive index, and $l_{\mathrm{L}} = 41.7\,\mathrm{m}$ is the fiber loop total length. An optical spectrum analyzer (OSA) is connected to the 10:90 OC.

3. USOC

Near wavelength of 1540 nm and below a critical temperature of about 10 K the measured optical spectrum exhibits narrow peaks at a sequence of wavelengths denoted by $\{\lambda_n\}$, where $n = 0, 1, 2, \cdots$ [see Fig. 1(b)]. For the data presented in Fig. 1 $\lambda_0 = 1540.629\,\mathrm{nm}$ and $\lambda_1 - \lambda_0 = 0.1661\,\mathrm{nm}$. The frequency f_n associated with wavelength λ_n is given by $f_n = c/\lambda_n$. The intensity of the USOC peak occurring at wavelength λ_n is denoted by I_n.

The normalized frequency sequence $i_n \equiv (f_0 - f_n)/f_{\mathrm{L}}$, and the normalized intensity sequence $s_n \equiv I_n/I_1$ are



.

Fig. 1. USOC (a) The experimental setup. (b) The measured optical spectrum with diode current $I_{\mathrm{D}} = 120\,\mathrm{mA}$. (c) Comparison between the measured normalized frequencies $i_n = (f_0 - f_n)/f_{\mathrm{L}}$ and the calculated values of $\nu \log p_n$ [see Eq. 1]. The dimensionless pre-factor ν is found by fitting to be given by $\nu = 5610$. (d) Comparison between the normalized intensities I_n/I_1 and the normalized wavelength gaps $(\lambda_{n+1} - \lambda_n)/(\lambda_1 - \lambda_0)$ [see Eq. 2].

well describe by the following empirical laws

$$i_n = \nu \log p_n \,, \tag{1}$$

$$s_n = \frac{\lambda_{n+1} - \lambda_n}{\lambda_1 - \lambda_0} \,, \tag{2}$$

where ν is a positive constant, and p_n is the n'th prime number. The comparison between the measured values of $i_n = (f_0 - f_n)/f_{\mathrm{L}}$ and the calculated values of $\nu \log p_n$ [see Eq. (1)] yields a good agreement [see Fig. 1(c)]. The level of agreement is quantified by the parameter $\varepsilon = n_{\mathrm{m}}^{-1} \sum_{n=1}^{n_{\mathrm{m}}} |(i_n - \nu \log p_n)/i_{n_{\mathrm{m}}}|$, where n_{m} is the number of peaks that can be reliably resolved. For the data shown in Fig. (1) $n_{\mathrm{m}} = 200$ and $\varepsilon = 0.0043$. The comparison between I_n/I_1 and $(\lambda_{n+1} - \lambda_n)/(\lambda_1 - \lambda_0)$ [see Eq. (2)] is shown in Fig. 1(d). The underlying mechanism responsible for USOC formation has remained mainly unknown. The connection between the normalized frequency sequence $i_n = (f_0 - f_n)/f_{\mathrm{L}}$ and the sequence of prime numbers [see Eq. (1)] is discussed in [5].

4. USOC tuning and optical memory

A detailed description of USOC tuning measurements will be given in a forthcoming publication. These measurements demonstrate several methods that allow tuning of the wavelengths at which multimode lasing occurs. The forthcoming publication also reports on measurements of USOC memory time. Future study will focus on systematically characterizing spectral hole burning in the system under study, in order to explore its performance for quantum memory applications.

References

1. S Yamashita and K Hotate, "Multiwavelength erbium-doped fibre laser using intracavity etalon and cooled by liquid nitrogen", *Electronics Letters*, vol. 32, no. 14, pp. 1298–1299, 1996.
2. Haochong Liu, Wei He, Yantao Liu, Yunhui Dong, and Lianqing Zhu, "Erbium-doped fiber laser based on femtosecond laser inscribed fbg through fiber coating for strain sensing in liquid nitrogen environment", *Optical Fiber Technology*, vol. 72, pp. 102988, 2022.
3. J Lopez, H Kerbertt, M Plata, E Hernandez, and S Stepanov, "Two-wave mixing in erbium-doped-fibers with spectral-hole burning at 77k", *Journal of Optics*, vol. 22, no. 8, pp. 085401, 2020.
4. Erhan Saglamyurek, Jeongwan Jin, Varun B Verma, Matthew D Shaw, Francesco Marsili, Sae Woo Nam, Daniel Oblak, and Wolfgang Tittel, "Quantum storage of entangled telecom-wavelength photons in an erbium-doped optical fibre", *Nature Photonics*, vol. 9, no. 2, pp. 83–87, 2015.
5. Eyal Buks, "Low temperature spectrum of a fiber loop laser", *Physics Letters A*, vol. 458, pp. 128591, 2023.

Super-resolution imaging

Analysis of tip-enhanced photoluminescence image of single molecule based on nonlocal response theory

Y. Tomoshige[1*], M. Tamura[1,2], T. Yokoyama[1], and H. Ishihara[1]

[1]Grad. Sch. Eng. Sci., Osaka Univ., Japan
[2]RILACS, Osaka Metro. Univ., Japan
[*]corresponding author: tomoshige.y@opt.mp.es.osaka-u.ac.jp

Abstract: Tip-enhanced photoluminescence (TEPL) can provide the spectroscopic image of photoluminescence with sub-nm resolution and probe the individual state of a single molecule. To discuss the microscopic optical response in the TEPL, we develop a theoretical framework based on nonlocal response theory and input-output theory. We can successfully obtain the photoluminescence intensity map reflecting the spatial distribution of transition dipole with distinguishing the different modes.

Tip-enhanced photoluminescence (TEPL) based on scanning probe microscopy enables to excite a sample locally and obtain an optical image with high resolution. The experiment demonstrated that TEPL could provide sub-nm resolution and the spectroscopic image of a single zinc phthalocyanine based on peak energy and line width of photoluminescence [1]. Imada et al. reported the capability to probe and control the individual state of a single molecule owing to the high space and energy resolution resulting from measuring the photoluminescence spectrum of a single phthalocyanine using a scanning tunneling microscope and tunable laser [2].

In this study, we propose the theoretical framework of TEPL based on the nonlocal response theory and input-output theory [3]. We self-consistently solve the molecular polarization and the electric field enhanced by the probe tip. The molecule is expressed with the nonlocal susceptibility based on the transition dipole of molecule. The electric field is expressed by the Green's function, where the presence of metallic structure is renormalized into the Green's function with the discrete dipole approximation [4]. Compared with the previous study on the theory of TEPL [5], we treat the Green's function with a dependency of frequency, and hence, we can correctly calculate photoluminescence even in the situation where the resonance level of the molecule shifts or splits due to the strong coupling between the gap plasmons sustained at the metal probe tip and the molecule.

Figure 1 shows the schematic model of TEPL calculation. The phthalocyanine molecule was located between the silver probe tip and the silver substrate. We considered the hemisphere with the minute protrusion as the silver probe. The Drude and critical points model was employed as the dielectric function of metal [6]. The transition

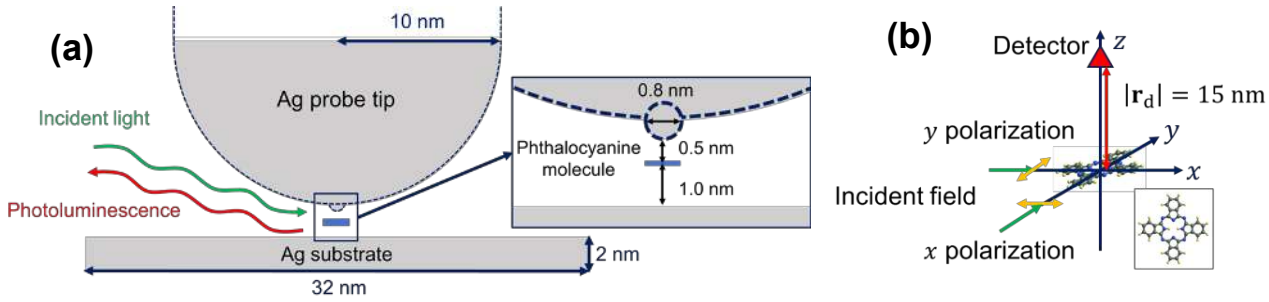


Figure 1 (a) Schematic model of TEPL. The inset shows the area in the vicinity of the protrusion. (b) The geometry of the incident field, the phthalocyanine molecule, and the detector. The inset shows the atomic structure of phthalocyanine.

dipole of the target molecule was obtained from the molecular orbit calculated by GEMASS [7]. We assumed the propagation and polarization direction of incident light for x and y as shown in Figure 1(b). As an elementary calculation at this time, we located the detector with the distance 15 nm from the sample above the tip and detected photoluminescence of the same energy as the incident light. Figure 2 shows a photoluminescence intensity map as a function of the probe tip position for optically allowed transition. Depending on the energy and polarization direction of the incident light, we can obtain the spatial distribution of the transition dipole of the selectively excited molecule. The effect of the nonlocality emerges especially in the case of optically forbidden transition with several nodes inside the molecule.

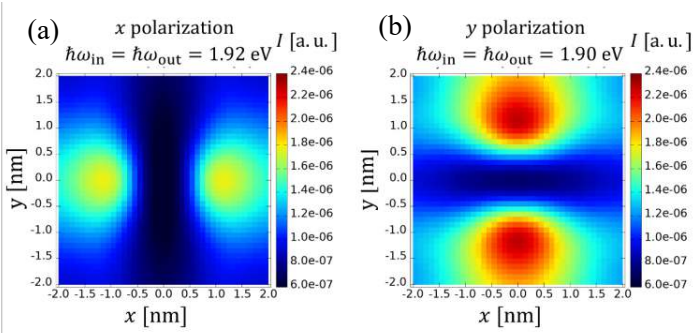


Figure 2 Photoluminescence intensity map in the case of the single molecule selectively excited by the incident field with (a) x and (b) y polarization.

In conclusion, based on the nonlocal response theory, we have constructed the theoretical framework of TEPL, which solved the electric field and the induced polarization of molecule self-consistently. By sweeping the probe tip location, we can successfully obtain the photoluminescence map of the phthalocyanine molecule. The obtained map indicated the selective excitation of molecule depending on the polarization of incident light. The theoretical framework will enable to explorer the physical properties inside of single molecules and contribute to the development of advanced technology of optical microscopy.

Acknowledgments: This work was supported by JSPS KAKENHI (Grant Numbers JP16H06504, JP21H05019, JP20K15196), JST-Mirai Program (Grant Numbers JPMJMI18GA and JPMJMI21G1), JST CREST (Grant Number JPMJCR1903), and JST SPRING (Grant Number JPMJSP2138).

References

1. Yang, B., Chen, G., Ghafoor, A. *et. al.*, "Sub-nanometre resolution in single-molecule photoluminescence imaging," Nature Photonics 14, 693, 2020.
2. Imada, H., Imai-Imada, M., Miwa, K. *et. al.*, "Single-molecule laser nanospectroscopywith micro–electron volt energy resolution," Science 373, 95, 2021.
3. Matsuda, T., Yokoshi, N., and Ishihara, H., "Upconverted photoluminescence induced by radiative coupling between excitons," Physical Review B 93, 155418, 2016.
4. Hoshina, M., Yokoshi, N., Okamoto, H., and Ishihara, H., "Super-Resolution Trapping: A Nanoparticle Manipulation Using Nonlinear Optical Response," ACS Photonics 5, 318, 2018.
5. Lyu, S., Zhang, Y., Zhang, Y., Chang, K., Zheng, G., and Wang, L., "Picocavity-Controlled Subnanometer-Resolved Single-Molecule Fluorescence Imaging and Mollow Triplets," The Journal of Physical Chemistry C 126, 11129, 2022.
6. Barchiesi, D. and Grosges T. "Fitting the optical constants of gold, silver, chromium, titanium, and aluminum in the visible bandwidth" Journal of Nanophotonics, 8, 083097, 2014.
7. Schmidt, M. W., Baldridge, K. K., Boatz, J. A. *et. al.*, "General atomic and molecular electronic structure system", The Journal of Computational Chemistry, 14, 1347-1363, 1993

META 2023, PARIS - FRANCE, JULY 18 – 21, 2023

Terahertz virtual superlens via evanescent amplification in the radiating near-field

Alessandro Tuniz[1] **and Boris T. Kuhlmey**[1]

[1] The University of Sydney, School of Physics and Institute of Photonics and Optical Science, Camperdown, Australia

*corresponding author: alessandro.tuniz@sydney.edu.au

Abstract: We present a universal method for amplifying evanescent waves in the radiating near field, reconstructing sub-wavelength images akin to a virtual superlens. We quantify the trade-off between noise and measurement distance, and demonstrate complex image reconstruction down to λ/7 with amplitude signal-to-noise ratios below 25 dB between 0.18-1.5 THz. Our procedure applies to any near field probe, greatly relaxes experimental requirements for subwavelength imaging at sub-optical frequencies, and opens the door to non-perturbing near-field scanning.

Although imaging objects with sub-wavelength resolution is now common in the visible spectrum, it is experimentally challenging to do so at lower frequencies (GHz, THz), where it is most needed due to the large wavelengths used [1], and where a tip or antenna are typically brought into very close vicinity to the object in order to measure evanescent waves with high spatial frequencies. This can often be problematic, because the probe can perturb the near-field distribution itself. We show that the information encoded in evanescent waves can be probed much further than previously thought, as minute modulations in the signal, so that a near-field image can be obtained through suitable amplification of evanescent waves - akin to a virtual "superlens" [2]. Figure 1 shows a schematic of our approach: we image a planar source object with subwavelength field E_{obj}. Propagating waves (Fig. 1, dashed) carry information via $E \propto e(i\mathbf{k}\cdot\mathbf{r})$, where $k_z = (k_0^2 - k_x^2 - k_y^2)^{1/2}$ emerging from spatial frequencies satisfying $k_x^2 + k_y^2 < k_0^2$, imposing a lower limit on the features *d* which can be resolved in the far field. Evanescent waves carry spatial frequencies satisfying $k_x^2 + k_y^2 > k_0^2$ but exponentially decay in free space. We reverse this process via the transformation (x, y, z) → (-x, -y, -z) over a subsequent length *L*, numerically reversing the phase accumulated by the propagating waves and amplifying the evanescent waves. Figure 1(b) shows a photograph of the experiment, and Figure 1(c) shows a microscope image of the terahertz probe used. A moveable, fiber-coupled near-field (NF) detector [3] module enables the measurement of the electric field at the output of the laser-machined samples that spell the letters "THZ". The near-field is spatio-temporally resolved at every point via a raster scan, and is frequency resolved through Fourier transform.

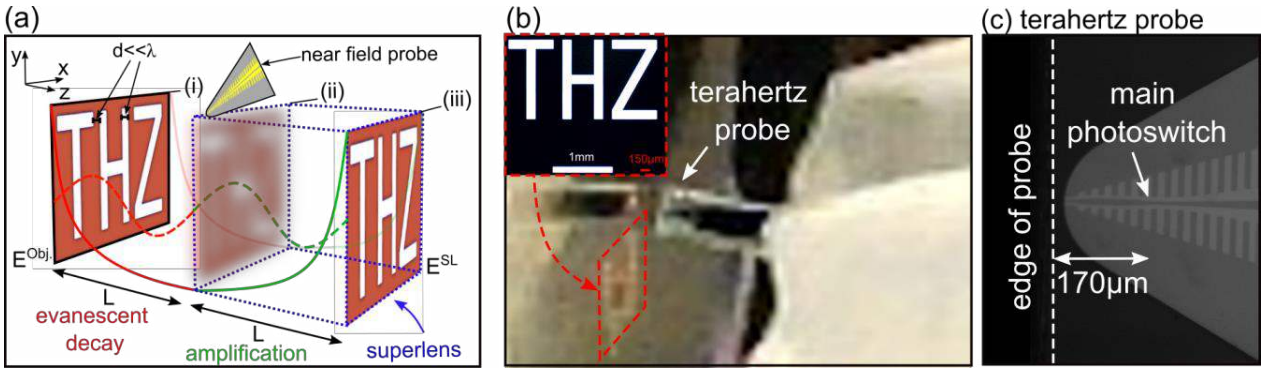


Figure 1. (a) Concept schematic of virtual superlens. (i) Sub-wavelength features are carried by evanescent waves which exponentially decay over L (red). (ii) The lower-resolution image is detected by a near field probe. The evanescent fields are then numerically amplified over L (green), leading to (iii) the original image, analogously to a superlens (blue). (b) Photograph of the near-field terahertz probe as it scans the surface of the sample. (e) Microscope image of the near-field terahertz probe, showing the location of its main photoswitch, which is at a nominal distance of 170 μm from the edge of the probe.

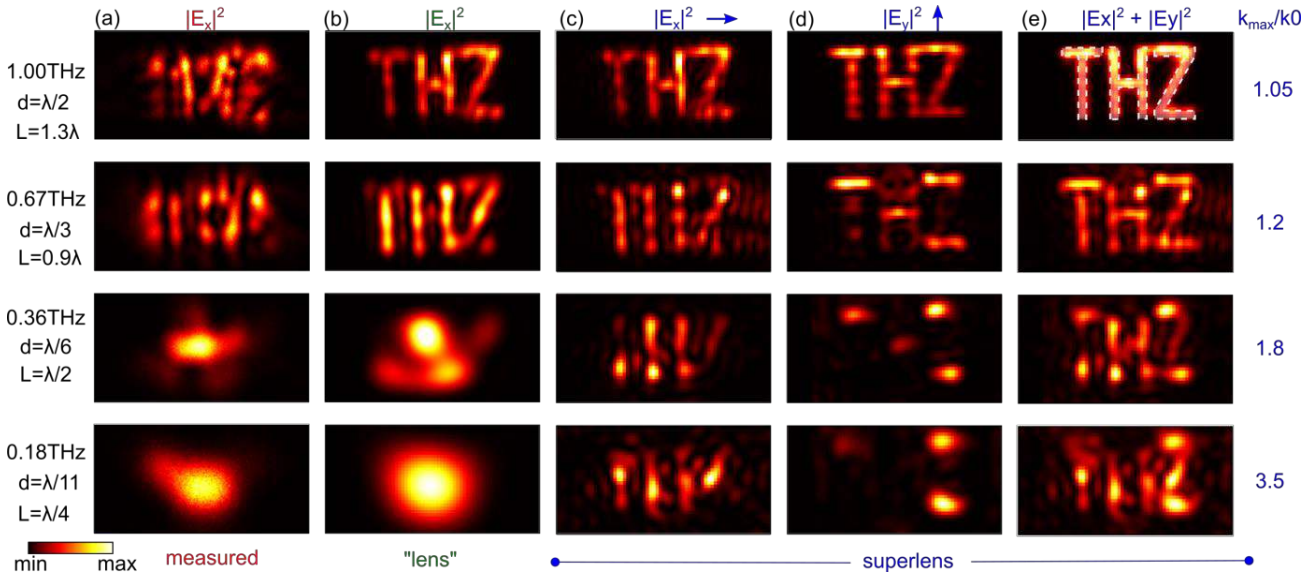


Figure 2. Superlens experiment, imaging the letters "THZ" (feature size: 150μm; detector distance: L = 440μm). (a) Raw measured $|E_x|^2$ at different frequencies labelled, with associated *d* and *L* in terms of λ. (b) Corresponding field after the superlens with maximum $k_{max} = k_0$ and (c) when $k_{max} > k_0$. (d) Reconstructed images using measured x- and y- polarized fields in (c),(d). k_{max}/k_0 for each row is shown on the right. Window area: 4mm × 2mm.

The gain applied to evanescent waves increases with spatial frequency, and is eventually dominated by noise. By equating the signal-to-noise ratio SNR with the amplification factor $\exp(k_z L)$ for a signal measured at a distance L, we obtain the maximum useful spatial frequency $k_{max}=k_0(1+\lambda/L\ \log 10/20\pi\ SNR)$ [4], which we use as a low-pass cut-off. We implement our procedure on a complex, large-area image formed by a laser-written metal sheet containing the letters "THZ" (minimum feature size: d=150μm; L = 440μm; SNR=15-25 dB, and k_{max}/k = 1-3.5) between 0.2-1 THz. Figure 2(a) shows the measured $|E_x|^2$ at different frequencies as labelled. Figure 2(b) shows the field after reversing the phase at different frequencies with $k_{max}=k_0$, i.e., conventional lens imaging. At 1.0THz (the diffraction limit) the letters can be discerned; at 0.67 THz, only the vertical features are resolved; lower frequencies do not provide a sufficiently sharp image to discern the finer features of the original image, with only a single large spot occurring at 0.18 THz. Figure 2(c) shows the corresponding retrieved intensity at different frequencies with k_{max}/k_0 as labelled in blue: vertical features are significantly sharpened. Note that horizontal features do not let E_x through. We repeat the above procedure for a polarization oriented in *y*, and plot the corresponding $|E_y|^2$ in Fig. 2(d) to resolve the horizontal features of each letter. The full image is obtained by summing the two contributions $|E_x|^2 + |E_y|^2$, shown in Fig. 2(e), revealing the letters "THZ" at all frequencies, down to λ/7. Our approach can be adapted to suit any near field experiment which measures amplitude and phase, immediately providing a pathway for increasing the imaging resolution of near field setups at any frequency.

Acknowledgements: ARC Discovery Early Career Researcher Award (DE200101041). ANFF (NSW).

References

1. A. J. L. Adam. "Review of near-field THz measurement methods and their applications" J. Infrared Milli. Terahz. Waves. **32** 976-1019 (2011).
2. J. Pendry, "Negative refraction makes a perfect lens", Phys. Rev. Lett. **85**, 3966 (2000)
3. A.Stefani et al."Flexible terahertz photonic light-cage modules for in-core sensing and high temperature applications."ACS Photonics **9** 2128 (2022).
4. A. Tuniz and B. T. Kuhlmey, " Subwavelength terahertz imaging via virtual superlensing in the radiating near field" arXiv:2211.11205 (2022)

Acoustic and seismic metamaterials

Sound insulation performance of ventilated labyrinthine metamaterial described by enriched homogenized continuum

Renan Liupekevicius, Hans van Dommelen, Marc Geers, and Varvara Kouznetsova
Eindhoven University of Technology, Netherlands
R.liupekevicius.carnielli@tue.nl, J.A.W.v.Dommelen@tue.nl, M.G.D.Geers@tue.nl, V.G.Kouznetsova@tue.nl

Abstract: Labyrinthine structures that increase the wave-path length can be used as an acoustic liner to attenuate sound in ducts while allowing net air flow. In this study, the performance of ventilated labyrinthine metamaterials is assessed utilizing a homogenized equivalent fluid continuum. The effective domain is a more computationally efficient way to compute the pressure field compared to direct numerical simulation thanks to a coarser mesh.

By coiling up the space, labyrinthine metamaterials are capable of interacting with large wavelengths compared to their unit cell size, in the so-called subwavelength regime. This attribute permits reducing the devices' dimensions, which is beneficial from a practical point of view considering they usually have to be integrated into larger engineering components. Ventilated sound silencers are one potential application of these metamaterials as demonstrated in [1], both attenuating sound and allowing airflow.

As the 3D printing resolution improves, fine-structured metamaterials can be created in non-trivial geometries and for large structures to explore designs with optimal sound attenuation. However, such engineered metamaterials pose computational problems because they tend to explode in the number of degrees of freedom that are needed to resolve the fine microstructure. Moreover, the processes at the microstructural level, such as coiling-up space and resonances, lead to a large-scale acoustic wave dispersion, giving rise to a multiscale phenomenon.

In this contribution, we develop a transient computational homogenization framework that gives rise to an enriched equivalent fluid continuum with additional field variables to capture the underlying localized resonances. Extending the approach proposed in [2] to quiescent fluid domains, the coupling between the scales is given by a variationally consistent averaging of the governing equations expressed in their weak form, i.e. a generalization of the Hill-Mandel condition. Numerical examples demonstrate the efficiency and suitability of the proposed two-scale approach paving the way to more affordable time-domain simulations of acoustic liners.

References

1. Chen, A., Zhao, X., Yang, Z., Anderson, S. and Zhang, X., 2022. "Broadband Labyrinthine Acoustic Insulator". *Phys. Rev. Appl.*, 18(6), p.064057.
2. Sridhar, A., Kouznetsova, V.G. and Geers, M.G., 2016. "Homogenization of locally resonant acoustic metamaterials towards an emergent enriched continuum". *Comput. Mech.*, 57, pp.423-435.

Reflection of ultrasound by underwater phase-gradient acoustic metasurfaces

J.-C. Hsu[1*], H. Alwi[1], K.-L. Liao[1], and J.-T. Huang[1]

[1]Department of Mechanical Engineering, National Yunlin University of Science and Technology, Taiwan
[*]corresponding author: hsujc@yuntech.edu.tw

Abstract: We numerically and experimentally study anomalous reflection of underwater ultrasound by phase-gradient acoustic metasurfaces. We conduct finite-element calculations to design the metasurfaces for desired phase gradient and simulate the reflected wave fields. The results exhibit anomalous reflection. We fabricate the metasurfaces with sub-mm meta-atoms and conduct pulsed ultrasound experiments to measure the azimuth distributions of the reflected waves. The experimental results agree well with the numerical results, confirming that anomalous reflection of underwater ultrasound can be achieved by the metasurfaces.

In the past decade, a family of two-dimensional artificial materials called acoustic metasurfaces has been quickly emerging. The acoustic metasurfaces enables manipulating acoustic waves in nonconventional ways by introducing the generalized Snell's law. Capability of tailoring efficient and diverse interfacial acoustic-structure interactions makes acoustic metasurfaces especially suitable to manipulate sound wave in air and water [1]. In this paper, we show underwater acoustic metasurfaces operating in the high frequency regime. Slit structures are utilized as the meta-atoms. We reveal the wave-steering features of ultrasound by the acoustic metasurfaces. We focus our study on the underwater reflection behaviors of the gradient-type metasurfaces. To validate the underwater acoustic metasurfaces working at 0.5 MHz, pulsed ultrasound experiments are conducted. However, well control of the phase change along the metasurface requires a dense array of fine meta-atoms. Therefore, we employed wire electrical-discharged cutting to fabricated the slit meta-atoms in the sub-mm scale.

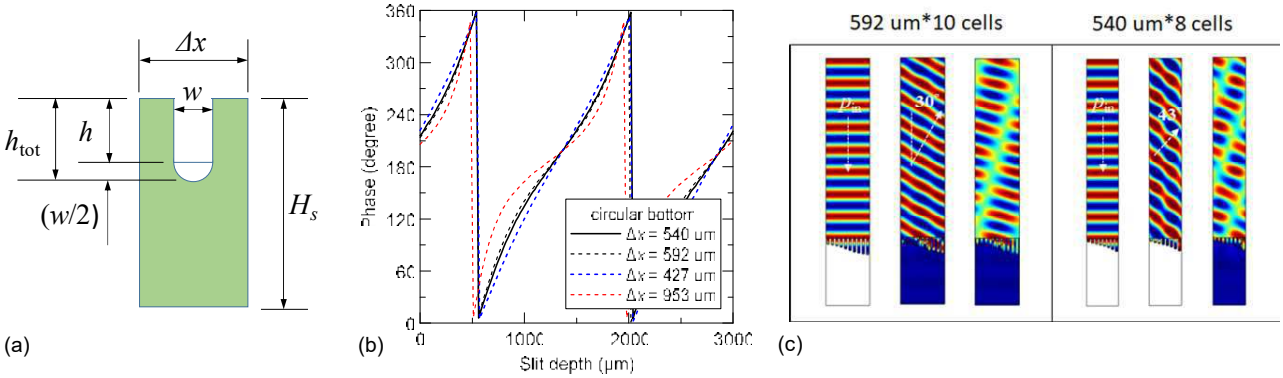


Figure 1 (a) Meta-atom. (b) Phase variation as a function of slit depth. (c) Simulated fields of designs I and II.

The meta-atom is made of stainless steel and has a circular-bottom slit of width w and depth h (Fig. 1(a)). Finite-element (FE) method is applied to design the acoustic metasurfaces and to simulate the propagation of the ultrasound in the system. We implement the numerical calculations using the commercial FE solver package COMSOL Multiphysics. Figure 1(b) shows the calculated reflected phase variation as a function of the slit depth, where the slit width w = 360 μm. To consider the influence of phase gradient, we build two different supercells (designs I and II) using the meta-atoms of a = 592 and 540 μm by following the strategy of engineering the phase profile to produce anomalous reflection with reflected angles of 30° and 43°, respectively. The calculated

normally incident, reflected, and total fields are shown in Fig. 1(c).

Figure 2 shows the full-wave results of plane-wave beam incident on the underwater metasurface. The used sound pressure beam width is 25 mm, which is about 8.4 times of the wavelength, covering about 42 and 46 unit cells of the design structures (corresponding to about 4.2 and 5.75 supercells). It can be observed from the results that reflected sound pressure beams with reflection angles of 30° and 43°are successfully generated, respectively. In addition to the sound pressure reflected back into the water, part of the sound wave energy penetrates into the material of the metasurface. Since the incident sound pressure is in the normal direction, it can be seen that the elastic wave penetrating into the solid mainly enters the steel solid in the form of bulk waves. Formation of the interface-coupled evanescent wave propagating to the left and right sides of the interface is not obvious.

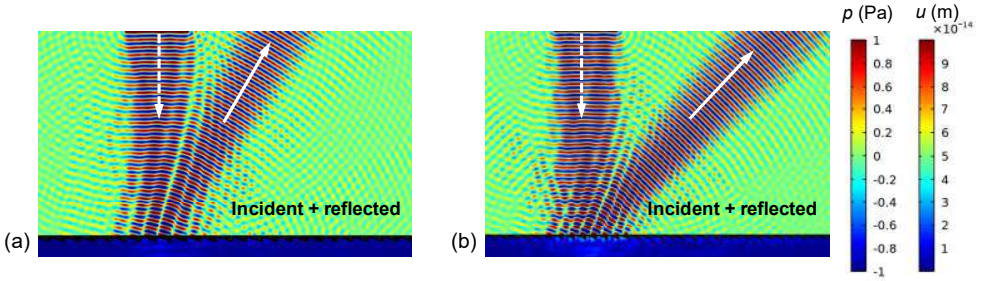


Figure 2 Full-wave results of plane waves incident on the underwater metasurface for designs I (a) and II (b).

In the experiments, we send ultrasound pulses and detect the ultrasound signals reflected by the underwater gradient metasurface in a water tank. Two identical immersion ultrasonic transducers of center frequency 0.5 MHz are properly positioned and oriented to emit and receive the ultrasound signals. A pulser-receiver is used to generates a high electric voltage pulse to be sent to the emitting transducer to excite the ultrasound pulse. The ultrasound pulse impinges on the underwater metasurface, and the reflected signal is detected by the receiving transducer and recorded by a digital oscilloscope. Figure 3 compares the calculation and measurement results of the azimuth distributions of the underwater ultrasonic reflection wave intensity. Briefly, the results of simulation and experiment show good agreement, which demonstrate that the designed and fabricated acoustic metasurface successfully produces the anomalous reflection of underwater ultrasonic waves.

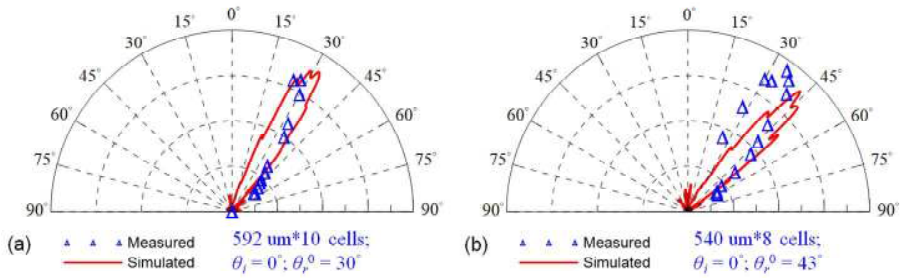


Figure 3 The azimuth distributions of the underwater ultrasonic wave intensity reflected by the metasurfaces.

This work was supported by the National Science and Technology Council, Taiwan (109-2221-E-224-004).

References

1. Assouar, B., Liang, B., Wu, Y., Li, Y., Cheng, J. C, and Jing, Y. (2018), “Acoustic metasurfaces,” Nat. Rev. Materi., Vol. 3, 460–472, 2018.

Acoustic anechoic coatings based on flexible honeycomb corrugated composite sandwich panel

Janghao Wu[1], Debao Ji[1], Yu Xie[1], Junyi Wang[1], Jiaming Hu[1], Yun Chen1[1*]

[1] State Key Laboratory of Application Specific Integrated Circuits (ASIC) and System, Department of Microelectronics, Fudan University, Shanghai, China

[*]corresponding author: chenyun@fudan.edu.cn

Abstract: The absorption of underwater acoustic waves and vibrations is of great importance for underwater applications. In this work, we propose a well-performance acoustic anechoic coating by adopting the perforated honeycomb-corrugation hybrid (PHCH) sandwich panels consisting of aluminum and rubber. The composite structure possesses a high absorption coefficient of the low-frequency acoustic wave under an oblique incidence range. With well pressure resistance ability, the structure has been used in the design and experiment of our underwater detection system.

With the constant consumption of resources, the exploration and utilization of marine resources have become one the important development directions, and various exploration vessels and underwater detectors have been widely used. However, the acoustic environment is also more complex due to the low-frequency mechanical noise or propeller noise from these growing ships. Therefore, it is necessary to explore the acoustic anechoic coating that is more suitable for the current working conditions. Since the invention of the PHCH structure[1], it has attracted attention from numerous fields. However, there has been a relative lack of research on underwater PHCH structures for oblique incidence conditions. Here, based on our previous study of PHCH structure[2], we demonstrate a novel composite PHCH structure for underwater low-frequency acoustic anechoic coatings and show its application in our underwater detector design and experiment.

As shown in Figure 1a, It consists of two perforated panels sandwiching a honeycomb-corrugation rectangular core. The top panel is perforated with micro-holes as MPPs, while the bottom panel is a sealed backing panel for sound reflection. The micro-holes are cylindrical and distributed above every cavity in the center, so the water from above the MPPs can fill in the cavities through the micro-holes. And details of the 2-D modal are shown in Figure 1b, the composite structure consists of two different materials, the green parts and the orange parts are set as rubber, while the partition boards are aluminum. This composite design preserves the sound absorption ability of the rubber for low-frequency sound, while the introduction of aluminum increases the pressure resistance of the overall structure.

We use COMSOL Multiphysics 5.6 to operate the finite element method(FEM) and run the numerical simulation. The result is shown in figure 1c, the main absorption peak frequency is about 500Hz with an absorption band of about 775Hz. The Vibration of perforated rubber plates contributes significantly to low-frequency sound absorption, thus greatly reducing the mismatch of acoustic impedance. under oblique incidence, the sound absorption coefficient of composite structures increases with the increase of angle in frequency range <200Hz but decreases slightly in frequency range >300Hz. The spectrum proves that the composite structure is a proper omnidirectional underwater sound absorber. Rubber is known as a non-resistant material to pressure, while, on the contrary, aluminum is considered a more rigid material. The aluminum partition boards support the whole structure from the lateral side and restrict deformation. As a result, while inheriting the pressure resistance of the PHCH structure, the composite structure ensures that the rubber parts are only slightly deformed, improving the ability of sound absorption[3].

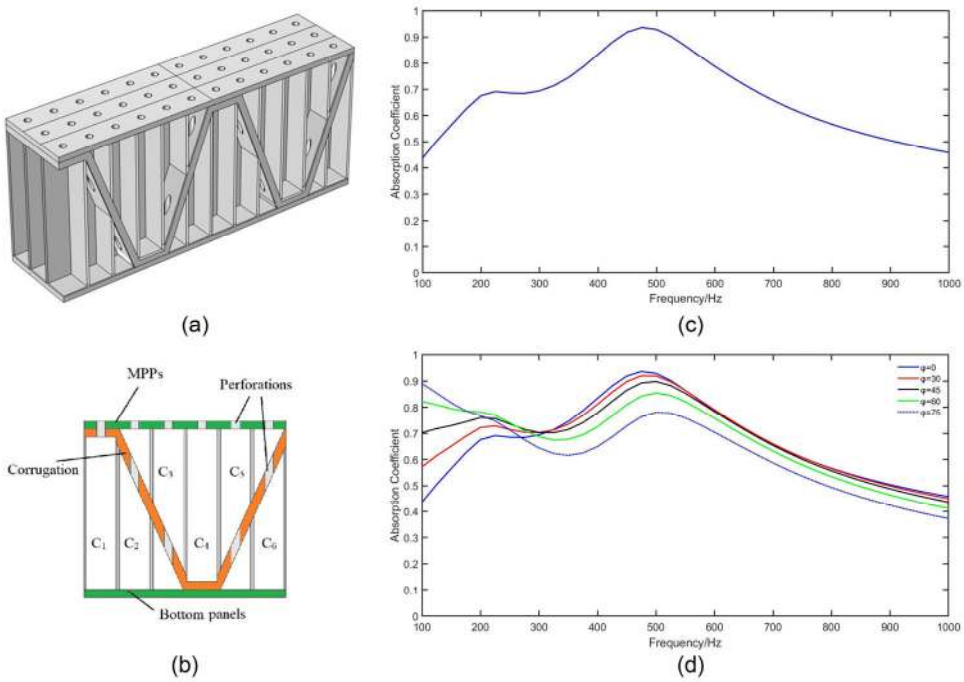


Figure 1: a) The geometry of the underwater PHCH structure. b) Details of the 2-D modal. c) Sound absorption coefficient of the composite structure underwater. d) Sound absorption coefficient under oblique incidence.

Based on the above characteristics, this composite structure has been used in the design and experiment of the underwater detection system. As the acoustic anechoic coating of the detector, it shows good resistance to compression, transverse deformation, and the generally good ability of sound absorption at different angles of incidence. Meanwhile, as the inner wall coating of the experimental water tank, the structure makes it possible to provide a relatively pure acoustic environment in the detector test. Therefore, it is more convenient to evaluate and contrast the performance of the detection system under different operating conditions. In addition, due to its deep subwavelength geometric design, this composite structure is expected to be more widely used as a lightweight and small-scale practical sound-absorbing material in other fields.

Acknowledgement

This work has received financial support from the National Natural Science Foundation of China under Grant 61774049, the National Key R&D Program of China under No.2019YFE0120700, and from Shanghai Municipal Commission of Economy and Informatization under Grant PKX2020-D10.

References

1. Tang Y, Li F, Xin F, et al. Heterogeneously perforated honeycomb-corrugation hybrid sandwich panel as sound absorber[J]. Materials & Design, 2017, 134: 502-512.
2. Hu J, Wang J, Xie Y, et al. Finite Element Analysis on Acoustic and Mechanical Performance of Flexible Perforated Honeycomb-Corrugation Hybrid Sandwich Panel[J]. Shock and Vibration, 2021, 2021: 1-14.
3. Wang J, Hu J, Chen Y. A composite perforated partitioned sandwich panel with corrugation for underwater low-frequency sound absorption[J]. Frontiers in Mechanical Engineering, 2021, 7: 679656.

Metamaterial Based Miniaturized Broad Band Acoustic Absorber

Santosh Dasila[1*], V Subramanian[1], and C V Krishnamurthy[2]

[1]Microwave Laboratory, Indian Institute of Technology, Madras, Chennai, India

[2] Indian Institute of Technology, Madras, Chennai, India

[*]corresponding author: santosh039@physics.iitm.ac.in

Abstract: A miniaturized, broadband (800 Hz - 5000 Hz) absorber with > 95% absorption is proposed and realized. The absorber is designed using quarter-wavelength resonator tubes coiled as a rectangular "meta-atom". The study describes the basic theoretical aspects of the absorber and compares it with the numerical simulations, fabrication, and experimental validation. The meta-atom, simple in design and made with fabrication-friendly materials, can provide greater spatial coverage through tiling over large surfaces.

Acoustic absorbers are essential for industrial and commercial applications that need to avoid noise pollution. In this work, we present an innovative structure based on a quarter wavelength resonator. Several air-filled quarter-wave resonators are arranged in parallel to achieve high absorption for a wide range of low-frequency sound. Numerous works have been reported on the resonator [1-5]. However, the unique structure and compact size with high absorption properties make it more applicable and cost-efficient. These resonator tubes show very high absorption at their resonance frequency. Since the absorption at resonance frequency is very sharp, a parallel arrangement of these tubes gives perfect absorption for a wide frequency range. The absorption coefficient is calculated using the formula given in Eq. (1)

$$\alpha = 1 - \left|\frac{Z_c/\phi - Z_0}{Z_c/\phi - Z_0}\right|^2 \quad (1)$$

Where Z_{eq} is the equivalent specific acoustic impedance can be obtained by using Eq. (2)

$$Z_{eq} = 1/\sum_{i=1}^{n} \frac{1}{Z_i} \quad (2)$$

(a) (b)

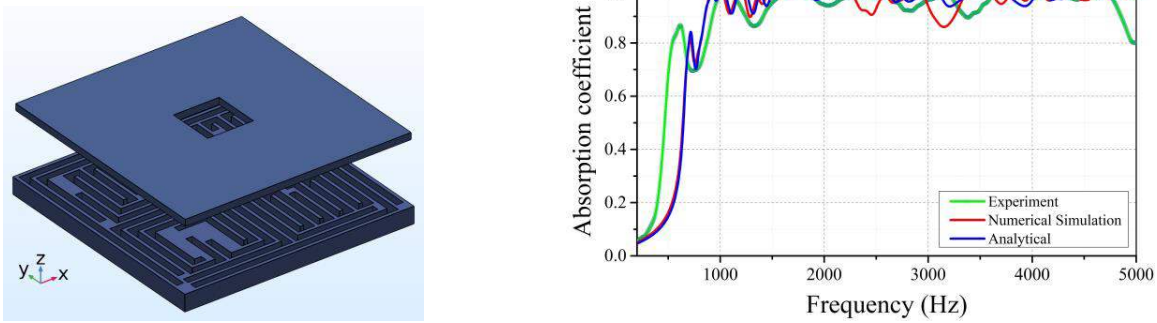


Figure 1: (a) Design of the unit cell of an acoustic metamaterial consisting of 20 resonant channels. (b) Absorption vs. frequency plot. The experimental results compare with the analytical and numerical results.

Highlights

- A unique and compact size sub-wavelength structure is proposed.
- The unit structure has a dimension of 70× 70× 8 mm^3.
- The lowest cutoff frequency (resonance frequency) is obtained at around 700Hz, decided by the longest tube in the structure.
- This 10 mm thick (including front and back penal) structure gives a very high absorption (more than 95%) spectrum for a wide range of frequencies (800 to 5000Hz).
- The experiment result is compared with theoretical and numerical outcomes. The agreement between experimental, numerical, and theoretical outcomes matches well.

References

1. Yang, Min, et al. "Optimal sound-absorbing structures." Materials Horizons 4.4 (2017): 673-680.

2. Y. Wang, H. Zhao, H. Yang, J. Zhong, J. Wen, A space-coiled acoustic metamaterial with tuneable low-frequency sound absorption, EPL (Europhysics Letters) 120 (5) (2018) 54001.

3. C. Chen, Z. Du, G. Hu, J. Yang, A low-frequency sound absorbing material with subwavelength thickness, Applied Physics Letters 110 (22) (2017) 221903.

4. H. Ryoo, W. Jeon, Perfect sound absorption of ultra-thin metasurface based on hybrid resonance and space-coiling, Applied Physics Letters 113 (12) (2018) 121903.

5. Zhang, Chi, and Xinhua Hu. "Three-dimensional single-port labyrinthine acoustic metamaterial: Perfect absorption with large bandwidth and tunability." Physical Review Applied 6.6 (2016): 064025.

Scattering of acoustic valley Hall modes through different turns

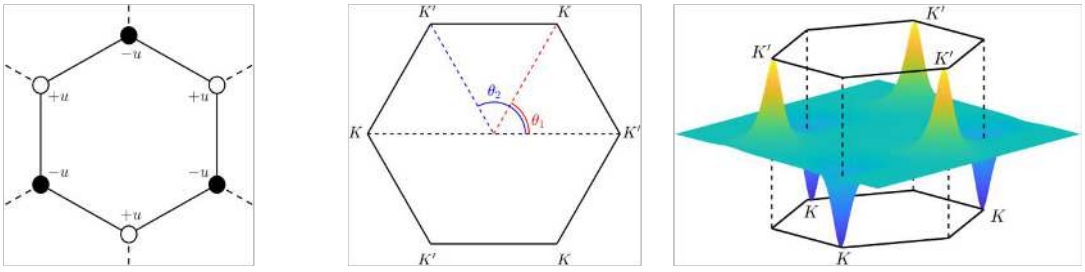
T. Torres[1*], A. Coutant[1], C. Bellis[1] and R. Cottereau[1]

[1]Aix Marseille Univ, CNRS, Centrale Marseille, LMA, Marseille, France
[*]Corresponding author: torres@lma.cnrs-mrs.fr

Abstract: This work studies the propagation of valley Hall modes through turns of different angles in a discrete model. The main goal of our study is the quantitative analysis of the transmission and reflection coefficients through different turns, and to relate our results with the topological argument of valley conservation which predicts high transmission for specific angles. Using the transfer matrix method, we solve the problem semi-analytically and reveal that some angles allow for a rich variety of scattering possibilities.

Two-dimensional topological insulators allow for the possibility to guide waves in a media without backreaction. Prime examples include the quantum Hall effect, where the perfect transmission is assured by the breaking of time-reversal symmetry, and the quantum spin Hall effect where the properties of the spin guarantee the modes' immunity to backscattering. The development of metamaterials opened the doors for the realization of two-dimensional topological insulators in a broad class of systems from mechanical to optical to acoustics system. However, for classical waves in such platforms, the protection of topological modes to backscattering relies on weaker mechanisms which implies that in most scattering scenarios some reflection will be present. While topological arguments might explain the quantitative behavior of the reflection, they are insufficient to quantitatively characterize the scattering in these cases, which remains an open question [1].

In this work, we focus on the quantitative analysis of the scattering of a type of topological modes in a metamaterial, namely valley Hall states realized in a graphene ribbon with zigzag edges. Our ribbon is composed of two regions of graphene with opposite on-site potential which opens a gap in the band structure. At the interface of these two regions, and in the bulk gap, a pair of topological modes exists. The modes propagate in opposite directions and carry with them a conserved valley index [2]. The graphene bulk structure on one side of the interface and the associated Brillouin zone are depicted in Fig.1a) and b) respectively. Fig.1c) shows the Berry curvature whose sign, different in each valley K and K', defines the valley index.



a) Graphene bulk structure b) Brillouin zone c) Berry curvature

Figure 1: Graphene structure and valleys. Panel a) shows the bulk graphene structure. Panel b) shows the Brillouin zone and the inequivalent Dirac point K and K'. Panel c) shows the Berry curvature, taking different signs in the two valleys.

Conservation of valley index suggests that scattering in certain direction are to be privileged. A scattering through an angle of $\pi/3$ changes the valley index while an angle of $2\pi/3$ conserves it, while backscattering also changes the valley index, see Fig. 1b). The topological argument therefore suggests that scattering through an angle of $2\pi/3$ will lead to high transmission but cannot illuminate the situation in the case of a $\pi/3$ angle.

Using the transfer matrix formalism [3], we solve semi-analytically the problem of the scattering of a valley mode through a $\pi/3$ and compute numerically the reflection and transmission coefficients. We show that this situation allows for a broad range of scattering possibilities and that an incoming interface mode can be transmitted with little backscattering, completely reflected or transmission to edge modes, depending on the energy range considered. Those three cases are represented in Fig.2 b), c) and d) respectively. We show that the qualitative behavior can be understood solely from the properties of the dispersion relation. A quantitative analysis is performed, and we compare the backscattering in this situation and with the case of an angle of $2\pi/3$.

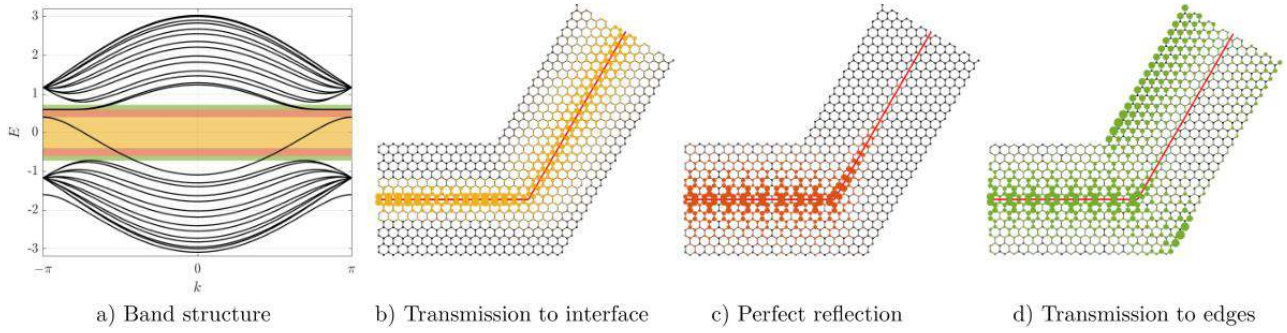


Figure 2: Band structure of graphene ribbon with bridge interface and scattering scenarios. Panel a) shows the band structure, revealing the topological band in the bulk gap. Panel b), c) and d) show the conversion through an angle of $\pi/3$ of a valley Hall mode coming from the left to another interface mode, evanescent modes and edge modes respectively.

Our results indicate that high transmission can be obtained even in cases where the scatterer changes the valley index. Our calculations are performed in a discrete model which while being simple remains general and can be applied to a variety of continuous systems. For example, our model can be seen as a tight-binding approximation or as a particular limit of an acoustic network [4]. We therefore believe that information about more general systems can be learned from our study, and we hope to trigger generalization of our results in continuous systems.

References

1. Orazbayec, B and Fleury, R. "Quantitative robustness analysis of topological edge modes in C6 and valley-Hall metamaterial waveguides," Nanophotonics, 8(8), 1433-1441, 2019.
2. Morpurgo, A. F. and Guinea, F. "Intervalley scattering, long-range disorder, and effective time reversal symmetry breaking in graphene", Phys. Rev. Lett. 97, 196804, 2006.
3. V. Dwivedi and V. Chua, "Of bulk and boundaries: Generalized transfer matrices for tight-binding models," Phys. Rev. B 93 no. 13, 134304, 2016.
4. Coutant, A., Sivadon, A., Zheng, L., Achilleos, V., Richoux, O., Theocharis, G., & Pagneux, V. "Acoustic Su-Schrieffer-Heeger lattice: Direct mapping of acoustic waveguides to the Su-Schrieffer-Heeger model". *Physical Review B*, *103*(22), 224309, 2021.

Superradiant Scattering from Nonlinear Wave-Mode Coupling

T. Pedergnana[1*] and N. Noiray[1*]

[1] CAPS Laboratory, Department of Mechanical and Process Engineering, ETH Zürich, 8092 Zürich, Switzerland
[*]corresponding authors: ptiemo@ethz.ch and noirayn@ethz.ch

Abstract: When waves are scattered at a resonant cavity, due to dissipation, the outgoing waves' energy is decreased compared to the incident waves. This limitation can be overcome if waves are instead scattered at a linearly unstable mode undergoing a limit cycle. Near the mode's eigenfrequency, synchronized self-oscillations feed energy to the outgoing waves, leading to superradiance, or amplification of incident harmonic waves. We derive a multiphysical theory of nonlinear wave-mode coupling and experimentally validate it on a superradiant aeroacoustic scatterer.

In this work, we show that waves scattered at a self-oscillating mode can exhibit superradiance. This exotic behavior, which arises from nonlinear coupling of the mode to the incident waves, is manifested by an amplification of an incident harmonic wave. On the theoretical side, we propose a generic, multiphysical theory of nonlinear mode-coupling, which is derived in analogy to the temporal coupled-mode theory of Fan et al.[1] Using the Moore-Penrose pseudoinverse, the scattering matrix can be explicitly expressed in terms of the incident and outgoing waves as

$$S = \frac{|s_{out}\rangle\langle s_{in}|}{\langle s_{in}|s_{in}\rangle}. \qquad (1)$$

The equations governing the nonlinear wave-mode coupling are shown in Fig. 1. Through the nonlinear term in the modal equation, the scattering matrix becomes dependent on the incident wave amplitude s_{in}. Theoretical predictions of the scattering matrix are shown in Fig. 2.

On the experimental side, a well-reproducible aeroacoustic realization of a superradiant scatterer was used to test the theory's predictions. The self-oscillating mode was achieved by subjecting a side cavity to a low-Mach mean flow, leading to a whistling phenomenon involving a purely acoustic longitudinal mode of the cavity.[2] Acoustic waves are sent from compression drivers located upstream and downstream of the cavity to obtain the scattering matrix. Repeated experiments on this carefully designed and characterized set-up demonstrate outstanding qualitative agreement between theory and experiment (see Fig. 3).

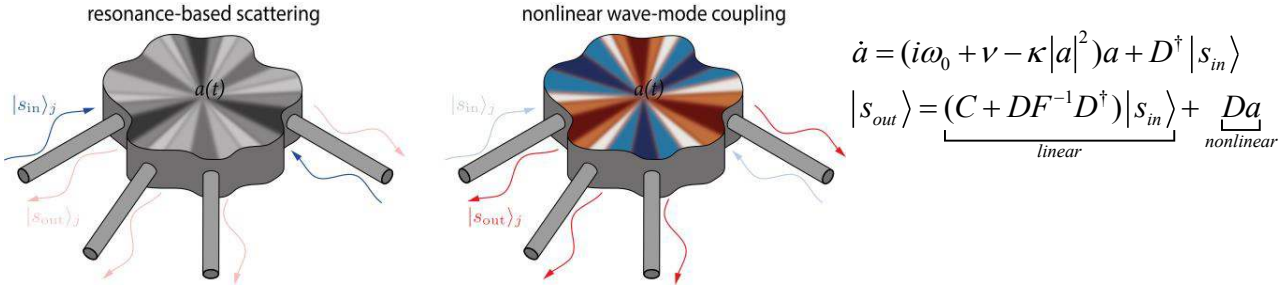


Figure 1. Left inset: In a classic resonant cavity, the energy of the incident waves always exceeds that of the outgoing waves. We show in this work that this limitation can be overcome by scattering waves at a self-oscillating mode, leading to nonlinear wave-mode coupling. Right inset: Equations describing the nonlinear wave-mode coupling.

We envision that the quasi-passive realization of superradiance presented in this work will find application in flow-based acoustic metamaterials and topological insulators, which often suffer from dissipation losses. Furthermore, the proposed theory can model a wide variety of nonlinear scattering problems and may be used in the future to develop novel non-acoustic lossless scatterers and metamaterials by exploiting the energy supplied by a self-oscillating mode.

This project is funded by the Swiss National Science Foundation under Grant agreement 184617.

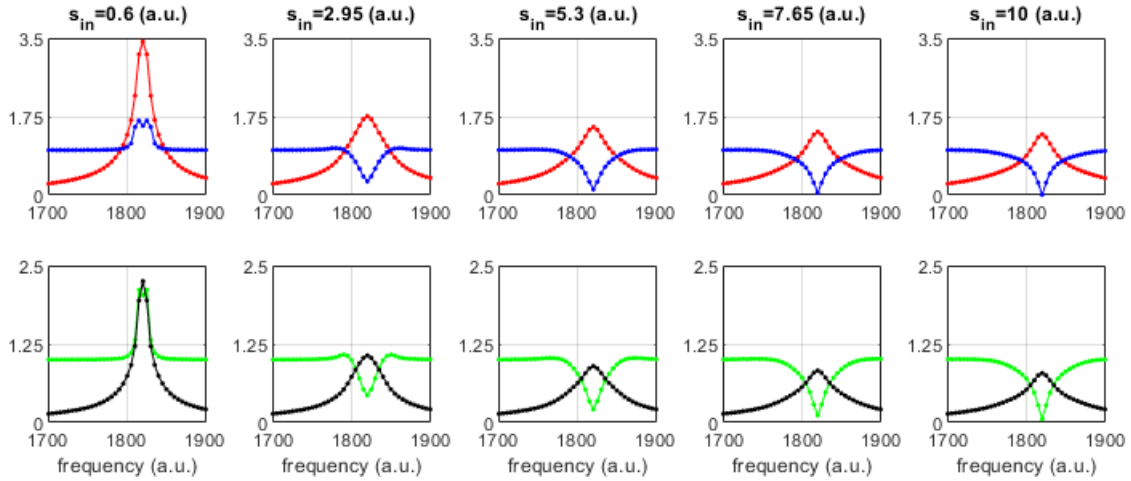


Figure 2. Theoretical prediction of the scattering matrix S. Shown are the entries S_{11} (red), S_{21} (blue), S_{12} (green) and S_{22} (black) over the incident wave frequency for different values of the normalized incident wave amplitude s_{in}.

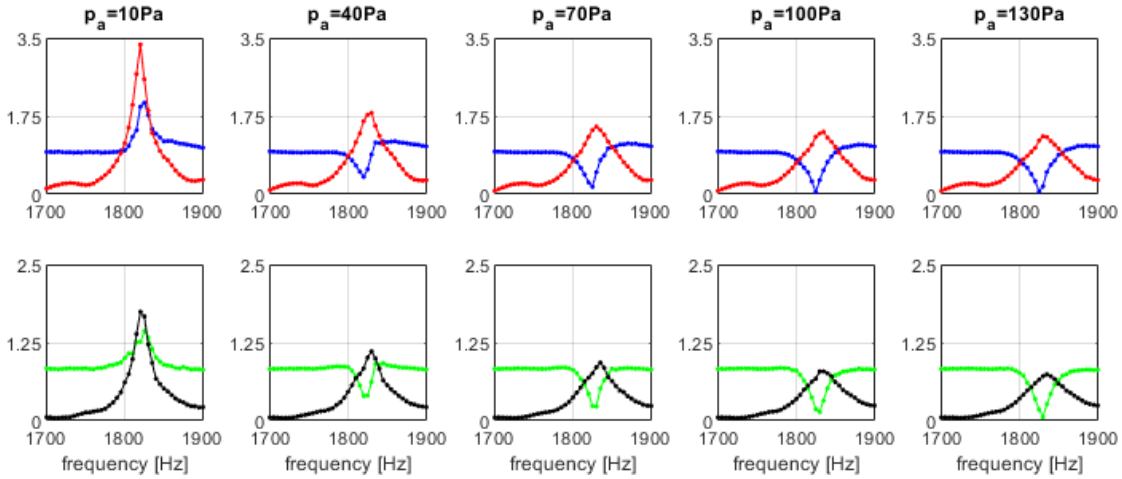


Figure 3. Experimental validation of the theoretical results shown in Fig. 2. The experiments were performed by sending acoustic waves to a whistling deep cavity in a wind channel biased by an imposed air flow. The acoustic amplitude of the wave just outside the cavity p_a was fixed for each measurement.

References

1. Fan, S., W. Suh and J. Joannopoulos, "Temporal coupled-mode theory for the Fano resonance in optical resonators" J. Opt. Soc. Am. A, Vol. 20, No. 3, 569-572, 2003.
2. Bourquard, C., A. Faure-Beaulieu and N. Noiray, "Whistling of deep cavities subject to turbulent grazing flow: intermittently unstable aeroacoustic feedback". J. Fluid Mech., Vol. 909, No. A19, 1-29, 2021.

Introduction to Functionally Graded Unit Cell of Nonlinear Metamaterial that Controls Harmonic Responses of Elastic Waves

P. R. Ghodake

Department of Mechanical Engineering, Indian Institute of Technology Bombay, India
mech7pkumar@gmail.com

Abstract: A unit cell of nonlinear functionally graded metamaterial is exploited in this study through multiple computational experiments. The manipulative capabilities of the nonlinear functionally graded unit cell sandwiched between linear elastic materials of the same impedance are exploited to control harmonic responses. Sensitivities of the parameters that control the spatial distribution of the nonlinear parameters will help to design novel functionally graded nonlinear metamaterials using forward, and inverse design approaches.

Introduction

The presence of harmonically scattered waves and their sensitivities toward various parameters motivates exploiting harmonically scattered waves from functionally graded nonlinear inclusions[1]. Limitations of theoretical techniques and experimental developments in nonlinear ultrasonics exploring harmonic scattering encourage us to explore the domain through numerical perspective[2,3]. Numerical experiments are conducted in this study using the finite element method. A schematic of the numerical model is shown in Figure 1, and the multiple distributions of functionally graded material are shown in Figure 2. As the power of the spatial term changes from ¼ to 1 and then to 0, the area under the curves changes, as seen in Figure 2. Murnaghan hyperelastic material model is considered for modeling functionally graded nonlinear material.

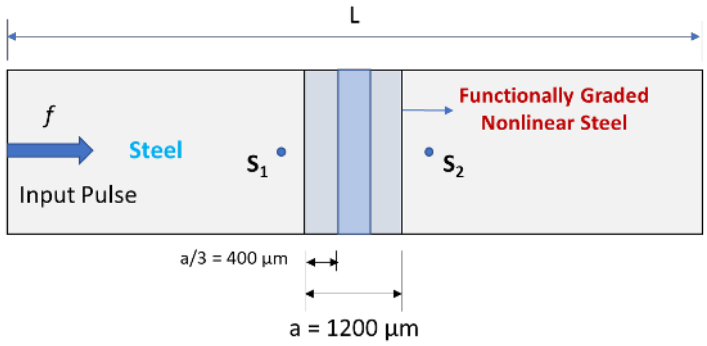


Figure 1. Schematics of three layered nonlinear functionally graded inclusion as a unit cell of the metamaterial to control nonlinear waves used for numerical modeling

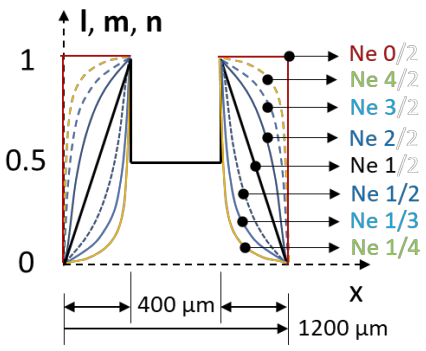


Figure 2. Multiple spatial distributions of nonlinear parameters over the length with different powers

Results and Conclusion

Static term (*0f* = 0 MHz) and 2nd harmonics (*2f* = 4 MHz) are generated due to harmonic scattering from a functionally graded unit cell. Figure 4 shows the increase in the amplitudes of 2nd harmonics and static term with a change in distribution curves from power Ne 4 to Ne 0. As the areas under curves increase from Ne 4 to Ne 0, amplitudes of harmonically forward (Figure 4) and backscattered (Figure 3) waves increase.

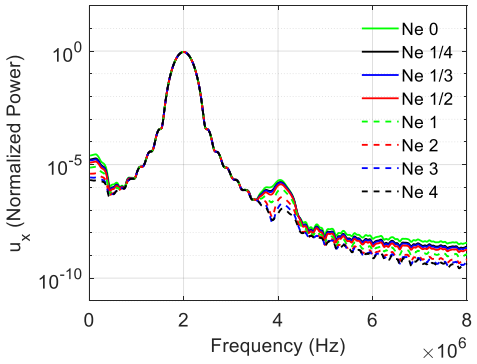


Figure 3. Harmonic responses of backscattered waves at S_1 with Ne 0 - 4 and 0.25(*l, m, n*) central layer

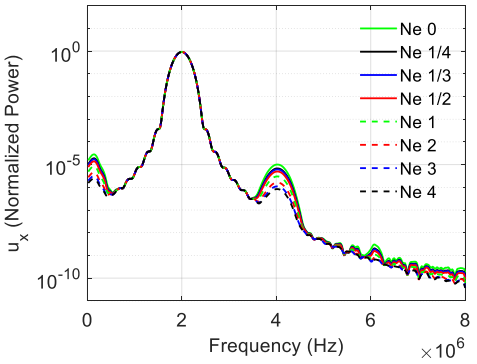


Figure 4. Harmonic responses of forward scattered waves at S_2 with Ne 0 - 4 and 0.25(*l, m, n*) central layer

Amplitudes of static terms (*0f*) of backscattered and forward scattered waves at any spatially distributed curves are the same, whereas amplitudes of 2nd harmonics of backscattered waves are always less than the forward scattered waves (Figure 3 and Figure 4). To understand the effect of the central layer of a unit cell, nonlinear parameters are varied from 0.25-1.00 multiples of (***l, m, n***). Amplitudes of forward scattered waves (*0f*, *2f*) increase (Figure 6) with an increase in the magnitude of middle layer nonlinear parameter from 0.25-1.00, whereas in contrast, the amplitude of 2nd harmonics (*2f*) of the backscattered wave decreases (Figure 5). But interestingly amplitude of the static term (*0f*) of backscattered waves increases (Figure 5) with an increase in parameter from 0.25-1.00, similar to forward scattered waves (Figure 6). These interesting behaviors will help us to design a unit cell by proposing novel functionally graded nonlinear metamaterials to manipulate nonlinear waves.

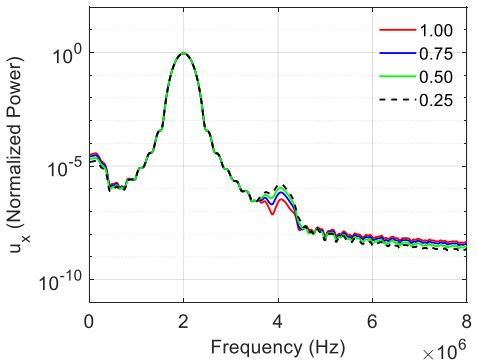


Figure 5. Harmonic responses of backscattered waves at S_1 with Ne 1/3 and various central layer parameters

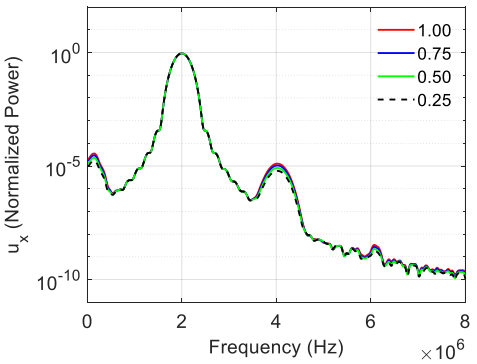


Figure 6. Harmonic responses of scattered waves at S_2 with Ne 1/3 and various central layer parameters

References

1. C. M. Kube, "Scattering of harmonic waves from a nonlinear elastic inclusion," *J. Acoust. Soc. Am.*, Vol. 141, No. 6, 4756–4767, 2017.
2. P. R. Ghodake, "Finite element studies to understand reflection of nonlinear waves in a continuous functionally graded material," *J. Acoust. Soc. Am.*, Vol. 152, No. 4, A294–A294, 2022.
3. P. R. Ghodake, "Nonlinear bulk wave in a functionally graded symmetric hysteretic material model—A numerical study," *J. Acoust. Soc. Am.*, Vol. 149, No. A138, 2021.

Fundamental Study of Elastic Wave Damping by Metamaterials with Local Resonant Structures in Electrical Systems

Kyogo SATO, Keisuke NISHIDA, Toshihiko SUGIURA*

Keio University, Japan
*corresponding author: sugiura@mech.keio.ac.jp

Abstract: Conventional acoustic metamaterials for elastic waves are mainly based on mechanical systems with local resonant structures, but this study aims to reduce vibration by replacing the unit cell with a resonant structure of a coupled electrical-structural system. As a basic study, we confirmed the vibration-damping property of acoustic metamaterials including electrical systems by numerical simulation and further clarified the resonance characteristics of unit cells by experiment.

1. Introduction

In recent years, acoustic metamaterials have been actively studied for waves in gases, liquids, and solids to help reduce noise [1]. Conventional research on acoustic metamaterials for waves in solids typically deals with vibration control methods that focus on the resonant structure of mechanical systems. However, we noted that such a system has installation restrictions on the structure and that it is necessary to change the resonant structure for each frequency to be attenuated. Therefore, we focused on coupled electrical and structural vibration systems based on resonant structures using electrical circuits and piezoelectric elements. In this study, we investigated the damping properties of acoustic metamaterials using electrical systems for wave propagation in solids by numerical simulation and the resonance properties of resonant structures by experiment.

2. Numerical simulation

Our metamaterial model consists of piezoelectric elements and resonant circuits periodically attached to the top surface of an aluminum beam, as shown in Figure 1. The thickness of the beam is 0.5 mm. The distance between the piezoelectric elements is also 0.5 mm, which is sufficiently shorter than the propagation wavelength. The resonant frequency of one circuit is set to 100.7 kHz. The resonant frequency of a unit cell was confirmed to be 101 kHz by eigenvalue analysis. In this model, the waves are transmitted in 10 kHz increments from 70 kHz to 160 kHz. The displacement of the top surface of the beam during wave propagation was determined by coupled electrical-structural finite element analysis and compared with the results for beams without piezoelectric elements and electrical circuits attached. Vertical displacements were obtained at three different locations on the top surface of the beam: point A, 100 mm from the transmission point and before the local resonant structure; point B, 170 mm from the transmission point and 100 unit cells away in the local resonant structure region; and point C, 200 mm from the transmission point and after passing the local resonant structure region.

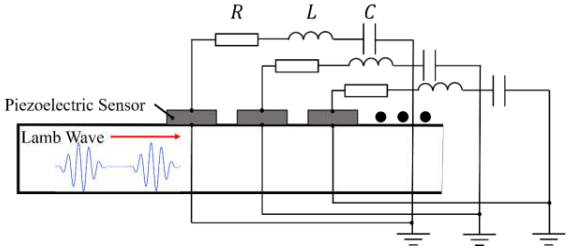


Figure 1. Periodic structures with local resonators as electrical systems

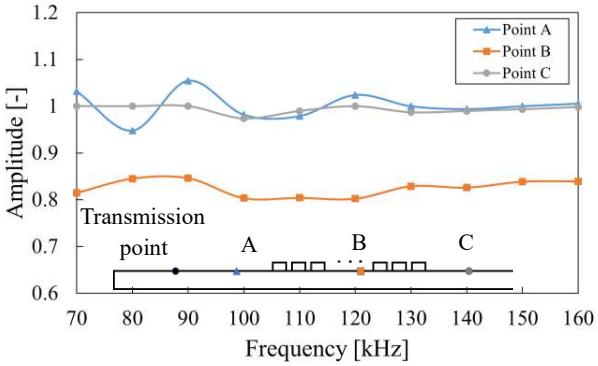


Figure 2. Amplitude of vertical displacement at three locations on the beam for each transmission frequency, obtained by FEM

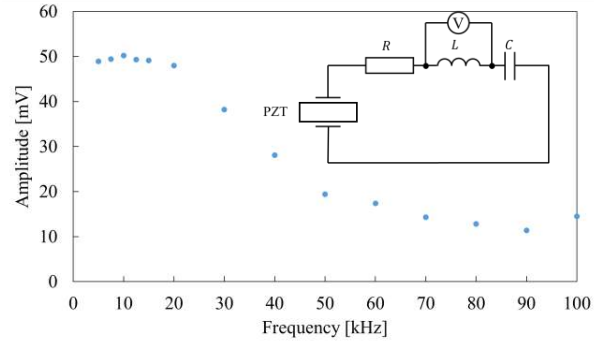


Figure 3. Measured amplitude of the electrical voltage depending on the frequency

Figure 2 shows amplitude of vertical displacement at three locations on the beam obtained by numerical simulation. The maximum amplitude on the vertical axis is the dimensionless value obtained by dividing by the maximum amplitude without the electrical system. The horizontal axis indicates the transmission frequency. As can be seen from this result, at point B in the local resonant structure region with the electrical system attached, the displacement amplitude is reduced by about 20%.

3. Experiment

In the experiment, 10 piezoelectric elements were placed on an aluminum plate at 5 mm intervals, and the resonant frequency of the circuit was set at 10.7 kHz. To investigate the resonant frequency of the coupled electrical-structural system, the voltage applied to the inductors of the circuit was measured. The measurement results obtained from the experiment are plotted in Figure 3, where the horizontal axis represents the excitation frequency, and the vertical axis represents the maximum amplitude of the voltage. The results show that the amplitude reaches its maximum value around 10 kHz, which is the resonant frequency of the circuit, and that the voltage amplitude is found to decrease in the frequency band away from this frequency. Thus, the voltage response due to mechanical excitation was confirmed and the resonance properties in the unit cell of the electrical metamaterial were also experimentally confirmed.

4. Conclusions

In the metamaterial containing a coupled electrical-structural system, numerical simulations confirmed the vibration-damping properties of the local resonant structure at locations near the unit cell. The resonance characteristics in the unit cell of the electrical system were also clarified by experiments.

References

1. Liu, J.Y., Guo, H.B. and Wang, T, “A review of acoustic metamaterials and phononic crystals,” Crystals, Vol. 10, No.4, 305, 2020.

META 2023, PARIS - FRANCE, JULY 18 – 21, 2023

High-resolution medical ultrasound focusing and temperature rise with acoustic metamaterial

Jiajie He[1], Xue Jiang[1*], and Dean Ta[1, 2]

[1] Center for Biomedical Engineering, School of Information Science and Technology, Fudan University, Shanghai, 200433, China.

[2] Department of Rehabilitation Medicine, Huashan Hospital, Fudan University, Shanghai, 200040, China.

[*]corresponding author: xuejiang@fudan.edu.cn

Abstract: We experimentally realize the medical ultrasound focusing based on the compact and passive metamaterial. The three-dimensional spot focusing is endowed with high spatial resolution (0.63λ FWHM and 2.75λ FLHM), broad effective bandwidth (0.5-1.4 MHz) and tunable focal length (18.5-71 mm). Ultrasound scalpel, which converge the acoustic energy within a sharp needle area, is demonstrated with an aspect ratio of 12.64. Additionally, we investigate the prominent temperature rise in the focal region and reveal the dependence on the ultrasound frequency.

Ultrasound focusing features superior penetrability, biocompatibility and non-radioactivity, enabling substantial applications in biomedical science and clinical medicine, such as medical imaging, non-invasive surgery and neurostimulation[1-3]. Conventional ultrasound focusing technologies face two urgent challenges. On the one hand, spatial resolution is the key indicator to evaluate the focusing performance. However, ultrasound has lower focusing resolution compared with light/electromagnetic wave. On the other hand, traditional ultrasound focusing relies on the active transducer array with complex circuit modulation, or curved lens with fixed focal length, which inevitably hinders the development of more precise and flexible focusing technology.

The advent of acoustic metamaterial/metasurface has provided new solutions to the freeform sound manipulation and improve focusing precision[4-7]. Currently, the metamaterial-based acoustic focusing is mainly implemented for airborne sound at a relatively low frequency (< 500 kHz). Due to the difficulties in the fabrication of complicated microstructures, underwater ultrasound focusing which plays a pivotal role in biomedical diagnosis and therapy still remains a challenging task.

In this work, we numerically and experimentally realize the underwater medical ultrasound focusing with sub-wavelength resolution and tunable focal length over a broad frequency band. The metamaterial is designed as an axisymmetric disk, which consists of spatially serrated units with specific tilted angles. Ultrasound energy is reflected by the structure and precisely converged at the target position, leading to the three-dimensional spot focusing and ultrasound focusing scalpel. Full width at half maximum (FWHM) and full length at half maximum (FLHM) are used to represent the spatial resolution. Figure 1 shows the measured underwater spot focusing, where the FWHM is 0.89λ and 0.63λ while the FLHM is 3.54λ and 2.75λ in measurements and simulations, respectively. Significantly, ultrasound focusing is effectively maintained within 0.5-1.4 MHz (1.5 octaves). The dynamic focal length presents an approximately linear relationship on the operating frequency. Ultrasound scalpel further enriches the focusing pattern by concentrating the energy inside a sharp needle area, with an aspect ratio of 12.64 in Fig. 2. Accompanied with the enhancement of ultrasound intensity, prominent temperture rise is also observed in the focal region. We investigate the simulated temperature rise and reveal the dependence on the ultrasound frequency in Fig. 3. Owning to the sub-wavelength focusing resolution, only the targeted focal region is heated by the ultrasound while the undesired region remains intact. Our proposal of the compact metasurface may offer a feasible approach for high-resolution medical ultrasound focusing, and possess fascinating prospects in biomedical imaging, diagnostic sonography and therapy.

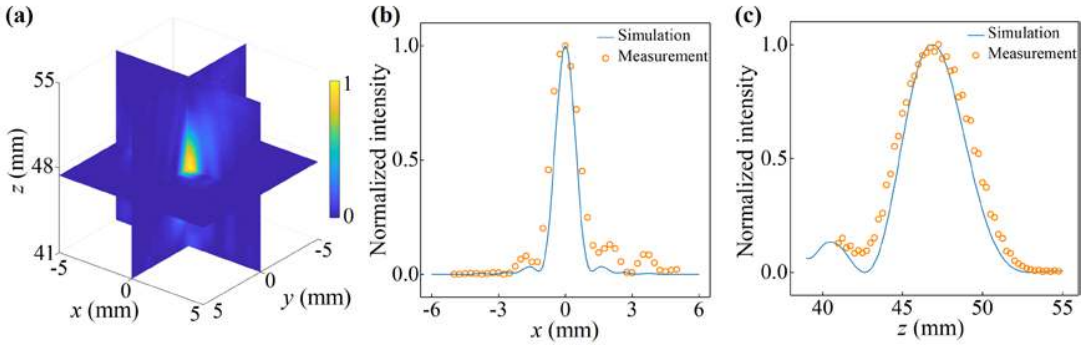


FIG. 1. High-resolution three-dimensional spot focusing.

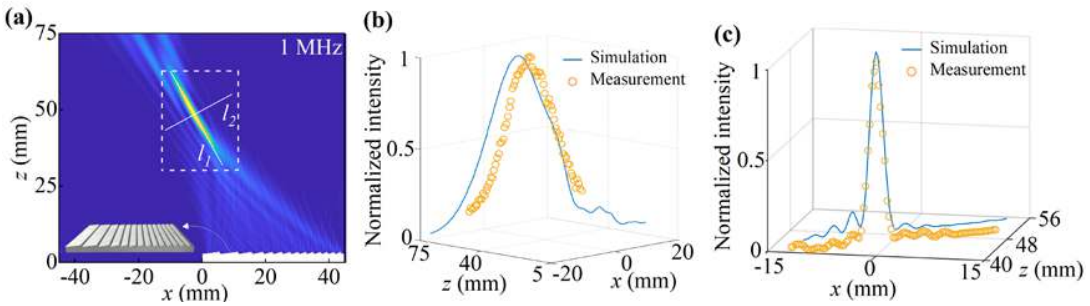


FIG. 2. Underwater ultrasound focusing scalpel.

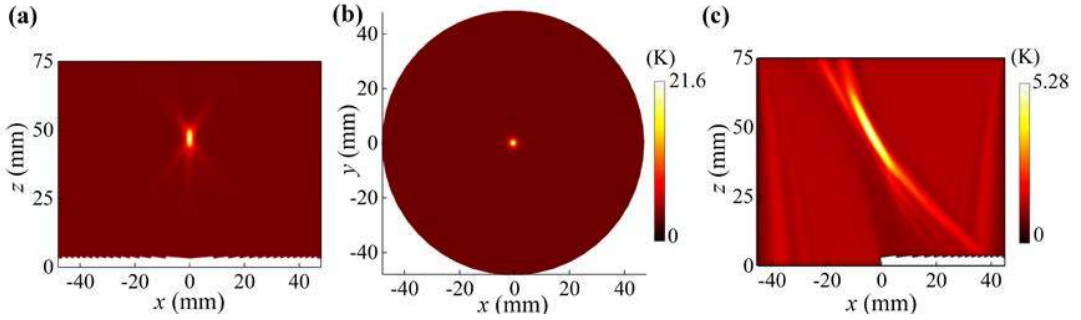


FIG. 3. Characterization of temperature rise effect.

References

1. Cox, B. and P. Beard, "Super-resolution ultrasound," Nature, Vol. 527, No. 7579, 451-452, 2015.
2. Legon, W., T. F. Sato, A. Opitz, J. Mueller, A. Barbour, A. Williams, and W. J. Tyler, "Transcranial focused ultrasound modulates the activity of primary somatosensory cortex in humans," Nat. Neurosci., Vol. 17, No. 2, 322-329, 2014.
3. King, R. L., J. R. Brown, and K. B. Pauly, "Localization of Ultrasound-Induced In Vivo Neurostimulation in the Mouse Model," Ultrasound Med. Biol., Vol. 40, No. 7, 1512-1522, 2014.
4. Guenneau, S., A. Movchan, G. Pétursson, and S. Anantha Ramakrishna, "Acoustic metamaterials for sound focusing and confinement," New J. Phys., Vol. 9, 399, 2007.
5. Zhang, S., L. Yin, and N. Fang, "Focusing Ultrasound with an Acoustic Metamaterial Network," Phys. Rev. Lett., Vol. 102, No. 19, 194301, 2009.
6. Chen J., J. Xiao, D. Lisevych, A. Shakouri, and Z. Fan, "Deep-subwavelength control of acoustic waves in an ultra-compact metasurface lens," Nat. Commun., Vol. 9, 4920, 2018.
7. Tang, H., Z. Hao, and J. Zang, "Nonplanar acoustic metasurface for focusing," J. Appl. Phys., Vol. 125, No. 15, 154901, 2019.

Chiral and hyperbolic metamaterials

Spin-momentum locking breakdown on plasmonic metasurfaces

F. Lorén[1,2*], and L. Martín-Moreno[1,2]

[1]Instituto de Nanociencia y Materiales de Aragón (INMA), CSIC-Universidad de Zaragoza, Zaragoza 50009, Spain

[2]Departamento de Física de la Materia Condensada, Universidad de Zaragoza, 50009 Zaragoza, Spain
[*]corresponding author: loren@unizar.es

Abstract: We have developed a detailed formalism to analyze the spin-momentum locking (SML) in structured plasmonic metasurfaces. It is valid for any unit cell where holes are placed at certain positions and angles. We can explain the SML emergence just from the unit cell configuration. Besides, there appear several breakdown terms spoiling the polarization landscape. We have studied systems with rotations along the unit cell but also with global symmetry of translation and rotation of the whole lattice, like Kagome lattice.

We revisit the optical properties of several plasmonic Berry metasurfaces. We focus on the spin-orbit coupling as a result of the local rotation of the coordinate system induced by the rotation of the nanoapertures, which is known to imprint a very strong polarization response in the far-field. In our work, we have studied a nanostructured metallic slab (gold), hosting certain nanoapertures or grooves configurations. The selection of a noble metal as the metallic slab is also important because they have positioned themselves as the most promising materials to host surface plasmon polaritons (SPPs) in the optical regime over the years. A properly hosting of these SPPs is fundamental for two reasons: the first one is because we want to use them to obtain a strong far-field response, and the second one is because we can place some 2D materials such as transition metal dichalcogenides (TMDs) above the metallic structure to enhance the coupling between the SPPs and the excitons from the TMDs. Finally, to trigger the spin-orbit coupling or spin-momentum locking, we have chosen two different configurations of grooves that lead to chiral behavior in the metasurface polarization response because of the positions and angles of their grooves.

To tackle theoretically this problem, we use the coupled-mode method, which consists of expanding the electromagnetic fields in a superposition of plane-wave modes in the region above the metasurface, and waveguide modes inside the sub-wavelength slits. We obtain the governing equations for the far-field landscape via the reflection coefficients, and we study in detail each element of these equations. We show that the interaction of the light with the metasurface allows for spin-to-momentum or momentum-to-spin conversions. We derive some selection rules which reveal a series of possible scattering processes for photons, that are associated with very specific changes in photon momentum and input/output polarizations. These selection rules are a theoretical confirmation of the spin-orbit Bragg's law, which is the momentum conservation of the spin-momentum locking. This is not the first time that a theoretical derivation for a system like this is implemented [1], but this is a simpler and more general way of exploring this kind of system. The most striking result is that the widely used spin-momentum locking is not perfect. We demonstrate that it suffers a breakdown. The circularly polarized photons that come in or out in the propagation direction get projected onto the planar metasurface, becoming elliptical in general. This breakdown causes more processes to be allowed and the polarization landscape to be spoiled. Besides, we observe that the less perpendicular-to-the-metasurface the propagation direction of the plane wave, the more relevant the effect, being critical when an SPP is excited.

The results for the first configuration are experimentally confirmed with Mueller polarimetry measurements, which allows for capturing the metasurface's full polarization, energy, and momentum response. Besides, these experimental results are

compared with numerical simulations and the agreement between both is excellent. Our results provide the much-needed microscopic understanding of this metasurface, which is already widely used for its distinct interaction properties with circularly polarized light. Furthermore, we have generalized the theoretical formalism and used it to explore the second of the configurations. This one is also called the Kagome lattice and it has been important in other works such as [1] because this distribution of grooves is invariant under combined translation and rotation of the whole lattice. We have found that the Kagome lattice also presents spin-momentum locking breakdown so, essentially, we demonstrate that the breakdown is ubiquitous and appears in any kind of nanostructured system.

These results are reported in [2] and are also under preparation for another paper.

References

1. N. Shitrit, I. Yulevich, E. Maguid, D. Ozeri, D. Veksler, V. Kleiner, and E. Hasman. Spin-Optical Metamaterial Rout to Spin-Controlled Photonics. Science 340(6133):724–726, May 2013.
2. F. Lorén, G. L. Paravicini-Bagliani, S. Saha, J. Gautier, M. Li, C. Genet, and L. Martín-Moreno. Microscopic analysis of the spin-momentum locking on a Geometric Phase Metasurface. arXiv:2205.10245v1

META 2023, PARIS - FRANCE, JULY 18 – 21, 2023

Engineering of a THz time-reversal symmetry breaking chiral metamaterial

L. Graziotto[1*], J. Andberger[1], L. Sacchi[1], M. Beck[1], G. Scalari[1], and J. Faist[1]

[1]Institute for Quantum Electronics, ETH Zürich, Auguste-Piccard-Hof 1, 8093 Zürich, Switzerland

[*]corresponding author: lgraziotto@phys.ethz.ch

Abstract: A metamaterial of resonators capable of sustaining circularly polarized electromagnetic modes has been developed and it is reported to give rise to chiral light-matter hybrid states when coupled to the cyclotron resonance of a two-dimensional electron gas. The cavity design, which is crucial to ultra-strongly couple to the solid-state system, could potentially be implemented to manipulate topological properties of materials, or to affect their transport behavior, about which one can gain insights via a circuit model that we have developed.

Ultra-strong coupling (USC) refers to the regime of light-matter interaction in which the magnitude of the coupling is of the order of the bare electromagnetic mode frequency. When the matter platform consists of the cyclotron resonance of electrons confined in GaAs/AlGaAs quantum wells (two-dimensional electron gas, 2DEG) in a perpendicular magnetic field one obtains light-matter hybrid modes called *Landau polaritons* [1], which have been investigated in the THz region via the use of split-ring resonators [2]. It has been recently demonstrated [3] the possibility of achieving circularly polarized Landau polaritons, which in addition to the characteristic anti-crossing of their energy dispersions do exhibit an energy-shift caused by the interaction with the counter-rotating component of the electromagnetic field, the so-called *vacuum Bloch-Siegert shift*. The cavity design is what is crucial to enable such exotic quantum states at equilibrium [4], at variance with the driven Floquet-engineered states [5] that being out of equilibrium suffer from dissipation, decoherence, and other scattering mechanisms.

Here we report on the implementation of a THz metamaterial capable of harnessing the inherently chiral behavior of the 2DEG in a magnetic field, thus leading to light-matter modes which break time-reversal symmetry. The unit cell of the structure (Fig. 1a) consists of two pairs of orthogonal antennas whose electric fields at resonance oscillate with 90 degrees phase difference, such that at their intersection a circularly polarized mode is

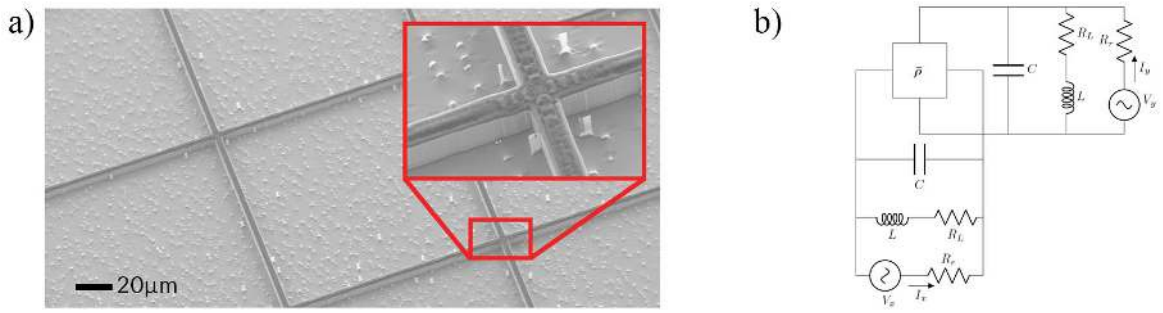


Figure 1. (a) SEM image of the chiral metamaterial. Inset: zoom in to the antenna gap, where the electromagnetic field interacts with the 2DEG. Notice the deep etch which suppresses the spurious capacitative effect. (b) Circuit model of the coupled system: the square represents the 2DEG, while the two antennas are represented by LC circuits.

sustained and coupled to the electron gas. We have characterized the system via THz time-domain spectroscopy (Fig. 2a): samples with different numbers of quantum wells have been investigated, and the coupling strength has been obtained by looking at the energy splitting at positive and negative magnetic field, which represents the hallmark of the chiral response. We have also developed a semi-classical circuit model (Fig. 1b) to get insights about the coupling mechanism and its limitations by cavity and material losses (Fig. 2b). The 2DEG gyrotropic response is calculated within Boltzmann's transport formalism, and the pairs of antennas are modelled via LC circuits. The model not only reproduces the results obtained via a formal Hamiltonian approach, but it is also applicable in general to planar resonators.

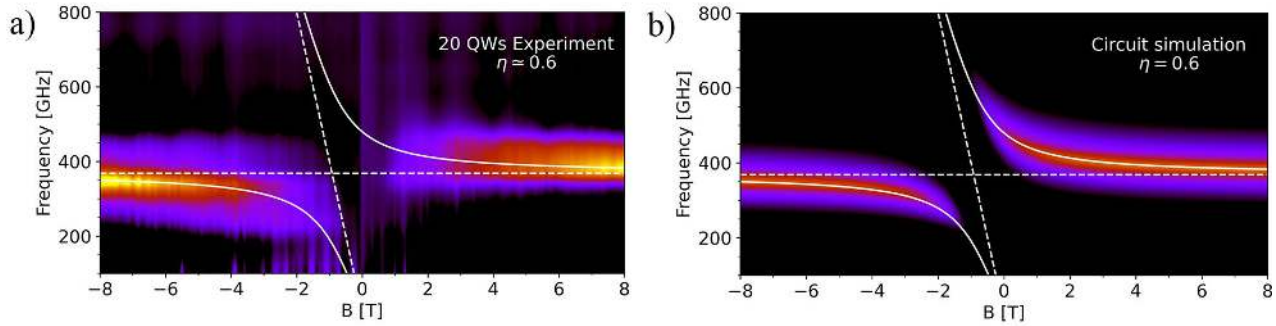


Figure 2. (a) Logarithm of transmission from a metamaterial sample coupled with 20 quantum wells, as a function of magnetic field and frequency of the excitation, as measured via THz time-domain spectroscopy. (b) Logarithm of transmission as simulated via a circuital approach. The dashed lines indicate the bare cavity frequency (horizontal) and cyclotron resonance (diagonal). η is the normalized coupling strength.

In conclusion, we have demonstrated a promising platform for exploring chiral states in condensed matter systems. Moreover, the cavity highly subwavelength interaction volume along with the strong polarizability of the solid-state platform pave the way for future magneto-transport experiments, which could access the USC ground state, whose chiral properties are still unexplored [6].

We acknowledge funding from the Swiss National Science Foundation (SNF).

References

1. Hagenmüller, David, Simone De Liberato, and Cristiano Ciuti. "Ultrastrong coupling between a cavity resonator and the cyclotron transition of a two-dimensional electron gas in the case of an integer filling factor." *Physical Review B* **81.23** (2010).
2. Scalari, G., et al. "Ultrastrong coupling of the cyclotron transition of a 2D electron gas to a THz metamaterial." *Science* **335.6074** (2012)
3. Li, Xinwei, et al. "Vacuum Bloch–Siegert shift in Landau polaritons with ultra-high cooperativity." *Nature Photonics* **12.6** (2018)
4. Hübener, Hannes, et al. "Engineering quantum materials with chiral optical cavities." *Nature materials* **20.4** (2021)
5. Oka, Takashi, and Sota Kitamura. "Floquet engineering of quantum materials." *Annual Review of Condensed Matter Physics* **10** (2019)
6. Garcia-Vidal, Francisco J., Cristiano Ciuti, and Thomas W. Ebbesen. "Manipulating matter by strong coupling to vacuum fields." *Science* **373.6551** (2021)

Machine learning for metamaterial design

Polarization holograms assisted with deep-learning

Jiawei Xi[1+], Jian Shen[1,2+], Man To Chow[1], Tan Li[3], Jack Ng[2*], Jensen Li[1*]

[1] Department of Physics, The Hong Kong University of Science and Technology, Clear Water Bay, Hong Kong
[2] Department of Physics, Southern University of Science and Technology, Shenzhen, Guangdong, China
[3] Centre for Advances in Reliability and Safety (CAiRS), Hong Kong Science Park, Pak Shek Kok, NT, Hong Kong, China

[*]corresponding author: jensenli@ust.hk, wuzh3@sustech.edu.cn

Abstract: We demonstrate an integrated deep-learning neural network that generates metasurface designs directly from independent polarization holograms, with a maximum of four different co- and cross- polarization conversion channels. This is achieved by extending the existing DeepCGH network with an inverse design component. Our approach enables a systematic design route for polarization holograms directly from an existing metamaterial library without requiring detailed knowledge of the constraints. Furthermore, it can be adapted for other multiplexing holograms that require automated designs.

Multiplexing holography with metasurfaces is a technology with emerging potential over a vast range of areas in science and technology, which include but are not limited to display technology and information storage [1]. Among different multiplexing approaches, polarization-multiplexed hologram is probably the most straightforward to use in practice. Recently, a planar metasurface has been demonstrated to increase the capacity for polarization multiplexing on various co-polarization channels by introducing the engineered noise [2]. However, such single-layered metasurfaces have a constrained form of Jones matrix being symmetric when expressed in terms of linear polarization: $t_{xy}=t_{yx}$. The incorporation of this degree of freedom (DOF) will further extend the usage of polarization holograms. On the other hand, the conventional iterative method for designing metasurface polarization holograms needs to consider the constraints on the multiple polarization channels, while it is not easily scalable to more variety of nanostructures (to break $t_{xy}=t_{yx}$) like the bianisotropic structures [3]. To overcome such issues and speed up the whole design process, it is beneficial to adopt a machine learning approach for generality.

Here, by extending the existing DeepCGH network [4] with an inverse design component, we developed a deep learning algorithm (DeepCGH-ID) to generate holograms and assist on the metasurface design. To fully utilize the polarization holograms, we take a bianisotropic metasurface as a template. As shown in the upper left panel of Fig.1(a), the designed bianisotropic structural unit with the silicon-made "fin" structure is embedded in glass in a square lattice of periodicity a = 1000 nm. The structure has two layers of L-shape bars (width w and thickness h = 250 nm) connected by a square pillar (width w and thickness t = 125 nm) in between. The two L-shapes break the mirror symmetry in the z-direction in generating bianisotropy. The size of the silicon structure in the y-direction is l = 637.5 nm. The vertical pillar is shifted by Δx and Δy relative to the two vertical middle planes of the unit cell (dashed line frames). This structure is defined as "right-handed", and the lower left panel in Fig.1(a) shows its mirrored structure (with mirror plane $x = y$), defined as the "left-handed" structure. The Jones matrix elements of the right-handed structure are obtained from simulations (with normal incidence (along positive z-direction) and a fixed wavelength of 1550 nm) with varied geometric parameters. All the phases can cover the full range of 2π, and t_{xy} is significantly different from t_{yx} as shown in the right panel of Fig.1(a). As the phase of t_{yy} does not change too much for the whole library, we add the orientation of the nanostructure as another geometric parameter, by rotating the structure in the counter-clockwise direction.

With the nanostructure library in place, an integrated deep neural network to design metasurface holograms is developed and shown in Fig.1(b). The whole network turns input target holograms B_{ki} (upper green box) to the

output geometric parameters of all nanostructures on the metasurface (the cyan box). Subscript k iterates the polarization channels (xx, xy, yx, yy or LL, LR, RL, RR for linear-polarization(LP) or circular-polarization(CP) holograms) and i iterates the pixels on the hologram. The decoder is pre-trained with supervised learning to turn geometric parameters to the Jones matrix elements. The encoder-decoder pair is an autoencoder variant to do inverse design of nanostructures from given Jones matrix elements. It is further embedded into the integrated network as an autoencoder in turning target holograms to geometry and to reconstructed holograms B'_{ki} with loss function being the reconstruction error. The integrated network trains the far-field predictor network and the encoder network with unsupervised learning [5]. Here, we generate 500 different configurations of polarization holograms with dice patterns (with the size of 64 by 64 pixels) to train the network, and each set consists of four independent holograms, which iterates four combinations of polarization conversion channels. After the network is well trained, a testing set with the dice patterns are chosen to test the network. The first row in Fig.1(c) lists the target holograms, and the second (third) row lists the generated holograms in the LP (CP) basis. Each column shows one of the four polarization channels with the first (second) arrow indicating the analyzing (incident) polarizations. The horizontal (vertical) arrow means x (y) polarization. The clockwise (counterclockwise) arrow means right (left)-handed CP. Pearson correlation coefficients between the reconstructed and the target holograms are shown in upper left corner of each hologram and are all higher than 0.8. It is worth to note that without detailed physical knowledge on the nanostructure constraints, this integrated network method can generate metasurface designs directly from the required complex polarization holograms.

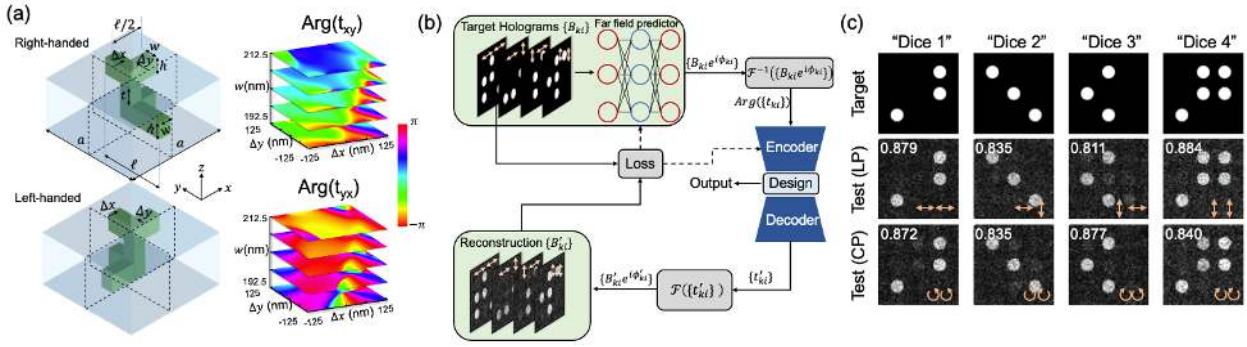


Figure 1. (a) Schematic of the unit cell in library, and the phases of t_{xy} and t_{yx} in the right-handed structure by scanning parameters w, Δx and Δy obtained from full-wave simulations. (b) Schematic of the integrated deep neural network. (c) Testing results of polarization holograms on the dice patterns.

Acknowledgements: The work is supported by Hong Kong RGC Grant No. C6013-18G, AoE/P-502/20. S.J. and J.N. are supported by NNSF of China (no. 12074169). T.L. is supported by AIR@ InnoHK Research Cluster.

References

1. R. Zhao et al., *Recent advances in multi-dimensional metasurfaces holographic technologies*, PhotoniX, 1, 1-24(2020).
2. B. Xiong et al, *Breaking the limitation of polarization multiplexing in optical metasurfaces with engineered noise*, Science, 379(6629), 294-299(2023).
3. C. Menzel, et al, *Asymmetric transmission of linearly polarized light at optical metamaterials,* Physical review letters, 104(25), 253902 (2010).
4. M. H. Eybposh et al, *DeepCGH: 3D computer-generated holography using deep learning*, Optics Express, 28(18), 26636-26650 (2020).
5. J. Xi, J. Shen, M. T. Chow, T. Li, J. Ng, J. Li, Deep-learning assisted Jones-matrix holograms, Adv. Opt. Mater. (accepted)

META 2023, PARIS - FRANCE, JULY 18 – 21, 2023

Machine Learning Techniques and Practical Advice for the Free-Form Inverse Design of Nanophotonic Devices

Timo Gahlmann* **and Philippe Tassin**

Department of Physics, Chalmers University of Technology, SE-412 96 Gothenburg, Sweden
*corresponding author: timo.gahlmann@chalmers.se

Abstract: The free-form inverse design of nanophotonic metasurfaces can be solved with a modified CGAN machine learning method that balances the accuracy of desired optical properties with experimental feasibility.

We will present several machine learning techniques that can be used for the inverse design of free-form nanophotonic devices, i.e., devices for the manipulation of light with subwavelength patterning [1]. Such devices allow us to control light at unprecedented levels, resulting in nontrivial scattering response, e.g., for holograms and retroreflectors. A nanophotonic device often consists of an array of scattering elements, each of which needs to have a specific transmission (or reflection) amplitude and phase. The challenge is, then, to find the shape and materials of meta-atoms with the desired scattering response. This engineering problem is called inverse design.

In this contribution, we will discuss how it is possible to address the computational and methodological difficulties emerging when using neural networks for the inverse design of metasurfaces [2]. Neural networks provide the big advantage that they can quickly generate a design for a meta-atom with most desired transmission amplitude and phase once they are trained. The training of the neural networks still requires a large number of simulations of the nanophotonic device (with different geometries), but they can be run in parallel on high-performance computer clusters. We will provide guidance for best practice and an overview of techniques that work well, illustrated by examples.

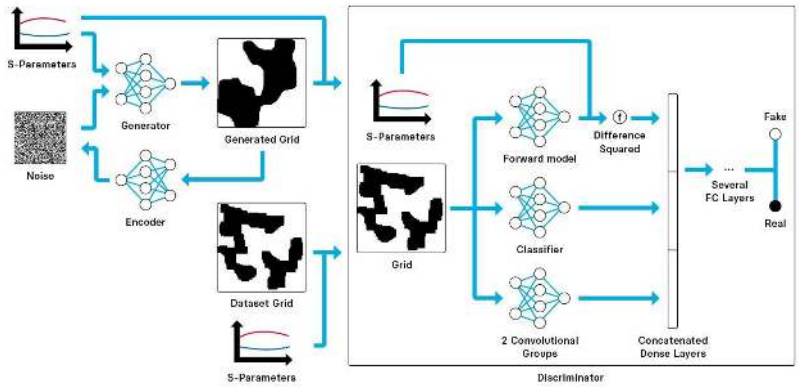


Figure 1: A conditional generative adversarial network model. The generator creates unit cell grids from noise and S parameters while the encoder prevents mode collapse. Two ”expert” networks (forward and classifier model) are integrated inside the discriminator.

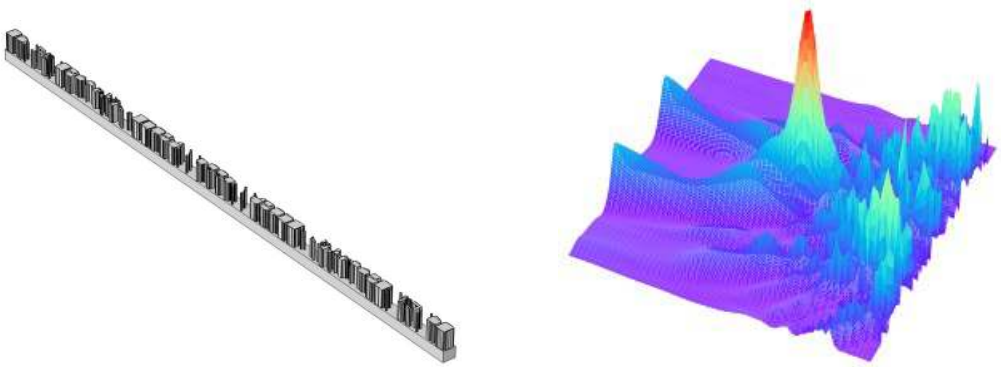


Figure 2: Left: Unit cell composition of a cylindrical lens as designed by the CGAN. Right: Intensity of the focused beam obtained from the CGAN-designed lens.

First we will show how to create a neural-network model mapping a random device geometry on an optical property of interest. Such a forward model is necessary as a surrogate model in the CGAN that we have built for the inverse design. Second, we will discuss methods to integrate fabrication feasibility into the inverse design method, e.g., by training a classifier network to distinguish between fabrication-feasible and unfeasible geometries. We will then proceed with presenting our CGAN model for the inverse design.

In a CGAN, a generator creates grids based on noise and labels (desired S parameters, aspect ratio, minimum resonances width and other criteria), while the discriminator is fed not only the grids produced by the generator and grids from the given data set, but also the respective labels. We will also show how the integration of "expert" networks into the discriminator can significantly improve the training speed and performance of the CGAN. Additionally, we will present a technique to prevent mode collapse in the generator, e.g., by using an additional encoder network. Finally, various other practical tricks to improve the stability, convergence, and outputs of the CGAN inverse-design network will be elaborated, e.g., data augmentation, use of dense ResNet [3], temporarily freezing the discriminator, data blurring, and noise to the different input channels.

We acknowledge support from the Chalmers Excellence Initiative Nano and from the Swedish Research Council under Grant No. 2020-05284. The numerical calculations and ANN training were performed on resources provided by the Swedish National Infrastructure for Computing (SNIC) at the Chalmers Centre for Computational Science and Engineering (C3SE), partially funded by the Swedish Research Council under Grant No. 2018-05973.

References

1. P. Genevet, F. Capasso, F. Aieta, M. Khorasaninejad, and R. Devlin. "Recent advances in planar optics: From plasmonic to dielectric metasurfaces," Optica, 4, 139–152, 2017.
2. T. Gahlmann and P. Tassin, "Deep neural networks for the prediction of the optical properties and the free-form inverse design of metamaterials," Phys. Rev. B, 106, 8, 2022.
3. G. Huang, Z. Liu, L. van der Maaten, and K. Q. Weinberger, "Densely Connected Convolutional Networks," 2017 IEEE Conference on Computer Vision and Pattern Recognition (CVPR), Honolulu, HI, USA, pp. 2261-2269, 2017. 3., arXiv:1608.06993.

Beyond Periodic pillar-wise library for metasurface: a stochastic approach

Loumi TREMAS[1*], and Mathys LE GRAND[1], Denis RIDEAU[2], Louis Henri FERNANDEZ-MOURON, Jeremy GREBOT, Bruce RAE, James DOWNING, Pascal URARD, Valérie SERRADEIL, Lucie DILHAN, Habib MOHAMAD, Gonzague DE CARPENTIER, Enrico Giuseppe CARNEMOLLA, Matteo FISSORE, Christophe SAUVAN

[1,2]STMicroelectronics, France [*]Corresponding author: loumi.tremas@st.com

Abstract: Most of the large scale metasurface are designed using pillar-wise periodic libraries [2]. However, in certain cases, resonances can appear which makes the relation between the desired phase and the corresponding pillar radius ambiguous. In the present abstract, we propose a new stochastic approach beyond pillar-wise periodic libraries.

The phase and transmission of the incident wave through the metasurface is studied with FDTD simulations. The studied systems are composed of pseudo-periodic assembly of pillars exhibiting a random radius variation obtained with a gaussian perturbation field (characterized by an RMS and a correlation length). Our metasurfaces are composed of scattering nano pillars. They are equally spaced on a grid and their radius can continuously vary in the interval $R \in [0.06; 0.18]\mu m$, their height is identical throughout all the experiment and have been simulated using a monochromatic source in the near infrared on a normal angle of incidence.

To study the impact of our system smoothness, a dataset of radius maps with different correlation length has been built. The correlation length translates how smooth the radius transition between neighboring pillars is. It is defined as $d_{corr} = N * \sigma$ where σ is the standard deviation of the gaussian perturbation and N the number of pillars. To create meta-surfaces with gaussian perturbations, a radius map M_i of NxN radii is generated from a uniform distribution. In this case $N = 21$. This radius map is then convoluted to several gaussian distributions parameterized by $\sigma = \{\sigma_1, \dots, \sigma_g\}\ with\ g \in \mathbb{N}$ to get g new

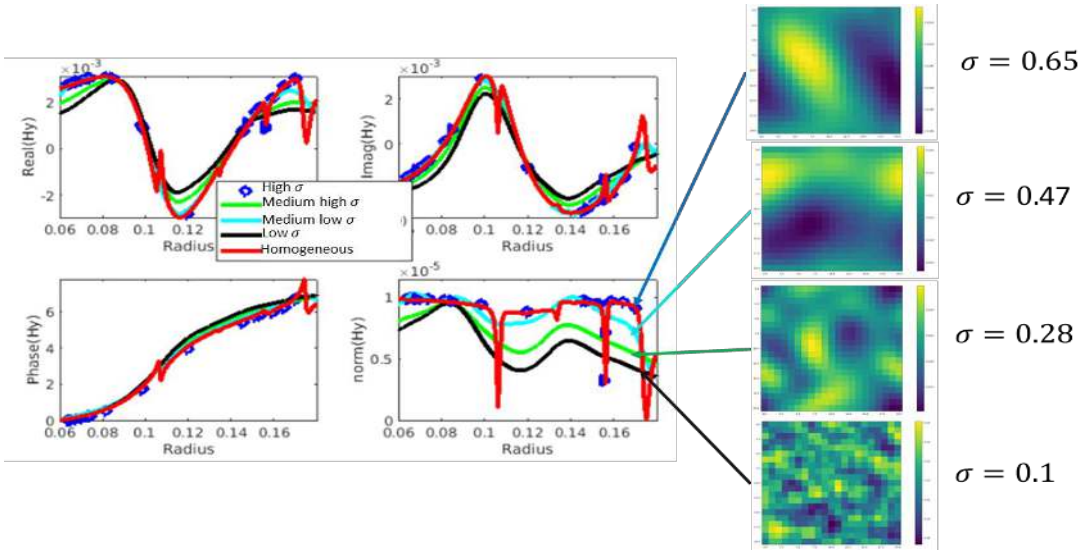


Figure 1: The relation between the phase and the radius is parameterized by the gaussian perturbation

ST Restricted

radius maps $M_i^{corr} = \{M_i^{\sigma_1}, \dots, M_i^{\sigma_g}\}$. By doing so with several M_i, a statical study on the correlation influence can be lead. Images on figure 1 show such radius maps.

Once the dataset inputs are generated, a Finite Time Difference Domain (FDTD) solver developed by Ansys to compute the near electromagnetic fields is used. The chosen nearfield distance for the study is 10 nanometer after the metamaterials in the z-axis.

The relation f between the pillar top radius and the local phase changed induced depends not only on the pillar parameters but also on the other pillars in his vicinity. There are electromagnetic couplings between pillars. And it is shown on figure 1 that when describing the neighborhood of a pillar with its correlation lengths, different relations f_{σ_i} are found. It appears that the resonance amplitudes decrease when the correlation lengths increase, and that the correlation length also affects the

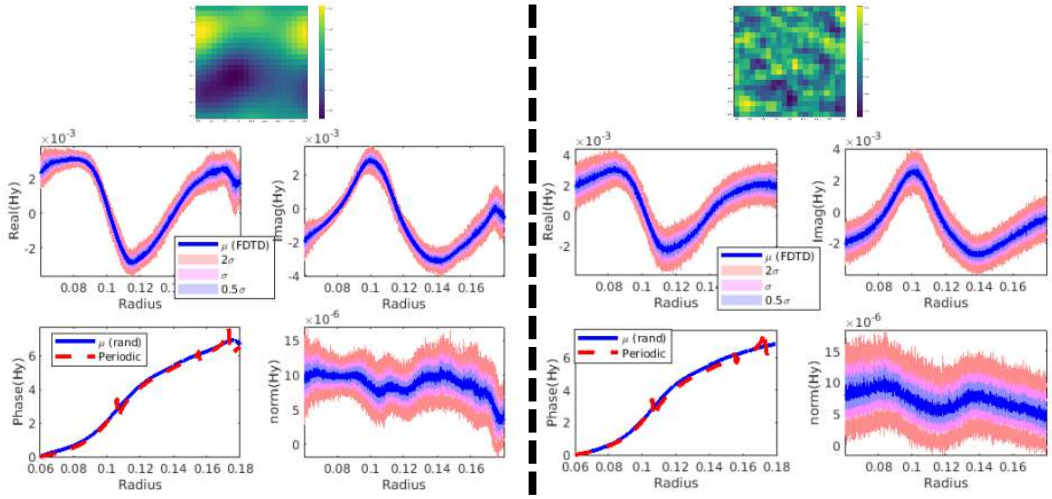


Figure 2:Statistical relation between phase/transmission and radius for two different perturbations

resonance localization [1-3]. This system makes possible a rigorous statistical analysis of the impact of neighboring pillars on a given individuation pillar. Additionally, an efficient AI-based convolutional model that can accurately reproduce the FDTD results (when these pseudo-random structures are correctly added in the training database) will be discussed in the conference. A further study has been conducted on the influence of the correlation length of a database on the training of an IA based solver with architectures like the ones introduced in [4-6].

References

1. M. Khokhar and R. V. Nair, "Engineering strong magnetic dipole resonance in all- dielectric metasurfaces," 2022 Workshop on Recent Advances in Photonics (WRAP), Mumbai, India, 2022, pp. 1-2, doi: 10.1109/WRAP54064.2022.9758271.
2. Lalanne, P., Chavel, P., Laser & Photonics Reviews 2017, 11, 1600295.
3. Babicheva, V. E., Evlyukhin, A. B., Laser & Photonics Reviews 2017, 11, 1700132. https://doi.org/10.1002/lpor.201700132
4. An, S., Zheng, B., Shalaginov, M. Y., Tang, H., Li, H., Zhou, L., Dong, Y., Haerinia, M., Agarwal, A. M., Rivero-Baleine, C., Kang, M., Richardson, K. A., Gu, T., Hu, J., Fowler, C., Zhang, H., Deep Convolutional Neural Networks to Predict Mutual Coupling Effects in Metasurfaces. Adv. Optical Mater. 2022, 10, 2102113. https://doi.org/10.1002/adom.202102113
5. Joowon Lim and Demetri Psaltis , "MaxwellNet: Physics-driven deep neural network training based on Maxwell's equations", APL Photonics 7, 011301 (2022) https://doi.org/10.1063/5.0071616
6. Mingkun Chen, Robert Lupoiu, Chenkai Mao, Der-Han Huang, Jiaqi Jiang, Philippe Lalanne, and Jonathan A. Fan "WaveY-Net: physics-augmented deep-learning for high-speed electromagnetic simulation and optimization", Proc. SPIE 12011, High Contrast Metastructures XI, 120110C (5 March 2022); https://doi.org/10.1117/12.2612418

ST Restricted

Metamaterial-based devices

Design of a beam-modulable vertical cavity using a dielectric metasurface with a full phase change encircling an exceptional point

Jaewon Jang and Yeonsang Park*

[1]Department of Physics, Chungnam National University, Daejeon 34134, Korea
[2]Institute of Quantum Systems, Chungnam National University, Daejeon 34134, Korea
*corresponding author: yeonsang.park@cnu.ac.kr

Abstract: We suggest dielectric metasurfaces that can have a 2π phase with high reflection. Suggested dielectric metasurfaces are designed to have high reflection and simultaneously have a 2π phase with transmitted light by encircling the phase singularity point. We confirmed by simulation that a vertical cavity with high quality factor can be formed by using metasurfaces as a top reflector in the cavity, and the beam shape emitted from this cavity is modulated with ease with the help of metasurfaces.

The Huygens' metasurfaces are well-known for their high transmittance and phase gradient achieved through the resonant overlapping.[1] In addition, dielectric metasurfaces can work as high reflectors with a single layer effectively.[2] Recently, Song et al. demonstrated that the wavefront of the reflected wave can be modulated by using plasmonic metasurfaces with a 2π phase change protected topologically around the exceptional point.[3]

Here, we propose a dielectric metasurface that has a very high reflectivity at the target wavelength of 980 nm and simultaneously enables a 2π phase change for a small amount of transmitted wave. Contrary to the existing Huygens' metasurfaces which focus on enhancing transmission, we investigated the possibility of obtaining high reflection while also modulating the phase of a small amount of transmitted light for the application of a resonant cavity. Through FDTD simulation, we found out the presence of an exceptional point in a cross-shaped a-Si nanostructure as shown in Fig. 1, and that a 2π phase change of the transmitted light could be obtained by encircling this exceptional point.

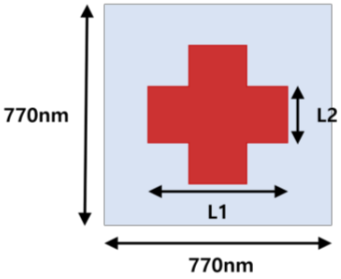


Figure 1. Schematic top view of a-Si nanostructure.

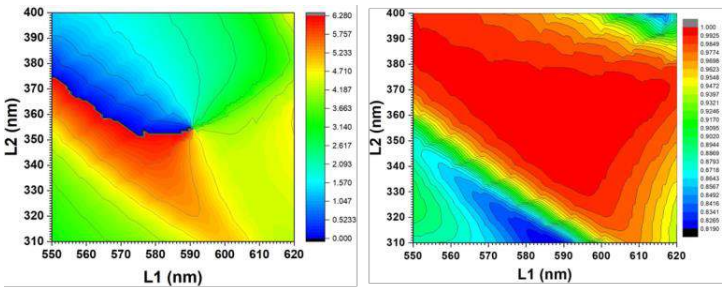


Figure 2. (a) Phase map and (b) Reflection map simulated while changing parameters of L1 and L2.

To confirm the function of the suggested metasurfaces, we simulated a metalens that shows high reflection to form the cavity with high quality factor and simultaneously controls the beam shape of the transmitted light. From Fig. 3, we could confirm that the most of light is reflected and a small amount of transmitted light is focused on the target focal distance with 20 μm. By integrating the simulated metalens with a bottom DBR, we developed a vertical cavity where the top DBR and the metasurface for controlling the emission beam shape are combined as a single layer. The suggested metasurfaces are expected to be used to form a vertical cavity as well as an external cavity for the application of optical communication, non-destructive biological imaging, endoscopy and beyond.

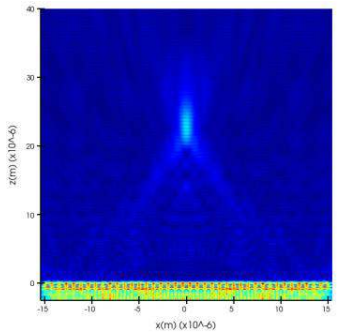


Figure 3. Simulated metalens made of suggested structures.

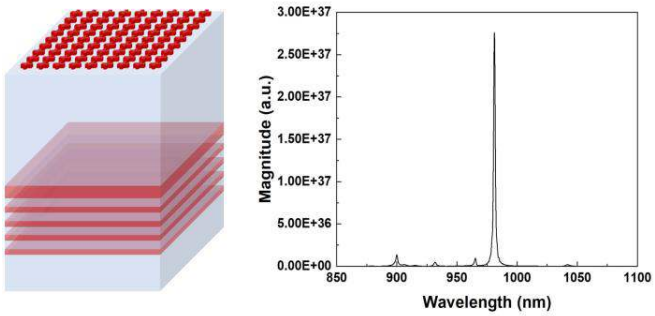


Figure 4. (a) Schematic of metasurface-integrated cavity (b) Simulated spectrum with 980 nm resonant wavelength.

This work was supported by the Ministry of Education of the Republic of Korea and the National Research Foundation of Korea (NRF-2021R1F1A1062182), a Basic Science Research Program through the National Research Foundation of Korea (NRF) funded by the Ministry of Education (NRF- 2020R1A6A1A03047771), and Korea Institute for Advancement of Technology (KIAT) grant funded by the Korea Government (MOTIE) (P0008458, The HRD Program for Industrial Innovation).

References

1. Decker, M., Staude, I., Falkner, M., Dominguez, J., Neshev, N. D., Brener, I., Pertsch, T., Kivshar, S. Y., “High-Efficiency Dielectric Huygens' Surfaces,” Adv. Opt. Mater., Vol. 3, No. 6, 813-820, 2015.
2. Moitra, P., Slovick, A. B., li, W., Kravchencko, I. I., Briggs, P. D., Krishnamurthy, S., Valentine, J., “Large-Scale All-Dielectric Metamaterial Perfect Reflectors,” ACS Photonics, Vol. 2, No. 6, 692-698, 2015.
3. Song, Q., Odeh, M., Zuniga-Perez, J., Kante, B., Genevet, P., “Plasmonic topological metasurface by encircling an exceptional point,” Science, Vol. 373, No. 6559, 1133-1137, 2021.

META 2023, PARIS - FRANCE, JULY 18 – 21, 2023

Converged wireless infrastructure with acoustic holography

Chuanxin Zhang[1], Xue Jiang[1,4,*] and Dean Ta[1,2,3,*]

[1]Center for Biomedical Engineering, School of Information Science and Technology, Fudan University, Shanghai, 200433, China

[2]Academy for Engineering and Technology, Fudan University, Shanghai 200433, China

[3]Department of Rehabilitation Medicine, Huashan Hospital, Fudan University, Shanghai, 200040, China

[4]PengCheng Laboratory, Shenzhen, 518055, China

[*] Email: xuejiang@fudan.edu.cn; tda@fudan.edu.cn

Abstract: Wireless technologies based on electromagnetic wave are crucial in the modern industry but nonoptimal in biomedical and underwater applications, where ultrasound has been proposed as an alternative approach. Here we construct a unified ultrasonic wireless infrastructure that supports multiple specific and separate functions, dubbed converged wireless infrastructure. The infrastructure based on ultrasound holography serves as the central hub to realize a series of wireless functions which is demonstrated with phased array and holograms.

The acoustic version of the wireless technology has been proposed and explored such as wireless powering. The piezoelectric energy harvesting of vibration [1] and ultrasound-based wireless power transfer (WPT) [2] are extended to be applied to charge biomedical electronics [3,4]. The existing research generally allows for single wireless function (e. g. wireless powering) and works for the single terminal. It is desired to develop a converged wireless infrastructure that integrates multiple mainstream wireless functions and allows the interaction among the various components, which yet remains an outstanding challenge. The difficulties lie in creating the complex control network and dynamically modulating the multiple control nodes.

Here we report the realization of acoustic-based converged wireless infrastructure by creating and modulating the control network consisting of multiple nodes with acoustic holography [5,6]. In the proposed wireless system, the holographic array serves as the central hub and integrates a series of mainstream wireless functions. We experimentally demonstrate those functions including the selective wireless power transfer, stable remote audio monitoring, dynamic programmable logic control, and parallel acoustic communication with 11 channels. The wireless system can also control multiple terminals even freely moving in 3D space. The immunity against EM and biological interference are also experimentally validated as unique features of acoustic wireless system. Considering the anti-interference performance and favorable underwater propagation ability, it is envisioned that the converged wireless system based on acoustic holographic array would perform a vital role in extreme environments such as the deep ocean. The converged wireless infrastructure represents a unified scheme to establish the integrated wireless network with different functions, which provides a promising strategy for wireless technologies performing in EM-restricted conditions.

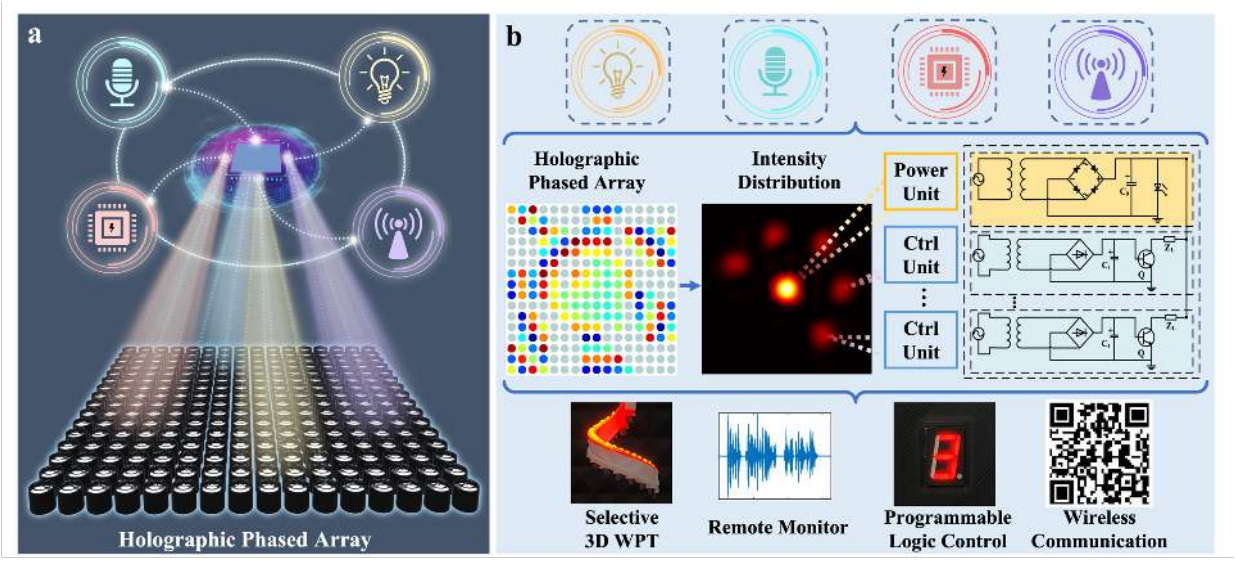


Figure 1. Converged wireless infrastructure based on acoustic holographic array. (a) Schematic of the converged wireless infrastructure which integrates mainstream wireless functions demonstrated in this work: selective 3D wireless powering of arbitrarily-distributed devices, remote audio monitoring, dynamic programable logic control of moving targets and wireless communication. Ultrasound holographic phased array (HPA) acts as the central hub to wirelessly assign commands and coordinate the individual devices. **(b)** Workflow diagram of the proposed acoustic wireless system. The HPA modulates control modes by specifying the acoustic intensity distribution according to the desired functions (top panel). Ultrasound energy is converted to the wireless power supplies by the power unit, or transferred into the control signals by the control unit, with the corresponding circuit diagrams shown on the right panel. Versatile wireless functions are realized by integrating those power and control units (bottom panel).

Acknowledgements: This work is supported by the National Natural Science Foundation of China (Grants No. 11904055, 12034005, and 11827808), the STCSM Science and Technology Innovation Plan of Shanghai Science and Technology Commission (Grant Nos. 20ZR1404200 and 21JC1400300), the Shanghai Chenguang Program (Grant No. 20CG02), the Program of Shanghai Academic Research Leader (Grant No. 19XD1400500).

References

1. Erturk A., J. Hoffmann, and D. J. Inman, “A piezomagnetoelastic structure for broadband vibration energy harvesting” Appl. Phys. Lett. Vol. 94, No. 25, 254102, 2009.
2. Jiang L., Y. Yang, Y. Chen, and Q. Zhou, “Ultrasound-induced wireless energy harvesting: From materials strategies to functional applications” Nano Energy Vol. 77, 105131, 2020.
3. Hinchet R., H.-J. Yoon, H. Ryu, M.-K. Kim, E.-K. Choi, D.-S. Kim, and S.-W.Kim, “Transcutaneous ultrasound energy harvesting using capacitive triboelectric technology” Science Vol. 365 No. 6452, 491, 2019.
4. Piech D. K., B. C. Johnson, K. Shen, M. M. Ghanbari, K. Y. Li, R. M. Neely, J.E. Kay, J. M. Carmena, M. M. Maharbiz, and R. Muller, “A wireless millimetre-scale implantable neural stimulator with ultrasonically powered bidirectional communication” Nat. Biomed. Eng. Vol. 4, No. 2, 207, 2020.
5. Marzo A., S. A. Seah, B. W. Drinkwater, D. R. Sahoo, B. Long, and S.Subramanian, Nat. Commun. Vol.6, No. 1, 8661, 2015.
6. Melde K., A. G. Mark, T. Qiu, and P. Fischer, “Holograms for acoustics” Nature Vol. 537, No. 7621, 518, 2016.

META 2023, PARIS - FRANCE, JULY 18 – 21, 2023

Atomic-level engineered transition-metal alloy photoanodes with record efficiency for solar water splitting

Fei Xiang[1], Ning Li[1], Arturo Burguete-Lopez[1], Zhao He[1], Maxim Elizarov[1], Andrea Fratalocchi[1*]

[1]PRIMALIGHT, King Abdullah University of Science and Technology (KAUST), Thuwal 23955-6900, Saudi Arabia
[*]corresponding author: andrea.fratalocchi@kaust.edu.sa

Abstract: We report a uniform transition-metal metamaterial alloy with atomic-level control on Si photoanodes for efficient and stable solar-assisted water splitting. This technique extends the lifetime of the photoelectrochemical device beyond 250 hours, achieving a record applied bias photon-to-current efficiency (ABPE) efficiency of 4.25%.

Harvesting solar energy for hydrogen production has attracted broad research interests as a sustainable conversion and storage pathway with zero carbon emission [1-3]. While the hydrogen evolution reaction at the device photocathode achieves high efficiency (ABPE up to 12% [4]), the water reaction at the photoanode suffers from poor kinetics, with best-reported ABPE efficiencies below 4% [4-6]. Studying new photoanodes with enhanced performances attracts the largest body of present research efforts [3, 7].

Besides the energy conversion efficiency, PEC photoanodes also need to improve their stability [8, 9]. For PEC devices with efficiencies above 3%, the reported stability under continuous working is generally below 100 hours [5]. For example, the a-Si/TiO_2 bilayer passivated n-c-Si/a-Si/TiO_2/Ni photoanode affords a ABPE of 3.9% with 30 hours stable operation [4]. The poor device lifetime for photoanodes originates from the structural instability of the semiconductor light absorber in the strong alkaline electrolyte (pH = 14) and the photo corrosion of the co-catalyst layer [7]. While additional protective layer coating, such as, e.g., SiO_x and Al_2O_3, prolongs the n-Si/Pt/Ni photoanode lifetime to around 200 hours, the water oxidation efficiency drops to 0.98% [6].

In this work, we report a conformal, atomic-level engineered nickel-iron (NiFe) metamaterial that simultaneously works as a co-catalyst and protective layer for the photoanodes (**Figure 1**). These self-protected photoanodes with 2 nm thickness of NiFe achieve an ABPE efficiency of up to 4.25% for the water oxidation reaction. Figure 1a-c report the scanning electron microscopy (SEM) and scanning transmission electron microscope (STEM) images of uniform and conformal coating of NiFe alloy deposited on the top surface of photoanodes. Figure 1d presents the *J-E* curves of fabricated PEC devices with varying thicknesses of NiFe. The best PEC device achieves a low onset potential of 1.08 V vs. RHE at the current density of 10 mA cm^{-2}. The system reaches a saturated current density I_{sat} = 39 mA cm^{-2}, close to the thermodynamic limit of the c-Si (Fig. 1d dashed line). Under continuous working conditions, the device operates with nearly 100% retention of its initial current for more than 40 hours (Fig. 1e). Figure 1f compares the performances of the NiFe PEC device implemented in this work against state of the art. These results open the design and implementation of highly efficient and durable PEC devices for large-scale solar hydrogen generation.

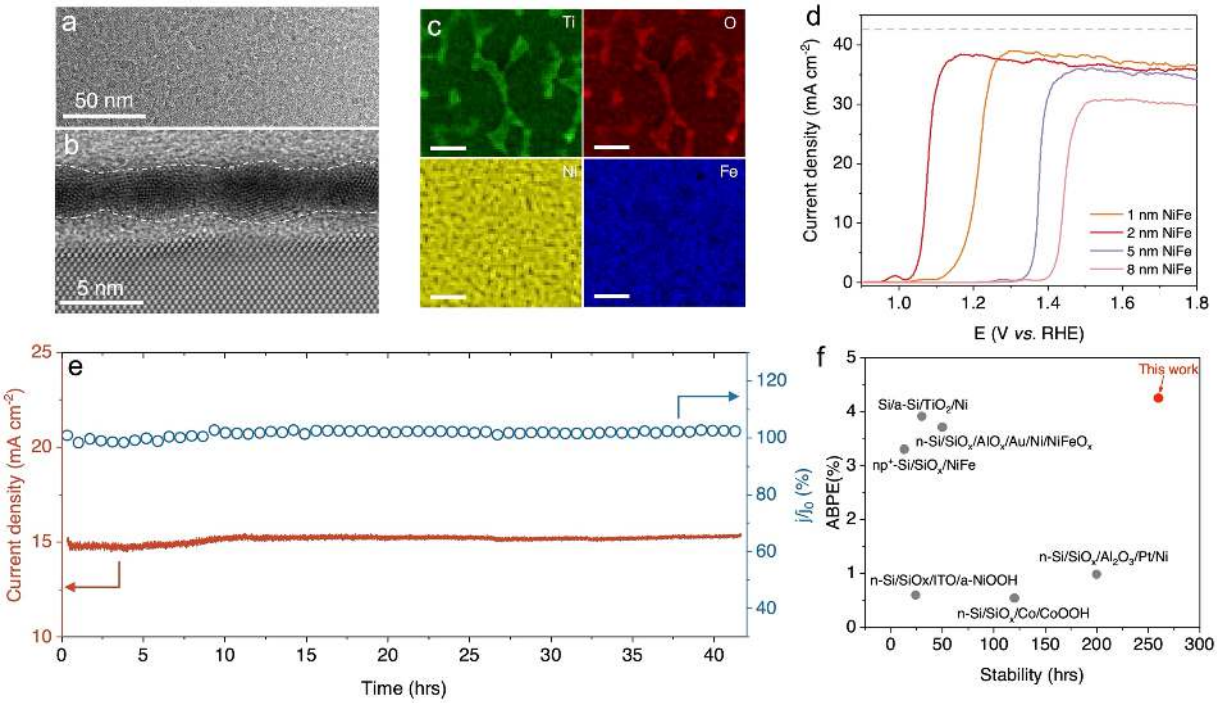


Figure. 1 (a) Top-view SEM image of the device surface. (b) Cross-sectional STEM image of the heterostructured PEC device (The region between the dash lines represents the NiFe alloy layer). (c) Top-view EDS mapping of the TiO_2 and NiFe nanofilms on the Si substrate (scale bars: 2 nm). (d) J-E curve of devices with different NiFe alloy thicknesses. (e) Long-term stability test of the device with an optimized thickness of NiFe nanolayer at initial current density of 15 mA cm^{-2}. (f) Applied bias photon-to-current efficiency and stability of the device compared with the state-of-the-art.

References

1. Kenney, M. J. et al. High-performance silicon photoanodes passivated with ultrathin nickel films for water oxidation. Science 342, 836–840 (2013).
2. Sun, K. et al. Enabling silicon for solar-fuel production. Chemical Reviews 114, 8662–8719 (2014).
3. Yang, J. et al. A multifunctional biphasic water splitting catalyst tailored for integration with high-performance semiconductor photoanodes. Nature Materials 16, 335–341 (2017).
4. Liu, B. et al. Bifacial passivation of n-silicon metal–insulator–semiconductor photoelectrodes for efficient oxygen and hydrogen evolution reactions. Energy & Environmental Science 13, 221–228 (2020).
5. Ma, J. et al. Identifying and Removing the Interfacial States in Metal-Oxide–Semiconductor Schottky Si Photoanodes for the Highest Fill Factor. Journal of the American Chemical Society 144, 17540–17548 (2022).
6. Digdaya, I. A., Adhyaksa, G. W., Trze´sniewski, B. J., Garnett, E. C. & Smith, W. A. Interfacial engineering of metal-insulator-semiconductor junctions for efficient and stable photoelectrochemical water oxidation. Nature Communications 8, 15968 (2017).
7. Chen, Y. W. et al. Atomic layer-deposited tunnel oxide stabilizes silicon photoanodes for water oxidation. Nature Materials 10, 539–544 (2011).
8. D¨oscher, H., Young, J. L., Geisz, J. F., Turner, J. A. & Deutsch, T. G. Solar-to-hydrogen efficiency: shining light on photoelectrochemical device performance. Energy & Environmental Science 9, 74–80 (2016).
9. Hill, J. C., Landers, A. T. & Switzer, J. A. An electrodeposited inhomogeneous metal–insulator–semiconductor junction for efficient photoelectrochemical water oxidation. Nature Materials 14, 1150–1155 (2015).

META 2023, PARIS - FRANCE, JULY 18 – 21, 2023

Breathalyzer-based Prompt Coronavirus Screening Test using Terahertz Spectroscopy of Viruses in LC-Resonant Metamaterial Nano-Antenna Array

Rudrarup Sengupta[1*], Heena Khand[1], and Gabby Sarusi[1]

[1]Department of Photonics and Electro-Optics Engineering, School of Electrical and Computer Engineering, Ben-Gurion University of the Negev, Beer Sheva, Israel. *corresponding author: rudrarup@post.bgu.ac.il

Abstract: We propose a tested, sensitive and prompt COVID-19 breath-screening method that takes less than one-minute. The non-biological method is based on detection of shift in terahertz resonance-frequency of a nano-engineered LC-resonant metamaterial chip, caused by viruses and related exhaled particles. The chip is enclosed in breathalyzer-like enclosure, which is shown to optically suppress Fabry-Pérot, for the first time. Low-scale clinical trials were conducted with asymptomatic, symptomatic coronavirus-patients and healthy individuals, where coronavirus-positive are effectively-screened with 87% accuracy, from healthy individuals.

Our proposed method is based on the detection of shift in resonance frequency of a nano-gap LC-resonant metamaterial chip, caused by viruses and mainly related exhaled particles, when performing a terahertz (THz) spectroscopy. The metallic nanostructure is physically designed as an inductor and capacitor element, where its fundamental resonant frequency is $F_0 = 1/2\pi\sqrt{LC}$. Here, L is the inductance and C is the capacitance. C is highly dependent on the effective dielectric constant (ε_{eff}) of the material introduced inside the capacitor gap. A change in the resonant frequency of the metamaterial structure can be brought about by any foreign substance deposited in the capacitive gap region, thereby changing the ε_{eff} and thus the capacitance, resulting in a redshift in the resonance frequency (ΔF) with respect to the pristine LC circuit in the array.

For the detection of COVID-19 carriers using metamaterial-based structures, we physically re-design the THz LC resonant geometry with the intention of maximizing the capacitor-gap-area. The capacitor gap (width) can be reduced in order in order to obtain the plasmonic enhancement that is associated with the nano-metric scale of such a capacitor gap. Placing the capacitor gaps at both geometric diagonals of a square inductor enables the exhaled viruses and particles to be detected in both S and P polarization states with a rectangular all-around singular inductor structure as shown in Figure 1(a, b), for its resonance detection. This improvement enables breathalyzer-based coronavirus and related particle detection by increasing the capacitive gap lengths compared to the basic SRR[1]; this effectively increases the sensitivity by increasing the probability of viruses/particles falling inside the capacitive gap and yet maintaining a sub-micron capacitor gap, thereby enabling pronounced resonance frequency shifts for breath samples even with a lower virus load. The 3D printed capsule enclosure for our metamaterial chip, is optically designed with layers having specific property to optically suppress the Si substrate's Fabry-Perot losses.

In our proposed coronavirus screening test with we detect a combination of viruses and related biological particles exhaled by an infected person, (e.g. virus debris, cytokines, cell debris and related proteins and fat molecules) which produces an effective change in dielectric constant of the resonant metamaterial at the capacitive gap regions. This phenomenon red shifts the resonance frequency (ΔF), which becomes the deterministic factor to effectively screen the infected patients from the healthy individual. We achieve a definite band of $\Delta F = 1.5\ GHz$ to $9\ GHz$ for infected individuals, with a linear relationship of increasing ΔF with increasing viral load as shown in Figure 2. In order to effectively differentiate between 'healthy' and 'SARS-CoV-2 infected' patients in terms of ΔF, we included only 'completely healthy' and 'sick of SARS-CoV-2' individual, in order to design a screening test only and not a diagnostic test. The simplicity of this cost-effective breathalyzer-based testing kit lies in its ease of handling, which does not require

a complex setup procedure. The entire testing and analysis are performed within 50 to 55 seconds, with 86.84% agreement with the RT-qPCR analysis (with both PPV and NPV values of 88.88%), based on the low scale verification clinical trials conducted at Soroka medical centre, Israel.

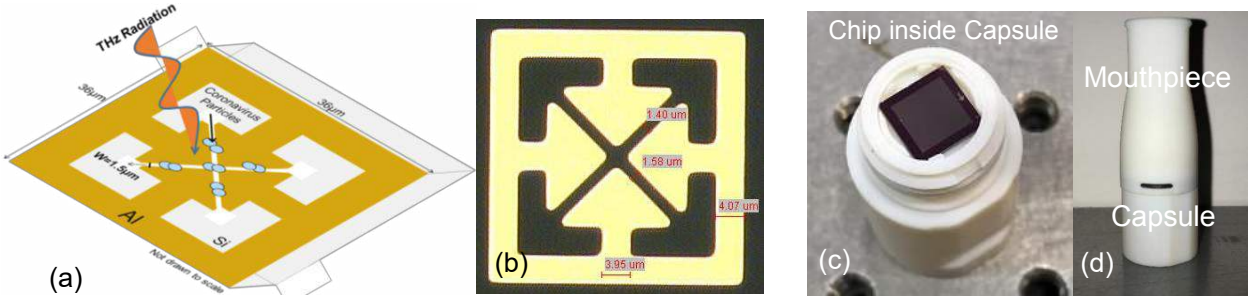


Figure 1. (a) 3D schematic model of the engineered cross-polarization four arrowhead LC resonant metamaterial structure with coronavirus particles positioned at the capacitive gap (W), changing the ε_{eff} (given dimensions not drawn to scale). (b) Microscopic image of the fabricated cross-polarization four arrowhead LC resonant metamaterial structure. (c) Snapshot of open capsule cover revealing chip inside the capsule; (d) snapshot of the entire breathalyzer kit assembly ready to be exhaled.

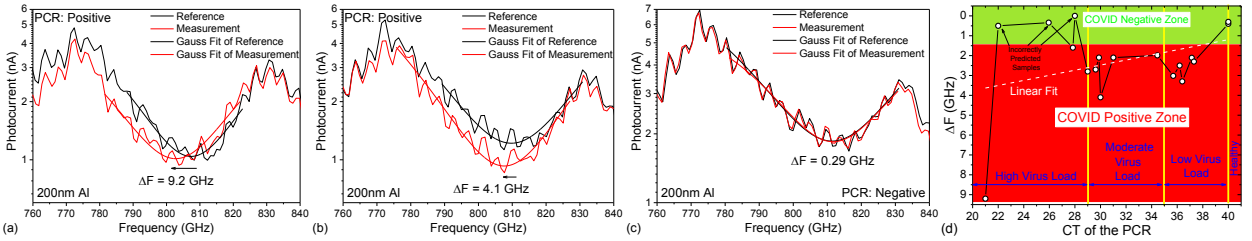


Figure 2. Experimental THz spectra (envelope) of healthy and infected patients. (a) Transmittance spectra of a coronavirus infected patient with CT value of 21 showing a ΔF of 9.2GHz. (b) Transmittance spectra of a coronavirus infected patient with CT value of 30 showing a ΔF of 4.1 GHz. (c) Transmittance spectra of a completely healthy individual with negligible ΔF. (d) Statistical representation of all the samples (positive and negative) showing the relation between ΔF and the viral load which is indicated by the CT value of the PCR. The data-set is linearly fitted which shows a clear linear dependence.

Table 1. Comparison of SARS-CoV-2 RT-qPCR and Breath Analyzer Rapid Test Results

	Breath Analyzer Rapid Test			
RT-qPCR Test	Positive	Negative	Total	Sens/Spec
Positive	13	3	16	Sens: 13/16 = 81.25%
Negative	2	22	24	Spec: 22/24 = 91.67%
Total	15	25	40	87.50% agreement with the RT-qPCR analysis
PPV/NPV	PPV: 13/15 = 86.67%	NPV:22/25 = 88.00%		

Sens:sensitivity; Spec:specificity; PPV:positive predictive value; NPV:negative predictive value; RT-qPCR:realtime quantitative polymerase chain reaction

References

1. Park, S. J.; Cha, S. H.; Shin, G. A.; Ahn, Y. H. 'Sensing Viruses Using Terahertz Nano-Gap Metamaterials'; Biomed. Opt. Express 2017, 8 (8), 3551. https://doi.org/10.1364/boe.8.003551.
2. Sengupta, R; Khand, H; and Sarusi, G; 'Terahertz Impedance Spectroscopy of Biological Nanoparticles by a Resonant Metamaterial Chip for Breathalyzer-Based COVID-19 Prompt Tests'; ACS Applied Nano Materials, 2022, 5 (4), 5803-5812, DOI: 10.1021/acsanm.2c00954.
3. Sarusi, G.; Sengupta, R.; 'Prompt Viruses Infection Detection Using THz Spectroscopy in a Breathalyzer-Like Configuration'; Patent WO2021199036A1, 2021.

Electronic beam steering using a reconfigurable metasurface

N. Meftah[1], B. Ratni[1], M. N. El Korso[2], and S. N. Burokur[1*]

[1]LEME, UPL, Univ Paris Nanterre, F92410 Ville d'Avray, France
[2]Université Paris-Saclay, CNRS, CentraleSupélec, Laboratoire des signaux et systèmes, 91192 Gif-sur-Yvette, France
[*]corresponding author: sburokur@parisnanterre.fr

Abstract: A 2D reconfigurable reflective metasurface with individually addressable unit cells incorporating voltage-controlled varactor diodes is proposed. This metasurface illuminated by a primary source is used as a reconfigurable parabolic reflector antenna, enabling an electronic control of beam steering by assigning the appropriate phase profile along the metasurface through capacitance modulation.

Metasurfaces have attracted great interest due to their ability to manipulate electromagnetic waves, such as radiation control [1-3], wavefront shaping [1,4], and polarization conversion [5]. The concept of reconfigurable metasurfaces has emerged in recent years to satisfy the changing requirements in practical applications and enable the integration of multiple functionalities into a single metasurface. In this paper, a fully programmable metasurface with individually addressable unit cells, enabling between -180° and 180° phase coverage, is designed for operation around 2.3 GHz by incorporating varactor diodes. The metasurface associated with a primary source is used as a 2D reconfigurable parabolic reflector antenna to achieve complete elevation and azimuth beam scanning.

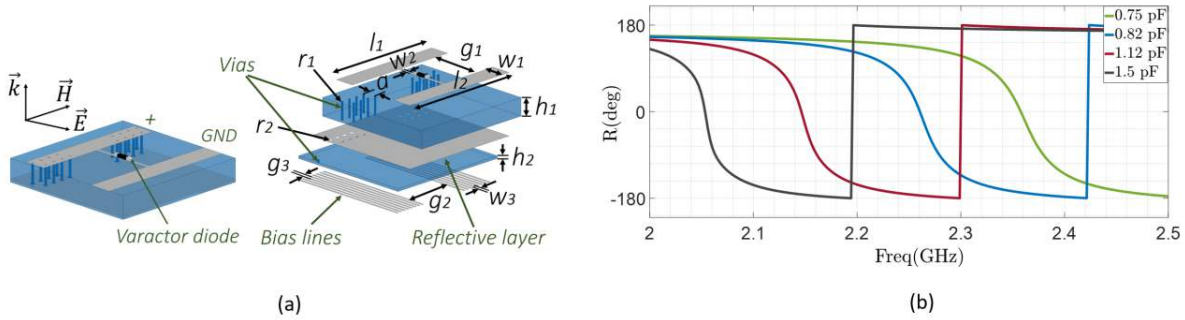


Figure 1. (a) Schematic design of the unit cell: l_1 = 24 mm, l_2 = 25 mm, w_1 = 4 mm, w_2 = 2 mm, w_3 = 0.4 mm, g_1 = 11 mm, g_2 = 9.85 mm, g_3 = 0.5 mm, a = 2 mm, r_1 = 0.4 mm, r_2 = 0.8 mm, h_1 = 3.5 mm and h_2 = 0.25 mm. (b) Simulated reflection phase responses for different capacitance values.

The proposed reconfigurable metasurface comprises 16x16 tunable unit cells. As shown in Fig. 1(a), the tunable unit cell is composed of three metal layers: the capacitive grid incorporating the varactor diode (SMV1405-040LF), the reflective ground plane and the voltage bias layer. The dielectric substrates used have relative permittivity ε_r = 2.2. 16 vias are integrated into the top dielectric substrate, where 15 are blind vias, and a single one is connected to the power supply to bias the varactor diode. From Fig. 1(b), it can be noted that the resonance frequency varies from 2.05 GHz to 2.36 GHz when the capacitance changes from 1.5 pF to 0.75 pF, enabling to achieve a phase gradient close to 360° at 2.3 GHz.

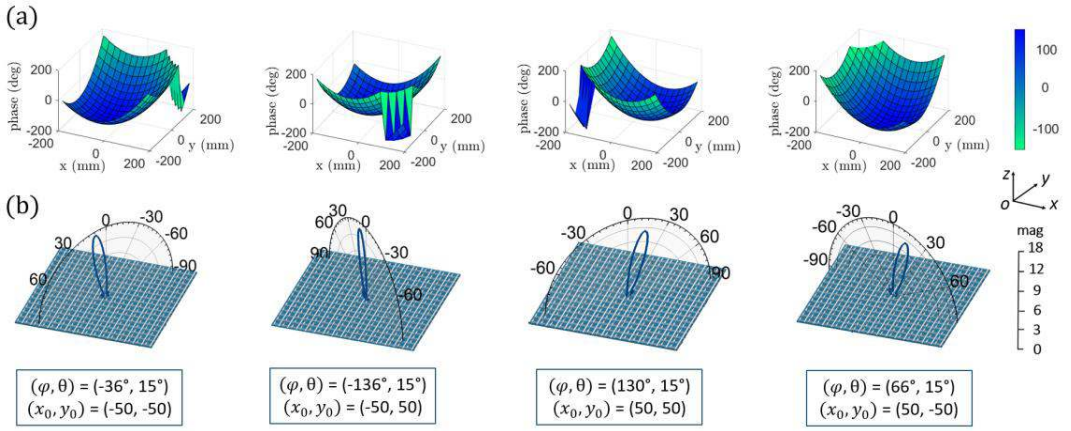


Figure 2. (a) 2D phase profiles for beam steering. (b) Simulated far-field radiation patterns for different (x0, y0) shifting.

The designed 2D reconfigurable metasurface is illuminated by a primary source to be used as a planar parabolic reflector to generate a fully controllable highly directional beam. The parabolic phase profile applied along the metasurface is calculated as:

$$\varphi(x,y) = \frac{2\pi}{\lambda}\left(\frac{(x-x_0)^2+(y-y_0)^2}{4F}\right) + \varphi_0 \qquad (1)$$

where λ is the free space operating wavelength, F (= 150 mm) is the focal distance, and φ_0 is the reflection phase at (x_0, y_0). A direct coaxial-fed microstrip patch antenna designed for 2.3 GHz operation is used as a primary source and is placed at the focal point. In order to control beam steering, the phase profile is electronically adjusted by shifting the reference reflection phase along the *x*-, *y*-direction or both, such that the feeding source is virtually displaced in the focal plane. The simulation results show directive radiation with more than 10 dB realized gain. A deflection of ±30° from the *z*-axis with 360° steering in the *xoy* plane (Fig. 2) is achieved.

The designed programmable metasurface has been used to design a 2D reconfigurable parabolic reflector antenna, where high directive beams and 360° beam steering flexibility and ±30° vertical scanning have been demonstrated in simulation by judiciously modifying the phase profile.

References

1. Ratni, B., A. de Lustrac, G.-P. Piau and S. N. Burokur, "Reconfigurable meta-mirror for wavefronts control: applications to microwave antennas," Opt. Express, Vol. 26, No. 3, 2613–2624, 2018.
2. Ratni, B., Z. Wang, K. Zhang, X. Ding, A. de Lustrac, G.-P. Piau, S. N. Burokur, "Dynamically controlling spatial energy distribution with a holographic metamirror for adaptive focusing," Phys. Rev. Appl., Vol. 13, No. 3, 034006, 2020.
3. De Lustrac, A., B. Ratni, G.-P. Piau, Y. Duval and S. N. Burokur, "Tri-state metasurface-based electromagnetic screen with switchable reflection, transmission, and absorption functionalities," ACS Appl. Electron. Mater., Vol. 3, No. 3, 1184–1190, 2021.
4. Feng, R., B. Ratni, J. Yi, H. Zhang, A. de Lustrac and S. N. Burokur, "Versatile metasurface platform for electromagnetic wave tailoring," Photon. Res., Vol. 9, No. 9, 1650–1659, 2021.
5. Ratni, B., A. de Lustrac, G.-P. Piau and S. N. Burokur, "Electronic control of linear-to-circular polarization conversion using a reconfigurable metasurface," Appl. Phys. Lett., Vol. 111, No. 21, 214101, 2017.

Modifying the integer quantum Hall effect with cavity vacuum fields

J. Enkner[1], F. Appugliese[1], G. L. Paravicini-Bagliani[1], M. Beck[1], C. Reichl[2], W. Wegscheider[2], G. Scalari[1], C. Ciuti[3], and J. Faist [1*]

[1]Institute of Quantum Electronics, ETH Zürich, Zürich 8093, Switzerland
[2]Laboratory for Solid State Physics, ETH Zürich, Zürich 8093, Switzerland
[3]CNRS, Laboratoire Matériaux et Phénomènes Quantiques, Université Paris Cité, F-75013 Paris, France
[*]corresponding author: jerome.faist@phys.ethz.ch

Abstract: As reported by Appugliese et al. [1] as you immerse a Hall bar into the cavity vacuum fields of a 2-dimensional metamaterial, a split ring resonator (THz), the interaction with vacuum fields not only modifies the finite resistances of the Shubnikov de Haas oscillations in the diffusive transport regime [2], but it also breaks the topological protection in the integer quantum hall regime. We quantify this loss of quantization as vacuum field induced resistivity that is directly linked to the Rabi frequency.

As a topological insulator the quantum Hall system is paradigmatic for being robust under the influence of short-range perturbations. We observe the loss the zero-resistance states in the longitudinal traces and quantization of the Hall plateaus due to the cavity induced long-range perturbations. The accompanying picture is called "cavity mediated electron hopping" [3]. It shows that with an anti-resonant process we can lift an electron occupying the disordered state ϕ_λ^n in the nth Landau level into the state $\phi_{\lambda''}^{n+1}$ in the (n+1)th with the emission of a virtual photon. The inverse process then drops the electron back into the nth Level, but into a different disordered state $\phi_{\lambda'}^n$ at a different location as the virtual photon gets also re-absorbed. Effectively, with this process electrons can now scatter between the topologically protected edge states via the insulating bulk and break topological protection. The effective coupling $\tilde{\Gamma}_{\lambda,\lambda'}^{(n)}$ between the disordered states ϕ_λ^n and $\phi_{\lambda'}^n$ is given by the expression

$$\tilde{\Gamma}_{\lambda,\lambda'}^{(n)} = \sum_{\lambda''} \frac{\tilde{g}_{\lambda,\lambda''}^{(n,n+1)} \tilde{g}_{\lambda',\lambda''}^{(n,n+1)}}{\epsilon_{n,\lambda} - \epsilon_{n+1,\lambda''} - \hbar\tilde{\omega}_{\mathrm{cav}}} \qquad (1)$$

Summing over all N_{deg} disordered states, where N_{deg} is the degeneracy of the Landau band and $g_{\lambda,\lambda''}^{(n,n+1)}$ is the single electron Rabi frequency that that is calculated through the overlap of the electronic wave functions of state ϕ_λ^n and state $\phi_{\lambda''}^{n+1}$.

We quantitatively characterize this loss of quantization as vacuum field induced resistivity ρ_{vac}^{xx}, a parameter we get from performing an adapted Landauer-Büttiker formalism [4], that describes the scattering that is causing the deviation from perfect quantization with a finite transmission t_i of the highest populated edge state [5]. With extracting the longitudinal resistance R_{xx} at the middle of each quantized plateau we can fit a value for the vacuum field induced scattering ρ_{vac}^{xx}.

When we plot ρ_{vac}^{xx} as a function of the cyclotron energy, first we find that the absolute values are higher for odd states than for even. This can be intuitively understood with the fact that each time an electron crosses the gap via an anti-resonant process, it also suffers an energy penalty related to the gap spacing. Since the Zeeman-split states are energetically smaller, higher rates of scattering are a consequence. Secondly, both odd and even states follow the same exponential decay, the characteristic energy E_{char} that hints towards $g_{\lambda,\lambda''}^{(n,n+1)}$ being the

controlling parameter.
In a study we alter the geometry of both Hall bar and cavity (complementary split ring resonator [6]) in a way that guarantees us the same coupling strength but different Rabi frequency (Figure 1a).
Two different samples processed on the same heterostructure display an exponential decay that aligned with the prediction of the characteristic energy in this system, therefore reinforcing the connection to the rabi frequency.

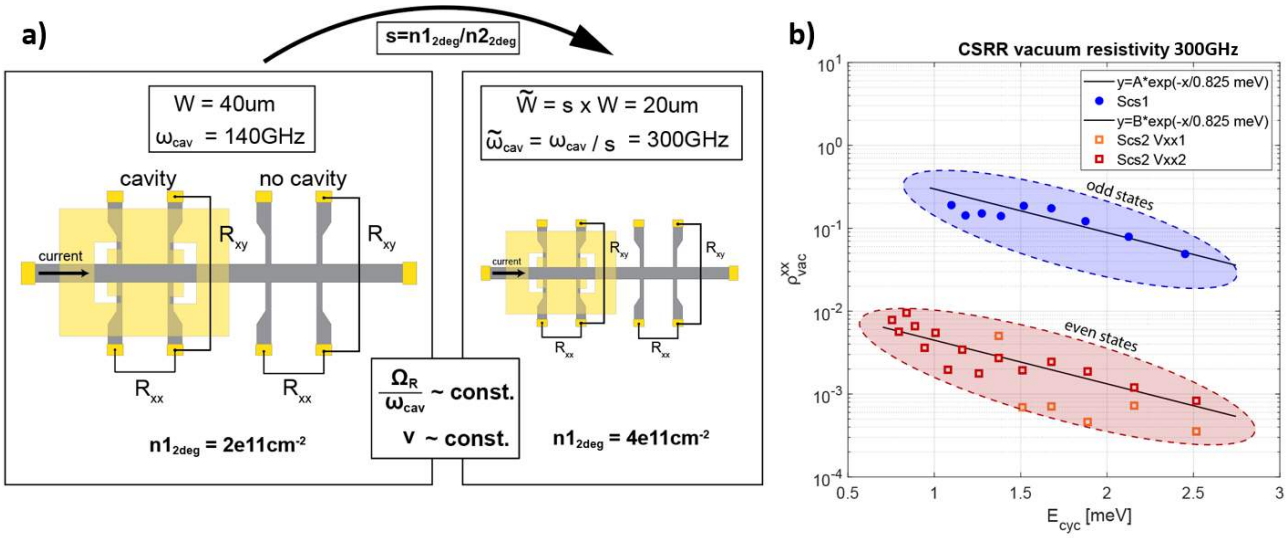


Figure 1: a) sketch illustrating the straight forwardness of scaling both Hall bar and CSRR down by factor 2, locking the coupling strength to the same value of Ω_R/ω_{cav} = 30% while keeping the field profile inside the cavity the same. The parameter changed is Rabi frequency Ω_R. b) two independent samples processed on the same heterostructure but with the same sample geometry and Rabi frequency now only display very comparable values for ρ_{vac}^{xx} but also show the same exponential decay, E_{char} =0.825, that again is directly proportional to the Rabi frequency.

In our work we present a deeper understanding and characterization of the effect reported in [1], while directly drawing the connection to the light matter coupled nature of the system.

References

1. F. Appugliese, et.al. Breakdown of topological protection by cavity vacuum fields in the integer quantum hall effect. Science, 375(6584):1030–1034, 2022.
2. Gian L Paravicini-Bagliani et al. Magneto-transport controlled by landau polariton states. Nature Physics, 15(2):186–190, 2019.
3. C. Ciuti. Cavity-mediated electron hopping in disordered quantum hall systems. Physical Review B, 104(15):155307, 2021.
4. M. Büttiker. Absence of backscattering in the quantum hall effect in multiprobe conductors. Physical Review B, 38(14):9375, 1988
5. PL McEuen et al. New resistivity for high-mobility quantum hall conductors. Physical review letters, 64(17):2062, 1990
6. G Scalari et al. Ultrastrong coupling of the cyclotron transition of a 2d electron

gas to a thz metamaterial. Science, 335(6074):1323–1326, 2012

Conductive coupling induced Dark multipole plasmon modes in hybrid cavities

Sukhvinder Kaur[1,*], R. K. Varshney[1], and Dibakar Roy Chowdhury[2]

[1]Department of Physics, Indian Institute of Technology Delhi, Hauz Khas, New Delhi, 110016, India

[2]Department of Physics, Ecole Centrale School of Engineering - Mahindra University, Jeedimetla, Hyderabad, Telangana, 500043, India

[*]Corresponding author: phz198496@physics.iitd.ac.in

Abstract: We have demonstrated the excitation of multipole plasmon modes in hybrid cavity consisting of a split ring resonator (SRR) in the vicinity of dipole cavity (hole array) via conductive coupling.

Localized surface plasmon resonances (LSPRs) are non-propagating surface plasmons, which can be excited via the interaction of electromagnetic wave with appropriately designed dipole cavities [**1**]. These plasmonic modes enhances the confinement of electromagnetic energy through strong light-matter interaction. Planar plasmonic structures support higher order plasmonic modes inherently but they consist of low scattering intensity in comparison to the dipolar plasmonic modes [**2**]. Hence, these higher order modes are not easy to excite in such structures. In this context, the coupling of dipole cavities with other plasmonic structures provides additional degree of freedom to tune the higher-order plasmon modes [**2-4**]. In the present study, we investigated the effect of conductive coupling of SRR and dipole cavity on the transmission characteristics of the hybrid structure.

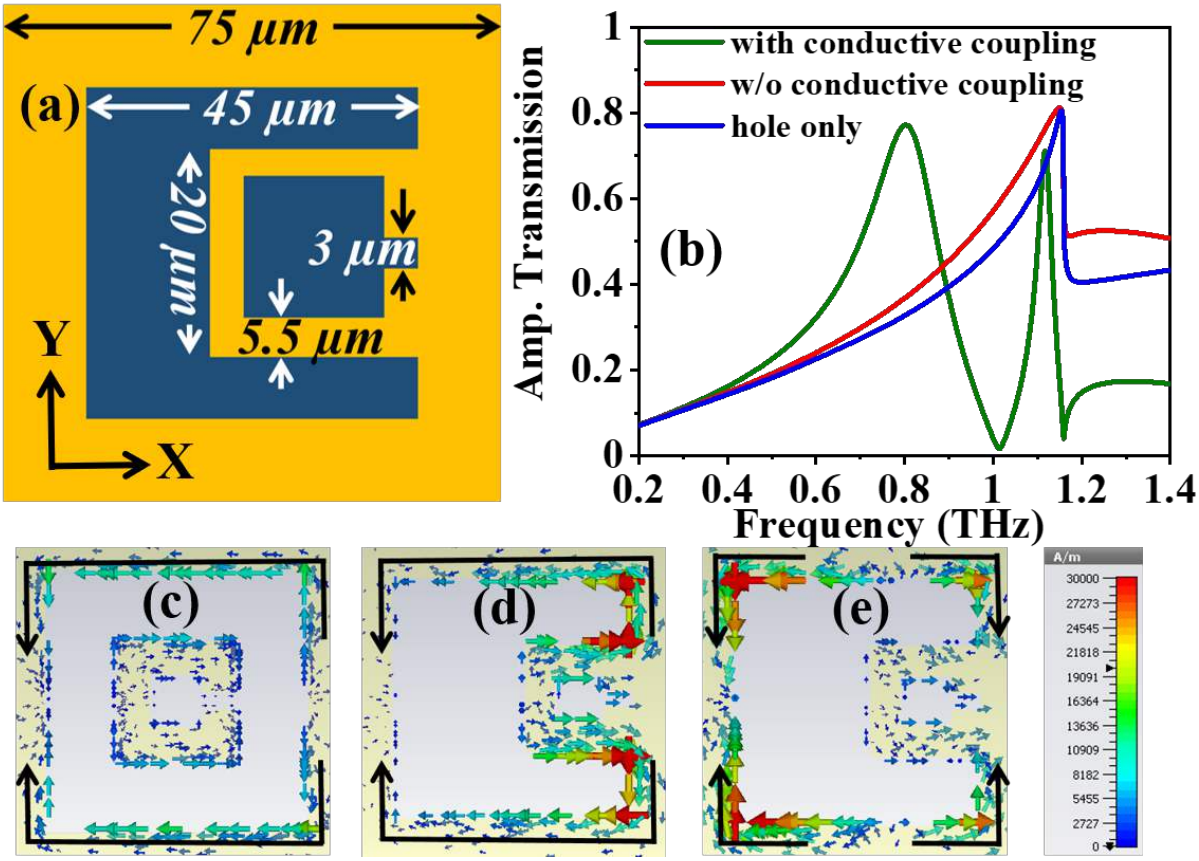


Fig. 1: (a) Unit cell of the proposed metamaterial structure displaying the geometrical parameters; (b) Transmission amplitude spectra depicting the evolution of new resonance peak for conductive coupling; Surface

current distribution (c) for "without" conductive coupling at $f = 1.15\,THz$; for "with" conductive coupling at (d) $f = 0.80\,THz$, and (e) $f = 1.12\,THz$.

The unit cell of the proposed structure along with the geometrical parameters is shown in Fig. 1(a). The structure is designed on an intrinsic silicon substrate of $25\,\mu m$ thickness. On the top of the Si substrate, a 200 nm thick perforated aluminum sheet consisting of a square cavity is placed and an SRR of same thickness is placed inside the cavity. We theoretically investigated the transmission characteristic of the hybrid resonant cavity for x-polarized terahertz radiations. The numerical analysis of the designed structure is done by using commercially available CST microwave studio. Unit cell boundary conditions are used in the x- and y-direction, whereas open boundary conditions are used in the z-direction.

Initially, we studied the transmission amplitude spectra of the uncoupled dipole cavity. As shown in Fig. 1(b), the transmission spectra of uncoupled dipole cavity consist of a dipole resonance peak at $f = 1.15\,THz$ due to the excitation of surface plasmons at metal-dielectric boundary. Subsequently, the SRR was introduced at the center of the cavity and the transmission spectra was recorded with x-polarized light. The structure is symmetric about x-axis, therefore the presence of SRR does not significantly affect transmission spectra (as shown in Fig. 1(b)) for x-polarized incident radiation. In order to introduce conductive coupling between the cavity and the SRR, the SRR is shifted along x-axis until it touches the cavity wall. The transmission spectra for such configuration (Fig. 1(b)) shows the excitation of an additional higher order plasmonic mode. The presence of higher order mode can be confirmed through surface current distribution at resonance frequency (Fig. 1(c-e)), where the direction of the surface current is indicated by the black arrows. Figure 1(c) shows the surface current distribution for the hybrid cavity at $f = 1.15\,THz$ where the SRR is placed at the center. It is clear from the figure that the contribution of SRR does not have significant contribution and the resonance peak is excited due to the cavity only. Figure 1(d, e) shows the surface current distribution for conductive coupling at $f = 0.80\,THz$ and $f = 1.12\,THz$, respectively. The current distribution shows the significant contribution of the SRR and cavity in the excitement of these resonance modes. The current distribution at $f = 0.80\,THz$ demonstrate a typical dipolar plasmon mode whereas, the current distribution at $f = 1.12\,THz$ confirms the excitation of quadrupole surface plasmon mode.

In summary, we demonstrated the excitation of the higher order plasmonic modes induced via conductive coupling between the SRR and the dipole cavity. Such higher order plasmonic modes may have various potential THz applications including filtering, sensing, spectral enhancement, etc.

Acknowledgements: Author SK acknowledges financial support from DST-INSPIRE.

References

1. Maier, S.A. "Plasmonics: fundamentals and applications," New York: springer, Vol. 1, p. 245, 2007.
2. Habteyes, T.G. "Theta-shaped plasmonic nanostructures: bringing "dark" multipole plasmon resonances into action via conductive coupling," Nano letters, 11(4), pp.1819-1825, 2011.
3. Li, L. "Fano-like resonances in the binary elliptical nanoring resonator array," Optical Materials Express, 8(8), pp.2131-2139, 2018.
4. Kaur, S. "Hybrid resonant cavities: A route towards phase engineered THz metasurfaces," Iscience, 25(4), p.104024, 2022.

Highly Sensitive Flexible Terahertz Metasensor for Thin Film Sensing

Parveen Joon, Sukhvinder Kaur, and R. K. Varshney*

Physics Department, Indian Institute of Technology Delhi, New Delhi-110016, India

* ravi@physics.iitd.ac.in

Abstract: We present a flexible terahertz metamaterial sensor that exhibits inductive capacitive (LC)/dipole resonance, and the effects of varying the thickness of a dielectric analyte on Split Ring Resonator/rod structure have been explored. The sensor is highly sensitive to even small (59.9 GHz/μm) environmental changes as the sensor's geometry results in enhanced localized electric fields.

Giving flexibility to metamaterials enables the wrapping of transparent and lightweight metamaterials around objects [1,2]. The dielectric environment present on the surface of the metamaterial structure affects the metamaterial's resonance frequency as it is highly sensitive to changes in the dielectric environment. The sensor is greatly miniaturized due to its subwavelength resonance, which also helps to increase sensitivity because high resonance is restricted to a small area [3]. Therefore, in the present study, we have studied the coupling of SRR and rod structure and demonstrated the excitation of LC/dipole resonance.

Our proposed terahertz metamaterial sensor consists of SRR/rod resonator unit and a flexible polyimide substrate. Figure 1(a) depicts the unit cell of sensing structure. The bottom is the dielectric flexible substrate of polyimide film (n=1.87), and the top is a metallic layer (Al) that produces electromagnetic resonance. The metallic layer encompasses SRR and rod structures. The dimensions are l_r = 20 μm, l_i = 45.5 μm, t_s = 25 μm and t_{al} = 0.2 μm (metallic layer thickness), t_r = 5.5 μm, g = d = 3 μm. The period is l = w = 75 μm and Δl is the change in length.

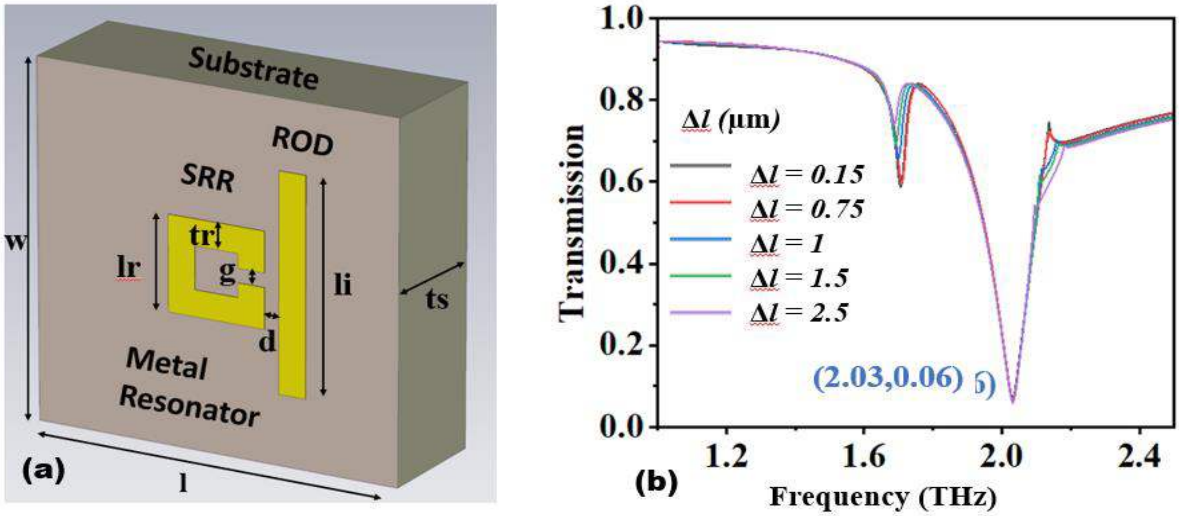


Fig.1. (a) Schematic diagram of SRR/Rod terahertz metamaterial sensor unit cell with parameters (b) Transmission spectra for change in dimensions of the SRR and rod

The transmission spectra, as shown in Figure 1(b), for change in length and width (keeping the area constant) of SRR and rod were obtained by using CST microwave studio to ascertain the flexibility of the structure. The dipole

and LC resonance appeared at 1.71 and 2.03 THz, respectively. It is evident from the transmission spectra that there is no significant shift in the resonance frequency on varying the length and width. Hence, the proposed structure is well-suited for applications that need conformal adhesion. Therefore, the terahertz metamaterial sensor was utilized for thin-film sensing of Mica with a constant refractive index (n)=2.44.

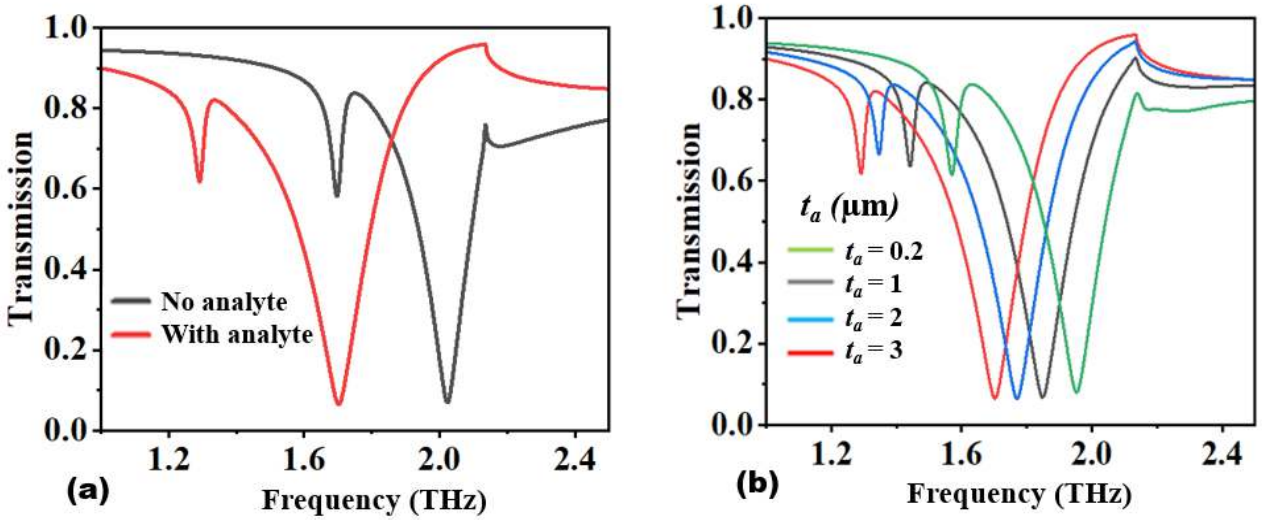


Fig.2. (a) Transmission spectra showing the shift of resonance frequency with and without analyte (b) Transmission spectra showing the shift in resonance frequency with change in Analyte thickness.

The transmission spectra were captured with and without an analyte, as shown in Figure 2(a). The shift in resonance frequency was found to be quite noticeable as evident from the plot. To comprehend the shift in resonance frequency with increasing analyte thickness, the thickness of the sample was increased from 0.2 to 3 μm. As the thickness of the analyte increases, effective capacitance of SRR increases, and hence the resonance frequency decreases leading to redshift [4] which can be seen in the transmission spectrum as shown in Figure 2(b). Hence, the proposed terahertz metamaterial sensor can be employed as thin film sensor and calculated sensitivity ($\frac{\Delta f}{\Delta t_a}$, where, Δf is change in resonance frequency and Δt_a is change in analyte thickness) is 59.9 GHz/μm, which is almost double of previously reported results.

References

1. Walia, "Flexible metasurfaces and metamaterials: A review of materials and fabrication processes at micro-and nano-scales." Applied Physics Reviews, 2(1), p.011303, 2015.
2. Tao, H., "Terahertz metamaterials on free-standing highly-flexible polyimide substrates." Journal of Physics D: Applied Physics, 41(23), p.232004, 2008.
3. Kaur, S., "Resonant toroidal metasurface as a platform for thin-film and biomaterial sensing." Applied Optics, 61(30), pp.9020-9027, 2022.
4. Han, N.R. "Broadband multi-layer terahertz metamaterials fabrication and characterization on flexible substrates," Optics express, 19(8), pp.6990-6998, 2011.

Engineering a multifunctional TiO_2 BIC metasurface

H. Hu[1], L. Hüttenhofer[1], O. Bienek[2], A. Wester[1], T. Weber[1], I. D. Sharp[2], S. A. Maier[1,3,4], E. Cortés[1], and A. Tittl[1*]

[1] Chair in Hybrid Nanosystems, Nanoinstitute Munich, Faculty of Physics, Ludwig-Maximilians-Universität München, Königinstraße 10, 80539 München, Germany
[2] Walter Schottky Institute and Physics Department, Technical University Munich, Am Coulombwall 4, 85748 Garching, Germany
[3] School of Physics and Astronomy, Monash University Clayton Campus, Melbourne, Victoria 3800, Australia
[4] The Blackett Laboratory, Department of Physics, Imperial College London, London SW7 2AZ, United Kingdom.

[*]corresponding author: Andreas.Tittl@physik.uni-muenchen.de

Abstract: We develop a multifunctional metasurface platform that leverages the combination of loss-engineered substoichiometric titanium oxide (TiO_{2-x}) and the emerging physical concept of optical bound states in the continuum (BICs) to boost photoinduced charge transfer (PICT) and provide broad spectral tunability, making this semiconductor metasurface not only a competitive platform for surface photocatalytic investigations, but also a promising candidate for boosting sensitivities in in semiconductor-based surface-enhanced Raman scattering (SERS) applications.

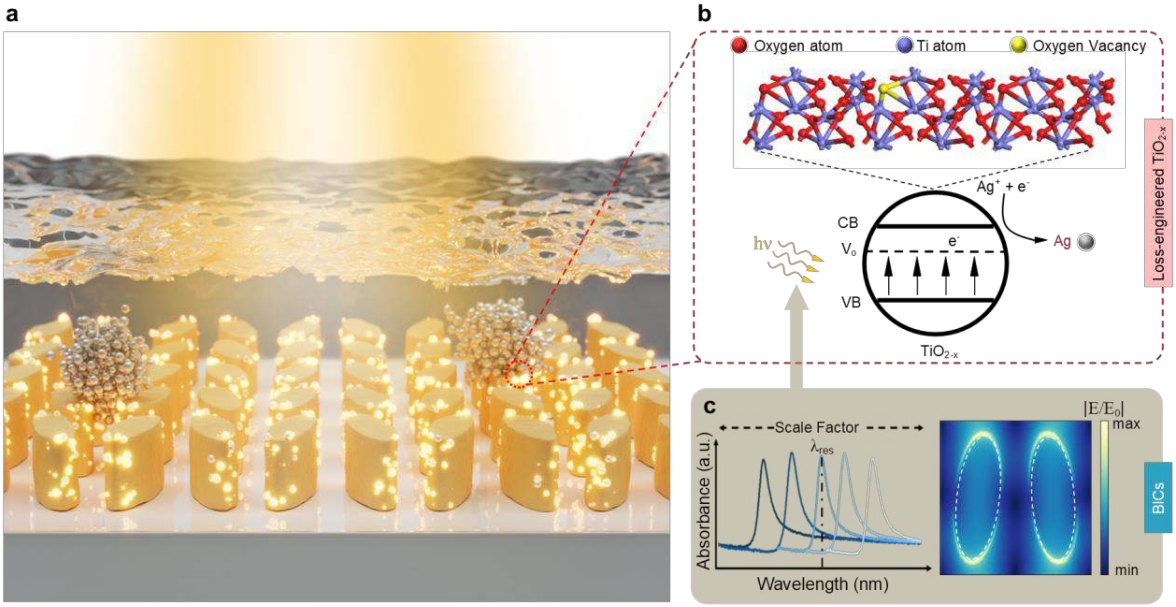


Figure 1. Catalytic metasurfaces driven by bound states in the continuum. a, Schematic of the TiO_{2-x}-based BIC metasurface platform for the photoreduction of silver ions. **b**, Schematic of oxygen vacancies acting as the defect energy level between the conduction band and valence band, which extends the light absorption to the visible region. The photo-excited electron exhibits strong reducing reactivity, resulting in the reduction of Ag^+ ions. **c**, The reduction rate of Ag^+ is increased via metasurface-enhanced light absorption at a given excitation wavelength. Spectral tunability of the catalytic metasurfaces is achieved by adjusting the scaling factor of the unit cell. Strong nanoscale light confinement and

enhancement of the local electromagnetic fields of the catalytic metasurface are provided by the BIC concept (right). This idea can be extended to other materials. Adapted from Ref. [5].

Recently, metasurfaces underpinned by the physics of photonic bound states in the continuum (BICs) with extremely high quality (Q) factors and strong enhancement of electromagnetic fields have received significant interest [1,2]. Most of the BIC-based systems demonstrated so far are constructed from high refractive index materials like Si [3], where pushing the operating range towards the blue part of the optical spectrum is still challenging due to significant dielectric losses associated with the band gaps. TiO_2 is a promising alternative because of its adjustable extinction coefficient [4], but has, so far, not been employed in the context of BIC-based systems.

Here, we present an ultrathin catalytic metasurface platform that leverages, the combination of loss-engineered substoichiometric titanium oxide (TiO_{2-x}) and the emerging physical concept of optical bound states in the continuum (BICs) to boost photocatalytic activity and provide broad spectral tunability (**Figure 1**). We demonstrate that our platform reaches the conditions of critical light coupling in a TiO_{2-x} BIC metasurface, providing at the same time a general framework for maximizing light-matter interactions in diverse photocatalytic materials. This approach can avoid long-standing drawbacks of many naturally occurring semiconductor-based ultrathin films applied in photocatalysis, such as poor spectral tunability and limited absorption manipulation [5].

Additionally, the enhanced photoinduced charge transfer (PICT) in TiO_2 metasurface systems reveals the great potential of this approach as a semiconductor SERS substrate, where PICT is shown to play a dominant role in our experiments. Significantly, we harness two additional benefits of our BIC platform: strong near-field electromagnetic field enhancement as well as broad spectral tunability, which are urgently needed for pushing the development of semiconductor SERS substrates.

Hence, our findings establish this multifunctional metasurface platform as a versatile and efficient means to enhance various photochemical processes and enable new opportunities for optoelectronic device applications.

References

1. Hsu, C. W., B. Zhen and A. D. Stone, et al. “Bound states in the continuum,” Nat. Rev. Mater., Vol. 1, No. 10, 1-13, 2016.
2. Marinica, D. C., A. G. Borisov* and S. V. Shabanov. “Bound states in the continuum in photonics,” Phys. Rev. Lett., Vol. 100, No. 18, 183902, 2008.
3. Tittl A, A. Leitis and H. Altug, et al. “Imaging-based molecular barcoding with pixelated dielectric metasurfaces,” Science, Vol. 360, No. 6393, 1105-1109, 2018.
4. Hüttenhofer L., F. Eckmann and S. A. Maier, et al. “Anapole Excitations in Oxygen-Vacancy-Rich TiO_{2-x} Nanoresonators: Tuning the Absorption for Photocatalysis in the Visible Spectrum” ACS Nano, Vol. 14, No. 1, 2456-2464, 2020.
5. Hu H., T. Weber and O. Bienek, et al. “Catalytic Metasurfaces Empowered by Bound States in the Continuum”. ACS nano, Vol. 16, No. 8, 13057-13068, 2022

META 2023, PARIS - FRANCE, JULY 18 – 21, 2023

Demonstration of an ultra-sharp bend in 1D grating waveguides based on inverse design

A. O. Sakin[1], A. C. Songur[1], H. A. Gunes[1], B. Akcay[1], and M. Unlu[1*]

[1] Dept. of Electrical and Electronics Engineering, TOBB University of Economics and Technology, 06510 Ankara, Turkey

[*]corresponding author: munlu@etu.edu.tr

Abstract: The design of sharp bends in 1D grating waveguides is a challenging problem as the Bloch mode profiles are being pushed towards the outer sidewall and becoming highly asymmetrical, as a result of the steep and high group velocity dispersion of the 1D grating waveguide. To overcome this problem, we propose a first-of-its-kind ultra-sharp bend design in an extensively corrugated 1D grating waveguide on silicon-on-insulator, based on pixelated metamaterials with an ultra-compact size of 2.1 × 2.2 μm^2.

Silicon Photonics Integrated Circuits (PICs) have been attracting tremendous interest due to their potential for meeting the growing need for ultra-high bandwidth data transmission, providing unique capabilities with their inherently broadband, high-speed, and low-loss nature. However, the challenge of achieving miniaturized, low-power photonic structures is ever-increasing as a result of the limitations of silicon, including the absence of a direct band gap and weak second-order nonlinearity, in response to the need for high-capacity photonic interconnects. An intriguing area of study in the field of photonics involves creating optical true time delay (TTD) lines for the purpose of steering antenna beams, modulating signals, and implementing advanced multiplexing techniques. In particular, the one-dimensional (1D) grating waveguide, comprising a periodically modulated pattern of index guiding in both vertical and horizontal directions, has been the focus of much attention as a consequence of its compact size, low loss, and ultra-high bandwidth [1-2]. For changing the direction of light propagation in 1D grating waveguides, sharp bends are an indispensable structure. The high refractive index contrast between the core and claddings in single-mode strip waveguides makes it simple to achieve ultra-sharp waveguide bends [3]. However, when it comes to bends in 1D grating waveguides, the scenario becomes notably different, resulting in both mode-mismatch loss and inter-mode crosstalk. This is because the Bloch mode profiles, a type of guided mode, are squeezed towards the outer sidewall and become highly asymmetrical due to the steeper dispersion relationship and higher group velocity dispersion of the 1D grating waveguide.

A widely used method for managing the difficulties posed by sharp bends in 1D grating waveguides is to gradually transform the taper from a 1D grating waveguide to a conventional strip waveguide at the bend and then tapering back to a 1D grating waveguide after the bend. Nevertheless, the tapering approach has the drawback of adding the extra loss and occupying valuable chip estate unnecessarily [4]. Additionally, the concept of bending in a 1D grating waveguide using modified Archimedean spirals with maximum radii of 59 μm has been proposed in order to achieve low excess losses and inter-mode crosstalk [5]. However, this method is only effective when the corrugation width is narrower, resulting in a more symmetrical Bloch mode profile with a lower group velocity dispersion [6]. Currently, the bends that have been shown are not sharp, and designing them with a wider corrugation to enhance group velocity dispersion is still not possible. Therefore, we propose, for the first time to the authors' best knowledge, an ultra-sharp bend based on pixelated metamaterials for an extensively corrugated 1D grating waveguide on silicon-on-insulator (SOI) with a footprint of only 2.1 × 2.2 μm^2. A sharp bend made of pixelated metamaterials is designed using a genetic algorithm, with the pixels being 100 nm by 100 nm. The material properties are binary, either silicon or silicon dioxide. As

schematically illustrated in Figure 1 (a), where turquoise pixels denote silicon dioxide cells, and the red area represents unetched silicon. These elements have been chosen after taking into account the feasibility of our electron beam lithography and dry etching processes. The metamaterial-assisted bends in Figure 1(a) have been optimized for 2.1 μm corrugation width, but they can also withstand narrower corrugations. Despite its ultra-compact design, the insertion loss is approximately -1.25 dB and tend to decrease when utilizing large footprints. Also, there exists no compromise of the high bandwidth characteristics of the 1D grating waveguide. The frequency response reveals that it can support ultra-wide-band operations over a 55 nm bandwidth range. (Ref. [7] contains the details and results of the 1D grating waveguide.) The fabrication process is still in progress, and the measurement results of the fabricated structure will be presented at the conference.

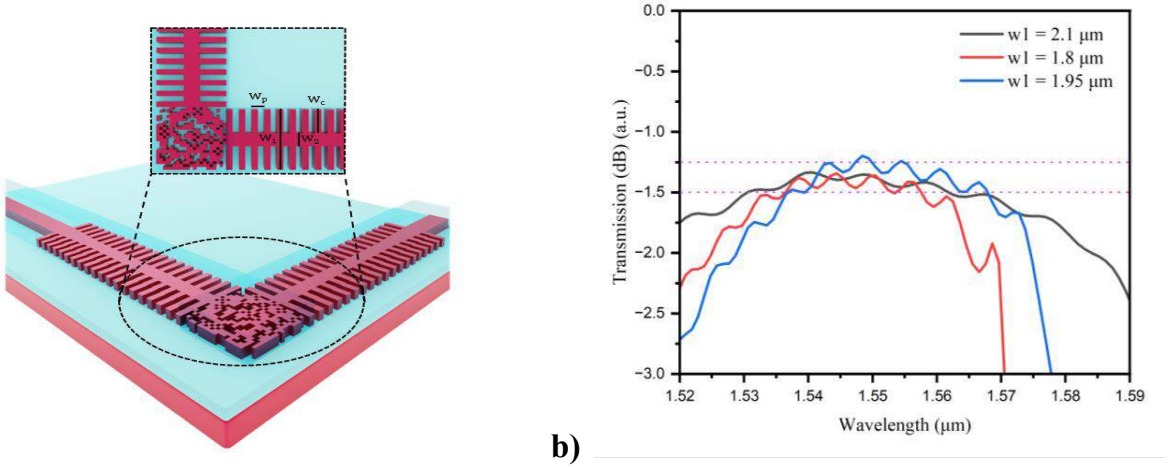


Figure 1. a) Schematic of ultra-sharp bend in the 1D grating waveguide and illustration of design parameters on the structure, **b)** The frequency response of the metamaterial-assisted bend structure, using 2.1, 1.8, and 1.95 μm corrugated grating configurations.

Acknowledgement

All authors acknowledge TUBITAK for their support with project numbers: 119E501. A.O. Sakin, H.A. Gunes, B. Akcay, and A.C. Songur acknowledge the support of the TUBITAK BIDEB 2210A grant.

References

1. Zhang, W., and J. Yao, "A fully reconfigurable waveguide Bragg grating for programmable photonic signal processing," Nature Communications, Vol. 9, No. 1, 1396, 2018.

2. Chung, C. J., X. Xu, G. Wang, Z. Pan, and R.T. Chen, "On-chip optical true time delay lines featuring one-dimensional fishbone photonic crystal waveguide," Applied Physics Letters, Vol. 112, No. 7, 071104, 2018.

3. Gabrielli, L. H., D. Liu, S.G. Johnson, and M. Lipson, "On-chip transformation optics for multimode waveguide bends," Nature Communications, Vol. 3, No. 1, 1217, 2012.

4. Oskooi, A., A. Mutapcic, S. Noda, J.D. Joannopoulos, S.P. Boyd, and S.G. Johnson, "Robust optimization of adiabatic tapers for coupling to slow-light photonic-crystal waveguides," Optics Express, Vol. 20, No. 19, 21558-21575, 2012.

5. Ma, M., Z. Chen, H. Yun, Y. Wang, X. Wang, N.A. Jaeger, and L. Chrostowski, "Apodized spiral Bragg grating waveguides in silicon-on-insulator," IEEE Photonics Technology Letters, Vol. 30, No. 1, 111-114, 2017.

6. Sun, Y., D. Wang, C. Deng, M. Lu, L. Huang, G. Hu, ... and Y. Cui, "Large group delay in silicon-on-insulator chirped spiral Bragg grating waveguide," IEEE Photonics Journal, Vol. 13, No. 5, 1-5, 2021.

7. Sakin, A. O., H. A. Gunes, H. Kurt, and M. Unlu, “Genetic algorithm based, on-chip, fishbone grating waveguide and transition design for time-domain operation,” Integrated Photonics Platforms II, Vol. 12148, pp. 113-118, 2022.

Metamaterial-Assisted Power Division: An Inverse Design Study in 1D Grating Waveguides

A. O. Sakin[1], B. Akcay[1], H. A. Gunes[1], A. C. Songur[1], and M. Unlu[1*]

[1] Dept. of Electrical and Electronics Engineering, TOBB University of Economics and Technology, 06510 Ankara, Turkey

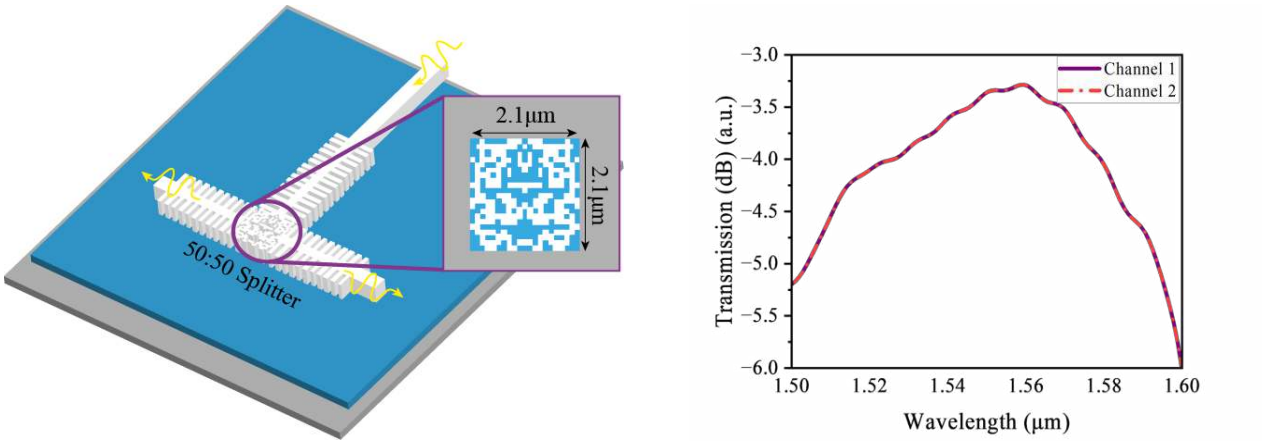
[*]corresponding author: munlu@etu.edu.tr

Abstract: Power dividers are vital components playing a crucial role in facilitating signal merging, routing, and division to ensure the efficient functioning of multi-channel systems in photonic integrated circuits. However, the use of bulky power splitters can occupy a significant amount of space on the chip. Therefore, we propose the utilization of a metamaterial-assisted ultra-low-loss T junction power divider, which integrates an input and two output grating waveguides, with a size of just 2.1 × 2.1 μm^2.

Silicon photonic integrated circuits (PICs) have the potential to revolutionize high-speed communication, sensing, computing, and quantum technologies through their low power consumption, compatibility with CMOS technology, and broadband capabilities [1]. In recent years, microwave photonic (MWP) devices, a type of PIC application, have seen increasing interest due to their exceptional qualities when compared to traditional microwave technologies, with the high intrinsic bandwidth of optical signals being the primary reason for their superiority. In particular, the true time delay line (TTDL) is an essential component for signal processing in microwave photonics and optical communications, as it can be utilized in various applications such as optical beamforming in phased array antennas, generating arbitrary waveforms, and reconfigurable MWP filters. There are several methods for designing TTDLs, including photonic crystal waveguides, ring resonators, one-dimensional (1D) grating waveguides, and subwavelength grating waveguides. 1D grating waveguides are highly suitable for communication and sensing applications due to their compact design, high bandwidth, and Bloch mode capability to achieve highly localized modes that enhance modulation efficiency through Kerr and Pockels effects [2]. In addition, the compact size of 1D grating waveguides makes them well-suited for multi-channel operations that require precise control over the time delay between multiple optical signals, particularly in applications such as antenna beam steering. Nevertheless, in traditional photonic interconnects, bulky power splitters are often favored to separate the power and direction of channels, whether in vertical or horizontal directions. The utilization of bulky power splitters to separate the power and direction of channels in traditional photonic interconnects, whether in the vertical or horizontal direction, can occupy valuable chip estate, and the dispersion effect of a unit silicon path can cause pulse broadening significantly [3].

Recent studies have shown that utilizing directional couplers with sidewall corrugated subwavelength grating waveguides can split power effectively for broadband add–drop grating waveguide filters [4]. However, power splitting between two 1D grating waveguides in the same path has not yet been demonstrated due to the challenge of achieving a suitable match between the 1D grating waveguide's unique band structure using a splitting structure, particularly in a high group velocity dispersion configuration. To overcome this problem, we present utilizing a metamaterial-assisted T junction power divider that integrates an input and two output grating waveguides on a silicon-on-insulator (SOI) substrate, with a footprint of only 2.1 × 2.1 μm^2. Moreover, the proposed T junction power divider is capable of executing the necessary 90-degree turn for multi-channel photonic interconnections. The design of a metamaterial topology that is both highly symmetric and efficient has

been achieved by optimizing it with a genetic algorithm and utilizing 3D finite difference time domain solutions, on a 2 μm buried oxide layer with a top silicon layer of 220 nm thickness, and 1 μm cladding layer. The silica layer is indicated by the blue portion while the silicon layer is denoted by the white portion, as illustrated in Figure 1(a). By setting the corrugation width of the 1D grating waveguide to 2.1 um, a high group velocity dispersion has been achieved, which has posed a challenge for the design of the splitter. (Further information about the implementation of the 1D grating waveguide can be found in Ref. [5]) The transmission efficiency of the TE polarization state, assuming that the input is also in the TE polarization, is considered the figure of merit (FOM) for our device. The device has been discretized into 21 by 21 square pixels, each with a size of 100 nm by 100 nm. With a per-channel insertion loss of -3.28 dB, the power divider has a total insertion loss of -0.275 dB and is able to support an ultra-high bandwidth ranging from 1,500 to 1,600 nm, as shown in Figure 1(b). The fabrication process is still in progress, and the measurement results of the fabricated structure will be presented at the conference.



(a) (b)

Figure 1. a) Schematic of power divider in the 1D grating waveguide b) The frequency response of the power divider

Acknowledgments

All authors acknowledge TUBITAK for their support with project numbers: 119E501. A.O. Sakin, H.A. Gunes, B. Akcay, and A.C. Songur acknowledge the support of the TUBITAK BIDEB 2210A grant.

References

1. Wang, J., F. Sciarrino, A. Laing and M. G. Thompson, “Integrated photonic quantum technologies,” Nature Photonics, Vol. 14, No. 5, 273-284, 2020.

2. Deng, C., L. Zhu, M. Lu, Y. Sun, L. Huang, D. Wang, G. Hu, B. Yun and Y. Cui, "Design and simulation of high modulation efficiency, low group velocity dispersion lithium niobate slow-wave electro-optic modulator based on a fishbone-like grating," Optics & Laser Technology, Vol. 158, 108769, 2023.

3. Zhang, F., J. Dong, Y. Zhu, X. Gao and X. Zhang, "Integrated optical true time delay network based on grating-assisted contradirectional couplers for phased array antennas," IEEE Journal of Selected Topics in Quantum Electronics, Vol. 26, No. 5, 1-7, 2020.

4. Kazanskiy, N. L., M. A. Butt and S. N. Khonina, "Silicon photonic devices realized on refractive index engineered subwavelength grating waveguides-A review," Optics & Laser Technology, Vol. 138, 106863, 2021.

5. Sakin, A. O., H. A. Gunes, H. Kurt, and M. Unlu, “Genetic algorithm based, on-chip, fishbone grating waveguide and transition design for time-domain operation,” Integrated Photonics Platforms II, Vol. 12148, 113-118, 2022.

META 2023, PARIS - FRANCE, JULY 18 – 21, 2023

Ultracompact Tapers & Splitter for Fishbone-Like Grating Waveguides

A. O. Sakin[1], H. A. Gunes[1], B. Akcay[1], A. C. Songur[1], and M. Unlu[1*]

Dept. of Electrical and Electronics Engineering, TOBB University of Economics and Technology, 06510 Ankara, Turkey

[*]corresponding author: munlu@etu.edu.tr

Abstract: The use of fishbone-like grating waveguides (FLGWs) in photonic integrated circuits (PICs) presents a challenge in terms of chip space utilization because it requires incorporating conventional, large components. Therefore, we propose the combination of three key elements - a long adiabatic waveguide taper, a power splitter, and a transition region for FLGWs - using digital metamaterials to allow for the effective utilization of FLGWs that are excited by ultrashort pulses in a compact footprint of only 5 × 14.1 μm^2.

Radio-over-fiber (RoF) technology, being the major branch of microwave photonics, provides high bandwidth, low-loss, and long-distance propagation capabilities, enabling a wide range of applications spanning from communications to wireless networks. The employment of ultrashort pulses as the optical carrier results in a further enhancement of the substantial capacity [1]. Moreover, in order to improve the capabilities of RoF systems, it is critical to design on-chip, compact, and high-performance electro-optic modulators (EOMs) and true time delay (TTD) lines excited by ultrashort pulses. Fishbone-like grating waveguides (FLGWs) have become increasingly popular in recent times as they have the potential to deliver a TTD, a broad bandwidth, and the ability to easily adjust the group velocity dispersion characteristic [2-3]. The relationship between the Bloch mode, a form of guided light in FLGWs, and the group velocity dispersion is interdependent and can be adjusted by changing the geometric parameters of the FLGWs [3]. This aspect is beneficial to both EOMs and TTD lines, due to the increased modulation efficiency and delay characteristic that can be achieved through the presence of highly localized modes in FLGWs [3-5]. Nevertheless, the use of FLGWs in photonic integrated circuits (PICs) is challenging from the perspective of chip estate utilization, as it requires the utilization of conventional, bulky components in terms of footprint size like a grating coupler (GC) to strip waveguide taper, power splitter, and transition region before the grating waveguide. As an example, to minimize loss during the transition between the classical GC and strip waveguide, the adiabatic waveguide taper must be at least 120 μm in length [6]. Additionally, the size of other components, such as the power splitter and the transition region of the grating waveguide, occupies a considerable amount of area on the chip.

The ever-increasing demand for higher integration density dictates more compact components. It is important to note that while various miniaturized grating couplers to taper & splitter designs have been proposed in the literature to reduce the footprint size [7-8], no solution has been found to connect an area-efficient grating coupler with FLGWs due to the complex and distinctive nature of its band structure and Bloch mode pattern that makes it challenging to match it with other components. Therefore, we present the merging of three key components - long adiabatic waveguide taper, power splitter, and transition region of FLGWs - by digital metamaterials to enable the efficient use of FLGWs excited by the ultrashort pulse in a compact footprint of only 5 × 14.1 μm^2. Hence, significant progress has been made in compensating for dispersion, specifically with ultrashort pulses, by utilizing a compact structure instead of larger silicon paths. In the study, we opt for larger grating coupler width (14 μm) compared to other studies [7-8] to assess the stability of the digitized metamaterial-based approach under non-optimal conditions. Decreasing the width of the grating coupler can also lead to an easier and more compact design of the structure with improved transmission characteristics. The

optimized design of the structure utilizing digital metamaterials has been accomplished using a genetic algorithm and includes 100 nm x 100 nm cells, which are compatible with the fabrication process. Algorithm decides whether a cell at a predetermined location should be SiO_2 or Si. The differential evolutionary approach of the algorithm creates unintuitive solutions to the determined figure of merit. As shown in Fig. 1 (a), the unified design does the work of 3 different on-chip components. The design is terminated with a fishbone waveguide and fishbone taper to a normal strip waveguide. According to Fig. 1 (b), the bandwidth of the design is greater than 100 nm and the transmission response of each channel is approximately -4.8 dB which is significantly high considering the ultra-compact topology.

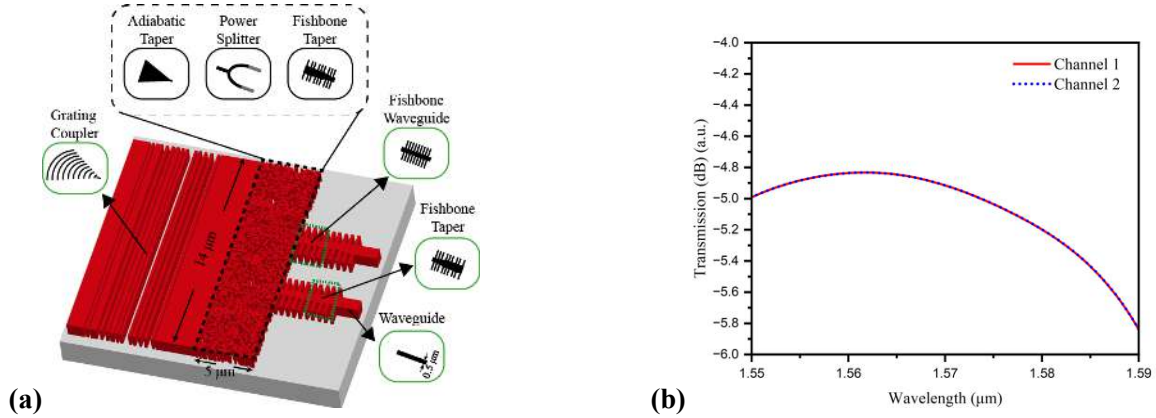


Figure 1. (a) Schematical illustration of unified taper-splitter for fishbone-like waveguides. **(b)** The simulated transmission efficiency of the proposed structure.

Acknowledgments

All authors acknowledge the TUBITAK for their support with project numbers: 119E501. A.O. Sakin, H.A. Gunes, B. Akcay, and A.C. Songur acknowledge the support of the TUBITAK BIDEB 2210A grant.

References

1. Jin, Y., Y. Yang, H. Hong, X. Xiang, R. Quan, T. Liu, et al., "Quantum microwave photonics in radio-over-fiber systems," Photonics Research, Vol. 10, No. 7, pp. 1669-1678, 2022.
2. Zhang, W., and J. Yao, "A fully reconfigurable waveguide Bragg grating for programmable photonic signal processing," Nature Communications, Vol. 9, No. 1, 1396, 2018.
3. Sakin, A. O., H. A. Gunes, H. Kurt, and M. Unlu, "Genetic algorithm based, on-chip, fishbone grating waveguide and transition design for time-domain operation," Integrated Photonics Platforms II, Vol. 12148, pp. 113-118, 2022.
4. Chung, C. J., X. Xu, G. Wang, Z. Pan, and R. T. Chen, "On-chip optical true time delay lines featuring one-dimensional fishbone photonic crystal waveguide," Appl. Phys. Lett., Vol. 112, No. 7, 071104, 2018.
5. Deng, C., L. Zhu, M. Lu, Y. Sun, L. Huang, D. Wang, ... and Y. Cui, “Design and simulation of high modulation efficiency, low group velocity dispersion lithium niobate slow-wave electro-optic modulator based on a fishbone-like grating. Optics & Laser Technology, Vol.158, 108769, 2023.
6. Hosseini, R. and K. Jamshidi, "Analysis of Kerr nonlinearity enhancement in silicon nitride waveguides using one-dimensional slow light structure," Optics Communications, Vol. 421, pp. 25-29, 2018.
7. Liu, Y., W. Sun, H. Xie, N. Zhang, K. Xu, Y. Yao, et al., "Adiabatic and ultracompact waveguide tapers based on digital metamaterials," IEEE Journal of Selected Topics in Quantum Electronics, Vol. 25, No. 3, pp. 1-6, 2018.
8. Huang, J., J. Yang, D. Chen, W. Bai, J. Han, Z. Zhang, et al., "Implementation of on-chip multi-channel focusing wavelength demultiplexer with regularized digital metamaterials," Nanophotonics, Vol. 9, No. 1, pp. 159-166, 2020.

META 2023, PARIS - FRANCE, JULY 18 – 21, 2023

Flexible metamaterial microwave absorbers with polymer nanocomposite as substrates

M. Anjali*, Kumaran Rengaswamy, Abhishek Ukey, Lincy Stephen, C. V. Krishnamurthy, and V. Subramanian

Microwave Laboratory, Department of Physics, Indian Institute of Technology Madras, Chennai 600036, India

*Email: anjalim@physics.iitm.ac.in

Abstract: In this work, we have demonstrated metamaterial absorbers operating at 9.88 GHz using novel epoxy/graphene nanoplatelets composites (E-GnP) as substrates. The substrate is systematically studied for different weight percentages of GnP in epoxy, which could result in variation of dielectric constant as well as loss tangent and hence the enhancement of bandwidth. Owing to the flexibility of the substrate, the metamaterial absorber could cater to conformal applications.

Using novel materials in the design of metamaterial microwave absorbers provides a holistic way of device design by leveraging the degrees of freedom in engineering unit cells. Polymer nanocomposites are useful in this regard as there are a variety of options to fabricate materials with desirable mechanical, thermal and dielectric properties depending on the choice of the matrix and filler. The present work involves the realization of flexible metamaterial absorber with epoxy/graphene nanoplatelets polymer composite (E-GnP) as substrates. The X-band dielectric permittivity varied from 3.4 for 1 wt% (E-GnP1) to 14.7 for 9 wt% (E-GnP9) of the composites. The absorption bandwidth of the metamaterial absorbers designed to operate at 9.88 GHz increased from 0.114 GHz for E-GnP1 to 0.350 GHz for the E-GnP9 substrate, owing to an increase in the substrate loss tangent. The user-controllable mechanical and dielectric properties of the E-GnP composites can overcome the constraints of commercial substrates and make them a good choice for designing metamaterial absorbers.

Reference:

M Anjali, Kumaran Rengaswamy, Abhishek Ukey, Lincy Stephen, C V Krishnamurthy, and V Subramanian “Flexible metamaterial based microwave absorber with epoxy/graphene nanoplatelets composite as substrate” J. Appl. Phys., Vol. 133, No. 063105, 1-9, 2023.

Active metasurface using Ag/ITO nano antenna for visible wavelength

C.-S. Hwang[1*], Y.-H. Kim, J. H. Yang, J. Y. Kim, K. H. Choi, J. Moon, J. H. Choi

[1]Electronics and Telecommunications Research Institute, S. Korea
[*]corresponding author: hwang-cs@etri.re.kr

Abstract: We propose double line nano antenna structure for the purpose of complex modulation in visible wavelength. RCWA simulation results show that the nano antenna with Ag/ITO outperform the stacked structure in that case the modulated active layers are vertically stacked.

We previously suggested the active metasurface for complex modulation in visible wavelength [1]. The structure consists of Al nano antenna and hyperbolic meta material including ITO/Ag multilayers as shown Fig, 1 (a). The carrier concentration of top and bottom ITO layers could be controlled independently to modulate the reflective wave for complex modulation. We suggest novel modification of the structure to enhance the modulation amplitude and to reduce the difficulties in fabrication. The voltage of each line of the antenna in Fig. 1 (b) and (c) could be controlled independently for the complex modulation. We found that the structure consists of double line of Ag nano antenna combined with patterned ITO layers (Fig. 1 (c)) results in better result compared with the structure consists of double Al nano antenna with un-patterned Ag layers. The performance of the structure, the modulated area in complex reflectance plane, was tested using RCWA simulation with the randomly distributed structure parameters [2]. As shown in Fig. 2, the performance of double line structure with Al nano antenna (double line type-1) was inferior to the single line structure, but the modified double line structure with Ag/ITO nano antenna (double line type-2) showed better performance.

Another merit of the novel structure is that the coupling with dielectric environment could be enhanced due to the strong local electrical field formed near the modulated region as shown in Fig. 3. The LC-coupled metasurface can be the example of the possible application with the double line metasurface [3].

This work was supported by the National Research Foundation of Korea (NRF-2021M3H4A1A04086553) and Electronics and Telecommunications Research Institute (ETRI) grant funded by the Korean government [23ZH1300, Research on hyper-realistic interaction technology for five senses and emotional experience] .

References

1. Kim, Y. -H., C.S. Hwang, J. H. Yang, J. Y. Kim, K. H. Choi, J. Moon and J. H. Choi, “Active metasurface using ITO device in visible wavelength,” META 2022.
2. Song, A.Y., P.B. Catrysse and S. Fan, “Broadband Control of Topological Nodes in Electromagnetic Fields,” Phys. Rev. Lett., Vol. 120, 193903, 2018.
3. Chang, X., M. Pivenko, P. Shrestha, W. Wu, W. Zhang and D. Chu, “Electrically tuned active metasurface towards metasurface-integrated liquid crystal on silicon (meta-LCoS) devices,” Optics Express, Vol. 31, No. 4, 5378–5387, 2023.

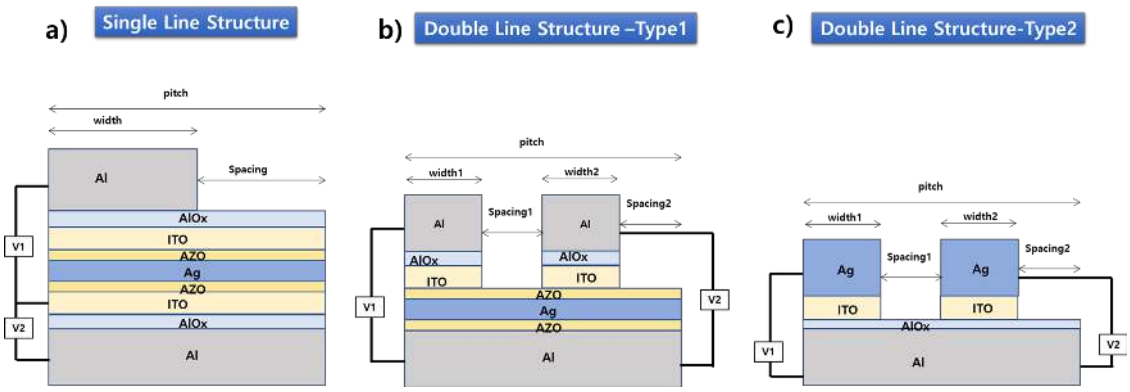


Figure 1. The cross section diagram of active metasurface for visible wavelength.

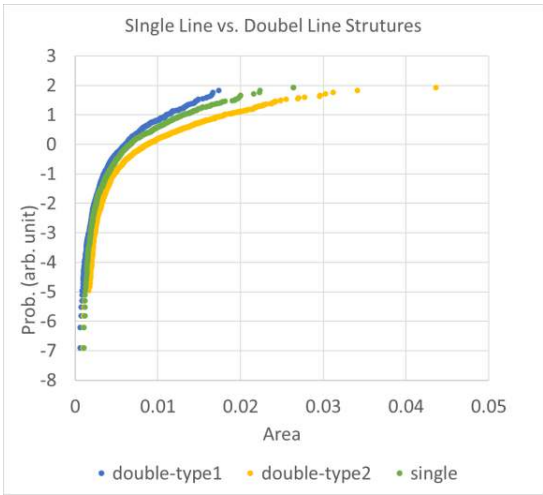


Figure 2. The simulated modulated area in complex reflectance plane using the randomly assigned parameter set for the structures shown in Fig. 1.

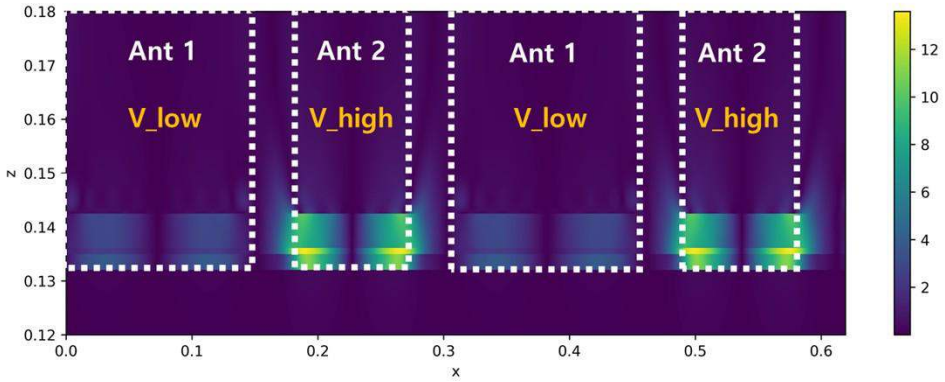


Figure 3. The simulated electrical field (vertical direction) of the structure shown in Fig. 1 (c) for the case of different voltages are applied at each nano wire.

META 2023, PARIS - FRANCE, JULY 18 – 21, 2023

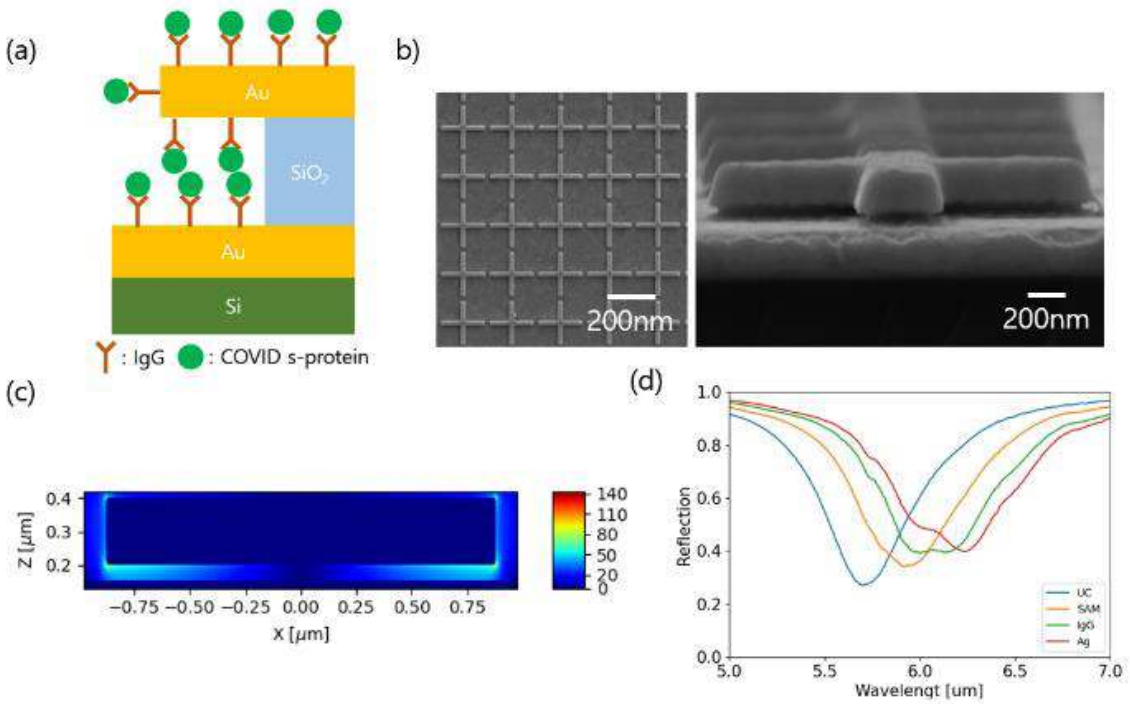
Label-Free Protein Detection based on Surface-Enhanced Infrared Absorption Spectroscopy with vertical nanogap

Mingyun Kim[1], Dohyun Kang[2], Jongwon Lee[1*] and Joo-Yun Jung[2,*]
[1]Department of Electrical Engineering, Ulsan National Institute of Science and Technology, Ulsan, 44919, Korea
[2]Nano-convergence Mechanical Systems Research Division, Korea Institute of Machinery and Materials, Dajeon, 305-343, Korea
* jjy2121@kimm.re.kr

Abstract: The COVID-19 pandemic increased the need for accurate and rapid detection of biomolecules, leading to the development of immunoassay-based biosensors. While label-binding can be time-consuming and costly, Label-free and highly sensitive biosensors using Mid-IR molecular fingerprint have been explored. Surface-Enhanced Infrared Absorption spectroscopy has emerged to enhance and measure vibrational modes in small amounts of analyte, and a metamaterial absorber was developed to increase the sensing area and enhance the SEIRA signal. SEIRA spectroscopy has the potential for biosensing device.

Due to the COVID-19 pandemic, there is a growing demand for the detection of biomolecules to identify infected individuals, particularly in high-risk areas like airports and medical facilities. It is crucial to detect biomolecules accurately and quickly to prevent the spread of infectious diseases. As a result, there is a rising interest in the development of immunoassay-based biosensors that utilize the antigen-antibody reaction for fast and precise biomolecule detection. The immunoassay approach allows for the identification and quantification of analytes using fluorescence or color change, with additional signal amplification through the binding of a label with an enzyme linked to the analyte. However, this label-binding process can be time-consuming and expensive, leading to the exploration of label-free and highly sensitive immunoassay-based biosensors. Label-free biomolecule sensing can be achieved through Mid-IR molecular fingerprint, which involves measuring the vibrational modes of different molecules, including biomolecules. These molecules have unique vibrational modes that can be used to determine specific molecular structures using spectroscopy.

Traditionally, molecular vibrational modes have been measured using spectroscopy with increasing interaction optical path as described by the Beer-Lambert law. However, this approach faces challenges in detecting small amounts of analyte in thin films due to the small scattering cross-section. To overcome this limitation, Surface-Enhanced Infrared Absorption (SEIRA) spectroscopy has been developed to enhance and measure vibrational modes in extremely small amounts of analyte. This technique involves analyzing the strongly coupled far-field spectra between the near-field generated by Localized Surface Plasmon Resonance (LSPR) and the vibrational mode of the analyte to identify and quantitatively measure the analyte. By spatially and spectrally overlapping the near-field and the vibrational modes of the analytes, the signal extracted from the spectrum can be enhanced. In this study, a metamaterial absorber (MA) was fabricated as a plasmonic resonance cavity with a vertical nanogap, and isotropic dry etching was performed to enhance the near-field generated by LSPR and increase the surface sensing area, thereby enhancing the SEIRA signal.[1] Using these biosensors, small amounts of biomolecules can be rapidly and accurately measured. As a result, SEIRA spectroscopy holds potential to become an important sensing device for preparing for future pandemics.



[Fig.1] (a) The schematic of antibody-antigen combined with MA. (b) SEM Image of MA fabricated by nano-imprint lithography. (c) The simulated near-field profile of undercut MA at resonance wavelength. (d) The spectrum of the undercut MA, SAM coated MA, antibody incubated MA, antibody-antigen incubated MA.

The immunoassay process involves combining the plasmonic MA structure with antibody-antigen for biomolecule detection. The schematic of the immunoassay process with Surface-Enhanced Infrared Absorption (SEIRA) is shown in Fig.1(a), while Fig.1(b) shows the scanning electron microscopy (SEM) image of the fabricated MA structure, and Fig.1(c) shows the simulated near-field distribution of the MA. The study increased the near-field enhancement and enlarged the sensing area by using MA fabricated through isotropic dry etching to undercut the spacer layer of the metal-insulator-metal structure. The SEIRA signal was confirmed by measuring the corona virus antibody and antigen with a peak splitting of 0.343μm. The concentration of antigen relates to the number of interacting molecules, and the peak splitting relates to the number of interacting molecules and effective mode volume. [2]

References

1. Hwang, I., et al. “Ultrasensitive molecule detection based on infrared metamaterial absorber with vertical nanogap”, Small Methods. 5,8 ,2021.
2. Li, Peining, et al. “Boron nitride nanoresonators for phonon-enhanced molecular vibrational spectroscopy at the strong coupling limit” Light: Sicence & Applications 7.4, 2018

Metasurface Augmented Camera for General Optical Metrology Applications

A. Burguete-Lopez[1*], M. Makarenko[1], Q. Wang[1] , F. Getman[1] A. Fratalocchi[1]

[1]PRIMALIGHT, Faculty of Electrical Engineering; Applied Mathematics and Computational Science,
King Abdullah University of Science and Technology, Thuwal 23955-6900, Saudi Arabia
*corresponding author: arturo.burguetelopez@kaust.edu.sa

Abstract: We present a general optical metrology platform that employs an information processing metasurface as the means for the measurement of observables. The approach, consisting of combining an information processing metasurface with an off-the-shelf CMOS sensor, permits rapid characterization of the properties of materials in a cost-effective and mass-producible package. We present initial results on the fabrication of a prototype of this system.

The technology of metasurfaces has attracted great interest over the past decade, with numerous works showing that optical elements such as lenses [1], polarizers [2], filters [3] and holograms [4] can be realized in highly integrated and compact sheets. More recent works in the field have begun exploring the realization of metasurface based instruments, with demonstrations of metasurface chains for spectroscopy [5], [6], orbital angular momentum measurement [7] and Bell states measurements [8]. As metasurface based instrumentation is an emerging field, existing works have focused on the design of devices for highly specific tasks, with little work available on the development of general purpose devices.

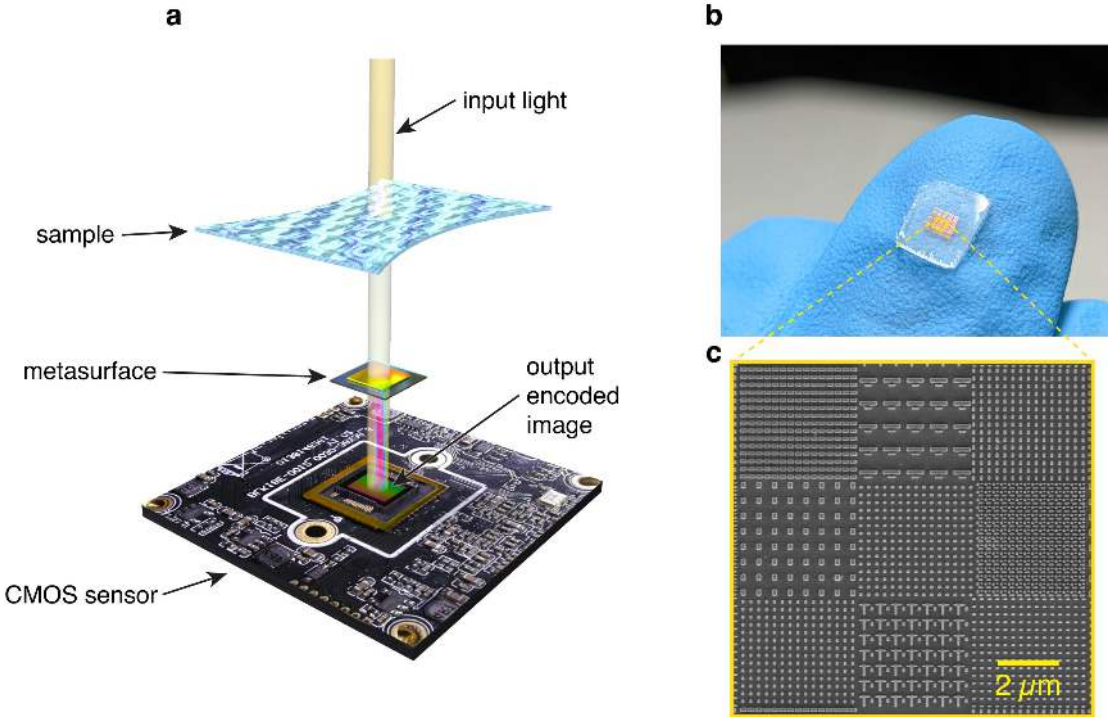


Figure 1: **Metrology system**. **a** An input light beam passes through a sample and propagates carrying information about the interaction. A suitably designed metasurface extracts this information, converting it to an encoded image that a CMOS sensor reads. **b** Photograph of fabricated information extracting metasurface. **c** scanning electron microscope image showing the structure of encoder arrays that conform the information processing metasurface.

In this work we aim to address this gap by introducing a general purpose metasurface based instrument for optical metrology. Figure 1a illustrates the concept. Light that interacts with a material, either through transmission or reflection, becomes a medium that carries information on the physical properties of the material. This information, encoded as amplitude, phase and polarization variations in the beam, can be extracted through the use of a suitably engineered metasurface sensitive to these changes. We design such metasurfaces following a data driven approach. Making use of an inverse design software that can

obtain designs for arbitrarily defined input-output optical responses. The metasurface converts the information encoded in the light beam into an intensity pattern, which is then read by a standard CMOS sensor as an encoded image.

Figure 1b presents a photograph of a prototype metasurface and fig. 1c a scanning electron microscope closeup of the metasurface structure. The design consists of a an array of nine patterns that repeats across the substrate area. These patterns are engineered to translate the information encoded in an input beam to amplitude signals. The metasurface is placed on the CMOS sensor in such a way that each of these patterns covers a sensor pixel, in a manner analogous to the Bayer array of color cameras.

Acknowledgements: This research received funding from KAUST (Award OSR-2016-CRG5-2995). Parallel simulations are performed on KAUST's Shaheen supercomputer. Sample fabrication is conducted in the KAUST Core Labs nanofabrication cleanroom.

References

[1] W. T. Chen, A. Zhu, e. Y, J. Sisler, Z. Bharwani, and F. Capasso, "A broadband achromatic polarization-insensitive metalens consisting of anisotropic nanostructures," *Nature Communications*, vol. 10, no. 1, p. 355, 2019.

[2] M. Makarenko, Q. Wang, A. Burguete-Lopez, F. Getman, and A. Fratalocchi, "Robust and Scalable Flat-Optics on Flexible Substrates via Evolutionary Neural Networks," *Advanced Intelligent Systems*, vol. 3, no. 11, p. 2 100 105, 2021.

[3] F. Getman, M. Makarenko, A. Burguete-Lopez, and A. Fratalocchi, "Broadband vectorial ultrathin optics with experimental efficiency up to 99% in the visible region via universal approximators," *Light: Science & Applications*, vol. 10, no. 1, pp. 1–14, 1 Mar. 4, 2021.

[4] L. Huang, S. Zhang, and T. Zentgraf, "Metasurface holography: From fundamentals to applications," *Nanophotonics*, vol. 7, no. 6, pp. 1169–1190, 2018.

[5] M. Faraji-Dana, E. Arbabi, A. Arbabi, S. M. Kamali, H. Kwon, and A. Faraon, "Compact folded metasurface spectrometer," *Nature Communications*, vol. 9, no. 1, p. 4196, 1 Oct. 10, 2018.

[6] M. Makarenko, A. Burguete-Lopez, Q. Wang, *et al.*, "Real-time Hyperspectral Imaging in Hardware via Trained Metasurface Encoders," in *2022 IEEE/CVF Conference on Computer Vision and Pattern Recognition (CVPR)*, Jun. 2022, pp. 12 682–12 692.

[7] T. Dinter, C. Li, L. Kühner, *et al.*, "Metasurface Measuring Twisted Light in Turbulence," *ACS Photonics*, vol. 9, no. 9, pp. 3043–3051, Sep. 21, 2022.

[8] Z. Gao, Z. Su, Q. Song, P. Genevet, and K. E. Dorfman, "Metasurface for complete measurement of polarization Bell state," *Nanophotonics*, vol. 12, no. 3, pp. 569–577, Feb. 1, 2023.

Attribute of attenuation band in smart negative indexed mechanical metamaterials

Ankur Dwivedi[1*] and S. A. R. Horsley[1]

[1]University of Exeter, United Kingdom
[*]corresponding author: A.Dwivedi@exeter.ac.uk

Abstract: Unique tailored geometry and pattern of engineered mechanical metamaterials are essential to accomplish unusual properties which are seldom observed in natural materials. Here we study the characteristic of the attenuation band in smart mechanical metamaterial having negative stiffness and mass properties. We derive critical physical parameters, which are essential in the formation of locally resonant attenuation band. We found the higher attenuation (HA1) region in the attenuation band has different attributes in case of negative stiffness and mass metamaterials.

Elastic mechanical metamaterials are the exemplars of periodic structures that exhibit interesting frequency-dependent properties like negative Young's modulus and negative mass in a certain frequency band due to emergence of local resonance. The structural arrangement of the individual unit-cells define the property of the material system and material property of the base material has little influence. Their precise shape, geometry, size, orientation, contact property and arrangement gives them their properties capable of manipulating acoustic waves by blocking, absorbing, enhancing, bending waves, to achieve objectives that are unrealizable with conventional materials. Embedding of the piezoelectric material empowers such systema to harvest the vibrational energy effectively along with simultaneously vibration attenuation. Based on the interesting physical properties exhibited by the mechanical metamaterials, they can be categorized as negative mass [1], negative stiffness [2], and other combinations also as shown in Figure 1.

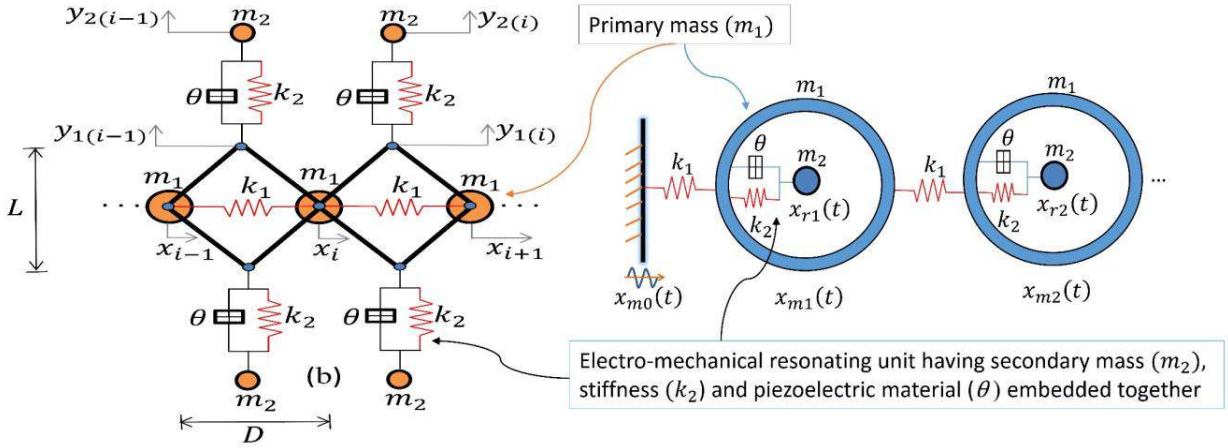


Figure 1: Piezo-embedded negative stiffness metamaterial (left), where a series of primary masses (m_1) attach to each other by springs and rocker mechanism (four rigid massless bars with friction revolute joints such that nodes connecting the primary masses traverse only horizontally). Piezo-embedded negative mass metamaterial (right), a mass-in-mass system where inside the primary mass (m_1) a resonating mass (m_2), is present. A piezoelectric material having an electromechanical coupling coefficient (θ) is embedded in the electromechanical resonating units in both metamaterials.

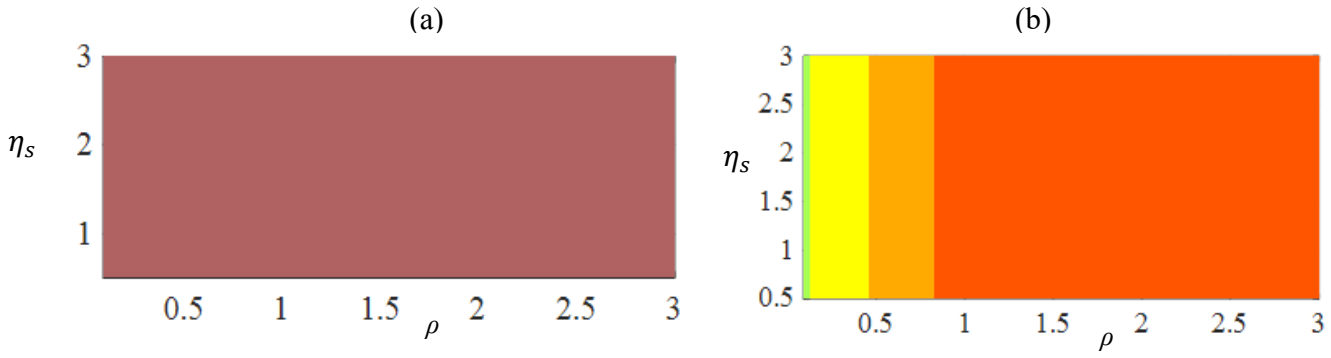


Figure: Contour plots for HA1, piezo-embedded negative (a) stiffness and (b) mass metamaterial for a set of value of capacitive parameter (c) and resistive parameter (r) in non-dimensional frequency domain (η_2).

The dynamics of piezo-embedded mechanical metamaterials gives the dispersion relationship which can be deduced by Bloch's formulation [3,4] and gives physical parameters stated in Eqn. (1).

$$\eta_s = \frac{\omega_2}{\omega_1}, \rho = \frac{m_2}{m_1}, c = \frac{\theta^2}{k_2 C^p}, r = \frac{R\omega_2\theta^2}{k_2} \tag{1}$$

where, ω = (k/m)$^{0.5}$ is natural frequency, R is resistance attached in the energy harvesting circuit and C_P is the capacitance of piezoelectric material.

We found for the negative stiffness metamaterial HA1 is independent of mass ratio (ρ) and structural frequency ratio (η_s), it depends only on the non-dimensional capacitive (c) and resistive parameter (r),whereas in case of negative mass metamaterial HA1 is constant for range of value of (ρ). Therefore, this investigation can suggest insight about identifying critical physical parameters and their range for optimal vibration attenuation and energy harvesting. It will be useful while designing the smart negative indexed mechanical metamaterials integrated with the piezoelectric material.

The authors would like to acknowledge the Royal Society TATA University Research Fellowship (RPG-2016-186) for funding and supporting this research.

References

1. Huang, H. H., C. T Sun and G. L. Huang, “On the negative effective mass density in acoustic metamaterials,” International Journal of Engineering Science, **47,** No. 4, 610-617, 2009.
2. Huang, H. H. and C. T. Sun, “Theoretical investigation of the behavior of an acoustic metamaterial with extreme Young's modulus,” Journal of the Mechanics and Physics of Solids, **59,** No.10, 2070-2081, 2011.
3. Dwivedi, A., A. Banerjee and Bishakh Bhattacharya, "Dynamics of piezo-embedded negative stiffness mechanical metamaterials: A study on electromechanical bandgaps," In ASME International Mechanical Engineering Congress and Exposition, Vol. **84478**, p. V001T01A015, American Society of Mechanical Engineers, 2020.
4. Dwivedi, A., A. Banerjee and Bishakh Bhattacharya, "Study of piezo embedded negative mass metamaterial using generalized Bloch theorem for energy harvesting system," In Active and Passive Smart Structures and Integrated Systems XIII, Vol. **10967**, pp. 656-666, SPIE, 2019.

META 2023, PARIS - FRANCE, JULY 18 – 21, 2023

Scanning Reflectance Anisotropy Microscopy: strain mapping of metasurfaces and beyond.

Fabian Haake[1*]
Joan Sendra[1]
Henning Galinski[1]
Ralph Spolenak[1]

[1]Author: Department of Materials ETH Zurich, Switzerland
[*]Corresponding author: fabian.haake@mat.ethz.ch

Abstract: Elastic deformation of materials leads to breaking of the lattice symmetry. One consequence of the deformation is the emergence of optical anisotropy. However, the capabilities to map local strain fields by optical microscopy are currently limited. Here, we introduce a broadband reflectance anisotropy microscope as a phase-sensitive optical platform for the sensing of elastic strain in materials. We demonstrate non-destructive mechanical characterization of strained metasurfaces, which can serve as strain markers, and amorphous dielectric photonic-like crystals.

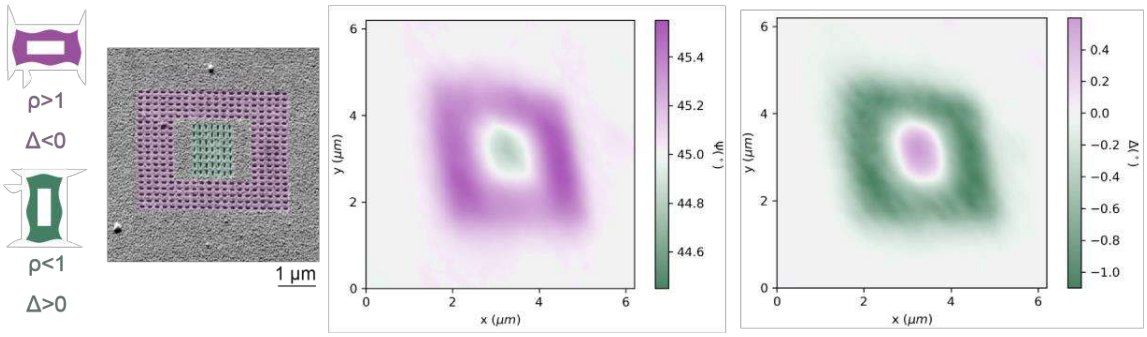


Figure 1: SEM image and SRAM measurements of a metasurface composed of dipolar slot antennas showcasing the sensitivity of the setup to the ellipsometric properties (phase Δ and amplitude Ψ) of the sample.[1]

Figure 1 shows a metasurface of nanoslot antennas (width: 100 nm height: 50 nm) that were milled with FIB in a 100 nm thick template stripped gold surface on polycarbonate. The SRAM measurements were carried out at the resonance frequency of the nanoslot array of 2.39 eV. These maps show the high phase sensitivity of SRAM at diffraction-limited resolution.[1]

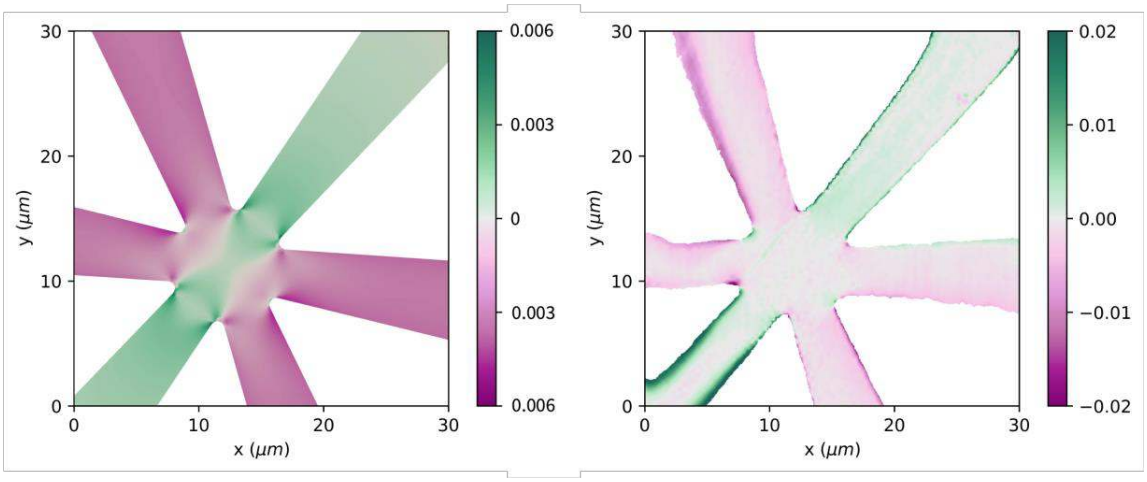


Figure 2: Simulated strain distribution ε_{xx}-ε_{yy} and measured SRAM map of an uniaxially strained photonic crystal-like structure.

Figure 2 shows the simulated strain distribution and measured SRAM map of a photonic crystal-like structure in a 500 nm thick amorphous germanium layer on Kapton. This structure consists of 6 concentrically aligned wedges that were milled with a FIB. A tensile stage introduces anisotropy between two wedges with a total strain of 0.2%. As shown the technique is able measure the local strain field distribution and can therefore be used for the optical characterization of large photonic crystals.

References

1. Sendra J., Haake F., Calvo M., Galinski H. and Spolenak R. “Scanning Reflectance Anisotropy Microscopy for Multi-Material Strain Mapping,” arXiv e-prints, arXiv:2302.04095, 2023.

Line modes in elastic mechanical metamaterials

Ankur Dwivedi[1*] and S. A. R. Horsley[1]

[1]University of Exeter, United Kingdom
[*]corresponding author: A.Dwivedi@exeter.ac.uk

Abstract: The one dimensional analogue of surface modes - line modes - have been recently found in electromagnetic materials, existing at the interface between surfaces of positive and negative reactance. Here we consider the mechanical analogue of line modes. Analytically we find they exist at the interface between two surfaces respectively pinned in vertical and in-plane directions, and we examine the conditions for their existence using the finite element method, tuning the line mode eigenfrequencies by varying the density and elastic moduli of the materials.

Elastic surface waves (SWs) bound to a planar interface can take the form of Rayleigh waves when the surface is traction free. Analogously, electromagnetic (EM) waves at a free-space interface take either the form of a surface plasmon, or a surface magneto-plasmon, depending on the sign of the surface reactance. It was recently found that EM surface waves could be further confined to propagate in only one-dimension (as "line waves") with a metasurface containing an interface between regions where the reactance has opposite sign [1, 2] (see Fig. 1). In this work we investigate the existence and properties of line waves on mechanical metasurfaces (in contrast to the sub-wavelength guiding structures of [3, 4])

We define the elastic surface reactance Y at an interface via $\sigma.n = Y.u$, where $n.\sigma$ is the normal stress, and u is the displacement. It is not straightforward to directly translate results from EM to elastic waves, due to the absence of longitudinal EM waves. We first give a simple case where we can analytically demonstrate the existence of elastic line modes. As shown in [2], the interface between a PEC ($\boldsymbol{E}$ field normal to surface) and PMC ($\boldsymbol{E}$ field parallel to surface) supports an EM line wave. Assuming a pure shear wave in a bulk elastic medium, which obeys (ρ is mass density, G is the shear modulus, and ω is angular natural frequency)

$$\nabla^2 u_T + \frac{\rho\omega^2}{G} u_T = 0 \qquad (1)$$

we can see that the boundary conditions $n.u = 0$ and $n \times u = 0$ are exactly equivalent to PEC and PMC conditions respectively. Therefore, as described in [2] these boundary conditions must support a line wave of the form $u_x = K_{1/2}(\kappa r)cos(\theta/2)exp(ik_z z)$, where $K_{1/2}$ is a modified Bessel function.

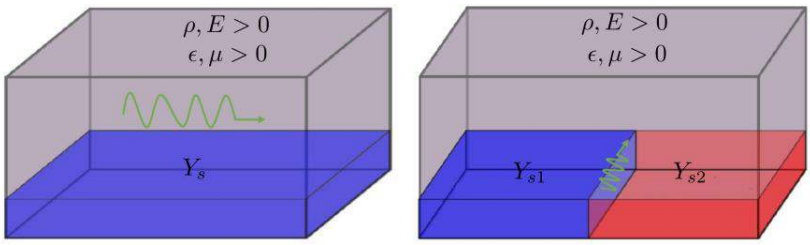
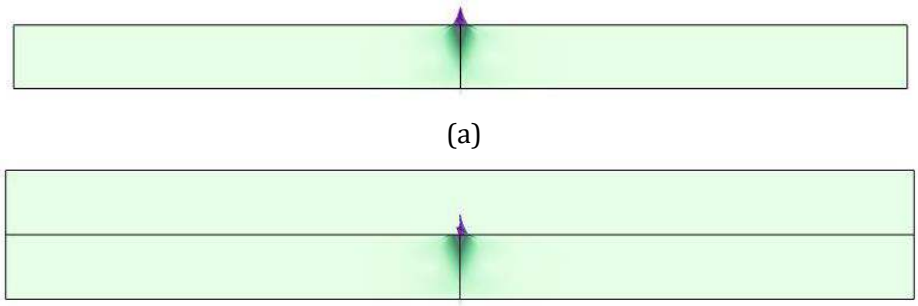


Figure 1: Both EM and elastic surface waves (SWs) can be seen (left) on an interface, with the properties of the SW depending on the surface admittance Y_s. The SWs turns to line wave (LW) at an interface between

surfaces of differing admittance.

We have further developed our understanding of elastic line modes via numerical simulations, varying both material parameters and boundary conditions. In Fig. 2 we show two examples where these modes are evident. we have taken fixed wave propagation constants $k_z > \sqrt{\rho\,\omega^2/G}$ along the z-axis and applied a fixed boundary condition along the edges of the simulation, mimicking the surface impedance conditions (1) with bulk media. We used an eigenmode analysis to solve for the frequency ω in a 2D model in COMSOL Multiphysics.



(a)

(b)

Figure 2: Eigenmodes shown for (a) two positive density materials with equal magnitude elastic modulus, but opposite sign. (b) three materials with upper material having positive density and elastic modulus. Lower two materials also have positive mass density but equal and opposite elastic modulus.

The authors would like to acknowledge the Royal Society TATA University Research Fellowship (RPG-2016-186) for funding and supporting this research.

References

1. S. A. R. Horsley and I. R. Hooper, "One dimensional electromagnetic waves on flat surfaces," Journal of Physics D: Applied Physics, **47**, No. 43, 2014.
2. J. B. Dia'aaldin and D. F. Sievenpiper, "Guiding waves along an infinitesimal line between impedance surfaces," Phys. Rev. Lett., **119**, No. 10, 2017.
3. A. Dwivedi, A. Banerjee and B. Bhattacharya, "Simultaneous energy harvesting and vibration attenuation in piezo-embedded negative stiffness metamaterial," Journal of Intelligent Material Systems and Structures, **31**, No. 8, 1076-1090, 2020.
4. J-J. Marigo, K. Pham, A. Maurel and S. Guenneau, "Effective model for elastic waves propagating in a substrate supporting a dense array of plates/beams with flexural resonances," Journal of the Mechanics and Physics of Solids, **143**, 2020.

Fabrication of two-dimensional magnonic crystal using yttrium iron garnets and non-magnetic metals

Kanta Mori[1, 2], Takumi Koguchi[1, 2], Toshiaki Watanabe[3], Mitsuteru Inoue[1], Kazushi Ishiyama[1] and Taichi Goto[1, *]

[1]Research Institute of Electrical Communication, Tohoku University, Japan
[2]Graduate School of Engineering, Tohoku University, Japan
[3]Shin-Etsu Chemical Co., Ltd, Japan
[*]taichi.goto.a6@tohoku.ac.jp

Abstract: Two-dimensional magnonic crystals (2D MCs) for forward volume spin waves were demonstrated using yttrium iron garnets (YIG) and copper disks. The 2D MCs with hexagonal lattice were fabricated on a 13 μm thick YIG on a gadolinium gallium garnet substrate by using photolithography and the wet etching and lift-off method. A bandgap was observed in a measured transmission spectrum. The frequency of the bandgap and the propagation band of spin waves were in good agreement with a calculation result.

Electronic devices have achieved high performance through miniaturization and high integration, but the growth rate of device performance is slowing down as the integration density approaches the physical limit. This is a problem arising from the principle of electronic devices that transmit information by transferring electric charges. For this reason, spin wave devices using phase waves created by magnetic moments are being developed as the next generation of information processing devices because of no charge transfer and functions utilizing the phase interference phenomenon. Recently, NAND devices based on spin wave interference have been demonstrated[1], and nano- and micro-scale integration technologies are being developed for chipping spin wave devices[2]. However, the technology to wire spin waves, like electrical wiring in electronic circuits, has not been established. Therefore, we have focused on magnonic crystals (MCs), in which the flow of spin waves can be controlled by using a periodic magnetic structure. MCs can be used to filter, confinement, and phase modulation for spin waves. These functions of MCs are essential for the development of spin wave integrated circuits, including logic gates. In these applications, the forward volume spin wave (FVSW) is suitable because of its in-plane isotropy. In addition, the waveguide comprising yttrium iron garnet (YIG) is useful because of the long propagation length of spin waves. One-dimensional (1D) MCs with a periodic magnetic structure have already been demonstrated as a configuration that can be chipped in principle, and the appearance of a bandgap has been observed[3]. However, two-dimensional (2D) MCs showing bandgaps for all directions in a plane need to be demonstrated to realize control of spin wave propagation in two dimensions. Hence, in this work, 2D MCs were fabricated using YIG, and non-magnetic metals and spin wave transmission spectra were measured.

First, 2D MCs were designed using a three-dimensional electromagnetic simulator (Dassault Systems, Simulia CST studio suite 2022) based on the finite integration technique. It was used because of its good agreement with experimental results in previous studies[2, 3]. The simulation model consists of a substrate with two microstrip lines (MSLs) and a YIG film placed on top of the MSLs. The substrate consists of a 170 mm × 170 mm × 0.6 mm glass epoxy (FR4) with an 18-μm thick Cu signal line (SL) on the top surface of FR4 and an 18-μm thick Cu ground plane on the bottom surface of FR4. The YIG is a 15 mm × 15 mm × 10 μm film. Cu disks with a diameter of 300 μm and a thickness of 1 μm were periodically located on the surface of the YIG between two SLs. A configuration type of 2D MC was a hexagonal lattice with a lattice constant of 450 μm.

30-nm thick Au films were located on one side of SLs to depress reflected spin waves from the edge of the YIG film[4]. The transmission spectra were calculated when the incident angles of the spin waves to the 2D MCs were varied by rotating the 2D MCs. The incident angle was varied from 0 to 30 degrees in a step of 5 degrees. Band gaps which were low transmission bands, were observed in the range of 10 to 30 degrees. And a frequency of the band gaps shifted to the lower frequency as the incident angle increased. At a frequency of 1.80 GHz, the band gaps were generated in the range of 10 to 30 degrees.

Based on the above calculation, 2D MC samples were fabricated on a 13 μm thick YIG on a gadolinium gallium garnet substrate by wet etching and lift-off method using photolithography. And a measurement system the same as the simulation model was constructed. The transmission spectra were measured using a vector network analyzer while applying a biased magnetic field perpendicular to the YIG film. A bandgap was observed in the measured transmission spectrum. The frequency of the bandgap and the propagation band of spin waves were in good agreement with the calculation result. From these results, 2D MC using YIG and non-magnetic metals was demonstrated.

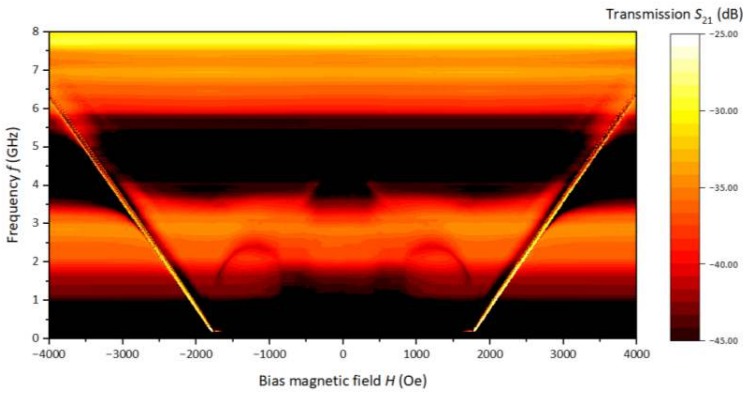


Figure 1. Measured spin wave spectroscopy when the incident angle was 5 degrees.

References

1. N. Kanazawa, T. Goto, K. Sekiguchi, A. B. Granovsky, C. A. Ross, H. Takagi, Y. Nakamura, H. Uchida and M. Inoue, “The role of Snell’s law for a magnonic majority gate”, Scientific Reports, 7, (2017).
2. T. Goto, T. Yoshimoto, B. Iwamoto, K. Shimada, C. A. Ross, K. Sekiguchi, A. B. Granovsky, Y. Nakamura, H. Uchida and M. Inoue, “Three port logic gate using forward volume spin wave interference in a thin yttrium iron garnet film”, Scientific Reports, 9, (2019).
3. T. Goto, K. Shimada, Y. Nakamura, H. Uchida and M. Inoue, “One-dimensional magnonic crystal with Cu stripes for forward volume spin waves”, Physical Review Applied, 11, (2019).
4. K. Shimada, T. Goto, N. Kanazawa, H. Takagi, Y. Nakamura, H. Uchida and M. Inoue, “Extremely flat transmission band of forward volume spin wave using gold and yttrium iron garnet”, Journal of Physics D: Applied Physics, 50, (2017).

Temporal modulation of Bound States in the Continuum at Mid-IR wavelengths

S. Kishen, P. Sahaan, J. Tapar and N.K. Emani*

Department of Electrical Engineering, Indian Institute of Technology, Hyderabad 502285, India
*corresponding author: naresh@ee.iith.ac.in

Abstract: The physics of time-varying media as a means of wave manipulation has resulted in the demonstration of several novel phenomena such as magnetic-free non-reciprocity, photonic time crystals, etc., to name a few. Here, we numerically demonstrate the excitation of BIC in a silicon metasurface without breaking the symmetry of the structure. By sinusoidally modulating the refractive index in time, using experimentally realizable parameters, we show the excitation, dynamic tuning, and restoration of BIC in mid-IR.

Introduction

Bound states in the continuum (BIC) are non-radiating localised waves coexisting within a continuum of propagating waves [1, 2]. Unlike a resonant state, a BIC cannot be excited using plane waves coming from infinity, i.e. BICs are dark states with infinite radiative lifetimes [3, 4]. Recently, there has been a growing interest in realizing an open cavity supporting a BIC that is accessible to broadband light for perpetual optical storage [5-7].

Here, we numerically demonstrate the excitation of BIC using an external broadband light source, in mid-IR, without breaking the structural symmetry. We perturb the BIC mode by modulating the refractive index of a silicon metasurface in time, using experimentally realisable modulation frequencies. The BIC can be dynamically tuned by changing the modulation frequency and hence can be used for optical trapping, sensing, etc.

Simulation and Results

The proposed structure consists of a 1 μm thick, two-dimensional silicon metasurface on a glass substrate ($\varepsilon_{SiO2} = 1.45$), as shown in fig. 1a. A unit cell of the metasurface consists of cylindrical nanoholes of diameter and height of 1 μm and an inter-cell periodicity of P_x and P_y in the x−, and y− directions, respectively. The structure is embedded in SiO_2 to provide a homogeneous environment. The permittivity of silicon is assumed to be dispersionless and taken to be $\varepsilon_{0,Si} = 11.9$ prior to modulation ($t < t_0$). We use the commercial FDTD solver, Lumerical FDTD™, to carry out the numerical study of the structure.

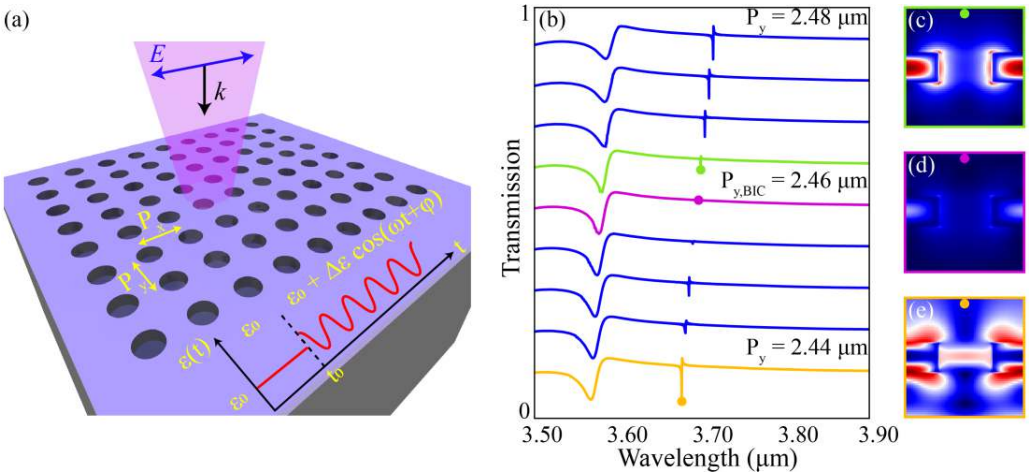


Fig 1: (a) Schematic illustration of 1 μm thick silicon metasurface on a glass substrate. The diameter of a cylindrical nanohole is 1 μm, with a periodicity of P_x and P_y in the respective directions. The scheme for permittivity modulation of silicon is shown in the figure. (b) The transmission spectra calculated for $P_x = 2.20$ μm and P_y varying from 2.44 μm to 2.48 μm. (c-e) Field profiles for (c) $P_y = 2.465$ μm, (d) $P_y = 2.46$ μm and (e) $P_y = 2.44$ μm.

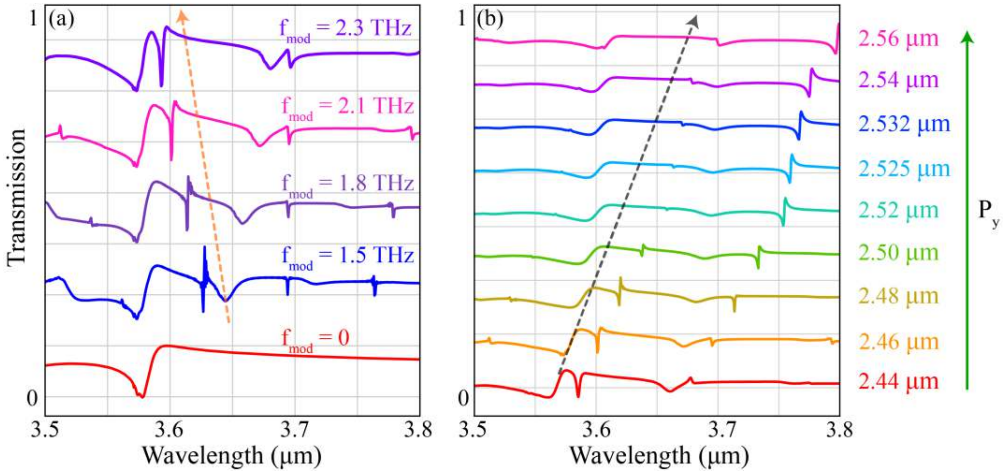


Fig. 2: (a) Transmission spectra as a function of wavelength and modulation frequency for a periodicity of P_x = 2.20 μm and P_y = 2.60 μm, and modulation depth of $\Delta\varepsilon$ = 0.5. (b) Transmission spectra for varying P_y when the metasurface is modulated at f_{mod} = 2.1 THz. The mode restores to BIC on varying P_y (dashed grey), thereby confirming the excitation of quasi-BIC in fig 2a (dashed orange).

The geometric parameters, P_x and P_y, are tuned to achieve the BIC condition. Figure 1b shows the evolution of normalised transmission spectra as a function of wavelength and periodicity P_y, with P_x = 2.20 μm. The incident beam is polarised along the x−direction for normal incidence. The figure shows two resonant transmission dips at wavelengths of 3.57 μm and 3.67 μm for P_y = 2.44 μm, with the dip at lower energy vanishing with increasing P_y. The BIC mode, therefore, occurs for a periodicity of P_x = 2.20 μm and P_y = 2.46 μm. The cross-sectional field profiles for P_y = 2.44 μm, 2.46 μm, and 2.465 μm are shown in Fig. 1c-e, respectively. The fields are highly localised within silicon for periodicities slightly detuned from the BIC (fig. 1c), are extremely leaky for periodicities away from BIC (fig. 1e), and vanish at BIC (fig. 1d).

We now modulate the permittivity of silicon in time with a modulation frequency f_{mod} and modulation depth $\Delta\varepsilon$ such that $\varepsilon_{Si} = \varepsilon_{0,Si} + \Delta\varepsilon \cos(2\pi f_{mod} t + \varphi)$ for $t > t_0$. Figure 2a shows the transmission spectra for modulated metasurface with the following parameters: $\Delta\varepsilon$ = 0.5, f_{mod} = 1.5 THz to 2.3 THz, and φ = 0. Compared to the unmodulated case (red curve), we see signatures of three distinct modes when f_{mod} = 1.5 THz. We focus on the transmission dip at 3.63 μm, which blue-shifts and broadens as f_{mod} increases. This dip corresponds to the perturbation of BIC and its subsequent conversion to a quasi-BIC mode. To verify that the excited mode is a quasi-BIC mode, we vary the periodicity P_y at a particular modulation frequency and observe the evolution of the mode. Figure 2b shows the transmission spectra at different periodicities for f_{mod} = 2.1 THz. As the periodicity increases, the mode at 3.58 μm red-shifts with reduced amplitude, vanishes for a periodicity of 2.52 μm and re-emerges on further increase in P_y. The mode restores to BIC on varying the periodicity, thereby confirming that the modulation resulted in excitation of a quasi-BIC mode.

In conclusion, we have demonstrated the coupling of BIC mode to external radiation by temporally modulating the refractive index of a silicon metasurface. The Q-factor of the mode can be controlled by varying the modulation frequency, and hence can be used for sensing, optical storage, etc.

References

[1] S. I. Azzam, et al., "*Advanced Optical Materials*", **2021**, 9, 2001469.

[2] C. W. Hsu, et al., "*Nature Reviews Materials*", **2016**, 1, 1.

[3] S. T. Ha, et al., "*Nature nanotechnology*", **2018**, 13, 1042.

[4] K. Koshelev, et al., "*Nanophotonics*", **2019**, 8, 725.

[5] E. Bulgakov, et al., "*Optics express*", **2015**, 23, 22520.

[6] Z. Hayran, et al., "*ACS Photonics*", **2021**, 8, 813.

[7] S. Lannebère, et al., "*Nature communications*", **2015**, 6, 8766.

META 2023, PARIS - FRANCE, JULY 18 – 21, 2023

Morphing design of Network of Beams to Maximize Absolute Bandgaps using Spectral Element Method

T. Bonneval[1*], M. Lanoy[2], L. Sanches[1], C. Lyszyk[3], R. Tanays[3], A. Pelat[2], G. Michon[1]

[1] Université de Toulouse, ICA, CNRS, INSA/UPS/ISAE-Supaero/IMT Mines Albi, Toulouse, France
[2] Laboratoire d'Acoustique de l'Université du Mans, CNRS, Le Mans, France
[3] Institut de Recherche Technologique Saint Exupéry, B612, Toulouse, France
[*]corresponding author: Theo.BONNEVAL2@isae-supaero.fr

Abstract: We propose a 3D lattice design (assembly of beams) that uses an optimization routine to generate forbidden frequency bands for all types of mechanical waves. The optimization step is performed using the Spectral Element Method (SEM) with a genetic algorithm. A specific example demonstrates the evolution of the unit cell structure over generations, resulting in a complete (relative to all wave polarizations) band gap opening. To verify the bandgap efficiency, wave propagation in an 8-unit cell periodic network is computed.

I. INTRODUCTION

Phononic crystals have demonstrated the effectiveness of Bragg or resonant band gaps in filtering, guiding, and manipulating acoustic waves [1]. Just like phononic crystals, lattice structures can be designed periodically to produce stopbands while ensuring good static rigidity [2]. A design study [3] showed that proper tuning of a 1D unit cell allows for the design of absolute bandgaps (i.e., relative to all mechanical wave polarizations). In this presentation, we propose the design of a 3D lattice unit cell modeled with SEM coupled with a genetic algorithm that searches for the optimal set of interconnected beams that opens the largest forbidden frequency band.

II. METHODOLOGY

We model the propagation of elastic waves in a set of interconnected beams using a semi-analytical computational algorithm called the Spectral Element Method (SEM). This algorithm provides exact theoretical frequency domain solutions and is faster than the finite element method, making it ideal for computing a wide variety of configurations [4]. The optimization is performed using a genetic algorithm. The cost function to be minimized is defined as the inverse of the frequency value of the largest bandgap calculated within the studied frequency range. The genes are linked to the ability to reshape the existing beams or add new ones.

III. RESULTS AND DISCUSSIONS

Figure 1 presents an optimization example. The first row shows the initial structure consisting of two beams on each side of the propagation axis. The flexural resonance of the lateral beams affects the propagation of torsional and bending waves, significantly reducing the structure's stiffness and thus the wave speed. We run the genetic algorithm for 14 iterations. After the fifth generation (second row in Fig. 1), the structure adopts a spring shape in the x direction, resulting in a significant drop in compressional (red dots) rigidity. The optimization lowers the propagation speed of compression waves, leading to the appearance of a complete forbidden frequency band. After 14 iterations (third row in Fig. 1), the structure remains similar to that of the 5th iteration, but the bandgap is significantly broader.

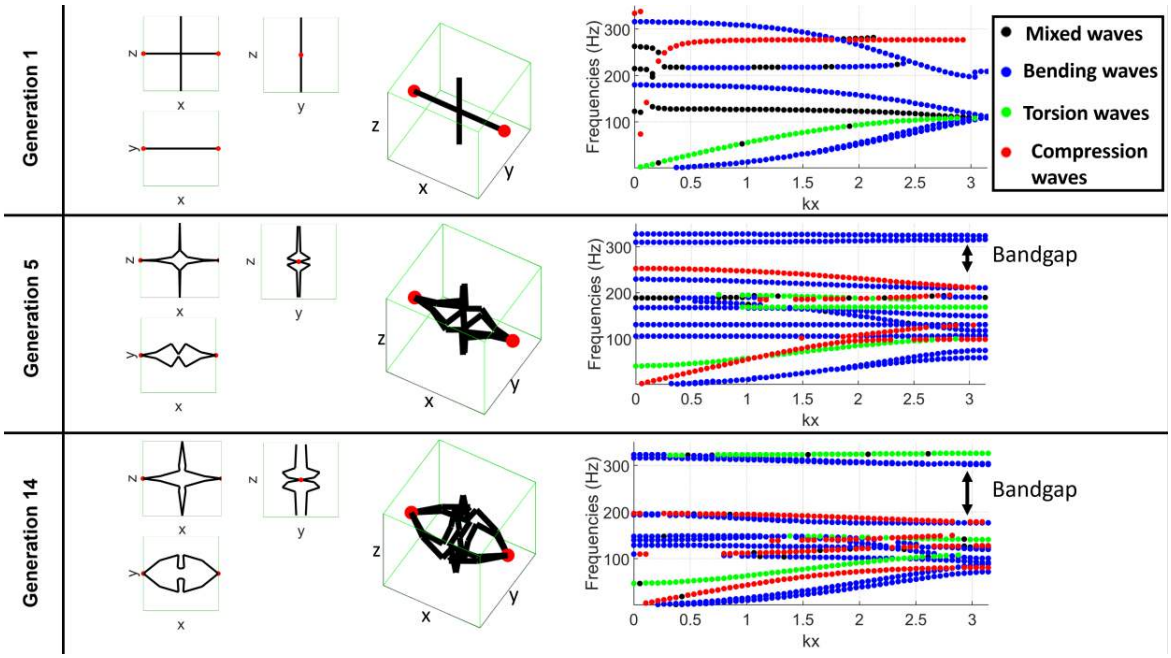


Fig. 1. The results of a genetic algorithm used to optimize a 3D structure composed of interconnected beams to maximize the stopband in a 1D periodic network are displayed on three lines, representing generations 1, 5, and 14 of the algorithm. On each line, the left side shows the different views of the unit cells selected at each generation. The right side of each line presents the dispersion diagrams associated with the unit cells computed with SEM. Each point on the diagram is colored according to the type of wave propagating in the network: compression waves are represented in red, torsion waves in green, bending waves in blue, and mixed waves in black.

IV. CONCLUSION

We have established a method that uses a genetic algorithm to modulate beam network structures to achieve forbidden frequency bands for all types of mechanical waves. The modeling was carried out semi-analytically using the Spectral Element Method (SEM), which allowed for faster computation than finite element methods. The presented optimization example shows the effectiveness of this method in achieving an absolute vibration filter and understanding how the structure evolves to control the propagation of mechanical waves within its periodic network. With the rise of additive manufacturing, this work will be extended to periodic networks that allow for multi-directional propagation of mechanical waves, with the goal of fabricating 3D-printed structural components that act as absolute vibration filters.

References

1. S. Cummer, J. Christensen, and A. Alù, "Controlling sound with acoustic metamaterials," Nat. Rev. Mater., vol. 1, p. 16001, 2016.
2. Xiyue An, Changliang Lai, Weiping He, Hualin Fan, "Three-dimensional meta-truss lattice composite structures with vibration isolation performance," Extreme Mech. Lett., vol. 33, 100577, 2019.
3. J. Plisson, A. Pelat, F. Gautier, V. Romero-Garcia, and L. Mevel, "Design of a Multiwaves Vibration Filtering," SAE Tech. Paper, 2020-01-1560, 2020.
4. Z.J. Wu, F.M. Li, and C. Zhang, "Vibration band-gap properties of three-dimensional Kagome lattices using the spectral element method," J. Sound Vib., vol. 341, pp. 162-173, 2015.

META 2023, PARIS - FRANCE, JULY 18 – 21, 2023

Numerical method for the inverse design of three-component metamaterial multilayers

T. Terao[1*]

[1]Department of Electrical, Electronic and Computer Engineering, Gifu university, Japan
[*]corresponding author: terao@gifu-u.ac.jp

Abstract: A numerical method for inverse design of three-component metamaterial multilayers was developed. Restart-tempering method was applied to optimize optical properties for three-component metamaterials multilayers. An algorithm suitable for accurately calculating the effective refractive index of these metamaterial multilayers was also demonstrated**.**

The design of metamaterials with arbitrary refractive indices is an important issue for the further practical development of metamaterial composites, and is useful for the creation of negative-refractive-index materials (NIMs) and epsilon-near-zero materials. In addition, it is also desirable to search for materials with the smallest possible imaginary part of the refractive index, as previously proposed metamaterial materials (especially in the optical domain) often have very strong optical absorption in the frequency region of interest. In my previous study,[1] I have proposed an original method called "restart tempering method", which is suitable for the inverse design of metamaterial multilayers consisting of two different types of layers with different dielectric constants and magnetic permeabilities. In this study, we discuss an inverse design method for a three-layer metamaterial multilayer film consisting of two different positive refractive index materials (PIMs) and a thin layer of PIMs or metals, in order to increase the degree of freedom in designing metamaterial composite materials (Figure 1).

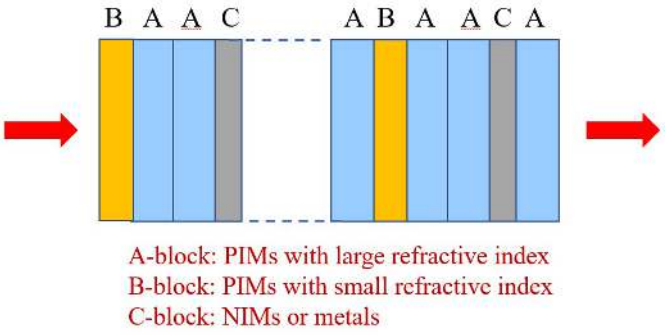


Figure 1. Metamaterial multilayers with three different components

Several attempts have been made to determine the (effective) complex refractive index n of the entire multilayer from the transmission coefficient t and reflection coefficient r of the multilayer. Experimental methods exist to determine the refractive index of a thin film, such as ellipsometry. In the case of conventional experimental refractive index measurement methods, the interior of the thin film is formulated as a homogeneous medium, but this is not strictly the same problem for metamaterial multilayers such as the present one, since the interior is not homogeneous. From the standpoint of numerical analysis, the method proposed by Ref. 2 is well known as a representative method. However, in this method, the complex refractive index is determined by inverse trigonometric functions which are multivalued functions. Therefore, there is a problem that the real part

of the refractive index is not uniquely determined, and no mathematical formula is given to give an integer that specifies the true solution from an infinite number of sequences. In addition, it is of interest to clarify whether the effective refractive index estimated for a metamaterial multilayer is transferable with respect to the angle of incidence.

In this study, the downhill simplex method was employed to estimate more accurately the effective refractive index n_{eff} of metamaterial multilayers and corresponding software to address the above problem. The problem of transferability of n_{eff} in multilayers was also numerically verified by comparing the case of perpendicular incidence with that of oblique incidence. In parallel, we extended the restart tempering method,[1] which was developed by our group, to the problem of three-component multilayer systems and applied it to the inverse design of these systems.

The author acknowledges the Supercomputer Center at the University of Tokyo, for the use of their facilities. This work was supported by JSPS KAKENHI Grant Number 20K11848.

References

1. T. Terao, “Numerical methods for design of metamaterial photonic crystals and random metamaterials,” EPJ Applied Metamaterials, Vol. 9, 1, 2022.
2. D. R. Smith, S. Schultz, P. Markos, and C. M. Soukoulis, “Determination of effective permittivity and permeability of metamaterials from reflection and transmission coefficients,” Physical Review B, Vol. 65, No. 19, 195104, 2002.

META 2023, PARIS - FRANCE, JULY 18 – 21, 2023

Twisted Polaritonic Crystals in Thin Anisotropic Van der Waals Slabs

N. Capote-Robayna[1*], O. Matveeva[2], V. S. Volkov[2], P. Alonso-González[3,4] and A. Y. Nikitin[1,5]

[1]Donostia International Physics Center (DIPC), Paseo Manuel de Lardizabal, 4, 20018, Donostia-San Sebastián, Spain
[2]XPANCEO, Bayan Business Center, DIP, 607-0406, Dubai, UAE
[3]Department of Physics, University of Oviedo, Oviedo, 3006, Spain
[4]Center of Research on Nanomaterials and Nanotechnology, CINN (CSIC-Universidad de Oviedo), El entrego, 33940, Spain
[5]IKERBASKE, Basque Foundation for Science, Bilbao, 48013, Spain
[*]nathaniel.capote@dipc.org

Abstract: Polaritons – hybrid light-mater excitations – are very appealing for the confinement of light at the nanoscale. Recently, a particular interest has been focused on thin anisotropic slabs of van der Waals (vdW)[1,2] materials supporting anisotropic polaritons which exhibit ultra-high momenta and strongly directional in-plane[3]. Here we introduce a concept of vdW slabs-based twisted polaritonic crystals (PCs) – lattices with periods comparable to the polariton wavelength rotated with respect to the natural vdW crystal axes – to efficiently excite and control in-plane anisotropic polaritons.

In this work we focus our study on PCs made out of thin biaxial slabs, such as, for instance, hole arrays made directly in the slab[4]. The periodic structure gives rise to Bragg resonances whose properties can be extracted from the polaritonic bandstructure provided by our theory. Such Bragg resonances can be efficiently tuned in frequency by twisting the lattice with respect to the crystallographic axes. We develop a simple theoretical approach to treat the diffraction of light by the twisted PCs and demonstrate its validity for realistic structures (e.g., hole arrays) by comparing analytical results with full-wave electromagnetic simulations. Our results open up a new research area of twisted polaritonic crystals, including those that support nontrivial topological polaritons. PCs may be very attractive for some practical use, such as in tunable sensors or photodetectors in a plethora of possible optical setups.

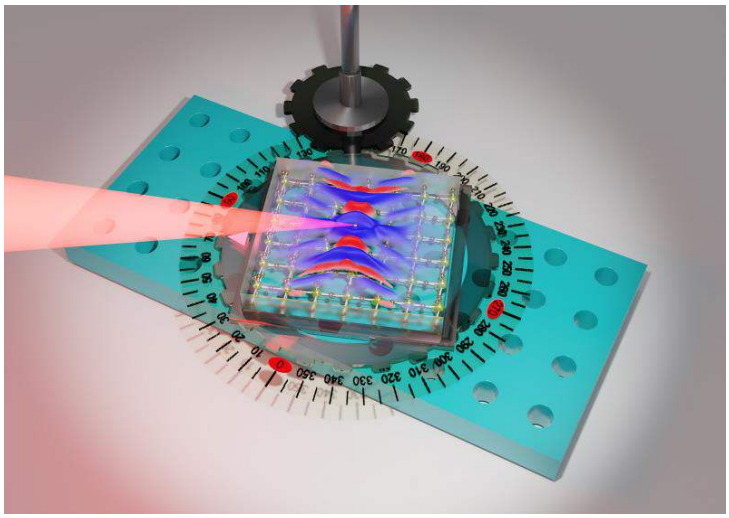


Figure 1: An artistic image of a potential twist-tunable PC structure. The polaritons inside the crystal can be efficiently controlled by twisting the axes of the periodic structure made in the substrate with respect to the natural axes of the anisotropic crystal slab.

References

1. Basov, D. N. “Polaritons in van der Waals materials” Science, Vol. 354, No. 6309, .aag1992, 2016.
2. Low, T. “Polaritons in layered two-dimensional materials” Nature Mat., Vol. 16, No. 2, 182-194, 2017.
3. Ma, W. “In-plane anisotropic and ultra-low-loss polaritons in a natural van der Waals crystal” Nature, Vol. 562, No. 557-562, 2018.
4. Capote-Robayna, N. “Twisted Polaritonic Crystals in Thin van der Waals Slabs” Laser & Photonics Reviews, Vol. 16, No. 2200428, 2022.

Arbitrarily-broadband dispersion compensation with ultrathin multiresonant metasurfaces

Odysseas Tsilipakos[1*] and Thomas Koschny[2]

[1] Theoretical and Physical Chemistry Institute, National Hellenic Research Foundation, GR-11635 Athens, Greece
[2] Ames Laboratory–U.S. DOE and Department of Physics and Astronomy, Iowa State University, Ames, Iowa 50011, USA
*corresponding author: otsilipakos@eie.gr

Abstract: We propose multiresonant metasurfaces exhibiting a broadband and purely quadratic spectral phase to be utilized for dispersion compensation and in general any application requiring temporal pulse shaping of broadband signals. The proposed metasurfaces require implementing a specific combination of Lorentzian resonances in the electric and magnetic surface conductivities. Our approach overcomes the fundamental limitations of both conventional, non-resonant approaches (too bulky) as well as modern, singly-resonant metasurfaces (too narrowband) and aspires to bring broadband dispersion engineering at ultrathin physical scales.

In recent years, metasurfaces (MSs) have been extensively studied for a myriad of applications. However, they have found limited use when it comes to broadband dispersion engineering and the temporal shaping of short pulses. This is because conventional, singly-resonant MSs are inherently narrowband and exhibit a specific spectral phase profile dictated by the resonance dispersion; for a single Lorentzian resonance centered at Ω it is of the form $\varphi(\omega) \propto \mathrm{atan}(\gamma(\omega - \Omega))$. The first example of a broadband, specifically-engineered spectral phase concerned a linear profile (spectrally-constant group delay), utilized to delay broadband pulses without distortion [1] and to perform achromatic wavefront manipulation (e.g., beam focusing and steering) [2,3]. However, a wider class of important applications requires a quadratic phase profile (linear group delay), namely, dispersion compensation, chirped pulse amplification, and more generally any application requiring control over the instantaneous frequency (chirp) and temporal duration of a broadband pulse through pulse chirping/de-chirping.

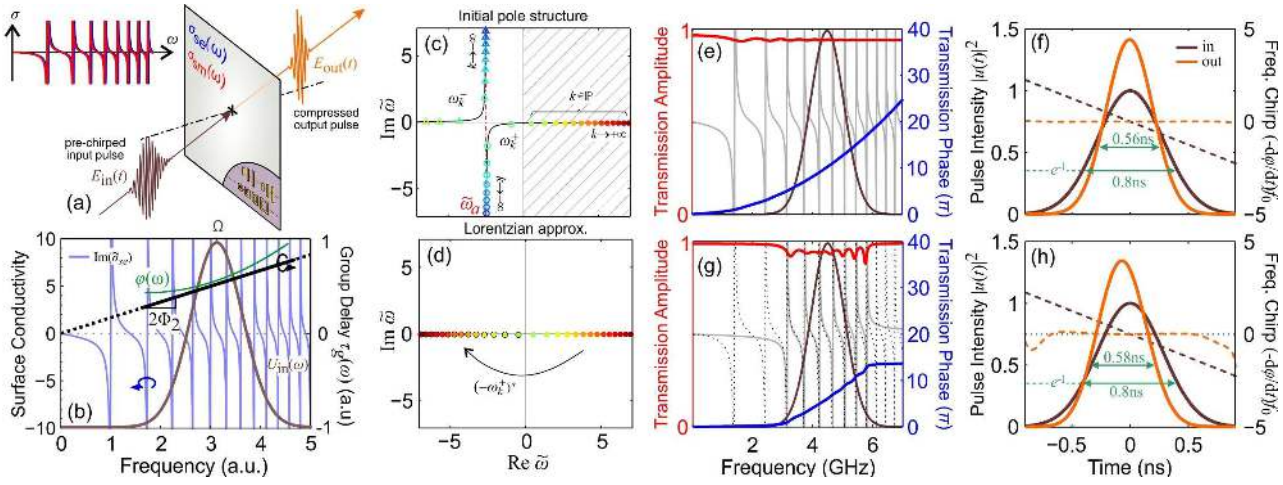


Figure 1: (a) Multiresonant metasurface with overlapping electric and magnetic surface conductivities for dispersion compensation in transmission. (b) The decreasing frequency spacing leads to positive group delay dispersion ($\Phi_2 > 0$). (c) Initial pole structure of required surface conductivity $\tilde{\sigma}_{se}(\omega)$. (d) Pole structure of the Lorentzian approximation $\tilde{\sigma}_{se}^{LA}(\omega)$. (e,f) Dispersion compensation example with an infinite Lorentzian resonance train. (g,h) The resonance train is truncated to seven resonances; the bandwidth becomes finite but the performance is not compromised.

Thus far, the approaches to dispersion compensation with MSs are either too narrowband or do not guarantee pulse integrity [4-6]. Here, we present a solution to this problem by constructing multiresonant MSs that implement a purely quadratic phase profile which is both arbitrarily strong (despite the ultrathin nature) and (almost) arbitrarily broadband, as controlled by the spacing and number of the implemented resonances, respectively. The main elements of our approach are illustrated in Fig. 1. A specific configuration of Lorentzian resonances in the electric and magnetic surface conductivities with decreasing(increasing) frequency spacing can lead to a purely quadratic phase $\varphi(\omega) = \Phi_2(\omega - \Omega)^2 + \Phi_1(\omega - \Omega) + \Phi_0]$ with positive(negative) group delay dispersion Φ_2 [Fig. 1(a),(b)].

In order to rigorously derive the required surface conductivities, we plug the desired transmission/reflection transfer function $H(\omega) = A\exp\{i\varphi(\omega)\}$ [$\varphi(\omega)$ is the quadratic phase and A allows for amplitude decay] in the expressions relating transmission/reflection plane-wave scattering coefficients with the surface conductivities of the MS [1]. The resulting prescription for the electric surface conductivity is found to be $\tilde{\sigma}_{se}(\omega) = -i\tan\{[\varphi(\omega) + i|\log A|]/2\}$. The poles of this complex function are depicted in Fig. 1(c). Subsequently, we keep only the poles with indices $k \in \mathbb{P}$ in Fig. 1(c) and complement them with their negative-conjugate counterparts [Fig. 1(d)] in order to end up with a Lorentzian approximation to the required conductivity. The Lorentzian approximation $\tilde{\sigma}_{se}^{LA}(\omega)$ is (i) characterized by poles residing only in the lower complex half-plane (as required by causality) and (ii) possesses the correct spectral symmetry (real part: even; imaginary part: odd) so that it translates into a real function in the temporal domain, as required for physical response functions.

As can be seen in Fig. 1(e), implementing the Lorentzian approximation $\tilde{\sigma}_{se}^{LA}(\omega)$ the metasurface can exhibit a broadband quadratic spectral phase with a fairly flat amplitude. This can be used for dispersion compensation of chirped signals [Fig. 1(f)]. For operation in transmission(reflection) electric and magnetic conductivities have to be spectrally overlapping(interleaved). In the example of Fig. 1(e),(f), the output pulse is completely de-chirped and compressed by a factor of $\sqrt{2}$, as intended. In practice, the resonance trains need to be truncated. Figure 1(g) investigates this scenario keeping seven resonances. The compression is only slightly affected and the residual output chirp is negligible along the duration of the output pulse [Fig. 1(h)].

This work was funded by the Hellenic Foundation for Research and Innovation (H.F.R.I.) under the "2nd Call for H.F.R.I. Research Projects to support Post-doctoral Researchers" (Project Number: 916, PHOTOSURF).

References

1. Tsilipakos, O., Zhang, L., Kafesaki, M., Soukoulis, C. M. and Koschny, T., "Experimental implementation of achromatic multiresonant metasurface for broadband pulse delay," ACS Photon., Vol. 8, 1649-1655, 2021.
2. Fathnan, A. A., Liu, M., Powell, D. A., "Achromatic Huygens' Metalenses with Deeply Subwavelength Thickness," Adv. Optical Mater. Vol. 8, 2000754, 2020.
3. Tsilipakos, O., Kafesaki, M., Economou, E. N., Soukoulis, C. M. and Koschny, T., "Squeezing a prism into a surface: emulating bulk optics with achromatic metasurfaces," Adv. Opt. Mater., Vol. 8, 2000942, 2020.
4. Dastmalchi, B., Tassin, P., Koschny, T. and Soukoulis, C. M., "Strong group-velocity dispersion compensation with phase-engineered sheet metamaterials," Phys. Rev. B, Vol. 89, 115123, 2014.
5. Decker, M., Staude, I., Falkner, M., Dominguez, J., Neshev, D. N., Brener, I., Pertsch, T., Kivshar, Y. S., "High-efficiency dielectric Huygens' surfaces," Adv. Opt. Mater., Vol. 3, 813−820, 2015.
6. Divitt, S., Zhu, W., Zhang, C., Lezec, H. J. and Agrawal, A., "Ultrafast optical pulse shaping using dielectric metasurfaces," Science, Vol. 364, 890-894, 2019.

ZrO_2 Holographic Metasurfaces for Biophotonics Applications

Mohammad biabanifard[1], Tomasz Plaskocinski[1], Jianling Xiao[1], and Andrea Di Falco[1]

[1]University of St Andrews, North Haugh, St Andrews, Fife, KY16 9SS, United Kingdom
*corresponding author: adf10@st-andrews.ac.uk

Abstract: We present zirconium dioxide holographic metasurfaces offering environmental independence operation, ease of fabrication, biocompatibility, and broadband functional nature. Here we show that this class of metasurfaces can be used for integrated optical trapping in the visible range.

Metasurfaces, artificial two-dimensional surfaces that are designed to manipulate the electromagnetic behavior of light, can be used to modulate the optical response of the incident light [1-2]. Holographic metasurfaces (MSs) have found utilization in virtual and augmented reality, encryption and security, sensing, imaging and digital art applications [3]. One of the key factors that determine the properties and scope of applications of metasurfaces-based devices is the material chosen for the meta-atoms. Titanium dioxide (TiO_2) and amorphous silicon are among the most prominent materials for practical metasurface applications in the visible range, due to their high refractive index and broadband transparency. However, they suffer from high-temperature fabrication (TiO_2) and low operational bandwidth in visible wavelengths (amorphous silicon).

Here, we discuss particularly the potential of zirconium dioxide (ZrO_2) as a suitable material for the practical use of metasurface technology, offering broadband operation across the whole visible range, as shown in Fig. 1a. Most importantly, ZrO_2 presents excellent resistance to corrosion and different chemicals, very high fracture toughness, high hardness and density, good frictional behavior, low thermal conductivity, and solid electrical insulation, which make it particularly attractive for real-world applications [4].

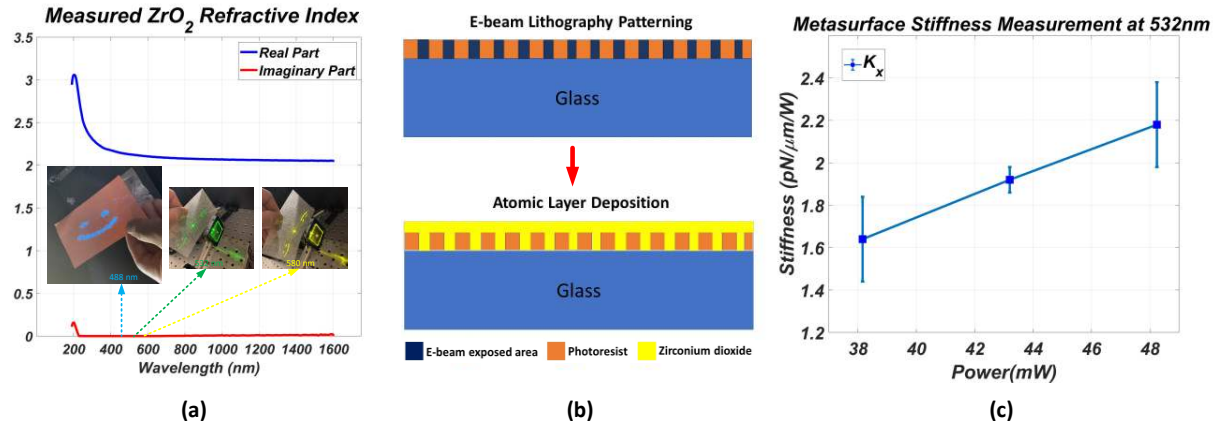


Fig. 1. (a) The measured refractive index of ZrO_2 with the inserted smile face holographic image working at 488nm, (b) the fabrication process, and (c) the measured trap stiffness operating at 532nm.

The platform was validated by fabricating holographic metasurfaces for on-chip optical trapping, which replaces the need for a costly and bulky high numerical aperture microscope objective. The meta-atoms were fabricated using electron beam lithography on a glass substrate, followed by low-temperature conformal coating of ZrO2 using atomic layer deposition, as depicted in Fig. 1b.

The design of the meta-atoms was optimized to cover a phase range of approximately 260 degrees at 532 nm, taking into account the refractive index of ZrO2 which is n=2.11. Although not complete, the achieved phase range was sufficient to design a high-quality focused spot with a focal distance of 40 micrometers and designed numerical aperture NA=1.2. The trap stiffness of a 2-micrometer silica particle trapped by a ZrO_2 MS, excited by a collimated beam at 532nm, is shown in Fig. 1c. These experimental results demonstrate the potential of ZrO_2 MSs for on-chip optical trapping applications.

The new fabrication technique used in this study does not require etching after atomic layer deposition, and it is a low-temperature process that results in a flat surface on top of the structure. These features make the technique particularly advantageous for biophotonics applications, where a smooth and uniform surface is often required. Additionally, the efficiency of the fabrication process could potentially reduce the cost and complexity of manufacturing metasurface devices for a variety of applications.

References

1. Yu Nanfang, and Federico Capasso. "Flat optics with designer metasurfaces." *Nature materials* 13, no. 2 (2014): 139-150.
2. Yu Nanfang, Patrice Genevet, Mikhail A. Kats, Francesco Aieta, Jean-Philippe Tetienne, Federico Capasso, and Zeno Gaburro. "Light propagation with phase discontinuities: generalized laws of reflection and refraction." *science* 334, no. 6054 (2011): 333-337.
3. Yan Libin, Jianling Xiao, Tomasz Plaskocinski, Mohammad Biabanifard, Saydulla Persheyev, Meisam Askari, and Andrea Di Falco. "Two-tier manipulation of holographic information." *Optics Express* 30, no. 11 (2022): 19145-19151.
4. Ahmed M. Walaa, Tom Troczynski, Anthony P. McCullagh, Chris CL Wyatt, and Ricardo M. Carvalho. "The influence of altering sintering protocols on the optical and mechanical properties of zirconia: a review." *Journal of Esthetic and Restorative Dentistry* 31, no. 5 (2019): 423-430.

META 2023, PARIS - FRANCE, JULY 18 – 21, 2023

Ray-based design of hybrid metalens refractive imaging systems

Yijun Ding[1*] and Bryan D. Stone[1]

[1]Synopsys Inc., 199 S. Los Robles Ave. Suite 400, Pasadena, CA 91101, USA
[*]corresponding author: joyding@synopsys.com

Abstract: The complexity of the design workflow is one of the main roadblocks for the adoption of metalenses in a hybrid imaging system that include both metalenses and conventional refracting or reflecting optical elements. This complexity is caused by the two significantly different length scales of lenses (macro-optics) and meta-atoms (micro-structures). To bridge the gap between the two scales, we propose a ray-based approach for designing hybrid imaging system and provide design examples for this approach.

Metalenses have the potential to become a powerful new tool in an optical engineer's toolbox, in light of its potential applications in AR/VR, biomedical imaging, and wearable consumer electronics [1–3]. One of the main roadblocks for the adoption of metalenses in optical design is the complexity of the design workflow. This complexity is caused by the two significantly different length scales involved in the design of a metalens. Meta-atoms, with a length scale of a few hundred nanometers, are often simulated with rigourous coupled-wave analysis (RCWA) or finite-difference time-domain (FDTD) method. However, these simulation methods alone are not suitable for the design of mm-scale metalenses, as the memory and computation time required for the simulation is prohibitive. A ray-based metalens analysis tool can bridge the gap between the metalens and the optical property of the meta-atoms, hence reducing the complexity of the metalens design workflow.

Because of the length-scale of the meta-atoms, ray-based methods for analysis and optimization may not be considered to be appropriate. However, by treating the imparted phase appropriately, ray-based method can be used to design and analyze optical systems that incorporate one or more meta lenses. In order for ray-based design methods to be generally successful, they must account for angular and wavelength dependence of the meta-atom optical properties. Prior work on multiscale optimization of hybrid imaging systems has applied a simple phase surface [4], Sweatt model [5], or effective medium theory [6] to simulate a metalens. We treat a metalens similar to a conventional diffractive surface [7, 8]. Compared to prior work, our approach considers the optical property dependence on wavelength and field of view, and it works for varying meta-atom types.

In our approach, there are two pieces of information that are required by the ray trace:

1. The ray directions following the meta surface.
2. The amount of energy (also called efficiency) that propagates in each of these orders.

We use the discontinuities in the meta-atom parameter to determine the ray directions for the diffracted order and Fourier Optics [9] to estimate the amount of energy that goes into the various orders for a given incident ray. This allows the ray direction and energy to be dependent on the wavelength and angle of incidence. The ray-based approach can still take into account the wave-nature of light, but rays are used as an integral part of the design and analysis process.

Our approach is not limited to a particular type of meta-atoms. The optical properties of the meta-atoms can be

calculated with RCWA or FDTD algorithms using local periodic approximation [10]. By varying the design parameter(s) of the meta-atoms, a lookup table can be generated in the form of a transfer-function library [11]. The angular and wavelength dependence can be included in the meta-atom library and hence considered in the ray-based design approach. We have implemented a ray-based metalens design tool that links to such a meta-atom library.

The proposed methods can be applied to imaging systems or illumination systems composed solely of meta lenses, or systems that incorporate a mix of meta lenses and conventional refractive, reflective, or diffractive optical elements. In this paper we discuss this ray-based approach and offer design examples that are used to validate this approach. For the validation, we compare the results of ray-based analysis with those found by a more rigourous wave-based analysis. Note that the ray-based approach can still take into account the wave-nature of light, but rays are used as an integral part of the design and analysis process. We find that the design process is greatly simplified by using the ray-based approach and that there is excellent agreement between the ray-based predictions and the wave-based analysis.

References

1. Khorasaninejad, M., W. T. Chen, R. C. Devlin, J. Oh, A. Y. Zhu, and F. Capasso, “Metalenses at visible wavelengths: Diffraction-limited focusing and subwavelength resolution imaging,” Science 352, 1190–1194 (2016).
2. Kamali, S. M., E. Arbabi, A. Arbabi, and A. Faraon, “A review of dielectric optical metasurfaces for wavefront control,” Nanophotonics 7, 1041–1068 (2018).Lastname, F. M. and F. M. Lastname, “Title of the journal paper,” Journal Title Abbreviation, Vol. 34, No. 10, 1064–1076, 1986.
3. Chen, W. T., A. Y. Zhu, and F. Capasso, “Flat optics with dispersion-engineered metasurfaces,” Nat. Rev. Mater. 5, 604–620 (2020).
4. Shalaginov, M. Y., An, S., Yang, F., Su, P., Lyzwa, D., Agarwal, A. M., ... & Gu, T. (2020). Single-element diffraction-limited fisheye metalens. Nano Letters, 20(10), 7429-7437.
5. Hon, P. W.C., S. Larouche, K. Fountaine, S. W. Lee, S. Wang, E. Bustamante, I. El-Kady, E. Poutrina, A. Urbas, “Multiscale Optimization of Metaoptic Hybrid Lenses”, Meta conference (2022).
6. Cuillerier, A. C., Borne, J., Dallaire, X., & Thibault, S. (2021, June). Toward hybrid refractive and metalens design. In International Optical Design Conference (p. 120781W). Optica Publishing Group.
7. Schake, M., "Examining and explaining the “generalized laws of reflection and refraction” at metasurface gratings," J. Opt. Soc. Am. A **39**, 1352-1359 (2022).
8. O'Shea, D. C., T. J. Suleski, A. D. Kathman; D. W. Prather, Diffractive Optics: Design, Fabrication, and Test (SPIE Press, 2003), Chapt 2.
9. Goodman, J.W., “Introduction to Fourier Optics”, 4th ed., W.H. Freeman and Company, (2017).
10. Arbabi, A., Y. Horie, A. J. Ball, M. Bagheri, and A. Faraon, “Subwavelength-thick lenses with high numerical apertures and large efficiency based on high-contrast transmitarrays,” Nat. communications 6, 1–6 (2015).
11. Bos, J., R. Scarmozzino, M. Bahl, E. Heller, and C. Xu, “A design automation and simulation flow for lens systems containing multiple metasurfaces,” in Proceedings of Meta 2022, (2022), pp. 1229–1231.

META 2023, PARIS - FRANCE, JULY 18 – 21, 2023

Metasurface-based optical concentrators monolithically integrated with Barrier infrared detectors

T. Wenger, R. Muller, C. J. Hill, A. Fisher, D. Z. Ting, D. Wilson, S. D. Gunapala, and A. Soibel*
Jet Propulsion Laboratory, California Institute of Technology, 4800 Oak Grove Dr., Pasadena, California 91011, USA
*asoibel@jpl.nasa.gov

Abstract: Recently developed metasurface technology enables optical concentrators that can be integrated with detectors. In this work we developed InAsSb-based infrared photodetectors monolithically integrated with metasurface lenses (metalenses) that act as optical concentrators. The metalenses are fabricated on the backside of a gallium antimonide substrate, and the photodetectors are fabricated on the frontside of the same substrate. The metalenses enhance the detector responsivity up to 10-fold and detectors retain the same detectivity at temperatures up to 40K higher.

Infrared (IR) detectors are widely used in medical, defense, and space applications. Recent IR detector advances such as nBn detectors have emerged with favorable high temperature performance. This makes them highly interesting for applications in space, especially for satellite concepts with small form factors where room for cooling hardware remains limited. Integration of photodetectors with optical concentrators enables detectors to collect a larger fraction of incident light, thereby increasing the responsivity of the detector and enabling operation at higher temperatures with the same performance. Such high-temperature detectors are attractive for instance in IR spectroscopy applications and gas analyzers.

We monolithically integrated metalenses as optical concentrators with single-pixel nBn detectors.[1] This was done by first fabricating the concentrators on the backside of a GaSb wafer with detector material grown on the frontside, followed by detector fabrication on the frontside. We investigated two separate metasurface designs, one annulus-shaped broadband design and one square narrowband design. Both metasurface designs are based on circular nanoposts, with post-post distance of 400 nm, that are etched 2 μm directly into the GaSb substrate. The metalens were designed to have a focal length of 500 μm (same as substrate thickness) for 4 μm light.

First, the detector material, $InAs_{0.915}Sb_{0.085}$, was grown using molecular-beam epitaxy (MBE) on the frontside of a GaSb substrate. Then metalens were fabricated on the backside of the detector wafer using electron-beam lithography and dry etching in both fluorine and chlorine chemistries. Next, the single pixel detectors with sides 100 μm were fabricated on the frontside using standard photolithography and a dry/wet etch. The metalens pattern contains alignment marks which were used for front-back alignment between metalenses and detectors. The alignment was performed with a maskless aligner.

We measured effective quantum efficiency (QE) for detectors with and without optical concentrators at T = 250 K. The bare detectors exhibit a fairly uniform response for 2−4 μm. Both metalens designs are effective in concentrating additional light onto the detector. The broadband design provides a more uniform performance enhancement, whereas the narrowband concentrator design has a peak in efficiency close to 4 μm. We found that QE enhancement is 3.5x for the broadband design and of 11x for the narrowband design. We evaluated the detectivity at the wavelength 3.75 μm with and without concentrators as a function of temperature. With the proper detectivity generalization, detectors with and without metalenses reach the same background-limited performance (BLIP) of 10^{12} cm Hz/W at low temperature. As the temperature increases, the dark current also increases and detectivity decreases. Importantly, the detectivity of the metalensed detectors falls off more slowly than detectors without metalenses, so these detectors can be operated at up to 40 K higher temperatures with the

©2023 California Institute of Technology. Government sponsorship acknowledged

same detectivity.

The research described in this publication was carried out at the Jet Propulsion Laboratory, California Institute of Technology, under a contract with the National Aeronautics and Space Administration (NASA). We would like to thank Parminder S. Ghuman, Sachidananda R. Babu, and Nikzad Toomarian for their encouragement and support. This work was partially funded by the ACT program NASA ESTO.

References

1. Wenger, T., Muller, R., Hill, C. J. *et al.* "Infrared nBn detectors monolithically integrated with metasurface-based optical concentrators," **Appl. Phys. Lett**. 121, 181109 (2022); https://doi.org/10.1063/5.0121643.

META 2023, PARIS - FRANCE, JULY 18 – 21, 2023

Phase sensing with meta-optical devices for wavefront recovery and biological imaging

L. Wesemann[1*], S. B. Sulejman[1], T. J. Davis[1], and A. Roberts[1]

[1] ARC Centre of Excellence for Transformative Meta-Optical Systems, School of Physics, University of Melbourne, Victoria 3010, Australia

[*]Corresponding author: lukas.wesemann@unimelb.edu.au

Abstract: Detection of the phase of an electromagnetic field is fundamental to applications including wavefront sensing in ophthalmology and precision telescopes as well as biological cell imaging. In contrast to readily detectable intensity variations, measuring phase usually requires more complex approaches. Conventional methods in this field suffer from drawbacks involving bulky and moving components, long propagation distances, computation time and energy consumption. Here we report on the use of nanophotonic devices used in transmission for phase-sensing and demonstrate their potential for ultra-compact wavefront recovery.

Detection of the phase of an electromagnetic field is fundamental to applications including biological cell imaging as well as wavefront recovery. While the intensity of a wavefield can be easily measured using conventional photodetectors, phase information is not directly accessible and requires application specific approaches. The field of wavefront sensing is concerned with extracting all relevant parameters of amplitude, phase, and polarisation from a wavefield. In this context, phase is for example used to draw conclusions about medical conditions in eye tests, or to compensate for aberrations in telescope images arising from atmospheric turbulences. A common approach to map phase modulations in the context of wavefront sensing is the use of Shack-Hartmann sensors as well interferometric approaches. Common methods for phase imaging in biology include Zernike phase imaging, DIC microscopy as well as other optical methods requiring computational post processing. These conventional phase detection methods commonly suffer from one or more disadvantages including bulky and moving components, macroscopic propagation distances as well as time and energy intensive computation. Recent work has demonstrated that all-optical image processing through meta-optical devices, including the visualisation of phase, has the potential to address these challenges [1]. These permit ultra-compact, real-time sensing of phase gradients via its conversion into readily measured intensity distributions. Initial demonstrations have demonstrated their applicability to phase imaging of unstained human cancer cells [2,3] as well as wavefront sensing [4]. We believe that nanophotonic approaches have significant potential to address the drawbacks of current phase sensing methods and we envisage new methods suitable for ultra-compact integration. Here we report on progress towards the application of meta-optical devices for all-optical, quantitative wavefront sensing. The quantification of phase can be used to determine quantities of interest such as the refractive index or dry mass of cells. We demonstrate recovery of the original wavefront through time-efficient computational post processing of the recorded data. We consider a subwavelength silver grating on top of a TiO_2 waveguiding layer sandwiched between a glass substrate and a PMMA superstrate (*c.f.* Fig. 1.a). This resonant waveguide grating device enables angle dependent coupling of incident radiation into guided modes, thereby filtering the spatial frequency content of the transmitted wavefield [2]. This permits optical computation of the first spatial derivative of the transmitted wavefield. For an incident wavefield with constant amplitude, but a modulation in phase, the intensity of the transmitted field is then proportional to the square of the first derivative of the phase. This all-optical conversion from phase into intensity underpins the

wavefront sensing method proposed here. In Fig. 1b first-order spatial derivatives along the *x*- and *y*-direction of an incident wavefield with a phase modulation in the shape of Zernike polynomials are optically computed by transmission through the device. Subsequently, we use the derivatives obtained along both spatial directions to computationally reconstruct the original wavefront through an iterative algorithm based on Fourier integration. Fig. 1.c shows a numerical example of reconstruction of the original wavefront from the spatial derivatives, as obtained upon transmission of the incident wavefield through the meta-optical device.

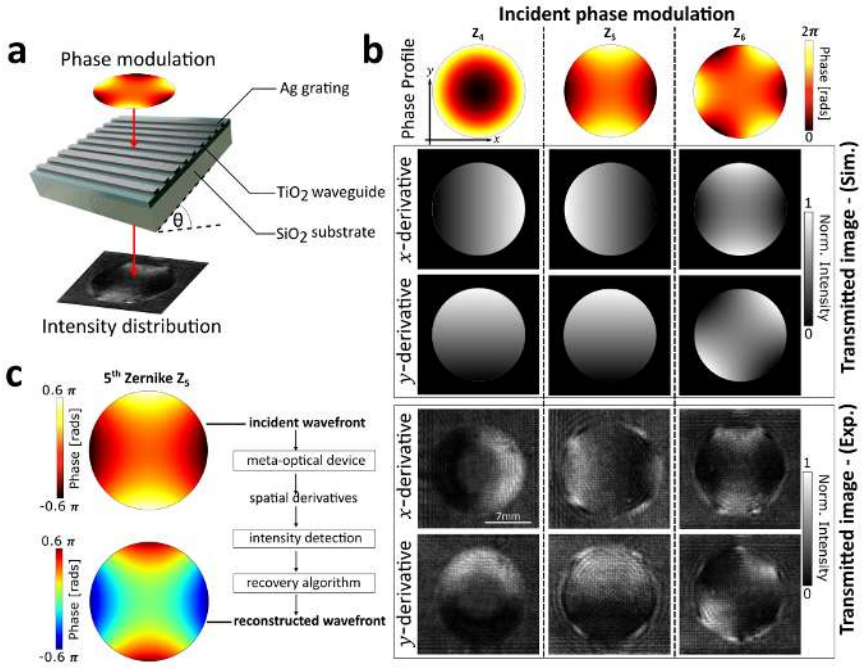


Fig.1 – a) Meta-optical device for phase visualisation in transmission at λ = 637 nm at a device tilt angle of θ = 3°. Subwavelength grating of Ag strips with period p = 400 nm on top of TiO_2 waveguid layer with a thickness of t = 150nm. b) Numerical and experimental optical computation of spatial derivatives of phase modulations along *x*- and *y*-direction via transmission through device using example of Zernike polynomials Z_4-Z_6. Experimental phase modulations of Z_4-Z_6 are imposed via a spatial light modultator (SLM) . c) Numerical simulation of meta-optical wavefront reconstruction based on integration of derivatives for the 5th Zernike polynomial Z_5.

In our presentation we will discuss application of the proposed method to quantitative phase-imaging of biological cells, and discuss devices that permit dynamic tuning of their processing capacity based on the incorporation of tuneable 2D materials.

This research was funded by the Australian Government through the Australian Research Council Centre of Excellence grant (CE200100010). S.B.S also gratefully acknowledges the support of the Ernst & Grace Matthaei Scholarship and the Australian Government Research Training Program Scholarship.

References

1. Wesemann, L., Davis, T. J., & Roberts, A. “Meta-optical and thin film devices for all-optical information processing” Applied Physics Reviews, Vol. 8 No. 3, 031309, 2021.
2. Wesemann, L., Rickett, J., Song, J., Lou, J., Hinde, E., Davis, T.J., Roberts, A. "Nanophotonics enhanced coverslip for phase imaging in biology" Light Sci. Appl., Vol. 10, No. 1, 98, 2021.
3. S.B. Sulejman, N. Priscilla, L. Wesemann, W. S. L. Lee, J. Lou, E. Hinde, T. J. Davis, A. Roberts, “Thin film notch filters as platforms for biological image processing,” arXiv:2209.09539, 2022.
4. Vohnsen, B., & Valente, D. “Surface-plasmon-based wavefront sensing” Optica, Vol. 2, No, 12, 1024-1027, 2015.

META 2023, PARIS - FRANCE, JULY 18 – 21, 2023

Metasurface enabled multifunctional microscopy

Muhammad Afnan Ansari[1*], Yuttana Intaravanne[1,2], Hammad Ahmed[1], Narina Bileckaja[3], Huabing Yin[3] and Xianzhong Chen[1]

[1]Institute of Photonics and Quantum Sciences, School of Engineering and Physical Sciences, Heriot-Watt University, EdinburghEH14 4AS, U.K.
[2]National Electronics and Computer Technology Center, National Science and Technology Development Agency, 112 Thailand Science Park, Phahonyothin Road, Khlong Nueng, Khlong Luang, Pathum Thani12120, Thailand.
[3]Biomedical Engineering Division, James Watt School of Engineering, University of Glasgow, GlasgowG12 8QQ, U.K.
[*]corresponding author: Muhammad_Afnan.Ansari@hw.ac.uk

Abstract: Edge and polarimetric imaging play an essential role in the enhancement of target detection and recognition performance. However, an imaging system with such multiple functionalities tend to be bulky and expensive because of the substantial footprint of their benchtop-based electronic and optical components. Here, we propose a multifunctional 3-in-1 microscope based on an ultrathin metasurface device which can concurrently perform polarimetric, edge and microscope imaging to visualize the multiple facets of transparent biological samples in real-time.

For microscopy imaging, typically biological samples are made very thin to avoid the scattering of light from various tissue structures. Without special image enhancement techniques, these tissue samples show little contrast under the conventional microscope, as these samples are usually transparent [1-3]. Precisely differentiating the edges, increasing the target detection, and enhancing the recognition performance of the imaging system are important for the study of such transparent biological samples [4-6]. The currently available imaging systems can only perform a single functionality at a time. In addition, only limited number of imaging systems are present to date which can perform multiple functionalities on the cost of expensive and substantial footprint of their benchtop-based electronic and optical components [7]. This reduces the portability and hinder their practical applications. Moreover, the application of standalone circular polarimetric microscopy in biological sciences is limited despite the useful information obtained from the circular polarization measurement. This is due to the challenging imaging techniques that require the frequent replacement of optical components for subsequent measurement for different polarization states [8].

To resolve the aforementioned challenges, here, a multifunctional 3-in-1 microscope is proposed based on a novel and compact optical device, which is impossible to achieve with conventional optical components. An ultrathin metasurface is incorporated into a microscopy setup, which can concurrently perform polarimetric imaging, edge imaging, and traditional microscope imaging. As a result, five images of the target sample are obtained with unique optical properties on the same imaging plane as shown in Figure 1. Although three different imaging functionalities are combined within the same microscope imaging system, the volume of the proposed 3-in-1 metasurface-based microscope does not increase. The proposed metasurface device is realized based on both spatial and polarization multiplexing techniques.

We experimentally demonstrate the capability of the proposed 3-in-1 metasurface-based microscope with various samples. Using the proposed device, the edge imaging enabled reliable and fast cell detection. The polarimetric imaging acquired the complete polarization information. This is used to resolve microstructures and

the anisotropic information, for example, their orientation and ordering. Edge and polarimetric information are complementary to that obtained through traditional microscopy imaging, allowing the visualization of multiple facets of the target samples in real-time.

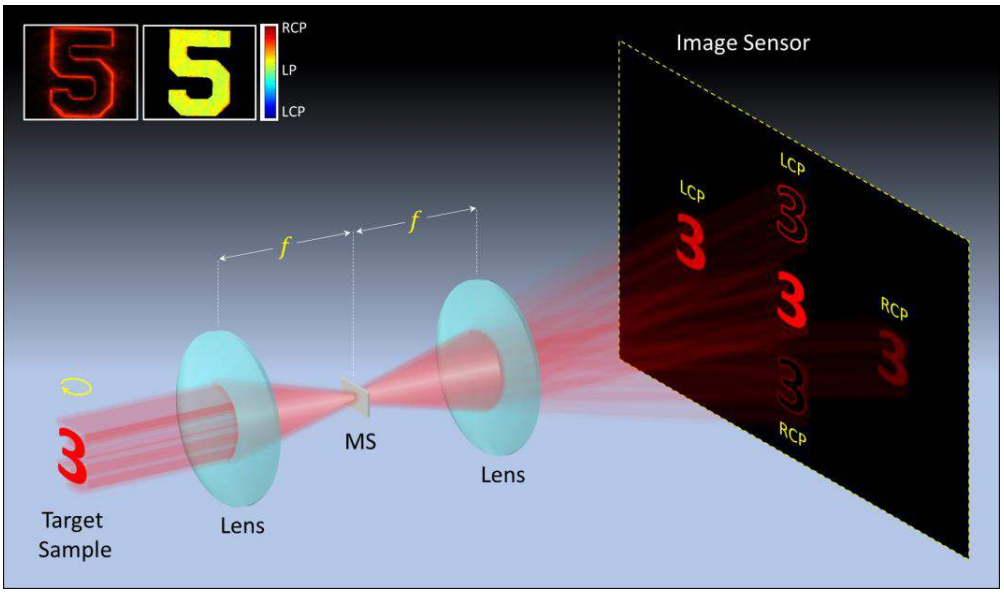


Figure 1. Metasurface enabled multifunctional microscopy. MS denotes the proposed metasurface.

Acknowledgements

This project was funded by the Leverhulme Trust (RPG-2021-145).

References

1. Zernike, F., How I Discovered Phase Contrast. Science 1955, 121 (3141), 345-349.
2. Popescu, G., Quantitative Phase Imaging of Cells and Tissues. First edition. ed.; McGraw-Hill Education: New York, 2011.
3. Park, Y.; Depeursinge, C.; Popescu, G., Quantitative phase imaging in biomedicine. Nat Photonics 2018, 12 (10), 578-589.
4. Huo, P.; Zhang, C.; Zhu, W.; Liu, M.; Zhang, S.; Zhang, S.; Chen, L.; Lezec, H. J.; Agrawal, A.; Lu, Y.; Xu, T., Photonic Spin-Multiplexing Metasurface for Switchable Spiral Phase Contrast Imaging. Nano Lett 2020, 20 (4), 2791-2798.
5. Zernike, F.; Stratton, F. J. M., Diffraction Theory of the Knife-Edge Test and its Improved Form, The Phase-Contrast Method. Mon Not R Astron Soc 1934, 94 (5), 377-384.
6. Normanski, G., Interferometry with Schlieren microscopy. J Phys Radium 1955, 16, 9-11.
7. Senarathna, J.; Yu, H.; Deng, C.; Zou, A. L.; Issa, J. B.; Hadjiabadi, D. H.; Gil, S.; Wang, Q.; Tyler, B. M.; Thakor, N. V.; Pathak, A. P., A miniature multi-contrast microscope for functional imaging in freely behaving animals. Nat Commun 2019, 10 (1), 99.
8. Le Gratiet, A.; Dubreuil, M.; Rivet, S.; Le Grand, Y., Scanning Mueller polarimetric microscopy. Opt Lett 2016, 41 (18), 4336-4339.

Dielectric polarization-insensitive metasurfaces for Bessel beam generation in light sheet microscopy

A. Archetti[1,2*], M. Bruzzone[1,3], G. Tagliabue[2] and M. dal Maschio[1,3*]

[1]Department of Biomedical Sciences, University of Padua, Padua, Italy
[2]École Polytechnique Fédérale de Lausanne (EPFL), 1015 Lausanne, Switzerland
[3]Padova Neuroscience Center - PNC, University of Padua, Padua, Italy
[*]corresponding authors: anna.archetti@unipd.it, marco.dalmaschio@unipd.it

Abstract: We present a method based on wave front engineering for rendering a Bessel Beam (BB) lattice with one single, flat, and lightweight optical element. According to this design, we fabricated and characterized a Silicon Nitride (SiNx) element using Meta-Surface (MS) technology encoding all the operations required to generate the designed BB lattice. Finally, we demonstrated its application in microscopy by integrating it along the excitation path of a light-sheet microscope (LSM) and recording neuronal activity from the zebrafish larva brain.

Laser beam shaping approaches are fundamental techniques adopted in a variety of applications such as microlithography, material processing, microscopy and optical tweezing, to increase the quality, the uniformity and speed of their beam-based processes by redistributing the irradiance and phase of the input beam[1]. Among the most frequently engineered and used beam shapes, Bessel beam profiles have been largely adopted due to their elongated depth-of-focus and self-healing features to drill high-aspect-ratio or narrow grooves[2,3], to manipulate microscopic particles[4], to illuminate samples with a thinner and wider light-sheet[5,6], and to produce patterns on glass[7].
Traditionally, arrays of Bessel beams are generated by combining an axicon phase profile and a spatial light modulator[8], or Dammann grating[9]. However, these approaches cannot avoid some of the following limitations, depending on the specific implementation: low numerical aperture (NA) of the single beams, a NA dependent on the grating orders and supercell period[9], the constraint of having all the beams in the array with the same optical features, the constrains of having a number of beams in the array limited by the grating order, the constraint on the input light polarization, or the limited intensity uniformity among all the beam spots included the zero-order one.
Here, we propose a method which exploits a novel, custom-designed Meta-Surface to generate an array containing an arbitrary number of BB with independent optical properties, focal position, and depth of focus. Finally, we show how we did integrate this novel Meta-Surface along an optical path to validate its performance in a challenging application: the recording of the neuronal activity from the zebrafish larva brain at cellular resolution.

ACKNOWLEDGEMENTS: This work was funded by European Union's Horizon 2020 research and innovation program under the Marie Sklodowska-Curie grant agreement No. 898315 (FLAMMES).

References

1. *Laser Beam Shaping: Theory and Techniques, Second Edition*. (CRC Press, 2017). doi:10.1201/b17140.
2. Yu, X., Trallero-Herrero, C. A. & Lei, S. Materials processing with superposed Bessel beams. *Appl. Surf. Sci.* **360**, 833–839 (2016).
3. Bhuyan, M. K. *et al.* High aspect ratio nanochannel machining using single shot femtosecond Bessel beams. *Appl. Phys. Lett.* **97**, 081102 (2010).

4. Sokolovskii, G. S. *et al.* Optical trapping with Bessel beams generated from semiconductor lasers. *J. Phys. Conf. Ser.* **572**, 012039 (2014).
5. Betzig, E. Excitation strategies for optical lattice microscopy. *Opt. Express* **13**, 3021 (2005).
6. Chen, B.-C. *et al.* Lattice light-sheet microscopy: Imaging molecules to embryos at high spatiotemporal resolution. *Science* **346**, 1257998 (2014).
7. Mikutis, M., Kudrius, T., Šlekys, G., Paipulas, D. & Juodkazis, S. High 90% efficiency Bragg gratings formed in fused silica by femtosecond Gauss-Bessel laser beams. *Opt. Mater. Express* **3**, 1862–1871 (2013).
8. Čižmár, T. *et al.* Generation of multiple Bessel beams for a biophotonics workstation. *Opt. Express* **16**, 14024–14035 (2008).
9. Lin, Z. *et al.* High-efficiency Bessel beam array generation by Huygens metasurfaces. *Nanophotonics* **8**, 1079–1085 (2019).

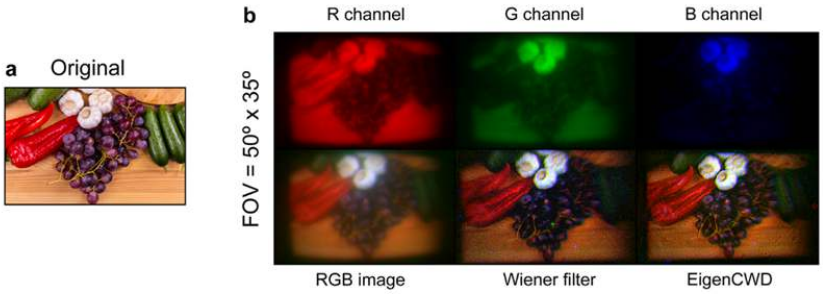
Large Field-of-View and Multi-Color Imaging with Quadratic Metalenses

Emmanuel Lassalle[1,*], **Anton V. Baranikov**[1], **Egor Khaidarov**[1], **Damien Eschimese**[1], **Joel Yeo**[1,2,3], **N. Duane Loh**[2,4], **Ramon Paniagua-Dominguez**[1], **Arseniy I. Kuznetsov**[1]

[1]*Institute of Materials Research and Engineering (IMRE), Agency for Science, Technology and Research (A*STAR), 2 Fusionopolis Way, Innovis # 08-03, Singapore 138634*
[2]*Department of Physics, National University of Singapore, Singapore 117551*
[3]*Integrative Sciences and Engineering Programme, NUS Graduate School, National University of Singapore, Singapore 119077*
[4]*Department of Biological Sciences, National University of Singapore, Singapore 117557*
[*]*corresponding author: emmanuel_lassalle@imre.a-star.edu.sg*

Abstract: In this talk, we will give a demonstration, based on a recently-developed class of metalenses, of a prototype that alleviates the challenges of chromatic and coma aberrations within a single-layer device, and achieves color imaging over a field-of-view of $\sim 100°$. The proposed approach opens venues for translating this emergent technology into commercial products.

Flat optics holds the promise to replace conventional optics in many user devices, such as in smartphone cameras. However, challenges like chromatic and coma aberrations have hindered so far spectral broadband and large field-of-view (FOV) imaging performances in most of metalenses. Based on a recent class of metalenses, called quadratic metalenses [1–3], we provide here a solution that overcomes simultaneously both challenges. While quadratic metalenses are exempted from coma aberrations and thus provide naturally a large FOV [1–3], their inherent spherical aberrations (i.e. elongation of the focal spot along the axial direction), were seen so far as a limitation leading to non-diffraction limited focusing and lower focusing efficiencies. Here, we show that the depth-of-focus coming from these spherical aberrations allows for broadband focusing, and we leverage on this effect to design a set of three R,G,B quadratic metalenses whose working bandwidths match with the filter bandwidths present in a color camera, to demonstrate white light and large FOV imaging. Combined with our own post-processing deconvolution algorithm (called "EigenCWD"), this solution offers high contrast and good color reproduction capability and a spatial resolution that are sufficient for most smartphone camera applications [4]. Moreover, these three metalenses are fabricated on a same substrate with a same height, allowing to be fabricated upon a one-step photolithography suitable with mass-production.



References

1. Pu Mingbo, Li Xiong, Guo Yinghui, Ma Xiaoliang, Luo Xiangang, "Nanoapertures with ordered rotations: symmetry transformation and wide-angle flat lensing", *Optics Express* **25**, 31471–31477 (2017).
2. Martins Augusto, Li Kezheng, Li Juntao, Liang Haowen, Conteduca Donato, Borges Ben-Hur V, Krauss Thomas F, Martins Emiliano R, "On metalenses with arbitrarily wide field of view", *ACS Photonics* **7**, 2073–2079 (2020).
3. Lassalle Emmanuel, Mass Tobias WW, Eschimese Damien, Baranikov Anton V, Khaidarov Egor, Li Shiqiang, Paniagua-Dominguez Ramon, Kuznetsov Arseniy I, "Imaging properties of large field-of-view quadratic metalenses and their applications to fingerprint detection", *ACS Photonics* **8**, 1457–1468 (2021).
4. Baranikov Anton V, Khaidarov Egor, Lassalle Emmanuel, Eschimese Damien, Yeo Joel, Loh N Duane, Paniagua-Dominguez Ramon, Kuznetsov Arseniy I, "Large field-of-view and multi-color imaging with quadratic metalenses", *In preparation* (2023).

Photonic bound states in the continuum in asymmetric bi-slot metasurfaces

Ti-Jung Hsu , Ruey-Lin Chern *

Institute of Applied Mechanics, National Taiwan University, Taipei 106, Taiwan
*corresponding author: chernrl@ntu.edu.tw

Abstract : We investigate the photonic bound states in the continuum (BICs) in dielectric metasurfaces composted of two asymmetric slots in the unit cell of a square lattice. Symmetry-protected (SP) BICs occur at the polarization vortex center (V point) with integer topological charge in the polarization state diagram when the structure is fully symmetric. By introducing the asymmetry between the two slots, accidental BICs or Friedrich-Wintgen (FW) BICs can be formed from the merging of two circular polarization points (C points) with half-integer topological charge.

Summary :

Bound states in the continuum (BICs) are non-leaky localized resonance modes that coexist with a continuous spectrum of radiating waves [1]. They are non-radiative waves and possess extremely large quality factors with vanishing spectral linewidths. As a concept introduced in quantum mechanics by von Neumann and Wigner in 1929, the existence of BICs was explained by Friedrich and Wintgen in 1985 as the result of destructive interference between two resonances coupled to the same radiation channel. In this study, we investigate the BICs in dielectric metasurfaces composed of asymmetric two rectangular slots in the unit cell of a square lattice. In particular, symmetry-protected (SP) BICs occur at the polarization vortex center (V point) with integer topological charge in the polarization state diagram when the two slots are identical, in which the topological charge is defined by the number of times the polarization vector winds around a BIC as [2]

$$q = \frac{1}{2\pi}\oint_C d\mathbf{k}\cdot\nabla_{\mathbf{k}}\phi(\mathbf{k}). \tag{1}$$

Here, $\phi(\mathbf{k}) = \arg[c_x(\mathbf{k}) + ic_y(\mathbf{k})]$ is the angle of the polarization vector, and C is a closed simple path in the momentum space that goes around the BIC in the counterclockwise direction. By introducing asymmetry between two rectangular slots, accidental BICs or Friedrich-Wintgen (FW) BICs can be formed by the merging of a pair of circular polarization points (C points) with half-integer topological charge [3], which is achieved by tuning the asymmetry parameter of the rectangular slot. In this situation, two modes are hybridized and the quality factors are greatly enhanced.

Referance :

1. Hsu, C. W., Zhen, B., Stone, A. D., Joannopoulos, J. D., & Soljačić, M. (2016). Bound states in the continuum. Nat. Rev. Mater., **1**, 1-13.
2. Zhen, B., Hsu, C. W., Lu, L., Stone, A. D., & Soljačić, M. (2014). Topological nature of optical bound states in the continuum. Phy. Rev. Lett., **113**, 257401.
3. Kang, M., Zhang, S., Xiao, M., & Xu, H. (2021). Merging bound states in the continuum at off-high symmetry points. Phy. Rev. Lett., **126**, 117402.

META 2023, PARIS - FRANCE, JULY 18 – 21, 2023

Highly angle-sensitive and efficient optical metasurfaces

N. Kim[1], M. Kim[1], J. Jung[1], T. Chang[1], S. Jeon[1], and J. Shin[1*]

[1]Department of Materials Science and Engineering, Korea Advanced Institute of Science and Technology, Daejeon 34141, Republic of Korea

[*]corresponding author: qubit@kaist.ac.kr

Abstract: Angle-multiplexed metasurfaces offer new degrees of freedom in multi-functional metasurfaces. However, they can suffer from trade-offs in transmission efficiency and angular sensitivity for paraxial rays. Here, we demonstrate a solution to the limitation by breaking mirror symmetries of single-layer metasurface structures. Using a theoretical model, we intuitively explain which material parameters affect the sensitivity and efficiency. Additionally, through the inverse design method, an angle-multiplexed beam deflector is proposed.

Angle-multiplexed metasurfaces have garnered much attention due to their ability to provide new optical functionalities that were not previously possible with conventional optical devices. Many studies have proposed angle-multiplexed metasurface designs with several different physical principles [1–2]. However, those proposals so far have a common problem that high angle sensitivity is achieved by at the expense of optical efficiency, especially for paraxial rays used in practical applications. Recently, we theoretically demonstrated that the problem is fundamental and inherent to angle-multiplexed metasurfaces with mirror symmetries, and proposed a new class of angle-multiplexed metasurface with broken mirror symmetry [3]. Here, we explicate the principle behind the proposed metasurfaces and show examples.

Assuming that the metasufaces consist of subwavelength fundamental building blocks and they are locally periodic, we can approximate each structure as a uniform anisotropic effective medium. In general, the effective optical axis of the material can be slanted with respect to axis normal to the substrate. The slanted crystal axis induces an off-diagonal component in the permittivity tensor, which can only be obtained by breaking the structural mirror symmetry. For two near-zero incidence waves propagating in the z-direction, Figure 1 compares complex transmission between anisotropic media with vertical and slanted crystal axes with varying a permittivity along the z-axis (ε_3). Most of points in the anisotropic medium with a vertical crystal axis have transmission amplitudes below the threshold despite certain permittivity values being able to produce a considerable phase difference (Fig. 1(a–b)). On the other hand, the medium with a slanted crystal axis can obtain both high transmission efficiency and large phase gradient for inputs. The medium can produce the phase difference of up to π while having transmission amplitudes above the threshold (Fig. 1(c–d)).

The reason behind this phenomenon is due to the dependence of the refractive index and wave impedance on incident angle and the permittivity (ε_3). Anisotropic media with a vertical crystal axis has a significant increase in the derivative of the refractive index with respect to incidence angle as the ε_3 approaches small values. However, the wave impedance and its derivative also increase dramatically, which makes it difficult to achieve both high angle-sensitivity and high transmission efficiency. In contrast, if the crystal axis is slanted, the changes in wave impedance and its derivative are less sensitive, allowing higher transmission efficiency (Fig. 1(e–f)).

Based on the theoretical analysis, we design the angle-multiplexed metasurfaces with high optical efficiency by spatially arranging the unit structures with broken mirror symmetry. We utilize a simple unit structure, slanted grating with a parallelogram-like cross section, which has minimal symmetry breaks. The angle-sensitive beam deflector is designed as an example of angle-multiplexed phase gradient metasurface (Fig. 2). The

optimized beam deflector directs the two incidence angles with a small angular separation, $\theta_1 = +5°$ and $\theta_2 = -5°$, in two very different directions, 39.2° and −7.3°, with a high relative transmission efficiency 93.8% and 88% (absolute efficiency: 83% and 56.3%) respectively. This indicates that not only the structures with broken mirror symmetries can induce large phase gradients at near-zero incidences, but they also can achieve asymmetric transmission with symmetric inputs.

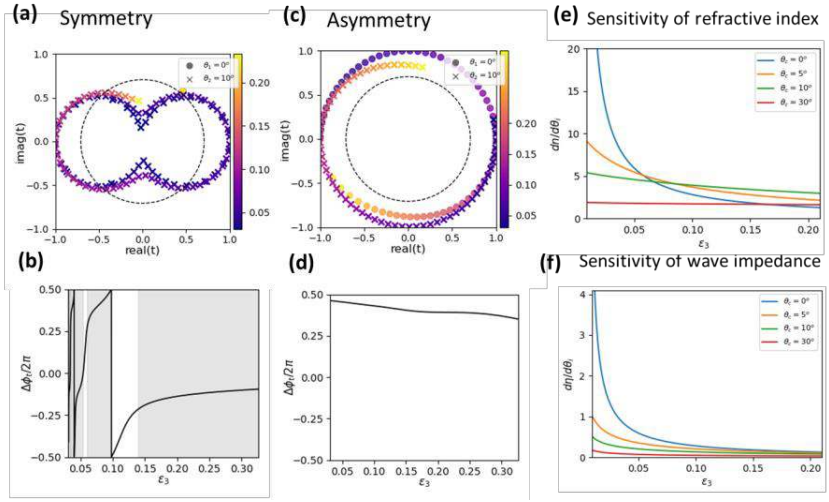


Fig. 1. Theoretical analysis based on effective medium. (a, c) The transmission coefficients of the anisotropic medium with different slanted optical axis (a) θ_c=0° (c) θ_c=15° in complex domain as a function of ε_3. The ε_1 is fixed to 15. (b, d) The corresponding phase difference. (e, f) Derivative of refractive index and wave impedance.

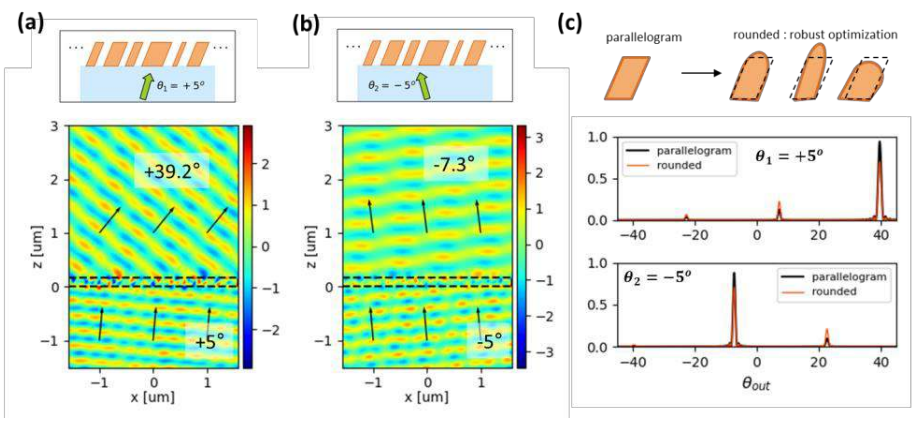


Fig 2. Optimized angle multiplexed beam deflector with symmetric input angles. The real part of electric field phasors for the incidences (a) θ_1=+5° (b) θ_2=+5°. The desired angles are 39.2° and –7.3°. (c) Result with robust optimization with consideration of fabrication errors.

References

1. Kamali, S. M., Arbabi, E., Arbabi, A., Horie, Y., Faraji-Dana, M. and Faraon, A., "Angle-Multiplexed Metasurfaces: Encoding Independent Wavefronts in a Single Metasurface under Different Illumination Angles," Phys. Rev. X, Vol. 7, No. 041056, 2017.
2. Haghtalab, M., Tamagnone, M., Zhu, A. Y., Safavi-Naeini, S. and Capasso, F., "Ultrahigh Angular Selectivity of Disorder-Engineered Metasurfaces," ACS Photonics, Vol. 7, No. 4, 991–1000, 2020.
3. Kim, N., Kim, M., Jung, J., Chang, T., Jeon, S., and Shin, J., "Highly angle-sensitive and efficient optical metasurfaces with broken mirror symmetry," Nanophotonics, 2023.

Acknowledgement

This work is supported by the National Research Foundation of Korea (2018M3D1A1058998, 2021R1A2C2008687)

Morphogenetic engineering of radiating metasurfaces

Thomas Fromenteze,[1,*] Okan Yurduseven,[2] Eric Arnaud,[1] David R. Smith,[3] and Cyril Decroze[1]

[1,*] University of Limoges, CNRS, XLIM, UMR 7252, F-87000 Limoges, France
[2] Centre for Wireless Innovation (CWI), Institute of Electronics, Communications and Information Technology (ECIT), Queen's University Belfast, Belfast, BT3 9DT, UK
[3] Center for Metamaterials and Integrated Plasmonics, Department of Electrical and Computer Engineering, Duke University, Durham, NC 27708, USA
[*] Corresponding author: thomas.fromenteze@unilim.fr

Abstract: A morphogenesis-inspired technique for the engineering of electromagnetic components is under development and finds new applications in the procedural generation of radiating metasurfaces. This method simulates the growth of structures capable of spatially self-organizing to respond to electromagnetic constraints. An application is presented with the automated synthesis of a morphogenetic metasurface radiating a field distribution constrained in frequency, in space, and in polarization.

Many inverse design techniques rely on a guided exploration of huge component spaces to find the best candidates able to satisfy desired functionalities [1]. However, these approaches are constrained by the exploitation of gradient descent of non-convex cost functions and involving a large number of design variables [2]. Inspired by the structuring of living organisms and Alan Turing's pioneering work on its numerical modeling [3], morphogenetic engineering is based on a decentralization of the designer's role [4], trying to define local rules guiding the self-organization of complex systems and ensuring the emergence of the desired functions at the macroscopic scale. It is thus proposed to develop a model capable of generating radiating metasurfaces (Fig. 1), simulating the growth of spatial structures capable of ensuring an efficient conversion between a surface wave excited by a coaxial guide and spatially constrained radiated waves, in frequency and polarization.

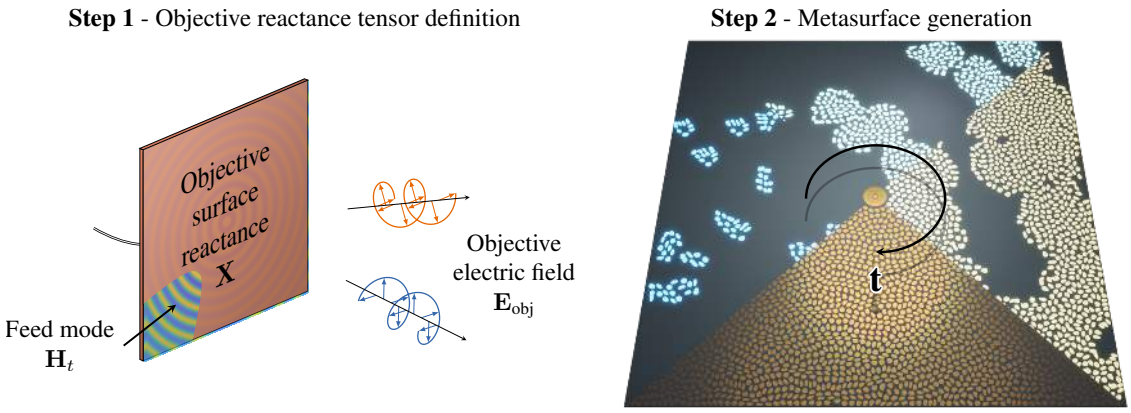


Figure 1: Design of a morphogenetic metasurface: (Left) Definition of electromagnetic constraints allowing the conversion of surface waves into radiated waves. (Right) Growth of elliptical patterns synthesizing the expected properties.

The generative model used here is based on the Gray-Scott reaction-diffusion model, defined by Eqs. (1) and (2), simulating the interaction between chemical species (called morphogens by Turing) progressively forming spatial structures used in this work. The synthesis of anisotropic properties required a modification of the original generative model, forcing the emergence of asymmetric patterns whose orientation can be controlled. Inspired by previous work on texture synthesis [5], the Gray-Scott system was thus altered as follows:

$$\frac{\partial \mathbf{U}}{\partial t} = \mathbf{d_u} \nabla \cdot (\underline{\underline{\mathbf{D}}} \nabla \mathbf{U}) - \mathbf{U}\mathbf{V}^2 + \mathbf{f}(1 - \mathbf{U}) \tag{1}$$

$$\frac{\partial \mathbf{V}}{\partial t} = \mathbf{d_v} \nabla \cdot (\underline{\underline{\mathbf{D}}} \nabla \mathbf{V}) + \mathbf{U}\mathbf{V}^2 - (\mathbf{f} + \mathbf{k})\mathbf{V}. \tag{2}$$

In this model, $\mathbf{U}$ and $\mathbf{V}$ represent the spatial concentrations of antagonistic morphogens, whose guided self-organization over time allows the formation of a metasurface. The resolution of this model by finite difference ensures the growth of spatial patterns controlled by the parameters $\mathbf{d_u}$, $\mathbf{d_v}$, $\mathbf{f}$, and $\mathbf{k}$. Finally, one can deform and control the local orientation of the generated patterns by modulating the anisotropy and the orientation of the eigenaxes of the tensors $\underline{\underline{\mathbf{D}}}$ guiding the diffusion of the morphogens. Following a characterization of the impedance properties synthesized using the finite element method, it was thus possible to directly convert the morphogenetic parameters guiding the emergence and the self-structuring of the patterns into electromagnetic properties. Fig. 2 depicts an holographic experiment based on the fabrication of a metasurface radiating a controlled field distribution at 20cm from the latter at 20.2 GHz. Following the radiation objectives translated into local rules guiding the morphogenetic synthesis, the measured electric field reveals both the letter "L" in left circular polarization and the letter "R" in right circular polarization.

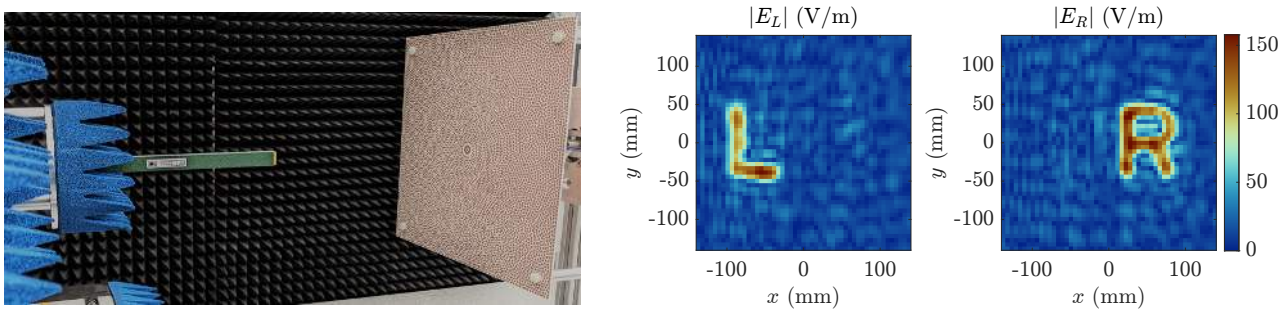


Figure 2: Fabrication and measurement of a morphogenetic metasurface generating a field distribution at 20.2 GHz revealing the letter "L" in left circular polarization ($|E_L|$) and the letter "R" in right circular polarization ($|E_R|$).

Many application perspectives of this generation technique still need to be explored, encouraged by the good performance of first demonstrations.

References

[1] Sean Molesky, Zin Lin, Alexander Y Piggott, Weiliang Jin, Jelena Vucković, and Alejandro W Rodriguez. Inverse design in nanophotonics. *Nature Photonics*, 12(11):659–670, 2018.

[2] Jiaqi Jiang and Jonathan A Fan. Simulator-based training of generative neural networks for the inverse design of metasurfaces. *Nanophotonics*, 9(5):1059–1069, 2020.

[3] Alan Mathison Turing. The chemical basis of morphogenesis. *Bulletin of mathematical biology*, 52(1-2):153–197, 1990.

[4] René Doursat, Hiroki Sayama, and Olivier Michel. *Morphogenetic engineering: toward programmable complex systems*. Springer, 2012.

[5] Andrew Witkin and Michael Kass. Reaction-diffusion textures. In *Proceedings of the 18th annual conference on Computer graphics and interactive techniques*, pages 299–308, 1991.

META 2023, PARIS - FRANCE, JULY 18 – 21, 2023

Enabling and perfectioning advanced large Area Metalens Nanofabrication by Electron Beam Lithography (EBL)

F. Nouvertné*, C. Aulbach, G. Piaszenski, J. Münchenberger and V. Boegli

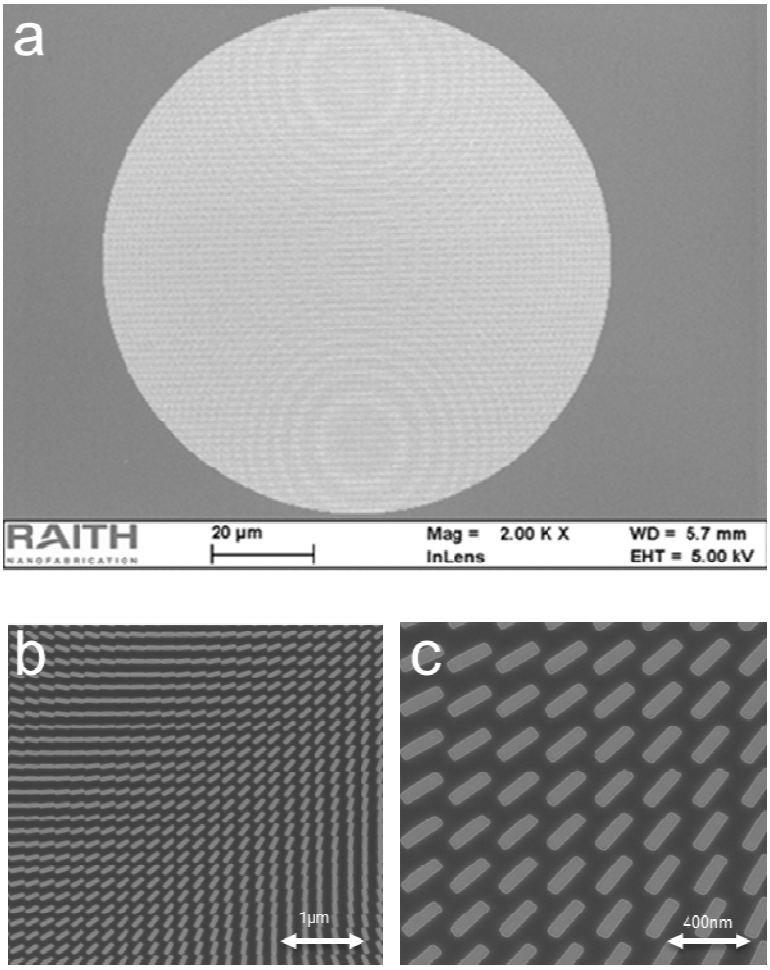
Raith GmbH Dortmund, Konrad-Adenauer-Allee 8, 44263 Dortmund
*corresponding author: frank.nouvertne@raith.de

Abstract: The geometric nature of a large ~cm^2-sized metalense with its many unique and individual design elements can lead to corresponding design data file sizes of several hundreds of GB. This makes it extremely challenging if not impossible to be processed with conventional EBL nanofabrication systems. We present an enabling, innovative, and extremely efficient EBL workflow that circumvents the necessity for generating CAD-design-data for EBL by exploiting the algorithmic (formula-based) description of metalens patterns for "on-the-fly" EBL exposure pixel stream generation.

Metalenses are based on a new lens technology that is very promising for sensing and imaging in consumer electronics, medical applications, autonomous vehicles, AR/VR displays, and more. Metalenses are "flat" (2D) and made by optical components that use metasurfaces to focus light without the need for bulky classical optical lenses thus allowing for miniaturization of all devices mentioned above. Typically, metalens patterns extend over multiple 10mm^2 if not cm^2 and consist of an extremely high number of separate, irregularly and individually arranged unique design elements like small rectangles, circles, ellipses or similar with a few 100nm in size.

Corresponding CAD designs thereof, e.g. in GDSII format, the standard used in EBL nanofabrication, can grow up to data file sizes of several hundreds of GB making it extremely challenging if not impossible to be handled efficiently with conventional EBL systems. Exemplarily, for a metalens with ~1cm^2 diameter and ~200nm sized elementary functional elements like nanofins, the entire design consists of several hundred million unique design elements, that cannot be treated hierarchically or in a repetitive way within the EBL system´s data handling architecture. They rather need to be sequentially and individually processed (including design fracturing, data transmission and exposure pixel sequence calculation) within the entire data processing path of the EBL system. This requires highest computational power and most efficient data transmission capabilities in both the system´s workstation as well as in its pattern generator, something that is still very challenging even in view of modern and powerful electronic infrastructure embedded in nowadays EBL systems.

Here, we present a lean, fast and extremely efficient, new and innovative EBL workflow that circumvents the necessity for generating a flat GDSII design by exploiting the algorithmic (formula-based) description of the metalens pattern. The pattern information contained in the mathematical formula is translated into an EBL job, that directly creates the relevant pixel stream for the pattern generator "on-the-fly" only as soon as the exposure has been started. This results in almost zero overhead and eliminates time consuming generation of intermediate GDSII design or machine code files – while not suffering from potential file size limits regarding the metalens dimension.



Figures a-c: Metalens pattern in resist, manufactured by using algorithmic patterning and metalens design as described in ref. [1]. a) Overview of an ~100µm diameter metalens. b) zoom in a; c) zoom in b.

References

1. Mohammadreza Khorasaninejad, Federico Capasso et al., "Metalenses at visible wavelengths: Diffraction-limited focusing and subwavelength resolution imaging", Science, Vol. 352, issue 6290, 1190–1194, 2016

META 2023, PARIS - FRANCE, JULY 18 – 21, 2023

Transmittance analysis of dielectric optical metasurfaces

Ivan Moreno*, Carlos Basilio-Ortiz

Universidad Autonoma de Zacatecas, Mexico
*corresponding author: imorenoh@uaz.edu.mx

Abstract: Metasurfaces that consist of a graded array of dielectric nano-posts arranged in a lattice are widely studied in optics and photonics. We analyze the light beam transmittance through such an optical metasurface at oblique incidences for visible wavelengths. We obtain the transmitted intensity through the dielectric metasurface versus the incident angle, for different phase gradients of the metasurface. These results are useful for designing efficient nonimaging metalenses. Finally, some concepts are presented for specifying directional transmittance of a dielectric metasurface.

Metalens technology based on dielectric metasurfaces is showing considerable optical performance while opening up new opportunities to thin, flat, lightweight optical devices [1,2]. Metalens applications in nonimaging optics require the optimization of the efficiency light propagation [3], and then to study the transmittance (transmitted intensity/incident intensity) of light beams at oblique incidence. Figure 1 shows the transmission of an input beam of light through a dielectric metasurface with constant phase gradient C, or phase profile $\Phi(x)=Cx$. This Figure shows a lateral view of a metasurface with nano-posts, and input angle θ_1 and output angle θ_2. Oblique incidence may introduce changes in the light propagation due to the finite height of the nano-posts, which height reduction is under research [4].

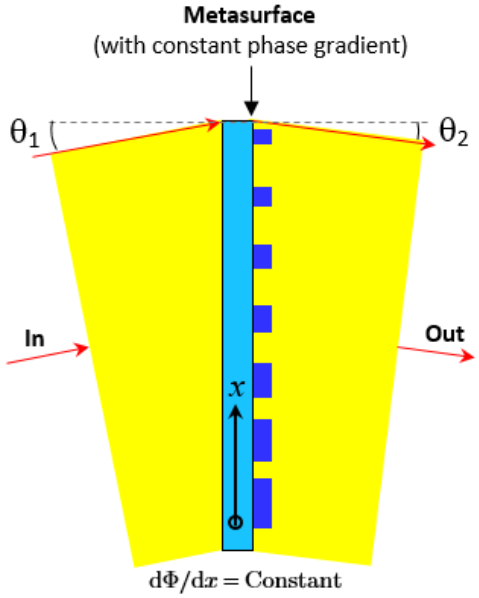


Figure 1: Transmission of an input beam of light through a dielectric metasurface with constant phase gradient C, or phase profile $\Phi(x)=Cx$. Figure shows a lateral view of a metasurface with nano-posts, and input angle θ_1 and output angle θ_2.

Therefore, here we analyze the light beam transmittance through an optical metasurface at oblique incidences for visible wavelengths. We obtain the transmitted intensity through the dielectric metasurface versus the incident angle, for different phase gradients of the metasurface. So that a relation between transmittance and phase gradient is obtained.

This work was financially supported by the Consejo Nacional de Ciencia y Tecnología (grant 316548).

References

1. W.T. Chen, A.Y. Zhu, F. Capasso, “Flat optics with dispersion-engineered metasurfaces,” Nat. Rev. Mater., pp. 1-17 (2020).
2. I. Moreno, “Optics of the metalens,” Eur. J. Phys. 43, 065302 (2022).
3. I. Moreno, M. Avendaño-Alejo, and C. P. Castañeda-Almanza, “Nonimaging metaoptics,” Opt. Lett. 45(10), 2744–2747 (2020).
4. J. Carlos Basilio-Ortiz and Ivan Moreno, "Multilayer dielectric metalens," Opt. Lett. 47, 5333-5336 (2022).

Pancake metalens for compact imaging systems

Chen Chen*, Shining Zhu, and Tao Li*

National Laboratory of Solid State Microstructures, Key Laboratory of Intelligent Optical Sensing and Manipulations, Jiangsu Key Laboratory of Artificial Functional Materials, College of Engineering and Applied Sciences, Nanjing University, Nanjing, 210093, China

*corresponding author: chenchen2021@nju.edu.cn; taoli@nju.edu.cn

Abstract: Metalenses have great potential for miniaturizing imaging systems due to the ultrathin and flat features. However, besides reducing lens thickness, folding/compressing the space between lens and image is also a dominating factor to obtain the utmost compactness. This work proposes a pancake metalens that folds the optical path at will using a metacavity consisting of a bifacial metasurface and a mirror. This pancake meta-optics framework could enable miniaturization of imaging systems and would provide insights for meta-device applications.

Metalenses have arrested tremendous research interest due to its ultra-thin and flat architecture that favor the compact imaging systems [1]. Nevertheless, the lens thickness itself determines little the whole devices size indeed. The occupation mainly accounts for the imaging distance of a certain lens. Therefore, to ultimately reduce the size of an imaging system, one needs to greatly fold/compress the imaging distance but not purely reduce the lens thickness. Unfortunately, few works paid attention to this goal in previous researches about the metalens.

In this work, we propose an ingenious method for on-demand compression of imaging systems based on a metacavity consisting of a bifacial metasurface and a parallel mirror. We first employed chiral meta-atoms [2] to compose a supercell to access the bifacial metasurface with asymmetric and independent functions. Next, incorporating the metasurface with a mirror, light experiences three times of reflection and four times of spin flip within the meta-cavity. Simulations under both normal and oblique incidences are performed to exhibit the polarized space-folding effect. Finally, imparted with specifically designed phase both in transmission and reflection, *pancake metalenses* with ultrathin element features and on-demand working distance cut are constructed and demonstrated with relatively good imaging performances [3]. This kind of design can be scaled up to a larger size and other wavelengths to benefit applications like landscape imaging and favor plenty of miniaturized optical devices.

References

1. Li, T., Chen, C., et al. “Revolutionary meta-imaging: from superlens to metalens,” Photonics Insights, in press, 2023.
2. Chen, C., et al., “Metasurfaces with planar chiral meta-atoms for spin light manipulation,” Nano Letters, Vol. 21, 1815, 2021.
3. Chen, C., et al., “Bifacial-metasurface-enabled pancake metalens with polarized space folding,” Optica, Vol. 9, 1314, 2022.

Investigating the Bound States in the Continuum Phenomenon in hBN Nano-antenna Arrays

Harsh Gupta[1, 2], James Edgar[3], Francesco De Angelis[1], Andrea Toma[1], Michele Tamagnone[1]

[1]Istituto Italiano di Tecnologia (IIT), via Morego 30, 16163 Genova, Italy.

[2]Dipartimento di Chimica e Chimica Industriale, Università di Genova, Genova, Italy.

[3]Department of Chemical Engineering, Kansas State University, Manhattan, U.S.A

Abstract: In this study, we present the study of phonon-polariton bound states in the continuum (BIC) modes in an array of elliptical hexagonal boron nitride (hBN) nanoantennas. Using both theoretical analysis and experimental verification, we demonstrate the existence of a red-shifted quasi-BIC (Q-BIC) mode with a high-quality factor along the x-polarization. Additionally, we uncover a novel concept of a blue-shifted Q-BIC mode with a high-quality factor along the y-polarization, which we also verify theoretically and experimentally.

Bound state in the continuum (BICs) is a fascinating phenomenon in the field of physics that has garnered significant attention from researchers over the years [1]. BICs refer to a special class of localized modes in open systems that exhibits resonance frequencies embedded within the continuous spectrum but do not radiate energy into the surrounding continuum. The use of bound states in the continuum (BIC) is, in particular, a very active research topic in photonics. One promising approach is the use of dielectric metasurfaces, for sensing applications. In fact, one of the main challenges is improving the quality factor Q by confining BICs, which is defined as,

$$\text{Quality Factor } (Q) = \frac{\text{Central Frequency of the Resonance } (f_0)}{\text{Full Width Half Maximum (FWHM) } (\Delta f)} \qquad [1]$$

We modeled phonon polaritons in hBN through the Lorentz model including the matrix tensor equations of direction-dependent permittivity which defined different values in x and z directions because of the uniaxial in-plane isotropic crystal property of hBN ($\varepsilon_{xx}=\varepsilon_{yy}\neq\varepsilon_{zz}$).

The system in our model comprises two elliptical hBN resonators arranged parallel to each other along the y-axis. We started by simulating the system without any rotation of the ellipses to establish the baseline for the Q-BIC properties within a frequency range of 40THz to 45THz. The main resonance of hBN was observed at 43.60THz/1454 cm^{-1} along x-polarization and 42.3THz/1411 cm^{-1} along y-polarization, inside the upper reststrahlen band of $h^{11}BN$ (Type II hyperbolic polariton). Although the BIC mode was present at this stage, it was not visible due to its non-radiative nature. To demonstrate the Q-BIC modes, we considered a cell of two ellipses and broke the symmetry, and rotated them in opposite directions by 25 degrees a (Fig.1a). This resulted in a new Q-BIC mode with a redshift in the resonance frequency to 41.95THz/1399.3 cm^{-1} are shown in Fig. 1c, along with x-polarization as a low-frequency dark mode and an increase in the quality factor of the quasi-BIC mode.. We achieved the enhancement in quality factor from 161.5 (main resonance) to 233.05 (Q-BIC) by nearly 44% calculated from eq. 1 along with x-polarization and a new Q-BIC blue shifted mode occurs along y-axis polarization at 43.95THz/1466cm^{-1} in our simulations, which can be explained by the band structure folding in the Q-BIC hBN resonators.

We conducted an experimental study to confirm our simulated findings on the BIC and Q-BIC modes in hBN

nano-antennas. To create our sample, we exfoliated natural $h^{11}BN$ onto a CaF_2 substrate, chosen for its UV-IR spectrum transparency, and patterned the meta-surfaces of elliptical resonators with e-beam lithography. After fabrication, SEM images were taken and presented in Figure 1b, which shows elliptical hBN nano-antenna resonators with a period size of 1.7µm. We used FTIR spectroscopy to measure the transmission spectrum under the IR-transmission regime of 1300 cm^{-1} -1350 cm^{-1} with an aperture size of 20µm. Our results indicate the presence of the Q-BIC mode, which is red-shifted at a frequency of 1383 cm^{-1} along the x-polarization, as shown by the red solid line in Figure 1d. We used a polarizer to separate out both modes along the x and y polarization, as shown in Figure 1d. Our findings also provide experimental evidence of the presence of band structure folding along y-polarization, as the Q-BIC along y-polarization is blue-shifted to 1437cm^{-1}, as shown by the blue solid line in Figure 1d. Finally, we achieved nearly a 39% enhancement in the red-shifted Q-factor from 143 (main resonance) to 198 (Q-BIC) along the x-polarization. This project has received funding from the European Research Council (ERC) under the European Union's Horizon 2020 research and innovation program (Grant Agreement No. 948250)

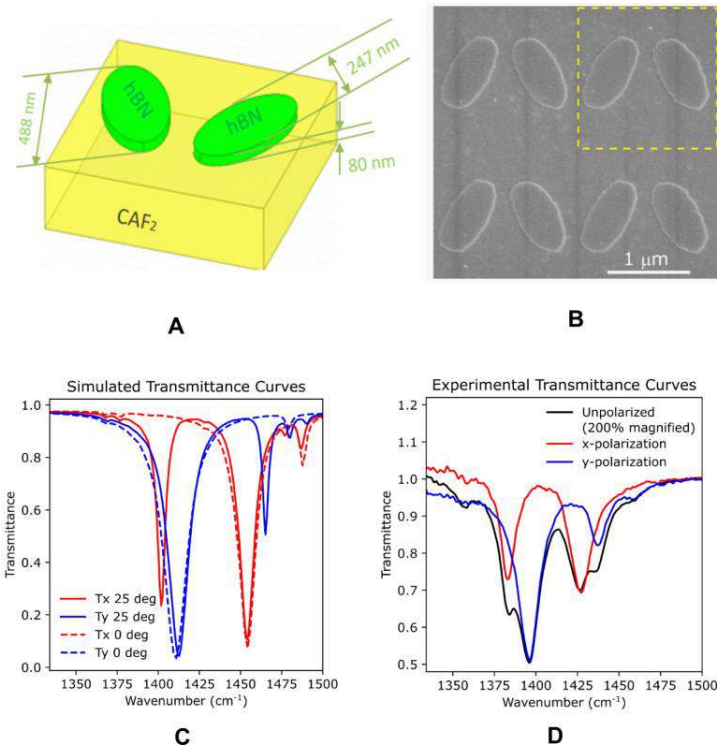


Figure 1 - hBN resonators with the major axis of 488nm, minor axis of 247nm, hBN thickness of 80nm over the CAF_2 substrate (1a), SEM image of the hBN resonators having a period size of 1.7µm with same measurements of simulated resonators (1b), Simulated transmitted curves shows the main resonances at zero degrees rotation by dotted lines and 25 degrees rotation curves by solid lines, red and blue color shows the x and y polarization respectively (1c), Experimental FTIR curves show by solid lines, black represents to the unpolarized curve (without polarizer), red and blue shows the transmission curves shows the x and y polarization respectively.

References

1. Joseph, Shereena, et al. "Bound states in the continuum in resonant nanostructures: an overview of engineered materials for tailored applications." Nanophotonics 10.17 (2021): 4175-4207.

Polarization Dichroic Fabry-Perot Cavities Enabled By Metasurface Structures

B. Semnani[1,2*], M. Soltani[1,2], S. Kuru[1], and M. Bajcsy[1,2]

[1]Institute for Quantum Computing (IQC), Waterloo, ON, Canada
[2]Department of Electrical & Computer Engineering, University of Waterloo, Waterloo, ON, Canada
[*]corresponding author: bsemnani@uwaterloo.ca

Abstract: Here we report on our experimental progress towards design, fabrication and experimental characterization of a new class of high performance confocal Fabry–Pérot cavities formed by dielectric metasurface structures. The metasurface structures are used to make the cavities stable, optimized their mode volume and also to make them polarization birefringent.

Fabry–Pérot cavities that operate in free-space are superb platforms to enhance light-mater interaction in various media, such as cold atoms and optically trapped single quantum emitters. Despite their significance, integrated confocal Fabry–Pérot cavities with accessible mode distribution in free space and ultra-stable behaviour have yet to be experimentally demonstrated [1,2]. In this work, we present new design strategies accompanied with our preliminary experimental results on confocal Fabry–Pérot cavities formed by (i) a pair of Pancharatnam-Berry phase reflecting metasurfaces [3] which reflect and focuses only one helical state of light and (ii) Multilayer polarization-birefringent metasurface structure which reflects one linear polarization state and transmits the orthogonal polarization state. The metasurface mirrors are vertically mounted in lithography-defined platforms with proper spacing to form confocal Fabry–Pérot cavities.

(I) Self-polarizing Chiral Cavity: The chiral metasurface structure is formed by a subwavelength array of 400nm tall round-corner rectangular nanofins arranged on one side of a 50nm thick Silver layer which plays the role of the back mirror (Fig.1a). The phase profile associated with a focusing mirror is imparted via rotation of each nanofin at a given coordinate (x,y) by an angle $\theta(x,y)=2\varphi(x,y)$ where φ is the desired phase . Since the array spacing is subwavelength, higher order Floquet modes can potentially excite lossy Plamsons. We thus introduce a thin layer of SiO2 to prevent field accumulation on the surface of the Silver. This minimizes depolarization (see Fig.1b) and loss. Therefore, higher Q factors can be achieved. Also, the design is optimized to maintain polarization purity for all rotation angles. Fig 1.b shows the geometric phase vs the angle of rotation for all nanofin ordinations. Another significant issue is the formation of nanoislands on the silver layer during PECVD deposition of amorphous Si. The film morphology spontaneously forms nanoislands. The nanoisland formation also occurs when the substrate temperature becomes high and local melting happens for the thin metal layer. It is a well-known process named "dewetting" [4]. To circumvent this issue, we used the magnetron sputtering method followed by a thin film of Silicon dioxide sputtering to prevent dewetting during the PECVD process of a-Si coating at high temperatures. The SEM images show the ability of this modified coating strategy compared to the conventional e-beam evaporation of Silver after the growth of 400nm a-Si using PECVD in 300C. So, not only the spacing layer prevents the field accumulation on the surface of Silver, it plays a crucial role in avoiding dewetting the thin Silver layer during PECVD deposition of amorphous silicon.

(II) Polarization-dichroic Fabry–Pérot cavity: Another cavity structure is formed by two vertically

mounted birefringent metasurface structures which operate in confocal lens/cavity modes. Each birefringent metasurface, as a whole, is composed of two flat planar dielectric structures with nano-scale patterns. The layers are responsible for polarization-selective reflection and focusing of light respectively. The phase-front of the light for the two orthogonal polarization states is independently controlled by using high aspect ratio symmetry broken dielectric metasurfaces [3]. A second layer of photonic-crystal slab acting as broadband dimerized high contrast grating (DHCG) [5] with near 100% polarization discrimination is used to switch between the lensing behavior to a metastructure which behaves as a focusing mirror. We used ray tracing to obtain independent phase profiles imparted by polarization dichroic metasurface so that the modes overlap properly. The cavity structure is used to build a single photon gate mediated by cold Cs atoms.

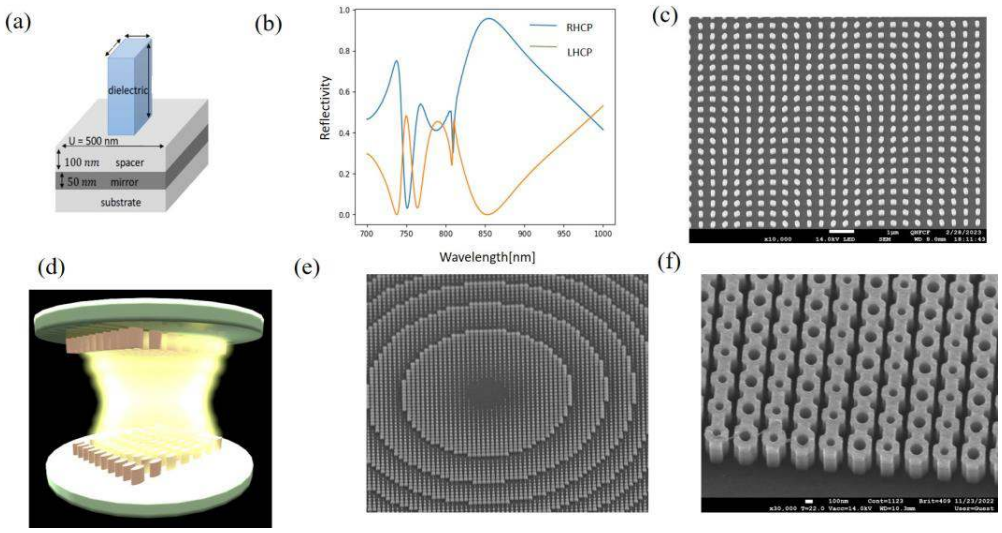


Figure 1. (a-c) Pancharatnam-Berry phase reflecting metasurfaces (a) Schematics of the multilayer metasurface. Nanofins are made of PECVD-grown α-Si.(b) Reflection spectrum upon purely right handed circularly polarized illumination. At 850nm the mirror becomes spin-preserving (c) fabricated metasurface **(d-f)** bilayer Polarization-dichroic metasurface structure (e) phase imparting layer (f) Dimerized high contras grating layer with near unity reflectivity discrimination for linear polarization of light.

References

1. Li, J, et al. "Strong optical confinement between nonperiodic flat dielectric gratings." Physical review letters, 106.19, 2011
2. Liao, C, T. Hu, and D. Wang, “Optical fiber fabry-perot interferometer cavity fabricated by femtosecond laser micro-machining and fusion splicing for refractive index sensing,” Optics express, vol. 20, no. 20, pp. 22813–22818, 2012.
3. Khorasaninejad, M, W. T. Chen, R. C. Devlin, J. Oh, A. Y. Zhu, and F. Capasso, “Metalenses at visible wavelengths: Diffraction-limited focusing and subwavelength resolution imaging,” Science, vol. 352, no. 6290, pp. 1190–1194, 2016.
4. Thompson, C.V, “Solid-state dewetting of thin films,” Annual Review of Materials Research, vol. 42, pp. 399–434, 2012.
5. Overvig, AC., S. Shrestha, and N. Yu. "Dimerized high contrast gratings." *Nanophotonics* 7.6 (2018): 1157-1168.

Three-dimensional varifocal device by mechanical tuning of metalens doublet and auxiliary visual alignment guiding hologram

Hyeonhee Kim[1], Joonkyo Jung[1], and Jonghwa Shin[1*]

[1]Department of Materials Science and Engineering, KAIST, Daejeon, 34141, Republic of Korea
[*]corresponding author: qubit@kaist.ac.kr

Abstract: In this study, we proposed an optical system including metalens doublet which can generate focus at an arbitrary location in three-dimensional space by simply tuning their distance or orientation angles. For fully exploiting 2-polarization channels of the unitary symmetric metasurfaces, a built-in hologram is embedded in the remaining channel, which visually guides rotational and positional alignment between two metalenses in real-time, without additional fabrication cost. The suggested hybrid optical system could apply to and widen many other studies.

Active metasurfaces with reconfigurable and tunable properties have attracted a lot of academic and industrial interest. By controlling the properties of the constituent material or environment surrounding the metasurfaces, one can tune the response of the metasurfaces[1]. However, a significant challenge in achieving high performance is the requirement for the size of independently tunable pixels to be on the same scale as the wavelength. Accordingly, mechanical reconfiguration of multiple metasurfaces also has been studied because of its simple and macroscopic tuning mechanism[2].

Here, using the polarization-multiplexing characteristic of the unitary symmetric metasurfaces, we demonstrate that the metalens doublet can work as a three-dimensional varifocal device for right-circularly polarized (RCP) light and generate a visual alignment-guiding hologram for left-circularly polarized (LCP) light.

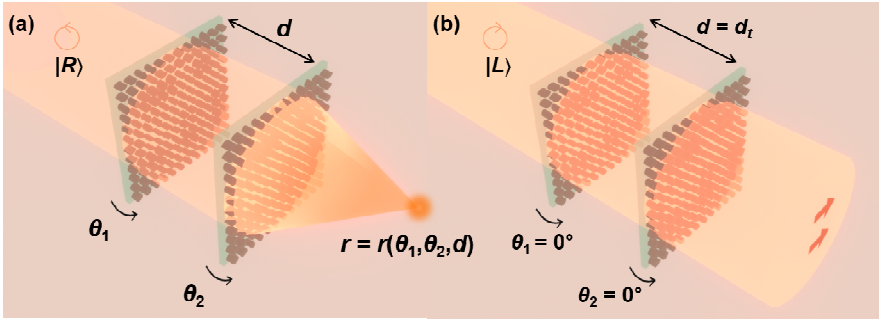


Figure 1. Schematic illustration of polarization-multiplexed metalens doublet. (a) Three-dimensional varifocal device for RCP incidence. The location of the hot spot can cover the three-dimensional space by simply rotating two metalenses or changing the distance between them. (b) Alignment-guiding hologram for LCP input light. Depending on the distance between two metalenses and the orientation of each metalens, the output holographic image is blurred, rotated, and shifted.

In Figure 1, The tunable metalens doublet consists of two optical elements, each of which is functionally a superposition of a beam-steerer and a lens for RCP incidence. According to imaging equation, the position of the hotspot can cover longitudinal displacement. The transversal displacement effect at the imaging plane can be analytically derived using Fresnel approximation, which is given as

$$\boldsymbol{\rho} = \frac{d_2}{k_0}\left(\boldsymbol{k}_{\parallel,2} + \frac{f_1}{d_1}\boldsymbol{k}_{\parallel,1}\right) \tag{1}$$

k_0 : vacuum wavevector
$\boldsymbol{k}_{\parallel,i}(i = 1,2)$: beam steering tangential wavevector of ith element
$\theta_i(i = 1,2)$: rotation angle of ith element

For LCP incidence, the first metasurface is designed to perform as a superposed device of a hologram and a convex lens, and the second metasurface is designed to be superposed of a concave lens, a grating, and a beam-steerer.

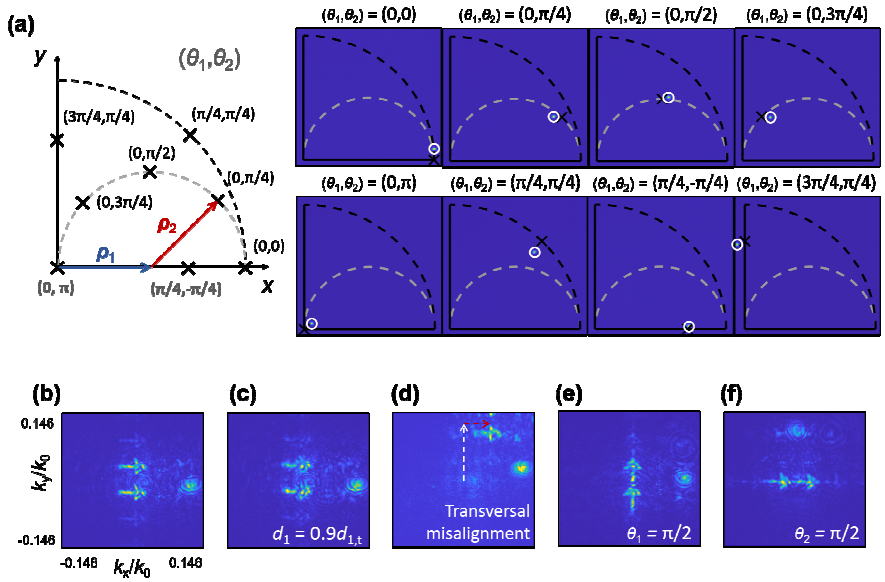


Figure 2. Experimentally measured device performance. (a) Transversal controllability of the hot spot. The left(right) panel represents the target(measured) focusing position. (b) Measured holographic image when the rotation angle of each metasurface is 0° and the metasurface aligned well to have target distance. (c-f) Measured holographic images with each kind of misalignment. (d) Measured holographic image with transversal misalignment along the vertical direction. The white arrow shows the intrinsic displacement caused by lens characteristics. The red arrow shows the extrinsic displacement caused by the spatially-varying beam-steering effect. This figure is adapted from Figure 5 and Figure 6 of reference 2.

We theoretically, numerically, and experimentally proved that by just manipulating their inter-distance and orientation angles, the resulting hot spot can be relocated arbitrarily. Figure 2(a) experimentally proves the transversal controllability of the focal spot and Figure 2(b)-(f) show the measured results of the built-in hologram. The tunable mechanism and the multifunctionality of our suggested device could be widely applied to a variety of research fields such as three-dimensional imaging, facial recognition, laser cutting, and distance sensing.

References

1. J. Park, J. -H. Kang, S. J. Kim, X. Liu, and M. L. Brongersma, "Dynamic reflection phase and polarization control in metasurfaces," *Nano Lett.*, Vol. 17, No. 1, 407-413, 2017.
2. J. Jung, H. Kim, and J. Shin, *Nanophotonics*, 2023. doi: 10.1515/nanoph-2022-0634

Fully Beam Scanning Transmissive Mechanical Metasurface with Polarization Conversion

Chhunheng Lor[1], and Sungjoon Lim[2*]

[1]School of Electrical Engineering, Chung-Ang University, Seoul, Korea
[2] School of Electrical Engineering, Chung-Ang University, Seoul, Korea
[*]corresponding author: sungjoon@cau.ac.kr

Abstract: A circular-polarization (CP) beam scanning metasurface is proposed to achieve fully transmission beam scanning of 28-degree for both positive and negative direction of the radiation pattern. The combination of plannar and non-plannar electromagnetic (EM) elements to enlarge the distance variation of spacing modulation metasurface for larger beam scanning range than the conventional active. The scanning ability is being controlled and optimized by integrated with the DC motor and is being verified through the numerical and measurement result.

Metasurface is the compose of periodic electromagnetic (EM) elements that can manipulate the electromagnetic wave. Recently proposed of reconfigurable metasurface has shown the limitations of integration functions for transmission beam scanning and polarization conversion due to the tuning ability [1], basing layer [2]. Phase and spacing modulation are two conventional designs for beam scanning metasurface that proceed by reconfiguring the phase delays and spacings between EM elements on a metasurface. Phase modulation metasurface commonly used active components to integrate with the FSS to adjust the phase delay of each unit cell (UC), which is costly and limited design. Therefore, spacing modulation is required, especially for transmission beam steering, and polarization conversion. In challenging to solve the design limitations for reconfigurable metasurface, we propose a transmissive CP metasurface with polarization conversion function that has large scanning range by the combination of planar and non-planar spacing modulation structure (Fig 1a).

Conventional spacing modulation metasurface has UC arrangement in planar where the distance variation is considered by the air gap between UC and ranging between the UC size at d = 0.5 UC size and the air gap where d > 0.5 UC size. To increase the distance variation range, we demonstrate rotatable UCs to achieve both plannar and non-plannar geometry for lowering the limited distance between UCs to smaller than the UC size (d < 0.5 UC size). Fig 1b shows the geometrical and characteristic of the distance variation and rotation angle of the rotatable UC.

To implementation the idea of the propose metasurface, we firstly designed a conventional 3-layer transmission polarization conversion UC to convert the EM wave polarization from Linear Polarization (LP) to CP and achieved 90-degree phase different at UC size of wavelength ($\lambda \sim 30$mm) at 10.5 GHz operation frequency. Fig 1c show the simulated average transmission magnitude over -3 dB and the phase shift of the 90-deg phase different UCs A, B, C, and D at different rotation state α = 0,10, and 20 deg. Fig 1d showing the simulated RHCP and LHCP beam scanning range from 22 to 50 deg of the metasurface in function of the distance variation. Respectively, the flip of the UC B and D could switch the RHCP and LHCP beam between positive and negative direction angle due to the phase gradient phenomena of the LP source [3]. Moreover, we measured the RHCP and LHCP beam angle at 22 and 37 deg and received good results confirming the performance of the proposed metasurface as shown in Fig 1e.

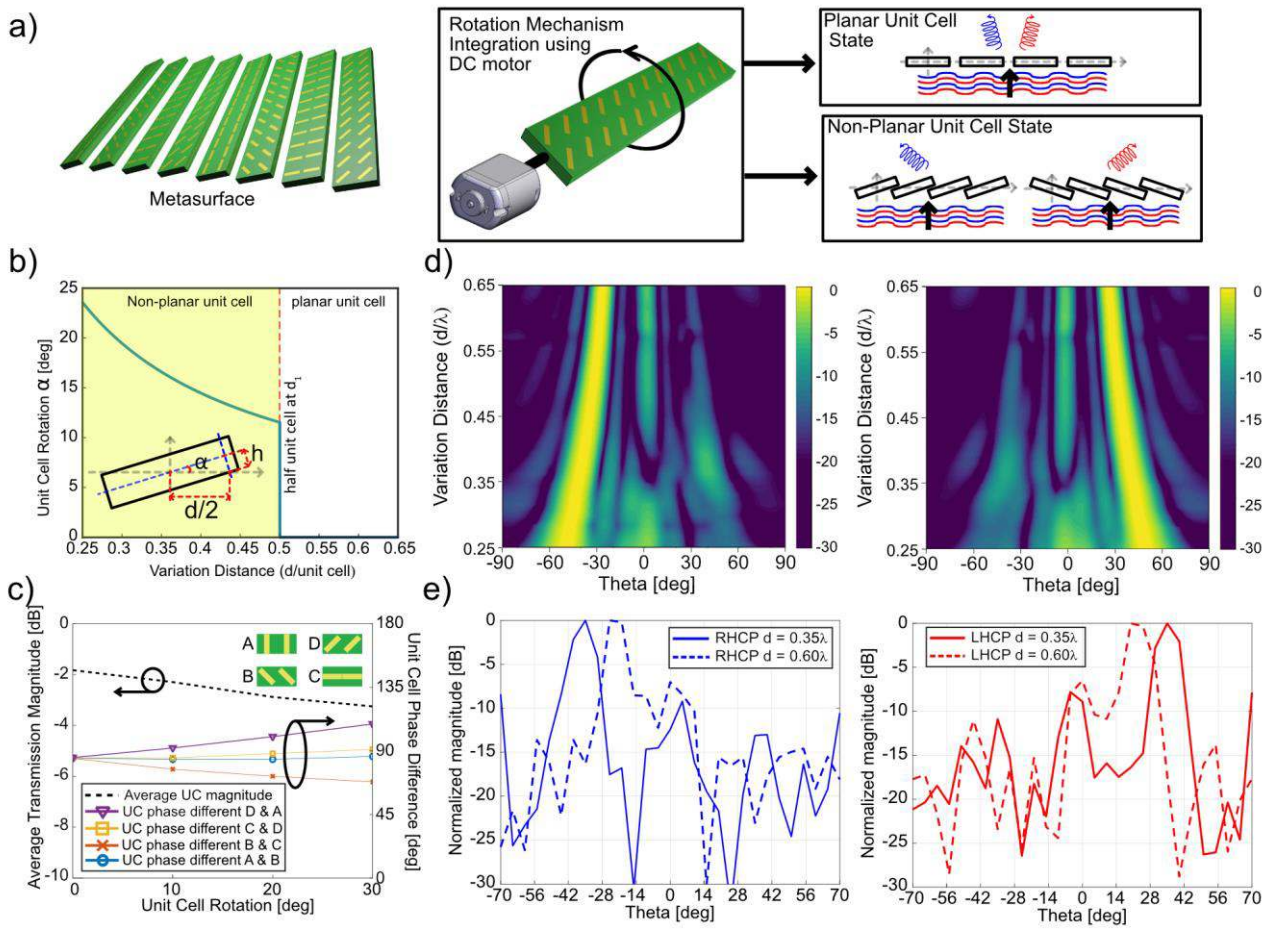


Figure 1 a) Metasurface illustration and mechanism. b) UC rotation and distance variation characteristics.
c) simulated UC average transmission magnitude and phase difference.
d) Simulated scanning range of RHCP (left figure) and LHCP beam (right figure)
e) Measurement result of RHCP (left figure) and LHCP (right figure) beam at 22 and 37-deg radiation angle

Inconclusion, in this summary we introduce a fully CP beam scanning transmission metasurface with mechanically integration of planar and non-planar UC reconfiguration that could achieved 28-deg transmission beam scanning range for either RHCP and LHCP in both positive and negative radiation pattern direction.

Acknowledgement, this research was supported by the National Research Foundation of Korea (NRF) grant funded by the Korea government (MSIT) (2021R1A2C3005239 and 2021R1A4A2001316).

References

1. Phon, R., Kim, Y., Park, E., Jeong, H., Lim, S., “Mechanical and Self-Deformable Spatial Modulation Beam Steering and Splitting Metasurface”, Adv. Optical Mater, Vol 9, No. 2100821, 2021.
2. Gao, W. H. Chen, M. Cui, T. J., “A 1-Bit Coding Metasurface with Polarization Conversion in X-Band”, Front. Mater, Vol 9, No. 914937, 2022.
3. Yoon, G. Lee, D. Nam, K. T. Rho, J., “Geometric metasurface enabling polarization independent beam splitting”, Sci Rep, Vol 8, No. 9468, 2018.

Angle sensitivity of extraordinary optical transmission and resonant spatial frequency filtering

Sun-Je Kim[1*] and Hanbyul Chang[2]

[1]Department of Physics, Myongji University, Republic of Korea
[2]Department of Electrical and Computer Engineering, Seoul National University, Republic of Korea
[*]corresponding author: sunjekim@mju.ac.kr

Abstract: In this paper, we propose a rigorous study on the angle-sensitivity of the extraordinary optical transmission resonances in subwavelength plasmonic silver nanogratings. The mechanism of angle sensitivity of the resonances is revealed in terms of the coupling between the cavity resonance and the propagating surface plasmon excitation. Based on the mechanism, strong and efficient monochromatic spatial filters are engineered by judicious tuning of the geometric parameters. The designed spatial filtering functions are also verified via experiments.

Plasmonic nanogratings have been widely studied over the decades since the first observation of the extraordinary optical transmission (EOT) resonances [1]. Majority of EOT research has been focused on understanding and utilizing complex spectral behaviors under a fixed incidence angle. In this paper, we suggest a rigorous study on incidence angle-sensitivity of the EOT and its use for resonant spatial frequency filtering [2, 3]. As can be seen in Fig. 1(a), according to the incidence angle, silver nanograting shows the strong angle-sensitivity with the red shift of the EOT (red box region in Fig. 1(a)). For the design of a finite Ag EOT nanograting with strong angle-sensitive cavity resonance, lowpass (Fig. 1(b)) and bandpass (Fig. 1(c)) spatial filtering is achieved at the different resonance wavelengths, respectively.

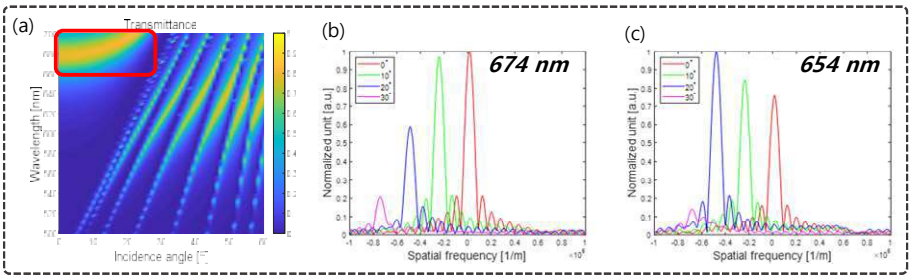


Figure 1. (a) Angle sensitive EOT spectrum. (b) lowpass and (c) bandpass spatial filtering at the wavelengths of 674 and 654 nm, respectively.

Acknowledgements This work was supported by the National Research Foundation of Korea (NRF) grant funded by the Korea government (MSIT) (No. 2021R1F1A1062368).

References

1. Ebbesen, T. W., H. J. Lezec, H. F. Ghaemi, T. Thio, and P. A. Wolff, “Extraordinary optical transmission through sub-wavelength hole arrays,” Nature, Vol. 391, No. 6668, 667-669, 1998.
2. Wesemann, L., T. J. Davis, and A. Roberts. "Meta-optical and thin film devices for all-optical information processing." Appl. Phys. Rev., Vol. 8, No. 3, 031309, 2021.
3. Kim, S.-J., J. Hong, S. Moon, J.-G. Yun, and B. Lee, “Full color angular filtering of visible transmission in tapered plasmonic metamaterial,” Plasmonics, Vol. 16, No. 1, 115-121, 2021.

Electrical tunning of metasurfaces via transparent conducting oxide micro heaters

Khosro Zangeneh Kamali[1], Lei Xu[2], Nikita Gagrani[1], Hark Hoe Tan[1], Chennupati Jagadish[1], Andrey Miroshnichenko[3], Dragomir Neshev[1], Mohsen Rahmani[2*]

[1] ARC Centre of Excellence for Transformative Meta-Optical Systems, Research School of Physics, The Australian National University,
Canberra, ACT 2600, Australia
[2] Advanced Optics and Photonics Laboratory, Department of Engineering, School of Science and Technology, Nottingham Trent University,
Nottingham NG11 8NS, United Kingdom
[3] School of Engineering and Information Technology, University of New South Wales, Canberra, ACT 2600, Australia
* corresponding author: mohsen.rahmani@ntu.ac.uk

Abstract: We demonstrate a rapid and programmable amplitude modulator based on the thermo-optical effect by integrating transparent conducting oxide micro-heaters with metasurfaces. The system exhibits sub-millisecond rise-time and 9 folds of amplitude modulation.

Metasurfaces have attracted much interest recently because of their exceptional light-scattering properties, thanks to their ability to manipulate light-matter interaction through their geometrical parameters and material properties. Currently, there is a quest to enable dynamic tuning of metasurface properties, particularly with fast tuning rate and programmable across multiple pixels [1]. However, the fixed geometry of the metasurfaces has been an obstacle to the tunability of their scattering properties.

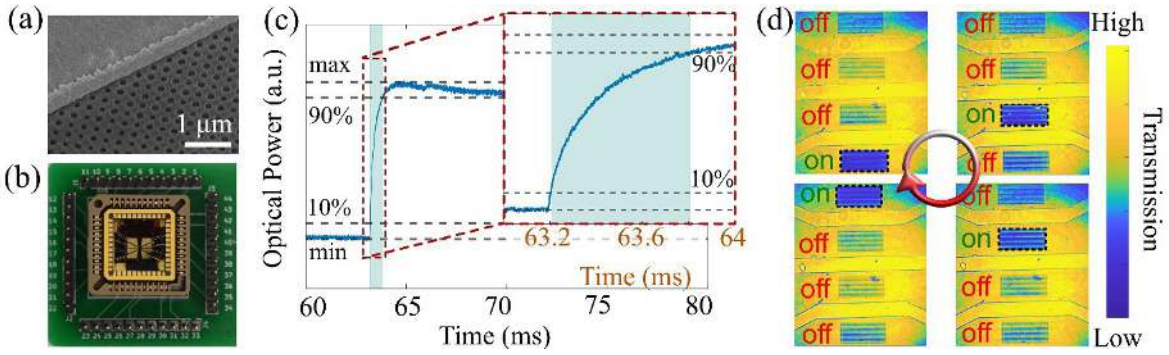


Fig. 1 (a) SEM of the Si hole-array metasurface embedded in ITO. (b) Picture of the printed circuit board (PCB) used for programming and electrically driving the metasurface. (c) Transmission intensity rise-time after electrically biasing the system. Insert is the magnified plot, indicating the switching rise-time (d) Addressable tuning of individual metasurfaces by controlling the micro-heaters.

Here, we demonstrate electrically tunable metasurfaces driven by thermo-optic effect and flash-heating in silicon [2]. Our device consists of a silicon hole array metasurface encapsulated by transparent conducting oxide as a localised heater (see Fig. 1a,b). We show a 9-fold change in transmission by < 5 V biasing voltage and the modulation rise-time of < 625 µs., which is about 20-fold faster than biasing the system with a step profile voltage

(Fig. 1c). As can be seen in Fig 1d, this method enables programming the spatially individual metasurfaces, on-demand. Some of the advantages of the proposed tuning method compared with other methods are the possibility to apply it for modulation in the visible and near-infrared region, large modulation depth, working at transmission regime, exhibiting low optical loss, low input voltage requirement, and operating with higher than video-rate switching speed. The device is furthermore compatible with modern electronic display technologies and could be ideal for personal electronic devices such as flat displays, virtual reality holography and light detection and ranging, where fast, solid-state and transparent optical switches are required.

Acknowledgements

This study was kindly supported by The Royal Society and the Wolfson Foundation (RSWF\FT\191022), as well as the Australian Research Council through TMOS Centre of Excellence (CE20010001), and Discovery Project (DP200101353). The authors appreciate using the Australian National Fabrication Facility (ANFF) - the ACT Node and acknowledge the use of NTU High-Performance Computing cluster Hamilton.

Acknowledgements, if any, including all funding information, should be gathered into a brief statement at the end.

References

1. Yang, J., Gurung, S., Bej, S., Ni, P. and Lee, H.W.H. “Active optical metasurfaces: comprehensive review on physics, mechanisms, and prospective applications”. Rep. Prog. Phys., Vol 85, No 3, 036101, 2022.
2. Zangeneh Kamali, K., Xu, L., Gagrani, N., Tan, H., Jagadish, C., Miroshnichenko, A., Neshev, D., and Rahmani, M. “Electrically-tunable solid-state metasurfaces via flash localised heating,” Light Sci. Appl Accepted, in Press, DOI: 10.1038/s41377-023-01078-6

Investigation of Field Effect Tuning of Refractive Index in Transparent Conducting Oxide Thin Film Fabry-Perot Cavity Structures.

Evan Roy[1], **Nishtha Shelly**[1], **Chris Murray**[1], **David McCloskey**[1]

[1]School of Physics, CRANN and AMBER, Trinity College Dublin, Dublin 2, Ireland

eroy@tcd.ie

Abstract: Electrical tuning of transparent conducting oxides (TCOs) can result in unity order change in refractive index at visible and NIR frequencies by blue shifting the plasma frequency ω_p within an interfacial accumulation layer. We used the Transfer Matrix Method (TMM) in MATLAB to simulate TCO heterostructures based on metal-insulator-metal (MIM) Fabry-Perot (FP) cavities. Our results demonstrate that large changes in transmitted and reflected light are achievable in MIM heterostructures in the visible at low voltages in the surface normal geometry.

Summary: A typical MIM FP device will have a thin transmissive metal on top to allow light in and another metal on the bottom to form two reflective surfaces. Different insulating or conducting layers can be added in between to manipulate the confined modes as well. By manipulating the thickness of these layers, one can fine tune the frequencies of the resonance modes and the internal field in the cavity. By simulating with the TMM in MATLAB we can predict the spectra of our heterostructures and fine tune them accordingly [1,2].

The placement of ultrathin (less than 10nm) absorbers like Mo, MoS_2, and Cr in the central high intensity region of the dielectric spacer helps to sharpen the MIM FP cavity resonance mode via coupling it with an additional absorption band. Mo and Cr are among the best broadband absorbers in the visible, reducing reflectivity and transmittance evenly across this range as a result. See figure 1(A, B). The idea of sharpening and suppressing higher order optical resonances using this particular MIM structure is based on the work of Korean researchers Junho Lee and Kyu-Tae Lee, among others, looking at high-color-purity structural color filters in transmittance and reflectance [3,4].

Indium tin oxide is a well-studied TCO that has shown promise in many different optoelectronic applications, including large field effect refractive index change. Recent literature has reported on unity order change in the local refractive index of ITO by applying an electrical bias up to 2.5 V across a metal-oxide-semiconductor (MOS) structure [5]. By applying a bias, an accumulation layer is created at the ITO-dielectric interface where the charge carrier density n can increase by factor of 10. Higher initial doping levels in the ITO shifts the strong refractive index change from the NIR to the visible range, creating greater sensitivity in the permittivity ε of ITO below 700 nm. See eq.(1) and figure 1(B, C).

$$\varepsilon = \varepsilon_\infty - \frac{\omega_p^2}{\omega^2 + i\omega\Gamma}; \quad \omega_p^2 = \frac{ne^2}{\varepsilon_\infty m^*} \tag{1}$$

Although a large change in the local refractive index is possible, the accumulation region in which this occurs is localized to within ~5nm of the ITO-oxide interface and is spatially characterized by a Poisson distribution. To create a large change in transmission or reflectivity upon bias there are two strategies that we used in tandem. The heterostructure can be optimized to enhance the matter light interaction by coupling an FP cavity mode to the absorption band of the central metal layer, and additional ITO and insulating layers can be added to multiply the effective shift in the spectra as shown in figure 1(E, F).

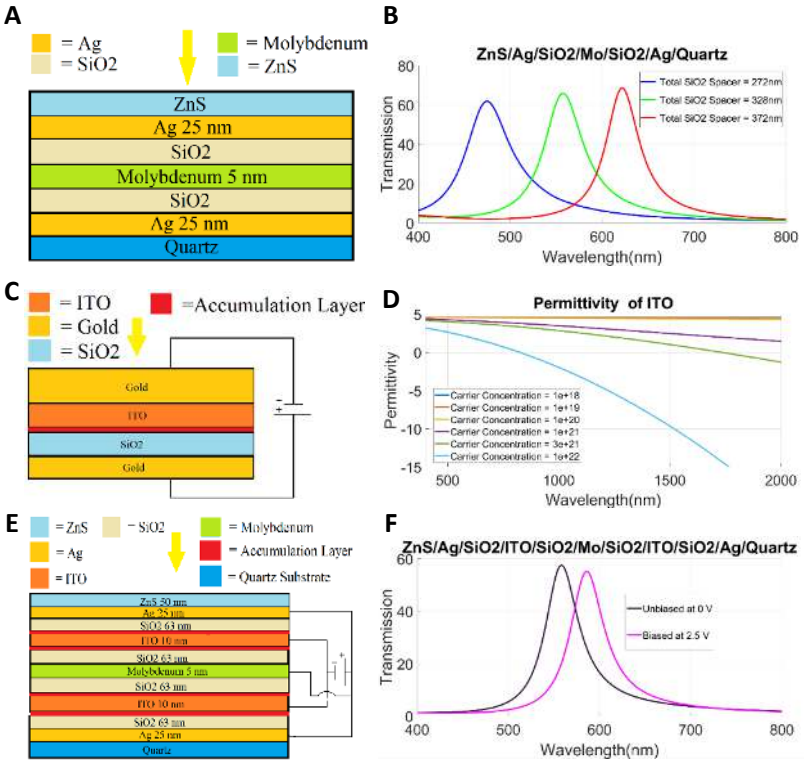


Figure 1(A, B). A MIM heterostructure with a 5 nm Mo layer central absorber. By changing the dielectric SiO_2 spacer thickness, the resonance peak position can be controlled. The result is a structural high-purity transmission filter, which can have useful applications in RGB display technology. Figure 1(C, D). The real permittivity of ITO in a MOS device relative to wavelength and carrier concentration as derived from the Drude-Lorentz model shown in equation (1). Changing n from $10^{21} - 10^{22}$ cm^{-3} creates a large change in ε in the accumulation layer in the visible range [5]. Figure 1(E, F). Simulated spectra of a large MIM FP heterostructure using a quartz substrate. The spectrum shifts when biased allowing for large change in transmission around the resonance mode peak.

Acknowledgements: This work is supported by Science Foundation Ireland (SFI) funded by the Irish government.

References:

[1] Katsidis, C. C., & Siapkas, D. I. General transfer-matrix method for optical multilayer systems with coherent, partially coherent, and incoherent interference. *Applied Optics*, *41*(19), 3978–3987. (2002).

[2] Kenneth J. Pascoe. Reflectivity and Transmissivity through Layered, Lossy Media A User-Friendly Approach. Graduate School of Engineering and Management Air Force Institute of technology Wright-Patterson Air Force base Ohio. (2001)

[3] Junho lee, Jaeyong Kim, & Myeonggkyu Lee. High-purity reflective color filters based on thin film cavities embedded with an ultrathin $Ge_2Sb_2Te_5$ absorption layer. Nanoscale Adv., (2020), **2**, 4930-4937.

[4] Lee, KT., Han, S.Y., Li, Z. *et al.* Flexible High-Color-Purity Structural Color Filters Based on a Higher-Order Optical Resonance Suppression. *Sci Rep* **9**, 14917 (2019).

[5] Feigenbaum, E., Diest, K., & Atwater, H. A. Unity-order index change in transparent conducting oxides at visible frequencies. *Nano Letters*, *10*(6), 2111–2116. (2010).

META 2023, PARIS - FRANCE, JULY 18 – 21, 2023

Optical Metasurfaces for Grafted Vortex Beams Generation

Hammad Ahmed[1*], Muhammad Afnan Ansari[1], Xianzhong Chen[1]

[1]Institute of Photonics and Quantum Sciences, School of Engineering and Physical Sciences, Heriot-Watt University, Edinburgh, EH14 4AS, UK.
[*]Corresponding author: ha2016@hw.ac.uk

Abstract: Inspired by plant grafting, the act of placing a portion of one plant (scion) on a branch or root of another (rootstock), grafted vortex beams (GVBs) can be formed through grafting two or more helical phase profiles of optical vortex beams. GVBs have attracted much attention due to their unique optical properties and potential applications. Here, we propose and demonstrate the coaxial superposition of GVBs without relying on the complicated optical setup. The coaxial superposition of GVBs can generate asymmetric singularity distribution, which can be modulated by introducing an initial phase difference in the metasurface design. Our work has provided a compact metasurface approach to complete the sophisticated task that is extremely challenging or impossible with conventional optics, opening opportunities for the study and applications of GVBs in a wide range of areas.

In conventional optical vortices, the OAM distribution on the doughnut-shaped intensity ring is uniform. This uniformity is not suitable for applications where versatile OAM distributions are required, e.g., multiparticle trapping and manipulation. Therefore, noncanonical optical vortices (non-uniform hollow circular OAM distributions, spiral OAM distributions)[1] are proposed to tackle these challenges. However, these OAM distributions are strongly dependent on the intensity and the local OAM modulation is impossible. A GVB, which is generated through grafting two or more spiral phase profiles of optical vortex beams, has a controllable OAM distribution and constant intensity. Recently, GVBS have attracted much attention due to their unique optical properties (e.g., versatile OAM distributions) and potential applications (e.g., more options for particle manipulation) [2]. However, the generation and manipulation of GPVBs are more challenging and complicated due to the involvement of an additional phase profile of a lens and that of an axicon. The optical setups currently being used for generating GPVBs are complex, requiring numerous optical components, including spatial light modulators, lenses, pinhole filters, polarizers, and dichroic mirrors, which result in large space requirement and high cost[3, 4]. These optical systems are impractical for many applications, and hence there is a pressing requirement for a compact, simple, and efficient approach to generating and manipulating GVBs.

To tackle the fundamental and technical challenges in more conventional optics, we propose and experimentally demonstrate (as shown in Figure 1) a metasurface-based approach to generating and manipulating GVBs. To the best of our knowledge, this is the first time that a single metasurface has been used to generate various GPVBs and realize the coaxial superpositions, without relying on the complex conventional optical setup. The uniqueness of this method is that the superimposed GPVBs have nonuniform OAM and asymmetric singularity distributions, which can be modulated by introducing initial phase difference in the metasurface design. The proposed metasurface approach can facilitate system integration and device miniaturization and has strong potential for novel applications that may not be possible with conventional optics.

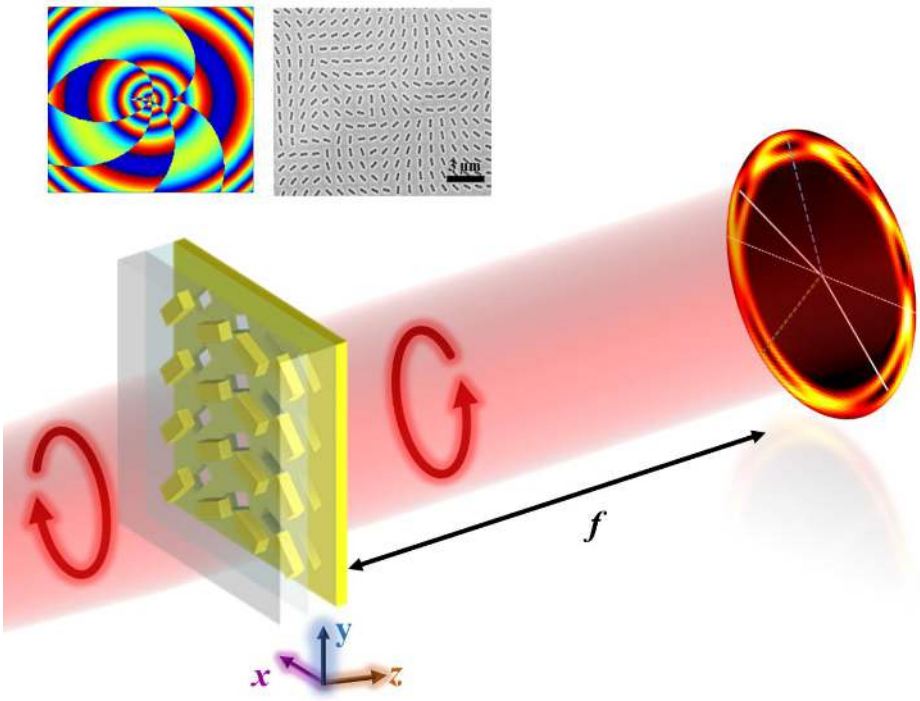


Figure 1: Schematic of GVB generating metasurface. Inset: calculated phase profile (left) and SEM image of fabricated metasurface (right)

Acknowledgements

This project was funded by the Engineering and Physical Sciences Research Council (EP/P029892/1), the Leverhulme Trust (RPG-2021-145), DASA Advanced Vision project (DSTLX1000147844)

References

1. Rodrigo, J.A. and T. Alieva, *Freestyle 3D laser traps: tools for studying light-driven particle dynamics and beyond.* Optica, 2015. **2**(9): p. 812-815.
2. Zhang, H., et al., *Grafted optical vortex with controllable orbital angular momentum distribution.* Optics express, 2019. **27**(16): p. 22930-22938.
3. Ahmed, H., et al., *Multichannel superposition of grafted perfect vortex beams.* Advanced Materials, 2022. **34**(30): p. 2203044.
4. Ming, Y., et al., *Creating composite vortex beams with a single geometric metasurface.* Advanced Materials, 2022. **34**(18): p. 2109714.

Performance Analysis of Patch-HIS Arrays for Visually Impaired Aid System

A. Flórez Berdasco[1], J. Laviada Martínez[1], M. E. de Cos Gómez[1] and F. Las-Heras Andrés[1]

[1]TSC Electrical Engineering Dept., Gijon, Spain
*corresponding author: florezalicia@uniovi.es

Abstract: A High Impedance Surface (HIS) metasurface has been designed to be combine with patch-based antennas to improve their radiation properties for the Electronic Travel Aid (ETA) application for which they are intended. A wearable patch and patch-HIS arrays antennas have been designed *ad hoc,* in the 24.05-24.25GHz frequency band. In order to evaluate the performance of the antennas, electromagnetic images have been obtained and a metric have been applied to compare their quality and evaluate their behavior for the application.

The traditional travel aids used by visually impaired people have been the white cane and the guide dog. However, these solutions are not enough for autonomous mobility. In this context, it seems that millimeter wave radars may be appropriate for obstacle detection, due to its great development in recent years and the relatively high frequency in which this technology operates, which allows obtaining compact radar modules. In order to improve the performance of the antennas (e.g., front-to-back ratio, gain, etc.), antennas surrounded by HIS unit cells have been proposed [1]. In this work, the effects of these nonideal radiators are analyzed for a short distance avoidance collision application. Electromagnetic images will be obtained by a flexible sum-and-delay algorithm:

$$\rho(\vec{r}) = \sum_{m=1}^{M}\sum_{n=1}^{N} S_r(m,n)\cdot e^{jk_m 2|\vec{r}-\overrightarrow{r_n}|} \quad (1)$$

Sr refers to the acquired data, *M* stands for the number of frequencies while *N* indicates the acquisition points. *km* represents the wavenumber at the m-frequency, $\vec{r}$ indicates the pixel where the reflectivity is going to be calculated and $\overrightarrow{r_n}$ refers to the n-measured position. This algorithm assumes that a perfect spherical wavefront is employed for calculating the reflectivity. However, if the waves are not created from the same position, dispersive behavior along frequency is expected, producing unwanted artifacts in images.

The performance of patch-based antennas, all of them designed in RO3003, have been analyzed for this application. A simple patch antenna (*Patch*), a two-element patch array with a wall of HIS unit cells between its elements to reduce the coupling (*Array-HIS Wall*) and including a row of unit cells surrounding the patches to reduce the possible surface waves (*Array-HIS Row*) have been evaluated. The fabricated prototypes are shown in Figure 1a. TABLE 1 summarizes the radiation properties of each antenna for the center frequency of the operating bandwidth. More details about the antennas and metasurface design can be found in [1].

Electromagnetic images have been obtained from a monostatic set-up (see Figure 1b). A simple target has been employed, as this kind of objects provides a simple response, which facilitates the analysis of the results. In this work a metal strip of 4x340mm is used as the target. It is placed over the antenna at a distance of 13.2cm, so that far-field conditions are met. The synthetic aperture length is set in 30 cm in the direction of the x-axis (see Figure 1b) and the sampling step has been established in order to satisfy the Nyquist theorem (~λ/4 at 24.25GHz). The data have been acquired with a Vector Network Analyzer (VNA) simulating a step-frequency continuous wave (SCFW) radar. Figure 1c, d and e show the electromagnetic images obtained with each antenna, where the contour of the object has been highlighted in magenta. In order to quantitatively compare the quality of the images

their entropy (IE) have been calculated according to [2], and the results are indicated in TABLE 1. The smaller the entropy value, the better quality of the image. It can be concluded that all the antennas detect the target (see Figure 1c, d and e). The *Array-HIS Row* design, which reduce the coupling between the array elements, improves the IE result with respect to the simple *Patch*. As it can be observed in Figure 1d, the spread energy around the target is lower than the other cases. However, surrounding the array by a row of unit cells does not improve the IE result obtained with the *Wall Array-HIS*, although it performs better than the *Patch*. Therefore, few unit cells in the middle of the array elements contribute to reduce the coupling between them, modifying the radiation diagram of the antenna, so that a better performance is reached for this application.

TABLE 1. Simulated and measured radiation properties of the antennas and TCR results.

	Simulated				Measured	IE
Antenna	G [dB]	D [dB]	η [%]	FTBR [dB]	G [dB]	
Patch	6.8	6.8	100	20.2	7.4	6.9
Array-HIS Wall	8	8	100	24.8	8.5	6.5
Array-HIS Row	7.9	7.9	100	36.7	7.9	6.8

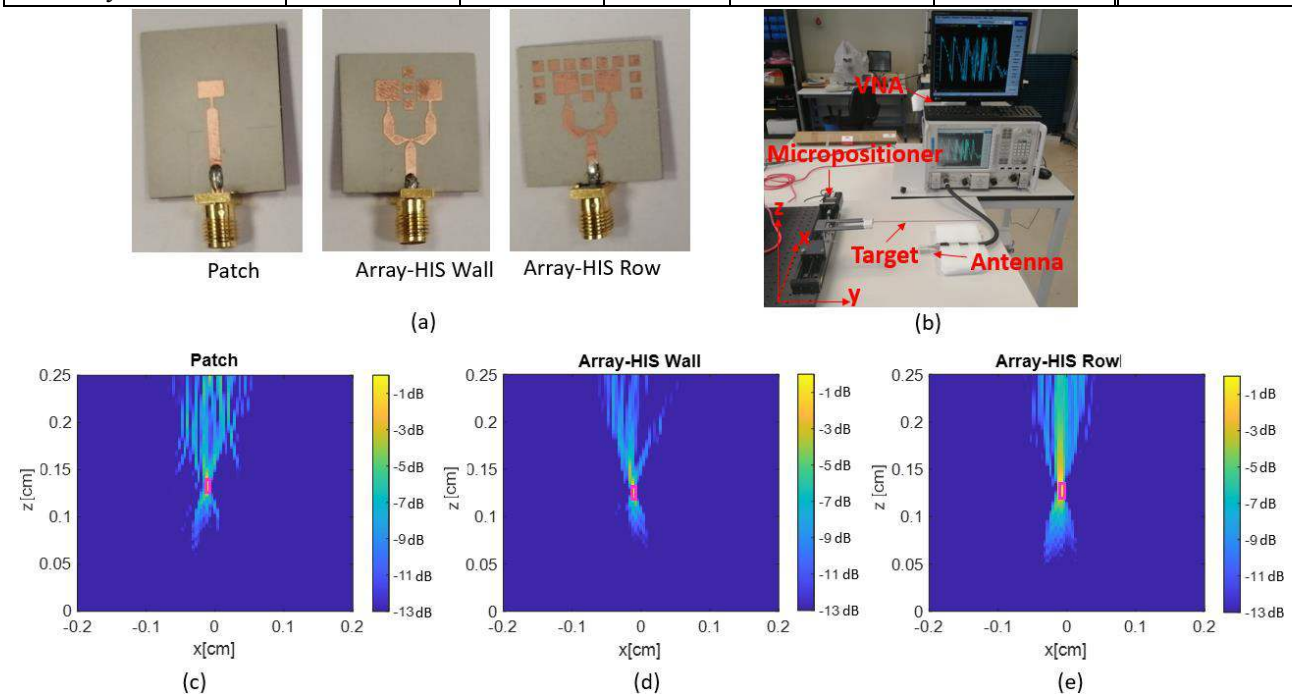


Figure 1. (a) Antennas under evaluation, (b) SAR measurement set-up, (c) Patch Electromagnetic Image, (c) Array-HIS Wall Electromagnetic Image, (e) Array-HIS Row Electromagnetic Image.

Acknowledgement

This research was funded by the Ministerio de Educación y Formación Profesional of Spain under the FPI Grant PRE2019-089912, by the Ministerio de Ciencia, Innovación y Universidades of Spanish Government under project META-IMAGER PID-2021-122697OB-100, and by Gobierno del Principado de Asturias under project AYUD-2021-51706.

References

1. A. F. Berdasco, M. E. de Cos Gómez, H. F. Álvarez and F. L. -H. Andrés, "Array Antenna with HIS Metasurface for mmWave Imaging Applications," EuCAP, Madrid, Spain, 2022, pp. 1-5, doi: 10.23919/EuCAP53622.2022.9769433.
2. Z. Hao; R. Wang; X. Dang; H. Yan; J. Peng, "mmSight: A Robust Millimeter-Wave Near-Field SAR Imaging Algorithm, " *Appl. Sci.* 2022, *12*, 12085. https://doi.org/10.3390/app122312085.

Silicon metalens using Fresnel zone plate with subwavelength gratings

W. Fraser[1*] and W. N. Ye[1]

[1]Silicon Micro/NanoPhotonics Group, Carleton University, Ottawa, Canada
[*]corresponding author: williamfraser3@cmail.carleton.ca

Abstract: Beam focusing metalenses have become an enabling technology for flat optic-integrated imaging and free-space communication systems. Traditional metalenses comprised of periodically arranged subwavelength building blocks rely on custom fabrication practices. We present a 500 nm silicon-on-insulator-compatible metalens based on the Fresnel zone plate capable of subwavelength focusing with a peak efficiency of 42.7% over a 389 nm bandwidth in the *C*-band.

Summary: All-dielectric metasurfaces [1-4] have attracted great interest for imaging and free-space communication applications. Typical beam focusing metalenses form a hyperbolic phase profile spanning the 0 to 2π range which converts planar wavefronts into converging spherical waves. This is achieved by varying the geometrical properties of subwavelength scattering elements arranged in a periodic array [5-18]. Phase accumulation requires lens thicknesses that are close to the operating wavelength [17] unless complex resonances are exploited, sacrificing the bandwidth [18]. Consequently, conventional all-dielectric focusing metalenses are incompatible with public silicon-on-insulator (SOI) foundries which slows integration with photonic systems. In this work [19], we present the design and simulation of a novel compact metalens that can be fabricated with a single full etch step on the 500 nm SOI platform. The proposed design uses silicon subwavelength grating (SWG) structures to form a binary phase Fresnel zone plate (BPFZP) that produces a subwavelength focal spot across the *C*-band.

The binary phase Fresnel zone plate consists of a set of concentric annular regions forming a circular aperture. The radii of these so-called Fresnel zones are calculated a focal length, f, and the wavelength, λ, using equation 1 [20]:

$$r_n = f\sqrt{\frac{n\lambda}{f} + \left(\frac{n\lambda}{2f}\right)^2} \tag{1}$$

where n is an integer representing the order of the zones counting out from the center of the aperture. The radii are such that the optical path length difference to the focal point between adjacent zones is a half-wavelength. Introducing a phase profile that alternates between 0 and π according to the Fresnel zones produces constructive interference at the focal point.

A diagram of the proposed design presented in this work is shown in Figure 1. Trapezoidal segmented subwavelength gratings [21] are etched into the even-numbered Fresnel zones to spatially vary the equivalent refractive index over the surfaces of the lens.

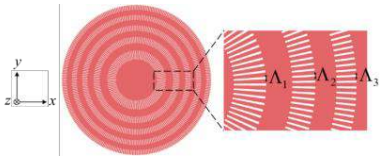


Figure 1. Top-view diagram of our proposed binary phase Fresnel zone plate using subwavelength gratings.

The duty cycle of the subwavelength gratings is optimized to satisfy the binary phase profile of the Fresnel zone plate. The circular symmetry of the lens enables polarization-insensitive operation. Near diffraction-limited focusing is demonstrated in simulations over a 389 nm bandwidth with a peak focusing efficiency of 42.7%.

References

1. Yu, A. and Capasso, F., "Flat optics with designer metasurfaces," Nat. Mater. Vol., 13, No. 2, 139-150, 2014.
2. Chen, H.-T., Taylor, A. and Yu, N., "A review of metasurfaces: Physics and applications," Reports on Prog. Phys., Vol. 79, No. 7, 076401, 2016.
3. Khorasaninejad, M. and Capasso, F., "Metalenses: Versatile multifunctional photonic components," Science, Vol. 358, No. 6367, 1-8, 2017.
4. Arbabi, A., Horie, Yu., Bagheri, M., and Faraon, A., "Dielectric metasurfaces for complete control of phase and polarization with subwavelength spatial resolution and high transmission," Nat. Nanotechnol., Vol. 10, No. 11, 937-943, 2015.
5. Chang, Y.-C. et al., "2D beam steerer based on metalens on silicon photonics," Opt. Express, Vol. 29, No. 2, 854-864 2021.
6. Pahlevaninezhad, H. et al., "Nano-optic endoscope for high-resolution optical coherence tomography in vivo," Nat. Photonics, Vol. 12, No. 9, 540-547, 2018.
7. Wang, Z., Li, Q. & Yan, F., "A high numerical aperture terahertz all-silicon metalens with sub-diffraction focus and long depth of focus," J. Phys. D: Appl. Phys., Vol. 54, No. 8, 085103, 2020.
8. Wang, Y. et al., "High-efficiency broadband achromatic metalens for near-ir biological imaging window," Nat. Commun., Vol. 12, No. 1, 5560, 2021.
9. Arbabi, A., Horie, Y., Ball, A., Bagheri, M. and Faraon, A., "Subwavelength-thick lenses with high numerical apertures and large efficiency based on high-contrast transmitarrays," Nat. Commun., Vol. 6, No. 1, 7069, 2015.
10. Wang, J., Yang, J. and Kang, G., "Achromatic focusing effect of metasurface-based binary phase Fresnel zone plate," Phys. Lett. A, Vol. 407, 127463, 2021.
11. West, P. et al., "All-dielectric subwavelength metasurface focusing lens," Opt. Express, Vol. 22, No. 21, 26212, 2014.
12. Wang, S. et al., "A broadband achromatic metalens in the visible," Nat. Nanotechnol., Vol. 13, No. 3, 227-232, 2018.
13. Aieta, F., Kats, M., Genevet, P. and Capasso, F., "Multiwavelength achromatic metasurfaces by dispersive phase compensation," Science, Vol. 347, No. 6228, 1342-1345, 2015.
14. Khorasaninejad, M. et al., "Metalenses at visible wavelengths: Diffraction-limited focusing and subwavelength resolution imaging," Science, Vol. 352, No. 6290, 1190-1194, 2016.
15. Fattal, D., Li, J., Peng, Z., Fiorentino, M. and Beausoleil, R., "Flat dielectric grating reflectors with focusing abilities," Nat. Photonics, Vol. 4, No. 7, 466-470, 2010.
16. Khorasaninejad, M. and Crozier, K., "Silicon nanofin grating as a miniature chirality-distinguishing beam-splitter," Nat. Commun., Vol. 5, No. 1, 5386, 2014.
17. Cai, H. et al., "Ultrathin transmissive metasurfaces for multi-wavelength optics in the visible," Appl. Phys. Lett., Vol. 114, No. 7, 071106, 2019.
18. Decker, M. et al., "High-efficiency dielectric Huygen's surfaces," Adv. Opt. Mater., Vol. 3, No. 6, 813-820, 2015.
19. Fraser, W. and Ye, W. N., "Fresnel zone plate metalens using silicon subwavelength gratings," In Proceedings of Photonics West, San Francisco, USA, 2023.
20. Pedrotti, F., Pedrotti, L. and Pedrotti, L., [Introduction to Optics], Pearson Prentice-Hall, New Jersey, 316-318, 2007.
21. Cheben, P., Halir, R., Schmid, J., Atwater, H. and Smith, D., "Subwavelength integrated photonics," Nature, Vol. 560, No. 7720, 565-572, 2018.

Optical matrix computation using programmable metalens array

Randy Stefan Tanuwijaya[1], **Hong Liang**[1], **Jiawei Xi**[1], **Tsz Kit Yung**, **Wing Yim Tam**[1], **and Jensen Li**[1*]

[1]Department of Physics, The Hong Kong University of Science and Technology, Clear Water Bay, Hong Kong, China
[*]corresponding author: jensenli@ust.hk

Abstract: We propose and experimentally demonstrate a programmable matrix computation in the optical domain using a spatial light modulator (SLM) and a metalens array. Our scheme encodes the programmable matrix to the metalens array by superimposing multiple phase gradients. Meanwhile, the SLM produces a phase-controlled spatial illuminated light which acts as our input vector. Then, the result can be extracted from the far-field interference pattern constructed by different metalenses using a pattern recognition method.

Introduction

Over the past decade, metasurfaces have shown remarkable capabilities in wavefront manipulation for various optical applications. Metalens, one of the metasurface applications, enables focusing at multiple points in space unlike conventional lens. Recent works in the field include tunable metalens [1,2], applications for imaging [3], spectroscopy [4], and quantum source generation [5]. Our work demonstrates the programmable capability of metalens array for optical matrix computation. We use a geometric-phase metasurface to realize our metalens array, which encodes specific matrix operations simultaneously. Our implementation utilizes phase-modulated light as the input vector, and the resulting vector can be obtained by analyzing the interference pattern formed on the camera. Our demonstration of optical matrix computation can be developed for more sophisticated applications, such as neural network computation at the speed of light, which involves larger-sized matrices.

Programmable metasurface

Fig. 1 illustrates the scheme for optical matrix computation using a metalens array. A Spatial Light Modulator (SLM) is used to selectively illuminate the area on the metalens array using phase gradient and encodes the input vector as different phase profiles. Then, the metalens array transforms the input vector with the transform matrix, and the resulting vector can be obtained from the far-field interference pattern using a pattern recognition method.

Programmable operations can be achieved by choosing which lenses to excite with corresponding the input amplitudes and phases. For example, we have designed a metalens array that by exciting the 2-by-2 upper left lenses, we can get a Grover-search operation. On the other hand, by exciting the 2-by-2 bottom left lenses, we can get a 4-bit FT operation.

Our metasurface design is composed of a 3-by-3 lens array which acts as 9 different input ports. Each metalens can deflect the beam to 9 output ports (3-by-3 spots in the far field) with designed amplitude and phase. Therefore, our system is a 9-by-9 programmable matrix transformation via setting the entries of the transform matrix T. Eq. (1) gives the complex profile of our metasurface design.

$$E_i(x,y) = \sum_j T_i^j \exp\left[ik_x^j\left(i\left(x-x_i\right) + ik_y^j\left(y-y_i\right)\right)\right] \exp\left[i\,k_0\sqrt{\left(x-x_i\right)^2+\left(y-y_i\right)^2+f^2}\right] \quad \textbf{(1)}$$

Here, i denotes input lens index and j denotes the output port index. The origin for each lens is given by the coordinate (x_i, y_i), and the target deflection angle or far-field output port coordinate is related by $\left(k_x^j, k_y^j\right)$. Additionally, we also added a focusing profile with a focal length f to facilitate the limited numerical aperture of the objective lenses. The transform matrix T, which encodes both Grover-search and FT operations at once, is given by Eq. (2).

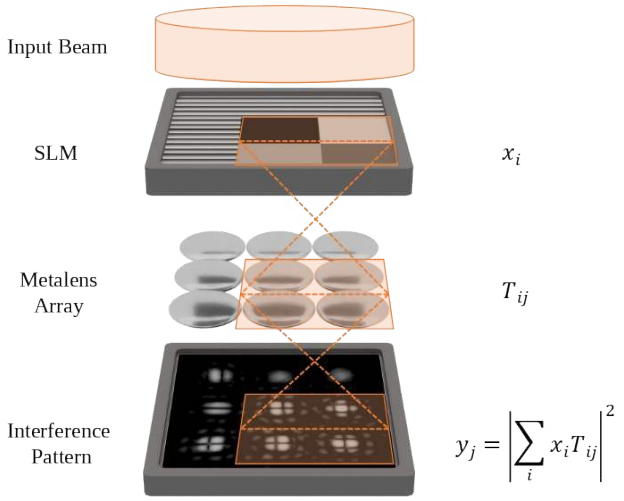


Figure 1. Schematic for optical matrix computation using metalens array for 4-bit Fourier transform computation.

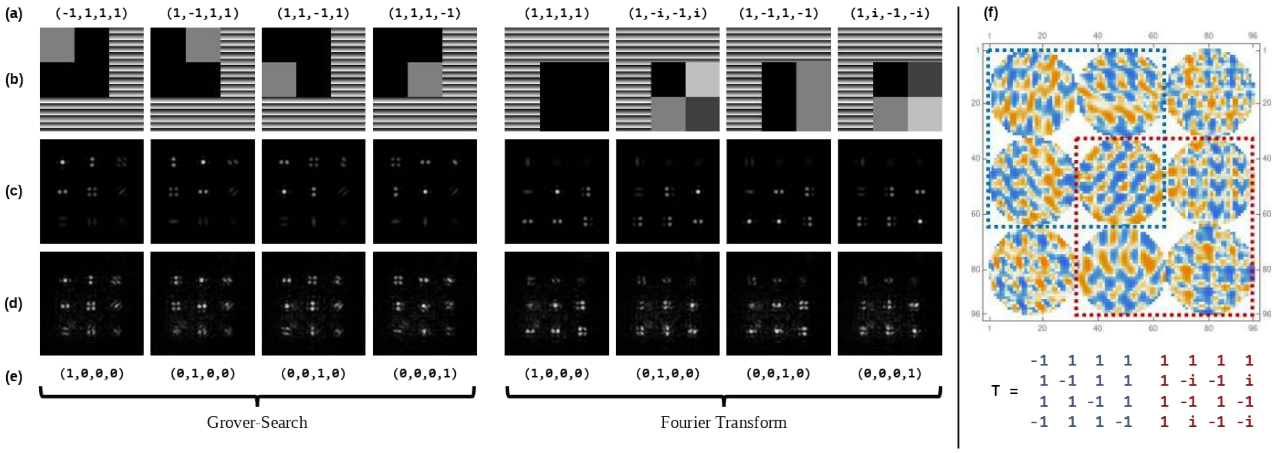


Figure 2. Experimental result for optical matrix computation using a programmable metalens array. (a) Input vector; (b) encoded SLM phase profile; (c) simulated far-field interference pattern; (d) experimental result; (e) normalized output vector (f) 96x96 unit cells metasurface design and transformation submatrices (blue: Grover-search, red: Fourier transform).

$$T = \begin{pmatrix} -1 & 1 & 1 & 1 & 1 & 1 & 0 & 0 & 0 \\ 1 & -1 & 1 & 1 & 1 & 0 & 1 & 0 & 0 \\ 1 & 1 & -1 & 1 & 0 & 0 & 0 & 0 & 1 \\ 1 & 1 & 1 & -1 & 1 & 0 & 0 & 1 & 0 \\ 1 & 1 & 0 & 1 & -1 & -1 & -1 & -1 & -1 \\ 1 & 0 & 0 & 0 & -1 & -i & 1 & 1 & i \\ 0 & 1 & 0 & 0 & -1 & 1 & -1 & -1 & 1 \\ 0 & 0 & 0 & 1 & -1 & 1 & -1 & -1 & 1 \\ 0 & 0 & 1 & 0 & -1 & i & 1 & 1 & -i \end{pmatrix} \quad (2)$$

The blue entries indicate the relevant submatrix for the Grover-search matrix, whereas the red entries indicate the submatrix for Fourier transform.

Experimental results

Fig. 2 shows the simulated and experimental result for different input vectors. Each column represents different input vector bases displayed by the SLM. After the transformation, the expected normalized output vector is either 1 or 0, corresponding to constructive or destructive interference at the center of each far-field spot. Constructive interference is represented by a single spot (bright center), while destructive interference is represented by multiple spots (dark center). In our experiment, we use a Single Photon Avalanche Diode (SPAD) camera to capture the interference patterns and analyze them to determine the output vector.

As an example, the first column in Fig. 2 is to illustrate one Grover-search operation, which is to find which variable in the input vector having an extra pi phase. In this case, we can focus only on the top-left part of the metasurface. We first encode the input vector $x = (-1,1,1,1)$ by taking its argument as the SLM phase profile. Then, we observe the patterns on the far field as: one constructive interference, followed by three destructive interference patterns; which yields the output vector $y = (1,0,0,0)$. For other input beams, we can determine the output vector by measuring the intensity at the center of each spot or by analyzing the interference pattern.

Conclusion

In conclusion, we experimentally demonstrate an optical matrix computation scheme using SLM and geometric-phase metalens array. The result can then be obtained by analyzing the interference pattern observed on the camera. Lastly, this scheme introduces the powerful capability of metasurface to the optical computational field. With a larger and more efficient metasurface, scaling up the size of the vectors will be possible, and further extension of this scheme can be applied for optical quantum computation and optical neural network.

Acknowledgements

The work is supported by the Hong Kong RGC (16304020, 16306521, C6013-18G, AoEP-502/20) and by Croucher Foundation (CAS20SC01).

[1] M. Y. Shalaginov et al., "Reconfigurable all-dielectric metalens with diffraction-limited performance," Nat Commun, vol. 12, no. 1, p. 1225, Feb. 2021, doi: 10.1038/s41467-021-21440-9.

[2] A. H. Dorrah and F. Capasso, "Tunable structured light with flat optics," Science, vol. 376, no. 6591, p. eabi6860, Apr. 2022, doi: 10.1126/science.abi6860.

[3] Z.-B. Fan et al., "A broadband achromatic metalens array for integral imaging in the visible," Light Sci Appl, vol. 8, no. 1, p. 67, Jul. 2019, doi: 10.1038/s41377-019-0178-2.

[4] R. C. Devlin, M. Khorasaninejad, W. T. Chen, J. Oh, and F. Capasso, "Broadband high-efficiency dielectric metasurfaces for the visible spectrum," Proc. Natl. Acad. Sci. U.S.A., vol. 113, no. 38, pp. 10473–10478, Sep. 2016, doi: 10.1073/pnas.1611740113.

[5] L. Li et al., "Metalens-array–based high-dimensional and multiphoton quantum source," Science, vol. 368, no. 6498, pp. 1487–1490, Jun. 2020, doi: 10.1126/science.aba9779.

META 2023, PARIS - FRANCE, JULY 18 – 21, 2023

Switching of Phase-Change Optical Metasurfaces via Remote Thermal Sources

G. Braid[1], C. Ruíz de Galarreta[1,2], A. Comley[3], J. Bertolotti[1], C. D. Wright[1*]

[1]Centre for Metamaterial Research and Innovation, University of Exeter, Exeter EX4 4QF, UK
[2]Instituto de Óptica, IO-CSIC, Madrid 28006, Spain
[3]AWE Aldermaston, Reading RG74PR, Berkshire, UK
[*]corresponding author: david.wright@exeter.ac.uk

Abstract: The application space for optical metasurfaces is increased if they are actively controllable. This can be achieved by including a phase-change material, whose optical properties can be changed by thermal stimuli. Such stimuli are often provided by laser excitation of the metasurface, or by embedded micro-heaters within the surface. Some metasurfaces may however not be suited to such approaches. In this work we explore the provision of suitable stimuli using a thermal source that is physically remote from the metasurface.

Metasurfaces offer precise control of optical wavefronts, which has led to the development of compact optical devices for applications such as perfect absorbers, polarisers, beam deflectors, holograms, and lenses, to name but a few [1,2]. The range of possible applications is further expanded if the metasurface can be actively controlled. Many methods have been explored for achieving this control, and one of the most promising is the incorporation of a chalcogenide phase-change material (PCM) layer in the design [1].

Chalcogenide PCMs have two solid phases—amorphous and crystalline—with substantially different physical properties. Both phases are stable at room temperature, and each can be switched to the other by a thermal stimulus [1]. The switching of PCM regions embedded within optical metasurfaces is not, however, always straightforward. For certain designs, direct laser excitation of the metasurface may not be feasible (e.g., in cases where the PCM layer/region is embedded within other materials that absorb strongly at the laser excitation wavelength). Similarly, the integration of micro-heaters into some metasurface designs can pose a significant engineering challenge. Here, therefore, we explore an alternative approach, that of switching PCM-based metasurfaces via a thermal source that is physically remote (separated) from the surface itself.

Han et al. [3] recently demonstrated fan-shaped thermal metamaterial-type heat guide structures that can provide near-uniform heating over extended regions by directed conduction of heat from a remote source. Although Han's designs were on the macroscale (sizes in the cm range), the approach is readily shrunk down to the microscale, as shown in Figure 1. Indeed, similar control and transfer of heat from a remote source can be obtained using considerably simpler structures, ones potentially more suited to use with typical PCM metasurfaces. In Figure 2, for example, we show a design in which the heat sources are linked to a central metasurface-containing region by four straight metal (here tungsten) arms. Upon exciting the end of one or more of these arms using a laser pulse, heat is conducted to the metasurface and, with appropriate design, sufficiently high temperatures and cooling rates can be obtained for successful crystallisation and amorphisation of commonly used PCMs.

In summary, in cases where direct heating of a PCM metasurface is not straightforward, we have shown that switching of the PCM layer/region can be achieved by heat conducted from thermal sources placed remotely from the metasurface itself. Various devices based on this concept of the switching of PCM metasurfaces via remote thermal sources are in the process of being fabricated and experimentally characterised.

(a) (b)

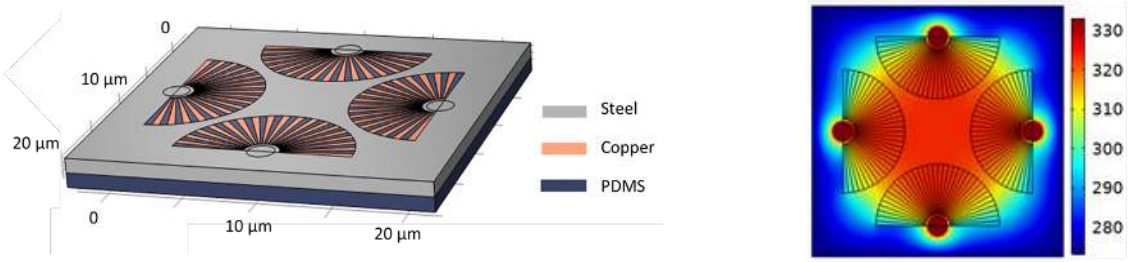


Fig. 1. (a) The fan-type thermal metasurface design from Han et al. [3] shrunk down to the microscale and providing uniform heating from remote heat sources (located in the circle at the base of each fan). (b) Finite-element (Comsol) simulated heat distribution for the structure in (a) with the heat sources assumed at a constant temperature of 333 K.

(a) (b)

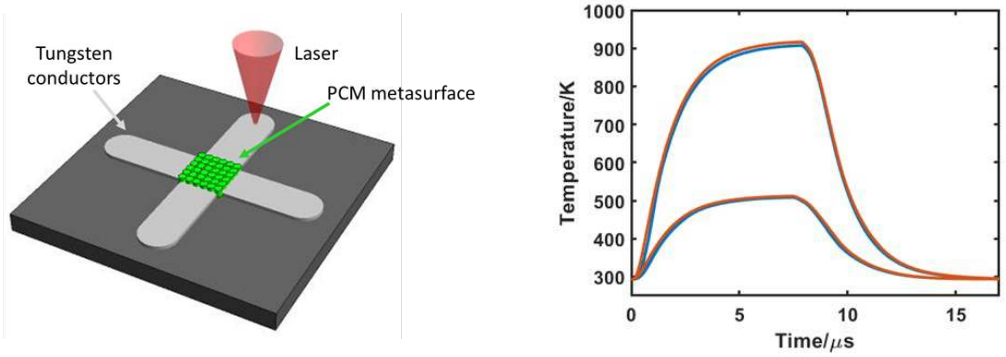


Fig. 2. (a) Schematic of a simplified structure for switching of a PCM metasurface via remote thermal stimulation. Lasers incident at the ends of the arms supply the heat needed to switch PCM. (b) Finite element simulation (Comsol) of the heating of a $Ge_2Sb_2Se_4Te_1$ (GSST) PCM metasurface (of the type used in [2]) via remote thermal excitation using a 400 nm laser. Temperatures suited to both fast crystallisation and to melting can be reached with practicable values of laser power. Moreover, cooling post-melting is relatively fast, implying successful amorphisation is achievable (for GSST) with the remote heating approach. Red and blue lines show maximum and minimum temperatures in the GSST regions of the metasurface (their closeness indicating uniformity of heating achieved).

Acknowledgements

Funding is acknowledged from EPSRC (EP/L015331/1) and AWE Ltd.

© British Crown Owned Copyright 2022/AWE applies to this article.

References

1. Ruiz de Galarreta C et al., “Tunable optical metasurfaces enabled by chalcogenide phase-change materials: from the visible to the THz”, Journal of Optics, Vol. 22, No. 11, 114001, 2020
2. Braid, G. et al., “Optical and Thermal Design and Analysis of Phase-Change Metalenses for Active Numerical Aperture Control,” Nanomaterials, Vol. 12, No. 15, 2689, 2022.
3. Han, T. et al., “Manipulating Steady Heat Conduction by Sensu-shaped Thermal Metamaterials,” Sci Rep, Vol. 34, 10242, 2015.

META 2023, PARIS - FRANCE, JULY 18 – 21, 2023

Metasurface-enabled molecular spectroscopy and machine learning resolve lipid membrane photoswitching

M. Barkey[1,§], R. Büchner[1,2,§], A. Wester[1], S. Pritzl[3,4], M. Makarenko[5], Q. Wang[5], T. Weber[1], S. A. Maier[6,7,1], A. Fratalocchi[5], T. Lohmüller[3], and A. Tittl[1,*]

[§]equal contribution

[1] Chair in Hybrid Nanosystems, Nanoinstitute Munich, Faculty of Physics, Ludwig-Maximilians-Universtität München, Königinstraße 10, 80539 München, Germany
[2] Nanophotonic Systems Laboratory, ETH Zürich, 8092 Zürich, Switzerland
[3] Chair for Photonics and Optoelectronics, Nanoinstitute Munich, Faculty of Physics, Ludwig-Maximilians-Universtität München, Königinstraße 10, 80539 München, Germany
[4] Department of Physics and Debye Institute for Nanomaterials Science, Utrecht University, Princetonplein 1, 3584 CC Utrecht, The Netherlands
[5] PRIMALIGHT, Faculty of Electrical Engineering, King Abdullah University of Science and Technology (KAUST), Thuwal 23955-6900, Saudi Arabia
[6] School of Physics and Astronomy, Monash University, Wellington Rd, Clayton VIC 3800, Australia
[7] The Blackett Laboratory, Department of Physics, Imperial College London, London, SW7 2AZ, United Kingdom

[*]corresponding author: andreas.tittl@physik.uni-muenchen.de

Abstract: We present an integrated platform for ultrasensitive in-situ biospectroscopy by combining all-dielectric pixelated metasurfaces and machine learning. Specifically designed metasurfaces with advanced sampling techniques probe the real-time dynamics of lipid membrane photoswitching in an aqueous environment in the mid-infrared, overcoming sensitivity limitations and strong water absorption associated with conventional infrared spectroscopy. Our platform combines metasurfaces, optofluidics, and artificial intelligence (AI) to extend the capabilities of dielectric metasurfaces for analyzing complex biological entities.

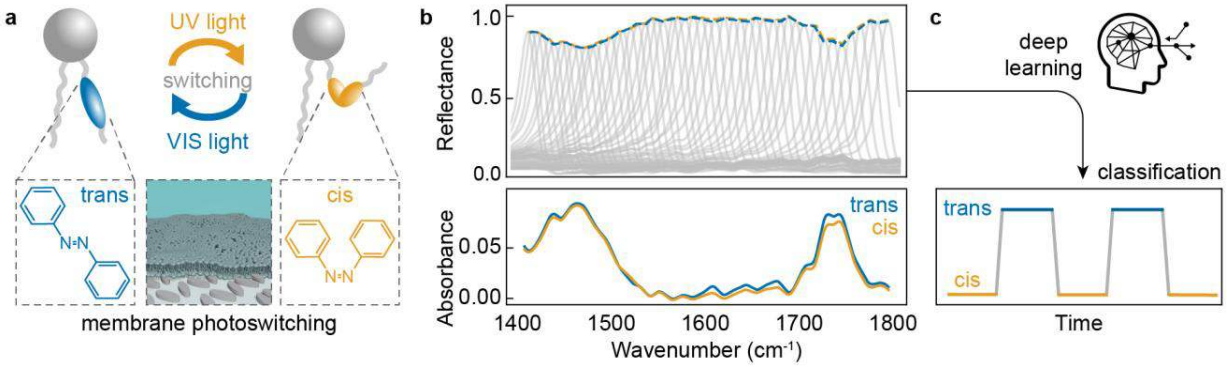


Figure 1. Metasurface-enabled biospectroscopy of photoswitachble lipid membranes aided by AI. **a,** Sketch demonstrating the photoinduced change of the azobenzene group from cis to trans conformation under UV or visible light. The lipid bilayer on the metasurface highlights the conformal coating. **b,** Reflectance spectra of a pixelated metasurface coated with lipid membranes in the cis and trans states (top). Retrieved absorbance spectra of the lipid membranes (bottom). **c,** The machine learning model classified the state of the membrane.

Surface-enhanced infrared absorption spectroscopy (SEIRA) is an important method for studying the molecular composition of analytes, overcoming the challenges due to the size difference between mid-infrared (mid-IR) wavelengths and nanometer-scale molecules [1]. While previous SEIRA implementations based on plasmonic resonators can suffer from Ohmic losses, emerging directions involve the use of all-dielectric nanostructures that support bound states in the continuum (BICs) to enhance sensitivity. BIC-driven metasurfaces with ultra-sharp high-Q resonances enable precise control over resonance position, line width, and magnitude of near-field enhancement [2]. By implementing such metasurface approaches in a pixelated arrangement for molecular barcoding [3], an unambiguous mapping between spectral information and spatial information can be created.

This technique allows the imaging-based readout of biomolecular fingerprints, which could aid in the study of the photoisomerization dynamics and interactions between synthetic photoswitchable lipids, or photolipids, and other membrane components in a supported lipid bilayer (SLB) setting without the requirement of an additional spectroscopic label. Photolipids, which contain an azobenzene unit in the lipid tail, allow the reversible control of membrane properties, such as bilayer fusion [4]. Machine learning models have demonstrated great potential in addressing the complexity of data analysis in metasurface-enhanced bioanalytical studies [5].

Our integrated platform combines metasurfaces, optofluidics, and AI for the in-situ real-time investigation of the composition and switching dynamics of photoswitchable lipid membranes (**Figure 1**). We engineered all-dielectric metasurfaces that support high-Q BIC resonances in an aqueous environment in the mid-infrared to enhance the capabilities of studying the minute spectroscopic absorption variations between the two photolipid membrane states, trans and cis, such as around 1735 cm^{-1}. Furthermore, machine learning was implemented for rapid and reliable data analysis and optimization of the metasurface design.

By adapting the metasurface based on the AI model results, the integrated platform can be tailored to other molecular analytes, allowing for the study of more complex molecular systems and processes in biology and environmental monitoring.

References

1. Neubrech, F., Huck, C., Weber, K., et al. “Surface-Enhanced Infrared Spectroscopy Using Resonant Nanoantennas,” Chem. Rev., 117 (7), 5110–5145, 2017.
2. Koshelev, K., Favraud, G. and Bogdanov, A., et al. “Nonradiating Photonics with Resonant Dielectric Nanostructures,” Nanophotonics, 8 (5), 725–745, 2019.
3. Tittl A, A. Leitis and H. Altug, et al. “Imaging-based molecular barcoding with pixelated dielectric metasurfaces,” Science, Vol. 360, No. 6393, 1105-1109, 2018.
4. Pritzl, S. D., Morstein, J., Kahler, S. and Konrad, et al. “Postsynthetic Photocontrol of Giant Liposomes via Fusion-Based Photolipid Doping,” Langmuir, 38 (39), 2022.
5. John-Herpin, A., Kavungal, D. and von Mücke, L., et al. ,” Infrared Metasurface Augmented by Deep Learning for Monitoring Dynamics between All Major Classes of Biomolecules,” Advanced Materials 2021, 33 (14), 2006054, 2021.

META 2023, PARIS - FRANCE, JULY 18 – 21, 2023

Tuning optical properties of individual Sb_2S_3 nanostructures

P. Kepič[1,2*], P. Liška[1], B. Idesová[1], F. Ligmajer[1,2], and T. Šikola[1,2]

[1] Institute of Physical Engineering, Faculty of Mechanical Engineering, Brno University of Technology, Czech Republic
[2] Central European Institute of Technology, Brno University of Technology, Czech Republic
[*] corresponding author: peter.kepic@ceitec.vutbr.cz

Abstract: Phase-change materials represent one of the main directions toward tunable nanophotonic devices. Even though a phase-changing antimony trisulfide (Sb_2S_3) has recently received tremendous attention due to its low absorption in the visible and near-infrared spectral region, its crystal phase transition is still not fully understood, especially at the nanoscale. Here, by observing the tuning of the optical properties of individual Sb_2S_3 nanostructures, we want to explain the gradual tunning of the future Sb_2S_3 metasurfaces.

Antimony trisulfide (Sb_2S_3) is a non-volatile phase-change material that goes through an amorphous–crystalline transition (~250°C) that can be achieved by simple heating and crystalline–amorphous transition (~600°C) that is based on a very fast (~10°C/ns) melt-quench process achieved by high-energy pulses [1]. Its most significant advantage lies in its lowest absorption and relatively large refractive index modulation in the visible and near-infrared spectral region. While several articles report tunable (multi-function) metasurfaces by continuously changing the phase of this or other phase-change materials [2, 3], those that describe if the tuning takes place at the nanostructure or is an average behavior of an array are missing. Observation of the transition in single and arrayed Sb_2S_3 nanostructures would help us better understand the phase transition process and its influence on the optical properties at the nanoscale.

First, we deposited a 160 nm Sb_2S_3 thin film on a fused silica substrate using a pulsed laser deposition. Before the investigation and crystallization, the film was coated by approx. 15 nm Al_2O_3 protective layer, using atomic layer deposition to prevent contamination and sulfur loss. The film was gradually crystallized on a 250°C hot plate and investigated in 30 s steps from amorphous to crystalline phase using microscopy images and spectroscopic ellipsometry. We observed a clear gradual crystallization during six crystallization steps (in 180s; see Figure 1a), where already after 60 s, more than 50% of the film was crystallized (Figure 1b). From the spectroscopic ellipsometry, we obtained the refractive index and absorption coefficient of each of these intermediate states (Figure 1c). Note that effect of individual anisotropic crystals is considered to be averaged. For the refractive index at 633 nm wavelength, we obtained the same S-shaped behavior as in the crystallized area graph (Figure 1b), in which curvature is most pronounced around 60 s of crystallization.

Using these gradually crystallized refractive indices, we simulated single scattering and absorption cross-section of Sb_2S_3 nanocylinders using FDTD simulation. In Figure 1d, we can see that the Mie resonance peak of the nanocylinder with a 200 nm diameter is transferred from one to the other when the film is continuously crystallized. However, this is just a simulation, and we would like to know if we can measure such gradual crystallization in individual Sb_2S_3 nanostructures. We fabricated single Sb_2S_3 nanostructures and nanostructure arrays in the same deposition process (160 nm film and 17 nm protective layer) to verify this hypothesis. We are about to crystallize and measure these nanocylinders using dark-field reflection spectroscopy. Whether the result is positive or negative, it will give a better inside into the crystallization process of phase-change tunable metasurfaces and ultimately improve such devices.

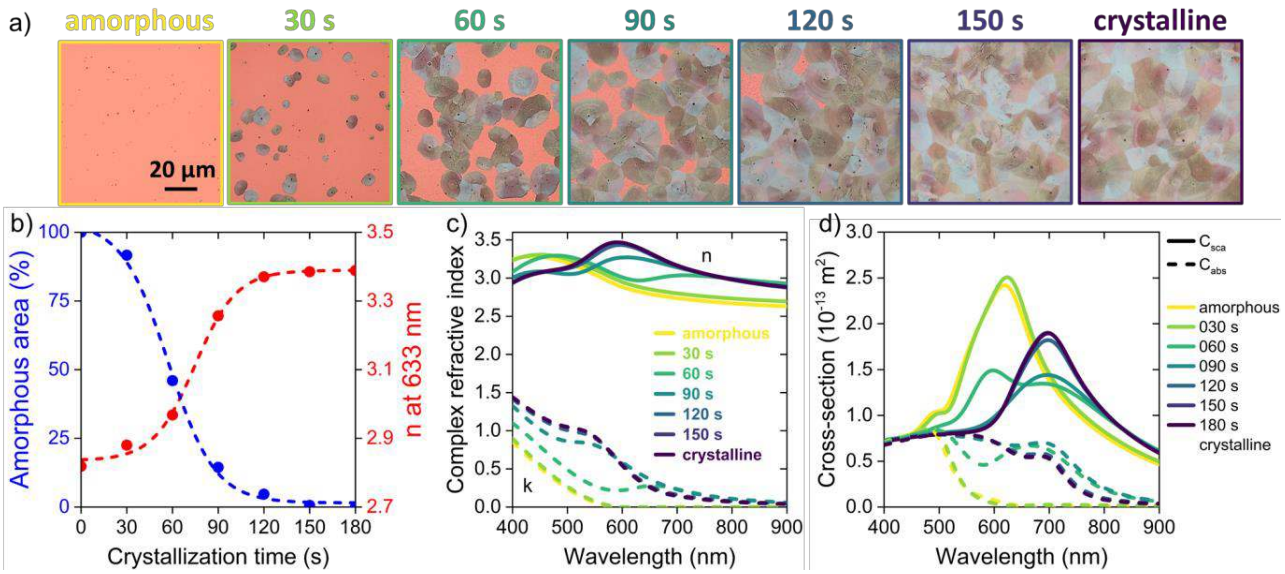


Figure 1. a) Microscopy images of Sb_2S_3 films gradually crystallized on 250°C hot plate from amorphous to crystalline phase by 30 s steps. b) Amorphous area and refractive index at 633 nm as a function of crystallization time of films from (a). c) Refractive index and absorption coefficient of Sb_2S_3 films in (a). d) Scattering and absorption cross-sections of the 160 nm Sb_2S_3 nanocylinder with 200 nm diameter on the fused silica substrate using refractive indices in (c).

This work is supported by the Grant Agency of the Czech Republic (21-29468S). The corresponding author is also supported by the Brno Ph.D. talent and Thermo Fisher Scientific scholarships. We also acknowledge CzechNanoLab Research Infrastructure supported by MEYS CR (LM2018110).

References

1. Lu, L., Z. Dong, R. J. Hong, H. Wang, S. D. Rezaei, Y. Wang, H. S. Leong, J. K. W. Yang and R. E. Simpson, "Reversible Tuning of Mie Resonances in the Visible Spectrum," ACS Nano, Vol. 15, No. 12, 19722-19732, 2021.
2. Leitis, A., A. Heßler, S. Wahl, M. Wuttig, T. Taubner, A. Tittl and H. Altug, "All-Dielectric Programmable Huygens' Metasurfaces," Adv. Fun. Mat., 30, 19, p. 1910259, 2020.
3. Kepič, P., F. Ligmajer, M. Hrtoň, H. Ren, L. S. Menezes, S. A. Maier and T. Šikola, "Optically tunable Mie resonance VO2 nanoantennas for metasurfaces in the visible," ACS Photonics, Vol. 8, No. 4, 1048–1057, 2021.

META 2023, PARIS - FRANCE, JULY 18 – 21, 2023

Efficient broadband mid-infrared linear-to-circular polarization conversion using a nanorod-based metasurface

H. Zou*, and G. R. Nash

Natural Sciences, University of Exeter, United Kingdom
*corresponding author: hz358@exeter.ac.uk

Abstract: In this work a nanorod-based metasurface is experimentally demonstrated to exhibit broadband linear-to-circular polarization conversion in the mid-infrared region of the spectrum. Measurement of the Stokes parameters confirms reflected light is circular polarization with average axial ratio of 0.75 across broadband from 3.5μm to 7.5μm. Such metasurfaces could not only replace conventional quarter wave plates, but also be used for circular dichroism spectroscopy allowing the characterization of important chiral molecules.

Circular polarization light is particularly useful for infrared circular dichroism spectroscopy. Under illumination with circularly polarized light, chiral molecules absorb different amounts dependent on their handedness, and important information about the structure of chiral biomolecules, such as proteins, can be obtained without labeling the analytes. This is particularly useful if this effect can be exploited in the infrared region of the spectrum, where many important biomolecules have strong vibrational fingerprints [1]. However, traditional quarter wave plate have fundamental problems including bulky size, single operating wavelength while metasurfaces have been investigated as a potential means of replacing bulk optic components due to their subwavelength thickness, and flexibly tailored operation wavelength. In addition, the strong near-fields associated with metasurfaces could also ultimately be exploited for high sensitivity biosensing.

Building on the work on metasurfaces for the terahertz region [2], a metasurface consisting of an array of nanorod resonators for efficient linear-to-circular convertor in the mid-infrared spectrum in reflection mode was investigated in this work [3]. Figure 1 (a) shows the schematic unit cell of metasurface with geometric parameters and a scanning electron microscope (SEM) photo of fabricated sample.

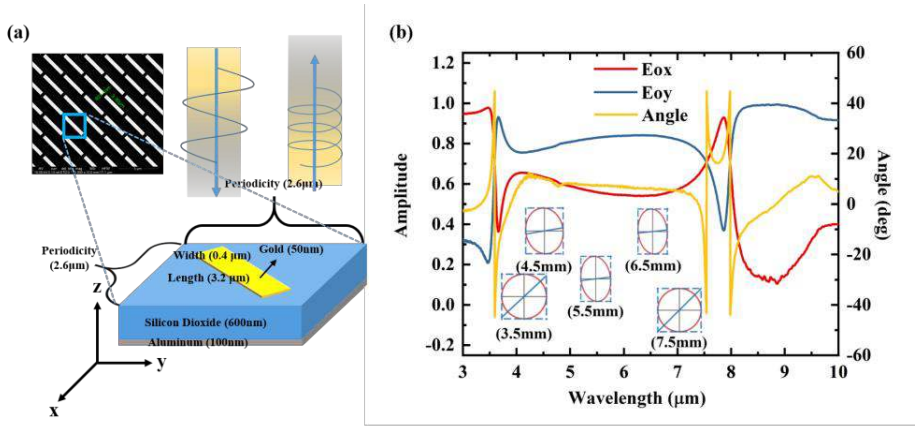


Fig. 1. (a) The schematic of one unit cell of nanorod-based metasurface. The device is placed on the x-y plane and light travels along z direction. Insert shows the SEM photo of fabricated sample. (b) Spectrum of ellipse parameters Eox Eoy and Angle of reflected beam. Inserts are polarization states of the beam at corresponding wavelength.

Samples were fabricated using electron beam lithography and characterized using a Fourier transform infrared (FTIR) spectrometer. The light source is filtered by a wire grid polarizer allowing only linearly polarized light to illuminate on samples. Reflected signal from the sample is collected by a liquid nitrogen cooled HgCdTe detector with a 2–12μm response at room temperature under ambient conditions. Ellipse parameters i.e. amplitude Eox, Eoy and Angle enabling to define the polarization of reflected beam can be calculated based on measured four Stokes parameters [4]. The calculated ellipse parameters as a function of wavelength is shown in Figure 1 (b). At resonances of 3.5μm and 7.5μm as indicated in inserts, the reflected beam is circular polarization with axial ratio of 1. The slope of Eox, Eoy and Angle show relatively flat features between 3.5μm and 7.5μm indicating that the polarization state keeps stable as elliptical with the evidence that the average axial ratio is 0.75. The insert ellipses show the polarization states are elliptical at 4.5μm, 5.5μm and 6.5μm, respectively. In conclusion, the rod-shaped metasurface features broadband linear-to-circular polarization conversion from 3.5-7.5μm. Compared with conventional bulky quarter wave plates, which only provide polarization conversion at a specific wavelength, the metasurface provides a working bandwidth of ~4μm, but with subwavelength thickness (~λ/4). Such metasurfaces could potentially be exploited for circular dichroism spectroscopy to characterize chiral molecules such as proteins in the mid-infrared region.

Acknowledgement We gratefully acknowledge the financial support of the China Scholarship Council, the University of Exeter and the EPSRC Prosperity Partnership "The Tailored Electromagnetic and Materials Accelerator" (Grant No. EP/R004781/1), which is a collaboration with QinetiQ Ltd.

References

[1] S. M. Kelly, T. J. Jess, and N. C. Price, "How to study proteins by circular dichroism," *Biochim. Biophys. Acta - Proteins Proteomics*, vol. 1751, no. 2, pp. 119–139, 2005.

[2] C. C. Chang, Z. Zhao, D. Li, A. J. Taylor, S. Fan, and H. T. Chen, "Broadband Linear-to-Circular Polarization Conversion Enabled by Birefringent Off-Resonance Reflective Metasurfaces," *Phys. Rev. Lett.*, vol. 123, no. 23, p. 237401, Dec. 2019.

[3] H. Zou and G. R. Nash, "Efficient mid-infrared linear-to-circular polarization conversion using a nanorod-based metasurface," *Opt. Mater. Express*, vol. 12, no. 12, p. 4565, 2022.

[4] B. Schaefer, E. Collett, R. Smyth, D. Barrett, and B. Fraher, "Measuring the Stokes polarization parameters," *Am. J. Phys.*, vol. 75, no. 2, pp. 163–168, 2007.

META 2023, PARIS - FRANCE, JULY 18 – 21, 2023

Complete linear control based on universal metasurfaces and their applications

Joonkyo Jung[1], Taeyong Chang[1], Sang-Hyeon Nam[1], Hyeonhee Kim[1], Jong Uk Kim[1], Nayoung Kim[1], Suwan Jeon[1], Minsung Heo[1], and Jonghwa Shin[1,*]

[1]Department of Materials Science and Engineering, KAIST, Daejeon, 34141, Republic of Korea
[*]corresponding author: qubit@kaist.ac.kr

Abstract: By virtue of their high degrees of freedom in manipulating optical properties of an incident light such as amplitude, phase, and polarization, dielectric metasurfaces have attracted a lot of attraction from academia and industry. However, they still suffer from the lack of complete controllability of amplitude, phase, and polarization. Here, we have theoretically, numerically and experimentally proven that the complete linear control of those properties can be possible by using bi-layer dielectric metasurfaces, which we named universal metasurfaces.

During the last decade, metasurfaces comprised of arrays of nanostructures with subwavelength scales have attracted a lot of interest from both academia and industry because of their unnatural capability of controlling an incident wave. In particular, since dielectric metasurfaces have the advantage of higher transmission compared to metallic counterparts, and full 2π phase coverage over two different linear polarization states, many research groups studied dielectric metasurfaces for a variety of applications such as optical imaging, hologram, quantum photonics, and so on. However, the known metasurface technique still has limitations in the range of controllability and the complete control of amplitude, phase, and polarization all at once has not been demonstrated yet. In this paper, we proved that bi-layer dielectric metasurfaces, which we named universal metasurfaces, theoretically suffice to control the amplitude, phase, and polarization of the incident wave based on the Jones matrix analysis. To support this, we have conducted numerical simulations and experiments.

To begin with, we approached the extended controllability of universal metasurfaces using the analysis based on the Jones matrix, with which a single layer of dielectric metasurface can be approximated as a unitary symmetric matrix, U_S where U_S is a unitary symmetric matrix. By stacking two layers, a bi-layer structure is created and the Jones matrix at each position can be given as a unitary matrix, denoted as $U=U_{S,A}U_{S,B}$ where U is a unitary matrix and the subscript A and B represent bottom and top layers. In addition, based on the singular value decomposition, any arbitrary matrix can be decomposed into the sum of two unitary matrices, $A=1/2(U_1+U_2)$ where A is an arbitrary matrix, and subscripts 1 and 2 represent the position. To physically realize this matrix operation, we used spatial homogenization of two types of bilayer unit cell structures. The details of the structure are depicted in Figure 1(a). We have confirmed numerically that this suggested structure can achieve any Jones matrix as shown in Figure 1(b). Using the arbitrary Jones matrices that can be supported by universal metasurfaces, we have created novel hologram applications that surpass existing functionalities. As a representative example, two independent vector holographic images are presented in Figure 2, where a pseudo-color space is utilized to visually display complex polarization states.

In summary, we have established the theoretical, numerical, and experimental validity of universal metasurfaces. We hope that the exceptional controllability provided by our universal metasurfaces will lead to novel applications in many other research fields.

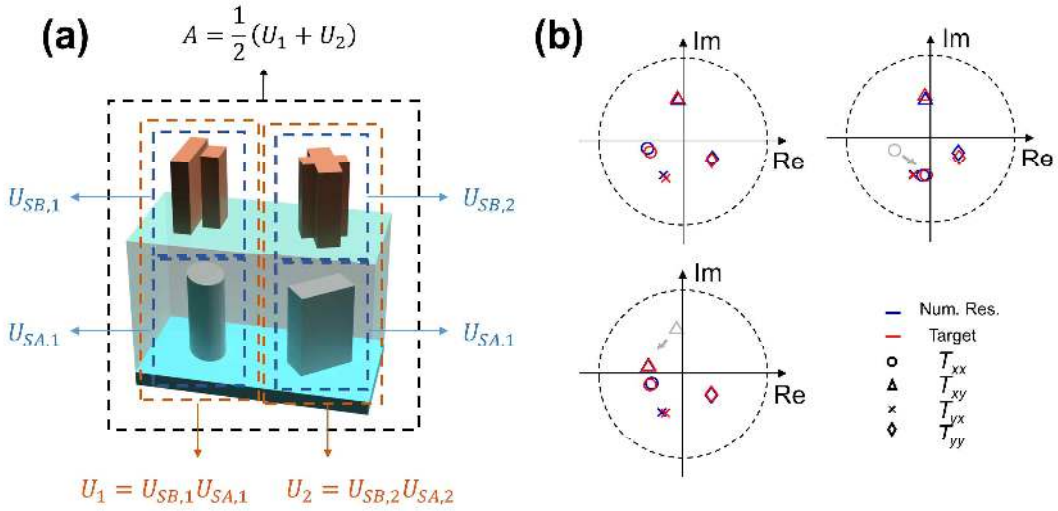


Figure 1. Universal metasurfaces. (a) Schematic illustration of universal metasurfaces. U, US, and A are unitary, unitary symmetric, and arbitrary matrices. The subscripts A and B represent the bottom and top layers. The subscript 1 and 2 represent the position. (b) Numerical verification of arbitrary Jones matrices using the finite-difference time-domain simulations.

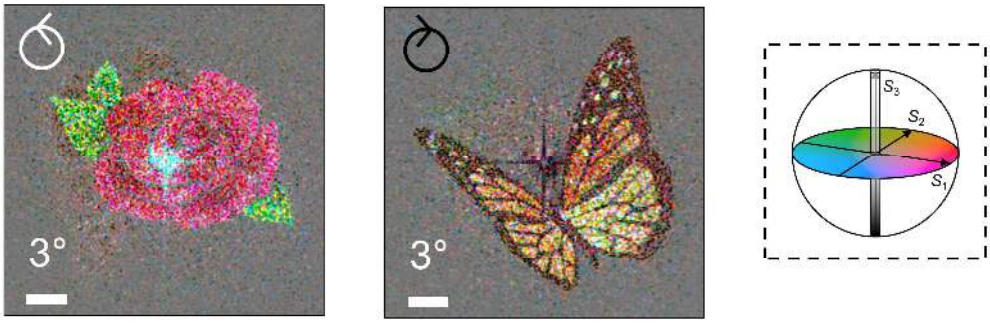


Figure 2. Polarization-multiplexed vector hologram examples. The right (left) panel shows the measured vector hologram where polarization states are inhomogeneous over the space; The right(left) panel is the result when the input polarization state is the right(left) circularly polarized state. The dashed box represents the mapping of Stokes parameter space into the pseudo-color space. The conversion relation is given as {L*, a*, b*} = {50(S_3+1), 100S_1, 100S_2}.

References

1. A. Arbabi, et al., "Dielectric metasurfaces for complete control of phase and polarization with subwavelength spatial resolution and high transmission", *Nat. Nanotechnol.*, **10**, 937-943 (2015).
2. J. P. B. Mueller, et al., "Metasurface Polarization Optics: Independent Phase Control of Arbitrary Orthogonal States of Polarization", *Phy. Rev. Lett.*, **118**, 113901 (2017).
3. T. Chang, et al., "Universal Metasurfaces for Complete Linear Control of Coherent Light Transmission", *Adv. Mater.*, **34**, 2204085 (2022).

Miniaturized Metamaterial Absorber Using Lossy Effective Dielectric-Medium and Resistive Metasurface

Jyoti Yadav [a, *], Mondeep Saikia [b], Kumar Vaibhav Srivastava [b], J. Ramkumar [c]
[a] IIT Kanpur, Material Science Program, Kanpur, India, 208016
[b] IIT Kanpur, Department of Electrical Engineering, Kanpur, India, 208016
[c] IIT Kanpur, Department of Mechanical Engineering, Kanpur, India, 208016

* Corresponding author email address: jyoti@iitk.ac.in

Abstract: Resistive frequency selective surface (FSS) based microwave absorbers have been widely reported but at lower frequency bands, reducing their unit cell size remains a challenge. In this paper, a resistive ink-based miniaturized passive metamaterial absorber is proposed for S- Band with stable absorption performance up to high oblique incidence angles. The periodicity of the unit cell is approximately λ/26 and the overall thickness is λ/20. The miniaturization of unit cell can be explained using effective medium theory.

The unit cell is based on a lossy cavity, in addition to conventional FSS. To fabricate the final prototype, resistive ink is to be coated on FR4 substrate stripes. The cavity can then be assembled by cutting narrow slits on these stripes and inserting them orthogonally through these slits to form a square shape. Resistive square ring metasurface patterns are printed separately and placed on the top of the cavities. A high absorption response is achieved which is stable up to 50º angle of incidence for both TE and TM mode. Use of spacing between FSS and ground plane reduces the periodicity as well as overall thickness of the absorber. Unlike conventional FSS, the resistive elements are designed on the transverse walls that ultimately results in an open cavity. This cavity-based structure is then merged with a resistive FSS top layer to control the resonance of overall structure. The unit cell diagram and absorption response for various oblique incident angles for TE mode are given in Fig 1.

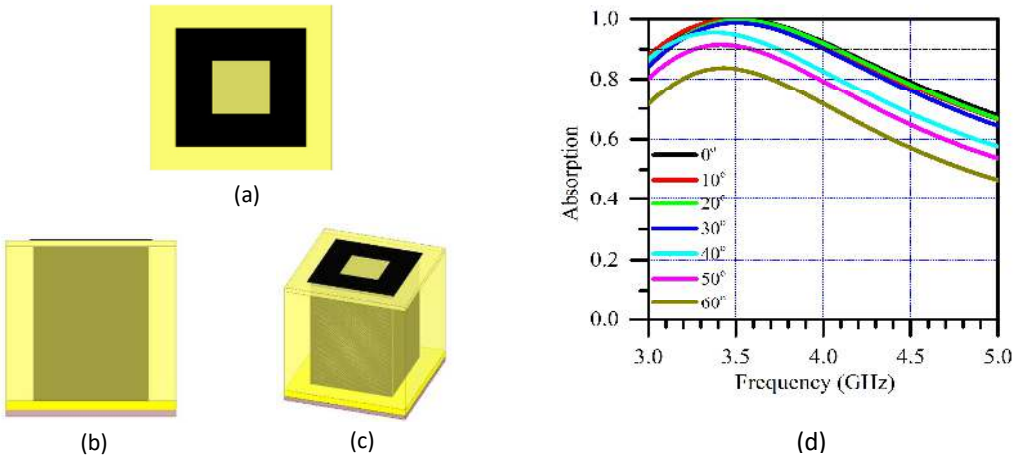


Fig 1: (a) Top view (b) Side view and (c) Perspective view of the miniaturized unit cell of the proposed microwave absorber for S-band and it's (d) Absorption response.

References

[1]] F. Costa, A. Monorchio, and G. Manara, "Analysis and design of ultra-thin electromagnetic absorbers comprising resistively loaded high impedance surfaces," *IEEE Trans. Antennas Propag.*, vol. 58, no. 5, pp. 1551–1558, May 2010.

[2] S. Ghosh, S. Bhattacharyya, D. Chaurasiya, and K. V. Srivastava, "Polarisation-insensitive and wide-angle multi-layer metamaterial absorber with variable bandwidths," *Electron. Lett.*, vol. 51, no. 14, pp. 1050–1052, Jul. 2015.

[3] T. Wei, B. Li, H. Li, L. Zhu and C. -H. Cheng, "Synthesis of 3-D Polarization-Rotating Surface Based on Orthogonally Inserted Parallel-Coupled Slotlines," in *IEEE Transactions on Antennas and Propagation*, vol. 70, no. 12, pp. 11957-11967, Dec. 2022, doi: 10.1109/TAP.2022.3211335.

Metasurface-Based Radome for Wearable Antenna at 24GHz

M. E. de Cos Gómez[1*], A. Flórez Berdasco[1], and F. Las-Heras Andrés[1]

[1] TSC, Electrical Engineering Department. Universidad de Oviedo. Gijón, Spain
[*]corresponding author: medecos@uniovi.es

Abstract: A metasurface-based radome (metaradome) is designed to protect a wearable grid array antenna (GAA) for imaging applications in 24.05GHz-24.25GHz. It provides high transmission and low reflection within the GAA operation frequency band in a wide angular range under oblique incidence. The GAA with metaradome. preserves the GAA operation band and radiation parameters. The overall device' size is 40 x 40 x 3.162 mm^3. The envisioned application is collision avoidance in aid to visually impaired people at medium-long distance.

A radome should protect the antenna with minimal impact on its performance. Ideally it should be electrically invisible, that is, fully transparent and lossless. In practice a radome must ensure high transmission and low reflection and absorption within the antenna operation frequency band. In addition, radiation scattered from the radome may elevate antenna sidelobes, which can lead to reduction in gain and directivity. In recent years it has been proposed to use metasurfaces to be combined with radomes to reduce their negative effects on antenna performance, or even as radomes themselves [1], giving rise to the term metaradome or metadome [2]. In this work, a metasurface-based radome has been designed to be located much closer to the antenna than a radome of the same material and without degrading the performance of the antenna. In this way, the antenna is protected while maintaining a lightweight, compact and fully operational design for the intended application. Figure 1 shows the metasurface unit cell geometry and dimensions on RO3003 dielectric substrate, the simulation set-up using Floquet ports and master-slave boundary conditions and the retrieved transmission and reflection coefficient for both TE and TM polarized incident plane-waves. It can be highlighted that very high transmission and very low reflection is achieved in the band of interest (24.05GHz-24.25GHz), as intended.

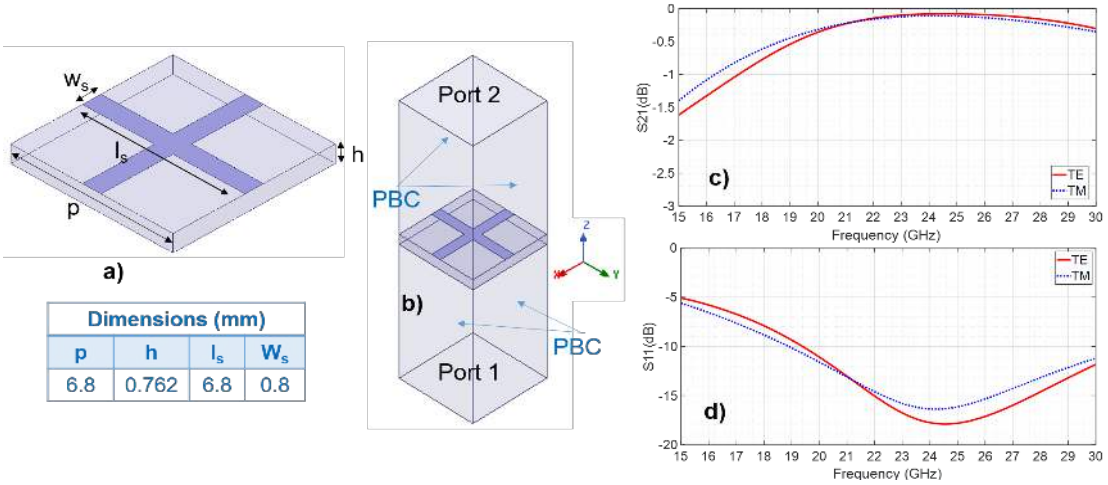


Figure 1. Metaradome: a) Unit cell; b) Simulation set-up; c) Transmission coefficient; d) Reflection coefficient

The angular stability of a metasurface usable as a radome is crucial. The designed metaradome is fully

angularly stable under oblique incident TE and TM polarized plane waves up to θ=45º and highly stable up to θ=50º, considering both transmission and reflection coefficients.

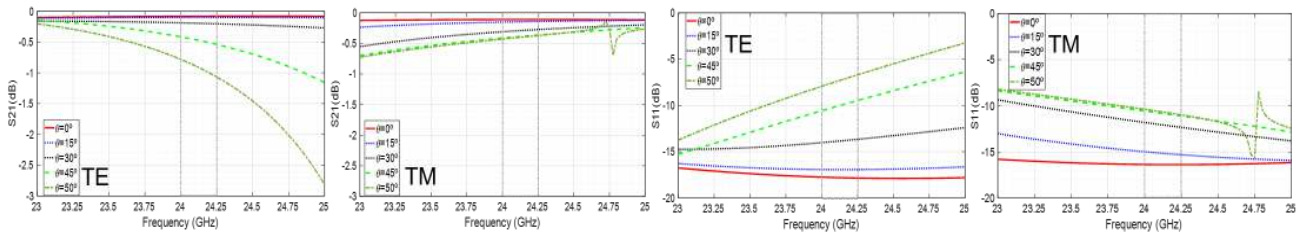
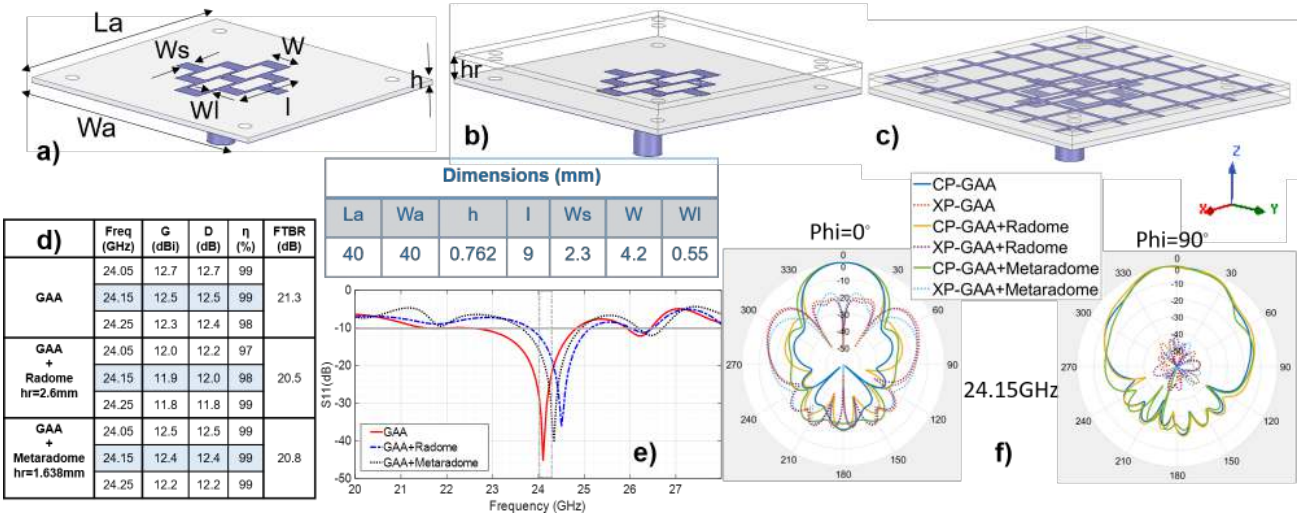


Figure 2. Angular stability of the metaradome for Phi=0º under TE and TM polarized incident plane waves

For the intended application a trade-off solution between-range and coverage area has to be adopted. A suitable Grid Array Antenna (GAA) [3] was designed on RO3003 substrate. In Figure 3 it can be observed that a metaradome can be arranged at closer distance from the GAA than a radome (1.638mm vs 2.6mm) and better preserving the operational properties of the GAA. Thus a protected and compact wearable antenna is achieved.



d)	Freq (GHz)	G (dBi)	D (dB)	η (%)	FTBR (dB)
GAA	24.05	12.7	12.7	99	21.3
	24.15	12.5	12.5	99	
	24.25	12.3	12.4	98	
GAA + Radome hr=2.6mm	24.05	12.0	12.2	97	20.5
	24.15	11.9	12.0	98	
	24.25	11.8	11.8	99	
GAA + Metaradome hr=1.638mm	24.05	12.5	12.5	99	20.8
	24.15	12.4	12.4	99	
	24.25	12.2	12.2	99	

Figure 3. GAA under study: a) GAA; b) GAA+radome; c) GAA+Metaradome; d) Radiation properties; e) Reflection coefficient S11(dB); f) Radiation pattern cuts.

This research was funded by Ministerio de Ciencia, Innovación y universidades of Spanish Government under project META-IMAGER PID-2021-122697OB-100 and by Gobierno del Principado de Asturias under project AYUD-2021-51706.

References

1. He, Y. and Eleftheriades, G. V., "A Thin Double-Mesh Metamaterial Radome for Wide-Angle and Broadband Applications at Millimeter-Wave Frequencies," in IEEE Trans. Antennas Propag, Vol. 68, No. 3, pp. 2176-2185, 2020.
2. Öziş, E., Osipov, A. V. and Eibert, T. F. "Metamaterials for Microwave Radomes and the Concept of a Metaradome: Review of the Literature", IJAP, Hindawi, Vol. 2017, Article ID 1356108, pp.1-13, 2017
3. Lin, Z., Wei, Z.X., Ping, Z.Y., "A microstrip grid array antenna for 24 GHz Doppler sensors". IEEE Asia-Pacific Conf. on Antennas and Propagation (APCAP), pp. 257– 258, 2012.

META 2023, PARIS - FRANCE, JULY 18 – 21, 2023

Active phase control with metasurfaces in the visible by electrochemistry

Junhyung Park[1], Min Gwan Jo[1], and Jonghwa Shin[1*]

[1]Department of Materials Science and Engineering, KAIST, Daejeon, Republic of Korea
[*]corresponding author: qubit@kaist.ac.kr

Abstract: Metasurfaces have been realized large control on properties of light, amplitude, phase, and polarizations with adequate design of meta-atoms. Nevertheless, such control is not yet fully achieved dynamically after fabrication. We show large dynamic change (over 180°) of phase of visible light with a single metasurface, which so far required the use of liquid crystals, based on simple electrochemistry. We believe our approaches will help realize dynamic beam control devices for visible light.

Temporal coupled mode theory, a simple and effective theoretical model for understanding optical scattering properties of resonators, provides viable design strategies for phase control of light with metasurfaces. ITO based active metasurfaces studies demonstrated that one resonator with background mirror can be simplified as one-port single resonance system and a small change of ratio between two resonator parameters, radiational loss and resistive loss, at perfect absorption condition will lead to large phase shift near 180° in the infrared [1]. Also, large resonance frequency changes can lead to large phase change with similar one-port single resonance systems, if the resistive loss is small[2]. In addition, achievable amount of phase change can be further increased over 360° with negligible amplitude change when the number of resonances increases [3]. There have been many papers that suggested and demonstrated large phase control up to 360° in the infrared with active materials. However, most of active materials used in for infrared active metasurfaces cannot be used for visible metasurfaces since their effectiveness becomes much smaller or material loss becomes too large in the visible regime. As a result, large dynamic phase control for visible light are typically done with liquid crystals, which are almost transparent and possess a large change of the refractive index depending on their orientation. Liquid crystals, however, suffer from pixel crosstalks due to coupling between neighboring liquid crystal molecules and have not achieved pixel resolution below 1μm, thus may not be suitable for high numerical aperture or large angle applications [4].

We suggest that by using electrochemistry approaches, large phase change of visible light can be achieved with metasurfaces with sub-micron unit cells. Electrodeposition, coating of metals by voltage appliance in electrolyte, and electrochromic materials, which change color or opacity when voltage and ions are applied, have mostly been used for dynamic color tunable metasurfaces [5], [6]. However, electrodeposition of metals, which have large optical losses at the visible regime, can effectively change resistive and radiational losses of nanoresonators, when it occurs between background channels and resonators. As a result, coupling condition of metausrfaces shifts during electrodeposition of metals and thus large phase shift follows as in ITO based dynamic metasurfaces in the infrared. Our suggested electrodeposition based metasurfaces can have further larger change of ratio between radiational and resistive loss, and thus perfect absorption at target wavelength is not necessary. When we design our metasurfaces to have perfect absorption at wavelength deviated from target wavelength and resonance frequency passing by target wavelength when resistive loss is smaller than radiational loss, our metasurfaces can have phase change larger than 180°, and smaller amplitude change. Secondly, we suggest one port double resonance reflective metasurfaces can be used in the visible regime to have phase change over 360° with well-known electrochromic materials, polyaniline. Phase-only change in double resonance system require the condition that each resonance frequency shifts with same direction, but different amount and thus one resonance

pass by the other resonance when material properties change. We designed such system by coupling Mie resonances and Fabry-Perot resonances. Resonance frequency shift is proportional to volume integral of multiplication of permittivity change and electric field intensity divided by mode volume. [7] Fabry-Perot resonances consist of active materials, polyaniline, dielectric Mie resonators are placed near Fabry-Perot resonances and both resonance frequencies are matched in the middle of permittivity change in our study and we achieved phase change over 360° with suppressed amplitude change even with material loss of polyaniline.

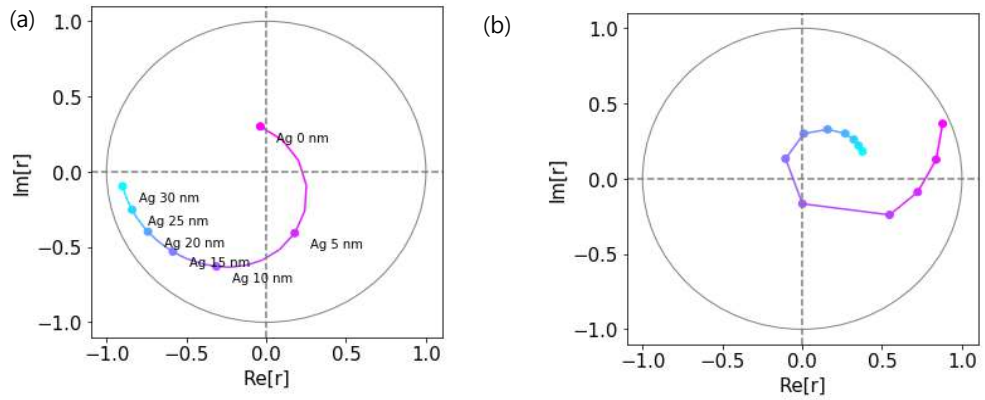


Figure 1: (a) Trajectory of reflection coefficients of electrodeposition based dynamic metasurfaces at 532nm (b) Trajectory of reflection coefficients of electrochromic material based dynamic metasurfaces at 545nm. Refractive index values are from 1.5 to 1.13 and intermediate index values are linearly interpolated [6]

This work is supported by National Research Foundation (NRF) grants (NRF-2021R1A2C2008687) funded by the Ministry of Science and ICT (MSIT), Republic of Korea

References

1. J. Park, J.-H. Kang, S. J. Kim, X. Liu, and M. L. Brongersma, “Dynamic reflection phase and polarization control in metasurfaces.” Nano Lett., 17, 1, 407–413, 2017.
2. J. Park, S. J. Kim, P. Landreman, and M. L. Brongersma, “An over-coupled phase-change metasurface for efficient reflection phase modulation.”, Adv. Optical Mater. 8, 2000745, 2020.
3. .J. Y. Kim, J. Park, G. R. Holdman, J. T. Heiden, S. Kim, V. W. Brar, and M. S. Jang, “ Full 2π tunable phase modulation using avoided crossing of resonances.” Nat. Commun, 13, 2103, 2022.
4. S.-Q. Li, X. Xu, R. M. Veetil, V. Valuckas, R. Paniagua-Dominguez, and A. I. Kuznetsov “Phase-only transmissive spatial light modulator based on tunable dielectric metasurface” Science, 364, 6445, 1087-1090, 2019.
5. C. W. Moon, Y. Kim, and J. K. Hyun, “Active electrochemical high-contrast gratings as on/off switchable and color tunable pixels.” Nat. Commun. 13, 3391, 2022
6. R. Kaissner, J. Li, W. Lu, X. Li, F. Neubrech, J. Wang, and N. Liu, “Electrochemically controlled metasufaces with high-contrast switching at visible frequencies”, Sci. Advances, 7, 19, eabd9450, 2021.
7. S. G. Johnson, M. Ibanescu, M. A. Skorobogatiy, O. Weisberg, J. D. Joannopoulos, and Y. Fink, “Perturbation theory for Maxwell’s equations with shifting material boundaries.”, Phys. Rev. E, 65,066611, 2002.

All metal 1D plasmonic metasurface broadband absorber for refractive index sensing in Mid-IR regime

S. K. Verma[1], S. K. Srivastava[1,2*]

[1]Department of Physics, Indian Institute of Technology Roorkee, Roorkee, Haridwar, Uttarakhand 247667, India
[2]Centre for Photonics and Quantum Communication Technology, Indian Institute of Technology Roorkee, India
[*]sachin.srivastava@ph.iitr.ac.in

Abstract: A one-dimensional all-metal, plasmonic metasurface absorber was fabricated from a compact disk by transferring a one-dimensionally patterned aluminium (Al) layer on transparent polymer. This plasmonic metasurface absorber was used for refractive index sensing in the mid-infrared region. A sensitivity of 10.708 µm/ RIU was achieved for the operating wavelength range 12-15 µm. This metasurface can be used in various photonics applications such as broadband light absorbers, filters, mode locking for mid-IR lasers, smart windows, photodetectors, etc.

Plasmonic multilayer structures having one-dimensional (1D) and 2D periodic nanostrucures are considered 1D or 2D plasmonic metasurfaces (PMs) [1]. PMs are used in various photonics applications such as refractive index (RI) sensors [2], surface enhanced IR absorption [3], light absorbers [4], etc. Generally, plasmonic metasurface absorbers (PMAs) are designed using a metal-insulator-metal (MIM) structure and the incident light gets absorbed in the insulator layer because of surface plasmon (SP) modes [5]. But the fabrication complexities of PMAs can be removed by designing all metal PMAs which support the confinement of light at the sharp edges of the plasmonic nanostructure [6]. Here, fabricated all-metal PMA was used for RI sensing.

A schematic of the fabricated PMA has been shown in Fig. 1 (a). The structure consists of 1D metallic aluminum (Al) grating lines having the period of 1450nm, grating width of 680nm, groove width of 770nm, and grating height of 120nm on a continuous Al layer which is 5 µm thick. The PMA has been fabricated using a commercially available compact disk (CD). PMA has been fabricated by transferring a one-dimensionally patterned aluminium (Al) layer on a transparent polymer. Fig. 1 (b), it has been shown the 3D top view of the fabricated all-metal PMA and it can be observed that the grating height is 120nm around; the period 1450nm; the grating width w=680nm; and the groove width a=770nm.

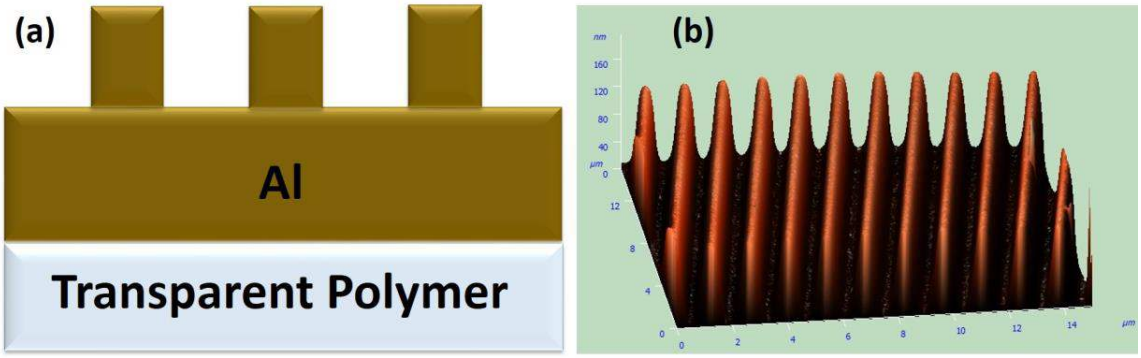


Fig. 1 (a) Schematic of the fabricated PMA, (b) 3D view of the PMA top surface by AFM characterization technique,

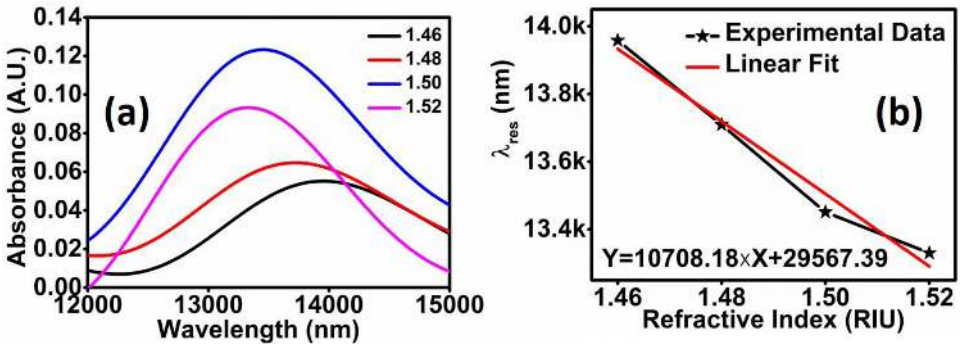


Fig. 2 (a) Absorption spectra for different RI of analyte medium, (b) Characteristics response curve of the sensor

Absorption of Mid-IR light in all metal PMA is achieved because of the confinement of light at the sharp edges of the plasmonic nanostructure and this confinement of light is due to SP modes which are excited at the metal-air interface. Fig. 2 (a), it has been shown an experimental absorption spectrum for different RI values of the analyte medium. The absorption spectra were recorded by using the Fourier transform infrared (FTIR) spectrometer integrated with an attenuated total reflection (ATR) accessory for TM polarized light. The absorption spectra for different RI values were recorded for the angle of incidence 83^0. It can be observed a blue shift in resonance wavelength ($\boldsymbol{\lambda}_{res}$) with the change of RI values from 1.46 to 1.52. The values of $\boldsymbol{\lambda}_{res}$ corresponding to different RI values have been extracted from Fig. 2(a) and plotted in Fig. 2(b). A sensitivity of 10.708 µm/ RIU has been estimated by linear fitting of the data points and calculating the slope.

In summary, an all-metal, flexible PMA has been fabricated as a wide-band absorber in the wavelength range of 12-15µm for refractive index sensing. A sensitivity of 10.708 µm/ RIU was achieved. This PMA can be used in various photonics applications such as Mid-IR photodetector, heat-absorbing flexible cover, biomedical sensors, etc.

Funding from MoE-STARS, and DST-BDTD grants are thankfully acknowledged. Sagar Kumar Verma thanks IITR and MoE for the Ph.D. fellowship.

References

1. Bin-Alam M. S., Reshef O., Mamchur Y., Alam M. Z., Carlow G., Upham J., Sullivan B. T., Ménard J. M., Huttunen M. J., Boyd R.W. and Dolgaleva K., "Ultra-high Q resonances in plasmonic metasurfaces,", Nat. Commun., Vol.12, No.974, 1-8, 2021.
2. Verma S. K. and Srivastava S. K., "Giant extra-ordinary near infrared transmission from seemingly opaque plasmonic metasurface: sensing applications", Plasmonics, Vol.17, 653-663, 2022.
3. Dintinger J., Klein S., and Ebbesen T.W., "Molecule–surface plasmon interactions in hole arrays: enhanced absorption, refractive index changes, and all-optical switching,", Adv. Mater., Vol.18, No.10, 1267-1270, 2006.
4. Li C., Zhu W., Liu Z., Yan S., Pan R., Du S., Li J., and Gu C., "Tunable near-infrared perfect absorber based on the hybridization of phase-change material and nanocross-shaped resonators," Appl. Phys. Lett., Vol.113, No.231103,1-6, 2018.
5. Ding F., Yang Y., Deshpande R. A., and Bozhevolnyi S. I., "A review of gap-surface plasmon metasurfaces: fundamentals," Nanophotonics, Vol.7, No.6, 1129-1156, 2018.
6. Maier S. A., Brongersma M. L., Kik P. G., Meltzer S., Requicha A. A. G., and Atwater H. A., "Plasmonics- A route to nanoscale optical devices," Adv. Mater., Vol.13, No.19, 1501-1505, 2001.

META 2023, PARIS - FRANCE, JULY 18 – 21, 2023

Metasurfaces for illumination and light concentration

Ivan Moreno*, C. P. Castañeda-Almanza, and Thaire V. Galvan

Universidad Autonoma de Zacatecas, Mexico
*corresponding author: imorenoh@uaz.edu.mx

Abstract: We show some methods for designing metalenses that deal with the optimal transfer of light energy, i.e. for light concentration and illumination applications. Owing to its compactness, flatness, and high design flexibility, metasurface-based flat optics may solve some problems in the nonimaging optics field, which deals with light concentration and illumination. We report our latest advances on this topic. We discuss two algorithms for uniform illumination design with metasurfaces: ray mapping method, and Monge–Ampere equation method. And we discuss the string method for efficient light concentration with flat optics.

Metalenses are finding new applications as nonimaging metalenses [1-3]. Therefore, here we describe the design of some types of metalenses for illumination and light concentration applications. We resume a simple method to design a metalens for uniform illumination, which is based on the ray mapping algorithm between a point source and a target [2]. Also, we explain the Monge–Ampere equation method for metasurfaces, which preserves the energy through the light propagation [3]. In addition, we introduce the string method for designing light concentrators with metasurfaces.

This work was financially supported by the Consejo Nacional de Ciencia y Tecnología (grant 316548).

References

1. I. Moreno, M. Avendaño-Alejo, and C. P. Castañeda-Almanza, “Nonimaging metaoptics,” Opt. Lett. 45(10), 2744–2747 (2020).
2. I. Moreno "An LED metalens for uniform illumination", Proc. SPIE 12217, Current Developments in Lens Design and Optical Engineering XXIII, 122170I (2022).
3. C. P. Castañeda-Almanza, and I. Moreno "Metalens for uniform rectangular illumination", Proc. SPIE 12220, Nonimaging Optics: Efficient Design for Illumination and Solar Concentration XVIII, 122200G (2022).

Analysis of Reliability of Flexible Microwave Absorbing Meta-Surface under Bending Stress

Doo-Sun Choi[1], Ji-Youn Kwak[2], Jun Sae Han[1], Eun-Ji Gwak[1]and Eun-chae Jeon[3*]

[1]Department of Nano Manufacturing Technology, Korea Institute of Machinery & Materials, Daejeon, Korea
[2]Department of Materials Science and Engineering, UNIST, Ulsan, Korea
[3]School of Materials Science and Engineering, University of Ulsan, Ulsan, Korea
[*]corresponding author: jeonec@ulsan.ac.kr

Abstract: We developed a simple method to predict the performances of absorbing microwaves under bending stress, and applied the method to a flexible meta-surface for assessing their reliability in this study. Since bending stress made severe damage immediately after bending and some damages were recovered after removing bending stress in flexible meta-surfaces, the reliability of flexible meta-surfaces should be evaluated under bending stress.

Meta-surfaces for absorbing microwaves can be used in various fields such as electronics, optics and militaries [1, 2]. Flexible meta-surfaces have much wider applications than flat and rigid meta-surfaces. Since the flexible meta-surfaces is attached on the targets which should be protected from microwaves, the flexible meta-surfaces experience continuous bending stress during whole life-time. Generally, the flexible meta-surfaces are manufactured and their performances are measured under flat state with no bending stress. However, the performances should be varied when the bending stress is first applied and can be varied with time. It is hard to measure variation of their performances with time (as known as reliability) because we need a large anechoic chamber and expensive measurement systems. We developed a simple method to predict the variations of microwave absorbing performances under bending stress in a general laboratory and with a simple measurement system, and applied this method to a flexible meta-surface for assessing their reliability in this study.

First, we manufactured several flexible meta-surfaces using metal molds, TPU(thermoplastic polyurethane) films and carbon-based conductive ink. The precise patterns for absorbing microwaves on the metal molds were machined by ultra-precision cutting technology. The electric properties of the meta-surfaces were measured under flat state without bending stress in order to obtain reference data. Then, we installed the flexible meta-surfaces in a customized bending system having designed bending radii. The electric properties measured shortly after the installation showed large degradation, which meant that bending stress could make severe damage immediately in flexible meta-surfaces. We maintained the bending state for 1,000hr, and measured the electric properties after certain elapsed time. The degradation of the electric properties showed little change under continuous bending stress. When we removed bending stress after 1,000hr, some degradation was recovered. This meant that the properties of flexible meta-surfaces should be evaluated under bending stress because they are not same under bending stress and at flat state. In summary, we suggested a simple method to assess reliability of flexible meta-surfaces, and verified the validity of the suggested method in this study.

This work was supported by the Center for Advanced Meta-Materials(CAMM) funded by the Ministry of Science and ICT as Global Frontier Project (CAMM- No. 2019M3A6B3031046)

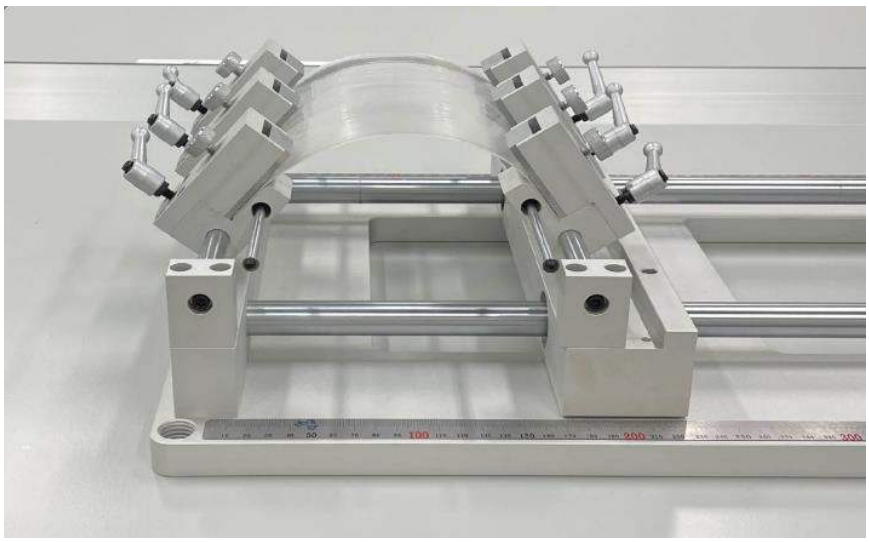


Figure 1. A customized bending system where a flexible meta-surface was installed in this study.

References

1. Zhang, W., Bie. S., Chen, H., Lu, Y. and Jiang J. "Electromagnetic and microwave absorption properties of carbonyl iron/MnO_2 composite," Journal of Magnetism and Magnetic Materials, Vol. 358-359, 1-4, 2014.
2. Afghahi, S. S. S., Jafarian, M., and Stergiou, C. A. "X-band microwave absorbing characteristics of multicomponent composites with magnetodielectric fillers," Journal of Magnetism and Magnetic Materials, Vol. 419, 386-393, 2016.

META 2023, PARIS - FRANCE, JULY 18 – 21, 2023

Reconfigurable On-Chip Waveguide-fed cELC-based Metasurface Antenna

K. Boubekeur[1*], N. Zerounian[1], and B. Ratni[2]**

[1]Centre de Nanosciences et de Nanotechnologies (C2N), CNRS, Université Paris-Saclay, 91120 Palaiseau, France

[2]LEME, UPL, Univ Paris Nanterre, F92410 Ville d'Avray, France

[*]corresponding author: khaled.boubekeur@c2n.upsaclay.fr

[**]corresponding author: badreddine.ratni@parisnanterre.fr

Abstract: The present paper describes the study and design of a Substrate Integrated Waveguide (SIW) Leaky Wave Antenna (LWA) that has a fixed frequency beam steering and is intended to be fabricated with microelectronic processes using polymers layers and metal deposition. The antenna is designed to operate between 58 GHz and 70 GHz, enabling MIMO communications. The radiation pattern of the antenna is reconfigurable using diodes connected to the capacitive gaps of Complementary Electric LC resonator (cELC) unit cells. The antenna is capable of scanning a beam range of 120° (-60° to 60°) and has a peak directivity of 9.13 dBi at 70 GHz, with a variation of less than 2 dB. The goal of the study is to design an integrated reconfigurable antenna.

Introduction: The rise of digital technology has led to a significant increase in data [1], requiring more transmission capacity to meet future needs. However, given the increased frequency range, such as mm-wave 5G or WiGig -around 60 GHz-, but also the terahertz range with 6G [2], short wavelengths require the design of miniaturized RF systems with low loss. Hence, the need to design efficient and agile antennas that can be integrated on-chips. In this article, we present a reconfigurable on-chip waveguide-fed cELC-based metasurface antenna, which operates in the 60 GHz range. The proposed antenna is composed of a SIW with resonant cells etched on its top with small lateral dimension ($< \lambda_0/5$, often $< \lambda_0/10$) and small distance between them ($\lambda_0/10$ to $\lambda_0/5$) of the free-space wavelength λ_0 [3]. It is crucial that each element couples weakly to the guided wave and do not contribute to the excitation of neighboring cells [4]. The antenna presented is designed on BenzoCycloButene (BCB) layer compatible with microelectronics processes [5,6], allowing a complete integration with existing microelectronics manufacturing.

Design and discussion: The scheme of the antenna is shown in Figure 1. On the top surface of the SIW, 18 cELC (2 x 9 cELC) are built as radiation elements with lateral dimensions of $\lambda_0/16$. The distance between each cell is about $\lambda_0/6$ at 60 GHz. The SIW is designed following the method presented in [7] on a BCB layer 60 µm thick. In order to add reconfigurability mechanism to the structure, varactor diodes are placed at both capacitive ends of each element. This allows to modify radiating properties by varying the capacitance of each unit cell. The bias via is located near the edge of the SIW to reduce its impact on the guided wave.

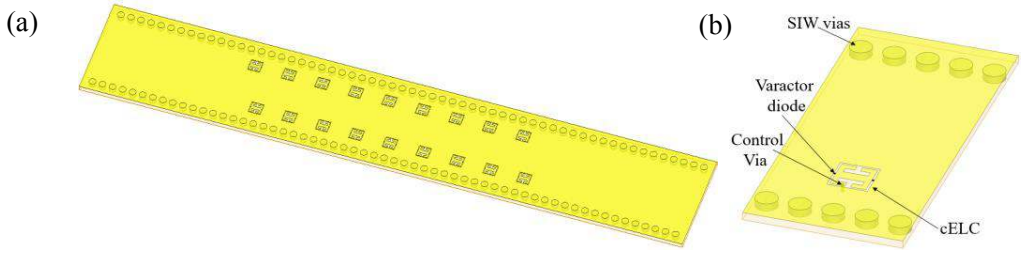


Figure 1: Schematic view of the design (a) SIW LWA, (b) cELC

EM simulations are carried out using HFSS software. The behavior of varactor diodes is emulated using the HFSS RLC boundaries. Figure 2(a) presents the radiation patterns at 60 GHz. We can observe that by varying the capacitance of the varactors, the radiation pattern, at a fixed frequency (60 GHz), can be steered up to 60°. Figure 2(b) presents the peak of directivity at different frequencies ranging from 58 GHz to 70 GHz with different steering angles. Antenna S-parameters are presented in Figure 3 and we can observe that for each case S_{11} is lower than -10 dB, thus ensuring the correct matching of the antenna. It should be noted that it is possible to lower the side lobe levels by applying a magnitude taper.

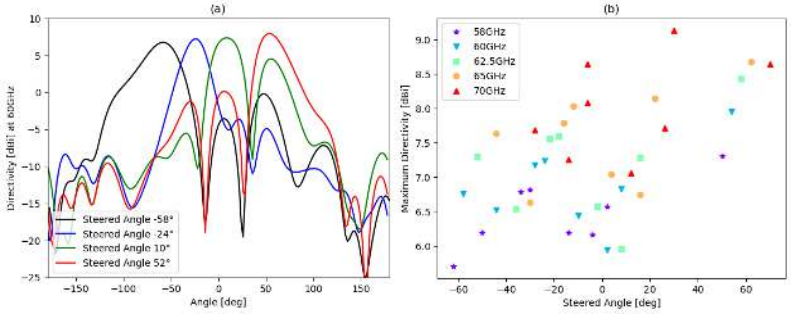


Figure 2: Radiation properties (a) Radiation Pattern at 60 GHz (b) Maximum Directivity Vs Steered Angle

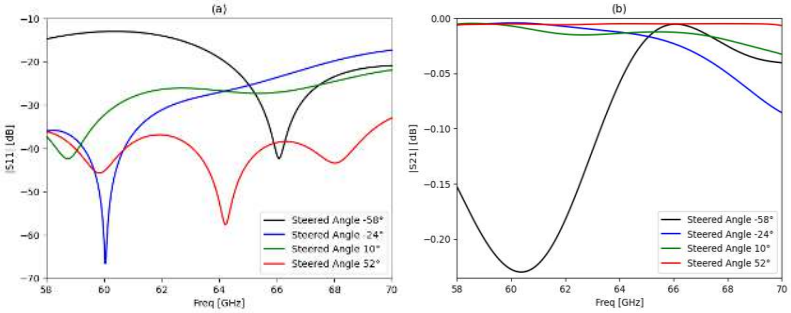


Figure 3: Scattering Parameters (a) $|S_{11}|$ (b) $|S_{21}|$

Conclusion: A reconfigurable on-chip antenna operating at 60 GHz is designed. The proposed antenna can allow to steer the main beam from -60° to 60° at different frequencies ranging between 58 and 70 GHz. Primary simulation results were presented to validate the structure.

References

1. Holst, A. "Volume of data/information created, captured, copied, and consumed worldwide from 2010 to 2025," Statista, June, 2021.
2. FCC. "FCC opens spectrum horizons for new services and technologies." www.fcc.gov/document/fcc-opens-spectrum-horizons-new-services-technologies.
3. Smith, D. R., et al. "An analysis of beamed wireless power transfer in the Fresnel zone using a dynamic metasurface aperture," Journal of Applied Physics, vol. 121, no. 1, 014901, 2017.
4. Sleasman, T., et al. "Waveguide-fed tunable metamaterial element for dynamic apertures," IEEE Antennas and Wireless Propagation Letters, vol. 15, p. 606-609, 2015.
5. Yeap, S. B., et al. "135GHz antenna array on BCB membrane backed by polymer-filled cavity," in Proceedings of the 6th European Conference on Antennas and Propagation (EuCAP), pp. 1337–1340, 2012.
6. Acri, G., et al. "BenzoCycloButene-based in-Package Substrate Integrated Waveguides for sub-THz Applications," in Proceedings of the 49th European Microwave Conference, Paris, France, 1-3 Oct. 2019.
7. Xu, F. and Wu, K. "Guided-wave and leakage characteristics of substrate integrated waveguide," IEEE Transactions on Microwave Theory and Techniques, vol. 53, no. 1, p. 66-73, 2005.

Dielectric metalens and polarization beam splitter for UV wavelengths

B. Idesová[1,2], K. Rovenská[1,2], O. Červinka[1,2], M. Hrtoň[1,2], F. Ligmajer[1,2*] and T. Šikola[1,2]

[1]Central European Institute of Technology, Brno University of Technology, Czech Republic
[2]Faculty of Mechanical Engineering, Brno University of Technology, Czech Republic
[*]corresponding author: filip.ligmajer@vutbr.cz

Abstract: Conventional optical elements used nowadays are usually bulky and heavy, while metasurfaces offer a promising solution allowing for miniaturization and multifunctionality. In this work, we use hafnium dioxide (HfO_2) for its high index of refraction and wide bandgap, both of which allow for fabrication of dielectric metasurfaces even for deep-UV wavelengths. We present a metalens and polarization beam splitter composed of high aspect-ratio nanopillars and analyze their functionality for wavelengths of 325 nm and 266 nm.

Manipulation of ultraviolet (UV) light presents a significant challenge for the optical industry not only due to inherent absorption present in the commonly used materials also for due to tight precision limits limiting fabrication of conventional optical elements such as lenses. Nanophotonics offers a promising solution in the form of metasurfaces, which are able to alter the phase, amplitude, and polarization of incident light [1]. The advantage of metasurfaces lies in their compact size, as well as in the possibility of implementation of multiple optical functions in a single device [2]. In order to sustain low absorption, which is the key requirement in many optical applications, dielectric Mie-resonant nanostructures are mainly used due to the significantly lower losses compared to the metallic plasmonically active nanostructures [3]. So far, for the UV wavelengths, HfO_2, Nb_2O_5, Si_3N_4 or AlN have been proposed as suitable materials. In this work, we choose HfO_2 for its high refractive index >2 and wide bandgap 5.7 eV, ensuring low losses down to the deep-UV wavelengths. Based on this material platform, metalenses, metaholograms and self-accelerating beam generators have been demonstrated [4], as well as integrated metalenses on a single-photon avalanche diode [5]. In our work, we demonstrate not only a prototypical HfO_2 metalens for UV, but also a polarization beam splitter suitable for wavelengths of 325 nm and 266 nm.

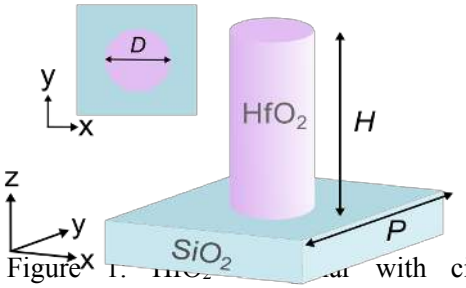
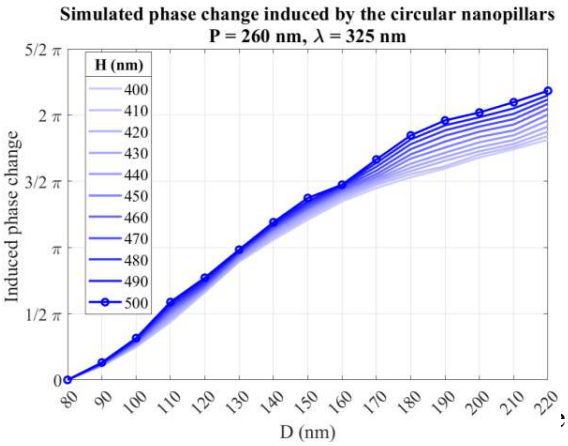


Figure 1. HfO_2 [illegible] with circular cross-section of height *H*, diameter *D,* and spacing between the nanopillars *P* on a fused silica substrate.



circular nanopillars with various diameters *D* and heights *H* when illuminated by a plane wave of 325 nm wavelength.

In the first step, finite-difference time-domain simulations were performed in order to estimate the phase of the light transmitted by the prospect metasurface building blocks — HfO_2 nanopillars with circular cross-sections on a fused silica substrate (Figure 1). In these simulations, we used periodic boundary conditions along the *x* and *y* axis, and perfectly matched layers in the *z* direction, while illuminating the nanostructure with a plane wave of 325 nm wavelength. The simulated phase alterations induced by such nanostructures of varying diameters *D* and heights *H,* with a constant spacing between the nanostructures (*P* = 260 nm) can be seen in Figure 2. The required 2π phase change, crucial for mimicking the phase profile of a lens, was reached only for nanostructures taller than 450 nm. These nanostructures of five different diameters were later considered in the metalens design shown in Figure 3. The subsequent fabrication of the metasurfaces consisted of multiple steps. In the first step, a resist mask with circular holes of the desired diameters was made via electron beam lithography into a positive resist. These holes were subsequently filled with HfO_2, employing atomic layer deposition, which ensures conformal coverage of the resist surface. In order to remove the resist in oxygen plasma, the top layer of HfO_2 must be etched away via argon ion etching. This fabrication process ensures high fabrication precision of the final nanostructures. Final metalens characterization was done by measuring the intensity profile of the focused spot. The design process of the polarization beam splitter, whose function schematic is shown in Figure 4, is very similar to the one of the metalens. The main difference is in the shape of the nanopillar cross-sections, which had to be rectangular in order to introduce the necessary polarization anisotropy. The phase profile of a beam splitter was then obtained through a geometric phase, where the individual building blocks were rotated to attain the desired phase profile.

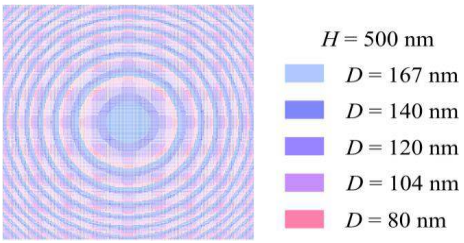


Figure 3: Proposed design of the final HfO_2 metalens based on nanopillars 450 nm tall with varying diameters *D*.

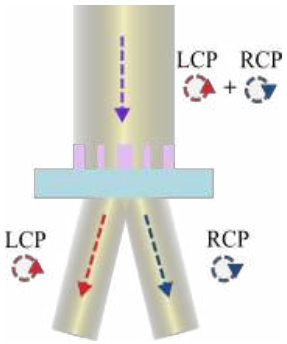


Figure 4: Schematics of polarization beam splitter employing HfO_2 nanopillars with a rectangular cross-section.

This work was supported by the Grant Agency of the Czech Republic (21-29468S). We also acknowledge CzechNanoLab Research Infrastructure supported by MEYS CR (LM2018110).

References

1. Neshev, D., Aharonovich, I., "Optical metasurfaces: new generation building blocks for multi-functional optics," Light Sci Appl, Vol 7, 58, 2018.
2. Ding, F., Chang, B., Wei, Q., et al., "Versatile polarization generation and manipulation using dielectric metasurfaces," Laser & Photonics Reviews, Vol 14, 2000116, 2020.
3. Genevet, P., Capasso, F., Aieta F., et al., "Recent advances in planar optics: from plasmonic to dielectric metasurfaces," Optica, Vol 4, 139, 2017.
4. Zhang, C., Divitt, S., Fan. Q., et al., "Low-loss metasurface optics down to the deep ultraviolet region," Light Sci Appl, Vol 9, 55, 2020.
5. Uenoyama, S., Ota, R., "Monolithic integration of metalens in silicon photomultiplier for improved photodetection efficiency," Advanced Optical Materials, Vol 10, 2102707, 2022.

META 2023, PARIS - FRANCE, JULY 18 – 21, 2023

Epsilon near zero metasurfaces (ENZ) at visible wavelengths

I.R.Alhamdan[1], **S.A.Schulz**[2]

[1]University of Saint Andrews, United Kingdom
[2]University of Saint Andrews, United Kingdome
[*]Corresponding author: sas35@st-andrews.ac.uk

Abstract: Here we present an Epsilon near zero (ENZ) metasurface in the visible range using a multilayer structure of silicon oxide (SiO_2), gold nanoantenna, and Indium tin Oxide (ITO). ITO is an ENZ material with distinguished optical properties and can control antenna resonances. Finite difference time domain (FDTD) simulations show high efficiencies for the proposed design in transmission and reflection modes. Our metasurface has promising potential for augmented reality and chemical sensing due to the flexibility of ITO's plasma frequency.

Epsilon near zero (ENZ) materials have a vanishing permittivity around a spectral point known as the epsilon near zero wavelength (λ_{ENZ}). In general, ENZ materials are engineered and designed using different mechanisms. One of these is the media mixing of a multilayered design of dielectric and metal layers [1]. Some transparent conductive Oxides (TCOs) are naturally occurring ENZ materials, for example Indium Tin Oxide (ITO) which has an λ_{ENZ} in the near-infrared region. This fact makes TCOs highly desirable in telecommunication applications and beam steering. One of the most important implementations of ITO is controlling the localized surface plasmon resonance (LSPR) of plasmonic antennas without having to alter their size or shape [2].

Harnessing the distinguished optical properties of ENZ material for controlling the propagation of light in the visible range will open the frontier for augmented reality applications and chemical sensing. The λ_{ENZ} of ITO can be flexibly tuned by simply changing the fabrication parameters where the carrier concentration of ITO is altered and hence the plasma frequency [3]. Therefore, ITO represents an optimum platform for shifting the operating wavelength of the metasurface to the visible wavelength, enabling the creation of imaging and holographic devices with unprecedented resolutions and capabilities. Achieving this could lead to advanced virtual reality experience and medical imaging technology.

We conducted a finite difference time domain (FDTD) simulation using a commercial software (lumerical), to showcase an ENZ metasurface at the visible range that incorporate ITO. In the transmission metasurface design, a nanostructured antenna is positioned on top of a thin layer of ITO that lies on a glass spacer (Figure 1. (a)). Our simulations indicate high efficiency in transmission as evidenced by the spectrum Figure 1. (b). Other parameters such as the spacer thickness and antenna thickness are optimized via a sweep simulation.

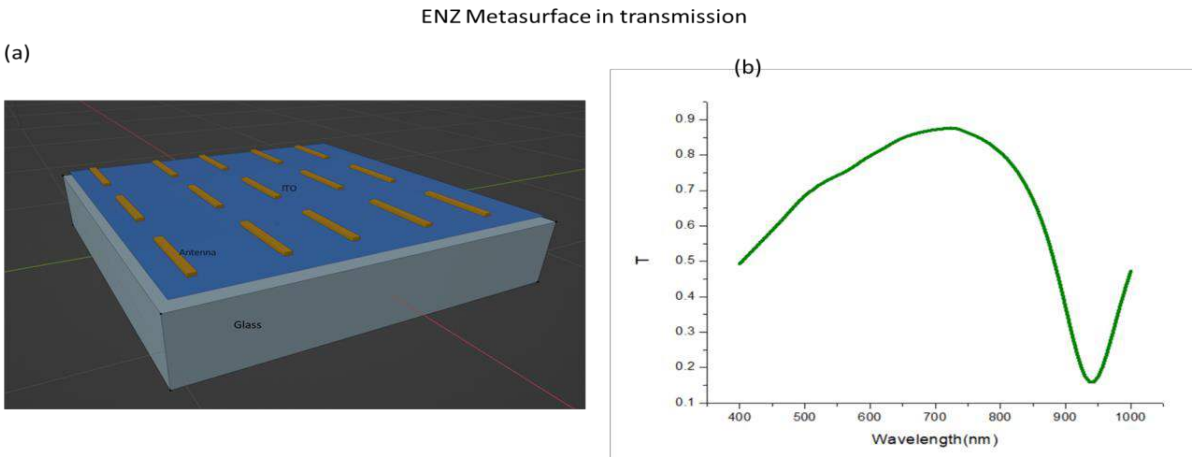


Figure 1: The metasurface in transmission as simulated in Lumerical (a) a perspective view of the design which contains an antenna nanostructure on a surface of an ITO and a glass spacer (b) the transmission spectrum of the structure.

In summary, the unique optical properties of ENZ materials hold great promise for manipulating light in the visible range, which can pave the way for the creation of highly advanced holographic devices. Our FDTD simulation has shown that our proposed metasurface design exhibits high efficiency, underscoring the potential of ENZ materials for use in augmented reality applications.

References

1. Jiaye Wu, Ze Tao Xie, Yanhua Sha, H. Y. Fu, and Qian Li, "Epsilon-near-zero photonics: infinite potentials," Photon. Res. 9, 1616-1644 (2021).

2. S. A. Schulz, L. C. Wynne and A. Di Falco, "Optical Metasurfaces Based on Epsilon-Near-Zero Materials: Towards Low Power Nonlinear Optics," 2020 22nd International Conference on Transparent Optical Networks (ICTON), Bari, Italy, 2020, pp. 1-4, doi: 10.1109/ICTON51198.2020.9203047.

3. Lian J, Zhang D, Hong R, Qiu P, Lv T, Zhang D. Defect-Induced Tunable Permittivity of Epsilon-Near-Zero in Indium Tin Oxide Thin Films. Nanomaterials (Basel). 2018 Nov 7;8(11):922. doi: 10.3390/nano8110922. PMID: 30405091; PMCID: PMC6267609.

Supercell Metasurfaces: Hierarchical Designs and Experimental Validation

Tatiana Contino[1,2]*, **Michele Tamagnone**[1]

[1]Fondazione Istituto Italiano di Tecnologia, via Morego 30, 16163 Genova, Italy

[2]Dipartimento di Chimica e Chimica Industriale, Università di Genova, Genova, Italy
*Corresponding author: tatiana.contino@iit.it

Abstract: In this work, we demonstrate a new concept of metasurfaces based on a generalization of supercells. In general, these supercells consist of a series of unit cells that combine with each other to achieve a specific function. We present hierarchical supercells (supercells of supercells) and we extend supercells to general 2D Bravais Lattice, providing a simple mathematical framework to describe the resulting metagratings.

Metasurfaces are artificial planar materials consisting of arrays of subwavelength-spaces nanostructures at an interface, allowing for unprecedented control over the properties of light like phase, amplitude, and polarization, and have allow multiple and versatile functionalities in a single device [1,2]. In general, metasurfaces are obtained through subwavelength unit cells designed to impart a local phase profile to light propagating through the cell. Multiple functions such as focusing, holograms, polarization functions, and beam shaping can be achieved by this technique. Using supercells (arrangements of multiple cells which can are optimized together in the design), it is possible to achieve multiple functions at same time[3]. When the supercell is repeated periodically, the device behaves as a grating, splitting the light in multiple diffraction orders (*metagrating*). The size of the supercells determines the number and direction of diffraction orders to be considered while the geometry of the nanostructures present in the unit cell determines the local effect of the metasurface on light.

In this work, we generalize the concept of supercells in two ways: (i) using hierarchies to create supercells of supercells and (ii) by means of general 2D integer Bravais lattices.

Hierarchies of supercells can be defined in the following way: starting from metasurfaces based on a single-unit cell that is repeated periodically on the plane, we define first-order supercells by joining several cells and then breaking the previous translational symmetry by creating differences among the various cells in the supercell. Second order supercells, similarly, are supercells of supercells, and so on for higher orders. Each time the supercell order is increased, new diffraction orders are obtained. By engineering the unit cells it is possible to obtain devices with different functions on each order (Figure 1A-C). The phase and amplitude of each order depend on the particular asymmetry introduced when the supercell is created, specifically the amplitude is proportional to the perturbation parameter in the small-perturbation limit.

In addition to considering supercells that extend horizontally or vertically on the plane, we consider here supercells that extend obliquely. It is possible to identify these supercells by means of an integer 2D Bravais lattice, defined by the points $\{n\bar{a} + m\bar{b}\}$, where $\bar{a}$ and $\bar{b}$ are 2D integer vectors. We can then define the supercell matrix L as

$$L = \begin{pmatrix} a_x & b_x \\ a_y & b_y \end{pmatrix} \in \mathbb{Z}^{2\times 2} \quad (1)$$

It is straightforward to show that the number of cells in the supercells is $|\det(L)|$. In Figure 1D,E we show an example of such a Bravais lattice (with $|\det(L)| = 4$), and we identify the associated supercell as a “Tetris-like” tile which fills the entire plane. The number of orders is also increased by a factor of $|\det(L)|$. Specifically, the diffraction orders for a metagrating with periodicity of P are given by:

$$\sum_{m,n} \delta\left(\bar{k} - \frac{2\pi}{P}\begin{bmatrix} m \\ n \end{bmatrix}\right) \tag{2}$$

while when the supercell is defined, the new diffraction orders (more numerous) are given by

$$\sum_{m,n} \delta\left(\bar{k} - \frac{2\pi}{P} L^{-1,H}\begin{bmatrix} m \\ n \end{bmatrix}\right) \tag{3}$$

In the presentation we will show concrete examples of devices based on these two concepts.

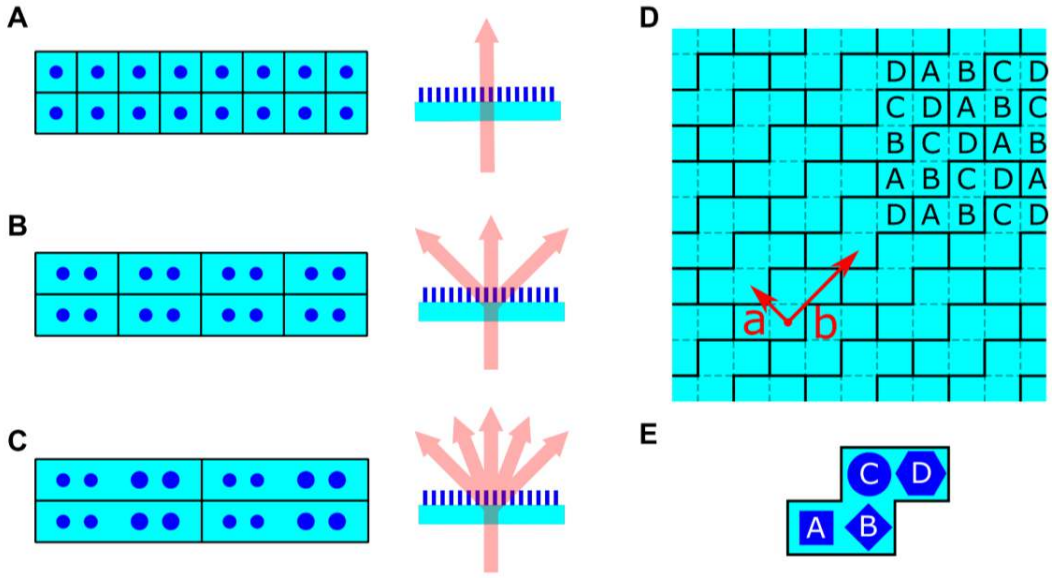


Figure 1: Generalized supercell metasurface concepts. A-C: Metagratings using supercells of increasing hierarchy. 0^{th} order supercells are just the unit cells of the metasurface, 1^{st} order are creating joining 0^{th} cells and so on. Increasing hierarchies generate an increased number of diffraction orders. **D**: An example of supercells based on a general integer Bravais lattice. **E**: Example of optical elements in a Bravais supercell.

This project has received funding from the European Research Council (ERC) under the European Union's Horizon 2020 research and innovation programme (Grant agreement No. 948250).

References

1. Khorasaninejad, Mohammadreza, Wei Ting Chen, Robert C. Devlin, Jaewon Oh, Alexander Y. Zhu, and Federico Capasso. "Metalenses at visible wavelengths: Diffraction-limited focusing and subwavelength resolution imaging." *Science* 352, no. 6290 (2016): 1190-1194.
2. Devlin, Robert C., Mohammadreza Khorasaninejad, Wei Ting Chen, Jaewon Oh, and Federico Capasso. "Broadband high-efficiency dielectric metasurfaces for the visible spectrum." *Proceedings of the National Academy of Sciences* 113, no. 38 (2016): 10473-10478.
3. Spägele, Christina, Michele Tamagnone, Dmitry Kazakov, Marcus Ossiander, Marco Piccardo, and Federico Capasso. "Multifunctional wide-angle optics and lasing based on supercell metasurfaces." *Nature Communications* 12, no. 1 (2021): 3787.

META 2023, PARIS - FRANCE, JULY 18 – 21, 2023

Non-Uniform Array of Polarizable Particles as a Locally Linear Space Invariant (LSI) Metasurface

J. Dugan[1*], T. J. Smy[1], João G. Nizer Rahmeier[1], and S. Gupta

[1]Carleton University, Canada
[*]corresponding author: jordandugan@cmail.carleton.ca

Abstract: Non-uniform metasurfaces are often analyzed as a locally Linear Space Invariant (LSI) system where the effective parameters of the surface at any given unit cell are equal to the parameters of an equivalent uniform surface composed of only that unit cell. This is often treated as an approximate method for modeling non-uniform surfaces, however, in this work we demonstrate that a non-uniform array of electrically polarizable particles can in fact be modeled as a local LSI system.

Non-uniform metasurfaces are essential in several applications, such as wireless channel engineering as well as electromagnetic cloaking and illusions. Much work has been done on homogenizing uniform metasurfaces, with non-uniform metasurfaces being assumed to be locally space invariant (LSI), i.e., the effective parameters of the non-uniform surface at a given unit cell are the same as an equivalent uniform metasurface constructed using that cell. In much of the literature, the LSI nature of metasurfaces is treated essentially as a perturbative approximation based on the assumption that the coupling between unit cells for a non-uniform surface is approximately the same as for a uniform surface[1]. The local LSI assumption has been shown to provide excellent results even for highly non-uniform metasurfaces[2]. In this work, we will investigate the validity of this assumption.

Consider a uniform array of polarizable particles with a polarizability α and a separation of d, excited with normal incidence. Following the derivation by Tretyakov[3], we can write the field at a given dipole as

$$\boldsymbol{E} = \boldsymbol{E}_s + \beta \boldsymbol{p}, \tag{1}$$

where $\boldsymbol{E_s}$ is the source field, $\boldsymbol{p}$ is the induced dipole moment, and β is the interaction coefficient which is determined by summing the fields produced by each dipole in the array assuming each dipole has the same dipole moment. Further, if we now replace the dipoles with an equivalent spatially averaged current $\hat{\mathbf{J}} = j\omega\widehat{\mathbf{P}}$ where $\widehat{\boldsymbol{P}} = \boldsymbol{p}/d^2$, we can write the averaged field at each dipole as

$$\boldsymbol{E}_{\text{avg}} = \boldsymbol{E}_s - \frac{\eta}{2}\hat{\boldsymbol{J}}, \tag{2}$$

where η is the free space impedance. Using (1) and (2), and $p = \alpha E$, we can write,

$$\boldsymbol{E}_{\text{avg}} = \left[\frac{d^2}{j\omega}\left(\frac{1}{\alpha} - \beta\right) - \frac{\eta}{2}\right]\hat{\boldsymbol{J}} \tag{3}$$

Identifying, $\boldsymbol{E}_{\text{avg}} = \boldsymbol{Z}\hat{\boldsymbol{J}}$, we obtain the effective sheet impedance as:

$$\boldsymbol{Z} = \left[\frac{d^2}{j\omega}\left(\frac{1}{\alpha} - \beta\right) - \frac{\eta}{2}\right] \tag{4}$$

Now we want to extend our analysis to non-uniform surfaces where the polarizability is a function of the position on the surface $\alpha(r, \phi)$. Similar to (1), we can write the field at the dipole location as:

$$\boldsymbol{E}(r, \phi) = \boldsymbol{E}_s + \hat{\beta}\{\boldsymbol{p}\} \tag{5}$$

Where $\hat{\beta}$ is now an LSI operator which again, is found by summing the fields produced by each dipole; only now each dipole can have a different dipole moment. Now, the spatially averaged current is non-uniform so the averaged field will have the following form

$$\boldsymbol{E}_{\text{avg}}(r,\phi) = \boldsymbol{E}_s(r,\phi) + \hat{L}\{\hat{\boldsymbol{J}}(r,\phi)\} \tag{6}$$

where $\hat{L}$ is now referred to as the LSI propagation operator given by,

$$\hat{L}\{\hat{\boldsymbol{J}}(r,\phi)\} = -j\omega\mu \int_S \frac{e^{-jk(r-r')}}{|r-r'|}\left[\hat{\boldsymbol{J}}(r',\phi') + \frac{1}{k^2}\nabla'\nabla'\cdot\hat{\boldsymbol{J}}(r',\phi')\right] dS', \tag{7}$$

describing the fields produced by a current $\hat{\boldsymbol{J}}$ at the source location (r',ϕ'), at the observation (r,ϕ).
Given $\boldsymbol{p}(r,\phi) = \alpha(r,\phi)\boldsymbol{E}(r,\phi)$, and using (5) and (6), we can obtain the position dependent sheet impedance *operator* as:

$$\hat{\boldsymbol{Z}}(r,\phi)\{\hat{\boldsymbol{J}}\} = \left[\frac{d^2}{j\omega}\left(\frac{\hat{I}}{\alpha(r,\phi)} - \hat{\beta}\right) - \hat{L}\right]\{\hat{\boldsymbol{J}}\} \tag{8}$$

Where $\hat{I}$ is the identity operator, defined as $\hat{I}\{\hat{\boldsymbol{J}}\} = \hat{\boldsymbol{J}}$. For a uniform surface with an arbitrary incident field, we get the following impedance operator,

$$\hat{\boldsymbol{Z}}(r,\phi)\{\hat{\boldsymbol{J}}\} = \left[\frac{d^2}{j\omega}\left(\frac{\hat{I}}{\alpha} - \hat{\beta}\right) - \hat{L}\right]\{\hat{\boldsymbol{J}}\} \tag{9}$$

which can be easily verified to lead to (4) for a constant $\hat{\boldsymbol{J}}$ across the surface. Comparing (8) and (9), we observe that at any given point, (r,ϕ), on the non-uniform surface, the impedance operator is equal to an equivalent uniform surface made up of dipoles of the same polarizability, and not dependent on the polarizabilities of the neighboring particles. This indicates that for an array of electric dipoles, local LSI is thus not an assumption but rather a fundamental property of the array.

In future works, we will perform this investigation for a general bi-anisotropic surface, as well as for a surface containing higher-order multipoles. We will further perform numerical demonstrations to conclusively demonstrate the validity of the local LSI model. We believe this can prove to be an important realization about the non-uniform surfaces, as the ability to treat a surface as locally LSI may greatly simplify the design and analysis of general non-uniform metasurfaces.

References

1. Asadchy, V. S., A. Díaz-Rubio, and S.A. Tretyakov, "Bianisotropic metasurfaces: physics and applications" Nanophotonics, vol. 7, no. 6, 2018, pp. 1069-1094
2. Dugan, J., J. G. N. Rahmeier, T. J. Smy and S. Gupta, "Part III - Spatially Dispersive Metasurfaces: Zero Thickness Modeling of Periodic and General Non-uniform Surfaces" TechRxiv. Preprint. 2022.
3. Tretyakov, S., "Analytical Modeling in Applied Electromagnetics." Norwood, MA, USA: Artech House, 2003.

META 2023, PARIS - FRANCE, JULY 18 – 21, 2023

Adjoint Optimized Mid-Wave Infrared Metalenses

J. Rollag[1,2], R. Wambold[1], R. Gibson[1*]
[1]Air Force Research Laboratory, Sensors Directorate, 2241 Avionics Circle, Wright-Patterson AFB, OH, 45433, USA
[2]KBR, Inc., 3725 Pentagon Blvd., Suite 210, Beavercreek, OH, 45431, USA
[*]corresponding author: ricky.gibson.2@us.af.mil

Abstract: Silicon metalenses with numerical apertures of 0.232 are designed for operation in the four to five micron wavelength range using adjoint optimization. The library element optimization allows for each freeform scatterer to be optimized for a given phase with feature size limitations suitable for standard fabrication. It is found that the silicon metalenses with the adjoint optimized scatterers perform better than traditional cylindrical scatterers in both bandwidth and focusing efficiency over the desired spectral range.

Many different optimization techniques for metasurface design have been studied recently. Broadly they fall in two categories where one can directly compute the performance of a particular meta-atom with an electromagnetic solver or rely on an inverse design technique [1]. While many variations of inverse design exist one that shows particular promise for metasurface design is adjoint optimization. Adjoint optimization has been used to enhance light extraction out of quantum emitters such as nitrogen vacancies in diamond [2] and increase coupling of defects in 2D materials coupled to photonic integrated circuits [3]. This technique has also been applied to develop robust metagratings that are insensitive to common fabrication imperfections [4] and with appropriate segmentation can be applied to freeform large-area metasurfaces [5]. This work is focused on adjoint optimization of individual freeform meta-atoms, or scatterers.

Using commercially available electromagnetic solver software [6] an algorithm is developed to optimize freeform meta-atom libraries. Each meta-atom is typically optimized in fewer than 400 iterations pushing the index of each meshed cell of the freeform element to either high or low index, corresponding to silicon or air, until the desired scattering phase is matched. The algorithm limits the feature sizes to be suitable for common fabrication techniques and from a desired phase profile distributes, the meta-atoms on a grid based on the scatterer phase nearest to that of the desired phase. The performance of metalenses with as few as four elements in the library show strong performance for millimeter scale apertures. While both the focusing efficiency and bandwidth improve with number of meta-atoms the trade-off between library size and performance levels off near 8 to 16 elements for silicon based MWIR lenses.

This method is shown to be an improvement over traditional cylindrical meta-atoms in terms of both bandwidth and focusing efficiency. This can be seen in Figure 1 where the electric field profile along the optical axis and at the focus are shown for an adjoint optimized metalens and a traditional cylindrical scatterer metalens, both constructed with eight meta-atoms and with NA ≈ 0.232. The focusing efficiency of the adjoint optimized metalens over the cylindrical scatterer metalens is 13.8% higher, where the focusing efficiency is defined at the percentage of $|E|^2$ within 3x the full-width half max [7], the FWHM at the focus is 13.9% smaller, and the average transmission 10.6% higher. Additionally, the transmission only varies by a few percent across the full-bandwidth for the adjoint optimized lenses whereas transmission varies by more than 15% for the cylindrical scatterer metalens. The adjoint optimized metalens outperforms in each of these metrics though a larger shift in the focal position across the $\lambda = 4 – 5$ μm range is observed. Larger aperture sizes, variations in NA, and variations in number of meta-atoms in each library will be presented for this design technique.

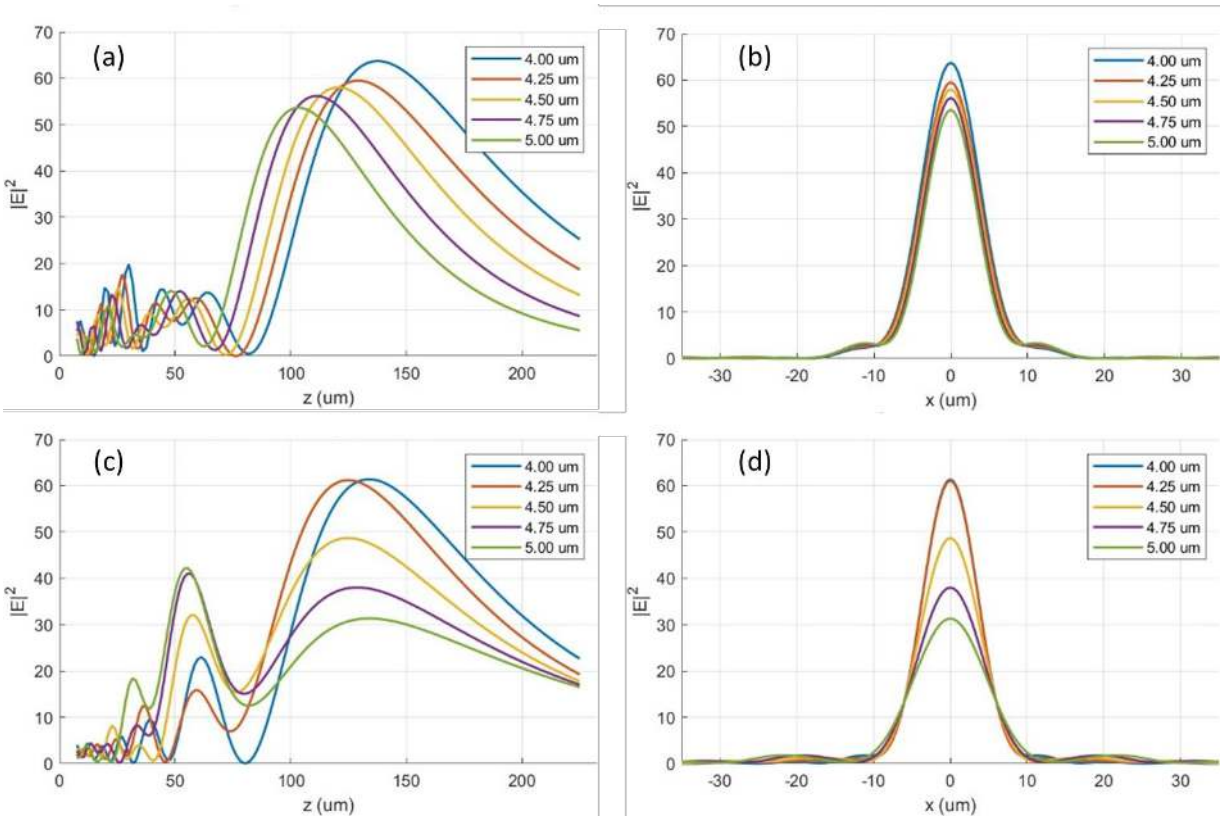


Figure 1. Comparison of performance in the λ = 4 – 5 μm range of metalenses designed by adjoint optimization (top row, (a) & (b)) and from direct computation (bottom row, (c) & (d)) with only eight elements each. The intensity profile along the optical axis is shown for the adjoint optimized design and direct computation in (a) & (c) while the intensity profile at the focus is shown in (c) & (d), respectively.

References

1. Elsawy, M. M., Lanteri, S., Duvigneau, R., Fan, J. A. and Genevet, P., "Numerical optimization methods for metasurfaces" Laser & Photonics Rev., Vol. 14, No. 10, 1900445, 2020.
2. Wambold, R. A., Yu, Z., Xiao, Y., Bachman, B., Jaffe, G., Kolkowitz, S., Choy, J. T., Eriksson, M. A., Hamers, R. J. and Kats, M. A., "Adjoint-optimized nanoscale light extractor for nitrogen-vacancy centers in diamond," Nanophotonics, Vol. 10, No. 1, 393-401, 2020.
3. Yesilyurt, O., Kudyshev, Z.A., Boltasseva, A., Shalaev, V.M. and Kildishev, A.V., "Efficient topology-optimized couplers for on-chip single-photon sources," ACS Photonics, Vol. 8, No. 10, 3061-3068, 2021.
4. Wang, E.vW., Sell, D., Phan, T. and Fan, J. A., "Robust design of topology-optimized metasurfaces," Opt. Mat. Exp., Vol. 9, No. 2, 469-482, 2019.
5. Lin, Z., Liu, V., Pestourie, R. and Johnson, S. G., "Topology optimization of freeform large-area metasurfaces," Opt. Exp., Vol. 27, No. 11, 15765-15775, 2019.
6. FDTD: 3D Electromagnetic Simulator, Lumerical Inc.
7. Engelberg, J. and Levy, U., "Standardizing flat lens characterization," Nature Photonics, Vol. 16, No. 3, 171-173, 2022.

Self-assembly of magnetoplasmonic nanowires for structural colors and chiral metasurfaces

My-Chi Nguyen, Huu-Quang Nguyen, and Jaebeom Lee*

Department of Chemistry, Chungnam Nation University, Republic of Korea
*corresponding author: nanoleelab@cnu.ac.kr

Abstract: A template-free and one-step synthesis of metal core-magnetic shell Au@Fe_xO_y nanowires with high aspect ratio was introduced. The magnetic field-induced aligned array film presents unique iridescent structural coloration in different observation and polarization modes. Furthermore, a helical metasurface is assembled resembling Bouligand structure which exhibits circular dichroism tunable by adjusting the magnetic field strength, number of layers, and helical pitch angle. These results demonstrate the capability of self-assembly metasurfaces as groundwork for optical and sensing devices.

A facile one-pot solvothermal synthesis method was developed for growing an anisotropic hybrid nanostructure composed of magnetic oxide nanoparticles coated on plasmonic gold nanowires (Au@Fe_xO_y MagPlas NWs). The effects of reaction temperature, time, reducing agent and precursor as well as post-synthesis treatment were optimized to produce highly uniform NWs in the aspect ratio of 25 ~ 82. The synthesized structures inherited the magnetic properties from the iron oxide layer and anisotropic localized surface plasmon resonance (LSPR) of the gold nanowires, which are potentially useful for a wide range of optical and sensing applications.

Especially, by exploiting the interaction of NWs with an external magnetic field, MagPlas NWs were aligned into 2D photonic surfaces with high periodicity, which can generate distinctive structural colors that are uniquely iridescent and polarization-sensitive. Furthermore, we demonstrated the fabrication of a bioinspired Bouligand-type chiral cholesteric metasurface, by stacking the 2D aligned microchains continuously with a rotating pitch angle. This film displays remarkable sensing capability with circular dichroism spectroscopy, which could detect the change of surface alignments upon the addition of analyte molecules. These intriguing properties of MagPlas anisotropic NWs and their self-assemblies could be consequently valuable for developing photonic, catalysts, and sensing applications.

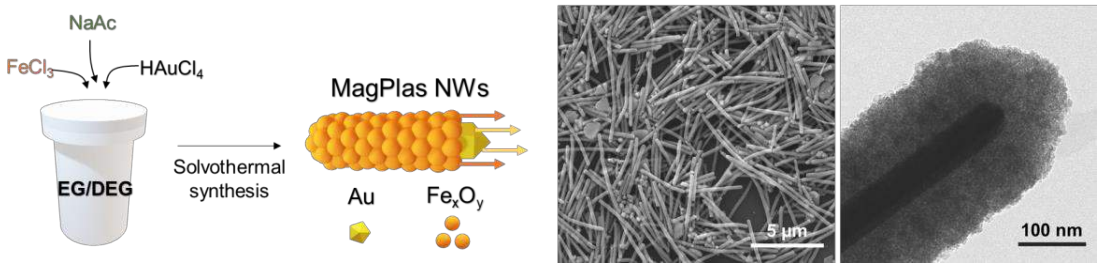


Figure 1. Schematics of the synthesis process and electron microscopic images of the synthesized MagPlas NWs

Acknowledgements

This work was financially supported by the National Research Foundation of Korea (NRF), grant number 2021K1A3A1A16096990, 2019K1A3A1A18116066 and 2019R1A2C2007825.

References

1. Nguyen, H-Q., D. Hwang, S. Park, M.-C. T. Nguyen, S. S. Kang, V. T. Tran and J. Lee, "One-Pot Synthesis of Magnetoplasmonic Au@FexOy Nanowires: Bioinspired Bouligand Chiral Stack," ACS Nano, Vol. 16, No. 4, 5795-5806, 2022.
2. Tran, VT., J. Kim, L. T. Tufa, S. Oh, J. Kwon and J. Lee, "Magnetoplasmonic Nanomaterials for Biosensing/Imaging and in Vitro/in Vivo Biousability," Anal. Chem., Vol. 90, No. 1, 225-239, 2018.

Dynamic phase-modulated metasurface for beam scanning antenna

Z. Zouhdi[1,2], B. Ratni[1], and S. N. Burokur[1*]

[1]LEME, UPL, Univ Paris Nanterre, F92410 Ville d'Avray, France
[2]Naval Group, Naval Research, Ollioules, France
[*]corresponding author: sburokur@parisnanterre.fr

Abstract: A directional high gain reconfigurable planar antenna is designed based on a phase-modulated metasurface. A prototype that operates around 5 GHz is designed, fabricated and tested. The metasurface is dynamically controlled by different bias voltages applied to the incorporated varactor diodes, thus allowing to control its phase characteristics. Different phase profiles have been tested allowing to firstly achieve a highly directive boresight radiation and secondly, to steer the main radiated beam towards an off-normal direction.

Metasurfaces have attracted great interest due to their ability to manipulate electromagnetic waves, such as radiation control [1-3], wavefront shaping [1,4], and polarization conversion [5]. In the field of antennas, metasurfaces have allowed to reduce the dimensions, particularly when they are used as partially reflective surfaces (PRS) in reflex-type Fabry-Perot (FP) cavity antennas to achieve high directivity from a single radiating element [6]. Flat lenses [7] and leaky-wave antennas [8] have also been designed based on the use of metasurfaces. The concept of reconfigurable metasurfaces has emerged in recent years to satisfy the changing requirements in practical applications and enable the integration of multiple functionalities into a single metasurface. In this work, a dynamic metasurface loaded with varactor diodes is exploited as a reconfigurable planar reflector with a parabolic phase profile in order to design a highly directive antenna at 5 GHz. Such antenna allows reconfigurability in frequency and further allows to control the direction of the radiated main beam in order to achieve beam steering.

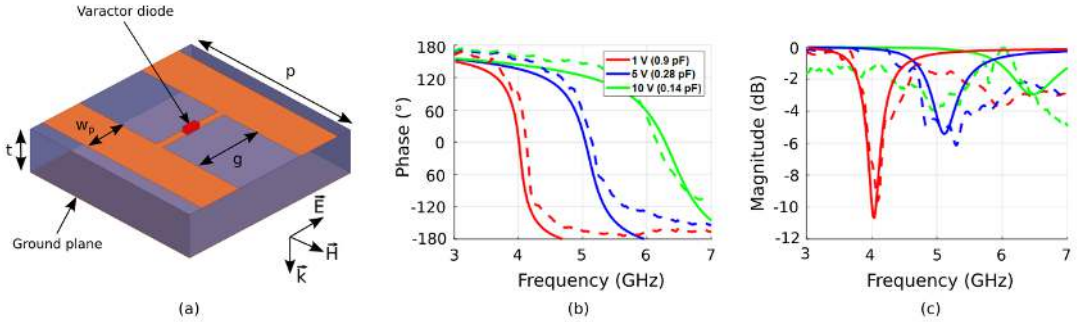


Figure 1. (a) Schematic design of the unit cell: p = 13 mm, w_p = 3 mm and g = 5 mm. The substrate used has a relative permittivity ε_r = 2.2 and a thickness t = 3 mm. Simulated and measured reflection responses for different applied stimuli signals: (b) phase and (c) magnitude.

The proposed reconfigurable metasurface comprises 30 columns, each containing 30 resonant unit cells (30 × 30 cells) and has lateral dimensions 390 mm × 390 mm. In this voltage bias configuration where a similar voltage will be applied to all the meta-atoms in a column, only a one-dimensional phase profile can be tailored. From Fig. 1(b), it can be noted that a high phase shift $\Delta\varphi$ (above 280°) is achieved within the 4.4 – 5 GHz due to the intrinsic design of the meta-atom.

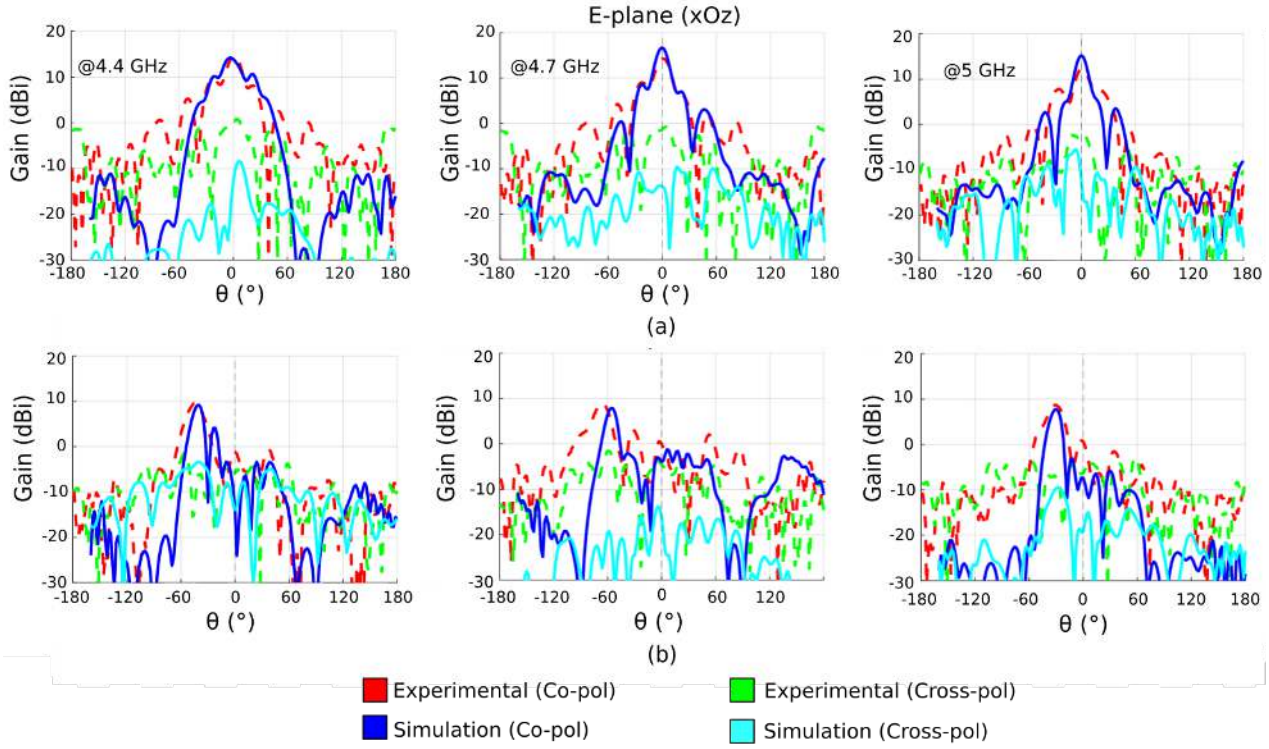


Figure 2. Simulation and experimental results. (a) Boresight radiation at different frequencies. (b) Beam steering (30°, 45° and 60°) at 4.7 GHz.

A Vivaldi radiating element is used to illuminate the metasurface reflector. This radiating element positioned at a certain distance in front of the metasurface will launch electromagnetic waves, which will be reflected by the meta-reflector. The cylindrical parabolic phase profile applied along the metasurface is calculated as:

$$\varphi(x,y) = \frac{2\pi}{\lambda}\left(\frac{(x-x_0)^2}{4F}\right) + \varphi_0 \qquad (1)$$

where λ is the free space operating wavelength, F (= 120 mm) is the focal distance, and φ_0 is the reflection phase at (x_0, y_0).

The cylindrical parabolic phase profiles allowing to obtain a boresight radiation at 4.4 GHz, 4.7 GHz and 5 GHz are applied to the metasurface by judiciously applying the correct bias voltage to each column of meta-atoms. The radiation patterns are presented in Fig. 2(a), and show a highly directive beam in the *E*-plane (*xOz* plane), where the phase profile is applied. The maximum gain reaches 16 dBi at the central frequency of 4.7 GHz. The half-power beamwidth of the antenna is found to be around 32°. The possibility of controlling the direction of the main radiated beam is also performed by introducing an offset x_0 in order to virtually move the parabola with respect to the source. In order to validate the beam-steering capabilities, the phase profile is shifted progressively. Three different beam steering angles (30°, 45° and 60°) are tested at 4.7 GHz. The results presented in Fig. 2(b) show high beam steering capabilities up to 60° with side-lobe levels (SLL) lower than 10 dB.

The resulting performances, particularly the directive nature of the antenna's radiated beam, open the way to several applications in the field of 5G, satellite, and naval communications. The high beam-steering capabilities allow a hemispheric coverage using a reduced number of antennas.

References

1. Ratni, B., A. de Lustrac, G.-P. Piau and S. N. Burokur, "Reconfigurable meta-mirror for wavefronts control: applications to microwave antennas," Opt. Express, Vol. 26, No. 3, 2613–2624, 2018.
2. Ratni, B., Z. Wang, K. Zhang, X. Ding, A. de Lustrac, G.-P. Piau, S. N. Burokur, "Dynamically controlling spatial energy distribution with a holographic metamirror for adaptive focusing," Phys. Rev. Appl., Vol. 13, No. 3, 034006, 2020.
3. De Lustrac, A., B. Ratni, G.-P. Piau, Y. Duval and S. N. Burokur, "Tri-state metasurface-based electromagnetic screen with switchable reflection, transmission, and absorption functionalities," ACS Appl. Electron. Mater., Vol. 3, No. 3, 1184–1190, 2021.
4. Feng, R., B. Ratni, J. Yi, H. Zhang, A. de Lustrac and S. N. Burokur, "Versatile metasurface platform for electromagnetic wave tailoring," Photon. Res., Vol. 9, No. 9, 1650–1659, 2021.
5. Ratni, B., A. de Lustrac, G.-P. Piau and S. N. Burokur, "Electronic control of linear-to-circular polarization conversion using a reconfigurable metasurface," Appl. Phys. Lett., Vol. 111, No. 21, 214101, 2017.
6. Ratni, B., W. A. Merzouk, A. de Lustrac, S. Villers, G.-P. Piau, and S. N. Burokur, "Design of phase-modulated metasurfaces for beam steering in Fabry-Perot cavity antennas," IEEE Antennas Wireless Propag. Lett., Vol. 16, 1401–1404, 2017.
7. Dhouibi, A., S. N. Burokur, A. de Lustrac and A. Priou, "Low-profile substrate-integrated lens antenna using metamaterials," IEEE Antennas Wireless Propag. Lett., Vol. 12, 43–46, 2013.
8. Minatti, G., F. Caminita, E. Martini, M. Sabbadini and S Maci, "Synthesis of modulated-metasurface antennas with amplitude, phase, and polarization control," IEEE Trans. Antennas Propag., Vol. 64, No. 9, 3907–3919, 2016.

Tuning of Fano resonance in mirrored array of split ring resonators

D. Seliuta[1,2,*], A. Kamarauskas[1], G. Šlekas[1], and Ž. Kancleris[1]

[1]Center for Physical Sciences and Technology, Sauletekio ave. 3, 10257 Vilnius, Lithuania
[2]Vilnius Gediminas Technical University, Sauletekio Ave. 11, 10223 Vilnius, Lithuania.
[*]corresponding author: dalius.seliuta@ftmc.lt

Abstract: Fano-type resonances in arrays of mirror-symmetric planar split-ring resonators (SRRs) are investigated using frequency-domain terahertz spectroscopy, numerical simulations, and analytical modeling. Special attention is paid to the guided substrate modes, which are responsible for the excitation of Fano-type peaks in the far-field transmission spectra. We find that the number, frequency, and amplitude of Fano resonances can be effectively tuned by varying the substrate thickness and array period.

Rapid progress in photonics and nanotechnology exposes many examples of resonant optical phenomena associated with Fano resonance [1]. Metasurface with mirror-symmetric SRRs serves as an excellent example of an artificial medium for Fano-type resonance to produce an appreciable transparency peak with enhanced quality factor [2]. In mirror-symmetric resonator array, Fano resonance emerges from the radiative coupling between resonators via the waveguide modes in a dielectric slab. In this work, to understand the behavior of Fano resonance in mirrored arrays, we investigate terahertz transmission of metasurfaces deposited on dielectric slabs of different thickness paying special attention to dispersion of the guided modes and configuration of electromagnetic fields in a dielectric substrate. We propose an original method – the analysis of the Fano resonance properties – to study the in-plane electromagnetic modes propagating along the substrate. We show a significant spectral narrowing and a rather large amplitude of Fano/EIT resonance in resonator arrays deposited on ultrathin dielectric films due to the reduction of ohmic and radiation losses. On the other hand, metasurface deposited on a thick dielectric substrate demonstrates excitation of higher-order guided modes resulting in multiple Fano resonances, which might be useful for various multichannel applications at terahertz frequencies.

The mirror-symmetric SRR array is shown in Fig. 1, and the relevant geometrical dimensions of the resonators are as follows: A = 500 μm, W = 50 μm, and G = 50 μm. The lattice constant L_y is changed from 525 to 800 μm, fixing all other parameters to study the dispersion of the diffracted waves along the dielectric plate. The substrate thickness d is varied in the range from 5 μm to 1200 μm. Numerical simulations are performed using a custom-made program based on the finite-difference time-domain method. An infinite metasurface is modeled by imposing the periodic boundary conditions at the sides of the unit cell. For experimental characterization, samples are fabricated

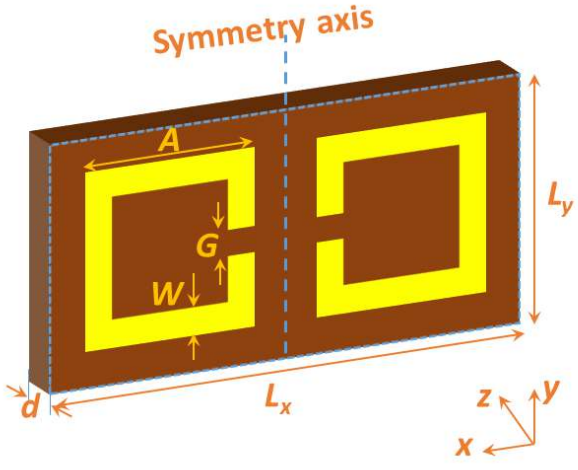


Figure 1. Schematic sketch of unit cell of mirror-symmetric SRR array. Period L_x is twice larger than L_y. Brown represents dielectric substrate, yellow indicates metallized surface.

on low-loss reinforced PTFE substrate of thickness 125 μm (Rogers RT/duroid 5880) and pure PTFE substrate of thickness 1000 μm. In the latter case, the PTFE substrate is metallized using SSAIL method [3]. Power transmission is measured using frequency-domain terahertz spectrometer Toptica Terascan 780. Metal resonators are patterned using conventional photolithography and wet etching techniques.

We observe that Fano-like resonance arises in the 200-300 GHz range due to the interference between the third-order plasmonic mode of SRRs and the guided substrate modes excited by the first-order diffraction of electromagnetic waves in the periodic resonator array [4]. We find that mirror-symmetric configuration of resonators allows excitation of fundamental guided mode in record thin ($\approx\lambda/40$) dielectric films. This is verified by the numerical simulation of electric and magnetic field amplitudes in the substrate. Also, the dispersion of Fano resonant frequency is studied analytically using the ray approach for guided modes and Fresnel formulas. The Fano frequency dispersion in the investigated structures is approximated using a modified waveguide dispersion model that includes an additional reflection phase shift at the substrate-resonator interface. The ultra-thin substrate is advantageous in that the coupling between the resonators is weak, leading to high Q factors and narrow Fano line widths.

On the other hand, as the substrate becomes thicker, the dielectric waveguide supports a more confined mode, resulting in stronger coupling between the resonators and stronger retardation of the in-plane electromagnetic modes, which lowers the Fano resonance frequency. In addition, the thick dielectric slab allows the propagation of higher-order guided modes that interfere with the plasmonic mode and induce three Fano peaks in the transmission spectrum. Theoretical simulations are confirmed by experimental results.

References

1. M. F. Limonov, M. V. Rybin, A. N. Poddubny, and Y. S. Kivshar, “Fano resonances in photonics,” Nat. Photonics, Vol. 11, No. 9, 543–554, 2017.
2. D. Seliuta, G. Šlekas, G. Valušis, and Ž. Kancleris, “Fano resonance arising due to direct interaction of plasmonic and lattice modes in a mirrored array of split-ring resonators,” Opt. Lett., Vol. 44, No. 4, 759–762, 2019.
3. A. Kamarauskas, D. Seliuta, G. Šlekas, M. Sadauskas, E. Kvietkauskas, R. Trusovas, K. Ratautas, and Ž. Kancleris, “Experimental demonstration of multiple Fano resonances in a mirrored array of split-ring resonators on a thick substrate,” Sci. Rep., Vol. 12, 15846, 2022.
4. D. Seliuta, G. Šlekas, A. Kamarauskas, and Ž. Kancleris, “Guided lattice modes in terahertz metasurface deposited on ultrathin dielectric substrate,” IEEE Trans. Terahertz Sci. Technol., Vol. 12, No. 4, 345–352, 2022.

Nonlinear metamaterials

Broadband Terahertz Emitter with All-Dielectric Metasurface Based on the Quasi-Bound States in the Continuum

Y. Guo[1,2*], L. Y. Hu[1,2], B. Wang[1], S. Du[1,2], and C. Z. Gu[1,2*]

[1] Beijing National Laboratory for Condensed Matter Physics, Institute of Physics, Chinese Academy of Sciences, Beijing, China

[2] School of Physical Sciences, CAS Key Laboratory of Vacuum Physics, University of Chinese Academy of Sciences, Beijing, China

[*]corresponding authors: yangguo@iphy.ac.cn, czgu@iphy.ac.cn

Abstract: We propose an all-dielectric metasurface supporting quasi-bound states in the continuum, by which terahertz emission is enhanced in a nonlinear lithium niobate ($LiNbO_3$) film under the excitation of femtosecond laser pulses. Our results show that the terahertz emission is enhanced up to 17 times by a silicon dioxide metasurface in the frequency range of 0.1–4.5 THz. This mechanism for the terahertz emission enhancement is attributed to the tight confinement of the pump field in the $LiNbO_3$ film.

Summary

In this study, we demonstrate an efficient terahertz emitter with an all-dielectric metasurface that enables up to 17 times enhancement of terahertz electric fields across a broad spectral range.[1] The metasurface is composed of patterned a silicon dioxide (SiO_2) layer and an $LiNbO_3$ film, supporting quasi-bound states in the continuum (BIC) induced by breaking the mirror and rotational symmetry.[2] The coupling between a magnetic-dipole mode and an electric-dipole one localizes the pump fields into the high-refractive-index $LiNbO_3$ film, and thus avoids the complicated process of $LiNbO_3$ etching.[3] As a result, the terahertz generation from $LiNbO_3$ is strikingly enhanced. Our work not only breaks the new ground for developing efficient broadband terahertz sources but also expands the application of all-dielectric metasurfaces.

The sample consists of an x-cut $LiNbO_3$ film on an insulating substrate (LNOI) capped a SiO_2 metasurface. We choose the x-cut LNOI to ensure that the orientation with the largest nonlinear coefficient (d33) is in-plane. The electric field of the pump light polarizes along the optic axis of $LiNbO_3$ (z-axis). As the metasurface building block, we select an L-shaped nanoresonator, formed by an in-plane perturbation on an $l \times l$ square (l = 250 nm) nanoresonator. An array of meta-atoms is arranged in a square lattice with the array pitch of p = 480 nm.

To reveal the mechanism of the THz emmission, we first calculated the electromagnetic eigenmodes of the unperturbed square nanoresonators. The square metasurface (SMS) supports a BIC (Mode 1) with an infinite Q factor at the point of the first Brillouin zone. The electric field distribution of Mode 1 presents a magnetic dipole nature polarizing along the x-axis (M_x). The BIC mode is prohibited from coupling with external electromagnetic waves and thus does not contribute to the enhancement of terahertz emission. An electric-dipole mode (mode 2) exists near the BIC mode, polarizing along the z-axis (P_z) with a finite Q factor (1758). The electric dipole mode nearly cannot boost the terahertz generation due to symmetry constraints, though it can slightly confine the pump fields inside the $LiNbO_3$ film.

In next, the L-shaped metasurface (LMS) is designed to break the mirror symmetry, resulting in the coupling between Mx and Pz. We calculated the eigenmode of the LMS. Two hybrid modes (Modes 3 and 4) are formed with both magnetic and electric dipole features. Mode 3 has a finite Q factor of 13768 at the Γ point of the

Brillouin zone, indicating that it is a quasi-BIC. The Q factor of the quasi-BIC approximately scales as an inverse square law with the asymmetry degree of the LMS, which is consistent with the previous report.[4] The quasi-BIC confines and enhances the optical electric fields inside the $LiNbO_3$. The enhanced optical electric field can enhance terahertz nonlinear polarization in $LiNbO_3$, which is the dominant mechanism for enhancing terahertz generation.

Finally, we illuminated our samples ($LiNbO_3$, $LiNbO_3$+SMS, and $LiNbO_3$+LMS) prepared by electron-beam lithography (EBL) technique, with NIR laser pulses (central wavelength 800 nm, repetition rate 80 MHz, duration 70 fs) and measured the terahertz generation by our homemade terahertz time-domain spectroscopy. We perform the Fourier transform of the terahertz pulses to investigate the enhancement further. Our results show that the enhancement of the terahertz amplitude spans the entire operating bandwidth of the detector (0.1–3 THz), but the detection frequency range is restricted by the thickness of ZnTe (2 mm). Utilizing a thinner ZnTe crystal (300 μm) as a detector, the detected enhanced bandwidth of the terahertz emission approaches 4.5 THz. The enhancement factor, terahertz amplitudes divided by the terahertz amplitude of $LiNbO_3$, reaches 17 around 0.7 THz for the LMS+ $LiNbO_3$ sample. Inversely, the enhancement factor for the SMS+ $LiNbO_3$ sample almost maintains 1 in the entire bandwidth of the detection. All of these findings show that our BIC-based all-dielectric metasurface can efficiently boost terahertz emission in the broadband range.

In conclusion, our experiment demonstrates that constructing metasurfaces on the $LiNbO_3$ film is an effective method to manipulate nonlinear processes, further releasing the potential of LNOI in nonlinear micro-nano photonics. The mechanism for enhancing terahertz generation is ascribed to the quasi-BIC induced by symmetry breaking, which strongly confines the pump electric fields in the $LiNbO_3$ films. The all-dielectric metasurface-based terahertz emitter features broadband, high efficiency, and small dimension, which paves the way for highly compact terahertz systems.

Acknowledgements

This work was supported by the National Natural Science Foundation of China under Grant Nos. 61888102, 11974386, 62174179, 12074420, U21A20140 and 61905274, the National Key Research and Development Program of China under Grant No. 2021YFA1400700, the Beijing Municipal Science & Technology Commission, Administrative Commission of Zhongguancun Science Park under Grant No. Z211100004821009, the Strategic Priority Research Program of Chinese Academy of Sciences (CAS) under Grant Nos. XDB33000000 and XDB28000000, the Key Research Program of Frontier Sciences of CAS under Grant Nos. QYZDJ-SSWSLH042 and XDPB22. and the Project for Young Scientists in Basic Research of CAS under Grant No.YSBR021. This work is also supported by the Synergic Extreme Condition User Facility, China.

References

1. Hu, L., B. Wang, Y. Guo, S. Du, J. Chen, et al. “Quasi-BIC Enhanced Broadband Terahertz Generation in All-Dielectric Metasurface,” Adv. Opt. Mater. 10, 2200193, 2022.
2. Yu, Z., Y. Y. Tong, H. K. Tsang and X. K. Sun, “High-dimensional communication on etchless lithium niobate platform with photonic bound states in the continuum” Nat. Commun. 11, 2602, 2020.
3. Sun, D., Y. Zhang, D. Wang, W. Song, X. Liu, et al. “Microstructure and domain engineering of lithium niobate crystal films for integrated photonic applications,” Light: Sci. Appl. 29, 197, 2020.
4. Koshelev, K., S. Lepeshov, M. Liu, A. Bogdanov and Y. Kivshar, “Asymmetric Metasurfaces with High-Q Resonances Governed by Bound States in the Continuum,” Phys. Rev. Lett. 121, 193903, 2018.

Nonlinear Effects of Linear Time-Dependent Metamaterials

P. R. Ghodake

Department of Mechanical Engineering, Indian Institute of Technology Bombay, India
mech7pkumar@gmail.com

Abstract: Nonlinear responses of linear time-dependent elastic metamaterials are demonstrated in this study through computational experiments. Manipulation capabilities of the time-varying metamaterials such as harmonic generation, controlling frequency combinations due to monochromatic wave and two-wave mixing by varying parameters time-dependent material property is explored in depth.

Introduction

Wave propagation in time-varying metallic materials is studied through a numerical perspective using the finite element method in this article. Recent developments in the photonics of time-varying media and multi-dimensional metamaterials motivated this research[1,2]. A Schematic of a numerical model is shown in Figure 1. The Young's modulus of the elastic material varies with respect to time (t) between t_1 and $t_2 + t_{pw}$, where t_1 and t_2 are the time required for the elastic waves to reach sensors S_1 and S_3, respectively, t_{pw} is the pulse width of the input monochromatic ($f = 2$ MHz) pulse, and f_0 is the oscillating frequency of the time-varying Young's Modulus (E) an elastic material property.

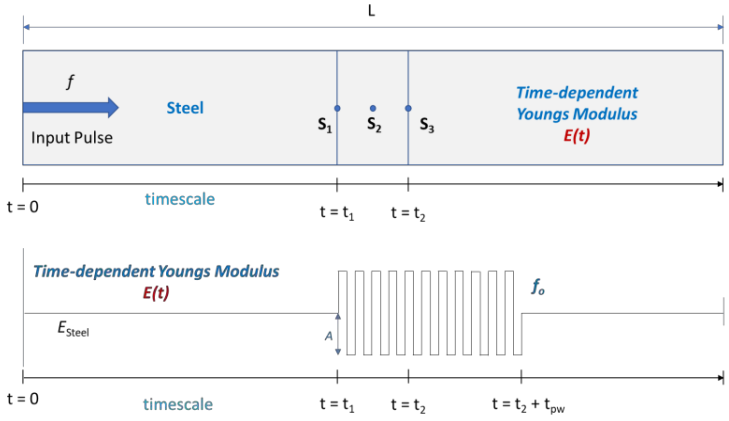


Figure 1. A schematic of the numerical model used to study the interaction of the elastic wave with the time-dependent metamaterial. The time variation of E_{steel} from t_1 to $t_2 + t_{pw}$ is shown.

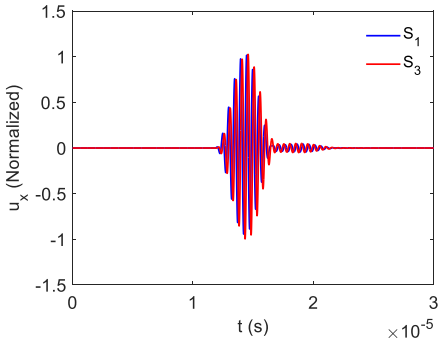


Figure 2. Time responses at S_1 and S_3 at amplitude $0.1E_{steel}$ (A) of the time-dependent material property when $f_0 = f$

Results and Discussion

Figure 2 shows the presence of scattered waves due to time-varying media and the input signal at both the sensors S_1 and S_3. Frequency responses from Figure 3 clearly show the presence of higher harmonics like $f + f_0 = |f - 3f_0| = 2f = \mathbf{4}$ MHz, $f + 3f_0 = |f - 5f_0| = 4f = \mathbf{8}$ MHz, and $|f - f_0| = \mathbf{0}$ MHz (static term) at low amplitude ($0.02E_{steel}$) of time-varying media. Interestingly as the amplitude of time-varying media increases from $0.02E_{steel}$ to $0.1E_{steel}$ the other frequency combinations like $f + 2f_0 = 3f = \mathbf{6}$ MHz shows their presence dominantly. Nonlinear harmonic responses of the linear time-varying materials show that linear materials behave as nonlinear materials due to the interaction of elastic waves when they are time-dependent.

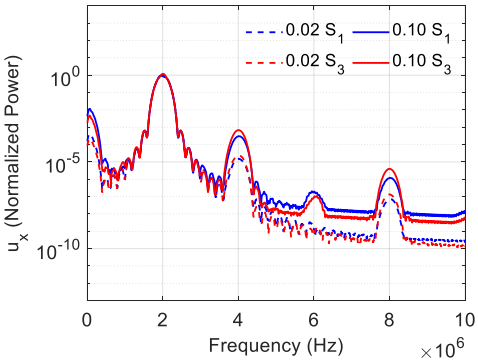


Figure 3. Frequency responses of the waves at S_1 and S_3 at $0.02E_{steel}$ and $0.10E_{steel}$ amplitudes (A) of time-dependent material properties when $f_0 = f$

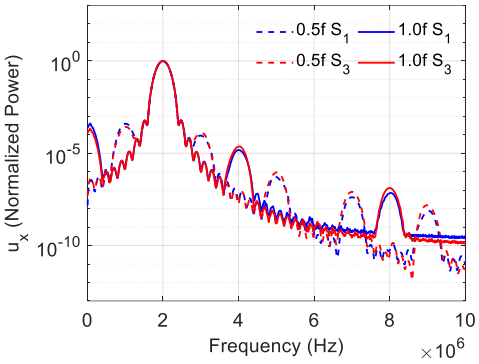


Figure 4. Frequency responses of the waves at S_1 and S_3 at $0.02E_{steel}$ amplitude (A) of time-dependent material properties and at $f_0 = 0.5f$ & $f_0 = 1.0f$

Similarly, when we change f_0 to $0.5f$, the different frequency combinations are observed such as $f + f_0 = |f - 5f_0| = 1.5f =$ **3** MHz, $f + 3f_0 = |f - 7f_0| = 2.5f =$ **5** MHz, $f + 5f_0 = 3.5f =$ **7** MHz, $f + 7f_0 = 4.5f =$ **9** MHz, and $|f - f_0| = |f - 3f_0| =$ **1** MHz as seen from Figure 4. Interestingly the static term ($0f =$ **0** MHz is not present when $f_0 = 0.5f$) only because of these particular combinations of the f and f_0 in comparison with when $f_0 = f$. Similar responses at $f_0 = 0.8f$, along with the frequency combinations during one-way two-wave mixing, are shown in Figure 5 and Figure 6. An increase in the amplitudes of all the frequency combinations during one-way two-wave mixing due to an increase in the amplitude (A) of the time-dependent material property from 0.02 to 0.10 can be seen in Figure 5. This study clearly shows the nonlinear manipulation of linear time-varying media that can be used as a nonlinear metamaterial to control elastic wave's harmonics. This study will help to expand the universe of time-dependent linear and nonlinear mechanical metamaterials to exploit their novel capabilities.

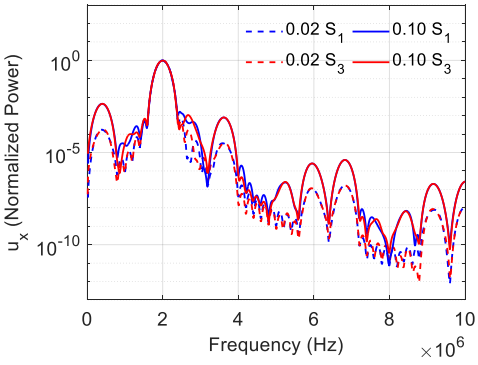


Figure 5. Frequency responses of the waves at S_1 and S_3 at $0.02E_{steel}$ and $0.10E_{steel}$ amplitudes (A) of time-dependent material properties when $f_0 = 0.8f$

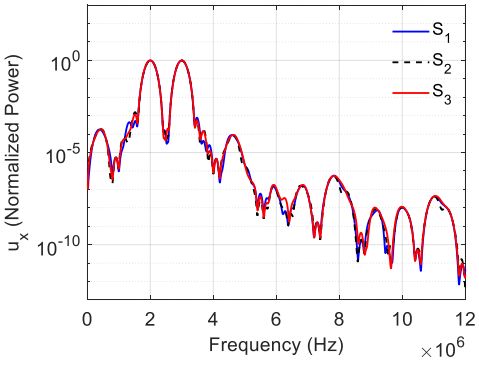


Figure 6. Frequency responses of the waves at S_1 and S_3 due to one-way two-wave mixing at $0.02E_{steel}$ amplitude (A) when $f_0 = 0.8f$

References

1. N. Engheta, "Metamaterials with high degrees of freedom: Space, time, and more," *Nanophotonics*, Vol. 10, No. 1, 639–642, 2021.
2. E. Galiffi *et al.*, "Photonics of time-varying media," *Adv. Photonics*, Vol. 4, No. 1, 1–32, 2022.

META 2023, PARIS - FRANCE, JULY 18 – 21, 2023

Nonlinear optics of quasistatic origin from a deep-subwavelength metallic meta-atomical system

Avi Niv[1]

[1]Department of Solar Energy and Environmental Physics, Jacob Blaustein Institutes for Desert Research, Ben-Gurion University of the Negev, Israel.

[*]Corresponding author: aviniv@bgu.ac.il

Abstract: Surprisingly, the exact macro-world nonlinear mechanisms known for decades are also invoked in nano-scale nonlinear optics. In this talk, we will present a nonlinear optical mechanism that can only be found once the spatial dimension of a system is below the electromagnetic penetration depth. We will describe our experiments with the second harmonic generation (SHG) and optical rectification and discuss future research directions such as third-order effects, high harmonic generation, and chaos.

Nonlinear optics (NLO) is a vibrant indispensable research field. Nonetheless, the fundamental mechanism responsible for parametric frequency mixing has been known for decades. These exact mechanisms are also considered in the nano-scale. An essential aspect of second-order optical nonlinearity is the necessity of inversion symmetry violation. Combined with the conventional view of NLO, only negligible nonlinearity is expected from systems whose spatial dimensions are below the electromagnetic penetration depth. This vanishing effect applies to bulk nonlinearity due to the system's inability to support the required field gradients or to the net response from surface sources due to the lack of a phase lag and the ensuing canceling effect at opposite-facing surfaces.

Recently we have studied a metallic dimer whose spatial dimensions are ~30nm – comparable to the EM penetration into its comprising silver and gold [1-3]. To our surprise, an appreciable SHG emerged and showed a qualitatively different behavior than what the existing theory predicts in this case. This observation promoted us to consider the consequence of an extreme subwavelength system: Since there is no possibility for an appreciable phase difference, charges in each material domain of the dimer oscillate uniformly – a fact that is also confirmed with simulations. In addition, since the entire dimer is also deeply subwavelength, quasistatic Coulomb interaction emerges. Under these circumstances, the inter-dimer interaction assumes the following form:

$$\propto \frac{Q}{\Delta^2(t)}, \qquad (1)$$

where Q is a fixed-charge-related property and $\Delta(t)$ is the instantaneous separation between the two bodies of oscillating charges. Notice that this Coulomb interaction differs from what is usually foreseen for a dipole interaction where the separation is fixed, and the charge-related property oscillates. The dynamic denominator of Eq. (1) endows a coupled oscillator model with such coupling a significant nonlinear character. NLO, in this case, emerges from the *interaction* between two optical systems that are otherwise strictly linear in their response to an external field due to their extreme subwavelength dimensions.

Figure 1(a) shows full-wave simulation results for a deep subwavelength silver-silver (Ag-Ag) dimer in blue, silver-gold (Ag-Au) dimer in green and gold-gold (Au-Au) in orange. The simulation of our most advanced understanding of the SHG from a dimer system predicts that the Ag-Ag dimer should have the upper hand in SHG, followed by the Ag-Au case and ending with the Au-Au dimer. In addition, the spectral lineshape follows the dimer's

linear absorption spectra (not shown). Fig. 1(b) shows the measured SHG from corresponding samples. It is seen that the Ag-Au dimer substantially surpasses the other cases in terms of its SHG strength and, in addition, has a spectral peak - both indicating that the dominant NLO mechanism is not as predicted. The results of an oscillator model with coupling terms following Eq. (1) are shown in a solid black line for the Ag-Au case and a dashed black line for the Ag-Ag and Au-Au cases. It is seen that an interaction-based model captures both Ag-Au supremacy and its spectral peak. We have also studied other NLO effects; Fig. 1 (c) shows the DC potential from a sample configured for parametric optical rectification in blue and the prediction of the interaction model in green. The model reproduces the measured signal, including the non-quadratic trend at the strong-excitation regime, which is not thermal. On the contrary, the conventional theory shown in the orange line is limited to quadratic lineshapes that missed essential aspects of the light-matter interaction in this case.

In summary, we discuss experimental proof for a nonlinear optical mechanism beyond what is considered conventional. In the talk, we will present our methods of investigation and discuss the unique properties of interaction-based nonlinear optics for third-order processes, high harmonics, and optical chaos.

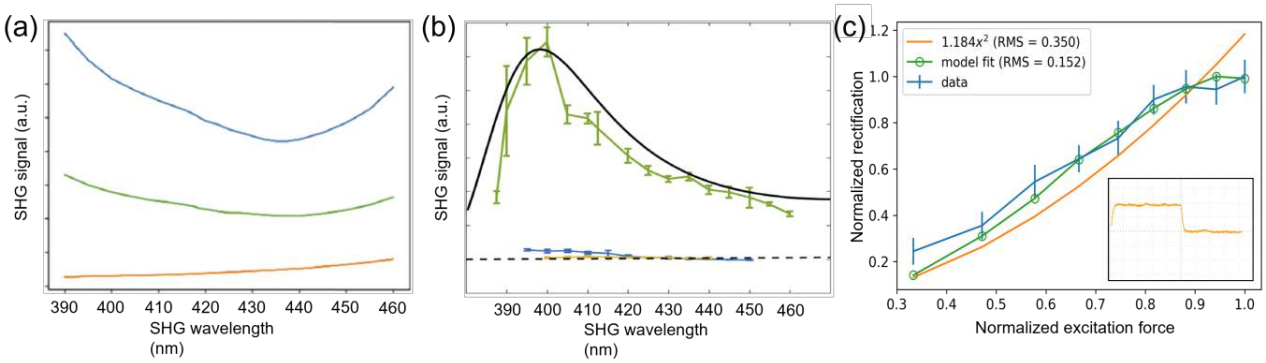


Figure 1: (a) Full-wave simulation of the dimer's SHG with blue, green, and orange lines depicting Ag-Ag, Ag-Au, and Au-Au dimers, respectively. (b) The experimental results from corresponding dimers. Notice that the Ag-Au case surpasses the Ag-Ag and the Au-Au dimers in contrast with the simulation results. Black lines depict the interaction model prediction for the Ag-Au case (solid) and for the Ag-Ag and Ag-Au cases (dashed). The proposed interaction-based nonlinear model reproduces the Ag-Au supremacy and its distinctive SHG peak. (c) Parametric rectification signal Vs. laser excitation force. Experimental results are shown in blue, the interaction model predictions are in green, and the best-case scenario of a conventional optical nonlinearity is in orange. It is seen that the model reproduces the non-quadratic trend of the rectified signal, which is a genuine interaction-based nonlinear effect and not a thermal one. Inset shows the parametric rectification signal for a single On-Off sequence of the excitation laser.

References

1. Levi, S., Samueli, R., Choudhary, M., and Niv, A., "Second-harmonic generation of electrostatic origin from extreme nanosized bi-metal structures," Optics Letters, Vol. 43, No. 15, 3662-3665, 2018.
2. Peled, M.H.S., Toledo, E., Shital, S., Maity, A., Pal, M., Sivan, Y., Schvartzman, M. and Niv, A., "Second-harmonic generation from subwavelength metal heterodimers," Optics Express, Vol. 28, No. 21, 31468-31479, 2020.
3. Pal, M. and Niv, A., "Parametric optical rectification due to the near-field interaction between nanosized metallic domains," Optics Express, Vol. 31, No. 3, 4873-4883, 2023.

Controlling High-Q Lattice Resonances in Bipartite Plasmonic Arrays through Nanoparticle Geometry and Orientation

Timo Stolt[1*], Jussi Kelavuori[1], Ali Panahpour[1] and Mikko J. Huttunen[1]

[1]Photonics Laboratory, Physics Unit, Tampere University, FI-33014 Tampere, Finland
[*]corresponding author: timo.stolt@tuni.fi

Abstract: We numerically investigated plasmonic nanoparticle (NP) arrays with bipartite lattice configuration. The lattice periodicities were selected to give rise surface lattice resonances (SLRs) at two separate wavelengths in the near-infrared region. We show that the quality factors of the SLRs can be considerably improved by modifying the NP geometry and mutual orientation. NP modification also impacted the local-field distributions associated with SLRs, which is expected to have a significant impact on the nonlinear responses of the studied structures.

Periodic arrays of plasmonic nanoparticles (NPs) show potential for realizing novel photonic devices, such as microscopic lenses, lasers, and nonlinear components [1-3]. The optical responses of such structures can be enhanced through collective resonances known as surface lattice resonances (SLRs), which are narrowband collective excitations associated with high quality-factors (Q-factors) and strong local-field enhancements [4]. Recently, structures exhibiting multiple SLRs have shown promise for tunable nonlinear metasurface devices [5,6]. However, different SLRs in such multiresonant designs often occur for orthogonal polarization states. This results in poor spatial overlap between different SLR modes, and consequently, weakened light–matter interaction. Here, we address this issue by designing plasmonic bipartite NP arrays exhibiting two SLRs for the same incident polarization. We show that by changing the NP geometry and orientation, the Q-factors and mutual mode-overlaps of the occurring SLRs can be improved, which is essential for enhancing nonlinear processes taking place in such NP arrays.

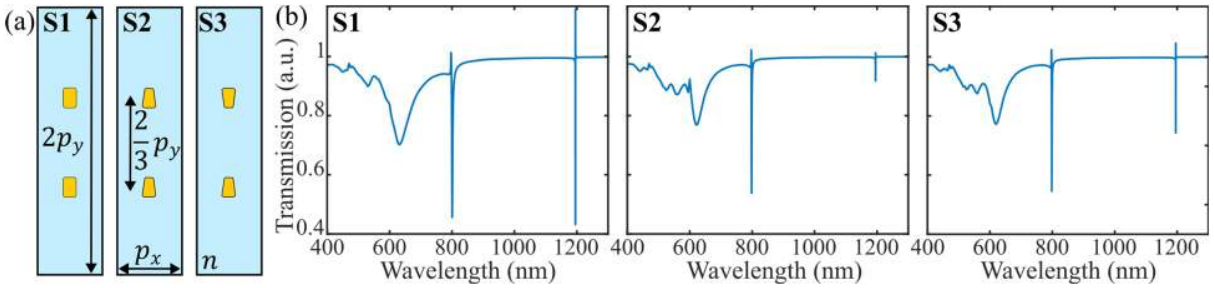


Figure 1: (a) The studied metasurface designs S1–S3 consisted of gold nanoparticles arranged in bipartite lattice. The arrays were embedded in homogeneous glass surroundings with refractive index $n = 1.45$. (b) Transmission spectra for x-polarized light for the studied sample designs. With p_y = 825 nm, the bipartite metasurfaces exhibit two SLRs near λ_1=800 nm and λ_2=1200 nm, respectively.

We numerically investigate (COMSOL Multiphysics) the optical properties of three metasurface designs consisting of gold NPs embedded in homogeneous glass surroundings ($n = 1.45$). Sample S1 consisted of rectangular NPs with thickness of 40 nm, length of 120 nm, and width of 80 nm (see Fig 1a). These NP dimensions give rise localized surface plasmon resonance (LSPR) near 625 nm (see Fig 1b). For samples S2 and S3, the width on one of sides of the NPs was shortened by 30 nm. In S2, the NPs were oriented in the same direction, while in

S3, every second NP was flipped so that the narrow ends of the NPs would point to each other. The narrowing of the NPs slightly blueshifts the LSPR to 620 nm and make it slightly narrower. The flipping of the NPs had no visible impact on LSPRs.

For all three designs, the lattice configuration was the same. Along the x-axis, each unit cell had one NP and periodicity of p_x = 400 nm. Along the y-axis, the total periodicity was $2p_y$ and two NPs were separated by $2/3p_y$ (see Figure 1a). With p_y= 825 nm, this lattice configuration gives rise two SLRs, named SLR1 and SLR2, near λ_1 = 800 nm and λ_2 = 1200 nm, respectively (see Figure 1b). The NP geometry and orientation do not significantly change these resonance wavelengths, but rather the Q-factor associated with the SLRs (see Figure 2). First, the narrowing of the NPs increases the Q-factor of SLR1 from 300 for S1 to roughly 1000 for S2 and S3. However, only narrowing the NPs decrease the Q-factor of SLR2 significantly: for S1 it is approximately 50 000, while for S2 it has decreased significantly to approximately 12 000. Interestingly, this effect can be compensated by flipping every second NP in the array. Thus, for S3, the SLR2 has a considerably high Q-factor of roughly 30 000. Furthermore, S3 has improved mode overlap between the two analyzed SLR modes, which is expected to boost nonlinear frequency-conversion processes, such as sum-frequency generation, difference-frequency generation, and four-wave-mixing.

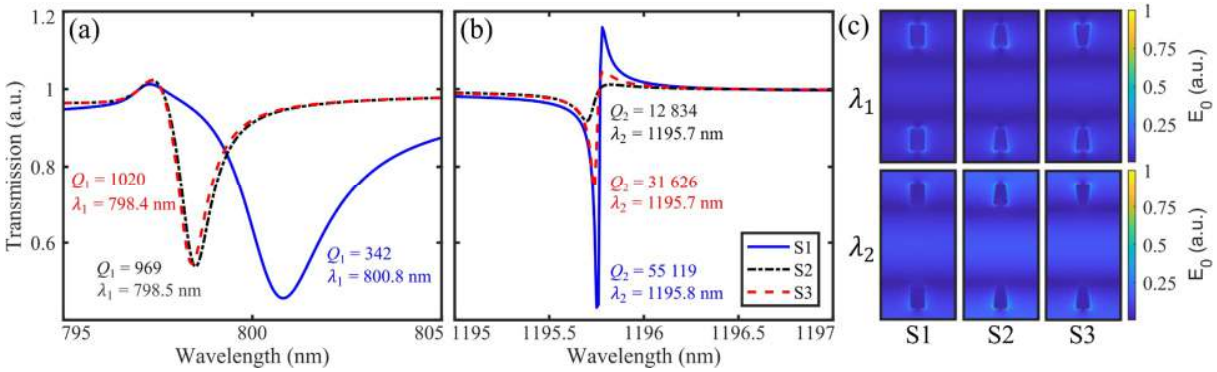


Figure 2: Transmission spectra for the investigated designs S1–S3 near (a) SLR1 wavelength $\boldsymbol{\lambda_1}$ and (b) SLR2 wavelength $\boldsymbol{\lambda_2}$. (c) Near-field distributions at $\boldsymbol{\lambda_1}$ and $\boldsymbol{\lambda_2}$.

We acknowledge the support the Flagship of Photonics Research and Innovation (PREIN) funded by the Academy of Finland (Grant No. 320165). T.S. acknowledges also Jenny and Antti Wihuri Foundation for a doctoral research grant.

References

1. J. Hu et al. “, Lattice-Resonance Metalenses for Fully Reconfigurable Imaging”, ACS Nano, Vol. 13, No. 4, 4613-4620 (2019).
2. T. K. Hakala et al. “, Lasing in dark and bright modes of a finite-sized plasmonic lattice”, Nat. Commun., Vol. 8, No. 13678 (2017).
3. L. Michaeli et al. “, Nonlinear Surface Lattice Resonance in Plasmonic Nanoparticle Arrays”, Phys. Rev. Lett., Vol. 118, No. 24, 243904, (2017).
4. M. S. Bin-Alam et al. “, Ultra-high-Q resonances in plasmonic metasurfaces”, Nat. Commun. Vol. 12,, No. 974 (2021).
5. T. Stolt et al. “, Multiply-resonant second-harmonic generation using surface lattice resonances in aluminum metasurfaces”, Opt. Express, Vol. 30, 3620–3631, (2022).
6. T. Lim et al. “, Fourier-Engineered Plasmonic Lattice Resonances”, ACS Nano, Vol. 16, No. 4, 5696–5703 (2022)

META 2023, PARIS - FRANCE, JULY 18 – 21, 2023

Enhanced Generation of Higher Harmonic from Halide Perovskite Metasurfaces

P. Tonkaev[1*], K. Koshelev[1], M. Masharin[2], S. Makarov[3], S. Kruk[1], and Yuri Kivshar[1]

[1] Nonlinear Physics Center, Research School of Physics, Australian National University, Canberra, ACT 2601, Australia

[2] Department of Electrical and Electronics Engineering and Department of Physics, UNAM-Institute of Materials Science and Nanotechnology, Bilkent University, Ankara 06800, Turkey

[3] Qingdao Innovation and Development Center, Harbin Engineering University, 266000 Qingdao, China

[*]corresponding author: pavel.tonkaev@anu.edu.au

Abstract: Many outstanding properties of halide perovskites provided their applications in optoelectronics. Perovskite films demonstrate outstanding nonlinear properties with large optical nonlinearities comparable to the nonlinear constants of conventional semiconductor materials. Meanwhile, nonlinear properties can be enhanced by the metaphotonic approach. Here we demonstrate a two-order enhancement of fifth-harmonic generation in halide perovskite nonlocal metasurfaces due to high-quality resonance at the generated harmonic wavelength in the visible frequency range.

Halide perovskites have many outstanding properties such as a tunable bandgap, pronounced exciton at room temperature, and high photoluminescence quantum yield [1]. Moreover, methylammonium lead halide perovskites have large nonlinear constants compared with conventional semiconductor materials [2] which provide a promising application for nonlinear metaphotonics. Their strong nonlinearities have provided high multiphoton absorption [3] and third-harmonic generation [4]. Engaging of metaphoric approach led to significant enhancement of two-photon photoluminescence and made it comparable to linear one [5]. Meanwhile, broken-symmetry nonlocal Si metasurfaces supporting a BIC demonstrated enhancement of high-harmonic generation [6]. Herein, we implement metaphotonics approach for the fifth harmonic generation in halide perovskite.

We designed and fabricated $MAPbBr_3$ metasurface that consists thin slab placed on a glass substrate and patterned with a shallow grating. Obtained metasurface supports two modes, a bound state in the continuum and guided-mode resonance, in the visible range. By pumping in the mid-IR range we observed third-harmonic generation in the near-IR range and fifth-harmonic generation in the visible range. The fifth-harmonic signal provided enhancement up to 90 in the range of pump wavelengths that generate harmonic in the visible range near the structure resonance of the metasurface. Our nonlinear simulations confirmed that the observed enhancement is due to the excitation of both modes of the structures. We believe our work paves the way toward efficient perovskite nonlinear metaphotonic devices.

This work was supported by the Australian Research Council (grants DE210100679 and DP210101292).

References

1. Tonkaev, P. et. al. “Multifunctional and Transformative Metaphotonics with Emerging Materials,” Chemical Reviews, Vol. 112, No. 19, 15414–15449, 2022.
2. Zhou, Y. et. al. “Nonlinear optical properties of halide perovskites and their applications,” Applied Physics Reviews, Vol. 7, No. 7, 041313, 2020.

3. Weng, G. et. al. “Picosecond random lasing based on three-photon absorption in organometallic halide CH3NH3PbBr3 perovskite thin films,” ACS Photonics Vol. 5, No 7, 2951–2959, 2018.
4. Abdelwahab, I. et. al. “Highly enhanced third-harmonic generation in 2D perovskites at excitonic resonances,” ACS Nano, Vol. 12, No. 1, 644–650, 2018.
5. Fan, Y. et al. “Enhanced multiphoton processes in perovskite metasurfaces,” Nano Letters Vol. 21, No. 17, 7191–7197, 2021.
6. Zograf, G., et al. “High-Harmonic generation from resonant dielectric metasurfaces empowered by bound states in the Continuum,” ACS Photonics, Vol. 9, No. 9, 567–574, 2022.

Optical bistability in Su-Schrieffer-Heeger lattice with Kerr nonlinearity

Ghada Alharbi, Sang Soon Oh*

School of Physics and Astronomy, Cardiff University, Cardiff CF24 3AA, UK
*E-mail: ohs2@cardiff.ac.uk

Abstract

We present a nonlinear 1D Su–Schrieffer–Heeger model that models an array of coupled ring resonators with Kerr nonlinearity. We theoretically demonstrate that spontaneous symmetry breaking can be observed by symmetrically pumping the array in the clockwise and counterclockwise directions. The optical bistability can be attributed to the different shift of resonance frequencies between the two counter-propagating modes.

In the recent years, the study of photonic topological insulators has rapidly grown as an interesting subject in the fields of nanophotonics and quantum optics. Researchers have applied topological insulator models to various photonic platforms, e.g., an array of optical waveguides and microring resonators, to explore unique properties related to zero-energy modes [1, 2, 3]. Topologically protected localization at one edge of the system is the unique characteristic of topological insulators. So far, most of studies have considered the photonic topological insulators in the linear regime with weak field intensities. This is partly due to the complexity in modelling nonlinear responses together with modulated couplings. In this work, we study optical bistabilities coming from the Kerr nonlinear effect in a one-dimensional lattice model, called Su-Schrieffer-Heeger (SSH) model.

First, we implement the SSH model in a photonic system by arranging coupled microring resonators with alternating coupling coefficients, v and w. Then, we introduce the Kerr nonlinearity in each ring resonator that leads to the change of refractive indices, called self-phase modulation (SPM) and cross-phase modulation (XPM). The first ring resonator in the array is pumped by the two input sources with the same amplitudes S_{in} in the opposite directions. Fig. 1(a) shows the SSH model consisting of $(N+1)$ unit cells, and each unit cell has two sites: a and b.

To theoretically describe the model, we use the temporal coupled mode theory where the time evolution of the circulating field amplitudes a_n and b_n are calculated in the time domain. Here, we consider the intensities of the modes circulating in the clockwise $(+)$ and counterclockwise $(-)$ directions at each ring resonator [4, 5].

$$\begin{aligned} \frac{da_{n,\pm}}{dt} &= -i\Big[\omega_0 + i\omega_0\kappa(|a_{n,\pm}|^2 + 2|a_{n,\mp}|^2) - i\gamma_n\Big]a_{n,\pm} + \gamma_c s_{in} + ivb_{n,\mp} + iwb_{n-1,\mp}, \\ \frac{db_{n,\pm}}{dt} &= -i\Big[\omega_0 + i\omega_0\kappa(|b_{n,\pm}|^2 + 2|b_{n,\mp}|^2) - i\gamma'_n\Big]b_{n,\pm} + iva_{n,\mp} + iwa_{n+1,\mp}, \end{aligned} \tag{1}$$

where n denotes the index site. Here, the parameters γ_n and γ'_n are defined as $\gamma_n = \gamma_0 + \gamma_c\delta_{n,1}$ and $\gamma'_n = \gamma_0$, where γ_0 is the damping coefficient and γ_c is the coupling coefficient between the input waveguide and the first ring resonator. $\omega_0 = \omega + \Delta$ is the resonance frequency, here ω is laser frequency and Δ is detuning. On the right hand side of Eq. (1), the first term describes the detuning, the second and third are nonlinear terms with Kerr coefficient κ and the fourth is a damping term. The fifth term is the input field that appears only for the first ring resonator because it is the only one pumped directly by the input sources. The other terms are related to the coupling between the ring resonators.

For convenience, we normalize the coefficients in Eq. (1) with respect to the damping coefficient γ_0. Then, the equation can be written as :

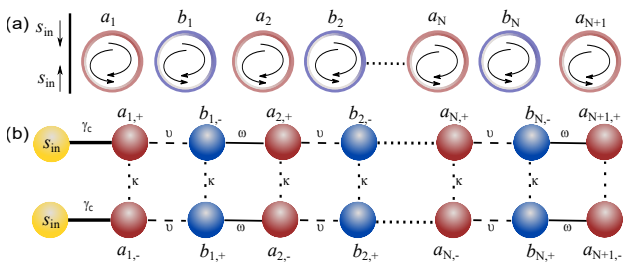


Figure 1: (a) A 1D array of coupled ring resonators with alternating gap sizes. (b) A schematic of the SSH model with resonators with Kerr nonlinearity coefficient κ.

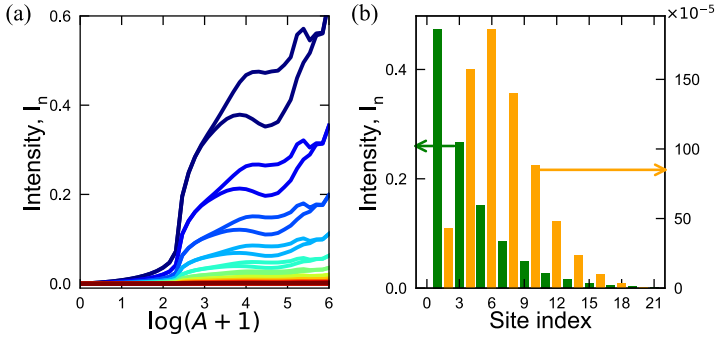


Figure 2: (a) Bistability observation for $M = 21$ ring resonators with detuning $\tilde{\Delta} = 1.85\tilde{\gamma_c}$, $\tilde{\gamma_c} = 10$, $\tilde{\kappa} = 10$ and $\gamma_0 = 0.001$. (b) The distribution of intensity on sites for $\log(A+1) = 4.15$ for odd sites (green color) and even site (orange color).

$$\begin{aligned} \frac{da_{n,\pm}}{d\tilde{t}} &= -\tilde{\gamma}_n - i\Big[1 + i\tilde{\kappa}(|a_{n,\pm}|^2 + 2|a_{n,\mp}|^2)\Big]a_{n,\pm} + \tilde{\gamma_c}s_{in} + i\tilde{v}b_{n,\mp} + i\tilde{w}b_{n-1,\mp}, \\ \frac{db_{n,\pm}}{d\tilde{t}} &= -\tilde{\gamma'}_n - i\Big[1 + i\tilde{\kappa}(|b_{n,\pm}|^2 + 2|b_{n,\mp}|^2)\Big]b_{n,\pm} + i\tilde{v}a_{n,\mp} + i\tilde{w}a_{n+1,\mp}, \end{aligned} \tag{2}$$

where the tilde denotes normalised quantities and we set the normalized frequency as the unity. Note that Eq. (2) is the Lugiato-Lefever equations [6] modified with additional couplings between the ring resonators and the input waveguides.

The circulating intensities for each ring resonator at different input amplitudes A are illustrated in Fig. 2(a). We observe the symmetry breaking of light intensities at the pump amplitude between $\log(A+1) = 3$ and $\log(A+1) = 5.8$. When the pump intensity goes above a certain level, the Kerr nonlinear effect shifts the resonance frequency of the modes and, along with some detuning, results in the optical bistabilities. As shown in Fig. 2(b), the field intensity becomes significant for odd sites only (sublattices a) and decreases exponentially in the right direction, which is the signature of the zero-energy edge modes.

In conclusion, we have theoretically shown that the spontaneous symmetry breaking in intensity between circulating optical modes can occur in a nonlinear coupled ring resonator even when symmetrically pumped in the clockwise and counterclockwise directions. We have shown that the Kerr effect starts to induce the resonance frequency shift between circulating modes at a certain value of the incident amplitude,

References

[1] J. Noh, S. Huang, K. P. Chen, and M. C. Rechtsman, "Observation of Photonic Topological Valley Hall Edge States," *Physical Review Letters*, vol. 120, p. 063902, feb 2018.

[2] M. A. Bandres, S. Wittek, G. Harari, M. Parto, J. Ren, M. Segev, D. N. Christodoulides, and M. Khajavikhan, "Topological insulator laser: Experiments," *Science*, vol. 359, p. eaar4005, mar 2018.

[3] Y. Gong, S. Wong, A. J. Bennett, D. L. Huffaker, and S. S. Oh, "Topological Insulator Laser Using Valley-Hall Photonic Crystals," *ACS Photonics*, vol. 7, pp. 2089–2097, aug 2020.

[4] H. H. Haus, *Waves and Fields in Optoelectronics*. Prentice Hall, 1983.

[5] W. Suh, Z. Wang, and S. Fan, "Temporal coupled-mode theory and the presence of non-orthogonal modes in lossless multimode cavities," *IEEE J. Quantum Electron.*, vol. 40, pp. 1511–1518, oct 2004.

[6] L. A. Lugiato and R. Lefever, "Spatial Dissipative Structures in Passive Optical Systems," *Physical Review Letters*, vol. 58, pp. 2209–2211, may 1987.

Large Enhancement in Visible to UV Nonlinear Frequency Conversion by a Plasmonic Gold Nanograting

S. Mukhopadhyay[1*], L. Rodriguez-Suné[1], C. Cojocaru[1], M. A. Vincenti[2], K. Hallman[3], G. Leo[4], M. Belchovski[2], D. de Ceglia[2], M. Scalora[5], and J. Trull[1]

[1] Department of Physics, Universitat Politècnica de Catalunya, Rambla Sant Nebridi 22, 08222 Terrassa (Barcelona), Spain
[2] Department of Information Engineering – University of Brescia, Via Branze 38, 25123 Brescia, Italy
[3] PeopleTec, Inc. 4901-I Corporate Dr., Huntsville, AL 35805, USA
[4] Lab. Matériaux et Phénomènes Quantiques, Université Paris Cité&CNRS, 10 rue Alice Domon et Léonie Duquet, 75013 Paris, France
[5] Aviation and Missile Center, US Army CCDC, Redstone Arsenal, AL 35898-5000, USA
[*]corresponding author: shroddha.mukhopadhyay@upc.edu

Abstract: We report a combined experimental/theoretical investigation on second and third harmonic generation from a plasmonic gold nanograting, resonant in the near infrared. The intense field localization leads to significant enhancement in nonlinear optical processes, more than three orders of magnitude herein, compared to flat gold nanolayer. The spectral and angular dependence (qualitative and quantitative) of the harmonics were experimentally recorded and validated within the framework of our microscopic, hydrodynamic model for linear and nonlinear material dispersion mechanisms of metals.

Theoretical and experimental study of nonlinear optical properties of metals, arches back to the beginning of nonlinear optics. Despite their high absorption in the visible and near infrared spectral ranges, metals are highly nonlinear materials and the study of NL optics from metal surfaces combined with plasmonics is a very active field of research with important applications in the fabrication of functional nano-photonic devices. However, the efficiency of harmonic generation from gold nanolayers and nanostructures is generally very low and is strongly limited in the wavelength range where absorption is present. Also, most of experimental results presented in literature often show only qualitative aspects of this enhancement, do not quantify the efficiency (presenting only arbitrary units) and are not in good agreement with the theoretical models set forward. It is crucial to understand and exploit the properties of light propagation and localization at the nanoscale to successfully design nano-antennas, filters and other devices whose geometrical features approach atomic size. At this scale light matter interaction display completely new and interesting physical phenomena and may not be well explained by conventional approximations.

Previously we were able to observe second (SH) and third harmonic (TH) generation from 20 nm and 70 nm-thick gold nano layers, to extract the basic physical intrinsic properties of the material [1]. Now we head towards structured nanomaterials, hence the grating, which promises enhanced nonlineartiy and more practical applications such as sensors, photonic circuits, high resolution imaging etc. Our approach consists of an expanded hydrodynamic model [2] that accounts for surface, magnetic and bulk nonlinearities extracted from equations of motion arising from free (Drude model) and bound electrons (Lorentz model) and contains different nonlocal effects such as convection and hot electrons.

The theoretical spectral response of the grating in reflection is calculated by means of rigorous coupled wave analysis (RCWA), also verified experimentally, and the reflectance map is shown in Figure 1(b). We fix the input wavelength at 800 nm, mapping the resonance at 16° incident angle (Figure 1(c)) for further measurements. The plasmonic structure confines the fields near the surface, producing an intense field close to the corners (Figure 1(d)), which in turn is responsible for pump absorption (resulting in near zero reflections) and the simultaneous enhancement of nonlinear interactions. Given the grating periodicity of ~610 nm, the SH (400 nm)

and TH (266 nm) produce several diffraction orders. The reflected SH efficiency from the grating, when summed over the different orders, is around 1.5×10^{-9}, which is about 1400 times the total SH efficiency from the planar gold part. Similarly, as shown in Figure 1(e), the total enhancement factor for the TH is of nearly 4000.

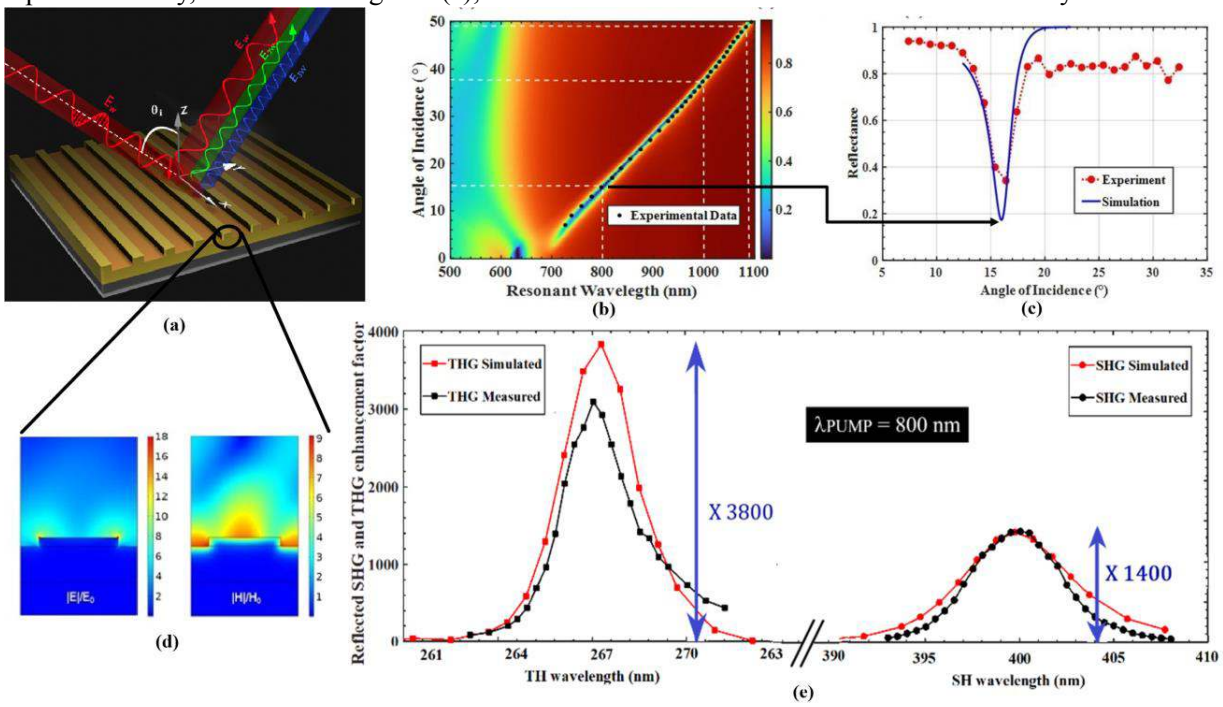


Fig. 1 (a) Schematic idea of the project. (b) Grating reflectance map, for TM incident polarization, as a function of incident angle and wavelength. The reflectance is normalized to 1 (100% reflection). Experimental measurements are shown as black dots on top of the simulations. (c) Reflectance as a function of incident angle for carrier wavelength tuned at 800 nm, normalized to the value obtained from the unpatterned gold layer: simulation (solid blue curve) and experimental measurements (dashed curve with red dots). The resonance is centered at 16º (d) Electric and magnetic field distributions at 800 nm and 16º angle of incidence around a single groove, normalized with respect to the incident electric and magnetic field amplitudes. (e) Simulated and measured enhancement of reflected SHG and THG, while pump wavelength is tuned at 800 nm and incident on the sample at 16°.

The reflected SH efficiency (0^{th} diffraction order) were also measured around 1000 nm (resonance at 37°), and around 1100 nm (resonance at 50°). The combined results of the three measured wavelengths depict conversion efficiencies of the same order of magnitude, although varying slightly due to different lab environments, different incident angles and penetration depths into the metal.

Based on the theoretical model, a large set of simulations were carried out, to obtain both SH and TH enhancements, varying incident pulse durations (FWHM) and using different grating geometries (channel and ridge widths). The results clearly show near-perfect agreement between theory and experimental observations of shape, spectral width, and maximum amplitude of the spectral response, and ways to enhance further the performance of the grating. The novelty of this work relays on the demonstration that a "mere" grating contains and displays a constellation of linear and nonlinear effects that require complex models, and should not be explained away using "effective" dielectric constants that may fit the observed spectra. Our results are not at all speculative, but demonstrate accurately a very good qualitative, and most importantly, quantitative agreement with our experimental results.

Acknowledgments

LRS, JT, and CC acknowledge Spanish Agencia Estatal de Investigación (project no. PID2019-105089GBI00/AEI/10.13039750110011033) and US Army Research Laboratory Cooperative Agreement Nº W911NF1920279 issued by US ARMY ACC-APG-RTP.

References

1. L. Rodriguez-Suñé, J. Trull, C. Cojocaru, et al, Optics Express 29, 8581 (2021).
2. M. Scalora, M. A. Vincenti, D. de Ceglia, et al, Phys. Rev. A 82, 043828 (2010).

META 2023, PARIS - FRANCE, JULY 18 – 21, 2023

Epsilon-Near-Zero coupled Surface Lattice Resonances as a Nonlinear Activation Function

D. Fomra[1], A. Ball[2], A. Agrawal[1], H. J. Lezec[1] and N. Kinsey[2]

[1]National Institute of Standards and Technology, Gaithersburg, MD 20899, USA.
[2]Department of Electrical and Computer Engineering, Virginia Commonwealth University, Richmond, VA 23284, USA.
*Corresponding Author: dnf4@nist.gov

Abstract: Photonics is a promising solution to meet the growing demand for data in defense, aerospace, and telecommunication sectors. However, current linear optical systems face limitations in performance and applicability due to the lack of nonlinear elements required for generalized computation. To address this challenge, that combines an ENZ film with a metasurface exhibiting a surface-lattice-resonance (SLR) has been developed. Simulations suggest that on optical excitation, the transmission of the film can be modulated by over 150% (27% to 71%).

The defense, aerospace and telecommunication sectors have a growing demand for data due to new edge technologies like 5G and AI, which is putting pressure on underlying technologies to scale [1]. To address this challenge, new methods of transmitting and processing information, such as quantum and neuromorphic systems, are being explored, with a promising approach being the use of optical technologies. Photonics offers fast terahertz-level computation, high parallelism, and direct compatibility with several optical technologies such as imaging systems, optical fibers, and numerous sensors. In essence, they offer the potential to exceed the performance of conventional systems by 1000× while reducing size, weight, and power constraints [2,3]. However, current linear optical systems face limitations in performance and applicability due to the lack of nonlinear elements required for generalized computation.

This work directly addresses this problem, by realizing a device that combines an epsilon-near-zero film (ENZ) with a metasurface exhibiting a surface-lattice-resonance (SLR). The large nonlinearities observed in ENZ films coupled to the highly sensitive SLR resonance offers a path towards realizing a nonlinear activation function at sub-GW/cm^2 levels, opening the potential for excitation with laser diodes and fiber optic systems.

The proposed nonlinear activation function (Fig. 1) is implemented via a plasmonic metasurface exhibiting high-Q (>500) surface lattice resonances (SLR), which are a hybridization between the localized surface plasmon resonances (LSPR) and propagating Rayleigh anomalies (RA). The designed metasurface consists of a rectangular array (1060 nm by 500 nm) of rectangular gold nanoantennae (150 nm by 160 nm) on a 65-nm thick ITO film on a glass substrate, cladded by oxide (Figs. 1(a,e)). The targeted SLR resonance occurs at a wavelength of 1550 nm, with a FWHM of 8 nm (Figs. 1(b,c)). Upon pumping the metasurface on resonance (incident peak power ~10 GW/cm^2), a 30x enhancement in pump absorption is observed along with detuning of the resonance which leads to a change in probe (1570 nm) transmission intensity (Fig. 1(d)) of over 150% (27% to 71%). The index change of the ITO film is a result of generation of hot electrons in the conduction band, which increases the average electron effective mass. This results in a more dielectric film (index increases), causing the SLR to red shift. The large modulation achieved with THz scale bandwidth, provides an avenue towards the realization of a low-cost and high-performance nonlinear activation function, an essential building block for the construction of true optical computing systems.

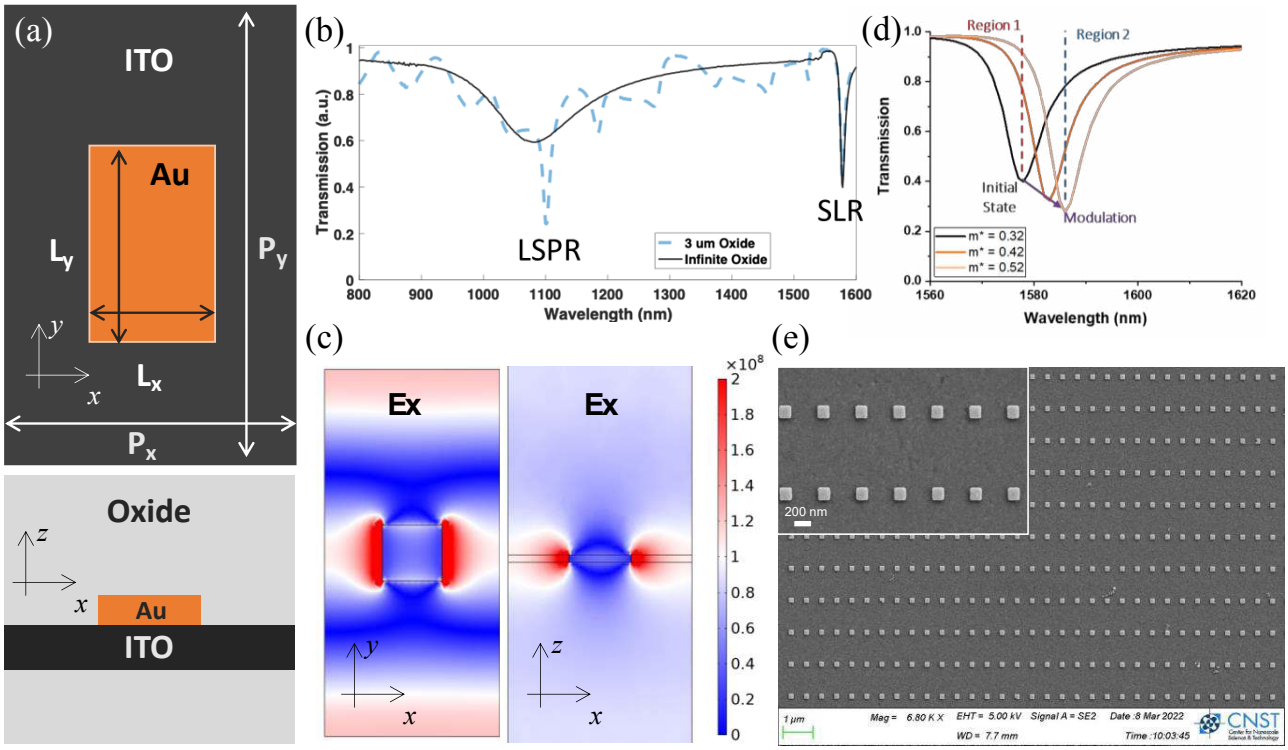


Figure 1: (a) Schematic of the SLR metasurface, top view and side view. Metasurface consists of Au nanoantenna (NA) fabricated on top of an ITO layer and cladded by an SiO_2 layer of thickness of a few microns. (b) Simulated transmission spectra exhibiting the LSPR and SLR resonance, for finite and infinite oxide thicknesses. The interference fringes due to reflections from the oxide/ air and Au NA/ oxide interface. (c) Simulated electric-field profiles within the metasurface at SLR resonance (left: top view, in the plane coinciding with ITO upper surface; right: side view, in the plane perpendicular to layer interfaces, through center of nanoantenna). (d) Calculated change in transmission as the average electron effective mass within ITO increases from 0.32 to 0.52. (e) SEM image of fabricated metasurface before oxide deposition. Inset: magnified view.

The authors acknowledge financial support from Air Force Office of Scientific Research, grant number: FA9550-18-1-0151 and FA9550-22-1-0383.

References

1. R. Umbrasas, *Monitoring Petabyte-Scale AI Data Lakes in Azure* (2017).
2. "Unlocking the True Potential of AI with In-Package Optical I/O - Ayar Labs," https://ayarlabs.com/unlocking-the-true-potential-of-ai-with-in-package-optical-i-o/.
3. H. Zhou, J. Dong, J. Cheng, W. Dong, C. Huang, Y. Shen, Q. Zhang, M. Gu, C. Qian, H. Chen, Z. Ruan, and X. Zhang, "Photonic matrix multiplication lights up photonic accelerator and beyond," Light: Science & Applications 2022 11:1 **11**, 1–21 (2022).

META 2023, PARIS - FRANCE, JULY 18 – 21, 2023

Suppression of filamentation in Kerr media by photonic crystals

Edvinas Aleksandravičius[1,*], Darius Gailevičius[1], Audrius Dubietis[1], Kęstutis Staliūnas[1,2,3]

[1]Vilnius University, Faculty of Physics, Laser Research Center, Saulėtekio ave. 10, LT-10223 Vilnius, Lithuania
[2]ICREA, Passeig Lluís Companys 23, 08010, Barcelona, Spain
[3]UPC, Dep. de Fisica, Rambla Sant Nebridi 22, 08222, Terrassa (Barcelona) Spain

[*]corresponding author: edvinas.aleksandravicius@ff.vu.lt

Abstract: We show the possibility of using photonic crystals to counteract the spatial Kerr effect, thus suppressing filamentation. Fine control of the spatial dispersion can be achieved by tuning the photonic crystal geometry and projecting to the appropriate Bloch mode branch. Chirped photonic crystals can be engineered with such geometry that the designed diffraction compensates for nonlinear focusing, suppressing beam filamentation.

Nonlinear propagation of intense ultrashort laser pulses in transparent materials produces a unique and spectacular phenomenon termed femtosecond filamentation. Femtosecond filamentation arises from a complex interplay between linear and a variety of nonlinear effects, which become coupled in space and time through material nonlinearity. This leads to a transformation of an ultrashort-pulsed laser beam into a light filament, which possesses an ultra-broadband spectrum, termed supercontinuum. In a sole spatial domain, the light filament emerges is a self-sustained structure that carries a limited amount of energy and power, which is of the order of critical power for self-focusing. In wide bandgap solid-state dielectric materials, in the near-infrared, P_{cr} is of the order of several MW [1]. However, many applications require high spectral energy density and high peak power, which is well above the typical values contained in a single filament.

Here we propose and substantialize an alternative idea that photonic crystals can efficiently suppress the emerging filamentation. It is well known that photonic crystals, can affect the overall diffraction of the beam [2]. The self-collimation effect is a thoroughly studied example of the effect of a photonic crystal on beam diffraction. This effect is caused by the flattening of the spatial dispersion curves that can be obtained for some photonic crystal geometries. Though this is of no particular use when it comes to suppressing filamentation, different geometries can be used to obtain other spatial dispersion regimes. For example, the reduced or increased curvature corresponds to weakened or strengthened diffraction. Another possibility is obtaining a spatial dispersion curve with a negative curvature corresponding to anti-diffraction. Considering this, we can infer that it is possible to devise a photonic crystal with such a geometry, that results in a spatial dispersion regime that can compensate for the nonlinear Kerr focusing of the beam, thus effectively suppressing filamentation.

Numerical simulations were performed using a forward beam propagation method, which approximates the envelope of the beam propagating in a slowly varying medium. The profile of refractive index modulation is chosen to be harmonic in both the transverse X and the longitudinal Z directions as shown in Figure 1a. The periodicities in both directions were varied to determine an optimal geometry, with the longitudinal period being tied to the transverse period through the Talbot length. It is convenient to introduce the geometric constant Q which is the inverse of the longitudinal period normalized to the Talbot length, the length at which self-imaging occurs:

$$Q = \frac{d_{Talbot}}{d_z} \cong \frac{2{d_x}^2}{\lambda d_z}$$

In the general case, for a photonic crystal with constant period and for all values of the geometric constant Q

that are close to 1, there are multiple dispersion curves corresponding to different Bloch mode branches. This is often undesirable since it makes it impossible to precisely control the diffraction of the beam, however this issue can be overcome by introducing an adiabatic chirp to the longitudinal period of the photonic crystal as seen in Figure 1a. We do this by starting at a longitudinal period corresponding to a geometric constant Q sufficiently far from 1 and slowly approaching the desired Q.

From the beam diameter evolutions shown in Figure 1b, we can see that in the homogeneous case (blue lines) the beam diameter first increases, but eventually the beam starts to converge and collapses at z = 2.84 mm. Using those same beam parameters but this time in a photonic crystal (yellow lines) we can see that the beam diameter again initially increases, however this time the beam does collapse, instead the beam converges only a little and the beam diameter asymptotically approaches some value for which the diffraction and nonlinear focusing are balanced. The initial divergence of the beams is likely because the initial beam used is elliptical.

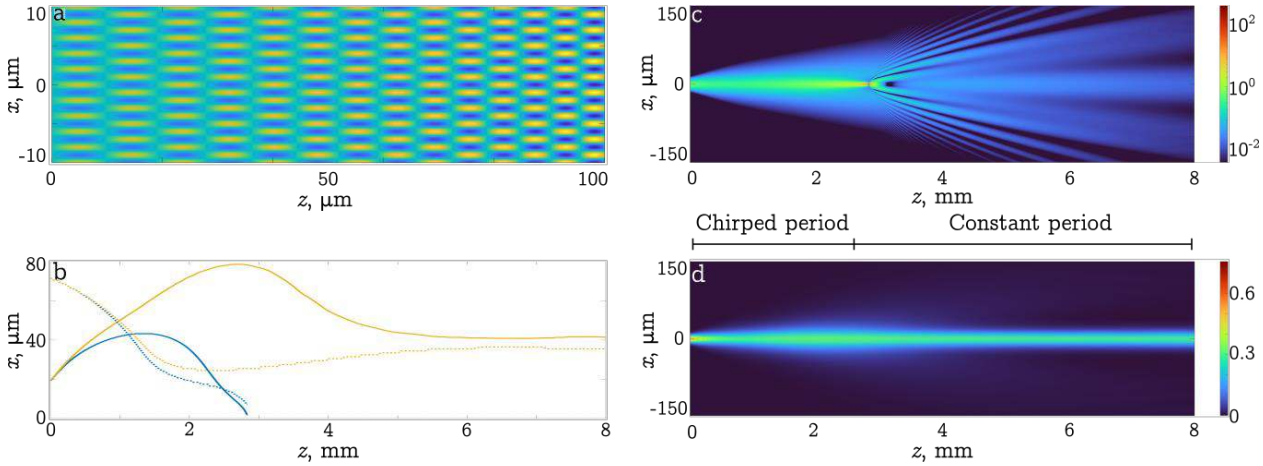


Figure 1. a – cross-section of the refractive index distribution in the modulated plane. b – beam diameter measured at e^{-2}; blue – unmodulated, yellow – modulated; solid – modulated plane, dotted – perpendicular plane. c and d – intensity distribution of the beam propagating in a homogeneous medium and photonic crystal, respectively.

The results show that using a photonic crystal with a geometry characterized by a value of Q close to 1 gives the desired result. In addition, using positive and negative chirp, both increased diffraction ($Q > 1$) and anti-diffraction ($Q < 1$) can be achieved.

In perspective, the current work created the framework for choosing advanced meta-structures that will be useful for super-continuum generation applications. Monolithic and compact devices that might replace the multi-plate systems might be enabled via future experimental tests.

This work has received funding from the Spanish Ministerio de Ciencia e Innovación under Grant PID2019-109175GB-C21, and the European Social Fund (Project No 09.3.3-LMT-K-712-17-0016) under a grant agreement with the Research Council of Lithuania (LMTLT).

References

1. A. Dubietis, G. Tamošauskas, R. Šuminas, V. Jukna, and A. Couairon, "Ultrafast supercontinuum generation in bulk condensed media." Lith. J. Phys. 57, 113–157 (2017).
2. H. S. Eisenberg, Y. Silberberg, R. Morandotti, and J. S. Aitchison, "Diffraction Management." Phys. Rev. Lett. 85, 1863–1866 (2000).

Stable periodic solutions in fractional dissipative systems with non-Hermitian modulation

Salim B. Ivars[1*], Muriel Botey[1], Ramon Herrero[1] and Kestutis Staliunas[1,2,3]

[1]Departament de Física, Universitat Politècnica de Catalunya (UPC), Rambla Sant Nebridi 22, 08222, Terrassa, Barcelona, Catalonia, Spain
[2]Institucio Catalana de Recerca i Estudis Avançats (ICREA), Passeig Lluís Companys 23, E-08010, Barcelona, Spain
[3]Vilnius University, Faculty of Physics, Laser Research Center, Sauletekio Ave. 10, Vilnius, Lithuania
[*]corresponding author: salim.benadouda@upc.edu

Abstract: New stable periodic solutions are uncovered in the fractional complex Ginzburg-Landau equation with the introduction of non-Hermitian potentials. This equation is known to be a general model for extended dissipative systems. A thorough analysis of the dynamics and stability of the system is conducted. The stabilisation is proven to be robust in a wide area in the parameters space, with potential applications to other physical systems. As an example the study provides results on the stabilisation of Class B lasers.

In this work we uncover new periodic solutions in non-linear dissipative systems. The study is based on the universal Complex Ginzburg Landau Equation (GCLE) and extended to its fractional counterpart and to more realistic models such as Class B lasers. We show how the introduction of a non-Hermitian (complex) potential can effectively stabilise these states for a wide range of parameters. In these systems, turbulence is a challenging subject not only for its theoretical understanding but for the practical consequences. For instance, for lasers, turbulence represents one of the main aspects limiting the output power. Different attempts to control the turbulence have been proved. From the introduction of a global delayed feedback on the system [1] or the effect of a gradient [2] to the recently proposed unidirectional mode coupling through the introduction of spatiotemporal non-Hermitian potential [3].

The current work consists on another approach. Here we propose the stabilisation of specific stationary solutions of the different systems by the addition of a complex spatial modulation. In optics, the introduction of this potential corresponds to a harmonic modulation of the gain and refractive index of the system in the form: $V(x) = \cos(2\pi x/L)e^{-i\vartheta}$. In Fig. 1a) we can see a selected family of unstable periodic solutions of the unmodulated CGLE and in b) the evolution of the turbulent field with the dynamic introduction of a modulation for a fixed value of φ. We see how the field gets fully stabilised after a transient state. In Fig. 1c) we display the amplitude of the modulation, m, and the growth rate of the stationary solution that gets stabilised as a function of time. Note that stable solutions correspond to $\Re(\lambda) \leq 0$.

The results show extended stabilisation areas for a wide range of periodicities L. Stabilisation is found even for every tiny modulation of the gain and refractive index, up to only a 5% modulation amplitude for some cases. This stabilising effect is proven for different parameters (higher nonlinearity and different fractional dispersion) and holds for higher dimension of the system [4].

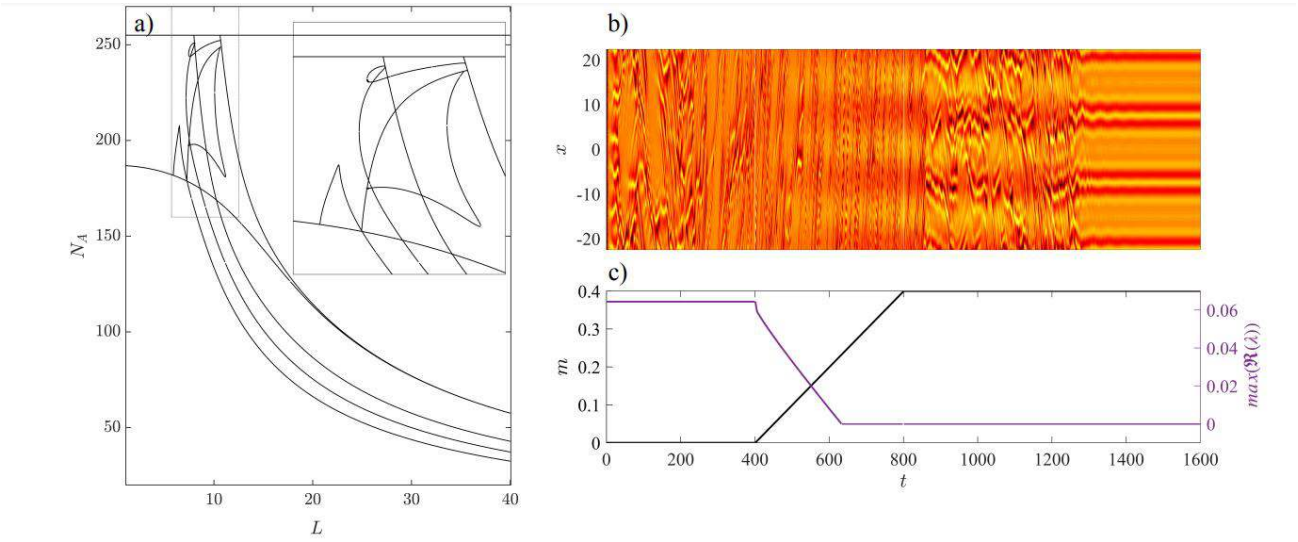


Fig. 1 a) Picture of the complexity of the unstable periodic solutions of the unmodulated CGLE. Inset corresponds to a zoom of some of the branches that are stabilised with the introduction of the non-Hermitian potential. NA corresponds to the norm of the solution. b) Transient evolution of the field profile from a turbulent state to the stable stationary state when the potential is applied. c) Profile of the potential amplitude and growth rate of the stationary solution

Moreover, the proposal holds also for Ginzburg-like models describing actual physical systems, for instance a 1D Vertical External-Cavity Surface Emitting Lasers, for which the dynamics of both the field and the carriers is considered. For this Class B lasers, the introduction of the non-Hermitian potential has shown to effectively stabilize the emission for highly unstable parameter ranges creating a large attractor basin.

References

1. Battogtokh, D., and A. Mikhailov. ”Controlling turbulence in the complex Ginzburg-Landau equation.” Physica D: Nonlinear Phenomena 90.1-2 (1996): 84-95Lastname, F. M. and F. M. Lastname, “Title of the journal paper,” Journal Title Abbreviation, Vol. 34, No. 10, 1064–1076, 1986.
2. Xiao, Jinghua, et al. ”Controlling turbulence in the complex Ginzburg-Landau equation.” Physical review letters 81.25 (1998): 5552
3. Ivars, Salim B., et al. ”Non-Hermitian control of optical turbulence in systems with fractional dispersion.” Chaos, Solitons Fractals 165 (2022): 112774
4. Ivars, Salim B., et al. ”Stabilisation of spatially periodic states by non-Hermitian potentials.” Chaos, Solitons Fractals 168 (2023): 113089

Laser and cavities

Hybrid External Cavity Laser based on a novel Si_3N_4 1D Photonic Crystal cavity for label-free on-chip sensing applications

Taynara Oliveira[1*], Simone Iadanza[3,4], Jesus Hernan Mendoza-Castro[5,6], Gautham Paikkath[1,5], Bernhard Lendl[6], Marco Grande[5] and Liam O'Faolain[1]

[1]Centre for Advanced Photonics and Process Analysis, Munster Technological University, Cork, Ireland
[3]Laboratiry of Nano and Quantum Technologies, Paul Scherrer Institut Forschungsstrasse, Switzerland
[4]IBM Research Zurich, Switzerland
[5]DEI, Politecnico di Bari, Bari, Italy
[6]TUW, Institute of Chemical Technologies and Analytics, Vienna, Austria
[*]corresponding author: taynara.oliveira@mycit.ie

Abstract: In this work we show the employment of a novel design photonic crystal (PhC) cavity in hybrid external cavity laser (HECL) configuration for refractive index sensing applications, with high sensitivity (145nm/RIU) and low detection limit (~10^{-5} RIU). The HECL RI sensor configuration exhibits a 16x improvement in the detection limit compared to the stand-alone photonic crystal cavity. In addition, the sensor is characterized by its compactness, high-power output, simplicity in fabrication, compatibility to integration process, and multi-sensing capability.

Recently optical biosensors have been developed to sense different analytes in real-time with high sensitivity and integration capabilities. For biomedical research, healthcare and environmental monitoring, the detection of ultralow concentrations of harmful compounds to human health is important. Therefore, sensors with detection limits (DLs) down to femtolitre [1] are very attractive for optical sensing applications.

In this work, we designed a novel PhC cavity based in 1D structure and optimized the cavity to work as laser mirror with very high Q-factors. Hence, by combining this 1D PhC cavity with III-V gain chips a new type of laser can be developed called Hybrid External Cavity Lasers (HECL). The HECL consists of a 250µm III/V reflective semiconductor optical amplifier (rSOA), and a Silicon Nitride (Si_3N_4) reflector. The reflector, consisting of a ridge waveguide and a side-coupled 1D PhC, is butt-coupled to the rSOA. To maximize optical coupling between the two components, the bus waveguide is designed with dimensions that match the area of the rSOA waveguide mode. This butt coupling approach has the advantage of designing, fabricating, testing, and optimizing the two components separately, ensuring optimal performance of both devices before packaging the laser. The laser characteristics were measured, and Figure 1 (a) shows the Light-Current (LI) curves for drive currents ranging from 0 to 100 mA, indicating high output power and low laser threshold. More than that, the HECL exhibits a mode-hop-free single-mode regime at telecom wavelengths for a wide range of drive currents (Figure 1 (b)), which is an important advantage for telecom and datacom applications.

As the laser mirror works as wavelength-selective feedback, the wavelength of the HECL is controlled by the 1D PhC cavity, and since part of mode supported by the PhC cavity exists in the cladding material, the lasing wavelength is strongly affected by the cladding refractive index (RI), making the laser a very precise RI sensor with high sensitivities [2]. The operation of the HECL as a RI sensor was studied by measuring the lasing wavelength shift in the presence of different upper-cladding materials (deionized water, i.e., "DI water", and sugar solution). Figures 1 (c) and 1 (d) demonstrate the experimental data of both optical spectral response, and calibration curve in terms of Δ_λ of the sensor with the standard deviations, respectively. Each data point was repeated multiple times to ensure the results repeatability. The HECL sensor exhibits a linear response when the

RI of the upper-cladding material increases. Furthermore, due to the lasing linewidth of the HECL being much narrower than that of the passive PhC resonance linewidth, the HECL improved the DL by a factor of ~16 to $6.6*10^{-5}$ RIU (limited value by the OSA resolution). We believe this is one of the first demonstrations using HECL for RI detection in which the experimental DL is much lower than the DL of its passive optical cavity, i.e., to the stand-alone photonic crystal cavity [2]. This promising result reinforces the advantage of hybrid lasers for refractive index sensing and not only for telecom/datacom applications. Moreover, the HECL-based RI sensor does not need an external light source, unlike the MMR RI sensor, which significantly reduces the system size and provides a better performance in terms of integration density.

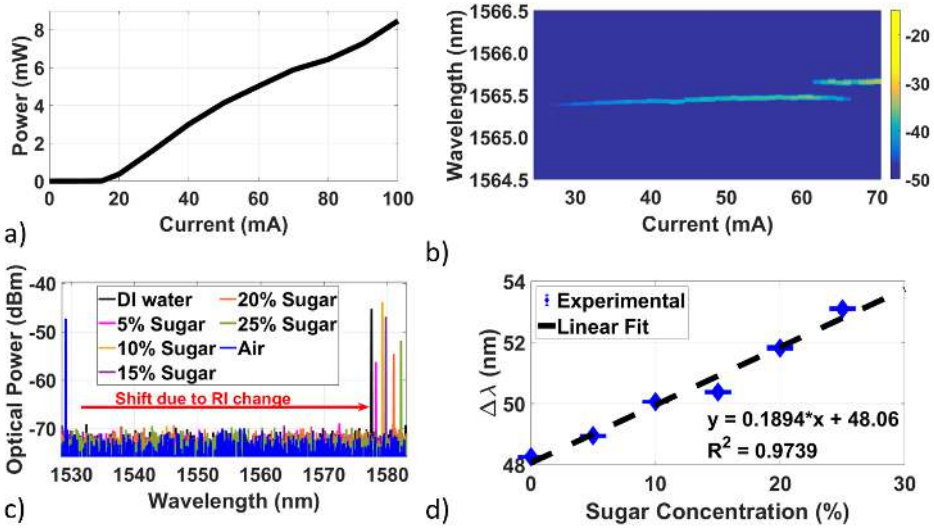


Figure 1. a) optical spectrum of the laser with different bias current; b) LI curve of the HECL; c) optical spectra of the sensor in the presence of different upper claddings; d) lasing wavelength shift when the upper cladding RI increases.

The main advantages that make HECL-based RI sensor attractive for optical biosensing can be summarized as follows: portability (lab-on-a-chip) and compactness, high power (mW range), high sensitivity, label-free detection (femtoliter detection), and simplicity in design and manufacturing (compared to 2D PhC). In addition, the HECL sensor presents important aspects from a commercialization point of view. These include the compatibility to integration process as Micro-Transfer Printing (mass sensor manufacturing capability) and the transparency from the visible to the NIR spectrum due the Si_3N_4 material, which opens the window for having sensors at different wavelengths on the same chip (multi-sensing capability).

References

1. X. Fan, I. M. White, S. I. Shopova, H. Zhu, J. D. Suter, and Y. Sun, "Sensitive optical biosensors for unlabeled targets: a review," Analytica Chimica Acta, vol. 620, pp. 8−26, 2008.
2. Iadanza, Simone, et al.. "High-Q asymmetrically cladded silicon nitride 1D photonic crystals cavities and hybrid external cavity lasers for sensing in air and liquids," Nanophotonics, vol. 11, no. 18, 2022, pp. 4183-4196.

Acknowledgements

The authors gratefully acknowledge Science Foundation Ireland (SFI) (16/ERCS/3838, SFI12/RC/2276) and he Marie Skłodowska-Curie grant No 860808 (OPTAPHI).

Integrated polariton condensate in SOI high contrast grating microcavities

P. Tassan[1,2*], D. Urbonas[1], B. Chmielak[2], T. Wahlbrink[2], R. F. Mahrt[1], and T. Stöferle[1]

[1]IBM Research Europe - Zurich, Switzerland

[2]ETH Zurich, Switzerland

[3]AMO GmbH, Germany

[*]corresponding author: tas@zurich.ibm.com

Abstract: A promising approach towards the next generation of computing architectures are all-optical logic gates[1]. Strong light-matter coupling based free space all-optical transistors have recently demonstrated showing ultra-fast switching at room-temperature[2]. Here, we use silicon-on-insulator high index contrast grating microcavities to demonstrate polariton condensation and strong light-matter interaction on a chip. This opens the door for integrated all-optical transistors with scalability towards more complex optical logic circuits operating at room temperature.

Summary: Today, one of the most important technological challenges consists in the development of alternatives to CMOS-based computers. In this sense, one of the potential technologies, which could outperform the classical transistor in terms of switching speed and energy efficiency, is photonic transistors[1]. Microcavity exciton-polaritons (polaritons) provide the physical properties required for an ultra-fast transistor[2], as they inherit the speed from their photonic component and the non-linear interaction from the excitonic part. Nevertheless, up to now, no device capable of operating at room-temperature with a THz switching frequency has shown the capability of being scalable on-chip[2]. Here, we use a Silicon-On-Insulator (SOI) platform to realize High Contrast Grating (HCG) microcavities[3] (Figure 1) that support strong light-matter coupling[4], and which could serve as building-block for realizing integrated all-optical circuits. We demonstrate on-chip strong light-matter interaction and polariton condensation by means of HCG cavities filled with optically active polymer material.

The HCG structures are realized by patterning an SOI wafer with electron beam lithography and reactive ion etching. The planar nanophotonic Fabry–Pérot-like resonator is then constituted by two arrays of silicon pillars which provide the micron-sized lateral light confinement due to constructive and destructive interference given by the refractive index contrast provided by the metamaterial. The vertical confinement is achieved by total internal reflection from the spin-coated MeLPPP (methyl substituted ladder-type polymer) layer, which serves as organic semiconductor.

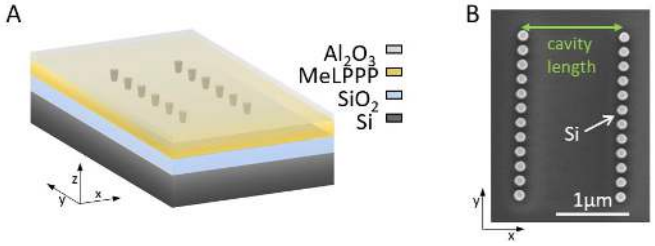


Figure 1. A) Top-view SEM image of an HCG cavity. B) Schematic of the HCG cavity.

We excited the cavities with a picosecond pulse at 400 nm in a micro-photoluminescence (µPL) setup. By varying the excitation fluence, we were able to observe polariton condensation, which gives rise to a narrow peak in the spectrum. Light-in-light-out characteristics (Figure 2.A) measured on a sample with cavity length L=1.82µm displays a polariton condensation threshold defined (grey bar at ≈81µJ/cm^2) by change in the slope.

Below the threshold, just PL is observed (violet in inset). Above threshold, a peak emerges on top of the PL signal, indicating polariton condensation (red in inset).

We fabricated multiple devices with different cavity lengths, allowing us to tune the cavity resonance and therefore the condensation energy (Figure 2.B). Comparing the experimental results (red circles) with Rigorous Coupled Wave Analysis (RCWA) simulations of the reflection of HCG cavities we observed that the experimental data and the RCWA simulation (solid yellow lines) are inconsistent for the weak light-matter coupling or purely photonic regime. By considering of the whole MeLPPP refractive index dispersion, the experimental data are well described by the RCWA simulation (greyscale map), showing anti-crossing of different longitudinal modes (i.e. lower polariton branches) at the excitonic energy (2.72 eV, dashed white line). This is an evidence of strong light-matter interaction regime. Furthermore, the definition of the resonances over a broad range of wavelengths (390-560nm) highlights the robustness of this metamaterial-based microcavities. The coupling-strength shows a record high value for MeLPPP-based cavities ($2\hbar\Omega$=350meV). The Hopfield coefficients, which determine the excitonic and photonic fractions of the constituting polaritons, are ~50%, establishing a record-high excitonic fraction for polariton condensates with this organic semiconductor.

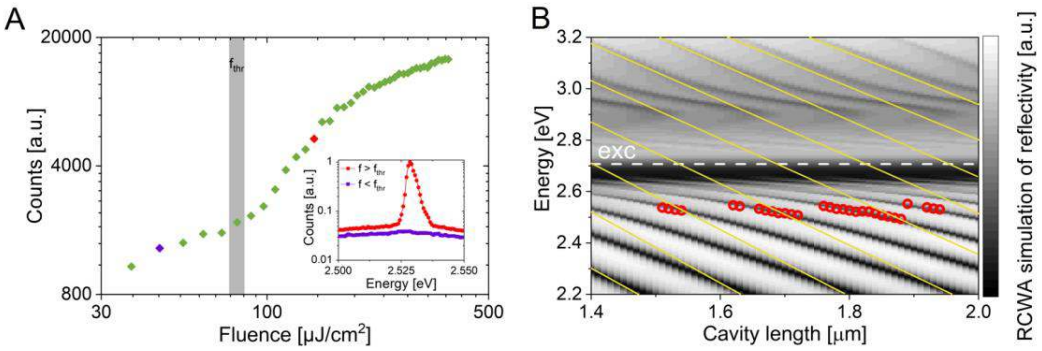


Figure 2. A) Light-in-light-out characteristic with polariton condensation above threshold. The inset shows the emission spectra below (violet) and above (red) threshold. B) RCWA simulations showing strong-coupling regime in the cavity detuning plot.

Conclusion: We have shown room-temperature polariton condensation on a photonic chip, paving the way to scalable polariton-based transistors. Progress of investigations of the coupling between multiple HCG cavities, which is central for establishing transistor action, will be reported.

Acknowledgement: All authors acknowledge support by EU H2020-FETOPEN project POLLOC (Grant No. 899141). P.T. acknowledges support by AppQInfo ITN EU H2020 project (Grant No. 956071).

References

1. Miller, D., "Are optical transistors the logical next step?", Nat. Phot., No 4, 3–5, 2010.
2. Zasedatelev, A.V., Baranikov, A.V., Urbonas, D. et al., "A room-temperature organic polariton transistor", Nat. Phot. No. 13, 378–383, 2019
3. Stöferle T., et al., "Ultracompact silicon/polymer laser with an absorption-insensitive nanophotonic resonator", Nano Lett., Vol. 10, No. 9, 3675-3678, 2010
4. Urbonas, D. "Tunable coupled microcavities for enhanced light-matter interaction", ETH Diss., No. 26125, 2019

META 2023, PARIS - FRANCE, JULY 18 – 21, 2023

Integrated Q-switched lasing element in the NIR with transition metal dichalcogenide gain and graphene saturable absorption

Georgios Nousios[1], Thomas Christopoulos[1*], Odysseas Tsilipakos[2], and Emmanouil E. Kriezis[1]

[1]School of Electrical and Computer Engineering, Aristotle University of Thessaloniki, GR-54124 Thessaloniki, Greece
[2]Theoretical and Physical Chemistry Institute, National Hellenic Research Foundation, GR-11635 Athens, Greece
[*]corresponding author: cthomasa@ece.auth.gr

Abstract: We propose and analyze an integrated passively Q-switched lasing element in the NIR based on a nanophotonic disk resonator and enhanced with the contemporary MoS_2/WSe_2 TMD hetero-bilayer and graphene monolayer to provide the optically-pumped gain and saturable absorption, respectively. The configuration is rigorously evaluated utilizing a temporal coupled-mode theory framework. Following a meticulous design process, the pulsed lasing source delivers mW peak power and ps duration pulses, with a repetition rate of tens of GHz for sub-mW pump power.

The development of highly efficient, monolithically integrated light sources in the technologically mature silicon-on-insulator (SOI) platform constitutes a key scientific and technological goal for future high-density integration photonic circuitry. A new avenue towards this goal has been opened by the exploitation of the novel luminescence and nonlinear properties of two-dimensional (2D) materials, such as the semiconducting transition metal dichalcogenides (TMDs) and the semi-metallic graphene [1]. In this work, we propose and computationally examine an integrated passively Q-switched lasing component in the near-infrared (NIR), based on a nanophotonic disk resonator where both the gain and the saturable absorption (SA) mechanisms are provided by 2D materials. The contemporary MoS_2/WSe_2 TMD hetero-bilayer is selected as the gain medium; it emits light at 1128 nm (1.1 eV) after being optically pumped at 740 nm (1.675 eV). To enhance the efficiency of the light source, the gain medium is pumped by appropriately exciting a whispering-gallery mode of the cavity near the pump wavelength using guided light. A graphene monolayer is additionally utilized to harness the required ultrafast and low-saturation-intensity SA effect. To numerically analyze and design the proposed light source, we rigorously develop a temporal coupled-mode theory (CMT) framework [2, 3], fed by linear finite element method (FEM) simulations. The lasing and pumping transitions of the three-level gain medium (MoS_2/WSe_2 heterostructure), are described by induced electric polarization fields which are incorporated in the CMT framework employing first order perturbation theory. The polarization fields follow equations of homogeneously broadened Lorentzian oscillators and the carrier dynamics are described by appropriate semiclassical rate equations. The latter are introduced in the CMT framework using only the standard slowly-varying envelope (SVEA) and rotating-wave (RWA) approximations. Overall, the developed CMT framework is capable of accurately evaluating the fundamental lasing characteristics, including the lasing frequency and the dynamic response, and allows to extract useful practical design guidelines as well as conduct a linear stability analysis to identify operation regimes of the pulsed lasing structure.

The proposed Q-switched lasing configuration is depicted in Figure 1(a) and consists of a silicon-rich nitride (SRN) disk resonator on silica substrate. A double bus waveguide scheme is employed to efficiently excite the pumping mode and extract the emitted light from the lasing mode. The MoS_2/WSe_2 bilayer and graphene monolayer are patterned in disks matching the resonator and placed on top of it, separated by a 60-nm layer of hexagonal boron nitride (h-BN). The geometric parameters of the structure are marked in Figure 1(b). The

heights of the disk resonator and the h-BN layer have been judiciously selected, in order to allow for the lasing mode to interact strongly with both the TMD bilayer and graphene monolayer, which is a key prerequisite for the lasing element to operate in the pulsed regime. Concurrently, the employed configuration enables the pumping mode to interact strongly only with the TMD bilayer, hence, leaving unaffected the nonlinear response of graphene. This is schematically illustrated in Figure 1(c, d), where the norm of the tangential to the 2D materials electric field is depicted in the $x-y$ plane for the two modes. Due to the highly efficient pumping scheme and the strong light-matter interaction between the 2D gain medium and the lasing mode, the lasing threshold is only $26\ \mu W$. In Figure 1(e) we depict the output peak power, the full-width half maximum (FWHM), and the repetition rate of the obtained Q-switched pulses as a function of the pump power. By increasing the pump power, the pulse width decreases, while the peak power and the repetition rate increase. The proposed Q-switched lasing element is capable of delivering pulsed light inside an integrated bus waveguide with mW peak power, ps duration and GHz repetition rate even for sub-mW pump power, rendering it promising for optical communication and sensing applications in the NIR. An individual Q-switched pulse for $P_p = 0.5$ mW is depicted in the inset of Figure 1(e), which has an asymmetric lineshape with slightly longer leading edge.

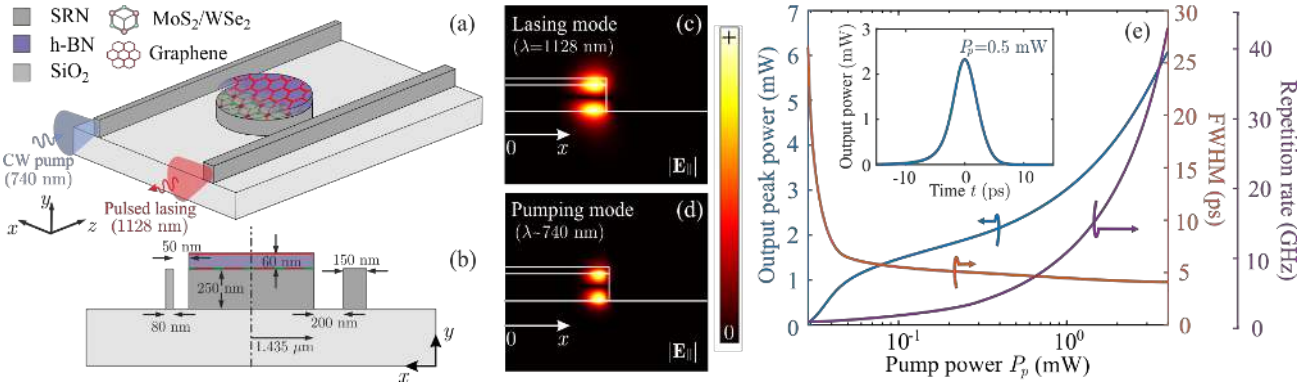


Figure 1. (a) Schematic of the proposed Q-switched lasing element consisting of a disk resonator comprising a MoS_2/WSe_2 TMD hetero-bilayer (gain) and a graphene monolayer (SA). The cavity is side-coupled to two dissimilar bus waveguides. (b) xy-plane cut of the structure with the geometric parameters. (c, d) Norm of the tangential to the 2D materials electric field for the (c) lasing and (d) pumping mode. (e) Output peak power, FWHM and repetition rate of the Q-switched pulses as a function of the pump power P_p. Inset: Individual Q-switched pulse for $P_p = 0.5$ mW.

Acknowledgements

This work was supported by the Hellenic Foundation for Research and Innovation, Project Number HFRI-FM17-2086.

References

1. D.-S. Liu, J. Wu, H. Xu, and Z. Wang, "Emerging Light-Emitting Materials for Photonic Integration," Adv Mater, Vol. 2021, No. 33, 2003733, 2021.
2. S.-L. Chua, Y. Chong, A. D. Stone, M. Soljacic, and J. Bravo-Abad, "Low-threshold lasing action in photonic crystal slabs enabled by Fano resonances," Opt Express, Vol. 19, No. 2, 1539–1562, 2011.
3. G. Nousios, T. Christopoulos, O. Tsilipakos, and E. E. Kriezis, "Integrated Lasers with Transition Metal Dichalcogenide Heterostructures: Analysis and Design Utilizing Coupled-Mode Theory for 2D Materials," submitted, 2022.

Tunable band structures coupled by spin-orbit interaction in self-organized photonic potential inside a liquid crystal optical microcavity

M. Muszyński[1], P. Oliwa[1], E. Oton[2], R. Mazur[2], P. Morawiak[2], W. Piecek[2], P. Kula[3], B. Piętka[1] and J. Szczytko[1*]

[1]Institute of Experimental Physics, Faculty of Physics, University of Warsaw, Poland
[2]Institute of Applied Physics, Military University of Technology, Poland
[3]Institute of Chemistry, Military University of Technology, Poland
[*]corresponding author: Jacek.Szczytko@fuw.edu.pl

Abstract: To obtain and control remarkable polarization properties of light, we consider a self-organizing, one-dimensional photonic potential inside a liquid crystal optical microcavity. Anisotropic modulation of the refractive index gives rise to two separated band structures for orthogonal, linear polarizations of light that interact with each other through spin-orbit coupling. The soft matter approach allows for efficient tuning of the bands with an external electric field.

Optical anisotropy in photonic structures typically grants greater control over system parameters, e.g. photon energy. In this case, the additional degree of freedom related to the polarization of light also distinguishes directions. Breaking the symmetry can lead to the spontaneous appearance of chirality in a system [1]. The introduction of an additional photonic potential may result in the appearance of photonic band gaps and states of light that inherit the polarization properties of the system [2].

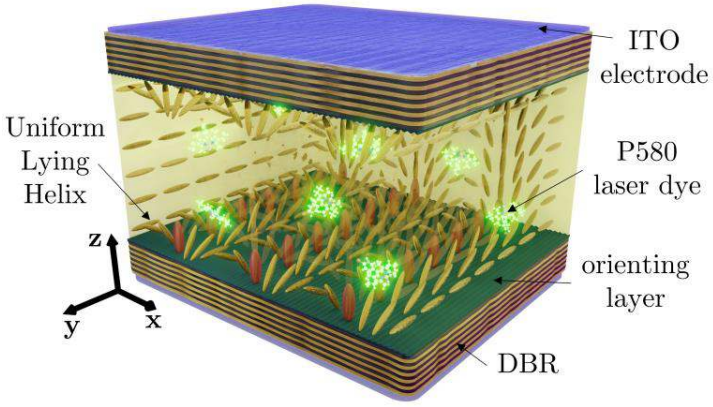


Figure 1. Schematic representation of the dye-doped optical microcavity with a stabilized ULH structure embedded within.

In this work, we propose a dye-doped liquid crystal optical microcavity with a built-in uniform lying helix (ULH) structure (Figure 1) that was induced in a chiral nematic liquid crystal matrix. Due to the birefringence of liquid crystals, a one-dimensional periodic modulation of the refractive index leads to the formation of two separate band structures with orthogonal linear polarization of light (Figures 2a, 2b). The inclination of the helix with respect to the plane of the cavity gives rise to the appearance of Rashba-Dresselhaus spin-orbit coupling for light, which couples the two bands together. As a result of the coupling, new states with strong circular polarizations are formed (Figure 2c).

An important aspect of the system is its technological advantages. A self-assembled one-dimensional well-oriented photonic potential based on ULH is formed in a macroscopic area (tens of micrometers). A special benefit of the use of soft matter is the easy dynamic tunability of the helix pitch (that is, the period of the

photonic potential) with an external electric field. In addition, due to doping the structure with light emitters, the system can transit to a non-linear regime with the laser light emitted from the sample [3].

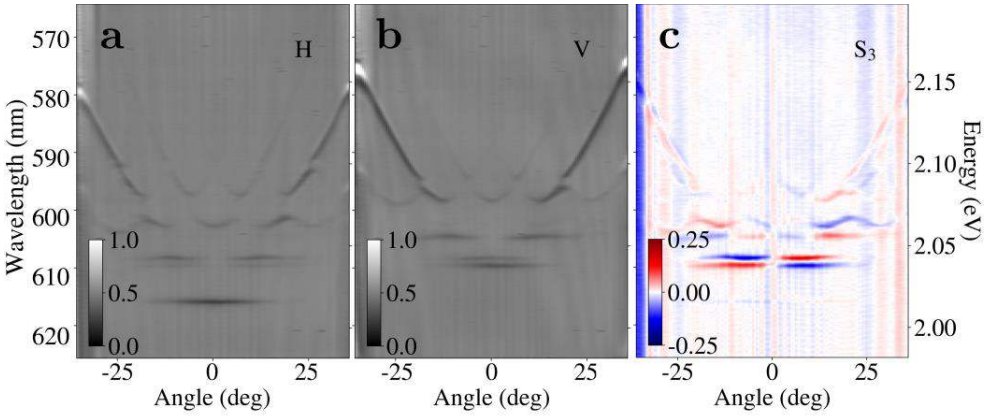


Figure 2. Angle-resolved reflectivity spectra of well-organized ULH in liquid crystal optical microcavity. Dispersion relation measured for orthogonal linear (a) horizontal H and (b) vertical V polarization of detected light. (c) Stokes parameter S_3 shows circularly polarized states of light caused by Rashba-Dresselhaus spin-orbit coupling.

To describe the dispersion relations observed experimentally, we propose a theoretical model based on effective Hamiltonians, which can be successfully applied to other optically anisotropic periodic structures. We believe that the phenomena presented here can be interesting and easily adapted not only in liquid crystal optical microcavities but also in fields such as photonics, metamaterials, or strong light-matter coupling.

References

1. Rechcińska, K. “Engineering spin-orbit synthetic Hamiltonians in liquid-crystal optical cavities” Science, Vol 366, Issue 6466, pp. 727-730 1076, 2019.
2. Muszyński M., et al. “Orthogonal band structures coupled by spin-orbit interaction in one dimensional self-assembled photonic potentials embedded in liquid crystal optical microcavities” (Manuscript in preparation)
3. Muszyński M., et. al (2022) “Realizing Persistent-Spin-Helix Lasing in the Regime of Rashba-Dresselhaus Spin-Orbit Coupling in a Dye-Filled Liquid-Crystal Optical Microcavity”, Phys. Rev. Applied **17**, 014041, 2022

Silicon Nitride Ring Resonators operating at 450nm

S. Jastan[1,2*], S. Iadanza [3], and L. O'Faolain[1,2]

[1]Munster Technological University, Ireland
[2]Tyndall National Institute, Ireland
[3]Paul Scherrer Institute (PSI), Switzerland
[*]corresponding author: samira.jastan@mycit.ie

Abstract: This study utilizes Low Pressure Chemical Vapor Deposition (LPCVD) to deposit a 190 nanometer layer of Silicon Nitride (Si_3N_4) on Silicon Dioxide (SiO_2) for the purpose of fabricating Micro Ring Resonators (MMRs). The MMRs are designed to operate in the deep blue wavelength region, specifically at 450 nm. The compact design of the MMRs, characterized by their small radius on the order of a few microns, allows for a reduced device footprint.

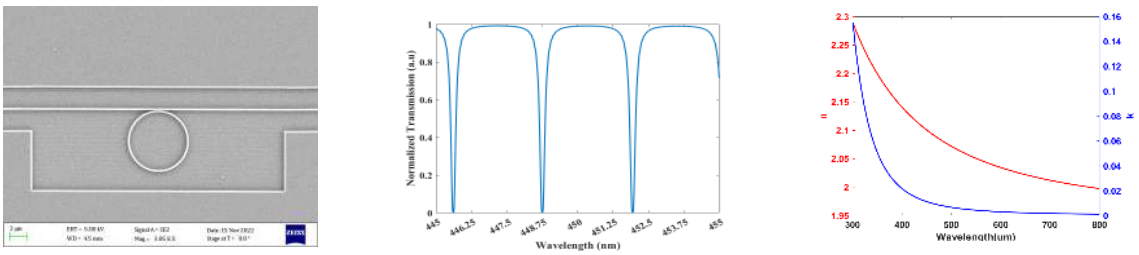
Recently, integrated ring resonators have gained popularity in the field of integrated optics and are now widely used in various applications. Their major application is for optical filtering and modulation. In addition, when combined with a broadband reflector, they can function as a wavelength-selective filter. A hybrid laser can be realized by coupling such a filter with a reflective semiconductor optical amplifier (RSOA) that will lase light at the same wavelength as the resonator. In order to obtain a narrow bandwidth laser, it is necessary to implement frequency-selective optical feedback, and a high Q factor ring resonator can fulfill this function. In this study, we are focusing on this application to develop narrow bandwidth lasers operating at 450 nm. Narrow linewidth light sources in the blue wavelength range are vital to applications ranging from Quantum Photonics to Raman spectroscopy to medical diagnostics. In particular, lasers at the wavelengths 461, 422, 407 and 396nm are important to compact atomic clocks, a rapidly emerging market, in which a narrow line-width blue laser source is used to target the atomic cooling transition. For designing the rings, we started with calculating the appropriate radius of the rings for 450 nm wavelength. In order for light to interfere constructively inside the ring resonator, the circumference of the ring must be an integer multiple of the wavelength of the light,

$$2\pi r n_{eff} = m\lambda \tag{1}$$

In this equation *r* is the ring radius, *m* is an integer, λ is our desired wavelength where we want to have a resonance, and n_{eff} is effective refractive index of the propagating mode. The quality factor (Q-factor) of a ring resonator is a parameter that determines how sharp the resonance is at the operating wavelength. If we define the resonance width as $\delta\lambda$, the Q-factor can be calculated using the following equation [1,2],

$$Q = \frac{\lambda}{\delta\lambda} \tag{2}$$

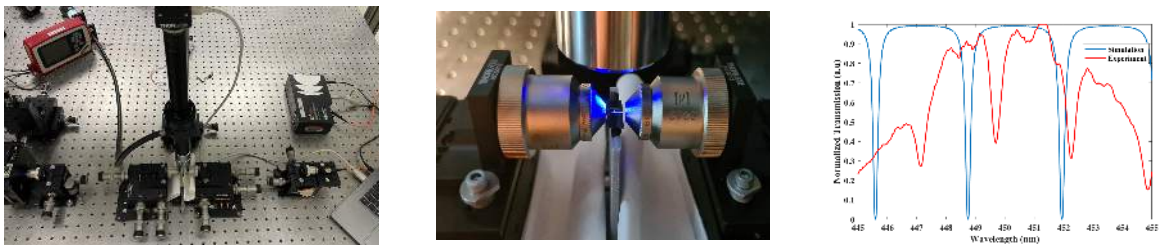
Utilizing VarFDTD module of the Lumerical software, we conducted simulations of the ring resonators. The Scanning Electron Microscopy (SEM) image of the ring structure (Figure 1a) and the transmission spectrum of the designed rings are depicted in Figure 1, illustrating our simulation outcomes. The challenge of working in the shorter wavelength range is due to the high loss characteristics of many materials in this spectrum. To assess material loss prior to fabrication, we deposited 190nm of SiN on Silicon Dioxide and conducted ellipsometry measurements. This allowed us to determine the absorption coefficient, as depicted in Figure 1c. Due to demand for high resolution, we employed Electron Beam



(a) **(b)** **(c)**

Figure 1: (**a**) SEM image and (**b**) Transmission spectrum of the designed ring resonator. (**c**) Ellipsometry data for loss calculation

Lithography (EBL) for fabrication and utilized a plasma etcher for the etching process. To characterize the fabricated rings, we used an endfire characterization setup which is shown in Figure 2. Also, Figure 2b shows the coupling method of light to the waveguides. In this setup, we used a broadband supercontinuum light source (400-2400 nm) which can be operated by a filter with tunability of 10 nm to 100 nm. In this experimental configuration, the light emitting from the



(a) **(b)** **(c)**

Figure 2: (**a**) Experimental setup for characterization of the fabricated ring resonators. (**b**) Coupling light to the waveguide. (**c**) Experimentally measured transmission spectrum of the rings and comparison with simulation

light source is coupled to the objective lens and propagates through the waveguides and ring resonators. On the opposite side of the chip, a second objective lens collects the light, which is then guided to a spectrometer for spectral analysis. The initial experimental results for the rings are presented in Figure 2c and compared to the simulation outcomes. The experimentally measured Q-factor was 1184, and the simulation Q-factor is 2000. These values are extracted directly from the FWHM of the resonance shape and using equation (3). Further enhancements will be pursued by modifying the ring structures and optimizing the fabrication process.

In summary, we have developed a simple method for fabrication and characterization of ring resonators that operate at 450 nm. The simulation of the ring resonators is described, which includes the display of the transmission spectrum of the designed rings. Additionally, the outcomes of the fabricated rings from experimentation are presented and compared to the simulation results. The initial results of the Q-factor of the ring structure are reported.

References

1. Rabus, Dominik G. Integrated ring resonators. Springer-Verlag Berlin Heidelberg, 2007.

2. Corato-Zanarella, Mateus, Andres Gil-Molina, Xingchen Ji, Min Chul Shin, Aseema Mohanty, and Michal Lipson. ”Widely tunable and narrow linewidth chip-scale lasers from deep visible to near-IR.” arXiv preprint arXiv:2109.08337 (2021).

Interlayer Exciton Lasing in Atomically Thin Heterostructures

Qiaoling Lin[1,3,4], Hanlin Fang[2], Yuanda Liu[5], Yi Zhang[6], Moritz Fischer[1,3,4], Juntao Li[7], Nicolas Stenger[1,3,4], Zhipei Sun[6], Martijn Wubs[1,3,4] and Sanshui Xiao[1,3,4,*]

[1]Department of Electrical and Photonics Engineering, Technical University of Denmark, DK-2800, Kongens Lyngby, Denmark.
[2]Department of Microtechnology and Nanoscience (MC2), Chalmers University of Technology, 41296, Gothenburg, Sweden.
[3]NanoPhoton - Center for Nanophotonics, Technical University of Denmark, DK-2800, Kongens Lyngby, Denmark.
[4]Centre for Nanostructured Graphene, Technical University of Denmark, DK-2800, Kongens Lyngby, Denmark.
[5]Institute of Materials Research and Engineering, Agency for Science Technology and Research (A*STAR), 2 Fusionopolis Way, 138634, Singapore.
[6]Department of Electronics and Nanoengineering and QTF Centre of Excellence, Aalto University, Espoo, 02150, Finland.
[7]State Key Laboratory of Optoelectronic Materials and Technologies, School of Physics, Sun Yat-Sen University, Guangzhou, 510275, China
*Corresponding author: saxi@dtu.dk

Abstract: We present an interlayer exciton laser composed of a MoS2/WSe2 heterostructure integrated with a silicon photonic topological microcavity with a quality factor of up to 10^4. We achieve excitonic lasing with ultra-low threshold, high side-mode suppression ratio and the longest emission wavelength to the telecommunication O-band.

Atomically thin heterostructures have attracted substantial attention in recent years due to their novel electronic and optical properties, and their ability for band structure engineering. Interlayer excitons (IX) with electrons and holes separated in different layers possess a long lifetime and have been used as an efficient gain medium for lasing [1,2]. However, IX lasing in optical communication wavelength has not been realized. Here, we report a room-temperature single-mode IX laser operating in the O-band (1260 – 1360 nm) [3]. Our observation is enabled by integrating a type-II heterostructure (MoS2/WSe2) with large band offset with a high-quality-factor topological silicon nanobeam cavity. We observe a single-mode lasing emission at 1320 nm with a linewidth of <~0.1 nm, the narrowest value reported for 2D material-based lasers. We highlight that the spectral resolution of our measurement setup limits the experimentally observed linewidth. Our work establishes IX as a practical gain medium for telecom lasing emission and highlights its potential for on-chip integration with silicon photonics platforms to develop compact, low-power, and high-speed optical communication systems.

References

1. Paik, E. Y. et al. ”Interlayer exciton laser of extended spatial coherence in atomically thin heterostructures. Nature 576, 80–84 (2019).
2. Liu, Y. et al., “Room temperature nanocavity laser with interlayer excitons in 2D heterostructures. Science Advances 5, eaav4506 (2019).
3. Lin, Q. et al., “A room-temperature moiré interlayer exciton laser”, arXiv:2302.01266, 2023.

Photonic bandgap structures

Fabrication of All-Garnet Bragg Mirror using Cerium Substituted Yttrium Iron Garnet

Yuki Yoshihara[1,2], Pang Boey Lim[2], Mitsuteru Inoue[1], Kazushi Ishiyama[1] and Taichi Goto[1]

[1]Research Institute of Electrical Communication, Tohoku University, Japan
[2]Toyohashi University of Technology, Japan
*taichi.goto.a6@tohoku.ac.jp

Abstract: A multilayer sample comprising cerium substituted yttrium iron garnet layer and gadolinium gallium garnet layer, which can act as a magnetooptical Bragg mirror, was fabricated on the yttrium aluminum garnet (YAG) substrate. The sample was fabricated by the ion beam sputtering method. Crystalline, optical, and magnetooptical properties were measured. The three-pair periodic structure was epitaxially grown on the YAG substrate with a lattice relaxation. An optical bandgap at a wavelength of 960 nm was observed, and magnetooptical responses were measured.

Magnetooptical Q-switch is a futuristic technology and is anticipated to realize high-power, tiny, and active Q-switched laser. Recently, the spin-controlled laser (SCL), which composed of a magnetooptical Q-switch and neodymium-doped $Y_3Al_5O_{12}$ (Nd:YAG) laser crystal, was demonstrated [1, 2]. Integration of components in the SCL is desired for the development of further practical devices. One of the great candidate materials for the integration of magnetooptical Q-switch is cerium-substituted yttrium iron garnet (Ce:YIG). Doped Ce into YIG enhances Faraday rotation angle at near-infrared wavelength region, which operates YAG laser with low optical absorption [3]. Ce:YIG has $a = 1.243$ nm lattice constant which is larger than $a = 1.201$ nm of YAG laser crystal. Such a large lattice mismatch between the film and substrate is supposed to involve dislocation defects and decreases magnetooptical behavior when Ce:YIG is grown directly on YAG. To prevent this issue $Gd_3Ga_5O_{12}$ (GGG) should be an effective material as the seed layer with $a = 1.238$ nm. Moreover, the Bragg mirror can be constituted by a difference in refractive index between Ce:YIG and GGG. In this report, we designed a three-pair periodic structure of Ce:YIG and GGG seed layer, working as a Bragg mirror, and fabricated it using by ion beam sputtering (IBS) method. Crystalline, optical, and magnetooptical properties of the fabricated sample were measured.

The periodic structure of $(Ce:YIG/GGG)^3/YAG$ substrate was designed by the matrix approach method [4]. Optical thicknesses of each layer d were determined so that the $\lambda = 4nd$, where λ is the center wavelength of the bandgap (1000 nm), n is the refractive index of the materials for each layer. From the calculation, d was determined as 132.3 nm and 113.6 nm for GGG and Ce:YIG, respectively. Ce:YIG and GGG films were deposited by a radio-frequency (RF) IBS system (RMTec, RM17-0010) on the YAG substrate. The substrate dimension was 10 mm x 10 mm x 0.5 mm with (111) surface orientation. The substrate temperature was held at 900°C during the deposition. The thickness of the film was measured by a stylus profilometer (Bruker Dektak XT-A). The crystalline structure was measured by an x-ray diffractometer (XRD, Rigaku Smartlab). Optical transmissivity was measured by spectrophotometer (Shimadzu UV-3150). The magnetooptical property was measured as Faraday rotation angle by the magnetooptical measurement system (JASCO J-1700FK).

The reciprocal space map (RSM) around the (336) diffraction point of the fabricated sample, which is shown in Figure 1, was measured to observe crystal structure. There are two films' peaks with the same in-plane q_x(-1

-1 2) coordinate, which means the in-plane lattice is well-matched between Ce:YIG and GGG. Although two film peaks deviated from the YAG substrate peak both in- and out-of-plane with broad peak supposed to lattice relaxation of the film from the substrate. Rocking curve measurement around (444) substrate peak was also performed, and there were no other peaks. The measured total thickness of the deposited film was 745 nm. Based on the single layer thicknesses of GGG and Ce:YIG deposited under the same condition, the expected thickness for GGG was 141.1 nm and for Ce:YIG was 112.3 nm. The transmissivity of the sample was 59% at the center wavelength of a bandgap of 960 nm. The Faraday rotation angle of the sample was –0.19° at λ = 1000 nm, 3.0 times larger than the epitaxial Ce:YIG film on YAG substrate. These results showed that a $(Ce:YIG/GGG)^n$ periodic structure can be grown epitaxially on a YAG substrate, and exhibits both magnetooptical response and Bragg mirror functionality. This suggested that the structure has the potential to be used in the development of integrated magnetooptical laser devices.

This work was partly supported by Grants-in-Aid for Scientific Research (KAKENHI) Nos. 20H02593, 20K20535 from the Japan Society for the Promotion of Science (JSPS), Bilateral Program No. JPJSBP120214807 from JSPS and No. 21-52-50006 from RFBR, New Energy and Industrial Technology Development Organization (NEDO) No. 20002157, Tohoku Initiative for Fostering Global Researchers for Interdisciplinary Sciences (TI-FRIS) fellowship, the Foundation for Technology Promotion of Electronic Circuit Board, and the Tanaka Kikinzoku Memorial Foundation.

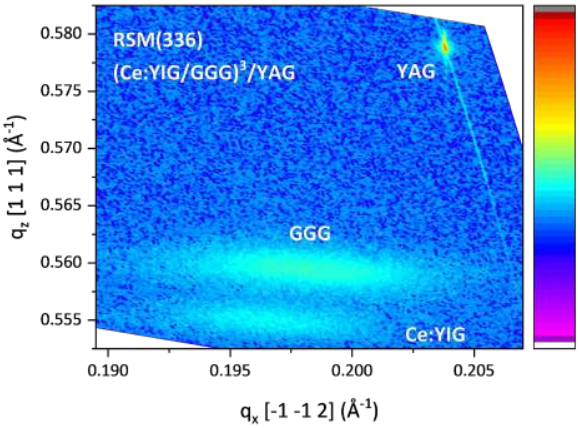


Figure 1. RSM around (336) diffraction points of $(Ce:YIG/GGG)^3$/YAG substrate. The film peaks are aligned for q_x (-1-12) direction, which indicates in-plane lattice matching though the film peaks are relaxed from the YAG substrate.

References

1 R. Morimoto, T. Goto, J. Pritchard, H. Takagi, Y. Nakamura, P. B. Lim, H. Uchida, M. Mina, T. Taira, M. Inoue, Magnetic domains driving a Q-switched laser, Scientific Reports 6 (2016) 1-7.

2 T. Goto, R. Morimoto, J. W. Pritchard, M. Mina, H. Takagi, Y. Nakamura, P. B. Lim, T. Taira, M. Inoue, Magneto-optical Q-switching using magnetic garnet film with micromagnetic domains, Optics Express 24(16) (2016) 17635-17635.

3 Y. Yoshihara, T. Sugita, P.B. Lim, Y. Tamba, H. Inoue, K. Ishiyama, M. Inoue, C.A. Ross, T. Goto, Thickness-dependent magnetooptical properties of ion beam sputtered polycrystalline $Ce_1Y_2Fe_5O_{12}$ films, Optical Materials 133 (2022) 112967.

4 M. Inoue, T. Fujii, A theoretical analysis of magneto-optical Faraday effect of YIG films with random multilayer structures, Journal of Applied Physics 81(8) (1997) 5659-5661.

Morphogenetic Design of Self-Organized Correlated Disordered Media

F. Chehami[1*], C. Decroze[1], and T. Fromenteze[1]

[1]University of Limoges, XLIM, UMR 7252, F-87000 Limoges, France
[*]corresponding author: fadhila.chehami@unilim.fr

Abstract: Recently, a new class of materials referred to as correlated disordered structures has emerged and gained growing attention offering a significant improvement in the control of scattering, transport and localization of light in matter. So far, the different protocols proposed to design such arrangements consist on gradient descent methods requiring high computational efforts. In this paper, we propose a new simple method, inspired by the Turing's morphogenesis theory, for designing self-organized correlated disordered media exhibiting isotropic photonic band gaps.

In the context of the emergence of structures exhibiting a correlated disorder, several numerical approaches have been proposed to generate such media [1, 2]. However, most are based on gradient descent algorithms evaluated on non-convex cost functions defined over extensive set of design parameters. In this paper, we propose a new design method inspired by the morphogenesis theory introduced by A. Turing [3], in an attempt to explain the formation of structure in nature. This generative technique defined as a *reaction-diffusion* system, is a mathematical model only following local interaction rules, making it easily adaptable to complex geometries and scalable to large domains. The Gray-Scott reaction-diffusion model [4] is considered in this work, based on a simple system of two chemical species diffusing and interacting with each other, governed by the two following differential equations defining the evolution of the concentration of each chemical species over time :

$$\frac{\partial A}{\partial t} = \left(d_A \nabla^2 A - AB^2 + f(1-A)\right) \qquad (1)$$

$$\frac{\partial B}{\partial t} = \left(d_B \nabla^2 B + AB^2 - B(f+k)\right) \qquad (2)$$

A and B correspond to the concentration of two chemical compounds considered, which Turing defined as morphogens. The parameters f and k control the spontaneous generation and extinction of A and B, respectively, determining population equilibria forming spatial clusters. We focus in this work on a specific class of Turing patterns forming circular spots. Their synthesis is provided by solving Eqs. (1) and (2) by the finite difference method (Fig. 1), revealing a self-replicating dynamic similar to mitosis.

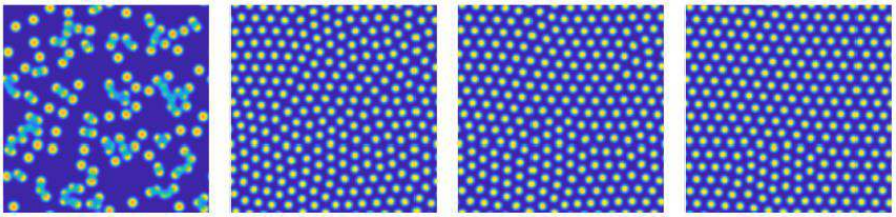


Figure 1: Generation steps of the self-replicating spots at different temporal iterations

Once the available space is filled with spots, the latter tend to optimize their compactness as the model iterates, transitioning from a disordered distribution to a quasi-crystalline arrangement. This model thus offers a way to generate disordered media whose degree of spatial correlation can be controlled. The self-structuring capability is

thus obtained through simple interaction rules defined at a local scale, without any form of cost function optimization.

To illustrate the ability of this generative model to synthesize correlated disordered media, an experiment of isotropic electromagnetic band gap formation is reproduced using this new technique [6] (Fig. 2).

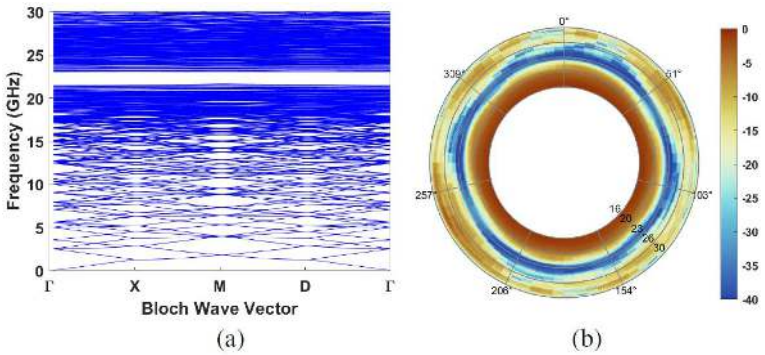


Figure 2: (a) Dispersion diagram and (b) Transmission measurements, over all incident angles, of the morphogenetic correlated disordered structure.

The computation of dispersion diagrams using the plane wave expansion method allowed the dimensioning of a structure based on acrylic rods of 3 mm radius (ϵ_r = 3), ensuring the formation of a band gap in the 18-26 GHz band. This structure was fabricated using commercial lollipop sticks of 15 cm length. A transmission measurement by means of a lens system forming a Gaussian beam allowed the extraction of attenuation coefficients in magnetic transverse excitation. Rotation of the sample revealed the formation of a quasi-isotropic band gap, characteristic of a structure with both periodic and random material properties.

This new morphogenetic generation method may offer flexibility, freedom and simplicity in the design of many components for applications in wave control devices such as freeform waveguides, polarizers and optical cavities with high quality factors.

References

1. Florescu, M., Torquato, S., Steinhardt, P. J., “Designer disordered materials with large, complete photonic band gaps”, PNAS, 106, 20658–20663, 2009.
2. Vynck, K., Pierrat, R., Carminati, R.; Froufe-Perez, L. S., Scheffold, F., Sapienza, R., Vignolini, S., Saenz, J. J., “Light in correlated disordered media”, arXiv preprint arXiv, 2106.13892, 2021.
3. Turing, A. M. “The chemical basis of morphogenesis,” Bull. Math. Biol, 52, 153–197, 1990.
4. Gray, P., Scott, S., “Autocatalytic reactions in the isothermal, continuous stirred tank reactor: isolas and other forms of multistability”, Chem. Eng. Sci, 38, 29–43, 1983.
5. Man, W., Florescu, M., Matsuyama, K., Yadak, P., Nahal, G., Hashemizad, S., Williamson, E., Steinhardt, P., Torquato, S., Chaikin, P., “Photonic band gap in isotropic hyperuniform disordered solids with low dielectric contrast”, Opt.Express, 21,19972–19981, 2013.

Directional emission enhancement measurements in terahertz photonic crystals

Kseniia Lezhennikova[1,2], Sahand Mahmoodian[3], Boris T. Kuhlmey[3], Redha Abdeddaim[1], Stefan Enoch[1], C Martijn de Sterke[3] and Alessandro Tuniz[3]

[1]Aix Marseille Université, CNRS, Centrale Marseille, Institut Fresnel, Institut Marseille Imaging, Marseille, France

[2]Multiwave Technologies AG, 3 Chemin du Pre Fleuri 1228, Geneva, Switzerland

[3]Institute of Photonics and Optical Science, School of Physics, University of Sydney, Camperdown, Australia

[*]corresponding author: alessandro.tuniz@sydney.edu.au

Abstract: We measure near-field directional emission in a terahertz photonic crystal slab near its quasi-TM band edge. We find that the direction of the emitted field dramatically differs for two neighbouring channels (0.445 THz and 0.465 THz) due to the underlying band structure, in agreement with simulations. We also find that the field is enhanced on the slab surface indicating a concentration of radiation. This platform has potential applications in alignment-free, chip-based 6G technologies.

Technologies operating at terahertz frequencies (i.e., sub-millimeter waves) will demand waveguides for chip-based connectivity to support emerging applications in 6G telecommunication, biosensing and spectroscopy [1]. On-chip waveguides can provide diffraction-free propagation, but coupling efficiency is sensitive to alignment. Photonic crystal (PHC) slabs and anisotropic metamaterials can support alignment-free self-collimation and directional emission via a tailored local density of states [2-5], but such effects have only been measured at near-IR and microwave frequencies [4-7].

Here we experimentally demonstrate directional emission in a terahertz PHC slab near its quasi-TM band edge through near-field excitation and imaging. Figure 1(a) shows a micrograph of the PHC, which is composed of a silicon slab (refractive index: n = 3.4; thickness: 250 µm) containing hexagonally arranged voids (pitch a=240 µm; radius r=0.3a). Figure 1(b) shows a detail of the experiment, where a *x*-polarized near-field terahertz emitter and moveable detector [8] (Protemics) are placed on each side of the PHC. The calculated band structure of the PHC (Fig. 1(c)) shows a quasi-TM band gap near ~0.45 THz (dashed line). An *x*-polarized electric dipole, placed externally to the PHC slab, most efficiently excites quasi-TE Bloch modes that have a wave vector component in *y*, and which are close enough to the light line that they can be excited. Figure 1(d) shows isofrequency contours at 0.435THz and 0.455THz, indicating that at each frequency emission direction of the Bloch modes (perpendicular to the contour) strongly differ. This highlights the sensitivity of PHCs to changes in frequency and the potential of harnessing their band structures for specific device applications, e.g., frequency selective signal routing.

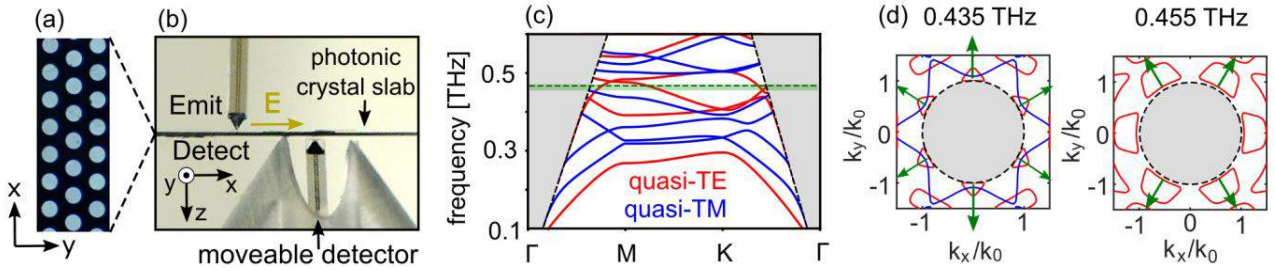


Figure 1. (a) Photonic crystal micrograph. Black: silicon; white: air. Period: a=240 µm; hole radius: r=72 µm. (b) Photograph of the terahertz emitter and detector on either side of the PHC slab. Yellow arrow: electric field direction. (c) Calculated photonic crystal band structure in the first Brillouin zone. (d) Calculated isofrequency contours (COMSOL) at 0.435 THz and 0.455 THz. Green arrows indicate preferred emission direction for the quasi-TE Bloch modes that are close to the light line (dashed line) to which we couple in our experiment.

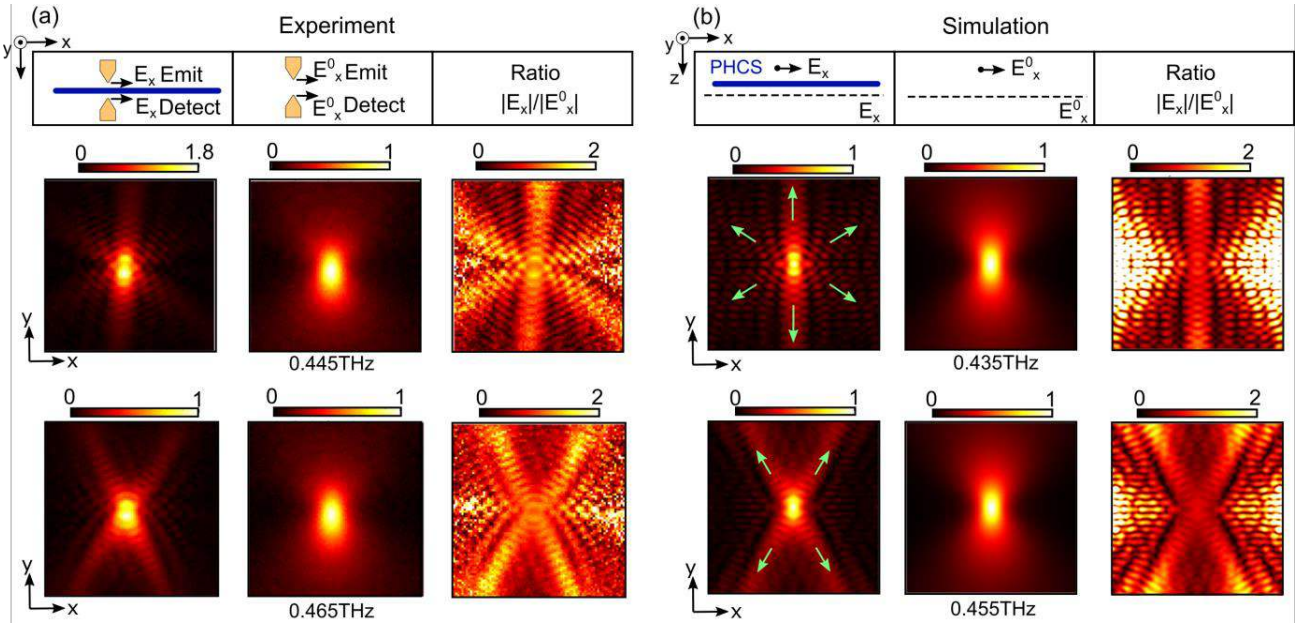


Figure 2. (a) Experiments of the transmitted electric field magnitude of an *x*-polarized electric dipole in near-contact with a PHC slab (left), without the slab (middle) and their ratio (right). (b) Corresponding simulations (CST). Green arrows are oriented as per Fig. 1(d).

Figure 2(a) show the experimental results: in the left column we show the *x*-polarized electric field magnitude distribution measured by scanning the moveable detector in *x* and *y*, transmitted by an *x*-polarized antenna located on the opposite side of the PHC, for two frequencies neighboring 0.45THz. The middle column shows the same experiment with the PHC removed. As expected from Fig 1(d), the field at lower frequency preferentially propagates along the *y* axis but splits in two across the diagonal at the higher frequency. The ratio between the first and second columns (third column) shows that for the same excitation, fields are locally increased due to the PHC in the vertical/diagonal regions of directional emission. FDTD simulation results, shown in Fig. 2(b), are in excellent agreement with simulations, with the same overall behaviour at frequencies within 2% of expectation. These experiments reveal that silicon photonic crystals can be harnessed to support frequency-selective directional emission of two neighboring sub-millimeter channels across spatially distinct pathways. We believe that this work provides a valuable addition to the limited library of chip-based functionalities of 6G technologies.

Acknowledgements

Australian Research Council Discovery Early Career Researcher Award (DE200101041). ANFF. LIA ALPhFA.

References

1. P. Yang, Y. Xiao, M. Xiao, and S. Li, "6G Wireless Communications: Vision and Potential Techniques", IEEE Network **33**, 70-75, 2019.
2. B. Gralak, S. Enoch, G. Tayeb, "Anomalous refractive properties of photonic crystals." J. Opt. Soc. Am. A **17**, 1012-1020, 2000.
3. A.F. Matthews, S.K. Morrison, Y. Kivshar, "Self-collimation and beam splitting in low-index photonic crystals" Opt. Commun. **279**, 313-319, 2007.
4. Z. Lu, et al.. "Experimental demonstration of self-collimation in low-index-contrast photonic crystals in the millimeter-wave regime." IEEE Trans. Microw. Theory Tech. **53**, 1362-1368, 2005.
5. Z. Lu, et al. "Experimental demonstration of self-collimation inside a three-dimensional photonic crystal." Phys. Rev. Lett. **96**, 173902, 2006.
6. Y. Yermakov et al. "Experimental observation of hybrid TE-TM polarized surface waves supported by a hyperbolic metasurface." Phys. Rev. B **98** 195404 (2018).
7. P. T. Rakich, et al. "Achieving centimeter-scale supercollimation in a large-area two-dimensional photonic crystal." Nat. Materials **5** 93-96 (2006).
8. A. Stefani et al. "Flexible terahertz photonic light-cage modules for in-core sensing and high temperature applications." ACS Photonics **9** 2128 (2022).

Nonlinear 2D Photonic Crystal Tunable Switch

A. Bounouioua[1*], A. Benmerkhi[1], and M. Bouchemat[1]

[1] Laboratoire de Microsystèmes et Instrumentation, Electronics Department,
Frères Mentouri Constanine1 university, Algeria
*corresponding author: bounouioua_amel@yahoo.fr

Abstract: In this study, we explored the effect of different tuned parameters in a 2D photonic crystal structure for all-optical switching based concept. The design based on a defect nonlinear ring resonator in a square lattice of silicon rods in air background is analyzed numerically. The outcomes of this investigation reveal very interesting switching characteristics by fitting the radius and position of the rods surrounding the center of the resonator. Furthermore, the device has multi-wavelength operation regime and fast response time with compact size.

NUMERICAL STUDY

In order to achieve the propagation of light with the c-band wavelength, we insert waveguides and ring resonator into the initial platform. The switching mechanism relays on the third order nonlinearity of a Kerr-like medium.

The calculation of band structure and simulation of the propagation of optical waves in the proposed structure were carried out using the plane wave expansion (PWE) and the finite difference time domain (FDTD) methods respectively. Simulation parameters such as the mesh sizes Δx and Δz in both X and Z directions and time step Δt were assumed $\Delta x = \Delta z = 50$ nm and $\Delta t = 0.1$ fs.

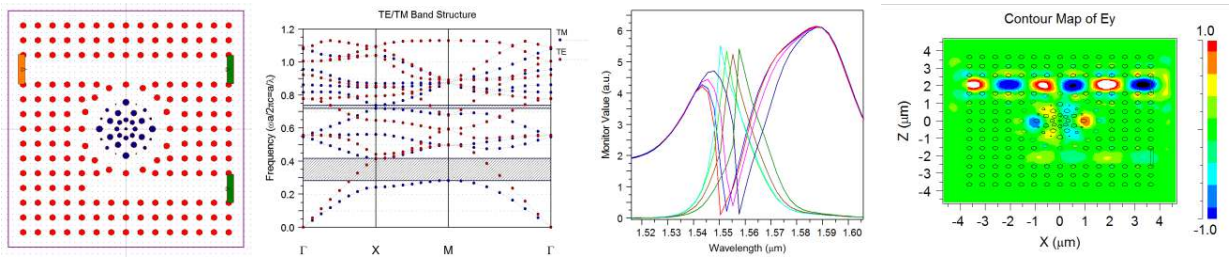
RESULTS AND DISCUSSION

Our platform is a square array of 15×15 silicon rods in air background. The Kerr-like medium is placed in the core of the ring resonator.

A photonic band gap (PBG) for TM mode was obtained in the range of $0.282 < a/\lambda < 0.417$.

By adjusting the radius and position of the rods surrounding the center of the resonator, we were able to adjust the operating wavelength to the desired point and produce a multi-wavelength operating design.

The effect of the previous parameters reveals the switching power threshold (<0.5w/µm), the response time (<1ps), the contrast ratio (>80% margin for logic 1).



(a) (b) (c) (d)

Fig. 1 (a) proposed structure, (b) Band diagram, (c) adjusting operating wavelength, (e) field propagation

CONCLUSION

By analyzing the obtained results and in comparison with works presented in the literature where for non-exhaustive example some focused on compactness of their structure [1] and some rather played attention to performing the switching parameters [2], we can say the one proposed in this paper gives a trade-off between all that and so it reveals a new area for 2D photonic crystal switches with tunable features.

References

1. Z. Mohebbi, N. Nozhat, and F. Emami, “High contrast all-optical logic gates based on 2D nonlinear photonic crystal,” Opt Commun., Vol. 355, pp. 130–136, 2015.
2. Bouaouina, M., M. Lebbal, M. Bouchemat, and T. Bouchemat, “Enhanced prompt trigger optical switching using nonlinear photonic crystal ring resonator for application on all-optical AND/NAND and OR/NOR logic function” Frequenz, Vol. 76 (Issue 3-4), pp. 145-155, 2021.

META 2023, PARIS - FRANCE, JULY 18 – 21, 2023

Nanophotonics with stratified architecture for bright phosphor-based nano LEDs.

Debapriya Pal[1*], Femius Koenderink[1]

[1]AMOLF, Amsterdam, The Netherlands
[*]Corresponding author: d.pal@amolf.nl

Abstract: In pc-LEDs, phosphor blends are illuminated by a blue “pump” LED (GaN die) to achieve the desired spectrum. Nano LEDs are envisioned as pixels for display. This constrains the lateral size and the distance between the phosphor layer & GaN die. We design thin spacers inserted between the phosphor and GaN die, which recover the waveguiding characteristics of the phosphor layer at emission wavelengths and facilitate the use of nanophotonic strategies to increase light absorption and extraction in specific directions.

In current phosphor-converted LEDs, white light is generated efficiently by using a blue "pump" LED to illuminate a phosphor blend that emits longer wavelengths. The phosphor materials absorb part of the incident blue photons and re-emit at larger wavelengths for, e.g., white light emission. Nanophotonic strategies, such as diffractive metasurfaces, to enhance pump absorption and emission directivity in this scenario work since the phosphor is far away from the blue emitting GaN, thereby avoiding that phosphor emission disappears into the LED [1]. In this work, we study the much more complex scenario of nano-LEDs, which are typically envisioned as pixels in a display. This constrains the lateral size and the distance between phosphor layer & GaN die, which is highly disadvantageous for light extraction.

We claim geometries in which the phosphor is concentrated in submicron sized layers and separated from the blue die chip by either (a) a micron-sized dielectric spacer with a refractive index lower than that of the phosphor (low index normal dielectric spacer) or (b) by a 1D dielectric multilayer stack of materials of alternating refractive index (Bragg stack dielectric spacer) as shown in Figure 1. The proposed geometry works via (A) recovering the waveguide mode characteristics of the phosphor layer, (B) avoiding tunneling of emission directly into GaN die, thereby promoting emission into the air, and (C) accelerating emission into the guided modes of the phosphor through the Purcell effect at expense of undesired emission into GaN. This geometry can be combined with plasmonic and dielectric nanophotonic strategies to increase pump light absorption and extract the guided light into specific directions in a nano-LEDs device architecture setting.

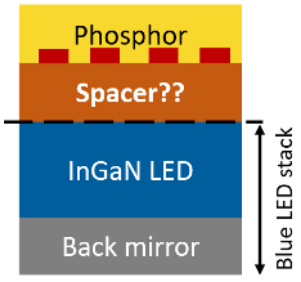


Figure 1: Schematic representation of the spacer inserted in between the phosphor layer and blue LED stack

with embedded corrugation (shown in red).

We present rigorous theoretical calculations to design the spacers which promote emission into the guided modes. We perform experiments confirming the benefits of inserting thin low index spacers combined with periodic corrugation to couple out those guided mode emission to far field using angle-resolved fluorescence microscopy experiments.

Acknowledgements: This work is part of the project NanoLED with project number 17100 of the research program High Tech Systems and Materials 2018, which is (partly) financed by the Dutch Research Council (NWO). This work is done in close collaboration with industrial partner Lumileds.

References

1. G. Lozano, D.J. Louwers, S.R.K. Rodriguez, S. Murai, O.T.A. Jansen, M.A. Verschuuren, and J. Gómez Rivas, Plasmonics for solid-state lighting: enhanced excitation and directional emission of highly efficient light sources, Light : Sci. Appl. 2, e66 1-7 (2013).

Emerging applications

Theoretical study of optomechanical effects by luminescence-induced optical force on micromechanical membranes

H. Arahari[1*], S. Konishi[2], S. Akita[2] and H. Ishihara[1]

[1]Dept. of Materials Engineering Science, Osaka University, Toyonaka, Osaka, 560-8531, Japan
[2] Dept. of Physics and Electronics, Osaka Metropolitan University, Sakai, Osaka, 599-8531, Japan
*corresponding author: arahari.h@opt.mp.es.osaka-u.ac.jp

Abstract: We have assumed a square-type optomechanical resonator formed with the luminescent nanofilm and a metallic mirror substrate, and then theoretically evaluated the luminescence-induced optical force (LiOF) on the emitting film. LiOF is enhanced at a specific cavity length due to the optical confinement effect of the resonator. We have shown theoretically that the enhanced LiOF could induce the mechanical frequency shift of the oscillator. This research provides new insights into the development of optomechanics using luminescence.

Light has momentum, and hence, force is exerted on the matter when the light is scattered or absorbed. This mechanism has been used for motion control of small particles in a wide range of fields, including molecular biology [1,2], photochemistry [3,4], and optomechanics [5]. 'Luminescence' of materials also causes a force on the matter. However, if it occurs isotropically, the exerted force is negligible. However, if the luminescence occurs anisotropically, it contributes to the motion of emitters. In this contribution, we focus on such luminescence-induced optical force (LiOF) causing mechanical motion, namely, we study an optomechanical cavity structure formed by a luminescent nanofilm and a metallic mirror substrate, as shown in Fig 1. We theoretically demonstrate that luminescence causes the mechanical motion of the emitters. If quantum states of the emitters can be coupled to mechanical modes via luminescence, we can realize quantum systems to control the luminescence properties of materials such as lasing [6].

As shown in Fig 1, we assumed organic-inorganic layered perovskites PhE-PbI_4 [7,8] as the luminescence film. This material is one of the promising light-emitting materials. By fabricating the luminescent film on a silicon nitride (SiN) membrane and transferring it onto the Al mirror substrate, the cavity structure is constructed. Here, the photoluminescence (PL) electric field in the cavity is enhanced or suppressed depending on the distance L between the film and the mirror due to the optical confinement effect. LiOF is caused by the spatial anisotropy of the PL electric field surrounding the emitter.

We evaluated the LiOF F_z^{inc} exerted on the luminescent film assuming the situation where only LiOF was exerted on the film by giving steady excitation energy to the luminescent film (see Fig. 2). As the steady-state excitation energy, we gave the interaction energy between the exciton polarization and the excitation light that corresponded to the energy when the luminescent film was irradiated

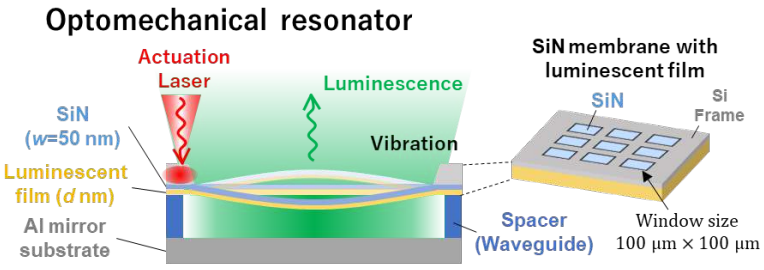


Figure 1. Model diagram of the optomechanical resonator. The size of the membrane window is 100 μm ×100 μm. As the luminescent film, we assumed organic-inorganic layered perovskites $(C_6H_5C_2H_4NH_3)_2PbI_4$, abbreviated here as PhE-PbI_4. The system is assumed to have a mechanical frequency $f_m = 1$ MHz and a film thickness of d=130 nm.

with excitation light of intensity I. Fig. 2 shows that, at a specific cavity length, the LiOF is enhanced. Such LiOF enhancement occurs at half the emission wavelength period (≅263 nm). The red line in Fig. 2 shows that the enhanced LiOF induces the mechanical frequency shift f_{opt} of the luminescent film from the given parameter f_{m} = 1 MHz,

$$f_{\mathrm{opt}} = f_{\mathrm{eff}} - f_{\mathrm{m}}, \ldots (1)$$

$$f_{\mathrm{eff}} = f_{\mathrm{m}}\sqrt{1 - \frac{\nabla_z F_z^{\mathrm{inc}}}{m_{\mathrm{eff}}\omega_{\mathrm{m}}^2}}, \ldots (2)$$

which is known as the optical spring effect [9]. We can confirm that LiOF influences the mechanical motion of the emitter by observing this effect in experiments.

The results of demonstrations indicate the potential of LiOF for unconventional optomechanical applications that convert the modes of luminescence into mechanical vibrational modes. We can use this mechanism to transmit the quantum properties of emitters to other quantum systems with different frequency regimes via the induced vibrational modes.

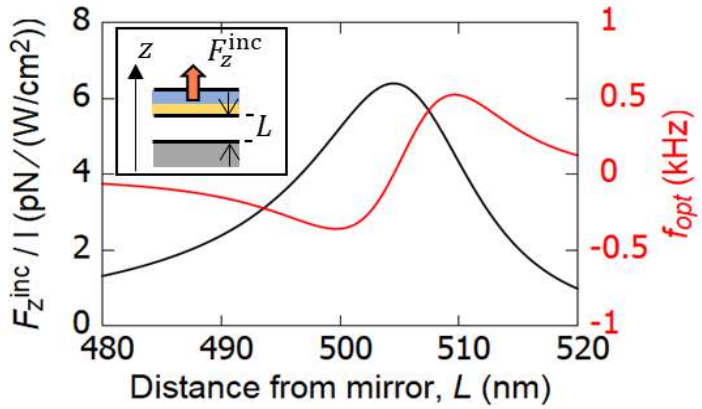


Figure 2. Black line: Cavity length L-dependence of LiOF F_z^{inc} when the luminescent film is given steady excitation energy. The results are normalized by I. Here, the excitation energy is the interaction energy between the exciton polarization and the excitation light field that corresponds to the energy when the luminescent film is irradiated with excitation light of intensity I. Red line: Mechanical frequency shift f_{opt} induced by LiOF under I=100 W/cm^2.

References

1. A. Ashkin, J. M. Dziedzic, J. E. Bjorkholm, and S. Chu, *Observation of a Single-Beam Gradient Force Optical Trap for Dielectric Particles*, Opt. Lett. **11**, 288 (1986).
2. S. Corsetti, and K. Dholakia, *Optical Manipulation: Advances for Biophotonics in the 21st Century*, J. Biomed. Opt. **26**, (2021).
3. S. Ito, Y. Tanaka, H. Yoshikawa, Y. Ishibashi, H. Miyasaka, and H. Masuhara, *Confinement of Photopolymerization and Solidification with Radiation Pressure*, J. Am. Chem. Soc. **133**, 14472 (2011).
4. A.-C. Cheng, H. Masuhara, and T. Sugiyama, *Evolving Crystal Morphology of Potassium Chloride Controlled by Optical Trapping*, J. Phys. Chem. C **124**, 6913 (2020).
5. M. Aspelmeyer, T. J. Kippenberg, and F. Marquardt, *Cavity Optomechanics*, Rev. Mod. Phys. **86**, 1391 (2014).
6. D. Yu and F. Vollmer, *Active Optomechanics*, Communications Physics **5**, 1 (2022).
7. X. Hong, T. Ishihara, and A. V. Nurmikko, *Dielectric Confinement Effect on Excitons in PbI4-Based Layered Semiconductors*, Phys. Rev. B **45**, 6961 (1992).
8. E. A. Muljarov, et al., *Excitons in Self-Organized Semiconductor/insulator Superlattices: PbI-Based Perovskite Compounds*, Phys. Rev. B Condens. Matter **51**, 14370 (1995).
9. B. S. Sheard, M. B. Gray, C. M. Mow-Lowry, D. E. McClelland, and S. E. Whitcomb, *Observation and Characterization of an Optical Spring*, Phys. Rev. A **69**, 051801 (2004).

Inverse design of fabrication-compatible monolithic metasurfaces for optically interfacing deeply embedded solid-state qubits

Amelia R. Klein[1*], Nader Engheta,[1] and Lee C. Bassett[1]

[1]Department of Electrical and Systems Engineering, University of Pennsylvania, Philadelphia, PA 19104, USA
[*]corresponding author: amklein@seas.upenn.edu

Abstract: We use adjoint shape optimization to design monolithic metasurfaces tailored exactly to maximize photon collection from a specific solid-state defect into a particular free-space collection angle. Our shape optimization manifestly adheres to fabrication constraints at every iteration. We show that our highly-tailored objective criteria result in performance superior to a structure optimized as a conventional focusing metalens. This flexible design approach will help realize scalable interfaces for developing quantum technologies.

Solid-state spin defects such as the nitrogen-vacancy (NV) center in diamond are platforms for many emerging quantum technologies. Applications of these systems require their single-photon emission to be collected as efficiently as possible. For deep defects (which are desirable for their improved spin and optical properties being free from surface interactions), total internal reflection at the surface of diamond is commonly overcome with a spherical solid immersion lens (SIL). However, fabricating SILs involves a complex etching process, and they must be combined with high-numerical aperture (NA) free-space optics. As a more scalable alternative, a metasurface fabricated on the diamond surface could collect light directly into an optical fiber. Recent work demonstrated such a metalens, using conventional phase-shift approximation techniques to design an array of pillars that approximate a Fresnel lens[1]. However, the metalens performance was limited due to the conventional, approximate design strategy. In the present work, we leverage modern photonic inverse design techniques tailored to the problem of maximizing the broadband photon collection efficiency from a NV center into a multi-mode optical fiber of given NA, while manifestly preserving manufacturing constraints through the constrained parameterization of our structure.

Inverse design photonics using adjoint-based gradient descent have been used extensively for a number of applications in nanophotonics. Topology-based adjoint methods in particular have recently been applied to related problems of enhancing collection from NV centers[2,3]; however, these designs focused on shallow defects, where the metastructure modifies both the near- and far-field emission properties. Moreover, obtaining fabricable structures from topology optimization requires a significantly longer computation time due to successive phases in the computational process of gradually applying filters to guarantee material binarization, smoothness, and a minimum feature size. With challenges of diamond fabrication in mind, we instead choose to perform a novel type of constrained shape optimization such that our design is composed only of elementary structures that remain within our chosen fabrication constraints at every iteration in the optimization.

Our design process uses custom code built on top of an existing open-source inverse design package for Lumerical FDTD[4]. Our metasurface is parameterized as an array of elliptical pillars of uniform height, each defined by five variable parameters: two center coordinates, two axes lengths, and an angle of rotation. Since the position of these pillars is variable as well as their size, we are still able to explore a broader possible design space than static unit-cell based designs. Fabrication constraints are made explicit via lower bounds on the pillar sizes and constraint functions between adjacent pillars that ensure a minimum spacing between them.

With a dipole source at the position of a desired NV center, the photon collection efficiency expressed is in

the objective function as the total normalized power above the diamond surface, filtered to include only the component propagating within a given acceptance angle. This function is also spectrally weighted according to the NV center's room-temperature emission spectrum. We include in Figure 1 a small-scale demonstrative example designing a 2µm x 2µm metasurface in diamond collecting from a 2µm-deep dipole into an acceptance NA of 0.2. We also perform a second optimization on the same initial geometry to design a more conventional lens that focuses a plane wave to a 2µm deep spot. Both are performed over the 600-800nm wavelength range. Tailoring our optimization for one mode of operation or another results in very different structures; each significantly outperforms the other in their designed use cases. Beyond the NV center, our technique is easily adapted to any choice of substrate, collection angle, emission spectrum, and dipole orientation.

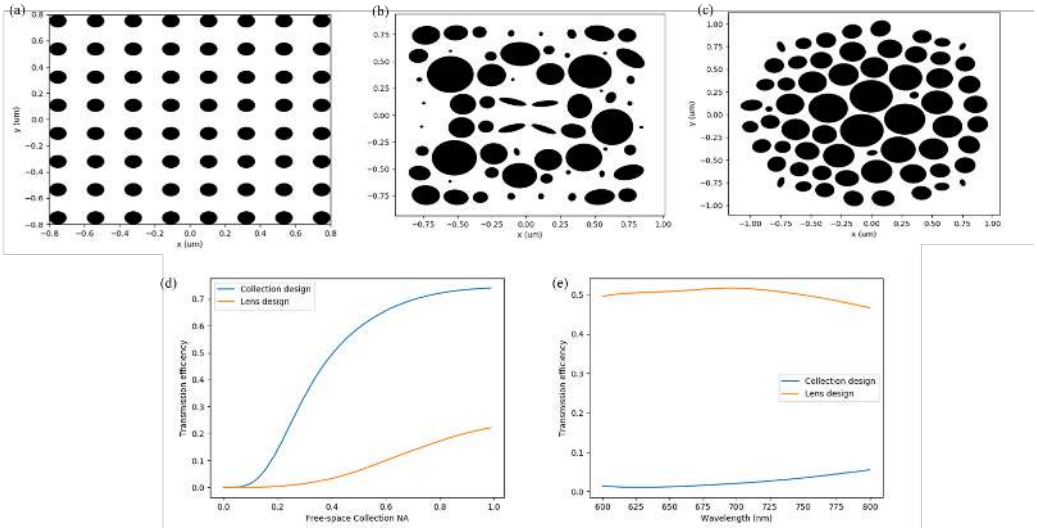


Figure 1: (a) A top-down view of the initial configuration used for subsequent optimizations. Diamond pillars are in black; air gaps are in white. **(b), (c)** Resulting structures after 100 iterations of optimization when optimized for **(b)** collecting from a 2µm deep dipole source into a fiber NA of 0.2 and **(c)** focusing a plane wave into a 2µm-deep spot. **(d)** Characterization of both simulated structures in transmitting light incident on the surface from a dipole source, as a function of free-space collection NA. **(e)** Characterization of both simulated structures in focusing a plane wave into a 500nm x 500nm square spot at the focus.

Acknowledgements

This work was supported by the National Science Foundation under award ECCS-1842655, and by the National Science Foundation Graduate Research Fellowship Program, Grant No. DGE-1845298 (A.R.K).

References

1. T.-Y. Huang, R. R. Grote, S.A. Mann, D.A. Hopper, A.L. Exharos, G.G. Lopez, A.R. Klein, E.C. Garnett, and L.C. Bassett "A monolithic immersion metalens for imaging solid-state quantum emitters," Nat. Commun. **10**, 2392 (2019).
2. R. A. Wambold, Z. Yu, Y. Xiao, B. Bachman, G. Jaffe, S. Kolkowitz, J. T. Choy, M. A. Eriksson, R. J. Hamers, and M. A. Kats. "Adjoint-optimized nanoscale light extractor for nitrogen-vacancy centers in diamond," Nanophotonics, Vol. 10 No. 1, 393-401, 2021.
3. S. Chakravarthi, P. Chao, C. Pederson, S. Molesky, A. Ivanov, K. Hestroffer, F. Hatami, A. W. Rodriguez, and K. C. Fu. "Inverse-designed photon extractors for optically addressable defect qubits," Optica 7, 1805-1811, 2020.
4. C.M. Lalau-Keraly, S. Bhargava, O.D. Miller, and E. Yablonovitch, "Adjoint shape optimization applied to electromagnetic design," Opt. Express 21, 21693-21701 (2013).

META 2023, PARIS - FRANCE, JULY 18 – 21, 2023

Applications of Eutectic Materials for 5G Technology

Hamid Reza Darabian[1]*, Jerzy Krupka[2], Bartłomiej Salski[3], Dorota Anna Pawlak[1,4,5]
[1] ENSEMBLE3 Centre of Excellence, ul. Wolczynska 133, 01-919 Warsaw, Poland
[2] Faculty of Electronics and Information Technology, Warsaw University of Technology, Koszykowa 75, 00-662 Warsaw, Poland
[3] Warsaw University of Technology Institute of Radioelectronics and Multimedia Technology Warsaw, Poland
[4] Chemistry Dept. University of Warsaw, Pasteura 1, 02-093 Warsaw, Poland
[5] Łukasiewicz Research Network – Institute of Microelectronics and Photonics, Wolczynska 133, 01-919 Warsaw, Poland
*corresponding author: hamid.reza.darabian@ensemble3.eu

Abstract: We utilize the micro-pulling down solidification technique with different pulling rates to tailor the dielectric permittivity and tangent loss for combination of TiO_2 and MgO for 5G applications. A set of measurements such as XRD and SEM have been conducted to study structural properties. The SEM images exhibit different crystalline sizes with the pulling rates. In addition, the dielectric permittivity measurements in the GHz range have been carried out for the samples revealing a dielectric dependency with pulling rates.

The growing interest in creating an internet-based network of different devices demands faster and more efficient communication. Such communications need to work at GHz and THz ranges [1]. Therefore, they trigger research areas for fabricating optimized dielectric materials which are the backbone of wireless communication [2]. Materials with minimum tangent loss, high-quality factor and high thermal stability are highly desired.

Recently eutectic materials attract lots of attention as materials for different applications including energy [4], metamaterials [5], plasmonics [6] and others [7]. In this work we investigate the potential of eutectic materials for the 5G Technology, particularly effects of growth parameters on dielectric values and losses.

TiO_2 is one the well-known dielectric materials due to its high permittivity and low loss [8]. Additionally, it has been shown that combination of TiO_2 with other oxides such as MgO and Al_2O_3 improves the thermal stability and reduces the loss.

In this project, we utilize the micro-pulling down solidification technique to control crystalline phases and interfaces and ultimately to reduce the tangent loss. TiO_2 and MgO have been selected as precursors and the composition percentages are selected based on two eutectic points in the phase diagram. The growth has been done at different pulling rates. A set of measurements have been conducted after the crystal growth, to study structural and dielectric properties. XRD measurements show the formation of TiO_2 and $MgTi_2O_5$ crystals. The SEM images exhibit partially formation of eutectic structures and different shapes with the pulling rates. In addition, the dielectric permittivity measurements in GHz range have been done for the samples showing a trend in the loss and permittivity values with pulling rates.

The authors thank the ENSEMBLE3 Project (MAB/2020/14) which is carried out within the International Research Agendas Programme (IRAP) of the Foundation for Polish Science co-financed by the European Union under the European Regional Development Fund and the Teaming Horizon 2020 programme of the European Commission.

References

1. Li, Z., Pan, J., Hu, H., & Zhu, H. (2022). Recent Advances in New Materials for 6G Communications. Advanced

Electronic Materials, 8(3), 2100978.

2. Sebastian M. T. (2010). Dielectric materials for wireless communication. Elsevier.
3. Kim, E. S., & Seo, S. N. (2010). Evaluation of microwave dielectric properties of MgO-TiO 2 system by dielectric mixing rules. Journal of the Korean Ceramic Society, 47(2), 163-168.
4. Kolodziejak. K, J. Sar, K. Wysmulek, P. Osewski, M. Warczak, A. Sadkowski, M. Radecka, D. A. Pawlak, *Journal of Catalysis* **2017**, 352, 93
5. Pawlak D. A, S. Turczynski, M. Gajc, K. Kolodziejak, R. Diduszko, K. Rozniatowski, J. Smalc, I. Vendik, *Adv. Funct. Mater.* **2010**, 20, 1116
6. Sadecka. K, M. Gajc, K. Orlinski, H. B. Surma, A. Klos, I. Jozwik-Biala, K. Sobczak, P. Dluzewski, J. Toudert, D. A. Pawlak, *Advanced Optical Materials* **2015**, 3, 381
7. Kulkarni. A. A, E. Hanson, R. Zhang, K. Thornton, P. V. Braun, *Nature* **2020**, 577, 355.
8. Kim, E. S., & Seo, S. N. (2010). Evaluation of microwave dielectric properties of MgO-TiO2 system by dielectric mixing rules. Journal of the Korean Ceramic Society, 47(2), 163-168.

Micro/Nano fabrication and characterization techniques

META 2023, PARIS - FRANCE, JULY 18 – 21, 2023

Sub-wavelength silicon nano-structuring with direct laser writing

Rana Asgari Sabet[1,2], Onur Tokel[1,2,*]

[1]Department of Physics, Bilkent University, Ankara, 06800, Turkey

[2]UNAM – National Nanotechnology Research Centre and Institute of Materials Science and Nanotechnology, Bilkent University, Ankara, 06800, Turkey

[*]corresponding author: otokel@bilkent.edu.tr

Abstract: We present a novel laser nano-lithography method inside the bulk of silicon. We exploit nanosecond laser pulses of 1.55-μm wavelength which are modulated with a spatial light modulator. The created Bessel beams enable direct and highly-controlled subsurface fabrication capability in Si. Using this technique, we demonstrate for the first time, the fabrication of sub-wavelength nano-modifications deep inside Si. We further illustrate nano-patterns of 200-nm width and of sub-micron separation. Such 3D control on sub-wavelength structures inside Si offer exciting possibilities for Si-photonics devices, meta-material and meta-surface in-chip technologies.

Direct laser writing (DLW) approaches have been widely used for 3D-structuring of transparent materials in recent years due to ease-of-operation, maskless nature, and rapid processing. Among different dielectrics, the high refractive index, low loss, and wide transparency window of silicon (Si) make it a great candidate for fabricating infrared sub-wavelength and resonant devices, potentially compatible with established electronic and photonic technologies. We recently demonstrated first subsurface Si photonics functionality and complete 3D fabrication capability with a resolution of 1 μm, created directly inside Si [1]. Numerous optical functionalities were shown in Si at this (or lower) resolutions [2], motivating us to overcome the challenges towards subsurface, sub-micron Si structuring. In order to accomplish this goal, we exploited nanosecond modulated beams. In spite of the progress made in nano-machining of other materials using femtosecond Bessel beams [3], attempts to apply this technique to Si have been unsuccessful due to limitations in the energy deposition of ultrafast pulses within the material [4].

Here we demonstrate volumetric (bulk) nano-structuring of Si using nanosecond Bessel beams, exploiting a spatial light modulator (SLM). The applied conical phase profile is in the form of $\phi(r) = e^{\pm\left(i2\pi\frac{r}{r_0}\right)}$, in which the r_0 parameter is correlated to conical angle of a physical axicon. The modulated beam is demagnified by a 4-*f* system and an aspheric lens with a focal point of 4.5 mm, and then directed to the wafer. Changing the applied phase pattern to the SLM, corresponding to different conical angles, and exploiting various polarization and pulse energies, we achieve sub-wavelength feature sized subsurface modifications, along with strong control on their position, feature size and architectures. By scanning the sample in a direction perpendicular to the laser propagation direction, planes with nano-scale one-dimensional-confinement are created inside Si (without altering the wafer surfaces). An optional selective chemical etching process reveals the nano-patterns. A representative cross-section SEM image of nano-scale lines with sub-micron separation is given in Figure 1(a). The nano-pattern is created with Bessel beam of $r_0 = 7$ pixels and pulse energy of $E_p = 5$ μJ. To reveal the nano-structures, the sample is briefly etched with a selective etchant [1]. The histogram shows the size distribution of these structures (Figure 1(b)).

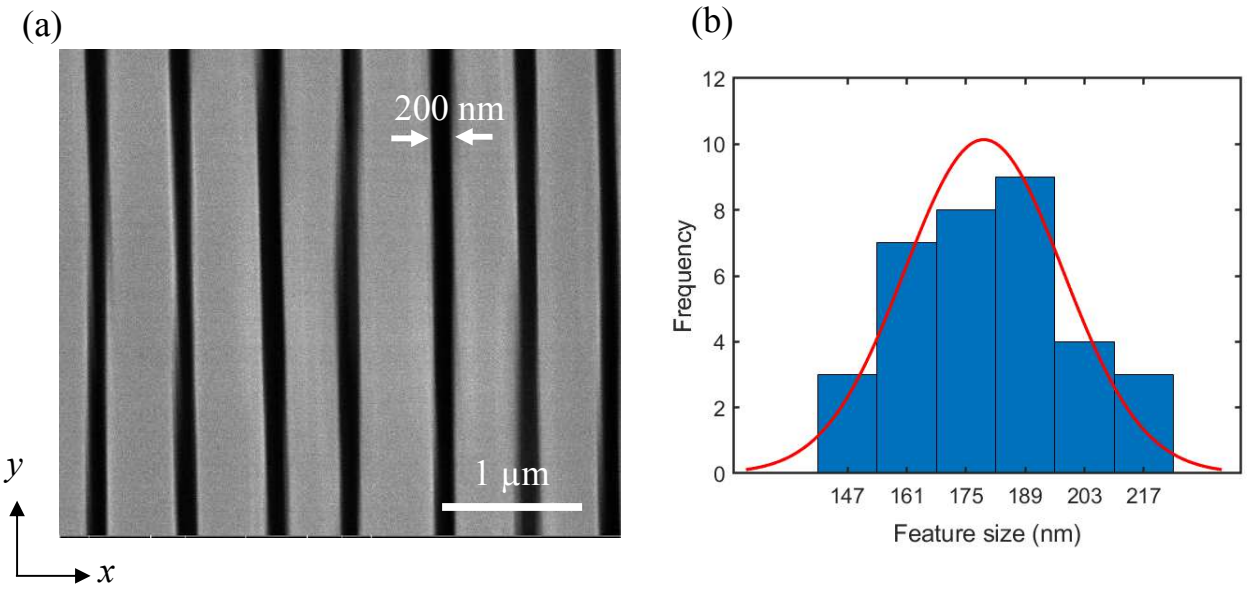


Figure 1. (a) Representative SEM image of nano-patterns created directly inside Si. The Bessel-type beam of y-polarization propagates along *z*-axis, whereas Si is scanned along *y*-axis. $r_0 = 7$, $E_p = 5$ μJ, and scanning speed = 1 mm/s. **(b)** Histogram of measured feature sizes indicates an average feature size of 180 nm ± 19 nm.

This new laser nano-structuring capability is unique, as the nanopatterning is performed directly and buried inside the Si wafer, with no surface damage. Such lithographic patterns can potentially be used as building blocks of sub-wavelength near- and mid-infrared photonic elements (potentially inside the bulk, or on the wafer surface). We anticipate that one may fabricate structures thinner than the current limit of 200 nm in Si with optimized parameters, leading to first subsurface sub-diffraction optical elements in Si, with significant consequences for sub-wavelength nano-photonics, metamaterials or metasurfaces.

References

1. Tokel, O. , et. al., "In-chip microstructures and photonic devices fabricated by nonlinear laser lithography deep inside silicon", *Nat. Photonics*. 11, 639, 2017.
2. Chambonneau, M., Grojo, D., Tokel, O., Ilday, F., Tzortzakis, S., Nolte, S., "In-volume laser direct writing of silicon-challenges and opportunities", *Laser & Photonics Reviews* **15,** 2021.
3. Velpula, P.K., Bhuyan, M.K, Courvoisier, F. , Zhang, H., Colombier, J.P., Stoian, R., "Spatio-temporal dynamics in nondiffractive Bessel ultrafast laser nanoscale volume structuring", *Laser Photonics Rev.* 10, 230–244 , 2016.
4. Grojo, D., Mouskeftaras, A., Delaporte, Ph., Lei, Sh., "Limitations to laser machining of silicon using femtosecond micro-Bessel beams in the infrared", *J. Appl. Phys.* 117, 2015.

META 2023, PARIS - FRANCE, JULY 18 – 21, 2023

MBE substrate deoxidation surveillance via RHEED image analysis with Deep-Learning

Abdourahman Khaireh-Walieh[1], Alexandre Arnoult[1], Sébastien Plissard[1] and Peter R. Wiecha[1]

[1]LAAS-CNRS, Université de Toulouse, CNRS, UPS, F-31400 Toulouse, France

[*]corresponding author:
akhairehwa@laas.fr

Abstract: In Molecular Beam Epitaxy (MBE), monitoring of the substrate deoxidation and in general, the entire crystal growth is crucial for precise crystal growth. Reflection High-Energy Electron Diffraction (RHEED) is a standard tool in MBE in-situ monitoring, providing complex real time information about the crystal surface. However, the diffraction patterns are often difficult to interpret, requiring experienced human operators[1]. We present an approach to automate the substrate deoxidation detection by analyzing RHEED video sequences by a deep-learning model.

Substrates used for crystal growth (gallium arsenide, GaAs, in our case) have usually a narrow layer of native oxide on their surface. This needs to be removed by heating before any crystal growth process can be done[2]. The deoxidation moment detection is crucial in order to avoid excessive heating and not to damage the substrate. RHEED is an in situ control method for MBE. An electron beam is directed towards the substrate surface under a narrow angle of a few degrees. The patterns on the RHEED screen are a result of diffraction of the electrons on the the crystal lattice at the substrate's surface, and thus contain information about the surface quality. RHEED is generally used to detect the deoxidation moment, but the exact deoxidation moment is not known in advance, and also the visual interpretation of the transition from oxidized to deoxidized in RHEED images is not trivial. Finally, the substrate is generally rotating, and the diffraction pattern is not necessarily visible at every rotation angle.

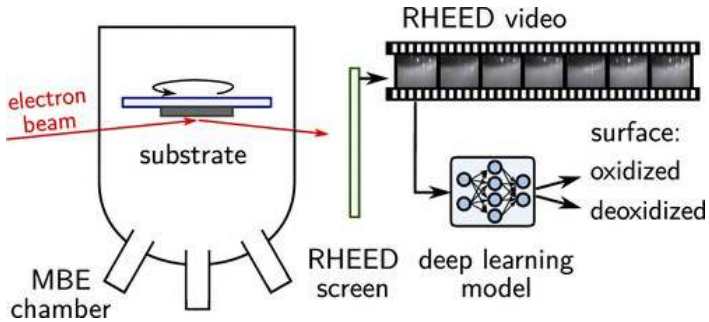


Figure 1: The e-beam is diffracted on the substrate surface forming a diffraction pattern on a fluorescent screen. Video sequences of these patterns are interpreted by a neural network.

The goal of our paper is to automate the deoxidation detection with a deep neural network model for the analysis of RHEED patterns. By analyzing sequences of images we furthermore

render the detection robust for rotating samples.
Our approach involves a two stage process. The first step consists in an autoencoder. During training, the input image is reconstructed through a bottleneck latent space by a decoder with the goal to minimize a loss function comparing the initial image and its reconstruction. After training, the encoder is used to extract the relevant information from the input image into a latent vector. These latent vectors will be stacked into sequences, representing the condensed content of entire video sequences. Those latent-sequences are finally fed into a convolution neural network classifier. We demonstrate that deoxidation detection works faithfully on experiments performed up to half a year after the training data acquisition, end despite visible RHEED screen deterioration[3].

Acknowledgements

This work was supported by the Toulouse HPC CALMIP (grant p20010). This study benefited from the support of both the LAAS-CNRS micro and nanotechnologies platform, a member of the French RENATECH network, and the EPICENTRE common laboratory between Riber and CNRS.

References

1. Kwoen, Arakawa, "Multiclass classification of reflection high-energy electron diffraction patterns using deep learning", Elsevier.

2. Bastiman, F.; Cullis, A. G. GaAs(001) planarization after conventional oxide removal utilising self-governed InAs QD site selection. Appl. Surf. Sci. 2010, 256 (13), 4269−4271.

3. Khaireh-Walieh, Arnoult, Plissard and R. Wiecha "Monitoring MBE Substrate Deoxidation via RHEED Image-Sequence Analysis by Deep Learning", Crystal growth and design.

Laser Anneal for Selective Crystallization of Magnetooptical Film

Hibiki Miyashita[1,2], Yuki Yoshihara[1,2], Takumi Koguchi[1,2], Pang Boey Lim[2], Mitsuteru Inoue[1], Kazushi Ishiyama[1], Taichi Goto[1,*]

[1]Research Institute of Electrical Communication, Tohoku University, Japan
[2]Toyohashi University of Technology, Japan
[*] taichi.goto.a6@tohoku.ac.jp

Abstract: A laser heating technique was used to selectively anneal a magnetic garnet film in a vacuum, which can be useful for integrating devices with other electronic or optical devices. The film was deposited on a synthetic fused silica substrate, and the laser was scanned in-plane to anneal the sample. Two types of periodical Ce:YIG structures were fabricated using the constructed laser annealing system, which could provide additional functionalities.

Magnetooptical (MO) effects exhibit many functionalities and have been applied in various devices, such as magnetophotonic crystals [1], magnonic crystals, MO isolators [2], MO spatial light modulators, and MO Q-switches. In these devices, MO garnet crystals or ceramics are widely used as MO materials because of their large MO response with low absorption. However, the high-temperature fabrication process of MO materials, which can reach over 700°C, is often an issue when integrating these devices with other electronic or optical devices. To address this issue, a laser heating technique can be used, which enables selective heating of a specific area. In this paper, we demonstrated the selective annealing of magnetic garnet film using a laser in a vacuum.

A 339-nm-thick film was deposited on a 5-mm square synthetic fused silica substrate using a radio frequency (RF) ion beam sputtering system with a sintered cerium-substituted yttrium iron garnet (Ce:YIG) target. The film thickness was measured by a stylus profilometer. The sample was placed on a sample stage in a vacuum chamber where no gases were introduced, and the pressure was 20 Pa. To anneal the sample, a laser was illuminated the sample, and the sample was scanned in-plane by the computer-controlled stage. The laser used for sample annealing was a continuous wave oscillation type, and an optical shutter was used to control the on/off timing of the laser annealing. The laser wavelength was 532 nm with a power of 2.0 W. The laser scanned the sample at the speed of 200 μm/s. Two types of laser scanning were conducted for annealing. The surfaces of the annealed samples were observed by microscopes, and magnetooptical responses (Faraday rotation angle) were measured.

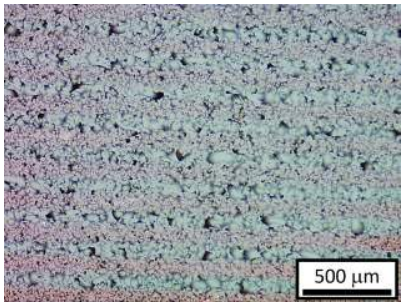


Figure 1. Microscope image of the stripe-type Ce:YIG surface annealing by scanning laser.

Figure 1 shows the stripe-patterned Ce:YIG structure. The bright area shows the crystallized part by the laser, and the dark parts are amorphous. The width of the stripe was about 100 μm, close to the spot size of the laser on the sample surface. The Faraday rotation angle was 0.27 degrees at a wavelength of 532 nm, 67% of the former-reported Ce:YIG film. Black points show the clacks or the pealed area of the sample because of the large difference in thermal expansion between the film and the glass substrate.

To decrease the clack or breakoff of the film, the stage temperature was increased by a heater at 200°C. The Faraday rotation angle was increased up to 0.34 degrees, corresponding to 0.1 degrees/micron. Figure 2 shows the periodical Ce:YIG dots fabricated by the constructed laser annealing system, combined with the optical shutter and the scanning stage. The laser was illuminated on one spot for 1 second, the optical shutter was closed, the sample was cooled for 10 seconds, and then the sample was moved at a 120 μm pitch. This sample is expected to work as two-dimensional magnetophotonic crystal or spatial light modulator by integrating with electronics.

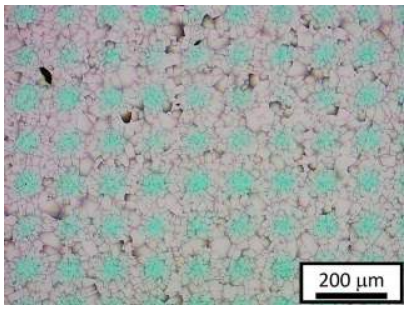


Figure 2. Periodical Ce:YIG dots fabricated by heater-assisted laser annealing.

Two types of periodical Ce:YIG structures were fabricated using a laser annealing system in this paper. The constructed laser annealing system would provide further complicated structures, demonstrating additional functionalities. In the symposium, the details of the magnetooptical responses will also be discussed.

This work was partly supported by Grants-in-Aid for Scientific Research (KAKENHI) Nos. 20H02593, 20K20535 from the Japan Society for the Promotion of Science (JSPS), Bilateral Program No. JPJSBP120214807 from JSPS and No. 21-52-50006 from RFBR, New Energy and Industrial Technology Development Organization (NEDO) No. 20002157, Tohoku Initiative for Fostering Global Researchers for Interdisciplinary Sciences (TI-FRIS) fellowship, the Foundation for Technology Promotion of Electronic Circuit Board, and the Tanaka Kikinzoku Memorial Foundation.

References

1. T. Goto, A. V. Dorofeenko, A. M. Merzlikin, A. V. Baryshev, A. P. Vinogradov, M. Inoue, A. A. Lisyansky, and A. B. Granovsky, "Optical Tamm states in one-dimensional magnetophotonic structures," Phys. Rev. Lett. 101, 113902 (2008).
2. T. Goto, M. C. Onbasli, D. H. Kim, V. Singh, M. Inoue, L. C. Kimerling, and C. A. Ross, "A nonreciprocal racetrack resonator based on vacuum-annealed magnetooptical cerium-substituted yttrium iron garnet," Opt. Express 22, 19047-19054 (2014).

Dyes emission mediated by plasmonic nanostructures revealed by SNOM

A. Mercedi [1*], L. Litti[1]

[1] Department of Chemical Sciences, University of Padova, v. Marzolo 1, 35131 Padova, Italy
[*]Corresponding author: anna.mercedi@studenti.unipd.it

Abstract: Looking at an object is the most direct approach to define and describe it. Scanning near field optical microscopy (SNOM) is part of the Scanning Probe Microscopy techniques. Its unique characteristic is to shed light in the nanoscale, overcoming the diffraction limit while simultaneously providing topographical images[1]. These reasons make this technique a powerful tool to directly correlate the complex mechanisms and structure/activity relationships that affect the emission properties of a fluorescent dye located in close proximity to a plasmonic nanostructure.

The interaction between a fluorescent dye and a plasmonic surface, can lead to a variety of different phenomena, such as Surface Enhanced Raman Scattering (SERS)[2,3], Surface Enhanced Fluorescence (SEF)[4], or even Surface Plasmon Amplification by Stimulated Emission of Radiation (SPASER)[5]. All these effects are most commonly studied in the far field regime, but they are strongly dependent on various local factors. For example, the distance between the fluorophore and the nanoparticle, the particles aggregation, as well as shape and composition of the plasmonic substrate. All these variables can be studied by SNOM techniques directly at the nanoscale. A direct correlation to the emission properties of the dyes is therefore eventually obtained. This could provide new insights into optical properties at the nanoscale and pave the way for new developments.

References

1 M. De Serio, R. Zenobi and V. Deckert, Looking at the nanoscale: scanning near-field optical microscopy, *TrAC Trends in Analytical Chemistry*, 2003, **22**, 70–77.

2 E. Lenzi, L. Litti, D. Jimenez de Aberasturi, M. Henriksen-Lacey and L. M. Liz-Marzán, SERSTEM: An app for the statistical analysis of correlative SERS and TEM imaging and evaluation of SERS tags performance, *Journal of Raman Spectroscopy*, 2021, **52**, 355–365.

3 L. B. Berganza, L. Litti, M. Meneghetti, S. Lanceros-Méndez and J. Reguera, Enhancement of Magnetic Surface-Enhanced Raman Scattering Detection by Tailoring Fe3O4@Au Nanorod Shell Thickness and Its Application in the On-site Detection of Antibiotics in Water, *ACS Omega*, 2022, **7**, 45493–45503.

4 A. R. Guerrero and R. F. Aroca, Surface-Enhanced Fluorescence with Shell-Isolated Nanoparticles (SHINEF), *Angewandte Chemie*, 2011, **123**, 691–694.

5 M. A. Noginov, G. Zhu, A. M. Belgrave, R. Bakker, V. M. Shalaev, E. E. Narimanov, S. Stout, E. Herz, T. Suteewong and U. Wiesner, Demonstration of a spaser-based nanolaser, *Nature*, 2009, **460**, 1110–1112.

META 2023, PARIS - FRANCE, JULY 18 – 21, 2023

Characterization of Optical Fourier Volumes made by Holographic Recording on Photo-reactive Polymers

K. Kim[1], Y. Lim[2], H. Son[1], S. J. Hong[3], C.-W. Shin[4], D. Baek[1], H. H. Kim[1], N. Kim[4], J. Bang[3], and S. Lee[1,2,5,6*]

[1]KU-KIST Graduate School of Converging Science and Technology, Korea University, Seoul 02841, Republic of Korea
[2]Department of Biomicrosystem Technology, Korea University, Seoul 02841, Republic of Korea
[3]Department of Chemical and Biological Engineering, Korea University, Seoul 02841, Republic of Korea
[4]School of Information and Communication Engineering, Chungbuk National University, Chungbuk 28644, Republic of Korea
[5]Department of Integrative Energy Engineering, Korea University, Seoul 02841, Republic of Korea
[6]KU Photonics Center, Korea University, Seoul 02841, Republic of Korea
[*]corresponding author: lee.seungwoo51@gmail.com

Abstract: Various researches have studied volume grating made of photo-reactive materials for optical elements due to their diffractive characteristics. However, investigation of optical features of volume grating still relies on the conventional Kogelnik's theory. Here, we analyzed the optical behaviors in detail and found out the conditions for noise-free diffraction by using Fourier-optics and computational simulations. Finally, we defined the optical Fourier volume (OFV) which has clear diffraction and experimentally validated our analytical results by using both photopolymer and photoaddressable polymer.

Since volume holograms were first developed by Gabriel Lippman (1), recording methods and recording materials of optical diffractive elements made of volume gratings have been extensively studied by many researchers. Currently, volume holograms are used in important components of AR/VR devices and Head-up-display not only simple optical elements such as lens and mirror.

The diffraction behaviors of volume grating such as transparency, diffraction efficiency and full-wave-half-maximum (FWHM) can be predicted by conventional coupled-wave theory (Kogelnik's theory). From Kogelnik's diffraction theory, we already knew that modulation range of refractive index (Δn) inside the volume grating and thickness determine the efficiency of first-order diffraction and FWHM. However, there are no established clear study for the condition of volume grating having noise-free ideal diffraction without interference of uninterested other frequencies. Thus, we analyzed the volume grating in perspective of Fourier Optics by using Fourier frequency analysis and rigorous coupled-wave analysis (RCWA) simulation, and then, we defined the Optical Fourier Volume (OFV) which exhibits the ideal diffraction behaviors (3).

In Fourier optical perspectives, one sine-wave component from Fourier decomposition of refractive index profile inside the volume grating leads to the one diffraction mode (4,5). In case of binary n profile that looks like a single grating lattice, it is decomposed into countless sine-wave functions by Fourier decomposition. Thus, those sine-wave functions produce the frequency interference from many diffraction modes (Fig. 1a). Additionally, in case of too large Δn, excessive phase accumulation of light inside the volume hologram can occur, then it results in decrease of diffraction efficiency and interference of frequencies (Fig. 1b). In conclusion, we found out that sine-wave n profile and proper phase accumulation determined by Δn and thickness are essential for ideal noise-free single diffraction of volume grating.

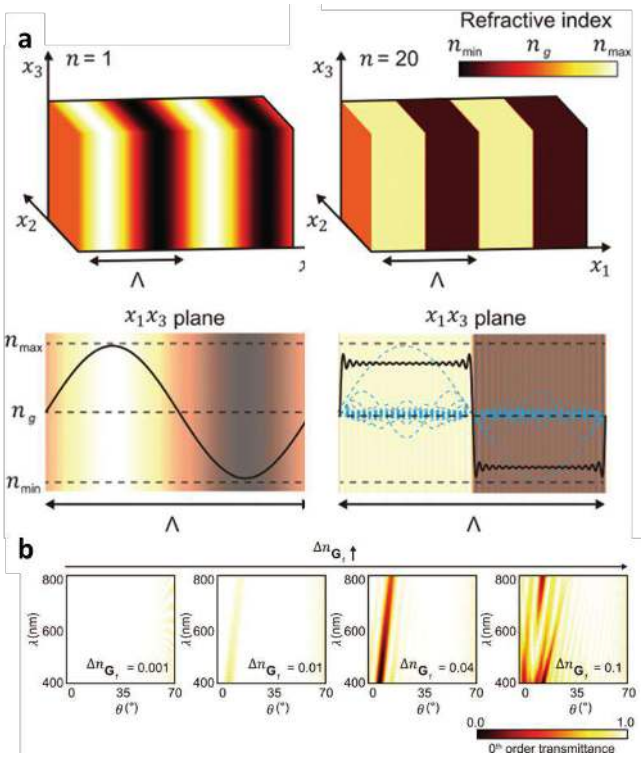


Fig1. a) The grating lattices having sin-wave and binary *n* profiles. b) Diffraction behaviors according to Δ*n*.

We experimentally validated our theoretical analysis of OFV by using two representative holographic polymers such as photopolymer and photoaddressable polymer. We confirmed that volume holograms made of both two holographic polymers exhibit the ideal OFV characteristics due to the sin-wave profile of *n* and under πd/2 value of phase accumulation. Some cases of photoaddressable polymers having high phase accumulations due to the thick film show the little degeneracies and frequency interferences.

References

1. Lippmann, G. "Sur la théorie de la photographie des couleurs simples et composées par la méthode interférentielle," J. Phys. Theor. Appl., Vol. 3, No. 1, 97–107, 1894.
2. Kogelnik, H. "Coupled Wave Theory for Thick Hologram Gratings," Bell Syst. Tech. J., Vol. 48, 2909–2947, 1969.
3. Kim, K., Y. Lim, H. Son, S. J. Hong, C.-W. Shin, D. Baek, H. H. Kim, N. Kim, J. Bang and S. Lee, "Optical Fourier Volumes: A Revisiting of Holographic Photopolymers and Photoaddressable Polymers," Adv. Opt. Mater., Vol. 10, 2201421, 2022.
4. Lassaline, N., R. Brechbühler, S. J. W. Vonk, K. Ridderbeek, M. Spieser, S. Bisig, B. le Feber, F. T. Rabouw and D. J. Norris, "Optical Fourier Surface," Nature, Vol. 582, 506-510, 2020.
5. Lim, Y., B. Kang, S. J. Hong, H. Son, E. Im, J. Bang and S. Lee, "A Field Guide to Azopolymeric Optical Fourier Surfaces and Augmented Reality," Adv. Func. Mater., Vol. 31, 2104105, 2021.

Rewritable Optical Fourier Volumes using Photoaddressable Polymers containing Azobenzene and Liquid Crystals

Heeju Son[1], Kwangjin Kim[1], Youngjun Lim[2], Seungjae Hong[3], Changwon Shin[5], Dongjae Baek[1], Hyeonho Kim[1], Nam Kim[5*], Joona Bang[3*], and Seungwoo Lee[1,2,4*]

[1]KU-KIST Graduate School of Converging Science and Technology, Korea University, Seoul 02841, Republic of Korea
[2]Department of Biomicrosystem Technology, Korea University, Seoul 02841, Republic of Korea
[3]Department of Chemical and Biological Engineering, Korea University, Seoul 02841, Republic of Korea
[4]Department of Integrative Energy Engineering and KU Photonics Center, Korea University, Seoul 02841, Republic of Korea
[5]School of Information and Communication Engineering, Chungbuk National University, Chungbuk 28644, Republic of Korea
[*]corresponding author: seungwoo@korea.ac.kr, joona@korea.ac.kr, nkim@cbnu.ac.kr

Abstract: Holographic Optical Elements (HOEs) based on the Fourier transform have to consist of the structures with sinusoidally modulated refractive index changes to avoid the mixing of undesired frequencies that can act as noise for the devices. In terms of the structure concepts, the optical Fourier volumes are appropriate for the HOEs due to their high diffraction efficiency, narrow angular selectivity. In this works, we synthesized the photoaddressable polymers and inscribed the optical Fourier volumes to confirm their properties as HOEs.

Holographic Optical Elements (HOEs) have used in many AR/VR devices to control the light to desired pathways. Among many types of holographic gratings, optical Fourier Volumes have appropriate structures to use as HOEs due to their high diffraction efficiency, narrow angular selectivity and enabling the control of the light with diverse pathways. However, in generally, optical Fourier Volumes have binary modulated structures produced by the lithography which can occur the noise appeared by mixing of undesired frequencies for the devices. In this reason, the optical Fourier Volumes are required to have sinusoidally modulated profiles of the refractive index to make higher signal-to-noise ratio. (Fig.1) [1]

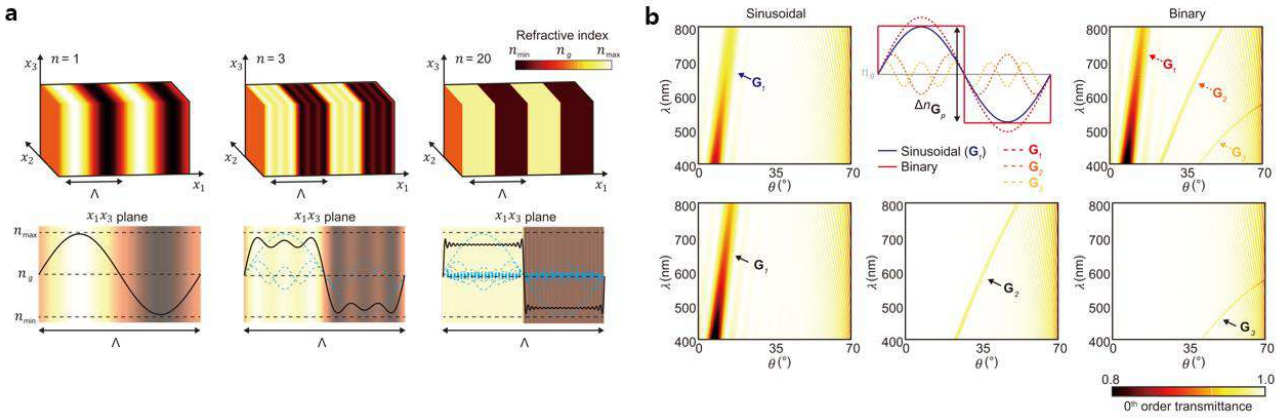


Fig. 1. The numerical calculations about 1D optical Fourier volumes through rigorous coupled-wave analysis (RCWA). (a) the spatial profiles of the refractive index according to the numbers of wave to be mixed. (b) The analysis of diffraction behaviors about sinusoidally and binary modulated optical Fourier volumes with the same values of the refractive index change through monitoring the 0th order transmission.

In this works, we synthesized the photoaddressable polymers consisting of azobenzene and liquid crystals to inscribe sinusoidally modulated optical Fourier Volumes and confirmed their properties as HOEs. The light-driven reorientation of the azobenzene molecules induced by the photochemical trans-cis-trans isomerization generates the sinusoidally modulated molecular alignments across the polarization directions of the interference pattern of two circular polarized lights.[2] The molecular alignments of the azobenzene molecules cause the refractive index changes sinusoidally and amplify them through the cooperative motions to align the neighboring liquid crystal molecules.[3]

We experimentally inscribed the two types of the sinusoidally modulated optical Fourier volumes, the transmissive and reflective volume gratings, and measured their characteristics such as diffraction efficiency, angular selectivity, and photonic band gaps which show that they can act as the optical Fourier volumes. (Fig.2) Each type of inscribed volume gratings has specific diffraction behaviors which well-match the Fourier spectrum without the noise from unwanted frequencies.

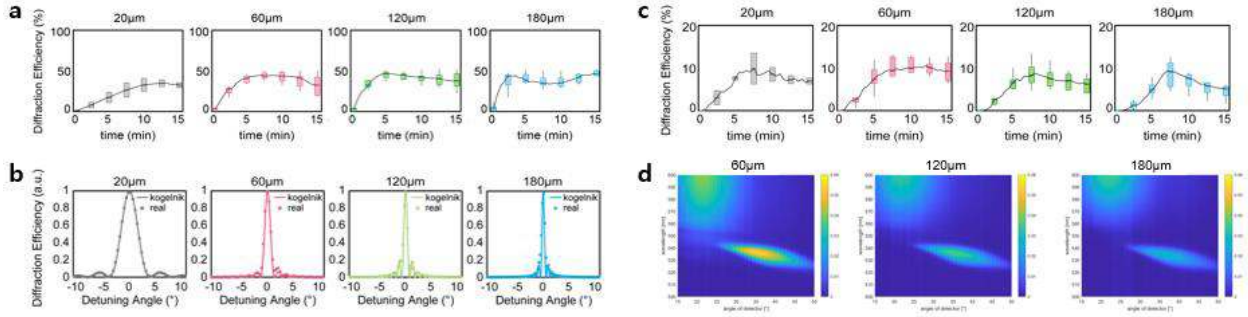


Fig. 2. The characteristics of each type of volume gratings. (a) Real-time measurement of diffraction efficiencies of each transmissive volume gratings along the thickness during the holographic inscription. (b) Angular selectivity of transmissive volume gratings measured by incident angle changing from the Bragg angle with the Kogelnik's fittings. (c) Real-time measurement of diffraction efficiencies of each reflective volume gratings along the thickness. (d) Photonic band gaps of each reflective volume gratings measured by FT-IR at the conditions fixing the incident angle at 20° and changing the angle of the detector.

Acknowledgement

This work was supported by the National Research Foundations of Korea (future technology laboratory program, project no. 2022M3H4A1A02074314), a Korea University grant, the KU-KIST School project, and the Future Research Grant (FRG) program at Korea University.

References

1. K. Kim, Y. Lim, H. Son, S. J. Hong, C. Shin, D. Baek, H. Kim, N. Kim, J. Bang and S. Lee, "Optical Fourier Volumes: A Revisiting of Holographic Photopolymers and Photoaddressable Polymers," Adv. Optical Mater., 10, 23, 2201421, 2022.
2. Y. Lim, B. Kang, S. J. Hong, H. Son, E. Im, J. Bang and S. Lee, "A Field Guide to Azopolymeric Optical Fourier Surfaces and Augmented Reality," Adv. Funct. Mater., 31, 39, 2104105, 2021.
3. S. L. Oscurato, M. Salvatore, P. Maddalena and A. Ambrosio, "From nanoscopic to macroscopic photo-driven motion in azobenzene-containing materials," Nanophotonics, 7, 8, 1387-1422, 2018.

Design and Fabrication for Optical Fourier Surfaces Reaching the Theoretical Upper Limit of Diffraction Efficiency

Yongjun Lim[1], Seung Jae Hong[2], Heeju Son[3], Joona Bang[2], and Seungwoo Lee[1,3,4*]

[1]Department of Biomicrosystem technology, Korea University, Seoul 02841, Republic of Korea
[2]Department of Chemical and Biological Engineering, Korea University, Seoul 02841, Republic of Korea
[3]KU-KIST Graduate School of Converging Science and Technology, Korea University, Seoul 02841, Republic of Korea
[4]Department of Integrative Energy Engineering and KU Photonics Center, Korea University, Seoul 02841, Republic of Korea

[*]corresponding author: seungwoo@korea.ac.kr

Abstract: Optical Fourier surfaces (OFSs), which are surface gratings having sinusoidally modulated profiles, can be minimized optical loss due to preventing the mixing of waves with undesired frequencies. In this work, we introduce a novel fabricated method for the perfect OFSs. Our method can generate perfect sinusoidal gratings with high throughput because it is based on holographic mass migration. Furthermore, we demonstrate that our OFSs can reach the theoretical upper limit of diffraction efficiency in the whole visible wavelength range.

Surface gratings, which are basic elements of diffractive optical elements (DOEs), have been widely used for various optical applications, especially augmented reality (AR) and virtual reality (VR) technologies. For the application of these optical devices, these diffractive gratings should be minimized optical loss. To this end, sinusoidally modulated surface profiles were required to prevent the mixing of waves with undesired frequencies. In terms of Fourier optics, diffractive gratings composed of entirely sinusoidal profiles can be categorized into optical Fourier surfaces (OFSs) [1].

Sinusoidally modulated surface profiles can be generated through lithographic approaches; recently, OFSs were successfully generated by scanning probe lithography (SPL) [2]. However, these conventional lithographic methods have limitations in fabricated area and throughput because of additional processes. In this work, we present a novel method for the fabrication of perfect OFSs through holographic mass migration rather than lithographic etching. In this process, the OFSs could be generated in a large area with high throughput compared to other fabricated methods [3,4].

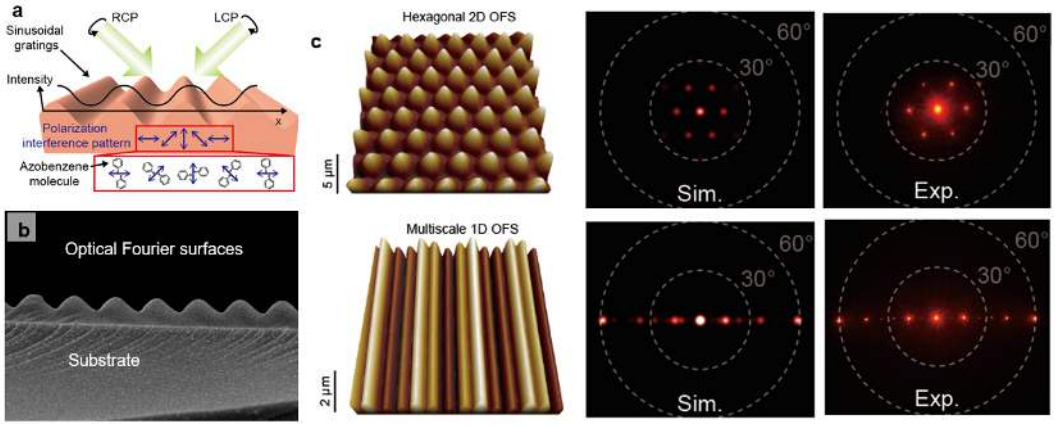


Figure 1. Optical Fourier surfaces (OFSs) through holographic mass migration. a) Schematic for holographic

mass migration. b) Scanning electron microscopy image of the perfect sinusoidally modulated profile of OFSs. c) Atomic force microscopy images and Fourier spectrum of complex 2D OFSs.

By the holographic inscription as depending on mass migration, we fabricated OFSs having a perfect sinusoidal profile which can be minimized the mixing of undesired frequencies. As a result, the experimental Fourier spectrums of not only 1D OFSs but complex 2D OFSs designed based on Fourier synthesis exactly match with numerical calculation (Figure 1). Another advantage of our OFSs was that can be easily transferred to other polymers, especially transparent materials with a high refractive index at visible wavelengths. We demonstrated that OFSs can reach the theoretical upper limit of diffraction efficiency in the whole visible wavelength range (Figure 2).

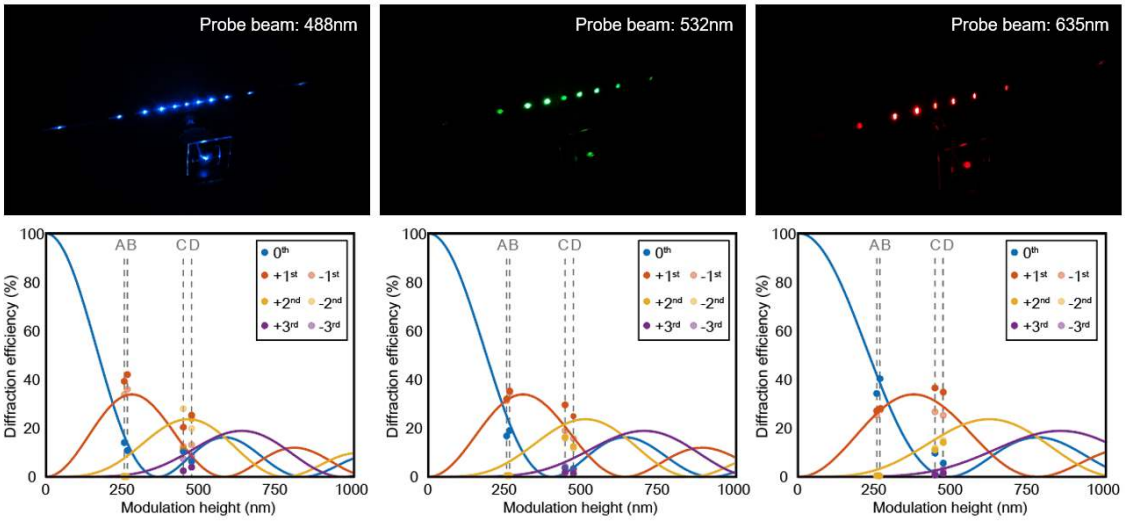


Figure 2. Full-color diffraction of OFSs reaching the theoretical upper limit of diffraction efficiency.

Acknowledgment

This work was supported by NRF-2022M3H4A1A02074314 (future technology laboratory program) funded by the National Research Foundation of Korea, the KU-KIST School Project, and a Korea University grant.

References

1. Y. Lim, H. Park, B. Kang, K. Kim, D. Yang, S. Lee, “Holography, Fourier optics, and Beyond Photonic Crystals: Holographic Fabrication for Weyl Points, Bound States in the Continuum, and Exceptional Points”, Adv. Photonic Res., 2 (8), 2100061, 2021.
2. N. Lassaline, R. Brechbuhler, S. J. W. Vonk, K. Ridderbeek, M. Spieser, S. Bisig, B. le Feber, F. T. Rabouw, D. J. Norris, “Optical Fourier Surfaces”, Nature, 582, 506, 2020.
3. Y. Lim, B. Kang, S. Lee, “Photo-Transformable Gratings for Augmented Reality”, Adv. Fucnt. Mater., 31, 2100839, 2021.
4. Y. Lim, B. Kang, S. J. Hong, H. Son, E. Im, J. Bang, S. Lee, “A Field Guide to Azopolymeric Optical Fourier Surfaces and Augmented Reality”, Adv. Funct. Mater., 31, 2104105, 2021.

Characterizing Far-Field Plasmonic Resonances of Au and $AuAl_2$ Structures using Dark Field Spectroscopy

T. McCaughery[1], A. Maity[1], R. Bowman[1]

[1]Queen's University, Belfast. United Kingdom

Abstract: Plasmonic materials such as Au and $AuAl_2$ have the ability to facilitate nanoscale heat generation and have attracted attention due to their relative availability [1,2]. In this work, these materials were patterned into various geometries. Dark field spectroscopy (DFS) was used to measure the far-field response of particles, along with 3D-FDTD modelling which calculated the field enhancement present within the structures. The experimental and simulated DF results were compared and showed good agreement for Au.

Au and $AuAl_2$ were fabricated by PVD (co-)sputtering sheet films onto a p-type silicon substrate, with subsequent photolithographic patterning and dry etching carried out, resulting in structures consisting of two 200nm discs connected by a nanowire (known as 'nanowire-bridged dimers'[3]). Single-particle DFS showed a spectral resonance at a wavelength of 668nm for the Au structure (see Fig. 1(a)). A monitor which was placed 5nm above the 'nanowire bridge' within the 3D-FDTD model showed a circular region of enhancement.

Having characterized the Au structure, the aim is to explore the effects of introducing Al into the system, maintaining the nanowire-bridged dimer design. Room temperature $AuAl_2$ has been co-sputtered and ellipsometry has been taken for both Au and $AuAl_2$ as shown in Fig.1(b). $AuAl_2$ nanowire-bridged dimers will be patterned and analyzed with increasing vacuum anneal temperature, in order to observe thermal robustness.

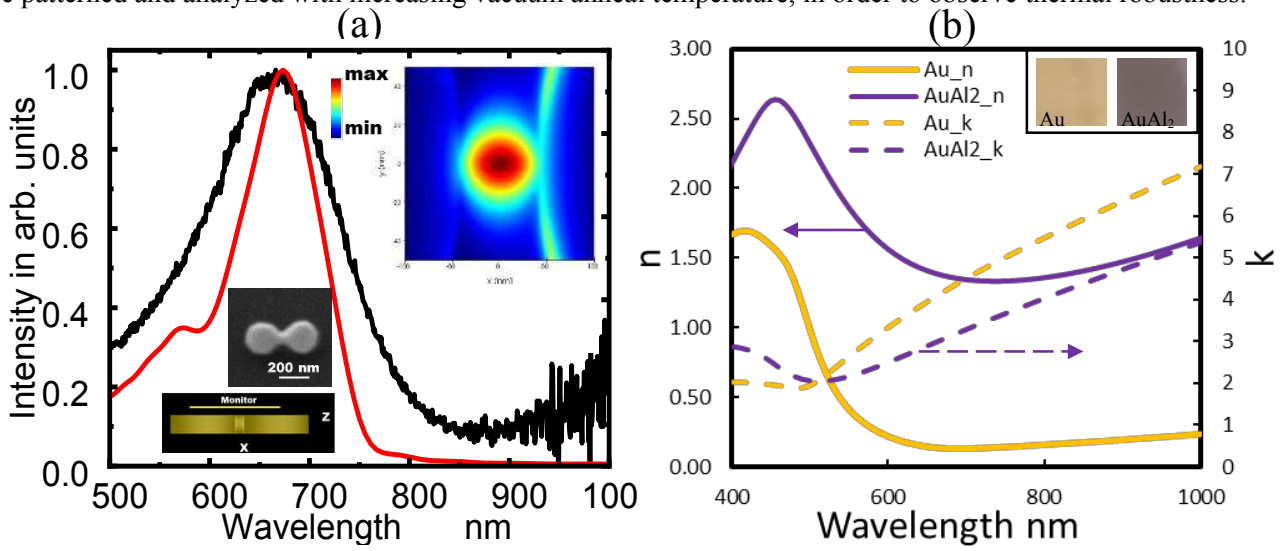


Fig. 1(a) Experimental **(black)** and calculated (**red**) DF Spectra of Au structure. **Inset top right**: FDTD showing field enhancement on top of nanowire. The incident light is propagated along z and polarization along x. **Inset bottom left**: Inline image of nanowire-bridged dimer with

References

1. Keast, V.J. "$AuAl_2$ and $PtAl_2$ as potential plasmonic materials," JAC, Vol. 577, Pg 581-586, 2013.
2. Jian, C, "Au-Al intermetallic compounds: A series of more efficient LSPR materials for hot carriers-based applications than noble metal Au," NE, Vol. 82, Pg 105763, 2021.
3. Wen, F., "Charge Transfer Plasmons: Optical Frequency Conductances and Tunable Infrared Resonances," ACS Nano, Vol. 9, Pg 6428-6435, 2015.

META 2023, PARIS - FRANCE, JULY 18 – 21, 2023

3D Micro-imprinted Flexible Plasmonic PDMS-based Platform for SPR-SERS Detection of the Formalin Contaminant

A. Campu[1*], M. Potara[1], S. Astilean[1,2] and M. Focsan[1]

[1]Nanobiophotonics and Laser Microspectroscopy Center, Interdisciplinary Research Institute in Bio-Nano-Sciences, Babes-Bolyai University, Treboniu Laurian No. 42, 400271 Cluj-Napoca, Romania
[2] Biomolecular Physics Department, Faculty of Physics, Babes-Bolyai University, Mihail Kogalniceanu No. 1, 400084 Cluj-Napoca, Romania
[*]corresponding author: andreea.campu@ubbcluj.ro

Abstract: One of the major concerns of the today's society is related to environmental monitoring and food safety, which have a great impact on the citizens well-being and health. In particular, food contamination is regarded as a severe public health problem due to the constant increase in food-borne diseases. A natural toxin, produced by living organisms and toxic to humans when ingested, is formaldehyde (FA), also known as formalin (37 % formaldehyde aqueous solution), which is a colour-less, highly volatile, with an irritating odour gas.

In this context, this work aims to develop and implement a new innovative miniaturized portable sensing platform for the dual-modal Surface Plasmon Resonance (SPR) – Surface Enhanced Raman Spectroscopy (SERS) detection of FA in beverages. Specifically, a sensor architecture is designed by combining the advantages of polydimethylsiloxane (PDMS), such as flexibility, optical transparency and chemical inertness, and gold thin films for FA monitoring by means of portable plasmon-based detection technologies. The developed flexible chip allows the efficient optical detection of glucose *via* SPR, but also its specific identification through SERS, by the modification of the PDMS' surface micro-roughness through an innovative simple method of micro-imprinting of the three-dimensional (3D) matrix of filter paper, thus, upon the deposition of the gold thin film, a rough surface suitable for SERS is obtained. Upon the optimization of the gold thin film thickness, the SPR and SERS sensitivities are evaluated using a well-known Raman reporter, specifically, 4-mercaptobenzoic acid. Further, the plasmonic platform will be functionalized with biomolecules in order to obtain at its surface primary amino groups, which are known to transform in imine groups as a result of their interaction with aldehydes, FA included. The dual implementation of SPR and SERS analysis techniques ensures both high sensitivity and specificity of the as-developed FA sensor, promoting portability and fast on-site detection capabilities, contributing thus to the progress of food pollutant monitoring by providing a real-world solution for the determination of life-threatening amounts of hazardous materials.

Acknowledgements: This work was supported by CNCS-UEFISCDI Romania, under the project number PN-III-P1-1.1-PD-2021-0175. Andreea Campu acknowledges the STAR-UBB Fellowships awarded by the Babes-Bolyai University, under the contract nr.21PFE/ 30.12.2021, ID: PFE-550-UBB.

META 2023, PARIS - FRANCE, JULY 18 – 21, 2023

Ion beam doping of phase-change materials: a platform for active metasurfaces

Martin Hafermann, Robin Schock, Annkathrin Köhler, Jacob Grandmontagne, and Carsten Ronning

Institute of Solid-State Physics, Friedrich Schiller University Jena, 07743 Jena, Germany
*corresponding author: martin.hafermann@uni-jena.de

Abstract: Phase-change materials (PCMs) have emerged to serve as active media for tunable plasmonic and photonic devices. They provide the ability of reversible, repeatable, and rapid switching between amorphous and crystalline states accompanied with drastic changes in the electronic and photonic properties. Impurity doping by means of ion implantation can be used to tailor the crystallization kinetics of PCMs. Here, we demonstrate that spatially selective ion beam doping of PCMs can serve as a platform in designing active metasurfaces.

The integration of active media into conventional metasurface designs enables the ability to control the optical response in-operando leading to dynamic switchable, tunable, and reconfigurable optical functionalities. While multiple material classes have been demonstrated to serve as such active media, particularly chalcogenide-based phase-change materials, such as $Ge_2Sb_2Te_5$ (GST), have emerged as one of the most promising materials for tunable plasmonic and photonic devices[1,2]. They provide the ability of reversible, repeatable, and rapid switching between amorphous and crystalline states upon external optical, electrical, or thermal stimuli and accompanied with drastic changes in the electronic and photonic properties.

In this work, we present that impurity doping via ion implantation can be utilized to modify the crystallization process of GST thin films[3]. Two opposing effects occur for the implantation of group V elements into GST thin films, which can be seen in Figure 1a. First, the crystallization process is facilitated by the reduction of homopolar bonds caused by ion beam induced lattice damage for low doping concentrations. This was corroborated by noble gas irradiations of as-deposited GST films, as no impurity doping effect is expected. Moreover, it was found that heavier ions have a more pronounced damaging effect that is accompanied with a higher reduction of the homopolar bonds destabilizing the amorphous phase. Second, the crystallization is retarded by higher contents of impurities, while various effects are proposed for different ion species. While light ions, like nitrogen, may induce a strain field due to their localization at tetrahedral interstitial sites, heavier ions may be able to substitute atoms from their lattice sites or fill the inherent vacancies in GST, which leads to the formation of additional covalent bonds inhibiting the crystallization process. Repeated re-amorphization via noble gas ion irradiation and thermal annealing of doped GST films was performed. The effect of induced lattice damage becomes similar for all ion species, as after multiple cycles only the contribution of Ar^+-ion irradiation used to re-amorphize GST is dominant. While the doping effect of the lighter ions diminishes, it is roughly constant for the heavier ions upon cycling. Enhancing the doping effect within As^+-doped GST by the introduction of a more uniform box-like implantation profile leads to well separated transitions of intrinsic (re-amorphized) and doped GST already for doping concentrations of 2 at.% (compare Figure 1b).

We further demonstrate how ion beam doping of GST combined with masking can serve as a platform for designing active photonic devices. As shown above, doping of GST with e.g. As can be utilized for stabilizing the amorphous phase by increasing the crystallization temperature. Thus, spatially selective doping based on ion implantation through lithographically patterned masks yields the ability to shift the crystallization temperature in

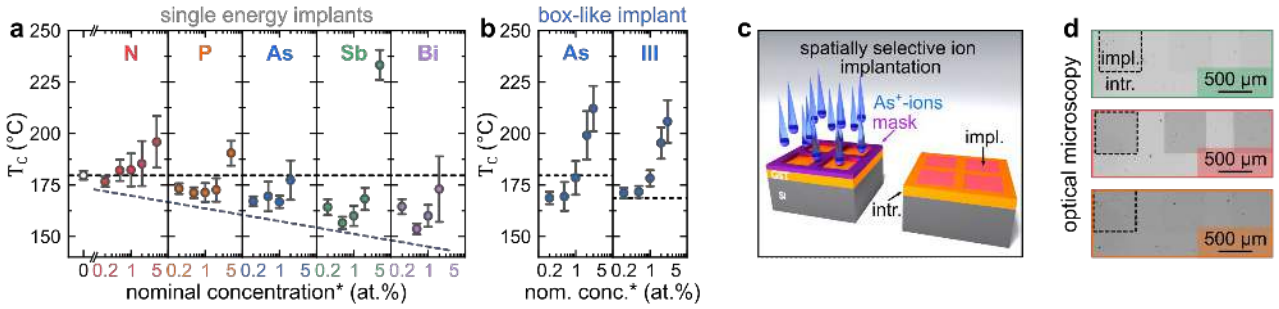


Figure 1 (a) Critical temperatures for crystallization T_C of various group V ion implanted GST thin films on Si substrates as a function of nominal dopant concentration for all ion species. Nominal concentration values correspond to peak values of ion depth distribution. Error bars correspond to the respective phase-transition width. (b) Critical temperatures for crystallization T_C of box-like As^+-ion implanted GST films as a function of nominal concentration. Subsequent to the first annealing step, each sample was repeatedly amorphized (using Ar^+-ion irradiation) followed by additional annealing steps (only step III shown). (c) Schematic of spatially selective ion implantation of As^+-ions through a lithographically patterned mask into GST film on Si. (d) Optical microscopy images of an area-selectively implanted GST film in the amorphous (orange box; both regions amorphous), partially annealed (red box; intrinsic is rock-salt, implanted is amorphous) and completely annealed (green box; both regions crystalline) states.

pre-defined, restricted regions (see Figure 1c). The separation between the phase transitions of intrinsic and implanted regions shown in Figure 1b was utilized to achieve artificial phase coexistence within a spatially selective implanted GST thin film by heating the sample to a temperature that is between the phase-change regimes of intrinsic and implanted regions. This was observed within an optical microscope, which is depicted in figure 1d for the three different states: amorphous (orange box; both regions amorphous), partially annealed (red box; intrinsic is rock-salt, implanted is amorphous) and completely annealed (green box; both regions crystalline). While the square structures are barely visible in the amorphous and completely annealed case, they are clearly distinguishable in the partially annealed state due to the distinct different reflectance of amorphous and crystalline GST in the visible spectral region.

Finally, we use e-beam lithography as masking technique that facilitates implanted regions with subwavelength dimensions. Appropriate switching between the states of these implanted and intrinsic regions enables active tuning of a lateral phase coexistence that can be accompanied with in- and out-tuning of an optical functionality. By this means, we demonstrate that spatially selective ion beam doping of a phase-change material can serve as a platform for designing active optical metasurfaces that are reconfigurable, switchable, and inherently flat.

References

1. Wang, Q. et al. Nature Photonics, 10, 60-65, 2016.
2. Li, P. et al. Nature Materials, 15, 870-875, 2016.
3. Gao, Q. and Chen, L. Applied Physics A, Vol. 125, No. 564, 2019.

Large area high-resolution nanostructure fabrication with focused ion beam for surface-enhanced Raman spectroscopy

L.Bikse[1*], R. Ignatans[1], J. Prikulis[2], A. Trausa[1] and K. Smits[1]

[1]Institute of Solid State Physics, University of Latvia, Latvia
[2]Institute of Chemical Physics, University of Latvia, Latvia
[*]corresponding author: liga.bikse@cfi.lu.lv

Abstract: The development of focused ion beam (FIB) has reached a point where its resolution and time-consumption are suitable for the fabrication of nanostructures. Various 100 nm diameter dumbbell-shaped pits were fabricated with FIB automation controlling the positions, depth, and gap of the dimer systems (Fig.1). Filling well-organized pits with gold nanoparticles (NP), can relieve whether random positioned NP can be a better solution for surface-enhanced Raman spectroscopy (SERS) than periodical positioned, and other related questions.

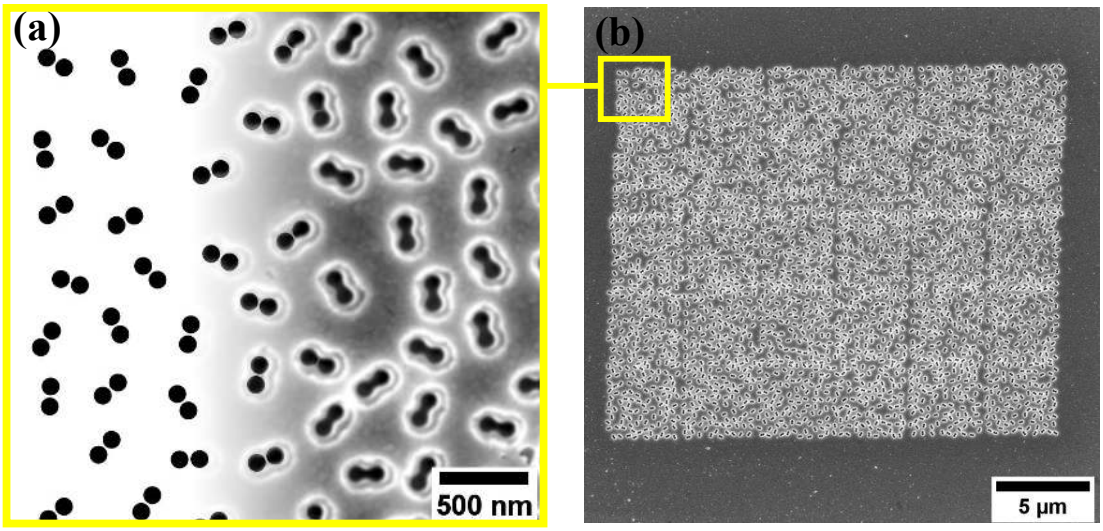


Fig.1. A bitmap of designed nanostructures on the left side of the and fabricated on the right side of (a) from a large area (b).

The authors gratefully acknowledge the financial support of the ERDF project Nr. 1.1.1.1/21/A/053 realised at the Institute of Solid State Physics, University of Latvia.

References

1. Han, X. X., Rodriguez, R. S., Haynes, C. L., Ozaki, Y., & Zhao, B. “Surface-enhanced Raman spectroscopy,” Nature Reviews Methods Primers, 1(1), 87, 2021.

META 2023, PARIS - FRANCE, JULY 18 – 21, 2023

Periodically modulated photonic structures for light manipulation

Julianija Nikitina[1,2*], Ceren Babayigit[3], Kęstutis Staliūnas[4,5], and Lina Grinevičiūtė[2]

[1]Center for Physical Sciences and Technology, Savanorių ave. 231, Vilnius LT-02300, Lithuania
[2]Laser Research Center, Vilnius University, Saulėtekio Ave. 10, Vilnius LT-10223, Lithuania
[3]University of California, Irvine, California 92697, United States
[4]ICREA, Passeig Lluís Companys 23, 08010, Barcelona, Spain
[5]UPC, Rambla Sant Nebridi 22, 08222, Barcelona, Spain
[*]corresponding author: julianija.nikitina@ff.vu.lt

Abstract: In this work the conformal deposition of high refractive index thin films on periodically micro-structured surfaces was investigated. The optical response of fabricated single-layer photonic structures demonstrates sharp sensitivity in both angle and wavelength domains, allowing to perform narrow-band spatial filtering and manipulate light polarization.

The modern tendency to miniaturize laser systems and enhance its laser power, evokes the need to create novel optical elements with periodically modulated inner nanostructure, such as photonic crystals. Artificially created refractive index modulation in such structures forms the allowed and forbidden energy bands, that are useful to manipulate light propagation in various ways. And yet, when the required periodicity of refractive index decreases to nano-scale, the possibilities of state-of-the-art lithography to fabricate such photonic crystals are restricted. Therefore, multidimensional photonic crystals are quite rare in practice.

One of the alternative fabrication methods is a conformal deposition of thin films on a structured surface, where every layer repeats initial surface modulation. The practical value of such complex multilayer nanostructures has been demonstrated in Ref. [1], however sharp optical characteristics deviate from theoretical predictions, due to various reasons, such as modulation extinction after the thickness of deposited layers reaches several microns, distortion of modulation form etc.

This work demonstrates the investigation of analogical structure, but consisting of a more simple architecture - of high refractive index single-layer deposited on a periodically modulated surface. When the periodically modulated single-layer structure with a high refractive index is surrounded by a low refractive index media, as shown in Fig. 1(a), it features Fano-like resonance phenomena due to the coupling of thin film waveguided modes with Fabry-Perot modes [2]. This phenomenon results in the appearance of extremely low transmittance lines in the transmittance (Θ, λ) maps, which are sensitive with respect to the angle and the wavelength of the incident light (Fig. 1(b)).

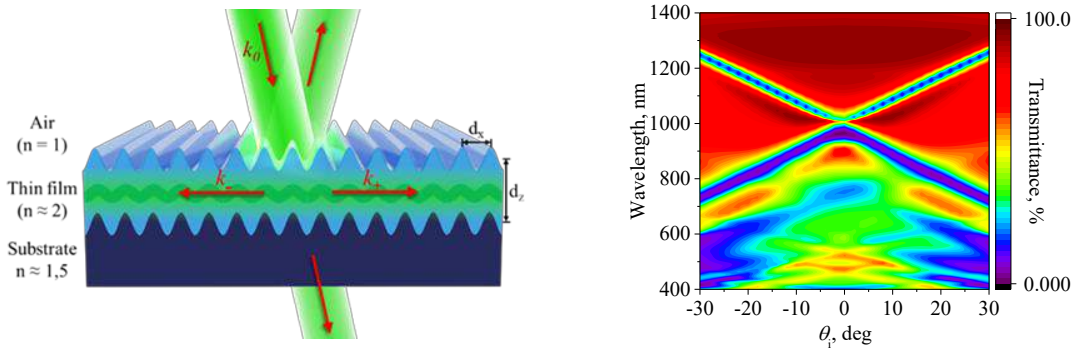


Figure 1. (a) The schematic representation of Fano-like resonance in periodically modulated single-layer photonic structure; (b) Transmission map in a plane (Θ, λ) for 0.2 μm thick tantalum oxide structured layer [2].

Moreover, as the fabricated single-layer photonic structure has refractive index modulation only in one direction, its optical response is also polarization dependent. As will be discussed during the presentation, the proposed single-layer photonic structure, featuring Fano-like resonances, can be considered as a potential spatial filtering or light-polarizing optical element suited for micro-laser systems.

This work received funding from the European Social Fund (Project No. 09.3.3-LMT-K712–17-0016) under grant agreement with LMTLT.

References

1. L. Grinevičiūtė, C. Babayigit, D. Gailevičius, M. Peckus, M. Turduev, T. Tolenis, M. Vengris, H. Kurt, K. Staliūnas, "Nanostructured Multilayer Coatings for Spatial Filtering", Adv. Optical Mater., 2001730, 2021.
2. L. Grinevičiūtė, J. Nikitina, C. Babayigit, K. Staliūnas, "Fano-like resonances in nanostructured thin films for spatial filtering" Applied Phys. Lett., 118, 131114, 2021.

META 2023, PARIS - FRANCE, JULY 18 – 21, 2023

Laser-Induced Nanostructuring of Material Phase and Shape for 3D Light Control

M.S. Elizarov*, N. Li, A. Fratalocchi

PRIMALIGHT, Faculty of Electrical Engineering, Applied Mathematics and Computational Science,
KAUST, Thuwal 23955-6900, Saudi Arabia
*corresponding author: maxim.elizarov@kaust.edu.sa

Abstract: We introduce a three-dimensional nanostructuring platform that utilizes light-induced control over nanomaterials' phase and geometry. We employ a heterogeneous oxide-polymer nanostructure as the fundamental component of our approach. By applying low-power (up to 15mW) CW lasers of varying intensity and exposure time, we achieve photothermal passivation and reshaping of the initial material. Resulting structures possess modified spectral response, enabling us to develop a technology for large-scale structural color laser printing with widest gamut reported.

The development of new nanofabrication techniques for controlling light at the nanoscale attracts considerable interest in research[1]. Recent advances in state-of-the-art methodologies, including nanopatterning, additive nanomanufacturing, and lithography, focus on processing specific geometrical patterns in a given material. Phase-changing media, on the contrary, have been reported to enhance the performance and response attainable at optical frequencies significantly. However, a technique that allows point-to-point controllability over the material phase and geometrical shape is unavailable. Addressing this problem can open new pathways for controlling materials' optical response, leading to new levels of performance of photonic devices.

Here we present a nanostructuring platform in which we explore nonlinear light-matter interactions to alter the material geometry and phase controllably. The cornerstone of this approach is laser-induced passivation and reshaping of oxide-polymer heterostructures deposited on rigid and flexible substrates. Figure 1a shows a cross-sectional TEM image with corresponding EDX elemental mapping for the initial heterostructure composed of polymer nanosphere with deposited partially oxidized material on top. Upon exposure to a tightly focused laser diode, we observe structural change involving polymer melting with the formation of fully oxidized hollow core-shell geometry (Fig.1c). Elemental mapping of this area (Fig.1d) confirms that the cavity of the newly formed nanostructure is void. We observe that the phase transition in these structures is a gradual process dependent on laser intensity and exposure time. The transformed system with partial to fully passivated material exhibits resonant behavior in the optical response. In the case of closely-packed two-dimensional arrays of an initial heterostructure, successive exposure to laser illumination over the larger sample area results in the generation of structural coloration at the microscale. We control this process by various parameters, including the laser power, exposure area, and exposure time.

We demonstrate this nanomaterial platform's effectiveness in the inkless laser color printing field, which recently attracted significant interest[2]. While resonant laser printing on a preprocessed photoactive material achieved subdiffraction limit resolution, it still lacks a wide color gamut and requires nonintegrated, high-energy, and high cost pulsed lasers. By using a low-power (15 mW) laser diode, we achieve laser printing at high-resolution (33000 DPI) images with the broadest gamut

reported. To the best of the authors' knowledge, the controllable gamut of color obtained with this technique also exceeds the best results currently available with inverse design. This new platform can open new applications of nanomaterial engineering for controlling light with nanoscale resolution[3].

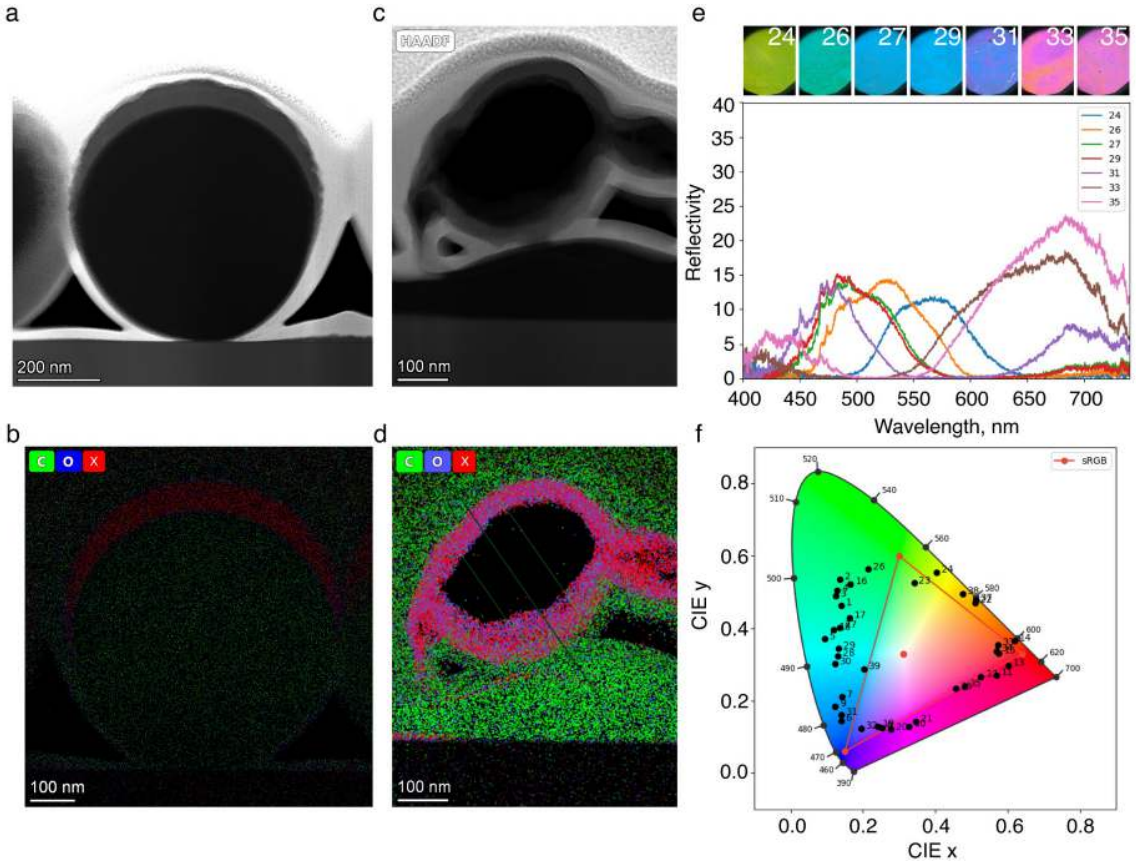


Fig.1. **a** - cross-sectional TEM image of initial heterostructure before laser illumination; **c** - cross-sectional TEM image of transformed heterostructure after laser illumination; **b,d** - corresponding elemental mappings; **e** - reflectivity spectra of structural color samples with corresponding optical photographs; **f** - CIE 1931 chromaticity diagram with plotted chromaticities of obtained samples.

References

1. Elizarov, M.S., Kivshar, Y.S., and A. Fratalocchi, “Inverse-designed metaphotonics for hypersensitive detection”, ACS Nanoscience Au, 2(5):422–432, 2022; doi.org/10.1021/acsnanoscienceau.2c00009
2. Fang, Z., Chen, R., Zheng, J., Khan, A. I., ... and Chen, E.,“Ultra-low-energy programmable non-volatile silicon photonics based on phase-change materials with graphene heaters,” Nat. Nanotechnol. 17, 842–848, 2022; doi.org/10.1038/s41565-022-01153-w
3. Zhu, X., Yan, W., Levy, U., Mortensen, N. A., and Kristensen, A., “Resonant laser printing of structural colors on highindex dielectric metasurfaces”, Sci. Adv. 3, e1602487, 2017; doi.org/10.1126/sciadv.1602487
4. Hao, Y., Liu, Y., Wu, T., Li, J., Sun, Y., ... and Ye, H, “Improved bidirectional networks for nanostructure color design”, Optics Communications, 520, 128419, 2022; doi.org/10.1016/j.optcom.2022.128419

Modeling and computational techniques

Micromagnetic Simulation of Sub-micron Scaled Magnetic Domains in Magnetic Garnet Films

Takumi Koguchi[1,2,3], Yuki Yoshihara[1,2,3], Pang Boey Lim[3], Mitsuteru Inoue[1], Kazushi Ishiyama[1] and Taichi Goto[1*]

[1]Research Institute of Electrical Communication, Tohoku University, Japan
[2]Graduate School of Engineering, Tohoku University, Japan
[3]Toyohashi University of Technology, Japan
[*]taichi.goto.a6@tohoku.ac.jp

Abstract: Magnetic garnet films have been widely used in magnetooptical devices because of their large Faraday rotation angle and low optical loss. For the development of magnetooptical devices such as spatial light modulators and spin-controlled lasers, controlling the magnetic domains is essential. However, predicting the behavior of magnetic domains can be challenging. In this research, we calculated the magnetic domains in the magnetic garnet film using a micromagnetic simulation.

Magnetic garnet films are widely used in magnetooptical devices because of their large Faraday rotation angles and low optical absorption. Cerium-substituted yttrium iron garnet (Ce:YIG, $Ce_1Y_2Fe_5O_{12}$)[1] particularly well-suited for use in magnetooptical modulators such as magnetooptical spatial light modulators[2] and magnetooptical Q-switch[3], due to its excellent magnetooptical response at near-infrared wavelengths. To be effective in such applications, Ce:YIG needs to exhibit perpendicular magnetic anisotropy in order to quickly control the magnetization direction. However, Ce:YIG films often exhibit magnetic domains with varying sizes and shapes, which presents a challenge in designing magnetooptical modulators. To address this issue, we used a large-scale parallel computing technique to perform micromagnetic simulations and calculate the magnetic domain structures of Ce:YIG films.

We employed a commercial micromagnetic simulator (EXAMAG, Fujitsu) to conduct our simulations, using a total of five nodes for parallel computing. The simulation process utilized 128 cores and 750 GB of memory. The model size was 5 microns × 5 microns × 0.2 microns (as shown in Figure 1) with a cell sizeof 10 nm × 10 nm × 10 nm. The entire model comprised 2.6×10^7 cells.

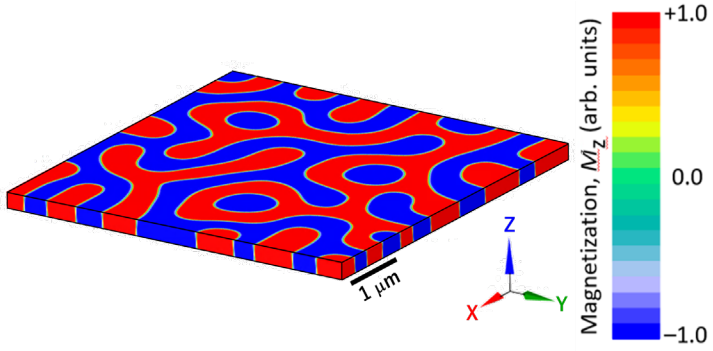


Figure 1. Steady simulation result of Ce:YIG, showing the perpendicular maze-like magnetic domains.

To obtain the initial magnetization state of the Ce:YIG film, we conducted simulations without an external magnetic field. We then utilized the energy minimization method to obtain a stable state of the magnetic moments, whereby the position and direction of magnetic moments are calculated so that the total energy of the entire model is minimized. In the simulation, we set the saturation magnetization of Ce:YIG to 225 mT and the exchange coupling constant to 3.5 pJ/m. The anisotropic magnetic field was set to 398.8 mT, with the field direction perpendicular to the film surface. These parameter values were determined based on experimental measurements.

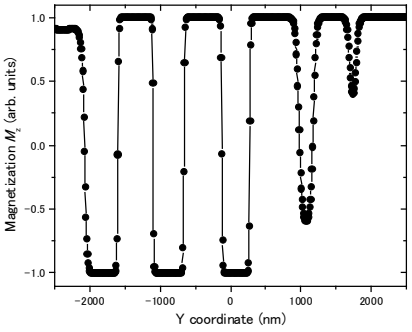


Figure 2. The plot of Z-component magnetization in Y direction.

Figure 1 shows the calculated result of the initial state of magnetization in the Ce:YIG. The maze-shaped magnetic domains were observed, with an average size of approximately 0.5 microns. Figure 2 shows the *z*-component of magnetization along the *y*-direction, where the average magnetic domains width was approximately 480 nm and the average domain wall width was approximately 12 nm. The observed domain wall type was the Bloch wall. These results suggest the presence of perpendicular maze-like magnetic domain in Ce:YIG. The next step is to calculate its magnetic properties and hysteresis loop. At the conference, we will report on the calculation of magnetic properties and other parameters, as determined from samples on another substrate.

This work was partly supported by Grants-in-Aid for Scientific Research (KAKENHI) Nos. 20H02593, 20K20535 from the Japan Society for the Promotion of Science (JSPS), Bilateral Program No. JPJSBP120214807 from JSPS and No. 21-52-50006 from RFBR, New Energy and Industrial Technology Development Organization (NEDO) No. 20002157, Tohoku Initiative for Fostering Global Researchers for Interdisciplinary Sciences (TI-FRIS) fellowship, the Foundation for Technology Promotion of Electronic Circuit Board, and the Tanaka Kikinzoku Memorial Foundation.

References

1. Y. Yoshihara, T. Sugita, P. B. Lim, Y. Tamba, H. Inoue, K. Ishiyama, M. Inoue, C. A. Ross, T. Goto, "Thickness-dependent magnetooptical properties of ion beam sputtered polycrystalline $Ce_1Y_2Fe_5O_{12}$ films", Optical Materials, 133, 112967, (2022).
2. W. E. Ross, D. Psaltis, and R.H. Anderson. "Two-dimensional magneto-optic spatial light modulator for signal processing," Optical Engineering, 22, 4, 22485, (1983).
3. T. Goto, R. Morimoto, J. W. Pritchard, M. Mina, H. Takagi, Y. Nakamura, P. B. Lim, T. Taira, and M. Inoue, "Magneto-optical Q-switching using magnetic garnet film with micromagnetic domains," Optics Express, 24, 16, 17635-17643, (2016).

META 2023, PARIS - FRANCE, JULY 18 – 21, 2023

Explaining Anomalous *Thermally Activated Delayed Fluorescence* (TADF) Response for a Phenothiazine Derivative through a TD-DFT Approach

L. Cascino[1,2*], A. Maggiore[2*], I. Rivalta[3,4], G. P. Suranna[5], R. Grisorio[5], D. Conelli[5], V. Maiorano[2*], and S. D'Agostino[1,2,6]

[1]Mathematics and Physics Department "*E. De Giorgi*", University of Salento, Lecce 73100, Italy

[2]Institute of Nanotechnology, National Research Council (CNR-NANOTEC), Lecce 73100

[3] Dipartimento di Chimica Industriale "Toso Montanari", Università di Bologna, 40136 Bologna, Italy

[4]ENSL, CNRS, Laboratoire de Chimie UMR 5182, 69364 Lyon France

[5] DICATECh, Politecnico di Bari, 70125 Bari, Italy.

[6]Center for Biomolecular Nanotechnologies, Istituto Italiano di Tecnologia, Arnesano (LE) 73010

[*]corresponding author: lucia.cascino@unisalento.it

Abstract: Thermally activated delayed Fluorescence (TADF) mechanism can occur by a complicated and fascinating route involving the triplet manifold. Here, we report a computational approach based on *Time Dependent Density Functional Theory* (TD-DFT) to shed light on the anomalous response of a phenothiazine derivative exhibiting efficient TADF only upon aggregation. The strong red-shifted peak in the photoluminescence spectrum of the molecule dispersed in a non-polar solvent (i.e. cyclohexane) is explained in terms of aggregation of monomers and dimer formation.

Molecular fluorescence is conventionally interpreted as a two-step process. An initial absorption induces an electronic transition to a singlet excited state of the quantum system, which then decays radiatively into the electronic ground state, with a certain quantum efficiency. In 2012, Adachi and co-workers [1] introduced the term TADF to indicate the phenomenon for which the singlet state can be populated-back by electrons coming from the nearest triplet state, according to what is called a reverse intersystem crossing (rISC) process. In order to achieve good TADF performance, an emitter must ensure a small enough triplet-singlet energy gap (less than 0.1 eV), [2] which allows to maximize the opportunity of harvesting triplet state by thermally activating the rISC process, i.e. high RISC rate in conjunction with minimum phosphorescence (k_P) and non-radiative (k_{ISC}) decay. Moreover, a high *Photo Luminescence Quantum Yield* is ensured trough a larger transition dipole moment between the singlet excited state and the ground state. The reduction of the singlet-triplet gap it has been shown to be achieved by charge transfer states that minimizes the exchange energy.

In this work, we investigated the TADF performance of a phenothiazine derivative consisting of a strong donor (phenothiazine) and an acceptor (fluorenone) in the quasi-equatorial conformation [3], see Fig. 1(a).

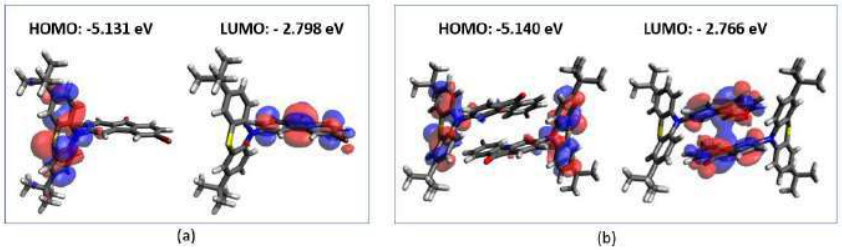


Fig. 1 (a) HOMO and LUMO orbitals of the phenothiazine derivative in the quasi-equatorial conformation. (b) HOMO and LUMO orbitals of the phenothiazine derivative excimer in the quasi-equatorial conformation relaxed in the dimer ground state.

All simulations were performed by using the ORCA 5.0 package. The geometry of the ground state was optimized in the gas phase by employing the B3LYP functionals and a TZVP basis set, with the def2/*J* auxiliary basis set for the RIJCOSX approximation to the Coulomb integrals [4]. Electronical and optical properties were analyzed for the monomer in the cyclohexane solvent, allowing identification of the first singlet (S_1) and triplet (T_3) charge transfer states. Coherently with experiments, revealing the appearance of a two-peak structure for the photoluminescence spectrum of the molecule in cyclohexane, we found out different TADF properties for the analyzed molecule in the monomer and excimer arrangements.

We performed several DFT simulations to select the most stable dimer conformation (relative orientation and distance between monomers), see Fig. 1(b), and compared its behavior to the monomer. A promising change in the relative position of the electronic states of interest for TADF and a red-shift of the emission peak, this being coherent with the appearance of an extra peak in the experimental PL spectrum (about 1 eV red-shift with respect to the monomer). The hypothesis of the formation of a dimer electronic state would, thus, explain the dependence of the TADF performance for such kind of phenothiazine derivative on the molecule concentration and aggregation conditions. This study could open new perspective toward an on-demand control and activation of the TADF phenomenon in molecules of interest for optoelectronics and nanomedicine applications.

This work was partially financed by the Research Project “PON ARS01_00951 ECOTEC_ ECO-sustainable and intelligent fibers and fabrics for TEChnic clothing (CUP B66C18000300005)”.

References

1. Uoyama, H., K. Goushi, K. Shizu, H. Nomura and C. Adachi, “Highly efficient organic light-emitting diodes from delayed fluorescence”, Nature, Vol. 492, No. 7428, 234-238, 2012.
2. Lv, L., K. Yuan, T. Zhao, and G. Dai, “Intrinsic Analysis of Thermally Activated Delayed Fluorescence (TADF) for Ag (I) Complex Based on the Path Integral Approach: Origin of the Effective Spin-Flipping Channel and Vibrational Spin-Orbit Coupling Effect”, J. Phys. Chem. A, Vol. 126, No. 38, 6695-6709, 2022.
3. Zhang, J., M. Zhu, Y. Lu, X. Zhang, S. Xiao, H. Lan and T. Yi, “Design of Stimuli-Responsive Phenothiazine Derivatives with Triplet-Related Dual Emission and High-Contrast Mechanochromism Guided by Polymorph Prediction”, Eur. J. Chem., Vol. 28, No. 29, 2022.
4. Neese, F., “The ORCA program system”, Wiley Interdiscip. Rev. Comput. Mol. Sci., Vol. 2, Issue 1, 73–78, 2012.

Inverse Design of Metalens Systems Including Refractive Lenses

Jan Bos[1], Evan Heller[2], Rob Scarmozzino[2], Mayank Bahl[2], Li-Ce Hu[3], and Chenglin Xu[2]*

[1]Synopsys Inc., Enschede, The Netherlands
[2]Synopsys Inc., Ossining, NY, USA
[3]Synopsys Inc., Hsinchu, Taiwan
*corresponding author: chenglin@synopsys.com

Abstract

The first fully automated design tool, MetaOptic Designer (MOD) [1] has been extended to design hybrid optical systems that combine metalenses with refractive lenses. In addition to metalenses, MOD can also model refractive lens accurately and efficiently. Hence, it can be used to design metalenses that correct various aberrations in existing optical system or to replace several refractive lenses in the system.

1. Introduction

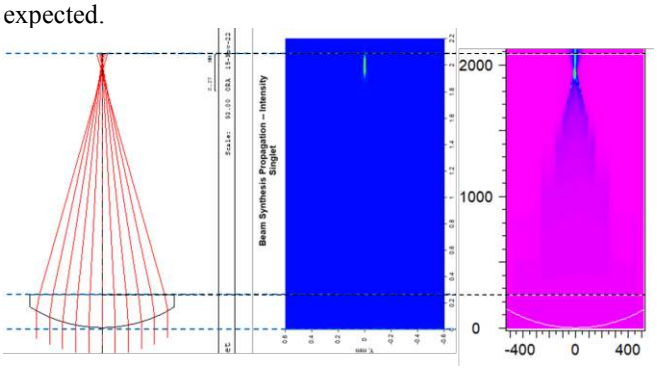
Because of their great potential to revolutionize optical products by replacing bulky curved lenses with thin, flat surfaces, metalenses have become a key enabling technology for the next generation of compact imaging, sensing, and display applications [2]. Because of the challenges in design and fabrication, however, it is difficult to replace traditional refractive lenses completely, especially for multi-functional optical systems like imaging lens systems which require both achromaticity and wide-angle. Therefore, adding metalenses to an existing optical system or partially replacing several of the bulky refractive lenses are now feasible solutions for correcting various aberrations or miniaturizing the optical system, as exemplified by Samsung [3] and LG [4].

Because of multi-scale optics involved, designing such hybrid optical systems is a challenging task. Synopsys provides leading design tools for both ray optics and electromagnetic optics and has developed a unique and proprietary technology to interface between the two optical domains seamlessly to model optical systems that combine metalenses and refractive lenses [5]. Refractive lenses designed in CODE V [6] can be directly loaded into MOD, and metalenses can be optimized subsequently within the hybrid lens system. In the following sections, we will first validate this hybrid algorithm, then apply it to hybrid optical systems.

2. Validation

The accuracy of MOD for metalenses/metasurfaces has been fully validated against rigorous FDTD for different applications [1]. Its handling of traditional refractive lenses, however, has not been verified. Therefore, it is necessary to validate MOD for refractive lens systems before applying it to hybrid optical systems.

We first apply MOD to a single plano-convex spherical lens as shown in Figure *1*. As indicted from the simulation results by different methods, the simple spherical lens suffers various aberrations and doesn't focus well as expected.



(a) (b) (c)

Figure 1: Simulation results of a simple spherical lens (a) Ray-tracing; (b) BSP; (c) MOD.

To make a quantitively comparison, the focus shift calculated by different methods is shown in Figure *2*. It is indicated that the MOD results are the same as BSP (Beam Synthesis Propagation) 0 results because both methods are based on physical optics with different base functions.

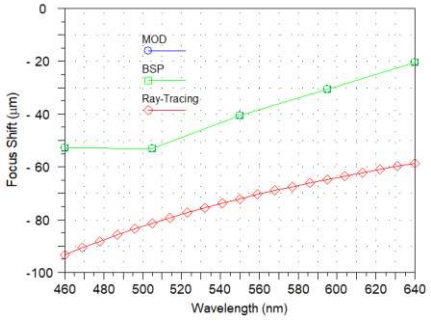


Figure 2: Focus shift of the spherical lens by different methods.

Compared with ray-tracing results, however, some discrepancy is observed. That is because different merit functions are used. In MOD and BSP, the intensity peak is used to determine the focal position, while wavefront error is used in ray-tracing. Hence, their results may differ, especially for systems with imaging aberrations.

The defocusing can be viewed more clearly in top-views zoomed around the focal position, as shown in Figure *3*. As can be observed, the simple spherical lens does not focus well over the entire visible range.

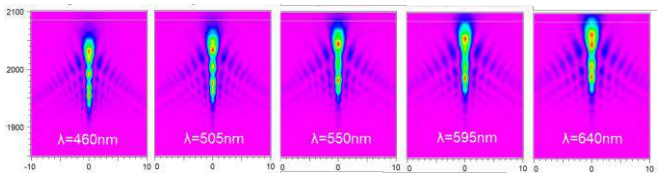


Figure 3: Defocusing over the at different wavelengths.

3. Metacorrector

To correct the chromatic and spherical aberrations, a metasurface is introduced into the optical system as shown in Figure *4*.

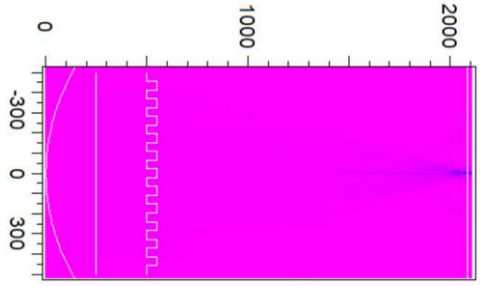


Figure 4: Hybrid optical system with both metalens and refractive lens.

A portion of the layout of the optimized metacorrector is shown Figure *5*.

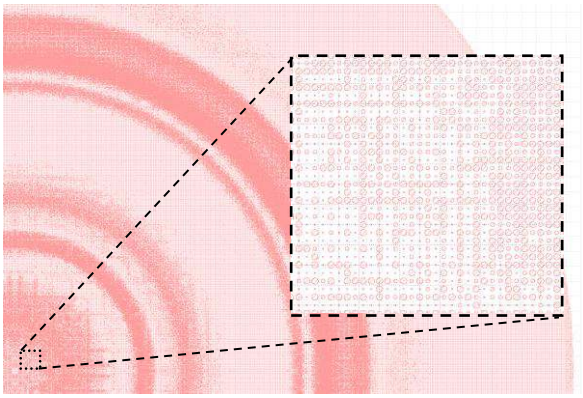


Figure 5: Layout of the optimized metacorrector.

Shown in Figure *6* are the focusing behavior of the hybrid optical system. Compared with Figure *3*, it shows the metacorrector improves the focusing significantly.

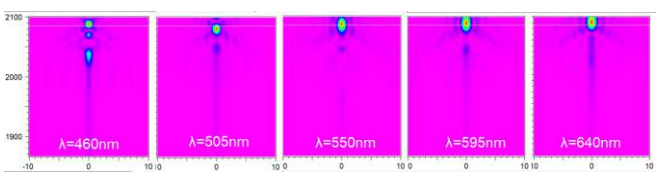


Figure 6: Focusing improvement with the metacorrector.

The focusing improvement can be compared quantitatively in focus shift as shown in Figure *7*. As observed, the metacorrector corrects both chromatic and spherical aberrations dramatically.

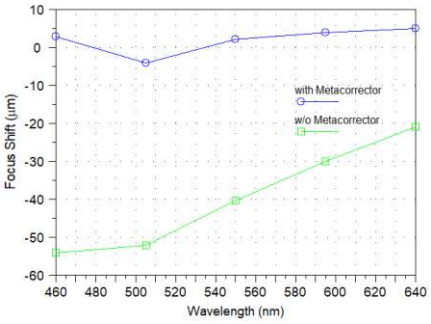


Figure 7: Comparison of the focus shift with and without metacorrector.

4. Conclusions

In summary, we have extended our inverse design tool, MetaOptic Designer to hybrid optical systems which includes both metalenses and refractive lenses. The validation showed MOD can handle refractive lenses well and that an optimized metalens can improve image quality significantly over a range of wavelenths. Furthermore, this approach can be applied to large and complex optical systems, such as those used in cellphone cameras.

References

[1] Bos, J., Scarmozzino, R., Bahl, M., Heller, E., Xu, C. "A Design Automation and Simulation Flow for Lens Systems Containing Multiple Metasurfaces", META, July 2022, Torremolinos Spain.

[2] Chen, W. T., Zhu, A. Y., & Capasso, F. (2020). Flat optics with dispersion-engineered metasurfaces. Nature Reviews Materials, 5(8), 604-620.

[3] Villas-Boas, A. (August 12, 2019). "*Samsung just unveiled the first smartphone camera that goes beyond 100 megapixels*. Business Insider". https://www.businessinsider.com/samsung-xiaomi-annonce-first-smartphone-camera-with-over-100-megapixels-2019-8?op=1

[4] Zlatev, D. (July 6, 2022). "*LG developing ultrathin camera metalens for compact and frugal electric vehicle self-driving kits"*. NotebookCheck. https://www.notebookcheck.net/LG-developing-ultrathin-camera-metalens-for-compact-and-frugal-electric-vehicle-self-driving-kits.633472.0.html

[5] Xu, C., Heller, E., Bos, J., Scarmozzino, R., Bahl, M., Hu, L-C., and Achuthan, N., " Fully Automated Inverse Design Solution for Metalenses/Metasurfaces." In *SPIE Photonics West,* pp. 12428-1. 2023

[6] https://www.synopsys.com/optical-solutions/codev.html https://www.synopsys.com/optical-solutions/codev/feature-closeup.html

Level-set optimization of non-reciprocal media

C. M. Cisowski[1*], R. Bennett[1]

[1]School of Physics and Astronomy, University of Glasgow, Glasgow, UK
[*]Corresponding author: clairemarie.cisowski@glasgow.ac.uk

Abstract: Non-reciprocal photonics holds transformative potential for energy harvesting and optical information processing. While computer assisted design techniques have become widespread approaches for tailoring and enhancing optical devices, devices based on non-reciprocal media constitute a missing entry in the growing catalogue of inverse-designed technology. In this work, we exploit a Green's tensor formalism to introduce a level-set method for the inverse design of a non-reciprocal material for the example of a point-based intensity optimization problem.

Inverse design engineering generates structures based on a set of desired properties and characteristics; it has gained in popularity in recent years due to its capacity to outperform traditional numerical techniques [1]. The majority of inverse design algorithms developed for optics exploit Lorentz reciprocity to reduce the time of the optimization process, making its implementation for non-reciprocal media an arduous process.

We propose a solution to this problem by basing our algorithm entirely on the use of electromagnetic dyadic Green's tensor, $\mathbf{G}(\mathbf{r},\mathbf{r}',\omega)$ which describes the propagation of a plane-wave electric field of frequency ω from a source point $\mathbf{r}'$ to an observation point $\mathbf{r}$ [2]**.** This method was introduced in [3] in the context of atomic interactions in external environments. Here we show that this method is particularly effective for tailoring non-reciprocal media. Using the finite difference time domain techniques, we demonstrate how our approach can be implemented to solve a three-dimensional point-based intensity optimization problem for the case of a gyrotropic medium. The inverse design technique used in our study is a topology optimization method.

This work unlocks new avenues for enhancing and tailoring nonreciprocal effects, enabling the development of a new set of optical devices with outstanding performances and functionalities, including optical isolators and circulators for photonics integrated circuits [4].

The authors acknowledge financial support from the UK Research and Innovation Council (UKRI) grant EP/W016486/1.

References

1. Molesky, S., et al. "Inverse design in nanophotonics" Nat. Photonics, Vol. 12, 659-670, 2018.
2. Asadchy, V. S et al. "Tutorial on Electromagnetic Nonreciprocity and its origins" Proc. IEEE, Vol. 108, 1984-1727, 2020.
3. Bennett, R., Buhmann, S. Y., "Inverse design of light–matter interactions in macroscopic QED," New J. Phys., Vol. 22, 093014, 2020.
4. Bi, L. "Materials for nonreciprocal photonics" MRS Bulletin, Vol. 43, No. 6, 408-412, 2018.

Ray-Optical Analysis for Optimization of Light Absorption in the Double-Junction III-V Solar Cells with Luminescent Solar Concentrators

Dongjae Baek[1], Shin Hyung Lee[2], Kwangjin Kim[1], Sung-Min Lee[2,3*] and Seungwoo Lee[1, 4, 5, 6*]

[1]KU-KIST Graduate School of Converging Science and Technology, Korea University, Seoul, Republic of Korea,
[2]School of Materials Science and Engineering, Kookmin University, 77 Jeongneung-ro, Seongbuk-gu, Seoul, South Korea
[3]Terasaki Institute for Biomedical Innovation, Los Angeles, California, United States
[4]Department of Biomicrosystem Technology, Korea University, Seoul, Republic of Korea,
[5]Department of Integrative Energy Engineering, Korea University, Seoul, South Korea
[6]KU Photonics Center, Korea University, Seoul, Republic of Korea
*corresponding author : S.-M.L. (sungminlee@kookmin.ac.kr), S.L. (seungwoo@korea.ac.kr)

Abstract: In order to enhance the light collection and absorption of III-V photovoltaic, the optimal cell geometry has been the subject of continuous research. For example, solar concentrators have been one of the attempts to increase the density of incident photon flux. However, as optic elements such as mirrors and lenses are inevitably required, There was an issue that not only the volume of the entire system but also the thermal density increased. In this work, we suggest the strategy to the optimal light-trapping structure for monolithic III-V double junction solar cell implemented with luminescence solar concentrator by systematic analysis, integrating ray-optical analysis with Shockley-queisser limit.

Luminescent Solar Concentrator has been attracting attention as an excellent alternative to solar concentrators. Unlike optical solar concentrator, it adopts luminophores that emit light omni-directionally in the multi-mode slab waveguide, so it does not only require bulky sun-tracker system and thermal cooler, but also it is much more advantageous in module assembly and shows excellent light collecting power in diffused sun light.

However, when this Luminescent Solar Concentrator was applied to double junction III-V, it suffered loss in photon energy due to energy downshifting, and it was difficult to achieve a great improvement in the increase of the collective output current of series-connected subcells.

In this study, we extend the geometrical optical absorption criterion of solar cells proposed by E. Yablonovitch to a structure containing a Luminescent Solar Concentrator, building a model based on ray optics, we could get a clue how the geometry and refractive index of a multimode slab waveguide affect the distribution of rays in the overall system[1].

Furthermore, we determined the quantum efficiency, absorption wavelength and emission wavelength of the luminophores to match the subcell absorption region of the double-junction solar cell while reflecting the full spectrum of sunlight and found the structural optimization conditions for the structure of the double junction III-V solar cell with Luminescent Solar Concentrator. This was possible through not only rigorous ray optical, but also the detailed balance analysis with our integrated modeling which can convert the light flux on photovoltaics into the electric properties of device, such as the short-curcuit current, open-circuit voltage and fill factor, etc[2].

As a result, the multi-junction solar cells were arranged co-planar with the multimode slab waveguide so that they could simultaneously take the directly illuminated solar photon flux and the light emitted from the luminophores. Then the thickness and refractive index of each slab were adjusted, the wave guided light was appropriately induced to the sub cell[3].

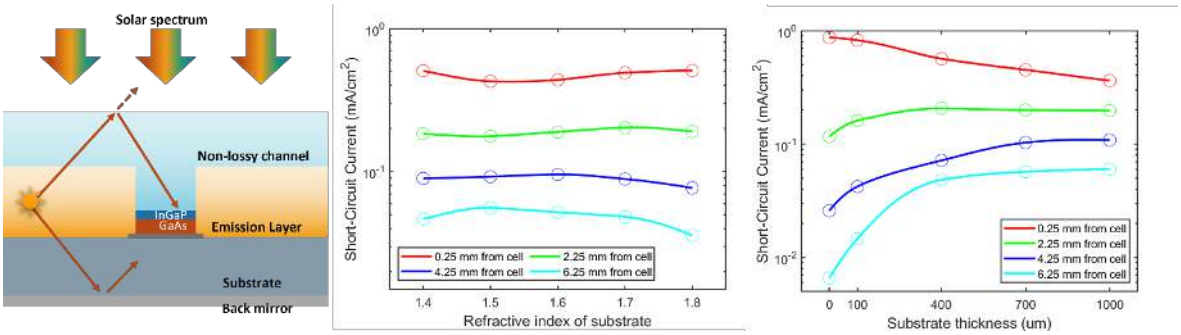


Figure 1: (a) Schematic of III-V Photovoltaic with Luminescent Solar Concentrator that condenses light from direct sunlight and luminophores. (b) Short circuit current increase due to induced light according to the refractive index of the substrate layer. (c) Short circuit current increase due to induced light according to the thickness of the substrate layer.

Acknowledgements, This work was supported by National Research Foundation of Korea (NRF) funded by the Ministry of Science, ICT under Grant NRF-2019R1A2C2004846 and NRF-2022M3H4A1A02074314. Also, This work was supported by the New & Renewable Energy Core Technology Program of the Korea Institute of Energy Technology Evaluation and Planning (KETEP) granted financial from the Ministry of Trade, Industry & Energy, Republic of Korea (No. 20203040010320).

References

1. E. Yablonovitch, "Statistical ray optics," *J. Opt. Soc. Am.* **72**, 899–907 (1982).
2. W. Shockley and H. J. Queisser, "Detailed Balance Limit of Efficiency of p-n Junction Solar Cells," Journal of Applied Physics 32, 510−519 (1961).
3. S. H. Lee, D. Baek, W. Cho, N. Lee, K. Kim, J.-H. Kim, H.-J. Kim, H. H. Kim, H. J. Kim, S. Lee, and S.-M. Lee, "Tailoring Luminescent Solar Concentrators for High-Performance Flexible Double-Junction III-V Photovoltaics," Advanced Functional Materials **33**, 2210357 (2023).

Band gap tuning based on adjustable stiffness of local resonators

H. Alimohammadi[1*], K. Vassilyeva[1], H. HosseinNia[2], and E. Petlenkov[1]

[1]Computer Systems Department, Tallinn University of Technology, 12618 Tallinn, Estonia
[2]Precision and Microsystems Engineering Department, Delft University of Technology, 2628 Delft, The Netherlands
[*]corresponding author: hossein.alimohammadi@taltech.ee

Abstract: This research explores the feasibility of using a cantilever-type resonator beam to achieve tunable and real-time control of vibration suppression. By varying the center of mass of the attached masses, the bandgap and transmittance response can be significantly impacted. The results suggest potential for improving resonator performance and optimizing metamaterial beams for vibration suppression applications.

Summary:

The method involves analyzing the propagation of acoustic waves through a phononic structure with one, two, and four beams connected to a non-uniform beam-type resonator. The frequency response of the tip of the Euler-Bernoulli beam is monitored to verify the outcomes found in the dispersion curves. The equation of motion is solved using a harmonic input force, with periodic boundary conditions and Floquet periodicity taken into account for accurate results. The study demonstrates the feasibility of using a cantilever-type resonator instead of a lumped mass spring for examining other modes of the resonator and tuning and controlling the bandgap characteristics of the beam in real-time experiments. A simulation is performed using finite element software.

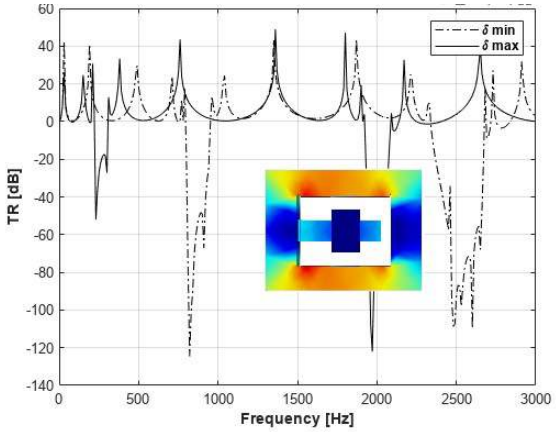


Fig.1. Transmittance responses of the first and second mode of resonator with μ=0.9 for different δ.

By using a cantilever-type resonator instead of a lumped mass spring, it becomes feasible to examine other modes of the resonator. Fig.1 shows the transmittance responses of the first and second mode of the resonator with a high mass ratio of μ=0.9 for different values of resonator center of mass (δ). The second mode is observed in the transverse vibration of the beam, and the attached mass on the resonator material is replaced from PLA to steel to decrease the natural frequency of the resonator to the desired frequency range. The result shows the same behaviour in the second mode as well, and the variation of δ changes the bandwidth and edge of bandgap similar to first mode.

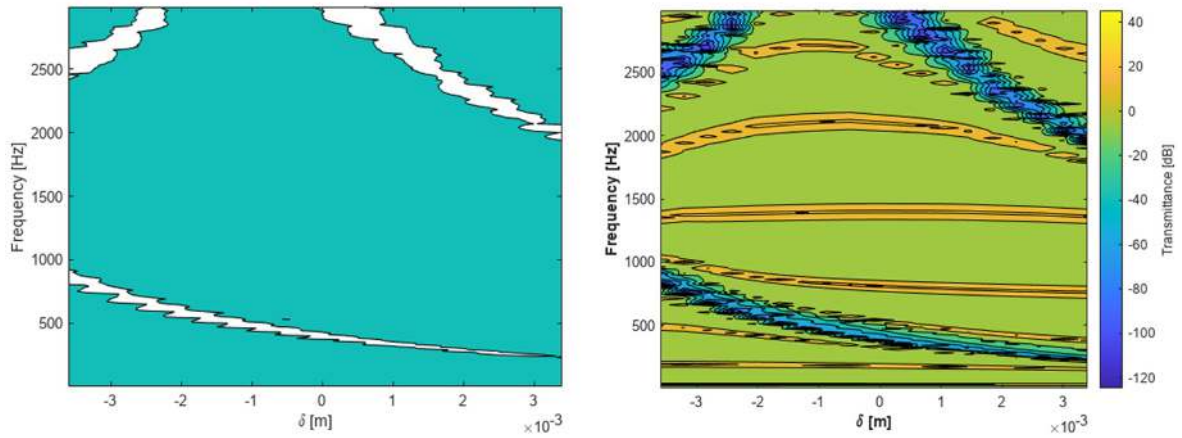


Fig.2. Contour and Image binarization of the transmittance using -40 dB as reference in response to the variation of δ, and μ=0.9.

Fig.2 shows the binary representation of the transmittance contour pattern evolution with changes in δ for a high mass ratio of μ=0.9. The image binary contour of the transmittance for μ=0.9 and -40 dB as reference is shown in Fig.2. The second mode of resonator creates an additional gap in higher frequencies, as shown in the top part of Fig.2. This result suggests that using a cantilever-type resonator instead of a lumped mass spring allows the study of other modes of the resonator. Moreover, the change in attached mass and mass ratio allows for tuning and controlling the bandgap characteristics of the beam in real-time experiments.

In conclusion, this research has examined the possibility of tuning the band gap of beam-type resonators based on adjustable stiffness to achieve broadband vibration suppression. Through the analysis of dispersion relations and the binary representation of transmittance contour patterns, it has been demonstrated that the center of masses of attached masses does not significantly affect the vibration suppression performance of the metamaterial beam. However, by using a cantilever-type resonator instead of a lumped mass spring, it has become possible to examine other modes of the resonator and to tune and control the bandgap characteristics of the beam in real-time experiments. This study has provided valuable insights into the design and optimization of graded metamaterial beams for vibration suppression applications.

Acknowledgment: This work has been partially conducted in the project "ICT programme" which was supported by the European Union through the European Social Fund. It was also supported by the Estonian Research Council grant PRG658.

References

1. X. Wu, Y. Li, and S. Zuo, “The study of a locally resonant beam with aperiodic mass distribution,” Appl. Acoust., vol. 165, 2020.

2. Z. Tao et al., “A novel auxetic acoustic metamaterial plate with tunable bandgap,” Int. J. Mech. Sci., vol. 226, p. 107414, Jul. 2022.

3. Y. Jian, L. Tang, G. Hu, Z. Li, and K. C. Aw, “Design of graded piezoelectric metamaterial beam with spatial variation of electrodes,” Int. J. Mech. Sci., vol. 218, 2022.